

# EUROPEAN AEROSOL CONFERENCE 2007

SEPTEMBER 9 – 14, 2007  
SALZBURG, AUSTRIA

**EAA**

European Aerosol Assembly



Gesellschaft für  
Aerosolforschung  
(GAeF)



**UNIVERSITÄT**  
SALZBURG

# European Aerosol Conference 2007

Salzburg, Austria, September 9 to 14, 2007

Organized by Gesellschaft für Aerosolforschung, Conference Chair: Prof. Werner Hofmann

## Contents

Foreword	pp. 4-5
Program, orals and posters	pp. 6-33 (orals), pp. 34-65 (posters)
Abstracts	
Plenary lectures	pp. 66-72
T01 Abstracts	pp. 73-134
T02 Abstracts	pp. 135-194
T03 Abstracts	pp. 195-198
T04 Abstracts	pp. 199-232
T05 Abstracts	pp. 233-243
T06 Abstracts	pp. 244-277
T07 Abstracts	pp. 278-295
T08 Abstracts	pp. 296-322
T09 Abstracts	pp. 323-383
T10 Abstracts	pp. 384-425
T11 Abstracts	pp. 426-477
T12 Abstracts	pp. 478-529
T13 Abstracts	pp. 530-530
T14 Abstracts	pp. 531-568
T15 Abstracts	pp. 569-587
T16 Abstracts	pp. 588-595
T17 Abstracts	pp. 596-616
T18 Abstracts	pp. 617-621
T19 Abstracts	pp. 622-696
T20 Abstracts	pp. 697-710
T21 Abstracts	pp. 711-723
T22 Abstracts	pp. 724-729
T23 Abstracts	pp. 730-740
T24 Abstracts	pp. 741-752

T25 Abstracts	pp. 753-786
T26 Abstracts	pp. 787-816
T27 Abstracts	pp. 817-825
T28 Abstracts	pp. 826-856
T29 Abstracts	pp. 857-884
T30 Abstracts	pp. 885-913
T31 Abstracts	pp. 914-934
T32 Abstracts	pp. 935-945
T33 Abstracts	pp. 946-957
WGLPI Abstracts	pp. 958-

# Foreword

# PREFACE

The European Aerosol Conference (EAC) is the annual European meeting place of the international research community working in the field of aerosol science and technology. These annual conferences are organised under the auspices of the European Aerosol Assembly (EAA), which selects the venue of the EAC for each year. In this year, the EAC 2007 is held in Salzburg, Austria, jointly organised by the Gesellschaft für Aerosolforschung (GAeF) and the University of Salzburg as the host institution.

The EAC 2007 in Salzburg is so far the largest in the history of the EAC with 811 submitted abstracts, including 5 plenary speakers. The submitted abstracts were reviewed by the EAA Working Groups and members of the Organising Committee and assigned to oral and poster sessions. Each day, from Monday through Friday, the conference starts with a plenary lecture, which covers a topic of general interest to everybody. The plenary lectures are followed by oral sessions, with 5 sessions running in parallel. In these 45 oral sessions, altogether 270 platform presentations will be given, with 6 presentations in each session. In addition, 3 special oral sessions, suggested by members of the EAA, address issues of interest to a specific group. The 534 posters are arranged in 2 poster sessions, covering a wide range of scientific topics, and the posters presented in a poster session will be on display for two days.

The importance of the Working Groups within the EAA, besides their role in reviewing the submitted abstracts, is illustrated by the individual sessions of the 10 Working Groups during the Conference. A special highlight of the EAC 2007 will be the public lecture of Prof. Andreae on Tuesday evening on the effects of aerosols on climate changes, which will also be open to the interested public.

The organisers of the EAC 2007 gratefully acknowledge the efforts of the EAA Working Groups, who were involved in the review process, and of the members of the Scientific Committee, who suggested plenary speakers and helped in setting up the various special sessions. We would also like to thank the Rector and the administration of University of Salzburg for providing the facilities of the NAWI for this conference. Finally, we are grateful to all sponsors and exhibitors for their financial support.

Werner Hofmann  
University of Salzburg  
Conference Chairman

# Program

**We have received in total 811 abstracts, 444 of them were submitted for oral presentation. At least we have in the five parallel sessions 270 slots for an oral presentation.**

[Sunday 9 September 2007](#)    [Monday 10 September 2007](#)    [Tuesday 11 September 2007](#)  
[Wednesday 12 September 2007](#)    [Thursday 13 September 2007](#)    [Friday 14 September 2007](#)  
[Saturday 15 September 2007](#)    [Poster Session Part I \(Tuesday\)](#)    [Poster Session Part II \(Thursday\)](#)

## [Sunday 9 September 2007](#)

08:00	Sound of Music Tour (organized by SEMACO)
15:00	Schloß Hellbrunn Tour (organized by SEMACO)

Sunday 9 September 2007	17:00 - 19:00	Pre-Registration
-------------------------	---------------	------------------

Sunday 9 September 2007	18:00 - 21:00	Welcome Party
-------------------------	---------------	---------------

[Top of Program](#)

## Monday 10 September 2007

Monday 10 September 2007	08:00 - 16:15	Registration
--------------------------	---------------	--------------

Monday 10 September 2007	08:30 - 10:00	AudiMax
--------------------------	---------------	---------

Opening Ceremony

Plenary Lecture I

Chair: Michael Shapiro

08:45	<a href="#">Plenary Lecture</a>	Materials Synthesis: Contributions and Challenges to Aerosol Science <i>Sotiris E. Pratsinis</i>
-------	---------------------------------	---

09:40	Obituary	Werner Stöber <i>Helmuth Horvath</i>
-------	----------	---

09:50	Obituary	Sheldon K. Friedlander <i>Sotiris E. Pratsinis</i>
-------	----------	---

Monday 10 September 2007	10:00 - 10:15	Coffee Break
--------------------------	---------------	--------------

Monday 10 September 2007	10:15 - 12:15	AudiMax
--------------------------	---------------	---------

<b>Atmospheric Aerosols - Nucleation</b>		
<b>Chairs: Amar Hamed and Michael Boy</b>		
10:15	<a href="#">T13A106</a>	<b>Mechanistic investigations on the formation of atmospheric H<sub>2</sub>SO<sub>4</sub>/H<sub>2</sub>O particles</b> <i>T. Berndt, O. Böge, and F. Stratmann</i>
10:35	<a href="#">T13A215</a>	<b>Formation of secondary organic aerosols by ozonolysis of plant-released volatiles</b> <i>J. Joutsensaari, P. Yli-Pirilä, D.M. Pinto, P. Tiiva, J. Heijari, A.-M. Nerg, J.K. Holopainen, P. Miettinen, P. Tiitta, J. Rautiainen, H. Kokkola, D.R. Worsnop, and A. Laaksonen</i>
10:55	<a href="#">T13A110</a>	<b>Investigating the composition of newly formed atmospheric aerosols with CPC battery</b> <i>H.E. Manninen, M. Kulmala, I. Riipinen, T. Petäjä, T. Grönholm, P.P. Aalto, M. Sipilä, and K. Hämeri</i>
11:15	<a href="#">T13A112</a>	<b>Comparison of H<sub>2</sub>SO<sub>4</sub> concentrations and new particle formation during 26 months in Hyytiälä, Finland</b> <i>T. Nieminen, M. Kulmala, I. Riipinen, M. Boy, and L. Laakso</i>
11:35	<a href="#">T13A239</a>	<b>Cosmic ray induced formation of atmospheric aerosol particles and cloud condensation nuclei: New insights from atmospheric trace gas and ion measurements and laboratory investigations of ion induced nucleation</b> <i>F. Arnold, V. Fiedler, H. Aufmhoff, T. Schuck, R. Nau, L. Pirjola, T. Jurkat, U. Reichel, A. Roiger, A. Sorokin, and H. Schlager</i>
11:55	<a href="#">T13A228</a>	<b>CCN properties of ambient aerosol particles during nucleation events</b> <i>U. Dusek, J. Curtius, G.P. Frank, F. Drewnick, A. Kürten, J. Schneider, M.O. Andreae, and U. Pöschl</i>
Back-up Paper	<a href="#">T13A144</a>	<b>A comparison of new particle formation events in Eastern Germany and in Northern East Italy based on a three-year-analysis</b> <i>A.Hamed, B.Weohner, W.Birmili, A.Wiedensohler, F.Cavalli, M.C.Facchini, J.Joutsensaari, and A.Laaksonen</i>

<b>Monday 10 September 2007</b>		<b>10:15 - 12:15</b>	<b>Blauer Hörsaal</b>
<b>Aerosol Chemistry - General I</b>			
<b>Chairs: Hans Puxbaum and Magda Claeys</b>			
10:15	<a href="#">T01A001</a>	<b>Imaging the chemical composition of the surface of atmospheric particles</b> <i>A. Krein, J.-N. Audinot, H.-N. Migeon, and L. Hoffmann</i>	
10:35	<a href="#">T01A010</a>	<b>Characterization of single urban dust particles from different urban location across UK</b> <i>M. Dall'Osto, R.M. Harrison, and A. Thorpe</i>	
10:55	<a href="#">T01A025</a>	<b>Heterogeneous reactions of unsaturated fatty acid aerosols with ozone: Reaction pathways and changes of particle mass, hygroscopicity and morphology</b> <i>A.K.Y. Lee and C.K. Chan</i>	
11:15	<a href="#">T01A045</a>	<b>Photochemical degradation study of pesticides adsorbed on atmospheric aerosols</b> <i>M. Pflieger, M. Goriaux, B. Temime, A. Monod, and H. Wortham</i>	
11:35	<a href="#">T01A046</a>	<b>Subcooled liquid saturation vapour pressures of C3-C6 dicarboxylic acids</b> <i>I. Riipinen, I.K. Koponen, M. Bilde, A. Hienola, and M. Kulmala</i>	
11:55	<a href="#">T04A049</a>	<b>Heterogeneous interactions of NO<sub>2</sub> with solid (NH<sub>4</sub>)<sub>2</sub>SO<sub>4</sub> surfaces</b> <i>C. Aghnatiou, S. Sobanska, F. Louis, and D. Petitprez</i>	
Back-up Paper	<a href="#">T01A024</a>	<b>Raman characterization of double salt formation from crystallization of mixed ammonium sulfate and ammonium nitrate particles</b> <i>T.Y. Ling and C.K. Chan</i>	

<b>Monday 10 September 2007</b>		<b>10:15 - 12:15</b>	<b>Grüner Hörsaal</b>
<b>Nanoparticles - Applications</b>			
<b>Chairs: Mansoo Choi and Knut Deppert</b>			
10:15	<a href="#">T09A002</a>	<b>Flame spray synthesis of nanostructured Perovskite-composites for fuel cell applications</b> <i>A. Heel, A. Vital, P. Holtappels, and T. Graule</i>	
10:35	<a href="#">T09A008</a>	<b>Enhancement of transport properties of Bi-2212 high temperature superconductor by</b>	

		<b>doping with MgO nanoparticles</b>
		<i>I.E. Agranovski, A.Y. Iluyshchkin, I.S. Altman, and M. Choi</i>
<b>10:55</b>	<b>T09A016</b>	<b>Characterisation of industrial aerosol nanoparticle generation process</b>
		<i>M. Aromaa, H. Keskinen, J.M. Mäkelä, M. Piispanen, L. Hupa, K. Deppert, S. Persson, M. Lang, P. Sandberg, G. Gunnarsson, J. Pimenoff, T. Kronberg, V. Pore, M. Ritala, M. Leskelä, and M. Raul</i>
<b>11:15</b>	<b>T09A023</b>	<b>Aerosol spray pyrolysis synthesis of spinel-supported catalysts for hydrogen production via solar-aided steam reforming of natural gas</b>
		<i>A. Zygianni, S. Lorentzou, P. Dimotikalis, C. Agrafiotis, and A.G. Konstandopoulos</i>
<b>11:35</b>	<b>T09A030</b>	<b>Fabrication of nanopillars for chemical analysis using deposited silica aerosol particles as etching mask</b>
		<i>J. M. Mäkelä, H. Keskinen, M. Aromaa, L. Sainiemi, L. Luosujärvi, T. Kotiaho, and S. Franssila</i>
<b>11:55</b>	<b>T09A049</b>	<b>Micro patterning sensors by flame spray aerosol deposition</b>
		<i>A. Tricoli, M. Graf, F. Mayer, S. Kühne, A. Hierlemann, and S. E. Pratsinis</i>
<b>Back-up Paper</b>	<b>T09A004</b>	<b>Air stable, carbon coated metal nanoparticles of sensor applications</b>
		<i>E.K. Athanassiou, R.N. Grass, and W.J. Stark</i>

<b>Monday 10 September 2007</b>	<b>10:15 - 12:15</b>	<b>Lecture Hall 414</b>
<b>Fundamental Aerosol Physics - Aerosol Dynamics</b>		
<b>Chairs:</b>	<b>Jose L. Castillo and Oliver Bischof</b>	
<b>10:15</b>	<b>T06A029</b>	<b>Cone-jet formation in nanospray atomisation</b>
		<i>S. Paredes-Egea and J. Rosell-Llompart</i>
<b>10:35</b>	<b>T06A027</b>	<b>Studies in electro-hydrodynamic spraying of water in standard CO<sub>2</sub></b>
		<i>B. Sersante and J. Rosell-Llompart</i>
<b>10:55</b>	<b>T06A032</b>	<b>Mobility of doublets of two different spheres in the transition regime</b>
		<i>Th. Weber, A. Maisels, and F.E. Krus</i>
<b>11:15</b>	<b>T06A021</b>	<b>Dynamics of porous aerosol particles under thermal gradients</b>
		<i>A. Perea, P.L. Garcia-Ybarra, and J.L. Castillo</i>
<b>11:35</b>	<b>T06A013</b>	<b>Particle deposition in a critical orifice</b>
		<i>S.C. Chen, C.J. Tsai, C.H. Wu, and A. Onischuk</i>
<b>11:55</b>	<b>T06A023</b>	<b>Simultaneous characterisation and manipulation of aerosol particles</b>
		<i>J.R. Butler, L. Mitchem, and P. Reid</i>
<b>Back-up Paper</b>	<b>T06A010</b>	<b>Investigation of the nanoparticles diffusion coefficient temperature dependence</b>
		<i>V.Y. Rudyak, S.N. Dubtsov, S.L. Krasnolytskii, and A.M. Baklanov</i>

<b>Monday 10 September 2007</b>	<b>10:15 - 12:15</b>	<b>Lecture Hall 421</b>
<b>Electrical Effects</b>		
<b>Chairs:</b>	<b>Jan Marijnissen and Tomasc Ciach</b>	
<b>10:15</b>	<b>T05A002</b>	<b>Reactive formation, charging, and deposition of nanosized TiO<sub>2</sub> particle</b>
		<i>H. Wiggers, P. Ifeacho, M. Barthel, B. Kock, and C. Schulz</i>
<b>10:35</b>	<b>T05A006</b>	<b>Structure of the deposits collected from EHD dispersion of carbon suspensions</b>
		<i>I.G. Loscertales, J.C. González, D. Galán, A. Perea, P.L. García-Ybarra, J.L. Castillo, M. Marquez, and A. Barrero</i>
<b>10:55</b>	<b>T05A007</b>	<b>Reduction of relaxation times during electro spraying</b>
		<i>U. Stachewicz, D. Burdinski, J.F. Dijkstra, and J.C.M. Marijnissen</i>
<b>11:15</b>	<b>T05A008</b>	<b>Aerosol mobility spectrometry based on diffusion charging</b>
		<i>L. Hillemann, A. Zschoppe, and R. Caldwell</i>
<b>11:35</b>	<b>T05A009</b>	<b>Evaluation of a drained DBD electrode apparatus for nano-particle charging</b>
		<i>M. Wild, J. Meyer, and G. Kasper</i>
<b>11:55</b>	<b>T05A010</b>	<b>Aerosol coatings for medical implants</b>

		<i>T. Ciach, W. Swierzkowski, and P. Grzybowski</i>
Back-up Paper	T05A004	<b>Novel wet space-charge electrostatic precipitator for fine particles</b>
		<i>A.M. Bologna, H.-R. Paur, H. Seifert, and K. Woletz</i>

<b>Monday 10 September 2007</b>	<b>12:15 - 13:45</b>	<b>Lunch Break</b>
<b>Monday 10 September 2007</b>	<b>12:15 - 13:45 (Meeting Room)</b>	<b>EAA Board Meeting</b>

<b>Monday 10 September 2007</b>	<b>13:45 - 15:45</b>	<b>AudiMax</b>
---------------------------------	----------------------	----------------

### Atmospheric Aerosols - Optical Properties

**Chairs:** Otmar Schmid and Lucas Alados-Arboledas

13:45	T13A010	<b>Retrieval of water vapor and of the optical-microphysical-chemical properties of tropospheric aerosols using a compact 6-wavelength Raman-lidar system</b> <i>A. Papayannis, R.E. Mamouri, A. Nenes, G. Avdikos, G. Chourdakis, G. Georgoussis, C. Böckmann, Kirsche, K. Eleftheriadis, G. Tsaknakis, and L. Schneidenbach</i>
14:05	T13A082	<b>Measurement of the optical and physical properties of light-duty and heavy-duty vehicle emissions</b> <i>A.W. Strawa, A.G. Hallar, T.W. Kirchstetter, G.A. Ban-Weiss, J.P. McLaughlin, R.A. Harley, M.M. Lunden, A.J. Kean, E.D. Stevenson, and G.R. Kendall</i>
14:25	T13A086	<b>Aerosol refractive index and extinction coefficient calculated from chemical data</b> <i>D. Benko, Á. Molnár and K. Imre</i>
14:45	T13A090	<b>Ambient single scattering albedo at the high alpine site Jungfraujoch</b> <i>M. Collaud Coen, E. Weingartner, R. Nessler, and U. Baltensperger</i>
15:05	T13A101	<b>Comparison of aerosol characteristics retrieved from scattering in local volume and extinction on horizontal path</b> <i>S.A. Terpugova, M.V. Panchenko, V.N. Uzhegov, T.A. Dokukina, and Y.A. Pkhalagov</i>
15:25	T13A046	<b>Refractive index measurements of size separated aerosol particles with a polar nephelometer</b> <i>F. Prodi, G. Santachiara, L. Di Matteo, F. Belosi, and M.R. Perrone</i>
Back-up Paper	T13A204	<b>Characterization of the atmospheric aerosol properties during ESTIO2005 field campaign: an interdisciplinary approach</b> <i>L. Alados-Arboledas, H. Horvath, X. Querol, F.J. Olmo, J.L. Guerrero-Rascado, H. Lyamani, M. Gangl, S. Castillo, and A. Alastuey</i>

<b>Monday 10 September 2007</b>	<b>13:45 - 15:45</b>	<b>Blauer Hörsaal</b>
---------------------------------	----------------------	-----------------------

### Aerosol Chemistry - General II

**Chairs:** Erik Swietlicki and Harald Saathoff

13:45	T01A054	<b>Ammonia uptake by organic aerosols and its effect on their water uptake properties</b> <i>E. Dinar and Y. Rudich</i>
14:05	T01A017	<b>Physicochemical characterization of nitrated and oxygenated polycyclic aromatic hydrocarbons in the atmospheres of two French alpine valleys</b> <i>A. Albinet, E. Leoz-Garziandia, H. Budzinski, E. Villenave, and J.-L. Jaffrezo</i>
14:25	T01A006	<b>Water soluble organic compounds of aerosols as metal complexing ligands</b> <i>G. Szentes, E. Schmidt, and A. Marton</i>
14:45	T01A014	<b>Secondary organic carbon in the urban area of Rome</b> <i>M. Manigrasso and P. Avino</i>
15:05	T01A026	<b>Oxygenated organic aerosols: bridging field and smog chamber observations</b> <i>M.R. Alfara, A.S.H. Prevot, J. Duplissy, A. Metzger, V. A.Lanz, C. Hueglin, J. Dommen, E. Weingartner, and U. Baltensperger</i>
15:25	T01A027	<b>Functional group monitoring in atmospheric particulate organic matter using tandem</b>

		<b>mass spectrometry: method developments and applications</b>
		<i>J. Dron, N. Marchand, M. Camredon B. Aumont, and H. Wortham</i>
Back-up Paper	<a href="#">T01A007</a>	<b>Crucial intermediates of benzaldehyde photolysis: Their roles in gas-to-particle conversion</b>
		<i>S.N. Dubtsov, G.G. Dultseva, and G.I. Skubnevskaya</i>

<b>Monday 10 September 2007</b>	<b>13:45 - 15:45</b>	<b>Grüner Hörsaal</b>
<b>Special Session: Fluctuations and Atmospheric Aerosols</b>		
<b>Chairs: Charles F. Clement and Jorma Jokiniemi</b>		
13:45	<a href="#">T21A004</a> invited	<b>Caustics, collisions and the Stokes trap in turbulent aerosols</b> <i>M. Wilkinson and B. Mehlig</i>
14:25	<a href="#">T22A001</a>	<b>Aerosol fluctuations and condensation</b> <i>C.F. Clement</i>
14:45	<a href="#">T22A002</a>	<b>Homogeneous nucleation in wake flows</b> <i>J. Pyykönen, S. Garrick, and J. Jokiniemi</i>
15:05	<a href="#">T13A043</a>	<b>Hot-air balloon measurements of vertical variation of boundary layer new particle formation</b> <i>L. Laakso, T. Grönholm, S. Haapanala, A. Hirsikko, T. Kurtén, M. Boy, A. Sogachev, I. Riipinen, M. Kulmala, L. Kulmala, E.R. Lovejoy, J. Kazil, D. Nilsson, and F. Stratmann</i>
15:25	<a href="#">T13A207</a>	<b>New statistical methods of analysis of atmospheric aerosols</b> <i>G. Gramotnev and D.K. Gramotnev</i>

<b>Monday 10 September 2007</b>	<b>13:45 - 15:45</b>	<b>Lecture Hall 414</b>
<b>Indoor Aerosols</b>		
<b>Chairs: Konstantinos Eleftheriadis and Joakim Pagels</b>		
13:45	<a href="#">T07A001</a>	<b>Removal of aerosol pollutants by portable ionic air purifiers in a well-ventilated room</b> <i>S.A. Grinshpun, T. Lee, J.H. Jung, and T. Reponen</i>
14:05	<a href="#">T07A003</a>	<b>Characterization of particulate matter during simulated indoor activities</b> <i>J. Ondráček, L. Džumbová, T. Glytsos, I. Kopanakis, and M. Lazaridis</i>
14:25	<a href="#">T07A013</a>	<b>Particles in various Swedish indoor environments: size distributions, number and mass concentrations</b> <i>A. Wierzbicka, A. Gudmundsson, J. Pagels, A. Dahl, J. Löndahl, E. Swietlicki, and M. Bohgard</i>
14:45	<a href="#">T07A016</a>	<b>Researchers exposure to particles in nanomaterial production laboratories</b> <i>E. Demou, S. Hellweg, W. Stark, and S. Pratsinis</i>
15:05	<a href="#">T07A007</a>	<b>Aerosol particles in a metropolitan underground railway station</b> <i>I. Salma, T. Weidinger, and W. Maenhaut</i>
15:25	<a href="#">T07A008</a>	<b>Feasibility study of LIDAR's measurements in an underground station</b> <i>A. Fortain, J.C. Raut, P. Chazette, K. Limam, and C. Cremezi Charlet</i>
Back-up Paper	<a href="#">T07A014</a>	<b>Physical and chemical properties of fine particles emitted from candles</b>
		<i>J. Pagels, A. Wierzbicka, A. Dahl, E. Swietlicki, and M. Bohgard</i>

<b>Monday 10 September 2007</b>	<b>13:45 - 15:45</b>	<b>Lecture Hall 421</b>
<b>Combustion Aerosols - Boilers</b>		
<b>Chairs: Christina Gutierrez-Canas and Mats Bohgard</b>		
13:45	<a href="#">T14A021</a>	<b>Filter test with soot generation from 7.5 nm up to 200 nm</b> <i>M. Schmidt and L. Mölter</i>
14:05	<a href="#">T14A009</a>	<b>Calculation of particle density of aerosol from wood combustion</b>

		<i>M. Lautenbach, R. Kunde, and M. Gaderer</i>
14:25	<a href="#">T14A032</a>	<b>Comparison of fine particle emissions from a modern small-scale biomass boiler and from a large-scale coal-firing power plant</b>
		<i>E. Lamminen and H. Isherwood</i>
14:45	<a href="#">T14A012</a>	<b>Measurements of size-segregated emission particles by a specially invented sampling system</b>
		<i>J. Turšič, I. Grgić, A. Berner, J. Škantar, and I. Cuhalev</i>
15:05	<a href="#">T14A026</a>	<b>Detailed particle analysis in the hot flue gas of a municipal waste incineration plant</b>
		<i>C. Deuerling, J. Maguhn, H. Nordsieck, R. Warnecke, and R. Zimmermann</i>
15:25	<a href="#">T14A037</a>	<b>Experiences with ultra fine particle monitoring in air quality monitoring networks in Europe</b>
		<i>C. Gerhart, T. Petry, T. Rettenmoser, A. Kranapeter, and H.P. Lötscher</i>
Back-up Paper	<a href="#">T14A024</a>	<b>Particle emissions from heating units operating on wood and heavy fuel oil</b>
		<i>O. Sippula, J. Hokkinen, P. Yli-Pirilä, H. Puustinen, and J. Jokiniemi</i>

<b>Monday 10 September 2007</b>	<b>15:45 - 16:15</b>	<b>Coffee Break and Exhibition</b>
---------------------------------	----------------------	------------------------------------

<b>Monday 10 September 2007</b>	<b>16:15 - 18:15</b>	<b>AudiMax</b>
---------------------------------	----------------------	----------------

### Atmospheric Aerosols - Urban Aerosols

**Chairs:** Lidia Morawska and Imre Salma

16:15	<a href="#">T13A036</a>	<b>Dispersion of fine and ultrafine particles near the Berlin urban motorway: Derivation of vehicular emission factors</b>
		<i>W. Birmili, B. Alaviippola, D. Hinneburg, O. Knoth, K. König, A. Sonntag, D. Bake, T. Tuch, S. Warwel, and J. Borcken</i>
16:35	<a href="#">T13A030</a>	<b>Monitoring the road traffic aerosol pollution in urban air: A comparative study between several aerosol concentration metrics</b>
		<i>S. Rodríguez, E. Cuevas, P.M. Romero, R. Ramos, X. Querol, and A. Alastuey</i>
16:55	<a href="#">T13A201</a>	<b>Characterization of different pollution levels in Beijing, China</b>
		<i>B. Wehner, F. Ditas, W. Birmili, A. Wiedensohler, Z. Wu, and M. Hu</i>
17:15	<a href="#">T13A017</a>	<b>Descriptive time series analysis of fine carbonaceous aerosol at Potsdam, NY</b>
		<i>R.S. Raman and P.K. Hopke</i>
17:35	<a href="#">T13A054</a>	<b>Nano/ultrafine particle behavior near intersection of busy roadway observed using a rapid type PM sizer</b>
		<i>H. Minoura, S. Terada, and T. Takada</i>
17:55	<a href="#">T13A199</a>	<b>Contribution of anthropogenic and biogenic aerosol sources in three Austrian cities</b>
		<i>P. Kotianová, I.L. Maar, and H. Puxbaum</i>
Back-up Paper	<a href="#">T13A162</a>	<b>UFIPOLNET: Concentration of particle number distributions at 4 stations in Europe</b>
		<i>H. Gerwig, G. Löschau, L. Hillemann, B. Wehner, A. Wiedensohler, A. Zschoppe, C. Peters, A. Rudolph, C. Johansson J. Cyrus, M. Pitz, R. Ruckerl, J. Novak, H.G. Horn, R. Caldow, and G.J. Sem</i>

<b>Monday 10 September 2007</b>	<b>16:15 - 18:15</b>	<b>Blauer Hörsaal</b>
---------------------------------	----------------------	-----------------------

### Nanoparticles - Synthesis

**Chairs:** Sotiris Pratsinis and Jean-Pascal Borra

16:15	<a href="#">T09A017</a>	<b>Formation of carbon aerosol particles in high-frequency discharge</b>
		<i>A.M. Baklanov, N.A. Ivanova, and G.A. Makhov</i>
16:35	<a href="#">T09A022</a>	<b>Tuning size-distribution of particles with filamentary discharges properties related to the nature of dielectric barriers in non-thermal plasma at atmospheric pressure</b>
		<i>J. Hou, N. Jidenko, J. P. Borra, and A. P. Weber</i>
16:55	<a href="#">T09A028</a>	<b>Production of metallic ions, atomic clusters and nano particles with hot wires</b>
		<i>M.B. Attoui and J. Fernández de la Mora</i>

17:15	<a href="#">T09A035</a>	<b>Formation of silicon particles using silane pyrolysis</b> <i>D.K. Woo, K.T. Nam, Y.G. Kim, K.S. Kim, Y.H. Kang, and T. Kim</i>
17:35	<a href="#">T09A051</a>	<b>Synthesis of terraced MgO nanoparticles using flame metal combustion method</b> <i>C.Kim, P.V. Pikhita, and M.Choi</i>
17:55	<a href="#">T09A052</a>	<b>Formation of Al<sub>2</sub>O<sub>3</sub> nanoparticles by combustion of single Al particles</b> <i>A.A. Onischuk, V.V. Karasev, and O.G. Glotov</i>
Back-up Paper	<a href="#">T09A024</a>	<b>Droplet size characterization in spray flames</b> <i>H. Keskinen, J.M. Mäkelä, M. Aromaa, M.C. Heine, and S.E. Pratsinis</i>

<b>Monday 10 September 2007</b>	<b>16:15 - 18:15</b>	<b>Grüner Hörsaal</b>
<b>Aerosol Modelling - Processes and Technical Applications</b>		
<b>Chairs: Bernhard Vogel and Elisabetta Vignati</b>		
16:15	<a href="#">T12A030</a>	<b>Oscillations of the parameters in finite system with condensation</b> <i>V.A. Zagaynov, A.K. Maslov, M. Bahtyreva, A. Lutsenko, and A.A. Lushnikov</i>
16:35	<a href="#">T12A006</a>	<b>Constructal view of dendritic growth of airborne particles</b> <i>A. H. Reis, A. F. Miguel, and A. Bejan</i>
16:55	<a href="#">T12A045</a>	<b>A stochastic Langevin model of particle dispersion in turbulent flows with active thermophoresis</b> <i>A. Dehbi</i>
17:15	<a href="#">T12A028</a>	<b>Particle size-separation and focusing in a flow through a channel with oscillating walls</b> <i>P. Vainshtein and M. Shapiro</i>
17:35	<a href="#">T12A040</a>	<b>Transport of fine aerosol particles in turbulent channel flow</b> <i>P.L. Garcia-Ybarra and A. Pinelli</i>
17:55	<a href="#">T12A042</a>	<b>Analytical modeling of diffusional nanoparticle deposition under low pressure conditions</b> <i>C. Asbach, H. Fissan, J. Wang, and D.Y.H. Pui</i>
Back-up Paper	<a href="#">T12A033</a>	<b>Numerical study of dynamics of growing droplets in Kelvin spectrometer</b> <i>S.K. Zaripov, R.S. Galeev, and W. Holländer</i>

<b>Monday 10 September 2007</b>	<b>16:15 - 18:15</b>	<b>Lecture Hall 414</b>
<b>PM10/PM2.5 - Characterisation</b>		
<b>Chairs: Willi Maenhaut and Jürgen Schnelle-Kreis</b>		
16:15	<a href="#">T19A026</a>	<b>Impact of ferrocene on the structure of diesel soot</b> <i>A. Braun</i>
16:35	<a href="#">T19A054</a>	<b>Characterization of traffic PM10 and PM2.5 by scanning electron microscopy</b> <i>K. Slezakova, M.C. Pereira, J.C.M. Pires, and M.C. Alvim-Ferraz</i>
16:55	<a href="#">T19A015</a>	<b>PM10 physical and chemical characterisation using high-time resolved samplings in an air pollution "hot-spot" area in Europe</b> <i>R. Vecchi, G. Valli, V. Bernardoni, D. Cricchio, A. D'Alessandro P. Fermo, A. Piazzalunga, C. Rigamonti, S. Nava, F. Lucarelli F. Mazzei, and P. Prati</i>
17:15	<a href="#">T19A018</a>	<b>A European quality assurance program on PM measurements</b> <i>L. Marelli, L. Emblico, F. Lagler, J. Theunis, D. Buzica, and A. Borowiak</i>
17:35	<a href="#">T19A037</a>	<b>PATOS: The first extensive field campaign for atmospheric aerosol characterisation in Tuscany (Italy)</b> <i>F. Lucarelli, F. Barzagli, S. Becagli, G. Calzolai, A. Cincinelli, M. Chiari, M. Giannoni, T. Martellini, L. Lepri, S. Nava, L. Paperetti, F. Rugi, R. Traversi, and R. Udisti</i>
17:55	<a href="#">T13A137</a>	<b>What about water uptake by mixtures of four of the most important atmospheric aerosol ions: NH<sub>4</sub><sup>+</sup>, Na<sup>+</sup>, SO<sub>4</sub><sup>2-</sup>, and Cl<sup>-</sup> ?</b> <i>B. Svenningsson, M. Bilde, J. Rissler, and E. Swietlicki</i>

Back-up Paper	<a href="#">T19A052</a>	<b>A novel sampler for large particles</b>
		<i>S.-R. Lee, T.M. Holsen, and S. Dhaniyala</i>

<b>Monday 10 September 2007</b>	<b>16:15 - 18:15</b>	<b>Lecture Hall 421</b>
---------------------------------	----------------------	-------------------------

<b>Special Sesion: UT/LS Aerosols and Clouds - Measurements and Modeling</b>
--

<b>Chairs:</b>	<b>Martina Krämer and Darrel Baumgardner</b>
----------------	--

16:15	<a href="#">T21A005</a> invited	<b>Do aircraft black carbon emissions affect cirrus clouds on the global scale?</b>
		<i>J. Hendricks, B. Kärcher, U. Lohmann, and M. Ponater</i>

16:35	<a href="#">T13A121</a>	<b>The meridional gradient of black carbon in the upper troposphere and lower stratosphere over Northern Europe</b>
		<i>D.G. Baumgardner, G.L. Kok, and M. Krämer</i>

16:55	<a href="#">T21A001</a>	<b>Dust aerosol-cloud interaction derived from A-train satellites and ground measurements</b>
		<i>J. Huang, P. Minnis, Y. Yi, J. Su, J. Bi, and K. Ayers</i>

17:15	<a href="#">T21A003</a>	<b>The Pacific Dust Experiment (PACDEX): Early results</b>
		<i>J.L. Stith and V. Ramanathan</i>

17:35	<a href="#">T21A007</a>	<b>Impact of aerosols and dynamics on cirrus clouds - measurements and model studies</b>
		<i>P. Spichtinger, S. Schlicht, C. Schiller, N. Spelten, M. de Reus, J. Curtius, H.-J. Vössing, S. Borrmann, and M. Krämer</i>

17:55	<a href="#">T21A002</a>	<b>Dynamics and ice nucleation behavior of water on kerosene soot, original and wetted by H<sub>2</sub>SO<sub>4</sub>: UT/LS implications</b>
		<i>B. Demirdjian, D. Ferry, J. Suzanne, O.B. Popovicheva, N.M. Persiantseva, and N.K. Shonija</i>

<b>Monday 10 September 2007</b>	<b>18:15</b>	<b>End of Conference Day</b>
---------------------------------	--------------	------------------------------

<b>Monday 10 September 2007</b>	<b>18:15 - ??</b>	<b>Journal of Aerosol Science- Editorial Board Meeting</b>
---------------------------------	-------------------	--

<b>Monday 10 September 2007</b>	<b>20:00 - 21:00</b>	<b>Concert in the Residenz State Rooms on Invitation by the Lord Mayor and the Governor of Salzburg</b>
---------------------------------	----------------------	---

[Top of Program](#)

## Tuesday 11 September 2007

<b>Tuesday 11 September 2007</b>	<b>08:00 - 16:15</b>	<b>Registration</b>
----------------------------------	----------------------	---------------------

<b>Tuesday 11 September 2007</b>	<b>08:45 - 09:45</b>	<b>AudiMax</b>
----------------------------------	----------------------	----------------

<b>Plenary Lecture II</b>
---------------------------

<b>Chair:</b>	<b>Wolfgang Kreyling</b>
---------------	--------------------------

08:45	<a href="#">Plenary Lecture</a>	<b>From nanoparticles to large expiratory droplets in indoor air</b>
		<i>Lidia Morawska</i>

<b>Tuesday 11 September 2007</b>	<b>09:45 - 10:15</b>	<b>Coffee Break and Exhibition</b>
----------------------------------	----------------------	------------------------------------

<b>Tuesday 11 September 2007</b>	<b>10:15 - 12:15</b>	<b>AudiMax</b>
----------------------------------	----------------------	----------------

<b>PM10/PM2.5 - Sources I</b>		
<b>Chairs: Philip K. Hopke and Luisa Marelli</b>		
10:15	<a href="#">T19A012</a>	<b>Source apportionment of PM10 in industrialized urban areas by automated electronmicroscopical particle analysis</b> <i>M. Ebert, N. Benker, K. Kandler, D. Müller-Ebert, and S. Weinbruch</i>
10:35	<a href="#">T03A001</a>	<b>Source apportionments and spatial variability of coarse particle during the regional air pollution study (RAPS)</b> <i>I.J. Hwang, Ph.K. Hopke, and J.P. Pinto</i>
10:55	<a href="#">T19A033</a>	<b>Source apportionment of fine and coarse aerosol in the Athens Metropolitan area</b> <i>A.A Karanasiou, P.A. Siskos, and K. Eleftheriadis</i>
11:15	<a href="#">T19A049</a>	<b>Gradients of PM10 mass concentrations analysed for major German conurbation areas</b> <i>U. Quass, U. Rating, A. Hugo, and T.A.J. Kuhlbusch</i>
11:35	<a href="#">T19A004</a>	<b>Positive matrix factorization on particulate matter daily data series</b> <i>F. Mazzei, A. D'Alessandro, F. Lucarelli, S. Nava, P. Prati, G. Valli, and R. Vecchi</i>
11:55	<a href="#">T19A044</a>	<b>Characterization of polycyclic aromatic hydrocarbons from different sources of urban areas in Germany</b> <i>M.A. Bari, G. Baumbach, G. Scheffknecht, and B. Kuch</i>
Back-up Paper	<a href="#">T19A031</a>	<b>Chemical composition and source apportionment of particulate matter in Elche, Spain</b> <i>J. Crespo, J. Nicolás, S. Caballero, E. Yubero, M. Chiari, F. Lucarelli, S. Nava, and I. García Orellana</i>

<b>Tuesday 11 September 2007</b>		<b>10:15 - 12:15</b>	<b>Blauer Hörsaal</b>
<b>Aerosol Chemistry - Secondary Organic Aerosols</b>			
<b>Chairs: Thorsten Hoffmann and NN</b>			
10:15	<a href="#">T01A018</a>	<b>Characterisation of organosulphates from the photo-oxidation of isoprene in ambient PM2.5 aerosol by LC/(-)ESI-linear ion trap mass spectrometry</b> <i>Y. Gómez González, R. Vermeylen, R. Szmigielski, J.D. Surratt, T.E. Kleindienst, M. Jaoui, M. Lewandowski, J.H. Offenberg, E.O. Edney, W. Maenhaut, and M. Claeys</i>	
10:35	<a href="#">T01A029</a>	<b>The influence of relative humidity on the SOA-formation at various temperatures</b> <i>R. Tillmann, T.F. Mentel, A. Kiendler-Scharr, and H. Saathoff</i>	
10:55	<a href="#">T01A030</a>	<b>Chamber studies of the stable carbon isotope composition of secondary organic aerosol formed by <math>\beta</math>-pinene ozonolysis</b> <i>R. Fisseha, A. Kiendler-Scharr, H. Spahn, R. Tillmann, R. Wegener, and A. Wahner</i>	
11:15	<a href="#">T01A005</a>	<b>Comparison of simulation chamber and field observations of biogenic SOA aerosol mass spectrometric signatures</b> <i>A. Kiendler-Scharr, Q. Zhang, T. Mentel, E. Kleist, T. Hohaus, M. Miebach, R. Tillmann, R. Uerlings, R. Fisseha, P. Griffiths, Y. Rudich, E. Dinar, and J. Wildt</i>	
11:35	<a href="#">T01A050</a>	<b>Secondary organic aerosol formation and on-line chemical composition analysis with a thermal desorption chemical ionisation aerosol mass spectrometer (TDCIAMS)</b> <i>G. Etylunent, A. Leperson, G. Solignac, N. Marchand, and A. Monod</i>	
11:55	<a href="#">T01A057</a>	<b>Characterization of oligomers in organic aerosols with ultra-high mass resolution and accurate mass measurements</b> <i>M. Kalberer, A. Reinhardt, C. Emmenegger, J. Dommen, B. Gerrits, and Chr. Pansé</i>	
Back-up Paper	<a href="#">T01A004</a>	<b>Secondary organic aerosol formation from plant emissions: Overview of the Jülich Plant chamber experiments</b> <i>A. Kiendler-Scharr, T. Hohaus, E. Kleist, M. Miebach, R. Tillmann, R. Uerlings, R. Fisseha, P. Griffiths, Y. Rudich, E. Dinar, J. Wildt, and T. Mentel</i>	

<b>Tuesday 11 September 2007</b>		<b>10:15 - 12:15</b>	<b>Grüner Hörsaal</b>
<b>Nanoparticles - Handling</b>			
<b>Chairs: Andreas Schmidt-Ott and Martin Seipenbusch</b>			

10:15	<a href="#">T09A019</a>	<b>Aerosol generation for exposure experiments</b> <i>S. Mülhopt, A. Kocheh Alavi, S. Diabaté, and H.-R. Paur</i>
10:35	<a href="#">T09A021</a>	<b>Fragmentation and bouncing of nanoparticles in low pressure impaction</b> <i>T. Wu and A.P. Weber</i>
10:55	<a href="#">T09A036</a>	<b>Control of the structure of deposits collected from aerosol particles</b> <i>D. Rodriguez-Perez, J. L. Castillo, and J. C. Antoranz</i>
11:15	<a href="#">T09A037</a>	<b>Synthesis of Ag-SnO<sub>x</sub> core-shell nanoparticles for gas sensor applications</b> <i>I. Aruna and F.E. Kruis</i>
11:35	<a href="#">T09A031</a>	<b>Aerosol processing and sintering of supported metal nanoparticles</b> <i>A. Binder, M. Seipenbusch, and G. Kasper</i>
11:55	<a href="#">T09A055</a>	<b>Development of a metal membrane filter with high filtration performance by the depostion and sintering of nanoparticle agglomerates</b> <i>S.J. Park and D.G. Lee</i>
Back-up Paper	<a href="#">T09A040</a>	<b>Thermal tweezers for effective manipulation of nano-particles on surfaces</b> <i>D.R. Mason, D.K. Gramotnev, and G. Gramotnev</i>

<b>Tuesday 11 September 2007</b>		<b>10:15 - 12:15</b>	<b>Lecture Hall 414</b>
<b>Aerosol Modelling - Processes and Technical Applications / Atmospheric Processes</b>			
<b>Chairs: Frank Stratmann and Karle Hämeri</b>			
10:15	<a href="#">T12A018</a>	<b>Simulation of carbon black formation in a solar thermal reactor for the decomposition of methane</b> <i>M. Kostoglu, G. Patrianakos, and A.G. Konstandopoulos</i>	
10:35	<a href="#">T12A014</a>	<b>Development of a kinetic model framework and master mechanism of aerosol surface chemistry and gas-particle interactions</b> <i>R.M. Garland, J.R. Scheintaub, and U. Pöschl</i>	
10:55	<a href="#">T12A039</a>	<b>Detailed process modelling of SOA formation: Kinetic vs. K-alpha approach</b> <i>K.-H. Naumann and H. Saathoff</i>	
11:15	<a href="#">T12A036</a>	<b>Modelling particle formation and growth from biogenic precursors measured in the Jülich plant chamber</b> <i>M. Dal Maso, T. Hohaus, A. Kiendler-Scharr, E. Kleist, M. Miebach, R. Tillmann, R. Uerlings, R. Fisseha, J. Wildt, and T. Mentel</i>	
11:35	<a href="#">T12A011</a>	<b>Influence of SO<sub>2</sub> on nucleation, growth rates and yield of secondary organic aerosol</b> <i>A. Metzger, B. Verheggen, J. Duplissy, J. Dommen, A.S.H. Prevot, U. Baltensperger</i>	
11:55	<a href="#">T11A012</a>	<b>New particle formation at rural sites simulated with MALTE (model to predict new aerosol formation in the lower troposphere)</b> <i>M. Boy, O. Hellmuth, H. Korhonen, A. Guenther, J. Kazil, E. Lovejoy, and M. Kulmala</i>	
Back-up Paper	<a href="#">T12A021</a>	<b>Modeling nitric acid adsorption in mixed-phase clouds</b> <i>J-P. Pietikäinen, J. Hienola, H. Kokkola, S. Romakkaniemi, K. Lehtinen, M. Kulmala, and A. Laaksonen</i>	

<b>Tuesday 11 September 2007</b>		<b>10:15 - 12:15</b>	<b>Lecture Hall 421</b>
<b>Combustion Aerosols - Engines</b>			
<b>Chairs: Heinz Burtscher and Horiaki Minoura</b>			
10:15	<a href="#">T14A003</a>	<b>Oil mist emission by crank case ventilation from medium speed 4-stroke diesel engines</b> <i>P. Lauer</i>	
10:35	<a href="#">T14A016</a>	<b>Direct comparison of four different measurement methods applied to particle emissions from diesel engines</b> <i>H.-G. Horn</i>	
10:55	<a href="#">T14A006</a>	<b>Particulate matter characterization for a commercial aircraft – The Delta Atlanta Hartsfield Jet Engine Exhaust Emissions Study</b> <i>D. Hagen, P. Whitefield, P. Lobo, and M. Trueblood</i>	

11:15	<a href="#">T14A017</a>	<b>Size distribution, morphology, fractal dimension, and elemental composition of soot particles emitted by commercial CFM-56 aircraft engines</b> <i>D. Delhaye, D. Ferry, E. Ruiz, J. Gouge, G. Rollin, B. Demirdjian, and J. Suzanne</i>
11:35	<a href="#">T14A034</a>	<b>Water uptake by exhaust soot and its transformation through the interactions in the humid atmosphere</b> <i>V.V.Tishkova, A.M.Voloshuk, O.B. Popovicheva, and N.K.Shonija</i>
11:55	<a href="#">T14A035</a>	<b>Gaseous sulphuric acid and volatile nanoparticle formation by modern diesel vehicles</b> <i>F. Arnold, T. Schuck, L. Pirjola, J. Keskinen, T. Rönkkö, T. Lähde, K. Hämeri, H. Aufmhoff, A. Sorokin, and D. Rothe</i>
Back-up Paper	<a href="#">T14A013</a>	<b>2D particle transport in a full dilution tunnel of diesel vehicle emissions</b> <i>L. Isella, B. Giechaskiel, P. Dilara, and Y. Drossinos</i>

<b>Tuesday 11 September 2007</b>	<b>12:15 - 13:45</b>	<b>Lunch Break</b>
----------------------------------	----------------------	--------------------

<b>Tuesday 11 September 2007</b>	<b>12:15 - 13:45 (Meeting Room)</b>	<b>GAeF Board Meeting</b>
----------------------------------	-------------------------------------	---------------------------

<b>Tuesday 11 September 2007</b>	<b>13:45 - 15:45</b>	<b>Poster and Exhibition Area</b>
----------------------------------	----------------------	-----------------------------------

<b>Poster Session Part I and Exhibition</b>		
---	--	--

<b>Tuesday 11 September 2007</b>	<b>15:45 - 16:15</b>	<b>Coffee Break and Exhibition</b>
----------------------------------	----------------------	------------------------------------

<b>Tuesday 11 September 2007</b>	<b>16:15 - 18:15</b>	<b>AudiMax</b>
----------------------------------	----------------------	----------------

<b>Aerosol Instrumentation I</b>		
----------------------------------	--	--

<b>Chairs:</b>	<b>Hans Georg Horn and Risto Hillamo</b>	
----------------	--	--

16:15	<a href="#">T02A008</a>	<b>In situ measurements of large atmospheric particles in mixed phase clouds using digital holography</b> <i>S.M.F. Raupach, J. Curtius, H.J. Voessing, and S. Borrmann</i>
-------	-------------------------	--

16:35	<a href="#">T02A012</a>	<b>Aerosol light scattering at high relative humidity</b> <i>R. Schmidhauser, G. Wehrle, T. Ulrich, E. Weingartner, and U. Baltensperger</i>
-------	-------------------------	---

16:55	<a href="#">T02A017</a>	<b>Condensation particle counting for particle diameters down to 1nm</b> <i>P.M. Winkler, G.W. Steiner, G.P. Reischl, A. Vrtala, and M. Kulmala</i>
-------	-------------------------	--

17:15	<a href="#">T02A030</a>	<b>Laser-based measurement system for size-dependent particle composition</b> <i>C. Fricke-Begemann, T. Kühlen, N. Strauß, and R. Noll</i>
-------	-------------------------	---

17:35	<a href="#">T02A036</a>	<b>Passive sampler sigma 2 as an inlet for an optical aerosol spectrometer</b> <i>F. Kohler, L. Mölter, E. Schultz, S. Schütz, V. Dietze, and H. Helm</i>
-------	-------------------------	--

17:55	<a href="#">T02A043</a>	<b>Wavelength and refractive index independent number concentration</b> <i>L. Vámos and P. Jani</i>
-------	-------------------------	--

Back-up Paper	<a href="#">T06A026</a>	<b>Direct measurements of the optical properties of humic and humic like substances (HULIS) by cavity ring down aerosol spectrometer</b> <i>E. Dinar, A.A. Riziq, C. Spindler, C. Erilic, G. Kiss, and Y. Rudich</i>
---------------	-------------------------	---

<b>Tuesday 11 September 2007</b>	<b>16:15 - 18:15</b>	<b>Blauer Hörsaal</b>
----------------------------------	----------------------	-----------------------

<b>Aerosol Chemistry - PM/Sources</b>		
---------------------------------------	--	--

<b>Chairs:</b>	<b>Mar Viana and Ernest Weingartner</b>	
----------------	---	--

16:15	<a href="#">T01A036</a>	<b>Chemical composition and mass closure for PM<sub>2.5</sub> and PM<sub>10</sub> aerosols at K-pusztá, Hungary, in summer 2006</b> <i>W. Maenhaut, N. Raes, X. Chi, J. Cafmeyer, and W. Wang</i>
-------	-------------------------	--

16:35	<a href="#">T01A043</a>	<b>Source apportionment of submicron organic aerosol during wintertime inversions: A new</b>
-------	-------------------------	--

		<b>factor analytical approach</b>
		<i>V.A. Lanz, M.R. Alfarra, U. Baltensperger, B. Buchmann, C. Hüglin, S. Weimer, and A.S.H. Prévôt</i>
16:55	T01A041	<b>Chemical composition and optical properties of megacity aerosols in Paris/Beijing/Cairo: A comparative study</b>
		<i>O. Favez, J. Sciare, and H. Cachier</i>
17:15	T01A053	<b>Intensive measurements and modelling of size segregated chemical composition of aerosols in June 2006 and January 2007 in EMEP</b>
		<i>W. Aas, M.R. Alfarra, E. Bieber, D. Ceburnis, T. Ellermann, M. Ferm, M. Frölich, R. Gehrig, H.C. Hansson, G. Kiss, U. Makkonen, N. Mihalopoulos, E. Nemitz, R. Otjes, N. Perez, C. Perrino, J.P. Putaud, G. Spindler, S. Tsyro, M. Vana, and K.E. Yttri</i>
17:35	T01A055	<b>Assessment of Diesel exhaust particulate exposure and surface characteristics in association with levels of oxidative stress biomarkers</b>
		<i>A. Setyan, J. Sauvain, M. Riediker, M.J. Rossi, and M. Guillemin</i>
17:55	T01A059	<b>Simultaneous on-line size and chemical analysis of gas phase and particulate phase of cigarette mainstream smoke</b>
		<i>J. McAughey, T. Adam, C. McGrath, C. Mocker, and R. Zimmerman</i>
Back-up Paper	T01A008	<b>Distributions and health risks of polycyclic aromatic hydrocarbons (PAHs) in atmospheric aerosols of the city of Chania (Greece)</b>
		<i>A. Pafitis, N. Pasadakis, I. Kopanakis, and E. Katsivela</i>

<b>Tuesday 11 September 2007</b>		<b>16:15 - 18:15</b>	<b>Grüner Hörsaal</b>
<b>Fundamental Aerosol Physics - Nucleation, Condensation and Evaporation</b>			
<b>Chairs: Ian Ford and Jiri Smolik</b>			
16:15	T06A009	<b>Heterogeneous nucleation on single microdroplets</b>	
		<i>A.K. Ray, J.L. Huckaby, and Y. Raja</i>	
16:35	T06A014	<b>The effect of carrier gas pressure on homogeneous nucleation of n-pentanol + helium in a laminar flow diffusion chamber</b>	
		<i>A.-P. Hyvarinen, D. Brus, V. Ždímal, J. Smolik, M. Kulmala, Y. Viisanen, and H. Lihavainen</i>	
16:55	T06A006	<b>Classical nucleation theory for pure water below 240 K</b>	
		<i>T. Nemeč, F. Maršik, and J. Hrubý</i>	
17:15	T06A018	<b>A method to evaluate the line tension in heterogeneous nucleation by molecular Monte Carlo simulations</b>	
		<i>A. Lauri, E. Zapadinsky, A. I. Hienola, H. Vehkamäki, and M. Kulmala</i>	
17:35	T06A004	<b>Heat transfer to a particle in the transition regime</b>	
		<i>A.A. Lushnikov and M. Kulmala</i>	
17:55	T06A011	<b>Stochastic birth and death equations to treat nucleation in small systems</b>	
		<i>I. Ford and C. Losert-Valiente Kroon</i>	
Back-up Paper	T06A005	<b>Critical behaviour of the particle mass spectra in gelling systems</b>	
		<i>A.A. Lushnikov</i>	

<b>Tuesday 11 September 2007</b>		<b>16:15 - 18:15</b>	<b>Lecture Hall 414</b>
<b>Remote Sensing</b>			
<b>Chairs: Helmuth Horvath and Tymon Zielinski</b>			
16:15	T20A002	<b>A low-cost, telemetric LIDAR for the monitoring of PBL aerosols</b>	
		<i>M. Del Guasta, F. Castagnoli, M. Baldi, and V. Venturi</i>	
16:35	T20A011	<b>On the relation between AOD and PM<sub>2.5</sub> at the research station of Cabauw, the Netherlands</b>	
		<i>M. Schaap, B. Henzing, A. Apituley, D.P.J. Swart, R. Koelmeijer, and G. de Leeuw</i>	
16:55	T20A004	<b>Local radiative forcing by Saharan dust and forest fire aerosols over Portugal</b>	
		<i>D. Santos, M.J. Costa, and A.M. Silva</i>	

17:15	<a href="#">T20A009</a>	<b>Water vapour column content derived from a star photometer at Granada, Spain</b> <i>D. Pérez-Ramírez, F.J. Olmo, L. Alados-Arboledas, and J.A. Aceituno</i>
17:35	<a href="#">T20A006</a>	<b>Aerosol optical properties in a rural site of South Italy from simultaneous measurements by CIMEL and Avantes radiometers</b> <i>G. Pavese, F. Esposito, L. Leone, M.R. Perrone, F. De Tomasi, A.M. Tafuro, L. Alados-Arboledas, and H. Lyamani</i>
17:55	<a href="#">T20A012</a>	<b>Influence of variability in aerosol vertical profile on retrievals of aerosol optical thickness from NOAA AVHRR measurements</b> <i>A. Rozwadowska</i>
Back-up Paper	<a href="#">T13A013</a>	<b>Aerosol physical properties as an important factor in remote sensing of coastal areas</b> <i>T. Zielinski and A. Ponczkowska</i>

<b>Tuesday 11 September 2007</b>	<b>16:15 - 18:15</b>	<b>Lecture Hall 421</b>
----------------------------------	----------------------	-------------------------

### Aerosol Filtration

**Chairs: Leon Gradon and Gerhard Kasper**

16:15	<a href="#">T11A006</a>	<b>Experimental determination of axial dispersion coefficients of aerosol particles in fibrous filters</b> <i>A. Jackiewicz, A. Balazy, and A. Podgórski</i>
16:35	<a href="#">T11A016</a>	<b>Filtration of aerosols with different shape on oil coated fibers</b> <i>L. Boskovic, I. Agranovski, and R. Braddock</i>
16:55	<a href="#">T11A026</a>	<b>Characterization of deposit structures on single dust-loaded filter fibers</b> <i>S. Schollmeier, J. Meyer, and G. Kasper</i>
17:15	<a href="#">T11A005</a>	<b>A mathematical model of the deposit on fibrous filters as a porous medium</b> <i>S.J. Dunnett and C.F. Clement</i>
17:35	<a href="#">T11A023</a>	<b>Deposition of ions and monomobile nanoparticles on wire screens</b> <i>M.B. Attoui, G. Mouret, D. Bémer, S. Callé-Chazelet, and D. Thomas</i>
17:55	<a href="#">T11A021</a>	<b>Pilot plant tests of a ceramic catalytic filter</b> <i>D. Sanz-Rivera, J.-J. Rodríguez-Maroto, J.L. Dorronsoro-Arenal, E. Rojas-García, L. Armesto-López, A. Bahillo-Ruiz, and R. Ramos-Casado</i>
Back-up Paper	<a href="#">T11A017</a>	<b>Application of Brownian dynamics approach to evaluate a fibrous filter efficiency</b> <i>A. Balazy and A. Podgórski</i>

<b>Tuesday 11 September 2007</b>	<b>18:15</b>	<b>End of Conference Day</b>
----------------------------------	--------------	------------------------------

<b>Tuesday 11 September 2007</b>	<b>18:25 - 19:00</b>	<b>General Assembly of GAeF</b>
----------------------------------	----------------------	---------------------------------

<b>Tuesday 11 September 2007</b>	<b>20:00 - ????</b>	<b>AudiMax</b>
----------------------------------	---------------------	----------------

### Public Lecture

**Chair: Werner Hofmann**

20:00	Public Lecture	<b>Interaction between aerosols, clouds and climate</b> <i>Meinrat Andreae</i>
-------	----------------	---

[Top of Program](#)

## Wednesday 12 September 2007

<b>Wednesday 12 September 2007</b>	<b>08:00 - 12:30</b>	<b>Registration</b>
------------------------------------	----------------------	---------------------

<b>Wednesday 12 September 2007</b>	<b>08:45 - 09:45</b>	<b>AudiMax</b>
------------------------------------	----------------------	----------------

### Plenary Lecture III

<b>Chair:</b>	<b>Urs Baltensperger</b>
---------------	--------------------------

<b>08:45</b>	<a href="#">Plenary Lecture</a>	<b>Particles from road traffic - emission trends, reduction measures and contribution to ambient particle concentrations</b>
		<i>Heinz Burtscher</i>

<b>Wednesday 12 September 2007</b>	<b>09:45 - 10:15</b>	<b>Coffee Break and Exhibition</b>
------------------------------------	----------------------	------------------------------------

<b>Wednesday 12 September 2007</b>	<b>10:15 - 12:15</b>	<b>AudiMax</b>
------------------------------------	----------------------	----------------

### Atmospheric Aerosols - Sources

<b>Chairs:</b>	<b>Janja Tursic and Anne Kasper-Giebl</b>
----------------	---

<b>10:15</b>	<a href="#">T13A103</a>	<b>Towards source apportionment of soot particles from wood and diesel combustion in ambient samples with X-ray microscopy</b>
		<i>M.G.C. Vernooij, M.Mohr, R.Kaegi, T. Huthwelker, G.Tzvetkov, and R.Gehrig</i>

<b>10:35</b>	<a href="#">T13A070</a>	<b>Wood smoke contribution to aerosol concentrations in Northern Italy: Levoglucosan determination by GC-MS and HPAEC-PAD</b>
		<i>P. Fermo, A. Piazzalunga, R. Vecchi, G. Valli, M. A. De Gregorio, and S. Marengo</i>

<b>10:55</b>	<a href="#">T13A047</a>	<b>Characterisation of the chemical composition of aerosol particles from wood burning emissions</b>
		<i>S. Weimer, M.R. Alfarra, D. Schreiber, M. Mohr, and A.S.H. Prévôt</i>

<b>11:15</b>	<a href="#">T13A168</a>	<b>The natural aerosol field over Northern Europe - Implications of important climate feedbacks</b>
		<i>P. Tunved, H.-C. Hansson, B. Svenningsson, V.-M. Kerminen, J. Ström, M. Dal Maso, H. Lihavainen, Y. Viisanen, P.P. Aalto, M. Komppula, and M. Kulmala</i>

<b>11:35</b>	<a href="#">T13A172</a>	<b>Coarse particles of probably volcanic origin collected with a passive sampler on NE-Greenland</b>
		<i>E. Schultz, V. Dietze, and B. Sittler</i>

<b>11:55</b>	<a href="#">T13A210</a>	<b>Processing of soot by controlled sulfuric acid and water condensation – Mass and mobility relationship and morphology</b>
		<i>J. Pagels, A. Khalizov, M. Emery, P.H. McMurry, and R.Y. Zhang</i>

<b>Back-up Paper</b>	<a href="#">T13A065</a>	<b>Wood burning aerosol during winter in an Alpine valley: Aethalometer and the Aerosol Mass Spectrometer measurements</b>
		<i>J. Sandradewi, M.R. Alfarra, A.S.H. Prévôt, E. Weingartner, M. Gysel, R. Schmidhauser, S. Szidat, and U. Baltensperger</i>

<b>Wednesday 12 September 2007</b>	<b>10:15 - 12:15</b>	<b>Blauer Hörsaal</b>
------------------------------------	----------------------	-----------------------

### Bioaerosols - General I

<b>Chairs:</b>	<b>Gedi Mainelis and Heidi Bauer</b>
----------------	--------------------------------------

<b>10:15</b>	<a href="#">T04A020</a>	<b>Comparison between ambient concentrations of the major birch allergen Bet v 1 and birch pollen count</b>
		<i>J. Buters, I. Weichenmeier, S. Ochs, W. Kreyling, J. Boere, W. Schober, and H. Behrendt</i>

<b>10:35</b>	<a href="#">T04A024</a>	<b>Modelling a birch pollen episode with a weather forecast model system</b>
--------------	-------------------------	--

		<i>H. Vogel, A. Pauling, and B. Vogel</i>
10:55	<a href="#">T04A028</a>	<b>Study of morphology and settling velocity of airborne pollen grains captured in a Paul trap</b>
		<i>F. Kohler, E. Schultz, and H. Helm</i>
11:15	<a href="#">T04A004</a>	<b>Factors affecting the performance of bioaerosol impactors</b>
		<i>S.A. Grinshpun, A. Adhikari, S.H. Cho, T. Reponen, G. Mainelis, and M. Yao</i>
11:35	<a href="#">T04A022</a>	<b>Real time analysis of bacillus species strain specific analysis by MALDI aerosol ToF mass spectrometry</b>
		<i>A.L. van Wuijckhuijse, C.E.A.M. Degenhardt, F.P.J. de Groot, B.L.M. van Baar, and Ch.E. Keintz</i>
11:55	<a href="#">T04A034</a>	<b>Concentrations and size distributions of fluorescent biological aerosol particles measured with an ultraviolet aerodynamic particle sizer (UVAPS)</b>
		<i>B. Treutlein and U. Pöschl</i>
Back-up Paper	<a href="#">T04A025</a>	<b>Effect of sampling time on the overall performance of portable microbial impactors</b>
		<i>G. Mainelis and M. Tabayoyong</i>

<b>Wednesday 12 September 2007</b>	<b>10:15 - 12:15</b>	<b>Grüner Hörsaal</b>
------------------------------------	----------------------	-----------------------

### Nanoparticles - Basics and Characterization

**Chairs:** Einar Kruis and Alfred P. Weber

10:15	<a href="#">T09A001</a>	<b>Iron doped carbon shell nanoparticles</b>
		<i>S. Yang, P.V. Pikhitsa, Y.-J. Kim, D. Kim, H. Lee, J. Yu, and M. Choi</i>
10:35	<a href="#">T09A007</a>	<b>Comparison of ultrafine particle surface area measurement with NSAM and SMPS</b>
		<i>C. Asbach, H. Kaminski, H. Fissan, C. Monz, D. Dahmann, and T.A.J. Kuhlbusch</i>
10:55	<a href="#">T09A025</a>	<b>Interparticulate forces in nanoparticle agglomerates</b>
		<i>M. Seipenbusch, S. Rothenbacher, A. P. Weber, and G. Kasper</i>
11:15	<a href="#">T09A046</a>	<b>Calculating the steady-state charge distribution for aerosols in the lower nm-range by the three body trapping method</b>
		<i>Y.G. Stommel and U. Riebel</i>
11:35	<a href="#">T09A050</a>	<b>Measuring hydrogen storage in individual nanoparticles</b>
		<i>V. Vons and A. Schmidt-Ott</i>
11:55	<a href="#">T09A053</a>	<b>The influence of carbon monoxide chemisorption on the magnetization of Fe<sub>3</sub>C nanoparticles</b>
		<i>A.A. Orischuk, N.A. Ivanova, S.V. Voxel, P.A. Purtov, N.T. Vasenin, V.F. Anufrienko, and V.N. Ikorski</i>
Back-up Paper	<a href="#">T09A039</a>	<b>Nanoparticle synthesis by gas-dynamically induced heating and quenching</b>
		<i>M. Dannehl, A. Maisels, W. Leibold, H. Olivier, A. Grzona, A. Weiß, A. Gülhan, T. Gawehn, G.H. Schnerr, N. Al-Hasan, A. Abdali, M.Y. Luong, H. Wiggers, C. Schulz, B. Weigand, J. Chun, W. Schröder, M. Meinke, T. Winnemöller, H. Nirschl, V. Goertz, K. Schaber, and T. Rakel</i>

<b>Wednesday 12 September 2007</b>	<b>10:15 - 12:15</b>	<b>Lecture Hall 414</b>
------------------------------------	----------------------	-------------------------

### Aerosol Instrumentation II

**Chairs:** Martin Schmidt and Christian Peters

10:15	<a href="#">T02A018</a>	<b>Performance and characterisation of a high-flow, high-resolution DMA: Particle losses and filtration efficiency measurements for particles below 20nm</b>
		<i>M. Heim, M. Attoui, and G. Kasper</i>
10:35	<a href="#">T02A041</a>	<b>A portable TEM sampler for quantitative single-particle analysis</b>
		<i>M. Fierz, R. Kaegi, and H. Burtscher</i>
10:55	<a href="#">T02A029</a>	<b>A DMA covering the 1-100 nm particle size range with high resolution down to 1 nm</b>
		<i>J. Fernández de la Mora and M.B. Attoui</i>
11:15	<a href="#">T02A004</a>	<b>Comparison of six H-TDMA systems: A laboratory study</b>

		<b>A. Massling, N. Kaaden, T. Hennig, E. Swietlicki, E. Nilsson, J. Löndahl, K. Hämeri, M. Ehn, P. Laj, P. Villani, G. McFiggans, N. Good, and A. Wiedensohler</b>
11:35	<a href="#">T02A039</a>	<b>Measurement instruments for optical absorption spectra of aerosol by photoacoustic spectroscopy</b> <i>C. Haisch, P. Menzenbach, and R. Niessner</i>
11:55	<a href="#">T02A011</a>	<b>Intercomparison study of different mobility particles sizers with NaCl, Diesel soot, and ambient aerosols</b> <i>C. Asbach, H. Kaminski, B. Stahlmecke, H. Fissan, C. Monz, D. Dahmann, S. Müllhopt, H.-R. Paur, H.J. Kiesling, F. Herrmann, M. Voetz, and T.A.J. Kuhlbusch</i>
Back-up Paper	<a href="#">T02A048</a>	<b>A new conception for environmental measurement of ultrafine particles</b> <i>A. Zschoppe, A. Rudolph, R. Caldow, B. Wehner, and L. Hillemann</i>

<b>Wednesday 12 September 2007</b>	<b>10:15 - 12:15</b>	<b>Lecture Hall 421</b>
------------------------------------	----------------------	-------------------------

### Aerosol Modelling - Atmospheric Applications

**Chairs:** Kari Lethinen and Pedro L. Garcia-Ybarra

10:15	<a href="#">T12A031</a>	<b>Effect of nucleation and secondary organic aerosol formation on cloud droplet number concentrations</b> <i>R. Makkonen, A. Asmi, H. Korhonen, H. Kokkola, S. Järvenoja, P. Räisänen, K.E.J. Lehtinen, A. Laaksonen, V.-M. Kerminen, H. Järvinen, and M. Kulmala</i>
10:35	<a href="#">T12A037</a>	<b>Closure study of aerosol cloud interactions using trajectory ensemble model</b> <i>S. Romakkaniemi, G. McFiggans, K. Bower, H. Coe, and T. W. Choularton</i>
10:55	<a href="#">T12A013</a>	<b>On the evaluation of modelled Black Carbon using both BC and EC measurements</b> <i>E. Vignati, F. Cavalli, and M. Karl</i>
11:15	<a href="#">T12A038</a>	<b>Predicting fine inorganic aerosols in Mexico City during winter 2005: deliquescence vs efflorescence branch</b> <i>M. Moya, C. Fountoukis, A. Nenes and E. Matías</i>
11:35	<a href="#">T11A015</a>	<b>Modeling the urban- and regional-scale dynamics of gaseous pollutants and aerosols</b> <i>V.O. Arutyunyan, A.E. Aloyan, and A. N. Yermakov</i>
11:55	<a href="#">T12A025</a>	<b>Aerosol properties in the spring and summer Arctic troposphere: a global model study</b> <i>H. Korhonen, D.V. Spracklen, K.S. Carslaw, and G.W. Mann</i>
Back-up Paper	<a href="#">T12A009</a>	<b>Estimating cloud droplet number concentration with particle number-to-volume concentration ratio</b> <i>N. Kivekäs, V.-M. Kerminen, T. Anttila, H. Korhonen, M. Komppula, and H. Lihavainen</i>

<b>Wednesday 12 September 2007</b>	<b>12:15 - 13:45</b>	<b>Lunch Break</b>
------------------------------------	----------------------	--------------------

<b>Wednesday 12 September 2007</b>	<b>12:15 - 13:45 (Meeting Room)</b>	<b>IARA Committee Meeting</b>
------------------------------------	-------------------------------------	-------------------------------

<b>Wednesday 12 September 2007</b>	<b>13:45</b>	<b>End of Conference Day</b>
------------------------------------	--------------	------------------------------

<b>15:00</b>	<b>Festung Hohensalzburg Tours (organized by SEMACO)</b>
--------------	--

<b>15:00</b>	<b>Residenz Salzburg and City Tour (organized by SEMACO)</b>
--------------	--

[Top of Program](#)

## Thursday 13 September 2007

Thursday 13 September 2007	08:00 - 16:15	Registration
----------------------------	---------------	--------------

Thursday 13 September 2007	08:45 - 09:45	AudiMax
----------------------------	---------------	---------

<b>Plenary Lecture IV</b>		
<b>Chair:</b>	Regina Hitzemberger	
08:45	<a href="#">Plenary Lecture</a>	<b>Biosphere-aerosol-cloud-climate interactions</b> <i>Markku Kulmala</i>

Thursday 13 September 2007	09:45 - 10:15	Coffee Break and Exhibition
----------------------------	---------------	-----------------------------

Thursday 13 September 2007	10:15 - 12:15	AudiMax
----------------------------	---------------	---------

<b>Atmospheric Aerosols - Cloud Properties and Hygroscopicity</b>		
<b>Chairs:</b>	Martina Krämer and Scot Martin	
10:15	<a href="#">T13A181</a>	<b>Partitioning of aerosol particles in mixed-phase clouds at a high alpine site</b> <i>E. Weingartner, J. Cozic, B. Verheggen, M. Gysel, U. Baltensperger, S. Mertes, K.N. Bower, I. Crawford, M. Flynn, P. Connolly, M. Gallagher, T. Choularton, U. Lohmann, D. Cziczo, J. Schneider, S. Walter, J. Curtius, S. Borrmann, and A. Petzold</i>
10:35	<a href="#">T13A014</a>	<b>The composition of ice residue in clean mixed phase clouds</b> <i>L. Keller, H. Herich, D.J. Cziczo, and U. Lohmann</i>
10:55	<a href="#">T13A225</a>	<b>Are the cloud condensation nuclei (CCN) properties in polluted air different from those in a remote region?</b> <i>D. Rose, G. P. Frank, U. Dusek, M. O. Andreae, and U. Pöschl</i>
11:15	<a href="#">T13A163</a>	<b>Measurement of size resolved hygroscopic and cloud activation aerosol properties</b> <i>N. Good, J. Crosier, P. Williams, H. Coe, G. McFiggans</i>
11:35	<a href="#">T13A151</a>	<b>Hygroscopic properties of secondary organic aerosol formed from plant emissions</b> <i>T. F. Mentel, E. Dinar, P. Griffiths, R. Tillmann, R. Fisseha, T. Hohaus, A. Kiendler-Scharr, E. Kleist, A. Mensah, M. Miebach, Y. Rudich, R. Uerlings, and J. Wildt</i>
11:55	<a href="#">T13A175</a>	<b>Hygroscopic properties of summertime central Arctic sub-micrometer aerosol particles and prediction of their CCN activity</b> <i>E. Swietlicki, J. Rissler, J. Zhou, E.K. Bigg, and C. Leck</i>
Back-up Paper	<a href="#">T13A154</a>	<b>Aerosol hygroscopicity as the function of the size and the chemical composition</b> <i>K. Imre, A. Molnár, and D. Benko</i>

Thursday 13 September 2007	10:15 - 12:15	Blauer Hörsaal
----------------------------	---------------	----------------

<b>High Temperature Aerosols</b>		
<b>Chairs:</b>	Hanns-Rudolf Paur and Franco Lucarelli	
10:15	<a href="#">T14A036</a>	<b>Formation of TiO<sub>2</sub> nanoparticles by combustion of single titanium particles</b> <i>V.V. Karasev, A.A. Onischuk, S. A. Khromova, and C.J. Tsai</i>
10:35	<a href="#">T16A005</a>	<b>Zinc aerosols from steelmaking EAF: Morphology and growth</b> <i>E. García, I. Lopez Baiñ, S. Astarloa, J.A. Legarreta, and C. Gutiérrez-Cañas</i>

10:55	<a href="#">T16A001</a>	<b>Characterisation of aerosols formed in high temperature experiments</b> <i>A. Pintér Csordás, P. Windberg, I. Nagy, Z. Hózer, and L. Matus</i>
11:15	<a href="#">T16A003</a>	<b>Aerosol synthesis as a route to metallic Ni-Mo alloys with enhanced mechanical properties</b> <i>E. K. Athanassiou, R.N. Grass, and W.J. Stark</i>
11:35	<a href="#">T16A006</a>	<b>Measurements of high temperature particle charge</b> <i>K. Reuter-Hack, J. Meyer, A. P. Weber, and G. Kasper</i>
11:55		

<b>Thursday 13 September 2007</b>	<b>10:15 - 12:15</b>	<b>Grüner Hörsaal</b>
<b>Special Session: COST 633 - Particulate Matter and Health Effects</b>		
<b>Chairs:</b>	<b>Thomas Kuhlbusch and Wilfried Winiwarter</b>	
10:15	<a href="#">T23A001</a>	<b>Cross-disciplinary approaches for critical issues in particulate air pollution</b> <i>R. Hitzenberger, J. Tursic, J.-P. Putaud, A. Berner, R.O. Salonen, W. Kreyling, T.A.J. Kuhlbusch, M. Amann, F. Cassee, W. Winiwarter, and COST633-Members</i>
10:35	<a href="#">T23A007</a>	<b>Differences and similarities in PM characteristics across Europe: Results of the COST633 data compilation activity</b> <i>J.P. Putaud, A. Alastuey, H. ten Brink, R. Hitzenberger, A. Jones, A. Kasper-Giebl, A. Kousa, A. Molnar, T. Moreno, F. Palmgren, C. Petaloti, I. Salma, J. Tursic, and M. Viana Rodriguez</i>
10:55	<a href="#">T13A075</a>	<b>Overview of source apportionment methods in selected European COST633 action member countries</b> <i>M. Viana, X. Querol, T.A.J. Kuhlbusch, A. Miranda, M. Valliu, A. Kasper-Giebl, S. Szidat, W. Winiwarter, and R.M. Harrison</i>
11:15	<a href="#">T23A004</a>	<b>Modelling exposure to atmospheric particulate matter – An overview</b> <i>C. Borrego, A.I. Miranda, J. Ferreira, O. Hänninen, T. Kuhlbusch, and W. Winiwarter</i>
11:35	<a href="#">T23A009</a>	<b>Heterogeneity in toxicity of particulate matter collected across Europe</b> <i>F.R. Cassee, E. Dybing, T. Sandström, and R.O. Salonen</i>
11:55	<a href="#">T23A002</a>	<b>Similarities and heterogeneities in exposure and health effects over Europe – Epidemiological results and research needs identified in COST action 633</b> <i>M. Riediker, N. Künzli, G. Hoek, J. Cyrus, A. Peters, and R.O. Salonen</i>
Back-up Paper	<a href="#">T23A005</a>	<b>Generation and quantification of organic peroxides in aerosols to study cellular responses on oxidative stress</b> <i>A.A.-M. Gaschen, A. Praplan, M. Savi, D. Lang, M. Geiser, and M. Kalberer</i>

<b>Thursday 13 September 2007</b>	<b>10:15 - 12:15</b>	<b>Lecture Hall 414</b>
<b>Aerosol Instrumentation III</b>		
<b>Chairs:</b>	<b>Wolfram Birmilli and Henna Isherwood</b>	
10:15	<a href="#">T02A020</a>	<b>Aerosols washout by a water spray in hostile environment: Experimental and numerical approaches</b> <i>D. Marchand, E. Porcheron, P. Lemaitre, G. Grehan, and W. Plumecocq</i>
10:35	<a href="#">T02A027</a>	<b>On-line measurements of industrial minerals' particle size during milling</b> <i>K. Tousimi, C. Pagoura, O. Makridou, C. Agrafiotis, A.G. Konstandopoulos, G. Zannis, and M. Founti</i>
10:55	<a href="#">T02A031</a>	<b>Intercomparison of measurement techniques for black or elemental carbon under urban background conditions in wintertime</b> <i>R. Hitzenberger, P. Reisinger, A. Wonaschuetz, A. Petzold, H. Bauer, N. Jankowski, H. Puxbaum, X. Chi, and W. Maenhaut</i>
11:15	<a href="#">T02A038</a>	<b>Development and characterization of an ion trap mass spectrometer for the on-line analysis of atmospheric aerosol</b> <i>J. Curtius, A. Kürten, A. Ehlerding, F. Helleis, and S. Bormann</i>

11:35	<a href="#">T02A049</a>	<b>Analysis of transfer functions of fast scanning DMAs</b> <i>P. Dubey and S. Dhaniyala</i>
11:55	<a href="#">T02A002</a>	<b>Uncertainty on experimental aerosol characterization: Calibration tests supporting aerosol studies under severe accident SGTR conditions</b> <i>F.J. Sánchez-Velasco, C. López del Prá, and L.E. Herranz</i>
Back-up Paper	<a href="#">T02A047</a>	<b>Modelling Ag-particle activation and growth in TSI CPC 3785</b> <i>F. Stratmann, T. Petäjä, and M. Kulmala</i>

<b>Thursday 13 September 2007</b>	<b>10:15 - 12:15</b>	<b>Lecture Hall 421</b>
-----------------------------------	----------------------	-------------------------

### Bioaerosols - General II

**Chairs: Ruprecht Jaenicke and Sergey Grinshpun**

10:15	<a href="#">T04A019</a>	<b>Seasonal variation of fungal spores and their contribution to organic carbon and to PM10 aerosols in Vienna, Austria</b> <i>H. Bauer, V. Bumberger, A. Caseiro, P. Pouresmaeil, A. Berger, and H. Puxbaum</i>
10:35	<a href="#">T04A008</a>	<b>Molecular genetics and diversity of bacteria and archaea in urban, rural and high alpine air</b> <i>V. Després, J. Nowoisky, M. Klose, R. Conrad, and J. Cimbali</i>
10:55	<a href="#">T04A009</a>	<b>To what extent can viable bacteria in atmospheric aerosols be dangerous for humans?</b> <i>A.S. Safatov, I.S. Andreeva, B.D. Belan, G.A. Buryak, E.K. Emelyanova, R. Jaenicke, M.V. Panchenko, N.I. Pechurkina, L.I. Puchkova, V.E. Repin, I.V. Saranina and, A.N. Sergeev</i>
11:15	<a href="#">T04A030</a>	<b>Total numbers and activity of environmental airborne bacteria</b> <i>R. Thyrrhaug, J.Einen, R-A. Sandaa, M. Heldal, and G.Bratbak</i>
11:35	<a href="#">T04A017</a>	<b>Disinfection of bioaerosols using filters saturated with tea tree</b> <i>R. Huang, B.J. Mullins, I. Agranovski, and O. Pyankov</i>
11:55	<a href="#">T04A010</a>	<b>Removal of bioaerosol by the combination of photocatalysis and negative air ion</b> <i>K.-P. Yu, W.-M. Lee, and S.-Y. Lin</i>
Back-up Paper	<a href="#">T04A029</a>	<b>Combined UV-fluorescence and background aerosol monitoring for detection of intentional release of airborne biological agents</b> <i>K. Janka, R. Reinivaara, J. Tikkanen, A. Rostedt, M. Putkiranta, J. Laaksonen, M. Marjamäki, J. Keskinen, and T. Humpi</i>

<b>Thursday 13 September 2007</b>	<b>12:15 - 13:45</b>	<b>Lunch Break</b>
-----------------------------------	----------------------	--------------------

<b>Thursday 13 September 2007</b>	<b>13:45 - 15:45</b>	<b>Poster and Exhibition Area</b>
-----------------------------------	----------------------	-----------------------------------

### Poster Session Part II and Exhibition

<b>Thursday 13 September 2007</b>	<b>15:45 - 16:15</b>	<b>Coffee Break and Exhibition</b>
-----------------------------------	----------------------	------------------------------------

<b>Thursday 13 September 2007</b>	<b>16:15 - 18:00</b>	
-----------------------------------	----------------------	--

### Working Group Sessions

<b>Thursday 13 September 2007</b>	<b>16:15 - 17:00</b>	<b>AudiMax</b>
-----------------------------------	----------------------	----------------

### Working Group: Atmospheric Aerosols

<b>Chair:</b>	<b>Lothar Schütz</b>
<b>Topics:</b>	The structure and content of the working group will be discussed in view of the developments in this research area during the last years. In addition, the elections of chairman and vice-chairman will be held.

<b>Thursday 13 September 2007</b>	<b>16:15 - 17:00</b>	<b>Blauer Hörsaal</b>
-----------------------------------	----------------------	-----------------------

**Working Group: PMx**

<b>Chair:</b>	<b>Harry ten Brink</b>
---------------	------------------------

<b>Topics:</b>	Chemical artefacts in filter-sampling of PM2.5 (speaker to be announced), followed by a discussion on the new/revised EU Air Quality Directive and FP7 with regard to possible implication on research activities. In addition, the elections of chairman and vice-chairman will be held.
----------------	---

<b>Thursday 13 September 2007</b>	<b>16:15 - 17:00</b>	<b>Grüner Hörsaal</b>
-----------------------------------	----------------------	-----------------------

**Working Group: Nanoparticles**

<b>Chair:</b>	<b>Alfred Weber</b>
---------------	---------------------

<b>Topics:</b>	The activities of the working group will be presented and current trends within the aerosol nanoparticle community such as the increasing orientation towards material applications will be discussed. In addition, the elections of chairman and vice-chairman will be held.
----------------	---

<b>Thursday 13 September 2007</b>	<b>16:15 - 17:00</b>	<b>Lecture Hall 414</b>
-----------------------------------	----------------------	-------------------------

**Working Group: Aerosol Modelling**

<b>Chair:</b>	<b>Bernhard Vogel</b>
---------------	-----------------------

<b>Topics:</b>	Discussion and possibility to present brief summaries (one slide) on new modelling projects (FP7), as well as discussion on future improvements of the EAC. In addition, the elections of chairman and vice-chairman will be held.
----------------	--

<b>Thursday 13 September 2007</b>	<b>16:15 - 17:00</b>	<b>Lecture Hall 421</b>
-----------------------------------	----------------------	-------------------------

**Working Group: Fundamentals**

<b>Chair:</b>	<b>Charles Clement</b>
---------------	------------------------

<b>Topics:</b>	Review of fundamental issues in aerosol science Solicitation of papers for special sessions
----------------	--

<b>Thursday 13 September 2007</b>	<b>17:15 - 18:00</b>	<b>AudiMax</b>
-----------------------------------	----------------------	----------------

**Working Group: Instrumentation**

<b>Chair:</b>	<b>Aladar Czitrovski</b>
---------------	--------------------------

<b>Topics:</b>	
----------------	--

<b>Thursday 13 September 2007</b>	<b>17:15 - 18:00</b>	<b>Blauer Hörsaal</b>
-----------------------------------	----------------------	-----------------------

**Working Group: Aerosol Chemistry**

<b>Chair:</b>	<b>Thomas Kuhlbusch</b>
<b>Topics:</b>	<b>Chemistry of secondary organic Aerosols (Thorsten Hoffman) followed by an open discussion on the future needs and research directions in Aerosol Chemistry</b>

<b>Thursday 13 September 2007</b>	<b>17:15 - 18:00</b>	<b>Grüner Hörsaal</b>
-----------------------------------	----------------------	-----------------------

**Working Group: Lung-Particle-Interaction**

<b>Chair:</b>	<b>Wolfgang Kreyling</b>
---------------	--------------------------

<b>T08A007</b>	<b>Size partitioning of airborne particles to compare their proinflammatory effect in airway epithelial cells</b> <i>K. Ramgolam, O. Favez, L. Martinon, H. Cachier, A. Person, A. Gaudichet, F. Marano, and A. Baeza-Squiban</i>
----------------	--

<b>T08A024</b>	<b>Prolonged retention of ultrafine carbon particles from human airways and the lung periphery</b> <i>W. Möller, K. Felten, K. Sommerer, G. Scheuch, G. Meyer, K. Häussinger, and W.G. Kreyling</i>
----------------	--

<b>Thursday 13 September 2007</b>	<b>17:15 - 18:00</b>	<b>Lecture Hall 414</b>
-----------------------------------	----------------------	-------------------------

**Working Group: High-Temperature-Aerosols**

<b>Chair:</b>	<b>Cristina Gutierrez-Canas</b>
---------------	---------------------------------

<b>Topics:</b>	<b>High-T high concentration aerosols sampling issues, followed by a discussion on research needs and future directions</b> Speaker to be confirmed In addition, the elections of chairman and vice-chairman will be held.
----------------	--

<b>Thursday 13 September 2007</b>	<b>17:15 - 18:00</b>	<b>Lecture Hall 421</b>
-----------------------------------	----------------------	-------------------------

**Working Group: Electrical Effects**

<b>Chair:</b>	<b>Tomasz Ciach</b>
---------------	---------------------

<b>Topics:</b>	
----------------	--

<b>Thursday 13 September 2007</b>	<b>18:00</b>	<b>End of Conference Day</b>
-----------------------------------	--------------	------------------------------

<b>Thursday 13 September 2007</b>	<b>19:00</b>	<b>Conference Dinner</b>
-----------------------------------	--------------	--------------------------

[Top of Program](#)

## Friday 14 September 2007

<b>Friday 14 September 2007</b>	<b>08:30 - 15:00</b>	<b>Registration</b>
---------------------------------	----------------------	---------------------

<b>Friday 14 September 2007</b>	<b>08:45 - 09:45</b>	<b>AudiMax</b>
---------------------------------	----------------------	----------------

<b>Plenary Lecture V</b>		
<b>Chair:</b>	<b>Leon Gradon</b>	
<b>08:45</b>	<b>Plenary Lecture</b>	<b>Therapeutic aerosols: Today and tomorrow</b>
		<i>Gerhard Scheuch</i>

<b>Friday 14 September 2007</b>	<b>09:45 - 10:15</b>	<b>Coffee Break and Exhibition</b>
---------------------------------	----------------------	------------------------------------

<b>Friday 14 September 2007</b>	<b>10:15 - 12:15</b>	<b>AudiMax</b>
---------------------------------	----------------------	----------------

### Atmospheric Aerosols - Transport and Physical Properties

**Chairs:** Sabine Wurzler and Vidmantas Ulevicius

<b>10:15</b>	<a href="#">T13A173</a>	<b>In-situ evidence for free-tropospheric long-range transport of a Siberian forest fire plume to the North Pole region</b>
		<i>E. Swietlicki, A. Wisthaler, M. Tjernström, A. Hansel, and C. Leck</i>
<b>10:35</b>	<a href="#">T13A076</a>	<b>Characterization by electronic microscopy of particulate matter in different places of Mexico influenced by different pollutants emissions</b>
		<i>A. Aragón, A.A. Campos, and G.J. Labrada</i>
<b>10:55</b>	<a href="#">T13A134</a>	<b>Observations of different events with high particle number size distributions at the coastal Atlantic area of south-west Spain</b>
		<i>M. Sorribas, V.E. Cachorro, B. Wehner, W. Birmili, N. Prats, J.F. López, A. Wiedensohler, A.M. De Frutos, and B.A. De la Morena</i>
<b>11:15</b>	<a href="#">T13A147</a>	<b>Density of boreal forest aerosol particles as a function of mode diameter</b>
		<i>J. Kannosto, A. Virtanen, T. Rönkkö, P.P. Aalto, and M. Kulmala</i>
<b>11:35</b>	<a href="#">T13A205</a>	<b>Ultrafine particle exposure control measurement techniques</b>
		<i>H. Fissan, C. Asbach, H. Kaminski, B. Stahlmecke, and T. Kuhlbusch</i>
<b>11:55</b>	<a href="#">T13A220</a>	<b>Influence of the mixing layer on the concentration and size distribution of particulate matter over Milan</b>
		<i>L. Ferrero, E. Bolzacchini, M. G. Perrone, S. Petraccone, G. Sangiorgi, C. Lo Porto, B.S. Ferrini, Z. Lazzati, A. Riccio, E. Previtali, M. Clemenza, F. Bruno, D. Cocchi, and F. Greco</i>
<b>Back-up Paper</b>	<a href="#">T13A031</a>	<b>Aerosols transport across the Central Mediterranean</b>
		<i>D. Đorđević, S. Rodríguez, J.J. Rodríguez, J.C. Guerra, M. Todorovic, D. Relić, A. Mihajilidi-Zelić, and D. Šegan</i>

<b>Friday 14 September 2007</b>	<b>10:15 - 12:15</b>	<b>Blauer Hörsaal</b>
---------------------------------	----------------------	-----------------------

### PM10/PM2.5 - Sources II

**Chairs:** Stephan Leinert and Harry M. ten Brink

<b>10:15</b>	<a href="#">T19A023</a>	<b>Impact of wood combustion on composition and concentrations of urban particulate matter</b>
		<i>J. Schnelle-Kreis, J. Orasche, M. Sklorz, J.J. Briedé, T.M. de Kok, and R. Zimmermann</i>
<b>10:35</b>	<a href="#">T19A040</a>	<b>Contribution of soft and hardwood combustion to the Austrian PM10</b>
		<i>P. Kotianová, A. Caseiro, and H. Puxbaum</i>
<b>10:55</b>	<a href="#">T19A034</a>	<b>Influence of tyre and pavement on PM10 and particle number emissions from road wear</b>
		<i>A. Gudmundsson, A. Dahl, E. Swietlicki, G. Blomqvist, P. Jonsson, and M. Gustafsson</i>
<b>11:15</b>	<a href="#">T19A048</a>	<b>Non-exhaust PM emission from highway traffic</b>
		<i>A.C. John, U. Quass, J. Lindermann, M. Beyer, M. &amp; M. Sulkowski, A.V. Hirner, A. Baum, and T.A.J. Kuhlbusch</i>
<b>11:35</b>	<a href="#">T13A026</a>	<b>Traffic contribution to PM in cities – size segregated characterization of EC/OC and organic species</b>
		<i>K. Müller, T. Gnauk, E. Brüggemann, G. Spindler, D. van Pinxteren, and H. Herrmann</i>
<b>11:55</b>	<a href="#">T19A016</a>	<b>Fireworks as a source of PM pollution: Results of a case study</b>
		<i>R. Vecchi, G. Valli, V. Bernardoni, A. D'Alessandro, P. Fermo, A. Piazzalunga, S. Nava, M. Chiari, and F. Lucarelli</i>

Back-up Paper	<a href="#">T19A047</a>	<b>Effectiveness of street cleaning for reducing ambient PM10 concentrations</b>
		<i>A.C. John, A. Hugo, H. Kaminski, A. Brandt, W. Kappert, E. Falkenberg, and T.A.J. Kuhlbusch</i>

<b>Friday 14 September 2007</b>	<b>10:15 - 12:15</b>	<b>Grüner Hörsaal</b>
<b>Lung-Particle-Interaction and Medical Aerosols</b>		
<b>Chairs: George Ferron and Imre Balásházy</b>		
10:15	<a href="#">T08A002</a>	<b>CFD modelling of transient aerosol transport and deposition in human airways</b> <i>M. Forman, M. Jicha, and J. Katolicky</i>
10:35	<a href="#">T08A004</a>	<b>In vitro cytotoxicity and quantitative models for the uptake of oxide nanoparticles into human lung cells</b> <i>L.K. Limbach, T.J. Brunner, R.N. Grass, P. Wick, A. Bruinink, D. Günther, and W.J. Stark</i>
10:55	<a href="#">T08A009</a>	<b>Calculation of diesel combustion particle deposition in the human respiratory tract</b> <i>B. Alfoldy, B. Giechaskiel, Y. Drossinos, and W. Hofmann</i>
11:15	<a href="#">T08A011</a>	<b>Respiratory tract deposition of fine particles in candle smoke</b> <i>J. Löndahl, J. Ådahl, C. Boman, and E. Swietlicki</i>
11:35	<a href="#">T08A013</a>	<b>Ultrafine particle deposition differs consistently between the developing and adult rat lung</b> <i>M. Semmler-Behnke, I. Bolle, W. Moeller, H. Schulz, S. Takenaka, A. Tsuda, and W.G. Kreyling</i>
11:55	<a href="#">T08A003</a>	<b>Human nasal passage fibrous particle deposition: the influence of particle length, flow rate and passage geometry</b> <i>Z. Wang and P.K. Hopke</i>
Back-up Paper	<a href="#">T08A014</a>	<b>Modelling deposition of hygroscopic particles in the human respiratory tract</b> <i>R. Winkler-Heil, G.A. Ferron, and W. Hofmann</i>

<b>Friday 14 September 2007</b>	<b>10:15 - 12:15</b>	<b>Lecture Hall 414</b>
<b>Atmospheric Aerosols - Desert Dust</b>		
<b>Chairs: Andreas Petzold and Lothar Schütz</b>		
10:15	<a href="#">T13A073</a>	<b>Desert aerosol size distributions and mass concentrations – Results from the Saharan Mineral Dust Experiment SAMUM 2006</b> <i>L. Schütz, K. Kandler, C. Deutscher, P. Knippertz, R. Jaenicke, S. Zorn, M. Ebert, S. Weinbruch, A. Maßling, A. Schladitz, and A. Wiedensohler</i>
10:35	<a href="#">T13A227</a>	<b>Saharan Mineral Dust Experiment SAMUM 2006: Vertical profiles of dust particle properties from airborne in-situ and LIDAR observations</b> <i>B. Weinzierl, K. Rasp, M. Fiebig, M. Esselborn, F. Wagner, A. Virkkula, and A. Petzold</i>
10:55	<a href="#">T13A035</a>	<b>State of mixing of the Saharan dust sub- and supermicrometer aerosol</b> <i>N. Kaaden, A. Massling, T. Müller, A. Schladitz, K. Kandler, L. Schütz, and A. Wiedensohler</i>
11:15	<a href="#">T13A032</a>	<b>Saharan dust observations in the Mediterranean - Adriatic confluence region</b> <i>S. Rodríguez and D. Đorđević</i>
11:35	<a href="#">T13A164</a>	<b>Temporal variation of chemical compositions for aerosol sample collected during an Asian dust storm event in 2006</b> <i>H. Hwang, E. Choi, S. Kang, Y. Park, H. Kim, and C.-U. Ro</i>
11:55	<a href="#">T13A029</a>	<b>The processes prompting the contrasting behavior between the aerosol mass and number concentrations at the Izaña GAW Observatory: New particles formation versus saharan dust inputs</b> <i>S. Rodríguez, E. Cuevas, R. Ramos, and P.M. Romero</i>
Back-up Paper	<a href="#">T13A222</a>	<b>Saharan Mineral Dust Experiment SAMUM 2006: Aerosol optical properties of dust from various source regions</b> <i>A. Petzold, K. Rasp, T. Hamburger, B. Weinzierl, M. Fiebig, and A. Virkkula</i>

<b>Friday 14 September 2007</b>	<b>10:15 - 12:15</b>	<b>Lecture Hall 421</b>
---------------------------------	----------------------	-------------------------

<b>Radioactive Aerosols</b>		
<b>Chairs: Denis Boulaud and Constantin Papastefanou</b>		
10:15	<a href="#">T10A001</a>	<b>Individual protection against inhalation of long living radioactive dust due to an uncontrolled release</b> <i>T. Streil, V. Oeser, R. Rambousky, and F.W. Buchholz</i>
10:35	<a href="#">T10A002</a>	<b>Residence time of atmospheric aerosols in association with radioactive nuclides</b> <i>C. Papastefanou and A. Ioannidou</i>
10:55	<a href="#">T10A012</a>	<b>Relationship between origin of air masses and <sup>137</sup>Cs activities in French aerosols, 2000-2006</b> <i>O. Masson, D. Piga, G. Le Roux, L. Bourcier, L. Saey, P. Paulat, and X. Cagnat</i>
11:15	<a href="#">T10A006</a>	<b>Experiments and modelling on the transport and speciation of ruthenium oxides</b> <i>T. Kärkelä, U. Backman, A. Auvinen, Y. Enqvist, R. Zilliacus, M. Lipponen, T. Kekki, U. Tapper, and J.K. Jokiniemi</i>
11:35	<a href="#">T10A010</a>	<b>Generation and measurement of aerosols for severe nuclear reactor accident research</b> <i>T.M. Lind, S. Danner, and S. Güntay</i>
11:55	<a href="#">T10A013</a>	<b>Removal of radon decay products using unipolar ionisers</b> <i>B.K. Sapra, A. Khan, P.S. Kothalkar, and Y.S. Mayya</i>

<b>Friday 14 September 2007</b>	<b>12:15 - 13:45</b>	<b>Lunch Break</b>
<b>Friday 14 September 2007</b>	<b>12:15 - 13:45 (Meeting Room)</b>	<b>Working Group Chairs Meeting</b>

<b>Friday 14 September 2007</b>	<b>13:45 - 15:45</b>	<b>AudiMax</b>
<b>Atmospheric Aerosols - Chemical Properties</b>		
<b>Chairs: Risto Hillamo and Martine van Poppel</b>		
13:45	<a href="#">T13A042</a>	<b>Air quality in background savannah in Southern Africa</b> <i>L. Laakso, T. Petäjä, H. Laakso, P.P. Aalto, E. Siivola, P. Keronen, S. Haapanala, M. Kulmala, H. Hakola, N. Kgabi, M. Molefe, D. Mabaso, K. Pienaar, and E. Sjöberg</i>
14:05	<a href="#">T13A093</a>	<b>Characteristic size distribution of sulphate aerosols influenced by Asian outflow</b> <i>N. Kaneyasu, A. Takami, and S. Hatakeyama</i>
14:25	<a href="#">T13A094</a>	<b>Chemical and morphological characterization of atmospheric particles in Mexico City and its classification in anthropogenic types</b> <i>G.J. Labrada-Delgado, J. Gladis, A. Aragón Piña, and A.A. Campos Ramos</i>
14:45	<a href="#">T13A100</a>	<b>Surface tension properties of aerosol water extract and atmospheric humic-like substances</b> <i>I. Salma, R. Ocskay, N. Peron, and I. Varga</i>
15:05	<a href="#">T13A105</a>	<b>Chemical characterization of all-year-round atmospheric aerosol at Dome C, East Antarctica</b> <i>R. Udisti, S. Becagli, E. Castellano, O. Cerri, F. Lucarelli, F. Marino, A. Morganti, S. Nava, F. Rugi, E. Salviotti, M. Severi, and R. Traversi</i>
15:25	<a href="#">T13A118</a>	<b>In-situ analysis of free tropospheric aerosol and small ice crystal residuals using a High Resolution Aerosol Mass Spectrometer (HR-ToF-AMS) at the Jungfrauoch during CLACE 5</b> <i>J. Schneider, S. Walter, J. Curtius, F. Drewnick, S. Borrmann, S. Mertes, E. Weingartner, M. Gysel, and J. Cozic</i>
Back-up Paper	<a href="#">T13A078</a>	<b>Long-term observations of aerosol mass and composition and trace gas concentrations in Pacific background airmasses at coastal atmospheric monitoring sites in Taiwan</b> <i>C. Junker and C.T. Lee</i>

<b>Friday 14 September 2007</b>	<b>13:45 - 15:45</b>	<b>Blauer Hörsaal</b>
<b>PM10/PM2.5 - Variability/Meteorology</b>		

<b>Chairs:</b>		<b>Gilmore Sem and NN</b>
13:45	<a href="#">T19A001</a>	<b>Size-segregated physical-chemical characterization of particles depending of air mass origin at German lowlands (Melpitz site)</b> <i>G. Spindler, E. Brüggemann, Th. Gnauk, A. Grüner, H. Herrmann, K. Müller, T.M. Tuch, B. Wehner, M. Wallasch, and A. Wiedensohler</i>
14:05	<a href="#">T19A003</a>	<b>Interannual variation of particulate matter over Europe with emphasis on North-Rhine-Westphalia: Impact of changing emissions and meteorological conditions</b> <i>S. Wurzler, J. Geiger, U. Hartmann, A. Brandt, U. Pfeffer, M. Memmesheimer, E. Friese, H.J. Jakobs, H. Feldmann, A. Ebel, and C. Kessler</i>
14:25	<a href="#">T19A021</a>	<b>Variations of particulate matter in dependence on climatic conditions</b> <i>V. Adamec, J. Huzlik, R. Licbinsky, and M. Schwarzova</i>
14:45	<a href="#">T19A053</a>	<b>Mobile laboratory measurements of PM9 and PM2.5 in Helsinki, Finland</b> <i>L. Pirjola, K. Kupiainen, and H. Tervahattu</i>
15:05	<a href="#">T13A020</a>	<b>Analysis of temporal patterns of turbulent fluxes of PM2.5 on the Venice lagoon</b> <i>A. Donato, D. Contini, D. Cesari, F. Belosi, and F. Prodi</i>
15:25	<a href="#">T01A037</a>	<b>Seasonal variability in atmospheric aerosol levels and composition during 2006 at Uccle, Belgium</b> <i>X. Chi, W. Maenhaut, W. Wang, N. Raes, H. De Backer, and A. Cheymol</i>
Back-up Paper	<a href="#">T19A010</a>	<b>High population density and heavy industry: The challenge for air quality management in North Rhine Westphalia: Are the measures effective?</b> <i>S. Wurzler, W. Kappert, D. Gladtko, P. Bruckmann, and M. Memmesheimer</i>

<b>Friday 14 September 2007</b>	<b>13:45 - 15:45</b>	<b>Grüner Hörsaal</b>
---------------------------------	----------------------	-----------------------

### Aerosol Instrumentation IV

<b>Chairs:</b>		<b>Athanasios Konstandopoulos and Christian Gerhart</b>
----------------	--	---

13:45	<a href="#">T02A033</a>	<b>Modification and characterization of an expansion condensation nucleus counter for nanometer-sized particles</b> <i>H. Saghaififar, A. Kürten, J. Curtius, and S. Borrmann</i>
14:05	<a href="#">T13A044</a>	<b>Fulvic acids and their sulfated and nitrated analogues in atmospheric aerosol - Determination by ultrahigh resolution electrospray mass spectrometry</b> <i>T. Reemtsma, A. These, M. Linscheid, P.K. Hopke</i>
14:25	<a href="#">T02A032</a>	<b>Analysis of uncertainty in particle mass measurement using an aerosol particle mass analyzer</b> <i>K. Ehara, H. Sakurai, A. Yabe, N. Tajima, and K. J. Coakley</i>
14:45	<a href="#">T02A021</a>	<b>Evaluation of neutral cluster and air ion spectrometer (NAIS)</b> <i>S. Mirme, A. Mirme, E. Tamm, and J. Uin</i>
15:05	<a href="#">T02A035</a>	<b>Generation of standard aerosols by electrical separation in a wide size range</b> <i>J. Uin, A. Mirme, S. Mirme, and E. Tamm</i>
15:25	<a href="#">T13A176</a>	<b>A new loading and scattering correction for the particle soot absorption photometer (PSAP)</b> <i>T. Müller, A. Schladnitz, A. Wiedensohler</i>
Back-up Paper	<a href="#">T02A037</a>	<b>Design and performance evaluation of a new non-collective electrical aerosol sensor</b> <i>K. Janka, V. Niemelä, E. Lamminen, J. Keskinen, A. Rostedt, and M. Lemmetty</i>

<b>Friday 14 September 2007</b>	<b>13:45 - 15:45</b>	<b>Lecture Hall 414</b>
---------------------------------	----------------------	-------------------------

### Industrial Aerosols

<b>Chairs:</b>		<b>Karl-Heinz Schaber and Helmuth Horvath</b>
----------------	--	---

13:45	<a href="#">T17A002</a>	<b>Fog formation during hydrogen bromide absorption in flue gas cleaning processes</b> <i>A. Wix, S. Sinanis, and K. Schaber</i>
14:05	<a href="#">T17A005</a>	<b>Real time wood dust sampling with particle size classification</b>

		<i>F. Belosi, F. Prodi, and G. Santachiara</i>
14:25	<a href="#">T17A008</a>	<b>Nanoparticulate construction materials via flame spray synthesis: Enhanced reactivity of nano-Portland cement and improved hardness of nano-gypsum</b> <i>S.C. Halim, N. Osterwalder, S. Loher, R.N. Grass, T.J. Brunner, L.K. Ludwig, M. Bohner, and W.J. Stark</i>
14:45	<a href="#">T17A014</a>	<b>The effect of hygroscopicity on inhaled dose for aerosol species measured in an industrial workplace</b> <i>C. Mitsakou, A. Karanasiou, S. Vratolis, K. Eleftheriadis, M. Lazaridis, and C. Housiadas</i>
15:05	<a href="#">T17A016</a>	<b>Physicochemical characterization of atmospheric particulate emissions from an iron and steel works</b> <i>H. Laversin, D. Hleis, D. Courcot, F. Ledoux, L. Courcot, E.A. Zhilinskaya, F. Cazier, S. Bouhsina, and A. Aboukais</i>
15:25	<a href="#">T17A017</a>	<b>Characterization of salt and acid aerosols using Raman spectroscopy</b> <i>S. Sinanis, M. Aleksandrova and K. Schaber</i>
Back-up Paper	<a href="#">T17A019</a>	<b>Experimental analysis of aerosol driven NOx reduction process assisted with ultraviolet irradiation</b> <i>Y. Emi, H. Takano, and M. Itoh</i>

<b>Friday 14 September 2007</b>	<b>13:45 - 15:45</b>	<b>Lecture Hall 421</b>
<b>Fine Particles</b>		
<b>Chairs:</b>	<b>Christof Asbach and NN</b>	
13:45	<a href="#">T15A003</a>	<b>Aerosol synthesis as a route to bulk nanocrystalline metals and composites with superior mechanical properties</b> <i>R.N. Grass and W.J. Stark</i>
14:05	<a href="#">T15A002</a>	<b>Characterization of aerosols produced by laser-matter interaction during paint stripping experiments by laser</b> <i>P. Dewalle, J. Vendel, J.M. Weulersse, P.Hervé, and G. Decobert</i>
14:25	<a href="#">T15A011</a>	<b>Particulate matter characterization by carbon isotopes</b> <i>C. Grassi, V. Campigli, L. Dallai, S. Nottoli, L. Tognotti, and M. Guidi</i>
14:45	<a href="#">T15A012</a>	<b>Chemical investigation of eight different types of carbonaceous particles using thermoanalytical techniques</b> <i>G. Matuschek, E. Karg, A. Schröppel, H. Schulz, and O. Schmid</i>
15:05	<a href="#">T15A010</a>	<b>Temporal variation of apparent particle density in an urban aerosol</b> <i>M. Pitz, W. Birmili, O. Schmid, J. Heinrich, R. Zimmermann, H.-E. Wichmann, A. Peters, and J. Cyrys</i>
15:25	<a href="#">T15A004</a>	<b>Capturing the effect of sulphur in diesel exhaust</b> <i>M. Lemmetty, L. Pirjola, E. Vouitsis, and J. Keskinen</i>
Back-up Paper	<a href="#">T15A009</a>	<b>Interaction between meteorological quantities and particle concentrations in the suburban/rural boundary layer during different weather episodes</b> <i>S. Weber</i>

<b>Friday 14 September 2007</b>	<b>15:45 - 15:00</b>	<b>AudiMax</b>
<b>Closing Remarks</b>		

<b>Friday 14 September 2007</b>	<b>15:00</b>	<b>End of Conference</b>
---------------------------------	--------------	--------------------------

[Top of Program](#)

# Saturday 15 September 2007

09:00

Lake and MountainTour (organized by SEMACO)

[Top of Program](#)

# Poster Session Part I

[Aerosol Chemistry](#)

[Indoor Aerosols](#)

[Aerosol Instrumentation](#)

[Lung-Particle-Interaction](#)

[Aerosol Modeling](#)

[Medical Aerosols](#)

[Aerosol Standards](#)

[Nanoparticles](#)

[Atmospheric Aerosols - Nucleation](#)

[PM10 / PM2.5](#)

[Atmospheric Aerosols - Urban Aerosols](#)

[Special Session: UT/LS Aerosols and Clouds  
- Measurements and Modeling](#)

[Electrical Effects](#)

[Aerosol Filtration#2](#)

<b>Tuesday 11 September 2007</b>	<b>13:45 - 15:45</b>	<b>Poster Area</b>
<b>Poster Session Part I</b>		

<b>Aerosol Chemistry</b>	
<a href="#">T01A002</a>	<b>The effect of Saharan dust outbreaks on particulate sulfate and nitrate levels in southeast Spain</b> <i>E. Yubero, N. Galindo, J. Nicolás, S. Caballero, C. Pastor, and J. Crespo</i>
<a href="#">T01A003</a>	<b>Size-segregated analysis of PM10 at a tandem rural-urban site combination</b> <i>J. Gietl, T. Tritscher, and O. Klemm</i>
<a href="#">T01A004</a>	<b>Secondary organic aerosol formation from plant emissions: Overview of the Jülich Plant chamber experiments</b> <i>A. Kiendler-Scharr, T. Hohaus, E. Kleist, M. Miebach, R. Tillmann, R. Uerlings, R. Fisseha, P. Griffiths, Y. Rudich, E. Dinar, J. Wildt, and T. Mentel</i>
<a href="#">T01A007</a>	<b>Crucial intermediates of benzaldehyde photolysis: Their roles in gas-to-particle conversion</b> <i>S.N. Dubtsov, G.G. Dultseva, and G.I. Skubnevskaya</i>
<a href="#">T01A008</a>	<b>Distributions and health risks of polycyclic aromatic hydrocarbons (PAHs) in atmospheric aerosols of the city of Chania (Greece)</b> <i>A. Pafitis, N. Pasadakis, I. Kopanakis, and E. Katsivela</i>
<a href="#">T01A009</a>	<b>Airborne copper, nickel and lead in northern Finland – Effects of the Kola metallurgical industry</b> <i>U. Makkonen, J. Paatero, K. Pyy, and M. Kulmala</i>
<a href="#">T01A011</a>	<b>TSP and heavy metals measurements in the roadside environment of the coastal city of Chania (Greece)</b> <i>V. Voudouri, N. Lydakakis-Simantiris, D. Pentari, and E. Katsivela</i>
<a href="#">T01A012</a>	<b>Modelling of the formation of metal oxide aerosols</b> <i>I. Alxneit and H.R. Tschudi</i>
<a href="#">T01A013</a>	<b>Polycyclic aromatic hydrocarbons and size distributions in Tehran, Iran</b> <i>F. Halek, M. Hashtroudi, and A. Kavousi</i>

<a href="#">T01A015</a>	<b>SPACCIM model studies of the multiphase chemistry processing of tropospheric aerosols</b> <i>A. Tilgner, R. Wolke, and H. Herrmann</i>
<a href="#">T01A016</a>	<b>Metal distribution from gasoline-fueled engine</b> <i>Y.F. Wang, H.R. Chao, L.C. Wang, H.H. Yang, and L.T. Hsieh</i>
<a href="#">T01A020</a>	<b>Characterisation, diel variation and mass size distributions of a-pinene oxidation products in ambient aerosol from K-pusztá, Hungary</b> <i>I. Kourtchev, M. Claeys, R. Szmigielski, P. Van der Veken, R. Vermeylen, W. Maenhaut, M. Jaoui, T.E. Kleindienst, M. Lewandowski, J.H. Offenberg, and E.O. Edney</i>
<a href="#">T01A021</a>	<b>Aerosol formation from isoprene</b> <i>B. Verheggen, A. Metzger, J. Duplissy, J. Dommen, E. Weingartner, A.S.H. Prevot, and U. Baltensperger</i>
<a href="#">T01A022</a>	<b>Identification of secondary inorganic and organic aerosol components in urban particulate matter samples</b> <i>A. Piazzalunga, P. Fermo, C. Rigamonti, R. Vecchi, G. Valli, and V. Bernardoni</i>
<a href="#">T01A023</a>	<b>Examples of SOA analysis by mass spectrometry from the PSI smog chamber</b> <i>J. Dommen, A. Metzger, A. Gascho, K. Gaeggeler, M.R. Alfara, A.S.H. Prevot, U. Baltensperger, M. Kalberer, D. Gross, and A. Brunner</i>
<a href="#">T01A024</a>	<b>Raman characterization of double salt formation from crystallization of mixed ammonium sulfate and ammonium nitrate particles</b> <i>T.Y. Ling and C.K. Chan</i>
<a href="#">T01A028</a>	<b>Effects of the wildfires in August 2006 on the air quality in south-eastern Finland</b> <i>U. Makkonen, P. Anttila, H. Hellén, and M. Ferm</i>
<a href="#">T01A031</a>	<b>Evaporation of multicomponent droplets</b> <i>I.K. Koponen, I. Riipinen, M. Kulmala, G. Frank, and M. Bilde</i>
<a href="#">T01A032</a>	<b>Ion composition in submicron aerosols in Helsinki area</b> <i>K. Teinilä, M. Aurela, H. Timonen, S. Kuokka, S. Saarikoski, K. Saarnio, O. Tolonen-Kivimäki, and R. Hillamo</i>
<a href="#">T01A033</a>	<b>Source contribution to high PM10 episodes in a residential area in the vicinity of two cement plants</b> <i>A. Carratala, E. Yubero, M. Santacatalina, J.F. Nicolas, and J. Crespo</i>
<a href="#">T01A034</a>	<b>Air concentrations of dioxins, PAHs and metals near two cement plants</b> <i>J. Conesa, A. Gálvez, M. Santacatalina, and A. Carratalá</i>
<a href="#">T01A035</a>	<b>Seasonal dependence of polar and non-polar organic compounds in aerosols in the atmosphere of a coastal city (NW Spain)</b> <i>D. García-Gacio, M. Piñero-Iglesias, E. Concha-Graña, P. López-Mahía, S. Muniategui-Lorenzo, and D. Prada-Rodríguez</i>
<a href="#">T01A038</a>	<b>Aerosol chemistry, chemical mass closure, and aerosol sources at two sites in Tanzania</b> <i>S. Mkoma, W. Wang, X. Chi, N. Raes, and W. Maenhaut</i>
<a href="#">T01A039</a>	<b>NMR Functional group analysis extended to carboxylic acids and ketones providing an insight into chemical ageing of SOA</b> <i>F. Moretti, E. Tagliavini, S. Decesari, M.C. Facchini, and S. Fuzzi</i>
<a href="#">T01A040</a>	<b>Phase changes during hygroscopic cycles in polyethylene glycol 400/ammonium sulfate system</b> <i>G. Ciobanu, C. Marcolli, U.K. Krieger, U. Weers, and T. Peter</i>
<a href="#">T01A042</a>	<b>Investigating the role of ammonia in atmospheric nucleation using quantum chemistry</b> <i>T. Kurtén, L. Torpo, H. Vehkamäki, M.R. Sundberg, K. Laasonen, V.-M. Kerminen, M. Noppel, M. Salonen, and M. Kulmala</i>
<a href="#">T01A044</a>	<b>On the beneficial effect of near-waterfall environment</b> <i>T.-E. Parts and A. Luts</i>
<a href="#">T01A047</a>	<b>Arsenic species levels of PM10 and PM2.5 in urban monitoring station (Huelva, SW Spain)</b> <i>A.M. Sánchez de la Campa, J.D. de la Rosa, D. Sánchez Rodas, V. Oliveira, A. Alastuey, and X. Quero</i>
<a href="#">T01A048</a>	<b>Polycyclic aromatic hydrocarbon in suspended particulate matter in southeastern Spain</b> <i>J. Gil-Moltó, M. Varea, N. Galindo, S. Caballero, R. Esclapez, C. Pastor, and J. Crespo</i>
<a href="#">T01A051</a>	<b>Dynamics of secondary organic aerosol from the ozonolysis of terpenes and isoprene: Results from aerosol chamber experiments and model analysis</b>

	<i>H. Saathoff, K.-H. Naumann, O. Möhler, A. Kiendler-Scharr, T. Mentel, R. Tillmann, Å. M. Jonsson, M. Hallquist, and U. Schurath</i>
<a href="#">T01A052</a>	<b>The effect of the surface coating grade of an organic insoluble substance onto hygroscopic particles</b>
	<i>P. Villani, V. Michaud, R. Weigel, D. Picard, K. Sellegri, S. Sjöegren, J. Duplissy, U. Baltensberger, E. Weingartner, and P. Laj</i>
<a href="#">T01A056</a>	<b>Aerosol catalysis: Size effects and metal support interactions on Pd nanoparticles</b>
	<i>F. Bacle, M. Seipenbusch, and G. Kasper</i>
<a href="#">T01A058</a>	<b>Influence of different sample preparations on the determined concentrations of selected trace metals in atmospheric particles</b>
	<i>H. Radic, J. Turšič, M. Kovacevic, and M. Veber</i>
<a href="#">T13A081</a>	<b>Effects of potassium nitrate on the polymorphic transformations of ammonium nitrate particles</b>
	<i>H.B. Wu, M.N. Chan, and C.K. Chan</i>
<a href="#">T13A148</a>	<b>Characterization of residual lignin polymers in particulate matter by LC-MS</b>
	<i>E. Bolzacchini, L. Ferrero, B. Ferrini, Z. Lazzati, M. Orlandi, C. Lo Porto, G. Perrone, G. Sangiorgi, S. Petraccone, and L. Zoia</i>
<a href="#">T13A149</a>	<b>Determination of oxygenated, nitrated and native polycyclic aromatic hydrocarbons (PAH) in aerosols using different, liquid chromatographic based methods</b>
	<i>J. Lintelmann, K. Fischer, M. Heil-Franca, and G. Matuschek</i>
<a href="#">T13A203</a>	<b>Optimization of high-resolution ICP-MS methods for determination of the “soluble” fraction of trace-metals in aerosol samples</b>
	<i>F. Rugi, S. Becagli, E. Castellano, M. Chiari, F. Lucarelli, F. Marino, S. Nava, M. Severi, R. Traversi, and R. Udisti</i>

[Top of Program](#)

[Top of Poster Session Part I](#)

<b>Aerosol Instrumentation</b>	
<a href="#">T02A001</a>	<b>An experimental study on relation of heterogeneous and homogeneous condensations in condensation aerosol generation</b>
	<i>Z. Zhang, L. Chen, and F. Jiang</i>
<a href="#">T02A003</a>	<b>Improving the detection efficiency of a condensation particle counter by means of pulse height analysis technique</b>
	<i>M. Sipilä, P.P. Aalto, and M. Kulmala</i>
<a href="#">T02A005</a>	<b>Configuration of air filters based on the constructal theory</b>
	<i>A.F. Miguel, A.H. Reis, and A. Bejan</i>
<a href="#">T02A006</a>	<b>Characterization of specific vertical aerosol fluxes by turbulent flux measurement and single particle mass spectrometry for micro-meteorological analysis</b>
	<i>E. Gelhausen, K.-P. Hinz, B. Spengler, A. Schmidt, and O. Klemm</i>
<a href="#">T02A007</a>	<b>Application of the method of Laser Doppler anemometry for aspiration measurement characteristics of the process of aerosol aspiration</b>
	<i>G.N. Lipatov and M.A. Yugov</i>
<a href="#">T02A009</a>	<b>Diffusion of charged particles in a DMA with inclined electric field</b>
	<i>J. Salm and U. Hörrak</i>
<a href="#">T02A010</a>	<b>A digital in-line holographic microscope (DIHM) for ice crystals</b>
	<i>P. Amsler, O. Stetzer, and U. Lohmann</i>
<a href="#">T02A013</a>	<b>Development of a thermal desorption chemical ionization ion trap mass spectrometer for the chemical characterization of ultrafine aerosol</b>
	<i>A. Held, J. Rathbone, and J. Smith</i>
<a href="#">T02A014</a>	<b>Numerical and experimental study on particle collection efficiency of polyurethane foam impactors</b>
	<i>C.-H. Huang</i>
<a href="#">T02A015</a>	<b>Design and performance evaluation of a three-stage impactor for rapid bioaerosol detection by ATP bioluminescence</b>
	<i>K.Y. Yoon, D. Park, J.H. Byeon, J. Hwang, J.H. Ji, and G.N. Bae</i>

<a href="#">T02A016</a>	<b>Formation of thick silver lines on a PET (polyethylene terephthalate) film patterned by a combined process of electrohydrodynamic printing and electroless deposition</b> <i>S.Y. Kim, J.H. Byeon, and J. Hwang</i>
<a href="#">T02A019</a>	<b>Photophoretic migration of monodispers aerosols</b> <i>C. Kykal, C. Haisch, and R. Niessner</i>
<a href="#">T02A022</a>	<b>Pressure controlled gas-to-gas humidification of HTDMAs</b> <i>E. Nilsson, E. Swietlicki, and D. Collins</i>
<a href="#">T02A023</a>	<b>Instrument characterization and first field test of the portable ice nucleation chamber PINC</b> <i>B. Sierau, O. Stetzer, and U. Lohmann</i>
<a href="#">T02A024</a>	<b>Analysis and calibration of a small cyclone at high flow rates</b> <i>J.M. Fernández-Díaz, I.A. SanJuan, M.A. Rodríguez-Braña, and M. Domat</i>
<a href="#">T02A025</a>	<b>Quality factors for the optimisation of electrical mobility based particle sizers</b> <i>J.M. Fernández-Díaz, M. Domat, M.A. Rodríguez-Braña, and I.A. SanJuan</i>
<a href="#">T02A026</a>	<b>Study of PM morphology using scanning electron microscopy</b> <i>R. Licbinsky, V. Adamec, J. Huzlik, and M. Schwarzova</i>
<a href="#">T02A028</a>	<b>Theory of optical differential mobility analyzer</b> <i>S.B.Kim, D.K. Song, and S.S. Kim</i>
<a href="#">T02A034</a>	<b>Calibration of a differential mobility spectrometer</b> <i>J.P.R. Symonds and K.St.J. Reavell</i>
<a href="#">T02A035</a>	<b>Generation of standard aerosols by electrical separation in a wide size range</b> <i>J. Uin, A. Mirme, S. Mirme, and E. Tamm</i>
<a href="#">T02A037</a>	<b>Design and performance evaluation of a new non-collective electrical aerosol sensor</b> <i>K. Janka, V. Niemelä, E. Lamminen, J. Keskinen, A. Rostedt, and M. Lemmetty</i>
<a href="#">T02A040</a>	<b>Robust portable, HH-TDMA for field use</b> <i>G.R. Johnson, C. Fletcher, N. Meyer, and Z.D. Ristovski</i>
<a href="#">T02A042</a>	<b>A method for measuring surface area concentration of ultrafine particles</b> <i>J. Wie, E. Kruis, and H. Fissan</i>
<a href="#">T02A044</a>	<b>Design and experimental evaluation of the dual wavelength optical particle spectrometer</b> <i>P. Gál, A. Nagy, A. Czitrovsky, and W. Szymanski</i>
<a href="#">T02A045</a>	<b>Design and evaluation of the KS-220 and KS-222 cascade impactors developed for PM10A/10B--&gt; PM2.5A/2.5B--&gt; PM1A/1B sampling</b> <i>A. Nagy, I. Kálmán, and C. Kálmán</i>
<a href="#">T02A047</a>	<b>Modelling Ag-particle activation and growth in TSI CPC 3785</b> <i>F. Stratmann, T. Petäjä, and M. Kulmala</i>
<a href="#">T02A048</a>	<b>A new conception for environmental measurement of ultrafine particles</b> <i>A. Zschoppe, A. Rudolph, R. Caldow, B. Wehner, and L. Hillemann</i>
<a href="#">T02A050</a>	<b>The construction of an optical particle counter with sub- and super-micron counting capability</b> <i>R.J. Greaney, O. Ryan, C.D. O'Dowd, and S.G. Jennings</i>
<a href="#">T02A051</a>	<b>Design of the Ice Optical Detector (IODE) for the Zurich Ice Nucleation Chamber (ZINC)</b> <i>M. Nicolet, O. Stetzer, and U. Lohmann</i>
<a href="#">T02A052</a>	<b>An experiment on performance evaluation of particle collection and gas removal of an air washer system for semiconductor manufacturing clean rooms</b> <i>S.-T. Park, K.-H. Yoo, K.-E. Tae, and S.-W. Son</i>
<a href="#">T02A053</a>	<b>Distortion of the SMPS size distribution associated with the diffusion broadening of the DMA transfer function</b> <i>A. Mamakos, L. Ntziachristos, and Z. Samaras</i>
<a href="#">T02A054</a>	<b>Improved inversion method for the scanning mobility particle sizer</b>

	<i>A. Mamakos, L. Ntziachristos, and Z. Samaras</i>
<a href="#">T06A026</a>	<b>Direct measurements of the optical properties of humic and humic like substances (HULIS) by cavity ring down aerosol spectrometer</b>
	<i>E. Dinar, A.A. Riziq, C. Spindler, C. Erilic, G. Kiss, and Y. Rudich</i>
<a href="#">T13A156</a>	<b>Counting particle measurement within the size range from soot to pollen</b>
	<i>M. Schmidt, S. Schütz, and L. Mölter</i>
<a href="#">T13A202</a>	<b>The new UFP 330: Comparison with a DMPS for ambient aerosols</b>
	<i>B. Wehner, T. Tuch, A. Wiedensohler, A. Zschoppe, L. Hillemann, and H. Gerwig</i>

[Top of Program](#)

[Top of Poster Session Part I](#)

<b>Aerosol Modeling</b>	
<a href="#">T11A014</a>	<b>Simulation of aerosol dynamics in forest fires</b>
	<i>A.E. Aloyan and V.O. Arutyunyan</i>
<a href="#">T12A001</a>	<b>Influence of car induced turbulence on PM dispersion along urban traffic paths</b>
	<i>J. Pospisil and M. Jicha</i>
<a href="#">T12A002</a>	<b>An improved model for heterogeneous nucleation</b>
	<i>A.Määttänen, H. Vehkamäki, A. Lauri, I. Napari, P.E. Wagner, and M. Kulmala</i>
<a href="#">T12A003</a>	<b>Two-component heterogeneous nucleation in the Martian atmosphere</b>
	<i>A.Määttänen, H. Vehkamäki, A. Lauri, I. Napari, and M. Kulmala</i>
<a href="#">T12A004</a>	<b>Evaporation and condensation of succinic acid and water: Model intercomparison</b>
	<i>J. Voigtländer, I. Riipinen, M. Kulmala, and F. Stratmann</i>
<a href="#">T12A005</a>	<b>A numerical study of calm air sampling</b>
	<i>S.J. Dunnett and X. Wen</i>
<a href="#">T12A007</a>	<b>Mass accommodation coefficient of water: Combined analysis of experimental data and computational fluid dynamics results</b>
	<i>J. Voigtländer, F. Stratmann, D. Niedermeier, and H. Wex</i>
<a href="#">T12A008</a>	<b>Aerosol model development for calculation of aerosol extinction in the coastal atmosphere surface layer</b>
	<i>G.A. Kaloshin</i>
<a href="#">T12A009</a>	<b>Estimating cloud droplet number concentration with particle number-to-volume concentration ratio</b>
	<i>N. Kivekäs, V.-M. Kerminen, T. Anttila, H. Korhonen, M. Komppula, and H. Lihavainen</i>
<a href="#">T12A010</a>	<b>Deposition of submicron aerosol on spruce needles; wind tunnel measurements</b>
	<i>K. Lamprechtová and J. Hovorka</i>
<a href="#">T12A015</a>	<b>Mathematical modelling of heat transport in aerosol systems with particles of complex geometry</b>
	<i>L.A. Uvarova</i>
<a href="#">T12A016</a>	<b>Experimental characterization and modelling of soot primary particles emitted by a CFM56 commercial aircraft engine</b>
	<i>D. Delhaye, D. Ferry, F. Moulin, S. Picaud, E. Ruiz, B. Demirdjian, P.N.M. Hoang, and J. Suzanne</i>
<a href="#">T12A017</a>	<b>An expression of particle dry deposition velocity for polydispersed particle using the moment method</b>
	<i>S.Y. Bae, C.H. Jung, and Y.P. Kim</i>
<a href="#">T12A019</a>	<b>Modeling and calculation of fractional efficiency of tangential flow cyclones</b>
	<i>Y. Ben-Shmuel and M. Shapiro</i>
<a href="#">T12A020</a>	<b>Source apportionment of submicron organic aerosol at an urban background site by positive matrix factorization (PMF) applied to aerosol mass spectra</b>
	<i>V.A. Lanz, M.R. Alfara, U. Baltensperger, B. Buchmann, C. Hüglin, and A.S.H. Prévôt</i>

<a href="#">T12A021</a>	<b>Modeling nitric acid adsorption in mixed-phase clouds</b> <i>J.-P. Pietikäinen, J. Hienola, H. Kokkola, S. Romakkaniemi, K. Lehtinen, M. Kulmala, and A. Laaksonen</i>
<a href="#">T12A022</a>	<b>OIO nucleation simulations</b> <i>H. Vuollekoski, M. Kulmala, V.-M. Kerminen, S.-L. Sihto, I. Riipinen, H. Korhonen</i>
<a href="#">T12A023</a>	<b>High PM1 and ozone levels in the Cadiz Gulf during the Galicia fires of summer 2006</b> <i>J.D. de la Rosa, A.F. Stein, Y. González-Castanedo, A. Alastuey, E. Mantilla, J. Contreras, X. Querol, and A. Sánchez de la Campa</i>
<a href="#">T12A024</a>	<b>Modeling and measurements of high arsenic levels in Southwestern Spain</b> <i>A.F. Stein, J.D. de la Rosa, A.M Sánchez de la Campa, X. Querol, and A. Alastuey</i>
<a href="#">T12A026</a>	<b>Modelling study on the connection of sulphuric acid and new particle formation</b> <i>S.-L. Sihto, H. Vuollekoski, J. Leppä, I. Riipinen, V.-M. Kerminen, H. Korhonen, K.E.J. Lehtinen, and M. Kulmala</i>
<a href="#">T12A027</a>	<b>A combined method for data processing in an elastic backscatter Lidar</b> <i>D. Nicolae, C. Talianu, A. Nemuc, E. Carstea, L. Belegante, and C. Radu</i>
<a href="#">T12A029</a>	<b>Modeling of atmospheric aerosol processing with consideration of non-ideal solutions and complex multiphase chemistry</b> <i>R. Wolke, J. Zoboki, A. Tilgner, and H. Herrmann</i>
<a href="#">T12A032</a>	<b>Evaluation of Brownian motion calculation using Discrete Phase Model of FLUENT</b> <i>D.K. Song and S. Dhaniyala</i>
<a href="#">T12A033</a>	<b>Numerical study of dynamics of growing droplets in Kelvin spectrometer</b> <i>S.K. Zaripov, R.S. Galeev, and W. Holländer</i>
<a href="#">T12A034</a>	<b>How reduction policies on emission scenarios can affect air quality in the Tuscany region</b> <i>C. Grassi and S. Verrilli</i>
<a href="#">T12A035</a>	<b>PBMR safety analysis: Aerosol modelling for Generation IV Nuclear Plants</b> <i>L. Naicker and A. Ramlakan</i>
<a href="#">T12A041</a>	<b>Sensitivity of urban and rural ammonium-nitrate particulate matter to precursor emissions in Southern Germany</b> <i>U. Uhmer, S. Drechsler, R. Wolke, P.J. Sturm, and A. Wiedensohler</i>
<a href="#">T12A043</a>	<b>Is the thermodynamic equilibrium an adequate approach for representing fine (PM1, PM2.5) inorganic aerosol behavior? ISORROPIA-II simulations under 2005 winter Mexico City conditions</b> <i>M. Moya, C. Fountoukis, A. Nenes, and E. Matías</i>
<a href="#">T12A044</a>	<b>Modelling on H<sub>2</sub>SO<sub>4</sub>-H<sub>2</sub>O particle formation and growth in the diluting diesel exhaust</b> <i>L. Pirjola, F. Arnold, T. Schuck, J. Keskinen, T. Rönkkö, T. Lähde, K. Hämeri, A. Sorokin, and D. Rothe</i>
<a href="#">T12A046</a>	<b>Application of mesoscale WRF-CHEM model for researching of vertical and horizontal inhomogeneous structure of pollutant concentration in the East Europe region</b> <i>D.P. Zinin, G.M. Teptin, and O.G. Khoutorova</i>
<a href="#">T12A047</a>	<b>Modelling of workplace nanoparticle exposure</b> <i>C. Asbach, H. Kaminski, U. Rating, H. Fissan, and T.A.J. Kuhlbusch</i>
<a href="#">T12A048</a>	<b>Particle deposition on a semiconductor wafer larger than 100 nm</b> <i>K.-H. Lee, G.-S. Song, K.-H. Yoo, and S.-K. Chae</i>
<a href="#">T13A152</a>	<b>Mixed effects regression model in the analysis of 50nm particle number concentration</b> <i>S. Mikkonen, K.E.J. Lehtinen, A. Hamed, J. Joutsensaari, and A. Laaksonen</i>

[Top of Program](#)

[Top of Poster Session Part I](#)

<b>Aerosol Standards</b>	
<a href="#">T03A002</a>	<b>Computational investigation of particle losses in random porous structures</b> <i>A. Serrenho, A.F. Miguel, and A.H. Reis</i>

<a href="#">T03A003</a>	<b>Influence of the stains on the Millikan-type plate electrode in the absolute size measurement of particle size standards by the electro-gravitational aerosol balance</b> <i>K. Takahata and K. Ehara</i>
<a href="#">T03A004</a>	<b>The EU project NANOTRANSPORT</b> <i>T. Rettenmoser, C. Gerhart, and H. Grimm</i>

[Top of Program](#)

[Top of Poster Session Part I](#)

<b>Atmospheric Aerosols - Nucleation</b>	
<a href="#">T13A079</a>	<b>Particle formation events observed at the King Sejong station, Antarctica</b> <i>Y.J. Yoon, B.Y. Lee, T.J. Choi, T.G. Seo, and S.S. Yum</i>
<a href="#">T13A080</a>	<b>Formation of particles in aircraft plumes using a multitrajectory box model and LES</b> <i>X. Vancassel, E. Maglaras, and E. Ruiz</i>
<a href="#">T13A087</a>	<b>Binary homogenous nucleation of sulfuric acid and water mixture: Experimental device and setup</b> <i>D. Brus, A.-P. Hyvärinen, H. Lihavainen, Y. Viisanen, and M. Kulmala</i>
<a href="#">T13A124</a>	<b>Air Ion Spectrometer measurements of marine/coastal secondary particle formation</b> <i>M. Ehn, T. Petäjä, H. Vuollekoski, P. Aalto, M. Vana, G. de Leeuw, D. Ceburnis, C. D. O'Dowd, and M. Kulmala</i>
<a href="#">T13A125</a>	<b>Observations of secondary particle formation above the North Atlantic</b> <i>M. Ehn, T. Petäjä, P. Aalto, G. de Leeuw, C. D. O'Dowd, and M. Kulmala</i>
<a href="#">T13A138</a>	<b>New particle formation above a sub-arctic wetland-forest mosaic: analysis of high growth rates</b> <i>B. Svenningsson, A. Arneth, S. Hayward, T. Holst, A. Massling, E. Swietlicki, A. Hirsikko, M. Vana, T. Bergman, I. Riipinen, M. Dal Maso, T. Hussein, and M. Kulmala</i>
<a href="#">T13A139</a>	<b>Aerosol particle and air ion number size distributions along the Trans-Siberian railroad</b> <i>E. Vartiainen, M. Kulmala, M. Ehn, T. Petäjä, S. Kuokka, R. Hillamo, A.I. Skorokhod, I.B. Belikov, N.F. Elansky, and V.-M. Kerminen</i>
<a href="#">T13A140</a>	<b>Aerosol particle and ion measurements in Queen Maud Land, Antarctica</b> <i>E. Vartiainen, M. Ehn, P.P. Aalto, A. Frey, A. Virkkula, R. Hillamo, A. Arneth, and M. Kulmala</i>
<a href="#">T13A141</a>	<b>Presence of cluster ions in low ambient temperatures</b> <i>A.-K. Viitanen, T. Mattila, and J.M. Mäkelä</i>
<a href="#">T13A144</a>	<b>A comparison of new particle formation events in Eastern Germany and in Northern East Italy based on a three-year-analysis</b> <i>A.Hamed, B.Wehtner, W.Birmili, A.Wiedensohler, F. Cavalli, M.C. Facchini, J. Joutsensaari, and A. Laaksonen</i>
<a href="#">T13A145</a>	<b>Nucleation events in Melpitz, Germany, as a source of cloud condensation nuclei</b> <i>A. Hamed, B. Wehtner, W. Birmili, T. Tuch, G. Spindler, A. Wiedensohler, J. Joutsensaari, and A. Laaksonen</i>
<a href="#">T13A157</a>	<b>Characterisation of air ions during a cruise over the Eastern Atlantic and Southern Ocean</b> <i>M. Vana, A. Virkkula, A. Hirsikko, P. Aalto, M. Kulmala, and R. Hillamo</i>
<a href="#">T13A160</a>	<b>Investigating ion-induced nucleation with an Ion-DMPS</b> <i>S. Gagné, T. Petäjä, L. Laakso, V.-M. Kerminen, P.P. Aalto, and M. Kulmala</i>
<a href="#">T13A166</a>	<b>Overview of nucleation events based on air ion measurements at Tahkuse observatory</b> <i>K. Komsaare, D. Singh, A. Mirme, and U. Hörrak</i>
<a href="#">T13A171</a>	<b>Atmospheric particle formation rates below 3 nm</b> <i>I. Riipinen, H.E. Manninen, T. Nieminen, M. Sipilä, T. Petäjä and, M. Kulmala</i>
<a href="#">T13A184</a>	<b>The effect of clouds on ion cluster concentrations and new particle formation at 1465 m. a.s.l.</b> <i>H. Venzac, K. Sellegri, and P. Laj</i>
<a href="#">T13A195</a>	<b>One-year observations of new particle formation at two stations in Central Siberia</b> <i>M. Dal Maso, L. Sogacheva, A. Vlasov, A. Staroverova, A. Lushnikov, M. Anisimov, V.A. Zagainov T.V. Khodzer, V.A. Obolkin, Yu.S. Lyubovtseva, I. Riipinen, and M. Kulmala</i>

<a href="#">T13A224</a>	<b>Aerosol composition after a clean air nucleation event in Hyytiälä, Finland</b> <i>T. Raatikainen, P. Vaattovaara, J. Rautiainen, P. Tiitta, A. Laaksonen, and D. Worsnop</i>
<a href="#">T13A238</a>	<b>Newly-formed nucleation mode particles composition change at boreal forest atmosphere</b> <i>P. Vaattovaara, T. Petäjä, D.R. Worsnop, and A. Laaksonen</i>
<a href="#">T13A243</a>	<b>Fine and ultrafine aerosol in southwestern Australia, influence of land surface, land use and vegetation on size and number distribution</b> <i>W. Junkermann, J. Hacker, T. Lyons, and U. Nair</i>
<a href="#">T20A005</a>	<b>Atmospheric fronts, cloudiness and aerosol particle formation in Hyytiälä, Southern Finland</b> <i>L. Sogacheva, L. Saukkonen, G. de Leeuw, and M. Kulmala</i>

[Top of Program](#)

[Top of Poster Session Part I](#)

## Atmospheric Aerosols - Urban Aerosols

<a href="#">T13A005</a>	<b>A gas/aerosol pollutant study in urban and rural atmosphere of Rome during the ITALIA campaigns. Monitoring and characterization</b> <i>P. Di Filippo, C. Riccardi, D. Pomata, F. Incoronato, S. Spicaglia, A. Cecinato, and C. Balducci</i>
<a href="#">T13A024</a>	<b>An inter-year climatology of urban aerosol and minor gas impurities in the east European region of Russia</b> <i>O.G. Khutorova and G.M. Teptin</i>
<a href="#">T13A038</a>	<b>Urban particle number size distributions of ambient-state and non-volatile aerosols in Augsburg, Germany</b> <i>K. Heinke, W. Birmili, M. Pitz, J. Cyrys, and A. Peters</i>
<a href="#">T13A053</a>	<b>Microscale variations of atmospheric particle number size distributions in a densely built-up city area: Implications for exposure to traffic particles</b> <i>M. Merkel, W. Birmili, A. Wiedensohler, D. Hinneburg, O. Knoth, T. Tuch, and U. Franck</i>
<a href="#">T13A064</a>	<b>Chemical characterization and source attribution of size-segregated aerosol collected at an urban site in Mediterranean basin</b> <i>M. Rinaldi, L. Emblico, V. Mancinelli, S. Decesari, M. C. Facchini, S. Fuzzi, and V. Librando</i>
<a href="#">T13A071</a>	<b>Determination of particulate carbonaceous species in an urban background aerosol in Nairobi, Kenya</b> <i>M. J. Gatari, M. D. Hays, R. J. Lavrich, and S. M. Gaita</i>
<a href="#">T13A077</a>	<b>A wintertime study of atmospheric aerosols collected in São Paulo, Brazil</b> <i>P.C. Vasconcellos, L. Ogura, W. Lopes, P.A. Pereira, J. Andrade, and O. Sanchez-Ccoyllo</i>
<a href="#">T13A162</a>	<b>UFIPOLNET: Concentration of particle number distributions at 4 stations in Europe</b> <i>H. Gerwig, G. Löschau, L. Hillemann, B. Wehner, A. Wiedensohler, A. Zschoppe, C. Peters, A. Rudolph, C. Johansson J. Cyrys, M. Pitz, R. Ruckerl, J. Novak, H.G. Horn, R. Caldow, and G.J. Sem</i>
<a href="#">T13A170</a>	<b>Time evolution of fine and ultrafine ambient particles in a Madrid suburban site</b> <i>M. Pujadas, F.J. Gómez-Moreno, J. Plaza, J. Rodriguez-Maroto, M. Sánchez, E. Coz, and B. Artíñano</i>
<a href="#">T13A213</a>	<b>Mixing state of non volatile particle fractions in two Chinese mega city areas</b> <i>B. Wehner, M. Berghof, P. Achtert, A. Nowak, A. Wiedensohler, Y.F. Cheng, M. Hu, Y.H. Zhang, and T. Zhu</i>
<a href="#">T13A217</a>	<b>Chloride ion in urban atmospheric aerosols</b> <i>A.F. Ferreira, P. Portela, C. Oliveira, L. Quintão, and M.F. Camões</i>
<a href="#">T13A221</a>	<b>On aerosol characterization at the research station of Cabauw, The Netherlands</b> <i>B. Henzing, M. Moerman, M. Schaap, and G. de Leeuw</i>
<a href="#">T13A229</a>	<b>Seasonal variation of submicron aerosol number size distributions at urban and suburban sites of Prague in 2004/2005</b> <i>J. Hovorka, V. Ždímal, J. Schwarz, Z. Wagner, P. Dohányosová, M. Braniš, and J. Smolík</i>
<a href="#">T14A025</a>	<b>Human basophils are target cells for urban aerosol-associated polycyclic aromatic hydrocarbons</b>

(PAHs)

*W. Schober, S. Lubitz, B. Belloni, G. Gebaue, B. Eberlein, J. Lintemann, H. Behrendt, and J. Buters*[Top of Program](#)[Top of Poster Session Part I](#)**Electrical Effects**

<a href="#">T05A001</a>	<b>Laboratory simulation of body charging by the flow with electrical charged water drops</b> <i>A. Vatazhin, D. Golentsov, and V. Likhter</i>
<a href="#">T05A003</a>	<b>A fixed site monitoring station to measure corona produced from a high voltage powerline</b> <i>J.C. Matthews, P.A. Keitch, J.P. Ward, and D.L. Henshaw</i>
<a href="#">T05A004</a>	<b>Novel wet space-charge electrostatic precipitator for fine particles</b> <i>A.M. Bologa, H.-R. Paur, H. Seifert, and K. Woletz</i>
<a href="#">T05A005</a>	<b>Dynamics of highly charged fine aerosols in between electrodes</b> <i>I.G. Loscertales, E.A. Rodríguez, D. Galán, M. Marquez, and A. Barrero</i>
<a href="#">T05A011</a>	<b>Numerical simulation of nanoparticle patterning via electrodynamic focusing</b> <i>S. You and M. Choi</i>
<a href="#">T13A050</a>	<b>Investigation of the associations between parameters characterizing the electrical environment near a strong corona ion emitting source</b> <i>F.O. J-Fatokun, E.R. Jayaratne, L. Morawska, R. Rachman, and D. Birtwhistle</i>
<a href="#">T02A046</a>	<b>Application of aerosol electrometer for ambient particle charge measurements</b> <i>F.O. J-Fatokun, E.R. Jayaratne, M. Jamriska, and L. Morawska</i>
<a href="#">T13A051</a>	<b>Lunar variation of precipitation supports links between solar activity and atmospheric ionization</b> <i>L. Hejkrlik</i>
<a href="#">T13A056</a>	<b>Corona ions from HV powerlines: measurements, theory and health implications</b> <i>A.J. Buckley, M.D. Wright, P.A. Keitch, J.C. Matthews, and D.L. Henshaw</i>

[Top of Program](#)[Top of Poster Session Part I](#)**Indoor Aerosols**

<a href="#">T07A002</a>	<b>Influence of source of heating and air movement on the particles and air parameters</b> <i>E. Jankowska and E. Walicka</i>
<a href="#">T07A004</a>	<b>Commuter exposure to particulate matter in transport microenvironments</b> <i>I. Colbeck and Z. Ahmad Nasir</i>
<a href="#">T07A005</a>	<b>Fine and coarse aerosol particles in a student's club before and after a smoking ban</b> <i>J. Hovorka, M. Braniš, P. Gadas, and T. Valchářová</i>
<a href="#">T07A006</a>	<b>Effect on indoor air ion enhancement and bacterial activity inhibition by evaporating selected essential oils</b> <i>C.H. Luo, Y. Shih, and S.B. Lian</i>
<a href="#">T07A009</a>	<b>Aerosol dynamics in a test chamber: experiment and modelling</b> <i>J. Smolík, A. Hruška, P. Dohányosová, T. Hussein, and J. Hemerka</i>
<a href="#">T07A010</a>	<b>Single-particle characterization of seasonal aerosol samples collected at a subway station platform in Seoul, Korea</b> <i>S. Kang, H. Hwang, M.S.I. Khan, Y. Park, E. Choi, H. Kim, and C.-U. Ro</i>
<a href="#">T07A011</a>	<b>Measurements of domestic UFP sources in a real life test chamber</b>

	<i>N. Bleux, P. Berghmans, F. Deutsch, S. Janssen, J. Vankekom, M. Van Poppel, and R. Torfs</i>
<a href="#">T07A012</a>	<b>Monitoring of aerosolized black carbon in a pulmonary hospital setting</b>
	<i>M. Vardjan, G. Mocnik, and A. Zrimec</i>
<a href="#">T07A014</a>	<b>Physical and chemical properties of fine particles emitted from candles</b>
	<i>J. Pagels, A. Wierzbicka, A. Dahl, E. Swietlicki, and M. Bohgard</i>
<a href="#">T07A015</a>	<b>Gravimetric and optical aerosol measurements in an industrial workplace and the impact of the measurement uncertainty on the calculated inhaled dose</b>
	<i>S. Vratolis, C. Mitsakou, K. Eleftheriadis, A. Karanasiou, C. Housiadas, and M. Lazaridis</i>
<a href="#">T07A017</a>	<b>The origin of indoor PM2.5 at a residence in Melbourne, Australia</b>
	<i>J.C. Powell and G.P. Ayers</i>

[Top of Program](#)

[Top of Poster Session Part I](#)

<b>Lung-Particle-Interaction</b>	
<a href="#">T08A001</a>	<b>Model for the deposition of fine and ultrafine aerosol particles in rat lungs</b>
	<i>G.A. Ferron, J. Gentry, E. Karg, O. Schmid, and S. Takena</i>
<a href="#">T08A005</a>	<b>A mechanical lung model to measure particle deposition</b>
	<i>P.A. Keitch, M.D. Wright, A.J. Buckley, and D.L. Henshaw</i>
<a href="#">T08A006</a>	<b>Regional deposition pattern of aerosol particles in the replica of upper airways</b>
	<i>T.R. Sosnowski, L. Gradon, and A. Moskal</i>
<a href="#">T08A008</a>	<b>Development of a decision support tool for estimation of human exposure to particles (STEDOM)– A presentation of the stand alone exposure and dosimetry modules</b>
	<i>V. Aleksandropoulou and M. Lazaridis</i>
<a href="#">T08A010</a>	<b>Number size distribution of atmospheric aerosol particles at urban and rural sites in Hungary with health implications</b>
	<i>R. Ocskay, I. Salma, P. Aalto, M. Kulmala, A. Gelencsér, G. Kiss, and I. Balásházy</i>
<a href="#">T08A012</a>	<b>Respiratory tract deposition measurements of aerosol particles with on-line techniques; review of sources of error and estimation of their impact</b>
	<i>J. Löndahl, E. Swietlicki, J. Pagels, and M. Bohgard</i>
<a href="#">T08A014</a>	<b>Modelling deposition of hygroscopic particles in the human respiratory tract</b>
	<i>R. Winkler-Heil, G.A. Ferron, and W. Hofmann</i>
<a href="#">T08A015</a>	<b>Deposition of polydisperse fibers in the human respiratory tract: Comparison between theoretical predictions and experimental data</b>
	<i>R. Sturm and W. Hofmann</i>
<a href="#">T08A016</a>	<b>A stochastic model for the deposition of nonspherical particles in the human respiratory tract</b>
	<i>R. Sturm and W. Hofmann</i>
<a href="#">T08A017</a>	<b>Lung deposition of particle aggregates: Theory and experimental data</b>
	<i>O. Schmid, W. Möller, E. Karg, K. Felten, G.A. Ferron, H. Fissan, W. Hofmann, H. Schulz, and W.G. Kreyling</i>
<a href="#">T08A018</a>	<b>A theoretical approach to the bronchial clearance of micrometer-sized nonspherical particles</b>
	<i>R. Sturm and W. Hofmann</i>
<a href="#">T08A019</a>	<b>The lung's structural asymmetry and its effect on ventilation and particle deposition</b>
	<i>D.M. Broday and Y. Agnon</i>
<a href="#">T08A020</a>	<b>Health effects of inhaled radon progenies in homes and mines</b>
	<i>I. Szoke, Á. Farkas, I. Balásházy, and W. Hofmann</i>
<a href="#">T08A021</a>	<b>Pulmonary deposition and chemical composition of biosoluble vitreous fibers</b>
	<i>R. Szoke, I. Sziklai-László, I. Balásházy, G. Kudela, and W. Hofmann</i>
<a href="#">T08A022</a>	<b>Effect of therapeutic salt aerosols on ambient particle concentrations and size distributions and</b>

	<b>related lung deposition</b>
	<i>F. Kwasny, P. Madl, and W. Hofmann</i>
<a href="#">T08A023</a>	<b>Analyses of size distribution and related lung deposition in the SELSONICS ultrasonic nebulization chamber</b>
	<i>P. Madl and W. Hofmann</i>
<a href="#">T08A024</a>	<b>Simulation of nano-particle deposition in human central airways</b>
	<i>M.C. Piglione and M. Vanni</i>
<a href="#">T13A022</a>	<b>Health risk from vehicle emissions and soot in urban area</b>
	<i>A. Schady, A. Gzella, J. Zwozdziak, A. Szczurek, I. Sowka, and A. Zwozdziak</i>
<a href="#">T13A059</a>	<b>Cardiovascular emergency calls associated to urban submicron aerosol fractions</b>
	<i>U. Franck, S. Odeh, T. Tuch, O. Herbarth, W.-H. Storch, A. Wiedensohler, and B. Wehner</i>

[Top of Program](#)

[Top of Poster Session Part I](#)

<b>Medical Aerosols</b>	
<a href="#">T18A001</a>	<b>Reentrainment and deaggregation of powder particles as a result of flow disarrangement</b>
	<i>T.R. Sosnowski, J. Gac, and L. Gradon</i>
<a href="#">T18A002</a>	<b>The effect of particle hygroscopicity on mouth and throat deposition</b>
	<i>C. Mitsakou, D. Mitrakos, and C. Housiadas</i>
<a href="#">T18A003</a>	<b>Numerical study of the transient behavior of cascade impactors</b>
	<i>M. Chiruta, D.L. Roberts, and F.J. Romay</i>
<a href="#">T18A004</a>	<b>Aerodynamic characterisation of new pharmaceutical inhalers</b>
	<i>H. Wachtel, Ö. Ertunc, C. Köksoy, and F. Durst</i>

[Top of Program](#)

[Top of Poster Session Part I](#)

<b>Nanoparticles</b>	
<a href="#">T01A019</a>	<b>Aerosol reaction engineering in flames: From oxides to salt and metal nanoparticles</b>
	<i>R.N. Grass, E.K. Athanassiou, and W.J. Stark</i>
<a href="#">T09A003</a>	<b>Formation process and chemical structure analysis of ionic-liquid nanoparticle</b>
	<i>M. Shigeyasu and H. Tanaka</i>
<a href="#">T09A004</a>	<b>Air stable, carbon coated metal nanoparticles of sensor applications</b>
	<i>E.K. Athanassiou, R.N. Grass, and W.J. Stark</i>
<a href="#">T09A005</a>	<b>Size and concentration control of nanoparticles in plasma using pulsed hydrogen gas</b>
	<i>K.-S. Kim, B.-H. Kim, and T. Kim</i>
<a href="#">T09A006</a>	<b>Urban and rural measurements of atmospheric small-ions and ultrafine particles</b>
	<i>M. D. Wright, A. J. Buckley, P. A. Keitch, and D. L. Henshaw</i>
<a href="#">T09A009</a>	<b>Deposition of composite aerosol particles and their subsequent evolution through surface diffusion</b>
	<i>M.J. Burchill, D.K. Gramotnev, T. Bostrom, D.R. Mason, and G. Gramotnev</i>
<a href="#">T09A010</a>	<b>Relations of discharge electrode form and ozone generation in ESP</b>
	<i>D. Yagishita, Y. Takagi, Y. Ehara, T. Takahashi, A. Zukeran, and K. Yasumoto</i>
<a href="#">T09A011</a>	<b>Collection of nanoparticles by improvement of charging section in ESP</b>
	<i>T. Okabe, Y. Takagi, Y. Ehara, A. Zukeran, and K. Yasumoto</i>

<a href="#">T09A012</a>	<b>Preparation of Co and Ni nanoparticles</b> <i>J. Forsman, A. Auvinen, J. Jokiniemi, and U. Tapper</i>
<a href="#">T09A013</a>	<b>Morphology and reactivity of carbon nanoparticles and nanotubes formed during co-pyrolysis of Fe(CO)<sub>5</sub> and propane</b> <i>N.A. Ivanova, A.A. Onischuk, S.V. Vosel, P.A. Purtov, A.M. Baklanov, L.V. Kulik, L.L. Rapatskiy, N.T. Vasenin, and V.F. Anufrienko</i>
<a href="#">T09A014</a>	<b>Flame synthesis of TiO<sub>2</sub> nanoparticles and their use as a photocatalyst</b> <i>G.W. Lee, S.M. Choi, and J. Park</i>
<a href="#">T09A015</a>	<b>A stable nano-generator based on the sublimation of tungsten oxide</b> <i>G. Steiner and G.P. Reischl</i>
<a href="#">T09A018</a>	<b>Production of novel Ag nanoparticle with C60 nanoparticle</b> <i>N. Hashimoto, S. Taguchi, and H. Tanaka</i>
<a href="#">T09A020</a>	<b>Effect of Nanoparticles on the respiratory epithelium in vitro: Role of chemical composition and particle size</b> <i>S. Boland, S. Hussain, M.A. Billon-Galland, J. Fleury-Feith, A. Baeza, L. Martinon, F. Moisan, J.C. Pairon, and F. Marano</i>
<a href="#">T09A024</a>	<b>Droplet size characterization in spray flames</b> <i>H. Keskinen, J.M. Mäkelä, M. Aromaa, M.C. Heine, and S.E. Pratsinis</i>
<a href="#">T09A026</a>	<b>Hydrogen storage behaviour of metallic nanoparticles generated by spark discharge</b> <i>N. Salman Tabrizi, W.J. Legerstee, S. Eijt, and A. Schmidt-Ott</i>
<a href="#">T09A027</a>	<b>Deposition of nanometric singly charged particles in cylindrical metallic and flexible conductive silicone tubes</b> <i>M.B. Attoui</i>
<a href="#">T09A029</a>	<b>Ni/NiO nanoparticle synthesis by MOCVD</b> <i>P. Moravec, J. Smolík, H. Keskinen, J.M. Mäkelä, and V.V. Levdansky</i>
<a href="#">T09A032</a>	<b>Ethylene flame: Effects of pressure on soot properties</b> <i>M. Maugendre, A. Coppalle, J. Yon, K. P.Geigle, and R. Stirn</i>
<a href="#">T09A033</a>	<b>Nanoinventory – results of a qualitative survey about nanoparticles in Swiss industries</b> <i>K. Schmid and M. Riediker</i>
<a href="#">T09A034</a>	<b>Effects of Ti<sup>4+</sup> concentration on crystal phase of TiO<sub>2</sub> powders synthesized by low-temperature hydrothermal method</b> <i>P.-S. Tsai, C.-H. Tsai, Y.-F. Lai, and Y.-M. Yang</i>
<a href="#">T09A038</a>	<b>Preparation and characteristic of Pt and Pt-Ru nanoparticles for utilized proton exchange membrane regenerative fuel cell</b> <i>Y.-C. Chiang, C.-C. Lin, and C.-C. Lee</i>
<a href="#">T09A039</a>	<b>Nanoparticle synthesis by gas-dynamically induced heating and quenching</b> <i>M. Dannehl, A. Maisels, W. Leibold, H. Olivier, A. Grzona, A. Weiß, A. Gülhan, T. Gawehn, G.H. Schnerr, N. Al-Hasan, A. Abdali, M.Y. Luong, H. Wiggers, C. Schulz, B. Weigand, J. Chun, W. Schröder, M. Meinke, T. Winnemöller, H. Nirschl, V. Goertz, K. Schaber, and T. Rakel</i>
<a href="#">T09A040</a>	<b>Thermal tweezers for effective manipulation of nano-particles on surfaces</b> <i>D.R. Mason, D.K. Gramotnev, and G. Gramotnev</i>
<a href="#">T09A041</a>	<b>Investigation of the charge distribution in a FePt nanoaerosol formed by pulsed laser ablation</b> <i>M. Rouenhoff, A. Nedic, and E. Kruis</i>
<a href="#">T09A042</a>	<b>The TSI N95-Companion™ – a convenient alternative in everyday nanoparticle classification?</b> <i>M.N.A. Karlsson, Z. Geretovszky and K. Deppert</i>
<a href="#">T09A043</a>	<b>NANOCAP : Nanotechnology Capacity Building NGOs</b> <i>I. Colbeck and A. Cox</i>
<a href="#">T09A044</a>	<b>Catalytic oxidation of carbon aerosols by Pt nanoparticles: Influence of the Pt-C interparticle contact configuration on the reaction rate</b> <i>P. Davoodi, M. Seipenbusch, A.P. Weber, and G.Kasper</i>
<a href="#">T09A045</a>	<b>The production of nanoparticles with a CO<sub>2</sub> laser driven aerosol process</b> <i>J.W.M. van Erven, Z. Fu, T.M. Trzeciak, and J.C.M. Marijnissen</i>

<a href="#">T09A047</a>	<b>Strategies for the determination of engineered nanoparticles – Examples from TiO<sub>2</sub> production</b> <i>T.A.J. Kuhlbusch, C. Asbach, H. Kaminski, and H. Fissan</i>
<a href="#">T09A054</a>	<b>Fabrication and size control of carbon nanotube on nano-scale Ni aerosol particles</b> <i>K. Bente, H. Takano, and M. Itoh</i>
<a href="#">T09A056</a>	<b>Study on the collection of nanometric powders by electro-static precipitators from iron and steel industry gases emission</b> <i>C. Grigoriu, I. Nicolae, C. Viespe, D. Dragulinescu, D. Martin, S. Jinga, R. Macarie, and P. Biswas</i>
<a href="#">T09A057</a>	<b>Nanoparticles in fine dust - development of modern measuring methods</b> <i>N. Sabbagh and W.W. Szymanski</i>
<a href="#">T09A058</a>	<b>Cyclone technology for nanopowder collection</b> <i>H.M. Chein and Y.-D. Hsu</i>
<a href="#">T09A059</a>	<b>On the particle size distributions by flame electrospray pyrolysis</b> <i>H. Oh and S. Kim</i>

[Top of Program](#)

[Top of Poster Session Part I](#)

<b>PM10 / PM2.5</b>	
<a href="#">T13A023</a>	<b>Urban dust – chemical composition of PM10 in Prague tunnels</b> <i>V. Tydlitát, B. Kotlík, J. Karban, and J. Janota</i>
<a href="#">T13A069</a>	<b>Chemical mass balance of PM10 at Sonnblick</b> <i>C. Effenberger, A. Kranabetter, G. Schauer, and A. Kasper-Giebl</i>
<a href="#">T13A072</a>	<b>The use of trajectory cluster analysis to interpret PM levels and composition at central Spain</b> <i>P. Salvador, B. Artíñano, and X. Querol</i>
<a href="#">T13A097</a>	<b>New sites for background air quality monitoring in Ireland</b> <i>S. Leinert and G. Jennings</i>
<a href="#">T13A114</a>	<b>Mobile air quality monitoring trailer for developing countries</b> <i>T. Petäjä, L. Laakso, T. Pohja, E. Siivola, H. Laakso, P.P. Aalto, P. Keronen, N.A. Kgabi, and M. Kulmala</i>
<a href="#">T13A127</a>	<b>Effects of particle hygroscopicity on fine particle mass concentration at Seoul, Korea</b> <i>E.K. Choi and Y.P. Kim</i>
<a href="#">T13A128</a>	<b>PM air pollution in urban agglomerations</b> <i>M. Schwarzova, M. Schmidt, R. Licbinsky, J. Huzlík, V. Adamec, and W. Goessler</i>
<a href="#">T13A129</a>	<b>Water soluble organic and inorganic compounds in PM10</b> <i>G.A. Blanco-Heras, M.C. Prieto-Blanco, M.I. Turnes-Carou, M. Piñeiro-Iglesias, P. López-Mañía, S. Muniategui-Lorenzo, and D. Prada-Rodríguez</i>
<a href="#">T13A165</a>	<b>Profiles of road dust and its contribution to PM10 atmospheric aerosol</b> <i>N. Jankowski, H. Puxbaum, and I.L. Marr</i>
<a href="#">T13A231</a>	<b>Some aspects of fine inorganic aerosols (PM1, PM2.5) in the metropolitan area of Mexico City during the winters of 2003, 2005 and 2006 (MIRAGE campaign).</b> <i>M. Moya</i>
<a href="#">T13A235</a>	<b>Concentration and the chemical characterization of PM10 and PM2.5 in all the Italian territory</b> <i>E. Bolzacchini, L. Ferrero, C. Lo Porto, M. G. Perrone, G. de Gennaro, P. Bruno, M. Caselli, P.R. Dambruoso, B.E. Daresta, C.M. Placentino, M. Tutino, M. Amodio, D. Baldacci, M. Stracquadanio, L. Tositti, S. Zappoli, D. Gullotto, V. Librando, Z. Minniti, G. Perrini, G. Trinalli, S. Becagli, A. Mannini, R. Udisti, C. Paradisi, A. Tapparo, P. Barbieri, L. Capriglia, F.Cozzi, E. Maran, E. Reisenhofer, V. Sicardi, P. Fermo, and A. Piazzalunga</i>
<a href="#">T13A236</a>	<b>Summer 2006 events and their effect on PM10 levels in Haifa Bay region, Israel</b> <i>Yuval and David M. Broday</i>
<a href="#">T19A002</a>	<b>PM10 in Ireland, 2002 to 2005</b>

	<i>S. Leinert, J. Finnan, and B. O'Leary</i>
<a href="#">T19A005</a>	<b>PM1 and trace element concentrations measured in Tito Scalo (Basilicata region, Southern Italy)</b>
	<i>S. Trippetta, R. Caggiano, M. Macchiato, M. Ragosta, S. Sabia, and G. Scardaccione</i>
<a href="#">T19A006</a>	<b>PM10 and PM2.5 in ambient soil dust: Elemental enrichment factor</b>
	<i>K. Trzepla-Nabaglo, R.G. Flocchini, and O.F. Carvacho</i>
<a href="#">T19A007</a>	<b>Statistical study of the secondary organic aerosol from countryside of Madrid (Spain)</b>
	<i>O. Pindado, R.M. Pérez, S. García, and A.I. Barrado</i>
<a href="#">T19A008</a>	<b>Monitoring of heavy metals Pb, Cd in fine particles PM10 in the Mitrovica urban atmosphere</b>
	<i>A.M. Syla, K. Berisha, and A. Veliu</i>
<a href="#">T19A009</a>	<b>The episode of high particle loads in Europe in January and February 2006 with emphasis on Germany</b>
	<i>S. Wurzler, W. Kappert, K. Mildenerger, M. Memmesheimer, H. Jakobs, G. Spindler, K. Drescher, and P. Bruckmann</i>
<a href="#">T19A010</a>	<b>High population density and heavy industry: The challenge for air quality management in North Rhine Westphalia: Are the measures effective?</b>
	<i>S. Wurzler, W. Kappert, D. Gladke, P. Bruckmann, and M. Memmesheimer</i>
<a href="#">T19A011</a>	<b>The ratio of PM2,5/PM10 concentrations of suspended particles at stations selected in the Czech Republic</b>
	<i>I. Brožová</i>
<a href="#">T19A013</a>	<b>Characteristics of atmospheric aerosols in Cheonan, Korea during 2006</b>
	<i>S. Oh</i>
<a href="#">T13A014</a>	<b>Modification of commercially available whole body exposure chambers for rodents for exposure to fine and ultrafine aerosols</b>
	<i>T.M. Tuch, U. Franck, M. Schilde, M. Wilde, V. Menzel, P. Portius, and O. Herbarth</i>
<a href="#">T19A017</a>	<b>Evaluation of the effectiveness of street sweeping on road dust removal</b>
	<i>S. Han, H. Jo, J.S. Kim, S.B. Lee, and Y.-W. Jung</i>
<a href="#">T19A019</a>	<b>Air Quality assessment at a Portuguese rural city using a TEOM instrument</b>
	<i>S.N. Pereira, F. Wagner, and A.M. Silva</i>
<a href="#">T19A020</a>	<b>Characteristics of atmospheric particles collected near a wax apple waste open burning site</b>
	<i>W.Y. Lin, S.J. Chen, K.L. Huang, C.C. Lin, and J.H. Tsa</i>
<a href="#">T19A022</a>	<b>Evaluation of PM10 sources in three coastal areas of the north-west of Spain</b>
	<i>M. Piñeiro-Iglesias, P.López-Mahía, S. Muniategui-Lorenzo, D. Prada-Rodríguez, and E. Fernández-Fernández</i>
<a href="#">T19A024</a>	<b>Concentrations of oxygenated PAH and other SVOC in relation to urban PM2.5 derived formation of reactive oxygen species</b>
	<i>M. Sklorz, J.J. Briedé, J. Schnelle-Kreis, Y. Liu, J. Orasche, J. Cyrys, T.M. de Kok, and R. Zimmermann</i>
<a href="#">T19A025</a>	<b>Air pollution and climate change - Who takes the blame ? C(1s) NEXAFS spectroscopy on fine particulates "Feinstaub" could provide answers</b>
	<i>A. Braun</i>
<a href="#">T19A027</a>	<b>PM10, PM2.5, PM1 fractions of particulate matter in Prague during year 2006</b>
	<i>L. Štefancová, J. Schwarz, and J. Smolík</i>
<a href="#">T19A028</a>	<b>Levels and chemical composition of PM10 and PM2.5 in "El Arenosillo" rural monitoring station (SW Spain)</b>
	<i>Y. González Castanedo, J.D. de la Rosa, A.M. Sánchez de la Campa, A. Alastuey, X. Querol, J.P. Bolívar, V. Cachorro, and M. Sorribas</i>
<a href="#">T19A029</a>	<b>PM10 and PM2,5 ambient levels in the Czech Republic</b>
	<i>I. Hunová</i>
<a href="#">T19A030</a>	<b>Spatial and temporal variability in PM10 data from Italian urban networks</b>
	<i>A. Di Menno di Bucchianico, S. Bartoletti, A. Gaeta, G. Gandolfo, A.M. Caricchia, and M.C. Cirillo</i>
<a href="#">T19A031</a>	<b>Chemical composition and source apportionment of particulate matter in Elche, Spain</b>
	<i>J. Crespo, J. Nicolás, S. Caballero, E. Yubero, M. Chiari, F. Lucarelli, S. Nava, and I. García Orellana</i>
<a href="#">T19A032</a>	<b>Urban contribution to trace metals in the PM10 in Salzburg and other Austrian cities</b>

	<i>M. Handler, H. Zbiral, H. Puxbaum, and A. Limbeck</i>
<a href="#">T19A035</a>	<b>Size-selective mass and elemental composition of fine particles in the vicinity of a major freeway</b> <i>D. Martuzevicius, S.A. Grinshpun, A.L. Kelley, H. St.Clair, L. Kliucininkas, and T.A. Cahil</i>
<a href="#">T19A036</a>	<b>Study of spatial variability of the particulate matter (PM) concentrations</b> <i>S. Stefan and C. Raicu</i>
<a href="#">T19A038</a>	<b>Atmospheric aerosol characterisation in Tuscany (PATOS project): identification of natural and anthropogenic episodes by PIXE analysis</b> <i>F. Lucarelli, G. Calzolai, M. Chiari, L. Lepri, S. Nava, L. Paperetti, and R. Udisti</i>
<a href="#">T19A039</a>	<b>On the methodology to identify the origin of air masses arriving in a receptor site and determine their contribution to PM levels. A 7-year study in SE Spain.</b> <i>M. Cabello, V. Galiano, and J.A.G. Orza</i>
<a href="#">T19A041</a>	<b>Vegetative input to the Austrian PM10</b> <i>P. Kotianová, A. Caseiro, I.L. Maar, H. Bauer, and H. Puxbaum</i>
<a href="#">T19A042</a>	<b>Speciation of semivolatile organics in the Veneto's bonfires aerosol</b> <i>A. Latella, L. Sporni, E. Rampado, and A. Benassi</i>
<a href="#">T19A043</a>	<b>Exceptional urban air pollution episode from biomass burning</b> <i>A. Latella, A. De Bortoli, G. Marson, E. Baraldo, P. Tieppo, and A. Benassi</i>
<a href="#">T19A045</a>	<b>Characterisation and size distribution of airborne particles in urban traffic and background sites at Stuttgart Neckartor</b> <i>K.B. Ang, G. Baumbach, M.A. Bari, G. Scheffknecht, W. Dreher, and P. Pesch</i>
<a href="#">T19A046</a>	<b>PM<sub>x</sub> mass and ionic composition of PM in the NW suburb of Prague in relation to meteorological conditions</b> <i>J. Schwarz, J. Smolík, and J. Hovorka</i>
<a href="#">T19A047</a>	<b>Effectiveness of street cleaning for reducing ambient PM10 concentrations</b> <i>A.C. John, A. Hugo, H. Kaminski, A. Brandt, W. Kappert, E. Falkenberg, and T.A.J. Kuhlbusch</i>
<a href="#">T19A050</a>	<b>Magnetic measurements of PM10 and their potential for monitoring environmental stress</b> <i>E. Petrovský, B. Kotlík, R. Zboril, J. Novák, A. Kapicka, and H. Fialová</i>
<a href="#">T19A051</a>	<b>HULIS over Vienna investigations into water and alkaline extractable Humic Like Substances in airborne particulate matter</b> <i>B. Klatzer, H. Bauer, I.L. Marr, and H. Puxbaum</i>
<a href="#">T19A052</a>	<b>A novel sampler for large particles</b> <i>S.-R. Lee, T.M. Holsen, and S. Dhaniyala</i>
<a href="#">T19A055</a>	<b>Chemical characterization of fine particulate matter in Bari and Taranto (South Italy)</b> <i>M. Amodio, P. Bruno, M. Caselli, P.R. Dambruoso, B.E. Daresta, G. de Gennaro, P. Ielpo, V. Paolillo, C.M. Placentino, L. Trizio, and M. Tutino</i>
<a href="#">T19A056</a>	<b>Rainfall influence on the relation between particulate matter and traffic flow</b> <i>M. Filice and P. De Luca</i>
<a href="#">T19A057</a>	<b>Chemical characterization of atmospheric PM sampled near an incinerator of urban solid waste located in Granarolo dell'Emilia, Bologna, Italy, and in the neighbours urban and rural areas of Bologna</b> <i>V. Poluzzi, C. Maccone, I. Ricciardelli, L. Passoni, M. Busetto, D. Lucchini, E. Errani, M. Ridolfi, S. Ruiba, S. Tamburini, P. Franceschi, I. Scaroni, and G. Castellari</i>

[Top of Program](#)

[Top of Poster Session Part I](#)

### Special Sesion: UT/LS Aerosols and Clouds - Measurements and Modeling

<a href="#">T13A034</a>	<b>Ice-nucleating ability of the most abundant mineral dust phases in the atmosphere</b> <i>F. Zimmermann, M. Ebert, St. Weinbruch, and L. Schütz</i>
-------------------------	--

<a href="#">T21A006</a>	<b>Nitric acid uptake and supersaturations in different types of cirrus clouds: model case and sensitivity studies</b> <i>I. Gensch, H. Bunz, D. Baumgardner, L.E. Christensen, J. Curtius, R.L. Herman, T. Peter, P. Popp, C. Schiller, H. Schlager, C. Voigt, C.R. Webster, J.C. Wilson, and M. Kraemer</i>
<a href="#">T21A008</a>	<b>Model calculations and experiments investigating freezing of UT/LS-aerosols</b> <i>H. Bunz, S. Benz, and O. Möhler</i>
<a href="#">T21A009</a>	<b>Aerosol impact on supersaturations in cirrus: Laboratory and field observations</b> <i>M. Krämer, S. Schlicht, C. Schiller, A. Mangold, O. Möhler, H. Saathoff, V. Ebert, and N. Sitnikov</i>
<a href="#">T21A010</a>	<b>Formation of large (100 microns) ice crystals near the tropopause</b> <i>E.J. Jensen, L. Pfister, T.V. Bui, P. Lawson, B. Baker, Q. Mo, D. Baumgardner, E.M. Weinstock, J.B. Smith, E.J. Moyer, T.F. Hanisco, D.S. Sayres, J.M. St.Clair, R.L. Herman, R.F. Troy, M.J. Alexander, O.B. Toon, and J.A. Smith</i>
<a href="#">T21A012</a>	<b>Particle chemical composition measured at a high alpine field station in Switzerland: Impact on the phase of cold clouds</b> <i>A.C. Targino, K. Bower, T.W. Chouarton, H. Coe, J. Crosier, I. Crawford, M.W. Gallagher, M. Flynn, J. Cozic, B. Verheggen, E. Weingartner, and U. Baltensperger</i>

[Top of Program](#)

[Top of Poster Session Part I](#)

<b>Aerosol Filtration#2</b>	
<a href="#">T11A025</a>	<b>Comparison of the loading characteristics onto filters of the particles entering the ceramic candle filter vessel through the normal or tangential inlet</b> <i>S.J. Park, K.S. Lim, and J.H. Lim</i>

[Top of Program](#)

[Top of Poster Session Part I](#)

# Poster Session Part II

[Atmospheric Aerosols - Chemical Properties](#)

[Bioaerosols](#)

[Atmospheric Aerosols - Cloud Properties](#)

[Combustion Aerosols](#)

[Atmospheric Aerosols - Desert Dust](#)

[Fine Particles](#)

[Atmospheric Aerosols - Hygroscopicity](#)

[Fundamental Aerosol Physics - Nucleation, Condensation and Evaporation](#)

[Atmospheric Aerosols - Optical Properties](#)

[High Temperature Aerosols](#)

[Atmospheric Aerosols - Physical Properties](#)

[Industrial Aerosols](#)

[Atmospheric Aerosols - Sources](#)

[Radiative Aerosols](#)

[Atmospheric Aerosols - Transport](#)

[Remote Sensing of Aerosols](#)

[Aerosol Filtration](#)

[Special Session: COST 633 - Particulate Matter and Health Effects](#)

Thursday 13 September 2007	13:45 - 15:45	Poster Area
Poster Session Part II		

Atmospheric Aerosols - Chemical Properties	
<a href="#">T13A002</a>	<b>Aerosol climatology of tropospheric aerosol profiles over Athens, Greece using an elastic-RAMAN lidar system (2000-2006)</b> <i>R. E. Mamouri, G. Tsaknakis, and A. Papayannis</i>
<a href="#">T13A004</a>	<b>Analysis of size-resolved atmospheric aerosol particle samples by Raman Microscopy</b> <i>N.P. Iivleva, U. McKeon, U. Pöschl, and R. Niessner</i>
<a href="#">T13A006</a>	<b>Single Particle Characterisation of Marine Aerosols at Mace, Ireland: Winter and Summer Data from the MAP Campaigns 2006</b> <i>C. Grüning, P. Cavalli, N.R. Jensen, D. Mira Salama, and F. Raes</i>
<a href="#">T13A018</a>	<b>Size resolved mass and elemental composition of ground collected aerosols over south-east Italy</b> <i>I. Carofalo and M.R. Perrone</i>
<a href="#">T13A025</a>	<b>Laminar Co-Flow Tube: A novel tool to study sulfuric acid – water nucleation</b> <i>P. Krejčí, T. Nemeč, J. Hrubý, and V. Ždímal</i>
<a href="#">T13A055</a>	<b>Characterization of ice residuals from the CLACE 5 experiment</b> <i>A. Worringer, N. Benker, M. Ebert, F. Zimmermann, S. Mertes, E. Weingartner, and S. Weinbruch</i>
<a href="#">T13A057</a>	<b>Aerosol elemental mass size distributions at Baia Terra Nova (Antarctica): Individual representations and intersample variability</b> <i>P. Mittner, D. Ceccato, V. Trovò, and F. Chiminello</i>

<a href="#">T13A058</a>	<b>Analysis of aerosol water-soluble organic compounds and humic-like substances by anion-exchange chromatography coupled to Total Organic Carbon determination</b> E. Finessi, S. Decesari, V. Mancinelli, M. Rinaldi, C. Carbone, M. Mircea, M. C. Facchini, and S. Fuzzi
<a href="#">T13A078</a>	<b>Long-term observations of aerosol mass and composition and trace gas concentrations in Pacific background airmasses at coastal atmospheric monitoring sites in Taiwan</b> C. Junker and C.T. Lee
<a href="#">T13A111</a>	<b>Characterization of aqueous solutions of atmospheric humic-like substances</b> R. Ocskay and I. Salma
<a href="#">T13A117</a>	<b>The atmospheric partitioning of PAHs and n-alkanes in urban (Milan) and remote (Alpe San Colombano, 2260 m) sites in Italy</b> G. Sangiorgi, L. Ferrero, Z. Lazzati, C. Lo Porto, M. G. Perrone, S. Petraccone, and E. Bolzacchini
<a href="#">T13A119</a>	<b>Season time modulation of Nitro-PAH in the air of Montelibretti RM, Italy</b> A. Cecinato, C. Balducci, G. Nervegna, G. Tagliacozzo, and A. Brachetti
<a href="#">T13A120</a>	<b>Detection and evaluation of cocaine in ambient air particulates</b> A. Cecinato and C. Balducci
<a href="#">T13A123</a>	<b>Size distributions of PAHs collected beside a heavily-trafficked road</b> C.C. Lin, S.J. Chen, K.L. Huang, and W.Y. Lin
<a href="#">T13A130</a>	<b>Spring monitoring of the aerosol precursor isoprene and other biogenic volatile organic compounds (VOC) in a suburban area of A Coruña (NW Spain)</b> D. Pérez-Rial, P.López-Mahía, S. Muniategui-Lorenzo, D. Prada-Rodríguez, and E. Fernández-Fernández
<a href="#">T13A132</a>	<b>Atmospheric aerosol characterization in Tuscany (PATOS project): n-alkanes, PAHs and Total Carbon</b> T. Martelini, A. Cincinelli, M. Giannoni, F. Barzagli, D. Vannucchi, L. Lepri, R. Udisti, and F. Lucarelli
<a href="#">T13A142</a>	<b>Single particle characterization in the coarse mode from local, regional and long range transport episodes in Madrid by CCSEM and FE-SEM</b> E. Coz, F.J. Gómez-Moreno, M. Pujadas, T. Lersch, G. Casuccio, and B. Artíñano
<a href="#">T13A158</a>	<b>The elemental analysis of size-fractionated particulate matter using TXRF - a tentative field study in Göteborg, Sweden -</b> A. Wagner and J. Boman
<a href="#">T13A169</a>	<b>Geochemical characterization of mineral aerosol reaching the East Antarctic Plateau</b> F. Marino, S. Becagli, E. Castellano, O. Cerri, F. Rugi, R. Traversi, S. Caporali, S. Nava, M. Chiari, F. Lucarelli, V. Maggi, and R. Udisti
<a href="#">T13A178</a>	<b>Single-particle characterization of aerosol samples collected over the Yellow Sea</b> Y. Park, H. Hwang, M.S.I. Khan, S. Kang, H. Kim, and C.-U. Ro
<a href="#">T13A192</a>	<b>Atmospheric aerosol characterization in Tuscany (PATOS project): ionic composition and "soluble" fraction of selected metals</b> S. Becagli, E. Castellano, O. Cerri, L. Lepri, F. Lucarelli, F. Marino, A. Morganti, F. Rugi, M. Severi, R. Traversi, and R. Udisti
<a href="#">T13A194</a>	<b>Sampling strategies and first results on chemical composition of size-segregated aerosol fractions at Dome C (Central East-Antarctica) during the 2006 winter-over campaign</b> O. Cerri, S. Becagli, E. Castellano, M. Chiari, F. Lucarelli, F. Marino, A. Morganti, S. Nava, F. Rugi, M. Severi, R. Traversi, and R. Udisti
<a href="#">T13A208</a>	<b>Annual semicontinuous monitoring of SPAH in the urban airshed</b> A. Latella and A. Benassi
<a href="#">T13A214</a>	<b>Alkali metal content of individual particles in Mexico City during the MILAGRO campaign in 2006</b> T.L. Gustafsson, J. Noda, and J.B.C. Pettersson
<a href="#">T13A218</a>	<b>Characterization of compositions and size distributions of dicarboxylic acids in background and suburban aerosols</b> Y.I. Tsai, T.-H. Weng, S.-C. Kuo, and L.-Y. Hsieh
<a href="#">T13A219</a>	<b>Long term measurements of inorganic, organic and radionuclides at the puy de Dôme, 1465 m a.s.l.</b> L. Bourcier, K. Sellegri, O. Masson, J.-M. Pichon, P. Chausse, P. Paulat, and P. Laj
<a href="#">T13A246</a>	<b>Chemical and size characteristics of particles in the Lower Fraser Valley, British Columbia, Canada</b>

[Top of Program](#)

[Top of Poster Session Part II](#)

## Atmospheric Aerosols - Cloud Properties

<a href="#">T13A008</a>	<b>Cubic and hexagonal ice and high humidity in low-temperature cirrus</b> <i>A. Bogdan</i>
<a href="#">T13A009</a>	<b>Nature of high relative humidity with respect to ice on cold cirrus</b> <i>A. Bogdan</i>
<a href="#">T13A074</a>	<b>Surface tensions of multi-component mixed inorganic/organic aqueous systems of atmospheric significance: Measurements, model predictions and importance for cloud activation</b> <i>D.O. Topping, G.B. McFiggans, G. Kiss, Z. Varga, M.C. Facchini, S. Decesari, and M. Mircea</i>
<a href="#">T13A083</a>	<b>The first aerosol-cloud experiment in the Puijo semi-urban measurement station</b> <i>A. Leskinen, T. Raatikainen, A.-P. Hyvärinen, A. Kortelainen, P. Miettinen, N. Pietikäinen, H. Portin, J. Rautiainen, R. Sorjamaa, P. Tiitta, P. Vaattovaara, A. Laaksonen, K.E.J. Lehtinen, H. Lihavainen, and Y. Viisanen</i>
<a href="#">T13A159</a>	<b>Observations of the role of organic aerosol in the initiation of ice and liquid clouds</b> <i>K. Bower, E. Weingartner, T.W. Choularton, M.R. Alfarra, M.W. Gallagher, H. Coe, J. Crosier, J. Allan, A.T. Argino, I. Crawford, P. Connolly, B. Verheggen, M. Gysel, S. Sjogren, U. Baltensperger, and J. Cozic</i>
<a href="#">T13A167</a>	<b>European Integrated Project on Aerosol Cloud Climate Air Quality Interactions - EUCAARI</b> <i>M. Kulmala, A. Asmi, and H. Lappalainen</i>
<a href="#">T13A244</a>	<b>Cloud condensation nucleus activity of secondary organic aerosol particles mixed with sulfate</b> <i>S.M. King, T. Rosenoern, J.E. Shilling, Q. Chen and S.T. Martin</i>

[Top of Program](#)

[Top of Poster Session Part II](#)

## Atmospheric Aerosols - Desert Dust

<a href="#">T13A039</a>	<b>Chemical and mineralogical composition of Saharan dust over south-east Morocco</b> <i>K. Kandler, C. Deutscher, M. Ebert, H. Hofmann, S. Jäckel, A. Petzold, L. Schütz, S. Weinbruch, B. Weinzierl, and S. Zorn</i>
<a href="#">T13A062</a>	<b>Reporting aerosol data about the most strong desert dust outbreak registered over the Iberina Peninsula mixed with a forest fire episode. Columnar properties with remote sensing techniques.</b> <i>V.E. Cachorro, N. Prats, M. Sorribas, C. Toledano, S. Mogo, A. Berjón, A.M. de Frutos, and B.A. de la Morena</i>
<a href="#">T13A179</a>	<b>Measurements of optical properties of dust particles during the Saharan Mineral Dust Experiment SAMUM 2006</b> <i>A. Schladitz, T. Müller, N. Kaaden, A. Maßling, and A. Wiedensohler</i>
<a href="#">T13A191</a>	<b>Size distribution vertical profiles of Saharan dust over the Eastern Atlantic during the 2005-2006 summer outbreaks from aircraft "in-situ" measurements</b> <i>J. Andrey, M. Gil, O. Serrano, and E. Cuevas</i>
<a href="#">T13A222</a>	<b>Saharan Mineral Dust Experiment SAMUM 2006: Aerosol optical properties of dust from various source regions</b> <i>A. Petzold, K. Rasp, T. Hamburger, B. Weinzierl, M. Fiebig, and A. Virkkula</i>

[Top of Program](#)

[Top of Poster Session Part II](#)

## Atmospheric Aerosols - Hygroscopicity

<a href="#">T13A015</a>	<b>LACIS-Measurements of hygroscopic growth and activation of sea-salt</b> <i>D. Niedermeier, H. Wex, and F. Stratmann</i>
<a href="#">T13A016</a>	<b>Comparison of the hygroscopic growth and activation of urban aerosol and HULIS</b> <i>M. Ziese, E. Nilsson, H. Wex, T. Hennig, I. Salma, and F. Stratmann</i>
<a href="#">T13A084</a>	<b>The effects of aerosol composition on the hygroscopicity of atmospheric aerosols collected at three sites in Taiwan</b> <i>C.-T. Lee and M.-J. Chen</i>
<a href="#">T13A092</a>	<b>Closure between chemical composition and hygroscopic growth of aerosol particles</b> <i>M. Gysel, J. Crosier, D.O. Topping, J.D. Whithead, K.N. Bower, M.J. Cubison, P.I. Williams, M.J. Flynn, G.B. McFiggans, and H. Coe</i>
<a href="#">T13A154</a>	<b>Aerosol hygroscopicity as the function of the size and the chemical composition</b> <i>K. Imre, A. Molnár, and D. Benko</i>
<a href="#">T13A174</a>	<b>Hygroscopic properties of sub-micrometer atmospheric aerosol particles measured with H-TDMA instruments in various environments - A review</b> <i>E. Swietlicki, H.-C. Hansson, A. Massling, T. Petäjä, P. Tunved, K. Hämeri, E. Weingartner, U. Baltensperger, P.H. McMurry, G. McFiggans, B. Svenningsson, A. Wiedensohler, and M. Kulmala</i>
<a href="#">T13A190</a>	<b>Mixing states and hygroscopicity of aerosol particles in West Africa: Based on AMMA aircraft campaign in summer 2006</b> <i>A. Matsuki, A. Schwarzenboeck, H. Venzac, P. Laj, O. Laurent, G. Momboisse, S. Crumeyrolle, L. Gomes, and T. Bourriane</i>

[Top of Program](#)

[Top of Poster Session Part II](#)

<b>Atmospheric Aerosols - Optical Properties</b>	
<a href="#">T13A011</a>	<b>Studies of the impact of Arctic aerosols on climate modifications</b> <i>T. Zielinski, J. Piskozub, T. Petelski, A. Rozwadowska, S. Malinowski, T. Stacewicz, K. Markowicz, R. Neuber, A. Jagodnicka, M. Posyniak, M. Gausa, and S. Blindheim</i>
<a href="#">T13A012</a>	<b>Impact of different aerosol sources on particle optical properties - Experiment SOAP</b> <i>T. Zielinski, J. Remiszewska, G. Chourdakis, and N. Mihalopoulos</i>
<a href="#">T13A033</a>	<b>Model-predicted and satellite-/sun photometer-derived aerosol optical properties in East Asia</b> <i>C.H. Song, Y. Lee, J.Y. Kim, Y.J. Kim, and K.H. Lee</i>
<a href="#">T13A041</a>	<b>Seasonal variability of vertical profiles of the single scattering albedo of submicron aerosol</b> <i>V.S. Kozlov and M.V. Panchenko</i>
<a href="#">T13A060</a>	<b>Aerosol optical properties measurements from two Chinese megacities, Beijing and Guangzhou</b> <i>R.M. Garland, H. Yang, O. Schmid, D. Rose, S.S. Gunthe, M. Hu, M. Shao, L. Zeng, Y. Zhang, T. Zhu, M.O. Andreae, and U. Pöschl</i>
<a href="#">T13A061</a>	<b>Preliminary estimations of Aerosol Optical Depth (AOD) over Spain obtained from the INM CIMEL sun-photometers measurements</b> <i>M.D. Gil, B. Navascúes, M. López, and A. Cansado</i>
<a href="#">T13A067</a>	<b>The angle-dependent light scattering by soot-water drops agglomerates</b> <i>S.S. Vlasenko, E.F. Mikhailov, and M.Y. Igonin</i>
<a href="#">T13A085</a>	<b>The estimation of light scattering coefficient of atmospheric aerosols using source area analysis for particle size distribution</b> <i>P. Kolmonen, V. Aaltonen, J. Hatakka, A. Hyvärinen, T. Kaurila, K.E.J. Lehtinen and H. Lihavainen</i>
<a href="#">T13A098</a>	<b>Comparison of surface and satellite derived aerosol optical depth measurements in Finland</b> <i>T. Mielonen, A. Arola, P. Kolmonen, H. Lihavainen, T. Kaurila, E. Parmes, and K.E.J. Lehtinen</i>
<a href="#">T13A107</a>	<b>Aerosol optical properties in Granada from simultaneous measurements by LIDAR, Nephelometer, CIMEL, Avantes and FieldSpec radiometers</b> <i>F. Esposito, M.R. Calvello, L. Leone, G. Pavese, R. Restieri, H. Lyamani, J.L. Guerrero-Rascado, F.J. Olmo, and L. Alados-Arboledas</i>
<a href="#">T13A113</a>	<b>Aerosol scattering and mass concentration for different aerosol types</b> <i>S.N. Pereira, F. Wagner, A.M. Silva, and N. Belo</i>

<a href="#">T13A116</a>	<b>Seasonal variability in the physical and optical properties of atmospheric aerosols over a coastal zone</b> <i>A. Saha, J. Piazzola, and S. Despiou</i>
<a href="#">T13A135</a>	<b>Study of inter-annual variability of atmospheric aerosol as assessed from the data of spectral measurements of aerosol extinction on near-ground path</b> <i>E.V. Makienko, Y.A. Pkhalagov, R.F. Rakhimov, and V.N. Uzhegov</i>
<a href="#">T13A146</a>	<b>MieCalc program for calculation of light scattering and absorption characteristics of particles continental and coastal aerosol</b> <i>G.A. Kaloshin, L. B. Kochneva, and S. V. Beresnev</i>
<a href="#">T13A153</a>	<b>Estimation of aerosol impact on extreme weather and climate</b> <i>A.V. Andronova, D.P. Gubanova, and V.M. Minashkin</i>
<a href="#">T13A185</a>	<b>CAPEX – AEROPOR Overview : objectives and first results</b> <i>A.M. Silva, M.J. Costa, F. Wagner, D. Bortoli, S. Pereira, N. Belo, L. Bugalho, L. Alados-Arboledas, H. Lyamani, J.L. Guerrero-Rascado, D. Kindred, and M. Smith</i>
<a href="#">T13A196</a>	<b>CAPEX-AEROPOR: Aerosol Measurements derived from airborne and ground-based measurements</b> <i>F. Wagner, S. Pereira, D. Bortoli, M.J. Costa, N. Belo, A.M. Silva, J.L. Guerrero-Rascado, H. Lyamani, L. Alados-Arboledas</i>
<a href="#">T13A200</a>	<b>Seasonal and diurnal variations of scattering and absorption properties of aerosols in an urban area, Granada, Spain</b> <i>H. Lyamani and L. Alados-Arboledas</i>
<a href="#">T13A204</a>	<b>Characterization of the atmospheric aerosol properties during ESTIO2005 field campaign: an interdisciplinary approach</b> <i>L. Alados-Arboledas, H. Horvath, X. Querol, F.J. Olmo, J.L. Guerrero-Rascado, H. Lyamani, M. Gangl, S. Castillo, and A. Alastuey</i>
<a href="#">T13A223</a>	<b>Arctic smoke – aerosol characteristics during a record air pollution event in the European Arctic and its radiative impact</b> <i>R. Treffeisen, P. Turnved, J. Ström, A. Herber, J. Barreis, A. Helbig, R. S. Stone, W. Hoyningen-Huene, R. Krejci, A. Stohl, and R. Neuber</i>
<a href="#">T13A233</a>	<b>Comparisons between the AERONET products and those derived from aerosols optic and chemistry in Beijing</b> <i>J.C. Roger, O. Dubovik, B. Guinot, M. Mallet, L. Lin, E. Vermote, H. Cachier, H. Chen, Y. Tong, and B. Holben</i>
<a href="#">T13A234</a>	<b>Results of spring aerosol campaigns in Hornsund, Spitsbergen, 2004 and 2007</b> <i>A. Rozwadowska, T. Petelski, K. Migala, T. Zielinski</i>

[Top of Program](#)

[Top of Poster Session Part II](#)

<b>Atmospheric Aerosols - Physical Properties</b>	
<a href="#">T13A001</a>	<b>Influence of clouds on aerosol particle number concentrations in the upper troposphere – results from the CARIBIC project</b> <i>A. Weigelt, M. Hermann, P.F.J. van Velthoven, C.A.M. Brenninkmeijer, J. Heintzenberg, and A. Wiedensohler</i>
<a href="#">T13A003</a>	<b>Thirty months of systematic measurements of tropospheric aerosol and ozone vertical profiles using a combined RAMAN-DIAL and a DOAS system over Athens, Greece (2005-2007)</b> <i>G. Tsaknakis, A. Papayannis, P.D. Kalabokas, I. Ziomas, G. Chourdakis, G. Georgousis, and P. Zanis</i>
<a href="#">T13A028</a>	<b>The size segregated mass concentrations of aerosols in the North Atlantic free troposphere: 5 observations at the Izaña Global Atmospheric Watch Observatory</b> <i>S. Rodríguez, E. Cuevas, P.M. Romero, X. Querol, A. Alastuey, N. Perez, and S. Castillo</i>
<a href="#">T13A037</a>	<b>Differences between marine aerosol backscatter and size-distribution in upwind and downwind conditions with respect to the ship</b> <i>M. Del Guasta, F. Castagnoli, and V. Venturi</i>
<a href="#">T13A040</a>	<b>Meteorological processes affecting the atmospheric particle number size distribution at the high Alpine observatory "Schneefernerhaus"</b> <i>K. König, W. Birmili, A. Sonntag, L. Ries, R. Sohmer, and A. Stohl</i>

<a href="#">T13A045</a>	<b>Physico-chemical characterization of Venice lagoon aerosol</b> <i>F. Prodi, L. Di Matteo, F. Belosi, G. Santachiara, S. Nava, R. Udisti, D. Contini, and A. Donateo</i>
<a href="#">T13A049</a>	<b>Atmospheric aerosol dynamics obtained by experiment using diffusion battery</b> <i>A.M. Baklanov, G.I. Gorchakov, and T.E. Ovchinnikova</i>
<a href="#">T13A063</a>	<b>Similarity between aerosol physico-chemical properties at a coastal station and the open ocean over the North Atlantic</b> <i>M. Rinaldi, C. Carbone, E. Finessi, S. Decesari, M. Mircea, M.C. Facchini, S. Fuzzi, D. Ceburnis, and C.D. O'Dowd</i>
<a href="#">T13A089</a>	<b>Mass distribution by gravimetric measurements in a rural site in South Italy</b> <i>M. Calvello, F. Esposito, L. Leone, and R. Restieri</i>
<a href="#">T13A091</a>	<b>Variability and long-term trends of aerosol parameters at the Jungfraujoch</b> <i>M. Collaud Coen, E. Weingartner, S. Nyeki, J. Cozic, B. Verheggen, and U. Baltensperger</i>
<a href="#">T13A096</a>	<b>Size distributions of atmospheric ions in the Baltic Sea region</b> <i>M. Komppula, M. Vana, V.-M. Kerminen, H. Lihavainen, Y. Viisanen, U. Hörrak, K. Komsaare, E. Tamm, A. Hirsikko, L. Laakso, and M. Kulmala</i>
<a href="#">T13A099</a>	<b>Comparison of columnar aerosol properties in Moscow and Moscow region</b> <i>M.A. Sviridenkov, N.Y. Chubarova, and P.P. Anikin</i>
<a href="#">T13A104</a>	<b>Real-time observation of deliquescence and efflorescence behaviour of individual aerosol particles</b> <i>S.M. Kim, J.H. Kuk, K.H. Ahn, S. Kang, H. Hwang, and C.U. Ro</i>
<a href="#">T13A109</a>	<b>Database driven web-application for atmospheric data visualization</b> <i>H. Junninen, M. Kulmala</i>
<a href="#">T13A126</a>	<b>Seasonal variation of particle size distributions of PAHs at Seoul, Korea</b> <i>J.Y. Lee, C.-H. Kang, and Y.P. Kim</i>
<a href="#">T13A150</a>	<b>The coating of soot with levoglucosan</b> <i>T. F. Mentel, A. Kiendler-Scharr, R. Tillmann, A. Kiselev, H. Wex, F. Stratmann, T. Hennig, J. Schneider, and S. Walter</i>
<a href="#">T13A177</a>	<b>The variability of the atmospheric aerosol in the planetary boundary layer for a subtropical, polluted environment in Southern China</b> <i>A. Nowak, A. Wiedensohler, W. Birmili, P. Achtert, M. Hu, and Y. Zhang</i>
<a href="#">T13A180</a>	<b>Comparison of the seasonal variation of the aerosol size distribution at high altitude research stations in France and Nepal</b> <i>H. Venzac, K. Sellegri, P. Villani, D. Picard, P. Bonasoni, and P. Laj</i>
<a href="#">T13A182</a>	<b>Latitudinal variation in aerosol size distribution in the Eastern Atlantic</b> <i>P.I. Williams, M.W. Gallagher, and G. McFiggans</i>
<a href="#">T13A187</a>	<b>Air quality, particle size distribution and trace metal composition of aerosols from an urban area near an iron smelting facility</b> <i>M.A. Barrero and L. Cantón</i>
<a href="#">T13A189</a>	<b>Integrating LIDAR profiles and surface particulate matter mass concentration for atmospheric aerosol characterization</b> <i>R. Caggiano, A. Boselli, M. Macchiato, L. Mona, G. Pappalardo, S. Sabia, and S. Trippetta</i>
<a href="#">T13A197</a>	<b>Weekly cycles of atmospheric variables and a possible link to the aerosol load</b> <i>D. Bäumer and B. Vogel</i>
<a href="#">T13A206</a>	<b>First results of a simple method for directional coarse particulate matter monitoring</b> <i>J.A.G. Orza, M. Cabello, and J. Mateo</i>
<a href="#">T13A212</a>	<b>Comparison of particle number concentrations and size distributions at Dome Concordia in the high Antarctic plateau and at Aboa in Queen Maud Land, Antarctica</b> <i>A. Virkkula, R. Hillamo, M. Busetto, V. Vitale, P. Aalto, and M. Kulmala</i>
<a href="#">T13A242</a>	<b>Mass balance of Total Suspended Particles over the coal burning power production area of western Macedonia, Greece</b> <i>E. Terzi, Ch. Anatolaki, R. Tsitouridou, and C. Samara</i>

<b>Atmospheric Aerosols - Sources</b>	
<a href="#">T13A021</a>	<b>The role of road transport and industrial emission sources in daily distribution of BTX concentrations in Wroclaw air</b> <i>J. Zwodziak, A. Zwodziak, I. Sowka, A. Gzella, and A. Schady</i>
<a href="#">T13A027</a>	<b>Source apportionment on time resolved particles number distributions</b> <i>F. Mazzei, F. Lucarelli, S. Nava, P. Prati, G. Valli, and R. Vecchi</i>
<a href="#">T13A052</a>	<b>An analysis of vehicular particle number emissions based on long-term roadside and urban background measurements</b> <i>S. Klose, W. Birmili, T. Tuch, B. Wehner, A. Wiedensohler, U. Franck, M. Ketzel</i>
<a href="#">T13A065</a>	<b>Wood burning aerosol during winter in an Alpine valley: Aethalometer and the Aerosol Mass Spectrometer measurements</b> <i>J. Sandradewi, M.R. Alfara, A.S.H. Prévôt, E. Weingartner, M. Gysel, R. Schmidhauser, S. Szidat, and U. Baltensperger</i>
<a href="#">T13A068</a>	<b>Chemical composition of primary marine aerosol: Results from the bubble bursting laboratory experiment during MAP</b> <i>C. Carbone, E. Finessi, M. Rinaldi, S. Decesari, M. Mircea, M.C. Facchini, S. Fuzzi, D. Nilsson, D. Ceburnis, and C. O'Dowd</i>
<a href="#">T13A088</a>	<b>Size distributions of aerosol particles in a food waste composting center</b> <i>J.H. Byeon, C.W. Park, K.Y. Yoon, J.H. Park, and J. Hwang</i>
<a href="#">T13A102</a>	<b>Road-side ultrafine particle and ion size distributions</b> <i>P. Tiitta, P. Miettinen, P. Vaattovaara, A. Laaksonen, J. Joutsensaari, and A. Hirsikko</i>
<a href="#">T13A122</a>	<b>Contribution of natural emissions to ambient aerosol concentration levels in the eastern Mediterranean</b> <i>A. Spyridaki, V. Aleksandropoulou, M. Latos, F. Flatoy, and M. Lazaridis</i>
<a href="#">T13A131</a>	<b>Particulate organic compounds in the atmosphere surrounding a waste water treatment plant (Aglia - Pistoia, Italy)</b> <i>T. Martellini, A. Cincinelli, M. Del Bubba, L. Misuri, A. Valentino, and L. Lepri</i>
<a href="#">T13A133</a>	<b>Monitoring station for ground based tropospheric aerosol properties in Southwest Spain</b> <i>M. Sorribas, S. Mogo, V.E. Cachorro, J. De la Rosa, N. Prats, J.F. López, A.M. Sánchez de la Campa, Y. González, A.M. De Frutos, B.A. De la Morena</i>
<a href="#">T13A136</a>	<b>The effect of remote fire smokes on spectral behavior of the scale height of the aerosol atmosphere</b> <i>V.N. Uzhegov, Y.A. Pkhalagov, D.M. Kabanov, and S.M. Sakerin</i>
<a href="#">T13A143</a>	<b>Determination of particle emission factors of individual vehicles under real-life conditions</b> <i>C. Hak, E. Ljungström, M. Hallquist, M. Svane, and J. Pettersson</i>
<a href="#">T13A155</a>	<b>Chemical composition of fine particles in two major biomass burning episodes observed in Helsinki, 2006</b> <i>S. Saarikoski, K. Saarnio, M. Sillanpää, H. Timonen, K. Teinilä, M. Sofiev, J. Kukkonen, and R. Hillamo</i>
<a href="#">T13A161</a>	<b>Traffic and meteorological influence on size segregated trace elements at a kerbside in Dresden, Germany</b> <i>H. Gerwig, E. Brüggemann, T. Gnauk, K. Müller, and H. Herrmann</i>
<a href="#">T13A183</a>	<b>Monitoring of atmospheric aerosols over Baikal Lake</b> <i>V.A. Zagaynov, T.V. Khodzher, Yu.G. Biryukov, V.A. Obolkin, J.S. Lyubovtseva, A.A. Lushnikov</i>
<a href="#">T13A186</a>	<b>Biomass burning traces in Antarctic ice</b> <i>R. Zangrando, A. Gambaro, C. Barbante, P. Gabrielli, W. Cairns, C. Turetta, and P. Cescon</i>
<a href="#">T13A193</a>	<b>Aerosol sources apportionment at Lampedusa island (Central Mediterranean Sea)</b> <i>S. Becagli, E. Castellano, M. Severi, R. Traversi, D.M. Sferlazzo, C. Bommarito, A. di Sarra, F. Lucarelli, F. Marino, S. Nava, F. Rugi, and R. Udisti</i>
<a href="#">T13A198</a>	<b>Annual variability of aerosol load and chemical composition in two sites at different anthropic</b>

	<b>impact in Sesto F.no area (Florence-Italy) - PASF Project</b>
	<i>R. Traversi, S. Becagli, E. Castellano, O. Cerri, M. Chiari, F. Lucarelli, F. Marino, A. Morganti, F. Rugi, M. Severi, and R. Udisti</i>
<a href="#">T13A209</a>	<b>Primary Marine Aerosol emissions on the North Atlantic MAP-cruise 2006: combining eddy covariance flux measurements with in situ laboratory tank experiments</b>
	<i>E. D. Nilsson, K. Hultin, E. M. Mårtensson, R. Krejci, D. Broman, Å. Hagström, K. Rosman, L. Bäcklin, M. C. Facchini, C. O'Dowd, G. de Leeuw</i>
<a href="#">T13A216</a>	<b>The boreal forest canopy and aerosol eddy covariance fluxes</b>
	<i>L. Ahlm, S. Launiainen, D. Nilsson, T. Grönholm, J. Rinne, M. Mårtensson, P. Aalto, S. van Ekeren, M. Kulmala, and T. Vesala</i>
<a href="#">T13A232</a>	<b>Sea spray emission function calculated from vertical aerosol concentration gradients over Arctic seas</b>
	<i>T. Petelski and A. Rozwadowska</i>
<a href="#">T13A237</a>	<b>Use of inventories of natural and artificial radionuclides in soils to estimate total aerosols deposition and origin in French mountains</b>
	<i>G. Le Roux, L. Pourcelot, O. Masson, C. Duffa, F. Vray, and P. Renaud</i>
<a href="#">T13A241</a>	<b>Characterisation of woodsmoke from distant forest fires</b>
	<i>T.H. Gan, P.J. Hanhela, W. Mazurek, and R. Gillett</i>

[Top of Program](#)

[Top of Poster Session Part II](#)

<b>Atmospheric Aerosols - Transport</b>	
<a href="#">T13A019</a>	<b>Influence of averaged vertical wind on transport of stratospheric aerosols</b>
	<i>V.I. Gryazin and S.A. Beresnev</i>
<a href="#">T13A031</a>	<b>Aerosols transport across the Central Mediterranean</b>
	<i>D. Đorđević, S. Rodríguez, J.J. Rodríguez, J.C. Guerra, M. Todorović, D. Relić, A. Mihajilidi-Zelić, and D. Šegan</i>
<a href="#">T13A048</a>	<b>Meteorological criteria for the accumulation, their transport and the range of a boundary layer of aerosols on the mesoscale</b>
	<i>K. Weinhold, W. Birmili, C. Engler, A. Sonntag, and A. Wiedensohler</i>
<a href="#">T13A066</a>	<b>Back trajectories classification with columnar aerosol properties in south-west Spain</b>
	<i>C. Toledano, V. Cachorro, B. Torres, N. Prats, R. Rodrigo, M. Sorribas, A. Berjón, and A. De Frutos</i>
<a href="#">T13A108</a>	<b>Vertical movement of strong absorbing particles for stratospheric pressures due to gravitophoretic force and their morphology</b>
	<i>O. Jovanovic and H. Horvath</i>
<a href="#">T13A226</a>	<b>Origin of the aerosol nanoparticles in the marine boundary layer over the south-eastern Baltic Sea</b>
	<i>V. Ulevicius, K. Plauškaite, N. Prokopciuk, N. Špirkauskaitė, T. Petelski, and T. Zielinski</i>
<a href="#">T13A245</a>	<b>Large-scale inhomogeneity of aerosol concentration at various humidity levels</b>
	<i>A.A. Jouralev and G.M. Teptin</i>

[Top of Program](#)

[Top of Poster Session Part II](#)

<b>Aerosol Filtration</b>	
<a href="#">T11A001</a>	<b>An experimental study on respirator penetration testing by sodium flame and aerosol photometer methods</b>
	<i>Z.Z. Zhang, F. Jiang, Z.Y. Zhang, and S.S. Ye</i>
<a href="#">T11A002</a>	<b>A discussion on filtration mechanism of moisture separator for nuclear reactor</b>
	<i>Z.Z. Zhang, F. Jiang, J.Y. Wie, and S.S. Ye</i>
<a href="#">T11A003</a>	<b>Image force effect on aerosol penetration through wire screen in the transition regime</b>

	<i>M. Alonso, F.J. Alguacil, N. Jidenko, and J.P. Borra</i>
<a href="#">T11A004</a>	<b>Filtration of fine particles by melt-blown nonwovens</b>
	<i>E. Jankowska and J. Kaluzka</i>
<a href="#">T11A007</a>	<b>Experimental determination of inhomogeneity factors of fibrous filters</b>
	<i>A. Jackiewicz, A. Zareba, A. Podgórski, and A. Balazy</i>
<a href="#">T11A008</a>	<b>Filtration of liquid aerosol particles in multilayer fibrous filters - Theoretical and experimental results</b>
	<i>T. Jankowski</i>
<a href="#">T11A009</a>	<b>Improvement of the most penetrating particles removal in fibrous filters with the use of bipolarly charged electrets or nanofibrous media</b>
	<i>A. Podgórski, A. Balazy, and L. Gradon</i>
<a href="#">T11A010</a>	<b>New experimental findings of nanoparticle filtration in fibrous filters</b>
	<i>A. Podgórski and A. Balazy</i>
<a href="#">T11A011</a>	<b>Filtration characteristics of polyacrylonitrile membrane filters</b>
	<i>S. Yang, H.-L. Huang, and Y.-C. Huang</i>
<a href="#">T11A013</a>	<b>The study on filtration characteristics of miniature electrostatic precipitator using alternating current</b>
	<i>C.W. Kuo, W.Y. Lin, and H.H. Hsu</i>
<a href="#">T11A017</a>	<b>Application of Brownian dynamics approach to evaluate a fibrous filter efficiency</b>
	<i>A. Balazy and A. Podgórski</i>
<a href="#">T11A018</a>	<b>Extension of the single fiber theory to inhomogeneous fibrous filters</b>
	<i>A. Balazy and A. Podgórski</i>
<a href="#">T11A019</a>	<b>Influence of a fibrous filter geometry on the spatial distribution of deposited particles - CFD modelling</b>
	<i>A. Balazy, A. Moskal, and A. Podgórski</i>
<a href="#">T11A020</a>	<b>Trimodal model for multicomponent aerosol dynamics</b>
	<i>S.B. Kim, S.K. Jeong, S.S. Kim, and P. Biswas</i>
<a href="#">T11A022</a>	<b>Most penetrating particle size in multiple fluid collectors</b>
	<i>C.H. Jung, H.S. Park, and K.W. Lee</i>
<a href="#">T11A024</a>	<b>Aerosol filtration with electrospun fiber filters</b>
	<i>H.-S. Park</i>
<a href="#">T11A027</a>	<b>Measurement of the collection efficiency of single dust-loaded fibers</b>
	<i>S. Schollmeier, J. Meyer, and G. Kasper</i>
<a href="#">T11A028</a>	<b>Generation of ultrafine aerosols from saturated oil-mist filters</b>
	<i>B.J. Mullins and G. Kasper</i>
<a href="#">T11A029</a>	<b>Automated fibre diameter and packing density measurements from SEM images of fibrous filters</b>
	<i>R.A. Cropp and B.J. Mullins</i>
<a href="#">T11A030</a>	<b>Fine particle removal by a vehicle air cleaner</b>
	<i>M.-H. Lee, G.S. Kim, S.B. Kim, Y.J. Kim, and B.H. Park</i>

[Top of Program](#)

[Top of Poster Session Part II](#)

<b>Bioaerosols</b>	
<a href="#">T04A001</a>	<b>Personal sampler for monitoring of viable viruses; Part I: Modelling of outdoor sampling conditions</b>
	<i>A.I. Borodulin, B.M. Desyatkov, N.A. Lapteva, A.N. Sergeev, and I. Agronovski</i>

<a href="#">T04A002</a>	<b>Personal sampler for monitoring of viable viruses; Part II: Modelling of indoor sampling conditions</b> <i>V.A. Shlychkov, A.I. Borodulin, B.M. Desyatkov, and I. Agranovski</i>
<a href="#">T04A003</a>	<b>Survey of bioaerosol emissions from Australian poultry buildings</b> <i>V. Agranovski, T. Reponen, and Z.D. Ristovski</i>
<a href="#">T04A005</a>	<b>Portable bio-aerosolspectrometer for quick detection of biological aerosols</b> <i>F. Schneider and H. Grimm</i>
<a href="#">T04A006</a>	<b>Fungal contribution to the ambient organic carbon</b> <i>J.Y.W. Cheng, A.P.S. Lau, and M. Fang</i>
<a href="#">T04A007</a>	<b>Measurement of size distributions and viability of nanobioaerosols</b> <i>A. Maißer, C. Laschober, G. Allmaier, and W.W. Szymanski</i>
<a href="#">T04A011</a>	<b>Correlation between the concentrations of biogenic components of atmospheric aerosol measured simultaneously in spaced points</b> <i>G.A. Buryak, A.S. Safatov, K.P. Koutsenogii, V.I. Makarov, V.V. Marchenko, S.E. Olkin, S.A. Popova, I.K. Peznikova, M.P. Shinkorenko, and B.S. Smolyakov</i>
<a href="#">T04A012</a>	<b>Avian influenza (subtype H5N1) transmission mechanisms</b> <i>A.S. Safatov, I.E. Agranovski, V.N. Mikheev, S.A. Kiselev, O.V. Pyankov, M.O. Skarnovich, V.A. Petrishchenko, G.A. Buryak, L.N. Shishkina, A.N. Sergeev, and I.G. Drozdov</i>
<a href="#">T04A013</a>	<b>Molecular genetics and diversity of fungi and plants in urban air</b> <i>J. Nowoisky, V. Després, J. Cimbal, M. Klose, R. Conrad, M.O. Andreae, and U. Pöschl</i>
<a href="#">T04A014</a>	<b>Laboratory and field characterization of (1-3)-<math>\beta</math>-D-glucan in aerosolized fungal fragments</b> <i>T. Reponen, S.-C. Seo, F. Grimsley, T. Lee, C. Crawford, and S.A. Grinshpun</i>
<a href="#">T04A015</a>	<b>Antimicrobial characteristics of ACF filter containing silver nano particles</b> <i>C.W. Park, K.Y. Yoon, J.H. Byeon, J.H. Park, R.H. Lee, and J. Hwang</i>
<a href="#">T04A016</a>	<b>Bioaerosols in the environment – should we apply reference values?</b> <i>R.L. Górny, G. Mainelis, J. Dutkiewicz, and E. Anczyk</i>
<a href="#">T04A018</a>	<b>Single particle mass spectrometry on bioaerosols</b> <i>W.A. Kleefsman, M.A. Stowers, and J.C.M. Marijnissen</i>
<a href="#">T04A021</a>	<b>Application of the flame spectrophotometry in the biological aerosol detection in the airborne particle, using statistical multi- and megavariate analysis</b> <i>D. Descroix and M.B. Attoui</i>
<a href="#">T04A022</a>	<b>Real time analysis of bacillus species strain specific analysis by MALDI aerosol ToF mass spectrometry</b> <i>A.L. van Wuijckhuijse, C.E.A.M. Degenhardt, F.P.J. de Groot, B.L.M. van Baar, and Ch.E. Keintz</i>
<a href="#">T04A023</a>	<b>Polymer containing respirator offers enhanced protection against airborne viruses</b> <i>St. Bourget, A. Staffa, M.-E.S. Cartier, and P.J. Messier</i>
<a href="#">T04A025</a>	<b>Effect of sampling time on the overall performance of portable microbial impactors</b> <i>G. Mainelis and M. Tabayoyong</i>
<a href="#">T04A026</a>	<b>Bioaerosols in public buildings in Warsaw</b> <i>E. Miaskiewicz-Peska, M. Lebkowska, P. Grzybowski, and E. Karwows</i>
<a href="#">T04A027</a>	<b>Bioaerosol generation in ventilation systems</b> <i>P. Grzybowski</i>
<a href="#">T04A029</a>	<b>Combined UV-fluorescence and background aerosol monitoring for detection of intentional release of airborne biological agents</b> <i>K. Janka, R. Reinivaara, J. Tikkanen, A. Rostedt, M. Putkiranta, J. Laaksonen, M. Marjamäki, J. Keskinen, and T. Humpi</i>
<a href="#">T04A031</a>	<b>Contribution of fungi to primary biogenic aerosols in the atmosphere</b> <i>W. Elbert, P.E. Taylor, M.O. Andreae, and U. Pöschl</i>
<a href="#">T04A032</a>	<b>Occurrence of microorganisms in bioaerosols</b> <i>L. Mateju, B. Kotlík, M. Brabec, and J. Keder</i>

<a href="#">T04A033</a>	<b>Patterning of protein via electrodynamic focusing for biological applications</b>
	<i>H. Lee, H. Shin, and M. Choi</i>

[Top of Program](#)

[Top of Poster Session Part II](#)

## Combustion Aerosols

<a href="#">T14A001</a>	<b>Raman microscopic analysis of changes in structure and reactivity of soot undergoing oxidation and gasification by oxygen</b>
	<i>M. Knauer, M. Carrara, R. Niessner, and N.P. Ivleva</i>

<a href="#">T14A002</a>	<b>Particle concentration and characteristics near a major freeway with heavy-duty diesel traffic</b>
	<i>L. Ntziachristos, N. Zhi, M.D. Geller, and C. Sioutas</i>

<a href="#">T14A004</a>	<b>Quantification of water uptake by combustion (soot) particles</b>
	<i>O.B. Popovicheva, N.M. Persiantseva, and N.K. Shonija</i>

<a href="#">T14A005</a>	<b>Some remarks about the nucleation mode in diesel exhaust</b>
	<i>D. Rothe</i>

<a href="#">T14A007</a>	<b>Mobile sources of atmospheric polycyclic aromatic hydrocarbons</b>
	<i>F. Halek, M. Mirmohammadi, and A. Kavousi</i>

<a href="#">T14A008</a>	<b>Black carbon concentration trends at urban site in Helsinki during ten years</b>
	<i>L. Järvi, H. Junninen, A. Karppinen, A. Virkkula, R. Hillamo, and M. Kulmala</i>

<a href="#">T14A010</a>	<b>Small angle and wide angle X-ray scattering for characterization of carbonaceous materials, aerosols, and particles</b>
	<i>A. Braun</i>

<a href="#">T14A011</a>	<b>Characterisation of soot particles collected at two different sites dominated by wood smoke and vehicle exhaust</b>
	<i>M. Pawlyta, J.-N. Rouzaud, S. Duber, and J. Sandradewi</i>

<a href="#">T14A013</a>	<b>2D particle transport in a full dilution tunnel of diesel vehicle emissions</b>
	<i>L. Isella, B. Giechaskiel, P. Dilara, and Y. Drossinos</i>

<a href="#">T14A014</a>	<b>Field measurements of fine particle and gas emissions from residential wood combustion appliances</b>
	<i>J.M. Tissari, K.H. Hytönen, T. Turrek, J. Lyyräinen, and J. Jokiniemi</i>

<a href="#">T14A015</a>	<b>Fractional efficiency in the submicron range and control of heavy metals emission by means of a hybrid filter</b>
	<i>S. Astarloa, E. Peña, Z. Elorriaga, E. García, J.A. Legarreta, C. Gutiérrez-Cañás, S.-C. Kim, and D.Y. Pui</i>

<a href="#">T14A018</a>	<b>Influence of the sample preparation on the aircraft engine soot primary particles size distribution determined by Scanning Electron Microscopy</b>
	<i>D. Delhaye, D. Ferry, E. Ruiz, B. Demirdjian, J. Suzanne, J. Gouge, and G. Rollin</i>

<a href="#">T14A019</a>	<b>In-situ analysis of diesel nano PM, THC and SOF using multi DMAs-CPCs and FID in transient engine conditions</b>
	<i>B. Han, H. J. Kim, and Y. J. Kim</i>

<a href="#">T14A020</a>	<b>Elemental content of traffic emitted PM<sub>2.5</sub></b>
	<i>S. Janháll, J. Boman, M. Hallquist, and E. Lakelayeh</i>

<a href="#">T14A022</a>	<b>Gas-particle distribution of PAH emission from masonry heater in wood combustion</b>
	<i>K. Hytönen, P. Yli-Pirilä, J. Tissari, and J. Jokiniemi</i>

<a href="#">T14A023</a>	<b>Fine particulate emissions from combustion of woods common in Austria</b>
	<i>C. Schmidl, A. Caseiro, H. Puxbaum, and I.L. Marr</i>

<a href="#">T14A024</a>	<b>Particle emissions from heating units operating on wood and heavy fuel oil</b>
	<i>O. Sippula, J. Hokkinen, P. Yli-Pirilä, H. Puustinen, and J. Jokiniemi</i>

<a href="#">T14A027</a>	<b>Traffic emissions and micrometeorology near a busy road</b> <i>G. Gramotnev, M.J. Burchill, and D.K. Gramotnev</i>
<a href="#">T14A028</a>	<b>Cross-correlations of particle modes at different distances from a busy road</b> <i>G. Gramotnev and D.K. Gramotnev</i>
<a href="#">T14A029</a>	<b>Exhausted particle concentration of charge injected two fluid combustion nozzle for non-conducting liquid</b> <i>J.H. Kim, Y. Choi, M. Park, and S.S. Kim</i>
<a href="#">T14A030</a>	<b>Real-world particle number emission factors from residential wood burning</b> <i>G. Olivares, C., Johansson, J., Ström, and L. Gidhagen</i>
<a href="#">T14A031</a>	<b>Fine particle emissions from solid biofuel combustion studied with single particle mass spectrometry</b> <i>J. Pagels, D.S. Gross, D.D. Dutcher, M.R. Stolzenburg, and P.H. McMurry</i>
<a href="#">T14A033</a>	<b>Particle emissions during pulsating combustion of biomass in a pilot reactor</b> <i>C. Boman, J. Hrdlicka, A. Dahl, S.-I. Möller, and E. Swietlicki</i>
<a href="#">T14A038</a>	<b>High-speed video observations of the alumina nanoparticle formation during combustion of Al microparticles</b> <i>E.V. Karaseva, A.A. Onischuk, V.V. Karasev, and C.J. Tsai</i>

[Top of Program](#)

[Top of Poster Session Part II](#)

<b>Fine Particles</b>	
<a href="#">T15A001</a>	<b>Copper a marker for non-tailpipe emissions from traffic?</b> <i>P. Molnár, T. Bellander, G. Sällsten, and J. Boman</i>
<a href="#">T15A005</a>	<b>Mobile inhalation system for exposure to diluted diesel exhaust</b> <i>J. Guénette, D.J. MacIntyre, K. Curtin, and R. Vincent</i>
<a href="#">T15A006</a>	<b>Synthesis of yellow emitting silicate phosphor particles for white LED</b> <i>H.S. Kang and S.B. Park</i>
<a href="#">T15A007</a>	<b>Synthesis of mesoporous SiO<sub>2</sub> using ultrasonic spray method</b> <i>L.H. Song and S.B. Park</i>
<a href="#">T15A008</a>	<b>Characteristics of aerosol formation from pulverized coal pyrolysis</b> <i>W.H. Chen and J.S. Wu</i>
<a href="#">T15A009</a>	<b>Interaction between meteorological quantities and particle concentrations in the suburban/rural boundary layer during different weather episode</b> <i>S. Weber</i>
<a href="#">T15A013</a>	<b>Measurements of particle number concentrations in Athens, Greece</b> <i>G. Grivas, A. Chaloulakou, and N. Spyrellis</i>
<a href="#">T15A014</a>	<b>Submicron aerosol particles in a small settlement near highway</b> <i>J. Hovorka and Z. Stanková</i>
<a href="#">T15A015</a>	<b>Characteristics of particulate matter deposition from port of Koper</b> <i>B. Poljšak, G. Jereb, B. Marzi, F. Cepak, and G. Dražić</i>
<a href="#">T15A016</a>	<b>Characteristics of the multiplexed grooved nozzles for high flow rate electrospray</b> <i>K. Kim, W. Kim, and S. Kim</i>
<a href="#">T15A017</a>	<b>Highway exhaust aerosols and their effects on alpine lichen populations</b> <i>E. Heinzlmann, P. Madl, and W. Hofmann</i>
<a href="#">T15A018</a>	<b>Electrical and mechanical properties of alumina-MWNT nanocomposite synthesized by spray pyrolysis and spark plasma sintering</b>

**Fundamental Aerosol Physics - Nucleation, Condensation and Evaporation**

<a href="#">T06A001</a>	<b>Thermophoresis of aerosols</b> <i>S.P. Bakanov</i>
<a href="#">T06A002</a>	<b>Surface tension of critical nuclei composed of molecules with orientational tendency</b> <i>I. Napari and A. Laaksonen</i>
<a href="#">T06A003</a>	<b>Influence of optical radiation on the homogeneous nucleation</b> <i>V.G. Chernyak and E.S. Evgrafova</i>
<a href="#">T06A005</a>	<b>Critical behaviour of the particle mass spectra in gelling systems</b> <i>A.A. Lushnikov</i>
<a href="#">T06A007</a>	<b>The rate of vapor condensation on clusters in ion-induced water cluster formation</b> <i>Y. Okada and Y. Hara</i>
<a href="#">T06A008</a>	<b>Fine particle losses in the sampling lines of Puijo tower measurement station</b> <i>H.J. Portin</i>
<a href="#">T06A010</a>	<b>Investigation of the nanoparticles diffusion coefficient temperature dependence</b> <i>V.Y. Rudyak, S.N. Dubtsov, S.L. Krasnolytskii, and A.M. Baklanov</i>
<a href="#">T06A016</a>	<b>The effect of surrounding vapour in homogeneous nucleation: a Monte Carlo study</b> <i>T.R. Bergman, A. Lauri, J. Merikanto, and H. Vehkamäki</i>
<a href="#">T06A017</a>	<b>Derivation of the first heterogeneous nucleation theorem including the line tension</b> <i>A. I. Hienola, H. Vehkamäki, A. Lauri, and M. Kulmala</i>
<a href="#">T06A019</a>	<b>Surface tensions of sodium chloride/succinic acid/water solutions</b> <i>J. Vanhanen, A.-P. Hyvärinen, H. Lihavainen, Y. Viisanen, and M. Kulmala</i>
<a href="#">T06A020</a>	<b>The gas-kinetic theory of gravitophoresis for stratospheric conditions and its experimental verification</b> <i>S.A. Beresnev and D.V. Suetin</i>
<a href="#">T06A022</a>	<b>Influence of size effects on condensation of vapor on small charged aerosol particles</b> <i>V.V. Levdansky, J. Smolik, V. Zdimal, and P. Moravec</i>
<a href="#">T06A024</a>	<b>Impact of aerosol microphysics on its optical properties</b> <i>E. Carstea, S. Stefan, and A. Nemuc</i>
<a href="#">T06A025</a>	<b>Critical analysis of the Fuchs "Boundary Sphere" method</b> <i>V.Y. Smorodin</i>
<a href="#">T06A030</a>	<b>Stochastic degradation-condensation processes in fractal aggregates with multiple bonds</b> <i>M.B. Flegg and D.K. Gramotnev</i>
<a href="#">T06A031</a>	<b>Freezing of evaporating oxalic acid solution droplets</b> <i>E.A. Svensson, S. Badiei, M. Hallquist, and J.B.C Pettersson</i>
<a href="#">T06A033</a>	<b>Evaporation from a planar surface at a maximum rate of entropy production</b> <i>I. Ford</i>
<a href="#">T06A034</a>	<b>Determination of the mean aspect ratio of aerosol particles from optical data</b> <i>M. Kocifaj</i>
<a href="#">T06A035</a>	<b>Exact solution for stochastic evaporation/degradation processes in a chain/ring aggregate with multiple bonds</b> <i>M. Flegg and D. Gramotnev</i>

<a href="#">T13A095</a>	<b>About photophoresis of aerosol particles in the stratosphere</b> <i>L.B. Kochneva and S.A. Beresnev</i>
<a href="#">T13A240</a>	<b>Restore of aerosol microstructure parameters and component composition by the method of Muller's matrix discrete elements</b> <i>A.B. Gavrilovich</i>

[Top of Program](#)

[Top of Poster Session Part II](#)

<b>High Temperatur Aerosols</b>	
<a href="#">T16A002</a>	<b>Behaviors of polycyclic aromatic hydrocarbons during vitrification in a coke bed furnace</b> <i>Y.M. Kuo, C.H. Tsai, and C.T. Wang</i>
<a href="#">T16A004</a>	<b>Identification of byproduct species for destructing sulfur hexafluoride using a high-temperature plasma torch</b> <i>C.-H. Tsai, Z.-Z. Kuo, Y.-C. Lin, and K.-C. Fang</i>

[Top of Program](#)

[Top of Poster Session Part II](#)

<b>Industrial Aerosols</b>	
<a href="#">T17A001</a>	<b>Characterization of aerosol emitted by impact of millimetric droplets onto a liquid film</b> <i>C. Motzkus, E. Gehin, and F. Gensdarmes</i>
<a href="#">T17A003</a>	<b>Effect of wastewater/heavy oil emulsified fuel on the emissions of polycyclic aromatic hydrocarbons from the industrial boiler</b> <i>C.-C. Chen, W.-J. Lee, and O.J. Hao</i>
<a href="#">T17A004</a>	<b>Wood dust particle size sampler: WODUSA</b> <i>F. Belosi, F. Prodi, S. Agostini, M. Casazza, and L. Di Matteo</i>
<a href="#">T17A006</a>	<b>Emission characteristics of polychlorinated dibenzo-p-dioxins and dibenzofurans in the stack flue gases of electric arc furnaces</b> <i>S.I. Shih, W.J. Lee, C.C. Chen, M.H. Liu, G.P. Chang-Chien, and L.C. Wang</i>
<a href="#">T17A007</a>	<b>Characterization of ultrafine aerosol particles from aluminium smelter potrooms by electron microscopy</b> <i>N. Benker, G. Miehe, M. Ebert, Y. Thomassen, and S. Weinbruch</i>
<a href="#">T17A009</a>	<b>Characteristics of oil mist control by corona discharge</b> <i>K.S. Hwang and D.N. Shin</i>
<a href="#">T17A010</a>	<b>Particle Collection Efficiency of a Vortex Scrubber with Opposing Nozzles</b> <i>K. S. Lim, S. H. Lee, H. S. Park</i>
<a href="#">T17A011</a>	<b>Nanoparticles measurement in two workplaces</b> <i>C.J. Tsai, C.S. Chang, C.H. Wu, Y.H. Cheng, S.C. Chen, T.S. Shih, and S.N. Uang</i>
<a href="#">T17A012</a>	<b>The influence of process conditions on the efficiency of non-steady filtration of aerosols</b> <i>T. Jankowski</i>
<a href="#">T17A013</a>	<b>A multi-scale characterization of PM10 at an urban and industrialised coastal site</b> <i>J. Rimetz-Planchon, E. Perdrix, S. Sobanska, and C. Brémard</i>
<a href="#">T17A015</a>	<b>Modeling of in-situ coated particles</b> <i>B.A. Buesser, M.C. Heine, and S.E. Pratsinis</i>
<a href="#">T17A018</a>	<b>Effect of SO<sub>x</sub> gas on NO<sub>x</sub> removal process by aerosol driven NTPT process</b> <i>E. Nishino, K. Grzybowski, H. Takano, and M. Itoh</i>

<a href="#">T17A019</a>	<b>Experimental analysis of aerosol driven NO<sub>x</sub> reduction process assisted with ultraviolet irradiation</b> <i>Y. Emi, H. Takano, and M. Itoh</i>
<a href="#">T17A020</a>	<b>Filter cleaning performance of a cyclone-baghouse dust collector</b> <i>H.-S. Park and K.S. Lim</i>

[Top of Program](#)

[Top of Poster Session Part II](#)

<b>Radioactive Aerosols</b>	
<a href="#">T10A003</a>	<b>The solubility of the aerosol – 137Cs and 60Co carrier – in the Ignalina Nuclear Power Plant region</b> <i>R. Jasiulionis and A. Rozkov</i>
<a href="#">T10A004</a>	<b>Variations of atmospheric 7Be and 210Pb depositions at Malaga, Spain</b> <i>C. Dueñas, M.C. Fernández, S. Cañete, and J. Pérez Barea</i>
<a href="#">T10A007</a>	<b>7Be, 210Pb and 210Po concentrations in aerosols in coastal areas of Southwest of Spain</b> <i>T. Terán, E.G. San Miguel, and J.P. Bolívar</i>
<a href="#">T10A008</a>	<b>On the comparison of 7Be activity, trace metal and aerosol mass size distributions</b> <i>K. Eleftheriadis, A.A. Karanasiou, P.A. Siskos, and C. Psomiadou</i>
<a href="#">T10A009</a>	<b>Influence of AMAD of industrial alpha-emitting aerosols on Pu dialysis kinetics</b> <i>V.V. Khokhryakov and S.V. Sytko</i>
<a href="#">T10A011</a>	<b>Numerical calculation for radioactive particle sampling in a nuclear stack</b> <i>S.B. Kim and S.S. Kim</i>
<a href="#">T13A188</a>	<b>Atmospheric radioactivity in Slovenia</b> <i>N. Leskovar, M. Bizjak, and M. Krizman</i>

[Top of Program](#)

[Top of Poster Session Part II](#)

<b>Remote Sensing of Aerosols</b>	
<a href="#">T13A013</a>	<b>Aerosol physical properties as an important factor in remote sensing of coastal areas</b> <i>T. Zielinski and A. Ponczkowska</i>
<a href="#">T20A003</a>	<b>CALIPSO and MISR aerosol data available for atmospheric research</b> <i>N.A. Ritchey, L.A. Hunt, and M.T. Ferebee</i>
<a href="#">T20A007</a>	<b>Atmospheric aerosol characterization by lidar and sun-photometer measurements</b> <i>A. Boselli, A. Amodeo, C. Cornacchia, G. D'Amico, F. Madonna, L. Mona, and G. Pappalardo</i>
<a href="#">T20A008</a>	<b>Analysis of aerosol extinction coefficient using lidar observation in urban area</b> <i>N. Boyouk, J.-F. Léon, and H. Delbarre</i>
<a href="#">T20A010</a>	<b>MODIS satellite observations and meteorological surface characterization to evaluate PM2.5 concentrations</b> <i>W. Di Nicolantonio, A. Cacciari, E. Bolzacchini, L. Ferrero, B. Ferrini, E. Pisoni, and M. Volta</i>
<a href="#">T20A013</a>	<b>Exact analytical solution of the vector radiative transfer equation for aerosols with arbitrary scattering matrix</b> <i>A.B. Gavrilovich</i>
<a href="#">T20A014</a>	<b>Mixing layer height determination by Lidar and radiosounding data</b> <i>F. Navas-Guzmán, J.L. Guerrero-Rascado, A.B. Fernández-Medina, J.A. Adame and L. Alados-Arboledas</i>

[Top of Program](#)

[Top of Poster Session Part II](#)

## Special Session: COST 633 - Particulate Matter and Health Effects

[T23A003](#) **Analysis of contribution of different sources to PM10 concentrations at three different locations in Slovenia**

*T. Bolte, J. Turšič, A. Šegula, and B. Gomišček*

[T23A005](#) **Generation and quantification of organic peroxides in aerosols to study cellular responses on oxidative stress**

*A.A.-M. Gaschen, A. Praplan, M. Savi, D. Lang, M. Geiser, and M. Kalberer*

[T23A008](#) **Seasonal variability of air pollution and mortality in the urban area of Katowice, Poland**

*M. Kowalska, J.E. Zejda, L. Osródka, K. Kleinowski, and E. Krajny*

[T23A010](#) **PM2.5 site/seasonal variability in Ireland: toxicological effects**

*D. Healy, V. Silviri, E. Pere-Trepat, J. Lopez, A. Whittaker, I. O'Connor, J. Sodeauand, and J. Heffron*

[Top of Program](#)

[Top of Poster Session Part II](#)

# **Abstracts**

## **Plenary lectures**

## Particles from road traffic - emission trends, reduction measures and contribution to ambient particle concentrations

H. Burtscher

Institute for Aerosol and Sensor Technology, University of Applied Sciences, Northwestern Switzerland, Klosterzelgstrasse, CH-5210, Windisch, Switzerland

Keywords: Diesel exhaust, Soot particles, Vehicles emissions

When talking about particulate air pollution, vehicle emissions, in particular those from diesel engines, are an important topic. The contribution of different engine types (spark ignition-, direct injection spark ignition-, diesel engines) is very different. Gasoline engines have considerable emissions during acceleration phases, but not during steady state operation, even at high speed and load. Due to their higher efficiency direct injection gasoline engines (lean engines) have been introduced in the past years. However, the reduction of fuel consumption is accompanied by a significant increase in particle emissions, in particular in low load conditions. Emissions from diesel engines depend on engine speed and load and may be high also under steady state operating conditions. The influence of operating conditions for the different engine types will be discussed.

Great effort has been taken to reduce gaseous and particulate vehicle emissions. This is done on the one hand by an optimization of the combustion process. In the case of diesel engines as main particle emitters means therefore are increased injection pressure, multiple injection, exhaust gas recirculation, improvement of fuel (mainly lower sulfur content) and lubricant oil. These measures allowed to reduce the total particle mass emissions significantly. However, the number concentration of the particles remained fairly constant. The main effect of optimization is a shift of the particle size distribution to smaller sizes.

Besides engine optimization aftertreatment devices as catalysts and particle traps are applied. Traps allow a dramatic reduction of mass and number concentration. If efficient wall flow filters are used (as introduced for passenger cars by PSA some years ago) the number concentration can be reduced by two to three orders of magnitude. Meanwhile 'open filters' are applied by some manufactures. These filters are by far less efficient, usually less than 60%. As the traps collect the particles, they have to be regenerated from time to time by burning the soot, accumulated in the trap. The main role of catalysts is assisting this regeneration process.

Applying aftertreatment devices not only reduces particle mass- or number concentration, but also changes the nature of the particles. The volatile fraction passes a particle trap in the gas phase, whereas the solid material is precipitated. For an effi-

cient trap this means that downstream the trap mainly volatile material remains, which may nucleate and form new particles when cooling down (Burtscher, 2005). Catalytically active devices may oxidize SO<sub>2</sub> and other species, which again increases the probability of nucleation. If nucleation occurs, the number concentration may be dominated by particles in the nucleation mode, which mainly consist of volatile material (sulfur compounds and hydrocarbons). An undesired side effect of catalysts may be the formation of NO<sub>2</sub> from NO which increases the emission of the more toxic NO<sub>2</sub>.

Most results for vehicle emissions are obtained from engine test bench and chassis dynamometer measurements of more or less well tuned and maintained engines. Not so many results from field measurements are available. However, there is strong evidence that few very high emitters (super-polluters) are responsible for a considerable part of the total emissions. The conclusion of a recent study by Kurniawan & Schmidt-Ott (2006) is that about 5% of (old or malfunctioning) cars cause 40% of particle emissions. An efficient measure to reduce total emissions would therefore be detecting and repairing these superpolluters.

Current legislation for emissions and ambient air particle concentrations only limits the total mass. As particles emitted by vehicles are very small, their contribution to PM<sub>10</sub> is small. Even in areas with high pollution, the contribution of vehicle emissions to PM<sub>10</sub> is only about 20%, but 50% to PM<sub>0.1</sub>. A study by Imhof et al. (2007) shows that the daily variation of PM<sub>10</sub> close to a road with heavy traffic is merely related to traffic density, whereas the number concentration shows a strong correlation. On the other hand in particular ultrafine particles from combustion are considered to cause severe health effects. This lead to a very controverse discussion on the relevance of vehicle emissions for the ambient air particle pollution on the one hand and what the appropriate metric is on the other hand. Recent suggestions for new European limits include a limitation of the number concentration of solid particles in addition to the existing mass limits.

Burtscher, H. (2005) *J. Aerosol. Sci.* 36, 896-932.

Imhof, D. (2007) Personal communication

Kurniawan, A., & Schmidt-Ott, A. (2006) *Environ. Sci. Technol.* 40, 1911-1915.

## **Biosphere-aerosol-cloud-climate interactions**

M. Kulmala

Department of Physical Sciences, P.O.Box 64, FI-00014 University of Helsinki, Finland

Keywords: Climate Change, Aerosol formation, Cloud microphysics, Biospheric processes.

Atmospheric aerosol particles and trace gases affect the quality of our life in many different ways. In polluted urban environments, they influence human health and deteriorate visibility. In regional and global scales, aerosol particles and trace gases have a potential to change climate patterns and hydrological cycle. Aerosol particles also influence the radiation intensity distribution that reaches the earth surface having a direct influence on the terrestrial carbon sink. Better understanding of the various effects in the atmosphere requires detailed information on how different sources (including those of biosphere) and transformation processes modify properties of aerosol particles and trace gases. Trace gases and atmospheric aerosols are tightly connected with each other via physical, chemical, meteorological and biological processes occurring in the atmosphere and at the atmosphere-biosphere interface. An important phenomenon as an example is atmospheric aerosol formation, which involves the production of nanometer-size particles by nucleation and their growth to detectable sizes. Human actions, such as emission policy, forest management and land use change and various natural feedback mechanisms involving the biosphere and atmosphere have an impact on the coupling between the aerosols and trace gases.

In 2001 and also in 2007, the Intergovernmental Panel on Climate Change (IPCC) estimated the global and annual radiative forcing due to greenhouse gases and aerosols, along with natural changes associated with solar radiation. Emphasis was placed on the complexity of the combined direct and indirect forcing from both aerosols and gases as well as on the importance of improving our understanding of the role that each of these three individual components plays in radiative forcing in an integrated system. Such knowledge would reduce the uncertainty in current estimates of radiative forcing and enable a better prediction of the effects of anthropogenic activity on global change. The most important issue to resolve is how the different components affecting radiative forcing interact with one another. We have recently proposed a mechanism that couples the effect of CO<sub>2</sub> and aerosol particles on climate. This suggestion is based on connections between photosynthesis, emissions of non-methane biogenic volatile organic compounds (BVOCs), and their ability to form aerosol particles.

Although observed all over the world, the understanding of atmospheric new particle formation is still far from complete. Altogether, most observations made so far support the idea that nucleation and subsequent particle growth are uncoupled under atmospheric conditions. The associations between formation rate and H<sub>2</sub>SO<sub>4</sub> vapour concentration are suggestive of the involvement of H<sub>2</sub>SO<sub>4</sub> in atmospheric nucleation. We have seen that ion-induced nucleation is taking place all the time, but its contribution is usually limited at least in the continental boundary layer. Observed growth rates of nucleated particles cannot usually be explained by the condensation of sulfuric and associated inorganic compounds (water and ammonia) alone. Organic compounds having a very low saturation vapor pressure would appear to be the most likely candidates for assisting the growth of nucleated particles, yet identity of these compounds remains to be revealed. Depending on the location, atmospheric aerosol formation is capable of increasing the concentrations of cloud condensation nuclei (CCN) by a factor more than two over the course of one day. Also we have seen that the contribution of BVOCs is significant in CCN production.

In future, the relative contribution of biogenic and anthropogenic emissions to atmospheric aerosol load should be investigated. While biogenic aerosol formation mechanisms are known for the most part because of the research carried out during the recent years, there is an urge for applying them in the global scale in the future. This calls for understanding and ability to observe how the biogenic formation mechanisms are linked to underlying ecosystem processes. At the same time it is important to make an integrated attempt to understand various, but inter-linked, biosphere-atmosphere interactions by using inter- and multi-disciplinary approaches in a coherent manner.

This work was done within the framework of Nordic Centre of Excellence BACCI (Research Unit on Biosphere – Aerosol – Cloud – Climate Interactions). The main objective of BACCI was to study the importance of aerosol particles on climate change.

## **FROM NANOPARTICLES TO LARGE EXPIRATORY DROPLETS IN INDOOR AIR**

Idia Morawska

School of Physical and Chemical Sciences, International Laboratory for Air Quality and Health, Queensland University of Technology, 2 George Street  
Brisbane, 4001 Australia

Keywords: nanoparticles, indoor aerosols

It is not a discovery that indoor aerosol, a mixture of outdoor aerosol, aerosol particles emitted by indoor sources and those formed indoors through physical and chemical reactions, presents significant scientific challenge, and in turn, challenges to control it at level acceptable in relation to health and well being of the building occupants. An additional complexity is that in order to avoid disruption to the indoor activities and inconvenience to the occupants, we are usually limited in the amount of time allowed for investigations, as well as in the type of instrumentation we can use indoors. Therefore there is still a lot to learn and discover about the dynamics of indoor aerosol and the processes driving it. For example how likely and how frequent are the events of nanoparticles formation indoors from the reactions involving for example terpenes from cleaning agents and ozone. It has been shown through controlled laboratory

experiments that such processes are likely to occur in residential or office environment. Do we detect particles from these or other nucleation processes in real indoor environments. On another end of the spectrum of particle sizes, what happens to the droplets introduced into the air by expiratory activities, including breathing, speaking, or coughing. The importance of these droplets is that they can carry infectious microorganisms, bacteria and viruses. Are they large and deposit on indoor surfaces within an arms length of emissions, as believed by respiratory physicians, or are they much smaller and can travel large distances within the building. The last few years witnessed a lot of progress in understanding of indoor aerosol and the dynamics of processes occurring in indoor air. The presentation will review the new findings and the current research directions in this field of indoor aerosol.

## Materials Synthesis: Contributions and Challenges to Aerosol Science

Sotiris E. Pratsinis

Particle Technology Laboratory, Institute of Process Engineering,  
Department of Mechanical and Process Engineering, ETH Zurich, 8092 Zurich, Switzerland

Keywords: agglomerates, coagulation, fractals, particle concentration.

Aerosol routes are very attractive for materials manufacture as they offer unique advantages over classic wet chemistry: fewer process steps resulting in high purity products (e.g. optical fibers), easier particle collection from gas rather than from liquid streams and no liquid by-products that require costly effluent cleaning (Pratsinis and Mastrangelo, 1989). Today a number of particulate and film commodities are made with flame (carbon blacks, fumed silica and titania) and hot-wall (zinc oxide, filamentary nickel and tungsten carbide) aerosol processes to name few.

Most of these products were developed with little, if any, formal aerosol science. As a result, early practitioners developed ingenious ways to characterize, control and handle industrial aerosol products. Some of the first attempts to characterize agglomerates were made by carbon black engineers in their effort to connect reinforcing performance to carbon black characteristics and eventually to their reactor operation. Medalia and Heckman (1969) found that the number of primary particles in agglomerates was related to agglomerate size by a power law, the so-called fractal dimension, that was introduced years later by Mandelbrot (1982). In fact, carbon blacks were frequently cited as applications of fractals by Mandelbrot and others. Ulrich (1971) at Cabot predicted that fumed silica attains a self-preserving size distribution and calculated it first in the free-molecular regime, a year ahead of Sai et al. (1972) who have been largely credited for it. Also, the self-preserving theory explained measured size distributions of flame-made titania at Tioxide in 1973 where thermophoretic sampling was used to explore the contribution of surface growth on TiO<sub>2</sub> formation, a technique systematically introduced by Dobbins and his colleagues in 1987, to effectively open up the black box of combustion aerosol synthesis of materials. Today aerosol science is used routinely in characterization and processing of aerosol-made materials in chemical, microelectronic and pharmaceutical industries.

The quest of synthesis of functional materials brings new challenges as their performance relies on particle composition and morphology. As with bulk commodities today, there is also keen interest to make nanorods and nanotubes in the gas-phase to facilitate and scale-up their manufacturing so the potential of nanoscale is realized economically. Characterizing such particles create new challenges to aerosol science. Making multicomponent particles

with spatially controlled component distribution is essential for developing the required functionalities of such materials. For example, particles with uniform Pt/Ba/alumina composition perform worst catalytic NO<sub>x</sub> storage-reduction than particles with segregated components (Strobel et al., 2006).

Aggregates or agglomerates of nanostructured particles occupy far more volume than their equivalent solid mass (Matsoukas and Friedlander, 1991). Though these particles may grow initially by surface growth and/or Brownian coagulation, very quickly grow to a state that is no longer covered by the Smoluchowski theory. This indicates that a transition from dilute to concentrated aerosol dynamics takes place (Heine and Pratsinis, 2006). As a result, there is less free gas volume per agglomerate, so the steady-state concentration profile away from the receiving particle surface during coagulation does not form showing the need for extending coagulation theory to high aerosol concentrations. At these conditions such particles are likely to restructure and eventually break-up.

Distinguishing between aggregates and agglomerates brings another challenge to aerosols. Even though conditions leading to synthesis of either state are known in case of coagulation and sintering (Tsantilis and Pratsinis, 2004), there is a need for their undisputable characterization. Aggregates are needed for catalysts and gas sensors to facilitate easy access to their surface while agglomerates are needed for nanocomposites to facilitate mix in polymer matrices for dental, optic, biomaterial and other applications.

- M. Heine & Pratsinis, S. E. (2006) *Langmuir*, **22**, 10238-10245.  
F.S. Sai, S.K. Friedlander, J. Pich, G.M. Hidy (1972) *J. Colloid Interface Sci.*, **39**, 395-405.  
B.B. Mandelbrot, *The Fractal Geometry of Nature*, Freeman, San Francisco, 1982.  
T. Matsoukas, S.K. Friedlander (1991) *J. Colloid Interface Sci.*, **146**, 495-506.  
AI Medalia, FA Heckman (1969) *Carbon*, **7**, 567-582  
S.E. Pratsinis, and S.V.R. Mastrangelo (1989) *Chem. Eng. Prog.*, **85**(5), 62-66.  
R. Strobel, M. Piacentini, M. Madler, M. Maciejewski, A. Baiker, S.E. Pratsinis (2006) *Chem. Mater.*, **18**, 2532-2537.  
S. Tsantilis, S.E. Pratsinis (2004) *Langmuir*, **20**, 5933-5939.  
G.D. Ulrich (1971) *Combust. Sci. Technol.*, **4**, 47-57.

# Therapeutic Aerosols: Today and Tomorrow

Gerhard Scheuch

Activaero, Wohraer Strasse 37, 35285, Gemuenden/Wohra, Germany

Keywords: Asthma treatment, Pulmonary Drug delivery, COPD, Insulin inhalation.

## Introduction

Many investigations have demonstrated that 4 out of 10 leading causes of mortality are due to lung diseases: low respiratory tract infections, chronic obstructive pulmonary disease, bronchial cancer and tuberculosis (Murray & Lopez 1997). In addition allergic asthma is one of the major increasing diseases in the developed and industrial countries. In some countries the incidence of getting asthma in children is already higher than 20%. In this context aerosol therapy becomes more and more important.

The efficacy of an inhaled medication is dependent on three major factors:

- the efficacy of the drug
- the aerosol parameters (device and particles)
- the compliance and breathing pattern of the patient

Only if all three factors are considered, the treatment will be successful.

## Devices

The modern inhalation therapy has started with the development of the first metered dose inhaler (MDI) in 1956. Different kind of jet nebulisers were used before. All these systems were developed to treat the different kind of lung diseases, mainly bronchial asthma.

About 25 years ago, it was recognized, that the use of CFC destroyed the ozone layer of our atmosphere. Therefore, the industry was asked to find alternatives for the CFCs which were used regularly in MDIs. This was the start signal of a new generation of therapeutic aerosol systems: the dry powder systems (DPI) were developed and improved. On the other hand alternative gases were developed which could be used in MDIs. Today almost all MDIs contain HFA. Asthma and COPD therapy uses DPI and MDIs in parallel.

The next generation of devices is already under development: intelligent aerosol delivery systems. These systems will not only deliver a more or less inhalable aerosol, but will additionally measure compliance (if and how often the patient takes the medication). These systems are able to manage the disease.

## Indications

The progress of therapeutic aerosols did not only happen on the device side, but also on the use of aerosols for different application (diseases). Today about 99% of the aerosol therapy is used to treat lung

diseases, mainly Bronchial Asthma and COPD. Bronchodilatation and anti inflammatory treatment is used, regularly. In future there will be other drugs used in aerosol form. Many drugs which are developed by the biotech companies cannot penetrate through the intestinal epithelium and must be injected. This is inconvenient for the patient. In future a variety of molecules will be delivered via the lungs into the blood circulation. Insulin for the treatment of diabetes is the first example. It was approved by the American and European regulatory agencies early 2006 for inhalation application. Discovered in 1922 Insulin was already tested as an aerosol in 1924 in men. But it took another 80 years to develop a formulation and a device, that was able to allow a reliable dosing and was comparable to the injectable form.

A variety of other drugs are recently investigated to be used in aerosol form. In table 1 a number of drug classes are listed, which are under investigation for aerosol use (Scheuch et al. 2006).

Table 1: Different substances investigated as aerosol treatment in different indications

Substance	Indication
Ergotamine	Migraine
Heparin	Deep venous thrombosis
Hormones	
Calcitonin	Osteoporosis
GM-CSF	Tumor
Growth hormone	Growth hormone deficiency
Insulin	Diabetes
Testosterone	Hormone replacement
Interferons	Hepatitis, MS
Interleukin-2	Tumour therapy
Opioids	Pain
Peptides/Proteins	
Factor I	Haemophilia B
Hirudine	Anticoagulant
Protein C	Thrombophilia
Prostaglandins	Pulmonary Hypertension
Tranquilizer	Sedation
Vaccines	Vaccination

Heubner, W., de Jongh, S.E., Jaeger, E. (1924).

*Dtsch. Med. Wochenschr.*, 51, 2342 – 2343.

Murray, C.J. & Lopez, A.D. (1997). *Lancet*, 349, 1498-1504.

Scheuch, G., Kohlhaeufel, M.J., Brand, P., Siekmeier, R. (2006). *Adv. Drug Deliv. Rev.*, 58, 996-1008.

## **T01 Abstracts**

## Imaging the chemical composition of the surface of atmospheric particles

A. Krein<sup>1</sup>, J. - N. Audinot<sup>2</sup>, H. - N. Migeon<sup>2</sup> and L. Hoffmann<sup>1</sup>

<sup>1</sup>Department of Environment and Agro-Biotechnologies, Public Research Centre Gabriel Lippmann, 41, rue du Brill, L-4422, Belvaux, Luxembourg

<sup>2</sup>Department Science and Analysis of Materials, Public Research Centre Gabriel Lippmann, 41, rue du Brill, L-4422 Belvaux, Luxembourg

Keywords: Instrumentation / chemical characterization, nanoparticles / characterization.

To what extent particles can penetrate the various areas of the lungs and be deposited there depends on the physical characteristics, on breathing patterns and the anatomy of the lung, which is subject to change as the result of growth or illness. Because of the contact between fine particles and lung tissue more information about the surface structure of the fines is required.

During February and March 2006 particles with an aerodynamic diameter smaller than 20 microns were gathered with a low volume sampler on Teflon air monitoring filters in the industrialized region of Esch sur Alzette in the Grand Duchy of Luxembourg (Krein *et al.*, 2007). The NanoSIMS50 ion probe (SIMS: secondary ion mass spectrometry) is used to image the elemental composition at the surface of sub-micrometer particles (Stern *et al.*, 2005).

The advantage of the technology is the ability to make direct observation of the distribution of any element (and all isotopes) occurring at the surface of a sample, without any specific labeling with a fluorescent or radioactive probe. SIMS analyze is based on the sputtering of secondary particles under the impact of high-energy primary ions. Upon the impact of these primary ions, atoms and polyatomic fragments are ejected from the most superficial atomic layers of the specimen (1 to 2 nm). In the ejection process, some of the atoms and clusters can be spontaneously ionized. In a SIMS instrument, these secondary ions are accelerated, separated in function of their mass/charge ratio and detected, which is giving the chemical information of the origin impact place at the particle. The characteristics of these ion microscopes are a high lateral resolution (smaller than 50 nm with cesium primary ions and smaller than 150 nm with oxygen primary ions), a capability to measure up to 5 masses in parallel, coming from the same micro volume ensuring perfect isotopic ratio from the same small volume or perfect image superimposition, and a good transmission, e.g. high sensitivity, even at high mass resolution. The keywords of this technique are the sensibility (ppm-ppb) and the mass resolution (discrimination between isobars masses, e.g. <sup>32</sup>S and <sup>16</sup>O<sub>2</sub>).

Figure 1 shows an airborne particle, which consists of different materials. An unstructured matrix containing sulphur and copper forms the main

body of the particle. By the top of the particle one recognizes needle-shaped crystalline structures with a small crystal at the end. The sulphur is adhered to the particle in the shape of a circle. Copper shows some concentration hot spots following the circular sulphur configuration.

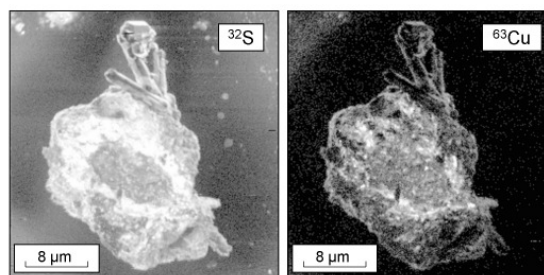


Figure 1. Sulphur and copper on the surface of a particle, respective concentrations of the different elements increase from black to white colouring.

Our results show that the atmospheric fine dust consists of a mixture of organic and inorganic compounds even on the nanometer scale. Particularly at the particles adhering heavy metals represent a potential threat for the human organism. According to our further work, the measurements of the isotopic ratio of chlorine, sulfur, and other elements, would allow to determine the origin of the particles collected on our filters. It is planned to fingerprint sources like vehicle engines, industrial combustion or local heating systems with the help of the NanoSIMS50.

The authors thank the National Research Fund of the Grand Duchy of Luxembourg for the funding of this study. The results were performed in the project with the title „Analyse d'échantillons environnementaux à l'échelle du nanometre”.

Krein, A., Audinot, J.-N., Migeon, H.-N. & Hoffmann, L. (2007). *Environmental Science and Pollution Research*, Online First (DOI: <http://dx.doi.org/10.1065/espr2006.10.356>).

Stern, R. A., Fletcher, I. R., Rasmussen, B., McNaughton, N.J. & Griffin, B.J. (2005). *Int J Mass Spectrom Ion Processes*, 224, 125-134.

## The effect of Saharan dust outbreaks on particulate sulfate and nitrate levels in southeast Spain

J. Nicolás, N. Galindo, E. Yubero, S. Caballero, C. Pastor and J. Crespo

División de Física Aplicada, Universidad Miguel Hernández, Avda. de la Universidad s/n, 03202, Elche, Spain

Keywords: PM2.5, PM10, mineral dust, particulate nitrate, sulfate.

Between October 2003 and September 2004 more than 300 twenty-four hour samples of PM10 and PM2.5 were analyzed for sulfate and nitrate content at an urban background station in Elche, 12 km from the southeast Spanish Mediterranean coast. To evaluate the influence that mineral dust has upon nitrate and sulfate levels we selected the months between March and September 2004, as the major portion of the Saharan dust episodes took place within this period.

Table 1 shows the average concentrations for both anions in PM10 and PM2.5 corresponding to normal days (ND) and intrusion days (ID). Normal days were those in which no event that has a special influence upon the particle levels or their chemical composition was detected (*e.g.* precipitation or high pollution episodes). The relative increase in nitrate and sulfate levels with respect to normal days is also indicated.

Table 1. Comparison of sulfate and nitrate levels on normal and intrusion days and the relative increase with respect to normal days.

	SO <sub>4</sub> <sup>2-</sup> (µg/m <sup>3</sup> )		NO <sub>3</sub> <sup>-</sup> (µg/m <sup>3</sup> )	
	PM10	PM2.5	PM10	PM2.5
ND	4.6	3.5	4.3	1.5
ID	7.4	5.7	6.1	1.7
Incr. (%)	61	63	42	13

The increase in nitrate concentrations in Saharan dust episodes is less than that recorded for sulfate, especially in PM2.5. The results indicate that mineral dust notably contributes to the formation of fine SO<sub>4</sub><sup>2-</sup> (< 2.5 µm), while for NO<sub>3</sub><sup>-</sup> the formation of coarse particles (2.5-10 µm) is more favored. The oxidation of sulfur dioxide and the neutralization of the formed sulfuric acid may occur on the surface of dust particles. These processes are more favored in smaller-size particles due to their greater surface area, which justifies the observed increase of the sulfate levels in PM2.5 (Zhang *et al.*, 2000). In the case of nitric acid, recent studies suggest that the neutralization on mineral dust takes place in the bulk phase, leading to the formation of coarse nitrate and increasing its PM10 concentration (Hodzic *et al.*, 2006).

These results have been confirmed by means of principal component analysis (PCA) with varimax

rotation (Table 2). This analysis was conducted on both intrusion days and normal days in order to identify the sources related with the formation of nitrate and sulfate in the fine (PM2.5) and coarse (PM2.5-10) fractions.

Table 2. Rotated principal component matrix (factor loadings smaller than +0.5 are not given).

	Normal Days		Intrusion Days	
	PC1	PC2	PC1*	PC2*
PM2.5-10		0.77		
PM2.5	0.87			0.83
Fine NO <sub>3</sub> <sup>-</sup>	0.90			0.92
Coarse NO <sub>3</sub> <sup>-</sup>		0.78	0.86	
Fine SO <sub>4</sub> <sup>2-</sup>	0.66		0.58	
Coarse SO <sub>4</sub> <sup>2-</sup>		0.77	0.73	

Two components with eigenvalues superior to 1 for both types of days were obtained. The first component (PC1) for normal days corresponds to the formation of fine ammonium nitrate and sulfate with an anthropogenic origin. The second one refers to the formation of coarse nitrate and sulfate by heterogeneous reactions of nitric and sulfuric acids, respectively, with soil particles or sea-salt particles of local origin. On intrusion days the first component (PC1\*) can be associated, just the same as the second on normal days (PC2), with the formation processes of coarse calcium and/or sodium sulfates and nitrates, but the production of both anions by reactions on mineral dust from the intrusion is also perceivable. It can be observed how, different from a normal day, the PC1\* component includes fine sulfate but not fine nitrate. The second component (PC2\*) shows the anthropogenic origin of the particulate matter during the Saharan dust outbreaks, which is very much influenced by the fine nitrate.

We thank the Elche City hall for allowing access to their facilities for the placement of the particle samplers and P. Nordstrom for his assistance in this work.

- Zhang, D., Shi, G.Y., Iwasaka, Y., Hu, M. (2000). *Atmospheric Environment*, 34, 2669-2679  
 Hodzic, A., Bessagnet, B., Vautard, R. (2006). *Atmospheric Environment*, 40, 4158-4171.

## Size-segregated analysis of PM<sub>10</sub> at a tandem urban – rural site combination

J. Gietl, T. Tritscher and O. Klemm

Institute of Landscape Ecology, University of Münster, Robert-Koch-Str. 26, 48149 Münster, Germany

Keywords: aerosol chemistry, cascade impactor, size-segregated aerosols

In January 2006, airborne particulate matter was collected simultaneously using two five stage Berner type impactors at two sites in Münster, NW Germany. Altogether 70 x 5 samples from those cascade impactors were analyzed. One site was located in the centre of Münster, next to a main road. The second one was situated 6 km to the North, in a bird nature protection area. Simultaneous samples were taken twice a day, with sample integration times between 4 and 6 hours. The goal was to identify the sources of particulate material (urban versus regional background) with the help of size- and time-resolved chemical characterization of the particle components. The main ions Ca<sup>2+</sup>, Cl<sup>-</sup>, Mg<sup>2+</sup>, Na<sup>+</sup>, NH<sub>4</sub><sup>+</sup>, NO<sub>3</sub><sup>-</sup> and SO<sub>4</sub><sup>2-</sup> were analyzed with an ion chromatograph, an atom-absorbing spectrometer, and a flow injection analyser. Carbon (OC, EC) was detected with an OCEC Lab Analyser.

The mean mass concentration of particulate matter over all stages (PM<sub>10</sub>) was considerably higher at the roadside (31 µg m<sup>-3</sup>) than in the rural area (24 µg m<sup>-3</sup>). The difference in average mass concentrations consisted exclusively in the carbon concentrations, see figure 1. The carbon amount in the city (mean 13 µg m<sup>-3</sup>) was on average 1.5 times higher than in the surrounding (mean 8.3 µg m<sup>-3</sup>).

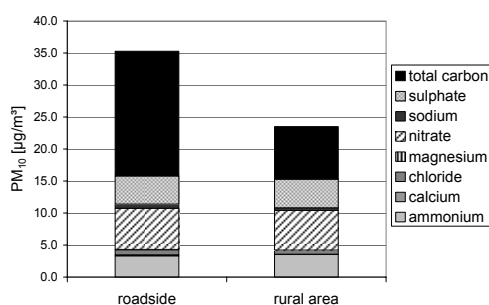


Figure 1: Average concentration over all stages, PM<sub>10</sub>, at two sites in Münster, Germany

It is particularly the elemental carbon concentration that is enhanced at the roadside, due to traffic and other combustion processes. In contrast to carbon, the average mass concentrations of the ions on the five stages do not show any clear differences between the sites. Only sodium, chloride, and calcium in coarse particles are enhanced at the urban site. The additional salt (NaCl), as measured at the roadside, is most likely

due to the use of de-icing salt, additional calcium due to dust dispersion from road traffic. Ca<sup>2+</sup>, a crustal element often found in particulate matter from roads (Finlayson-Pitts & Pitts, 2000), can be used as an indicator for traffic.

The highest mass concentration was determined for particulate matter in the accumulation range, with an equivalent aerodynamic diameter (EAD) of 0.6-0.7 µm. At the roadside, carbon dominates the total concentrations in every aerosol size class. At the rural site, carbon dominates only in the finer PM fraction.

EC was predominantly found in the small fraction, with a maximum at around 0.1 µm EAD. The secondary particulate compounds NH<sub>4</sub><sup>+</sup>, NO<sub>3</sub><sup>-</sup> and SO<sub>4</sub><sup>2-</sup> were mainly found at EAD of 0.6-0.7 µm. Na<sup>+</sup>, Cl<sup>-</sup>, and Mg<sup>2+</sup>, and also crustal elements such as Ca<sup>2+</sup>, were typically found in coarse particles. The amount of salt varied during the winter time, but still the ions (Na<sup>+</sup>, Cl<sup>-</sup>, and Mg<sup>2+</sup>) are highly correlated. All of these elements show a unimodal distribution.

Differences between the two sites were more significant at daytime than during the nights. During the day at the roadside, the mean mass concentration of each size range was predominantly higher than during nights. On the other hand, in the rural area, the concentrations are slightly higher during night, primarily caused by enhanced NH<sub>4</sub><sup>+</sup> and NO<sub>3</sub><sup>-</sup> concentrations. This phenomenon is also found at the roadside and described in Stelson & Seinfeld (1982). The effect of the decreasing carbon and Ca<sup>2+</sup> in all five size ranges in the centre of Münster at night is higher than the nightly increase of the secondary particle compounds at the rural site.

The difference in mass concentrations consisted in carbon. Other matters, produced by traffic, as NH<sub>3</sub> and NO<sub>x</sub>, do not seem to have enough time to clearly influence the particle formation and growing.

This work was supported by the municipality of Münster.

- Finlayson-Pitts, B. J. & Pitts, J. N (2000). *Chemistry of the upper and lower atmosphere*. San Diego, USA: Academic Press.
- Stelson, A. W. & Seinfeld, J. H. (1982). *Atmospheric Environment*, 16, 2507-2514.

## Secondary organic aerosol formation from plant emissions: overview of the Jülich Plant chamber experiments

A. Kiendler-Scharr<sup>1</sup>, T. Hohaus<sup>1</sup>, E. Kleist<sup>1</sup>, M. Miebach<sup>1</sup>, R. Tillmann<sup>1</sup>, R. Uerlings<sup>1</sup>, R. Fisseha<sup>1</sup>, P. Griffiths<sup>2</sup>, Y. Rudich<sup>3</sup>, E. Dinar<sup>3</sup>, J. Wildt<sup>1</sup>, and T. Mentel<sup>1</sup>

<sup>1</sup>Institut für Chemie und Dynamic der Geosphäre, Forschungszentrum Jülich, D-52425 Jülich, Germany

<sup>2</sup>Cambridge University, Center of Atmospheric Science, Cambridge, UK

<sup>3</sup>Weizmann Institute of Science, Department of Environmental Science, 76100 Rehovot, Israel

Keywords: Aerosol Yield, CPC, DMA, Nucleation Rate, SOA

A considerable fraction of the organic aerosol component is of secondary origin, meaning it is formed through oxidation of volatile organic compounds (VOCs). Plant emissions, e.g. monoterpenes and sesquiterpenes, are a major source of VOCs in the troposphere (Guenther et al., 1995). VOC emissions commonly depend on light and temperature (Guenther et al., 1995). So far most laboratory investigations on the potential to form secondary organic aerosols (SOA) from plant emissions focused on single VOCs such as  $\alpha$ -pinene which is probably the most investigated monoterpene (e.g. Saathoff et al., 2003). In this study we investigated the formation of SOA from the mixture of VOCs emitted by spruce, pine and birch trees by oxidation with ozone and OH.

The experiments were performed in the Jülich plant chamber in order to provide well defined conditions for plants. A fraction of the air carrying plant emissions was transferred from the plant chamber to a reaction chamber. The chamber was operated as a continuously stirred tank reactor. SOA formation from the VOCs introduced into the reaction chamber was initiated by UV-photolysis of ozone. VOC measurements were conducted simultaneously with a Proton-Transfer-Reaction Mass Spectrometer (PTR-MS, IONICON, Lindiger et al. 1998) to determine the emission kinetics, and an online-GC-MS system for compound identification. VOC mixing ratios were in the lower ppbv to pptv range. Identification by GC-MS was based on mass spectra and retention times of pure chemicals (Fluka / Aldrich, purity > 93 %). The total number of particles formed was measured with a TSI Model 3025A Ultrafine CPC. The size distribution of the aerosols in the chamber was measured by a TSI SMPS 3936. The resulting SOA was analysed with an Aerodyne aerosol mass spectrometer (Q-AMS).

We derived nucleation rates of  $0.04$  to  $260 \text{ cm}^{-3} \text{ s}^{-1}$  from the uCPC data during these experiments which is high compared to ambient observations which range from  $0.01 - 10 \text{ cm}^{-3} \text{ s}^{-1}$  (Kulmala, Vehkamäki et al. 2004). Growth rates of  $3$  to  $29 \text{ nm h}^{-1}$  were calculated from the SMPS size distributions. This compares reasonably well with growth rates observed in mid latitudes with a range of  $1-20 \text{ nm h}^{-1}$  (Kulmala, Vehkamäki et al. 2004).

The maximum SOA volume produced during VOC oxidation was used as the quantity determining the SOA formation potential. We compared these results to those obtained using  $\alpha$ -pinene as single VOC. Spruce, pine and birch were used as model plants representing the boreal forest. Changing temperature in the plant chamber led to changes of VOC emissions and furthermore, to changes of the maximum SOA volumes in the reaction chamber. Plots of maximum SOA volumes versus the total amount of carbon fed into the reaction chamber led to approximately linear relationships. The intercepts of these plots were seen as threshold for SOA formation. It was observed that this threshold was lower for the mixture of VOCs emitted from spruce, pine, and birch than for  $\alpha$ -pinene as single compound. We therefore conclude that the threshold for SOA formation from real plant mixtures may be much lower than the threshold obtained from laboratory experiments that were focussed on single VOCs.

Guenther, A., et al., 1995, A global model of natural volatile organic emissions, *J. Geophys. Res.*, 100, 8873-8892

Jayne, J.T., Leard, D.C., Zhang, X., Davidovits, P., Smith, K.A., Kolb, C.E., and Worsnop, D.R. (2000). Development of an Aerosol Mass Spectrometer for Size and Composition Analysis of Submicron Particles, *Aerosol Science and Technology*, 33, 49-70.

Kulmala, M., Vehkamäki, H., et al. (2004). Formation and growth rates of ultrafine atmospheric particles: a review of observations, *Journal of Aerosol Science*, 35(2), 143-176

Lindinger, W., Hansel, A., Jordan, A., (1998). On-line monitoring of volatile organic compounds at ppt levels by means of proton-transfer-reaction mass spectrometry (PTR-MS) medical applications, food control and environmental research, *Int. J. Mass Spec. and Ion Processes*, 173, 191-241.

Saathoff, H., et al., (2003) Coating of soot and  $(\text{NH}_4)_2\text{SO}_4$  particles by ozonolysis products of  $\alpha$ -pinene, *Aerosol Science and Technology*, 1297-1321

## Water soluble organic compounds of aerosols as metal complexing ligands

G. Szentes, E. Schmidt and A. Marton

Atmospheric Research Group of the Hungarian Academy of Sciences, University of Pannonia, Veszprem, H-8201, Veszprem, Hungary

Keywords: organic matter, metal complexation, metal binding capacity.

Volatile organic components (VOC) of the atmosphere are mostly non-polar compounds of natural and/or human origin. On the effect of the reactive species of the atmosphere (mostly hydroxyl radicals) the components of the VOC undergo various oxidation reactions known only partially today and becoming more and more polar compounds until they are finally converted to water and carbon dioxide. Beside the oxidation processes, however, even less well understood polymerization reactions may also take place leading to the formation of a large number of secondary organic compounds of which many are polar, water soluble (WSOC). The WSOC usually amounts to 20 – 70% of the fine (0,1-1  $\mu\text{m}$ ) fraction of the tropospheric aerosol collected by the usual sampling impactors. A further treatment of the WSOC fractions with solid phase extraction proved that 20 – 50% of these compounds are humic-like substances (Krivacsi *et al.*) often referred to as HULIS in the literature (Havers *et al.*).

Atmospheric aerosol has both direct and indirect effects on the climate. A direct effect is shown up in the absorption and scattering of the solar radiation. The indirect effect is represented by the fact that these particles are acting as condensation nuclei for the cloud formation. The latter process is modelled by the Kohler equation (or its more sophisticated versions) where surface tension plays an important role. The air - water interfacial tension, however, is markedly controlled by the WSOC content of the aerosol. The efficient surface activity lowering effect of the WSOC was proved in our earlier work (Szentes *et al.*, 2005).

In connection with the chemical characterization of the aerosols our current work is concerned with the determination of the stability constant as well as the copper(II) ion binding capacity of the WSOC components. According to our best knowledge no similar studies were reported earlier in the aerosol literature. Electroanalytical studies were performed by using the competing ligand exchange technique of the adsorption stripping voltammetry (CLE – AdSV). Competing ligand exchange is used here to avoid the problem caused by the poorly characterized complex forming ligands of the WSOC. As a competing ligand salicylaldehyde was used. Our results indicated that the WSOC components of the fine aerosol (typically the HULIS)

forms stable complexes with Cu(II)-ions. Stability constants of the various aerosol samples ( $\log K = 16.0 - 16.5$ ) were calculated from the data of the CLE – AdSV experiments by using the *van den Berg – Ruzic* equation (Ruzic, 1982). The applied method of calculation yields also an estimate for the metal ion binding capacity of the WSOC. The obtained capacity values were in between 6.6 – 39 nM Cu(II) / mgC for the aerosols collected in various seasons.

Comparing the above data to the stability constants of the Cu(II) with well defined monodentate, bidentate, chelating and naturally occurring ligands it is concluded that the WSOC forms almost as stable complex as the chelating ligands. Metal ion binding capacity values were compared with the complexing capacities of the various types of natural waters published in the literature. In order of magnitude, the metal ion binding capacities of the aerosols are comparable to that of the natural waters although exact comparison would require the actual TOC values of the waters. The developed technique is being used for the study of complexation of the WSOC with further metal ions of atmospheric importance (like iron, nickel, zinc *etc.*).

Our understanding of the atmospheric significance of the metal ion complexation is still in infancy. Nonetheless, the following aspects may be worth mentioning: in the global cycle of elements the copper ion is transported through the atmosphere in the form of a rather stable complex, its toxicity is highly reduced as compared to that of the non complexed copper species, complexation reduces the catalytic effect of the metal played in the oxidation processes maintained by the hydroxyl or other atmospheric radicals.

This work was supported by the National Scientific Research Council under grant T 048556.

Havers, N., Burba, P., Lambert, J. & Klockow, D. (1998), *J. Atmos. Chem.*, 29, 45 – 54.

Krivacsi, Z., Hoffer, A., Sarvari, Z., Temesi, D., Baltensprenger, U., Nyeki, S., Weingartner, E., Kleefeld, S. & Jennings, S. G. (2001), *Atmos. Environ.* 35, 6231 – 6235.

Ruzic, I. (1982), *Anal. Chim. Acta*, 140, 99 – 113.

Szentes, G., Schmidt, E., Kiss, Gy. & Marton, A. (2005). in *Faraday Discuss.*, 130, *Atmospheric Chemistry* (RSC, London), p. 529.

## Crucial intermediates of benzaldehyde photolysis: their roles in gas-to-particle conversion

S.N. Dubtsov, G.G. Dultseva and G.I. Skubnevskaya

Institute of Chemical Kinetics and Combustion, Siberian Branch of the Russian Academy of Sciences, 630090, Novosibirsk, Russia

Keywords: aerosol formation, photochemical processes, SOA

Aldehydes, reactive intermediate products of the atmospheric photooxidation of hydrocarbons, attract attention as photoactive compounds able to produce particulate matter under irradiation by sunlight. We showed in our previous investigations that even the simplest aldehydes, formaldehyde and acetaldehyde, form nanometer-sized aerosol particles when irradiated by the UV light ( $\lambda < 330$  nm). However, the yield of particulate matter from aldehyde photolysis is low. So, the trace amounts of gaseous intermediates may be expected to play key roles in the processes of gas-to-particle conversion in aldehyde vapour.

Benzaldehyde is known to produce a photopolymer under UV photolysis; so, the expected yield of photoaerosol should be much higher than for the cases of HCHO or CHCHO, and thus benzaldehyde  $C_6H_5CHO$  is a convenient compound to master the procedures for the investigation of minor (trace) gaseous photolysis products and to follow the routes leading to particulate matter.

We studied the photolysis of  $C_6H_5CHO$  in a flow photochemical reactor irradiated with a middle-pressure Hg lamp. Photolysis both in an inert gas (argon) and in the air was investigated. We have previously reported on the kinetics of aerosol formation in this system. Now we carried out a thorough analysis of stable intermediates and short-lived free radicals, either generated photolytically or arising in secondary transformations of the primary radicals. Thorough analysis of the minor intermediates present in trace amounts in the gas phase after photolysis was carried out by means of HPLC (high-performance liquid chromatography), IR spectroscopy (after concentrating in a proper solvent), and qualitative chemical tests (to establish the presence of definite functional groups). Short-lived free radicals were identified by means of spin trapping in combination with the counter-synthesis to prove the structure of radicals trapped (Dultseva *et al.*, 1996). In addition to  $C_6H_5$ , HCO (in argon) and  $C_6H_5O$  (in the air), we detected free radicals containing two and three aromatic rings. This fact proves that benzaldehyde photopolymerization and photonucleation both are initiated and proceed through the free radical mechanism in the gas phase.

The roles of intermediates on the pathways to particulate matter were revealed by testing the aerosol-forming abilities of free radicals generated additionally by independent procedures, e.g. HCO – by glyoxal photolysis,  $C_6H_5CO$  by benzophenone photolysis, etc.. It was observed that HCO does not give rise to particulate matter, while the radicals containing the aromatic ring are efficient initiator of photonucleation. Detection of glyoxal among the photolysis products in the air suggests that the fate of HCO radical is not the interaction with oxygen to form  $HO_2$ . A possible reason may be the formation of HCO in the interaction of an excited benzaldehyde molecule with a ground-state one, so that  $(CHO)_2$  is formed before HCO has time to react with  $O_2$ . Thus HCO terminates the chain sequences that otherwise could result in the formation of particulate matter. Chemical analysis of aerosol products allows to supplement the scheme as shown in Fig. 1.

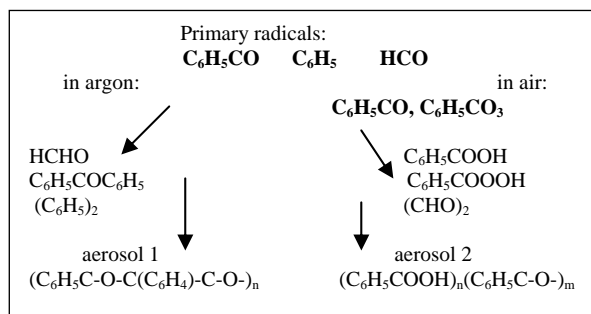


Figure 1. A chart of intermediates of  $C_6H_5CHO$  photolysis.

Thus, investigation of reactive intermediates proves that photonucleation in  $C_6H_5CHO$  vapour is a process driven by the free radical polymerization.

This work was supported by CRDF under grant No. RC1-2330-NO-02.

Dubtsov, S.N., Dultseva, G.G., Dultsev, E.N., & G. I. Skubnevskaya, G.I. (2006). *J. Phys. Chem. B*, 110, 645-649.

Dultseva, G. G., Skubnevskaya, G. I., Volodarsky, L. V., Tikhonov, A. Ya., & Mazhukin, D. G. (1996). *J. Phys. Chem.*, 100, 17523-17527.

## Distributions and health risks of polycyclic aromatic hydrocarbons (PAHs) in atmospheric aerosols of the city of Chania (Greece)

A. Pafitis<sup>1</sup>, N. Pasadakis<sup>2</sup>, I. Kopanakis<sup>3</sup> and E. Katsivela<sup>1</sup>

<sup>1</sup>Department of Natural Resources and Environment, Technological Educational Institute of Crete, Romanou 3, 73133 Chania, Crete, Greece

<sup>2</sup>Department of Mineral Resources Engineering, Technical University of Crete, Polytechnioupolis, 73100 Chania, Crete, Greece

<sup>3</sup>Department of Environmental Engineering, Technical University of Crete, Polytechnioupolis, 73100 Chania, Crete, Greece

Keywords: aerosol chemistry, health effects of aerosols, PAHs, TSP, urban pollution.

The main objective of the present work was to study the variation of particulate PAHs (EPA priority components) in the urban area of the coastal city Chania (Western Crete, Greece), as well as in its suburban area (Kounoupidiana, Akrotiri) and to estimate the health risks, according to the toxicity equivalency factors (TEFs) (Nisbet & LaGoy, 1992). Duplicates of samples of total suspended particles (TSP) (12 campaigns in total) were collected using a portable high volume sampler (GT2200 Tripod Sampler, Andersen Instruments Inc., Georgia, USA) on glass fiber filters during November and December 2005. Sampling duration was 12 hours (8 a.m. to 8 p.m.) and the air sample volume was approximately 950 m<sup>3</sup>. Sampling in the urban and suburban area was performed at a height of 1.2 m from the ground level, whereas a background (ambient) sample was collected at a location 1 km away from the city centre and at a height of 7 m above the ground level. Sampling filters were stored in fast plastic bags. Prior to the extraction, parts of the filters (11 cm x 9 cm) were spiked with the recovery standards d<sub>10</sub>-phenanthrene, d<sub>10</sub>-pyrene and d<sub>12</sub>-perylene (final concentration 3.3 ng/μL each) as well as n-hexadecane (final concentration 10 ng/μL). The spiked filters were extracted in an ultrasound bath (Branson Ultrasonics Corporation, Connecticut, USA) for 30 minutes with cyclohexane (Riedel-de-Haen, Germany). The sample extracts, after filtration, were concentrated to 800 μL by a rotary evaporator, spiked with the internal standard 1-chlorooctadecane and analysed using gas chromatography/mass spectrometry (GC-MS). PAHs were determined in the full scan mode (50-400 m/z) as well as using selected ion monitoring (SIM) at the nominal molecular weight and at the characteristic mass fragments. As reference material was used a standard solution containing the 16 EPA PAHs (Sigma-Aldrich, Germany).

As shown in figure 1, the main particulate PAHs in the urban area were those of higher molecular weight (HMW) (Benzo[a]anthracene, Benzo[b] fluoranthrene, Benzo[k]fluoranthrene, Benzo[a] pyrene, Indeno[1,2,3-cd]pyrene and Benzo[ghi] perylene) and their mean concentrations

varied from 0.74 to 4.6 ng/m<sup>3</sup>. In contrast, in the suburban area high concentrations of both lower molecular weight (LMW) (Fluorene: 0.12 ng/m<sup>3</sup>; Phenanthrene: 0.16 ng/m<sup>3</sup>) and HMW PAHs (0.12-0.47 ng/m<sup>3</sup>) were observed. The total PAHs concentration at the suburban area (2.23 ng/m<sup>3</sup>) was 7.4 lower than in the urban area (16.45 ng/m<sup>3</sup>). In comparison, the total PAHs concentration at the background was 18 times lower (0.94 ng/m<sup>3</sup>), whereas the LMW PAH Phenanthrene had the highest concentration (0.17 ng/m<sup>3</sup>).

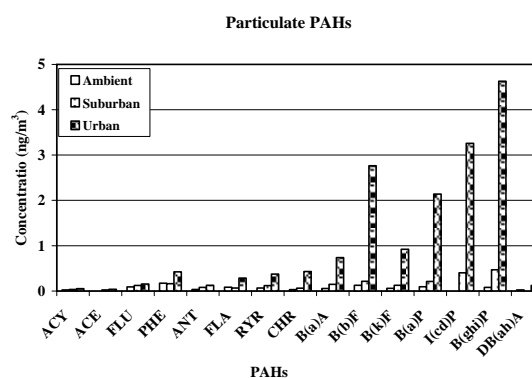


Figure 1. PAHs distributions in urban aerosols. ACY: Acenathylene; ACE: Acenaphthene; FLU: Fluorene; PHE: Phenanthrene; ANT: Anthracene; FLA: Fluoranthrene; RYR: Pyrene; CHR: Chrysene; B(a)A: Benzo[a]anthracene; B(b)F: Benzo[b]fluoranthrene; B(k)F: Benzo[k]fluoranthrene; B(a)P: Benzo[a]pyrene; I(cd)P: Indeno[1,2,3-cd]pyrene; B(ghi)P: Benzo[ghi]perylene; DB(ah)A: Dibenzo(a,h)anthracene

The conversion of the individual PAHs concentrations in benzo(a)pyrene equivalents (B(a)P<sub>eq</sub>) based on the TEFs (Nisbet & LaGoy, 1992) was used in the current work to estimate their relative toxicity. Thus, the total B(a)P<sub>eq</sub> concentration calculated is equal to 3.57 and 2.23 ng/m<sup>3</sup> for the urban and suburban areas, respectively.

Nisbet, I. C. T., & LaGoy P. K. (1992). *Regulatory Toxicology and Pharmacology*, 16, 290-300.

## Airborne Copper, Nickel and Lead in Northern Finland – Effects of the Kola Metallurgical Industry

U. Makkonen<sup>1</sup>, J. Paatero<sup>1</sup>, K. Pyy<sup>1</sup>, and M. Kulmala<sup>2</sup>

<sup>1</sup>Finnish Meteorological Institute, Air Quality Research, P.O.Box 503, FI-00101 Helsinki, Finland

<sup>2</sup>Department of Physical Sciences, P.O.Box 64, FI-00014 University of Helsinki, Finland

Keywords: Atmospheric Aerosols, Trace elements, Air Pollution.

The mining and metallurgical industry at Kola peninsula, north-west Russia is the most important source of air pollution next to Norilsk in the Arctic. Especially the nickel, copper and cobalt smelters at Monchegorsk, Nickel and Zapoljarnij emit huge quantities of sulphur dioxide, metals and inhalable particles to the atmosphere. These gas- and particle-phase pollutants have a serious impact on the atmosphere at Kola peninsula and Finnish Lapland (Virkkula *et al.*, 1995)

In this work we collected aerosol samples with teflon filters at two monitoring stations in northern Finland. Värriö (67°45'N, 29°37'E) is located close to the Finnish-Russian border 140 km west of Monchegorsk. Pallas (68°00'N, 24°15'E) is located 30 km east of the Finnish-Swedish border and 350 km west of Monchegorsk. At Pallas weekly samples were collected while at Värriö three samples per week with filter changes on Mondays, Wednesdays, and Fridays were collected. The filters were analysed for nickel, copper and lead with ICP-MS.

The occasional high concentrations of nickel and copper at Värriö compared to those at Pallas are related to the emissions at metallurgical plants at Kola peninsula (Figures 1 and 2). On average, the concentrations at Värriö are twice higher than at Pallas (Table 1). On the other hand, lead concentrations at Värriö and Pallas are quite similar indicating that airborne lead in northern Finland originates from different sources than nickel and copper, e.g. from Central Europe (Figure 3).

Table 1. Copper, nickel, and lead concentrations in the air (ng/m<sup>3</sup>) at Värriö and Pallas April-December 2006.

Station	parameter	Cu	Ni	Pb
Värriö	average	1.14	1.39	0.84
	min	0.011	0.013	0.013
	max	14.6	15.7	6.1
	n	114	114	114
Pallas	average	0.49	0.44	0.78
	min	0.0040	0.0043	0.052
	max	1.8	1.9	4.2
	n	37	37	37

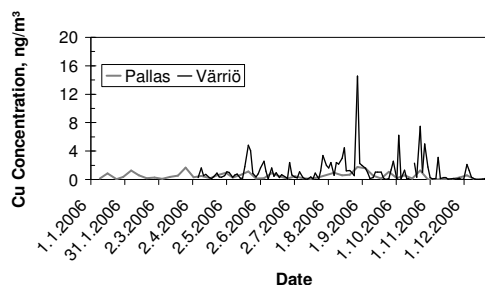


Figure 1. Airborne copper at Pallas (grey line) and Värriö (black line), northern Finland in 2006.

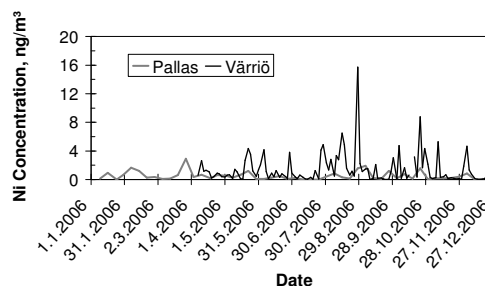


Figure 2. Airborne nickel at Pallas (grey line) and Värriö (black line), northern Finland in 2006.

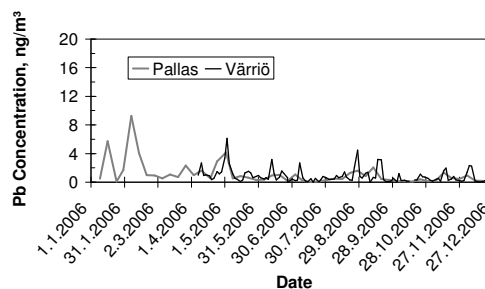


Figure 3. Airborne lead at Pallas (grey line) and Värriö (black line), northern Finland in 2006.

This work was financially supported by the Finnish Ministry of Environment as a part of the "Russia in Flux" research programme of the Academy of Finland.

Virkkula, A., Mäkinen, M., Hillamo, R. and Stohl, A., 1995. Atmospheric aerosol in the Finnish Arctic: particle number concentrations, chemical characteristics, and source analysis. *Water, Air, & Soil Poll.*, 85, 1997-2002.

## Characterization of single urban dust particles from different urban location across UK

Manuel Dall'Osto\*, Roy M. Harrison and Alistair Thorpe

\*Division of Environmental Health and Risk Management, University of Birmingham, Edgbaston; Birmingham, B15 2TT United Kingdom (mxd266@bham.ac.uk)

Keywords: chemical composition, dust, on-line measurements, PM and source apportionment, single particle analysis

The aerosol time-of-flight mass spectrometer (ATOFMS; TSI-Model 3800) provides information on a polydisperse aerosol, acquiring precise aerodynamic diameter ( $\pm 1\%$ ) within the range 0.1 to 3 micrometres and individual particle positive and negative mass spectral data in real time (Gard et al. 1997).

The ATOFMS has been deployed in several different urban locations (background, roadside and tunnel site at London and Birmingham, UK) during several different field studies spread over four years. More than half million particles were detected by the ATOFMS and the positive and negative single particle spectra were recorded in real time.

In addition, various dust samples were analyzed in the laboratory, including brake dust, soil, vegetative dust and road dust collected around Birmingham. Moreover, about 50 road dust samples were collected in four different roads in London in 2006 during the REPARTEE field study. The roads presented very different amount of traffic, ranging from few hundreds up to 80,000 vehicles per day.

Specific fingerprints for different types of dust were determined in the laboratory and were used to identify different classes of dust detected during the field studies.

Differences among collected vegetative dust samples were minimal. The average spectrum highlights the intense potassium signal ( $m/z$  39;  $[K]^+$ ) observed in the majority of spectra, as well as a very strong peak  $[PO_3^-]$  at  $m/z$  -79. Road dust was found to be similar to soil samples. Soil samples contain a range of metal components, the most intense peaks being due to lithium, sodium, aluminium, potassium, calcium and iron at  $m/z$  7, 23, 27, 39, 40 and 56, respectively. The negative spectra also show a dominant set of peaks occurring at  $m/z$  = -17, -26, -42, -63 and -79. These indicate the presence of  $OH^-$ ,  $CN^-$ ,  $CNO^-$ ,  $PO_2^-$  and  $PO_3^-$ , respectively. Aluminum and calcium often constituted the two most commonly detected cations. Dust particles attributed to brake dust often exhibited specific peaks at  $m/z$  -88  $[FeO_2]^-$  and 138  $[Ba]^+$ . Moreover peaks due to copper ( $[Cu]^+$ ,  $m/z$  63 and 65), antimony ( $[SbO_2]^{+/-}$ ,  $m/z$  +/- 153 and 155,  $[SbO_4]^{+/-}$ ,  $m/z$  -185/-187) and fluorine compounds ( $m/z$  -19  $[F]^-$  and  $m/z$  - 32  $[CHF]$ ) were seen in about a quarter of the brake dust particles analysed.

The road dust samples collected at the four London roads showed clear trends. ART-2a area matrix of ATOFMS single particle positive and negative mass spectra (Song et al. 1999; Allen 2007) with strong peaks at  $m/z$  39  $[K]^+$  and  $m/z$  -79  $[PO_3^-]$  were apportioned to vegetative debris. These particle types were found mainly on roads within parks. Fewer particle types belonging to vehicle sources were found on lightly trafficked roads.

In the Queensway tunnel (UK), most of the Fe-rich dust particles were due to brake dust (about 90%) and only a minor proportion to road dust (about 10%) when expressed as the number of particles in the size range 0.3-3.0  $\mu m$ . At the roadside site, the abundance of the two types was far more equal, probably reflecting greater inputs of soil to road dust and different driving modes. It appears that a major quantity of vehicle-generated dust such as brake dust is suspended directly and dispersed in the atmosphere, with only a minor amount deposited on the road and resuspended.

The set of road dust samples collected at London also seem to confirm that vehicle-generated dust (in particular brake dust) is suspended directly and dispersed in the atmosphere.

Allen, J. O. (2007). YAADA, Yet Another ATOFMS Data Analyzer. <http://www.yaada.org/index.html>.

Gard, E., J. E. Mayer, B. D. Morrical, T. Dienes, D. P. Fergenson and K. A. Prather (1997). "Real-time analysis of individual atmospheric aerosol particles: Design and performance of a portable ATOFMS." *Analytical Chemistry* 69(20): 4083-4091.

Song, X. H., P. K. Hopke, D. P. Fergenson and K. A. Prather (1999). "Classification of single particles analyzed by ATOFMS using an artificial neural network, ART-2A." *Analytical Chemistry* 71(4): 860-865.

## TSP and heavy metals measurements in the roadside environment of the coastal city of Chania (Greece)

V. Voudouri<sup>1</sup>, N. Lydakakis-Simantiris<sup>1</sup>, D. Pentari<sup>2</sup> and E. Katsivela<sup>1</sup>

<sup>1</sup>Department of Natural Resources and Environment, Technological Educational Institute of Crete, Romanou 3, 73133 Chania, Crete, Greece

<sup>2</sup>Department of Mineral Resources Engineering, Technical University of Crete, Polytechnioupolis, 73100 Chania, Crete, Greece

Keywords: aerosol chemistry, trace elements, TSP, urban pollution.

The current study considers the spatial variability of the concentrations of eight trace metals (Cd, Cr, Cu, Fe, Mn, Ni, Pb and Zn) in aerosol at the roadside environment of the urban area of the coastal city of Chania (Western Crete, Greece), as well as in one of its suburbs (Kounoupidiana, Akrotiri).

Duplicates of samples of total suspended particles (TSP) (12 samplings in total) were collected using a portable high volume sampler (GT2200 Tripod Sampler, Andersen Instruments Inc., Georgia, USA) on glass fibre filters. Sampling duration was 12 hours (8 a.m. to 8 p.m.) and the air sample volume was approximately 950 m<sup>3</sup>. Samplings in the urban and suburban areas were performed alongside of roads at a height of 1.1 m during November and December 2005. Sampling filters were stored in airtight plastic bags. Parts of the filters (11 cm x 9 cm) were digested with 30 mL of concentrated HCl (37% w/v, suprapur grade, Merck, Germany) in an ultrasound bath (Branson Ultrasome Corporation, Connecticut, USA), for 30 min. After decantation, the filters were washed 3 times for 15 min each, with 30 mL of ultra pure water (millipore) in the ultrasound bath. The filtrates were concentrated by evaporation at 100 °C and dissolved in 15 mL HCl (12.3% w/v), in which 5 drops of concentrated HNO<sub>3</sub> (65%) (Riedel de Haen, Germany), were added. The concentrations of the trace elements were determined with a Perkin Elmer AA100 atomic absorption spectrometer using acetylene-air flame. The detection wavelength was 228.8 nm for Cd, 357.9 nm for Cr, 324.8 nm for Cu, 248.3 nm for Fe, 279.5 nm for Mn, 332 nm for Ni, 283.3 nm for Pb and 213.9 nm for Zn. Calibration curves for all the determinations were constructed using standards (Merck, Germany). Solutions prepared as mentioned above, using clean glass fibre filters were used as blanks.

Figure 1 shows the distribution of the seven trace metals examined, in the urban and suburban areas. As expected, all trace metals showed higher concentrations in the urban area (less than 40% contribution in the suburban area). In particular, Cd and Ni were under the detection limits in the suburban area, whereas the particulate concentrations of Cu, Fe, Pb and Mn contributed in the suburban area lower than 20% of their concentrations in the urban area. Only Cr and Zn showed relatively high

concentrations in the suburban area, their contribution ranging from 28% for Cr to 37% for Zn.

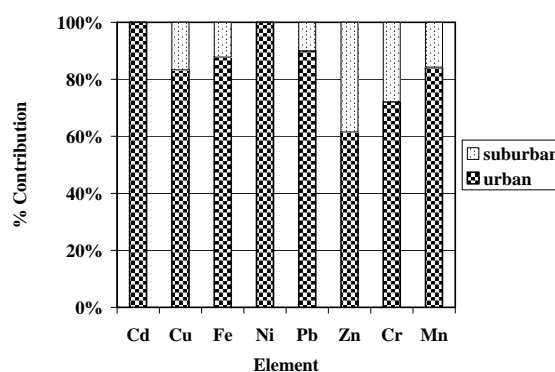


Figure 1. Concentration distributions for the eight trace elements in TSP in the urban and suburban areas of the city of Chania

In Table 1, we present the enrichment factors ( $EF_{\text{crust}}$ ) (Finlayson-Pitts & Pitts, Jr., 2000; Taylor & McLennan, 1995), as they were calculated using Fe concentration as reference. From the eight trace metals examined, only Cu, Pb, and Zn were enriched in the aerosols of urban as well as in the suburban areas.

Table 1. Enrichment factors of trace metals in aerosols using Fe as reference in the urban and suburban areas of the city of Chania.

Element	Urban $EF_{\text{crust}}$	Suburban $EF_{\text{crust}}$
Cd	0.29	0
Cr	0.88	2.44
Cu	52.84	76.28
Fe	1.0	1.0
Mn	2.21	2.97
Ni	1.89	0
Pb	177.92	141.99
Zn	113.07	510.65

Finlayson-Pitts, B. J., & Pitts, Jr. J. N. (2000). *Chemistry of the Upper and Lower Atmosphere*. California, USA: Academic Press.

Taylor, S. R., & McLennan S. M. (1995). *Rev. Geophys.* 33, 241-265.

## Modelling the Formation of Metal Oxide Aerosols

I. Alxneit and H.R. Tschudi

Solar Technology Laboratory, Paul Scherrer Institute, 5232 Villigen PSI, Switzerland

Keywords: Aerosol formation, chemical composition, elemental composition, numerical simulation

The formation of aerosols by homogeneous nucleation and subsequent growth of the particles by condensation can be well described if atoms or stable molecules are considered the precursors. Aerosols formed in this way exhibit the identical chemical composition as their precursors. In the case of metal oxides, such as e.g.  $\text{TiO}_2$ ,  $\text{SiO}_2$ , or  $\text{Al}_2\text{O}_3$ , this assumption is questionable as the predominant binary gas phase species are usually the molecular monoxides (MO). Only including these precursors in the reaction will fail to predict to the correct chemical composition of the products. Similarly, the correct average chemical composition of the product of the reaction of zinc vapor and oxygen, zinc oxide (ZnO) and bulk zinc, is not obtained with the traditional approach. Moreover, not even the formation of ZnO is correctly described: Although molecular ZnO exists (Chertihin & Lester 1997), its formation from the elements is endergonic.

Here, we report on a model and its implementation that allows to treat the formation of metal oxide aerosols and to predict their properties such as chemical composition, or particle size distribution. The model includes: homogeneous nucleation of the metal (1), addition of metal atoms to the (liquid) metal surface (2), addition of oxygen molecules to the metal surface (3) to form an oxide mono-layer, and the addition of zinc atoms onto the oxide mono-layer (4). With this last process, a MO unit at the surface of the cluster is converted into a bulk MO unit. Any suitable expression for the steady state homogeneous nucleation rate can be applied for the rate of reaction (1). The rates for reactions (2), (3), and (4) are based on the collision frequency of an ideal gas with the corresponding surfaces and properly chosen values for the sticking probabilities  $\zeta_{\text{M-M}}$ ,  $\zeta_{\text{O}_2\text{-M}}$ , and  $\zeta_{\text{M-MO}}$ .

In the thermochemical ZnO/Zn cycle studied in our laboratory for the production of solar hydrogen (Steinfeld 2002) zinc has to be separated from a stoichiometric mixture of zinc vapor and oxygen with minimum reoxidation. We applied our model to study the influence of process parameters on the extent of reoxidation to be expected.

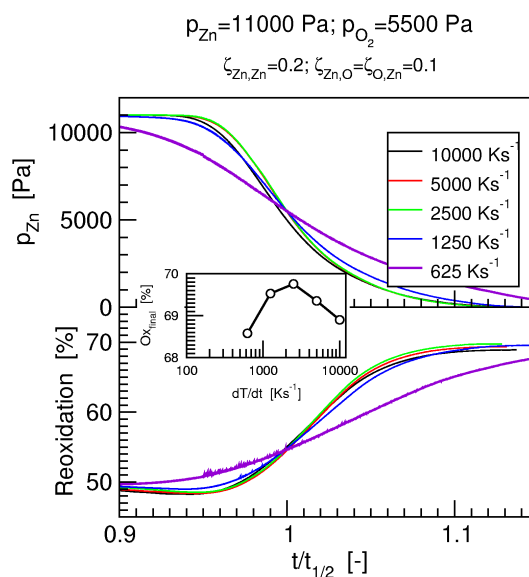


Figure 1. Time evolution of  $p_{\text{Zn}}$  (top) and the average degree of oxidation of the product (bottom) for various quench rates. The insert shows the final degree of oxidation as function of the quench rate.

In Figure 1 we report the influence of the quench rate on the product composition when a stoichiometric mixture of zinc vapor and oxygen is subjected to a quench. For an easier comparison the time axis is scaled by  $t_{1/2}$ , the time at which the zinc partial pressure decreases to 50% of its initial value. The time evolution of the zinc partial pressure and of the average degree of oxidation almost coincides for the various quench rates down to a quench rate of  $625 \text{ Ks}^{-1}$  when the process begins to markedly slow down. Interestingly, the average degree of oxidation of the final product, as show in the inset, remains almost constant at a value around 70%.

This work was supported by the Swiss Federal Office of Energy .

Chertihin, G. V., & Andrews, Lester (1997). *J. Chem. Phys.*, 106, 3457-3465.  
Steinfeld, A. (2002). *Int. J. Hydrogen Energy*, 27, 611-619.

## Polycyclic aromatic hydrocarbons and size distributions in Tehran's atmosphere, Iran

F. Halek, M. Hashtroudi, A. Kavousi

Materials & Energy Research Center, P.O. Box 14155-4777, Tehran, IRAN

Keywords: Atmospheric aerosols; PAHs; Particle characterization; human carcinogenic

Polycyclic aromatic hydrocarbons (PAH<sub>s</sub>) a group of organic compounds made up of two or more fused benzene rings in linear, angular or cluster arrangements. Most carcinogenic PAH<sub>s</sub> occur almost exclusively in the long-lived particulate phase. It is known that PAH<sub>s</sub> are rapidly absorbed and can be activated in the lung. PAH are present in ambient air as gases or absorbed onto particles, both of which can be inhaled into the lungs. Tehran with population of more than 10 million has faced air pollution for a long time.

Suspended particulate matter samples were collected by impactor samplers in different sites to characterize the mobile source emissions for polycyclic aromatic hydrocarbons (PAH<sub>s</sub>).

An orifice uniform deposit Impactor was used to measure the size distributions of the aerosols. Motor vehicles are the major source of atmospheric PAH<sub>s</sub> in Tehran. Mobile source PAH emission estimates were generated from the Particle and vapor phase samples collected in the sites and agree with emission resulted from previously studies. PAH<sub>s</sub> in the atmosphere have been collected as PM on glass-fiber filters (GF<sub>s</sub>) by using high volume impactor samplers. The samples extracted by ultrasonic and subsequently analyzed by using Knaver high-performance liquid chromatography ( HPLC ) .Results of PAH analysis indicated existence of several of the higher molecular weight PAH<sub>s</sub> (Benzo(α)Anthracene , Chrysene ,

Benzo[b]fluoranthene , Benzo[k]fluoranthene , Benzo[α]Pyrene) Benzo[ghi]Perylene , Indeno(1,2,3-cd) Pyrene that confirm role of gasoline fueled emissions in Tehran's atmosphere.

Sanderson, E. G. ; Raqbi, A. ; Vyskocil, A. ; Farant, J. P., (2004) *Comparison of particulate Polycyclic Aromatic Hydrocarbon profiles in different regions of Canada*. Atmospheric Environment, 38: 3417-3429.

Thongsanit, P.; Jinsart, W.; Hopper, B.; hopper, Martin; Limpaseni, W.( 2003): *Atmospheric particulate matter and polycyclic aromatic hydrocarbon for pm<sub>10</sub> and size-generated samples in Bangkok*; Journal of Air & Waste Manage. Assoc., 53, 1490-1498.

Pollution Control Department Annual Report, Situation and management of air and noise pollution in Thailand; Pollution Control Department, ministry of science, technology and environment: Bangkok, Thailand, 1998, pp 16-45.

Chen, L. W. A. , Doddridge, B. G, Dickerson, R. R. , Chow, Henry, J. C R. C., (2002) *Origins of fine aerosol mass in the Baltimore-Washington Corridor*. Atmospheric Environment, 36: 4541-4554.

Kiss, G.; Vargr puchony, Z.; Rohrbacher, G.; Hiavay, J. (1998) *Distribution of polycyclic aromatic hydrocarbon on atmospheric aerosol particles of different sizes*; Atms. Res., 46, 253-261.

---

\* E-mail: [f-halek@merc.ac.ir](mailto:f-halek@merc.ac.ir)  
[fhalek@yahoo.com](mailto:fhalek@yahoo.com)

Cite abstract as Author(s) (2007), Title, European Aerosol Conference 2007, Salzburg, Abstract T01A013

## Secondary organic carbon in the urban area of Rome

M. Manigrasso and P. Avino

DIPIA ISPESL, via Urbana 184, 00184, Rome, Italy

Keywords: carbonaceous particles, organic carbon, SOA, urban areas

In urban areas carbonaceous particulate matter (TC) represents an important fraction of the atmospheric aerosol. It is usually classified in two fractions: elemental carbon (EC) and organic carbon (OC). While EC is a primary pollutant emitted during incomplete combustion processes, OC can be split in two forms: primary OC ( $OC_{pri}$ ) and secondary OC ( $OC_{sec}$ ).  $OC_{pri}$  is directly emitted into the atmosphere from both anthropogenic (combustion) and biogenic sources.  $OC_{sec}$  derives from the atmospheric oxidation of reactive organic gasses (ROG) emitted by many anthropogenic and natural sources. Secondary organic aerosol (SOA) arises from a two-step process: oxidation of ROGs with production of semi-volatile organic carbon (SVOCs) and partition of SVOCs to the aerosol phase.

In order to investigate the contribution of  $OC_{sec}$  to the carbonaceous fraction of atmospheric particulate, a campaign of measurements of TC, OC and EC was performed in January-July 2005.

The measurements were carried out, simultaneously at ground level and at 20 m-height, with a 10  $\mu$ m-sampling head, by an ACP Monitor 5400 (Rupprecht & Patashnik, NY). The study was performed at the ISPESL's Pilot Station, located in downtown Rome, in an area characterized by anthropogenic sources (autovehicular traffic and domestic heating) and light vegetation. The  $OC_{sec}$  fraction was assessed using EC as a tracer of  $OC_{pri}$  (Turpin et al, 1995; Castro et al., 1999) by the equation:

$$OC_{sec} = OC_{total} - \left( \frac{OC}{EC} \right)_{pri} \times EC$$

The  $(OC/EC)_{pri}$  ratios were estimated with subsets of data points with the lowest OC/EC values and having a EC vs OC correlation with  $R^2 > 0.9$ : such values were 0.7 and 1.4 in winter and 0.5 and 2.2 in summer, at ground level and at 20 m height, respectively.

At ground level the EC/OC ratio is always above 1, while it becomes opposite in altitude where the atmospheric remixing properties favour the pollutant dilution and other sources and persistent species becomes preponderant.

The % contribution of  $OC_{sec}$  to OC is different depending on both seasons and vertical distribution (46% at 20 m and 36% at ground level in summer and 44% at 20 m and 29% at ground level in winter). These results are coherent with the expected higher radical oxidative activity in summer and in altitude.

As shown in figures 1 and 2, the average contribution of  $OC_{sec}$  to TC during the nocturnal hours is higher in winter than in summer, both at ground level and at 20 m. Such trends can be related to the reduction of the vapour pressures of SVOCs due to the lower temperatures in winter than in summer, favouring the formation of SOA. A role can be played also by the increase of relative humidity during nocturnal hours that could favour acid-catalyzed heterogeneous reactions leading to the formation of SOA (Jang et al., 2002).

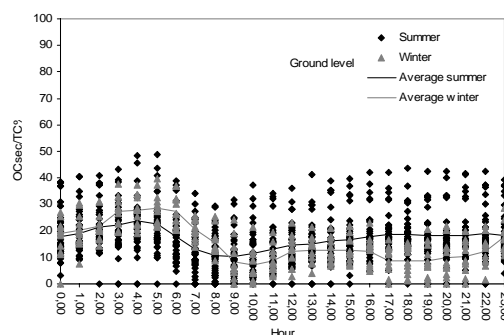


Figure 1. Contribution of  $OC_{sec}$  to TC at ground level in summer and in winter.

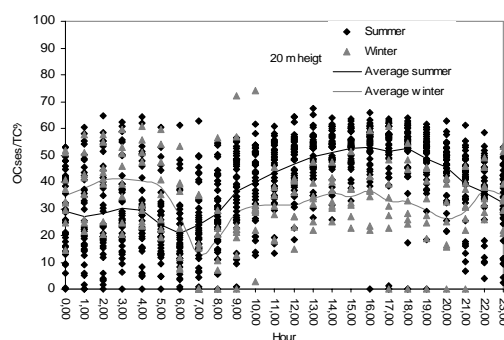


Figure 2. Contribution of  $OC_{sec}$  to TC at 20 m in summer and in winter.

Turpin, B.J., Huntzicker, J.J. (1995). *Atmospheric Environment*, 29, 3527-3544

Castro, L.M., Pio, C.A., Harrison, R.M., Smith D.J.T. (1999). *Atmospheric Environment*, 33, 2771-2781.

Jang, M., Czoschke, N.M., Lee, S., Kamens, R.M. (2002). *Science*, 298, 5594, 814-817.

## SPACCIM model studies of the multiphase chemistry processing of tropospheric aerosols

A. Tilgner<sup>1</sup>, R. Wolke<sup>1</sup> and H. Herrmann<sup>1</sup>

<sup>1</sup>Leibniz-Institut für Troposphärenforschung, Permoserstr. 15, D-04318 Leipzig, Germany

Keywords: modelling, multiphase chemistry, aerosol cloud interaction

The parcel model SPACCIM (Spectral Aerosol Cloud Chemistry Interaction Model / Wolke et al., 2005) has been applied to investigate the effect of multiphase processing of tropospheric aerosol particles and trace gases based on more realistic meteorological non-permanent cloud model scheme. The applied model includes a complex microphysical and a detailed multiphase chemistry model. The applied multiphase chemistry mechanism with about 1100 processes consists of an extended version of the gas phase mechanism RACM-MIM2 (Karl et al., 2006) coupled to the detailed aqueous phase mechanism CAPRAM 3.0i (Herrmann et al., 2005). The chemical mechanism incorporates a detailed description of the multiphase chemistry based on time-dependent size-resolved aerosol/cloud spectra.

The model was initialised with chemical and physical aerosol data (Poppe et al., 2001) for three different atmospheric conditions (urban, remote, marine). Simulations were carried out for a meteorological scenario including 8 cloud passages and an intermediate aerosol state at a 90 % relative humidity level by neglecting the effects of non-ideal solutions. Simulation has been performed with and without aqueous phase chemistry to study the effect of aerosol-cloud interaction on the tropospheric multiphase system. The model results have been analysed including time resolved source and sinks studies focused particularly on multiphase phase radical as well as non-radical oxidants and multiphase oxidations of C<sub>2</sub>-C<sub>4</sub> organic compounds.

The model studies shows significant effects of multiphase cloud droplet and aqueous aerosol interactions on the tropospheric oxidation budget for polluted and remote environmental conditions as well as influenced VOC's oxidation due to the changed oxidation budget within the clouds. Furthermore, the simulations implicate the potential role of deliquescent particles to act as a reactive chemical medium due to the in-situ aqueous phase production of radical oxidants such as OH and non-radical oxidants such as H<sub>2</sub>O<sub>2</sub>. Moreover, the model study shows the importance of the aqueous phase for the formation of higher oxidised organic compounds such as substituted mono- and diacids like pyruvic acid and tartaric acid. In particular, the aqueous phase oxidations of methylglyoxal and 1,4-butenedial have been identified as important OH radical sinks under polluted environmental conditions contributing to the production of less volatile organic compounds

and thus the organic aerosol particle mass. For pyruvic acid, in-cloud productions of about 130 ng m<sup>-3</sup> and 35 ng m<sup>-3</sup> have been modelled under remote conditions in a day and a night cloud, respectively. Further, the in-cloud oxidation of methylglyoxal and its oxidation products represents an efficient sink for NO<sub>3</sub> radicals in the aqueous phase particularly under urban as well as remote conditions.

Moreover, the model studies have been focused on the total organic mass productions resulting from the aerosol-cloud chemistry interactions. The model results show in-cloud organic mass productions up to about 1 µg m<sup>-3</sup> preferably under polluted day time cloud conditions mainly due to OH initiated multiphase oxidation processes. Additionally, corresponding size-resolved organic mass productions restricted to the size interval of about 100 – 800 nm have been modelled including spectral particle size processing mainly by reason of inorganic chemical processes. Finally, the sum of the results implicates the importance of the aqueous phase processes to be considered in future higher scale chemistry transport models.

This study was supported by the scholarship programme of the German Federal Environmental Foundation (DBU).

- Herrmann, H., Tilgner, A., Barzaghi, P., Majdik, Z., Gligorovski, S., Poulain, L. & Monod, A., (2005). *Towards a more detailed description of tropospheric aqueous phase organic chemistry: CAPRAM 3.0*. Atmospheric Environment 39 (23-24), 4351-4363.
- Karl, M., Dorn, H.-P., Holland, F., Koppmann, R., Poppe, D., Rupp, L., Schaub, A. & Wahner, A., (2006). *Product study of the reaction of OH radicals with isoprene in the atmosphere simulation chamber SAPHIR*. Journal of Atmospheric Chemistry 55 (2), 167-187.
- Poppe, D., Aumont, B., Ervens, B., Geiger, H., Herrmann, H., Röth, E. P., Seidl, W., Stockwell, W. R., Vogel, B., Wagner, S. & Weise, D., (2001). *Scenarios for modeling multiphase tropospheric chemistry*. Journal of Atmospheric Chemistry 40, 77-86.
- Wolke, R., Sehili, A.M., Simmel, M., Knoth, O., Tilgner, A. & Herrmann, H., (2005). *SPACCIM: A parcel model with detailed microphysics and complex multiphase chemistry*. Atmospheric Environment 39 (23-24), 4375-4388.

## Metal Distribution from Gasoline-Fueled Engine

Y. F. Wang,<sup>1\*</sup> H. R. Chao,<sup>2</sup> L. C. Wang<sup>3</sup>, H. H. Yang<sup>4</sup> and L.T. Hsieh<sup>2</sup>

<sup>1</sup>Department of Bioenvironmental Engineering, Chung Yuan Christian University, Chung-Li 320, Taiwan

<sup>2</sup>Department of Environmental Science and Engineering, National Pingtung University of Science and Technology, Pingtung 912, Taiwan

<sup>3</sup>Department of Chemical Engineering, Cheng Shiu University, Kaohsiung 833, Taiwan

<sup>4</sup>Department of Environmental Engineering and Management, Chaoyang University of Technology, Taichung 413, Taiwan

Keywords: metal, motorcycle, gasoline engine

Gasoline and diesel vehicles are major sources of urban air pollution. A large amount of particulate matters (PM) and volatile organic compounds (VOCs) are emitted, which might lead to respiratory and mutagenic diseases, such as lung and bladder cancer. However, it should be further noted that the engine exhausts also contain various metal contents attaching on to fine granular matters in the engine exhaust. Because of their fine particle sizes, they can penetrate into the deep respiratory tract and cause respiratory diseases (Sagai et al., 1996). Valavanidis et al. (2000) indicated that the deposition of metals (especially Fe) on the lower airway firstly will generate hydroxyl radicals (in aqueous buffered solutions, in the presence of hydrogen peroxide), then trigger the production of oxygen free radicals, and finally cause both acute and chronic lung damages. Therefore it is expected that, beside the organic contents and particulate matters, the investigation of metal contents in the engine exhaust is important for assessing health effects associated with vehicular metal emissions

Taiwan has highest motorcycle density in the world. An estimated 700,000 motorcycles were sold in the local market in 2005. In this study, eighteen particulate samples (including every six samples from 92, 95, 98 unleaded gasoline-fueled engines, respectively) collected with tube filter from the exhaust of the motorcycle engine were analyzed for twenty metal contents (Al, Ag, As, Ba, Ca, Cd, Cr, Cu, Fe, Hg, Mg, Mn, Mo, Ni, Pb, Si, Sr, Ti, V, Zn). Each particulate sample was treated with acid extraction and pressurized digestion. The digested samples were then measured for metal elements using inductively coupled plasma/atomic emission spectrometry (ICP-AES).

The metal contents were further classified into the crust and anthropogenic element categories (Wang et al., 2003). The former consisted of five elements – Al, Ca, Fe, Mg, and Si, while the latter included Ag, As, Ba, Cd, Cr, Cu, Hg, Mn, Mo, Ni, Pb, Sr, Ti, V and Zn. Table 1 showed that the metal composition of exhaust from 92, 95, 98 unleaded gasoline-engines. The metal compositions from 98 unleaded gasoline-engines were the lowest except As, V and Zn. Furthermore, the top four metal compositions of anthropogenic elements of exhaust

from 92, 95 and 98 unleaded gasoline-fueled engines are all the same, as follows: Ba, Sr, Zn and Cr. Comparing with the data of Wang et al. (2003), it's interesting to find the ratios of metal composition in exhaust from diesel engines to motorcycles gasoline engines are over 50 for Cr, Cu, Mn, Mo, Ni, Ti, V and Zn. Accordingly, it warrants further investigation for health effects exposed to such highly populated vehicular exhaust in Taiwan in the future.

Table 1 The metal composition (mg/g) of exhaust from 92, 95 and 98 unleaded gasoline-fueled engines

metal		92 (mg/g)	95 (mg/g)	98 (mg/g)
crust elements	Al	7.72	6.52	5.48
	Ca	18.1	17.2	13.5
	Fe	2.58	3.12	2.64
	Mg	7.76	6.39	6.32
	Si	5.08	4.12	3.54
anthropogenic elements	Ag	0.03	0.02	0.02
	Ba	3.26	3.14	2.54
	Cd	0.02	0.01	0.01
	Cr	0.05	0.05	0.04
	Cu	0.02	0.03	0.02
	Mn	0.03	0.03	0.03
	Mo	0.04	0.05	0.03
	Ni	0.03	0.02	0.02
	Pb	0.03	0.03	0.02
	Sr	0.69	0.52	0.41
	Ti	0.04	0.04	0.03
	V	0.93(μg/g)	1.06(μg/g)	1.53(μg/g)
	Zn	0.07	0.05	0.08
	As	31.2 (μg/g)	35.7(μg/g)	35.4(μg/g)
	Hg	0.26(μg/g)	0.33(μg/g)	0.16(μg/g)

Sagai, M., Furuyama, A., Ichinose, T., (1996). *Free Radical Biology & Medicine* 21, 199-209.

Valavanidis, A., Salika, A., Theodoropoulou, A., (2000). *Atmospheric Environment* 34, 2379-2386.

Wang, Y. F., Huang, K. L., Li, C. T., Mi, H. H., Luo, J. H. and Tsai, P. J., (2003) *Atmospheric Environment*, 37, 4637-4643.

## Physicochemical characterization of nitrated and oxy- polycyclic aromatic hydrocarbons in the atmospheres of two French alpine valleys

A. Albinet<sup>1</sup>, E. Leoz-Garziandia<sup>1</sup>, H. Budzinski<sup>2</sup>, E. Villenave<sup>3</sup>, J.-L. Jaffrezo<sup>4</sup>

<sup>1</sup>Institut National de l'Environnement industriel et des RISques (INERIS), Parc technologique Alata BP2, 60550 Verneuil en Halatte, France

<sup>2</sup>Laboratoire de Physico-& Toxicologie Chimie des systèmes naturels (LPTC), UMR 5472 CNRS, Université Bordeaux 1, 33405 Talence, France

<sup>3</sup>Laboratoire de Physico-Chimie Moléculaire (LPCM), UMR 5803 CNRS, Université Bordeaux 1, 33405 Talence, France

<sup>4</sup>Laboratoire de Glaciologie et Géophysique de l'Environnement (LGGE), UMR 5183 CNRS, Université Grenoble 1, 38402 Saint Martin d'Hères, France

Keywords: PAHs, NPAHs, OPAHs, ambient aerosols, field measurements

The objective of this study was to characterize the NPAHs and OPAHs in ambient air on various sites (traffic, suburban, rural and altitude). Atmospheric concentrations of these classes of compounds are of interest because they include potential mutagens and carcinogens.

Samplings were performed within the framework of the French research program POLLUTION des Vallées Alpines (POVA) during the winter 2002-2003 and the summer 2003. Both, ambient air particulate and gas phases were collected and particle size distribution was also studied.

Results show that, OPAH concentration levels were of the same order of magnitude as PAHs while NPAH concentrations were one to two orders of magnitude lower (Figure 1).

Study of source specific ratios (2-nitrofluoranthene/1-nitropyrene) clearly showed these compounds had a primary origin at the sites close to the sources of pollution whereas production of secondary NPAHs by gas phase reactions was prevalent at the rural sites far to the direct sources of pollution. Because a weak formation of secondary NPAHs by gas reaction in winter, the relative contribution of NPAHs from primary sources increased during this season. Nevertheless, in winter under specific conditions, evidence of secondary NPAH formations was observed at suburban and traffic sites (snowfalls) and rural site (pollutants accumulation and snowfalls).

Despite their lower atmospheric concentrations, carcinogenic risk (estimated using toxic equivalent factors) attributed to the NPAHs could reach 20% of the total risk. This risk becomes more critical on the sites away from pollution sources, where the formation of the secondary compounds like NPAHs, have been highlighted.

The fraction of PAHs, OPAHs and NPAHs associated with the particle phase was strongly depending on their vapour pressure and the ambient conditions.

During both seasons, PAHs, OPAHs and NPAHs were mainly associated (>80%) with fine particles ( $D_p < 1.3 \mu\text{m}$ ). The differences of

physicochemical properties of the classes of compounds could account in their particle size distribution.

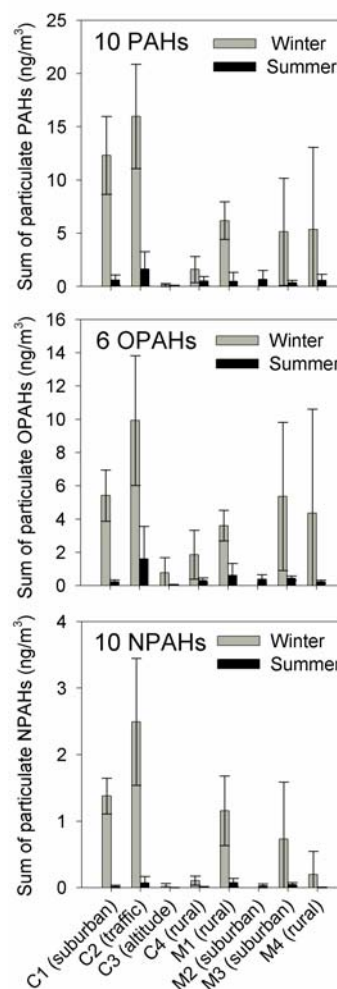


Figure 1. Average sum of particulate PAH, OPAH and NPAH concentrations during the winter and summer field campaigns according to the sampling site.

This work was supported by the French Ministry of Ecology and Sustainable Development (MEDD), the ADEME agency and the PRIMEQUAL-2 program.

## Characterisation of organosulphates from the photo-oxidation of isoprene in ambient PM<sub>2.5</sub> aerosol by LC/(-)ESI-linear ion trap mass spectrometry

Y. Gómez González<sup>1</sup>, R. Vermeylen<sup>1</sup>, R. Szmigielski<sup>1</sup>, J.D. Surratt<sup>2</sup>, T.E. Kleindienst<sup>3</sup>, M. Jaoui<sup>4</sup>, M. Lewandowski<sup>3</sup>, J.H. Offenberg<sup>3</sup>, E.O. Edney<sup>3</sup>, W. Maenhaut<sup>5</sup> and M. Claeys<sup>1</sup>

<sup>1</sup>Dept. of Pharmaceutical Sciences, Univ. of Antwerp (Campus Drie Eiken), Universiteitsplein 1, BE-2610 Antwerp, Belgium

<sup>2</sup>Dept. of Chemistry, California Institute of Technology, Pasadena, CA 91125, U.S.A.

<sup>3</sup>Nat. Exposure Research Lab., Environ. Protection Agency (EPA), Research Triangle Park, NC 27711, U.S.A.

<sup>4</sup>Alion Science and Technology, P.O. Box 12313, Research Triangle Park, NC 27709, U.S.A.

<sup>5</sup>Dept. of Anal. Chemistry, Inst. for Nuclear Sciences, Ghent Univ., Proeftuinstraat 86, BE-9000, Gent, Belgium

Keywords: aerosol chemistry, secondary organic aerosols, mass spectrometry, PM<sub>2.5</sub>, organosulphates.

Field observations of certain aerosol compounds, i.e., diastereoisomeric 2-methyltetrols and 2-methylglyceric acid, attributable to isoprene oxidation, and the experimental observation that isoprene under highly acidic conditions can lead to the formation of oligomeric, humic-like substances through heterogeneous reactions, re-opened the issue of secondary organic aerosol (SOA) formation from isoprene. In this context, a recent laboratory chamber study demonstrated that oligomeric, humic-like substances, i.e., organosulphates, are formed from the photo-oxidation of isoprene in the presence of sulphate seed aerosol (Surratt *et al.*, 2007). In the present study, liquid chromatography/electrospray ionisation – linear ion trap mass spectrometry (LC/ESI-MS) was used to examine the presence of organosulphates from the photo-oxidation of isoprene in PM<sub>2.5</sub> samples collected at K-puszta, Hungary, a mixed deciduous/coniferous forest site, during a 2003 summer field campaign. A motivation for re-examining these samples was that relatively high concentrations of isoprene SOA compounds, i.e., 2-methyltetrols and 2-methylglyceric acid, were measured in a previous study (Ion *et al.*, 2005). For comparison purposes, PM<sub>2.5</sub> aerosol collected during a laboratory irradiation experiment of an isoprene/air/NO<sub>x</sub> mixture in the presence of SO<sub>2</sub> was also examined (Edney *et al.*, 2005).

For LC/ESI-MS analysis, an LXQ linear ion trap instrument (ThermoElectron) was used in the negative ion mode. Archived aerosol samples collected on quartz fibre filters (in the case of ambient samples) or a Teflon filter (in the case of isoprene SOA) were extracted with methanol. The extract residues were analysed without prior sample purification. LC separation was achieved with a dC18 Atlantis column (Waters).

Organosulphates were identified on the basis of a *m/z* 97 ion [HSO<sub>4</sub><sup>-</sup>], while organonitrates were identified by a neutral loss of 63 u (HNO<sub>3</sub>), in their [M – H]<sup>-</sup> product ion spectra. Organosulphates from the following isoprene SOA products were characterised: 2-methyltetrols, 2-methylglyceric acid, and 2-methyltetrol mono-nitrates. The organosulphates of the 2-methyltetrols showed two partially resolved

peaks, while those of 2-methylglyceric acid showed one peak, and those of the 2-methyltetrol mononitrates, which are more hydrophobic, revealed six later-eluting partially resolved peaks.

In addition to organosulphates from the photo-oxidation of isoprene, organosulphates of hydroxycarboxylic acids, i.e., malic and tartaric acid sulphates, were also tentatively identified in the ambient PM<sub>2.5</sub> samples. The latter compounds have similar hydrophilic properties as the organosulphates of 2-methyltetrols and 2-methylglyceric acid.

It is likely that organosulphate formation is important for biogenic volatile organic compounds other than isoprene, which is consistent with recent field and laboratory studies showing evidence for organosulphate formation in SOA produced from  $\alpha$ -pinene (Gao *et al.*, 2006; Surratt *et al.*, 2007), and may be important in the formation of humic-like substances in ambient aerosol.

Research at the Universities of Antwerp and Ghent was supported by the Belgian Federal Science Policy Office and the Research Foundation - Flanders. Although this work was reviewed by the EPA and approved for publication, it may not necessarily reflect official Agency policy.

Edney, E. O., et al. (2005). *Atmos. Environ.*, 39, 5281-5289.

Gao, S., et al. (2006). *J. Geophys. Res.*, 111, D14314, doi:10.1029/2005JD006601.

Ion, A. C., et al. (2005) *Atmos. Chem. Phys.*, 5, 2947-2971.

Surratt, J. D., et al. (2007). *Environ. Sci. Technol.*, 41, 517-527.

## Characterisation, diel variation and mass size distributions of $\alpha$ -pinene oxidation products in ambient aerosol from K-puszt, Hungary

I. Kourtchev<sup>1</sup>, M. Claeys<sup>1</sup>, R. Szmigielski<sup>1</sup>, P. Van der Veken<sup>1</sup>, R. Vermeylen<sup>1</sup>, W. Maenhaut<sup>2</sup>, M. Jaoui<sup>3</sup>, T.E. Kleindienst<sup>4</sup>, M. Lewandowski<sup>4</sup>, J.H. Offenberg<sup>4</sup> and E.O. Edney<sup>4</sup>

<sup>1</sup>Dept. of Pharmaceutical Sciences, Univ. of Antwerp (Campus Drie Eiken), Universiteitsplein 1, BE-2610 Antwerp, Belgium

<sup>2</sup>Dept. of Anal. Chemistry, Inst. for Nuclear Sciences, Ghent Univ., Proeftuinstraat 86, BE-9000, Gent, Belgium

<sup>3</sup>Alion Science and Technology, P.O. Box 12313, Research Triangle Park, NC 27709, U.S.A.

<sup>4</sup>Nat. Exposure Research Lab., Environ. Protection Agency (EPA), Research Triangle Park, NC 27711, U.S.A.

Keywords: aerosol chemistry, mass spectrometry, PM<sub>2.5</sub>, secondary organic aerosols, biogenic particles.

It has been firmly established that monoterpenes give rise to secondary organic aerosol (SOA) through reactions of ozone, OH, and NO<sub>3</sub> radicals. Most laboratory studies of formation of SOA from monoterpenes have focused on investigations of SOA ozonolysis products of  $\alpha$ -pinene, including pinic, norpinic, pinonic, and norpinonic acids with pinic acid as a major reaction product, and, conversely, field studies mainly concerned the measurement of the latter compounds. The SOA ozonolysis products of  $\alpha$ -pinene were also reported for the OH radical initiated photo-oxidation of  $\alpha$ -pinene; however, in recent smog chamber experiments chemical analysis of irradiated  $\alpha$ -pinene/NO<sub>x</sub> mixtures that involve reactions of  $\alpha$ -pinene with OH and NO<sub>3</sub> as well as with ozone revealed the presence of highly oxidized, acyclic, polar compounds along with the ozonolysis products (Edney *et al.*, 2003; Jaoui *et al.*, 2005).

Here, we consider the identification of these compounds detected in PM<sub>2.5</sub> field samples collected in K-puszt, Hungary, a rural site with a mixed deciduous/coniferous vegetation. Based on chemical considerations, the synthesis of reference compounds, and the interpretation of mass spectra, the structures of the compounds, all hydroxydicarboxylic acids, were identified with greater confidence than could be achieved in the study of Jaoui *et al.* (2005) (Claeys *et al.*, 2007). The structures of the identified compounds, i.e., 3-hydroxyglutaric acid (3-HGA), 3-hydroxy-4,4-dimethylglutaric acid, and 2-hydroxy-4-isopropyladipic acid (2-HIPAA), are given in Figure 1. In addition, diel variations and mass size distributions of the identified compounds have also been investigated.

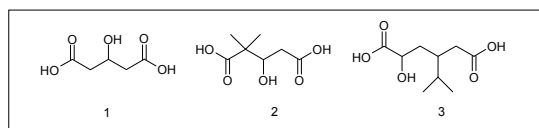


Fig. 1. Structures of the  $\alpha$ -pinene SOA tracer compounds; (1) 3-HGA, (2) 3-hydroxy-4,4-dimethylglutaric acid, and (3) 2-HIPAA.

The field campaign at K-puszt took place from 4 June to 10 July 2003 and separate daytime and nighttime samples were taken. The PM<sub>2.5</sub> aerosol samples were collected using a high-volume (Hi-Vol) dichotomous sampler. The size-fractionated aerosols were collected with a 10-stage micro-orifice uniform deposit impactor (MOUDI). All PM<sub>2.5</sub> filter samples were analysed for organic carbon (OC) and elemental carbon (EC) by a thermal-optical transmission technique. Sections of the PM<sub>2.5</sub> samples and selected MOUDI samples were acidified with 0.1% formic acid, extracted with methanol, derivatised to trimethylsilyl derivatives and analysed with gas chromatography/mass spectrometry (GC/MS).

The atmospheric OC concentration for the PM<sub>2.5</sub> samples was, on average, 4.0  $\mu\text{g m}^{-3}$  (range: 1.9 – 6.8  $\mu\text{g m}^{-3}$ ). The median concentrations of the  $\alpha$ -pinene oxidation products in daytime PM<sub>2.5</sub> aerosol samples were 16.8 ng m<sup>-3</sup> for 3-HGA, 14.9 ng m<sup>-3</sup> for 2-HIPAA and 2.3 ng m<sup>-3</sup> for pinic acid. Among the detected acids, only pinic acid exhibited a strong diel pattern, with highest concentrations during nighttime. Analysis of size-segregated aerosol samples collected at night showed that pinic acid and 2-HIPAA were mainly associated with the accumulation mode (0.1–1.0  $\mu\text{m}$  aerodynamic diameter), consistent with their secondary formation from gaseous precursors.

Research at the Universities of Antwerp and Ghent was supported by the Belgian Federal Science Policy Office and the Research Foundation - Flanders. Although this work was reviewed by the EPA and approved for publication, it may not necessarily reflect official Agency policy.

Claeys, M., *et al.* (2007). *Environ. Sci. Technol.*, 41, in press, doi:10.1021/es0620181.

Edney, E. O., *et al.* (2003). *Atmos. Environ.*, 37, 3947-3965.

Jaoui, M., *et al.* (2005). *Environ. Sci. Technol.*, 39, 5661-5673.

## Aerosol Formation from Isoprene

B. Verheggen<sup>1,2</sup>, A. Metzger<sup>2</sup>, J. Duplissy<sup>2</sup>, J. Dommen<sup>2</sup>, E. Weingartner<sup>2</sup>, A.S.H. Prevot<sup>2</sup> and U. Baltensperger<sup>2</sup>

<sup>1</sup>Institute for Atmospheric and Climate Science, ETH Zürich, 8092 Zürich, Switzerland

<sup>2</sup>Laboratory of Atmospheric Chemistry, Paul Scherrer Institut, 5232 Villigen PSI, Switzerland

Keywords: aerosol formation, growth, isoprene, nucleation rate, SOA.

Due to its high source strength, there has been considerable interest in the potential of isoprene to contribute to the formation of Secondary Organic Aerosol (SOA). Measurements of aerosol formation and growth following isoprene oxidation have been performed in the PSI smog chamber (27 m<sup>3</sup> teflon bag) to address this issue. Using only the measured aerosol size distributions as input, we determined empirical particle nucleation and growth rates.

Aerosol size distributions were measured using a twin-SMPS system, one with a short classifier and a TSI 3786 UWCPC (4-150 nm) and one with a long classifier and a TSI 3022 CPC (16-700 nm). From these we made composite size distributions covering the whole size range from 4 to 700 nm diameter which we used for further analysis.

The experiment was started by producing particles through ozonolysis of isoprene. This aerosol was diluted to reduce the particle concentration to around 500 cm<sup>-3</sup>. We then injected 350 ppbv of isoprene in the presence of NO and turned on all chamber lights. An hour later, the pre-existing particle mode started to significantly grow in size, indicative of condensation. Another two hours later a modest nucleation event occurred, producing approximately 4000 new particles cm<sup>-3</sup>. A contourplot of the measured size distributions is shown in Figure 1.

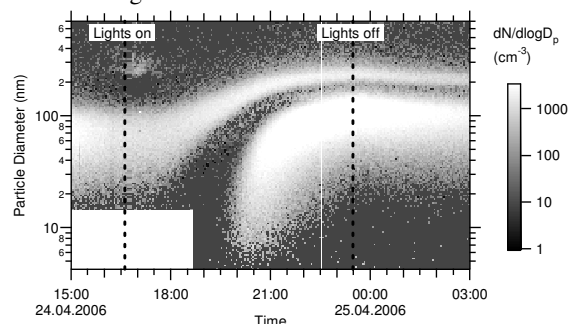


Figure 1. Measured size distributions following isoprene oxidation.

The condensational growth rate is found by regression analysis of the General Dynamic Equation, using the PARGAN procedure (Verheggen and Mozurkewich, 2006). The effects of particle wall loss and coagulation are taken into account. The growth rate provides an indirect measure of the concentrations of the condensing species, offset by

their vapor pressures. Diameter growth rates and the equivalent vapor mixing ratios are shown in Figure 2.

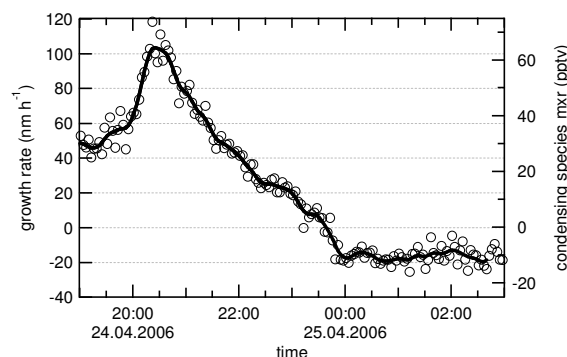


Figure 2. Particle growth rate during photo-oxidation of isoprene. Solid line is seven-point running mean. The equivalent mixing ratio of the condensing vapor (in excess of saturation) can be read off the right axis.

After the lights had been turned off (23:30), the aerosol evaporated continuously at a rate of 17 nm h<sup>-1</sup>. This corresponds to a mixing ratio in the chamber of 10 pptv below saturation. Therefore 10 pptv is a lower limit for the effective saturation vapor pressure of the condensable products of isoprene.

The growth rate is then used to estimate the time of nucleation for particles in each measured size bin, defined as the time when their calculated diameter surpassed 1 nm. Their number density at the time and size of nucleation is determined by integrating the particle losses that occurred in the time interval between nucleation and measurement. The nucleation rate is then given by the rate at which particles grow past the critical cluster size, assumed to be 1 nm diameter. The nucleation rate reaches 1 cm<sup>-3</sup> s<sup>-1</sup>, which is relatively small compared to other chemical systems involving terpenes and/or SO<sub>2</sub>. This suggests that at atmospheric conditions isoprene is not likely to induce nucleation, but it could contribute to SOA formation by condensation on existing aerosol. The yield was 0.8% at an aerosol mass of 5.5 μg m<sup>-3</sup> (assumed density of 1.4 g cm<sup>-3</sup>).

This work was supported by the Swiss NSF well as the EC projects EUROCHAMP and POLYSOA.

Verheggen, B., and Mozurkewich M. (2006), An inverse modeling procedure to determine particle growth and nucleation rates, *Atmos. Chem. Phys.*, 6, 2927-2942.

## Identification of secondary inorganic and organic aerosol components in urban particulate matter samples

A. Piazzalunga<sup>1</sup>, P. Fermo<sup>1</sup>, C. Rigamonti<sup>1</sup>, R. Vecchi<sup>2</sup>, G. Valli<sup>2</sup>, V. Bernardoni<sup>2</sup>

<sup>1</sup>Dep. Inorganic, Metallorganic and Analytical Chem., University of Milan, Via Venezian 21, 20133, Milan, Italy

<sup>2</sup>Institute of General Applied Physic, University of Milan, Via Celoria 16 20133, Milan, Italy

Keywords: SOA, organic carbon, particulate matter, ammonium nitrate, ammonium sulfate

Atmospheric aerosols in urban areas contain a significant fraction of both carbonaceous material and inorganic ions such as nitrate, ammonium and sulphate. Most of these pollutants are of secondary origin. Organic carbon (OC) can be emitted directly into the air or formed in the atmosphere through chemical reactions of reactive organic gases and subsequent gas-to-particle conversion (Secondary Organic Aerosol, SOA). In the present study PM10 samples collected in Milan during a wintertime and a summertime campaign, with a 4-hours time resolution, have been chemically characterized.

Secondary organic carbon can be estimated by subtracting the expected primary OC from the total observed ambient OC. Primary OC can be estimated using different approaches (Turpin et al., 1995; Plaza et al., 2006; Salma et al., 2004; Strader et al., 1999):

$$OC_{\text{prim}} = (OC/EC)_{\text{prim}} EC$$

or:  $OC_{\text{prim}} = a + bEC$

where  $a$  and  $b$  are the intercept and the slope, respectively, of the best fit line. The intercept  $a$  is considered to be the primary OC background concentration originating from non-combustion sources. It is supposed that primary OC and EC have the same source, and therefore there is a representative OC/EC ratio for the primary aerosol (EC is only primary in origin). Since  $(OC/EC)_{\text{prim}}$  emission rates vary by source (vehicles, fireplaces, heating, etc.) and are influenced by meteorological conditions, it is mandatory to estimate a local and seasonal value for the ratio. These values can be calculated when SOA is expected to be low (low local photochemical activity, i.e. low  $O_3$  concentration and high values for  $NO_2/NO_x$  ratio).

In this study six different criteria, some of which already used in the literature, have been employed to estimate  $(OC/EC)_{\text{prim}}$ . It represents the slope of the linear regressions obtained: (1) choosing the interval time 4-8 a.m. (low photochemical activity and, during summer, traffic as the only active source); (2) low values for  $NO_2/NO_x$  ratio; (3) low  $SO_4^{2-}$  concentrations; (4) low values for OC/EC; (5) low values of both  $SO_4^{2-}$  and OC/EC; (6) low  $SO_4^{2-}$  and  $C_2O_4^{2-}$  concentrations. It is worth noting that both sulphate and oxalate are typically secondary components deriving respectively from  $SO_2$  and VOCs oxidations.

Depending on the criteria  $OC_{\text{sec}}$  resulted to vary during the hot and the cold season as shown in table1.

	$OC_{\text{sec}}/OC_{\text{tot}}$ (%)	$OC_{\text{sec}}/PM$ (%)
Summer	15 – 40	3 – 9
Winter	20 – 30	5 – 7

Table1:  $OC_{\text{sec}}$  concentration range

During summer, when  $O_x$  ( $O_x=O_3+NO_2$ ) concentrations are higher, a fair agreement with  $OC_{\text{sec}}$  concentrations has been observed (figure 1).

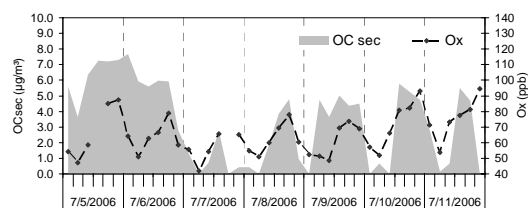


Figure 1:  $O_x$  and  $OC_{\text{sec}}$  concentrations during summer

Comparing the hot and the warm season  $NO_3^-$  was higher in winter because of the low temperatures which favor ammonium nitrate formation while during summer it is partially loosened for volatilization.  $SO_4^{2-}$  is higher in summer because of the photochemical activity (figure 2).

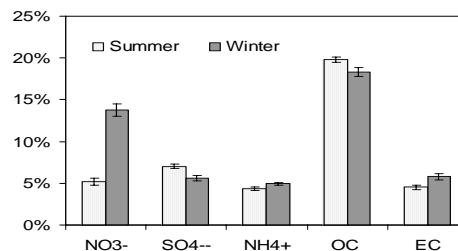


Figure 2 – principal ionic components, OC and EC concentrations in summer and winter

Plaza J. et al. (2006). *Atmos. Environ.*, 40, 1134-1147.

Salma I. et al. (2004). *Atmos. Environ.*, 38, 27-36

Strader R. et al. (1999). *Atmos. Environ.*, 33, 4849-4863

Turpin, B. J. et al. (1995). *Atmos. Environ.*, 29, 3527-3544.

## Examples of SOA analysis by mass spectrometry from the PSI smog chamber

J. Dommen<sup>1</sup>, A. Metzger<sup>1</sup>, A. Gascho<sup>1</sup>, K. Gaeggeler<sup>1</sup>, M.R. Alfarra<sup>1</sup>, A.S.H. Prevot<sup>1</sup>, U. Baltensperger<sup>1</sup>, M. Kalberer<sup>2</sup>, D. Gross<sup>3</sup>, A. Brunner<sup>4</sup>

<sup>1</sup>Laboratory of Atmospheric Chemistry, Paul Scherrer Institute, 5232 Villigen, Switzerland

<sup>2</sup>Department of Chemistry and Applied Biosciences, ETH Zurich, 8092 Zurich, Switzerland

<sup>3</sup>Department of Chemistry, Carleton College, Northfield, Minnesota 55057, USA

<sup>4</sup>Research Station Agroscope Reckenholz-Tänikon ART, Zurich, Switzerland

Keywords: aerosol mass spectrometry, aerosol characterization, aerosol chemistry, aerosol measurements, smog chamber.

Organic compounds account for 20-90 % of the total fine particle mass concentration in a wide variety of atmospheric environments. Secondary organic aerosol (SOA) is formed from reactions of volatile organic compounds with hydroxyl radicals, ozone and nitrate radicals where the resultant low vapor pressure oxidation products partition between the gas and aerosol phase. Recent studies have shown that a substantial fraction of organic aerosol mass is composed of oligomers (Kalberer et al., 2004; Surratt et al., 2006). The heterogeneous reactions of relatively volatile carbonyls in the aerosol phase are estimated to have great importance on the formation of high molecular weight products via oligomerization. Several reactions have been postulated to contribute to the formation of high molecular weight compounds in SOA, including hemiacetal and acetal formation, condensation, peroxy-hemiacetal formation and esterification. Recently, various mass spectrometric methods for determination of organics in particles have been developed. At the PSI smog chamber joint experiments with such new instruments were performed. The goal of this effort was to test the potential of various mass spectrometric techniques for the investigation of the chemical composition of SOA and the formation of oligomers therein.

The following instruments were involved:

- Matrix-assisted laser desorption/ionization MS (MALDI-MS): SOA particles were sampled on impactor plates for 1-4 h.
- TSI Single particle Aerosol Time of Flight Mass Spectrometer (ATOFMS, TSI 3800): Complete positive and negative ion mass spectra are generated on-line from single particles.
- Aerodyne Aerosol Mass Spectrometer: An aerodynamic lens produces a collimated particle beam that impacts on a surface heated typically to 550°C causing the particles to flash vaporize. The vapour plume is immediately ionised.
- Proton-transfer-reaction MS (PTR-MS) and GC-PTR-MS: The gas phase is stripped off by a charcoal denuder and the aerosols are thermally evaporated. Aerosol samples were also taken onto a cartridge and analysed on a GC-FID coupled to a PTR-MS.

-Ion Chromatography-MS: The gas and particle phase were sampled with a wet effluent diffusion denuder/ aerosol collector (WEDD/AC). Detection was done with a conductivity detector and a single quadrupole mass detector (Dionex, MSQ™) in series.

-FT-ICR-MS (Thermo Electron): Filter sampled SOA was extracted and electrosprayed into a high resolution, accurate mass LTQ-FT mass spectrometer and analyzed for high mass compounds.

The formation of oligomers was shown by the on-and off-line mass spectrometric methods laser desorption/ionization MS (LDI-MS), ATOFMS and FT-ICR-MS. The high-mass ions occur with a characteristic spacing of 14 and 16 Da, indicative of oligomeric species. A comparison between the (matrix-assisted) laser desorption/ ionization mass spectra and those of the ATOFMS showed good agreement. A similar result was observed by comparing spectra from the FT-ICR-MS and MALDI-MS. Temporal trends of peak families and individual mass peaks were analyzed and compared. The lower mass species in the particles and the gas phase were investigated and compared using PTR-MS and IC-MS.

This work was supported by the Swiss National Science Foundation (No. 2169-061393), by ETHZ (No. TH-10./01-2), the European Commission (EUROCHAMP, No. FP6-505968) and the Swiss Bundesamt für Bildung und Wissenschaft (ACCENT, No. 03.0430-1; EU No. GOCE-CT-2004-505337).

Kalberer, M., Paulsen, D., Sax, M., Steinbacher, M., Dommen, J., Prevot, A. S. H., Fisseha, R., Weingartner, E., Frankevich, V., Zenobi, R. & Baltensperger, U. (2004). *Science*, 303, 1659-1662.

Surratt, J. D., Murphy, S. M., Kroll, J. H., Ng, N. L., Hildebrandt, L., Sorooshian, A., Szmigielski, R., Vermeylen, R., Maenhaut, W., Claeys, M., Flagan, R. C. & Seinfeld, J. H. (2006). *J. Phys. Chem.*, 110, 9665-9690.

## Raman characterization of double salt formation from crystallization of mixed ammonium sulfate and ammonium nitrate particles

Tsz Yan Ling and Chak K. Chan

Department of Chemical Engineering, Hong Kong University of Science and Technology, Clear Water Bay, Hong Kong

Keywords: aerosol chemistry, aerosol thermodynamics, ammonium nitrate, ammonium sulfate

Ammonium sulfate (AS) and ammonium nitrate (AN) are ubiquitous components of atmospheric aerosols. Tani *et al.* (1983) observed nitrate present as double salts in ambient sampling. Thermodynamic predictions by the Aerosol Inorganic Model (AIM) also show the formation of both pure salts (AS and AN) and double salts (2AN\*AS and 3AN\*AS) in solid phase for the ammonium-sulfate-nitrate system.

In this study, single particle levitation by an electrodynamic balance (EDB) coupled with Raman spectroscopy was applied to investigate the chemical composition of crystals formed from AN/AS mixed droplets. We observed chemical transformation of the solids.

Reference Raman spectra for the two double salts were obtained for comparison with single particle Raman results, as shown in Figure 1. They show distinguishable signatures for each salt from nitrate signal at  $\sim 1050\text{cm}^{-1}$ .

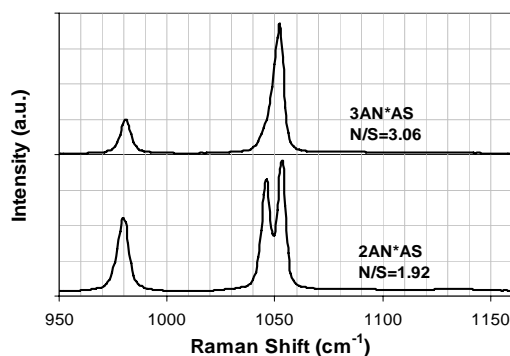
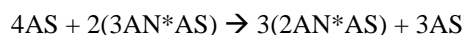


Figure 1. Raman spectra for 2AN\*AS and 3AN\*AS.

In single particle experiments, a droplet consisting of equal molar AN and AS was levitated in an EDB, which was then crystallized at its Crystallization RH (CRH) at  $\sim 30\%$ . The RH of the EDB chamber was then increased step-wise and the crystallized particle was allowed to attain equilibrium in the EDB for  $\sim 2$  hours until the Deliquescence RH (DRH) was reached. Single particle Raman spectra were measured at each equilibrium RH, using a 514.5nm argon ion laser as the excitation source, and a 1200g/mm grating of monochromator (Acton SpectraPro 500) with a CCD detector (Andor

Technology DV420-OE) attached. The resolution of the spectra was about  $2\text{cm}^{-1}$ .

Figure 2 shows the single particle Raman results. The double peaks or shoulder indicate the presence of 2AN\*AS, while the relatively stronger signal at  $1052\text{cm}^{-1}$  suggests the presence of 3AN\*AS at the same time. The gradual change in Raman signals with RH suggests the following chemical transformation has taken place.



Temporal and RH effects on the changes will be discussed.

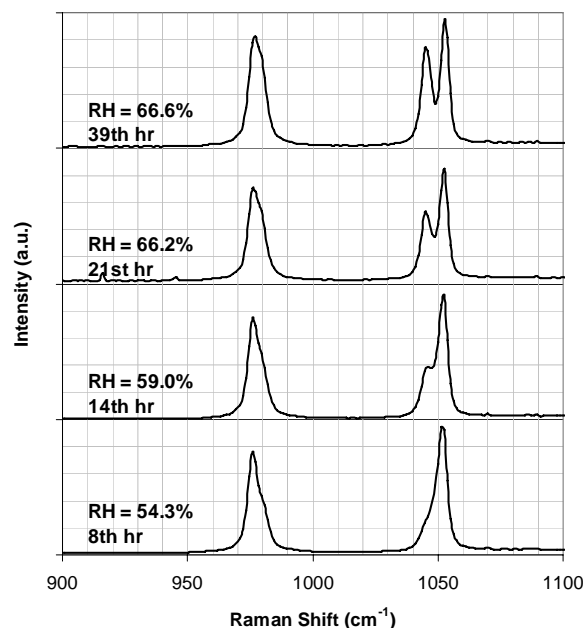


Figure 2. Raman spectra of solid AN/AS mixed particle equilibrated at various RHs.

This work was supported by the Research Grants Council Earmarked Grant of Hong Kong Special Administrative Region, China under grant 600303.

Tani, B., Siegel, S., Johnson, S. A. and Kumar, R. K. (1983). X-Ray diffraction investigation of atmospheric aerosols in the 0.3-1.0  $\mu\text{m}$  aerodynamic size range, *Atmos. Environ.*, 17, 2277-2283.

## Heterogeneous reactions of unsaturated fatty acid aerosols with ozone: Reaction pathways and changes of particle mass, hygroscopicity and morphology

Alex K. Y. Lee and Chak K. Chan

Department of Chemical Engineering, Hong Kong University of Science and Technology,  
Clear Water Bay, Kowloon, Hong Kong

Keywords: Aerosol chemistry, hygroscopicity, organic aerosols

Atmospheric aerosols experience various physical and chemical aging processes throughout their atmospheric lifetime. In particular, organic species in atmospheric particles are susceptible to reactions with gas phase atmospheric oxidants, such as ozone, OH and NO<sub>3</sub> radicals. Recently, ozonolysis of oleic acid has been emerged as a model system to better understand the chemistry of heterogeneous reactions of organic aerosols and their environmental effects. Linoleic acid and linolenic acid are poly-unsaturated fatty acids that have similar to oleic acid except for their degree of unsaturation. Since these two acids contain more carbon-carbon double (C=C) bonds in their hydrocarbon skeletons, they are expected to be more reactive than oleic acid under ozone exposure. While ozone molecules can directly attack the C=C bonds of linoleic acid and linolenic acid, it is particularly important to note that ozone can also initiate another oxidative pathway, so called autoxidation, of these poly-unsaturated fatty acids efficiently (Pryor, 1994). However, to the best of our knowledge, the autoxidation of poly-unsaturated fatty acids has not yet been reported in the literature of atmospheric chemistry. The significance of this specific oxidation pathway needs to be investigated.

In this study, the combination of electrodynamic balance (EDB) and single particle Raman system was utilized to investigate the heterogeneous reactions of linoleic acid and linolenic acid with ozone under ambient temperature (22–24 °C) and dry condition (RH<5%) (Lee and Chan, 2007). One of the distinct advantages of using EDB/Raman system for studying heterogeneous reactions is that long duration exposure of particles to gas phase reactants at concentrations relevant to atmospheric applications are possible as the particles can be trapped inside the EDB for an extended period of time (days). The primary objective of this study is to study the possible reaction pathways involved when the linoleic acid and linolenic acid particles expose to 200–250ppb of ozone. Extremely high ozone concentration (~10 ppm) was also applied in order to compare with the results obtained from the low ozone concentration experiments. The changes in particle mass, hygroscopicity and morphology due to ozone exposure are also reported.

Raman measurements provide spectroscopic evidences that ozone-induced autoxidation, in addition to direct ozonolysis, is also a plausible pathway in the reactions between ozone and linoleic acid and linolenic acid particles. The significance of this specific oxidation pathway, however, depends on the ozone concentrations applied in the experiment. At low ozone concentration (~200–250 ppb) with longer exposure period (20 hrs), it is more favorable for the particles to undergo autoxidation pathways since extremely high ozone concentration (~10 ppm) may force most of the unsaturated fatty acids to react with ozone in relatively short period of time. Direct particle mass measurements show that heterogeneous oxidations of organic aerosols can modify the particle mass yields in different extents depending on the molecular structures of chemical species. In the low ozone concentration experiments, the mass of the ozone-processed linoleic acid and linolenic acid particles increased by about 2–3% and 10–13%, respectively. Hygroscopic measurements confirm that the reaction products that remained in the particles are more hygroscopic than the hydrophobic parent molecules. The mass ratios (mass at RH≈85% /mass at RH<5%) of the ozone-processed linoleic acid and linolenic acid particles increased by about 2–3% and 3–4% respectively. Based on the particle morphology and laser-illuminated light scattering pattern, both pure and ozone-processed linoleic acid and linolenic acid particles were in liquid state and no phase transition were observed in the low ozone exposure experiments. On the contrary, there were some solid materials coated on the surface of the particles, making the particle shape irregular in the high ozone concentration experiments.

This work was supported by the Research Grants Council of the Hong Kong Special Administrative Region, China (Project No. HKUST600303).

Pryor, W. A. (1994), *Free Radical Biology and Medicine*, 17 (5), 451-465.

Lee, A. K. Y. & Chan, C. K. (2007), *Single particle Raman spectroscopy for investigating atmospheric heterogeneous reactions of organic aerosols*, submitted.

**Oxygenated organic aerosols: Bridging field and smog chamber observations**M.R. Alfarra<sup>1</sup>, A.S.H. Prevot<sup>1</sup>, J. Duplissy<sup>1</sup>, A. Metzger<sup>1</sup>, V. A. Lanz<sup>2</sup>, C. Hueglin<sup>2</sup>, J. Dommen<sup>1</sup>, E. Weingartner<sup>1</sup>, U. Baltensperger<sup>1</sup><sup>1</sup>Laboratory of Atmospheric Chemistry, Paul Scherrer Institut, 5232 Villigen PSI, Switzerland<sup>2</sup>Empa, Swiss Federal Laboratories for Materials Testing and Research, 8600 Dübendorf, Switzerland

Keywords: Aerosol chemistry, Aerosol mass spectrometry, Secondary organic aerosol, Biogenic particles

Two types of oxygenated organic aerosols (OOA I and OOA II) have recently been identified at urban locations in Europe (Lanz *et al.*, 2006) and North America (Ulbrich *et al.*, 2006) using the Aerodyne Mass Spectrometer (AMS) and based on multivariate statistical analysis methods. During a summer study in Zurich, Switzerland, OOA I was characterised by a relatively high  $m/z$  44 to total organic ratio and it had a mass spectral signature similar to that of fulvic acid (a model compound for aged and oxygenated organic aerosols and also for humic-like substances, HULIS). It was also found to have a similar temporal behaviour to the sulphate component of the aerosols. On the other hand, OOA II was found to be less aged than OOA I and it was characterised by a relatively high  $m/z$  43 to total organic ratio. It also had a similar temporal behaviour to the nitrate component of the aerosol and it was sensitive to ambient temperature (i.e. more volatile than OOA I). In this paper, we investigate the chemical composition of secondary organic aerosol (SOA) generated in a smog chamber from the photooxidation of the biogenic precursor ( $\alpha$ -pinene) and compare it to the ambient spectra of OOA I and OOA II. In particular, we present results showing the effect of the initial precursor concentration on the mass spectral signature of the SOA produced and on its chemical and physical properties.

Our findings suggest that the partitioning, in the smog chamber, is precursor concentration dependent. Results show that starting with lower precursor concentration, close to ambient conditions, leads to the formation of SOA particles that have a mass spectral signature representative of organic aerosols measured at rural and remote locations (Alfarra *et al.*, 2006). These findings are illustrated for SOA particles produced from the photooxidation of  $\alpha$ -pinene using a range of initial concentrations in the presence of  $\text{NO}_x$  (while keeping the  $\text{VOC}/\text{NO}_x$  ratio constant). Results in Figure 1 show that using lower initial precursor concentrations leads to the production SOA which is more similar to the ambient OOA I type (described above). On the other hand, SOA produced from the photooxidation of high initial precursor concentrations is more similar to the ambient OOA II type. In other words, lower initial precursor concentrations leads to the formation of SOA, which has a mass spectrum that is dominated by  $m/z$  44 and has a signature similar to that of fulvic acid, while the SOA produced using higher initial

precursor concentrations has a mass spectrum that is rich in  $m/z$  43 and appears to be relatively more volatile. These findings will be compared to results obtained using other precursors such as isoprene and 1,3,5-trimethylbenzene (1,3,5-TMB).

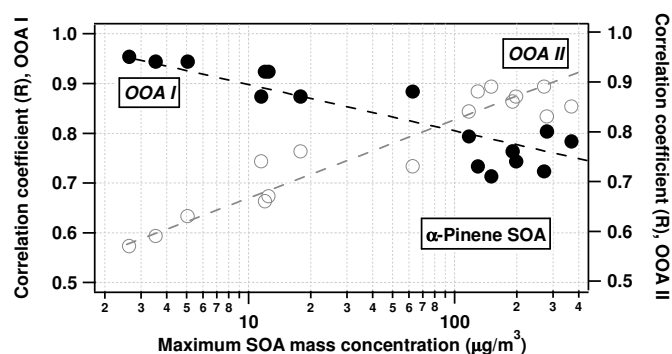


Figure 1: Correlations of the mass spectra of  $\alpha$ -pinene SOA produced using various precursor concentrations with the mass spectra of the ambient OOA I and OOA II aerosol components measured during a summer study in Zurich.

- Alfarra, M. R., Paulsen, D., Gysel, M., Garforth, A. A., Dommen, J., Prévôt, A. S. H., Worsnop, D. R., Baltensperger, U. and Coe, H. (2006), A mass spectrometric study of secondary organic aerosols formed from the photooxidation of anthropogenic and biogenic precursors in a reaction chamber, *Atmos. Chem. Phys.*, 6, 5279–5293.
- Lanz, V. A., Alfarra, M. R., Baltensperger, U., Buchmann, B., Hueglin, C. and Prevot, A. S. H. (2006), Source apportionment of submicron organic aerosols at an urban site by linear unmixing of aerosol mass spectra, *Atmos. Chem. Phys. Discuss.*, 6, 11681–11725.
- Ulbrich, I., Brinkman, G., Hannigan, M., Milford, J., Jimenez, J. and Zhang, Q. (2006), Source apportionment of aerosol mass spectrometer data in Pittsburgh and Mexico City using positive matrix factorization and other time-series analysis methods. *International Aerosol Conference, St. Paul, Minnesota, USA*, p1779.

## Functional group monitoring in atmospheric particulate organic matter using tandem mass spectrometry: method developments and applications

J. Dron<sup>1</sup>, N. Marchand<sup>1</sup>, M. Camredon<sup>2</sup>, B. Aumont<sup>2</sup> and H. Wortham<sup>1</sup>

<sup>1</sup>LCE, University Aix-Marseille 1, 3 place Victor Hugo, 13331, Marseille Cedex 3, France

<sup>2</sup>LISA, UMR CNRS 7583, University Paris 7 and Paris 12, 94010 Créteil Cedex, France

Keywords: Aerosol characterization, Chemical composition, Mass spectrometry, Modelling.

Particulate organic matter (POM) in atmospheric aerosols results from primary emissions as well as in situ formation through oxidative processes of gas-phase organic compounds, and contributes in approximately 20 to 50% of the total fine aerosol mass at continental mid-latitude (Kanakidou, 2005). It has been well established that this class of particulate material has a high potential impact on both human health and climate change. In order to better estimate the influence of organic aerosols, a good knowledge of their organic fraction in terms of composition and reactivity is required. However, considering the degree of complexity of POM, conventional analytical methods lead to its incomplete characterization (Jacobson, 2000).

Functional group determination is a complementary approach between molecular identification and organic carbon measurements which enables the characterization of a larger fraction of the aerosol mass and provides valuable information on its chemical composition. This analytical technique being besides the best suited for modelling purposes, it appears imperative to improve its performances. Also, Fourier Transform Infrared spectroscopy (FT-IR) suffers from poor robustness (Blando, 2001), proton nuclear magnetic resonance (H-NMR) (Tagliavini, 2006) requires heavy instrumentation, and both have a relatively low sensibility.

The aim of this work is to propose a new method for the analysis of functional groups and to highlight its relevance for atmospheric chemistry purposes. The analytical method is based on tandem mass spectrometry operating in the constant neutral loss scanning mode (CNLS-MS/MS). The quantification of the functional groups relies on the ability of the compounds bearing the same functional group to lose an identical and characteristic neutral fragment into the MS collision cell. Analytical procedures were developed for the determination of carboxylic acids, and carbonyl and hydroxyl compounds. Compared to FT-IR and H-NMR, this analytical strategy offers major benefits, providing (i) a molecular weight distribution of the detected compounds (ii) high accuracy quantification of the targeted moieties (iii) low detection limits suited to environmental measurements.

The methodology was successfully applied to carboxylic group quantification into POM collected

in July 2006 in Marseille, France. For that purpose, the carboxylic functionalities were derivatized into their corresponding methyl esters and the loss of the methanol neutral fragment was monitored. Figure 1 compares two mass spectra obtained before and after derivatization. The upper one characterizes qualitatively the initial methyl ester and methoxy content of the sample while the lower one provides a quantitative measurement of the carboxylic concentration. Carboxylic concentrations ranged from 8 to 12 nmol/m<sup>3</sup> for respectively night and day sampling. The monitoring of the major oxygenated functional groups (i.e. carboxylic, carbonyl and hydroxyl) during photooxidation experiments of n-decane in the EUPHORE (Valencia, Spain) simulation chamber and the comparison of the analysis results with what calculated by a Self Generator of Master Mechanisms model (Aumont, 2005) also permitted to investigate the formation pathways of these functionalities.

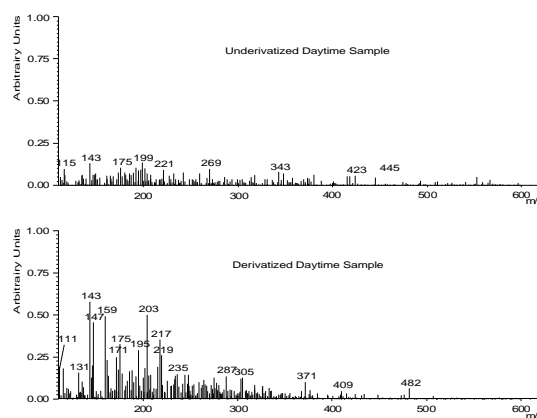


Figure 1. Mass spectra obtained for the neutral loss analysis of methanol ( $m/z$  32) of the same sample before and after derivatization.

Aumont, B. Et al. (2005). *Atmos. Chem. Phys.*, 5, 2497-2517.

Blando, J. D. et al. (2001). *Aerosol Sci. Technol.*, 35, 899-908.

Jacobson, M. C. et al. (2000). *Rev. Geophys.*, 38, 267-294.

Kanakidou, M. et al. (2006). *Atmos. Chem. Phys.*, 5, 1053-1123.

Tagliavini, E. et al. (2006). *Atmos. Chem. Phys.*, 6, 1003-1019.

## Effects of the wildfires in August 2006 on the air quality in south-eastern Finland

U. Makkonen<sup>1</sup>, P. Anttila<sup>1</sup>, H. Hellén<sup>1</sup> and M. Ferm<sup>2</sup>

<sup>1</sup>Finnish Meteorological Institute, Air Quality Research, P.O. Box 503, FI-00101 Helsinki, Finland

<sup>2</sup>IVL Swedish Environmental Research Institute, P. O. Box 5302, 400 14 Gothenburg, Sweden

Keywords: Atmospheric Aerosols, PM10, PM2,5/PM1, Trace Elements, PAH

In August 2006 several wildfires in north-western Russia affected widely the air quality at the surrounding areas. During these fires enhanced aerosol measurements of different fractions (PM10, PM2,5 and PM1,0) were carried out at the Virolahti background station in southeastern Finland, about 5 kms from the Russian border.

At the Virolahti station (N 60°32', E 27°41'), PM10, PM2,5 and PM1,0 aerosol particles were collected with three parallel collectors. The PM10 sampler was supported with the sampling head (Digitel DPM10/2,3/01, 2,3 h/m<sup>3</sup> according to EN12341) and the PM2,5 sampler with a MCZ PM2,5-sampling head. For collecting the smallest particles an IVL-made PM1,0 sampling head (flow 17.8 l/min) was used. The particles were collected on polytetrafluoroethylene (PTFE) filters. The chemical composition of the particulate matter was investigated by ion chromatography (main ions), inductively coupled plasma mass spectrometry (trace elements) and gas chromatography mass spectrometer (polyaromatic hydrocarbons).

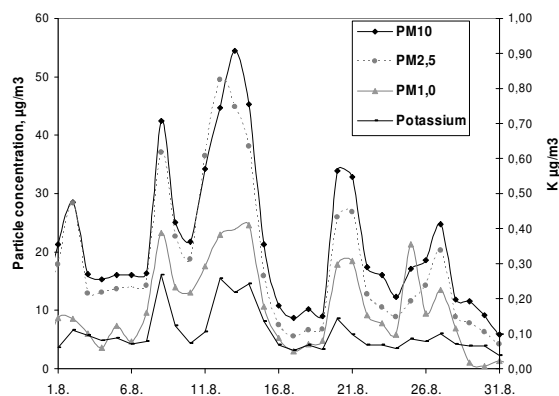


Figure 1. The mass concentrations of PM10 (black line), PM2,5 (dot line), PM1,0 (grey line) and potassium at Virolahti southeastern Finland in August, 2006.

During this one month period the measured PM10 value exceeded the 24h limit value (50 µg/m<sup>3</sup>) once. The ratio PM2,5/PM10 was 0.79, and the proportion of PM1,0 rose up to as high as 60 % of the mass of the PM10 (Fig.1).

The highest concentrations of PAHs (11 ng/m<sup>3</sup>) were measured from the PM10 fraction on 13<sup>th</sup> August simultaneously with the PM10 maximum (Fig. 2). This high PAH concentrations are

characteristic rather to wintery traffic environments. Potassium concentration followed the particulate mass concentration closely and the measured concentrations exceeded 0,2 µg/m<sup>3</sup> on 8<sup>th</sup> and 12-15<sup>th</sup> August.

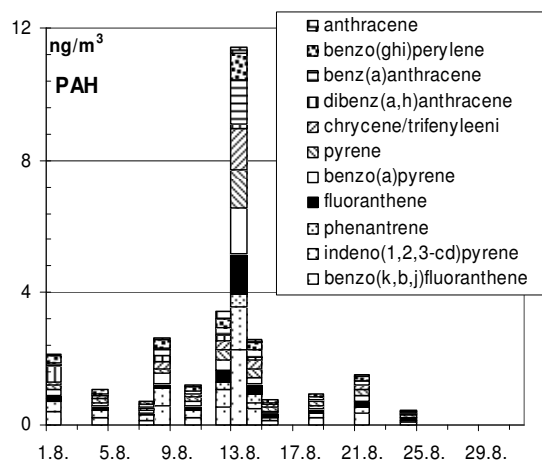


Figure 2. The concentrations of polyaromatic hydrocarbons from PM10 at Virolahti in August, 2006

Also the concentrations of trace elements rose during the episode (Fig 3). The most abundant trace elements were Zn and Pb. However the concentrations of the regulated elements As, Cd and Ni remained well below their annual EU limit value levels.

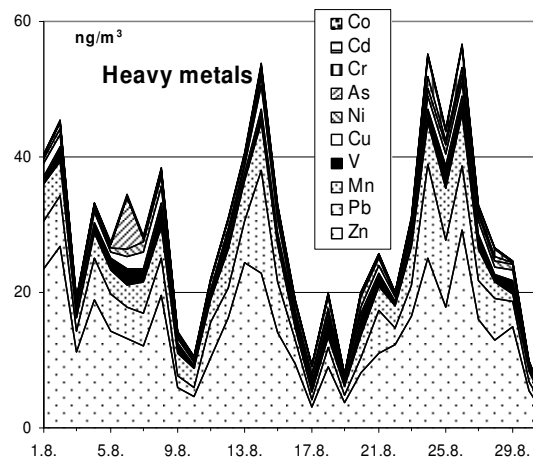


Figure 3. The concentrations of trace elements from PM10 at Virolahti in August, 2006.

## The influence of relative humidity on the SOA-formation at various temperatures

R. Tillmann<sup>1</sup>, Th.F. Mentel<sup>1</sup>, A. Kiendler-Scharr<sup>1</sup>, and H. Saathoff<sup>2</sup>

<sup>1</sup>Institute for Chemistry and Dynamics of the Geosphere, ICG II: Troposphere, Research Centre Jülich, 52425 Jülich, Germany

<sup>2</sup>Institute of Meteorology and Climate Research, Forschungszentrum Karlsruhe, POB 3640, 76021 Karlsruhe, Germany

Keywords: SOA, aerosol formation, VOC(s), smog chamber.

Monoterpenes represent a significant fraction of biogenic originated volatile organic compounds in the atmosphere. The oxidation of monoterpenes by ozone, OH- and NO<sub>3</sub>-radicals has been identified as a significant source for secondary organic aerosols (SOA) in the atmosphere (Griffin *et al.*, 1999).

SOA-yields are dependent on a variety of parameters like organic precursors, oxidants, relative humidity, temperature and pre-existing particulate organic mass for the absorption of the respective oxidation products.

We investigated the SOA-yields of the ozonolysis of  $\alpha$ -pinene and limonene under dry and humid conditions in the aerosol chamber AIDA (Saathoff *et al.*, 2003) at temperatures of 303 and 253 K. All experiments were carried out in the presence of 500 ppm cyclohexane to scavenge OH-radicals produced during the reaction. Ozone has been used in excess of the monoterpene concentration. The monoterpene was added stepwise into the chamber in amounts up to 50 ppb after complete consumption of the monoterpene of the previous step. This way the SOA-yield for increasing organic aerosol mass was determined.

The monoterpenes and their oxidation products in the gas phase were measured by proton-transfer-reaction mass-spectrometry (PTR-MS, IONICON). The composition of the aerosol phase was characterized by means of an aerosol mass spectrometer (Q-AMS, Aerodyne Research Inc.). Size distributions of the organic aerosol were measured with differential mobility particle sizers (DMA 3071 & CPC 3010, TSI) outside and inside the thermostated housing of the AIDA chamber.

SOA-masses were calculated from the measured size distributions using an aerosol density of 1 g/cm<sup>3</sup>. SOA-mass-concentrations were set in relation to the consumed monoterpene providing a time dependent growth function (Fig. 1). Data is provided with a time resolution of 5 minutes.

We observed smaller SOA-yields for  $\alpha$ -pinene and limonene under dry conditions at a temperature of 253 K (Tab. 1 and Fig. 1). At room temperature no significant humidity dependance of the SOA-yield was observed. The AMS measurements reveal, that partitioning of water to the aerosol phase is small under humid conditions and cannot account for the

increase in SOA-yields as determined from the measured size distributions.

Table 1. Mean SOA-yields under dry and humid conditions.

Monoterpene	T [K]	SOA-Yield (dry)	SOA-Yield (humid)
$\alpha$ -Pinene	303	0.15	0.18
$\alpha$ -Pinene	253	0.53	0.86
Limonene	253	0.75	1.42

PTR-MS measurements reveal, that the molar yield of the  $\alpha$ -pinene oxidation product pinonaldehyde at 303 K is significantly lower under dry conditions. At 253 K pinonaldehyde is exclusively found in the condensed phase due to its low vapor pressure. The lower molar yield of pinonaldehyde under dry conditions therefore lowers the SOA-yield at 253 K. Thus water plays an important role in the reaction mechanisms of the  $\alpha$ -pinene ozonolysis. The presence of water vapor leads to the production of low volatile products resulting in higher SOA-yields under humid conditions.

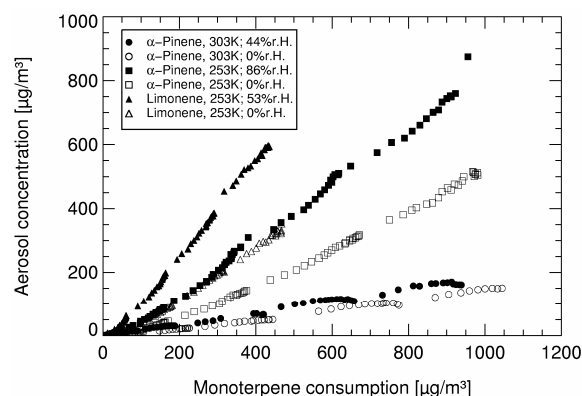


Figure 1. Humidity- and temperature dependent growth functions of SOA-concentrations formed from the ozonolysis of  $\alpha$ -pinene and limonene.

Griffin, R. J., Cocker, D. R., Flagan, R. C. & Seinfeld, J. H. (1999). *J. Geophys. Res. - Atmos.*, 104, 3555-3567.

Saathoff, H., Moehler, O., Schurath, U., Kamm, S., Dippel, B., Mihelcic, D. (2003). *J. Aerosol Science*, 34, 1277-1296.

## Chamber studies of the stable carbon isotope composition of secondary organic aerosol formed by $\beta$ -pinene ozonolysis

R. Fisseha<sup>1</sup>, A. Kiendler-Scharr<sup>1</sup>, H. Spahn<sup>1</sup>, R. Tillmann<sup>1</sup>, R. Wegener<sup>1</sup>, and A. Wahner<sup>1</sup>

<sup>1</sup>Institut für Chemie und Dynamik der Geosphäre, ICG-II: Troposphäre, Forschungszentrum Jülich, Jülich, Germany

Keywords: SOA, Aerosol chemistry, smog chamber, stable carbon isotope, organic aerosols.

Atmospheric aerosols impact the global radiation budget, the hydrologic cycle and human health. The organic aerosol component which is composed of numerous species with a variety of functionalities poses a big challenge in determining aerosol sources, physical properties and their influence in climate change. The formation of secondary organic aerosols (SOA) via oxidation of volatile organic compounds (VOCs) emitted from plants is one important source of organic aerosols in the atmosphere (Finlayson-Pitts and Pitts, 2000). Several techniques are used to determine the formation pathways of SOA.

Stable isotopes of carbon have been widely used for trace analysis and source apportionment in different environments. In atmospheric studies, the stable carbon isotope composition, expressed as  $\delta^{13}\text{C}$ , has provided invaluable information on temporal evolution of  $\text{CO}_2$  and other carbon containing greenhouse gases (Flanagan *et al.*, 2005). Recently it was shown that concurrent measurements of the mixing ratio and  $\delta^{13}\text{C}$  values of atmospheric VOCs can be used to provide information on the extent of chemical processing these VOCs have undergone in the troposphere (Rudolph *et al.*, 2003). As an extension to this approach we combine the measurement of gas phase and particulate phase  $\delta^{13}\text{C}$  values to study the formation of SOA from the ozonolysis of  $\beta$ -pinene which were performed in the Jülich large indoor chamber.

$\beta$ -Pinene and ozone were injected into a large indoor chamber and let to react. No OH scavenger was used during the experiments implying that part of the oxidation was due to OH formed in ozonolysis reactions. Gas phase samples were collected in SilcoSteel canisters (SilcoCan), with a time interval of 2h. Aerosol samples were collected on quartz fiber filters (Whatman) at a flow rate of 15l/min for 3h. All filters were pretreated at a temperature of 600 °C overnight before sampling. A customized thermal desorption system combined with cryofocusing (from Gerstel) was used for desorbing the compounds from the filter and sampling the gas phase compounds. 2-D gas chromatography coupled with isotope ratio mass spectrometry (GC-IRMS) was used for investigations of the stable carbon isotope ratios of selected VOCs in both the gas phase and particulate phase. The concentration of  $\beta$ -pinene together with some

reaction products was monitored using a proton transfer mass spectrometer (PTRMS).

In first test measurements, nopinone was found in both the gas and particulate phase with a higher  $\delta^{13}\text{C}$  values compared to  $\beta$ -pinene. The nopinone  $\delta^{13}\text{C}$  value for the particulate phase was also found to be higher than the corresponding gas phase value. In addition acetone with a lower  $\delta^{13}\text{C}$  value compared to  $\beta$ -pinene was found from the filter samples.

The data indicates the potential of stable carbon isotope measurements in studying SOA formation and characterization. The general viability of the combined measurements of  $\delta^{13}\text{C}$  in gas phase and particulate phase atmospheric samples for source apportionment and studies of the extent of chemical processing in the atmosphere will be discussed in more detail.

Finlayson-Pitts, B. J. & Pitts, J. N. (2000). *Chemistry of the upper and lower atmosphere*. Academic Press, San Diego.

Flanagan, B., Ehleringer, J.R., & Pataki, D.E. (2005). *Stable Isotopes and Biosphere Atmosphere Interactions: Process and Biological Controls*. Elsevier, Great Britain.

Rudolph, J., Anderson, R.S., Czapiewski, K.V., Czuba, E., Ernst, D., Gillespie, T., Huang, J., Rigby, C., & Thompson, A.E. (2003). *Journal of Atmospheric Chemistry*, 44 (1), 39-55.

## Evaporation of multicomponent droplets.

I.K. Koponen, I. Riipinen, M. Kulmala,  
G. Frank, and M. Bilde

Department of Chemistry, University of Copenhagen, Universitetsparken 5, DK-2100 Copenhagen,  
Denmark

Department of Physical Sciences, Division of Atmospheric Science, P.O.Box 64,  
FIN-00014 University of Helsinki, Finland

Keywords: organic compounds, vapor pressure, evaporation, condensation

Water-soluble organic compounds constitute a significant fraction of the organic atmospheric aerosol (Saxena et al., 1995). These organic compounds participate in condensation and evaporation processes in the atmosphere. Therefore thermodynamic data related to aerosol formation and growth are crucially needed for developing a truly predictive capability for anthropogenic effects on e.g. studies of climate change. Previously, evaporation rates of a series of aqueous solution droplets containing water soluble organic compounds have been determined experimentally (Riipinen et al., 2006 Koponen et al., submitted). Experimental data were incorporated into a model for multicomponent condensational growth and/or evaporation of droplets in the atmosphere (Kulmala et al., 1991). In this study we have extended our goal to make an effort to measure evaporation rates of mixed particles. Our first attempt is to measure evaporation of droplet containing succinic acid and sodium chloride.

Using a laminar flow chamber evaporation rates of droplets at the initial size 100 nm were measured at relative humidities above their crystallization relative humidity. Experiments were performed at room temperature. Vapor pressures will be determined from these experiments using a mass transfer model for evaporation of binary/ternary aerosol particles. A more detailed description of the measurement set up and the model is presented in the paper Riipinen et al., 2005.

In Figure 1 evaporation rates of aqueous succinic acid and succinic acid NaCl droplets as a function of time are presented. The initial sizes of the droplets after DMA were 100 nm, but only data obtained inside the laminar flow reactor (10-60 s.) the 3<sup>rd</sup> and 6<sup>th</sup> points will be used in the modeling studies.

For pure succinic glutaric and malonic acids experimental and modeling studies are already

done (Riipinen et al., 2006 and Koponen et al., submitted.) and studies of the mixtures are in progress.

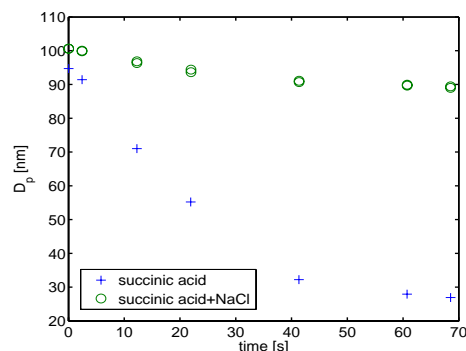


Figure 1. Measured evaporation rates of the succinic acid and mixture of succinic acid(72 %) and NaCl(28 %) solution droplets are presented.

This work is supported by the Carlsberg Foundation and the Danish Natural Science Research Council.

Saxena, P., Hildemann, M., Seinfeld, J. Organics alter the hygroscopic behavior of atmospheric particles. *J. Geophys. Res.* 100, 18, 1995, 18,555-18,770.

Koponen I.K., Riipinen I., Frank G., Markku Kulmala and Bilde M., Thermodynamic properties of succinic, glutaric and malonic acids: evaporation rates and saturation vapor pressures. *Environ. Sci. Technol.*, submitted.

Kulmala, M., Vesala, T. Condensation in the continuum regime. *J. Aerosol Sci.* 1991, 22, 337- 346

Riipinen, I., Svenningsson, B., Bilde, M., Gaman, A., Ehtinen, K.E.J. and Kulmala M., A method for determining thermophysical properties of organic material in aqueous solutions: succinic acid, *J. Atmos. Res.* 2006, 82, 579-590.

## Ion composition in submicron aerosols in Helsinki area

K. Teinilä, M. Aurela, H. Timonen, S. Kuokka, S. Saarikoski, K. Saarnio, O. Tolonen-Kivimäki, and R. Hillamo

Finnish Meteorological Institute, Air Quality Research, Erik Palménin auku 1, FIN-00560, Helsinki, Finland

Keywords: Aerosol chemistry, measurements, PM<sub>1.0</sub>

Aerosol composition was studied in Helsinki city area between Feb. 10, 2006 and Nov. 28, 2006. Ion concentration was measured with continuous PILS-IC system. The PILS-IC system consists the PILS sampler (Particle Into Liquid Sampler, Orsini *et al.*, 2003) coupled with two Dionex ICS-2000 ion chromatographs. The PILS sampler was connected to a virtual impactor which divides aerosol particles into two size fractions (cut size 1.0 µm). The submicron fraction of the sample was fed into the PILS sampler. Denuders were installed upstream of the sampling line to remove acidic gases and ammonia from the sampled air. Concentration of sulphate, nitrate, ammonium, potassium, sodium, chloride and oxalate was measured with 15 minutes time resolution.

PM<sub>1.0</sub> sampler was used to collect aerosol samples on a quartz fibre filter for subsequent analysis by the IC. The sampling time was typically 24 hours, except during the weekends when it was 72 hours.

The ion concentrations obtained from the PILS-IC system were averaged for each PM<sub>1.0</sub> sampler measurements in order to compare the concentrations obtained from these two methods. The calculated correlation coefficients were 0.85 for sulphate, 0.80 for nitrate, 0.75 for ammonium, 0.69 for potassium and 0.48 for oxalate. Comparison were not made for sodium and chloride since their concentrations are typically low in submicron particles, and the sodium blank was quite high for the quartz fibre filters.

The average PILS to PM<sub>1.0</sub> sampler ratio for sulphate was 0.82 during the campaign (standard deviation std.=0.23). PILS measurements give slightly lower concentrations compared to the PM<sub>1.0</sub> sampler measurements, but this ratio is still reasonable good. The lower PILS results may be due to some internal losses of aerosol particles inside the PILS sampler. For ammonium this ratio was 1.25 (std. 0.46) and for nitrate 1.77 (std. 1.92). The ratios above unity indicate possible evaporation of nitric acid and ammonium nitrate from the quartz fibre filters during the samplings.

The PILS to PM<sub>1.0</sub> ratio for potassium was 0.81 (std. 0.49) and for oxalate 0.34 (std. 0.52). The concentration of oxalate was often near the detection limit, which can partly explain this lower ratio for it. However the measured potassium concentrations were typically in the same level than the oxalate

concentrations, so there may be also other reasons for this low ratio. One possible explanation is the evaporation of oxalate inside the PILS sampler.

The results showed that there are differences between the two measurement techniques. For sulphate which is non-volatile, the results obtained from the PILS system are lower compared to the PM<sub>1.0</sub> measurements. However, if nitric acid and ammonium nitrate are evaporated during the samplings from the quartz fibre filter, the concentrations obtained from PILS-IC measurements could be more accurate than those obtained from the PM<sub>1.0</sub> measurements.

Although there may be some uncertainties in the PILS-IC measurement, its good time resolution gives valuable information on short lasting episodes and temporary high concentration levels. Also diurnal variations of different ions can be obtained from these kinds of measurements.

Potassium can be used as a tracer for biomass burning. During the campaign there were often temporary high potassium concentrations which were probably due to local biomass burning in residential heating. During the spring and summer 2006 couple of long lasting wildfire episodes were observed in Helsinki. During these episodes the concentration of potassium and also oxalate were at high level for a long time period. Nitrate concentrations showed their lowest values during June and July. This can be partly due to evaporation of nitric acid from the aerosol particles in the atmosphere during the warm season. It may also indicate that the main source of particulate nitrate is traffic emissions. The use of automobiles in Helsinki area is in its minimum during the summer months.

This work was supported by the Finnish Funding Agency for Technology and Innovation (grant no. 40531/04) and Magnus Ehrnrooths Foundation.

Orsini, D., Ma, Y., Sullivan, A., Sireau, B., Baumann, K., and Weber, R., (2003). *Atmos. Environ.* 37, 1243-1259.

## Source contribution to high PM<sub>10</sub> episodes in a residential area in the vicinity of two cement plants

A. Carratala<sup>1</sup>, E. Yubero<sup>2</sup>, M. Santacatalina<sup>1</sup>, J.F.Nicolas<sup>2</sup>, J. Crespo<sup>2</sup>

<sup>1</sup>Dept. de Ingenieria Química, Universidad de Alicante. 03080 Alicante, Spain

<sup>2</sup>CA, Laboratorio de Contaminación Atmosférica  
Div. de Física Aplicada, Universidad Miguel Hernández de Elche. 03202 Elche, Spain

Keywords: aerosols, PM<sub>10</sub>, chemical composition, source apportionment, cement

The objective of the present work was to know the main sources and their contribution to high PM<sub>10</sub> episodes in a residential area located in the vicinity of two cement plants where the responsibility of high pollution episodes is a matter of concern. The sampling has been done at the University of Alicante (southeastern Spain), which is situated in between the growing residential areas of two main cities, Alicante and San Vicente (of 350,000 and 35,000 inhabitants, respectively), and next to cement plants. The study period covers more than one year (June 2004 to July 2005). 84 samples with high PM<sub>10</sub> levels have been selected. These episodes correspond to specific meteorological situations such as advections and stable conditions. The average level of PM<sub>10</sub> of samples analysed was 46.9 µg/m<sup>3</sup>.

The analysis of NO<sub>3</sub><sup>-</sup>, SO<sub>4</sub><sup>-2</sup>, and Cl<sup>-</sup> were made by ionic chromatography on water extracts of a quarter of fibre quartz filters. NH<sub>4</sub><sup>+</sup> was analysed in water extracts by indophenol method. For the metal analysis, half of the filter was digested using an acidic oxidant digestion (HNO<sub>3</sub> (65%) H<sub>2</sub>O<sub>2</sub> (30%)) on a microwave oven reaching high temperature (170 C) and analysed by ICP-Mass spectrometry. C was determined directly on the filters by a ECO CN analyser.

The results from factor analysis performed on the dataset is summarised in Table 1. Only elements with factor loadings >0.5 are shown. Five factors were found. The first factor has as main tracers Mg, Al, Fe, K, Mn, this suggest a mineral origin of the atmospheric particles, probably originated from natural sources (regional-scale re-suspension and African Outbreaks). The tracers of the second factor are V, Ni, Ca, Sr. V and Ni are generally known as tracers for oil combustion emissions and Ca and Sr are cement compounds. In the surroundings of the sampling site is found two cements plants. Hereby this factor suggests cement plant emissions as the underlying PM source. The third factor represents a traffic source (traced by Cu, Pb and C). Cu is a known tracer of break-wear and carbonaceous particles are tracers of exhaust emissions (mostly diesel). In factor 4, SO<sub>4</sub><sup>-2</sup> is the main tracer and thus suggests that this source was associated with secondary aerosols and regional- or long-range air

mass transport, given the long atmospheric residence time of (NH<sub>4</sub>)<sub>2</sub>SO<sub>4</sub>. Furthermore, secondary aerosols may also originate from local NO<sub>x</sub> and SO<sub>2</sub> from industry or traffic on a city scale (regional-scale). Finally, the last factor may be easily identified as sea salt with Cl and Na as main tracers.

	Mineral	Cement Plant	Traffic	Sec. Aerosol	Sea-salt
g					
l					
e					
n					
i					
Ca					
r					
Cu					
o					
b					
C					
Cl					
a					

Table 1. Factor analysis results

quantification of the sources contributions to PM<sub>10</sub> described above was carried out by means of M RA. A good correspondence was achieved between the modelled and the gravimetric PM<sub>10</sub> results with R<sup>2</sup> value 0.85. Mineral source constitutes the major source of PM<sub>10</sub> with a 36 (~17µg/m<sup>3</sup>) of the PM<sub>10</sub> mass. Cement plant contribution constitutes the second highest PM<sub>10</sub> fraction with a percentage of 17 (~10µg/m<sup>3</sup>). The traffic source accounted for 15 of the PM<sub>10</sub> mass with ~7µg/m<sup>3</sup>. The secondary aerosol source represents only 8 (~3.5µg/m<sup>3</sup>) of the mass due to the selection of the days explained above. Finally, sea-salt accounted for 4 the mass (~2µg/m<sup>3</sup>).

## Iron concentrations, dioxins and metals near two cement plants

J. A. Conesa A. G. Ivez M. Santacatalina A. Carratal

Dept. de Ingenieria Química, Universidad de Alicante. 03080 Alicante, Spain

Keywords: aerosols, PM10, chemical composition, dioxin, cement

Levels of PM10 particles were measured at the University of Alicante, situated close to two cement plants and in between the growing residential areas of two important towns (populations 350,000 and 65,000), where public concern about air quality is increasing. The objective of this study was to determine the levels of the toxic pollutants (metals, PCDDs/Fs and PAHs) in the highest PM10 episodes that occurred along a one-year period (June 2004 to July 2005), in order to inspect the most dramatic situations and the possible influences from different sources: anthropogenic (cement production, traffic) or natural, like Saharan intrusion. The average level of PM10 for the one-year period was 43.90  $\mu\text{g}/\text{m}^3$  and the PM10 average of the samples analysed was 61.11  $\mu\text{g}/\text{m}^3$ .

The analyses of the dioxin and furan levels in the quartz fibre filters that contained the particulate matter were done following the U.S.EPA 1613 method. Dioxin and furans tetra to octachlorinated by isotopic dilution, and using high resolution gas chromatography (HRGC) with a high resolution mass spectrometer (HRMS) as detector. For the PAH analysis, a gas chromatograph with a mass spectroscopy detector was employed. Metal analysis was performed using an acidic oxidant digestion ( $\text{HNO}_3$  (65%)  $\text{H}_2\text{O}_2$  (30%)) in a microwave oven at a high temperature (170 C) and then analysed by ICP-Mass spectrometry. The analysis for  $\text{NO}_3^-$ ,  $\text{SO}_4^{2-}$ , and  $\text{Cl}^-$  was made by ionic chromatography of water extracts from a quarter of the fibre quartz filters. Water extracts were analysed for  $\text{NH}_4^+$  by the indophenol method.

The different analyses (inorganic ions, heavy metals, PCDDs/Fs and PAH) were performed on daily filters from high episodes that correspond to three common meteorological conditions. Tables 1 and 2 show the results for total PCDDs/Fs and PAH. The average levels detected in the different analyses were approximately 10 times less than the limits or objective values stipulated in the directives or WHO recommendations.

The comparison of major ion content with that of urban and industrial environments show that pollution levels of secondary ions are in the lower end of the range of heavy urban and industrial environment levels, whereas calcium content is far above the range for those polluted environments.

Also, the levels of V, Tl and to a lesser extent Ni are found to be higher than the reference environments. Dioxin and furan levels are similar to those obtained in urban environments, both in concentration (approx. 50 fg I-TE / $\text{m}^3$ ) and congener distribution. Polyaromatic hydrocarbon (PAH) analysis shows that the major compounds are naphthalene and fluoranthene but levels are even lower than those found in some rural areas.

With respect to meteorological conditions, advective conditions causing high PM10 episodes present lower levels of V, Ca, Sr, Ni and PCDDs/Fs compared to stable meteorological conditions where local emissions accumulate.

Table 1. Results of dioxin analysis (total I-TE values) analysis made in the laboratory of Dioxins of CSIC (Barcelona)

Sample	Dioxin concentrations (fg/ $\text{m}^3$ )
1	5.36
2	40.7
3	59.4
4	6.43
5	85.56
6	61.80
7	45.32
8	32.18
9	6.69

Table 2. Concentrations of PAHs in filter samples

	Concentration ng/m		
aphthalene	46,56	1,77	0,35
cenaphthylene	0,14	n.d.	n.d.
cenaphthene	n.d.	n.d.	n.d.
luorene	0,17	n.d.	n.d.
henanthrene	0,11	0,19	0,06
anthracene	n.d.	n.d.	n.d.
fluoranthene	0,51	0,59	0,14
benzofluoranthene	0,55	0,67	0,14
benzo[a]anthracene	1,34	1,03	0,50
Chrysene	1,51	1,74	0,38
benzo[b]fluoranthene	n.d.	0,22	0,07
benzo[k]fluoranthene	n.d.	0,66	0,17
benzo[a]pyrene	0,31	0,37	0,73
indeno[1,2,3-cd]perylene	0,34	0,55	0,18
benzo[e]anthracene	0,05	0,06	0,02
benzo[ghi]perylene	0,36	0,61	0,21

## Seasonal dependence of polar and non-polar organic compounds in aerosols in the atmosphere of A Coruña City (NW-Spain)

D. García-Gacio<sup>1</sup>, M. Piñeiro-Iglesias<sup>2</sup>, E. Concha-Graña<sup>1</sup>, P. López-Mahía<sup>1,2</sup>, S. Muniategui-Lorenzo<sup>1</sup> and D. Prada-Rodríguez<sup>1,2</sup>

<sup>1</sup>Department of Analytical Chemistry, University of A Coruña, Campus da Zapateira s/n. 15071, A Coruña.

<sup>2</sup>Institute of Environment, University of A Coruña, Pazo de Lóngora, Liáns, 15179, A Coruña.

Keywords: aerosol characterization, organic compounds, primary organic compounds, SOA, urban aerosols.

The major aerosol components include inorganic substances such as sulphates and carbonaceous species. The carbonaceous aerosol is formed by a complex mixture of organic compounds and a mass of carbon atoms with a graphitic-like structure that is black in colour and is normally called soot or black carbon. However, there is a general consensus that the organic composition of atmospheric aerosol should be understood to correctly describe the multiphase atmospheric system and to evaluate its environmental and health effects (Alves et al., 2006).

The main goal of this work was the quantification of non-polar and polar compounds present in PM<sub>10</sub> and PM<sub>2.5</sub> aerosols from an urban site and the study of their evolution during one year (May 2004-May 2005).

The most relevant solvent extractable organic compounds (SEOC) identified classes were fatty acids at both fractions. In PM<sub>10</sub> fatty acids and aliphatics constituted, respectively, 67% and 16% of the identified SEOC, whereas in PM<sub>2.5</sub> these compounds constituted, respectively, 57% and 27% of the identified SEOC.

n-Alkanes and fatty acids displayed the same seasonal variations in yield: the lowest concentration was found in the spring/summer samples while the highest loading was observed in the autumn/winter samples. The concentrations of n-alkanols in the samples recollected in warm months are similar to the cold ones.

There are some parameters that help us to assign the origin of the organic compound series. The C<sub>max</sub> (Carbon number maximum) for n-alkanes is minor in PM<sub>10</sub> samples (C<sub>25</sub>) than in PM<sub>2.5</sub> (C<sub>29</sub>). For n-alkanols the C<sub>max</sub> is C<sub>26</sub>-OH for PM<sub>10</sub> samples, while for PM<sub>2.5</sub> is C<sub>18</sub>-OH. The most abundant fatty acid is C<sub>16:0</sub> for PM<sub>10</sub> samples, while for PM<sub>2.5</sub> the linoleic acid is the most relevant. There are no differences between the two periods of year.

The CPI (Carbon Preference Index) for n-alkanes equal to one indicates the characteristics of petroleum residues. CPI values suggest that the relative petroleum residue contribution to the n-alkanes in autumn/winter samples was higher than in spring/summer. Besides, the lowest values of CPI for the PM<sub>2.5</sub> samples indicate a higher petrogenic origin than for PM<sub>10</sub> samples. For n-alkanols the average of CPI values in cold months for PM<sub>10</sub> samples is minor

than the average for warm months samples. Nevertheless, the CPI values for PM<sub>2.5</sub> samples are similar during the whole year, indicating high biogenic contributions for PM<sub>2.5</sub> samples, and a mixed origin of alkanols for the PM<sub>10</sub> samples, having in the cold months the greatest petrogenic contributions. The CPI values for acidic fraction increase from spring/summer samples to autumn/winter samples, which implies that the latter were affected by more biogenic contributions. The highest anthropogenic contributions are present in the PM<sub>2.5</sub> samples as the lowest values of CPI for fatty acids indicate (Wang and Kawamura, 2005).

Normally, the PM<sub>10</sub> samples show two UCMs (Unresolved complex mixture), the first one with the maximum in the alkane C<sub>16</sub> due to diesel emissions and the other one, centred on the alkane C<sub>26</sub> corresponding to combustion gases. Furthermore, the PM<sub>2.5</sub> samples do not usually have UCM, but five of the forty-six samples analyzed do, all of them in coldest months.

The average U:R (Unresolved/resolved) loadings for PM<sub>10</sub> samples are similar for the two periods of year. Nevertheless, the first UCM is higher in the autumn/winter samples, and for the spring/summer ones the second UCM is the greatest.

The ratio between oleic acid and stearic acid (C<sub>18:1</sub>/C<sub>18:0</sub>) is used as an indication of the aging of aerosols. Bigger values of this parameter for the samples recollected in the cold months are showed. Moreover, the PM<sub>10</sub> samples present lower values (0.54 and 1.18) than PM<sub>2.5</sub> samples (0.70 and 2.45). Low values of this parameter suggest that the aerosols in the air were aged and could be from the fast reactions with radicals. Higher ratios suggest that there were more fresh aerosols and less degradation of the fatty acids due to atmospheric conditions.

The authors thank financial support from Ministerio de Ciencia y Tecnología (REN2003-08603-C04-01) and to SAI (Universidade da Coruña) for technical support. Also, they are acknowledged to P. Esperón and V. Juncal for their assistance and to National Meteorological Institute (Centro Zonal de A Coruña).

Alves C., Pio, C., Carvalho A., Santos A. (2006). *Chemosphere*, 63, 153-164.

Wang G., Kawamura K. (2005) *Environ. Sci. Technol.*, 39, 7430-74.38.

## Chemical composition and mass closure for PM<sub>2.5</sub> and PM<sub>10</sub> aerosols at K-puszta, Hungary, in summer 2006

W. Maenhaut, N. Raes, X. Chi, J. Cafmeyer and W. Wang

Institute for Nuclear Sciences, Ghent University, Proeftuinstraat 86, B-9000 Gent, Belgium.

Keywords: atmospheric aerosols, PM<sub>10</sub>/PM<sub>2.5</sub>, supersite, chemical composition, chemical mass closure.

A comprehensive chemical aerosol characterisation study was carried out at the European Supersite of K-puszta, Hungary, from 24 May until 29 June 2006. The study showed similarity to, but extended on an earlier study at the same site in summer 2003 (Maenhaut *et al.*, 2004; Ion *et al.*, 2005). During the 2006 study, several filter samplers were deployed in parallel, typically for separate day and night collections, and 68 parallel collections were made. Among the samplers were two PM<sub>2.5</sub> samplers (one with a 0.4 µm pore size Nuclepore polycarbonate filter, the other with two pre-fired Whatman QM-A quartz fibre filters in series) and two PM<sub>10</sub> samplers (with the same filter types as the PM<sub>2.5</sub> samplers). All filters had a diameter of 47 mm, and the four samplers operated at a flow rate of 17 L per min. The purpose of the second quartz fibre filter was to assess artifacts (i.e., adsorption of volatile organic compounds and losses of semi-volatile organic compounds) in the collection of carbonaceous aerosols.

The particulate mass (PM) was obtained from weighing each filter before and after sampling with a microbalance. All quartz fibre filters were analysed for organic carbon (OC) and elemental carbon (EC) by a thermal-optical transmission (TOT) technique. The Nuclepore filters were analysed for 29 elements (from Na to Pb) by particle-induced X-ray emission spectrometry and for major anions and cations by ion chromatography (Maenhaut *et al.*, 2005). Particulate OC was obtained as the difference between the OC on the front and back quartz fibre filters.

Whereas it was very hot and dry during the entire duration of the 2003 study, during the 2006 campaign there was substantial variation in weather conditions. From the start of the campaign until 11 June, it was unusually cold with daily maximum temperatures between 13 and 23°C, but from 12 June onward higher temperatures were noted with daily maxima from 23 to 35°C. The concentrations of the PM and OC followed the ambient temperature, with higher levels during the warm period. For example, for the PM<sub>2.5</sub> PM the median (and concentration ranges) were 7.6 (2.7-15.6) µg/m<sup>3</sup> and 17.4 (7.2-32) µg/m<sup>3</sup> during the cold and warm periods, respectively. The average ratio PM<sub>2.5</sub>/PM<sub>10</sub> for the PM (average over all samples) was 0.67±0.08.

Aerosol chemical mass closure calculations were done for the PM<sub>2.5</sub> and PM<sub>10</sub> aerosol, and this for each individual sampling. As gravimetric PM data we used the data from the Nuclepore polycarbonate filters. For reconstituting this PM, eight aero-

sol types (or components) were considered (Maenhaut *et al.*, 2004; 2005). The average concentrations of the various aerosol types (and of the unexplained gravimetric PM) are shown in Figure 1, and this separately for the PM<sub>2.5</sub> and PM<sub>10</sub> aerosol and for the cold and warm periods. For 6 of the 8 components, higher average levels are observed in the warm period than in the cold one. The two exceptions are nitrate and sea salt. The lower levels of nitrate during the warm period have to be attributed to transfer of nitrate from the particulate to the vapour phase at elevated temperature. For sea salt, the difference may be due to difference in air mass origin. The percentage contributions of the various components to the average gravimetric PM were also calculated. Organic matter (OM), calculated as 1.8 OC, contributed by far the most to the PM<sub>2.5</sub> and PM<sub>10</sub> PM; it was responsible for 40-50% of the average PM during both the cold and warm periods. Noteworthy were the much larger percentages of crustal matter during the warm period than during the cold one. In the PM<sub>2.5</sub> aerosol, crustal matter accounted for 17% of the average PM during the warm period, but only for 3.1% during the cold period. For the PM<sub>10</sub> aerosol, the percentages were 28% in the warm period and 10% in the cold one.

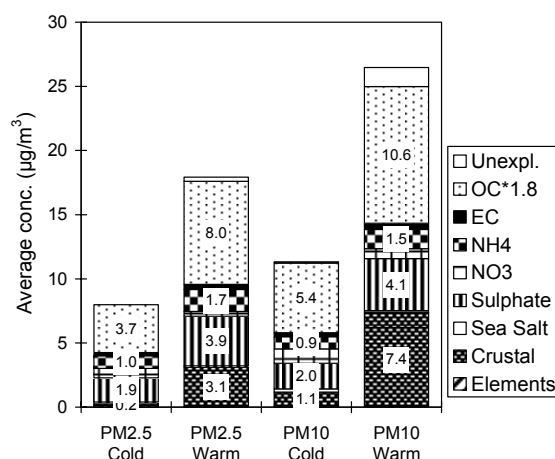


Fig. 1. Average concentrations of 8 aerosol types during the 2006 summer campaign at K-puszta.

Ion, A. C., *et al.* (2005). *Atmos. Chem. Phys.*, 5, 1805-1814.

Maenhaut, W., *et al.* (2004). *J. Aerosol Sci.*, Abstracts EAC 2004, S799-S800.

Maenhaut, W., *et al.* (2005). *X-Ray Spectrom.*, 34, 290-296.

## Aerosol chemistry, chemical mass closure, and aerosol sources at two sites in Tanzania

S. Mkoma<sup>1,2</sup>, W. Wang<sup>2</sup>, X. Chi<sup>2</sup>, N. Raes<sup>2</sup> and W. Maenhaut<sup>2</sup>

<sup>1</sup>Faculty of Science, Sokoine University of Agriculture, P.O. Box 3038, Morogoro, Tanzania.

<sup>2</sup>Institute for Nuclear Sciences, Ghent University, Proeftuinstraat 86, B-9000 Gent, Belgium.

Keywords: atmospheric aerosols, PM10, chemical composition, chemical mass closure, aerosol sources.

Three aerosol sampling campaigns were conducted at two sites in Tanzania, first in the 2005 wet season (May-June), which was actually rather dry, then in the 2005 dry season (July-September), and finally in the 2006 wet season (March-May). The sites were at Dar es Salaam (a kerbside, with a paved road and the samplers at 8 m above street level) and at Morogoro (a rural site; on the main campus of the university), about 200 km to the west of Dar es Salaam. A Gent PM10 stacked filter unit (SFU) sampler with sequential Nuclepore polycarbonate filters, providing coarse (2-10  $\mu\text{m}$  diameter) and fine (<2  $\mu\text{m}$ ) size fractions, and PM2.5 and PM10 samplers with two pre-fired Whatman QM-A quartz fibre filters in series were deployed. Depending upon the season and the location, either 24-hour collections or separate day-time and night-time samplings were performed. The samples were analysed for the particulate mass (PM) by gravimetry, organic carbon and elemental carbon (OC and EC) by a thermal-optical transmission technique, major inorganic cationic and anionic species by ion chromatography, and 28 elements (from Na to Pb) by particle-induced X-ray emission spectrometry (PIXE) (Maenhaut *et al.*, 2005).

The median levels of the PM10 PM for the 3 campaigns were 23, 45, and 13  $\mu\text{g}/\text{m}^3$  at Morogoro and 46, 58, and 40  $\mu\text{g}/\text{m}^3$  at Dar es Salaam. The average percentages of the PM10 mass in the fine (PM2) size fraction during the 3 campaigns were 35, 49, and 37% at Morogoro and 31, 27, and 33% at Dar es Salaam. OC, EC, sulphate, ammonium, and  $\text{K}^+$  were mostly present in the fine size fraction. In contrast, most elements measured by PIXE were predominantly associated with the coarse size fraction; notable exceptions were S, K, and Pb, and at Dar es Salaam also V, suggesting that these elements originated mainly from anthropogenic sources. Some typical anthropogenic elements, such as Zn and Pb, exhibited 20-70 higher median PM10 levels at Dar es Salaam than at Morogoro.

Aerosol chemical mass closure calculations were made for the fine (PM2), coarse (2-10  $\mu\text{m}$ ) and PM10 size fractions, and this for each individual sampling. As gravimetric PM data we used the data from the SFU sampler. For reconstituting this PM, eight aerosol types (or components) were considered (Maenhaut *et al.*, 2005). The average concentrations of the various aerosol types (and of the unexplained gravimetric PM) in PM10 for each campaign at Dar es Salaam are shown in Figure 1.

At Morogoro the PM10 aerosol consisted, on average, of 48% organic matter (calculated as 1.8 OC) and 36% crustal matter. The contributions of sea salt, EC, non-sea-salt sulphate, nitrate, and ammonium were 4.1, 2.5, 3.6, 2.2, and 0.9%, resp., and 2.3% remained unexplained. At the Dar es Salaam kerbside, the PM10 aerosol consisted, on average, of 37% organic matter (calculated as 1.6 OC) and 33% crustal matter. Sea salt, EC, non-sea-salt sulphate, nitrate, and ammonium contributed with 10, 8.7, 2.9, 1.2, and 0.27%, respectively, and 6.0% was unexplained. The crustal matter at this site is undoubtedly mostly resuspended road dust. Its concentration followed a strong diurnal pattern, with 3-5 times higher levels during the day than during the night.

Biomass burning is likely a major contributor to the fine organic matter at both sites and in both seasons. This is suggested by the data for fine K, a typical indicator for biomass burning. Its crustal enrichment factors were, on average, around 10, which is similar to that at sites that are heavily impacted by biomass burning. Furthermore, OC was well correlated with water-soluble  $\text{K}^+$ . By comparing the OC/ $\text{K}^+$  ratio with those for the global emissions of biofuel burning, charcoal burning, and burning of agricultural residues (Andreae & Merlet, 2001), and assuming that all of the  $\text{K}^+$  is derived from biomass burning, it is estimated that, on average, between 30% and 100% of the OC at the two sites is derived from biomass burning.

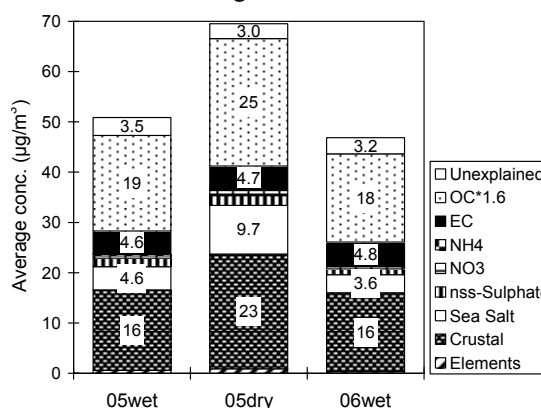


Fig. 1. Average concentrations of 8 aerosol types in PM10 at Dar es Salaam during the 3 campaigns.

Andreae, M. O., & Merlet, P. (2001) *Global Biogeochem. Cycles*, 15, 955-966.

Maenhaut, W., et al. (2005). *X-Ray Spectrom.*, 34, 290-296.

## NMR Functional group analysis extended to carboxylic acids and ketones providing an insight into chemical ageing of SOA

F. Moretti<sup>1</sup>, E. Tagliavini<sup>1</sup>, S. Decesari<sup>2</sup>, M.C. Facchini<sup>2</sup> and S. Fuzzi<sup>2</sup>

<sup>1</sup> Dipartimento di Chimica "G. Ciamician", via Selmi, 2 40126 Bologna and  
Centro Interdipartimentale di Ricerca in Scienze Ambientali, via S. Alberto, 163 48100 Ravenna. Italy

<sup>2</sup> Istituto di Scienze dell'Atmosfera e del Clima, Consiglio Nazionale delle Ricerche,  
via Gobetti, 101, 40129 Bologna, Italy

Keywords: chemical analysis, organic aerosol, SOA, water soluble compounds, HNMR spectroscopy.

Organic aerosols can be classified on the basis of their source type into primary organic aerosols (POA) constituted of compounds directly emitted in the atmosphere, and secondary organic aerosol (SOA) made of compounds formed through *in-situ* reaction from gaseous precursors. The chemical composition of organic particles can be further modified by photochemical and polymerization reactions occurring during aerosol transport and ageing. Such chemical transformation of organic aerosol ("chemical ageing") leads to formation of more oxidized compounds containing carbonyl, carboxyl groups and possibly of high molecular weight species. These organic compounds exhibit a high surface activity and can play a key role in cloud drops formation. Their chemical composition, however, has eluded characterization by coupled chromatographic/spectroscopic methods so far.

Recently, <sup>1</sup>H NMR spectroscopy in D<sub>2</sub>O solution was exploited for functional group analysis of water extractable organic aerosols (Decesari et al. 2000), providing quantitative results for alkylic, alcoholic, ethereal and aromatic moieties. Other functional groups like ketones and Carboxylic acids are not directly visible in the <sup>1</sup>H NMR spectra and must be converted to H-containing groups through chemical derivatization.

Carboxylic groups (COOH) were converted to methyl esters with diazomethane, according to the procedure described by Tagliavini et al. (2006). In the present study we also obtained first quantitative measurements of total carbonylic groups by applying a new specific derivatization method. Carbonylic groups were converted by reaction with methoxyamine to oximes which are detected in the NMR spectrum in the 3.2-4.4 ppm ( $\delta_H$ ) region. In this way, we were able to quantify the most important oxygenated organic functional groups in the samples: the carboxylic, carbonylic hydroxylic and alkoxylic groups.

PM10 samples were collected on the roof of ISAC institute building (40°31'25"N, 11°20'17"E) in Bologna, Italy with high-volume sampler at 1.13 m<sup>3</sup>/min on 24-27 May 2006 and on 28 June 2006. Sampling time varied from 4 to 9 hours. The days of 24 and 25 May were characterised by atmospheric instability, while a photochemical smog episode

started to onset on 26 – 27 May. 28 June was a typical summer day with high pressure conditions

All samples were extracted by ultrapure (MilliQ) water and aliquots of the solution were employed for water soluble organic carbon (WSOC) analysis, H NMR analysis and for the derivatization reactions. Filter punches were used for total carbon (TC) analysis, too.

Looking at the changes in the functional group distribution between samples, three different trends can be observed: 1) the carboxylic (COOH) and carbonylic (C=O) groups are higher in last three samples, characterised by a higher photochemistry, 2) the aromatic (A-H) and hydroxylic (HC-O) functions show an opposite behaviour with a maximum in the first two days, 3) the aliphatic saturated (H-C) and unsaturated (HC-C=) groups show no significant trends (Figure 1)

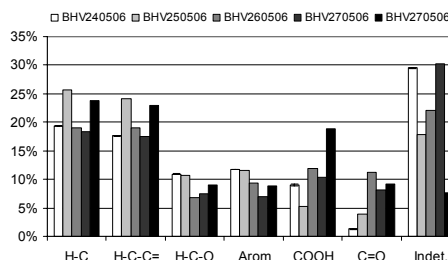


Figure 1. Functional groups distributions

These preliminary results indicate that <sup>1</sup>H NMR spectroscopy coupled with chemical derivatization can be fruitfully employed to trace the effects of SOA formation and chemical ageing processes on the chemical composition of ambient organic aerosol particles.

Decesari S., M.C. Facchini, S. Fuzzi, and E. Tagliavini, (2000). *Characterization of water-soluble organic compounds in atmospheric aerosol: A new approach*. J. Geophys. Res. 105, 1481-1489.

Tagliavini E., Moretti F., Decesari S., Facchini M. C., Fuzzi S., and Maenhaut W. (2006). *Functional group analysis by H NMR/chemical derivatization for the characterization of organic aerosol from the SMOCC field campaign*. Atmos. Chem. Phys. 6, 1003-1019.

## Phase changes during hygroscopic cycles in polyethylene glycol 400/ammonium sulfate system

Gabriela Ciobanu, Claudia Marcolli, Ulrich K. Krieger, Uwe Weers and Thomas Peter

Institute for Atmospheric and Climate Science, ETH Zurich, 8092, Zurich, Switzerland

Keywords: organics, relative humidity, polyethylene glycol 400, ammonium sulfate

### Introduction

Atmospheric aerosols are complex mixtures of inorganic and organic components, whereof organics typically account for 20-50% of the total fine aerosol mass at continental mid-latitudes. The presence of organics impacts the heterogeneous chemistry, CCN activity, hygroscopicity, and the interaction with light of aerosol particles (Kanakidou *et al.*, 2005).

The phases of mixed organic/inorganic aerosol particles are influenced by physical and chemical properties of both components, but also by temperature and relative humidity. An understanding of the phases is required to quantify the impact of aerosols on climate, visibility and atmospheric chemistry (Parsons *et al.*, 2004).

### Experimental procedure

Single droplets of polyethylene glycol 400/ammonium sulfate were produced from bulk solutions by a droplet generator with a modified ink jet print cartridge and deposited on a hydrophobically coated slide in a heating/cooling stage. The relative humidity over the particle was varied by passing a continuous flow of dry and humidified nitrogen at different ratios, through the cell. The particle's phases were monitored with a microscope and their composition determined by Raman spectroscopy.

### Results and Conclusions

With a 50:50 wt% mixture of polyethylene glycol 400/ammonium sulfate we have performed several humidity cycles at 293 K for different particle sizes. For all the particles we have observed a liquid-liquid phase separation when the ammonium sulfate deliquesced. This separation of phases was also observed in bulk measurements performed on the same system (Marcolli & Krieger, 2006). The presence of two liquid phases in a  $\sim 70 \mu\text{m}$  particle is shown in Figure 1. Based on Raman spectra collected from the particle, the ammonium sulfate was found to be in the inner sphere, meanwhile the polyethylene glycol was present in the outer sphere.

By increasing the relative humidity in the heating/cooling stage, the two liquid phases merge into one liquid phase, corresponding to a polyethylene glycol/ammonium sulfate aqueous solution. A decrease in relative humidity leads to

liquid-liquid phase separation, which starts at about 90% RH and lasts until ammonium sulfate effloresces.

Such phase separation might be very common in tropospheric aerosol particles and in consequence may be an important factor affecting the climate by influencing heterogeneous and multiphase chemistry, gas/particle partitioning and the aerosol's hygroscopicity.

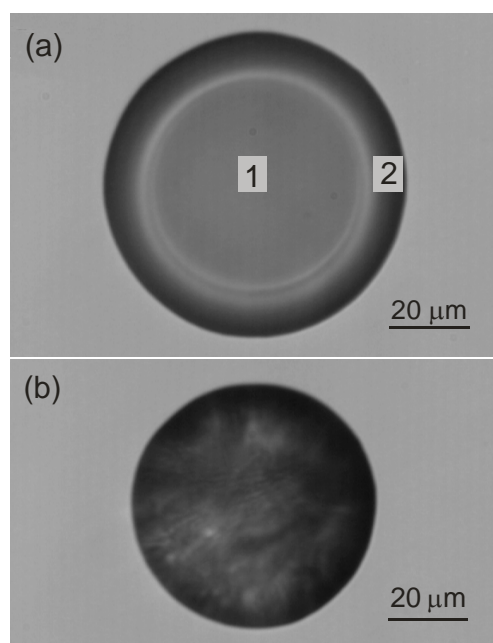


Figure 1. (a) Liquid-liquid phase separation for the polyethylene glycol 400/ammonium sulfate system (50:50 wt %); 1) aqueous ammonium sulfate solution; 2) mainly PEG 400. (b) effloresced particle.

This work was supported by the Swiss National Foundation, project No. 200020-103651/1.

### References

- Kanakidou, M. *et al.* (2005), *Atmos. Chem. Phys.*, 5, 1053-1123.
- Marcolli, C. & Krieger U. K. (2006), *J. Phys. Chem. A*, 110, 1881-1893.
- Parsons, M. T. *et al.* (2004), *J. Phys. Chem. A*, 108, 11600-11608.

## **Chemical Composition and Optical properties of Megacity Aerosols in PARIS/BEIJING/CAIRO: A comparative study.**

O. Favez, J. Sciare and H. Cachier

Laboratoires des Sciences du Climat et de l'Environnement (LSCE), 91191-Gif sur Yvette, France

Keywords: megacity, carbonaceous particles, water soluble compounds, size distribution, light scattering.

The part of the world population living in urban area, which was around 30% in 1950, is now about 50% and is expected to reach nearly 75% in 2030. The world urban population would thus extent from less than 1 billion in 1950 to more than 5 billions in 2030. Most of this increase will occur in less developed countries, where urban centres are expanding rapidly. The subsequent concentration of people and their activities in megacities leads to the formation of intense air pollutant emission sources and heat islands, with impacts at urban, regional and global levels. Among air pollutants, airborne particles are of major concern, especially because of their potential adverse health effects and their climatic impacts.

This study investigates the aerosol chemical composition and related optical properties in three selected megacities: Paris (France), Beijing (P.R. China) and Cairo (Egypt). These various urban areas were chosen as case studies to explore contrasted situations and assess aerosols properties from the perspective of "low" polluted atmosphere met in occidental industrialised countries (Paris) against two of the most polluted cities in industrialising countries (Beijing and Cairo).

For each of these case studies, an experimental protocol, based on size-segregated particulate mass and number, was set up in order to study multi-pollutant situations. Particles were sampled on different substrates and the size separation (ultra-fine/fine/coarse modes) was achieved using Stack Filter Units, sharp cut cyclones and low pressure cascade impactors. Chemical mass balance of size selected aerosol was achieved through exhaustive chemical analyses: elemental composition, major inorganic soluble species, carbonaceous compounds (Black Carbon, Organic Carbon, and Water Soluble Organic Carbon). The use of one-field analyzers (TEOM, Aethalometers, Nephelometers, and Optical Particles Counters) allowed the investigation of fast changes in key characteristics of the aerosol mixture.

Besides long-term monitoring, intensive field measurement campaigns were performed in various periods of the year in each investigated megacities: winter/summer for Paris and Beijing, autumn/spring for Cairo. Measurements and sampling took place at city center background sites and, for Beijing and Cairo, at upwind/downwind sites.

Results indicate particulate pollution levels increasing from Paris to Beijing and then to Cairo, with particulate mass (PM<sub>10</sub>) being about 4 times higher in Beijing compared to Paris and about 6 times higher in Cairo than in Paris. Aerosol mixture complexity was found to increase following the same way, leading to strong seasonal and diurnal variability in Beijing and Cairo. Elevated regional air pollution backgrounds and specific meteorological conditions (photochemistry, humidity) were identified as major factors responsible for strong formation of secondary inorganic aerosols in Beijing. The case of Cairo, which represents a very interesting case study for aerosol mixture (due to the multiplicity of sources: intense mobile and industrial sources, biomass burning in the Nile Delta, Saharan dust emissions) are emphasized here. In particular, a "black cloud" event (dark pollution plume hovering the city during the fall season for about a decade), was fully characterized and the contribution of post-harvesting rice straw burning evaluated. Interactions between mineral dust and anthropogenic emissions (e.g. scavenging of acidic species by dust particles) during dust storm events were also observed.

The major role of carbonaceous particles, in particular within the ultra-fine and fine aerosol fractions (representing more than 50% of the mass in these modes), is pointed out. Seasonal variations and mass size distribution of Water Soluble Organic Carbon (WSOC) are presented here. Due to photochemical oxidation processes, the ratio WSOC/OC was for instance found to reach more than 80% within the fine mode (0.1-1 $\mu$ m) during summer afternoon in Paris.

Finally, the contribution of each chemical species to light scattering coefficient was evaluated for the three investigated megacities.

This work was supported by ADEME (Agence de l'Environnement et de la Maitrise de l'Energie), CNRS (Centre National de la Recherche Scientifique) and CEA (Commissariat à l'Energie Atomique).

## Investigating the role of ammonia in atmospheric nucleation using quantum chemistry

T. Kurtén<sup>1</sup>, L. Torpo<sup>1</sup>, H. Vehkamäki<sup>1</sup>, M. R. Sundberg<sup>2</sup>, K. Laasonen<sup>3</sup>, V.-M. Kerminen<sup>4</sup>, M. Noppel<sup>5</sup>, M. Salonen<sup>1</sup> and M. Kulmala<sup>1</sup>

<sup>1</sup>Department of Physical Sciences, University of Helsinki, PL 64, 00014 Helsingin yliopisto, Finland

<sup>2</sup>Department of Chemistry, University of Helsinki, PL 55, 00014 Helsingin yliopisto, Finland

<sup>3</sup>Department of Chemistry, University of Oulu, PL 3000, 90014 Oulun yliopisto, Finland

<sup>4</sup>Finnish Meteorological Institute, PL 503, 00101 Helsinki, Finland

<sup>5</sup>Institute of Environmental Physics, University of Tartu, 18 Ülikooli Str, 50090 Tartu, Estonia

Keywords: atmospheric nucleation, sulfuric acid, ammonia, quantum chemistry

The role of ammonia in atmospheric sulfuric acid - water nucleation is controversial. Earlier quantum chemical studies (Ianni and Bandy, 1999) predicted the NH<sub>3</sub>:H<sub>2</sub>SO<sub>4</sub> mole ratio of nucleating clusters to be close to zero, while state of the art thermodynamics (Clegg *et al.*, 1998) predicted extensive ammonium bisulfate formation (Vehkamäki *et al.*, 2004), corresponding to a ratio of 1:1.

We have recently computed formation free energies for small sulfuric acid - water - ammonia clusters at the RI-MP2/aug-cc-pV(T+d)Z//MPW1B95/aug-cc-pV(D+d)Z (Weigend and Häser, 1997; Zhao and Truhlar, 2004) level. The results show that ammonia enhances the addition of sulfuric acid molecules to sulfuric acid - water clusters. The importance of this effect increases with the number of acid molecules already present in the cluster. In the simulated distributions of one- and two-acid clusters, the role of ammonia is not yet apparent, as water tends to out-compete it due to mass balance effects. However, in atmospheric conditions ammonia will significantly assist the growth of two-acid clusters to three-acid clusters. This implies a lower limit of 1:3 for the NH<sub>3</sub>:H<sub>2</sub>SO<sub>4</sub> mole ratio.

The presence of water affects the acid - ammonia binding relatively weakly (Kurtén *et al.* 2007a, Ianni and Bandy, 1999). The effects that do exist are mostly systematic, with the addition of multiple water molecules decreasing the binding of ammonia to the clusters. This observation can be used to set an upper limit to the NH<sub>3</sub>:H<sub>2</sub>SO<sub>4</sub> ratio of atmospheric clusters by studying only the acid-ammonia "core" of the clusters, without explicitly including water molecules. Our recent RI-MP2/aug-cc-pV(T+d)Z//RI-MP2/aug-cc-pV(D+d)Z calculations (Kurtén *et al.*, 2007b) on such cluster cores indicate that the formation of small ammonium sulfate clusters (NH<sub>3</sub>:H<sub>2</sub>SO<sub>4</sub> ratio 2:1) in atmospheric conditions can probably be ruled out. Even the formation of ammonium bisulfate clusters (1:1) requires either quite high (over 10 ppb) NH<sub>3</sub> concentrations or low temperatures. Sensitivity analysis calculations indicate that errors in the computational method might lead to an overestimation of the NH<sub>3</sub> concentration required for ammonium bisulfate to form by at most 2 orders of magnitude. The finding that ammonium sulfate

molecular clusters do not form in the atmosphere is insensitive even to relatively large systematic errors.

Based on our results, we can conclude that the NH<sub>3</sub>:H<sub>2</sub>SO<sub>4</sub> ratio of nucleating atmospheric clusters is probably between 1:3 and 1:1. This is lower than the typical experimental values measured for larger (> 10 nm in diameter) particles (see *e.g.* Feng and Penner, 2007). This indicates that the chemical composition of nucleating clusters may differ significantly from that of larger particles.

RI-MP2/aug-cc-pV(D+d)Z calculations (Kurtén *et al.*, 2007c) on ion clusters show that NH<sub>3</sub> binds very weakly to the HSO<sub>4</sub><sup>-</sup> ion. This implies that ammonia will probably not play a major role in ion-induced nucleation of the sulfuric acid - water system. All computations have been done using the Gaussian 03 (Frisch *et al.*, 2004) and Turbomole (Ahlrichs *et al.*, 1989; v. 5.8.) programs.

The authors thank the Scientific Computing Center (CSC) in Espoo, Finland for computing time

- Ahlrichs, R., Bär, M., Häser, M., Horn, H. & Kölmel, C. (1989). *Chem. Phys. Lett.*, 162, 165-169.
- Clegg, S. L., Brimblecombe, P. & Wexler, A. S. (1998). *J. Phys. Chem. A*, 102, 2137-2154.
- Feng, Y. & Penner, J. E. (2007). *J. Geophys. Res.*, 112, D01304, doi:10.1029/2005JD006404.
- Frisch, M. J. *et al.* (2004). Gaussian 03, Revision C.02, Gaussian, Inc., Wallingford CT, U.S.A.
- Ianni, J. C. & Bandy, A. R. (1999). *J. Phys. Chem. A*, 103, 2801-2811.
- Kurtén, T., Torpo, L., Ding, C.-G., Vehkamäki, H., Sundberg, M. R., Laasonen, K. & Kulmala, M. (2007a). *J. Geophys. Res.*, in press.
- Kurtén, T., Torpo, L., Sundberg, M. R., Kerminen, V.-M., Vehkamäki, H. & Kulmala, M. (2007b). *Atmos. Chem. Phys. Discuss.*, submitted.
- Kurtén, T., Noppel, M., Vehkamäki, H., Salonen, M. & Kulmala, M. (2007c). *Boreal Env. Res.*, submitted.
- Vehkamäki, H., Napari, I., Kulmala M. & Noppel, M. (2004). *Phys. Rev. Lett.*, 93, 148501.
- Weigend, F. & Häser, M (1997). *Theor. Chem. Acc.*, 97, 331-340.
- Zhao, Y. & Truhlar, D. G. (2004). *J. Phys. Chem. A*, 108, 6908-6918.

## Source apportionment of submicron organic aerosol during wintertime inversions: A new factor analytical approach

V.A. Lanz<sup>1</sup>, M.R. Alfarra<sup>2</sup>, U. Baltensperger<sup>2</sup>, B. Buchmann<sup>1</sup>, C. Hüglin<sup>1</sup>, S. Weimer<sup>1,2</sup>, and A.S.H. Prévôt<sup>2</sup>

<sup>1</sup>Empa, Swiss Federal Laboratories for Materials Testing and Research, CH-8600, Dübendorf, Switzerland

<sup>2</sup>Paul Scherrer Institute, Laboratory for Atmospheric Chemistry, Villigen, CH-5342, Villigen PSI, Switzerland

Keywords: aerosol mass spectrometry, aerosol modelling, PM1, source apportionment.

Real-time measurements of submicron aerosol were performed during three weeks at an urban background site (Zürich, Switzerland) in January 2006. A new hybrid receptor model (solved by the Multilinear Engine, ME-2; Paatero, 1999) was applied to highly time-resolved organic aerosol mass spectra measured by an Aerodyne aerosol mass spectrometer (AMS) during temperature inversions in wintertime.

Low temperatures, low photochemical activity, and fog episodes are typical conditions of Swiss Plateau winters. During high pressure conditions, inversions can extend over several days and lead to smog formation: aerosol mass concentrations are strongly influenced by meteorology rather than by variation of source strengths in such episodes of winter smog (Gehrig and Buchmann, 2003). Unlike in summer (Lanz et al., 2006), *a priori* known source composition was needed in receptor modelling to resolve different aerosol sources and components here.

Sensitivity of source apportionments to incorporating *a priori* knowledge was studied. Three sources of submicron organic aerosols were identified. The major component was oxygenated organic aerosol (OOA), representing highly aged and secondary particles, accounting on average for 52-57% of the particulate organic mass. OOA estimates were strongly correlated with measured particulate ammonium. Particles from wood combustion (35-40%) plus 3-13% traffic-related hydrocarbon-like organic aerosol (HOA) fractions accounted for the other half of measured organic matter (OM) and were found to be somewhat enriched during a high particulate matter (PM) episode.

Estimated source profiles were verified by measured emission profiles and modelled source strengths by time series of indicative tracer species from collocated instruments. High correlations were found between computed source activities and indicative species from collocated instruments: *e.g.* wood burning activities are correlated with measured carbon monoxide CO ( $R^2=0.78$ ; Fig. 1), a gaseous tracer for incomplete combustion; significant fractions of organic particles from wood combustion sources are emitted under poor burning conditions (Khalil and Rasmussen, 2003). Emission factors for modelled HOA to measured nitrogen oxides ( $\text{NO}_x$ )

and OM from wood burning to levoglucosan from filter analyses were found to be consistent with values retrieved from literature.

In future studies, incorporating *a priori* given profiles of oxidized primary particles (*e.g.* from smog chamber studies) into this hybrid model may be useful when aerosol ageing is to be studied under environmental conditions.

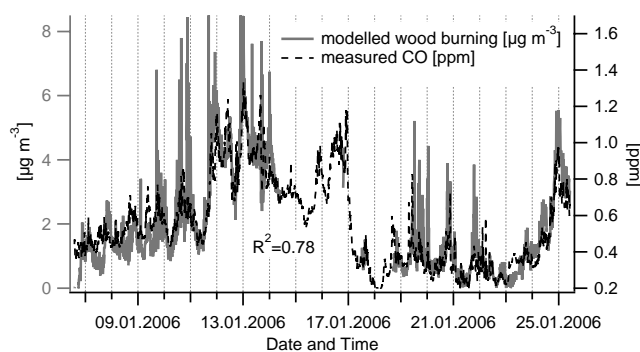


Figure 1. ME-2 modelled wood burning particles (organic fraction) versus measured carbon monoxide (CO, a tracer for incomplete combustion) during wintertime inversions at an urban background site.

Gehrig, R., & Buchmann, B. (2003). Characterising seasonal variations and spatial distribution of ambient PM10 and PM2.5 concentrations based on long-term Swiss monitoring data. *Atmos. Environ.*, *37*, 2571-2580.

Khalil, M.A.K., & Rasmussen, R.A. (2003). Tracers of wood smoke, *Atmos. Environ.*, *37*, 1211-1222.

Lanz, V. A., Alfarra, M. R., Baltensperger, U., Buchmann, B., Hueglin, C., & Prévôt, A. S. H. (2006). Source apportionment of submicron organic aerosols at an urban site by linear unmixing of aerosol mass spectra. *Atmos. Chem. Phys. Discuss.*, *6*, 11681-11725.

Paatero, P. (1999) The multilinear engine - A table-driven, least squares program for solving multilinear problems, including the n-way parallel factor analysis model, *J Comp Graph Stat*, *8*, 854-888.

## On the beneficial effect of near-waterfall environment

T.-E. Parts and A. Luts

Institute of Environmental Physics, University of Tartu, Ülikooli 18, 50090 Tartu, Estonia

Keywords: aerosol formation, chemical composition, modelling, health aspects of aerosol.

The environment influences our health through exposures to many physical, chemical and biological risk factors. Air pollution is one of the most studied adverse factors. On the other hand some environment condition are especially healthy. People like to be at the beach, in the mountains, in the country, in pine forests, near waterfalls, and feel good after visit them.

In this work we highlight the possible beneficial health effect that can be result from exposure to negatively charged ultrafine (cluster-size, nanometers range) particles generated in the air due to an additional source of ions – falling water.

It is proposed that high levels of negative air ions may positively affect our health due to the stimulating the cells that regulate our body resistance to disease (Ryushi *et al.*, 1998). The chemical composition of such ions remains unclear.

Recently Laakso *et al.*, 2006 provide new evidence for waterfall-modified air ion size distribution in comparison with common tropospheric air. The measurements revealed several times increased concentration of intermediate negative ions, about 10 nanometers in size. The enhanced concentration of small ions (cluster ions in size below 1.5 nm) was also observed.

Though, physical characterization does not render any information about the ion's chemical composition, the simulation of air ions evolution can provide possible candidates for unknown negative ions.

Commonly, air ion evolution is considered an evolution of ion nature (as transformations of ion cores). Now, it is proposed that water chemistry can interfere air particle formation channels more effectively than previously thought.

The simulation of air ion evolution in the troposphere begins from primary ions, formed mainly by cosmic radiation and radiation from radioactive elements such as radon. The concentrations of chemical species involved into evolution scheme are known as average ones (Luts&Parts, 2002). For negative ions  $\text{NO}_3^-$  and/or  $\text{HSO}_4^-$  cluster ion families are established as dominant steady state ions (final ions aged about hundred seconds). The effect of water clusters on air ion evolution is not completely understood.

Waterfalls can produce a lot of  $\text{OH}^-$  core ions due to autoionization of water

$$(\text{H}_2\text{O})_n \rightarrow \text{H}_3\text{O}^+(\text{H}_2\text{O})_{n-m} + \text{OH}^-(\text{H}_2\text{O})_{m-2}, \text{ where } m \text{ is much lesser than } n.$$

The contribution of hydroxyl ions into air ions evolution scheme results in the changes of the composition of negative ions, see Fig. 1.  $\text{HCO}_3^-$ -cluster ions became dominating.

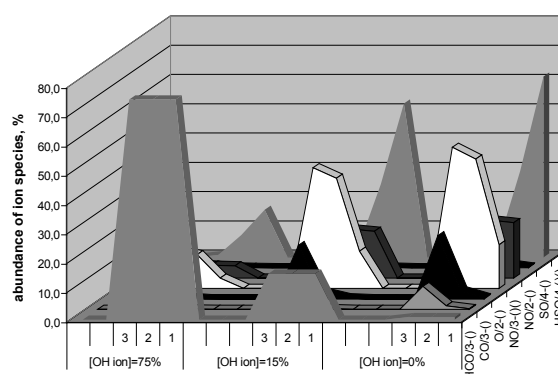


Figure 1. The abundances of ion families at different initial concentration of hydroxyl ions. Cases A –  $[\text{OH}^-] = 0\%$ ; cases B – 15%; cases C – 75%.

The reaction  $\text{OH}^- + \text{CO}_2 \rightarrow \text{HCO}_3^-$  constitutes a stage of the reversible hydration of carbon dioxide, a process involved in transportation of  $\text{CO}_2$  in living organisms (Nemukhin *et al.*, 2002).

So, we can assume that negatively charged water clusters  $\text{OH}^-(\text{H}_2\text{O})_m$  directly produced by the evaporation of falling water and  $\text{HCO}_3^-$  cluster ions revealed in our simulation results should bear some beneficial effect.

This work was supported by the Estonian Science Foundation grants no. 6223 and 6988.

Laakso, L.; Hirsikko, A.; Grönholm, T.; Kulmala, M.; Luts, A., & Parts, T. (2006). *ACPD*, 6, 9297-9314.

Luts, A., and Parts, T., (2002). *J. Atm. Sol.-Terr. Phys.*, 64, 763-774.

Nemukhin, A.V., Topol, I.A., Grigorenko, B.L., & Burt, S.K. (2002). *J. Phys. Chem. B*, 106, 1734-1740.

Ryushi, T., Kita, I., Sakurai, T., Yasumatsu, M., Isokawa, M., Aihara, Y., & Hama, K. (1998). *Int. J. Biometeorol.* 41, 132-136.

## Photochemical degradation study of pesticides adsorbed on atmospheric aerosols

M. Pflieger, M. Goriaux, B. Temime, A. Monod and H. Wortham

LCE, University Aix-Marseille 1, 3 place Victor Hugo (case 29), 13331, Marseille Cedex 3, France

Keywords: Aerosol chemistry, organic compounds, PAH(s), SOA

The intensive use of pesticides has led to an ubiquitous contamination of the environment. These semi volatile organic compounds have been identified in the Arctic ecosystem and in a variety of other remote areas (Li *et al.*, 2006). During agricultural treatments, an important part of these compounds transfers into the atmosphere (30 to 50%) (Van den Berg *et al.* 1999). Thereby the atmosphere is rated as the most important vector for pesticides dissemination at local, regional and global scales. A comprehensive knowledge of the behaviour of these compounds in the atmosphere is absolutely necessary in order to understand their environmental fate.

In the atmosphere, pesticides are found essentially in the particulate phase. However, their life times are calculated from the available gas phase kinetic data. This is due to the few particulate phase kinetic data available. The disagreement between calculated (some hours to some days) (Howard *et al.*, 1991) and measured (several weeks) (Chernyak *et al.*, 1996) atmospheric residence times results probably from the lack of information.

In order to improve the scientific knowledge towards pesticides atmospheric fate, applying a flow photoreactor we investigate the heterogeneous reactivity of four herbicides (Alachlor, Diflufenicanil, Terbutylazin, Trifluralin) and one PAH (Naphthalene for the experimental validation) with the atmospheric oxidants such ozone and OH radicals under simulated conditions.

The flow photoreactor was designed to study heterogeneous photooxydation under simulated atmospheric conditions. Its walls are covered with a thin layer of the representative (silica) atmospheric aerosol particles. A constant gaseous flow of pesticides (from a permeation cell) passes through the reactor, permitting the adsorption of the compounds on the aerosol's surface. The kinetic heterogeneous reactions of ozone towards the adsorbed pesticides are studied as a function of time and ozone concentration. After each experiment, the flow tube reactor is opened, and the remaining pesticides and their degradation products are extracted prior to analysis. The analysis of pesticides is performed using a gas chromatograph equipped with a flame ionisation detector and/or mass spectrometer. A large volume

injector is used to avoid a pre-concentration step that generates compounds losses.

The experimental set up has been validated with the ozonolysis of naphthalene. The results obtained from this study are in agreement with the previous results from our laboratory and elsewhere (Perraudin, 2004). These results clearly show that the reaction of ozone with the naphthalene adsorbed on the aerosols surfaces proceeds faster in comparison with the corresponding gas phase reactivity. On the other hand, although the applied concentration of ozone was 40 ppm the four pesticides concerned in this study show no degradation in a period of 6 hours. These first results indicate that the atmospheric life time of those pesticides in regard to ozone reactions can be greater than 8 months.

These results are so far preliminary and as further experimental data becomes available, in particular the OH reactivity a more complete picture on the degradation mechanisms of these pesticides will be revealed.

Photo induced degradation processes in presence of oxidants on atmospheric aerosol surfaces are an emerging research topic as these processes have the potential to directly affect air quality, the tropospheric oxidation capacity and/or the aerosol-cloud-climate issues.

This work is financially supported by the French Environmental Department (Primequal program) and ADEME (Agence de l'Environnement et de la Maîtrise de l'Energie).

- Chernyak, S. M., Rice, C. P., & McConnell (1996). *Marine Pollution Bulletin*, 32, 410-419.
- Howard, P.H., Boethling, R. S., Jarvis, W. F., Meylan, W. M., & Michalenko, E. M. (1991). *Handbook of Environmental Degradation Rates*, Lewis Publishers.
- Li, J., Zhu, T., Wang, F., Qiu, X.H., & Lin, W.L. (2006). *J. Ecotoxicology and Environmental Safety*, 63, 33-41.
- Perraudin, E (2004). *PhD Thesis*. University of Bordeaux I.
- Van den Berg, F., Kubiak, R., & Benjey, W.G. (1999). *J. Water, Air, and Soil Pollution*, 115, 195-218.

## Subcooled liquid saturation vapour pressures of C3-C6 dicarboxylic acids

I. Riipinen<sup>1</sup>, I.K. Koponen<sup>2</sup>, M. Bilde<sup>2</sup>, A. I. Hienola<sup>1</sup> and M. Kulmala<sup>1</sup>

<sup>1</sup>Department of Physical Sciences, University of Helsinki, P.O. Box 64, FI-00014, University of Helsinki, Finland

<sup>2</sup>Department of Chemistry, University of Copenhagen, Universitetsparken 5, DK-2100, Copenhagen Ø, Denmark

Keywords: atmospheric aerosols, vapour pressure, organics, condensation/evaporation.

Dicarboxylic acids, such as malonic, succinic, glutaric and adipic acid are organic acids which are typically found in atmospheric aerosol samples (see e.g. Kanakidou *et al.*, 2004). This suggests that they might have a role in the formation and growth of new atmospheric aerosol particles. However, in order to make quantitative analysis on the role of organics in particle formation and growth, information on thermodynamic properties of these compounds is needed.

Riipinen *et al.* (2006) have recently described a method that is suitable for determining thermophysical properties, such as saturation vapour pressures, of organic compounds in aqueous solutions. The method combines the use of well-defined evaporation experiments and accurate binary evaporation modelling.

In this work we have applied the method for determining the saturation vapour pressures of malonic (C3), succinic (C4), glutaric (C5) and adipic (C6) acids in aqueous solutions. All of the pure acids are solid in atmospheric conditions, but once deliquesced, they stay in liquid solutions at relative humidities even below 60% (e.g. Peng *et al.*, 2001). The subcooled liquid vapour pressures are therefore one of the key properties describing the formation and growth behaviour of droplets consisting of these compounds.

The evaporation rates of binary droplets containing water and the investigated acids were measured with TDMA technique at temperatures near the room temperature (295 – 301 K), and relative humidities above the deliquescence points of the acids. The droplet sizes considered in this study were typically 80 – 130 nm.

The saturation vapour pressures were derived from the evaporation rates by analysing the experimental data with a numerical condensation/evaporation model BCOND (see Vesala *et al.*, 1997). Model input parameters, such as relative humidities, temperatures and droplet concentrations, were obtained from the experiments. The mass and thermal accommodation coefficients were assumed to be unity. The UNIFAC Dortmund model was used for the activity coefficient predictions.

The obtained subcooled liquid vapour pressures at  $T = 299$  K for the investigated C3-C6 dicarboxylic

acids are presented in Figure 1 (black curve). The solid state vapour pressures determined by Bilde *et al.* (2003) are also presented for comparison (grey curve). For all the investigated dicarboxylic acids, the obtained liquid state vapour pressures are higher than or similar to the solid state values. Also, the even-odd alternation visible for the solid state vapour pressures is not observed for the subcooled liquid phase.

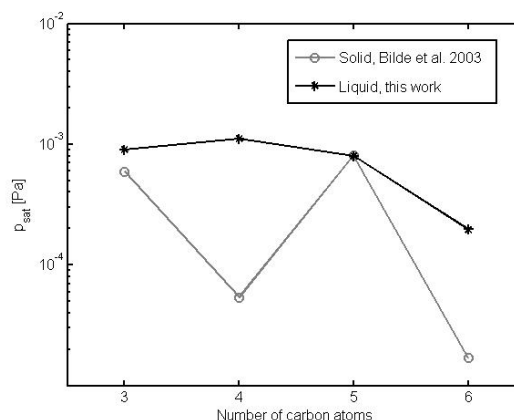


Figure 1. The saturation vapour pressures of C3-C6 dicarboxylic acids at 299 K. Black curve: subcooled liquid phase (this work); Grey curve: solid phase (Bilde *et al.*, 2003).

- Bilde, M., Svenningsson, B., Mønster, J. & Rosenørn, T. (2003). *Environ. Sci. Technol.*, 37, 1371-1378.
- Kanakidou, M., Seinfeld, J.H., Pandis, S.N., Barnes, I., Dentener, F.J., Facchini, M.C., Van Dingenen, R., Ervens, B., Nenes, A., Nielsen, C.J., Swietlicki, E., Putaud, J.P., Balkanski, Y., Fuzzi, S., Horth, J., Moortgat, G.K., Winterhalter, R., Myhre, C.E.L., Tsigaridis, K., Vignati, E., Stephanou, E.G. & Wilson, J. (2005). *Atmos. Chem. Phys.*, 5, 1053-1123.
- Peng, C., Chan, M.N. and Chan, C.K. (2001). *Environ. Sci. Technol.*, 35, 4495-4501.
- Riipinen, I., Svenningsson, B., Bilde, M., Gaman, A., Lehtinen, K.E.J. & Kulmala, M. (2006). *Atmos. Res.*, 82, 579-590.
- Vesala, T., Kulmala, M., Rudolf, R., Vrtala, A. & Wagner, P.E. (1997). *J. Aerosol Sci.*, 28, 565-598.

## Arsenic species levels of PM10 and PM2.5 in urban monitoring station (Huelva, SW Spain)

A.M. Sánchez de la Campa<sup>1,2</sup>, J.D de la Rosa<sup>2</sup>, D. Sánchez-Rodas<sup>3</sup>, V. Oliveira<sup>3</sup>, A. Alastuey<sup>4</sup>, X. Querol<sup>4</sup> and J.L. Gómez Ariza<sup>3</sup>.

<sup>1</sup>Department of Environment and Planning, University of Aveiro, Campus Univ. de Santiago, 3810 Aveiro, Portugal

<sup>2</sup>Department of Geology, University of Huelva, Campus Univ. El Carmen 21071 Huelva, Spain

<sup>3</sup>Department of Chemistry and Science of Material, University of Huelva, Campus Univ. El Carmen 21071 Huelva, Spain

<sup>4</sup>Institute of Earth Sciences “Jaume Almera”, CSIC, C/ Lluís Sole i Sabaris s/n, 08028 Barcelona, Spain

Keywords: arsenic, speciation, urban aerosol, Huelva.

An arsenic speciation study has been performed in PM10 and PM2.5 samples collected on a fortnight basis in an urban background monitoring station (Manuel Lois) of the city of Huelva during 2001 and 2002. Previously, the high levels of arsenic found in PM10 and PM2.5 have been interpreted due to the emissions of a nearby copper smelter (Querol *et al.*, 2002, Alastuey *et al.* 2006). The rural background levels of arsenic around Huelva are rather high, in comparison to other rural or urban areas in Spain, showing a relatively high atmosphere residence time of arsenic. (Sánchez de la Campa *et al.*, 2007, Sánchez-Rodas *et al.*, 2007).

The arsenic species were extracted from the PM10 and PM2.5 filters using a  $\text{NH}_2\text{OH} \cdot \text{HCl}$  solution and sonication, and determined by HPLC–HG–AFS (Oliveira *et al.*, 2005).

The mean bulk As concentration of the samples analyzed during 2001 and 2002 slightly exceed the mean annual  $6 \text{ ng m}^{-3}$  target value proposed by the European Commission for 2013, being arsenate [As(V)] responsible for the high level of arsenic. The speciation analyses showed that As(V) was the main arsenic species found, followed by arsenite [As(III)] (mean  $7.3$  and  $5.9 \text{ ng m}^{-3}$  for As(V), mean  $1.6$  and  $1.1 \text{ ng m}^{-3}$  for As(III), in PM10 and PM2.5, respectively). The ratio of As in PM2.5/As in PM10 was 0.83.

During Atlantic advection days, the mean concentration of As was low ( $2.6 \text{ ng m}^{-3}$ ) and the As(III)/As(V) in PM2.5 and PM10 high (0.92 and 1.15, respectively (Figure. 1). However, in the anthropogenic sceneries, under synoptic conditions in which the winds with S and SW components transport the contaminants from the main emission source, the As mean concentration were highest ( $25.7 \text{ ng m}^{-3}$ ), with low As(III)/As(V) ratio in both PM2.5 (0.05) and PM10 (0.06) samples (Figure. 1). In the anthropogenic more african outbreak episodes, the concentration of As was intermediate between the two Atlantic and anthropogenic episodes ( $9.9 \text{ ng m}^{-3}$ ). The frequent African dust outbreaks over Huelva may result in an increment of mass levels of PM, but

do not represent a significant input of arsenic in comparison to the anthropogenic source.

Furthermore, the Figure 1 show the situation of chemical equilibrium among the ratios As(III)/As(V) in PM2.5 and PM10 (correlation coefficient  $R^2=0.79$ ).

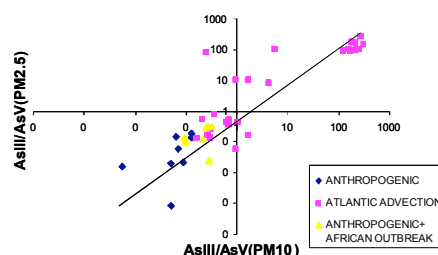


Figure 1. As(III)/As(V) in PM2.5 vs. As(III)/As(V) in PM10 for anthropogenic, Atlantic advection, and anthropogenic more african outbreak days in the period 2001–2002.

In this work we have showed the importance of arsenic speciation in studies of aerosol chemistry, due to the presence of arsenic species [As(III) and As(V)] with distinct toxicity, and the implications in future EU air quality Directive.

- Alastuey, A., Querol, X., Plana, F., Viana, M., Ruiz, C.R., Sánchez de la Campa, A., de la Rosa, J., Mantilla, E., & García dos Santos, S. (2006). *J. of Air Waste Management*, 56, 993–1006.
- Oliveira, V., Gómez-Ariza, J.L., & Sánchez-Rodas, D. (2005). *Analytical Bioanalytical Chemistry*, 382, 335–340.
- Querol, X., Alastuey, A., de la Rosa, J., Sánchez de la Campa, A., Plana, F., Ruiz, C.R. (2002). *Atmospheric Environment* 36, 3113–3125.
- Sánchez de la Campa, A. M., De la Rosa, J. D., Querol, X., Alastuey, A., & Mantilla, E. (2007). *Environmental Research*, 103, 305–316.
- Sánchez-Rodas, D., Sánchez de la Campa, A.M., de la Rosa, J.D., Oliveira, V., Gómez-Ariza, J.L., Querol, X., & Alastuey, A. (2007). *Chemosphere*, 66, 1485–1493.

## Polycyclic Aromatic Hydrocarbon in Suspended Particulate Matter in Southeastern Spain

J. Gil-Moltó, M. Varea, N. Galindo, S. Caballero, R. Esclapez, C. Pastor and J. Crespo

Physics Department, Miguel Hernández University, Avda. de la Universidad s/n, 03202, Elche, Spain

Keywords: PAH, TDS-GS-MS, particulate matter, source identification

The polycyclic aromatic hydrocarbon (PAH) levels associated with different fractions of suspended particulate matter (PM<sub>10</sub>, PM<sub>2.5</sub> and TSP) were studied during 2006 in an area of southeast Spain.

Samples of atmospheric particles were collected during representative periods of each season of the year using intercalibrated low and medium-volume gravimetric samplers. Twenty four hours samples were collected onto quartz fiber filters at three types of locations simultaneously: rural (MO), semi-industrial (UA) and urban (AY).

The samples were analyzed without previous extraction by means of thermal desorption coupled with gas chromatography and mass spectrometry (TD-GC-MS). Sixteen PAH categorized by the EPA as being priority contaminants were quantified in a total of 160 samples.

The presence of high levels of benzo[*g,h,i*]perylene (BghiP), indeno[1,2,3-*cd*]pyrene (IP), fluoranthene (Ft), pyrene (Pyr), benzo[*b*]fluoranthene (BbFt) and benzo[*k*]fluoranthene (BkFt), along with chrysene (Chry), with respect to the remaining PAH indicates that motor vehicle traffic is the primary source of these compounds at the studied locations (Figure 1).

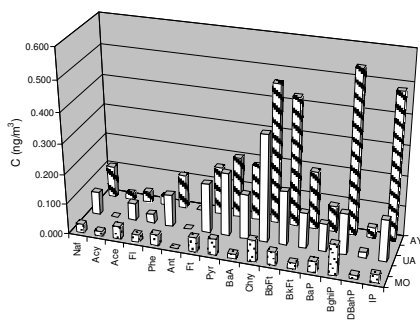


Figure 1. PAH concentration in PM<sub>10</sub> at each sampling point type

In order to determine their origins, the concentration ratios of some PAH in PM<sub>10</sub> were studied. The [Ft/(Ft+Pir)], [Phe/(Phe+Ant)] and [IP/(IP+BghiP)] ratios calculated for the three locations, semi-industrial, rural and urban, oscillate around 0.40, 0.98 and 0.45, respectively. This

confirms the previously obtained result (Simcik *et al.*, 1999; Sicre *et al.*, 1987).

Furthermore, it can also be seen in figure 1 that the primary difference between each sampling point is the PAH levels obtained, being lowest in the rural location as may be expected.

In all the samples the concentrations of benzo(a)pyrene (0.013-0.20 ng/m<sup>3</sup>) were found to be lower than the annual limit value (1 ng/m<sup>3</sup>) fixed by European Directive 2004/107/CE.

Upon comparing the PM<sub>2.5</sub>/PM<sub>10</sub> ratios for different PAH at the semi-industrial location, values superior to 0.6 can be observed in all cases. This indicates that these compounds accumulate in the size range inferior to 2.5 μm, just as has been demonstrated in previous studies (Aceves & Grimalt, 1993).

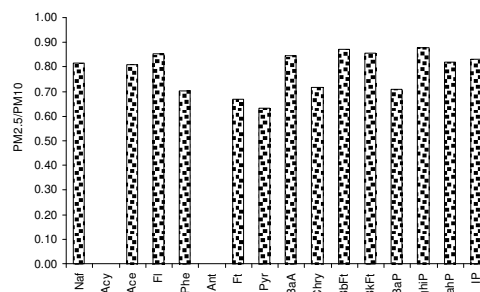


Figure 2. PM<sub>2.5</sub>/PM<sub>10</sub> Ratio for PAH in the semi-industrial location

This work was supported by the Generalitat Valenciana, GV05/086 ECOPAS project. We wish to thank A. Carratalá, M. Santacatalina and P. Nordstrom for their assistance in this work.

Sicre, M. A., Marty, J. C., Saliot, A., Aparicio, X., Grimalt, J., Albaiges, J. (1987). *Atmospheric Environment*, 21, 2247-2259.

Simcik, M. F., Eisenreich, S. J., Liyo, P.J. (1999). *Atmospheric Environment*, 33, 5071-5079.

Aceves, M., Grimalt, J.O. (1993). *Environmental Science & Technology*, 27, 2896-2908.

## Heterogeneous interactions of NO<sub>2</sub> with solid (NH<sub>4</sub>)<sub>2</sub>SO<sub>4</sub> surfaces

Carole Aghnati<sup>1</sup>, Sophie Sobanska<sup>2</sup>, Florent Louis<sup>1</sup>, and Denis Petitprez<sup>1</sup>

<sup>1</sup>PhysicoChimie des Processus de Combustion et de l'Atmosphère (PC2A), UMR CNRS 8522, FR CNRS 2416 Centres d'Etudes et de Recherche Lasers et Applications (CERLA), Université des Sciences et Technologies de Lille, 59655 Villeneuve d'Ascq Cedex, France.

<sup>2</sup>Laboratoire de Spectrochimie Infrarouge et Raman (LASIR), UMR CNRS 8516, FR CNRS 2416 Centres d'Etudes et de Recherche Lasers et Applications (CERLA), Université des Sciences et Technologies de Lille, 59655 Villeneuve d'Ascq Cedex, France.

Keywords: aerosol chemistry, ammonium sulphate, multiphase processes, NO<sub>x</sub>.

### INTRODUCTION

For many years, gas-phase atmospheric chemistry has been the main field of research. However, it is well known nowadays that the atmosphere is a multiphase system where solid and liquid particles coexist in addition to the gas phase.

Although their concentration in the air is relatively low, mineral particles are known to be very critical to the environment; their effect on the atmosphere and the climate has been of great scientific interest recently. In fact, these particles can affect the photochemical and optical properties of the troposphere and in addition, they present reactive surfaces for trace gases where heterogeneous reactions could take place.

The uptake of trace gases molecules by these particles is a critical step in atmospheric processes and it can lead to the removal and the transformation of many species as well as to the clarification of some reaction schemes that can not be explained solely with gas-phase reactions (Krueger et al., 2004). Although many studies were investigated on the interaction of NO<sub>2</sub> on mineral particles such as alkali halides (Finlayson-Pitts, 2003), little is known about its interaction on ammonium and sulphate salts. Thus, an understanding of this heterogeneous chemistry is important because it could play a role in the chemical balance of the troposphere.

In the present work, we focused our study on the interaction between gaseous NO<sub>2</sub>, one of the major components of air pollution, and ammonium sulphate (NH<sub>4</sub>)<sub>2</sub>SO<sub>4</sub> which is a dominant component in continental mineral particles.

### EXPERIMENTAL

The interaction of nitrogen dioxide with the solid phase was investigated at different relative humidities using a gas flow reactor and a mobile rod covered by a thin film of ammonium sulphate. The gas-phase composition was followed in real time with FTIR spectroscopy and mass spectroscopy. In the same time, the solid surfaces were characterized using the Environmental Scanning Electronic Microscopy (ESEM - Quanta 200 FEI instrument) and Raman

microspectrometry and imaging techniques (Labram Jobin Yvon SA). We have also conducted additional experiments where powders of (NH<sub>4</sub>)<sub>2</sub>SO<sub>4</sub> particles are exposed to NO<sub>2</sub> in a Teflon cell located in the sampling compartment of the FTIR spectrometer.

### RESULTS

We observed the consumption of NO<sub>2</sub> from the gas-phase as well as the formation of products in the different phases. Exposition were done at a total pressure of 1 bar and with different relative humidity (RH = 0, 50 and 80 %). After 2 hours of exposition to NO<sub>2</sub>, ammonium nitrate was identified, in the deliquescent phase, on the solid phase of ammonium sulphate. The size and the morphology of the surface particles were drastically changed. As expected, relative humidity is a key parameter governing the reactivity in all phases (Schlenker and Martin, 2005).

The formation of new products, in both the gas and the condensed phases, leads us to conclude on the presence of heterogeneous reactivity between nitrogen dioxide and ammonium sulphate in the solid phase.

### REFERENCES

- Finlayson-Pitts, B. J., (2003). *The tropospheric chemistry of Sea Salt : A molecular-Level view of the chemistry of NaCl and NaBr*. Chem. Rev. (103), 4801-4822.
- Krueger, B. J., Grassian, V. H., Cowin, J. P., Lakin, A., (2004).. *Heterogeneous chemistry of individual mineral dust particles from different dust source regions: the importance of particle mineralogy*. Atmospheric Environment (38), 6253-6261.
- Schlenker, J. C., Martin, S. T., (2005).. *Crystallization Pathways of Sulfate-Nitrate-Ammonium Aerosol Particles*. The Journal of Physical Chemistry A (109), 9980-9985.

## Secondary Organic Aerosol formation and on-line chemical composition analysis with a Thermal Desorption Chemical Ionisation Aerosol Mass Spectrometer (TDCIAMS)

G. Eyglunet<sup>1,2</sup>, A. Leperson<sup>2</sup>, G. Solignac, N. Marchand<sup>1</sup> and A. Monod<sup>1</sup>

<sup>1</sup>Laboratoire de Chimie et Environnement, Université de Provence, 3, place Victor Hugo, 13331, Marseille, France

<sup>2</sup> Now at Institut de Combustion, Aérothermique, Réactivité et Environnement, CNRS, 1C, Avenue de la Recherche Scientifique, 45071 Orléans Cedex 2 - France

Keywords: Aerosol Mass Spectrometry, SOA, Chemical composition, Aerosol Formation.

Atmospheric aerosols may have an important impact on climate and also human health. Aerosol Organic fraction, of which a major part is potentially of secondary origin, could play a significant role in these two effects. Formation mechanisms of Secondary Organic Aerosols are complicated phenomena which are nowadays not completely understood, and the chemical composition of SOA is difficult to determine because of its complexity and temporal variability. This work presents the application of an aerosol mass spectrometer using thermal desorption and chemical ionisation: the TDCIAMS, which allows on-line analysis of Secondary Organic Aerosol chemical composition and the study of secondary organic aerosol formation and aging.

The instrument was developed from the modification of a commercial APCI/MS/MS Varian 1200L. Characterisation of its performances has shown that the particle transmission efficiency is higher than 85%, and the gas trapping efficiency is higher than 90% in the inlet. The particles volatilisation efficiencies are higher than 90%, and the optimisation of the detection/ionisation step has allowed to obtain calibration lines with a repeatability higher than 90% for standard products of  $\alpha$ -pinene ozonolysis. It has been shown that the TDCIAMS is well adapted to on-line analysis of the chemical composition of organic particles for diameter of several hundred nanometers, and for a concentration range of 5 to 1000  $\mu\text{g}\cdot\text{m}^{-3}$ .

SOA have been produced from the ozonolysis of  $\alpha$ -pinene, in a Teflon Atmospheric Simulation Chamber, equipped with in situ FTIR for the gas phase analysis and a SMPS for the particles' granulometric distribution. The TDCIAMS was directly connected to the chamber, in order to analyse on-line the chemical composition of particles. Two experiments were performed, with the same initial reactant concentrations, with and without the addition of formic acid. This compound was used in the 2<sup>nd</sup> experiment to inhibit nucleation (Bonn *et al.*, 2002 and Lee & Kamens, 2005), and the comparison between both experiments allowed us to study the early stage of the reaction.

The addition of formic acid induced a particle nucleation inhibition, with a decrease of the particle

number, a conservation of the produced SOA mass and an increase of the diameter of the particles, in good agreement with previous studies. The new results consisted in the on-line analysis of SOA chemical composition. The results have shown that this composition does not qualitatively change in the presence of formic acid. However, the contribution of the main products (pinic, pinonic, norpinic acids and pinonaldehyde) and their molar yield decrease with formic acid. Furthermore, their concentration ratios are significantly modified, showing a modification of the SOA chemical composition and a modification of the chemical mechanisms. The results will be presented, as well as the proposed mechanism to explain the early stage of particle's formation.

This work was supported by the PRIMEQUAL program and the French ministry of research.

Bonn, B., Schuster, G. & Moortgat, G.K (2002). *The Journal of Physical Chemistry A*, 106, 2869-2881.

Lee, S. & Kamens, R.M. (2005). *Atmos. Environ.*, 39, 6822-6832.

## Dynamics of secondary organic aerosol from the ozonolysis of terpenes and isoprene: Results from aerosol chamber experiments and model analysis

H. Saathoff<sup>1</sup>, K.-H. Naumann<sup>1</sup>, O. Möhler<sup>1</sup>, A. Kiendler-Scharr<sup>2</sup>, T. Mentel<sup>2</sup>, R. Tillmann<sup>2</sup>, Å. M. Jonsson<sup>3</sup>, M. Hallquist<sup>3</sup>, and U. Schurath<sup>1</sup>

<sup>1</sup>Institute for Meteorology and Climate Research, Forschungszentrum Karlsruhe, Hermann-von-Helmholtz-Platz 76344 Eggenstein-Leopoldshafen, Germany

<sup>2</sup>Institute of Chemistry and Dynamic of the Geosphere, Forschungszentrum Jülich, Leo-Brandt-Str. 52428 Jülich, Germany

<sup>3</sup>Department of Chemistry, Atmospheric Science, Göteborg University, SE 412 96 Göteborg, Sweden

Keywords: SOA, aerosol chemistry, aerosol modelling, aerosol formation, biogenic particles

Secondary organic aerosols (SOA) from the oxidation of biogenic volatile organic compounds (BVOC) are a large fraction of the tropospheric aerosol especially over tropical continental regions. Dominant SOA forming processes are the reactions of monoterpenes with OH radicals, NO<sub>3</sub> radicals, and ozone forming SOA mass in highly variable yields. The ozonolysis of monoterpenes is supposed to be one of the major atmospheric sources of SOA (Griffin et al., 1999). Although isoprene is the most abundant BVOC its contribution to the formation of SOA is still unclear. SOA yields depend mainly on the type of organic precursor molecules, the mass of organic aerosol that can serve as solvent for condensing organic compounds, the acidity of and chemical reaction in the particulate phase, the humidity, and the temperature controlling the phase equilibrium of the semi volatile organics but also influencing the reaction pathways leading to condensable molecules. So far the influence of temperature on SOA yields is one of the major uncertainties. Model calculations show that a substantial amount of SOA mass from oxidation of BVOCs may be formed in the free troposphere and hence at lower temperatures.

Therefore we investigated the yield of SOA material from the ozonolysis of  $\alpha$ -pinene, limonene, and isoprene under simulated tropospheric conditions in the large aerosol chamber AIDA (Saathoff et al., 2003) on time scales of up to 30 hours and at temperatures between 243 and 313 K. The organic aerosol was generated by controlled oxidation with an excess of ozone and the aerosol yield is calculated from size distributions measured with differential mobility analysers. During the experiments trace gases were measured with PTR-MS, aerosol mass and composition with an aerosol mass spectrometer (AMS) and changes in particle volatility with a volatility tandem differential mobility analyser (VTDMA). On the basis of the measured initial particle size distribution and evolution of hydrocarbon and ozone concentrations model calculations were done using the aerosol model COSIMA (Naumann, 2003), supplemented by a recently developed SOA module.

Figure 1 shows the evolution of SOA mass in the AIDA chamber as measured independently by a SMPS and a DMPS system as well as the corresponding results of model calculations. The model assumed in this case the SOA particles to consist of two products with different vapour pressure.

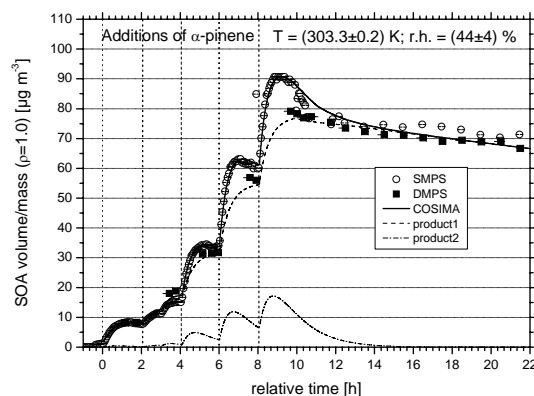


Figure 1. SOA mass evolution for subsequent oxidation of increasing amounts of  $\alpha$ -pinene with an excess of ozone in the AIDA chamber. The measurements (symbols) by SMPS and DMPS are compared to results of calculations with the COSIMA model.

This paper discusses the aerosol yields as function of temperature, humidity, and organic aerosol mass using different model attempts.

Griffin, R.J., Cocker III, D.R., Flagan, R.C., and Seinfeld, J.H. (1999). *J. Geophysical Research*, 104, 3555-3567.

Naumann, K.-H. (2003) *J. Aerosol Science*, 34, 1371-1397.

Saathoff, H., Möhler, O., Schurath, U., Kamm, S., Dippel, B., Mihelcic, D. (2003). *J. Aerosol Science*, 34, 1277-1296.

Tsigradis, K., Lathiere, J., Kanakidou, M., Hauglustaine, D. A. (2005). *Atmospheric Chemistry and Physics*, 5, 1891-1904.

## The effect of the surface coating grade of an organic insoluble substance onto hygroscopic particles

P. Villani<sup>1</sup>, V. Michaud<sup>1</sup>, R. Weigel<sup>1</sup>, D. Picard<sup>1</sup>, K. Sellegri<sup>1</sup>, S. Sjoegren<sup>2</sup>, J. Duplissy<sup>2</sup>, U. Baltensberger<sup>2</sup>, E. Weingartner<sup>2</sup> and P. Laj<sup>1</sup>

<sup>1</sup>Laboratoire de Météorologie Physique (LaMP), Observatoire de Physique du Globe de Clermont-Ferrand, Université Blaise Pascal, F-63170 Clermont-Ferrand, France

<sup>2</sup>Paul Scherrer - Institute, CH-5232 Villigen PSI, Switzerland

Keywords: aerosol cloud interaction, HTDMA, hygroscopicity, volatility.

The activation of atmospheric aerosol into cloud droplets due to condensation of water vapor is strongly linked to the hygroscopic properties of certain aerosol species. Indeed, the condensational growth of hygroscopic aerosol particles already occurs outside of clouds at values of relative humidity (RH) below 100%. By several experimental studies and numerical analyses, the deliquescent RH which affects the sudden solution of hygroscopic particles, for e.g. Ammonium Sulphate  $[(\text{NH}_4)_2\text{SO}_4]$  or Sodium Chloride  $[\text{NaCl}]$  is well known to be  $80\% \pm 1\%$  Hämeri et al. 2001(a) and  $75\% \pm 1\%$ , respectively Hämeri et al. 2001(b).

However, a quantitative influence of the internal mixture of different chemical aerosol compounds on the physico-chemical aerosol property is not well known, neither by experimental nor by theoretical studies. In this study, different fractions of organic substances were used to coat a NaCl core and their hygroscopicity was measured in laboratory experiments (Figure 1).

The goal was to investigate whether the hygroscopicity of an inorganic/organic mixture could be predicted from the known individual pure substances hygroscopic properties. For this purpose, the activity coefficient, surface tension, and density of the mixtures were calculated with thermodynamical models and the modeled hygroscopicity compared to the experimentally determined.

Finally, measurements were performed with a Volatility/Hygroscopicity – Tandem Differential Mobility Analyzer V/H-TDMA in order to evidence the surface effect of gradual coating of insoluble organic substances onto hygroscopic particles in terms of influencing the physico-chemical behavior of the hygroscopic bulk.

The use of the V/H-TDMA technique aims at the modification of the particles surface by exposing the aerosol to changed conditions of temperature and relative humidity. A complete study with the V/H-TDMA related to one specific aerosol size consists of quantifying the shift of the aerosol size distributions maximum obtained after heating (Volatility-Scan at temperatures of up to  $110^\circ\text{C}$ ), then the size-change due to exposure to enhanced humidity (Humidity-

Scan at  $\sim 90\%$  RH), and the shift due to heating followed by humidifying (Volatility-Humidity-Scan).

This technique brings new information on our understanding on how the surface of the particles influences their growth rate when they are exposed to a humid environment.

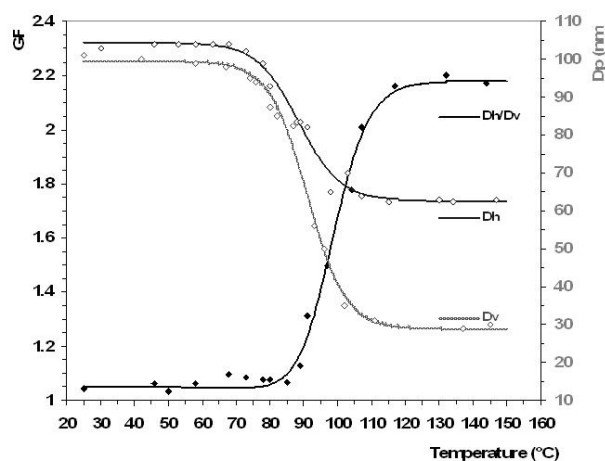


Figure 1: Particle Diameter (right ordinate) as a function of volatilization temperature, for the Volatility-Scan only ( $D_V$ ) and for the Volatility-Humidity-Scan ( $D_H$ ), as well as the resulting ratio of both as Growth Factor (GF – left ordinate) versus volatilization temperature ( $D_H/D_V$ ).

This work was supported by French Centre National de la Recherche Scientifique CNRS and PRIMEQUAL.

Hämeri, K.; Väkevä, M.; Hansson, H.-C.; Laaksonen, A.; 2001(a); Hygroscopic growth of ultrafine sulphate aerosol measurements using an ultrafine tandem differential mobility analyzer; *Journal of Geophysical Research*, Vol.105, 22 231 – 22242.

Hämeri, K.; Laaksonen, A.; Väkevä, M.; Suni, T.; 2001(b); Hygroscopic growth of ultrafine sodium chloride particles; *Journal of Geophysical Research*, Vol.106, 20 749 – 20757.

## Intensive measurements and modelling of size segregated chemical composition of aerosols in June 2006 and January 2007 in EMEP

W. Aas<sup>1</sup>, M.R. Alfarra<sup>2</sup>, E. Bieber<sup>3</sup>, D. Ceburnis<sup>4</sup>, T. Ellermann<sup>5</sup>, M. Ferm<sup>6</sup>, M. Frölich<sup>7</sup>, R. Gehrig<sup>8</sup>, H.C. Hansson<sup>9</sup>, G. Kiss<sup>10</sup>, U. Makkonen<sup>11</sup>, N. Mihalopoulos<sup>12</sup>, E. Nemitz<sup>13</sup>, R. Otjes<sup>14</sup>, N. Perez<sup>15</sup>, C. Perrino<sup>16</sup>, J.P. Putaud<sup>17</sup>, G. Spindler<sup>18</sup>, S. Tsyro<sup>19</sup>, M. Vana<sup>20</sup>, K.E. Yttri<sup>1</sup>

<sup>1</sup>Norwegian Institute for Air Research (NILU), Box 100 2027 Kjeller, Norway, [waa@nilu.no](mailto:waa@nilu.no)

<sup>2</sup>Paul Scherrer Institute (PSI), Villigen, Switzerland

<sup>3</sup>Umweltbundesamt, Dessau, Germany

<sup>4</sup>National University of Ireland, Galway, Ireland

<sup>5</sup>National Environmental Research Institute (NERI), Roskilde, Denmark

<sup>6</sup>Swedish Environmental Research Institute (IVL), Gothenburg, Sweden

<sup>7</sup>Umweltbundesamt, Vienna, Austria

<sup>8</sup>Air Pollution, Environmental Technology EMPA, Dübendorf, Switzerland

<sup>9</sup>The Department of Applied Environmental Science (ITM), Stockholm University, Sweden

<sup>10</sup>University of Veszprém, Veszprem, Hungary

<sup>11</sup>Finnish Meteorological Institute (FMI), Helsinki, Finland

<sup>12</sup>University of Crete, Heraklion, Greece

<sup>13</sup>Centre for Ecology and Hydrology (CEH) Edinburgh, UK

<sup>14</sup>Energy Centre of the Netherlands (ECN), Petten, Netherlands

<sup>15</sup>The Institute of Earth Sciences Jaume Almera (ICTJA-CSIC)

<sup>16</sup>CNR, The Institute for Atmospheric Pollution, Italy

<sup>17</sup>European Commission – DG Joint Research Centre, Ispra, Italy

<sup>18</sup>Leibniz Institute for Tropospheric Research (IFT) Leipzig, Germany

<sup>19</sup>Norwegian Meteorological Institute, Oslo, Norway

<sup>20</sup>The Czech Hydrometeorological Institute (CHMI), Prague, Czech Republic

Keywords: ambient aerosols, chemical composition, long-range transport, number size distribution

In the EMEP Monitoring Strategy (EB.AIR/GE.1/2004/5) it is stated that advanced aerosol measurements at super sites (Level 2 and 3) should be included as a regular part of the monitoring programme in Europe. It is however not realistic to require full daily chemical speciation or continuous measurements 365 days a year. Coordinated intensive measurements have therefore been recommended, and the first sampling periods were set for June 2006 and January 2007. The main focus was on size-resolved chemical speciation (i.e. PM<sub>10</sub>, PM<sub>2.5</sub> and PM<sub>1</sub>) and the gas/aerosol partitioning of inorganic aerosol. In addition, number size distribution was measured at several sites. Both continuous and manual measurements were used. In table 1 there is an overview of what have been measured.

These new data are very valuable for further EMEP model verification. The measurements have been compared with calculations from the EMEP Unified model, facilitating evaluation of the model performance with respect to PM size distribution and chemical speciation.

The results show clear regional differences. In the Nordic countries the average PM<sub>1</sub> mass as well as the chemical composition is very similar as to that of PM<sub>2.5</sub> in summer. While in central and southern Europe the ration varies more from day to day, dependent on source areas. For the

intensive hourly measurements there is a distinct difference between the nitrogen rich air in NL compared with the other sites.

Table 1. Measurement programme.

Sites	Mass	D	I	O	M	C	I
		I	N	R	T	R	N
		S	O	G	A	A	T
		T	R		L	S	E
		G	G			T	N
AT02	PM10,PM2.5,PM1		X	X			
CH02	PM10,PM2.5,PM1	X	X	X			X
CZ03	PM10,PM2.5			X	X		
DK41	PM10,PM2.5, PM1			Element anal.			
DE02	PM10,PM2.5,PM1						
DE03	PM10, PM2.5	X					
DE07	PM10,PM2.5				X		
DE44	PM10,PM2.5,PM1	X	X	X			X
ES31	PM10,PM2.5, PM1		X	X	X	X	
FI17	PM10,PM2.5,PM1		X				
HU02	PM10			X			
IE31	PM10,PM2.5,PM1	X	X	X			X
IT01	PM10,PM2.5	X	X	X		X	
IT04	PM10,PM2.5	X	X	X			X
NL11							X
NO01	PM10,PM2.5,PM1	X	X	X			
SE12	PM10,PM2.5,PM1	X		X			
GR02	PM10		X	X			
GB36							X
GB40							X

\* DIST means number size distribution while INTEN means continuous measurements using the AMS or MARGA/GRAEGOR systems. Some measurements were only done in one period. ORG may be either or both EC and OC.

## Ammonia uptake by organic aerosols and its effect on their water uptake properties

E. Dinar and Y. Rudich

Department of Environmental Sciences, Weizmann Institute of Science, 76100, Rehovot, Israel

Keywords: Aerosol chemistry, Aerosol cloud interaction, CCN, Hygroscopicity, Organic aerosols.

Atmospheric aerosols play an important role in Earth's radiation balance. They can be directly responsible for scattering and absorbing of both incoming short wave radiation and outgoing long wave radiation. Indirectly, aerosols can alter Earth's radiation balance through the modification of cloud microphysics by acting as Cloud Condensation Nuclei (CCN). Understanding and predicting aerosol particles' influence on cloud microphysics and its effect upon local and global climatic changes requires knowledge of their hygroscopic properties, which are a result of the chemical nature of the aerosol components.

Until recently most studies focused on how soluble and insoluble inorganics species such as ammonium sulfate and mineral dust, respectively, can influence aerosols cloud interactions. Recently, an increasing attention is directed for understanding the role of organic species in aerosol-cloud interactions and their influences on cloud microphysics. Moreover, new evidence from various field studies suggests that coupling between inorganic and organic chemistry in atmospheric aerosols exist, mainly through the formation of short and long lived organic ammonium salts.

Ammonia is a known player in the atmosphere; it is the only species that neutralizes acidic compounds formed from oxidation of sulfur dioxide and nitrogen oxides. These reactions result in the formation of ammonium-containing fine aerosols which can be either stable ( $(\text{NH}_4^+)_2\text{SO}_4^{2-}$ ) or less stable ( $\text{NH}_4^+\text{NO}_3^-$ ).

In contrast to other pollutants (such as sulfur compounds), ammonium concentrations in precipitation in the United States increased over the past 20 years and ammonia's mixing ratios range between few ppb up to a few ppm (depending on location, sources and on meteorological conditions). This is also the reason why atmospheric ammonia is a growing environmental and human health concern.

It was recently found that the observed CCN activity of biomass burning aerosols can be explained only if organic acids present in the particles are present in the form of ammonium salts [Mircea, *et al.*, 2005; Trebs, *et al.*, 2005]. Moreover, new evidence shows that near livestock farms, ammonia plays a significant role in the formation of secondary organic aerosols that can act as CCN [Lammel, *et al.*, 2004].

In the present study we show that gas phase ammonia can interact with aerosols containing atmospherically relevant organic compounds such as adipic acid, glutaric acid, suberic acid, humic substances and humic like substances (HULIS) extracted from collected atmospheric particles. The reactive uptake of ammonia by these organic aerosols results in a dramatic decrease in their diameter of activation ( $D_{50}$ ) to cloud droplets (as can be seen in Figure 1 for adipic acid) at all supersaturations thereby making them better CCN. We will discuss a mechanism by which ammonia acts as a non-destroying reactant upon organics with high vapor pressure. We will also suggest a mechanism by which ammonia can be recycled.

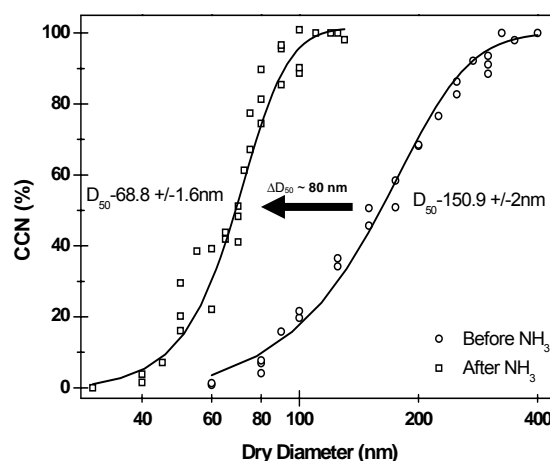


Figure 1. The influence of <125 ppm ammonia on adipic acid aerosols activation to droplets (measured at supersaturation of 0.64%).

Lammel, G., *et al.*: Aerosols emitted from a livestock farm in southern Germany, *Water Air Soil Pollut.*, 154, 313-330, 2004.

Mircea, M., *et al.*: Importance of the organic aerosol fraction for modeling aerosol hygroscopic growth and activation: A case study in the Amazon basin, *Atmos. Chem. Phys. Discuss.*, 5, 1-46, 2005.

Trebs, I., *et al.*: The  $\text{NH}_4^+\text{-NO}_3\text{-Cl-SO}_4\text{-H}_2\text{O}$  aerosol system and its gas phase precursors at a pasture site in the Amazon basin: How relevant are mineral cations and soluble organic acids? *J. Geophys. Res.*, 110, 2005.

## Assessment of Diesel exhaust particulate exposure and surface characteristics in association with levels of oxidative stress biomarkers

Ari Setyan<sup>1</sup>, Jean-Jacques Sauvain<sup>1</sup>, Michael Riediker<sup>1</sup>, Michel J. Rossi<sup>2</sup>, Michel Guillemin<sup>1</sup>

<sup>1</sup> Institute for Occupational Health Sciences, Rue du Bugnon 19, CH-1005 Lausanne, Switzerland

<sup>2</sup> Swiss Federal Institute of Technology, Air and Soil Pollution Laboratory, CH-1015 Lausanne, Switzerland

Keywords: Diesel exhaust, Aerosol sampling, Aerosol size distribution, Aerosol-surface reactions, Health effects of aerosols.

Exposure to PM<sub>10</sub> and PM<sub>2.5</sub> (particulate matter with aerodynamic diameter smaller than 10 µm and 2.5 µm, respectively) is associated with a range of adverse health effects, including cancer, pulmonary and cardiovascular diseases. Surface characteristics (chemical reactivity, surface area) are considered of prime importance to understand the mechanisms which lead to harmful effects. A hypothetical mechanism to explain these adverse effects is the ability of components (organics, metal ions) adsorbed on these particles to generate Reactive Oxygen Species (ROS), and thereby to cause oxidative stress in biological systems (Donaldson *et al.*, 2003). ROS can attack almost any cellular structure, like DNA or cellular membrane, leading to the formation of a wide variety of degradation products which can be used as a biomarker of oxidative stress.

The aim of the present research project is to test whether there is a correlation between the exposure to Diesel Exhaust Particulate (DEP) and the oxidative stress status. For that purpose, a survey is conducted in real occupational situations where workers are exposed to DEP (bus depots).

Different exposure variables have been considered:

- particulate number, size distribution and surface area (SMPS);
- particulate mass - PM<sub>2.5</sub> and PM<sub>4</sub> (gravimetry);
- elemental and organic carbon (coulometry);
- total adsorbed heavy metals - iron, copper, manganese (atomic adsorption);
- surface functional groups present on aerosols (Knudsen flow reactor). (Demirdjian *et al.*, 2005)

Several biomarkers of oxidative stress (8-hydroxy-2'-deoxyguanosine and several aldehydes) have been determined either in urine or serum of volunteers.

Results obtained during the sampling campaign in several bus depots indicated that the occupational exposure to particulates in these places was rather low (40-50 µg/m<sup>3</sup> for PM<sub>4</sub>). Size distributions indicated that particles are within the nanometric range. Surface characteristics of sampled

particles varied strongly, depending on the bus depot. They are usually characterized by high carbonyl and low acidic sites content.

Among the different biomarkers which have been analyzed within the framework of this study, mean levels of 8-hydroxy-2'-deoxyguanosine and several aldehydes (hexanal, heptanal, octanal, nonanal) increased during two consecutive days of exposure for non-smokers.

In order to bring some insight into the relation between the particulate characteristics and the formation of ROS by-products, biomarkers levels will be discussed in relation with exposure variables.

This project is financed by the Swiss State Secretariat for Education and Research. It is conducted within the framework of the COST Action 633 "Particulate Matter – Properties Related to Health Effects".

Demirdjian B., Rossi M. J. (2005). *Atmos. Chem. Phys. Discuss.*, 5, 607 – 654.

Donaldson K., Stone V., Borm P. J., Jimenez L. A., Gilmour P. S., Schins R. P., Knaapen A. M., Rahman I., Faux S. P., Brown D. M., MacNee W. (2003). *Free Radical Biol. Med.*, 34, 1369-1382.

## Aerosol Catalysis: Size effect and Metal support interaction on Pd Nanoparticles

F. Bacle, M. Seipenbusch and G. Kasper

Institut für Mechanische Verfahrenstechnik und Mechanik, Universität Karlsruhe (TH), 76128 Karlsruhe, Germany

Keywords: nanoparticles, aerosol catalysis, nanoparticles characterization

Due to their large specific surface according to their small size, nanoparticles are particularly interesting for catalysis. Using Fourier Transformation IR Spectroscopy, we have investigated the influence of metal-support interaction on aerosol catalysis. Ethylene hydrogenation served as a test reaction for a Pd aerosol catalyst. Aim of this project is to show the variation and the effect on reactivity between supported and non-supported catalyst aerosol.

Bos and Westerterp (1993) have shown the hydrogen's ability of dissociation on Pd. Many parameters have been studied, mainly concerning reaction temperature, gas pressure and Pd structure (Molero, Bartlett and Tysoe, 1999). Due to the structural dependence of adsorption energy, catalysis strongly depends on the particle size. It has been demonstrated that the number of high energy sites decreases with increasing primary particle size (Shaikhutdinov, Heemeier, Bäumer, Lear, Lennon, Oldman, Jackson and Freund, 2001). This shows the importance of the particle size (particularly for aerosol). Apart from size effects, metal support interactions can have a great influence on catalytic activity (Weber, Davoodi, Seipenbusch and Kasper, 2006). Interactions can be of different natures, such as diffusion inhibition, electronic and spill-over interaction.

To study size effects and metal support-interactions it is necessary to avoid wall-effects and observe impacts on isolated particles. For this purpose aerosol catalysis is of unique tool.

The unsupported catalyst aerosol is a continuous stream, composed of isolated Pd nanoparticles produced by spark discharges, carried by an inert gas. The aerosol catalyst is mixed with the reaction gases and passes through the reactor. The product gas was analysed online with FTIR, while the aerosol particles were characterised by a SMPS offline method. Primary particles agglomerated together as shown in Figure 1.

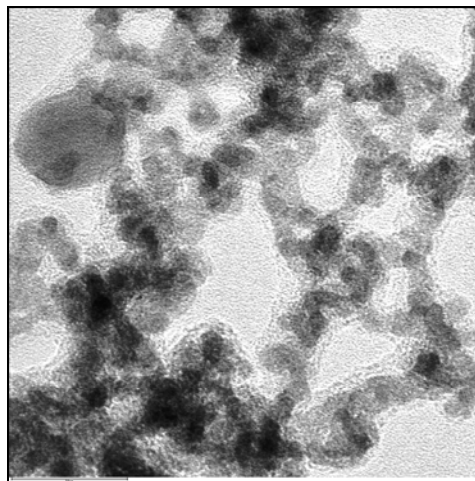


Figure 1. TEM image of agglomerated particles of Pd

The agglomerate size can be changed varying the supporting gas flow rate and the discharge frequency of the aerosol generator. Primary particle size can be influenced by controlled sintering.

The supported catalyst aerosol is composed of nanoparticles of Pd dispersed on the surface of SiO<sub>2</sub> sintered particles.

Non-supported and supported interactions have been investigated to show correlations between structure and function of aerosols.

- A. N. R. Bos and K. R. Westerterp, *Chem. Engineering and Processing*, 32 (1993) 1-7
- H. Molero, B. F. Bartlett and W. T. Tysoe, *J. of Catalysis*, 181 (1999) 49-56
- Sh. Shaikhutdinov, M. Heemeier, M. Bäumer, T. Lear, D. Lennon, R. J. Oldman, S. D. Jackson and H.-J. Freund, *J. of Catalysis*, 200 (2001) 330-339
- A.P. Weber, P. Davoodi, M. Seipenbusch, G. Kasper, *J. of Nanoparticle Research*, 8 (2006), 445-453

## Characterization of oligomers in organic aerosols with ultra-high mass resolution and accurate mass measurements

M. Kalberer<sup>1</sup>, A. Reinhardt<sup>1</sup>, C. Emmenegger<sup>1</sup>, J. Dommen<sup>2</sup>, B. Gerrits<sup>3</sup>, Christian Panse<sup>3</sup>

<sup>1</sup>Department of Chemistry and Applied Biosciences, ETH Zurich, 8093 Zurich, Switzerland

<sup>2</sup>Laboratory of Atmospheric Chemistry, Paul Scherrer Institut, 5232 Villigen PSI, Switzerland

<sup>3</sup>Functional Genomics Center Zurich, UZH / ETH Zurich, Winterthurerstrasse 190, 8057 Zurich, Switzerland

Keywords: Aerosol chemistry, Chemical analysis, Mass spectrometry, Smog chamber, SOA.

The chemical nature of a large fraction of organic aerosols is not known. It has been shown that high molecular weight compounds make up a significant fraction (20-50%) of the water-soluble organic carbon (WSOC) in ambient aerosols. To better understand formation processes of secondary organic aerosol (SOA) mass and estimate their influence on climate and health related issues a more complete knowledge of the SOA components is necessary.

High resolution mass spectrometry, such as Fourier transform ion cyclotron resonance mass spectrometry (FTICR-MS), allows to determine unambiguously the elemental composition of compounds. SOA samples generated in a smog chamber under different conditions (e.g., terpene and aromatic precursors, ozonolysis or photolysis conditions) were analyzed with FTICR-MS. These laboratory generated SOA analyses are compared with ambient aerosol samples.

Several hundred peaks in a mass range between  $m/z$  200-700 were detected. Often within a few millidalton 2-3 peaks with totally different elemental composition are measured emphasizing the necessity for high resolution measurements to elucidate the components in complex samples such as SOA.

The mass spectrum is clearly divided in a range with low-molecular weight compounds ( $m/z < 300$ ) and a high molecular weight (or oligomer) range ( $m/z > 300$ ). In the oligomer mass range a dimer and trimer range is distinguishable.

Using advanced data analysis techniques (e.g., the Kendrick mass analysis) the elemental composition of the majority of all peaks in the entire mass spectrum could be assigned.

Van Krevelen diagrams show that most of the compounds in  $\alpha$ -pinene-ozonolysis-SOA have high O:C ratios in the range of 0.4 - 0.6. Monomers have on average a higher O:C ratio than dimers and trimers, suggesting a condensation reaction leading from the monomers to the small co-oligomers as shown in Figure 1 (Reinhardt et al., 2007).

A program developed in-house, MonomerHunter, was used to calculate the abundance of exact mass differences throughout the spectrum to find potential monomers. A majority of the peaks measured in the low mass region of the spectrum ( $m/z < 300$ ) is also found in the calculated results of the MonomerHunter, indicating that this mathematical

procedure gives mostly chemically meaningful results.

For the first time ultra-high resolution MS data from aerosol samples were analyzed for a wide mass range ( $m/z$  200-700) with advanced data analysis methods to examine the elemental composition of monomers and oligomers and to investigate possible oligomer formation mechanisms in secondary organic aerosols.

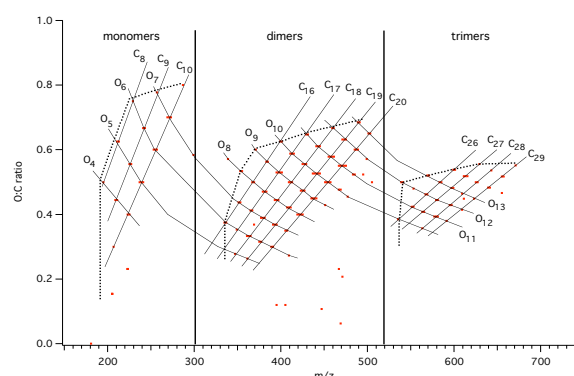


Figure 1. O:C ratio as a function of  $m/z$  for all compounds  $> m/z 200$  for  $\alpha$ -pinene-ozonolysis-SOA. Dimers and trimers have a lower maximum O:C ratios than monomers suggesting condensation reactions as possible formation pathways of SOA oligomers as indicated with the dotted lines. Compounds with the same number of carbon and oxygen atoms are connected with solid lines.

The Functional Genomics Center is greatly acknowledged for providing their infrastructure. This work was supported by ETH Grant TH-14/04-2, the Swiss National Science Foundation (No. 200020-108095) and the EC project POLYSOA (Polymers in Secondary Organic Aerosols).

Reinhardt et al. (2007). *Anal. Chem.* Accepted.

## Influence of different sample preparations on the determined concentrations of selected trace metals in atmospheric particles

H. Radič<sup>1</sup>, J. Turšič<sup>1</sup>, M. Kovačević<sup>1</sup> and M. Veber<sup>2</sup>

<sup>1</sup>Laboratory for Analytical Chemistry, National Institute of Chemistry, Hajdrihova 19, SI-1000 Ljubljana, Slovenia

<sup>2</sup> Faculty of Chemistry and Chemical Technology, University of Ljubljana, Aškerčeva cesta 5, Ljubljana, Slovenia

Keywords: urban aerosols, PM10, trace elements, soluble fraction

Trace metals are released into the atmosphere as a result of anthropogenic and natural emissions. The main anthropogenic sources are combustion of fossil fuels and wood, as well as high temperature industrial processes and waste incineration. Natural emissions result from a variety of processes acting on crustal minerals, from forest fires and the oceans (Allen *et al.*, 2001).

There is a general agreement on the existence of significant statistical relation between airborne particulate matter and adverse effects on human health (Pope, 2000). Toxicological studies have frequently implicated the metal content (particularly water soluble part) as a possible harmful component of atmospheric particles (Heal *et al.*, 2005).

There are many different methods of sample preparation of ambient particulate matter. One of the widely used is microwave-assisted digestion of filter based samples. However, the choice of digestion reagents is an important consideration for determination of multiple elements in complex matrix containing carbonaceous and crustal material, sulphates, nitrates. The most problematic are silicon-containing compounds and the elements bonded to siliceous material (Perkney and Davidson, 2005).

The aim of our work was to determine the fraction of water soluble metals and compare it to the amounts of metals obtained with two different digestion procedures.

Sampling of PM10 was performed at urban background location in Ljubljana, Slovenia in spring 2005. After weighting, filters with deposit were cut into three sub-samples. For the determination of water soluble parts, filters were sonicated at room temperature for 30 min in Milli-Q water. First digestion procedure was performed in microwave oven using HNO<sub>3</sub> and H<sub>2</sub>O<sub>2</sub> according to SIST EN 14902 (Ambient Air Quality – Standard method for the measurement of Pb, Cd, As and Ni in the PM10 fraction of suspended particulate matter). As second digestion procedure decomposition by mixture of HF, HCl and HNO<sub>3</sub> was applied. For testing the recovery rates, certified reference material (SRM 1648 Urban Particulate Matter) was used. Concentrations of selected trace metals (V, Cr, Ni, Cu, Zn, As, Cd, and Pb) were determined by collision cell ICP-MS, using He as a collision gas.

Results of analysis of certified reference material showed that both applied digestion procedures give recovery rates higher than 90 % for Cu, Zn, As, Cd and Pb. The most pronounced difference between two procedures was observed in the case of Cr, where digestion according to SIST EN 14902 resulted in recovery rate of about 25 %, while recovery after digestion by mixture of HF, HCl was much higher (80 %). Higher recoveries using mixture of HF, HCl and HNO<sub>3</sub> were observed also for V, Ni and Sb.

Average fractions of trace metals after different sample preparation in PM10 collected in Ljubljana are shown in table 1.

Table 1 Average fractions of trace metals in PM10 particles collected in Ljubljana after different sample preparation - dissolution in water, digestion 1 (SIST EN 14902) and digestion 2 (mixture of HF, HCl and HNO<sub>3</sub>).

Trace metal	Dissolution in water [µg g <sup>-1</sup> ]	Digestion 1 [µg g <sup>-1</sup> ]	Digestion 2 [µg g <sup>-1</sup> ]
V	47	59	58
Cr	29	172	286
Ni	8	121	179
Cu	192	432	466
Zn	1390	1460	1700
As	19	23	27
Cd	20	26	27
Pb	192	735	845

This work was supported by the Slovenian Research Agency and was done in the frame of COST-633 Action.

Allen A.G., Nemitz E., Shi J.P., Harrison R.M., Greenwood J.C. (2001). *Atmos. Environ.* 35, 4581-4591

Heal M.R., Hibbs L. R., Aginus R. M., Beverland I.J. (2005). *Atmos. Environ.* 39, 1417-1430

Perkney N.J., Davidson C. I. (2005). *Anal. Chim. Acta* 540, 269-277

Pope C.A. (2000). *Aerosol Sci. Technol.* 32, 4-14

## Simultaneous on-line size and chemical analysis of gas phase and particulate phase of mainstream tobacco smoke

J. McAughey<sup>1</sup>, T. Adam<sup>2,3</sup>, C. McGrath<sup>1</sup>, C. Mocker<sup>2,3</sup>, R. Zimmermann<sup>2,3,4</sup>

<sup>1</sup>British American Tobacco, Group R&D Centre, Southampton SO15 8TL, United Kingdom

<sup>2</sup>Analytical Chemistry, Institute of Physics, University of Augsburg, 86159 Augsburg, Germany

<sup>3</sup>Institute of Ecological Chemistry, GSF - National Research Center for Environment and Health, 85764 Neuherberg, Germany

<sup>4</sup>BIfA - Bavarian Institute of Applied Environmental Research and Technology GmbH, Environmental Chemistry, 86167 Augsburg, Germany

Keywords: mass spectrometry, on-line measurement, chemical composition, particle size, tobacco smoke

Tobacco smoke is a complex and dynamic matrix consisting of gaseous compounds and particulate material, in which about 4800 constituents have been identified (Baker, 1999). The chemical composition and partition between both phases of the smoke can change continuously and is strongly influenced by time, temperature, chemistry and dilution of smoke. Therefore, in order to gain dosimetric predictions of smoke components relevant for human smokers, it is helpful to investigate both phases simultaneously in real time, in fresh rather than aged smoke. In this paper we present an experimental set-up consisting of gas phase and particulate phase on-line instrumentation for comprehensive analysis of cigarette mainstream smoke, that is, the smoke that emerges from the mouth end of the cigarette during a puff.

The smoke is provided by a smoking engine and diluter (Model MD-19E, Matter Engineering, Wohlen, Switzerland), which can be set to a square-wave smoking profile controlling puff volume, puff duration, and puff frequency. A rotating disk diluter allows a 50:1 real-time dilution of the whole smoke, prior to particle diameter and concentration measurement by an electrical mobility spectrometer at 10 Hz resolution in the range 5 – 1000 nm (Model DMS-500, Cambustion, Cambridge, UK) (Reavell *et al.*, 2002).

The excess non-diluted smoke was sampled directly, again in real-time, for mass spectrometry where two soft ionisation techniques based on photoionisation were applied. These avoid fragmentation, and allow improved interpretation and quantification of spectra of highly complex matrices such as smoke.

The resonance-enhanced multi-photon ionisation (REMPI) technique uses at least two ultraviolet (UV) photons for photoionisation, which takes place via an optical resonance absorption step. In practice, REMPI is highly sensitive for aromatic compounds. The single photon ionisation (SPI) technique uses vacuum ultraviolet (VUV) photons for ionisation. With SPI, additional compounds e.g. aliphatic hydrocarbons, carbonyl compounds and nitrogen-containing substances are accessible. In principle, both ionisation methods can be applied in

an alternating mode with a time-resolution of up to 10 Hz. Combining REMPI and SPI with time-of-flight mass spectrometry (TOFMS) results in a fast measurement system for trace compounds in complex gaseous matrices (Mitschke, 2005)

Cigarettes were smoked at two flow regimes of 1.05 and 2.10 l.min<sup>-1</sup> over eight puffs of 2s duration and 60s intervals. Cigarettes consisted solely of Burley, Virginia or Oriental tobacco and were filter ventilated at 0, 35 or 70%.

Count median diameter (CMD) averaged over the cigarette varied from 182 – 260 nm and increased with increasing filter ventilation and lower puff flow rates; a consequence of increasing smoke residence time and coagulation within the rod. Puff-by-puff data showed increasing particle concentration and decreasing diameter as the tobacco was consumed and the coagulation period decreased.

Initial mass spectrometry data show that most smoke constituents feature a continuous increase from the first to the last puff. This behaviour is due to a gradual reduction in tobacco length as the cigarette is consumed, which results in a decrease in filtration by the tobacco rod for species in the particulate phase of smoke and a decrease in air dilution and outward gaseous diffusion. However, there are some substances, in particular unsaturated hydrocarbons e.g. butadiene, isoprene, and propyne, which show a completely different behaviour by having the highest amounts in the first puff. This is likely to be related to the different combustion and pyrolysis conditions when the cigarette is lit (Adam, 2006).

Adam, T. *et al.* (2006). *Chem. Res. Toxicol.*, 19, 511 - 520.

Baker, R.R. (1999). *Smoke Chemistry*. In *Tobacco: Production, Chemistry, and Technology*; Blackwell: Oxford, U.K.; 398 - 439.

Mitschke, S. *et al.* (2005). *Anal. Chem.*, 77, 2288-2296.

Reavell, K. *et al.* (2002). *A fast response particulate spectrometer for combustion aerosols*. SAE Technical Paper, 2002-01-2714

## Effects of potassium nitrate on the polymorphic transformations of ammonium nitrate particles

HongBo Wu, ManNin Chan and Chak K. Chan

Department of Chemical Engineering, Hong Kong University of Science and Technology, Clear Water Bay, Kowloon, Hong Kong, China

Keywords: ammonium nitrate, potassium nitrate, polymorph, phase transition, Raman spectroscopy.

### INTRODUCTION

Solid ammonium nitrate ( $\text{NH}_4\text{NO}_3$ ) exists in five stable polymorphic forms below its melting point at  $170^\circ\text{C}$  (Hendricks et al., 1932). Phase IV is known to be stable from  $-17^\circ\text{C}$  to  $32^\circ\text{C}$  and can transform to phase III at  $32\text{--}50^\circ\text{C}$  or to phase II at  $50\text{--}55^\circ\text{C}$ . Little attention of the possible importance of these polymorphic transformations in atmospheric aerosols has been paid until recently (Chan and Chan, 2004). Our new results show that solid and pure  $\text{NH}_4\text{NO}_3$  particles only exhibit the  $\text{IV}\leftrightarrow\text{II}$  phase transition at around  $50^\circ\text{C}$  (Wu et al., 2007). However, the transition paths and temperatures have been found to change by a small amount of doping potassium salts. For example, Campbell and Campbell (1946) reported that 2wt% of potassium nitrate ( $\text{KNO}_3$ ) in  $\text{NH}_4\text{NO}_3$  powder samples lowers the  $\text{IV}\rightarrow\text{III}$  transition temperature from  $32^\circ\text{C}$  to  $28.4^\circ\text{C}$ . In this study, the effects of  $\text{KNO}_3$  on the  $\text{IV}\rightarrow\text{III}$  and  $\text{IV}\rightarrow\text{II}$  transitions of  $\text{NH}_4\text{NO}_3$  particles were investigated using in-situ Micro-Raman spectroscopy.

### METHODS

Solid  $\text{KNO}_3/\text{NH}_4\text{NO}_3$  particles were generated by the efflorescence of their solution droplets on a PTFE surface. Typically, the experiments started in an airflow at feed  $\text{RH}=60\%$  at around  $23^\circ\text{C}$ , and the samples were heated and cooled at a rate of  $0.18^\circ/\text{min}$ . Raman spectra were recorded in situ at every  $2^\circ\text{C}$  in this thermal cycle using microscopic Raman spectroscopy (Renishaw, Model 1000).

### RESULTS

As shown in Fig. 1, the phase transition paths and temperatures of  $\text{KNO}_3/\text{NH}_4\text{NO}_3$  particles are influenced by the  $\text{KNO}_3$  concentration and particle size. Pure  $\text{NH}_4\text{NO}_3$  particles only experience  $\text{IV}\rightarrow\text{II}$  phase transition at above  $50^\circ\text{C}$ , independent of the particle size. When the  $\text{KNO}_3$  concentration is less than 6wt%, small  $\text{KNO}_3/\text{NH}_4\text{NO}_3$  particles (40–60  $\mu\text{m}$ ) exhibit the  $\text{IV}\rightarrow\text{II}$  transition at above  $45^\circ\text{C}$ . However, when the  $\text{KNO}_3$  concentration increases to 8wt%, the  $\text{IV}\rightarrow\text{III}$  transition, instead of  $\text{IV}\rightarrow\text{II}$ , takes place at around  $35^\circ\text{C}$ . The  $\text{IV}\rightarrow\text{III}$  transition temperature decreases and becomes close to, or even below the ambient temperatures, when the  $\text{KNO}_3$  concentration decreases further.

The bigger particles (around 250, 450 and 650  $\mu\text{m}$ , respectively) show similar trends of the transition path and temperature as the small particles. However, the lower  $\text{KNO}_3$  concentration limit for the change in the transition path from  $\text{IV}\rightarrow\text{II}$  to  $\text{IV}\rightarrow\text{III}$  decreases with increasing particle size. For the biggest  $\text{KNO}_3/\text{NH}_4\text{NO}_3$  particles (around 650  $\mu\text{m}$ ) examined in our experiments, the  $\text{IV}\rightarrow\text{III}$  transitions were observed at only 2wt% of  $\text{KNO}_3$  concentration.

These results suggest that the  $\text{IV}\rightarrow\text{III}$  transition may potentially take place under ambient conditions, when  $\text{NH}_4\text{NO}_3$  aerosol particles are mixed with relatively high concentrations (e.g.  $>20\text{wt}\%$ ) of  $\text{KNO}_3$ .

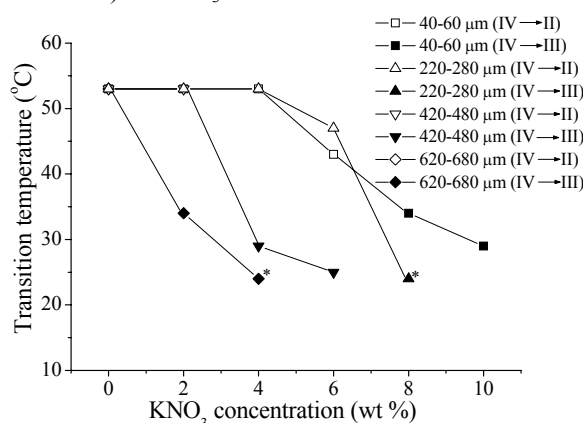


Figure 1. The phase transition paths and temperatures of  $\text{KNO}_3/\text{NH}_4\text{NO}_3$  particles as a function of  $\text{KNO}_3$  concentration and particle size. (\* indicates that the solid particles directly formed in phase III at ambient temperatures)

This work was supported by the Research Grants Council Earmarked Grant of Hong Kong Special Administrative Region, China under grant 600304.

- Hendricks, S. B., Posnjak, E., & Kracek, F. C. (1932). *J. Amer. Chem. Soc.*, 54, 2766-2786.  
 Chan, C. K., & Chan, M. N. (2004). *Atmos. Environ.*, 38, 1387-1388.  
 Campbell, A. N., & Campbell, A. J. R., (1946). *Can. J. Res. B*, 24, 176-185.  
 Wu, H. B., Chan, M. N., & Chan, C. K. (2007). *Aerosol Sci. Tech.*, accepted.

## Characterization of residual lignin polymers in particulate matter by LC-MS

E. Bolzacchini<sup>1</sup>, L. Ferrero<sup>1</sup>, B. Ferrini<sup>1</sup>, Z. Lazzati<sup>1</sup>, M. Orlandi<sup>1</sup>, C. Lo Porto<sup>1</sup>, G. Perrone<sup>1</sup>, G. Sangiorgi<sup>1</sup>, S. Petraccone<sup>1</sup>, L. Zoia<sup>1</sup>,

<sup>1</sup>Department of Environmental Science, University of Milano-Bicocca, Piazza della Scienza 1, 20026, Milan, Italy

Keywords: coagulation, HPLC-MS, lignin, markers, particulate matter

The composition of particulate matter comprehends a monomeric and polymeric unknown organic fraction (Cappiello et al 2003).

These molecules are important because of their roles in the nucleation and coagulation of chemicals; like reactive substrate and/or inhibitor of some reactions; like markers for the determination of view, transport and aging of the carrier (Rogge et al 1993).

The lignin (Fig. 1) is the second aromatic biopolymer more abundant in nature.

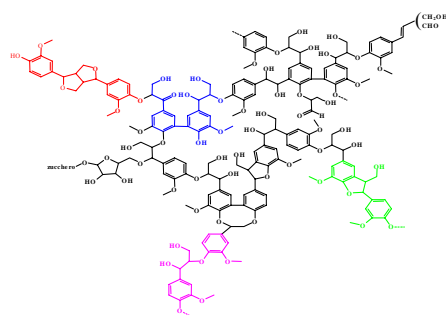


Figure 1. Lignin structure.

It's composite of phenylpropanoidic unit bonded of different type of C-H and C-O (Fig. 2). In Fig. 2 there show the oligomers of lignin. The most abundant intermonomeric bond in the lignin-structure is the  $\beta$ -O-4 (Crestini et al 2006).

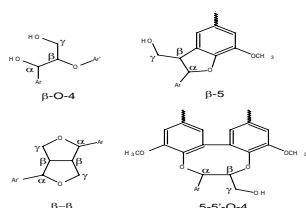


Figure 2. Intermonomeric bonds of lignin.

The lignin pyrolysis biosynthetic products were show by Atmospheric pressure chemical ionization mass spectrometry (APCI-MS). The lignin fraction was diluted in methanol and the sample was introduced in the APCI source at an eluent (MeOH : H<sub>2</sub>O 50:50), flow rate of 1 ml/min. Positive ion APCI-MS spectra were acquired (Shimadzu 2010) with a mass range 100-2000 amu (Fig.3) (Crestini et al 2006).

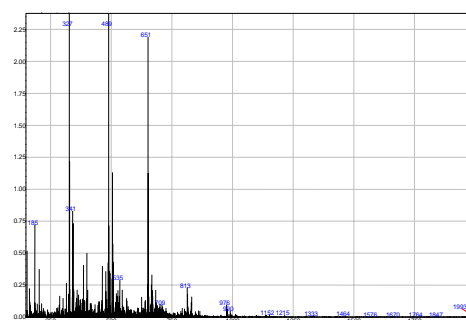


Figure 3. Mass Spectra of a lignin biopolymer.

The APCI mass spectrum (Fig.3) showed resolved signals of protonated  $\beta$ -5 (MW= 326) and  $\beta$ -O- 4 (MW=343) (Fig.4)  $[M+1]^+ = 327$ ;  $[M]^+ = 343$  respectively (Fig.5).

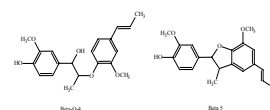


Figure 4. Dimers  $\beta$ -5 and  $\beta$ -O- 4.

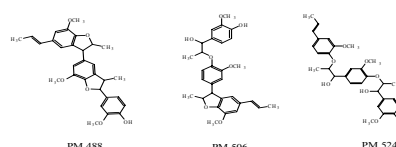


Figure 5. Thrimers.

- A. Cappiello, E. De Simoni, C. Fiorucci, F. Mangani, P. Palma, M.C. Facchini, S. Fuzzi, (2003). *Env. Science and Tech.*, 37, 1229-1240.
- W.F. Rogge, M.A. Mazurek, L.M. Hildemann and G.R. Cass, B.R.T. Simonet (1993). *Atmosph. Env.*, 27A, 1309-1330.
- M. Kalberer, D. Paulsen, M. Sax, M. Steinbacher, J. Dommen, A.S.H. Prevot, R. Fisseha, E. Weingartner, V. Frankevich, R. Zenobi, U. Balensperger (2004). *Science*, 303, 1659-1662.
- C. Crestini, M. Orlandi, E-L Tolppa, L. Zoia, R. Saladino. Characterisation of lignin by different spectroscopic and aromatic techniques. COST E41, Analysis Effort on wood and fiber characterisation. Vienna 31-agosto-1 settembre 2006.

## Determination of oxygenated, nitrated and native Polycyclic Aromatic Hydrocarbons (PAH) in Aerosols using different, liquid chromatographic based methods

J. Lintelmann, K. Fischer, M. Heil-Franca, G. Matuschek

Institute of Ecological Chemistry, GSF-National Research Center for Environment and Health, Ingolstädter Landstr.1, D-85764 Neuherberg

Keywords: HPLC-MS, organic compounds, PAH(s), urban aerosols

Fine and ultrafine particles are probably responsible for numerous health effects, but so far it is still unclear whether and to which extent the particle itself or organic compounds which are adsorbed or condensed on the particle are responsible for the effects observed. Important classes of particle bound substances are the Polycyclic Aromatic Hydrocarbons (PAH) as well as their oxygenated and nitrated derivatives. To improve the tools for the chemical characterization of particulate matter, analytical methods for the determination of those substances in aerosol samples were developed and applied. The methods are based on high performance liquid chromatographic (HPLC) separation coupled with fluorescence (FD) or tandem mass spectrometric detection (MS/MS) (Lintelmann et al., 2005).

15 EPA-PAH were analysed using reversed phase separation (MZ-PAH C-18, 5  $\mu$ m, 250 x 3 mm I.D., 0.5 ml/min) and time-programmed fluorescence detection of the PAH. Eluents were acetonitrile/water and the injection volume was 10  $\mu$ l.

The same chromatographic principle could be applied for the determination of four nitro-PAH (1-; 2-nitropyrene, 2-; 3-nitrofluoranthene). The analytes were separated on a reversed phase column (MZ-PAH C-18, 5  $\mu$ m, 250 x 4 mm I.D., 1 ml/min, 20  $\mu$ l injection volume with a methanol gradient. Because nitro-PAH are non-fluorescent, a post-column reduction on an additional column (Pt/ $\gamma$ -Al<sub>2</sub>O<sub>3</sub>, 5% Pt, 50 x 4 mm I.D., 90 °C) was integrated into the HPLC-system allowing the sensitive detection of the resulting fluorescent amino-PAH.

6 isomeric benzo[a]pyrene-diones, two isomeric chrysene-diones, phenanthrene-9,10-dione and a further oxy-benzo[a]pyrene derivate were quantified with an HPLC-MS/MS method. Chromatographic separation of the oxy-PAH was achieved by use of a methanol gradient (methanol / ammonium acetate, 10 mmol) on a reversed phase column (LiChroCart 250 x 4 mm I.D., Superspher 100 C18, 0.7 ml/min, 10  $\mu$ l injection volume). The HPLC-eluent was introduced into the on-line coupled mass spectrometer via an atmospheric pressure chemical ionization interface. The qualification and quantification of the analytes was performed in the multiple reaction monitoring mode (MRM).

Validation studies demonstrated good reliability, high precision and selectivity as well as low detection limits (< 10 pg/m<sup>3</sup>) for the methods described.

During 2005 and 2006 aerosol samples were collected at two sites; the Munich city center (2006) and the Munich city border (2005): Fine particulate matter (PM<sub>2.5</sub>) was collected on quartz fiber filters with a high-volume sampler (HVS) which was operated for 24 h at a flow rate of ca. 700 l/min. Additionally, some meteorological data like temperature and global radiation were documented.

For the determination of PAH and nitro-PAH in the samples, one third of the filter was extracted using accelerated solvent extraction (ASE) with hexane/acetone as solvents. The extract was divided and each part was separately processed and analyzed with the HPLC-FD-systems. For the quantification of PAH-diones another third of the filter was ultrasonically extracted with ethylacetate, processed and analyzed by HPLC-MS/MS.

The results obtained show a significant correlation with meteorological conditions (e.g.ambient temperature). More and over the sampling site and therefore potential sources of the pollutants considered influence their concentrations found in the samples.

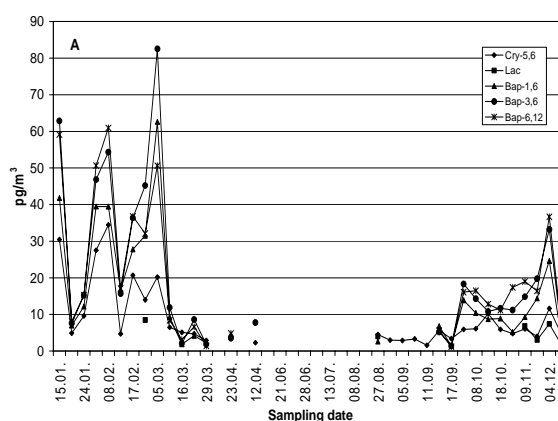


Figure 1. PAH-diones in the course of 2005

Lintelmann, J., Fischer, K., Karg, E., Schröppel, A. (2005). Anal. Bioanal. Chem., 381, 508-519

## Optimization of High-Resolution ICP-MS methods for determination of the “soluble” fraction of trace-metals in aerosol samples.

F. Rugi<sup>1</sup>, S. Becagli<sup>1</sup>, E. Castellano<sup>1</sup>, M. Chiari<sup>2</sup>, F. Lucarelli<sup>2</sup>,  
F. Marino<sup>1,3</sup>, S. Nava<sup>2</sup>, M. Severi<sup>1</sup>, R. Traversi<sup>1</sup>, R. Udisti<sup>1</sup>.

<sup>1</sup>Department of Chemistry, University of Florence, Sesto F.no (FI), I-50019, Italy

<sup>2</sup>Department of Physics, University of Florence and INFN, Sesto F.no (FI), I-50019, Italy

<sup>3</sup>Department of Environmental Science, University of Milano Bicocca, Milano I-20126, - Italy.

Keywords: Aerosol characterization, ICP-MS, Metal content, PIXE, Soluble fraction

Accurate and reproducible determination of metals in environmental samples and discrimination between natural and anthropic contributions are basic in understanding the impact of metal-cycle components on human health and on eco-systems healthiness and preservation. In this optic, the development and optimization of analytical methods able to give a reliable quantification of the concentration of several metals at sub-ppb level in a simultaneous way is one goal not yet completely achieved.

Here, we present the optimization of methods for the contemporaneous determination of 13 trace-metals (Al, As, Cd, Cr, Cu, Fe, Hg, Mn, Mo, Ni, Pb, V and Zn) in aerosol samples at concentration ranging from few ppt to some ppb by High-Resolution Inductively Coupled Plasma Mass-Spectrometry (HR-ICP-MS).

The methods were applied to the analysis of aerosol collected on one quarter of 47 mm Teflon filters by impactors working for 24 h at the flow of 2.3 m<sup>3</sup>/h (EN 12341 directive) with cutoff heads PM10, PM2.5 and PM1.

We determined by HR-ICP-MS the metal fraction soluble at pH=1.5, as an indicator of a easily mobile fraction in the environment. These results were compared with the analysis of the total content of each metal, determined in the same filter by Particle Induced X-ray Emission (PIXE), in order to evaluate the percentage contribution of the “soluble” fraction of metals emitted in the atmosphere by natural and anthropic sources in different eco-systems. Aerosol measurements were carried out on several hundreds of filters collected in 10 sites with different anthropic impact located in Tuscany (Central Italy) and in the Lampedusa Island (Sicily Channel, Mediterranean Sea, Italy).

Tuscany sampling stations were chosen in the framework of PATOS (Particolato Atmosferico in Toscana) and PASF (Particolato Atmosferico in Sesto Fiorentino) Italian programs and the Lampedusa sampling activity was carried out accordingly the MAIL (Marine Aerosol in the Island of Lampedusa) project (udisti@unifi.it).

The possibility to select three different mass resolution (300, 4000 and 10,000) allowed to choose, for each metal, the most suitable isotopic species, taking into account isotopic abundance, isobaric interferences and concentration levels.

Method accuracy for Al, As, Cd, Cu, Pb and Ni was evaluated by analysis of reference materials (CRM 609 and CRM 610 for low and high concentrations, respectively). Accuracy for As, Cd, Cr, Cu, Hg, Mn, Pb and Zn was also checked by using certificate material ERM-CE278. For Fe, Mo and V, accuracy was evaluated by analysing certified standard solutions and by comparison with GFAAS measurements. Percentage errors were always lower than 10%. Measurements on aerosol samples were carried out by standard addition method (adding three standard solutions to each sample), because external calibration or internal standards gave non accurate results. Self-purified nitric acid was obtained by sub-boiling distillation of per-analysis HNO<sub>3</sub> using all PFA materials. Detection limits ranged from 1.6 ppt (Cd) to 71.4 ppt (Zn). Considering we are analysing a quarter of filter extracted with about 10 ml of suprapure water and sampling volumes were about 55 m<sup>3</sup>, detection limits expressed as atmospheric concentrations were at least two order of magnitude lower than values measured in real samples. Filter blank evaluation revealed that atmospheric concentrations were at least 10 times higher than operative blanks.

The analysis of the 13 selected metals on the PATOS, PASF and MAIL samples allowed to evaluate the atmospheric concentrations of their soluble fraction in the different stations (urban traffic, urban background, rural background, anthropized marine, remote marine), enlightening temporal trends and possible seasonal pattern. Concentration spikes were interpreted as a result of the formation of atmospheric inversion layers (checked by Rn-family measurements), particular anthropic inputs or long-range transport events (such as Saharan Dust transport). Particular attention was devoted to the temporal profiles of As, Cd, Ni and Hg, for which references values for air quality were indicated in the EU 2004/107/CE Directive, because of their high toxicity.

PCA statistical analysis allowed to group metals as a function of common sources (crustal, anthropic) or transport processes. The comparison with total metal content, measured by PIXE, revealed that metals mainly coming from anthropic sources showed higher soluble percentages than crustal metals.

## **T02 Abstracts**

## An experimental study on relation of heterogeneous and homogeneous condensations in condensation aerosol generation

Z.Z. Zhang, L. Chen and F. Jiang

Institute of Nuclear and New Energy Technology, Tsinghua University, 100084, Beijing, China

Keywords: heterogeneous and homogeneous, condensation, aerosol generation, monodisperse.

Stable and reproducible monodisperse aerosols are required in many research fields, such as calibration and assessment of aerosol measurement instruments, gas-particle fluid dynamics studies, filter efficiency testing, and human lung inhalation studies, etc. Condensation aerosol generation (abbreviated as CAG), which means aerosols formed by condensation of vapor, is one of the most advanced methods. Particle size distribution and concentration are primary parameters of aerosol. They are recorded by count median diameter (CMD), geometric standard deviation (GSD) and number concentration (N). GSD is used to illustrate the monodispersity of aerosol. The more GSD is adjacent to 1, the better the monodispersity is.

There are two condensation mechanisms of CAG method, heterogeneous and homogeneous condensations. In the former, aerosols are formed by condensing vapor onto condensation nuclei. The latter happens at higher level of vapor supersaturation, and clusters from molecular collisions perform as condensation nuclei of the heterogeneous type.

The heterogeneous type is preferred because it can produce aerosols much more monodisperse than the other. High concentration nuclei can suppress the homogeneous condensation process. Thereby, it's important to study the relation of heterogeneous and homogeneous condensations to improve the monodispersity of produced aerosols.

A condensation aerosol generator (Model 3475 Condensation Monodisperse Aerosol Generator, TSI Incorporated, St. Paul, MN) was used in this study. Experimental results were detailed in Figure 1.

From experimental results, when the nuclei concentration is above  $1.1 \times 10^6 \text{ cm}^{-3}$ , GSD is a constant value of 1.32 and the total concentration is  $1.1 \times 10^6 \text{ cm}^{-3}$ . This means the homogeneous condensation process is suppressed, and the CMD of aerosols increases along with the increase of vapor quality.

While the nuclei concentration is below  $3.6 \times 10^5 \text{ cm}^{-3}$ , the homogeneous condensation process is no longer suppressed, the concentration and GSD as well as the CMD of the right peak where aerosols was formed by heterogeneous condensation didn't change much, but the concentration and GSD as well as the CMD of the left peak where aerosols was formed by homogeneous condensation increases along with the increase of vapor quality.

So, a high number concentration of nuclei is necessary to suppress the homogeneous condensation, otherwise the more vapor quality doesn't result in the increase of the CMD but the increase of GSD, That also means enough nuclei whose concentration is above a critical value are required to acquire monodisperse aerosols with a larger CMD.

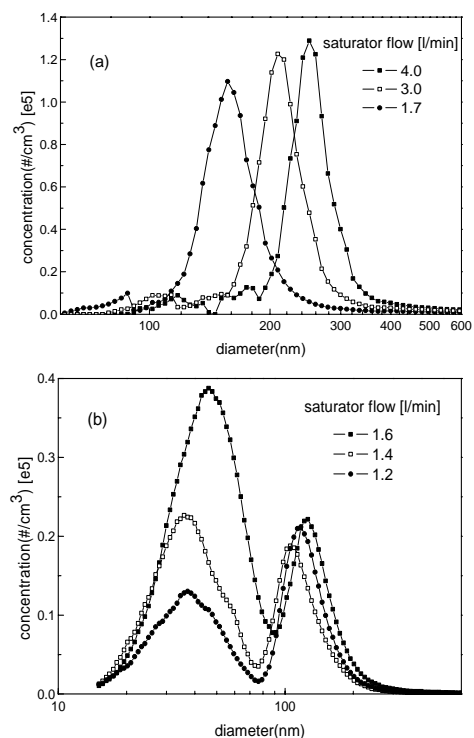


Figure 1. Size distributions of aerosols by CAG method.

(a) total flow rate = 4.8 l/min, screen flow rate = 3.0 l/min,  $N \approx 1.1 \times 10^6 \text{ cm}^{-3}$ ,  $GSD \approx 1.32$ ; (b) total flow rate = 3.0 l/min, screen flow rate = 2.2 l/min,  $N \approx 3.6 \times 10^5 \text{ cm}^{-3}$ ,  $GSD \approx 1.35$  (for the right peak).

This work was supported by the National Natural Science Foundation of China (No.50608044).

Perry, D. G., & Smaldone G. C. (1985). *Factors Affecting Aerosol Production from a Modified Sinclair-LaMer Aerosol Generator*. *J. Aerosol Science*, 16, 427-436.

Ristovski, Z. D., Morawska, L., & Bofinger, N. D. (1998). *Investigation of a Modified Sinclair-LaMar Aerosol Generator in the Submicrometer Range*. *J. Aerosol Science*, 29, 799-809.

## Uncertainty on Experimental Aerosol Characterization: Calibration Tests Supporting Aerosol Studies under Severe Accident SGTR Conditions

F.J.S. Velasco, C. López del Prá, Luis E. Herranz

Unit for Nuclear Safety Research, CIEMAT Research Center, Av. Complutense, 22, 28040, Madrid, Spain

Keywords: aerosol surface interaction, deposition efficiency, instrumentation, measurements errors, nuclear aerosols.

The Pressurized nuclear water reactors rely on shell-and-tube heat exchangers to generate the steam that expands in the turbine stage of a Rankine cycle. Under the highly unlikely conditions of a reactor core melt accident, a tube rupture in the heat exchanger could result in a release of radioactive particles to the environment. This scenario, generally called severe accident Steam Generator Tube Rupture (SGTR), is of an outstanding importance in nuclear safety. Previous investigations (Auvinen et al., 2005) showed that the most challenging condition would be the absence of water in the secondary side of the steam generator. Nevertheless, even under these circumstances, a fraction of particles carried by the gas would be deposited on the tubes near the breach (Herranz et al., 2006).

In order to explore the severe accident SGTR scenario, an ambitious international research program is being led by PSI. As a contribution to the ARTIST program, an experimental series aimed at measuring the aerosol retention in the secondary side of a dry steam generator around the tube breach has been initiated by CIEMAT (CAAT, CIEMAT Artist Aerosol Tests). In particular, the influence of particle size characterization (mono- and poly-disperse; AMMD=1-4  $\mu\text{m}$ ), aerosol nature ( $\text{TiO}_2$  and  $\text{SiO}_2$ ) and inlet gas mass flow rate (75-250 kg/h) will be investigated. To do so, a mock-up facility consisting of a tube bundle of 11x11 rows will be used to simulate the break stage of the SG (Quarini, 1999). Characterization of incoming and outgoing particles will be done by multiple devices based on different fundamentals: OPC, APS and ELPI for online measurements, and cascade impactors and membrane filters for post-test analyses.

Previous to CAAT experiments, a calibration campaign has been carried out to find out possible correlations among OPC, APS and ELPI measurements. This paper summarizes the main observations derived from comparisons set between different devices and it discusses strengths and weaknesses of each technique. Comparisons have been based on the fraction of particle counted in each bin per unit of diameter logarithm. As an example, Figure 2 shows an APS® and ELPI® comparison. Both qualitative and quantitative differences can be observed. Important uncertainties would affect the description of aerosols with a particle size distribution. The discussion will assess the feasibility

of using these devices to characterize inlet and outlet particles size distributions in the CAAT tests.

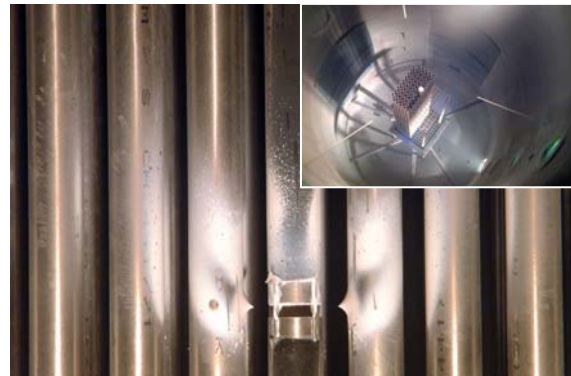


Fig. 1. Experimental set-up of the bundle in the PECA vessel for the CAAT experiments (up). Aerosol deposition in the near field of a guillotine breach after a CAAT test (down).

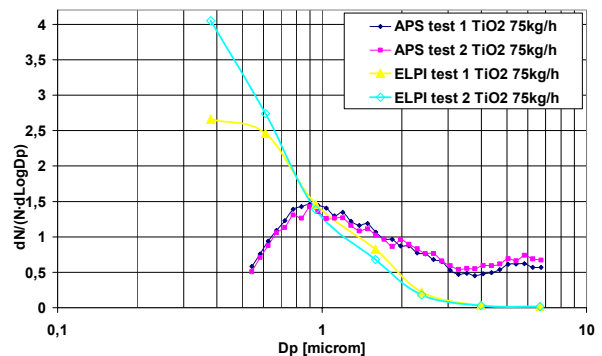


Fig. 2. Measured aerodynamic particle size distribution by APS® and ELPI® for a  $\text{TiO}_2$  aerosol.

This work has been financially supported by the Spanish Nuclear Council in the frame of the International ARTIST project.

Auvinen, A., Jokiniemi, J.K., Lähde, A., Routamo, T., Lundström, P., Tuomistob, H., Dienstbierec, J., Guntay, S., Suckow, S., Dehbi, A., Sloomane, M., Herranz, L., Peyres, V. and Polo, J., (2005). *Nucl. Eng. Des.*, 235, pp. 457-472.  
Herranz, L., Velasco, F.J.S., Del Prá, C.L. (2006). *Nucl. Tech.*, 154, pp. 85-94.  
Quarini, J., (1999). ARTIST-01/99, Paul Scherrer Institut.

## Improving the detection efficiency of a condensation particle counter by means of pulse height analysis technique.

M. Sipilä, P. P. Aalto and M. Kulmala

Department of Physical Sciences, University of Helsinki, P.O. Box 64, 00014 Univ. Helsinki, Finland.

Keywords: CPC, Aerosol instrumentation, Ultrafine particles, Cut-off diameter.

To solve the detailed pathways of atmospheric aerosol particle formation, the measurements of newly formed nanometric particles are necessary. Most powerful instruments in that size range are condensation particle counters (CPCs). However, the lowest detectable particle diameters of commercially available instruments start from 3nm, which is far above the sizes where the initial steps of nucleation take place. Pulse height analysis (PHA) of white light scattered from the droplets nucleated on existing aerosol particles in CPC condenser has been used in size distribution measurements between 3 and 10 nm (Weber et al., 1998) as well as to determine the composition of freshly nucleated nanoparticles (O'Dowd et al., 2002). Here we report on the application of PHA-technique together with modified commercial CPC (model TSI-3025A) to extend the measurable particle size range below 2 nm.

The PHA-CPC comprises TSI-3025A CPC, in which the detector laser is replaced by the white light source, and the pulse height analyzer. Butanol supersaturation needed to activate the particle inside the CPC condenser is determined by particle size (Kelvin effect and the contact angle for heterogeneous nucleation) and composition. Supersaturation field is not homogeneous inside the condenser and thus the physico-chemical properties of entering particle determine the position where it will be activated for growth. Larger particles activate first and they have more time for growth yielding to larger droplet sizes and thus the higher pulses in the detector.

At normal operation conditions the supersaturation inside the TSI-3025A condenser is not high enough to activate particles smaller than ca. 2.5 nm. We increased the supersaturation by adjusting the temperature difference between the condenser and the saturator from 27 °C to 34 °C. This led to homogeneous nucleation of butanol vapour. However, the pulse height from homogeneously nucleated droplets is much smaller than pulse height from the droplets formed by heterogeneous nucleation (Fig. 1.). This fact allowed us to use extremely high supersaturations and still distinguish between homogeneous and heterogeneous nucleation.

Preliminary results show the huge potential of this method to improve the detection efficiency in sub-3 nm range. The cut-size of the instrumental setup for negatively charged WO<sub>x</sub>-particles is well below 2 nm, which should be compared to the cut-size of 3 nm at standard operation conditions.

Calibration with neutral particles at this size range is very complicated because of the lack of the reference instrument. The promising results suggest that with this method the lowest detectable particle size will be rather determined by particle transport efficiency and other factors related to instrument design than the particle activation and the ability to distinguish between homogeneously and heterogeneously nucleated droplets.

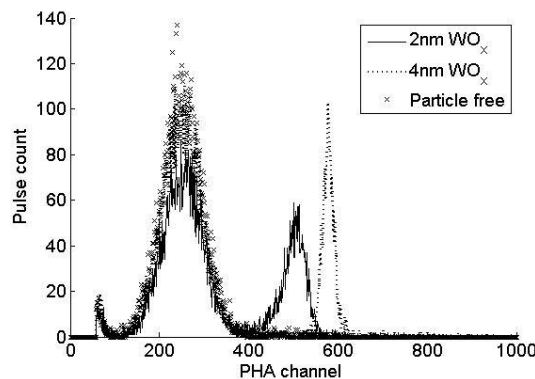


Figure 1. Homogeneously nucleated droplets (mode on the left hand side) in the pulse height spectrum are clearly distinguishable from heterogeneously nucleated droplets even at initial particle size of 2 nm.

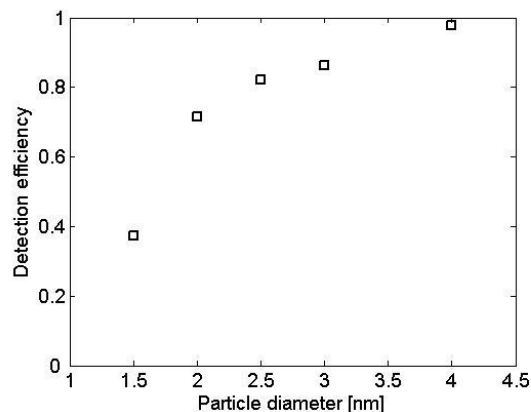


Figure 2. Detection efficiency of TSI-3025A for negatively charged WO<sub>x</sub>-particles at 34°C temperature difference between the saturator and the condenser.

Weber, R. J., Stolzenburg, M. R., Pandis, S. N., & McMurry, P. H. (1998). *J. Aerosol Sci.*, 29, 601-615.

O'Dowd, C. D., Aalto, P., Hämeri, K., Kulmala, M. & Hoffmann, T. (2002). *Nature*, 416, 497-498.

## Comparison of six H-TDMA systems: a laboratory study

A. Massling<sup>1</sup>, N. Kaaden<sup>1</sup>, T. Hennig<sup>1</sup>, E. Swietlicki<sup>2</sup>, E. Nilsson<sup>2</sup>, J. Löndahl<sup>2</sup>, K. Hämeri<sup>3</sup>, M. Ehn<sup>3</sup>, P. Laj<sup>4</sup>, P. Villani<sup>3</sup>, G. McFiggans<sup>5</sup>, N. Good<sup>5</sup> and A. Wiedensohler<sup>1</sup>

<sup>1</sup>Department of Physics, Leibniz-Institute for Tropospheric Research, Leipzig, Germany

<sup>2</sup>Department of Physics, Lund University, Lund, Sweden

<sup>3</sup>Department of Physical Sciences, University of Helsinki, Helsinki, Finland

<sup>4</sup>Laboratoire de Météorologie Physique, Clermont Ferrand, France

<sup>5</sup>Department of Atmospheric and Environmental Science, University of Manchester, Manchester, United Kingdom

Keywords: aerosol characterization, aerosol instrumentation, growth, HTDMA, hygroscopicity.

### INTRODUCTION

Hygroscopic properties of aerosol particles are crucial parameters for the determination of the understanding of the particle's impact on regional and global climate. One of the most common methods to examine these properties is the H-TDMA (Hygroscopicity-Tandem Differential Mobility Analyzer) technique. The principle of the H-TDMA has been used for more than twenty years to investigate hygroscopic properties of submicrometer aerosol particles with high temporal resolution. In general, these systems are home-made set-ups and show substantial differences in technical details, used quality criteria, and applied data evaluation.

### METHODS

A workshop comparing six European H-TDMA systems was held in February 2006 at the Leibniz-Institute for Tropospheric Research in Leipzig, Germany. It was the aim of this study to intercompare the performance of those systems in terms of particle dry sizing, RH (Relative Humidity) control and RH stability (certainty of growth factor determination), and determination in observed number fractions in case of external mixtures. For this reason, four different experiments were prepared (Table 1).

Table 1. Experiments and measurements performed within the H-TDMA workshop in Leipzig.

Ex-periment	Generated aerosol	Measurement
1	Ammonium sulfate	Growth factor at RH < 30%
2	Ammonium sulfate	Growth factor at RH = 90%
3	Ammonium sulfate	Growth factor at 75% < RH < 85% (DRH)
4	Ammonium sulfate + soot	Number fraction determined at RH = 90%

All data were evaluated using the individual evaluation procedure of the operating institute. Additionally, the data were processed using the internal evaluation procedure developed by the Leibniz-Institute for Tropospheric Research.

### RESULTS

In general, all systems showed good results in terms of particle dry sizing. Particle sizing of all systems was within 4% of relative uncertainty.

When comparing the theoretical DRH (Deliquescence Relative Humidity) of ammonium sulfate particles with the observed DRH of five systems, it was found out, that all systems were underestimating the theoretical value of 80% DRH (ammonium sulfate). Results of this evaluation are shown in Figure 1.

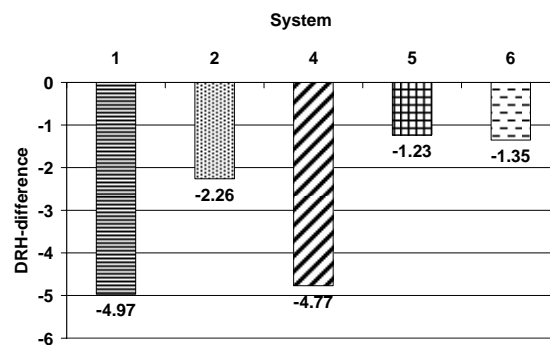


Figure 1. Evaluated DRH difference (ammonium sulfate) for five H-TDMA systems.

A comparison in determined number fractions observing a mixture of ammonium sulfate and soot particles showed variations within +/- 15% of the six systems independently of the type of evaluation.

This work was supported by ACCENT (The European Network of Excellence).

Liu, B. Y. H., Pui, D. Y. H., Whitby, K. T., Kittelson, D. B., Kousaka, Y., McKenzie, R. L. (1978). The aerosol mobility chromatograph: a new detector for sulfuric acid aerosols. *Atmos. Environ.* 12, 99-104.

## Configuration of air filters based on the constructal theory

A. F. Miguel<sup>1</sup>, A. H. Reis<sup>1</sup> and A. Bejan<sup>2</sup>

<sup>1</sup>Department of Physics and Geophysics Centre of Evora, University of Évora, 7000-671 Évora, Portugal

<sup>2</sup>Department of Mech. Eng. and Materials Science, Duke University, Durham, NC 27708-0300, USA

Keywords: air filters, design, constructal law.

Filtration is one of the simplest and most effective ways to separate particulate matter from fluid and filters find diverse application. The filter design is a critical aspect because it impacts performance.

The constructal theory is about the generation of flow architecture both in engineered and natural flow systems, as evidenced by numerous applications (e.g. Bejan, 2000; Bejan & Lorente 2006). According to constructal law, the system shape and internal flow architecture do not develop by chance, but result from the permanent struggle for better performance and therefore must evolve in time.

In this study we apply the constructal law to filter design with a geometry that is optimized for the capture of submicrometre aerosols which are particularly hazardous.

Filters operate at low Reynolds numbers. Their principle of operation is this: an air stream containing particles with concentration  $C_{in}$  is forced through a set of collecting elements (e.g. fibres, beds). Particles approaching the collectors are then transferred from the air stream to the collector surface. The global purpose is that particle concentration at the outlet is the smallest possible. This means that the purpose of the flow architecture is to maximize deposition rate and volumetric density.

If the collecting elements are very close to each other (e.g., in the small-porosity limit). The corresponding particle transfer density ( $m_{el}$ ) is (Reis *et al.*, 2006)

$$m_{\varepsilon_l} = \frac{s\varepsilon^3 d^2 \Delta p (C_{in} - C_o)}{\mu(1-\varepsilon)^2 L^2} = \frac{s\varepsilon^3 Be D_{dif} (C_{in} - C_o)}{(1-\varepsilon)^2 L^2}$$

where  $s$  is a constant,  $\varepsilon$  is porosity,  $L$  is filter thickness,  $d$  is the filter collector characteristic length,  $D_{dif}$  is diffusivity of particles in the air,  $C_o$  is the outlet concentration of aerosol particles,  $\mu$  is dynamic viscosity,  $\Delta p$  is pressure drop and  $Be$  is the Bejan number for mass transfer ( $=L^2 \Delta p / (\mu D_{dif})$ ).

In the opposite limit (large-porosity spacing) the particle transfer density ( $m_{eh}$ ) is

$$m_{\varepsilon_h} = \frac{\xi(1-\varepsilon) D_{dif} (C_{in} - C_o)}{d^2} = \frac{\xi(1-\varepsilon) \Delta p (C_{in} - C_o)}{\mu Be}$$

where  $\xi$  is a geometric parameter.

Next, we identify the geometric factors that maximize the rate of deposition in the filter. These

factors can be determined by using the method of intersecting the asymptotes (Bejan, 2000). According to this method, the intersection of two highly dissimilar trends ( $m_{el}$  and  $m_{eh}$ ) determines the optimal internal structure (Figure 1).

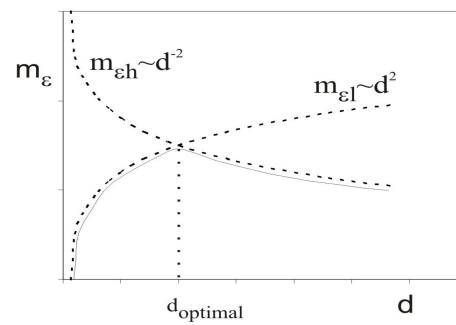


Figure 1. The intersection of asymptotes' method.

If the aim is to obtain the filter design based on collector element and thickness optimization, then from  $m_{el}$  and  $m_{eh}$  it follows that

$$\left(\frac{d}{L}\right)_{\text{optimal}} = \left[\frac{s\varepsilon^3 Be}{\xi(1-\varepsilon)^3}\right]^{1/2}$$

If the goal is the porosity optimization, then

$$(\varepsilon)_{\text{optimal}} = \left(\frac{\xi d}{sLBe}\right)^{1/3} \left[1 + \left(\frac{\xi d}{sLBe}\right)^{1/3}\right]^{-1}$$

These equations show the optimal geometrical groups that form such that the deposition of particles in the filter is maximum. Another study regarding the optimal geometry of air cleaning devices composed of parallel-plate channels and by tubes can be found in Reis *et al.* (2006).

This work was supported by Foundation for Science and Technology (FCT) project POCTI/EME/59909/2004.

Bejan, A. (2000). *Shape and Structure, from Engineering to Nature*. Cambridge, U.K.: Cambridge University Press.

Bejan, A. & Lorente S. (2006). *J. Appl. Phys.*, 100, 041301

Reis, A. H., Miguel, A. F. & Bejan A. (2006). *J. Physics D*, 39, 2311-2318.

## Characterization of specific vertical aerosol fluxes by turbulent flux measurement and single particle mass spectrometry for micro-meteorological analysis

E. Gelhausen<sup>1</sup>, K.-P. Hinz<sup>1</sup>, B. Spengler<sup>1</sup>, A. Schmidt<sup>2</sup> and O. Klemm<sup>2</sup>

<sup>1</sup>Institute of Inorganic and Analytical Chemistry, Justus Liebig University Giessen, Schubertstr. 60, Giessen, D-35392, Germany

<sup>2</sup>Institute for Landscape Ecology - Climatology, University of Muenster, Robert-Koch-Str. 26, D-48149 Muenster

Keywords: Chemical composition, Mass spectrometry, Single particle analysis, Atmospheric aerosols

Transportable on-line mass spectrometer instruments are well proven to determine the chemical composition of single aerosol particles during ambient measurements. Size-resolved chemical analysis of ambient particles offers detailed information within the aerosol particle population with high temporal resolution. Parallel determination of the vertical wind vector component enables the characterization of flux directions for specific chemical compounds in the atmosphere. A fast response of both measuring techniques, wind measurement and chemical single particle analysis is an essential approach under highly variable ambient conditions to better understand natural and anthropogenic impacts on environmental and climate changes.

The mobile, bipolar on-line laser mass spectrometer LAMPAS 2 (Laser Mass Analyzer for Particles in the Airborne State; Trimborn *et al.*, 2000) provides for chemical and physical characterisation of individual airborne particles in the sub-micron and super-micron size range. The instrument uses an impact-free particle inlet system with a differentially pumped nozzle/skimmer system to directly introduce the particles into the mass spectrometer. Inside the instrument particles are detected by two cw laser beams and their size is determined. An actively triggered, pulsed UV-Laser (wavelength  $\lambda = 337$  nm) evaporates and ionizes the particles followed by bipolar time-of-flight mass spectrometry to analyze the generated ions chemically.

In a parallel measurement the vertical wind vector is determined using an ultrasonic anemometer (YOUNG Inc.). The combination of this technique with single particle analysis allows the detailed characterization of the deposition of particle constituents (Held *et al.*, 2003).

Particle mass spectra are sorted and classified by means of a fuzzy clustering algorithm (Hinz *et al.*, 1999). It allows a "soft" attribution of individual particles to classes (groups of chemically similar particles) using membership degrees of similarity. A chemical assignment of the particle classes and their abundances are determined by the algorithm.

The second step of the data evaluation sorts the particles and particle groups with respect to the measured vertical wind vector and correlates specific

particle compounds to the deposition/emission conditions.

In December 2006 a joint test experiment was performed over a period of nine hours using both techniques in an ambient measurement. During this time period 681 single particle spectra were registered. The measurement of turbulent wind fluxes with the ultrasonic anemometer was performed with a time resolution of 1/10 s. The resulting classes are shown in Table 1.

Table 1. Abundances of five particle classes determined with fuzzy clustering for the particle population measured during a test campaign in Giessen, December 2006.

chemical class	class abundance[%]
C + sec	7,3
C+mineral+sec	12,2
C+sec+org	4,9
mineral+C+sec1	16,4
mineral+C+sec2	59,2

Methodology and results of the combined measurements of time-correlated wind data and single particle compounds will be presented.

This work was supported by the Deutsche Forschungsgemeinschaft (DFG), Germany, Grant No. HI 857/4-1.

Held, A., Hinz, K.-P., Trimborn, A., Spengler, B. Klemm, O. (2003). *Geophys. Res. Lett.* 30, 2016  
Hinz, K.-P., Greweling, M., Drews, F., Spengler, B. (1999). *J. Am. Soc. Mass Spectrom.* 10:648-660.  
Trimborn, A., Hinz, K.-P., Spengler, B. (2000). *Aerosol Sci. Technol.* 33, 191-201.

## **Application of the method of Laser Doppler anemometry for measurement characteristics of the process of aerosol aspiration**

G.N. Lipatov, M.A. Yugov

Department of Physics, National University, Dvoryanskaya 2, 65026, Odessa, Ukraine

Keywords: fundamental aerosol physics, aerosol dynamics, aerosol sampling, measurements, Laser Doppler anemometry.

In most cases, the measurement of parameters of the disperse components of multiphase media is carried out not in the system itself but within samples being selected by different ways.

In this case, the question about the accordance of the measured parameters to those taking place in the system under the investigation arises. The problem of the sample selection challenged either theoretical or experimental interest (Grinshpun et al., 1990). However, some questions of the aerosol aspiration from low-velocity flows (when the flow velocity is comparable with the velocity of particle sedimentation) as well as interaction of particles with external and internal surfaces of nozzle are studied insufficiently (Lipatov et al., 1988).

Essence of the proposed method consists in measuring of the field of velocities as gas near-by a cylindrical probe by Laser Doppler anemometry so direct measuring of parameters of trajectories of aerosol particles.

In this paper, the central attention is spared to next problems:

- a) The measurement of the velocity field in certain points of the system.
- b) The measurement of the parameters of the aerosol particle trajectories.

### Conclusions

The method proposed in the present paper rather good reflects physical regularities of single

particle dynamics and can be applied for the investigation of the aspiration processes. The obtain results are in good accordance with those obtained by the known methods of the investigation of the aspiration processes (Lipatov , 1989).

Grinshpun, S.A., Lipatov, G.N., & Sutugin, A.G. (1990). Sampling errors in cylindrical nozzles. *Aerosol Science and Technology*, 12, 716-740.

Grinshpun, S.A., Lipatov, G.N., Semenyuk, T.I. & Sutugin, A.G. (1988) Secondary Aspiration of Aerosol Particles into Thin Walled Nozzles Facing the Wind, *J. Atmospheric Environment*, 22(8), 1721-1727.

Lipatov, G.N., (1989) Experimental coarse aerosol research: the "thread-of-droplet" technique. *J. Aerosol Science*, 20(6), 721-722.

## In situ measurements of large atmospheric particles in mixed phase clouds using digital holography

S.M.F. Raupach (1), J. Curtius (1), H.J. Voessing (1), and S. Borrmann (1,2)

(1) Johannes Gutenberg-Universität Mainz, Institut für Physik der Atmosphäre, Joh.-Joachim-Becher-Weg 21, D-55099 Mainz, Germany

(2) Max Planck-Institut für Chemie, Joh.-Joachim-Becher-Weg 27, D-55020 Mainz, Germany

Keywords: digital holography, CLACE, ice cloud, particle shape, optical instrumentation

Atmospheric ice particles show a rich variety of shapes and sizes, which can be investigated by imaging them in situ. Imaging can also be used to look e.g. for effects revealing the coexistence of ice crystals and cloud droplets in mixed phase clouds like riming. In contrast to techniques based on measuring the angular intensity of scattered light, imaging does not involve presumptions concerning the particles' shapes. One drawback of current instruments, however, is their limited depth of focus, which requires the particles to be located in a well-defined plane in space in order to be imaged sharply. Among the different techniques, holography is a versatile tool as it allows for imaging particles in a deep volume without being restricted by the typically small depth of focus. Thereby it offers the advantage of gaining not only information on the particles' shapes and sizes over a large range of distances, but also on the particles' relative position in space.

At Johannes Gutenberg-Universität Mainz, within a PhD-project a digital-holographic camera system is currently being developed which is capable of imaging airborne atmospheric particles, ranging in size from tens of microns to several millimetres, yielding an *in situ* nanosecond-snapshot of an atmospheric volume of about 20cm<sup>3</sup>. The computer-reconstructed images of the particles can be used to investigate their sizes, shapes, habits, and possibly their macroscopic structures and three-dimensional interparticle distances.

On the High Altitude Research Station Jungfraujoch, situated at about 3500m a.s.l. in the Swiss Alps, the prototype underwent a

first field test within the "CLACE5" experiment in early 2006. A modified version of the instrument was deployed again on the Jungfraujoch in December 2006. Several tens of thousands of holograms of ice crystals were obtained successfully and are under analysis.

Additionally, in spring 2007 the system will be used for measurements at the cloud simulation facility AIDA in Karlsruhe/Germany.

Besides a presentation of the current system, digital holograms of atmospheric particles obtained on the Jungfraujoch and of particles grown under controlled conditions in the laboratory will be presented along with their reconstructions and preliminary analyses.

This work is supported by "Deutsche Forschungsgemeinschaft (DFG)" as part of the collaborative research centre SFB641.

### References:

Raupach, S.M.F. et al. (2006). *J. Opt. A: Pure Appl. Opt.*, 8, 796-806.

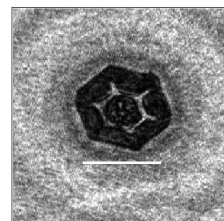


Fig. 1 Digital reconstruction of a hologram showing an atmospheric ice crystal imaged on the Jungfraujoch (length of scalebar approx. 300 $\mu$ m).

## Diffusion of charged particles in a DMA with inclined electric field

J. Salm and U. Hörrak

Institute of Environmental Physics, University of Tartu, 18 Ülikooli St., 50090, Tartu, Estonia

Keywords: DMA, size analysis, diffusion, measurement errors.

In general lines, a differential mobility analyser (DMA) has air inlet(s), air outlet(s), electrodes, and collector(s) of electric current. Diffusion distortions in a simple DMA have been studied in (Salm, 2000). We will demonstrate that the method developed in the above paper is applicable also for a more complicated DMA. In particular, we consider the design of DMA with inclined electric field, which has certain advantages with respect to resolution (Loscertales, 1998; Tammet, 1999). The principle of inclined velocities was developed in an analyser by Tammet (2003).

In this abstract we systematically refer to the paper (Salm, 2000) and the corresponding equation numbers. Figure 1 of this paper is retained, only the traverse electric field strength  $\mathbf{E}$  is replaced by two components  $\mathbf{E}_x$  and  $\mathbf{E}_y$ , where  $\mathbf{E}_x$  is directed against the airflow  $\mathbf{u}$ .

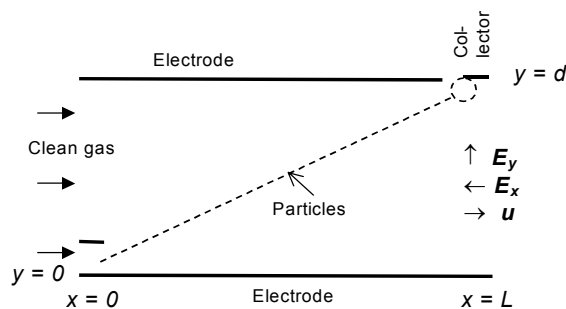


Figure 1. Schematic representation of the DMA.

Thus the horizontal velocity of charged particles is

$$\mathbf{u} - Z_1 \mathbf{E}_x,$$

where  $Z_1$  is the mobility of entering aerosol particles.

Equation (12) for the characteristic (limiting) mobility is replaced by a modified equation

$$Z_0 = \frac{u - Z_1 E_x}{E_y} \frac{d}{L}.$$

We will consider here the case  $\mathbf{E}_x \propto \mathbf{E}_y$ . Let us express  $\mathbf{E}_x = k \mathbf{E}_y$ , where  $k$  is the coefficient of proportionality.

The following derivation of equations is quite similar to that in (Salm, 2000), with understandable replacements. In Equation (14) the flow velocity  $\mathbf{u}$  is retained, since the horizontal electric field  $\mathbf{E}_x$  does not influence the inlet. The entering aerosol is characterized by the differential distribution of polar

charge density of particles by mobility or the mobility spectrum  $\rho(Z_1)$ . In Equation (15) the electric field strength  $\mathbf{E}$  is replaced by  $\mathbf{E}_y$  etc. The derivation results in the normalized apparent spectrum  $w^*(Z, Z_1)$ . Equation (27) in (Salm, 2000) is replaced by the following equation:

$$w^*(Z, Z_1) = \frac{\text{Pe} Z_1}{2\pi Z^2 \left(1 + \frac{k Z_1 d}{ZL}\right)} \times \exp \left( \frac{\text{Pe}}{2} \left( \frac{L}{d} + \left(1 - k \frac{L}{d}\right) \frac{\frac{Z_1 d}{ZL}}{1 + \frac{k Z_1 d}{ZL}} \right) \right) \times K_0 \left( \frac{\text{Pe}}{2} \sqrt{ \left( 1 - 2 \frac{k \frac{Z_1 d}{ZL}}{1 + \frac{k Z_1 d}{ZL}} + (1 + k^2) \frac{\left(\frac{Z_1 d}{ZL}\right)^2}{\left(1 + \frac{k Z_1 d}{ZL}\right)^2} \right) \left(1 + \frac{L^2}{d^2}\right) } \right)$$

where  $Z$  is the variable mobility,  $\text{Pe}$  is the Peclet number,  $K_0(\zeta)$  is the Macdonald's function.

Rough estimations of the influence of diffusion on the resolution of mobility spectrometers are possible also by means of simpler methods. However, a precise knowledge of the apparent spectrum opens a way to the improvement of resolution by calculations.

If we know the normalized apparent spectrum  $w^*(Z, Z_1)$  for one mobility  $Z_1$ , then the apparent spectrum  $\rho^*(Z)$  for any general case is expressed as

$$\rho^*(Z) = \int w^*(Z, Z_1) \rho(Z_1) dZ_1. \quad (*)$$

In many cases the apparent spectrum  $w^*(Z, Z_1)$  depends on the ratio  $Z/Z_1$ . Then, using a simple exponential transformation, it is possible to express Equation (\*) in the shape of convolution, and to solve the convolution equation by means of the Fourier transform.

This work was supported by the Estonian Science Foundation under grants 6223 and 6988.

- Loscertales, I. G. (1998). *J. Aerosol Sci.*, 29, 1117-1139.  
 Salm, J. (2000). *Aerosol Science and Technology*, 32, 602-612.  
 Tammet, H. (1999). in *Proc. 11th Int. Conf. Atmos. Electr.*, Alabama (NASA, MSFC), 626-629.  
 Tammet, H. (2003). in *Proc. 12th Int. Conf. Atmos. Electr.*, Versailles, 399-402.

## A Digital In-line Holographic Microscope (DIHM) for ice crystals

P. Amsler, O. Stetzer, U. Lohmann

Institute for Atmospheric and Climate Science, ETH Zurich, 8092 Zurich, Switzerland  
peter.amsler@env.ethz.ch

Keywords: Ice nuclei, Ice crystals, Crystal habits, Holographic microscopy.

In Atmospheric Science, the ability of aerosols to act as ice nuclei (IN) is the subject of intense investigations. Much has been learned about ice nucleation and its importance in cloud microphysical processes (Schaefer, 1947; Vali, 1985; Lohmann & Feichter, 2005). Nevertheless, as there is still a lack of a comprehensive theory for heterogeneous ice nucleation (Cantrell & Heymsfield, 2005), laboratory experiments and field measurements are necessary to help understand ice nucleation processes. The Zurich Ice nucleation Chamber (ZINC), which is a continuous flow diffusion chamber, was built in our group to investigate the nucleation potential of atmospheric aerosols. The ice crystals which form in the ZINC instrument have a size of roughly  $2\text{--}8\ \mu\text{m}$  and their habit is dependent on the temperature and relative humidity they experienced during formation and growth. Within the ZINC we are able to create a controlled ice supersaturated environment in order to investigate the deposition freezing mechanism at different temperatures (Stetzer & Lohmann, submitted 2007). The flow through the ZINC instrument is laminar and the velocities of the particles can reach values of about  $2\text{m/s}$  at the bottom of the chamber.

The detection of ice particles coming from ZINC is currently made by sizing the particles with an optical particle counter. However, this technique does not allow for determining the crystal habits. Holographic microscopy will be used because the principle of this technique allows for producing 2D images and 3D shapes with reduced resolution of ice crystals throughout the whole observing volume but this information can only be obtained when the hologram is recorded with a camera. This camera is mounted to a small detection chamber ( $3\text{ cm} \times 6\text{ cm} \times 9\text{ cm}$ ) such that it is in line with a point source of light (see Figure 1). A *laser* pulse with a wavelength of  $532\text{ nm}$  is going to be coupled into a single mode fiber (not shown) of  $1\ \mu\text{m}$  core diameter. This fiber produces the point source of light. The coherent light is scattered off an object inside the light cone, defined by the divergence of the point source, resulting in a coherent interference pattern on the *camera* sensor. Therefore, the DIHM consists only of a *laser*, an optical fiber and a *camera*.

With this newly-installed setup, we are able to determine both the size and the shape of ice crystals coming from the *ice crystal inlet* because the

resolution of a DIHM can be calculated very precisely (Jericho *et al.*, 2006). It has been shown in a proof of concept study that latex spheres of  $1\ \mu\text{m}$  diameter were clearly resolvable (Kreuzer *et al.*, 2001).

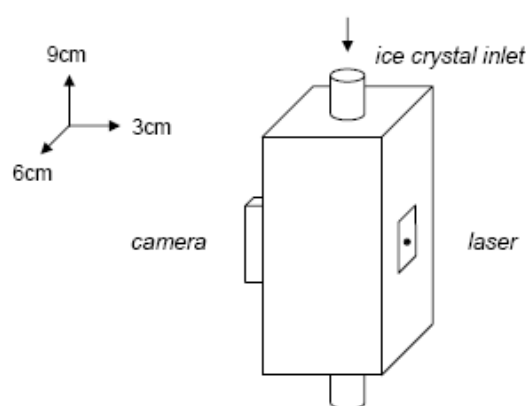


Figure 1. Schematic view of the detection chamber carrying the DIHM (*laser*, fiber (not shown) and *camera*).

The characterization of the newly-installed DIHM at this detection chamber will be presented.

This work was supported by the ETH Zurich research grant TH-39/05-1 “Development of an in-line Holographic Microscope for Ice Crystals”.

- Cantrell, W., & Heymsfield, A. (2005). *Bull. Amer. Meteor. Soc.*, 795-807.
- Jericho S. K., Garcia-Sucerquia J., Xu W., & Kreuzer H. J. (2006). *Review of Scientific Instruments*, **77**, 043706
- Kreuzer H. J., Jericho H. H., Meinertzhagen I. A., & Xu W. (2001). *Journal of Physics: Condensed Matter*, **13**, 10729-10741.
- Lohmann U., & Feichter J. (2005). *Atmos. Chem. Phys.*, **5**, 715-737.
- Schaefer V. J. (1947). *Trans Amer. Geophys. union*, **28**, 557.
- Stetzer O., & Lohmann U. (2007). Submitted to: *Aerosol Science and Technology*.
- Vali G. (1985). *J. Rech. Atmos.*, **19**, 105-115.

## Intercomparison study of different mobility particle sizers with NaCl, Diesel soot, and ambient aerosols

Christof Asbach<sup>1</sup>, Heinz Kaminski<sup>1</sup>, Burkhard Stahlmecke<sup>1</sup>, Heinz Fissan<sup>1</sup>, Christian Monz<sup>2</sup>, Dirk Dahmann<sup>2</sup>, Sonja Mülhopt<sup>3</sup>, Hanns R. Paur<sup>3</sup>, Heinz J. Kiesling<sup>4</sup>, Friedhelm Herrmann<sup>4</sup>, Matthias Voetz<sup>4</sup>, and Thomas A.J. Kuhlbusch<sup>1</sup>

<sup>1</sup> Institut für Energie- und Umwelttechnik (IUTA), Bliersheimer Str. 60, 47229 Duisburg, Germany

<sup>2</sup> Institut für Gefahrstoffforschung (IGF), 44789 Bochum, Waldring 97, Germany

<sup>3</sup> Forschungszentrum Karlsruhe, Herrmann-von-Helmholtz Platz 1, 76344 Eggenstein-Leopoldshafen, Germany

<sup>4</sup> Bayer Technology Services GmbH, 51368 Leverkusen, Germany

Keywords: SMPS, FMPS, NaCl, diesel soot, agglomerate

Mobility particle sizers are being used as a standard tool for physical characterization of airborne particles. For nanoparticles, these devices comprise scanning mobility particle sizers (SMPS's) or fast mobility particle sizers (FMPS's) that measure the number size distribution of airborne particles. These instruments are usually calibrated for spherical particles. The response, however, can be affected by particle morphology, due to different particle charging in neutralizers (Wen *et al.*, 1984a & 1984b) and drag force experienced e.g. by agglomerates (Chan & Dahneke, 1981; Dahneke, 1982). A model to predict particle number and surface size distribution of chain-like agglomerates based on electrical mobility data has recently been published by Lall & Friedlander (2006).

In industrial hygiene, mobility particle sizers can provide useful means to assess human exposure to nanoparticles, e.g. in nanotechnology workplaces, where nanoparticles are produced, handled, or processed. Intercomparability studies under various conditions concerning particle morphology, instrument settings and operators among these instruments from different manufacturers are therefore crucial in view of standardization.

In this study, we challenged altogether five instruments (4 different SMPS's, 1 FMPS) with both intentionally produced and ubiquitous ambient particles. Intentionally produced particles included sodium chloride (NaCl) and Diesel soot that were mixed with dilution air in a wind tunnel and sampled from a 25 m<sup>3</sup> sedimentation chamber. The sample conditioning assured a homogenous distribution of the particles such that all instruments could be assumed to sample identical aerosols. Diesel soot and NaCl were chosen as test materials as these exhibit very different particle morphologies which might affect the measurement. While NaCl usually forms cubic particles, Diesel soot particles are complex agglomerates. Ambient particles were sampled over night directly from room air with no activities within the room. Size distributions of the different test aerosols are illustrated in Fig. 1.

Mode and median diameter, geometric standard deviation, and peak concentration of the size distributions, as well as the size resolved ratios of the concentration values were subject to a detailed intercomparison study. The total number concentrations obtained from the different size distributions were compared with concentrations measured with two handheld Condensation Particle Counters (CPC's) within the size detection limits of the CPC's. The results of this comparison study will be presented and the implications of the resulting uncertainties discussed towards implementation into standardization.

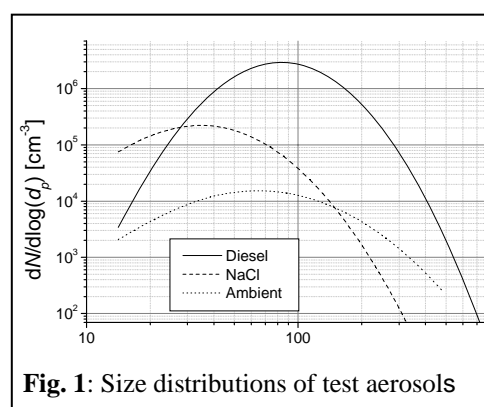


Fig. 1: Size distributions of test aerosols

This work was supported by the German Federal Ministry of Education and Research (BMBF) as part of the NanoCare project.

Chan, P. & Dahneke, B. (1981) *J. Appl. Phys.* **52**:3106

Dahneke, B. (1982) *Aerosol Sci. Technol.* **1**: 179

Wen, H.Y.; Reischl G.P. & Kasper, G. (1984a) *J. Aerosol Sci.* **15**:89

Wen, H.Y.; Reischl G.P. & Kasper, G. (1984b) *J. Aerosol Sci.* **15**:103

Lall, A.A. & Friedlander, S.K. (2006) *J. Aerosol Sci.* **37**: 260

## Aerosol light scattering at high relative humidity

R. Schmidhauser, G. Wehrle, T. Ulrich, E. Weingartner and U. Baltensperger

Laboratory of Atmospheric Chemistry, Paul Scherrer Institut, 5232, Villigen PSI, Switzerland

Keywords: Light scattering, relative humidity, optical properties, nephelometer.

Aerosol light scattering is strongly dependent on relative humidity (RH) as shown by model calculations in Nessler *et al.* (2005). Nevertheless it is recommended within the Global Atmosphere Watch aerosol monitoring network to measure aerosol light scattering coefficients  $b_{\text{scat}}$  at relative humidities (RH) below 40%, in order to be able to compare results from different locations. As ambient RH values are typically higher, we built a humidification system for a nephelometer (TSI model 3563) that allows for measurement of  $b_{\text{scat}}$  at a defined and controlled RH in the range 20-90%.

Figure 1 shows a rough set-up of the system. First, the aerosol enters a humidifier, which is controlled by a first temperature and RH sensor. After that the aerosol passes through a dryer and its efficiency is controlled by a second sensor. The dryer can be operated without drying the air. Then, the light scattering coefficient of the aerosol particles is measured by the nephelometer at a controlled temperature and RH.

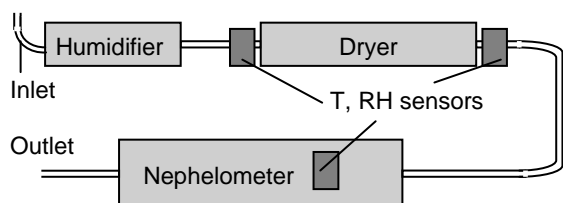


Figure 1. Set-up of the humidified nephelometer.

The humidifier (a heatable Gore-Tex tube) is able to increase the RH to values up to 99% at a flow rate of 15 liters per minute. In the nephelometer the maximum RH is at about 90%, because irradiation by the lamp heats the aerosol by about 1°C. The dryer (based on Nafion) is capable of reducing the RH from 85% to 20%. If the particles hygroscopic properties experience a hysteresis behaviour, the upper and lower branch of this hysteresis curve can be measured by varying the humidifier RH and dryer settings.

First measurements were performed to test the new instrument with sodium chloride (NaCl) particles produced by nebulization of an aqueous solution. An SMPS (Scanning Mobility Particle Sizer) was running in parallel to the humidified nephelometer, in order to monitor the development of the particle size distribution in the diameter size range 7-300 nm (median diameter: 31 nm, standard deviation: 1.8).

Figure 2 shows preliminary results of the scattering enhancement factor  $b_{\text{scat}}(\text{RH})/b_{\text{scat}}(\text{dry})$  vs. the RH in the nephelometer, where the RH of the humidifier was limited to a maximum of 85%. The measured scattering coefficients were normalized to the integrated particle surface area density, given by the SMPS, to be able to adjust the scattering coefficients for slightly varying particle sizes and concentrations.  $b_{\text{scat}}$  is up to six times higher at high RH than for dry conditions.

The theoretical curve according to Biskos *et al.* (2006) is added in Figure 2. In this preliminary analysis, the median diameter of the size distribution was taken for the calculation. A more detailed analysis is expected to reduce the discrepancy between experimental and theoretical values. Efflorescence occurred at RH between 40 and 50%, in good agreement with theory. Due to the higher temperature in the nephelometer, the deliquescence RH cannot be measured in the nephelometer.

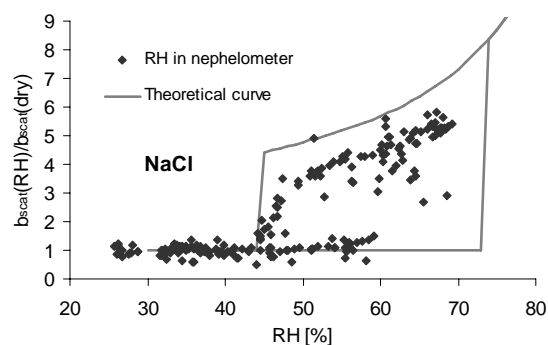


Figure 2. Scattering enhancement factor  $b_{\text{scat}}(\text{RH})/b_{\text{scat}}(\text{dry})$  at the RH in the nephelometer plus theoretical scattering enhancement factor, measured and calculated at 450 nm wavelength.

The presented result is a first laboratory measurement, but the humidified nephelometer is mainly designed to be operated in the field, where the enhanced scattering coefficients of ambient aerosol particles will be measured at different locations.

This work was supported by the EU-funded project EUSAAR.

Biskos, G., Malinowski, A., Russell, L.M., Buseck, P.R. & Martin, S.T. (2006). *Aerosol Sci. and Tech.* 40, 97-106.

Nessler, R., Weingartner, E. & Baltensperger, U. (2005). *Environ. Sci. Technol.*, 39 (7), 2219-2228.

## Development of a Thermal Desorption Chemical Ionization Ion Trap Mass Spectrometer for the Chemical Characterization of Ultrafine Aerosol

A. Held, G. Rathbone and J. Smith

Atmospheric Chemistry Division,  
National Center for Atmospheric Research, Boulder, CO 80301, USA

Keywords: Instrumentation/chemical char., Mass spectrometry, Particle formation, Ultrafine particles

Rapid online measurements of the chemical composition of ultrafine aerosol particles (< 100 nm diameter) are a key component to investigate health effects of particulate matter, atmospheric heterogeneous chemistry, and atmospheric particle nucleation and growth. Recently, a triple quadrupole thermal desorption chemical ionization mass spectrometer (TDCIMS) was successfully employed to measure chemical compounds of atmospheric aerosol in the 6-20 nm diameter range (Smith et al., 2004).

Here, we report advances in the development of a new TDCIMS instrument using a quadrupole ion trap mass spectrometer and a modified inlet design. The main improvements of this new instrument are its reduced size and weight, faster and more efficient passage of particles through the instrument, and the analytical versatility of an ion trap mass spectrometer.

The basic principles of the TDCIMS technique (Voisin et al., 2003) will be briefly described: Ambient aerosol particles entering the instrument are charged, a size-segregated subsample of the aerosol is selected with a differential mobility analyzer (DMA), and the monodisperse aerosol is collected on an electrostatic precipitator. In order to improve instrument sensitivity, the charged particles cross the flow of a clean sheath gas that prevents contamination of the collector from the ambient gas. Finally, the collected sample is thermally desorbed in the ion source region of the mass spectrometer and analyzed for characteristic ions.

The new instrument configuration has been designed for fast and efficient transport of ultrafine particles from the particle inlet to the electrostatic precipitator. Reduced volumes of the sampling lines and the electrostatic precipitator minimize sample mixing to allow for conditional sampling procedures. In addition, radial DMAs with simple outlet geometries are applied to reduce loss of particles in the DMA exit regions. Overall, the compact design of an ion trap mass spectrometer facilitates transportation and application of the instrument in field studies.

Ion trap mass spectrometry is a versatile technique to analyze ions generated from the thermal desorption of aerosol particles. In a first step, ions are trapped in a superposition of oscillating and static electric fields. In a second step, the stored ions are

ejected from the trap according to their mass-to-charge ratio by changing the electric field. Depending on the studied ions, storage and ejection times allow fast scanning of mass spectra. In typical laboratory experiments, we record 1 to 10 spectra per second. Thus, changes in the ion composition during thermal desorption with a temperature ramp can easily be followed.

During storage, ions can be manipulated in various ways. In order to reduce background interferences, unwanted ions are ejected from the ion trap through multiple-frequency resonance ejection. In preliminary laboratory experiments, we applied a filtered noise field (FNF) in order to increase the signal-to-background ratio. On this basis, multi-dimensional MS analysis of individual compounds by resonant excitation of isolated ions will be further investigated. This approach shows promise to characterize organic molecules in ultrafine aerosol particles through mass spectral analysis of parent and daughter molecules in multiple fragmentation steps.

First experimental results of the new thermal desorption chemical ionization ion trap mass spectrometer will be presented and discussed.

A BEACHON instrument development grant is gratefully acknowledged. AH is supported by a research fellowship of the German Research Foundation (DFG).

Smith, J.N., Moore, K.F., McMurry, P.H., and Eisele, F.L. (2004) Atmospheric measurements of sub-20 nm diameter particle chemical composition by thermal desorption chemical ionization mass spectrometry. *Aerosol Sci. Technol.* 38, 100-110.

Voisin, D., Smith, J.N., Sakurai, H., McMurry, P.H., and Eisele, F.L. (2003) Thermal desorption chemical ionization mass spectrometer for ultrafine particle chemical composition. *Aerosol Sci. Technol.* 37, 471-475.

## Numerical and experimental study on particle collection efficiency of polyurethane foam impactors

C.-H. Huang

Department of Environmental Engineering and Health, Yuanpei University, Hsinchu, Taiwan

Keywords: inertial impactor, particle collection efficiency, polyurethane foam.

Polyurethane foam avoids adhesive coating and chemical interference on the substrate of the inertial impactors. Moreover, particle bounce, re-entrainment and particle over-loading can be neglected. But, the use of the polyurethane foam as the substrate of the impactor causes some changes in the particle collection characteristic. In this study, the particle collection efficiency of the single-round nozzle impactor with polyurethane foam was investigated numerically and experimentally. The numerical results of the impactor with polyurethane foam were compared to those of the experimental data at different flow rates.

Both oleic acid and KCl particles with the various aerodynamic diameters were generated by using an ultrasonic atomizing nozzle. Solid particles were used to test if particle bounce occurs on the substrates. The aerosols were dried in the upper section of the test chamber by mixing with dried filtered air and were further neutralized in the middle section of the test chamber. The aerodynamic particle sizer was used to measure the aerosol number concentrations at the inlet and outlet of the impactor installed in the lower section of the test chamber to determine the particle collection efficiency. The particle wall loss in the impactor was also determined using monodisperse oleic acid particles tagged with fluorescein. At the end of each sampling period of five minutes, particles on the impaction substrate, the downstream filter, and the other portions of the impactor were extracted. A fluorometer was used to measure the wall loss of the inertial impactor with polyurethane foam.

The flow field in the impactor with polyurethane foam was simulated by solving the Navier-Stokes equations in the cylindrical coordinate. The fluid flow in the inertial impactor with polyurethane foam was assumed steady, incompressible and laminar. The governing equation was discretized by means of the finite volume method. After obtaining the flow field, the particle equations of motion were solved numerically to obtain particle trajectories in the inertial impactor with polyurethane foam. The particle collection efficiency of the single-round nozzle impactor with polyurethane foam can be defined as one minus the outlet particle concentration divided by the inlet particle concentration.

Figure 1 plots the comparison of the numerical particle collection efficiency of impactor with the polyurethane foam and the experimental data at the

sampling flow rates of 1.5 L/min and 2.0 L/min for the nozzle diameter of 0.26 cm. The results demonstrate that the numerical results of the particle collection efficiency of the impactor with the polyurethane foam are close to the experimental data. The numerical results can be used to calculate the particle collection efficiency of the impactor with the polyurethane foam at various conditions.

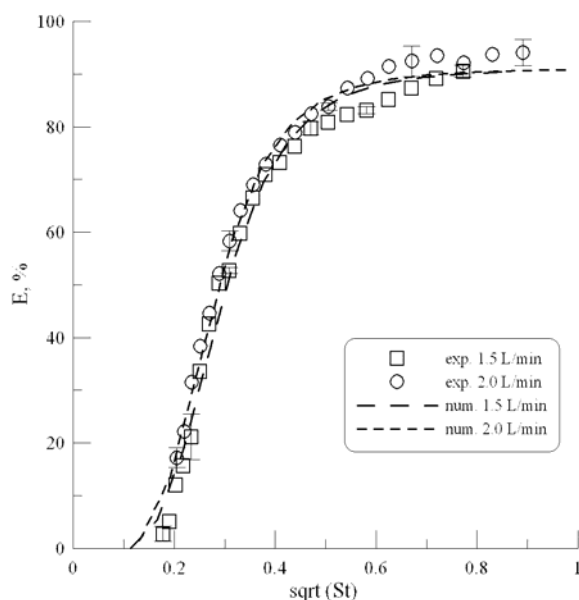


Figure 1. Relationship between the numerical and experimental particle collection efficiency of the impactor with polyurethane foam at different sampling flow rates.

This work was supported by the Taiwan National Science Council of the Republic of China under the contract number : NSC 95-2221-E-264 -012 -MY3

Huang, C. H., Chang, C. S., Chang, S. H., Tsai, C. J., Shih, T. S. & Tang, D. T. (2005). *J. Aerosol Science*, 36, 1373-1386.

## Design and performance evaluation of a three-stage impactor for rapid bioaerosol detection by ATP bioluminescence

K.Y. Yoon<sup>1</sup>, D. Park<sup>1</sup>, J.H. Byeon<sup>1</sup>, J. Hwang<sup>1</sup>, J.H. Ji<sup>2</sup>, G.N. Bae<sup>3</sup>

<sup>1</sup>Department of Mechanical Engineering, Yonsei University, Seoul 120-749, Korea

<sup>2</sup>Digital Appliance R&D Center, Samsung Electronics, Suwon 443-742, Korea

<sup>3</sup>Hazardous Substance Research Center, Korea Institute of Science and Technology, Seoul 136-791, Korea

Keywords: cascade impactor, bioaerosol, ATP

Monitoring of biological aerosols is required for controlling air quality, for exposure assessment in health risk evaluation, for investigating dispersion of bioaerosols in atmosphere, or for other research purposes (Agranovski et al., 2004). The conventional method for monitoring of bioaerosols is colony counting after sampling and culturing. This culture-based method requires at least 24 hours to provide the results.

ATP bioluminescence is generally used to measure the approximate number of living organisms by determining the essential metabolite, intracellular ATP. ATP bioluminescence is one of the most popular rapid detection methods in microbiology (Sakakibara et al., 2003). The main objective of this study is development of the methodology for determining the concentration of bioaerosols collected on impaction plate of impactor by using ATP bioluminescence.

Prior to applying ATP bioluminescent method for rapid detection of bioaerosols, three-stage impactor with aerodynamic cutoff diameters of 1, 2.5, and 10  $\mu\text{m}$  was designed and its performance was evaluated. For designing and performance testing of stages 1 and 2 of the impactor, a vibrating orifice aerosol generator (VOAG, TSI model 3450) was used to generate monodisperse oleic acid or sodium chloride (NaCl) aerosols of diameter larger than 2  $\mu\text{m}$ . For stage 3 of the impactor, polystyrene latex (PSL) particles smaller than 2  $\mu\text{m}$  in diameter were generated from an atomizer. The gravimetric method was used for stages 1 and 2, and the counting method for stage 3.

The particle collection efficiency curve of an impactor can be characterized by the  $Stk_{50}$ , which is the Stokes number at 50-% collection efficiency. For a circular nozzle, Eq. (1) gives the cutoff diameter in terms of  $Stk_{50}$ .

$$d_{50} = \sqrt{\frac{9 \mu D Stk_{50}}{\rho_p U C_c}} \quad (1)$$

We designed a three-stage impactor to provide aerodynamic cutoff diameters of 1, 2.5, and 10  $\mu\text{m}$  at a flow rate of 30 L/min. The initial square root of the Stoke number,  $\sqrt{Stk_{50}}$ , was assumed as 0.49 for all

stages. Then, we carried out a performance test for each stage and revised the values of  $\sqrt{Stk_{50}}$  by using the experimental particle collection efficiency curves. Figure 1 shows the particle collection efficiency curves of revised impactor.

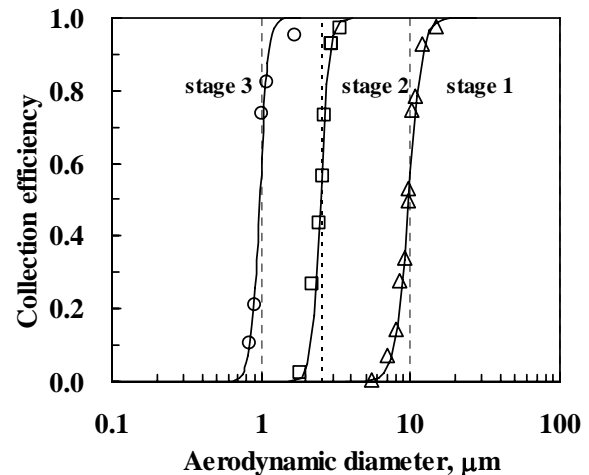


Figure 1. Particle collection efficiency curves of the revised impactor.

This work was supported by grant No. R01-2005-000-10723-0 from the Basic Research Program of the Korea Science & Engineering Foundation. This work was also supported by Seoul R&D Program.

Agranovski, V., Ristovski, Z.D., Ayoko, G.A., & Morawska, L. (2004). *Aerosol Science and Technology*, 38, 354-364.

Sakakibara, T., Murakami, S., & Imai, K. (2003). *Analytical Biochemistry*, 312, 48-56.

## Formation of Thick Silver Lines on a PET(polyethylene terephthalate) Film Patterned by a Combined Process of Electrohydrodynamic Printing and Electroless Deposition

Kim, S.Y., Byeon, J.H., and Hwang, J.

Department of Mechanical Engineering, Yonsei University, Shinchon-dong, 120-749, Seoul, Korea

Keywords: Electrohydrodynamic printing(EHDP), electroless deposition(ELD), cone-jet mode, silver line

Direct writing technology(DWT) is the most recent and novel approaches of forming a fine pattern whose line width ranges from the meso to the nano scale. The term direct write refers to any technique or process capable of depositing, dispensing, or processing different types of materials on various surfaces following a preset pattern or layout(Pique and Chrisey, 2002). With a direct-write approach, patterns or structures can be obtained directly without the use of various fabrication processes, masks, and liquids for etching. Direct write technologies, therefore, are the low cost, high speed, non-contact, and environmental-friendly processes(Chrisey, 2000).

Electrohydrodynamic printing(EHDP) is one of the novel printing methods for direct writing technology. EHDP has the advantage of being able to generate monodispersed droplets and to control the size of generated droplets by controlling the flow rate or electrical conductivity of the liquid(Calvo et al., 1995). In this system, the nozzle size has no effect on droplet size. Since the generation of droplets is in the assistance of an electric field, the droplets size can be much finer than the used nozzle diameter. Also high viscose liquids or metal particle suspension with high concentration(above 20%) is available for fine droplet generation without any clogging problem.

In this study, we carried out the formation of silver lines by using the cone-jet mode of EHDP. Experiments were carried out by using Ag particles of 10 nm in diameter. They were dispersed in a mixture of DI water with a surfactant and a dispersant for a stable cone-jet mode of EHDP. The physical properties of suspension are shown in Table 1.

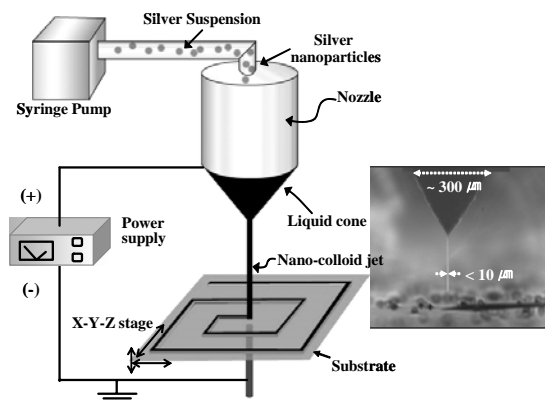


Figure 1. Scheme of experimental set-up.

Table 1. Physical properties of suspension

Silver particle diameter (nm)	Silver particle conc. (wt%)	Viscosity (mPa-s)	Surface tension (mN/m)	Conductivity (mS/m)
10	20	112	41	65

Figure 1 shows a scheme of the equipment set-up used for the cone-jet mode of EHDP. The system consisted of a liquid supplying system, an electrical power supplying system, and a moving stage system.

For the improvement of silver line's thickness, electroless deposition(ELD) employed. This combined process can yield mechanically durable fine Ag metal lines layers with high aspects ratio. Silver lines as fine as 32~165  $\mu\text{m}$  in width and 0.3~5  $\mu\text{m}$  in thickness were obtained onto the PET(polyethylene terephthalate) film by a stable cone-jet mode of EHDP. With electroless deposition, we obtained 400~450  $\mu\text{m}$  in thickness onto the PET film in Fig. 2.

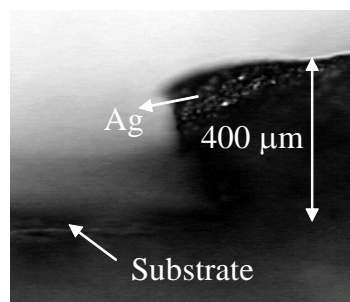


Figure 2. Cross-sectional image of silver line using combined process of EHDP and ELD.

This work was supported by grant NO. 013-071-052 from the Eco-Technopia 21 Project of the Korea Institute of Environmental Science and Technology.

- A. M. Ganan-Calvo, J. Davila and A. Barreo (1995). *J. Aerosol Science*, 28, 249-275.  
 Chrisey, D. B. (2000). *Science*, 289, 879-881.  
 Poon, H. F. (2002). Ph. D. Thesis, Dept. Chem. Eng.: Princeton University.  
 Alberto Pique, Douglas B. Chrisey (2002). Academic Press

## Condensation particle counting for particle diameters down to 1 nm

P. M. Winkler<sup>1</sup>, G.W. Steiner<sup>1</sup>, G. P. Reischl<sup>1</sup>, A. Vrtala<sup>1</sup>, M. Kulmala<sup>2</sup>, P. E. Wagner<sup>1</sup>

<sup>1</sup> Fakultät für Physik, Universität Wien, Boltzmanngasse 5, A-1090 Wien, Austria

<sup>2</sup> Department of Physical Sciences, University of Helsinki, P.O.Box 64, FIN-00014 Helsinki, Finland

Keywords: CPC, aerosol instrumentation, heterogeneous nucleation, nanoparticles, ions.

The particle size dependent response of condensation particle counters has been the object of numerous experimental studies (see, e.g. Reischl & Wagner 2002). So far it has usually been assumed that only particles with sizes beyond the prediction by the Kelvin equation are activated by vapour nucleation (Rebours et al., 1996). Accordingly, the lower limit for the cut-off diameter has been expected around 2 nm. In recent experiments we have observed heterogeneous nucleation already well below the Kelvin prediction (Winkler et al. 2006; Hienola et al. 2007). Therefore somewhat smaller cut-off diameters may be expected for condensation particle counting.

In the present study we show that significantly smaller cut-off diameters down to about 1 nm can be achieved, if the measuring method provides sufficient time resolution. We have used a fast-expansion chamber together with the Constant-Angle Mie Scattering (CAMS) method (Wagner et al., 2003). Propanol was used as the working fluid. WO<sub>x</sub> nanoparticles as well as ions obtained from an <sup>241</sup>Am aerosol charger were considered. As can be seen from Fig. 1, heterogeneous can only be separated from homogeneous nucleation, if the droplet concentration measurement is performed at the *first* Mie maximum, occurring already 2 ms after expansion. However, concentration measurement at the *ninth* Mie maximum, occurring about 8 ms after expansion, is already influenced by the onset of homogeneous nucleation.

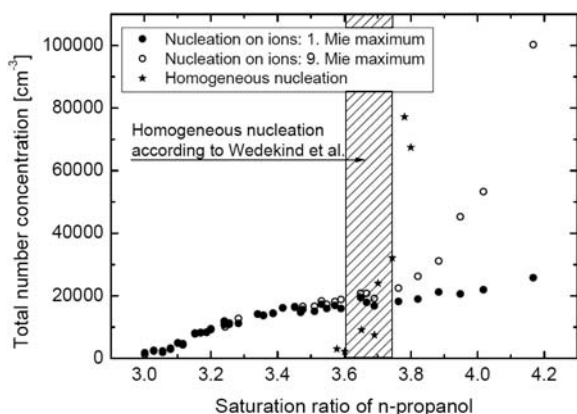


Figure 1. Time resolved detection of droplet number concentration allowing distinction between heterogeneous and homogeneous nucleation.

Furthermore, for concentration measurement of particles with diameters below about 2 nm ion-induced nucleation becomes increasingly important. In Fig. 2 we show, for the first time, the simultaneous nucleation by WO<sub>x</sub> particles (diameter 2 nm) and by ions (diameter 1 nm). Particles in the size range below 2 nm can only be uniquely detected, if ions are previously removed. Work will continue with the study of different chemical compounds.

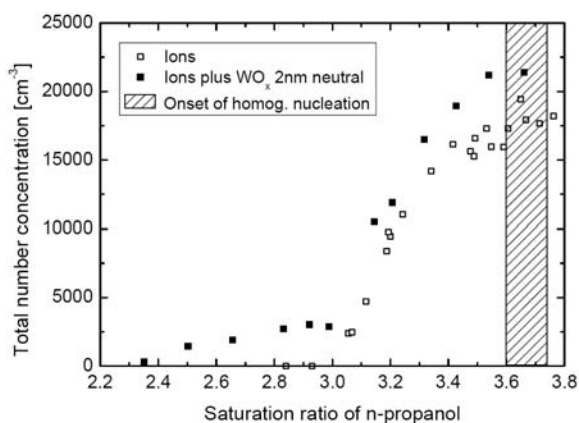


Figure 2. Transition from heterogeneous nucleation on WO<sub>x</sub> seed particles to ion-induced nucleation.

This work was supported by the Austrian Science Foundation (FWF, Project No. P16958-N02).

- G. P. Reischl, P. E. Wagner (Eds.) (2002), *Aerosol Number Concentration Measurement*, Atmospheric Research **62**, Special Issue.
- A. Rebours, D. Boulaud, A. Renoux (1996), *J. Aerosol Sci.* **27**, 1227.
- P. M. Winkler, G. Steiner, G. P. Reischl, A. Vrtala, P. E. Wagner, A. I. Gaman, H. Vehkamäki, M. Kulmala (2006), in *Proc. 7<sup>th</sup> Int. Aerosol Conf.*, St. Paul (P. Biswas, D.-R. Chen, S. Hering, Eds.), p. 1615.
- A. I. Hienola, P. M. Winkler, P. E. Wagner, H. Vehkamäki, A. Lauri, I. Napari, M. Kulmala (2007), *J. Chem. Phys.*, accepted.
- P. E. Wagner, D. Kaller, A. Vrtala, A. Lauri, M. Kulmala, A. Laaksonen (2003), *Phys. Rev.* **E67**, 021605.
- J. Wedekind, K. Iland, P. E. Wagner, R. Strey, (2004), in *Nucleation and Atmospheric Aerosols*, Kyoto, (Kyoto University Press), 49-52.

## Performance and characterisation of a high-flow, high-resolution DMA: Particle losses and filtration efficiency measurements for particles below 20 nm.

M. Heim<sup>1</sup>, M. Attoui<sup>2</sup> and G. Kasper<sup>1</sup>

<sup>1</sup>Institut für Mechanische Verfahrenstechnik und Mechanik, Universität Karlsruhe, 76128, Karlsruhe, Germany

<sup>2</sup>Faculté des Sciences, Université Paris II - Val de Marne, 94010, Créteil, France

Keywords: Nano-DMA, Nanoparticles, Aerosol filtration, TDMA

Several different DMA designs have been developed in the last 30 years, however only two have received widespread use - due to their commercialization. The first one is the so called Minnesota design, which is described in detail in the work of Knutson and Whitby, the second design is the Vienna DMA, which was optimized for the low nanometer size range by shortening the residence time of the aerosol within the instrument. Recently an improved design of the original Vienna DMA developed by Rosser and de la Mora (2005) was used at flow rates as high as 3800 l/min - while still working in the laminar regime.

The DMA used for this work (figure 1) is comparable to the one of Rosser and de la Mora, but is using an improved sheath gas exhaust system that produces essentially no pressure drop, permitting sheath gas flow rates well above 4000 l/min. This device, termed the Attoui DMA, has been developed by Fernandez de la Mora and Attoui (2007). The design allows aerosol flow rates of 100 l/min, but has been tested only up to 30 l/min, with excellent performance.

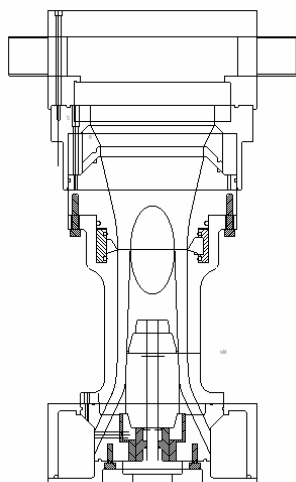


Figure 1 – Sketch of the Attoui Vienna DMA.

Compared to other high resolution Nano-DMAs, this instrument can also be used at much lower flow rates, enabling a useful operating particle size range between 1 and at least 30 nm at high resolution.

The extended size range, the attainable high aerosol flow rate and the high resolution make this DMA an ideal instrument for the characterization of

particle losses in the size range below 20 nm. In the first part of this work, the performance of the DMA is shown by the measurements of monodisperse ions produced by an electrospray generator. In a second part, different applications are presented.

One application is the measurement of particle penetration in the low nanometer size range. We measured the penetration through a wire screen in the size range below 10 nm and compared the results to the well known theory of Cheng and Yeh. Comparable to a previous work of Heim et al. (2005), we found no deviation between the measurements and the theory, but extended the examined size range down to 1.3 nm. Below this size, artifacts caused by nearly monodisperse ions could be observed.

Another application shown is the determination of particle losses in differential mobility analyzers. Therefore Tandem-DMA measurements have been performed and the losses of a short Vienna DMA were measured. The measured transmission efficiency is shown in figure 2.

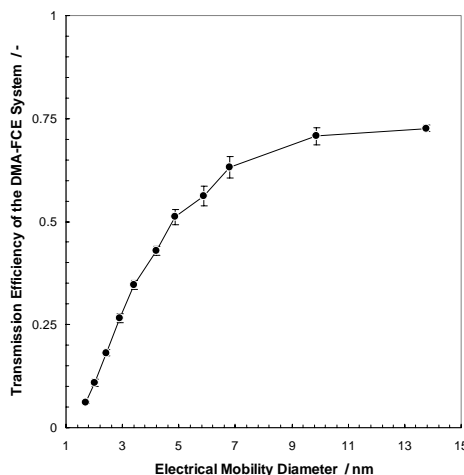


Figure 2 – Transmission Efficiency of a short Vienna DMA at a flow ratio of 6:60 l/min.

S. Rosser and J. Fernandez de la Mora (2005), *Aerosol Sci. and Technology*, 39, 1191-1200.

M. Heim, B. Mullins, M. Wild, J. Meyer and G. Kasper (2005), *Aerosol Sci. and Technology*, 39, 782-789.

J. Fernandez de la Mora and M. Attoui (2007), Abstract submitted to the EAC 2007 (this issue).

## Photophoretic Migration of Monodisperse Aerosols

C. Kykal, C. Haisch and R. Niessner

Chair for Analytical Chemistry, Technische Universität München,  
Marchioninistrasse 17, D-81373, Munich, Germany

Keywords: Photophoresis, thermo-photophoresis, separation, aerosol

Photophoresis (PP) denotes the phenomenon that small particles suspended in gas (aerosols) [1] or liquid (hydrocolloids) start to migrate when illuminated by a sufficiently intense beam of light. PP motion can occur in the direction of light beam (positive PP) or in the opposite direction (negative PP). In case the particle is transparent and the index of refraction is larger than the one of the surrounding medium, the particle moves away from the light source due to momentum transfer from absorbed and scattered photons. When the particle absorbs the incident light, a temperature gradient is generated which causes the migration according to its thermal and optical properties and is termed Thermo-PP.

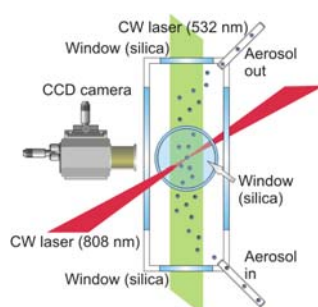


Figure 1. Cross flow setup: flow cell with silica windows, laser for illumination (CW,  $P = 20\text{mW}$ ,  $\lambda = 532\text{ nm}$ ) and for separation (CW,  $P = 1\text{W}$ ,  $\lambda = 808\text{ nm}$ )

In conventional separation techniques, aerosols and colloids are separated by means of electrical, thermal or flow fields. In our approach, the application of light is tested as a means to separate particles due to their optical properties. Such a separation technique would allow e.g. the separation of organic from inorganic particles of the same size. We aim to develop a continuous flow separation system for aerosols regarding the optical properties of the particles [2].

Table 1. Photophoretic properties of differently coloured and sized PSL particles (cross flow setup).

Size [ $\mu\text{m}$ ]	Particle colour	Photophoretic velocities [ $\text{mm/s}$ ]
0.99	white	$0.112 \pm 0.014$
1	red [606 nm]	$0.113 \pm 0.018$
1	yellow [514 nm]	$0.144 \pm 0.014$
1.9	white	$0.172 \pm 0.025$
2.88	white	$0.259 \pm 0.034$

Table 1 summarizes the observed PP velocities in ascending order for a set of PSL

particles differing in size and colour. The experimental system essentially consists of a flow cell with rectangular cross section ( $1\text{ cm}^2$ , length  $25\text{ mm}$ ), where the aerosol stream is pumped through in vertical direction at ambient pressure. Two different configurations were compared, one where the laser beam and hence the PP force is directed orthogonally to the aerosol flow and one, where the PP force and the gas flow counteract in opposite directions. PP force in both cases is generated by a diode laser. Migration of the particles is observed by a CCD camera. From the image series the PP velocities of every single particle is obtained by a special particle imaging velocimetry algorithm.

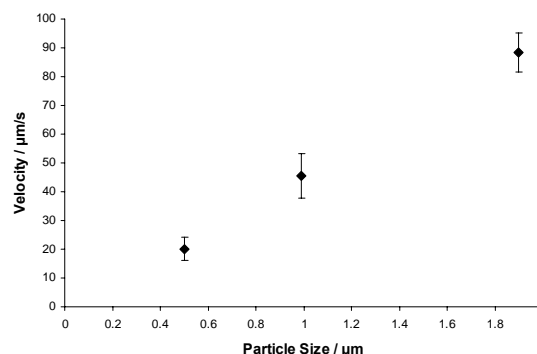


Figure 2. Dependency of PP velocities on particle size of monodisperse white polystyrene lattices ( $I = 1.6 \cdot 10^3\text{ W/cm}^2$ ).

Experiments with polystyrene lattices (Figure 2) verify the theoretically predicted linear correlation between the particle size and the measured velocities induced by PP. In other experiments we found the same correlation between laser power and PP velocities for a constant particle size. For monodisperse soot particles with a very low thermal conductivity and therefore a high temperature gradient across the particle the highest PP velocities were found. No gradient PP force in radial direction of the laser beam was observed. Therefore, the flow-generated force on the one hand and the PP force on the other hand can be superposed in any desired direction, which allows the construction of a continuous separation system. This work is financially supported by the DFG grant Ni 261/16-1.

- 1.: Ehrenhaft, F. (1918), *Annalen der Physik*, 56, 81-132
- 2.: Zaho, B.S., Koo, Y.M., Chung, D.S.. (2006), *Analytical Chimica Acta*, 556,1, 97-103.

## Aerosols washout by a water spray in hostile environment: experimental and numerical approaches

D. Marchand<sup>1</sup>, E. Porcheron<sup>1</sup>, P. Lemaitre<sup>1</sup>, A. Nuboer<sup>1</sup>, W. Plumecocq<sup>3</sup> and G. Grehan<sup>2</sup>

<sup>1</sup>Institut de Radioprotection et de Sûreté Nucléaire - DSU/SERAC, Laboratoire d'Expérimentations en Confinement, Epuration et Ventilation, BP 68, 91192 Gif-sur-Yvette Cedex, FRANCE

<sup>2</sup>UMR 6614 CORIA-CNRS, Laboratoire d'Electromagnétisme des Systèmes Particulaires, Site universitaire du Madrillet, Avenue de l'Université BP 12, 76 801 Saint Etienne du Rouvray Cedex, France

(3) Institut de Radioprotection et de Sûreté Nucléaire DPAM/SEMIC, BP 3, 13115 St Paul-Lez-Durance.

E-mail : [denis.marchand@irsn.fr](mailto:denis.marchand@irsn.fr)

Keywords: collection efficiency, airborne particles, aerosol measurements, optical particle counter, modelling.

This work lies within the general framework of the studies and researches on the nuclear Pressurized Water Reactors (PWR) safety. During a hypothetical severe accident in a PWR, the containment building can be pressurized by steam released from a break of the primary circuit. The loss of coolant then leads to the degradation of the nuclear core, which would release fission products (FP) under aerosols and gaseous forms. Consequences of an overheating reactor accident can be limited by a cold-water spray injection into the reactor containment building. To preserve the integrity of the PWR containment, the primary function of the spray is to remove heat and to condense steam on spray droplets in order to reduce pressure and temperature levels in the reactor containment. In addition, the spray will also washout airborne FP and will distribute them into the containment by convection flows according to steam wall condensation and spray entrainment, from the containment vessel towards the sump (Grist 1982). The modelling of phenomena involved in FP washout by spray water and the estimation of the aerosols removal rate is of great importance for source term assessment

In order to simulate typical accidental thermal-hydraulic conditions, the Institut de Radioprotection et de Sûreté Nucléaire (IRSN) has developed the TOSQAN facility. The TOSQAN facility which is a large vessel (7 m<sup>3</sup>) suitable for optical diagnostics (Porcheron et al. 2004) allows to study the physical phenomena involved in the aerosols washout by water droplets for thermal hydraulic conditions representative of a severe accident. Concerning aerosols measurements, an optical particle counter (WhitE-Light Aerosol Spectrometer) is provided in order to determine aerosols size distribution and concentration in air, and a turbidimeter allows to measure the aerosols concentration collected by droplets and drained out of the vessel. A previous study (Marchand et al. 2006) under atmospheric conditions shows that droplets don't perturb the measurements with the WELAS.

Measurements of aerosols characteristics in gas, such as aerosols concentration and size, coupled

with measurements of spray characteristics, such as droplets size and velocity, will provide detailed informations for a better understanding of collection mechanisms. To date, previous studies described in the literature, undertaken on a large scale, were based on old technologies of measurements and few experiments were interested in these phenomena under well-controlled thermodynamic conditions. The aim of this work is to present results about aerosols collection efficiency by water droplets in well-controlled conditions and to compare them to the ones coming from simulations.

This paper is divided in three parts. The first one is devoted to describe the TOSQAN experimental facility and the instrumentation associated for aerosols washout characterization is presented with its qualification under severe conditions. The second part presents the results of airborne concentration and aerosols diameter evolution obtained for various configurations tests studying the influence of several parameters on the aerosols washout, such as the characteristics of the spray (water flow, droplets size), the characteristics of aerosols (size, mass injected), as well as the gases characteristics (pressure, temperature, mixture composition). Finally, the experimental results are compared to calculations performed with the severe accident code ASTEC (Accident Source Term Evaluation Code) concerning airborne mass and diameter evolution of aerosols.

Grist, D. R. Spray removal of fission products in PWR containments. *SRD-R-267*, United Kingdom Atomic Energy Authority (1982)

Marchand, D., Porcheron, E., Lemaitre, P. and Grehan, G. Characterization of the washout of aerosols by spraying water for thermal hydraulic conditions representative of a severe accident in nuclear reactor containment. *ICLASS 2006*, Kyoto, Japan (2006)

Porcheron, E., Brun, P., Cornet, P., Lemaitre, P., Malet, J., Nuboer, A. and Vendel, J. Experimental study of water spray interaction with air/steam mixture using optical diagnostic, applied to nuclear reactor safety in TOSQAN facility. *ICMF'04*, Yokohama (2004)

## Evaluation of Neutral Cluster and Air Ion Spectrometer (NAIS)

S. Mirme, A. Mirme, E. Tamm and J. Uin

Institute of Environmental Physics, University of Tartu, Estonia, 50090, Tartu, Estonia

Keywords: aerosol spectrometry, aerosol measurement, instrumentation, air ions, cluster ions

A Neutral cluster and Air Ion Spectrometer NAIS developed by Airel Ltd., Estonia is based on air cluster ion spectrometer AIS (Mirme et al., 2007). NAIS can be used to simultaneously measure electrical mobility distribution of positive and negative air ions (mobilities in the range of  $3.2$  to  $1.2 \cdot 10^{-3} \text{ cm}^2 \text{ V}^{-1} \text{ s}^{-1}$  and  $-3.2$  to  $-1.2 \cdot 10^{-3} \text{ cm}^2 \text{ V}^{-1} \text{ s}^{-1}$ ). NAIS can also measure size distribution of aerosol particles in the particle size range about  $0.8$  to  $40$  nm (Millikan diameter). Ions and particles can be measured almost simultaneously by running the instrument alternately in the corresponding operating modes with a 1 minute period (minimum).

NAIS consists of two mobility analyzers with 21 parallel measurement channels each. In ion measurement mode the air sample is measured without any treatment. If running in aerosol measurement mode, chargers placed in front of the analyzers are also activated.

The calibration of NAIS includes the verification of sizing and concentration measurements in both ions and particles modes. The instruments are verified using the calibration setup of the University of Tartu (Mirme, 2007).

Silver particles in the size range of  $2$  to  $40$  nm were generated with an oven type generator. The mobility classified particles were used directly as single charged ions for ions mode calibrations. The classified particles were neutralized for particles mode calibrations.

The calibration has been made on the basis of the mathematical model of the instrument. The particle/ion loss factor and charging efficiency were assessed from experimental data.

Measurement performance of a prototype of NAIS was extensively tested with the facilities of University of Tartu. In cluster ion range (ion mobility  $> 0.3 \text{ cm}^2/\text{V/s}$ ) the measured concentration agrees well with an ion counter at concentrations ranging from  $50\,000$  to ambient background level of  $600 \text{ #}/\text{cm}^3$ . NAIS was tested in ions mode using mobility classified aerosol as single charged air ions in the particle diameter range of  $1.4$  to  $20$  nm. In particles mode the mobility classified and neutralized aerosol was measured. The sizing and the concentration estimates agreed with the expected values also quite well down to particle size of  $3$  nm (Figure 1). At  $2$  nm size and below the distribution of cluster ions of the NAIS charger and the distribution of the calibration particles overlap and skew the estimate. It is possible to detect particles with diameters of  $2$  nm and less with fine adjustment of NAIS filtering.

The measurement of  $10$  nm classified aerosol produced a quite regular distribution for both polarities (Figure 2). The tail at  $5$  to  $15$  nm may be caused by imperfections of the classifier, turbulence in the analyzer or undercompensation of multiple charges on particles.

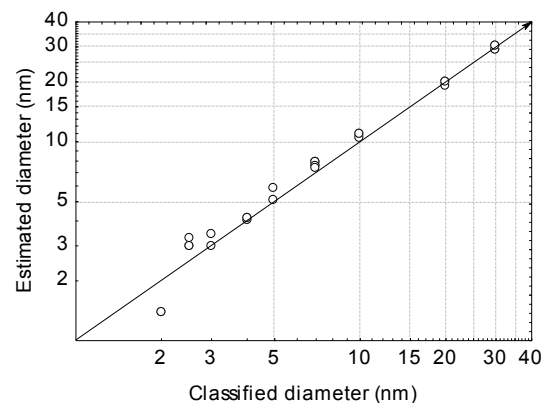


Figure 1. Sizing of aerosol particles by NAIS and by aerosol classifier

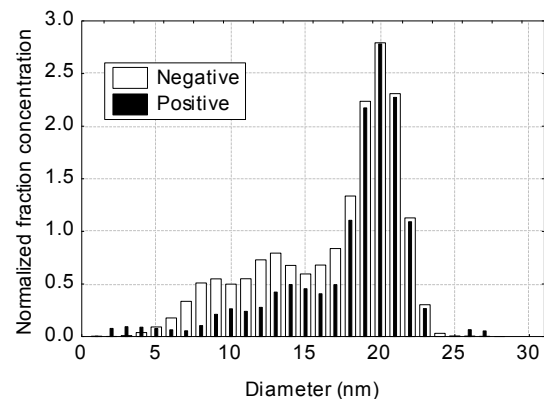


Figure 2. Sizing of mobility classified  $10$  nm aerosol measured simultaneously with negative and positive analyzers

This work was supported by the Estonian Science Foundation grants no. 5387, 5855 and 6988.

Tammet, H., Mirme, A., Tamm, E. (2002) Electrical aerosol spectrometer of Tartu University. *Atmos. Res.* 62, 315–324. doi:10.1016/S0169-8095(02)00017-0.

Mirme, A., Tamm, E., Mordas, G., Vana, M., Uin, J., Mirme, S., Bernotas, T., Laakso, L., Hirsikko, A., Kulmala, M. (2007) A wide range multi-channel Air Ion Spectrometer. *Boreal Env. Res.* (submitted).

## Pressure controlled gas-to-gas humidification of HTDMA:s

Erik Nilsson<sup>1</sup>, Erik Swietlicki<sup>1</sup> and Don Collins<sup>2</sup>

<sup>1</sup>Division of Nuclear Physic, Lund University, P.O. Box 118, SE-221 00 Lund, Sweden

<sup>2</sup>Departement of Atmospheric Sciences, Texas A&M University, 3150 TAMU  
College Station, TX 77843-3150

Keywords: HTDMA, Aerosol instrumentation

Measurements of the hygroscopic properties of sub-micrometer atmospheric aerosol particles using H-TDMA instruments (Hygroscopic Tandem Differential Mobility Analyzers) have until now been limited to short field campaigns of maximum a few months in duration, since these instruments have not been suitable for unattended long-term operation. One limitation has been the humidification of the aerosol and sheath air flows entering the second DMA. The aim of this work is to investigate the efficiency of a gas-to-gas humidification system based on Nafion dryers, similar to that previously used by Santarpia *et al.* (2004).

For long-term measurements, for which simplicity is of essence, a closed-loop DMA sheath air flow system is preferred, giving the possibility of only humidifying the aerosol line. Relative humidity (*RH*) control with a dew point sensor implies that both the dew point temperature and the temperature of the second DMA are needed to obtain the DMA *RH*. *RH* fluctuations corresponding to double the precision of the temperature sensors are therefore acceptable (this corresponds to  $\sim \pm 0.5\%$  for ammonium sulphate at *RH* = 90%).

For this study, the response time and stability of the humidification system shown in Figure 1 was investigated. The principle is to control the *RH* by regulating the pressure of the purge flow of the second Nafion dryer (Permapure MD-110 series) with a mass flow controller between bubbled air with an *RH* close to 100% and a vacuum source. The humidification is done in two steps, allowing both deliquescence and efflorescence (*RH* hysteresis) measurements of the aerosol. The DMA tested in this study was a 50 cm Vienna type, and a small (pulse free) lamella pump for a minimal dead volume was used in the loop. There was no temperature stabilization except the lab air conditioning system.

The response time in the aerosol line is  $\sim 6$  minutes for *RH* values between 35% and 90% (around 20 min from 90% to 25%) and the long term stability of the aerosol *RH* before the DMA is well within  $\pm 0.5\%$ . In addition to this, the dead volume in the closed loop gives a significant buffering effect for the *RH* experienced by the particles passing through the DMA, adding further stabilization of the *RH*. The response time of the system going from 80% to 40% ( $\sim 20$  min) is seen

in Figure 2. Even though the *RH* stabilized, there is a constant offset of about 1.5%, which is most likely due to a temperature difference between the two measurement points.

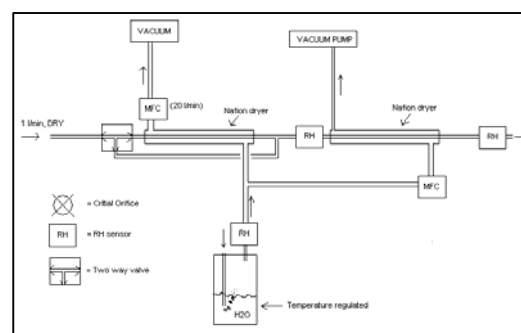


Figure 1. Humidification system.

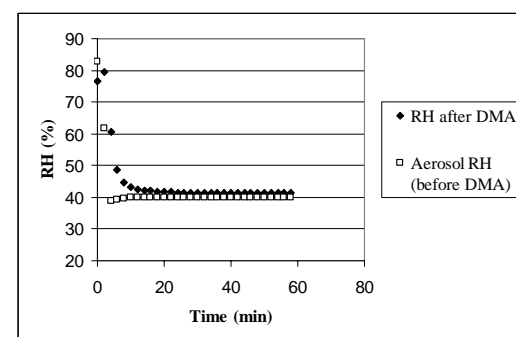


Figure 2. Response time of aerosol before and after DMA.

It was concluded that the system is capable of keeping the *RH* within the desired  $\pm 0.5\%$ , even without rigorous temperature stabilization, and the response time is acceptable for most long-term H-TDMA measurement applications.

This work was carried out within the frameworks of the EU FP6 Infrastructure Project EUSAAR and the NOS-N Nordic Centre of Excellence BACCI.

### REFERENCES

Joshua L. Santarpia, Runjun Li, and Don R. Collins 2004, *Direct measurement of the hydration state of ambient aerosol Populations*, Journal of Geophysical Research, vol. 109, D18209.

## Instrument characterization and first field test of the Portable Ice Nucleation Chamber PINC

B. Sierau, O. Stetzer, and U. Lohmann

Institute for Atmospheric and Climate Science, ETH Zurich, 8092, Zurich, Switzerland

Keywords: Aerosol-cloud interaction, Aerosol instrumentation, Atmospheric aerosol, Ice nuclei.

Ice nuclei (IN) are aerosol particles that catalyze the formation of ice crystals in clouds. Ice nuclei and ice processes are of major importance in the atmosphere as they determine the microphysical properties (e.g. concentration, shape and phase of cloud particles) and radiative properties (e.g. scattering, absorbance) of clouds and thus the earth's radiative balance.

The investigation of the role of IN in cloud processes and to understand under which conditions particles initiate ice formation is a major task of recent experimental and modelling studies. However, in situ studies of IN are rare as measurements has to be performed in/close to ice or mixed phase clouds, i.e. mostly at higher altitudes. Therefore, the **Portable Ice Nucleation Chamber (PINC)** was constructed at the ETH Zurich which is particularly designed to fulfill the requirements of aircraft and field site deployment. The PINC is a further development of the laboratory instrument ZINC (Stetzer et al., 2007) and is based on the Continuous Flow Diffusion Chamber for airborne IN measurements introduced by Rogers et al., 2001. We will present results related to the characterization of the PINC with emphasis on data obtained during a first field test of the instrument at the high altitude research station Jungfraujoch in the Swiss Alps in summer 2007.

The PINC design is based on that of the ZINC instrument which has been already deployed during a field campaign at the Jungfraujoch (CLACE-5, Feb-Mar 2006). The IN-counter consist of two main parts: The main chamber where the aerosol is exposed to a defined temperature and supersaturation with respect to ice, and a detector that counts the ice crystals that had formed in the chamber. The chamber itself consists of two opposing parallel plates held at different temperatures below the melting point of water and covered with a thin layer of ice. The temperature gradient between the chamber walls induces a supersaturation (with respect to ice) of the carrier gas with water vapour. This leads to the formation of ice crystals in case the sampled particles show the ability to act as ice nuclei at that certain temperature and supersaturation.

A schematic of the PINC set-up is shown in Figure 1: The sample flow is layered between to particle-free sheath flows to constrain the temperature and humidity the particles are exposed

to. Sheath and sample flow are controlled using mass flow controllers. Main constructional modifications of the portable instrument PINC compared to the lab version ZINC are a) the down-scaled vertical length of the main body, and b) a newly designed, two-stage lightweight cooling system. This system consists of a compressor stage and thermoelectric modules instead of open bath cryostats using a cooling liquid directly exposed to the walls.

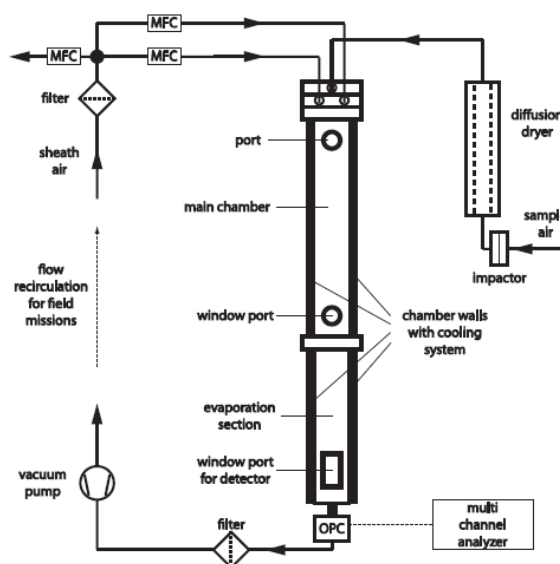


Figure 1. Schematic of the PINC set-up.

The high altitude research station Jungfraujoch is very well suited for studies of mixed-phase and ice clouds due to its elevation and a yearly cloud exposure of 37%. The results from the Jungfraujoch first have to be interpreted in the framework of a feasibility study for measuring IN in-situ using the new, modified version of the ZINC. However, the results should also give insight into the abundance of ice nuclei under the given meteorological conditions during the field campaign.

This work is supported by the Swiss GAW program and MeteoSwiss.

Rogers, D. C., et al. (2001). *J. Atmos. Ocean. Tech.*, 18, 725-741.

Stetzer, O., and Lohmann, U. (2007), submitted to *J. Aero. Sci. Tech.*

## Analysis and calibration of a small cyclone at high flow rates

J.M. Fernández-Díaz, I.A. SanJuan, M.A. Rodríguez-Braña, M. Domat

Department of Physics, University of Oviedo, C/Calvo Sotelo, s/n, E-33007 Oviedo, SPAIN

Keywords: Cyclone, respirable aerosol, aerosol cleaners

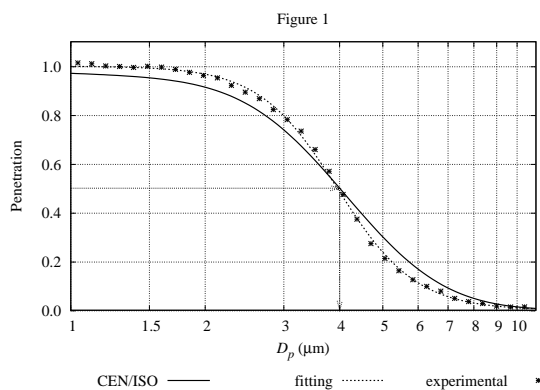
Cyclones are today very used in the aerosols field, mainly due to their easy design and making. In some cases their use is as respirable aerosol samplers; in others, as polluted air cleaners.

Despite their conceptual simplicity, the behaviour of cyclones is a partially open subject, due to turbulence and the interactions among the several parts in the flow in their non-split inside.

One of the unknowns is the behaviour of the small cyclones for high flow rates. Normally, over 20 lpm the use of the respirable aerosol samplers is not common.

Kenny and Gussman (1997) have analysed several configurations and we have chosen one of these (GK type with 56 mm internal diameter) to be made and calibrated. The prototype has been made of nylon.

We have calibrated it for 20 lpm flow rate, by using a TSI APS 3321. The results are in Fig. 1.

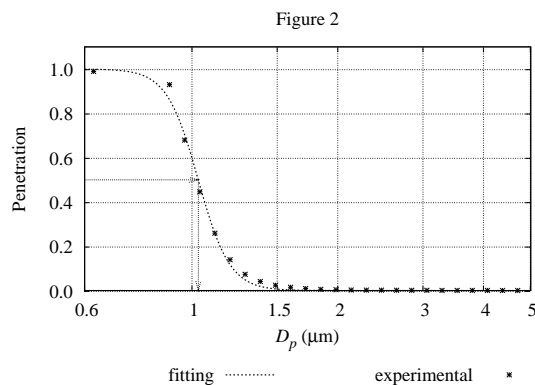


Besides, a fitting of the penetration (with two adjustable parameters,  $a$  and  $b$ ) of the form:

$$p(D_p) = \left[ 1 + a(D_p)^b \right]^{-1},$$

has been done (with a good agreement). This fitting, apart from describing the penetration curve for the cyclone in an efficient way, serves for an easy determination of the 50% cut diameter:  $D_{50} = a^{-1/b}$ . The obtained value is  $4.0 \mu\text{m}$ , in agreement with its making premise (a possible use as a respirable aerosol sampler). The curve CEN/ISO showed in the Fig. 1 has been taken from Soderholm (1989).

We have also done a calibration for a flow rate of 155 lpm. The penetration curve is shown in Fig. 2.



The experimental value for  $D_{50}$  is  $1.03 \mu\text{m}$ , far away the value of  $0.51 \mu\text{m}$  obtained with the empirical formula proposed for Kenny and Gussman ((1) in their article) for this cyclone geometry. This formula (KG(1)) proposes a very different behaviour vs. flow rates and internal cyclone diameters from the simple theory (ST) (Reist, 1993): an exponent 2 for KG vs. 1.5 for ST for the internal diameter; an exponent  $-1$  for KG vs.  $-1/2$  for ST for the flow rate.

As conclusions, this lead us to affirm that KG(1) formula is not valid for high flow rates, and that more work has to be done to explain the behaviour of GK type cyclones for high flows.

Nonetheless, we have to calibrate our cyclone for intermediate flows for ensure the different performance at high flow rates. Also an analysis with some CFD codes are in our goals to explain the behaviour of the cyclone.

We thank the Ministerio de Educación y Ciencia of Spain for support under the project MEC05CGL2005-05244/CLI.

Kenny and Gussman. Characterization and modelling of a family of cyclone aerosol preseparators. *J. Aerosol Sci.*, 28:677–688, 1997.

Reist. *Aerosol Science and Technology*. McGraw-Hill, 1993.

Soderholm. Proposed international conventions for particle size-selective sampling. *Ann. Occup. Hyg.*, 33:301–320, 1989.

## Quality factors for the optimisation of electrical mobility based particle sizers

J.M. Fernández-Díaz, M. Domat, M.A. Rodríguez-Braña, I.A. SanJuan

Department of Physics, University of Oviedo, C/Calvo Sotelo, s/n, E-33007 Oviedo, SPAIN

Keywords: particle sizers, electrical mobility, quality factor

Differential mobility analysers are one of the most important instruments in the aerosol field. In some systems they are coupled with CPC to count particles. In other cases the electrical current created in a discrete set of electrometers are continuously measured. We will focus in the latter.

With the aim of improve the instruments existing nowadays, some parameter is necessary to be used in the optimisation process.

The general formula to describe the measurement behaviour of an instrument is done by Voutilainen (2001). Applied to our case, the electrical current measured in electrometer  $j$  is done by

$$I_j = \int_{D_{p, \text{inic}}}^{D_{p, \text{fin}}} K_j(D_p) h(D_p) dD_p,$$

where  $h(D_p)$  is the particle size distribution density function and  $K(D_p)$  is the kernel of the instrument. Alofs and Balakumar (1982) provide a formula for this:

$$K_j(D_p) = e Q \sum_{n=1}^{\infty} n \phi(n, D_p) F_r(D_p, n, j),$$

where  $e$  is the unit charge,  $Q$  the flow rate,  $\phi$  a function depending on the charging mechanism and  $F_r$  the fraction of particles that arrive to the counter (in our case an electrometer). We use an auxiliary set of parameters, which depends on the kernels:

$$\sigma_{ij} = \int_{-\infty}^{\infty} K_i(\log D_p) K_j(\log D_p) d \log D_p.$$

The values of  $\sigma_{ij}$  form a sparse matrix with negligible values far away the main diagonal (see Fig. 1). We define the quality factor as:

$$g = \sum_i \sum_{j < i} \frac{\sigma_{ij}}{\sqrt{\sigma_{ii} \sigma_{jj}}}$$

We have also analysed others possible definitions, but this is the better we found: it diminishes as the ‘interaction’ among electrometers decreases, and as the current measured in each electrometer increases.

For some geometrical design, results for several electrometer configurations are presented in Fig. 2, vs. the flow rate, for constant voltage. As we can see the positioning and size of the electrometers is a very important factor: the case with all electrometers constant on size is similar to a random one;

the better configuration is with electrometers increasing in size from the entrance of the flow, following a quadratic or cubic function.

This is an important conclusion for improving the current designs of these instruments, which should be modified accordingly.

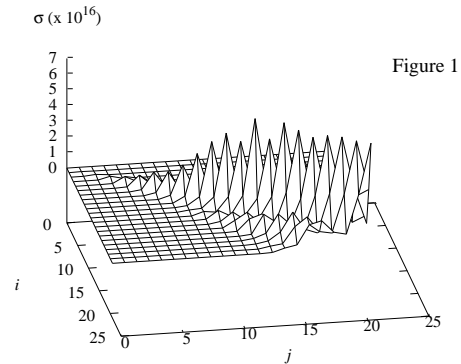


Figure 1

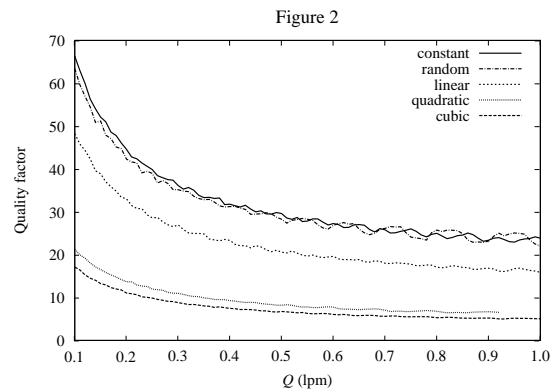


Figure 2

We thank the Ministerio de Educación y Ciencia of Spain for support under the project MEC05CGL2005-05244/CLI.

Alofs and Balakumar. Inversion to obtain aerosol size distributions from measurements with a DMA. *J. Aerosol Sci.*, 8:513–527, 1982.

Voutilainen. *Statistical inversion methods for the reconstruction of aerosol size distributions*. PhD thesis, University of Kuopio, Finland, 2001.

## Study of PM morphology using Scanning electron microscopy

R. Licbinsky<sup>1</sup>, V. Adamec<sup>1</sup>, J. Huzlik<sup>1</sup> and M. Schwarzova<sup>1</sup>

<sup>1</sup>Transport Research Centre, 636 00 Brno, Czech Republic

Keywords: morphology, particulate matter, scanning electron microscopy, shape, traffic

Information about physical properties of particulate matter (PM) is important for behaviour characterisation, source identification and possible effects on human health. The diameter and shape are the most discussed in this point of view. Some groups of particles have except typical chemical composition also the specific shape reflecting the way of formation, so it is possible to conclude the source.

Imaging of PM was done by using Scanning electron microscope VEGA TS 5136 LSU that permits both low vacuum and high vacuum mode of measurements with resolution up to 3.5 nm. PM air samples were taken on the special filters Millipore made of polycarbonate membrane (Isopore) with the 0.4  $\mu\text{m}$  size of pores. Filters are designed specially for the scanning electron microscopy (SEM) purposes with the perfectly smooth surface. Several measuring and imaging modes were tested. The image of particles smaller than 15  $\mu\text{m}$  could not be obtained for non-plated sample in the low vacuum mode of measuring. Particles became electric charged fast due to incident electron beam and they were released from the non-plated filter during the measurements of samples in high vacuum mode. PM imaging of samples with plated surface in the high vacuum mode was chosen as the most suitable way. Plated surface of the exposed filter divert the arising charge from the place of impact of the electron beam. This allows achieving the image of PM magnification at 150 thousand in the very good quality when you can precisely determine the shape of PM with diameter about 100 nm. This size correspond to the diameter of particles emitted from gasoline and diesel engines that coagulate to larger aggregates with size more than 300 nm.

Separate particles and also their aggregates were observed on filters exposed on locality with high traffic intensity where road traffic is considered to be the dominant source of air pollution. Spherical particles with diameter about 100 nm coagulated to the larger aggregates are shown in figure 1. These particles were the most frequent ones on this locality. The other particle shapes except the spherical particles were often observed on the locality that represents the wide opened area with the lot of trees. Sharp-edged particles probably of geological origin (soils) and larger spherical or elongated particles of biological origin (spore) were also often observed on the filters from this locality. The interpretation of the source only on the basis of the particle morphological

characteristics without any knowledge about chemical composition is in some cases inaccurate.

The results correspond with the data published in literature (McCullum & Kindzierski, 2001; Zongping et al., 2003; Weinbruch & Ebert, 2004), where the same shape of PM was observed and was assigned to the specific source also on the basis of chemical composition. Next step in this field of research will be aimed to the taking samples on localities with more exactly defined source of particles.

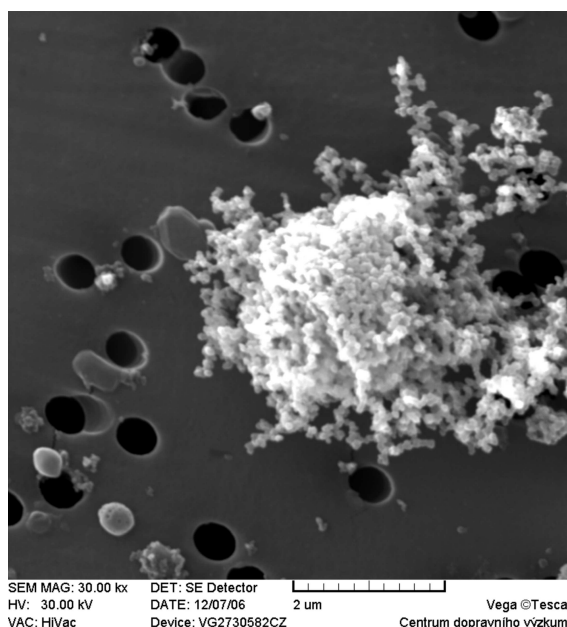


Figure 1 Spherical aggregates of particles from combustion process

McCullum, K. & Kindzierski, W. (2001) Analysis of particulate matter origin in ambient air at High Level, Alberta. Department of Civil & Environmental Engineering, University of Alberta, Edmonton, Alberta.

Weinbruch, S. & Ebert, M. (2004) Source apportionment of atmospheric aerosols based on electron microscopy, Technical University of Darmstadt.

Zongping, P., Baoping, H., Hanhu, L., Xiaoyan, J., Hongyan, H., Yunjian, L. (2003) Study on Application of SEM in Source Apportionment for Urban Ambient Particulate Matter, China University of Mining & Technology, Xuzhou.

## On-line measurements of industrial minerals' particle size during milling

K.Tousimi<sup>1</sup>, C.Pagkoura<sup>1</sup>, O.Makridou<sup>1</sup>, C.Agrafiotis<sup>1</sup>, A.G.Konstandopoulos<sup>1</sup>, G.Zannis<sup>2</sup>, M.Founti<sup>2</sup>

<sup>1</sup>Aerosol and Particle Technology Laboratory (APTL), Center for Research and Technology-Hellas, Chemical Process Engineering Research Institute (CERTH/CPERI), Greece

<sup>2</sup>Laboratory of Heterogeneous Mixtures and Combustion Systems, Thermal Engineering Section, Mechanical Engineering Department, National Technical University of Athens (NTUA), Greece

Keywords: on-line measurements, particle size distribution, optical particle counter, industrial minerals, milling

During the industrial process of minerals' size reduction, it is very important to monitor end-product specifications, such as size distribution, in order to improve, not only the final quality of the product, but also the efficiency of the process, resulting in a lower energy consumption and a more cost-effective production. The use of reliable, non-intrusive experimental techniques, especially in the micro-scale, is essential for the on-line measurement of powders particle size. Particle Counter Sizer Velocimeter (PCSV, Process Metrix), developed for on-line measurements of aerosols in industrial environments, is an individual particle counting instrument, measuring the scattered light in the near forward direction. In the present study, the applicability of PCSV for on-line particle size measurements was investigated, for the case of milling of olivine ores. The milled olivine powders are used for the development of catalysts for the treatment of noxious gas effluent streams.

Two grades of olivine, of initial particle size <0.75mm and <0.1mm respectively, were ground in a pilot-scale ring mill under various process parameters, in order to investigate their effect on particles' size reduction. Three feeding rates of the raw material, 10kg/h, 30kg/h and 50 kg/h and three rotational speeds of the mill's motor, 600 rpm, 800 rpm and 1000 rpm, were applied. PCSV was adapted to a bypass of the suction pipe transporting pneumatically the air-suspended milled materials from the exit of the mill to the airbag of the system. The results were evaluated using the Sauter Mean Diameter  $D(3,2)$  and the normalized log-normal volume distribution  $dV(dp)/d(\ln dp)$ , where  $dp$  is the particle diameter.

The obtained results, in terms of  $D(3,2)$  of olivine as a function of its feeding rate at constant mill's rotational speed and as a function of the mill's power consumption at constant feeding rate, showed that there is a linear dependence of particles' size with the above parameters.  $D(3,2)$  becomes higher as the feeding rate increases, indicating that, when a constant power is provided to the system, the grinding effect varies inversely with the quantity of the materials to be milled. On the other hand, it was shown that finer final particle size can be achieved at the expense of extra energy consumption.

In terms of distributions, the corresponding geometric diameters of the 4-peak normalized log-normal volume distributions were calculated, using the theoretical probability density function (PDF), for different mill's rotational speeds and olivine feeding rates. It was found that the milling of all samples has resulted in their particle size reduction from hundreds to tens of micrometers in less than 15s. Moreover it was found that, for the same milling conditions, the final size of the milled particles depends on the raw material's initial size distribution.

Finally, in order to confirm the results of the on-line / in-situ PCSV measurements, "ex-situ" particle size measurements were performed on representative samples, taken at the exit of the mill and corresponding to each set of the milling parameters, using the following instruments: a) Low Angle Laser Light Scattering Analyzer (LALLS, Malvern Mastersizer-S and Mastersizer 2000), b) Particle Size Distribution Analyser (PSD 3603, TSI) and c) Particle Counter Sizer Velocimeter (PCSV). Scanning Electron Microscope (SEM) Image Analysis was also performed. An agreement among the ex-situ techniques was observed, with small differences attributed to their different operating principles.

A good agreement between in-situ and ex-situ measurements was found. Only in some cases on-line measurements resulted in higher sizes than the ex-situ ones. These differences were attributed to the sampling process of the milled materials, driven through the PCSV, as well as to the bypass's air flow/ dilution system and indicate the possible points of improvement during on-line monitoring in industrial environments.

This work has been funded in part by the Greek General Secretariat for Research and Technology through the VALORMIN – 2003 EPAN program.

G. Zannis, M. Founti, P. Makris (2006) in *Proc. QIRT 2006*, Padova, Italy

D. Holve, S.A. Self (1979). *Applied Optics*, 18, 1632-1645.

F-M Etzler, M. Sanderson (1995). *Part. Part. Syst. Charact.*, 12, 278-282.

K. Willeke, P. Baron (1993). *Aerosol Measurement*, John Wiley & Sons, Inc., USA

## Theory of optical differential mobility analyzer

S. B. Kim<sup>1</sup>, D. K. Song<sup>2</sup> and S. S. Kim<sup>1</sup>

<sup>1</sup>Department of Mechanical Engineering, KAIST, 373-1 Guseong-dong, 305-701, Daejeon, South Korea

<sup>2</sup>Department of Environmental Engineering, Kumoh National Institute of Technology,  
1 Yangho-dong, 730-701, Gumi, South Korea

Keywords: optical instrumentation, optical properties, refractive index, size measurement, trajectory.

In the present study, we propose and discuss the possibility of developing an optical mobility analyzer and provide a theoretical description for classifying colloidal particles under selected operating conditions. For this purpose, the concept of optical mobility in a radiation field is defined and the derivation of the probability function (or the transfer function) for finding a colloidal particle having a specific optical mobility in an optical differential mobility analyzer (ODMA) is presented. As a result, we describe an ODMA that can be easily adapted for use in the current and widely-used microfluidic lab-on-a-chip system.

Kim et al. calculated trajectories of particles in the radiation field and derived retention distance. Figure 1 shows their results. When particles pass through radiation field, the positions of particle deviate from their initial position and remain at the retention distance. The retention distances depend on optical mobility of particles.

Based on these results, we derived concept of optical differential mobility analyzer. In optical differential mobility analyzer, the radiation field acts as electric field in the conventional electrical mobility analyzer. Therefore we can find similarity between optical and electrical mobility analyzer. To show the similarity, we derived transfer function of optical mobility analyzer. As shown in figure 2, the transfer function of the optical differential mobility analyzer has same shape and property with electrical mobility analyzer.

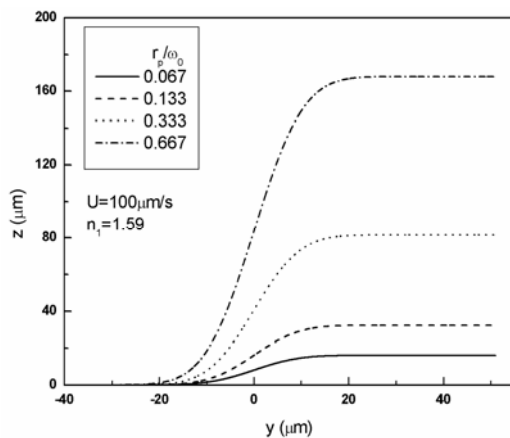


Figure 1. Trajectories of particles of different size in the optical differential mobility analyzer.

The optical mobility analyzer has many advantages as a biological cell separation device. Due to its non-contact property, radiation force can be applied to cell separation without mechanical damages on living cells. And, in optical differential mobility analyzer uses laser light as source of radiation force, we can also measure scattering signal from particles. Therefore particle size, optical property and mobility of particle can be determined simultaneously.

Furthermore, the optical mobility analyzer can be used in microfluidic lab-on-a-chip since it can be miniaturized easily.

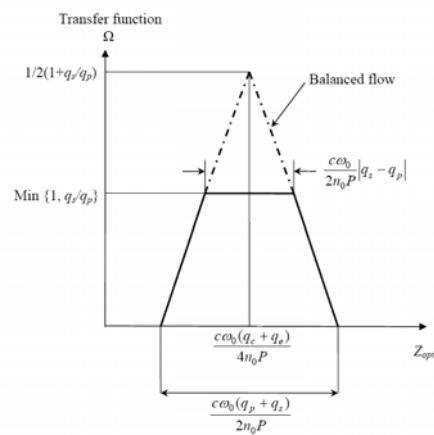


Figure 2. Transfer function of the optical differential mobility analyzer.

The authors express their gratitude for support through a grant from the Brain Korea 21 program of the Ministry of Education. This work was partially supported by the Korea Research Foundation Grant funded by the Korean Government (MOEHRD, KRF-2006-214-D00015).

Kim, S. B., Kim, J. H. & Kim, S. S. (2006). *Appl. Opt.* 45, 6917-6924.

Kim, S. B. & Kim, S. S. (2006). *J. Opt. Soc. Am B*, 23, 897-903.

Knutson, E. O. & Whitby, K. T. (1975). *J. Aerosol Sci.*, 6, 443-451.

**A DMA covering the 1-100 nm particle size range with high resolution down to 1 nm**

Fernández de la Mora, J. Yale University, Mechanical Engineering Department, USA.

Attoui, M., Département de Physique, Université Paris 12, France

Key word : nanoparticles, DMA, wide size range

The DMA sketched in fig 1 has been built and tested with an aim to cover the particle diameter range from 1 nm to 100 nm, while achieving narrow peak widths even at 1 nm (FWHM < 0.04). While DMAs with a size range below 20 nm have shown considerably narrower transfer functions (~ 1%), this is the first DMA having both full size range and excellent resolving power at 1 nm. Its dimensions are comparable to those of the Vienna DMA, though a conical inner electrode similar to that previously used by Rosser and Fernandez de la Mora (2005) enables laminar operation at high Reynolds numbers, even with a relatively long working section. We use a new widely open sheath gas exhaust system that produces essentially no pressure drop, permitting sheath gas flow rates  $Q$  well above 4000 lit/min. The DMA is operated in a "safe" mode with the inner electrode at high negative voltage, and a "leaky" insulator connector bringing the sample aerosol back to ground voltage. Several such leaky insulator designs have been tested. The transmission with particles (ions) 1nm in diameter is indistinguishable from that of a metallic tube of the same length in a stand alone voltage change system. But, for unclear reasons, a similar performance in the DMA requires aerosol outlet flow rates several times larger. The DMA is designed to accept aerosol flow rates of 100 lit/min, but has been tested only up to 30 Lit/min, with excellent performance.

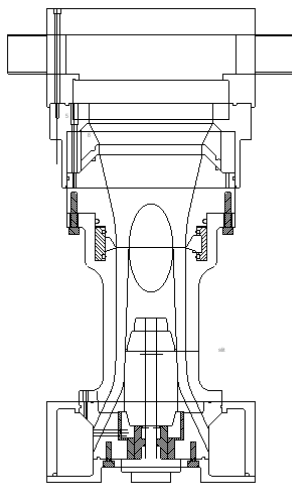


**Figure 1:** Sketch of the DMA

The performance of the instrument has been tested at varying  $Q$  with monomobile ions generated by electrospray. Figure 2 shows to the left (filled symbols) the mobility spectrum from tetraheptyl ammonium bromide, where a monomer ( $Z_1 = 0.95 \text{ cm}^2/\text{V/s}$ ) and a dimer peak ( $Z_1/Z_2 \sim 1.5$ ) are well resolved from each other at  $Q = 290 \text{ Lit/min}$ . This

spectrum reveals a DMA constant  $ZV/Q = 0.061 \text{ cm}^{-1}$ . The open data to the right are for the pure ion Heptyl $_4\text{N}^+$ , each peak corresponding to a different  $Q$ , varying from left to right from 990 to 2160 L/min.

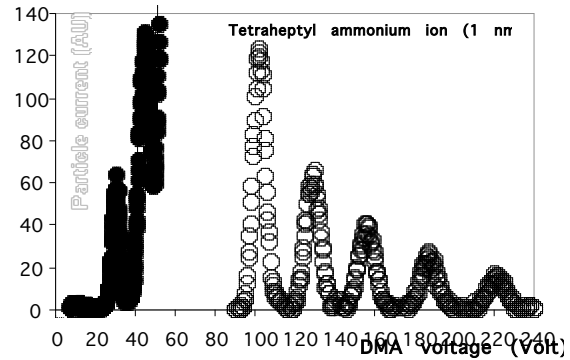
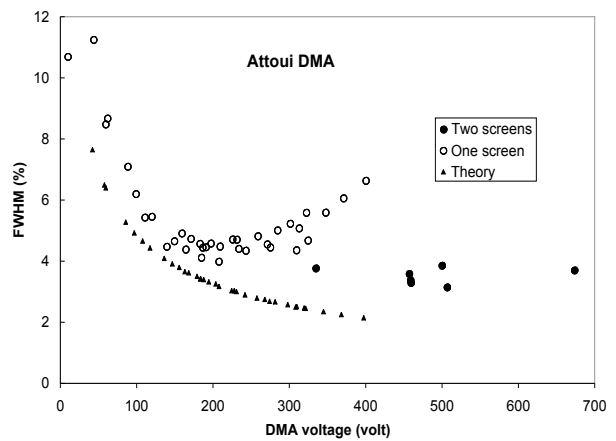


**Figure 2** Tests of the DMA performance with monomobile ions, with  $290 < Q \text{ (Lit/min)} < 2160$ . FWHM = 4.6% for the rightmost peak.

An extended performance test of has been carried out with  $Q$  in excess of 4000 lit/min, and with other ions, the largest of which is the dimer of tetradodecyl ammonium bromide ( $Z = 0.5 \text{ cm}^2/\text{V/s}$ ). The results are shown in figure 3, where the theory line is for Brownian broadening alone. One can see that use of two laminarization screens is necessary for best performance (FWHM < 3.7%), but the resolution is otherwise reasonably close to theory.

**Figure 3:** Performance tests at  $Q$  in excess of 4000



Lit/min, including data with larger ions.

In conclusion, thanks to its large dimensions and an unconventionally large sheath gas flow rate, this DMA covers the full 1-100 nm size range with exceptional resolution at 1 nm

S. Rosser and J. F. de la Mora (2005) Vienna-type DMA of high resolution and high flow rate, *Aerosol Sci. and Technology*, 39 (12): 1191-1200.

## **Laser-based measurement systems for size-dependent particle composition**

C. Fricke-Begemann<sup>1</sup>, T. Kuhlen<sup>1</sup>, N. Strauß<sup>1</sup> and R. Noll<sup>1</sup>

<sup>1</sup>Fraunhofer-Institut für Lasertechnik, Steinbachstr. 15, 52074 Aachen, Germany

Keywords: chemical analysis, elemental composition, optical instrumentation, ELPI, DMA.

Laser-based measurement techniques have been developed to measure size-dependently the elemental composition of fine and ultrafine aerosol particles.

Laser-induced breakdown spectroscopy (LIBS) is a measurement technology for chemical analysis which uses a focussed pulsed laser beam that evaporates and thermally excites a small amount of material. The radiation emitted from the excited material is measured with a spectrometer and due to the characteristic spectral lines of the elements it allows to determine the composition of the material under investigation. LIBS can be applied directly to solids, liquids and gases, and it is used in a wide range of applications. The applicability of LIBS for rapid online analysis offers the possibility to employ this method for real-time in situ aerosol analysis.

To measure the composition of particles using LIBS, we demonstrate the realisation of two different approaches. Firstly, the particles are collected in size-fractions ranging from 30 nm to 10 µm using an electrical low pressure impactor, which measures the size distribution at the same time. These samples are analysed consecutively using LIBS. The measurements are calibrated with artificially produced aerosols from defined aqueous solutions. First analyses of emission samples show a good agreement with ICP-MS analysis.

For direct analysis of airborne particles a different technique is demonstrated. The LIBS method is applied to aerosols which are transferred by a gas stream into a measurement chamber where they are evaporated in the gas stream into a laser-induced plasma. The short response time of the instrument allows measurements with a time resolution below one second. When the aerosol gas stream is guided previously through an electrostatic classifier, the particle composition is determined with respect to the particle size.

Our first measurements focussed on the abundance of heavy metals, e.g., cadmium, copper and zinc, in particles from industrial emissions and show a strong size-dependence of the concentrations of most elements. This is dependent on the source of the particles and enables the source apportionment and assessment of emissions.

This work was supported by the EU Research Fund for Coal and Steel under contract number RFS-CR-04049.

## Intercomparison of measurement techniques for black or elemental carbon under urban background conditions in wintertime

R. Hitzenberger<sup>1\*</sup>, P. Reisinger<sup>1</sup>, A. Wonaschuetz<sup>1</sup>, A. Petzold<sup>2</sup>, H. Bauer<sup>3</sup>, N. Jankowski<sup>3</sup>, H. Puxbaum<sup>3</sup>, X. Chi<sup>4</sup>, W. Maenhaut<sup>4</sup>

<sup>1</sup> Faculty of Physics, University of Vienna, Boltzmannngasse 5, A-1090 Vienna, Austria. <sup>2</sup> Institut für Physik der Atmosphäre, DLR Oberpfaffenhofen, Germany.

<sup>3</sup> Inst. for Chem. Technologies and Analytics, Vienna University of Technology, Getreidemarkt 9, A-1060 Vienna, Austria. <sup>4</sup> Institute for Nuclear Sciences, Ghent University, Proeftuinstraat 86, B-9000 Gent, Belgium.

Keywords: Black Carbon (BC), Elemental Carbon (EC), wood combustion.

Black carbon (BC) and elemental carbon (EC) are important fractions of the atmospheric aerosol because of their light absorbing properties (IPCC, 2001) and possible health effects. Despite all the efforts during the past 20 years, however, no globally accepted standard measurement methods exist. At this time, measured values of BC and EC concentrations are still method specific and can differ widely (e. g., Schmid *et al.*, 2001; ten Brink *et al.*, 2004).

In an earlier study at the same site under summer conditions, the agreement between optical and thermal measurement methods was quite good (Hitzenberger *et al.*, 2006). Campaign average values determined with different methods agreed within their standard deviations.

In order to investigate the effect of the different measurement methods on BC (or EC) concentrations also under winter aerosol conditions, the present study was performed in February and March 2006 on the roof (35 m above ground) of the building of the Institute for Experimental Physics, which is located in downtown Vienna. Ambient urban aerosol was sampled on filters (pre-heated quartz fibre filters and MSI polycarbonate filters with 0.2 µm pore size). Sampling times were approximately 24 hours. The sampling substrates were analyzed for EC using a thermal-optical method (Schmid *et al.*, 2001), the Cachier method (Cachier *et al.*, 1989) and a thermal-optical transmission method using two different temperature protocols, one commonly used in Sunset instruments (Birch & Cary, 1996) and one with a lower temperature in the first phase (Schauer *et al.*, 2003). The filters were analyzed for BC using a filter transmission method similar to the aethalometer (Hansen *et al.*, 1984), the multi-angle absorption photometer MAAP (Petzold & Schönlinner, 2004) and the integrating sphere method (Hitzenberger & Tohno, 2001). Total carbon (TC) was determined with the method developed by Puxbaum and Rendl (1983) and also with the thermal-optical transmission method.

In this study, agreement between the methods was found to be much worse, with largest differences between the thermal methods. The optical methods

agreed reasonably well during the whole campaign. On days with low temperatures, the differences in the methods (especially in the thermal methods) were found to be more than a factor of 2. Lowest concentrations were always measured with the thermal-optical transmission methods. During warmer periods, the agreement was better and comparable to the agreement in the summer study. If the BC data obtained with the integrating sphere (IS) method are corrected for the influence of biomass combustion aerosol ("brown" carbon), the agreement between corrected IS data and data measured with the thermal-optical transmission methods becomes acceptable.

Birch, M. E., & Cary, R. A. (1996). *Aerosol Sci. Technol.*, 25, 221-241.

Cachier, H., et al. (1989). *Tellus*, 41B, 379-390.

IPCC (2001). *Climate Change 2001 - The Scientific Basis*, Cambridge, UK: Cambridge University Press.

Hansen, A. D. A., et al. (1984). *Sci. Total Environ.*, 36, 191-196.

Hitzenberger, R., & S. Tohno (2001). *Atmos. Environ.*, 35, 2089-2100.

Hitzenberger, R., et al. (2006). *Environ. Sci. Technol.*, 40, 6377-6383.

Petzold, A., & Schönlinner, M. (2004). *J. Aerosol Sci.*, 35, 421-441.

Puxbaum, H., & Rendl, J. (1983). *Mikrochim. Acta*, 1983 I, 263-272.

Schauer, J. J., et al. (2003). *Environ. Sci. Technol.* 37, 993-1001.

Schmid, H., et al., (2001). *Atmos. Environ.*, 35, 2111-21221.

ten Brink, H., et al. (2004). *Atmos. Environ.*, 38, 6507-6519.

This work was supported by the Belgian Federal Science Policy Office and by internal projects of the Vienna University of Technology.

## Analysis of uncertainty in particle mass measurement using an aerosol particle mass analyzer

K. Ehara<sup>1</sup>, H. Sakurai<sup>1</sup>, A. Yabe<sup>1</sup>, N. Tajima<sup>2</sup>, and K. J. Coakley<sup>3</sup>

<sup>1</sup>National Institute of Advanced Industrial Science and Technology, Tsukuba, Ibaraki 305-8563, Japan

<sup>2</sup>Kanomax Japan Inc., 2-1 Shimizu, Suita, Osaka 565-0805, Japan

<sup>3</sup>National Institute of Standards and Technology, 325 Broadway, Boulder, CO 80305, USA

Keywords: aerosol instrumentation, particle mass measurement, aerosol particle mass analyzer, uncertainty.

The aerosol particle mass analyzer (APM) classifies aerosol particles according to their mass-to-charge ratio (Ehara *et al.*, 1996). Particle mass can be measured by use of the APM in combination with a condensation particle counter. Being a balance method, this technique is expected to attain such accuracy as required in certifying the mass and/or diameter of standard particles for instrument calibration. In the present study, we have analyzed the uncertainty in APM particle mass measurement.

The center of the mass band of particles selected by an APM,  $m$ , is given by

$$mr_c\omega^2 = \frac{qV}{\ln(r_2/r_1)}, \quad (1)$$

where  $\omega$  is the rotational velocity of the APM electrodes;  $q$  is the charge carried by the particles;  $V$  is the applied voltage;  $r_1$  and  $r_2$  are the inner and outer radii, respectively, of the annular electrode gap; and  $r_c = (r_1 + r_2)/2$ . From Eq. (1) we obtain

$$\left[\frac{u(m)}{m}\right]^2 \cong \left[\frac{u(V)}{V}\right]^2 + \left[\frac{u(r_c)}{r_c}\right]^2 + \left[2\frac{u(\omega)}{\omega}\right]^2 + \left[\frac{u(\delta)}{\delta}\right]^2, \quad (2)$$

where  $u(x)$  denotes the standard uncertainty of quantity  $x$ , and  $\delta = (r_2 - r_1)/2$ . In deriving Eq. (2), we have assumed  $\delta/r_c \ll 1$ . Substituting typical parameter values into Eq. (2), we find that the most dominant contribution to  $u(m)$  comes from  $u(\delta)$ .

In order to evaluate  $u(\delta)$ , we need to know: (a) the gap profile over the entire electrode space when the electrodes are at rest, and (b) the profile of the electrode distortion due to the centrifugal force. We have constructed an APM such that the gap profile after the electrodes are assembled can be estimated. In this design, there are four small holes bored on each of the top and bottom plates of the cylindrical electrodes, through which the gap can be measured on eight positions of the electrode space by means of ball gauges. Prior to assembling the electrodes, the geometrical profiles of the inner and outer surfaces of the outside and inside electrodes, respectively, were measured by a dial gauge, a height gauge, and a three dimensional coordinate measuring machine. From these two set of data, we have estimated the deviation of the gap from its design value of 2 mm to be smaller than 25  $\mu\text{m}$  over the entire electrode space. If we roughly assume the deviation to obey a uniform distribution with 25  $\mu\text{m}$  half width, it will result in a contribution to  $u(m)/m$  of at most 1.3 %.

Estimate of the distortion of the electrodes due to rotational motion was conducted by a numerical calculation using a finite element method program ANSYS. On the outer face of the inside electrode, we have four thin grooves parallel to the axis which accommodate partitioning rods that ensure a sample aerosol to rotate exactly at the same velocity as the electrodes. A distortion pattern obtained in the numerical calculation is given in Figure 1, which shows that a notable distortion occurs locally around a groove. At 5000 rpm, the deviation of  $r_2 - r_1$  from its design value of 2 mm is smaller than 10  $\mu\text{m}$  as seen in Figure 2, which will cause the uncertainty in  $m$  of at most 0.5 %.

The uncertainty components that are not covered by Eq. (2) include the effect of Brownian diffusion for relatively small particles, and the reproducibility in measurements. A Monte Carlo simulation of particle motion within the electrodes shows that Brownian diffusion does not significantly shift the location of the APM transfer function, even when its effect on broadening is notable. An experiment to evaluate the reproducibility in measurements is underway.

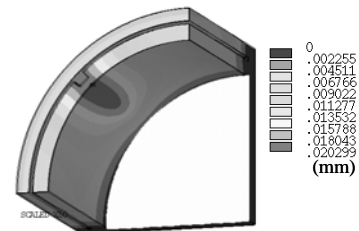


Figure 1. Profile of electrode distortion due to the centrifugal force at 5000 rpm.

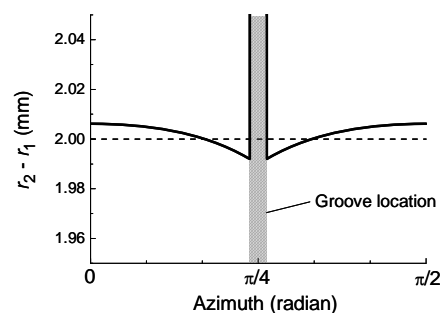


Figure 2. The electrode gap at  $z = 125$  mm when the rotational velocity is 5000 rpm.

## Modification and characterization of an expansion condensation nucleus counter for nanometer-sized particles

H. Saghafifar<sup>1,2</sup>, A. Kürten<sup>2</sup>, J. Curtius<sup>3</sup> and S. Borrmann<sup>2,3</sup>

<sup>1</sup> Physics Group, Faculty of Science, University of Isfahan, Isfahan, Iran

<sup>2</sup> Max Planck Institute for Chemistry, Particle Chemistry Group, Mainz, Germany

<sup>3</sup> Johannes Gutenberg University, Institute for Atmospheric Physics, Mainz, Germany

Keywords: Number Concentration, Supersaturation, Condensation, Cut-off diameter, CPC.

Number concentration measurements of ultrafine particles are necessary for a number of purposes like health related studies, combustion characterization, air quality issues, as well as for studies of cloud formation and climate related aerosol effects. One suitable instrumental technique presented here is that of a newly developed type of expansion condensation nucleus counter (ECNC). This ECNC operates based on fast adiabatic expansion followed by a specifically devised way of optically measuring and deriving the particle number density for particles with sizes above a few nm [1]. As such, ultrafine particles are too small to be detected through their direct light scattering, and therefore they are first grown to sufficiently large sizes. For this the aerosol particles are humidified and pumped into a measurement chamber of length  $L$ , where they are cooled down by fast adiabatic expansion. This expansion is generated by connecting the measurement chamber to a second, partially evacuated chamber through a solenoid valve which can be opened very fast. Condensable vapors such as water -among others- cause growth of the particles to reach sizes comparable to the light wavelength of the adopted laser where Mie theory becomes applicable. In the presented ECNC setup the scattered light is continuously detected during the entire expansion. The high resolution time series of the scattering cross sections measured during the expansion process exhibits a particular "step structure". This means the monotonous increase in measured (scattered) light intensity during particle growth is interspersed with several short disjunctive periods of intensity stagnation although the particles still grow. Exploiting these features the particle number density can be derived for each of the "stagnation steps" independently by using the equation:

$$N = \frac{E \cdot I(n)}{C_{sca,p}(n) \cdot L \cdot I_0}$$

where  $E$  is expansion factor and  $C_{sca,p}(n)$  denotes the Mie theory derived particle scattering cross section at the known size of a particular "step"  $n$ .  $I_0$  stands for the initial laser light intensity,  $I(n)$  for the scattered light intensity measured at "step"  $n$  and  $L$  is the length of expansion chamber. Consequently this counter principle provides an absolute measurement

of the number density of ultrafine particles, without need for calibration factors. The particle growth rate depends on the amount of supersaturation attained during expansion inside the measurement chamber. By measuring pressure before and after expansion (utilizing an additional pressure sensor at the chamber) it is possible to observe the pressure variation as function of time and obtain the expansion ratio. Since the supersaturation is dependent on the relative humidity, a corresponding sensor is included in a bypass used for providing a quasi-continuous flow through the counter. The amount of supersaturation determines the smallest particle size detectable by the ECNC. A precise orifice behind the vacuum chamber allows control of the desired expansion values. Thus different cut-off sizes are obtained corresponding to different supersaturations. Laboratory experiments with nanoparticles consisting of tungsten oxide and sulfuric acid are presented for defining the ECNC cut-off sizes at various supersaturations. It is shown that the lowest cut-off sizes can be less than 3 nm for a high expansion ratio while it can be higher (e.g. 7 nm) at lower adjusted expansion ratios. This opens options for size distribution measurements. The Kelvin diameters can be determined experimentally and compared with theoretical curves for the measured values of relative humidity.

The newly designed ECNC is capable of detecting particles smaller than 3 nm in diameter was also used for measurements in ambient air concurrent data from this instrument and a TSI UCPC 3025A are presented. The results show an excellent correspondence and agreement over long periods of time.

1- Kürten A., Curtius, J., Nillius, B., Borrmann, S.(2005), " Characterization of an automated, water-based expansion condensation nucleus counter for ultrafine particles", *Aerosol Science and Technology*, 39, 1174-1183.

## Calibration of a differential mobility spectrometer.

J.P.R. Symonds and K.St.J. Reavell

Cambustion Ltd, J6 The Paddocks, 347 Cherry Hinton Road, Cambridge CB1 8DH, U.K.

Keywords: Instrumentation, Aerosol Measurement, Charged Particles, Soot Agglomerates, Size Distribution

The Cambustion DMS500 (Reavell *et al.*, 2002) and DMS50 (Rushton *et al.*, 2007), along with the TSI EEPs and FMPS, are fast response differential mobility spectrometers, which classify aerosol particles by electrical mobility with 22 electrometers after charging with a unipolar diffusion charger (Figure 1).

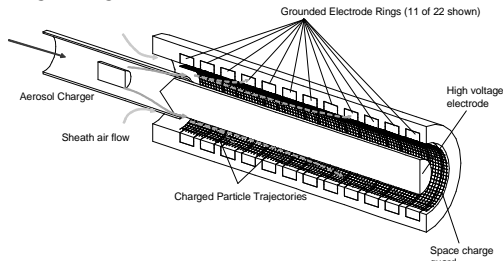


Figure 1. DMS500 schematic

The starting calibration for the DMS is achieved using a Monte-Carlo simulation of the trajectory of particles in the classifier, based upon an assumed charge distribution. Size calibration is then adjusted using traceable polystyrene latex (PSL) spheres for  $D_p > 50$  nm, and checked after calibration for certification with PSL ( $D_p > 50$  nm) and by comparison with an SMPS using sulphuric acid and salt aerosols ( $7 < D_p < 50$  nm). As well as a discrete spectral output, the DMS series offers a real-time multi-lognormal fit giving CMD,  $\sigma_g$ , and concentration for each aerosol mode (Symonds *et al.*, 2007). This proves invaluable for calibration, as an unambiguous peak position is returned (even with a large surfactant mode present), as well as giving much improved spectral resolution for PSL aerosol measurement, down to  $\sigma_g = 1.05$  (Figure 2).

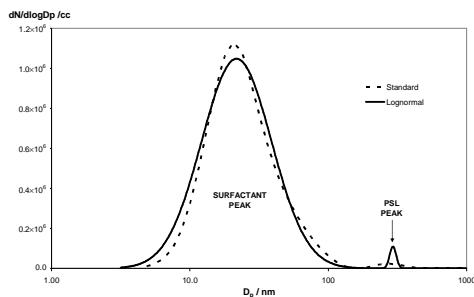


Figure 2. Resolution of PSL aerosol

Any gain calibration adjustment is made by sampling DMA charged and cut aerosol into both the DMS and

an electrometer (a similar method to the calibration of CPCs).

Even for a bipolar charging based device (such as the SMPS), differences in particle charging can cause inaccuracies when agglomerates are sampled with a device calibrated for spherical aerosols (Lall & Friedlander, 2006). A comparison with DMA cut engine agglomerates reveals some differences in size classification (for  $D_{me} > 100$  nm) between a unipolar diffusion charging electrical mobility instrument (e.g. DMS) and the bipolar charging DMA (Figure 3).

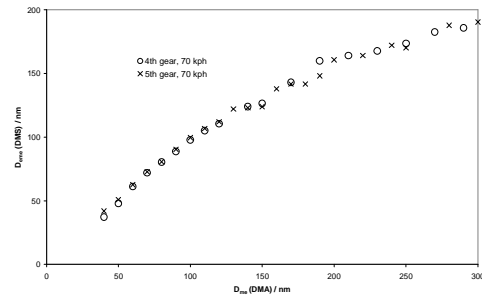


Figure 3. Comparison of DMA mobility classified and electrical mobility classified diesel agglomerates.

These differences are consistent with agglomerates gaining more charge than would be expected for spheres. This is also reflected in the gain for agglomerate particles larger than 100 nm.

The DMS's lognormal data inversion allows for separate calibrations for each mode in the spectrum to account for these effects. For example, for Diesel emissions, the assumed spherical nucleation mode and the agglomerate accumulation mode can have different calibrations.

Finally, the possibility of a direct particle mass calibration using a Centrifugal Particle Mass Analyser is examined.

Lall, A.A. & Friedlander, S.K. (2006), *J. Aerosol Science*, 37, 260–282

Reavell, K., Hands, T. & Collings, N. (2002). *SAE Technical Paper*, 2002-01-2714.

Rushton, M.G., Symonds, J.P.R., Nickolaus, C.D. & Reavell, K.St.J. (2007), *proc. 17<sup>th</sup> CRC On-Road Vehicle Emissions Workshop*.

Symonds, J.P.R., Reavell, K.St.J., Olfert, J.S.,

Campbell, B.W. & Swift, S.J. (2007), *J. Aerosol Science*, 38, 52–68.

## Generation of standard aerosols by electrical separation in a wide size range

J. Uin, A. Mirme, S. Mirme and E. Tamm

Institute of Environmental Physics, University of Tartu, Ülikooli 18, 50090, Tartu, Estonia

Keywords: aerosol generation, aerosol instrumentation, aerosol size distribution, DMA.

Standard aerosols (SA) are needed for many purposes, especially for the calibration of the particle size spectrometers. Usually the quasimonodispersed aerosols are used with known mean (median, modal) diameter  $d_m$  of the particles, particle concentration  $c_p$  and some parameter of the spectrum width. For generation of the SA, electrical classification of the particles from a polydispersed aerosol (PA) is one of the most applicable methods. A steady-state charge distribution of the particles of PA is created in the symmetrically bipolar atmosphere of the light air ions and the particles in a narrow interval of their electrical mobility are separated by electrical classifier (Liu & Pui, 1974).

For small particles ( $d_m < 50$  nm) this method is correct and almost only usable method. But in case of bigger particles the multiple electronic charges on a fraction of the particles are unavoidable, and SA comprises a fraction of the bigger particles. Tamm (1992) formulated the requirements for PA, to minimize the effect of the multiple charges.

Here we describe a method for the perfect elimination of the effect of multiple charges. The steady-state charge distribution was created on the small particles from the condensation generator, and these nuclei were grown in the modified La Mer type condensation generator (growth chamber). As the small nuclei are singly charged, the final SA contains only singly charged particles.

In the experiments silver particles with  $d_m \approx 30$  nm (nuclei) were generated and then passed through a DOP growth chamber and a  $^{239}\text{Pu}$  neutralizer. The grown particles with diameters about 110 nm were then led to a Vienna design based DMA and a Faraday cup electrometer. The experiments were conducted using two different setups of the instruments. In the first configuration the neutralizer was placed before the DOP chamber so that the nuclei were charged. In the second configuration the neutralizer was connected after the DOP chamber, so that already grown particles were charged this time (standard configuration). In both setups the mobility distribution of the particles was then determined with the DMA.

From the mobility distribution from the first instrument configuration, the density distribution of all particles, charged and uncharged, was calculated using the charging probability for the nuclei. From this the expected mobility distributions of 1, 2 and 3 times charged particles and the total distribution were found as shown on Figure 1.

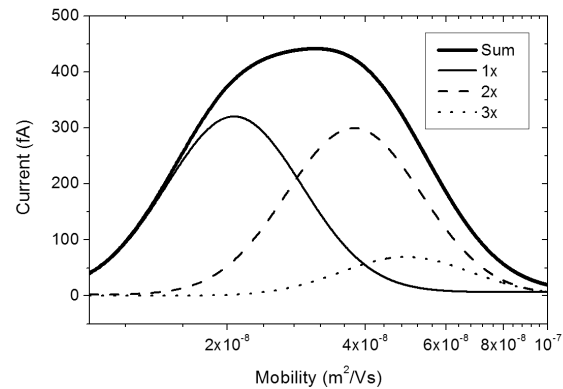


Figure 1. Expected distributions of  $n=1,2,3$  times charged particles and the total distribution.

The expected total distribution was then compared to the particles mobility distribution obtained from the second experiment configuration. Figure 2. shows the expected total distribution, the measured distribution from the second configuration and the distribution from the first configuration with mobilities normalized to the peak mobilities of the distributions. As we can see, by standard configuration we can separate the SA only from the bigger particles “tail” of the PA, the  $c_p$  of the SA is low.

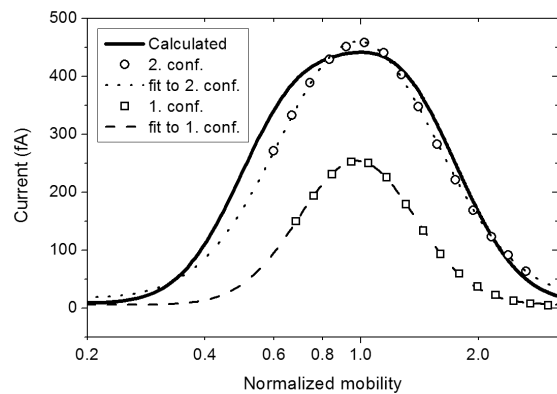


Figure 2. The mobility distributions from the 1. and 2. configuration and the calculated distribution.

This work was supported by the Estonian Science Fund under grant GFKKF 6988 and by the Doctorate School of Ecology and Environmental Sciences of the University of Tartu.

Liu, B. Y. H., & Pui, D. Y. H. (1974). *J. Coll. Interf. Science*, 47, 155-171.

Tamm, E. (1992). *J. Aerosol Science*, 23, S285-S288.

## Passive Sampler Sigma-2 as an Inlet for an Optical Aerosol Spectrometer

Felix Kohler<sup>1,2</sup>, Leander Mölter<sup>3</sup>, Eckart Schultz<sup>2</sup>, Volker Dietze<sup>2</sup>, Sven Schütz<sup>3</sup>, Hanspeter Helm<sup>1</sup>

- <sup>1</sup> Molecular and Optical Physics, Institute of Physics, University of Freiburg, 79104 Freiburg, Germany  
<sup>2</sup> Deutscher Wetterdienst (DWD), Department of Human Biometeorology, 79104 Freiburg, Germany  
<sup>3</sup> Palas<sup>®</sup> GmbH, 76229 Karlsruhe, Germany

Keywords: inlets, optical particle counter, aerosol sampling, collection efficiency, passive sampler

The sampling efficiency of an aerosol sampler considerably depends on the geometry of the inlet and meteorological conditions, in particular wind velocity. The importance of these effects grows with increasing particle size and decreasing sampling volume. Optical aerosol spectrometers typically have low sampling volumes. Reliable coarse particle measurement with an optical aerosol spectrometer therefore needs an inlet suitable for low air flows and minimizing wind effects.

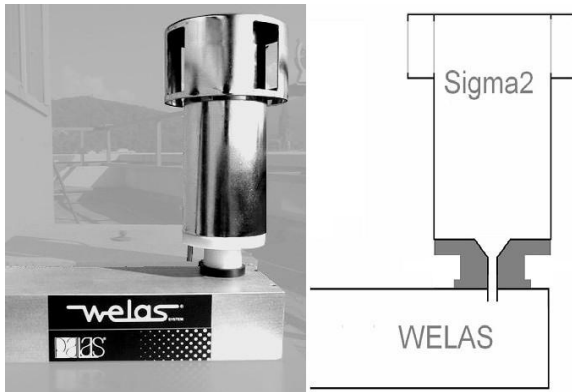


Figure 1. Sigma 2 as an inlet for the Palas<sup>®</sup> aerosol spectrometer Welas<sup>®</sup>.

For this purpose, standard sampling heads were tested: the passive sampler Sigma-2 according to VDI 2119-4, and the TSP head of the MiniVolume Sampler MiniVS (Leckel GmbH). Both were used as air inlets of the Palas<sup>®</sup> aerosol spectrometer Welas<sup>®</sup>. For comparison the Welas<sup>®</sup> was operated in parallel without sampling head, but only equipped with the unprotected nozzle. The TSP head and the Sigma-2 give shelter against settling dust and rain. The Sigma-2 additionally acts as a stilling chamber at the entrance to the Welas<sup>®</sup> nozzle.

Ratios of number concentration in Figure 2 demonstrate an increasing efficiency of collection for particles above 2  $\mu\text{m}$  in diameter if the Welas<sup>®</sup> is operated with a Sigma-2.

In a next step, settling conditions in the Sigma-2 were studied by comparing particle deposition occurring at the bottom of the Sigma-2. Deposition in the Sigma-2 was compared by using it as a passive sampler and in parallel as an inlet for the Welas<sup>®</sup>. Size segregated microscopic particle analysis showed no difference. From this result it was

concluded that the calming effect in the Sigma-2 is not affected if used as an air intake of the Welas<sup>®</sup>.

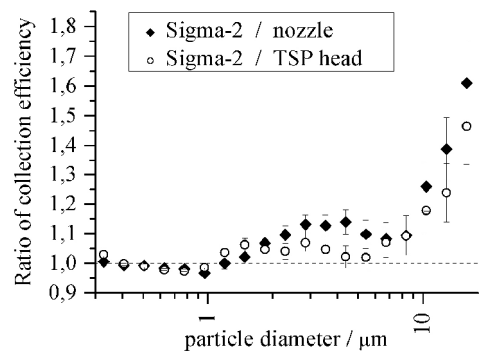


Figure 2. Ratio of collection efficiencies of the Welas<sup>®</sup> operated with different inlets determined in summer under low wind conditions.

Size fractionated coarse particle concentration was determined by active measurement with the Welas<sup>®</sup> and calculated from number deposition rate derived from microscopic particle data. Both aerosol size distributions agree pretty well (Figure 3).

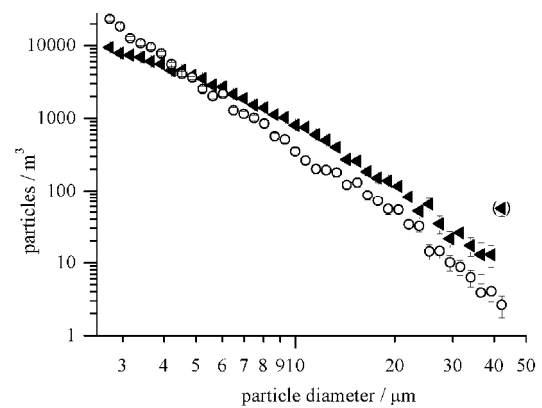


Figure 3. Particle size distributions determined with active Welas<sup>®</sup> ( $\blacktriangle$ ) and calculated from passive (collection plate in Sigma-2) (O) measurement.

From these results it is concluded, that the use of the Sigma-2 as an inlet for aerosol sampling (1) provides a calmed air volume in front of the air intake, (2) overcomes the shortcoming of a low air flow typical for optical counters and (3) by this, extends the applicability of the Palas<sup>®</sup> aerosol spectrometer Welas<sup>®</sup> to outdoor measurements.

## Design and performance evaluation of a new non-collective electrical aerosol sensor

K. Janka<sup>1</sup>, V. Niemelä<sup>1</sup>, E. Lamminen<sup>1</sup>, J. Keskinen<sup>2</sup>, A. Rostedt<sup>2</sup>, M. Lemmetty<sup>2</sup>

<sup>1</sup>Dekati Ltd., Osuusmyllynkatu 13, FIN-33700 Tampere, Finland

<sup>2</sup>Tampere University of Technology, Department of Physics, Aerosol Physics Laboratory,  
PO Box. 692, FIN-33101 Tampere, Finland

Keywords: Aerosol measurement, Corona discharge, Diesel exhaust

Dekati Ltd., together with Tampere University of Technology, Aerosol physics laboratory, Tampere, Finland and various other partners has developed a new particle charger-sensor for aerosol measurements. In this device particles are flying through a charging chamber where particles obtain a known level of electrical charge, and after this they fly away from the detector. A sensitive electrometer is used to measure the electrical charge that is leaving the detector with the particles.

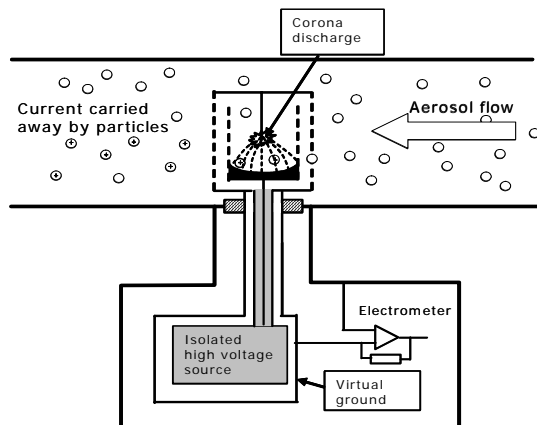


Figure 1: Simplified operational picture of the new particle sensor

In this design a corona needle is kept at zero potential (virtual ground) and the counter electrode is connected to an isolated high-voltage power supply. Inner charging chamber is a cylindrical tube with perforated walls allowing particles to go into and out from the chamber. Outer chamber walls are also perforated, but this part is kept at zero potential together with the needle. This acts as an ion trap preventing ions flying out from the sensor being detected.

Unlike in traditional aerosol chargers or surface area monitors particles are not collected into the device, therefore a term flow-through sensor can be used to describe the sensor.

When looking at the charger characteristics,  $Nt$  –product ( $N$  being ion density,  $t$  residence time inside the charging region) and theoretical charging

efficiency it is seen that the charger response depends on the aerosol flow rate in a non-linear way.

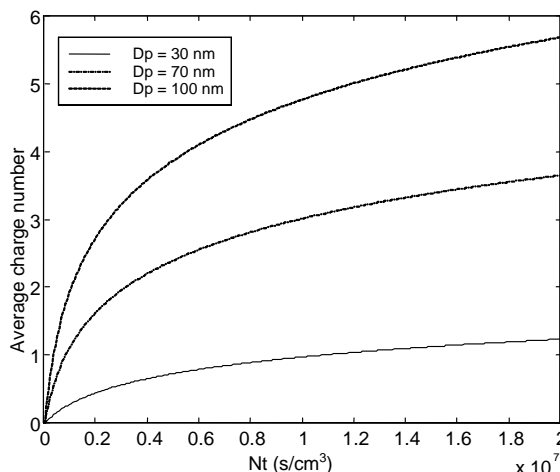


Figure 2: Theoretical diffusion charging efficiency as a function of  $Nt$  for selected particle sizes. Field charging is not taken into account

At first phase of the development the device was used in laboratory conditions where the signal was compared to other aerosol measuring equipment. Correlation with condensation nuclei counter and Electrical Low Pressure Impactor data verifies the linear response and good sensitivity of this new sensor.

Design of the instrument is done so that it can be used in very difficult environments. In first application it is used for diesel vehicle tailpipe PM emission measurements where the simplicity and robustness are important features. The whole sensor and also the charging process are inside the vehicle tailpipe. Here the flow rate is not constant and must be taken into account when data is analysed and compared to other instruments.

In this work we present the operation principles of this new instrument, laboratory data on the size- and flow rate dependent charging efficiency measurements, as well as field measurement data from diesel engines.

Finally we discuss other possible applications where this kind of detection principle can be used.

## Development and characterization of an ion trap mass spectrometer for the on-line analysis of atmospheric aerosol

J. Curtius<sup>1</sup>, A. Kürten<sup>2</sup>, A. Ehlerding<sup>2</sup>, F. Helleis<sup>2</sup> and S. Borrmann<sup>1,2</sup>

<sup>1</sup>Institute for Atmospheric Physics, Johannes Gutenberg University, Mainz, 55099 Mainz, Germany

<sup>2</sup>Max Planck Institute for Chemistry, Mainz, 55128 Mainz, Germany

Keywords: aerosol chemical composition, aerosol mass spectrometry, ion trap, aerosol instrumentation.

A novel Aerosol Ion Trap Mass Spectrometer (AIMS) for atmospheric particles has been developed and characterized. With this instrument the chemical composition of the non-refractory component of aerosol particles can be measured quantitatively. The set-up makes use of the well-characterized inlet and vaporization/ionization system of the Aerodyne Aerosol Mass Spectrometer (AMS, Jayne *et al.*, 2000). While the AMS uses either a linear quadrupole mass filter (-AMS) or a time-of-flight mass spectrometer (ToF-AMS) as the mass analyzer, the AIMS utilizes a three dimensional quadrupole ion trap (Figure 1).

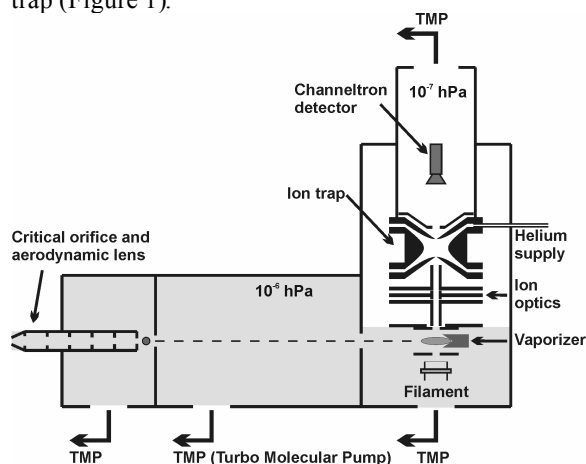


Figure 1. Schematics of the AIMS instrument.

The main advantages of an ion trap are the possibility of performing MS<sup>n</sup> experiments as well as ion-molecule-reaction studies. A filtered-noise-field can be applied to the end caps of the ion trap to remove unwanted ions from the trap. The mass analyzer has been built in-house together with major components of the electronics. The AIMS can be used as a field instrument due to its compact size. Calibrations with laboratory-generated monodisperse aerosol particles such as ammonium nitrate, ammonium sulfate and organic particles indicate a strictly linear relationship between signal response and generated aerosol mass concentration (Figure 2). The detection limits for the different chemical compounds are currently determined to be well below 1 µg m<sup>-3</sup> and we expect to be able to lower these limits by further modifications of the instrument.

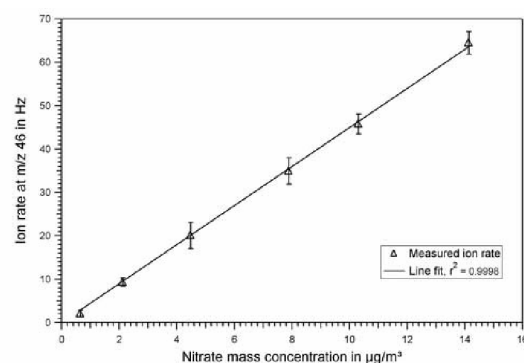


Figure 2. Calibration of the AIMS instrument with laboratory-generated ammonium nitrate aerosol. A strictly linear relationship ( $r^2 = 0.9998$ ) between the ion rate and the generated nitrate mass concentration is observed.

Our studies demonstrate the suitability of the AIMS to measure the chemical composition of the non-refractory fraction of atmospheric aerosol particles. The AIMS can be operated with a large mass range (1000 amu) to detect large molecular ions. Additionally, it can be operated with high mass resolution (1500), allowing, for example, the differentiation between ions of identical integer m/z ratio such as C<sub>3</sub>H<sub>7</sub> (m/z 43.054754) and C<sub>2</sub>H<sub>3</sub>O (m/z 43.018342). The inter-comparison of the AIMS with a regular Aerodyne -AMS in urban air yields good agreement.

The application of soft ionization methods such as low energy electron impact and VUV ionization in combination with the MS/MS-method using collision-induced dissociation (CID) for the identification of specific organic aerosol compounds will be presented.

Support by the German Research Foundation within the Interdisciplinary Research Training Group Program 826 Trace analysis of elemental species: Development of methods and applications and by the Swedish Research Council is greatly acknowledged.

Jayne, J. T., Kürten, A., Curtius, J., Davidovits, P., Smith, K. A., Kolb, C. E., and Worsnop, D. R. (2000), *Aerosol Sci. Technol.*, 33, 49 - 70.

## Measurement Instruments for Optical Absorption Spectra of Aerosol by Photoacoustic Spectroscopy

C. Haisch, P. Menzenbach, R. Niessner

Chair for Analytical Chemistry, Technische Universität München,  
Marchioninistrasse 17, D-81373, Munich, Germany

Keywords: photoacoustic, absorption coefficient, instrumentation

Optical properties of aerosol particles play an important role for the radiation balance of the earth's atmosphere. Light scattering can be monitored routinely on different wavelengths by several commercial instruments. Light transmission measurements only allow for determination of optical extinction and, thus, only indirectly reveal the optical absorption. Only photoacoustic (PA) spectroscopy directly measures the optical absorption. Absorption of pulsed or modulated optical radiation by the aerosols leads to warming of the particle and the surrounding gas atmosphere. The resulting expansion of the gas atmosphere leads to formation of pressure waves, which can be detected by means of a microphone. The microphone signal is directly proportional to the absorbed light power. Hence, it depends only on the applied laser power and the absorption. To amplify the acoustical signal, the absorption can be carried out in an acoustical resonator.

We present two different approaches of PA instrumentation for a continuous monitoring of aerosol absorption. One system is based on a modulated diode laser and measures at wavelengths of 532 nm and 806 nm. It is optimized for extremely low absorption values and for automated long-time measurements. The limit of detection for this instrument is as low as  $2 \cdot 10^{-7}$  cm. Both wavelengths are detected in parallel in two separate PA cells. The background absorption of the cells is determined periodically and taken in account by the control software.

As the system is meant for routine operation, a focus was set on handling and service qualities of the instrument. The PA cells can easily be replaced and cleaned within minutes. Time resolution can be varied from some seconds to averaging times of some minutes. We present results with the instrument compared to light scattering measurements with a commercial system under different atmospheric conditions.

The other system works with a pulsed laser system, consisting of a Nd-YAG laser with 10 Hz repetition rate and a emission wavelength of 355 nm. This laser is coupled to a OPO (Optical Parametrical Oscillator), which allows automated wavelength

tuning from 420 nm to 780 nm (signal) and 820 nm to 2500 nm (idler). The instrument combines six resonant PA cells to allow parallel measurements at 355 nm and a tunable signal and idler wavelength. At each chosen wavelength a differential measurement of filtered and unfiltered air is carried out in order to eliminate the influence of gaseous absorbers. The filter can be switched to each cell to determine the cell-specific back-ground (see Fig. 1).

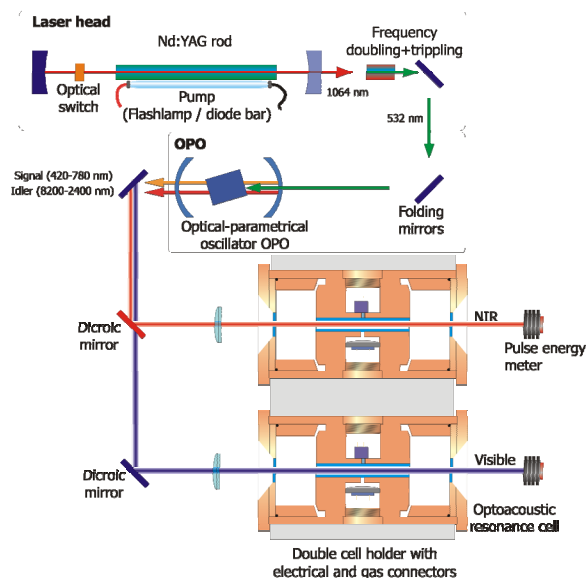


Figure 1 Schematic set-up of the tuneable pulsed PA system, here with only two PA cells.

For this PA system, a special OPO-Laser combination with extremely low beam divergency, homogeneous energy distribution over the circular laser beam was constructed by Innolas GmbH, Krailling, Germany. It delivers pulses with 5 ns length and a pulse energy in the mJ range. It is possible either to scan over the complete spectral range available, i.e. the signal range and the idler range are recorded simultaneously together with 355 nm. Alternatively, a chosen list of relevant wavelengths can be measured step-wise.

## Robust portable, HH-TDMA for field use

<sup>1</sup>G.R. Johnson, <sup>1</sup>C. Fletcher, <sup>1,2</sup>N. Meyer, <sup>1</sup>Z. D. Ristovski.

<sup>1</sup>International laboratory for Air Quality and Health, Queensland University of Technology, GPO Box 2434, Brisbane 4001, Australia.

<sup>2</sup>Now at Institute for Aerosol and Sensor Technology, FHNW, Switzerland.

Keywords: HTDMA, Hygroscopicity, Instrumentation, particle characterisation, relative humidity.

A new design for a hygroscopicity tandem differential mobility analyser system is presented which is both light-weight and portable, while permitting accurate hygroscopic growth and deliquescence measurements for aerosols over a very wide, seamless continuous relative humidity range without reconfiguration. This range can in principle be from 0 to 99.1%.

The method achieves this through three significant advances in H-TDMA design:

Firstly, the approach regulates humidification by controlling the fraction of time air flows through two alternate paths: saturator or dryer. Rapid switching of the flow path is controlled by a Labview™ PID algorithm which takes humidity data from a chilled mirror humidity sensor. This results in a very simple and robust humidity regulation process.

Secondly, the system incorporates a unique two stage Nafion™ humidifier which allows a continuous range of aerosol humidification from dry to greater than 99% relative humidity without pre wetting the aerosol or changing the system configuration. The monodisperse aerosol, exiting the preclassifier, are humidified in the first Nafion™ by the wet excess air from the second classifier. Afterwards it passes through the second Nafion™ where it's humidity is further increased and equalised to the humidity of the sheath air. In this way the aerosol entering the second classifier and the sheath air are at exactly the same humidity which has been shown (Biskos et al 2006) to be an essential prerequisite for reliable hygroscopic growth factor measurements.

Thirdly the humidifier Nafion™ assembly temperature is directly thermally coupled to that of the second DMA by enveloping the humidifier in the wet DMA excess air flow and by keeping the Nafion™ and second classifier in a thermally isolated chamber.

The design is shown schematically in figure 1, while figure 2 shows the extremely well regulated, constant humidity exiting the HDMA, in spite of an increasing ambient temperature in the system.

The rapid response of the system after a step changes in set-point is shown in figure 3.

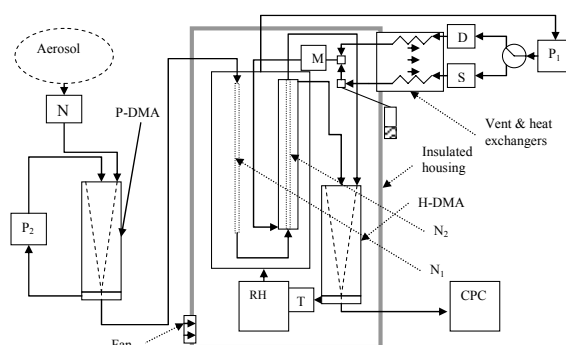


Figure 1. Schematic diagram of the H-TDMA. P-DMA: Preclassifier DMA. H-DMA: Humidified aerosol DMA, N<sub>1</sub>, N<sub>2</sub>: Nafion™ tubes, P<sub>1</sub>, P<sub>2</sub>: pumps, D: dryer, S: saturator, M: mixing chamber, N: neutraliser, RH: humidity sensor, T: temperature sensor for RH measurement.

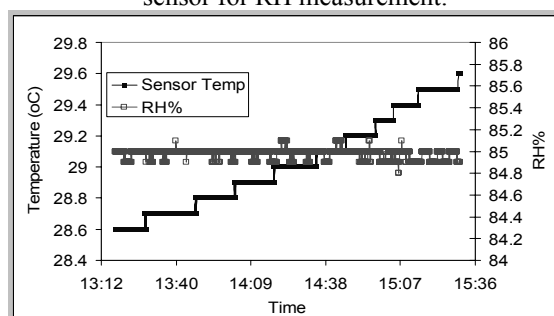


Figure 2. Stability of the relative humidity of the aerosol exiting the H-DMA under conditions of changing temperature.

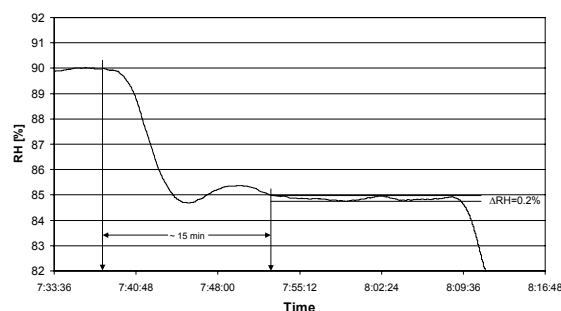


Figure 3. Response to a step change in the RH set-point.

Biskos, G., D. Paulsen, et al. (2006). "Prompt deliquescence and efflorescence of aerosol nanoparticles." *Atmospheric Chemistry and Physics* **6**: 4633-4642.

## A portable TEM sampler for quantitative single-particle analysis

M.Fierz<sup>1</sup>, R.Kaegi<sup>2,3</sup> and H.Burtscher<sup>1</sup>

<sup>1</sup>University of Applied Sciences, Northwestern Switzerland, 5210 Windisch, Switzerland

<sup>2</sup>Swiss Federal Institute for Environmental Science and Technology (Eawag), Ueberlandstrasse 133, 8600 Dübendorf, Switzerland

<sup>3</sup>Swiss Federal Institute for Materials Science and Technology (Empa), Ueberlandstrasse 129, 8600 Dübendorf, Switzerland

Keywords: Aerosol instrumentation, Aerosol sampling, Electron microscopy, Single particle analysis

Recent studies provide evidence of an increased toxicity of ultrafine particles (e.g. Gilmour et al., 2004 etc), which is not correlated with PM10 mass, but rather depends on size, number concentration, chemistry and/or adsorbed substances. Therefore, there is a pressing need to characterize ultrafine particles in more detail, which should lead to an improved understanding of their toxicity. The transmission electron microscope (TEM) is one of the most powerful methods to study individual ultrafine particles – it is the only instrument to simultaneously provide information on particle size, morphology and chemistry. It has been used extensively to study the composition of individual particles, however, due to the nature of the aerosol samplers involved, these studies remain largely qualitative in nature.

We have developed and calibrated a portable instrument where particles are sampled directly onto a TEM grid. Such samplers have already been described in the literature (e.g. Morrow and Mercer, 1964; Dixkens and Fissan, 1999, etc), however, none of these samplers was properly characterized. In general, two types of sampling bias are possible in a sampler: 1) particles of different sizes are sampled with different efficiency (size bias) and 2) particles are not deposited uniformly on the TEM grid (uniformity bias). Our sampler is similar to the Dixkens and Fissan design, but more compact. It is also battery-powered to allow sampling in remote locations where no line voltage is available. The sampler consists of three functional units:

1. Particles are positively charged in a Hewitt-type unipolar diffusion charger
2. Particles are deposited on the TEM grid by an electric field in a rotationally symmetric deposition zone, ensuring at least a rotational symmetry in the deposition pattern on the TEM grid.
3. An electrometer after the deposition zone measures the diffusion charging signal of the charged particles when the electric field for deposition is not applied, thus giving an estimate of the sampling time necessary. A direct measurement of the current produced by particles precipitated on the TEM grid is in progress.

To calibrate our sampler, we operated it in parallel with a CPC or an SMPS, and challenged these systems with both monodisperse (CPC) and polydisperse aerosols (SMPS). From the monodisperse experiments, we could derive a calibration curve, which gives us the deposition efficiency of the sampler for a particular particle size. This calibration was used to in combination with image analysis to recover the size distribution of the polydisperse particles. In addition, finite element calculations made with a commercial package (Comsol multiphysics) were performed, with a satisfactory agreement between experimental and theoretical efficiency (Figure 1).

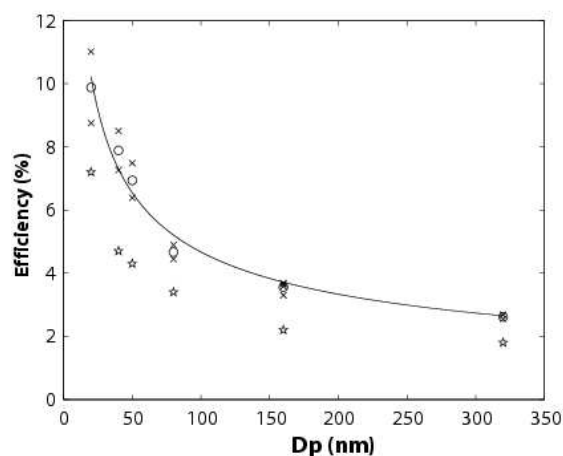


Figure 1: Experimentally measured (crosses; circles = average) and theoretically calculated deposition efficiency (stars) as function of particle size.

Dixkens, J. and Fissan, H. (1999). Development of an electrostatic precipitator for off-line particle analysis. *Aerosol Science and Technology*, 30: 438-453.

Gilmour, P. S. et al. (2004). Pulmonary and systemic effects of short-term inhalation exposure to ultrafine carbon black particles. *Toxicology and Applied Pharmacology*, 195: 35-44.

Morrow, P. E. and Mercer, T. T. (1964). A point-to-plane electrostatic precipitator for particle size sampling. *American Industrial Hygiene Association Journal*, 25: 8-14.

## A method for measuring surface area concentration of ultrafine particles

J. M. Wei<sup>1</sup>, F. E. Kruis<sup>1</sup> and H. Fissan<sup>2</sup>

<sup>1</sup>Institute for Nanostructures and Technology, University of Duisburg-Essen,  
Bismarckstr. 81, 47057 Duisburg, Germany

<sup>2</sup>Institute of Energy and Environmental Technology (IUTA), Bliersheimerstr. 60, 47229 Duisburg, Germany

Keywords: ultrafine particles, surface area concentration, charging efficiency, deposition efficiency, current

The surface area concentration of ultrafine particles has become the focus of attention of recent studies due to their close relationship with human health (Donaldson et al., 1998). A novel method of measuring surface concentration of ultrafine particles in the size range 20-100nm, based on a three-step approach, including particle diffusion charging, ion precipitation and particle deposition, is proposed in this paper. Instead of using an absolute filter in a Faraday cage, our method uses an electrical precipitator to sample the charged particles (Fig. 1) and further derive the particle surface area concentration from the measured current caused by the deposited particles.

Based on the designed prototype, experiments were carried out to measure the particle charging efficiency  $\eta_c$ , mean charge acquired on the particle  $q_p$  and deposition efficiency  $\eta_d$ . With these parameters experimentally determined, the equation for describing the signal current can be established. The equation is further verified by comparing the theoretical current calculated on the basis of the size distribution obtained by a SMPS with the measured current using both monodisperse and polydisperse aerosol (Fig. 2). Furthermore, the relationship between the current  $I$  and particle diameter has been established:

$$I \propto \eta_c \cdot \eta_d \cdot q_p$$

$$I \propto d_p^{\beta_1 + \beta_2 + \beta_3}$$

with  $\beta_1$ ,  $\beta_2$  and  $\beta_3$  to be determined experimentally.  $\beta_3$  can be varied and adjusted such that  $\beta_1 + \beta_2 + \beta_3 = 2$ . In the present experiment the strategy of changing the deposition voltage ( $HV2$ , Fig. 1) was adopted to regulate the value of  $\beta_3$  to let it satisfy above condition. In this circumstance, the particle surface area concentration can be obtained by measuring the current at this voltage. Furthermore, the particle surface area concentration estimated from the measured current was compared to that derived from the SMPS. The results show that they agree with each other very well.

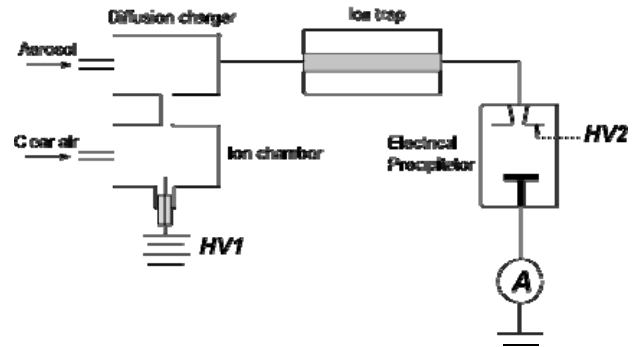


Figure 1. Proposed prototype for measuring particle surface area concentration. ( $HV1=3.76kV$ , aerosol flow 1l/min, clean air 1l/min)

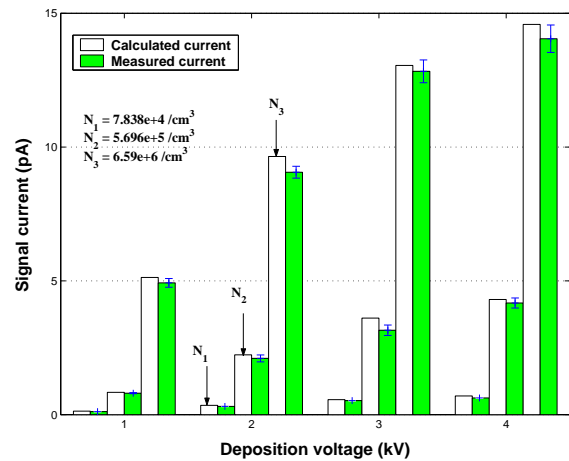


Figure 2. Comparison between measured and calculated current as function of deposition voltages  $HV2$ , with parameters listed in Table 1.

Table 1. Parameters of the particle size distribution obtained from the SMPS

$i$	$d_g$ (nm)	$\sigma_g$	$N_i$ ( $1/cm^3$ )
1	77.55	2.04	$7.839 \times 10^4$
2	68.35	2.08	$5.696 \times 10^5$
3	60.22	1.65	$6.596 \times 10^6$

Donaldson, K., Li, X. Y. & MacNee, W. (1998). *J. Aerosol Science*, 29, 533-560

## Wavelength and refractive index independent number concentration determination algorithm for ensemble of aerosol particles

L. Vámos, P. Jani

Research Institute for Solid State Physics and Optics, 29-33. Konkoly-Thege str. H-1525. Budapest, Hungary

Keywords: light scattering, modelling, number concentration, optical instrumentation

The size determination of aerosol particles can be divided into two main classes: methods based on single particle and methods based on particle ensemble scattering experiments. Both methods are useful for aerosol characterisation including size, refractive index, concentration, composition. In an earlier work (Jani *at all*, 2002) we have shown that the ratio of the mean intensity,  $\bar{I}$ , to the standard deviation of scattered intensity,  $\sigma_I$ , on the particle ensemble is a constant, depending on the number of the scattering particles:

$$\frac{\bar{I}}{\sigma_I} = \sqrt{N} \frac{\bar{I}_1}{\sqrt{\sigma_{I_1}^2 + \bar{I}_1^2}}, \quad (1)$$

where  $\bar{I}_1$  mean value and  $\sigma_{I_1}$  is the standard deviation of intensity scattered on single particles. Strictly speaking for a monodisperse ensemble of particles the  $\sigma_{I_1}$  can be neglected so the second term on the right side of the equation is near to 1, so the  $\bar{I}/\sigma$  ratio is independent of the refractive index and wavelength.

In a simulation we investigated this feature by computing the scattered intensity of the ensemble from an appropriate direction. In the simulation we assume the particle number to follow Poissonian and the size lognormal distribution. This created ensemble is illuminated with an impulse train and the scattered light is computed for each individual particle with Mie algorithm in an appropriate direction. The scattered intensities are summed up to get  $I$ . After shooting the particle ensemble  $k$  times, we compute the mean value ( $\bar{I}$ ) and standard deviation ( $\sigma_I$ ).

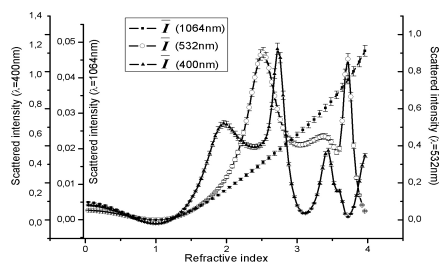


Figure 1. Mean of the scattered in the function of the refractive index for monodisperse ensemble. The distribution was computed for the 5-sigma size range. In the monodisperse case  $\bar{N} = 1000$

particles and  $k = 1000$  impulses were chosen and the ratio  $\bar{I}/\sigma$  was computed for a scattering angle  $\Theta=20^\circ$ . The particle ensemble of homogeneous sphere water droplets ( $n=1.33$ ) has the mean particle number 200nm and the standard deviation 2.2nm. It is not surprising that the range and shape scattered intensity curves are very different as it is seen in fig. 1.

In fig. 2.  $\bar{I}/\sigma$  ratio is plotted in the function of the refractive index for three wavelengths.

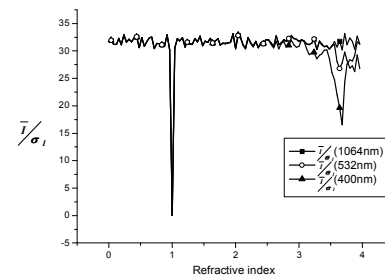


Figure 2. Ratio of the scattered intensity and standard deviation in the function of refractive index for different wavelengths for 1000 particles

In the relevant refractive index values the ratio is constant, and independent of the refractive index and the wavelength, except for a narrow region where the particle is indistinguishable from the air. In other normal parts of the curve its value is very close to the square root of the number of particles – in our case  $\sqrt{N} = \sqrt{1000} = 31.62$  – as it is suggested by equation (1).

It was verified for different particle ensembles with different mean particle number and standard deviation.

In conclusion we notice that the algorithm developed contains a refinement to the method proposed in (Jani *at all*, 2002), that is by a simple measurement of the scattered intensity constructed its mean value and standard deviation particle number is assessed. Implicitly the inverse problem also can be solved namely in case of known number of generated particles: their standard size deviation can be measured.

- Jani P., Konioreczyk M., Nagy A., Lipp Z., Bartal B., Laszlo A. and Czitrovsky A., Probability distribution of scattered intensities, J. Aer. Sci., Vol. 33., pp 694-707, 2002

## Design and experimental evaluation of the Dual Wavelength Optical Particle Spectrometer

P. Gál<sup>1</sup>, A. Nagy<sup>1</sup>, A. Czitrovsky<sup>1</sup>, W. Szymanski<sup>2</sup>

<sup>1</sup>Research Institute for Solid State Physics and Optics,  
Konkoly Thege M. st. 29-33., H-1121 Budapest, Hungary

<sup>2</sup>Faculty of Physics, University of Vienna,  
Boltzmanngasse 5, A1090 Vienna, Austria

Keywords: size distribution, single particle analysis, index of refraction, light scattering.

Numerical and experimental study showed the feasibility of the Dual Wavelength Optical Particle Spectrometer method (Nagy *et al.*, 2007), which was introduced recently for the real time measurement of the size and the complex refractive index of aerosol particles (Szymanski *et al.*, 2002). The method is based on the principles of single optical particle counters. Each particle passing the sensing volume is illuminated by two laser beams with different wavelength. The scattered light is collected over four angular ranges, forward and backward scattering directions compared to the two illumination laser light beams. The measured and digitized quartet is then compared to a pre-computed table calculated using the Mie scattering theory. The rows of the table contain a size, a complex refractive index and the corresponding four scattered signals from the four angular ranges.

In order to perform a proper calibration, first a scaling factor must be determined for each detector to link the scattered intensities calculated using the Mie theory with the detector signals. PSL particles with sizes 0.5 and 2.0  $\mu\text{m}$  were used to obtain these scale factors.

To evaluate the performance of the method particles were generated from a suspension using pneumatic atomization and electrostatic classification with a DMA were used to obtain monodisperse distribution. These particles were then introduced to the DWOPS measuring volume after aerodynamic focusing. The four signals from the four detectors were catch by a four channel peak detection system which utilises certain logic to minimise the effects of possible crosstalk between channels. The detected signals were digitized and using the scale factors a search was performed in the evaluation table to obtain the particle size and complex refractive index. Figure 1 demonstrates the achieved signal quality and the resolution of the channels.

PSL particles with different sizes from aqueous suspension, DEHS particles generated from an Isopropyl Alcohol-DEHS solution, Paraffin oil and carbon-like absorbing particles generated from black ink diluted in pure distilled water were used for the test measurements.

Using the "36-19-21" size evaluation table (Nagy *et al.*, 2005) ~20000particles/sec. evaluation

speed was achieved which corresponds to 1.2million particles/litre concentration for 1 lit./min sample flow rate.

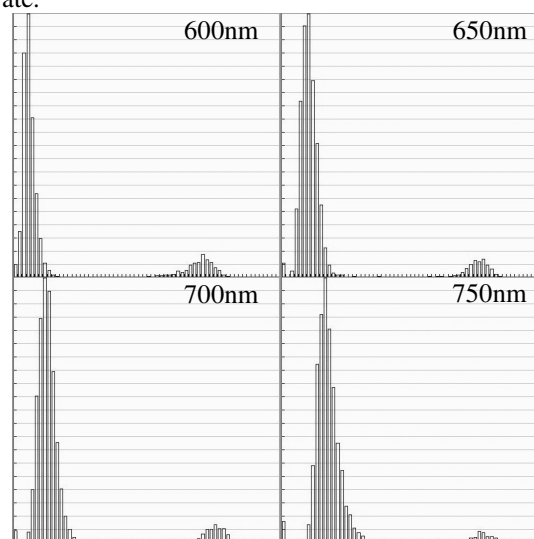


Figure 1. Measured amplitude distributions of the forward scattered signal from the generated calibration aerosol particles with sizes 600 - 750 nm at 808 nm illumination wavelength during the calibration procedure. The X axis correspond to the amplitudes and the Y axis show the counts.

This work was supported in part by the National Research and Development Program NRDP3 Proj. Nr. 3A/089/2004, by the ÖAD-WTZ, Proj. Nr. A17/2005 and by the Austrian Science Foundation, Proj. Nr. P15619.

Nagy, A., Szymanski, W.W., Gál, P., Golczewski, A., Czitrovsky, A. (2007) Numerical and experimental study of the performance of the Dual Wavelength Optical Particle Spectrometer (DWOPS), accepted for publication in the *Journal of Aerosol Science*

Szymanski, W.W., Nagy, A., Czitrovsky, A., Jani, P. (2002). *Measurement Science and Technology*, 13, 303-307.

Nagy, A., Szymanski, W.W., Golczewski, A., Gál, P., Czitrovsky, A., (2005) The effects of the evaluation table dimensions on the DWOPS sizing accuracy, p.298 Proceedings of EAC2005.

## Design and evaluation of the KS-220 and KS-222 cascade impactors developed for $PM_{10A/10B} \rightarrow PM_{2.5A/2.5B} \rightarrow PM_{1A/1B}$ sampling

A. Nagy<sup>1</sup>, I. Kálmán<sup>2</sup>, Cs. Kálmán<sup>2</sup>

<sup>1</sup>Research Institute for Solid State Physics and Optics,  
Konkoly Thege M. st. 29-33., H-1121 Budapest, Hungary  
<sup>2</sup>Kálmán System Ltd., Trencsényi u. 16., H-1125 Budapest, Hungary

Keywords: cascade impactor, PM measurement, aerosol sampling, aerosol instrumentation.

Cascade impactors are widely used instruments for sampling and fractionation of aerosol particles according to their aerodynamic size. The KS-200 and KS-220 impactors are the improved version of the patented OH-610-B type cascade impactor. The aim of the development was to design and produce an instrument which fulfils the requirements of the new environmental protection regulations. In this contribution we present the result of this development, the design of the KS-220 and KS-222 cascade impactors and show their performance evaluation together with application examples.

These impactors utilize the double stage layout, where the two corresponding stages have the same characteristic curves, which ensures sharper collection efficiency curves and reduces the carry-over effect. They are capable of gravimetric fractionation of  $PM_{10A/10B} \rightarrow PM_{2.5A/2.5B} \rightarrow PM_{1A/1B}$  particles and require new evaluation methods.

New construction solutions were applied to increase the impaction efficiency and to decrease the size of the instrument, e.g. the particles are accelerated to the necessary impaction speed through annular nozzles instead of through the many small sized round nozzles. The impactors consist of well separated chamber like stages for weighing to decrease the reproduction error caused by the different adhesiveness of the particles. The outstanding advantage of the new type impactors is that they can be used “in-stack” in small size flue gas pipes.

The KS-220 cascade impactor consists of a standard suction pipe, a diffuser inlet, three consecutive double stages and a backup filter. The KS-222 model was developed mainly for sampling in chimneys with thick wall. Different catch plates can be used depending on the actual application.

Calibration of the impactor showed sharp characteristic curves and that the stage cut-off sizes are close to the values predicted by impactor theory (Fig. 1). Fig. 2 shows the measurement site of an application example and fig. 3 shows the measured sample, the exposed catch plates of the 3x2 impactor stages and the backup filter.

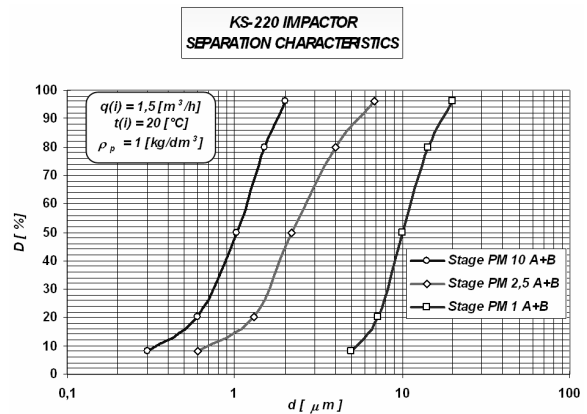


Figure 1. The separation characteristics of the KS-220 impactor.



Figure 2. Measurement site.

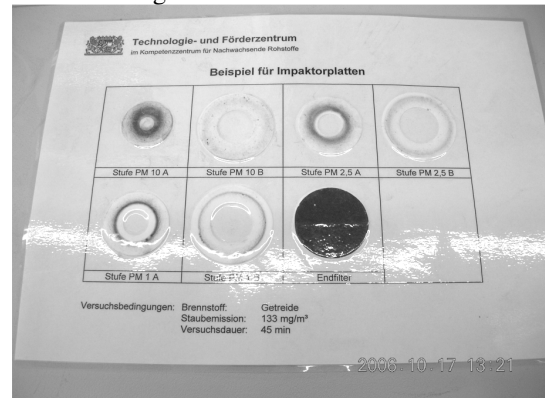


Figure 3. Exposed catch plates of the 3x2 stages and the backup filter.

## Modelling g- article ctivation and rowth in C C

F. Stratmann<sup>1,2</sup>, T. Petä ä<sup>1</sup> and M. Kulmala<sup>1</sup>

<sup>1</sup>Department of Physical Sciences, University of Helsinki, Helsinki, Finland  
<sup>2</sup>eibniz Institute for Tropospheric Research (IfT), eipzig, Germany

Keywords: Aerosol Dynamics, CPC, Heterogeneous Nucleation, Instrumentation, Modelling

The question of how heterogeneous nucleation processes affect the behaviour of condensational particles counters (CPCs) has been around for years and has become increasingly important due to the fact that the CPC counting efficiencies are currently being pushed down to new lower limits (e.g. Petä ä et al., 2006). Therefore in this work, the activation and dynamic growth inside a TSI 3785 WCPC, i.e. a CPC using water as working fluid, will be investigated numerically. In addition, results from the numerical model will be compared to experimental data.

For modelling fluid flow, heat/mass transfer and particle dynamics inside the WCPC, the Fine Particle Model (FPM) (particle dynamics, 2005), together with the Computational Fluid Dynamics (CFD) Code F UENT was used. Particles were assumed to initially be and stay monodisperse during activation and growth. Describing particle/droplet activation and dynamic growth, the heterogeneous nucleation process was modelled as suggested in e.g., azaridis (1991) and the condensational growth was considered according to Barrett and Clement (1988). Using this model, velocity, temperature, vapour mass fraction distributions together with the total particle/droplet number and mass (insoluble seed and water) concentration fields inside the CPC were determined. In the solution process, multi-component and thermal diffusion, vapour source at the wall and vapour sink due to particle/droplet condensation, and vapour latent heat release were accounted for. To avoid numerical diffusion, the laminar velocity profile inside the CPC was prescribed and radial particle/transport due to diffusion and thermophoresis was neglected.

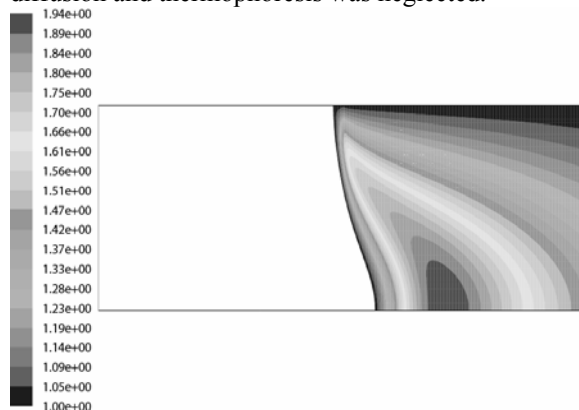


Figure 1: Modeled saturation ratio distribution inside a TSI 3785 WCPC.

Figure 1 depicts the saturation distribution inside the TSI 3785 WCPC. Here the temperatures of the saturator and the condenser were set to default operation temperatures of 293.15 K and 333.15 K, respectively. As illustrated in Figure 1, the saturation distribution is highly inhomogeneous and peak supersaturations occur in the tube centre.

Figure 2 depicts a comparison of numerically and experimentally (Petä ä et al., 2006) determined CPC counting efficiencies.

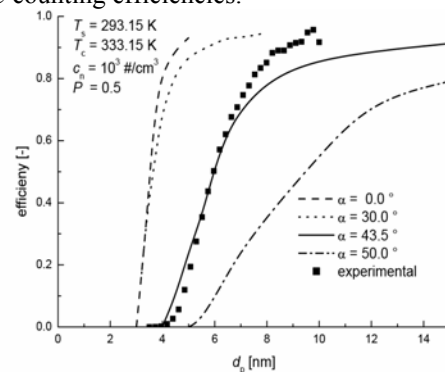


Figure 2: Experimental and modelled counting efficiencies as function of particle size for different contact angles.

As to be seen from Figure 2, good agreement between theoretical and experimental results can be observed, if a contact angle of 43.5 is assumed.

In addition, the investigations showed that CPC counting efficiencies maybe strongly affected by heterogeneous nucleation processes and that heterogeneous nucleation theory is not able to consistently explain the experimental observations. Furthermore it will be shown that particle number concentration does not affect the CPC counting efficiency, if monodisperse seed aerosol is assumed. For a polydisperse aerosol, however, number concentration might influence counting efficiency. Also results concerning the effects of homogeneous nucleation will be presented.

Barrett, J.C. and Clement (1988), *J. Aerosol Sci.* 19, 223-242.

azaridis, M., Kulmala, M. and aaksonen, A. (1991), *J. Aerosol Sci.* 22, 823-830.

particle dynamics (2005), *Fine Particle Model (FPM) for FLUENT*, particle dynamics GmbH, eipzig, Germany. ([www.particle-dynamics.de](http://www.particle-dynamics.de))

Petä ä et al. (2006) *Aerosol Sci. Technol.* 40, 1090-1097.

## A new conception for environmental measurement of ultrafine particles

A. Zschoppe<sup>1</sup>, A. Rudolph<sup>1</sup>, R. Caldow<sup>2</sup>, B. Wehner<sup>3</sup> and L. Hillemann<sup>4</sup>

<sup>1</sup>Topas GmbH, Wilischstr. 1, D-01279 Dresden, Germany

<sup>2</sup>TSI Incorporated, 500 Cardigan, MN 55126 Shoreview, USA

<sup>3</sup>Leibniz-Institute for Tropospheric Research, Permoserstraße 15, D-04318 Leipzig, Germany

<sup>4</sup>Institute of Process Engineering and Environmental Technology, TU Dresden, D-01062 Dresden, Germany

Keywords: instrumentation, measurement

It is well known that ultrafine particles have an impact on human health. Consequently it is necessary to monitor the exposure in cities and urban areas. There are some instruments commercially available for this task like SMPS, DMPS or FMPS but their original field of application is contradictory to the utilization in air pollution monitoring networks.

These sensitive devices had been developed primarily for scientific purposes in the lab environment, they are servicing-intensive and delicate to handle. The use of radioactive sources in the charger complicates the transport of the devices. Furthermore a compromise has to be found between the necessary accuracy in the field of air monitoring and the costs of the devices. The high accuracy of these devices is not needed within the scope of air pollution monitoring and lead to too high costs.

Based on the requirements of monitoring networks a new concept was developed and tested in the project UFIPOLNET – using of a diffusion charger instead of a radioactive source and an electrometer instead a CPC:

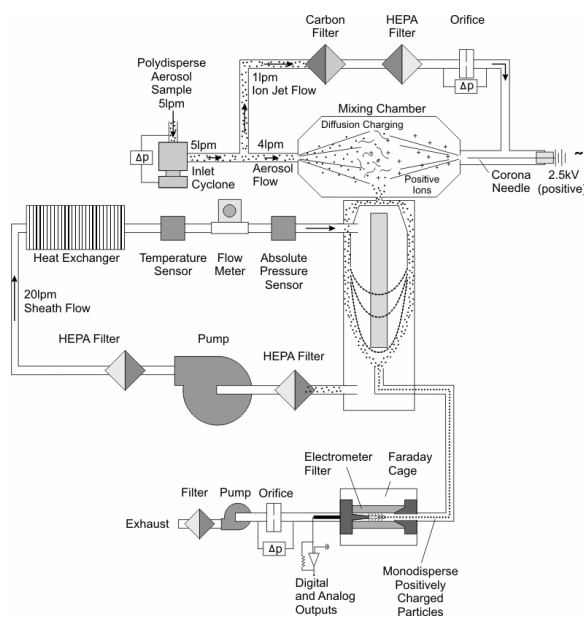


Figure 1. Schematic of the new particle monitor for ultrafine particles series UFP.

Additional components are a long DMA (TSI 3081) with sheath air circuit, a complete control unit (PCB)

and a single board computer for data processing and a database driven data storage.

The data inversion delivers the particle number concentration in the following size classes:

CH1 (nm)	CH2 (nm)	CH3 (nm)	CH4 (nm)	CH5 (nm)	CH6 (nm)
20...30	30...50	50...70	70...100	100...200	>200

In the field of environmental aerosols particular attention has to be paid to the sampling system.. Basically it consists of a PM1-inlet, a membrane dryer and an equalizing tank. The membrane dryer requires no maintenance and induces only minimal particle losses.

In comparison measurements between the new spectrometer and a DMPS at a street canyon site in Leipzig a good correlation was found:

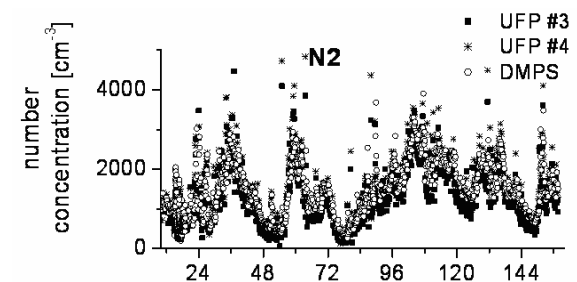


Figure 2. Comparison measurements between the new spectrometer and a DMPS (30 – 50 nm).

Within the project UFIPOLNET at four measurement stations in Europe prototypes were installed with identical sampling systems. The instruments are running over a longer period and experiences of the users will also be presented.

UFIPOLNET ([www.ufipolnet.eu](http://www.ufipolnet.eu)) is financed by the LIFE financial instrument of the European Community under No. LIFE04 ENV/DE/000054.

## Analysis of transfer functions of fast scanning DMAs

Praney Dubey and Suresh Dhaniyala

<sup>1</sup>Department of Mechanical Engineering, Clarkson University, Potsdam, 13699, NY, USA

Keywords: DMA, Scanning, Fast, Transfer function.

The revolution in the field of particle sizing came with the design of an instrument popularly known as the DMA (Differential mobility analyzer). The transfer function and working procedure of a DMA was explained by Knutson and Whitby (1975). The transfer function developed by Knutson and Whitby was for non-diffusive particle, with the DMA operated in a stepping mode. The instrument if used in stepping mode takes several minutes to measure the wide spectrum of particle sizes. Wang and Flagan (1990) showed that this instrument can be used in scanning mode, and if used with exponential voltage ramp, the shape of transfer function through out the scan remains unchanged. Theoretical or numerical-based calculations of transfer functions for scanning mode DMA remained untouched for more than a decade. Recently, Collins et al (2004) analyzed the transfer function for a scanning mode using Monte Carlo simulations. The transfer function for scan times of 20s to 3600s were shown in that work.

In order to determine the DMA transfer functions as a function of particle mobility and scan times, the particle trajectory equations must be solved for a time varying field. The trajectory equations for the scanning DMA are complicated, making it difficult to get closed form solutions for this operation. While the previous approach (Collins, et al., 2004) used Monte Carlo simulations., that approach is expensive and difficult to deploy in a near real-time basis. Here, we adopt a hybrid approach to obtain the transfer function, by combining analytical solution with time-stepping simulations. In this approach, first we solve the trajectory equations analytically for the up scan. Using the analytical solution for particle trajectory, simulations are performed with particles injected at the entrance over small time intervals. This simulates continuous particle injection into the DMA. The sampling rate of particles of different mobility and their residence time (up to certain accuracy) has been obtained and these results are used to calculate the instrument transfer function. The hybrid approach reduces the simulation time considerably, making repeated calculations with high time resolution feasible.

The results suggest that for moderate scan times, the transfer function widths increased along with decrease in the maximum transfer function height. For very low scan time, particles injected from outer most radial locations could never be sampled while

particles injected at other locations could be sampled. This further decreased the transfer function height. The injection locations that contribute to the sampled particle stream depend on the scan time and particle mobility. Thus, the transfer functions for a scanning DMA are a function of the mean sampled particle mobilities.

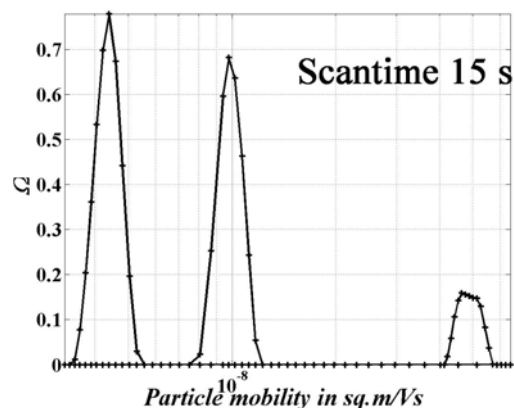


Figure 1. This Figure shows the difference in transfer function heights for different particle mobilities for a fast scan.

Operating DMAs at very low scan times also put limitations on the lowest mobility that could be sampled. This lower sampled size limit depends on the particle residence time. In fact, lower mobility particles have residence times greater than the scan times when very fast scans are performed. These limitations constrain the range of particle mobilities that can be analyzed as the scan rate is increased. These limitations and distortions in the transfer function shape make fast scans less accurate and in some case completely impractical. The distorted transfer function if accurately known can reduce the estimation error. In combination with advanced inversion routines, size distribution analysis with fast scans should be possible. This presentation will outline the limitations of currently existing scanning DMAs and provide a basis for designing new fast scanning DMAs.

This work was supported by the National Science Foundation under grant ATM 0548036

### REFERENCES:

- Collins, et al., (2004), *Aer. Sci. and Tech.*, 38:833.
- Knutson, E. O., and Whitby, K. T. (1975). *J. Aer. Sci.* 6:443-451
- Wang and Flagan (1990) *Aer. Sci. Tech.* 13: 230-240.

## The construction of an optical particle counter with sub- and super-micron counting capability.

R.J. Greaney, O. Ryan, C.D O'Dowd, S.G. Jennings.

Department of Physics & Environmental Change Institute,  
National University of Ireland, Galway, University Road, Galway, Ireland.

Keywords: Optical particle counter, Forward scatter, Backscatter.

### Abstract

An Optical Particle Counter (OPC) has been designed with a single ellipsoid reflector as the main optical element. Photodiodes with low noise transimpedance are used to detect forward and backscatter responses of particles scattering laser light (685 nm) at the ellipsoid focus. The OPC has been designed using Zemax® to yield light collection efficiency. The design process has included modeling the optical response of various lenses, reflector coatings, and laser wavelengths, on forward and backscatter responses. The simulations show that the single ellipsoid reflector design is suitable for our purpose of collecting forward and backscattered light.

A modified scattered light modeling program based on that devised by Garvey and Pinnick [1983] is used to calculate the cross section scattering coefficient of particles over a range of particle diameters, from sub-micron to super-micron (Figure. 1). For example A 100nm diameter particle has a scattering cross section response of  $6.32 \times 10^{-13} \text{cm}^2$  per particle at 685nm.

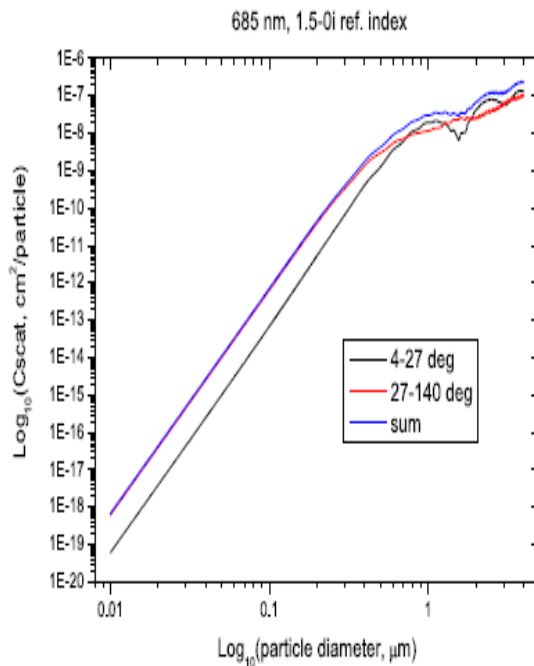


Figure 1. Scattering cross section of particles versus particle diameter (10nm - 4µm) for refractive index of 1.5 - 0i, at 685nm.

An oscilloscope-captured real time pulse response for a random sized particle is shown in (Figure 2).

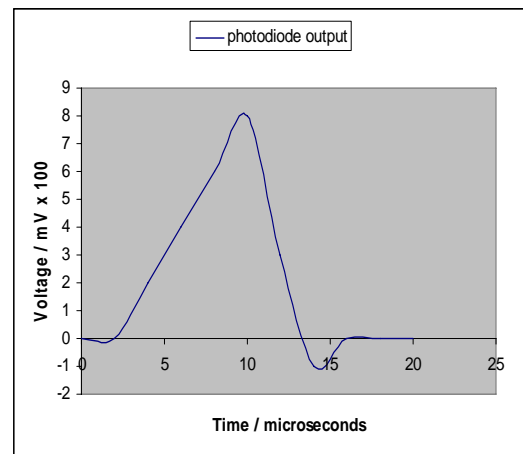


Figure 2. This figure shows the backscatter response (where zero is the threshold level) for a random particle being scattered by the 685nm laser using the single ellipsoid mirror to collect the backscattered light onto the photodiode.

Other avenues of development are being explored for the further improvement of the instrument. The OPC is being calibrated with monodisperse particles of known particle size and constant concentration.

### References:

Garvey, D. M., and Pinnick, R. G. (1983). Response characteristics of the Particle Measuring System Active Scattering Aerosol Spectrometer Probe (ASASP-X). *J.Aerosol Sci. and Technol.*, **2**, 477-488.

Pinnick, R.G. and Auvermann, H.J. (1979). Response characteristics of Knollenberg lightscattering aerosol counters. *J.Aerosol Sci.* **10**:55-74

## Design of the Ice Optical Detector (IODE) for the Zurich Ice Nucleation Chamber (ZINC)

M. Nicolet, O. Stetzer and U. Lohmann

Institute for Atmosphere and Climate Science, ETH Zurich, 8092 Zurich, Switzerland

Keywords: aerosol measurements, nucleation, depolarization, optical properties, light scattering.

Ice particles are an important factor for climate since their presence affects the radiative properties of clouds as well as their lifetimes. Ice nucleation is also one of the uncertainties in climate forcing. The Zurich Ice Nucleation Chamber (ZINC) was built to perform laboratory experiments and field measurements to help understand the ice nucleation processes. The ice particles need to be detected at the exit of the ZINC chamber with an optical ice detector using the property of depolarization.

Both liquid and solid phases may coexist in the ZINC chamber. Depolarization is used because the principle of this technique is to differentiate between water droplets and ice crystals. Water droplets are assumed to be spherical, causing no significant depolarization, whereas ice crystals induce depolarization due to their nonsphericity (Sassen & Liou, 1979). The central question is to know how much depolarization we might expect from the ice particles generated in the ZINC chamber as single particle detection has to be done. Ice crystals grown in the chamber tend to be randomly oriented (Hallett, 1987) and to grow nearly isometrically ( $\chi \sim 1$ ) (Young, 1993) in the case of small crystals ( $d=1-10\mu\text{m}$ ). To calculate the depolarization ratio, the T-matrix code for non-spherical particles in a fixed orientation by Mishchenko (2000) was used. The following plot shows the evolution of the depolarization ratio with the size parameter  $x$ . The values are integrated over all orientations and the bars show the standard deviation (Nicolet *et al.*, 2007):

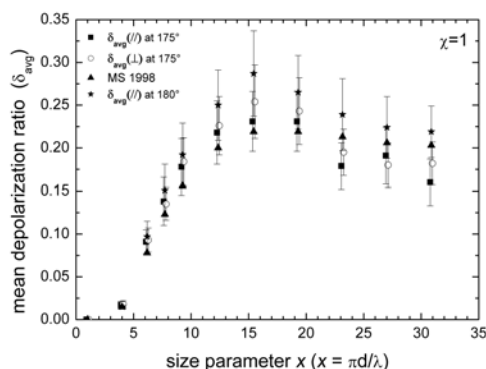


Figure 1. Evolution of the depolarization ratio with increasing particle size parameter  $x$ .

For first measurements and tests with the IODE detector, a simulation chamber which has the same dimensions as the ZINC chamber was used.

Particles are injected from the top of the chamber. For tests with spherical particles, PSL latex spheres were produced with an atomizer. A fluidized bed aerosol generator was used to create a polydisperse distribution of dust particles (kaolinite) to test the detector with non-spherical particles. An aerodynamic particle sizer was connected at the bottom of the chamber to obtain size distributions and to create a straight flow at the level of the overlap region of the detector. An example of a test experiment is shown in Fig. 2. It illustrates measurements made with kaolinite in order to obtain the depolarization ratio for non-spherical aerosols on a particle by particle basis:

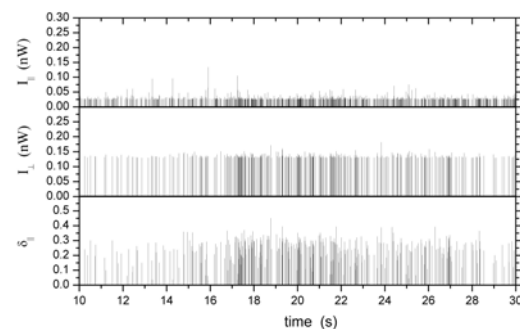


Figure 2. Intensities and depolarization ratio for kaolinite particles.

The modelling part gives us information about the depolarization ratio expected from the ice particles grown in the ZINC chamber. With the optical ice detector, it is therefore possible to distinguish between water droplets and ice crystals and thus to determine the efficiency of different aerosols to act as ice nuclei.

This work was supported by the Swiss National Science Foundation under grant 200021-107663/1.

Hallett, J. (1987). *J. Opt. Soc. Am. A*, 4, 581-588.

Mishchenko, M. I. (2000). *Appl. Opt.*, 39, 1026-1031.

Sassen, K., and Liou K. N. (1979). *J. Atmos. Sci.*, 36, 838-861.

Young, K. C. (1993). *Microphysical Processes in Clouds*. Oxford, New-York: Oxford University Press.

Nicolet, M., Stetzer, O., & Lohmann, U. (2007). *Appl. Opt.* (accepted for publication).

## An experiment on performance evaluation of particle collection and gas removal of an air washer system for semiconductor manufacturing clean rooms

Sang-Tae Park<sup>1</sup>, Kyung-Hoon Yoo<sup>1</sup>, Kyung-Eung Tae<sup>2</sup> and Seung-Woo Son<sup>3</sup>

<sup>1</sup> Aerosol and Contamination Control Laboratory, Korea Institute of Industrial Technology(KITECH),  
35-3, Hongcheon-Ri, Ibjang-Myun, Cheonan-Si, 330-825, South Korea

<sup>2</sup> Daehan PNC Co., Seoul 153-775, South Korea, <sup>3</sup> Sungrim PS Co., Seoul 153-802, South Korea

Keywords: heat recovery type air washer, L/G(gravimetric ratio of water/air), gas removal, particle collection.

In recent semiconductor manufacturing clean rooms, in order to improve clean room air quality, air washers are used to remove airborne gaseous contaminants such as NH<sub>3</sub>, SO<sub>x</sub> and organic gases from the outdoor air introduced into clean room. In the present study, an experiment was conducted to investigate particle collection and gas removal efficiencies for two kinds of air washer systems, direct atomization type and fin-coil type ones, as shown in Fig. 1 and Fig. 2.

The present experimental apparatus for evaluating particle collection and gas removal efficiencies of the air washer was used with DOS aerosols and Ammonia gas, respectively. The efficiencies are determined by the following equation.

$$\eta = \frac{C_{inlet} - C_{outlet}}{C_{inlet}} \quad (1)$$

where  $C_{inlet}$  is the total particle number (or gas volume) concentration at the inlet of the air washer and  $C_{outlet}$  is that at the outlet of the air washer, respectively.

Figure 3 shows the variation of gas removal efficiency with respect to L/G. It is seen that the removal efficiencies for two kinds of air washer

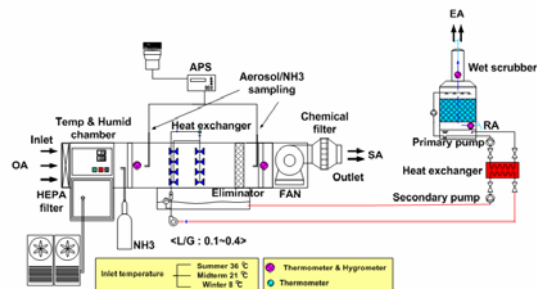


Fig. 1. Schematic diagram of the experimental apparatus for the present heat recovery direct atomization type air washer.

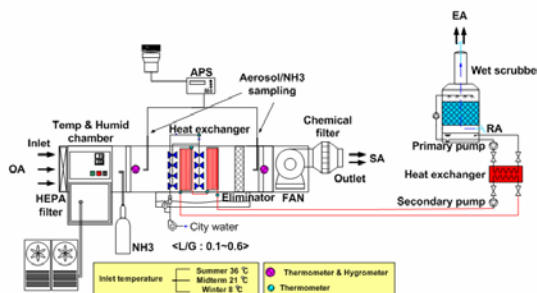


Fig. 2. Schematic diagram of the experimental apparatus for heat recovery fin-coil type air washer.

systems become more than 80% for L/G of greater than about 0.3. Figure 4 shows the variations of collection efficiencies of air washer systems for both direct atomization type and fin-coil type with respect to particle size for various L/G. The particle sizes on the abscissas are the geometric mean diameters of the DOS aerosols at the inlet of the air washer. It can be seen that when L/G and particle size are increased the collection efficiencies increase significantly.

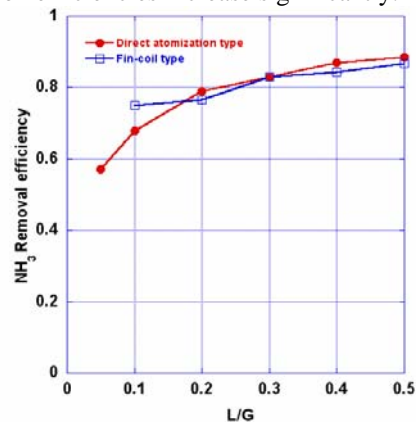


Fig. 3. Variation of NH<sub>3</sub> removal efficiency with respect to L/G.

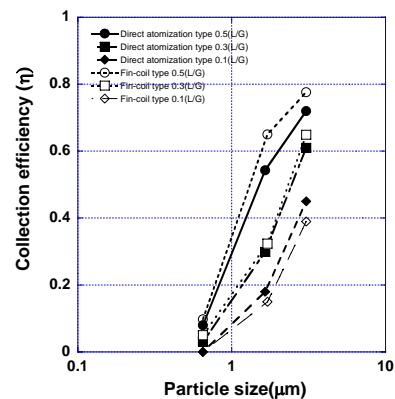


Fig. 4. Variations of the collection efficiencies with respect to particle size for various L/G.

This work was supported by the Korean Energy Management Corporation.

Fujisawa, S., Moriya, M., Yosa, K., Nishiwaki, S., Yamamoto, H., Katsuki, T., Nabeshima, Y., & Oda, H.(2002)., in *Proc. 20 th Annual Technical Meeting on Air Cleaning and Contamination Control*, Tokyo, 162-165(in Japanese).

## Distortion of the SMPS size distributions associated with the diffusion broadening of the DMA transfer function

A. Mamakos, . Ntziachristos and . Samaras

laboratory of Applied Thermodynamics, Mechanical Engineering Department, Aristotle University, Thessaloniki, GR 54124, Greece

Keywords: Aerosol instrumentation, diffusion, DMA, particle size distribution.

Despite the fact that there exists an analytical expression for the diffusion broadened transfer function (Stolzenburg, 1998), the validity of which was recently verified by Mamakos et al., (2007), most commonly the diffusion is neglected in the inversion of the Scanning Mobility Particle Sizer (SMPS) data. In this study we investigate the extent to which this simplification affects the recovered size distributions, in the case of the TSI s 3936 10 SMPS.

The error associated with the neglect of particle diffusion in the recovery of SMPS signal was quantified by means of numerical simulations with lognormal size distributions. Starting from a given distribution, the TSI s 3936 10 SMPS response was simulated using Stolzenburg s transfer function. Then the simulated SMPS signal was inverted using the triangular transfer function, characteristic of non-diffusive particles (Knutson & Whitby, 1975). The Twomey algorithm (Twomey, 1975) was employed for the data inversion since the use of noise-free distributions eliminated the need of smoothing the solution. Calculations have been performed for a sheath over sample flow ratio of 10 lpm:1 lpm.

Figure 1, shows the error in the recovered distributions in terms of the peak number concentration ( $N_{max}$ ), the geometric standard deviation ( $\sigma_g$ ) and the geometric mean diameter ( $d_g$ ). Results are shown for geometric mean diameters below 50 nm and geometric standard deviations smaller than 1.2 since differences above these values were minimal. As a frame of reference, the geometric standard deviation of the DMA transfer function at the lowest detectable size (7 nm) in the setup examined is 1.05. The larger peak of the triangular transfer function, compared to the diffusion broadened one, results in a consistent underestimation of the peak number concentration. The error increases with decreasing the width and the median diameter of the distribution, ranging between 12% for  $d_g$  12 nm and  $\sigma_g$  1.05, and -0.1% for  $d_g$  50 nm and  $\sigma_g$  1.2. The geometric standard deviation is slightly overestimated (up to 0.8%), since the use of the narrower triangular transfer function falsely extends the size range corresponding to the measured SMPS signal. The overestimation of the true distribution width results also in a subtle underestimation of the geometric mean diameter (up to 0.6%) that is associated with the decrease of the

charging and detection efficiencies with decreasing particle size. Collectively, the results indicate that the error is insignificant for size distributions being a few times wider than the transfer function.

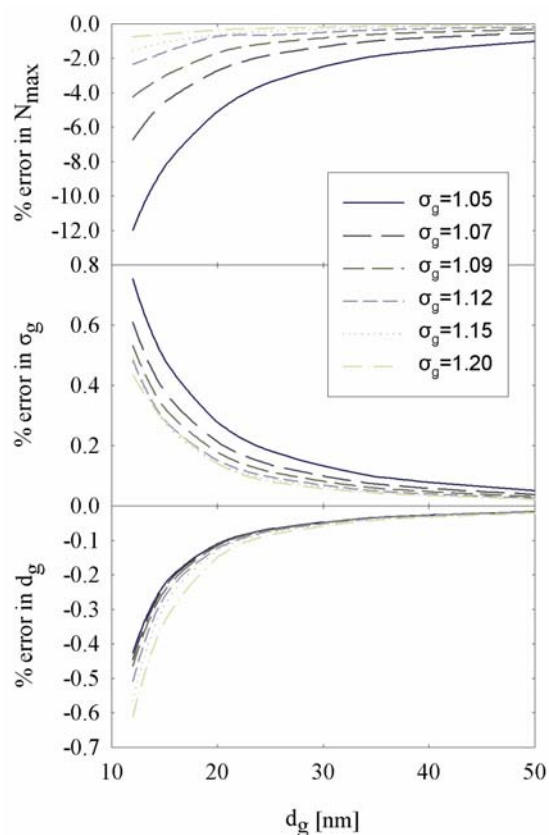


Figure 1. Errors in the recovered size distributions (in terms of  $N_{max}$ ,  $\sigma_g$  and  $d_g$ ) resulting when the diffusion broadening of the transfer function is neglected.

- Knutson, E. & Whitby, K. (1975), *J. Aerosol Science*, 6, 443-451.
- Kousaka, Y., Okuyama, K. & Adachi, M. (1985), *Aerosol Science & Technology*, 4, 209-225.
- Mamakos, A., Ntziachristos, . & Samaras, . (2007), *J. of Aerosol Science*, doi: 10.1016/j.aerosci.2007.1005.1004.
- Stolzenburg, M. (1988). *An Ultrafine Aerosol Size Distribution Measuring System*, University of Minnesota, Minnesota.
- Twomey, S. (1975), *Journal of Computational Physics*, 18, 188-200.

## Improved inversion method for the Scanning Mobility Particle Sizer

A. Mamakos, Ntziachristos and Samaras

laboratory of Applied Thermodynamics, Mechanical Engineering Department, Aristotle University, Thessaloniki, GR 54124, Greece

Keywords: Aerosol instrumentation, SMPS, particle size distribution.

For an accurate inversion of the SMPS signal it is important to precisely characterize the DMA transfer function and to accurately ascribe the CPC particle counts to transmitted electrical mobilities. The complications arising from the non-uniform velocity profile inside the DMA classification region and in the transfer line from the DMA outlet to the optical detector inside the CPC (Collins et al., 2004) have been neglected in the practical application of the instrument.

In the present study, an improved inversion method is presented for the calculation of the SMPS size distributions. The inversion is performed in a two stage procedure in an approach similar to that suggested by Collins et al., (2002). First, the recorded CPC counts are corrected for smearing effects inside the transport lines from the DMA outlet to the optical detector inside the CPC. In the case of the TSI s 3010 CPC considered here, the first order dynamic model suggested by Mamakos et al., (2007a) has been employed, which also considers the plumbing used to connect the CPC to the DMA. In a second step, the  $\beta$ -curve method (Hansen & O'earry, 1993) is employed to numerically solve the system of Fredholm integral equations relating the corrected particle fluxes to the underlying size distribution (Wolfenbarger & Seinfeld, 1990). For the inversion, the scanning DMA transfer functions derived by Mamakos et al., (2007b) are employed.

The performance of the inversion method was evaluated in the measurements of thermally treated diesel exhaust aerosol with a TSI s 3936 10 SMPS, operating on a sheath over sample flow ratio of 10 lpm:1 lpm. Figure 1a shows the size distributions obtained with the TSI s application for three consecutive SMPS scans (45, 300 and 45 s). Compared to the 300 s result, the 45 s distributions are consistently shifted towards larger sizes, exhibiting 10% larger geometric mean diameters and 4% lower total number concentrations. A much better agreement was obtained between the 45 and 300 s distributions determined with the proposed inversion method (Figure 1b). The geometric mean diameters differed by less than 2% while the total number concentrations agreed within 0.2%. The smoothness of the recovered size distributions was also improved since the  $\beta$ -curve method more effectively controls the measurement noise.

Conclusively, an improved inversion method is presented that utilizes a more accurate expression

for the scanning DMA transfer function and also accounts for the dynamic characteristics of the CPC. Application of the algorithm to experimental data from a diesel engine verifies its superior performance compared to the simplified inversion algorithm supplied by the manufacturer.

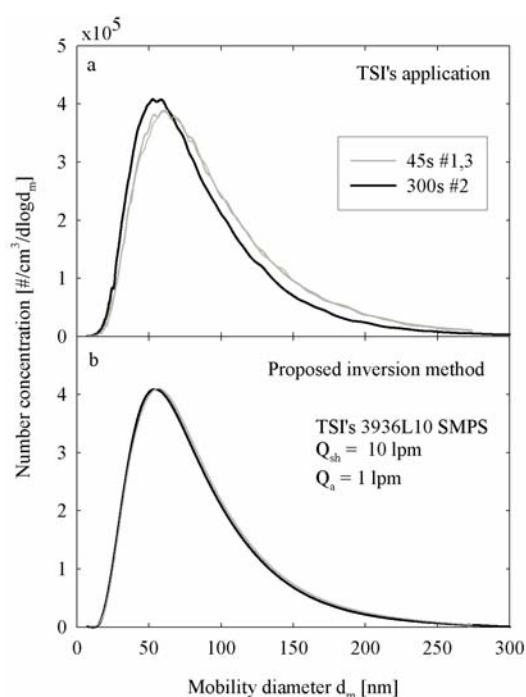


Figure 1. Diesel exhaust size distributions determined with the TSI s algorithm and the proposed inversion method in three consecutive upscans.

- Collins, D., Flagan, R. & Seinfeld, J. (2002), *Aerosol Science & Technology*, 36, 1-9.
- Collins, D., Cocker, D., Flagan, R. & Seinfeld, J. (2004), *Aerosol Science & Technology*, 38, 833–850.
- Hansen, P. & O'earry, D. (1993), *SIAM Journal on Scientific Computing*, 14, 1487-1503.
- Mamakos, A., Ntziachristos, N. and Samaras, N. (2007a), *Aerosol Science & Technology*, submitted for publication.
- Mamakos, A., Ntziachristos, N. and Samaras, N. (2007b), *Journal of Aerosol Science*, submitted for publication.
- Wolfenbarger, J. and Seinfeld, J. (1990), *J. Aerosol Science*, 21, 227-247.

## Direct measurements of the optical properties of Humic and Humic Like Substances (HULIS) by cavity ring down aerosol spectrometer

E. Dinar<sup>1</sup>, A.A. Rizit<sup>1</sup>, C. Spindler<sup>1</sup>, C. Erilic<sup>2</sup>, G. Kiss<sup>3</sup>, and Y. Rudich<sup>1</sup>

<sup>1</sup>Department of Environmental Sciences, Weizmann Institute of Science, 76100, Rehovot, Israel

<sup>2</sup>Department of Atmospheric Sciences, The Hebrew University of Jerusalem, 91904, Jerusalem, Israel

<sup>3</sup>Air Chemistry Group, The Hungarian Academy of Sciences, Veszprem, Hungary

Keywords: Optical properties, Organic aerosols, Refractive index, Light absorption, Light extinction,

Atmospheric aerosols can alter Earth's radiation balance **indirectly** throughout the modification cloud microphysics or **directly** by scattering and absorbing incoming short wave radiation and outgoing long wave radiation.

Although organic species account for a significant fraction of total atmospheric particulate mass, until recently most attention was directed towards studying how aerosols composed from inorganics such as ammonium sulfate, mineral dust and carbon soot ( $C_s$ ) can influence the direct effect of aerosols. Moreover, evaluations of direct radiative forcing by organic aerosol components in the atmosphere have typically assumed that organic components behave similarly towards solar radiation as do sulfate type aerosols, meaning that they do not absorb in the visible part of the spectrum.

The optical properties of "brown carbon" ( $C_{\text{brown}}$ , which includes all light absorbing carbonaceous (LAC) species excluding  $C_{\text{soot}}$ ) were not studied in details and it was recently suggested that the assessment of absorption of solar radiation by  $C_{\text{brown}}$  may not be sufficient, since both measurements and modeling did not take into account the fact that  $C_{\text{brown}}$  exhibit strong absorption spectral dependence, especially in UV range [Andreae and Gelencser, 2006; Kirchstetter, et al., 2004].

It is convenient to classify organic aerosol species on the basis of water solubility, with the water soluble organic carbon (WSOC) portion making up the major mass contribution to atmospheric organic matter. Between 20–70 wt% of WSOC fraction is composed of high molecular weight (HMW) polycarboxylic acids, which are heterogeneous mixture of structures containing aromatic, phenolic and acidic functional groups [Graber and Rudich, 2006]. These aerosol-associated compounds resemble humic substances (HS) from terrestrial and aquatic sources and therefore, they are termed HUMic-Like Substances (HULIS). HULIS probably comprise a major fraction of LAC or the "brown carbon" ( $C_{\text{brown}}$ ). However, the optical properties of HULIS material are not well known, mostly due to difficulties in sampling and collection of high quantities of atmospheric HULIS for detailed laboratory measurements. The lack of material raised the need to search for proxy material, such as

commercial available HS from aquatic and terrestrial sources.

Herein we used a dual wavelength Cavity Ring Down Aerosol Spectrometer (CRD-AS) in the visible (532 nm) and in the ultraviolet (390 nm) regions to measure the size-dependent extinction efficiency,  $Q_e$ , of laboratory generated aerosols composed from molecular weight-fractionated SRFA and HULIS. The measured extinction coefficients were compared to Mie scattering calculations enabling to derive the complex refractive indices (see example in Figure 1) and allowed to differentiate between the scatter and the absorber components. The complex refractive indices were further used to derive the particles' single scattering albedo and scattering and absorption mass extinction coefficients. The possible radiative impacts of HULIS in mixed aerosols are also given.

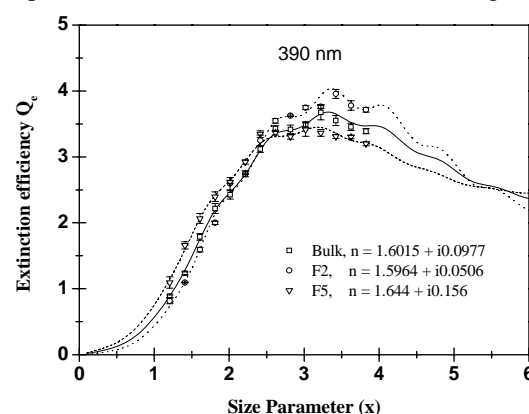


Figure 1. An example illustrating the extinction efficiency as function of size parameter (at 390 nm) for three fulvic acids samples. For each dataset the best Mie fit was used to derive the complex refractive index.

Andreae, M. O., and Gelencser, A.: Black carbon or brown carbon? The nature of light-absorbing carbonaceous aerosols, *Atmos. Chem. Phys.*, 6, 3131-3148, 2006.

Graber, E. R., and Rudich, Y.: Atmospheric hulis: How humic-like are they? A comprehensive and critical review, *Atmos. Chem. Phys.*, 6, 729–753, 2006.

Kirchstetter, T. W., Novakov, T., and Hobbs, P. V.: Evidence that the spectral dependence of light absorption by aerosols is affected by organic carbon, *J. Geophys. Res.*, 109, 2004.

## Fulvic Acids and their sulfated and nitrated analogues in atmospheric aerosol – Determination by Ultrahigh Resolution Electrospray Mass Spectrometry

T. Reemtsma<sup>1</sup>, A. These<sup>1</sup>, M. Linscheid<sup>2</sup> and P.K. Hopke<sup>3</sup>

<sup>1</sup>Department of Water Quality Control, Technical University of Berlin, Sekr KF 4, Str des 17 Juni 135, 10623 Berlin, Germany

<sup>2</sup>Department of Chemistry, Humboldt-Universität zu Berlin, Brook-Taylor-Strasse 2, 12489 Berlin, Germany

<sup>3</sup>Center for Air Resources Engineering and Science, Clarkson University, Box 5708, Potsdam, NY 13699-5708, USA

Keywords: LC-MS, ultrahigh resolution mass spectrometry, organic matter, PM<sub>2.5</sub>, SOA.

The occurrence of humic acid like substances (HULIS) in the atmospheric aerosol is well documented. As long as individual humic acid molecules were not analytically amenable it was impossible to clarify whether the HULIS fraction was only similar to humic acids or whether compounds were identical to those found in terrestrial or aquatic humic or fulvic acid isolates.

Fourier Transform Ion Cyclotron Resonance mass spectrometry (FTICR-MS) with its ultrahigh mass resolution ( $m/\Delta m > 100.000$ ) can fully resolve the molecules in natural organic matter isolates such as humic and fulvic acids in a mass range up to approx. 500 Da.

We have used FTICR-MS to investigate the water soluble organic matter fraction of PM<sub>2.5</sub> aerosol samples collected in Riverside, CA, USA (Reemtsma *et al.*, 2006). Mass spectra in the mass range  $m/z$  200 to  $m/z$  600 were dominated by a few strong signals. This work focused on the vast majority of „background“ signals occupying each nominal mass. Molecular formulas for about 1000 signals in the mass range 200 – 420 were calculated (Fig.1) and could be ascribed to four classes of organic matter.

(I) About 460 molecular formulas consisted solely of C, H and O and were identical to molecular series found in aquatic fulvic acids. Product ion spectra confirmed that these molecules are dominated by carboxylate groups with other functional groups being almost absent. This is the first identification of fulvic acids outside of the soil/water environment.

(II) The 210 sulfur-containing molecules showed the same intensity pattern as the fulvic acids. Product ion spectra confirmed the presence of sulfate groups. We, therefore, propose that these are sulfated fulvic acid analogues. However, the presence of sulfonate groups cannot be ruled out.

(III and IV) Furthermore a series of nitrogen-containing analogues were found and, finally a series where S and N were present in the same molecules. For the nitrogenous molecules the presence of nitrate groups was proven by their product ion spectra.

The identification of fulvic acids together with three series of sulfated, nitrated and mixed sulfated and nitrated molecules in the atmospheric aerosol raises the question as to their origin. From the particle size of the aerosol ( $< 2.5 \mu\text{m}$ ) investigated

here and owing to the fact that sulfated and nitrated analogues of fulvic acids have never been reported to occur in soils we conclude that this was secondary organic aerosol (SOA).

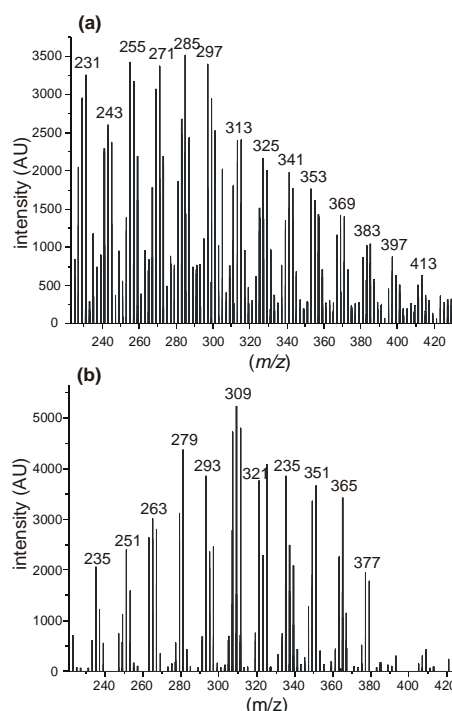


Figure 1. Mass spectra showing (a) fulvic acids and (b) sulfated fulvic acids determined by FTICR-MS in atmospheric aerosol.

We do not yet know whether oxidative transformation of primary biological material or free radical oligomerization of the oxidation products of primary volatile organic compounds led to the formation of fulvic acids. Further investigations will also have to elucidate whether sulfate and nitrate were introduced after SOA was formed or whether they were incorporated as part of the (acid catalyzed) SOA formation.

FTICR-MS will be an inevitable tool to study processes of SOA formation and their products.

Reemtsma T., These A., Venkatachari P., Xia X., Hopke P.K., Springer A. & Linscheid M. (2006) *Anal. Chem.* 78: 8299-8304

## Counting particle measurement within the size range from soot to pollen

Sven Schütz, Martin Schmidt, Leander Mölter  
 Palas® GmbH, Greschbachstr. 3b, 76229 Karlsruhe, Germany

**Keywords:** atmospheric aerosols, bioaerosols, environmental particles, nanoparticles, single particle analysis

In many gaseous multi-phase systems, like in the atmosphere, in exhaust gases etc., there are particles which are too small to be measured directly by conventional detection mechanisms with regard to their number and to their size. The time-resolved detection of these parameters is however important because the particle size and particle number can have a substantial influence on the health e.g. in the breathing air, or they may affect the efficiency and the lifetime of filters e. g. in technology.

To measure the number of small particles within the range of 5 nm to 1 µm condensation nucleus counters, so called CNCs, are used. These CNCs are developed usually for laboratory measurements and are sensitive in relation to fluctuations of the temperature and of the air pressure in the atmosphere.

**A new particle measuring system was developed, which consists of the combination of an aerosol spectrometer with a CNC-module.** Due to the combination of the welas® system with the new CNC-module, the number of smallest particles down to 10 nm can, for the first time, be accurately determined with a counting procedure also in concentrations up to 10<sup>5</sup> particles/cm<sup>3</sup>. Therefore, the new device combination is suitable particularly for measurements in the outside air, the more so as the number concentration of atmospheric particles < 100 nm can increase easily up to 10<sup>5</sup> particles/cm<sup>3</sup>.



Figure 1. CNC-06 with two welas® sensors for measurement within the system welas® 3000

The combination of a new condensation module, the CNC, with the white light aerosol spectrometer welas® and the passive collector Sigma-2 allows an almost accurate time-resolved determination of the particle number within the range of < 10 nm to 40 µm.

An interesting possibility for many measuring tasks is the combination of the CNC-module with the system welas® 3000 which measures quasi simultaneously with two sensors at two different measuring points or in combination with the new CNC module at the same measuring point. Both sensors are connected to only one light source, one photo-multiplier and one control unit. Therefore the transient characteristics of the two sensors are identical and the measurements are very reliable.

Since for the high-resolved size and quantity determination of particles > 0.3 µm one uses the same device as for the counting of the up-condensed smaller particles, both measurements are identical concerning the counting efficiency. Therefore, the measurement results can be clearly combined computationally.

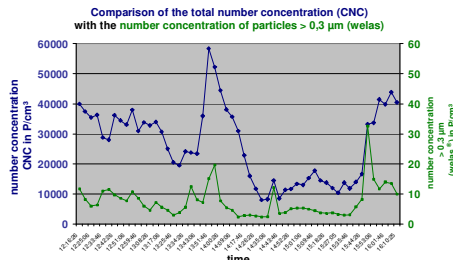


Figure 2. Quasi simultaneous measurements with welas® 3000 and CNC-module: comparison of total number concentration (CNC, upper curve) with the number concentration of particles > 0,3 µm (welas®, lower curve)

Furthermore, this new device combination offers an automatic coincidence detection which is particularly important also for the accurate concentration determination of small particles.

Due to the new evaporator technology of the CNC module, the vertical structure and the plane evaporator surface, an automatic and fast adjustable activation and deactivation of the liquid to be evaporated is possible. Due to the robust structure and the simple handling, the system should be optimally suitable for continuous use over months with high availability. In this paper we will describe the complete system and validate its function with measurement results.

## A new Loading and Scattering Correction for the Particle Soot Absorption Photometer (PSAP)

T. Müller, A. Schladitz, A. Wiedensohler

Leibniz Institute for Tropospheric Research, Permoserstr. 15, 04318, Leipzig, Germany

Keywords: Absorption coefficient, Atmospheric aerosols, Aerosol instrumentation.

Scattering and absorption of light due to particles are major parameters for calculating the net effect of atmospheric aerosol on the radiation balance of Earth. While the measurement of the particle scattering coefficient is a well understood technique (nephelometers), the measurement of the particle absorption coefficient is still affected by large uncertainties.

Most systems for determining the particle absorption coefficient are based on the measurement of light transmission of a particle loaded filter. This measurement technique depends on a well-defined calibration, which has to account for the total loading of the filter (loading correction) and for a cross sensitivity to particle scattering (scattering correction). Both effects can not be addressed independently. The correction of the cross sensitivity to scattering requires the measurement of the particle scattering coefficient.

One often used absorption photometer, the particle soot absorption photometer (PSAP; Radiance Research, Inc., Seattle, WA, USA), was calibrated to correct both effects (Bond, 1999) but the scattering correction is merely a first order correction. An additional restriction of this correction is the limitation to low filter loading.

Loading and scattering correction functions commonly result from calibration experiments. We present a new hybrid approach which is based on simulations of the radiative transfer of particle filter and an experimental calibration. The radiative transfer calculations were done using ray-tracing simulations (Müller, 2006). In order to calculate the “true” absorption the modelled correction function was modified using data from an experimental calibration.

The absorption coefficient is calculated by:

$$\sigma_{abs}(t) = \frac{-\ln(\tau(t)) \cdot \frac{A}{V \cdot \Delta t}}{K(\tau(t), \omega_0^\Sigma)}$$

where  $\tau(t)$  is the actual transmission<sup>1</sup> of the filter,  $A$  is the size of the sample spot, and  $V$  is the aerosol flow sucked through the filter during the time interval  $\Delta t$ . The correction function  $K$  depends on the actual transmission and the single scattering albedo of all particles collected on the filter:  $\omega_0^\Sigma = \sigma_{sca}^\Sigma / \sigma_{ext}^\Sigma$ . The

<sup>1</sup> The transmission is set to unity for an unloaded filter.

new correction method and the correction of Bond (1999) result in nearly the same values for low single scattering albedos ( $\omega_0 = \sigma_{sca} / \sigma_{ext} < 0.6$ ). For higher single scattering albedos the new correction method results in lower absorption coefficients.

An example is shown in Figure 1) for data collected during the SAMUM<sup>2</sup> field experiment. The effect of the new correction can easily be seen when plotting the time series of the SSA. Using the correction scheme of Bond (1999), we obtained a saw tooth like run of the single scattering albedo (dots). Using the new correction scheme (open circles) the saw tooth structure disappears even for high loadings (DOY 145).

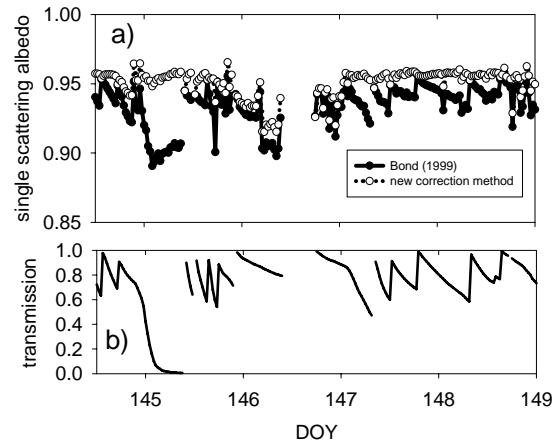


Figure 1. a) Single scattering albedo during the SAMUM campaign. b) Transmission of light through the particle filter.

Bond, T. C., T. L. Anderson, et al. (1999) Calibration and intercomparison of filter-based measurements of visible light absorption by aerosols, *Aerosol Sci. Technol.*, 30, 582-600.

Müller, T., Hallbauer, E. and J. Pelzer (2006) Characteristics and Calibration of a Spectral Online Absorption Photometer, *Proceedings of the Seventh International Aerosol Conference*, 431.

This work was supported by the Deutsche Forschungsgemeinschaft under grant MU 2669/1-1.

<sup>2</sup> SAMUM: The „Saharan Mineral dust experiment“ took place in southern Morocco in May/June 2006.

## The new UFP 330: Comparison with a DMPS for ambient aerosols

B. Wehner<sup>1</sup>, T. Tuch<sup>1</sup>, A. Wiedensohler<sup>1</sup>,  
A. Zschoppe<sup>2</sup>, L. Hillemann<sup>3</sup>, H. Gerwig<sup>4</sup>

<sup>1</sup>Leibniz-Institute for Tropospheric Research, 04318 Leipzig, Germany

<sup>2</sup>Topas GmbH, 01279 Dresden, Germany

<sup>3</sup>UBG – Staatliche Umweltbetriebsgesellschaft, Radebeul, Germany

<sup>4</sup>LfUG - Saxon State Agency for Environment and Geology, Section Air Quality, 01109 Dresden, Germany

Keywords: number concentration, instrument development, comparison, network operation

Several epidemiological studies have shown a relationship between high number concentrations of ultrafine particles (< 100 nm) and adverse health effects. However, most routine measurements of particulate matter are limited to the mass concentration, e.g. PM<sub>10</sub> or PM<sub>2.5</sub>. One major reason for this is that commercially available measurement technique is relatively expensive and needs more maintenance than in the routine network operation can be provided. Within the frame of the project UFIPOLNET a new instrument to measure ultrafine particle number concentrations has been developed which is easy to handle and needs less maintenance than e.g. available SMPS systems.

The new instrument (Ultrafine Particle Monitor, UFP330) consists of a Corona Charger, a DMA, and an electrometer. The measured current is online transferred to a number size distribution (20 – 500 nm) and locally stored. Within routine networks the number of measured parameters which might be saved continuously is limited. Thus, number size distributions are usually replaced by integral concentrations within certain size classes. For the UFP330 the size classes have been defined as follows:

name	range
<b>N1</b>	20 - 30 nm
<b>N2</b>	30 – 50 nm
<b>N3</b>	50 – 70 nm
<b>N4</b>	70 – 100 nm
<b>N5</b>	100 – 200 nm
<b>N6</b>	> 200 nm

Within the frame of UFIPOLNET 4 prototypes of the instrument have been built and are operated at 4 stations in Europe. To ensure the data quality and comparability the UFPs have been operated in parallel to a DMPS system in a street canyon, representing a typical measurement site within an urban network. Number size distributions obtained by DMPS have been converted to size classes according to N1 – N6.

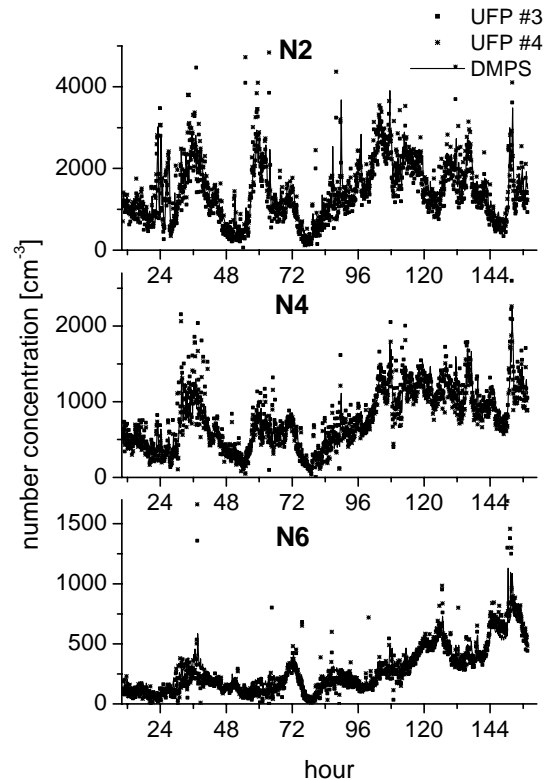


Figure 1: Number concentrations measured in parallel with two new UFP and one DMPS in the street canyon site

Figure 1 shows the results of three selected size channels for parallel measurements between two UFP prototypes and one IfT-operated DMPS. In the first view they show a good correlation, only a few outliers have been registered. In general, the correlation for the size classes N2 – N5 is higher than for the largest and smallest one. The result is nearly independent on the concentration at this site.

In February 2007 the instruments have been set up at four measurement sites within Europe. Three of them measure there parallel to another size spectrometer such as SMPS or DMPS. These results will give more information about the data quality at differently polluted sites and also over a longer period.

This project ([www.ufipolnet.eu](http://www.ufipolnet.eu)) is financed by the LIFE financial instrument of the European Community under No. LIFE04 ENV/D/000054.

## **Intercomparison of instrumentation for atmospheric aerosol measurements. DAMOCLES campaign**

J.A. Martínez-Lozano<sup>1</sup>, L. Alados-Arboledas<sup>2</sup>, B. de la Morena<sup>3</sup>, V. Estellés<sup>1</sup>, F.J. Exposito<sup>4</sup>, J. Pey<sup>5</sup>, M. Sicard<sup>6</sup>  
and M. Sorribas<sup>3</sup>

<sup>1</sup>Department of Earth Physics, University of Valencia, 46100, Burjassot (Valencia), Spain

<sup>2</sup>Department of Applied Physics, University of Granada, 18071, Granada, Spain

<sup>3</sup>Atmospheric Sounding Station, INTA, 21130, Mazagón, (Huelva), Spain

<sup>4</sup>Department of Fundamental Physics, University of La Laguna, 38200, La Laguna (Tenerife), Spain

<sup>5</sup>Instituto Ciencias de la Tierra "Jaume Almera", CSIC, 08028, Barcelona, Spain

<sup>6</sup>Department of Signal Theory and Communications, Univ. Politècnica de Catalunya, 08038, Barcelona, Spain

Keywords: Atmospheric aerosols, Aerosol instrumentation

The DAMOCLES network is a thematic network, started in 2004, whose main objective is the establishment of a link among the different groups that perform research on atmospheric aerosols in Spain. Under the DAMOCLES coordination, a field campaign was held in summer 2006 at the INTA installations (El Arenosillo, Huelva, in southern Spain) for the intercomparison of different kind of instruments devoted to in-situ and columnar aerosol measurement. The Atmospheric Sounding Station 'El Arenosillo' (37.1° N, 6.7°W, 40 m a.s.l.) is an exceptional platform to measure different atmospheric parameters for temporary or continuous monitoring. Ground-based meteorological parameters are routinely measured at the station.

The field campaign took place from 27<sup>th</sup> June to 4<sup>th</sup> July 2006. 13 European institutions, mostly Spanish, participated on it. During this field campaign, two daily meteorological soundings were carried out at midday and midnight for characterisation of the atmospheric condition. A plane was also flown by the National Institute of Aerospace Technology (INTA), to carry airborne sensors for measuring different atmospheric factors: meteorological parameters, ozone with a 2B Tech analyzer, and aerosol particle size distributions in the range (0.01-2)  $\mu\text{m}$ , by using a PCASP probe.

A total number of five LIDAR instruments were deployed on the site: two laboratories LIDAR from Barcelona and Madrid, a Raymetrics LR321 from Granada, a CIMEL Electronique CAML CE370-2 from Valencia and an Elight UV11 from Cartagena. The measurement protocols were twofold: a) continuous daytime measurements between 0800 and 2000 UTC, and b) 2-hour nighttime measurements starting at 2130 UTC for the Raman channel. The campaign was also twofold as far as lidars were concerned: identification (i) of the hardware problems and limitations of each system, and (ii) of the limitations of the pre-processing softwares used by each group.

The columnar aerosol optical depth was also measured by 7 CIMEL CE318 sunphotometers. All these instruments were previously calibrated in the

same site. The calibration was performed for direct and diffuse radiance. In order to get the aerosol radiative properties from the CE318 data (aerosol optical depth, Ångström wavelength exponent, single scattering albedo, etc...) software developed by the Universidad de Granada was applied based on the Skyrad.pack version 2 algorithm.

For in situ aerosol characterisation, high volume collectors (DIGITEL and MCV) with DIGITEL for PM<sub>10</sub>, PM<sub>2.5</sub> and PM<sub>1</sub> measurement were also deployed, with two cascade impactors for particulate matter measurement in 7-8 granulometric fractions. For the PM<sub>10</sub>, PM<sub>2.5</sub> and PM<sub>1</sub> measurement, quartz fiber filters of 150 mm diameter were adapted. The measurement was recorded every campaign day, by changing the filters twice per day for each granulometric fraction (1000 – 2200 and 2200 – 1000 UTC) intended for the separate characterisation of daytime and nighttime aerosols.

Other in situ deployed instrumentation was a Scanning Mobility Particle Sizer, (SMPS, Model 3936), two Aerodynamic Particle Sizer (APS, Model 3321) and a Grimm Spectrometer (Models #190) used to measure ground base particle size distributions at discrete size interval almost continuously. For nephelometric characterisation of aerosols at ground level, three integrating nephelometers TSI-3563, with capabilities to determine the scattering and backscattering coefficients at three wavelengths were also deployed. Additionally the University of Vienna team operated a polar nephelometer that determines the angular scattering function at 670 nm, from 10 to 170°. Absorption coefficient has been measured continuously at 670 nm by using a Multi Angle Absorption Photometer, while accumulated values for twelve hours period have been determined at several wavelengths, by the Integrating Plate technique.

The Spanish Ministry of Education and Science (MCYT) is thanked for the Complimentary Action CGL2006-27108-E/CLI.

## **T03 Abstracts**

## Computational investigation of particle losses in random porous structures

A. Serrenho<sup>1</sup>, A. F. Miguel<sup>1,2</sup> and A. H. Reis<sup>1,2</sup>

<sup>1</sup>Geophysics Centre of Évora, Rua Romão Ramalho 59, 7000-671 Évora, Portugal

<sup>2</sup>Department of Physics, University of Évora, 7002-554 Évora, Portugal

Keywords: particle losses, particle residence time, porous structure.

Processes involving aerosols are used in the production of many advanced materials, in such a way that a number of recent chemical engineering techniques involve dynamics of aerosols. Micro-reactor technology seems to be very effective in rapid mixing of aerosol streams with the purpose of producing more uniform dispersions (Heim *et al.*, 2006). This work studies the influence of random porous structures with different porosities on mixing of aerosol particle streams with clean gas streams. Two key quantities were used to characterize the process: particle losses (deposition) within the porous structure and residence time distribution of the particles.

A Lagrangian simulation for aerosol dynamics in random porous structures was carried out. Flow conditions in the porous geometries were assumed to be isothermal, incompressible and laminar, and solid spherical particles ranging from 0.2 to 10  $\mu\text{m}$  were considered. A detailed description of the numerical model can be found in Aydın *et al.* (2005). Examples of random porous structures used in the numerical simulations are shown in Figure 1.

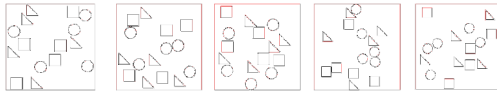


Figure 1. Schematic representation of random porous structures with same porosity.

The study was performed in porous structures with porosities ranging from 0.8 to 0.9. The simulations were carried out in such a way that the mean fluid velocity inside of these porous structures (intrinsic velocity) was always  $10^{-4}$  m/s.

The fraction of lost particles in the porous structures is documented in Table 1.

Table 1. Particle losses within the porous structure (mean percentage and standard deviation)

Porosity	Particle size 0.2 $\mu\text{m}$ (%)	Particle size 2 $\mu\text{m}$ (%)	Particle size 10 $\mu\text{m}$ (%)
0.80	4.6 $\pm$ 1.9	4.4 $\pm$ 1.7	3.7 $\pm$ 2.0
0.85	3.2 $\pm$ 1.4	3.2 $\pm$ 1.4	3.1 $\pm$ 1.0
0.90	1.4 $\pm$ 1.0	1.7 $\pm$ 0.8	1.9 $\pm$ 1.2

It is observed that particle losses decrease with porosity as expected. For a porosity of 0.85 the particle losses are almost the same for the three different particle sizes. For a porosity of 0.8 the losses of submicrometer particles are larger than for micrometer particles (2 and 10  $\mu\text{m}$ ), the inverse occurring for porosities of 0.9.

We analyzed also pressure drop through the porous structure in relation with particle losses (Figure 2). For a constant fluid speed increase in pressure means decrease in porosity.

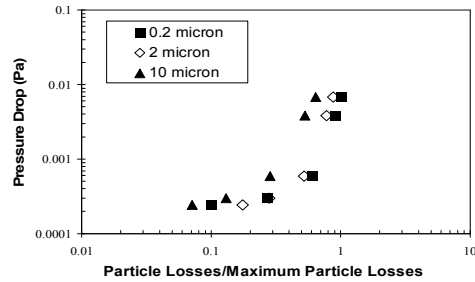


Figure 2. Pressure drop versus fraction of lost particle for porous structures with porosity 0.85.

It was found that particles losses increase with pressure drop increase. Similar results were obtained for porosities of 0.8 and 0.9. The residence time inside porous structures is listed in Table 2. It seems that residence time is strongly dependent on particle size. For particles with 0.2  $\mu\text{m}$ , the residence time decrease with the porosity while for micrometer particles (2 and 10  $\mu\text{m}$ ) it is almost independent of the porosity.

Table 2. Mean residence time distribution within porous structures

Porosity	Particle size 0.2 $\mu\text{m}$ (s)	Particle size 2 $\mu\text{m}$ (s)	Particle size 10 $\mu\text{m}$ (s)
0.80	79	46	36
0.85	72	44	36
0.90	61	42	35

This work was supported by Foundation for Science and Technology (FCT) project POCTI/EME/59909/2004.

Aydın, M., Balik, G., Miguel, A. F. & Reis, A. H. (2005). *J. Mech. Eng.*, 51, 495-500

Heim, M., Wengeler, R., Nirschl, H. & Kasper, G. (2006). *J. Micromech. Microeng.*, 16, 70-76

## Influence of the stains on the Millikan-type plate electrodes in the absolute size measurement of particle size standards by the electro-gravitational aerosol balance

K. Takahata and K. Ehara

National Metrology Institute of Japan (NMIJ), National Institute of Advanced Industrial Science and Technology (AIST), 1-1-1 Umezono, Tsukuba, Ibaraki 305-8563, Japan

Keywords: standard for calibration, size measurement, electro-gravitational aerosol balance.

Polystyrene latex (PSL) particles have been widely used as particle size standards to calibrate or inspect various types of aerosol measurement instruments. The traceable calibration service for the manufacturer of PSL particles to determine the number average diameter of monodisperse PSL particles in the size range of 100 nm to 1 μm has been provided by NMIJ/AIST for several years. The adopted sizing method is the absolute size measurement method called electro-gravitational aerosol balance (EAB) using Millikan-type plate electrodes (Ehara et al. 2006a, 2006b). In the EAB measurement, charged sample PSL particles are introduced into parallel plate electrodes, and the particle survival rate after a certain holding time is measured as a function of applied voltage. The number average diameter is determined by fitting a theoretical curve based on the solution to the diffusion equation to experimental data. At the present time, the stains on the electrodes are visible to the naked eyes and can not be wiped off, because the electrodes had been used intermittently since 1996. It is therefore supposed that the stains might cause the difference in the work function between the electrode surfaces, and then the bias voltage corresponding to the particle size change. The new electrodes are being developed in order to investigate the influence of the stains and to maintain high quality calibration service. In the present study, details of the new electrodes which are the most important components are described.

Figure 1 shows top and side views of the electrodes under development. Two flat plate electrodes made of stainless steel with a corrosion resistance, 250 mm in diameter and 10 mm in thickness, are separated by alumina annulus having a nominal height of 15 mm which was determined by a micrometer. The flatness of the electrode surfaces and the annulus surfaces were evaluated with a flatness interferometer. The space between the electrodes is sealed by alumina annulus without silicon-gel O-rings. The inside diameter of the annulus is 200 mm, and hence the volume of the sealed space amounts to 471.2 cm<sup>3</sup>. There are 12 holes bored on the side of the annulus, five of which serve as aerosol inlets, five as clean air inlets, and the remaining two as aerosol outlets. One of the aerosol outlets functions to exhaust the aerosol before the holding time has started, and the other to feed the

aerosol to a particle counter after the holding time has elapsed. The voltage of the upper electrode relative to the lower one was chosen to be negative, and hence positively charged particles were the target of our measurement. The applied voltage was monitored with a digital multimeter.

One of the most important functions of the new electrodes is can be turned upside down. The direction of the additional electrostatic force caused by the difference in the work function between the two electrode surfaces will be reversed if the electrodes are turned upside down. It is then expected that the influence of the additional electrostatic force would be determined from a pair of survival rate spectra obtained by reversing the electrodes.

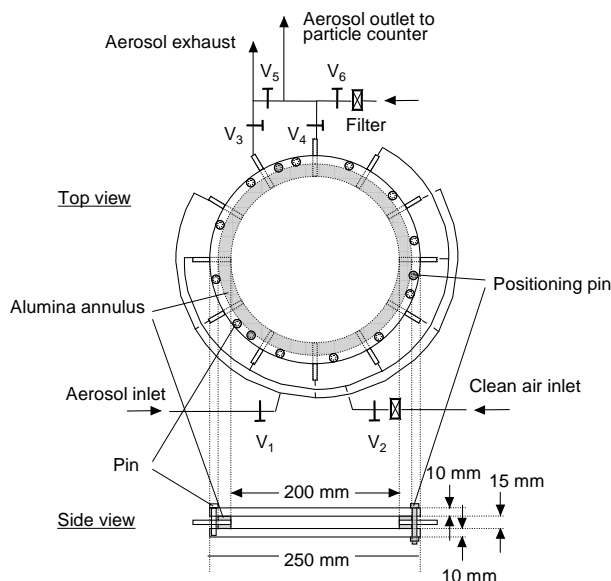


Figure 1. The new Millikan-type plate electrodes under development.

This work was performed as a part of the Nanotechnology Material Metrology Project supported by New Energy and Industrial Technology Development Organization.

Ehara, K., Takahata, K., and Koike, M. (2006a). *Aerosol Sci. Technol.*, 40, 514-520.

Ehara, K., Takahata, K., and Koike, M. (2006b). *Aerosol Sci. Technol.*, 40, 521-535.

## The EU project NANOTRANSPORT

T. Rettenmoser<sup>1</sup>, C. Gerhart<sup>1</sup> and H. Grimm<sup>1</sup>

<sup>1</sup>Grimm Aerosol Technik GmbH & Co. KG, Ainring, 83404, Germany

Keywords: aerosol characterisation, aerosol generation, nanoparticles, particle size distribution, size-segregated aerosols

The EU project NANOTRANSPORT brings together leading expert organisations in risk management, aerosol monitoring, filtration, nanoparticle technology and online particle characterization fields that are critical for the success of the project. The NANOTRANSPORT participants, Det Norske Veritas, GRIMM Aerosol Technik and University of Karlsruhe - Institut für Mechanische Verfahrenstechnik und Mechanik, will collectively contribute with deep insight in their respective fields of competence.

The proposed pre-normative study has the objective of bringing into light and to document the need for standardised test aerosols adapted to the scope of nanotoxicology and occupational health studies. State-of-the-art nanoparticle generation and aerosol monitoring equipment will be used to show that the properties (such as size, size distribution, surface chemistry, surface charge, concentration) of aerosols formed by manufactured nanoparticles experience dramatic changes when released in the ambient air compared to their initial properties within the reactor. The project will provide introductory experimental results that will be used to develop recommendations and guidelines for the European Commission.

Based on NANOTRANSPORT results, the Commission will have the necessary background information to prioritise and initiate research to develop standard test aerosols adapted to specific studies/tests/validations/investigations. It will contribute to determine the toxicological and epidemiological hazards posed by nanopowders in a systematic way reflecting exposure levels likely to be encountered in industry.

Also new standards and particularly adequate test aerosols for testing and guaranteeing suitability of filtration and respiratory protection for use in nanoparticles/nanopowders production or processing sites will be identified and described. Promote a more effective use of research funding by providing a framework of correct methodologies that will contribute to provide meaningful and comparable results which will help the development of risk assessment tools for released nanoparticles and also help gaining public and stakeholder acceptance regarding safe production and use of manufactured nanoparticles.

The aim of is to help define realistic test conditions in terms of test aerosols characteristics

(particle size distribution, concentration and surface chemistry) for use within nanotoxicology investigations but also to test and certify the efficiency of existing engineering control systems of manufacturing equipment (such as air cleaning systems, personal protective equipment).

An overview about the continuous methods for nanoparticle production (aerosol process) will be prepared to show which industries are involved in that field and which production methods are used to give a first impression of the different production methods and production conditions. This could be e.g. flame process, spray process, milling or ablation process in different temperature, pressure and concentration conditions. This would give a first feeling on critical exposure situations to the workplace and the environment and relevant scenarios will be developed.

Based on these scenarios and the state-of-the-art study where the most critical experimental parameters governing aerosols behaviour will have been identified, a tailor-made experimental programme will be defined. Nanoparticles will be generated in a controlled manner in terms of size distribution, composition, material and concentration and the formed aerosols will be released in exposure chambers with controlled atmosphere (temperature, pressure and relative humidity). State-of-the-art equipment will be used to monitor the behaviour of the released aerosols. Interaction between nanoparticles, surface contamination and interaction with existing ambient aerosols will be investigated function of time. The properties of aerosols released to ambient air from manufactured nanoparticle will be compared to those of the initial nanoparticles aerosols.

GRIMM will contribute to the execution of the experimental work. As the leading scientific instrumentation company providing products for continuous aerosol monitoring for environmental and occupational use in Europe GRIMM has unique facilities which will be used during the project. Top of the line pieces of equipment to generate nanoparticles in a controlled manner (size from a few nanometres up to several hundred nanometres, concentration, composition) and to monitor numerous properties of the formed aerosols in exposure chambers with controlled atmosphere offer a unique opportunity to conduct the study proposed in NANOTRANSPORT.

## **T04 Abstracts**

## Personal Sampler for Monitoring of Viable Viruses; Part 1: Modelling of Outdoor Sampling Conditions

A.I. Borodulin<sup>1</sup>, B.M. Desyatkov<sup>1</sup>, N.A. Lapteva<sup>1</sup>, A.N. Sergeev<sup>1</sup>, I. Agranovski<sup>2</sup>

<sup>1</sup> State Research Center of Virology and Biotechnology "Vector", Koltsovo, Novosibirsk region, 630559 Russia

<sup>2</sup> Faculty of Environmental Sciences, Griffith University, Brisbane, 4111, QLD, Australia

Keywords: bioaerosol, personal monitoring, viable microorganisms, collection efficiency, air pollution modelling, optimal sampling locations.

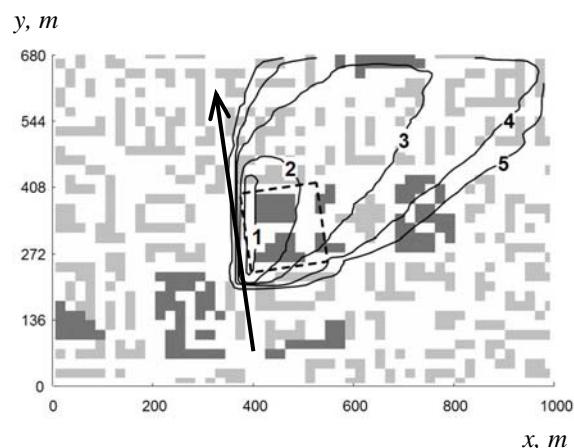
A new personal aerosol sampler has recently been developed and verified to be very efficient for monitoring of viable bioaerosol bacteria, fungi and viruses (Agranovski *et al.* 2002). The operational principle is based on passing of air sample through porous medium submerged into a layer of collecting liquid. As the result, during passing through narrow and tortuous channels inside the porous medium, the air stream is split into a multitude of very small bubbles with the particulates are being scavenged by these bubbles and, thus, effectively removed before the effluent air leaves the device. Bioaerosol particles are being accumulated in the collecting liquid during the entire process of sampler operation. The experimental verification of the sampler on monitoring of common viruses (Influenza, Mumps, Measles, Vaccinia and SARS) with different levels of sensitivity to physical and biological stresses showed that it can recover up to 25% of rather labile Influenza virus, whilst a very robust and stable Vaccinia virus is being recovered at the level of 90% (Agranovski *et al.* 2004).

This presentation derives a mathematical model for determination of concentration of airborne bioaerosols in analyzed air sample based on the number of live particles detected in the collecting liquid after sampling. The minimal concentration of live airborne microorganisms measurable by the device was also evaluated (Borodulin *et al.* 2006).

The possibility of obtaining reliable values of virus-containing aerosol concentrations under real conditions of the sampler operation was demonstrated taking as an example the simulated hypothetical "terrorist act" involving viral material under city outdoor conditions. A hypothetical episode concerned with music concert in the central square of Novosibirsk is considered in the calculations. The concert was held from 3 p.m. to 4 p.m. local time under meteorological conditions typical for the middle of July. South-western wind with the velocity of 2 m/s was preset in the calculations. According to the legend, during the concert the "terrorists" performed concealed use of a preparation of a highly pathogenic viral strain in aerosol form. A car with the aerosol source was running along the central street of

the city crossing the square at the speed of 18 km/hour (shown by arrow). The spraying line was 250 m long. A total of 250 g of the preparation with the concentration of viral particles of  $5 \cdot 10^{10}$  per g was discharged into the atmosphere along the spraying line at the height of 2 m above the underlying surface. The spraying started at 3 p.m. It lasted for 40 s.

Figure below show the scheme of the calculation template with the isolines of mathematical expectation of the measured concentration of virus-containing aerosols for the height  $z = 1.5$  m. Numbers 1-5 respectively correspond to the values of measured concentration  $2.5 \cdot 10^7$ ,  $5 \cdot 10^6$ ,  $5 \cdot 10^5$ ,  $5 \cdot 10^4$ ,  $5 \cdot 10^3$  virus particles per  $m^3$ . The territory of concert marked by dotted line.



The minimal reliably measurable concentration of bioaerosol for the sampler in our case is  $4.2 \cdot 10^2$  viruses per  $m^3$ . Consequently, in the case under consideration all data obtained by samplers within the area shown with a dotted line can be considered as reliable.

Agranovski I. *et al.* (2004). *Atmospheric Environment*. 36, 889-898.

Agranovski I. *et al.* *Applied Environmental Microbiology*. 70, 6963-6967.

Borodulin A.I. *et al.* *Atmospheric Environment*. (2006). 40 (35), 6687-6695.

## Personal Sampler for Monitoring of Viable Viruses; Part II: Modelling of Indoor Sampling Conditions

V.A. Shlychkov<sup>1</sup>, A.I. Borodulin<sup>1</sup>, B.M. Desyatkov<sup>1</sup>, I. Agranovski<sup>2</sup>

<sup>1</sup> State Research Center of Virology and Biotechnology “Vector”, Koltsovo, Novosibirsk region, 630559 Russia

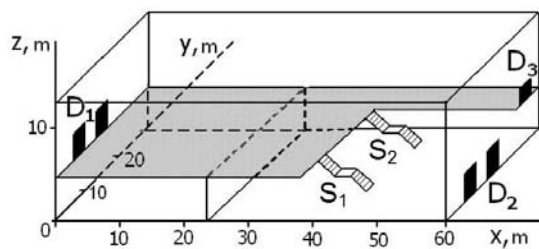
<sup>2</sup> Faculty of Environmental Sciences, Griffith University, Brisbane, 4111, QLD, Australia

Keywords: bioaerosol monitoring, personal sampling, air pollution modelling.

A new personal aerosol sampler has recently been developed and verified to be very efficient for monitoring of viable bioaerosol bacteria, fungi and viruses (Agranovski *et al.* 2002). The operational principle is based on passing of air sample through porous medium submerged into a layer of collecting liquid. As the result, during passing through narrow and tortuous channels inside the porous medium, the air stream is split into a multitude of very small bubbles with the particulates are being scavenged by these bubbles and, thus, effectively removed before the effluent air leaves the device. Bioaerosol particles are being accumulated in the collecting liquid during the entire process of sampler operation. The experimental verification of the sampler on monitoring of common viruses with different levels of sensitivity to physical and biological stresses showed that it can recover up to 25% of rather labile Influenza virus, whilst a very robust and stable Vaccinia virus is being recovered at the level of 90% (Agranovski *et al.* 2004).

This presentation describes the development of a mathematical model for evaluation of particle concentration for indoor air conditions. The results of modeling could be used to predict particle concentration in an ambient air, taking into account space geometry and ventilation/air conditioning created air streams (Shlychkov *et al.* 2007).

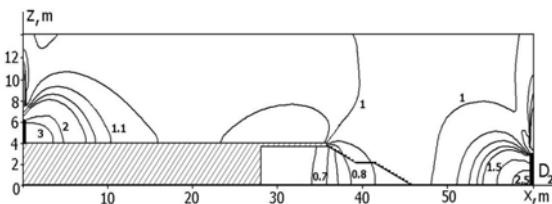
Two case studies were then undertaken to determine the particle concentration at hypothetical shopping centre, see fig. below,



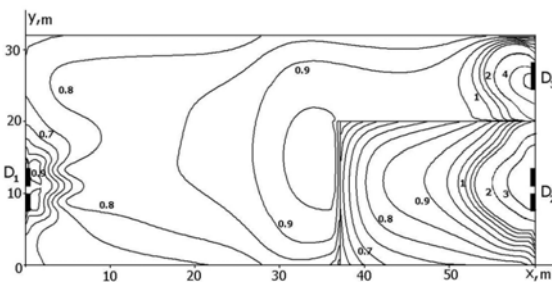
where D<sub>1</sub>, D<sub>2</sub> – the doors; S<sub>1</sub>, S<sub>2</sub> – the stairs.

The calculations were made for the situations when: the ambient air movement is created by a local

ventilation system, and besides the local ventilation, the outdoor air enters the space influencing particle distribution situation due to mixing with ventilation created air streams. The next figure shows the isolines of normalized concentration values of virus-containing particles at the section  $y = 9$  m under “no external wind” conditions.



And the last figure shows isolines of normalized values of virus-containing particles concentration at the height of 1.5 m from the floor calculated for the presence of the wind pressure on the building.



The results of modeling were used to evaluate the minimal source concentration of virus-containing aerosols measurable by the personal bioaerosol sampler moving along various routes during certain time intervals. It was found that the minimal concentration is relatively high for naturally occurring viral particles, however could be achieved during some event (for example bio-terrorists attack).

Agranovski I. *et al.* (2004). *Atmospheric Environment*. 36, 889-898.

Agranovski I. *et al.* *Applied Environmental Microbiology*. 70, 6963-6967.

Shlychkov V.A. *et al.* *Aerosol Science & Technology*. 2006.

## Survey of Bioaerosol Emissions from Australian Poultry Buildings

V. Agranovski<sup>1</sup>, T. Reponen<sup>2</sup>, and Z. D. Ristovski<sup>1</sup>

<sup>1</sup>International Laboratory for Air Quality and Health, Institute of Health and Biomedical Innovation, Queensland University of Technology, Brisbane, Australia.

<sup>2</sup>Center for Health-Related Aerosol Studies, University of Cincinnati, OH, USA

Keywords: bioaerosols, dust, emissions, health effects, chicken farm

Bioaerosol emissions from poultry sheds may represent a risk to the health of farmers and rural residents living in close proximity to the farms. Pathogen and allergen emissions in exhaust plumes from chicken sheds and their potential to cause human disease are increasingly raised as an issue by environmental lobby groups. Tunnel ventilated sheds are of a particular concern as they produce the most concentrated plumes and consequently may cause the most significant health impacts. While it is commonly known that a diverse range of biological agents is present in the exhaust air from the sheds, the potential for human health impacts does not necessarily follow, as aspects such as the specific characteristics of the bioaerosols are important.

The objective of this study was to evaluate the risks of developing respiratory allergies due to environmental exposure to bioaerosols emitted from tunnel ventilated broiler sheds. Bioaerosol emissions from typical Australian (specifically, sub-tropical Queensland) broiler sheds were assessed over a range of operational conditions, including bird age, stocking density and ventilation rates. Aerosols were sampled isokinetically from a duct connected to one of the exhaust fans. The sampling probe was inserted to the center of the duct, approximately seven diameters downstream from the fan. The measured gas velocity (at the center of the duct) was multiplied by the cross-sectional area of the duct to get the volumetric flow rate at the probe entrance.

Weekly measurement campaigns were conducted twice a year (in winter and summer), over the entire growing periods (up to 40-55 days). Measurements were also taken from empty sheds (no birds, litter only) and a day or so before and after birds were placed into or removed from the sheds. Aerosols were monitored continuously with the UV-APS. Bacterial and fungal samples were collected with AGI-30 impingers and Andersen microbial impactors (1, 2 and 6-stage) and then subjected to cultivation on a range of agars: TSA and R2A for total bacterial heterotrophs; half-strength TSA and Nutrient agar for thermophilic actinomycetes; MCA and EMBA for gram-negative bacteria; MEA, DRBC, SDA and DG-18 for fungi. Potato glucose agar was occasionally used to assist in the identification of fungi.

Based on the UV-APS data, approximately 95 % of both total and biological (fluorescent) particles emitted from the sheds were respirable (< 7 µm) and

approximately 60 % of total and 50 % of bio-particles were within the fine particles size range (< 2.5 µm). All particles larger than 6 µm carried biological agents (including viable microorganisms, feed materials, skin debris or dander, and broken feather fragments). Overall, 80 ± 3 % of the particles emitted from the sheds (so called "percent fluorescence", PF) contained biological/ fluorescent agents. It indicates that PF can be used as a marker for the particles emitted from chicken sheds, e.g., for tracing the particles over the distances from the sheds.

Particle emissions increased with the increase of ventilation rates and were dependent on birds' age. The highest particle emissions were detected when the birds were 4-5 weeks old (prior to first pick-up).

The concentration of bioaerosols measured with the UV-APS was 1-2 orders of magnitude higher than the concentration of cultureable microorganisms.

The concentration of bacteria ranged from  $1.12 \times 10^5$  to  $6.38 \times 10^6$  CFU/m<sup>3</sup> (mean =  $2.89 \times 10^5$  CFU/m<sup>3</sup>). Approximately 85% of bacteria were gram-positive species. Maximum bacterial emissions reached  $1.1 \times 10^9$  CFU/h.

No thermophilic actinomycetes were detected in the airborne dust emitted from the sheds.

Concentrations of airborne fungi ranged from  $4.4 \times 10^3$  to  $6.2 \times 10^5$  CFU/m<sup>3</sup> (mean =  $3.32 \times 10^4$  CFU/m<sup>3</sup>). The maximum emission rates of fungi reached  $1.9 \times 10^8$  CFU/h (typically, were around  $9.5 \times 10^7$  CFU/h). The species identified include (in order of prevalence): *Cladosporium*, *Aspergillus*, *Penicillium*, *Scopulariopsis*, *Fusarium*, *Epicoccum*, *Mucor*, *Trichophyton*, *Alternaria*, *Ulocladium*, *Basidiospores*, *Acremonium*, *Aurobasidium*, *Drechslera*, *Pithomyces*, *Crysosporium*, *Geomyces*, *Rhizomucor*. The majority of these species are known to be potential respiratory allergens.

In conclusion, the results indicate that particles emitted from chicken sheds may contain a considerable amount of airborne allergens. Humans, particularly sensitive individuals, exposed to fungal aerosols at the concentrations we measured in this study may be at a health risk. The health risks to humans exposed at distances from the sheds is, however, uncertain as there would be dispersion of aeroallergens over distance.

Authors express their gratitude to Nic Meyer for the technical support with field measurements.

## Factors affecting the performance of bioaerosol impactors

S.A. Grinshpun<sup>1</sup>, A. Adhikari<sup>1</sup>, S.H. Cho<sup>1</sup>, T. Reponen<sup>1</sup>, G. Mainelis<sup>2</sup>, M. Yao<sup>2</sup>

<sup>1</sup>Center for Health-Related Aerosol Studies, University of Cincinnati, Cincinnati, OH 45267, USA

<sup>2</sup>Department of Environmental Sciences, Rutgers University, New Brunswick, NJ 08901 USA

Keywords: bioaerosols, collection efficiency, inertial impactor, cut-off diameter, particle deposition.

While different principles are utilized for sampling biological aerosol particles, impaction appears to be the most common for collecting bacteria and fungi. This method is used for total and culture-based microbial enumeration. For instance, the total number of viable and non-viable airborne spores is conventionally counted under a microscope after collecting them on a slide of a single-stage impactor, e.g., Air-O-Cell sampling cassette (Zefon Analytical Instruments, Inc., USA), the Burkard Personal Volumetric Air Sampler (Burkard Manufacturing Co. Ltd., U.K.) and Allergenco-D (Environmental Monitoring Systems, Inc., USA) to mention a few. Available bioaerosol impactors are usually equipped with either circular or rectangular (slit) inlets. Some impactors have a single nozzle as an inlet, e.g., Air-O-Cell, while others have hundreds of nozzles, e.g., Millipore Air Tester (Millipore Corp., USA). More importantly, they differ from one another with respect to their ability to efficiently collect bio-particles of specific sizes as well as by the particle deposit uniformity on a substrate (the latter is often critical for applying certain microbial enumeration protocols). The collection efficiency is characterized by the cut-off size,  $d_{50}$  that depends on the flow velocity through the nozzle, nozzle size (W), nozzle shape, non-dimensional jet-to-plate distance (S/W), and other factors.

In this study, we have tested the physical performance of eleven bioaerosol impactors. The collection efficiency and the bio-particle deposit characteristics were determined in the laboratory using a real-time particle size selective aerosol spectrometer and different microscopic enumeration methods. The test impactors were challenged with non-biological polydisperse NaCl aerosol, monodisperse polystyrene latex (PSL) particles, and aerosolized bacterial and fungal spores (*Bacillus subtilis*, *Cladosporium cladosporioides*, *Aspergillus versicolor*, and *Penicillium melinii*). The total number of spores,  $N_{MICROSCOPE}$ , collected on the slide deposition area,  $A_{DEP}$ , was counted and then related to the number of aerosol particles of a specific size range recorded by an aerosol spectrometer (Model 1.108, Grimm Technologies, Inc., Germany) upstream of the impactor over the time  $t$ . Thus, the actual collection efficiency of some of the tested impactors was calculated as

$$E_{ACTUAL} = \frac{N_{MICROSCOPE}}{C_{UP}Qt} \times 100 \%$$

where  $C_{UP}$  is the upstream aerosol concentration and  $Q$  is the sampling flow rate. The overall physical collection efficiency was also determined for biological and non-biological particles from the ratio of the aerosol concentration up- and downstream of the impactor. Consequently,  $d_{50}$  was obtained for each tested impactor as presented in the table below.

Design and collection characteristics of the tested impactors.

Impactor	Jet shape	No of jets	Q, l/min	W, mm	S/W	$d_{50}$ , $\mu\text{m}$
Air-O-Cell	slit	1	15	1.0	1.0	2.5
Allergenco-D	slit	1	15	1.0	0.89	1.7
Burkard	slit	1	10	1.0	1.0	2.4
CyClex	round	1	20	4.4	0.1	1.8
Micro-5	round	1	5	2.1	0.12	$\leq 1$
SMA	round	12	141.5	6.3	0.8	4.8
BioCulture	round	380	120	2.3	0.75	7
MAS-100	round	400	100	0.7	4	1.7
Microflow	round	378	120	2.5	0.84	8.8
SAS Super 180	round	401	180	0.8	2.7	2.1
Millipore Air Tester	round	1000	140	0.46	12.7	2.3

The data demonstrate how much the samplers differ by the cut-off size ( $d_{50}$  varies within a decade). Some impactors appear to significantly undersample airborne fungi, and almost all of the tested samplers have clear limitations to efficiently collect bacteria. Statistical modeling was applied to determine the role of different impactor design parameters in the bioaerosol collection and enumeration process. The study revealed that a relatively small change in the bioaerosol impactor design (e.g., Allergenco-D versus Air-O-Cell) may significantly improve its collection characteristics, decreasing the cut-off size so that practically all fungal species are collected on the substrate. The dimensionless jet-to-plate distance was confirmed to be influential for reducing the  $d_{50}$  of single-nozzle impactors. For some multi-nozzle impactors, we found that the collection efficiency is improved substantially if S is decreased by increasing the amount of agar on the collection plate. As to the microscopic enumeration of spores, the deposit uniformity and the count variability differ considerably from one sampler to the other. For several impactors, however, we found that the three methodologies – the entire impaction trace count, 40-field random partial count, and 20-traverses partial count – produced the same results ( $p > 0.05$ ).

## **Portable BIO-AEROSOLSPECTROMETER for Quick Detection of BIOLOGICAL AEROSOLS**

Dr. Friedhelm Schneider<sup>1</sup> and Hans Grimm<sup>1</sup>

<sup>1</sup>Grimm Aerosol Technik GmbH & Co. KG, Ainring, 83404, Germany

Keywords: Bioaerosols, Fluorescence, Instrumentation, Particle size distribution

The new system consist of a unique BIO-AEROSOLSPECTROMETER with integrated bio-impactor and a LED fluorescence microscope. All equipment is portable both the BIO-AEROSOLSPECTROMETER (2.5 kg with battery and internal pump) and the LED fluorescence microscope (1.7 kg) or AC powered. The system is able to detect in real time particle number, surface area or mass concentration and test the collected aerosol particles for existing biological material, e.g. bacteria or fungal spores much faster than existing techniques with petri dishes and incubation. Due to the compact and robust design the #1.209 BIO-AEROSOLSPECTROMETER can be used at nearly all locations indoor and outdoor.

The #1.209 BIO-AEROSOLSPECTROMETER records particle number, particle surface area or particle mass concentration in 31 size channels ( $0.25 \mu\text{m} < D < 32 \mu\text{m}$ ) in real time. The optical particle detection is based on  $90^\circ$  scattering light technique with a 683 nm diode laser. An internal, volume-controlled pump delivers the sampling air. All detected particles are collected in the same device on a glass slide for a rapid further investigation (staining and fluorescence microscopy).

The user can interact with the spectrometer by display/keypad or PC. All spectrometer data are stored on the data storage card and are online available also via PC.

The portable LED microscope can be used in transmission mode (peak wavelength  $\lambda = 565 \text{ nm}$ ) or fluorescence mode (with different wavelength) for rapid test of biological particle components. The microscope is equipped with a CCD camera and a imaging and data analysis software.

The BIO-AEROSOLSPECTROMETER also can be equipped with different isokinetic sampling inlets for special workplaces or in stack sampling and external sensors for air temperature, relative humidity and velocity. The whole system can be decontaminated after measurements in critical locations.

First results and tests confirm the precise particle detection and particle sampling with the bio-impactor, the easy handling pf the whole system and the possibility of getting results within minutes. The system can be used for monitoring e.g. indoor air quality, bioaerosol studies, respiratory studies, animal mass production, production inspection and decontamination control.

## Fungal contribution to the ambient organic carbon

Jessica Y.W. Cheng<sup>1</sup>, Arthur P.S. Lau<sup>1</sup> and Ming Fang<sup>2</sup>

<sup>1</sup>Institute for the Environment, <sup>2</sup>Department of Chemical Engineering,  
Hong Kong University of Science and Technology, Clear Water Bay Road, Kowloon, Hong Kong

Keywords: fungi, organic carbon, bioaerosol, ambient aerosol.

### Introduction

Organic carbon (OC) consists of a wide range of compounds and is a major component in atmospheric aerosols. Biological contribution to ambient aerosols can be substantial (Graham *et al.*; 2003). The fungi are a prevalent group in ambient air and their contribution to the ambient OC will be of great interest. The authors had established a weighted-average conversion factor, CF, (0.197 pg ergosterol/spore) of the biomarker, ergosterol, to spore number concentration (Cheng, 2006). This paper presents an approach employing this CF and individual species OC content in assessing the fungal contribution to the ambient OC.

### Materials and Methods

Common ambient fungal strains were collected from the field, isolated and sub-cultured on Malt Extract Agar (MEA) plates. Spores were collected from matured colonies with sterilized water. Spore concentrations were determined by counting with a hemocytometer. Different amounts of the spores were dried and their OC contents were determined using the Solid Sample Module of the Shimadzu total organic carbon (TOC) analyzer. The OC was oxidized to CO<sub>2</sub> at 900°C. The CO<sub>2</sub> was measured by a Non-Dispersive Infra-Red detector. The OC content per spore of each species studied was determined from the slope of the respective regression line.

Ambient aerosols with aerodynamic diameter smaller than 10µm were collected on quartz filters using a high volume sampler. Ergosterol contents on the filters were quantified with GC-MS and the number concentrations of spores (n) in the air were estimated with the CF (Cheng, 2006). The total carbon (TC) and total inorganic carbon (TIC) contents in the ambient air were determined by the TOC analyzer described earlier for the fungal spores. Portions of the filter were combusted at 900°C to yield the TC. Other portions of the filter were pre-combusted at 340°C for 2 hours under a helium flow in a muffle oven to remove OC contents before combusting at 900°C to give the TIC content. The OC<sub>ambient</sub> contents of the filters were determined as the differences between TC and TIC. The fungal contributions to organic aerosols (%OC<sub>fungi</sub>) were calculated as:

$$\%OC_{\text{fungi}} = \frac{n \sum f_i C_i}{OC_{\text{ambient}}} \times 100\% \quad (1)$$

where n was the number concentrations of spore, f<sub>i</sub> and C<sub>i</sub> were the number fraction determined from the viable sampling and the OC content of the group fungi i determined in the laboratory, respectively.

### Results and Discussion

The OC contents of spores/yeast cells are summarized in Table 1. With the relative contribution (f) of different fungi from the viable sampling, their OC contents (C) and according to equation (1), the average fungal contribution to ambient OC was 0.25% (n = 29; 95% CI: 0.19% - 0.32%) at a suburban area in Hong Kong. In rainfall period when spore dispersion is favored, the fungal OC contribution could be up to 7.4% of the ambient OC (mean: 3.69%; range: 1.01% - 7.43%; n = 5). The results indicate that the biological contribution to organic aerosols cannot be overlooked.

Table 1: Organic carbon contents of different fungal spores/yeast cells (95% confidence interval)

Fungal species	Carbon content (pg C/spore or cell)
<i>Alternaria sp.</i>	201.0 (161.9 – 240. 2)
<i>Aspergillus niger</i>	13.0 (9.6 – 16.4)
<i>Candida sp.</i>	4.0 (3.3 – 4.7)
<i>Cladosporium sp.</i>	6.5 (5.2 – 7.8)
<i>Paecilomyces sp.</i>	9.5 (7.9 – 11.1)
<i>Penicillium chrysogenum</i>	5.5 (4.1 – 6.7)
<i>Penicillium sp. (A)</i>	3.6 (2.5 – 4.7)
<i>Penicillium sp. (B)</i>	4.0 (3.0 – 5.1)
<i>Penicillium sp. (C)</i>	4.3 (2.5 – 6.2)
<i>Penicillium sp. (D)</i>	3.8 (2.3 – 5.3)
<i>Rhodotorula sp.</i>	5.8 (4.3 – 7.3)

The study was supported by the Hong Kong Research Grant Council (DAG03/04.ATC01).

Graham, B., Guyon, P., Taylor, P. E., Artaxo, P., Maenhaut, W., Glovsky, M. M., Flagan, R. C. & Andreae, M. O. (2003). *J. Geophysical Research*, 108(D24), 4766.

Cheng, Y. W. (2006). Ergosterol to Fungal Spore Concentration Conversion Factors: Determination and Application to Ambient Aerosols. Master Thesis, HKUST.

## Measurement of size distributions and viability of nano-bioaerosols

Anne Maißer<sup>1</sup>, Christian Laschober<sup>1,2</sup>, Günter Allmaier<sup>2</sup> and Wladyslaw W. Szymanski<sup>1</sup>

<sup>1</sup>Faculty of Physics, University of Vienna, Strudlhofgasse 4, 1090, Vienna, Austria

<sup>2</sup>Faculty of Technical Chemistry, Vienna University of Technology, Getreidemarkt 9, 1060, Vienna, Austria

Keywords: Bioaerosols, Collection Efficiency, Nano-DMA, Nanoparticles, Particle shape

In the recent decade differential mobility analyzers (DMA) became a major apparatus for size classification of nanoaerosols. This technique, combined with a soft method for aerosol generation from solution, such as nano-Electrospray (n-ES), allows to characterize according to their size important biological species, such as proteins, protein complexes, DNA, bacteriophages, viruses, or virus fragments.

However, size spectra from DMAs alone are frequently insufficient for satisfactory analysis and data interpretation, especially from bioaerosols.

Substantial features of DMAs are the operation under ambient pressure and the fact that investigated bioaerosols are intact after DMA sizing (Laschober, et al. 2007), which opens specific prospects for the DMA technique.

Based on this rationale, a parallel-DMA (PDMA) was constructed (Fig.1) enabling simultaneous recording of the size distribution of particles in question and selection/sampling of a specific size fraction for further purposes.

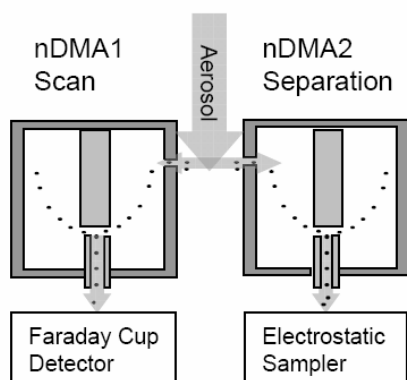


Figure 1. PDMA – schematic diagram

For sampling a selected size fraction, two different devices were designed. The first one is an electrostatic sampler (ELS) (Fig.2a) which was built for sampling directly on a microscopic target. This sampler consists of a flow chamber where a transmission electron microscope (TEM) support grid is imbedded in the insulating holder and connected to high voltage. The charged particles entering the flow chamber are thus deflected by the electrical field and deposited onto the TEM grid.

The second sampler (Fig.2b) is an electrostatic biosampler (EBS) designed as a glass impinger with a high voltage applied to the impaction

surface, which is a conducting liquid that also provides physiological conditions for bioparticles in order to preserve biological activity of the sampled biomaterial.

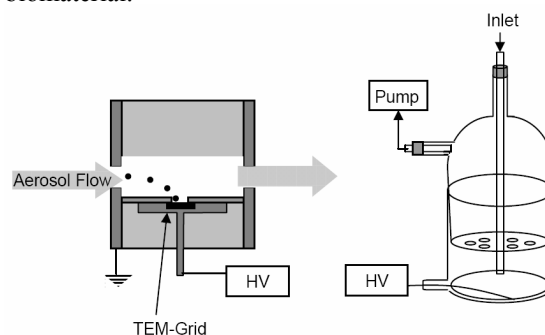


Figure 2. a) Electrostatic Sampler (ELS)  
b) Electrostatic Biosampler (EBS)

The ELS was applied to sample tobacco mosaic viruses (TMV). The intact virus particle is cylindrically shaped, with a diameter of 20 nm and a length of 300 nm. The TMV aerosol was generated using an nano-electrospray aerosol generator (n-ES). A specific size fraction was chosen for sampling and subsequently analyzed by TEM to investigate if this procedure has any effect on the virus particle.

The EBS was first characterized for its collection efficiency by using different aerosol particles in the size range from 5 to 800 nm. The influence the nozzle outlet to liquid surface distance, the nozzle diameter and the applied electrical field was investigated. The feasibility of the EBS to preserve biological activity after measurement and sampling was confirmed with an enzyme ( $\beta$ -Galactosidase), which was electrosprayed, size-selected and collected in the liquid used for soft landing in the EBS. The experimental data will be presented and discussed.

This work was supported by the Austrian Science Foundation (FWF), Project No. P16185-N02.

Laschober, C., Wruss J., Blaas D., G. Allmaier and W.W. Szymanski, Gas Phase Electrophoretic Molecular Mobility Analysis of Size and Stoichiometry of Complexes of a Common Cold Virus with Antibodies, submitted to Biotechniques (2007)

## Molecular genetics and diversity of *Bacteria* and *Archaea* in urban, rural and high alpine air

V. Després<sup>1,2</sup>, J. Nowoisky<sup>1,2</sup>, M. Klose<sup>3</sup>, R. Conrad<sup>3</sup>, J. Cimbal<sup>1</sup>, M.O.Andreae<sup>1</sup>, U.Pöschl<sup>1</sup>

<sup>1</sup>Biogeochemistry, Max Planck Institute for Chemistry, P.O. Box 3060, D-55020 Mainz, Germany

<sup>2</sup>General Botany, Johannes Gutenberg University, Saarstraße 1, D-55099 Mainz, Germany

<sup>3</sup>Biogeochemistry, Max Planck Institute for Terrestrial Microbiology, Karl-von-Frisch-Straße, D-35043, Germany

Keywords: Bacteria, Archaea, DNA, T-RFLP

This study explores the applicability of molecular genetic methods for the characterization of primary biogenic aerosol (PBA) particles in the atmosphere, focusing on *Bacteria* and *Archaea*. Samples of fine (<2.5 µm), coarse (>2.5 µm), and total suspended particulates were collected at four different German sampling locations: Mt. Zugspitze (high alpine, 2962 m a.s.l.), Hohenpeissenberg (rural, 990 m a.s.l.), Munich and Mainz (urban, 550 m and 150 m a.s.l.).

Investigations of blank and background samples showed that filter materials have to be decontaminated prior to use, and that the sampling and handling procedures have to be carefully controlled to avoid artifacts in the genetic analyses.

From filter aliquots loaded with about one milligram of air particulate matter, DNA could be extracted and genetic sequences could be determined for *Bacteria* and *Archaea* in Mainz, and only for *Bacteria* in the three other locations. Molecular techniques (e.g., DNA sequencing, T-RFLP) were used to determine the identity of the microorganisms, and to estimate their diversity and relative abundances.

Mass fractions of DNA in fine particulate matter (PM<sub>2.5</sub>) were found to be around ~0.05 % in all sampled locations. The average concentration of DNA determined for urban air was on the order of ~7 ng m<sup>-3</sup>, indicating that human adults may inhale about one microgram of DNA per day (corresponding to ~10<sup>5</sup> haploid human genomes).

There was no obvious difference in the composition of *Bacteria* present in fine and coarse particulate matter. Most of the bacterial sequences belong to the phyla of *Proteobacteria*, *Actinobacteria*, *Bacteroidetes* and *Firmicutes*. Among the *Proteobacteria* all four classes (*Alpha*-, *Beta*-, *Gamma* -, and *Deltaproteobacteria*) were present in varying amounts (Figure 1).

T-RFLP analysis on bacteria was performed for all locations. Over 80% of the bacterial PM<sub>2.5</sub> sequences of Munich, Hohenpeissenberg and Mt. Zugspitze could be matched with about 40% of the T-RF peaks (ranging from 58 to 494 base pairs in length). These results demonstrate that the T-RFLP analysis covered more of the bacterial diversity than the sequence analysis. For the coarse particle

samples from Mainz, preliminary results indicate a more diverse bacterial composition than for the other locations.

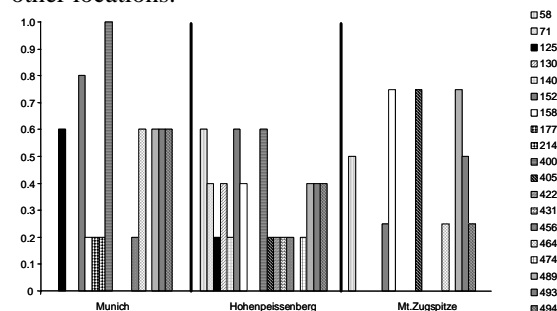


Figure 1. The x-axis represents different sampling locations and measured T-RF peak positions (number of base pairs, bp). The y-axis specifies the fraction of filter samples on which the T-RF peaks were found at each location.

Archaeal DNA was detected on the coarse particle samples from Mainz but could not yet be retrieved from other samples. First sequence analyses point to high similarities with Archaea and *Crenarchaeota* environmental sample sequences in the databank of the National Center for Biotechnology Information (NCBI). Besides Pro- and Eukaryotes, Archaea represent the third domain of life and are potentially the most abundant organism group on Earth. They are bacteria-like microorganisms which are mostly found under extreme environmental conditions and have the capability of living in almost all kinds of environments, including ocean water and sediments.

### Acknowledgements

The German Research Foundation, the LEC Geocycles (Contribution No.25), and the Max Planck Society are gratefully acknowledged for funding.

### References

Després, V., Nowoisky, J., Klose, M., Conrad, R., Andreae, M.O., Pöschl, U. (2007) *Biogeosciences Discussions*, 349-384.

## To what extent can viable bacteria in atmospheric aerosols be dangerous for humans?

A.S. Safatov<sup>1</sup>, I.S. Andreeva<sup>1</sup>, B.D. Belan<sup>2</sup>, G.A. Buryak<sup>1</sup>, E.K. Emel'yanova<sup>1</sup>, R. Jaenicke<sup>3</sup>, M.V. Panchenko<sup>2</sup>, N.I. Pechurkina<sup>1</sup>, L.I. Puchkova<sup>1</sup>, V.E. Repin<sup>1</sup>, I.V. Saranina<sup>1</sup>, A.N. Sergeev<sup>1</sup>

<sup>1</sup>Federal State Research Institution State Research Center of Virology and Biotechnology "Vector", Novosibirsk Region, 630559, Koltsovo, Russia;

<sup>2</sup>Institute of Atmospheric Optics SB RAS, 634055, Tomsk, Russia

<sup>3</sup>Johannes Gutenberg - Universitat Mainz, Institut für Physik der Atmosphäre, D-55099, Mainz, Germany

Keywords: bioaerosols, atmospheric aerosols, culturable microorganisms, health effects of aerosols.

Microorganisms present in atmospheric aerosols are a potential danger for humans. To study this 4 groups of tests for quantitative evaluation of this potential danger for the whole complex of viable microorganisms detected in atmospheric aerosols are proposed. Firstly, these microorganisms must be pathogenic or conventionally pathogenic for humans. Secondly, bioaerosols are the more dangerous the higher the concentration of viable microorganisms and the larger the portion of microorganisms pathogenic or conventionally pathogenic for humans they contain. Thirdly, the hazard of concrete microorganisms increases when they display high resistance to unfavorable environmental factors causing microorganism inactivation. And, fourthly, when potentially pathogenic microorganisms, which were not inactivated in the environment, affect humans, microorganisms being drug resistance represent the greatest danger.

Conventional pathogenicity of bacteria can be determined *in vitro* by erythrocyte hemolysis and plasmacoagulation reactions, fibrinolytic, hemolytic and gelatinolytic activities. Concentrations of different viable microorganisms can be determined with standard microbiological methods. High resistance to unfavorable environmental factors is characterized by the ability of microorganisms to grow at high salt concentration (which usually increases when the particle dries out), the presence of various enzymatic activities such as lipolytic, phosphatase, letinase, lipase, etc. (note that such activities also characterize potential conventional pathogenicity of bacteria), the presence of restriction exo- and endonucleases, plasmid DNAs, etc. And finally, drug resistance can be evaluated by resistance to a number of antibiotics. Carrying out such experimental evaluation of characteristics of microorganisms, which are present in atmospheric aerosols, allows us to draw a valid conclusion about their potential danger for humans.

More than 500 bacterial strains isolated from atmospheric aerosols of Southwestern Siberia in summer and fall 2006 had low conventional pathogenicity: 34-80% of the tested strains did not display any of the above characteristics of conventional pathogenicity; 16-59% displayed one, 0-32 % - two, 5 bacterial strains – three, and none of

them displayed 4 types of these characteristics simultaneously.

The ability to grow at high salt concentration was as follows: 21-75 % of the microorganisms displayed the ability to grow at 5% NaCl concentration, and 21-39% grew at 10% salt concentration. 20-27% of microorganisms isolated from atmospheric air in August – October 2006 possessed lipolytic activity, 5% had exonucleases and 9% - endonucleases. Alkaline phosphatase was found in 52% of microorganisms and plasmid DNAs - in 24%. Thus, the tested microorganisms possess a rather high "protective potential" providing survival in the environment.

Approximately one-third of bacteria are not resistant to all the 15 studied antibiotics. 25 % are resistant to more than one antibiotic. Most often the tested bacteria are resistant to polymyxin (60%) and lincomycin (29%). No bacteria resistant to all the 15 antibiotics simultaneously, were detected.

Taking into account that a cubic meter of atmosphere contains approximately  $10^3$  of viable microorganisms, it can be concluded that the atmosphere of Southwestern Siberia contains a considerable number of microorganisms, presenting a potential threat to human health. Note that the potential danger of microorganisms isolated from atmospheric air samples in fall 2006 for humans is considerably higher than that determined for microorganisms isolated in summer 2006.

The work was partially supported by ISTC, project #3275.

## Removal of bioaerosol by the combination of photocatalysis and negative air ion

K.-P. Yu<sup>1</sup>, W.M. Lee<sup>2</sup> and S.-Y. Lin<sup>2</sup>

<sup>1</sup> Institute of Chemistry, Academia Sinica, 128 Academia Rd., Nankang District, 11529, Taipei, Taiwan

<sup>2</sup> Graduate Institute of Environmental Engineering, National Taiwan University, 71 Chou-Shan Rd., 106, Taipei, Taiwan

Keywords: bioaerosols, filters, indoor air quality, ions, reaction chamber.

Recently the outburst of SARS (severe acute respiratory syndrome), increasing occurrence of asthma and diseases related to respiratory tract, and the deterioration of indoor air quality are relevant to the airborne bioaerosols (Gustavsson, 1999).

In this study, *E. coli*, yeast, and  $\lambda$  vir phage were selected as the model strain of bacteria, fungi, and virus, respectively. We used a reactor equipped with photocatalytic filter (PCO/filter) and a negative air ion (NAI) generator to investigate the bioaerosols removal efficiency and factors affecting the removal efficiency. The *E. coli*, yeast, and  $\lambda$  vir phage bioaerosols removal efficiency of different controlling methods were shown as Figure 1.

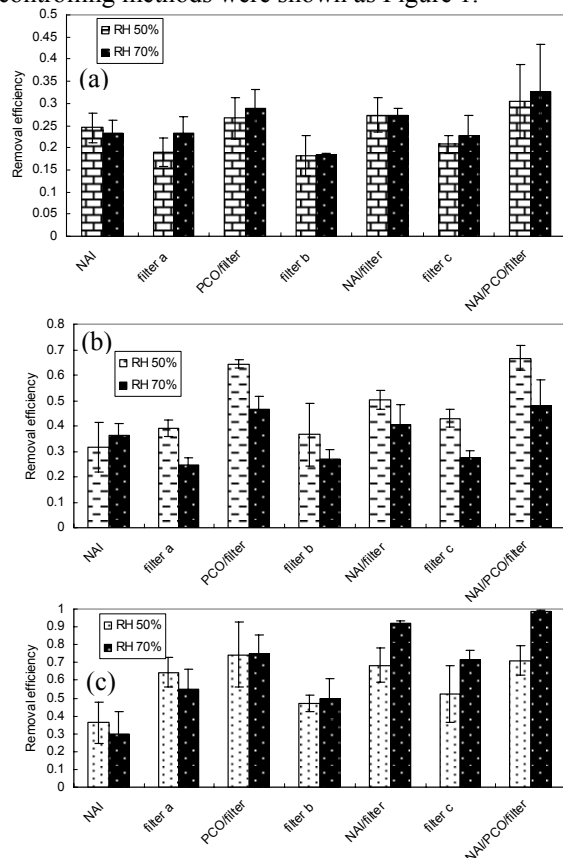


Figure 1. (a) *E. coli* (b) yeast (c)  $\lambda$  vir phage bioaerosols removal efficiency

According to the results of ANOVA (analysis of variance), the differences of removal efficiency between different controlling methods (NAI/PCO/filter, NAI/filter, PCO/filter, NAI, and

filter) were significant. When the relative humidity was 50%, the *E. coli*, yeast, and  $\lambda$  vir phage bioaerosols removal efficiency of different controlling methods ranged from 0.182 to 0.304, 0.314 to 0.667, and 0.327 to 0.724, respectively. When the relative humidity was 70%, *E. coli*, yeast, and  $\lambda$  vir phage bioaerosols removal efficiency ranged from 0.183 to 0.326, 0.247 to 0.476, and 0.354 to 0.983, respectively. The effect of relative humidity on *E. coli* bioaerosols removal efficiency was insignificant. Yeast bioaerosols removal efficiency was higher under 50% of relative humidity, and  $\lambda$  vir phage bioaerosols removal efficiency was higher under 70% of relative humidity. The order of *E. coli* bioaerosols removal efficiency of the controlling methods was NAI/PCO/filter > NAI/filter  $\approx$  PCO/filter > NAI > filter. The order of yeast bioaerosols removal efficiency of the controlling methods was NAI/PCO/filter > PCO/filter > NAI/filter > NAI  $\approx$  filter, and that of  $\lambda$  vir phage bioaerosols removal efficiency was NAI/PCO/filter > NAI/filter > PCO/filter > filter > NAI.

The bioaerosols removal efficiency of NAI/PCO/filter for 5-hour continuous experiments decreased with time elapsed as shown in Figure 2, and the 5-hour bioaerosols removal efficiency capacities were as the following: *E. coli*: 4466 CFU/cm<sup>2</sup>, yeast: 881 CFU/cm<sup>2</sup>, and  $\lambda$  vir phage: 3191 PFU/cm<sup>2</sup>.

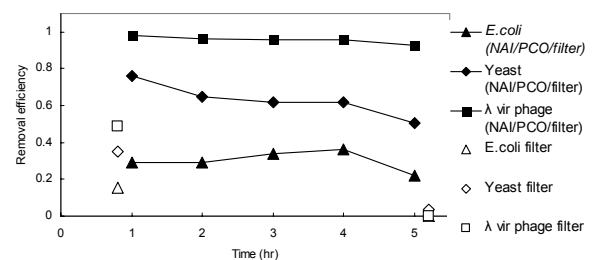


Figure 1. 5-hour continuous bioaerosols removal efficiency

This work was supported by the National Science Council of R.O.C. under grant NSC 94-2211-E-002 - 019 -.

Gustavsson, J. (1999), *Filtration and Separation*, 36, n2, 20-25.

## Correlation between the concentrations of biogenic components of atmospheric aerosol measured simultaneously in spaced points

G.A. Buryak<sup>1</sup>, A.S. Safatov<sup>1</sup>, K.P. Koutsenogii<sup>3</sup>, V.I. Makarov<sup>3</sup>, V.V. Marchenko<sup>1</sup>,  
S.E. Olkin<sup>1</sup>, S.A. Popova<sup>3</sup>, I.K. Peznikova<sup>1</sup>, M.P. Shinkorenko<sup>2</sup>, B.S. Smolyakov<sup>2</sup>

<sup>1</sup>Federal State Research Institution State Research Center of Virology and Biotechnology “Vector”, Novosibirsk Region, 630559, Koltsovo, Russia

<sup>2</sup>Institute of Inorganic Chemistry SB RAS, 3, Lavrent’ev Blvd, 630090, Novosibirsk, Russia

<sup>3</sup>Institute of Chemical Kinetics and Combustion SB RAS, 3, Institutskaya street, 630090, Novosibirsk, Russia

Keywords: atmospheric aerosols, bioaerosols, measurements, monitoring.

The construction of the mathematical model of the biogenic background in the atmosphere requires data describing space and time variation of its components. Previously we presented detailed dynamics of time variation of the concentrations of total protein and viable microorganisms in atmospheric aerosol of the near-ground atmospheric layer and at the heights up to 7000 m (Safatov *et al.*, 2006). The goal of the present work is the analysis of data on space variation of total protein concentrations in atmospheric aerosol. This variation was evaluated by comparing the results of measurements of total protein concentration in atmospheric aerosol performed simultaneously in spaced points.

The measurements were carried out on three sites: FSRI SRC VB Vector (**A**), Klyuchi settlement (**B**, different seasons of 2001 – 2006) and Zav’yalovo settlement (**C**, the summers of 2005 and 2006). The distance between the sites of FSRI SRC VB Vector and Klyuchi settlement was approximately 11 km, and that from these sites to Zav’yalovo settlement was approximately 80 km. Daily aerosol samplings were performed on the sites of Klyuchi and Zav’yalovo settlements and four 6-hour samplings were performed for 24 hours on the site of FSRI SRC VB Vector on fibrous filters AFA-HA-20, after which the mass of total protein on the filters was determined in a laboratory according to the method described in You *et al.*, (1997).

The results of the performed comparison are summarized in Table 1. As it follows from these results, mass aerosol concentration on Site **A** tends to exceed that measured on **C** and on **B**, and the concentration measured on **C** tends to exceed that measured on **B**. It should be noted that the observed differences are statistically indistinguishable due to insufficiency of data. The concentrations and the portions of total protein in the full mass of aerosol on Site **A** also tend to exceed those measured on **C**, which is more than that on **B**. However, like for mass aerosol concentrations, the observed differences are statistically indistinguishable.

Compared sites	Value ratio*	The number of pair measurements and correlation coefficients
<b>A and B</b> , 2001 – 2006	MA 1.0 */÷ 1.9	17 points, +0.52
<b>A and B</b> , 2001 – 2006	MP 1.9 */÷ 5.5	21 points, +0.39
<b>B and C</b> , 2005	MA 0.9 */÷ 1.8	15 points, -0.10
<b>B and C</b> , 2005	MP 0.5 */÷ 2.0	15 points, -0.19
<b>B and C</b> , 2005	P 0.5 */÷ 2.1	15 points, +0.05
<b>B and C</b> , 2006	MA 0.9 */÷ 2.0	17 points, -0.20
<b>B and C</b> , 2006	MP 0.6 */÷ 1.8	17 points, -0.08
<b>B and C</b> , 2006	P 0.6 */÷ 2.2	17 points, -0.02

\*Note: MA = mass aerosol concentration, MP = mass concentration of total protein and P = portion of total protein in aerosol mass

Table 1. Comparison of pairs of values measured simultaneously on different sites.

The obtained preliminary data on space variation of the concentration of atmospheric bioaerosols in the region show that, on the whole, their concentrations can be considered constant at the distances up to 80 km. This might be caused by the absence of powerful local sources of bioaerosols in the studied region.

The work was partially supported by ISTC, project # 3275.

Safatov, A. S. et al., (2006). *Chemical Engineering Transactions*, 10, 401-406.

You, W. W., et al., (1997). *Annal. Biochem.*, 244, 277-282.

## Avian influenza (subtype H5N1) transmission mechanisms

A.S. Safatov<sup>1</sup>, I.E. Agranovski<sup>2</sup>, V.N. Mikheev<sup>3</sup>, S.A. Kiselev<sup>1</sup>, O.V. Pyankov<sup>1,2</sup>, M.O. Skarnovich<sup>1</sup>,  
V.A. Petrishchenko<sup>1</sup>, G.A. Buryak<sup>1</sup>, L.N. Shishkina<sup>1</sup>, A.N. Sergeev<sup>1</sup>, I.G. Drozdov<sup>1</sup>

<sup>1</sup>Federal State Research Institution State Research Center of Virology and Biotechnology "Vector", Novosibirsk Region, 630559, Koltsovo, Russia

<sup>2</sup>School of Environmental Engineering at Griffith University, Nathan Campus, Qld 4111, Brisbane, Australia

<sup>3</sup>Administration of Rospotrebnadzor in Novosibirsk region, Bd. 7A, Cheluskintsev street, 630132, Novosibirsk, Russia

Keywords: bioaerosols, health aspects of aerosols, avian influenza virus, virus aerosol transmission, aerosol infectivity

The epidemic of avian influenza A subtype H5N1 caused a great economic damage in Asian and European countries. More than 150 million infected birds were slaughtered. According to the WHO data for the beginning of 2007, this subtype of influenza virus killed more than 150 humans. However, in spite of the fact that influenza viruses are respiratory ones, there are no literature data on aerosol way of transmission of infection caused by influenza A subtype H5N1. Moreover, there is evidence that aerosol way of infection transmission is not the main one for this subtype of influenza virus

The infection pathogenesis at different ways of infecting hens with influenza A virus subtype H5N1 was studied in the work experimentally; the possibility of infecting hens with the virus aerosol as well as the virus transmission with aerosol from infected hens to healthy birds and the virus stability in aerosol were checked.

Experiments were performed with avian influenza *virus* strain A/Chicken/Suzdalka/Nov-11/2005 (H5N1) obtained from the collection of FSRI SRC VB "Vector". The virus biological activity was determined on MDCK cell culture in tissue cytopathic doses per 1 ml of virus-containing suspension (TCPD<sub>50</sub>/ml).

SPF *Hens* weighing 200 to 600 g were used in the experiments.

**Aerosol experiments.** All aerosol experiments were performed in a dynamic aerosol chamber. At *aerosol infection* of hens the experiment was performed as follows. The virus aerosol was generated with a nebulizer. After mixing with clean airflow, aerosol was supplied to the chamber with birds where the latter were exposed to the virus for the required time period with simultaneous sampling into samplers to determine the virus doses received by hens. The same dynamic aerosol chamber was used in experiments on investigating the possibility of *aerosol transmission of infection from diseased birds to healthy one*, but the virus was not dispersed for the birds to be in clean airflow.

**The carried out work** revealed 3 – 4 times lower survival of avian influenza virus in aerosol state (at the level of approximately 1%) as compared

with that of human influenza virus A/Aichi/2/68 strain (H3N2) and more than 50 times lower as compared with that of one of the most resistant viruses – vaccinia virus.

Data on hens' sensitivity to avian influenza virus indicate that at intravenous, intranasal and aerosol infection the virus displays high infectivity level comparable with that for mice infected with human influenza virus adapted to animals. **Aerosol 50% infective dose** is estimated in 2 TCPD<sub>50</sub>.

The study of the infection development in hens after intranasal infection with avian influenza virus at the dose of 3-5 LD<sub>50</sub> allowed us to reveal the following dynamics of the virus accumulation in different organs of birds. The site of initial virus replication is nasal cavity of birds, in which the virus is detected at a considerable concentration already 24 hours post infection in hens and disappears from it within 36 - 60 hours. The virus from nasal cavity obviously penetrates into lungs where the virus concentration reaches 5.8 log<sub>10</sub> TCPD<sub>50</sub>/ml 60 hours post infection and stomach and, at the same time, might spread throughout the organism through blood and lymph causing infection with maximal accumulation of the virus in gastroenteric tract and excrements (up to 6.5 log<sub>10</sub> TCPD<sub>50</sub>/ml).

**Aerosol transmission of infection from diseased birds to healthy ones** can occur both through aerosol excreted from respiratory tract of infected birds and aerosol generated from birds' excrements. Experiments allowing the evaluation of each of the ways separately demonstrated the possibility of both ways of infection transmission.

Thus, there are two main ways of infection transmission: **by aerosol** (site of entry - upper and lower sections of respiratory tract) when infection occurs through them and **fecal-oral rote** (site of entry - upper sections of respiratory tract) when infection occurs through nasal cavity. It should be noted that from our point of view the second way has higher probability than the first one.

This work was partially supported by RF Government grant #820-R.

## Molecular genetics and diversity of *Fungi* and *Plants* in urban air

J. Nowoisky<sup>1,2</sup>, V. Després<sup>1,2</sup>, J. Cimbal<sup>1</sup>, M. Klose<sup>3</sup>, R. Conrad<sup>3</sup>, M.O. Andreae<sup>1</sup>, U. Pöschl<sup>1</sup>

<sup>1</sup>Biogeochemistry, Max Planck Institute for Chemistry, P.O. Box 3060, D-55020 Mainz, Germany

<sup>2</sup>General Botany, Johannes Gutenberg University, Saarstraße 1, D-55099 Mainz, Germany

<sup>3</sup>Biogeochemistry, Max Planck Institute for Terrestrial Microbiology, Karl-von-Frisch-Straße, D-35043, Germany

Keywords: Fungi, Plants, Insects, DNA

Aerosol particles are of central importance for atmospheric chemistry and physics, climate and public health. A significant fraction of the particles in the atmosphere is of biological origin like plant fragments, pollen, spores, bacteria, fur fibres, skin fragments, fungi and more. So far, however, the abundance, diversity, sources, properties and effects of biological particles in the atmosphere have not been well characterized. The use of molecular genetic methods resolves many limitations of traditional detection methods for the analysis of biological aerosol particles (Després et al., 2007).

In this study, air filter samples were collected with a High Volume Sampler separating fine and coarse particles (aerodynamic cut-off diameter 2.5µm) for one year 2006/2007 in Mainz (130 m a.s.l.), Germany. The samples were analyzed for the presence of fungal, plant and insect DNA. All PCR products were cloned and several clones sequenced. The obtained sequences were blasted in the National Center for Biotechnology Information database to find the closest match and determine the taxonomic identity of the organisms from which the DNA on the filter samples had most likely originated.

Fungal DNA was detected on coarse and fine particle filters. Preliminary results show high taxonomic diversity for the 168 fungal sequences obtained from coarse particle samples. The sequences were characteristic for different groups of *Basidiomycota* (30%) and *Ascomycota* (70%), which are known to actively discharge spores into the atmosphere. Ten genera within the phylum *Basidiomycota* were found. Eight of them belong to the class *Homobasidiomycetes* and some of them include species which can act as plant pathogens or human allergens (e.g. *Stereum*). Few sequences belong to the genus *Iterosporium* within the class of the *Heterobasidiomycetes*. Among them are typical plant pathogens. Further the allergenic genus *Sporobolomyces* was detected from the *Basidiomycota* class *Urediniomycetes*. The sequences within the *Ascomycota* belong e.g. to the genera *Cladosporium* (an important allergen) and *Epicoccum* (a soil and litter fungus and allergen) as well as

to some other genera which include also plant pathogen species (e.g. *Stemphylium*).

The plant sequences could be attributed to green plants, within the families *Betulaceae* (e.g. birch), *Poaceae* (e.g. barley), *Plantagiaceae* (e.g. plantain), *Urticaceae* (e.g. nettle), *Taxaceae* (e.g. yew), *Cupressaceae* (e.g. fir), and mosses within the *Bryophyta* moss superclasses II and V. The fact that most of these plant sequences results from core genome amplification of the 18S RNA gene and that they were found in samples collected during the pollen season in spring and summer time, suggests that the DNA was likely recovered from pollen or spores (Bryophytes) rather than tissue fragments. Pollen and spores are known and designed to resist environmental stress and survive atmospheric transport, whereas DNA in plant tissue fragments may be rapidly degraded by atmospheric photooxidants. However, the additionally positive detection of the *rbcL*- and 16S RNA gene of chloroplast DNA suggests that also leaf fragments from different plants are present in the air. As most plants do not transport chloroplasts within the pollen chloroplast DNA likely stems from leaf material.

As animals in general are too diverse to be amplified with a single universal primer pair, we concentrated on the amplification of insect DNA. First PCR results with insect specific primers within the 18S RNA gene indicate the presence of insects in 93 % of the coarse filter samples.

The German Research Foundation, the LEC Geocycles (Contribution No.25), and the Max Planck Society are gratefully acknowledged for funding.

Després, V., Nowoisky, J., Klose, M., Conrad, R., Andreae, M.O., Pöschl, U. (2007) *Biogeosciences Discussions*, 349-384.

## Laboratory and field characterization of (1-3)- $\beta$ -D-glucan in aerosolized fungal fragments

T. Reponen<sup>1</sup>, S.-C. Seo<sup>1</sup>, F. Grimsley<sup>2</sup>, T. Lee<sup>1</sup>, C. Crawford<sup>1</sup>, S.A. Grinshpun<sup>1</sup>

<sup>1</sup>Center for Health-Related Aerosol Studies, University of Cincinnati, Cincinnati, OH 45241, USA

<sup>2</sup>Department of Environmental Health Sciences, Tulane University, LA 70112, USA

Keywords: Bioaerosols, Fine particles, Indoor aerosols, Size-segregated aerosol

Earlier studies have shown that large quantities of fungal fragments are released together with intact spores from contaminated surfaces.<sup>1,2</sup> Fine fungal fragments may contribute to mold-related health effects. The lack of suitable methods, however, has hindered the exposure assessment to fungal fragments. We have recently developed a field-compatible method for the sampling and analysis of airborne fungal fragments. The sampling system consists of two sharp-cut cyclones and an after-filter. The particles are separated into three size fractions: (i) >2.25  $\mu\text{m}$  (spores); (ii) 1.05-2.25  $\mu\text{m}$  (mixture); and (iii) < 1.0  $\mu\text{m}$  (submicrometer fragments). Samples are analyzed for (1-3)- $\beta$ -D-glucan using the kinetic chromogenic *Limulus* Amebocyte lysate assay (LAL). (1-3)- $\beta$ -D-glucan was selected as a surrogate of fungal biomass as it is a stable component of fungal cell-wall and does not depend on the viability or metabolic state of the fungi. This new methodology was utilized for characterizing fungal fragments in aerosol samples collected in laboratory and field conditions.

In the laboratory investigation, two fungal species, *Aspergillus versicolor* (*A.ver*) and *Stachybotrys chartarum* (*S.cha*), were grown for six months at a relative humidity of 97-99% on malt extract agar, ceiling tile, and gypsum board. Fungal particles were released from surfaces by air flow and collected with the new sampling system. For comparison, the number concentration of particles in the first size fraction (spores) was measured by two optical particle counters (Model 1.108, Grimm Technologies, Inc. Germany); one upstream and the other downstream of the PM<sub>2.5</sub> cyclone.

The field investigation was conducted in five mold-contaminated homes. Three homes, located in New Orleans, were flooded during the hurricane Katrina. Two others, located in Southern Ohio, had suffered water-damage in the basement. Fragment sampling was performed in all these homes during the summer of 2006 and repeated in two homes in the winter. Traditional fungal spore enumeration was performed by collecting spores onto polycarbonate filters using the Button Sampler (SKC, Inc.) and analyzing the filters by microscopic counting. The fragment fractions were also observed under a microscope to confirm the absence of spores.

The geometric mean concentrations of (1-3)- $\beta$ -D-glucan in the laboratory tests were much higher than in the field tests (Tables 1 and 2), which was

attributed to the difference in the sampling protocols. In the laboratory tests, fungi were grown at high humidity and released from the surface directly into the experimental system. In the field, the release was not controlled, and the particles had time to be diluted and settle down before sampled from the air. The fragment to spore ratio for (1-3)- $\beta$ -D-glucan varied from 0.001 to 0.670 in the laboratory tests, and from 0.011 to 2.163 in the field tests. Surprisingly, this ratio was higher in the field than in the laboratory tests. In many field samples, the (1-3)- $\beta$ -D-glucan mass in the fragment fraction was equal to that in the spore fraction.

Our previous laboratory study showed that the number concentration of fragments was as much as 500 higher than that of spores.<sup>2</sup> For the field sampling, the number concentration of fragments can be estimated based on the mass. If we assume that the mass concentration of fragments and spores is equal and the spore size is 3  $\mu\text{m}$ , the number ratio (fragments/spores) would be 10<sup>3</sup> and 10<sup>6</sup>, if fragment size is 0.3 and 0.03  $\mu\text{m}$ , respectively. These results indicate that the actual (field) contribution of fungal fragments to the overall exposure may be much higher than it was earlier estimated in the laboratory studies.

Table 1. Results from the laboratory study.

	GM of Particles <sup>a</sup> ( $\times 10^6$ particles/m <sup>3</sup> )	GM of (1-3)- $\beta$ -D-glucan (ng/m <sup>3</sup> )		Average F/S ratio <sup>b</sup>
		Fragment fraction	Spore fraction	
<i>A.ver.</i>	90.7	59.2	7,224.5	0.018
<i>S.cha</i>	10.6	10.9	1,374.7	0.105

<sup>a</sup>Geometric mean of particle concentration in spore size fraction.

<sup>b</sup> $\beta$ -glucan in fragment fraction  $\div$   $\beta$ -glucan in spore fraction

Table 2. Results from the field study.

	GM of Spores <sup>a</sup> ( $\times 10^3$ spores/m <sup>3</sup> )	GM of (1-3)- $\beta$ -D-glucan (ng/m <sup>3</sup> )		Average F/S ratio <sup>b</sup>
		Fragment fraction	Spore fraction	
Summer	8.1	0.121	1.620	0.277
Winter	2.6	0.419	0.569	1.017

<sup>a</sup>Geometric mean of spore concentration from the Button sampler

<sup>b</sup> $\beta$ -glucan in fragment fraction  $\div$   $\beta$ -glucan in spore fraction

This work was supported by the NIEHS Center for Environmental Genetics Pilot Project Program (grant #PO30ES006096).

<sup>1</sup>Górný, R.L., Reponen, T., Willeke, K., Robine, E., Boissier, M., Grinshpun, S.A. *App. Environ Microbiol* 68:3522-3531, 2002.

<sup>2</sup>Cho, S.-H., Seo, S.-C., Schmechel, D., Grinshpun, S.A., Reponen, T. *Atmos Environ* 39:5454-5465, 2005.

## Antimicrobial Characteristics of ACF Filter Containing Silver Nano Particles

C.W. Park<sup>1</sup>, K.Y. Yoon<sup>1</sup>, J.H. Byeon<sup>1</sup>, J.H. Park<sup>1</sup>, R.H. Lee<sup>1</sup> and J. Hwang<sup>1</sup>

<sup>1</sup>Department of Mechanical Engineering, Yonsei University, 120-749, Seoul, Korea

Keywords: Bioaerosols, Activated carbon fiber, Antimicrobial, Silver.

### Introduction

Bioaerosols are present in the atmosphere in the form of pollens, fungal spores, bacteria, viruses, and any fragments from plants and animals (Jones & Harrison, 2004). In suitable hosts, bioaerosols can cause adverse effects such as headaches, nausea, allergies on humans (Maus et al., 1997).

Activated carbon fiber (ACF) filter is widely used in air cleaning to remove hazardous gaseous pollutants because of their extended surface area and high adsorption amount. However, bacteria preferably adhere to solid supports made of carbon materials, indicating that ACF filters have good biocompatibility. Bacteria may breed on the ACF filters, so that the ACF filters themselves becomes a source of bioaerosols (Park & Jang, 2003). In order to avoid such a problem, antimicrobial ACF filters are required.

Our previous study (Yoon et al., 2006), we had known static antimicrobial characteristics of ACF filter containing metal (silver, copper) nano particles by modified Kirby-Bauer method. In this study, the object is evaluation of time-dependent antimicrobial characteristics of ACF filter containing silver nano particles.

### Materials and Methods

Silver was deposited on the ACF filter (KF-1500, Toyobo, Japan) by an electroless deposition method. The samples denoted in ACF/Ag-10, ACF/Ag-20 and ACF/Ag-30 were prepared without the use of electric current at different deposition times of 10, 20 and 30 minutes, respectively, with silver metal solution.

*E. coli* (ATCC 11775) was chosen in this study. *E. coli* was prepared by culturing again 0.1 mL of an overnight culture inoculated in 15 mL of nutrient broth for 18 hours. The culture was then diluted with nutrient broth to obtain suspensions with O.D. (optical density) of 0.1 at 600nm of wavelength. O.D. was measured by spectrophotometer (SP-300, Optima, Japan).

Time-dependent antimicrobial characteristics were investigated by separating bacteria from test filters after contact for predetermined periods.  $10^7$  cells were inoculated onto the test filter media and leaved for the contact time of 0, 2, 5, and 10 min. After the contact time, test filter media were immersed into 50 mL of deionized water in sterilized plastic bag, BagLight (Interscience), and the bags were stocked by BagMixer (400VW, Interscience)

for 3 min at the speed of 9 strokes/sec. The samples containing *E. coli* were diluted with deionized water. After then, 0.1 mL from the diluted samples were spread on the nutrient agar plates and analyzed by colony counting after incubation of 24 hours.

### Results and Discussion

Our results were summarized in Figure 1. Colony ratio is the number of colony of 0 min contact time divided by each the number of colony of other contact time.

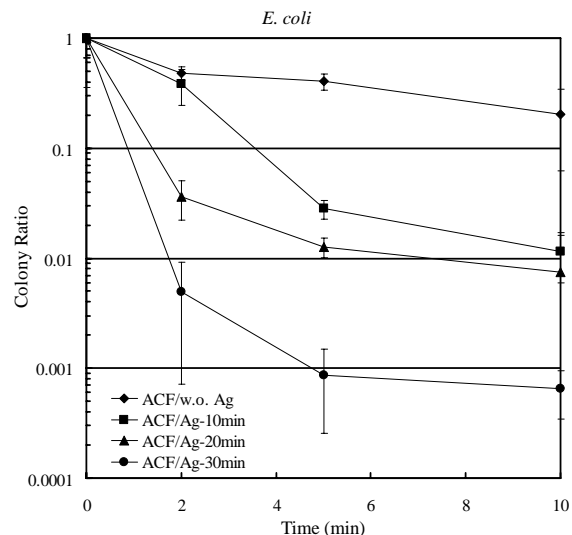


Figure 1. Time-dependent colony ratio

The number of colony was in inverse proportion to the contact time and duration time of electroless plating.

This work was supported by grant NO. 013-071-052 from the Eco-Technopia 21 Project of the Korea Institute of Environmental Science and Technology.

Jones, A. M., & Harrison, R. M. (2004). *Science of the Total Environment*, 326, 151-180.

Maus, R., Goppelsröder, A., & Umhauer, H. (1997). *Atmospheric Environment*, 31, 2305-2310.

Park, S. J., & Jang, Y. S. (2003). *Colloid Interf. Sci.*, 261, 238-243.

Yoon, K. Y., Byeon, J. H., Ko, B. J., Park, J. H., Park, C. W., Hwang, J., & Yoon, H. S. (2006). *Materials Science Forum*, 544, 191-194.

## Bioaerosols in the environment – should we apply reference values?

R.L. Górny<sup>1</sup>, G. Mainelis<sup>2</sup>, J. Dutkiewicz<sup>3</sup> and E. Anczyk<sup>4</sup>

<sup>1</sup>Department of Biohazards, <sup>4</sup>Department of Health Policy, Institute of Occupational Medicine and Environmental Health, 13 Koscielna Street, 41-200 Sosnowiec, Poland

<sup>2</sup>Department of Environmental Sciences, Rutgers - The State University of New Jersey, 14 College Farm Road, New Brunswick, New Jersey 08901-8551, USA

<sup>3</sup>Department of Occupational Biohazards, Institute of Agricultural Medicine, 2 Jaczewskiego Street, 20-950 Lublin, Poland

Keywords: bioaerosols, indoor air quality, hygienic standards, limit values

Exposure to airborne biological agents very often leads to adverse health effects in susceptible individuals. However, in majority of cases the dose-response relationships either do not exist or, if available, are controversial in many aspects. Such problems of hygienic indoor environmental evaluations could be at least partially solved by using a strategy that takes into account (1) the type of the environment, (2) the type of contaminated medium (Figure 1) and is supported by an adequate quantitative and qualitative assessment of biological agents (Górny, 2004).

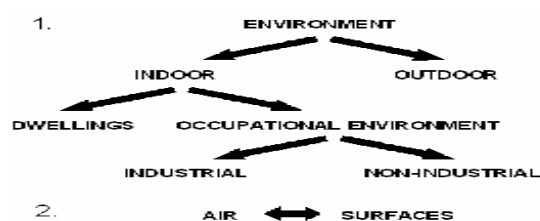


Figure 1. Strategy of hygienic standard elaboration taking into account environmental parameters.

The strategy of providing environmental hygiene standards for biological aerosols should take into account environmental parameters, discuss limitations of available recommendations, and should help with decision making and data interpretation issues. To ensure the reliability and accuracy of bioaerosol measurement methods and their proper interpretation, it is first of all necessary to unify the measurement methodology. For each specific method, the reference limit values for widely measured agents (i.e., bacteria, fungi, and endotoxin), should be recognized by the international scientific community. Such categorization, especially in indoor bioaerosol studies, should describe the parameters for data interpretation and analysis.

If a solid link between the concentration of investigated parameters and resulting adverse health effect cannot be effectively established, then, based on the biological agent concentration measurements, the reference values should enable evaluation of the quality of the environment, as well as determination of “what is typical and acceptable” and “what is atypical or not acceptable”

for a specific type of setting.

Based on these assumptions, several Polish proposals for occupational exposure limits (OEL) (Dutkiewicz & Górny, 2002), public service (PSLV) and residential limit values (RLV) (Górny, 2004) for various bioaerosol components were suggested (Table 1). In addition to these values, it should also be generally assumed that for certain indoor exposures, especially for sensitive individuals, microbial pathogens may be a cause of health problems even at concentrations substantially below the proposed reference limits. In addition, the presence of microorganisms from the risk groups 3 and 4 (Directive 2000/54/EC), independently of their concentration, should always be inadmissible and result in preventive action.

Table 1. Polish proposals for OEL and PSLV/RLV for various bioaerosols (volumetric methods).

Type of setting	Bioaerosol component	OEL, PSLV, RLV proposals
Industrial settings	Mesophilic bacteria	$1 \times 10^5$ CFU/m <sup>3</sup>
	Gram-neg. bacteria	$2 \times 10^4$ CFU/m <sup>3</sup>
	Thermophilic actinomycetes	$2 \times 10^4$ CFU/m <sup>3</sup>
	organic dust	
	Fungi	$5 \times 10^4$ CFU/m <sup>3</sup>
	Endotoxin	$2 \times 10^3$ EU/m <sup>3</sup>
Public service and residential buildings	Mesophilic bacteria	$5 \times 10^3$ CFU/m <sup>3</sup>
	Gram-neg. bacteria	$2 \times 10^2$ CFU/m <sup>3</sup>
	Thermophilic actinomycetes	$2 \times 10^2$ CFU/m <sup>3</sup>
	Fungi	$5 \times 10^3$ CFU/m <sup>3</sup>
	Endotoxin	$5 \times 10^1$ EU/m <sup>3</sup>

CFU – colony forming unit. EU – endotoxin unit.

This research was supported in part by the US National Academies' Twinning Program.

Directive 2000/54/EC on the protection of workers from risk related to exposure to biological agents at work. *Official J. Eur. Communities*, 17.10.2000, L262/21–45.

Dutkiewicz, J. & Górny, R. (2002). *Med. Pr.*, 53, 29-39.

Górny, R. (2004). *Princip. Methods Assess. Work Environ.*, 3, 17-39.

## Disinfection of Bioaerosols using Filters Saturated with Tea Tree Oil.

Ruth Huang<sup>1</sup>, Benjamin J. Mullins<sup>2</sup>, Igor E. Agranovski<sup>1</sup>, and Oleg V. Pyankov<sup>1</sup>

1. Faculty of Engineering and Information Technology, Griffith University, Nathan, 4111 Australia.  
2. Centre of Excellence in Cleaner Production, Curtin University, GPO Box U1987, WA, 6845, Australia.

Keywords: Bioaerosol, disinfectant, filter, nebuliser.

Filters with the potential to deactivate bioaerosols – usually via photocatalysis – have received significant attention recently (Vohra et al. 2006). Such filters, however, are often expensive, complex, difficult to produce, and may produce toxic by-products such as phosgene as part of the catalytic decomposition process.

The essential oil of *Melaleuca alternifolia*, commonly referred to as tea tree oil (TTO), is widely used as a topical antiseptic, and also as a complementary medicine for bacterial and fungal infections. Several investigations have confirmed the in-vitro activity of TTO against a wide range of Gram-positive, Gram-negative bacteria and fungi (May et al. 2000), however with “kill times” of minutes to hours using a 5% solution of TTO.

This study examines the possibility of producing a simple, low-cost disinfecting filter by saturating a conventional fibrous filter with a solution of mineral oil (MO – (Sigma Chemicals M3516) - biologically inactive) and TTO. Filters are commonly used for oil mist filtration (Mullins and Kasper 2006), and it was considered that the ability of filters to retain oil through capillarity could be of benefit for bioaerosol filtration when conventional mineral oil is substituted with TTO.

Low-efficiency fibrous filters were wetted to equilibrium saturation (approx. 25% of void space) by dipping in oil mixtures, ranging from 0% TTO (100% MO) - to 100% TTO (0% MO). Each filter was then tested in a conventional test apparatus for their ability to disinfect *Escherichia coli* aerosols generated via a nebuliser (OMRON CX3). The aerosol was sampled before and after the filter using the Agranovski personal sampler (Agranovski et al. 2002). The liquor from the samplers was then cultured, along with a sample of the wetting liquid from the filter.

Figure 1 shows the ratio of viable airborne *Escherichia coli* after the filter, to before the filter (corrected for filtration efficiency). The increasing concentration of TTO appears to provide some low level of deactivation of transient aerosols, however only slightly above the baseline (0% TTO). More experimentation is required to verify if TTO is able to disinfect transient bioaerosols, and if increasing residence time will increase rate of disinfection.

Figure 2 shows the ability of the wetting liquid to deactivate captured *Escherichia coli* aerosols – in

relation to the proportion of viable aerosols before the filter and the filtration efficiency. Here, there is a clear trend that aerosol particles completely wetted by the TTO solution are deactivated effectively, which supports previous work (May et al. 2000).

It can be concluded that this new filtration technology shows significant potential, as it would in theory be able to provide complete disinfection of bacteria, if the filter was 100% efficient, and possibly also some disinfection of transient aerosols.

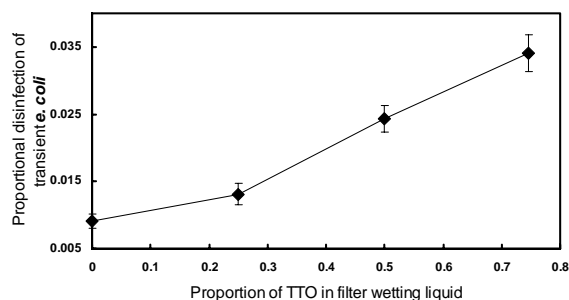


Figure 1 – Disinfection of transient bioaerosols (not captured by filter) as a function of TTO conc.

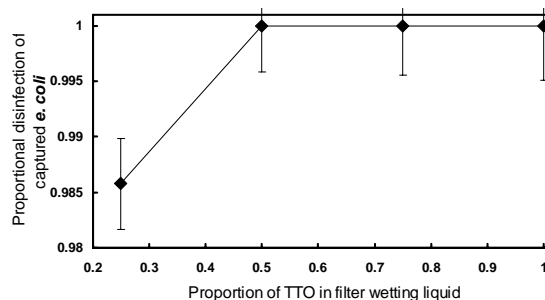


Figure 2 – Disinfection of captured bioaerosols as a function of TTO conc.

I. Agranovski, V. Agranovski, T. Reponen, K. Willeke, and S. Grinshpun, (2002). *Atmos. Env.* 36(5): 889-898.  
J. May, C. Chan, A. King, L. Williams, and G. French, (2000). *J. Antimicrobial Chemotherapy* 45(5): 639-643.  
B. Mullins, and G. Kasper, (2006). *Chem. Eng. Sci.* 61(18): 6223-6227.  
A. Vohra, D. Goswami, D. Deshpande, and S. Block, (2006). *App. Catalysis B-Environmental* 64(1-2): 57-65.

## Single particle mass spectrometry on bio-aerosols

W.A. Kleefsman<sup>1</sup>, M.A. Stowers<sup>1</sup>, P.J.T. Verheijen<sup>1</sup> and J.C.M. Marijnissen<sup>1</sup>

<sup>1</sup> Faculty of Applied Sciences, Nanostructured Materials, Delft University of Technology, 2628 BL, Delft, The Netherlands

Keywords: Aerosol characterization, Aerosol mass spectrometry, Bioaerosols, Fluorescence, Instrumentation.

Aerosol mass spectrometry is a common analyzing technique for the characterization of aerosol particles. Aerosol MALDI (matrix-assisted laser desorption/ionization) mass spectrometry can be seen as a subcategory within aerosol mass spectrometry. For several years, our group at the Delft University of Technology is developing an aerosol MALDI mass spectrometer (van Wuijckhuijse *et al.*, 2005). The primary goal of the project is the on-line analysis of bacteria-containing single aerosol particles.

The aerosol MALDI mass spectrometer can be divided into three main parts: the aerosol sample preparation, the particle detection, sizing and selection and thirdly the mass spectrometer section. In the particle detection, sizing and selection part, aerosol particles originating at ambient pressure form a particle beam in the vacuum chamber of a time-of-flight mass spectrometer. The particles are intercepted by two continuous laser beams (detection) and the particle velocity is determined (sizing). The wavelength of one laser beam is 266 nm, the wavelength that excites the amino acid tryptophan, present in all bacteria. The emitted fluorescence is recorded and only the fluorescing particles are further investigated. This detection scheme reserves the system only for the particles of interest (selection) (Stowers *et al.*, 2006). Based on the particle velocity information obtained, an Excimer laser pulse is generated to initiate ion formation. These ions are accelerated and identified based on their time of flight.

MALDI mass spectrometry is a commonly used method for bulk analysis of biological materials, like proteins and bacteria. In MALDI mass spectrometry a matrix compound is used, which allows the ionization of high mass molecules. The matrix compound absorbs the ionising laser light and subsequently causes soft ionization of the intact high mass molecules of interest.

The fundamentals of the mechanism of the MALDI-process are and have been subject of research of many groups. All of them agree on the importance of sample preparation on the quality of the mass spectrum. The choice of matrix compound, the analyte (proteins of bacteria) and the solvent used, as well as the interaction of above-mentioned factors, determine the peaks (that can be) obtained in the mass spectrum.

In on-line aerosol MALDI mass spectrometry the sample preparation also plays an important role. The sample preparation has to be imitated on a much smaller scale, i.e. on single aerosol particles. Due to the smaller sizes the effects and interactions of the necessary components are different. This paper will report on the effects of sample preparation in aerosol MALDI, for proteins and bacteria particles. An example of the effect of the solvent in aerosol MALDI is shown in figure 1. Figure 1a is a mass spectrum of 50 particles of the protein ubiquitin premixed with the matrix sinapinic acid in the solvent ethylene glycol is given. Figure 1b is also a mass spectrum of 50 particles made from the same compounds, except for the solvent, which was ethylene glycol with 10% (v/v) glycerol. The volatility of the latter solvent is very low, resulting in a long drying time of the aerosol particles, therefore affecting the crystal growth of the matrix. The slower crystal growth might be the reason that signals observed in figure 1b are more intense.

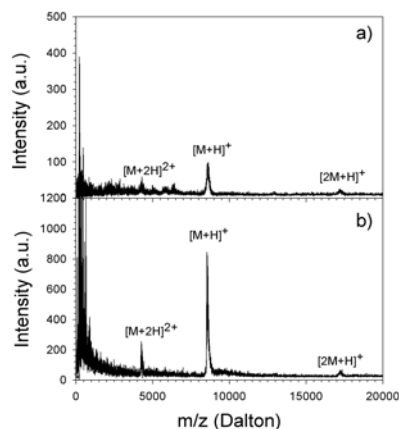


Figure 1. Mass spectra of 50 ubiquitin-containing aerosol particles, originating from solutions of different volatility.

This work was supported by TNO Defence, Security and Safety and the Dutch Ministry of Defence.

Van Wuijckhuijse, A.L., Stowers, M.A., Kleefsman, W.A., Baar, B.L.M. van, Kientz, Ch.E. & Marijnissen, J.C.M. (2005). *J. Aerosol Science*, 36, 677-687.

Stowers, M.A., van Wuijckhuijse, A.L., Marijnissen, J.C.M., Kientz, Ch.E. & Ciach, T. (2006) *Applied Optics*, 45, 8531-8536

## Seasonal variation of fungal spores and their contribution to organic carbon and to PM10 aerosols in Vienna, Austria

H. Bauer, V. Bumberger, A. Caseiro, P. Pournesmaeil, A. Berger, H. Puxbaum  
Institute for Chemical Technologies and Analytics, Vienna University of Technology, A-1060 Vienna, Austria

*Keywords: Bioaerosols, Fungal spores, Organic Carbon, Atmospheric aerosols.*

### INTRODUCTION

Fungal spores are not only important because of their property of causing allergies, they are also major contributors to the organic carbon in atmospheric aerosols. Quantitative assessments in terms of the amount of biogenic carbon in relation to the organic carbon fraction of the aerosol have been reported for primary bio-components such as cellulose (Kunit & Puxbaum, 1996; Puxbaum & Tenze-Kunit, 2003), bacteria (Sattler *et al.* 2001, Bauer *et al.*, 2002a), fungal spores (Bauer *et al.*, 2002a,b; Womiloju *et al.*, 2003, Bauer *et al.*, 2007). Earlier publications refer mainly to cultivable micro-organisms and their potential health risks.

The aim of this study was to investigate the annual trend of airborne fungal spores and their contribution to PM10 aerosol and to the organic carbon balance.

### EXPERIMENTAL

Sampling was performed from January 2004 to July 2005 at two suburban and two urban sites, which belong to the air quality network of Vienna, Austria. In a smaller set of 50 samples aerosols for the analysis of fungal spores were collected with an AGI-4 impinger, the suction pipe of which was positioned next to the inlet tube of a High Volume sampler collecting aerosols on quartz fiber filters for chemical analyses. The filter samples were analyzed for PM<sub>10</sub> aerosol mass, total, organic, elemental and carbonate carbon, polyols and ions (major ions and organic acids). In this set of samples the number concentrations of fungal spores were determined by direct enumeration by epifluorescence microscopy after staining with SYBR-Gold. The carbon content of the fungal biomass was calculated using the conversion factor of 13 pg C spore<sup>-1</sup> (Bauer *et al.*, 2002a,b, Bauer *et al.*, 2007).

In the second set of samples the fungal marker arabinol was used to derive the. Arabinol was determined using high pH anion exchange and pulsed amperometry (HPAE-PAD).

Organic carbon was determined as the difference of total carbon minus elemental carbon using thermal methods described by Schmid *et al.* (2001).

### RESULTS AND DISCUSSION

Our first results show surprisingly high contributions of fungal spores during the growing season (up to 21% of OC and 13% of PM10 at the suburban and 10% of OC and 5% of PM10 at the urban sites). Highest concentrations of fungal spores and highest contributions to OC and PM10 were measured in July. It can thus be concluded that fungal spores may make a considerable contribution to the carbon mass balance.

This work was supported by internal projects of the Vienna University of Technology.

### REFERENCES

- Bauer, H., Kasper-Giebl, A., Löflund, M., Giebl, H., Hitzenberger, R., Zibuschka, F., & Puxbaum, H. (2002a). *Atmos. Res.*, 64, 109-119.
- Bauer, H., Kasper-Giebl, A., Zibuschka, F., Kraus, G. F., Hitzenberger, R., & Puxbaum, H. (2002b). *Anal. Chem.*, 74, 91-95.
- Bauer, H., Schüller, E., Weinke, G., Berger, A., Hitzenberger, R., Marr, I., Puxbaum, H. (2007) Significant contributions of fungal spores to the organic carbon balance of the urban atmospheric aerosol. *Environ. Sci. Technol.* Submitted
- Kunit, M., & Puxbaum, H. (1996). *Atmos. Environ.* 30, 1233-1236.
- Puxbaum, H., & Tenze-Kunit, M. (2003). *Atmos. Environ.* 37, 3693-3699.
- Sattler, B., Puxbaum, H., & Psenner, R. (2001). *Geophys. Res. Lett.*, 28/2, 239-242
- Schmid, H., Laskus, L., Abraham, H. J., Baltensperger, U., Lavanchy, V., Bizjak, M., Burba, P., Cachier, H., Crow, D., Chow, J., Gnauk, T., Even, A., ten Brink, H. M., Giesen, K. P., Hitzenberger, R., Hueglin, C., Maenhaut, W., Pio, C., Carvalho, A., Putaud, J.-P., Toom-Sauntry, D., & Puxbaum, H. (2001). *Atmos. Environ.* 35, 2111-2121.
- Womiloju, T. O., Miller, J. D., Mayer, P. M., & Brook, J. R. (2003). *Atmos. Environ.* 37, 4335-4344.

## Comparison between ambient concentrations of the major birch allergen Bet v 1 and birch pollen count

J. Buters<sup>1</sup>, I. Weichenmeier<sup>1</sup>, S. Ochs<sup>1</sup>, W. Kreyling<sup>2</sup>, J. Boere<sup>3</sup>, W. Schober<sup>1</sup>, H. Behrendt<sup>1</sup>

<sup>1</sup>Division of Environmental Dermatology and Allergy GSF/TUM, AUM- Center for Allergy and Environment Munich, Munich, Germany

<sup>2</sup>GSF-Focus: Aerosols and Health, Institute for Inhalation Biology, Neuherberg, Germany

<sup>3</sup>National Institute for Public Health and the Environment, Centre for Environmental Health Research, Dept. Toxic Effects of Air Pollution, Bilthoven, Netherlands

Keywords: biogenic particles, health effects of aerosols, outdoor aerosols, PM10, PM2.5.

**Background:** Exposure to allergens like Bet v 1, the major birch pollen allergen, is generally deduced from birch pollen counts in ambient air. Proof is lacking that pollen counts reflect exposure to this allergen (Schäppi 1997, Rantio-ethimaki 1994).

**Methods:** At the hospital campus in Munich, Germany, 562 m above sea level, 1.8 m above ground, we monitored simultaneously birch pollen counts with a standard Burkard pollen trap, and Bet v 1 in ambient air with a Chemvol High-Volume sampler (900 l/min). Bet v 1 was extracted from the filters with 0.1 M  $\text{NH}_4\text{HCO}_3$  and quantitated with a Bet v 1 specific EISA.

**Results:** Peak birch pollen count in 2004, 2005, and 2006 were 729, 3522 and 1681 pollen/m<sup>3</sup>/24h, respectively (see figure 1). At the same time peak Bet v 1 concentration was 148, 364 and 1390 pg Bet v 1/m<sup>3</sup>, respectively. According to pollen count, 2005 showed the strongest exposure to allergens. In 2006, when pollen counts were half of 2005, Bet v 1 concentration in ambient air was about 4-fold higher than 2005, indicating that the release of Bet v 1 per pollen was 8-times higher than in 2005. Also, later in the season when pollen counts were low, Bet v 1 persisted at high concentrations in ambient air. No other pollen, like *Fraxinus* or *Quercus* as another source of Bet v 1 in ambient air, was detected.

**Conclusion:** Exposure to birch pollen allergens is dependent on the amount of pollen released in a particular year (pollen flight). On top of that is also the difference in allergen release of that pollen between years. The allergen release of pollen can differ 8-fold between years. Thus birch pollen counts do not necessarily reflect birch allergen exposure, especially later in the season.

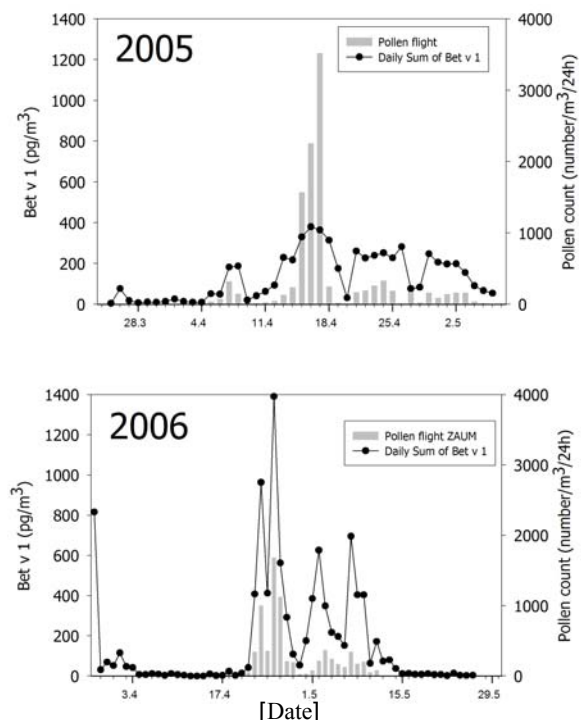


Figure 1. Concomitant determination of birch pollen and their major allergen Bet v 1 in Munich.

Schäppi, G. F., Suphioglu, C., Taylor, P. E., & Knox, R. B. Concentrations of the major birch tree allergen Bet v 1 in pollen and respirable fine particles in the atmosphere. *J Allergy Clin Immunol* 1997, 100, 656-661.

Rantio-ethimaki, A., Viander, M., & Koivikko, A. Airborne birch pollen antigens in different particle sizes. *Clin Exp Allergy* 1994, 24, 23-28.

## APPLICATION OF THE FLAME SPECTROPHOTOMETRY IN THE BIOLOGICAL AEROSOL DETECTION IN THE AIRBORNE PARTICLE, USING STATISTICAL MULTI- AND MEGAVARIATE ANALYSIS.

D. DESCROIX<sup>1</sup>, M.B. ATTOU<sup>2</sup>

<sup>1</sup> CEB, BP N° 3, 91710 Vert le Petit, France.

<sup>2</sup> Département de Physique, UFR Sci, UPVM, 94010 Créteil, France. [attoui@univ-paris12.fr](mailto:attoui@univ-paris12.fr)

**Keywords:** Atmospheric aerosols, flame spectrophotometry, principal component analysis, bioaerosols

The aim of our study is the biological aerosol detection by flame emission photometry. We must determine the essential parameters to bacterium detection and to define limits of sensitivity for atoms which are present into these microorganisms. We analyze bacteria through the emission lines, mainly alkaline metals. Our first step has led us to put in place measurement tools and data processing around a flame spectrophotometer. This device is developed to monitor, to sample continuously and to analyze in real time the airborne particle. This device analyzes on spectral range from 340 to 800 nm. Our study took place in three steps: the optimization of the sampling parameters (1, 2), the particle analysis by flame spectroscopy and the statistical treatment by multi-and megavariate data analysis (3). The device which we used, allows to sample inhaled particles and to concentrate them according to their size. The optimization of the parameters of the device (burner, optics), allowed to obtain limits of sensitivity about the femtogram for sodium and potassium. With these limits, it is possible to detect bacteria, the mass of which is about 1 picogram. In addition to elementary analysis capabilities, we have shown that flame spectrophotometry allows to

estimate ratios between atoms in a bacterium. They are constant and characteristic of a bacterial strain, grown and dispersed in the same conditions. Using specific algorithms, we show that it is possible to differentiate some biological agents from the non-biological particles. Statistical multi-and megavariate data analytical methods (PLS : Partial Least Square, PCA : Principal component analysis) allows real time data processing.

This work was supported by the Centre d'Etude du Bouchet.

- 1 - Descroix, D., H. Lancelin, K. Scurrah, and M. B. Attoui. 2003. Presented at the European Aerosol Conference, Madrid, September.
- 2 - Descroix, D., H. Lancelin, K. Scurrah, and M. B. Attoui. 2004. Presented at the European Aerosol Conference, Budapest, September.
- 3 - Descroix, D., I. Gustafson, H. Lancelin, G. Olofsson, S. Rännar, and T. Tjärnhage. 2004. Presented at the 8th CBW Protection Symposium, Gothenburg Sweden, June 2-6.

## Real Time Analysis of *Bacillus species* Strain specific analysis by MALDI Aerosol ToF Mass Spectrometry

A.L. van Wuijckhuijse, C.E.A.M. Degenhardt, F.P.J. de Groot, B.L.M. van Baar, Ch.E. Kientz  
TNO Defence, Security and Safety, P.O. Box 45, 2280 AA Rijswijk, The Netherlands

Keywords : bioaerosols, MALDI, aerosol mass spectrometry,  
*Bacillus spores*

### INTRODUCTION

Bioaerosol particles such as micro-organisms *e.g.*, spores, bacteria and viruses can be health-threatening, especially when dealing with terrorist threats. Techniques for rapid and accurate microbial identification are crucial for recognizing bio warfare threats and a wide range of environmental and medical applications. Matrix Assisted Laser Desorption/Ionization Time-of-Flight Mass Spectrometry (MALDI-TOFMS) has emerged as a reliable generic laboratory technique, suitable for toxins, viruses, bacteria and spores including whole cells. However in case of bioaerosols MALDI-TOFMS involves sampling by deposition; the material has to be collected on a suitable substrate before it can be analyzed.

A joint effort of the TNO Defence, Security and Safety and Delft University of Technology has recently shown that it is possible, in principle, to apply real-time aerosol MALDI-TOFMS to bioaerosols (van Wuijckhuijse 2005). With the prototype instrument mass spectra can be obtained from single biological aerosol particles. The present paper describes recent results obtained with the prototype at TNO.

### RESULTS

To characterize the discriminative power of the current state of the system two *Bacillus cereus* strains and the species: *B. cereus*, *B. thuringiensis* and *B. globigii* have been tested under several circumstances, like *e.g.* growth medium and culture age. The results of these tests are very promising since even strains of *Bacillus cereus* spores can be discriminated (Figure 1). Dependencies of the growth medium and sample age on the mass spectrum will be presented.

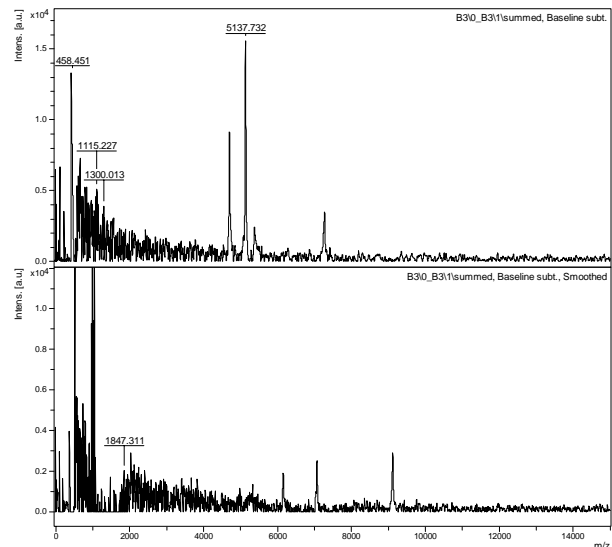


Figure 1: Real-time MALDI Aerosol ToF spectra of two *Bacillus cereus* strains

### CONCLUSION

On-line MALDI Aerosol ToF Mass Spectrometry is able to discriminate among *Bacillus species*. Hereby the system offers the potential to be developed in the first specific near real time detector for bioaerosol agents.

### ACKNOWLEDGEMENTS

The authors gratefully acknowledge financial support from the Netherlands Ministry of Defence. The authors also gratefully acknowledge J.C.M. Marijnissen, M.A. Stowers and W.A. Kleefsmann of Delft University of Technology for their support in the instrument development.

### REFERENCES

van Wuijckhuijse, A.L. *et al* (2005). *J. Aerosol Science*, 36, 677.

## Polymer Containing Respirator Offers Enhanced Protection against Airborne Viruses

S. Bourget<sup>1</sup>, A. Staffa<sup>1</sup>, M.E. Sans Cartier<sup>1</sup> and P.J. Messier<sup>1</sup>

<sup>1</sup>Triosyn Research, 14163 abelle blvd., J7J 1M3, Mirabel, Canada

Keywords: aerosol filtration, bioaerosol, airborne particles, respirators.

Several airborne viral pathogens present a worldwide threat to the health of communities: SARS outbreak, pending influenza pandemic, as well as smallpox and other pathogenic viruses as possible bioterrorism agents. These events have brought increasing attention to the level of respiratory protection available against aerosolized viruses.

Devices such as Self-Contained Breathing Apparatus (SCBAs) or Powered-Air Particulate Respirators (PAPRs) provide the highest possible level of respiratory protection, but do not allow easy stockpiling and its use might not be realistic in all situations. Therefore, recommendations mostly aim at more practical and available solutions such as particulate respirators.

Occupational health authorities typically recommend the use of CE certified (FFP2, FFP3) respirators in situations suspected of involving an airborne infectious microbial hazard. Such certifications require particulate filtration efficiencies of 94 to 99 against an aerosol of inert particles with a mean particle size of 0.6  $\mu\text{m}$ . As electrostatics enhances filtration efficiency, most respirators are manufactured using electrostatically charged filter media. It was recently reported (Balazy *et al.*, 2006) that the most penetrating particle size through such charged media shifts toward the nano-sized range. Most viruses of pathogenic concern are nano-sized particles.

An iodinated polymer was developed and combined with the mechanical filtration equivalent of a standard respirator in the aim of providing for a higher level of filtration efficiency against viral agents. A self-contained testing system was also designed to evaluate full-scale respiratory protection devices against live aerosolized viruses.

Alongside commercial CE-rated respirators, the Iodinated Polymer Containing (IPC) FFP3 respirator was evaluated for their Viral Reduction Efficiency (VRE) using the Bio-Aerosol Test System (BATS). Suspensions of either a surrogate (MS2 coliphage, 0.025  $\mu\text{m}$ ) or an animal virus (influenza A H1N1, 0.08–0.12  $\mu\text{m}$ ) were aerosolized using Collison nebulizers. Full-sized respirators were attached to sampling ports (one port was kept empty to determine the challenge level) and connected to All-Glass Impingers (AGIs). In this closed system, the bioaerosol is drawn through the test articles at an air flow of 85.0  $\text{PM}$  and collected in AGIs containing phosphate buffer. To assess performance in various environmental conditions representing

end-use situations, testing can be performed at different levels of temperature and humidity.

At ambient conditions, the IPC respirator reduced aerosolized concentrations of MS2 coliphage by 3 to 4 logs, translating into VRE results of 99.9 to 99.99. For comparison, standard FFP2 and FFP3 respirators showed VRE values comprised between 97 and 99.9. Similar results were obtained against an aerosol of influenza A.

The BATS apparatus has proven to be an efficient tool in assessing the VRE of respiratory protection devices against live aerosolized viruses. The inclusion of a biocidal polymer has been shown to improve the VRE performance of the IPC respirator.

Balazy, A., Toivola, M., Reponen, T., Podgorski, A., immer, A., & Grinshpun, S. A. (2006). *Manikin-Based Performance Evaluation of N95 Filtering-Facepiece Respirators Challenged with Nanoparticles*. *Ann. Occup. Hyg.*, vol. 50 (3), pp. 259-269.

## Modelling a birch pollen episode with a weather forecast model system

H. Vogel<sup>1</sup>, A. Pauling<sup>2</sup>, B. Vogel<sup>1</sup>

<sup>1</sup> Institut für Meteorologie und Klimaforschung, Forschungszentrum Karlsruhe/Universität Karlsruhe, Postfach 3640, 76021 Karlsruhe, Germany

<sup>2</sup> Bio- and Environmental Meteorology, Climate Division, MeteoSwiss, Krähbühlstr. 58, 8044 Zürich, Switzerland

Keywords: Bioaerosols, Aerosol Modelling, PM.

We developed a new model system for the calculation of reactive gas traces and aerosols. For this purpose we coupled the CTM model DRAIS/Madesoot (Riemer et al., 2003) with the meteorological model LM of the German Weather Service (DWD). The LM is a non hydrostatic mesoscale model and is part of the forecast system of the DWD. The standard model domain covers whole Europe. In contrast of several other CTM model systems our model system is fully online coupled, that means that for the transport processes consistent numerical methods for all variables are used. It has a modular structure and therefore it is easily possible to run it in a forecast mode. Several modules were implemented to describe the primary emission of aerosols which are a function of different meteorological variables like temperature and wind speed. To describe the emissions flux of pollen model was extended by the parameterisation of Helbig et al. (2004).

The basic idea of our parameterization is that the vertical flux of pollen grains  $F_e$  at the top of the vegetation is proportional to the product of a characteristic concentration and a characteristic velocity. It is obvious that the available pollen grains cannot be emitted into the atmosphere, if the meteorological conditions are unfavorable. This behavior is taken into account by a meteorological adjustment factor. To calculate the settling velocity a parameterization of Aylor (2002) was used, which takes into account that the pollen grains can hydrate or dehydrate. The advantage of the simultaneous calculation of the transport and dispersion of all components is that it is possible to describe interactions of example between pollen grains and nitrogen oxides or soot.

To validate the implemented parameterizations a birch pollen episode was simulated that lasts from 19.04. to 23.04.2006 and took place in Switzerland. In order to determine the flux of pollen grains into the atmosphere, it is necessary to have information on the percentage contribution of alder trees for each grid point of the model domain. For that purpose a data set of birch trees in Switzerland was built with a horizontal resolution of 7 km using

all available information. For comparison with measurements we used the data from the national pollen network of Switzerland. By default there were only daily mean values of the pollen concentration available but for 4 stations we had data in a temporal resolution of 2 hours. Additionally to the pollen concentration also meteorological variables are measured. Figure 1 shows the simulated horizontal distribution of the pollen concentration and the according wind field for April, 21, 11 UTC. The development of secondary circulations systems caused by the topography has a strong influence of the distributions of the pollen concentrations and lead to a transport over large distances. Otherwise low wind speeds inhibit the emission of pollen grains. The comparison of the simulated temporal development of the pollen concentrations with the observed one will be presented and the capability of using such a model system for the pollen forecast will be discussed.

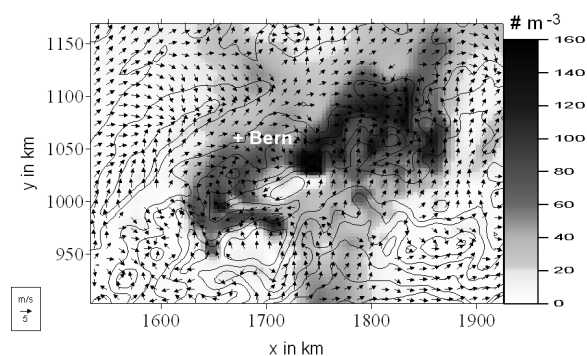


Figure 1. Pollen concentration and according wind field for Switzerland, April, 21, 11 UTC.

Aylor, D.E. (2002). *J. Aerosol Science*, 33, 1601-1607.

Helbig, N., Vogel, B., Vogel, H. & Fiedler, F. (2004). *Aerobiologia*, 20, 3-19.

Riemer N., Vogel, H., Vogel, B. & Fiedler, F. (2003). *J. Geophys. Res.*, 109, 4601, doi:10.1029/2003JD003448

## Effect of sampling time on the overall performance of portable microbial impactors

G. Mainelis and M. Tabayoyong

Department of Environmental Sciences, Rutgers - The State University of New Jersey,  
14 College Farm Road, New Brunswick, New Jersey 08901-8551, USA

Keywords: aerosol sampling, bioaerosols, cascade impactor, collection efficiency, environmental particles

Exposure to airborne bacteria and fungi has been linked to various negative health effects. Portable microbial samplers are being increasingly used for monitoring presence of viable bioaerosols; however, data about their performance characteristics are only starting to appear. This study is a continuation of our efforts to analyze and determine various performance characteristics of several portable microbial impactors: SMA MicroPortable, BioCulture, Microflow, Microbiological Air Sampler (MAS-100), Millipore Air Tester, SAS Super 180, and RCS High Flow when collecting bacteria and fungi both indoors and outdoors. All these samplers collect biological particles on agar media and their built-in sampling flow rates range from 30 to 180 L/min. According to our previous studies, the impactors' cut-off size, or  $d_{50}$ , range from 1.2 to 7.0  $\mu\text{m}$  (Yao and Mainelis, 2006). In this part of the study, we analyzed whether the sampling time affects the overall performance of the portable impactors.

The experiments were performed with seven portable impactors and a BioStage impactor (Andersen N-6 equivalent), which served as a reference sampler. The bacterial and fungal samples were collected indoors and outdoors with portable impactors operating simultaneously and collecting samples for different sampling periods:  $t_s = 2, 5, 10,$  and 30 minutes. During all four different sampling periods, the reference BioStage collected samples for  $t_r = 2$  minutes only. Overall, nine replicates for both bacteria and fungi were collected for each sampling time and environment. The collected samples were incubated at room temperature and the formed Colony Forming Units (CFUs) were counted after 24, 48 and 72 hours. Tryptic soy agar (TSA) was used for collection of bacteria, while Malt Extract Agar (MEA) was used to collect fungi. To determine the effect of sampling time, the Concentration Ratio,  $CR(t_s, i)$ ,

was determined as 
$$CR(t_s, i) = \frac{C(t_s, i)}{C_r(t_s = 2 \text{ min})}$$

where  $C(t_s, i)$  is a concentration determined by a test sampler  $i$  during sampling time  $t_s$ , and the  $C_r$  is a concentration measured by a reference sampler. This procedure was applied for both bacteria and fungi and for both sampling environments.

The indoor bacterial and fungal concentrations measured by the reference BioStage impactor was generally below 100 CFU/m<sup>3</sup>. The average CR for

the portable impactors at  $t_s = 2$  min when sampling bacteria was 0.3 and decreased to 0.15 for  $t_s = 30$  min. The values for fungi were 0.44 and 0.27, respectively. Both the effect of sampling time  $t_s$  and the impactor model were statistically significant ( $p < 0.0005$ ).

The preliminary outdoor sampling experiments indicated that for most of the samplers, sampling times above 5 min caused CFU overload, therefore the procedure was modified in the following way: all samplers were operated for 2 min outdoors and then were brought into a clean environment where they sampled clean air only (no particles present) for  $t_s = 2$  min. This experiment was designed to investigate a potential desiccation effect, once the microorganisms are already deposited on agar.

According to the reference sampler, the outdoor bacterial concentrations ranged from 200 to 2,000 CFU/m<sup>3</sup>, while fungal concentrations ranged from 600 to 8,000 CFU/m<sup>3</sup>. The average CR for the portable impactors at  $t_s = 2$  min when sampling bacteria was 0.43 and decreased to 0.03 for  $t_s = 30$  min. The values for fungi were 0.27 and 0.02, respectively. Both the effect of sampling time  $t_s$  and the impactor model were statistically significant ( $p < 0.0005$ ).

This research shows that sampling time may play a significant and substantial role in both indoor and outdoor environments when determining bioaerosol concentration. Due to desiccation of already collected microorganisms by the air passing through the samplers, their recovery could be reduced by a factor as high as 10.

This research was supported by CDC/NIOSH grant DHHS-CDC1-K01-OH008029. The technical assistance by EMD Chemicals, Inc. (Gibbstown, NJ), A.P. BUCK Inc. (Orlando, FL), Veltek Associates, Inc. (Phoenixville, PA), Bioscience International, Inc., (Rockville, MD), Millipore Corp., (Billerica, MA), and Biotest Diagnostics Corp., (Denville, NJ) is appreciated.

Yao, M. and Mainelis, G. (2006) Investigation of Cutoff Sizes and Collection Efficiencies of Portable Microbial Samplers, *Aerosol Science and Technology*, 40(8): 595-606.

## Bioaerosols in public buildings in Warsaw.

E. Miaśkiewicz-Pęska<sup>1</sup>, M. Łebkowska<sup>1</sup>, P. Grzybowski<sup>2</sup> and E. Karwowska<sup>1</sup>

<sup>1</sup>Faculty of Environmental Engineering, Warsaw University of Technology, 20 Nowowiejska str.  
00-653 Warsaw, Poland

<sup>2</sup>Faculty of Chemical and Process Engineering, Warsaw University of Technology, 1 Waryńskiego str.,  
00-645, Warsaw, Poland

Keywords: bioaerosol, ventilation system, filtration, sick house syndrome.

The level of airborne particles of biological nature, bioaerosols, is one of the comfort and health parameters describing the air quality. Public buildings are nowadays equipped with ventilation/air conditioning systems providing air to all the rooms. It happens too that the only air available inside the building come from the ventilation system. People who work all the week for eight hours a day in an office where the air quality is poor may suffer chronic diseases, allergies and other caused by the bioaerosols they breath in. Sick House Syndrome (SHS) is stated to be developed when 30% of the population of the building declare discomfort or health problems.

The bioaerosols may be generated inside the ventilation systems when find there conditions good for growing. Old and not cleaned channels covered inside with a deposit suitable as a fertilizer for microorganisms may act as bioaerosol generators. The aim of the study was to check the concentrations of the airborne bioaerosol particles at various places inside the public buildings in Warsaw. The tests were conducted in one high building with offices and in one theatre. The air sampling was made with the use of MASS 100 Merc impactor. The samples were collected on the Peltier dishes and further analysed according to the microbiological technics. The numbers of the developed colonies were recalculated into the concentrations of the bioaerosol in the air. The results of the measurements are shown in Tables 1-4.

Table 1. Office Building, 5<sup>th</sup> July 2006

Place of sampling	Psychroph. bacteria [cfu/m <sup>3</sup> ]	Mesoph. bacteria [cfu/m <sup>3</sup> ]	Moulds [cfu/m <sup>3</sup> ]
outdoor	134	59	765
ventilation chamber	51	24	130
room inlet	18	123	27
room, middle	26	121	44

Table 2. Theater, 10<sup>th</sup> July 2006

Place of sampling	Psychroph. bacteria [cfu/m <sup>3</sup> ]	Mesoph. bacteria [cfu/m <sup>3</sup> ]	Moulds [cfu/m <sup>3</sup> ]
outdoor	29	8	64
ventilation chamber	38	16	79
room inlet	50	55	7
room, middle	79	55	10

Place of sampling	Psychroph. bacteria [cfu/m <sup>3</sup> ]	Mesoph. bacteria [cfu/m <sup>3</sup> ]	Moulds [cfu/m <sup>3</sup> ]
outdoor	94	31	799
ventilation chamber	5	14	196
room inlet	11	4	170
room, middle	99	80	525

Table 3. Office Building, 7<sup>th</sup> November 2006

Place of sampling	Psychroph. bacteria [cfu/m <sup>3</sup> ]	Mesoph. bacteria [cfu/m <sup>3</sup> ]	Moulds [cfu/m <sup>3</sup> ]
outdoor	278	30	243
ventilation chamber	160	121	509
room inlet	42	4	37
room, middle	199	219	410

Table 4. Theater, 7<sup>th</sup> November 2006

Place of sampling	Psychroph. bacteria [cfu/m <sup>3</sup> ]	Mesoph. bacteria [cfu/m <sup>3</sup> ]	Moulds [cfu/m <sup>3</sup> ]
outdoor	278	30	243
ventilation chamber	160	121	509
room inlet	42	4	37
room, middle	199	219	410

cfu – colony forming units

### Conclusions

The concentrations of the bioaerosols found during the described tests show low or medium levels of biocontamination in all places checked. The fungi (moulds) and bacteria were relatively well stooped in ventilation systems. The increase of the concentrations in the middle of the room was due to the people presence itself and had anthropogenic source. The concentrations of bioaerosols in the office building sampled in autumn are higher to those from the summer while in the theatre the summer concentrations are lower to those from the autumn.

### ACKNOWLEDGMENT

This work was supported by funds of Ministry of Education and Science designated for the science in the years 2005-2007 as a research project.

## Bioaerosol generation in ventilation systems

P. Grzybowski

Faculty of Chemical and Process Engineering, Warsaw University of Technology, 1 Warynskiego str., 00-645, Warsaw, Poland

Keywords: bioaerosol, ventilation system, filtration, aerosol generation.

The ventilation system ducts may become bioaerosol generators in certain circumstances. Old and not cleaned ducts have the walls covered with a deposit layer. Among regular, mineral dust particles there exist also organic elements which serve as a fertilizer for the fungi and bacteria. While the temperature and humidity are adequate the microorganisms grow and produce spores and hyphae which may contaminant the air passing in the ducts. The reaerosolization of the deposit matter is the another source of airborne particles. In the case when such particles contain bacteria of fungi present in the deposit layer they become bioaerosol. It may even happen that the concentration of a given species forming bioaerosol is greater at the outlet of the ventilation system than at its inlet. Presence of bioaerosols inside the buildings may lead to SBS (Sick Building Syndrome) development. Experiments on collecting of bioaerosols in ventilation systems in real buildings in Warsaw in July 2006 (Table 1) show up to intermediate levels of the biocontaminations (Table 2).

Table 1. Bioaerosols concentrations.

building #	Psychroph bacteria [cfu/m <sup>3</sup> ]	Mesoph bacteria [cfu/m <sup>3</sup> ]	Moulds [cfu/m <sup>3</sup> ]	Yeast [cfu/m <sup>3</sup> ]
I.	18-134	24-123	27-765	4-49
II.	5-99	4-80	170-799	app.1

Table 2. Guidelines of Commission of the European Communities for non-industrial indoor air.

Bacteria concentration [cfu/m <sup>3</sup> ]	Fungi concentration [cfu/m <sup>3</sup> ]	Guideline
< 50	< 50	very low
50÷100	50÷200	low
100÷500	200÷1000	intermediate
500÷2 000	1000÷10 000	high
> 2 000	> 10 000	very high

The mathematical modelling of the grow of the microorganisms on the inner wall of the air channel was conducted for a straight, horizontal pipe (Fig.1.)

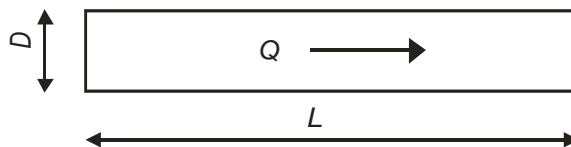


Fig.1 Model of the ventilation channel.

As a result it was possible to predict changes of the concentration of the bioaerosol in the time of the pipe conducting air stream Q [m<sup>3</sup>/h] for a given air humidity and temperature. The local grow of the fungi colony was described by a set of equations (1-6) and example calculations results at fig.2 :

$$\mu = \frac{1}{X} \cdot \frac{dX}{dt} \quad (1)$$

$$\mu(X, S) = \mu_{\max} \cdot \frac{S}{K + S} \quad (2)$$

$$\frac{1}{X} \cdot \frac{dX_L}{dt} = \mu_L \quad (3)$$

$$\mu_L = \mu_{L\max} \cdot \left(1 - \frac{S}{K_L + S}\right) \quad (4)$$

$$\frac{dZ}{dt} = 0 \quad \text{for } t < 3 \text{ days} \quad (5)$$

$$\frac{dZ}{dt} = \eta \cdot \frac{dX}{dt} \quad \text{for } t \geq 3 \text{ days} \quad (6)$$

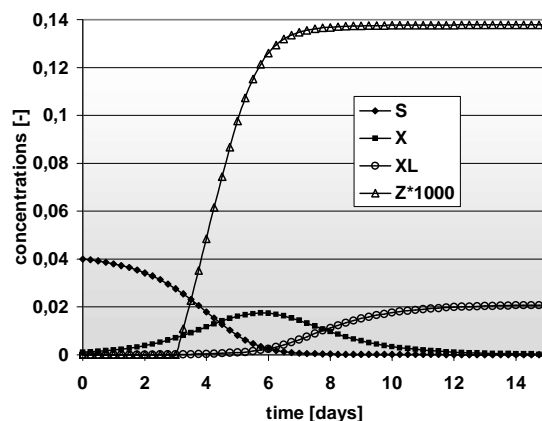


Fig.2. Changes of the fertilizer (S), alive biomass (X), non alive biomass (XL) and spores (Z) concentrations with time.

### ACKNOWLEDGMENT

This work was supported by funds of Ministry of Education and Science designated for the science in the years 2005-2007 as a research project.

## Study of morphology and settling velocity of airborne pollen captured in a Paul trap

Felix Kohler<sup>1,2</sup>, Eckart Schultz<sup>2</sup>, Hanspeter Helm<sup>1</sup>

<sup>1</sup> Molecular and Optical Physics, Institute of Physics, University of Freiburg, 79104 Freiburg, Germany

<sup>2</sup> Deutscher Wetterdienst, Department of Human Biometeorology, 79104 Freiburg, Germany

Keywords: single particle analysis, bio-aerosols, agglomerates, levitation, morphology

Only little is known about the alteration of airborne pollen in morphology and settling velocity after their release from plants due to varying meteorological conditions. However, this information is an important parameter for reliably modelling the atmospheric dispersal of pollen.

We describe the design, operation, and the characteristics of an electrodynamic levitation cell for long-term studies of a single airborne pollen grain in a specified gaseous environment. We report on first measurements of settling velocity of pollen by exploiting the sensitivity of the trapping stability on the aerodynamic drag of the pollen.

The pollen is levitated in a Paul trap and can be observed through a light microscope as well as from a lateral CCD camera. If the adequate AC and DC voltages are applied to the trap electrodes the levitated pollen is captured practically motionless at the trap center. Highly focused images (50x objective magnification) of the airborne pollen can then be recorded. Temperature and humidity in the levitation chamber are monitored by a sensor adjacent to the trap center. By balancing the gravitational force with an electric force we can determine the ratio of charge to mass of the trapped pollen grain.

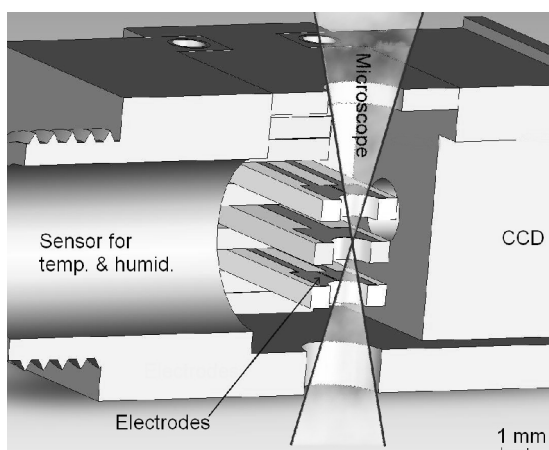


Figure 1. Levitation cell.

Figure 1 gives a cross-sectional view of the levitation cell. The electrodes and the trapping chamber are designed for incident and transmitted light microscopy. The stability of the pollen in the trap depends on the parameters  $\epsilon$  and  $\delta$  which are reduced quantities related to the trap parameters and

the properties of the trapped object. A simulated stability diagram for our trap is shown in Figure 2. We examined the stability boundaries of the Paul trap by monitoring the transition from stability to instability of the trapped pollen when varying the AC frequency and amplitude.

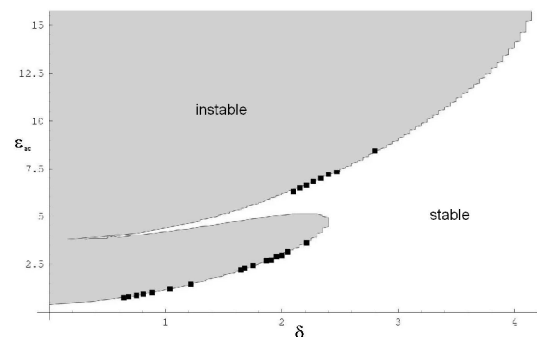


Figure 2. The stability domain of our trap. Black squares indicate measurements of the transition to instability as recorded for a single birch pollen.

Owing to the sensitivity of the stability boundary on aerodynamic parameters of the pollen, the settling velocities of single as well as of clustered pollens can be determined directly. On the basis of 18 experiments we determined the mean settling velocity of single birch pollen to be  $1.57 \pm 0.14$  cm/s at room temperature and at a relative humidity of 40%. This result is in very good agreement with the results of a classical settling experiment in a sedimentation cell, where we obtained an average settling speed of 1.58 cm/s for single birch pollen under similar atmospheric conditions.

We demonstrate that the adaptation of this Paul trap is highly suitable for microscopic studies of airborne pollen grains. By this approach pollen morphology and settling velocity can be determined under defined micro-environmental conditions.

This work was supported by Palas<sup>®</sup> GmbH, Karlsruhe, Germany.

Hartung, W. H., and C. T. Avedisian (1992). *On the electrodynamic balance*. Proc. Roy. Soc. London A, 437, 237–266.

Laucks, R. (1999). *Physical and chemical (Raman) characterization of bio-aerosols – pollen* J. Aerosol Science, 145-146

## Combined UV-fluorescence and background aerosol monitoring for detection of intentional release of airborne biological agents

K. Janka<sup>1</sup>, R. Reinivaara<sup>1</sup>, J. Tikkanen<sup>1</sup>, A. Rostedt<sup>2</sup>, M. Putkiranta<sup>2</sup>, J. Laaksonen<sup>2</sup>, M. Marjamäki<sup>2</sup>, J. Keskinen<sup>2</sup> and T. Humppi<sup>3</sup>

<sup>1</sup>Dekati Ltd., P.O. Osuusmyllynkatu 13, FI-33700, Tampere, Finland

<sup>2</sup>Aerosol Physics Laboratory, Tampere University of Technology, P.O.Box 692, FI-33101, Tampere, Finland

<sup>3</sup>Finnish Defence Forces Technical Research Centre, Paroistentie 20, FIN-34110 Lakiala, Finland

Keywords: aerosol characterization, bioaerosols, fluorescence, light scattering

The biggest challenge in real time detection of airborne biological threat agents (ABTA) is to distinguish the benign natural or man made bioaerosols from intentional release of ABTA (Pan *et al.* 2004; Sivaprakasam *et al.*, 2004).

No single available real-time detection technique gives a satisfactory criterion for detection. Thus the reliable biodection have to rely on more than one detection technology giving diverse information from aerosol background, concentration, size distribution and intrinsic fluorescence.

The most commonly used techniques are based on the measurement of intrinsic UV-fluorescence and size of bioparticles. For any reliable alarming criteria the timely behaviour of the measured parameters compared to normal conditions is significant. Utilizing the timely behaviour of the particle concentrations requires fast response detection of the particles. Because extremely low concentrations of harmful bio agents can cause infection, sensitivity in terms of agent containing particles per liter air (ACPLA) is of a crucial importance.

The sensitivity of the detector can be improved by concentrating the aerosol stream prior to feeding it to the sensing volume of the detector. Because there is usually a background of bioaerosols giving response to these detectors, the alarming algorithms have an important role. The timely deviation of the detector signal(s) is important factor for interpreting the origin of aerosols detected (natural or artificially spread). In addition to the background bioaerosol, other aerosols (i.e. soot from diesel engines) may yield also fluorescent response. The timely behaviour or this kind background aerosol typically resembles that of artificially spread bioaerosols. For that reason it is extremely difficult to distinguish using only software based algoritms. Pan *et al.* (2004) and Sivaprakasam *et al.* (2004) refer the major challenges of biodetection techniques.

This paper describes a concept combining UV-fluorescence detection optics for bioaerosols and a special background-aerosol detector system (figure 1.) The light source for this fluorescence is a CW semiconductor diode laser with 405 nm wavelength. The optical system detects both fluorescence and

scattered light, giving indication on both the fluorescence tendency and concentration of particles. The practical system includes also a particle concentrator concentrating the bioaerosol for the UV-fluorescence unit by factor of 500. The background aerosol detection system measures the concentration of particles causing typically false signals for UV-fluorescence detection unit. Characteristics for this technique are fast response time and sensitivity. It can be easily integrated into a robust biodetector for field operation. The practical realisation of the developed biodetector, as well as, the experimental results are presented.

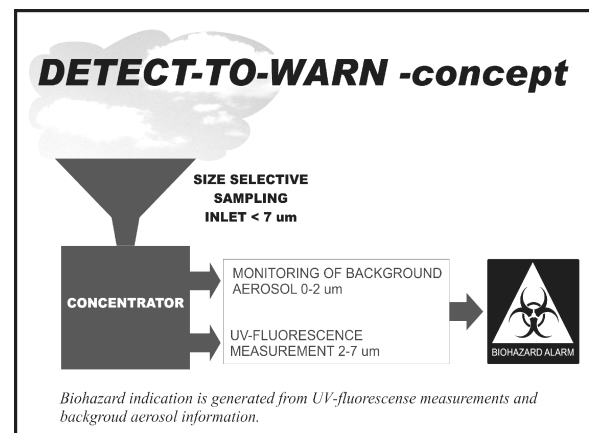


Figure 1. The basic concept of the biodetector.

Pan, Y.-L., Boutou, V., Bottiger, J. R., Zhang, S. S., Wolf, J.-P., & Chang, R. K. (2004). *J. Aerosol Science*, 38, 598-602.

Sivaprakasam, V., Huston, A. L., & Eversole, J. D. (2004). *Optics Express*, 12, 4457-4466.

## Total numbers and activity of environmental airborne bacteria

R. Thyrrhaug, J.Einen, R-A. Sandaa, M. Heldal, G.Bratbak

<sup>1</sup>Department of Biology, University of Bergen, Jahnebakken 5, 5020 Bergen, Norway

Keywords: bioaerosols, Flow cytometry, RT-PCR, bacterial activity

Reliable methods for total enumeration and activity measurements of environmental airborne microorganisms are generally lacking. In other environmental habitats, like sea water, fresh water and soil, in general less than 1 % of bacterial populations are easily cultivated on agar plates. However, most bacteria may be alive in such environments, their activity are assumed to be limited i.e. by nutrient availability.

We collected samples using a XMX-CV particle collector (Dycor Technologies Ltd) as well as rain. The bacterial concentrations in these liquid samples were measured using Flow cytometry, RT-PCR and agar plates. Samples collected for flow cytometric analysis was fixed by glutaraldehyde, stained by SYBRGreen I (Molecular Probes) and diluted in PBS before analysis (i.e. Marie et al 1999). RT-PCR was performed according to different DNA rinsing protocols including commercially available kits, as well as direct analysis of samples. Agar plates were used to quantify the easily culturable bacterial fraction.

Generally flow cytometric and RT-PCR analysis of airborne bacterial yielded comparable results. The use of some of the kits resulted in too high background noise to get reliable results. As expected, only a small proportion was growing on agar plates.

Bacterial production was analysed according to Smith and Azam (1992). In general, production per bacteria in collected rain drops were at the same level as in marine samples.

More results as well as the methodical and ecological questions will be further discussed.

### References

Marie, D., C. P. D. Brussaard, R. Thyrrhaug, G. Bratbak, and D. Vault. 1999.

Enumeration of viruses in marine samples by flow cytometry. *Appl. Environ. Microbiol.* 65:45-52.

Smith, D. C., and F. Azam. 1992. A simple, economical method for measuring bacterial protein synthesis rates in seawater using <sup>3</sup>H-leucine. *Mar. Microb. Food Webs* 6:107-114.

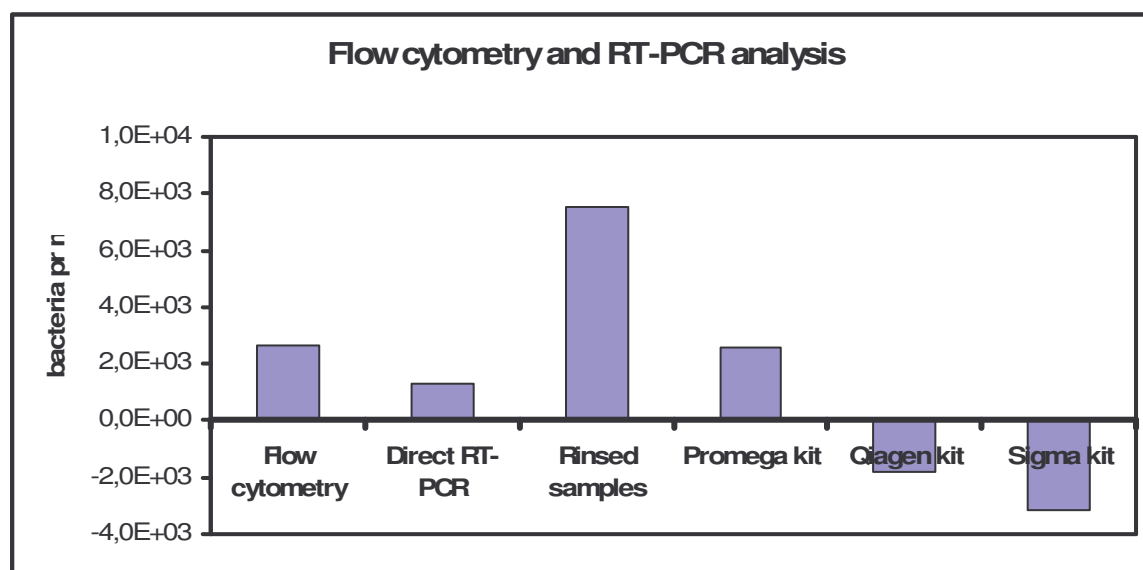


Fig 1. Comparison of bacterial counts (mL<sup>-1</sup> corresponding to around 0.7 m<sup>3</sup> air) using flow cytometry and RT-PCR following collection of airborne bacteria using XMX-CV particle collector.

## Contribution of fungi to primary biogenic aerosols in the atmosphere

W. Elbert<sup>1</sup>, P. E. Taylor<sup>2</sup>, M. O. Andreae<sup>1</sup>, U. Pöschl<sup>1</sup>

<sup>1</sup>Max Planck Institute for Chemistry, Biogeochemistry Department, PO Box 3060, 55020 Mainz, Germany

<sup>2</sup>Chemistry and Chemical Engineering, California Institute of Technology, Pasadena, CA 91125, USA,

Keywords: bioaerosols, biogenic particles, emission, PM and source apportionment, primary organic aerosols

Spores and related chemical compounds from actively spore-discharging Ascomycota (AAM) and actively spore-discharging Basidiomycota (ABM) are primary biogenic components of air particulate matter (characteristic size range: 1–10  $\mu\text{m}$ , characteristic boundary layer concentrations:  $\sim 10^3$ – $10^4$   $\text{m}^{-3}$ ). Measurement results and budget calculations based on investigations in Amazonia (Balbina, Brazil, July 2001) indicate that the forcible discharge of fungal spores may account for a large proportion of coarse air particulate matter in tropical rainforest regions during the wet season (0.7–2.3  $\mu\text{g m}^{-3}$ ). For the particle diameter range of 1–10  $\mu\text{m}$ , the estimated proportions are  $\sim 25$  % during day-time,  $\sim 45$  % at night, and  $\sim 35$  % on average. For the sugar alcohol, mannitol, the budget calculations indicate that it is suitable for use as a molecular tracer for actively discharged basidiospores (ABS), and that the literature-derived emission ratio of about 5 pg per ABS may be taken as a representative average. ABM emissions may account for most of the atmospheric abundance of mannitol (10–68  $\text{ng m}^{-3}$ ), and can explain the observed diurnal cycle (higher abundance at night). ABM emissions of hexose carbohydrates might also account for a significant proportion of glucose and fructose in air particulate matter (7–49  $\text{ng m}^{-3}$ ), but the literature-derived ratios are not consistent with the observed diurnal cycle (lower abundance at night). AAM emissions appear to account for a

large proportion of potassium in air particulate matter over tropical rainforest regions during the wet season (17–43  $\text{ng m}^{-3}$ ), and they can also explain the observed diurnal cycle (higher abundance at night). The results of our investigations and budget calculations for tropical rainforest aerosols are consistent with measurements performed at other locations.

Based on the average abundance of mannitol in particulate matter, which is consistent with the above emission ratio and the observed abundance of ABS ( $\sim 10^3$ – $10^4$   $\text{m}^{-3}$ ), we have also calculated a value of  $\sim 17$   $\text{Tg yr}^{-1}$  as a first estimate for the global average emission rate of ABS over land surfaces. Comparisons with estimated rates of emission and formation of other major types of organic aerosol ( $\sim 47$   $\text{Tg yr}^{-1}$  of anthropogenic primary organic aerosol; 12–70  $\text{Tg yr}^{-1}$  of secondary organic aerosol) indicate that emissions from actively spore-discharging fungi should be taken into account as a significant source of organic aerosol. Their effects might be particularly important in tropical regions, where both physicochemical processes in the atmosphere and biological activity at the Earth's surface are particularly intense, and where the abundance of fungal spores and related chemical compounds are typically higher than in extratropical regions.

## Occurrence of microorganisms in bioaerosols

L.Mateju<sup>1</sup>, B. Kotlik<sup>1</sup>, M.Brabec<sup>1</sup>, J. Keder<sup>2</sup>

<sup>1</sup> National Institute of Public Health, CZECH REPUBLIC

<sup>2</sup> Czech Hydrometeorologic Institute, CZECH REPUBLIC

Keywords: bioaerosols, culturable microorganisms, frequency

Airborne pollution includes bioaerosols, aside from airborne dust and chemical pollutants. Bioaerosols or organic dust particles can contain both pathogenic and non-pathogenic bacteria, moulds, viruses, high-molecular weight allergens, bacterial endotoxins, peptoglycans,  $\beta(1\rightarrow3)$ -glucanes, pollen, vegetable fibres etc. Effects of such aerols are detrimental to health and cause ailments including infections, acute toxic reactions, allergies and cancer (Douwes et al., 2003).

Systematic data concerning incidence and effects of bioaerosols, particularly in localities prone to their presence are not as yet known in the Czech Republic.

Determination of microorganisms is based on various types of samplers. The selection of samplers and sampling methods will influence the results received and none of the available methods for sampling airborne bioaerosols is ideal, and all contain various inaccuracies (Grinshpun, 2002, Kelly, 2005).

The aim of the measurements was to acquire bioaerosol frequency sampling data, and hence determine the significance of changes of microorganism incidence over the course of a day in ambient air, using a simple and accessible method. The Merck MAS 100 sampler was selected for this purpose. Total bacteria count (TBC), yeast and mould count (MC) and pathogenic mould count (PMC) were monitored. Bioaerosol sampling proceeded in regular intervals (every 15 mins on 3 petri dishes in random order). Sampling was conducted twice over a 48-hour period in two subsequent years. Results were statistically evaluated.

Analysis of dispersion of pertinent data reveals that differences among daily values are statistically significant (TBC = 0,0129, MC = 0,0072 and PMC = 0,6699). The incidence of microorganisms in bioaerosol is diurnal. The frequency of changes over a 24-hour period are shown in Figs. 1,2, and 3. The spectrum is characterised by a periodogram with detrending and subsequent annullment. The frequency of changes detected allows estimation of sampling frequency, so as to record significant differences in bioaerosol microorganism incidence. Sampling for TBC determination would be performed with frequency 1.36 per hour, determination of MC with frequency

1.56 per hour and all changes in PMC would be sampled with frequency 1.72 per hour.

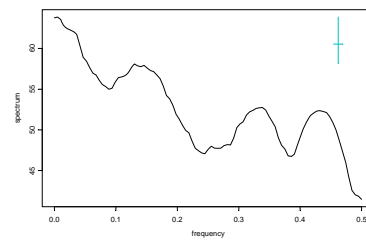


Figure 1 Spectrum of TBC levels

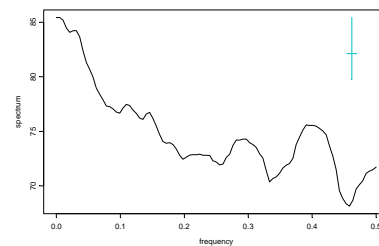


Figure 2 Spectrum of MC levels

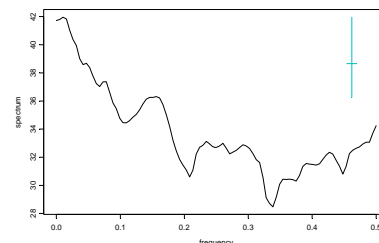


Figure 3 Spectrum of PMC levels

**Douwes, J., Thorne, P., Pearce, N., Heederick, D. (2003):** Bioaerosol Health Effects and Exposure Assessment: Progress and Prospects, *Ann.Occup.Hyg.*, **47**(3):187–200

**Grinshpun, S.A. (2002):** Sampling of bioaerosols: what are the special features? Bioaerosols: A view from Different Perspectives, Forschungszentrum Karlsruhe in der Helmholtz-Gemeinschaft, Center for Advanced Technological and Environmental Training Leopoldshafen, 2002

**Kelly, J. (2005):** Microbiological Air Samplers and ISO 14698-1/2, Categories of air samplers and actors to consider when choosing one, *Controlled Environemnts™ Magazine*, www accessed 120606 <http://www.cemag.us/articles.asp?pid=522>

## Patterning of Protein via Electrodynamic Focusing for Biological Applications

H. Lee, H. Shin, M. Choi\*

National CRI Center for Nano Particle Control, School of Mechanical and Aerospace Engineering, Seoul National University, Seoul 151-742, Korea.

\*Email : mchoi@snu.ac.kr

Keywords: nanoparticle patterning, electrodynamic focusing, electrospray, protein patterning

Biomaterials selective deposition on large surfaces is very important to realize future nano-bio device such as DNA chip, protein chip, and lab on a chip. Here, we show focused patterning of protein over large surface area is possible.

Focused deposition experiment consists of two main steps. First step is the ion shower on substrate. Ion shower is required to remove noise particles and develop focusing effect. Ions accumulated on prepatterned PR or SiO<sub>2</sub> film develop electrostatic lenses which guide protein particles into the desired location and prevent the generation of noise particles (Kim et al. 2006, Choi et al. 2005). Second step is the deposition of protein(Human-IgG) on prepatterned substrate using electrospray method under the given electric potential difference. In electrospray method, protein with high number of elementary charge are generated even if some of them may be lost in the solvent evaporation process. This highly charged protein particles have high inertia effect so that they don't follow the electric field line well. So, we use neutralizer (Po-210) to reduce number of elementary charge of protein. In this case, neutral proteins and negatively charged proteins may be also generated despite of very small numbers compared to the positively charged protein particles. But the neutral proteins and negatively charged proteins are not affected by electric field, thus they will be removed by carrier gas.

Fig.1 shows one example of the focused deposition of Human-IgG on prepatterned PR film. Human IgG particles formed about 350nm width line structure consisting of many Human IgG particles. The protein pattern size is much smaller than PR pattern size due to focusing effect. This focusing effect is due to the ion accumulation on PR substrate by ion shower and electrospray.

The activity of Human-IgG was confirmed by fluorescence detection. Human-IgG deposited prepatterned SiO<sub>2</sub> pattern are reacted with anti-human IgG-Alexa Fluor 488 for one hour. And then, we observe the image of this pattern by CLSM(Confocal Laser Scanning Microscope).

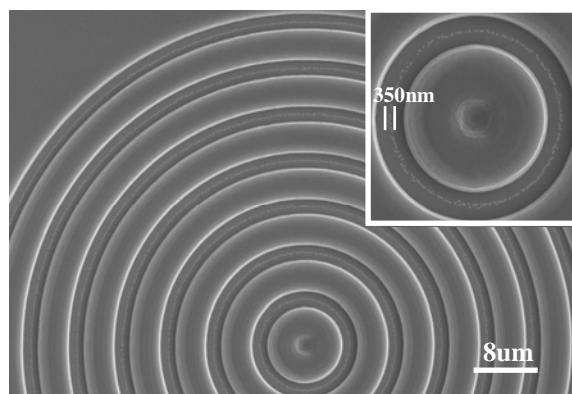


Figure 1. Focused deposition of Human-IgG on silicon surface

In summary, nanostructured deposition of proteins in gas phase was investigated experimentally. We could obtain focused structure of nanoparticles assembly by electrospray method and ion accumulation on PR substrate. And through the antibody-antigen reaction, we showed that our method can be applied to biological device manufacturing.

This work was funded by Creative Research Initiatives program sponsored by Korea Ministry of Science and Technology.

H. Kim, J. Kim, H. Yang, J. Suh, T. Kim, B. Han, D. S. Kim, S. Kim, Peter V. Pikhitsa and M. Choi (2006). *Nature Nanotechnology*, vol. 1, no. 2, 117-121

M. Choi, J. Kim, H. Yang (2005). *Korea Patent Application 2005-30239 and USA Patent Application (11/346, 401)*.

## **T05 Abstratcs**

## Application of aerosol electrometer for ambient particle charge measurements

F.O. J-Fatokun, L. Morawska, M. Jamriska and E.R. Jayaratne,

International Laboratory on Air Quality and Health.

Queensland University of Technology. GPO Box 2434, Brisbane 4001. Australia.

Key words: Ambient aerosols, charged particles, Aerosol electrometer, charge measurement.

The charge of ambient atmospheric particles is an important parameter in investigations on particle dynamics. Yet, there is only limited knowledge available on it, mainly due to the lack of instrumentation for its direct measurements. Though several studies were conducted on the bipolar and unipolar charging of aerosol particles, very few were directed at measuring charged ambient aerosols, which are presently regarded as a form of large air ions and measured with the aid of hand held air ion counters (IEEE 1990a).

One instrumental technique, with a potential for application in the investigations of ambient aerosol charge is the aerosol electrometer (AE). But till date, its use has been limited to instrument calibration, particle counting and ionic current measurement (Banse, Esfeld et al. 2001; Camata and Atwater 1996; Hameri, Koponen et al. 2002).

The aims of this study were to explore the AE as a direct instrument for measuring ambient particle charges, thereby extending its use beyond the current applications; and through a set of experimental investigations establish its limitation and optimal operating conditions for ambient charge particle measurement. Therefore, the AE was used under various conditions, to measure the net charge of unipolar and bipolar aerosol particles in a typical outdoor environment.

Results indicated the net unipolar and bipolar aerosol particle concentration, in a typical outdoor air were low and undetectable by the AE. As all the values obtained were within the instrument's zero readings (i.e when AE is switched on, but no flow is passing through) of  $\pm 5$  mV.

To establish this, conditions with very high concentrations of aerosol particles in an equilibrium state of charge were created. By passing some laboratory generated NaCl aerosols, (mobilities in the 30 - 100 nm particle size range) through a bipolar charger and using the AE, the particle charge concentration and number of elementary (fraction of single and multiple) charges on the NaCl particles were determined. Experimental results obtained with the NaCl particles were within 2% of values predicted for particles in a state of charge equilibrium by Maxwell Boltzmann and the approximation of Fuchs (1963) theory presented in Wiedensohler (1988). Proving the concentration of charged aerosol particles in a typical outdoor air are below the AE's detection limit.

The AE was then used to determine the net charge on particles in close proximity of a strong ion emitting source. As shown by the graphic presentation of particle charge, measured by the instrument in a (i) typical outdoor, and (ii) highly charged air environment (Figure 1); the mean unipolar particle charge concentration near the ion emitting source was  $-1663 \pm 839$  ions  $\text{cm}^{-3}$ , while that of a typical outdoor air was within the AE's zero readings, and less than 500 ions  $\text{cm}^{-3}$ .

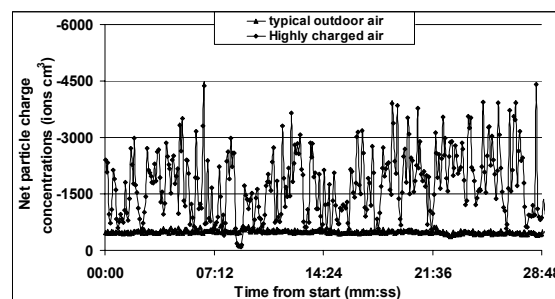


Figure 1 Ambient particle charge concentration

Operating the electrometer under various conditions showed (i) the instrument is only suitable for field measurement studies, where charged particle concentrations are elevated (near a strong ion emitting source); and (ii) it's stability and operations are highly sensitive to variations in humidity; hence the AE is only suitable for use under conditions of relative humidity below 60%.

This work was supported by the Australian Research council (ARC) funded Discovery project (Project identification number DP0558409).

- Banse, D. F., K. Esfeld, et al. (2001). "Particle counting efficiency of the TSI CPC 3762 for different operating parameters." *Journal of Aerosol Science* **32**: 157-161.
- Camata, R. P. and H. A. Atwater (1996). "Size classification of silicon nanocrystals." *Applied Physics Letters* **68**( 22): 3162, 3p, 5 diagrams, 2 graphs;
- Fuchs, n. A. (1963). "On the stationary Charge Distribution on Aerosol Particles in a Bipolar Ionic Atmosphere." *Geophys. Pur a Appl.* **56**: 185.
- Hameri, K., I. K. Koponen, et al. (2002). "The particle detection efficiency of the TSI-3007 condensation particle counter." *Journal of Aerosol Science* **33**(10): 1463-1469.
- IEEE (1990a). "IEEE guide for the measurement of DC electric-field strength and ion related quantities." *IEEE Std 1227-1990*.
- Wiedensohler, A. and H. J. Fissan (1988). "Aerosol Charging in High Purity Gases." *Journal of Aerosol Science* **19**(7): 867-870.

## Laboratory simulation of body charging by the flow with electrical charged water drops

A. Vatazhin, D. Golentsov, V. Likhter

Central Institute of Aviation Motors, Aviamotornaya St. 2, 111116, Moscow, Russia

Keywords: corona discharge, charged particles, body electrization

In ambient disperse medium there are regions both negatively and positively charged. The carriers of charge may be water drops (e.g. negatively charged drops in the atmospheric cloud bottom). In passing through these regions, a body (aircraft element) gets electric charge much greater than in a neutral flow.

The main problem of laboratory simulation of the phenomenon mentioned above is the creation of the vapour-air flow with charged water drops. In our researches the corona discharge was used to charge effectively the drops in the vapour-air flow (see also [1]). The condensation develops very intensively in the presence of ions ("electric" condensation) and the electric charge on the arisen drops increases continuously due to their charging by ions in the presence of the electric field. The following processes in the region between corona discharge electrodes are considered: homogeneous and "electric" condensation, kinetic processes of growth of the water drops, their diffusive and inductive charging by ions, motion of charged drops and ions in the external and induced electrical fields.

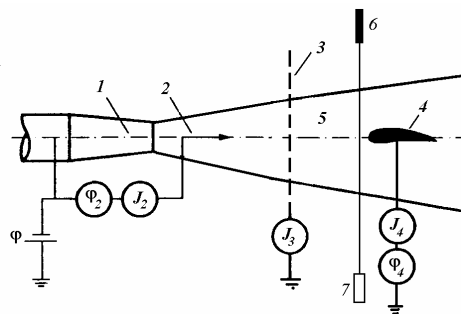


Figure 1. Experimental set-up

The laboratory set-up is shown in fig. 1. Water vapour jet exhausts from a heated nozzle 1 with the velocity at the nozzle exit  $v_o = 250$  m/s. The needle 2 is fixed downstream the nozzle exit on the axes of the jet and creates the corona discharge. The grounded grid 3 (the second corona electrode) is at a distance 100 mm downstream from the needle. It accumulates corona ions but lets the charged drops pass. The charged body 4 that is flowed round by the jet 5 with the charged drops is at a distance 100 mm downstream from the grid. Laser 6 and photomultiplier 7 are used to estimate the size and the concentration of the drops by measuring of decay and scattering of the laser light. The velocity and temperature fields in the jet are determined on the base of theory of gasdynamic turbulent jets.

The basic parameters influencing on condensation intensity are: the jet temperature  $T_o$  at the nozzle exit, the ambient medium temperature  $T_\infty$  and the needle potential  $\phi_2$ . For example, at  $|\phi_2| > 0$  the condensation appears even if it was absent at  $|\phi_2| = 0$ .

Two species of electric conditions for the body were investigated. The first one – the grounded ( $\phi_4 = 0$ ) body and measuring of the charge current  $J_4$  onto it. The second one – the body is under floating potential  $\phi_4$  and its measuring. The last case simulates the charge accumulation on the aircraft which moves in charged clouds. The charging current onto the body equals to the current that "flows down" the body into surrounding space. (In practice it is the current of the electric dischargers, fixed on aircraft surface.)

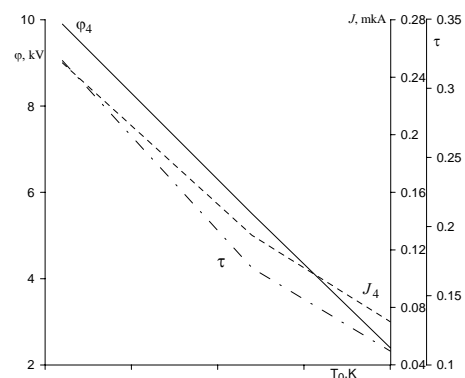


Figure 2. Body electrization potential  $\phi_4$  and current  $J_4$ , and optical layer thickness  $\tau$  vs temperature  $T_o$

In fig. 2 the values of  $\phi_4$ ,  $J_4$  and  $\tau$  (the optical thickness of the jet just before the body) depending on the operating rates (various  $T_o$ ) are presented. The negative corona discharge was used. In increasing of  $T_o$  the intensity of electric condensation decreases that results in both the concentration of charged drops and optical thickness  $\tau$  decrease. The consequence of it is the body falling off charging intensity.

This work was supported by the Russian Foundation for Basic Research (project No. 05-01-00394) and by the Russian Support Foundation for leading scientific schools (project No. 1635.2003.1)

[1] Vatazhin A. et al. (1995) *J. Aerosol Science*, 26, 71-93.

## Reactive formation, charging, and deposition of nanosized TiO<sub>2</sub> particles from the gas phase

H. Wiggers, P. Ifeacho, M. Barthel, B. Kock, C. Schulz

Institut fuer Verbrennung und Gasdynamik IVG,  
University of Duisburg-Essen, D-47057 Duisburg, Germany

Keywords: Nanoparticles, Charged particles, Electrostatic precipitators,  
Particle deposition, Deposition efficiency

TiO<sub>2</sub> films consisting of nanocrystals with anatase crystal structure are of important interest due to their outstanding photocatalytic activity. A promising way to produce thin films with high photocatalytic activity pursues the combination of forced nanoparticle deposition and CVD. Therefore, electrostatic assisted charging and subsequent deposition of nanosized TiO<sub>2</sub> particles, synthesized in a hot wall reactor were investigated using an oscillating electric field corona charger, and an electrostatic precipitator. The particle synthesis temperature varied between 650 and 900°C in steps of 50°C. It was observed that above 700 °C there is a strong reduction in the CMD due to a change in the particle formation process.

The amount of particles charged were influenced by gas velocity, particle concentration and discharge current. The changes in particle concentration, size distribution and charge concentration were monitored with a differential mobility analyzer (DMA)<sup>[1,2]</sup> and an electrometer connected to the reactor system. Using a combination of negative corona and positive potential, a deposition rate of up to 80 % was observed with enhanced deposition of bigger particles due to higher charging/deposition efficiency.

Furthermore, the deposition efficiency within the electrostatic precipitator was found to increase with decreasing gas flow velocity and increasing electric field strength. Lower deposition rates were observed for same corona and precipitator polarity, while particle percolation and loss in the corona charger were identified as functions of the corona polarity.

A simple model has been used to interpret the charging efficiency of larger particles with respect to the forces acting on a charged particle as well as the effect of Brownian motion. Electrostatic deposition of particles on surfaces can be potentially applied to generation of thin films on surfaces based on nanoparticles.

### References

- Knutson, E. O., Whitby, K., T. (1975). *Journal of Aerosol Science*, 6, 443–451.
- Krinke, T. J., Deppert, K., Magnusson, M.H., Schmidt, F., Fissan, H. (2002). *Journal of Aerosol Science*, Vol. 33, 1341-1359

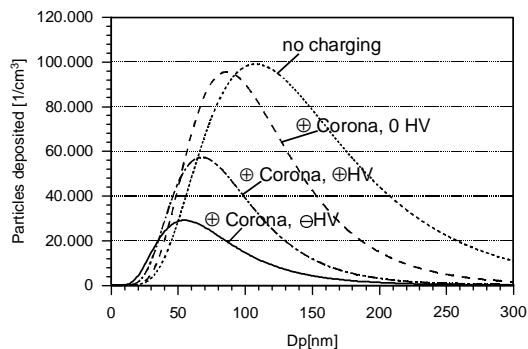


Figure 1: Influences of various combinations of corona polarity and electrostatic precipitator potential on residual TiO<sub>2</sub> particle size distribution.

## A fixed site monitoring station to measure corona produced from a high voltage powerline.

J.C. Matthews, P. A. Keitch, J. P. Ward and D.L. Henshaw

H. H. Wills Physics Laboratory, Bristol University, Tyndall Avenue, Bristol, BS8 1TL, UK

Keywords: charged particles, corona discharge, field measurements, ions.

Corona ions produced by high voltage powerlines escape the line and are carried by the wind in largely unipolar clouds of space charge. These clouds can affect the DC electric field of the Earth as measured from the ground. It is known that the clouds of unipolar ions are predominantly positive in fair weather and predominantly negative in wet weather.

The Earth's natural fair weather field (dry with a blue sky) is found to be around  $100 \text{ V m}^{-1}$  but measurements by ground based field mill meters downwind of a powerline in a crosswind have shown the field modified above or below this value (Fews *et al* 2002). The time variant traces of such fields have a distinctive rise and fall and can fluctuate between hundreds of volts per metre in a short space of time, rates of change of  $100 \text{ V m}^{-1} \text{ s}^{-1}$  have been seen regularly. These measurements have thus far been limited to small time windows on fair weather days so a fixed site monitoring station has been created to measure the corona ion induced electric field continuously and in all weathers. This will enable the amount of corona production and propagation to be better understood.

The fixed site monitoring station contains a field mill meter connected to a data logger which records the vertical electric field every second with limits at  $\pm 1000 \text{ V m}^{-1}$ . A weather station records the average and peak wind strength and direction and temperature as well as rainfall, humidity, pressure and solar energy every ten minutes. The station is powered from batteries trickle charged from solar and wind energy. It is situated 175 metres North East from a 400 kV powerline and over 500 m away from major roads and buildings.

The monitoring station has been running almost continuously since December 2006, with some loss of data due to power loss. Early results show the distinctive corona trace when the monitoring station is downwind from the powerline and shows a flat trace when it is upwind. The most changeable electric fields occur when there are strong winds and precipitation.

Figure 1 shows the time variant DC electric field measured from the field mill meter on two consecutive days. The dominant wind direction on the 21<sup>st</sup> January was West South West while the average windspeed was  $3.8 \text{ m s}^{-1}$ , the dominant wind direction on the 22<sup>nd</sup> January was North East and the average windspeed was  $4.9 \text{ m s}^{-1}$ . Rainfall was

recorded between 06:30 and 07:30 and between 21:30 and 22:30 on the 21<sup>st</sup> January.

The difference between the North East and West South West winds is obvious, there is a far greater variability of electric field and the peak values are far greater when the monitoring station is downwind of the monitoring station. Rainfall makes a great difference

An unexpected result was the large swings from high positive to high negative values in the same hour, such as at 6 am on the 21<sup>st</sup> January, when it was raining, which included a change from  $1000$  to  $-1000 \text{ V m}^{-1}$  in 40 s. This shows that both positive and negative corona are being produced and propagated in unipolar clouds. It is known that negative ions are produced in wet weather but it seems as if a large number of positive ions are still produced. New equipment is being developed to measure exactly the time when rain begins.

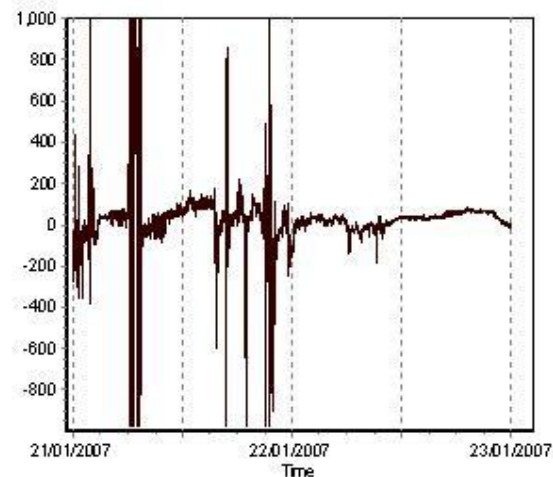


Figure 1. Time varying electric field recorded at the fixed site monitoring station on the 21<sup>st</sup> and 22<sup>nd</sup> January 2007.

This work was supported by Children with Leukaemia, Registered Charity No. 298405. The authors would also like to thank Miss Alison Buckley and Mr Matthew Wright for assistance in creating and maintaining the monitoring station.

Fews, A. P., Wilding, R. J., Keitch, P. A., Holden, N. K. & Henshaw, D. L. (2002). *Atmos. Res.*, 63, 271-289.

## Novel wet space-charge electrostatic precipitator for fine particles

A.M. Bologna, H.-R. Paur, H. Seifert and K. Woletz

Institut für Technische Chemie, Forschungszentrum Karlsruhe, Eggenstein-Leopoldshafen, 76344, Germany

Keywords: space-charge electrostatic precipitator, wet gases, fine aerosol, collection efficiency

Different industrial processes require efficient removal of fine aerosols from raw gases. This task is made difficult if particles are sticky or when the gas stream is humid (Light, 1988). Wet electrostatic precipitators (WESP) are the most effective control device for fine aerosol from the humid gases.

There are two steps in the conventional electrical precipitation of particles. First, the particles are charged, usually by impact of the ions generated by corona discharge. Second, particles are collected, usually under the influence of electric field. In the Space Charge Precipitator (SCP) unipolar charged particles are precipitated due to the field of their own space charge (Melcher, 1977).

A novel space-charge electrostatic precipitator is developed in the Forschungszentrum Karlsruhe (Bologna, 2005). It consists of a high intensity ionizing stage and a grounded field-free collection stage (Fig.1). The ionizing stage consists of a nozzle plate, grounded tube shell-electrodes and disk-shaped high voltage electrodes. Particles are charged in the DC negative corona discharge. The grounded collection stage consists of tower packing column.

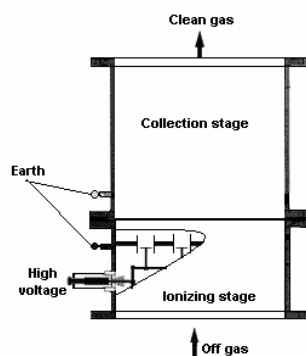


Figure 1. One-field SCP electrostatic precipitator

The SCP differs from the conventional WESP by a high velocity of the gas flow in the ionizing stage (over 20 m/s) and by absence of the external electric field in the collection stage. From the Venturi scrubber with high ionizing stage, the SCP differs by low velocity in the collection stage (< 3 m/s) and by low pressure drop. In comparison with Ionizing Wet Scrubber, in the SCP the velocity of the gas is much higher in the ionizing stage and there is no plenum chamber between the ionizing and collection stages. The new approaches of the SCP design allow to develop compact and cost-effective wet gas cleaning technology for fine particles.

The laboratory and pilot one- and two-field SCP precipitators were used for collection of HCl, H<sub>2</sub>SO<sub>4</sub>, (NH<sub>4</sub>)<sub>2</sub>SO<sub>4</sub> and (NH<sub>4</sub>)Cl aerosols. It was shown that the absence of plenum chamber between the ionizing and collection stages and the use of high velocity gas flow in the ionizing stage increase the spark-over voltage and operation corona current of the SCP. When the plenum chamber is used, the aerosol space charge suppresses the corona discharge and provokes “spark-over” discharges in the plenum chamber. The high velocity gas flow transports the space charge into the collection stage and increases both mechanical and electrostatic collection of particles inside of the tower packing column.

The results of the use of laboratory two-field SCP precipitator for collection of HCl are presented in the Fig.2. In both ionizing stages, which consisted from a single nozzle, the air flow rate was 80 m<sup>3</sup>/h. About 4 kg/h of water vapour was introduced into the air flow. The velocity of the gas in the electrode gap was 18 m/s. The operation parameters of the 1<sup>st</sup> stage were: voltage U<sub>1</sub>=12 kV and corona current I<sub>1</sub>=0,8 mA. The 2<sup>nd</sup> stage was characterised by U<sub>2</sub>= 13 kV and I<sub>2</sub>=1,0 mA. The mass concentration of the HCl in gas phase was 0,5-3 mg/Nm<sup>3</sup> depending on operation conditions.

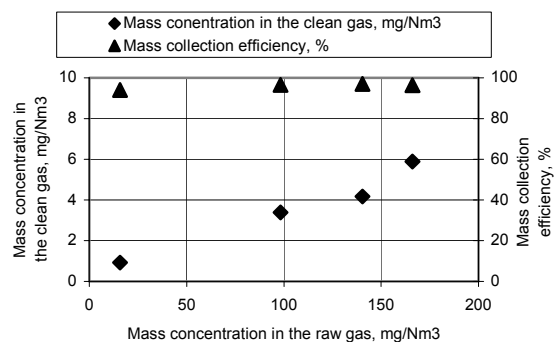


Figure 2. Mass collection efficiency of a two-field laboratory SCP precipitator

- Light, W. (1988). *Air Pollution Control Engineering: Basic calculations for particulate collection.*, Marcel Dekker, Inc. New York and Basel.
- Melcher, J.R., Sachar, K.S. Warren, E.P. (1977). *Proceedings of the IEEE*, 65 (12), 1659-1669.
- Bologna, A.M., Paur, H.-R., Seifert, H., Wäscher, Th. (2005). *IEEE Transactions on Industry Applications*, 41 (4), 882-890.

## Dynamics of highly charged fine aerosols in between electrodes

I.G. Loscertales<sup>1</sup>, E.A. Rodríguez<sup>1</sup>, D. Galán<sup>2</sup>, M. Marquez<sup>3</sup> and A. Barrero<sup>4</sup>

<sup>1</sup>ETS Ingenieros Industriales, Universidad de Málaga, Málaga, Spain

<sup>2</sup>Yflow SL, Marie Curie 4-12, Parque Tecnológico de Andalucía, Campanillas, Málaga, Spain

<sup>3</sup>Harrington Dep. Bioengineering, Arizona State University, Tempe, AZ 85287-9709, USA

<sup>4</sup>Escuela Superior de Ingenieros, Universidad de Sevilla, Sevilla, Spain.

Keywords: electrospray, aerosol dynamics, electrical effects.

The electrohydrodynamic atomization in the so called steady cone-jet mode has become a process broadly used to generate fine and ultrafine, highly charged aerosols. During the last 25 years, an intense research has been aimed at unravelling the complex dynamics of this process, including, the Taylor cone formation, the charge and mass emissions through a micro jet ejected from the tip of the cone, the break up of such micro jet and, finally, the evolution of the charged aerosol (electrospray) from its inception to a certain counter electrode. Most of the available literature focuses on the charge and size of the jet, but very little is reported on the dynamics of the electrospray. In this regard, one of the first works on the evolution of the spray (Gañán-Calvo *et al.*, 1994) describes it using a Lagrangian approach. This scheme may also be used to describe the evolution of the electrospray in more different configurations, such those in which a third electrode (i.e. extractor) is used in between the collector and the needle tip. In this work we focus on describing the evolution of the electrospray in a region limited by two infinite parallel conducting plates separated a length  $L$ .

One of the key features of the electrospray is the strong space-charge provoked by the aerosol itself. To account for it in the Lagrangian approach, the above referenced authors split the total electric field acting on a droplet, as the sum of two fields: the one coming from electrostatic solution of the needle-to-plate geometry without aerosol, and a field consisting of the sum of the field exerted by each charged droplet, considered as an isolated charged point. Although this scheme seems correct, the direct addition of the second electric field *breaks down* the equipotential conditions that must satisfy the needle and the plate. The correct solution of the Laplace equation satisfying the boundary conditions along the plates may be explicitly written by using the *image charge approach*. Since there are two parallel plates, an infinite set of image charges are needed for each aerosol particle. These additional terms give rise to electric forces that are of the same order of those considered by Gañán-Calvo *et al.*, and must be considered to properly describe the dynamics of the aerosol.

Figure 1 shows two steady-state aerosol distributions, calculated without (a) and with (b) the effect of the image charges. Both radial and axial coordinates are made dimensionless with the

extractor to collector distance  $L$  ( $\rho/L$  and  $z/L$ ). For the sake of clarity, the particles plotted are those contained in a centered  $\rho$ - $z$  slice of dimensionless thickness 0.1. The aerosol properties are: droplet diameter of  $1.38\mu\text{m}$ , droplet charge of  $6.75 \cdot 10^{-18}\text{C}$ , which roughly corresponds to an electrospray of ethylene glycol seeded with  $\text{NaCl}$  (electric conductivity= $10^{-3}\text{S/m}$ ) injected at a flow rate of  $0.895\mu\text{l/min}$ . In this case,  $L=10\text{mm}$  and the voltages at extractor and collector plates are 0 and 3000 volts respectively.

Aside of the obvious change in aerosol structure, the most noticeable difference is related to the transport of the droplets. In (a) 100% of the injected droplets reaches the collector, whereas only 60% does so in (b). The other 40% flies back towards the extractor, where they get lost.

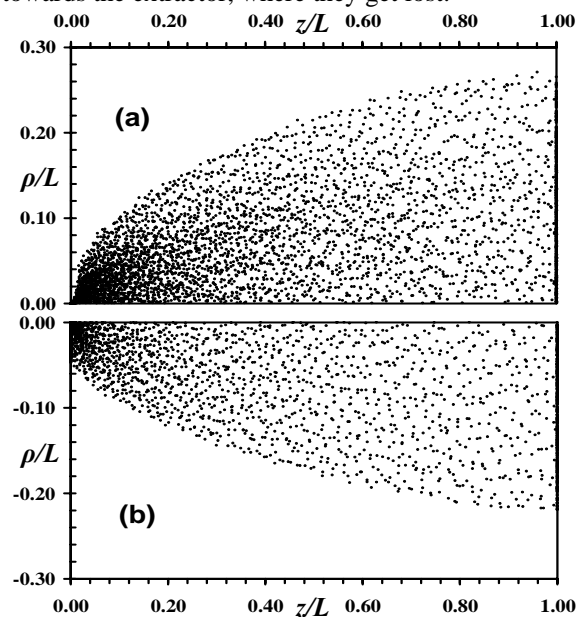


Figure 1. Sections of the aerosol distribution: (a) without image charge; (b) with image charge

This work has been partially supported by the Spanish Ministry of Education and Science, under projects DPI2004-05246-C03-C04 and NAN2004-09312-C03, and by Yflow SL

Gañán-Calvo, A. M., Lasheras, J. C., Dávila, J., & Barrero, A. (1994). *J. Aerosol Science*, Vol. 25, No. 6, pp. 1121-1142.

## Structure of the deposits collected from the EHD dispersion of carbon suspensions

I.G. Loscertales<sup>1</sup>, J.C. González<sup>1</sup>, D. Galán<sup>2</sup>, A. Perea<sup>3</sup>, P.L. García-Ybarra<sup>3</sup>, J.L. Castillo<sup>3</sup>, M. Marquez<sup>4</sup> and A. Barrero<sup>5</sup>

<sup>1</sup>ETS Ingenieros Industriales, Universidad de Málaga, Málaga, Spain

<sup>2</sup>Yflow SL, Marie Curie 4-12, Parque Tecnológico de Andalucía, Campanillas, Málaga, Spain

<sup>3</sup>Dep. Física Matemática y Fluidos, UNED, Madrid, Spain

<sup>4</sup>Harrington Dep. Bioengineering, Arizona State University, Tempe, AZ 85287-9709, USA

<sup>5</sup>Escuela Superior de Ingenieros, Universidad de Sevilla, Sevilla, Spain.

Keywords: electrospray, dry deposition, morphology, electrical effects.

Many industrial processes involve the use of catalysts. The way through which those catalysts are prepared and dispersed on a substrate may have important effects on the reactions that must occur. Furthermore, the morphology of the catalyst layer itself may also influence the rates of these reactions. In this scenario, the morphology of the catalyst layer may depend on the process selected to disperse it. From a general standpoint, the morphology must be such that (1) all the catalyst is exposed to the reactants, (2) the reactants and products can easily access or leave the catalyst, and (3) the catalyst should be homogeneously dispersed.

The electrohydrodynamic atomization in the steady cone-jet mode has been proposed as a convenient mean to disperse liquid suspensions to form structured layers on substrates (Chen et al. 1995 and 1999, Benítez et al. 2005 among many others). In this work, we have experimentally studied the morphology of the layers formed from the electro

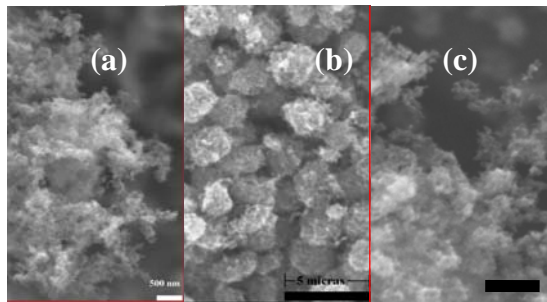


Figure 1. Morphologies: (a) fractal, (b) spheroids and (c) mixed. Scale bars: 0.5, 5 and 1 micron, respectively.

atomization of suspensions. The suspensions consist of carbon nanoparticles (~30 nm in diameter), both with and without catalyst, dispersed in ethanol and stabilized with the help of polymers. The load of carbon ranged from 1 to 10 mg/cc. The conductivity does not vary much for the suspensions without platinum, being always between  $0.7 \times 10^{-3}$  to  $1.5 \times 10^{-3}$  S/m. It increases a factor of 4 when carbon containing 10% in mass of platinum. The low polymer content (less than few %) does not affect the conductivity. All the suspensions were electrosprayed in the steady cone-jet mode. The needle to collector distance was 10 cm, and the

potential difference was 10 kV. The collector was a  $2 \times 2$  cm<sup>2</sup> piece of graphite mat. The operating conditions allowed for complete drying of the aerosol while airborne. The morphology of the structured layers, shown in figure 1, was classified as: (a) fractal-like, (b) spheroids and (c) mixed. The main parameters determining this structure are the particle concentration in the suspension,  $C$ , and the flow rate  $Q$  injected through the electrospray. Their combined effect is shown in figure 2. When either  $C$  or  $Q$  is large enough, the layer is formed by spheroids with characteristic diameters in the microns range. These are the residues left after solvent evaporation from the droplets. For a given  $C$ , there are flow rates small enough such that the structure presents no characteristic size in the micron range, belonging to a fractal-like type. The same can be observed for a given  $Q$ . For intermediate values of  $C$  and  $Q$ , the structured presents both features, being of type (c). The same behaviour is obtained when platinum is present.

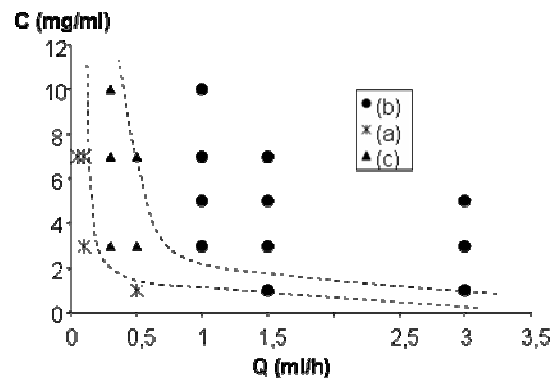


Figure 2. Structure type as a function of flow rate and concentration.

This work has been partially supported by the Spanish Ministry of Education and Science, under projects DPI2004-05246-C03-C04 and NAN2004-09312-C03, and by Yflow SL.

Chen, C.H., Buysman, A.A.J., Kelder, E.M. & Schoonman, J. (1995). *Solid State Ionics*, 80, 1.

Chen, C.H., Kelder, E.M. & Schoonman, J. (1999). *Thin Solid Films*, 342, 35-41.

Benítez, R., Soler, J., Daza, L. (2005). *J. Power Sources*, 151, 18-24.

## Reduction of relaxation times during electro spraying

U. Stachewicz<sup>1a,2</sup>, D. Burdinski<sup>1b</sup>, J.F. Dijkstra<sup>1a</sup>, J.C.M. Marijnissen<sup>2</sup>

<sup>1</sup>Department of Healthcare Devices and Instrumentation (a) and Department of Biomolecular Engineering (b), Philips Research Europe, High Tech Campus, 5656 AE Eindhoven, The Netherlands

<sup>2</sup>Nano Structured Materials, DelftChemTech, Faculty of Applied Sciences, Delft University of Technology, Julianalaan 136, 2628 BL Delft, The Netherlands

Keywords: electro spray, anti-wetting coating, relaxation time

Electrospraying, often referred to as electrohydrodynamic atomization (EHDA), is a technique to generate an aerosol of fine droplets through electric forces. Besides many other applications, electro spraying is used as a deposition method for a wide range of materials. The advantage of electro spraying over ink jet deposition techniques is the possibility to generate jets and/or droplets that are much smaller than the inner diameter of the nozzle (Liu 2000). We have observed that the wetting properties of different fluids affect the shape and size of the meniscus. Furthermore they influence the natural vibration of the pending droplet and its hydrodynamic relaxation time.

In our electro spraying set-up an electric potential gradient is applied between a nozzle of a liquid filled glass pipette and a grounded counter electrode placed at a 1-2 millimeter distance. We use a pulsed field superposed on a DC field to control the droplet generation process (Stachewicz *et al.* 2007). A high voltage power source is connected to the glass capillary, which encloses a metal wire.

In order to confine the wetted area to the rim of the nozzle, we modified the outer surface close to the orifice of the glass capillary with an anti-wetting coating. To achieve this, the nozzle front was contacted with a poly(dimethylsiloxane) (PDMS) stamp impregnated with a solution of octadecyl-trichlorosilane (OTS, 10 mM in n-hexane). The amphiphilic OTS molecules form a densely packed self-assembled monolayer (SAM) on the glass surface only in the area of contact at the outer rim of the nozzle (Figure 1). Although the SAM is not thicker than the length of individual OTS molecules (~2 nm), it is characterized by a generally high chemical and mechanical stability (Onclin *et al.* 2005).

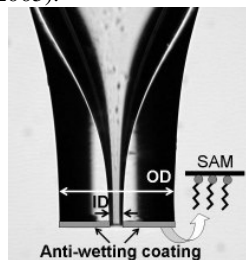


Figure 1. Anti-wetting coating on the glass capillary defines the wetted area close to the orifice of the nozzle. The inner diameter ID is 50  $\mu\text{m}$ , the outside diameter OD is 600  $\mu\text{m}$ .

Comparing the behaviour of the liquid in the absence and presence of the anti-wetting coating

(Table 1), it was seen that the volume of the fluid in its equilibrium state was much smaller for the modified capillary. The volume was at least 10 times smaller; therefore the relaxation time of ethylene glycol and water solutions was reduced from ms to  $\mu\text{s}$ . Since the system capacity became smaller, from 2.5 fF to 0.0174 fF, the RC time got 100 times shorter.

Table 1. Electro spraying examples of ethylene glycol and water solution (70/30).

Glass nozzle	Meniscus shape in equilibrium state	Electrospraying in cone-jet mode (different picture scales)
without coating		
with anti-wetting coating		

Moreover, during our experiments a reduction of the jet and droplet diameter was observed, when the meniscus became confined to the inner diameter of the capillary.

This study offers a new approach to reduce the block of fluid size hanging at the nozzle, which causes a shorter hydrodynamic relaxation time. The surface tension becomes a dominant force and the importance of the viscous drag is reduced. The generation of jets and droplets becomes easier to control.

This study is supported by the European research program, Marie Curie Actions, Early Stage Fellowship; project number MEST-CT-2004-505006 and Philips Research Europe.

Liu, H. (2000), *Science and Engineering of Droplets* New York: Noyes Publication, 49.

Stachewicz U., Dijkstra J.F. & Marijnissen J.C.M. (2007), *Electrostatic 2007, Journal of Physics: Conference Series*, to be published.

Onclin, S, Ravoo, B.J., Reinhoudt, D.N. (2005), *Angew. Chem. Int. Ed.* 44, 6282-6304.

## Aerosol mobility spectrometry based on diffusion charging

L. Hillemann<sup>1</sup>, A. Zschoppe<sup>2</sup> and R. Caldw<sup>3</sup>

<sup>1</sup>Institute of Process Engineering and Environmental Technology, TU Dresden, D-01062 Dresden, Germany

<sup>2</sup>Topas GmbH, Wilischstr. 1, D-01279 Dresden, Germany

<sup>3</sup>TSI Incorporated, 500 Cardigan, MN 55126 Shoreview, USA

Keywords: electrical effects, charged particles, instrumentation, measurement

Aerosol spectrometers employed in the nanometer range base their measurement on the classification of charged particles in an electric field. Accurate measurement requires a well-defined charge status for the aerosol which is usually achieved by ionization of gas in the presence of radioactive sources such as Kr<sup>85</sup> (Liu, 1974). Diffusion charging has also been used for this purpose, but it generates a much higher charge level of the particles making the data inversion more difficult.

The aim of this paper is to model a particular diffusion charger and to evaluate the feasibility of using this charger in an aerosol spectrometer. The applicability of the device for environmental aerosols will be shown by comparing parallel measurements with an SMPS-system.

Charging of particles by means of an electrical field or corona-generated ions has been known for many years. Whitby and Clark introduced the diffusion charging of an aerosol by preventing the particles from undergoing strong field charging. This mechanism was used to produce a monotonic decreasing relationship between size and electrical mobility of the aerosol particles (Whitby, 1966). More recently this principle inspired the design of the so-called "corona-jet-charger" which attaches ions on particles by diffusion and forced convection in a mixing chamber (Medved, 2000).

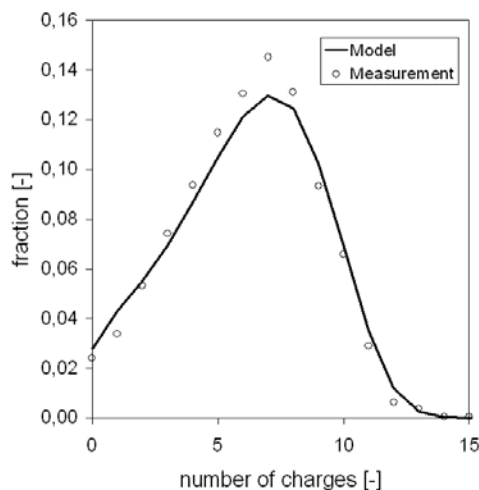


Figure 1. Calculated charge distribution compared to measured data (particle size 227 nm)

The charge distribution generated by this device can be calculated by applying Fuchs' limiting sphere

theory to the flow regime in the mixing chamber (taken from Biskos et. al., 2005). It is also possible to measure the charge distribution of particles leaving the charger by classifying monodisperse particles after the charger according to their charge status. An example of the comparison between model and measurement is shown in Figure 1.

By combining the corona-jet-charger with a DMA and an electrometer, a new aerosol spectrometer similar to an EAA and DMPS was developed. The advantage of this device is its simple set-up and the stability and robustness of the components. More problematic is the superposition of the mobility spectra of different particle size fractions due to their broad charge distribution. This leads to a lower size resolution compared to the SMPS. However, it is sufficiently precise for environmental aerosol quantification in air pollution networks.

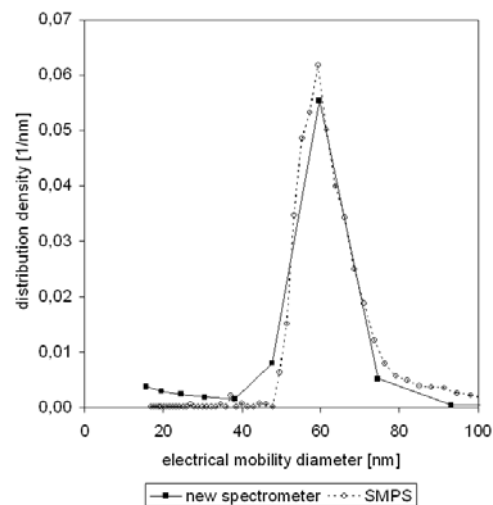


Figure 2. Distribution of 60-nm test aerosol showing SMPS and the developed spectrometer

UFIPOLNET ([www.ufipolnet.eu](http://www.ufipolnet.eu)) is financed by the LIFE financial instrument of the European Community under No. LIFE04 ENV/D/000054.

Liu, B. Y. H., Pui, D. Y. H. (1974). *J. Aerosol Science*, 5, 465-472.

Whitby, K. T., Clark, W. E. (1966). *Tellus*, 18, 573

Medved A., Dorman F., Kaufman, S. L. (2000). *J. Aerosol Science*, 31 SUPP/1, 616-617.

Biskos G., Reavell K., Collings N. (2005). *J. Aerosol Science*, 36, 247-265.

## Evaluation of a Drained DBD Electrode Apparatus for Nano-Particle Charging

M. Wild, J. Meyer and G. Kasper

Institut für Mechanische Verfahrenstechnik und Mechanik, Universität Karlsruhe (TH), Karlsruhe, 76131, Karlsruhe, Germany

Keywords: dielectric barrier discharge, particle charging, electrical effects, charged particles, nanoparticles.

This work deals with a concentric Dielectric Barrier Discharge (DBD) electrode arrangement (see Fig. 1). Its basic electrical behaviour was determined. Furthermore, the electrical conditions were investigated by means of numerical simulations and suitable operating conditions were identified. Based on these parameters the charging behaviour for nano-scaled particles was investigated.

Compared to classical corona wire electrodes, the evaluated setup provides an additional degree of freedom. The emission of charges can be controlled by the magnitude of DBD-excitation with a separately applied AC high voltage. Therefore the excitation can be influenced independently from the static electric field which is predominantly responsible for the particle losses in the charger. The charger carriers produced by the DBD are drained out of the generation area to the charging zone by a superposed DC HV (drained dielectric barrier discharge; dDBD).

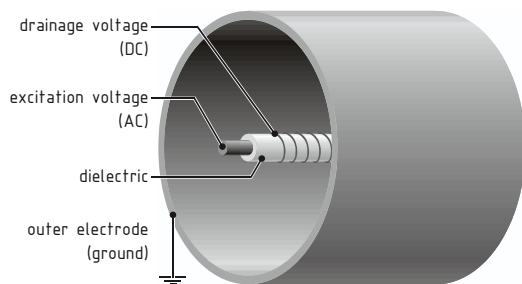


Figure 1. Schematic of the dDBD charger and the connection of applied voltages.

The charger employs a coaxial design. The outer electrode consists of an aluminium tube. Regular corona wire electrodes as well as DBD electrodes can be mounted concentrically. The latter consists of the metallic central excitation electrode (AC HV), a surrounding tubular dielectric and a metallic outer winding (DC HV), which provides the discharge interface and also acts as the drainage electrode (Masuda, 1978). The electrical field in the charger was investigated by means of FEM simulations (Comsol Multiphysics). The electric behaviour was also investigated experimentally in particle free conditions with respect to parameters of the different voltages and the dielectric (frequency, voltages, material, design). Thus, proper operating parameters for the subsequently conducted charging experiments could be determined.

The charging experiments were performed using monodisperse, electrically neutral Di-(2-Ethylhexyl)-Sebacate (DEHS) particles as test aerosol. The aerosol was generated by an evaporation and condensation method. The obtained average particle charge as well as the total loss in the charger was determined using a Faraday Cup Electrometer and Condensation Particle Counters (TSI Model 3010). The DBD charger performed well despite its slightly increased loss for the same amount of charge per particle compared to the regular wire discharge (Fig. 2).

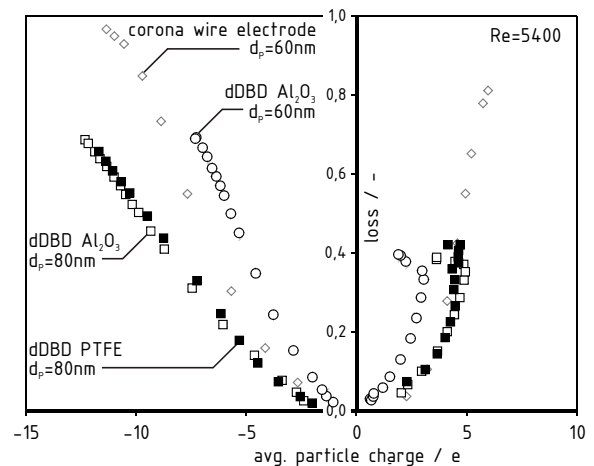


Figure 2. dDBD charging results for different particle sizes compared to corona wire electrode results (corona charging data from Marquard (2006))

The capability for charging particles with an excitation based method of charge emission could be confirmed experimentally. Further research will deal with non negligible particle space charge conditions at which regular wire electrodes suffer from corona quenching. For the dDBD electrode a superior performance is expected, since the electric field in the gap isn't crucial for the charge carrier release. The Authors would like to thank the DFG (Deutsche Forschungsgemeinschaft <http://www.dfg.de>) for their financial support of this project.

Masuda, S., M. Washizu, M., Mizuno A., and Akutsu K. (1978), *Conf. Rec. IEEE/IAS Ann. Meeting Vol. 1B*, pp. 16-22

Marquard (2006), *PhD Thesis*, University of Karlsruhe

## **T06 Abstracts**

## Thermophoresis of aerosols.

### (The state of the problem of today)

S.P.Bakanov

99423, Weimar, Germany

Keywords: aerosol fundamentals, fundamental aerosol physics, thermophoresis

For today in the field of thermophoresis of aerosols it is possible to consider as firmly established positions of the theory the following:

1. Expression for velocity of thermophoresis of small particles - Bakanov-Deraguin (1959) and Waldmann (1959) equations. Both expressions are fair at  $Kn = \lambda/R \rightarrow \infty$  ( $1/R \rightarrow 0$ ).

2. Expression for velocity of thermophoresis of large bodies (particles)  $v_{Ep}$  - Epstein's formula adjusted for size of thermal slip coefficient. Instead of Maxwell's numerical value  $3/4$  it is necessary to use a function  $k_{TS}(\varepsilon)$  ( $\varepsilon$  - accommodation coefficient of an impulse of molecules at their interaction with a surface of a particle). Maxwell's value corresponds to a special case of specular reflection ( $\varepsilon = 0$ ).

It is necessary to emphasize especially, that the velocity  $v_{Ep}$  is proportional to the first power of Knudsen number, calculated concerning the length scale of variation of gas temperature (width of a slit, diameter of a pipe etc), instead of the size of particle  $R$ .

The formula is fair at  $Kn = \lambda/R \rightarrow 0$ .

3. Expression for velocity of thermophoresis  $v_{th}$  at  $Kn \ll 1$  as usual has a form

$$v_{th} = v_{Ep} + Kn\Phi(\varepsilon, \alpha, \xi), \quad (1)$$

where  $\Phi(\varepsilon, \alpha, \xi)$  - some function of the kinetic coefficients depending from character of accommodation of an impulse and energy of molecules at collision with a surface of a particle, as well as the relation  $\xi$  of heat conductivities of a particle and gas. Depending on values of these parameters it can change a sign. At  $\xi \ll 1$  the second term of Eq. (1) becomes prevailing, that explains a deviation observed experimentally from Epstein's formula. For high-heat-conducting particles change of a sign  $\Phi(\varepsilon, \alpha, \xi)$  especially essential for specifies an opportunity negative thermophoresis.

Here is the well-time to make the important remark. In papers of many authors expression for  $v_{th}$  in this approximation has much more complex appearance. In our opinion it is the mistake consisting in excess of accuracy of result. Analytical solution of a problem should be made within the limits of that approach which has been incorporated in its most statement. In this case it is a question of the solution in approach of a  $Kn$  number power not above the first. Therefore more complex equations it is necessary to expand in a power series of the  $Kn$  number, having kept only the first

power, i.e. to the form (1), for all other coefficients of the resolution are doubtful.

4. Talbot's *et al.* equation (1980) represents itself no more than based on Brock's formula - semi-empirical interpolation between expressions for velocity of thermophoresis at  $Kn \ll 1$  and  $Kn \gg 1$ . It cannot serve as criterion of an estimation of results of measurements, and itself requires experimental definition of its coefficients.

5. The thermal slip coefficient (creep)  $k_{TS}(\varepsilon)$  is calculated by a number of authors. And though calculations were conducted by different methods using of various models, they have shown, that  $k_{TS}(\varepsilon)$  can vary only in an interval of values from  $3/4$  (at  $\varepsilon = 0$ ) up to approximately 1.2 (at  $\varepsilon = 1$ ).

6. The linear approximation of the measured values of velocity of thermophoresis at  $Kn \ll 1$  should cross an ordinate axis in a point  $v_{th} = v_{Ep}$ . It is the main criterion of reliability of experiment. The intersection point defines  $k_{TS}(\varepsilon)$  and, hence,  $\varepsilon$ ,  $\Phi(\varepsilon, \alpha, \xi)$  being the slope. That, in turn, allows to define  $\alpha$ .

Any of results of measurements known to us, except for a paper of Rosenblatt & Maer (1946), do not satisfy to this criterion. The consent marked by much authors with Talbot's formula in intermediate area of values of number  $Kn$  of anything neither proves, nor denies.

7. Bakanov *et al.* (1979) found out the phenomenon of thermal polarization of bodies in a rarefied gas flow. It is an alternative method of research in a considered field of knowledge. Bakanov *et al.* (1982) succeed also to measure the effect. This method is represented to us especially perspective for low-heat-conducting bodies as allows receiving rather simply results at as much as small values of  $Kn$  numbers.

Not less attractive, though also more dear, is the method of measurements in conditions of microgravitation which has started to be applied during the latest time.

Bakanov, S. P., & Deraguin, B. V. (1959). *Koll. Zhurnal*, 21, 377-384.

Bakanov, S. P., & Roldughin, V. I. (1979). *J. Coll. Interface Science*, 72, 428-441.

Bakanov, S. P., Vysotsky, V. V., Deraguin, B. V., & Roldughin, V. I. (1983). *J. Non-Equilibrium Thermodynamics*, 6, 75-84.

## Surface tension of critical nuclei composed of molecules with orientational tendency

I. Napari<sup>1</sup> and A. Laaksonen<sup>2,3</sup>

<sup>1</sup>Department of Physical Sciences, University of Helsinki, P.O. Box 64, FI-00014 Helsinki, Finland

<sup>2</sup>Department of Applied Physics, University of Kuopio, P.O. Box 1627, FI-70211 Kuopio, Finland

<sup>3</sup>Finnish Meteorological Institute, P.O. Box 503, FI-00101 Helsinki, Finland

Keywords: homogeneous nucleation, surface tension, density functional theory

One of most important causes for the discrepancies between classical nucleation theory (CNT) and nucleation experiments is the assumption that the critical clusters in CNT have the properties of bulk fluid. Especially troublesome is surface tension  $\gamma$ , because the particle number and the formation energy  $W^*$  of the critical cluster have cubic dependence on  $\gamma$  in CNT. No universal theory exists for the cluster surface tension, although the general features of radial behaviour are well known for simple one-component fluids.

In this work we use density functional theory (DFT) to investigate surface tension of clusters consisting of molecules composed of two or three atomic sites with varying degree of asymmetry in the attractive interaction between the atomic sites. The diatomic models (“dimers”) are numbered according to the asymmetry and behaviour at the liquid-vapour interface: DI (identical sites, no molecular orientation at the interface), DII (modest orientation with the weakly interacting sites pointing toward vapour), DIII (strongly oriented surface layer), DIV (multiple oriented layers). The special feature of these dimer fluids is that they have the same equation of state.

Surface tension of clusters  $\gamma_s(R)$  is obtained in a thermodynamically consistent manner with the aid of the thermodynamic expression for  $W^*$  and the Laplace equation with supplementary data from DFT (Laaksonen & Napari, 2001).

Figure 1 shows the ratio  $\gamma_s/\gamma_\infty$  as a function of the radius of surface of tension  $R_s$ . Fluids DI and DII behave in a similar manner and the overall radial dependence resembles closely to that of monoatomic fluids (Koga *et al.*, 1998). On the other hand, the curves for models DIII and DIV show intriguing humps which are related to the orientational reordering in the cluster. The intersection of the curves at  $R_s = 4.4\sigma$  is attributable to cluster geometry.

The most baffling feature in Fig. 1 is that the cluster surface tension is lower than the planar surface tension even at  $R_s = 100\sigma$  for the models DIII and DIV (the cluster contains here approximately  $10^6$  molecules). The reason for this behaviour can be found by examining the density of cluster. The densities of the largest clusters in our study are still slightly above the bulk value, which enhances the molecular orientation at the surface and, consequently, lowers the surface tension.

Nevertheless, the ratio  $\gamma_s/\gamma_\infty$  is expected to approach unity for very large droplets.

The observed behaviour of models DIII and DIV suggests that real molecular systems showing layered structures at interfaces might behave similarly. Such systems are e. g. diblock copolymers and metals. Indeed, surface tension of metal clusters has been shown to deviate strongly from the planar value (Onischuk *et al.*, 2006).

The radial dependence of cluster surface tension in fluid systems having little or no surface structure seems to follow the same the qualitative trend, which implies that a (simple) generic correction to planar surface tension might be found to give better estimate of the formation energy in nucleation. For fluids with layered interfaces this may not be possible, because the layered zone itself complicates the thermodynamic description of the droplet.

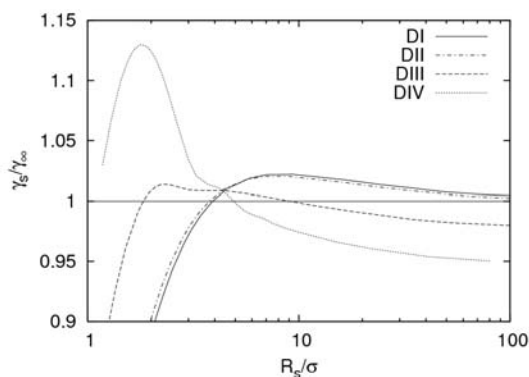


Figure 1. The ratio of cluster surface tension and surface tension of planar interface as function of the radius of surface of tension. The radius is scaled with the Lennard-Jones site length parameter.

This work was supported by the Academy of Finland.

Koga, K., Zeng, X. C., & Shchekin, A. K. (1998). *J. Chem. Phys.*, 109, 4063-4070.

Laaksonen, A. & Napari, I. (2001). *J. Phys. Chem. B.*, 105, 11678-11682.

Onischuk, A. A., Purtov, P. A., Baklanov, A. M., Karasev, V. V. & Vosel S. V. (2006). *J. Chem. Phys.*, 124, 104506.

## Influence of optical radiation on the homogeneous nucleation

V.G. Chernyak and E.S. Evgrafova

Department of Physics, Ural State University, 620083, Yekaterinburg, Russia

Keywords: vapour, aerosol formation, radiation, homogeneous nucleation, nucleation rate.

The physical and mathematical model of homogeneous nucleation kinetics in a supersaturated vapor in an optical radiation field has been developed. It is of interest for the modern atmosphere research techniques and also from the standpoint of partial control of the nucleation process. A feature of this problem lies in the fact that the temperature of nucleus differs from the equilibrium temperature of a vapor, a fact that can be explained either by the absorption of the light by the particle or by removal of the latent heat of phase transition.

Expression for change of the free energy has the form

$$\Delta\Phi = \Delta\Phi_0 + c(T_0 - T_p), \quad (1)$$

where  $\Delta\Phi_0$  is the isothermal work of nucleation,  $c$  is the heat capacity of particle,  $T_0$  is the equilibrium temperature of a vapor,  $T_p$  is the temperature of nucleus. The second term in Eq. (1) takes into account the change of free energy due to the absorption of the radiation by the particle and due to the removal of the latent heat of phase transition.

The temperature of the nucleus was defined from the solution of the heat conductivity equation considering the absorption of radiation by the particle. It has allowed taking into account the thermal physical and optical properties of the nucleus.

It has been considered for the free-molecular regime, in which the mean free path of molecules is much greater than the radius of nucleus. In addition, it has been assumed that the radius of the particle is much less than the wavelength of radiation. In this case for change of the free energy the following expression has been obtained

$$\Delta\Phi(r, T_p) = \Delta\Phi_0(r, T_0) + cT_0\gamma \frac{4\pi}{3v_m} r^4, \quad \gamma \sim IK, \quad (2)$$

where  $r$  is the radius of the nucleus,  $v_m$  is the volume per condensed phase molecule,  $I$  is the radiation intensity,  $K$  is the efficiency factor of the radiation absorption by the nucleus.

For further calculations the Frenkel - Zeldovich's classical method was used (E.M. Lifshitz and L.P. Pitaevskii, 1981) and the expressions for radius of a critical nucleation center and nucleation rate have been obtained. Dependencies of these quantities on intensity and frequency of radiation,

optical properties of the nucleus and thermophysical parameters of a vapor have been calculated. It is shown that with a increase of intensity or frequency of radiation, the radius of a critical nucleus value also increases, however the nucleation rate value decreases.

We made some numerical estimates for water vapor under typical experimental conditions. The source of light is a tunable dye CO<sub>2</sub> – laser with wave length  $\sim 10.6 \mu\text{m}$ . The result of calculation for relative nucleation rate  $J/J_0$  ( $J_0$  is the isothermal nucleation rate at  $I=0$ ) depending on radiation intensity is presented in Fig.1.

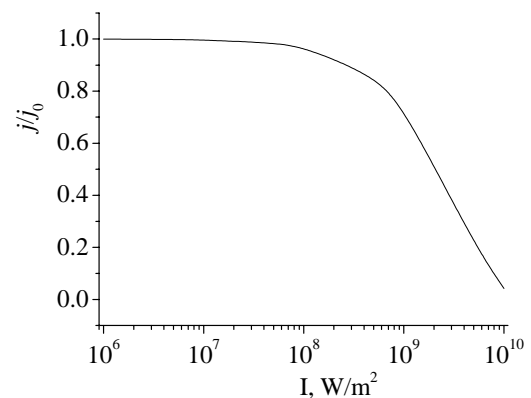


Figure 1. The nucleation rate in supersaturated water vapor as a function of the radiation intensity.

As is seen from the Figure1, the influence of radiation becomes essential at  $I > 10^8 \text{ W/m}^2$ . If at intensity  $10^8 \text{ W/m}^2$  the radiation practically does not influence on the nucleation rate, then at intensity  $10^{10} \text{ W/m}^2$  the nucleation rate decreases approximately by two orders of magnitude.

This work was supported by the Russian Foundation for Basic Research under grant 06-01-00594.

Lifshitz, E. M., & Pitaevskii, L. P. (1981). *Physical Kinetics: Course of Theoretical Physics by L. Landau and E.M. Lifshitz*. Oxford: Pergamon, Vol. 10.

## Heat transfer to a particle in the transition regime

A.A. Lushnikov and M. Kulmala

Department of Physical Sciences, University of Helsinki, P.O. Box 64, FI-00014, Helsinki, Finland

Keywords: aerosol thermodynamics, fine particles, heat and mass transfer, mechanisms.

In contrast to condensation and evaporation no simple formulas exist so far describing heat transfer to (from) an aerosol particle in the transition regime. We mean the formulas describing the heat transfer efficiency (HTE) of the particles with sizes comparable to the mean free path of the carrier gas molecules. The attempts grounded on the numerical solution of the Boltzmann equation presented in Williams & Loyalka, 1991 are too complicated for everyday use. It is very desirable to have something similar to the Fuchs-Sutugin formula for the condensational efficiency of aerosol particles. Below we present our attempt to derive such a formula. To this end we apply the scheme developed in Lushnikov & Kulmala, 2004.

Let  $J(a)$  be the energy flux onto the particle of radius  $a$ . We introduce the particle heat transfer efficiency  $\gamma(a)$  as follows:

$$J(a) = \gamma(a)(T_a - T_\infty), \quad (1)$$

where  $T_r$  is the temperature at the distance  $r$  from the particle centre. We can also write

$$J(a, R) = \gamma(a, R)(T_a - T_R), \quad (2)$$

with  $\gamma(a, R)$  being a generalised heat transfer efficiency of the particle which allows us to find the energy flux, once the temperature at a finite distance  $R$  from the particle centre is known.

Let us assume now that we know the exact temperature profile corresponding to the given energy flux  $J(a)$ . Then

$$J(a) = \gamma(a, R)(T_a - T_R^{exact}) \quad (3)$$

Now we choose  $R$  sufficiently large for the continuous approximation to reproduce the exact temperature profile. This profile is well known,

$$T_R^{exact} = T_\infty - \frac{J(a)}{4\pi\Lambda R}. \quad (4)$$

Here  $\Lambda$  is the thermal conductivity of the particle material. On substituting eq. (4) to eq. (3) yields the

equation for  $J(a)$ . We then solve this equation and use definition eq. (1). The result is,

$$\gamma(a) = \frac{\gamma(a, R)}{1 + \frac{\gamma(a, R)}{4\pi\Lambda R}}. \quad (5)$$

This expression is exact, but we know neither  $\gamma(a, R)$  nor the matching distance  $R$ . In order to find these functions we call upon two approximations: i. we approximate  $\gamma(a, R)$  by its free-molecule expression, and ii. we define  $R$  by requiring the continuity of radial derivative of the temperature profile at  $r = R$

In order to find  $\gamma_{fm}(a, R)$  (subscript *fm*. is deciphered as free-molecule) we solved the collisionless Boltzmann equation with the Maxwell boundary condition, i.e. we consider that part of molecules elastically reflects from the particle surface while the rest equilibrates and acquires the temperature of the particle surface. Thus found velocity distribution function serves for calculating the temperature profile. Then we can find the final expression for the thermal response of the particle

$$\gamma(a) = \gamma_{fm}(a)Q(a), \quad (6)$$

where  $\gamma_{fm}$  is the heat transfer efficiency in the free molecule regime and the modifier  $Q(a)$  is:

$$Q(a) = [1 + \frac{a^2}{4R^2}(\frac{R}{R+R_0} + \frac{4R}{R_0})]^{-1} \quad (7)$$

Here  $a$  is the particle radius,  $R^2 = R_0^2 + a^2$ ,  $R_0 = 2\Lambda/v_T$ , and  $v_T$  is the molecular thermal velocity. The result eqs (6) and (7) reproduces limiting values of the heat transfer coefficient in the free molecule and continuous regimes.

Lushnikov, A.A., & Kulmala, M. (2004) *Phys. Rev. E* 70, 046413-1 – 9.

Williams, M.M.R. & Loyalka, S.K. (1991). *Aerosol Science. Theory & Practice*, Oxford, New York, Seoul, Tokyo, Pergamon P ress.

## Critical behaviour of the particle mass spectra in gelling systems

A.A. Lushnikov

Department of Physical Sciences, University of Helsinki, P.O. Box 64, FI-00014, Helsinki, Finland

Keywords: agglomerates, coagulation, particle formation and growth, particle size distribution.

The phenomenon of coagulation is well known to everyone who encountered physics of fractals, cloud physics, kinetics of nanoaerosols and formation of large agglomerates from small aerosol particles. Theory of coagulation deals with the systems of particles that can coalesce producing larger and larger agglomerates. The process continues until the moment when only one particle remains in the system. The kinetics of coagulation is described by the well known Smoluchowski equation whose solution defines the time evolution of the particle mass spectrum. It seems from the first sight that if we have sufficiently power computers then we are able to answer all questions concerning the time evolution of any coagulating system. Not all, however, is so cloudless. The point is that the Smoluchowski equation operates in terms of concentrations, i.e., it describe thermodynamically large systems wherein the particle population numbers are macroscopically large. This thermodynamical consideration thus ignores the particles whose population numbers grow slower than the total volume of the whole system. The fact that the particle spectra found from the Smoluchowski equation do not conserve the total particle mass concentration was known since very long ago (see extensive citations in Leyvraz, 2003). This strange effect was attributed to the formation of an invisible infinite agglomerate (the gel) whose mass was equal to the deficit of mass remained in the sol fraction.

Very recently I tried to answer the question what is the gel and how does it form (Lushnikov, 2007). To this end I exploited the truncated model of coagulation proposed in Lushnikov & Piskunov (1982). This model considers the coagulating system with an instantaneous sink of large particles. The particles with masses exceeding a cutoff mass  $G$  are assumed to form a passive deposit, i.e., they do not interact with the rest coagulating sol particles.

This presentation reports on the exact post-gel solution of the truncated Smoluchowski equation for the family of coagulation kernels of the form:

$$K(g, l) = \frac{1}{2} (g^\alpha l^\beta + g^\beta l^\alpha),$$

where  $g, l$  are the masses of two coalescing particles and  $1 > \alpha + \beta \leq 2$ ,  $0 < |\alpha - \beta| < 1$ .

The main results of the present analysis can be summarized as follows:

The coagulating systems considered here reveal a phase transition. Before the critical time  $t = t_c$  the total mass concentration of the sol fraction is conserved. The spectrum contains a damping exponent whose scale grows as  $g_0 \propto (t - t_c)^{-2/(1+\mu)}$  in approaching to the critical time. Here  $\mu = |\alpha - \beta|$ .

At the critical point the spectrum becomes the algebraic function of the particle mass,

$$c_g \propto g^{-(3+\lambda)/2}$$

with  $\lambda = \alpha + \beta$ .

At the post-critical stage the sol spectrum drops down with time as  $t^{-1}$  and acquires rather unusual dependence on the particle mass,

$$c_g \propto t^{-1} g^{-(3+\lambda)/2} e^{\xi_g/G}$$

The sol spectrum now contains the *growing* exponent of the particle mass.

The spectrum of the deposit is also found as the function of time and the particle mass. The critical time is independent of the value of the cutoff mass  $G$  and is expressed in terms of the exponents  $\lambda$  and  $\mu$ . It is essential to emphasize that neither of above mentioned dependencies contains matching parameters that should be found from a numerical solution of the Smoluchowski equation for the initial stage of coagulation.

Leyvraz, F. (2003). *Phys. Rep.* 383, 95 -212 .

Lushnikov, A.A. & Piskunov, V.N. (1982). *Dokl. Akad. Nauk SSSR (Sov. Phys. Doklady)*, 267, 127 . 130.

Lushnikov, A.A. (2007). *J. Phys. A: Math. Theor.*, 40, F119 – F125.

## Classical nucleation theory for pure water below 240 K

T. Němec, F. Maršík and J. Hrubý

Institute of Thermomechanics ASCR, v.v.i., Dolejškova 1402/5, 182 00 Prague 8, Czech Republic

Keywords: homogeneous nucleation, ice nuclei, nucleation rate.

It is a known flaw of the Classical Nucleation Theory (CNT) that its predictions of the nucleation rate, not only in the case of pure water, do not coincide with the experimentally measured nucleation rates at some specific temperatures. Nucleation experimentalists noticed (Wölk *et al.*, 2002) that the classical Becker-Döring (BD) nucleation-rate formula considerably underestimates the measured nucleation rate of pure water at temperatures under roughly 240 K. Moreover, there is a significant feature of this underestimation as it progresses with decreasing temperature reaching roughly 5 orders of magnitude around 220 K. Above 240 K, on the other hand, the tendency of the discrepancies is not that obvious; nucleation rate is overestimated of only few orders of magnitude which can be ascribed to the fact that the CNT treats water as an ideal gas. Therefore, we turn our attention to the region below 240 K in this work.

There have been many attempts to improve the accuracy of the CNT predictions in the past – starting with empirical modifications to the BD formula, adding various terms to the expression for the nucleation work, adjusting the thermophysical properties of water used in the CNT formulas, or questioning the applicability of the capillary approximation and developing a completely different approach. Nevertheless, a fit to the experimental data still remains the most reliable method of calculating nucleation rates for engineering purposes (Holten *et al.*, 2005).

We tackled this problem by reconsidering the nucleation work of water clusters at temperatures below 240 K. Although the current opinion (Labetski *et al.*, 2004), a result of an ongoing discussion among nucleation researchers, is that the nuclei in pure-water nucleation do not freeze during nucleation experiments at temperatures as low as 205 K, our assumption is that this happens at roughly 235 K. This temperature suspiciously coincides with the so called homogeneous ice nucleation limit (~ 235 K, Koop, 2004) which is the minimum temperature to which liquid water can be undercooled without freezing. Below this temperature liquid water freezes instantaneously which we believe is also the case of the nucleation processes under consideration. Our idea is further supported by the fact that by freezing the droplet the heat of melting is released. A release of the melting heat has an effect of lowering the nucleation work of a particular cluster. As a consequence of lower nucleation work, the nucleation rate is enhanced which can restore the agreement with experimental nucleation-rate data.

We attempted to describe the above-mentioned ideas in terms of the CNT. We used the usual CNT treatment with an alternative expression for the chemical potential that enables to account for the release of the heat of melting by the newly formed droplet. The results of our calculations are illustrated in Fig. 1 where the (log-scaled) ratio of our “freezing-enabled” CNT nucleation rate to the original BD nucleation rate is shown. We found that our new description increases the nucleation rates at temperatures below 240 K, reaching a very good agreement with experimental data. Moreover, at temperatures above 240 K, the new treatment slightly lowers the nucleation rates as it accounts for the non-ideality of water as well.

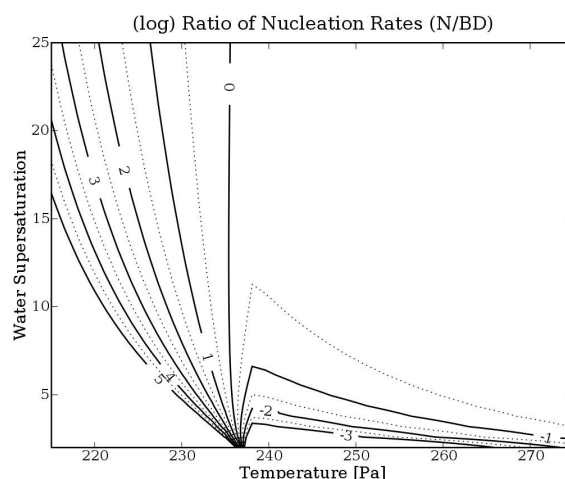


Figure 1. A log-scaled ratio of our predicted nucleation rate of pure water (N) to the nucleation rate calculated according to the Becker-Döring theory (BD).

This work was supported by the Grant Agency of the Academy of Sciences of the Czech Republic grant KJB400760701.

Becker, R., & Döring, W. (1935). *Ann. Phys.*, 4, 719-752.

Holten, V., Labetski, D. G. & Van Dongen, M. E. H. (2005). *J. Chem. Phys.*, 123, 104505.

Koop, T. (2004). *Z. Phys. Chem.*, 218, 1231-1258.

Labetski, D. G., Holten, V. & Van Dongen, M. E. H. (2004). *J. Chem. Phys.*, 120, 6314-6314.

Wölk J., Strey, R., Heath, C. H. & Wyslouzil, B. E. (2002). *J. Chem. Phys.*, 117, 4954-4960.

## The Rate of Vapor Condensation on Clusters in Ion-induced Water Cluster Formation

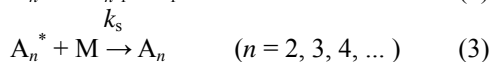
Yoshiki Okada and Yuta Hara

Kansai University, 3-3-35 Yamate-cho, suite-shi, Osaka 564-8680, Japan

Key Words: water cluster, vapor condensation rate, cluster formation, sticking probability.

In this study the rate of water vapor condensation on a water cluster is determined from the values of the sticking probability of the water molecule on the cluster and the collision cross section between the molecule and cluster. We investigate the reasons for enhancement of the vapor condensation rate on a water cluster ion compared with that on a neutral water cluster.

In the early stages of cluster formation, the monomer ( $A_1$ ) attachment produces, at an incorporation rate constant  $k_f$ , unstable clusters which possesses sufficient energy for dissociation as expressed by Eq. (1). The dissociation of a monomer  $A_1$  from the vibrationally excited cluster ( $A_n^*$ ) generates a stable cluster ( $A_{n-1}$ ) at a dissociation rate constant  $k_d$  in Eq. (2). In parallel with this dissociation path, deactivating collisions of the vibrationally excited cluster with inert gas atoms (M) results in the formation of a stable cluster ( $A_n$ ) at a stabilization rate constant  $k_s$ , as given by Eq. (3).<sup>1)</sup>



The vapor condensation rate  $r_c$  in the cluster formation stage corresponds to the production rate of  $A_n$ . When the sticking probability  $P_s$  is defined as the ratio of the production rate of  $A_n$  in Eq. (3) to the collision rate between  $A_{n-1}$  and  $A_1$  on the left-hand side of Eq. (1),  $r_c$  is given by the product of  $P_s$  and the collision rate between  $A_{n-1}$  and  $A_1$  as follows,

$$r_c = P_s \sigma_{\text{coll}} v c_m \quad (4)$$

where  $\sigma_{\text{coll}}$  is the collision cross section between  $A_{n-1}$  and  $A_1$ ,  $v$  is the relative velocity between  $A_{n-1}$  and  $A_1$ ,  $c_m$  is the molecular concentration of  $A_1$ , and  $\sigma_{\text{coll}} v c_m$  gives the collision rate between  $A_{n-1}$  and  $A_1$ .

The collision cross sections between a water cluster ion  $H^+(H_2O)_n$  at the cluster size  $n$  and a water molecule,  $\sigma_{\text{coll},i}$ , and between a neutral water cluster  $(H_2O)_n$  and a water molecule,  $\sigma_{\text{coll},h}$ , can be calculated by the method<sup>2)</sup> based on the Langevin theory. Figure 1 shows the ratio of  $\sigma_{\text{coll},i}$  to  $\sigma_{\text{coll},h}$  as a function of  $n$  at 273

K. The ratio was as large as 2.0 at  $n = 1$ , decreased with increasing  $n$ , and was about 1.1 at  $n = 100$ .

According to the pseudo steady state assumption on the concentration of  $A_n^*$ ,  $P_s$  is given by the following equation with the dissociation rate constant  $k_d$  and stabilization rate constant  $k_s$ .

$$P_s = \{k_s / (k_d + k_s)\} P_i, \quad (5)$$

where  $P_i$  is the incorporation probability defined as the ratio of the production rate of  $A_n^*$  to the collision rate between  $A_{n-1}$  and  $A_1$ . The incorporation probability of a water molecule into a water cluster was found<sup>3)</sup> to be equal to unity below about 1000 K for the cluster sizes ranging from 2 to  $10^4$ . The values of  $k_d$  and  $k_s$  for formation of both water cluster ion  $H^+(H_2O)_n$  and neutral water cluster  $(H_2O)_n$  can be calculated by the methods<sup>4)</sup> based on the RRK theory and  $V \rightarrow T$  relaxation rate equation, respectively. Figure 2 shows the ratio of the sticking probabilities for water cluster ions,  $P_{s,i}$ , to that for neutral water clusters,  $P_{s,h}$ , as a function of cluster size  $n$  at 273 K. The ratio was as large as approximately 7 at  $n = 3$ , decreased with increasing  $n$ , and was about unity at  $n > 20$ .

When the enhancement factor  $F_e$  for the rate of water vapor condensation on water clusters is defined as the ratio of the vapor condensation rate for water cluster ions,  $r_{c,i}$  to that for neutral water clusters,  $r_{c,h}$ ,  $F_e$  is given as the ratio of the product  $P_{s,i} \sigma_{\text{coll},i}$  to  $P_{s,h} \sigma_{\text{coll},h}$  from Eq. (4). Figure 3 shows  $F_e$  as a function of cluster size  $n$  at 273 K.  $F_e$  was as large as approximately 13 at  $n = 2$ , decreased with increasing  $n$ , and was about 1.1 at  $n > 20$ . The large values of  $F_e$  in the small cluster-size region was found to be caused by the large values of both  $\sigma_{\text{coll},i} / \sigma_{\text{coll},h}$  and  $P_{s,i} / P_{s,h}$  in this size region.

1) Okada, Y., Yamaguchi, S., Takeuchi, K. (2001), *Appl. Phys.* **B72**, 507.

2) Okada, Y., Yamaguchi, S., Takeuchi, K. (2003), *J. Aerosol Research, Japan*, **18**, 47.

3) Okada, Y., Yamaguchi, S., Kawai, Y., Orii, T., Takeuchi, K. (2003), *Chem. Phys.*, **294**, 37.

4) Okada, Y.: submitted to *J. Aerosol Research, Japan*

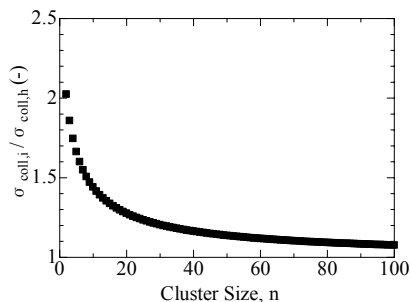


Fig. 1 Ratio of the collision cross sections as a function of water cluster size

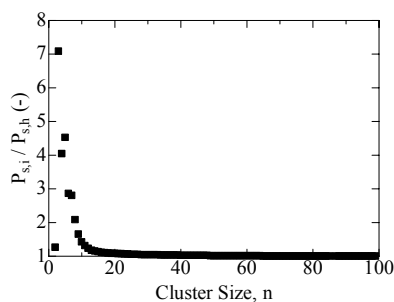


Fig. 2 Ratio of the sticking probabilities

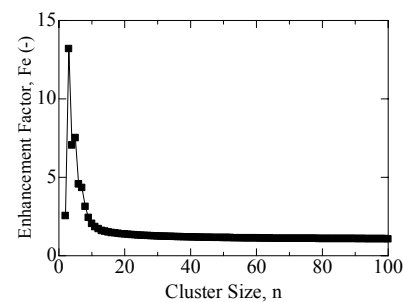


Fig. 3 Enhancement factor for the rate of water vapor condensation on water clusters

## Fine particle losses in the sampling lines of Puijo tower measurement station

H.J. Portin<sup>1</sup>, A.P. Leskinen<sup>1</sup> & K.E.J. Lehtinen<sup>1,2</sup>

<sup>1</sup>Finnish Meteorological Institute, Kuopio unit, P.O. Box 1627, FI-70211, Kuopio, Finland

<sup>2</sup>University of Kuopio, Department of Physics, P.O. Box 1627, FI-70211, Kuopio, Finland

Keywords: deposition, diffusion, measurement errors, penetration.

Recently, a new measurement station for aerosol-cloud interactions was established in Kuopio, Finland. The measurement station is located on top of the Puijo observation tower, which offers good conditions for particle and cloud measurements (Leskinen *et al.*, 2006).

Because of some practical issues, the sampling lines of the station had to be made quite long. There are two sampling lines, one with a PM<sub>10</sub> inlet (inner diameter 6 cm, flow rate 50 lpm) and one with a PM<sub>2.5</sub> cyclone (inner diameter 3.3 cm, flow rate 16.7 lpm). The lengths of the sampling lines are about 6 m and 8 m, respectively. In addition, there is also a 2 m long line connecting the main lines with the measurement instruments (inner diameter 0.4 cm, flow rate 1-2 lpm).

Because of the length of the sampling lines, some particle losses were expected to occur. To obtain reliable data from the station, it would be necessary to consider this problem. In the first part of the research, actual particle losses were calculated by using monodisperse aerosol. In the second part, these results were compared with some mathematical models.

In the measurements, 6 sizes of monodisperse aerosol were used: sodium chloride particles with diameters of 30, 50, 100 and 200 nm and latex particles with diameters of 0.6 and 1.36  $\mu\text{m}$ . Two condensation particle counters were used to measure the number concentration in both ends of the lines. It was observed that penetration for smaller particles was considerably lower than that of larger particles. For 30 nm particles the penetration in PM<sub>10</sub> line was about 80 % and in PM<sub>2.5</sub> line only 73 %.

In theoretical calculations it was assumed that diffusion, sedimentation and inertial losses in bends are the most important deposition mechanisms. Other mechanisms, such as thermophoresis and electrostatic deposition, were omitted. In total, 4 diffusion models (Baron & Willeke, 2001; Davies, 1966; Ingham, 1975; Hinds, 1999), 2 sedimentation models (Hinds, 1999; Wang, 1975) and 3 models for bend losses (Baron & Willeke, 2001; Hinds, 1999; Cheng & Wang, 1981) were considered.

There were no significant differences between various combinations of models; all results are within a few percent. Only exception is Davies's diffusion model, which deviates significantly from the other models and will be ignored in further analysis.

When theoretical and measured penetrations are compared, it can be seen that they differ somewhat, the difference being biggest for smaller particles. On the other hand, the correlation between measured and theoretical values is good, ranging between 0.81 and 0.87. One example of results is given in figure 1, where measured values are shown together with theoretical predictions. The calculations in this example are based on the diffusion model by Ingham, sedimentation model by Wang and bend loss model by Hinds.

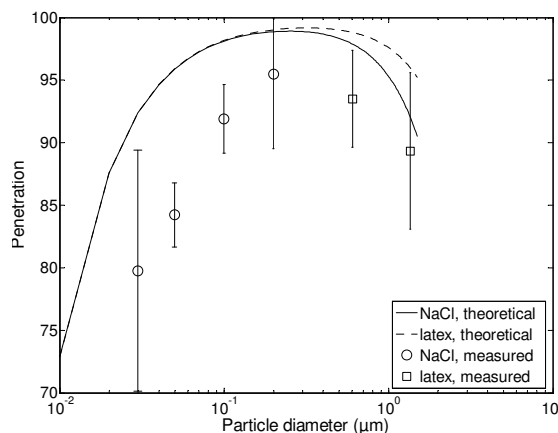


Figure 1. Measured and theoretical penetrations for the PM<sub>10</sub> line. Theoretical calculations are based on the diffusion model by Ingham, sedimentation model by Wang and bend loss model by Hinds.

- Baron, P.A. & Willeke, K. (2001). *Aerosol measurement. Principles, Techniques and Applications*. New York, USA: Wiley Interscience.
- Cheng, Y.S. & Wang, C.S. (1981). *Atmopheric. Enviroment.*, 15, 301-306.
- Davies, C.N. (1966). *Aerosol Science*. London, U.K.: Academic Press.
- Hinds, W.C. (1999). *Aerosol Technology. Properties, Behavior and Measurement of Airborne Particles*. New York, USA: Wiley Interscience.
- Ingham, D.B. (1975). *J. Aerosol Science*, 6, 125-132.
- Leskinen, A.P., Lehtinen, K.E.J., Portin, H.J., Laaksonen, A., Miettinen, P., Lihavainen, H., Komppula, M. & Viisanen, Y. (2006). *Report Series in Aerosol Science*, 83, 212-213.
- Wang, C. S. (1977). *J. Aerosol Science*, 8, 289-295.

## HETEROGENEOUS NUCLEATION ON SINGLE MICRODROPLETS

A. K. Ray, J. L. Huckaby and Y. Raja

Department of Chemical Engineering, University of Kentucky, Lexington, KY 40506-0046, USA

Keywords: heterogeneous nucleation, growth, light scattering, single particle analysis.

We have examined heterogeneous nucleation on droplets that were exposed to vapors of various immiscible compounds. Experiments were conducted on single droplets that were suspended in an electrodynamic balance mounted inside a thermal diffusion cloud chamber. By placing a pool of liquid at the bottom plate of the cloud chamber a well defined one-dimensional vapor concentration field as a function of position was created inside the chamber. The concentration profile is defined by the temperature difference between the top and bottom plates, and the vapor concentration around a suspended droplet was increased from unsaturated to supersaturated levels in small steps by altering the temperature difference. A suspended droplet was illuminated by a tunable ring-dye laser that was scanned to obtain a scattering intensity versus wavelength spectrum. Resonances observed in the spectrum were used to characterize the droplet (Huckaby et al., 1994). We have examined dioctyl phthalate (DOP) droplets exposed to water vapor, Santovac droplets (i.e., five ring polyphenyl ether) to invol 90 (i.e., straight chain alkane) vapor, hexadecane vapor and Fomblin (i.e., perfluorinated polyether) vapor.

Results show that when a droplet is exposed to an environment that is supersaturated with an immiscible vapor, heterogeneous nucleation occurs through three possible ways: by dropwise condensation, nucleation inside the droplet, and nucleation leading to the formation of a layer. High surface tension compounds (e.g., water vapor on DOP droplets) do not form layers. We also observed that when a Santovac droplet is exposed to invol 90 vapor, above a certain supersaturation level a second phase forms by nucleation inside the droplet phase, and nuclei grow to form an emulsion in the droplet. The emulsion remains stable and persists for days. Nucleation of low surface tension compounds on a droplet results in the formation of a layer, and transpires in the absence of any significant supersaturation. Results show that the formation of an adsorbed layer depends on the surface and interfacial tensions. For example, hexadecane layers form on Santovac droplets at hexadecane saturation ratios in the range 1.005 to 1.02. Below  $S=1.005$ , a droplet absorbs hexadecane vapour, while the droplet remains homogeneous. Figure 2 shows the thickness of hexadecane layer on a Santovac droplet as a function of time. The layer thickness was determined from the shifts of transverse magnetic (TM) and transverse electric (TE) mode resonances from their positions before the formation of the layer (Huckaby and Ray,

1995). The results show that after the formation of a layer on a droplet, the layer initially grows slowly, but the growth rate increases as the layer thickness increases. Above a certain thickness, the layer behaves like a macroscopic phase whose growth rate can be described by mass transfer equations.

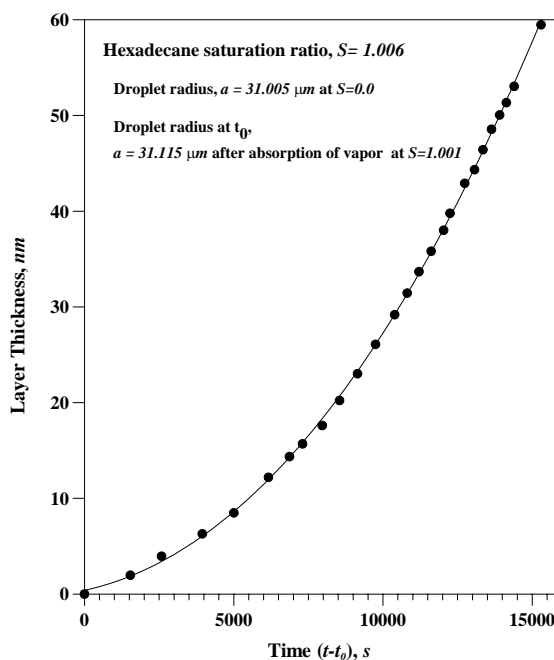


Figure 1. Hexadecane layer thickness on a Santovac droplet as a function of time.

This work was supported by the National Science Foundation (grant # CTS-0130778), Kentucky Science & Engineering Foundation (grant # KSEF-456-RDE-005), and DOE National Institute for Climatic Change Research (grant# 06-SC-NICCR-1066).

Huckaby, J. L., Ray, A. K., & Das, B. (1994) *Applied Optics*, 33, 7112-7125.

Huckaby, J. L., & Ray, A. K. (1995) *Langmuir*, 11, 80-86.

## Investigation of the nanoparticles diffusion coefficient temperature dependence

V. Ya. Rudyak<sup>1</sup>, S.N. Dubtsov<sup>2</sup>, S.L. Krasnolytskii<sup>1</sup> and A.M. Baklanov<sup>2</sup>

<sup>1</sup>Novosibirsk State University of Architecture and Civil Engineering, 113, Leningradskaya str., 630008, Novosibirsk, Russia

<sup>2</sup>Institute of Chemical Kinetics and Combustion SB RAS, 3, Institutskaya str., 630090, Novosibirsk, Russia

Keywords: aerosol fundamentals, diffusion, nanoparticles

The dependence of the aerosol particles diffusion coefficient on temperature is one of their key characteristics. According to Einstein theory, the temperature dependence of diffusion coefficient for such particles is determined by the carrier gas viscosity. This dependence is described by experimental Canningam – Milliken – Davis (CMD) correlation for rarefied gases. CMD-correlation is widely used for many applications. In paper (Rudyak *et al.*, 2001) significant difference of the dependence of nanoparticles diffusion coefficient on temperature from CMD correlation was predicted.

The systematic investigation of the dependence of nanoparticles diffusion coefficient on temperature is the main objective of this presentation. This dependence was experimentally studied for WO<sub>x</sub> and NaCl particles (the particle sizes are varied from 4 to 30 nm) in the temperature range from 295 to 570 K. Hot – wire generator (Baklanov, 1993) and Collisson-type nebulizer were used to produce WO<sub>x</sub> and NaCl nanoparticles respectively. Automated Diffusion Battery (Ankilov *et al.*, 2002) was used to measure nanoparticles concentration and size distribution. The diffusion coefficient was calculated from the penetration coefficient using Chen and Yeh (1980) method. In order to obtain unbiased experimental data, the nanoparticle diameters were measured by both the Diffusion Battery method and transmission electron microscope. The obtained data are essentially different (about 20 or 30 %) for small aerosol particles (see also paper (Rudyak, 2002)).

The typical experimental data of the diffusion coefficient dependence on temperature of carrier gas is presented in Figure 1 for WO<sub>x</sub> nanoparticles. Here the diffusion of particles WO<sub>x</sub> in air at normal pressure was studied. The size of these nanoparticles is  $4.2 \pm 0.2$  nm.

The experimental data have been compared with values of diffusion coefficient calculated by the kinetic theory. We use the Boltzmann kinetic theory for special interaction potential of the aerosol particles with carrier gas molecules was offered in papers (Rudyak, 2001; 2002). It is shown that the kinetic theory describes good the experimental data. On the other hand the CMD-correlation is applicable only in narrow temperature range. At higher temperatures, the CMD-formula leads to strongly underestimated diffusion coefficient and thus cannot be applied.

In conclusion the simple analytical correlation of the nanoparticles diffusion coefficient dependence on carrier gas temperature is proposed.

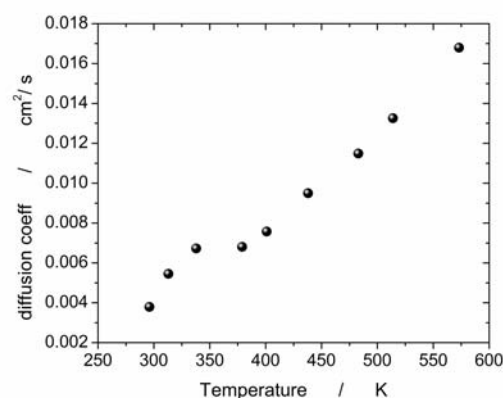


Figure 1. Temperature dependence of  $4.2 \pm .2$  nm WO<sub>x</sub> particles diffusion coefficient.

This work was supported in part by the Russian Foundation for Basic Researches (grant No. 07-08-00106) and the Program “Development of scientific potential of higher schools” of Ministry of Education and Science of the Russian Federation (project No. PHC 2.1.1.474).

- Ankilov, A., Baklanov, M. *et al.* (2002). *Atmospheric Research*, 62, 177-207.
- Baklanov, A. M., & Dubtsov S. N. (1993). *J. Aerosol. Science*, 24, Suppl. 1. P. S237-S238.
- Cheng Y.S., & Yeh H.C. (1980). *J. Aerosol. Science*, 11, 313-320.
- Rudyak, V.Ya., & Krasnolutskii, S.L. (2001). *Doklady Physics*, 46, 897-899.
- Rudyak, V.Ya., Krasnolutskii, S.L., Nasibulin, S.G., & Kauppinen, E.I. (2002). *Doklady Physics*, 47, 758-761.
- Rudyak, V.Ya., & Krasnolutskii, S.L. (2002). *Technical Phys.*, 47, 807-813.

## Stochastic birth and death equations to treat chemistry and nucleation in small systems

Christiane Losert-Valiente Kroon and Ian Ford

Department of Physics and Astronomy, University College London, Gower Street, London, WC1E 6BT, UK

Keywords: nucleation, fundamental aerosol physics, aerosol chemistry, Monte Carlo simulations

Chemical and nucleation processes taking place in very small open systems do not necessarily proceed at the scaled down rates of similar processes taking place in large systems. For example, reactions taking place on the surface of a particle of area  $1 \text{ nm}^2$  will not proceed at one millionth of the rate of the same process on a particle of area  $1 \mu\text{m}^2$ . In making this claim, we are not appealing to differences in surface properties, such as curvature. The crucial difference is that the populations of reactants in the smaller system are lower, and therefore more susceptible to statistical fluctuations which can alter the reaction rate in an important way. Normal classical chemical kinetics fail, as do the usual Becker-Döring birth and death equations for nucleation. The chemical and activation properties of ultrafine aerosols can therefore differ from expectations. The effect of this small system stochasticity was explored by Lushnikov, Bhatt and Ford (2003) and Bhatt and Ford (2003).

The reaction  $A+A \rightarrow C$  can provide a simple illustration of the reason for the failure of traditional kinetics. The rate for such a two-body process is proportional to the square of the population of reactant A. The mean reaction rate is therefore proportional to the time-average of the squared reactant population. However, traditional kinetic equations employ the square of the mean reactant population, rather than the mean of the square, and these quantities differ for small systems. Mathematically, the evolution of  $N$ , the mean population of A-molecules, is given by

$$\frac{dN}{dt} = j - \lambda N - \frac{1}{2} \kappa N^2 \quad (1)$$

where  $\kappa$  is the reaction rate to form product C, and the first two terms describe gain and loss rates to and from the open system, respectively. For nucleation, the growth rate of a molecular cluster is normally taken to be proportional to the product of mean populations of monomer and cluster, and this assumption is similarly flawed.

In order to treat population fluctuations correctly, we can replace mean population dynamics with a description using master equations. These describe the evolution of the full probability distribution of the reactant population. However, except in some special cases, the equations are too complicated to be solved

exactly, and numerical methods are very cumbersome. We have therefore explored a procedure to reduce master equations to traditional rate equations, but with additional stochastic terms that take account of fluctuations. The methods used are similar to treatments of quantum mechanical systems, where the fluctuations are due to quantum uncertainty, rather than the population uncertainty associated with a small, open, classical system.

The master equations may be cast in the form of a path integral (Doi 1976), which is a weighted sum of contributions from all possible time-histories of a complex quantity  $\phi(t)$ . The path integral plays a similar role to the partition function in equilibrium statistical mechanics, in that it provides a means for calculating average quantities, such as mean populations and reaction rates. The key step (Tauber et al 2005) is then to convert the weighted integration over all paths into an averaging of system quantities over histories of  $\phi(t)$  computed according to a stochastic differential equation

$$\frac{d\phi}{dt} = j - \lambda\phi - \frac{1}{2} \kappa\phi^2 + \zeta \quad (2)$$

where  $\zeta(t)$  is a complex white noise term.

The correspondence between equations (1) and (2) is quite clear and suggests that the real part of  $\phi(t)$  averaged over all noise histories corresponds to the mean population  $N$ . Fluctuations are described by the noise term in the rate equation.

The formalism provides a simplified means for solving master equation kinetics, using Monte Carlo sampling of stochastic histories. The systems that can be described include cases of heterogeneous chemistry as well as much more complicated mechanisms for nucleating systems.

This work was supported by the Leverhulme Trust under grant F/07134/BV.

Bhatt, J.S. and Ford, I.J. (2003) *J. Chem. Phys.* 118, 3166-3176.

Doi, M. (1976) *J. Phys. A: Math. Gen.* 9, 1465-1477

Lushnikov, A.A., Bhatt, J.S. and Ford, I.J. (2003). *J. Aerosol Sci.* 34, 1117.

Tauber, U.C., Howard, M. and Vollmayr-Lee, B.P. (2005) *J. Phys. A: Math. Gen.* 38, R79-R131

## article deposition in a critical orifice

S.C. Chen<sup>1</sup>, C.J. Tsai<sup>1</sup>, C.H. Wu<sup>1</sup> and A. Onischuk<sup>2</sup>

<sup>1</sup> National Chiao Tung University, Institute of Environmental Engineering,  
No.75, Poai St., Hsin-Chu 300, Taiwan

<sup>2</sup> Siberian Branch of the Russian Academy of Sciences, Institute of Chemical Kinetics and  
Combustion, 630090, Novosibirsk, Russia

Keywords: critical orifice, particle deposition, inertial impaction, trajectory

Orifices are widely used to control flow rate, or as a pressure reducing device for high purity gas sampling or used in a particle focusing apparatus. In these applications, it is desirable to have particle loss in the orifice as minimum as possible so that particle concentration in the pipe flow can be measured accurately. Lee et al. (1993) reviewed particle deposition mechanisms in orifice-type pressure reducers including inertial impaction at the front side and the back side of the orifice (OP), and on the tube wall downstream of the orifice (TAO).

In this study, particle deposition in different parts of a critical orifice assembly was studied numerically and experimentally. The investigated orifice was the O'Keefe E-9 (O'Keefe Control Co.) orifice whose inner diameter was 0.231 mm and critical flow rate was 0.455 slpm. At the upstream and downstream of the orifice, there is an inlet tube (inner diameter 10.4 mm, length 90 mm) and outlet tube (inner diameter 6.2 mm, length 60 mm), respectively. In the numerical study, an axisymmetric laminar flow field of the orifice assembly was first obtained by solving the Navier-Stokes equations. After obtaining the flow field, diffusion loss of nanoparticles was calculated by solving the convection-diffusion equation. Inertial impaction and interception loss of 2-10  $\mu\text{m}$  particles was calculated by tracing particle trajectories in the flow field. In the experimental study, monodisperse NaCl (20-800 nm) and fluorescein oleic acid (2-10  $\mu\text{m}$ ) particles were generated to test particle deposition efficiency by introducing particles into the orifice. Deposition efficiency was determined by recovering the deposited particles and measuring the concentration of  $\text{Cl}^-$  and fluorescein, respectively. The numerical results agree the experimental data very well.

Fig. 1 shows the comparison of the present experimental data with simulated deposition efficiencies at OP, and previous results of literatures. The present simulated results are in very good agreement with the data which almost fall on the curve of Pich (1964).

Fig. 8 shows the comparison of the particle deposition efficiency at TAO between the present experimental data, simulated results and the previous results of Pui et al. (1998). The simulated results are seen in good agreement with the experimental data with a maximum difference of about 10%.

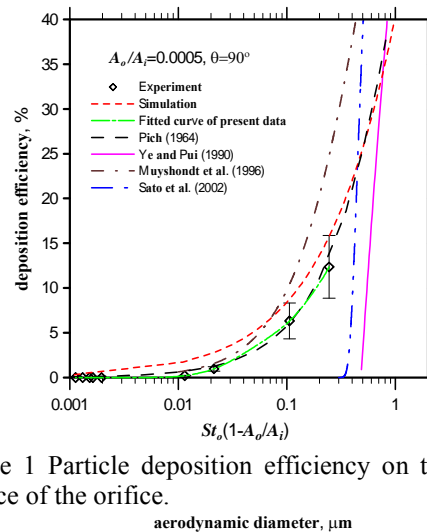


Figure 1 Particle deposition efficiency on the front surface of the orifice.

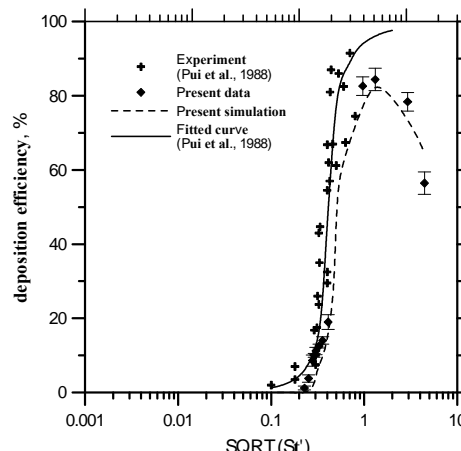


Figure 2 Particle deposition efficiency at TAO.

The present data and simulated results are in agreement with the results of Pui et al. (1998) when the  $SQRT(St')$  is less than 1 while the disagreement exist as  $SQRT(St') > 1$ .

- Lee, J. K., K. S. Rubow, D. Y. H. Pui and B. Y. H. Liu. (1993). *Aerosol. Sci. Technol.*, 19, 215-226.  
 Muyschondt, A., A. R. McFarland and N. K. Anand. (1996). *Aerosol. Sci. Technol.*, 24, 205-216.  
 Pich, J. (1964). *Colln. Czech. Chem. Commun.* 29, 2223-2227.  
 Pui, D. Y. H., Y. Ye and B. Y. H. Liu. (1988). *in Proc. 9th Int. Symp. on Contamination Control*, Los Angeles, CA, September 26-30.

## The effect of carrier gas pressure on homogeneous nucleation of *n*-pentanol + helium in a laminar flow diffusion chamber

A.-P. Hyvärinen<sup>1</sup>, D. Brus<sup>1,2</sup>, V. Ždímal<sup>2</sup>, J. Smolík<sup>2</sup>, M. Kulmala<sup>3</sup>, Y. Viisanen<sup>1</sup>, H. Lihavainen<sup>1</sup>

<sup>1</sup> Finnish Meteorological Institute, Erik Palménin aukio 1, P.O. Box 503, FI-00101 Helsinki, Finland

<sup>2</sup> Laboratory Aerosol Chemistry and Physics, Institute of Chemical Process Fundamentals, Academy of Sciences of the Czech Republic, Rozvojová 135, 165 02 Prague 6, Czech Republic

<sup>3</sup> University of Helsinki, Dept. Physical Sciences, P.O. Box 64, 00014 Univ. of Helsinki, Finland

Keywords: homogeneous nucleation, nucleation rate, laminar flow diffusion chamber, pressure effect

### INTRODUCTION

Homogeneous vapor-to-liquid nucleation refers to the formation of liquid particles from condensable vapor without pre-existing surfaces. As nucleation has many applications in science and technology, it has received a considerable amount of interest both from theoretical and experimental points of view.

In vapor-liquid nucleation experiments, the condensable vapor is typically dispersed in a large background of inert carrier gas. Its main function is to serve as a heat-bath for the latent heat release during condensation. It was generally assumed that the presence of a non-condensable carrier gas does not influence the clustering process, but several experimental and theoretical studies implicate that both the type and pressure of the carrier gas can affect the measured nucleation kinetics.

According to recent studies, nucleation rates decrease with the increase of total pressure (negative effect) measured in different diffusion based devices (etc. Brus *et al.*, 2006, Hyvärinen *et al.* 2006). Comparison between measurements is still difficult due to different compounds and thermodynamic conditions applied in the experiments.

In this work, we have measured the homogeneous nucleation rates of *n*-pentanol in a laminar flow diffusion chamber (LFDC) using helium as a carrier gas.

### EXPERIMENTAL METHODS

The LFDC used in this work is based on design of Lihavainen and Viisanen (2001) and was modified to sustain both under- and over-pressure in the range of 50 kPa to 400 kPa. The correct and stable operation of the device was rigorously tested (Hyvärinen *et al.* 2006).

### RESULTS

Figure 1 presents nucleation rates measured as a function of pressure at constant saturation ratio. For the first time, the pressure effect was observed to be both negative and positive with the same substance, depending on temperature. A transition concerning the pressure dependence occurs at 280 K. A positive pressure effect is observed at temperatures below 280 K and a negative effect above it. This is in

accordance with results presented by Anisimov *et al.* (2000) below 270 K. The pressure effect is always more notable at lower pressures.

Nucleation rates were also measured as a function of saturation ratio at constant temperature and pressure. The critical cluster sizes were determined from these measurements with the nucleation theorem (Kashchiev 1996). Increasing pressure in the measurements was observed to decrease the number of molecules in a critical cluster. Similar pressure dependence has also been observed with *n*-butanol (Hyvärinen *et al.* 2006).

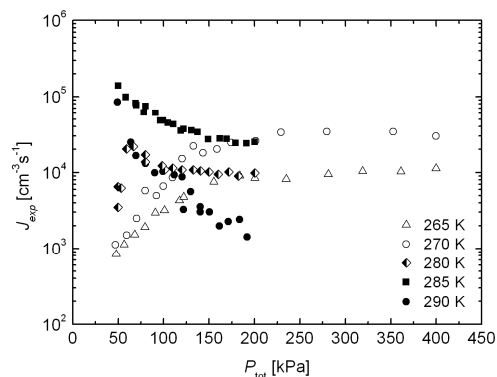


Figure 1. Nucleation rates  $J_{exp}$  as a function of pressure  $P_{tot}$  at constant saturation ratios for temperatures between 265 and 290 K.

This work was supported by Maj and Tor Nessling foundation.

Anisimov M.P., Hopke P.K., Shandakov S.D., Shvets I.I. (2000) *J. Chem. Phys.* 113, 1971.

Brus D., Ždímal V., and Stratmann F., (2006) *J. Chem. Phys.* 124, 164306.

Hyvärinen A.-P., Brus D., Ždímal V., Smolík J., Kulmala M., Viisanen Y., Lihavainen H. (2006) *J. Chem. Phys.* 124, 224304.

Kashchiev D. (1996) *J. Chem. Phys.* 104, 8671.

Lihavainen H., Viisanen Y. (2001) *J. Phys. Chem. B* 105, 11619.

## The effect of surrounding vapour in homogeneous nucleation: a Monte Carlo study

T. R. Bergman, A. Lauri, J. Merikanto and H. Vehkamäki

Department of Physical Sciences, University of Helsinki, FI-00014 University of Helsinki, Finland

Keywords: aerosol fundamentals, homogeneous nucleation, Monte Carlo simulations.

We have carried out molecular Monte Carlo (MC) simulations of homogeneous nucleation of argon in a surrounding gas. We chose argon for our model substance mainly for two reasons. First, intermolecular interactions of argon as well as other noble gases are described fairly well by simple and computationally feasible Lennard-Jones potential models. Second, the relatively few experimental studies of argon nucleation have given contradictory results when compared to the classical nucleation theory (CNT) results or molecular simulation results. For argon, the CNT generally predicts lower energy barriers and thus nucleation rates several orders of magnitude higher than those gained from Monte Carlo simulations. Controversially, some experimental results show a good agreement with the results of the CNT, whereas in some cases the experimental nucleation rates show a better match with the nucleation rates calculated from MC simulation results.

Almost all of the reported nucleation experiments of argon have been carried out either in supersonic nozzle flows (see e.g. Wu *et al.*, 1978) or using shock tubes (see e.g. Zahoransky *et al.*, 1999). The question of possible effects of the carrier gas and/or the surrounding, highly supersaturated argon vapour arises in both of these cases. However, the studies of the surrounding vapour effect on nucleation are sparse and few in number (see e.g. Wyslouzil *et al.*, 1994; Senger *et al.*, 1999; Oh & Zeng, 2000).

In our molecular simulations we employed the growth/decay method (Vehkamäki & Ford, 2000; Merikanto *et al.*, 2004), based on the Metropolis MC algorithm, to evaluate formation free energies of argon clusters. The surrounding vapour was considered to be argon as well. We applied the cluster definition of Stillinger, and put in a cubic simulation box, each side 100 Å long, a cluster of 1-79 argon molecules and 72-190 molecules not belonging to the cluster. Periodical boundary conditions were applied on the sides of the simulation box. During the simulation, both cluster and vapour molecules were moved according to the Metropolis algorithm.

The critical formation free energy barriers obtained from the simulations at two different temperatures, 80 K and 85 K, both including and excluding the surrounding vapour effect, are shown in Fig. 1 for saturation ratios 4-8. As the figure shows, the surrounding vapour enhances the

nucleation rate by decreasing the energy barrier height. The differences between the critical free energies of formation in 80 and 85 K are between  $0.8kT$  and  $2kT$ , respectively, depending on the saturation ratio. The temperature dependence is minimal. Inclusion of the surrounding gas in the calculations increases the predicted nucleation rates by a factor 2-7.

The approach of Oh & Zeng (2000) results in similar behaviour, but the magnitude of the surrounding gas effect on the formation free energy obtained in our study is approximately twice as strong as in their approach.

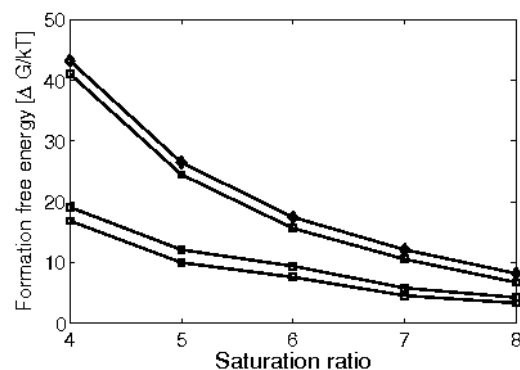


Figure 1. Formation free energies calculated by MC simulations in 80 K (upper curve pair) and 85 K (lower curve pair). In both curve pairs, the lower curve corresponds to the case where the surrounding vapour is effective; the upper curve represents the free energy barrier where the surrounding vapour effect is neglected.

- Merikanto, J., Vehkamäki, H., & Zapadinsky, E. (2004). *J. Chem. Phys.*, 121, 914-924.
- Oh, K. J., & Zeng, X. C. (2000). *J. Chem. Phys.*, 112, 294-300.
- Senger, B., Schaaf, P., Corti, D. S., Bowles, R., Pointu, D., Voegel, J.-C., & Reiss, H. (1999). *J. Chem. Phys.*, 110, 6438-6450.
- Vehkamäki, H., & Ford, I. J. (2000). *J. Chem. Phys.*, 112, 4193-4202.
- Wu, B. J. C., Wegener, P. P., & Stein, G. D. (1978). *J. Chem. Phys.*, 69, 1776-1777.
- Wyslouzil, B. E., Wilemski, G., Beals, M. G., & Frish, M. B. (1994). *Phys. Fluids*, 6, 2845-2854.
- Zahoransky, A., Hörschele, J., & Steinwandel, J. (1999). *J. Chem. Phys.*, 110, 8842-8843.

## Derivation of the first heterogeneous nucleation theorem including the line tension

A. I. Hienola, H. Vehkamäki, A. Lauri and M. Kulmala

Department of Physical Sciences, University of Helsinki, FI-00014 University of Helsinki, Finland

Keywords: aerosol fundamentals, aerosol thermodynamics, heterogeneous nucleation.

The nucleation theorems (Kashchiev, 2000) give a theory-independent insight to nucleation phenomena beyond experimental limits. Earlier, we have introduced a way to interpret an experimentally achievable quantity in heterogeneous nucleation, namely the nucleation probability, in terms of the nucleation theorems (Vehkamäki *et al.*, 2007).

In the present study we include the concept of line tension in the analysis, and derive the first nucleation theorem for one-component systems.

Gretz (1966) was the first to realize the effect of line tension in heterogeneous nucleation. Since then, several others have followed (see e.g. Navascues & Mederos, 1982; Lazaridis, 1993; Hienola *et al.*, 2007a), and it has been commonly recognized that line tension should be included in the theoretical considerations of heterogeneous nucleation.

The inclusion of line tension produces an extra term to Young's equation:

$$\cos \theta = \frac{\sigma_{sg} - \sigma_{sl}}{\sigma_{lg}} - \frac{\sigma_l}{\sigma_{lg} R \tan \phi}.$$

For angles  $\phi$  and  $\theta$ , see Fig. 1.  $\sigma_{ij}$  represents the interfacial tension between phases  $i$  and  $j$  (subindexes  $g$ ,  $l$  and  $s$  correspond to vapour, liquid, and substrate phases, respectively);  $\sigma_l$  is line tension, the reversible work needed to expand a unit length of the three phase contact line isothermally, and  $R$  is the radius of the seed particle.

The critical formation free energy in heterogeneous nucleation, including line tension, is given by (Lazaridis, 1993)

$$\Delta G_{\text{het}}^* = f_g \Delta G_{\text{hom}}^* - \frac{\sigma_l A_{sg}}{R \tan \phi} + 2\pi R \sigma_l \sin \phi,$$

where  $f_g$  is a geometric factor (see e.g. Vehkamäki, 2006), and  $A$  is surface area.

Assuming that the equimolar surface coincides with the surface of tension, and applying the Gibbs adsorption isotherm in one dimension, the nucleation theorem in terms of critical free energy of formation becomes (Hienola *et al.*, 2007b)

$$\left[ \frac{\partial \left( \frac{\Delta G_{\text{het}}^*}{kT} \right)}{\partial \ln S} \right]_T = \Delta N_{\text{het}}^*,$$

where  $\Delta N_{\text{het}}^*$  is the number of molecules in the critical cluster, similarly as in the homogeneous case.

Furthermore, in terms of the usual measurable quantity in heterogeneous nucleation, nucleation

probability  $P = 1 - \exp(-J\tau)$ , where  $J$  is the nucleation rate, and  $\tau$  is nucleation time, the nucleation theorem is given by

$$\left[ \frac{\partial \ln \left( \ln \frac{1}{1-P} \right)}{\partial S} \right]_T = \Delta N_{\text{het}}^* + k,$$

where  $k$  is the (minor) contribution of the kinetic prefactor.

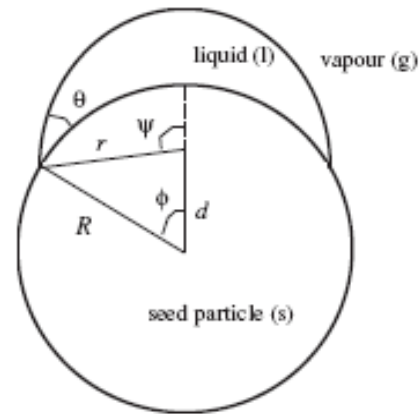


Figure 1. The geometry of the cross section of an embryo of radius  $r$  heterogeneously nucleating on the surface of a sphere of radius  $R$ .

- Gretz, R. D. (1966). *Surf. Sci.*, 5, 239-251.  
 Hienola, A. I., Winkler, P. M., Wagner, P. E., Lauri, A., Napari, I., Vehkamäki, H., & Kulmala, M. (2007a). *J. Chem. Phys.*, accepted.  
 Hienola, A. I., Vehkamäki, H., Lauri, A., & Kulmala, M. (2007b). *J. Chem. Phys.*, submitted.  
 Kashchiev, D. (2000). *Nucleation: Basic Theory with Applications*. Oxford, U.K.: Butterworth-Heinemann.  
 Lazaridis, M. (1993). *J. Colloid Interf. Sci.*, 155, 386-391.  
 Navascues, G., & Mederos, L. (1982). *Surf. Tech.*, 17, 79-84.  
 Vehkamäki, H. (2006). *Classical Nucleation Theory in Multicomponent Systems*, Berlin, Germany: Springer.  
 Vehkamäki, H., Määttänen, A., Lauri, A., Kulmala, M., Winkler, P. M., Vrtala, A., & Wagner, P. E. (2007). *J. Chem. Phys.*, submitted.

## A method to evaluate the line tension in heterogeneous nucleation by molecular Monte Carlo simulations

A. Lauri, E. Zapadinsky, A. I. Hienola, H. Vehkamäki and M. Kulmala

Department of Physical Sciences, University of Helsinki, FI-00014 University of Helsinki, Finland

Keywords: aerosol fundamentals, heterogeneous nucleation, Monte Carlo simulations.

Line tension is a quantity describing the effect of the energy bound in the contact line between the three phases usually present in the heterogeneous nucleation phenomenon: vapour, nucleating embryo and insoluble substrate surface. Line tension as a concept in heterogeneous nucleation has been a matter of discussion during the past decades. Gretz (1966) was the first to notice the significance of the three-phase interface in theoretical considerations of heterogeneous nucleation. Since then, it has been commonly agreed that line tension should be taken into account in order to have a thermodynamically correct description of heterogeneous nucleation, and the line tension concept has been successfully used to explain experimental results (Hienola *et al.*, 2007).

It has, however, proved to be very difficult to make quantitative estimates of the magnitude, or even the sign of the line tension to be utilized in computational model calculations. In this study we present a new approach for the calculation of an estimate of line tension from molecular simulations.

If line tension is not considered, the formation free energy in heterogeneous nucleation is given by

$$\Delta G_{\text{het}} = \rho_l (\mu_l - \mu_v) V_{\text{het}} + \sigma_{\text{lg}} A_{\text{lg}} + (\sigma_{\text{sl}} - \sigma_{\text{sg}}) A_{\text{sl}},$$

where  $\rho$  is density,  $\mu$  is chemical potential,  $\sigma$  is surface tension,  $V$  is volume, and  $A$  is surface area. Subindexes  $g$ ,  $l$  and  $s$  correspond to vapour, liquid, and substrate phases, respectively. Including the effect of line tension, an extra term is added to the free energy formula (Lazaridis, 1993):

$$\Delta G_{\text{het}}^t = \Delta G_{\text{het}} + 2\pi r \sigma_l \sin \theta,$$

where  $r$  is the radius of the cluster, and  $\theta$  is the contact angle between the surfaces of the nucleating embryo and a flat substrate.

Earlier we have derived the difference between the formation free energy of an  $n$ -cluster in heterogeneous and homogeneous nucleation (Lauri *et al.*, 2006). It is straightforward to include the extra term including the line tension in the derivation:

$$\Delta G_{\text{het}}^t(n) - \Delta G_{\text{hom}}(n) = \alpha (f^{1/3} - 1) n^{2/3} + \left[ \frac{24\pi^2 (1+m)^2}{\rho_l (2+m)(1-m^2)^{1/2}} \right]^{1/3} \sigma_l n^{1/3},$$

where  $\alpha = (36\pi)^{1/3} \rho_l^{-2/3} \sigma_{\text{lg}}$ ,  $f$  is a geometrical factor, and  $m = \cos \theta$ .

The overlapping distribution Monte Carlo method (Bennett, 1976) enables one to evaluate the

difference in formation free energy of a heterogeneous and homogeneous  $n$ -cluster numerically (Zapadinsky *et al.*, 2005):

$$\Delta G_{\text{het}}^t(n) - \Delta G_{\text{hom}}(n) = [F_{\text{het}}(n) - F_{\text{hom}}(n)] - [F_{\text{het}}(1) - F_{\text{hom}}(1)],$$

where  $F(n)$  is the Helmholtz free energy of an  $n$ -cluster, given by the simulations.

We simulated molecular clusters consisting of 1-200 argon molecules in the presence of an fcc(111) monolayer of platinum atoms at  $T=60$  K. The formation free energy differences obtained from the simulations are plotted as a function of  $n^{1/3}$  in Fig. 1. A second order polynomial function fit is also shown. The sign and magnitude of line tension can be calculated from the first order term in the fit, resulting in a positive value of the line tension,  $\sigma_l = 1.2 \times 10^{-12}$  N.

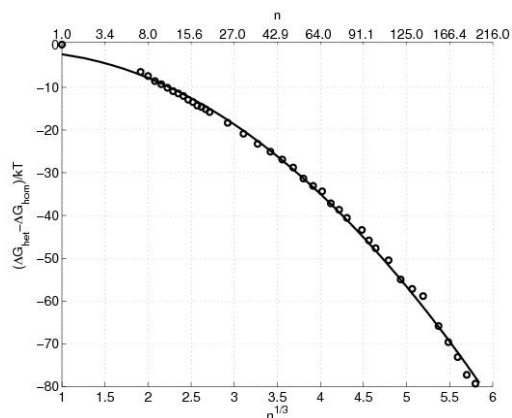


Figure 1. The formation free energy difference of an  $n$ -cluster in heterogeneous and homogeneous nucleation, showing both Monte Carlo simulation results (circles) and a fit function (solid line).

- Bennett, C. H. (1976). *J. Comput. Phys.*, 22, 245-268.
- Gretz, R. D. (1966). *Surf. Sci.*, 5, 239-251.
- Hienola, A. I., Winkler, P. M., Wagner, P. E., Lauri, A., Napari, I., Vehkamäki, H., & Kulmala, M. (2007a). *J. Chem. Phys.*, accepted.
- Lauri, A., Zapadinsky, E., Vehkamäki, H., & Kulmala, M. (2006). *J. Chem. Phys.*, 125, 164712.
- Lazaridis, M. (1993). *J. Colloid Interf. Sci.*, 155, 386-391.
- Zapadinsky, E., Lauri, A., & Kulmala, M. (2005). *J. Chem. Phys.*, 122, 114709.

## Surface tensions of sodium chloride/succinic acid/water solutions

J. Vanhanen<sup>1</sup>, A.-P. Hyvärinen<sup>1</sup>, H. Lihavainen<sup>1</sup>, Y. Viisanen<sup>1</sup>, M. Kulmala<sup>2</sup>

<sup>1</sup>Finnish Meteorological Institute, Erik Palménin aukio 1, 00560, Helsinki, Finland

<sup>2</sup>Department of Physical Sciences, University of Helsinki, P.O. Box 64, FIN-00014 Helsinki, Finland

Keywords: Aerosol thermodynamics, surface tension.

Activation of aerosol particles into cloud droplets depends on the surface tension of the droplet (Anttila *et al.* 2002). In most cases the surface tension of multicomponent particles is not known, and surface tension of water is used for example in cloud- and condensation models.

Surface tensions of bulk liquids can be measured in laboratory conditions. While knowing the exact composition of activating particles is difficult due to the vast amount of organic species, it can be estimated with a few general, representative compounds. In this study we measured and modelled the surface tension of ternary mixture of sodium chloride/succinic acid/water. Sodium chloride is typically transported inland with marine air masses, while succinic acid is an abundant compound in the aerosol phase.

Surface tensions were measured using a capillary rise technique. The sample was placed in a double-walled glass. The temperature of the sample was controlled by letting thermostated liquid to flow between the walls (LAUDA RC6 CS). Capillary tube was mounted to the glass by using a teflon stopper. The height of the liquid in the capillary tube was measured with a caliper. Uncertainty of the surface tension measurements was estimated to be less than 1%.

In figure 1 the surface tension of sodium chloride/succinic acid/water-mixture is presented as a function of the mole fraction of succinic acid, as the temperature and mole fraction of sodium chloride is kept constant. It can be seen that the surface tension increases when sodium chloride is added and decreases when succinic acid is added. Surface tension increases quite linearly as a function of the sodium chloride concentration while succinic acid tends to lower it rather strongly. Temperature dependence of the surface tension is presented in figure 2.

We found also that presence of sodium chloride enhances surface tension lowering of succinic acid. Same kind of behaviour is found previously with ammonium sulphate and HULIS by Kiss *et al.* (2005). This is because salt ions tend to force the acid molecules to partition to the surface (Kiss *et al.* 2005).

To make our measurements useful for the numerical models, results were fitted to equation derived by Chunxi *et al.* (2000). Also the surface tensions of pure substances were used as data points.

This way the surface tension of the mixture could be estimated beyond the measured values.

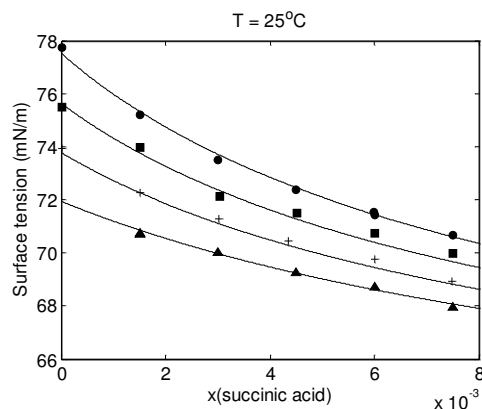


Figure 1. Surface tension of ternary solution of sodium chloride/succinic acid/water as a function of mole fraction (x) of succinic acid. Symbols ●, ■, + and ▲ represent sodium chloride mole fractions 0.06, 0.04, 0.02 and 0 respectively.

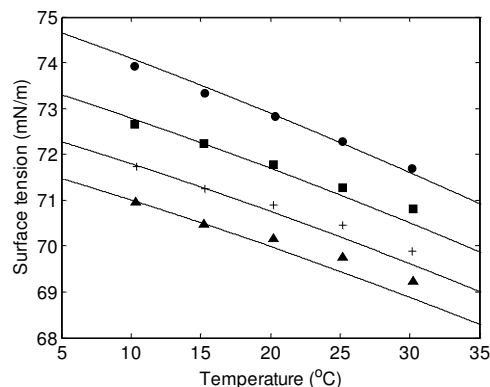


Figure 2. Surface tension of ternary solution of sodium chloride/succinic acid/water as a function of temperature. Symbols ●, ■, + and ▲ represent succinic acid mole fractions 0.0015, 0.003, 0.0045 and 0.006 respectively. Mole fraction of sodium chloride is kept constant ( $x(\text{NaCl}) = 0.02$ )

Anttila, T., Kerminen, V.-M. (2002) *J. Geophys. Res.*, 107, 4662-4674.

Chunxi, L., Wenchuan, W., & Zihao W. (2000). *Fluid Phase Equilibria*, 175, 185-196.

Kiss, G., Tombácz E., Hansson, H.-C., *J. Atm. Chem.* (2005) 50, 279-294.

## The gas-kinetic theory of gravitophoresis for stratospheric conditions and its experimental verification

S.A. Beresnev, D.V. Suetin

Aerosol Physics Laboratory, Ural State University, 620083, Ekaterinburg, Russia

Keywords: Aerosol dynamics, Fundamental aerosol physics, Stratospheric aerosols, Gravitophoresis.

In 1951 Ehrenhaft and Reeger reported about observation of so-called “transversal photophoresis” for graphite powder particles in argon at low gas pressures. Particles at their illumination by horizontal light beam showed various trajectories of movement, including vertical lifting against gravity. This phenomenon (occurrence of vertical force and vertical particles velocity in a field of arbitrary directed radiation) has been termed gravitophoresis. The further experimental investigations (both qualitative, and quantitative) were carried out by Rohatschek (1984, 1985) and by Horvath & Jovanovic (2000, 2001, 2006). The theoretical description of phenomenon is based on known semi-empirical model developed for many years by Rohatschek (1995, 1996, 2000). The spherical high-conductivity particle is in a field of the directed unilateral radiation. Frontal to radiation and back hemispheres are characterized by the asymmetry of surface properties (difference of energy accommodation coefficients). In the free-molecular regime the arising force has form:

$$F_{\text{gph}} = \frac{\pi R}{4 M} \rho_g R_p^2 (T_s - T_g) \Delta\alpha_E. \quad (1)$$

The received results predict high efficiency of the gravitophoresis in vertical transport of aerosols against a gravity in stratosphere and mesosphere.

In this paper the new gas-kinetic theory of gravitophoresis in the free-molecular regime and experimental attempt of force measurements by a technique of model thermal-physics experiment with macroparticles are presented. The obtained expression for gravitophoretic (accommodation) force (with neglect of radiative transfer from particle surface - that is allowable in stratospheric and mesospheric conditions - has the form:

$$F_{\text{acc}} = \frac{\pi}{8} R_p^2 \frac{1}{\bar{v}_g} I Q_{\text{abs}} \Delta A_n, \quad (2)$$

where  $Q_{\text{abs}}$  – absorption efficiency factor, and

$$\Delta A_n = \alpha_n(2) / [1 - \frac{9\pi}{32} (1 - \alpha_n(2))] - \alpha_n(1) / [1 - \frac{9\pi}{32} (1 - \alpha_n(1))].$$

It is possible to show, that Eq. (2) is reduced to Eq. (1). However, instead of a difference of energy accommodation coefficients  $\Delta\alpha_E$  in (1) the complex  $\Delta A_n$  responsible for normal momentum accommodation of gas molecules on various particle hemispheres appears. The reason of this basic distinction is discussed in detail.

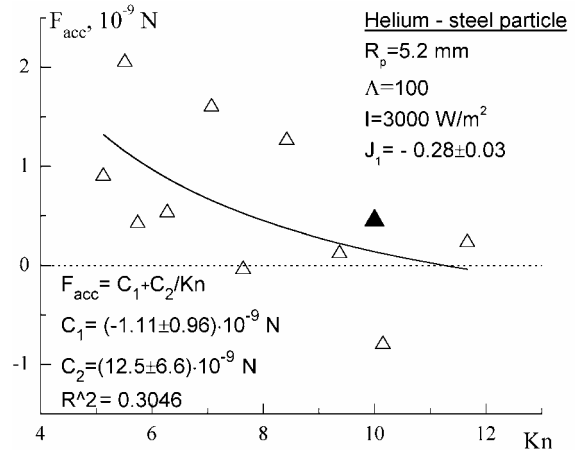


Fig.1. Difference of forces acting on homogeneous rough and bilateral (rough and polished) steel particle in helium. Light triangles – experimental data, black triangle – independent theoretical calculation at  $Kn=10$ , solid curve – approximation of experimental data by dependence  $F_{\text{acc}} = C_1 + C_2/Kn$ .

Estimations of the relations of “accommodation” forces to a gravity forces and to radiometric photophoresis forces have been carried out at characteristic values of necessary parameters. These estimations have shown, that “accommodation” forces can be significant for vertical stratospheric aerosol transport, but do not surpass the gravity forces. Comparison of characteristic values for “accommodation” forces with the forces of radiometric photophoresis allows to hope for their direct detection by a technique of model thermal-physics experiment with macroparticles (which was applied earlier in investigations of photophoresis). As object for measurements the steel particle in helium has been chosen at low pressures corresponding to the free-molecular regime ( $Kn=5\div 15$ , Fig.1). Corresponding measurements with various particles in air did not give appreciable effect.

The ratio of “accommodation” force to the radiometric photophoresis forces in experiment does not exceed 3 %. The estimations show that action of the investigated force is not capable to provide effective vertical transport of aerosol particles against a gravity at altitudes of the lower and middle stratosphere.

This work was supported by the Russian Foundation for Basic Research (RFBR) under grant 06-01-00669.

## Dynamics of porous aerosol particles under thermal gradients

A. Perea, P. . Garcia-Ybarra and J. . Castillo

Dept. de Física Matematica y de Fluidos, Facultad de Ciencias, UNED, Senda del Rey 9, Madrid 28040, Spain

Keywords: aerosol dynamics, physical properties, thermophoresis, slip correction.

Porous aerosol particles are very common in many practical applications (as material processing) and environmental problems (as particulate emissions from combustion). On the other hand, larger aggregates can be modelled as pseudo-porous particles. The dynamics of these particles is affected by the flow penetrating through the particle which modifies the gas streamlines and the viscous stresses on the particle surface. In a recent paper (Garcia-Ybarra *et al.*, 2006), a theoretical analysis provided a general framework for solving the velocity field in the gas and the penetration flow inside the particle. The matching of both flow fields at the particle outer surface allows to determine the viscous drag on the porous aerosol particle.

Moreover, aerosol particles under strong temperature gradients are driven by thermophoresis (Rosner *et al.*, 1992) that pushes the aerosol toward the cooler gas regions. Here, a previous work (Perea *et al.*, 2005) is extended to describe the dynamics of a porous aerosol particle under thermal gradients.

In the outer gas, the Stokes equation relates the velocity field ( $\mathbf{v}$ ) and the pressure distribution ( $p$ )

$$\nabla p = \mu \nabla^2 \mathbf{v}$$

where  $\mu$  is the dynamic viscosity. Inside the particle, a modified Brinkmann equation holds

$$\frac{\mu}{c} \nabla^2 \mathbf{v} - \mathbf{v}_{trans} = \frac{1}{c} \nabla p$$

is the permeability of the porous aerosol particle and  $\mathbf{v}_{trans}$  is the transpiration velocity induced by the gas thermal slip at the walls of the pores

$$\mathbf{v}_{trans} = \frac{1}{6t} C_S \frac{\mu}{r T_0} \nabla T$$

$f$  is the solid fraction,  $t$  the tortuosity,  $C_S$  the slip coefficient,  $r$  the gas density, and  $T_0$  the mean particle temperature. These equations are solved together with the equations for the temperature field in both (gas and porous) media and imposing the appropriate boundary conditions.

At the particle surface, the normal component of the velocity should be continuous, but there is a slip in the tangential velocity ( $v_t$ ), such that

$$v_t^{gas} = v_t^{porous} + C_S f \frac{\mu}{r T_0} \nabla_s T \quad \text{at } r = R$$

where  $\nabla_s$  stands for the surface gradient.

The forces acting on the aerosol particle are the drag (proportional to the aerosol velocity relative to the gas) and the thermophoretic force (proportional

to the temperature gradient,  $\nabla T$ ). The balance between both forces provides the value of the particle thermophoretic velocity, which can be written as

$$\mathbf{v}_T = \frac{\mathbf{a} \nabla T}{T}$$

Where  $\mathbf{a}$  is the thermophoretic strength factor for a solid particle of the same size,  $\nu$  the gas kinematic viscosity ( $\nu = \mu / r$ ) and  $\mathbf{e}$  the thermophoretic strength correction due to the particle porosity.

The thermophoretic strength factor  $\mathbf{a}$  depends on the particle-gas interactions (Garcia-Ybarra & Castillo, 1997). In the studied limit,  $\mathbf{a}$  is given by

$$\mathbf{a} = 2C_S \frac{I}{I + 2I_p}$$

Here,  $I$  and  $I_p$  are the gas and particle thermal conductivity, respectively. Moreover, the thermophoretic strength correction due to the aerosol porosity results

$$\mathbf{e} = \frac{1-f}{4t} \frac{1-3k \tanh 1/k}{1-k \tanh 1/k} \mathbf{f}$$

with the permeability parameter

$$k = c^{1/2} / R$$

$k$  provides a dimensionless measurement of the aerosol permeability. As expected,  $\mathbf{e}$  tends to one for low porosity particles (in the limit  $f \rightarrow 1$ ,  $k \rightarrow 0$ ).

The first term in  $\mathbf{e}$  (proportional to the void fraction,  $1-f$ ) comes from the transpiration flow through the particle, whereas the second term accounts for the reduction of the thermal slip due to the existence of pores at the particle surface.

This work was supported by the Ministerio de Educacion y Ciencia, Spain, under grants DPI2005-04601 and ENE2005-09190-C04-02, and also by Comunidad de Madrid under grant S-505/ENE/0229.

Garcia-Ybarra, P. . & Castillo, J. . (1997) *J. Fluid Mech.*, 336, 379-409.

Garcia-Ybarra, P. ., Castillo J. . & Rosner, D.E. (2006). *J. Aerosol Sci.*, 37, 413-428.

Perea, A., Garcia-Ybarra, P. . & Castillo, J. ., (2005) *Abstracts of the EAC2005*, 115.

Rosner, D.E., Mackowski, D.W., Tassopoulos, M., Castillo, J. . & Garcia-Ybarra, P. . (1992). *Ind. Eng. Chem. Res.* 31, 760-769.

## Influence of size effects on condensation of vapor on small charged aerosol particles

V. V. Levdansky<sup>1</sup>, J. Smolik<sup>2</sup>, V. Zdimal<sup>2</sup> and P. Moravec<sup>2</sup>

<sup>1</sup>Heat and Mass Transfer Institute NASB, 15 P. Brovka Str., 220072 Minsk, Belarus

<sup>2</sup>Institute of Chemical Process Fundamentals AS CR, Rozvojova 135, 165 02 Prague 6, Czech Republic

Keywords: condensation, evaporation, charged particles.

It is known that charged small aerosol particles enhance the condensation of vapor (Reist, 1993). Size effects in the condensational growth of the charged particle are related in particular to dependence of the effective energy evaporation of molecules from the particle  $E_{\text{eff}}$  on the particle size due to dependence of  $E_{\text{eff}}$  on the Kelvin effect and the particle charge. The condensation coefficient  $\alpha_c$  and the surface tension  $\sigma$  can also depend on the size of the particle. Moreover, transfer of vapor molecules to the particle surface generally depends on the particle size. The paper deals with the joint influence of above-mentioned effects on the density of the resulting flux of vapor molecules into the particle. Further we for simplicity do not consider the effect related to influence of the particle charge on the vapor concentration of polar molecules near the particle surface (Nadykto *et al.*, 2003).

Taking into account (Levdansky *et al.*, 2006) the density of the resulting flux of vapor molecules into the particle with the elementary charge  $q$  in the general case when the condensation coefficient  $\alpha_c$  and the surface tension  $\sigma$  depend on the particle size can be written as

$$I = \frac{P_\infty}{(2\pi mkT)^{1/2}} \frac{\alpha_{\text{cf}} \exp(-\phi) - \frac{P_e}{P_\infty} \alpha_e \exp(\phi)}{1 + \alpha_{\text{cf}} \exp(-\phi) - \frac{3}{4\text{Kn}}}, \quad (1)$$

$$\phi = \frac{V_m}{kT} \frac{6\sigma_f}{d + 4\delta}, \quad (2)$$

$$\phi = \frac{V_m}{kT} \left[ \frac{4\sigma_f}{d + 4\delta} - \frac{q^2}{2\pi^2 \varepsilon_0 d^4} \left( \frac{1}{\varepsilon_g} - \frac{1}{\varepsilon_p} \right) \right]. \quad (3)$$

Here  $d$  is the particle diameter, Kn is the Knudsen number,  $m$  is the molecule mass,  $V_m$  is the volume per molecule,  $T$  is the temperature,  $k$  is the Boltzmann constant,  $\sigma_f$  is the surface tension for a flat surface,  $\varepsilon_p$  and  $\varepsilon_g$  are respectively the relative permittivity of the particle and the gas phase,  $\varepsilon_0$  is the vacuum permittivity,  $\alpha_{\text{cf}}$  is the condensation coefficient for a flat surface,  $\alpha_e$  is the evaporation

coefficient,  $\delta$  is the Tolman's length,  $P_e$  is the saturation vapor pressure over a flat surface,  $P_\infty$  is the partial pressure of the vapor at infinity distance from the particle.

Figure 1 shows dependence of the density of the dimensionless flux of vapor molecules into the water drop  $I' = I(2\pi mkT)^{1/2} (P_\infty)^{-1}$  on its diameter at  $T = 273 \text{ K}$ ,  $P_\infty / P_e = 15$ ,  $\alpha_c = \alpha_e = 1$ ,  $\sigma = \sigma_f$ .

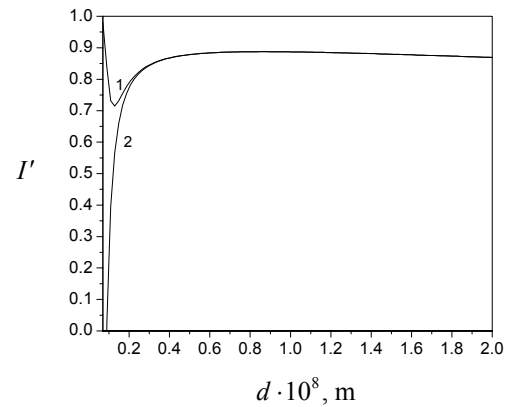


Figure 1. Dependence of the density of the dimensionless resulting flux of vapor molecules into the water drop on the drop diameter: 1 – drop with elementary charge, 2 – uncharged drop.

It is seen that the function  $I'(d)$  in the case of charged particle is characterized by minimum for small values of  $d$ . This is related to different influence of the Kelvin effect and the particle charge on the flux density of vapor molecules into the particle. In some region of the particle size  $I'(d)$  has a maximum that is related to the increase in the resistance for the transport of vapor molecules to the particle surface due to the Knudsen number decrease.

This work was supported in part by GACR projects 101/05/2214, 101/05/2524 and 104/07/1093.

Reist, P. C. (1993). *Aerosol Science and Technology*. New York: McGraw-Hill.

Nadykto, A. B., Makela, J. M., Yu, F., Kulmala, M., & Laaksonen, A. (2003). *Chem. Phys. Lett.*, 382, 6-11.

Levdansky, V. V., Smolik, J., & Moravec, P. (2006). *J. Eng. Phys. Thermophys.*, 79, 217-221.

## Simultaneous characterisation and manipulation of aerosol particles

J.R. Butler, L. Mitchem and J.P. Reid

Department of Chemistry, University of Bristol, Bristol, BS8 1TS, United Kingdom

Keywords: aerosol characterisation, cavity enhanced Raman spectroscopy, holographic optical tweezers, hygroscopicity, relative humidity.

Optical tweezing is an established method of characterising 1-15 $\mu\text{m}$  aerosol particles (Hopkins, *et al.*, 2004). The simultaneous trapping and probing of a single laser beam combined with the surface-less environment of the trap provides a non-intrusive method of direct aerosol study in a good approximation of relevant environments.

It has been demonstrated that Köhler theory, which describes the equilibrium hygroscopic nature of liquid droplets, is well adhered to by simple inorganic aqueous aerosols such as the NaCl-H<sub>2</sub>O system (Mitchem, *et al.*, 2006a).

The equilibration time of such droplets is on the order of seconds (Chan and Chan, 2005), and can therefore provide high accuracy information on the relative humidity (RH) of a system over a large range (Mitchem, *et al.*, 2006b), when compared to commercially available alternatives.

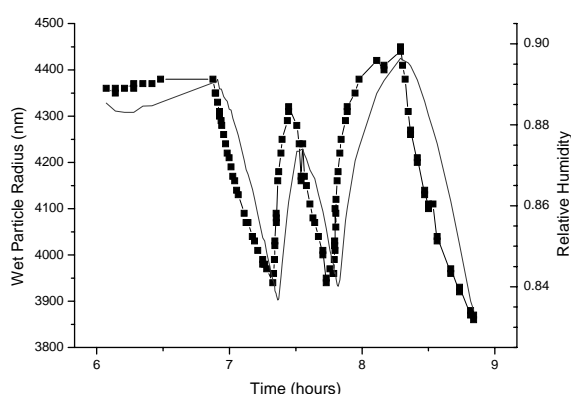


Figure 1. Variation in measured droplet size (line and symbol) with time compared to the reported RH from a commercially available probe.

Using optical tweezers, the hygroscopic behaviour of (NH<sub>4</sub>)<sub>2</sub>SO<sub>4</sub>-H<sub>2</sub>O droplets have been compared to that of droplets which contain, in addition, Glutaric or Maleic acid. These measurements probe the variation in hygroscopicity due to the acid component.

It has been shown that generation of holographic arrays of optical traps using a spatial light modulator (SLM) offers more diversity and control of the manipulation of liquid aerosols (Burnham and McGloin, 2006; (Sinclair, *et al.*, 2004).

To use a droplet of simple as a relative humidity probe in proximity to a more complex droplet, a stringent method for controlling the composition of each droplet is required. An array of optical traps, with 'picket fence' arrangements, offers a potential solution to this and an SLM has been used to create arrays of optical traps to test the feasibility of this proposal.

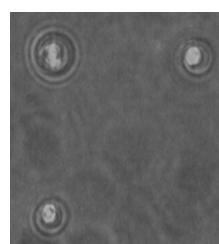


Figure 2. Droplets held in an array.

A holographic array of traps can be manipulated with relative ease and facilitates a large variety of experiments which would otherwise be difficult to realise.

Scaled down reactions are of interest in situations with limited sample sizes and studies of such micro-reactions using an SLM would complement results from other methods, such as electrode array devices (Taniguchi, *et al.*, 2002).

This work is supported by EPSRC (EP/D003326/1) and NERC.

Hopkins, R. J., Mitchem, L., Ward, A. D. & Reid, J. P. (2004). *Physical Chemistry Chemical Physics*, 6, 4924-4927.

Mitchem, L., Buajarern, J., Hopkins, R. J., Ward, A. D., Gilham, R. J. J., Johnston, R. L. & Reid, J. P. (2006a). *Journal of Physical Chemistry A*, 110, 8116 - 8125.

Chan, M. N. & Chan, C. K. (2005). *Atmospheric Chemistry and Physics*, 5, 2703-2712.

Mitchem, L., Hopkins, R. J., Buajarern, J., Ward, A. D. & Reid, J. P. (2006b). *Chemical Physics Letters*, 432, 362 - 366.

Burnham, D. R. & McGloin, D. (2006). *Optics Express*, 14, 4175-4181.

Sinclair, G., Jordan, P., Courtial, J., Padgett, M., Cooper, J. & Laczik, Z. J. (2004). *Optics Express*, 12, 5475-5480.

Taniguchi, T., Torii, T. & Higuchi, T. (2002). *Lab on a Chip*, 2, 19-23.

## Impact of aerosol microphysics on its optical properties

E.Carstea<sup>1</sup>, S. Stefan<sup>2</sup> and A. Nemuc<sup>1</sup>

<sup>1</sup> National Institute for Optoelectronics, P.O.Box MG 5, Bucharest-Magurele, Romania

<sup>2</sup> University of Bucharest, Faculty of Physics, Dept. of Atmospheric Physics, Bucharest-Magurele, Romania

Keywords: mass concentration, urban aerosol, number size distribution, absorption and extinction coefficient

The aerosol number or mass concentration is a key parameter in studies of radiative effects. Stefan and Iorga (2004) have shown for a marine aerosol consisting of pure ammonium sulphate and a rural aerosol, consisting of a mixture of ammonium sulphate and mineral dust, that optical properties of clouds are strongly correlated with the characteristics of aerosols. The aerosol types used in this study were rural and urban. The size distributions of these aerosol types were derived from measurements (Whitby, 1978; Jaenicke, 1988). Also, the chemical composition of the aerosol is based on measurements reported in literature, which show that the continental aerosol contains 15-30% sulphate and clearly most of the sulphate for both types of aerosol can be found in the accumulation mode. The aerosol number size distribution is assumed to be described by a lognormal distribution:

$$\frac{dn_r}{d \ln r} = \sum_{i=1}^3 \frac{n_{r,i}}{\sqrt{2\pi} \ln \sigma_i} \exp\left(-\frac{[\ln(r/r_{m,i})]^2}{2(\ln \sigma_i)^2}\right)$$

where  $n_{r,i}$ ,  $r_{m,i}$  and  $\sigma_i$  are the total number concentration, geometric mean radius, and geometric standard deviation of aerosol mode  $i$ , respectively. The modes are:  $i = 1$  nucleation mode,  $i = 2$  accumulation mode and  $i = 3$  coarse mode. The coefficients in equation are given in Table 1 for urban aerosol. The chemical composition of the rural aerosols is assumed to be a mixture of ammonium sulphate (75%) and mineral dust (25%) as reported by Bott (2000).

The corresponding coefficients of the aerosol number size distributions are also reported in the paper.

The Table 1 contains the modal parameters of the urban aerosols as given by Whitby (1978) and Jaenicke (1988).

In this paper Mie theory is used for estimation of specific aerosol optical properties (extinction and absorption coefficients and single scatter albedo) using 10 wavelengths between 0.3 and 10.0  $\mu\text{m}$ .

Table 1. Modal parameters of number size distributions for urban aerosols.

	$n_{r,i} (\text{cm}^{-3})$	$r_i (\mu\text{m})$	$\log \sigma_i$
W	$2120 \cdot 10^3$	0.006	0.240
	$37 \cdot 10^3$	0.031	0.297
	4.9	0.540	0.328
J	$9.93 \cdot 10^4$	0.006	0.245
	$1.11 \cdot 10^3$	0.007	0.666
	$3.64 \cdot 10^4$	0.025	0.337

Optical properties are also estimated for high relative humidity values (60%, 70%, 80% and 90%). Optical properties of the aerosols vary depending on increasing relative humidity values and on two other parameters: particle dimension and refractive index. If the water component of the aerosol increases then the radiation extinction decreases due to lower absorption. The radiation extinction reaches the maximum value in urban areas where anthropogenic sources are present.

This work has been done during the national research program CEEEX No.112/2005 IMPAERO.

Stefan S., G. Iorga., 2004: *Effects of aerosol on the optical properties of clouds*; The 14th International Conference on Clouds and Precipitation, Bologna, Italia July 2004; pg. 235-238

Whitby, K.T., 1978: *The physical characteristics of sulfur aerosol*, Atmos. Environ., 12, 135-159.

Jaenicke, R., (1988): *Aerosol physics and Chemistry*, in Landolt-Boernstein (Ed.), Zahlenwerte und Funktionen aus Naturwissenschaften und Technik, Vol. 4b, Springer, 391-457

## Critical Analysis of the Fuchs “Boundary Sphere” Method

V.Y.Smorodin

Climate Change Institute, 303 Edward T. Bryand Global Sciences Center,  
University of Maine, Orono, ME 04469-5790, USA  
Email: [Vladimir.Smorodin@gmail.com](mailto:Vladimir.Smorodin@gmail.com)

Keywords: aerosol fundamentals, coagulation, Fuchs’ “boundary layer” method, Knudsen layer

We present some results of our critical analysis of the Fuchs’ initial hypothesis that the boundary layer (BL) near the “probe” sphere is “free” from any other molecules (particles) [1]. For the analysis we have employed the Poisson’s probabilistic distribution (PBD).

As known, a probability,  $P(x)$ , to find  $N$  particles (molecules) in a finite volume,  $V$ , at the given molecule concentration,  $n$ , can be calculated using the PBD:

$$(1) \quad P(x) = \frac{e^{-\mu} \mu^x}{x!}$$

Here  $P(x)$  is the probability of  $x$  occurrences in an interval of space (or time),  $\mu$  is the average number (or expected value) of occurrences in the specified interval. At the given free molecular path,  $l$ , the mean molecule concentration in air is evaluated as:  $n \approx l^{-3}$ ; then the average number of all molecules,  $\mu$ , in a cylindrical particle “track” of the radius  $R_0$  between the moving particle and the “probe” particle of the same radius is presented as:

$$(2) \quad \mu_a \leq \mu \leq \mu_b,$$

$$\text{where } \mu_a = V_{\min} n \approx \pi / Kn^2,$$

$$\text{and } \mu_b = V_{\max} n \approx 2\pi \sqrt{(1 + 0.5Kn)^2 - 1} / Kn^3$$

Then a probability to find at least one molecule in the BL is estimated as:

$$(3) \quad P_{\min}(1, Kn) \leq P(1, Kn) \leq P_{\max}(1, Kn),$$

$$\text{where } P_{\min}(1, Kn) = \text{Min}\{\mu_a e^{-\mu_a}, \mu_b e^{-\mu_b}\},$$

$$\text{and } P_{\max}(1, Kn) = \text{Max}\{\mu_a e^{-\mu_a}, \mu_b e^{-\mu_b}\}$$

Calculations by the formula (3) show that, e.g., for  $Kn \in [1, 10]$ ,  $P(1, Kn)$  has a finite value with a maximum  $P_{\max}(1, Kn) \approx 0.38$ . Thus a dilute gas space in the BL cannot be regarded as empty “vacuum”, as it is treated by the Fuchs “boundary sphere” method (FBSM).

**Conclusions.** (A) Since at any space range, including the free path scale, a moving particle can meet another one with a finite probability, there is no criterion to separate a space using the FBSM, as well as any its modifications. Therefore an initial assumption of the FBSM about the “empty” BL near the “probe” particle is not correct. This conclusion could support a hypothesis about the Maxwell-Boltzmann distribution of particle rates inside the BL.

(B) Conventional methods of solving the coagulation problem based on a combination of separate regarding the diffusion approximation at “large” distances from the “probe” particle and the kinetic one at “short” distances and their next “sewing” are not physically justified.

(C) A practical efficacy of Fuchs’ method can be explained by its overlapping both diffusion and kinetic flow regimes; empirically choosing boundary conditions one can fairly approximate any experimental data near intermediate regime.

(D) The FBSM has to be replaced with proper boundary conditions defining the particle flux onto the “probe” particle (see our complementary paper on this subject).

**Refs:** [1] Fuchs, N.A. *The Mechanics of Aerosols*. Pergamon Press, New York, 1964.

## Studies in electro-hydrodynamic spraying of water in standard CO<sub>2</sub>

B. Sersante<sup>1</sup> and J. Rosell-Llompart<sup>1,2</sup>

<sup>1</sup>Department of Chemical Engineering, Universitat Rovira i Virgili, 43007 Tarragona, Spain

<sup>2</sup>ICREA (Catalan Institution of Research and Advanced Studies), 08010 Barcelona, Spain

Keywords: EHDA, electrospray, aerosol generation, corona discharge.

Water is a solvent of obvious importance and the electro-spraying of water into uniformly sized droplets is therefore of significant interest. Due to its high surface tension, however, the appearance of corona discharges precludes a corona-free, steady-flow cone-jet structure in air (Cloupeau, 1994). One option is to operate at the high field-high flow mode called “cone-jet glow” mode described by Borra *et al.* (1999) where spraying coexists with a corona. Precluding gas discharges in air at 1 atm is possible by reducing the size of the capillary to an outer diameter under 50 or so micro-meters (Lopez-Herrera *et al.* 2004). Another option to achieve corona-free cone-jets is to raise the ambient pressure (an inconvenience, usually), or to replace the ambient air with a gas with higher dielectric strength, such as CO<sub>2</sub>. Tang and Gomez (1995) studied water spraying into CO<sub>2</sub> and encountered steady cone jets in two distinct modes (figure 1): a low-current mode of normal electrospray, and a high-current one, with smaller droplets, and which, they argued, was assisted by a corona (invisible in CO<sub>2</sub>).

We have carried out an investigation of the following “macroscopic” system responses of steady water cone-jets in CO<sub>2</sub>: stability domains in flow rate–capillary voltage plane, transmitted current (DC and AC), and geometry of the meniscus.

Figure 1 shows the stability domain from this study compared to those by Tang and Gomez for similar capillary diameter (~200 μm) as well as distance to the counter electrode (~30 mm). Because these authors used a coaxial tube around their capillary (for feeding CO<sub>2</sub>), they require higher voltages. And, the minimum flow rate in our domain resembles theirs in “corona-assisted” mode. However, we have not found two separate domains, but just one. Figure 2 shows that, while our DC current values are somewhat smaller than for the “corona-assisted” mode, the current is in both cases higher than expected for corona-free cone-jets (Fernandez de la Mora & Loscertales, 1994; Ganán-Calvo, 2004).

We are currently investigating the effects of electrical conductivity and electrode geometry.

This work was supported by the European Commission (MIRG-CT-2004-511310), the Catalan Government (2005SGR-00735), the Spanish Government (FIS2005-07194, CTQ2004-22275-E-PPQ).

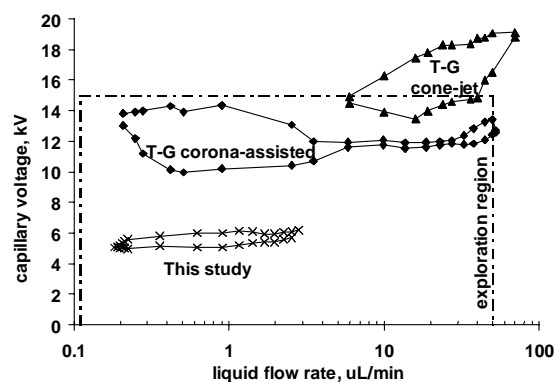


Figure 1. Existence domains of steady cone-jets of low conductivity water ( $k \sim 1 \text{ uS/m}$ ) in CO<sub>2</sub>.

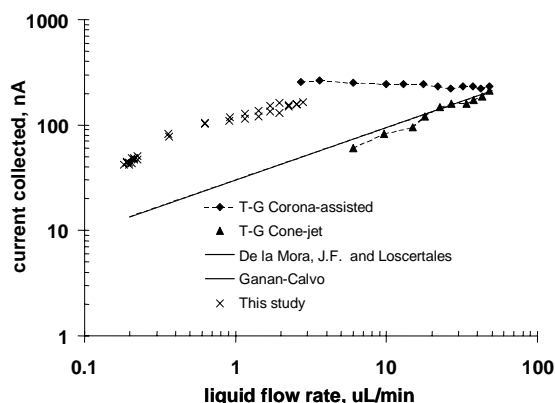


Figure 2. DC current collected on the ground electrode.

- Borra, J.P., *et al.* (1999). *J. Aerosol Science*, 30, 913-925.
- Cloupeau, M. (1994). *J. Aerosol Science*, 25, 1143-1157.
- Fernandez de la Mora, J. & Loscertales, I.G. (1994). *J. Fluid Mech.*, 260, 155-184.
- Gañán-Calvo, A.M., (2004). *J. Fluid Mech.*, 507, 203-212.
- Lopez-Herrera, J.M., *et al.* (2004) *J. Am. Soc. Mass Spectr.*, 15, 253-259.
- Tang, K.Q. & Gomez, A. (1995). *J Colloid Interf. Sci.*, 175, 326-332.

## Cone-jet formation in nanospray atomisation

S. Paredes-Egea<sup>1</sup> and J. Rosell-Llompart<sup>1,2</sup>

<sup>1</sup>Department of Chemical Engineering, Universitat Rovira i Virgili, 43007 Tarragona, Spain

<sup>2</sup>ICREA (Catalan Institution of Research and Advanced Studies), 08010 Barcelona, Spain

Keywords: EHDA, electrospray, aerosol generation, HPLC-MS, nanospray.

The method of electrostatic spraying, also called electro-hydrodynamic atomisation or simply electrospray (ES), distinguishes itself from other methods of atomisation by its unusually narrow size distributions (Fdez. de la Mora, 2007). Applicability of this methodology for materials production (in particle or thin layer form) is limited, however, in part because of the low flow rates involved, but also because a relatively narrow window of liquid electrical conductivities is required to achieve any given droplet diameter. Consequently, a need exists for approaches that can relieve these constraints.

In connection with the second constraint, we became interested in a report by Wilm & Mann (1996) that explains how narrowing the capillary exit diameter from conventional sizes, typical of ES (of order  $\sim 100$   $\mu\text{m}$ ), down to just a few microns resulted in reduced droplet diameter by a factor of 2 or 3. While this phenomenon has not been studied in detail, it has become popular in the field of mass spectrometry, where it is known as “nanospray” (nES) owing to the nano-liter-per-minute flows it employs. To the best of our knowledge, ours is the first quantitative investigation of the electro-hydrodynamic behaviour of nES.

We have thus carried out an investigation of how the nES flows depend on the following independent variables: electrical conductivity (solute concentration, [LiCl]), solvent composition (tri(ethylene)glycol “3EG” or 2-propanol-water mixtures), ambient gas ( $\text{CO}_2$  or  $\text{N}_2$ ), starting liquid column length, flow rate, and capillary electric potential. Borosilicate glass tubes (1 mm OD) are pulled using a P-97 Sutter micropipette puller, and are characterized by Environmental-SEM (figure 1). The pressure of the liquid inside these tubes is adjusted by a  $\text{N}_2$  source, while the tube lays horizontally on a purpose-made Teflon platen that is attached to a metallographic microscope fitted with a long-working distance ( $\sim 8$  mm) 20X lens. Facing the pulled end of the tube at about 3 mm, is a counter electrode (a metal frit disk 9.5 mm in diameter) that is connected to the electrical ground through a homemade nano-amp-meter. Images focused onto a CCD camera sensor through the scope’s photo tube are captured by a PC.

We have encountered robust steady cone-jet formation across the range of conductivities studied (0.0005 and 0.014 S/m). In fact, all patterns found were analogous to those of conventional electrospray

sources (i.e. pulsatile cone-jet, steady cone-jet, multi-jet). We have also confirmed the reduction in flow rate and in jet diameter observed by Wilm & Mann relative to ES. Figure 2 shows that the current-flow rate relationships of both regimes appear to match. These observations suggest that the system responses (i.e. stability domains features, current, meniscus appearance, jet size, etc) are continuous functions, rather than discontinuous ones, of the capillary tip diameter, as it is changed between  $\sim 100$ ’s of  $\mu\text{m}$  typical of ES down to a few  $\mu\text{m}$ ’s necessary for nES, and that a narrow capillary somehow permits access to lower flow rates than possible in ES sources.

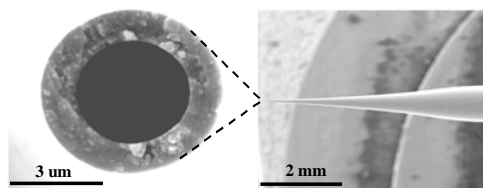


Figure 1. Front and side views of a pulled glass tube.

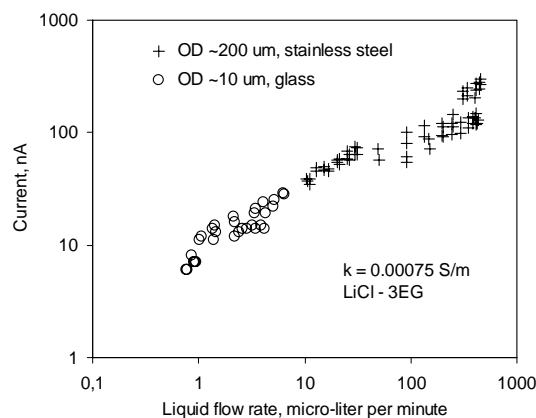


Figure 1. Electrical current for ES (+) and nES (o).

This work was supported by the European Commission (MIRG-CT-2004-511310), the Catalan Government (2005SGR-00735), the Spanish Government (FIS2005-07194, CTQ2004-22275-E-PPQ).

Fernandez de la Mora, J. (2007). *Ann. Rev. Fluid Mech.*, 39, 217–243.

Wilm, M. & Mann, M. (1996). *Anal. Chem.*, 68, 1-8.

## Stochastic Degradation-Condensation Processes in Fractal Aggregates with Multiple Bonds.

M. B. Flegg and D. K. Gramotnev

Applied Optics Program, School of Physical and Chemical Sciences,  
Queensland University of Technology, GPO Box 2434, Brisbane, QLD 4001, Australia

Keywords: Thermal fragmentation, Fractals, Fundamental aerosol physics, Particle size distribution.

As has been suggested in (Gramotnev & Gramotnev, 2005), thermal fragmentation of nano-particle aggregates may play a significant role in evolution of combustion aerosols. The model was based on the assumption that primary particles in a fractal aggregate may be bonded by means of volatile molecules, evaporation of which will result in weakening interaction between the primary particles, and these particles may eventually fragment from the aggregate (similar to evaporation of water molecules from a droplet). Theoretical analysis of fragmentation of fractal structures should thus be based on degradation kinetics of multiple bonds (each volatile bonding molecule representing one bond).

The analysis of degradation/evaporation processes in nano-particle aggregates and polymer-like systems with multiple bonds has so far been conducted for an arbitrary chain and ring-like aggregates with arbitrary numbers of bonds and primary particles (Gramotnev & Gramotnev, accepted, Flegg & Gramotnev, to be published). Though these structures represent a reasonable approximation for combustion aggregates consisting of a small number of primary particles, the developed model may be oversimplified when considering fragmentation of larger fractal aggregates with diameters of  $\sim 100$  nm or more (Gramotnev & Gramotnev, 2007). Furthermore, the approach described in (Gramotnev & Gramotnev, accepted, Flegg & Gramotnev, to be published) neglects possible condensation processes, assuming that bonding molecules (bonds) can only stochastically evaporate from between the primary particles.

Therefore, this paper extends the developed approaches and analysis of thermal fragmentation due to stochastic evaporation/degradation of multiple bonds to a fractal branching aggregate (network) with the possibility of stochastic bond restoration (condensation of volatile molecules). The elements of the branching fractal are assumed to be chain and/or ring aggregates, the "primary particles" of which also consist of chains and/or rings, etc. The analysis is based on the theory of thermal fragmentation of chains and rings of particles with multiple bonds (Flegg & Gramotnev, to be published) and self-similarity of the branching fractal structure.

Stochastic condensation (restoration) of multiple bonds between the particles is taken into account by introducing a continuous time Markov

process to describe the evolution of a single link with multiple bonds between the particles or elements of a fractal branch. We also assume that restoration of bonds (condensation of volatile molecules) may only occur for a link between the particles (fractal elements) with non-zero number of bonds. A link with zero number of bonds (disconnected or fragmented particles) cannot be restored, which is equivalent to neglecting coagulation processes. Thus, the aim is to find the probability for fractal to be in a state with at least some of the links to have zero number of bonds, which eventually should lead to fragmentation (Flegg & Gramotnev, to be published).

The analysis is conducted on an example of degradation of a ring/chain fractal structure (Fig. 1).

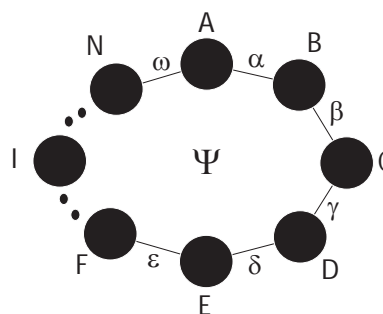


Figure 1. A ring N-mer structure  $\Psi$  (consisting of N nodes) with different numbers of bonds represented by the Greek letters in each link. Each node represents a fractal aggregate.

The nodes of the ring/chain are represented by further branching systems. The size of the successive inner systems are determined from the fractal parameters such as dimension (typically varying between 1.3 and 2) and fractal prefactor. As a result, an analytic expression for the average particle size distributions during fractal fragmentation are found.

- M. B. Flegg and D. K. Gramotnev, *Phys Rev E* (to be published).  
D. K. Gramotnev and G. Gramotnev (2005), *J. Aerosol Sci.*, vol.36, pp.323-340.  
D. K. Gramotnev and G. Gramotnev, *J. Appl. Phys.* (accepted).  
G. Gramotnev, D. K. Gramotnev, *Atm. Env.* (online 30/01/2007; doi:10.1016/j.atmosenv.2007.01.007).

## Freezing of evaporating oxalic acid solution droplets

E.A. Svensson, S. Badii, M. Hallquist and J.B.C Pettersson

Department of Chemistry, Atmospheric Science, Göteborg University, Sweden

Keywords: levitation, freezing, oxalic acid, ice nuclei

The conversion of supercooled water to ice is of major importance for a number of atmospheric processes, including precipitation formation and the influence of clouds on the atmospheric radiation budget. The optical properties of clouds are quite different for clouds containing liquid water and ice. Understanding and predicting precipitation and radiative effects of clouds and how anthropogenic activities can influence them rely on knowing how ice forms.

Various theories for heterogeneous freezing mechanisms have been advanced, but the processes that actually occur in the atmosphere have not been firmly established. Progress has been plagued by a host of complex issues, including the precise mode of action of ice nuclei (IN) and in situ modification of IN activity by various substrate coatings. Numerous aerosol species of anthropogenic origin have been identified as effective ice initiators. In addition, there is the possibility that secondary aerosol constituents such as aliphatic alcohols or dicarboxylic acids could coat inactive particles and thus transform them into efficient IN. In a recent study Zobrist et al. (2006) showed that precipitates of oxalic acid dihydrate may act as heterogeneous ice nuclei in aqueous droplets immersed in oil. Modeling showed that oxalic acid (OA) in the upper troposphere may well have a climatic effect.

In the present study a new levitation set-up was used to investigate the freezing of evaporating OA solution droplets. An electrodynamic balance (EDB) traps a single droplet which can be studied for a long period. The surroundings are temperature controlled (-50 to +40°C). The droplet is illuminated by a HeNe laser (633 nm) and monitored by two cameras. One of the cameras records the light scattering pattern. As long as a levitated particle is liquid it is also spherical, and the droplet size may be determined using Mie scattering theory.

Droplets were generated and electrically charged by a syringe with a charged injection needle. The produced droplet sizes varied in the diameter range 50-100  $\mu\text{m}$ . The double ring EDB trapped particles with diameters ranging between 5 and 150  $\mu\text{m}$ . Experiments with pure water

droplets were initially performed and the observed homogeneous nucleation rates were in agreement with results from earlier studies (Cantrell and Heymsfield, 2005).

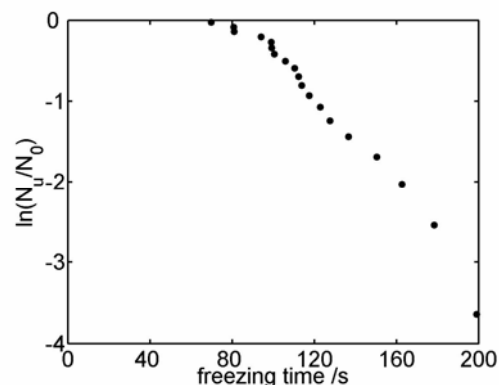


Figure 1. Analysis of freezing times of oxalic acid solution droplets at  $-24^\circ\text{C}$ .  $N_i$  is the number of unfrozen droplets at a certain time and  $N_0$  is the total number of droplets.

The experiments show freezing of OA solution droplets at temperatures as high as  $-20^\circ\text{C}$ . Figure 1 shows typical results at a temperature of  $-24^\circ\text{C}$ . The freezing is delayed, which excludes the possibility of contamination of some preexisting ice nuclei. This delay is interpreted as the time for formation of a precipitate. After a droplet is trapped in the EDB it evaporates and the OA concentration increases. At some concentration a precipitate forms, and this precipitate acts as a heterogeneous ice nucleus. At  $-37^\circ\text{C}$ , close to the homogeneous freezing temperature, 10 of 25 droplets studied froze quickly (0-80 s) while the others froze after a period of evaporation (290-470 s). These two groups are interpreted as homogeneous and heterogeneous freezing respectively. Results from studies at different temperatures will be presented and discussed.

Zobrist B. et al (2006). *Atmos. Chem. Phys.*, 6, 3115-3129

Cantrell W. and Heymsfield A. (2005). *Bull. Am. Met. Soc.* 6, 795-807

## Mobility diameters of doublets of two different spheres in the transition regime

T. Weber<sup>1</sup>, A. Maisels<sup>2</sup> and F. E. Kruis<sup>1</sup>

<sup>1</sup>Institute for Nano Structures and Technology, University Duisburg-Essen, 47057 Duisburg, Germany

<sup>2</sup>Degussa, Process Technology & Engineering, Particle Processing, 63457 Hanau, Germany

Keywords: fundamental aerosol physics, nanoparticles, particle shape.

**Doublets** of spheres are bodies comprising exactly two spheres in contact. Their mobility is of interest in aerosol technology (e.g. Kasper, 1985), as they constitute the transition from spheres to chains and aggregates of spheres. Besides, asymmetrical doublets may serve as a rather simple model for non-spherical particles.

Many publications have dealt with the drag of doublets, which is essential for their physical behaviour – not lastly in DMA measurements. However, most of the authors presumed continuum regime or treated symmetrical doublets (e.g. Götz, 2005).

To produce nano-doublets, we used a facility for **bipolar aggregation** (Fig. 1) which was precisely described, e.g. in Maisels *et al.* (2000). This set-up makes it possible to produce gas borne doublets, the two spheres of each having a specified diameter between 10 nm and 100 nm (Fig. 2a–c). The doublets (Fig. 2d) reside in the transition regime at  $0.2 < Kn_D < 2.0$ . The used substances were gold and silver.

In the first step of the process, aerosol is generated by evaporating and condensing the selected material. Its particles are then transferred into spherical shape by a heat treatment. The adjacent size selection using DMAs delivers singly and likely charged monodisperse nano-spheres. After that, two such aerosol flows are joined with the spheres in one branch charged positively and those in the second one charged negatively. Well-defined doublets then form by pairwise collisions which are induced by Coulomb forces.

The **measurements** included the mobility diameters of both each sphere and the resulting doublet. A first set of experiments was conducted with doublets of equal spheres. The results for gold and silver (Fig. 3) are on one straight line. A fit of the data gives a slope of 1.32 which conforms to Hutchins & Dahneke (1994) and Götz (2005).

For another test series, doublets of differently sized spheres were produced. In dimensionless representation, a general scaling law has been found. As expected, the mobility diameter of a doublet tends towards the diameter of its larger sphere.

Unlike reported by Kousaka *et al.* (1996), expanded measurements did not reveal any influence of the field strength on the mobility diameters of the doublets.

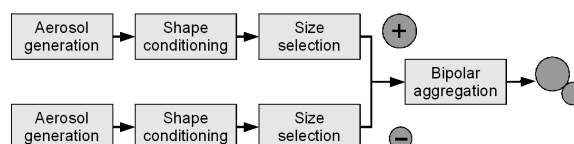


Figure 1. The making of nano-doublets.

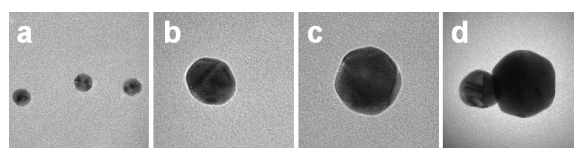


Figure 2. TEM photographs of silver spheres of **a** 20 nm, **b** 60 nm, and **c** 100 nm diameter, and **d** of a doublet comprising silver spheres of 60 nm and 100 nm diameter.

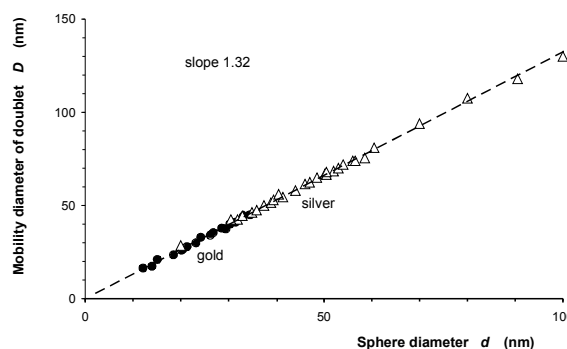


Figure 3. Measured mobility diameters of doublets of equal spheres for  $0.2 < Kn_D < 2.0$ .

This work was financially supported by the DFG in the framework of the special research program *Nanoparticles from the gas phase: formation, structure, properties* (SFB 445).

Maisels, A., Kruis, F. E., Fissan, H., Rellinghaus, B., & Záhres, H. (2000). *Appl. Phys. Lett.*, 77, 4431–4433.

Kasper, G. (1985). *J. Aerosol Sci.*, 16, 535–556.

Götz, T. (2005). *J. Comput. Appl. Math.*, 175, 415–427.

Hutchins, D. K., & Dahneke, B. E. (1994). *J. Chem. Phys.*, 100, 7903–7915.

Kousaka, Y., Endo, Y., Ichitsubo, H., & Alonso, M. (1996). *Aerosol Sci. Tech.*, 24, 36–44.

## Evaporation from a planar surface at a maximum rate of entropy production

Ian Ford

Department of Physics and Astronomy, University College London, Gower Street, London, WC1E 6BT, UK

Keywords: fundamental aerosol physics, evaporation

The second law of thermodynamics states that irreversible (that is to say almost all) processes that occur in a macroscopic system are accompanied by entropy production. These processes include the conduction of heat, the transfer of momentum, the mixing of components and the progress of chemical reactions. Entropy production only ceases when the system settles down in equilibrium, which is the state of the system with the maximum value of entropy consistent with any constraints, such as volume, temperature etc. This principle is the basis for all of equilibrium thermodynamics and statistical mechanics.

But what about the rate at which entropy is produced as the state of equilibrium is approached? There are suggestions in the literature (Ozawa et al 2001, Martyushev and Seleznev 2006) that some systems approach equilibrium at a rate which maximises the rate of production of entropy. In other words, the system tries to equilibrate as rapidly as possible, given the physical constraints.

The most intriguing application of this principle, as far as environmental physics is concerned, is a study of the distribution of global temperature and cloud cover (Paltridge 1975, 1978). Energy is transported in the atmosphere in such a way as to maximise the entropy production associated with heat flows, it is claimed. Perhaps aerosol dynamics also reaches a similar steady state, on some suitable timescale?

In a rather less speculative application, the production of entropy may be studied in a situation relevant to the evaporation of aerosol droplets.

I consider a situation where a condensed phase evaporates into a vacuum across a planar interface. I have carried out a revised treatment of an earlier study (Ford and Lee 2001) to show that a principle of maximum entropy production requires the vapour to stream away from the surface at precisely the speed of sound, which is in remarkable agreement with detailed calculations made using microscopic gas dynamics, which require considerable computational and mathematical resources.

The study centres on a search for the velocity distribution functions  $f(v)$ , for molecules at and far away from the surface, which maximise the (negative) production of Boltzmann's  $H$ -function:

$$H = \int f(v) \ln f(v) dv$$

which is the negative of the entropy for a rarified gas.

Together with constraints which ensure the conservation of molecules, momentum and energy, maximising entropy production may be achieved through simple use of variational calculus and some straightforward numerical searching. The entropy production rate as a function of the most interesting parameter, the Mach number of the evaporating flow, is shown in Figure 1. The maximum lies at  $Ma=1$ .

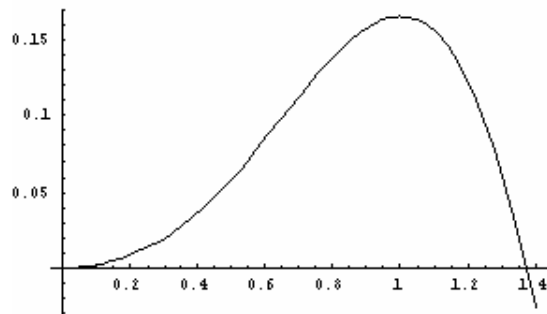


Figure 1. Entropy production rate, in arbitrary units, against Mach number of evaporating flow (horizontal axis).

A rigorous proof for a principle of maximum entropy production does not exist, though some interesting studies have been published (Dewar 2003, 2005). If it proves in practice to hold, even approximately, then its use would simplify calculations of many non-equilibrium processes, including aerosol condensation and evaporation, especially far from equilibrium. It might even cast light on the dynamics of aerosol nucleation, which is a statistical process particularly far-from-equilibrium. On a broader scale, it might simplify the modelling of global climate dynamics, though this is perhaps straying too far towards speculation, if not wishful thinking.

- Ford, I J and Lee, T-L (2001) *J. Phys. D: Appl. Phys.* 34, 413  
Dewar, R (2003) *J. Phys. A: Math. Gen.* 36, 631  
Dewar, R (2005) *J. Phys. A: Math. Gen.* 38, L371  
Martyushev, L M and Seleznev, V D (2006) *Phys. Rep.* 426, 1  
Ozawa, H, Shimokawa, S and Sakuma, H (2001) *Phys. Rev. E* 64 026303  
Paltridge, G W (1975) *Q. J. R. Met. Soc.* 101, 475  
Paltridge, G W (1978) *Q. J. R. Met. Soc.* 104, 927

## Determination of the mean aspect ratio of aerosol particles from optical data

M. Kocifa

Department of Interplanetary Matter, Astronomical Institute, Slovak Academy of Sciences, D bravsk 9, 845 04 Bratislava, Slovak Republic, astromir savba.sk

Keywords: Aspect ratio, aerosol optics, size distribution, inverse problems.

Airborne aerosol particles coexist in complex systems with variable size distributions, shape distributions, and orientation distributions as well (Mishchenko et al., 1997). Shape of the particles can vary from nearly spherical (like water droplets or water soluble aerosols Buseck and P sfai, 1999) to highly irregular (e.g. desert dust Volten et al., 2001). Solid particles made up of deliquescent materials become solution droplets at high humidity. Under low relative humidity conditions the solid materials can in preference form the morphology of the aerosols. Basically, it is impossible to describe the realistic shapes and shape distributions of ambient aerosols (but in some cases the exact modelling of aerosol morphologies is required e.g. for correct interpretation of measured data or for accurate modelling of the optical properties of irregularly shaped particles Hellmers and Wriedt, 2004). Instead, it is more convenient to characterize the prevailing morphology of aerosols by means of aspect ratio, which relates the largest and smallest characteristic sizes of arbitrarily shaped particle. Except rare extreme cases, the tropospheric aerosols have predominately moderate aspect ratios with typical values between 1 and 2.3 (Mishchenko et al., 1995).

The shape of aerosol particles is one of key factors influencing the optical properties of atmospheric environment. Therefore it is rather evident, that optical measurements of scattered and attenuated light can provide valuable information on microphysical properties of aerosol polydispersions (uirantes and Delgado, 1998). Retrieval of the aspect ratio from optical data is an ill-posed problem which requires an existence of subsidiary *a-priori* information (e.g. on particle chemistry). Assuming the mean refractive index of the particles is known, the solution of the inverse problem is possible.

During field campaigns we measured the phase function and aerosol optical thickness in Bratislava (capital of Slovakia) and interpreted the results in terms of surface distribution function and mean effective aspect ratio of aerosol particles. In general, the aspect ratio of aerosol particles is still scarcely evaluated quantity and it was never recovered in Bratislava by means of optical methods. Obtained behaviour of aspect ratio in Bratislava was compared with that obtained in Vienna. In context of a general picture it is of high interest to compare a city with long experience in fighting pollution (i.e.

Vienna) with a city at the beginning of cleaning process (i.e. Bratislava). Comparing the aerosol properties in both cities we found that particles in Bratislava are larger whenever, and non-deliquescent to a great extent. While aspect ratio of Viennese aerosols is typically small (quite frequently it is less than 1.2), the aerosol particles in atmosphere of Bratislava are more non-spherical (the aspect ratio may reach the value about 1.4).

This work was supported by the Scientific Grant Agency VEGA (grant No. 1/3074/06).

Buseck, P. R. & P sfai, M.. (1999). in *Proc. Natl. Acad. Sci. USA*, 96, 3372-3379.

Hellmers, J., Wriedt, Th. (2004). *J. Quant. Spectrosc. Rad. Transfe,r* 89, 97-110.

Mishchenko, M. I., acis, A. A., Carlson, B. E., Travis, . D. (1995). *Geophys. Res. Lett.*, 22, 1077-1080.

Mishchenko, M. I., Travis, . D., Kahn, R. A., West, R. A. (1997). *J. Geoph. Res.*, 102, 16831-1684.

uirantes, A., Delgado, A. (1998). *J. Quant. Spectrosc. Rad. Transfer*, 60, 463-474.

Volten, H., Mu oz, O., Rol, E., de Haan, J. F., Vassen, W., Hovenier, J. W. (2001). *J. Geophys. Res.*, 106, 17375-17401.

## Exact Solution for Stochastic Evaporation/Degradation Processes in a Chain/Ring Aggregate with Multiple Bonds

M. B. Flegg and D. K. Gramotnev

Applied Optics Program, School of Physical and Chemical Sciences,  
Queensland University of Technology, GPO Box 2434, Brisbane, QLD 4001, Australia

Keywords: Nanoparticle aggregates, Particle fragmentation, Evaporation, Degradation, Aerosol evolution.

It has been shown that thermal fragmentation of nano-particle aggregates can explain a number of the observed unusual features of evolution of combustion aerosols (Gramotnev & Gramotnev, 2005). Nano-particle aggregates are polymer-like systems in which monomers (primary particles) are bonded by multiple bonds (bonding volatile molecules). Stochastic evaporation of these bonds eventually leads to aggregate fragmentation.

Figure 1 shows an example of an aggregate in which links with quadruple indistinguishable bonds hold together monomers (primary particles) to form a chain-like 3-mer.

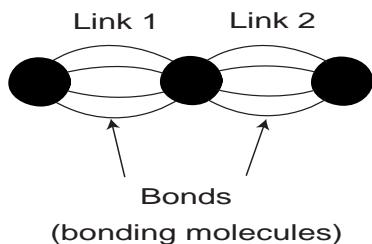


Figure 1. A chain 3-mer (consisting of three primary particles/monomers) with indistinguishable quadruple bonds in each link.

The analysis of degradation in such aggregates was attempted in (Gramotnev & Gramotnev, accepted). Bonds (bonding molecules) in one link were assumed to interact with each other, e.g., by means of weak van der Waals forces. Therefore, the energy that is required for a bond to evaporate generally increases with increasing number of bonds in a link. Degradation of such a system caused by stochastic evaporation of bonds can be represented by a random graph, the vertices of which show possible intermediate states of the aggregate, while the graph edges represent possible evaporation processes (Gramotnev & Gramotnev, accepted). However, generalisation of the obtained results to an arbitrary initial state of the aggregate was difficult.

Therefore, here, we present a new statistical approach for the analysis of degradation processes in chain or ring aggregates with multiple bonds. An exact solution describing fragmentation processes is obtained for a general aggregate with arbitrary numbers of primary particles and indistinguishable interacting bonds between them.

In particular, it is demonstrated that degradation and fragmentation of a nano-particle aggregate strongly depends on the numbers of bonds in the links between the primary particles. Increasing evaporation energy per one bond (or bonding molecule) due to mutual interactions between the bonds is demonstrated to be one of the key factors for substantial differences in the aggregate fragmentation processes. As a result, aggregates having identical number of primary particles but different number of bonds are shown to evolve in a significantly different ways. For example, typical time-dependent numbers of aggregates in the intermediate fragmenting states are shown in Fig. 2 for 4-mer ring aggregates in the initial state with 2 indistinguishable bonds (bonding molecules) per each link in the presence of weak interaction between the bonds (dashed curves) and in the absence of such interaction (solid curves).

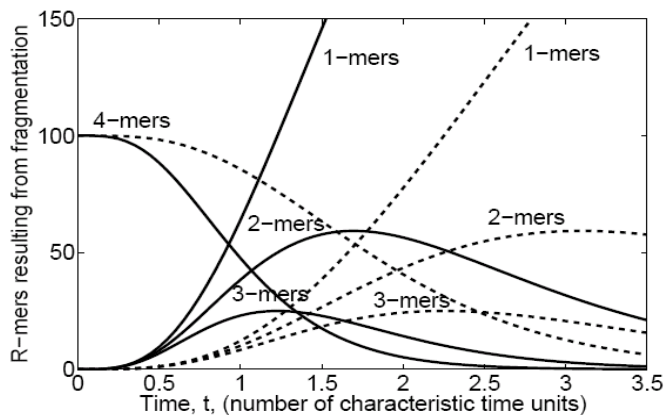


Figure 2. Typical time dependencies of particle numbers in different fragmentation states for 4-mer ring aggregates with (dashed) and without (solid) interaction between multiple bonds in a link.

Substantial variations in the life time for intermediate states (Fig. 2), accumulation of aggregates in some intermediate modes and their relationship to evolution of combustion aerosols are analysed and discussed. The results are applicable to any polymer-like systems/aggregates with multiple bonds.

D. K. Gramotnev and G. Gramotnev (2005), *J. Aerosol Sci.*, 2005, vol.36, pp.323-340.

D. K. Gramotnev and G. Gramotnev, *J. Appl. Phys.* (accepted).

## About photophoresis of aerosol particles in stratosphere

L.B. Kochneva, S.A. Beresnev

Aerosol Physics Laboratory, Ural State University, 620083, Ekaterinburg, Russia

Keywords: Aerosol dynamics, Atmospheric aerosols, Carbonaceous particles, Photophoresis.

One of possible mechanisms of vertical transport of aerosol particles in stratosphere can be radiometric photophoresis. The developed by authors theory of atmospheric aerosol photophoresis predicts that for the certain types of carbonaceous aerosol the negative “solar” photophoresis (motion of particles in a field of shortwave solar radiation) can lead to the vertical lifting and levitation for sub-micrometer particles at altitudes of the lower and middle stratosphere at the assumption of stationary atmosphere (without vertical wind action). Similar opportunities demonstrates the positive “thermal” photophoresis (motion of particles in a field of outgoing longwave radiation) for the micrometer carbonaceous particles.

In this paper the results for calculated characteristics of photophoretic motion of some types of atmospheric aerosols are presented: dependences for photophoretic forces and velocities on atmospheric altitudes (Figs.1 and 2); full particles velocities taking into account the photophoresis and gravitational sedimentation; the estimations of characteristic times for particles lifting up to levitation altitudes and particles subsidence from set altitude up to tropopause boundary under action of photophoretic and gravitation forces (Fig. 3). The characteristic times for particles lifting under action of negative “solar” photophoresis from Earth’ surface up to levitation altitudes make 25÷30 years. In the case of “thermal” photophoresis the carbonaceous particles in the range up to 2 μm achieve levitation altitudes for a little bit smaller times 20÷25 years (Fig. 3).

Thus, the radiometric photophoresis (both “solar”, and “thermal” photophoresis) it is possible to consider as the sufficiently effective mechanism of vertical transport for strong-absorbing, light and low-conductivity atmospheric aerosol particles in the lower and middle stratosphere on the global time scale. The photophoretic forces can compete to gravity forces up to altitudes 30÷35 km for sub-micrometer and micrometer particles. It is shown, that in some important cases the photophoretic velocities of particles are quite comparable to averaged velocities of vertical wind transport in stratosphere.

This work was supported by the Russian Foundation for Basic Research (RFBR) under grant 06-01-00669.

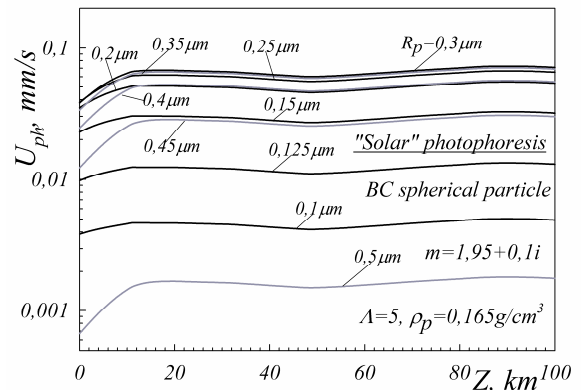


Fig. 1. The velocities of carbonaceous particles motion in stationary stratosphere and mesosphere under action of negative “solar” photophoresis.

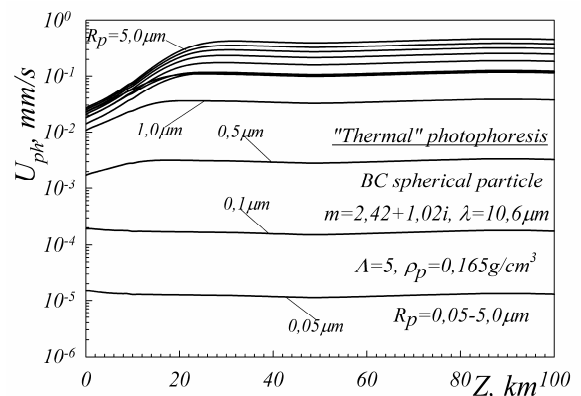


Fig. 2. The velocities of carbonaceous particles motion in stationary stratosphere and mesosphere under action of positive “thermal” photophoresis.

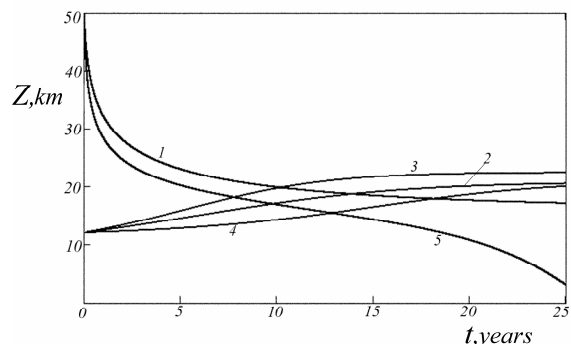


Fig. 3. The times of subsidence for particles with  $R_p=1 \mu\text{m}$  (1) and  $R_p=2 \mu\text{m}$  (5) from altitude of 50 km and times of lifting of particles with  $R_p=1.3, 1.5$  and  $1.8 \mu\text{m}$  from altitude of 12 km (curves 2, 3 and 4 accordingly) up to levitation altitudes in field of outgoing longwave radiation.

## Restore of aerosol microstructure parameters and component composition by the method of Muller's matrix discrete elements.

A. B. Gavrilovich

Institute of Physics, National Academy of Sciences,  
68, Nezavisimosti Prosp., 220072, Minsk, Belarus

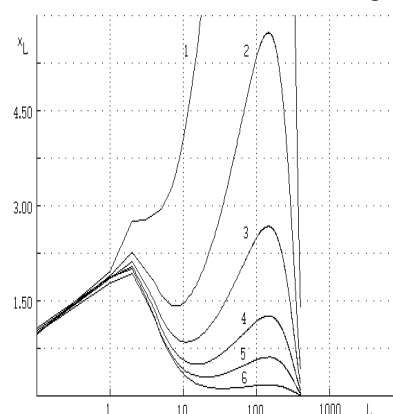
Keywords: atmospheric aerosols, industrial aerosol, aerosol microstructure, aerosol component composition, light-scattering matrix.

Aerosols of the Earth atmosphere recommended by the Radiation Commission of the International Association on Meteorology and Atmospheric Physics was investigated in this report. The different stages of aerosol dynamics were considered through the concentration changes of the main aerosol components: D- water-insoluble dust particles, W- water-soluble particles, and S- carbon antropogenic aerosol.

We have considered an inverse problem of restore of aerosol microstructure and its component composition from scattering light by the method of Muller's matrix discrete elements. This problem pertains to class very complex incorrect problems for integral equation of the Fredholm type. The known approximate methods of reconstruction (the small angles method, diffusion, nefelometric, and others) associate with loss of a great volume information because of limited angular interval. Our method is free from these defects since it uses whole information concluded in light-scattering Muller's matrix in the full angular interval.

We have converted the angular elements of the Muller's matrix in their equivalent analogues depended on discrete variables. For this purpose, we have executed the projection of each element of scattering matrix on corresponding axis of the certain Gillbert's space and have got the collection of the important discrete functionals. These distributions of functionals reflect the information about aerosol microstructure and its component composition in the suitable demonstration form. Namely, we have realized transition from the continuous optical parameters to the aerosol parameters of the discrete form. We will name them as the discrete elements of Muller's matrix, and method is as the method of Muller's matrix discrete elements. The several local maximums on the curved distribution are indicating that the investigation aerosol has a mixture which is consisting of corresponding different components. In given private example, it points that in the industrial aerosol there are the components of type D, W, and

S which have the different effective sizes of particles.



For example on the figure 1 there is the first Muller's matrix discrete functional element depended from an argument L. Argument L is linked to either the diffraction parameter or the size of particles.

Figure.1. The first Muller's matrix discrete element for aerosol models.

The positions L of maxima are related to the effective radius of particles for components  $r_{ef} = c \lambda L$ , where  $c = 0.11 - 0.14$ ,  $\lambda = 0.55 \mu$  is the wavelength of light. For the components W and S, (the first maximum) a ratio of particle sizes is small so they are insufficient for the separating. The second maximum points to presence in aerosols a large - dispersion component of type D. Amplitudes of maxima define to the volume concentration of D-aerosol component.

### Conclusion

Results of statistical modeling of possible errors in the input parameters shows that the method of Muller's matrix discrete elements may be used for restore of real aerosol parameters.

## **T07 Abstracts**

## Removal of aerosol pollutants by portable ionic air purifiers in a well-ventilated room

S.A. Grinshpun, T. Lee, J.H. Jung, T. Reponen

Center for Health-Related Aerosol Studies, University of Cincinnati, Cincinnati, OH 45267, USA

Keywords: indoor aerosols, ions, electrostatic precipitators, air pollution, ozone.

Numerous techniques have been developed to reduce the exposure to indoor aerosol particles. Some of them aim solely at the aerosol concentration reduction; others are designed to inactivate viable bioaerosol particles. The basic principles utilized in air purification techniques include mechanical filtration, electrostatic precipitation, ion emission, photocatalytic reactions, ozone generation, UV irradiation, and others. While portable indoor air cleaners operate in tens of million homes, there is still a big controversy about their effectiveness to reduce aerosol and bioaerosol exposure and concerns about some potentially unhealthy by-products, which may be formed in the process (such as ozone).

Ion-based air purifiers are becoming increasingly popular worldwide. They utilize one of the two particle removal mechanisms: (i) charging airborne particles by ions and letting them pass through an electrostatic precipitator (ESP) where they are, at least partially, deposited on the charged plates, and (ii) ion emission (IE) into an indoor air environment so that the airborne particles interact with these ions, acquire charges, and are finally removed due to either migration to surfaces or coagulation. Many available papers and reports fail differentiating between the above two mechanisms. We have previously evaluated the ESP- and IE-based air purifiers in indoor test chambers of different sizes in the absence of air exchange. The present study aims at evaluating the particle removal efficiency of these purifiers in a room with high air exchange rate, in which case a portable unit competes with the room/building ventilation and air filtration system.

A furnished, non-occupied, room (volume = 36.2 m<sup>3</sup>) ventilated through a double-filter setting was used for the testing at an air exchange of 4-6 ACH. An electrical low pressure impactor (ELPI, Dekati, Finland) was used to determine the concentration and the aerodynamic particle size distribution in real-time. In addition, an OPC (1.108, Grimm Technologies Inc., Germany) and a CNC (P-Trak, TSI Inc., USA) operated in parallel to the ELPI. Two challenge aerosols, smoke and NaCl, were utilized to represent an *indoor pollutant*. The measurements were conducted without the portable air purifier (natural decay) and with it operating in the room. The tested units were obtained from three manufacturers: EcoQuest International, Sharper Image, and Wein Products. To quantify the particle removal efficiency exclusively due to the purifier, the air cleaning factor (ACF) was determined for every

particle size as the ratio of the concentration measured at a specific time point during the natural decay to the concentration measured at the same time point when the air purifier was operating. The purifier's performance was also characterized by answering the following question: once an air pollutant is introduced in the environment, how long would it take to restore the initial background aerosol concentration level. This question was answered for two situations: when the air purifier operated in the room and when it was off. The ratio of the above time intervals represents the contribution of the portable air cleaner in restoring the "status-quo."

The tested ESP- and IE-based purifiers demonstrated different abilities to reduce the aerosol concentration after the pollutant was introduced. We have shown that the ion output and voltage, the particle size and their ability to acquire electric charges, as well as other factors affect the air cleaning efficiency. While the ACF values in the ventilated room appears to be not as high as those observed in the calm air test chamber with the same units, the aerosol reduction effect was still significant for some purifiers, see Figure 1.

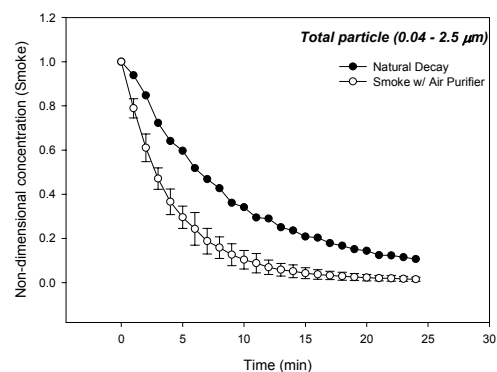


Fig. 1. Non-dimensional decays for smoke aerosols.

The best unit (IE) reduced the concentration of smoke particles ranging from 0.04 to 2.5 μm (PM<sub>2.5</sub>) faster than the natural decay by a factor of ~4 in 10 min and ~9 in 25 min, as found from the ELPI data (p<0.0001). The data collected with the OPC and CNC confirmed the trends revealed by the ELPI measurements. The ozone level in the room was < 0.05 ppm during the 24-hour test period.

The information generated in this study seems crucial for selecting and developing methods and devices that can effectively reduce the exposure to indoor aerosol pollutants.

## Influence of source of heating and air movement on the particles and air parameters

E.Jankowska and E.Walicka

Department of Chemical and Aerosol Hazards, Central Institute for Labour Protection  
 – National Research Institute, Czerniakowska 16, 00-701 Warsaw, Poland

Keywords: indoor air, particle concentration, size distribution, air parameters

The source of heating and air movement, for example a typical local thermofan in the room, can have a significant influence on the change of the particles concentration in indoor air.

This article presents the results of investigation of the concentration and size distribution of particles in three situations:

- A – thermofan was switched off,
- B – thermofan was switched on only in the option for heating,
- C – thermofan was switch on in both options heating and air movement.

The changes of air parameters (air temperature, air humidity and air velocity) in situations A, B and C are shown in Table 1.

Table 1. Air parameters in three situations A, B, C.

Situation	Air temperature (°C)	Air humidity (%)	Air velocity (m/s)
A	23.9	53	0.05
B	26.4	39	0.08
C	27.7	40	0.16

Measurements of particles concentrations were conducted with:

- DUST TRAK 8520 (TSI) - mass concentration (mg/m<sup>3</sup>) of particles in range the 0.1–10 µm,
- P-TRAK 8525 (TSI) - number concentration (particles/m<sup>3</sup>) of particles in the range 0.02–1 µm,
- SMPS (CPC 3022A and DMA 3080L, TSI) - number concentration (particles/m<sup>3</sup>) and size distribution of particles in the range 0.017–0.6 µm.

The results of measurements of particles concentration and size distribution are shown in Figures 1, 2 and 3.

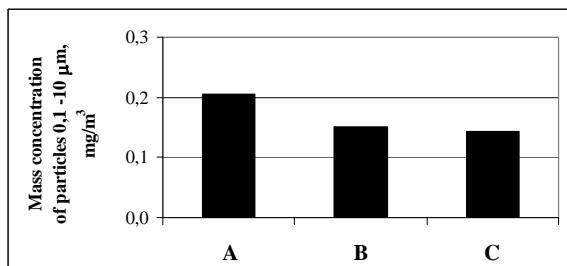


Figure 1. Mass concentration of particles in the 0.1–10 µm range determined with DUST-TRAK.

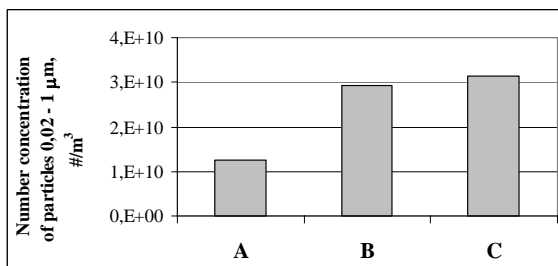


Figure 2. Number concentration of particles in the 0.02–1 µm range determined with P-TRAK.

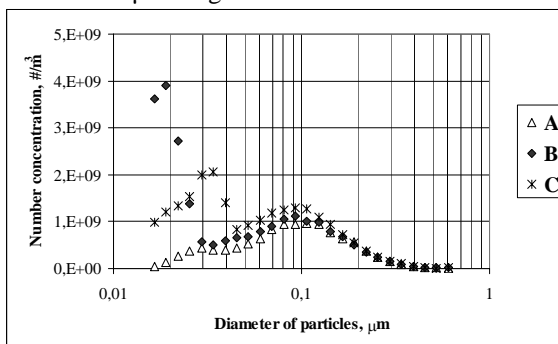


Figure 3. Number concentration and size distribution of particles in the 0.017–0.6 µm range determined with SMPS (CPC and DMA).

During heating (situation B), air temperature increased by 2.5°C, the air humidity decreased by 14% and air velocity increased by 0.03m/s. Mass concentration decreased by 0.0543 mg/m<sup>3</sup> (DUST-TRAK) but number concentrations increased significantly by 1.7 E+10 #/m<sup>3</sup> (P-TRAK). In the air, close to the thermofan, the number of very small particles in the range 0.017–0.045 µm (figure 3 – SMPS results) increased rapidly.

Compared to situation B, in situation C, when both options of the thermofan were used (heating and air movement) mostly air velocity increased. Air temperature, air humidity and mass (Figure 1) and number concentrations (Figure 2) changed less. But in situation C the number of very small particles in the range 0.017–0.026 µm (figure 3) in air decreased significantly.

This study has been prepared within National Programme “Adaptation of Working Conditions in Poland to EU Standards”, supported in 2005–2007 by the State Committee for Scientific Research of Poland. CIOP-PIB has been the Programme main coordinator.

## Characterization of particulate matter during simulated indoor activities

J. Ondráček<sup>1,2</sup>, L. Džumbová<sup>1,2</sup>, T. Glytsos<sup>1</sup>, I. Kopanakis<sup>1</sup> and M. Lazaridis<sup>1</sup>

<sup>1</sup>Laboratory of Atmospheric Aerosols, Department of Environmental Engineering, Technical University of Crete, 73100, Chania, Crete, Greece

<sup>2</sup>Laboratory of Aerosol Chemistry and Physics, Institute of Chemical Process Fundamentals, Academy of Sciences of the Czech Republic, Rozvojová 135, 16502, Prague 6, Czech Republic

Keywords: indoor sources, mass and number concentration, number size distribution.

In recent years numerous research efforts were focused in the examination of the relationship between the exposure of humans to the particulate matter (PM) and consecutive adverse health effects (Schwartz, 1994). The quality of air in the indoor environment has become of great importance as people nowadays spend about 80% of their time indoors. Moreover a large portion of their time is spent at home and thus they are exposed to particulate matter emitted during different indoor activities. The PM concentration during indoor activities can reach elevated values (up to tenfold compared to the situation without the sources) for short or even for longer periods of time (He et al., 2004). The determination of physical characteristics of emitted PM from different indoor sources is important for determining the indoor air quality and furthermore the fraction of particles that can enter the human respiratory tract.

In the current paper indoor measurements including several simulated indoor sources are presented. All the measurements were conducted in the empty laboratory, where only the measurement devices and laboratory furniture were present. The PM<sub>2.5</sub> mass concentration was measured using a DustTrak Aerosol Monitor (TSI, Model 8520), while the approximately PM<sub>1</sub> number concentration was measured using P-Trak Ultrafine Particle Counter (TSI, Model 8525). The PM<sub>2.5</sub> mass concentration was measured simultaneously indoors and outdoors. The GRIMM SMPS+C system (GRIMM, CPC, Model 5.403 and LONG Vienna DMA) measured the number size distribution in the range between 11.1 – 1083.3 nm. The indoor conditions (temperature and relative humidity) were monitored as well.

Typical indoor activities, which were chosen as aerosol sources in this study, include candle burning (1), water boiling (2), onion frying (3), vacuuming (4), hair spraying (5), hair drying (6), smoking (7) and burning of incense stick (8). The indoor conditions during these activities were kept constant. All the sources were repeated several times keeping the same indoor conditions. The AMANpsd algorithm was used to evaluate the modal structure of measured particle number size distribution data (Ondracek & Lazaridis, 2006).

Selective results of particle number and mass concentration measurements are shown in Table 1.

Table 1. Number (approx. PM<sub>1</sub>) and mass (PM<sub>2.5</sub>) average maximum concentrations measured during different indoor activities (1-8).

Source	N conc. [ #/cm <sup>3</sup> ]		M conc. [ µg/m <sup>3</sup> ]	
	Av. Max.	St. Dev.	Av. Max.	St. Dev.
1	56457	27309	530	264
2	2036	559		
3	73791	10215	296	268
4	3459	2045		
5	6983	1772	793	225
6	40219	46798		
7	112407	3668	1264	209
8	70674	14549	631	49

Finally, Figure 1 shows the evolution of the number size distribution during candle burning. The modal structure of particle number size distribution shifts towards the bigger particle diameter within the time.

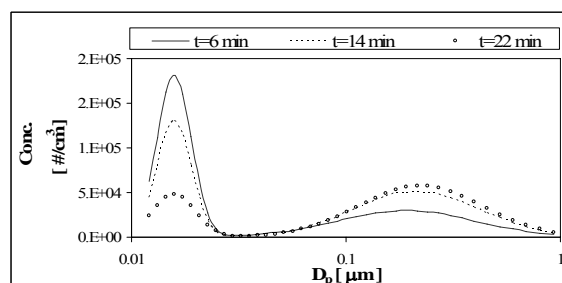


Figure 1. Particle number size distributions during candle burning.

The project is co-funded by the European Social Fund & Natural Resources – EPEAK II – IRAKLITOS and Marie-Curie TOK project MTKD-CT-2004-513849.

He, C., Morawska, L., Hitchins, J., Gilbert, D., (2004). *Atmospheric Environment*, 38, 3405-3415.

Schwartz, J. (1994). *Fundamental and Applied Toxicology*, 64, 26-35.

Ondracek, J. & Lazaridis, M. (2006). in *Proc. of 8th Int. Conf. "Protection and Restoration of the Environment VIII"*, Chania, Crete, Greece, 581.

## Commuter exposure to particulate matter in transport microenvironments

Ian Colbeck and Zaheer Ahmad Nasir

Department of Biological Sciences, University of Essex, Colchester, CO4 3SQ, UK

Keywords: PM measurements, transport, railways, cars.

A large proportion of the working population spends a significant time commuting. The information regarding the exposure of the commuter to particulate air pollution is potentially important but studies of journey time exposure to particulate matter are relatively rare. Most of these studies have focused on exposure of PM in motorized transport or bicyclists. Data on particulate matter inside trains is rare and only a few studies have been reported. Seaton et al., (2005) assessed the hazards associated with exposure to dust on the London Underground. Their study showed that concentrations of PM<sub>2.5</sub> at the platform were 270 - 480  $\mu\text{g}/\text{m}^3$  against to 130 - 200  $\mu\text{g}/\text{m}^3$  inside the driver's cabin. In the United Kingdom, although rail is a highly efficient mode of transport, no study to date has been reported with regards to particulate matter inside railway coaches

To investigate the situation of PM<sub>10</sub>, PM<sub>2.5</sub> and PM<sub>1</sub> inside railway coaches and cars sampling was carried out during 2004 - 2006. Four train companies serving all around the UK were selected and multiple journeys were made on them throughout this period. These included, One Railway, GNER, Northern and Southern. All the rail tracks were electrified and the coaches were air-conditioned, except Northern (non air conditioned). On the other hand, measurements inside a car were carried out on a route in a typical town of South East England (Colchester). Two journeys were made in one day using the same route - one in morning and other in evening.

The mass concentration of particles was monitored using two different GRIMM analysers i) Model 1.108 ii) Model 1.101 (Grimm Aerosol Technik GmbH, Ainring, Germany). For air conditioned rail coaches the concentration of PM<sub>10</sub> ranged from 20  $\mu\text{g}/\text{m}^3$  to 47  $\mu\text{g}/\text{m}^3$  followed by a concentration of 3  $\mu\text{g}/\text{m}^3$  to 17  $\mu\text{g}/\text{m}^3$  for PM<sub>2.5</sub> and 2  $\mu\text{g}/\text{m}^3$  to 10  $\mu\text{g}/\text{m}^3$  for PM<sub>1</sub>. On the other hand, in non air conditioned coaches, the concentration of PM<sub>10</sub> rose to 95  $\mu\text{g}/\text{m}^3$  followed by 14  $\mu\text{g}/\text{m}^3$  to 30  $\mu\text{g}/\text{m}^3$  and 6  $\mu\text{g}/\text{m}^3$  to 19  $\mu\text{g}/\text{m}^3$  for PM<sub>2.5</sub> and PM<sub>1</sub>, respectively (Fig. 1). The relationship among PM<sub>10</sub>, PM<sub>2.5</sub> and PM<sub>1</sub> revealed that PM<sub>10</sub> always stayed well above PM<sub>2.5</sub> and PM<sub>1</sub>. However PM<sub>2.5</sub> levels were well correlated with PM<sub>1</sub> ( $r^2=0.92$ ), no matter which category of train.

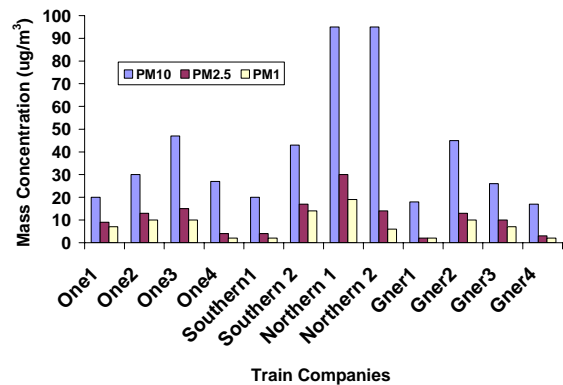


Figure 1. Particulate matter inside the rail coaches in United Kingdom

Most of the particulate matter inside the car was recorded in PM<sub>10</sub> fraction (17  $\mu\text{g}/\text{m}^3$  - 47  $\mu\text{g}/\text{m}^3$ ) during both morning and evening journeys.. High levels of PM<sub>10</sub> were observed during busy times, while PM<sub>2.5</sub> and PM<sub>1</sub> stayed normal. However, during a particular week PM<sub>2.5</sub> and PM<sub>1</sub> rose to 40  $\mu\text{g}/\text{m}^3$  and 38  $\mu\text{g}/\text{m}^3$  respectively. A comparison of these measurements to a local fixed site monitoring of PM revealed that PM<sub>2.5</sub> was very high all around the south east of England. A good correlation between PM<sub>2.5</sub> and PM<sub>1</sub> was documented for both morning ( $r^2=0.94$ ) and evening ( $r^2=0.88$ ) journeys (Fig.2).

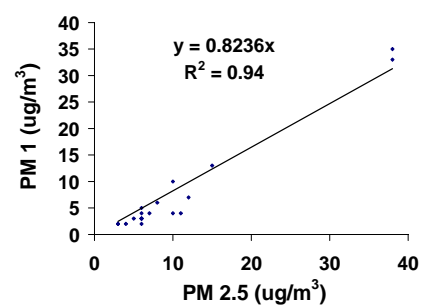


Figure 2. Relationship of PM<sub>2.5</sub> to PM<sub>1</sub> in car (morning).

In general the mass concentration of particulate matter in air conditioned trains and in car microenvironments were almost the same (20  $\mu\text{g}/\text{m}^3$  - 47  $\mu\text{g}/\text{m}^3$  for PM<sub>10</sub>). However, high PM levels were found in non air conditioned rail coaches and during busy times in road traffic.

Seaton, A., Cherrie, J., Dennekamp, M., Donaldson, K. Hurley, J.F. and Tran, C.L. 2005. The London Underground: dust and hazards to health. *Occupational Environ. Med.* 62, 3555 - 362.

## Fine and coarse aerosol particles in a student's club before and after a smoking ban

J. Hovorka, M. Braniš, P. Gadas, T. Valchářová

Institute for Environmental Studies, Charles University in Prague, Albertov 6, 128 43 Prague 2, Czech Republic

Keywords: PM<sub>1</sub>, PM<sub>2.5</sub>, PM<sub>10</sub>, ETS, indoor air quality,

In contrast to USA and most of the EU countries, smoke-free restaurants, bars and cafes are still rare in the Czech Republic. However, stricter regulations have been recently applied to minimize adverse effects of smoking on human health. We took the advantage of changes in the smoking rules on the university premises and performed two short campaigns to ascertain differences in aerosol mass-size concentrations in a students club "Dead Fish" at the Faculty of Science, Charles University - FSCU in Prague. We hypothesized that smoking ban will have a significant effect on particle concentrations. The main aim of the study was to ascertain which particle sizes will be primarily affected.

Five minute integrates of number-size distribution of particles in the range of 0.524 to 20µm measured by an APS-3321 (TSI) was used in the study. One campaign (6 days) was performed under "smoking regime" in the spring 2005, the second campaign (19 days) in winter 2006 after the ban.

Diurnal variation of PM mass concentrations exhibited, during both campaigns, almost the same pattern corresponding to the presence of customers. Also the congruency of exponential decrease of PM<sub>10</sub> mass concentration after closing time at 2:30 AM indicated quite similar ventilation conditions (Fig.1.).

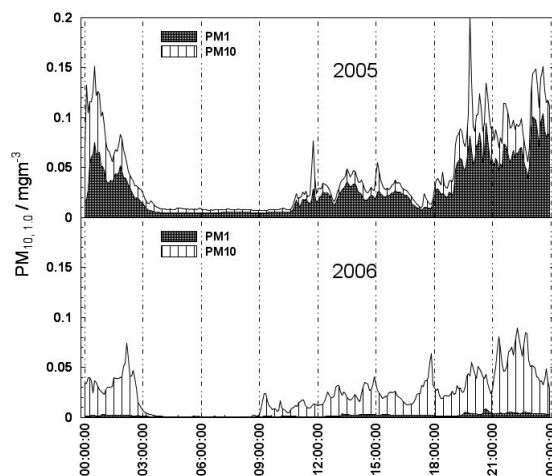


Figure 1. Diurnal variation of PM<sub>1</sub> and PM<sub>10</sub> in the club before (2005) and after (2006) a smoking ban.

Contrary to temporal variations, medians of PM mass concentrations during the measurement periods differed remarkably (Tab. 1.). After the ban

PM<sub>10</sub> concentrations decreased, on average, by 25% while PM<sub>1</sub> and PM<sub>2.5</sub> dropped by more than 50%. The proportion of PM<sub>1</sub> (PM<sub>2.5</sub>) to PM<sub>10</sub> decreased from 57% (74%) to 38% (56%) between 2005 and 2006 respectively.

Table 1. Campaign medians of PM<sub>10</sub>, PM<sub>2.5</sub> and PM<sub>1</sub> mass concentrations ( $\rho=1.5\text{gcm}^{-3}$ )

	2005	2006
PM <sub>1</sub> / $\mu\text{g m}^{-3}$	12	5
PM <sub>2.5</sub> / $\mu\text{g m}^{-3}$	18	9
PM <sub>10</sub> / $\mu\text{g m}^{-3}$	23	17

Higher decrease of relative and absolute PM<sub>1</sub> (PM<sub>2.5</sub>) values in comparison to PM<sub>10</sub> mass concentrations agrees with changes in mass size distributions during opening hours. In 2005, mass size distributions were bi-modal with the first mode in the region of fine (GMD 0.6 µm) particles and the second mode in the region of coarse (GMD 6 µm) particles. Particles of the fine mode were seemingly produced by smoking. They formed the majority of PM<sub>1</sub> and PM<sub>2.5</sub> mass. Termination of smoking resulted in a large drop of PM<sub>1</sub> and PM<sub>2.5</sub> mass concentrations. The first (fine) mode disappeared and the recorded distributions became mono-modal (GMD 6 µm). The mass concentrations of coarse particles (PM<sub>10</sub> – PM<sub>1</sub>) did not change significantly because their principal source was most probably resuspension caused by movement of people, which contrary to smoking has not changed significantly compared to the before-ban period.

Our measurements are generally in accord with other studies addressing problems connected with smoking on public (Ott, 1996, Repace, 2006) and hospitality business spaces (Mulcahy, 2005) but bring new insight in size distribution of aerosol in these types of indoor environments.

The research was carried out under the Institute for Environmental Studies of FSCU in Prague institutional support.

- Ott, W., Switzer, P., Robinson, J. (1996) *J. Air & Waste Manage. Assoc.* 46(12)1120-1134  
 Mulcahy, M., Evans, D. S., Hammond, S. K., Repace J. L., Byrne, M., (2005) *Tobacco Control*, 14, 384-388  
 Repace J. L., Hyde, J. N., and Brugge, D. (2006) *BMC Public Health*, 6, 266-281

## Effect on indoor air ion enhancement and bacterial activity inhibition by evaporating selected essential oils

C.H. Luo<sup>1</sup>, Y. Shih<sup>2</sup> and S.B. Lian<sup>1</sup>

<sup>1</sup>Department of Environmental Engineering, Hungkuang University, 34 Chung Chie Road, 43302, Taichung, Taiwan

<sup>2</sup>Department of Applied Cosmetology, Hungkuang University, 34 Chung Chie Road, 43302, Taichung, Taiwan

Keywords: bioaerosols, air ions, essential oils, indoor air quality, indoor aerosols.

Essential oils are highly concentrated, volatile, aromatic products extracted from various natural plants. Considering chemical constituents, essential oils consist of hormones, vitamins, and other elements that work at different levels, such as antimicrobial activity (Su, et al., 2006; Dusan, et al., 2006) and enhancement of air ions (Luo, et al., 2004). Especially, mostly volatile compounds in essential oils are named as environmental essence which provides indoor environment distinctive aroma and potential impacts on indoor air quality.

Air ions are defined as airborne atomic or molecular clusters with separated positive or negative charges. The lifetime of natural air ions is up to 100-1000 seconds, but the lifetime of artificial air ions is precisely shorter. High frequency of their birth and death induces a sharp fluctuation of concentration ratio between the negative and positive ions. The high amount of airborne negative ions implies that a healthy occurrence of environmental interest may happen. Several compounds in essential oils can increase the lifetime of existent air ions in atmosphere.

Essential oils have long served as antibacterial agents due to their versatile content of antimicrobial compounds, they possess potential as natural agents for airborne bacterial activity inhibitors. Their antimicrobial activity is assigned to a number of small molecular terpenoids and phenolic chemicals, which activity is also confirmed in pure form.

In this study, an environmental box, an indoor simulation, combined with an air ion detector and a 6-stage bioaerosol deposit impactor was used to investigate the effect on enriching air ions and inhibiting airborne bacteria by evaporating selected essential oils. The ventilation ratios of approximately 0.5-5 h<sup>-1</sup> were set to represent low, moderate, and high average values of typical residences. Negative and positive ions were counted in ions/c.c. (air), then the relative ratio was calculated automatically. Duplicate samples of airborne bacteria were collected, cultured, and calculated as CFU/m<sup>3</sup>.

The results showed that evaporation velocity of essential oils was a major factor for enhancing the concentration of air ions. No matter what kind of air ions, their lifetime expansion was achieved. Furthermore, highly volatile elements in essential oil provided a large concentration of air ions. On the other hand, the existence of specific compounds in essential oils dominated inhibition effect on airborne bacteria. We will develop a screening model to suggest a formula of essential oils which can provide an effective inhibition on airborne microbes for indoor environment.

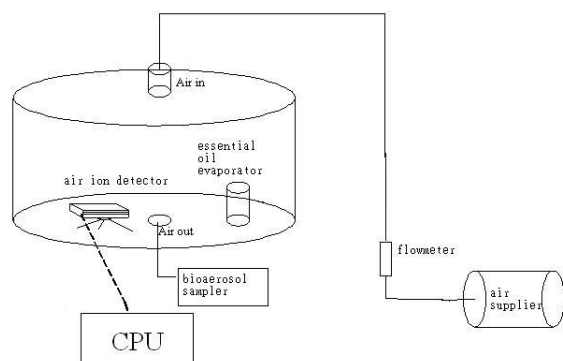


Figure 1. Experimental setup.

- Su, H.J., Chao, C.J., Chang, H.Y. & Wu, P.C. (2006). *Atmospheric Environment*, 41, 1230-1236.
- Dusan, F., Marian, S., Katarina, D. & Dobroslava, B. (2006). *Toxicology in Vitro*, 20, 1435-1445.
- Luo, C.H., Shih, Y. (2004). in *Proc. 11th Int. Conf. on Aerosol Science and Technology*, Taichung, Taiwan, 44.

## Aerosol particles in a metropolitan underground railway station

Imre Salma<sup>1</sup>, Tamás Weidinger<sup>2</sup>, Willy Maenhaut<sup>3</sup>

<sup>1</sup> Eötvös University, Institute of Chemistry, H-1518 Budapest, P.O. Box 32, Hungary

<sup>2</sup> Eötvös University, Department of Meteorology, H-1518 Budapest, P.O. Box 32, Hungary

<sup>3</sup> Ghent University, Institute for Nuclear Sciences, Proeftuinstraat 86, B-9000 Ghent, Belgium

Keywords: aerosol characterization, health aspects of aerosols, indoor air quality, traffic sources.

The metropolitan underground railway in Budapest is one of the oldest underground transport systems. Mass concentration, its temporal variation, elemental composition of the aerosol particles, their residence time, and sources in the metro were examined in one of its central stations (Astoria) by in situ aerosol measurements and sample collections.

The temporal variation of the PM<sub>10</sub> mass concentration (MC), horizontal wind speed and wind direction were determined with time resolutions of 30 and 4 s by a tapered element oscillating microbalance and wind monitor, and aerosol samples were collected by a stacked filter unit in the PM<sub>10-2.0</sub> and PM<sub>2.0</sub> size fractions on the platform. The samples were analyzed by gravimetry for the particulate mass, particle-induced X-ray emission spectrometry for elements, and light reflectometry for black carbon.

The diurnal variation of the PM<sub>10</sub> mass concentration exhibited two peaks, one at about 7:00, the other at about 17:00. The mean PM<sub>10</sub> mass concentration and standard deviation for the working hours were  $(155 \pm 55) \mu\text{g}/\text{m}^3$ . Iron, Mn, Ni, Cu, and Cr exhibited concentrations that were larger than outside by factors between 5 and 20, and these elements were substantially enriched with respect to both the average crustal rock composition and outside average aerosol composition, while black carbon showed a smaller concentration inside than outside. Iron made up for 40 and 46% of the PM<sub>10-2.0</sub> and PM<sub>2.0</sub> masses, respectively, and 72% of the PM<sub>10</sub> mass was associated with the PM<sub>10-2.0</sub> size fraction. Mechanical wear and friction of the electric cables and collectors, rails, and wheels, and resuspension were identified as the primary sources, which is consistent with the high time resolution MC measurement (see Fig. 1). The composition of the aerosol in the metro station is quite different from the average outside downtown aerosol above. Table 1 demonstrates that all underground railways presented uniformly exhibit significantly larger concentrations than the daily ambient (outside) EU PM<sub>10</sub> limit, and than that for the outside areas just above. Possible health implications for the passengers and workers in the metro will also be discussed.

This work was supported by the Hungarian Scientific Research Fund under grant K061193, and by the Belgian Federal Science Policy Office under contrs. EV/02/11A and BL/02/CR01.

Table 1. Ranges and averages of particulate mass concentration in the coarse and fine size fractions for different underground railways.

City	Range ( $\mu\text{g}/\text{m}^3$ )	Mean ( $\mu\text{g}/\text{m}^3$ )
Prague	—	103
Berlin	—	147
Budapest	85–234	180
Rome	71–877	407
Stockholm	212–722	469
London	500–1120	795
Cairo	794–1096	938

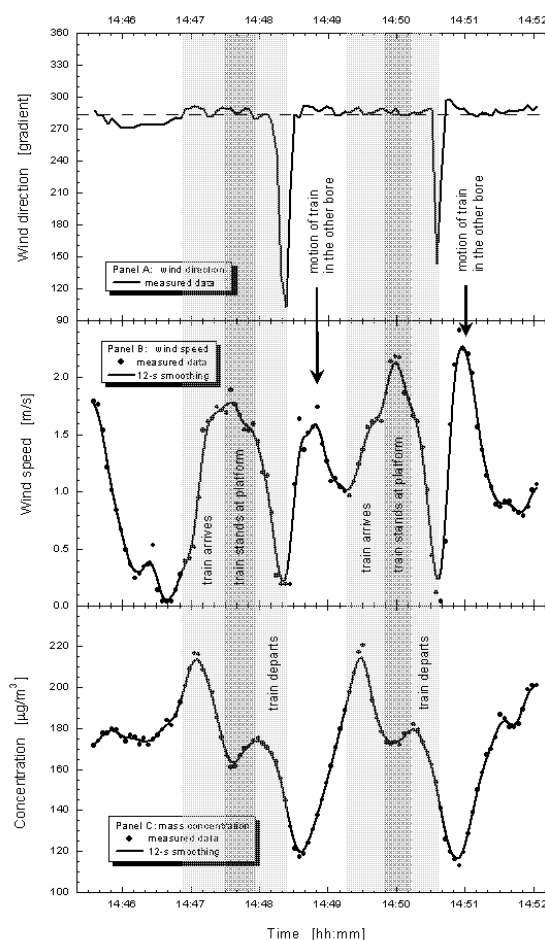


Figure 1. Temporal variation of wind direction, horizontal wind speed, and PM<sub>10</sub> mass concentration on 21 April 2006 at the Astoria metro station, Budapest.

## Feasibility study of LIDAR's measurements in an underground station

A.Fortain<sup>1,3</sup>, J.C.Raut<sup>2</sup>, P.Chazette<sup>2</sup>, K.Limam<sup>3</sup>, C.Cremezi Charlet<sup>1</sup>

1 SNCF, Direction de l'Innovation et de la Recherche 45 rue de Londres 75379 Paris cedex 8

2 CEA, Laboratoire des Sciences du Climat et de l'Environnement Centre de Saclay – DSM/LSCE bat. 706 - 91191 Gif-sur-Yvette Cedex

3 LEPTAB, Pôle sciences et technologies, avenue M.Crépeau 17042 La Rochelle CEDEX 01

Keywords: Aerosol measurement, Extinction coefficient, Indoor particle, Lidar, Particle concentration.

Indoor air quality has been studied for years especially in buildings, schools or industrial environments. Small enclosed spaces like offices, room or flat, start to be well known unlike underground station. As it presents particularly characteristics (big volume with complex air velocity distribution, typical aerosol...) traditional measurements devices are not sufficient to better understand what kind of phenomenon influence aerosol distribution. That's why a new technology is needed.

The development of LIDAR techniques for atmospheric sciences permit to significantly improved it so that it became a reference technical measurement in atmospheric research studies (Chazette, 2005). Because of its own operation, lidar can't be used in small volumes like offices or rooms but it can be interesting to test it in a bigger volume like an underground train station. That's why a measurement campaign has been realized during one week in a SNCF's enclosure with LAUV (Lidar Aerosol Ultra Violet) developed by LSCE.

The campaign took place on the platform of an underground station of Paris. Different measurements have been performed: aerosol extinction coefficient profile, PM<sub>10</sub> and PM<sub>2.5</sub> mass concentrations, size distribution (0.028 to 10µm), black carbon concentration, scattering and backscattering coefficient at 450, 550 and 700 nm, aerosol chemical composition in term of ionic and carbon concentration and temperature, pressure and relative humidity.

First results give good correlation between PM mass concentration and scattering coefficient (figure 1). All measurement device show day and night transitions due to traffic "on and off" periods. These transitions have also been observed in other studies in Stockholm (Johansson, 2002), Helsinki (Aarnio, 2005) and London, as the mass concentration's variations due to the alternation of rush hour and off-peak period.

Our study permit to show the aerosol size distribution variations. During traffic period, the

proportion of big particles is higher than during the night when traffic stopped.

Fine aerosol chemical composition is also different during day or night. It is mainly formed with dust and organic compounds but the proportion of these ones increase during night.

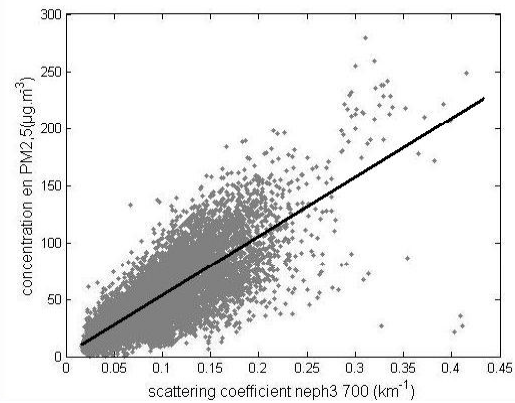


Figure 1 : correlation between PM<sub>2,5</sub> concentration and scattering coefficient at 700nm

The paper will present how LIDAR technology can be qualified for indoor air quality. It will also detailed measurements analysis that will permit to conclude about the interest of developing a lidar for indoor air quality.

Chazette P., P. Couvert, H. Randriamiarisoa, J. Sanak, B. Bonsang, P. Moral, S. Berthier, S. Salanave and F. Toussaint, *Three dimensional survey of pollution during winter in French Alps valleys*, Atmosph. Env., 39, 1345-1047, 2005

C.Johansson, *Particulate matter in the underground of Stockholm*, Atmospheric Environment 37, october 2002

P.Aarnio, *The concentrations and composition of and exposure to fine particles (PM<sub>2,5</sub>) in the Helsinki subway system*, Atmospheric Environment 39, may 2005

## Aerosol dynamics in a test chamber: experiment and modelling

J. Smolík<sup>1</sup>, A. Hruška<sup>2</sup>, P. Dohányosová<sup>1</sup>, T. Hussein<sup>3</sup> and J. Hemerka<sup>2</sup>

<sup>1</sup>The Laboratory of Aerosol Chemistry and Physics, ICPF AS CR, Rozvojová 2/135,  
165 02, Prague 6, Czech Republic

<sup>2</sup>Faculty of Mechanical Engineering CTU in Prague, Department of Environmental Engineering, Technická 4,  
166 07, Prague 6, Czech Republic

<sup>3</sup>Institute of Applied Environmental Science, Stockholm University, Frescativägen 54a,  
SE-10691 Stockholm, Sweden

Keywords: indoor particles, deposition, coagulation, modelling.

Aerosol particle contaminants in the indoor environment are considered to be one of the major pollutants of the atmosphere. Since human population is exposed to particulate matter mainly indoors, understanding of indoor aerosol behaviour is strongly required. Air filtration and ventilation are the mechanisms considered to be most important for reducing particle concentrations indoors. However, only limited information is available about other natural mechanisms such as deposition and coagulation, which are important especially in the buildings with low air-exchange rates. Particle deposition on the walls and other inner surfaces decreases the indoor aerosol concentration in any case, on the contrary coagulation, which reduces particle number and causes particle growth, affects aerosol especially in higher concentrations. Mechanism such as aerosol nucleation, evaporation, and condensation are considered to be of lesser significance in terms of affecting indoor processes.

Particle deposition onto indoor surfaces has been extensively studied by many researches (e.g. Byrne *et al.*, 1995, Thatcher & Layton, 1995, Mosley *et al.*, 2001 etc.), but in most of these works only monodisperse aerosol was involved. In this paper we present experimental results of monodisperse, bimodal and polydisperse aerosol. For experiments with polydisperse aerosol the influence of the initial particle concentration to coagulation has been examined.

A rectangular 1x1x1 m aluminium chamber was constructed for this study. The dimensions are small enough to provide a stable and manageable work size and large enough to provide insight into particle behaviour in a full-size room. The chamber is equipped with ports for filling the chamber by aerosol, sampling of aerosol, adjustment of the ventilation rate, and of temperature, pressure and relative humidity measurements. A mixer providing various mixing speeds, corresponding to friction velocities 1-12 cm/s, is mounted in the chamber. The construction is electrically grounded to avoid the electrical field. The temperature profiles inside the chamber have been monitored, the velocity turbulence intensity profiles was mapped out by a hot-wire anemometer. The chamber is relatively air-

tight, air consumed by used particle counters is compensated by an air pump to maintain pressure equilibrium.

The set of three different aerosol generation systems (AGK-2000 Palas, MAG 3000 Palas and flow-tube reactor) has enabled to produce monodisperse and/or polydisperse particles of various sizes from 8nm to 8µm. The experiments were based on particle loss measuring, which was carried out by monitoring the decay of the particle number concentration inside the chamber with SMPS 3934 or 3936, and/or APS 3021 (all TSI). A simple mass balance model based on "well-mixed" zonal approach (Wallace *et al.*, 2004) was used to determine the loss rates. The experimental results were compared with theoretical predictions of deposition model developed by Lai & Nazaroff (2000).

Indoor aerosol dynamics model (MC-SIAM) (Hussein *et al.*, 2005) was validated and evaluated with the chamber measurements. We found that self-coagulation process is negligible for nano-particles (below 50 nm) with concentrations below 30000 cm<sup>-3</sup>. However, the coagulation process strongly enhances with the presence of the coarse particle mode.

This model evaluation experience gave us good confidence in the chamber measurements and the performance of MC-SIAM model.

This work was supported by the GA CR under grant GA101/07/1361.

- Byrne M. A., Goddard A. J. H., Lange C., Roed J. (1995), *J. Aerosol Sci.*, 26 (4), 645-653.  
Hussein T, Korhonen H, Herrmann E, Hämeri K, Lehtinen K, Kulmala M. (2005) , *Aerosol. Sci. Tech.*, 39 (11), 1111-1127.  
Lai A. C. K., Nazaroff W. W. (2000), *J. Aerosol Sci.*, 31 (4), 463-476.  
Mosley R. B., et al. (2001), *Aerosol Science and Technology*, 34 (1), 127-136.  
Thatcher T. L. and Layton D. W. (1995), *Athmos. Environ.* 29(13), 1487-1497.  
Wallace L. A., Emmerich S. J. and Howard-Reed C. (2004), *Environ. Sci & Technol.* 38, 2304-2311.

## Single-particle characterization of seasonal aerosol samples collected at a subway station platform in Seoul, Korea

S. Kang, H. Hwang, M.S.I.Khan, Y. Park, E. Choi, H. Kim and C.-U. Ro

Department of Chemistry, Inha University, YonghyunDong, NamGu, 402-751, Incheon, Korea

Keywords: chemical analysis, field measurements, instrumentation, single particle analysis.

As people stay inside longer than outside, concern on air quality in indoor environment is increasing nowadays. Among various indoor environments, subway stations have some unique characteristics, i.e. they are very much closed place with various aerosol sources. Aerosols in subway stations can be generated by the movement of trains and passengers and also possibly by shopping activities at nearby underground stores. And thus the aerosol particles might be accumulated in this somewhat closed environment, resulting in the high concentration of particulate matters in the indoor air. PM<sub>10</sub> concentrations in subway station mainly depend on ventilation systems and train traffic intensity.

In this study, a single particle analytical technique, named low-Z EPMA (low-Z particle EPMA), was applied for the characterization of samples collected at a subway station platform in Seoul, Korea. The low-Z particle EPMA utilizes SEM/ED instrument, where the ED  $\gamma$ -ray detector is equipped with an ultra-thin window, and the technique can perform the quantitative determination of concentrations of low-Z elements such as C, N, and O as well in individual particles of micrometer size. The capability of the quantitative determination of low-Z elements in individual environmental particles improves the applicability of single particle analysis many environmentally important atmospheric particles (e.g. sulfates, nitrates, ammonium salt and carbonaceous particles) contain low-Z elements. Therefore, this low-Z particle EPMA is expected to provide more conclusive and detailed analysis on the chemical composition of the subway aerosols.

Eight samples were collected in the subway station (twice for each season in 2004-2005), using a seven-stage May cascade impactor. Cut-off diameters of May impactor from stages 1-5 are 16, 8, 4, 2, and 1  $\mu$ m, respectively. Major chemical species observed for the samples are carbonaceous particles such as carbon-rich and organic particles, aluminosilicates (notated as AlSi), AlSi/C, CaCO<sub>3</sub>, SiO<sub>2</sub>, and Fe<sub>2</sub>O<sub>3</sub> (see Figure 1). Fe-containing particles that come from frictions of brake block, subway train wheel, and electric contact materials, are the most abundantly encountered both in coarse and fine fractions: the relative abundances of the Fe-containing particles are in the range of 50-70%, and those particles exist in the chemical forms of Fe<sub>2</sub>O<sub>3</sub>, Fe<sub>2</sub>O<sub>3</sub>/C, (Si, Fe)O<sub>x</sub>, (Si, Fe)O<sub>x</sub>/C and etc. The iron-containing particles are well known to be main chemical species in the

underground subway micro-environment, and it was reported that those particles might adversely influence human health. Some particles such as carbonaceous and soil-derived particles might come from the outdoor. However, reacted sea-salts and ammonium sulfate particles must come from the outdoors, and it is possible, even roughly, to estimate the extent of outdoor influence on subway aerosols by observing the amount of the apparent outdoor aerosols. In this study, it is observed that there exist no significant seasonal variations of chemical compositions for the samples (see Figure 2).

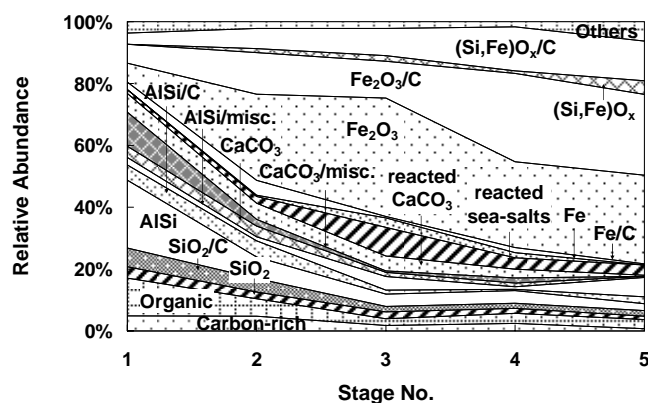


Figure 1. An exemplar size-segregated relative abundances of chemical species observed in a underground aerosol sample collected at HyeHwa (Seoul, Korea) subway station platform on Nov. 23, 2005.

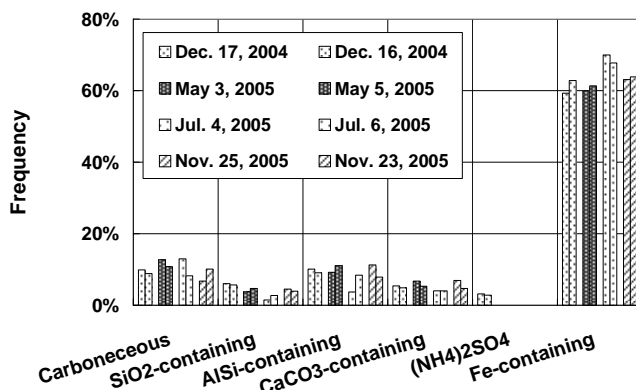


Figure 2. Overall relative abundances of significantly encountered particle types.

## Indoor measurements of domestic UFP sources

N. Bleux; P. Berghmans; F. Deutsch ; S. Janssen; J. Vankerkom; M. Van Poppel; R. Torfs

<sup>1</sup> VITO – Flemish Institute for Technological Research Boeretang 200, B-2400 Mol, Belgium

Keywords: Indoor aerosols, ultrafine particles, generation of nanoparticles, aerosol modelling.

Indoor dust concentrations and ultra fine particles in ambient air are currently two topics which are receiving increasing amounts of attention.

In order to validate a new indoor dispersion model, a number of experiments were performed in a test chamber. simulating the exposure of ultra fine particles generated by domestic activities.

A test chamber of 36 m<sup>3</sup> was modified using controllable fans in order to regulate the refresh rate of the room. Real life conditions were obtained using indoor sources like burning of candles (different types), oil lamps, incense, smoking cigarettes, gas cooking, frying meat and making French fries (Table 1).

source	UFP concentration* (#/cc)	Size** (nm)
Meat frying	620 000	60
French fries	30 000 – 50 000	200 - 250
Gas cooking	6000	20
Candles***	3 000 – 40 000	20 - 40
Oil lamps	175 000 - 350 000	230
Cigarette	160 000 – 350 000	75 - 100
Incense	120 000 – 250 000	100 - 120

Table 1. Comparison of different indoor UFP sources.

\* test were performed several times under different working conditions.

\*\* Size: modus of the size distributions (number concentration based).

\*\*\* 3 different candle types were used.

During 2 weeks of intense testing we used an extensive array of equipment. Temperature, relative humidity and ventilation speeds (refresh rates) were monitored for later use in the dispersion model. Ultra

fine particles were measured with a SMPS (model 3080 from TSI) while fine dust concentrations were measured with an optical dust monitor (Grimm 1.108 Dust Monitor). TVOC and NO<sub>x</sub> were monitored continuously and specific VOC (benzene, toluene, ...) were sampled for offline analyses.

Both number concentration and size distribution varied significantly between different indoor sources, but also between different tests of the same type of source (Table 1 and Figure 1). In a similar test set-up, different brands of tea light candles were measured, showing a concentration range of 3000 vs. 40 000 particles/cc.

Different cooking activities were performed without the use of a cooker hood, simulating a worst case scenario of indoor concentrations. The results demonstrate that some cooking activities like meat frying emit higher concentrations of particles compared to the smoking of cigarettes (see Figure 1).

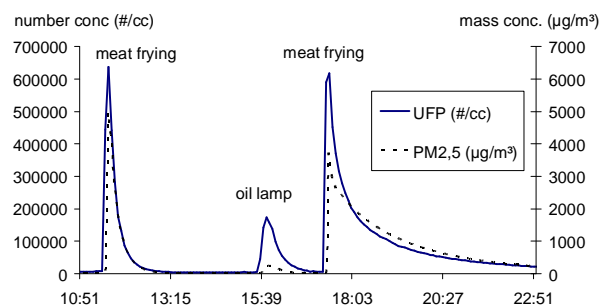


Figure 1. comparison for fine dust (mass based) and ultra fine dust concentrations (number based).

## Monitoring of aerosolized black carbon in a pulmonary hospital

M. Vardjan<sup>1</sup>, G. Močnik<sup>1</sup> and A. Zrimec<sup>2</sup>

<sup>1</sup>Optotek d.o.o., Stegne 13a, SI-1000 Ljubljana, Slovenia

<sup>2</sup>Institute of Physical Biology, Veliko Mlačevo 59, SI-1290 Grosuplje, Slovenia

Keywords: Aerosol measurement, Black carbon, Indoor/outdoor particles, Hospital.

Fine particulate matter has adverse effects on human health and is more strongly associated with mortality than coarse particles (Dockery *et al.*, 1993). Black carbon (BC) is associated with severe health effects (Jansen *et al.*, 2005).

Black carbon concentrations in indoor and outdoor air were measured at a pulmonary hospital in Golnik, Slovenia. Three Aethalometer™ (Magee Scientific, USA) instruments were installed to sample air from the parking lot (L), ward hall (W) and a patient room (R). The Aethalometer samples aerosols on filter tape and measures BC concentration with optical transmission (Hansen *et al.*, 1984). Size selective cyclones (BGI, USA) were attached to measure particles with aerodynamic diameter of 2 µm or less. Measurements were carried out continuously for 44 days during October and November 2006. Due to sensitive hospital environment and prolonged campaign, special care was taken to cause as little disturbance as possible. This included operating at a very low flow rate, which resulted in increased measurement noise and subsequent digital signal processing was required.

BC concentration according to the day of week was analysed. On weekdays, the morning peak associated with the traffic is very distinct (Fig. 1). On weekends, the morning peak is delayed and less distinct, possibly due to different time characteristics of traffic and domestic heating (Fig. 2).

Inside and outside concentrations were cross correlated in time for both infra red (IR) and ultra violet (UV) channel separately. Both results are consistent and show that indoor concentrations follow the outdoor concentration with time lag of about 30 minutes.

Immediately after this campaign, the same instruments were used to measure BC concentrations in the city of Ljubljana, about 30 km from the hospital. The measured BC concentrations were about 3 times higher than those at the hospital, which confirmed the standing, but not yet quantitatively proven reputation of Golnik clean air.

This work was partially supported by the Ministry of Higher Education, Science and Technology of Slovenia (3211-05-000548) and Technology Agency of RS (TP MIR 06/RR/02). Authors wish to thank the staff and patients at KOPA Golnik for their help and patience, and Anthony Hansen for instrumentation.

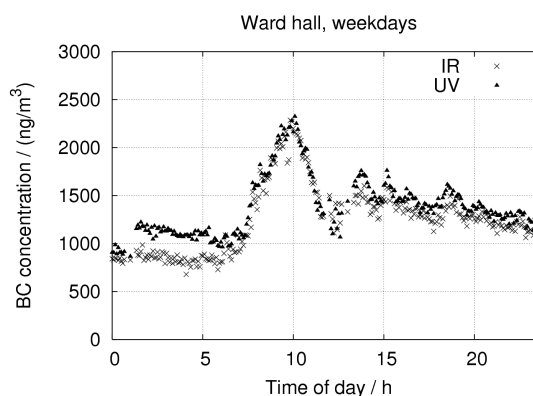


Figure 1. Monday-Friday indoor BC concentrations, calculated as median of all weekdays.

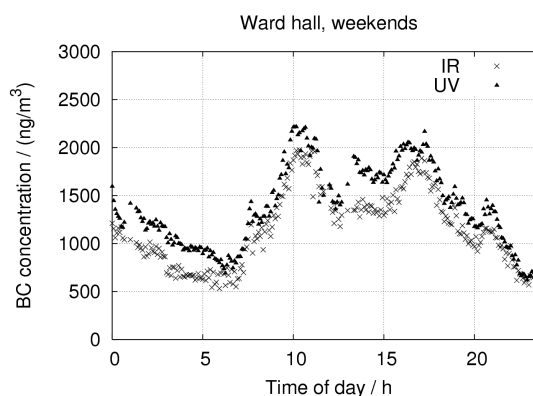


Figure 2. Saturday-Sunday indoor BC concentrations, calculated as median of all weekends.

Jansen, K. L., Larson, T. V., Koenig J. Q., Mar T. F., Fields, C., Stewart, J., Lippmann, M. (2005). *Associations between Health Effects and Particulate Matter and Black Carbon in Subjects with Respiratory Disease*. Thorax, 60, 455-461.

Hansen, A. D. A., Rosen, H., Novakov, T. (1984). *The Aethalometer - An instrument for the real-time measurement of optical-absorption by aerosol-particles*. Science of the Total Environment, 36, 191-196.

Dockery, D. W., Pope, C. A. 3rd, Xu, X., Spengler, J. D., Ware, J. H., Fay, M. E., Ferris, B. G. Jr, Speizer, F. E. (1994). *An association between air pollution and mortality in six U.S. cities*. New England Journal of Medicine, 329, 1753-1759

## Particles in various Swedish indoor environments: size distributions, number and mass concentrations

A. Wierzbicka<sup>1</sup>, A. Gudmundsson<sup>1</sup>, J. Pagels<sup>1</sup>, A. Dahl<sup>1</sup>, J. Löndahl<sup>2</sup>, E. Swietlicki<sup>2</sup> and M. Bohgard<sup>1</sup>

<sup>1</sup>Division of Ergonomics and Aerosol Technology (EAT), Lund University, Box 118, SE-221 00, Lund, Sweden

<sup>2</sup>Division of Nuclear Physics, Lund University, Box 118, SE-221 00, Lund, Sweden

Keywords: indoor particles, indoor air quality

Even though people on average spend at least 85% of their time inside buildings, the concentration and characteristics of particles in indoor environments are not well known. Until recently most research was focused on ambient air particles. Indoor particles originate from indoor sources, penetrate from ambient air or are formed indoors as secondary aerosol (e.g. chemical reactions of ozone and terpenes). Indoor sources of coarse particles have been identified as sweeping, hoovering, dusting, resuspension from clothes and carpets (Howard-Reed et al., 2003; Ogulei et al., 2006), while the fine fraction was identified to come from cooking, gas stoves, electric ovens or toaster ovens, gas-powered clothes dryers, burning candles and incense (Wallace, 2006). The aim of this study was to gain information about particle loads and their characteristics in various Swedish indoor non-industrial environments, namely: in the school, fast food restaurant, supermarket, residential apartment close to busy road in a polluted city and residential house in a remote area. Results from the first three locations are presented here.

Measurements were performed for seven consecutive days in each location between September 2006 and February 2007. Log books of activities during the measurement period were created for the identification of particles' sources. Measurements were recorded continuously with the following instruments: an aerodynamic particle sizer TSI APS 3321, a scanning mobility particle sizer (SMPS), (consisting of differential mobility analyzer (TSI DMA 3071) and condensation particle counter (TSI CPC 3010)), and two DustTracks TSI model 8520. Into the sampling system a valve was incorporated enabling alternate measurements of indoor and outdoor, or indoor and supplied ventilation air by the SMPS. The two DustTracks were used for indirect mass concentration measurements of particles smaller than 2.5  $\mu\text{m}$  (PM<sub>2.5</sub>) down to 0.1  $\mu\text{m}$ , they enabled simultaneous measurement of indoor and outdoor mass concentration. PM<sub>2.5</sub> were also collected on quartz filters for organic and elemental carbon analysis.

The highest average PM<sub>2.5</sub> mass concentration was measured in the school (39  $\mu\text{g}/\text{m}^3$ ), while the lowest in the supermarket (20  $\mu\text{g}/\text{m}^3$ ). In the school fine particles (smaller than 1  $\mu\text{m}$ ) mirrored the outdoor number concentration

and size distribution, it could be explained due to lack of indoor sources of fine particles (no cooking, candle burning etc.) and high penetration ratios. In the fast food restaurant and in the supermarket differences in the fine mode concentration and size distribution between indoor and supplied ventilation air are visible which indicates presence of strong indoor sources. Daily average number size distributions for the school, fast food restaurant and supermarket are given in Figure 1.

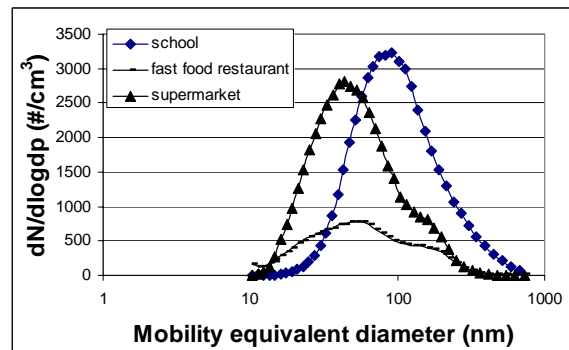


Figure 1. Daily average number size distribution of fine particles in the school, fast food restaurant and supermarket.

The average total number concentration of fine particles in the size range from 10 to 800 nm were 2100, 1900 and 700  $\#/\text{cm}^3$  for the school, supermarket and fast food restaurant, respectively. This indicates that removal of fine particles in the fast food restaurant ventilation system was more efficient than in the school.

This study shows that mass and number concentrations of particles in different indoor environments can vary to a great extent. To gain knowledge about typical levels of particles in various indoor environments more data is needed as this study is limited to just few locations at specific time.

Acknowledgements: This study was supported by the Swedish Research Council FORMAS.

Howard-Reed C., Wallace L.A., Emmerich S.J. (2003) *Atmospheric Environment* 37, 5295-5306.

Ogulei D., Hopke P.K. & Wallace L.A. (2006) *Indoor Air*, 16, 204-215.

Wallace L., (2006) *Aerosol Science and Technology*, 40, 348-360.

## Physical and Chemical Properties of Fine Particles Emitted from Candles

J. Pagels<sup>1</sup>, A. Wierzbicka<sup>1</sup>, A. Dahl<sup>1</sup>, E. Swietlicki<sup>2</sup> and M. Bohgard<sup>1</sup>

<sup>1</sup>Div. of Aerosol Technology (EAT), and University, SE-221 00, P.O. Box 118, and, Sweden

<sup>2</sup>Division of Nuclear Physics, and University, and, Sweden

Keywords: Indoor Particles, Candles, Hygroscopicity, Volatility, Combustion Particles

Candles have appeared as a source of fine and ultrafine particles in indoor air (e.g. Hussein et al. 2006). Fine et al. (1999), found high Organic Carbon (OC) emissions connected to the extinction of the candle and high EC concentrations when the flame was burning unsteady. ai et al. (2006) identified three different particle types from size distribution analysis. However, the connection between the chemical composition and the physical particle properties remains unclear. The aim of this work was to gain more insight into the physical and chemical properties and the formation mechanisms of the different particle types emitted from candles.

The experiments comprised candles of ten different brands, including paraffin, stearin, bees wax and scented fuels. Emissions were studied in a 25 m<sup>3</sup> air-tight steel-chamber where the background particle concentration was lower than 100 cm<sup>-3</sup>. The air exchange ratio was 2 h<sup>-1</sup>. A fan was used to ensure mixing in the chamber. In a typical experiment a candle was lighted and let burn continuously for approximately 3 hours. Particle size distributions in the room were measured using two SMPS system (10-1000 nm). A TEOM was used to determine the average effective density by combining the SMPS and TEOM data. Samples for morphology were collected using an electrostatic precipitator and the morphology was studied with Transmission Electron Microscopy. Particles were separated according to volatility and hygroscopicity using Tandem Differential Mobility Analyzers (TDMAs). The chemical composition was determined from filter and low pressure impactor samples analyzed using Ion Chromatography (IC water soluble ions), Particle Induced -ray Emission (PI E metals) and Evolving Gas Analysis (OC/EC).

High concentrations (10<sup>6</sup> cm<sup>-3</sup>) of ultrafine particles were detected during steady burning of a single candle. Particles aged 2-5 min were in the range of 10 to 25 nm. These particles acted as coagulation sink and a bimodal size distribution developed with one mode of fresh particles and a mode of larger aged particles (up to 100 nm). Dependent on candle type, two different categories of particles were detected during steady burning using the volatility and hygroscopicity analysis.

Type 1a particles had hygroscopic growth factors (*G<sub>f</sub>*) of around 1.8 at 90 RH and were volatilized at 400 C in the Thermodesorber in the VTDMA analysis. These particles were rich in Potassium and

Nitrate and contained relatively high concentrations of metals such as Cu and Sn.

Type 1b particles had hygroscopic growth factors of around 1.6 at 90 RH and were volatilized at 150°C in the VTDMA analysis. These particles were rich in phosphate and contained less metals.

**Table 1.** Physical and chemical properties of the different particle types emitted from candles.

Type	Mean Particle Size (nm)	G <sub>f</sub> (90 %)	Evaporation in TD (°C)	Main Components	Morphology
1a	15-30	1.8	400	K <sup>+</sup> , NO <sub>3</sub> <sup>-</sup>	Compact
1b	10-25	1.6	150	K <sup>+</sup> , PO <sub>4</sub> <sup>3-</sup>	Compact
2	200-250	1.05	600	Soot	Aggregate
3	30-100	low	70	OC	Compact

When the flame was exposed to increased air flows, the flame started flickering. A larger sized mode appeared in the size distribution. These particles (Type 2) were essentially non volatile (up to 600° C) and hydrophobic. TEM analysis revealed highly agglomerated carbon rich particles. The average effective density was 0.3 g/cm<sup>3</sup>. These are features similar to soot from other sources such as diesel exhaust.

As the candle was extinguished white smoke appeared. These particles (Type 3) were volatile at around 70 C. This indicates organic components from evaporation and condensation of the fuel, as has been described previously (Fine et al. 1999).

In conclusion distinctly different particle types are emitted from candles. The water soluble particles emitted during steady (optimal) combustion may need to be treated differently from soot particles in future health risk estimates of fine and ultrafine particles in indoor air.

**Acknowledgements:** This study was supported by the Swedish Research Council FORMAS.

Fine PM, Cass GR and Simoneit BRT. (1999) *Env. Sci. & Techn.* 33: 2352-2362.

Hussein T, Glytsos T, Ondracek J, Dohanyosova P, dimal V, Hameri K, azaridis M, Smolik J and Kulmala M. (2006). *Atmos. Env.* 40: 4285-4307.

ai S, hen H and Jia-Song W. (2006) *J. Aerosol Sci.* 37: 1484-1496.

## Gravimetric and optical aerosol measurements in an industrial workplace and the impact of the measurement uncertainty on the calculated inhaled dose

S. Vratolis<sup>1</sup>, Mitsakou C<sup>1</sup>, K. Eleftheriadis<sup>1</sup>, A. Karanasiou<sup>1</sup>, C. Housiadas<sup>1</sup>, M. Lazaridis<sup>2</sup>

<sup>1</sup>Institute of Nuclear Technology and Radiation Protection, N.C.S.R. “Demokritos”, Ag. Paraskevi, Attiki, 15310, Greece

<sup>2</sup>Technical University of Crete, Department of Environmental Engineering, 73100 Chania, Crete, Greece

Keywords: Indoor aerosols, Lung deposition, Instrumentation/Phys. characterisation

PM<sub>10</sub> and size distribution measurements were carried out in a detergent factory. A Berner impactor and a DataRAM 4 (DR4) nephelometer were used amongst other instruments. In order to estimate the uncertainty introduced into the calculation of the inhaled dose when the PM<sub>10</sub> mass obtained by an optical instrument is employed, calculations of the lung deposition were performed applying a Eulerian model with a sectional representation of aerosol size distribution.

The industrial sampling site is located in Athens area. Apart from its own emissions, it is influenced by other industries in the area and motorway traffic. The measurements were carried out on July 2005. Inside the factory, the average relative humidity during July 2005 was 47 ±16% and the temperature was 30 °C ±4%. A Berner impactor was employed with 50 % cut off aerodynamic diameters at 0.026, 0.062, 0.110, 0.173, 0.262, 0.46, 0.89, 1.77, 3.4, and 6.8 µm. The DR4 two-wavelength nephelometer utilising two light beams at 660 and 880 nm within a confined space with active air sampling was also employed. Based on the ratio of the signals detected at 660 and 880 nm the volume median particle diameter is determined and the PM<sub>10</sub> mass is computed, when a lognormal mass size distribution and constant particle density value at 2.6 g cm<sup>-3</sup> is assumed. The sampling point was on a rack, at a height of 2 meters. A typical aerosol mass size distribution measured by the Berner impactor and inferred by the DR4 nephelometer is presented in Figure 1.

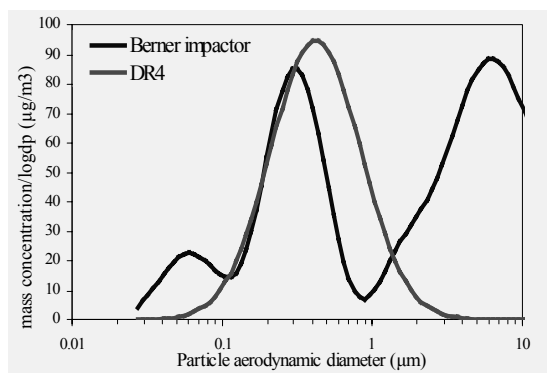


Figure 1: Measured size Distribution of aerosol mass concentration during working hours The mass size distribution can be approximated by two

lognormal modes with parameters ( $\sigma_g$ =geometric standard deviation,  $d_p$ =geometric mean aerodynamic diameter).shown in table 1.

Table 1: Characteristics of the aerosol size distribution on 6/7/2005

$\sigma_{g1}$	$d_{p1}$	Mass <sub>1</sub>	$\sigma_{g2}$	$d_{p2}$	Mass <sub>2</sub>
1.61	0.30	43.19	2.37	6.38	79.92

In order to assess the difference in lung deposition of the above measured mass concentrations, a mechanistic inhalation dosimetry model, which includes aerosol dynamics (Mitsakou et al., 2005), was used. The model solves numerically the aerosol general dynamic equation (GDE) along the flow direction, as the aerosol passes through the regions of the respiratory tract. The thoracic geometry is described by Weibel’s model “A” – the respiratory tract has the form of an airway tree, where the airways branch dichotomously from generation 0 (trachea) to generation 23.

The deposited mass on lung regions, namely, ET: extrathoracic region, TB: tracheobronchial region (Generations 0-15), AI: Alveolar region (Generations 16-23) is given on Table 2

Table 2: Deposited Mass in ng per breath.

6/7/2005	ET	TB	AI
Berner	66	186	316
DR4	4	268	490

It is observed that a modest deviation between measurements by DR4 and Berner impactor in the fine mode, may result in significant under or over estimations of the inhaled dose.

### Reference

Mitsakou, C., Helmis, C., Housiadas, C., “Eulerian modelling of lung deposition with sectional representation of aerosol dynamics”, J. Aerosol Sci., 36, 75-94, 2005

## Researchers exposure to particles in nanomaterial production laboratories

Evangelia Demou<sup>1</sup>, Stefanie Hellweg<sup>1</sup>, Wendelin J. Stark<sup>2</sup>, Sotiris E. Pratsinis<sup>3</sup>

<sup>1</sup>Institute of Environmental Engineering, ETH Zurich, Zurich, CH-8093, Switzerland

<sup>2</sup>Institute of Chemical and Bioengineering, ETH Zurich, Zurich, CH-8093, Switzerland

<sup>3</sup>Institute of Process Engineering, ETH Zurich, Zurich, CH-8092, Switzerland

Keywords: indoor particles, exposure, number size distribution, PM1

The number of researchers working in laboratories producing or using nanomaterials are increasingly exposed to particles. Therefore, studies analyzing such exposure situations are required.

Condensation Particle Counters (CPC) and aerosol monitors in parallel with a Scanning Mobility Particle Sizer<sup>TM</sup> (SMPS) were used to quantify real-time size and number concentrations in nanoparticle production laboratories. All sites used the same technology to generate particles of different composition and size, under various production conditions. Spatial and temporal analysis of the particle concentrations and sizes were performed. Characterization of concentrations near the source of emission, i.e., breathing zone, and those at secondary stations were quantified. Additionally, the influence of environmental conditions was investigated.

The results show that researchers in nanoparticle production laboratories may be exposed to elevated concentrations during the production process. Number concentrations can be more than an order of magnitude higher than background levels, while maximum concentrations recorded were over 150,000 cm<sup>-3</sup>. Further, the size distribution showed that primary particle production leads to airborne nanoparticle and submicron particle exposure (Figure 1).

Current research suggests that size by itself may be one determinant of toxicity. Current occupational thresholds are mass based, while studies evaluating possible threshold metrics suggest particle number and possibly surface area as better indicators of exposure (Aitken et al. 2004). Therefore, mass and number concentrations of the airborne particles were analyzed. In many cases (Figure 1) these followed the same profile and correlated with production activities. However, the pattern of mass concentration was not always consistent

with number concentrations. In particular, some very significant rises in number concentrations were not reflected by the mass-concentration measurements. These findings question the appropriateness of mass concentration as a monitoring metric.

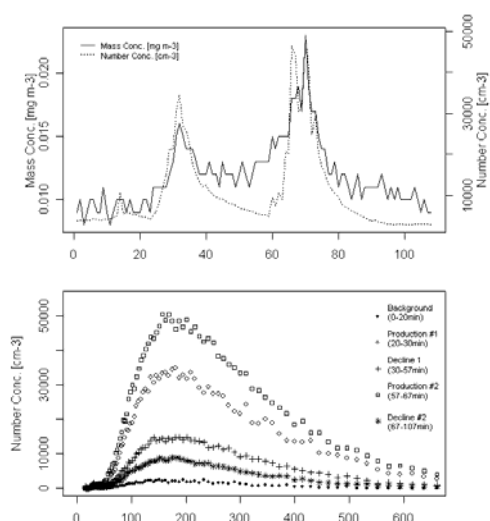


Figure 1. Number and mass concentration during background and production conditions (above). Corresponding particle size distributions (below).

Further exposure determinates, such as common laboratory practice and workers' behavior were investigated, and suggestions for good laboratory practice for nanomaterial production facilities were made.

This work is relevant for health officials, companies and those working in the field of nanoparticle production, as it allows for minimization of risks and provides indications for a safe occupational environment.

Aitken RJ, Creely KS, Tran CL. 2004. Nanoparticles: An Occupational Hygiene Review. Edinburgh: Institute of Occupational Medicine (IOM).

## **The origin of indoor PM<sub>2.5</sub> at a residence in Melbourne, Australia**

J.C. Powell<sup>1</sup>, G.P. Ayers

<sup>1</sup>CSIRO Marine and Atmospheric Research, Aspendale, 3195, Melbourne, Australia

Keywords: PM<sub>2.5</sub>, Indoor air quality, Indoor/outdoor particles.

Australians may spend 90% or more of their time indoors, particularly in their house. It is often assumed that indoor households provide a level of protection against exposure to outdoor pollutants such as PM<sub>2.5</sub>, but contributions from indoor sources can result in higher indoor concentrations than outdoors. A greater understanding of the contributions of indoor and outdoor sources to indoor PM<sub>2.5</sub> offers improved exposure estimates for health studies and helps to identify the major influences on exposure to PM<sub>2.5</sub> indoors.

To quantify the contribution to indoor PM<sub>2.5</sub> from indoor and outdoor sources, a measurement campaign was carried out at a suburban Melbourne house over a 7-week period in winter. The campaign included real-time measurements of indoor and outdoor aerosol light-scattering, meteorological conditions and 24-hour average gravimetric PM<sub>2.5</sub>.

A time-activity diary was used to identify periods of no activity within the household. It was assumed that during these periods, indoor PM<sub>2.5</sub> originated only from outdoor sources. This assumption was tested using measured outdoor PM<sub>2.5</sub> concentrations in a mass-balance model to predict indoor PM<sub>2.5</sub> during periods of no activity. The best-fit model output provided a correlation of R=0.98, indicating that during periods of no household activity most PM<sub>2.5</sub> originated outdoors. The difference between the best-fit model predictions and measured PM<sub>2.5</sub> during periods of household activity was then used to determine the contribution from indoor sources resulting from activities such as cooking and cleaning.

This poster presents results on the contributions from indoor activities and outdoor sources to indoor PM<sub>2.5</sub>.

## **T08 Abstracts**

## Model for the deposition of fine and ultrafine aerosol particles in rat lungs

G.A.Ferron<sup>1</sup>, J. Gentry<sup>2</sup>, E. Karg<sup>1</sup>, O. Schmid<sup>1</sup> and S. Takenaka<sup>1</sup>

<sup>1</sup>Institute for Inhalation Biology, GSF – National Research Centre for Environment and Health, D-85758 Neuherberg/Munich; Germany

<sup>2</sup>Department of Chemical and Nuclear Engineering, University of Maryland, ML, USA

Keywords: health aspects of aerosols, particle deposition, modelling, rat lungs

Rats are commonly used for studies on the health effects of aerosols. Since airways offer the main entranceway for particles into the organism, lung-deposition models of inhaled particles are an important aspect for these studies (Anjilvel & Asgharian, 1995, MPPD model, 1999). Here a model for man (Ferron et al., 1988) is adapted to the rat lung using structure analysis of the lung and the nasal cavity of rats (Yeh et al., 1979, Schreider & Raabe, 1981). Calculated particle deposition using this model is compared with results from the MPPD model as well as with experimental data for fine particles (aerodynamic diameters  $d_a > 0.2 \mu\text{m}$ : Raabe et al., 1988; and others) and recent data for ultrafine particles (volume equivalent diameter  $d_e < 0.1 \mu\text{m}$ : Takenaka et al., 2004) including nasal deposition data ( $d_e < 0.2 \mu\text{m}$ : Gerde et al., 1991).

Standard respiration conditions are a tidal volume of  $2.1 \text{ cm}^3$  and a respiration frequency of  $102 \text{ min}^{-1}$  (Anjilvel & Asgharian, 1995) for a rat with body weight of 330 g. Spherical monodisperse particles were assumed to have a density of  $2 \text{ g cm}^{-3}$  as frequently used in animal studies.

Total particle deposition is shown in Figure 1 calculated with the present model, the MPPD model and experimental data from literature. The present model differs by more than 20% from the MPPD model for  $0.2 < d_a < 1.5 \mu\text{m}$ , which is smaller than the variations of the experimental data.

Since considerable uncertainties are present in the input parameters of the model, we used this model to investigate the sensitivity of total particle lung deposition. We varied the parameters by a factor of 2 (unless stated otherwise) and list the size range for which changes in excess of 20% in total deposition (Figure 1) are found:

- size of the nose for  $d_e < 0.01 \mu\text{m}$ ,
- size of the alveolar ducts and sacs for  $0.2 < d_a < 1.5 \mu\text{m}$ ,
- total lung volume for  $0.02 < d_a < 1.5 \mu\text{m}$ ,
- most respiration conditions for  $d_a < 3 \mu\text{m}$ ,
- particle density less than 0.5 for  $d_a < 1.5 \mu\text{m}$  and for  $d_e > 0.3 \mu\text{m}$ ,
- geometric standard deviation larger than 1.6.

On the other hand, total deposition calculated for different body weights corrected for changes in

tidal volume and respiration frequency (Guyton, 1949) and resting conditions do not change more than 20% for all.

Finally, we note that total deposition for  $d_e < 0.03 \mu\text{m}$  and  $0.03 < d_a < 2 \mu\text{m}$  is dominated by losses in the nose and alveolar ducts, respectively. The sizes of nose and alveolar ducts can be used to optimize the present deposition model.

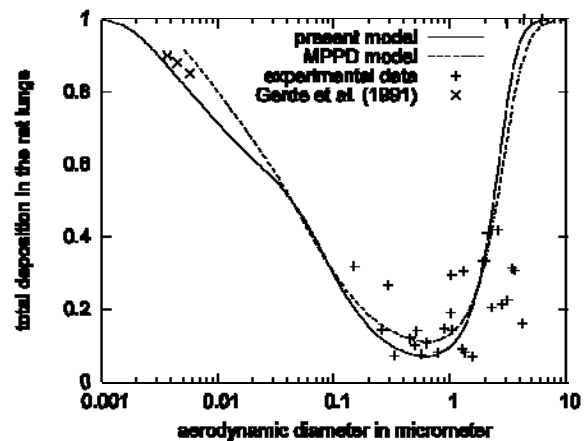


Figure 1. Total deposition of monodisperse aerosol particles in the rat lungs.

- Anjilvel, S. & Asgharian, B. (1995). *Fund. Appl. Toxicol.*, 28, 41-50.
- Ferron, G. A., et al. (1988). *J. Aerosol Sci.*, 19, 343-363 & 611-633.
- Gerde, P., et al. (1991). *Fund. appl. Toxicol.*, 16, 330-336.
- Guyton, A. C. (1947). *Am. J. Physiol.*, 150, 78-83.
- MPPDep (1999). Multiple-path Particle Deposition Model, MPPDep v1.11. the Chemical Industry Institute of Toxicology (CIIT), USA, and the National Institute of Public Health and the Environment (RIVM), the Netherlands.
- Raabe, O. G., et al. (1988). *Ann. occup. Hyg.*, 32, Suppl. 1, 53-63.
- Schreider, J. P. & Raabe, O. G. (1981). *Anatomical Record* 200, 195-205.
- Takenaka, S., et al. (2004). *Inhal. Toxicol.*, 16 (Suppl. 1), 83-92.
- Yeh, H. C., et al. (1979). *Anat. Rec.* 195, 483-492.

## CFD modelling of transient aerosol transport and deposition in human airways

M. Forman, M. Jicha, J. Katolicky

Faculty of Mechanical Engineering, Brno University of Technology, Technicka 2, 61669, Brno, Czech Republic

Keywords: Aerosol modelling, CFD, lung deposition

The paper presents results of computational modeling of aerosol transport and deposition of three different size classes in the upper human airways down to 6<sup>th</sup> bifurcation. As a geometrical model, a real CT scan of a living human was acquired from St. Anna University hospital in Brno – see Fig.1. The scan was transported into \*.stl format, then smoothed and cleaned off unnecessary details and by means of an automatic mesh generator, first the surface and then the volume mesh were created.



Fig.1 CT scan of human airways

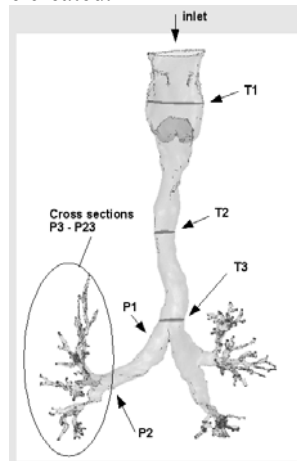


Fig.2 Solution domain

For modeling purposes, the nasal/oral cavity was omitted and the inlet to the airways was above the glottis. The solution domain with selected planes in which results were analyzed is in Fig.2 (human front view). The model contains 3 millions of control volumes. Commercial CFD code StarCD was used.

Two regimes, namely resting conditions and maximum exercise were simulated with the inlet conditions given in Tab.1. Both regimes were calculated in the transient mode inspiration /expiration that followed a sinusoidal curve.

Tab.1 Inlet conditions

	Resting conditions	Maximum exercise
Tidal volume $V_t$ [liter]	0.5	3.33
Flow rate [l/min]	7.5	120
Frequency [Hz]	0.25	0.8
Period [s]	4	1.25

Three size classes were assumed in the inlet to the trachea according to Tab.2.

Tab.2 Aerosol characteristics

Particle diameter [ $\mu\text{m}$ ]	Concentration [ $\mu\text{g}/\text{m}^3$ ]
10	25
5	9
1	16

Calculations were done using standard k- $\epsilon$  model of turbulence and Euler-Lagrange Eddy Interaction Model for particles transport; inlet conditions were ascribed as “inlet”, outlet as pressure conditions with identical relative pressure in all airways terminations.

Results show a strong asymmetry in the flow rate distribution between the left and right airways under the resting conditions (only 17% of air goes to the right airways); at the maximal exercise the asymmetry almost vanishes. This asymmetry could be partially attributed to the model itself, partially to the flow pattern above the plane T3 (see Fig.2). A transverse vortex forms behind the bend upstream the plane T3 that partially blocks the flow into the right airways. The PM deposition results from the flow field, so we can see strongly asymmetric deposition between the left and right airways for resting conditions. Sums of the left and right airways deposition (in % of the inlet) of the individual size classes is in Fig.3. We can see quite different deposition for resting and maximum conditions on one hand and on the other hand a very different deposition of PM1 at resting conditions compared with PM5 and PM10.

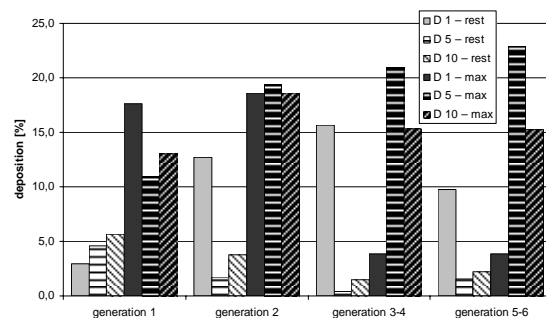


Fig.3 Aerosol deposition under resting conditions and maximum exercise for 3 size classes

The work was supported by the Czech Ministry of Education and Youth under COST project 1P05OC028.

## Human nasal passage fibrous particle deposition: the influence of particle length, flow rate and passage geometry

Zuocheng Wang, Philip K. Hopke

Center for Air Resources Engineering and Science, Clarkson University, 13699, Potsdam, NY, USA.

Keywords: fibrous particle deposition, human nasal passage, glass fiber, head loss.

The filtration efficiency of the nose during nasal inhalation determines the fraction of airborne particles reaching the lung. Recent research has shown that fibrous particles have higher penetration through human respiratory airway compared with equivalent spherical particles. In this study, human nasal models were constructed from MRI files of human nasal passage using a stereolithography system. Airborne glass fibers were passed into these models to investigate the effect of particle length, flow rate and passage geometry on nasal deposition efficiency. A dielectrophoretic fiber classifier (Baron *et al.*, 1994; Wang *et al.*, 2005) was used to produce an aerosol with the fibers within a specific length range. This study found that the fiber deposition increases with increasing flow rates and the deposition efficiency generally increases with increasing fiber length. It was noted that the deposition efficiency was generally proportional to total head loss across the nasal model. The pressure drop across the model can be calculated from geometrical sizes of the nasal passage.

The experimental setup consists of the aerosol generation system, the humidifier and classifier, flow distribution system, and nasal deposition section. The classifier generated length segregated glass fibers and that were then introduced into a dilutor where additional clean air was added to reach the desired flow rate passing through the nasal model. A thin layer of oil was applied to the inner wall of the model to mimic the mucous layer in the nose and capture the deposited fibers. A membrane filter was placed at the end of the model to collect the fibers that penetrated through the model. After each run, the nasal model was divided into sections and washed with solvent using sonication. The resulting solution was filtered through a Millipore AA type membrane. The membrane was cleared with vaporized acetone from a QuickFix. The number of the deposited fibers was determined using phase contrast microscopy. A leak test was performed before each experiment to assure the proper sealing of the nasal model. Pressure drops across the nasal model under different flow rates were also measured.

JM-100 glass fibers made from JM-475 glass were used in the study. The average diameter of the fiber is approximately 1  $\mu\text{m}$ . The density of the glass is 2.56  $\text{g/cm}^3$ .

The regional deposition efficiency is defined as a percentage of the total fiber number entered the region of the nasal model. The results indicate that

deposition efficiency for glass fibers is higher in the middle section where the presence of the nasal valve and turbinates create secondary flow and local eddies. The deposition increased with an increase in fiber length.

Increasing flow rate generally increased the deposition efficiency. It should be noted that the decrease in the deposition efficiency for the posterior section at a high flow rate (15 l/min) might also result from particle re-entrainment even with the oil layer.

The geometry of nasal airway is a key factor in determining particle deposition efficiency. An empirical equation of particle deposition efficiency (PDE) was proposed as following:

$$PDE = 1 - \exp[-(ad_a^2 + bl^2)Q\Delta H]$$

where  $a$ ,  $b$  are constants,  $d_a$  is the aerodynamic diameter of the fibrous particle,  $l$  is the length of glass fiber,  $Q$  is flow rate and  $\Delta H$  is the total head loss.

The total head loss is part of pressure drop across the nasal passage. The relationship between pressure drop and flow is described by a second order equation,

$$\Delta p = k_1 Q + k_2 Q^2$$

where  $k_1$  and  $k_2$  are constants which can be determined from the geometry sizes of the passage.

The "hot spot" of glass fiber deposition is located in the middle region of the nasal passage. Increases in fiber length and flow rate generally enhanced the deposition efficiency. The complex geometry of nasal airway and the varying flow fields determine the intersubject variations in particle deposition. An empirical equation can be used to predict the aerosol deposition efficiency in nasal passage.

This work is supported by the National Institute for Occupational Safety and Health (NIOSH) under grant R01 OH003900.

Baron, P. A., Deye, G. J. and Fernaback, J. (1994). Length separation of fibers. *Aerosol Science and Technology*, 21: 179-192.

Wang, Z., Hopke, P. K., Baron P. A., Ahmadi G., Cheng Y. S., Deye G. and Su, W. C. (2005). Fiber classification and the influence of average air humidity. *Aerosol Science and Technology*, 39: 1056-1063.

## In vitro cytotoxicity and quantitative models for the uptake of oxide nanoparticles into human lung cells

L.K. Limbach<sup>1</sup>, T.J. Brunner<sup>1</sup>, R.N. Grass<sup>1</sup>, P. Wick<sup>2</sup>, A. Bruinink<sup>2</sup>, D. Günther<sup>3</sup> and W.J. Stark<sup>1</sup>

<sup>1</sup>Institute for Chemical and Bioengineering, ETH Zurich, Zurich, 8093, Switzerland

<sup>2</sup>Materials and Tissues for Medicine Group, EMPA St. Gallen, St. Gallen, Switzerland

<sup>3</sup>Laboratory for Inorganic Chemistry, ETH Zurich, Zurich, 8093, Switzerland

Keywords: health effects of aerosols, penetration, surface activity, lung/particles interaction, flame spray pyrolysis.

Rapidly growing reports on novel applications of nanoparticles fail to alleviate the often cited public unease towards the invisible technology. Spectacular findings of nano-materials in the bodies of rats after exposure to carbon nanotubes or titania nanoparticles are in sharp contrast to a series of successful market introductions of consumer goods and slow legislation. This discrepancy urgently calls for quantitative studies on the toxicity and uptake of nanoparticles into humans.

### Nanoparticle uptake

We have therefore developed an analytical method to measure nanoparticle uptake in living human lung fibroblasts at physiologically relevant concentrations ( $100 \text{ ng ml}^{-1}$ ). The uptake of oxide nanoparticles was analyzed in time dependence with different size ranges and different exposure concentrations. (Fig. 1)

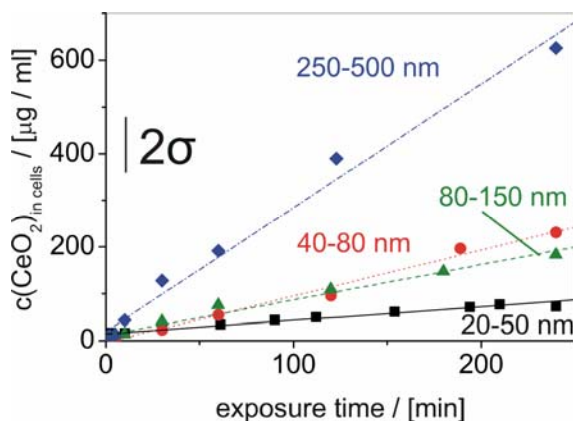


Fig 1: Amount of ceria taken up by human lung fibroblasts vs. exposure time

Based on these quantitative measurements, the role of agglomeration, surface change and protein adsorption was incorporated into a quantitative uptake model (Limbach et al. 2005).

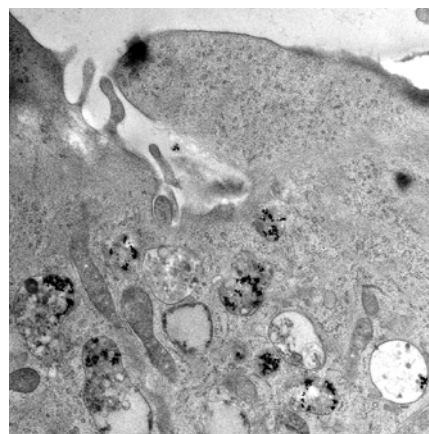


Fig 2: Transmission electron micrograph of ceria nanoparticles entering a fibroblast cell.

### Cytotoxicity of nanoparticles

Nanoparticle product design suffers from the uncertainty involved in potential adverse health effects. Early risk indicators should therefore provide a relative measure for cytotoxicity of nanomaterials in comparison to existing toxicological data. We have therefore evaluated a human mesothelioma and a rodent fibroblast cell line for in vitro cytotoxicity tests using industrially important nanoparticles. Their response in terms of metabolic activity and cell proliferation of cultures exposed to 0 to 30 ppm nanoparticles ( $\mu\text{g g}^{-1}$ ) was compared to the effects of non-toxic amorphous silica and toxic crocidolite asbestos (Brunner et al. 2006).

This work was supported by the Swiss Federal Office of Public Health (BAG, decision number 05.001872)

### References

- Limbach, L.K., Li, Y., Grass, R. N., Brunner, T. J., Hintermann, M. A., Muller, M., Gunther, D., & Stark, W. J. (2005). *Environ. Sci. Tech.*, 39, 9370-9376.
- Brunner T. J., Wick, P., Manser, P., Spohn, P., Grass, R. N., Limbach, L. K., Bruinink, A., & Stark, W. J. (2006). *Environ. Sci. Technol.*, 40 (14), 4374-4381.

## A mechanical lung model to measure particle deposition

Paul A. Keitch, Matthew D. Wright, Alison J. Buckley and Denis L. Henshaw

H. H. Wills Physics Laboratory, University of Bristol, Tyndall Avenue, Bristol, BS8 1TL. UK

Keywords: lung deposition, DMA, mechanical model lung, submicron particles

There has been much concern about the health effects of air pollution, with particular interest in nano-aerosols, size range 20 – 200 nm. Particulate air pollution has been associated with a number of adverse health effects from chronic as well as acute exposure. The smallest aerosols, which penetrate deeply into the lung, are thought to be the most harmful due to their larger specific surface area. In ambient atmospheric conditions, lung deposition on inhalation of 200 nm particles is around 30% (ICRP 1994), but has been shown to increase if the particles become charged. Therefore additional charging could increase the health risks associated with nano-aerosols.

To eliminate biological variation and ethical difficulties, a mechanical lung was built to study the deposition of aerosols in the respiratory tract. The mechanical model is based on the symmetric adult lung model of Weibel (1963). The first four branches of the bronchial tree are made from earthed metal piping at the correct size and branching angle. After the fourth generation, which has 128 tubes, this technique is no longer a viable engineering option and the lower generations are represented by earthed wire meshes. Four wire cloths with different mesh sizes are used to represent the small bronchioles and alveoli. A highly idealised nose and mouth has been added following the work of Zhang *et al.* (2004).

The set up of the mechanical lung is shown in Figure 1. Due to the considerable short term variation in atmospheric aerosol concentration it is necessary to alternate between lung and control measurements. Valves are used to switch between the two at periodic intervals (approximately 3 minutes). Sample air is drawn one way through the lung into a Sequential Mobility Particle Sizer + Classifier (SMPS+C), which measures particles of diameter of 10 – 1100 nm. The airflow through the lung is controlled externally and can be set between 4 and 16 l min<sup>-1</sup>.

The ICRP (1994) lung deposition model shown in Figure 2 is for a reference adult male Caucasian engaged in light work, breathing through his nose with an assumed breathing rate of 20 l min<sup>-1</sup>. Figure 2 compares this with laboratory measurements in ambient air taken over 6 hours. The airflow was 7.0 ± 0.25 l min<sup>-1</sup> which has been shown to follow the ICRP (1994) model. Also plotted in Figure 2 is the experimental work of Kim and Jaques (2000) which was carried out on human volunteers.

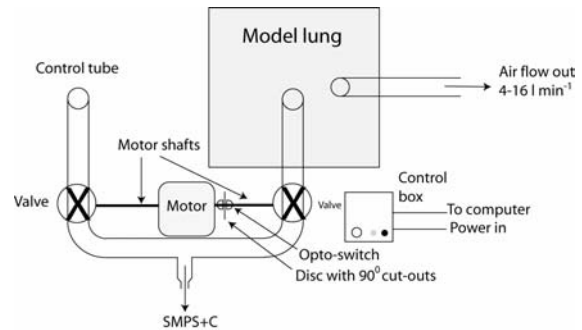


Figure 1. Schematic diagram of mechanical lung.

Variations in deposition efficiency in different exposure environments, including indoor and outdoor locations and near to sources of aerosols and ions will be presented. Factors affecting day to day variation, such as charge state and size distribution of aerosols, will be discussed. The ICRP (1994) model also includes deposition efficiencies for different breathing patterns which will be compared to the mechanical lung results.

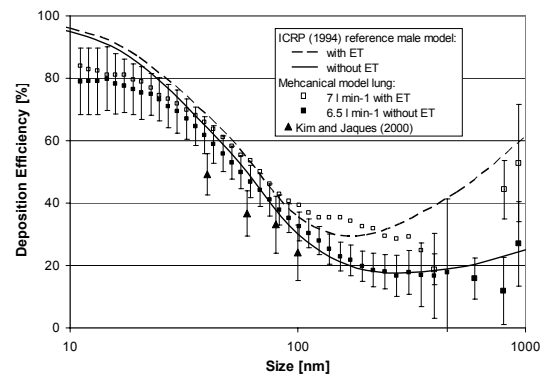


Figure 2. Deposition efficiency in mechanical lung compared with ICRP (1994) and Kim & Jaques (2000). Errors not shown for mechanical lung with ET (extrathoracic) but are similar to without ET.

This work was supported by CHILDREN with LEUKAEMIA, registered charity No. 298405 (UK)

ICRP publication 66 (1994) *Ann. ICRP* (UK), vol. 24 Nos. 1-3, Pergamon

Kim, C.S. and Jaques, P.A. (2000). *Phil Trans R Soc London* **358** 2693-2705

Weibel, E.R. (1963) *Morphology of the human lung*. Academic Press, New York

Zhang, Y., Finlay, W.H. and Matida, E.A. (2004). *J Aerosol Sci* **35** 789-803

## Regional deposition pattern of aerosol particles in the replica of upper airways

T.R. Sosnowski, L. Gradoń, and A. Moskal

Faculty of Chemical and Process Engineering, Warsaw University of Technology, Waryńskiego 1, 00-645 Warsaw, Poland

Keywords: inhalation, deposition, replica cast, variable flow

Drug delivery by aerosol inhalation is the preferable method of treatment of lung diseases such as COPD or asthma. It becomes also popular for administration of drugs with systemic action (e.g., insulin, growth hormone, vaccines), which are absorbed to the blood after deposition of aerosol particles on the lung surface. Although mouth-breathing is suggested during aerosol therapy to minimize particle deposition in the extra-thoracic region, always a certain amount of drug particles are captured in the oro-pharynx. As demonstrated recently, deposition efficiency in that part of the respiratory system depends not only on particle size but also on dynamics of breathing, which univocally determines the aerosol behavior in the airways, Sosnowski et al (2006). The aim of this work is to compare the experimental deposition of aerosol particles in three regions of sample extra-thoracic geometry (mouth, throat and pharynx) under constant flow rate and two variable inspiratory flows.

The measurements of regional deposition of aerosol particles in the sample replica of human oro-pharynx were done in the system depicted in Fig.1. Aerosol of sodium chloride was produced from 20% aqueous solution by pneumatic atomization (1, Sidestream nebulizer operated at 1.5 bar). Aerosol was suspended in the chamber (2), and then it was drawn through the silicone-rubber replica cast (3) and the filter (4) by the computer-driven piston pump (5). Studies were done for two sinusoidal-like inhalation patterns (Sosnowski et al., 2006) and five fixed values of flow rate (30-90 LPM). The replica cast was constructed as an assembly of three parts: mouth (M), throat (T) and pharynx (P), according to the geometry presented by Sosnowski et al. (2006).

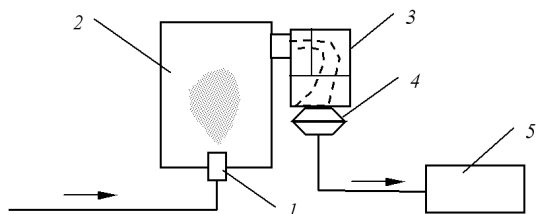


Figure 1. Scheme of the experimental set-up.

After the experiment, each part of the cast and the final filter were washed with 20 ml of de-ionized water, and all collected samples were analyzed conductometrically. Initial particle size distribution generated by the atomizer (1) was determined with

Andersen Cascade Impactor in separate experiments, and indicated that the majority of particles was less than 10  $\mu\text{m}$  (MMD  $\approx$  3  $\mu\text{m}$ ).

The results show (Fig.2) that the total and regional particle deposition in the studied geometry strongly depend on aerosol flow pattern.

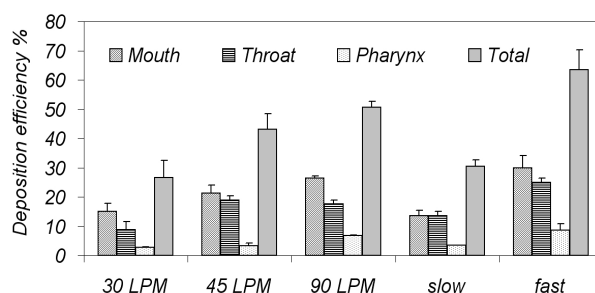


Figure 2. Experimental regional deposition data for the selected aerosol flow rates.

It can be found that, in general, deposition efficiency in each segment increases at higher flow rates, however both the overall efficiency and the deposition distribution are noticeably different at constant flows in comparison to the corresponding non-steady sinusoidal flows. The latter are denoted as "slow" (with the time-averaged flow rate equal 45 LPM), and "fast" (60 LPM). Sinusoidal "fast" flow results in the highest deposition efficiency in each segment of the replica cast, which suggest that dynamic effects associated with flow variations strongly enhance the deposition, especially in the mouth-throat region. On the other hand, such variations in the case of "slow" inhalation result in lower deposition efficiencies than found for the constant flow with the rate equal to the time-averaged rate for the given pattern (i.e. 45 LPM).

The results of presented experimental studies confirm that the pattern of flow variations is important for local aerosol flow and deposition efficiencies in the oro-pharynx, which was also suggested recently by results of CFD simulations (Sosnowski et al., 2006).

This work was supported by the budget sources for science in the years 2005-2008 (MEiN grant 3 T09C 028 29).

Sosnowski, T.R., Moskal, A., & Gradoń L. (2006). *Inhal. Toxicology*, 18, 787-801.

## Size partitioning of airborne particles to compare their proinflammatory effect in airway epithelial cells.

K. Ramgolam<sup>1</sup>, O. Favez<sup>2</sup>, L. Martinon<sup>3</sup>, H. Cachier<sup>2</sup>, A. Person<sup>4</sup>, A. Gaudichet<sup>5</sup>, F. Marano<sup>1</sup> and A. Baeza-Squiban<sup>1</sup>

1 : Laboratoire de Cytophysiologie et Toxicologie Cellulaire (LCTC), Université Paris 7, 75005 Paris, France

2 : Laboratoires des Sciences du Climat et de l'Environnement (LSCE), 91191- Gif sur Yvette, France

3 : Laboratoire d'Etude des Particules Inhalées (LEPI), 11 rue Georges Eastman, 750013-Paris, France

4 : Laboratoire d'Hygiène de la Ville de Paris (LHVP) 11 rue Georges Eastman, 750013-Paris, France

5 : Laboratoire Interuniversitaire des Systèmes Atmosphériques (LISA), Université Paris 12, Créteil, France

Keywords: urban aerosols, fine and ultrafine fractions, lung-particle interactions, health effects of aerosols.

Paris background aerosol is almost exclusively composed of fine (PM 2.5; PM 1) and ultra fine (PM 0.1) particles, originating mainly from combustion processes including traffic exhausts. Epidemiological and experimental investigations underlined the role of the aerosol size, in particular the ultra fine one.

The aim of the present study was to investigate which size-fraction of the urban particulate matter is the most relevant regarding to the biological effect considering the proinflammatory response of airway epithelial cells *in vitro*. This response is characterized by the release of mediators that would explain the inflammation observed in exposed subjects.

Human bronchial epithelial cells (16HBE) and primary cultures of nasal epithelial cells (HNE) that are the main target cells of airborne particles were exposed to the different size-fractions. The release of GM-CSF, a cytokine involved in allergic process was used as a proinflammatory biomarker of PM exposure and the cytochrome P450 1A1 (CYP1A1) that metabolizes xenobiotics, which activity was used as a biomarker of polyaromatic hydrocarbon (PAH) bioavailability.

Downtown Paris, four co-located 13-stage Dekati cascade impactors running in parallel were used to selectively collect particles from 30nm to 10µm on polycarbonate filters and were allocated to biological and physico-chemical (black carbon, particulate organic matter and water soluble organic compounds, major ions, PAH) investigations. 11 samplings were conducted in order to investigate whether the seasonal variability (summer and winter) and diurnal evolution related to photochemistry of the urban aerosol composition modulate the biological effects of some or all size-fractions.

*In vitro* biological assays were conducted with particles from pooled stages (1 to 3 representing ultra fine fraction [0.1-0.03µm], 4 to 7 the [1-0.1µm], 8 to 9 the [2.5-1µm] fine fraction and 10 to 13 the [10-2.5µm] coarse fraction). Particles were recovered from collection filters by brief sonications directly in the same volume of cell culture medium for each

size-fractions. Two experimental strategies were used: cells were exposed for 24 hours either at isovolume of particles suspension in order to respect the proportion of the different size-fraction in the sampled-air volume or at isomass.

When cells are exposed to an isovolume of particles suspension, the highest GM-CSF secretion was induced by PM1-0.1 that is the most important fraction in Paris background aerosol (up to 71% of the total PM10 mass). With a cell exposure at an isomass of particles, GM-CSF secretion was significantly induced by fine and ultra-fine particles with a dose-dependent increase from 1µg/cm<sup>2</sup> (5µg/mL) to 10µg/cm<sup>2</sup>, without inducing any cytotoxicity. Whatever the season or diurnal sampling, the finer the aerosol fraction, the higher the GM-CSF secretion was, whereas coarse particles displayed no or fewer effect. Moreover, endotoxins were not involved in the ultrafine particle-induced GM-CSF secretion whereas they partially contributed to the fine particle ones as assessed by the use of endotoxin neutralizing recombinant protein. Considering PAH bioavailability, PM1-0.1 from winter samples induced the higher CYP1A1 activity whereas the CYP 1A1 activity increases as the size decreases with summer samples.

Chemical analyses enlightened the major presence of carbonaceous species in Paris aerosols especially in the ultra-fine and fine fractions where PAH are also predominant (90% in these fractions).

To conclude, we observed that the proinflammatory response of bronchial epithelial cells *in vitro* was closely related to particle size with ultrafine particles exhibiting the highest effect.

This work was supported by ADEME, the french environmental agency, under the PRIMEQUAL grant n° 0462C0056.

## Development of a decision support tool for estimation of human exposure to particles (STEDOM) – A presentation of the stand alone exposure and dosimetry modules

V. Aleksandropoulou and M. Lazaridis

Department of Environmental Engineering, Technical University of Crete, Crete, GR- 73100, Chania, Greece

Keywords: Lung deposition, inhalation, chemical composition, PM.

Adverse health effects such as morbidity and mortality have been associated with exposure to particulate matter. In the past years several exposure models have been developed (e.g. IEM, Wu *et al.*, 2005; MENTOR, Georgopoulos *et al.*, 2006). A simple and user friendly integrated tool for estimating the PM actual human exposure and dose (STEDOM), taking into account the chemical characteristics of particles, is currently being developed at the Laboratory of Atmospheric Aerosols of Technical University of Crete, Greece. The model is developed in a modular way, with independent modules for data input (pollution sources and emissions, map of the modelled area, meteorological, air pollution and terrain data, building characteristics and exposed population characteristics), for dispersion, microenvironmental, exposure and dose modelling and a statistical module all combined under a graphical user interface with GIS capabilities (MapObjects by ESRI). The model will be used as a decision support tool for air quality management in urban areas.

In this work the stand alone exposure and dosimetry modules (EXDOM) are presented. The modules have been developed and combined under a graphical user interface. The estimation of the applied and internal dose is based on the HRTM of the ICRP (ICRP, 1994) and the respiratory tract clearance model by Gradon *et al.*, 1996. The user is asked to provide the exercise level, the exposed subject and the particulate matter characteristics as input or choose from data stored in a database and the model estimates and provides in graphical form the exposure and dose profiles.

A comparison of the deposition module results with results from HRTM of ICRP (ICRP, 1994) and MPPD (Multiple Path Particle Model – Price *et al.*, 2002) models are presented in Table 1 for polydisperse 5 µm particles (typical individual and exposure scenario; ICRP, 1994). Values in brackets correspond to fraction of particles deposited in the nose and trachea and bronchi.

Table 1. Regional deposition fractions of polydisperse 5 µm particles.

RT region	EXDOM	HRTM	MPPD
ET	76.25 (35.03)	73.29 (39.39)	84.1
TB	2.71 (1.81)	2.9 (1.8)	2.8
AI	4.53	5.3	5.6
Total	83.49	82	92.5

The EXDOM has been applied in the estimation of exposure and dose of chemically speciated particles in a suburban area of Oslo, Norway. In Figures 1 and 2 example calculations of inorganic ions dose and retention in the lungs of an individual on 03/06/2002 are presented (activity: “light exercise”, clearance: “fast”; ICRP, 1994).

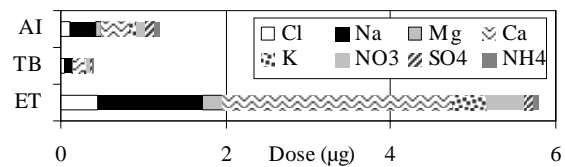


Figure 1. Dose of inorganic components of particles.

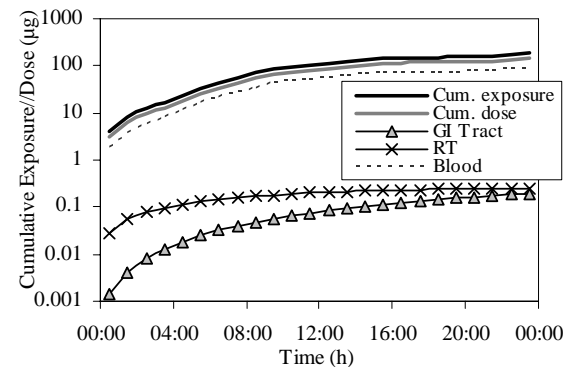


Figure 2. Cumulative exposure, dose and mass of particles retained at the RT or transferred to GI Tract and Blood.

This work was supported by the Research Committee of Technical University of Crete and the European Commission under the grant EVK4-CT-2000-00018.

International Commission on Radiological Protection (ICRP) (1994). *Human Respiratory Tract Model for Radiological Protection*, Pergamon, Oxford.

Georgopoulos, P. G., & Liou, P. J. (2006). *J. Tox. & Environ. Health, Part B*, 9, 457–483.

Gradon, L., Pratsinis, E., Prodigorski, A., Scott, S. & Panda, S. (1996). *J. Aerosol Sci.*, 27, 487 – 503.

Price, OT., Asgharian, B., Miller, F. J., Cassee, F. R., & Winter-Sorkina, R. (2002). *Multiple Path Particle Dosimetry model (MPPD v1.0): A model for human and rat airway particle dosimetry*. RIVM rapport 650010030.

Wu, J., Lurmann, F., Winer, A., Lu, R., Turco, R., & Funk, T. (2005). *Atmos. Environ.*, 39, 259 – 273.

## Calculation of diesel combustion particle deposition in the human respiratory tract

B. Alföldy<sup>1,2</sup>, B. Giechaskiel<sup>2</sup>, Y. Drossinos<sup>2</sup>, W. Hofmann<sup>3</sup>

<sup>1</sup>Hungarian Academy of Sciences KFKI Atomic Energy Research Institute, POB 49, H-1525, Budapest, Hungary

<sup>2</sup>European Commission, Joint Research Centre, I-21020 Ispra (Va), Italy

<sup>3</sup>University of Salzburg, A-5020 Salzburg, Austria

Keywords: diesel soot particles, ultrafine particles, nucleation mode, lung deposition.

The primary particles generated during diesel fuel combustion are soot granules. As the exhaust fumes dilute and cool in the atmosphere the primary particles aggregate to form a well defined log-normal size distribution accumulation mode (AM). In addition, under certain conditions a nucleation mode (NM) is formed. The generation and the characteristics of the NM depend sensitively on engine operating conditions, on the sulfur content of the fuel, and on the presence of a diesel particulate filter (DPF) or oxidative catalyst.

Although most authors agree that particle surface plays a key role in lung-particle interaction (Oberdorster, 2000), current legislation regulates only the total mass emissions. DPF reduces the emission of AM, and accordingly the total mass, but it does not affect the NM emission since it originates from SO<sub>2</sub> nucleation after the DPF. Therefore, although DPF decreases total mass emissions with high efficiency, the total surface of the emitted particles remains considerable because nucleation-mode particles contribute significantly to it.

Since during cooling volatile hydrocarbon species (VOC, PAH) condense onto particles, the total emitted particle surface may be considered a measure of transport of carcinogenic compounds. Moreover, the slightly soluble AM soot particles upon interaction with the lung fluid cause the generation of oxidative agents that induce oxidative stress on lung cells. Thus, in oxidative stress processes, as well, particle surface becomes the determining factor.

The main goal of this work is to investigate lung deposition efficiency of diesel combustion particles generated under different conditions. The mass and surface area of the particles deposited in the human respiratory tract was calculated with a stochastic lung deposition model (Koblinger and Hofmann, 1990). Emissions from Euro 3 and 4 light duty vehicles were measured: the generated particle size distributions were measured by SMPS according to the PARTICULATES project protocol (Ntziachristos et al., 2004). Diesel fuels were used with varying sulfur content of 10, 38 and 280 ppm. The vehicle speed varied between 50, 100 and 120 km/h. Moreover, the effect of DPF was investigated.

Total particle surface deposited in the human lung was calculated for 12 cases. In Fig. 1 deposited particle surface is shown as a function of mass

concentration of the inhaled particles. One breath was considered under sitting breathing conditions. Each symbol in the figure represents an emission measurement, different conditions corresponding to different symbols.

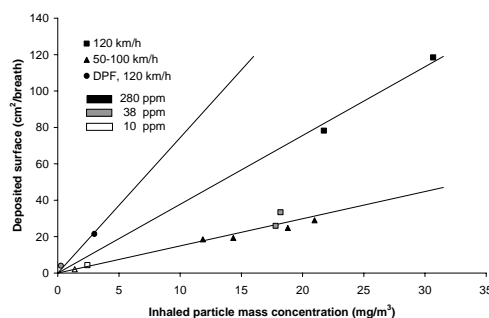


Fig. 1. Deposited particle surface in the human lung.

Total deposited surface calculations can be classified into three groups depending on the size distribution of the inhaled particles. The first group is associated with DPF emissions that are dominated by NM. The second group corresponds to high speed (120 km/h) emissions, where NM and AM are of the same order of magnitude. The third corresponds to moderate speeds (50-100 km/h), or reduced sulphuric fuel (10 and 38 ppm) that are dominated by AM. All three groups can be fitted by straight lines with zero intercept, manifesting that deposition is proportional to inhalation. The slope is largest for DPF emissions implying that percentage deposition is highest, even though total inhaled mass is low. The results reflect the importance of the size distribution of the emitted particles, in particular their surface area, because a given inhaled mass concentration may lead to different deposited surface in the lung, and hence, possibly, to different health effects.

The authors thank the Laboratory of Applied Thermodynamics, Aristotle University, Thessaloniki, Greece for kindly providing the size distributions used in this work.

- Koblinger, L., Hofmann, W., (1990). *J. Aerosol. Sci.* 21. 661-674.  
Ntziachristos, L., Giechaskiel, B., Pistikopoulos, P., Samaras, Z., Mathis, U., Mohr, M., Ristimäki, J., Keskinen, J., Mikkanen, P., Casati, R., Scheer, V., Vogt, R. (2004), in *SAE 2004-01-1439*.  
Oberdorster, G. (2000). *Phil. Trans. R. Soc. Lond. A*, 258, 2719-2740.

## Number size distribution of atmospheric aerosol particles at urban and rural sites in Hungary with health implications

Rita Ocskay<sup>1</sup>, Imre Salma<sup>1</sup>, Pasi Aalto<sup>2</sup>, Markku Kulmala<sup>2</sup>, András Gelencsér<sup>3</sup>, Gyula Kiss<sup>3</sup>, Imre Balásházy<sup>4</sup>

<sup>1</sup>Eötvös University, Institute of Chemistry, H-1518 Budapest, P.O. Box 32, Hungary

<sup>2</sup>University of Helsinki, Department of Physical Sciences, FIN-00014, Helsinki, P.O. Box 64, Finland

<sup>3</sup>University of Pannonia, Department of Earth and Environmental Sciences, and Air Chemistry Group of HAS, H-8200 Veszprém, P.O. Box 158, Hungary

<sup>4</sup>Atomic Energy Research Institute, H-1525 Budapest, P.O. Box 49, Hungary

Keywords: DMPS, number size distribution, health effects of aerosols.

Number size distributions of atmospheric aerosol particles in the mobility diameter range from 10 nm through 1  $\mu\text{m}$  were measured by a differential mobility particle sizer (DMPS), and aerosol ion spectrometer (AIS) at the continental background site of K-puszta, Hungary since 5 May 2006. Similar measurements were performed by the DMPS in the campus of the Eötvös University in Budapest, Hungary in November 2006.

From the measured data, time evolution of the number size distributions was derived to identify new aerosol particle formation processes, and average or typical number size distributions were calculated for deposition modelling purposes. Further objectives are to study the variability in the concentration of the cluster air ions, and to reveal the relationship between the local meteorology and the characteristics of the size distributions.

One of the new particle formation events observed by the DMPS at the K-puszta site is shown in Figure 1. Similar events were observed quite frequently, almost every day. The new particle formation was approved by the AIS as well in all cases. An example of the AIS spectra is displayed in Figure 2. At the urban site, the concentration level of the nucleation mode particles was shifted to larger values, and hence, the identification of the new particle formation events became more difficult. Nevertheless, some occasions were identified in the urban environments as well. The evaluation and interpretation of the data are in progress.

The average number size distributions were further utilized in the stochastic lung deposition model IDEAL as input data to derive the deposition of ultrafine particles in the compartments of the human respiratory system. Deposition probabilities for the urban and rural locations will be presented and intercompared.

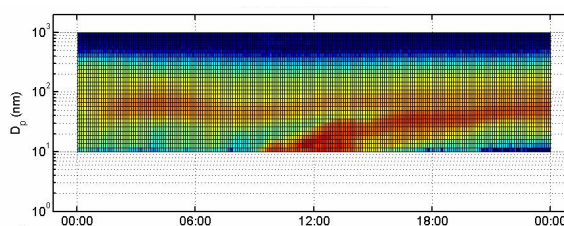


Figure 1. Time evolution of the number size distribution of aerosol particles derived from the DMPS at the K-puszta site on 6 June 2006.

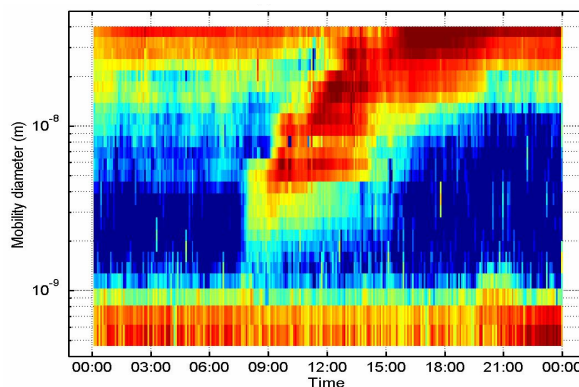


Figure 2. Time evolution of the number size distribution of negative aerosol ions derived from the AIS at the K-puszta site on 6 June 2006.

This work was supported by the Hungarian Scientific Research Fund under grant K061193.

## Respiratory tract deposition of fine particles in candle smoke

J. Löndahl, J. Ådahl, C. Boman and E. Swietlicki

Div. of Nuclear Physics, Lund University, P.O. Box 118, S-221 00, Lund, Sweden

Keywords: lung deposition, lung/particle interaction, indoor particles, health aspects of aerosols

Candles are common sources of both ultrafine and fine particles in indoor environments (Zai *et al.*, 2006). Pagels *et al.* (2007) have shown that ultrafine candle smoke particles grow by absorption of water in a humid environment. As the relative humidity (RH) in the respiratory tract is high, this would alter the deposition from that of the models, which often only include insoluble particles (Löndahl *et al.* 2007). There are few or none published measurements of respiratory tract deposition of any indoor particle source apart from tobacco smoke. This work presents preliminary results from measurements of respiratory tract deposition fraction (DF) of particles emitted from tea light candles.

Three tea light candles were lit in a 0.5 m<sup>3</sup> box. In order to establish an increased and “controlled” generation of soot, the candle flames were cooled by a plate of stainless steel. A fan was used to mix and dilute the aerosol. Number concentrations ranged from 6000-30000 cm<sup>-3</sup> and the size-distribution basically had two modes; the first with a geometric mean diameter (GMD) around 50 nm and the second with a GMD around 300 nm. An instrument, incorporating a scanning mobility particle sizer (SMPS), has previously been developed to measure the respiratory tract deposition of polydisperse aerosols (RESPI, Löndahl *et al.* 2006). In this experiment it was used to determine the size-resolved DF in the range 20-400 nm on 2 healthy, non-smoking male subjects breathing spontaneously. The size shift of the particles at an RH > 90% was measured with a tandem differential mobility setup.

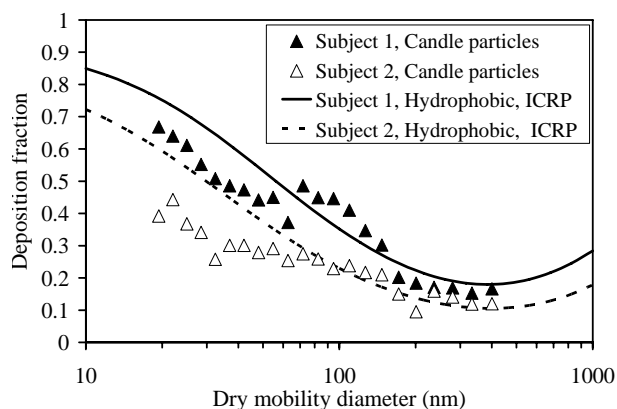


Figure 1. Respiratory tract deposition fraction (DF) of particles from tea light candles and calculated DF for insoluble particles.

DF for the subjects is shown in Figure 1. The tidal volume and breathing frequency was 0.8 L respectively 10 min<sup>-1</sup> for subject 1 and 0.4 L respectively 25 min<sup>-1</sup> for subject 2. Figure 1 also show DF calculated for the subjects with the ICRP model (1995) for insoluble particles. The particles shrank about 1% during inhalation, which indicate limited agglomeration. However, the shift was taken into account in the deposition measurement.

The ultrafine particles below 80 nm had a lower DF than calculated with the ICRP model. This indicates growth by water uptake in the respiratory tract and is in agreement with the hygroscopic growth measurements by Pagels *et al.* (2007). The larger particles (GMD around 300 nm) presumably consist to a large extent of soot, which also is discussed by Pagels *et al.* (2007). These are most likely water insoluble with little or no growth at high RH. The measured DF for these is similar to the calculated DF for hydrophobic particles, which confirm the assumption of low solubility.

As a first test, the measurements demonstrate the deposition behaviour of candle smoke particles. Further, the importance of including hygroscopicity in respiratory tract deposition estimates is clearly stressed. Ultrafine combustion particles could contain a substantial amount of salt, which lead to a decreased DF.

In the near future respiratory tract deposition of diesel exhaust aerosols will be measured for a larger group of subjects. The performed measurements are partly made as a pre-study to identify experimental difficulties and improve the technique.

Acknowledgements: This study was supported by the Swedish Emissions Research Programme, EMFO.

ICRP Publication 66. 1995., 66. International Commission on Radiological Protection.

Löndahl, J., Pagels, J., Swietlicki, E., Zhou, J., Ketzel, M., Massling, A. and Bohgard, M., (2006), *Journal of Aerosol Science* 37:1152-1163

Löndahl, J., Massling, A., Pagels, J., Swietlicki, E., Vaclavik, E. and Loft, S. (2007), *Inhalation Toxicology* 19:109-116

Pagels J, Wierzbicka A., Dahl A., Swietlicki E. and Bohgard M. (2007) *Proceeding of the European Aerosol Conference 2007, Salzburg*

Zai S, Zhen H and Jia-Song W. (2006) *J. Aerosol Sci.* 37: 1484-1496.

## Respiratory tract deposition measurements of aerosol particles with on-line techniques; review of sources of error and estimation of their impact

J. Löndahl<sup>1</sup>, E. Swietlicki<sup>1</sup>, J. Pagels<sup>2</sup> and M. Bohgard<sup>2</sup>

<sup>1</sup>Div. of Nuclear Physics, Lund University, P.O. Box 118, S-221 00, Lund, Sweden

<sup>2</sup>Div. of Aerosol Technology (EAT), Lund University, P.O. Box, 118, S-221 00, Lund, Sweden

Keywords: lung deposition, measurement errors, instrumentation

A common method to measure the respiratory tract deposition fraction (DF) of aerosol particles is to compare the particle concentration in the inhaled and exhaled air. Tyndall made the first study with this approach 1870. Since then the technique has been improved and a variety of sources of errors have been identified and discussed to improve the technique.

In this work experimental difficulties and systematic errors in respiratory tract deposition measurements are reviewed, both to improve the quality of future measurements and to facilitate comparison between experiments and models. The review is essentially based on 33 publications, whereof most are summarized by Löndahl (2006).

Some difficulties are general. Others are specific for monodisperse experiment, where one size is measured at a time and others for polydisperse experiments, where the complete size distribution is studied at once.

### General difficulties

A. Losses (e.g. electrostatic) in the measurement equipment may be interpreted as an increased deposition. This is especially complicated for bag-systems since the losses depend on the volume in the bags.

B. Pressure variations caused by the breathing may give errors in the particle counting.

C. Temperature and relative humidity could be higher in exhaled than inhaled air leading to particle loss or diameter change by evaporation or condensation.

D. The air trapped in the dead space in the mouthpiece after exhalation is inhaled again. Thereby the inhaled concentration is lower than measured.

E. The finite response time of particle counters delay and smear the signal, thereby decreasing the difference between measured inhaled and exhaled concentration.

F. Only one of the studies present a lowest acceptable concentration limit due to counting statistics or an upper concentration limit, e.g. due to particle coagulation. Some studies may use too high concentration.

G. If inhaling dry or room temperature aerosol, the volume of the exhaled air is larger than the inhaled because of the temperature and humidity change. This dilutes the exhaled air and decreases concentration, thereby seeming to increase DF.

I. An error may arise if the concentration of the inhaled particles is varying. This is in particular impor-

tant for polydisperse measurements because the size distribution could change too much between the scans. Scan times must be short, measurement time long or the concentration stable.

J. Hygroscopicity may alter deposition.

### Specific difficulties

a. If monodisperse particles are separated in an electric field (e.g. with a DMA) they will have similar electrical mobility but different mechanical mobility because of multiple charges. It is the mechanical mobility that determines the deposition.

b. The polydisperse techniques are sensitive to small size shifts of the dried diameter between the inhaled and exhaled sample. If not taken into account, this could render substantial errors.

c. Polydisperse techniques are also sensitive to smearing of the output signal in the SMPS mainly caused by the finite CPC response time. This distorts the size-classification and is of significance if the scan time is too short and no correction is made.

### Discussion and conclusion

Table 1 Estimated impact of errors

Error	Deviation from true DF*
A.	+ 1 – 20%
B.	- 0 – -3%
C.	+ 0 – 10%
D.	- -1 – -5%
E.	- 0 – -5%
F.	- 0 – -5%
G.	- 0 – -10%
I.	-/+ -0.1 – 0.1 in DF
b.	-/+ -0.2 – 0.2 in DF

\* Note that some errors are relative and therefore given in percentage while others are absolute and given as deviation from true DF.

Table 1 shows estimates of the impact of the errors, if not taken into account, on the measured DF. Especially error D and G are well known but often not mentioned in publications, which make it probable that some experiments systematically underestimate DF. Errors may mask the real variability of DF and make comparisons of experimental results difficult.

Löndahl (2006), *Licentiate Dissertation*, Div. of Nuclear Physics, Lund University

## Ultrafine particle deposition differs consistently between the developing and adult rat lung

M. Semmler-Behnke, DVM<sup>1</sup>, I. Bolle, DVM<sup>1</sup>, W. Moeller, PhD<sup>1</sup>, H. Schulz, MD<sup>1</sup>, S. Takenaka, DVM<sup>1</sup>, A. Tsuda<sup>3</sup> and W.G. Kreyling, PhD<sup>1,2</sup>

GSF - National Research Center for Environment and Health, <sup>1</sup>Institute of Inhalation Biology, <sup>2</sup>Focus Network Aerosols and Health, D-85746 Neuherberg / Munich, Germany, <sup>3</sup>Physiology Program, Harvard School of Public Health, Boston, Massachusetts 02115, USA

Keywords: lung deposition, ultrafine particles, inhalation, insoluble particles, lung/particle interaction

Rodent animal models are frequently used for toxicological studies after inhalative exposure to particulate matter. Total and regional particle deposition is an essential prerequisite for extrapolation of toxicological results to assess human health risk. Very limited data on total and regional deposition in rodents exist for ultrafine particles in the size range of 10-100 nm. In addition, no deposition data exist for the developing lungs of rats which may serve as a first estimate for the human developing lungs.

We have determined total and regional deposition of 20 and 80 nm radio-labeled ultrafine insoluble iridium particles (UFP) in 7, 14 and 21 days old WKY baby rats and adult rats. Animals were exposed by spontaneous breathing (nose-only) for one hour following an inhalation protocol described earlier (Kreyling et al. 2002; Semmler et al., 2004). The breathing frequency of the animals was recorded using pressure transducers attached to the animal holding tubes and the median breathing frequency was calculated. The average median breathing frequency was used for further calculations. The tidal volume was calculated by the individually determined median breathing frequency of each rat and the regression line of tidal volume versus breathing frequency. The latter data were determined by measurements of spontaneous breathing rates of each age category in the BUXCO-System<sup>®</sup> (Bolle et al., 2006). The total breathing volume was the product of the tidal volume, the median breathing frequency and the aerosol inhalation time.

Directly and 24 hours after inhalation rats were killed and all organs, tissues, the remaining carcass as well as excreta were quantitatively collected and were radio-analysed for <sup>192</sup>Ir content using gamma spectroscopy in a lead-shielded well-type geometry. The data obtained from the radioactive animal samples directly after the nose only inhalation were corrected for radiation background, physical decay of <sup>192</sup>Ir and importantly for their pelt contamination.

Total deposition in the entire respiratory tract was determined after 0-hour and 24-hour retention. Airway deposition was assessed by the fraction which had been cleared from the respiratory tract within the first 24 hours. Alveolar deposition was

evaluated by the fraction which was retained in the lungs after 24h. Similar to total deposition, data of alveolar deposition and airway deposition were corrected for external pelt contamination.

Results: Compared to the other age groups total deposited fractions were maximal in 21 days old rats (79% or 52% of inhaled UFP) after the inhalation of 20nm or 80nm <sup>192</sup>Ir-particles, respectively. Total deposited fractions after inhalation of 20nm <sup>192</sup>Ir-particles increased from 14% to 44% and 79% with the age of the baby rats and decreased to 62% for adult rats. The total deposited fractions after inhalation of 80nm <sup>192</sup>Ir-particles were 28%, 29%, 52% and 20% at the ages of 7, 14 and 21 days and adult. Using the 24 h clearance data total deposition was separated into airway and alveolar deposition. The alveolar deposition was almost always higher by factor 2 or more than the airway deposition after inhalation of 20nm or 80nm <sup>192</sup>Ir-particles. Only in adult rats alveolar and airway deposition of 20 nm UFP was nearly the same (44% vs. 46%). In particular, the very low deposition fraction of UFP in the airways of 7-days-old rats suggests large airway calibres and demonstrates the lower efficiency of diffusional deposition. It is quite striking that the maximal total deposition observed in 21-day-old rats results from both maximum alveolar and maximum airway deposition rather than from one region. During lung development air spaces in bronchioli and alveoli at the age of 2-3 weeks appear to be narrower compared to younger and older lungs. As a result the diffusion dominated deposition of 20 and 80 nm UFP reaches a maximum.

Conclusion: particle deposition in the developing lungs cannot simply be estimated by scaling down anatomy and function of the adult lungs but requires thorough experimental analysis on particle dynamics and lung morphology.

This work was partly supported by the EU FP6 PARTICLE\_RISK 012912 (NEST), and U.S. NIH Grant HL070542.

Bolle et al., (2006), in *Pneumologie*, Georg Thieme Verlag KG Stuttgart-New York, 60:89-90, ISSN 0934-8387

Kreyling WG, Semmler M, et al. 2002. *J. Tox. Environ. Health-Part A* 65(20):1513-1530.

Semmler M, Seitz J, et al.. 2004. *Inhal Toxicol* 16(6-7):453-9.

## Modelling deposition of hygroscopic particles in the human respiratory tract

R. Winkler-Heil<sup>1</sup>, G.A. Ferron<sup>2</sup> and W. Hofmann<sup>1</sup>

<sup>1</sup>Department of Materials Engineering and Physics, University of Salzburg, 5020 Salzburg, Austria

<sup>2</sup>Institute for Inhalation Biology, GSF – National Research Center for Environment and Health, 85764 Neuherberg/Munich, Germany.

Keywords: lung deposition, hygroscopicity, inhalation, modelling.

Upon penetration into the human respiratory tract, inhaled hygroscopic particles experience increasing humidity and temperature, thereby gradually growing in diameter until reaching an equilibrium diameter. Through the uptake of water molecules, however, the initial density of the particles decreases in a likewise fashion, reducing gradually their aerodynamic diameters. In the present study, salt aerosol particles were used to simulate the effect of hygroscopic growth on total particle deposition.

Growth of sodium chloride in the human airways was calculated using a model for the growth of a single aerosol particle in humid air (Ferron *et al.*, 1988a), which includes both water vapour and heat transport corrected for slip, and a model describing the transport of water vapour and heat in the upper human airways (Ferron *et al.*, 1988a). The resulting growth curves for different breathing patterns as a function of the time after inhalation through nose or mouth were then used as input for the deposition calculations.

These growth curves for different breathing patterns as a function of the time after inhalation through nose or mouth data were used to calculate total lung deposition with a stochastic, asymmetric deposition model (Hofmann & Koblinger, 1990; Hofmann & Koblinger, 1990). At the midpoint of each airway, the time elapsed since inhalation was computed and the diameter of the inhaled particle increased by the diameter ratio (hygroscopic vs. non-hygroscopic) at that time, until the particle is finally exhaled.

Experimental data of the growth of sodium chloride particles in the human lungs have been published by Gebhart *et al.* (1990) for a tidal volume of 1000 cm<sup>3</sup> at constant in- and exhalation air flows of 250 cm<sup>3</sup>s<sup>-1</sup> for dry particle sizes between 0.3 and 2 µm. To facilitate comparison with these experimental data, the same oral breathing conditions were assumed for the simulations.

Total oral deposition data for hygroscopic and non-hygroscopic particles are plotted in Figure 1 for initial aerodynamic particle diameters ranging from 0.1 to 10 µm. Because of particle growth, deposition for small particles decreases due the less efficient diffusion, while the more efficient impaction and sedimentation mechanisms increase deposition of

larger particles. Due to the asymmetric, stochastic structure of the lung morphology and the resulting variability in pathway lengths, the effect of hygroscopic growth varies significantly along randomly selected particle paths.

The stochastic results are compared in Figure 1 with previously published calculations with a symmetric, deterministic deposition model (Ferron *et al.* (1988b) and with experimental data for human test subjects (Anselm, 1989). Despite significant differences in lung morphology and modeling techniques, both models predict the same general trend, consistent with the experimental evidence.

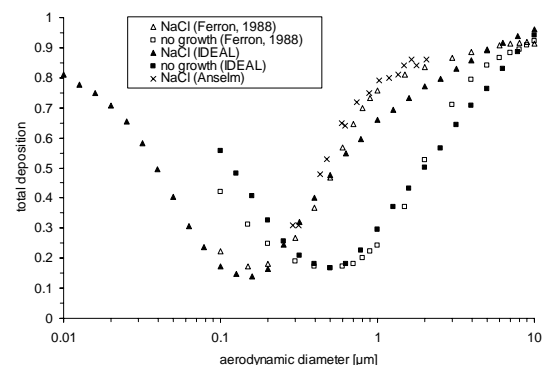


Figure 1. Total oral deposition for hygroscopic (NaCl) and non-hygroscopic particles. Stochastic model predictions are compared to previous deterministic calculations and experimental data.

- Anselm, A.F. (1989). Dissertation, University of Frankfurt.
- Ferron, G.A., Haider, B., & Kreyling, W.G. (1988a). *J. Aerosol Science*, 19, 343-363.
- Ferron, G.A., Kreyling, W.G., & Haider, B. (1988b). *J. Aerosol Science*, 19, 611-631.
- Gebhart, J., Anselm, A., Ferron, G.A., Heyder, J., & Stahlhofen, W. (1990). in *Aerosols, Proc. Third Int. Aerosol Conf.*, Kyoto (Pergamon Press, Oxford), 1298-1302.
- Hofmann, W., & Koblinger, L. (1990). *J. Aerosol Science*, 21, 675-688.
- Koblinger, L., & Hofmann, W. (1990). *J. Aerosol Science*, 21, 661-674.

## Deposition of polydisperse fibers in the human respiratory tract: comparison between theoretical predictions and experimental data

R. Sturm and W. Hofmann

Division of Physics and Biophysics, Department of Materials Engineering & Physics,  
University of Salzburg, A-5020 Salzburg, Austria

Keywords: Fibers, lung deposition, inhalation, modelling.

Fibers are elongated particles with an aspect ratio (i.e. the ratio of the length to the diameter) greater than 3. In the past, asbestos fibers were classified as significant occupational hazards, leading to their prohibition in many countries. Today, asbestos is partly substituted by so-called man-made vitreous fibers (MMVFs). These particles, however, seem to produce biological effects similar to those of the original material (Su & Cheng, 2006). Therefore, studies on the deposition of fibrous particles in the human respiratory tract have obviously the same relevance as one or two decades ago. In the study presented here, lung deposition of carbon fibers polydisperse in length is simulated, and results obtained from the computations are compared with the experimental data of Su & Cheng (2006).

Deposition of fibers is affected by four main physical mechanisms, i.e. diffusion, sedimentation, inertial impaction, and interception, whereby the predominance of one mechanism chiefly depends upon the fiber length. For a theoretical approach of fiber deposition in the respiratory system, the aerodynamic diameter concept introduced by Stöber (1972) is frequently applied. By using this mathematical concept, a distinction between various fiber orientations in extrathoracic and tracheobronchial airways is enabled. In this study, random aerodynamic diameters,  $d_{ae(r)}$ , of fibers (specific weight:  $1.83 \text{ g/cm}^3$ ) with a uniform diameter of  $3.66 \mu\text{m}$  and a length between  $10$  and  $70 \mu\text{m}$  are calculated and used for deposition computations performed with the Monte Carlo program IDEAL (Koblinger & Hofmann, 1990). Concerning air flow and lung volume parameters, respective values outlined by Su & Cheng (2006) are used. These authors measured fiber deposition in a realistic cast of the extrathoracic region and upper airways, thereby considering inspiratory flow rates of  $15 \text{ l/min}$  and  $43.5 \text{ l/min}$ , which correspond to sitting breathing and light-working breathing conditions, respectively.

Concerning the first deposition scenario using an inspiratory flow rate of  $15 \text{ l/min}$  and fibers with a length of  $10$  to  $20 \mu\text{m}$ , good correspondence between experiment and model is obtained for airway generations 0 to 4+ (Fig. 1A). Significant differences can be observed for the extrathoracic region, where model data exceed experimental results by a factor of 3. This effect causes a higher experimental fiber deposition in the trachea and the following airway bifurcations. In the second scenario, an inspiratory flow

rate of  $43.5 \text{ l/min}$  and fibers with a length between  $60$  and  $70 \mu\text{m}$  were selected. In this case, only insignificant discrepancies between model and experiment can be noticed. For the extrathoracic region, theoretical deposition only slightly exceeds the experimental value (Fig. 1B). In generation 0 to 4+ experimental values are only insignificantly higher than respective results from theoretical computations. From these preliminary results it can be concluded that the agreement between model and experimental data partly is quite satisfactory, but also requires some model refinement in the future.

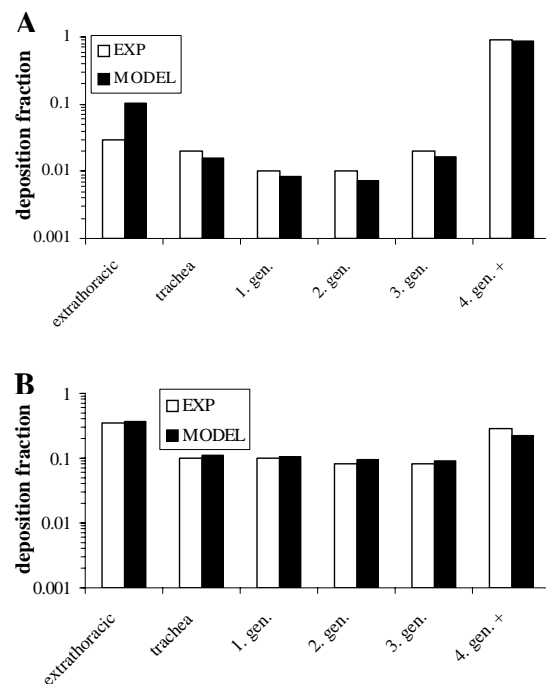


Figure 1. Comparison of fiber deposition data obtained from model and experiment (Su & Cheng, 2006). A. Scenario assuming an inspiratory flow rate of  $15 \text{ l/min}$  and a fiber length between  $10$  and  $20 \mu\text{m}$ , B. Scenario assuming an inspiratory flow rate of  $43.5 \text{ l/min}$  and a fiber length between  $60$  and  $70 \mu\text{m}$ .

Koblinger, L. & Hofmann, W. (1990). *J. Aerosol Sci.*, 21, 661-674.

Su, W. C. & Cheng, Y. S. (2006). *J. Aerosol Sci.*, 37, 1429-1441.

Stöber, W. (1972). in *Assessment of airborne particles* (Thomas, Springfield), 249-289.

## A stochastic model for the deposition of nonspherical particles in the human respiratory tract

R. Sturm and W. Hofmann

Division of Physics and Biophysics, Department of Materials Engineering & Physics,  
University of Salzburg, A-5020 Salzburg, Austria

Keywords: Nonspherical particles, lung deposition, inhalation, modelling.

Nonspherical particles, including fibers and platelets, may be regarded as notorious occupational hazards. In the past, especially the exposure to airborne asbestos fibers was found to increase the incidence of lung cancer. Therefore, enhanced scientific interest was concentrated on this particle category, and important findings regarding the extrathoracic and tracheobronchial deposition behaviour of particles with aspect ratios  $> 3$  were published (Su & Cheng, 2006). Concerning platelets, representing the preferential shape of dust aerosols and being characterized by aspect ratios  $\ll 1$ , similar studies are still missing, although the exact knowledge of dust deposition in the lung would mean a tremendous progress in aerosol sciences and lung medicine. In the study presented here, preliminary attempts regarding a more appropriate description of nonspherical particle deposition in the lung are made.

Deposition calculations were conducted on the basis of the aerodynamic diameter concept previously introduced by Dai & Yu (1998). Generally, this parameter is defined as follows:

$$d_{ae} = \sqrt{\frac{1}{3} (b_{\parallel} + 2b_{\perp}) \frac{\rho}{\rho_0} d_v^2} \quad (1)$$

In Eq. (1),  $b_{\parallel}$  and  $b_{\perp}$  denote the normalized mobilities of the particles moving parallel and perpendicular to the flow,  $\rho$  and  $\rho_0$  the particle mass density and unit density, and  $d_v$  represents the equivalent volume diameter. Mobilities of fibers and platelets were derived from high-order polynomial fit functions, setting the aspect ratio and related slip correction factor as independent variables (Tab. 1).

Table 1. Normalized mobilities for fibers and platelets with unit-density (a. r. = aspect ratio).

Mobility	Fiber ( $d = 1 \mu\text{m}$ , a. r. = 10)	Platelet ( $d = 10 \mu\text{m}$ , a. r. = 0.1)
$b_{\parallel}$	1.138	1.352
$b_{\perp}$	0.621	1.063

Deposition calculations were carried out assuming unit-density particles and sitting breathing conditions with a tidal volume of  $500 \text{ cm}^3$  and a flow rate of  $250 \text{ cm}^3/\text{s}$ . Regional deposition as well as deposition per airway generation were computed using the Monte Carlo computer code IDEAL outlined by Koblinger & Hofmann (1990).

In general, the deposition behaviour of fibers and platelets with the particle properties listed in Tab. 1 exhibits significant differences. While platelets are preferentially deposited in the trachea and more proximal bronchi, fibers, like spheres with comparable diameter, are chiefly accumulated in the more distal bronchi and alveoli (Fig. 1A). Platelets are to a high extent filtered in the extrathoracic region and exhibit a total deposition  $> 90\%$ , whereas fibers have a total deposition of ca. 10% and are only marginally deposited in nose or mouth (Fig. 1B). In future studies, probable consequences of nonspherical particle deposition will be discussed more in detail.

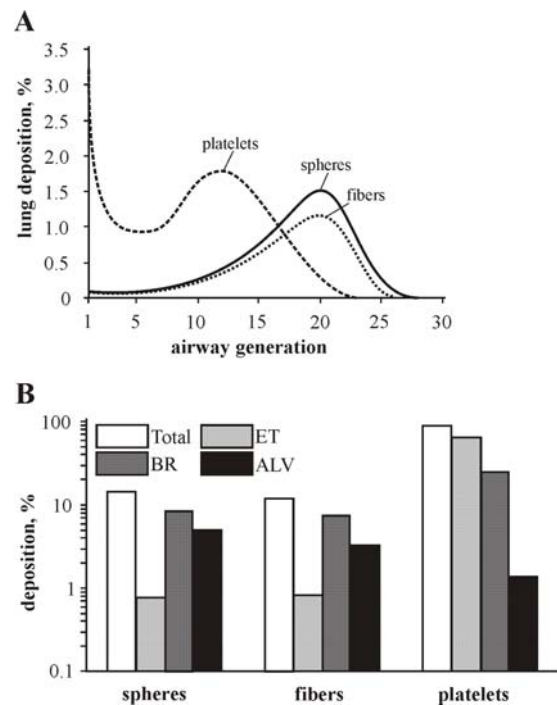


Figure 1. Preliminary results of the deposition calculations. A. Deposition per airway generation, B. Total and regional deposition (ET = extrathoracic, BR = bronchial, ALV = alveolar).

Dai, Y. T. & Yu, C. P. (1998). *J. Aerosol Med.*, 11, 247-258.

Koblinger, L. & Hofmann, W. (1990). *J. Aerosol Sci.*, 21, 661-674.

Su, W. C. & Cheng, Y. S. (2006). *J. Aerosol Sci.*, 37, 1429-1441.

## Lung deposition of particle aggregates: Theory and experimental data

O. Schmid<sup>1</sup>, W. Möller<sup>1</sup>, E. Karg<sup>1</sup>, K. Felten<sup>1</sup>, G. A. Ferron<sup>1</sup>, H. Fissan<sup>2</sup>, W. Hofmann<sup>3</sup>, H. Schulz<sup>1</sup>, and W. G. Kreyling<sup>1</sup>

<sup>1</sup>Institute for Inhalation Biology, GSF-National Research Center for Environment and Health, 85764, Neuherberg/Munich, Germany

<sup>2</sup>Institute for Energy and Environmental Technology, IUTA e.V., Bliersheimerstr. 60, 47229, Duisburg, Germany

<sup>3</sup>Department of Materials Engineering & Physics, University of Salzburg, Hellbrunner Strasse 34, 5020 Salzburg, Austria,

Keywords: Aerosol measurement, aerosol modelling, agglomerates, inhalation, nanoparticles.

The lungs are the main entranceway of aerosol particles into the human organism. Hence, reliable assessment of aerosol-related health effects requires accurate knowledge of particle deposition efficiencies into the lungs. While this issue has been studied experimentally for spherical particles, the database on non-spherical particles (e.g. soot agglomerates) is scarce. In this study we experimentally determine the lung-deposition of fractal-like carbon agglomerates and compare it to standard deposition models adjusted for shape effects based on the effective density concept (Schmid et al. 2007).

The regional and total deposition efficiencies for fractal-like agglomerates were determined experimentally on four healthy subjects using an aerosol bolus inhalation device (respiratory aerosol probe, RAP). DMA-selected, neutralized carbon agglomerates (Technegas, <sup>99m</sup>Tc-radioactively labelled, Möller et al., 2006) in the diameter range between about 30 and 230 nm were inhaled without breath holding by healthy non-smokers using the RAP. Preferred airway (AW) or alveolar (AL) targeting was achieved by inhalation of shallow or deep 100 mL aerosol boli (with phase 1 dead space or 800 mL as bolus front depth, respectively) (Möller et al., 2004). In addition, 1.0 L single breaths (SB) were inhaled for measurements of total particle deposition. Deposition efficiencies were determined from the difference in radioactivity (~particle concentration) on filter samples from the inhaled and exhaled air stream. Total and regional deposition efficiencies were calculated using the ICRP deposition model (Luddep, Version 2.0; ICRP 1994) and a stochastic lung model (USBG, Hofmann et al. 1990), respectively, assuming spherical particles with an effective mobility density between 2.3 g/cm<sup>3</sup> and 0.4 g/cm<sup>3</sup> for limiting diameters of 30 nm and 250 nm, respectively.

As seen from Fig. 1 the SB aerosol inhalation shows an increase of deposition with decreasing particle diameter and is in good agreement with the ICRP model. AW (shallow) bolus inhalation gives very low particle deposition reflecting the large airway structures. AL (deep) bolus inhalation gives higher deposition than SB due to the enhanced particle residence time and the large surface-to-volume ratio of alveolar structures. The simulations

of the bolus inhalation using the USBG model also reflect this principal behaviour and show good agreement with the experimental data. Using a constant particle density of 2.3 g/cm<sup>3</sup> (i.e., shape effects are neglected) induces a maximum change of +5% in modelled deposition at 230 nm. This indicates that our data belong to the diffusion dominated regime, where sedimentation and impaction losses are negligible.

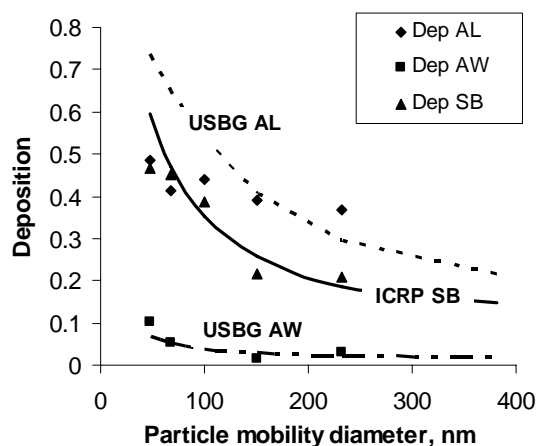


Figure 1: Measured and calculated particle lung deposition in one subject after inhalation of the deep (AL) and shallow bolus (AW), and after 1.0 L single breath (SB) aerosol inhalation.

To our knowledge the data presented here represent the first measurements of regional (AL, AW) lung deposition of agglomerates. The results for carbon agglomerates confirm that standard deposition models are applicable without adjustment for shape effects for particle sizes up to about 250 nm.

Hofmann, W., and Koblinger, L. (1990). *J. Aerosol Sci.*, 21, 675-688.

ICRP Publication 66 (1994). Human respiratory tract model for radiological protection. *Ann. ICRP*, 24, 1-482.

Möller, W., Häussinger, K., Winkler-Heil, R., et al., (2004). *J. Appl. Physiol.*, 97, 2200-2206.

Möller, W., Felten, K., Seitz, J., et al., (2006). *J. Aerosol Sci.*, 35, 631-644.

Schmid, O., Karg, E., Hagen, D.E., Whitefield, P.D., and Ferron, G.A. (2007). *J. Aerosol Sci.*, in print.

## A theoretical approach to the bronchial clearance of micrometer-sized nonspherical particles

R. Sturm and W. Hofmann

Division of Physics and Biophysics, Department of Materials Engineering & Physics, University of Salzburg, A-5020 Salzburg, Austria

Keywords: nonspherical particles, inhalation, bronchial clearance, modelling.

Recently, several theoretical approaches concerning the clearance of insoluble particles from the tracheobronchial tree of the human lung have been published, thereby distinguishing between a fast clearance phase represented by the mucociliary escalator and several slower clearance phases (e.g. Hofmann & Sturm, 2004; Sturm & Hofmann, 2004). The main simplification of all models published so far is that clearance computations are routinely carried out for spherical particles. In the contribution presented here, the multicompartmental clearance model introduced by Sturm & Hofmann (2006a) is applied to two categories of unit-density nonspherical particles, i.e. fibers and platelets. Differences in the tracheobronchial clearance behaviour between these specific particles and spheres are discussed.

For the computations, fibers with a diameter of 1  $\mu\text{m}$  and a length of 10  $\mu\text{m}$  and platelets with a diameter of 10  $\mu\text{m}$  and a thickness of 1  $\mu\text{m}$  were assumed. Corresponding aerodynamic diameters were derived from respective fit functions and yielded 1.16  $\mu\text{m}$  for the fibers and 10.23  $\mu\text{m}$  for the platelets. Deposition was computed using the computer program FIBROS (Sturm & Hofmann, 2006b) and the Monte Carlo code IDEAL (Koblinger & Hofmann, 1990), assuming sitting breathing conditions (ICRP 1994). For the clearance computations, slow bronchial clearance fractions of 0% for the platelets and 65% for the fibers were assumed. Transfer rates between single compartments were selected according to the suggestions of Sturm & Hofmann (2006a) and the ICRP (1994).

The primary difference between platelet and fiber clearance is the participation of mucociliary transport and uptake of deposited particles by airway macrophages. While platelets are to a high extent cleared by the gel layer, clearance of fibers is chiefly carried out by macrophages immigrating into the airways from the alveoli or the lamina propria (Fig. 1). As a consequence, 24-hour retention increases from 0.24 for platelets to 0.70 for fibers. Spherical particles with a diameter of 1  $\mu\text{m}$  show a 24-hour retention of 0.66 and thus behave similar to fibers with the geometry used here. From the preliminary findings it may be concluded that bronchial clearance of nonspherical particles is characterized by significant variations, which will be investigated in more detail in future studies.

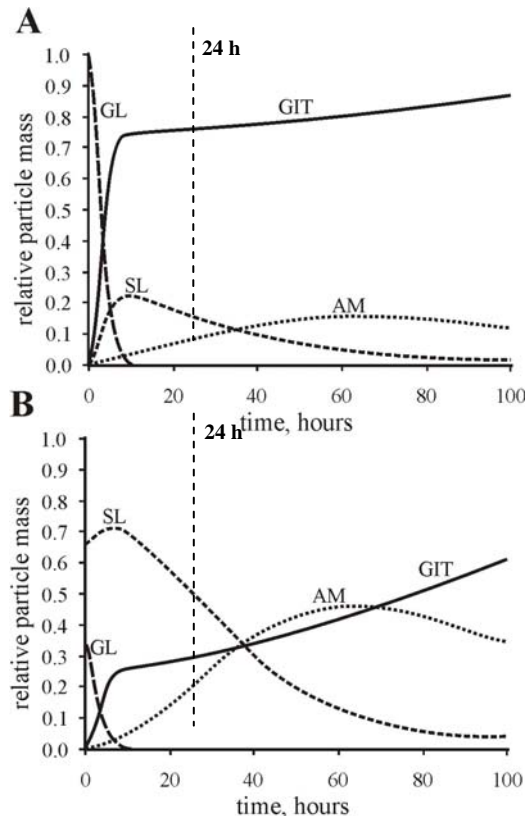


Figure 1. Results of the clearance calculations for platelets (A) with a diameter of 10  $\mu\text{m}$  and an aspect ratio of 0.1, and fibers (B) with a diameter of 1  $\mu\text{m}$  and an aspect ratio of 10. Abbreviations: AM = airway macrophages, GIT = gastrointestinal tract, GL = gel layer, SL = sol layer (Sturm & Hofmann 2006a).

Hofmann, W. & Sturm, R. (2004). *J. Aerosol Med.*, 17, 73-89.

Koblinger, L. & Hofmann, W. (1990). *J. Aerosol Sci.*, 21, 661-674.

International Commission on Radiological Protection (1994), *Human respiratory tract model for radiological protection*. Oxford, U.K.: Pergamon Press.

Sturm, R. & Hofmann, W. (2004). *Rad. Prot. Dosim.*, 118, 384-394.

Sturm, R. & Hofmann, W. (2006a). *Rad. Prot. Dosim.*, 118, 384-394.

Sturm, R. & Hofmann, W. (2006b). *Comp. Biol. Med.*, 36, 1252-1267.

## **The lung's structural asymmetry and its effect on ventilation and particle deposition**

David M. Broday and Yehuda Agnon

Civil and Environmental Engineering, Technion, Haifa, Israel

Keywords: Inhomogeneity, lung deposition, Fractals

Normally, the morphological model of the respiratory tract used in mechanistic inhalation dosimetry simulations follows a relatively simple structure, with the lungs represented by a set of straight tubes or a sequence of bifurcating Y-shaped units. The most common lung model is Weibel's scheme, which assumes a symmetric (hence complete) dichotomously branching airway tree. However, this model does not permit structural variability of the respiratory system among people. Moreover, it can not explain the substantial spatial heterogeneity in ventilation, which is oftentimes suggested to be linked to the complexity of the lung's architecture. An alternative lung model, which emphasizes the asymmetric morphology of the airway tree, has been promoted by Horsfield and coworkers. We implemented Horsfield's deterministic asymmetrical lung scheme to study the effect of the lung's structure on ventilation asymmetry and on the regional variation in particle deposition. Model results show that the fractal dimension that describes the ventilation variability in our simulations is very close to that reported experimentally, and is only weakly

dependent on the nature of the asymmetry. Particle deposition variability is affected by the same processes that affect airflow distribution within the lung and, therefore, closely follows the ventilation variability.

## Health effects of inhaled radon progenies in homes and mines

István Szöke<sup>1</sup>, Árpád Farkas<sup>1</sup>, Imre Balásházy<sup>1</sup>, and Werner Hofmann<sup>2</sup>

<sup>1</sup>Hungarian Academy of Sciences KFKI Atomic Energy Research Institute  
1525 Budapest, P.O. Box 49, Hungary

<sup>2</sup>Department of Material Science, Division of Physics and Biophysics, University of Salzburg  
Hellbrunner Str. 34, 5020 Salzburg, Austria

Keywords: health effects of aerosols, lung deposition, lung/particle interaction.

Inhalation of radon progenies may be an important factor of the occurrence of lung cancer. The progenies of radon may adhere to the surface of the ambient aerosols in a very short time. The percent of the unattached fraction of the radon daughters depends on the isotope and the aerosol composition of the ambient air. High concentration of radon can be found in mines in general and in uranium mines especially. Radon, on the other hand, is also present in the air of homes. The concentration of radon in homes is generally much lower, however, in some cases radon concentration nears the concentrations measured in mines. The isotope composition and the ratio of the attached and unattached portion of the isotopes are different in homes and in uranium mines. The question, how the distribution of radiation burden among bronchial epithelial cells and the biological consequences of radon exposure alters in mines and homes has not yet appropriately been answered. The aim of the present study is to investigate and compare the distribution of radiation burden and primary biological consequences originating from radon inhalation in case of a typical home exposure and in case of exposure conditions characteristic of uranium mines. A CFPD (Computational Fluid and Particle Dynamics) approach was employed in this study to determine the deposition distribution of the inhaled attached and unattached radon progenies (Balásházy *et al.* 2003).

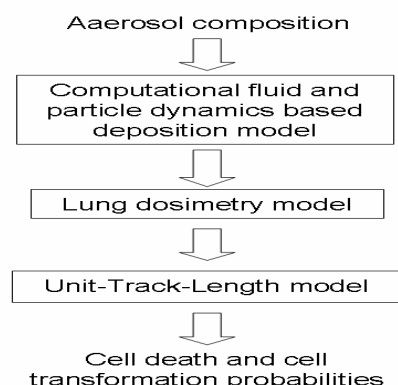


Figure 1. Structure of a complex microdosimetric model for the prediction of primary biological outcome of radon progeny inhalation.

Based on the deposition pattern of radioactive sources a biophysical mechanisms based, microdosimetric model was applied in order to calculate the cellular doses of the exposed epithelium. The biological outcome of the damage caused by the alpha-particles was predicted by the Unit-Track-Length Model of Hofmann and Koblinger (Crawford-Brown and Hofmann 2001). This model calculates cell inactivation and cell transformation probabilities based on microdosimetric values. The structure of the complex microdosimetric model employed in this work is demonstrated in Figure 1.

A typical radio-aerosol composition in homes was generated by averaging the aerosol data measured in 2000 homes. The results of the measurements were taken from the literature. In case of uranium mines, the data measured in the well documented New Mexico uranium mine were utilized.

Our calculations demonstrate that the local distribution of radon deposition and consequently the distribution of radiation burden among epithelial cell nuclei are highly nonuniform in both homes and uranium mines. In spite of the distributions of the local burden were very similar in the two cases, significant differences were experimented in all the maxima of calculated microdosimetric parameters. The probability of multiple cell nuclei hit and the maximum value of cell nuclei dose were significantly higher in mines. The probability of multiple cell nuclei hit was  $0.9 \times 10^{-5}$  in mines and only  $0.34 \times 10^{-5}$  in homes inhaling 10 million particles.

This research was supported by the CEC Contract no. 016987 (FI6R), CEC Contract no. FI6R-2003-508842 (RISC-RAD), the Hungarian NKFP-3/A-089/2004, NKFP-1/B-047/2004 and GVOP-3.1.1-2004-05-0432/3.0 Projects.

Balásházy, I., Farkas, Á., Szöke, I., Hofmann, W. and Sturm, R. (2003). *Radiation Protection Dosimetry*, 105, 129-132.

Crawford-Brown, D. J. and Hofmann, W. (2001) *Radiation Environment Biophysics* 40, 317-323.

## Pulmonary deposition and chemical composition of biosoluble vitreous fibers

R. Szőke<sup>1</sup>, I. Sziklai-László<sup>1</sup>, I. Balásházy<sup>1</sup>, G. Kudela<sup>2</sup>, W. Hofmann<sup>3</sup>

<sup>1</sup>KFKI Atomic Energy Research Institute, P.O. Box 49, H-1525 Budapest, Hungary

<sup>2</sup>Technoorg-Linda Co. Ltd., H-1077 Budapest, Rózsa u. 24.

<sup>3</sup>Division of Physics and Biophysics, University of Salzburg, Hellbrunner Str. 34, 5020 Salzburg, Austria

Keywords: vitreous fibers, pulmonary deposition, INAA/ENAA, elemental composition.

### INTRODUCTION

How inhaled fibers may cause cell damage related to tumor formation is presently not exactly known, although there are several hypotheses about it. *In vivo* studies have provided evidences that the most important parameters to determine the carcinogenicity and the toxicity of fibers are the dimensions, the local doses and the particles' chemical compositions. Fiber length and alveolar geometry appear to be important limiting factors for the submersion of vitreous fibers into the lungs' surface lining layer. Fiber dimensions are considered to be important because the macrophages that normally remove particles from the lungs cannot engulf fibers much longer than the macrophage diameter. The chemical composition of fibrous materials plays an important role in fiber-induced toxicity, while fiber biodurability directly correlates with pathogenic potential as it was observed in rodents (Jäckel et al, 2005). The main objectives of this study were to determine the deposition pattern of inhaled fibers in the human respiratory system and the concentration of macro- and microcomponents.

### METHODS

Fiber depositions in the human respiratory system of a Caucasian-type healthy adult male and 10 years-old child under different physical exertions were computed by the updated version of the stochastic lung deposition model of Koblinger and Hofmann (1990). The computations by the stochastic lung deposition model were performed on the polydisperse system. The extrathoracic model applies the empirical formula of Stahlhofen. Chemical composition was studied by panoramic instrumental and epithermal neutron activation analysis (INAA, ENAA). The accuracy of the analyses was tested by co-analyses of "NIST 613 Trace Elements in Glass" standard reference material.

### RESULTS

The highest deposition values were obtained for the extrathoracic region, more than 80%, and only a small fraction of the inhaled fibers reached the tracheobronchial tree and the acinar region, less than 12.4%. Interception contributes significantly to fiber deposition, particularly in the pulmonary part (Szőke et al, 2007). The number and the mass fraction of the inhaled vitreous fibers deposited in different regions of the human lung at resting activity and light

physical exercise breathing conditions are presented in Table 1.

Table 1. Number and mass fraction of inhaled biosoluble vitreous fibers deposited in different pulmonary regions.

Physical exertion	Interception	Bronchial region	Acinar region	ET
<i>Number distribution %</i>				
resting	3.38	4.06	4.93	81
active	1.98	1.29	1.98	91
<i>Mass distribution %</i>				
resting	0.73	2.36	1.63	94
active	0.01	0.47	0.31	99

Note: resting= resting activity; active= light physical exercise.  
ET- extrathoracic region.

The deposition fractions are strongly influenced by the level of physical exertion. Deposition in the lungs decreased with rising flow rate. The high percentage of extrathoracic deposition originates from the nose breathing conditions.

The biosoluble glass wool is characterized by a low amount of alumina (~1 wt% Al<sub>2</sub>O<sub>3</sub>) and a high amount of boron trioxide (~12 wt% B<sub>2</sub>O<sub>3</sub>). CaO, MgO, Na<sub>2</sub>O, B<sub>2</sub>O<sub>3</sub>, and BaO increase the dissolution rate; in contrast to this, Al<sub>2</sub>O<sub>3</sub> has a negative coefficient, meaning that increasing amounts of this oxide decreases the dissolution rate in borosilicate glass composition. No significant differences between the analyzed glass wool samples were found for Ag, Cs, and Sb; however, the Co (0.29 ± 0.02 µg/g) and Zn (20.56 ± 1.13 µg/g) concentrations were highest in one sample. The concentration of As varied between 2.33-30.17 ppm. Although the chemical composition of fibers is purportedly not responsible for the carcinogenic effect, it can play a potential role in the induction of related health effects due to their toxic components.

This research was supported by the Hungarian NKFP-3/A-089/2004, NKFP-1/B-047/2004 and GVOP-3.1.1-2004-05-0432/3.0 Projects.

### References

- Koblinger, L., Hofmann, W. (1990). *J. Aerosol Sci.*, 21: 661-674.
- Jäckel, M., Sáfrány, Á., Hargittai, P., Szőke, R., Pott, F., Kerényi, T. (2005). *AARMS*, 4: 275-283.
- Szőke, R., Alföldy, B., Balásházy, I., Hofmann, W., Sziklai-László, I. (2007). *Inhal. Toxicol.*, 19:1-8.

## Effect of therapeutic salt aerosols on ambient particle concentrations and size distributions and related lung deposition

F. Kwasny, P. Madl and W. Hofmann

Department of Materials Engineering & Physics, University of Salzburg, 5020 Salzburg, Austria

Keywords: salt aerosol, inhalation, modeling, lung deposition

The investigated “Gradierwerk” (GW) is a covered open-air saltwater inhalation spa in Bad Reichenhall, Southern Germany, close to Salzburg. Almost  $400 \times 10^3$  L of alpine brine per day trickle down the 13 m high wall made of stacks of hawthorn and blackthorn twigs. Dripping occurs at the luv-side of the GW, allowing the wind to press the nebulized brine through the twigs onto the lee-side of the GW, where patients are supposed to stand for therapeutic inhalation. The park is surrounded by a major road to the north-west, a residential area to the north-east and a pedestrian district on the remaining sides with the GW being located at the center.

The SMPS-sampling campaign investigated the suspended particle number in the range below  $1 \mu\text{m}$ . A repetitive series of measurement was carried out at selected sites in the vicinity of the GW to obtain a realistic picture of the particle distribution around the GW and the adjacent spa garden. A comparison of the aerosol inventory was made when the GW was turned on and when it was turned off for maintenance reasons. During operation, a peak at around  $100 \text{ nm}$  occurred. Under almost identical meso-climatic conditions, a significantly higher amount of nano-particles was present below the  $20 \text{ nm}$  range when the GW was turned off (Figure 1).

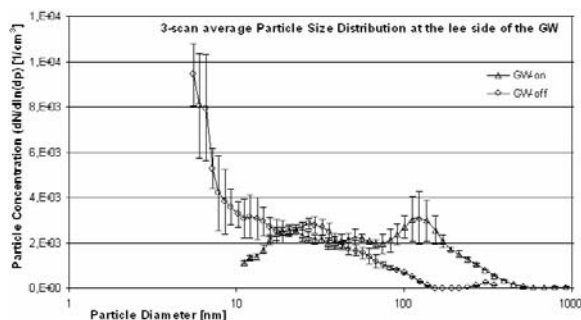


Figure 1. Difference in particle size distribution during on / off cycles at the lee sides of the GW.

To assign the observed agglomeration peak during on-site measurements to the brine aerosol, a lab-experiment was conducted which confirmed that nebulized brine did indeed level out over time towards the characteristic agglomeration peak at around  $100 \text{ nm}$ .

Investigating the fate of inhaled particles, the stochastic lung particle deposition model IDEAL-2 (Koblinger and Hofmann, 1990; Hofmann and

Koblinger, 1990) was used. Applying the scanned particle spectrum of the GW under the two operational conditions, revealed a significantly higher total lung deposition when the GW was turned off (Figure 2). Calculations with the spectral data when the GW was in operation, total pulmonary deposition decreased somewhat. However, a further reduction was obtained when introducing an equilibrium hygroscopic growth factor (HGF) of 5 for the inhaled brine aerosol (Heyder et al., 2004) to reflect the almost super-saturated conditions within the human respiratory tract.

Besides the well-known therapeutic effects of nebulized brine aerosol, a significant reduction of nanometer-sized particles (probably traffic-related) in the ambient air could be observed.

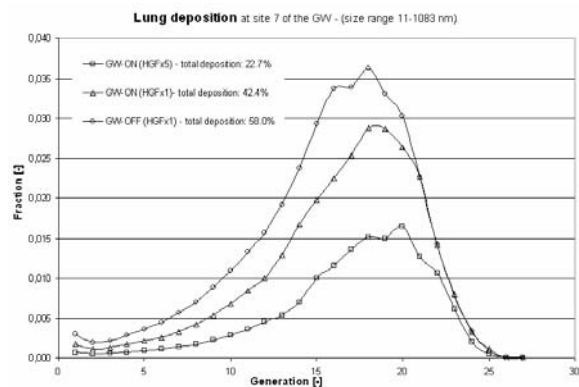


Figure 2. Computed particle deposition patterns of the nebulized brine aerosol in the various lung generations.

This research was made possible by the Kur GmbH Bad Reichenhall / Bayerisch Gmain. Climatic data were kindly provided by the Salzburg Airport and the Deutscher Wetterdienst.

Heyder, J., Gebhart, J. Roth, C., & Ferron, G. (2004). in Gradon L., Marijnissen, J.C. (eds.). *Optimization of Aerosol Drug Delivery*. Heidelberg, FRG: Springer Verlag, 139-147.

Hofmann, W., & Koblinger, L. (1990). *J. Aerosol Science*, 21, 675-688.

Koblinger, L., & Hofmann, W. (1990). *J. Aerosol Science*, 21, 661-674.

## Analyses of size distribution and related lung deposition in the *SELSONICS* Ultrasonic Nebulization Chamber

P. Madl and W. Hofmann

Department of Materials Engineering & Physics, University of Salzburg, 5020 Salzburg, Austria

Keywords: health aspects of aerosols, inhalation, lung deposition, particle formation, size distribution.

Vitamin-C enriched sodium-chloride (15% NaCl solution) from the Dead Sea and organically grown and extracted olive-oil samples with traces of supplemented Vitamin-D (5mL each) were separately nebulized by ultrasound atomizers in a therapeutic aerosol cabin constructed by Selsonics GmbH. Particle growth dynamics from aerosol processing reactions were measured with a Scanning Mobility Particle Sizer (SMPS) immediately after a 3 minutes long sample injection sequence. Scanning times with the SMPS covered a potential exposure window of at least 10 minutes in the size range of 0.01 to 1.1  $\mu\text{m}$ . Based on the data obtained from the SMPS measurements, the stochastic lung particle deposition model IDEAL-2 (Koblinger & Hofmann, 1990; Hofmann & Koblinger, 1990) was applied. As expected, two very different particle deposition patterns were obtained based on the hydrophilic / hydrophobic nature of the aerosol samples involved.

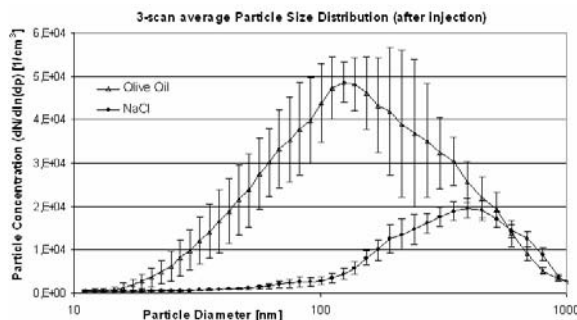


Figure 1. Size distributions of olive-oil and NaCl aerosols.

Figure 1 reveals a polydisperse distribution with the geometric mean located at around 140 nm. Particle concentrations of the olive-oil (NaCl) peaked at around  $103 \times 10^3 \pm 26 \times 10^3$  ( $30 \times 10^3 \pm 4.8 \times 10^3$ ) particles  $\text{cm}^{-3}$  and gradually decreased afterwards due to agglomeration to larger clusters.

To investigate the fate of inhaled olive-oil and NaCl particles with unit density, we used the stochastic lung deposition model to predict particle deposition patterns. For the deposition calculations, the 44 size classes of the SMPS were grouped into 20 size classes to facilitate the computations. Considering the elevated humidity level within the pulmonary region, an equilibrium hygroscopic growth factor (HGF) of 5 was assigned to the NaCl aerosol (Heyder et al. 2004). Predicted deposition

patterns of the samples within the human lung are exhibited in figure 2. The generation-numbers plotted on the abscissa correspond to the different lung regions (trachea: generation 0), where generations 1 to 15 are associated with the bronchial region, and generation numbers greater than 15 correspond to the alveolar region (Yeh & Schum, 1980).

In conclusion, deposition from both olive-oil and NaCl particles is higher in the alveolar region, and to a lesser extent within the bronchial region, where ciliary motion would promptly translocate deposited particles (clearance). Hence, from a therapeutic perspective, alveolar deposition may be associated with an increased imuno-response activity by alveolar macrophages (Donaldson et al., 1998).

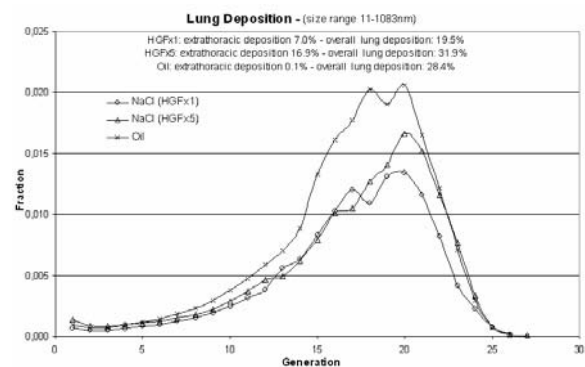


Figure 2. Particle deposition of the nebulized oil and NaCl samples in the various lung generations.

The authors wish to thank the Selsonics GmbH for their kind assistance, in particular to *P. Huber*, Technical Officer and to *P. Richter*, Managing Director of Selsonics GmbH.

- Donaldson, K., Li, X.Y., & MacNee, W. (1998). *J. Aerosol Science*, 29, 553-560.
- Heyder, J., Gebhart, J., Roth, C., & Ferron, G. (2004). in Gradon L., Marijnissen, J.C. (eds.). *Optimization of Aerosol Drug Delivery*. Heidelberg, FRG: Springer Verlag, 139-147.
- Hofmann, W., & Koblinger, L. (1990). *J. Aerosol Science*, 21, 675-688.
- Koblinger, L., & Hofmann, W. (1990). *J. Aerosol Science*, 21, 661-674.
- Yeh, H. C. & Schum, G. M. (1980). *Bull Math Biol.*, 42, 461-480.

## Simulation of Nano-Particle Deposition in Human Central Airways

Maria Chiara Piglionne and Marco Vanni

Dipartimento di Scienza dei Materiali e Ingegneria Chimica, Politecnico di Torino,  
Corso Duca degli Abruzzi 24, 10129 Torino, Italy

Keywords: lung deposition, lung-particle interaction, modelling, nanoparticles

The purpose of this study is to investigate transport and deposition of spherical nano-particles inside human central airways during the inhalation phase, using the Computational Fluid Dynamics code Fluent. The attention was focused on generations G3 to G15 (referring to Weibel's A lung model, 1963), considering particles having diameters ranging from 1 to 50 nm.

In order to simulate particle deposition we created a symmetric single bifurcation grid, basing its geometry on Weibel's lung classification scheme and also referring to results obtained by Hammersley & Olson (1992). This grid was characterized by a branching angle of  $70^\circ$ , a diameter to length ratio of 0.30 and a branching diameter ratio between two subsequent generations of 0.80.

The numerical method used for simulations considers a two phase problem and assumes the particle suspension as dilute due to the low mass loading ratio at the oral/nasal inlet. A simplified Eulerian-Eulerian approach was used: due to small size of the considered particles the particulate phase is modeled as a solute which is transported by the air flow and obeys a standard convection-diffusion equation with diffusivity expressed by the Stokes-Einstein equation. Two different breathing conditions were considered, resting and light activity (corresponding respectively to breathing rates of 15 L/min and 30 L/min). We also chose to examine two different kinds of boundary conditions for the outlet sections of bifurcations: first the condition of pressure outlet, implying uniform pressure at both outlets, secondly the condition of outflow, implying the outlet flux is the same on the two sides. In order to simplify settings for the simulations it was decided to consider bifurcations separately and sequentially: a uniform profile both for airflow and for particle flow was introduced in the third bifurcation, then velocity and concentrations profiles located at the end of the bifurcation were turned by  $90^\circ$  and introduced as inlet conditions for the subsequent bifurcation, after interpolation on the new nodes. The same thing was repeated for each bifurcation until the sixteenth one in order to reproduce a sequence of mutually orthogonal bifurcations, as described by Fontana and Vanni (2007). Simulations' results confirmed that velocity profiles changed considerably from the 3<sup>rd</sup> to the 15<sup>th</sup> generation. Initially velocity distributions are highly skewed, due to the presence of strong secondary flows; then, progressively, they become

axi-symmetric, evolving to a parabolic profile (corresponding to the 10<sup>th</sup> bifurcation). The velocity flow range depended on the conditions chosen for each simulation. For all four cases, the deposition fraction of the smallest particles increases with each subsequent bifurcation, until it levels off at the maximum of 1 in correspondence of generation 13<sup>th</sup>. On the contrary, as the diameter of the particles increases, the value of the deposition fraction decreases and never reaches the maximum possible value of 1. Considering the same flow rates, results showed that the maximum values of deposition fraction are slightly larger for the condition of pressure outlet than the maxima obtained with the condition of outflow. Figure 1 shows an example of the values of deposition fraction for particles of different diameters during resting conditions. Also the places of strongest deposition of particles inside every bifurcation were investigated, noticing that in the first examined bifurcations particles tend to deposit on the carinal ridge, and then, progressively, they tend to deposit more uniformly in the subsequent bifurcations.

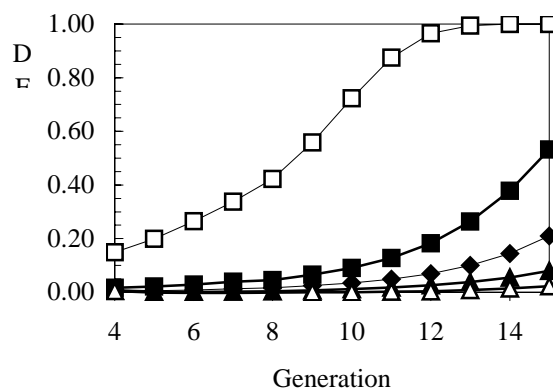


Figure 1. Deposition fraction for particles of different diameters for flow rate of 15 L/min, *outflow* chosen as boundary condition. □: 1 nm; ■: 5 nm; ◆: 10 nm; ▲: 20 nm; △: 50 nm.

Weibel, E. R. (1963). *Morphometry of the Human Lung*. New York, U.S.A.: Academic Press.

Hammersley, J. R., & Olson D.E., (1992). *J. App. Physiol.* 72(6), 2402-2414.

Fontana, D., & Vanni, M. (2007). Submitted to *J. Aerosol Sci.*

## Health risk from vehicle emissions and soot in urban area

A Schady<sup>1</sup>, A. Gzella<sup>2</sup>, J. Wozdzia<sup>2</sup>, A. Szczurek<sup>2</sup>, I. Sowka<sup>2</sup> and A. Wozdzia<sup>2</sup>

<sup>1</sup> Institut für Physik der Atmosphäre, DLR-Oberpfaffenhofen, D-82234 Weßling, Germany

<sup>2</sup> Ecological and Atmosphere Protection Division, Institute of Environment Protection Engineering, Wrocław University of Technology, Wyb. Wyspińskiego 27, 50-370, Wrocław, Poland

Keywords: traffic, fine particles, modelling.

Increased emissions through the stop and go at traffic junctions in combination with surrounding buildings may lead to accumulation of pollutants and multiply the harmful impact on human health. Inhalation is the major route of exposure to benzene and fine soot particles in cities.

The microscale model MIMO (developed at the Department of Technical Thermodynamics, University of Karlsruhe and described by Winkler, 1995 and Erhard (2000)) was applied for simulation the dispersion of inert gases and fine aerosols (soot) under different wind regimes. The simulation was based on the common rules which govern wind flow and dispersion in built up areas. However, a different approach to urban air pollution modeling was developed. At first, we concentrated on long term means (monthly). Secondly, we determined the most polluted zones which arise and persist stationary as a result of air flow around buildings near the traffic junction. Samples were exposed to air pollution for one month, thus finally the model results have been weighed according to wind rose in that time.

At the beginning, a GIS-spatial data base was created in which the results from measurements campaigns were included. The simulation region is located near the main traffic junction at Square region w, in the center of Wrocław. Wrocław is situated in southwestern Poland, it has ca. 720 000 inhabitants.

There were 827 point sources, each in a mesh of 3 x 3 m, the total length of a line source about 2500 m. Typical emission scenarios for heavy traffic roads is presented in Table 1, hence total soot emission should be 10 mg/s or 36000 mg/h. For the evaluation run a value of 3000 mg/h has been used. As for an example, the spatial soot concentrations for east wind conditions are presented in Figure 1.

The spatial analysis confirmed that concentrations of vehicle pollutants are not homogeneously distributed along street canyons and also impact on backyards. This method could be used for evaluation of urban inhabitants exposure to vehicle emissions and thus it seems to be an effective tool for urban management.

Table 1. Typical emission scenarios and values for heavy traffic roads.

	Benzene	Soot
Emission factor g/kg/PKW	0.3	0,015 automobiles 0,3 trucks
Emission density mg/m/s	0.006	0.004
Avg. of a polluted road g/m <sup>3</sup>	4.1 – 6.5	3.0 – 4.9

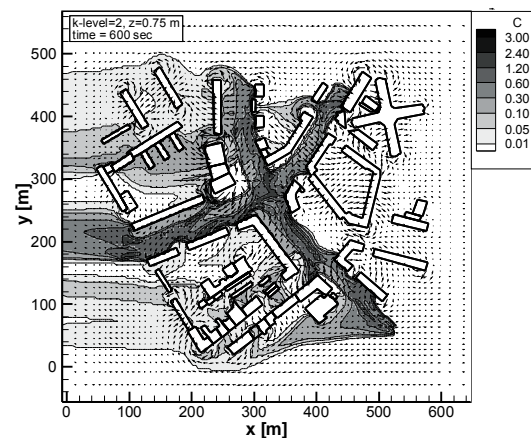


Figure 1. The wind field and spatial soot concentration distribution for east wind conditions.

This work was supported by the Polish Ministry of Science and Education under grant 3T09D06927.

Winkler, C. (1995). *n*  
*n n n n n n*  
 Fortschr.-Ber. VDI Reihe 7 Nr. 268. Düsseldorf: VDI-Verlag.  
 Ehrhard, I.A., Khatib, C., Winkler, R., Kunz, N., Moussiopoulos & Ernst G. (2000). *n*  
*n n n n n In n*,  
 85, 163-176.

## Cardiovascular Emergency Calls Associated to Urban Submicron Aerosol Fractions

U. Franck<sup>1</sup>, S. Odeh<sup>1</sup>, W.-H. Storch<sup>2</sup>, Th. Tuch<sup>1</sup>, A. Wiedensohler<sup>3</sup>, B. Wehner<sup>3</sup>, and O. Herbarth<sup>1,4</sup>

<sup>1</sup>Department Human Exposure and Epidemiology, Helmholtz Centre for Environmental Research – UFZ, Permoserstraße 15, 04318 Leipzig, Germany

<sup>2</sup>Ärztlicher Leiter Rettungsdienst - Brandschutzamt der Stadt Leipzig, Goerdeleerring 7, 04092 Leipzig, Germany

<sup>3</sup>Leibniz-Institute for Tropospheric Research, Permoserstraße 15, 04318 Leipzig, Germany

<sup>4</sup>Department of Environmental Hygiene and Epidemiology, Medical Faculty, University of Leipzig, Liebigstraße 27, 04103 Leipzig, Germany

Keywords: Health effects of aerosols, submicron particles, size distribution, urban areas

**Introduction:** It is well known that high concentrations of airborne particles are associated with the development of various environment related diseases and the exacerbation of various diseases. Since middle of the nineties epidemiologists found more and more indications that in addition to respiratory illnesses cardiovascular illnesses seem to be associated to airborne particulates. Recently, ultrafine particles have come under special scientific scrutiny. Usually, these particles do not contribute significantly to the mass concentration PM10 but they dominate particle number concentration. Especially, cardiovascular diseases are under suspicion to be evoked and exacerbated by particles significantly smaller than one micrometer.

This study is primarily aiming at two questions:

One aim is to investigate the influence of “rather low” common urban concentrations on the health state of city dwellers, who are not occupationally exposed.

Secondly, this study is quantifying risk differences for selected cardiovascular diseases associated with different size fractions of submicrometer particles, PM2.5 and PM10.

**Material and Methods:** The study was carried out in the city of Leipzig. This city is located in the Leipzig basin with no significant elevations in and around the city. Leipzig has approx. 500,000 inhabitants. There is no significant pollution by industry. In the City of Leipzig urban traffic is a very important source of airborne particles.

Aerosol measurements were carried out at the Leibniz Institute for Tropospheric Research using TDMPMS (twin differential mobility sizer system) working detecting particles with diameters from 3 to 800 nm. The measuring site can be regarded as urban background. Additionally, PM10 and PM2.5 data of public authorities were used for comparison of the health effects of these coarser particles with the effects of the smaller ones.

Cardiovascular emergency calls were selected from the total number of emergency calls for a time period of 12 month within the City of Leipzig.

Therefore, there is no bias produced by the selection of areas within the city.

**Results:** Table 1 lists the urban particle concentrations of different size fractions found during the measuring period.

Size Fractions (Dp nm; PM µg/m <sup>3</sup> )	Mean	Median	Min	Max
Dp<100	12094	10893	1487	34650
100<Dp<500	1919	1723	334	18668
Dp>500	28.54	17.91	2.107	280
Dp<800	14043	13111	2450	35338
PM10	32.48	28.56	6.829	109.7
PM2.5	20.61	18.18	1.375	84.06

Table 1. Statistics of daily averages of particle number concentrations during the measuring period.

In total 5326 cardiovascular emergency calls were used for epidemiologic analysis. Generally, there is no significant difference in incidence between the weekdays and weekends. There are 22.74% and 22.44 % of cardiovascular emergency calls, respectively.

We found:

- a significant positive correlation between the risk for cardiovascular emergency calls and the particle number concentrations,
- a time lag of 1 to 8 days for the health effect of the particles,
- differences in effect for different particle size fractions,
- differences in effect on different cardiovascular diseases.

Significant effects could be found despite of the great inner urban differences in the concentrations of some particle fractions (Tuch *et al.* 2006).

Tuch, Th., Herbarth, O., Franck, U., Peters, A., Wehner, B., Wiedensohler, W., Heintzenberg, J. (2006). *J Expo Sci Environ Epidemiol*, 16, 486-490.

## **T09 Abstracts**

## Chemical aerosol reaction engineering in flames: from oxide production to salts and metal nanoparticles

R. N. Grass, E. K. Athanassiou and W. J. Stark

Department of Chemistry and Applied Biosciences, ETH Zurich, Wolfgang-Pauli-Strasse 10, 8093, Zurich, CH

Keywords: generation of nanoparticles, combustion synthesis, reducing flame synthesis, salt nanoparticles, metal nanoparticles

The enhanced properties of nanoscale metal and salt nanoparticles has triggered a wealth of research on their applications in electronics, magnetics and optics. Unfortunately, the availability of larger amounts ( $> 100$  g) of metal and salt nanoparticles at high purity is still an open technical problem. Currently, gas-phase flame technology is applied for the large scale manufacture of silica and titania yielding more than 2 million metric tons of nanoparticles per year. Alternatives in the liquid phase suffer from contamination from residual surfactants and solvents but can give rise to more complex materials. Recently, the introduction of flame spray technology further allowed the synthesis of complex mixed metal oxides and biomaterials. (Loher et al., 2005). It would be most advantageous, however, to actually use flame spray technology for a much broader range of materials.

This contribution will how flame-based aerosol methods can even be extended for the synthesis of complex inorganic salts and metal nanoparticles by influencing the reaction chemistry in the flame.

**Metal halide nanoparticles** (Grass and Stark, 2005) (Fig 1): Nanoparticles consisting of  $\text{BaF}_2$ ,  $\text{CaF}_2$ ,  $\text{SrF}_2$  and even  $\text{NaCl}$  could be prepared at production rates of above 10 g / h using a standard flame spray reactor. The high purity of the produced nanoparticles and the possibility of rare earth metal doping suggests application of the materials in optics.

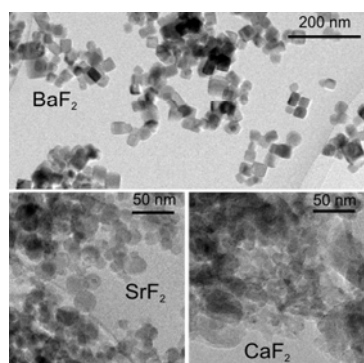


Figure 1. Transmission electron micrograph of barium- strontium – and calcium fluoride nanoparticles produced by flame synthesis.

**Cobalt nanoparticles** (Grass and Stark, 2006) (Fig 2): Nanoparticles of 20 - 60 nm in diameter consisting of metallic face-centered-cubic cobalt were synthesized in one-step process by reducing flame synthesis operated in an oxygen free environment. The material was highly magnetic with promising properties for application in electronics.

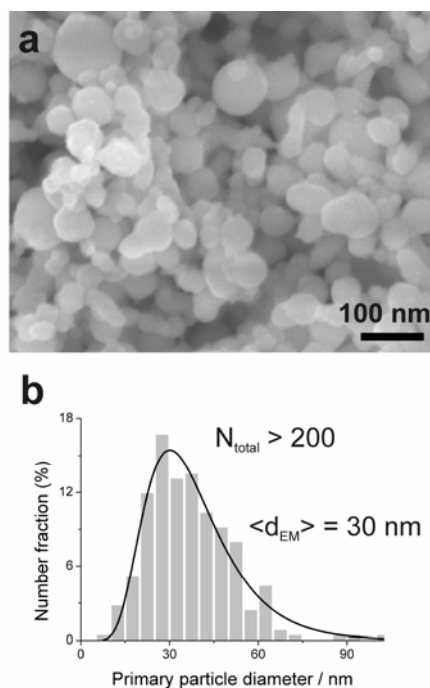


Figure 2. Scanning electron image of as-prepared cobalt nanoparticles with an average particle diameter of 30 nm and a narrow particle size distribution.

### References

- Grass, R. N., & Stark, W. J. (2005). *Chem. Commun.*, 14, 1767-1769.
- Grass, R. N., & Stark, W. J. (2006). *J. Mater. Chem.* DOI: 10.1039/b601013j.
- Loher, S., Stark, W. J., et al. (2005). *Chem. Mater.*, 17, 36-42.

## Iron Doped Carbon Shell Nanoparticles

S. Yang<sup>1,2</sup>, P. V. Pikhitsa<sup>1</sup>, Y.-J. Kim<sup>1</sup>, D. Kim<sup>1</sup>, H. Lee<sup>3</sup>, J. Yu<sup>3</sup>, and M. Choi<sup>1</sup>

<sup>1</sup>National CRI Center for Nano Particle Control, School of Mechanical and Aerospace Engineering, Seoul National University, Seoul 151-742, Korea

<sup>2</sup>Powder Materials Research Center, Korea Institute of Machinery and Materials, Changwon 641-831, Korea

<sup>3</sup>Department of Physics and Astronomy And Center for Strongly Correlated Materials Research, Seoul National University, Seoul 151-742, Korea

Keywords: Nanoscale carbon particles, nanoparticles, generation, composition, physical properties.

CW CO<sub>2</sub> laser irradiation of pure acetylene flow preheated with a diffusion oxy-hydrogen flame was shown to generate carbon shell nanoparticles at a sufficient laser power (Choi *et al.*, 2004). Later we found that preheating is not necessary. In complete absence of oxygen continuous carbon shells can be generated at lower laser power by self-sustained laser-assisted chemical reactions producing C<sub>2</sub> from acetylene and the process is governed by both acetylene concentration and laser power. Metastable amorphous carbon (and even nanodiamonds) is created from fast condensation of carbon dimers and then, in 1 msec, it may be transformed into carbon shells under laser irradiation (Pikhitsa *et al.*, 2005).

This peculiar carbon shell generation method allows achieving transition metal doping of carbon shells. The iron ions obtained with iron pentacarbonyl admixture into acetylene flow are first trapped into the metastable carbon. Then, the metastable carbon rapidly transforms into continuous layer polyhedral carbon shell nanoparticles under the same laser beam. The iron ions remain sandwiched between carbon shells, presumably in topological defects (Pikhitsa *et al.*, 2005a) as DFT computer calculations suggest.

Magnetic measurements of Fe doped shells with 260 ppmw of iron revealed ferromagnetism. Electron spin resonance confirmed presence of Fe<sup>1+</sup> ions in a 3d<sup>7</sup> state.

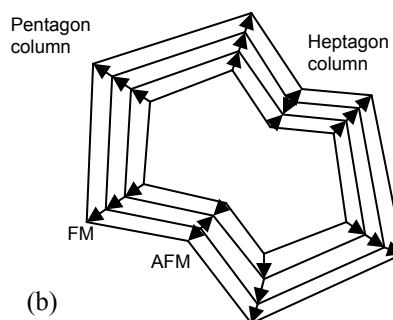
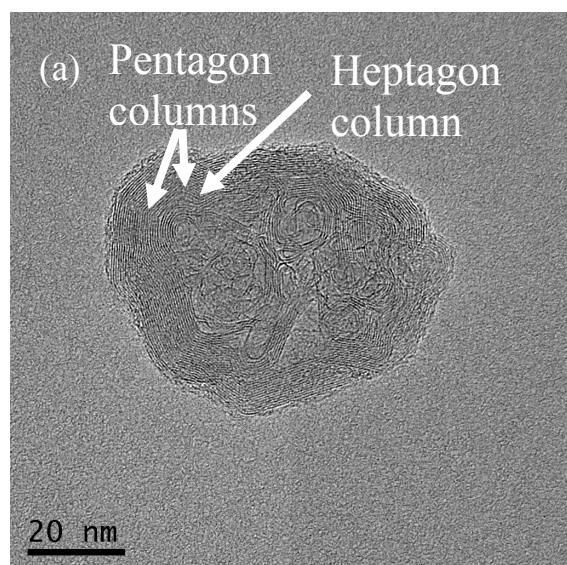


Figure 1. An iron-doped carbon nanoparticle. (a) Topological defects are indicated with arrows; (b) a schematic of the nanoparticle with pentagon and heptagon columns; arrows indicate computed spin alignment of iron ions in the columns which can be ferromagnetic or antiferromagnetic in pentagon and heptagon columns, correspondingly.

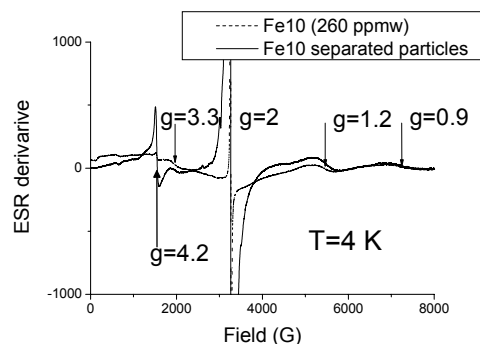


Figure 2. Electron spin resonance from individual Fe<sup>1+</sup> ions in iron doped carbon shells.

This work was funded by the Creative Research Initiatives Program supported by the Korea Ministry of Science and Technology.

Choi, M., Altman I.S., Kim Y. J., Pikhitsa P.V., Lee S., Park G., Jeong T.&Yoo J. (2004) *Adv. Mater.* 16, 1721-1725.

Pikhitsa P. V., Kim Y.J. & Choi M. (2005), in *Proc. 4<sup>th</sup> Asian Aerosol Conference*, Mumbai (R.V. Enterprises, Mumbai ), 18-19.

Pikhitsa P.V., Kim Y.J., Kim M.W., S. Yang, Noh T.W.&Choi M. (2005a) *Phys. Rev. B*71, 073402(1-4).

## Flame Spray Synthesis of Nanostructured Perovskite-Composites for Fuel Cell Applications

A. Heel, A. Vital, P. Holtappels, T. Graule

Empa, Swiss Federal Laboratories for Materials Testing and Research, Laboratory for High Performance Ceramics, Überlandstrasse 129, CH-8600 Dübendorf, Switzerland

Keywords: nano, composite, perovskite, flame spray synthesis, fuel cell

Solid oxide fuel cells (SOFCs) are an up-and-coming technology for high efficiency and environmentally-friendly power generation. Lowering the operating temperature from 800-1000°C to intermediate temperatures of around 500-600°C is one of the primary scientific aims in the fuel cell community. This has the advantage of decreasing the thermal requirements of the materials and increases the life time, which is limited due to diffusion effects in the fuel cell materials. On the one hand alternative materials have to be developed but on the other hand a nanostructured material offers the prospect to reach a higher performance at lower operating temperatures.

For the cathodes of a SOFC, mainly mixed oxides with an  $ABO_3$  crystal structure (perovskite) are used, where the A and/or B side is substituted by multi valent cations to increase the oxygen transport. The nanostructured powder morphology is expected to affect the catalytic and electrochemical properties of these materials (Weber & Ivers-Tiffée, 2004). Those particles show a significant higher number of reactivity sites, while bulk conductivity plays a minor role and at the same time lower sintering temperatures can be applied. Additionally, new processing routes can be adopted to improve the desired highly electrochemical reactive SOFC layers.

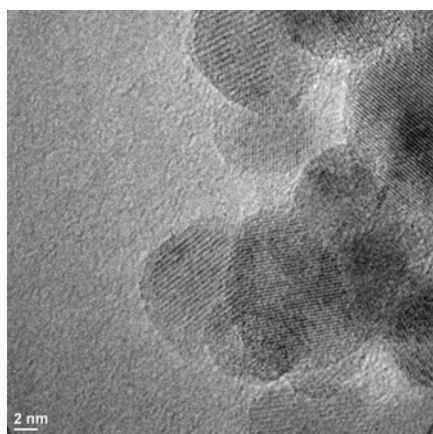


Figure 1. HR-TEM of high-crystalline  $La_{0.8}Sr_{0.2}MnO_3$  composite, necessary for electrochemical applications.

Flame spray synthesis (FSS) is an adequate method to reach a high throughput and allows the usage of

cost-extensive and uncritical precursors. This is significant for large scale industrial applications. Here, a one-step gas phase process is presented, where high-crystalline nanomaterials are generated by a liquid-fed flame spray process and which allows detailed control of the particle stoichiometry.

Three different promising cathode materials with the following stoichiometry were synthesised  $La_{0.8}Sr_{0.2}MnO_3$  (LSM),  $La_{0.6}Sr_{0.4}Co_{0.2}Fe_{0.8}O_3$  (LSCF) and  $Ba_{0.5}Sr_{0.5}Co_{0.8}Fe_{0.2}O_3$  (BSCF) (Ried *et al.*, 2006) by FSS. We will show the influence of process parameters on the morphology of the powders (HR-TEM, BET), desired crystal structure/size (XRD) and element stoichiometry (ICP-AES). The nanostructured powders (figure 1) are investigated by dilatometry in terms of the sintering and shrinkage behaviour (figure 2) and coefficient of thermal expansion (CTE) as a function of particle size.

The results are compared to conventional multi-step processed microscale materials. Furthermore, electrochemical performance of the powders will be shown with respect to its application in a SOFC at intermediate temperatures.

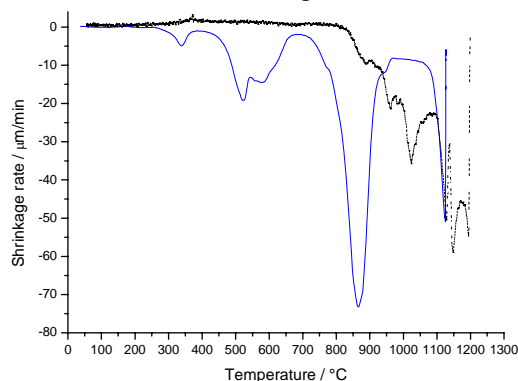


Figure 2. Sintering and shrinkage behaviour of nano (lined) and conventional submicron (dashed)  $Ba_{0.5}Sr_{0.5}Co_{0.8}Fe_{0.2}O_3$ .

This work was supported by EU Funding under grant SOFC600 (SES6-020089).

Ried, P., Bucher, E., Preis, W., Sitte, W., Holtappels, P. (2006). *Proc. of SOFC-X, Nara, Japan*.

Weber, A., Ivers-Tiffée, E. (2004). Materials and concepts for solid oxide fuel cells (SOFCs) in stationary and mobile applications. *J. Power Sources* 127 (1-2), 273-283.

## Formation process and chemical structure analysis of ionic-liquid nanoparticle

M. Shigeyasu, H. Tanaka

Institute of Science and Engineering, Chuo Univ., 1-13-27 Kasuga, Bunkyo-ku, 112-8551, Tokyo, Japan

Keywords: ionic liquid, nanoparticle, DMA, PS, homogeneous nucleation mechanism

It has been widely investigated on nanoparticles composed of ionic-crystal salts such as NaCl, CsCl *etc.*, of which melting temperatures are usually high. On the other hands, recently, ionic liquids of which melting temperatures are extremely low have attracted much attention because of their novelty and their specific properties. In this study, we investigated the formation process of ionic-liquid nanoparticle with measurements of its diameter using a differential mobility analyzer (DMA). In addition, we also analyzed the ionic-liquid nanoparticle using an X-ray photoelectron spectroscopy (PS) in order to elucidate whether its chemical structure was decomposed or not.

$C_4\text{mpyr}rr\text{NTf}_2$ , 1-butyl-1-methylpyrrolidinium bis(trifluoromethanesulphonyl)imide, loaded on an alumina boat was heated at 250 °C by a furnace. Vaporized molecules were then cooled and admitted into an  $^{241}\text{Am}$  neutralizer for ionization with  $\text{N}_2$  gas. Negatively ionized particles were diameter-analyzed by a DMA and current of the ions was measured by a Faraday cup electrometer. The pressure in the particle generator and in the DMA was regulated at 270 hPa. Diameter spectrum was obtained by measuring of the current as a function of the diameter. On the other hand, diameter-selected nanoparticles were electrically collected on a silicon substrate and were analyzed by using an PS in order to elucidate the chemical structure of the nanoparticles.

Figure 1 shows diameter distribution of nanoparticle produced from  $C_4\text{mpyr}rr\text{NTf}_2$  heated at 250 °C. A symmetrical single peak was observed at 4.9 nm. It is plausible that the observed

nanoparticle is originated from  $C_4\text{mpyr}rr\text{NTf}_2$  because the peak was only observed with heated  $C_4\text{mpyr}rr\text{NTf}_2$ . Shape of the peak indicates that the observed nanoparticle is produced by simple aggregation process. The stoichiometry of the produced nanoparticle was confirmed as  $C_4\text{mpyr}rr\text{NTf}_2$ ,  $\text{C}_{11}\text{H}_{20}\text{F}_6\text{N}_2\text{O}_4\text{S}_2$ , by relative intensities of the observed photoelectron peaks in an XPS spectrum. Ionic structure of the produced nanoparticle was also confirmed by analyzing chemically shifted peaks in the N 1s and the C 1s spectra. In summary, the  $C_4\text{mpyr}rr\text{NTf}_2$  nanoparticle was formed by the homogeneous nucleation mechanism, and was composed of an ionic-liquid structure.

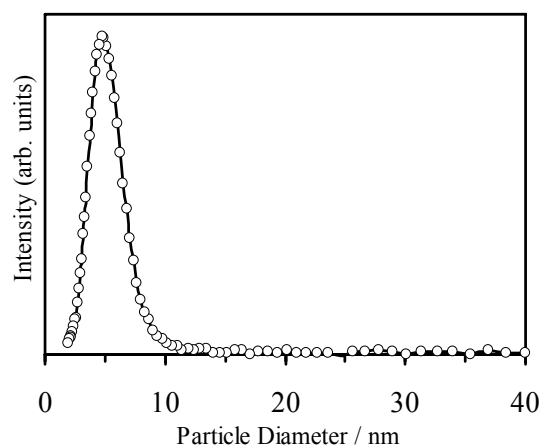


Figure 1. Particle diameter distribution of nanoparticle produced from  $C_4\text{mpyr}rr\text{NTf}_2$  heated at 250 °C.

## Air stable, carbon coated metal nanoparticles for sensor applications

E. K. Athanassiou, R. N. Grass and W. J. Stark

<sup>1</sup>Department of Chemistry and Applied Biosciences, ETH Zurich, Wolfgang-Pauli-Strasse 10, 8093, Zurich, CH

Keywords: copper, reducing flame synthesis, metal nanocomposite, thermal sensors, pressure sensors

Inexpensive, reliable temperature and pressure sensors are a crucial part in most manufacturing processes. The current demand for increasingly more integrated consumer products has created a strong need for ultra low cost materials with exceptional sensitivity and mechanical or thermal stability. At present, temperature sensing is based on composite oxides of transition metals or advanced spinel compositions and account for most negative temperature coefficient (NTC) thermistors (Rousset et al., 1994).

Among metallic nanoparticles copper has attracted considerable interest because of its optical, catalytic, mechanical and electrical properties, resulting in a wide range of applications in the field of metallurgy, catalysis, nano- and optoelectronics (Dhas et al., 1998).

Here, we use most recently developed reducing flame spray synthesis for the preparation of 1 nm carbon coated metallic copper nanoparticles (10 to 20 nm) at up to 10 g h<sup>-1</sup>. The carbon coating protected the zero-valent copper particles from oxidation in air. Transmission electron microscopy images showed that the average thickness of the layers was about 1-2 nm (Figure 1a). Raman and solid state <sup>13</sup>C magic angle spinning spectroscopy revealed that the carbon layers consisted of a sp<sup>2</sup> – hybridized carbon modification in the form of graphene stacks (Figure 1b) (Athanassiou et al., 2006a; Athanassiou et al., 2006b).

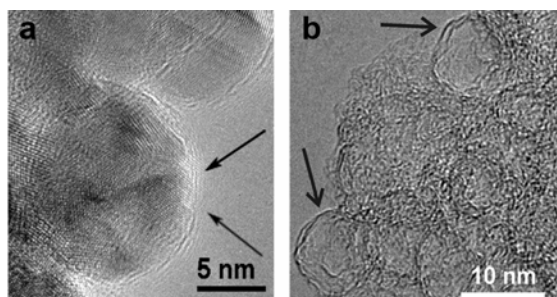


Figure 1. Electron microscopy images of C/Cu nanoparticles (a) produced by reducing flame synthesis. Treatment with nitric acid removed the copper core and resulted in empty carbon shells (b).

Bulk pills of pressed carbon/copper nanoparticles were pressed and examined by four point resistivity measurements. They displayed a highly pressure- and temperature dependent electrical

resistivity. The negative temperature coefficient (NTC) behavior of the material revealed a characteristic material constant  $\beta$  of above 4500 K (Table 1). The core/shell nanocomposite therefore exhibited a similar or greater sensitivity than today's commercially applied ceramic sensing materials (Table 1) (Athanassiou et al., 2006a; Yue et al., 2002; Lee & Yoo, 2002; Metzmacher et al., 2000).

Table 1. NTC properties of C/Cu nanoparticles and metal oxides spinels.

Sensing material	$\beta$ (K)	$E_a$ (meV)	T range (K)
C/Cu	4550	392	298 – 373
Mn-Zn-Ni Spinel	4260	367	298 – 673
Mn-Co-Ni Spinel	4800	414	298 – 358
Mn-Ni-In Spinel	4050	349	298 – 423

These properties suggest the use of the insulator/conductor nanocomposite as novel, low cost temperature sensing material and offer a metal-based alternative to the currently used brittle metal oxide based spinels and perovskites.

### References

- Rousset, A., Legros, R., & Lagrange, A. (1994). *J. Eur. Ceram. Soc.*, 13, 185-195.
- Dhas, N. A., Raj, C. P., & Gedanken, A. (1998). *Chem. Mater.*, 10, 1446-1452.
- Athanassiou, E. K., Grass, R. N., & Stark W. J. (2006a). *Nanotechnology*, 17, 1668-1673.
- Athanassiou, E. K., Mensing, C., & Stark, W.J. (2006b). *Sens. Actuators, A*, submitted.
- Yue, Z., Qie, X. W., Wang, X. H., Zhou, J., Gui, Z. L., & Li, L. T. (2002). *J. Mater. Sci. Lett*, 21, 375-377.
- Lee, M., & Yoo, M. (2002). *Sens. Actuators, A*, 96, 97-104.
- Metzmacher, C., Groen, W. A., & Reaney, I.M. (2000). *Phys. Status Solidi A*, 181, 369-386.

## Size and concentration control of nanoparticles in plasma using pulsed hydrogen gas

Kwang-Su Kim<sup>1</sup>, Byung-Hoon Kim<sup>2</sup> and T. Kim<sup>3</sup>

<sup>1</sup>School of nanoscience and nanotechnology (SAINT)

<sup>2</sup>School of mechanical engineering

<sup>3</sup>School of mechanical engineering & Sungkyun Advanced Institute of NanoTechnology, Sungkyunkwan University, Cheoncheon-dong, 440-746, Suwon, Korea

Keywords: CVD, Electron microscopy, Particle formation and growth, Size analysis.

Silicon nanoparticles are widely studied as one of the building blocks for novel devices and nanostructured materials. For successful applications, it should be easy to synthesize large amount of silicon nanoparticles with accurate size control. Several groups reported synthesis method for silicon nanoparticles for this purpose. (Koliopoulou et al., 2006; Oda, 2003; Ostraat, 2000).

In this paper, we investigated size and concentration control characteristics of SiH<sub>x</sub> nanoparticles using hydrogen gas pulse which had been proposed by Oda (2003). An inductively-coupled plasma chamber with RF power (13.56 MHz) was designed for this study. To increase the particle collection efficiency while avoiding the film formation, DC-bias is applied between the substrate and the grid made with stainless steel mesh. Experiments were performed with various hydrogen gas on time between 0.1 to 0.9 sec, with 0.2 sec step. The size of synthesized nanoparticles was measured using scanning electron microscopy (SEM) and analyzed using Image J software from NIST.

With the use of hydrogen gas pulse, the separation of the nucleation (hydrogen-on) and the growth process (hydrogen-off) can be achieved. During the hydrogen-off time, the radicals tend to contribute to the growth of particles which are already nucleated rather than to the creation of new nuclei (Oda, 2003). Therefore, the particle growth mainly occurs. However, when the hydrogen gas is introduced into the plasma in which the particle are being grown, hydrogen gas drives the grown particles out of the plasma region to the substrate and nucleation occurs simultaneously. Particle nucleation dominates in this case. Thus we can control the size of nanoparticles effectively with the use of hydrogen gas pulse.

In Figure 1, the geometric mean size of particles increased as the hydrogen-on time decreased. In addition, the particle concentration increased as the hydrogen-on time increased. It is because the particle nucleation mainly occurs with hydrogen-on, as was speculated by Oda (2003). If the hydrogen-on time becomes too long, the growth due to coagulation between the nuclei or slightly grown particles can occur, which leads to the lower uniformity of particle size. This effect is shown in

Figure 2. Especially, all the particles formed agglomerates when the hydrogen pulse on time is over 0.5 sec (over duty 0.5).

In this study, it was found that the size and concentration of silicon nanoparticles could be controlled with the precise control of hydrogen gas pulse.

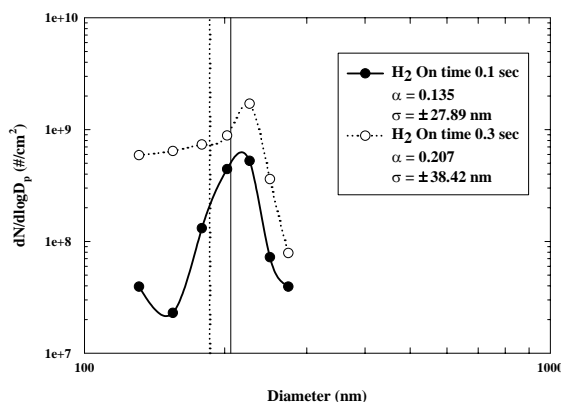


Figure 1. The comparison of size distribution between hydrogen-on time 0.1 and 0.3 sec.

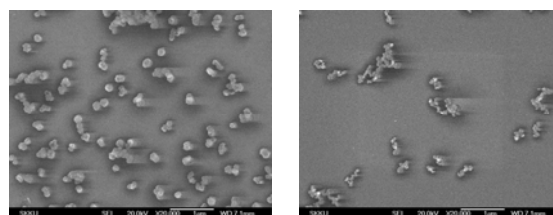


Figure 2. SEM images of the synthesized nanoparticles with different hydrogen-on time; (left) 0.3 sec & (right) 0.5 sec.

- Koliopoulou, S., Dimitrakis, P., Goustouridis, D., & et al. (2006). *Microelectronic engineering*, 83, 1563-1566.
- Oda S. (2003). *Materials science & Engineering B*, 101, 19-23.
- Ostraat, M.L., De Blauwe, J.W, Green, M.L. (2001). *J. of the Electrochemical society*, 148(5), G265-G270.

## Urban and rural measurements of atmospheric small-ions and ultrafine particles

M. D. Wright<sup>1</sup>, A. J. Buckley<sup>1</sup>, P. A. Keitch<sup>1</sup>, D. L. Henshaw<sup>1</sup>.

<sup>1</sup>H. H. Wills Laboratory, University of Bristol, Tyndall Avenue, Bristol, BS8 1TL, U.K.

Keywords: urban aerosols, ions, ultrafine particles, indoor/outdoor particles, particle size distribution

The ultrafine fraction of atmospheric aerosols is increasingly linked with adverse health effects (Oberdörster *et al.*, 2005). Characterisation of aerosol properties in exposure environments is therefore vital to understanding and reducing the potential health risk. An estimated 73% of the population of Europe live in urban areas in which they are exposed to high concentrations of anthropogenic aerosols. Recently, Knox (2006) linked 'hot-spots' of pollution, including transportation facilities such as bus and railway stations and major roads, with initiation of childhood leukaemia.

This study aims to add to the body of knowledge regarding ultrafine particles in urban areas, in several indoor and outdoor locations such as roadside, industrial, residential, office and domestic sites in the Bristol (UK) area, with comparison to rural background locations away from the city. In addition, measurements of both aerosol and small-ion concentrations allows examination of the relationship between aerosol size distribution and ion concentration under different environmental conditions (Hörrak, 1998).

Measurements are made using custom-built aspiration condenser ion mobility spectrometers (ACIMS) in the diameter range 0.4 - 30 nm (Fews *et al.*, 2005) and a sequential mobility particle sizer and classifier (SMPS+C) in the diameter range 10 - 1100 nm. The ACIMS is based on the 'Gerdien' design, where air is drawn through a cylindrical capacitor and the voltage applied across the capacitor is varied from 0 to  $\pm 1000$  V. Charged particles deflect in the electric field and are deposited on a central electrode where the current is measured with a sensitive electrometer. The time taken for one voltage cycle is around 15 minutes.

Initial indoor measurements in a fourth-storey room in the Department of Physics, University of Bristol were taken with windows open and with windows closed. A typical indoor ACIMS mobility spectrum is shown in Figure 1 and SMPS+C size distributions (taken overnight) for larger aerosols in Figure 2. Urban ion and aerosol concentrations vary considerably depending on the time of day and day of the week. A peak in aerosol concentration, as measured indoors, is seen at around 9 a.m. on working days, coincident with the morning 'rush-hour'. The size distribution is also shifted to smaller sizes. Fluctuations are reduced but not eradicated by closing the windows as the room is not environmentally enclosed. Aerosol concentrations

were reduced by around 70% after windows were closed, while ion concentrations remained unchanged. At the rural locations, ion concentrations were higher than at any of the urban locations, and small aerosol (< 15 nm) counts were 2 to 3 times lower than usually observed indoors.

The poster will present further results from these and additional locations, including in the open air on the Department roof (20 m above ground level) and outside the entrance to the Department at ground level, to examine the vertical ion/aerosol profile at the building, at various sites around Bristol and at rural locations.

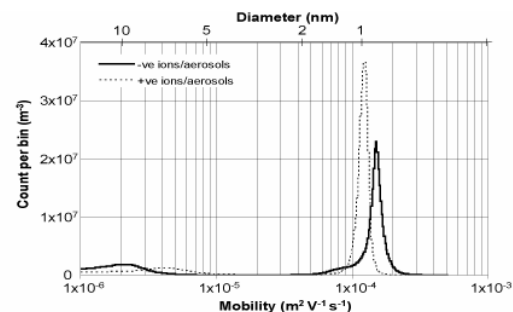


Figure 1. Typical indoor ACIMS mobility spectrum.

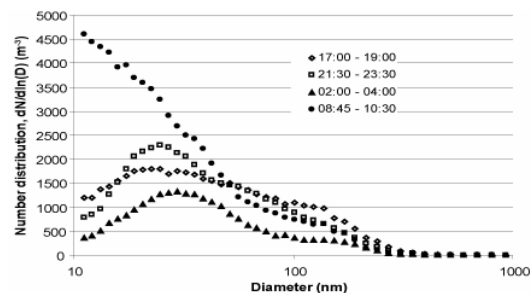


Figure 2. SMPS+C indoor size distributions obtained at different times of day

This work is supported by CHILDREN with LEUKAEMIA, registered charity No. 298405 (U.K.).

- Fews, A. P., Holden, N. K., Keitch, P. A. and Henshaw, D. L. (2005). *Atmos. Res.*, 76, 29-48.  
 Hörrak, U., Mirme, A., Salm, J., Tamm, E. and Tammet, H. (1998). *Atmos. Res.*, 46, 233-242.  
 Knox, E. G. (2006). *J. Epidemiol. Community Health*, 60, 136-141.  
 Oberdörster, G., Oberdörster, E. and Oberdörster, J. (2005). *Environ. Health Perspect.*, 113, 823-839.

## Comparison of Ultrafine Particle Surface Area Measurement with NSAM and SMPS

Christof Asbach<sup>1</sup>, Heinz Kaminski<sup>1</sup>, Heinz Fissan<sup>1</sup>, Christian Monz<sup>2</sup>, Dirk Dahmann<sup>2</sup>, and Thomas A.J. Kuhlbusch<sup>1</sup>

<sup>1</sup> Institut für Energie- und Umwelttechnik (IUTA), Bliersheimer Str. 60, 47229 Duisburg, Germany

<sup>2</sup> Institut für Gefahrstoffforschung (IGF), 44789 Bochum, Waldring 97, Germany

Keywords: SMPS, NSAM, NaCl, diesel soot particles, agglomerate

Health effects of inhaled ultrafine particles have been reported to correlate better with particle surface area (e.g. Oberdörster, 1996) rather than with particle number or mass. Direct measurement of the particle surface area is impossible, but several approaches have been made to assess this parameter indirectly. For powders, the surface area is commonly determined by means of gas adsorption, but for airborne particles, the determination of particle surface area remains challenging.

One approach to estimate the surface area of airborne particles is based on electrical mobility analysis of the particles, e.g. with a scanning mobility particle sizer (SMPS). The particles are assumed to be spherical with the mobility diameter as their physical diameter. Lall & Friedlander (2006) recently developed a model that allows more accurate assessment of the surface area distribution of chain like agglomerates, based on measured mobility distributions delivered by an SMPS. Their model is based on several assumptions and therefore only valid for very specific agglomerates. In order to assess the amount of particle surface area that deposits in the lung, the surface area size distributions can be weighted with lung deposition curves (e.g. by James *et al.*, 2000), which allow differentiation into the deposition in different compartments of the human lung. These distributions of lung-deposited surface area can be integrated within the particle size limits of interest to obtain the total lung-deposited surface area. The total lung deposited surface area can be used as a single value that determines the health relevance of inhaled ultrafine particles.

The Nanoparticle Surface Area Monitor (NSAM) is an instrument that uses diffusion charging of particles followed by a manipulated ion trap to measure the electric current, induced by the deposition of the charged particles. It has been shown that the current can be correlated with the total particle surface area deposited in either the alveolar or tracheobronchial region, depending on the ion trap setting (Fissan *et al.*, 2007; Shin *et al.*, 2007). Like the SMPS, the NSAM has been calibrated for spherical particles and shows very good agreement with the surface area derived from SMPS mobility data as long particles with diameters  $\geq 400$  nm do not significantly contribute to the total surface area (see Figure 1). Due to different device concepts, deviations in the measured surface area

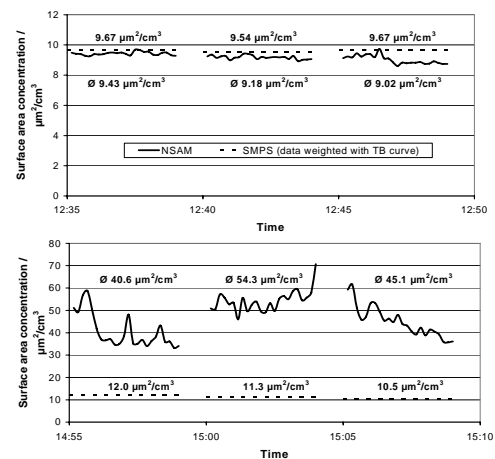


Fig. 1: Time series of surface area concentrations measured with SMPS and NSAM for mainly  $d_p < 400$  nm (top) and significant amount  $> 400$  nm (bottom)

concentrations are likely, when the instruments are challenged with particle morphologies other than spherical.

To compare the surface area measurements with SMPS and NSAM, the two instruments have been used side by side, sampling simultaneously from the same NaCl (cubic), Diesel soot (agglomerate), or ambient (mixture) aerosols. The results of this comparison study will be presented and the implications of particle morphology on the surface area measurement with NSAM and SMPS discussed.

This work was supported by the German Federal Ministry of Education and Research (BMBF) as part of the *NanoCare* project.

Oberdörster, G. (1996) *Particulate Sci. Technol.*

**14**:135

Lall, A.A. & Friedlander, S.K. (2006) *J. Aerosol Sci.*

**37**: 260

James, A.C.; Bailey, M.r.; Dorrian, M.D, (2000)

LUDEP Software, *RPB, Chilton, OXON, UK*

Fissan, H.; Neumann, S.; Trampe, A.; Pui, D.Y.H.,

Shin, W.G. (2007) *J.Nanop. Res.* **9**: 53-59

Shin, W.G.; Pui, D.Y.H.; Fissan, H.; Neumann, S.;

Trampe, A. (2007) *J. Nanop. Res.* **9**: 61-69

## Enhancement of transport properties of Bi-2212 high temperature superconductor by doping with MgO nanoparticles

I.E.Agranovski<sup>1</sup>, A.Y. Ilyushechkin<sup>2</sup>, I.S.Altman<sup>1,3</sup> and M. Choi<sup>3</sup>

<sup>1</sup>Griffith School of Engineering, Griffith University, Brisbane, 4111, QLD, Australia

<sup>2</sup>CSIRO, Pullenvale, 4069, QLD, Australia

<sup>3</sup>Institute of Advanced Machinery and Design, Seoul National University, Seoul 151-742, Korea

Keywords: MgO nanoparticles, high temperature superconductor.

It is well known that critical current densities of Bi<sub>2</sub>Sr<sub>2</sub>CaCu<sub>2</sub>O<sub>y</sub> (Bi-2212) bulk and tapes can be enhanced by improvement grain alignment, reduction of weak links and fraction volume of secondary phases, and by addition of pinning centers. One of the possible ways to introduce flux-pinning centres in superconductors is using addition MgO particles, which are incorporated into Bi-2212 matrix. In this work, we investigated the effect of the addition of ultra-fine MgO particles on the microstructure and superconducting properties of Bi-2212/Ag tapes. Ultra-fine MgO particles with cubic morphology were obtained by burning out a single Mg particle in air as described elsewhere (Altman *et al.*, 2004). The average MgO particle size is about 40 nm. Then, the MgO particles synthesized by the Mg particle combustion could be alternative candidates for use in Bi-2212 tapes instead of commercially available MgO powders.

When MgO is embedded into the Bi-2212 tapes by direct deposition onto the surface of the coated tape, the MgO is mainly distributed as individual (loose) particles with original cubic shape kept. Typical surface of that tape is shown in Figure 1a. Appearance of the MgO particles in the tapes was found different for the tapes classically prepared from the slurry with initially mixed MgO particles. It was observed, that for this scenario, MgO particles formed agglomerates within the Bi-2212 matrix and such agglomerated clusters are shown in Figure 1b. Also, for both types of the tape, the MgO particles did not react with the Bi-2212 matrix and preserve their appearance, as clearly seen in the photographs.

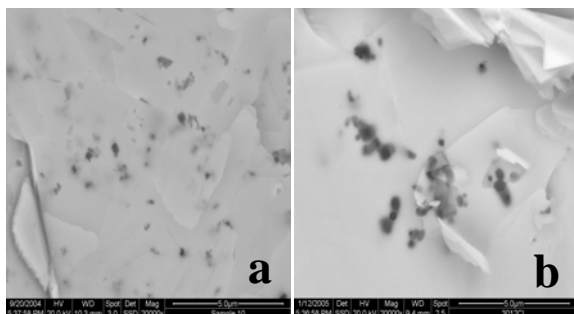


Figure 1. SEM images of the Bi-2212+MgO, prepared by MgO deposition on the surface of coated tape (a); and by MgO mixed in the slurry (b).

For the study of magnetic field dependence, three samples with the same thickness (45-50 μm) were chosen: undoped Bi-2212/Ag tapes, Bi-2212+MgO/Ag tape with the MgO particles added in the slurry (“MgO clusters”); and Bi-2212+MgO/Ag tape with MgO particles deposited directly from the flame (“MgO loose”). Figure 2 shows the  $J_c - H$  curves for all three samples at 2 K. As it was expected, all samples shows degradation of critical current densities with increasing of applied field.  $J_c$ 's of the tape with MgO loose particles are constantly higher than those for the tape without MgO by a factor of 1.3-1.4 in all magnetic fields. Degradation of  $J_c$  in the sample with MgO clusters occurs more dramatically with increasing the field strength.

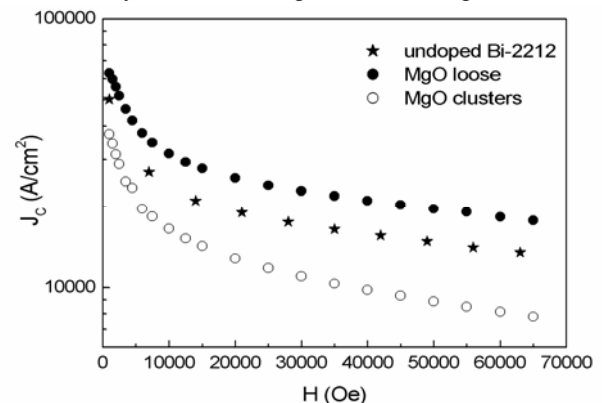


Figure 2. Dependence of the critical current density ( $J_c$ ) on magnetic field ( $H$ ) in the MgO-doped and undoped tapes at 2 K.

A significant enhancement in magnetization hysteresis can be achieved only if MgO ultrafine particles are individually dispersed in the Bi-2212 matrix. The largest improvement over undoped Bi-2212 tapes is achieved at 25 K and magnetic field of 1 T.

Altman, I. S., Agranovski, I. E. & Choi, M. (2004) *Appl. Phys. Lett.*, 84, 5130

Ilyushechkin, A., Agranovski, I., Altman, I., Rasha, N. & Choi, M. (2005). *Supercond. Sci. Tech.* 18, 1123-1128.

Agranovski, I., Ilyushechkin, A., Altman, I., Bostrom, T. & Choi, M. (2006). *Physica C.* 434: 115–120.

## Deposition of composite aerosol particles and their subsequent evolution through surface diffusion

M. J. Burchill, D. K. Gramotnev, T. E. Bostrom, D. R. Mason, G. Gramotnev

Applied Optics Program, School of Physical and Chemical Sciences, Queensland University of Technology,  
GPO Box 2434, Brisbane, QLD 4001, Australia

Keywords: Particle deposition, Composite nanoparticles, Surface activity, Electron microscopy

This paper investigates deposited particles, and their surface evolution, both theoretically and experimentally. Combustion particles from near a busy road are deposited onto thin metal films and highly oriented pyrolytic graphite (HOPG). Analysis of the samples is then performed using scanning electron microscopy.

The results obtained show a significant dependence on the surface conditions. In particular, particles tend to group around areas of structural imperfection, such as cracks and rough areas, while large smooth areas often appear entirely particle free. The process of dry deposition has no dependence on surface conditions; it is a process dependent only on the efficiency of impaction, gravitational settling and Brownian diffusion through the laminar layer. Therefore it is evident that the deposition patterns observed must be caused by surface evolution of the particles, after and/or during deposition.

One of the most prolific structures observed on the metal films are rings and halos. These structures usually contain a central NaCl crystal, which is confirmed by X-ray microanalysis. Outer rings are made up of smaller nano-crystal salts, clusters of organic compounds, or both. A typical example of such a structure with non-crystalline halos is shown in Figure 1.

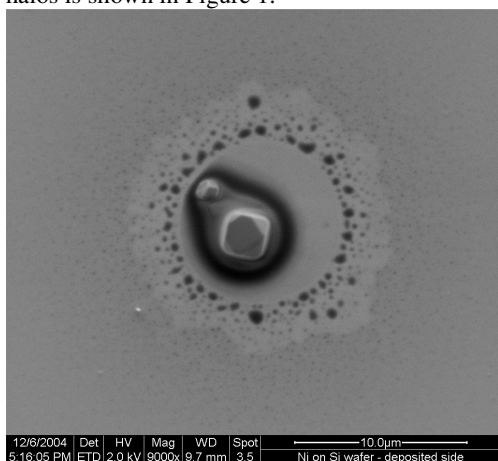


Figure 1. A typical SEM image showing a central salt particle, surrounding halos and multiple black dots of presumably organic compounds.

The formation of such structures has been explained by the deposition of composite particles,

containing two immiscible liquids, such as water and oil, possibly surrounding a central salt crystal. After deposition, the water evaporates, leaving behind any salt dissolved within, and the oil and/or other organic substances diffuse away from the centre forming series of halos and multiple dot structures (Figure 1).

In order to confirm this explanation, numerical modelling of the surface diffusion process, based upon a random walk of an individual particle/molecule, in the presence of adsorbing centres distributed randomly on the surface, is conducted. The diffusing particles can move randomly along the surface only until they hit a surface defect (adsorbing centre), after which the particle sticks permanently to the defect. Many such particles near the same defect form a big circular cluster with the area that is equal to the total area of all the particles adsorbed by the considered defect. The resultant distribution and size of the immobile clusters (Figure 2) demonstrates the same qualitative pattern as that shown in the SEM analysis (Figure 1).

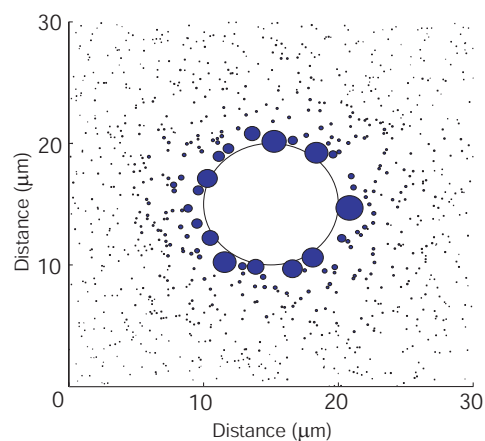


Figure 2. Numerical modelling of surface diffusion.

Further image analysis provides reasonable quantitative comparison between the model used and SEM observations. Using the presented model of surface pattern formation and typical deposition rates, estimates of particle dimensions ( $\sim 1 - 2.5 \mu\text{m}$ ) and their concentration in the ambient air have been determined, thus providing a relation between the observed SEM images and composition of combustion aerosols.

## Relations of Discharge Electrode Form and Ozone Generation in ESP

D. Yagishita<sup>1</sup>, Y. Takagi<sup>1</sup>, Y. Ehara<sup>1</sup>, T. Takahashi<sup>1</sup>, A. Zukeran<sup>2</sup>, and K. Yasumoto<sup>2</sup>

<sup>1</sup>Musashi Institute of Technology, Setagaku Tamazutumi 1-28-1, 158-0087, Tokyo, Japan

<sup>2</sup>Fuji Electric Systems Co.,Ltd., Shinagawaku Osaki 1-11-2, 141-0032, Tokyo, Japan

Keywords: Electrostatic Precipitator, Ozone, Electrode Shape, Dissociation Area

Electrostatic precipitator (ESP) is used in a tunnel to remove a particle included in diesel exhaust gas. ESP generates ozone necessarily to use an electric discharge, but it is designed to hold down the ozone density low. However, further restraint is expected. As for the discharge electrode of charging section in ESP, the monotonous electrode which was an end face saw-tooth type is commonly used now. In this study, we changed shape of this saw-tooth type electrode and examined relations with the generation ozone density.

The gas exhausted from the diesel engine of load 0.5kW were diluted with the atmosphere and introduced into ESP. The gas rate is 7m/s uniformly. An electrode structure of the ESP was shown in Fig.1. The charging section was structure to sandwich in a high voltage saw-tooth electrode between the grounded plate electrodes. The gap was 9mm. The collecting section had a parallel-plates configuration. The shape of a saw-tooth electrode used three kinds of 2.5, 5, 10mm at ditch length for 5mm in pitch length, thickness 0.1mm uniformity. The applied voltage of collecting section was DC7.5kV uniformity. The ozone concentration behind ESP was measured. We performed electric field analysis in each electrodes and compared it with the ozone concentration.

Ozone concentrations in the case of each electrode as a function of discharge current are shown Fig 2. The ozone concentration is lower a sharp electrode with deep ditch. Secondly, we

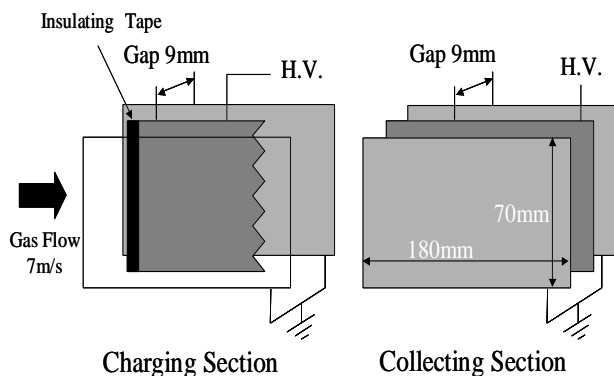


Figure 1. Structure of electrodes.

demand an electric field of each electrode by electric field analysis. It is ionized at electric field strength 30kV/cm by corona discharge. Ionization energy of oxygen molecule is 12.2kV/cm. Therefore, an electric field strength of 12.5kV/cm is necessary to have dissociation energy 5.1eV of oxygen molecule<sup>[1]</sup>. An ozone concentration as a function of area more than 12.5kV/cm is shown in Fig 3. The ozone concentration increase with increasing an oxygen dissociation area in any electrode.

### REFERANCE

[1] I. Takakura et al, IEJ Vol.25, No.2, pp.101-104 (2001)

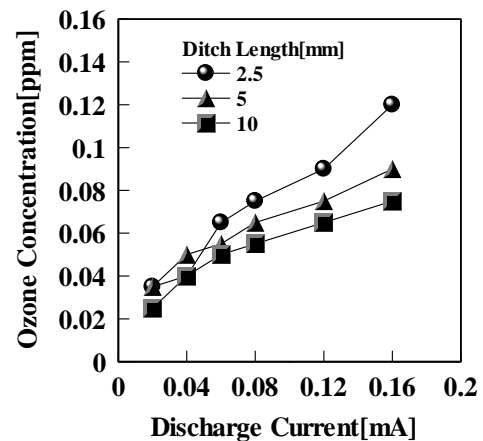


Figure 2. Ozone concentration as a function of discharge current.

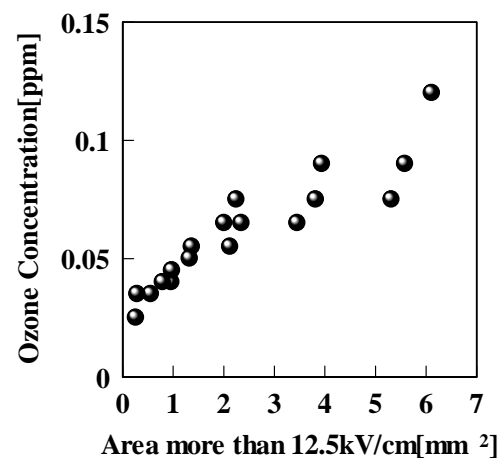


Figure 3. Ozone concentration as a function of area more than 12.5kV/cm.

## Collection of nanoparticles by improvement of charging section in ESP

T.Okabe<sup>1</sup>, Y.Takagi<sup>1</sup>, Y.Ehara<sup>1</sup>, A.Zukeran<sup>2</sup>, K.Yasumoto<sup>2</sup>

<sup>1</sup>Musashi Institute of Tecnology, 1-28-1 Tamazutsumi, Setagaya-ku, Tokyo, 158-8557, Japan

<sup>2</sup>Fuji Electric Co.Ltd., 2-11-2 Osaki, Shinagawa-ku, Tokyo, 141-0032, Japan

Keywords: nano-particles, electrostatic precipitator,

When diesel-exhaust-particles (DEP) deposit on cameras, lamp covers, and walls, etc, the distinction of sight at tunnel observation points become difficult. Two-stage-type electrostatic precipitator (ESP) is used to remove DEP from the air in the tunnel. However, ESP has low collection efficiency of a nano-particles. In past research, when saw-tooth-electrode applied to charging section, Current densities increase, and charging efficiency improves. In this work, single-saw-tooth-electrode (SSTE) and double-saw-tooth-electrode (DSTE) are applied to charging section, and the improvements collecting efficiency of nano-particles is experimented.

Two-stage-type ESP composed of a precharger and a collecting section is used. Electrode structure is shown Fig.1. SSTE, DSTE and wire electrode are applied as charging electrode, a collection electrode is plate electrode. Each gap between electrodes is 9mm. Distance of tooth is 2.5, 5, 10mm. A high voltage of rectangle AC 15kVp-p was applied the collecting section. The mean gas flow velocity is fixed at 7m/s. Particle concentrations are measured by particle counter and scanning mobility particle sizer (SMPS) in the upstream and downstream ESP.

Collection efficiency as a function of discharge current at SSTE is shown Fig.2(SSTE2.5~10: distance of tooth is 2.5, 5, 10mm in SSTE, W1:one wire). Collection efficiency of SSTE is lower than wire in the case of low current. An electric discharge point is located in saw-tooth-electrode when discharge current is low. However, when electric currents increase, there becomes little localized influence. Therefore collection efficiency increase. In addition, localized influence comes to have little even that distance of the tooth becomes small.

Collection efficiency by a difference of an electrode type is shown Fig.3(W2:two wire). A DSTE showed the highest collection efficiency. This is because diffusion charging with electricity quantity increased. Diffusion charging with electricity quantity increases so that  $E_D/J(E_D)$ : electric field strength of charging section,  $J$ :current density) is small<sup>[1]</sup>. A number of an electric discharge point doubles in DSTE. Therefore an electric field strength is small with the same electric current value. Furthermore, a current density rises so that an electric discharge point is located. As a result, diffusion

charging with electricity quantity increases, and it is thought that a collection efficiency improved.

Reference

[1]HANDBOOK OF ELECTROSTATIC, chap4, pp96-99(1981)

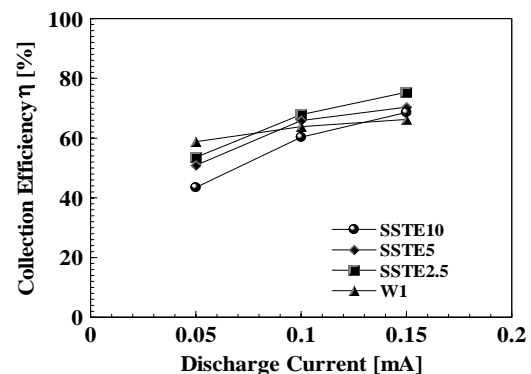
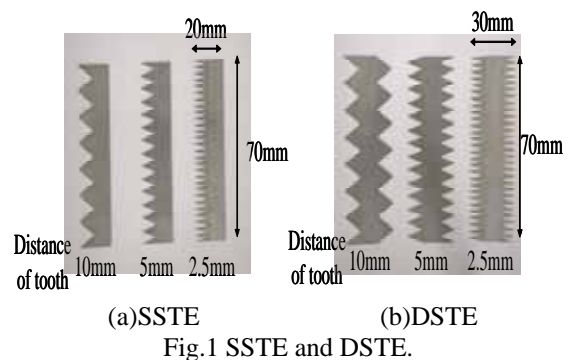


Fig.2 Collection efficiency as a function of discharge current at SSTE.(Particle size 100nm)

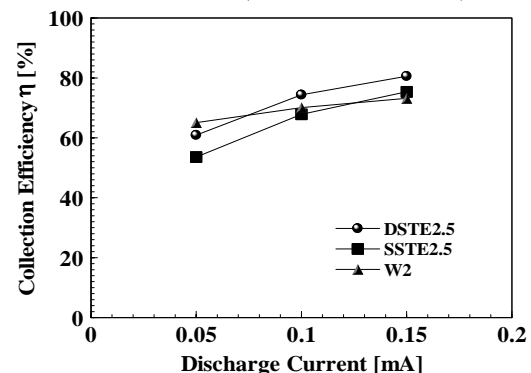


Fig.3 Collection efficiency by a difference of an electrode type. (Particle size 100nm)

## Preparation of Co and Ni nanoparticles

J. I. Forsman<sup>1</sup>, A. Auvinen<sup>1</sup>, J. Jokiniemi<sup>1,2</sup>, U. Tapper<sup>1</sup>

<sup>1</sup>Fine particle team, VTT Technical Research Institute of Finland, 02044-VTT, Espoo, Finland

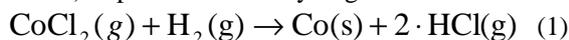
<sup>2</sup>Department of Environmental Sciences, University of Kuopio, Fine Particle and Aerosol Technology Laboratory, 70211 Kuopio, Finland

Keywords: Generation of nanoparticles, CVD, Aerosol formation

Cobalt and nickel nanoparticles have applications for example as catalysts, in conducting inks and polymers, magnetorheological devices and multilayer capacitors. Currently in many of these applications, particle size is around 0.3 – 5 µm. Replacing these with smaller particles could reduce costs and improve performance. The lack of suitable commercial nanoparticles restrains the transition.

Cobalt and nickel nanoparticles have been prepared by a variety of methods, including laser evaporation, flame synthesis, spray pyrolysis, sonochemical and chemical vapour synthesis (Trzeciak et al. 2004, Che et al. 1999, Koltypin et al. 1996, Syukri et al. 2003, Jang et al. 2003). Few of the methods have been or may become commercialised.

In this work chemical vapour synthesis (CVS) is used. Cobalt and nickel chlorides reduce in presence of hydrogen at high temperature (around 900°C) to pure metal and hydrogen chloride as



Production of cobalt and nickel nanoparticles by hydrogen reduction method has been reported by Jang et al (2004). In this work we describe a method for producing cobalt nanoparticles based on the same chemical reaction but with significantly better design, high yield and online measurements during the experiments.

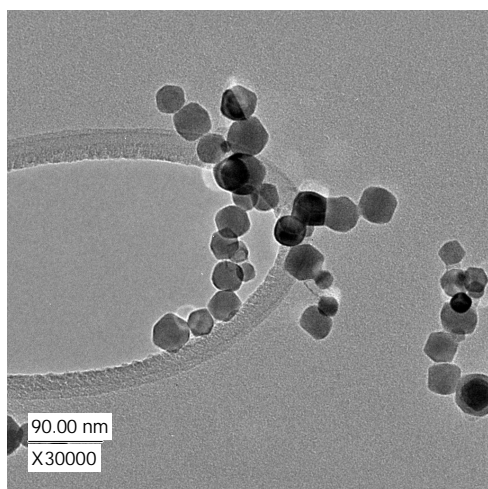


Figure 1. Nickel particles produced at reaction temperature 900°C. Evaporation temperature of NiCl<sub>2</sub> was 650°C.

The particles were studied with a transmission electron microscope equipped with EDS analyser, semi quantitative x-ray fluorescence, BET, ICP and TGA. Fourier-transform infrared spectroscopy (FTIR) was used to determine the hydrogen chloride content of the gas flow. Mass concentration of particles was measured with filter samples.

High mass concentrations of high-purity cobalt and nickel nanoparticles with primary particle diameter below 100 nm were produced with aerosol method. An example of the produced nickel particles is illustrated in Figure 1. The size distribution of the primary particles was narrow. The particles were mostly well faceted single crystals with fcc structure. The oxidation of the particles was slow. Chain-like agglomerates were formed.

This work was supported by OMG Kokkola Chemicals Ltd.

- Trzeciak T. M., Cherbański R., Marijnissen J. C. M., Podgórski A. and Gradon L. (2004) Design of an improved laser aerosol reactor. Partec 2004.
- Che S.-L., Takada K., Takashima K., Sakurai O., Shinozaki K. and Mizutani N. (1999) *Journal of Materials Science* **34**, 1313-1318.
- Koltypin Y., Katabi G., Cao X., Prozorov R. and Gedanken A. (1996) *Journal of Non-Crystalline Solids* **201** 159-162
- Syukri, Ban T., Ohya Y. and Takahashi Y. (2003) *Materials Chemistry and Physics* **78** 645-649
- Jang ,H.D., Hwang, D.W., Kim, D.P., Kim, H.C., Lee, B.Y., Jeong, I.B. (2004) *Materials Research Bulletin*, **39**, 63-70.

## Morphology and reactivity of carbon nanoparticles and nanotubes formed during co-pyrolysis of $\text{Fe}(\text{CO})_5$ and propane

N.A. Ivanova<sup>1</sup>, A.A. Onischuk<sup>1</sup>, S.V. Vosel<sup>1</sup>, P.A. Purto<sup>1</sup>, A.M. Baklanov<sup>1</sup>, L.V. Kulik<sup>1</sup>, L.L. Rapatskiy<sup>1</sup>, N.T. Vasenin<sup>2</sup>, V.F. Anufrienko<sup>2</sup>

<sup>1</sup>Institute of Chemical Kinetics and Combustion SB RAS, 630090, Novosibirsk, Russia,

<sup>2</sup>Boreskov Institute of Catalysis SB RAS, 630090, Novosibirsk, Russia

Keywords: nanotubes, nanoparticles, aerosol formation, high temperature aerosol, nanoparticles characterization

The every year increase of nanomaterials production has raised a problem of air contamination due to the nanoparticle and nanotube release to the atmosphere. The toxic effect from the exhausted aerosol is governed by the particle morphology as well as the radical concentration and their location in particles. In this work we investigate the morphology and radical centers of particles formed during pyrolysis of  $\text{C}_3\text{H}_8 + \text{Fe}(\text{CO})_5 + \text{Ar}$  (with initial molar fraction -  $[\text{C}_3\text{H}_8]_0 = 8.0 \times 10^{-2}$  and  $[\text{Fe}(\text{CO})_5]_0 = 0 - 5.0 \times 10^{-5}$ ) mixture in a flow reactor. We measured the decomposition degree for  $\text{Fe}(\text{CO})_5$  and propane using IR-spectroscopy and gaseous chromatography methods, respectively. Figs. 1a and b show inlet  $\text{Fe}(\text{CO})_5$  and  $\text{C}_3\text{H}_8$  to particle conversion ratio as a function of temperature. One can see that the decomposition of  $\text{Fe}(\text{CO})_5$  occurs at much lower temperatures (440 – 500 K) than that for  $\text{C}_3\text{H}_8$  (1000 – 1100 K). The particle and nanotube morphology was studied by High Resolution Transmission Electron Microscopy (HR TEM). In case of propane pyrolysis ( $[\text{Fe}(\text{CO})_5]_0 = 0$ ) soot primary particles are formed (Fig. 2a), and during co-pyrolysis of  $\text{C}_3\text{H}_8 + \text{Fe}(\text{CO})_5$  the aerosol evolve from single Fe particles to Fe/C aggregates and finally to very long carbon nanotubes (Fig. 2b,c) covered by amorphous carbon (Fig. 2b(1)). The XRD analysis showed that the only crystalline phase present in the samples is  $\text{Fe}_3\text{C}$ . The  $\text{Fe}_3\text{C}$  particles can be seen in HR TEM images (Fig. 2b).

The location of radical centers of carbonaceous particles and oxygen influence on it were analyzed by Electron Paramagnetic Resonance (EPR). Particles for the EPR analysis were placed to a sealed glass tube. EPR spectrum of soot samples after evacuation ( $P < 10^{-4}$  torr) was presented as a narrow signal with Lorentz shape. The line width and g-value for this spectrum are  $\Delta B_{pp} = 0.18$  mT and  $g = 2.0026 \pm 0.0002$ , respectively. To observe the oxygen effect to the EPR spectrum we put the  $\text{O}_2(20\%) + \text{Ar}(80\%)$  mixture to the sample tube. The resulting signal consisted of two Lorentz components – narrow ( $\Delta B_{pp} = 0.18$  mT) and broad ones. The integral intensity for each component did not depend on the partial oxygen pressure in the test tube. The ratio between the integral intensities of narrow and broad components was 1/3 regardless of the oxygen pressure. The width of the narrow component was independent on the oxygen pressure  $P_{\text{O}_2}$ , while that of the broad component was a function of  $P_{\text{O}_2}$  (Fig. 3a). The  $\Delta B_{pp}$  vs.  $P_{\text{O}_2}$  dependence follows the oxygen adsorption isotherm. The broad component line width was found to be dependent on the measurement temperature as well. Two kinds of experiments were carried out: slow (0.3 K/min) and quick ( $10^3$  K/min) cooling of sample (Fig. 3b). In the former case one observed monotonous increase of the line width with temperature decreasing, while

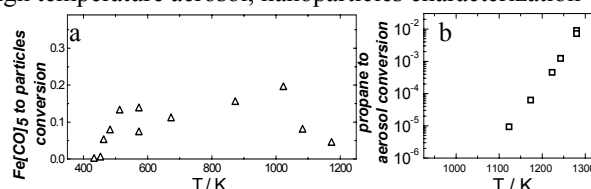


Fig. 1.  $\text{Fe}(\text{CO})_5$  (a) and  $\text{C}_3\text{H}_8$  (b) conversion to aerosol.

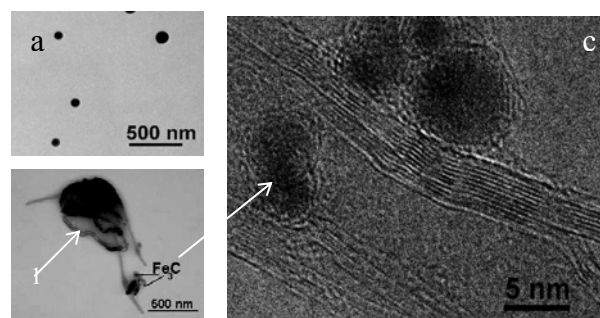


Fig. 2. HR TEM images of soot nanoparticles (a) and carbon nanotubes (b,c) covered by amorphous carbon (b).

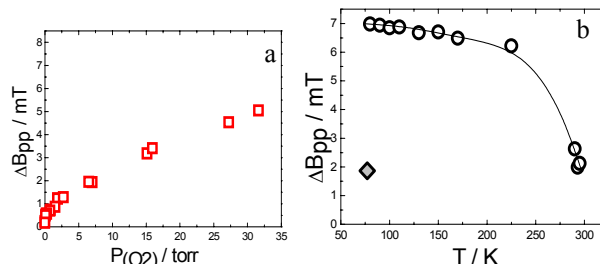


Fig. 3. Line width of EPR soot spectrum vs. the oxygen pressure (a) and sample temperature (b). b: Circles – slow cooling, diamond – quick cooling.

in the last case there was no difference between the room temperature and liquid nitrogen temperature measurements. It is natural to assume that the diffusion of oxygen through a system of interconnected microvoids and microchannels plays a role in the oxygen effect.

EPR spectrum of amorphous carbon covering nanotubes consist of a single narrow signal with line width  $\Delta B_{pp} = 0.24$  mT (evacuated sample) and  $g = 2.0026 \pm 0.0002$ . When putting oxygen inside the sample tube the line width was equal to  $\Delta B_{pp} = 0.33$  mT independently of the oxygen pressure. Thus, we observed a weak oxygen effect for these samples, while all the centers were accessible to the air as in contrast to the soot. The increase of  $\text{Fe}(\text{CO})_5$  in the inlet  $\text{C}_3\text{H}_8 + \text{Ar}$  mixture leads to an increase of line width of EPR signal. Shape and g-value of these spectrum were irrespective of  $\text{Fe}(\text{CO})_5$  concentration.

Financial support for this work was provided by RFBR 05-03-90576-NSC\_a, NSC\_Taiwan-RFBR No. 94WFA0600016\_Contract No. RP05E15.

## Flame synthesis of titanium nanoparticles and their use as a photocatalyst

G.W. Lee<sup>1</sup>, S.M. Choi<sup>1</sup> and J. Park<sup>2</sup>

<sup>1</sup>Division of Mechanical and Aerospace System Engineering, Chonbuk National University, Jeonju 561-756, South Korea

<sup>2</sup>CNF Inc., Jeonju Machinery Research Center 205, Jeonju 561-844, South Korea

Keywords: Flame synthesis, TiO<sub>2</sub> nanoparticles, Photocatalyst.

Titania (TiO<sub>2</sub>) nanoparticles are well known photocatalyst materials. They mostly crystallize into two polymorphic forms: anatase and rutile. Anatase is a metastable phase that transforms into rutile at high temperatures (Nair et al., 2001). Anatase titania particles have been proven to be more active photocatalysts in environmental remediation than rutile particles are (Fox & Dulay, 1993), while rutile particles have been used as a white pigment. Because of the photocatalytic properties of anatase particles, much research has been focused on the application of these particles to the treatment of wastewater (Naskar et al., 1998), and the degradation of gas phase organic compounds (Andersson et al., 1997) and mercury (Lee & Hyun, 2006).

In this work, we synthesized TiO<sub>2</sub> nanoparticles with using N<sub>2</sub>-diluted and O<sub>2</sub>-enriched coflow, hydrogen, diffusion flames. We investigated the effects of the flame temperature on the crystalline phases of the TiO<sub>2</sub> nanoparticles that were formed. Also the use of these nanoparticles as a photocatalyst to decompose the methylene blue solution was done.

The burner used in this study consisted of four concentric tubes with 3.87, 10.22, 16.57, and 22.10mm inner diameters. The argon gas used as a carrier gas for the precursor was delivered through the central tube via the evaporator of the TTIP (titanium tetraisopropoxide) precursor (0.5 liters/min.). The oil bath surrounding the evaporator was maintained at a temperature 80°C. The fuel, hydrogen, was supplied through the second tube (3.3 liters/min.). The oxygen (3.8 liters/min.) was premixed with nitrogen (8.9 liters/min.), and then the mixture passed through the outer tube, which was the fourth tube. The amounts of oxygen were enriched to

increase the flame temperature.

The temperature distributions were measured along the axial distance from the burner. The measured maximum temperature was 1,976K at 65mm from the burner tip along the centerline. Spherical shaped with diameter about 50 to 60 nm sized titania nanoparticles that had clear boundaries were formed.

X-ray diffraction patterns, as shown in Fig. 1, were used to examine the crystalline phases of the TiO<sub>2</sub> nanoparticles formed for the several flame conditions. The strongest peaks for the anatase and rutile phases are located at  $2\theta = 25.3^\circ$  for the (101) reflection and  $27.5^\circ$  for the (110) reflection. Based on the XRD analysis, most of the TiO<sub>2</sub> nanoparticles that were synthesized were of the anatase phase.

Figure 2 shows the photocatalytic decomposition of the methylene blue by using the synthesized TiO<sub>2</sub> nanoparticles with UV light (365 nm). Data were compared with the result of commercial TiO<sub>2</sub> particles (P-25, Degussa).

This work was supported by the Automobile Hi-Technology Research Center, Engineering Research Institute of CNU.

- Fox, M.A., & Dulay, M.T. (1993). *Chemical Reviews*, 93, 341-357.  
 Andersson, P.-O., Berggren, H., Andersson, A., & Augustsson, O. (1997). *Catalyst Today*, 35, 137-144.  
 Lee, T.G., & Hyun, J.E. (2006). *Chemosphere*, 62, 26-33.  
 Naskar, S., Pillay, S.A., & Chanda, M. (1998). *J. Photochem. Photobiology A: Chemistry*, 113, 257-264.  
 Nair, S., Seraphimova, R., Bocquet, J.F., Colbeau-Justin, C., & Pommier, C. (2001). *Materials Research Bulletin*, 36, 811-825.

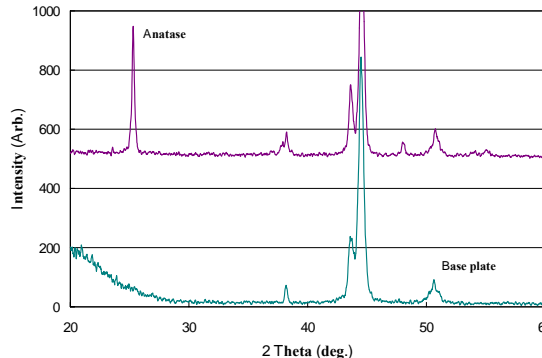


Figure 1. X-ray diffraction patterns of the flame synthesized TiO<sub>2</sub> nanoparticles.

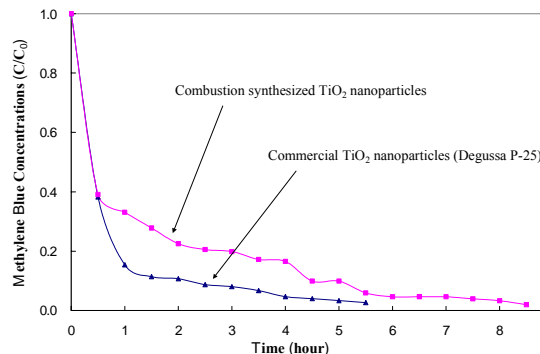


Figure 2. Decomposition of methylene blue by the TiO<sub>2</sub> nanoparticles and 365 nm UV light.

## A stable nano-particle generator based on the sublimation of tungsten oxide

G. Steiner<sup>1</sup>, G.P. Reischl<sup>1</sup>

<sup>1</sup> Fakultät für Physik, Universität Wien, Boltzmanngasse 5, A-1090 Wien, Austria

Keywords: Aerosol generation, Nanoparticles, Number size distribution, Molecular clusters, WO<sub>x</sub>

A newly developed tungsten oxide heating wire particle generator (WO<sub>x</sub>-Generator) allows the generation of aerosols with diameters in the size range of 1-10 nm. Its first prototype was built at the Institute of Chemical Kinetics and Combustion in Novosibirsk (Ankilov et al. 2002, Reischl et al. 1997). We improved the generator performance (particle size range, the range of possible particle concentrations as well as the temporal stability of the number size distributions) by applying numerical methods to optimize the design. In cooperation with Grimm-Aerosoltechnik GmbH & Co. KG, a second prototype of the WO<sub>x</sub>-Generator was built and evaluated in several experiments.

The principle of operation of the WO<sub>x</sub>-Generator is based on the sublimation of tungsten oxide. Heated tungsten reacts in dry clean air to several oxides and nitrates of different valences (0, +2, +3, +4, +5 and +6). A heating wire around the WO<sub>x</sub> coils provides a temperature of approximately 900°C; the sublimation temperature of WO<sub>3</sub>. Tungsten oxide sublimates into a controlled fraction of the carrier gas and is immediately diluted when exiting the heated zone by a flow of purified gas (air) (see Figure. 1).

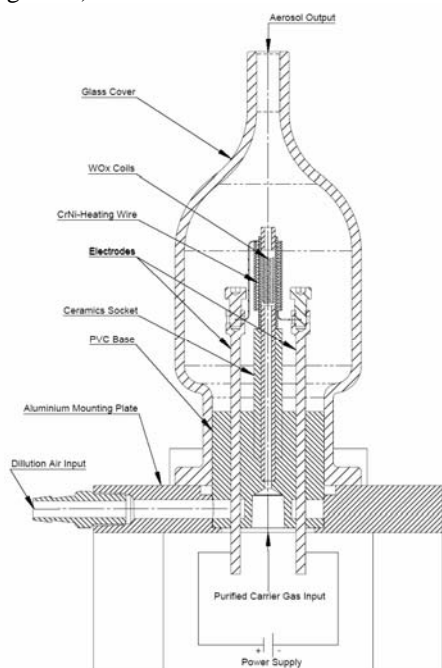


Figure. 1: Sketch of the WO<sub>x</sub>-Generator 2005

To be able to measure the number size distribution (NSD) of the nano-particles provided by the WO<sub>x</sub>-Generator, newly developed DMAs (NDMA 2003 and NDMA 2005) with a channel length of 15.5 mm, have been used. For the analysis of the generated aerosol, a detailed knowledge of the size and concentration of the ionic molecular clusters involved in the charging process is of crucial importance, since WO<sub>3</sub> monomers (232 amu) are expected to have a mobility equivalent diameter of 1.25nm (see Kilpatrick 1971).

An extensive evaluation of the NSD of ionic molecular clusters, produced by the ionizing radiation in the charger, has been performed in previous experiments. The NSD for negative ions has its peak at a diameter of D<sub>p</sub>=0.93nm, the NSD for positive ions at a diameter of D<sub>p</sub>=1.12nm.

A typical number size distribution of the aerosol, produced by the WO<sub>x</sub>-Generator, is shown in Figure 2.

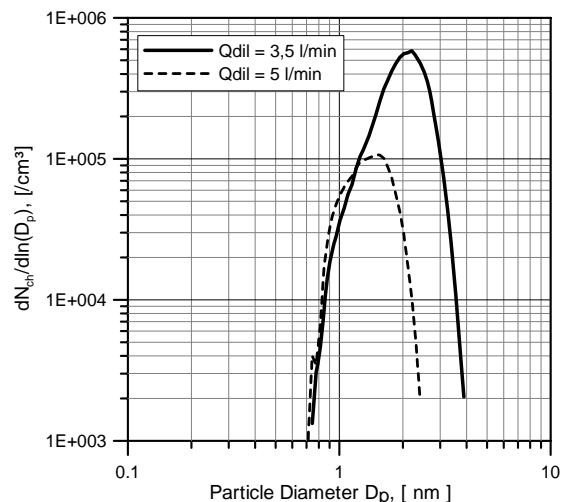


Figure 2: Typical WO<sub>x</sub>-Generator NSD

Ankilov, A. et al. (2002) Particle size dependent response of aerosol counters. *Atmospheric Research* 62(3-4), 209-237.  
 Kilpatrick, W.D. (1971), An Experimental Mass-Mobility Relation For Ions in Air at Atmospheric Pressure. In *Proc. Ann. Conf. Mass Spectrosc. 19<sup>th</sup>*, pages 320-326.  
 Reischl, G.P., Mäkelä, J.M. and Nucid, J. (1997), Performance of Vienna Type Differential Mobility Analyzer at 1.2-20 Nanometer. *Aerosol Sci. Technol.* 27, 651-672

## Characterisation of industrial aerosol nanoparticle generation process

M. Aromaa<sup>1</sup>, H. Keskinen<sup>1</sup>, J.M. Mäkelä<sup>1</sup>, M. Piispanen<sup>2</sup>, L. Hupa<sup>2</sup>, K. Deppert<sup>3</sup>, S. Persson<sup>4</sup>, M. Lang<sup>4</sup>, P. Sandberg<sup>4</sup>, G. Gunnarsson<sup>5</sup>, J. Pimenoff<sup>6</sup>, T. Kronberg<sup>7</sup>, V. Pore<sup>8</sup>, M. Ritala<sup>8</sup>, M. Leskelä<sup>8</sup>, M. Raulio<sup>9</sup>, M.S. Salkinoja-Salonen<sup>9</sup> and V.M. Airaksinen<sup>10</sup>.

<sup>1</sup>Aerosol Physics Laboratory, Institute of Physics, Tampere University of Technology, Tampere, Finland.

<sup>2</sup>Process Chemistry Centre, Åbo Akademi University, Turku, Finland.

<sup>3</sup>Nanocrystals Group, Lund University, Lund, Sweden

<sup>4</sup>Glasforskningsinstitutet, Växjö, Sweden

<sup>5</sup>Technological Institute of Iceland, Reykjavik, Iceland

<sup>6</sup>Beneq Ltd, Vantaa, Finland

<sup>7</sup>IDO Bathroom Ltd, Tammissaari, Finland

<sup>8</sup>Laboratory of Inorganic Chemistry, Department of Chemistry, University of Helsinki, Helsinki, Finland.

<sup>9</sup>Department of Applied Chemistry and Microbiology, University of Helsinki, Helsinki, Finland.

<sup>10</sup>Micronova, Helsinki University of Technology, Espoo, Finland

Keywords: nanoparticle, nHALO, Liquid Flame Spray, anti-microbial coating

Flame methods are widely used in nanoparticle generation for industrial purposes. In this study we introduce a process called nHALO (Hot Aerosol Layering Operation), also known as Liquid Flame Spray (LFS) (Aromaa *et al* 2007). In nHALO liquid precursor is fed into a turbulent hydrogen-oxygen flame. nHALO can be used in production of nanoparticles which are deposited on a substrate (Figure 1). nHALO is an optimal process to make composite nanoparticles.

In nHALO process the liquid droplets evaporate in the flame the evaporated material may decompose thermally to form different molecules. After that it nucleates and re-condensates to form nanoparticles. The process parameters such as combustion gas velocities, precursor feed rate and concentration can be used to control the particle size (Aromaa *et al.* 2007).

nHALO can be utilised in many applications. In this study we apply an anti-microbial titania-silver nanoparticle coating on ceramic tiles (Figure 2.) (Keskinen *et al.* 2006). Multicomponent nanoparticles composed of titania and silver are generated in one-step process using a precursor solution of TTIP (Titanium(IV) isopropoxide) in isopropanol. Silver nitrate is also soluted in this solution. The amount of silver in the solution is 1 wt% of pure titanium.

In the composite nanoparticles, silver is on top of titania particles as only a few nanometre-sized spheres (Keskinen *et al.* 2006). The coatings are characterised using electron microscopy (SEM and TEM) and contact angle tests. Also the anti-microbial effect of the coating is studied in bacterial tests.

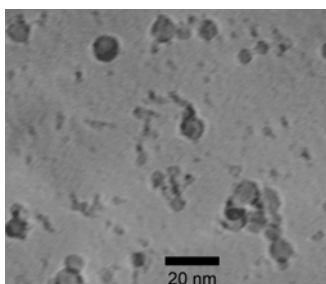


Figure 2. TEM image titania-silver nanoparticles

Aromaa M, Keskinen H. and Mäkelä, J.M. (2007) The Effect of Process Parameters on the Liquid Flame Spray Generated Titania Nanoparticles, Accepted, to be published in *Biomolecular Engineering*

Keskinen H. et al. (2006) Deposition of Titania and Titania-Silver Nanoparticles by Liquid Flame Spray and Their Application as a Photocatalyst, *Catalysis Letters*, vol. 111, pp.127-132.

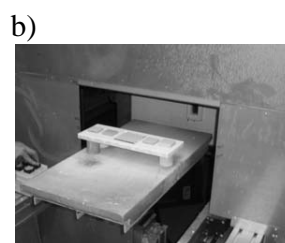
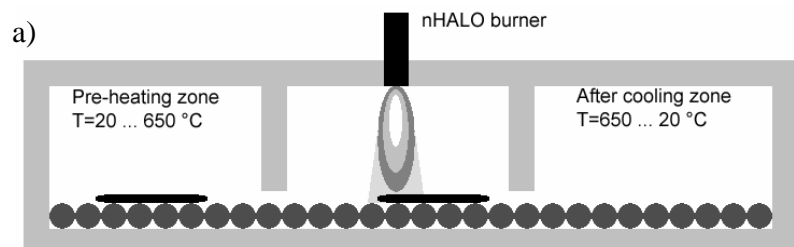


Figure 1. a) Schematic of nHALO in coating process. In the process ceramic tiles move from left to right in the coating furnace. b) tiles entering the furnace

## Formation of carbon aerosol particles in high-frequency discharge

A.M. Baklanov, N.A. Ivanova and G.A. Makhov

Institute of Chemical Kinetics and Combustion SB RAS, 630090, Novosibirsk, Russia,

Keywords: Nanoparticles, measurements, particle size distribution, particle concentration, particle formation and growth

Formation of carbon aerosol nanoparticles is studied during decomposition of propane with argon as a carrier gas in a high-frequency discharge. Gaseous intermediates from propane thermal decomposition ( $\text{CH}_4$  and  $\text{C}_2\text{H}_6$ ) are monitored by Gas Chromatography. Figs. 1a,b shows the concentrations of propane and gaseous intermediates at the outlet of the reactor as a function of the inlet molar fraction of propane. The aerosol morphology is studied by Transmission Electron Microscopy (TEM) and High Resolution TEM. The aerosol particle concentration and size distribution are measured by an Automated Diffusion Battery (ADB). The propane decomposition produces the formation of single carbon particles (Fig. 2) with typical radius spectrum with mode centered about 12 nm as measured by the ADB spectrometer and shown in Fig. 3. The size distribution is good described by the log-normal function with the standard geometric deviation  $\sigma_g \approx 1.20$ . Fig. 4 shows the mean arithmetic radius of the carbon particles and the particle number concentration at the reactor outlet vs. the propane molar fraction. Particle radius is measured to increase with increasing propane relative concentration, whereas the particle concentration increases only at low  $\text{C}_3\text{H}_8$  concentration, and does not change in the whole concentration range with propane relative concentration in this range.

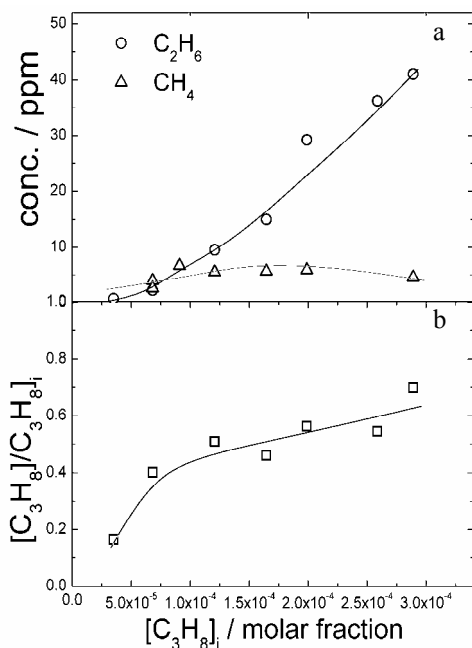


Fig. 1a,b. The relative gaseous concentrations of intermediates (a) and propane (b) in the mixture sampled at the outlet of reaction zone vs. the inlet molar fraction of propane.

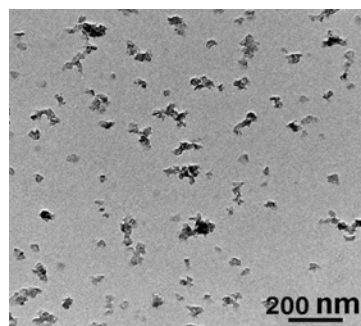


Fig. 2. TEM image of carbon nanoparticles formed during the decomposition of  $\text{Ar} + \text{C}_3\text{H}_8$  mixture in high-frequency discharge.

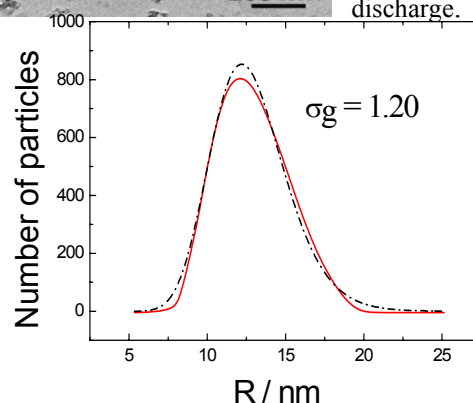


Fig. 3. Size distribution of carbon nanoparticles formed decomposition of  $\text{C}_3\text{H}_8 + \text{Ar}$  mixture. Solid line – ADB data; dotted line corresponds to Log-normal function with the standard geometric deviation  $\sigma_g = 1.20$ .

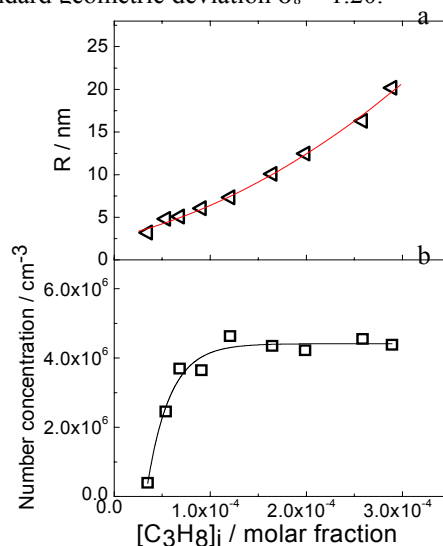


Fig. 4. Mean arithmetic radius  $R$  (a) and number concentration (b) of carbon nanoparticles as measured at the outlet of reaction zone vs. the inlet molar fraction of propane.

Financial support for this work was provided by RFBR 05-03-90576-NSC\_a, grant of SD RAS No 78, NSC\_Taiwan-RFBR No. 94WFA0600016\_Contract No. RP05E15.

## Production of novel Ag nanoparticle with C<sub>60</sub> nanoparticle

N. Hashimoto<sup>1</sup>, S. Taguchi<sup>2</sup>, H. Tanaka<sup>1,2</sup>

Institute of Science and Engineering, Chuo Univ.<sup>1</sup>, Faculty of Science and Engineering, Chuo Univ.<sup>2</sup>,  
1-13-27 Kasuga, Bunkyo-ku, 112-8551, Tokyo, Japan

Keywords: Ag nanoparticle, C<sub>60</sub> nanoparticle, DMA, PS, Ag-C<sub>60</sub> composite nanoparticle

Fabrication of novel nanomaterials has been extensively investigated by using a fullerene as a size-specific reaction medium. Especially, production of metallic nanoparticle with the fullerene has attracted much attention because the fullerene may be enabled to produce size-specific functional metallic nanoparticle. In this study, we examined to produce novel nanoparticle from Ag vapor interacted with C<sub>60</sub> nanoparticle. Particle diameter of the produced nanoparticle was measured by a differential mobility analyzer (DMA), and composition of the produced nanoparticle was analyzed by an X-ray photoelectron spectroscopy (PS).

C<sub>60</sub> powder was vaporized at 420 °C with N<sub>2</sub> gas flow by a furnace. Vaporized C<sub>60</sub> was cooled and ionized by an <sup>241</sup>Am neutralizer. The produced C<sub>60</sub> nanoparticle ion was passed through silver vapor formed by a vaporization of silver grains at 1050 °C in another furnace. The produced nanoparticle ion was size-analyzed by a DMA. Particle diameter of the nanoparticle was obtained from a peak position of the diameter spectrum thus measured. In this experiment, the pressure in the furnace and the DMA was maintained at atmospheric pressure. On the other hand, a Si substrate was prepared by electrical collection of the nanoparticle size selected by the DMA, and was analyzed by the PS.

Figure 1 shows the diameter spectrum. Particle diameter for the nanoparticle thus produced was obtained at 5.6 nm while that for the nanoparticle produced by only Ag vapor was observed at 9.0 nm. The observed particle diameter apparently became small when the C<sub>60</sub> vapor was used for the production

of the nanoparticle. Therefore, diameter difference suggests that C<sub>60</sub> vapor played an important role in the production process of the nanoparticle. The particle diameter tended to increase monotonically from 4 nm to 8 nm, as the Ag-vapor temperature increased from 1000 °C to 1100 °C. On the other hand, diameter difference between the nanoparticle with and without the C<sub>60</sub> vapor was almost constant at 3 nm as the Ag-vapor temperature increased. These results suggest that the C<sub>60</sub> nanoparticle produced from the C<sub>60</sub> vapor worked as a reaction medium for the production of the nanoparticle. In addition, it was confirmed by PS measurements that the nanoparticle thus produced contained Ag atoms.

In summary, the nanoparticle thus produced was composed of the C<sub>60</sub> nanoparticle behaved as a nucleus indicated by the DMA measurements, and was composed of Ag atoms confirmed by the PS measurements. Consequently, it is considered that Ag-C<sub>60</sub> composite nanoparticle was produced by the present method.

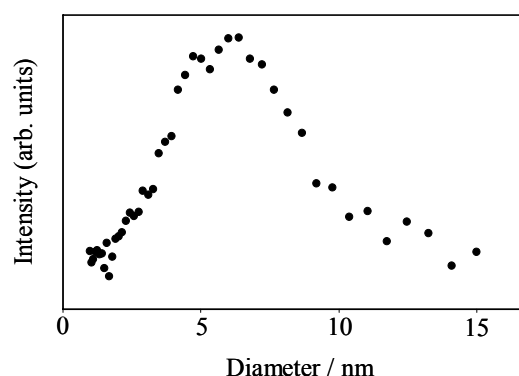


Figure 1. Diameter spectrum of the nanoparticle produced with C<sub>60</sub> vapor and Ag vapor.

## AEROSOL GENERATION FOR EXPOSURE EXPERIMENTS

<sup>1</sup>S. Mühlhopt, <sup>1</sup>A. Kocheck Alavi, <sup>2</sup>S. Diabaté, <sup>1</sup>H.-R. Paur

<sup>1</sup>Institute for Technical Chemistry, Thermal Waste Treatment Division,  
Forschungszentrum Karlsruhe, 76344, Karlsruhe, Germany

<sup>2</sup>Institute for Toxicology and Genetics,  
Forschungszentrum Karlsruhe, 76344, Karlsruhe, Germany

Keywords: Aerosol generation, Health effects of aerosols, Human lung cell,  
Nanoparticles characterization, Ultrafine particles

Epidemiological studies show an association between the concentration of fine and ultrafine particles (PM<sub>10</sub>, PM<sub>2.5</sub>, PM<sub>0.1</sub>) in the atmosphere and the rate of mortality or morbidity due to respiratory and cardiovascular disease. The assessment of the risk of airborne nanoparticles in workplaces is therefore an urgent task. The causes of the toxicological effects of ultra fine and nanoparticles to the human organism are yet unknown. Besides the chemical composition, the physical properties of the particles seem to be of particular importance for the effects. For the quantitative assessment of the toxicity of airborne nanoparticles the dose – response relationship is essential.

A technique was developed to expose human lung cells in vitro to analyse in particles with respect to their effects on human health which were determined by a special bioassay. For testing different particles for their lung toxicity the reproducible generation of aerosols by suspension is necessary.

Titanium oxide nanoparticles (21 nm) and quartz particles (Min-U-Sil 5) were suspended in cleaned air and carried to the exposure system containing the human lung cell cultures. In the first step dry and wet dispersion methods were tested and compared. For dry dispersion a rotating brush disperser (RBG 1000, Palas, Karlsruhe) was used.

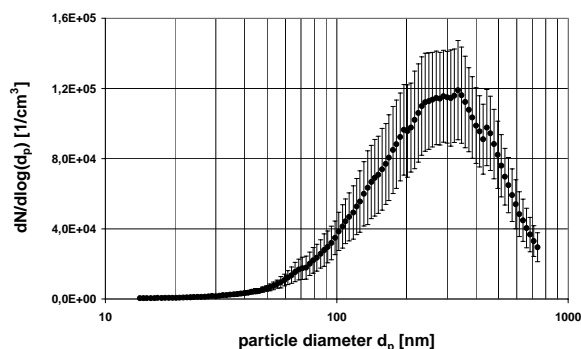


Figure 1. Dispersion of Min-U-Sil 5 quartz by RBG 1000

For wet dispersion suspensions of the particles in ultra pure water were sprayed into a reactor by a two phase nozzle (Typ S4, Schlick, Coburg) with

pressured air as gas phase. The reactor is surrounded by a mantle of Silicagel for drying the aerosol.

As shown in figure 1 the dry dispersion method produces particles in the size range of 300 nm. The wet dispersion yielded a size distribution at 35 nm. The reason for finding nanosized particles in the quartz aerosol is not cleared yet. Figure 2 shows the influence of the mass concentration in suspension to the particle size distribution of the titanium oxide aerosol.

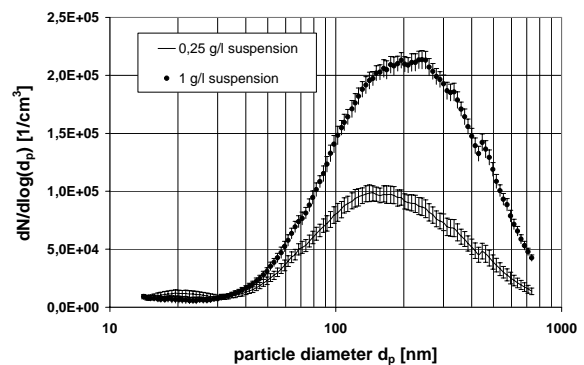


Figure 2. Wet dispersion of titanium oxide, different mass concentration in suspension

After generation of the aerosol the first steps of the exposure system are the separation of particles bigger than 1 µm and the humidification of the aerosol. Afterwards the human lung cell cultures are subjected to a constant flow of the conditioned aerosol. By this procedure an exposure of cell cultures at the air liquid interface is achieved, which resembles the conditions in the human lung. After exposure the responses of the cells were analyzed by measuring the viability (LDH, AlamarBlue) as well as the release of Interleukin-8 (IL-8) as a marker for pro-inflammatory changes.

The exposure method and the lung specific bioassay seem to be an appropriate model to screen the biological effects of different industrial particles.

Mühlhopt, S., Paur, H.R., Diabaté, S., Krug, H.F. (2007). Advanced Environmental Monitoring. Heidelberg, Springer, in press.

Diabaté, S., Mühlhopt, S., Paur, H.-R., Krug, H.F. (2002) *Ann. Occup. Hyg.* 46, 382-385.

## **Effect of Nanoparticles on the respiratory epithelium *in vitro*: Role of chemical composition and particle size**

*Boland S.<sup>1</sup>, Hussain S.<sup>1</sup>, Billon-Galland M.A.<sup>2</sup>, Fleury-Feith J.<sup>2</sup>, Baeza A.<sup>1</sup>, Martinon L.<sup>2</sup>, Moisan F.<sup>2</sup>,  
Pairon J.C.<sup>2,3</sup> and Marano F.<sup>1</sup>.*

<sup>1</sup> Laboratoire de Cytophysiologie et Toxicologie Cellulaire, Université Paris 7 Denis Diderot, case 7073, 2 Place Jussieu, 75 251 Paris cédex 05, France

<sup>2</sup> Laboratoire d'Etude des Particules Inhalées, 11 rue George Eastman, 75013 Paris, France

<sup>3</sup>INSERM Unité 841, 94000 Créteil, France

Keywords: Nanoscale carbon particles, Oxides nanoparticles, Agglomerates, Health effects of aerosols, Human lung cells.

Research development in the field of nanotechnologies which represent around 3000 milliard of euros on world scale will lead to an important production of nanoparticles (NP) and consequently to a potential human exposure. The effects of these NP on health are still unknown especially on the respiratory tract, which is the main route of exposure to NP. The aim of this work was to study according to the NP-physico-chemical characteristics (size, chemical composition, surface reactivity) the abilities and mechanisms of NP-internalisation in respiratory epithelial cells and their oxidative effects susceptible to drive cytotoxic and/or inflammatory effects which may lead to lung diseases such as asthma and chronic obstructive pulmonary disease (COPD).

For this purpose we used the human bronchial epithelial cell line 16HBE, which we exposed to NP (carbon black, titanium dioxide and zinc oxide) of different sizes. Transmission electron microscopy using JEOL 1200 EXII fitted with energy X ray spectrometry (EDS Link ISIS 300) was used to study NP behavior in culture medium and NP internalization (number, cumulative surface, site of accumulation).

All these particles were taken up by epithelial cells in a time and dose dependent process. The cytotoxic effect of the particles was related to their chemical composition as well as to the particle size with the smallest being the most toxic and zinc oxide having the lowest LC50. This cell death is the result of early apoptosis (4 hours) as shown by annexin/propidium iodide double staining. Furthermore, this cytotoxicity is due to the generation of an oxidative stress, which was quantified by flow cytometry using the fluorescent dye dihydroethidium. Thereby, the use of the antioxidants catalase allows rescuing cells from death.

Exposure to titanium dioxide NP at non-toxic concentrations leads to a pro-inflammatory response characterized by GM-CSF release correlated to the induction of mRNA expression. This GM-CSF induction seems to be more specific to TiO<sub>2</sub> and is size dependent with the smallest particles having a greater inflammatory potential.

To conclude, we have shown that the biological effects of NP depend on their chemical composition as well as particle size. NP are taken up by bronchial epithelial cells inducing oxidative stress leading to cell death by apoptosis. A strong pro-inflammatory response could be induced by TiO<sub>2</sub> particles.

*This work was supported by ANR grant n° 05 9 9-05 SET 024-01*

## Fragmentation and bouncing of nanoparticles in low pressure impaction

T. Wu and A.P. Weber

Institute for Mechanical Process Engineering, Clausthal University of Technology,  
Leibnizstraße 19, D-38678, Clausthal-Zellerfeld, Germany

Keywords: nanoparticle deagglomeration, nanoparticle disperser, bouncing, charge exchange

Airborne nanoparticles produced at high concentrations or after redispersion of nanopowders in a carrier gas are usually highly agglomerated. Many attempts to reduce the particle size down to the primary particles by external forces encountered a lower limit in the range of a few hundred nanometers [Meyer et al., 2002]. However, for optoelectronic applications individual nanoparticles are demanded to preserve the physical properties.

Recently, it was shown by TEM analysis that nanoparticle agglomerates can be disassembled down to the primary nanoparticles using low pressure impaction [Seipenbusch et al. 2002]. However, so far the nanoparticles remained on the surface, which may be employed in surface coating processes but which prevents further treatment of the nanoparticles. For special systems such as titania it was observed that the impaction fragments bounce off of the impaction surface at very high impaction velocities. This was the starting point for the present study in which the influence of the inclination of the impaction plate and of the particle velocity on the bouncing phenomenon was investigated. The experimental setup is shown schematically in Fig.1.

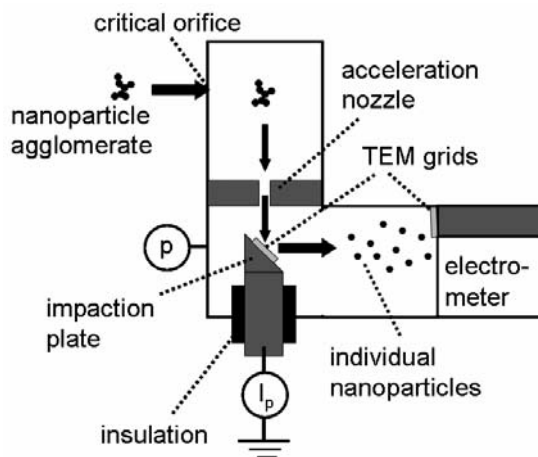


Figure 1. Schematic diagram of the experimental setup to study the bouncing of nanoparticle fragments.

Nanoparticle agglomerates enter a low pressure chamber through a critical orifice and are accelerated towards an impaction plate by a nozzle. The agglomerates are singly charged and size-

selected by a DMA before entering the low pressure impactor. The impaction efficiency is measured with an aerosol electrometer as indicated in Fig.2. TEM grids are placed on the impaction plate and further downstream. From these techniques the three processes which may take place in parallel (impaction, deagglomeration, bouncing) can be distinguished.

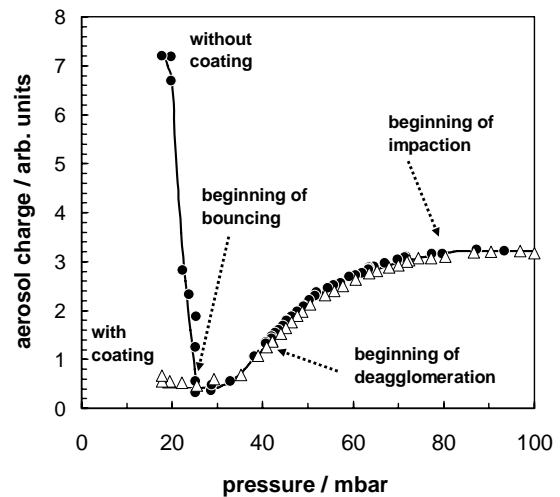


Figure 2. Behavior of agglomerates of titania nanoparticles as a function of chamber pressure for perpendicular incident

In Fig.2 the influence of a grease film on the impaction plate is also shown. It is obvious that bouncing may be effectively suppressed by increasing adhesion forces and offering new channels for energy dissipation. The results for different commercial nanopowders will be presented. In particular the influence of the plate inclination angle on the deagglomeration and bouncing will be discussed.

Meyer, J., (2002) PhD thesis, University of Karlsruhe  
Seipenbusch, M., Froeschke, S., Weber, A. P., and Kasper, G., (2002). *J. Proc. Mech. Eng.*, 216, 219-225

## Tuning size-distribution of particles with filamentary discharges properties related to the nature of dielectric barriers in Non-Thermal Plasma at atmospheric pressure

J. Hou<sup>1</sup>, N. Jidenko<sup>2</sup>, J.P. Borra<sup>2</sup> and A. P. Weber<sup>1</sup>

<sup>1</sup>Institute for Mechanical Process Engineering, Clausthal University of Technology, Leibnizstraße 19, 38678, Clausthal-Zellerfeld, Germany

<sup>2</sup>Lab. de Phys. Gaz & Plasmas (UMR 8578 CNRS Univ Paris-Sud Orsay, F-91405) Supélec, F-91192 Gif

Keywords: nanoparticle production, cold plasma, DBD (Dielectric Barrier Discharge), atmospheric pressure

Many of the classical techniques for the production of nanoparticles suffer from limitations regarding the choice of carrier gas, pressure and scale up potential. In this project, a Non-Thermal Plasma (NTP) process has been developed for the production of nanoparticles from any material in nitrogen at atmospheric pressure. One of the main goals of this project is to investigate the potential for scale up of this method. Figure 1 shows the schematic diagram of the experimental setup.

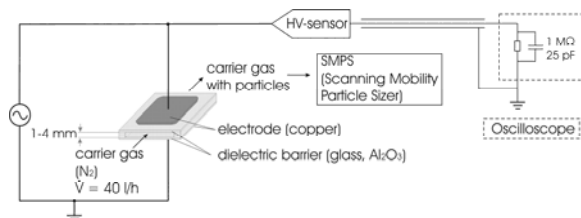


Figure 1. experimental setup

Plane-to-plane DBD, made of parallel glass or alumina dielectric barriers are tested. The gap length varies between 1 and 4 mm. Nitrogen is used as carrier gas with a gas flow rate of 40 l/h. The AC voltage is recorded with a high voltage probe and the current with an oscilloscope. The AC power supply delivers up to 20 kV at 50 kHz. The particle size distributions are measured with a SMPS (Scanning Mobility Particle Sizer).

Figures 2 and 3 show preliminary size distributions of particles produced by filamentary discharges interaction with the surface of dielectric barriers, glass or alumina respectively.

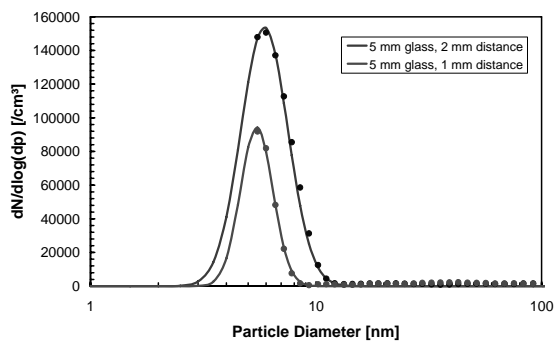


Figure 2. Particle size distributions from 5 mm thickness alumina DBD (gap=1 or 2 mm).

Fig. 3 shows that, with glass DBD, particles with narrow size distribution below 10 nm are produced. The number concentration of particles increases with the gap length, related to the increase of both the energy per filament deposited on surface and the power density ( $W \cdot m^{-2}$ ).

Fig. 4 shows that with alumina DBD as well, primary nucleated nano-particles below 10 nm are produced. However, for similar gap lengths with thinner alumina barriers (dielectric permittivity,  $\epsilon_r \sim 8$ ), the energy per filament is about ten times higher than with thicker glass barriers ( $\epsilon_r \sim 4$ ). Besides, for similar applied voltage, the voltage drop in the dielectric barriers is higher with glass than with alumina, implying a lower field in the gas and a smaller number a filament per half-cycle. Thus, with more energetic and more numerous filamentary discharges with alumina than with glass DBD, the particle concentration and the related mean size resulting from coagulation of primary nano-particles, both increase.

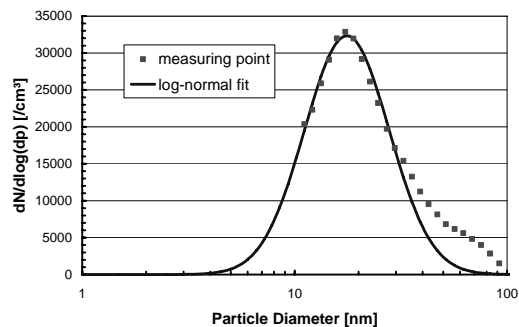


Figure 3. Particle size distributions from 1 mm thickness Alumina DBD (gap=1 mm).

Depending on the power density and energy per filament, which is higher with thicker glass barrier than with alumina, the size distribution can vary from nearly monodisperse 5 to 10 nm with low particle concentration up to a few tens of nanometers with a second coagulation mode around 70 nm, with higher power density.

The influence of the running parameters (voltage, gas flow rate, temperature etc.) on size and structure of the so-produced nano-particles as well as on the long term stability of the production is investigated. The first results of the study are presented.

## Aerosol Spray Pyrolysis Synthesis of spinel-supported catalysts for Hydrogen Production via Solair-aided Steam Reforming of Natural Gas

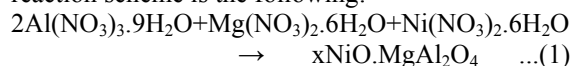
A. Zygogianni, S. Lorentzou, P. Dimotikalis, C. Agrafiotis and A.G. Konstandopoulos

Aerosol and Particle Technology Laboratory (APTL), Center for Research and Technology-Hellas, Chemical Process Engineering Research Institute (CERTH/CPERI), Greece

Keywords: aerosol chemistry, aerosol spray pyrolysis, nanoparticles, steam reforming, hydrogen.

Current state-of-the-art catalytic systems used for hydrogen production via hydrocarbons steam reforming are based on either expensive precious metals (Rh) supported on  $\text{Al}_2\text{O}_3$  or on much less expensive Ni-metal supported on mixed oxides ( $\text{MgAl}_2\text{O}_4$ ,  $\text{CaAl}_2\text{O}_4$ ). The latter are conventionally produced by high temperature calcination, followed by reduction of NiO to “active” Ni, by firing at 500 - 700°C under  $\text{H}_2$  flow. In the present study, Aerosol Spray Pyrolysis (ASP) was employed for the synthesis of such catalytic systems in one step, within very short times.

The synthesis experiments took place in an aerosol reactor consisting of a stainless steel tube ( $\varnothing$  3 in, length 40 in), heated between 350-1000 °C. A filter holder at the end of the reactor was used to collect the synthesized particles. Metal nitrates (of Al, Mg, Ca and Ni) were used as precursor materials employing two kinds of aqueous solutions: “plain” and citric acid-additized (the latter to facilitate metal ions complexation and avoid selective precipitation). The solution was atomized with the aid of an in-house atomizer (droplet mean diameter  $\approx 2 \mu\text{m}$ ) and the droplets formed pass through the heated tubular reactor, where the evaporation of the solvent and the reaction between the precursors take place. A typical reaction scheme is the following:



The effects of the synthesis parameters (kind of precursor solution, synthesis temperature and atmosphere) on final product properties such as particle size, phase composition, specific surface area, catalytic activity and resistance to coke poisoning were investigated. XRD spectra of ASP products showed that the main product phases are Mg-Al spinel ( $\text{MgAl}_2\text{O}_4$ ) or Ca-Al spinel ( $\text{CaAl}_2\text{O}_4$ ) and MgO. SEM photographs of the synthesized powders showed that the particles are always spherical, with a high percentage being of submicron size whereas the EDS elemental microanalysis and mapping (Figure 1) show that the particles are homogeneous containing all three metal components, Al, Ca (or Mg) and Ni.

The catalytic performance of such spinel-supported Ni-metal systems for methane steam reforming was studied in an in-house built test rig.

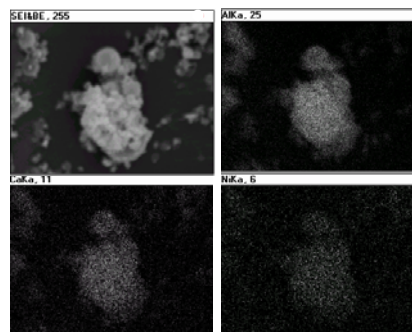


Figure 1: Mapping of a typical particle at  $\text{CaAl}_2\text{O}_4$  ASP product.

Typical conversion behavior achieved from such ASP products, synthesized at temperatures of 900°C and 1000°C during a thermo-programmed steam reforming cycle, is shown in Figure 2.

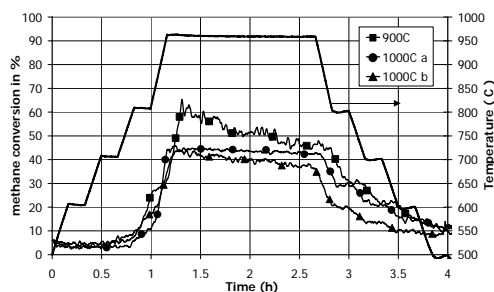


Figure 2:  $\text{CH}_4$  conversion achieved from ASP products.

It can be seen that such ASP-synthesized systems are in principle capable for Hydrogen production via steam reforming. Current research efforts are targeted on improving their conversion - currently being within 40-60 % depending on the synthesis conditions - and of the deposition of such materials on SiC foams to be used as solar receivers/reactors for solar-aided steam reforming.

This work has taken place within the SOLREF project, financed in part by the EU Commission (CONTRACT No.: 502829).

S. Lorentzou, K.Karadimitra, C.Agrafiotis, A.G.Konstandopoulos (2004), *Proceedings of PARTEC*, Nuremberg, Germany, March 16-18.  
A.A. Lemonidou, I.A.Vasalos (1989), *Applied Catalysis*, A 54, 119.

## Droplet size characterization in spray flames

Helmi Keskinen<sup>1</sup>, Jyrki M. Mäkelä<sup>1</sup>, Mikko Aromaa<sup>1</sup>, Martin C. Heine<sup>2</sup> and Sotiris E. Pratsinis<sup>2</sup>

<sup>1</sup> Institute of Physics, Aerosol Physics Laboratory, Tampere University of Technology, P.O. Box 692, FIN-33101, Tampere, Finland.

<sup>2</sup> Particle Technology Laboratory, Institute of Process Engineering, Department of Mechanical and Process Engineering, ETH Zürich, 8092 Zürich, Switzerland.

Keywords: droplets, size distribution, spray, flame, zirconia

Flame methods have been developed during the last decades to produce complex composite nanoparticles. These methods can be up-scaled as shown for FSP (Mueller *et al.* 2004) and are also very promising in deposit preparation (Keskinen *et al.*, 2007). Recently, droplet atomization and dynamics in different spray flames have been studied by phase-Doppler anemometry (PDA) non-intrusively by Heine & Pratsinis (2005) and Heine *et al.* (2006) during synthesis of ZrO<sub>2</sub> nanoparticles. In this work atomization, droplet size evolution, evaporation, and dynamics in liquid spray (LS, without the flame) and Liquid Flame Spray (LFS) are compared at on spray nozzle modification.

Droplets, dry salt particles and ceramic zirconia nanoparticles were generated using a specific spray nozzle for liquid atomization. In LS water, ethanol and salt water solution were dispersed to generate droplets and dried salt particles. In LFS a solution of 0.5 M zirconium propoxide in ethanol was combusted with a stoichiometric H<sub>2</sub>/O<sub>2</sub> flame. The liquid was atomized with Q<sub>a</sub> = 20 (low flow) and 40 (high flow) l/min pressurized air (LS) or H<sub>2</sub> (LFS). The zirconia production rate was 4 to 60 g/h assuming complete precursor conversion. Droplets and particles produced by LS and LSF were characterized by PDA (TSI Inc., USA), Electrical Low Pressure Impactor (ELPI; Dekati), Scanning Mobility Particle Sizer (SMPS) (DMA; TSI model 3071A and CPC; TSI model 3025A), Transmission Electron Microscopy (TEM; JEM 2010 from JEOL, Tokyo, Japan) (including Selected Area Electron Diffraction, SAED) and X-ray Diffraction (XRD; Kristalloflex D-500, Siemens).

In LS sub-micron to super-micron droplet size distributions were determined by combining the results of SMPS, ELPI and PDA (Figure 1). Spraying produced droplets with a number mean diameter at sub-micron size range and both mass mean and Sauter mean droplet diameter (SMD) at super-micron size range.

In LFS studies on zirconia particle morphology indicated that at lower atomization gas flow rate, the precursor decomposition was not complete. At this gas flow rate, PDA measurements showed that the gas velocities were substantially low (60 m/s) and Sauter mean droplet diameters derived from droplet measurements were larger.

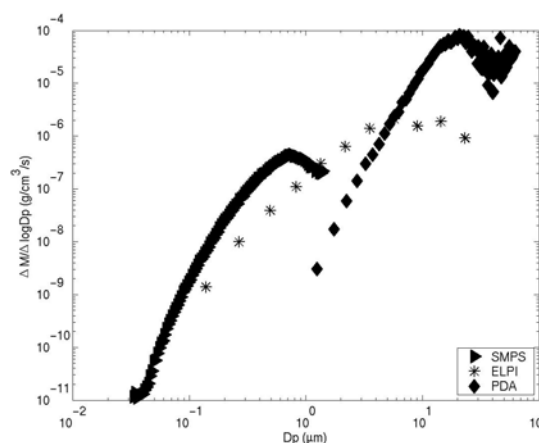


Figure 1. Droplet mass size distributions for gas flow rates of Q<sub>a</sub> = 40 l/min at liquid feed rate of 2 ml/min of water derived from PDA, ELPI, and SMPS measurements number size distributions (in LS).

At higher atomization gas flow rate, the droplet size was smaller than expected. The gas velocities reached a maximum of 140 m/s with zirconia particle production. The zirconia particle morphology was also more uniform.

This work was supported in part by Tekes (The National Technology Agency, Project Shine Pro/Pinta), Tampere University of Technology and Finnish Academy of Science and Letters and by the Swiss National Science Foundation (SNF). We gratefully thank M. Sc. Mari Honkanen and M. Sc. Juha-Pekka Nikkanen from Institute of Materials Science, Tampere University of Technology for TEM and XRD studies.

Heine M. C., & Pratsinis S. E. (2005). *Ind. Eng. Chem. Res.*, 44, 6222-6232.

Heine M. C., Mädler L., Jossen R., & Pratsinis S. E. (2006). *Combust. Flame*, 144, 809-820.

Keskinen H., Mäkelä J. M., Aromaa M., Keskinen J., S. Areva, C. V. Teixeira, J. B. Rosenholm, V. Pore V., Ritala M., Leskelä M., Raulio M., Salkinoja-Salonen M., Levänen E., & Mäntylä T. (2006). *Cat. Lett.* 111, 127-132.

Mueller R., Jossen R., Pratsinis S. E., Watson M., & Akhtar M. K. (2004). *J. Am. Ceram. Soc.*, 87, 197-202.

## Interparticle forces in Nanoparticle Agglomerates

M. Seipenbusch<sup>1</sup>, S. Rothenbacher<sup>1</sup>, A. P. Weber<sup>2</sup>, G. Kasper<sup>1</sup>

<sup>1</sup>Institut für Mechanische Verfahrenstechnik und Mechanik, Universität Karlsruhe, Am Forum 8, 76131 Karlsruhe, Germany

<sup>2</sup>Institut für Mechanische Verfahrenstechnik, Technische Universität Clausthal, Leibnizstrasse 19, 38678 Clausthal-Zellerfeld, Germany

Keywords: interparticle forces, agglomerates, nanoparticles characterization, photochemical processes, materials synthesis

Due to the high surface energy of nanoparticles their tendency to form agglomerates is quite strong. Upon contact the primary particles of an agglomerate form bonds which can be of different nature. Sintering and monomer adsorption from the surrounding atmosphere can lead to solid state necks. Chemical bonds between the particle surfaces may also form and magnetic dipole forces can potentially contribute to the interparticulate forces. As a baseline of bond energy *van der Waals forces* are always present. The strength of these interparticle bonds determines to a large part their physical properties and applicability in materials synthesis. On one hand, there are nanomaterials that have to be applied in single particle form, e. g. in electronics, optics and optoelectronics applications. In these cases the energy needed for particle deagglomeration is an important parameter. In filled polymers however, the elasticity of nanoparticle chain aggregates seems to contribute to the mechanical properties of the composite material, thus the strength of the interparticle forces is of importance in a positive way (Bandyopadhyaya *et al.*, 2004).

To determine the bond energies of primary particles within agglomerates the method of impact fragmentation was adapted to the nanoscale (Seipenbusch *et al.*, 2002). Defragmentation patterns of agglomerates impacted in a single stage low pressure impactor where analysed in the transmission electron microscope (TEM). A variety of materials was tested, ranging from metal particles and oxides to polymer particles. Particle size effects were analyzed for the separate materials, revealing the different origins of the interparticle bonds. For some materials near van der Waals behaviour was found. For Nickel the onset of additional *magnetic forces* were observed for larger particle sizes, when the superparamagnetic behaviour of particles smaller than ~12 nm transforms into permanent magnetic dipoles. Another strong effect on the magnitude of agglomerate strength seems to be surface purity, which is qualitatively determined from aerosol photoemission spectroscopic analysis.

Chemical surface adducts like hydroxyl groups can form *chemical bonds* between the primary particles, e. g. by way of a condensation reaction. Therefore

the bond energy can be manipulated by influencing the density of these groups on particle surfaces prior to agglomeration. Using photochemical reactions on aerosol polymer nanoparticles generated from a polystyrene /CCl<sub>4</sub>- solution particles this manipulation was carried out in both directions of the bond energy scale, as shown in Fig. 1. The alteration of the surface groups and the corresponding change in bond energy was correlated to the dose of irradiation.

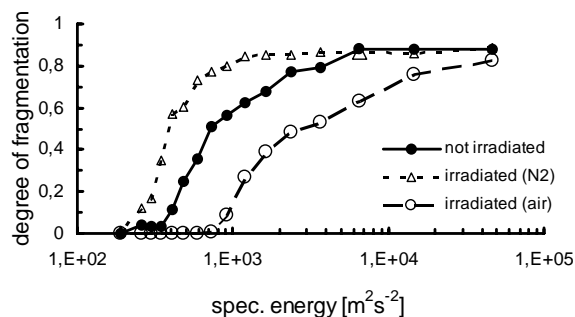


Fig. 1: Fragmentation efficiency of polystyrene particles: the effect of photochemical surface alteration

In this contribution the fragmentation results for the different nanoparticle systems (metals, metal oxides and polymers) will be presented and ways of tailoring the interparticle forces will be outlined. In particular, the effects of chemical surface reactions and tempering on the bond strength will be discussed.

Bandyopadhyaya, R., Rong, W., Friedlander S. K., (2004). *Chem. Mater.*, 16, 3147-3154.

Seipenbusch, M., Froeschke, S., Weber, A. P., and Kasper, G., (2002). *J. Proc. Mech. Eng.*, 216, 219-225

## Hydrogen Storage Behaviour of Metallic Nanoparticles Generated by Spark Discharge

N. S. Tabrizi<sup>1</sup>, W.J. Legerstee<sup>2</sup>, S. Eijt<sup>2</sup>, A. Schmidt-Ott<sup>1</sup>

<sup>1</sup>Nanostructured Materials, DelftChemTech, TUDelft, Julianalaan 196, 2628 BL, Delft, The Netherlands

<sup>2</sup>RRR/Fund. Asp. of Mat.&Energy, TUDelft, Mekelweg 15, 2629 JB, Delft, The Netherlands

Keywords: spark discharge, nanoparticles, hydrogen storage.

Metal hydrides are potentially good candidates for hydrogen storage applications due to their high storage capacity. However, light metal hydrides show sluggish H<sub>2</sub> adsorption/ desorption kinetics (Zaluska, 1998) and the reaction occurs at elevated temperatures (350-400° C). Recent investigations report that the hydrogen storage properties of metals can be improved by increasing the surface activity induced by reduction in particle size. The grain size can affect thermodynamic properties like plateau pressures and phase boundary envelopes as well as the kinetics. Therefore, nanocrystalline metals are targets of many studies.

In this work, magnesium and palladium nanoparticles of few nanometers in diameter, depicted in Figure 1, are produced in the gas phase by the spark discharge method (Schwyn, 1988) and some preliminary tests on their H<sub>2</sub> adsorption/ desorption behaviour were carried out in a thermal desorption setup. Since most metallic nanoparticles have a high affinity to oxygen and a surface layer of oxide can act as a barrier for H<sub>2</sub> diffusion, the production process has to be very clean and the collected particles should be handled in an inert atmosphere i. e. a glove box. In practice, formation of a thin layer of oxide at the surface of particle is usually unavoidable. Therefore the sample often needs annealing which can result in the activation of the sample and breakage of the oxide layer due to the difference in the thermal expansion coefficients of pure metal and metal oxide at elevated temperature.

Figure 2 shows the hydrogen desorption behaviour of magnesium nanoparticles. The particles are charged under 4 and 8 bar of hydrogen pressure for different periods of time, then their hydrogen discharge in vacuum (0.1 Pa) at various temperatures is measured. All curves show the maximum hydrogen release at almost the same temperature around 180°C. This is quite promising, because this temperature is significantly lower than reported for larger particles. In comparison with magnesium, palladium is chemically more resistant with high hydrogen solubility over a wide range of pressures and temperatures. Figure 3 shows the accumulative hydrogen desorption of the palladium nanoparticles. It can be seen that the maximum weight percentage of hydrogen stored is very near to the theoretical maximum value (0.566 %) and releases around 250°K. Detailed study on the kinetics and thermodynamics of these systems is in progress.

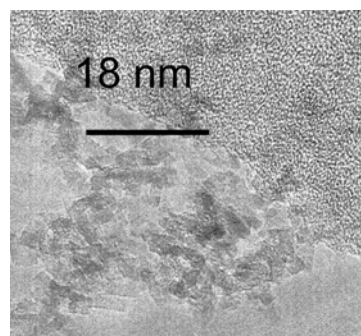


Figure 1- TEM micrograph of Mg nanoparticles

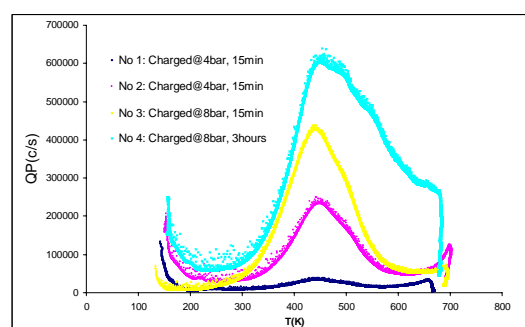


Figure 2- Desorption behaviour of Mg nanoparticles

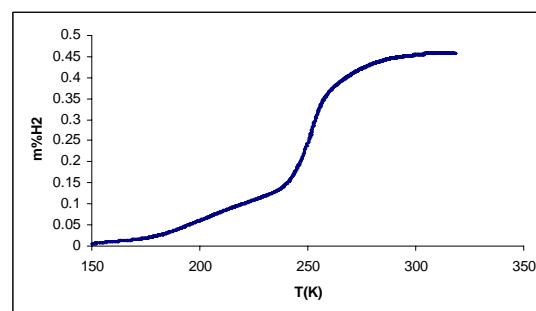


Figure 3- Accumulative hydrogen desorption of Pd nanoparticles

### References:

- A. Zaluska, L. Zaluski, J. O. Strom-Olsen, Nanocrystalline Magnesium for Hydrogen Storage, *Journal of Alloys and Compounds* Volume 288, 1999, Pages 217-225.
- S. Schwyn, E. Garwin, A. Schmidt-Ott, Aerosol Generation by Spark Discharge, *Journal of Aerosol Science*, Volume 19, No. 5, 1988, Pages 639-642.

## Deposition of nanometric singly charged particles in cylindrical metallic and flexible conductive silicone tubes

M.B. ATTOUI

Département de Physique, Faculté des Sciences, Université Paris XII ; France. [attoui@univ-paris12.fr](mailto:attoui@univ-paris12.fr)

Keyword : nanoparticles, deposition,

The deposition of nanoparticles in tubes is of a great interest in many fields: aerosol science, spectrometry ..... In aerosol science the particle deposition is used in metrology (diffusion batteries for example). However the deposition of the particles in tubes is on the first interest in term of 'losses' in experimental measurement (size, concentration). Below 10 nm the diffusion losses are prevailing. Metallic tubes are widely used to prevent electrostatic deposition. Commercialized silicone conductive (flexible) tubes started to be widely used thanks to their comfort of using. Classical theoretical treatments for diffusional deposition of particles in tube flow describe the losses within straight tubes. Gormley and Kennedy (1949) first derived the penetration efficiency for diffusional particles in fully developed laminar flow through a circular tube with a uniform inlet particle concentration. particle penetration through straight tubes is well studied with particles larger than 3 nm with the size limit of the aerosol metrology detection and generation. Electro spray atomisers have opened the road for generating aerosols of arbitrarily 'small' particles down to sub nanometric range. In the other hand short DMAs capable of resolving power 1/FWHH) in excess of 50 with 1 nm particles are introduced by J. Fernandez de la Mora and his team at Yale University and now commercialized. ES-DMA instrument used in this study produce standards ions with known mobility diameter, mass and charge state from 1 nm to beyond 3 nm from tetra alkyl ammonium halides (Ude, Fernandez de la Mora 2006). Home made aerosol electrometer (université paris XII electrometer) used as a detector has a maximum of 50 l/min and lower detection limit close to 1 fA. In this paper we present the results of the penetration fraction measurements in cylindrical tubes for singly charged particles and ions of 1 nm and below. Tetra heptyl ammonium bromide (THABr) salt dissolved in ethanol is atomised by electro spray to produce singly charged standards ions of 1,47 nm (mobility diameter) for the monomer (first pic on the figure 1), 1,78 nm for the dimer and 1,197 nm for the trimer (3d pic).

TSI and Grimm silicone conductive tube, stainless tube and cooper are tested for different flowrate. Figure 1 and 2 give the results of the upstream and downstream concentrations of TSI tubes (0,41 and 0,31" ID and 24,5 cm length) at respectively 8 and 6 l/min.

The spectrum transmission (upstream and downstream) of the THABr in figure 1 and 2 show 3 well defined measurable pics with known mobility of the singly charged monomer, dimer and trimer, for the 2 tubes of TSI at 8 and 6 l/min.

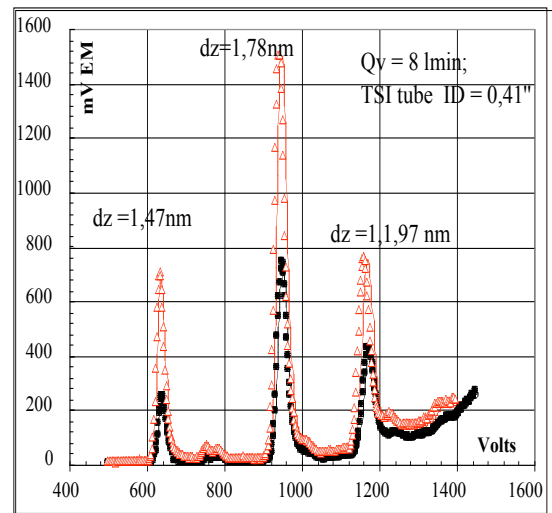


Figure 1 Transmission by TSI 0,41'' ID tube at 8 l/min

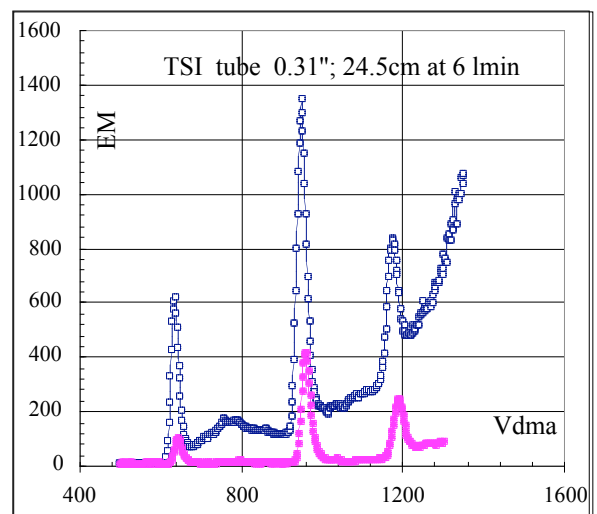


Figure 2 Transmission of ions by TSI 0,31'' ID TSI tube at 6 l/min.

The transmission is a strong function of the flow rate and size as we can see it on the both figures. The trimer is well transmitted (28%) even at 6 l/min compared to the monomer. The transmission of the same trimer at 8 l/min is close to 50%. The lower transmission is for the monomer (13 % at 6 l/min and 33% at 8 l/min).

### References :

Ude, S. Fernandez de la Mora, J. (2005) : Molecular monodisperse mobility and mass standards from electro sprays of tetra-alkyl ammonium halides. J. Aerosol Sci 35, p 1224-123

## Production of metallic ions, atomic clusters and nano particles with hot wires

M.B. Attoui, J. Fernandez de la Mora

Département de Physique Université Paris XII, France; Mechanical Engineering Department, Yale University USA

Key words : nanoparticles, ions, nucleation

Several prior studies from Schmidt-Ott's group have noted that heated metal wires used as condensation aerosol generators produce naturally charged particles. Their explanation involves the evaporation of impurity ions from the metal surface, followed by vapor condensation on the ions. This generator must therefore be able to supply nanoparticles covering a size range from single atoms or small clusters (the evaporated ions) up to relatively large sizes. The combination is therefore ideal for basic studies covering the full nanoparticle size range. Our objective here is to characterize the transition from ion to particle formation in heated wires of several metals by means of a high resolution Herrmann DMA (HDMA) specially designed to cover the 1-20 nm size range with high resolution (Herrmann et al. 2000)

The wire generator is made mostly of standard stainless steel UHV parts. As previously described

(Peineke 2006), it is inexpensive and easy to build. The wire is held in a four way cross by a current feed-through with an embedded gas inlet. The wire is resistively heated by a DC low voltage/high current supply. Palladium, Platinum, Tungsten, Nickel Chrome alloy and stainless steel wires were used in this study with air and or nitrogen.

The setup for measuring particle mobility distributions of the aerosol charged particles (ions + particles) is a classical set up (DMA+ Detector). The detector is a home-made electrometer (Université Paris XII electrometer), with 1 fA limit detection. Since the external electrode of the HDMA is at high voltage (the internal is grounded) the wire is powered with 12 Volts car battery with a voltage controller which gives a maximum of 5 Volts. The wire diameters (0,3 to 0,8 mm) used in this study with lengths of 10 cm give a resistors from 0,2 to 0,8 Ohms at room temperature.

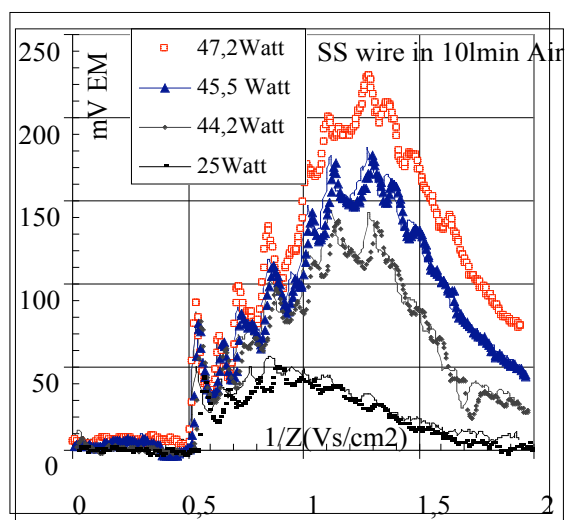
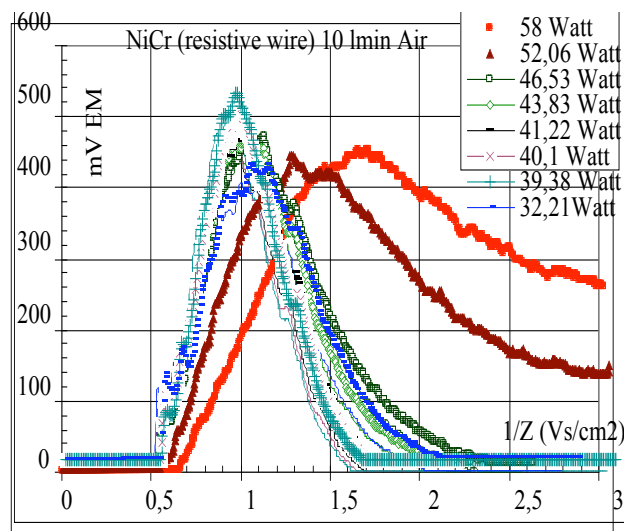


Figure 1: Mobility spectra of ions (sharp picks) and particles (continuous spectrum) from NiCr and SS heated wires at different temperatures.

Figure 1 shows the mobility spectra of positive ions and particles generated by nickel-chrome and stainless steel wires in 10 l/min clean air (breathing quality) at different temperature. Essentially purely ionic signatures are generated at relatively low temperatures. The largest inverse mobilities observed of  $2 \text{ cm}^2/\text{Vs}$  correspond to very small objects in the polarization limit, possibly metallic ions. Peineke et al. have previously interpreted sharp observed peaks as magic numbers in the series of metal clusters. Because we did not bake the system, our own sharp peaks may be due to impurities from organic vapours, which pick up the charge from the smaller ions originally evaporated

from the wire. The onset of ion-induced nucleation observed at increasing temperatures (left), immediately removes the sharp peaks, though with only slight mobility changes. This must be due initially to modest metal vapour attachment to the smaller primary ions, while the larger ions nucleate more readily and produce the tails of much large particles seen.

### References

Herrmann W., et al. (2000). Abstract of the annual conference of the AAAR, St Louis, Missouri.

Peineke, C., Schmidt-Ott, A. (2006) Abstract 7<sup>th</sup> international aerosol conference Minneapolis, 686-687

Peineke, C., Attoui, M.B., Schmidt Ott, A. (2006) J. Aerosol Science 37, 1651-1661.

## Ni/NiO nanoparticle synthesis by MOCVD

P. Moravec<sup>1</sup>, J. Smolík<sup>1</sup>, H. Keskinen<sup>2</sup>, J.M. Mäkelä<sup>2</sup> and V.V. Ievdanský<sup>3</sup>

<sup>1</sup> laboratory of Aerosol Chemistry and Physics, Institute of Chemical Process Fundamentals AS CR, 165 02, Prague, Czech Republic

<sup>2</sup>Institute of Physics, Tampere University of Technology, FIN-33101, Tampere, Finland

<sup>3</sup>Heat and Mass Transfer Institute NASB, 220072, Minsk, Belarus

Keywords: CVD, Generation of nanoparticles, Nickel acetylacetonate, Particle characterization.

Nickel and nickel oxide nanoparticles show many peculiar optical, magnetic, electrical and catalytic properties with high potential of application in such areas as sensors, magnetic data storage and catalysis. In our laboratory we synthesized Ni/NiO nanoparticles by metal organics CVD using nickel acetylacetonate (NiAA) as a precursor.

Particles were prepared in an externally heated glass tube flow reactor of the length 55 cm and i.d. 27 mm. Deoxidized, dry and particle free nitrogen was used as a carrier gas. Particles production was studied by various decomposition processes: (i) thermal decomposition in an inert atmosphere, (ii) hydrothermal decomposition and (iii) reduction in the presence of hydrogen in the carrier gas. Besides the chemistry of precursor decomposition, the influence of precursor concentration ( $c_{\text{NiAA}}$ ), reactor temperature ( $T_R$ ), flow rate ( $Q_R$ ) and concentration of hydrogen ( $c_H$ ) on particle production and characteristics was also investigated. Precursor vapour pressure was controlled both by the flow rate of the carrier gas through the saturator and, predominantly, by variation of saturator temperature ( $T_S$ ). The vapour pressure was calculated on the basis of experimental data of Götze *et al.* (1970). Samples for TEM, SAED (JEO 2010) and EDS (Noran Vantage) analyses were deposited onto carbon coated grids and PTFE filters.

The particle generation was observed already at reactor temperature 400 °C. Number concentration and particle size strongly increased with increasing  $T_R$  and  $T_S$ , and they were also affected by  $Q_R$ , while concentration of hydrogen had greater impact on morphology, crystalline structure and composition than on the size and shape of particle size distribution curves. Particles prepared by pyrolysis and hydrolysis of NiAA had shell-like structure, size well below 50 nm and they were agglomerated into clusters and/or chains. They were possibly contaminated by carbon (dark grey deposit on PTFE filters) from incomplete decomposition of precursor. Electron diffraction patterns (EDP) were due to the size of particles rather weak and were composed predominantly of the rings of FCC Ni EDP.

Particles produced by reduction of NiAA had broader size distribution (from 10 to cca 50 nm), were less agglomerated and shell-like structure

almost disappeared. Electron diffraction patterns of big particles (50 nm) corresponded with FCC Ni, while those from clusters of small particles contained rings from both Ni and NiO crystalline structures. The deposit of particles prepared by reduction had silver colour. TEM image of the sample of particles prepared by reduction and EDP of the cluster of nanoparticles is shown in Figure 1.

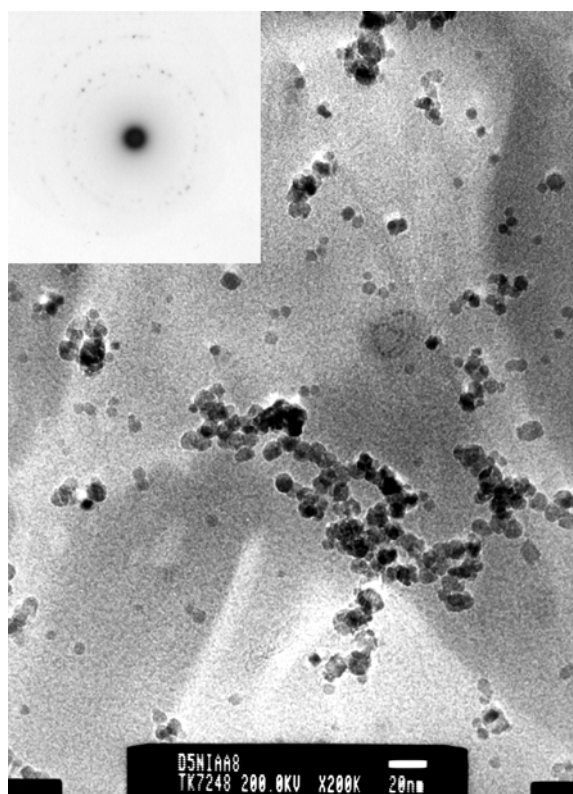


Figure 1. TEM image and electron diffraction pattern of the sample of particles prepared at  $P_{\text{NiAA}}$  2.9 Pa,  $T_R$  500 °C,  $Q_R$  800 cm<sup>3</sup>/min,  $Q_{\text{CF}}$  20 cm<sup>3</sup>/min,  $Q_R$ ,  $c_H$  7 %.

This work was supported by the Grant Agency of the CR No. 104/07/1093 and by Finnish Academy of Sciences and Letters. TEM/EDS analyses were performed by Tomi Kanerva, Institute of Material Science, Tampere University of Technology.

Götze, H.-J., Bloss, K., & Molketin, H. (1970). *Zeitschrift Phys. Chem. Neue Folge*, 73, 314-320.

## Fabrication of nanopillars for chemical analysis using deposited silica aerosol particles as etching mask

J. M. Mäkelä<sup>1</sup>, H. Keskinen<sup>1</sup>, M. Aromaa<sup>1</sup>, L. Sainiemi<sup>2</sup>, L. Luosujärvi<sup>3</sup>, T. Kotiaho<sup>3,4</sup>, and S. Franssila<sup>2</sup>

<sup>1</sup>Aerosol Physics Laboratory, Institute of Physics, Tampere University of Technology, Tampere, Finland

<sup>2</sup>Micro and Nanosciences Laboratory, Helsinki University of Technology, Helsinki, Finland

<sup>3</sup>Laboratory of Analytical Chemistry, University of Helsinki, Finland

<sup>4</sup>Division of Pharmaceutical Chemistry, Department of Pharmacy, University of Helsinki, Finland

Keywords: Liquid Flame Spray, nanopillar, deep reactive ion etching

Aerosol particle deposits with coverage less than 100 %, can be used as a etch mask to fabricate patterns on a silicon wafer. Nanoparticles, deposited on a silicon wafer, create a shadow when etching the wafer by deep reactive ion etching (DRIE). The technique has been used for several applications creating sophisticated patterns on the substrate (e.g. Maximov *et al.*, 2002, Villanueva *et al.*, 2006).

Here, separate randomly displaced ~100 nm sized silica particles are used as the etch mask. The particle deposits are prepared using Liquid Flame Spray (LFS) technique, with liquid TEOS as the precursor (Figure 1). The substrate is swept through the flame, total exposure time being 1-2 seconds. Particle number density of 1-10 particles/ $\mu\text{m}^2$  is conveniently obtained.

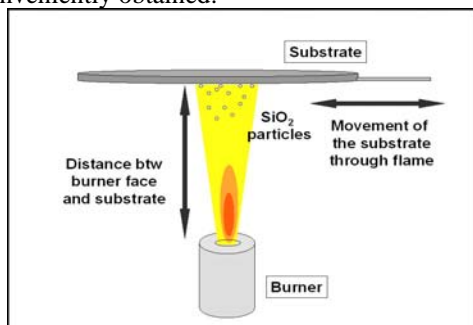


Figure 1. Preparation of the LFS-generated nanoparticle deposits on a silicon wafer. Distance from burner face 10 cm, precursor TEOS, particle production rate 76g/h (see Pitkänen *et al.*, 2005).

The etching is performed using the Plasmalab System 100 (Oxford Instruments) reactor, relying on inductively coupled  $\text{SF}_6/\text{O}_2$  plasma chemistry. During the etching process, the silicon wafer material is removed from aside of the particles thus, a 'forest' of high narrow nanopillars appears on the wafer. The silica particles remain on the location of deposit, but the Si-wafer material has been removed in the process chamber due to the chemical reactions and bombarding ions (Figure 2). The removal occurs vertically, with minimum amount undercutting underneath the particles. The height of the nanopillar is proportional to the etching time. Specific surface area of the pillars is in the order of  $1 \text{ m}^2/\text{m}^2$  (of wafer) depending on the initial coverage and etching time. The whole 100 mm wafer can be processed at once.

This new technique combines LFS and DRIE and has potential to be scaled up even for larger areas.

High surface-to-volume ratio is desirable in many fluidic applications (e.g. liquid chromatography (LC) and desorption-ionization on silicon mass spectrometry (DIOS-MS)). Pillars are used to increase surface-to-volume ratio in chemical concentrators and fluidic structures. In applications where the concentrator activation can be performed using laser illumination (such as DIOS-MS), a pillar array type of structure on the surface is advantageous compared to ordinary porous material.

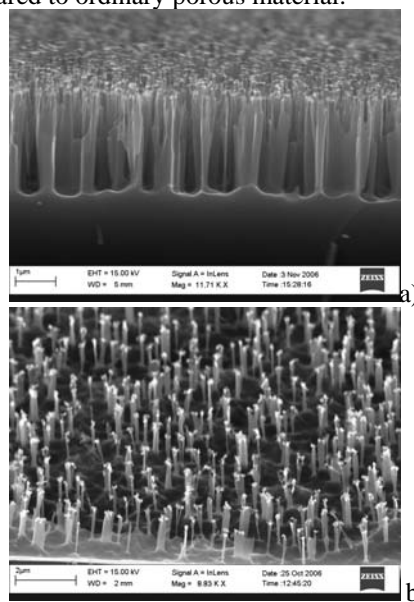


Figure 2. SEM-image of the surface with ~100 nm thick nanopillars with aspect ratio 20:1, after 150 sec etching. a) From aside b) Tilted image

Maximov *et al.* (2002) Fabrication of Si-based nanoimprint stamps with sub-20 nm features, *Microelectronic Engineering*, 61-62, 449-454.

Pitkänen *et al.* (2005) Numerical Study of Silica Particle Formation in Turbulent  $\text{H}_2/\text{O}_2$  Flame.

*IFRF Combustion Journal*, Article No 200509

Villanueva *et al.* (2006) Deep reactive ion etching and focused ion beam combination for nanopillar fabrication, *Materials Science and Engineering: C*, 26, 164-168

## Aerosol Processing and Sintering of Supported Metal Nanoparticles

A. Binder<sup>1</sup>, M. Seipenbusch<sup>1</sup> and G. Kasper<sup>1</sup>

<sup>1</sup> Institut für Mechanische Verfahrenstechnik und Mechanik, Universität Karlsruhe (TH), 76131, Karlsruhe, Germany

Keywords: CVD, Pd/SiO<sub>2</sub>, sintering, Low Pressure Impactor

The preparation of heterogeneous catalysts remains a complex process, specifically with regard to adjusting the dispersion, concentration and the surface area of the active phase. Catalysts are often generated using wet phase processes such as impregnation, which involves many process-steps, including intensive cleaning, solvent removal, drying, washing and calcination, all of which are not required in aerosol-based production processes. It has been shown, that chemical vapour deposition (CVD) is a suitable method to prepare highly dispersed, functionalised nanoparticles in the gas phase (Heel and Kasper, 2005). Since the loss of catalytic activity by sintering is one of the main causes of deactivation of supported metal catalysts subjected to high temperatures, the sintering behaviour of supported metal nanoparticles was investigated in the aerosol state. The metal-support interactions of different oxide carrier particles with respect to the stability of dispersion of the supported metal particles were studied.

In this work, highly dispersed palladium was deposited on oxide nanoparticles like silica (SiO<sub>2</sub>), titanium dioxide (TiO<sub>2</sub>) or aluminium oxide (Al<sub>2</sub>O<sub>3</sub>) from metal-organic precursors by a continuous gas phase process at atmospheric pressure. The support particles were generated by chemical vapour synthesis (CVS) using tetraethyl(ortho)silicate (TEOS), titantetraisopropoxide (TTIP) and Aluminium-sec-butoxide, respectively, in a nitrogen-oxygen mixture in a hot-wall reactor. Downstream, the carrier particles were directly coated with palladium in the aerosol state. The functionalisation of the support particles was carried out by CVD, using ( $\eta^3$ -allyl)( $\eta^5$ -cyclopentadienyl)palladium [Pd(allyl)Cp].

The carrier particles were functionalised using various amounts of Pd, whereas the rate of deposition and the Pd island size could be controlled by the concentration of the Pd precursor in the gas phase. The degree of deposition is measured online in the aerosol state by a single-stage low pressure impactor (SS-LPI) in the pressure scanning mode (Seipenbusch *et al.*, 2002) and in conjunction with a Faraday Cup Electrometer. The surface number density and size distributions of the palladium nanodots on the support particles were measured by HR-TEM analysis. The Pd island size ranged from 1.3 nm to 3.0 nm with narrow size distributions denoted geometric standard deviations of  $\sigma_g = 1.2$ .

The surface concentrations were found to be between 6 and 12 Pd particles per 100 nm<sup>2</sup>.

The number of Pd nanodots was also controlled by varying the concentration of hydroxyl groups on the support particle surface, which are necessary for the first deposition step of the palladium precursor (Wu *et al.*, 2005). This surface concentration could be controlled by varying process parameters in the CVS process, within a typical range of 3 up to 8 Pd nanodots per 100 nm<sup>2</sup>. The hydroxyl group surface density was verified by TG analysis (Binder, 2007).

In order to study the sintering kinetics of the Pd particles, the functionalised particles were fed through an oven directly after the coating reactor and sintered in the aerosol state. The sintering behaviour of the Pd/Al<sub>2</sub>O<sub>3</sub>, Pd/SiO<sub>2</sub> (Fig. 1) and Pd/TiO<sub>2</sub> were investigated by HR-TEM image analysis and the kinetic data were compared.

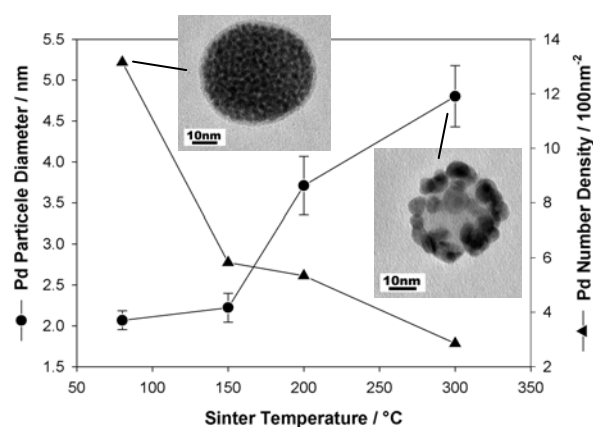


Figure 1. Resulted Pd particle size and Pd number density after online sintering of Pd/SiO<sub>2</sub> (t = 47s).

This project was funded by German Research Foundation (DFG) in SPP 1119.

- Binder, A., Heel, A., Kasper, G. (2007) *Chem. Vap. Deposition*, 13, 48–54.  
 Heel, A., Kasper, G. (2005). *Aerosol Sci. Technol.*, 39, 1027-1037.  
 Seipenbusch, M., Heel, A., Weber, A.P., Kasper, G. (2002). *Chem. Eng. Technol.*, 25, 77-82.  
 Wu, Q.-H., Gunia, M., Strunskus, T., Witte, G., Muhler, M., Wöll, C. (2005), *Chem. Vap. Deposition*, 11, 355-361.

## Ethylene flame : effects of pressure on soot properties

M. Maugendre<sup>1</sup>, A. Coppalle<sup>1</sup>, J. Yon<sup>1</sup>, K. P.Geigle<sup>2</sup> and R. Stirn<sup>2</sup>

<sup>1</sup>Coria UMR 6614, Avenue de l'Université, 76801 Saint-Etienne du Rouvray, France

<sup>2</sup>German Aerospace Center (DLR), Institute of Combustion Technology, Stuttgart, Germany

Keywords : combustion aerosol, refractive index, size distribution

This work inserts in the framework of the “Toward Lean Combustion” European project, whose aim is to decrease aircraft pollutant emissions. In order to improve quantitative characterization of soot particles using optical methods like Laser Induced Incandescence (LII) (Schoemacker, 2002), soot optical refractive index  $m = n - ik$  is required especially for infrared light. This optical property has been widely studied for gaseous flames in the visible range (Dalzell & Sarofim, 1969 ; Lee & Tien, 1981) but there is a lack of knowledge for infrared wavelengths and for under-pressure flames. Recently measurements of the optical index were conducted in IR on acetylene, PMMA, toluene (Ouf, 2006).

In order to gain a better understanding of pressure effects on soot properties, sampling has been conducted on ethylene flame in a high pressure burner. Measurements were made at 3 and 5 bars for different equivalent ratios. Several soot properties were analysed, such as morphology and light extinction and scattering at infrared wavelength ( $\lambda = 1.064 \mu\text{m}$ ). Total particle size distributions were measured with a Scanning Mobility Particle Sizer (SMPS).

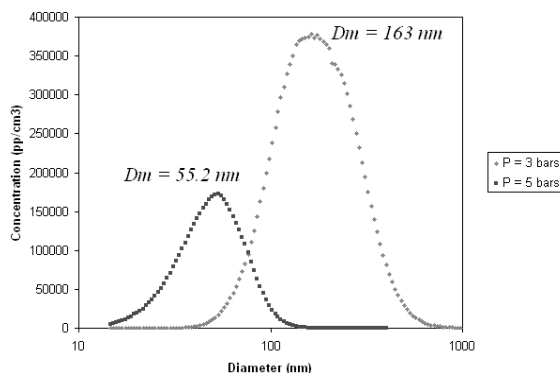


Figure 1. Size distributions for two pressure conditions

Size distributions were satisfactorily fitted by a log normal equation (Figure 1) ; modal diameters, total particle concentrations and geometric standard

deviation were compared in different flame conditions (Figure 2).

Images obtained from transmission electron microscopy were analysed to check an eventual dependency of the soot morphology (fractal dimension, primary particles diameter) on pressure conditions.

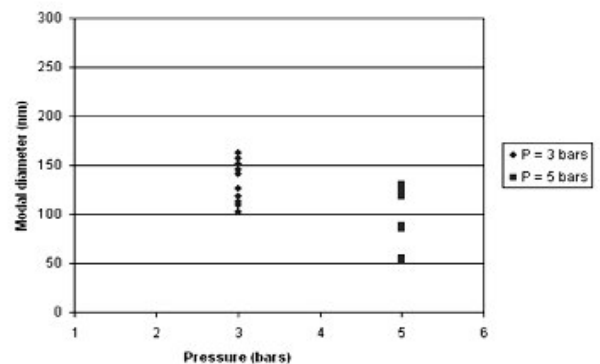


Figure 2. Modal diameter as a function of pressure

Finally, measurements of extinction and scattering properties parsed with Rayleigh scattering theory for fractal aggregates (RDG – FA) lead to the determination of the functions  $E(m)$  and  $F(m)$  of the refractive index. The refractive index is then deduced in IR for each pressure.

Schoemacker Moreau C. (2002). Thesis, University of Lille.

Dalzell W.H., Sarofim A.F. (1969). *Journal of Heat Transfer*, 91, 100-104.

Lee S.C., Tien C.L. (1981). *18<sup>th</sup> Symposium on Combustion*, 1159-1166.

Ouf FX. (2006). Thesis, University of Rouen.

## «Nanoinventory – results of a qualitative survey about nanoparticles in Swiss industries»

Kaspar Schmid<sup>1</sup>, Michael Riediker<sup>1</sup>

<sup>1</sup>Institute for occupational health sciences, University of Lausanne, rue du Bugnon 19, 1005, Lausanne, Switzerland

Keywords: indoor particles, nanoparticles applications, occupational exposures.

A large number of applications with manufactured nanoparticles <100nm are currently being introduced into industrial processes and consumer products<sup>1</sup>. Manufactured nanoparticles might cause similar negative health effects as micro- and nanosized ambient particulate matter (PM)<sup>2</sup>. There is an urgent need to evaluate the risks of these particles to ensure their safe production, handling, use, and disposal. However, we currently lack information about types and quantity of industrially used manufactured nanoparticles and the exposure to them in Switzerland.

The pilot study of the Swiss Nanoinventory was an evaluation of the knowledge of production and safety managers in most types of industries about nanoparticles and safety measures. A telephone survey was conducted among 200 Swiss companies to evaluate the nanoparticle applications with regard to types and quantities of nanoparticles, protective measures and numbers of potentially exposed workers.

The following nanoparticles were found to be used in considerable quantities (>1000kg/a per company): Ag, Al-Ox, Fe-Ox, SiO<sub>2</sub>, TiO<sub>2</sub> and ZnO, but the majority of nanoparticle applications were on a small production scale.

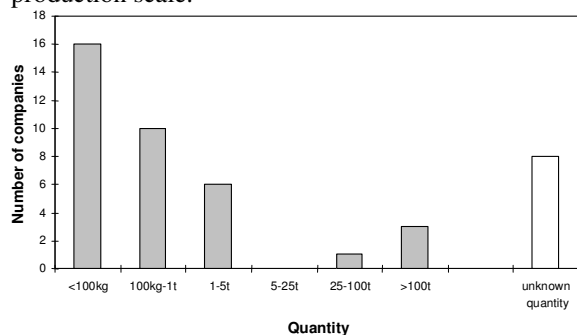
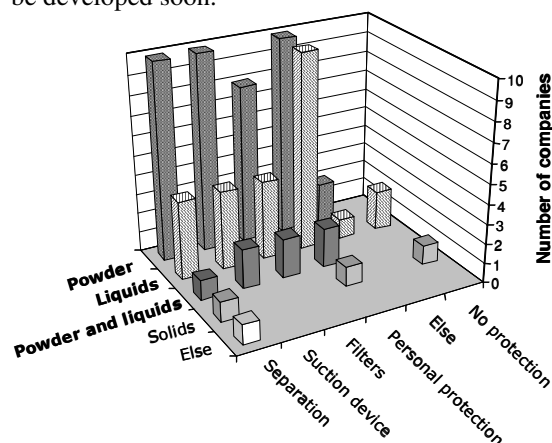


Chart 1: Number of companies in the different quantity classes of nanoparticles used per year (n=44). The applications were identified in the following fields: coating, cosmetics, food, paintings, powder-production, and surface-treatment. The survey showed that nanoparticles are used in many Swiss industrial sectors, outside typical nanotechnology industries.

Safety managers as well as top management put strong emphasis on safety measures. They used their own experience to develop a protection strategy.

However, they had many open questions about best practices. Guidelines and protection strategies should be developed soon.



Graph 1: Type of protection measures used for the different application types, (n=44)

The study showed that the use of nanoparticles is not fiction but already reality in the Swiss industry and it allowed an identification of industrial sectors with an established nanoparticle-use.

It gave us valuable information about the knowledge of safety managers concerning the handling of nanoparticles in their companies. It will form the basis for a detailed representative inventory, which eventually will be an important element for risk evaluation and prevention strategies regarding nanoparticles and health in Swiss industries.

Chaudhry M. Q.; Boxall A. B.; Aitken R.J.; Hull M. (2005). *A Scoping Study into the Manufacture and Use of Nanomaterials in the UK*. London, UK, Department for Environment Food and Rural Affairs.

Hoet P.H., Bruske-Hohlfeld I. and Salata O.V., *Nanoparticles - known and unknown health risks*. (2005) *J. Nanobiotechnology*, 2, 12

Acknowledgements: This work was supported by the Swiss Federal Offices for Health (OFSP), Environment (OFEV) and Economy (SECO), the Swiss National Accident Insurance (SUVA) and the French Agency for Environmental and Occupational Health Safety (AFFSET).

## Effects of $Ti^{4+}$ concentration on crystal phase of $TiO_2$ powders synthesized by low-temperature hydrothermal method

Ping-Szu Tsai<sup>1,2,\*</sup>, Cheng-Hsien Tsai<sup>1</sup>, Yu-Feng Lai<sup>1</sup> and Yu-Min Yang<sup>2</sup>

<sup>1</sup>Department of Chemical and Material Engineering, National Kaohsiung University of Applied Sciences, Kaohsiung 807, Taiwan.

<sup>2</sup>Department of Chemical Engineering, National Cheng Kung University, Tainan 701, Taiwan.

Keywords: air pollution, generation of nanoparticles, indoor aerosols, sintering, photocatalyst.

Crystalline  $TiO_2$  powders with an anatase phase have been commonly used as a photocatalyst for photodecomposition of harmful air pollutants and aerosols, sterilization of bioaerosols, and solar energy conversion, and gas sensor because of its high photoactivity [Larson & Falconer, 1994]. Generally,  $TiO_2$  powders are fabricated by chloride process, such as hydrothermal method, while a higher temperature or pressure with a sequent sintering process is usually needed. Hence, a low temperature (below boiling point of water) without sintering stage by adding solvent and inorganic acid has been demonstrated in this study.

Crystalline  $TiO_2$  fabrication procedure was as follows.  $TiCl_4$  of 0 °C was slowly added into a container with distill water ice pieces and stirred to precede hydrolysis reaction. Lots of heat and hydrogen chloride were released during the reaction, as well as yellow cakes of  $TiO(OH)_2$  were formed by accompanying with the slow melting of ice pieces. Subsequently, the transparent  $TiOCl_2$  solution was formed via the overall reaction of  $TiCl_2 + H_2O \rightarrow TiOCl_2 + 2HCl$ .

Then, amorphous  $TiO_2$  precipitation was formed by adding NaOH into the  $TiOCl_2$  solution at pH = 7 following to wash with distill water by three times, and drying by oven. For fabricating anatase phase, amorphous  $TiO_2$  with 30 ml 3 M of  $HNO_3$  and 50 ml  $C_3H_7OH$  were mixed, then the solution was at 90 °C to precede crystallization after different reaction time (6-48 hr). The crystal structures of  $TiO_2$  were determined by XRD spectroscopy with  $CuK_{\alpha}$  radiation that scanned from 20 to 80° (2 $\theta$ ).

Fig. 1 showed that the characteristic peak (at  $2\theta = 25.3^\circ$ ) intensity of anatase  $TiO_2$  increased with increased reaction time regardless of  $[Ti^{4+}]$ . Moreover, the higher peak intensity could be achieved at a lower  $[Ti^{4+}]$  with a shorter reaction time. At  $[Ti^{4+}] = 0.16$  M, the higher peak intensity has been found at reaction time = 6 hr, to much higher than  $[Ti^{4+}] = 0.33$  M or 0.49 M, even 12 hr was passed to reach a higher and stable peak intensity at a higher  $[Ti^{4+}]$ .

In addition, the anatase  $TiO_2$  powders synthesized at  $[Ti^{4+}] = 0.16$  M were analyzed via the  $N_2$  adsorption-desorption method to determine the BET specific areas ( $S_{BET}$ ) at 77 K. Table 1 showed

that the effects of reaction time on the FWHM (full width at half maximum) of characteristic peak (average = 2.179) and the crystalline size (mean = 3.92 nm) were not obvious, while had an apparent influence on the  $S_{BET}$ . The results showed that when a longer reaction time (> 12 hr) with a greater  $S_{BET}$  (average = 173.0  $m^2/g$ ) was achieved, such as the  $S_{BET}$  equaled 203.0  $m^2/g$  at 12 hr. The higher  $S_{BET}$  can provide more surface areas to apply on the photocatalytic reaction to remove the air pollutants and indoor aerosols.

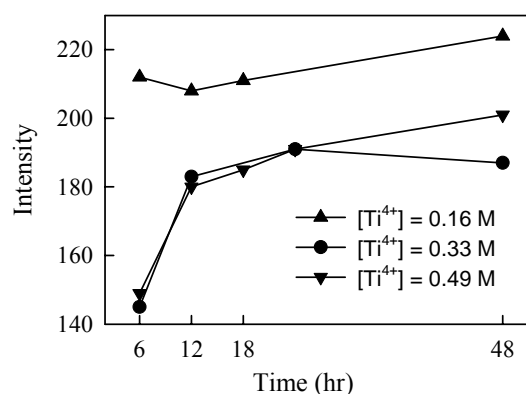


Figure 1. The intensity of characteristic peak for various reaction time and  $[Ti^{4+}]$ .

Table 1. Analyses of  $TiO_2$  powders for various reaction time (90 °C, PH = 7).

Time (hr)	FWHM (at 25.3°)	Crystalline size (nm)	$S_{BET}$ ( $m^2/g$ )
6	2.150	3.94	114.3
12	2.312	3.73	203.0
18	2.147	3.98	194.2
48	2.106	4.02	180.4
Average	2.179	3.92	173.0

In sum, the addition of organic solvent and nitric acid with a lower  $[Ti^{4+}]$  can synthesize anatase  $TiO_2$  powders at a lower temperature with a short reaction time. Moreover, the powders that have enough intensity of characteristic peak do not need further sintering process. This easy process precedes the promotion of pollution control and aerosol removal techniques.

Larson, S. A., Falconer, J. L. (1994). *Appl. Catal. B*:

Cite abstract as Author(s) (2007), Title, European Aerosol Conference 2007, Salzburg, Abstract T09A034

*Env.*, 4, 325-342.

## Formation of Silicon Particles Using Silane Pyrolysis

D.K. Woo<sup>1</sup>, K.T. Nam<sup>2</sup>, Y.G. Kim<sup>2</sup>, K.S. Kim<sup>1</sup>, Y.H. Kang<sup>3</sup> and T. Kim<sup>1,2</sup>

<sup>1</sup>School of nanoscience and nanotechnology (SAINT)

<sup>2</sup>School of Mechanical Engineering

Sungkyunkwan University, Cheoncheon-dong, 440-746, Suwon, Korea

<sup>3</sup>Samsung Advanced Institute of Technology, Nongseo-dong, 446-712, Yongin, Korea

Keywords: Pyrolysis, Particle formation, SMPS, Size distribution

The particle formation using pyrolysis has many advantages over other particle manufacturing techniques. The particles produced by this method have relatively uniform size and chemical composition. Also, we can easily produce high-purity particles using pyrolysis. Ostraat et al (2001) reported nano floating gate memory device using nanoparticles which were produced using pyrolysis.

Figure 1 shows a schematic of pyrolysis system. There are two furnaces (pyrolysis furnace & oxidation furnace) which have 3 heaters respectively, Scanning Mobility Particle Sizer (SMPS) for particle size distribution measurement and particle deposition system for particle collection. 50 % silane in argon (0.1 SCCM) and N<sub>2</sub> (500 SCCM) flow into the pyrolysis furnace (heater temperature: 800, 800 and 800 °C) simultaneously. Then, O<sub>2</sub> (1000 SCCM) is added in the oxidation furnace (heater temperature: 750, 700 and 650 °C). The operation pressure is atmospheric. The aerosol flow from furnaces is separated into two ways. One is to the SMPS (TSI 3080 model) for particle size distribution measurement. The other is to the particle deposition system. The produced Si nanoparticles are directly deposited on the wafer in deposition chamber.

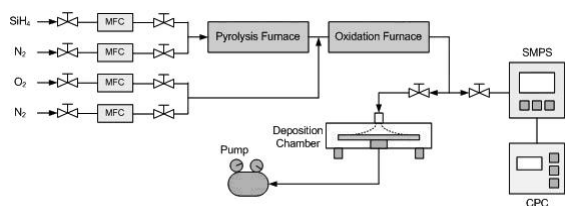


Figure 1. The schematic of pyrolysis system.

In the pyrolysis furnace, silicon nanoparticles have been generated by pyrolysis of silane and in the oxidation furnace, surface of Si nanoparticles obtains oxide coating layer to suppress further growth. The particle size distribution measured by SMPS is shown in Figure 2. The mean diameter is 63.93 nm with geometric standard deviation of  $\pm 1.45$  nm and the total concentration is  $2.69 \times 10^6$  #/cm<sup>3</sup>. Figure 3 shows the SEM image of Si nanoparticles which were deposited on the wafer. The spherical Si particles are between 40 and 100 nm, which is in good agreement with SMPS measurement result. We

also confirmed that the surface of Si particles has oxide layer by using EDS analysis.

In this paper, a pyrolysis system was used to synthesize spherical particles which were generated by thermal decomposition of SiH<sub>4</sub> gas. Si particles produced in this study will be useful for improved flash memory devices and 2<sup>nd</sup> generation battery electrode.

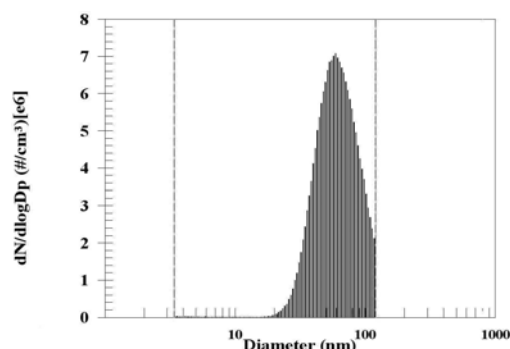


Figure 2. The size distribution of particles.

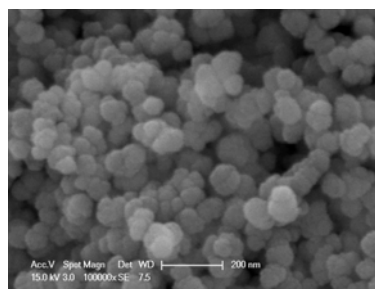


Figure 3. SEM image of Si nanoparticles.

This work was supported by the Samsung Advanced Institute of Technology.

Ostraat, M. L., & De Blauwe, J. W. et al. (2001). *Journal of Electrochemical Society*, 148, G265-G270.

Colbeck, I., & Kamlag, Y. (1996). *J. Aerosol Science*, 27, S395-S396.

Wiggers, H., Starke, R., & Roth, P. (2001). *Chem. Eng. Technol*, 24, 261-264.

## Control of the structure of deposits collected from aerosol particles

D. Rodríguez-Perez, J. Castillo and J.C. Antoranz

Dept. de Física Matemática y de Fluidos, Facultad de Ciencias, UNED, Senda del Rey 9, Madrid 28040, Spain

Keywords: particle deposition, deposition, deposit morphology, Monte Carlo simulations, aerosol dynamics.

Aerosol particles can be driven towards neighboring walls by different transport mechanisms leading to the formation of structured particle deposits on the surfaces exposed to particle-laden gas streams. In areas such as material synthesis from nanoparticles or surface fouling by particles in combustion processes, there is a need of controlling the structure of such deposits collected by aerosol particles. For collecting particles which attach to the deposit at the first reached active location (that is, in the absence of surface diffusion and of any type of deposit sintering or restructuring after the particle arrival) the deposit grows as the particle arrive without the influence of any further physicochemical process. Under these circumstances, the deposit morphology would only depend on the particle dynamical behaviour near the surface.

In this work, we simulate the evolution of deposits formed by different particle arrival mechanisms to obtain the bulk deposit properties (density) and surface features (roughness) as a function of the particle dynamics. Monte Carlo simulations for the particle motion using a discretized on-lattice space were performed (Rodríguez-Perez *et al.*, 2005, 2007).

The particle motion can be split in two contributions: a mean drift velocity  $V$  (due to sedimentation or any phoretic particle motion as electrophoresis, photophoresis, or thermophoresis, García-Ybarra & Castillo, 1997) and a Brownian random motion with a diffusion coefficient  $D$ . Thus, the particle dynamics becomes characterized by a single parameter, the Peclet number

$$Pe = \frac{V a}{D}$$

where  $a$  is the characteristic length (the side of the lattice cell which is chosen equal to the particle diameter). Particles are assumed monodisperse, the  $Pe$  number remains fixed along each Monte Carlo deposit growth simulation, and the results are averaged over ten deposit samples.

Figure 1 depicts the deposit density (number of deposited particles at a given height divided by the number of lattice sites at this height) for different values of  $Pe$ . In all the cases, the lattice is  $400 \times 400$  cells<sup>2</sup> on the horizontal directions and the simulations stop when the maximum deposit height is 200 cells. The points represent the Monte Carlo results and the lines account for correlation laws based on scaling arguments (Rodríguez-Perez *et al.*, 2005, 2007).

The density profiles of the deposits formed by particles arriving to an initially flat wall become structured in three regions. A near-wall region (where the density is relatively high and decreases with height) affected by the compact flat surface. The uniform region corresponds to the consolidated part of the deposit free from external influences, here the mean density is uniform and depends only on  $Pe$ . Finally, the outermost deposit region is the active region where new particles may still arrive, here the density decreases vanishing at the top of the deposit. Higher Peclet numbers (corresponding to particles with low diffusion and following almost ballistic trajectories) lead to denser deposits with thinner active regions, whereas in the low Peclet number limit (very diffusive particles) sparser tree-like branched deposits are formed.

The lines in figure 1 are correlation laws (Rodríguez-Perez *et al.*, 2005, 2007) set in terms of the known behaviour in the two extreme cases: pure ballistic deposition and diffusion-limited deposition.

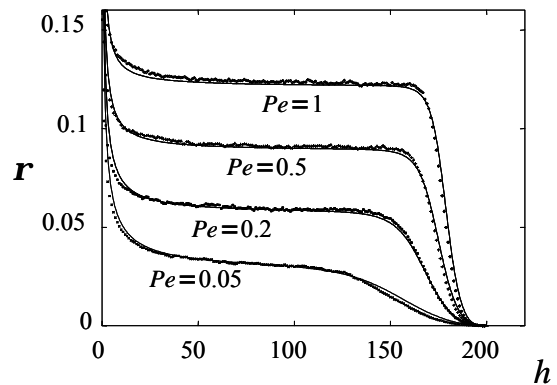


Figure 1. Deposit density profiles for different values of the particle Peclet number,  $Pe$ .

This work was supported by the Ministerio de Educación y Ciencia, Spain, under grants DPI2005-04601 and ENE2005-09190-C04-02, and also by Comunidad de Madrid under grant S-505/ENE/0229.

Rodríguez-Perez, D., Castillo, J. & Antoranz, J. C. (2005) *Phys. Rev. E*, 72, 021403.  
 Rodríguez-Perez, D., Castillo, J. & Antoranz, J. C. (2007) *Phys. Rev. Letters*, submitted.  
 García-Ybarra, P. & Castillo, J. (1997) *J. Fluid Mech.*, 336, 379-409.

## Synthesis of Ag-SnO<sub>x</sub> core-shell nanoparticles for gas sensor applications

I. Aruna and F.E. Kruis

Institute for Nano Structures and Technology, Faculty of Engineering, University of Duisburg-Essen,  
Bismarckstr. 81, 47057, Duisburg, Germany

Keywords: Tin oxide, silver, core-shell nanoparticle, heterogeneous nucleation, gas sensor.

SnO<sub>x</sub> nanoparticle gas sensors have become the archetypal semiconductor oxide based gas sensors since Ogawa et al. (1981) observed the advantages of exploiting the modified properties of tin oxide at nanodimensions. Enhancement in the sensitivity and selectivity by using metal additives has also been widely explored (Yamazoe, 1991). Recently SnO<sub>x</sub>/Ag composite nanoparticle layers, deposited from homogeneously mixed separately synthesized monodispersed SnO<sub>x</sub> and Ag nanoparticle aerosols of well defined shape and size, were observed to exhibit significantly improved sensor characteristics.

The present study is an attempt to synthesize Ag-SnO<sub>x</sub> core-shell nanoparticles utilizing gas phase synthesis for gas sensor applications. The schematic diagram of the set up is shown in Figure 1.

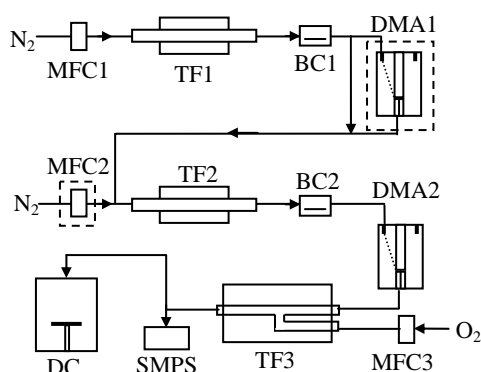


Figure 1. Schematic diagram of the synthesis setup for Ag-SnO<sub>x</sub> core-shell nanoparticles. The details of various components are discussed in the text.

It contains mass flow controllers (MFC), tube furnaces (TF), bipolar chargers (BC), differential mobility analysers (DMA), scanning mobility particle sizer (SMPS) and the deposition chamber (DC). Ag nanoparticles are synthesized by evaporating Ag in TF1 in the presence of a carrier gas, followed by cooling leading to nucleation and coagulation. Radioactive  $\beta$  source (Kr<sup>85</sup>) acts as bipolar charger, DMA is used for size classification and SMPS for particle size and concentration measurement. The as-synthesized Ag nanoparticle aerosol is fed to the SnO furnace (TF2) to act as the nuclei for the heterogeneous nucleation of SnO. These can then be size selected and fed to another tube furnace (TF3) for sintering and crystallization of Ag-SnO core-shell nanoparticles. The total gas flow is kept 1.0 l/min by means for MFC's and the system

is operated at atmospheric pressure. In TF3, a flow of O<sub>2</sub> is added to oxidize the Ag-SnO core-shell nanoparticles to Ag-SnO<sub>x</sub> nanoparticles ( $x > 1$ ).

Figure 2 shows the effect of the SnO furnace (TF2) temperature on the size distribution of Ag-SnO<sub>x</sub> core-shell nanoparticles.

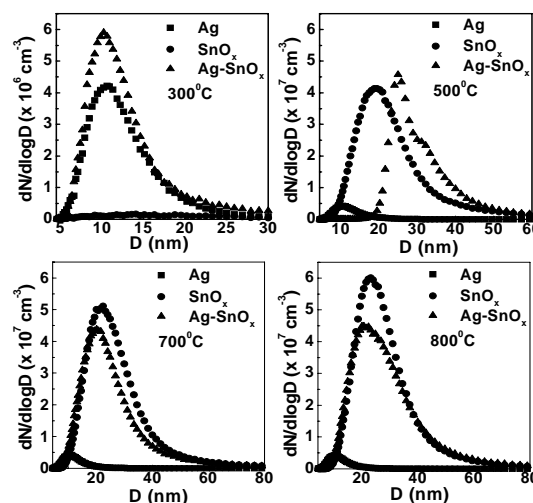


Figure 2. Size distribution of the polydispersed Ag nanoparticle aerosol which is fed into TF2 and SnO<sub>x</sub> nanoparticles with embedded Ag formed at different temperatures of TF2. For comparison the concentration profile of the SnO<sub>x</sub> nanoparticles that would have been synthesized at the particular furnace temperature are also given.

Clearly, a very small concentration of the initial Ag nuclei allows the modification in the size distribution of SnO<sub>x</sub> nanoparticles. It is interesting to note that at a particular TF2 temperature the competing processes of heterogeneous and homogeneous nucleation of SnO are evident. To synthesize core-shell particles the conditions for dominance of heterogeneous nucleation are optimised and the sensing properties studied.

This work is supported by Deutsche Forschungsgemeinschaft (DFG) in the framework of the special research program "Nanoparticles from the gas phase: formation, structure, properties" (SFB445).

Ogawa, H., Abe, A., Nishikawa M. & Hayakawa S. (1981), *J. Electrochem. Soc.* 128, 685-689.

Yamazoe, N. (1991), *Sensors and Actuators B*, 5, 7-18.

## Preparation and Characteristic of Pt and Pt-Ru Nanoparticles for Utilized Proton Exchange Membrane Regenerative Fuel Cell

Yu-Chun Chiang<sup>1</sup>, Chien-Chih Lin<sup>1</sup> and Chien-Cheng Lee<sup>2</sup>

<sup>1</sup> Department of Mechanical Engineering Yuan e Fuel Cell Center, Yuan e University. 135 Yuan-Tung Rd., Chung- i, Taoyuan 320, Taiwan, ROC.

<sup>2</sup> Department of Communications Engineering, Yuan e University. 135 Yuan-Tung Rd., Chung- i, Taoyuan 320, Taiwan, ROC.

Keywords: nanoparticles, generation, characterization.

Unitized regenerative fuel cell (URFC) system combines fuel cell and water electrolyzer with advantages of lower cost, weight, and volume (Ioroi et al., 2000). The possible applications of URFCs can be for space and military uses, on-site energy storage systems or renewable energy. Up to date, the key technical problem for developing the URFC is optimization of the structure and composition of oxygen electrode for water electrolysis and fuel cell operations. The carbon-supported platinum nanoparticles (Pt/C) have been widely used in fuel cell electrodes. However, due to the corrosion of carbon materials by oxygen evolved during water electrolysis, the Pt/C electrocatalyst is not suitable for the oxygen electrode of URFC. Besides, the alloys of Pt and oxophilic metals, giving rise to a bi-functional mechanism, are known to be superior to Pt-only catalysts. Therefore, in this study, Pt and Pt-Ru nanoparticles were prepared and characterized.

Referring to Deivara and Lee (2005) and according to the preliminary results, the impregnation method (Kim and Mitani, 2006) could give a more homogeneous particle distribution. Therefore, 0.52 M of 50 mM of H<sub>2</sub>PtCl<sub>6</sub>·6H<sub>2</sub>O (Alfa Aesar) was diluted with 10 M deionized water. Next, 40 mg of NaBH<sub>4</sub> (Fluka) was dissolved in 25 M deionized water, and then this solution was introduced into the above solution. Stirring was lasted for 2 h to make the solids deposited. Then the solution was centrifuged and the recovered solids were washed with ethanol. Finally the Pt solids were vacuum dried. For the preparation of Pt-Ru particles, follow the above procedures, but 5.3 mg RuCl<sub>3</sub> (Fluka) was dissolved in 10 M deionized water before adding the H<sub>2</sub>PtCl<sub>6</sub>·6H<sub>2</sub>O. The effects of pH, the atmosphere, and the heat treatment were discussed. The properties of the products were probed by ICP-AES, TGA, HRTEM, XRD and XPS.

Table 1 shows the yield, purity and recovery of all Pt samples, where almost had a purity over 94%. A higher pH seemed to improve the purity, but the effects of the atmosphere and heat treatment were insignificant. The TGA data also reflected the high purity of the nanoparticles. From HRTEM images, the particle size of Pt and Pt-Ru samples were uniformly distributed, ranging from 10 to 20 nm. The XRD patterns for Pt and Pt-Ru samples (e.g., Figure 1) all showed three characteristic f.c.c. Pt peaks,

indexed as Pt (1 1 1), Pt (2 0 0), and Pt (2 2 0). There were no peaks assigned to h.c.p. Ru or its oxides, which was consistent with the result reported by Deivara and Lee (2005). XPS data indicated that C and O still remained on the surface of nanoparticles. Heat treatment tended to decrease C1s without the removal of O1s. The addition of NaOH to increase pH enhanced the O 1s. H<sub>2</sub> atmosphere eliminated the impurities and eased the noises in the XPS spectra.

Table 1. Yield, purity and recovery of Pt nanoparticles.

Sample	Yield (wt. %)	Purity (wt. %)	Recovery (%)
Pt-H10	74.0	94.1	69.6
Pt-A10	79.0	96.9	76.5
Pt-H13	88.9	99.9	88.8
Pt-A13	118.5	97.5	115.5
Pt-H10T	69.1	95.4	65.9
Pt-A10T	118.5	84.4	100
Pt-H13T	49.4	95.3	47.07
Pt-A13T	44.5	96.0	42.7

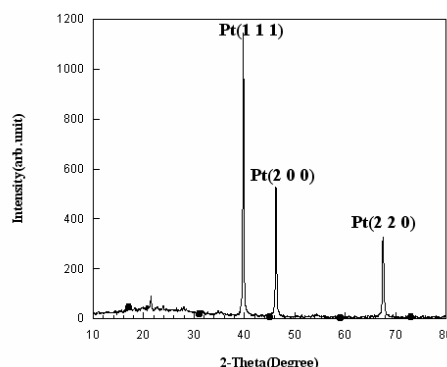


Figure 1. XRD pattern of Pt-Ru-H10T nanoparticles (synthesized under H<sub>2</sub> atmosphere, pH = 10, and heat-treated at 400 °C for 90 min under N<sub>2</sub>)

This work was supported by Ministry of Education, Taiwan, ROC. and Yuan e Fuel Cell Center.

Deivara, T. C. and Lee, J. Y. (2005) *Journal of Power Sources*, 142, 43-49.

Ioroi, T., Kitazawa, N., Yasuda, K., Yamamoto, Y. and Takenaka, H. (2000) *Journal of Electrochemical Society*, 147(6), 2018-2022.

Kim, Y. T. and Mitani, T. (2006) *Journal of Catalysis*, 238(2), 394-401.

## Nanoparticle synthesis by gas-dynamically induced heating and quenching

M. Dannehl<sup>1</sup>, A. Maisels<sup>1</sup>, W. Eibold<sup>2</sup>, H. Olivier<sup>3</sup>, A. Grzona<sup>3</sup>, A. Weis<sup>3</sup>, A. G. Ihan<sup>4</sup>, T. Gawehn<sup>4</sup>, G.H. Schneringer<sup>5</sup>, N. Al-Hasan<sup>5</sup>, A. Abdali<sup>6</sup>, M.Y. Luong<sup>6</sup>, H. Wiggers<sup>6</sup>, C. Schulz<sup>6</sup>, B. Weigand<sup>7</sup>, J. Chun<sup>7</sup>, W. Schröder<sup>8</sup>, M. Meinke<sup>8</sup>, T. Winnemöller<sup>8</sup>, H. Nirschl<sup>9</sup>, V. Goertz<sup>9</sup>, K. Schaber<sup>10</sup>, T. Rakek<sup>10</sup>

<sup>1</sup>Process Technology & Engineering, Particle Processing, Degussa, 63457 Hanau-Wolfgang, Germany

<sup>2</sup>IPW, 63457 Hanau-Wolfgang, Germany

<sup>3</sup>Shock Wave Laboratory, RWTH Aachen, 52056 Aachen, Germany

<sup>4</sup>German Aerospace Center, Wind Tunnel Section, 51147 Cologne, Germany

<sup>5</sup>Lehrstuhl für Fluidmechanik, Fachgebiet Gasdynamik, TU Munich, 85748 Garching, Germany

<sup>6</sup>IVG, University Duisburg-Essen, Campus Duisburg, 47057 Duisburg, Germany

<sup>7</sup>Institute of Aerospace Thermodynamics, University of Stuttgart, 70569 Stuttgart, Germany

<sup>8</sup>Institute of Aerodynamics, RWTH Aachen, 52056 Aachen, Germany

<sup>9</sup>Mechanical Engineering and Mechanics, University of Karlsruhe, 76128 Karlsruhe, Germany

<sup>10</sup>ITTK, University of Karlsruhe, 76131 Karlsruhe, Germany

Keywords: Aggregates high-temperature aerosol material synthesis nanoparticles, generation supersonic flow.

Different procedures for gas-phase nanoparticle synthesis can be found in scientific literature, measurement technology, and industry (Pratsinis, 1998; Granqvist et al., 2004; Buxbaum & Pfaff, 2005). While considering synthesis procedures of comparably high mass throughput (flame reactors, hot-wall reactors, laser ablaters), it can be found, that the morphology of the synthesized nanoparticles nearly does not vary significantly: most of them are aggregates with fractal dimension of 1.8 – 1.9, while the geometric standard deviation of the aggregate size distribution is in the range of 1.5 – 1.7.

Numerous studies have been carried out to investigate the origin of nanoparticle morphology in gas-phase nanoparticle reactors (Skillas et al., 2005). Most of them point on the influence of the homogeneity of the flow field and temperature profile on the width of the particle size distribution. Previous work also indicates the importance of rapid heating and quenching for achieving narrow size distributions and low aggregation. Though flow conditions in gas-phase particle reactors can be optimized, usual gas-phase particle reactors have limitations with respect to heating and, especially, to quenching rates.

The current work proposes a nanoparticle synthesis reactor based on unconventional for particle synthesis heating and quenching mechanisms and optimized flow conditions, namely a gas-dynamic reactor with two supersonic nozzles (Fig. 1).

The gaseous nanoparticle precursor is injected in the converging part of the first nozzle (cross-section  $A_1^*$ ) in a high-enthalpy gas flow (inlet conditions:  $p_{01}$  10 bar,  $T_{01}$  1400 K). As shown by 3-D Navier-Stokes simulations, the acceleration of the gas flow in the converging and partly in the diverging part of the first nozzle cools the flow down to 900 K before the first shock arises, as shown by temperature profile in Fig. 1. In the first shock, gas flow heats up to 1211 K within 70  $\mu$ s. Such quasi-instantaneous heating leads to precursor decay with additional subsequent heating through reaction heat and to particle formation at slightly non-adiabatic conditions

through wall cooling. The expansion in the second supersonic nozzle (cross-section  $A_2^*$ ) rapidly cools the flow down to 617 K within 80  $\mu$ s. Water injection (not considered in simulations) in the diverging part of the second nozzle determines the final flow temperature of 473 K at a pressure of 1.3 bar.

Since gasdynamic heating and quenching occur much more rapidly than conventional heating and cooling strategies in usual particle synthesis reactors, narrower particle size distributions and lower aggregation grades are expected.

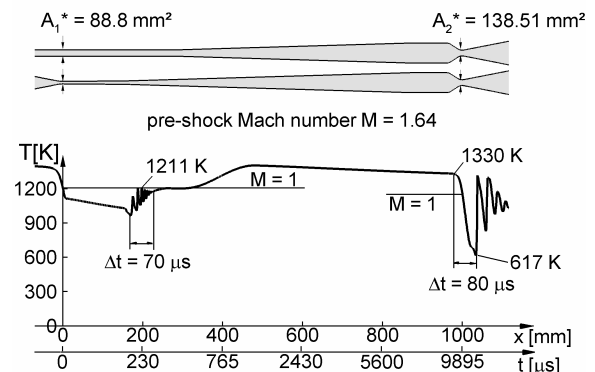


Figure 1. Reactor geometry and simulated temperature profile

This work is supported by Deutsche Forschungsgemeinschaft (DFG) as PAK 75/1.

Buxbaum, G. & Pfaff, G. (2005). *In* *In* *n* *n*. WI EY-VCH Verlag GmbH & Co KGaA, Weinheim.

Granqvist, C. Kish, . Marlow, W. (2004) *n* *n*, Springer.

Pratsinis, S.E. (1998), *Flame Aerosol Synthesis of Ceramic Powders*. *n* . 197-219.

Skillas, G., Becker, C., M hlenweg, H., Benesch, J., (2005) *Simulation of Particulates in a Carbon Black Reactor*. *n* ., 15-27.

## Thermal Tweezers for Effective Manipulation of Nano-Particles on Surfaces

D. R. Mason, D. K. Gramotnev, G. Gramotnev

Applied Optics Program, School of Physical and Chemical Sciences,  
Queensland University of Technology, GPO Box 2434, Brisbane, QLD 4001, Australia

Keywords: Nanoparticles, Surface diffusion, Thermophoresis, Nanoparticle applications, Material synthesis.

Optical tweezers are the well-developed tool for manipulation and trapping of microscopic particles. The principles of this manipulation and trapping are based on optically induced forces on a particle, which may result in transfer of significant translational momentum to the particle, or prevent its random drift due to Brownian motion. However, it is known that optical trapping of small nanoparticles may be difficult, because of rapidly decreasing optical and increasing Brownian forces exerted on the particle with decreasing its diameter and mass. Therefore, effective optical trapping may usually be achieved only for particles that are larger than  $\sim 100$  nm. At the same time, the development of modern nano-technology requires effective tools for manipulation of much smaller particles (e.g., of  $\sim 10$  nm or smaller). In addition, for the same purpose, it is important to be capable of manipulating nanoparticles on surfaces and interfaces, rather than in a liquid suspension.

Therefore, in this paper we develop and investigate theoretically a new approach to manipulation and trapping of nanoparticles, using optically induced strong temperature gradients on surfaces and interfaces (thermophoresis on a surface) [1]. Surface temperature modulation is achieved by means of the holographic approach with two or more interfering short laser pulses. The pulse duration is in pico- and nano-second range, which enables substantial temperature gradients on the surface (with hundreds of degrees of temperature difference between hot and cold regions).

Diffusion of nanoparticles is analyzed numerically and statistically by means of the Langevin equation and random walk approach with effective friction experienced by the moving particle, periodic potential of interaction between the particle and the crystal lattice of the substrate, and random Brownian force represented by white noise. An alternative approach is based on the direct (less numerically intensive) solution of the Fokker-Plank equation in the presence of periodic potential of interaction with the substrate.

Strong re-distribution (with the concentration ratio of up to  $\sim 100$ ) of nanoparticles on a surface is predicted with the predominant diffusion occurring from hot to cold regions. As a result a new technique called thermal tweezers for surface manipulation of nano-particles has been described. The major new features of thermal tweezers include:

- The trapping efficiency of thermal tweezers rapidly increases with decreasing size of the particles (contrary to optical tweezers).
- Surface features with dimensions as small as  $\sim 10 - 50$  nm are demonstrated to be achievable using laser radiation in the visible range of frequencies.
- Typical concentration modulations for particles on a surface are shown to be  $\sim 2$  orders of magnitude higher than those in a bulk medium (e.g., liquid or air). This is due to additional periodic potential of interaction between the particles and the crystalline substrate.
- Feasibility of new all-optical technological processes with simultaneous laser ablation, deposition of nano-particles from an aerosol, and their controlled re-arrangement of the surface into required nano-structures with precisely engineered electronic and optical properties.

The probabilities of finding a particle in the cold and hot regions in the steady-state regime of diffusion are shown to strongly depend on temperature gradients, energy and duration of the laser pulses, interaction between the particles and surface, coefficient of effective friction, and background temperature. It is also demonstrated that a special super-resolution technique may be used to achieve surface structures with the typical period that is at least three times smaller than the period of surface temperature modulation, which leads to truly nano-scale resolution of thermal tweezers [1]. Optimization of structural parameters, determination of statistical errors and interpretation of the obtained results are also presented. Typical average translational momentum that can be transferred to a particle is calculated. Applicability conditions for the developed approaches are determined and discussed. In particular, it has been suggested that the obtained efficiencies of particle re-distribution of the surface are rather underestimates of the expected concentration modulations, because interaction between the particles (coagulation and cluster formation on the surface) should result in further significant increase of the re-distribution and trapping efficiency.

D. K. Gramotnev, D. R. Mason, G. Gramotnev, A. J. Rasmussen (2007), *Appl. Phys. Lett.* vol.90, 054108.

## Investigation of the charge distribution in a FePt nanoaerosol formed by pulsed laser ablation

M. Rouenhoff, A. Nedic, F.E. Kruis

Institute for Nanostructures and Technology, University of Duisburg-Essen, Bismarck 81, 47057, Duisburg, Germany

Keywords: DMA, SMPS, electrical effects, electrostatic precipitator, laser ablation

In this paper, we present experimental results about the electrical charge distribution generated by a Nd: YAG laser, which ablated a Fe<sub>53</sub>Pt<sub>47</sub> rod as target with the second (532 nm) or fourth harmonic (266 nm) pulsed with a duration of 10 ns. The FePt nanoparticles were carried away from the ablation cell with nitrogen as carrier gas and later on fractionated by using a differential mobility analyzer (DMA). We have followed the method of measuring the charge distribution of nanosized aerosols as reported by Kim *et al.* (2005), in which a TDMA measurement leads to the charge fraction of nanosized aerosol particles as a function of equivalent mobility particle diameter.

Apart from the wavelength of the laser beam, the laser power and the velocity of the carrier gas were varied as well. The stoichiometry of the generated FePt nanoparticles was checked with EDX and found out to be the same as the target material.

In all charge measurements the nanoparticles were not heat treated after passing away from the ablation cell and thus thermal charging did not affect the electrical charge of the nanoparticles.

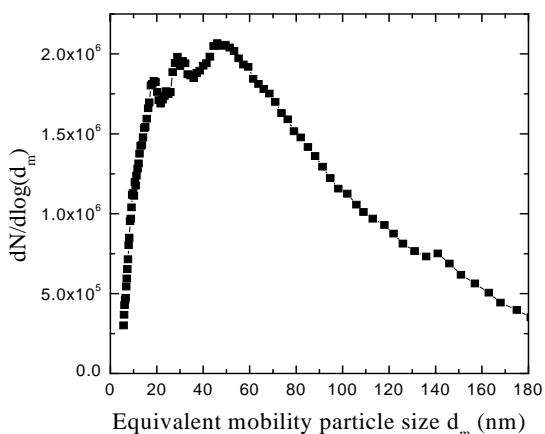


Figure 1. Number size distribution of FePt nanoaerosol for equivalent mobility particle sizes measured with the SMPS at a laser power of 185 mW.

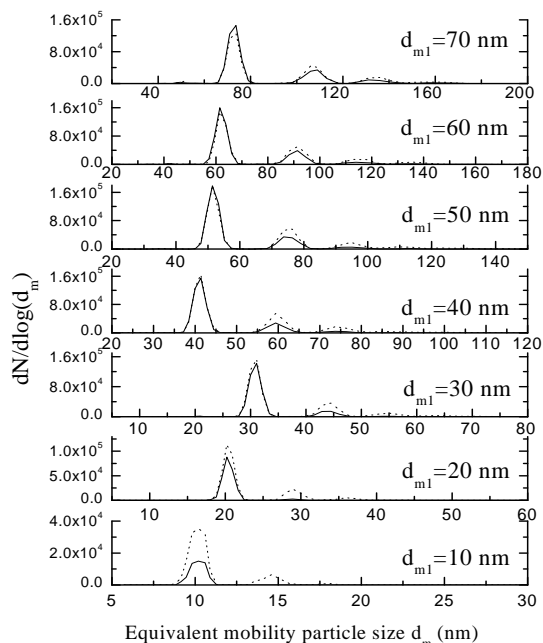


Figure 2. Spectra of negatively (solid lines) and positively (dotted lines) charged particle size distributions at a laser power of 185 mW and preselected equivalent mobility particle sizes  $d_{m1}$

The total charging efficiency of laser ablation was found out by relating the number concentration of charged nanoparticles to the total number concentration by means of an ultrafine condensation particle counter (UCPC) and an electrostatic precipitator (ESP) that filtered out the charged nanoparticles.

This work is financially supported by the Deutsche Forschungsgemeinschaft (DFG) in the framework of the special research program “Nanoparticles from the gas phase: formation, structure, properties” (SFB 445).

Kim, S. H., Woo, K. S., Liu, B. Y. H., & Zachariah, M. R. (2005). *J. Colloid Interface Sci.*, 282, 46-57.

## The TSI N95-Companion™ – a convenient alternative in everyday nanoparticle classification?

M.N.A. Karlsson<sup>1</sup>, Zs. Geretovszky<sup>2</sup> and K. Deppert<sup>1,\*</sup>

<sup>1</sup>Solid State Physics, Lund University, Box 118, S-221 00 LUND, Sweden

<sup>2</sup>Department of Optics and Quantum Electronics, University of Szeged, Dóm tér 9, H-6720, SZEGED, Hungary

\*Corresponding author: knut.deppert@ftf.lth.se

Keywords: nanoparticles, DMA, size classification

Nanometre-sized particles (1–100 nm) are receiving growing attention in wide areas of aerosol research due to their unique properties and possible applications. This growing interest drives the need for convenient and operator friendly size classifications of aerosol nanoparticles. Size classification by differential mobility analyzers (DMAs) is a well-known and widespread method. The method utilizes an electrical field for size selection of charged aerosol particles. There are different types of DMA geometries, e.g., cylindrical or radial. Here, we investigate the performance of a radial-type DMA hidden in the TSI N95-Companion™ (Model 8095), hereby referred to as the Companion DMA. This DMA is compact in size, which could be useful in certain applications.

We compared the characteristics of a Vienna-type cylindrical DMA, hereby referred to as the Vienna DMA, and the Companion DMA using a standard tandem DMA setup. The investigated DMAs were connected in parallel in the first DMA position downstream of an evaporation/condensation Au nanoparticle generator. The experimental setup made it possible to easily change the route of the aerosol flow, via the DMAs to be compared, between consecutive measurements. The carrier gas was nitrogen, at 0.7 l/min. The Companion DMA was run by its internal closed loop pump and the Vienna DMA by a separate vacuum pump. The sheath flow of the Vienna DMA was 10 l/min. In order to select particles with a diameter of 40 nm the voltage of the Companion DMA was 1.0 kV, as recommended by TSI. The Vienna DMA was therefore also set to select 40 nm particles. Another Vienna DMA was placed in the second position of the tandem DMA setup downstream of the investigated first DMA. Finally, a home-built electrometer was used to measure the particle number concentration of the aerosol leaving the second DMA. By increasing the voltage of the second DMA stepwise and simultaneously measuring the concentration, the size distribution of the aerosol passing the first DMA was obtained. In Fig. 1 two such distributions are shown.

These preliminary results indicate that the size distribution of the Vienna DMA is narrow with a log-normal shape, as expected. In comparison, the Companion DMA exhibits somewhat broader distribution, which is not log-normal in shape. The

peak diameter selected by the Companion DMA is about 42 nm, which correlates well with its specifications (40 nm in diameter). The discrepancy could be explained by the fact that the preset parameters may not be optimized for individual processes, regarding flow rates and voltage settings. There is also a small diameter discrepancy in the Vienna DMA distribution, peaking at 43 nm, which might be associated with the fact that this DMA was not calibrated. The flows through the Vienna DMA were not optimal in these experiments, which explain the relatively low throughput. When run at optimal settings, the Vienna DMA throughput is approximately 10 times higher.

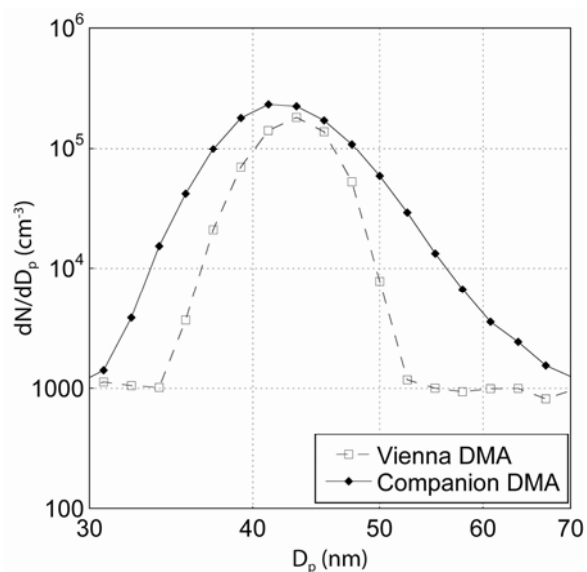


Figure 1. Particle size distributions measured with a Vienna-type DMA and a Companion-type DMA.

To conclude, our results indicate that the compact Companion DMA could in some cases be a convenient alternative in everyday size classifications. Its distribution is narrow enough for some applications, and the throughput could possibly be made higher. With a higher throughput this DMA would be suitable for our particle generator setup.

The authors thank TSI Aachen, Germany for lending us the TSI N95-Companion™.

## NANOCAP : Nanotechnology Capacity Building NGOs

Ian Colbeck and Alison Cox

Centre for Environment and Society, University of Essex, Colchester, CO4 3SQ, UK

Keywords: nanoparticles, exposure, risk

Nanotechnology is a major growth area in research and industry. Applications of nanotechnology include advanced materials, textiles, prosthetic implants, food and drugs. However, there is also a serious debate about the potential hazards of nano-particles (<100 nm), when introduced into the environment and the workplace.

NANOCAP (acronym for “Nanotechnology Capacity Building NGOs”) is a European project, financed by the European Commission within the 6<sup>th</sup> Framework Programme. NANOCAP is a consortium of 5 environmental NGOs, 5 trade unions and 5 universities from different EU-areas covering a large part of Europe. It aims to deepen the understanding of environmental, occupational health and safety risks and ethical aspects of nanotechnology via a structured discussion between NGOs, academic researchers and other stakeholders (see Figure 1). NANOCAP will enable environmental NGOs and trade unions to participate in a debate on nanotechnology at the European level. It will improve their understanding of this new technological field and, supported by scientific input, it will give them the opportunity to formulate their positions within the context of the actual science and society policy and the political background of the organisation, to inform their members and the general public, and to discuss the various issues.

Of particular interest are environmental concerns. There are a number of studies going on into the health and environmental impacts of many applications of nanotechnology. Although such technology could have significant effects on the environment such considerations have not historically been given a large priority in new developments compared to commercial considerations. Various research organisations and committees have considered the issues of environmental risks of nanoparticles. Most highlight the lack of information on nanoparticles entering the environment, and what health risks and consequences to the environment these particles could have. It is evident from NANOCAP that many workers are concerned about the absence of scientific clarity and the impact of this on an assessment of the risk involved. Hence the ethical questions and the potential hazards, both real and imaginary, need to be dealt with to facilitate the acceptance of both nanotechnology-based products and the processes that lead to their production.

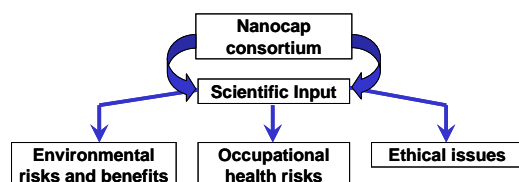


Figure 1 Structure of NANOCAP

In addition to enhancing the capacities of NGOs and trade unions, NANOCAP will develop recommendations to enable public authorities to address the health, safety and environmental risk issues related to the rapid introduction of nanotechnology into society. At the same time it is the goal of this project to give industry the tools to introduce a “responsible nanotechnology”, i.e. to stimulate industrial and academic R&D performers to focus on source reduction of emitted nano-particles and to make risk assessment an important dimension in their work.

## Catalytic oxidation of carbon aerosols by Pt nanoparticles: Influence of the Pt-C interparticle contact configuration on the reaction rate

Parisa Davoodi<sup>1,2</sup>, Martin Seipenbusch<sup>1</sup>, Alfred Weber<sup>2</sup>, Gerhard Kasper<sup>1</sup>

<sup>1</sup>Institute for Mechanical Process Technology and Applied Mechanics, University of Karlsruhe, Germany

<sup>2</sup>Institute for Mechanical Process Engineering, Technical University of Clausthal-Zellerfeld, Germany

Keywords: Nanoparticles, Nano contact, Aerosol catalysis, Carbon oxidation

There are different strategies to remove soot generated from combustion processes. Two of these are the use of Fuel Borne Catalysts in the aerosol state or oxidation of deposited soot particles on diesel particle filters (DPF). The relevant mechanisms of catalytic carbon oxidation in both cases are not entirely understood. There are several investigations on the catalytic carbon oxidation at low temperatures, which shows a strong interaction between carbon and catalyst particles (Van Setten et al., 2001) (Hinot et al., 2006).

In this work an investigation of the catalytic carbon oxidation for different contact types between carbon and platinum particles was performed in the gas phase. Five contact types of platinum particles with carbon were implemented according to the experimental configuration:

1. Pt nano sphere in a *single contact* with a carbon nano sphere.
2. Pt nano sphere in a *single contact* with a carbon nano agglomerate.
3. Pt nano sphere contact in *multiple contact* with a carbon nano agglomerate.
4. Pt nano sphere partially *embedded* in a carbon nano agglomerate.
5. Pt nano agglomerate *coated* with carbon using a CVD process.

Two sample results of TEM images are demonstrated in Figure 1.

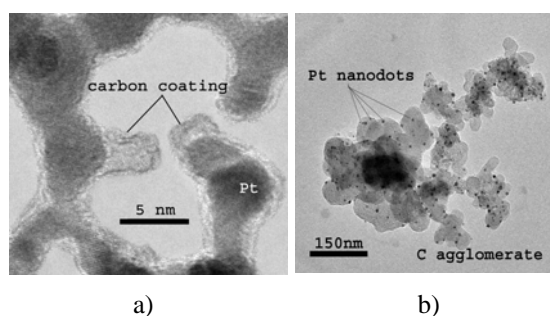


Figure 1. TEM images of Pt-C nano particles:  
a) case 4, b) case 5

different contact intensity. According to this diagram, higher catalytic activity was obtained in the case of multiple contact. In addition, the lowest catalytic activity was observed in the case of partially embedded Pt nano spheres.

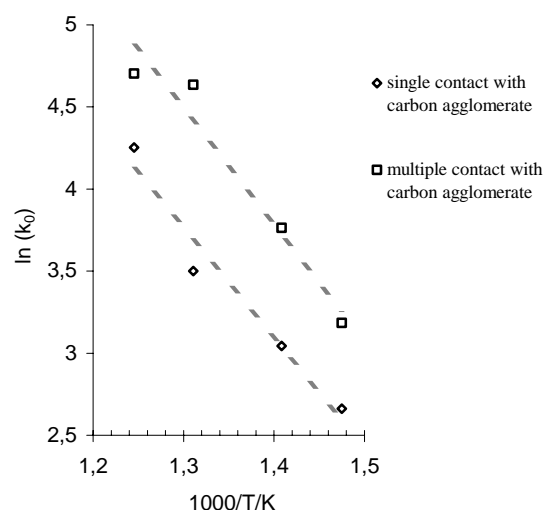


Figure 2: Velocity coefficient ( $k_0$ ) versus reverse of temperature in Kelvin ( $1/T$ ) for three different particle contact cases

The results show an improvement in the reaction rate with increasing intensity of contact represented by the velocity coefficient ( $k_0$ ) and a constant value of activation energy ( $E_a$ ) for all cases.

This work is part of the project "Einfluss des Partikelkontaktes auf die katalytische Kohlenstoff-oxidation" supported by DFG.

Van Setten, B. A.A.L; Makkee, M.; Moulijn, J.L.; Appl. Catal., B: 43(4), 489-564 (2001)

Hinot, K.; Burtscher, H.; Weber, A.P.; Kasper, G.; J. Appl. Catal. B: 71 (2006)

Figure 2 shows a comparison of the velocity coefficient between different configurations based on

## The production of nanoparticles with a CO<sub>2</sub> laser driven aerosol process

J.W.M. van Erven<sup>1</sup>, Z. Fu<sup>2</sup>, T.M. Trzeciak<sup>1</sup>, J.C.M. Marijnissen<sup>1</sup>

<sup>1</sup>NanoStructured Materials, Delft University of Technology, Julianalaan 136, 2628 NL Delft, The Netherlands

<sup>2</sup>DEMO, Mekelweg 4, 2628 CD, Delft, The Netherlands

Keywords: Laser pyrolysis, nanoparticle production, carbon, ethylene.

Full dense ceramics are of interest because of their high temperature strength, higher hardness, lower density and lower thermal conductivity compared to metals. The sensitivity of structural ceramics to small defects, leading to a lower strength, is a disadvantage. The powder has to have certain characteristics to achieve superior properties and avoiding defects in the sintered product. The powders should be spherical, not agglomerated, highly pure and need to have a narrow size distribution in the nanorange (Haggerty and Cannon, 1981).

Haggerty and Cannon (Haggerty & Cannon, 1981) started to develop a laser synthesis process in the late 1970's to produce silicon containing nanoparticles (e.g., Si, SiC, Si<sub>3</sub>N<sub>4</sub>). Many other researchers continued in that direction, however, the majority of the research was focussed on the development of new materials and not on the design of the reactor. A schematic of a classic design is shown in figure 1.

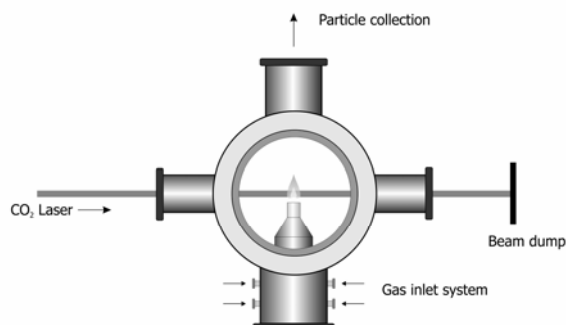


Figure 1. Classic laser assisted aerosol reactor

In this research a new CO<sub>2</sub> laser assisted aerosol reactor was built, with the focus on the design. Several parts have been changed compared to the original design. One of the new features is the rectangular design of the nozzle. Combined with a sheet of a CO<sub>2</sub> laser beam, which is also a new feature, this can lead to a more uniform reaction zone. The reactor also includes a wide range of optical access for analysing purposes. The details of the design can be found elsewhere (van Erven *et al.*, 2006).

The construction of the reactor is completed and currently the first experiments are done. This includes the production of carbon nanoparticles from ethylene. Production rates of several grams per hour can be established. After the successful performance of these experiments, highly interesting materials

such as silicon, siliconcarbide and siliconnitride will be produced. The results of the particle production with this system are presented on the conference.

Haggerty, J. S. and Cannon, W. R. (1981) 3. *Sinterable powders from laser-driven reactions* in *Laser-Induced Chemical Processes* 165-241. (ed by Steinfeld, J. I.). New York: Plenum Press.

Van Erven, J.W.M., Trzeciak, T.M., Fu, F., Marijnissen, J.C.M. (2006). *Design of a Laser Assisted Aerosol Reactor for Production of Nanoparticles on Semi-Industrial Scale*. Proceedings of the World Congress on Particle Technology V 2006, Orlando USA. Paper nr. 202D.

## Calculating the steady-state charge distribution for aerosols in the lower nm-range by the three body trapping method

Y.G. Stommel<sup>1</sup> and U. Riebel<sup>2</sup>

<sup>1</sup>Degussa GmbH, Process Technology, 63457 Hanau, Germany

<sup>2</sup>Chair for particle technology, Technical University of Cottbus, 03013 Cottbus, Germany

Keywords: Charged particles, submicron particles, aerosol instrumentation, aerosol modeling, diffusion.

In numerous fields of aerosol technology the charge on the gas-borne particles is of great significance. When exposed to bipolar gaseous ions and in absence of an external electrical field for  $n_i \tau \geq 6 \cdot 10^{12} \text{ s} \cdot \text{m}^{-3}$  (with  $n_i$  being the ion number concentration and  $\tau$  the charging time), the particles attain a statistical charge distribution which does no longer change with increasing  $n_i \tau$  (Hinds, 1999). This process is termed aerosol neutralization.

One of the most important applications of aerosol neutralization is as a processing step before classification in the Differential Mobility Analyzer (DMA), which is incorporated in the Scanning Mobility Particle Sizer (SMPS) for measuring the size distribution of submicron particles. Accurate knowledge of the charge distribution on the aerosol particles is necessary in order to relate the electrical mobility distributions to size distributions.

The neutralized state is governed by the ion-particle attachment coefficients, which are a function of the ion species and the particle charge and diameter (assuming spherical particles). After obtaining the ion-particle attachment coefficients, the charge distributions can be calculated according to the procedure outlined by f. e. Reischl et al. (1996).

While various theories for calculating the ion-aerosol attachment coefficients lead to similar results for particles in the continuum regime, the existing theories for small particles (particles with diameters in the order of magnitude of the ionic mean free path) are still debated. To this day, the theory of Fuchs (1963) – albeit with some minor corrections (Hoppel and Frick, 1986) – is widely used even for this size range, in spite of the no longer valid assumptions used in the named theory.

In order to overcome the deficiencies of the original Fuchs theory, Hoppel and Frick (1986) developed a different calculation method of the ion-particle attachment rate, called three body trapping (TBT), which is applicable for small particles down to the size of ions and of opposite polarity to the ion. The calculation method was laid out in the 1986 paper, a further improvement was hinted to in a 1990 paper. However, recalculation by Stommel (2006) showed, that some of the published equations were wrongly printed and some mistakes were made while calculating the so-called ion-aerosol trapping distances. Aim of the presentation will be to correct

these errors, to provide some additional information on the calculation method and to define a new range of applicability of TBT based on new calculations.

The recalculation of the charge distributions for small particles based on three-body trapping shows a pronounced difference in comparison to data calculated solely according to the theory of Fuchs. For positive and negative ion masses of 100 and 130 amu respectively and positive and negative ion mobilities of  $1.4 \cdot 10^{-4}$  and  $1.9 \cdot 10^{-4} \text{ m}^2/\text{s}$ , calculations after Fuchs show an inversion: The positive particle fraction overtakes the negative one for small particles. This, however, can not be observed in experiments. The calculated data according to TBT does not show this crossover and seems to coincide nicely with data published by f. e. Reischl et al. (1996).

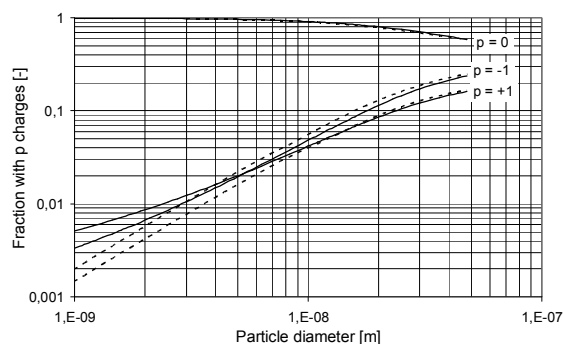


Figure 1: Charge fractions calculated according to Fuchs (dotted lines) and Hoppel and Frick (TBT for ions of opposite particle polarity)

The authors wish to express their gratitude to Mr. W. Hoppel for his assistance in preparing this paper.

- Fuchs, N. (1963). *Geofis. Pura Appl.* 56: 185-192.  
Hinds, W. (1999). *Aerosol technology*, John Wiley & Sons, Inc., ISBN 0471194107.  
Hoppel, W., Frick, G. (1986). *J. Aerosol Sci.* 5: 1-21.  
Hoppel, W., Frick, G. (1990). *Aerosol Sci. Technol.* 12: 471-496.  
Reischl, G., Mäkelä, J., Karch, R., Nucid, J. (1996). *J. Aerosol Sci.* 27: 931-949.  
Stommel, Y. (2006). *Neutralisation submikroner Aerosole durch hochfrequente Corona-Entladung*, Dissertation, Cuvillier Verlag Göttingen.

## Strategies for the determination of engineered nanoparticles in workplace environments – Examples from TiO<sub>2</sub> production

T.A.J. Kuhlbusch, C. Asbach, H. Kaminski, H. Fissan

Airborne Particles / Air Quality Unit, IUTA, 57229, Duisburg, Germany

Keywords: Nanoparticle, Measurements, Instrumentation, Exposure, Workplace

Developments in Nanotechnology have been very fast during the last decade and a vast number of applications of nanomaterials in new products are foreseen. One of the building blocks in Nanotechnology is particles in the nanometre size range. Even though some of them have been produced for more than a century (e.g. carbon black) already, these particles are nowadays discussed to possibly cause health effects. A recent review on possible health effects and current knowledge related to exposure is given e.g. by Borm et al. (2006). Some of the mayor research needs seen are related to

- the lack of understanding of the mechanisms and particle properties causing health effects,
- the uncertainties in the assessment of possible exposure,
- the large variety in engineered nanoparticles and subsequently the variety in nanoparticle properties,
- the high uncertainties in any risk assessment resulting from the uncertainties in the exposure and toxicological assessments,
- the lack of sound life cycle assessments of nanoparticles.

In order to improve the necessary knowledge to assess the possible environmental implications of nanoparticles it is necessary to be able to detect and quantify nanoparticles in the corresponding matrix; soil, water, and air in the ambient and/or workplace environment. Different measurement and sampling techniques are necessary as well as task specific strategies to identify and quantitatively determine nanoparticles.

This presentation focuses on measurement strategies for the determination of excess engineered nanoparticles in workers' environments to avoid data misinterpretation. Figure 1 gives an example on how particles may influence the work atmosphere, with the upper time series in the top part of the figure representing particle number concentrations at a site directly outside of the work area and the lower time series the same type of measurement in the work area with no work activity. Also sources other than the product nanoparticle may cause elevated nanoscale particle concentrations in the work areas besides outside sources. Hence specific measurement strategies including the choice of instrumentation and the set up are necessary to properly assess nanoparticle exposure at work places.

The importance and need of such measurement strategies, including workplace analysis, will be shown and a possible strategy as currently being employed at several work places will be discussed using the example of measurements at a TiO<sub>2</sub>-workplace.

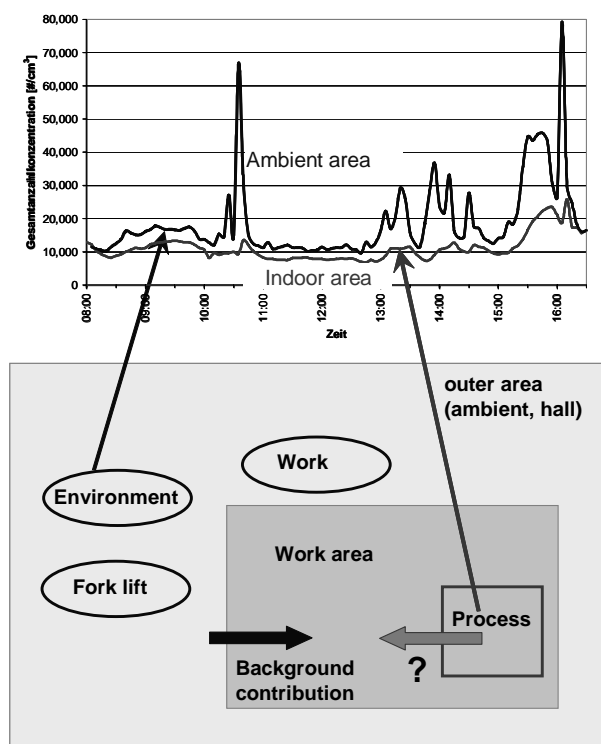


Figure 1. Influence of outside ultrafine particles onto workplace atmospheres (Kuhlbusch et al., 2006)

This work has been supported by the federal state government of North Rhine Westphalia and the European Union under grant number 005-0406-0004. The financial support is gratefully acknowledged.

Borm, PJA, Robbins R, Haubold S, Kuhlbusch TAJ, Fissan H, Donaldson K, Schins RPF, Stone V, Kreyling W, Lademann J, Krutmann J, Warheit D, Oberdorster E (2006) *Particle and Fibre Toxicology* 3:11.

Kuhlbusch, T.A.J., Kaminski, H., Fissan, H., Asbach, C. Strategies and Examples on the Determination of Nanoparticles at Workplaces, in preparation, 2007.

## Micro-patterning sensors by flame spray aerosol deposition

A. Tricoli<sup>1</sup>, M. Graf<sup>2</sup>, F. Mayer<sup>2</sup>, S. Kühne<sup>3</sup>, A. Hierlemann<sup>3</sup> and S. E. Pratsinis<sup>1</sup>

<sup>1</sup>Particle Technology Laboratory, <sup>3</sup>Physical Electronics Laboratory,  
ETH Zurich, CH-8092 Zurich, Switzerland

<sup>2</sup>Sensirion AG, CH-8712 Stäfa Zürich, Switzerland

Keywords: deposition, sintering, electrical effects, metal-oxide gas sensors, combustion synthesis.

The development of low-cost, portable, metal-oxide gas sensors with high sensitivity, selectivity and material stability bears considerable scientific and commercial potential (Eranna *et al.*, 2004). Highly sensitive nano-material synthesis by direct, aerosol-based methods offer unique advantages in comparison to wet-routes including crack-free, highly pure deposits, and the fact that only few process steps are required (Madler *et al.*, 2006). Sputtering, spray pyrolysis, cluster beam deposition, spray pulverization, combustion chemical vapor deposition (Liu *et al.*, 2005) and, recently, flame spray pyrolysis (FSP) have been applied to yield nanostructured sensing layers. The FSP freshly-deposited layers, in particular, consist of highly-porous (98%), loosely interconnected, soft nanostructures (Madler *et al.*, 2006). These, however, can be easily destroyed under mechanical stress and require stabilization.

Here we present a CMOS-compatible, two-step method for deposition and *in-situ* mechanical stabilization of gas sensitive, metal-oxide microlayers on wafer-level. Lace-like highly porous, Pt-doped SnO<sub>2</sub> nanostructured layers are deposited at wafer-level on 69 microsensors. Second, these layers are converted in well-adhered, cauliflower-like structures (figure 1b, inset). The resulting sensor layer performance is characterized using the analytes CO and EtOH on microsensor devices.

Figure 1 shows the resistance of a microsensor (inset a) with a nanostructured, transparent SnO<sub>2</sub>/Pt layer ( $d_{\text{XRD}} = 21.9 \text{ nm}$ ) (inset b) at different CO concentrations by heating the substrate surface at 450 °C. Below 20 ppm the microsensor response was in the range of seconds and a stable resistance was reached promptly (Fig. 1). Higher CO concentrations led to destabilization of the baseline due to the strong interaction between CO and Pt-doped SnO<sub>2</sub> nanoparticle. The microsensor had a response of 1.7 for 1 ppm and 5.4 for 20 ppm CO.

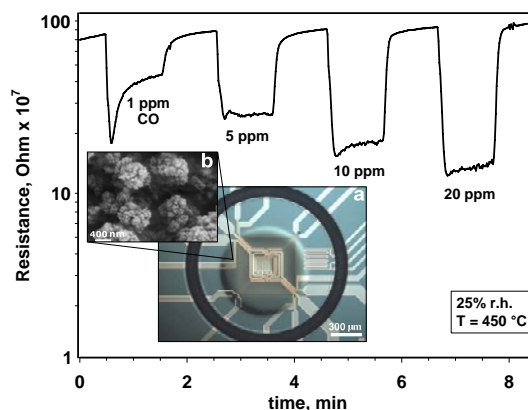


**figure** Microsensor (inset a) response featuring a SnO<sub>2</sub>/Pt 0.2 wt% transparent layer (inset b) upon alternating exposure to increasing CO concentrations.

Uniform, regular, macroporous Pt/SnO<sub>2</sub> layers have been patterned simultaneously on microsensors on wafer-level down to a diameter of 100 μm at 20 μm resolution. Gas microsensors showed a detection limit to CO of 1 ppm and fast response and recovery times. The layers had a large response also to EtOH ranging from 60 to 120 for concentrations varying from 10 to 50 ppm at 220 °C. Recent studies have reduced this to 100 ppb.

Financial support was provided from the Swiss Commission for Technology and Innovation KTI under grant 7745.1 and the ETH CCMX-NANCER program.

Eranna, G., Joshi, B.C., Runthala, D.P., & Gupta, R.P. (2004). *Crit. Rev. Solid State Mat. Sci.*, 29, 111-188.

Madler, L., Roessler, A., Pratsinis, S.E., Sahm, T., Gurlo, A., Barsan, N., & Weimar, U. (2006). *Sens. Actuators, B*, 114, 283-295.

Liu, Y., Koep, E., & Liu, M.L. (2005). *Chem. Mat.*, 17, 3997-4000.

## Measuring Hydrogen Storage in Individual Nanoparticles

V. Vons<sup>1</sup>, A. Schmidt-Ott<sup>1</sup>

<sup>1</sup> Nanostructured materials, DelftChemTech, Delft University of Technology, Julianalaan 136, 2628BL Delft, The Netherlands

Keywords: nanoparticles, UV electron emission, metalhydrides

Nanoparticulate metal hydrides (Zaluski et al., 1997) offer an interesting possibility for hydrogen storage on board of vehicles (Schlapbach & Zuttel, 2001). In this report we propose a new method for the *in-situ* analysis of hydrogen storage characteristics of *separate* metal hydride nanoparticles, using UV-light stimulated electron emission.

Nanoparticles in an aerosol emit electrons when exposed to UV-light of a high enough energy (Schmidt-Ott & Siegmann, 1978, Schmidt-Ott et al., 1980). The amount of emitted electrons and thus the charge state of the particles depends on the difference between the photon energy and the photoemission threshold (the energy barrier valence electrons must overcome to escape a solid, Cardona & Ley, 1978). When transforming from a metal to a metal hydride the photoemission threshold of a material changes drastically. This results in a change of the charge state of the particles after photoemission, which can be detected using an aerosol electrometer (AEM).

Particles from a glowing wire generator (GWG) are size selected with a differential mobility analyser (DMA). After the DMA the particles are exposed to hydrogen at a given temperature. Subsequently they are exposed to the UV light of low-pressure mercury lamps, with a wavelength of 185 nm. After the UV lamp the particle charge is measured with an AEM (figure 1).

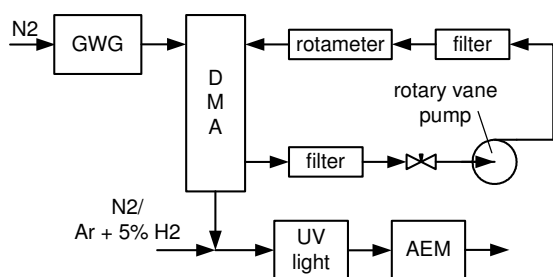


Figure 1: Experimental setup.

The AEM measures the current  $I$  caused by deposition of charged particles on its filter. The current with ( $I_{UV}$ ) and without ( $I_{total}$ ) the UV light turned on is measured. As the particles studied are very small ( $<30$  nm), it can be assumed that they are all singly charged, and therefore  $I_{total}$  is a measure of the total amount of particles, and  $I_{total} - I_{UV}$  is a measure of the total amount of electrons

that are emitted and lost to the walls. Therefore the average number of electrons lost per particle ( $n_{loss}$ ) can be calculated as  $n_{loss} = (I_{total} - I_{UV}) / I_{total}$ .

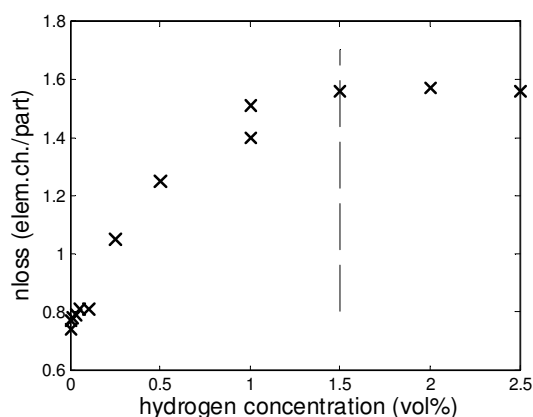


Figure 2:  $n_{loss}$  as a function of hydrogen concentration. Particle size is 16.5 nm. The dashed line indicates the equilibrium pressure for palladium and hydrogen at 20°C.

In figure 2  $n_{loss}$  is plotted for different hydrogen concentrations, for 16.5 nm particles. As can be seen, the addition of hydrogen has a distinct influence on the behaviour of the particles under UV light, up until the point that the equilibrium (plateau) pressure of palladium and hydrogen (based on Flanagan & Oates, 1991) at the given temperature (20 °C) is reached. After this the lost amount of electrons stabilizes. We conclude that the transition from the pure metal to the metal hydride can be detected by the proposed technique

L. Zaluski, A. Zaluska, J.O. Strom-Olsen (1997). *J. Alloys Comp.*, 253-254, 70-79.

L. Schlapbach, A. Zuttel (2001). *Nature*, 414, 353-358

A. Schmidt-Ott, H.C. Siegmann (1978). *Appl. Phys. Lett.*, 42, 710-713.

A. Schmidt-Ott, P. Schurtenberger, H.C. Siegmann (1980). *Phys. Rev. Lett.*, 45, 1284-1287.

M. Cardona, L. Ley (1978). Introduction. In M. Cardona, L. Ley (ed.) *Topics in Applied Physics: Photoemission in Solids I*. Springer Verlag, Berlin, p. 16-17.

T.B. Flanagan, W.A. Oates (1991). *Annu. Rev. Mater. Sci.*, 21, 269-304.

## Synthesis of Terraced MgO Nanoparticles Using Flame Metal Combustion Method

C. Kim, P.V. Pikhitsa and M. Choi

<sup>1</sup>National CRI Centre for Nano Particle Control, School of Mechanical and Aerospace Engineering, Seoul National University, 151-742, Seoul, Korea.

Keywords: Flame metal combustion, MgO Nanoparticles, Terrace, CL, UV

Magnesium oxide has been used and studied for many applications such as plasma display panels (PDP). UV emission from magnesia is considered as a dominant property to improve PDP performance (Motoyama *et al.* 2004, Uhm *et al.* 2002). To make UV emission particles, some researchers tried to dope magnesia (Karner *et al.* 2000). However, we synthesized UV emitting MgO nanoparticles without doping by a novel flame metal combustion method.

The experimental set-up fed Mg micropowder into oxy-hydrogen diffusion flame. The growth process of solid MgO nanoparticles was the result of condensation of MgO gas molecules produced in the combustion.

MgO nanoparticles synthesized by the flame metal combustion method had high purity without contamination by precursor Mg, which was proven by an XRD analysis. Size distribution and morphology changed according to conditions while the phase did not change. Size distribution was affected by concentration, temperature and the residence time. Concentration varied with precursor feeding rates; temperature and residence time were controlled by gas flow rates. Average particle sizes ranged from 30nm to 65nm.

MgO nanoparticles synthesized by other methods (*e.g.* Mg burning in air or a sol-gel method) have the cubic shape. On contrast, MgO nanoparticles produced by the novel metal combustion have two types of morphology: pure cubic and terraced with step-like edges (Fig. 1). The proportion of terraced and cubic nanoparticles can be also controlled by gas flow rates.

Cathodo-luminescence (CL) spectra in Fig.1 (b) demonstrated that MgO particles have UV emission (260nm) that cannot be seen in MgO nanoparticles prepared by other methods. A more intense UV peak existed at edges of terraced nanoparticles. Correlation between UV and oxygen vacancy bands in terraced nanoparticles ( $F^0$  (490nm) and  $F^+$  (420nm) centers) was revealed and theoretically explained. This result demonstrates that oxy-hydrogen diffusion flame plays a significant role in making oxygen vacancies -  $F^0$  and  $F^+$  centers - related to UV emission.

MgO nanoparticles emitting UV light were synthesized by novel flame metal combustion method. Moreover, through changing conditions, we could control the proportion of UV emitting nanoparticles as well as size distributions.

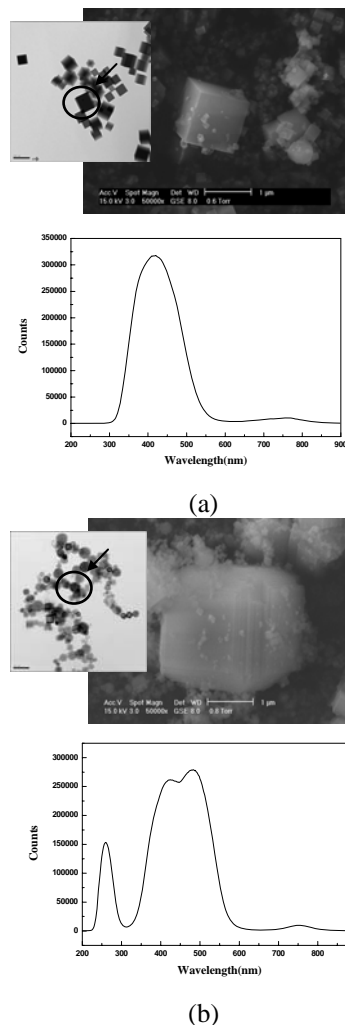


Figure 1. Morphologies and CL spectra of (a) Cubic and (b) Terraced MgO Nanoparticles

This work was funded by Creative Research Initiatives program sponsored by Korea Ministry of Science and Technology.

Motoyama Y., Hirano Y., Ishii K., Murakami Y. & Sato F. (2004), *J. Appl. Phys.* 95, 8419-8424.

Uhm H. S., Choi E. H. & Lim J. Y. (2002), *Appl. Phys. Lett.* 80, 737-739.

Karner T., Dolgov S., Krim M., Liblik P., Lushchik A., Maaros A. & Nakonechnyi S. (2000) *Nuclear Instruments and Methods in Physics Research B* 166-167, 232-237.

## Formation of $Al_2O_3$ nanoparticles by combustion of single Al particles

A.A. Onischuk, V.V. Karasev, O. G. Glotov

Institute of Chemical Kinetics and Combustion SB RAS, 630090, Novosibirsk, Russia,  
 Keywords:  $Al_2O_3$  agglomerates, aluminum oxide nanoparticles, metal particle combustion

The investigations of single metal droplets combustion are inspired by both fundamental interest and possible applications. In particular the combustion of metal powder can be an effective way of synthesis of semiconductor and ceramic oxide nanoparticles. Metal powders are of interest as ingredients for high energetic formulations. Aluminum powders are added to propellants and explosives to boost their combustion enthalpy. Metal oxide nanoparticles are a product of maternal metal particle combustion. However the mechanism of nanoparticles formation is not understood completely yet, partially, due to the lack of experimental data.

In this work the formation of metal oxide nanoparticles was studied during combustion of Al particles moving in the air at the velocity of 5 - 10 m/s. The radius of maternal droplets was in the range 1-200  $\mu m$ . The metal oxide aerosol was formed as fractal aggregates with the size of 0.1 - 10  $\mu m$  which consist of primary particles with the diameter of 5 - 50 nm. The aggregate size and morphology was analyzed by a Transmission Electron Microscope.

The high speed video microscopy were used to observe the combustion process in detail (Fig. 2). It was observed that aluminum oxide nanoparticles are formed in the reaction zone detached from the droplet surface.

Both the ratio  $\frac{R}{r}$  between the radius  $R$  of the

reaction zone and the radius  $r$  of maternal Al particle) and the radius of primary particles in  $Al_2O_3$  aggregates are functions of the maternal particle radius (Figs. 3, 4). An analytical model based on the solution of the heat and mass transition equations is in a reasonable agreement with the experimental data.

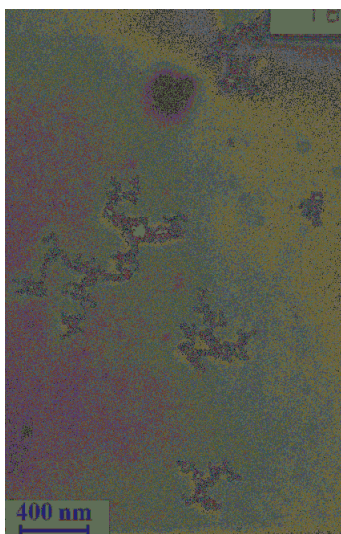


Fig. 1. TEM image  $Al_2O_3$  aggregates.

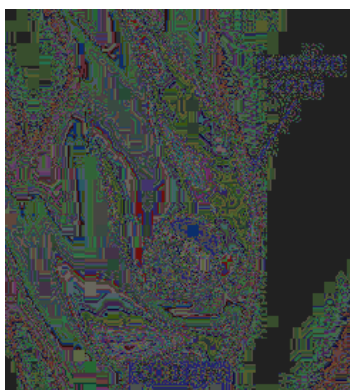


Fig. 2. High speed video observation of burning Al particle

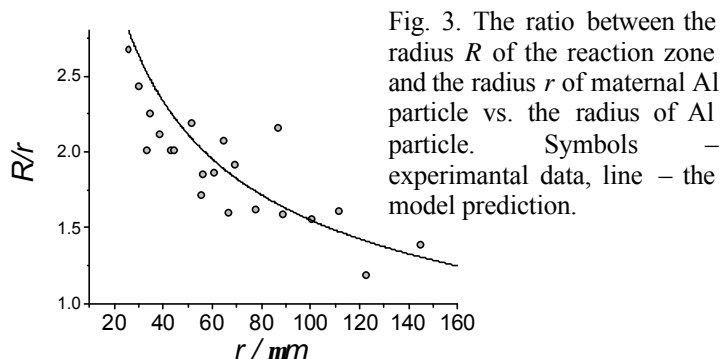


Fig. 3. The ratio between the radius  $R$  of the reaction zone and the radius  $r$  of maternal Al particle vs. the radius of Al particle. Symbols – experimental data, line – the model prediction.

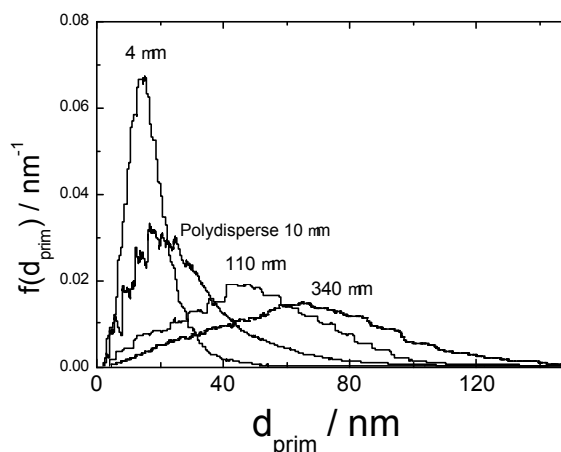


Fig. 4. Size distributions of primary particles for Al maternal particles of different diameters (shown above the distribution curves).

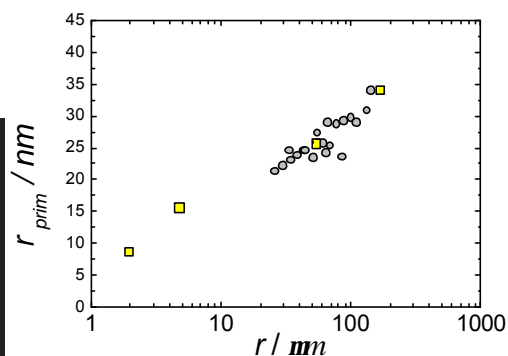


Fig. 5. The mean arithmetic radius of primary particles in  $Al_2O_3$  aggregates vs. the radius of maternal Al particle. Squares – experimental data, circles – calculation results.

Financial support for this work was provided by RFBR 05-03-90576-NSC a, grant of SD RAS No 78, NSC Taiwan-RFBR No. 94WFA0600016 Contract No. RP05E15.

## The Influence of Carbon Monoxide Chemisorption on the Magnetization of Fe<sub>3</sub>C nanoparticles

A. A. Onischuk<sup>1</sup>, N. A. Ivanova<sup>1</sup>, S. V. Vosel<sup>1,3</sup>, P. A. Purtov<sup>1</sup>,  
N. T. Vasenin<sup>2</sup>, V. F. Anufrienko<sup>2</sup>, V. N. Ikorski<sup>4</sup>

<sup>1</sup>Institute of Chemical Kinetics and Combustion SB RAS, 630090, Novosibirsk, Russia,

<sup>2</sup>Boriskov Institute of Catalysis SB RAS, 630090, Novosibirsk, Russia

<sup>3</sup>Institute of Geology and Mineralogy SB RAS, 630090, Novosibirsk, Russia

<sup>4</sup>International Tomography Center, SB RAS, 630090, Novosibirsk, Russia,

Keywords: Cementite, carbon monoxide chemisorption, magnetization, nanoparticles, pyrolysis.

The development of nanoscience and nanotechnology has resulted in various application of magnetic nanoparticles including magnetic targeting in drug delivery, medical imaging, gas sensing, magnetic storage technology. This paper is devoted to the ESR and magnetic measurements of Fe<sub>3</sub>C nanoparticles covered by a carbon structure. The samples were prepared by co-pyrolysis of C<sub>3</sub>H<sub>8</sub> Fe(CO)<sub>5</sub> diluted by Ar at atmospheric pressure and temperature 1280 K. A flow quartz reactor with the outer resistive heating was used. The propane and iron pentacarbonyl decomposition degree were analysed by the gas-chromatography and IR spectrometry, respectively. The outlet particles were sampled thermophoretically to be analyzed by a Transmission Electron Microscope (TEM) and a High Resolution Transmission Electron Microscope (HRTEM). The phase composition studied by means of the X-ray diffraction (XRD). A typical TEM images of particles sampled at the reactor outlet are shown in Fig. 1. The only phase observed by the

XRD method was Fe<sub>3</sub>C. Fig. 2 compares ESR and magnetic measurements data. The ESR spectrum from the as-prepared sample is demonstrated in Fig. 2a. One can see the line from carbon radical centers (marked as

Carbon) and other broad lines which are related to the Fe<sub>3</sub>C phase. The ESR spectrum has changed essentially after the sample being treated by the water vapor (at T = 723 K, P<sub>H<sub>2</sub>O</sub> = 20 Torr, exposure time t = 1 hour) or CO (at T = 573 K, P<sub>CO</sub> = 4 Torr, t = 2 hours). Note, the water exposure at T = 723 K has resulted in the sample treatment by CO which was formed via the reaction H<sub>2</sub>O + C = CO + H<sub>2</sub>.

On the other hand, the CO exposure has resulted in the strong decrease of ferromagnetism of the sample (compare Figs 2e and f). The further air exposure of this sample during 10 days has restored the magnetization up to the initial value of 0.2 Gs cm<sup>3</sup>g<sup>-1</sup> (see Fig. 2g), and the ESR spectrum has become about the same as the initial one (Figs. 2a and d). Thus, there is no correlation between the ESR spectra and the specific magnetization curves. Therefore we assume that the ESR signals are not related directly with the ferromagnetism of Fe<sub>3</sub>C particles. On the other hand, the spectrum observed can not be attributed to the paramagnetic resonance from Fe<sup>0</sup> or Fe<sup>2+</sup> ions, because these species have a very short relaxation time at the room temperature i.e. the line width is very broad to observe the ESR spectrum (the concentration of Fe<sup>3+</sup> ions is negligible in the samples under consideration). Therefore, we attribute the ESR signals to the are caused superparamagnetic Fe<sub>3</sub>C particles. The chemisorbed CO

has demagnetized the surface layers of Fe<sub>3</sub>C particles resulting to the transition of some of Fe<sub>3</sub>C nanoparticles from ferromagnetic to superparamagnetic state and other particles from superparamagnetic to paramagnetic state. The following air exposure has removed CO from the surface and restored the magnetization.

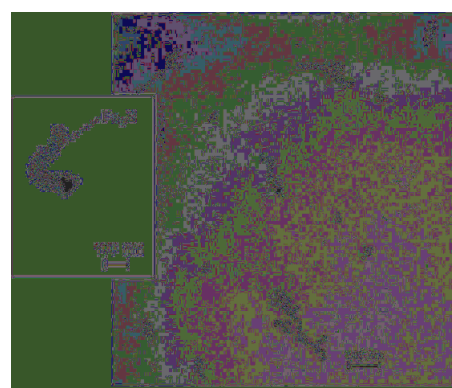


Fig. 1. Typical TEM images of the samples used in magnetic and ESR measurements

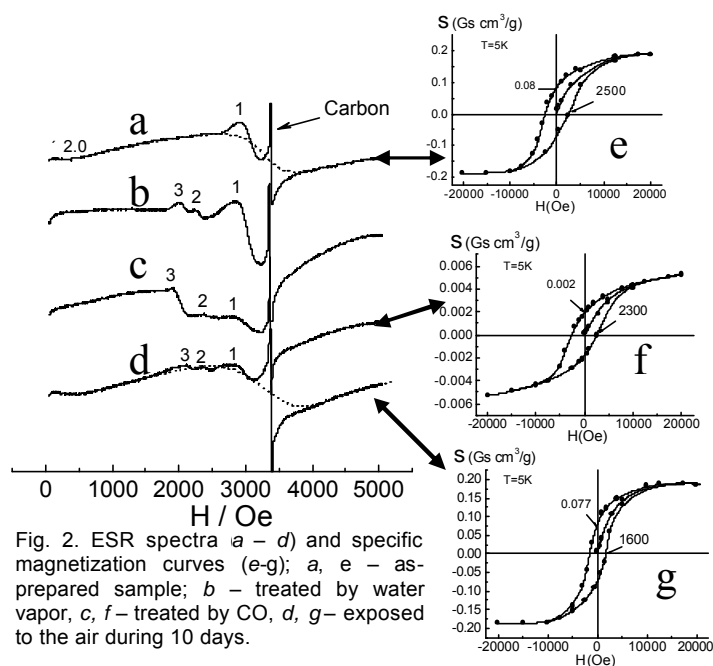


Fig. 2. ESR spectra (a – d) and specific magnetization curves (e-g); a, e – as-prepared sample; b – treated by water vapor, c, f – treated by CO, d, g – exposed to the air during 10 days.

Financial support for this work was provided by RFBR 05-03-90576-NSC a, grant of SD RAS No 78, NSC Taiwan-RFBR No. 94WFA0600016 Contract No. RP05E15.

## Fabrication and size control of carbon nanotube on nano-scale Ni aerosol particles

Katsunori Bente, Hiroshi Takano and Masayuki Itoh

Department of Chemical Engineering and Materials Science  
Doshisha University, Kyoto 610-0321, Japan

Keywords: Nanotubes, middle power CO<sub>2</sub> laser, carbon micro-beads, nickel particle size

Carbon nanotubes are an allotrope of carbon. They take the form of cylindrical carbon molecules and have novel properties that make them potentially useful in a wide variety of applications in nanotechnology, electronics, optics and other fields of materials science. Recently the size control of CNTs is often tried with metallic nano-particles as a catalysis. In this report, the relationship between the particle size and nano-tube diameter was investigated for the CNTs fabricated from carbon micro-beads by laser ablation using CO<sub>2</sub> CW laser.

The experimental setup is shown in Figure 1. The PBN crucible filled with carbon micro beads (3.9µm in diameter) and Ni micro-beads (4.µm in diameter) was set at the center of the chamber and pre-heated up to 750K with a heater to stabilize the ablation condition. After the chamber was evacuated less than  $1.0 \times 10^{-4}$ Pa by a rotary pump and diffusion pump, He (99.9999%) gas was filled in as the diffuser of vapors up to the pressure of 11000 Pa.

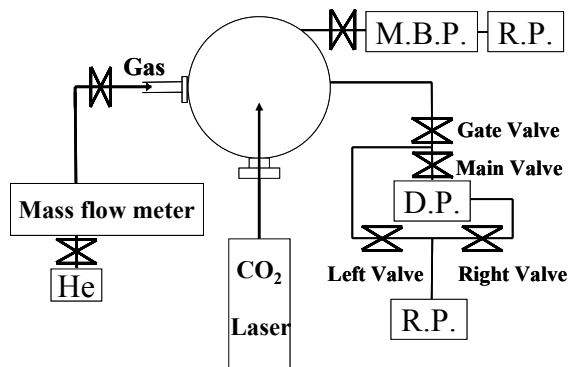


Figure 1. Experimental setup for the laser ablation with a. medium power CW CO<sub>2</sub> laser.

The laser beam (10.6µm) of power density about 430MW/m<sup>2</sup> was focused onto the target and irradiated for 5 minutes to produce Ni nano-particles and carbon vapor with heating and ablation. The produced carbonaceous materials were collected on a carbon plate placed at the upper side of the crucible. The produced carbonaceous materials were observed and characterized by a transmission electron microscopy (TEM).

The soot collected on the chamber wall was mostly in the form of powder-like soot exhibiting a rubbery texture. Most CNT showed clear tube, but

some were complex carbon needles. Figure 2 shows typical TEM micrographs of carbon nanotubes growing on nickel particles as nuclei. Sato et al. reported that the diameter of CNT produced with such metallic catalysts showed a good coincidence with size of nuclei. Figure 3 shows the clear linear relationship or coincidence between the size of Ni nano-particles and that of the growing CNT of our case.

In the case of pure graphite target, multi wall carbon nanotubes would be synthesized. But uniform single wall carbon nanotubes could be synthesized if a mixture of graphite with Co, Ni, or Fe was used instead of pure graphite. Our results prove that single wall CNTs can be fabricated with a medium power CO<sub>2</sub> laser from carbon micro-beads and the size can be controlled easily with the diameter of metallic particles using as nuclei and catalysts.

S. Sato. A. Kawabata, M. Nihei, Y. Awano, (2003), CPL, **382**, 361.

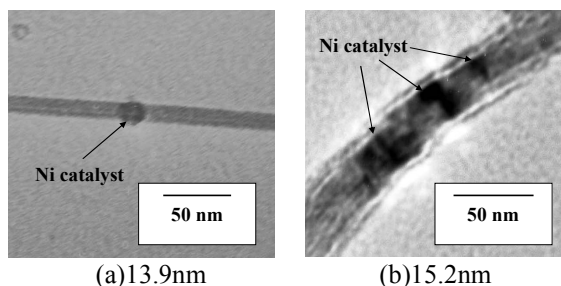


Figure 2. TEM micrographs of carbon nanotubes synthesized by carbon micro-beads on nickel particles.

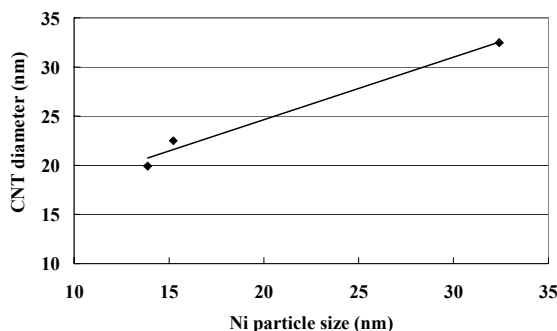


Figure 3. The relation between Ni particle diameter and CNT diameter.

## Development of a metal membrane filter with high filtration performance by the deposition and sintering of nanoparticle agglomerates

S.J. Park<sup>1</sup> and D.G. Lee<sup>2</sup>

<sup>1</sup>Clean Air Technology Research Center, Korea Institute of Energy Research,  
71-2 Jang-dong, Yuseong-gu, 305-343, Daejeon, Republic of Korea

<sup>2</sup>Department of Mechanical Engineering, Chungnam National University,  
220 Gung-dong, Yuseong-gu, 305-764, Daejeon, Republic of Korea

Keywords: aerosol filtration, agglomerates, filters, nanoparticles applications, sintering.

Metal filters are typically divided into two classes: metal fiber sintered filters and metal powder sintered filters. The metal fiber sintered filter is made by felting woven or nonwoven micro-fibers and sintering them to bind each other, which large pores are formed in, so that the filtration efficiency is low but the gas permeability is high. The metal powder sintered filter is made by packing micro-powders densely and sintering them, which tiny pores are developed in, so that the filtration efficiency is considerably excellent but the gas permeability is too low. Therefore, the metal powder sintered filter is applied to the hot gas cleanup process to require significantly high filtration efficiency in spite of high pressure drop. If a high efficient metal filter that can be operated at low pressure drop is developed, it is easier to prevent serious air pollution caused by the particulate matters emitted from automobiles and to cleanup the hot gas produced from advanced power plants such as IGCC and PFBC (Chaudhuri *et al.*, 1994).

This study suggests the method to fabricate new metal filter media with high filtration efficiency at low pressure drop by depositing metal nanoparticle agglomerates on a conventional micro-fibrous metal filter and sintering them on the surface. The nanoparticle agglomerates of dendrite structure with lower fractal dimension may be used to fabricate the higher porous layer structure (Houriet *et al.*, 1999).

The nanoparticles are generated from stainless steel metal plate by laser ablation. The experimental apparatus is consisted of carrier gas supply, laser ablation chamber including a sample target rotated by a motor, high power Nd:Yag laser (Continuum, Surelite III-10), a focusing lens moved by optical rail, a filter holder, and an exhaust. Nitrogen gas of 1 slm is supplied into the ablation chamber to carry synthesized nanoparticles. Nanoparticles are generated by the homogeneous nucleation and growth of the vapor molecules evaporated from the surface of solid target by the focused high power laser beam of Nd:Yag laser. Wavelength of used laser is 532 nm and laser energy is 200 mJ/pulse. Most of nanoparticles are coagulated as soon as generated because their concentration is significantly high. The coagulated nanoparticle-agglomerates are transported to a micro-fibrous metal filter contained

as a support filter in the filter holder. The nanoparticle agglomerates deposit on the filter surface and form the porous layer composed of nanoparticles until the pressure drop is 20 mbar at 4.2 cm/s in face velocity. The porous layer composed of nanoparticle agglomerates is sintered on the support filter for 30 min in the hot argon gas atmosphere of 300 – 800 °C. The porous structure formed on the filter is observed by SEM (scanning electron microscope, HITACHI S-4700). The penetration of 100 nm NaCl test particles at 3 cm/s in face velocity is measured by DMA (differential mobility analyzer, TSI 3081) and UCPC (ultra condensational particle counter, TSI 3025A).

The pressure drop of the fabricated filter decreases with sintering temperature, which means that the pores of the porous layer composed of deposited nanoparticles are larger because the nanoparticles contacted each other are sintered and the agglomerates shrink. Especially, the pressure drop lowers dramatically at 800 °C by the breakup of porous layer. The penetration rate through the filter does not show significant difference when the temperature for sintering the nanoparticle-deposited porous layer is below 700 °C. Therefore, this fabricated filter may be used stably below 700 °C.

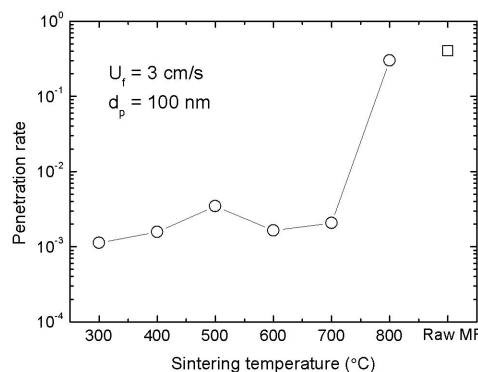


Figure 1. Penetration rates through the filters with nanoparticle-porous-layers sintered at different temperature.

Chaudhuri, M., Verma, S. R. and Gupta, A. (1994). *J. Environ. Eng.*, 120, 1646-1651.

Houriet, R., Vacassy, R., & Hofmann, H. (1999). *NanoStr. Mater.*, 11, 1155-1163.

## Study on the collection of nanometric powders by electrostatic precipitators from iron and steel industry gases emission

C.Grigoriu<sup>1</sup>, I.Nicolae<sup>1</sup>, C.Viespe<sup>1</sup>, D.Dragulinescu<sup>1</sup>, D.Martin<sup>1</sup>, S.Jinga<sup>2</sup>, R. Macarie<sup>3</sup>, and P.Biswas<sup>4</sup>

<sup>1</sup>Lasers and Accelerators Department, National Institute of Laser, Plasma and Radiation Physics, Atomistilor 409, 077125, Bucharest-Magurele, Romania

<sup>2</sup>Oxidic Materials Science & Engineering, Nanomaterials, Politehnica University of Bucharest, Spl. Independentei 313, 060042, Bucharest, Romania

<sup>3</sup>ICPET ECO SA, Sos. Berceni 104, 041919, Bucharest, Romania

<sup>4</sup>Department of Energy, Environmental and Chemical Engineering, Washington University in St. Louis, One Brookings Drive, Campus Box 1180, MO 63130-4899, St. Louis, USA

Keywords: environmental particles, industrial aerosols, electrostatic precipitators, submicron particles, nanoparticles characterization

In recent years the scientific community has been concerned about the toxicity of emitted nanoparticles (Maddalena et al., 2004; European Commission, 2005). A significant effort has been devoted to the control of emissions of submicrometer and nanometer sized particles.

The electrostatic precipitators (ESPs) which are in operation in the present industry have low capture efficiencies in certain size ranges. The collection efficiency is lower for submicron particles by 12-15 % than for microsized particles. Therefore, the capture of submicron particles with a high efficiency is an important challenge for the scientific community. Due to these lower efficiencies, other methods have been proposed for capture of nanosized particles, such as particle agglomeration or utilizing of adhesive means, etc. (Sug et al., 2006).

This study is aimed at investigating: (a) the constitutional species, the morphological and structural characteristics, and surface composition of the submicrometer sized powders emitted in the atmosphere from iron and steel foundries (equipped with electrostatic precipitators); (b) the capture of submicrometer particles in a standard ESP and a hybrid one equipped with an additional ionizing source (laboratory models).

The particle characterization methods include determination of structure, morphology, composition and size based on X ray diffraction (XRD), scanning electron microscopy (SEM), and transmission electron microscopy (TEM), laser granulometry and X ray photoelectron spectroscopy (XPS), and on line differential mobility analysis (DMA).

The powders used in this study were collected at the agglomeration furnace before and after the de-dusting equipments. The de-dusting equipment had a flow rate of 610,196 m<sup>3</sup>/h, at gas temperatures of 110 °C and a efficiency of around 98%. A specially designed capture system was utilized to collect the samples from the sintering point. The approximate particle concentration prior to the stack was 150 mg/m<sup>3</sup>.

The powder consisted of agglomerates, with the size of most particles below 1 micrometer. The

clusters, were composed of primary particles less than 100 nm, as is illustrated in Figure 1.

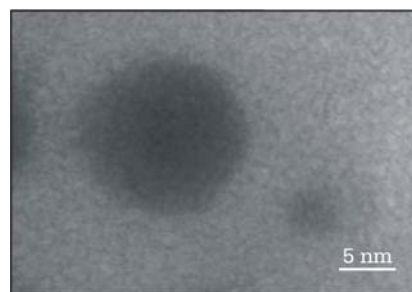


Figure 1. Primary nanoparticles collected after ESP.

The majority of the species consisted mainly of a crystalline mixture of Fe<sub>3</sub>O<sub>4</sub> and  $\gamma$ -Fe<sub>2</sub>O<sub>3</sub>. The surface composition of the particles, are related to the oxidic compounds of the iron. Other important constituents such as carbon, calcium, aluminum, silicon, were also identified.

The work investigated the capture performance of a standard laboratory ESP and a hybrid one which uses a supplementary photo-ionizer, a soft X ray source (Kukami et al., 2002). In both cases, the performance was determined under the DC and pulsed voltage regimes. The powder capture efficiency and particle size distribution was investigated. Details will be presented at the Conference.

This work was supported by the National Authority for Scientific Research / AMCSIT, under grant 54/10.2005.

Maddalena R., MacLeod M., McKone T., Sohn M. (2004) –*Proc. Soc. Environmental Toxicology and Chemistry Conf.*; Pensacola, FL, USA  
European Commission - *Nanotechnology for Health*; (2005), ISBN 92-894-9599-5  
Sug B.J., Aly A., Takashima K., Kastura S., Mizuno A., (2006) *Plasma Process. Polym.*, 3, 661-667  
Kulkarni P., Namiki N., Otani Y., Biswas P., (2002) *J. Aerosol. Sci.* 33 1279-1298

## Nanoparticles in fine dust – development of modern measuring methods

Nayla Sabbagh<sup>1</sup>, Wladyslaw W. Szymanski<sup>1</sup>

<sup>1</sup>Faculty of Physics, University of Vienna, Strudlhofgasse 4, 1090 Vienna, Austria

Keywords: Ultrafine particles, PM1.0 and PM0.1, Air quality, Health effects, Virtual impactor

Airborne particulate matter (PM), its health and environmental impact are strongly associated with aerosol size distributions and concentrations next to the chemical composition of particles in question. There is a large number of studies, which established links between concentration of ambient aerosols, levels of air pollution and adverse health and environmental effects. For the description of air quality the term particulate matter (PM) has been coined. PM10 particle size fraction represents mass concentration of particles with aerodynamic diameters below 10 micrometers. Similarly, the PM2.5 rule was established in the United States, however formally not yet in the European Union. It is a broad understanding now that the PM10 and PM2.5 measurement provide very important steps towards air quality assessment but there is also no doubt that more accurate descriptors of the actual environmental burden are still needed. However, there is broad consensus that PM1.0 and PM0.1 would be more suitable size than PM 2.5 for health related aerosol sampling. Though, there is still relatively limited amount of data for the PM1.0 and PM0.1 fraction available. Very recently an increasing volume of scientific contributions mirrors the enormous importance and very likely, health hazard due to nanoparticles.

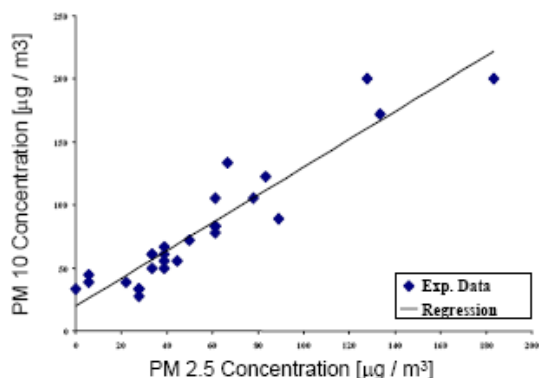


Figure 1. Relationship between PM10 and PM2.5 of urban aerosol measured on a major traffic route.

For that reason we develop a sampling/sizing system – allowing a combined aerosol mass, surface and number size distribution measurement: cascade virtual impactor (LCVI) allowing time-integrated, size-resolved measurements: PM10, PM2.5, PM1 and PM0.1. Those measurements will be carried out as a function of key environmental parameters along with chemical post-sampling characterization of the collected particulate matter focussing particularly on carbon (total, organic, elemental). The sampling and characterization of PM0.1, PM1, PM2.5 and PM10 will be conducted concurrently with the time- and size-resolved measurement of particle number and surface distributions in these size fractions. The mass information (PM) will then be linked with two additional descriptors of airborne particles, which are meant to be of decisive importance in determining the health and environmental impact - number and surface - covering the airborne particle size range starting from 10nm. This approach provides a better understanding of the relationship and interaction between nanoparticles and larger PM constituents. First results obtained with this hybrid measuring system will be presented and discussed.

Edwards, L., Limit values in urban air pollution . European Aspects ( Fenger, Herstel, Palmgren, Eds.), Kluwer Acad. Publishers (1998).

Pressertachato, T., A. Podgorski, J.H. Luckner, M. Furuuchi, L. Gradon, S. Suvachittanont and W.W. Szymanski, Sampling and characterization of PM-fractions of ambient particulate matter in Bangkok utilizing a cascade virtual impactor, *Aerosol Air Qual.Res.* 6:67-81 (2006).

## Cyclone Technology for Nanopowder Collection

HungMin Chein and Yu-Du Hsu  
 Energy and Environment Research Laboratories  
 Industrial Technology Research Institute  
 Room 1128, Building. 51, No. 195, Section 4, Chung Hsing Road, 310, Chutung, Hsin Chu, Taiwan, R.O.C.  
 Tel: +886-3-5913853; Email: hmchein@itri.org.tw

Keywords: cyclone, nanoparticle, nanopowder, collection.

Nanotechnology is expected to bring a new industry revolution. Nanopowder production is one of the key technologies. Particle separation and collection plays a very important role in the production process. Meanwhile, nanoparticle contamination is affecting product yield of semiconductor and opto-electronic manufacturing in addition to creating clogging problem of pumping line. ITRI has developed a new generation of cyclone system (Figure1) to separate and collect nanopowders, which has collection efficiency larger than 90% for 100 nm particles. The cyclone system is proved to separate the nanoparticles efficiently and, therefore, enhance the production and market value.

The cyclone system designed and evaluated in Energy and Environment Lab (EEL) has a collection efficiency of 20% and 98% for 100 nm particles at 13 and 6 torr, respectively. This is the first report of cyclone applied to collect nanometer size range of particles (Tsai et. al, 2004). The slip correction factor increases as the operating pressure decreases and hence lowers the cutoff aerodynamic diameter. The cutoff aerodynamic diameter is adjusted with the flow Reynolds number. The cyclone has been evaluated at various conditions both experimentally and theoretically (Hsu and Chein, 2005). A universe curve is established for particle collection efficiency as shown in figure 2. The collection efficiency can be expressed as following:

$$\eta = 1 - \exp(-d_{pa}'^2 / d_{pa50}'^2)$$

where  $d_{pa50}' = d_{pa50} / \sqrt{\ln 2}$ .



Fig. 1. Nanopowder Separation & Collection System

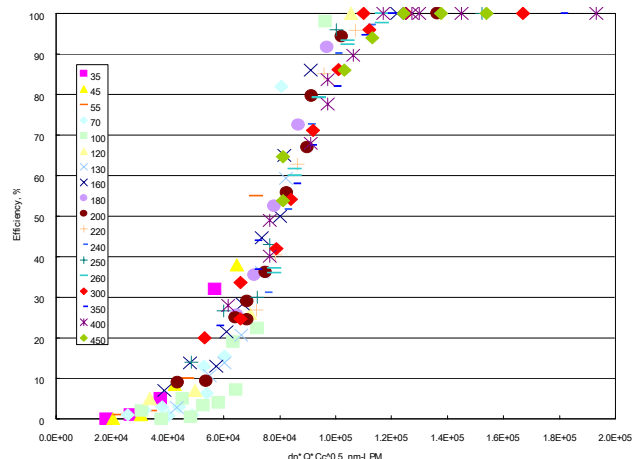
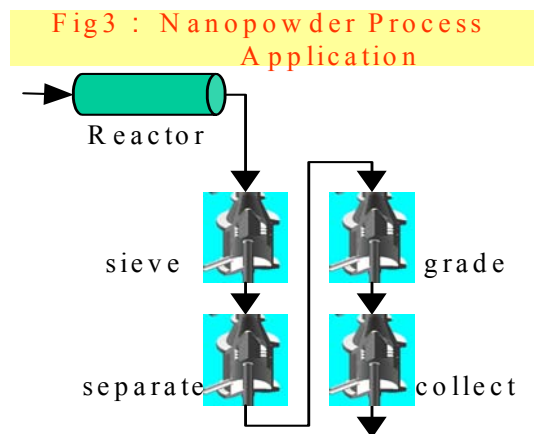


Fig.2. Universe curve for particle collection efficiency at various conditions

The cyclone has a great application in nanopowder separation and collection in the production process (Figure 3). In addition, it can be applied to remove fine and ultrafine particles emitted from semiconductor or opto-electronic manufacturing process.



Hsu, Yu-Du, HungMin Chein, Tzu Ming Chen, and Chuen-Jinn Tsai (2005), Environmental Science & Technology 39, 1299-1308  
 Tsai, Chuen-Jinn, Daren-Ren Chen, HungMin Chein, Sheng-Chieh Chen, Jian-Lun Roth, Yu-Du Hsu, Biswas Pratim, Weiling Li (2004), Journal of Aerosol Science, vol. 35 (9), 1105-1118

## On the particle size distributions by flame electrospray pyrolysis

Hyuncheol Oh<sup>1</sup> and Sangsoo Kim<sup>1</sup>

<sup>1</sup>Department of Mechanical Engineering, KAIST, Guseong-Dong, Yuseong-Gu, 305-701, Daejeon, Rep. of Korea

Keywords: trimodal size distribution, flame, electrospray, pyrolysis

Of the emerging methods available for the production of metal oxide powders, spray pyrolysis has been widely used to prepare continuously spherical, high-purity, multicomponent products, because of its low cost and versatility. Generally, in the spray pyrolysis technique, three types of atomizer are used to spray precursor into droplets; ultrasonic, pneumatic, and electrospray. Electrospray pyrolysis has attracted attention because it can produce submicron, highly-charged droplets. Electrospraying refers to a process in which a liquid jet breaks up into droplets under influence of electrical forces. The charges on the droplets eventually minimize the coagulation process, which is a severe problem for powder production via aerosol routes.

Most studies of electrospray pyrolysis have used a hot-walled furnace as an energy source for the chemical reaction to produce functional particles. Recently, a new process for flame electrospray pyrolysis was presented for synthesizing CeO<sub>2</sub> nanoparticles with dense morphology, high crystallinity and nanometer size (Oh & Kim, 2006).

In this study, the particle size distributions generated by flame electrospray pyrolysis were investigated. The experimental set-up has been described elsewhere (Oh & Kim, 2006). Hydrated cerium nitrate precursor dissolved in ethanol/diethylene glycol butyl ether mixtures was injected into the CH<sub>4</sub>/Air premixed flame by the electrospray method. The electrospray nozzle used a stainless steel capillary (Upchurch, USA) that had outer and inner diameters of 0.785 and 0.45 mm, respectively. An electric potential between 3.2 and 3.7 kV was used. The precursor solution was delivered to the spray nozzle at a flow rate of 0.3 ml/h.

The number size distributions of the as-prepared particles were trimodal as shown in Figure 1. When the applied voltage was increased, the resulting particle size distribution was almost unchanged. This means that droplet size is almost independent of the applied voltage for the cone-jet mode. The fine mode was about one order of magnitude smaller than the coarse mode. It was suggested that the particles for the fine mode were formed by Rayleigh disintegration of charged precursor droplets during droplet evaporation. Rayleigh disintegration occurs when electric force overcomes the liquid surface tension. The particles for the coarse and middle modes might come from primary and secondary droplets respectively, which were formed simultaneously during atomization

process. The possibility of precursor evaporation and droplet explosion for the origin of fine and middle mode should be further considered.

Figure 2 shows the particle size distribution measured at three different locations in the flame. From the spray center to the spray edge, the number concentration for the fine mode increased, while the coarse mode decreased. This implies size segregation effects (Tang & Gomez, 1994).

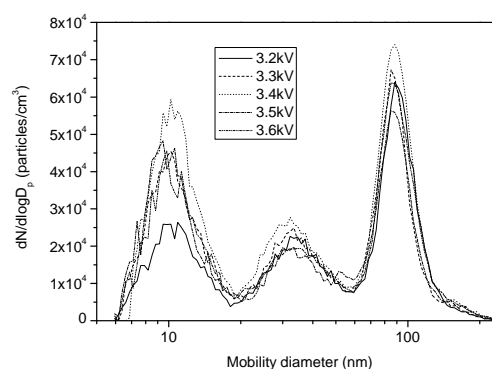


Figure 1. Particle size distributions for the different applied voltage at a precursor flow rate of 0.3 ml/h.

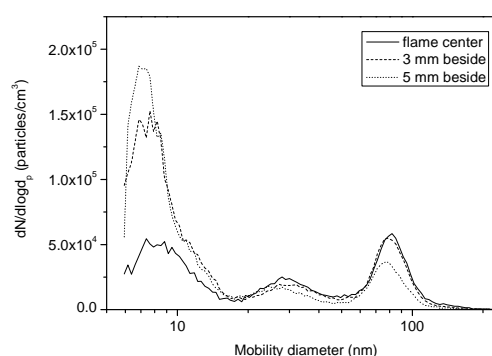


Figure 2. Particle size distributions for the different sampling position at an applied voltage of 3.3 kV and a precursor flow rate of 0.3 ml/h

This work was supported by the BK21 program of the Korean Ministry of Education & Human resources.

Tang K., & Gomez, A. (1994). *Phys. Fluids*, 6, 2317-2332.

Oh, H., & Kim S. (2006). In *Proc. 7th Int. Aerosol Conf.*, 32.

## **T10 Abstracts**

## Individual protection against inhalation of long living radioactive dust due to an uncontrolled release

Streil, T<sup>1</sup>, V. Oeser<sup>1</sup>, R. Rambousky<sup>2</sup> and F.W. Buchholz<sup>2</sup>

<sup>1</sup> SARAD GmbH, Wiesbadener Str. 10-20, D-01159 Dresden, Germany

<sup>2</sup> Armed Forces Scientific Institute for Protection Technologies- NBC Protection  
PO.Box 1142, 29633 Munster, Germany

Keywords: aerosol instrumentation, inhalation, nuclear aerosols, radioactive particles, radon decay products

Individual protection against inhalation of long living radioactive dust (LLRD) saves human life and health. LLRD may occur in natural environment ( NORM materials like Thorium, Uranium, and Radium) as well as in case of nuclear accident or military (DU- munitions) and terrorist attacks (dirty bombs). **MyRIAM** is the acronym for **My Radioactivity In Air Monitor** and points out that the device was designed for **personal use to detect any radioactivity in the air at the place and at the moment of the danger**. Therefore, it is the unique way to detect dangerous exposures in time to warn the person and the public. The active air sampling process enables a detection limit several orders of magnitude below that of Gamma detectors. But in any case, the immediate warning of the population is from major meaning. Keep in mind: it is very easy to avoid LLRD inhalation - but you have to recognise the imminent danger. The increasing terrorist activities focus on the problem of using nuclear or radioactive material by terrorists. In the US and EU many high level security systems were implemented or are being installed. However the best-performed security system cannot ensure 100% protection against the multiple possibilities of terror offences. Therefore, the following question arises: How will the terrorists apply this material and what's to do in order to protect the population? We believe, one of the most likely scenarios is the injection of radioactive material into the ambient air by dirty bombs or simple aerosol generators. Compared with the assembling of nuclear weapons, this kind of use is very easy to realise without detailed technical knowledge, infrastructure and transport logistics, which is needed to create and use nuclear bombs. Furthermore, beside the Plutonium and High Enriched Uranium (HEU), also the extremely radioactive and easy to acquire isotopes Radium and Thorium and other radioactive isotopes from medical applications or from radioactive waste, like **Sr-90, I-131, Cs-137, Co-60 etc.** could be used. In the US as well as in the EU, only wide meshed networks of high volume air samplers with very low detection limits for environmental monitoring exist. Because of their size and power consumption, such samplers are usually installed in observation

containers or institutes which are not the typical objects of interest for terrorists. Therefore, incidences inside buildings will not be detected and most small-scale outdoor events will be visible only in case of injured persons. The only way to close this security gap is to equip persons who will likely be exposed to radiological terrorist attacks. Such persons could be members of fire brigades and military task forces, police officers as well as bodyguards of politicians, or staff of public utilities.

The MyRIAM, containing an internal pump with a continuous air flow of 0.25 l/min, samples the nuclides on a Millipore filter with excellent spectroscopic resolution. A 1.5 cm<sup>2</sup> light protected ion-implanted silicon detector analyses the  $\alpha$ - and  $\beta$ - radiation on the filter. This small detector head contains also the pre amplification and pulse processing unit. The  $\alpha$ - and  $\beta$ - radiation of the radon progeny and the long-lived  $\alpha$ - and  $\beta$ - nuclides are analysed by a 60-channel spectrometer. The energy resolution of the online analysed filter spectrum is in the order of 150 keV. Mechanical and electronic design enables one to distinguish the long-lived  $\alpha$ - and  $\beta$ -nuclides from the Radon and Thoron progeny very easily. The threshold energy for the analyses of the  $\beta$ - nuclides is 120 KeV. Using a special algorithm we correct the influence of the tailing of the radon progeny to the long-lived  $\alpha$ - nuclides and take into consideration possible interference in determining the long lived  $\alpha$ - nuclides. Also we correct the  $\beta$ - radiation of natural radon/thoron progeny to the artificial nuclides. Because of the air sampling volume of nearly 15 l/h, the system has a high efficiency. The detection limit by 2 hours sampling time is 0.05 Bq/m<sup>3</sup>  $\alpha$ - nuclide concentrations.

The paper demonstrates the possibility to design small and low cost air samplers, which can be used as personal, alarm dosimeters and fulfil the requirements mentioned above. The system is able to warn with a time resolution of 1 min in the order of 10 % of the yearly radiation limit of 20 mSv/y. Several test measurements taken by a mobile phone sized MyRIAM, shall be used to demonstrate the correctness of this statement.

## Residence Time of Atmospheric Aerosols in Association with Radioactive Nuclides

C. Papastefanou and A. Ioannidou

Atomic and Nuclear Physics Laboratory, Aristotle University of Thessaloniki, Thessaloniki 54124, Greece

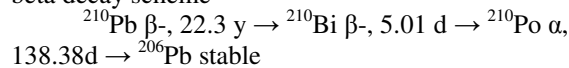
Keywords: Ambient aerosols, Atmospheric aerosols, Radioactive particles, Radon decay products

A method for estimating the residence time of tropospheric aerosol particles associated with the cosmic-ray produced radionuclides, such as  $^7\text{Be}$  is based on the aerosol particle growth rate, that is the change of particle diameter in respect of time, which was estimated to be 0.004 or 0.005  $\mu\text{m h}^{-1}$  (McMurry & Wilson, 1982) and the difference between the activity median aerodynamic diameter, AMAD of a radionuclide, e.g.  $^7\text{Be}$  and the size of Aitken nuclei in the size distribution of aerosol particles, which is 0.015  $\mu\text{m}$  (NRC, 1979). The AMAD for all radionuclides is in the accumulation mode of the size distribution of atmospheric aerosol particles which ranges between 0.1 and 2.0  $\mu\text{m}$  (NRC, 1979). The residence time,  $\tau_R$  is described by the formula

$$\tau_R = \frac{AMAD_{mean} - Size_{Aitken\ nuclei}}{Mean\ particle\ growth\ rate} \quad (1)$$

Taking into account that the AMAD of aerosol particles associated with  $^7\text{Be}$  varied from 0.76 to 1.18  $\mu\text{m}$  as determined from the measured activity size distribution of this radionuclide based in twelve measurements of aerosol samplings carried out during an 1 1/2 - year period, thus including all seasons of a year, then, according to Eq.1 the residence time of atmospheric aerosols will vary between 7.4 and 8.9 days (average 8.0 days) at Thessaloniki region (40°38'N, 22°58'E), Northern Greece, with dry (precipitation-free) climate at temperature latitude.

Another method for estimating the residence time of tropospheric aerosol particles associated with the radon decay product radionuclides is based on the radioactivity of a pair of genetically related radioisotopes, such as  $^{210}\text{Pb}$ ,  $^{210}\text{Bi}$  or  $^{210}\text{Pb}$ ,  $^{210}\text{Po}$  according to the sequential disintegrations in the beta decay scheme



The residence time,  $\tau_R$  based in the first pair of  $^{210}\text{Pb}$  and  $^{210}\text{Bi}$  is described by the formula

$$\tau_R = \frac{1}{\lambda_{Bi}} \frac{\lambda_{Bi} N_{Bi}}{\lambda_{Pb} N_{Pb} - \lambda_{Bi} N_{Bi}} \quad (2)$$

where,  $\lambda_{Bi} N_{Bi}$  is the activity of  $^{210}\text{Bi}$ ,  $\lambda_{Pb} N_{Pb}$  is the activity of  $^{210}\text{Pb}$  in air and  $\lambda_{Bi}=0.138\text{ d}^{-1}$  is the decay constant of  $^{210}\text{Bi}$ . The Eq.2 was derived from the equation of the production and removal of radionuclides assuming a steady state equilibrium

$$\frac{dN_{Bi}}{dt} = \lambda_{Pb} N_{Pb} - (\lambda_{Bi} - \lambda_R) N_{Bi} = 0 \quad (3)$$

where,  $\lambda_R=1/\tau_R$  is the first-order rate constant for the removal of aerosols from the atmosphere by all processes, that is the inverse of residence time,  $\tau_R$ . The ratio of the activities  $\lambda_{Bi} N_{Bi} / \lambda_{Pb} N_{Pb}$  in Eq.2 varied from 0.48 to 0.68 (this work) or from 0.42 to 0.85 (Moore et al., 1972).

Taking into account the  $^{210}\text{Bi}/^{210}\text{Pb}$  ratios as determined in twenty one measurements of aerosol samplings carried out during an annual period, thus included all seasons of a year at Oak Ridge, Tennessee (35°58'N, 84°17'W) at temperate latitude with high precipitation (wet climate), the estimated residence time of tropospheric aerosols in the boundary layer varied from 4.8 to 15.3 days (average 8.2 days).

McMurry, P.H. & Wilson, J.C. (1982), Growth laws for the formation of secondary ambient aerosols: Implications for chemical conversion mechanisms. *Atmospheric Environment* 16, 121-134.

Moore, H.E., Poet, S.E., & Martell, E.A. (1972). Tropospheric aerosol residence times indicated by radon-daughter concentrations. In *Natural Radiation Environment II*. (edited by Adams, J.A.S., Lowder, W.M. and Gessel, T.F.). CONF-720805-P2, pp. 775-786. Technical Information Center/U.S. Department of Energy, Washington D.C.

NRC. (1979). National Research Council. *Airborne Particles*. University Park Press, Baltimore (USA).

## The solubility of the aerosol – $^{137}\text{Cs}$ and $^{60}\text{Co}$ carrier – in the Ignalina Nuclear Power Plant region

R. Jasiulionis, A. Rozkov

Nuclear and Environmental Radioactivity Research Laboratory, Institute of Physics, 02300 Vilnius, Lithuania

Keywords: Ignalina NPP, modelling (regional), radioactive aerosol, soluble fraction

The study of physical and chemical properties of the aerosol – carrier of artificial radionuclides – is of a great importance in the modelling of the radionuclide migration and accumulation in the elements of the biosphere (Jasiulionis & Rozkov, 2006).

The aim of our work was to study the solubility in water of the aerosol – carrier of  $^{60}\text{Co}$  and  $^{137}\text{Cs}$  – in the effluents of the Ignalina Nuclear Power Plant (Ignalina NPP) and in the ground-level air. Experimental data were used to evaluate the radionuclide internal dose in the 30 km Ignalina NPP observation zone.

$^{137}\text{Cs}$  and  $^{60}\text{Co}$  activity concentrations were measured in aerosol samples collected in ventilation stacks of the Ignalina NPP (N 55°36'18" E 26°33'44") Unit 1 and Unit 2 in December 2005 – January 2006. The ground-level air aerosol was collected in 2004-2006 at the monitoring station of the Institute of Physics (PhI station) (N 55°34'34" E 26°35'25"). Gammas energy spectra of samples were obtained using low background HPGe detector.

The solubility in water of aerosol samples was determined as a ratio between the radionuclide activity in the water soluble fraction and that total. The percentage quantities of the water soluble fraction of the Ignalina NPP origin aerosol and that collected at the PhI station were compared.

In certain sampling periods, coinciding with the  $^{137}\text{Cs}$  activity concentration increases in the air, the solubility of the ground level air aerosol – carrier of the radiocaesium – was higher than in other periods. The backward air mass transport trajectories were calculated using the Hybrid Single-Particle Lagrangian Trajectory (HYSPLIT) model (Draxler & Hess, 1998). The observed increase in the aerosol solubility, probably, can be explained by the impact of the atmospheric aerosol of the different origin that was transported into the Ignalina NPP region from distant sources (e.g. due to the resuspension from the Chernobyl NPP accident polluted areas).

The experimental  $^{137}\text{Cs}$  and  $^{60}\text{Co}$  activity concentrations in the air were compared with the Ignalina NPP origin radionuclide activity concentrations that were calculated using the HYSPLIT model. The distribution of radionuclides in deposition was modelled for both water soluble and insoluble fractions of the aerosol. These results were used to determine input parameters in the

radionuclide dynamics equation in the Ignalina NPP region.

Internal radiation doses of  $^{60}\text{Co}$  (about  $0.05 \mu\text{Sv y}^{-1}$ ) and  $^{137}\text{Cs}$  ( $0.5 \mu\text{Sv y}^{-1}$ ) were calculated using the INTERRAS software (IAEA, 1997) and compared with internal radiation doses caused by the naturally occurring  $^7\text{Be}$  ( $100 \mu\text{Sv y}^{-1}$ ). Calculation results were compared with internal radiation doses for the water soluble fraction of the aerosol – carrier of radionuclides.

The authors are grateful to M. and T. Litvinovs for their assistance in sampling of the Ignalina NPP aerosol and Envinet Ltd. (Czech Republic) for the technical assistance.

Draxler R. & Hess D. (1998). *Aust. Meteorol. Mag.*, 47, 295-308.

IAEA (1997). *International Radiological Assessment System (InterRAS), version 1.2.*

Jasiulionis R. & Rozkov A. (2006). *Central European J. Phys.*, 4 (4), 417-428.

## VARIATIONS OF ATMOSPHERIC $^7\text{Be}$ AND $^{210}\text{Pb}$ DEPOSITIONS AT MALAGA, SPAIN

C. Dueñas, M.C. Fernández, S. Cañete and J. Pérez Barea

Department of Applied Physics I, Faculty of Sciences, University of Málaga. 29071 Málaga (SPAIN)

E-mail: [mcduenas@uma.es](mailto:mcduenas@uma.es)

Keywords: atmospheric aerosol, deposition, radioactive particles

**INTRODUCTION.**-Beryllium-7 is one of the radionuclide produced by spallation reactions of cosmic rays with light atmospheric nuclei.  $^7\text{Be}$  rapidly associates primarily with submicron-sized aerosol particles. Gravitational settling and precipitation processes largely accomplish transfer to the earth's surface. Lead-210 which is one of the natural radionuclide of the  $^{238}\text{U}$  decay series is widely used as a tracer.  $^{210}\text{Pb}$  depositional pattern gave us information on continental aerosols in lower troposphere. These two radionuclides with their different sources and therefore are useful to understand the mechanisms of aerosol removal from the atmosphere. These radionuclides have measured routinely in many places of the world in order to study the description of environmental processes such as aerosol transit and residence times in the troposphere, aerosol deposition velocities and aerosol trapping by ground vegetation. The behaviour of the attached radionuclides is determined to a large extent by the physical behaviour of the aerosol particles in the atmosphere. The bulk atmospheric deposition of  $^7\text{Be}$  and  $^{210}\text{Pb}$  has been measured at Málaga, south-eastern Spain, during a period of two years (2005-2006)

**MATERIAL AND METHODS.**- The sampling site is one of the environmental radioactivity monitoring network stations operate by the Spanish Nuclear Security Council (CSN). The sampling point was located above the ground, on the roof of the Faculty of Sciences, University of Málaga ( $4^\circ 28' 80'' \text{W}$ ;  $36^\circ 43' 40'' \text{N}$ ). Precipitation samples are collected on a monthly basis with a bulk rain collector. Monthly precipitation and dry fallout samples were routinely collected using a steel tray  $1\text{m}^2$  in area as a collecting system and polyethylene vessels of 50 l capacity for rainwater samples reservoirs. Measurements by gamma spectrometry were performed to determine the  $^7\text{Be}$  and  $^{210}\text{Pb}$  activities of the samples using an intrinsic REGe detector. The peak analysis of  $^7\text{Be}$  ( $I = 10.52\%$ , 477.7 KeV) and  $^{210}\text{Pb}$  ( $I = 4\%$ , 45 KeV) was done using SPECTRAN AT peak analysis software. The counting time was 172800s

**RESULTS** The results from depositions of  $^7\text{Be}$  and  $^{210}\text{Pb}$  were analyzed to derive the statistical estimates characterizing the distributions. Table 1 provides arithmetic mean (AM) and related statistical information such as geometric mean (GM), standard deviation (SD), dispersion factor of geometric mean (DF), maximum and minimum values and the

coefficient of variation (CV). These values are given in  $\text{Bq/m}^2\text{xmonth}$ .

	AM	GM	SD	DF	Max	Min	CV
$^7\text{Be}$	66.5	38.8	16.6	22	339.5	4.0	122
$^{210}\text{Pb}$	7.9	5.4	1.5	2.6	30.0	1.4	93

Table 1. Statistical parameters.

The AM of deposition monthly of  $^7\text{Be}$  is  $66.5 \text{ Bq/m}^2\text{xmonth}$  and varied widely between 339.5 and  $4.0 \text{ Bq/m}^2\text{xmonth}$ . The annual deposition is  $798 \text{ Bq/m}^2$ . The AM of deposition monthly of  $^{210}\text{Pb}$  is  $7.9 \text{ Bq/m}^2\text{xmonth}$ , ranged from 1.4 to  $30 \text{ Bq/m}^2\text{xmonth}$ .

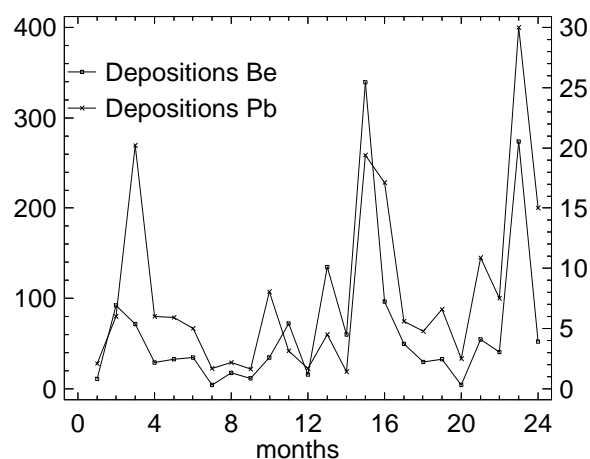


Fig. 1 shows the monthly results for two years. The depositions in 2006 are higher than 2005. Also the precipitations in 2006 are higher than 2005.

The depositions of  $^7\text{Be}$  and  $^{210}\text{Pb}$  are correlated with the magnitude of precipitation with correlation coefficients ( $r$ ) of 0.85 and 0.72 respectively ( $p < 0.001$ ). Such relations have been commonly observed and explained by the fact that rainfall constitutes the major depositional pathway of these radionuclides. As previously observed, correlation of rainfall with  $^7\text{Be}$  seems better than with  $^{210}\text{Pb}$  (Caillet et al., 2001) likely due to a relatively greater contribution of  $^{210}\text{Pb}$  from dry deposition.

Caillet, S., P. Arpagaus, F. Monna and J. Dominik (2001). Factors controlling  $^7\text{Be}$  and  $^{210}\text{Pb}$  atmospheric deposition as revealed by sampling individual rain events in the region of Geneva, Switzerland. *J. Environ. Radioactivity* 53, 241-256.

## Small scale experiments on aerosol resuspension in the nuclear fusion safety field

F. Parozzi<sup>1</sup>, M. T. Porfiri<sup>2</sup>

<sup>1</sup>CESI Ricerca, via Rubattino 54, I-20134, Milano, Italy

<sup>2</sup>ENEA ERG-Fusion Safety & Environment, via Enrico Fermi 45, I-00044 Frascati (Roma), Italy

Keywords: dust, mobilization, resuspension, tokamak, accident.

The ongoing process for the licensing of the International Tokamak Fusion Reactor (ITER) highlights the main safety concerns for this kind of devices. As regards the radiological source term that can be associated to accident scenarios, the aerosol transport process plays a significant role. The presence of airborne particles is due to the mixing of dust and steam as a consequence of a loss of coolant accident, or dust and air moisture if a loss of vacuum accident occurs. The dust settled inside the vacuum chamber is due to several processes like the erosion caused by the plasma (spallation), or by the arcing that locally deposits large amounts of energy onto the surface and induces material evaporation from the walls. Edge Localized Modes (ELM's), Vertical Displacement Events (VDE's) and disruptions, by means of the same mechanism of plasma energy deposition on exposed surfaces, rapidly heat the walls causing the melting and vaporization of the material. Another important origin of dust production is the abrasion for the cut of the components during normal maintenance activities for replacement.

The knowledge about the aerosol transport phenomena inside nuclear installations is quite large thanks to the theoretical and experimental programs carried out in the field of fission reactors safety along these last decades, but it is still weak in the peculiar conditions of the fusion machines. As a matter of fact, the temperature field inside the plasma chamber, the vacuum conditions and the high energy fields involved and the type of dust depositions are likely to be responsible for a quite different behavior of particulate deposits from those investigated for nuclear fission plants, because particles are made of completely different chemical compounds, lifted at much lower pressures and much higher temperatures.

In order to improve the computational tools for the aerosol simulation in case of accident in the fusion machines, possibly starting from the existing nuclear fission background, simple experiments have been managed to investigate the behavior of representative dust samples under conditions reproducing the very fast fluid-dynamic transients expected in fusion reactor accidents.

The lifting of thick dust deposits of different materials subjected to fully turbulent gas flows was directly observed and quantified in the experiments SOFFIA performed at CESI Ricerca (Figure 1); that lifting was obtained with nitrogen flow within a

plexiglass square duct at velocities ranging from 0 to 80 m/s at room conditions (Parozzi, 2006)

In the experimental campaign STARDUST, managed at ENEA, the influence of a sudden inflow of air stream on a dust layer was studied, both starting from atmospheric pressure and from conditions near vacuum (Figure 2) (Paci *et al.*, 2005).

The paper reports the main results of both campaigns and points out the main differences between fission and fusion aerosol features (type, composition, behavior and environment) as regards their expected resuspension behavior to be modelled in the nuclear safety computer codes.

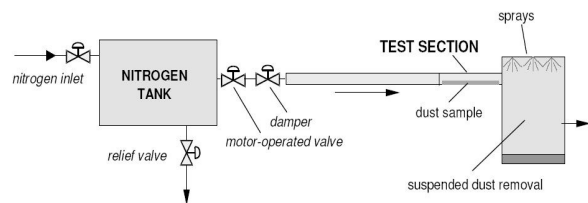


Figure 1. Scheme of the apparatus SOFFIA, with transparent duct operating at room conditions.

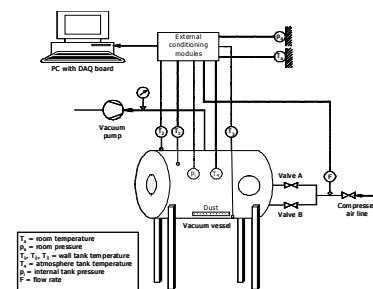


Figure 2. Scheme of the experimental apparatus STARDUST, operating also in vacuum conditions.

This work has been financed by ENEA FUS, EURATOM and by the Research Fund for Italian Electrical System established with Ministry of Industry Decree DM 26/1/2000.

Paci, S. et al. (2005). *Bases for dust mobilization modelling in the light of STARDUST experiments*. Nuclear Eng. and Design 235, 1129-1138.

Parozzi, F. (2006). *Resuspension of multi-layered dust deposits*. AIDIC – Advanced Atmospheric Aerosol Symp. Milan, Italy, 12-15 November.

## Experiments and modelling on the transport and speciation of ruthenium oxides

T. Kärkelä<sup>1</sup>, U. Backman<sup>1</sup>, A. Auvinen<sup>1</sup>, Y. Enqvist<sup>1</sup>, R. Zilliacus<sup>2</sup>, M. Lipponen<sup>2</sup>, T. Kekki<sup>2</sup>,  
U. Tapper<sup>1</sup> and J.K. Jokiniemi<sup>1,3</sup>

<sup>1</sup>VTT Technical Research Centre of Finland, Fine Particles, P.O.Box 1000, FIN-02044 VTT, Finland

<sup>2</sup>VTT Technical Research Centre of Finland, Accident Management, P.O.Box 1000, FIN-02044 VTT, Finland

<sup>3</sup>University of Kuopio, Department of Environmental Sciences, Fine Particle and Aerosol Technology Laboratory, 70211 Kuopio, Finland

Keywords: high temperature aerosols, nuclear aerosols, oxides nanoparticles, radioactive particles

During routine nuclear reactor operation, ruthenium will accumulate in the fuel in relatively high concentrations. In an accident in a nuclear power plant, it is possible that air gets into contact with overheated reactor core. In this case ruthenium may oxidise and form volatile ruthenium species, RuO<sub>3</sub> and RuO<sub>4</sub>, which can be transported into the containment. In order to estimate the amount of gaseous ruthenium species, it is of interest to know, how it is formed and it behaves.

A tubular flow reactor with a high purity alumina tube was applied to oxidise RuO<sub>2</sub> powder at high temperature. The amount of produced gaseous ruthenium oxides was quantified by weighting the oxidation crucible. Non-condensable gas flow through the furnace was set to 5 l/min (0°C, 101325 Pa). Water was added to the gas stream either by saturating air in a temperature controlled bubbler or by adding superheated steam through critical orifice directly into the gas stream. In some experiments, gaseous RuO<sub>4</sub> was produced in a distillation flask and mixed with a carrier gas instead of using a RuO<sub>2</sub> powder sample. The resulting gas mixture was then fed through the tubular flow reactor.

As the gas exited the reactor, it cooled down either in a stainless steel or in an alumina tube. A large fraction of gaseous ruthenium oxides decomposed to RuO<sub>2</sub> particles or reacted on the surface. Aerosol particles were filtered from the gas at 106 cm from the reactor outlet. Gaseous RuO<sub>4</sub> was trapped downstream of the filter in 1 M NaOH-water solution. Mass of ruthenium in filters and in the bubbler was determined with instrumental neutron activation analysis (INAA).

Gas-phase sampling was done at 74 cm downstream of the reactor. Number size distribution of the particles was measured with differential mobility analyser (DMA) and condensation nucleus counter (CNC). RuO<sub>2</sub> particles were also collected on copper grids with electrostatic precipitator (ESP) and analysed with transmission electron microscope (TEM). The ruthenium aerosol deposit samples were analysed with x-ray photoelectron spectroscopy (XPS) in Surface Science group lead by Docent Jouko Lahtinen in Helsinki University of Technology.

In some experiments RuO<sub>2</sub> powder sample contained  $\gamma$ -active <sup>103</sup>Ru isotope. In those experiments ruthenium transport kinetics as well as deposition profile could accurately be measured.

Ruthenium release rate increased from 0.11 to 19.4 mg/min as temperature increased from 1100 K to 1700 K. According to results, the release rate decreased as oxygen partial pressure was decreased. Increasing steam partial pressure while keeping the oxygen partial pressure constant seemed to have no effect on the release rate.

The fraction of ruthenium transported through the facility ranged from 0.6% to 35% depending on experiment. In all experiments most of the released ruthenium deposited as RuO<sub>2</sub> on the surfaces. Gaseous RuO<sub>3</sub> decomposed thermally to RuO<sub>2</sub> as temperature decreased below approximately 800°C. Retention of gaseous RuO<sub>4</sub> on stainless steel depended significantly on whether the surface was metallic or oxidised. In addition, the surface temperature and deposited RuO<sub>2</sub> particles influenced decomposition of RuO<sub>4</sub> to RuO<sub>2</sub>.

The fraction of ruthenium transported as gaseous RuO<sub>4</sub> into trapping bubbler ranged from ~ 0 to 89%. Due to very low release rate, the transport of RuO<sub>4</sub> was lowest at 1100 K. The highest transport rate was measured at 1300 K. The addition of steam into the gas stream increased the fraction of gaseous ruthenium oxides. However, when the temperature of the furnace exceeded 1300 K, the fraction of gaseous ruthenium decreased substantially. At the same time, ruthenium transport as RuO<sub>2</sub> particles increased.

As a conclusion of the study, it can be said that if ruthenium is released from the fuel during an air ingress accident, a significant amount of it is expected to be released from the primary circuit in gaseous form. The most likely mechanism for the release of gaseous ruthenium would be revaporisation of RuO<sub>2</sub> particles deposited on tube surfaces.

This work is supported by Finnish Research Programme on Nuclear Power Plant Safety (SAFIR2010), Fortum Nuclear Services Ltd (FNS) and the Nordic Nuclear Safety Research (NKS-R).

## $^7\text{Be}$ , $^{210}\text{Pb}$ and $^{210}\text{Po}$ concentrations in aerosols in coastal areas of Southwest of Spain

T. Ter n, E. G. San Miguel, J.P. Bol var

Dpto F sica Aplicada. Universidad de Huelva. Facultad de Ciencias Experimentales. 21071-Huelva, Spain

Keywords:  $\text{PM}_{10}$ , TSP, Radioactive particles, Particulate matter.

$^7\text{Be}$ ,  $^{210}\text{Pb}$  and  $^{210}\text{Po}$  are useful to understand the mechanisms of aerosol removal from the atmosphere. They have been used to estimate aerosol residence times in the troposphere and aerosol deposition velocities worldwide (Due as et al., 2005).

$^7\text{Be}$ ,  $^{210}\text{Pb}$  and  $^{210}\text{Po}$  activities have been determined in the  $\text{PM}_{10}$  and TSP fractions of surface aerosols at three different locations of Huelva province (South west of Spain). The monitoring stations were classified, according to their surrounding anthropogenic activities, as follows: 1) Rural background: monitoring station located in the countryside far away from anthropogenic PM emission sources and urban nuclei (INTA) 2) Urban monitoring station located at certain distance from traffic emission sources (El Carmen) 3) Industrialized area: monitoring stations under the influence of industrial particulate matter emissions ( a Rabida).

The aerosols have been collected simultaneously in the three monitoring stations. The sampling was performed at a rate of 1 sample (from 48 to 72 h) every fifteen days.

$^7\text{Be}$  and  $^{210}\text{Pb}$  activities were obtained through gamma spectrometry while  $^{210}\text{Po}$  activities by alpha-particle spectrometry. The present study reports two years measurements (2004–2006) of  $^7\text{Be}$ ,  $^{210}\text{Pb}$  and  $^{210}\text{Po}$  concentrations in surface air samples at these sampling stations. Nevertheless the sampling period can be sub-divided in two ones: 1) from July 2004 to July 2005 in this period we have determined  $^7\text{Be}$  and  $^{210}\text{Pb}$  activities in  $\text{PM}_{10}$  (INTA and El Carmen monitoring stations) and TSP ( a Rabida and INTA monitoring stations) 2) from December 2005 to December 2006 in this period we have determined  $^7\text{Be}$ ,  $^{210}\text{Pb}$  and  $^{210}\text{Po}$  activities only in  $\text{PM}_{10}$  at the three monitoring stations.

The  $^{210}\text{Pb}$  and  $^7\text{Be}$  activities per unit volume and  $^7\text{Be}/^{210}\text{Pb}$  activity ratios for the different sampling stations in  $\text{PM}_{10}$  and TSP fraction of the aerosol are displayed in Figure 1 for the first period of sampling (July 2004–July 2005).

From this figure it can be seen that the levels of  $^7\text{Be}$  are similar to those ones found in other areas of Northern Hemisphere (Due as et al., 2005 and references therein).

The specific objectives of the work are: 1) to know the temporal variation of  $^7\text{Be}$ ,  $^{210}\text{Pb}$  and  $^{210}\text{Po}$  in surface aerosol samples at these stations, 2) to investigate if there are anthropogenic inputs of  $^{210}\text{Pb}$

and  $^{210}\text{Po}$  in aerosols from the area, and 3) to estimate the mean aerosol residence time based on  $^{210}\text{Po}/^{210}\text{Pb}$  activity ratios.

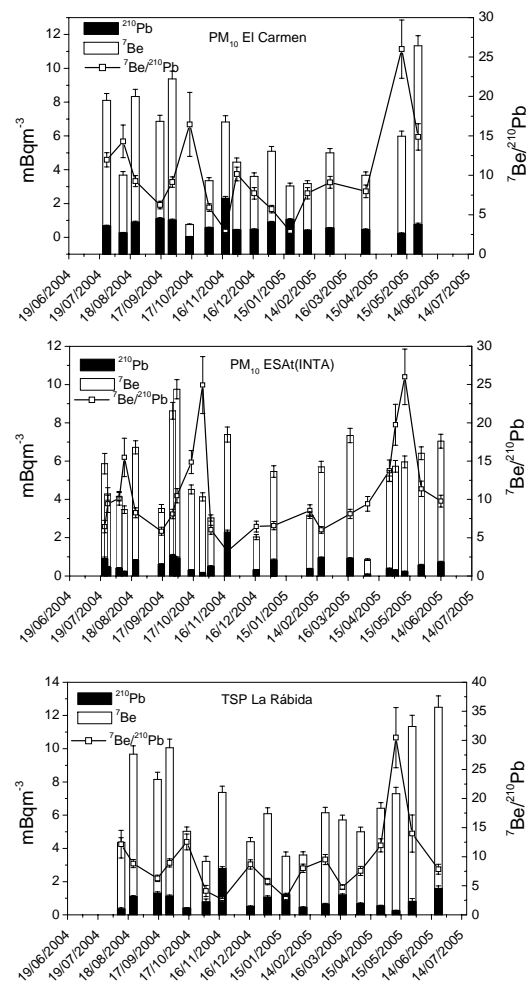


Fig. 1.  $^7\text{Be}$  and  $^{210}\text{Pb}$  activities per unit volume in  $\text{PM}_{10}$  at El Carmen and ESAt (INTA) and in TSP at a Rabida.  $^7\text{Be}/^{210}\text{Pb}$  activity ratios are also shown. The dates are expressed as dd/mm/yy.

This work has been supported by the Spanish Dept. Sci. Tech. under research projects REN2003-04942, CTM2006-08148/MAR.

C. Due as, M.C. Fern ndez, J. Carretero, E. iger, S. Ca ete, *Atmospheric Environ.* 39 (2005) 6897.

## On the comparison of <sup>7</sup>Be activity, trace metal and aerosol mass size distributions.

K. Eleftheriadis<sup>1</sup>, A.A Karanasiou<sup>1,2</sup>, P.A. Siskos<sup>2</sup> and C. Psomiadou<sup>1</sup>

<sup>1</sup>Institute of Nuclear Technology and Radiation Protection, Environmental Radioactivity Laboratory, N.C.S.R. "Demokritos", Ag. Paraskevi, Attiki, 15310, Greece

<sup>2</sup>Department of Chemistry, Laboratory of Analytical Chemistry, National and Kapodistrian University of Athens, Panepistimiopolis, 15771, Athens, Greece

Keywords: <sup>7</sup>Be, size distribution, aerosol characterization, radioactive particles, trace elements

<sup>7</sup>Be is a cosmogenic radionuclide produced by spallation reactions mainly occurring in the stratosphere. Once <sup>7</sup>Be is formed, it is rapidly attached to submicron aerosol particles (Papastefanou and Ioannidou, 1995). <sup>7</sup>Be is a good tracer of vertical transport of stratospheric air masses. The objective of this study was to examine the size distribution of <sup>7</sup>Be and reveal possible correlations with aerosol mass distribution and other aerosol constituents such as characteristic trace metals.

Aerosol sampling was performed over 24 h periods during May-October 2003 at the city of Volos in Central Greece. The size distributions of <sup>7</sup>Be, aerosol mass and trace metals were measured simultaneously using a six-stage Andersen cascade impactor. The cut-off diameters (at 50% collection efficiency) were: 8.8, 3.6, 1.8, 1.2, 0.62, and 0.35 μm at a flow rate of 752 l min<sup>-1</sup>. Aerosol particles collected on cellulose filters were digested in a microwave oven with HNO<sub>3</sub> and HF for the extraction of the total metal content. The solutions obtained were analysed for Cd, Pb, V, Ni, Mn, Cr, Cu, Fe, Al, Ca, Mg, K and Na by atomic absorption spectrometry (AAS). The measurements of <sup>7</sup>Be activity were carried out in two gamma-spectrometry systems each comprised of a HpGe Detector with relative efficiencies of 90% and 20% and a resolution of 2.1 keV at 1.33 MeV. The HpGe detector was connected to a multi-channel analyzer (Canberra Genie 2000). The <sup>7</sup>Be activity was determined by the gamma peak at 477 keV. The measurement duration was 70000 seconds.

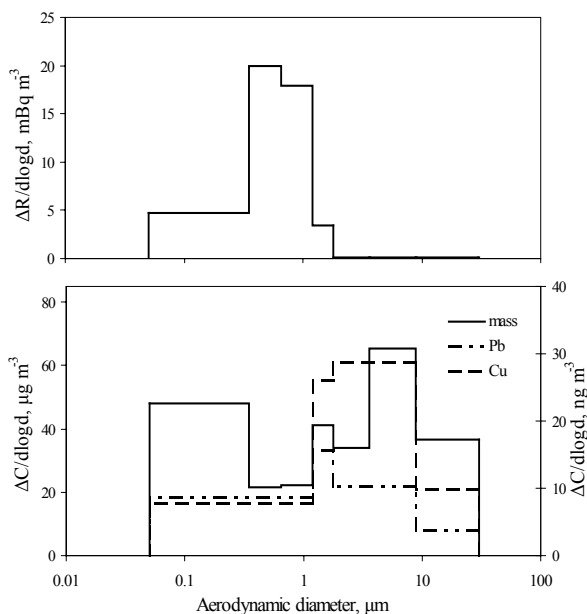
<sup>7</sup>Be concentrations were higher than the mean annual values reported by Gerasopoulos et al., (2003) for Northern Greece. However, this is in line with the fact that during the warm season tropopause height is increased and more efficient vertical mixing is favoured. Moreover according to the 11-year periodicity, <sup>7</sup>Be concentrations during 2003 were expected to approach the maximum of this cycle.

Figure 1 shows the activity size distribution of <sup>7</sup>Be radionuclide, the aerosol mass and the size distribution for two trace metals characteristic of anthropogenic activity. <sup>7</sup>Be showed a unimodal distribution and was exclusively associated with aerosol particles in the accumulation mode ranging from 0.05 to 1.2 μm. The activity median aerodynamic diameter AMAD calculated by the

lognormal function was 0.47 μm. On the other hand aerosol mass followed a bimodal size distribution, with AMDs for the fine and coarse modes at 0.1 and 5.86 μm respectively. This feature is an indication that <sup>7</sup>Be and associated aerosol particles are externally mixed with the aerosol particles derived from ground sources.

The activity median diameter was also anti-correlated to <sup>7</sup>Be activity. For high <sup>7</sup>Be concentrations indicative of stratospheric intrusions, smaller AMD values were calculated. <sup>7</sup>Be activity concentration displayed negative correlation with aerosol mass concentration and against concentrations of most of the determined metals. A positive correlation was found between <sup>7</sup>Be and each of the metals Al, Mg and K.

Figure 1. Activity size distribution of <sup>7</sup>Be and aerosol



mass and trace metal size distributions

### References

- Papastefanou, C., & Ioannidou, A., (1995). *J. Environ. Radioact.* 26, 273–283  
 Gerasopoulos, E., Zerefos, C.S., Papastefanou, C., Zanis, P., & O'Brien K., (2003). *Atmos Environ.* 37, 1745–1756

## Influence of AMAD of industrial alpha-emitting aerosols on Pu dialysis kinetics

V.V. Khokhryakov, S.A.Sypko  
Southern Urals Biophysics Institute, Ozyorsk, Chelyabinsk Region, 456780 Russia

Key words: aerosol size distribution, radioactive aerosols, industrial aerosols, lung/particle interaction

The main factor of internal radiation exposure to workers at radiochemical and chemical-metallurgical facilities is plutonium incorporation as a result of inhalation intake of this radionuclide. Absorption of radioactive substance from respiratory tract into blood (dissolution) plays the most important role in the process of lung clearance. The method adopted in Russia for objective classification of plutonium aerosols based on their transportability that utilizes procedure for radionuclide dialysis through semipermeable membrane, does not account for such an important factor as aerosol particle size. The aim of this study is to clarify the influence of particle size on dialysis kinetics for alpha-emitting aerosols such as plutonium.

Air sample containing industrial alpha-emitting aerosols was collected at a workplace at nuclear fuel reprocessing plant. Aerosols were collected at AFA-RMP20 filters placed at impactor stages. Dialysis procedure was conducted in Ringer's saline during 7 days. Solution was exchanged with clean one after 1, 2, and 4 hours and then 1, 2, 3, 4, 5, 6 and 7 days. Activity of all plutonium isotopes present in substrates obtained in the course of the experiment was determined with radionuclide co-precipitation with bismuth phosphate and subsequent measurement of alpha-activity of precipitate mixed with powdered ZnS scintillator at alpha-radiometer.

Dialysis kinetics presented in Fig.1 is characterized by two fractions: rapid and slow.

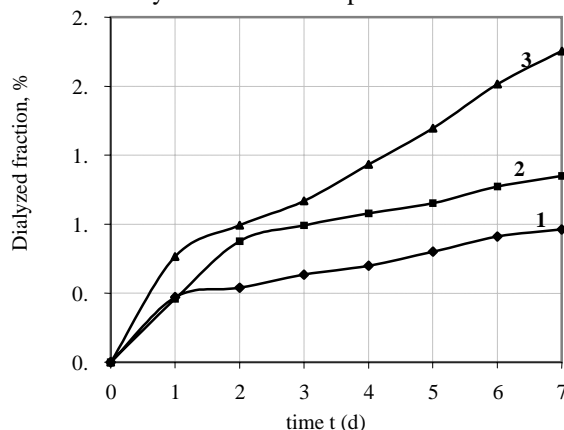


Fig. 1. Pu dialysis kinetics in Ringer's solution for I, II and III impactor stages.

Stage # 1 – AMAD >10 μm); Stage # 2 – AMAD = 7,5μm; Stage # 3 – AMAD = 5 μm.

Plutonium dialysis rate pertaining to aerosols of different AMAD essentially differs. Dialysis rate is inverse proportional to aerosol particle size. International Commission on Radiological Protection (ICRP) recommends Mercer's model to

describe processes of transfer of radioactive substance from solid phase into bodily fluids as follows:

$$\frac{dM}{dt} = -K \cdot S = -K \alpha_s D^2 = -\frac{K \alpha_s M^{2/3}}{(\rho \alpha_v)^{2/3}}$$

where  $M$  - particle mass  
 $S$  - particle surface area  
 $K$  - dissolution rate constant  
 $D$  - particle diameter  
 $\rho$  - density of aerosol solid phase  
 $\alpha_s$  - surface shape factor of aerosol particle calculated by the equation:

$$\alpha_s = \frac{S}{D^2}$$

$\alpha_v$  - volume shape factor of aerosol particle:

$$\alpha_v = \frac{M}{\rho D^3}$$

Experimental validation of Mercer's model showed its inadequacy. Calculated model values for relative rate of plutonium transfer from aerosol solid phase to Ringer's saline differed qualitatively from experimentally observed ones.

The data obtained show the need to conduct more comprehensive study of processes of plutonium transfer from aerosol particle solid phase into bodily fluids.

## Generation and measurement of aerosols for severe nuclear reactor accident research

T.M. Lind, S. Danner and S. Guntay

Paul Scherrer Institut, Villigen, CH-5232 Villigen PSI, Switzerland

Keywords: Aerosol generation, nuclear aerosols, fluidized bed, monodisperse aerosol

Steam generators (SG) in pressurized water reactors (PWR) are subject to research and development due to material degradation leading to a possibility of a tube leakage or rupture (Auvinen *et al.*, 2005). In the unlikely event of a severe accident, steam generator tube rupture may lead to the escape of radio nuclides from the primary circuit to the secondary side, containment bypass, and subsequent emissions to the environment. Generally, no retention of radio nuclides is presumed to occur in the secondary side. However, the steam generator offers ample surface where fission products may be deposited by impaction, thermophoresis, and turbulent deposition. Such deposition would significantly reduce the emissions of the radioactive aerosols.

Due to the complex geometry of the steam generators in PWRs, modeling of deposition of the fissions products in aerosol form is difficult. Even though the main deposition mechanisms are known, turbulent deposition is still not fully characterized. In addition, despite intensive research, resuspension of particles from surfaces can not be modeled for diverse surface and particle characteristics. For this reason, experimental investigation of particle retention in a steam generator is carried out in the ARTIST research program (Guntay *et al.*, 2004). Different types of aerosol particles are used to determine particle retention in a steam generator in several experimental conditions. For modeling purposes, also monodisperse spherical particles were used for the work.

Aerosol was generated using a fluidized bed aerosol generator (FBG) to disperse SiO<sub>2</sub> particles. Commercial SiO<sub>2</sub> powder (Seahostar, by Nippon Shokubai) had particle sizes of 1.0 and 2.6 μm as provided by the manufacturer. The size of the particles was confirmed by SEM micrographs. For feeding with FBG, SiO<sub>2</sub> powder was mixed with 0.2-0.3 mm diameter glass beads that acted as bed material. SiO<sub>2</sub> powder with glass beads was filled into the generator on top of 3 mm glass beads which were used in the bottom of the generator to provide an even air distribution. The gas velocity in FBG was 11 – 18 cm/s.

Aerosol particle size distributions and concentrations were determined at the outlet of the fluidized bed generator using Berner-type low-pressure impactors (BLPI), optical particle counters (OPC, Palas PCS 2010), electrical low-pressure impactors (ELPI), and filter measurements. The

aerosol coming from the fluidized bed generator was mixed with an air flow of 360 kg/h. Then the aerosol flow continued into the aerosol measurement devices. For the steam generator retention tests, the aerosol was then directed into the steam generator test section after the first aerosol measurement location. For calibration purposes, the aerosol was directed to the gas cleaning with a scrubber after aerosol measurements.

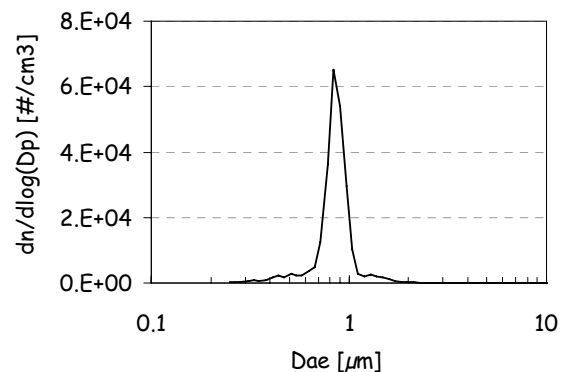


Figure 1. Aerosol size distribution at the outlet of the fluidized bed generator as determined by the optical particle counter.

The results show that almost monodisperse aerosol was generated using FBG and spherical SiO<sub>2</sub> particles. The particle size distributions showed a single particle mode and no agglomerates, Figure 1. The mass concentration of the aerosol as determined by filters, low-pressure impactors, ELPI and OPC agreed well with each other when assuming a spherical shape and the density of 2.0 g/cm<sup>3</sup> to convert number distributions from OPC and ELPI to mass distributions. The particle feed rates up to 17 g/hour were used, corresponding to mass concentration of 60 mg/Nm<sup>3</sup>.

This work was funded through research program ARTIST. The funding by all the partners is acknowledged.

Auvinen, A., Jokiniemi, J.K., Lähde, A., Routamo, T., Lundström, P., Tuomisto, H., Dienstbier, J., Guntay, S., Suckow, D., Dehbi, A., Sloopman, M., Herranz, L., Peyres, V. & Polo (2005). *J. Nuclear Eng. Design*, 235, 457-472.

Guntay, S., Suckow, D., Dehbi, A. & R. Kapulla (2004). *Nuclear Eng. Des.*, 231, 109-121.

## Numerical calculation for radioactive particle sampling in a nuclear stack

S. B. Kim and S. S. Kim

Department of Mechanical Engineering, KAIST, 373-1 Guseong-dong, 305-701, Daejeon, South Korea

Keywords: aerosol sampling, monitoring, numerical simulation, particle deposition, radioactive particles.

To protect environment from radioactive intimidation, monitoring of radioactive particles releasing from nuclear stack is very important. In the monitoring system of nuclear stack, sampling system should deliver a representative sample to detector or collector.

ANSI (American National Standard Institute) reported criteria of sampling position in nuclear stack, to make representative sampling, in ANSI/HPS N13.1-1999. The criteria of sampling position of radioactive particle are as following:

1. In velocity profile, COV (Coefficient of Variation) shall not exceed 20% over the center region of the stack that encompasses at least 2/3 of the stack area.
2. The average swirl angle shall be less than 20°
3. COV of particle concentration shall not be exceed 20 % over the center region of the stack that encompasses at least 2/3 of the stack area.

In present study, the COV and swirl angle along the stack height were determined numerically. Using present calculation, the sampling position can be predetermined. Therefore, the sampling line from probe to detector can be minimized to reduce deposition loss. The calculation geometry was similar to Rodgers *et al.* (Rodgers *et al.*, 1996). The disturbance is occurred at the interface between rectangular duct and stack. Merge angle between duct and stack is 45°.

Calculation was performed for Reynolds number of  $10^5$ ,  $3 \times 10^5$  and  $5 \times 10^5$  which cover normal and abnormal operating condition of nuclear facilities. Standard k-ε model was used to include turbulence effect and flow field was calculated using finite volume method.

Figure 1 shows COV as function of stack height. D is diameter of stack. As shown in figure 1, COV decreases as height increases and COV is not significantly affected by Reynolds number. This result is consistent with experimental results of Rodgers *et al.* COV was satisfied the criteria at distance around 4D from the disturbance. The COV can be expressed following fitting equation

$$COV(\%) = 5.56 + 117.26 \exp\left(-0.58 \frac{z}{D}\right)$$

From above equation, the proper sampling position can be determined easily before sample system is installed.

The average swirl angle was also calculated in same Reynolds number range. For all cases, the average swirl angle was satisfied the criteria.

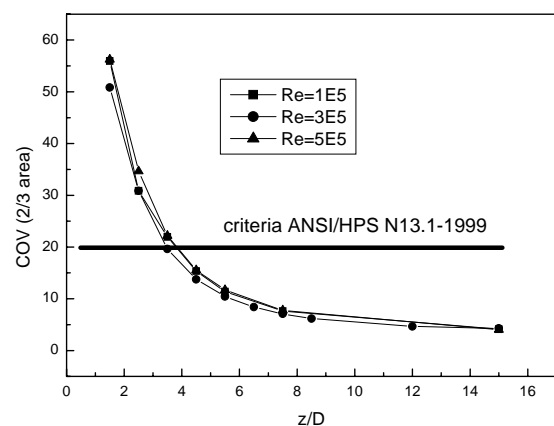


Figure 1. COV as function of height of stack.

This work was supported by the Ministry of Science and Technology (0200-0210-0214-B060601). The authors express their gratitude for support through a grant from the Brain Korea 21 program of the Ministry of Education.

American National Standard Institute. *Guide to sampling airborne radioactive materials in nuclear facilities*. ANSI Standard N13.1-1969. New York: American National Standard Institute, 1969

American National Standard Institute. *Sampling and monitoring releases of airborne radioactive substances from the stacks and ducts of nuclear facilities*. ANSI Standard N13.1-1999. New York: American National Standard Institute, 1999

Chapman, D. H. (1975). *J. Aerosol Science*, 36, 3456-3467.

Rodgers, J. C, Fairchild, C. I., Wood, G. O., Ortiz, C. A., Muyschondt, A. & McFarland, A. R. (1996). *Health Phys.*, 70, 25-35.

## Relationship between origin of air masses and $^{137}\text{Cs}$ activities in French aerosols, 2000-2006

O. Masson, D. Piga, G. Le Roux, L. Bourcier, L. Saey, P. Paulat, X. Cagnat

Institut de Radioprotection et Sûreté Nucléaire, DEI/SESURE

Laboratoire d'Etude Radioécologique du milieu Continental et Marin,

CEN Cadarache Bât. 153 BP 3,13115 St Paul lez Durance

Keywords: aerosol characterization, long-range transport, trajectory, soil re-suspension, tropospheric particles

Atmospheric  $^{137}\text{Cs}$  activities are no more largely decreasing in collected French aerosols since 2000, with actual values between 0.2 et 0.3  $\mu\text{Bq}\cdot\text{m}^{-3}$ . After the large decrease of purely atmospheric, tropospheric or/and stratospheric, inputs of artificial radionuclides, variability of  $^{137}\text{Cs}$  in air is now explained by re-suspension (i.e. soil erosion), re-emission (i.e. fires) of contaminated soils and vegetation coming from more or less remote areas.

Thanks to the sampling stations of the network OPERA ("Observatoire PERmanent de la Radioactivité": Permanent Observatory of the Radioactivity), even small inputs of  $^{137}\text{Cs}$  due to local re-suspension of low-contaminated French soils (1000 to 10 000  $\text{Bq}\cdot\text{m}^{-2}$ ) or incoming of contaminated aerosols transported on a continental scale can be detected.

Our aim was to precise the origin of the past 6y. variability of  $^{137}\text{Cs}$  in the air using a combination of measurements in 6 stations in France and modelling of back-trajectories using Hysplit. More than 14 000 daily back-trajectories were calculated in order to establish a relationship between  $^{137}\text{Cs}$  in the air and the origin of the air masses.

Analysis of back-trajectories highlights quasi-systematic correlations between high  $^{137}\text{Cs}$  in air and continental origin of air masses (Fig.1). Only exceptions are Saharan-dust events increasing aerosol load and importing aerosols from African contaminated soils by global fallout of Nuclear Weapons Tests. This is a combination of re-suspension of contaminated soil and long-distance transport, which can explain the largest observed variability. Oceanic air masses are, them, associated with lower  $^{137}\text{Cs}$  activities (Fig.2).

Combination of our measurements of  $^{137}\text{Cs}$  in aerosols, modelled back-trajectories and also our knowledge of the repartition of the contamination of soils in France and more remote areas, but largely contaminated areas, allows us to calculate the parts of local and long-distance re-suspension and transport in observed  $^{137}\text{Cs}$  activities in the air.

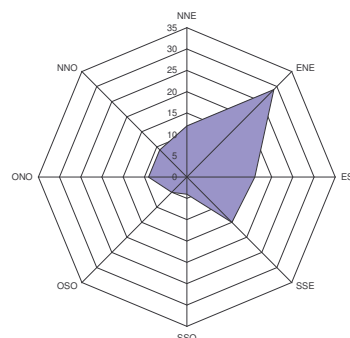


Figure 1. Repartition of the origin of the air masses correlated with high (percentile 90)  $^{137}\text{Cs}$  activities in Charleville-Mézière

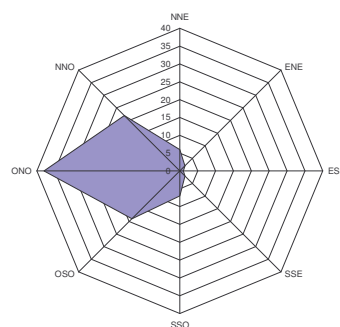


Figure 2. Repartition of the origin of the air masses correlated with low (percentile 10)  $^{137}\text{Cs}$  activities in Charleville-Mézière

### Acknowledgment

The authors gratefully acknowledge the NOAA Air Resources Laboratory (ARL) for the provision of the HYSPLIT transport and dispersion model used in this publication.

## Removal of radon decay products using unipolar ionisers

B.K. Sapra\*, Arshad Khan, Pallavi.S. Kothalkar and Y.S. Mayya

Environmental Assessment Division, Bhabha Atomic Research Centre; Mumbai- 400 085. INDIA.

\*Email: [bsapra@barc.gov.in](mailto:bsapra@barc.gov.in)

Key words – radon decay products, reduction, unipolar ioniser, modelling.

Unipolar ionisers have been used in indoor environments for reduction of particulate levels, in general and radon and thoron decay products, in particular, leading to lowered inhalation doses in the latter case (Sheets and Thompson 1995; Li and Hopke 1991 and Hopke et al, 1993). There are not many studies which model the possible mechanisms leading to this reduction. Mayya et al. (2004) made an attempt at formulating such a model for aerosol particles by considering various processes responsible for aerosol removal in the presence of ionisers. The present study quantifies the reductions obtained in radon progeny concentrations in a confined environment by the use of unipolar ionisers and extends the model proposed by Mayya et al. (2004) to include the radon decay product removal mechanisms.

Experiments were carried out in a 10 m<sup>3</sup> test vessel in which ionisers were suspended in airspace and Ra-226 planchettes (5.85 KBq) were placed at the bottom of the vessel as sources of radon. The radon concentration in the vessel was measured using on-line radon monitor AlphaGuard while the aerosol number concentration was measured on-line in 15 size channels using the Grimm 1.108 Optical Particle Counter. The progeny concentrations inside the vessel were estimated by alpha counting of the Millipore filter paper samples (using a counting protocol of sampling time 5 min, delay time 1 min, and counting time 500 s) collected from the vessel at regular intervals at a flow rate of 10 lpm. The above measurements were made both prior to and post-ioniser operation.

The steady state radon concentration in the vessel was found to be 350-400 Bq/m<sup>3</sup>. As expected, radon being a gas, ioniser operation did not affect its concentration in the vessel. On the other hand, there was a rapid fall in the alpha counts obtained due to the radon progeny when the ionisers were switched on. Within about 300 mins of operation, the steady background levels in the vessel were reached. Reversibly, on switching off the ionisers, these background counts reached the initial peak steady value within 200 min. The progeny concentrations

decreased by a factor of about 10 with a mean life ( $\tau$ ) of about 35 min. Similarly, the total number concentration of all particles > 0.3  $\mu$ m, also showed considerable reduction after the ionisers were switched on.

A mathematical model has been developed for estimating the various fractions of the progeny concentrations in the presence of the ioniser. The possible progeny mechanisms accounted for in this model are radioactive disintegration, attachment to aerosol particles, deposition or plate out on the walls and recoil after attachment. The results of the model compared well with the experimental results. (See Fig. 1). This study has a possible application for reducing progeny concentrations in U mines at local scales and specific working areas such as Uranium mines.

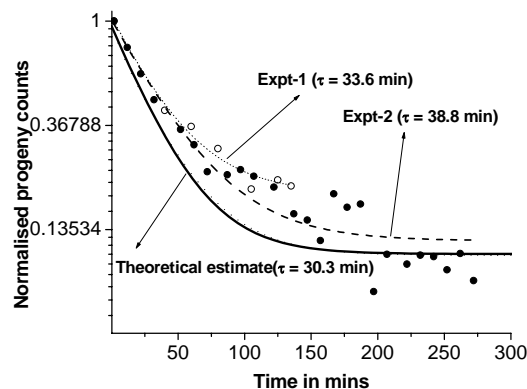


Fig. 1: Comparison of theoretical and experimental results of radon progeny reduction with ionisers

- Y. S. Mayya, B. K. Sapra, Arshad Khan, Faby Sunny (2004). *J. Aerosol Science*, 35, 923-941.  
R.W. Sheets, C. C. Thompson, (1995). *J. of Radioanal. and Nucl.Chem.*, 193(2), 301-308.  
Li, C.S., & Hopke, P.K. (1991). *Health Phys.*, 61, 785-797.  
Hopke, P.K., Montassier, N., & Wasiolek, P.(1993). *Aerosol Sci. and Technol.*, 19, 268-278.

## Atmospheric radioactivity in Slovenia

N. eskovar<sup>1</sup>, Mirko Biz ak<sup>1</sup> and M. Kri man<sup>2</sup>

<sup>1</sup>University of l ubl ana, University College for Health Studies, Pol anska 23a, SI-1000 l ubl ana, Slovenia

<sup>2</sup>Slovenian Nuclear Administration, elezna 16, SI-1000 l ubl ana, Slovenia

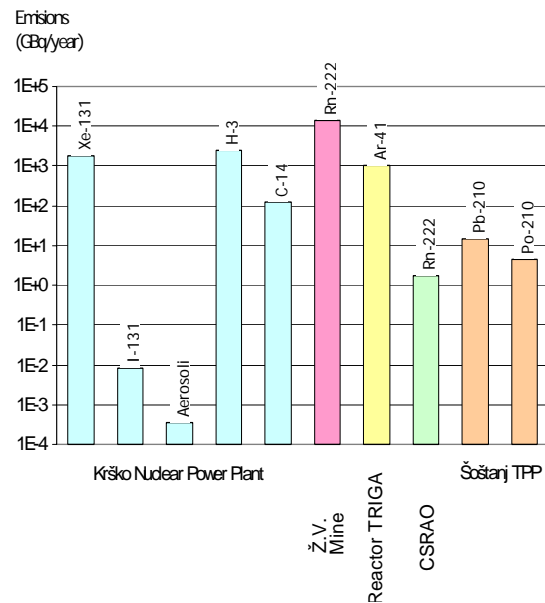
**Keywords:** atmospheric aerosols, radioactive properties, radioactive particles, health effects of aerosols, natural and artificial radioactivity, nuclear explosions tests, nuclear reactor, uranium mine, accidents.

The atmosphere consists of gases, water vapour, and dust particles and beside them also of radioactive substances the latter are mostly gases and solid particles by their composition. Radioactive substances consist of unstable nuclei of various chemical elements and during their radioactive decay into stable nuclei they emit alpha or beta particles and gamma rays. The ma or part of the atmospheric radioactivity is of a natural origin, but some radioactive isotopes in the air are the consequence of the past and current human activities. The largest source of natural radioactivity of the atmosphere is radioactive elements in the Earth crust (uranium, thorium and potassium). Cosmic radiation is less important source and creates radioactive isotopes in the upper layers of the atmosphere through nuclear reactions. Regarding artificial radioisotopes, the most important ones are the long-lived Cesium and Strontium isotopes (<sup>137</sup>Cs, <sup>90</sup>Sr), that resulted from atmospheric nuclear explosions tests in the fifties and sixties of the past century. The biggest radioactive contamination of the atmosphere was caused by the accident at the nuclear power plant in Chernobyl (Ukraine). In much lesser extent, locally the atmosphere is additionally contaminated by operation of nuclear reactors (Table 1) and by uranium mining and other installations (Fig.1).

Table 1: Gaseous releases from the Kr ko Nuclear Power Plant in the period 2002- 2004

ISOTOPE	DISCHARGES GBq/year		
	2002	2003	2004
Noble gases ( <sup>133</sup> e equivalent) <sup>(1)</sup>	0,89.10 <sup>3</sup>	0,12.10 <sup>3</sup>	1,87.10 <sup>3</sup>
Iodine isotopes ( <sup>131</sup> I-equivalent) <sup>(1)</sup>	0,60.10 <sup>-3</sup>	0,22.10 <sup>-3</sup>	8,4.10 <sup>-3</sup>
Aerosols ( <sup>60</sup> Co, <sup>137</sup> Cs,...)	0,76.10 <sup>-3</sup>	0,03.10 <sup>-3</sup>	0,34.10 <sup>-3</sup>
Tritium ( <sup>3</sup> H)	1,25.10 <sup>3</sup>	1,22.10 <sup>3</sup>	2,42.10 <sup>3</sup>
Carbon ( <sup>14</sup> C)	0,084.10 <sup>3</sup>	0,11.10 <sup>3</sup>	0,123.10 <sup>3</sup>

Figure 1: Annual discharges of radio nuclides from individual nuclear or radiation facilities in Slovenia



This paper presents the data on natural and artificial radioactivity concentration in the atmosphere in Slovenia. Natural and artificial radioactive isotopes in the atmosphere are separately quoted, together with their characteristic concentration values, measured or estimated for the Slovenian territory. Radiation exposures for human beings due to inhalation of radioactive substances are also mentioned, together with possible harmful health effects of atmospheric radioactivity on a human body.

This work was done as diploma thesis by N. eskovar in 2005. The support of Slovenian Nuclear Administration is acknowledged.

European Commission DG ENV (2001). *Environmental Radioactivity in the European Community 1995*. Luxembourg: Radiation Protection No.126 2001: 9-51.

Slovenian Nuclear Safety Administration (2005). *Report on Radiation Protection and Nuclear Safety in the Republic of Slovenia in 2004*, extended version of the report, l ubl ana, No. DP-079/2004, l ubl ana, 7/2005, 51-123

## An experimental study on respirator penetration testing by sodium flame and aerosol photometer methods

Z.Z. Zhang<sup>1</sup>, F. Jiang<sup>1</sup>, Z.Y. Zhang<sup>2</sup> and S.S. Ye<sup>1</sup>

<sup>1</sup>Institute of Nuclear and New Energy Technology, Tsinghua University, 100084, Beijing, China

<sup>2</sup>First Affiliated Hospital of Tsinghua University, 100084, Beijing, China

Keywords: sodium flame method, aerosol photometer method, aerosol measurement, respirator, penetration.

According to EN143-2000, two kinds of methods are used for respirator penetration testing, Sodium Flame (also Flame Photometer) and Aerosol Photometer (also Laser Photometer) methods.

In China, Sodium Flame method has been successfully used for the filtration efficiency (100 percent minus penetration) testing of HEPA filter and HEPA filter media for thirty years. In November 2006, Model KZNJ-1 tester is invented by Tsinghua University of China on basis of Sodium Flame aerosol measurement technology. In USA, one tester has been developed for the testing of respirator filtration efficiency which is based on the principle of Aerosol Photometer aerosol measurement technology and named TSI 8130 (TSI Incorporated, St. Paul, MN, USA).

In improved Model KZNJ-1 tester, which is different from previous design (Jiang *et al.*, 2006), the NaCl aerosol shall be generated from 1% solution of NaCl, the atomizer is composed of one Collision Type nozzle and works at a pressure of 2.6 bar. The particle size distributions which are measured by TSI SMPS3936L22 (TSI Incorporated, St. Paul, MN, USA) are shown in Figure 1.

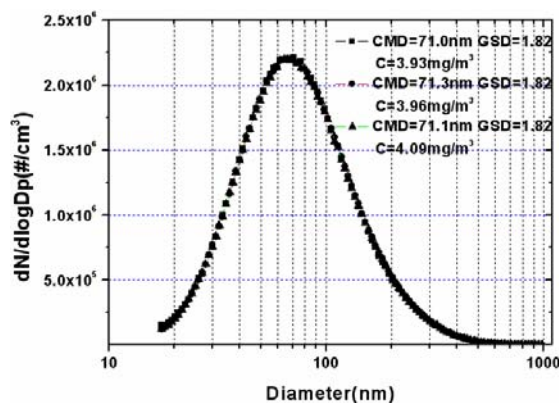


Figure 1. Particle size distribution of NaCl aerosol.

19 pieces of media are tested at 14.2cm/s of face velocity (flow rate is 85l/min, filtration area is 100cm<sup>2</sup>) by one KZNJ-1 tester and two TSI 8130 testers. The experimental results of KZNJ-1 and TSI 8130 are given in Figure 2.

The results show the penetrations have well consistent between KZNJ-1 and TSI 8130 for the media whose penetrations are higher than 0.01%.

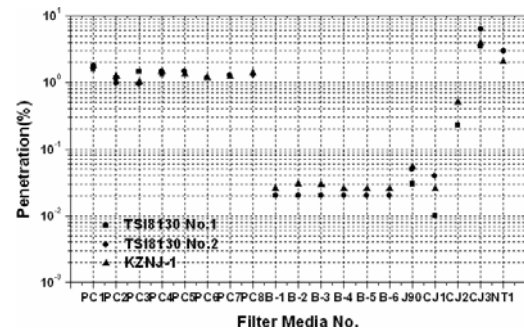


Figure 2. Results comparison of media penetration which are tested by KZNJ-1 and TSI 8130.

Others media are tested at different face velocities (from 1 cm/s to 16.7 cm/s) by one KZNJ-1 tester and one TSI 8130 tester. The experimental data are given in Figure 3.

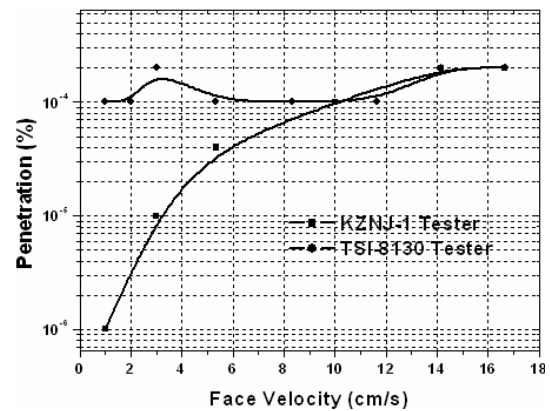


Figure 3. Results comparison of media penetration which are tested by KZNJ-1 and TSI 8130.

From the experimental data, for the media whose penetrations are lower than 0.01%, the accuracy of TSI 8130 is lower. All of the experimental results show the good agreement with those described in EN143.

European Committee for Standardization. (2000). *EN143:Respiratory Protective Device - Particle Filters - Requirements, Testing, Marking.*

Jiang, F., Zhang, Z. Z., & Ye, S. S. (2006). *An Measurement for Filtration Efficiency of Respirator by Sodium Flame Method.* 7th International Aerosol Conference.

## A Discussion on Filtration Mechanism of Moisture Separator for Nuclear Reactor

Z.Z. Zhang, F. Jiang, J.Y. Wei and S.S. Ye

Institute of Nuclear and New Energy Technology, Tsinghua University, 100084, Beijing, China

Keywords: filtration, moisture separator, aerosol measurement, droplets, modelling..

Moisture Separator is a kind of specific particle filter and used in the Nuclear Air Cleaning System of Nuclear Reactor for removing the water droplets whose diameters are larger than  $5\mu\text{m}$ . It consists of wire screens and mixed screens made of wire and glassfiber whose configuration is similar to HEPA filter. But its filtration principle is multilayer filtration which is different from HEPA filter's monolayer filtration.

The schematic diagram of Moisture Separator is shown in Figure 1. Multilayer screens rank in series and can be divided into three groups: the upstream group includes sheets of wire screens which are only weakly hydrophilic but effective in trapping big droplets whose diameters are larger than  $10\mu\text{m}$  and getting them out quickly. The middle group consists of both wire screens and mixed screens. The mixed screens are more strongly hydrophilic and the smaller droplets snatched by them whose diameters are between  $5\mu\text{m}$  and  $10\mu\text{m}$  can stay on the fiber and form the bigger, stable droplets which will significantly influence the filtration process and enhance the filtration efficiency. The downstream group was also made of sheets of wire screens and it will trap almost all the big droplets in the air flow and get them out from the bottom.

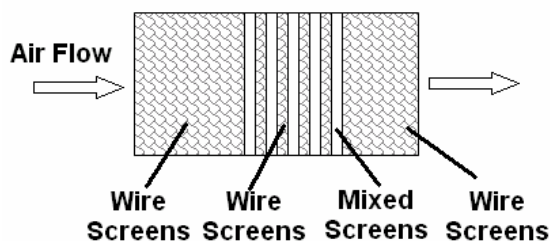


Figure 1. Schematic diagram of Moisture Separator

Table 1. Comparison between theoretical calculations and experimental measurements.

Diameter ( $\mu\text{m}$ )	Measured efficiency (%)	Calculated efficiency (%)
5	89.37	96.85
7	99.57	99.98
10	99.96	$\approx 100$
5~10	99.84	

One experimental system has been set up for testing the filtration efficiency of Moisture Separator by Cascade impactor sampling and microscope measuring method (Huang *et al.*, 2006).

One physical and numerical model has been set up based on the experimental analysis. For the wire screens, we can get the inertial impaction efficiency by a step-by-step particle tracking in a Kuwabara flow field and then calculate the total filtration efficiency of the wire screen. But for a mixed screen, the meshes can be classified into three types: standard meshes, bur meshes and middle meshes (Hung *et al.*, 1999 and 2002).

For standard type, the glassfiber is smooth-faced. For bur type, the surface of glassfiber has many burs and the burs make the mesh size more small. Middle type is one whose bur number is between that of standard type and bur type. The proportions of them are respectively about 30%, 20% and 50% by statistical analysis.

The developing trend and the critical size of the droplets for each kind of meshes are studied with the correction for horizontal air flow. Then we can get the inertial impaction efficiency in an around-flat flow field so as to calculate the efficiency of the mixed screen. At last, we get the total efficiency of Moisture Separator according to the theory of the filtration efficiency for filters in series. The calculation and experiment results under the rated running condition ( $1700\text{m}^3/\text{h}$ ) are given in Table 1.

In consideration of disintegration of the larger droplets during the filtration process, the theoretical result is well consistent with the experimental data. These proved that the computational model is successful.

In order to get more accurate result, two possible factors should be took in account in succedent research: on the one hand, we should have a more accurate consideration of the burr meshes; on the other hand, we should describe the disintegration of droplets in air flow field and during the filtration process.

Huang, Y. F., Zhang, Z. Z., Jiang, F., & Ye, S. S. (2006). *Measurement for Moisture Separator Efficiency. Nuclear Power Engineering*, 27(1), 70-72.

Hung, L. S., & Yao, S. C. (1999). *Experimental Investigation of the Impaction of Water Droplets on Cylindrical Objects. International Journal of Multiphase Flow*, 25, 1545-1559.

Hung, L. S., & Yao, S. C. (2002). *Dripping Phenomena of Water Droplets Impacted on Horizontal Wire Screens. International Journal of Multiphase Flow*, 28, 93-104.

## Image Force Effect on Aerosol Penetration through Wire Screen in the Transition Regime

M. Alonso<sup>1</sup>, F.J. Alguacil<sup>1</sup>, N. Jidenko<sup>2</sup> and J.P. Borra<sup>2</sup>

<sup>1</sup>Centro Nacional de Investigaciones Metalúrgicas (CSIC), 28040 Madrid, Spain

<sup>2</sup>Lab. de Phys. Gaz & Plasmas (UMR 8578 CNRS Univ Paris-Sud Orsay, F-91405) Supélec, F-91192 Gif

Keywords: aerosol filtration, wire screen, image force, charged particles, penetration

An experimental investigation has been carried out to examine the effect of image force on the penetration of multiply-charged aerosol particles through wire screens.

In the experiments, neutral monodisperse ZnCl<sub>2</sub> aerosol particles were charged in a corona ionizer, and classified by means of a DMA into fractions of monodisperse particles having +1, +2 and +3 elementary charges. The neutral and charged aerosols were passed alternatively through two geometrically identical cylinders, one of them equipped with four wire screens. Penetrations were determined from comparison of the concentrations measured at the outlet of both cylinders. Particle number concentrations were kept below 10<sup>4</sup> cm<sup>-3</sup> so as to rule out space-charge effects.

Experiments were carried out for particle diameter between 25 and 65 nm (transition regime) and aerosol flow rates of 1, 1.5 and 2 lpm. The results for 1 and 2 lpm are shown in Figures 1 and 2, respectively. The curves shown in the Figures were calculated by means of the correlation

$$P = \exp[-nS(\eta_D + \eta_{IM})], \quad (1)$$

where  $n$  is the number of screens (four),  $S$  is the screen parameter (= 1.437 in our case), and  $\eta_D$  and  $\eta_{IM}$  are the single fiber efficiency for the mechanisms of diffusion and image force, respectively. The diffusional efficiency was calculated with the expression (Cheng and Yeh, 1980)

$$\eta_D = 2.7Pe^{-2/3},$$

where  $Pe$  is the Peclet number. The single fiber efficiency for the mechanism of image force has been taken to be of the form (Brown, 1993)

$$\eta_{IM} = aK_{IM}^{1/2},$$

where  $a$  is a constant, and

$$K_{IM} = \left( \frac{\epsilon_r - 1}{\epsilon_r + 2} \right) \frac{Cp^2e^2}{12\pi^2\mu\epsilon_0d_p d_f^2}$$

is the dimensionless number accounting for the image force effect (Shapiro et al., 1988). In the last expression,  $C$  is the slip correction factor,  $pe$  the

particle charge,  $\mu$  the air viscosity,  $d_p$  the particle diameter,  $d_f$  the fiber diameter, and  $\epsilon_r$  the relative permittivity of the grid. From the analysis of experimental data the value  $a = 7.73$  was obtained for a relatively good agreement between the calculated and experimental data.

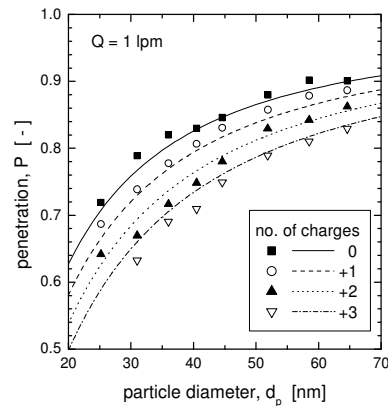


Figure 1. Comparison between experimental results (symbols) and Eq.(1). Aerosol flow rate = 1 lpm.

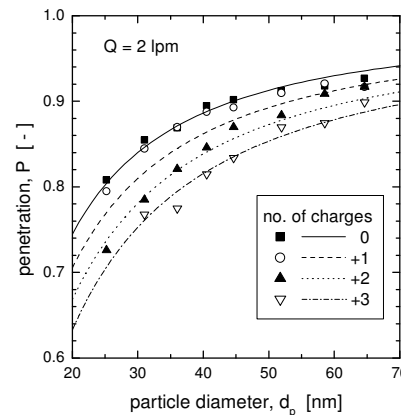


Figure 2. Comparison between experimental results (symbols) and Eq.(1). Aerosol flow rate = 2 lpm.

Cheng, Y. S., & Yeh, H. C. (1980). *J. Aerosol Science*, 11, 313-320.

Shapiro, M., Gutfinger, C., & Laufer, G. (1988). *J. Aerosol Science*, 19, 651-677.

Brown, R.C. (1993). *Air Filtration*, Pergamon Press.

## Filtration of fine particles by melt-blown nonwovens

E.Jankowska<sup>1</sup> and J.Kaluźka<sup>2</sup>

<sup>1</sup>Department of Chemical and Aerosol Hazards, Central Institute for Labour Protection  
– National Research Institute, Czerniakowska 16, 00-701 Warsaw, Poland

<sup>2</sup>Polymer Laboratory, Textile Research Institute, Brzezińska 5/15, 92-103 Łódź, Poland

Keywords: melt-blown nonwovens, fine particles, filtration, fractional efficiency.

Melt-blown nonwovens are widely used for air cleaning from fine particles because this technology allows making filtering materials with a small diameter of fibres (Gradoń *et al.*, 2006).

This article presents the results of investigation of fractional efficiency of melt-blown nonwovens made of polypropylene Borealis Borflow HL 608 FB (melt flow rate - MFR - 800g/10min). In the Textile Research Institute melt-blown nonwovens with different average diameter of elementary fibres were made by changing, in control conditions, two parameters (polymer feed rate and output of hot compressed air). The parameters of these nonwovens are shown in Table 1.

Table 1. Parameters of nonwovens made with the melt-blown technology.

No	Average diameter of fibres (µm)	Area weight (g/m <sup>2</sup> )	Thickness (mm)
1	1.99	37	0.74
2	2.13	74	1.47
3	2.31	72	1.13
4	3.83	102	0.84

The microscope views of the surface of nonwovens with average fibres diameters 1.99 µm and 3.83 µm are shown in Figure 1.

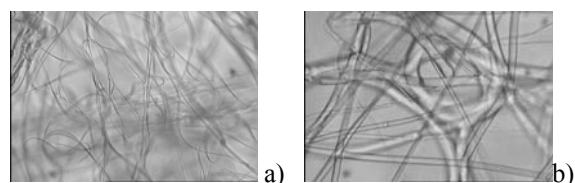


Figure 1. The microscope view of surface of nonwovens with average fibres diameter:  
a) 1.99 µm, b) 3.83 µm.

The fractional efficiency of nonwovens was determined in the Central Institute for Labour Protection-PIB with a condensation particle counter (CPC 3022A, TSI), equipped with an electrostatic classifier (DMA 3080L, TSI). Atmospheric aerosol was used as the test aerosol. The results of investigation of fractional efficiency of nonwovens for particles from the range 27 nm to 274 nm and air velocity 5 cm/s and 10 cm/s are shown in Figure 2.

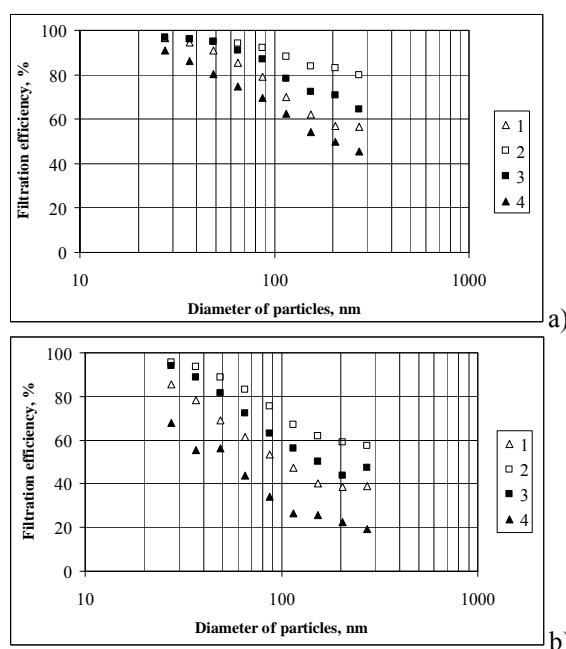


Figure 2. Fractional efficiency of nonwovens for different air velocity: a) 5 cm/s, b) 10 cm/s.

Fractional efficiency of made nonwovens were higher for air velocity 5 cm/s than for 10 cm/s, especially for particles with bigger diameter.

Nonwoven No.1 with smaller average diameter of fibres 1.99 µm and area weight 37 g/m<sup>2</sup> has higher fractional efficiency than nonwoven No.4 with bigger average diameter of fibres 3.83 µm and area weight 102 g/m<sup>2</sup>.

Area weight and thickness of nonwoven No.2 - about two times bigger than for nonwoven No.1 - significant influence on fractional efficiency (both nonwovens have similar average diameter of fibres). For example, for atmospheric aerosol particles with diameter 87 nm the efficiency of nonwoven No.2. was 13 % higher for air velocity 5 cm/s and 23 % higher for 10 cm/s than for nonwoven No.1.

This study was supported by the Polish Scientific Committee under grant 3 T08E 035 30.

Gradoń, L., Bałazy, A., & Podgórski, A. (2006). Nanofibrous media – promising tools for filtration of nanosized aerosol particles. in *Proceeding of the Seventh International Aerosol Conference*, St. Paul, Minnesota, 319-320.

## A mathematical model of the deposit on fibrous filters as a porous medium.

Sarah J. Dunnett<sup>1</sup>, Charles F. Clement<sup>2</sup>

<sup>1</sup>Department of Aeronautical and Automotive Engineering, Loughborough University, Loughborough, Leics. LE11 3TU, U.K.

<sup>2</sup>15 Witan Way, Wantage, Oxon, OX12 9EU, U.K.

Keywords: filtration, numerical simulation

### INTRODUCTION

Fibrous filters are widely used to separate particles from fluid flow. They generally consist of many threadlike fibres which are positioned more or less normal to the direction of the fluid flow. The flow passes through the regions between the fibres and some of the particles contained within the flow may be removed by deposition onto the fibres surface. The deposit builds up on the fibres until in the limit clogging takes place. Neglecting the influence of electric effects the main mechanisms by which particles are removed are interception, impaction, diffusion and gravitational settling. The dominant mechanism for any application will depend upon the size of the particles being considered.

Although the performance of clean filters is now well understood, the feedback effects particulate deposit has upon further deposit and filter performance is less so. In earlier work by the authors, Dunnett and Clement (2006), the effects of diffusive deposition on the efficiency of fibrous filters was studied by considering the deposit to form a smooth solid layer on the fibre surface. In the work described here that model is extended by assuming the deposit forms a porous layer.

### NUMERICAL MODEL

As in Dunnett and Clement (2006) a cell model has been developed where the equations of motion are solved in a two dimensional 'cell' surrounding a single fibre, where the boundary conditions applied on the cell boundaries take into account the presence of neighbouring fibres. In order to account for the porous deposit on the fibre the 'cell' is divide into two regions I and II, see figure 1. Region II is the porous deposit and region I is the area outside the deposit.

Considering the outer region I, as the Reynolds number for the fluid flow through a filter is generally very small the Navier-Stokes equations of motion reduces to the biharmonic equation for the stream function,  $\psi$ ,

$$\nabla^4 \psi = 0 \quad (1)$$

In region II, assuming a small porosity, the flow can be represented by the Darcy equation for pressure P,

$$\nabla P = -\frac{\mu}{k} \underline{V} \quad (2)$$

where  $\mu$  is the fluid viscosity,  $k$  is the permeability of the medium and  $\underline{V}$  is the fluid velocity.

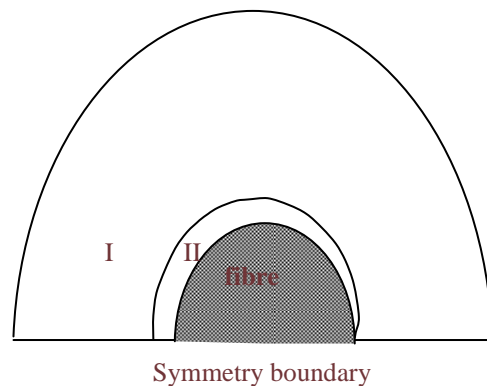


Figure 1. Cell considered.

Equations (1) and (2) are solved subject to appropriate boundary conditions using the Boundary Element Method (BEM). The advantage of the BEM technique is that only the boundary of the fibre needs to be divided into elements, hence requiring lower computer resources than other available numerical methods. The effect of allowing region II to be porous is that the boundary between it and region I is divided into two parts: a part A where flow is into the deposit and a part B where flow is out of the deposit.

Once the flow field for a particular deposit has been obtained the equations of motion of the particles are solved and the feedback effects of the deposit upon further deposition investigated. In this work small particles are modelled to allow capture by interception and diffusion. Relative to the non-porous case, deposition is enhanced along boundary A, but decreased for boundary B. The efficiency of the filter as the deposit grows is also investigated.

The present work is intended to provide a practical means of investigating the effects of aerosol deposition on fibres upon the immediate flow field and hence further deposition.

### REFERENCES

Dunnett, S.J. and Clement, C.F. (2006) *J.Aerosol Science*, 37, 1116-1139.

## Experimental determination of axial dispersion coefficients of aerosol particles in fibrous filters

A. Jackiewicz, A. Bałazy and A. Podgórski

Faculty of Chemical and Process Engineering, Warsaw University of Technology, Waryńskiego 1, 00-645 Warsaw, Poland

Keywords: dispersion, fibrous filters, filtration.

Fibrous filters are very efficient for sub- and micrometer particles' removal. Fractional penetrations for a wide size range of solid aerosol particles through such five filters made by us utilizing the melt-blown technique were determined using the modular filter test system (model MFP-2000, Palas GmbH, Germany). The experiments were carried out for several different air velocities in the range  $U=0.08-0.2$  m/s. To describe data obtained for multilayer sets of fibrous filters composed of up to nine layers of the same filter, the axial dispersion model was applied. This model predicts a non-exponential decrease of aerosol penetration with filter thickness,  $L$ . The solution of the standard axial dispersion model for aerosol filtration in fibrous filters with Danckwerts' boundary conditions has the following form:

$$\frac{1}{P} = \frac{\left(1 + \sqrt{1 + \frac{4d_F \lambda}{Bo}}\right)^2}{4\sqrt{1 + \frac{4d_F \lambda}{Bo}}} \exp\left[-\left(1 + \sqrt{1 + \frac{4d_F \lambda}{Bo}}\right) \frac{LBo}{2d_F}\right] + \frac{\left(1 - \sqrt{1 + \frac{4d_F \lambda}{Bo}}\right)^2}{4\sqrt{1 + \frac{4d_F \lambda}{Bo}}} \exp\left[-\left(1 - \sqrt{1 + \frac{4d_F \lambda}{Bo}}\right) \frac{LBo}{2d_F}\right]$$

where the Bodenstein number is defined as follows:  
 $Bo = Ud_F / \epsilon D_x$ .

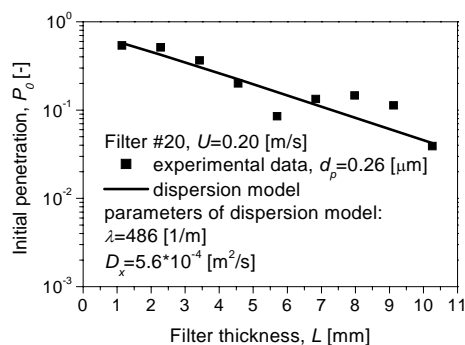


Figure 1. Application of the dispersion model to fit the experimental data of particles' penetration through the nine layers of the filter #20.

Dispersion model contains two parameters,  $\lambda$  and  $D_x$ , which were evaluated on the basis of the experimental data.  $\lambda$  is the filter coefficient which is related to the single fiber efficiency,  $E$ , the fiber diameter,  $d_F$ , and the filter porosity,  $\epsilon$ , as:  $\lambda = 4E(1-\epsilon) / \pi \epsilon d_F$ .

For the first ever time the axial dispersion coefficients in fibrous filters were determined. It was found that the coefficients of axial dispersion,  $D_x$ , are a few orders of magnitude greater than the values of the Brownian diffusion coefficients,  $D$ , determined for the same particle diameters. The ratio of the dispersion coefficient,  $D_x$ , to the coefficient of Brownian diffusion,  $D$ , was found to be nearly proportional to the Peclet number,  $Pe$ , see Fig. 2. This suggests predominance of the convective dispersion mechanism in highly porous fibrous filters, which have always more or less inhomogeneous internal structure. Inhomogeneity of the fibrous filters causes a tunneling effect of the aerosol flow. It means that there are preferential flow paths through the areas of a higher local porosity. We can conclude that the mass dispersion may be significant phenomenon in fibrous filters, especially in these ones having a high porosity, a low thickness and a high degree of the structure inhomogeneity.

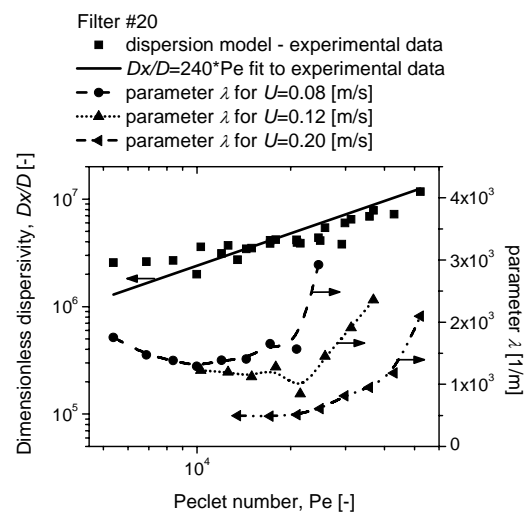


Figure 2. Dimensionless dispersivity,  $D_x/D$ , and  $\lambda$  parameter vs the Peclet number for the filter #20 ( $\epsilon=82.2\%$ ,  $d_F=12.47 \pm 7.64 \mu\text{m}$ ,  $L=1.14$  mm) for the several air velocities.

## Experimental determination of inhomogeneity factors of fibrous filters

A. Jackiewicz, A. Zaręba, A. Podgórski and A. Bałazy

Faculty of Chemical and Process Engineering, Warsaw University of Technology,  
Waryńskiego 1, 00-645 Warsaw, Poland

Keywords: inhomogeneity factor, fibrous filters, filtration.

Real filters are inhomogeneous and the degree of nonuniformity depends on the manufacturing method used. Performance of twelve filters made by us utilizing the melt-blown technique were determined using the modular filter test system (model MFP-2000, Palas GmbH, Germany). The experiments were carried out for air velocity  $U=0.2$  m/s.

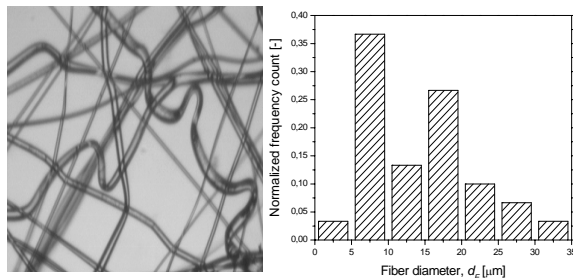


Figure 1. Fiber size distribution of the filter #3.

A degree of the fibers' polydispersity can be characterized by the coefficient of variation,  $CV$ , defined as a ratio of standard deviation,  $SD$ , to the mean fiber diameter,  $d_F$ :  $CV=SD/d_F$ .

Table 1. Characteristics of the analyzed filters.

Filter No.	Fiber diameter, $d_F \pm SD$ [ $\mu\text{m}$ ]	Packing density, $\alpha$ [-]	Thickness, $L$ [mm]
1	26.2 $\pm$ 11.2	0.145	1.26
2	15.3 $\pm$ 6.7	0.154	1.35
3	14.5 $\pm$ 7.5	0.160	1.25
5	6.1 $\pm$ 3.5	0.0361	3.77
6	8.4 $\pm$ 4.9	0.0527	2.22
7	3.9 $\pm$ 1.8	0.0386	5.20
8	29.7 $\pm$ 9.0	0.235	10
9	28.1 $\pm$ 10.2	0.198	10
10	14.8 $\pm$ 6.7	0.183	10
11	27.1 $\pm$ 11.7	0.218	10
12	27.4 $\pm$ 13.4	0.227	10
14	17.3 $\pm$ 7.3	0.258	10

The inhomogeneity in a filter media may be quantified by comparing theoretical predictions of filter performance with experimental data, c.f., Fig. 2. The inhomogeneity factor for the pressure drop is defined as  $A_p = \Delta p / \Delta p_{hom}$ , and the inhomogeneity factor for the penetration as  $A_E = \ln P / \ln P_{hom}$ , where  $\Delta p_{hom}$  and  $P_{hom}$  are calculated using classical single-fiber theory based on the Kuwabara flow model. We can observe in Fig. 3 that  $A_E$  can be either greater or

lower than one, depending on the filter structure and particle diameter, and that it reaches a local maximum for the range of particle diameter 0.4-0.7  $\mu\text{m}$ . Contrary to that, the values of  $A_p$  were found to be always below one, see Fig. 4. It seems, however, that a single parameter, like  $CV$ , characterizing filter inhomogeneity, is insufficient to describe precisely of a real filter performance from the idealized, homogeneous medium, and the distribution of fiber sizes should be rather analyzed.

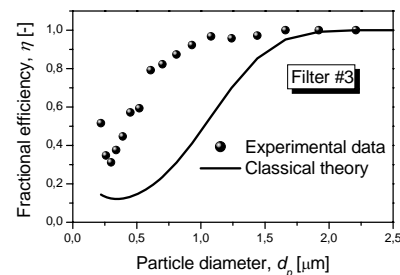


Figure 2. Example of comparison of the experimental data with results of classical theory.

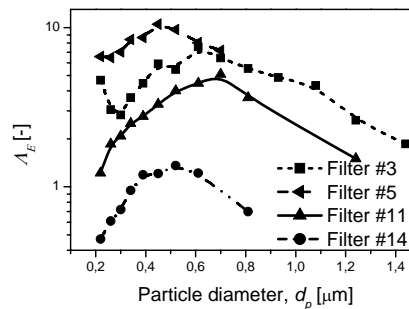


Figure 3. Effect of particle diameter,  $d_p$ , on  $A_E$ .

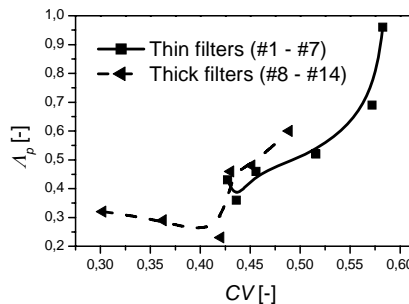


Figure 4.  $A_p$  vs  $CV$  for all filters.

## Filtration of liquid aerosol particles in multilayer fibrous filters – theoretical and experimental results

T. Jankowski

Department of Chemical and Aerosol Hazards, Central Institute for Labour Protection – National Research Institute, 00-701 Warsaw, Poland

Keywords: aerosol filtration, fibrous filters, filtration efficiency, SMPS

According to Brown's (1993) classic theory of depth filtration, changes in structural parameters and aerosol flow conditions influence the filtration efficiency of fibrous filters. The filtration efficiency ( $\eta_i$ ) of fibrous filters is considered as a sum of single fibre efficiencies, which make up a fibrous filter of known thickness ( $L$ ), according to the formula:  $\eta_i = 1 - \exp(-\lambda \cdot L)$ , wherein filter coefficient ( $\lambda$ ) depends on the efficiency of particle deposition on a single fibre ( $E$ ), the fibre diameter ( $d_f$ ) and the filter porosity ( $\epsilon$ ).

According to Podgórski (2003), changes in the thickness and porosity of two-layer filters have a significant influence on the filtration efficiency of solid aerosol particles through the composition of the raw material of nonwovens.

This article compares empirical results of an investigation of filtration efficiency of liquid aerosol particles through multilayer fibrous filters to Brown's (1993) theoretical results.

The experiments were carried out using commercial needled nonwovens manufactured from polyester fibres. The sebacic acid-bis (2-ethylhexyl) ester (DEHS) test was used for measuring filtration efficiency of aerosol particles through multilayer fibrous filters. The DEHS aerosol was generated in a cumulative concentration of  $2.68 \cdot 10^5$  particles/cm<sup>3</sup>. Filtration efficiency of multilayer fibrous filters was determined on the basis of the measurement of particle number concentration at the inlet and at the outlet of the filtration structure. The experiments were conducted using a SMPS 3936 scanning mobility particle sizer (TSI Inc., USA), which consists of a DMA 3080L differential mobility analyzer and a CPC 3022A condensation particle counter. Particle number concentration was measured in the range of particle size from 40 to 300 nm. The experiments were carried out at four different face velocities ( $U=5, 10, 15$  and  $20$  cm/s).

Figure 1 and 2 illustrate the results of experimental and theoretical changes in filtration efficiency depending on the thickness of multilayer fibrous filters, at four aerosol velocities.

It was found that filtration efficiency of liquid aerosol particles increases as the thickness of filters increases and as aerosol velocity decreases.

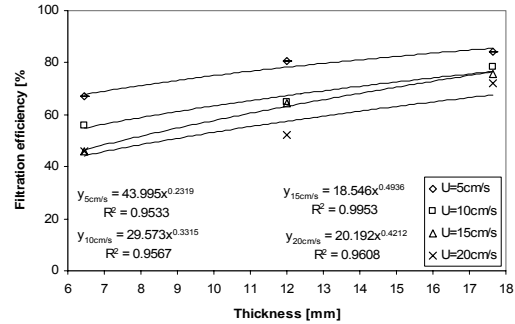


Figure 1. Filtration efficiency measured with the DEHS test.

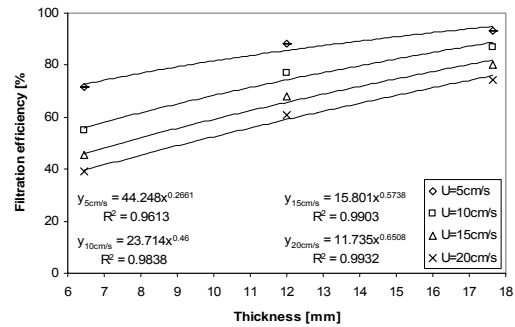


Figure 2. Filtration efficiency determined according to Brown's (1993) theory.

For all aerosol velocities ( $U$ ), the changes in filtration efficiency depending on the thickness of filters ( $L$ ) can be expressed with an exponential function as:  $\eta_e = c \cdot L^n$ . In each analyzed case experimental data fit Brown's (1993) theoretical formula. The results show compatibility of the directional coefficients from the theoretical and experimental equations (for aerosol velocity of 5 cm/s:  $c_e=44.00$  and  $n_e=0.23$  according to experimental data;  $c_t=44.25$  and  $n_t=0.27$  according to theoretical data). Moreover, the results also show that coefficients of regression ( $R^2$ ) were higher than 0.95 at all velocities.

This study was part of the statutory activity of the Central Institute for Labour Protection – National Research Institute, Warsaw, Poland.

Brown R.C. (1993). Air filtration. Pergamon.

Podgórski A. & Bałazy A. (2003). J. Aerosol Sci, vol. II, 1197-1198.

## Improvement of the most penetrating particles removal in fibrous filters with the use of bipolarly charged electrets or nanofibrous media

A. Podgórski, A. Bałazy, L. Gradoń

Faculty of Chemical and Process Engineering, Warsaw University of Technology,  
Waryńskiego 1, 00-645, Warsaw, Poland

Keywords: aerosol filtration, electret, fibrous filters, nanofibers

Conventional mechanical filters, made of fibers with a few or a few dozen micrometers, are very effective in the removal of aerosol particles larger than several hundreds or smaller than a hundred nanometers in diameter. In the intermediate size range, between 100 and 700 nm, a local minimum of fractional filtration efficiency is usually observed, and the particle diameter around 300nm is commonly referred to as the most penetrating particle size (*MPPS*). The central problem is therefore to develop filter structures with enhanced collection efficiency of *MPPS* particles with the pressure drop kept at an acceptable level. To achieve this, either use of electret or nanosized fibers seems to be the most promising and both these cases are studied in this work. Filtration efficiency in bipolarly charged electret filters was determined using the Brownian dynamics method. Exemplary results of the single fiber efficiency,  $E$ , obtained for the filter packing density  $\alpha=0.069$ , gas velocity  $U=0.129\text{m/s}$ , fiber diameter  $d_f=7.84\mu\text{m}$ , and for particles with diameters in the range  $d_p=0.01\text{--}1\mu\text{m}$  are shown in Fig. 1 for a neutral fiber and for 7 charged fibers with linear charge density  $q_f$  in the range  $0.1\text{--}13\text{nC/m}$ . As can be seen a significant increase of  $E$  is observed with increasing  $q_f$  and it is accompanied by a shift of the *MPPS* towards smaller sizes.

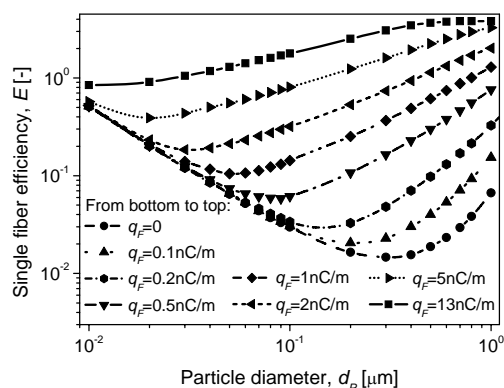


Fig. 1. Effect of  $q_f$  on the single fiber efficiency.

These calculations were repeated for other values of  $\alpha$ ,  $U$  and  $d_f$ . The difference  $\Delta E_{el}=E_{el}-E_{mech}$  between the single fiber efficiency for an electret filter,  $E_{el}$ , and that one for identical mechanical filter,  $E_{mech}$ , was determined. Then it was fitted vs. the Kuwabara number,  $Ku=-0.5\ln\alpha+\alpha-0.25\alpha^2-0.75$ , and vs. the polarization force parameter, which is defined as:

$$N_{\sigma 0} = \frac{2(\varepsilon_p - 1)d_p^2 q_f^2 C_C}{3\varepsilon_0(\varepsilon_p + 2)(1 + \varepsilon_F)^2 \mu U d_f^3}, \quad (1)$$

wherein  $\varepsilon_0$  is vacuum permittivity,  $\varepsilon_F$  and  $\varepsilon_p$  – fiber and particle dielectric constants,  $C_C$  – Cunningham’s factor and  $\mu$  – gas viscosity. It was possible to obtain a simple correlation describing an increase of the single fiber efficiency due to polarization force:

$$\Delta E_{el}(Ku, N_{\sigma 0}) = 0.77 N_{\sigma 0} / [1 + 0.97(Ku N_{\sigma 0})^{0.785}]. \quad (2)$$

Correctness of this formula was proven comparing its predictions with experimental data. Application of nanofibrous media was also studied theoretically and experimentally. Fig. 2 shows sample results of fractional efficiency,  $\eta$ , measured for conventional microfibrinous filter (depicted “BL”; it was made of fibers with the mean diameter  $d_{f,mean}=18\mu\text{m}$ ) and for BL layer covered with one, two, or three nanofibrous layers (denoted “NL1”;  $d_{f,mean}=0.74\mu\text{m}$ ). An increase of the efficiency and a shift of *MPPS* towards smaller particles can be observed when subsequent nanofibrous layers are added. Simultaneously, the quality factor  $QF=-\ln(1-\eta)/\Delta p$  (where  $\Delta p$  is the pressure drop) increases with the increase of the number of NL1 layers and it is greater than  $QF$  for BL layer alone. Several other nanofibrous media were also investigated yielding similar results. One can draw a conclusion that utilization of nanofibers or electrically charged fibers is especially profitable to enhance filtration of particles that are usually considered to be the most penetrating, resulting in the increase of  $\eta$  and  $QF$  and in the *MPPS* reduction.

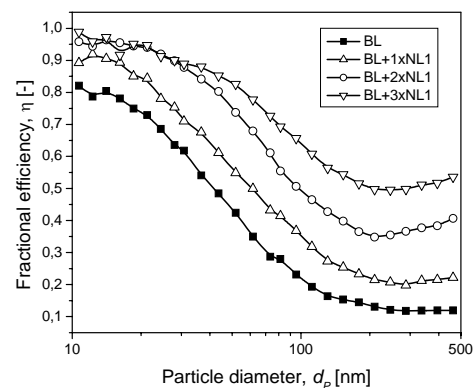


Fig. 2. Efficiency of the microfibrinous filter BL and BL covered with 1, 2 or 3 nanofibrous layers NL1.

The work was financed from the budget means for science in 2006-2009 as a research project.

## New experimental findings of nanoparticle filtration in fibrous filters

A. Podgórski, A. Bałazy

Faculty of Chemical and Process Engineering, Warsaw University of Technology,  
Waryńskiego 1, 00-645, Warsaw, Poland

Keywords: aerosol filtration, fibrous filters, nanoparticles

Our previous experimental studies performed using the fibrous filters (Bałazy et al., 2004) suggested a possible gradual drop of collection efficiency of nanoparticles with a particle size decrease starting from about 20 nm in diameter. Unfortunately, those results were distorted by an improper operation of a particle spectrometer used in the experiments (Wide-Range Particle Spectrometer, WPS 1000XP-B). After upgrade of the instrument by the manufacturer (MSP Corp., USA), such a trend was no longer observed. Typical results of filtration efficiency of DEHS nanoparticles in a commercial fibrous filter obtained with two different experimental protocols are shown in Fig. 1. The filter efficiency,  $\eta$ , was then recalculated into the single fiber efficiency,  $E$ , and plotted in a log-log graph as a function of the Peclet number,  $Pe$ . A perfect fit to a straight line was obtained for the particles with diameters 40-200 nm, Fig. 2, that confirms predominance of diffusional deposition mechanism.

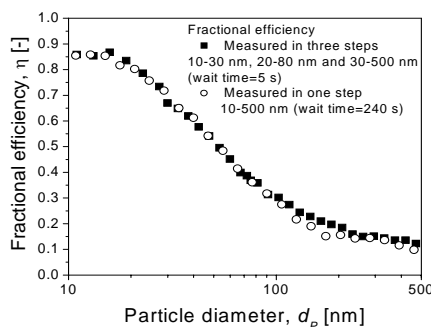


Fig. 1. Collection efficiency of DEHS nanoparticles obtained using two various experimental procedures.

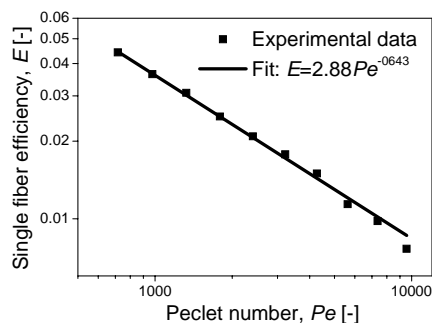


Fig. 2. Fit of the experimental data of  $E$  to the power function of  $Pe$  for particle size range  $40 < d_p < 200$  nm.

However, extrapolating this fit beyond the fitting domain we can observe that the actually measured efficiency is lower for particles smaller than 40 nm,

Fig. 3. We postulate that this may be caused by thermal rebound and thermal resuspension of the nanoparticles. Ratio of the measured single fiber efficiency to the efficiency predicted by the extrapolated fit in Fig. 3 determines the total adhesion efficiency ( $TAE$ ) for a given particle size.

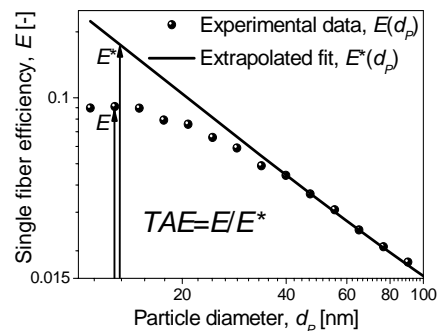


Fig. 3. Determination of experimental  $TAE$  values.

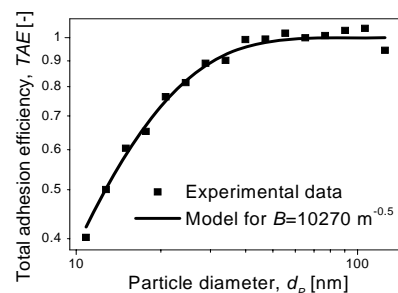


Fig. 4. Model comparison with experimental data.

Assuming that a particle adhesion to a fiber is caused by van der Waals forces, so that a particle critical adhesion velocity  $v_{Cr}$  is inversely proportional to its diameter  $d_p$ ,  $v_{Cr} = Cd_p^{-1}$ , we formulated a statistical-mechanical model of thermal rebound and resuspension. It predicts that  $TAE$  is given by:

$$TAE = \text{erf}(\sqrt{\bar{d}_p}) \left[ \text{erf}(\sqrt{\bar{d}_p}) - 2\sqrt{\bar{d}_p} / \pi \exp(-\bar{d}_p) \right],$$

where  $\bar{d}_p = d_p B^2$  and  $B = C(\pi \rho_p / 12kT)^{1/2}$ , wherein  $\rho_p$  is a particle density,  $k$  is Boltzmann constant and  $T$  – absolute temperature. In Fig. 4 we can observe a perfect agreement between the model values of  $TAE$  and the experimental data. Similar results were obtained for other filters and other particle material.

The work was financed from the budget means for science in 2006-2009 as a research project.

Bałazy, A., Podgórski, A., Gradoń, L. (2004). *J. Aerosol Sci. (EAC'04 Abstracts)*, 35S1, 967-968.

## Filtration characteristics of polyacrylonitrile membrane filters

S.H. Yang<sup>1</sup>, H.L. Huang<sup>2</sup> and Y.C. Huang<sup>3</sup>

<sup>1</sup>Department of Leisure and Recreation Management, Toko University, 51 University Rd., Sec. 2, Pu-tzu City, Chia Yi County 613, Taiwan, R.O.C

<sup>2</sup>Department of Occupational Safety and Health, Chia Nan University of Pharmacy & Science, Tainan 717, Taiwan, R.O.C.

<sup>3</sup>Graduate Institute of Environmental Engineering, National Taiwan University, Taipei 106, Taiwan, R.O.C.

Keywords: filtration, penetration, negative air ions, fibrous filter.

Generally, the filters used to sample or collect aerosols can be classified as fibrous filters, fabric filters, membrane filters or granular filters. The purposes of these various kind filters govern their structure, pore size, packing fraction, fiber diameter, thickness, felting methods and the air resistance across the filter. In the aspect of particle sampling, the fibrous filters are applied first in sampling particles. Recently, the membrane filters have been widely used to sample particles in the fields of environmental hygiene and occupational hygiene (Hoek et al., 1997), since they can sustain higher pressure and provide high-speed filtration performance. Moreover, the particles collected on the membrane filters can be weighed and chemically analyzed (Cohen and Hering, 1995).

The polymer membrane filters made from organic material have the widest available range of pore sizes, supporting high pressure and filtering at high face velocity. Hence, the polymer membrane filters can be usefully and economically applied to aerosol sampling and air purification. Therefore, The Polyacrylonitrile (PAN) membrane filters were applied to investigate the filtration efficiency of aerosols in this work. Polydisperse aerosols were generated from a Collision Atomizer. Then, the polydisperse aerosol was electrically classified using a Differential Mobility Analyzer to obtain monodisperse aerosol. A condensation particle counter measured the upstream and downstream aerosol concentrations and the pressure gauge measured the pressure drop. Thereafter, the filtration efficiency of the PAN membrane filter was determined by the difference of the numbers of the aerosols and the difference of pressure after filtration.

The results demonstrate that the aerosol penetrations through the 10% and 15% PAN membrane filters were around 13% and 7%. Results indicate that penetration through PAN membrane filters fell as the concentration- casting solution increased, because the pore size of the PSF membrane filters declines as the concentration of the casting solution rises. The most penetrating size of the PAN membrane filters was around 0.05  $\mu\text{m}$ .

Moreover, the penetration of solid aerosols through PAN membrane filters exceeds that of liquid

aerosols. Penetration through the PAN membrane filters increases obviously with the face velocity when aerosol smaller than 0.21  $\mu\text{m}$ . When aerosol larger than 0.3  $\mu\text{m}$ , the variations of penetration through the PAN membrane filters become smaller at different face velocity. The relative humidity does not influence the performance of the PAN membrane filters.

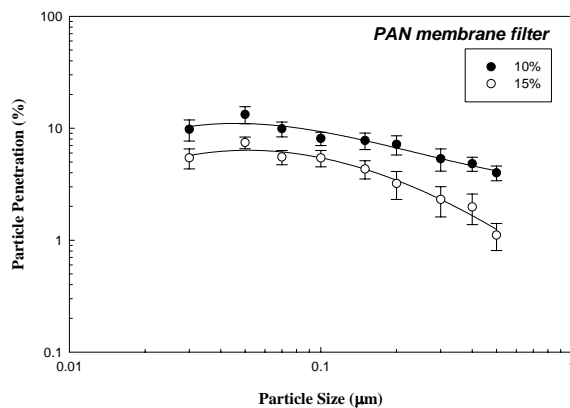


Figure 1. Penetration through the different concentration (10% and 15%) PAN membrane filters at face velocity of 0.1 m/s.

The authors would like to thank the National Science Council of Republic of China for financially supporting this research under Contract No. NSC 94-2211-E-041-006-.

Cohen, B. S., and Hering, S. V. (1995). Air Sampling Instruments for Evaluation of Atmospheric Contaminants. 8th Edition, ACGIH: Cincinnati, Ohio.

Hoek, G., Forsberg, B., Borowska, M., Hlawiczka, S., Vaskovi, E., Welinder, H., Branis, M., Benes, I., Kotesovec, F., Hagen, L. O., Cyrus, J., Jantunen, M., Roemer, W., and Brunekreef, B. (1997). Wintertime PM<sub>10</sub> and black smoke concentrations across Europe: Results from the PEACE study. Atmospheric Environment, 31, 3341–3349.

## The study on filtration characteristics of miniature electrostatic precipitator using alternating current

C.W. Kuo, W.Y. Lin and H.H. Hsu

Institute of Environmental Engineering and Management, National Taipei University of Technology, 1, Sec. 3, Chung-Hsiao E. Rd., 10608, Taipei, Taiwan

Keywords: aerosol measurement, charged particle, collection efficiency, ozone, SMPS.

Electrostatic precipitator (ESP) is high efficiency dust collector, which utilizes electric energy to remove particulate pollutant. The capital cost of ESP is relatively more expensive than general dust collectors. However, due to its small pressure-drop flow characteristics, the operational cost of ESP is usually lower than other particulate control devices (Lim et al., 1998). As a result, ESP is widely used in industry and in indoor air quality improvement. According to the principle of operation, air cleaners are sorted into filtration type, electrostatic type and mixing type. Offerman (1985) experimented with 11 commercial air cleaners, the results indicated that the electrostatic type had better efficiency at removing cigarette particles. Additionally, Don (2003) studied 4 kinds of commercial air cleaners (electrostatic type), the results indicated that collection efficiency, discharge current and ozone generation decreased over 18~26 days.

A two-stage miniature ESP has been set up in this study (Figure 1). A high-voltage AC power supply was used to provide the energy for corona discharge and to produce high concentration single polarity ions. The alternating electric field discharge electrode range is 0 –kV to 11.2 –kV. The objectives of this research included studying the filtration characteristics of ESP using AC fields and the

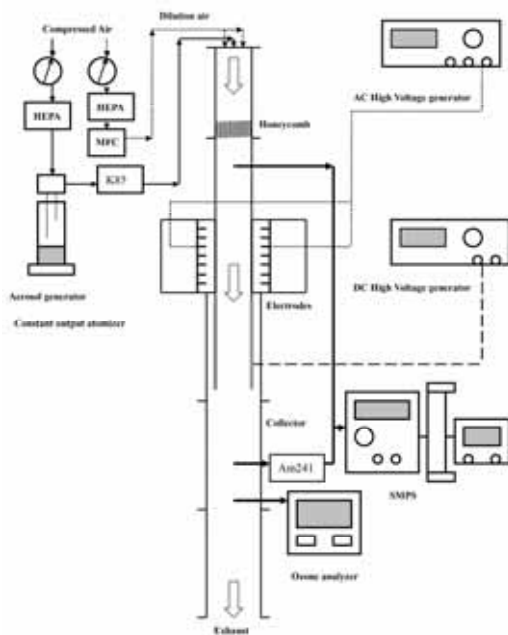


Figure 1. Experimental set-up.

influence of particle size, filtration speed, distance between electrodes, and voltage on aerosol collection efficiency and ozone generation. This study also investigated the particulate loading effect of the performance of the ESP.

Aerosol penetration of particle diameter under different operating voltage was showed in Figure 2. When the voltage went up, the penetration went down. The diameters with higher penetration were in the range between 200 to 500nm. Moreover, we noticed that under whatever operating conditions, if the diameters were smaller than 40nm, the penetration went up. This was mainly because the particles were not usually charged enough and would not be attracted by the Coulomb force of the electric field.

The experimental results indicated that the aerosol penetration through the ESP decreased as increasing voltage of the discharge electrode, decreasing the flow rate, lengthening the collector, and shortening the distance between electrodes. The characteristics of electric field and power consumption of AC electric field chargers were also compared.

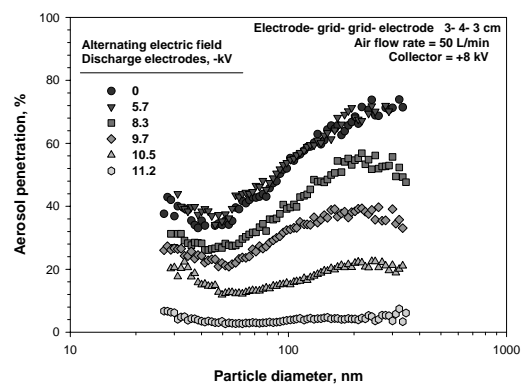


Figure 2. Aerosol penetration of particle diameter under different operating voltage.

Don, M. R. (2003). *The study of the particle collection efficiency of electrical precipitator air cleaners*. Taipei, R.O.C.: National Taiwan University Press.

Lim, H. C., Yatsuzuka, K., & Asano, K. (1998). *Proc. Inst. Electrostat.* 22 (3), 15-152.

Offerman, F. J., & Sextro, R. G. (1985). *Atmospheric Environment*, 19 (11), 1761-1771.

## Filtration of aerosols with different shape on oil coated fibers

L. Boskovic, I. E. Agranovski and R. D. Braddock

Griffith School of Engineering, Griffith University, Brisbane, 4111 QLD, Australia

Keywords: aerosol filtration, collection efficiency, fibrous filter, particle shape.

It has been shown that perfectly spherical polystyrene latex (PSL) particles have higher filtration efficiency compared to cubic magnesium oxide (MgO) particles (Boskovic *et al.*, 2005). This difference becomes more obvious with an increase of particle size from 50nm to 300nm. All experiments were conducted at 2cm/s filtration velocity to avoid the influence of inertial effects. This disparity was ascribed to the different nature of the motion of the spherical and cubic particles along the fiber surface, following the initial collision (Boskovic *et al.*, 2005). The experimental work has also been extended to include sodium chloride (NaCl) particles of intermediate shape (cubic particles with rounded edges) and tested all three types of particles at a range of filtration velocities from 5 to 20cm/s (Boskovic *et al.*, 2007). Particles of NaCl are being captured with efficiencies lower than those for PSL particles but higher than the efficiencies of cubic MgO particles, at the lowest filtration velocity. The difference between the filter efficiencies for collection of MgO and NaCl particles decreases with an increase in velocity. With velocity increase, the filtration efficiency of the cubic MgO particles, exceeds the filtration efficiency for the intermediate shaped NaCl particles, due to the dominating inertial effects of the denser MgO particles of similar size.

In this project, a thin coating of the polypropylene filter with a mineral oil was used, to absorb the energy of collision and, respectively, to minimize the particle bounce. Coating surfaces with oil or grease increases the adhesion energy, the

intermediate NaCl particles was measured in the same size range as before (50-300nm), for 10 and 20 cm/s filtration velocity. It was found that tested particles, regardless of shape, have very similar

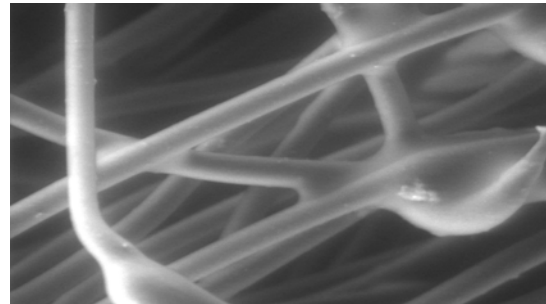


Figure 2. Photograph of coated fibre.

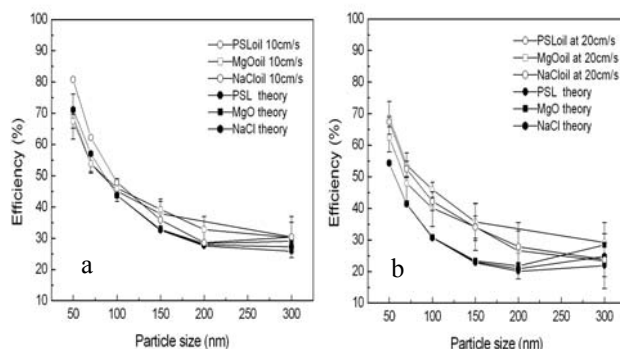


Figure 1. Efficiency of the filter coated with light mineral oil at velocities 10cm/s (a), and 20 cm/s (b)

deformation, and the dissipative energy and greatly reduces the problem of bounce (Hinds 1999). The filtration efficiency of spherical PSL, cubic MgO and

filtration efficiencies, as is clearly seen in Figure 1 for 10 and 20cm/s filtration velocities respectively. The curves are all close together and the standard deviations have overlap, showing insignificant discrepancy in the results compared to our previous findings (Boskovic *et al.*, 2005, 2007). We also compared our experimental results with theoretical filter efficiency estimated according to the classic approach (Hinds, 1999). For calculations, all parameters of filter had to be adjusted to take into account the alterations, due to fibre coating. To measure precisely the diameter of oil coated fiber, we used FEI Quanta 200 Environmental SEM (ESEM) which allows operation at moderate vacuum level and can be used for samples with slightly evaporative liquid (see Figure 2). It was found that the thickness of the fibre was increased by 7.4% and, correspondingly, packing density by 14.9%. The theoretical results are also shown in Figure 1. As is clearly seen, the theoretical predictions are in good agreement with our experimental results. The emission of oil was not influencing the process, as was verified by “zero” emission from the coated filter in absence of test aerosol supply. We have shown that the oil coating minimizes the amount of particle motion along the fibre after initial collision, making results for all particle shapes similar.

Boskovic, et al., (2005). *Aerosol Sci. Tech.*, 39, 1184-1190

Boskovic, et al., (2007) *Aerosol Sci. Tech.*, (submitted)

Hinds, W. C. (1999) *Aerosol technology: Properties, behaviour and measurement of airborne particles.* New York, John Wiley and Sons

## Application of Brownian dynamics approach to evaluate a fibrous filter efficiency

A. Bałazy, A. Podgórski

Faculty of Chemical and Process Engineering, Warsaw University of Technology,  
Warynskiego 1, 00-645, Warsaw, Poland

Keywords: Aerosol filtration, Agglomerates, Brownian dynamics, Particle deposition.

Brownian dynamics (BD) is a method where the collection efficiency is calculated considering simultaneously different forces acting on the particle during its motion in a fiber vicinity. At the same time the following forces can be taken into consideration: drag and resistance force, stochastic Brownian force, and external forces (gravitational force, van der Waals force, electrostatic force, etc.). This approach can be used instead of the classical single fiber (SF) theory, which is commonly utilized, but it does not take into consideration the interactions between various mechanisms. The aim of this work is to present the usefulness of the BD method for theoretical estimation of aerosol filtration efficiencies in fibrous filters. We performed the calculations for spherical particles and fractal-like aggregates. In the case of spherical particles, the simulations were made for neutral and bipolarly charged fibers. The values of the filter efficiency determined utilizing the BD method have been compared with the experimental data or the values obtained using the SF theory.

In Fig. 1 the experimental data for a HEPA filter, Gougeon et al (1996), are compared with the filter efficiencies determined using the BD approach and the SF theory. It can be observed that the values obtained using the former method are much closer to the experimental data in a wide range of particle sizes. The SF theory is in a good agreement with the experimental values for diffusional and deterministic ranges, but in the transition regime it significantly underestimates the measured efficiency.

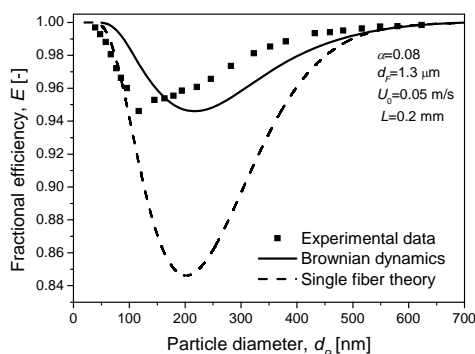


Fig. 1. Comparison of efficiencies determined using the BD and SF methods with the experimental data.

Also in the case of nonspherical particles, such as fractal-like aggregates, SF theory gives lower values of the efficiency in the transition regime – see Fig. 2.

Moreover, for the first ever time the BD approach was used to determine the particles' deposition efficiencies on bipolarly charged fibers. Fig. 3 shows a comparison of the experimental data obtained for an electret filter and the results of calculations carried out using the BD approach. As can be seen, a quite good agreement was obtained for the fiber charge density between 1.2 and 1.3 nC/m.

The results presented here indicate that the Brownian dynamics is a powerful tool, enabling one a more accurate evaluation of a filter efficiency than the commonly used classical single fiber theory.

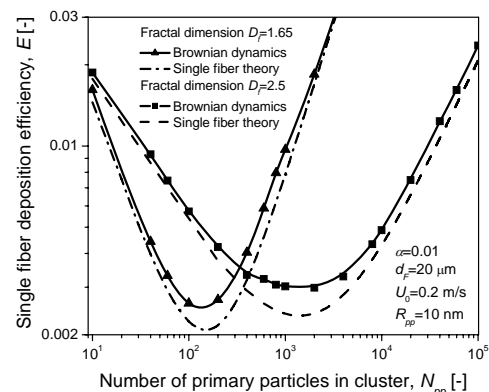


Fig. 2. Deposition efficiencies of aggregates calculated using the BD approach and the SF theory.

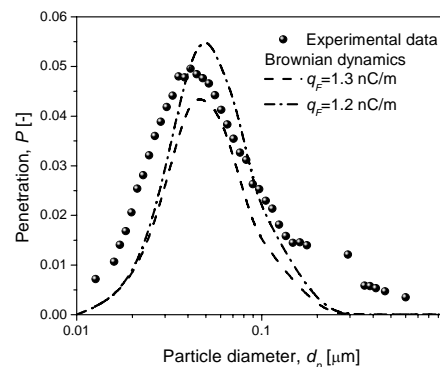


Fig. 3. Penetrations calculated using the BD method and experimental data obtained for an electret filter.

This work was supported by Cummins Filtration, USA.

Gougeon, R., Boulaud, D., Renoux, A. (1996). *Chem. Eng. Comm.*, 151, 19-39

## Extension of the single fiber theory to inhomogeneous fibrous filters

A. Bałazy, A. Podgórski

Faculty of Chemical and Process Engineering, Warsaw University of Technology,  
Waryńskiego 1, 00-645, Warsaw, Poland

Keywords: Aerosol filtration, Collection efficiency, Inhomogeneity.

Classical single fiber theory is based on the assumption that a fibrous filter is homogeneous, which means that it contains fibers of the same diameters and the pore sizes are equal in the entire volume of the filter. However, the real fibrous filters are usually more or less inhomogeneous and it should be taken into consideration when a filter performance is estimated. To take into account polydispersity of fibers, an equivalent fiber diameter can be used in calculations, e.g., the fiber diameter obtained from the Davies model,  $d_{FD}$  (Davies, 1973) or based on the Kuwabara cell model with slip,  $d_{FK}$  (Brown, 1993). However, in the case of some filters also inhomogeneity related to the spatial distribution of a filter porosity should be considered and this issue is investigated in this work.

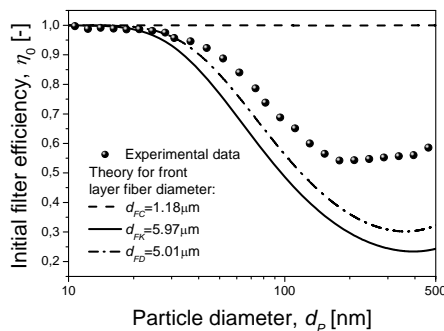


Fig. 1. Comparison of the experimental data with the single fiber theory for various equivalent fiber diameters assuming uniform filter porosity.

The experimental data were compared with the values of filter efficiencies predicted theoretically using the single fiber theory for bilayer set of filters. The back layer was composed of fibers with mean count diameter  $d_{FC}=18\mu\text{m}$ . For this filter a good agreement between the experimental and theoretical values of efficiency was obtained when  $d_{FK}=23.1\mu\text{m}$  was used in calculations. The front layer contained much thinner fibers ( $d_{FC}=1.18\mu\text{m}$ ) and was more inhomogeneous. It can be seen in Fig. 1 that the efficiencies determined on the basis of  $d_{FC}$  for the front filter layer considerably overestimate the filter efficiency measured experimentally. However, the theoretical values of the efficiency were underestimated when the equivalent fiber diameters were used ( $d_{FK}$  and  $d_{FD}$ ). To extend the single fiber theory in order to take into consideration a filter inhomogeneity, we used a theoretical model proposed by Dhaniyala & Liu (2001). The authors

consider a filter as a set of parallel cells with different packing densities and with various gas velocities, whereas the pressure drop across each cell is the same. The resultant aerosol penetration,  $\bar{P}$ , through a filter having mean packing density  $\bar{\alpha}$  can be determined from the individual single fiber efficiencies  $E[\alpha, U(\alpha)]$  corresponding to the cells of local packing densities  $\alpha$ . The final formula reads as:

$$\bar{P} = \frac{\int_0^1 \exp\left(-\frac{4\alpha E[\alpha, U(\alpha)]L}{\pi d_F}\right) \frac{\text{Ku}(\alpha)}{\alpha^2} \exp\left[-\frac{(\ln \alpha - \ln \bar{\alpha})^2}{2(\ln \sigma_{g\alpha})^2}\right] d\alpha}{\int_0^1 \frac{\text{Ku}(\alpha)}{\alpha^2} \exp\left[-\frac{(\ln \alpha - \ln \bar{\alpha})^2}{2(\ln \sigma_{g\alpha})^2}\right] d\alpha}$$

where  $U(\alpha) = U_0 \bar{\alpha} \text{Ku}(\alpha) / [(1-\alpha)\alpha \text{Ku}(\bar{\alpha})]$  is the gas velocity in a cell,  $U_0$  is superficial gas velocity and  $\text{Ku}$  is the Kuwabara number:  $\text{Ku} = -0.5 \ln \alpha + \alpha - 0.25 \alpha^2 - 0.75$ . The penetrations through the considered set of filters obtained using this model are shown in Fig. 2. The best fit to the experimental data was achieved when the geometric standard deviation of the assumed log-normal distribution of packing densities,  $\sigma_{g\alpha}$ , was taken to be between 1.5 and 1.75 and the agreement with the experimental data is much better than that one for homogeneous media.

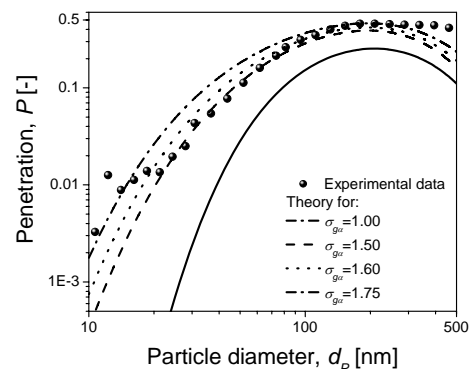


Fig. 2. Comparison of the experimental data of penetration with theoretical results obtained for nonuniform packing density of the filter.

The work was financed from the budget means for science in 2006-2009 as a research project.

- Brown, R. C. (1993). *Aerosol Filtration*. Pergamon Press, Oxford.  
 Davies, C. N. (1973). *Air Filtration*. Academic Press, London.  
 Dhaniyala, S., Liu, B.Y.H. (2001). *Aerosol Sci. Technol.*, 34, 170-178.

## Influence of a fibrous filter geometry on the spatial distribution of deposited particles – CFD modelling

A. Bałazy, A. Moskal and A. Podgórski

Faculty of Chemical and Process Engineering, Warsaw University of Technology,  
Warynskiego 1, 00-645, Warsaw, Poland

Keywords: Aerosol filtration, CFD, Fibrous Filter, Particle deposition.

Depending on the filtration system, various geometries of fibrous filters are applied. In our study we considered the following geometries: 1) flat filter located in the center of cubic box perpendicularly to air flow direction; 2) “filter M” – left picture in Fig. 1; 3) “filter W” – right picture in Fig. 1. The pleated filters have larger filter area ( $0.1332\text{m}^2$ ) comparing to the flat one ( $0.0324\text{m}^2$ ), which gives slower filter loading at the same aerosol concentration and lower air facial velocity at the same volumetric flow rate. However, designing a filter geometry one should consider if entire filter surface is utilized effectively. Fig. 1 shows the contours of absolute pressure in the cross-sections of these systems, where the filters are additionally presented (3D structures). The direction of air flow is from left to right. Using Fluent CFD Package we investigated distribution of deposited particles over a filter surface. The simulations were performed for the air superficial velocity  $0.1\text{m/s}$ .

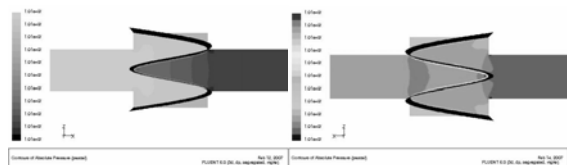


Fig. 1. Contours of absolute pressure for two filter geometries: “filter M” (left) and “filter W” (right).

In order to investigate where the particles deposit, a few thousands particles were injected into the system from the surface  $80\text{cm}$  distant from the box with a filter. The trajectories of particles were tracked and the places of their deposition were registered at the moment when particles hit the filter surface.

The distributions of number of deposited particles with the diameter  $1\mu\text{m}$  along Z-axis obtained for filters of various geometries are compared in Fig. 2. It can be seen that in the case of all filters much more particles are deposited on the central filter surfaces, whereas this distribution is a bit more even for a flat filter. The map of deposition of 200 particles of diameter  $1\mu\text{m}$  onto the surfaces of the “filter W” is shown graphically in Fig. 3.

We also investigated spatial distribution of deposited particles for three particle diameters:  $0.01$ ,  $0.1$  and  $1\mu\text{m}$ . The results indicate that in the case of the pleated filters (“filter M” and “filter W”) a considerable fraction of particles deposits onto two

filter faces located centrally. However, the number of particles that reach outermost filter surfaces increases with the particle diameter decrease.

The geometry of the considered system was based on the typical elements used in the ventilation systems. However, it seems that utilizing a pleated filter placed in such a box, the outermost filter surfaces remain almost clean, whilst these ones located centrally may be heavily loaded. Thus, when designing a filtration system, not only a filter performance and its area are of importance, but also a filter holder geometry plays a key role, and it should ensure quite uniform air flow field and aerosol concentration over a filter surface.

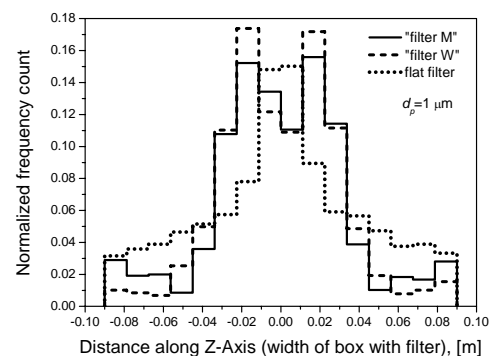


Fig. 2. Comparison of the distributions of number of deposited particles along Z-axis for various filter geometries;  $d_p=1\mu\text{m}$ .

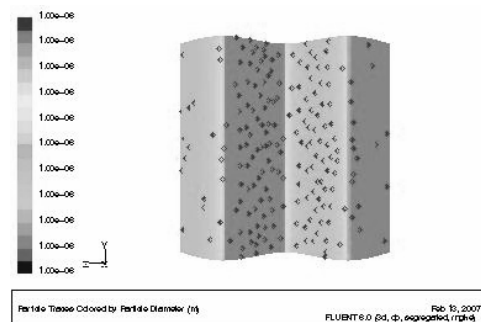


Fig. 3. Particles deposited onto the “filter W”; 200 particles of  $d_p=1\mu\text{m}$ .

The work was financed from the budget means for science in 2005-2006 as a research project.

## Trimodal model for multi-component aerosol dynamics

S. B. Kim<sup>1</sup>, S. K. Jeong<sup>2</sup>, S. S. Kim<sup>1</sup> and P. Biswas<sup>3</sup>

<sup>1</sup>Department of Mechanical Engineering, KAIST, 305-701, Daejeon, South Korea

<sup>2</sup>Korea Institute of Energy Research, 305-701, Daejeon, South Korea

<sup>3</sup>Environmental Engineering Science Program, Washington University in St. Louis, St. Louis, MO 63130, USA

Keywords: aerosol modeling, coagulation, nucleation mode, numerical simulation, particle size distribution.

To predict particle growth and morphology for gas to particle conversion, several simple numerical methods have been developed. Kruis et al. (1993) derived the monodisperse model. The monodisperse model gives good agreement with detailed sectional model. However, the monodisperse model can not reflect polydisperse character due to monodisperse assumption. To resolve this problem, Jeong & Choi (2001) proposed simple bimodal monodisperse model. The bimodal monodisperse model consists of nucleation mode and accumulation mode. Therefore, the polydisperse character of simulated aerosol can be included. This bimodal monodisperse model assumed no nucleation barrier. That is, monomer can be thought as stable particle.

In present study, the nucleation barrier is considered. Present trimodal monodisperse model consists of three modes, monomer, nucleation and accumulation modes. By separating the monomer and nucleation mode, the condensation, coagulation and coalescence effects are included. And present model can be applied multi-component aerosol dynamics. For example, two-component aerosol dynamics can be evaluated as shown in Figure 2.

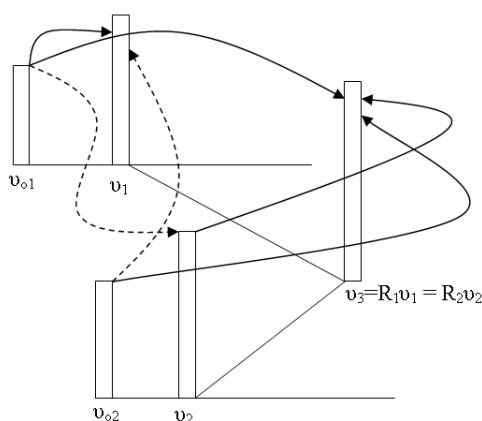


Figure 1. Schematics of trimodal model for two component aerosol dynamics. Dot lines describe heterogeneous condensation.

The present model can also be generalized to m-components aerosol dynamics by increasing number of monomer and nucleation modes. Comparing to detailed discrete sectional method, computation load of the present model is considerably low. Figure 2 shows calculation results

of the present model. In figure 2, the experimental results and discrete sectional calculation are also presented. The calculation model system is the sorbent capture of toxic metal species in the incinerator. In the incinerator, PbO vapour concentration increases by chemical reaction and decreases down stream due to nucleation. With SiO<sub>2</sub> sorbent, the PbO vapour concentration decreases more rapidly due to scavenging by SiO<sub>2</sub> particles. As shown in figure 2, the present model gives good agreement with discrete sectional calculations and experimental results.

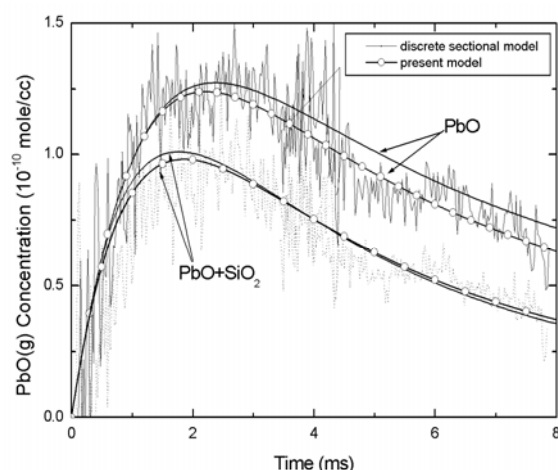


Figure 2. Comparison among results of experimental, discrete sectional model and present trimodal model. The experimental results are quoted from Biswas & Zachariah (1997) and discrete sectional calculations are referred from Wu & Biswas (1997)

The authors express their gratitude for support through a grant from the Brain Korea 21 program of the Ministry of Education. And this work was partially supported by the Korea Research Foundation Grant (KRF-2005-000-10038-0).

Biswas, P. & Zachariah, M. R. (1997). *Environ. Sci. Technol.*, 32, 2455-2463

Jeong, J. I. & Choi, M. (2001). *J. Aerosol Sci.*, 32, 565-582.

Kruis, F. E., Kussters, K. A., & Pratsinis, S. E. (1993). *Aerosol Sci. Technol.*, 19, 514-526.

Wu, C. Y. & Biswas, P. (1997). *Aerosol Sci. Technol.*, 29, 359-378.

### Pilot plant tests of a ceramic catalytic filter

D. Sanz-Rivera<sup>1</sup>, J. J. Rodríguez-Maroto<sup>1</sup>, J. Dorronsoro-Arenal<sup>1</sup>, E. Ros-García<sup>1</sup>, Armesto-pez<sup>2</sup>, A. Bahillo-Ruiz<sup>2</sup>, R. Ramos-Casado<sup>2</sup>

<sup>1</sup> Departamento de Medioambiente, CIEMAT, Avda. Complutense 22, 28040, Madrid, Spain

<sup>2</sup> Departamento de Energía, CIEMAT, Avda. Complutense 22, 28040, Madrid, Spain

Keywords: filtration, combustion particles, measurement

Catalytic filter, designed for selective catalytic reduction (SCR) of nitrogen oxides, are currently under development. These filters are based on ceramic materials, suitable for the high operating temperature needed for satisfactory reaction yield. Dry scrubbing of acid gases, such as sulphur dioxide or hydrogen chloride, by means of sodium bicarbonate in action is a well known method. SCR and dry scrubbing can be combined in a single process for simultaneous removal of particulate matter and pollutant gases in effluents. CIEMAT, SO VAY, PA-SCHUMACHER, KARSRUHE UNIVERSITY, INESCOP and CARE, cooperated in a project for pilot scale testing of this process (Armesto, 2005).

Pilot scale tests were preceded by laboratory investigations (Schaub, 1999; Döring, 2005; Nacken, 2007).

A pilot scale filterhouse was designed. It was connected to a 3.5 MWth bubbling fluidised bed combustion plant. The combustion plant was fed with a mixture of coal and *oruji* (a residue from olive oil production) and part of the flue gas was conducted to the filterhouse through a by-pass line.

Nine ceramic candles, with a filtration surface of 0.26 m<sup>2</sup> each, were installed in the filter. Two tests were done, 20 and 43 hour long. Filtration velocity was 2.5 cm/s on both tests. Operating temperature of the filter was 300 °C.

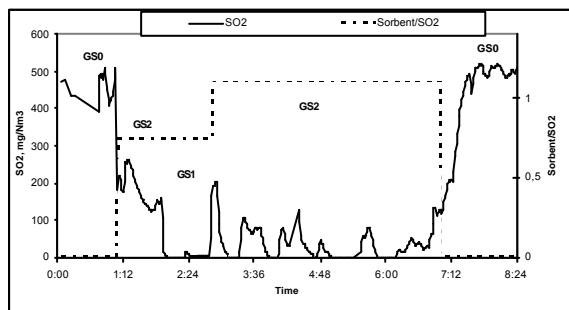


Figure 1. SO<sub>2</sub> concentration at GSO, GS1 and GS2 at different Sorbent/SO<sub>2</sub> stoichiometric ratios.

Figure 1 shows SO<sub>2</sub> concentration at GSO, GS1 (before and after the sorbent in action) and GS2

(downstream the filterhouse) at different Sorbent/SO<sub>2</sub> stoichiometric ratios. Obviously, SO<sub>2</sub> conversion depends on Sorbent/SO<sub>2</sub> ratio. To reach SO<sub>2</sub> conversion higher 90%, it is necessary to use Sorbent/SO<sub>2</sub> ratio higher 1

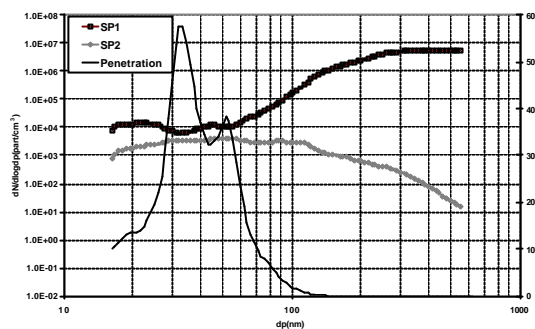


Figure 2. Particle size distributions upstream and downstream filter and penetration as a function of a particle diameter.

Experimental penetration of particles through the filter (Figure 2) determine that approximately 60% in the 30-40 nm particle size range will pass through the ceramic material but the most particles bigger than 200 nm will be retained in the candles.

The authors acknowledge the cooperation of all the project partners and the financial support by the European Union under contract ENK5-CT-2001-00523.

Armesto, J. (2005) Final report of the CE project BioWaRe (No. NNE-2001-00078)

Schaub, G. et al, (1999) *Chemical Engineering and Processing*, 42 (5), p. 365.

Döring, N. et al, (2005) *Proceedings of the 6th International Symposium on Gas Cleaning at High Temperatures, Osaka, Japan, October 20-22*, p 488-495

Nacken, M. et al (2007) *Applied Catalysis B: Environmental* 70 (1-4), pp. 370-376

## Most Penetrating Particle Size in Multiple Fluid Collectors

C.H. Jung<sup>1</sup>, H. S. Park<sup>2</sup>, and K.W. Lee<sup>3</sup>

<sup>1</sup>Department of Environmental Health, Kyungin Women's College, 407-740, Incheon, Korea

<sup>2</sup>Clean Air Technology Research Center, Korea Institute of Energy Research, 305-343, Daejeon, Korea

<sup>3</sup>Department of Environmental Science and Engineering, GIST, 500-712, Gwangju, Korea

Keywords: Filtration, Multiple fluid sphere, Most penetrating particle size, Harmonic mean.

The Filtration of aerosol particles, via spherical collectors, including granules, water droplets, and bubbles, has been the subject of a host of both theoretical and experimental studies. The underlying principles of particle capture by fluid spheres ensembles can be applied directly to the problem of wet scrubbers, the scavenging of atmospheric aerosol, or to particle capture by bubbles. One of the most important practical problems in filtration studies is the determination of the most penetrating particle size. An increase in particle size will induce increased collection efficiency as the result of interception, gravitation and inertial impaction mechanisms, whereas a reduction in the size of the particles will result in an augmentation of the efficacy of Brownian diffusion. Jung and Lee (1998) extended the flow field contained in Kuwabara's cell model for multiple fluid sphere systems, and obtained collection efficiencies for diffusion, interception, and gravitation. In this study, we obtained an approximated analytical solution for the most penetrating particle size in a multiple fluid sphere system based on the extended flow field for multiple fluid systems.

The most penetrating particle size ( $d_{p,min}$ ) can be obtained by differentiating the collection efficiency ( $\eta$ ) with regard to particle diameter ( $d_p$ ).

$$\frac{d\eta}{dd_p} = \xi_1 d_p^{-5/3} + \xi_2 d_p^{-3/2} + \xi_3 d_p + \xi_4 = 0 \quad (1)$$

Here,  $\xi_1$ ,  $\xi_2$ ,  $\xi_3$  and  $\xi_4$  are coefficients representative of diffusion, interception and gravitation for the fluid-type collecting spheres.

In this study, the general type of approximated solution for most penetrating particle size was obtained using the following harmonic mean type combination of simplified solutions (Jung and Lee, 2007).

$$d_{p,min} = \sqrt{\frac{1}{\frac{1}{d_{s1}^2} + \frac{1}{d_{s2}^2}} + \frac{1}{\frac{1}{d_{s3}^2} + \frac{1}{d_{s4}^2}}} \quad (2)$$

$$\text{where } d_{s1} = \left(-\frac{\xi_1}{\xi_3}\right)^{3/8}, d_{s2} = \left(-\frac{\xi_1}{\xi_4}\right)^{3/5}, d_{s3} = \left(-\frac{\xi_2}{\xi_3}\right)^{2/5},$$

$$\text{and } d_{s4} = \left(-\frac{\xi_2}{\xi_4}\right)^{2/3} \quad (3)$$

In Eq. (2), diffusion ( $\xi_1$  and  $\xi_2$ ), interception and gravitation ( $\xi_3$ ) contribute to  $d_{s1}$  and  $d_{s3}$ . Diffusion ( $\xi_1$

and  $\xi_2$ ) and interception ( $\xi_4$ ) contribute to  $d_{s2}$  and  $d_{s4}$ . As each term in Eq. (3) operates predominantly at different size ranges, it can be estimated that the solution for Eq. (1) can be approximated as a combination of the simplified solutions shown in Eq. (2). Figure 1 and 2 shows a comparison of most penetrating particle size values, between the numerical and approximated solutions, in the case of bubble and water droplet collectors. Both approximated and numerical solution show good agreement. As is shown in Figure 1 and 2, the harmonic mean type solution appears appropriate for the acquisition of a simplified approximated solution for most penetrating particle size.

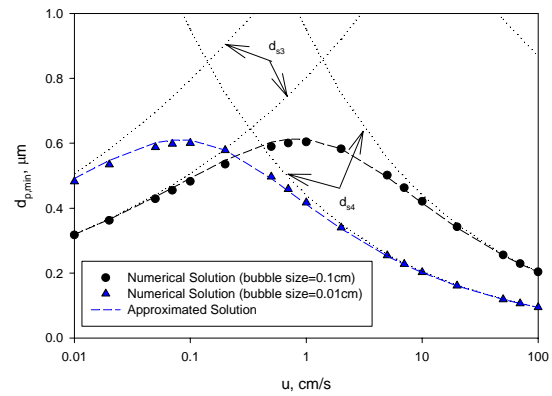


Figure 1. Comparison of the Most penetrating particle size between Numerical and Approximated solution in bubble case.

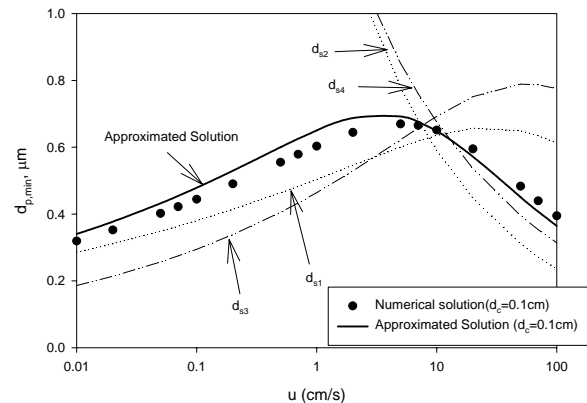


Figure 2. Comparison of the most penetrating particle size between numerical and analytic solution in liquid droplets ( $\sigma=\mu_l/\mu_g=70$ ).

Jung, C. H., and Lee, K. W. (1998). *Aerosol Sci. and Tech.*, 29:389-401.

Jung, C. H., and Lee, K. W. (2007). *Environmental Engineering Science*, 24(3), in press.

## Deposition of Ions and Monomobile Nanoparticles on Wire Screens

M.B. Attoui<sup>1</sup>, G. Mouret<sup>2</sup>, D. Bémer<sup>3</sup>, S. Callé-Chazelet<sup>2</sup>, D. Thomas<sup>2</sup>

<sup>1</sup> Département de Physique - Université Paris XII - Val de Marne, 94010 Créteil France

<sup>2</sup> Nancy-Université/LSGC/CNRS – 1, rue Grandville – BP 20451 – 54001 Nancy Cedex, France

<sup>3</sup> INRS – Ingénierie des Procédés – Avenue de Bourgogne 54501 Vandoeuvre les Nancy Cedex, France

Key words: nanoparticles, ions, penetration, filtration

We present in this paper experimental results of fractional penetration of ions and monomobile nanoparticles in the size range below 2 nm mobility diameter, with filtration velocity until 35 cm/s. Two metallic grids (SS75 & SS150) are used in this study. Their characteristics are given in table 1.

		SS 75	SS 150
fiber diameter $d_f$	$\mu\text{m}$	50	100
screen opening	$\mu\text{m}$	75	150
solid fraction $\alpha$	/	0.31	0.31

Table 1 - Characteristics of the grids tested in the study

The penetration is measured with ions of tetra heptyl ammonium bromide (THABr). The ions (singly charged) are produced by electrospray atomisation of a solution (~1mM) of THABr dissolved in 50/50 in volume ethanol+water (Ude & Fernandez de la Mora 2005). This ammonium halide salt produces a series of sharp peaks (fig. 1) of singly charged cations. The spectrum given in this figure is based on the mobility diameters based on Millikan's conventional size vs. mobility relation are 1.47 nm for the first peak (monomer), 1.78 nm for the second singly charged peak (dimmer) and 1.97 nm for the third singly charged peak (trimmer).

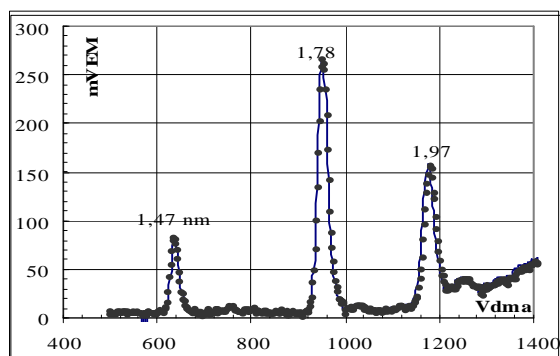


Figure 1 - Mobility spectra of electrosprayed cluster ions of tetra-heptyl ammonium ions in air at room temperature and atmospheric pressure

The doubly charged ions gives a minuscule signal which was not detected by the electrometer downstream of the grid even at very high flowrate. An axisymmetric DMA of the Herrmann type (Herrmann, Eichler, Bernardo & Fernández de la Mora, 2000) capable of a resolving power (1/FWHH) in excess of 50 with 1 nm particles and a

classical experimental filtration set up are used in this study. The ions leaving the DMA are alternately passed through either holder filter with 32 mm grid diameter or through geometrically identical 'empty' holder (dummy unit). Particle concentration is measured with a single aerosol electrometer (University Paris 12 EM) which can run at very high flowrate (up to 50 l.min<sup>-1</sup>) with an input bias current of 2 fA. The peaks of THABr are characterised in terms of *mobility size*. The penetration coefficient, ratio between downstream signal to the upstream, will be compared to the penetration given by theoretical models. These models use *size standard* not mobility size. All the point is to find a correct relation between size and mobility for the size range below 3 nm. Such a relation is presently not firmly established (Tammet, 1995; Li & Wang, 2003; Ude, 2004).

Table 2 give the first measured penetration values for the SS75 screen, at 19.5 and 35.1 cm/s, for both the monomer and dimmer.

$d_p$	filtration velocity	
	19.5cm/s	35.1 cm/s
nm		
1,47	0,17	0,41
1,78	0,20	0,52

Table 2 - Experimental penetration for grid SS75

### References:

- Herrmann W., et al. (2000). Abstract of the Annual Conference of the AAAR, St Louis, Missouri.
- Li, Z. G., & Wang, H. (2003). Drag force, diffusion coefficient, and electric mobility of small particles. II. Application. *Physical Review E*, 68(6), Art. no. 061207.
- Tammet, H. (1995). Size and Mobility of Nanoparticles, Clusters and Ions. *J. of Aerosol Science*, 26, 459–475.
- Ude, S. (2004). Measurement and Properties of Nanometer Particles in the Gas Phase. Ph.D. thesis, Yale University.

## Aerosol Filtration with Electrospun Fiber Filters

Hyun-Seol Park

<sup>1</sup>Department of Energy Conversion Research, Korea Institute of Energy Research, 71-2 Jang-dong, Yuseong-gu, 305-343, Daejeon, Korea

Keywords: Air Filter, Electrospun Fiber, Filtration, Collection Efficiency

Electrospinning is a method to produce extremely fine fibers from polymer solutions. The process applies a high electric voltage onto a spinning nozzle (polymer solution) as can be expected from its name. Since the electrospun fiber mats have higher specific surface area, they have lots of advantages as a filter medium.

In this work, we have investigated the filtration properties of electrospun fiber filters. The filter media were manufactured with various spinning conditions by a lab-scale electrospinning apparatus. The process parameters of electrospinning influences on fiber size distribution and pore size distribution of filters. Therefore, the filters electrospun under different conditions reveal their own filtration characteristics. In this study, the collection efficiency, pressure drop, and dust holding capacity of electrospun filters were measured and compared with a commercial air filter media composed of glass fibers.

Nylon 6,6 was used as a polymer material, and dissolved in formic acid. The Nylon 6,6 solution was spun by an electrospinning apparatus depicted in Fig. 1. The applied voltage was ranged from 20 to 50 kV, and the distance between the nozzle tip and collector was fixed as 110 mm. The morphology of the electrospun fibers was analyzed using a scanning electron microscopy (SEM). Based on the SEM images, the size distribution of electrospun fibers was obtained. The pressure drop across the tested electrospun filters was measured using a micro-manometer, and aerosol collection efficiency was calculated by measuring the aerosol concentration before and after passing through the filters. Monodisperse NaCl particles of 50, 70, 100, 150, 200, 300, and 400 nm in diameter were used as a test aerosol.

Fig. 2 is the SEM image of an electrospun fiber filter, showing average fiber diameter of 250 nm. The fractional collection efficiencies of electrospun filters manufactured at various electric potentials were plotted in Fig. 3. A typical aerosol collection efficiency curves were obtained. The minimum efficiency exists in the particle size of 150 nm. Higher voltage makes thinner fibers, resulting in higher efficiency as shown in Fig. 3. In Fig.4, the collection efficiency of an electrospun filter media was compared with that of a glass fiber filter media having 98% tentative efficiency for 0.3 $\mu$ m particles. The pressure drops at filtration velocity of 5 cm/s

were 28.4 mmAq for electrospun filter and 38.3 mmAq for glass fiber filter, respectively. On the other hand, the collection efficiencies of both filters were almost same, which indicates higher filtration performance of electrospun filters.

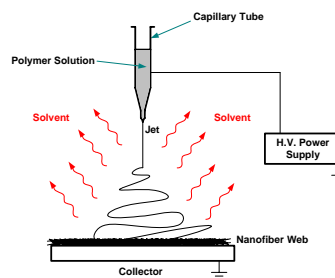


Figure 1. Electrospinning Process

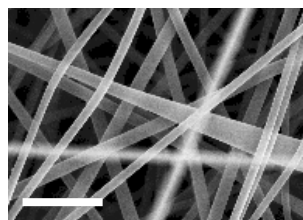


Figure 2. Electrospun fiber mat (scale bar: 2 $\mu$ m).

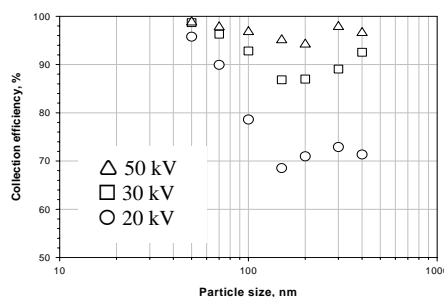


Figure 3. Collection efficiency of electrospun filters

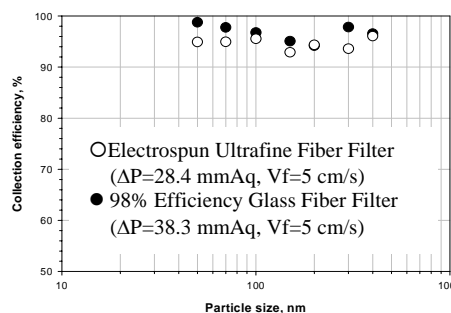


Figure 4. Comparison of collection efficiency with a commercial glass fiber filter.

## Comparison of the loading characteristics onto filters of the particles entering the ceramic candle filter vessel through the normal or tangential inlet

S.J. Park , K.S. Lim and J.H. Lim

Clean Air Technology Research Center, Korea Institute of Energy Research,  
71-2 Jang-dong, Yuseong-gu, 305-343, Daejeon, Republic of Korea

Keywords: aerosol filtration, CFD, filters, particle deposition, trajectory.

A ceramic candle filter is usually applied to hot gas filtration. The hot gas filtration is an essential technology for the successful working of the advanced power plants such as pressurized fluidized bed combustion (PFBC) and integrated gasification combined cycle (IGCC) promising coal-fired generation of electricity with substantially greater thermodynamic efficiencies and reduced particulate pollutant emissions (Ito *et al.*, 1998; Pastila *et al.*, 2001). The filtration protects gas turbine blades from the erosion and corrosion by particulate matter and improves the performance of a heat exchanger by decreasing particle deposition. A number of hot gas filtration systems have been developed and tested. Reviews of gas cleanup at high temperatures including ceramic candle filters were provided by Thamimuthu (1993) and Clift & Seville (1993). The candle filters generally have very high filtration efficiency of the order of 99.8%. There are, however, various unresolved problems such as the buildup of dust cake on the filters, the ash bridging between filters and the thermal fatigue and failure of filters. These problems are connected to the deposition onto filter surface of large amount of particles and the porous characteristics of dust cake formed on filter surface, which influences the non-uniform regeneration of filters by back-pulsing. To solve these problems, it is required to reduce originally the loading amount onto the filter surface of particles entering a filter vessel and to control the characteristics of dust cake.

In this study, the computational simulations were performed with *Fluent* CFD program to know the particle loading onto filters in the ceramic candle filter vessel of the particles entering through a tangential inlet or conventional normal inlet in Figure 1. Particles mixed with air enter the filter vessel through the inlet. Some particles are deposited on the wall surfaces in the vessel and the inner tube. The others are collected on the filter or penetrated through the filters in the real. However, it was assumed to simplify the simulation that all of the other particles are collected on the filter surface.

As shown in Figure 2, the particle loading is much lower through the tangential inlet than through the normal inlet. Especially, the difference of the loading of fine particles is greater. Therefore, the particle inflow through the normal inlet is more helpful at the earlier filtration time after the filter

regeneration because the depth filtration of fine particles is reduced and the regeneration efficiency is improved. After the dust cake composed of coarse and fine particles is formed, the particle loading may be decreased by turning the particle inflow to the tangential inlet, so that the rising rate of pressure drop is slowed down and the time gap between back-pulsings is reduced.

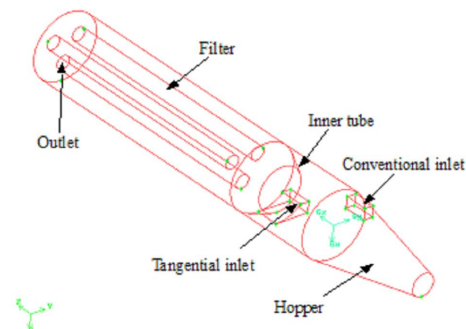


Figure 1. Filtration system configuration.

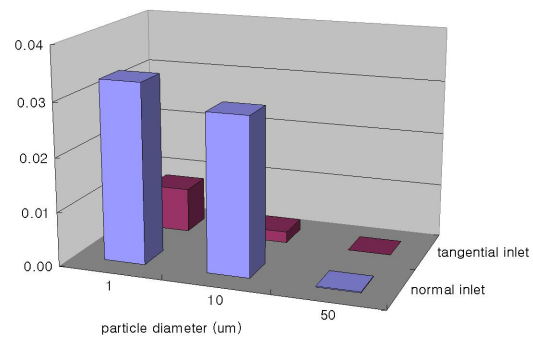


Figure 2. Loading rates onto filters of particles entering the filter vessel through the different inlet.

This work was supported by KEMCO KNREC, Ministry of Commerce, Industry and Energy under grant no. 2006-N-CO12-P-04-3-020.

- Clift, R. and Seville, J. P. K. (1993). Blackie Academic & Professional, New York.
- Ito, S., Tanaka, T. and Kawamura, S. (1998). *Powder Technol.* 100, 32-40.
- Pastila, P., Helanti, V., Nikkila, A. P. and Mantyla, T. (2001). *J. Eur. Ceram. Soc.*, 21, 1261-1268.
- Thambimuthu, K. V. (1993). IEA Coal Res., London, IEACR/53.

## Characterization of deposit structures on single dust-loaded filter fibers

S. Schollmeier, J. Meyer, G. Kasper

Institut für Mechanische Verfahrenstechnik und Mechanik, Universität Karlsruhe, Karlsruhe, Germany

Keywords: aerosol filtration, single fiber and particles, particle deposition, Confocal Laser Scanning Microscopy, Fibrous filter

Particulate structures on single fibers influence further particle deposition and gas flow passing the fibers. Knowledge of structure built-up at different conditions can be used in filter models to predict the filtration behavior depending on the increasing dust load. Characterization of particulate structures was done with Confocal Laser Scanning Microscopy: two scan modes allow visualizations longitudinal to the fiber axis as well as in cross sectional direction.

Different loading conditions lead to significant changes in structure built-up. Figure 1 shows the built-up of particulate structures in cross sectional direction at different velocity. At low velocity (top), some of the structures are orientated upstream, some others sideward to flow direction. Figure 2, top, illustrates the significant change of structure along the fiber axis at low velocity.

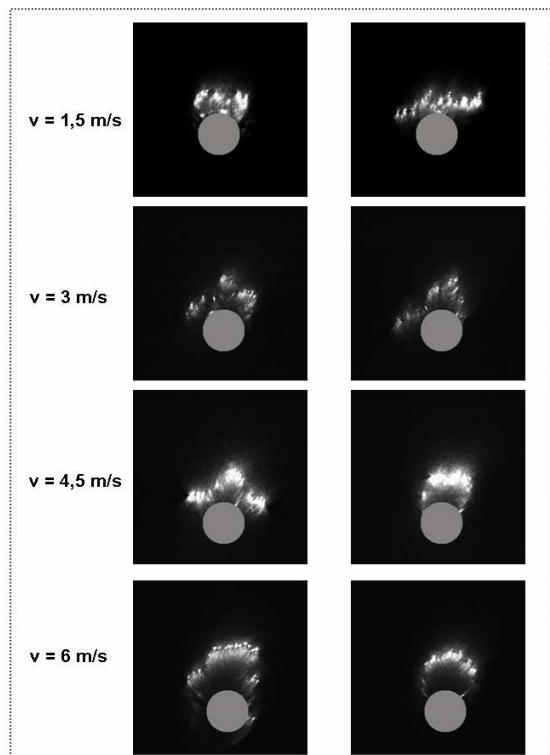


Figure 1. cross sectional view of particulate structures at different flow velocity

At increased velocity (3 m/s), structures are less sideward orientated and some of the structures show sideward arms. (Figure 1,  $v=3$  m/s, image on the left). These arms occur more often for further

increase of velocity, due to bounce of particles on the upstream orientated part of the structure. This effect was also recognized in modeling attempts (Lehmann, 2005). At high velocity the sideward orientated arms vanish and upstream orientated structures remain. Particles bounce strongly and do not deposit on other areas sideward. Regular, homogenous structures are built-up, shown in Figure 2, bottom.

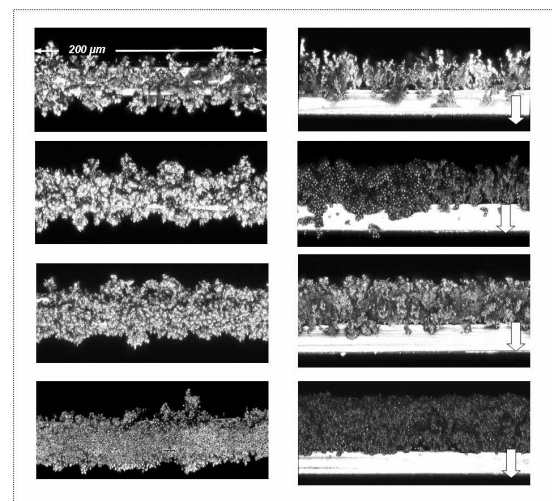


Figure 2. longitudinal (along fiber axis) view of particulate structures with increasing velocity (top to bottom, velocities see Figure 1); view in flow direction (left side) and perpendicular to flow direction (right side)

Kanaoka (1986) introduced a scheme, which describes the structure built-up at different values of the Stokes inertia parameter  $St$ : low  $St$  lead to sideward-, high  $St$  to upstream orientated structures. This was also observed in this work for low and high velocity (Figure 1, top, right side and bottom, right side). At constant particle size and fiber diameter, an increase of  $St$  is equivalent to an increase of velocity.

This work was supported by the Deutsche Forschungsgemeinschaft (DFG) under grant Ka1373/13-1.

Kanaoka, C. et al (1986). *Morphology of particulate agglomerates on a cylindrical fiber and a collection efficiency of a dust loaded fiber*. 2<sup>nd</sup> International Aerosol Conference.

Lehmann, M. J. (2005). *Untersuchungen zur Struktur und zur Beladungskinetik von Tiefenfiltern*. Dissertation, Universität Karlsruhe.

## Measurement of the collection efficiency of single dust-loaded filter fibers

S. Schollmeier, J. Meyer, G. Kasper

Institut für Mechanische Verfahrenstechnik und Mechanik, Universität Karlsruhe, Karlsruhe, Germany

Keywords: aerosol filtration, collection efficiency, fibrous filter, optical particle counter, single fiber and particles

Filtration efficiency of fibrous air filters can be predicted as a function of increasing dust loading by calculations with filter models. Some of these models are based on single fiber data. Therefore, single fiber efficiency  $\varphi$  can be obtained as a function of particle loading by measuring the particle concentrations upstream and downstream a single fiber with optical particle counters.

At all conditions single fiber efficiency rises with increasing particle loading  $M$  (mass of deposited particles / fiber length in  $\mu\text{g}/\text{mm}$ ), strong at low loading stages, which slows down at higher loading. Fig. 1 shows the efficiency increase at different velocities, alternatively Stokes inertia parameter ( $St$ ). First, with rising of  $St$ , stronger increase of efficiency was found as a function of  $M$ . Further increase of  $St$  leads to the lower increase of efficiency due to slim structures and increased bounce of particles on deposited particles.

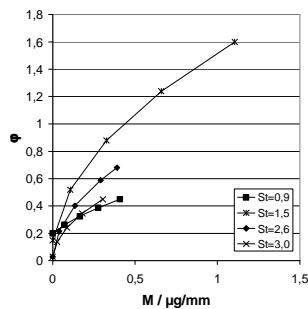


Figure 1. increase of single fiber efficiency  $\varphi$  with increasing loading  $M$ ;  $d_F = 30 \mu\text{m}$ ;  $d_p = 2,6 \mu\text{m}$

The increase of single fiber efficiency can be described by power law functions:

$$\frac{\varphi}{\varphi_0} = 1 + b \cdot \tilde{M}^c, \quad \tilde{M} = \frac{M}{\mu\text{g}/\text{mm}}$$

Values for  $c$  are about 0.65 over a wide range of conditions. The efficiency raising factor  $b$  as a function of the initial single fiber efficiency  $\varphi_0$  is presented in Fig.2. Combined with data for  $\varphi_0$  as a function of  $St$  (Rembor *et al.*, 1999), the efficiency raising factor can be determined.

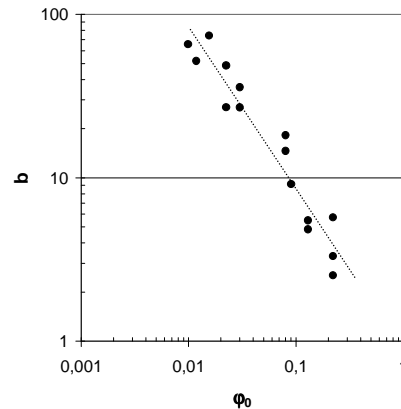


Figure 2. efficiency raising factor  $b$  as a function of initial single fiber efficiency  $\varphi_0$

The efficiency raising factor  $\lambda$  introduced by Kanaoka (1984) also decreases with  $\varphi_0$  but at higher values for each given  $\varphi_0$ .  $\lambda$  is the slope of the linear increase of  $\varphi$  with mass load. Kanaoka determined single fiber efficiencies from results of efficiency measurements on filters. Linear increase of efficiency as a function of deposited mass can also be observed in measurements of single fiber efficiency of fibers in fiber rows. In both cases flow and deposition of particles on fibers is influenced by adjacent fibers.

At low loading stages, the mass loading dependency of  $\varphi$  is linear, which is in agreement with literature (Billings, 1966).

This work was supported by the Deutsche Forschungsgemeinschaft (DFG) under grant Ka1373/13-1.

Billings, C. E. (1966). *Effects of particle accumulation in aerosol filtration*. PhD, Caltech University.

Kanaoka, C. *et al* (1984). *Experimental observation of collection efficiency of a dust loaded fiber*. Journal of Aerosol Science, Vol. 5, No. 4, pp. 483-489.

Rembor H.J. *et al* (1999). *Measurements of single fibre efficiencies at critical values of the Stokes number*. Part. Part. Syst. Charact 16, pp. 54-59.

## Generation of Ultrafine Aerosols from Saturated Oil-Mist Filters.

Benjamin J. Mullins<sup>1</sup>, Gerhard Kasper<sup>2</sup>.

1. Centre of Excellence in Cleaner Production, Curtin University, GPO Box U1987, WA, 6845, Australia.
2. Institute for Mechanical Process Engineering and Mechanics, Universität Karlsruhe, 76128, Karlsruhe, Germany.

Keywords: Oil-mist, Ultrafine aerosols, Generation, Re-entrainment.

Oil-mist or coalescing filters are widely used in a range of industries to remove liquid aerosol particles from air streams. These filters collect aerosol particles (usually oil-mist in the fine and ultrafine ranges), and coalesce them into larger droplets on the fibres (Raynor and Leith 2000).

Although the coalesced droplets should ideally drain from the filter as soon as possible, in practice they do not drain significantly until the pressure drop across the filter becomes high enough, whereupon a combination of drag and gravitational forces induce drainage (Mullins, Agranovski et al. 2004).

In practice then, such filters attain a “steady state” oil saturation, for a given set of operating conditions, whereupon the rate of influent oil captured and the drainage rate become equal. Modern oil-mist filters have become as compact as possible (due to space constraints) and utilise filter material with fine fibres, with packing densities up to 0.05. Therefore, for oleophilic filters, the quantity of oil which will be held in the filter at steady state in the filter is quite high (due to capillarity), and when no air is flowing through the filter, it is possible for some filters to fill all or nearly all of the void space with oil. This oil must then be forced out of the filter when the airflow is recommenced – either by drainage or re-entrainment. For industrial filters – such effects are very significant, as it is rare that they would operate continuously, or always at the same airflow rate.

The current work studied the re-entrainment of oil from a typical oil mist filter of approx 10cm diameter, located in a filter chamber with a plastic supporting mesh. The filter material was allowed to saturate itself through capillary effects, via a small bath of oil located in the bottom of the filter chamber. Once the filter had attained an equilibrium saturation state (for no airflow), airflow through the filter chamber (without aerosol) was commenced, and the reentrainment of aerosol particles from the filter was measured using an Optical Particle Counter (A10, Universitaet Karlsruhe) and an SMPS system (TSI 3010CPC and Hauke Long DMA) both of which received aerosol particles sampled through an isokinetic sampling point.

It was noted that on commencement of the airflow, the air bubbled through the media, and the

rupture of the air bubbles (surrounded by a thin oil film), is thought to account for the generated oil-mist being mostly in the ultrafine range – with a mean diameter of approximately 250nm, with a maximum recorded particle diameter of 2.9 $\mu$ m.

Figure 1 shows the mass-generation rates of re-entrained oil over time for 5 different face velocities using the same filter (re-saturated between experiments).

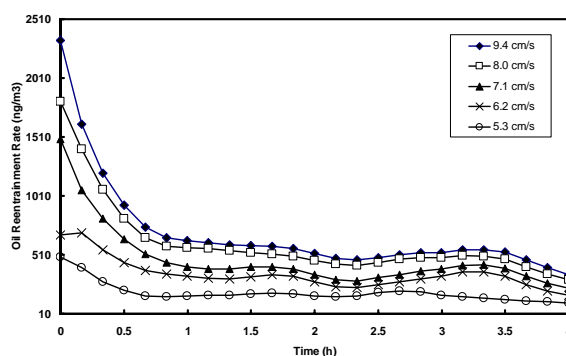


Figure 1 – Mass-based re-entrainment of oil-aerosol over time.

It will be noted that the shape of each curve is relatively constant, with higher airflow velocities inducing higher reentrainment rates. It will also be noted that the reentrainment continues for a significant time, due to the time needed for the filter to establish a new equilibrium.

These findings mean that the overall efficiency of an oil mist filter may be limited not by the rate of capture of aerosol particles, but rather by the rate of reentrainment. This would especially be true for filters which are operating at highly variable flow rates, or regularly stopping and restarting.

B. Mullins, I. Agranovski, et al. (2004). *J Coll. Int. Sci.* **269**(2): 449-458.

B. Mullins, and G. Kasper, (2006). *Chem. Eng. Sci.* **61**(18): 6223-6227

P. Raynor, and D. Leith (2000). *J. Aerosol Sci.* **31**(1): 19-34.

## Automated Fibre Diameter and Packing Density Measurements from SEM Images of Fibrous Filters.

Roger A. Cropp<sup>1</sup>, Benjamin J. Mullins<sup>2</sup>

1. Centre for Environmental Systems Research, Faculty of Environmental Science, Griffith University, Nathan, 4111 Australia.
2. Centre of Excellence in Cleaner Production, Curtin University, GPO Box U1987, WA, 6845, Australia.

Keywords: Filter, Fibre, SEM, Measurement.

Models of fibrous filter performance require accurate data on the fibre diameter, packing density, and (increasingly) homogeneity and fibre orientation of the filter media. Issues of fibre orientation are specially important in liquid aerosol filtration (Mullins and Kasper 2006).

There exists some excellent work on the 3D tomography of filters to obtain packing density and fibre orientation information (Hoferer et al. 2006). Such methods, however, are not able to produce accurate measurements of fibre diameter – particularly of the fine fibres which are used in modern filters.

Information on fibre diameters are typically obtained from manual or semi automated (point and click) analysis of Scanning Electron Microscope (SEM) images, which is usually tedious and time consuming.

This work aims to create an automated tool to measure both fibre diameter and (2D) packing density from SEM images of fibrous filters.

The tool has been programmed in MATLAB, using the Image Processing Toolbox. The image must first be read into MATLAB, and preliminary processing performed. The image is then “seeded” with a matrix of “dots”. The dots which fall on a blank area are discarded, while the dots which fall on a fibre are grown incrementally. When one side of the dot reaches the edge of a fibre, the drop is moved in the opposite direction. This process of growth and movement is continued until each dot reaches a fibre edge on both sides.

The resulting output (besides an image covered in dots!) is a histogram of dot size distributions. For a filter with uniform/monomodal fibre diameters, the resultant plot has a mode which corresponds to the fibre diameter. As could be expected, the distribution is relatively broad, as some dots are included which have grown on fibres which have been partially superimposed over one another in the 2D image. Nevertheless, for monomodal fibres it is relatively easy to determine the actual fibre diameter.

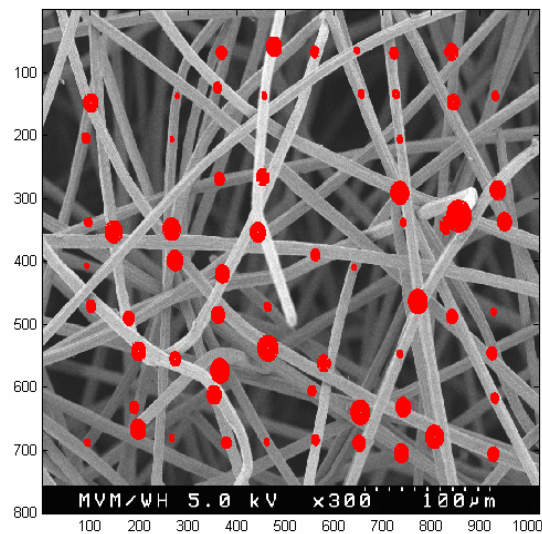


Figure 1 – SEM image of Bekaert stainless steel fibre filter with seeded dots (please note this is a preliminary image and some bugs were present which prevent the “dots” from ceasing their growth at the correct point).

However, expanding the work to filters with broad or bimodal fibre size distributions has not yet been performed, and it remains to be seen if reliable information on each mode can be obtained.

As mentioned, a further aim of the work is to obtain 2D measurements of filter packing density, and fibre angle, then to ascertain if a relationship exists between these measurements and 3D packing density measurements.

It is hoped that once this tool has been fully developed and tested, it will be beneficial to those working in the fibrous filtration field.

J. Hoferer, et al., (2006). Chem. Eng. And Tech. 29(7): 816:817.

B. Mullins, and G. Kasper, (2006). Chem. Eng. Sci. 61(18): 6223-6227.

## Fine particle removal by a vehicle air cleaner

Myong-Hwa Lee, Gyung Soo Kim, Sang Bum Kim, Yong Jin Kim, Byung Hyun Park  
Environment and Energy Division, Korea Institute of Industrial Technology, South Korea

Keywords: airborne particles, collection efficiency, filtration, fine particles, PM10

There is a growing interest in protecting human health and a precision instrument from air pollutants. Air cleaner which is one of the commonly used instrument, is essential to protect a vehicle engine from airborne particles. However, although it can prevent an engine abrasion, used material itself causes a waste treatment problem. Therefore, the development of an environmentally benign air cleaner with high performance is essential. In this study, an eco-friendly air cleaner using a polyurethane filter media was developed available in a remanufacturing process.

Two kinds of polyurethane filter media, a coarse(Filter-A) and a fine filter media(Filter-B), are used to protect a vehicle engine from airborne particles. In order to improve the collection performance of the filters(Filter-A, Filter-B), an oil coating technology on the filter surface was introduced.

As a result, inertial force is a dominant collection mechanism for a dry filter media, so that collection efficiency increases with increasing filtration velocity. However, intra-structure change of an oil-coated filter media influences on the collection mechanism, which shows a non-linear collection efficiency curve in terms of filtration velocity. Pressure drop,  $\Delta P$ , is another evidence of intra-structure change of an oil-coated filter media. In general, pressure drop increases with the amount of coated oil on the filter surface. However, the pressure drop of an oil-coated filter media shows opposite trend.

Furthermore, in order to use this oil coated filter as an air cleaner, the oil loss on a filter surface should be considered. Oil loss was not observed at all test filtration velocities.

In addition, the value of filter quality of an oil coated filter is higher than that of an uncoated filter at low filtration velocity.

In conclusion, the developed polyurethane filter media are eco-friendly and effective to protect a vehicle engine from airborne particles especially at low filtration velocity. Therefore, its usage is strongly recommended in all type of vehicles.

This work was financially supported by the Ministry of Commerce, Industry and Energy, Korea.

D. W. Dockery, J. Cunningham, A. I. Damokosh, L. M. Neas, J. D. Spengler, P. Koutrakis, J. H. Ware, M. Raizenne, & F. E. Speizer (1996). *Environ Health Perspect*, 104(5), 5500-505.

W. R. Stahel (1994). *The greening of industrial ecosystems*, Washington DC: National academy press, 178-191

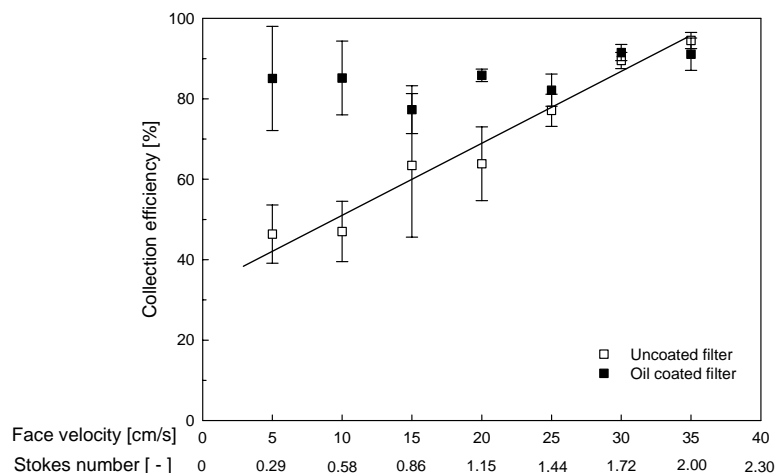


Figure 1. Collection efficiency of a Filter-AB with a face velocity and stokes number.

## **T11 Abstracts**

## New particle formation at rural sites simulated with MALTE (model to predict new aerosol formation in the lower troposphere)

M. Boy<sup>1</sup>, O. Hellmuth<sup>2</sup>, H. Korhonen<sup>3</sup>, A. Guenther<sup>4</sup>, J. Kazil<sup>5</sup>, E.R. Lovejoy<sup>5</sup> and M. Kulmala<sup>1</sup>

<sup>1</sup>Department of Physical Sciences, University of Helsinki, P.O. Box 64, 00014 University of Helsinki, Finland

<sup>2</sup>Leibniz Institute for Tropospheric Research, Permoserstrasse 15, 04 318 Leipzig, Germany

<sup>3</sup>Finnish Meteorological Institute, Air Quality Research, Sahaajankatu 20 E, FIN-00880 Helsinki, Finland

<sup>4</sup>ACD, NCAR, 3450 Mitchell Lane, Boulder, CO 80301, USA

<sup>5</sup>NOAA Earth System Research Laboratory, 325 Broadway, Boulder, CO 80305, USA

Keywords: aerosol formation, modelling, nucleation, organics, tropospheric aerosol.

New secondary particle formation has been observed at almost all places where both particle number concentrations and size distributions have been measured; a comprehensive summary of these studies is given in Kulmala et al. (2004). Although many field campaigns, laboratory experiments and new modelling approaches have led to increased understanding, detailed mechanisms responsible for the formation of new particles in the troposphere and their influence on health, environment and climate have still not been completely elucidated.

In MALTE (Model to predict new Aerosol formation in the Lower Troposphere) individually developed codes from different institutes around the globe merged into a one-dimensional model including aerosol dynamics, boundary layer meteorology, biology and chemistry in order to investigate the formation and growth processes of Secondary Organic Aerosols (SOA) under realistic atmospheric conditions.

Recently published field and laboratory studies showed that sulphuric acid is one key parameter concerning the formation of new particles. Comparison of modelled and measured H<sub>2</sub>SO<sub>4</sub> concentrations showed a satisfactory agreement for this compound (Boy et al., 2006). Further, the results indicate that the model is able to predict the on- and offset of new particle formation as well as the total aerosol number concentrations that were in good agreement with the observations by using the kinetic nucleation mechanism presented in Sihto et al. (2006).

The simulations showed that at a certain transitional particle diameter (2-9 nm), organic molecules can begin to contribute significantly to the growth rate compared to sulphuric acid (Figure 1). At even larger particle sizes, organic molecules can dominate the growth rate on days with significant monoterpene concentrations. Similar results were published by Wehner and co-authors (Wehner et al., 2005) recently. They calculated that new particles needed to reach a size range between about 7 – 20 nm before it becomes apparent that organic vapours can contribute significantly to the growth rate. However, their observations were from a more urban site in Germany with up to twice as much H<sub>2</sub>SO<sub>4</sub>.

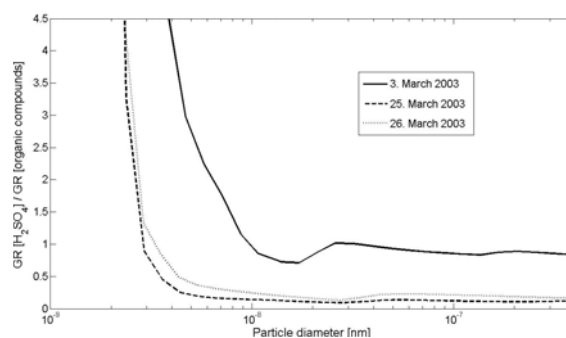


Figure 1: Ratio of the growth rate by sulphuric acid to that of organic vapours on 3 event days.

The intraday vertical evolution of new formed aerosols in the size range 3-6 nm calculated for an event day in March 2003 agreed well with measured vertical profiles reported by O'Dowd et al. (2005). The measurements and the model simulations showed high number concentrations of particles from about 100 m (lowest flight height) up to 500 m and a decrease above.

The contribution of particles below 10 nm inside the mixed layer produced by ion-induced nucleation over the boreal forest in Northern Europe seems to play a minor role compared to the total observed number concentration.

Boy, M., Hellmuth, O., Korhonen, H., Nillson, D., ReVelle, D., Turnipseed, A., Arnold, F. and Kulmala, M. (2006), *Atmos. Chem. Phys.*, 6, 4499–4517.

O'Dowd, C. D., Yoon, Y. J., Junkermann, W., Aalto, P. P. and Lihavainen, H. (2005), *Report Series in Aerosol Science*, Nr. 76, ISBN 952-5027-63-5, p. 162-173.

Sihto, S.-L., Kulmala, M., Kerminen, V.-M., Dal Maso, M., Petäjä, Riipinen, T., I., Korhonen, H., Arnold, F., Janson, R., Boy, M., Laaksonen, A. and Lehtinen, K. E. J (2006), *Atmos. Chem. Phys. Discuss.*, 6, 4079-4091.

Wehner, B., Petaja, T., Boy, M., Engler, C., Birmili, W., Tuch, T., Wiedensohler, A. and Kulmala, M. (2005), *Geo. Res. Lett.*, Vol. 32, L17810, doi:10.1029/2005GL023827.

## Simulation of aerosol dynamics in forest fires

A.E. Aloyan and V.O. Arutyunyan

Institute of Numerical Mathematics, Russian Academy of Sciences, Gubkin str. 8, 119333, Moscow, Russia

Keywords: aerosol dynamics, aerosol modeling, atmospheric aerosols, combustion particles, nucleation.

A complex mathematical model for aerosol dynamics has been developed for forest fire conditions. The model incorporates atmospheric hydrodynamics (accounting for atmospheric compressibility), condensation / evaporation, coagulation, gas- and aqueous-phase chemistry. More details of the model can be found in (Aloyan & Piskunov, 2004). The aerosol dynamics is based on the equation

$$\begin{aligned} & \frac{\partial \varphi_g}{\partial t} + \text{grad} \varphi_g + \frac{\partial (v_g \varphi_g)}{\partial g} \\ & = F + J(t)(g - g(t)) \\ & + \frac{1}{2} \int_0^g K(g, g_1) \varphi_{g-g_1} \varphi_{g_1} dg_1 \\ & - \varphi_g \int_0^\infty K(g, g_1) \varphi_{g_1} dg_1 + \frac{\partial k_{ij}}{\partial x_i} \frac{\partial \varphi_g}{\partial x_i}, \end{aligned}$$

where  $\varphi_g$  is the concentration of particles with masses between  $g$  and  $g + dg$ .  $K(x, y)$  is the coagulation kernel,  $J(t)$  is the nucleation rate,  $v_g$  is the rate of condensational growth.

The numerical calculations were performed for the Irkutsk area (East Siberia, Russia) which is known to suffer from forest fires. The dimensions of the computational grid are 60 x 60 x 20. The problem of condensation and coagulation includes 30 aerosol size bins starting from 0.05 up to 5  $\mu\text{m}$ . The surface heat flux was given to grow up to 50  $\text{kWt/m}^2$ , with a following no-flame combustion (smoldering). The total mass of combustible forest materials was assumed to be 3  $\text{kt/m}^2$ , which is in line with experimental data.

A detailed sensitivity analysis of the particle-size distribution to the capacity of these materials was performed. The results of numerical experiments indicate that the particle number concentration decreases with height much quicker than the mass concentration. This effect can be explained by an analysis of the particle-size distribution at different heights. It was found that near the source particles with doubled mass (0.65  $\mu\text{m}$ ) are generated rather quickly and then coagulate with only fine aerosol particles, thus decreasing the concentration of primary particles.

The variation of aerosol particles was investigated for nucleation, accumulation, and coarse modes as function of ageing. With going far from the source, the concentration of nucleation-mode particles with a radius of between 0.1 and 0.8  $\mu\text{m}$  quickly decreases, which is well consistent with the measurement data given in Radke *et al.* (1995). The decrease in the particle volume the nucleation mode occurs due to fast coagulation in the accumulation mode. Figure 1 shows the variation in the number concentration of coarse particles with a radius of 2  $\mu\text{m}$ . It can be seen that the concentration is much higher than in the fire point area.

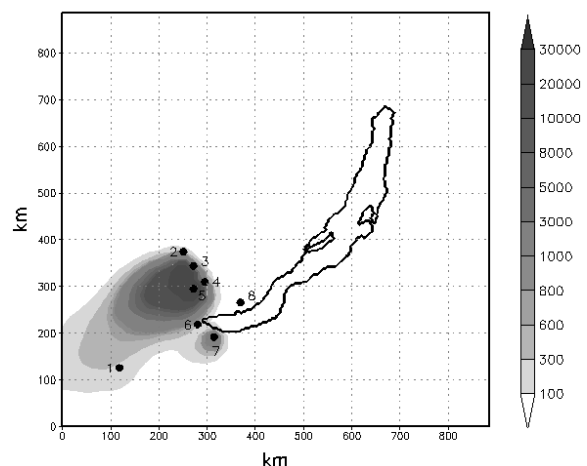


Figure 1. Concentration of aerosol particles ( $\text{m}^{-3}$ ) with a radius of 2  $\mu\text{m}$  in Lake Baikal region.

This work was supported by the RFBR, under projects 06-05-65184 and 06-05-66861.

Aloyan, A. E., & Piskunov, V. N. (2005). *Izv. RAN: Fizika atmosfery i okeana*, 41(3), 328–340.

Radke, J. F., Hegg, A. S., Hobbs, P. V., & Penker, J. E. (1995). *Atmospheric Research*, 38, 315–332.

## Modeling the urban- and regional-scale dynamics of gaseous pollutants and aerosols

V.O. Arutyunyan<sup>1</sup>, A.E. Aloyan<sup>1</sup>, and A. N. Yermakov<sup>2</sup>

<sup>1</sup>Institute of Numerical Mathematics, Russian Academy of Sciences, Gubkin str. 8, 119333, Moscow, Russia

<sup>2</sup>Institute of Energy Problems of Chemical Physics, Russian Academy of Sciences, Leninski pr. 38/2, 119334, Moscow, Russia

Keywords: aerosol chemistry, aerosol dynamics, aerosol modeling, atmospheric aerosols, ions.

A new 3D numerical model has been developed for gas and aerosol dynamics in the regional and urban scales. The main modules of the model are atmospheric hydrodynamics, gas- and aqueous-phase chemistry, binary/ternary nucleation, condensation/evaporation, and coagulation (Aloyan & Piskunov, 2004).

The chemical model includes some 300 chemical reactions, and 44 gas-phase and 51 aqueous-phase chemical species. The kinetic models of condensation and coagulation use a non-equilibrium particle-size distribution function. The number of particle size bins in the model is 30, ranging from 0.05 to 1.5  $\mu\text{m}$ . Using this model, numerical experiments were performed for condensation both on natural aerosol particles (Junge distribution) and on particles originated from binary/ternary nucleation.

The urban-scale calculations were performed for the industrial towns of Irkutsk (Russia) and Antwerp (Belgium). Along with photochemical transformation, the emphasis was on the possible formation of nucleation mode particles from precursor gases through the mechanisms of binary and ternary nucleation. The numerical calculations show that enhanced  $\text{SO}_2$  emission levels in these towns contribute to the formation of nucleation-mode particles, with its rate being essentially dependant on seasons of the year. Then, the nucleation rate is used in the right-hand side of the kinetic equation of condensation and coagulation to solve the problem of aerosol dynamics.

The regional-scale numerical calculations were performed for the Lake Baikal area in Russia, using emission data of local industrial sources. The emphasis was on the variability of atmospheric gaseous pollutants and formation of aerosol particles having regard to their ion composition (Yermakov *et al.*, 2007).

The calculated and measured data were compared for time periods when ammonium-sulfate particles had been registered. The numerical results show a good agreement between the calculated and measured data for the concentration of free protons in these particles. The oxidized  $\text{SO}_2$  is largely (around 98 %) stabilized in the atmosphere in the form of sulfate ions, while only some 2 % is found as gaseous molecules of  $\text{H}_2\text{SO}_4$ .

An additional thermodynamic estimation of the ion composition of aerosols indicated that the specific volume of liquid water in equilibrium particles (gas-particle equilibrium) was  $7 \times 10^{-10} \text{ l/m}^3$ . It follows from here that the acidity of ammonium-sulfate particles was very large (15 mole/l), which justifies the assumption that the acidity of aerosol particles collected during this episode is controlled exceptionally by the acidity of ammonium-sulfate particles. The agreement between kinetic calculations and observations is quite satisfactory for the mass concentration of nitrate ions (0.37 and  $0.25 \mu\text{g/m}^3$ , respectively).

Some discrepancy between calculated and observed data can be explained by the fact that there were no data of  $\text{NH}_3$  natural emissions available at the Mondy background station and that remote sources of  $\text{SO}_2$  outside the Baikal region may exist.

This work was supported by the RFBR, under projects 06-05-65184 and 06-05-66861.

Aloyan, A. E., & Piskunov, V. N. (2005). *Izv. RAN: Fizika atmosfery i okeana*, 41(3), 328–340.

A. N. Yermakov, A. E. Aloyan, T. V. Khodzer, I. P. Golobokova, and V. O. Arutyunyan (2007). *Izv. RAN: Fizika atmosfery i okeana*, 43(2), 20–35.

## Influence of car induced turbulence on PM dispersion along urban traffic paths

J. Pospisil, M. Jicha

Faculty of Mechanical Engineering, Brno University of Technology, Technicka 2, 61669, Brno, Czech Republic

Keywords: PM, modeling, traffic, urban areas

This paper presents the results of a case study utilizing small scale numerical modeling for expression of the relation between the moving cars induced kinetic energy of turbulence and the PM10 concentration along the street canyon in the central part of the city of Brno.

The influence of moving cars plays a significant roll in PM dispersion processes along traffic paths. Moving vehicles enhance both micro- and large-scale mixing processes in the environment by inducing additional turbulence and by entraining masses of air in the direction of vehicle movement.

The CFD code StarCD was used as a convenient modeling tool. A model based on Eulerian - Lagrangian approach to moving objects (Jicha et al., 2000) has been used for inclusion of traffic dynamic. The governing equations for the continuous phase were solved using the finite volume procedure. The set of equations for the conservation of mass and momentum was solved for unsteady incompressible turbulent flow. The equation for a general variable  $\phi$  has the form

$$\frac{\partial(\rho\phi)}{\partial t} + \frac{\partial}{\partial x_i}(\rho u_i \phi) = \frac{\partial}{\partial x_i} \left( \Gamma \frac{\partial \phi}{\partial x_i} \right) + S_\phi \quad (1)$$

Variable  $\phi$  stands for velocity components and  $S_\phi$  represents additional source terms. The standard  $k-\varepsilon$  model of turbulence was used.

As it is known, moving objects induce a strong kinetic energy of turbulence that was added as an additional source to the  $k$  equation. From different studies e.g. Eskridge and Hunt (1979) and Sedefian et al. (1981) it follows that turbulence is induced mainly in the wake behind the vehicle. Therefore the additional source of kinetic energy of turbulence  $S_k$  was assigned in the control volumes passed by moving cars.

$$S_k = C_c (U_{car} - U_\infty)^2 \dot{Q}_{car} \quad (2)$$

Where  $C_c$  is model constant (Sedefian et al., 1981) and  $\dot{Q}_{car}$  is traffic intensity.

The studied street canyon is located at the centre of the city of Brno (population 350000). Five-story buildings (20 m high) form both sides of the street canyon. Width of the street is 22 m. Two-way traffic in total four traffic lanes is present in the street. The day highest traffic rate is 1530 cars/hour.

The set of calculations was carried out on the numerical model of the studied area. During the calculations, the traffic rate was changed step-by-step from the day highest value to the situation without

traffic. All other parameters remained unchanged. Predicted PM10 concentrations were evaluated in 9 receptor points located in the studied street and perpendicular side-streets.

The figure 1 shows graphical expression of obtained results. Higher traffic rate causes higher PM10 concentrations in all considered receptor points. But, the relation between traffic rate and PM10 concentration is not strictly linear. Increasing traffic causes a more intensive transport of particulate matter from the line source, located in the middle of the studied street canyon, to the positions of the receptor points. This behavior is influenced by the actual value of kinetic energy of turbulence in the vicinity of the line source. Higher traffic rate causes higher value of kinetic energy of turbulence above a road surface. Intensive mixing of air intensifies transport of PM in the perpendicular direction to the street. That results in the presented progressive increase of PM concentrations with increasing traffic.

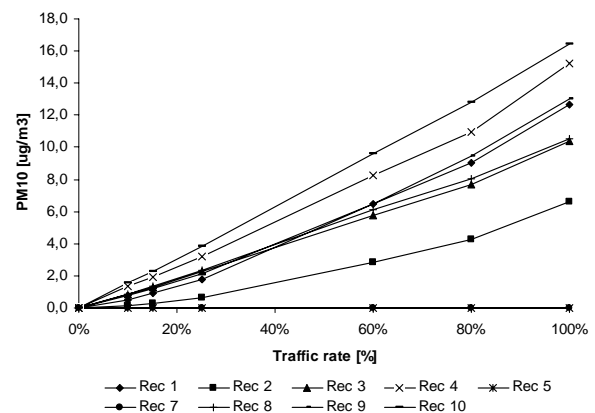


Figure 1. Relation between traffic rate and PM10 concentrations (1530 cars/hour = 100%)

The Czech Ministry of Transport financially supported this work under the grant 1F54H/098/520.

Eskridge, R. E.; Hunt, J. C. R. (1979) *Highway modelling. Part I* J. of Applied Meteorology, vol.18, pp. 387-392.

Sedefian, L.; Rao, S. T.; Czapski, U. (1981) *Effects of traffic-generated turbulence on near-field dispersion*. Atmos. Environ., vol. 15, pp. 527-535.

Jicha M., Katolicky J., Pospisil J. (2000), *Dispersion of pollutants in street canyon under traffic induced flow and turbulence*, J. Environmental Monitoring and Assessment, vol. 65, 343-35.

## An improved model for heterogeneous nucleation

A.Määttänen<sup>1,2</sup>, H. Vehkamäki<sup>1</sup>, A.Lauri<sup>1</sup>, I.Napari<sup>1</sup>, P.E.Wagner<sup>3</sup> and M.Kulmala<sup>1</sup>

<sup>1</sup>Department of Physical Sciences, University of Helsinki, P.O.Box 64, FI-00014, Helsinki, Finland

<sup>2</sup>Finnish Meteorological Institute, Space Research, P.O.Box 503, FI-00101, Helsinki, Finland

<sup>3</sup>Institut für Experimentalphysik, Universität Wien, Boltzmannngasse 5, A-1090, Wien, Austria

Keywords: Aerosol dynamics, modelling, nucleation, particle formation.

We have developed a model of two-component steady-state heterogeneous nucleation based on a homogeneous binary nucleation model. The heterogeneous nucleation part includes the exact calculation of the kinetic prefactor with the correct heterogeneous Zeldovich factor for a two-component system. The model has been tested with a water-*n*-propanol system and compared with measurements and a previously developed model.

We tested the kinetically correct model described in Noppel *et al.* (2002) with added heterogeneity using the surface diffusion approach (hereafter Model 1) with water-*n*-propanol system. We compared the results with experiments and a previous model that includes an approximative Zeldovich factor and uses the direct vapour deposition approach in the heterogeneous growth matrix terms. The second model (Kulmala *et al.*, 2001) is based on the approach of Kulmala and Laaksonen (1990) and Lazaridis *et al.* (1991). Results of the Kulmala *et al.* (2001) model (hereafter Model 2) have proved to compare reasonably well with the measurements (Wagner *et al.*, 2003).

For the comparison we ensured that both models have the same method for the calculation of the exponential part of the nucleation rate, since the comparison was to be made only between the calculation of the kinetic prefactor in the models. The largest difference in the calculation is originated in the difference between the theoretical approaches in the cluster growth model.

The other main issue is the Zeldovich factor, which is calculated very differently in the two models. Model 1 calculates the kinetic prefactor (including the Zeldovich factor) in a kinetically correct way, whereas Model 2 uses an approximation of a virtual monomer, which could be described as an "average" monomer colliding with the cluster, the volume of which is calculated as the sum of molecular volumes weighed with the respective mole fractions. The difference between the two Zeldovich factors can be several orders of magnitude. This is, however, not expected to have a significant effect on the nucleation probabilities.

We compared the models with an experimental dataset (Wagner *et al.*, 2003) and to each other. We chose three experiments conducted for oxidized Ag particles of 8 nm radii (non-monodisperse) with constant propanol liquid mass fractions (0.446, 0.763 and 0.926). We used a monodisperse condensation nucleus distribution. The thermodynamic and other

data used for the Model 2 can be found from Kulmala *et al.* (2001). The data for Model 1 is partly extracted from Model 2 (activities, surface tensions, etc.), and the values required for the surface diffusion method (energies for desorption and surface diffusion) have been mostly derived from the Model 2 values.

Model 1, the new, kinetically correct steady-state binary heterogeneous nucleation model gave surprisingly similar results compared to the Model 2 containing the approximative Zeldovich factor.

We gratefully acknowledge funding from the Academy of Finland and the Kordelin foundation.

Kulmala, M., and Laaksonen, A. (1990). Binary nucleation of water-sulfuric acid system: Comparison of classical theories with different H<sub>2</sub>SO<sub>4</sub> saturation vapor pressures. *J. Chem. Phys.*, 93, 696-701.

Kulmala, M., Lauri, A., Vehkamäki, H., Laaksonen, A., Petersen, D., and Wagner, P. E. (2001). Strange predictions by binary heterogeneous nucleation theory compared with a quantitative experiment. *J. Phys. Chem. B.*, 105, 11800-11808.

Lazaridis, M., Kulmala, M., and Laaksonen, A. (1991). Binary heterogeneous nucleation of a water-sulphuric acid system: the effect of hydrate interaction. *J. Aerosol Sci.*, 22, 823-830.

Noppel, M., Vehkamäki, H., and Kulmala, M. (2002). An improved model for hydrate formation in sulfuric-acid water nucleation. *J. Chem. Phys.*, 116, 218-228.

Pruppacher, H. R., and Klett, J. D. (1997). *Microphysics of Clouds and Precipitation*. Kluwer Academic.

Wagner, P. E., Kaller, D., Vrtala, A., Lauri, A., Kulmala, M., and Laaksonen, A. (2003). Nucleation probability in binary heterogeneous nucleation of water-*n*-propanol vapor mixtures on insoluble and soluble nanoparticles. *Phys. Rev. E*, 67, 021605.

## Two-component heterogeneous nucleation in the Martian atmosphere

A.Määttänen<sup>1,2</sup>, H. Vehkamäki<sup>1</sup>, A.Lauri<sup>1</sup>, I.Napari<sup>1</sup> and M.Kulmala<sup>1</sup>

<sup>1</sup>Department of Physical Sciences, University of Helsinki, P.O.Box 64, FI-00014, Helsinki, Finland

<sup>2</sup>Finnish Meteorological Institute, Space Research, P.O.Box 503, FI-00101, Helsinki, Finland

Keywords: Aerosol dynamics, modelling, nucleation, particle formation.

We have used a two-component nucleation model (another abstract Määttänen *et al.*) to model binary nucleation in the Martian atmosphere (Määttänen *et al.*, 2007).

The water - carbon dioxide system has not been modelled before. The Martian atmosphere is 95.3% carbon dioxide, and there is no liquid phase for the nucleating substances. Clouds are presumed to form from either water or CO<sub>2</sub> ice crystals, and this is the first study of binary nucleation on Mars. There is no thermodynamic data available for the ice mixture properties.

We calculated, as a first approximation, the thermodynamic data (surface energy, ice density) for the mixture assuming ideal mixing. For ideal mixture, the solid phase activities equal the mole fractions of the respective species. We tested the behavior of the system by using the activity coefficients of water - n-propanol mixture for the water - carbon dioxide mixture. The activities of the water - n-propanol system are thought to realistically mimic the behavior of the H<sub>2</sub>O - CO<sub>2</sub> system since both CO<sub>2</sub> and n-propanol are nonpolar molecules.

The nonisothermal coefficient (important in nucleation occurring in a near-pure substance) is calculated using the formulation of Feder *et al.* (1966) as was also done in Määttänen *et al.* (2005).

Our results show that the CO<sub>2</sub> concentration is not the limiting factor for the initiation of binary nucleation, but the water amount is. The results show that the onset of binary nucleation happens at slightly lower activities than the onset of unary nucleation of water. We looked at the numbers of molecules in the critical cluster in these cases, and noticed that the cluster is mainly composed of water molecules. In some cases with low amount of water vapor (1 ppm), the number of CO<sub>2</sub> molecules stays fairly large (tens of molecules) in a larger range of temperatures (about one degree), but for 300 ppm of water even in the first critical (binary) cluster the number of CO<sub>2</sub> molecules is only 2-3 and after that drops to less than one (which implies unary water nucleation). So theoretically at the onset of water nucleation on Mars it seems that binary nucleation might have a role in facilitating the process, but the number of CO<sub>2</sub> molecules in the critical clusters is so small, that particle formation process is nearly pure water nucleation. The nonisothermal coefficient was 0.02-0.03 for the range where the critical molecular numbers of both substances were greater than one. This is in the same range as was acquired for unary CO<sub>2</sub> nucleation in Määttänen *et al.* (2005).

According to our results we can presume that in the present Martian atmosphere ice clouds do form one component at a time, as described in our earlier paper (Määttänen *et al.*, 2005). and several other authors (e.g., Michelangeli *et al.*, 1993, Colaprete *et al.*, 1999, Colaprete & Toon 2002, Montmessin *et al.*, 2002). However, we can not completely rule out the possibility of binary nucleation of the CO<sub>2</sub> - H<sub>2</sub>O mixture, possibly at the very first stages of unary water nucleation. This result is naturally dependent on the assumptions made for the system (for example the ideal mixture assumption) and validating the results will have to wait until there are data or experiments for the real thermodynamic properties of the system.

We gratefully acknowledge funding from the Academy of Finland and the Kordelin foundation.

Colaprete, A., O.B. Toon, and J.A. Magalhaes (1999), Cloud formation under Mars Pathfinder conditions, *J. Geophys. Res.*, 104(E4), 9043-9054.

Colaprete, A., and O.B. Toon (2002), Carbon dioxide snow storms during the polar nights on Mars, *J. Geophys. Res.*, 107(E7), 5051, doi:10.1029/2001JE001758.

Feder, J., K.C. Russell, J. Lothe and G.M. Pound (1966), Homogeneous nucleation and growth of droplets in vapours. *Adv. Phys.*, 15, 111-178.

Michelangeli, D.V., O.B. Toon, R.M. Haberle and J.B. Pollack (1993), Numerical simulations of the formation and evolution of water ice clouds in the Martian atmosphere, *Icarus*, 100, 261-285.

Montmessin, F., P. Rannou and M. Cabane (2002), New insights into Martian dust distribution and water-ice cloud microphysics, *J. Geophys. Res.*, 107(E6), 5037, doi:10.1029/2001JE001520.

Määttänen, A., H. Vehkamäki, A. Lauri, S. Merikallio, J. Kauhanen, H. Savijärvi, and M. Kulmala (2005), Nucleation studies in the Martian atmosphere, *J. Geophys. Res.*, 110, E02,002.

Määttänen, A., H. Vehkamäki, A. Lauri, I. Napari, and M. Kulmala (2007), Two-component nucleation: A Martian test case. *Journal of Chemical Physics*, submitted.

## Evaporation and condensation of succinic acid and water: Model intercomparison

J. Voigtländer<sup>1</sup>, I. Riipinen<sup>2</sup>, M. Kulmala<sup>2</sup>, F. Stratmann<sup>1</sup>

<sup>1</sup>Leibniz Institute for Tropospheric Research, Leipzig, Germany

<sup>2</sup>Department of Physical Sciences, University of Helsinki, Finland

Keywords: condensation, evaporation, modelling, organics, succinic acid.

Organic compounds represent a significant fraction of all particulate matter in the atmosphere. A substantial fraction of the organic material is water soluble, e.g. dicarboxylic acids. Succinic acid ( $C_4H_6O_4$ ) is one of these dicarboxylic acids that are often found. Due to its atmospheric relevance, hygroscopic growth and CCN activation of succinic acid have been measured and theoretical modelled.

In this study we investigate the condensational growth and evaporation of droplets containing water and succinic acid by comparing to numerical model approaches. Both models simulate binary condensation and/or evaporation by combining basic mass and heat transfer theories in inert gas where no chemical reactions take place.

The first model is a numerical box model BCOND (Vesala, 1997), which allows an accurate thermodynamic description of the condensation/evaporation process. The model has been validated with experiments, and the model results are in a good agreement with observations, assuming that the thermophysical properties of the investigated compound are well-defined. Recently Riipinen et al. (2006) have used the model together with Tandem Differential Mobility Analyzer (TDMA) measurements obtain information about the thermodynamical properties succinic acid – water droplets.

The second model, called Fine Particle Model (FPM, Wilck, 2002), is an Eulerian model. It is fully integrated into the commercial three dimensional computational fluid dynamics (CFD) code FLUENT. The model is designed to describe coupled fluid flow and particle dynamical processes. In the FPM, condensation and evaporation are described by the simplified droplet growth law given by Barrett & Clement (Barrett & 1988). Therein, droplet temperature is included implicitly in linearized mass flux expressions, whereas in BCOND it is solved for separately during each time step. The FPM/FLUENT is applied to model experiments, which are performed on the Leipzig Aerosol Cloud Interaction Simulator (LACIS, Stratmann, 2004).

With the comparison of the models, the applicability of the FPM calculating hygroscopic growth and CCN activation of organic compounds can be validated.

For the model comparison, all relevant thermodynamical properties (temperature, system pressure, diffusion coefficients, activity models, densities, thermal conductivity, particle dry diameter,

parameterization of the surface tension, accommodation coefficients) were synchronized. Missing model descriptions, e.g. the UNIFAC Dortmund activity model, were implemented into the FPM.

The results for hygroscopic growth (at 293.15 K and 1000 hPa) of succinic acid particles with a dry diameter of 100 nm are shown in Fig. 1. The results produced by the compared models agree well. The simpler description of particle dynamics in the FPM/FLUENT model is therefore able to describe the particle growth and evaporation by succinic acid and water in a proper way.

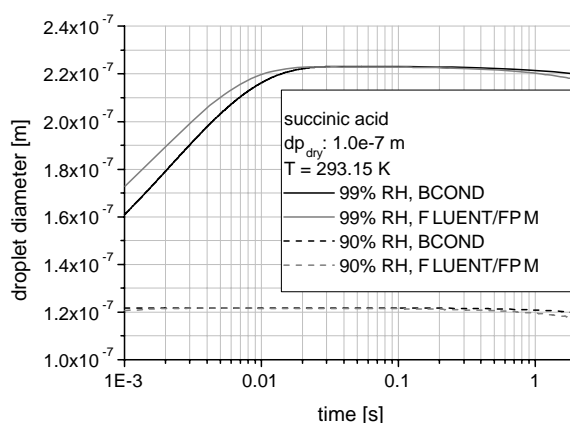


Figure 1. Comparison of the model results for succinic acid particles with 100 nm in diameter.

- Barrett, J.C. & Clement, C.F. (1988). *J. Aerosol Sci.*, 19(2), 223-242.
- Stratmann, F., Kiselev, A., Wurzler, S., Wendisch, M., Heintzenberg, J., Charlson, R.J., Diehl, K., Wex, H. & Schmidt, S. (2004). *J. Atmos. Oceanic Tech.*, 21, 876-887.
- Riipinen, I., Svenningsson, B., Bilde, M., Gaman, A., Lehtinen, K.E.J. & Kulmala, M. (2006). *Atm. Res.*, 82, 579-590.
- Wilck, M., Stratmann, F. & Whitby, E.R. (2002). in *Proc. Sixth Int. Aerosol Conf.*, Taipei, Taiwan, 1269-1270.
- Vesala, T., Kulmala, M., Rudolf, R., Vrtala, A. & Wagner, E. (1997). *J. Aerosol Sci.*, 28, 565-598.

## A numerical study of calm air sampling

Sarah J Dunnett<sup>1</sup>, Xianyun Wen<sup>2</sup>

<sup>1</sup>Department of Aeronautical and Automotive Engineering, Loughborough University, Loughborough, Leics., LE11 3TU, U.K.

<sup>2</sup>Environment, School of Earth and Environment, University of Leeds, Leeds LS2 9JT, U.K.

Keywords: aerosol sampling, numerical simulation

### INTRODUCTION

Aerosol samplers are widely used to determine the aerosol concentration in an environment. Due to many factors, such as the physical presence of the sampler and the action of withdrawing air through the sampler opening, the aerosol sample collected is not always a true representation of the aerosol concentration in the environment. Over the years much research has been carried out on understanding how samplers perform when operating under different conditions. Due to this work our knowledge of sampler behaviour for various situations is good, however one area in which our understanding is still not complete is sampling in calm air. This is when the only motion of the air is caused by the action of withdrawing air through the sampling inlet. It is of increasing importance as many airflows in modern workplaces are low, of order  $10^{-1}$  or less. Hence they can be approximated by the limiting calm air situation. In this work the study undertaken by Dunnett et al (2006) is extended to consider general expressions for the aspiration efficiency of a sampler operating under various conditions in calm air.

### METHOD AND RESULTS

Numerical models have been developed to determine the aspiration efficiency,  $A$ , of thin-walled samplers and blunt spherical samplers. This efficiency is defined as the ratio of the concentration of particles passing across the sampling inlet to the concentration in the undisturbed air away from the sampler. The numerical models have been validated using the experimental data available. Three different orientations of the samplers have been considered:

- i) inlet facing vertically upwards
- ii) inlet facing vertically downwards
- iii) inlet facing horizontally

Values of  $A$  have been determined numerically for all three orientations for various values of the operating parameters  $St_c$ ,  $R_c$   $B$ . Where  $St_c$  is the Stokes number,  $R_c$  the relative settling velocity, and  $B$  the sampler 'bluntness' defined as the ratio of the sampler body diameter to the sampling inlet diameter. For the thin-walled sampler  $B=1$ . Using the results obtained empirical formulae have been developed for  $A$  based upon physical reasoning.

As expected it was found that the effects of the sampler bluntness upon aspiration are negligible for orientation (i) but are of increasing importance as the inlet moves away from facing vertically upwards.

An example of some of the results obtained and the empirical formula developed are shown in figure 1 where the case of the sampler oriented with its inlet facing downwards, case ii), is considered.

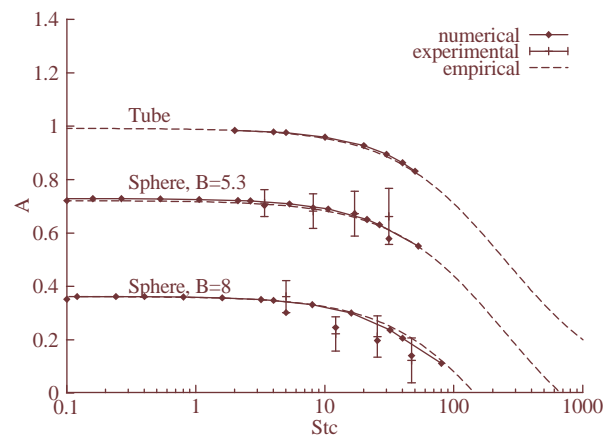


Figure 1.  $A$  as a function of  $St_c$  for case ii), showing the numerical, experimental and empirical formula.

In this case the empirical formula developed is given by

$$A = \frac{1 - R_c}{1 + (a * R_c + b) * St_c} - R_c (B^2 - 1)$$

$a$  and  $b$  are fitted coefficients.

In the work presented various situations are considered and a general formula for  $A$  developed.

### REFERENCES

Dunnett, S.J., Wen, X., Zaripov, S.K., Galeev, R.S. and Vanunina, M.V. (2006) *Aerosol Science and Technology*, 40, pp 490-502.

## Constructal view of dendritic growth of airborne particles

A. H. Reis<sup>1</sup>, A. F. Miguel<sup>1</sup> and A. Bejan<sup>2</sup>

<sup>1</sup>Department of Physics and Geophysics Centre of Evora, University of Évora, 7000-671 Évora, Portugal

<sup>2</sup>Department of Mech. Eng. and Materials Science, Duke University, Durham, NC 27708-0300, USA

Keywords: particle growth, shape, constructal law.

Agglomerates of aerosol particles often have dendritic shapes that can be observed experimentally or based on numerical simulations. Is dendritic shape the prevalent and natural form of particle agglomeration? If so, why do aggregates of particles exhibit this particular shape?

Here we address these issues in the framework provided by constructal theory (Bejan, 1996, 2000). The constructal law requires the architecture of the aggregate of particles to evolve in time in such a way that the global rate of accumulation of the particles is maximized. The generation of optimized architectures should bring the entire flow system (ambient + particles) to equilibrium in the fastest way. Among other phenomena, constructal theory was also applied to predicting atmospheric and oceanic circulation driven by heating from the sun (Reis and Bejan, 2006).

Electrical bonds may occur through interactions of various types (e.g. charge-charge, charge-dipole, dipole-dipole, etc.). However, charge-charge interactions cancel the existing surface charge, and only the charge-dipole interaction ensures a steady and continuing process of deposition, because a dipole-charge bond leaves the total charge amount invariant.

After having compared spherical to conical shaped agglomeration dynamics (Reis *et al*, 2006), and by invoking the constructal law we found that that the agglomerate first must grow as a sphere, and change to the conical shape at a critical

time  $t_c = \frac{9.9}{K} \left( \frac{\mu}{q} \right)^{3/2}$  because for  $t > t_c$  the conically

shaped agglomerate is more efficient as a particle collector than the spherically shaped

agglomerate.  $K = \frac{C_p \sigma c_c v_p}{6\pi^2 \varepsilon_0 \eta d_p} (q\mu)^{1/2}$  is a constant

where  $C_p$  is the concentration of dipolar particles in the vicinity of the surface,  $\sigma$  is surface density of charge,  $c_c$  is the Cunningham correction factor,  $v_p$  is particle volume,  $\varepsilon_0$  is electric permittivity of the air,  $\eta$  is dynamic viscosity,  $d_p$  is particle diameter,  $q$  is charge, and  $\mu$  is particle dipolar moment.

It is also interesting to compare the growth speeds of cone diameter ( $\dot{d}$ ) and cone tip ( $\dot{L}$ )

$\frac{\dot{d}}{\dot{L}} = \left( \frac{36}{K} \right)^{1/3} \left( \frac{\mu}{q} \right)^{1/2} t^{-1/3}$  which decreases as  $t^{-1/3}$ .

This means that at later stages the agglomerate grows as a needle, the geometry of which is given by

$d = \left( \frac{9}{\pi} \right)^{2/3} \left( \frac{\mu}{q} \right)^{1/3} L^{2/3}$  One interesting aspect of the

predicted geometry is that it depends only on the dipole moment  $\mu$ . This means that weakly dipolar molecules will agglomerate in a needle that is more slender than the needle formed by strongly dipolar molecules.

Another noteworthy aspect is that the critical time for switching from spherical to needle shaped growth depends only on the dipole strength. We calculated the critical diameter of the original sphere as  $D_{crit} \sim 6 \frac{\mu}{q} \sim 6a$  and predicted that a universal

behaviour of particle agglomeration must exist: when the sphere diameter reaches 6 particle diameters, the agglomerate (of  $(\pi/6) \cdot 6^3 \sim 113$  particles) must switch from spherical to needle-shaped growth as a preferential mode of particle agglomeration. This result agrees qualitatively with what is observed in nature. However, one needs precise measurements on particle growth to fully confirm the above predictions.

In summary, the constructal law enables us to predict important features of shape generation and architecture of particle agglomeration. In the very beginning the agglomerate grows as a sphere, because at short times this shape is more effective in collecting particles from the environment. At a critical time  $t_c$  the agglomerate switches to needle growth because for  $t > t_c$  this shape is more effective in collecting particles from the environment.

This work was supported by Foundation for Science and Technology (FCT) project POCTI/EME/59909/2004.

Bejan, A. (1997). *Advanced Engineering Thermodynamics*, 2nd ed., New York, U.S.: Wiley

Bejan, A. (2000). *Shape and Structure, from Engineering to Nature*. Cambridge, U.K.: Cambridge University Press.

Reis, A. H. & Bejan, A. (2006) *Int. J. Heat Mass Transfer* 49, 1957-1875

Reis, A. H., Miguel, A. F. & Bejan A. (2006). *J. Physics D*, 39, 2311-2318.

## Mass accommodation coefficient of water: Combined analysis of experimental data and computational fluid dynamics results

J. Voigtländer<sup>1</sup>, F. Stratmann<sup>1</sup>, D. Niedermeier<sup>1</sup>, H. Wex<sup>1</sup>

<sup>1</sup>Leibniz Institute for Tropospheric Research, Leipzig, Germany

Keywords: accommodation coefficient, mass accommodation, modelling

The mass accommodation coefficient  $\alpha_{\text{mass}}$  of water vapour into NaCl solutions has been studied at realistic lower atmospheric conditions (saturation ratio between 1.0 and 1.03,  $p = 1000$  hPa). For determination of  $\alpha_{\text{mass}}$ , a combination of experimental data and computational fluid dynamics (CFD) modelling has been applied. In contrast to previous studies (e.g. Winkler, 2006), we used a different experimental technique. Experiments were performed at the Leipzig Aerosol Cloud Interaction Simulator (LACIS, Stratmann, 2004), a laminar flow diffusion chamber for measurements of both, hygroscopic growth and cloud condensation nuclei (CCN) activation. Quasi-monodispersed sodium chloride particles with 54 nm and 108 nm have been used as condensation nuclei. Thereby, a shape factor of 1.08 was assumed. Measurements were performed at least three times for each measurement point and statistical tested using a Shapiro-Wilks-Test. The data are normal distributed with a significance level of 5 percent. Mean values and standard deviation have been calculated for each data point. The experimental uncertainty is given in terms of the standard deviation of the measurements.

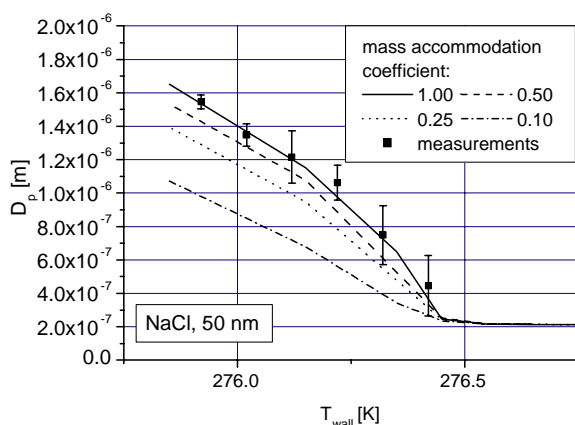


Figure 1. Comparison between measurements and calculation results. Inlet temperature was 293.15 K, dew point was 292.15 K, air pressure was 1000 hPa. Different values of  $T_{\text{wall}}$  correspond to different maximum saturation ratios inside the tube.

Experiments have been modelled using the Computational Fluid Dynamics Code (CFD-Code) FLUENT6 combined with a particle model (Fine

Particle Model (FPM), Wilck, 2002). Both, measurements results and calculations are shown in figure 1.

For determination of the mass accommodation coefficient  $\alpha_{\text{mass}}$ , measured droplet diameters were compared with calculated ones. The mass accommodation coefficient in the calculations was varied to achieve a quantitative comparison between model and measurement results. According to previous studies (Winkler, 2006), the thermal accommodation coefficient was set to unity in the calculations. With our experimental setup, we are not able to determine both coefficients simultaneously.

Our experimental data are consistent with a mass accommodation coefficient  $\alpha_{\text{mass}} > 0.30$  (figure 2), which agrees well with previous studies (e.g. Winkler, 2006). Therefore, we could confirm the results from previous studies using a different experimental technique.

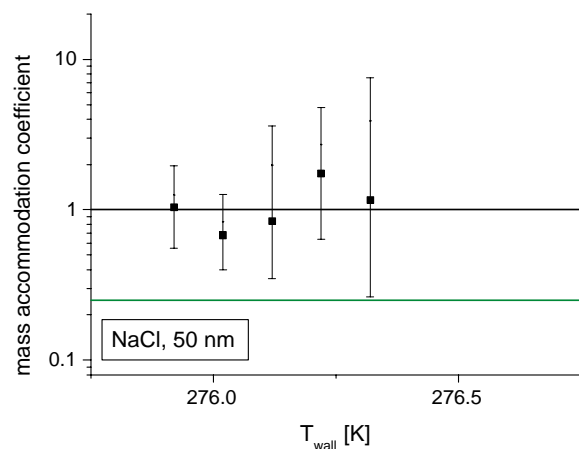


Figure 2. Measured mass accommodation coefficient.

Stratmann, F. & Kiselev, A. & Wurzler, S. & Wendisch, M. & Heintzenberg, J. & Charlson, R.J. & Diehl, K. & Wex, H. & Schmidt, S. (2004). *J. Atmos. Oceanic Tech.*, 21, 876-887.

Wilck, M. & Stratmann, F. & Whitby, E.R. (2002). in *Proc. Sixth Int. Aerosol Conf.*, Taipei, Taiwan, 1269-1270.

Winkler, P.M. & Vrtala, A. & Rudolf, R. & Wagner, P.E. & Riipinen, I. & Vesala, T. & Lehtinen, K.E.J. & Viisanen, Y. & Kulmala, M. (2006). *J. Geophys. Res.*, 111, D19202, doi:10.1029/2006JD007194.

## Aerosol model development for calculation of aerosol extinction in the coastal atmosphere surface layer

G.A. Kaloshin

V.E. Zuev Institute of Atmospheric Optics SB RAS,  
1, Academicheskii ave., 634055, Tomsk, Russia

Keywords: aerosol model, extinction, wind speed, fetch.

Extinction of radiation in the marine boundary layer is dominated by scattering and absorption due to atmospheric aerosol. This is important to optical retrievals from satellite, remote sensing at environmental monitoring, backscatter of light to space (including climate forcing), cloud properties etc. In unpolluted regions the greatest effects on near shore scattering extinction will be a result of sea-salt from breaking waves and variations in relative humidity. The role of breaking waves appears to be modulated by wind, tide, swell, wave spectra and coastal conditions. These influences will be superimposed upon aerosol generated by open ocean sea-salt aerosol that varies with wind speed.

The focus of our study is the extinction and optical effects due to aerosol in a specific coastal region. This involves linking coastal physical properties to oceanic and meteorological parameters in order to develop predictive algorithms that describe 3-D aerosol structure and variability.

The aerosol microphysical model of the marine and coastal atmosphere surface layer is considered. The model is made on the basis of the long-term experimental data received at researches of aerosol sizes distribution function ( $dN/dr$ ) in the band particles sizes in 0.01 - 100  $\mu\text{k}$ . The model is developed by present time for the band of heights is 0 - 25 m. Bands of wind speed is 3 - 18 km/s, sizes fetch is up to 120 km, RH = 40 - 98 %.  $dN/dr$  of the model is characterized by the four modified lognormal functions with modal radiuses, equal  $r_1 = 0,03$ ;  $r_2 = 0,24$ ;  $r_3 = 2$ ;  $r_4 = 10 \mu\text{k}$  (Piazzola, Kaloshin, 2005, 2006).

The model distinctive feature is parameterization of amplitude and width of the modes as functions of fetch and wind speed. In the paper the  $dN/dr$  behavior depending at change meteorological parameters, heights above sea level, fetch (X), wind speed (U) and RH is show. The received results are compared to available microphysical models NAN and ANAM.

On the basis of the developed model with usage of Mie theory for spheres the description of the last version of developed code MaexPro 5.0 (Marine Aerosol Extinction Profiles) for spectral profiles of aerosol extinction coefficients  $\alpha(\lambda)$  calculations in the wavelength band, equal  $\lambda = 0.2 - 12 \mu\text{m}$ , with step  $\Delta\lambda = 0.0001 \mu\text{m}$  is presented.

In Fig. 1 the composite window "extinction spectra" of the code MaexPro 5.0 is submitted on

which aerosol extinction spectra for chosen input meteorological parameters are resulted. Here with use of a service command "the switch OverPlot" aerosol extinction spectra  $\alpha(\lambda)$  calculated on a basis  $dN/dr$  are resulted which can be received with the help of aerosol counter AZ-5 with a range of aerosol particles measurement on radius  $\Delta r = 0.4 - 10$  microns and dust counter OMPN-10.0 (OPTEK Spb), carrying out the control of fractions in standard PM 10, PM 2.5 and PM 1. Fig. 1 shows that for three spectra of the aerosol sizes in wavelength band  $\Delta\lambda = 2 - 12 \mu\text{m}$   $\alpha(\lambda)$  differ approximately twice and in wavelength band  $\Delta\lambda = 0.2 - 2 \mu\text{m}$  of distinction in values  $\alpha(\lambda)$  reach 10 and more.

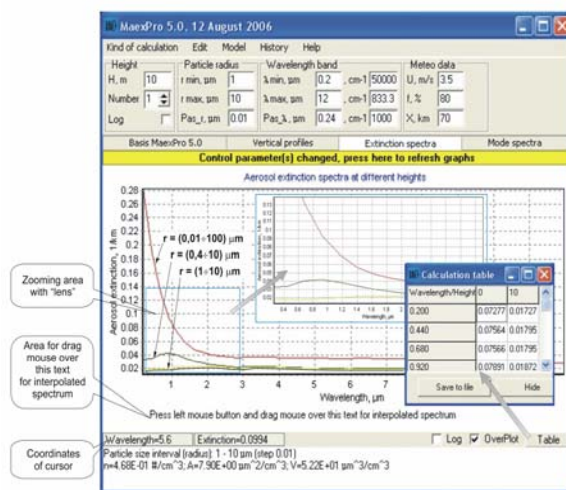


Figure 1. Composite window "Extinction spectra" including service commands

Also  $\alpha(\lambda)$  profiles for various wind modes (combinations X and U) calculated by MaexPro 5.0 code are given. Results of  $\alpha(\lambda)$  profiles calculations are presented at change RH = 40 - 98 % and heights H = 0 - 25 m. The calculated spectrums of  $\alpha(\lambda)$  profiles are compared with experimental data of  $\alpha(\lambda)$  received by a transmission method in various geographical areas.

J. Piazzola, G. Kaloshin. Performance evaluation of the coastal aerosol extinction code "MEDEX" with data from the Black Sea, J. of Aerosol Science. 36(3), pp. 341 - 359(2005).

G. Kaloshin, J. Piazzola. The Coastal Aerosol Microphysical Model, Proc. of the 23<sup>rd</sup> International Laser Radar Conf., Nara, Japan, pp. 423-426(2006).

## Estimating cloud droplet number concentration with particle number-to-volume concentration ratio

N. Kivekäs, V.-M. Kerminen, T. Anttila, H. Korhonen, M. Komppula and H. Lihavainen

Finnish Meteorological Institute, PO box 503, Helsinki, Finland

Keywords: Aerosol cloud interaction, Modelling, Aerosol size distribution.

In atmospheric aerosol systems, the number of particles >70-120 nm in diameter is related closely to the number of particles able to act as cloud condensation nuclei (CCN). Many large-scale atmospheric models, however, have the particle mass or volume concentration as the only prognostic variable.

The aim of this study is to investigate how accurate the estimation of cloud droplet number concentration (CDNC) would be if an empirical relation between the number concentration of CCN-size particles and particle volume (or mass) concentration was available. The relation used here is

$$R(d_c) = \frac{N(d > d_c)}{V_{tot}}, \quad (1)$$

where  $N(d > d_c)$  is the number concentration of submicron particles with dry diameter larger than a cut-off diameter  $d_c$  and  $V_{tot}$  is the total volume concentration of all submicron particles (Kivekäs *et al.*, 2007).

With an adiabatic air parcel model (Korhonen *et al.*, 2005, Anttila *et al.*, 2002) we simulated the activation of particles to cloud droplets in rising air. We varied the particle number size distribution parameters, the soluble fraction of particle mass ( $\varepsilon$ ) and the updraft velocity of the air parcel ( $v_{up}$ ). Then we fitted the numerical parameters to make the parameterization fit the simulated values as well as possible. The resulting formula was

$$CDNC = \left( a_1 \times \frac{R(0.1)}{d_c} \right) \times V_{tot} - a_2, \quad (2)$$

where

$$d_c = (b_1 \times \ln V_{tot} + b_2 \times \ln R(0.1) + b_3) \times \varepsilon^{b_4} \times v_{up}^{b_5}. \quad (3)$$

In the formulas above the numerical constants are  $a_1=0.10$ ,  $a_2=6\text{cm}^{-3}$ ,  $b_1=0.014$ ,  $b_2=0.008$ ,  $b_3=0.016$ ,  $b_4=-0.19$  and  $b_5=-0.32$ . The units are  $\text{cm}^{-3}$  for CDNC,  $\mu\text{m}^{-3}$  for  $R(d_c)$  and  $R(0.1)$ ,  $\mu\text{m}$  for  $d_c$ ,  $\mu\text{m}^3/\text{cm}^3$  for  $V_{tot}$  and m/s for  $v_{up}$ .  $\varepsilon$  is dimensionless.  $R(0.1)$  in the formula stands for  $R$  with  $d_c=0.1\mu\text{m}$ .

The parameterization was tested against measured cloud droplet activation data from Pallas GAW station in northern Finland (Komppula *et al.*, 2005). There were 33 clouds where particle activation was measured during the years 2000-2002. The soluble fraction of the particle mass was estimated to be 50% based on campaign

measurements at the same site during falls 2004 and 2005. There was no updraft velocity data available, so we decided to set  $v_{up}$  equal to 0.43m/s for all the cloud events.

The parameterized vs measured values of cloud droplet number concentration are shown in figure 1. The correlation coefficient between those two data sets was 0.76 and the largest offsets produced by the parameterization were within 50% of the measured value.

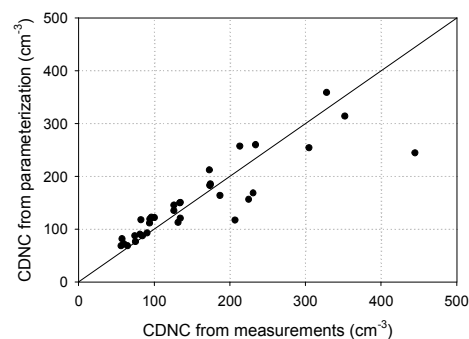


Figure 1. The parameterized vs measured cloud droplet number concentrations at Pallas during 33 cloud events.

The concept of parameterizing cloud droplet number concentrations (CDNC) with number-to-volume concentration ratios ( $R(d_c)$ ) works in Pallas, which is a station representing continental background air. If  $R(0.1)$  is known or can be parameterized, this kind of a parameterization would be a computationally efficient way to estimate the aerosol impact on cloud formation in large scale models. This demonstrates the benefit achievable from investigating parameterizations for  $R(0.1)$  or for some other  $R(d_c)$ .

- Anttila, T. and Kerminen, V.-M. (2002). *J. Geophys. Res.*, 107(D22), 4662, doi:10.1029/2001JD001482.
- Kivekäs N., Kerminen V.-M., Engler C., Lihavainen H., Komppula M., Viisanen Y. and Kulmala M. (2007), *J. Geophys. Res.*, accepted for publication
- Komppula M., Lihavainen H., Hatakka J., Aalto P.P., Kulmala M., and Viisanen Y. (2003), *J. Geophys. Res.*, 108(D9), 4295, doi:10.1029/2002JD002939.
- Korhonen, H., Kerminen, V.-M., Lehtinen, K. E. J. and Kulmala, M. (2005), *Atmospheric Chemistry and Physics*, 5, 2561- 2570.

## Deposition of submicron aerosol on spruce needles; wind tunnel measurements

K. Lamprechtová, J. Hovorka

Institute for Environmental Studies, Charles University in Prague, Benátská 2,  
128 01, Prague 2, Czech Republic

Keywords: aerosol-surface interaction, deposition, air pollution

Atmospheric aerosol deposition onto a plant surface is an efficient mechanism of its removal from the atmosphere. Rate of aerosol deposition strongly depends on thickness of laminar sublayer covering plant surface. The layer thickness is altered by vegetal surface morphology (Erisman, 2003) and by deposited aerosol. Additionally, deposited aerosol may increase stomatal conductance (Burkhardt, 2001), which lead to an unwanted increase of water transpiration during water stress periods. Conifers are periodically subjected to water stress during winter, when water supply is blocked due to frozen soil, and increased transpiration may affect conifer winter survival. To study an aerosol deposition under controlled conditions onto leaves of conifers, needles, we performed with needles series of measurements of aerosol deposition in a closed-circulation wind tunnel.

The tunnel construction (Volume-0,36 m<sup>3</sup>, Surface-3,73 m<sup>2</sup>, S/V=10.4) allows precise regulation of wind speed in the range of 0.5-6 ms<sup>-1</sup>. Monomodal aerosol (CMD, 0.69 μm) from aerosol generator (AGK 2000, Palas) was introduced into the tunnel and its disappearance measured by Aerodynamic Particle Sizer (APS-3321, TSI) within the size range of 0.524-10 μm. Spruce twigs with needles of the same age were fixed on the ceiling and bottom in 8 lines in the experimental section (0.71 m length, cross-section 0.18x0.18 m).

The timing of the measurements was as follows: aerosol injection into the tunnel for approx 1.5 min (total N<sub>max</sub><10<sup>4</sup> cm<sup>-3</sup>), aerosol plateout measurements for 90 minutes (6 s integrations were recorded), waiting period for 120 minutes of circulation under higher wind speed to lower aerosol concentration (total N<sub>0</sub><5 cm<sup>-3</sup>). Then the next measurements could start.

To evaluate recorded number size distributions, basic model of the aerosol deposition was applied (Okuyama, 1986). Bearing in mind complexity of turbulent deposition (Beneš, 1996) we suppose the deposition rate coefficients β under constant S/V changes due to the laminar sublayer modification. It was shown by experiments with fluorescein (Belot, 1994), that changes in epicuticular waxes covering plant surface, though the dimension of tubular wax structure is near order of magnitude smaller than the sublayer thickness, may strongly influence rate of aerosol deposition.

The β deposition rate constants of aerosol to needles calculated from consecutive measurements were usually in the range of 0.5-5 10<sup>-4</sup> (Fig.1) and are very accurate (RSTD <1.2%). Such accuracy allows detailed study of changes of the β caused by changes of laminar sublayer altered by needle age, epicuticular wax weathering and deposited aerosol.

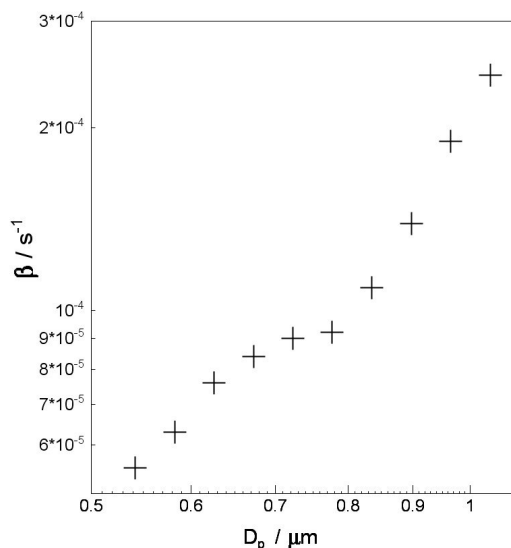


Figure 1. Deposition rate constant β of submicron particles to spruce twigs of two vegetative year old needles under wind speed of 1.1 ms<sup>-1</sup>

Financial support of the study by the Institute for Environmental Studies, Faculty of Science, Charles University in Prague is greatly acknowledged.

- Belot, Y., Camus, H., Gauthier, D., Caput, C. (1994), *Sci.Total Environ.*, 157, 1-6
- Beneš, M., Holub, R.F. (1996) *Envir. Int.*, 22, S883-S889
- Burkhardt, J., Kaiser, H., Kappen, L., Goldbach, H.E. (2001). *Basic Appl.Ecol.*, 2, 351-364.
- Erisman, J.W., Draaijers, G. (2003). *Environ. Pollut.*, 124, 379-388.
- Okuyama, K., Kousaka, Y., Yamamoto, S., and Hosokawa, T. (1986) *J.Colloid.Interface Sci.*, 110, 214-223

## Influence of SO<sub>2</sub> on nucleation, growth rates and yield of secondary organic aerosols

A. Metzger<sup>1</sup>, B. Verheggen<sup>2</sup>, J. Duplissy<sup>1</sup>, J. Dommen<sup>1</sup>, A.S.H. Prevot<sup>1</sup>, U. Baltensperger<sup>1</sup>

<sup>1</sup>Laboratory of Atmospheric Chemistry, Paul Scherrer Institute, 5232 Villigen, Switzerland

<sup>2</sup>Institute for Atmospheric and Climate Sciences, ETH, 8092 Zurich, Switzerland

Keywords: nucleation, yield, secondary organic aerosols

Binary nucleation of sulphuric acid and water was observed to occur in laboratory experiments at atmospherically relevant concentrations (Berndt et al.; 2005). In addition, laboratory experiments show that the nucleation of sulphuric acid is considerably enhanced in the presence of organic acids due to the formation of a stable aromatic acid-sulphuric acid complex, which reduces the nucleation barrier (Zhang et al.; 2004). Several laboratory studies have examined the role of acidic aerosols in enhancing the uptake of carbonyl compounds through acid catalyzed reactions (Jang et al.; 2003) and the influence on the SOA yield (Kleindienst et al.; 2006).

A laboratory study was carried out to investigate the secondary organic aerosol formation of 1,3,5-trimethylbenzene (TMB) in the presence of SO<sub>2</sub>. Several experiments were carried out using SO<sub>2</sub> concentrations between 0.2 and 20 ppb for TMB concentrations of 150, 300, 600 and 1200 ppb, while keeping all the other parameters constant. Aerosol size distributions were measured using a twin SMPS system. The first is a nano SMPS composed of a short DMA column and a TSI UWPCPC, while the second one consisted of a long DMA column and a TSI 3022CPC. This combination of instruments provided measurements of the size distributions over the size range from 4 to 700 nm diameter. VOC concentrations were measured using a Proton Transfer Reaction-Mass Spectrometer (PTRMS) while organic acids and SO<sub>2</sub> concentrations were measured using a wet effluent diffusion denuder/aerosol collector (WEDD/AC) connected to IC-MS. The particle chemical composition was measured using an Aerosol Time Of Flight Mass Spectrometer (ATOFMS, TSI, USA).

The empirical particle nucleation and growth rates were determined using only the aerosol size distribution as input, using the recently developed inverse modelling procedure PARGAN (Particle Growth and Nucleation) (Verheggen and Mozurkewich 2006). Growth rates were determined by regression analysis of the General Dynamic Equation. The empirical growth rates were then used to estimate the time of nucleation for particles in each size bin, defined as the time when their diameter surpassed 1 nm. Their number density at the time and size of nucleation were determined by integrating the particle losses that occurred in the time interval between nucleation and measurement. The nucleation rate was then given by the rate at which particles

grow past the critical cluster size, assumed to be 1 nm.

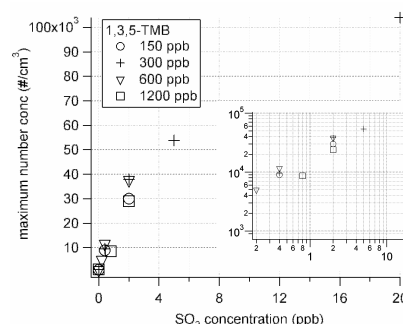


Figure 1. Experimentally observed maximum particle number concentrations (TSI CPC 3025) for a range of SO<sub>2</sub> and 1,3,5-TMB concentrations.

Figure 1 demonstrates the effect of SO<sub>2</sub> on nucleation. With higher initial SO<sub>2</sub> concentrations the maximum particle number concentration is increased from 800 to ~1.1x10<sup>5</sup> particles/cm<sup>3</sup> (0 to 20ppb SO<sub>2</sub>), while there is only a minor influence of 1,3,5-TMB on the maximum number concentration.

The observed nucleation and growth rates will be discussed with regard to SO<sub>2</sub>/sulphuric acid as well as TMB concentrations. The effect of SO<sub>2</sub> on the SOA yield and SOA composition, as measured with ATOFMS, will be discussed.

- Berndt, T., O. Boge, et al. (2005). "Rapid formation of sulfuric acid particles at near-atmospheric conditions." *Science* **307**(5710): 698-700.
- Jang, M. S., B. Carroll, et al. (2003). "Particle growth by acid-catalyzed heterogeneous reactions of organic carbonyls on preexisting aerosols." *Environmental Science & Technology* **37**(17): 3828-3837.
- Kleindienst, T. E., E. O. Edney, et al. (2006). "Secondary organic carbon and aerosol yields from the irradiations of isoprene and alpha-pinene in the presence of NO<sub>x</sub> and SO<sub>2</sub>." *Environmental Science & Technology* **40**(12): 3807-3812.
- Verheggen, B. and M. Mozurkewich (2006). "An inverse modeling procedure to determine particle growth and nucleation rates from measured aerosol size distributions." *Atmospheric Chemistry and Physics* **6**: 2927-2942.
- Zhang, R. Y., I. Suh, et al. (2004). "Atmospheric new particle formation enhanced by organic acids." *Science* **304**(5676): 1487-1490.

## On the evaluation of modelled Black Carbon using both BC and EC measurements

E. Vignati, F. Cavalli, M. Karl

European Commission DG Joint Research Centre, Institute for Environment and Sustainability, I-21020 Ispra, Italy

Keywords: black carbon, modelling, measurements, elemental carbon.

Black Carbon (BC) has a significant influence on air quality as well as on global climate. To evaluate the effect of future emission reductions the amount of BC in the atmosphere should be well quantified. To assess the impact of BC at global scale Chemistry Transport Models and General Circulation Models are applied carrying large uncertainties due to BC emissions and the treatment of physical and chemical processes.

To estimate atmospheric BC concentrations the TM5 model is applied. The TM5 model is an off-line global transport chemistry model (Krol *et al.*, 2005) that uses the meteorological data calculated by the ECMWF model. It has a spatial global resolution of 6°x 4° and a two-way zooming algorithm that allows resolving regions (e.g. Europe, N. America, Africa and Asia) with a finer resolution of 1°x 1°. The algorithm gives the advantage of a local high resolution for the locations where measurements are taken. The anthropogenic emissions are from Bond *et al.* (2004) and biomass burning from Van der Werf (2003). TM5 treats BC as external mixture and it is assumed to be accumulation particle for the wet and dry deposition processes. Modeled concentrations are compared with an extensive data set of observation distinguished by measurement methodology, season and region, containing network measurements (EMEP, IMPROVE), long-term and campaign measurements (Figure1).

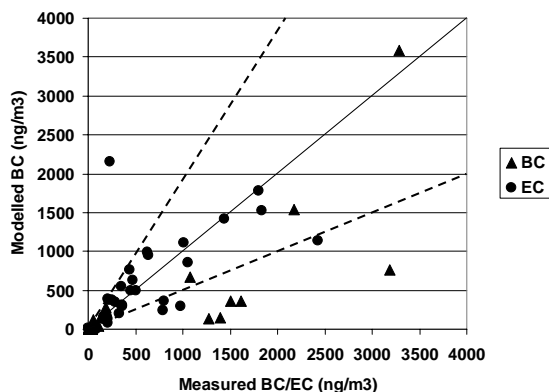


Figure 1. Comparison of BC/EC measurements with TM5 results

Due to sparse measurements available at global scale the data-set contains measurements of both BC and Elemental Carbon (EC). BC and EC are

operational definitions obtained by measurement methods which make use of different key properties of atmospheric soot: ie., light-absorbing and refractory character, respectively. Not surprisingly, comparison of EC and BC values, obtained at the same time, can show large discrepancies despite good correlations (ten Brink *et al.*, 2004; Jeong *et al.*, 2004). It is a common problem for models running at global scale to use a mixed set of data for the model evaluation. A more careful analysis of the emission inventories used in TM5 suggests an inhomogeneity of the measurement methods at sources which introduces an uncertainty in the emitted BC. Therefore a comparison done as in Figure 1 does not contain the right information on the model capability of reproducing BC.

Ideally, the methods used to measure atmospheric soot should be the same both at sources and in the atmosphere. The results –both measured and modelled values– will be critically interpreted in terms of their relation with a reference “definition” agreed upon.

- Bond, T., Streets, D., Yarber, K., Nelson, S., Wo, J.-H., & Klimont, Z. (2004), *J. Geophys. Res.*, 109, D14203, doi:10.1029/2003JD003697.
- Jeong C-H, Hopke P. K., Kim E., & Lee D-W. (2004). *Atmos. Environ.*, 38, 5193-5200.
- Krol, M., Houweling, S., Bregman, B., van den Broek, M., Segers, A., van Velthoven, P., Peters, W., Dentener, F., & Bergamaschi P. (2005). *Atmos. Chem. Phys.*, 5, 417-432.
- ten Brink H., Maenhaut W., Hitzenberger R., Gnauk T., Splindler G., Even A., Chi X., Bauer H., Puxbaum H., Putaud J.-P., Tursic J., & Berner A. (2004). *Atmos. Environ.*, 38, 6507-6519.
- Van der Werf, G. R., Randerson, J. T., Collatz, G. J., and Giglio, L. (2003), *Global Change Biology*, 9(4), 547-562.

## Development of a kinetic model framework and master mechanism of aerosol surface chemistry and gas-particle interactions

RM Garland<sup>1</sup>, JR Scheintaub<sup>1</sup>, and U Pöschl<sup>1</sup>

<sup>1</sup>Max Planck Institute for Chemistry, Department of Biogeochemistry, Mainz, Germany

Keywords: Aerosol modeling, aerosol-surface interactions, aerosol-surface reactions

Atmospheric aerosols are ubiquitous in the atmosphere. They have the ability to impact cloud properties, radiative balance and provide surfaces for heterogeneous reactions. The uptake of gaseous species on aerosol surfaces impacts both the aerosol particles and the atmospheric budget of trace gases. These subsequent changes to the aerosol can in turn impact the aerosol chemical and physical properties. However, this uptake, as well as the impact on the aerosol, is not fully understood. This uncertainty is due not only to limited measurement data, but also a dearth of comprehensive and applicable modeling formalizations used for the analysis, interpretation and description of these heterogeneous processes. Without a common model framework, comparing and extrapolating experimental data is difficult. In this study, a novel kinetic model framework was developed to describe the uptake and interactions of gas phase species and particles (Ammann & Pöschl, 2005; Pöschl *et al.*, 2005).

Integrated into this consistent and universally applicable kinetic and thermodynamic process model are the concepts, terminologies and mathematical formalizations essential to the description of atmospherically relevant physicochemical processes involving organic and mixed organic-inorganic aerosols. Within this process model framework, a detailed master mechanism, simplified mechanism and parameterizations of atmospheric aerosol chemistry are being developed and integrated in analogy to existing mechanisms and parameterizations of atmospheric gas-phase chemistry.

One of the key aspects to this model is the defining of a clear distinction between various layers of the particle and surrounding gas phase as seen in Figure 1 for compound “Z<sub>k</sub>”. The system can be described by six separate layers: gas phase, near-surface gas phase, sorption layer, quasi-static surface layer, near-surface bulk and bulk.

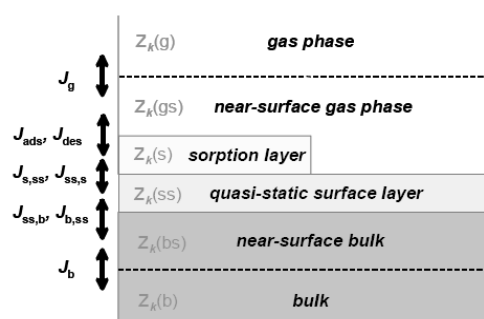


Figure 1: Representation of resolution of particle and gas layers in the model.

The processes occurring at each layer can be fully described using known fluxes and kinetic parameters. Using this system there is a clear separation of gas phase, gas-surface and surface bulk transport and reactions. The compound described in Figure 1, compound “Z<sub>k</sub>”, is semi-volatile and thus found in all layers. Its partitioning can be calculated using the various flux values (J) shown in Figure 1. By describing these layers unambiguously and precisely, the interactions of all species in the system can be appropriately modeled.

Using this framework, various systems have been modeled. Results of the uptake of various gas phase species into both liquid and solid particles will be discussed.

This work was supported by the European Integrated project on Aerosol Cloud Climate and Air Quality Interactions (EUCARRI).

Ammann, M. and Pöschl, U (2005) *Atmospheric Chemistry and Physics Discussions*, 5, 2193-2246.

Pöschl, U., Rudich, Y and Ammann, M. (2005) *Atmospheric Chemistry and Physics Discussions*, 5, 2111-2191.

## Mathematical modelling of heat transport in aerosol systems with particles of complex geometry

L.A. Uvarova

Department of Applied Mathematics, Moscow State University of Technology  
 "STANKIN", 3a Vadkovskii line, 127994, Moscow, Russia

Keywords: aerosol modelling, agglomerates, atmospheric aerosols, environmental particles, fractals.

At present problems of a dynamics and accompanied processes in aerosol systems are actual problems owing to the fact that the increase of the spreading of anthropogenic and bioaerosols in the atmosphere takes place. In general case such aerosol particles can have an arbitrary form.

For clusters and agglomerates the geometry factor is of great importance too.

The particles formation may be conditioned by different mechanisms, such as evaporation, nucleation, coagulation, thermal destruction under the influence of heat sources of the electromagnetic nature (Krivenko & Uvarova, 2004; Ivannikov, 2006) and other mechanisms. Now is considered the new mechanism - thermal fragmentation of nanoparticles (D. Gramotnev & G. Gramotnev, 2005).

As a rule for the mathematical description of the aerosol systems with particles of the "fine" forms (spherical, cylindrical, ellipsoid forms) the classic methods of the differential and integral calculus are used.

In case of the consideration the particles of the complex form one from most famous methods lies in the calculation of the fractal dimensions of the particles and of the further transition to the particles of the "fine" forms with new radiuses. This method develops on the base the fractal geometry (Feder, 1989; Schroeder). The cluster or agglomerate dimensions may be determined with the help methods of the quantum chemistry, for example with the help the density functional theory (Nadykto *et al.*, 2006).

In this paper we consider the transport processes in the aerosol systems with particles of an arbitrary form on the basis of the mathematical theory of objects of different dimensions (Pokornyi *et al.*, 2004). The parameters of the problem can be found with help methods of the quantum chemistry.

We consider the heat transport in aerosol systems with particles a complex form. In the quasi-stationary approximation heat transport equation and the boundary condition on the particle surface  $S$  have follows view:

$$\nabla(\lambda \nabla T) = -q, T_e = T_S + K_T \frac{\partial T_e}{\partial \vec{v}}, \quad (1)$$

where  $T$  is a temperature (index  $e$  relates to environment, index  $S$  relates to the particle surface),

$\lambda$  is a thermal conductivity coefficient,  $q$  is a heat source,  $\vec{v}$  is the normal vector,  $K_T$  is thermal jump coefficient. The equation (1) takes place for the stratified set (a totality of finite number of varieties of different dimensions) too. In this case equation (1) written for the potential  $\varphi = \int \lambda \delta T$  transforms to the follows form:

$$\Delta_p \varphi \equiv \frac{1}{\sqrt{h}} \frac{\partial}{\partial x^i} (p \sqrt{h} h^{ij} \frac{\partial \varphi}{\partial x^j}) + \sum_{\sigma_{kj} > \sigma_{k-1i}} p \frac{h^{ki}}{\sqrt{h^{kk}}} \vec{E} \frac{\partial \phi}{\partial x^i} = -q(\varphi), \quad (2)$$

where  $\sigma_{ki}$  is strat,  $\sigma_{kj} > \sigma_{k-1i}$  signifies that

$\sigma_{k-1i}$  adjoins to  $\sigma_{kj}$ .  $p$  is dimension,  $h^{ij}$  are contravariant metric components.

In particular, the numerical calculations carried out with the help this model (with the heat source of the electromagnetic nature (Uvarova *et al.*, 2006)) showed that the local overheating in such systems can exceed to a significant degree the local overheating in analogous systems with geometrically homogeneous particles.

This work was supported by the Russian Foundation for Basic Research (Grant No. 06-01-00548-a).

- Krivenko, I.V., & Uvarova, L.A. (2004). *Russ. J. Phys. Chem.*, 78, 894-898.
- Ivannikov, A.F. (2006). in *Proc. 9 Conf. MSUT "STANKIN"*, Moscow (Yanus -K, Moscow), 19-22. (in Russian).
- Gramotnev, D.K., & Gramotnev, G. (2005). *J. Aerosol Science*, 36, 323-340.
- Feder, J. (1989). *Fractals*. New York - London: Plenum Press.
- Schroeder, M. (2005). *Fractals, chaos, power laws*. Moscow -Ijevsk: R&C Dynamics.
- Nadykto, A.B., et al. (2006). *Physical Review Letters*, 96, 125701-4.
- Pokornyi, Yu. V., et al. (2004). *Differential Equations on geometrical graph*. Moscow: Fizmatlit. (in Russian).
- Uvarova, L.A., Krivenko, I.V. & Smirnova, M.A. (2006). *Chemical Engineering Transactions*, 10, 251-256.

## Experimental characterization and modelling of soot primary particles emitted by a CFM-56 commercial aircraft engine.

D. Delhaye<sup>1</sup>, D. Ferry<sup>2</sup>, F. Moulin<sup>3</sup>, S. Picaud<sup>3</sup>, E. Ruiz<sup>1</sup>, B. Demirdjian<sup>2</sup>, P.N.M. Hoang<sup>3</sup>, and J. Suzanne<sup>2</sup>.

<sup>1</sup>ONERA, DMPH / EAG, BP72, F-92322, Châtillon, France

<sup>2</sup>CRMC-N / CNRS, Campus de Luminy, Case 913, F-13009, Marseille, France

<sup>3</sup> Institut UTINAM, UMR CNRS 6123, Université de Franche-Comté, F-25030 Besançon Cedex, France

Keywords: Soot particle, Particle characterization, Modelling, Heterogeneous nucleation.

We present here a set of experiments that is combined with a modelling study to understand the water adsorption on soot primary particles at room temperature.

Soot particles are collected by direct impaction on polycarbonate membranes and transmission electron microscope (TEM) grids that are located at 27 m behind an aircraft engine during Landing/Take-Off (LTO) cycles. A CFM56-5C engine is used on an aero-engine bench at the SNECMA Villaroche center (France). Scanning and Transmission Electron Microscopy (SEM and TEM) allow us to determine the primary particles size distribution and show that it follows a lognormal law. It also enable us to observe the ‘onion-like’ structure of these particles (cf. figure 1) and to determine interplane distances through electron diffraction. Elemental composition and surface functional groups are investigated by Energy Dispersive X-ray Spectrometry (EDXS) and Fourier Transform Infrared Spectroscopy (FTIR).

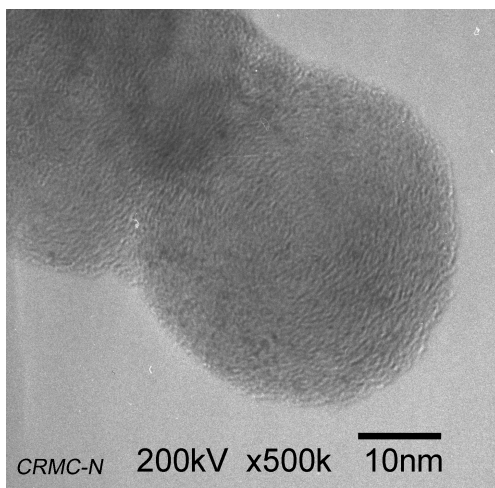


Figure 1. Soot primary particle observed by TEM

Despite its atmospheric importance, a detailed theoretical understanding of the water nucleation dynamics on soot at the molecular level remains challenging. First, we have combined quantum calculations and classical molecular dynamics simulations to model the interaction between water molecules and a partially oxidised soot particle

modelled by anchoring several COOH or OH active groups on a large graphite cluster.

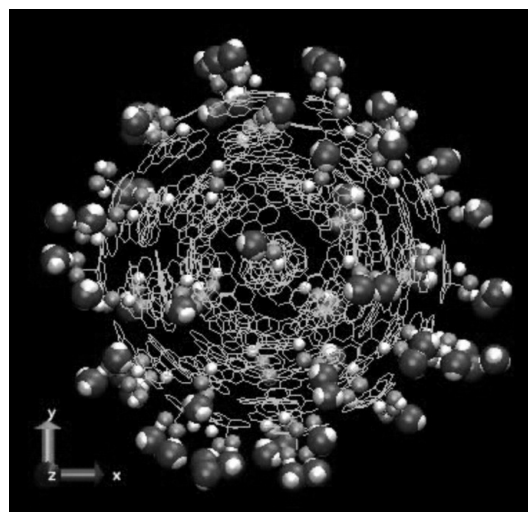


Figure 2. water molecules adsorbed around a partially oxidized soot particle. Snapshot taken from from Grand Canonical Monte Carlo simulations at 298 K

Our results indicate a preferential adsorption of water on graphite surfaces containing COOH rather than OH groups. Then, the influence of the soot morphology on the adsorption of water has been investigated by means of grand canonical Monte-Carlo (GCMC) calculations. The GCMC method allowed us to simulate a real adsorption experiment around a soot particle of spherical shape at 298 K (cf. figure2). This soot was made of carbon atoms only, or contained a certain amount of hydrophilic sites. The calculated adsorption isotherms illustrated the competitive influence of both soot morphology and chemical composition on water adsorption

Collignon, B., Hoang, P.N.M., Picaud, S. & Rayez, J.C., (2005). *Chem. Phys. Lett.*, 406, 431; ib. (2005). *Comp. Lett.*, 1, 277.

Picaud, S., Collignon, B., Hoang, P.N.M., & Rayez, J.C., (2006). *J. Phys. Chem.*, 110, 8398.

Moulin, F., Picaud, S., Hoang, P.N.M., Partay, L., & Jedlovsky, P., (2006). *Mol. Sim.*, 32, 487.

Moulin, F., Picaud, S., Hoang, P.N.M., Partay, L., & Jedlovsky, P., (2007). *Carbon*, submitted.

## An expression of particle dry deposition velocity for polydispersed particle using the moment method

S.Y. Bae<sup>1</sup>, C.H. Jung<sup>2</sup> and Y.P. Kim<sup>1</sup>

<sup>1</sup>Department of Environmental Science and Engineering, Ewha Womans University, Seoul, 120-750, Korea

<sup>2</sup>Department of Environmental Health, Kyungin Women's College, Incheon, 407-740, Korea

Keywords: aerosol size distribution, deposition, modelling.

Dry deposition is one of the most efficient particle sinks in the air. The dry deposition flux of particles is usually defined as the product of the local atmospheric concentration at a reference height by the deposition velocity. The particle dry deposition velocity representation has advantage that all the complexities of the dry deposition processes are combined into a single parameter. However, it is difficult to measure dry deposition velocity directly and to represent it as a function of particle size. The expression by Wesely (1989) has been widely used. However, it is hard to use the formula in the moment method representation of aerosol dynamics.

Raupach et al. (2001) reported a simple model based on antecedents for single-layer models. The deposition velocity is treated as a bulk conductance made up of three component bulk conductance acting in parallel: gravitational settling, impaction, and Brownian diffusion. Although this model is a great simplification of the real, multi-layer physics, it has advantages. It includes enough physics to capture the dependence of the three major processes on particle diameter and wind speed. Also, its two empirical coefficients are sufficient to permit matching to experimental reality but not enough to introduce parameterization problems.

In this study, the equation of Raupach et al. (2001) is approximated and an expression for dry deposition process is developed in the modal aerosol dynamics approach.

The dry deposition velocity proposed by Raupach et al. (2001) is as follows:

$$V_d = V_t + G[f_{form} a_f E + (1 - f_{form}) a_v Sc^{-2/3}]$$

$$\text{where, } V_t = \frac{\rho_p d_p^2 g C c}{18 \mu_a}, \quad G = \frac{u_*^2}{u_r}$$

$$E = \left( \frac{St}{St + 0.8} \right)^2, \quad St = \frac{\rho_p d_p^2 u_*^2}{18 \mu_a \nu}$$

$$Sc = \frac{\mu_a}{\rho_a D_{diff}}, \quad D_{diff} = \frac{k_b T C c}{3 \pi \mu_a d_p}$$

$$f_{form} = 0.75, \quad a_f = 2, \quad a_v = 8.$$

The expression of  $E$  was further approximated:

$$E = \left( \frac{St}{St + 0.8} \right)^2 \cong \frac{1}{\frac{1}{0.33 St^{6/5}} + 1}$$

Figure 1 shows the comparison of the particle deposition velocities for Wesely (1989) modified for particles, Raupach et al. (2001), and approximated equation obtained in this study. Three dry deposition velocities show similar trend and values.

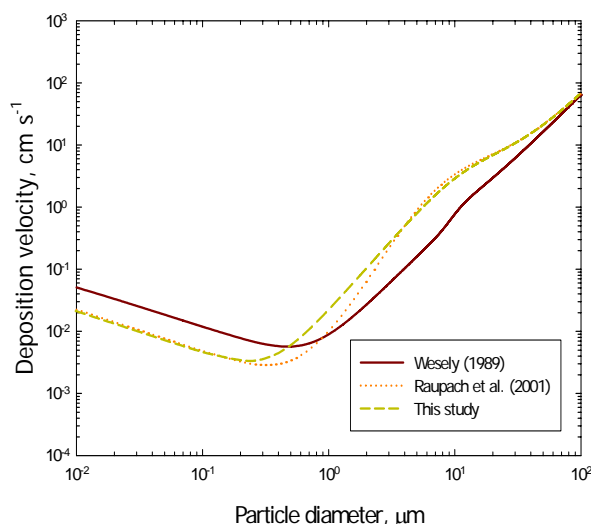


Figure 1. Comparison of the particle deposition velocities for Wesely (1989), Raupach et al. (2001), and approximated equation (this study).

This work was supported by the Korea Science and Engineering Foundation (KOSEF) through the National Research Lab. Program funded by the Ministry of Science and Technology (No. M10600000221-06J0000-22110) and Climate Environment System Research Center, an SRC program.

Raupach, M. R., Briggs, P. R., Ahmad, N., & Edge, V. E. (2001). *J. Environ. Qual.* 30, 729-740.

Wesely, M. L. (1989). *Atmos. Environ.* 23, 1293-1304.

## Simulation of Carbon Black Formation in a Solar Thermal Reactor for the Decomposition of Methane

M. Kostoglou<sup>1,2</sup>, G. Patrianakos<sup>1</sup> and A.G. Konstandopoulos<sup>1</sup>

<sup>1</sup>Aerosol and Particle Technology Laboratory (APTL), Center for Research and Technology-Hellas, Chemical Process Engineering Research Institute (CERTH/CPERI), Greece

<sup>2</sup>Department of Chemistry, Aristotle University, Thessaloniki, Greece

Keywords: Black carbon, Industrial aerosols, Numerical simulation, Particle formation and growth, Particle size distribution.

In making the transition from fossil fuel based energy systems to sustainable, hydrogen based energy systems, an unconventional route for hydrogen production is being developed. This involves the solar thermal decomposition of natural gas for the co-production of hydrogen and Carbon black (a high-value nano-material) with the bonus of zero CO<sub>2</sub> emissions. The SOLHYCARB project aims at developing a pilot industrial scale solar reactor for this purpose. As part of this work, a mathematical model has been developed to simulate the formation of Carbon black (CB) and hydrogen in the reactor. The key feature of this process is the need of very small residence times to avoid CB deposition. Conventional heat transfer routes are not efficient for the small residence times of the process so Carbon particles are added to the gas feed as heat adsorbers in order to ensure fast temperature rise and ignition of the reaction.

The mathematical model of the process consists of a population model of the CB aerosol and a 1D model of the reactor. A simple rate expression is assumed for the homogenous decomposition of CH<sub>4</sub> in order to compute the nucleation rate of Carbon atoms. Mass conservation in the CB population is applied to a range of particle size bins in order to describe the rate of production of the particles in each bin in terms of the various sources of generation and loss of these particles (kinetically controlled particle formation). The mechanism that is assumed for the generation and loss of the particles in each bin is Brownian coagulation. The Fuchs coagulation kernel (Seinfeld & Pandis, 1998) that is valid in the free molecular, transition and continuum regimes is used. Two populations are modeled: a population of fresh CB particles that evolves from the nucleated Carbon atoms and a population of seed Carbon particles that is fed to the reactor and which grows via coagulation with the fresh particles. In the 1-D reactor model an ideal CH<sub>4</sub>/H<sub>2</sub> gas mixture is assumed. Mass conservation is applied to the gas phase in order to model the volume expansion that occurs because of the stoichiometry of the decomposition reaction. Heat transfer (radiative and convective) to and from the CB particles, is also modeled.

As a first step, a simple tubular solar thermal reactor (indirect solar heating) for which an

experimental intrinsic kinetic has been reported by Dahl *et al* (2002), is modeled. A typical evolution of the fresh CB and seed Carbon-CB populations along the reactor is illustrated in Figure 1.

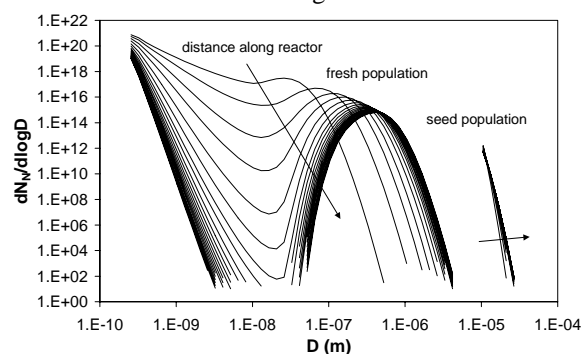


Figure 1. Number frequency distribution for the fresh and seed particle populations along the reactor.

Along the reactor the rate of CH<sub>4</sub> decomposition decreases as the concentration of CH<sub>4</sub> decreases and therefore so does the rate of nucleation of Carbon atoms. The many fresh Carbon atoms that are nucleated near the inlet gradually coagulate into a separate population of larger and fewer fresh CB particles and the number of small fresh CB particles decreases. At the same time, particles from the fresh population coagulate with the seed particles and the seed population grows slightly. The growth of the seed population is only slight because of the large size of the seed particles compared to the fresh particles.

The computational method that has been developed enables important characteristics of the CB produced by a reactor (such as the number of particles and their size distribution) to be related in a simple way to the operating conditions of the reactor.

This work was supported by the SOLHYCARB project, financed in part by the EU Commission under the 6<sup>th</sup> Framework Programme.

Seinfeld J.H., & Pandis S.N. (1998). *Atmospheric Chemistry and Physics: From Air Pollution to Climate Change*. Wiley, New York.

Dahl J.K., Barocas V.H., Clough D.E., & Weimer A.W. (2002). *Int. J. Hydrogen Energy*, 27, pp. 377 – 386.

## Modelling and calculation of fractional efficiency of tangential flow cyclones

Y. Ben-Shmuel, M. Shapiro

Laboratory of Transport Processes in Porous Materials  
Faculty of Mechanical Engineering, Technion-Israel Institute of Technology, 32000, Haifa, Israel

Keywords: cyclone separators, particle grade efficiency, mesh builder, CFD

Cyclones are commonly employed in industry for removal of dust dispersed solid particles. The advantages of cyclones are in their low cost and simplicity of construction, operation and relatively energy consumption. The cyclones are efficient in removal of relatively large particles, namely with diameters exceeding 2-5 $\mu\text{m}$ . Improvement of cyclone operation may be achieved by the rational design based on adequate modelling of the flow field and particle transport within these devices. Cyclone manufacturing had become a relatively straightforward operation. Yet, rational design of cyclones, including selection of geometry and dimensions to achieve the desired performance, is a difficult task. For this purpose semi-empirical models (e.g. of Barth, Stairmand etc), are normally used for air flow velocity calculation in a cyclone and its grade efficiency (Hoffman and Stein, 2002). CFD flow field simulations had been shown to be a promising design tool. This research employs this technique to examine the effects of cyclone geometry and physical boundary conditions on the fractional efficiency of tangential flow cyclones.

We used the three-dimensional Reynolds Stress Transformation Model (RSTM) implemented via the finite volume method (FLUENT commercial solver) to calculate the turbulent flow field in a cyclone. A special effort is made to appropriately define the flow region and generate the adequate mesh in order to capture the flow peculiarities. This is done by a special interface mesh/geometry builder, that we developed using GAMBIT pre-processor. As a result the pressure drop in a tangential flow cylinder-on-cone cyclone is calculated in agreement (within 5%) with the experimental data (see Fig. 1).

Basing on the computed flow field, a Lagrangian particle tracking method is employed to calculate the particle grade efficiency using a stochastic tracking (random walk) model accounting for instantaneous turbulent velocity fluctuations on the particle motion. We investigated the influence of cyclone design parameters (length, diameter, shape and geometry) and showed that the flow field boundary conditions at the secondary outlet (zero flow rate versus zero velocity conditions) have a significant effect on the fractional efficiency. Figure 2 shows a comparison of these results for 0.3 – 3.5  $\mu\text{m}$  PSL particles with the experimental data of Gottschalk and Bohnet (1998). In the range 1-3.5  $\mu\text{m}$  calculations agree with the measurements within 20%. Calculations with zero flowrate boundary

condition at the secondary outlet overestimate the grade efficiency, especially for submicron particles. With the secondary outlet extended as tubular or cone-like shape the agreement improves mainly for micron particles.

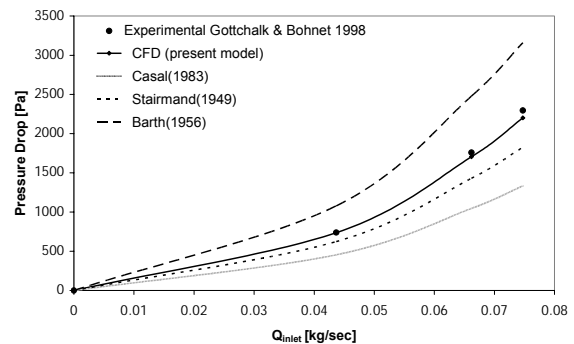


Figure 1. Pressure drop in a standard cylinder-on-cone cyclone with diameter 225 mm and inlet  $Re=10^6$ .

Further steps in development of the particle capture model are contemplated in order to improve the agreement especially for submicron particles, where the model still overpredicts the experimental grade efficiency. At the present stage the developed CFD model has good predictive capacity allowing establishing the relative merits of the existing computational models in rational cyclone design.

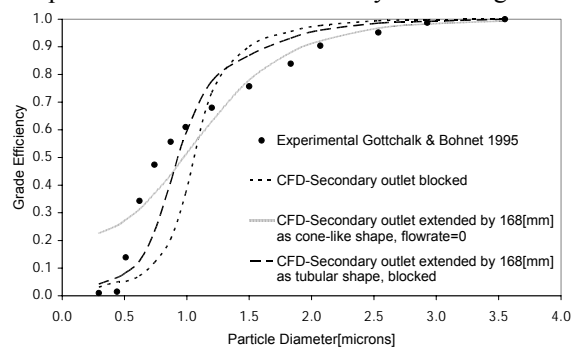


Figure 2. Comparison of the calculated grade efficiency with experimental data

1. A.C. Hoffmann, L.E. Stein, "Gas Cyclones and Swirl Tubes" Springer-Verlag, Berlin (2002)
2. M.D. Slack et al, "Advances in Cyclone modeling using unstructured grids". *Trans. Ind Chem E.* 78 part A 1098-1104 (2000)
3. O. Gottschalk, M. Bohnet, *Chem Eng. Technol. PARTEC* 95 22-37 (1995)
4. O. Gottschalk, M. Bohnet, *Chem Eng. Technol. PARTEC* 98 94-109 (1998)

## Source apportionment of submicron organic aerosols at an urban background site by positive matrix factorization (PMF) applied to aerosol mass spectra

V. A. Lanz<sup>1</sup>, M. R. Alfarra<sup>2</sup>, U. Baltensperger<sup>2</sup>, B. Buchmann<sup>1</sup>, C. Hüglin<sup>1</sup>, A. S. H. Prévôt<sup>2</sup>

<sup>1</sup>Empa, Swiss Federal Laboratories for Materials Testing and Research, CH-8600 Dübendorf, Switzerland

<sup>2</sup>PSI, Paul Scherrer Institute, CH-5232 Villigen PSI

Keywords: aerosol mass spectrometry, aerosol modelling, SOA, PM1, source apportionment.

Submicron ambient aerosol was characterized in summer 2005 at an urban background site in Zürich (Switzerland) during a three-week measurement campaign. Highly time-resolved samples of non-refractory aerosol components were analyzed with an Aerodyne quadrupole aerosol mass spectrometer (Q-AMS).

The quantification of different types of organic aerosols (OA) such as primary organic aerosols (POA) and secondary organic aerosols (SOA), or more classes if possible, was identified as an important research activity (Fuzzi *et al.*, 2006) as it is a necessary first step in the development of mitigation strategies.

Positive matrix factorization (PMF; Paatero, 1997) was used for the first time for aerosol mass spectra to identify the main components of the total organic aerosol and their sources. The PMF retrieved factors were compared to measured reference mass spectra from literature and were correlated with tracer species of the aerosol and gas phase measurements from collocated instruments.

Six factors were found to explain virtually all variance in the data and could be assigned either to sources or aerosol components such as oxygenated organic aerosol (OOA). Our analysis suggests that at the measurement site only a small (<10%) fraction of organic PM<sub>1</sub> originates from freshly emitted fossil fuel combustion. Other primary sources identified to be of similar or even higher importance are charbroiling (10–15%) and wood burning (~ 10%).

The fraction of all identified primary sources is considered as primary organic aerosol (POA). This interpretation is supported by calculated ratios of the modelled POA and measured primary pollutants such as elemental carbon (EC), NO<sub>x</sub>, and CO, which are in good agreement to literature values.

A high fraction (60–69%) of the measured organic aerosol mass is OOA which is interpreted mostly as secondary organic aerosol (SOA). The oxygenated organic aerosol could be separated into a highly aged fraction, OOA I, (40–50%) with low volatility and a mass spectrum similar to fulvic acid (a model compound that describes the chemical functionality of aged, oxygenated aerosol), and a more volatile and probably less processed fraction, OOA II (on average 20%).

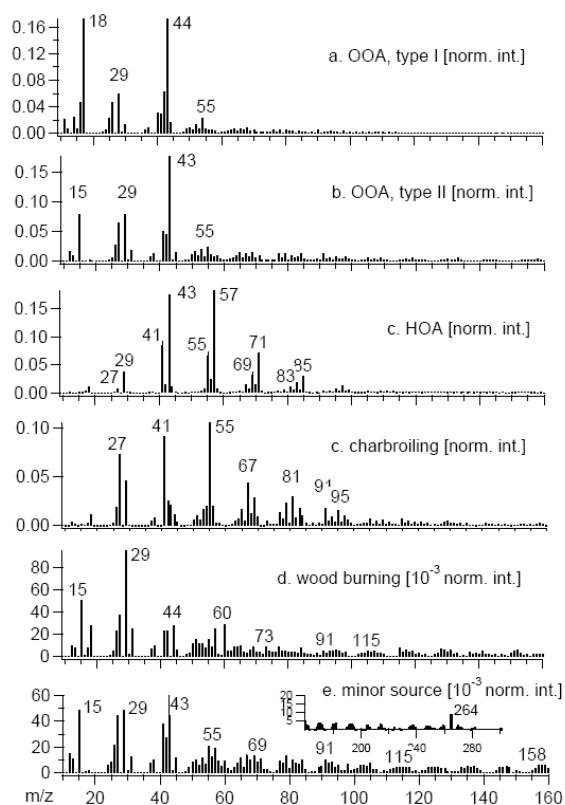


Figure 1. Normalized spectra of all estimated PMF factors (interpreted as the denoted source profiles) as calculated by the 6-factorial model. Only for the minor source the full mass range up to 300 m/z is shown because it is the only source or component with significant features in the high mass region.

The AMS measurements were supported by the Swiss Federal Office for the Environment (FOEN).

Fuzzi, S., Andreae, M. O., Huebert, B. J., et al. (2006). Critical assessment of the current state of scientific knowledge, terminology, and research needs concerning the role of organic aerosols in the atmosphere, climate, and global change. *Atmos. Chem. Phys.*, 6, 2017–2038.

Paatero, P. (1997). Least squares formulation of robust non-negative factor analysis. *Chemom. Intell. Lab. Syst.*, 37, 23–35.

### Modeling nitric acid adsorption in mixed-phase clouds

J-P. Pietikäinen<sup>1</sup>, J. Hienola<sup>2</sup>, H. Kokkola<sup>3</sup>, S. Romakkaniemi<sup>4</sup>, K. Lehtinen<sup>3</sup>, M. Kulmala<sup>2</sup> and A. Laaksonen<sup>1</sup>

<sup>1</sup>Department of Physics, University of Kuopio, P.O.B. 1627, FI-70211, Kuopio, Finland

<sup>2</sup>Department of Physical Sciences, University of Helsinki, P.O.B. 64, FIN-00014, Helsinki, Finland

<sup>3</sup>Finnish Meteorological Institute, University of Kuopio, P.O.B. 1627, FIN-70211, Kuopio, Finland

<sup>4</sup>Centre for Atmospheric Science, School of Earth, Atmospheric and Environmental Science, University of Manchester, P.O.B. 88 M60 1QD, Manchester, United Kingdom

Keywords: adsorption, ice clouds, ice nuclei, modeling, nitric acid.

Cirrus clouds play an important role in the Earth's energy balance. The ability to scatter and absorb both solar and Earth radiation makes cirrus clouds interesting part of climate. Moreover, cirrus clouds play an important role in redistributing HNO<sub>3</sub> via uptake and sedimentation in the upper troposphere. (Ullerstam *et al.*, 2005).

The adsorption of nitric acid is one of the most studied mechanisms for HNO<sub>3</sub> uptake (Ullerstam *et al.*, 2005). Adsorption models are equilibrium models, and different kind of isotherms for the adsorption is available. Adsorbed nitric acid can change the properties of ice particles, for example, it can affect the condensation of water and as an effect of this, prevent the ice/vapor system to gain equilibrium (Gao *et al.* 2004).

Using a microphysical cloud model we have compared different mechanisms for HNO<sub>3</sub> uptake to ice particles. Furthermore, different forms of Langmuir's isotherm for adsorption have been tested. We compare measurements from Gao *et al.* (2004) to the results from our model. Two mechanisms for HNO<sub>3</sub> uptake had been used. Nitric acid either stays in the particles during freezing or adsorpts to the surface of the particles.

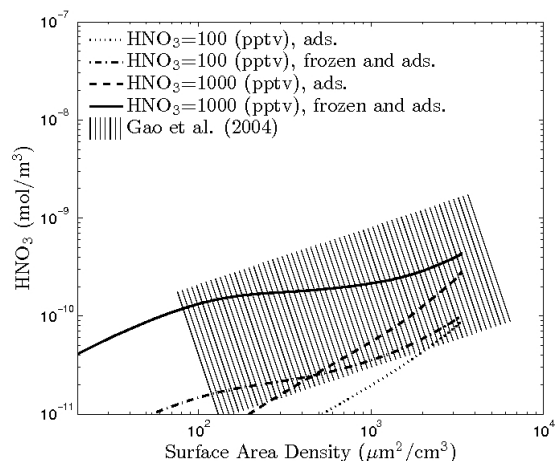


Figure 1. Concentration of nitric acid HNO<sub>3</sub> as a function of surface area density. Different lines represent the lower (100 ppt) and upper (1000 ppt) limits for initial gas phase nitric acid volume mixing ratio for cases where nitric acid is frozen or evaporated. The dissociative form for nitric acid adsorption has been used.

When the ice particles are formed, adsorption of HNO<sub>3</sub> is based on the Langmuir's isotherm:

$$\Theta = \frac{(K_{eq} P)^{\nu}}{1 + (K_{eq} P)^{\nu}}, \quad (1)$$

where  $\Theta$  is the surface coverage,  $K_{eq}$  is the equilibrium adsorption constant and  $P$  is the partial pressure on HNO<sub>3</sub> and  $\nu$  is the heterogeneity parameter. In the dissociative form of Langmuir's isotherm the  $\nu = 1/2$  and in the non-dissociative form  $\nu = 1$ .

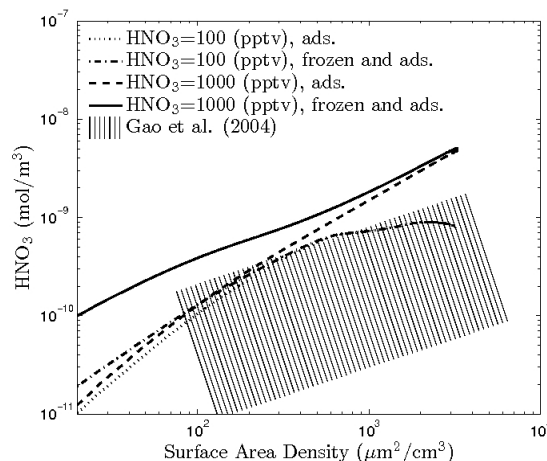


Figure 2. Like Figure 1 but the non-dissociative form for nitric acid adsorption has been used.

The figures 1 and 2 shows preliminary results of the difference between dissociative and non-dissociative form of Langmuir isotherm. Also, figures 1 and 2 represent measured values from Gao *et al.* (2004). The results show that if dissociative form of Langmuir's isotherm is used, the adsorption of nitric acid can not explain the measured values. However, if the non-dissociative form is used, adsorption by itself can explain the measured values. In the future, the difference between these two forms of Langmuir's isotherm will be studied further.

Gao *et al.* (2004). *Science*, 303, 516-520

Popp *et al.* (2004). *J. Geophys. Res.* 10, D06302

Ullerstam, M., Thornberry, T. and Abbatt, J. P. D. (2005). *Faraday Discuss.*, 130, 211-226

## OIO nucleation simulations

H. Vuollekoski<sup>1</sup>, M. Kulmala<sup>1</sup>, V.-M. Kerminen<sup>2</sup>, S.-L. Sihto<sup>1</sup>, I. Riipinen<sup>1</sup> and H. Korhonen<sup>3</sup>

<sup>1</sup>Division of Atmospheric Sciences, Department of Physics, University of Helsinki, P.O. Box 64, FI-00014, University of Helsinki, Finland

<sup>2</sup>Climate and Global Change Unit, Finnish Meteorological Institute, P.O. Box 503, FI-00101, Helsinki, Finland

<sup>3</sup>School of Earth and Environment, University of Leeds, LS2 9JT, Leeds, UK

Keywords: aerosol modelling, marine aerosols, nucleation, particle formation and growth, iodine dioxide.

Observations of coastal new particle formation have been made e.g. on the west coast of Ireland (O'Dowd *et al.*, 2005). The phenomenon overlaps with low tide, during which algae are exposed to ozone in air and emit iodine vapours. Various chemical reactions result in large amounts of iodine dioxide (OIO) in the atmosphere, which is believed to be a nucleating vapour.

We have simulated new particle formation with University of Helsinki Multi-component Aerosol model (UHMA, Korhonen *et al.*, 2004), which is a sectional multi-component aerosol dynamics box-model that simulates tropospheric aerosol particle populations and has all basic aerosol dynamical mechanisms implemented: nucleation, condensation, coagulation and dry deposition. For this study we have modified the model to marine conditions and to include iodine specific dynamics.

So far three nucleation mechanisms have been tested: the nucleation rate of one nanometer particles is assumed either linearly dependent (so called activation mechanism, Kulmala *et al.*, 2006) or squarely dependent (kinetic type nucleation) on OIO concentration, or activation type multiplied by the concentration of sulphuric acid. The nucleated particles grow by coagulation and condensation of both OIO and sulphuric acid.

The simulated box is moving with the wind from the Atlantic Ocean. At this point the model has no OIO chemistry, as OIO is injected into the system during low tide (9 o'clock), lasting 10 minutes, roughly corresponding to the time of influence with the coastal algae. A model simulating stationary measurement site is being developed. The present simulations do not include organic vapors.

An example of simulated new particle formation event can be seen in Figure 1, in which activation type nucleation was implemented with activation coefficient  $0.0001 \text{ s}^{-1}$ . Related gas and particle concentrations are illustrated in Figure 2. The parameterization used results in a particle concentration peak of  $500,000 \text{ cm}^{-3}$ .

We will perform sensitivity studies by varying model parameters, some of which are currently poorly known. More experimental data is needed for comparison with our results in order to achieve more accurate parameterization for coastal nucleation.

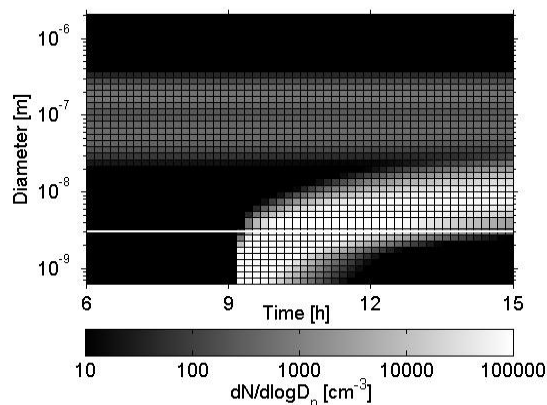


Figure 1. Particle size distribution as a function of time using activation type nucleation mechanism.

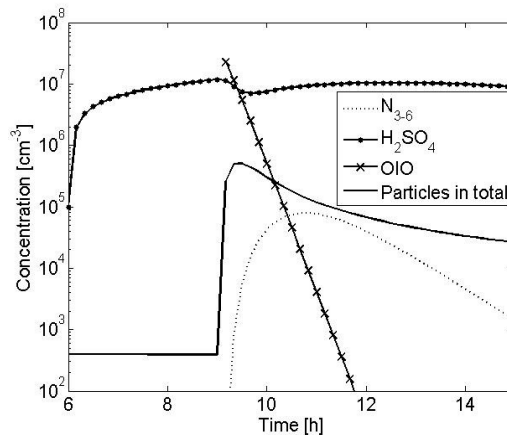


Figure 2. Gas, 3–6 nm particle and total particle concentrations during the simulation of Figure 1.

Korhonen, H., Lehtinen, K. E. J. and Kulmala, M. (2004). Multicomponent Aerosol Dynamics Model UHMA: Model Development And Validation, *Atmos. Chem. Phys.*, 4, 757-771

Kulmala, M., Lehtinen, K. E. J. and Laaksonen, A. (2006). Cluster Activation Theory as an Explanation of the Linear Dependence Between Formation Rate of 3 nm Particles and Sulphuric Acid Concentration, *Atmos. Chem. Phys.*, 6, 787-793.

O'Dowd, C. D. and Hoffmann, T. (2005). Coastal New Particle Formation: A Review of the Current State-Of-The-Art, *Environ. Chem.*, 2, 245-255.

## High PM1 and ozone levels in the Cadiz Gulf during the Galicia fires of Summer 2006

J.D. de la Rosa<sup>1</sup>, A.F. Stein<sup>2</sup>, Y. González-Castanedo<sup>3,1</sup>, A. Alastuey<sup>4</sup>, E. Mantilla<sup>5</sup>, J. Contreras<sup>6</sup>, X. Querol<sup>4</sup> and A. Sánchez de la Campa<sup>7,1</sup>

<sup>1</sup>Department of Geology, University of Huelva, Huelva, Spain.

<sup>2</sup>Earth Resources and Technology on assignment to NOAA's Air Resources Laboratory, MD, USA.

<sup>3</sup>Instituto Nacional de Técnica Aeroespacial, Esat El Arenosillo, Huelva Spain

<sup>4</sup>Institute of Earth Sciences "Jaume Almera", CSIC, C/ Lluís Sole i Sabaris s/n, 08028 Barcelona, Spain

<sup>5</sup>Centro de Estudios Ambientales del Mediterráneo (CEAM), 46980 Paterna, Valencia, Spain

<sup>6</sup>Department of Environment, Andalusia Government, C/ Manuel Siurot 41071 Sevilla Spain

<sup>7</sup>Department of Environment and Planning, University of Aveiro, 3810 Aveiro, Portugal

Keywords: PM1, ozone, HYSPLIT model, vegetation fires, Spain

During the month of August of 2006, the province of Galicia (NW of Spain) has suffered a high period of fire activity derived of forest burning. Concurrently, maximums in PM1 and ozone have been registered in several air quality network monitoring stations of the Andalusia Government (S of Spain).

On August 12<sup>th</sup> 2006, historic maximums of ozone levels have been measured in monitoring stations of the province of Huelva, for example La Rábida (191  $\mu\text{g}/\text{m}^3$ ), Campus El Carmen (210  $\mu\text{g}/\text{m}^3$ ), Doñana (160  $\mu\text{g}/\text{m}^3$ ), Valverde del Camino (176  $\mu\text{g}/\text{m}^3$ ), Cartaya (201  $\mu\text{g}/\text{m}^3$ ), Mazagón (266  $\mu\text{g}/\text{m}^3$ ), and El Arenosillo (275  $\mu\text{g}/\text{m}^3$ ). This last one was the maximum of ozone registered in all the air quality network of Huelva.

The maximum levels of ozone occurred simultaneous with maximum levels in PM1 and CO and low levels in NO<sub>2</sub>, for example Mazagón (1315  $\mu\text{gCO}/\text{m}^3$ ), and Campus Universitario (1932  $\mu\text{gCO}/\text{m}^3$ ). Also, the levels of PM10, PM2.5 and PM1 measured with a GRIMM 1107 monitor located in the city of Huelva, Los Barrios, and La Linea in the Gibraltar Straits show high concentrations during the night of August 12<sup>th</sup>- to 13<sup>th</sup> of 2006.

Between August 10<sup>th</sup> and 13<sup>th</sup>, a deep high pressure center was located W of Great Britain, and a Low pressure system was situated between the Iberian Peninsula and N of Africa. Under this scenery, N-NE winds were dominant.

Aerosol models such as NAAPS and satellite images (MODIS) (Figure 1 a and b) show high concentration of smoke in the W of the Iberian Peninsula, impacting the Gulf of Cádiz and Gibraltar Strait, which were associated to the Galicia fires.

In order to further assess the origin of the high levels of pollutants registered in the SW of Spain the HYSPLIT (Draxler and Hess, 1998) model has been utilized. The model was set to emit lagrangian particles to represent the fire emissions in Galicia. Since no information about the emissions strength was available, an emission of 1 unit per hour was assumed. Figure 1c shows the geographical distribution of the lagrangian particles. As can be

inferred from the figure, the pollutants emitted from Galicia were transported to the area of Huelva.

Since 1960, several works have shown that increments in ozone levels may be associated to vegetation burning. The formation of ozone in plumes originated from emissions derived from vegetation fires have the same physic-chemical behavior that the smog in the cities because they produce ozone precursors, such as NO<sub>x</sub> and organics, which under the influence of the ultraviolet light generate ozone as secondary product. As illustrated in this case study high levels of ozone, PM and CO can be linked to the long range transport of air masses originated from areas strongly influenced by forest fires.

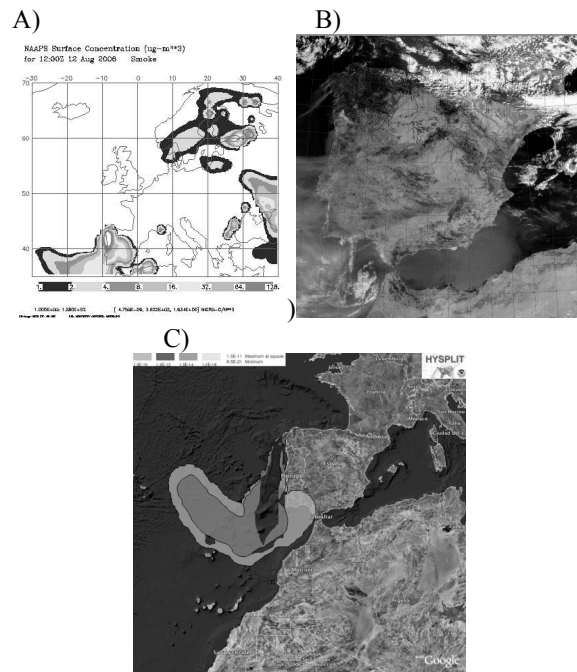


Figure 1. (a) NAAPS model, (b) Modis Images and (c) HYSPLIT 4 model for 12th August 2006 of the Iberian Peninsula

Draxler, R.R. & Hess, G.D. (1998) *Aust. Met. Mag.*, 47, 295-308.

## Modeling and Measurements of High Arsenic Levels in Southwestern Spain

A.F. Stein<sup>1</sup>, J.D. de la Rosa<sup>2</sup>, AM Sánchez de la Campa<sup>2</sup>, X. Querol<sup>3</sup> and A. Alastuey<sup>3</sup>

<sup>1</sup>Earth Resources and Technology on assignment to NOAA's Air Resources Laboratory, MD, USA.

<sup>2</sup>Department of Geology, University of Huelva, Huelva, Spain.

<sup>3</sup>Institute of Earth Sciences "Jaume Almera", CSIC, C/ Lluís Sole i Sabaris s/n, 08028 Barcelona, Spain

Keywords: HYSPLIT model, Aerosol measurement, Aerosol modeling, Modeling (regional).

The city of Huelva (SW Spain) is characterized by high levels of arsenic (Querol et al. 2002). The origin of the arsenic is predominantly industrial (Alastuey et al. 2006; Sánchez de la Campa 2007).

Arsenic concentrations have been modeled using the Hybrid Single Particle Lagrangian Integrated Trajectory (HYSPLIT) model (Draxler and Hess, 1998). Emissions include several major industrial sources in the area of Huelva, Spain. For this application, the HYSPLIT model has been configured to release 5000 three-dimensional lagrangian particles per hour to represent the dispersion and transport of As. The meteorological data used by the model are based on outputs from the Mesoscale Meteorological model version 5 (MM5) using four nested grids with the highest horizontal resolution of 2 km.

HYSPLIT has been run for three different summer days, namely August 10 and 15, 2003 and June 14, 2004, and compared with field measurements. Figure 1 shows the geographical distribution of the concentration of Arsenic as calculated by the model. On August 10 2003 and June 14 2004, the typical summertime sea breeze transports the pollutant inland increasing the concentrations in the city of Huelva. Conversely, on August 15 2003 during the passage of a frontal zone the pollutant plume is directed toward the South East preventing the buildup of As in the area of Huelva.

Table 1 shows a comparison between the model outputs and the measurements for the El Carmen site. The model is able to predict whether the source impacts at the measurement site; however it underpredicts the Arsenic concentrations. This underprediction could be due, among other factors, to the uncertainty in the emissions since they have been derived from annual averages and they can experience daily variations.

Table 2. Comparison of 24-hour averaged As concentrations at the El Carmen site.

Date	Model [ng/m <sup>3</sup> ]	Measurement [ng/m <sup>3</sup> ]
Aug 10, 2003	4.92±8.72	7.44
Aug 15, 2003	0.0±0.0	0.8
June 14, 2004	1.27±3.83	10.05

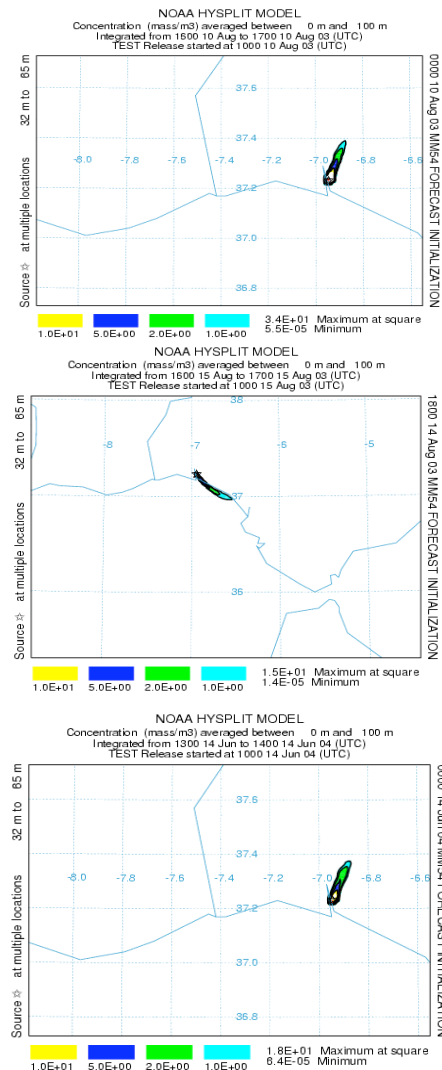


Figure 1. Geographical distribution of As levels (ng/m<sup>3</sup>) for (a) August 10, 16:00 UTC, 2003, (b) August 15, 16:00 UTC, 2003, and (c) June 14, 13:00 UTC, 2004.

Alastuey A et al. (2006). *J. of Air and Waste Manag. Assoc.* 56, 993-1006.

Draxler, R.R. and G.D. Hess (1998), *Aust. Met. Mag.*, 47, 295-308.

Querol et al. (2002). *Atmos. Environ.* 36, 3113-3125.

Sánchez de la Campa et al. (2007). *Environmental Research* 103, 305-316

## Aerosol properties in the spring and summer Arctic troposphere: a global model study

H. Korhonen, D. V. Spracklen, K. S. Carslaw and G. W. Mann

School of Earth and Environment, University of Leeds, Leeds, LS2 9JT, United Kingdom

Keywords: atmospheric aerosols, aerosol modelling, Arctic aerosol

The Arctic environment is particularly vulnerable to the global climate change and recent climate simulations have predicted the highest temperature rises on the globe for this region. Quantifying the future aerosol radiative effects in the Arctic is, however, very challenging as we do not currently fully understand the mechanisms that control the particle size distribution and cloud droplet concentration at these high latitudes. The picture is further complicated by many unique features of the Arctic, e.g. high surface albedo, strong seasonal variation in incoming solar radiation and spring time peak in long range transport from anthropogenic pollution sources, which influence the climate impact of the atmospheric particles.

We present an assessment of the current state of understanding of Arctic boundary layer aerosol based on comparison of observed and modelled aerosol properties. We use long term size distribution measurements from Spitsbergen and Finnish Lapland as well as summer time campaign measurements from high Arctic (Heintzenberg *et al.*, 2006) together with a global aerosol microphysics model GLOMAP (Spracklen *et al.*, 2005). GLOMAP is an extension to the TOMCAT 3D chemical transport model (Stockwell & Chipperfield, 1999) and has been shown by Spracklen *et al.* (2006) to capture the general features of the marine boundary layer aerosols at lower latitudes.

The simulations concentrate on the spring and summer period (February to July) when the observations show a shift from polluted Arctic haze conditions to clean summer conditions with low particle mass concentration. In the simulations the primary particle sources in addition to sea salt are natural and anthropogenic sulphate and OC/BC. Secondary particle formation occurs through binary nucleation which in the model takes place predominantly in the upper troposphere.

Although the model captures well the high SO<sub>2</sub> concentration in March and April and its decrease towards the summer, the basic runs fail to reproduce the change from accumulation mode dominated particle size distribution in spring to Aitken mode dominated distribution in the summer (e.g. Strom *et al.*, 2003). Instead, the shape of the modelled distribution remains very similar throughout the simulated period. Sensitivity simulations show that the description of the clouds in the model and their effect on the particle size distribution are crucial in determining the concentration of accumulation mode particles and therefore the sink for the condensing vapours and small clusters formed in the upper troposphere.

For the subarctic measurement sites in Finnish Lapland the model predicts realistic particle concentrations and general features of distribution in early spring. Towards summer the modelled particle concentrations are, however, significantly lower than the measured ones. In April and May this is partly due to lack of a boundary layer nucleation mechanism in the model but this mechanism may not be able to explain the discrepancy in the summer when new particle formation events are not frequently observed in Lapland.

Further work will be carried out to validate the model results with available chemical and meteorological measurements. Based on this we aim to improve the description of aerosol-cloud interactions in the high latitudes. We will also study the influence of boundary layer nucleation and SOA formation to our results especially in the subarctic regions.

This work was supported by the UK Natural Environment Research Council

- Heintzenberg, J., Leck, C., Birmili, W., Wehner, B., Tjernstrom, M. & Wiedensohler, A. (2006). *Tellus*, 58B, 41-50.
- Spracklen, D., Pringle, K., Carslaw, K. & Chipperfield, M. (2005). *Atmos.Chem. Phys.*, 5, 2227-2252.
- Spracklen, D., Pringle, K., Carslaw, K., Mann, G., Manktelow, P. & Heintzenberg, J. (2006). *Atmos.Chem. Phys.*, 6, 8871-8915.
- Stockwell, D. & Chipperfield, M. (1999). *Q. J. R. Meteorol. Soc.*, 125, 1747-1783.
- Strom, J., Umegard, J., Torseth, K., Tunved, P., Hansson, H.-C., Holmen, K., Wisma, V., Herber, A. & Konig-Langlo, G. (2003). *Phys. Chem. of the Earth*, 28, 1181-1190.

## Modelling study on the connection of sulphuric acid and new particle formation

S.-L. Sihto<sup>1</sup>, H. Vuollekoski<sup>1</sup>, J. Leppä<sup>2</sup>, I. Riipinen<sup>1</sup>, V.-M. Kerminen<sup>2</sup>, H. Korhonen<sup>3</sup>, K.E.J. Lehtinen<sup>4</sup> and M. Kulmala<sup>1</sup>

<sup>1</sup>University of Helsinki, Department of Physical Sciences, P.O. Box 64, FI-00014 Univ. of Helsinki, Finland

<sup>2</sup>Finnish Meteorological Institute, Climate and Global Change, P.O. Box 503, FI-00101 Helsinki, Finland

<sup>3</sup>University of Leeds, School of Earth and Environment, Leeds LS2 9JT, United Kingdom

<sup>4</sup>Finnish Meteorological Institute and University of Kuopio, Department of Applied Physics, P.O. Box 1627, FI-70211 Kuopio, Finland

Keywords: aerosol dynamics, modelling, nucleation rate, particle formation and growth, sulfuric acid.

Field measurements in e.g. Hyytiälä, Finland, indicate that atmospheric particle formation seems to be a function of sulphuric acid concentration to the power from one to two (Weber *et al.*, 1997; Riipinen *et al.*, 2006). To explain these dependences, the so called activation and kinetic nucleation mechanisms have been proposed (Kulmala *et al.*, 2006). We have performed a series of simulations with an aerosol dynamics box model to study the connection between sulphuric acid and new particle formation and the processes affecting the relationship in detail. In particular, we tried to find conditions which would yield the observed linear or square dependence between the number concentration of freshly nucleated particles and sulphuric acid.

Aerosol dynamics model UHMA (University of Helsinki Multicomponent Aerosol model, Korhonen *et al.*, 2004) is a sectional box model that has all the basic aerosol dynamical mechanisms implemented: nucleation, condensation, coagulation and dry deposition. For nucleation we assumed either activation or kinetic mechanism:

$$J_{act} = A[H_2SO_4]$$

$$J_{kin} = K[H_2SO_4]^2,$$

where for the nucleation coefficients  $A$  and  $K$  we used values given by Riipinen *et al.* (2006).

We studied the correlation of the simulated number concentration of 3–6 nm particles ( $N_{3-6}$ ) and formation rate of 3 nm particles ( $J_3$ ) with the modelled sulphuric acid concentration ( $[H_2SO_4]$ ):

$$N_{3-6} \sim [H_2SO_4]^{n_{N_{3-6}}} (t - \Delta t_{N_{3-6}})$$

$$J_3 \sim [H_2SO_4]^{n_{J_3}} (t - \Delta t_{J_3}).$$

The correlation exponents  $n$  and the time delays  $\Delta t$  were determined numerically by searching through pairs of  $(n, \Delta t)$  a combination that would give the maximum correlation coefficient between the curves.

The exponent for  $J_3$  correlation was greater or equal than the exponent for  $N_{3-6}$ , and the time delay for  $J_3$  shorter than for  $N_{3-6}$ , which results are in line with those by Riipinen *et al.* (2006). The time shift analysis has been used to estimate the growth rate of 1–3 nm sized particles from the measurement data (e.g. Sihto *et al.*, 2006). Comparison with the growth rates calculated from the simulated volume change

rate showed that the time delay for  $N_{3-6}$  gives on average a reasonable estimate for the growth rate of freshly nucleated particles.

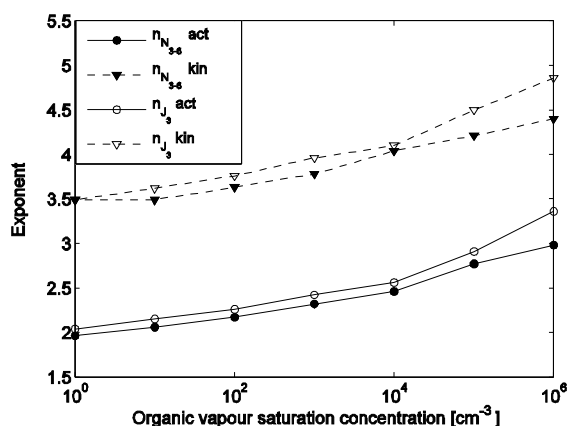


Figure 1. Correlation exponents for  $N_{3-6}$  and  $J_3$  as a function of organic vapour saturation concentration using activation and kinetic nucleation mechanisms.

The most important factor affecting the dependence on sulphuric acid at 3–6 nm was the growth process, including the amount of condensable vapours (sulphuric acid and an organic vapour), their diurnal profiles, and the saturation vapour pressure of organics. The exponents decreased as the saturation concentration of the condensable organic vapour was lowered (Fig. 1). In order to preserve the exponent in nucleation rate (either 1 or 2), the growth below 3 nm must be fast and not limited by saturation vapour pressure. In addition to general simulations, we performed case studies of some selected days with exponent 1 and 2 dependence.

Korhonen, H., Lehtinen, K.E.J. and Kulmala, M. (2004) *Atmos. Chem. Phys.*, 4, 757-771.

Kulmala, M., Lehtinen, K.E.J. and Laaksonen, A. (2006) *Atmos. Chem. Phys.*, 6, 787-793.

Riipinen, I., *et al.* (2006) *Atmos. Chem. Phys. Discuss.*, 6, 10837-10882.

Sihto, S.-L., *et al.* (2006) *Atmos. Chem. Phys.*, 6, 4079-4091.

Weber, R. J., *et al.* (1997) *J. Geophys. Res.*, 102, 4375-4385.

## A combined method for data processing in an elastic backscattered Lidar

D. Nicolae<sup>(\*)</sup>, C. Talianu<sup>(\*)</sup>, A. Nemuc<sup>(\*)</sup>, E. Carstea<sup>(\*)</sup>,  
L. Belegante<sup>(\*)</sup>, C. Radu<sup>(\*)</sup>

<sup>(\*)</sup> National Institute of R&D for Optoelectronics, Bucharest, Romania

Keywords: lidar ratio, remote sensing, particle characterization, vertical distribution

Atmospheric aerosols have large influence on earth's radiation budget. Very little is known about the aerosol vertical distribution, the climatology and air mass modification. Therefore, vertically resolved aerosol data represent an urgent need to obtain a statistically significant database on the aerosol variability. The laser remote sensing technique is a unique tool able to provide the vertical distribution of aerosols in the atmosphere with very high temporal and spatial resolution.

The simplest lidar systems used for vertical profiling of suspended particles in the lower atmosphere are based on the elastic backscattering process [1]. Unfortunately, few qualitative information can be directly obtained from elastic backscatter measurements. More information become available if the lidar system has additional receiving channels (Raman, depolarization). To derive the aerosol microphysical properties a 3 (elastic) + 2 (Raman) channels system is necessary [2].

In any case, the accuracy of obtained information is dependent on technical performances of the system and on the sensibility of data processing method, which can be critical in some cases. The need for compact, robust systems that can work in field campaigns limits the number of receiving channels and the power of the laser beam, so the improvements of a specific system's hardware are likely to be considered. On the other hand, more data processing algorithms which include complementary data can be foreseen based on new laboratory or theoretical studies of aerosols.

This paper will present the basic characteristics of a Lidar system, and particularly of the backscatter Lidar used for measurements. The advantages of a backscatter Lidar measurement system and the drawbacks will be underlined. Because the data inversion problem has a non-unique solution for this type of lidar systems, the quantitative data that can be derived from lidar signals is supposed to be limited to the backscattering coefficient profile of aerosols.

The paper will present an iterative hybrid regularization algorithm for elastic backscatter lidar data processing, developed by the Laser remote sensing group in Bucharest. This algorithm is meant to evaluate the microphysical properties of the suspended matter particles in the air if complementary data are available. In our study, a

simplified model of the atmosphere is used to deliver the meteorological parameters profiles (temperature, pressure, humidity), but real data can only improve the expected results. To initiate the iterations, some characteristics of the aerosols at ground level must be considered: refractive index, average radius, soot proportion, number distribution. For that we used the Ackermann model [3] which will be detailed in the extended paper.

The algorithm basically combines iteratively the Mie direct problem [4] with the inversion Fernald-Klett method [4, 5] to determine the microphysical parameters of the atmospheric particles for which the theoretical and the experimental outputs are corresponding. One important contribution of the algorithm is to eliminate uncertainties from using a constant value of the lidar ratio [6]. By an iterative approach, the vertical lidar ratio profile will be determined and then used in data processing.

Several results obtained using this algorithm and synthetic lidar signals will be presented, as well as the advantages and the limitations of the method.

1.Measures R.M., *Laser Remote Sensing. Fundamentals and Applications*, Krieger Publishing Company, Malabar, Florida, 1992.

2.Bockmann, C., Hybrid regularization method for the ill-posed inversion of multiwavelength lidar data in the retrieval of aerosol size distributions. *Appl. Opt.*, 40(9): p. 1329-1342, 2001

3.Ackermann J., *Two-frequency lidar inversion algorithm for a two-component atmosphere*, *Appl. Opt.* 36, 5134-5143, 1998

4.Mie G., *Ann. de Phys.*, Leipzig, 25, pg. 377, 1908

5.Fernald, F.G., Herman, B.M., and Reagan J.A., *Determination Of Aerosol Height Distribution By Lidar*, *J. Appl. Meteorol.* 11, 482-489, 1972

6.Klett J.D., *Stable Analytical Inversion Solution For Processing Lidar Returns*, *Appl. Opt.* 20, 211-220, 1981

7.Doina Nicolae, C.P. Cristescu, "*Laser remote sensing of tropospheric aerosol*", *J.Optoelectron.Adv.Mater.*, vol. 8, no. 5, October 2006, p.1781-1795

## Particle size-dependent focusing in a flow through a channel with oscillating walls

P. Vainshtein and M. Shapiro

Faculty of Mechanical Engineering, Technion – Israel Institute of Technology, Haifa, Israel

Keywords: particle, motion, channel, oscillations

We consider two-dimensional motion of aerosol particles in a long semi-infinite channel of height  $h$  walls of which perform harmonic oscillations  $y = h + 2b \cos \omega t$  with angular frequency  $\omega$  and amplitude  $b$  to-and-fro the channel axis. It is known that in the absence of imposed flow field, such walls' oscillations create flow field that induces particle drifting motion in compressible fluid<sup>1</sup>.

To calculate the incompressible flow field within the channel, we use the Poiseuille inlet velocity profiles  $U = U_0 [1 - (y/h)^2]$ . To find the disturbed velocity flow field, we employ the method of asymptotic expansions using dimensionless parameters  $\varepsilon = b/h$  and Womersley parameter,  $W = h(\omega/2\nu)^{1/2}$ . The obtained velocity field contains oscillating components and secondary streaming components, both arising from the wall oscillations<sup>2</sup>. The secondary streaming velocity near the axis is directed in the downstream direction. Its intensity increases linearly with  $x$ . The characteristic value of intensity depends on parameter  $\varepsilon W$ .

The micrometer and submicron particle trajectories are computed from the equation

$$\frac{d\mathbf{u}_p}{dt} = \frac{\mathbf{u} - \mathbf{u}_p}{\tau}, \quad \tau = \frac{2}{9} \frac{a^2 C}{\nu \Pi_\rho}, \quad (1)$$

where  $\mathbf{u}$  and  $\mathbf{u}_p$  are the velocities of fluid and particles, respectively,  $\tau$  is the Stokes relaxation time,  $a$  is the particle radius,  $\nu$  is the fluid kinematic viscosity,  $\Pi_\rho$  is the fluid-to-particle-density ratio and  $C$  is the Cunningham's slip correction factor.

For moderate and large Stokes numbers,  $S = \omega\tau$ , particle trajectories are computed numerically, using the solution for the flow velocity field. For small particle Stokes numbers, we obtain analytical expressions for particles' time averaged trajectories.

Figure 1 shows particles trajectories in the coordinates  $X=x/h$ ,  $Y=y/h$ . Particles are seeded at  $X_0 = 0$ ,  $Y_0 = 0.1$  with the initial velocity coinciding with that of air. It is shown that due to the walls' oscillations particles experience drifting motions (i) upstream in  $X$  direction toward the channel inlet and (ii) towards the axis (in  $Y$  direction). Intensity of the upstream drifting motion increases linearly with  $X$ . However, the effect of downstream motion caused by the secondary streaming always dominates over the effect of the particle upstream drifting motion. Therefore secondary streaming together with imposed main flow drives particles downstream. It is

shown that if Stokes number is smaller than some critical value, namely if  $\omega\tau < \zeta/\varepsilon^2$ , the particle approaches the axis asymptotically at infinite  $X$  (curve 1). Generally the value of parameter  $\zeta$  depends on the secondary streaming characteristic intensity. In particular, if  $W\varepsilon \gg 1$  (as in Fig. 1) one has  $\zeta = 0.33$ . In other important case when  $W\varepsilon \sim 1$  one has  $\zeta = 0.66$ . Trajectory behavior, presented by curve 1, is reminiscent of systems aerodynamic focusing in periodic nozzle systems<sup>3</sup> and in a channel with slightly corrugated walls<sup>4</sup>. It is shown that at sufficiently high amplitude and frequency of walls' oscillations their effect on focusing is more pronounced than that of walls' corrugation.

If  $\omega\tau > \zeta/\varepsilon^2$ , particle trajectory behavior turns out to be non-monotonic near the channel axis (curve 2). The amplitude of particle trajectory oscillations near the axis decays as  $X$  tends to infinity.

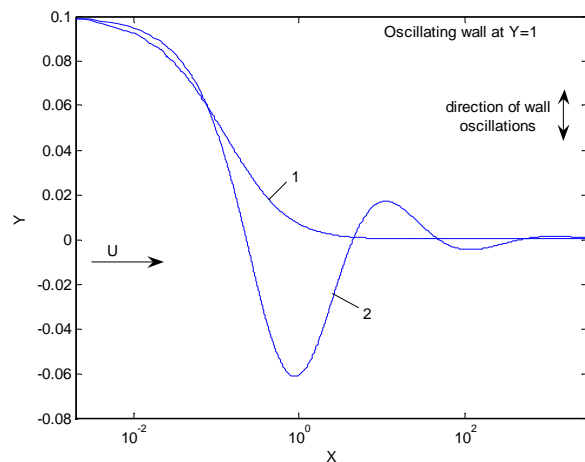


Figure 1. Particles' trajectories in the channel  $h = 10^{-2}$  m,  $U_0 = 0.1$  m/sec,  $f = \omega/2\pi = 1$  kHz  $\varepsilon = 0.1$ ,  $W = 144$ . 1 -  $a = 30 \mu\text{m}$ ; 2 -  $a = 100 \mu\text{m}$ .

<sup>1</sup> Dain, Y., Fichman, M., Gutfinger, C., Pnueli, D. and Vainshtein, P. (1995). *J. Aerosol Sci.*, 26, 575-594.

<sup>2</sup> Secomb, T.W. (1978). *J. Fluid Mech.*, 88, 273-288.

<sup>3</sup> Wang, X., Gidwani, A., Girshick, S.L. and McMurry, P.H. (2005). *Aerosol Sci. Technol.*, 39, 624-636.

<sup>4</sup> Fernandez de la Mora, J. (2006). *J. Aerosol. Sci.*, 37, 323-339.

## Modelling of atmospheric aerosol processing with consideration of non-ideal solutions and complex multiphase chemistry

R. Wolke, J. Zoboki, A. Tilgner and H. Herrmann

Leibniz Institute for Tropospheric Research, Permoserstr. 15, 04318 Leipzig, Germany

Keywords: aerosol modelling, aerosol cloud interaction, multiphase chemistry, aerosol thermodynamics, chemical composition.

In multi-component systems phase transfer processes take place, which can influence the particle and droplet formation as well as particle growth. In the modelling of such multiphase processes it is necessary to consider non-ideal conditions in deliquescent particles. Here we find highly concentrated solutions which are typical in the initial stage of the droplet formation, when only small amounts of water are available. The behaviour of these non-ideal mixed solvent-electrolyte solutions including inorganics and organics is not yet described satisfyingly in existing multiphase models. The aim of our work is to improve the description of such complex systems by the implementation of different activity coefficient calculation methods into the Spectral Aerosol Cloud Chemistry Interaction Model (SPACCIM) (Wolke et al., 2005).

This parcel model has been developed for the description of cloud microphysical processes with the consideration of complex multiphase chemistry for a size-resolved particle/drop spectrum. Microphysics is coupled with a chemical model, so meteorological and microphysical parameters needed for the chemistry can be taken from the microphysical model. Changes in the chemical composition feed back on the microphysical processes. The non-ideality of highly concentrated solutions is described by activity coefficients. In ideal (well diluted) case these coefficients are unity. An extended version (included ions) of UNIFAC coupled with the Pitzer method was implemented. The new SPACCIM version is able to simulate the physico-chemical processes of the particles/droplets also at lower relative humidities.

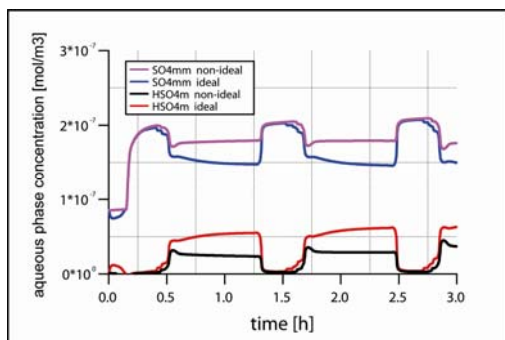


Figure 1. Sulfate concentration (accumulated over the spectrum) for the urban scenario.

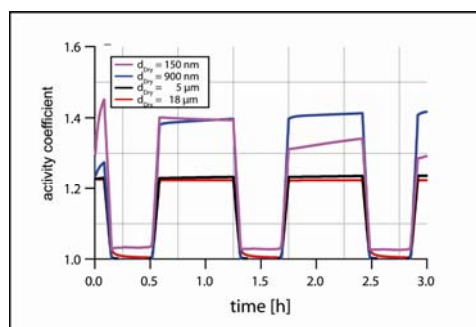


Figure 2. Activity coefficient of glycolic acid for different size bins and the urban scenario.

For the model studies, a reduced version of the multiphase mechanism CAPRAM 3.0 (Herrmann et al., 2005) is used. The simulations were carried out for a meteorological scenario in which an air parcel moves along a predefined trajectory including three cloud passages and intermediate aerosol state at a 90% relative humidity level. Simulations have been performed for marine, remote and urban conditions. Feed back effects of the multiphase chemistry on microphysics are considered.

Figure 1 shows the sulphate evolution of the urban scenario in ideal and non-ideal case. In general, the deviations from ideal solutions are not negligible. The feedback of non-ideality on microphysics is also clearly recognizable. In urban case, the consideration of non-ideality leads to a lower pH value during the interstitial aerosol states. However, the observed differences vary over the size spectrum and in dependence on the particle composition. This behaviour is illustrated for the activity coefficients of glycolic acid in Figure 2. A more detailed analysis shows that also the number of activated particles (especially during the second and third cloud passage) depends strongly on the consideration of non-ideality. The proposed approach leads to an appropriate modelling of complex solutions occurring atmospheric aerosols.

Herrmann, H., Tilgner, A., Barzaghi, P., Majdik, Z., Gligorovski, S., Poulain, L., & Monod, A. (2005). *Atmospheric Environment*, 39 (23-24), 4351-4363.

Wolke, R., Sehili, A.-M., Tilgner, A., & Herrmann, H. (2005). *Atmospheric Environment*, 39 (23-24), 4375-4388.

## Oscillations of the parameters in finite system with condensation and evaporation

V.A. Zagaynov<sup>1</sup>, A.K. Maslov<sup>2</sup>, M. Bahtyreva<sup>3</sup>, A. Lutsenko<sup>3</sup>, A.A. Lushnikov<sup>1</sup>

<sup>1</sup>Karpov Institute of Physical Chemistry, 10, Vorontsovo Pole str., 105064, Moscow, Russia

<sup>2</sup>Department of Numerical Mathematics of Moscow State University, Moscow, Russia

<sup>3</sup>Moscow State Industrial University, 16, Autozavodskaya, Moscow, Russia

Keywords: condensation, evaporation, nucleation, aerosol modelling.

The processes of nucleation and condensation – evaporation play a very important role in formation and evolution of aerosol particle concentration levels and particle size distributions (Friedlander, 2000). At the same time there are several approaches for modelling nucleation, condensation and evaporation. Nucleation is a process, which is responsible for the birth of disperse phase. As is known, using different methods for the description of this process one can come to inconsistent results. Most important part of the nucleation in the atmosphere is the formation of dimers and molecular clusters composed of 3-7 molecules.

For the description of the initial stage of the particle formation process we use the set of differential equations describing the nucleation- condensation-evaporation process:

$$\begin{aligned} \frac{\partial c_1}{\partial t} &= I - \alpha_1 c_1^2 - c_1 \sum_{i=1}^G \alpha_i c_i + \sum_{i=2}^G \beta_i c_i \\ \frac{\partial c_i}{\partial t} &= \alpha_{i-1} c_{i-1} c_{i-1} - \alpha_i c_i c_i - \beta_i c_i + \beta_{i+1} c_{i+1} \quad (1) \\ i &\leq G. \end{aligned}$$

Here  $c_i$  is the concentration of  $i$ -mers,  $I$  is the production rate of monomers,  $\alpha_i$  is the collision frequency of monomers and  $i$ -mers,  $\beta_i$  is the frequency of monomer escape from an  $i$ -mer, and  $G$  is a cut-off particle mass. The particles with the mass exceeding  $G$  are assumed to be instantly removed from the system and do not take a part in condensation and evaporation processes.

Solutions to differential equations (1) with initial conditions

$$c_i(t=0) = 0 \quad (2)$$

show that the particle concentrations oscillate and damp with time. As time grows the concentrations stabilize. When evaporation is neglected the explicit steady state solution can be obtained;

$$c_i = \sqrt{\frac{I}{\alpha_i(G+1)}} \quad c_i = \frac{1}{\alpha_i} \sqrt{\frac{\alpha_i I}{G+1}} \quad \text{for } i < G+1$$

This steady state solution is shown to be an attractor. The eigenvectors of the steady state equations have negative real parts and all eigenvectors form complex conjugated pairs. Figure 1 demonstrates the changes of particle concentrations with time (time and concentrations are dimensionless). In this example we solved 200 equations ( $G=200$ ) for

$I=1$  and took  $\alpha_i = i^{\frac{1}{3}}$ . It was shown, that initial conditions does not effect on position of attractor. The phase trajectories are spiral type curves.

It is clear, that condensation part of the differential equations (1) gives rise to oscillations due to its nonlinear form, whereas the evaporation part of the equations contributes to damping these oscillations. As was found, the general period of oscillation grows with  $G$

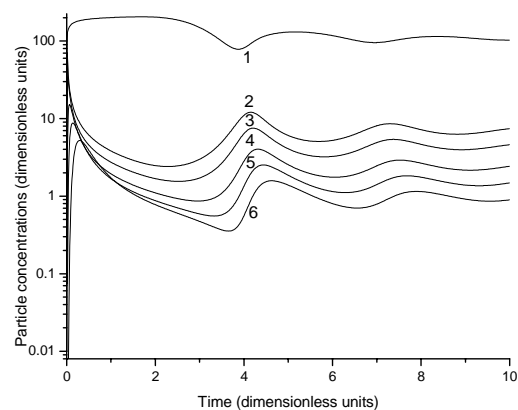


Figure 1. The variations of particle concentrations with time for different particle sizes: 1 – total particle concentration, 2 – concentrations of monomers, 3 – dimers, 4 – particle contained 5 monomers, 5 – 10 monomers, 6 – 20 monomers.

The analysis of the solution shows that period of oscillations grows with  $G$  and damping grows in increasing the evaporation rate.

This approach can be used to explain experimental results cited in Friedlander (2000).

This work was supported by International Science and Technology Center, project # 1908.

Friedlander, S.K. (2000). *Fundamental of Aerosol Dynamics*. New York, Oxford, Oxford University Press.

## Effect of Nucleation and Secondary Organic Aerosol formation on Cloud Droplet Number Concentrations

R. Makkonen<sup>1</sup>, A. Asmi<sup>1</sup>, H. Korhonen<sup>2</sup>, H. Kokkola<sup>3</sup>, S. Järvenoja<sup>4</sup>, P. Räisänen<sup>4</sup>, K.E.J. Lehtinen<sup>5</sup>,  
A. Laaksonen<sup>5</sup>, V.-M. Kerminen<sup>4</sup>, H. Järvinen<sup>4</sup> and M. Kulmala<sup>1</sup>

<sup>1</sup>Department of Physical Sciences, University of Helsinki, FI-00014, Helsinki, Finland

<sup>2</sup>School of Earth and Environment, University of Leeds, LS2 9JT, Leeds, United Kingdom

<sup>3</sup>Finnish Meteorological Institute, FI-70211, Kuopio, Finland

<sup>4</sup>Finnish Meteorological Institute, FI-00101, Helsinki, Finland

<sup>5</sup>Department of Physics, University of Kuopio, FI-70211, Kuopio, Finland

Keywords: nucleation, SOA, atmospheric aerosols, modelling, organic aerosols.

The continental biosphere emits large quantities of volatile organic compounds (VOCs) capable of forming secondary organic aerosols (SOA). By acting effectively as cloud condensation nuclei (Hartz et al., 2005), these aerosols have the potential to influence clouds and thereby climate. The climatic effects of biogenic SOA are, however, extremely poorly known. Reasons for this include the large uncertainties associated with the magnitude and variability of biogenic VOC emissions, as well as our incomplete understanding on the chemistry and processes responsible for the formation and growth of aerosol particles from these emissions. Biogenic VOC emissions may increase substantially in the future as a result of global warming, in addition to which there are potentially complex feedback mechanisms between biogenic VOC emission, aerosols, clouds and climate. As a result, the climatic effects of biogenic VOC emissions cannot be quantified without an Earth System Model that couples the biosphere and atmosphere and treats the microphysical processes associated with biogenic SOA formation.

We introduce the implementation of a simple computationally effective SOA distribution scheme into a global climate model. The scheme has a mechanistic description of aerosol formation and growth processes related to biogenic organic vapours; instead of treating SOA as primary emission, we model the condensation of organic vapour onto pre-existing particles. Additionally, we have compared four nucleation mechanisms using ECHAM5-HAM: two binary parameterizations as well as kinetic and activation type nucleation. Kinetic and activation type nucleation seem to produce more particles in the boundary layer than binary parameterizations.

Aerosol modelling was done with the HAM-module within the ECHAM5 atmospheric general circulation model (Stier *et al.*, 2005). HAM uses seven modes to describe aerosol population. In standard ECHAM5-HAM, nucleation of new particles is parameterized

using a binary nucleation scheme and secondary organic aerosols from biogenic VOCs are treated as primary organic aerosol emissions.

Coupling the aerosol distributions to a cloud activation model shows that just by changing the nucleation mechanism, the cloud droplet number concentrations can change substantially especially over land (Figure 1). This effect clearly shows the potential importance of nucleation on cloud properties. Explicit SOA formation can enhance cloud droplet number concentrations even more.

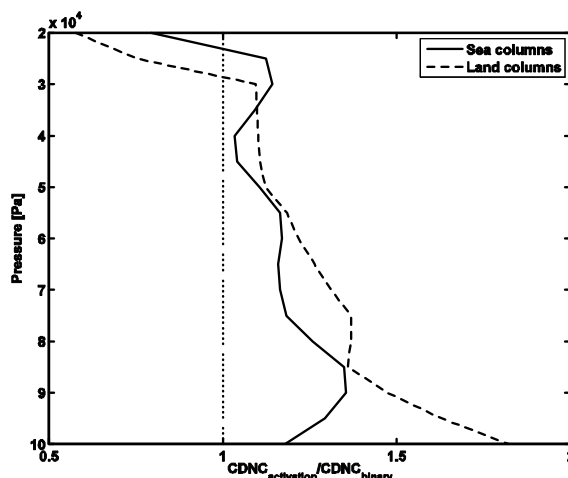


Figure 1. Ratio of cloud droplet number concentrations between simulations with activation – type and binary nucleation. Values are yearly averages from northern hemisphere, separately for land and sea areas.

Hartz, K. E. H., Rosenorn T., Ferchak S. R., Raymond T. M., Bilde M., Donahue N. M. and Pandis S. N. (2005). *J. Geophys. Res.*, 110, D14208.

Stier P., Feichter J., Kinne S., Kloster S., Vignati E., Wilson J., Genzeverld L., Tegen I., Werner M., Balkanski Y., Schultz M., Boucher O., Minikin A. and Petzold A. (2005). *Atmos. Chem. Phys.* 5, 1125-1156.

## Evaluation of Brownian motion calculation using Discrete Phase Model of FLUENT

D.K. Song<sup>1</sup> and S. Dhaniyala<sup>2</sup>

<sup>1</sup>Department of Environmental Engineering, Kumoh National Institute of Technology, 1, Yangho-dong, Gumi, Gyeongbuk, 730-701, Republic of Korea

<sup>2</sup>Department of Mechanical & Aeronautical Engineering, Clarkson University, Potsdam, NY 13699, USA

Keywords: Brownian diffusion, nanoparticle, trajectory, FLUENT.

Computational fluid dynamics (CFD) has played an important role in the development of instruments to measure and characterize physical properties of nanoparticles. As the target size of airborne particles has decreased to the nanometre size range, Brownian motion of nanoparticles has become the dominant characteristic describing their behaviour. In this study, we evaluate Brownian motion of particles by using Discrete Phase Mode in a popular commercial CFD tool, FLUENT (Fluent Inc., NH).

Particles move randomly by colliding with gas molecules and result in having a spatial distribution. Generally this distribution can be assumed as a Gaussian distribution with a standard deviation given by

$$\sigma = \sqrt{2Dt} = \sqrt{(2k_B T C_c t) / (3\pi\mu D_p)} \quad (1)$$

which is known as the Stokes-Einstein relation.

Fig. 1 shows a computational domain used for evaluation. To account for particle dispersion only by Brownian motion, no fluid flow is considered. A number of particles (N = 500) were started from the origin of the computation domain for each test case (Table 1). In calculations, the tracking parameters in FLUENT were set as: Maximum number of steps: 100,000; and the length scale: 10<sup>-8</sup> m. After particle trajectories are calculated (Fig. 1), particle positions were recorded as a function of time.

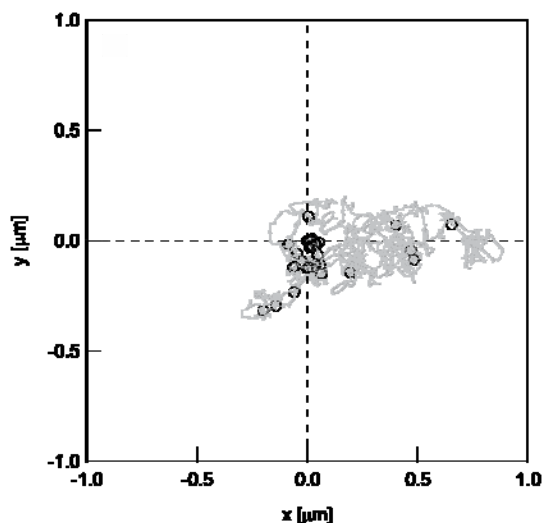


Figure 1. Computation domain and sample particle trajectory. Symbols represent particle position at observation time.

Table 1. Tracking schemes used for calculations.

Case	Tracking Scheme	Accuracy Control Scheme	
		Lower Order	Higher Order
00 <sup>†</sup>	-	-	-
01	Implicit		
02	Analytic		
03	Trapezoidal		Off
04	Runge-Kutta		
05		Analytic	Runge-Kutta
06	Off	Implicit	Runge-Kutta
07		Implicit	Trapezoidal
08		Analytic	Trapezoidal
09	Implicit		
10	Analytic		
11	Trapezoidal		On
12	Runge-Kutta		

<sup>†</sup> In this case, FLUENT v6.1.22 was used while v6.2.16 was used for all the other cases.

The standard deviation of particle position is calculated from the observed positions as shown in Fig. 2. For all cases, standard deviations of particle positions obtained from calculations with Brownian motion using FLUENT are much smaller compared to that from the Stokes-Einstein relation. It is important to recognize these possible errors in the calculations of nanoparticle motion using commercial codes.

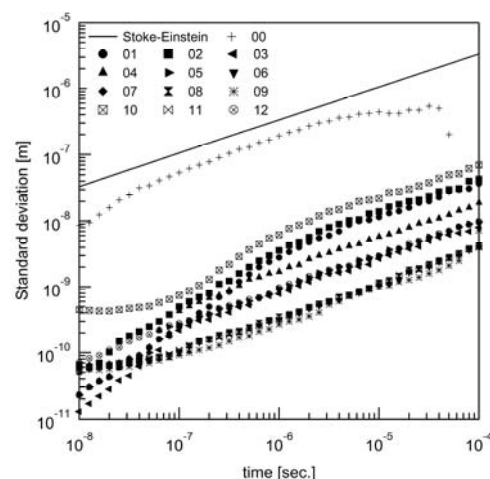


Figure 2. Comparison results from calculation.

This work was supported by the National Science Foundation under grant CTS-0508390 and the Korea Research Foundation Grant funded by the Korean Government (MOEHRD, KRF-2006-214-D00015).

## Numerical study of dynamics of growing droplets in Kelvin spectrometer

S.K. Zaripov<sup>1</sup>, R.S.Galeev<sup>1</sup>, W.Holländer<sup>2</sup>

<sup>1</sup>Institute of Mathematics and Mechanics, Kazan State University, Universitetskaya St., 17, Russia, 420008

<sup>2</sup>Fraunhofer Institute Toxikologie und Experimentelle Medizin  
Nikolai-Fuchs-Str. 1, D-30625, Hannover, Germany

Keywords: aerosol modelling, condensation, evaporation, deposition, growth.

Instruments capable of measuring droplet concentrations at given supersaturations are called Kelvin spectrometers. They are important for reliably characterizing atmospheric particles (Holländer et.al., 2002). The rapid pressure drop in measuring chamber of cylindrical cross section is accompanied by an adiabatic temperature decrease, which may lead to sufficient supersaturation followed by droplet formation due to heterogeneous nucleation. The growing droplets move in the chamber, and part of them will deposit on the walls or evaporate with time. Heat conduction and natural convection flow due to the difference between the wall and volume gas temperatures will increase the interior temperature and reduce the supersaturation that in turn affects droplets growth and deposition.

We developed a mathematical model describing the transient thermal convection flow and deposition of growing droplets in the expansion-type Kelvin spectrometer. The model includes the Navier-Stokes equations to describe the gasdynamic processes and droplet growth model with account for vapor depletion due to condensation and release of latent heat. Numerical calculations of gas flow by means of Fluent CFD software show that the evolution of processes inside the spectrometer chamber can be divided into two main stages. The first stage is the adiabatic gas expansion. During it the pressure in the chamber establishes very quickly. The gas temperature falls down practically uniformly in the entire volume of the chamber. The next stage is characterized by a slow temperature increase beginning from regions near the walls. The temperature gradient causes the development of a gas flow upwards near the wall in the course of time transforms into a global vortex flow inside the chamber. The values of the thermal convection flow velocity magnitude can achieve  $\sim 0.05\text{m/s}$ . To study the droplet dynamics we neglect the expansion stage in view of its small duration and calculate the temperature and convection flow development starting with the uniform temperature distribution inside the chamber and a constant wall temperature larger than the interior gas temperature. Using the gas flow velocity and temperature distribution from CFD calculation in the spectrometer chamber we calculate the droplets paths taking into account their growth resulting from the local super-saturation. The time

dependencies of the droplet deposition rate were found from numerical calculations. The deposition rates with and without convection flow influence are compared.

The relative droplet concentrations obtained taking into account the main processes in the measuring chamber (droplet growth by condensation, sedimentation, heat conduction, thermal convection, droplet evaporation) and without gravity influence ( $g=0$ ) are shown in fig.1. Curves obtained without gravity allow estimating the concentration dynamics due to the evaporation only. For the smaller initial saturation the losses of droplets generated by nucleation is determined mainly by evaporation. But for larger initial saturation sedimentation becomes main mechanism of droplet losses in the measuring chamber. In last case the vortex flow formed by thermal convection will reduce the deposition rate.

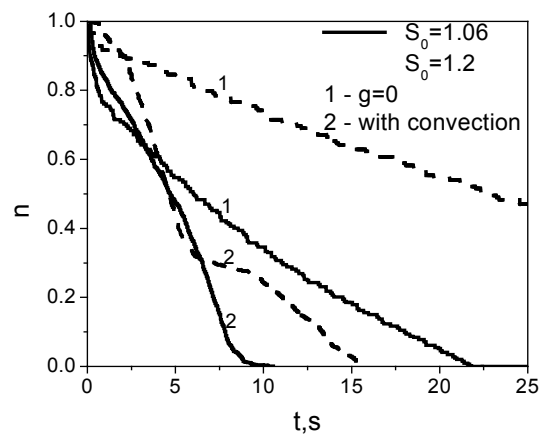


Figure 1. The relative droplet concentration for  $N=1000\text{ cm}^{-3}$  and various initial saturations  $S_0$

The work was supported by RFBR (project 05-01-00794).

Holländer W., Dunkhorst W., Lödding H., Windt H., 2002, Theoretical simulation and experimental characterization of an expansion-type Kelvin Spectrometer with intrinsic calibration, Journal of Atmospheric and Oceanic Technology 19, 1811-1825.

## How reduction policies on emission scenarios can affect air quality in the Tuscany region

C. Grassi<sup>1</sup>, S. Verrilli<sup>2</sup>, L. Tognotti<sup>2</sup>

<sup>1</sup>Department of Mechanical, Nuclear and Production Engineering, University of Pisa, 56100, Pisa, Italy

<sup>2</sup>Department of Chemical Engineering, University of Pisa, 56100, Pisa, Italy

Keywords: Air Pollution, Aerosol Modelling, Photochemical Processes, Emissions

The need to determine the more suitable policies to obtain significant reduction of the air quality pollutants concentration suggest to configure and test an advance modeling system for the Tuscany region to verify and understand the relative contribution of the long range transport of pollutants, emissions, physical and chemical atmospheric processes.

The CAMx multi-scale three dimensional photochemical grid model [Environ2004] was configured to the Tuscany region scenario: regional domain of center Italy comprising the Tuscany region with an horizontal master grid of 46 x 44 cells (6km x 6km) and 17 vertical levels of variable thickness form 20m up to 3600m agl. Regional emission inventory data were elaborated for pollutants emission and detailed VOC and PM<sub>2.5</sub> speciation was applied [Passant, 2002, SCC2004]. In addition three different emission scenarios were prepared, based on regional inventory and IASA projections, to assess the impact of the possible environmental policies on air quality. The meteorological input fields were elaborated from MM5 prognostic meteorological model data [Cetemps]. The IC and BC concentrations were provided by chemistry transport model CHIMERE [Cetemps].

The simulations were performed to reconstruct the air quality pollution in the Tuscany region during the months of October and May 2005.

Table 1. Measured and predicted ozone an PM<sub>10</sub> concentrations [ $\mu\text{g}/\text{m}^3$ ], Tuscany air quality network.

			PISA		FIRENZE		AREZZO		LIVORNO		LUCCA	
			Sub.Back.	Urb.Back.	Urb.Back.	Urb.Back.	Sub.Back.	Sub.Back.	Sub.Back.	Sub.Back.		
PM <sub>10</sub>	MAY	PREDICT	25.9	30.4	31.7	18.9	28.3					
		OSSERVED	27.5	22.1	20.1	17.8	22.1					
		RMSE	4.2	10.4	11.7	5.1	7.6					
	OCT	PREDICT	24.4	27.3	34.6	28.6	23.2					
		OSSERVED	30.6	23.0	30.6	15.3	25.9					
		RMSE	8.6	11.5	10.9	10.4	11.6					
O <sub>3</sub>	MAY	PREDICT	93.8	102.6	105.9	105.3	104.5					
		OSSERVED	97.8	107.4	100.8	104.6	85.1					
		RMSE	11.7	21.9	10.3	7.0	24.0					
	OCT	PREDICT	79.6	58.2	67.1	77.0	88.1					
		OSSERVED	45.9	28.8	35.9	70.0	49.8					
		RMSE	40.4	32.3	36.0	35.3	44.7					

The predicted time series of hourly ozone and daily PM concentration were found to be in good agreement to observed ones; the root mean square error between observed and predicted concentration were shown in table 1 together with the averaged concentration values.

The daily time series showed significant differences between costal and continental or

northern and southern sites, confirming the spatial and temporal observed PM<sub>10</sub> levels. Important results are related to the PM<sub>2.5</sub> and PM<sub>10</sub> concentration ratio that showed variable values from 60% for rural locations to 86% in urban or industrial sites. Significant difference were shown also between the two periods, in fact the 76% in October and 53% during may, indicating a major contribution of crustal component to the coarse fraction of the PM<sub>10</sub>.

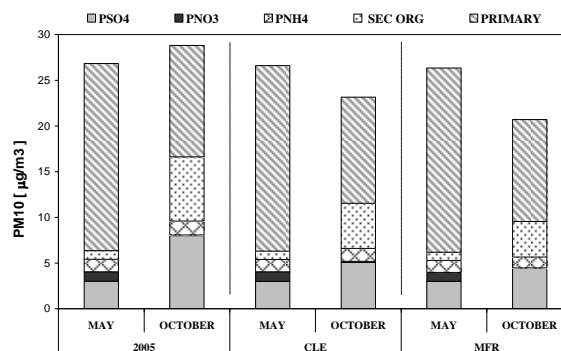


Figure 1. Average PM composition calculated by the models for the three emission scenarios.

The results related to the application of emission reduction as calculated by IASA for CLE2010 (Current Legislation) and MFR2010 (Most Feasible Reduction) to the regional emission inventory are shown in figure 1. The main difference in the effects of emission reduction occurred in the month of October when the secondary organic and ammonium sulphate concurred to the 50% of PM predicted mass concentration. The same reduction applied on the emission of primary particles and gaseous precursors have basically no effects in May related to the contribution of primary crustal particles that concurred up to 70% of the PM concentrations.

CETEMPS Center of Excellence 2005 - Experimental Chemical Weather Forecast over Italy, University of L'Aquila.

ENVIRON 2004, USER'S GUIDE (CAMx) version 4.03, International Corporation.

Passant N.R., Speciation of UK emissions of NMHC VOCs, AEAT/ENV/0545 1, February 2002.

## PBMR Safety Analysis: Aerosol Modelling for Generation IV Nuclear Plants

L. Naicker and A.Ramlakan

Department of Nuclear Engineering Analysis, Pebble Bed Modular Reactor (Pty) Ltd, Centurion, 0046, Gauteng, South Africa

Keywords: Aerosol Chemistry, Aerosol Modelling, Nuclear Aerosols, Radioactive Particles

The Pebble Bed Modular Reactor (PBMR) is a 400MW<sub>th</sub> Generation IV High Temperature Gas Reactor (HTGR). The PBMR core utilizes about 451000 low enriched uranium TRIPLE coated ISOTropic (TRISO) fuel spheres ('pebbles') in an annular fuel region that is surrounded by a fixed central graphite reflector and an outer graphite reflector.

The annular core of pebbles acts as a fixed bed through which the Helium coolant gas passes. The core is continuously loaded at the top and unloads at the bottom, maintaining a pebble inventory, and resulting in downward migration of pebbles. Pebble-to-pebble and pebble-to-reflector abrasion is expected, as well as abrasion of pebbles within the fuel handling and storage system that services the core. Abraded graphite dust can be transported through the cooling loop together with small amounts fission products which manage to escape the fuel spheres. Modelling the transport of graphite dust and fission products allows prediction of the radiological burden imposed on workers and public under accident conditions and is imperative for licensing of the design.

Our present modelling ability involves the use of the thermo-hydraulic code FLOWNEX and the RADAX code to model primary circuit aerosol processes using input from FLOWNEX. Under an accident condition, considered to be a rupture in the primary circuit, a release through the confinement compartments to the venting shaft is modelled using FLOWNEX for thermo-hydraulics and NAUA for aerosol processes.

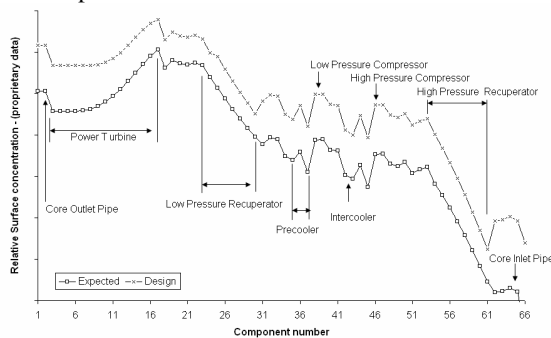


Figure 1. Ag110m primary circuit concentration after 36a

The work discussed here is part of a longer term collaborative modelling effort towards a PBMR specific code that can be generalized to model

accident scenarios in HTGRs. Future code development plans include fully coupled aerosol and thermal-hydraulic modules, a mechanistic account of dust and fission product interaction, chemical interaction between fission products all of which are important improvements to the model especially when re-suspension is considered in the primary circuit (figure 2) depressurization scenarios. In addition, multi-components effects are being investigated.

Isotopes such as Ag, Cs, I and Sr are expected to circulate in the primary loop over the plants lifetime. The primary loop chemical environment is considerably different from LWR and PWR conditions. We discuss the predicted chemical interactions occurring and the kind of uncertainties involved in modelling these reactions. Further discussions will include the licensing framework and release limits for the different accident scenarios, the physical conditions in the primary circuit and confinement building and how these relate to the amount and size distribution of graphite dust, more detailed results from primary circuit and confinement analysis, the aerosol phenomena that are expected to dominate in HTGR accidents, knowledge gained from the AVR(Arbeitsgemeinschaft VersuchsReactor GmbH) and its applicability to PBMR, the experiments required as part of the rigorous verification and validation framework to improve our modelling inputs.

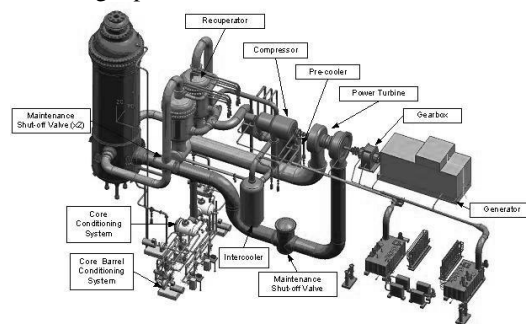


Figure 2. PBMR primary circuit

Stassen, L. (2006). *Validation of the plate-out model in the RADAX code used for plate-out and dust activity calculations at PBMR*. PHYSOR-2006.

Slabber, J. (2006). *Technical Description of the PBMR Demonstration Power Plant*. T016956, Revision 4, Internal PBMR document.

## Modelling Particle Formation and Growth from Biogenic Precursors Measured in the Jülich Plant Chamber

M. Dal Maso<sup>1</sup>, T. Hohaus<sup>1</sup>, A. Kiendler-Scharr<sup>1</sup>, E. Kleist<sup>1</sup>, M. Miebach<sup>1</sup>, R. Tillmann<sup>1</sup>, R. Uerlings<sup>1</sup>, R. Fisseha<sup>1</sup>, J. Wildt<sup>1</sup>, T. Mentel<sup>1</sup>

<sup>1</sup>Institut für Chemie und Dynamic der Geosphäre, Forschungszentrum Jülich, D-52425 Jülich, Germany

Keywords: Aerosol Formation, SOA, Aerosol Modelling, Nucleation

Biogenic volatile organic compounds (BVOC) are major participants in atmospheric chemistry, both due to their large emissions (Guenther *et al.*, 1995) and their influence on O<sub>3</sub> and OH radical budgets. In addition to affecting the oxidising capacity of the atmosphere, their chemical degradation leads to the formation of semi- or non-volatile compounds that considered to be a major source of tropospheric aerosol mass, and also to play an important part in growing recently formed particles to sizes where they can act as cloud condensation nuclei, CCN (see eg. Tunved *et al.*, 2006). Atmospheric aerosol size distribution measurements have shown that atmospheric particle formation, often involving biogenic organics, can be a significant aerosol source (Kulmala *et al.*, 2004).

In the Jülich plant chamber a series of experiments with a system consisting of a plant chamber and a reaction chamber have been carried out. In the experiments, varying plants were placed in the plant chamber in controlled conditions. The VOC mixture emitted from these plants was taken to a stirred reaction chamber which was continuously flushed with O<sub>3</sub>. At the reaction chamber an UV light could be switched on and off to initiate photolysis of O<sub>3</sub> to produce OH. This led to a short nucleation peak, producing a rapid increase in particle number. After the nucleation peak, no new particles are produced and the condensable vapours condense on the existing particle surface.

The setup, with inflow of VOC-laden air from the plant chamber and outflow from the reactor chamber to the instrumentation, leads to dilution of the aerosol concentration over time, with the aerosol lifetime being of the order of 70 min. As the particle concentration decreases, also the available condensation surface, or condensation sink (Kulmala *et al.*, 2001), decreases and in several cases, a new burst of nucleation can be observed.

To understand the processes leading to the observed SOA yields, and whether the VOC oxidation products condense on existing particles or form new particles, we have developed a model for the plant chamber. The model assumes a continuously stirred tank reactor (CSTR, see e.g. Schmidt, 1998), that is, that there exists perfect mixing inside the tank volume. Aerosol dynamic equations are solved simultaneously with the gas phase chemistry.

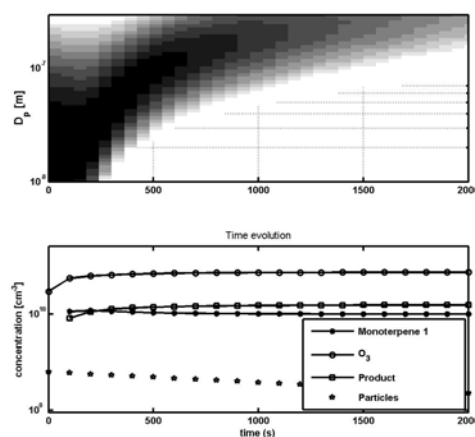


Figure 1. An example model run with the stirred reactor aerosol dynamical model, depicting ozonolysis of a model monoterpene and the resulting growth of the aerosol size distribution. The reactor goes into steady state after ca. 1000 s.

The model can be used to investigate the condensation sink threshold of new particle formation, as well as the e.g. the timescale needed to achieve steady state in the reactor chamber (see figure 1). It is also a valuable tool in estimating the effect of condensing vapour properties on the nucleation and growth rates during nucleation events.

- Guenther, A., et al., 1995, A global model of natural volatile organic emissions, *J. Geophys. Res.*, 100, 8873-8892
- Kulmala, M., *et al.*, (2004) Formation and growth rates of ultrafine atmospheric particles: A review of observations *Aerosol Science* 35, 143-176.
- Tunved, P. *et al.*, (2006) High Natural Aerosol Loading over Boreal Forests *Science* 14, 261-263
- Schmidt, Lanny D. (1998). *The Engineering of Chemical Reactions*. Oxford University Press, New York.

## Closure study of aerosol cloud interactions using trajectory ensemble model

S. Romakkaniemi, G. McFiggans, K. Bower, H. Coe, and T. W. Choulaton

Centre for Atmospheric Science, School for Earth, Atmospheric and Environmental Science, University of Manchester, Manchester M60 1QD, UK

Keywords: aerosol-cloud interactions, aerosol modelling

A closure study of the cloud aerosol interactions in stratocumulus cloud was carried out. In this study we use LEM (Large Eddy Model) to produce similar conditions to those observed during CLOPAP (Cloud Processing of regional Air Pollution advecting over land and sea) project flights. During CLOPAP the NERC / Met Office BAE 146 aircraft was used to conduct measurements in the stratocumulus capped boundary layer in order to study the evolution of polluted aerosols. LEM is further employed to produce a set of trajectories that can be used to run a detailed cloud parcel model, which includes differential equations describing condensation/evaporation of different gases, coagulation, and chemical reactions in the liquid and gas phases. In simulations, the cloud parcel model is initialised with the out-of-cloud aerosol compositional data from the AMS-measurements, and observed/estimated gas phase concentrations of water soluble gases. The existing adiabatic cloud parcel model is modified so that instead of an adiabatic expansion, the temperature and total water concentration are taken from LEM produced trajectories and the change in water saturation ratio is calculated based on these values. The method used is similar to one used by Stevens *et al.* (1996) and Feingold *et al.* (1998).

In Figure 1 an example of the comparison between measured and modelled cloud droplet number concentrations is shown. The measured data is from the CLOPAP flight 9 studying the plume originating from London and advecting to east at 30.9.2005. The cloud droplet number concentration data presented in Figure 1 is measured with FSSP and consist of 26 minutes of in-cloud measurements in the stratocumulus capped boundary layer with liquid water content between 0.05 and 0.4g/kg. The simulation data consist of an ensemble of 1000 trajectories produced with LEM. Measured potential temperature profile is slightly adjusted to get an agreement between measured and LEM simulated updraft velocities. As a measure of agreement we compared the standard deviation of vertical velocity distribution (0.22m/s in this case).

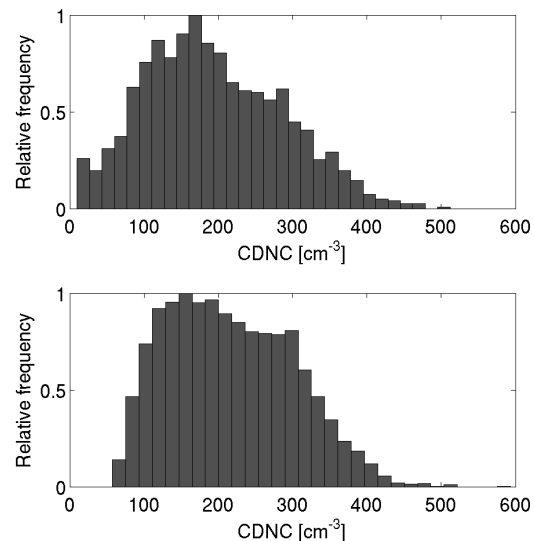


Figure 1. Upper: measured distribution of cloud droplet number concentration. Lower: Modeled cloud droplet number distribution.

As can be seen from Figure 1, the modelled and simulated cloud droplet number concentrations are in a good agreement with the mean value of simulated cloud droplet number concentration being less than 10% higher than the measured concentration. The total number concentration of accumulation mode aerosol particles in this simulation is  $712\text{cm}^{-3}$  with the mean diameter of 120nm. With these values even a small widening of probability density function of the LEM simulated updraft velocities can lead to a remarkable overestimation of the cloud droplet number concentration. Also variations in chemical composition of aerosol particles and the amount of condensable gases in the atmosphere are affecting the modeled results. Thus the work will be continued to conduct the closure that takes account the aging of aerosol due to the cloud processing.

This work was supported by the UK Natural Environment Research Council. S.R. was supported by the Helsingin sanomain 100-vuotissäätiö.

Feingold, G., Kreidenweis, S.M., Zhang, Y. (1998). *J. Geophys. Res.*, 103, 19527-19542  
Stevens, B., Feingold, G., Cotton, C.R., and Walko, R.L. (1995). *J. Atmos. Sci.*, 53, 980-1006

## Predicting fine inorganic aerosols in Mexico City during winter 2005: deliquescence branch.

M. Moya<sup>1</sup>, C. Fountoukis<sup>2</sup>, A. Nenes<sup>2,3</sup>, E. Matías<sup>4</sup>

<sup>1</sup>Centro de Ciencias de la Atmosfera, Universidad Nacional Autonoma de Mexico, Ciudad Universitaria, 04511, Mexico City, Mexico.

<sup>2</sup>School of Chemical and Biomolecular Engineering, Georgia Institute of Technology, 311 Ferst Drive, Atlanta, GA 30332-0100, USA

<sup>3</sup>School of Earth and Atmospheric Sciences Georgia Institute of Technology, 311 Ferst Drive, Atlanta, GA 30332-0100, USA

<sup>4</sup>Posgrado en Ciencias Químicas, Universidad Nacional Autonoma de Mexico, Ciudad Universitaria, 04511, Mexico City, Mexico.

*Keywords:* thermodynamic equilibrium, deliquescence, crustal species

### INTRODUCTION

Atmospheric pollution in the Mexico City Basin (MC) due to high levels of ozone (O<sub>3</sub>) and aerosols (particulate matter, PM) has become a significant issue for its nearly 20 million of inhabitants (Molina and Molina, 2002). PM levels exceed the Mexican PM<sub>10</sub> (PM with aerodynamic diameter  $\leq 10 \mu\text{m}$ ) 24-h standard on most of the days of the year (Edgerton et al., 1999). Although the Mexican PM<sub>2.5</sub> (PM with aerodynamic diameter  $\leq 2.5 \mu\text{m}$ ) 24-h standard of  $65 \mu\text{g m}^{-3}$  has been introduced very recently (November, 2005), PM<sub>2.5</sub> levels have been recorded well above acceptable limits. Atmospheric aerosols reduce local visibility, air quality and have adverse effects on human health. As the chemical composition of fine PM is also important in this respect, knowledge of these two parameters (size/composition) is essential to assess their role in several atmospheric processes occurring in the atmosphere. Airborne PM is composed by inorganic salts, organic material, crustal elements and trace metals. Inorganics may account up to 50% or more of total fine particulate matter. It has been commonly assumed that in the coarse fraction of PM (particles with  $dp > 2.5 \mu\text{m}$ ), where dust is an important constituent of airborne PM, crustal species, such as Ca, K, and Mg are abundant (Ansari and Pandis, 2000). It has been shown, however, in recent studies in this megacity (Moya et al., 2006) that these constituents are of relevance in the PM<sub>2.5-1</sub> size fraction as well.

Simulating the aerosol size and composition is an invaluable tool in increasing our understanding of aerosol behavior and in determining its role in several atmospheric processes. Measurements of the chemical composition of aerosols and their gas-phase precursors in this polluted area are essential to

provide information regarding the aerosol partitioning between the gas and particulate phases and to validate aerosol models.

In this work predictions of the partitioning of nitrate and ammonium between the gas and aerosol phases, under Mexico City conditions and applying SCAPE thermodynamic model are presented.

### RESULTS

Overall, four-hour average PM<sub>1</sub>, PM<sub>2.5</sub> nitrate and ammonium concentrations are predicted within 30-60% for cases where the relative humidity (RH) is within moderate values (40-70%). For the afternoon sampling periods (RHs: 20-35%), the deliquescence branch seems to introduce some errors in predicting aerosol behavior. By considering an updated water activity database, model performance significantly improves for these conditions.

### ACKNOWLEDGEMENTS

This work has been funded by the National Oceanic and Atmospheric Administration (NOAA-US) under contract NMRAC000-5-04017 (A. Nenes) and by the National Council for Science and Technology (CONACyT-Mexico) under contract J51782 (M. Moya). Support of PAPIIT-UNAM grant (reference: IN107306) is also acknowledged.

### REFERENCES

- Ansari, A. and Pandis, S.N. (2000) Atmospheric Environment 34, 157-168.
- Edgerton et al., 1999. Journal of the Air & Waste Management Ass. 49, 1221-1229.
- Molina, M. and Molina, J.T. (2002) Air quality in the Mexico Megacity: An integrated assessment. Kluwer Academic Publishers, Dordrecht.
- Moya, M. et al. (2006) Proceeding of the 2006 American Geophysical Union Fall Conference.

## Detailed process modelling of SOA formation: Kinetic vs. K- $\alpha$ approach

K.-H. Naumann, H. Saathoff

Research Centre Karlsruhe, Institute for Meteorology and Climate Research, Atmospheric Aerosol Research, POB 3640, 76021 Karlsruhe, Germany

Keywords: SOA, VOC(s), aerosol formation, aerosol modelling, aerosol dynamics.

The aerosol behaviour code COSIMA (Naumann, 2003), which has been developed originally to simulate the time evolution of structure, dynamics, optics and heterogeneous chemistry of fractal like agglomerate particles is supplemented by a module treating the formation and dynamics of secondary organic aerosol. While pure SOA particles are compact spheres, the fractal approach is required to account for the restructuring of agglomerates induced by coating with low volatile organic material, which does not necessarily lead to the formation of completely compact cores (Saathoff et al., 2003).

The COSIMA code is currently employed to analyse and to interpret the experimental results obtained during two extensive SOA campaigns conducted at the AIDA facility of Research Centre Karlsruhe in 2005 and 2006 in collaboration with several external partners. As a typical example Figure 1 compares the time evolution of the SOA mass concentration as determined by a SMPS device with the COSIMA predictions. Here the simulations are based on the simplifying assumption that the particle composition can be described by only two product proxies with highly different volatilities (denoted as comp. 1 and comp. 2 in Figure 1). Please note, however, that COSIMA is principally capable to account for much more detailed product distributions provided the relevant parameters are known or can be extracted from the experimental data.

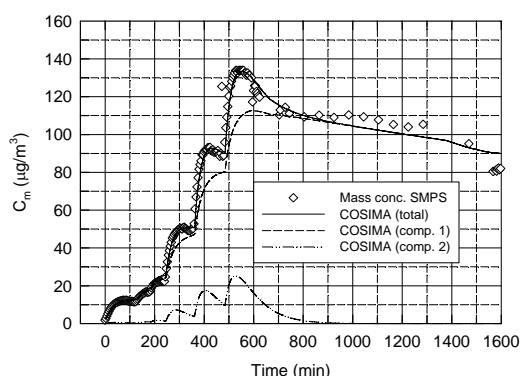


Figure 1. SOA mass evolution during ozonolysis of stepwise increased amounts of  $\alpha$ -pinene in the AIDA chamber and in the long time regime. Comparison between SMPS measurements (symbols) and COSIMA simulation (lines).

The COSIMA model treats the transport of gaseous compounds to and away from the particle surface (including condensation and evaporation as special cases) kinetically, using Dahneke's approach (Dahneke, 1983) to interpolate between the continuum and free molecular regimes. Therefore, non-equilibrium situations e.g. due to transport limitations are properly accounted for.

However, a large amount of work still relies on the assumption that in the course of SOA formation equilibrium is rapidly established between gas and particle phase. A very popular convenient concept has been devised by Pankow, see e.g. Seinfeld and Pankow (2003). In his K- $\alpha$  approach the aerosol yield  $Y = M_0/\Delta HC$  is given by

$$Y = \sum_i Y_i = M_0 \sum_i \frac{\alpha_i K_i}{1 + K_i M_0}$$

where  $M_0$  represents the particle mass concentration produced from the fraction  $\Delta HC$  of the total precursor concentration  $HC$ ,  $\alpha_i$  denotes the mass stoichiometric factor and  $K_i$  the gas phase/particle partitioning constant of component  $i$ , respectively.

A potential drawback of the K- $\alpha$  approach associated with the neglect of non-equilibrium processes could arise from the size dependence of the vapour pressure of small particles due to the Kelvin effect. During the early stages of chamber experiments on SOA formation, for example, constant  $K_i$  values will definitively prove inadequate to describe the observed aerosol dynamics.

Besides introducing the extended capabilities of the COSIMA model by means of simulations of selected recent AIDA SOA experiments, this paper will focus on the predictive efficiency of the K- $\alpha$  approach compared to detailed kinetic process modelling with particular emphasis on the analysis of results from aerosol chamber studies.

Dahneke, B. (1983). in *Theory of dispersed multiphase flow* (Academic Press) 97-133.

Naumann, K.-H. (2003). *J. Aerosol Science*, 34, 1371-1397.

Saathoff, H., Naumann, K.-H., Schnaiter, M., Schöck, W., Möhler, O., Schurath, U., Weingartner, E., Gysel, M., & Baltensperger, U. (2003). *J. Aerosol Science*, 34, 1297-1321.

Seinfeld, J. H., & Pankow, J. F. (2003). *Annu. Rev. Phys. Chem.*, 54, 121-140.

## Transport of fine aerosol particles in turbulent channel flow

A. Pinelli<sup>1</sup> and P.L. Garcia-Ybarra<sup>2</sup>

<sup>1</sup>Unidad de Modelizacion de Procesos, CIEMAT, Av. Complutense 22, Madrid 28040, Spain

<sup>2</sup>Dept. de Fisica Matematica y de Fluidos, Facultad de Ciencias, UNED, Senda del Rey 9, Madrid 28040, Spain

Keywords: aerosol modelling, particle deposition, numerical simulation, turbulence.

The transport & deposition properties of small diffusing aerosol particles very dilute in a channel turbulent flow have been theoretically analyzed by means of an Eulerian description. Aerosol inertia is accounted for by expanding the governing equations in terms of the Stokes number and retaining the first correction (Fernandez de la Mora, 1982). When the Schmidt number  $Sc$  is a large parameter, aerosol deposition on the walls is driven by Brownian and turbulent dispersion in a thin layer of thickness  $Sc^{-1/3}$ , with respect to the viscous sublayer (Garcia-Ybarra & Pinelli, 2006). In the channel core region, the Reynolds-averaged aerosol transport equation across the channel states the counterbalance between turbophoresis and turbulent dispersion (Garcia-Ybarra & Pinelli, 2005).

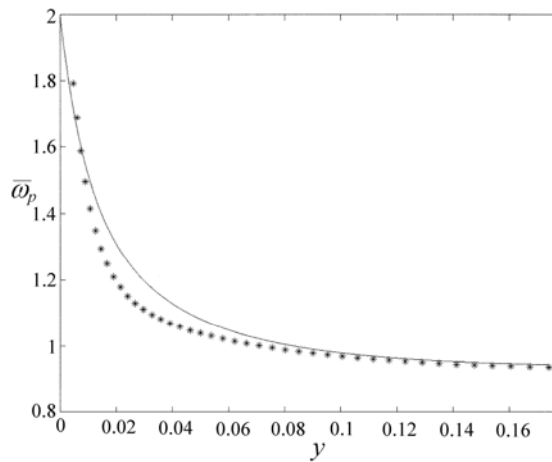


Figure 1. Average profile of aerosol mass fraction. Points (\*): Computed by DNS. Line (—): Predicted by theory with  $Sc_T = 1$ .

When the gradient-diffusion model is used, a profile is obtained with vanishing net flux and high values on the walls (Fig. 1), which enhance aerosol deposition in the thin diffusional layer.

Predictions for the average aerosol distribution with the turbulent Schmidt number (viscous eddy diffusivity to mass eddy diffusivity)  $Sc_T = 1$ , have been compared to DNS results (for  $Re = 3,250$ ). Agreement is not fully satisfactory due to the inadequacy of the constant  $Sc_T$  hypothesis, which close to the wall peaks like the average aerosol mass fraction (Fig. 2 & 3). Variable  $Sc_T$  models are presently being considered.

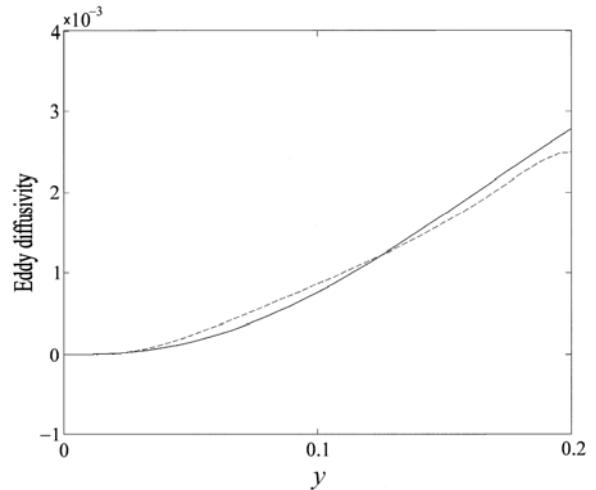


Figure 2. Eddy diffusivities of fluid momentum (—) and aerosol mass fraction (---) near the wall.

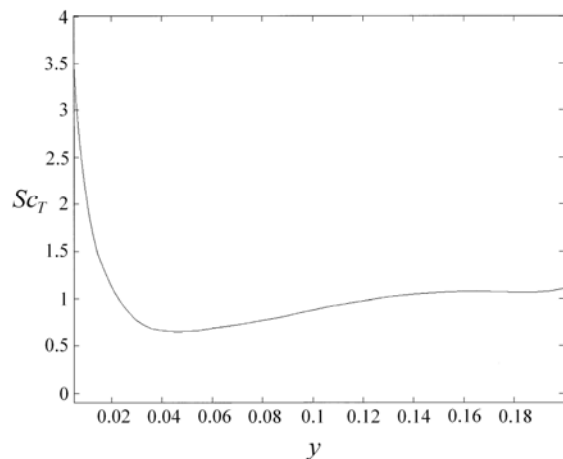


Figure 3. Variation of the turbulent Schmidt number approaching the wall.

This work was supported by Comunidad de Madrid under grant S-505/ENE/0229, and also by the Ministerio de Educacion y Ciencia, Spain, under grants DPI2005-04601 and ENE2005-09190-C04-02.

Fernandez de la Mora, J. (1982). *Phys. Rev. A*, 25, 1108-1122.

Garcia-Ybarra, P.L., & Pinelli, A. (2005). in *Abstract of the EAC 2005*, (Maenhaut Ed.), Ghent, 112.

Garcia-Ybarra, P.L., & Pinelli, A. (2006). *C. R. Mecanique*, 334, 531-538.

## Sensitivity of urban and rural ammonium-nitrate particulate matter to precursor emissions in southern Germany

U. Uhrner<sup>1</sup>, S. Drechsler<sup>2</sup>, R. Wolke<sup>3</sup>, P.J. Sturm<sup>1</sup> and A. Wiedensohler<sup>3</sup>

<sup>1</sup>Traffic and Environment, VKM-THD, Technical University of Graz, Inffeldgasse 81, 8010, Graz, Austria

<sup>2</sup>LUBW, Hertzstrasse 173, 76187, Karlsruhe, Germany

<sup>3</sup>IfT, Permoserstrasse 15, 04318, Leipzig, Germany

Keywords: Particulate Mass, Ammonium nitrate, Aerosol modelling, Emissions, Growth

Fine particulate matter (PM<sub>10</sub>, PM<sub>2.5</sub>) is considered as one of the most important pollutants regarding health effects. European standards for PM<sub>10</sub> (40 µg/m<sup>3</sup> annual mean, max. 35 days above 50 µg/m<sup>3</sup> as daily mean; 2<sup>nd</sup> daughter directive EC/30/99) are difficult to meet in most European cities. During winter time, a significant fraction of PM<sub>10</sub> consists of inorganic species, in particular ammonium nitrate and ammonium sulphate. An inorganic fraction of approximately one third is frequently found in PM<sub>10</sub> probes. During an air pollution episode, the inorganic fraction exceeded 40 µg/m<sup>3</sup> at a busy road in the city centre of Stuttgart in February 2005 (Drechsler et al., 2006). The inorganic fraction was mainly composed of ammonium nitrate and to a lesser extent of sulphate, indicating a major impact of NO<sub>x</sub> emissions and photochemical reactions on secondary aerosol formation.

The sensitivity of secondary ammonium nitrate formation was investigated using a box model approach for the urban area of Stuttgart and the neighbouring rural area Rems-Murr Kreis. The model was used to simulate atmospheric chemistry (Stockwell et al., 1997) and gas/particle partitioning of inorganic compounds (Nenes et al., 1999). Emissions from the detailed UMEG (2004) emission inventory were used. The evolution of the simulated urban particulate matter (PM) ammonium nitrate was found to be highly sensitive to changes in ammonia emissions (see Figure 1). Ammonia, rather than nitric acid was the limiting reagent in urban ammonium nitrate PM formation. In contrast, NO<sub>x</sub> emissions and hence nitric acid was the limiting reagent in the rural case (see Figure 2). Another important parameter in the sensitivity studies is the assumed well mixed layer used within these box model simulations. Decreasing mixing layers lead to stronger ammonium nitrate formation.

The overall behaviour of these model sensitivity studies agrees qualitatively well with composition resolved PM<sub>10</sub> measurements taken next to a busy road (ATV ~80000) in Stuttgart and mixing height computations for the aforementioned episode.

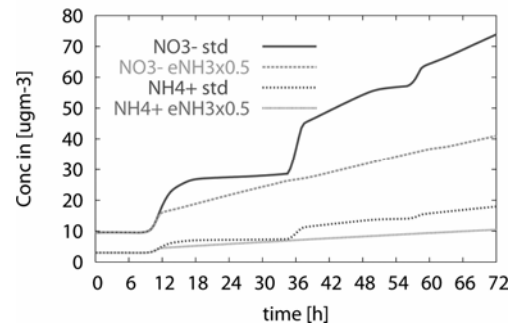


Figure 1. Simulated evolution particulate NO<sub>3</sub> & NH<sub>4</sub> for base run (std) and for 50% reduced NH<sub>3</sub> emissions (eNH<sub>3</sub>x0.5), Stuttgart case.

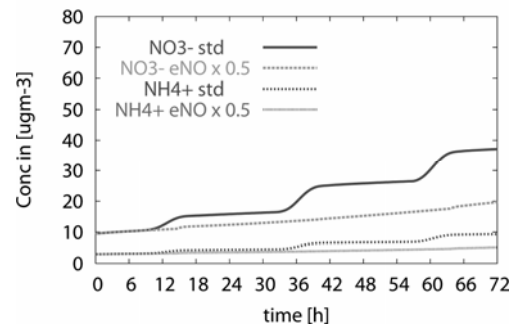


Figure 2. PM NO<sub>3</sub> & NH<sub>4</sub> for base run (std) and for 50% reduced NO<sub>x</sub> emissions (eNO<sub>x</sub> x 0.5), Rems-Murr district case.

Drechsler, S., Ahrens, D., Lump, R., Holst, T. und Uhrner, U., Hohe Feinstaubbelastung als Folge sekundärer Aerosolbildung, Zeitschrift „Immissionsschutz, 06/2006.

Nenes, A., Pandis, S. N., and Pilinis, C., Continued development and testing of a new thermodynamic aerosol module for urban and regional air quality models, Atmos. Environ. 33, 1553-1560, 1999.

Stockwell, W. R., Kirchner, F., Kuhn, M., and Seefeld, S., A new mechanism for regional atmospheric chemistry modeling, JGR, 102, D22, 25847-25879, 1997.

UMEG (2004) Bericht-Nr.4-04/2004 Luftschadstoff-Emissionskataster Baden-Württemberg (air pollution emission data base) 2002.

## Analytical Modeling of Diffusional Nanoparticle Deposition under Low Pressure Conditions

Christof Asbach<sup>1</sup>, Heinz Fissan<sup>1</sup>, Jing Wang<sup>2</sup>, David Y.H. Pui<sup>2</sup>

<sup>1</sup> Institut für Energie- und Umwelttechnik (IUTA), Bliersheimer Str. 60, 47229 Duisburg, Germany  
<sup>2</sup> University of Minnesota, 111 Church Street, Minneapolis, MN 55455, USA

Keywords: Diffusion, Nanoparticle, Contamination

The deposition of nanoparticles can be a major concern, e.g. for clean processing. The manufacture of the next generation of semiconductor chips requires a very clean environment and a low pressure level around 50 mTorr (6.7 Pa) or even below. The lithographic photomasks used are particularly vulnerable because common pellicles can no longer be installed to protect the masks. Several schemes have been developed to protect the photomasks from particle contamination (Asbach *et al.*, 2006) and a fully analytical model to describe the inertial particle motion under low pressure conditions (Asbach *et al.*, 2005) has been established. Diffusional deposition was not included in this model, but estimation revealed that under low pressure conditions diffusional nanoparticle contamination can be a major risk for the cleanliness of the photomasks (Asbach *et al.*, 2007). Based on the existing inertia model, which has been experimentally verified (Kim *et al.*, 2006) and the subsequent estimation of the diffusional particle deposition, an analytical extension of the model has been developed that determines the risks of nanoparticle contamination at low pressure under the influence of gravity, electrophoresis, thermophoresis and drag force. As a first approach the model assumes that inertial and diffusional transport can be decoupled and treated separately. The inertial transport is solved first in the shape of the particle stopping distance using the existing inertia model (Asbach *et al.*, 2005). It is assumed that the diffusional contribution to the stopping distance is negligible, which is justified in most cases, where the stopping distance is much larger than the simultaneous diffusional displacement. The location where the particle stops is taken as the starting point for the diffusion model, as it is assumed that the particle, once stopped, starts to diffuse. When no external forces act on the particle, it

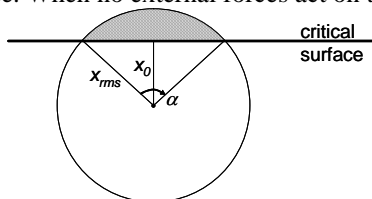


**Figure 1:** Assessment of deposition risk on a critical surface due to Brownian motion

can move in any direction with the same probability. The time dependent root mean square of the probability function can then be expressed as

$$x_{rms} = \sqrt{2Dt}$$

where  $D$  is the diffusion coefficient. The probability of a particle being within a sphere with radius  $x_{rms}$  (see Fig. 1) can thus be determined from the probability density function. The risk of a particle depositing on a critical surface is given by means of the hatched area in Fig. 1.

When external forces, such as gravity, electrophoresis and/or thermophoresis act on the particle, the shape of the sphere is changed to an ellipsoidal shape as illustrated in Fig. 2. However, the principle for the determination of the risk of particle contamination remains the same.

The approach for the model will be presented along with initial comparisons with experimental results.

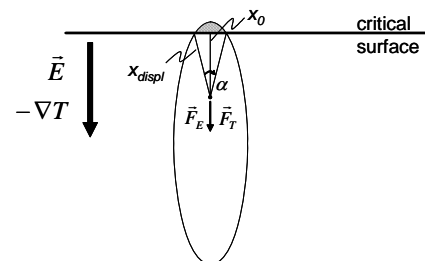


**Figure 2** Assessment of deposition risk on a critical surface due to Brownian motion with thermal and electrical gradient

This work was supported by the Deutsche Forschungsgemeinschaft (DFG).

### References

- Asbach, C.; Fissan, H.; Kim, J.H.; Yook, S.J.; Pui, D.Y.H. (2006), *J. Nanop. Res.* **8**: 705-708  
 Asbach, C.; Kim, J.H.; Yook, S.J.; Pui, D.Y.H.; Fissan, H. (2005), *Appl. Phys. Lett.* **87**: 234111  
 Asbach, C.; Fissan, H.; Kim, J.H. Yook, S.J.; Pui, D.Y.H (2007) *J. Vac. Sci. Technol.* **B25**:47-53  
 Kim, J.H.; Fissan, H.; Asbach, C.; Yook, S.J.; Orvek, K.; Ramamoothy A.; Pui, D.Y.H. (2006) *J. Vac. Sci. Technol.* **B24**: 1178-1184

## **Is the thermodynamic equilibrium an adequate approach for representing fine (PM<sub>1</sub>, PM<sub>2.5</sub>) inorganic aerosol behavior?: ISORROPIA-II simulations under 2005 winter Mexico City conditions.**

**M. Moya<sup>1</sup>, C. Fountoukis<sup>2</sup>, A. Nenes<sup>2,3</sup>, E. Matías<sup>4</sup>**

<sup>1</sup>Centro de Ciencias de la Atmosfera, Universidad Nacional Autonoma de Mexico, Ciudad Universitaria, 04511, Mexico City, Mexico.

<sup>2</sup>School of Chemical and Biomolecular Engineering, Georgia Institute of Technology, 311 Ferst Drive, Atlanta, GA 30332-0100, USA

<sup>3</sup>School of Earth and Atmospheric Sciences Georgia Institute of Technology, 311 Ferst Drive, Atlanta, GA 30332-0100, USA

<sup>4</sup>Posgrado en Ciencias Químicas, Universidad Nacional Autonoma de Mexico, Ciudad Universitaria, 04511, Mexico City, Mexico.

*Keywords:* thermodynamic equilibrium, efflorescence, crustal species

### *INTRODUCTION*

Atmospheric aerosols (particulate matter, PM) reduce local visibility, air quality and have adverse effects on human health. Chemical composition (and size) of PM are important aspects to assess their role in several atmospheric processes occurring in the atmosphere, such as visibility reduction, cloud formation, climate forcing and gas-particle interactions. Simulating the aerosol size and composition is an invaluable tool in increasing our understanding of aerosol behavior and in determining its role in several atmospheric processes.

There have been two main approaches in predicting the partitioning of semi-volatile species between the gas and particulate phases. The first of them uses a fully dynamic mass transfer while the second assumes that the two phases are in thermodynamic equilibrium. Both approaches have been extensively discussed in the literature and arguments have been provided in supporting or not the bulk equilibrium approach. In this work we attempt to provide new information in this regard by applying the recent developed thermodynamic model, ISORROPIA-II (Fountoukis and Nenes, 2007) over Mexico City ambient conditions, characterized for an important diurnal variability of parameters such as T and RH as well as other features e.g. low to-high aerosol nitrate concentrations. In this work, we will be referring to a field study conducted in 2005 (Moya et al., 2007).

### *MODELING FRAMEWORK*

ISORROPIA-II is the new version of ISORROPIA (Nenes et al., 1998). It includes the thermodynamics of crustal species which has been pointed in recent studies in this megacity (Moya et al., 2006, 2007) as relevant in the (PM<sub>2.5-1</sub>) size

fraction. The model considers both branches of aerosol behavior (deliquescence, efflorescence) and an updated water activity dataset. Details of ISORROPIA are depicted in Fountoukis and Nenes, 2007.

### *RESULTS*

ISORROPIA-II predicts adequately fine particulate (PM<sub>1</sub>, PM<sub>2.5</sub>) ammonium (within 30% of error). PM<sub>2.5</sub> nitrate is predicted adequately for RH cases with moderate RH (40-70%) by applying the deliquescence branch of aerosol behavior. For low RH cases (20-30%), the metastable approach of aerosol behavior is more adequate in representing particulate concentrations. Under conditions of this megacity (high T, very low RHs), the consideration of both branches should be taken into account, depending on the history of the particle, as first suggested by Seinfeld and Pandis (1998).

### *ACKNOWLEDGEMENTS*

This work has been funded by the National Oceanic and Atmospheric Administration (NOAA-US) under contract NMRAC000-5-04017 (A. Nenes) and by the National Council for Science and Technology (CONACyT-Mexico) under contract J51782 (M. Moya). Support of PAPIIT-UNAM grant (reference: IN107306) is also acknowledged.

### *REFERENCES*

- Fountoukis, C. and Nenes, A.* 2007. ACPD, 7, 1893-1939.
- Moya et al.* 2006. Proceeding of the 2006 American Geophysical Union Fall Conference.
- Moya et al.*, 2007. Analysis of fine inorganic particulate matter during the 2003, 2005, 2006 field studies in downtown Mexico City. Work in progress.
- Nenes et al.* 1998. Aquatic Geochem. 4, 123-152.

## Modelling on H<sub>2</sub>SO<sub>4</sub>-H<sub>2</sub>O particle formation and growth in the diluting diesel exhaust

L. Pirjola<sup>1,2</sup>, F. Arnold<sup>3</sup>, T. Schuck<sup>3</sup>, J. Keskinen<sup>4</sup>, T. Rönkkö<sup>4</sup>, T. Lähde<sup>4</sup>,  
K. Hämeri<sup>1,5</sup>, A. Sorokin<sup>3</sup>, and D. Rothe<sup>6</sup>

<sup>1</sup>Department of Physical Sciences, University of Helsinki, P.O. Box 64, FIN-00014 Helsinki, Finland

<sup>2</sup>Department of Technology, Helsinki Polytechnic, P.O. Box 4020, FIN-00099 Helsinki, Finland

<sup>3</sup>Atmospheric Physics Division, Max Planck Institute for Nuclear Physics (MPIK), P.O. Box 103980, D-69029 Heidelberg, Germany

<sup>4</sup>Aerosol Physics Laboratory, Institute of Physics, Tampere University of Technology, P. O. Box 692, FIN-33101 Tampere, Finland

<sup>5</sup>Department of Physics, Finnish Institute of Occupational Health, Topeliuksenkatu 41, FIN-00250 Helsinki, Finland

<sup>6</sup>MAN Nutzfahrzeuge AG, Abt. MTVN, Abgasnachbehandlung / Partikelmesstechnik, Vogelweiherstr. 33, D-90441 Nürnberg, Germany

Keywords: nucleation, sulphuric acid, filters, number concentration, size distribution.

Formation of particles in the cooling exhaust is still poorly understood. Evidence for homogeneous H<sub>2</sub>SO<sub>4</sub>-H<sub>2</sub>O nucleation has been shown, but also some other mechanisms such as condensation of volatile organics onto the core particles formed in the combustion process have been suggested. Particle formation depends on driving parameters, fuel and lubricant oil properties as well as exhaust after-treatment systems. Diesel particle filters (DPF) remove soot mode but due to lowered condensation sink of gaseous sulphuric acid (GSA), nucleation is promoted (e.g. Graves, 1999). On the other hand, oxidizing catalysts may enhance GSA formation.

In this work, diesel exhaust particle formation was studied by a sectional atmospheric chemistry and aerosol dynamics box model AEROFOR (Pirjola, 1999; Pirjola & Kulmala, 2001). The model includes gas phase chemical reactions, formation of thermodynamically stable clusters by homogeneous H<sub>2</sub>SO<sub>4</sub>-H<sub>2</sub>O nucleation (Vehkamäki *et al.*, 2003), condensation of H<sub>2</sub>SO<sub>4</sub>, H<sub>2</sub>O and an organic vapour onto particles, temperature cooling and dilution profiles (Lemmetty *et al.*, 2006), as well as wall losses in the ageing chamber. In this work 100 size sections were used. Besides the classical H<sub>2</sub>SO<sub>4</sub>-H<sub>2</sub>O nucleation mechanism also a kinetic model by Sorokin *et al.* (2005) is studied.

The input values were taken from the measurements made at the MAN laboratory by testing a heavy duty EUROIV standard diesel engine with different after-treatment systems and different engine loads. Fuel sulphur contents (FSC) of 7 and 36 ppmM were used. GSA was measured by a CIMS instrument (Arnold *et al.*, 2007) and number concentration of particles larger than 3 nm (N<sub>3</sub>) by a SMPS. The final dilution ratio at the end of the ageing chamber was 12. Temperature was measured in the raw exhaust and just before the ageing chamber, from which the time constant for cooling was found to be around 0.28 s. The free parameter was time constant for dilution. The total simulation time was 2.7 s.

Figure 1 shows the formed N<sub>3</sub> and particle volume concentration at the end of the ageing chamber as a function of the initial GSA. Variation in the GSA reflects different FSC and engine loads when a coated catalytic DPF was used. Huge number of particles were mostly formed, however, if GSA is less than 2x10<sup>11</sup> cm<sup>-3</sup>, no particle formation was observed.

The modelled concentrations and size distributions are compared with the measurements. Differences in the volume concentrations give some elucidation of the role of organic vapours in the particle growth which will be discussed.

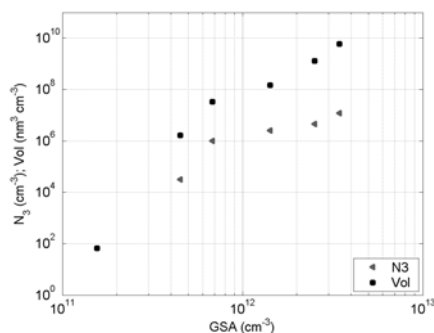


Figure 1. Particle number and volume concentration as a function of raw exhaust GSA

Arnold, F. et al. (2007) *This issue*.

Graves, R.L. (1999) *SAE Technical Paper Series*, No. 1999-01-2245.

Lemmetty, M., Pirjola, L., Mäkelä, J.M., Rönkkö, T., and Keskinen, J. (2006) *J. Aerosol Sci*, 37, 1596-1604.

Pirjola, L. (1999) *J. Aerosol. Sci.*, 30, 355-367.

Pirjola, L. and Kulmala, M. (2001) *Tellus*, 53B, 491-509.

Sorokin, A., Vancassel, X., and Mirabel, P. (2005) *J. Chem. Phys.*, 123, 22508.

Vehkamäki, H., Kulmala, M. and Lehtinen, K.E.J. (2003) *Environ. Sci. Technol.* 36, 283-289.

## A stochastic Langevin model of particle dispersion in turbulent flows with active thermophoresis

A. Dehbi

Department of Nuclear Energy and Safety, 5232 Villigen PSI, Switzerland

Keywords: continuous random walk, Langevin equation, inhomogeneous turbulence, thermophoresis

Recent Direct Numerical Simulations (DNS) (Marchioli *et al.*) and experimental data (Wang *et al.*) have shown that inertial particles exhibit concentration peaks in isothermal turbulent boundary layers. It is therefore expected that turbulence will significantly enhance thermophoretic deposition in flows where walls are colder than the carrier gas. To correctly capture turbulent particle dispersion with active thermophoresis, a Lagrangian continuous random walk (CRW) model is developed. The particle tracking model uses 3D mean flow data obtained from the Fluent CFD code, as well as Eulerian statistics of instantaneous quantities computed from DNS databases. The turbulent fluid velocities at the current time step are related to those of the previous time step through a Markov chain based on the normalized Langevin equation (Iliopoulos & Hanratty 1999) which takes into account turbulence inhomogeneities. The model includes a correction to reduce the “spurious drift” of tracer-like particles which manifests itself in isothermal flows as an unphysical preferential concentration of fluid-like particles near the walls. This correction involves the addition of a “drift velocity” (Bocksell & Loth 2006) and yields improved results in isothermal flows such that tracer-like particles retain approximately uniform concentrations if introduced uniformly in the domain, and the deposition velocity of tracer particles is vanishingly small, as it should be.

The mean thermophoretic force is added as a body force on the particle and follows the formulation by Talbot *et al.* (1980), which gives the best agreement with a large set of data.

The 3D geometry is subdivided into a bulk region where isotropic turbulence is predominant, and a boundary layer region where anisotropic effects are significant. In the boundary layer, arbitrary geometries are tackled by first computing at each time step the rms values of velocities in a “local” particle coordinate system constructed from the mean velocity vector  $I$  (stream-wise component), the wall-normal component  $J$ , and the span-wise component given by the cross product  $I \times J$ . The rms values in the local coordinates are transformed back to the computational coordinates to perform the particle tracking one additional time step. In this procedure, it is assumed that the rms velocity values in general geometries can locally be approximated by the DNS

data of fully developed flows in channel geometry. While clearly an approximation, the latter assumption provides a closer prediction of reality than taking turbulence to be isotropic all the way to the wall.

Benchmarks of the model are performed against recent integral thermophoretic deposition in long pipes ( $L/D=275$ ) at  $Re=6500$  (Tsai *et al.*) as well as the TUBA tests (Dumaz *et al.*) with their detailed local deposition measurements (see Figure 1). In both cases, the agreement with the data is quiet good.

Overall, it is shown that Lagrangian CRW, coupled with DNS data of Eulerian statistics and CFD data of the mean flow field, is able to accurately predict the dispersion and hence thermophoretic deposition of particles in turbulent flows.

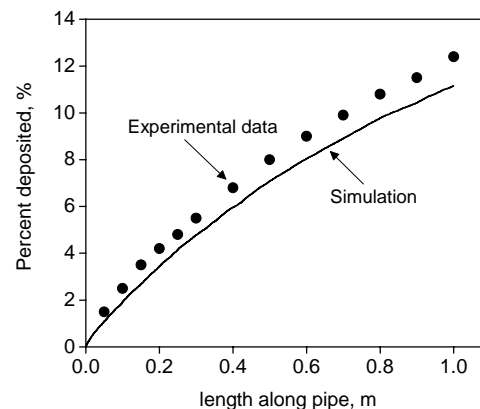


Figure 1. Comparison between CRW model predictions and the TUBA TT28 test

- Marchioli, C., Soldati, A. (2002). *J. Fluid Mech.*, 468, 283-315.
- Wang, J., Levy, E. (2006). *Experimental Thermal and Fluid Science*, 30, 473-483.
- Iliopoulos, I., Hanratty, T.J. (1999). *J. Fluid Mech.*, 392, 45-71.
- Talbot, L., Cheng, R., Schefer, R., Willis, D. (1980). *J. Fluid Mech.*, 101, 737-758.
- Bocksell, T.L., Loth, E. (2006). *Int. J. Multiphase Flow*, 32, 1234-1256.
- Tsai, C.-J., Lin, J.-S., Aggarwal, S.G., Chen, D.-R., (2004). *Aerosol Science and Technology*, 38, 131-139.
- Dumaz, P., Drossinos, Y., Areia Capito, J., Drosik, I. (1993). in *ANS Proc. 1993 National Heat Transfer Conference*, Atlanta, GA, 48-358.



## Modelling of Workplace Nanoparticle Exposure

Christof Asbach, Heinz Kaminski, U. Rating, Heinz Fissan, and Thomas A.J. Kuhlbusch

Institut für Energie- und Umwelttechnik (IUTA), Bliersheimer Str. 60, 47229 Duisburg, Germany

Keywords: Occupational Health, Exposure, Nanoparticles, CFD

The inhalation of particles at nano-scale is currently being discussed to induce adverse health effects such as inflammation. Particles in this size range can either originate from unintended anthropogenic or natural generation processes (e.g. combustion, nucleation) or can be intentionally engineered nanoparticles. Especially exposure to engineered nanoparticles in workplaces has recently raised increased interest (e.g. SCENIHR 2005) as these particles are usually produced in high concentrations and inhaled particle concentrations can thus be very high in case of (accidental) release. Monitoring of nanoparticle exposure at workplaces in the nanotechnology industry is thus an important issue for assessing the safety of workers.

Only very few studies have been published that report actual workplace measurements (e.g. Kuhlbusch *et al.* 2004 & 2006). However, for an expedient investigation of possible workplace exposure as well as save work place design it is essential to understand the behaviour and dispersion of particles within a workplace. Precise modelling of particle dispersion and physical reactions can therefore help to improve work place design, identify hot spots within the room, and give guidance for the definition of suited measurement locations. Furthermore, such simulations can provide a three dimensionally resolved picture of the exposure scenario. Therefore exposure can also be inferred from the model based on the posture of the worker, e.g. whether he is sitting or standing.

In this work, three exemplary, realistic workplaces have been simulated using the commercial computational fluid dynamics (CFD) code FLUENT, along with the Fine Particle Model (FPM). A software platform has been developed that simplifies the set up of common workplace geometries. The modelled scenarios comprise 1) a welding workplace, 2) a large hall with several pipes and a reactor with nanoparticles trickling from a conveyor belt, and 3) a hall with a leak in a slightly pressurized transport pipe of freshly formed nanoparticles. Besides convective transport of the particles and dilution with background air (assumed to be particle free), the considered physical processes also comprised sedimentation and coagulation. The welding workplace modelled was a real workplace that was subject to measurements of the particle size distributions (unpublished). The modelling results were compared with the measured data and found to be in good agreement. Scenario 2 included only

minor air movements and exemplarily showing the distribution of nanoparticles almost within the entire room. Scenario 3 was used to study the behaviour of particles, particularly when released at high concentrations and thus prone to coagulation. It was assumed that 50 nm particles ( $\sigma_g = 1.1$ ) were released at a very high concentration of  $10^{19} \text{ m}^{-3}$  from a leak in a slightly pressurized transport pipe 1.5 m above ground into a 10 m x 10 m x 5 m hall with two open windows on the sides and three apertures in the roof. Exposure was investigated at levels of 1.0 m and 1.50 m above ground to mimic the breathing height of a sitting and standing worker, respectively. It was found that exposure can vary significantly depending in the breathing height and location within the hall (Figure 1). The changes in the particle size that can be seen in the graph were caused by coagulation, whereas additionally dilution caused the concentration to drop by several orders of magnitude.

Results from the different simulated scenarios will be presented along with recommendations for representative and conclusive modelling of workplace exposure to nanoparticles.

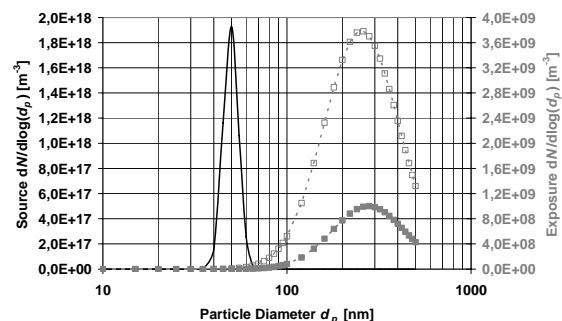


**Figure 1:** Simulated size distribution changes from source (left peak, primary axis) to exposure (1.5 m (■) and 1.0 m (□) above ground, secondary axis) near a window (1.5 m above ground)

This work has been supported by the government of Northrhine Westfalia and the European Union under grant number 005-0406-0004.

Kuhlbusch, T.A.J., H. Fissan (2006): *J. Occ. Env. Hyg.* **3**: 558-567

Kuhlbusch, T.A.J., S. Neumann, H. Fissan (2004): *J. Occ. Env. Hyg.* **1**: 660-671

SCENIHR (2005). [http://europa.eu.int/comm/health/ph\\_risk/committees/04\\_scenihr/docs/scenihr\\_o\\_003.pdf](http://europa.eu.int/comm/health/ph_risk/committees/04_scenihr/docs/scenihr_o_003.pdf)

## Particle deposition on a semiconductor wafer larger than 100 mm in diameter

Kun-Hyung Lee<sup>1</sup>, Gun-Soo Song<sup>2</sup>, Kyung-Hoon Yoo<sup>2</sup> and Seung-Ki Chae<sup>1</sup>

<sup>1</sup> Micro Contamination Control Group, Manufacturing Technology Center, Semiconductor Business, SAMSUNG Electronics, San #16, Banwol-Ri, Taean-Eup, Hwasung-Si, 445-701, South Korea

<sup>2</sup> Aerosol and Contamination Control Laboratory, Korea Institute of Industrial Technology (KITECH), 35-3, Hongcheon-Ri, Ibjang-Myun, Cheonan-Si, 330-825, South Korea

Keywords: deposition velocity, semiconductor wafer, wafer diameter.

Since the year of 2000, the semiconductor wafer diameter has been changed from 200 mm to 300 mm. However, so far, there have not been sufficient theoretical studies on particle deposition on a semiconductor wafer larger than 100 mm in diameter. In the present study, the characteristics of particle deposition velocity on the upper surface of 100, 200 mm sized wafers were investigated both experimentally and numerically.

Figure 1 shows the schematic diagrams of the present experimental apparatus and numerical calculation domain, respectively. Experiments were conducted in an ISO class 2 clean room of the line 14 fab of SAMSUNG Electronics Co. The wafer diameter and particles in the present experimental study were 200 mm and PSL particles, respectively. The governing equations of gas flow, energy and particle concentration for steady, incompressible and axis symmetric laminar flow with constant properties were considered in the present numerical study. For the details of the present numerical methods, readers can refer to those of 100 mm-diameter wafer by Yoo & Oh(2005).

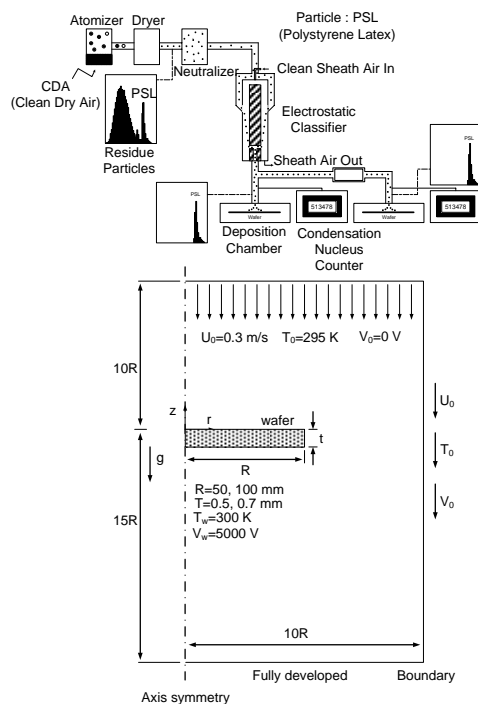


Figure 1. Schematic diagrams of the present experimental apparatus and calculation domain.

Figure 2 shows variations of the averaged deposition velocities on the upper surface of wafer with respect to particle size. It can be seen in the figure that the deposition velocity of 200 mm wafer is larger than that of 100 mm wafer. The increase of wafer diameter causes the fluid velocity boundary layer to be much thinner. This thinner fluid velocity boundary layer causes the particle concentration boundary layer to become much steeper and leads to consequent increase in the deposition velocities for the diffusion-dominant particle sizes generally less than  $0.1 \mu\text{m}$ . While in the particle sizes larger than  $1 \mu\text{m}$  no difference is found because of gravitational settling dominance. It is also shown that in the curves for the charged wafer with 5000V the particle deposition velocities are rapidly increased in the particle size range generally less than  $1.0 \mu\text{m}$ . Meanwhile, the present numerical results show relatively good agreement with the present experimental results and those of Ye et al.(1991) and Opiolka et al.(1994).

Yoo, K. H., & Oh, M. D. (2005). *J. Aerosol Science*, 36, 235-246.

Opiolka, S., Schmidt, & Fissan H. (1994). *J. Aerosol Science*, 25, 4, 656-671.

Ye, Y., Pui, D.Y.H., Liu, B.Y.H., Opiolka, S., Blumhorst, S. & Fissan, H. (1991). *J. Aerosol Science*, 22, 63-72.

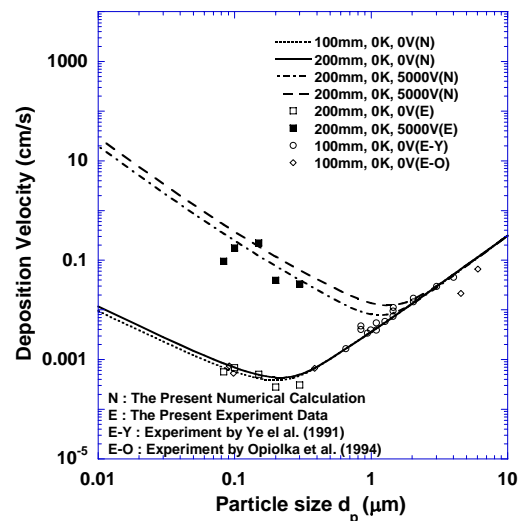


Figure 2. Variation of the averaged deposition velocity with respect to particle size.

## Mixed effects regression model in the analysis of 50nm particle number concentration

S. Mikkonen<sup>1</sup>, K. E. J. Lehtinen<sup>1,2</sup>, A. Hamed<sup>1</sup>, J. Joutsensaari<sup>3</sup> and A. Laaksonen<sup>1</sup>

<sup>1</sup>Department of Physics, University of Kuopio, P.O.B 1627, FIN-70211 Kuopio, Finland

<sup>2</sup>Finnish meteorological institute, P.O.B 1627, FIN-70211 Kuopio, Finland

<sup>3</sup>Department of Environmental Sciences, University of Kuopio, P.O.B 1627, FIN-70211 Kuopio, Finland

Keywords: Atmospheric aerosols, particle concentration, mixed effects regression.

It is well known, that atmospheric aerosols have a great effect on radiation budget, formation of clouds and on climate change. Despite of several years of research, many of the factors affecting the new particle formation and the growth of new formed particles remain unclear. Kulmala et al. (2004) studied several physical and chemical properties affecting particle growth and suggested that the factors affecting new particle formation and growth vary between locations.

Our dataset consists of measurements made between 24.3.2002 - 30.4.2005 at San Pietro Capofiume (SPC) station in the Po Valley area, Italy. The concentration of particles was measured by using a twin Differential Mobility Particle Sizer (DMPS) system. More details of the measurements can be found in Hamed et al. (2007).

The aim of our study was to predict the number of 50nm particles with various different factors, i.e. to find the factors affecting the growth of freshly nucleated particles to 50nm size. Most of our models were combinations from hourly averages of gas and meteorological parameters measured at SPC, including temperature, relative humidity, radiation, O<sub>3</sub>, SO<sub>2</sub>, NO<sub>2</sub>, condensation sink, wind speed and -direction and the probability that the day is a nonevent day i.e. a day when significant new particle formation cannot be seen. The probability of a nonevent day (PrNE) was calculated with discriminant analysis, details of the method can be found from Mikkonen et al. (2006). PrNE was favoured instead of probability of event day due to better predicting ability. The calculated nonevent probability was used instead of observed event classification because otherwise we would have had to exclude the unclassified days, which would have subsidised the data drastically. In addition, the probabilities of a nonevent day can be estimated also for those days where the event classification has not been made at all.

Due to complex structure of processes affecting to concentration of small particles it is not reasonable to use general linear effect models in the analysis. We chose to use generalized linear models with logarithmic link function and combine it with mixed model structure (McCulloch and Searle, 2001). The main idea of a mixed model is to estimate, not only the mean of the measured response

variable  $y$ , but also the variance-covariance structure of the data.

We found out that RH, PrNE and the concentration of SO<sub>2</sub> had significant additional variance components for different times of year. When the additional variance is taken into account, the model suggests that the effect of RH is negative in January and in December and positive for the rest of the year. The decreasing effect of PrNE is on its highest in January, June and July, and the effect of SO<sub>2</sub> concentration is negative in winter months (from Nov. to Apr.) and positive for the rest of the year.

Significant weekend effects have been reported for several pollutants (e.g. Marr and Harley, 2002). This reflects also to particle concentrations: Tuesday, Wednesday and Thursday seem to have the highest effects on the concentration of 50nm particles. Effect varies slightly between months.

Wind direction showed out to have a significant effect on the behaviour of some of the predictor variables. The effect of local wind speed is mainly positive, i.e. the particle number is higher when the wind speed is higher, except for the winds coming from northeast, south and southwest. The effect of Condensation Sink is on its lowest on north, northwest and west, respectively. These are the directions to the highly populated areas but also the directions to the mountains.

Effect of Ozone varies within the day; positive effect can be detected on daytime and negative effect on night. The coefficient of determination R<sup>2</sup> for the model is 0.61 which indicates that the model explains roughly 61% of the total variation of the particle concentration.

This work was supported by Graduate school in Physics, Chemistry, Biology and Meteorology of Atmospheric composition and climate change

Hamed, A., *et al.* (2007). *Atmos. Chem. Phys.*, 7, 355-376

Kulmala, M., *et al.* (2004). *J Aerosol Sci*, 35,143-176

Marr L.C. and Harley R.A. (2002). *Atmospheric Environment*, Vol. 36, 2327-2335.

McCulloch, C. and Searle, S. R. (2001). *Generalized, Linear, and Mixed Models*, New York: Wiley.

Mikkonen, S., *et al.* (2006): *Atmos. Chem. Phys.*, 6, 5549-5557.

## **T12 Abstracts**

## New particle formation at rural sites simulated with MALTE (model to predict new aerosol formation in the lower troposphere)

M. Boy<sup>1</sup>, O. Hellmuth<sup>2</sup>, H. Korhonen<sup>3</sup>, A. Guenther<sup>4</sup>, J. Kazil<sup>5</sup>, E.R. Lovejoy<sup>5</sup> and M. Kulmala<sup>1</sup>

<sup>1</sup>Department of Physical Sciences, University of Helsinki, P.O. Box 64, 00014 University of Helsinki, Finland

<sup>2</sup>Leibniz Institute for Tropospheric Research, Permoserstrasse 15, 04 318 Leipzig, Germany

<sup>3</sup>Finnish Meteorological Institute, Air Quality Research, Sahaajankatu 20 E, FIN-00880 Helsinki, Finland

<sup>4</sup>ACD, NCAR, 3450 Mitchell Lane, Boulder, CO 80301, USA

<sup>5</sup>NOAA Earth System Research Laboratory, 325 Broadway, Boulder, CO 80305, USA

Keywords: aerosol formation, modelling, nucleation, organics, tropospheric aerosol.

New secondary particle formation has been observed at almost all places where both particle number concentrations and size distributions have been measured; a comprehensive summary of these studies is given in Kulmala et al. (2004). Although many field campaigns, laboratory experiments and new modelling approaches have led to increased understanding, detailed mechanisms responsible for the formation of new particles in the troposphere and their influence on health, environment and climate have still not been completely elucidated.

In MALTE (Model to predict new Aerosol formation in the Lower Troposphere) individually developed codes from different institutes around the globe merged into a one-dimensional model including aerosol dynamics, boundary layer meteorology, biology and chemistry in order to investigate the formation and growth processes of Secondary Organic Aerosols (SOA) under realistic atmospheric conditions.

Recently published field and laboratory studies showed that sulphuric acid is one key parameter concerning the formation of new particles. Comparison of modelled and measured H<sub>2</sub>SO<sub>4</sub> concentrations showed a satisfactory agreement for this compound (Boy et al., 2006). Further, the results indicate that the model is able to predict the on- and offset of new particle formation as well as the total aerosol number concentrations that were in good agreement with the observations by using the kinetic nucleation mechanism presented in Sihto et al. (2006).

The simulations showed that at a certain transitional particle diameter (2-9 nm), organic molecules can begin to contribute significantly to the growth rate compared to sulphuric acid (Figure 1). At even larger particle sizes, organic molecules can dominate the growth rate on days with significant monoterpene concentrations. Similar results were published by Wehner and co-authors (Wehner et al., 2005) recently. They calculated that new particles needed to reach a size range between about 7 – 20 nm before it becomes apparent that organic vapours can contribute significantly to the growth rate. However, their observations were from a more urban site in Germany with up to twice as much H<sub>2</sub>SO<sub>4</sub>.

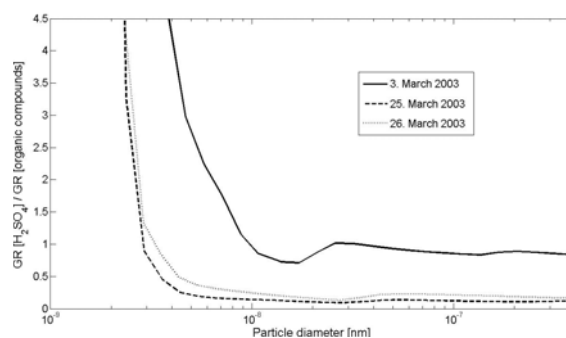


Figure 1: Ratio of the growth rate by sulphuric acid to that of organic vapours on 3 event days.

The intraday vertical evolution of new formed aerosols in the size range 3-6 nm calculated for an event day in March 2003 agreed well with measured vertical profiles reported by O'Dowd et al. (2005). The measurements and the model simulations showed high number concentrations of particles from about 100 m (lowest flight height) up to 500 m and a decrease above.

The contribution of particles below 10 nm inside the mixed layer produced by ion-induced nucleation over the boreal forest in Northern Europe seems to play a minor role compared to the total observed number concentration.

Boy, M., Hellmuth, O., Korhonen, H., Nillson, D., ReVelle, D., Turnipseed, A., Arnold, F. and Kulmala, M. (2006), *Atmos. Chem. Phys.*, 6, 4499–4517.

O'Dowd, C. D., Yoon, Y. J., Junkermann, W., Aalto, P. P. and Lihavainen, H. (2005), *Report Series in Aerosol Science*, Nr. 76, ISBN 952-5027-63-5, p. 162-173.

Sihto, S.-L., Kulmala, M., Kerminen, V.-M., Dal Maso, M., Petäjä, Riipinen, T., I., Korhonen, H., Arnold, F., Janson, R., Boy, M., Laaksonen, A. and Lehtinen, K. E. J (2006), *Atmos. Chem. Phys. Discuss.*, 6, 4079-4091.

Wehner, B., Petaja, T., Boy, M., Engler, C., Birmili, W., Tuch, T., Wiedensohler, A. and Kulmala, M. (2005), *Geo. Res. Lett.*, Vol. 32, L17810, doi:10.1029/2005GL023827.

## Simulation of aerosol dynamics in forest fires

A.E. Aloyan and V.O. Arutyunyan

Institute of Numerical Mathematics, Russian Academy of Sciences, Gubkin str. 8, 119333, Moscow, Russia

Keywords: aerosol dynamics, aerosol modeling, atmospheric aerosols, combustion particles, nucleation.

A complex mathematical model for aerosol dynamics has been developed for forest fire conditions. The model incorporates atmospheric hydrodynamics (accounting for atmospheric compressibility), condensation / evaporation, coagulation, gas- and aqueous-phase chemistry. More details of the model can be found in (Aloyan & Piskunov, 2004). The aerosol dynamics is based on the equation

$$\begin{aligned} & \frac{\partial \varphi_g}{\partial t} + \text{grad} \varphi_g + \frac{\partial (v_g \varphi_g)}{\partial g} \\ & = F + J(t)(g - g(t)) \\ & + \frac{1}{2} \int_0^g K(g, g_1) \varphi_{g-g_1} \varphi_{g_1} dg_1 \\ & - \varphi_g \int_0^\infty K(g, g_1) \varphi_{g_1} dg_1 + \frac{\partial k_{ij}}{\partial x_i} \frac{\partial \varphi_g}{\partial x_i}, \end{aligned}$$

where  $\varphi_g$  is the concentration of particles with masses between  $g$  and  $g + dg$ .  $K(x, y)$  is the coagulation kernel,  $J(t)$  is the nucleation rate,  $v_g$  is the rate of condensational growth.

The numerical calculations were performed for the Irkutsk area (East Siberia, Russia) which is known to suffer from forest fires. The dimensions of the computational grid are 60 x 60 x 20. The problem of condensation and coagulation includes 30 aerosol size bins starting from 0.05 up to 5  $\mu\text{m}$ . The surface heat flux was given to grow up to 50  $\text{kWt/m}^2$ , with a following no-flame combustion (smoldering). The total mass of combustible forest materials was assumed to be 3  $\text{kt/m}^2$ , which is in line with experimental data.

A detailed sensitivity analysis of the particle-size distribution to the capacity of these materials was performed. The results of numerical experiments indicate that the particle number concentration decreases with height much quicker than the mass concentration. This effect can be explained by an analysis of the particle-size distribution at different heights. It was found that near the source particles with doubled mass (0.65  $\mu\text{m}$ ) are generated rather quickly and then coagulate with only fine aerosol particles, thus decreasing the concentration of primary particles.

The variation of aerosol particles was investigated for nucleation, accumulation, and coarse modes as function of ageing. With going far from the source, the concentration of nucleation-mode particles with a radius of between 0.1 and 0.8  $\mu\text{m}$  quickly decreases, which is well consistent with the measurement data given in Radke *et al.* (1995). The decrease in the particle volume the nucleation mode occurs due to fast coagulation in the accumulation mode. Figure 1 shows the variation in the number concentration of coarse particles with a radius of 2  $\mu\text{m}$ . It can be seen that the concentration is much higher than in the fire point area.

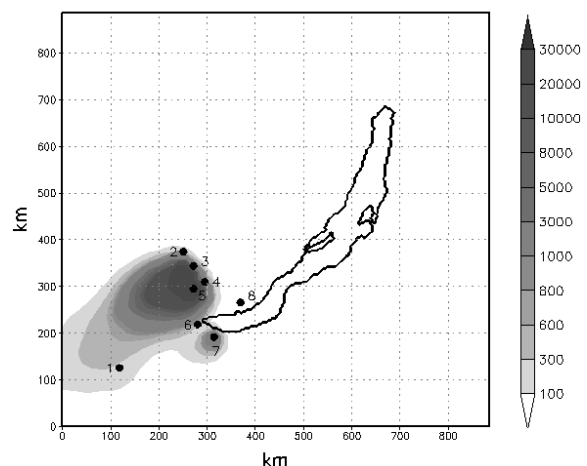


Figure 1. Concentration of aerosol particles ( $\text{m}^{-3}$ ) with a radius of 2  $\mu\text{m}$  in Lake Baikal region.

This work was supported by the RFBR, under projects 06-05-65184 and 06-05-66861.

Aloyan, A. E., & Piskunov, V. N. (2005). *Izv. RAN: Fizika atmosfery i okeana*, 41(3), 328–340.

Radke, L. F., Hegg, A. S., Hobbs, P. V., & Penker, J. E. (1995). *Atmospheric Research*, 38, 315–332.

## Modeling the urban- and regional-scale dynamics of gaseous pollutants and aerosols

V.O. Arutyunyan<sup>1</sup>, A.E. Aloyan<sup>1</sup>, and A. N. Yermakov<sup>2</sup>

<sup>1</sup>Institute of Numerical Mathematics, Russian Academy of Sciences, Gubkin str. 8, 119333, Moscow, Russia

<sup>2</sup>Institute of Energy Problems of Chemical Physics, Russian Academy of Sciences, Leninski pr. 38/2, 119334, Moscow, Russia

Keywords: aerosol chemistry, aerosol dynamics, aerosol modeling, atmospheric aerosols, ions.

A new 3D numerical model has been developed for gas and aerosol dynamics in the regional and urban scales. The main modules of the model are atmospheric hydrodynamics, gas- and aqueous-phase chemistry, binary/ternary nucleation, condensation/evaporation, and coagulation (Aloyan & Piskunov, 2004).

The chemical model includes some 300 chemical reactions, and 44 gas-phase and 51 aqueous-phase chemical species. The kinetic models of condensation and coagulation use a non-equilibrium particle-size distribution function. The number of particle size bins in the model is 30, ranging from 0.05 to 1.5  $\mu\text{m}$ . Using this model, numerical experiments were performed for condensation both on natural aerosol particles (Junge distribution) and on particles originated from binary/ternary nucleation.

The urban-scale calculations were performed for the industrial towns of Irkutsk (Russia) and Antwerp (Belgium). Along with photochemical transformation, the emphasis was on the possible formation of nucleation mode particles from precursor gases through the mechanisms of binary and ternary nucleation. The numerical calculations show that enhanced  $\text{SO}_2$  emission levels in these towns contribute to the formation of nucleation-mode particles, with its rate being essentially dependant on seasons of the year. Then, the nucleation rate is used in the right-hand side of the kinetic equation of condensation and coagulation to solve the problem of aerosol dynamics.

The regional-scale numerical calculations were performed for the Lake Baikal area in Russia, using emission data of local industrial sources. The emphasis was on the variability of atmospheric gaseous pollutants and formation of aerosol particles having regard to their ion composition (Yermakov *et al.*, 2007).

The calculated and measured data were compared for time periods when ammonium-sulfate particles had been registered. The numerical results show a good agreement between the calculated and measured data for the concentration of free protons in these particles. The oxidized  $\text{SO}_2$  is largely (around 98 %) stabilized in the atmosphere in the form of sulfate ions, while only some 2 % is found as gaseous molecules of  $\text{H}_2\text{SO}_4$ .

An additional thermodynamic estimation of the ion composition of aerosols indicated that the specific volume of liquid water in equilibrium particles (gas-particle equilibrium) was  $7 \times 10^{-10} \text{ l/m}^3$ . It follows from here that the acidity of ammonium-sulfate particles was very large (15 mole/l), which justifies the assumption that the acidity of aerosol particles collected during this episode is controlled exceptionally by the acidity of ammonium-sulfate particles. The agreement between kinetic calculations and observations is quite satisfactory for the mass concentration of nitrate ions (0.37 and  $0.25 \mu\text{g/m}^3$ , respectively).

Some discrepancy between calculated and observed data can be explained by the fact that there were no data of  $\text{NH}_3$  natural emissions available at the Mondy background station and that remote sources of  $\text{SO}_2$  outside the Baikal region may exist.

This work was supported by the RFBR, under projects 06-05-65184 and 06-05-66861.

Aloyan, A. E., & Piskunov, V. N. (2005). *Izv. RAN: Fizika atmosfery i okeana*, 41(3), 328–340.

A. N. Yermakov, A. E. Aloyan, T. V. Khodzer, I. P. Golobokova, and V. O. Arutyunyan (2007). *Izv. RAN: Fizika atmosfery i okeana*, 43(2), 20–35.

## Influence of car induced turbulence on PM dispersion along urban traffic paths

J. Pospisil, M. Jicha

Faculty of Mechanical Engineering, Brno University of Technology, Technicka 2, 61669, Brno, Czech Republic

Keywords: PM, modeling, traffic, urban areas

This paper presents the results of a case study utilizing small scale numerical modeling for expression of the relation between the moving cars induced kinetic energy of turbulence and the PM10 concentration along the street canyon in the central part of the city of Brno.

The influence of moving cars plays a significant roll in PM dispersion processes along traffic paths. Moving vehicles enhance both micro- and large-scale mixing processes in the environment by inducing additional turbulence and by entraining masses of air in the direction of vehicle movement.

The CFD code StarCD was used as a convenient modeling tool. A model based on Eulerian - Lagrangian approach to moving objects (Jicha et al., 2000) has been used for inclusion of traffic dynamic. The governing equations for the continuous phase were solved using the finite volume procedure. The set of equations for the conservation of mass and momentum was solved for unsteady incompressible turbulent flow. The equation for a general variable  $\phi$  has the form

$$\frac{\partial(\rho\phi)}{\partial t} + \frac{\partial}{\partial x_i}(\rho u_i \phi) = \frac{\partial}{\partial x_i} \left( \Gamma \frac{\partial \phi}{\partial x_i} \right) + S_\phi \quad (1)$$

Variable  $\phi$  stands for velocity components and  $S_\phi$  represents additional source terms. The standard  $k-\varepsilon$  model of turbulence was used.

As it is known, moving objects induce a strong kinetic energy of turbulence that was added as an additional source to the  $k$  equation. From different studies e.g. Eskridge and Hunt (1979) and Sedefian et al. (1981) it follows that turbulence is induced mainly in the wake behind the vehicle. Therefore the additional source of kinetic energy of turbulence  $S_k$  was assigned in the control volumes passed by moving cars.

$$S_k = C_c (U_{car} - U_\infty)^2 \dot{Q}_{car} \quad (2)$$

Where  $C_c$  is model constant (Sedefian et al., 1981) and  $\dot{Q}_{car}$  is traffic intensity.

The studied street canyon is located at the centre of the city of Brno (population 350000). Five-story buildings (20 m high) form both sides of the street canyon. Width of the street is 22 m. Two-way traffic in total four traffic lanes is present in the street. The day highest traffic rate is 1530 cars/hour.

The set of calculations was carried out on the numerical model of the studied area. During the calculations, the traffic rate was changed step-by-step from the day highest value to the situation without

traffic. All other parameters remained unchanged. Predicted PM10 concentrations were evaluated in 9 receptor points located in the studied street and perpendicular side-streets.

The figure 1 shows graphical expression of obtained results. Higher traffic rate causes higher PM10 concentrations in all considered receptor points. But, the relation between traffic rate and PM10 concentration is not strictly linear. Increasing traffic causes a more intensive transport of particulate matter from the line source, located in the middle of the studied street canyon, to the positions of the receptor points. This behavior is influenced by the actual value of kinetic energy of turbulence in the vicinity of the line source. Higher traffic rate causes higher value of kinetic energy of turbulence above a road surface. Intensive mixing of air intensifies transport of PM in the perpendicular direction to the street. That results in the presented progressive increase of PM concentrations with increasing traffic.

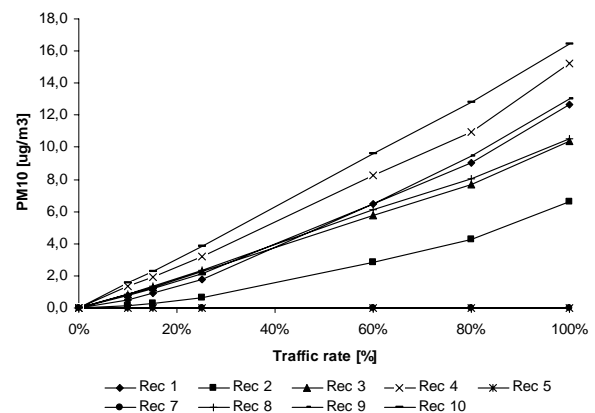


Figure 1. Relation between traffic rate and PM10 concentrations (1530 cars/hour = 100%)

The Czech Ministry of Transport financially supported this work under the grant 1F54H/098/520.

Eskridge, R. E.; Hunt, J. C. R. (1979) *Highway modelling. Part I* J. of Applied Meteorology, vol.18, pp. 387-392.

Sedefian, L.; Rao, S. T.; Czapski, U. (1981) *Effects of traffic-generated turbulence on near-field dispersion*. Atmos. Environ., vol. 15, pp. 527-535.

Jicha M., Katolicky J., Pospisil J. (2000), *Dispersion of pollutants in street canyon under traffic induced flow and turbulence*, J. Environmental Monitoring and Assessment, vol. 65, 343-35.

## An improved model for heterogeneous nucleation

A.Määttänen<sup>1,2</sup>, H. Vehkamäki<sup>1</sup>, A.Lauri<sup>1</sup>, I.Napari<sup>1</sup>, P.E.Wagner<sup>3</sup> and M.Kulmala<sup>1</sup>

<sup>1</sup>Department of Physical Sciences, University of Helsinki, P.O.Box 64, FI-00014, Helsinki, Finland

<sup>2</sup>Finnish Meteorological Institute, Space Research, P.O.Box 503, FI-00101, Helsinki, Finland

<sup>3</sup>Institut für Experimentalphysik, Universität Wien, Boltzmannngasse 5, A-1090, Wien, Austria

Keywords: Aerosol dynamics, modelling, nucleation, particle formation.

We have developed a model of two-component steady-state heterogeneous nucleation based on a homogeneous binary nucleation model. The heterogeneous nucleation part includes the exact calculation of the kinetic prefactor with the correct heterogeneous Zeldovich factor for a two-component system. The model has been tested with a water-*n*-propanol system and compared with measurements and a previously developed model.

We tested the kinetically correct model described in Noppel *et al.* (2002) with added heterogeneity using the surface diffusion approach (hereafter Model 1) with water-*n*-propanol system. We compared the results with experiments and a previous model that includes an approximative Zeldovich factor and uses the direct vapour deposition approach in the heterogeneous growth matrix terms. The second model (Kulmala *et al.*, 2001) is based on the approach of Kulmala and Laaksonen (1990) and Lazaridis *et al.* (1991). Results of the Kulmala *et al.* (2001) model (hereafter Model 2) have proved to compare reasonably well with the measurements (Wagner *et al.*, 2003).

For the comparison we ensured that both models have the same method for the calculation of the exponential part of the nucleation rate, since the comparison was to be made only between the calculation of the kinetic prefactor in the models. The largest difference in the calculation is originated in the difference between the theoretical approaches in the cluster growth model.

The other main issue is the Zeldovich factor, which is calculated very differently in the two models. Model 1 calculates the kinetic prefactor (including the Zeldovich factor) in a kinetically correct way, whereas Model 2 uses an approximation of a virtual monomer, which could be described as an "average" monomer colliding with the cluster, the volume of which is calculated as the sum of molecular volumes weighed with the respective mole fractions. The difference between the two Zeldovich factors can be several orders of magnitude. This is, however, not expected to have a significant effect on the nucleation probabilities.

We compared the models with an experimental dataset (Wagner *et al.*, 2003) and to each other. We chose three experiments conducted for oxidized Ag particles of 8 nm radii (non-monodisperse) with constant propanol liquid mass fractions (0.446, 0.763 and 0.926). We used a monodisperse condensation nucleus distribution. The thermodynamic and other

data used for the Model 2 can be found from Kulmala *et al.* (2001). The data for Model 1 is partly extracted from Model 2 (activities, surface tensions, etc.), and the values required for the surface diffusion method (energies for desorption and surface diffusion) have been mostly derived from the Model 2 values.

Model 1, the new, kinetically correct steady-state binary heterogeneous nucleation model gave surprisingly similar results compared to the Model 2 containing the approximative Zeldovich factor.

We gratefully acknowledge funding from the Academy of Finland and the Kordelin foundation.

Kulmala, M., and Laaksonen, A. (1990). Binary nucleation of water-sulfuric acid system: Comparison of classical theories with different H<sub>2</sub>SO<sub>4</sub> saturation vapor pressures. *J. Chem. Phys.*, 93, 696-701.

Kulmala, M., Lauri, A., Vehkamäki, H., Laaksonen, A., Petersen, D., and Wagner, P. E. (2001). Strange predictions by binary heterogeneous nucleation theory compared with a quantitative experiment. *J. Phys. Chem. B.*, 105, 11800-11808.

Lazaridis, M., Kulmala, M., and Laaksonen, A. (1991). Binary heterogeneous nucleation of a water-sulphuric acid system: the effect of hydrate interaction. *J. Aerosol Sci.*, 22, 823-830.

Noppel, M., Vehkamäki, H., and Kulmala, M. (2002). An improved model for hydrate formation in sulfuric-acid water nucleation. *J. Chem. Phys.*, 116, 218-228.

Pruppacher, H. R., and Klett, J. D. (1997). *Microphysics of Clouds and Precipitation*. Kluwer Academic.

Wagner, P. E., Kaller, D., Vrtala, A., Lauri, A., Kulmala, M., and Laaksonen, A. (2003). Nucleation probability in binary heterogeneous nucleation of water-*n*-propanol vapor mixtures on insoluble and soluble nanoparticles. *Phys. Rev. E*, 67, 021605.

## Two-component heterogeneous nucleation in the Martian atmosphere

A.Määttänen<sup>1,2</sup>, H. Vehkamäki<sup>1</sup>, A.Lauri<sup>1</sup>, I.Napari<sup>1</sup> and M.Kulmala<sup>1</sup>

<sup>1</sup>Department of Physical Sciences, University of Helsinki, P.O.Box 64, FI-00014, Helsinki, Finland

<sup>2</sup>Finnish Meteorological Institute, Space Research, P.O.Box 503, FI-00101, Helsinki, Finland

Keywords: Aerosol dynamics, modelling, nucleation, particle formation.

We have used a two-component nucleation model (another abstract Määttänen *et al.*) to model binary nucleation in the Martian atmosphere (Määttänen *et al.*, 2007).

The water - carbon dioxide system has not been modelled before. The Martian atmosphere is 95.3% carbon dioxide, and there is no liquid phase for the nucleating substances. Clouds are presumed to form from either water or CO<sub>2</sub> ice crystals, and this is the first study of binary nucleation on Mars. There is no thermodynamic data available for the ice mixture properties.

We calculated, as a first approximation, the thermodynamic data (surface energy, ice density) for the mixture assuming ideal mixing. For ideal mixture, the solid phase activities equal the mole fractions of the respective species. We tested the behavior of the system by using the activity coefficients of water - n-propanol mixture for the water - carbon dioxide mixture. The activities of the water - n-propanol system are thought to realistically mimic the behavior of the H<sub>2</sub>O - CO<sub>2</sub> system since both CO<sub>2</sub> and n-propanol are nonpolar molecules.

The nonisothermal coefficient (important in nucleation occurring in a near-pure substance) is calculated using the formulation of Feder *et al.* (1966) as was also done in Määttänen *et al.* (2005).

Our results show that the CO<sub>2</sub> concentration is not the limiting factor for the initiation of binary nucleation, but the water amount is. The results show that the onset of binary nucleation happens at slightly lower activities than the onset of unary nucleation of water. We looked at the numbers of molecules in the critical cluster in these cases, and noticed that the cluster is mainly composed of water molecules. In some cases with low amount of water vapor (1 ppm), the number of CO<sub>2</sub> molecules stays fairly large (tens of molecules) in a larger range of temperatures (about one degree), but for 300 ppm of water even in the first critical (binary) cluster the number of CO<sub>2</sub> molecules is only 2-3 and after that drops to less than one (which implies unary water nucleation). So theoretically at the onset of water nucleation on Mars it seems that binary nucleation might have a role in facilitating the process, but the number of CO<sub>2</sub> molecules in the critical clusters is so small, that particle formation process is nearly pure water nucleation. The nonisothermal coefficient was 0.02-0.03 for the range where the critical molecular numbers of both substances were greater than one. This is in the same range as was acquired for unary CO<sub>2</sub> nucleation in Määttänen *et al.* (2005).

According to our results we can presume that in the present Martian atmosphere ice clouds do form one component at a time, as described in our earlier paper (Määttänen *et al.*, 2005). and several other authors (e.g., Michelangeli *et al.*, 1993, Colaprete *et al.*, 1999, Colaprete & Toon 2002, Montmessin *et al.*, 2002). However, we can not completely rule out the possibility of binary nucleation of the CO<sub>2</sub> - H<sub>2</sub>O mixture, possibly at the very first stages of unary water nucleation. This result is naturally dependent on the assumptions made for the system (for example the ideal mixture assumption) and validating the results will have to wait until there are data or experiments for the real thermodynamic properties of the system.

We gratefully acknowledge funding from the Academy of Finland and the Kordelin foundation.

Colaprete, A., O.B. Toon, and J.A. Magalhaes (1999), Cloud formation under Mars Pathfinder conditions, *J. Geophys. Res.*, 104(E4), 9043-9054.

Colaprete, A., and O.B. Toon (2002), Carbon dioxide snow storms during the polar nights on Mars, *J. Geophys. Res.*, 107(E7), 5051, doi:10.1029/2001JE001758.

Feder, J., K.C. Russell, J. Lothe and G.M. Pound (1966), Homogeneous nucleation and growth of droplets in vapours. *Adv. Phys.*, 15, 111-178.

Michelangeli, D.V., O.B. Toon, R.M. Haberle and J.B. Pollack (1993), Numerical simulations of the formation and evolution of water ice clouds in the Martian atmosphere, *Icarus*, 100, 261-285.

Montmessin, F., P. Rannou and M. Cabane (2002), New insights into Martian dust distribution and water-ice cloud microphysics, *J. Geophys. Res.*, 107(E6), 5037, doi:10.1029/2001JE001520.

Määttänen, A., H. Vehkamäki, A. Lauri, S. Merikallio, J. Kauhanen, H. Savijärvi, and M. Kulmala (2005), Nucleation studies in the Martian atmosphere, *J. Geophys. Res.*, 110, E02,002.

Määttänen, A., H. Vehkamäki, A. Lauri, I. Napari, and M. Kulmala (2007), Two-component nucleation: A Martian test case. *Journal of Chemical Physics*, submitted.

## Evaporation and condensation of succinic acid and water: Model intercomparison

J. Voigtländer<sup>1</sup>, I. Riipinen<sup>2</sup>, M. Kulmala<sup>2</sup>, F. Stratmann<sup>1</sup>

<sup>1</sup>Leibniz Institute for Tropospheric Research, Leipzig, Germany

<sup>2</sup>Department of Physical Sciences, University of Helsinki, Finland

Keywords: condensation, evaporation, modelling, organics, succinic acid.

Organic compounds represent a significant fraction of all particulate matter in the atmosphere. A substantial fraction of the organic material is water soluble, e.g. dicarboxylic acids. Succinic acid (C<sub>4</sub>H<sub>6</sub>O<sub>4</sub>) is one of these dicarboxylic acids that are often found. Due to its atmospheric relevance, hygroscopic growth and CCN activation of succinic acid have been measured and theoretical modelled.

In this study we investigate the condensational growth and evaporation of droplets containing water and succinic acid by comparing to numerical model approaches. Both models simulate binary condensation and/or evaporation by combining basic mass and heat transfer theories in inert gas where no chemical reactions take place.

The first model is a numerical box model BCOND (Vesala, 1997), which allows an accurate thermodynamic description of the condensation/evaporation process. The model has been validated with experiments, and the model results are in a good agreement with observations, assuming that the thermophysical properties of the investigated compound are well-defined. Recently Riipinen et al. (2006) have used the model together with Tandem Differential Mobility Analyzer (TDMA) measurements obtain information about the thermodynamical properties succinic acid – water droplets.

The second model, called Fine Particle Model (FPM, Wilck, 2002), is an Eulerian model. It is fully integrated into the commercial three dimensional computational fluid dynamics (CFD) code FLUENT. The model is designed to describe coupled fluid flow and particle dynamical processes. In the FPM, condensation and evaporation are described by the simplified droplet growth law given by Barrett & Clement (Barrett & 1988). Therein, droplet temperature is included implicitly in linearized mass flux expressions, whereas in BCOND it is solved for separately during each time step. The FPM/FLUENT is applied to model experiments, which are performed on the Leipzig Aerosol Cloud Interaction Simulator (LACIS, Stratmann, 2004).

With the comparison of the models, the applicability of the FPM calculating hygroscopic growth and CCN activation of organic compounds can be validated.

For the model comparison, all relevant thermodynamical properties (temperature, system pressure, diffusion coefficients, activity models, densities, thermal conductivity, particle dry diameter,

parameterization of the surface tension, accommodation coefficients) were synchronized. Missing model descriptions, e.g. the UNIFAC Dortmund activity model, were implemented into the FPM.

The results for hygroscopic growth (at 293.15 K and 1000 hPa) of succinic acid particles with a dry diameter of 100 nm are shown in Fig. 1. The results produced by the compared models agree well. The simpler description of particle dynamics in the FPM/FLUENT model is therefore able to describe the particle growth and evaporation by succinic acid and water in a proper way.

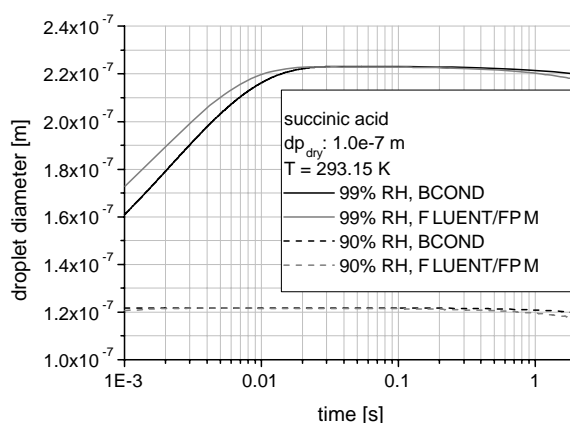


Figure 1. Comparison of the model results for succinic acid particles with 100 nm in diameter.

- Barrett, J.C. & Clement, C.F. (1988). *J. Aerosol Sci.*, 19(2), 223-242.
- Stratmann, F., Kiselev, A., Wurzler, S., Wendisch, M., Heintzenberg, J., Charlson, R.J., Diehl, K., Wex, H. & Schmidt, S. (2004). *J. Atmos. Oceanic Tech.*, 21, 876-887.
- Riipinen, I., Svenningsson, B., Bilde, M., Gaman, A., Lehtinen, K.E.J. & Kulmala, M. (2006). *Atm. Res.*, 82, 579-590.
- Wilck, M., Stratmann, F. & Whitby, E.R. (2002). in *Proc. Sixth Int. Aerosol Conf.*, Taipei, Taiwan, 1269-1270.
- Vesala, T., Kulmala, M., Rudolf, R., Vrtala, A. & Wagner, E. (1997). *J. Aerosol Sci.*, 28, 565-598.

## A numerical study of calm air sampling

Sarah J Dunnett<sup>1</sup>, Xianyun Wen<sup>2</sup>

<sup>1</sup>Department of Aeronautical and Automotive Engineering, Loughborough University, Loughborough, Leics., LE11 3TU, U.K.

<sup>2</sup>Environment, School of Earth and Environment, University of Leeds, Leeds LS2 9JT, U.K.

Keywords: aerosol sampling, numerical simulation

### INTRODUCTION

Aerosol samplers are widely used to determine the aerosol concentration in an environment. Due to many factors, such as the physical presence of the sampler and the action of withdrawing air through the sampler opening, the aerosol sample collected is not always a true representation of the aerosol concentration in the environment. Over the years much research has been carried out on understanding how samplers perform when operating under different conditions. Due to this work our knowledge of sampler behaviour for various situations is good, however one area in which our understanding is still not complete is sampling in calm air. This is when the only motion of the air is caused by the action of withdrawing air through the sampling inlet. It is of increasing importance as many airflows in modern workplaces are low, of order  $10^{-1}$  or less. Hence they can be approximated by the limiting calm air situation. In this work the study undertaken by Dunnett et al (2006) is extended to consider general expressions for the aspiration efficiency of a sampler operating under various conditions in calm air.

### METHOD AND RESULTS

Numerical models have been developed to determine the aspiration efficiency,  $A$ , of thin-walled samplers and blunt spherical samplers. This efficiency is defined as the ratio of the concentration of particles passing across the sampling inlet to the concentration in the undisturbed air away from the sampler. The numerical models have been validated using the experimental data available. Three different orientations of the samplers have been considered:

- i) inlet facing vertically upwards
- ii) inlet facing vertically downwards
- iii) inlet facing horizontally

Values of  $A$  have been determined numerically for all three orientations for various values of the operating parameters  $St_c$ ,  $R_c$   $B$ . Where  $St_c$  is the Stokes number,  $R_c$  the relative settling velocity, and  $B$  the sampler 'bluntness' defined as the ratio of the sampler body diameter to the sampling inlet diameter. For the thin-walled sampler  $B=1$ . Using the results obtained empirical formulae have been developed for  $A$  based upon physical reasoning.

As expected it was found that the effects of the sampler bluntness upon aspiration are negligible for orientation (i) but are of increasing importance as the inlet moves away from facing vertically upwards.

An example of some of the results obtained and the empirical formula developed are shown in figure 1 where the case of the sampler oriented with its inlet facing downwards, case ii), is considered.

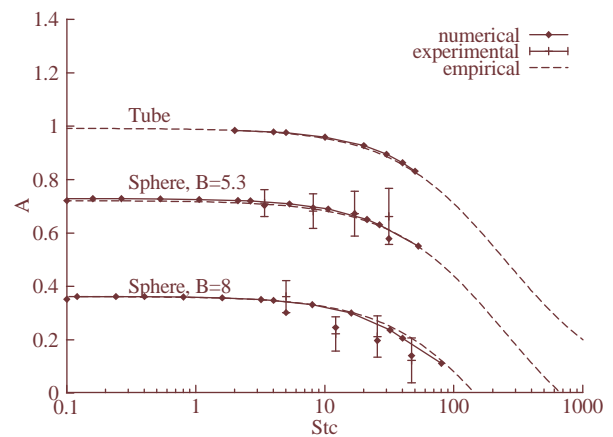


Figure 1.  $A$  as a function of  $St_c$  for case ii), showing the numerical, experimental and empirical formula.

In this case the empirical formula developed is given by

$$A = \frac{1 - R_c}{1 + (a * R_c + b) * St_c} - R_c (B^2 - 1)$$

$a$  and  $b$  are fitted coefficients.

In the work presented various situations are considered and a general formula for  $A$  developed.

### REFERENCES

Dunnett, S.J., Wen, X., Zaripov, S.K., Galeev, R.S. and Vanunina, M.V. (2006) *Aerosol Science and Technology*, 40, pp 490-502.

## Constructal view of dendritic growth of airborne particles

A. H. Reis<sup>1</sup>, A. F. Miguel<sup>1</sup> and A. Bejan<sup>2</sup>

<sup>1</sup>Department of Physics and Geophysics Centre of Evora, University of Évora, 7000-671 Évora, Portugal

<sup>2</sup>Department of Mech. Eng. and Materials Science, Duke University, Durham, NC 27708-0300, USA

Keywords: particle growth, shape, constructal law.

Agglomerates of aerosol particles often have dendritic shapes that can be observed experimentally or based on numerical simulations. Is dendritic shape the prevalent and natural form of particle agglomeration? If so, why do aggregates of particles exhibit this particular shape?

Here we address these issues in the framework provided by constructal theory (Bejan, 1996, 2000). The constructal law requires the architecture of the aggregate of particles to evolve in time in such a way that the global rate of accumulation of the particles is maximized. The generation of optimized architectures should bring the entire flow system (ambient + particles) to equilibrium in the fastest way. Among other phenomena, constructal theory was also applied to predicting atmospheric and oceanic circulation driven by heating from the sun (Reis and Bejan, 2006).

Electrical bonds may occur through interactions of various types (e.g. charge-charge, charge-dipole, dipole-dipole, etc.). However, charge-charge interactions cancel the existing surface charge, and only the charge-dipole interaction ensures a steady and continuing process of deposition, because a dipole-charge bond leaves the total charge amount invariant.

After having compared spherical to conical shaped agglomeration dynamics (Reis *et al*, 2006), and by invoking the constructal law we found that that the agglomerate first must grow as a sphere, and change to the conical shape at a critical

time  $t_c = \frac{9.9}{K} \left( \frac{\mu}{q} \right)^{3/2}$  because for  $t > t_c$  the conically

shaped agglomerate is more efficient as a particle collector than the spherically shaped

agglomerate.  $K = \frac{C_p \sigma c_c v_p}{6\pi^2 \epsilon_0 \eta d_p} (q\mu)^{1/2}$  is a constant

where  $C_p$  is the concentration of dipolar particles in the vicinity of the surface,  $\sigma$  is surface density of charge,  $c_c$  is the Cunningham correction factor,  $v_p$  is particle volume,  $\epsilon_0$  is electric permittivity of the air,  $\eta$  is dynamic viscosity,  $d_p$  is particle diameter,  $q$  is charge, and  $\mu$  is particle dipolar moment.

It is also interesting to compare the growth speeds of cone diameter ( $\dot{d}$ ) and cone tip ( $\dot{L}$ )

$\frac{\dot{d}}{\dot{L}} = \left( \frac{36}{K} \right)^{1/3} \left( \frac{\mu}{q} \right)^{1/2} t^{-1/3}$  which decreases as  $t^{-1/3}$ .

This means that at later stages the agglomerate grows as a needle, the geometry of which is given by

$d = \left( \frac{9}{\pi} \right)^{2/3} \left( \frac{\mu}{q} \right)^{1/3} L^{2/3}$  One interesting aspect of the

predicted geometry is that it depends only on the dipole moment  $\mu$ . This means that weakly dipolar molecules will agglomerate in a needle that is more slender than the needle formed by strongly dipolar molecules.

Another noteworthy aspect is that the critical time for switching from spherical to needle shaped growth depends only on the dipole strength. We calculated the critical diameter of the original sphere as  $D_{crit} \sim 6 \frac{\mu}{q} \sim 6a$  and predicted that a universal

behaviour of particle agglomeration must exist: when the sphere diameter reaches 6 particle diameters, the agglomerate (of  $(\pi/6) \cdot 6^3 \sim 113$  particles) must switch from spherical to needle-shaped growth as a preferential mode of particle agglomeration. This result agrees qualitatively with what is observed in nature. However, one needs precise measurements on particle growth to fully confirm the above predictions.

In summary, the constructal law enables us to predict important features of shape generation and architecture of particle agglomeration. In the very beginning the agglomerate grows as a sphere, because at short times this shape is more effective in collecting particles from the environment. At a critical time  $t_c$  the agglomerate switches to needle growth because for  $t > t_c$  this shape is more effective in collecting particles from the environment.

This work was supported by Foundation for Science and Technology (FCT) project POCTI/EME/59909/2004.

Bejan, A. (1997). *Advanced Engineering Thermodynamics*, 2nd ed., New York, U.S.: Wiley

Bejan, A. (2000). *Shape and Structure, from Engineering to Nature*. Cambridge, U.K.: Cambridge University Press.

Reis, A. H. & Bejan, A. (2006) *Int. J. Heat Mass Transfer* 49, 1957-1875

Reis, A. H., Miguel, A. F. & Bejan A. (2006). *J. Physics D*, 39, 2311-2318.

## Mass accommodation coefficient of water: Combined analysis of experimental data and computational fluid dynamics results

J. Voigtländer<sup>1</sup>, F. Stratmann<sup>1</sup>, D. Niedermeier<sup>1</sup>, H. Wex<sup>1</sup>

<sup>1</sup>Leibniz Institute for Tropospheric Research, Leipzig, Germany

Keywords: accommodation coefficient, mass accommodation, modelling

The mass accommodation coefficient  $\alpha_{\text{mass}}$  of water vapour into NaCl solutions has been studied at realistic lower atmospheric conditions (saturation ratio between 1.0 and 1.03,  $p = 1000$  hPa). For determination of  $\alpha_{\text{mass}}$ , a combination of experimental data and computational fluid dynamics (CFD) modelling has been applied. In contrast to previous studies (e.g. Winkler, 2006), we used a different experimental technique. Experiments were performed at the Leipzig Aerosol Cloud Interaction Simulator (LACIS, Stratmann, 2004), a laminar flow diffusion chamber for measurements of both, hygroscopic growth and cloud condensation nuclei (CCN) activation. Quasi-monodispersed sodium chloride particles with 54 nm and 108 nm have been used as condensation nuclei. Thereby, a shape factor of 1.08 was assumed. Measurements were performed at least three times for each measurement point and statistical tested using a Shapiro-Wilks-Test. The data are normal distributed with a significance level of 5 percent. Mean values and standard deviation have been calculated for each data point. The experimental uncertainty is given in terms of the standard deviation of the measurements.

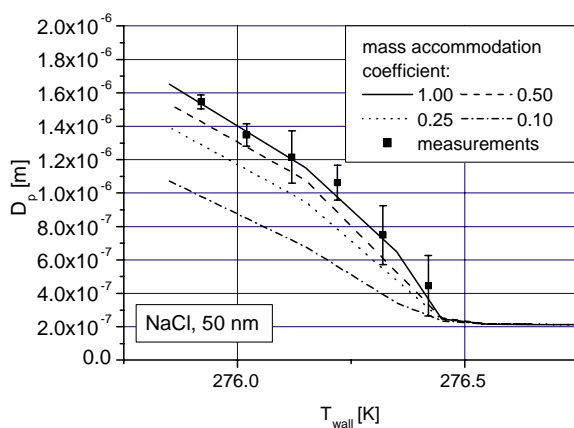


Figure 1. Comparison between measurements and calculation results. Inlet temperature was 293.15 K, dew point was 292.15 K, air pressure was 1000 hPa. Different values of  $T_{\text{wall}}$  correspond to different maximum saturation ratios inside the tube.

Experiments have been modelled using the Computational Fluid Dynamics Code (CFD-Code) FLUENT6 combined with a particle model (Fine

Particle Model (FPM), Wilck, 2002). Both, measurements results and calculations are shown in figure 1.

For determination of the mass accommodation coefficient  $\alpha_{\text{mass}}$ , measured droplet diameters were compared with calculated ones. The mass accommodation coefficient in the calculations was varied to achieve a quantitative comparison between model and measurement results. According to previous studies (Winkler, 2006), the thermal accommodation coefficient was set to unity in the calculations. With our experimental setup, we are not able to determine both coefficients simultaneously.

Our experimental data are consistent with a mass accommodation coefficient  $\alpha_{\text{mass}} > 0.30$  (figure 2), which agrees well with previous studies (e.g. Winkler, 2006). Therefore, we could confirm the results from previous studies using a different experimental technique.

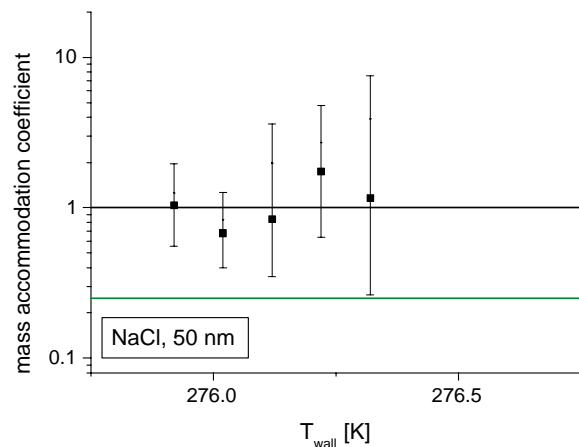


Figure 2. Measured mass accommodation coefficient.

Stratmann, F. & Kiselev, A. & Wurzler, S. & Wendisch, M. & Heintzenberg, J. & Charlson, R.J. & Diehl, K. & Wex, H. & Schmidt, S. (2004). *J. Atmos. Oceanic Tech.*, 21, 876-887.

Wilck, M. & Stratmann, F. & Whitby, E.R. (2002). in *Proc. Sixth Int. Aerosol Conf.*, Taipei, Taiwan, 1269-1270.

Winkler, P.M. & Vrtala, A. & Rudolf, R. & Wagner, P.E. & Riipinen, I. & Vesala, T. & Lehtinen, K.E.J. & Viisanen, Y. & Kulmala, M. (2006). *J. Geophys. Res.*, 111, D19202, doi:10.1029/2006JD007194.

## Aerosol model development for calculation of aerosol extinction in the coastal atmosphere surface layer

G.A. Kaloshin

V.E. Zuev Institute of Atmospheric Optics SB RAS,  
1, Academicheskii ave., 634055, Tomsk, Russia

Keywords: aerosol model, extinction, wind speed, fetch.

Extinction of radiation in the marine boundary layer is dominated by scattering and absorption due to atmospheric aerosol. This is important to optical retrievals from satellite, remote sensing at environmental monitoring, backscatter of light to space (including climate forcing), cloud properties etc. In unpolluted regions the greatest effects on near shore scattering extinction will be a result of sea-salt from breaking waves and variations in relative humidity. The role of breaking waves appears to be modulated by wind, tide, swell, wave spectra and coastal conditions. These influences will be superimposed upon aerosol generated by open ocean sea-salt aerosol that varies with wind speed.

The focus of our study is the extinction and optical effects due to aerosol in a specific coastal region. This involves linking coastal physical properties to oceanic and meteorological parameters in order to develop predictive algorithms that describe 3-D aerosol structure and variability.

The aerosol microphysical model of the marine and coastal atmosphere surface layer is considered. The model is made on the basis of the long-term experimental data received at researches of aerosol sizes distribution function ( $dN/dr$ ) in the band particles sizes in 0.01 - 100  $\mu\text{k}$ . The model is developed by present time for the band of heights is 0 - 25 m. Bands of wind speed is 3 - 18 km/s, sizes fetch is up to 120 km, RH = 40 - 98 %.  $dN/dr$  of the model is characterized by the four modified lognormal functions with modal radiuses, equal  $r_1 = 0,03$ ;  $r_2 = 0,24$ ;  $r_3 = 2$ ;  $r_4 = 10 \mu\text{k}$  (Piazzola, Kaloshin, 2005, 2006).

The model distinctive feature is parameterization of amplitude and width of the modes as functions of fetch and wind speed. In the paper the  $dN/dr$  behavior depending at change meteorological parameters, heights above sea level, fetch (X), wind speed (U) and RH is show. The received results are compared to available microphysical models NAN and ANAM.

On the basis of the developed model with usage of Mie theory for spheres the description of the last version of developed code MaexPro 5.0 (Marine Aerosol Extinction Profiles) for spectral profiles of aerosol extinction coefficients  $\alpha(\lambda)$  calculations in the wavelength band, equal  $\lambda = 0.2 - 12 \mu\text{m}$ , with step  $\Delta\lambda = 0.0001 \mu\text{m}$  is presented.

In Fig. 1 the composite window "extinction spectra" of the code MaexPro 5.0 is submitted on

which aerosol extinction spectra for chosen input meteorological parameters are resulted. Here with use of a service command "the switch OverPlot" aerosol extinction spectra  $\alpha(\lambda)$  calculated on a basis  $dN/dr$  are resulted which can be received with the help of aerosol counter AZ-5 with a range of aerosol particles measurement on radius  $\Delta r = 0.4 - 10$  microns and dust counter OMPN-10.0 (OPTEK Spb), carrying out the control of fractions in standard PM 10, PM 2.5 and PM 1. Fig. 1 shows that for three spectra of the aerosol sizes in wavelength band  $\Delta\lambda = 2 - 12 \mu\text{m}$   $\alpha(\lambda)$  differ approximately twice and in wavelength band  $\Delta\lambda = 0.2 - 2 \mu\text{m}$  of distinction in values  $\alpha(\lambda)$  reach 10 and more.

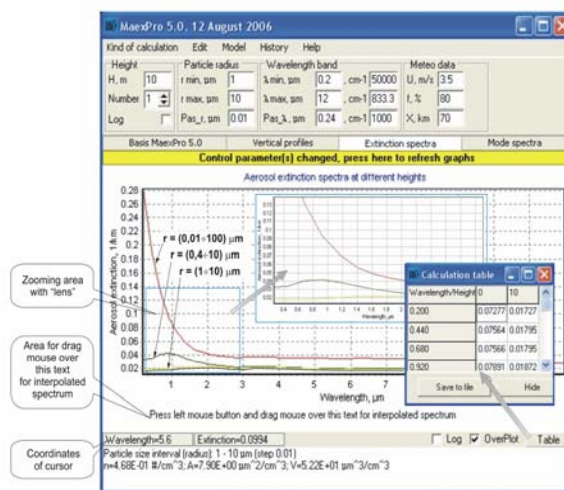


Figure 1. Composite window "Extinction spectra" including service commands

Also  $\alpha(\lambda)$  profiles for various wind modes (combinations X and U) calculated by MaexPro 5.0 code are given. Results of  $\alpha(\lambda)$  profiles calculations are presented at change RH = 40 - 98 % and heights H = 0 - 25 m. The calculated spectrums of  $\alpha(\lambda)$  profiles are compared with experimental data of  $\alpha(\lambda)$  received by a transmission method in various geographical areas.

J. Piazzola, G. Kaloshin. Performance evaluation of the coastal aerosol extinction code "MEDEX" with data from the Black Sea, J. of Aerosol Science. 36(3), pp. 341 - 359(2005).

G. Kaloshin, J. Piazzola. The Coastal Aerosol Microphysical Model, Proc. of the 23<sup>rd</sup> International Laser Radar Conf., Nara, Japan, pp. 423-426(2006).

## Estimating cloud droplet number concentration with particle number-to-volume concentration ratio

N. Kivekäs, V.-M. Kerminen, T. Anttila, H. Korhonen, M. Komppula and H. Lihavainen

Finnish Meteorological Institute, PO box 503, Helsinki, Finland

Keywords: Aerosol cloud interaction, Modelling, Aerosol size distribution.

In atmospheric aerosol systems, the number of particles >70-120 nm in diameter is related closely to the number of particles able to act as cloud condensation nuclei (CCN). Many large-scale atmospheric models, however, have the particle mass or volume concentration as the only prognostic variable.

The aim of this study is to investigate how accurate the estimation of cloud droplet number concentration (CDNC) would be if an empirical relation between the number concentration of CCN-size particles and particle volume (or mass) concentration was available. The relation used here is

$$R(d_c) = \frac{N(d > d_c)}{V_{tot}}, \quad (1)$$

where  $N(d > d_c)$  is the number concentration of submicron particles with dry diameter larger than a cut-off diameter  $d_c$  and  $V_{tot}$  is the total volume concentration of all submicron particles (Kivekäs *et al.*, 2007).

With an adiabatic air parcel model (Korhonen *et al.*, 2005, Anttila *et al.*, 2002) we simulated the activation of particles to cloud droplets in rising air. We varied the particle number size distribution parameters, the soluble fraction of particle mass ( $\varepsilon$ ) and the updraft velocity of the air parcel ( $v_{up}$ ). Then we fitted the numerical parameters to make the parameterization fit the simulated values as well as possible. The resulting formula was

$$CDNC = \left( a_1 \times \frac{R(0.1)}{d_c} \right) \times V_{tot} - a_2, \quad (2)$$

where

$$d_c = (b_1 \times \ln V_{tot} + b_2 \times \ln R(0.1) + b_3) \times \varepsilon^{b_4} \times v_{up}^{b_5}. \quad (3)$$

In the formulas above the numerical constants are  $a_1=0.10$ ,  $a_2=6\text{cm}^{-3}$ ,  $b_1=0.014$ ,  $b_2=0.008$ ,  $b_3=0.016$ ,  $b_4=-0.19$  and  $b_5=-0.32$ . The units are  $\text{cm}^{-3}$  for CDNC,  $\mu\text{m}^{-3}$  for  $R(d_c)$  and  $R(0.1)$ ,  $\mu\text{m}$  for  $d_c$ ,  $\mu\text{m}^3/\text{cm}^3$  for  $V_{tot}$  and m/s for  $v_{up}$ .  $\varepsilon$  is dimensionless.  $R(0.1)$  in the formula stands for  $R$  with  $d_c=0.1\mu\text{m}$ .

The parameterization was tested against measured cloud droplet activation data from Pallas GAW station in northern Finland (Komppula *et al.*, 2005). There were 33 clouds where particle activation was measured during the years 2000-2002. The soluble fraction of the particle mass was estimated to be 50% based on campaign

measurements at the same site during falls 2004 and 2005. There was no updraft velocity data available, so we decided to set  $v_{up}$  equal to 0.43m/s for all the cloud events.

The parameterized vs measured values of cloud droplet number concentration are shown in figure 1. The correlation coefficient between those two data sets was 0.76 and the largest offsets produced by the parameterization were within 50% of the measured value.

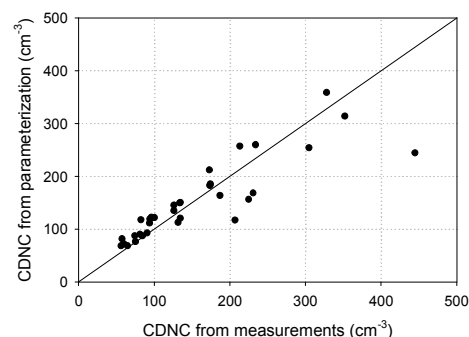


Figure 1. The parameterized vs measured cloud droplet number concentrations at Pallas during 33 cloud events.

The concept of parameterizing cloud droplet number concentrations (CDNC) with number-to-volume concentration ratios ( $R(d_c)$ ) works in Pallas, which is a station representing continental background air. If  $R(0.1)$  is known or can be parameterized, this kind of a parameterization would be a computationally efficient way to estimate the aerosol impact on cloud formation in large scale models. This demonstrates the benefit achievable from investigating parameterizations for  $R(0.1)$  or for some other  $R(d_c)$ .

- Anttila, T. and Kerminen, V.-M. (2002). *J. Geophys. Res.*, 107(D22), 4662, doi:10.1029/2001JD001482.
- Kivekäs N., Kerminen V.-M., Engler C., Lihavainen H., Komppula M., Viisanen Y. and Kulmala M. (2007), *J. Geophys. Res.*, accepted for publication
- Komppula M., Lihavainen H., Hatakka J., Aalto P.P., Kulmala M., and Viisanen Y. (2003), *J. Geophys. Res.*, 108(D9), 4295, doi:10.1029/2002JD002939.
- Korhonen, H., Kerminen, V.-M., Lehtinen, K. E. J. and Kulmala, M. (2005), *Atmospheric Chemistry and Physics*, 5, 2561- 2570.

## Deposition of submicron aerosol on spruce needles; wind tunnel measurements

K. Lamprechtová, J. Hovorka

Institute for Environmental Studies, Charles University in Prague, Benátská 2,  
128 01, Prague 2, Czech Republic

Keywords: aerosol-surface interaction, deposition, air pollution

Atmospheric aerosol deposition onto a plant surface is an efficient mechanism of its removal from the atmosphere. Rate of aerosol deposition strongly depends on thickness of laminar sublayer covering plant surface. The layer thickness is altered by vegetal surface morphology (Erisman, 2003) and by deposited aerosol. Additionally, deposited aerosol may increase stomatal conductance (Burkhardt, 2001), which lead to an unwanted increase of water transpiration during water stress periods. Conifers are periodically subjected to water stress during winter, when water supply is blocked due to frozen soil, and increased transpiration may affect conifer winter survival. To study an aerosol deposition under controlled conditions onto leaves of conifers, needles, we performed with needles series of measurements of aerosol deposition in a closed-circulation wind tunnel.

The tunnel construction (Volume-0,36 m<sup>3</sup>, Surface-3,73 m<sup>2</sup>, S/V=10.4) allows precise regulation of wind speed in the range of 0.5-6 ms<sup>-1</sup>. Monomodal aerosol (CMD, 0.69 μm) from aerosol generator (AGK 2000, Palas) was introduced into the tunnel and its disappearance measured by Aerodynamic Particle Sizer (APS-3321, TSI) within the size range of 0.524-10 μm. Spruce twigs with needles of the same age were fixed on the ceiling and bottom in 8 lines in the experimental section (0.71 m length, cross-section 0.18x0.18 m).

The timing of the measurements was as follows: aerosol injection into the tunnel for approx 1.5 min (total N<sub>max</sub><10<sup>4</sup> cm<sup>-3</sup>), aerosol plateout measurements for 90 minutes (6 s integrations were recorded), waiting period for 120 minutes of circulation under higher wind speed to lower aerosol concentration (total N<sub>0</sub><5 cm<sup>-3</sup>). Then the next measurements could start.

To evaluate recorded number size distributions, basic model of the aerosol deposition was applied (Okuyama, 1986). Bearing in mind complexity of turbulent deposition (Beneš, 1996) we suppose the deposition rate coefficients β under constant S/V changes due to the laminar sublayer modification. It was shown by experiments with fluorescein (Belot, 1994), that changes in epicuticular waxes covering plant surface, though the dimension of tubular wax structure is near order of magnitude smaller than the sublayer thickness, may strongly influence rate of aerosol deposition.

The β deposition rate constants of aerosol to needles calculated from consecutive measurements were usually in the range of 0.5-5 10<sup>-4</sup> (Fig.1) and are very accurate (RSTD <1.2%). Such accuracy allows detailed study of changes of the β caused by changes of laminar sublayer altered by needle age, epicuticular wax weathering and deposited aerosol.

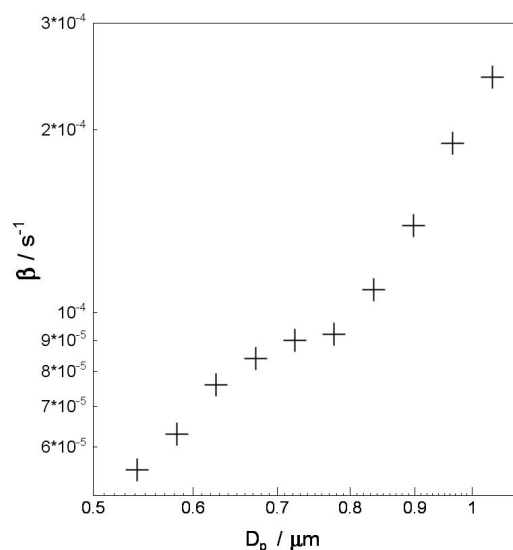


Figure 1. Deposition rate constant β of submicron particles to spruce twigs of two vegetative year old needles under wind speed of 1.1 ms<sup>-1</sup>

Financial support of the study by the Institute for Environmental Studies, Faculty of Science, Charles University in Prague is greatly acknowledged.

Belot, Y., Camus, H., Gauthier, D., Caput, C. (1994), *Sci.Total Environ.*, 157, 1-6

Beneš, M., Holub, R.F. (1996) *Envir. Int.*, 22, S883-S889

Burkhardt, J., Kaiser, H., Kappen, L., Goldbach, H.E. (2001). *Basic Appl.Ecol.*, 2, 351-364.

Erisman, J.W., Draaijers, G. (2003). *Environ. Pollut.*, 124, 379-388.

Okuyama, K., Kousaka, Y., Yamamoto, S., and Hosokawa, T. (1986) *J.Colloid.Interface Sci.*, 110, 214-223

## Influence of SO<sub>2</sub> on nucleation, growth rates and yield of secondary organic aerosols

A. Metzger<sup>1</sup>, B. Verheggen<sup>2</sup>, J. Duplissy<sup>1</sup>, J. Dommen<sup>1</sup>, A.S.H. Prevot<sup>1</sup>, U. Baltensperger<sup>1</sup>

<sup>1</sup>Laboratory of Atmospheric Chemistry, Paul Scherrer Institute, 5232 Villigen, Switzerland

<sup>2</sup>Institute for Atmospheric and Climate Sciences, ETH, 8092 Zurich, Switzerland

Keywords: nucleation, yield, secondary organic aerosols

Binary nucleation of sulphuric acid and water was observed to occur in laboratory experiments at atmospherically relevant concentrations (Berndt et al.; 2005). In addition, laboratory experiments show that the nucleation of sulphuric acid is considerably enhanced in the presence of organic acids due to the formation of a stable aromatic acid-sulphuric acid complex, which reduces the nucleation barrier (Zhang et al.; 2004). Several laboratory studies have examined the role of acidic aerosols in enhancing the uptake of carbonyl compounds through acid catalyzed reactions (Jang et al.; 2003) and the influence on the SOA yield (Kleindienst et al.; 2006).

A laboratory study was carried out to investigate the secondary organic aerosol formation of 1,3,5-trimethylbenzene (TMB) in the presence of SO<sub>2</sub>. Several experiments were carried out using SO<sub>2</sub> concentrations between 0.2 and 20 ppb for TMB concentrations of 150, 300, 600 and 1200 ppb, while keeping all the other parameters constant. Aerosol size distributions were measured using a twin SMPS system. The first is a nano SMPS composed of a short DMA column and a TSI UWPCPC, while the second one consisted of a long DMA column and a TSI 3022CPC. This combination of instruments provided measurements of the size distributions over the size range from 4 to 700 nm diameter. VOC concentrations were measured using a Proton Transfer Reaction-Mass Spectrometer (PTRMS) while organic acids and SO<sub>2</sub> concentrations were measured using a wet effluent diffusion denuder/aerosol collector (WEDD/AC) connected to IC-MS. The particle chemical composition was measured using an Aerosol Time Of Flight Mass Spectrometer (ATOFMS, TSI, USA).

The empirical particle nucleation and growth rates were determined using only the aerosol size distribution as input, using the recently developed inverse modelling procedure PARGAN (Particle Growth and Nucleation) (Verheggen and Mozurkewich 2006). Growth rates were determined by regression analysis of the General Dynamic Equation. The empirical growth rates were then used to estimate the time of nucleation for particles in each size bin, defined as the time when their diameter surpassed 1 nm. Their number density at the time and size of nucleation were determined by integrating the particle losses that occurred in the time interval between nucleation and measurement. The nucleation rate was then given by the rate at which particles

grow past the critical cluster size, assumed to be 1 nm.

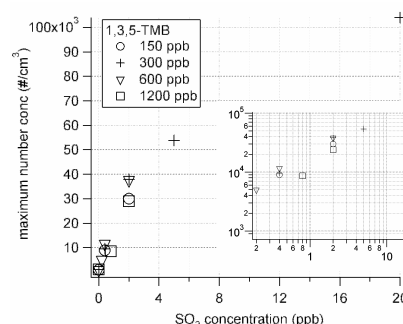


Figure 1. Experimentally observed maximum particle number concentrations (TSI CPC 3025) for a range of SO<sub>2</sub> and 1,3,5-TMB concentrations.

Figure 1 demonstrates the effect of SO<sub>2</sub> on nucleation. With higher initial SO<sub>2</sub> concentrations the maximum particle number concentration is increased from 800 to ~1.1x10<sup>5</sup> particles/cm<sup>3</sup> (0 to 20ppb SO<sub>2</sub>), while there is only a minor influence of 1,3,5-TMB on the maximum number concentration.

The observed nucleation and growth rates will be discussed with regard to SO<sub>2</sub>/sulphuric acid as well as TMB concentrations. The effect of SO<sub>2</sub> on the SOA yield and SOA composition, as measured with ATOFMS, will be discussed.

- Berndt, T., O. Boge, et al. (2005). "Rapid formation of sulfuric acid particles at near-atmospheric conditions." *Science* **307**(5710): 698-700.
- Jang, M. S., B. Carroll, et al. (2003). "Particle growth by acid-catalyzed heterogeneous reactions of organic carbonyls on preexisting aerosols." *Environmental Science & Technology* **37**(17): 3828-3837.
- Kleindienst, T. E., E. O. Edney, et al. (2006). "Secondary organic carbon and aerosol yields from the irradiations of isoprene and alpha-pinene in the presence of NO<sub>x</sub> and SO<sub>2</sub>." *Environmental Science & Technology* **40**(12): 3807-3812.
- Verheggen, B. and M. Mozurkewich (2006). "An inverse modeling procedure to determine particle growth and nucleation rates from measured aerosol size distributions." *Atmospheric Chemistry and Physics* **6**: 2927-2942.
- Zhang, R. Y., I. Suh, et al. (2004). "Atmospheric new particle formation enhanced by organic acids." *Science* **304**(5676): 1487-1490.

## On the evaluation of modelled Black Carbon using both BC and EC measurements

E. Vignati, F. Cavalli, M. Karl

European Commission DG Joint Research Centre, Institute for Environment and Sustainability, I-21020 Ispra, Italy

Keywords: black carbon, modelling, measurements, elemental carbon.

Black Carbon (BC) has a significant influence on air quality as well as on global climate. To evaluate the effect of future emission reductions the amount of BC in the atmosphere should be well quantified. To assess the impact of BC at global scale Chemistry Transport Models and General Circulation Models are applied carrying large uncertainties due to BC emissions and the treatment of physical and chemical processes.

To estimate atmospheric BC concentrations the TM5 model is applied. The TM5 model is an off-line global transport chemistry model (Krol *et al.*, 2005) that uses the meteorological data calculated by the ECMWF model. It has a spatial global resolution of 6°x 4° and a two-way zooming algorithm that allows resolving regions (e.g. Europe, N. America, Africa and Asia) with a finer resolution of 1°x 1°. The algorithm gives the advantage of a local high resolution for the locations where measurements are taken. The anthropogenic emissions are from Bond *et al.* (2004) and biomass burning from Van der Werf (2003). TM5 treats BC as external mixture and it is assumed to be accumulation particle for the wet and dry deposition processes. Modeled concentrations are compared with an extensive data set of observation distinguished by measurement methodology, season and region, containing network measurements (EMEP, IMPROVE), long-term and campaign measurements (Figure1).

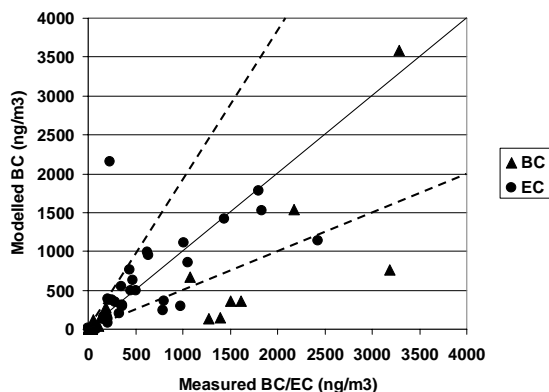


Figure 1. Comparison of BC/EC measurements with TM5 results

Due to sparse measurements available at global scale the data-set contains measurements of both BC and Elemental Carbon (EC). BC and EC are

operational definitions obtained by measurement methods which make use of different key properties of atmospheric soot: ie., light-absorbing and refractory character, respectively. Not surprisingly, comparison of EC and BC values, obtained at the same time, can show large discrepancies despite good correlations (ten Brink *et al.*, 2004; Jeong *et al.*, 2004). It is a common problem for models running at global scale to use a mixed set of data for the model evaluation. A more careful analysis of the emission inventories used in TM5 suggests an inhomogeneity of the measurement methods at sources which introduces an uncertainty in the emitted BC. Therefore a comparison done as in Figure 1 does not contain the right information on the model capability of reproducing BC.

Ideally, the methods used to measure atmospheric soot should be the same both at sources and in the atmosphere. The results –both measured and modelled values– will be critically interpreted in terms of their relation with a reference “definition” agreed upon.

- Bond, T., Streets, D., Yarber, K., Nelson, S., Wo, J.-H., & Klimont, Z. (2004), *J. Geophys. Res.*, 109, D14203, doi:10.1029/2003JD003697.
- Jeong C-H, Hopke P. K., Kim E., & Lee D-W. (2004). *Atmos. Environ.*, 38, 5193-5200.
- Krol, M., Houweling, S., Bregman, B., van den Broek, M., Segers, A., van Velthoven, P., Peters, W., Dentener, F., & Bergamaschi P. (2005). *Atmos. Chem. Phys.*, 5, 417-432.
- ten Brink H., Maenhaut W., Hitzenberger R., Gnauk T., Splindler G., Even A., Chi X., Bauer H., Puxbaum H., Putaud J.-P., Tursic J., & Berner A. (2004). *Atmos. Environ.*, 38, 6507-6519.
- Van der Werf, G. R., Randerson, J. T., Collatz, G. J., and Giglio, L. (2003), *Global Change Biology*, 9(4), 547-562.

## Development of a kinetic model framework and master mechanism of aerosol surface chemistry and gas-particle interactions

RM Garland<sup>1</sup>, JR Scheintaub<sup>1</sup>, and U Pöschl<sup>1</sup>

<sup>1</sup>Max Planck Institute for Chemistry, Department of Biogeochemistry, Mainz, Germany

Keywords: Aerosol modeling, aerosol-surface interactions, aerosol-surface reactions

Atmospheric aerosols are ubiquitous in the atmosphere. They have the ability to impact cloud properties, radiative balance and provide surfaces for heterogeneous reactions. The uptake of gaseous species on aerosol surfaces impacts both the aerosol particles and the atmospheric budget of trace gases. These subsequent changes to the aerosol can in turn impact the aerosol chemical and physical properties. However, this uptake, as well as the impact on the aerosol, is not fully understood. This uncertainty is due not only to limited measurement data, but also a dearth of comprehensive and applicable modeling formalizations used for the analysis, interpretation and description of these heterogeneous processes. Without a common model framework, comparing and extrapolating experimental data is difficult. In this study, a novel kinetic model framework was developed to describe the uptake and interactions of gas phase species and particles (Ammann & Pöschl, 2005; Pöschl *et al.*, 2005).

Integrated into this consistent and universally applicable kinetic and thermodynamic process model are the concepts, terminologies and mathematical formalizations essential to the description of atmospherically relevant physicochemical processes involving organic and mixed organic-inorganic aerosols. Within this process model framework, a detailed master mechanism, simplified mechanism and parameterizations of atmospheric aerosol chemistry are being developed and integrated in analogy to existing mechanisms and parameterizations of atmospheric gas-phase chemistry.

One of the key aspects to this model is the defining of a clear distinction between various layers of the particle and surrounding gas phase as seen in Figure 1 for compound “Z<sub>k</sub>”. The system can be described by six separate layers: gas phase, near-surface gas phase, sorption layer, quasi-static surface layer, near-surface bulk and bulk.

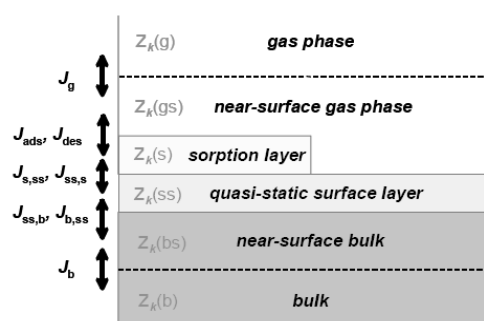


Figure 1: Representation of resolution of particle and gas layers in the model.

The processes occurring at each layer can be fully described using known fluxes and kinetic parameters. Using this system there is a clear separation of gas phase, gas-surface and surface bulk transport and reactions. The compound described in Figure 1, compound “Z<sub>k</sub>”, is semi-volatile and thus found in all layers. Its partitioning can be calculated using the various flux values (J) shown in Figure 1. By describing these layers unambiguously and precisely, the interactions of all species in the system can be appropriately modeled.

Using this framework, various systems have been modeled. Results of the uptake of various gas phase species into both liquid and solid particles will be discussed.

This work was supported by the European Integrated project on Aerosol Cloud Climate and Air Quality Interactions (EUCARRI).

Ammann, M. and Pöschl, U (2005) *Atmospheric Chemistry and Physics Discussions*, 5, 2193-2246.

Pöschl, U., Rudich, Y and Ammann, M. (2005) *Atmospheric Chemistry and Physics Discussions*, 5, 2111-2191.

## Mathematical modelling of heat transport in aerosol systems with particles of complex geometry

L.A. Uvarova

Department of Applied Mathematics, Moscow State University of Technology  
 "STANKIN", 3a Vadkovskii line, 127994, Moscow, Russia

Keywords: aerosol modelling, agglomerates, atmospheric aerosols, environmental particles, fractals.

At present problems of a dynamics and accompanied processes in aerosol systems are actual problems owing to the fact that the increase of the spreading of anthropogenic and bioaerosols in the atmosphere takes place. In general case such aerosol particles can have an arbitrary form.

For clusters and agglomerates the geometry factor is of great importance too.

The particles formation may be conditioned by different mechanisms, such as evaporation, nucleation, coagulation, thermal destruction under the influence of heat sources of the electromagnetic nature (Krivenko & Uvarova, 2004; Ivannikov, 2006) and other mechanisms. Now is considered the new mechanism - thermal fragmentation of nanoparticles (D. Gramotnev & G. Gramotnev, 2005).

As a rule for the mathematical description of the aerosol systems with particles of the "fine" forms (spherical, cylindrical, ellipsoid forms) the classic methods of the differential and integral calculus are used.

In case of the consideration the particles of the complex form one from most famous methods lies in the calculation of the fractal dimensions of the particles and of the further transition to the particles of the "fine" forms with new radiuses. This method develops on the base the fractal geometry (Feder, 1989; Schroeder). The cluster or agglomerate dimensions may be determined with the help methods of the quantum chemistry, for example with the help the density functional theory (Nadykto *et al.*, 2006).

In this paper we consider the transport processes in the aerosol systems with particles of an arbitrary form on the basis of the mathematical theory of objects of different dimensions (Pokornyi *et al.*, 2004). The parameters of the problem can be found with help methods of the quantum chemistry.

We consider the heat transport in aerosol systems with particles a complex form. In the quasi-stationary approximation heat transport equation and the boundary condition on the particle surface  $S$  have follows view:

$$\nabla(\lambda \nabla T) = -q, T_e = T_S + K_T \frac{\partial T_e}{\partial \vec{v}}, \quad (1)$$

where  $T$  is a temperature (index  $e$  relates to environment, index  $S$  relates to the particle surface),

$\lambda$  is a thermal conductivity coefficient,  $q$  is a heat source,  $\vec{v}$  is the normal vector,  $K_T$  is thermal jump coefficient. The equation (1) takes place for the stratified set (a totality of finite number of varieties of different dimensions) too. In this case equation (1) written for the potential  $\phi = \int \lambda \delta T$  transforms to the follows form:

$$\Delta_p \phi \equiv \frac{1}{\sqrt{h}} \frac{\partial}{\partial x^i} (p \sqrt{h} h^{ij} \frac{\partial \phi}{\partial x^j}) + \sum_{\sigma_{kj} > \sigma_{k-1i}} p \frac{h^{ki}}{\sqrt{h}^{kk}} \bar{E} \frac{\partial \phi}{\partial x^i} = -q(\phi), \quad (2)$$

where  $\sigma_{ki}$  is strat,  $\sigma_{kj} > \sigma_{k-1i}$  signifies that

$\sigma_{k-1i}$  adjoins to  $\sigma_{kj}$ .  $p$  is dimension,  $h^{ij}$  are contravariant metric components.

In particular, the numerical calculations carried out with the help this model (with the heat source of the electromagnetic nature (Uvarova *et al.*, 2006)) showed that the local overheating in such systems can exceed to a significant degree the local overheating in analogous systems with geometrically homogeneous particles.

This work was supported by the Russian Foundation for Basic Research (Grant No. 06-01-00548-a).

- Krivenko, I.V., & Uvarova, L.A. (2004). *Russ. J. Phys. Chem.*, 78, 894-898.
- Ivannikov, A.F. (2006). in *Proc. 9 Conf. MSUT "STANKIN"*, Moscow (Yanus -K, Moscow), 19-22. (in Russian).
- Gramotnev, D.K., & Gramotnev, G. (2005). *J. Aerosol Science*, 36, 323-340.
- Feder, J. (1989). *Fractals*. New York - London: Plenum Press.
- Schroeder, M. (2005). *Fractals, chaos, power laws*. Moscow -Ijevsk: R&C Dynamics.
- Nadykto, A.B., et al. (2006). *Physical Review Letters*, 96, 125701-4.
- Pokornyi, Yu. V., et al. (2004). *Differential Equations on geometrical graph*. Moscow: Fizmatlit. (in Russian).
- Uvarova, L.A., Krivenko, I.V. & Smirnova, M.A. (2006). *Chemical Engineering Transactions*, 10, 251-256.

## Experimental characterization and modelling of soot primary particles emitted by a CFM-56 commercial aircraft engine.

D. Delhaye<sup>1</sup>, D. Ferry<sup>2</sup>, F. Moulin<sup>3</sup>, S. Picaud<sup>3</sup>, E. Ruiz<sup>1</sup>, B. Demirdjian<sup>2</sup>, P.N.M. Hoang<sup>3</sup>, and J. Suzanne<sup>2</sup>.

<sup>1</sup>ONERA, DMPH / EAG, BP72, F-92322, Châtillon, France

<sup>2</sup>CRMC-N / CNRS, Campus de Luminy, Case 913, F-13009, Marseille, France

<sup>3</sup> Institut UTINAM, UMR CNRS 6123, Université de Franche-Comté, F-25030 Besançon Cedex, France

Keywords: Soot particle, Particle characterization, Modelling, Heterogeneous nucleation.

We present here a set of experiments that is combined with a modelling study to understand the water adsorption on soot primary particles at room temperature.

Soot particles are collected by direct impaction on polycarbonate membranes and transmission electron microscope (TEM) grids that are located at 27 m behind an aircraft engine during Landing/Take-Off (LTO) cycles. A CFM56-5C engine is used on an aero-engine bench at the SNECMA Villaroche center (France). Scanning and Transmission Electron Microscopy (SEM and TEM) allow us to determine the primary particles size distribution and show that it follows a lognormal law. It also enable us to observe the ‘onion-like’ structure of these particles (cf. figure 1) and to determine interplane distances through electron diffraction. Elemental composition and surface functional groups are investigated by Energy Dispersive X-ray Spectrometry (EDXS) and Fourier Transform Infrared Spectroscopy (FTIR).

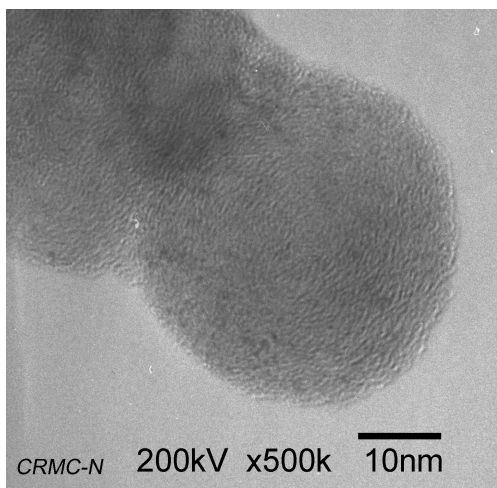


Figure 1. Soot primary particle observed by TEM

Despite its atmospheric importance, a detailed theoretical understanding of the water nucleation dynamics on soot at the molecular level remains challenging. First, we have combined quantum calculations and classical molecular dynamics simulations to model the interaction between water molecules and a partially oxidised soot particle

modelled by anchoring several COOH or OH active groups on a large graphite cluster.

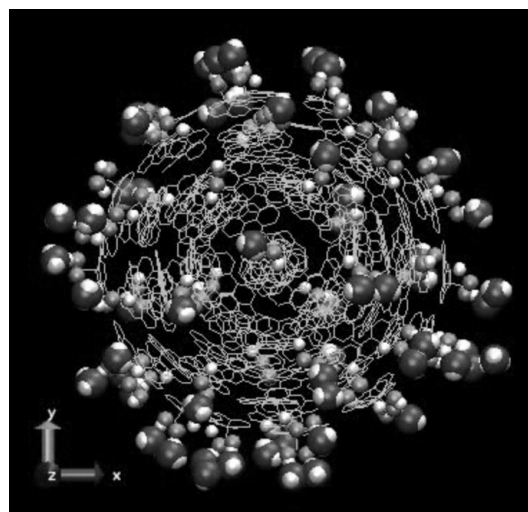


Figure 2. water molecules adsorbed around a partially oxidized soot particle. Snapshot taken from from Grand Canonical Monte Carlo simulations at 298 K

Our results indicate a preferential adsorption of water on graphite surfaces containing COOH rather than OH groups. Then, the influence of the soot morphology on the adsorption of water has been investigated by means of grand canonical Monte-Carlo (GCMC) calculations. The GCMC method allowed us to simulate a real adsorption experiment around a soot particle of spherical shape at 298 K (cf. figure2). This soot was made of carbon atoms only, or contained a certain amount of hydrophilic sites. The calculated adsorption isotherms illustrated the competitive influence of both soot morphology and chemical composition on water adsorption

Collignon, B., Hoang, P.N.M., Picaud, S. & Rayez, J.C., (2005). *Chem. Phys. Lett.*, 406, 431; ib. (2005). *Comp. Lett.*, 1, 277.

Picaud, S., Collignon, B., Hoang, P.N.M., & Rayez, J.C., (2006). *J. Phys. Chem.*, 110, 8398.

Moulin, F., Picaud, S., Hoang, P.N.M., Partay, L., & Jedlovsky, P., (2006). *Mol. Sim.*, 32, 487.

Moulin, F., Picaud, S., Hoang, P.N.M., Partay, L., & Jedlovsky, P., (2007). *Carbon*, submitted.

## An expression of particle dry deposition velocity for polydispersed particle using the moment method

S.Y. Bae<sup>1</sup>, C.H. Jung<sup>2</sup> and Y.P. Kim<sup>1</sup>

<sup>1</sup>Department of Environmental Science and Engineering, Ewha Womans University, Seoul, 120-750, Korea

<sup>2</sup>Department of Environmental Health, Kyungin Women's College, Incheon, 407-740, Korea

Keywords: aerosol size distribution, deposition, modelling.

Dry deposition is one of the most efficient particle sinks in the air. The dry deposition flux of particles is usually defined as the product of the local atmospheric concentration at a reference height by the deposition velocity. The particle dry deposition velocity representation has advantage that all the complexities of the dry deposition processes are combined into a single parameter. However, it is difficult to measure dry deposition velocity directly and to represent it as a function of particle size. The expression by Wesely (1989) has been widely used. However, it is hard to use the formula in the moment method representation of aerosol dynamics.

Raupach et al. (2001) reported a simple model based on antecedents for single-layer models. The deposition velocity is treated as a bulk conductance made up of three component bulk conductance acting in parallel: gravitational settling, impaction, and Brownian diffusion. Although this model is a great simplification of the real, multi-layer physics, it has advantages. It includes enough physics to capture the dependence of the three major processes on particle diameter and wind speed. Also, its two empirical coefficients are sufficient to permit matching to experimental reality but not enough to introduce parameterization problems.

In this study, the equation of Raupach et al. (2001) is approximated and an expression for dry deposition process is developed in the modal aerosol dynamics approach.

The dry deposition velocity proposed by Raupach et al. (2001) is as follows:

$$V_d = V_t + G[f_{form} a_f E + (1 - f_{form}) a_v Sc^{-2/3}]$$

$$\text{where, } V_t = \frac{\rho_p d_p^2 g C c}{18 \mu_a}, \quad G = \frac{u_*^2}{u_r}$$

$$E = \left( \frac{St}{St + 0.8} \right)^2, \quad St = \frac{\rho_p d_p^2 u_*^2}{18 \mu_a \nu}$$

$$Sc = \frac{\mu_a}{\rho_a D_{diff}}, \quad D_{diff} = \frac{k_b T C c}{3 \pi \mu_a d_p}$$

$$f_{form} = 0.75, \quad a_f = 2, \quad a_v = 8.$$

The expression of  $E$  was further approximated:

$$E = \left( \frac{St}{St + 0.8} \right)^2 \cong \frac{1}{\frac{1}{0.33 St^{6/5}} + 1}$$

Figure 1 shows the comparison of the particle deposition velocities for Wesely (1989) modified for particles, Raupach et al. (2001), and approximated equation obtained in this study. Three dry deposition velocities show similar trend and values.

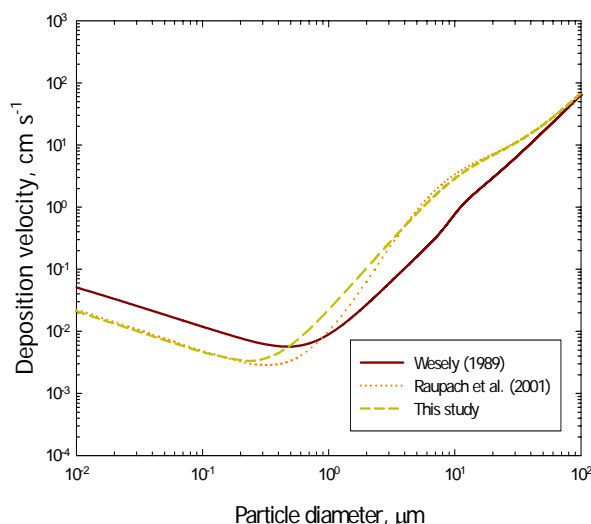


Figure 1. Comparison of the particle deposition velocities for Wesely (1989), Raupach et al. (2001), and approximated equation (this study).

This work was supported by the Korea Science and Engineering Foundation (KOSEF) through the National Research Lab. Program funded by the Ministry of Science and Technology (No. M10600000221-06J0000-22110) and Climate Environment System Research Center, an SRC program.

Raupach, M. R., Briggs, P. R., Ahmad, N., & Edge, V. E. (2001). *J. Environ. Qual.* 30, 729-740.

Wesely, M. L. (1989). *Atmos. Environ.* 23, 1293-1304.

## Simulation of Carbon Black Formation in a Solar Thermal Reactor for the Decomposition of Methane

M. Kostoglou<sup>1,2</sup>, G. Patrianakos<sup>1</sup> and A.G. Konstandopoulos<sup>1</sup>

<sup>1</sup>Aerosol and Particle Technology Laboratory (APTL), Center for Research and Technology-Hellas, Chemical Process Engineering Research Institute (CERTH/CPERI), Greece

<sup>2</sup>Department of Chemistry, Aristotle University, Thessaloniki, Greece

Keywords: Black carbon, Industrial aerosols, Numerical simulation, Particle formation and growth, Particle size distribution.

In making the transition from fossil fuel based energy systems to sustainable, hydrogen based energy systems, an unconventional route for hydrogen production is being developed. This involves the solar thermal decomposition of natural gas for the co-production of hydrogen and Carbon black (a high-value nano-material) with the bonus of zero CO<sub>2</sub> emissions. The SOLHYCARB project aims at developing a pilot industrial scale solar reactor for this purpose. As part of this work, a mathematical model has been developed to simulate the formation of Carbon black (CB) and hydrogen in the reactor. The key feature of this process is the need of very small residence times to avoid CB deposition. Conventional heat transfer routes are not efficient for the small residence times of the process so Carbon particles are added to the gas feed as heat adsorbers in order to ensure fast temperature rise and ignition of the reaction.

The mathematical model of the process consists of a population model of the CB aerosol and a 1D model of the reactor. A simple rate expression is assumed for the homogenous decomposition of CH<sub>4</sub> in order to compute the nucleation rate of Carbon atoms. Mass conservation in the CB population is applied to a range of particle size bins in order to describe the rate of production of the particles in each bin in terms of the various sources of generation and loss of these particles (kinetically controlled particle formation). The mechanism that is assumed for the generation and loss of the particles in each bin is Brownian coagulation. The Fuchs coagulation kernel (Seinfeld & Pandis, 1998) that is valid in the free molecular, transition and continuum regimes is used. Two populations are modeled: a population of fresh CB particles that evolves from the nucleated Carbon atoms and a population of seed Carbon particles that is fed to the reactor and which grows via coagulation with the fresh particles. In the 1-D reactor model an ideal CH<sub>4</sub>/H<sub>2</sub> gas mixture is assumed. Mass conservation is applied to the gas phase in order to model the volume expansion that occurs because of the stoichiometry of the decomposition reaction. Heat transfer (radiative and convective) to and from the CB particles, is also modeled.

As a first step, a simple tubular solar thermal reactor (indirect solar heating) for which an

experimental intrinsic kinetic has been reported by Dahl *et al* (2002), is modeled. A typical evolution of the fresh CB and seed Carbon-CB populations along the reactor is illustrated in Figure 1.

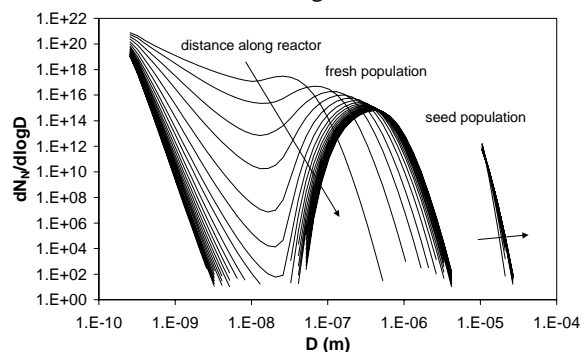


Figure 1. Number frequency distribution for the fresh and seed particle populations along the reactor.

Along the reactor the rate of CH<sub>4</sub> decomposition decreases as the concentration of CH<sub>4</sub> decreases and therefore so does the rate of nucleation of Carbon atoms. The many fresh Carbon atoms that are nucleated near the inlet gradually coagulate into a separate population of larger and fewer fresh CB particles and the number of small fresh CB particles decreases. At the same time, particles from the fresh population coagulate with the seed particles and the seed population grows slightly. The growth of the seed population is only slight because of the large size of the seed particles compared to the fresh particles.

The computational method that has been developed enables important characteristics of the CB produced by a reactor (such as the number of particles and their size distribution) to be related in a simple way to the operating conditions of the reactor.

This work was supported by the SOLHYCARB project, financed in part by the EU Commission under the 6<sup>th</sup> Framework Programme.

Seinfeld J.H., & Pandis S.N. (1998). *Atmospheric Chemistry and Physics: From Air Pollution to Climate Change*. Wiley, New York.

Dahl J.K., Barocas V.H., Clough D.E., & Weimer A.W. (2002). *Int. J. Hydrogen Energy*, 27, pp. 377 – 386.

## Modelling and calculation of fractional efficiency of tangential flow cyclones

Y. Ben-Shmuel, M. Shapiro

Laboratory of Transport Processes in Porous Materials  
Faculty of Mechanical Engineering, Technion-Israel Institute of Technology, 32000, Haifa, Israel

Keywords: cyclone separators, particle grade efficiency, mesh builder, CFD

Cyclones are commonly employed in industry for removal of dust dispersed solid particles. The advantages of cyclones are in their low cost and simplicity of construction, operation and relatively energy consumption. The cyclones are efficient in removal of relatively large particles, namely with diameters exceeding 2-5 $\mu\text{m}$ . Improvement of cyclone operation may be achieved by the rational design based on adequate modelling of the flow field and particle transport within these devices. Cyclone manufacturing had become a relatively straightforward operation. Yet, rational design of cyclones, including selection of geometry and dimensions to achieve the desired performance, is a difficult task. For this purpose semi-empirical models (e.g. of Barth, Stairmand etc), are normally used for air flow velocity calculation in a cyclone and its grade efficiency (Hoffman and Stein, 2002). CFD flow field simulations had been shown to be a promising design tool. This research employs this technique to examine the effects of cyclone geometry and physical boundary conditions on the fractional efficiency of tangential flow cyclones.

We used the three-dimensional Reynolds Stress Transformation Model (RSTM) implemented via the finite volume method (FLUENT commercial solver) to calculate the turbulent flow field in a cyclone. A special effort is made to appropriately define the flow region and generate the adequate mesh in order to capture the flow peculiarities. This is done by a special interface mesh/geometry builder, that we developed using GAMBIT pre-processor. As a result the pressure drop in a tangential flow cylinder-on-cone cyclone is calculated in agreement (within 5%) with the experimental data (see Fig. 1).

Basing on the computed flow field, a Lagrangian particle tracking method is employed to calculate the particle grade efficiency using a stochastic tracking (random walk) model accounting for instantaneous turbulent velocity fluctuations on the particle motion. We investigated the influence of cyclone design parameters (length, diameter, shape and geometry) and showed that the flow field boundary conditions at the secondary outlet (zero flow rate versus zero velocity conditions) have a significant effect on the fractional efficiency. Figure 2 shows a comparison of these results for 0.3 – 3.5  $\mu\text{m}$  PSL particles with the experimental data of Gottschalk and Bohnet (1998). In the range 1-3.5  $\mu\text{m}$  calculations agree with the measurements within 20%. Calculations with zero flowrate boundary

condition at the secondary outlet overestimate the grade efficiency, especially for submicron particles. With the secondary outlet extended as tubular or cone-like shape the agreement improves mainly for micron particles.

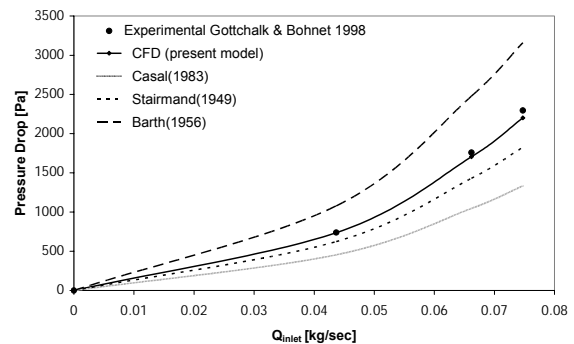


Figure 1. Pressure drop in a standard cylinder-on-cone cyclone with diameter 225 mm and inlet  $Re=10^6$ .

Further steps in development of the particle capture model are contemplated in order to improve the agreement especially for submicron particles, where the model still overpredicts the experimental grade efficiency. At the present stage the developed CFD model has good predictive capacity allowing establishing the relative merits of the existing computational models in rational cyclone design.

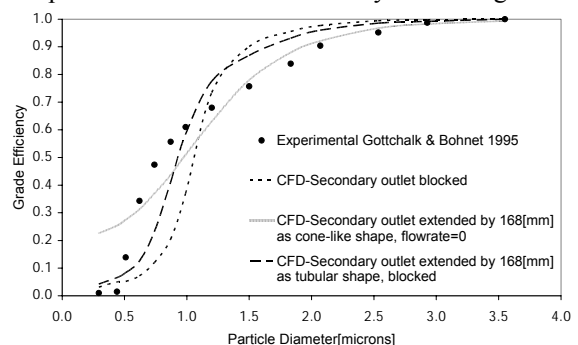


Figure 2. Comparison of the calculated grade efficiency with experimental data

1. A.C. Hoffmann, L.E. Stein, "Gas Cyclones and Swirl Tubes" Springer-Verlag, Berlin (2002)
2. M.D. Slack et al, "Advances in Cyclone modeling using unstructured grids". *Trans. Ind Chem E.* 78 part A 1098-1104 (2000)
3. O. Gottschalk, M. Bohnet, *Chem Eng. Technol. PARTEC* 95 22-37 (1995)
4. O. Gottschalk, M. Bohnet, *Chem Eng. Technol. PARTEC* 98 94-109 (1998)

## Source apportionment of submicron organic aerosols at an urban background site by positive matrix factorization (PMF) applied to aerosol mass spectra

V. A. Lanz<sup>1</sup>, M. R. Alfarra<sup>2</sup>, U. Baltensperger<sup>2</sup>, B. Buchmann<sup>1</sup>, C. Hüglin<sup>1</sup>, A. S. H. Prévôt<sup>2</sup>

<sup>1</sup>Empa, Swiss Federal Laboratories for Materials Testing and Research, CH-8600 Dübendorf, Switzerland

<sup>2</sup>PSI, Paul Scherrer Institute, CH-5232 Villigen PSI

Keywords: aerosol mass spectrometry, aerosol modelling, SOA, PM1, source apportionment.

Submicron ambient aerosol was characterized in summer 2005 at an urban background site in Zürich (Switzerland) during a three-week measurement campaign. Highly time-resolved samples of non-refractory aerosol components were analyzed with an Aerodyne quadrupole aerosol mass spectrometer (Q-AMS).

The quantification of different types of organic aerosols (OA) such as primary organic aerosols (POA) and secondary organic aerosols (SOA), or more classes if possible, was identified as an important research activity (Fuzzi *et al.*, 2006) as it is a necessary first step in the development of mitigation strategies.

Positive matrix factorization (PMF; Paatero, 1997) was used for the first time for aerosol mass spectra to identify the main components of the total organic aerosol and their sources. The PMF retrieved factors were compared to measured reference mass spectra from literature and were correlated with tracer species of the aerosol and gas phase measurements from collocated instruments.

Six factors were found to explain virtually all variance in the data and could be assigned either to sources or aerosol components such as oxygenated organic aerosol (OOA). Our analysis suggests that at the measurement site only a small (<10%) fraction of organic PM<sub>1</sub> originates from freshly emitted fossil fuel combustion. Other primary sources identified to be of similar or even higher importance are charbroiling (10–15%) and wood burning (~ 10%).

The fraction of all identified primary sources is considered as primary organic aerosol (POA). This interpretation is supported by calculated ratios of the modelled POA and measured primary pollutants such as elemental carbon (EC), NO<sub>x</sub>, and CO, which are in good agreement to literature values.

A high fraction (60–69%) of the measured organic aerosol mass is OOA which is interpreted mostly as secondary organic aerosol (SOA). The oxygenated organic aerosol could be separated into a highly aged fraction, OOA I, (40–50%) with low volatility and a mass spectrum similar to fulvic acid (a model compound that describes the chemical functionality of aged, oxygenated aerosol), and a more volatile and probably less processed fraction, OOA II (on average 20%).

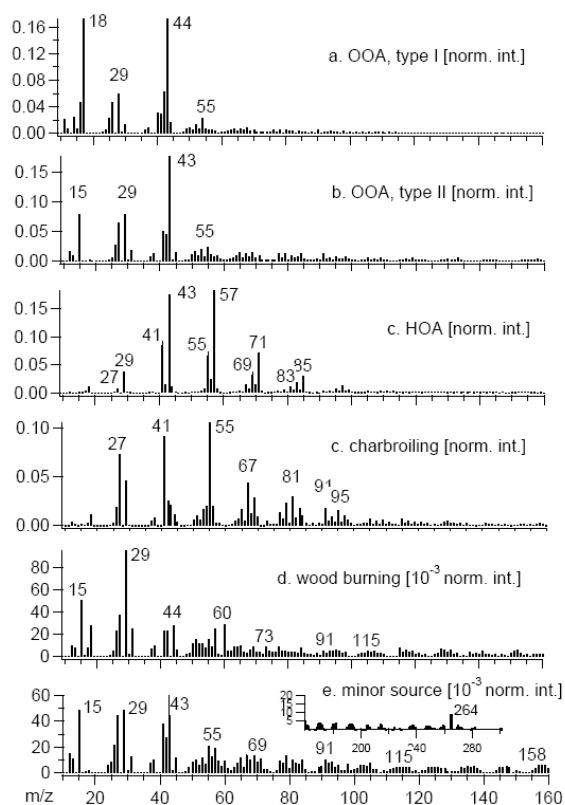


Figure 1. Normalized spectra of all estimated PMF factors (interpreted as the denoted source profiles) as calculated by the 6-factorial model. Only for the minor source the full mass range up to 300 m/z is shown because it is the only source or component with significant features in the high mass region.

The AMS measurements were supported by the Swiss Federal Office for the Environment (FOEN).

Fuzzi, S., Andreae, M. O., Huebert, B. J., et al. (2006). Critical assessment of the current state of scientific knowledge, terminology, and research needs concerning the role of organic aerosols in the atmosphere, climate, and global change. *Atmos. Chem. Phys.*, 6, 2017–2038.

Paatero, P. (1997). Least squares formulation of robust non-negative factor analysis. *Chemom. Intell. Lab. Syst.*, 37, 23–35.

## Modeling nitric acid adsorption in mixed-phase clouds

J-P. Pietikäinen<sup>1</sup>, J. Hienola<sup>2</sup>, H. Kokkola<sup>3</sup>, S. Romakkaniemi<sup>4</sup>, K. Lehtinen<sup>3</sup>, M. Kulmala<sup>2</sup> and A. Laaksonen<sup>1</sup>

<sup>1</sup>Department of Physics, University of Kuopio, P.O.B. 1627, FI-70211, Kuopio, Finland

<sup>2</sup>Department of Physical Sciences, University of Helsinki, P.O.B. 64, FIN-00014, Helsinki, Finland

<sup>3</sup>Finnish Meteorological Institute, University of Kuopio, P.O.B. 1627, FIN-70211, Kuopio, Finland

<sup>4</sup>Centre for Atmospheric Science, School of Earth, Atmospheric and Environmental Science, University of Manchester, P.O.B. 88 M60 1QD, Manchester, United Kingdom

Keywords: adsorption, ice clouds, ice nuclei, modeling, nitric acid.

Cirrus clouds play an important role in the Earth's energy balance. The ability to scatter and absorb both solar and Earth radiation makes cirrus clouds interesting part of climate. Moreover, cirrus clouds play an important role in redistributing HNO<sub>3</sub> via uptake and sedimentation in the upper troposphere. (Ullerstam *et al.*, 2005).

The adsorption of nitric acid is one of the most studied mechanisms for HNO<sub>3</sub> uptake (Ullerstam *et al.*, 2005). Adsorption models are equilibrium models, and different kind of isotherms for the adsorption is available. Adsorbed nitric acid can change the properties of ice particles, for example, it can affect the condensation of water and as an effect of this, prevent the ice/vapor system to gain equilibrium (Gao *et al.* 2004).

Using a microphysical cloud model we have compared different mechanisms for HNO<sub>3</sub> uptake to ice particles. Furthermore, different forms of Langmuir's isotherm for adsorption have been tested. We compare measurements from Gao *et al.* (2004) to the results from our model. Two mechanisms for HNO<sub>3</sub> uptake had been used. Nitric acid either stays in the particles during freezing or adsorpts to the surface of the particles.

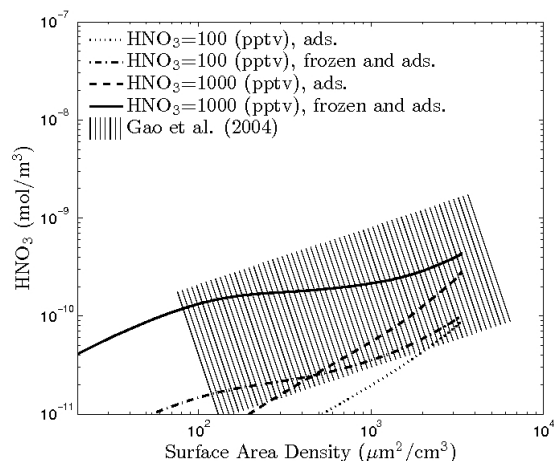


Figure 1. Concentration of nitric acid HNO<sub>3</sub> as a function of surface area density. Different lines represent the lower (100 ppt) and upper (1000 ppt) limits for initial gas phase nitric acid volume mixing ratio for cases where nitric acid is frozen or evaporated. The dissociative form for nitric acid adsorption has been used.

When the ice particles are formed, adsorption of HNO<sub>3</sub> is based on the Langmuir's isotherm:

$$\Theta = \frac{(K_{eq} P)^v}{1 + (K_{eq} P)^v}, \quad (1)$$

where  $\Theta$  is the surface coverage,  $K_{eq}$  is the equilibrium adsorption constant and  $P$  is the partial pressure on HNO<sub>3</sub> and  $v$  is the heterogeneity parameter. In the dissociative form of Langmuir's isotherm the  $v = 1/2$  and in the non-dissociative form  $v = 1$ .

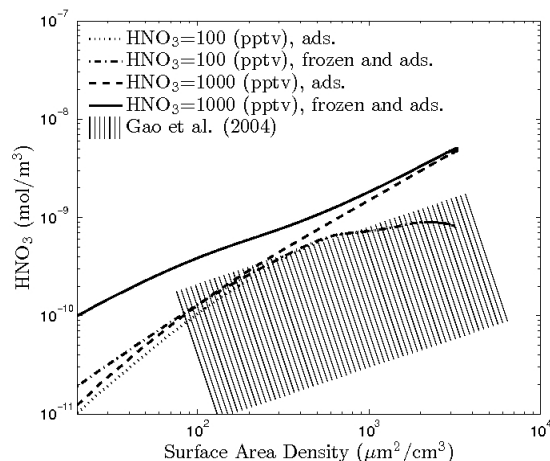


Figure 2. Like Figure 1 but the non-dissociative form for nitric acid adsorption has been used.

The figures 1 and 2 shows preliminary results of the difference between dissociative and non-dissociative form of Langmuir isotherm. Also, figures 1 and 2 represent measured values from Gao *et al.* (2004). The results show that if dissociative form of Langmuir's isotherm is used, the adsorption of nitric acid can not explain the measured values. However, if the non-dissociative form is used, adsorption by itself can explain the measured values. In the future, the difference between these two forms of Langmuir's isotherm will be studied further.

Gao *et al.* (2004). *Science*, 303, 516-520

Popp *et al.* (2004). *J. Geophys. Res.* 10, D06302

Ullerstam, M., Thornberry, T. and Abbatt, J. P. D. (2005). *Faraday Discuss.*, 130, 211-226

## OIO nucleation simulations

H. Vuollekoski<sup>1</sup>, M. Kulmala<sup>1</sup>, V.-M. Kerminen<sup>2</sup>, S.-L. Sihto<sup>1</sup>, I. Riipinen<sup>1</sup> and H. Korhonen<sup>3</sup>

<sup>1</sup>Division of Atmospheric Sciences, Department of Physics, University of Helsinki, P.O. Box 64, FI-00014, University of Helsinki, Finland

<sup>2</sup>Climate and Global Change Unit, Finnish Meteorological Institute, P.O. Box 503, FI-00101, Helsinki, Finland

<sup>3</sup>School of Earth and Environment, University of Leeds, LS2 9JT, Leeds, UK

Keywords: aerosol modelling, marine aerosols, nucleation, particle formation and growth, iodine dioxide.

Observations of coastal new particle formation have been made e.g. on the west coast of Ireland (O'Dowd *et al.*, 2005). The phenomenon overlaps with low tide, during which algae are exposed to ozone in air and emit iodine vapours. Various chemical reactions result in large amounts of iodine dioxide (OIO) in the atmosphere, which is believed to be a nucleating vapour.

We have simulated new particle formation with University of Helsinki Multi-component Aerosol model (UHMA, Korhonen *et al.*, 2004), which is a sectional multi-component aerosol dynamics box-model that simulates tropospheric aerosol particle populations and has all basic aerosol dynamical mechanisms implemented: nucleation, condensation, coagulation and dry deposition. For this study we have modified the model to marine conditions and to include iodine specific dynamics.

So far three nucleation mechanisms have been tested: the nucleation rate of one nanometer particles is assumed either linearly dependent (so called activation mechanism, Kulmala *et al.*, 2006) or squarely dependent (kinetic type nucleation) on OIO concentration, or activation type multiplied by the concentration of sulphuric acid. The nucleated particles grow by coagulation and condensation of both OIO and sulphuric acid.

The simulated box is moving with the wind from the Atlantic Ocean. At this point the model has no OIO chemistry, as OIO is injected into the system during low tide (9 o'clock), lasting 10 minutes, roughly corresponding to the time of influence with the coastal algae. A model simulating stationary measurement site is being developed. The present simulations do not include organic vapors.

An example of simulated new particle formation event can be seen in Figure 1, in which activation type nucleation was implemented with activation coefficient  $0.0001 \text{ s}^{-1}$ . Related gas and particle concentrations are illustrated in Figure 2. The parameterization used results in a particle concentration peak of  $500,000 \text{ cm}^{-3}$ .

We will perform sensitivity studies by varying model parameters, some of which are currently poorly known. More experimental data is needed for comparison with our results in order to achieve more accurate parameterization for coastal nucleation.

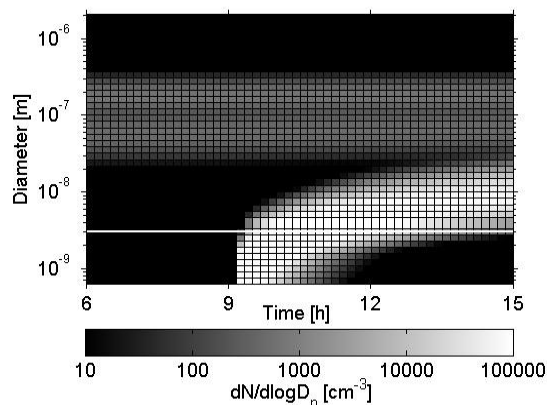


Figure 1. Particle size distribution as a function of time using activation type nucleation mechanism.

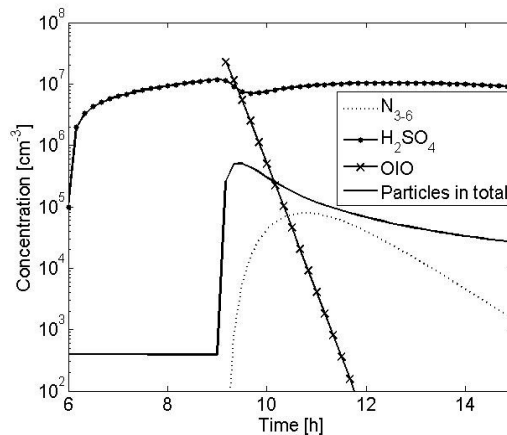


Figure 2. Gas, 3–6 nm particle and total particle concentrations during the simulation of Figure 1.

Korhonen, H., Lehtinen, K. E. J. and Kulmala, M. (2004). Multicomponent Aerosol Dynamics Model UHMA: Model Development And Validation, *Atmos. Chem. Phys.*, 4, 757-771

Kulmala, M., Lehtinen, K. E. J. and Laaksonen, A. (2006). Cluster Activation Theory as an Explanation of the Linear Dependence Between Formation Rate of 3 nm Particles and Sulphuric Acid Concentration, *Atmos. Chem. Phys.*, 6, 787-793.

O'Dowd, C. D. and Hoffmann, T. (2005). Coastal New Particle Formation: A Review of the Current State-Of-The-Art, *Environ. Chem.*, 2, 245-255.

## High PM1 and ozone levels in the Cadiz Gulf during the Galicia fires of Summer 2006

J.D. de la Rosa<sup>1</sup>, A.F. Stein<sup>2</sup>, Y. González-Castanedo<sup>3,1</sup>, A. Alastuey<sup>4</sup>, E. Mantilla<sup>5</sup>, J. Contreras<sup>6</sup>, X. Querol<sup>4</sup> and A. Sánchez de la Campa<sup>7,1</sup>

<sup>1</sup>Department of Geology, University of Huelva, Huelva, Spain.

<sup>2</sup>Earth Resources and Technology on assignment to NOAA's Air Resources Laboratory, MD, USA.

<sup>3</sup>Instituto Nacional de Técnica Aeroespacial, Esat El Arenosillo, Huelva Spain

<sup>4</sup>Institute of Earth Sciences "Jaume Almera", CSIC, C/ Lluís Sole i Sabaris s/n, 08028 Barcelona, Spain

<sup>5</sup>Centro de Estudios Ambientales del Mediterráneo (CEAM), 46980 Paterna, Valencia, Spain

<sup>6</sup>Department of Environment, Andalusia Government, C/ Manuel Siurot 41071 Sevilla Spain

<sup>7</sup>Department of Environment and Planning, University of Aveiro, 3810 Aveiro, Portugal

Keywords: PM1, ozone, HYSPLIT model, vegetation fires, Spain

During the month of August of 2006, the province of Galicia (NW of Spain) has suffered a high period of fire activity derived of forest burning. Concurrently, maximums in PM1 and ozone have been registered in several air quality network monitoring stations of the Andalusia Government (S of Spain).

On August 12<sup>th</sup> 2006, historic maximums of ozone levels have been measured in monitoring stations of the province of Huelva, for example La Rábida (191  $\mu\text{g}/\text{m}^3$ ), Campus El Carmen (210  $\mu\text{g}/\text{m}^3$ ), Doñana (160  $\mu\text{g}/\text{m}^3$ ), Valverde del Camino (176  $\mu\text{g}/\text{m}^3$ ), Cartaya (201  $\mu\text{g}/\text{m}^3$ ), Mazagón (266  $\mu\text{g}/\text{m}^3$ ), and El Arenosillo (275  $\mu\text{g}/\text{m}^3$ ). This last one was the maximum of ozone registered in all the air quality network of Huelva.

The maximum levels of ozone occurred simultaneous with maximum levels in PM1 and CO and low levels in NO<sub>2</sub>, for example Mazagón (1315  $\mu\text{gCO}/\text{m}^3$ ), and Campus Universitario (1932  $\mu\text{gCO}/\text{m}^3$ ). Also, the levels of PM10, PM2.5 and PM1 measured with a GRIMM 1107 monitor located in the city of Huelva, Los Barrios, and La Linea in the Gibraltar Straits show high concentrations during the night of August 12<sup>th</sup>- to 13<sup>th</sup> of 2006.

Between August 10<sup>th</sup> and 13<sup>th</sup>, a deep high pressure center was located W of Great Britain, and a Low pressure system was situated between the Iberian Peninsula and N of Africa. Under this scenery, N-NE winds were dominant.

Aerosol models such as NAAPS and satellite images (MODIS) (Figure 1 a and b) show high concentration of smoke in the W of the Iberian Peninsula, impacting the Gulf of Cádiz and Gibraltar Strait, which were associated to the Galicia fires.

In order to further assess the origin of the high levels of pollutants registered in the SW of Spain the HYSPLIT (Draxler and Hess, 1998) model has been utilized. The model was set to emit lagrangian particles to represent the fire emissions in Galicia. Since no information about the emissions strength was available, an emission of 1 unit per hour was assumed. Figure 1c shows the geographical distribution of the lagrangian particles. As can be

inferred from the figure, the pollutants emitted from Galicia were transported to the area of Huelva.

Since 1960, several works have shown that increments in ozone levels may be associated to vegetation burning. The formation of ozone in plumes originated from emissions derived from vegetation fires have the same physic-chemical behavior that the smog in the cities because they produce ozone precursors, such as NO<sub>x</sub> and organics, which under the influence of the ultraviolet light generate ozone as secondary product. As illustrated in this case study high levels of ozone, PM and CO can be linked to the long range transport of air masses originated from areas strongly influenced by forest fires.

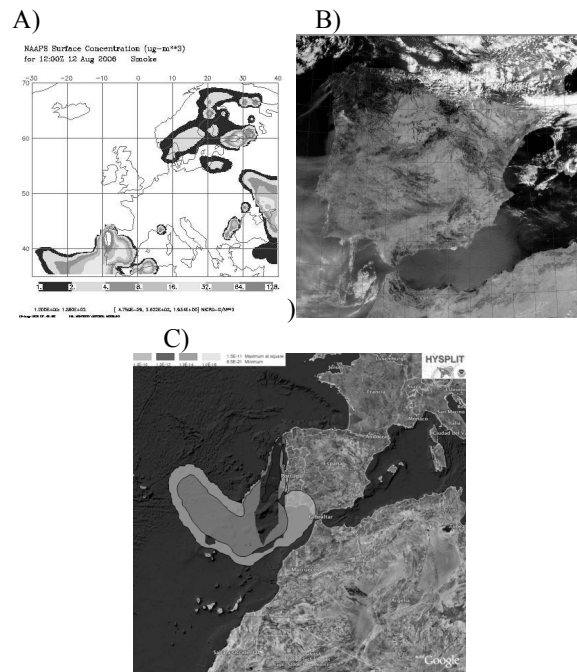


Figure 1. (a) NAAPS model, (b) Modis Images and (c) HYSPLIT 4 model for 12th August 2006 of the Iberian Peninsula

Draxler, R.R. & Hess, G.D. (1998) *Aust. Met. Mag.*, 47, 295-308.

## Modeling and Measurements of High Arsenic Levels in Southwestern Spain

A.F. Stein<sup>1</sup>, J.D. de la Rosa<sup>2</sup>, AM Sánchez de la Campa<sup>2</sup>, X. Querol<sup>3</sup> and A. Alastuey<sup>3</sup>

<sup>1</sup>Earth Resources and Technology on assignment to NOAA’s Air Resources Laboratory, MD, USA.

<sup>2</sup>Department of Geology, University of Huelva, Huelva, Spain.

<sup>3</sup>Institute of Earth Sciences ‘‘Jaume Almera’’, CSIC, C/ Lluís Sole i Sabaris s/n, 08028 Barcelona, Spain

Keywords: HYSPLIT model, Aerosol measurement, Aerosol modeling, Modeling (regional).

The city of Huelva (SW Spain) is characterized by high levels of arsenic (Querol et al. 2002). The origin of the arsenic is predominantly industrial (Alastuey et al. 2006; Sánchez de la Campa 2007).

Arsenic concentrations have been modeled using the Hybrid Single Particle Lagrangian Integrated Trajectory (HYSPLIT) model (Draxler and Hess, 1998). Emissions include several major industrial sources in the area of Huelva, Spain. For this application, the HYSPLIT model has been configured to release 5000 three-dimensional lagrangian particles per hour to represent the dispersion and transport of As. The meteorological data used by the model are based on outputs from the Mesoscale Meteorological model version 5 (MM5) using four nested grids with the highest horizontal resolution of 2 km.

HYSPLIT has been run for three different summer days, namely August 10 and 15, 2003 and June 14, 2004, and compared with field measurements. Figure 1 shows the geographical distribution of the concentration of Arsenic as calculated by the model. On August 10 2003 and June 14 2004, the typical summertime sea breeze transports the pollutant inland increasing the concentrations in the city of Huelva. Conversely, on August 15 2003 during the passage of a frontal zone the pollutant plume is directed toward the South East preventing the buildup of As in the area of Huelva.

Table 1 shows a comparison between the model outputs and the measurements for the El Carmen site. The model is able to predict whether the source impacts at the measurement site; however it underpredicts the Arsenic concentrations. This underprediction could be due, among other factors, to the uncertainty in the emissions since they have been derived from annual averages and they can experience daily variations.

Table 2. Comparison of 24-hour averaged As concentrations at the El Carmen site.

Date	Model [ng/m <sup>3</sup> ]	Measurement [ng/m <sup>3</sup> ]
Aug 10, 2003	4.92±8.72	7.44
Aug 15, 2003	0.0±0.0	0.8
June 14, 2004	1.27±3.83	10.05

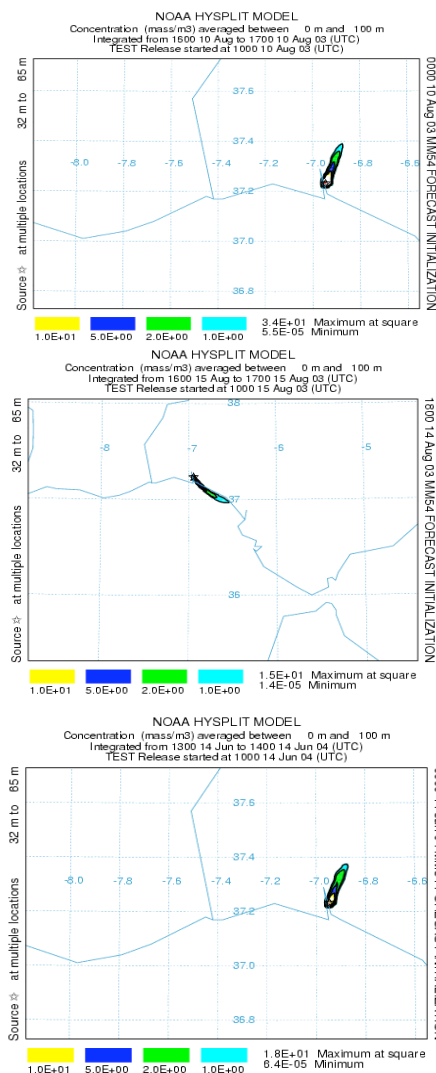


Figure 1. Geographical distribution of As levels (ng/m<sup>3</sup>) for (a) August 10, 16:00 UTC, 2003, (b) August 15, 16:00 UTC, 2003, and (c) June 14, 13:00 UTC, 2004.

Alastuey A et al. (2006). *J. of Air and Waste Manag. Assoc.* 56, 993-1006.  
 Draxler, R.R. and G.D. Hess (1998) , *Aust. Met. Mag.*, 47, 295-308.  
 Querol et al. (2002). *Atmos. Environ.* 36, 3113-3125.  
 Sánchez de la Campa et al. (2007). *Environmental Research* 103, 305-316

## Aerosol properties in the spring and summer Arctic troposphere: a global model study

H. Korhonen, D. V. Spracklen, K. S. Carslaw and G. W. Mann

School of Earth and Environment, University of Leeds, Leeds, LS2 9JT, United Kingdom

Keywords: atmospheric aerosols, aerosol modelling, Arctic aerosol

The Arctic environment is particularly vulnerable to the global climate change and recent climate simulations have predicted the highest temperature rises on the globe for this region. Quantifying the future aerosol radiative effects in the Arctic is, however, very challenging as we do not currently fully understand the mechanisms that control the particle size distribution and cloud droplet concentration at these high latitudes. The picture is further complicated by many unique features of the Arctic, e.g. high surface albedo, strong seasonal variation in incoming solar radiation and spring time peak in long range transport from anthropogenic pollution sources, which influence the climate impact of the atmospheric particles.

We present an assessment of the current state of understanding of Arctic boundary layer aerosol based on comparison of observed and modelled aerosol properties. We use long term size distribution measurements from Spitsbergen and Finnish Lapland as well as summer time campaign measurements from high Arctic (Heintzenberg *et al.*, 2006) together with a global aerosol microphysics model GLOMAP (Spracklen *et al.*, 2005). GLOMAP is an extension to the TOMCAT 3D chemical transport model (Stockwell & Chipperfield, 1999) and has been shown by Spracklen *et al.* (2006) to capture the general features of the marine boundary layer aerosols at lower latitudes.

The simulations concentrate on the spring and summer period (February to July) when the observations show a shift from polluted Arctic haze conditions to clean summer conditions with low particle mass concentration. In the simulations the primary particle sources in addition to sea salt are natural and anthropogenic sulphate and OC/BC. Secondary particle formation occurs through binary nucleation which in the model takes place predominantly in the upper troposphere.

Although the model captures well the high SO<sub>2</sub> concentration in March and April and its decrease towards the summer, the basic runs fail to reproduce the change from accumulation mode dominated particle size distribution in spring to Aitken mode dominated distribution in the summer (e.g. Strom *et al.*, 2003). Instead, the shape of the modelled distribution remains very similar throughout the simulated period. Sensitivity simulations show that the description of the clouds in the model and their effect on the particle size distribution are crucial in determining the concentration of accumulation mode particles and therefore the sink for the condensing vapours and small clusters formed in the upper troposphere.

For the subarctic measurement sites in Finnish Lapland the model predicts realistic particle concentrations and general features of distribution in early spring. Towards summer the modelled particle concentrations are, however, significantly lower than the measured ones. In April and May this is partly due to lack of a boundary layer nucleation mechanism in the model but this mechanism may not be able to explain the discrepancy in the summer when new particle formation events are not frequently observed in Lapland.

Further work will be carried out to validate the model results with available chemical and meteorological measurements. Based on this we aim to improve the description of aerosol-cloud interactions in the high latitudes. We will also study the influence of boundary layer nucleation and SOA formation to our results especially in the subarctic regions.

This work was supported by the UK Natural Environment Research Council

- Heintzenberg, J., Leck, C., Birmili, W., Wehner, B., Tjernstrom, M. & Wiedensohler, A. (2006). *Tellus*, 58B, 41-50.
- Spracklen, D., Pringle, K., Carslaw, K. & Chipperfield, M. (2005). *Atmos.Chem. Phys.*, 5, 2227-2252.
- Spracklen, D., Pringle, K., Carslaw, K., Mann, G., Manktelow, P. & Heintzenberg, J. (2006). *Atmos.Chem. Phys.*, 6, 8871-8915.
- Stockwell, D. & Chipperfield, M. (1999). *Q. J. R. Meteorol. Soc.*, 125, 1747-1783.
- Strom, J., Umegard, J., Torseth, K., Tunved, P., Hansson, H.-C., Holmen, K., Wisma, V., Herber, A. & Konig-Langlo, G. (2003). *Phys. Chem. of the Earth*, 28, 1181-1190.

## Modelling study on the connection of sulphuric acid and new particle formation

S.-L. Sihto<sup>1</sup>, H. Vuollekoski<sup>1</sup>, J. Leppä<sup>2</sup>, I. Riipinen<sup>1</sup>, V.-M. Kerminen<sup>2</sup>, H. Korhonen<sup>3</sup>, K.E.J. Lehtinen<sup>4</sup> and M. Kulmala<sup>1</sup>

<sup>1</sup>University of Helsinki, Department of Physical Sciences, P.O. Box 64, FI-00014 Univ. of Helsinki, Finland

<sup>2</sup>Finnish Meteorological Institute, Climate and Global Change, P.O. Box 503, FI-00101 Helsinki, Finland

<sup>3</sup>University of Leeds, School of Earth and Environment, Leeds LS2 9JT, United Kingdom

<sup>4</sup>Finnish Meteorological Institute and University of Kuopio, Department of Applied Physics, P.O. Box 1627, FI-70211 Kuopio, Finland

Keywords: aerosol dynamics, modelling, nucleation rate, particle formation and growth, sulfuric acid.

Field measurements in e.g. Hyytiälä, Finland, indicate that atmospheric particle formation seems to be a function of sulphuric acid concentration to the power from one to two (Weber *et al.*, 1997; Riipinen *et al.*, 2006). To explain these dependences, the so called activation and kinetic nucleation mechanisms have been proposed (Kulmala *et al.*, 2006). We have performed a series of simulations with an aerosol dynamics box model to study the connection between sulphuric acid and new particle formation and the processes affecting the relationship in detail. In particular, we tried to find conditions which would yield the observed linear or square dependence between the number concentration of freshly nucleated particles and sulphuric acid.

Aerosol dynamics model UHMA (University of Helsinki Multicomponent Aerosol model, Korhonen *et al.*, 2004) is a sectional box model that has all the basic aerosol dynamical mechanisms implemented: nucleation, condensation, coagulation and dry deposition. For nucleation we assumed either activation or kinetic mechanism:

$$J_{act} = A[H_2SO_4]$$

$$J_{kin} = K[H_2SO_4]^2,$$

where for the nucleation coefficients  $A$  and  $K$  we used values given by Riipinen *et al.* (2006).

We studied the correlation of the simulated number concentration of 3–6 nm particles ( $N_{3-6}$ ) and formation rate of 3 nm particles ( $J_3$ ) with the modelled sulphuric acid concentration ( $[H_2SO_4]$ ):

$$N_{3-6} \sim [H_2SO_4]^{n_{N_{3-6}}} (t - \Delta t_{N_{3-6}})$$

$$J_3 \sim [H_2SO_4]^{n_{J_3}} (t - \Delta t_{J_3}).$$

The correlation exponents  $n$  and the time delays  $\Delta t$  were determined numerically by searching through pairs of  $(n, \Delta t)$  a combination that would give the maximum correlation coefficient between the curves.

The exponent for  $J_3$  correlation was greater or equal than the exponent for  $N_{3-6}$ , and the time delay for  $J_3$  shorter than for  $N_{3-6}$ , which results are in line with those by Riipinen *et al.* (2006). The time shift analysis has been used to estimate the growth rate of 1–3 nm sized particles from the measurement data (e.g. Sihto *et al.*, 2006). Comparison with the growth rates calculated from the simulated volume change

rate showed that the time delay for  $N_{3-6}$  gives on average a reasonable estimate for the growth rate of freshly nucleated particles.

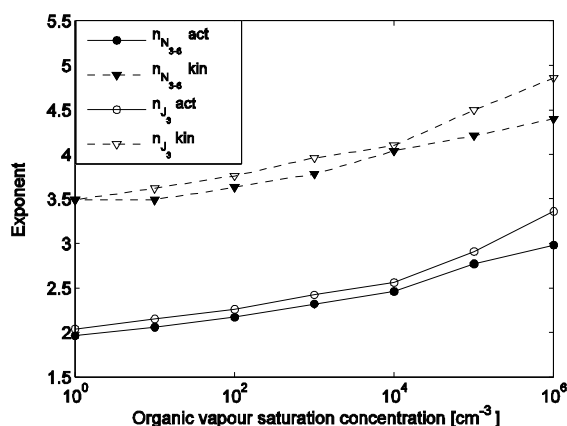


Figure 1. Correlation exponents for  $N_{3-6}$  and  $J_3$  as a function of organic vapour saturation concentration using activation and kinetic nucleation mechanisms.

The most important factor affecting the dependence on sulphuric acid at 3–6 nm was the growth process, including the amount of condensable vapours (sulphuric acid and an organic vapour), their diurnal profiles, and the saturation vapour pressure of organics. The exponents decreased as the saturation concentration of the condensable organic vapour was lowered (Fig. 1). In order to preserve the exponent in nucleation rate (either 1 or 2), the growth below 3 nm must be fast and not limited by saturation vapour pressure. In addition to general simulations, we performed case studies of some selected days with exponent 1 and 2 dependence.

Korhonen, H., Lehtinen, K.E.J. and Kulmala, M. (2004) *Atmos. Chem. Phys.*, 4, 757-771.

Kulmala, M., Lehtinen, K.E.J. and Laaksonen, A. (2006) *Atmos. Chem. Phys.*, 6, 787-793.

Riipinen, I., *et al.* (2006) *Atmos. Chem. Phys. Discuss.*, 6, 10837-10882.

Sihto, S.-L., *et al.* (2006) *Atmos. Chem. Phys.*, 6, 4079-4091.

Weber, R. J., *et al.* (1997) *J. Geophys. Res.*, 102, 4375-4385.

## A combined method for data processing in an elastic backscattered Lidar

D. Nicolae<sup>(\*)</sup>, C. Talianu<sup>(\*)</sup>, A. Nemuc<sup>(\*)</sup>, E. Carstea<sup>(\*)</sup>,  
L. Belegante<sup>(\*)</sup>, C. Radu<sup>(\*)</sup>

<sup>(\*)</sup> National Institute of R&D for Optoelectronics, Bucharest, Romania

Keywords: lidar ratio, remote sensing, particle characterization, vertical distribution

Atmospheric aerosols have large influence on earth's radiation budget. Very little is known about the aerosol vertical distribution, the climatology and air mass modification. Therefore, vertically resolved aerosol data represent an urgent need to obtain a statistically significant database on the aerosol variability. The laser remote sensing technique is a unique tool able to provide the vertical distribution of aerosols in the atmosphere with very high temporal and spatial resolution.

The simplest lidar systems used for vertical profiling of suspended particles in the lower atmosphere are based on the elastic backscattering process [1]. Unfortunately, few qualitative information can be directly obtained from elastic backscatter measurements. More information become available if the lidar system has additional receiving channels (Raman, depolarization). To derive the aerosol microphysical properties a 3 (elastic) + 2 (Raman) channels system is necessary [2].

In any case, the accuracy of obtained information is dependent on technical performances of the system and on the sensibility of data processing method, which can be critical in some cases. The need for compact, robust systems that can work in field campaigns limits the number of receiving channels and the power of the laser beam, so the improvements of a specific system's hardware are likely to be considered. On the other hand, more data processing algorithms which include complementary data can be foreseen based on new laboratory or theoretical studies of aerosols.

This paper will present the basic characteristics of a Lidar system, and particularly of the backscatter Lidar used for measurements. The advantages of a backscatter Lidar measurement system and the drawbacks will be underlined. Because the data inversion problem has a non-unique solution for this type of lidar systems, the quantitative data that can be derived from lidar signals is supposed to be limited to the backscattering coefficient profile of aerosols.

The paper will present an iterative hybrid regularization algorithm for elastic backscatter lidar data processing, developed by the Laser remote sensing group in Bucharest. This algorithm is meant to evaluate the microphysical properties of the suspended matter particles in the air if complementary data are available. In our study, a

simplified model of the atmosphere is used to deliver the meteorological parameters profiles (temperature, pressure, humidity), but real data can only improve the expected results. To initiate the iterations, some characteristics of the aerosols at ground level must be considered: refractive index, average radius, soot proportion, number distribution. For that we used the Ackermann model [3] which will be detailed in the extended paper.

The algorithm basically combines iteratively the Mie direct problem [4] with the inversion Fernald-Klett method [4, 5] to determine the microphysical parameters of the atmospheric particles for which the theoretical and the experimental outputs are corresponding. One important contribution of the algorithm is to eliminate uncertainties from using a constant value of the lidar ratio [6]. By an iterative approach, the vertical lidar ratio profile will be determined and then used in data processing.

Several results obtained using this algorithm and synthetic lidar signals will be presented, as well as the advantages and the limitations of the method.

1.Measures R.M., *Laser Remote Sensing. Fundamentals and Applications*, Krieger Publishing Company, Malabar, Florida, 1992.

2.Bockmann, C., Hybrid regularization method for the ill-posed inversion of multiwavelength lidar data in the retrieval of aerosol size distributions. *Appl. Opt.*, 40(9): p. 1329-1342, 2001

3.Ackermann J., *Two-frequency lidar inversion algorithm for a two-component atmosphere*, *Appl. Opt.* 36, 5134-5143, 1998

4.Mie G., *Ann. de Phys.*, Leipzig, 25, pg. 377, 1908

5.Fernald, F.G., Herman, B.M., and Reagan J.A., *Determination Of Aerosol Height Distribution By Lidar*, *J. Appl. Meteorol.* 11, 482-489, 1972

6.Klett J.D., *Stable Analytical Inversion Solution For Processing Lidar Returns*, *Appl. Opt.* 20, 211-220, 1981

7.Doina Nicolae, C.P. Cristescu, "*Laser remote sensing of tropospheric aerosol*", *J.Optoelectron.Adv.Mater.*, vol. 8, no. 5, October 2006, p.1781-1795

## Particle size-dependent focusing in a flow through a channel with oscillating walls

P. Vainshtein and M. Shapiro

Faculty of Mechanical Engineering, Technion – Israel Institute of Technology, Haifa, Israel

Keywords: particle, motion, channel, oscillations

We consider two-dimensional motion of aerosol particles in a long semi-infinite channel of height  $h$  walls of which perform harmonic oscillations  $y = h + 2b \cos \omega t$  with angular frequency  $\omega$  and amplitude  $b$  to-and-fro the channel axis. It is known that in the absence of imposed flow field, such walls' oscillations create flow field that induces particle drifting motion in compressible fluid<sup>1</sup>.

To calculate the incompressible flow field within the channel, we use the Poiseuille inlet velocity profiles  $U = U_0 [1 - (y/h)^2]$ . To find the disturbed velocity flow field, we employ the method of asymptotic expansions using dimensionless parameters  $\varepsilon = b/h$  and Womersley parameter,  $W = h(\omega/2\nu)^{1/2}$ . The obtained velocity field contains oscillating components and secondary streaming components, both arising from the wall oscillations<sup>2</sup>. The secondary streaming velocity near the axis is directed in the downstream direction. Its intensity increases linearly with  $x$ . The characteristic value of intensity depends on parameter  $\varepsilon W$ .

The micrometer and submicron particle trajectories are computed from the equation

$$\frac{d\mathbf{u}_p}{dt} = \frac{\mathbf{u} - \mathbf{u}_p}{\tau}, \quad \tau = \frac{2}{9} \frac{a^2 C}{\nu \Pi_\rho}, \quad (1)$$

where  $\mathbf{u}$  and  $\mathbf{u}_p$  are the velocities of fluid and particles, respectively,  $\tau$  is the Stokes relaxation time,  $a$  is the particle radius,  $\nu$  is the fluid kinematic viscosity,  $\Pi_\rho$  is the fluid-to-particle-density ratio and  $C$  is the Cunningham's slip correction factor.

For moderate and large Stokes numbers,  $S = \omega\tau$ , particle trajectories are computed numerically, using the solution for the flow velocity field. For small particle Stokes numbers, we obtain analytical expressions for particles' time averaged trajectories.

Figure 1 shows particles trajectories in the coordinates  $X=x/h$ ,  $Y=y/h$ . Particles are seeded at  $X_0 = 0$ ,  $Y_0 = 0.1$  with the initial velocity coinciding with that of air. It is shown that due to the walls' oscillations particles experience drifting motions (i) upstream in  $X$  direction toward the channel inlet and (ii) towards the axis (in  $Y$  direction). Intensity of the upstream drifting motion increases linearly with  $X$ . However, the effect of downstream motion caused by the secondary streaming always dominates over the effect of the particle upstream drifting motion. Therefore secondary streaming together with imposed main flow drives particles downstream. It is

shown that if Stokes number is smaller than some critical value, namely if  $\omega\tau < \zeta/\varepsilon^2$ , the particle approaches the axis asymptotically at infinite  $X$  (curve 1). Generally the value of parameter  $\zeta$  depends on the secondary streaming characteristic intensity. In particular, if  $W\varepsilon \gg 1$  (as in Fig. 1) one has  $\zeta = 0.33$ . In other important case when  $W\varepsilon \sim 1$  one has  $\zeta = 0.66$ . Trajectory behavior, presented by curve 1, is reminiscent of systems aerodynamic focusing in periodic nozzle systems<sup>3</sup> and in a channel with slightly corrugated walls<sup>4</sup>. It is shown that at sufficiently high amplitude and frequency of walls' oscillations their effect on focusing is more pronounced than that of walls' corrugation.

If  $\omega\tau > \zeta/\varepsilon^2$ , particle trajectory behavior turns out to be non-monotonic near the channel axis (curve 2). The amplitude of particle trajectory oscillations near the axis decays as  $X$  tends to infinity.

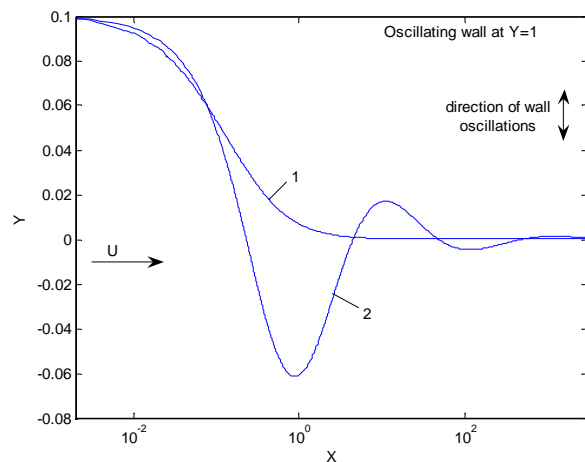


Figure 1. Particles' trajectories in the channel  $h = 10^{-2}$  m,  $U_0 = 0.1$  m/sec,  $f = \omega/2\pi = 1$  kHz  $\varepsilon = 0.1$ ,  $W = 144$ . 1 -  $a = 30 \mu\text{m}$ ; 2 -  $a = 100 \mu\text{m}$ .

<sup>1</sup> Dain, Y., Fichman, M., Gutfinger, C., Pnueli, D. and Vainshtein, P. (1995). *J. Aerosol Sci.*, 26, 575-594.

<sup>2</sup> Secomb, T.W. (1978). *J. Fluid Mech.*, 88, 273-288.

<sup>3</sup> Wang, X., Gidwani, A., Girshick, S.L. and McMurry, P.H. (2005). *Aerosol Sci. Technol.*, 39, 624-636.

<sup>4</sup> Fernandez de la Mora, J. (2006). *J. Aerosol. Sci.*, 37, 323-339.

## Modelling of atmospheric aerosol processing with consideration of non-ideal solutions and complex multiphase chemistry

R. Wolke, J. Zoboki, A. Tilgner and H. Herrmann

Leibniz Institute for Tropospheric Research, Permoserstr. 15, 04318 Leipzig, Germany

Keywords: aerosol modelling, aerosol cloud interaction, multiphase chemistry, aerosol thermodynamics, chemical composition.

In multi-component systems phase transfer processes take place, which can influence the particle and droplet formation as well as particle growth. In the modelling of such multiphase processes it is necessary to consider non-ideal conditions in deliquescent particles. Here we find highly concentrated solutions which are typical in the initial stage of the droplet formation, when only small amounts of water are available. The behaviour of these non-ideal mixed solvent-electrolyte solutions including inorganics and organics is not yet described satisfyingly in existing multiphase models. The aim of our work is to improve the description of such complex systems by the implementation of different activity coefficient calculation methods into the Spectral Aerosol Cloud Chemistry Interaction Model (SPACCIM) (Wolke et al., 2005).

This parcel model has been developed for the description of cloud microphysical processes with the consideration of complex multiphase chemistry for a size-resolved particle/drop spectrum. Microphysics is coupled with a chemical model, so meteorological and microphysical parameters needed for the chemistry can be taken from the microphysical model. Changes in the chemical composition feed back on the microphysical processes. The non-ideality of highly concentrated solutions is described by activity coefficients. In ideal (well diluted) case these coefficients are unity. An extended version (included ions) of UNIFAC coupled with the Pitzer method was implemented. The new SPACCIM version is able to simulate the physico-chemical processes of the particles/droplets also at lower relative humidities.

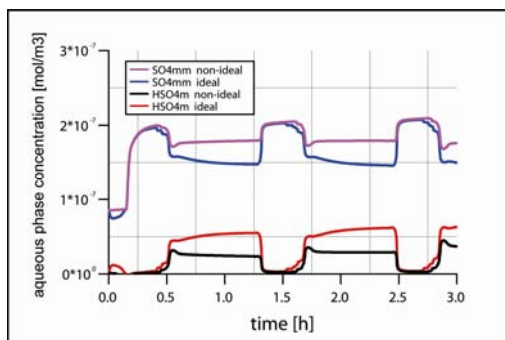


Figure 1. Sulfate concentration (accumulated over the spectrum) for the urban scenario.

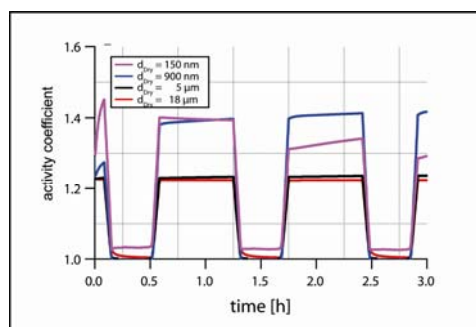


Figure 2. Activity coefficient of glycolic acid for different size bins and the urban scenario.

For the model studies, a reduced version of the multiphase mechanism CAPRAM 3.0 (Herrmann et al., 2005) is used. The simulations were carried out for a meteorological scenario in which an air parcel moves along a predefined trajectory including three cloud passages and intermediate aerosol state at a 90% relative humidity level. Simulations have been performed for marine, remote and urban conditions. Feed back effects of the multiphase chemistry on microphysics are considered.

Figure 1 shows the sulphate evolution of the urban scenario in ideal and non-ideal case. In general, the deviations from ideal solutions are not negligible. The feedback of non-ideality on microphysics is also clearly recognizable. In urban case, the consideration of non-ideality leads to a lower pH value during the interstitial aerosol states. However, the observed differences vary over the size spectrum and in dependence on the particle composition. This behaviour is illustrated for the activity coefficients of glycolic acid in Figure 2. A more detailed analysis shows that also the number of activated particles (especially during the second and third cloud passage) depends strongly on the consideration of non-ideality. The proposed approach leads to an appropriate modelling of complex solutions occurring atmospheric aerosols.

Herrmann, H., Tilgner, A., Barzaghi, P., Majdik, Z., Gligorovski, S., Poulain, L., & Monod, A. (2005). *Atmospheric Environment*, 39 (23-24), 4351-4363.

Wolke, R., Sehili, A.-M., Tilgner, A., & Herrmann, H. (2005). *Atmospheric Environment*, 39 (23-24), 4375-4388.

## Oscillations of the parameters in finite system with condensation and evaporation

V.A. Zagaynov<sup>1</sup>, A.K. Maslov<sup>2</sup>, M. Bahtyreva<sup>3</sup>, A. Lutsenko<sup>3</sup>, A.A. Lushnikov<sup>1</sup>

<sup>1</sup>Karpov Institute of Physical Chemistry, 10, Vorontsovo Pole str., 105064, Moscow, Russia

<sup>2</sup>Department of Numerical Mathematics of Moscow State University, Moscow, Russia

<sup>3</sup>Moscow State Industrial University, 16, Autozavodskaya, Moscow, Russia

Keywords: condensation, evaporation, nucleation, aerosol modelling.

The processes of nucleation and condensation – evaporation play a very important role in formation and evolution of aerosol particle concentration levels and particle size distributions (Friedlander, 2000). At the same time there are several approaches for modelling nucleation, condensation and evaporation. Nucleation is a process, which is responsible for the birth of disperse phase. As is known, using different methods for the description of this process one can come to inconsistent results. Most important part of the nucleation in the atmosphere is the formation of dimers and molecular clusters composed of 3-7 molecules.

For the description of the initial stage of the particle formation process we use the set of differential equations describing the nucleation- condensation-evaporation process:

$$\begin{aligned} \frac{\partial c_1}{\partial t} &= I - \alpha_1 c_1^2 - c_1 \sum_{i=1}^G \alpha_i c_i + \sum_{i=2}^G \beta_i c_i \\ \frac{\partial c_i}{\partial t} &= \alpha_{i-1} c_{i-1} c_{i-1} - \alpha_i c_i c_i - \beta_i c_i + \beta_{i+1} c_{i+1} \quad (1) \\ i &\leq G. \end{aligned}$$

Here  $c_i$  is the concentration of  $i$ -mers,  $I$  is the production rate of monomers,  $\alpha_i$  is the collision frequency of monomers and  $i$ -mers,  $\beta_i$  is the frequency of monomer escape from an  $i$ -mer, and  $G$  is a cut-off particle mass. The particles with the mass exceeding  $G$  are assumed to be instantly removed from the system and do not take a part in condensation and evaporation processes.

Solutions to differential equations (1) with initial conditions

$$c_i(t=0) = 0 \quad (2)$$

show that the particle concentrations oscillate and damp with time. As time grows the concentrations stabilize. When evaporation is neglected the explicit steady state solution can be obtained;

$$c_i = \sqrt{\frac{I}{\alpha_i(G+1)}} \quad c_i = \frac{1}{\alpha_i} \sqrt{\frac{\alpha_i I}{G+1}} \quad \text{for } i < G+1$$

This steady state solution is shown to be an attractor. The eigenvectors of the steady state equations have negative real parts and all eigenvectors form complex conjugated pairs. Figure 1 demonstrates the changes of particle concentrations with time (time and concentrations are dimensionless). In this example we solved 200 equations ( $G=200$ ) for

$I=1$  and took  $\alpha_i = i^{\frac{1}{3}}$ . It was shown, that initial conditions does not effect on position of attractor. The phase trajectories are spiral type curves.

It is clear, that condensation part of the differential equations (1) gives rise to oscillations due to its nonlinear form, whereas the evaporation part of the equations contributes to damping these oscillations. As was found, the general period of oscillation grows with  $G$

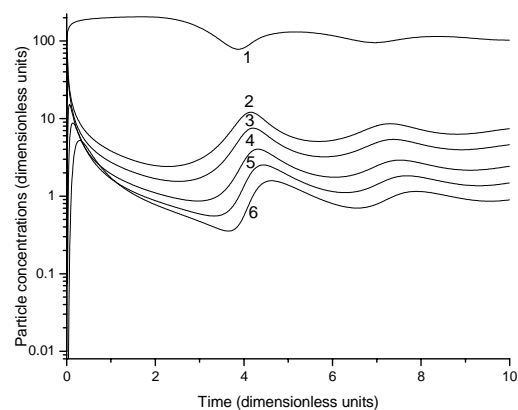


Figure 1. The variations of particle concentrations with time for different particle sizes: 1 – total particle concentration, 2 – concentrations of monomers, 3 – dimers, 4 – particle contained 5 monomers, 5 – 10 monomers, 6 – 20 monomers.

The analysis of the solution shows that period of oscillations grows with  $G$  and damping grows in increasing the evaporation rate.

This approach can be used to explain experimental results cited in Friedlander (2000).

This work was supported by International Science and Technology Center, project # 1908.

Friedlander, S.K. (2000). *Fundamental of Aerosol Dynamics*. New York, Oxford, Oxford University Press.

## Effect of Nucleation and Secondary Organic Aerosol formation on Cloud Droplet Number Concentrations

R. Makkonen<sup>1</sup>, A. Asmi<sup>1</sup>, H. Korhonen<sup>2</sup>, H. Kokkola<sup>3</sup>, S. Järvenoja<sup>4</sup>, P. Räisänen<sup>4</sup>, K.E.J. Lehtinen<sup>5</sup>, A. Laaksonen<sup>5</sup>, V.-M. Kerminen<sup>4</sup>, H. Järvinen<sup>4</sup> and M. Kulmala<sup>1</sup>

<sup>1</sup>Department of Physical Sciences, University of Helsinki, FI-00014, Helsinki, Finland

<sup>2</sup>School of Earth and Environment, University of Leeds, LS2 9JT, Leeds, United Kingdom

<sup>3</sup>Finnish Meteorological Institute, FI-70211, Kuopio, Finland

<sup>4</sup>Finnish Meteorological Institute, FI-00101, Helsinki, Finland

<sup>5</sup>Department of Physics, University of Kuopio, FI-70211, Kuopio, Finland

Keywords: nucleation, SOA, atmospheric aerosols, modelling, organic aerosols.

The continental biosphere emits large quantities of volatile organic compounds (VOCs) capable of forming secondary organic aerosols (SOA). By acting effectively as cloud condensation nuclei (Hartz et al., 2005), these aerosols have the potential to influence clouds and thereby climate. The climatic effects of biogenic SOA are, however, extremely poorly known. Reasons for this include the large uncertainties associated with the magnitude and variability of biogenic VOC emissions, as well as our incomplete understanding on the chemistry and processes responsible for the formation and growth of aerosol particles from these emissions. Biogenic VOC emissions may increase substantially in the future as a result of global warming, in addition to which there are potentially complex feedback mechanisms between biogenic VOC emission, aerosols, clouds and climate. As a result, the climatic effects of biogenic VOC emissions cannot be quantified without an Earth System Model that couples the biosphere and atmosphere and treats the microphysical processes associated with biogenic SOA formation.

We introduce the implementation of a simple computationally effective SOA distribution scheme into a global climate model. The scheme has a mechanistic description of aerosol formation and growth processes related to biogenic organic vapours; instead of treating SOA as primary emission, we model the condensation of organic vapour onto pre-existing particles. Additionally, we have compared four nucleation mechanisms using ECHAM5-HAM: two binary parameterizations as well as kinetic and activation type nucleation. Kinetic and activation type nucleation seem to produce more particles in the boundary layer than binary parameterizations.

Aerosol modelling was done with the HAM-module within the ECHAM5 atmospheric general circulation model (Stier *et al.*, 2005). HAM uses seven modes to describe aerosol population. In standard ECHAM5-HAM, nucleation of new particles is parameterized

using a binary nucleation scheme and secondary organic aerosols from biogenic VOCs are treated as primary organic aerosol emissions.

Coupling the aerosol distributions to a cloud activation model shows that just by changing the nucleation mechanism, the cloud droplet number concentrations can change substantially especially over land (Figure 1). This effect clearly shows the potential importance of nucleation on cloud properties. Explicit SOA formation can enhance cloud droplet number concentrations even more.

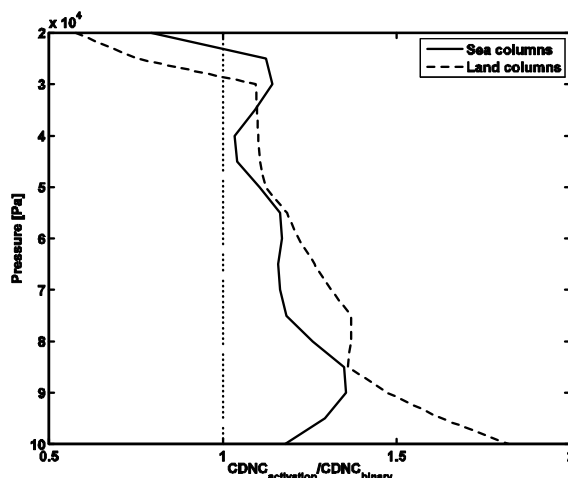


Figure 1. Ratio of cloud droplet number concentrations between simulations with activation – type and binary nucleation. Values are yearly averages from northern hemisphere, separately for land and sea areas.

Hartz, K. E. H., Rosenorn T., Ferchak S. R., Raymond T. M., Bilde M., Donahue N. M. and Pandis S. N. (2005). *J. Geophys. Res.*, 110, D14208.

Stier P., Feichter J., Kinne S., Kloster S., Vignati E., Wilson J., Genzeverld L., Tegen I., Werner M., Balkanski Y., Schultz M., Boucher O., Minikin A. and Petzold A. (2005). *Atmos. Chem. Phys.* 5, 1125-1156.

## Evaluation of Brownian motion calculation using Discrete Phase Model of FLUENT

D.K. Song<sup>1</sup> and S. Dhaniyala<sup>2</sup>

<sup>1</sup>Department of Environmental Engineering, Kumoh National Institute of Technology, 1, Yangho-dong, Gumi, Gyeongbuk, 730-701, Republic of Korea

<sup>2</sup>Department of Mechanical & Aeronautical Engineering, Clarkson University, Potsdam, NY 13699, USA

Keywords: Brownian diffusion, nanoparticle, trajectory, FLUENT.

Computational fluid dynamics (CFD) has played an important role in the development of instruments to measure and characterize physical properties of nanoparticles. As the target size of airborne particles has decreased to the nanometre size range, Brownian motion of nanoparticles has become the dominant characteristic describing their behaviour. In this study, we evaluate Brownian motion of particles by using Discrete Phase Mode in a popular commercial CFD tool, FLUENT (Fluent Inc., NH).

Particles move randomly by colliding with gas molecules and result in having a spatial distribution. Generally this distribution can be assumed as a Gaussian distribution with a standard deviation given by

$$\sigma = \sqrt{2Dt} = \sqrt{(2k_B T C_c t) / (3\pi\mu D_p)} \quad (1)$$

which is known as the Stokes-Einstein relation.

Fig. 1 shows a computational domain used for evaluation. To account for particle dispersion only by Brownian motion, no fluid flow is considered. A number of particles (N = 500) were started from the origin of the computation domain for each test case (Table 1). In calculations, the tracking parameters in FLUENT were set as: Maximum number of steps: 100,000; and the length scale: 10<sup>-8</sup> m. After particle trajectories are calculated (Fig. 1), particle positions were recorded as a function of time.

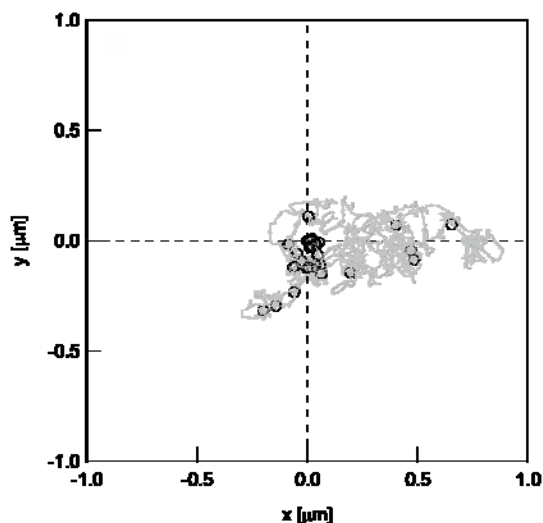


Figure 1. Computation domain and sample particle trajectory. Symbols represent particle position at observation time.

Table 1. Tracking schemes used for calculations.

Case	Tracking Scheme	Accuracy Control Scheme	
		Lower Order	Higher Order
00 <sup>†</sup>	-	-	-
01	Implicit		
02	Analytic		
03	Trapezoidal		Off
04	Runge-Kutta		
05		Analytic	Runge-Kutta
06	Off	Implicit	Runge-Kutta
07		Implicit	Trapezoidal
08		Analytic	Trapezoidal
09	Implicit		
10	Analytic		
11	Trapezoidal		On
12	Runge-Kutta		

<sup>†</sup> In this case, FLUENT v6.1.22 was used while v6.2.16 was used for all the other cases.

The standard deviation of particle position is calculated from the observed positions as shown in Fig. 2. For all cases, standard deviations of particle positions obtained from calculations with Brownian motion using FLUENT are much smaller compared to that from the Stokes-Einstein relation. It is important to recognize these possible errors in the calculations of nanoparticle motion using commercial codes.

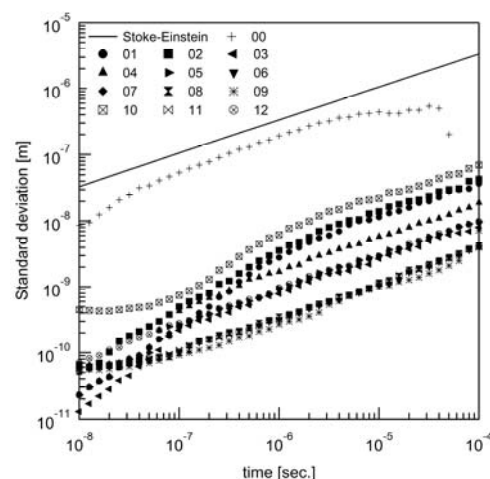


Figure 2. Comparison results from calculation.

This work was supported by the National Science Foundation under grant CTS-0508390 and the Korea Research Foundation Grant funded by the Korean Government (MOEHRD, KRF-2006-214-D00015).

## Numerical study of dynamics of growing droplets in Kelvin spectrometer

S.K. Zaripov<sup>1</sup>, R.S.Galeev<sup>1</sup>, W.Holländer<sup>2</sup>

<sup>1</sup>Institute of Mathematics and Mechanics, Kazan State University, Universitetskaya St., 17, Russia, 420008

<sup>2</sup>Fraunhofer Institute Toxikologie und Experimentelle Medizin  
Nikolai-Fuchs-Str. 1, D-30625, Hannover, Germany

Keywords: aerosol modelling, condensation, evaporation, deposition, growth.

Instruments capable of measuring droplet concentrations at given supersaturations are called Kelvin spectrometers. They are important for reliably characterizing atmospheric particles (Holländer et.al., 2002). The rapid pressure drop in measuring chamber of cylindrical cross section is accompanied by an adiabatic temperature decrease, which may lead to sufficient supersaturation followed by droplet formation due to heterogeneous nucleation. The growing droplets move in the chamber, and part of them will deposit on the walls or evaporate with time. Heat conduction and natural convection flow due to the difference between the wall and volume gas temperatures will increase the interior temperature and reduce the supersaturation that in turn affects droplets growth and deposition.

We developed a mathematical model describing the transient thermal convection flow and deposition of growing droplets in the expansion-type Kelvin spectrometer. The model includes the Navier-Stokes equations to describe the gasdynamic processes and droplet growth model with account for vapor depletion due to condensation and release of latent heat. Numerical calculations of gas flow by means of Fluent CFD software show that the evolution of processes inside the spectrometer chamber can be divided into two main stages. The first stage is the adiabatic gas expansion. During it the pressure in the chamber establishes very quickly. The gas temperature falls down practically uniformly in the entire volume of the chamber. The next stage is characterized by a slow temperature increase beginning from regions near the walls. The temperature gradient causes the development of a gas flow upwards near the wall in the course of time transforms into a global vortex flow inside the chamber. The values of the thermal convection flow velocity magnitude can achieve  $\sim 0.05\text{m/s}$ . To study the droplet dynamics we neglect the expansion stage in view of its small duration and calculate the temperature and convection flow development starting with the uniform temperature distribution inside the chamber and a constant wall temperature larger than the interior gas temperature. Using the gas flow velocity and temperature distribution from CFD calculation in the spectrometer chamber we calculate the droplets paths taking into account their growth resulting from the local super-saturation. The time

dependencies of the droplet deposition rate were found from numerical calculations. The deposition rates with and without convection flow influence are compared.

The relative droplet concentrations obtained taking into account the main processes in the measuring chamber (droplet growth by condensation, sedimentation, heat conduction, thermal convection, droplet evaporation) and without gravity influence ( $g=0$ ) are shown in fig.1. Curves obtained without gravity allow estimating the concentration dynamics due to the evaporation only. For the smaller initial saturation the losses of droplets generated by nucleation is determined mainly by evaporation. But for larger initial saturation sedimentation becomes main mechanism of droplet losses in the measuring chamber. In last case the vortex flow formed by thermal convection will reduce the deposition rate.

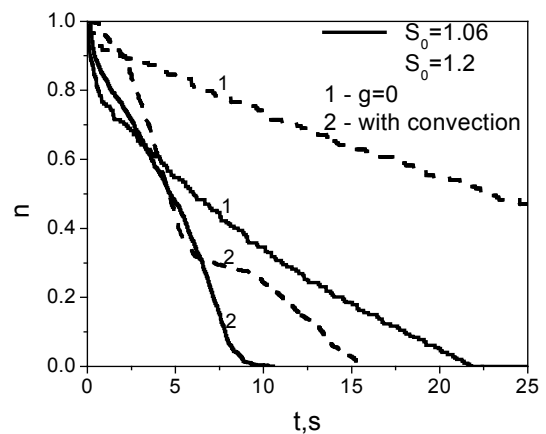


Figure 1. The relative droplet concentration for  $N=1000\text{ cm}^{-3}$  and various initial saturations  $S_0$

The work was supported by RFBR (project 05-01-00794).

Holländer W., Dunkhorst W., Lödding H., Windt H., 2002, Theoretical simulation and experimental characterization of an expansion-type Kelvin Spectrometer with intrinsic calibration, Journal of Atmospheric and Oceanic Technology 19, 1811-1825.

## How reduction policies on emission scenarios can affect air quality in the Tuscany region

C. Grassi<sup>1</sup>, S. Verrilli<sup>2</sup>, L. Tognotti<sup>2</sup>

<sup>1</sup>Department of Mechanical, Nuclear and Production Engineering, University of Pisa, 56100, Pisa, Italy

<sup>2</sup>Department of Chemical Engineering, University of Pisa, 56100, Pisa, Italy

Keywords: Air Pollution, Aerosol Modelling, Photochemical Processes, Emissions

The need to determine the more suitable policies to obtain significant reduction of the air quality pollutants concentration suggest to configure and test an advance modeling system for the Tuscany region to verify and understand the relative contribution of the long range transport of pollutants, emissions, physical and chemical atmospheric processes.

The CAMx multi-scale three dimensional photochemical grid model [Environ2004] was configured to the Tuscany region scenario: regional domain of center Italy comprising the Tuscany region with an horizontal master grid of 46 x 44 cells (6km x 6km) and 17 vertical levels of variable thickness form 20m up to 3600m agl. Regional emission inventory data were elaborated for pollutants emission and detailed VOC and PM<sub>2.5</sub> speciation was applied [Passant, 2002, SCC2004]. In addition three different emission scenarios were prepared, based on regional inventory and IASA projections, to assess the impact of the possible environmental policies on air quality. The meteorological input fields were elaborated from MM5 prognostic meteorological model data [Cetemps]. The IC and BC concentrations were provided by chemistry transport model CHIMERE [Cetemps].

The simulations were performed to reconstruct the air quality pollution in the Tuscany region during the months of October and May 2005.

Table 1. Measured and predicted ozone and PM<sub>10</sub> concentrations [ $\mu\text{g}/\text{m}^3$ ], Tuscany air quality network.

			PISA	FIRENZE	AREZZO	LIVORNO	LUCCA
			Sub.Back.	Urb.Back.	Urb.Back.	Sub.Back.	Sub.Back.
PM <sub>10</sub>	MAY	PREDICT	25.9	30.4	31.7	18.9	28.3
		OBSERVED	27.5	22.1	20.1	17.8	22.1
		RMSE	4.2	10.4	11.7	5.1	7.6
	OCT	PREDICT	24.4	27.3	34.6	28.6	23.2
		OBSERVED	30.6	23.0	30.6	15.3	25.9
		RMSE	8.6	11.5	10.9	10.4	11.6
O <sub>3</sub>	MAY	PREDICT	93.8	102.6	105.9	105.3	104.5
		OBSERVED	97.8	107.4	100.8	104.6	85.1
		RMSE	11.7	21.9	10.3	7.0	24.0
	OCT	PREDICT	79.6	58.2	67.1	77.0	88.1
		OBSERVED	45.9	28.8	35.9	70.0	49.8
		RMSE	40.4	32.3	36.0	35.3	44.7

The predicted time series of hourly ozone and daily PM concentration were found to be in good agreement to observed ones; the root mean square error between observed and predicted concentration were shown in table 1 together with the averaged concentration values.

The daily time series showed significant differences between costal and continental or

northern and southern sites, confirming the spatial and temporal observed PM<sub>10</sub> levels. Important results are related to the PM<sub>2.5</sub> and PM<sub>10</sub> concentration ratio that showed variable values from 60% for rural locations to 86% in urban or industrial sites. Significant difference were shown also between the two periods, in fact the 76% in October and 53% during may, indicating a major contribution of crustal component to the coarse fraction of the PM<sub>10</sub>.

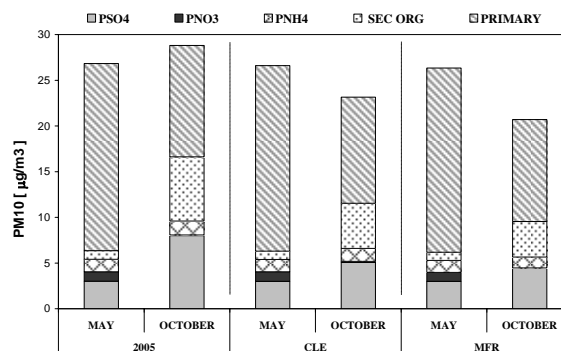


Figure 1. Average PM composition calculated by the models for the three emission scenarios.

The results related to the application of emission reduction as calculated by IASA for CLE2010 (Current Legislation) and MFR2010 (Most Feasible Reduction) to the regional emission inventory are shown in figure 1. The main difference in the effects of emission reduction occurred in the month of October when the secondary organic and ammonium sulphate concurred to the 50% of PM predicted mass concentration. The same reduction applied on the emission of primary particles and gaseous precursors have basically no effects in May related to the contribution of primary crustal particles that concurred up to 70% of the PM concentrations.

CETEMPS Center of Excellence 2005 - Experimental Chemical Weather Forecast over Italy, University of L'Aquila.

ENVIRON 2004, USER'S GUIDE (CAMx) version 4.03, International Corporation.

Passant N.R., Speciation of UK emissions of NMHC VOCs, AEAT/ENV/0545 1, February 2002.

## PBMR Safety Analysis: Aerosol Modelling for Generation IV Nuclear Plants

L. Naicker and A.Ramlakan

Department of Nuclear Engineering Analysis, Pebble Bed Modular Reactor (Pty) Ltd, Centurion, 0046, Gauteng, South Africa

Keywords: Aerosol Chemistry, Aerosol Modelling, Nuclear Aerosols, Radioactive Particles

The Pebble Bed Modular Reactor (PBMR) is a 400MW<sub>th</sub> Generation IV High Temperature Gas Reactor (HTGR). The PBMR core utilizes about 451000 low enriched uranium TRIPLE coated ISOTropic (TRISO) fuel spheres ('pebbles') in an annular fuel region that is surrounded by a fixed central graphite reflector and an outer graphite reflector.

The annular core of pebbles acts as a fixed bed through which the Helium coolant gas passes. The core is continuously loaded at the top and unloads at the bottom, maintaining a pebble inventory, and resulting in downward migration of pebbles. Pebble-to-pebble and pebble-to-reflector abrasion is expected, as well as abrasion of pebbles within the fuel handling and storage system that services the core. Abraded graphite dust can be transported through the cooling loop together with small amounts fission products which manage to escape the fuel spheres. Modelling the transport of graphite dust and fission products allows prediction of the radiological burden imposed on workers and public under accident conditions and is imperative for licensing of the design.

Our present modelling ability involves the use of the thermo-hydraulic code FLOWNEX and the RADAX code to model primary circuit aerosol processes using input from FLOWNEX. Under an accident condition, considered to be a rupture in the primary circuit, a release through the confinement compartments to the venting shaft is modelled using FLOWNEX for thermo-hydraulics and NAUA for aerosol processes.

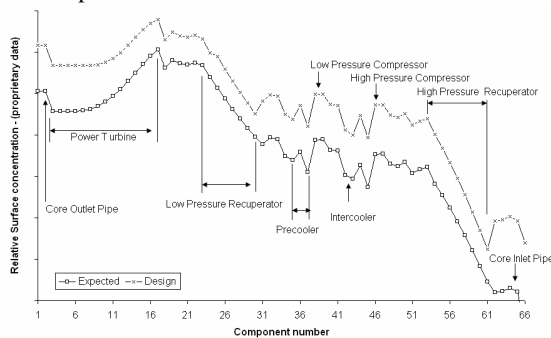


Figure 1. Ag110m primary circuit concentration after 36a

The work discussed here is part of a longer term collaborative modelling effort towards a PBMR specific code that can be generalized to model

accident scenarios in HTGRs. Future code development plans include fully coupled aerosol and thermal-hydraulic modules, a mechanistic account of dust and fission product interaction, chemical interaction between fission products all of which are important improvements to the model especially when re-suspension is considered in the primary circuit (figure 2) depressurization scenarios. In addition, multi-components effects are being investigated.

Isotopes such as Ag, Cs, I and Sr are expected to circulate in the primary loop over the plants lifetime. The primary loop chemical environment is considerably different from LWR and PWR conditions. We discuss the predicted chemical interactions occurring and the kind of uncertainties involved in modelling these reactions. Further discussions will include the licensing framework and release limits for the different accident scenarios, the physical conditions in the primary circuit and confinement building and how these relate to the amount and size distribution of graphite dust, more detailed results from primary circuit and confinement analysis, the aerosol phenomena that are expected to dominate in HTGR accidents, knowledge gained from the AVR(Arbeitsgemeinschaft VersuchsReactor GmbH) and its applicability to PBMR, the experiments required as part of the rigorous verification and validation framework to improve our modelling inputs.

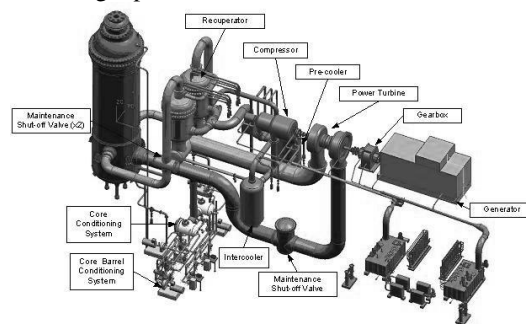


Figure 2. PBMR primary circuit

Stassen, L. (2006). *Validation of the plate-out model in the RADAX code used for plate-out and dust activity calculations at PBMR*. PHYSOR-2006.

Slabber, J. (2006). *Technical Description of the PBMR Demonstration Power Plant*. T016956, Revision 4, Internal PBMR document.

## Modelling Particle Formation and Growth from Biogenic Precursors Measured in the Jülich Plant Chamber

M. Dal Maso<sup>1</sup>, T. Hohaus<sup>1</sup>, A. Kiendler-Scharr<sup>1</sup>, E. Kleist<sup>1</sup>, M. Miebach<sup>1</sup>, R. Tillmann<sup>1</sup>, R. Uerlings<sup>1</sup>, R. Fisseha<sup>1</sup>, J. Wildt<sup>1</sup>, T. Mentel<sup>1</sup>

<sup>1</sup>Institut für Chemie und Dynamic der Geosphäre, Forschungszentrum Jülich, D-52425 Jülich, Germany

Keywords: Aerosol Formation, SOA, Aerosol Modelling, Nucleation

Biogenic volatile organic compounds (BVOC) are major participants in atmospheric chemistry, both due to their large emissions (Guenther *et al.*, 1995) and their influence on O<sub>3</sub> and OH radical budgets. In addition to affecting the oxidising capacity of the atmosphere, their chemical degradation leads to the formation of semi- or non-volatile compounds that considered to be a major source of tropospheric aerosol mass, and also to play an important part in growing recently formed particles to sizes where they can act as cloud condensation nuclei, CCN (see eg. Tunved *et al.*, 2006). Atmospheric aerosol size distribution measurements have shown that atmospheric particle formation, often involving biogenic organics, can be a significant aerosol source (Kulmala *et al.*, 2004).

In the Jülich plant chamber a series of experiments with a system consisting of a plant chamber and a reaction chamber have been carried out. In the experiments, varying plants were placed in the plant chamber in controlled conditions. The VOC mixture emitted from these plants was taken to a stirred reaction chamber which was continuously flushed with O<sub>3</sub>. At the reaction chamber an UV light could be switched on and off to initiate photolysis of O<sub>3</sub> to produce OH. This led to a short nucleation peak, producing a rapid increase in particle number. After the nucleation peak, no new particles are produced and the condensable vapours condense on the existing particle surface.

The setup, with inflow of VOC-laden air from the plant chamber and outflow from the reactor chamber to the instrumentation, leads to dilution of the aerosol concentration over time, with the aerosol lifetime being of the order of 70 min. As the particle concentration decreases, also the available condensation surface, or condensation sink (Kulmala *et al.*, 2001), decreases and in several cases, a new burst of nucleation can be observed.

To understand the processes leading to the observed SOA yields, and whether the VOC oxidation products condense on existing particles or form new particles, we have developed a model for the plant chamber. The model assumes a continuously stirred tank reactor (CSTR, see e.g. Schmidt, 1998), that is, that there exists perfect mixing inside the tank volume. Aerosol dynamic equations are solved simultaneously with the gas phase chemistry.

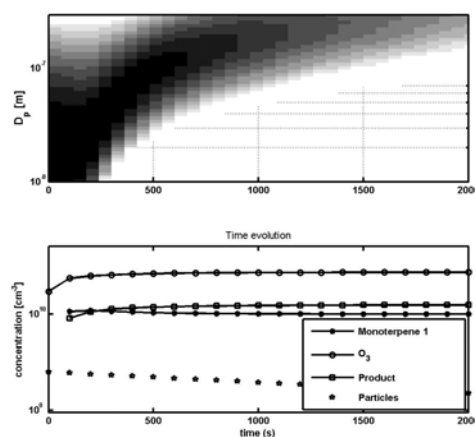


Figure 1. An example model run with the stirred reactor aerosol dynamical model, depicting ozonolysis of a model monoterpene and the resulting growth of the aerosol size distribution. The reactor goes into steady state after ca. 1000 s.

The model can be used to investigate the condensation sink threshold of new particle formation, as well as the e.g. the timescale needed to achieve steady state in the reactor chamber (see figure 1). It is also a valuable tool in estimating the effect of condensing vapour properties on the nucleation and growth rates during nucleation events.

- Guenther, A., et al., 1995, A global model of natural volatile organic emissions, *J. Geophys. Res.*, 100, 8873-8892
- Kulmala, M., *et al.*, (2004) Formation and growth rates of ultrafine atmospheric particles: A review of observations *Aerosol Science* 35, 143-176.
- Tunved, P. *et al.*, (2006) High Natural Aerosol Loading over Boreal Forests *Science* 14, 261-263
- Schmidt, Lanny D. (1998). *The Engineering of Chemical Reactions*. Oxford University Press, New York.

## Closure study of aerosol cloud interactions using trajectory ensemble model

S. Romakkaniemi, G. McFiggans, K. Bower, H. Coe, and T. W. Chouarton

Centre for Atmospheric Science, School for Earth, Atmospheric and Environmental Science, University of Manchester, Manchester M60 1QD, UK

Keywords: aerosol-cloud interactions, aerosol modelling

A closure study of the cloud aerosol interactions in stratocumulus cloud was carried out. In this study we use LEM (Large Eddy Model) to produce similar conditions to those observed during CLOPAP (Cloud Processing of regional Air Pollution advecting over land and sea) project flights. During CLOPAP the NERC / Met Office BAE 146 aircraft was used to conduct measurements in the stratocumulus capped boundary layer in order to study the evolution of polluted aerosols. LEM is further employed to produce a set of trajectories that can be used to run a detailed cloud parcel model, which includes differential equations describing condensation/evaporation of different gases, coagulation, and chemical reactions in the liquid and gas phases. In simulations, the cloud parcel model is initialised with the out-of-cloud aerosol compositional data from the AMS-measurements, and observed/estimated gas phase concentrations of water soluble gases. The existing adiabatic cloud parcel model is modified so that instead of an adiabatic expansion, the temperature and total water concentration are taken from LEM produced trajectories and the change in water saturation ratio is calculated based on these values. The method used is similar to one used by Stevens *et al.* (1996) and Feingold *et al.* (1998).

In Figure 1 an example of the comparison between measured and modelled cloud droplet number concentrations is shown. The measured data is from the CLOPAP flight 9 studying the plume originating from London and advecting to east at 30.9.2005. The cloud droplet number concentration data presented in Figure 1 is measured with FSSP and consist of 26 minutes of in-cloud measurements in the stratocumulus capped boundary layer with liquid water content between 0.05 and 0.4g/kg. The simulation data consist of an ensemble of 1000 trajectories produced with LEM. Measured potential temperature profile is slightly adjusted to get an agreement between measured and LEM simulated updraft velocities. As a measure of agreement we compared the standard deviation of vertical velocity distribution (0.22m/s in this case).

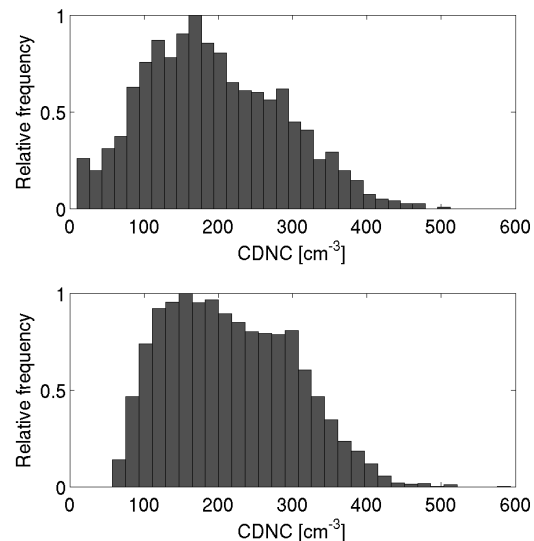


Figure 1. Upper: measured distribution of cloud droplet number concentration. Lower: Modeled cloud droplet number distribution.

As can be seen from Figure 1, the modelled and simulated cloud droplet number concentrations are in a good agreement with the mean value of simulated cloud droplet number concentration being less than 10% higher than the measured concentration. The total number concentration of accumulation mode aerosol particles in this simulation is  $712\text{cm}^{-3}$  with the mean diameter of 120nm. With these values even a small widening of probability density function of the LEM simulated updraft velocities can lead to a remarkable overestimation of the cloud droplet number concentration. Also variations in chemical composition of aerosol particles and the amount of condensable gases in the atmosphere are affecting the modeled results. Thus the work will be continued to conduct the closure that takes account the aging of aerosol due to the cloud processing.

This work was supported by the UK Natural Environment Research Council. S.R. was supported by the Helsingin sanomain 100-vuotissäätiö.

Feingold, G., Kreidenweis, S.M., Zhang, Y. (1998). *J. Geophys. Res.*, 103, 19527-19542  
Stevens, B., Feingold, G., Cotton, C.R., and Walko, R.L. (1995). *J. Atmos. Sci.*, 53, 980-1006

## Predicting fine inorganic aerosols in Mexico City during winter 2005: deliquescence branch.

M. Moya<sup>1</sup>, C. Fountoukis<sup>2</sup>, A. Nenes<sup>2,3</sup>, E. Matías<sup>4</sup>

<sup>1</sup>Centro de Ciencias de la Atmosfera, Universidad Nacional Autonoma de Mexico, Ciudad Universitaria, 04511, Mexico City, Mexico.

<sup>2</sup>School of Chemical and Biomolecular Engineering, Georgia Institute of Technology, 311 Ferst Drive, Atlanta, GA 30332-0100, USA

<sup>3</sup>School of Earth and Atmospheric Sciences Georgia Institute of Technology, 311 Ferst Drive, Atlanta, GA 30332-0100, USA

<sup>4</sup>Posgrado en Ciencias Químicas, Universidad Nacional Autonoma de Mexico, Ciudad Universitaria, 04511, Mexico City, Mexico.

*Keywords:* thermodynamic equilibrium, deliquescence, crustal species

### INTRODUCTION

Atmospheric pollution in the Mexico City Basin (MC) due to high levels of ozone (O<sub>3</sub>) and aerosols (particulate matter, PM) has become a significant issue for its nearly 20 million of inhabitants (Molina and Molina, 2002). PM levels exceed the Mexican PM<sub>10</sub> (PM with aerodynamic diameter  $\leq 10 \mu\text{m}$ ) 24-h standard on most of the days of the year (Edgerton et al., 1999). Although the Mexican PM<sub>2.5</sub> (PM with aerodynamic diameter  $\leq 2.5 \mu\text{m}$ ) 24-h standard of  $65 \mu\text{g m}^{-3}$  has been introduced very recently (November, 2005), PM<sub>2.5</sub> levels have been recorded well above acceptable limits. Atmospheric aerosols reduce local visibility, air quality and have adverse effects on human health. As the chemical composition of fine PM is also important in this respect, knowledge of these two parameters (size/composition) is essential to assess their role in several atmospheric processes occurring in the atmosphere. Airborne PM is composed by inorganic salts, organic material, crustal elements and trace metals. Inorganics may account up to 50% or more of total fine particulate matter. It has been commonly assumed that in the coarse fraction of PM (particles with  $dp > 2.5 \mu\text{m}$ ), where dust is an important constituent of airborne PM, crustal species, such as Ca, K, and Mg are abundant (Ansari and Pandis, 2000). It has been shown, however, in recent studies in this megacity (Moya et al., 2006) that these constituents are of relevance in the PM<sub>2.5-1</sub> size fraction as well.

Simulating the aerosol size and composition is an invaluable tool in increasing our understanding of aerosol behavior and in determining its role in several atmospheric processes. Measurements of the chemical composition of aerosols and their gas-phase precursors in this polluted area are essential to

provide information regarding the aerosol partitioning between the gas and particulate phases and to validate aerosol models.

In this work predictions of the partitioning of nitrate and ammonium between the gas and aerosol phases, under Mexico City conditions and applying SCAPE thermodynamic model are presented.

### RESULTS

Overall, four-hour average PM<sub>1</sub>, PM<sub>2.5</sub> nitrate and ammonium concentrations are predicted within 30-60% for cases where the relative humidity (RH) is within moderate values (40-70%). For the afternoon sampling periods (RHs: 20-35%), the deliquescence branch seems to introduce some errors in predicting aerosol behavior. By considering an updated water activity database, model performance significantly improves for these conditions.

### ACKNOWLEDGEMENTS

This work has been funded by the National Oceanic and Atmospheric Administration (NOAA-US) under contract NMRAC000-5-04017 (A. Nenes) and by the National Council for Science and Technology (CONACyT-Mexico) under contract J51782 (M. Moya). Support of PAPIIT-UNAM grant (reference: IN107306) is also acknowledged.

### REFERENCES

- Ansari, A. and Pandis, S.N. (2000) Atmospheric Environment 34, 157-168.
- Edgerton et al., 1999. Journal of the Air & Waste Management Ass. 49, 1221-1229.
- Molina, M. and Molina, J.T. (2002) Air quality in the Mexico Megacity: An integrated assessment. Kluwer Academic Publishers, Dordrecht.
- Moya, M. et al. (2006) Proceeding of the 2006 American Geophysical Union Fall Conference.

## Detailed process modelling of SOA formation: Kinetic vs. K- $\alpha$ approach

K.-H. Naumann, H. Saathoff

Research Centre Karlsruhe, Institute for Meteorology and Climate Research, Atmospheric Aerosol Research, POB 3640, 76021 Karlsruhe, Germany

Keywords: SOA, VOC(s), aerosol formation, aerosol modelling, aerosol dynamics.

The aerosol behaviour code COSIMA (Naumann, 2003), which has been developed originally to simulate the time evolution of structure, dynamics, optics and heterogeneous chemistry of fractal like agglomerate particles is supplemented by a module treating the formation and dynamics of secondary organic aerosol. While pure SOA particles are compact spheres, the fractal approach is required to account for the restructuring of agglomerates induced by coating with low volatile organic material, which does not necessarily lead to the formation of completely compact cores (Saathoff et al., 2003).

The COSIMA code is currently employed to analyse and to interpret the experimental results obtained during two extensive SOA campaigns conducted at the AIDA facility of Research Centre Karlsruhe in 2005 and 2006 in collaboration with several external partners. As a typical example Figure 1 compares the time evolution of the SOA mass concentration as determined by a SMPS device with the COSIMA predictions. Here the simulations are based on the simplifying assumption that the particle composition can be described by only two product proxies with highly different volatilities (denoted as comp. 1 and comp. 2 in Figure 1). Please note, however, that COSIMA is principally capable to account for much more detailed product distributions provided the relevant parameters are known or can be extracted from the experimental data.

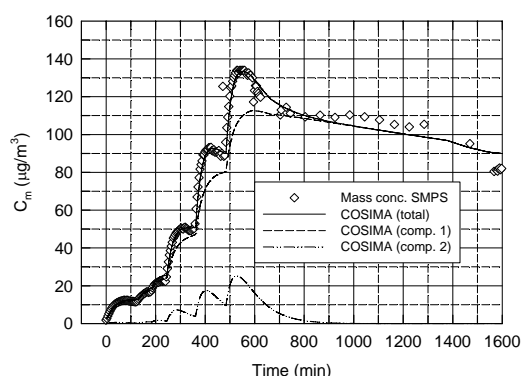


Figure 1. SOA mass evolution during ozonolysis of stepwise increased amounts of  $\alpha$ -pinene in the AIDA chamber and in the long time regime. Comparison between SMPS measurements (symbols) and COSIMA simulation (lines).

The COSIMA model treats the transport of gaseous compounds to and away from the particle surface (including condensation and evaporation as special cases) kinetically, using Dahneke's approach (Dahneke, 1983) to interpolate between the continuum and free molecular regimes. Therefore, non-equilibrium situations e.g. due to transport limitations are properly accounted for.

However, a large amount of work still relies on the assumption that in the course of SOA formation equilibrium is rapidly established between gas and particle phase. A very popular convenient concept has been devised by Pankow, see e.g. Seinfeld and Pankow (2003). In his K- $\alpha$  approach the aerosol yield  $Y = M_0/\Delta HC$  is given by

$$Y = \sum_i Y_i = M_0 \sum_i \frac{\alpha_i K_i}{1 + K_i M_0}$$

where  $M_0$  represents the particle mass concentration produced from the fraction  $\Delta HC$  of the total precursor concentration  $HC$ ,  $\alpha_i$  denotes the mass stoichiometric factor and  $K_i$  the gas phase/particle partitioning constant of component  $i$ , respectively.

A potential drawback of the K- $\alpha$  approach associated with the neglect of non-equilibrium processes could arise from the size dependence of the vapour pressure of small particles due to the Kelvin effect. During the early stages of chamber experiments on SOA formation, for example, constant  $K_i$  values will definitively prove inadequate to describe the observed aerosol dynamics.

Besides introducing the extended capabilities of the COSIMA model by means of simulations of selected recent AIDA SOA experiments, this paper will focus on the predictive efficiency of the K- $\alpha$  approach compared to detailed kinetic process modelling with particular emphasis on the analysis of results from aerosol chamber studies.

Dahneke, B. (1983). in *Theory of dispersed multiphase flow* (Academic Press) 97-133.

Naumann, K.-H. (2003). *J. Aerosol Science*, 34, 1371-1397.

Saathoff, H., Naumann, K.-H., Schnaiter, M., Schöck, W., Möhler, O., Schurath, U., Weingartner, E., Gysel, M., & Baltensperger, U. (2003). *J. Aerosol Science*, 34, 1297-1321.

Seinfeld, J. H., & Pankow, J. F. (2003). *Annu. Rev. Phys. Chem.*, 54, 121-140.

## Transport of fine aerosol particles in turbulent channel flow

A. Pinelli<sup>1</sup> and P.L. Garcia-Ybarra<sup>2</sup>

<sup>1</sup>Unidad de Modelizacion de Procesos, CIEMAT, Av. Complutense 22, Madrid 28040, Spain

<sup>2</sup>Dept. de Fisica Matematica y de Fluidos, Facultad de Ciencias, UNED, Senda del Rey 9, Madrid 28040, Spain

Keywords: aerosol modelling, particle deposition, numerical simulation, turbulence.

The transport & deposition properties of small diffusing aerosol particles very dilute in a channel turbulent flow have been theoretically analyzed by means of an Eulerian description. Aerosol inertia is accounted for by expanding the governing equations in terms of the Stokes number and retaining the first correction (Fernandez de la Mora, 1982). When the Schmidt number  $Sc$  is a large parameter, aerosol deposition on the walls is driven by Brownian and turbulent dispersion in a thin layer of thickness  $Sc^{-1/3}$ , with respect to the viscous sublayer (Garcia-Ybarra & Pinelli, 2006). In the channel core region, the Reynolds-averaged aerosol transport equation across the channel states the counterbalance between turbophoresis and turbulent dispersion (Garcia-Ybarra & Pinelli, 2005).

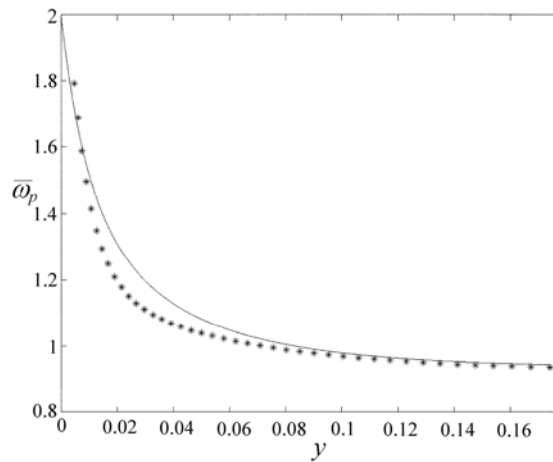


Figure 1. Average profile of aerosol mass fraction. Points (\*): Computed by DNS. Line (—): Predicted by theory with  $Sc_T = 1$ .

When the gradient-diffusion model is used, a profile is obtained with vanishing net flux and high values on the walls (Fig. 1), which enhance aerosol deposition in the thin diffusional layer.

Predictions for the average aerosol distribution with the turbulent Schmidt number (viscous eddy diffusivity to mass eddy diffusivity)  $Sc_T = 1$ , have been compared to DNS results (for  $Re = 3,250$ ). Agreement is not fully satisfactory due to the inadequacy of the constant  $Sc_T$  hypothesis, which close to the wall peaks like the average aerosol mass fraction (Fig. 2 & 3). Variable  $Sc_T$  models are presently being considered.

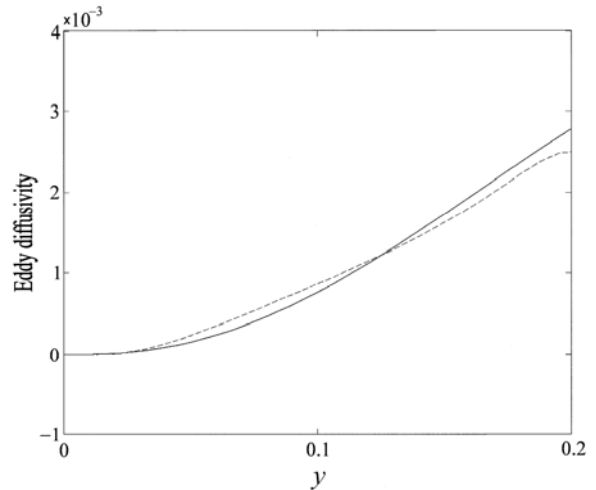


Figure 2. Eddy diffusivities of fluid momentum (—) and aerosol mass fraction (---) near the wall.

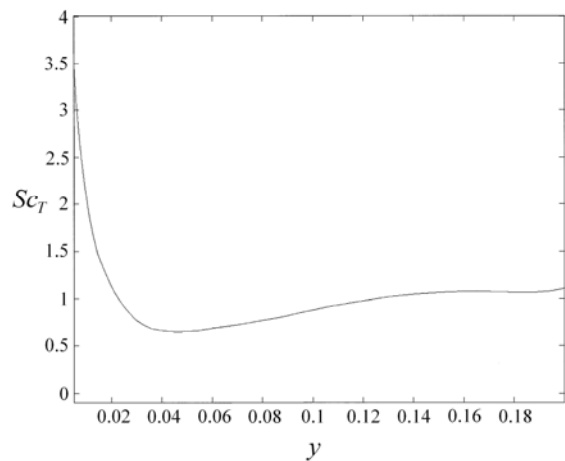


Figure 3. Variation of the turbulent Schmidt number approaching the wall.

This work was supported by Comunidad de Madrid under grant S-505/ENE/0229, and also by the Ministerio de Educacion y Ciencia, Spain, under grants DPI2005-04601 and ENE2005-09190-C04-02.

Fernandez de la Mora, J. (1982). *Phys. Rev. A*, 25, 1108-1122.

Garcia-Ybarra, P.L., & Pinelli, A. (2005). in *Abstract of the EAC 2005*, (Maenhaut Ed.), Ghent, 112.

Garcia-Ybarra, P.L., & Pinelli, A. (2006). *C. R. Mecanique*, 334, 531-538.

## Sensitivity of urban and rural ammonium-nitrate particulate matter to precursor emissions in southern Germany

U. Uhrner<sup>1</sup>, S. Drechsler<sup>2</sup>, R. Wolke<sup>3</sup>, P.J. Sturm<sup>1</sup> and A. Wiedensohler<sup>3</sup>

<sup>1</sup>Traffic and Environment, VKM-THD, Technical University of Graz, Inffeldgasse 81, 8010, Graz, Austria

<sup>2</sup>LUBW, Hertzstrasse 173, 76187, Karlsruhe, Germany

<sup>3</sup>IfT, Permoserstrasse 15, 04318, Leipzig, Germany

Keywords: Particulate Mass, Ammonium nitrate, Aerosol modelling, Emissions, Growth

Fine particulate matter (PM<sub>10</sub>, PM<sub>2.5</sub>) is considered as one of the most important pollutants regarding health effects. European standards for PM<sub>10</sub> (40 µg/m<sup>3</sup> annual mean, max. 35 days above 50 µg/m<sup>3</sup> as daily mean; 2<sup>nd</sup> daughter directive EC/30/99) are difficult to meet in most European cities. During winter time, a significant fraction of PM<sub>10</sub> consists of inorganic species, in particular ammonium nitrate and ammonium sulphate. An inorganic fraction of approximately one third is frequently found in PM<sub>10</sub> probes. During an air pollution episode, the inorganic fraction exceeded 40 µg/m<sup>3</sup> at a busy road in the city centre of Stuttgart in February 2005 (Drechsler et al., 2006). The inorganic fraction was mainly composed of ammonium nitrate and to a lesser extent of sulphate, indicating a major impact of NO<sub>x</sub> emissions and photochemical reactions on secondary aerosol formation.

The sensitivity of secondary ammonium nitrate formation was investigated using a box model approach for the urban area of Stuttgart and the neighbouring rural area Rems-Murr Kreis. The model was used to simulate atmospheric chemistry (Stockwell et al., 1997) and gas/particle partitioning of inorganic compounds (Nenes et al., 1999). Emissions from the detailed UMEG (2004) emission inventory were used. The evolution of the simulated urban particulate matter (PM) ammonium nitrate was found to be highly sensitive to changes in ammonia emissions (see Figure 1). Ammonia, rather than nitric acid was the limiting reagent in urban ammonium nitrate PM formation. In contrast, NO<sub>x</sub> emissions and hence nitric acid was the limiting reagent in the rural case (see Figure 2). Another important parameter in the sensitivity studies is the assumed well mixed layer used within these box model simulations. Decreasing mixing layers lead to stronger ammonium nitrate formation.

The overall behaviour of these model sensitivity studies agrees qualitatively well with composition resolved PM<sub>10</sub> measurements taken next to a busy road (ATV ~80000) in Stuttgart and mixing height computations for the aforementioned episode.

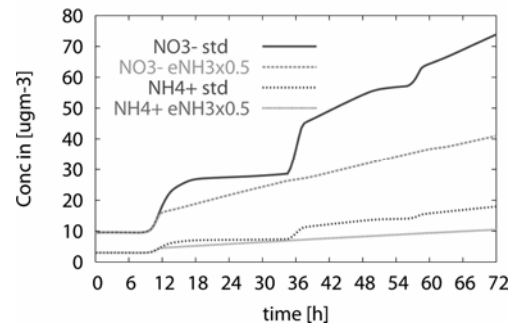


Figure 1. Simulated evolution particulate NO<sub>3</sub> & NH<sub>4</sub> for base run (std) and for 50% reduced NH<sub>3</sub> emissions (eNH<sub>3</sub>x0.5), Stuttgart case.

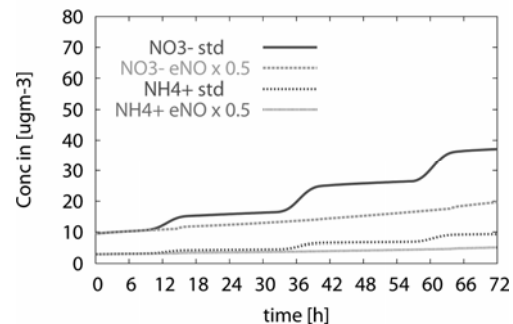


Figure 2. PM NO<sub>3</sub> & NH<sub>4</sub> for base run (std) and for 50% reduced NO<sub>x</sub> emissions (eNO<sub>x</sub> x 0.5), Rems-Murr district case.

Drechsler, S., Ahrens, D., Lump, R., Holst, T. und Uhrner, U., Hohe Feinstaubbelastung als Folge sekundärer Aerosolbildung, Zeitschrift „Immissionsschutz, 06/2006.

Nenes, A., Pandis, S. N., and Pilinis, C., Continued development and testing of a new thermodynamic aerosol module for urban and regional air quality models, Atmos. Environ. 33, 1553-1560, 1999.

Stockwell, W. R., Kirchner, F., Kuhn, M., and Seefeld, S., A new mechanism for regional atmospheric chemistry modeling, JGR, 102, D22, 25847-25879, 1997.

UMEG (2004) Bericht-Nr.4-04/2004 Luftschadstoff-Emissionskataster Baden-Württemberg (air pollution emission data base) 2002.

## Analytical Modeling of Diffusional Nanoparticle Deposition under Low Pressure Conditions

Christof Asbach<sup>1</sup>, Heinz Fissan<sup>1</sup>, Jing Wang<sup>2</sup>, David Y.H. Pui<sup>2</sup>

<sup>1</sup> Institut für Energie- und Umwelttechnik (IUTA), Bliersheimer Str. 60, 47229 Duisburg, Germany  
<sup>2</sup> University of Minnesota, 111 Church Street, Minneapolis, MN 55455, USA

Keywords: Diffusion, Nanoparticle, Contamination

The deposition of nanoparticles can be a major concern, e.g. for clean processing. The manufacture of the next generation of semiconductor chips requires a very clean environment and a low pressure level around 50 mTorr (6.7 Pa) or even below. The lithographic photomasks used are particularly vulnerable because common pellicles can no longer be installed to protect the masks. Several schemes have been developed to protect the photomasks from particle contamination (Asbach *et al.*, 2006) and a fully analytical model to describe the inertial particle motion under low pressure conditions (Asbach *et al.*, 2005) has been established. Diffusional deposition was not included in this model, but estimation revealed that under low pressure conditions diffusional nanoparticle contamination can be a major risk for the cleanliness of the photomasks (Asbach *et al.*, 2007). Based on the existing inertia model, which has been experimentally verified (Kim *et al.*, 2006) and the subsequent estimation of the diffusional particle deposition, an analytical extension of the model has been developed that determines the risks of nanoparticle contamination at low pressure under the influence of gravity, electrophoresis, thermophoresis and drag force. As a first approach the model assumes that inertial and diffusional transport can be decoupled and treated separately. The inertial transport is solved first in the shape of the particle stopping distance using the existing inertia model (Asbach *et al.*, 2005). It is assumed that the diffusional contribution to the stopping distance is negligible, which is justified in most cases, where the stopping distance is much larger than the simultaneous diffusional displacement. The location where the particle stops is taken as the starting point for the diffusion model, as it is assumed that the particle, once stopped, starts to diffuse. When no external forces act on the particle, it

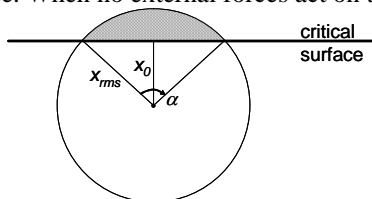


**Figure 1:** Assessment of deposition risk on a critical surface due to Brownian motion

can move in any direction with the same probability. The time dependent root mean square of the probability function can then be expressed as

$$x_{rms} = \sqrt{2Dt}$$

where  $D$  is the diffusion coefficient. The probability of a particle being within a sphere with radius  $x_{rms}$  (see Fig. 1) can thus be determined from the probability density function. The risk of a particle depositing on a critical surface is given by means of the hatched area in Fig. 1.

When external forces, such as gravity, electrophoresis and/or thermophoresis act on the particle, the shape of the sphere is changed to an ellipsoidal shape as illustrated in Fig. 2. However, the principle for the determination of the risk of particle contamination remains the same.

The approach for the model will be presented along with initial comparisons with experimental results.

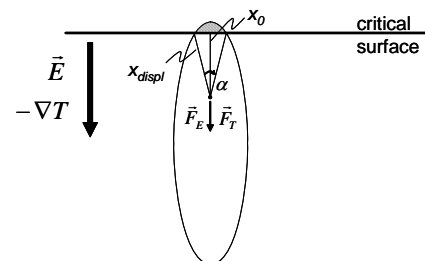


**Figure 2** Assessment of deposition risk on a critical surface due to Brownian motion with thermal and electrical gradient

This work was supported by the Deutsche Forschungsgemeinschaft (DFG).

### References

- Asbach, C.; Fissan, H.; Kim, J.H.; Yook, S.J.; Pui, D.Y.H. (2006), *J. Nanop. Res.* **8**: 705-708  
 Asbach, C.; Kim, J.H.; Yook, S.J.; Pui, D.Y.H.; Fissan, H. (2005), *Appl. Phys. Lett.* **87**: 234111  
 Asbach, C.; Fissan, H.; Kim, J.H. Yook, S.J.; Pui, D.Y.H (2007) *J. Vac. Sci. Technol.* **B25**:47-53  
 Kim, J.H.; Fissan, H.; Asbach, C.; Yook, S.J.; Orvek, K.; Ramamoothy A.; Pui, D.Y.H. (2006) *J. Vac. Sci. Technol.* **B24**: 1178-1184

## **Is the thermodynamic equilibrium an adequate approach for representing fine (PM<sub>1</sub>, PM<sub>2.5</sub>) inorganic aerosol behavior?: ISORROPIA-II simulations under 2005 winter Mexico City conditions.**

**M. Moya<sup>1</sup>, C. Fountoukis<sup>2</sup>, A. Nenes<sup>2,3</sup>, E. Matías<sup>4</sup>**

<sup>1</sup>Centro de Ciencias de la Atmosfera, Universidad Nacional Autonoma de Mexico, Ciudad Universitaria, 04511, Mexico City, Mexico.

<sup>2</sup>School of Chemical and Biomolecular Engineering, Georgia Institute of Technology, 311 Ferst Drive, Atlanta, GA 30332-0100, USA

<sup>3</sup>School of Earth and Atmospheric Sciences Georgia Institute of Technology, 311 Ferst Drive, Atlanta, GA 30332-0100, USA

<sup>4</sup>Posgrado en Ciencias Químicas, Universidad Nacional Autonoma de Mexico, Ciudad Universitaria, 04511, Mexico City, Mexico.

*Keywords:* thermodynamic equilibrium, efflorescence, crustal species

### *INTRODUCTION*

Atmospheric aerosols (particulate matter, PM) reduce local visibility, air quality and have adverse effects on human health. Chemical composition (and size) of PM are important aspects to assess their role in several atmospheric processes occurring in the atmosphere, such as visibility reduction, cloud formation, climate forcing and gas-particle interactions. Simulating the aerosol size and composition is an invaluable tool in increasing our understanding of aerosol behavior and in determining its role in several atmospheric processes.

There have been two main approaches in predicting the partitioning of semi-volatile species between the gas and particulate phases. The first of them uses a fully dynamic mass transfer while the second assumes that the two phases are in thermodynamic equilibrium. Both approaches have been extensively discussed in the literature and arguments have been provided in supporting or not the bulk equilibrium approach. In this work we attempt to provide new information in this regard by applying the recent developed thermodynamic model, ISORROPIA-II (Fountoukis and Nenes, 2007) over Mexico City ambient conditions, characterized for an important diurnal variability of parameters such as T and RH as well as other features e.g. low to-high aerosol nitrate concentrations. In this work, we will be referring to a field study conducted in 2005 (Moya et al., 2007).

### *MODELING FRAMEWORK*

ISORROPIA-II is the new version of ISORROPIA (Nenes et al., 1998). It includes the thermodynamics of crustal species which has been pointed in recent studies in this megacity (Moya et al., 2006, 2007) as relevant in the (PM<sub>2.5-1</sub>) size

fraction. The model considers both branches of aerosol behavior (deliquescence, efflorescence) and an updated water activity dataset. Details of ISORROPIA are depicted in Fountoukis and Nenes, 2007.

### *RESULTS*

ISORROPIA-II predicts adequately fine particulate (PM<sub>1</sub>, PM<sub>2.5</sub>) ammonium (within 30% of error). PM<sub>2.5</sub> nitrate is predicted adequately for RH cases with moderate RH (40-70%) by applying the deliquescence branch of aerosol behavior. For low RH cases (20-30%), the metastable approach of aerosol behavior is more adequate in representing particulate concentrations. Under conditions of this megacity (high T, very low RHs), the consideration of both branches should be taken into account, depending on the history of the particle, as first suggested by Seinfeld and Pandis (1998).

### *ACKNOWLEDGEMENTS*

This work has been funded by the National Oceanic and Atmospheric Administration (NOAA-US) under contract NMRAC000-5-04017 (A. Nenes) and by the National Council for Science and Technology (CONACyT-Mexico) under contract J51782 (M. Moya). Support of PAPIIT-UNAM grant (reference: IN107306) is also acknowledged.

### *REFERENCES*

- Fountoukis, C. and Nenes, A.* 2007. ACPD, 7, 1893-1939.
- Moya et al.* 2006. Proceeding of the 2006 American Geophysical Union Fall Conference.
- Moya et al.*, 2007. Analysis of fine inorganic particulate matter during the 2003, 2005, 2006 field studies in downtown Mexico City. Work in progress.
- Nenes et al.* 1998. Aquatic Geochem. 4, 123-152.

## Modelling on H<sub>2</sub>SO<sub>4</sub>-H<sub>2</sub>O particle formation and growth in the diluting diesel exhaust

L. Pirjola<sup>1,2</sup>, F. Arnold<sup>3</sup>, T. Schuck<sup>3</sup>, J. Keskinen<sup>4</sup>, T. Rönkkö<sup>4</sup>, T. Lähde<sup>4</sup>,  
K. Hämeri<sup>1,5</sup>, A. Sorokin<sup>3</sup>, and D. Rothe<sup>6</sup>

<sup>1</sup>Department of Physical Sciences, University of Helsinki, P.O. Box 64, FIN-00014 Helsinki, Finland

<sup>2</sup>Department of Technology, Helsinki Polytechnic, P.O. Box 4020, FIN-00099 Helsinki, Finland

<sup>3</sup>Atmospheric Physics Division, Max Planck Institute for Nuclear Physics (MPIK), P.O. Box 103980, D-69029 Heidelberg, Germany

<sup>4</sup>Aerosol Physics Laboratory, Institute of Physics, Tampere University of Technology, P. O. Box 692, FIN-33101 Tampere, Finland

<sup>5</sup>Department of Physics, Finnish Institute of Occupational Health, Topeliuksenkatu 41, FIN-00250 Helsinki, Finland

<sup>6</sup>MAN Nutzfahrzeuge AG, Abt. MTVN, Abgasnachbehandlung / Partikelmesstechnik, Vogelweiherstr. 33, D-90441 Nürnberg, Germany

Keywords: nucleation, sulphuric acid, filters, number concentration, size distribution.

Formation of particles in the cooling exhaust is still poorly understood. Evidence for homogeneous H<sub>2</sub>SO<sub>4</sub>-H<sub>2</sub>O nucleation has been shown, but also some other mechanisms such as condensation of volatile organics onto the core particles formed in the combustion process have been suggested. Particle formation depends on driving parameters, fuel and lubricant oil properties as well as exhaust after-treatment systems. Diesel particle filters (DPF) remove soot mode but due to lowered condensation sink of gaseous sulphuric acid (GSA), nucleation is promoted (e.g. Graves, 1999). On the other hand, oxidizing catalysts may enhance GSA formation.

In this work, diesel exhaust particle formation was studied by a sectional atmospheric chemistry and aerosol dynamics box model AEROFOR (Pirjola, 1999; Pirjola & Kulmala, 2001). The model includes gas phase chemical reactions, formation of thermodynamically stable clusters by homogeneous H<sub>2</sub>SO<sub>4</sub>-H<sub>2</sub>O nucleation (Vehkamäki *et al.*, 2003), condensation of H<sub>2</sub>SO<sub>4</sub>, H<sub>2</sub>O and an organic vapour onto particles, temperature cooling and dilution profiles (Lemmetty *et al.*, 2006), as well as wall losses in the ageing chamber. In this work 100 size sections were used. Besides the classical H<sub>2</sub>SO<sub>4</sub>-H<sub>2</sub>O nucleation mechanism also a kinetic model by Sorokin *et al.* (2005) is studied.

The input values were taken from the measurements made at the MAN laboratory by testing a heavy duty EUROIV standard diesel engine with different after-treatment systems and different engine loads. Fuel sulphur contents (FSC) of 7 and 36 ppmM were used. GSA was measured by a CIMS instrument (Arnold *et al.*, 2007) and number concentration of particles larger than 3 nm (N<sub>3</sub>) by a SMPS. The final dilution ratio at the end of the ageing chamber was 12. Temperature was measured in the raw exhaust and just before the ageing chamber, from which the time constant for cooling was found to be around 0.28 s. The free parameter was time constant for dilution. The total simulation time was 2.7 s.

Figure 1 shows the formed N<sub>3</sub> and particle volume concentration at the end of the ageing chamber as a function of the initial GSA. Variation in the GSA reflects different FSC and engine loads when a coated catalytic DPF was used. Huge number of particles were mostly formed, however, if GSA is less than 2x10<sup>11</sup> cm<sup>-3</sup>, no particle formation was observed.

The modelled concentrations and size distributions are compared with the measurements. Differences in the volume concentrations give some elucidation of the role of organic vapours in the particle growth which will be discussed.

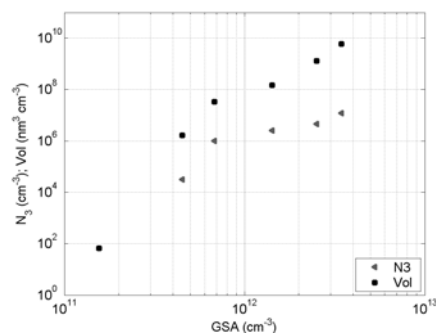


Figure 1. Particle number and volume concentration as a function of raw exhaust GSA

Arnold, F. et al. (2007) *This issue*.

Graves, R.L. (1999) *SAE Technical Paper Series*, No. 1999-01-2245.

Lemmetty, M., Pirjola, L., Mäkelä, J.M., Rönkkö, T., and Keskinen, J. (2006) *J. Aerosol Sci*, 37, 1596-1604.

Pirjola, L. (1999) *J. Aerosol. Sci.*, 30, 355-367.

Pirjola, L. and Kulmala, M. (2001) *Tellus*, 53B, 491-509.

Sorokin, A., Vancassel, X., and Mirabel, P. (2005) *J. Chem. Phys.*, 123, 22508.

Vehkamäki, H., Kulmala, M. and Lehtinen, K.E.J. (2003) *Environ. Sci. Technol.* 36, 283-289.

## A stochastic Langevin model of particle dispersion in turbulent flows with active thermophoresis

A. Dehbi

Department of Nuclear Energy and Safety, 5232 Villigen PSI, Switzerland

Keywords: continuous random walk, Langevin equation, inhomogeneous turbulence, thermophoresis

Recent Direct Numerical Simulations (DNS) (Marchioli *et al.*) and experimental data (Wang *et al.*) have shown that inertial particles exhibit concentration peaks in isothermal turbulent boundary layers. It is therefore expected that turbulence will significantly enhance thermophoretic deposition in flows where walls are colder than the carrier gas. To correctly capture turbulent particle dispersion with active thermophoresis, a Lagrangian continuous random walk (CRW) model is developed. The particle tracking model uses 3D mean flow data obtained from the Fluent CFD code, as well as Eulerian statistics of instantaneous quantities computed from DNS databases. The turbulent fluid velocities at the current time step are related to those of the previous time step through a Markov chain based on the normalized Langevin equation (Iliopoulos & Hanratty 1999) which takes into account turbulence inhomogeneities. The model includes a correction to reduce the “spurious drift” of tracer-like particles which manifests itself in isothermal flows as an unphysical preferential concentration of fluid-like particles near the walls. This correction involves the addition of a “drift velocity” (Bocksell & Loth 2006) and yields improved results in isothermal flows such that tracer-like particles retain approximately uniform concentrations if introduced uniformly in the domain, and the deposition velocity of tracer particles is vanishingly small, as it should be.

The mean thermophoretic force is added as a body force on the particle and follows the formulation by Talbot *et al.* (1980), which gives the best agreement with a large set of data.

The 3D geometry is subdivided into a bulk region where isotropic turbulence is predominant, and a boundary layer region where anisotropic effects are significant. In the boundary layer, arbitrary geometries are tackled by first computing at each time step the rms values of velocities in a “local” particle coordinate system constructed from the mean velocity vector  $I$  (stream-wise component), the wall-normal component  $J$ , and the span-wise component given by the cross product  $I \times J$ . The rms values in the local coordinates are transformed back to the computational coordinates to perform the particle tracking one additional time step. In this procedure, it is assumed that the rms velocity values in general geometries can locally be approximated by the DNS

data of fully developed flows in channel geometry. While clearly an approximation, the latter assumption provides a closer prediction of reality than taking turbulence to be isotropic all the way to the wall.

Benchmarks of the model are performed against recent integral thermophoretic deposition in long pipes ( $L/D=275$ ) at  $Re=6500$  (Tsai *et al.*) as well as the TUBA tests (Dumaz *et al.*) with their detailed local deposition measurements (see Figure 1). In both cases, the agreement with the data is quiet good.

Overall, it is shown that Lagrangian CRW, coupled with DNS data of Eulerian statistics and CFD data of the mean flow field, is able to accurately predict the dispersion and hence thermophoretic deposition of particles in turbulent flows.

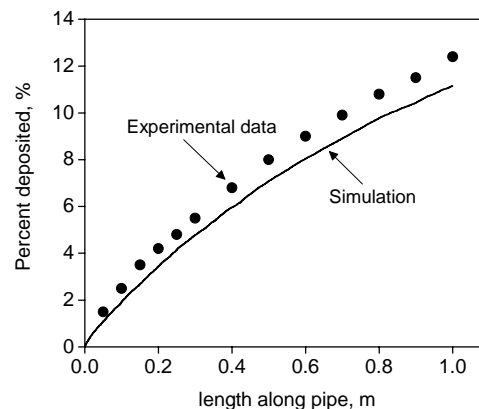


Figure 1. Comparison between CRW model predictions and the TUBA TT28 test

- Marchioli, C., Soldati, A. (2002). *J. Fluid Mech.*, 468, 283-315.
- Wang, J., Levy, E. (2006). *Experimental Thermal and Fluid Science*, 30, 473-483.
- Iliopoulos, I., Hanratty, T.J. (1999). *J. Fluid Mech.*, 392, 45-71.
- Talbot, L., Cheng, R., Schefer, R., Willis, D. (1980). *J. Fluid Mech.*, 101, 737-758.
- Bocksell, T.L., Loth, E. (2006). *Int. J. Multiphase Flow*, 32, 1234-1256.
- Tsai, C.-J., Lin, J.-S., Aggarwal, S.G., Chen, D.-R., (2004). *Aerosol Science and Technology*, 38, 131-139.
- Dumaz, P., Drossinos, Y., Areia Capito, J., Drosik, I. (1993). in *ANS Proc. 1993 National Heat Transfer Conference*, Atlanta, GA, 48-358.



## Modelling of Workplace Nanoparticle Exposure

Christof Asbach, Heinz Kaminski, U. Rating, Heinz Fissan, and Thomas A.J. Kuhlbusch

Institut für Energie- und Umwelttechnik (IUTA), Bliersheimer Str. 60, 47229 Duisburg, Germany

Keywords: Occupational Health, Exposure, Nanoparticles, CFD

The inhalation of particles at nano-scale is currently being discussed to induce adverse health effects such as inflammation. Particles in this size range can either originate from unintended anthropogenic or natural generation processes (e.g. combustion, nucleation) or can be intentionally engineered nanoparticles. Especially exposure to engineered nanoparticles in workplaces has recently raised increased interest (e.g. SCENIHR 2005) as these particles are usually produced in high concentrations and inhaled particle concentrations can thus be very high in case of (accidental) release. Monitoring of nanoparticle exposure at workplaces in the nanotechnology industry is thus an important issue for assessing the safety of workers.

Only very few studies have been published that report actual workplace measurements (e.g. Kuhlbusch *et al.* 2004 & 2006). However, for an expedient investigation of possible workplace exposure as well as save work place design it is essential to understand the behaviour and dispersion of particles within a workplace. Precise modelling of particle dispersion and physical reactions can therefore help to improve work place design, identify hot spots within the room, and give guidance for the definition of suited measurement locations. Furthermore, such simulations can provide a three dimensionally resolved picture of the exposure scenario. Therefore exposure can also be inferred from the model based on the posture of the worker, e.g. whether he is sitting or standing.

In this work, three exemplary, realistic workplaces have been simulated using the commercial computational fluid dynamics (CFD) code FLUENT, along with the Fine Particle Model (FPM). A software platform has been developed that simplifies the set up of common workplace geometries. The modelled scenarios comprise 1) a welding workplace, 2) a large hall with several pipes and a reactor with nanoparticles trickling from a conveyor belt, and 3) a hall with a leak in a slightly pressurized transport pipe of freshly formed nanoparticles. Besides convective transport of the particles and dilution with background air (assumed to be particle free), the considered physical processes also comprised sedimentation and coagulation. The welding workplace modelled was a real workplace that was subject to measurements of the particle size distributions (unpublished). The modelling results were compared with the measured data and found to be in good agreement. Scenario 2 included only

minor air movements and exemplarily showing the distribution of nanoparticles almost within the entire room. Scenario 3 was used to study the behaviour of particles, particularly when released at high concentrations and thus prone to coagulation. It was assumed that 50 nm particles ( $\sigma_g = 1.1$ ) were released at a very high concentration of  $10^{19} \text{ m}^{-3}$  from a leak in a slightly pressurized transport pipe 1.5 m above ground into a 10 m x 10 m x 5 m hall with two open windows on the sides and three apertures in the roof. Exposure was investigated at levels of 1.0 m and 1.50 m above ground to mimic the breathing height of a sitting and standing worker, respectively. It was found that exposure can vary significantly depending in the breathing height and location within the hall (Figure 1). The changes in the particle size that can be seen in the graph were caused by coagulation, whereas additionally dilution caused the concentration to drop by several orders of magnitude.

Results from the different simulated scenarios will be presented along with recommendations for representative and conclusive modelling of workplace exposure to nanoparticles.

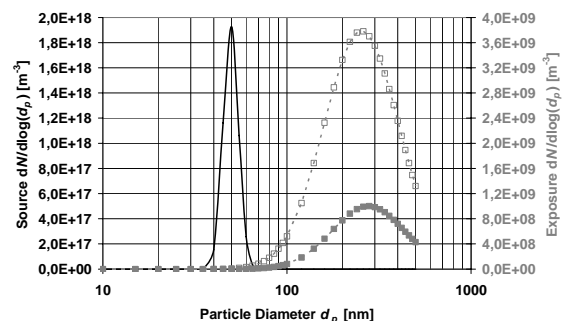


**Figure 1:** Simulated size distribution changes from source (left peak, primary axis) to exposure (1.5 m (■) and 1.0 m (□) above ground, secondary axis) near a window (1.5 m above ground)

This work has been supported by the government of Northrhine Westfalia and the European Union under grant number 005-0406-0004.

Kuhlbusch, T.A.J., H. Fissan (2006): *J. Occ. Env. Hyg.* **3**: 558-567

Kuhlbusch, T.A.J., S. Neumann, H. Fissan (2004): *J. Occ. Env. Hyg.* **1**: 660-671

SCENIHR (2005). [http://europa.eu.int/comm/health/ph\\_risk/committees/04\\_scenihr/docs/scenihr\\_o\\_003.pdf](http://europa.eu.int/comm/health/ph_risk/committees/04_scenihr/docs/scenihr_o_003.pdf)

## Particle deposition on a semiconductor wafer larger than 100 mm in diameter

Kun-Hyung Lee<sup>1</sup>, Gun-Soo Song<sup>2</sup>, Kyung-Hoon Yoo<sup>2</sup> and Seung-Ki Chae<sup>1</sup>

<sup>1</sup> Micro Contamination Control Group, Manufacturing Technology Center, Semiconductor Business, SAMSUNG Electronics, San #16, Banwol-Ri, Taean-Eup, Hwasung-Si, 445-701, South Korea

<sup>2</sup> Aerosol and Contamination Control Laboratory, Korea Institute of Industrial Technology (KITECH), 35-3, Hongcheon-Ri, Ibjang-Myun, Cheonan-Si, 330-825, South Korea

Keywords: deposition velocity, semiconductor wafer, wafer diameter.

Since the year of 2000, the semiconductor wafer diameter has been changed from 200 mm to 300 mm. However, so far, there have not been sufficient theoretical studies on particle deposition on a semiconductor wafer larger than 100 mm in diameter. In the present study, the characteristics of particle deposition velocity on the upper surface of 100, 200 mm sized wafers were investigated both experimentally and numerically.

Figure 1 shows the schematic diagrams of the present experimental apparatus and numerical calculation domain, respectively. Experiments were conducted in an ISO class 2 clean room of the line 14 fab of SAMSUNG Electronics Co. The wafer diameter and particles in the present experimental study were 200 mm and PSL particles, respectively. The governing equations of gas flow, energy and particle concentration for steady, incompressible and axis symmetric laminar flow with constant properties were considered in the present numerical study. For the details of the present numerical methods, readers can refer to those of 100 mm-diameter wafer by Yoo & Oh(2005).

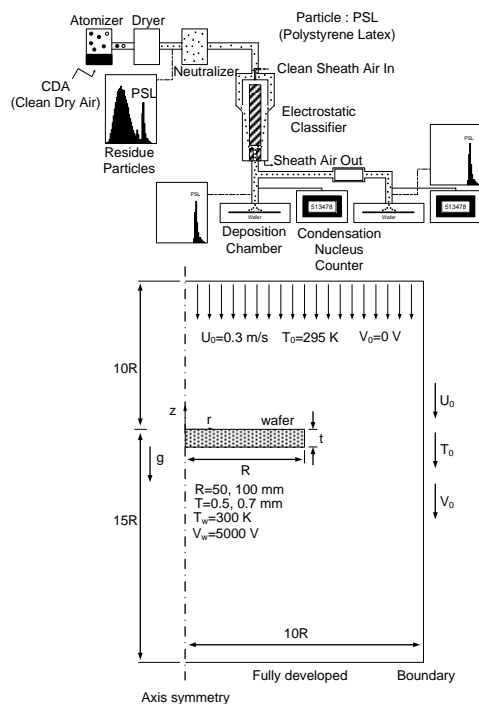


Figure 1. Schematic diagrams of the present experimental apparatus and calculation domain.

Figure 2 shows variations of the averaged deposition velocities on the upper surface of wafer with respect to particle size. It can be seen in the figure that the deposition velocity of 200 mm wafer is larger than that of 100 mm wafer. The increase of wafer diameter causes the fluid velocity boundary layer to be much thinner. This thinner fluid velocity boundary layer causes the particle concentration boundary layer to become much steeper and leads to consequent increase in the deposition velocities for the diffusion-dominant particle sizes generally less than  $0.1 \mu\text{m}$ . While in the particle sizes larger than  $1 \mu\text{m}$  no difference is found because of gravitational settling dominance. It is also shown that in the curves for the charged wafer with 5000V the particle deposition velocities are rapidly increased in the particle size range generally less than  $1.0 \mu\text{m}$ . Meanwhile, the present numerical results show relatively good agreement with the present experimental results and those of Ye et al.(1991) and Opiolka et al.(1994).

Yoo, K. H., & Oh, M. D. (2005). *J. Aerosol Science*, 36, 235-246.

Opiolka, S., Schmidt, & Fissan H. (1994). *J. Aerosol Science*, 25, 4, 656-671.

Ye, Y., Pui, D.Y.H., Liu, B.Y.H., Opiolka, S., Blumhorst, S. & Fissan, H. (1991). *J. Aerosol Science*, 22, 63-72.

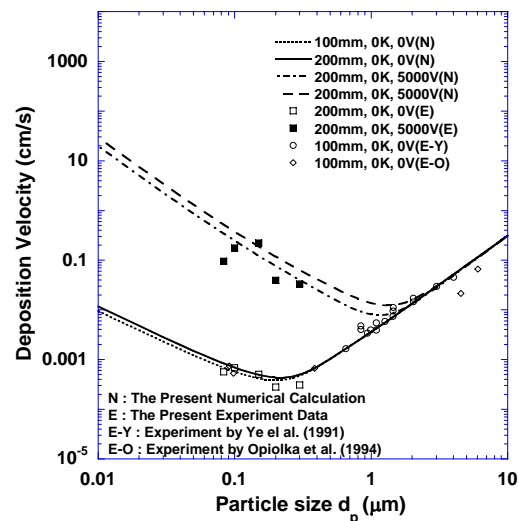


Figure 2. Variation of the averaged deposition velocity with respect to particle size.

## Mixed effects regression model in the analysis of 50nm particle number concentration

S. Mikkonen<sup>1</sup>, K. E. J. Lehtinen<sup>1,2</sup>, A. Hamed<sup>1</sup>, J. Joutsensaari<sup>3</sup> and A. Laaksonen<sup>1</sup>

<sup>1</sup>Department of Physics, University of Kuopio, P.O.B 1627, FIN-70211 Kuopio, Finland

<sup>2</sup>Finnish meteorological institute, P.O.B 1627, FIN-70211 Kuopio, Finland

<sup>3</sup>Department of Environmental Sciences, University of Kuopio, P.O.B 1627, FIN-70211 Kuopio, Finland

Keywords: Atmospheric aerosols, particle concentration, mixed effects regression.

It is well known, that atmospheric aerosols have a great effect on radiation budget, formation of clouds and on climate change. Despite of several years of research, many of the factors affecting the new particle formation and the growth of new formed particles remain unclear. Kulmala et al. (2004) studied several physical and chemical properties affecting particle growth and suggested that the factors affecting new particle formation and growth vary between locations.

Our dataset consists of measurements made between 24.3.2002 - 30.4.2005 at San Pietro Capofiume (SPC) station in the Po Valley area, Italy. The concentration of particles was measured by using a twin Differential Mobility Particle Sizer (DMPS) system. More details of the measurements can be found in Hamed et al. (2007).

The aim of our study was to predict the number of 50nm particles with various different factors, i.e. to find the factors affecting the growth of freshly nucleated particles to 50nm size. Most of our models were combinations from hourly averages of gas and meteorological parameters measured at SPC, including temperature, relative humidity, radiation, O<sub>3</sub>, SO<sub>2</sub>, NO<sub>2</sub>, condensation sink, wind speed and -direction and the probability that the day is a nonevent day i.e. a day when significant new particle formation cannot be seen. The probability of a nonevent day (PrNE) was calculated with discriminant analysis, details of the method can be found from Mikkonen et al. (2006). PrNE was favoured instead of probability of event day due to better predicting ability. The calculated nonevent probability was used instead of observed event classification because otherwise we would have had to exclude the unclassified days, which would have subsidised the data drastically. In addition, the probabilities of a nonevent day can be estimated also for those days where the event classification has not been made at all.

Due to complex structure of processes affecting to concentration of small particles it is not reasonable to use general linear effect models in the analysis. We chose to use generalized linear models with logarithmic link function and combine it with mixed model structure (McCulloch and Searle, 2001). The main idea of a mixed model is to estimate, not only the mean of the measured response

variable  $y$ , but also the variance-covariance structure of the data.

We found out that RH, PrNE and the concentration of SO<sub>2</sub> had significant additional variance components for different times of year. When the additional variance is taken into account, the model suggests that the effect of RH is negative in January and in December and positive for the rest of the year. The decreasing effect of PrNE is on its highest in January, June and July, and the effect of SO<sub>2</sub> concentration is negative in winter months (from Nov. to Apr.) and positive for the rest of the year.

Significant weekend effects have been reported for several pollutants (e.g. Marr and Harley, 2002). This reflects also to particle concentrations: Tuesday, Wednesday and Thursday seem to have the highest effects on the concentration of 50nm particles. Effect varies slightly between months.

Wind direction showed out to have a significant effect on the behaviour of some of the predictor variables. The effect of local wind speed is mainly positive, i.e. the particle number is higher when the wind speed is higher, except for the winds coming from northeast, south and southwest. The effect of Condensation Sink is on its lowest on north, northwest and west, respectively. These are the directions to the highly populated areas but also the directions to the mountains.

Effect of Ozone varies within the day; positive effect can be detected on daytime and negative effect on night. The coefficient of determination R<sup>2</sup> for the model is 0.61 which indicates that the model explains roughly 61% of the total variation of the particle concentration.

This work was supported by Graduate school in Physics, Chemistry, Biology and Meteorology of Atmospheric composition and climate change

Hamed, A., et al. (2007). *Atmos. Chem. Phys.*, 7, 355-376

Kulmala, M., et al. (2004). *J Aerosol Sci*, 35,143-176

Marr L.C. and Harley R.A. (2002). *Atmospheric Environment*, Vol. 36, 2327-2335.

McCulloch, C. and Searle, S. R. (2001). *Generalized, Linear, and Mixed Models*, New York: Wiley.

Mikkonen, S., et al. (2006): *Atmos. Chem. Phys.*, 6, 5549-5557.

## **T13 Abstracts**

(no T13 Abstracts)

## **T14 Abstracts**

## Raman microscopic analysis of changes in structure and reactivity of soot undergoing oxidation and gasification by oxygen

M. Knauer, M. Carrara, R. Niessner and N.P. Ivleva

Technical University of Munich, Institute of Hydrochemistry, Marchioninstr. 17, D-81377 Munich, Germany

Keywords: Soot particles, soot structure, soot reactivity, Raman Microscopy (RM)

Soot particles from diesel engines have become recently an important subject in environmental, scientific, and political discussions. Soot particles are hazardous environmental pollutants and account for a major fraction of fine air particulate matter in urban areas. They can cause and enhance respiratory, cardiovascular, and allergic diseases, and they influence atmospheric chemistry, physics, and climate (Oberdörster, *et al.*, 2005).

Efforts in reduction of soot particulate from diesel engine exhaust can be achieved by use of after-treatment systems. These technologies generally require a regeneration method, which efficiently oxidises and gasifies soot deposits in the filter or catalyst structures. A prerequisite for further technical improvement of soot particulate after-treatment systems is comprehensive information about the microstructure, and oxidative behaviour of soot originating from diesel engines. Usually high resolution electron microscopy (HRTEM), thermal gravimetry (Su *et al.*, 2004) and kinetic experiments (Messerer *et al.*, 2005) are used to investigate the microstructure and oxidation behaviour of the soot particles. These investigations have shown that differences in the oxidation behaviour of different types of soot are associated with the different microstructures.

Our recent study has demonstrated that Raman microscopy (RM) can be applied to investigate changes in the structure and reactivity of soot upon oxidation and gasification by nitrogen oxides and oxygen in a diesel exhaust after-treatment model system at 523 and 573 K (Ivleva *et al.*, 2006). RM provides fingerprint spectra, which allow the distinction of a wide range of chemical substances with the spatial resolution of an optical microscope. The first-order Raman spectra of soot are generally characterized by two broad and strongly overlapping peaks with intensity maxima near 1580 (G or "Graphite" peak) and 1350  $\text{cm}^{-1}$  (D or "Defect" peak). Based on experimental observations and theoretical calculations, up to five bands corresponding to different vibration modes in the sample have been suggested to account for the observed spectra (Sadezky *et al.*, 2005).

We have applied RM to follow structural changes in spark discharge (GfG) soot and light duty diesel vehicle (LDV) soot upon oxidation and gasification by oxygen (5%  $\text{O}_2$  in  $\text{N}_2$ ) at 473 – 773 K with a heating rate of 5 K/min. Raman spectra have

been recorded before and during the oxidation process, and spectral parameters have been determined by curve fitting (Sadezky *et al.*, 2005) with five bands (G, D1-D4). Figure 1 shows the evolution (narrowing of peaks) in the spectra of GfG soot in the oxidation process (473 – 773 K with 50 K step). Analysis of spectral parameters showed pronounced decrease of the relative intensity of the D3 band for GfG soot, which suggests rapid preferential oxidation of a highly reactive amorphous carbon fraction. Moreover width of D1 band exhibited a pronounced decrease with increasing temperature, indicating an increase of structural order and decrease of chemical heterogeneity in GfG soot undergoing oxidation. In our future work we plan to combine RM, kinetic experiments, and HRTEM to obtain precise information about structure-reactivity-relationship for different soot samples.

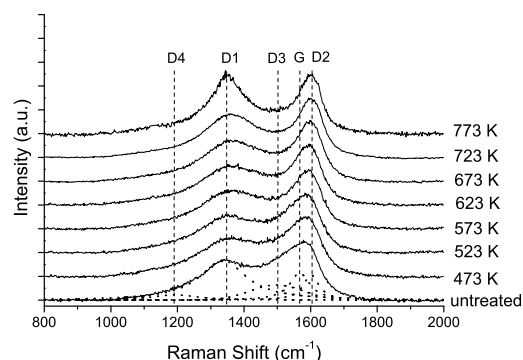


Figure 1. Raman spectra ( $\lambda_0 = 514 \text{ nm}$ ) of partially oxidized (473 – 773 K) and untreated GfG soot with five band fit (dotted lines).

- Ivleva, N. P., Messerer, A., Yang, X., Niessner, R., & Pöschl, U. (2006) *Environmental Science and Technology*, in press.
- Messerer, A., Niessner, R., & Pöschl, U. (2006) *Carbon*, 44, 307-324.
- Oberdörster, G., Oberdörster, E., & Oberdörster, J. (2005) *Environmental Health Perspectives*, 113, 823-839.
- Sadezky, A., Muckenhuber, H., Grothe, H., Niessner, R., & Pöschl, U. (2005) *Carbon*, 43, 1731-1742.
- Su, D. S., Jentoft, R. E., Müller, J. O., Rothe, D., Jacob, E., Simpson, C. D., Tomovic, Z., Müllen, K., Messerer, A., Pöschl, U., Niessner, R., & Schlögl, R. (2004) *Catalysis Today*, 90, 127-132.

## PARTICLE CONCENTRATION AND CHARACTERISTICS NEAR A MAJOR FREEWAY WITH HEAVY-DUTY DIESEL TRAFFIC

Leonidas Ntziachristos, Ning Zhi, Michael D. Geller and Constantinos Sioutas  
 Department of Civil and Environmental Engineering, University of Southern California,  
 Los Angeles, California 90089, USA

Keywords: diesel emissions, ultrafine particles, urban aerosols

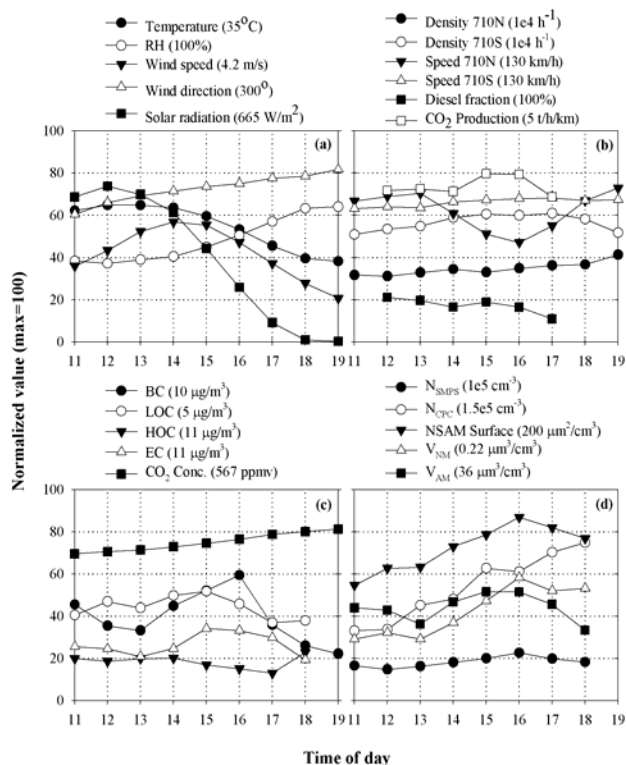
In this study, detailed information is provided on the physical and chemical characteristics of particles originating from a major freeway during the winter season, with a significant heavy-duty vehicle (HDV) fraction. This was accomplished by measuring semi-continuous and time-integrated particle number, surface area, mass and chemistry adjacent to I-710 from February to April 2006. The results are compared to previous studies, after correcting for the dilution ratio in different sampling locations, and a regression analysis is conducted to reveal the effect of meteorology and traffic conditions on the observed particle concentrations.

The I-710 freeway is a 26 m wide eight-lane highway connecting the ports complex of Long Beach and San Pedro to the shipping yards in East Los Angeles. For this reason, as much as 25% diesel traffic has been reported on this freeway. Total traffic counts are also very high, with between 150,000-200,000 vehicles per day passing the sampling location. Both gaseous and particulate pollutant concentrations were measured with various continuous and time-integrated instruments, approximately 10 m from the shoulder of the freeway. The prevailing southwesterly winds transported the fresh freeway emissions to the sampling location.

Figure 1 shows the averaged diurnal trends of the various parameters categorized as (a) meteorological and (b) traffic conditions, and (c) particle chemical and (d) physical properties. The y-axis is the normalized value of the different parameters with  $y = 100$  equal to the values listed in brackets for each parameter. The x-axis in the figures shows the sampling hour, which ranges from 11:00 to 19:00. As the day progressed, relative humidity increased while the temperature and solar radiation decreased. Wind speed was consistent throughout the day with a small peak in the early afternoon while total traffic volume on the freeway was consistent during the sampling period, with slight increases during morning and afternoon rush hours

Our study made it possible to compare particle concentrations measured next to the freeway to concentrations measured in roadway tunnels and in vehicle exhaust. In addition to the effect of the dilution ratio on the measured particle concentrations, multivariate linear regressions showed that light and heavy organic carbon

concentrations are positively correlated with the particle volume in the nucleation and accumulation modes respectively. Solar radiation was also positively correlated with the particle surface concentration and the particle volume in the accumulation (40-638 nm) mode, presumably as a result of secondary particle formation. The methods developed in this study may be used to decouple the effect of sampling position, meteorology and fleet operation on particle concentrations in the proximity of freeways, roadway tunnels and in street canyons.



This research was supported by the Southern California Particle Center (SCPC), funded by EPA under the STAR program through Grant RD-8324-1301-0 to the University of Southern California. The research described herein has not been subjected to the agency's required peer and policy review and therefore does not necessarily reflect the views of the agency, and no official endorsement should be inferred. Mention of trade names or commercial products does not constitute an endorsement or recommendation for use.

## Oil mist emission by crank case ventilation from medium speed 4-stroke Diesel engines

P. Lauer<sup>1</sup>

<sup>1</sup>MAN Diesel SE, Stadtbachstrasse 1, 86224 Augsburg, Germany

Keywords: Oil mist, VOC(s), Organic carbon, PM measurements, Diesel exhaust.

Besides reduction of exhaust gas emissions like nitrogen oxides (NO<sub>x</sub>), carbon monoxide (CO), sulfur oxides (SO<sub>x</sub>), hydrocarbons (HC) and particulate matter (PM) from large medium speed four stroke Diesel engines (Lauer, 2005), also volatile organic compounds (VOC) may be considered. Up to now there is only limited knowledge available of VOC emission from large Diesel engines. Oil mist may be considered as VOC emission therefore detailed measurements and chemical analysis have been performed.

The major source of oil mist is the crank case ventilation of the engine and the turbo charger sealing air. A minor source is the ventilation of the lube oil tank. These gases are usually vented to the atmosphere. Direct measurement techniques for VOC do not exist, therefore indirect methods had to be used.



Figure 1: PM dilution system for Diesel exhaust gas.

The characteristics of the oil mist depend on different formation mechanisms. Coarse oil droplets are centrifuged off moving parts of the engine like crankshaft or piston. Fine droplets are nebulized by the blowby gas passing through the piston ring package. Finally micro droplets condense from vaporized lube oil. A dilution system (figure 1) according to ISO-8178 was used for the measurements. The collected PM filters have been analyzed chemically. Size distribution was measured by optical particle counter (OPC) and differential mobility analyzer (DMA).

Oil mist size distribution (figure 2) and concentration (figure 3) is mainly influenced by the engine load. Major differences can be seen in the size range between 0.1 to 1µm in the order of one magnitude. The chemical analysis confirmed that the crank case gas aerosols are mainly composed of organic carbon. Furthermore different treatment devices e.g. cyclone, electrostatic precipitator, rotating disk separator and filtration have been investigated.

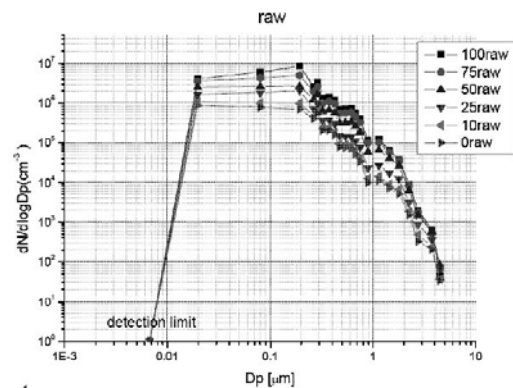


Figure 2: Oil mist size distribution at different loads.

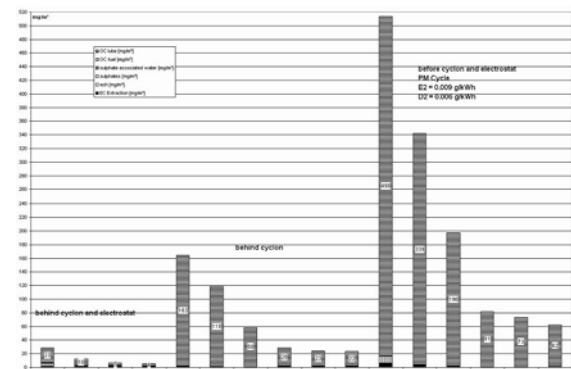


Figure 3: Oil mist concentration and composition at different loads and for different treatment devices.

### Acknowledgements:

Germanischer Lloyd, 20459 Hamburg, Germany, for chemical analysis of the PM filters.

Institut für Physik der Atmosphäre, DLR Oberpfaffenhofen, 82234 Wessling, Germany, for PM size distribution measurement.

Lauer, P. (2005). *Particulate emission and composition from marine Diesel engines for different fuels*: European Aerosol Conference 2005, Gent.

## Quantification of water uptake by combustion (soot) particles

O.B. Popovicheva<sup>1</sup>, N.M.Persiantseva<sup>1</sup> and N.K.Shonija<sup>2</sup>

<sup>1</sup>Institute of Nuclear Physics, Moscow State University, 119 992, Moscow, Russia

<sup>2</sup>Department of Chemistry, Moscow State University, 119 992, Moscow, Russia

Keywords: black carbon, soot particles, chemical properties, hygroscopicity, organic carbon

Carbonaceous (soot) aerosols emission from transport systems, industry, biomass burning and its indirect effect on the atmosphere is currently acknowledged to be the largest source of uncertainties in understanding the anthropogeneous aerosol impact on the global climate. The main reason is the significant role playing by soot aerosol in cloud formation, from one side, and a deep lack in the knowledge of water uptake by original soot particles, from the other side. It was recently concluded that soot appears to be the most important aerosol impacting clouds formation from aviation.

Soot particles emitted into atmosphere from a great variety of combustion sources have a wide range of a natural variability, including the ability to uptake water. Soot produced in urban regions is assumed to be hydrophobic, totally black carbon (BC), and present in an external mixture until their hygroscopic quality change due to the condensation of water-soluble material in the atmosphere (Riemer et al., 2004). The assumption about initial hydrophobic nature of aircraft engine-generated soot was also accepted between modelers but recent experimental studies of engine combustor particles (Demirdjian et al., 2007) proved the significant role of organic matter and sulfates in original soot hygroscopicity. It leads to necessity to link physico-chemical properties of emitted soot particles with soot-water interaction both for really hydrophobic and fully hydrophilic soots.

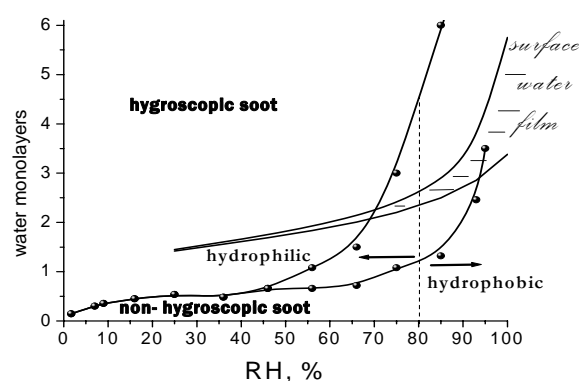
This report is devoted to the systematic analysis of the water uptake by laboratory soots proposed for atmospheric studies and the identification of water-soot interaction mechanisms in relation to surface chemistry and structure parameters. The purpose is the definition of a *quantification measure* to separate hygroscopic and non-hygroscopic soots, and the identification of hydrophilic and hydrophobic particles between non-hygroscopic atmospheric aerosols.

Soot is complex material composed from organic and elemental carbon with inorganic contaminations. In the limiting case of organic absence soot may be considered as black carbon. In general case two mechanisms of water interaction, namely the bulk dissolution into water soluble coverage (*absorption mechanism*) and the water molecule adsorption on active sites (*adsorption mechanism*) govern the water-soot interaction process. Comparative analysis of water uptake

isotherms on soots of various composition, from black carbons to complex composites with large water-soluble fraction, allow us suggesting a *concept of quantification*. Figure 1 demonstrates the scheme isotherm plot for this concept. The isotherm for a water film extended over the surface is suggested as a *quantification measure* which separates hygroscopic from non-hygroscopic soot. Water uptake of hygroscopic soot significantly exceeds the surface water film isotherm. If soot particles made mostly from EC and/or the organic coverage is totally water insoluble, we assume non-hygroscopic soot with isotherm less (hydrophobic soot) or approach the surface water film one (hydrophilic soot) (see Fig.1).

Water uptake measurements coupled with comprehensive soot characterization have shown that aircraft engine combustor soot and wood combustion soot are representatives of hygroscopic soots due to high water soluble fraction and multilayer water uptake. Spark discharge (Palas) soot demonstrates the features of hydrophobic black carbons because low water uptake. While TC1 kerosene flame and CAST burner soots are classified as hydrophilic between non-hygroscopic soots because water film formation on their surface before capillary condensation is happen for coalescence soot particles.

Fig.1. Scheme plot for a concept of quantification.



This work is supported by EC Quantify-TTC project under contract №003893.

Demirdjain.B., Ferry.D., Suzanne, Popovicheva. O.B., Persiantseva. N.M. & Shonija.N.K. (2007), *J.Atmos. Chem.*,56, 83-103  
Riemer N.,Vogel.H.&Vogel.B.(2004).*Atmos. Chem. Phys* , 4, 1885-1893

## Some remarks about the nucleation mode in diesel exhaust

D. Rothe<sup>1</sup>

<sup>1</sup>Motorenvorentwicklung, Abgasnachbehandlung  
MAN Nutzfahrzeuge Aktiengesellschaft,  
Vogelweiherstr. 33, D-90441 Nürnberg; Germany

Keywords: diesel exhaust, particle size distribution, nucleation mode, particle counting

While determining the particle size distribution in the exhaust of modern heavy-duty vehicles with an SMPS (Scanning mobility particle sizer), often two modes appear:

The nucleation mode in the area around 10 nm, which consists before or without oxidation catalysts usually of un- and/or partly burnt hydrocarbons (from fuel and engine oil).

As well as the accumulation mode in the area between 40 and 80 nm, the actual soot mode.

The nucleation mode is strongly influenced by the type of sampling, especially by the dilution. When falling below a certain dilution ratio, the hydrocarbons can nucleate homogeneous. In addition ash particles, which came from the engine oil, can serve as condensation particles.

The toxicological effect in the lung may differ based on the different composition and solubility of that of the soot mode. Both modes should separate valued become therefore with respect to their toxicological effect.

In this work, different factors (dilution, operating materials and exhaust after treatment) influencing the formation of the nucleation mode are introduced and discussed.

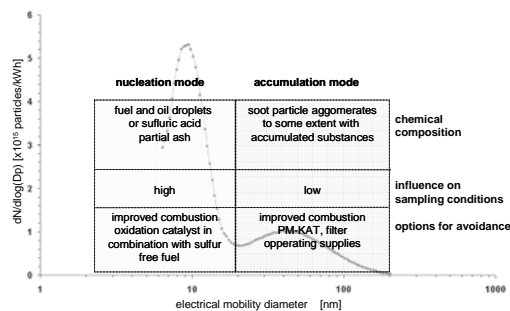


**Figure 1 Typical bimodal particle size distribution in heavy-duty-diesel-exhaust with sources and measures for reduction**

The different factors influencing the nucleation mode can be summarized in the following figure. There you can clearly see the strong influence of the nucleation mode by the sampling conditions, the engine operating parameters and exhaust gas after treatment devices.

It exists endeavour to establish a new additional emission limit of sides of the EU for the diesel exhaust. Next to the well known and in the last years drastically tightened particle mass limit, the establishment of a particle number limit is presently in the discussion. There are many open questions?

- 
- Is there a correlation between mass and number
- Is there a correlation between health effects and number
- What about the nucleation mode particles
- What about sampling artefacts (i. e. ash)
- What about the chemical composition of both modes

So it is questionable which relevant information this additional particle number limit will bring.

For the determination of this new particle number limit, a costly particle sampling and treatment is necessary to separate the solid from the volatile particles.

This is far from real world conditions.

Burtscher, H. (2005). *J. Aerosol Science*, 36, .896-932

Mohr, M., L. W. Jaeger, et al. (2001) *MTZ Motor-technische Zeitschrift*, 62, 686-692

Kittelson, D. B. (1998), *J. Aerosol Science*, 29, 575-588

Rothe, D. (2006), *Physikalische und chemische Charakterisierung der Rußpartikelemission von Nutzfahrzeugdieselmotoren und Methoden zur Emissionsminderung*, Ph. D. Thesis, Technische Universität München

## **Particulate Matter Characterization for Commercial Aircraft – The Delta Atlanta Hartsfield Jet Engine Exhaust Emissions Study**

D. Hagen, P. Whitefield, P. Lobo, and M. Trueblood

Center of Excellence for Aerospace Particulate Emissions Reduction Research, University of Missouri, Rolla, Missouri 65409, USA

Keywords: Combustion particles, soot particles, field measurements, emission factor, measurement (combustion aeros.)

There is a growing international concern about the environmental impact of jet engine exhaust emissions. Recent studies have shown an increasing number of environmental effects from aviation related activities such as impact on climate (Penner et al., 1999) and local air quality (Waitz et al., 2004). An accurate assessment requires that the number density and size of the aerosols within engine exhaust and aging plumes be well characterized. In the fall of 2004, the mobile laboratories operated by University of Missouri-Rolla, Aerodyne Research, Inc. and National Oceanic and Atmospheric Administration were deployed at the maintenance facilities of Delta Airlines to undertake on-wing exhaust emissions sampling from a variety of commercial aircraft at known power conditions. UMR focused on the particulate component of the emissions and used its mobile laboratory facility (Schmid, 2004).

Particle-laden exhaust is extracted directly from the combustor/engine exhaust flow through probes and supplied to the measurement devices. The primary probe for collecting exhaust samples is positioned within 1 meter of the exhaust nozzle exit plane, as this position is representative of the engine signature and the certification data in the International Civil Aviation Organization (ICAO) database. The UMR MASS method uses a variety of instruments to characterize the extracted sample and measure the following fundamental physical parameters: (1) Total particulate concentration using condensation nucleus counting and single-particle light scattering, (2) Total particulate size distributions for particulate diameters from 3.2 nm to 25  $\mu\text{m}$  using differential mobility analyzers (DMA) for particulate diameters < 1000 nm and a laser particle counter (LPC) for particulate diameters > 700 nm, (3) Carbon dioxide ( $\text{CO}_2$ ) concentrations using several non-dispersive infrared (NDIR) detectors of varying ranges from 0-3000 ppm to 0 to 10%  $\text{CO}_2$ , (4) Diameter of primary soot particles and particle morphology using transmission electron microscopy, and (5) Dew point. Based on these direct measurements and estimates of particulate density the following particulate physical characteristics can be derived: total concentration, mean geometric diameter, half width, emission index with respect to particle number, surface area, and mass. Combined with concomitant gas phase measurements and

source operating parameters (combustor inlet temperature and pressure, combustor exit temperature and pressure, engine exit temperature and air velocity, fuel flow rate, fuel composition, fuel properties, and bypass ratio) the UMR MASS measurements can provide an essential contribution to further understand and optimize the combustion process in gas turbine engines.

Emission measurements were performed for engine types JT8D-219, GE CF6-80, and PW 2037, with thrusts ranging from 93 to 258 kN. Two samples of each engine type were measured to study engine-engine variability. Data was acquired for a typical cycle involving the following engine power conditions – 4%, 7%, 30%, 50%, 70%, 85% and 100%. In case of the larger engines on 767 and 757 aircraft, the total number of engine conditions visited was limited to the low power conditions because the probe stand appeared to be unstable at the higher power settings. Both the geometric mean diameter and standard deviation were found to increase with power, ranging from ~13 nm and ~1.3 at idle to ~44nm and ~1.8, respectively, at maximum power conditions. All of the engines exhibited no significant engine-engine variability, except for the PW 2037 which did for its mass based emissions index.

Penner, J. E., Lister, D. H., Griggs, D. J., Dokken, D. J., and McFarland, M. (eds.) (1999). *Aviation and the global atmosphere*, IPCC Report: Cambridge University Press, Cambridge, UK, p. 373.

Schmid, O., Hagen, D.E., Whitefield, P.D., Trueblood, M.B., Rutter, A.P., and Lilienfeld, H.V., (2004) "Methodology for Particle Characterization in the Exhaust Flows of Gas Turbine Engines", *Aerosol Sci. Technol.*, 38, 1108-1122

Waitz, I. A., Townsend, J., Cutcher-Gershenfeld, J., Greitzer, E. M., and Kerrebrock, J. L. (2004) "Aviation and the Environment: A National Vision Statement, Framework for Goals and Recommended Actions," *Report to the United States Congress*, on behalf of the U.S. DOT, FAA and NASA.

## Mobile Sources of Atmospheric Polycyclic Aromatic Hydrocarbons

<sup>1</sup>F. Halek, <sup>2</sup>M. Mirmohammdi, <sup>1</sup>A. Kavousi

Environment Department, Materials & Energy Research Center, Tehran, IRAN

<sup>2</sup>Environmental Faculty, Tehran University, Tehran, IRAN

Keywords: Vehicles emission; Fine particles; PAHs; Organic compounds; Urban aerosols

Epidemiological studies have shown an association between respiratory-related mortality and morbidity and levels of ambient PM with diameter of <10 µm or PM10. Among the organic compounds of anthropogenic origin, the Polycyclic Aromatic Hydrocarbons (PAHs) make up a significant group first because of the way they endanger people's health and also because of the impact they have on the chemistry of the troposphere. Sources and composition patterns of PAH emissions is important because some of these compounds are mutagenic. PAHs are markers for emissions from various types of combustion sources. In Tehran vehicle fleet that uses petrol, consists of four-stroke engine cars and light-duty gasoline vehicles and heavy-duty diesel vehicles.

The contribution of petrol vehicles and diesel vehicles, were evaluated by measurement of 16 PAHs that are present in the atmosphere. 16 PAH compound were found (Naphthalene, Acenaphthylene, Acenaphthene, Fluorene, Phenanthrene, Anthracene, Fluoranthene, Pyrene, Benzo(α) Anthracene, Chrysene, Benzo (b) Fluoranthene, Benzo (k) Fluoranthene, Benzo(α) Pyrene, Dibenzo (a,h) Anthracene, Benzo (ghi) Perylene, Indeno (1,2,3-cd) Pyrene). The samples collected during intervals of high gasoline fueled vehicles traffic (06:00 am – 18:00 pm). Mobile source PAH emission were generated from the

particle and vapor phase samples collected in the different sites. High Performance Liquid Chromatography (HPLC) was employed to isolate and quantify individual PAHs in acetonitrile extracts of SKC adsorption tube and glass-fiber filters. The average concentrations ranged from 0.13 – 234.3 ng/m<sup>3</sup>.

This study has shown Fluoranthene and pyrene are emitted from both petrol and diesel vehicles with additional Indeno (123-cd) pyrene from petrol vehicles and chrysene, benzo (b) fluoranthene and benzo (k) fluoranthene from diesel powered vehicles.

Chen, L. W. A. , Doddridge, B. G, Dickerson, R. R. , Chow, Henry, J. C R. C., 2002. *Origins of fine aerosol mass in the Baltimore-Washington Corridor*. Atmospheric Environment, 36: 4541-4554.

Venkataraman C. and Friedlinder S.,(1994) *Source resolution of fine particulate polycyclic aromatic hydrocarbons using a receptor model modified for reactivity*. J. Air & Waste Manage. Assoc., 44:1103 -1108.

Chow, G. C., Watson J. G., Crow D., Lowenthal D. H., Merrifield T., 2001. *Comparison of improve and NIOSH carbon measurements*. Aerosol Science and Technology, 34(1), 1-12.

---

\* E-mail: [f-halek@merc.ac.ir](mailto:f-halek@merc.ac.ir)  
[fhalek@yahoo.com](mailto:fhalek@yahoo.com)

Cite abstract as Author(s) (2007), Title, European Aerosol Conference 2007, Salzburg, Abstract T14A007

Sanderson, E. G. ; Raqbi, A. ; Vyskocil, A. ; Farant, J. P., (2004). *Comparison of particulate Polycyclic Aromatic Hydrocarbon profiles in different regions of Canada*. *Atmospheric Environment*, 38: 3417-3429.

## Black carbon concentration trends at urban site in Helsinki during ten years

L. Järvi<sup>1</sup>, H. Junninen<sup>1</sup>, A. Karppinen<sup>2</sup>, A. Virkkula<sup>2</sup>, R. Hillamo<sup>2</sup> and M. Kulmala<sup>1</sup>

<sup>1</sup>Department of Physical Sciences, University of Helsinki, P.O. Box 64, FIN-00014, Helsinki, Finland

<sup>2</sup>Finnish Meteorological Institute, Erik Palménin Aukio 1, 00560 Helsinki, Finland

Keywords: black carbon, traffic, urban areas, vehicles emission

Black carbon (BC) is one of the main constituents in particulate matter, especially in particles originating from urban anthropogenic sources. Majority of BC is generated in incomplete combustion of fossil and biomass fuels, includes residential heating and traffic, especially diesel powered (e.g. Watson et al. 1994). BC has an important role in global climate change since it absorbs sun radiation at the atmosphere (Jacobson, 2001). Small carbonaceous particles have also severe health effects including cardiopulmonary and respiratory diseases (e.g. Stoeger et al., 2006).

The purpose of this study is to investigate the BC trends in Helsinki between 1996 and 2005. Measurements were made during three campaigns at the same site, which represents typical urban area in Helsinki. One of the main roads leading to Helsinki center is situated 13 m away from site, and traffic has been identified to be the main source of BC at the site (Pakkanen et al., 2000). All measurements were made with aethalometers (Magee Scientific Aethalometer). The first campaign lasted from Nov 1996 to Jun 1997, the second from Sep 2000 to May 2001 and the third from Mar 2004 to Oct 2005. Same amount of data was selected from all campaigns, total of 82 days.

That, how much of the BC concentration changes can be explained by improved traffic technology and how much by sole meteorology, are studied via multivariable analysis. Hourly traffic rates from the road next to the site are used and the meteorological data (including Obukhov length and mixing height) is computed by meteorological pre-processing model (MPP-FMI, Karppinen et al., 2000).

Table 1. The median BC concentrations and quartile deviations, and average daily traffic rates and standard deviations during different campaigns.

	BC ( $\mu\text{g}/\text{m}^3$ )	Traffic rates (vehicles/day)
Campaign 1	1.11 (0.60)	25 600 (5790)
Campaign 2	0.93 (0.4)	25 400 (6090)
Campaign 3	1.00 (0.56)	26 400 (5940)

The BC concentrations have had slightly decreasing trend, from 1.11 to 1.00  $\mu\text{g}/\text{m}^3$ , between campaigns 1 and 3 (Table 1). However, the

concentrations were lowest during campaign 2. At the same time, traffic rates have increased from 1996 to 2005, suggesting decreased emissions per vehicle.

The diurnal cycle of BC showed a clear rush hour related pattern during weekdays (Fig. 1a). Lowest daytime concentrations were measured during campaign 2 and highest during campaign 1, following the mean concentrations in table 1. The deviations of weekend concentrations were smaller between the campaigns with lowest values during campaign 3.

The BC concentrations seem to have decreased between campaign 1 and 3, with lowest concentrations during campaign 2. In the presentation, results from the multivariable analysis are also shown.

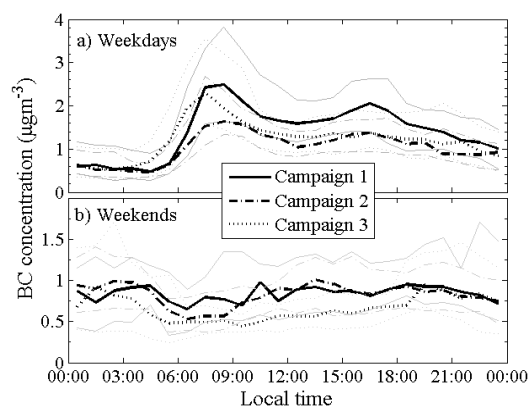


Figure 1. BC concentration during different campaigns: median diurnal variation at a) weekdays and b) weekends. Notice different scales for BC.

This work was supported by the Research Foundation of the University of Helsinki and National Technology Agency (TEKES, Grant # 40462/03).

- Jacobson, M. Z. (2001). *Nature*, 409, 844-850.  
 Karppinen, A., Joffre, S. M. & Kukkonen, J. (2000). *Int. J. Environ. Poll.*, 14, 565-572  
 Pakkanen, T., Kerminen, V.-M., Ojanen, C., Hillamo, R., Aarnio, P., & Koskentalo, T. (2000). *Atmos. Env.*, 34, 1497-1506.  
 Stoeger, T., Reinhard, C., Takenaka, S., Schroepfel, A., Karg, E., Ritter, B., Heyder, J., & Schulz, H., (2006). *Environ. Health Perspect.*, 114, 328-333.  
 Watson, J. G., Chow, J. C., Lowenthal, D. H., Pritchett, L. C., & Frazier, C. A. (1994). *Atmos. Env.*, 28, 2493-2505.

## Calculation of Particle Density of Aerosol from Wood Combustion

M. Lautenbach<sup>1</sup>, R. Kunde<sup>1</sup> and M. Gaderer<sup>1</sup>

<sup>1</sup>Bavarian Center for Applied Energy Research, Garching, D-85748, Germany

Keywords: combustion aerosol, wood combustion, particle characterization, particle density.

The prescriptive limits of particulate matter in ambient air are defined in microgram per cubic meter. Concerning health relevance besides mass also size and number of particles are important parameters. To draw conclusions from the size and the number of particles to mass relating values the density of the particles is an important information.

By means of data from on-site measurements at small-scale wood firing systems particle density was calculated using the coherence of aerodynamic diameter and mobility diameter.

Particulate matter emissions of three wood pellet heating systems with 15 to 30 kW power were measured. Additionally the emissions of a light fuel oil system were recorded. A TSI SMPS system including an electrostatic classifier and condensation particle counter and an electrical low pressure impactor (ELPI) were used. The SMPS system provides the number distribution of particles as a function of mobility diameter. ELPI gives the number distribution as a function of aerodynamic diameter.

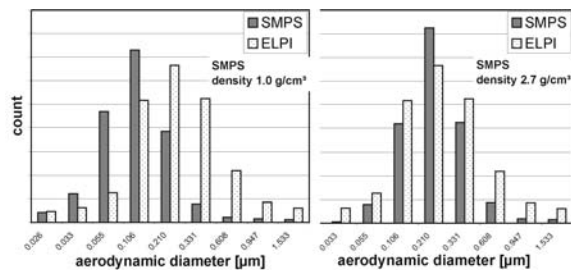


Figure 1. Distributions, left: shifted distributions; right: fitted distributions.

The calculation of particle density is based on the well-known mechanism of measuring particles with the electrical low pressure impactor. The charging of the particles in the corona charger can be calculated as well as their separation by impaction in the impactor. To determine the density of the particles the charging and the impaction in the ELPI are simulated with the number distribution given by the SMPS, which is a function of mobility diameter. The result is a distribution which is shifted versus the measured ELPI distribution in the diameter axis. Figure 1 shows the shift of the distribution. In the left diagram the measured ELPI distribution and the calculated SMPS distribution do not match, because the density of the particle differs from the standard density of 1 g/cm<sup>3</sup>.

By changing the density, the density with the best analogy of the two distributions is found. The right diagram shows the two distributions with the SMPS distribution calculated with a density of 2.7g/cm<sup>3</sup>, which shows the best analogy. This density is the average density of all particles in the considered diameter range from 15 nm to 10 µm.

The results of the density calculation are shown in table 1.

Table 1. Results of the density calculation

Firing System	Power [kW]	Density [g/cm <sup>3</sup> ]
wood pellets A	30	2.2-2.6
wood pellets B	14.9	2.7-3.4
wood pellets C	14.9	3.4
light fuel oil	35	1.5

The average calculated particle density of all observed wood firing systems was 2.9 g/cm<sup>3</sup>. A strong dependency of the density on the CO concentration in flue gas was noticed. With a higher CO concentration the calculated density was lower than under conditions with good burnout and low CO emissions. There is also a dependency on flue gas temperature. The density of the particles from the oil firing system is clearly lower than the results from the wood firing system. Published values of the density of particles from diesel engines, which are using the same fuel, are in the range of 1.0 to 1.5 g/cm<sup>3</sup>. These values are in line with the calculations carried out in this study. The higher density of particles from wood combustion is caused by the mineral constituents in the ash of wood firing system.

- Ristimäki, J. et al., (2002). *On-line measurement of size distribution and effective density of submicron aerosol particles*. J. of Aerosol Science, 33, 1641-1557.
- Marjamäki, M. et al., (2005). *ELPI Response and Data Reduction I: Response Functions*, Aerosol Science and Technology, 39, 575-582.
- Virtanen, A., (2004). *Physical Characterization of Diesel Soot Particles*. Tampere University of Technology.
- Lautenbach, M., (2006). *Messung der Feinstaubemissionen bei Biomassefeuerungen und Bestimmung der Partikeldichte*. Master Thesis, TU-Berlin/ZAE Bayern.

## Small angle and wide angle X-ray scattering for characterization of carbonaceous materials, aerosols, and particles

A. Braun<sup>1,2</sup>

<sup>1</sup>University of Kentucky, Dept. of Chemical and Materials Engineering, and Consortium for Fossil Fuel Sciences, University of Kentucky, Lexington KY 40506, USA

<sup>2</sup>EMPA – Swiss Federal Laboratories for Materials Testing & Research, Laboratory for High Performance Ceramics, CH-8600 Dübendorf, Switzerland

Keywords: SAXS, WAXS, Carbon, aerosols.

Small angle X-ray scattering (SAXS) provides quantitative information on surface areas, porosity, particle size, void size distributions, surface roughness and fractal dimension of surfaces, interfaces and particles and aggregate structures. In-situ and ex-situ, SAXS even permits to derive kinetic parameters for chemical reactions and transformations. Homogeneous systems such as soot can be studied with SAXS, and carbonaceous materials have been widely used to develop this technique. Wide-angle X-ray scattering (WAXS) measures crystallite sizes and to distinguish aromatic and aliphatic structures in carbon materials. WAXS was particularly applied for coal research. We present here studies on diesel exhaust for combustion engineering and environmental science, and studies on model systems such as glassy carbon (pore size and connectivity evolution) and aerogels. The scattering pattern of soot experiences systematic changes upon pressurizing, in particular a shift of the aggregate size signature which can be used to characterize the stiffness of the aggregates. Powder and pellets show characteristic aggregate structure at small scattering vectors. Scattering curves of the pellets show a shift of the aggregate size related scattering feature towards larger scattering vectors for increasing pressure. For the highest pressures, this aggregate structure vanished, while the primary particle scattering became visible as the asymptote of the aggregate scattering structure. Pressing soot into pellets eliminates scattering from aggregation of primary particles and provides a good route to reveal the otherwise inaccessible primary particle scattering. Without extracting volatiles, it is ultimately not possible to quantify the impact of the volatiles like lubricants and fuel on the compaction behaviour of the soot under pressure. This remains particularly unclear for idle soot, which contains more volatiles than load soot but yet strongly

resists pressure. The USAXS technique combined with pressing pellets is valuable for the study of materials which are built from aggregates of primary particles, providing robust and statistically representative data.

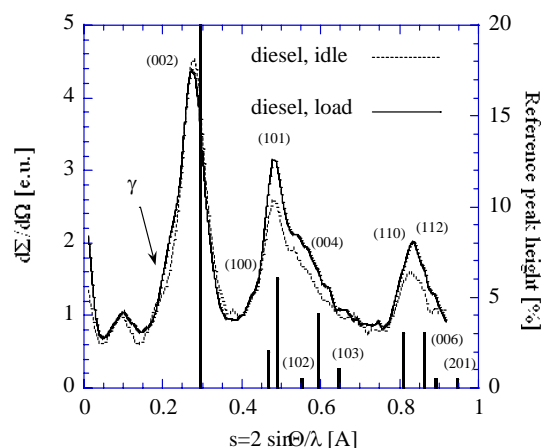


Figure 1. WAXS curves from diesel soot prepared from load and idle engine conditions.

Financial support by National Science Foundation grant # CHE-0089133.

A. Braun, Comment on soot oxidation, *Carbon* 2006, 44(7), 1313-1315.

A. Braun, S. Wirick, C. Jacobsen, F.E. Huggins, S.B. Mun, N. Shah. *Carbon* 43 (2005) 117-124.

A. Braun, J. Ilavsky, S. Seifert, P. R. Jemian. *J. Appl. Phys.* 98, 073513 (2005).

A. Braun, F. E. Huggins, S. Seifert, J. Ilavsky, K. Kelly, A. Sarofim, G. P. Huffman. *Combustion & Flame* 137 (1/2) pp. 63-72 (2004).

A. Braun, M. Bärtsch, R. Kötze, O. Haas, H.-G. Haubold, G. Goerigk. *J. Non-Cryst. Sol.* 260 (1-2), 1-14 (1999).

W. Gille and A. Braun. *Journal of Non-crystalline Solids* (2003) 321:89-95.

## Characterisation of soot particles collected at two different sites dominated by wood smoke and vehicle exhaust

M. Pawlyta<sup>1</sup>, J.-N. Rouzaud<sup>2</sup>, S. Duber<sup>1</sup> and J. Sandradewi<sup>3</sup>

<sup>1</sup> Faculty of Earth Sciences, University of Silesia, 60, Bedzinska St., 44-200, Sosnowiec, Poland

<sup>2</sup> Laboratoire de Géologie, Ecole Normale Supérieure, 24, rue Lhomond, 75231 Paris Cedex 5, France

<sup>3</sup> Laboratory of Atmospheric Chemistry, Paul Scherrer Institut, CH-5232 Villigen PSI, Switzerland

Keywords: black carbon, carbonaceous particles, soot particles, optical properties, electron microscopy

Black carbon (BC) the main constituent of soot is the main light absorbing component in the atmospheric aerosol. Soot particles show diverse morphology, depend on their sources. Soot emitted by cars includes chain-like aggregates, formed from fine (20-35nm) primary particles (Kittelson, 1998). Soot particles from wood smoke have significantly larger primary particles. The microstructures of such particles are also definitely better ordered than vehicle exhaust soot (Kocbach et al., 2006). The aim of this work was to compare the morphology and microstructure of combustion generated carbonaceous particles collected at two different sites using transmission electron microscopy (TEM).

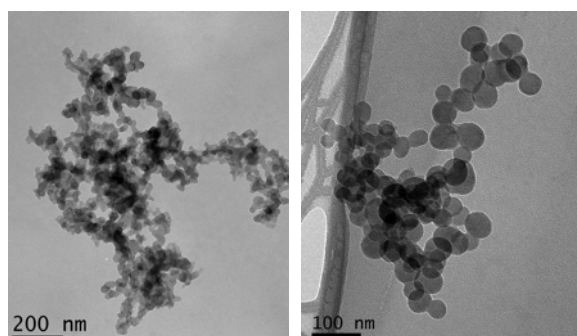


Figure 1. TEM micrograph of soot particle collected in Moleno. Structure similar to diesel soot, primary particle diameter  $d_p$   $26 \pm 6$  nm (left).

Soot particle collected in Roveredo in winter. Structure similar to soot from wood burning, primary particle diameter  $d_p$   $46 \pm 9$  nm (right).

The field samples were collected on quartz filter using a high volume (HIVO) sampler. The

Roveredo samples were taken in a village located in an Alpine valley in Switzerland with population ca. 2000. In winter, more than 70% of the houses in this village use wood stoves for heating. The

Moleno samples were taken from a parking area next to the St. Gotthard highway, which connects Canton Ticino and Italy to the northern part of Switzerland and Europe.

In all examined samples soot aggregates were a widespread component. Individual aggregates showed diverse morphology. Chain-like aggregates formed from fine primary particles, similar to diesel

soot (like the one in Fig.1a) were abundant soot type in all samples. Only in samples collected in Roveredo in winter we observed aggregates with perfectly spherical and significantly larger (than for diesel soot) primary particles (Fig.1b). Because such aggregates did not occur in other samples, we hypothesize that they are from wood burning. The nanostructure of such a spherical primary particle is visible in Fig.2. Space, where carbon layers are ordered (BSU), are significantly larger than in diesel soot (not shown). As discussed by Bond and Bergstrom (2006) a change in BSU (space where carbon layers are almost perfectly straight and parallel, spaced about 0.35 nm) size affects the optical properties of BC particles. In our example the Moleno samples included mainly diesel soot (poorly organized). Samples collected in Roveredo, included particles from wood burning (better organized). It is also visible that combustion particles from vehicle exhaust are characterised by a larger specific surface area as compared to wood burning particles.

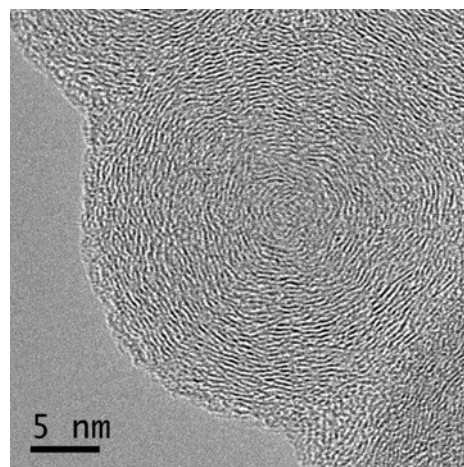


Figure 2. HRTEM micrograph of soot particle collected in Roveredo in winter.

Bond, T. C., & Bergstrom, R. W. (2006). *Aerosol Science and Technology*, 40(1), 27-47.

Kittelson, D.B. (1998). *Journal of Aerosol Science*, 29(5): 575-588.

Kocbach, A., Li Y., Yttri, K.E., Cassee, F.R., Schwarze, P.E., & Namork, E. (2006). *Particle and Fibre Toxicology*,

[www.particleandfibretoxicology.com/content/3/1/1](http://www.particleandfibretoxicology.com/content/3/1/1)

## Measurements of size-segregated emission particles by a specially invented sampling system

J. Turšič<sup>1</sup>, I. Grgič<sup>1</sup>, A. Berner<sup>2</sup>, J. Škantar<sup>3</sup> and I. Čuhalev<sup>3</sup>

<sup>1</sup>Laboratory for Analytical Chemistry, National Institute of Chemistry, Hajdrihova 19, SI-1000 Ljubljana, Slovenia

<sup>2</sup>Institute for Experimental Physics, University of Vienna, Boltzmanngasse 5, A-1090 Vienna, Austria

<sup>3</sup>Environmental Department, Electrolnstitute Milan Vidmar, Hajdrihova 2 SI-1000 Ljubljana, Slovenia

Keywords: Combustion particles, Emission, Mass size distribution, Size-segregated aerosols, PM10/PM2.5.

One of the more pernicious problems in air quality is the persistence of fine suspended particulate matter. Until recently, the total mass concentration of airborne particulate matter (TSP) was the only standard for particulates used for air quality assessment. New developments in aerosol measurement techniques enabled size-dependent analyses of aerosol particles, thus better classifications and more comprehensive studies of the effect of ambient aerosols were feasible. Exposure to elevated concentrations of respirable ambient aerosols has been associated with various health problems (Pope *et al.*, 2002).

Among the combustion sources that have the most significant relative contribution to air pollution are power and industrial plants, while coal is the most commonly used fuel for commercial power generation (Xu *et al.*, 2003). Formerly, emissions at the sources have been monitored by measuring TSP, and for the determination of mass size distribution of particles, measurements were performed by cascade impactors or cascade cyclones. Recently, a new PM<sub>10</sub>/PM<sub>2.5</sub> cascade impactor for in-stack measurements was developed (John *et al.*, 2003).

In this work, a special sampling system for measurements of size segregated particles directly at the source of emission will be presented. To prove the feasibility and capability of this newly developed system, it was employed for size segregated sampling of particles at the largest coal-fired power station in Slovenia.

Measurements of size-segregated emission particles were performed in June 2005 and May 2006. Sampling was conducted from the 50 m platform on the stack using the existing sample ports. The central part of our system is a ten stage low-pressure cascade impactor (Berner type, size ranges from 15 nm to 16 μm), which was positioned outside the chimney stack, while a sampling probe was placed into the chimney. The sampling probe was designed in a way that it is feasible to sample also with dilution by clean air. In order to prevent water condensation on the particles, the impactor was heated to the temperature of flue-gas (about 100 °C) before sampling and this temperature was maintained constant during sampling. The sampling times were from 10 min to 1 hour (without dilution), and 5 hours

when dilution was introduced. The impaction plates were covered with annular Tedlar foils., and on top of these folded aluminium foils were placed. This arrangement enabled simultaneous determination of mass and chemical size distribution with one impactor only.

The results of mass size distribution of particles emitted from the coal-fired power plant are shown in Fig. 1. The most pronounced mass peak is observed in the size range between 1 and 2 μm.

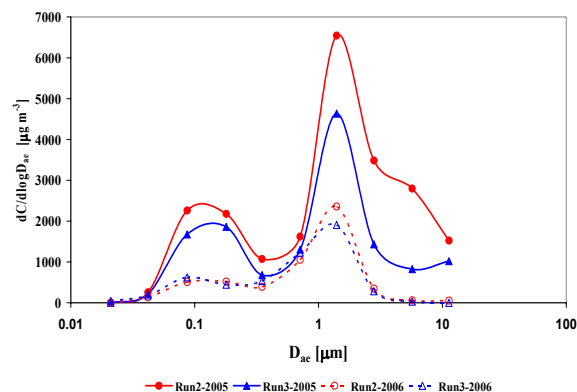


Figure 1. Mass size distribution of particles collected at the coal-fired power plant during sampling in 2005 and 2006. Concentrations are expressed at normal conditions (273 K, 1013 mbar).

This work was supported by the Slovenian Research Agency (Contract no. L1-6100-0104 and P1-0034-0104) and the Thermo-Power Plant Šoštanj..

Pope, C.A., Burnett, R.T., Thun, M.J., Calle, E.E., Krewski, D., Ito, K., & Thurston, G.D. (2002). *JAMA-J. Am. Med. Assoc.* 287, 1132-1141.

Xu, M., Yan, R., Zheng, C., Qiao, Y., Han, J. & Sheng, C. (2003). *Fuel Process. Technol.* 85, 215-237.

John, A.C., Kuhlbusch, T.A.J., Fissan, H., Bröker, G., & Geueke, K.-J. (2003). *Aerosol Sci. Technol.* 37, 694-702.

## 2D Particle Transport in a Full Dilution Tunnel of Diesel Vehicle Emissions

L. Isella, B. Giechaskiel, P. Dilara and Y. Drossinos

European Commission, Joint Research Centre, I-21020 Ispra (Va), Italy

Keywords: diesel exhaust, dilution, numerical simulation, size distribution, turbulence.

Current EU legislation establishes particulate-mass emission limits for diesel vehicles, but limits on particle number emissions are also under consideration due to concerns about the adverse health effect of fine particles.

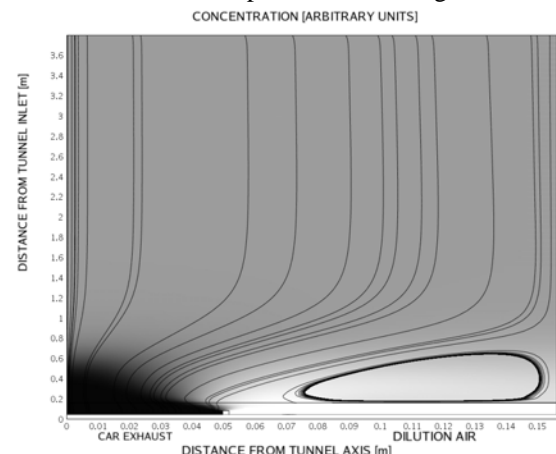
We study the turbulent transport of light-duty diesel engine exhaust particles in a standard emission facility. We investigate particle transport from the tailpipe to the sampling point both by experimental measurements and two-dimensional modeling. The experiments were performed at the VELA-2 laboratories at JRC, Italy. The experimental setup consists of a long flexible cylindrical tube (anaconda) connected to the car exhaust pipe that conducts the exhaust fumes into a wider cylindrical duct [dilution tunnel (DT)]. As a first step, only tests at steady vehicle velocity were conducted. While the dilution air and exhaust flow rates were approximately constant, temperature transients were often observed in the core region. The walls of the anaconda were kept at a constant temperature of 70°C, whereas constant room temperature was assumed for those of the DT. For simplicity, the experimental manifold is modeled as axisymmetric (the anaconda has a bend with a large curvature radius before reaching the DT). The modeling of the experiments differs from previous works [e.g. Vouitsis *et al.* (2005)] as it relies on a 2D calculation for the fluid flow, the temperature and concentration.

The flow field in the bulk region is calculated by a standard k- $\epsilon$  implementation in the finite-element PDE solver Comsol Multiphysics (Comsol Multiphysics, 2006). The wall boundary layer is not resolved at this stage, but we determine the velocity and temperature fields close to the wall by using law-of-the-wall functions to match the CFD solution (Housiadas & Drossinos, 2005). The use of turbulent conductivity and mass diffusivity in the bulk accounts for the effect of turbulence on heat and mass transport. An accurate treatment of the boundary layer is also fundamental for the modelling. Indeed the high resistance of the near-wall region to heat and mass transfer has a dramatic effect on the concentration and temperature profiles.

From experiments performed at VELA-2, we investigate the concentration and temperature profiles along the experimental manifold. The measured particle size distribution shows only the accumulation mode: the fitted mean mobility diameter of the distribution at the DT inlet ranged from 60 to 80 nm with a geometric standard

deviation of a few nm, depending on car speed and dilution ratio. The relaxation time  $\tau_p$  of such soot particles is of the order of  $10^{-8}$  s. The fluid characteristic time  $\tau_f$  is fixed by turbulence.

Analytical estimates (valid for a circular pipe) and numerical simulations determine the fluid turbulent time scale to be in the range  $10^{-3}$  to  $10^{-4}$  s. Consequently, the Stokes number is  $St = \tau_p / \tau_f \approx 10^{-5} - 10^{-4}$  s, and the soot particles can be treated as inertialess particles following the fluid.



In the figure we plot the particle concentration inside the DT (the dark shades stand for high concentration) along with the particle streamlines. In the simulated case the car speed is 120 Km/h, and the nominal Venturi flow rate is  $6.2 \text{ m}^3/\text{min}$  with an exhaust dilution ratio around three. One notices the area of low concentration past the diaphragm corresponding to a region of dilution air flow recirculation. At the sampling point, the concentration radial profile becomes relatively flat (a similar conclusion holds for the temperature profile), thus ensuring the robustness and repeatability of measurements of particle concentration. Mass losses along the anaconda (neglecting thermophoresis), estimated both from numerical simulations and the 1D correlation used by Vouitsis *et al.* (2005), amount at most to 1%.

Housiadas C. & Drossinos Y. (2005), *Aerosol Science and Technology*, 39, 304-318.

Vouitsis E., Ntziachristos L. & Samaras Z. (2005), *Atmospheric Environment*, 39, 1335-1345.

Comsol Multiphysics (2006), *Chemical Engineering Module User's Guide*, September 2005.

## Field measurements of fine particle and gas emissions from residential wood combustion appliances

J.M. Tissari<sup>1</sup>, K.H. Hytönen<sup>1</sup>, T. Turrek<sup>1</sup>, J. Lyyränen<sup>2</sup> and J. Jokiniemi<sup>1,2</sup>

<sup>1</sup>Department of Environmental Sciences, University of Kuopio, P. O. Box 1627, 70211, Kuopio, Finland

<sup>2</sup>VTT, Technical research Centre of Finland, Fine Particles, P.O. Box 1000, 02044, VTT, Espoo, Finland

Keywords: biomass burning, combustion particles, elemental carbon, emission, organic matter.

Residential wood combustion (RWC) is widely used for heating in many countries during winter, and is increasing due to its CO<sub>2</sub>-neutrality. However, RWC is an important source of both gaseous and particulate pollutants, such as fine particles (PM<sub>2.5</sub>) and carbon monoxide (CO).

The aims of this study were to define the range of the emission factors for fine particle and gaseous emissions in the field environment, where the different combustion appliances, operators and fuels are involved. The measurements were carried out in the suburb of the city of Kuopio, in Finland. The emissions were measured from seven wood combustion appliances typically used in Finland: a modern masonry heater (MMH), three conventional masonry heaters (CMH), a baking oven (BO), a sauna stove (SS) and semi-storing stove (S). The oldest appliance was built in 1990 and the latest in

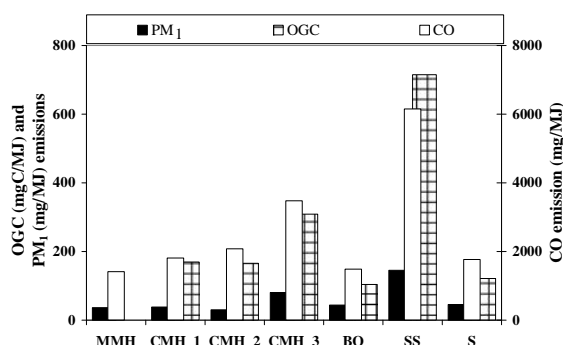


Figure 1. Average PM<sub>1</sub>, CO and OGC emissions from different combustion appliances.

2004. The quality of the fuels (mainly birch wood) burned was rather good. The moisture content was low, from 10.1 to 17.5% as well as ash contents from 0.2 to 0.8% of dry fuel. The operators used their appliances as they were used to, and there was quite a large variation in the operational practices. E.g. total mass of fuel burned varied from 5 to 17 kg and were combusted in 1 to 6 sequential batches.

Main gas components (NO<sub>x</sub>, CO, CO<sub>2</sub>, H<sub>2</sub>O) as well as the light organic gaseous substances (OGC) were measured continuously with a Fourier Transform Infrared (FTIR, Gasmeter Technologies Ltd.) analyzer. The oxygen concentration was measured with a separate CrO-cell. For particle measurements the sample flow was first diluted with a porous tube diluter (Lyyränen *et al.*, 2004) and

further with an ejector diluter, giving a total dilution ratio of 27–71. Particle number emissions and number size distributions were measured with an ELPI (Dekati Ltd.) and a FMPS (TSI 3091). The PM<sub>1</sub> samples for gravimetric and elemental analyses were collected on 47 mm Teflon membrane filters and the samples for organic and elemental carbon analysis were collected in parallel line on quartz fiber filters.

The emissions from the SS were clearly higher than from the other measured appliances due to its very simple combustion technology (Fig. 1). The emissions from different masonry heaters were fairly similar despite the large variety in their age and type of the heaters except for CMH<sub>3</sub>, where too large loading of wood to firebox was used. PM<sub>1</sub> emission composed mainly of organic matter and soot (Fig. 2). However, these emissions decreased notably from batch to batch in contrast to ash compounds that increased from batch to batch, probably due to increasing of combustion temperatures in the firebox in the sequential batches. Nearly similar results were also observed in our laboratory study (Tissari *et al.*, 2007).

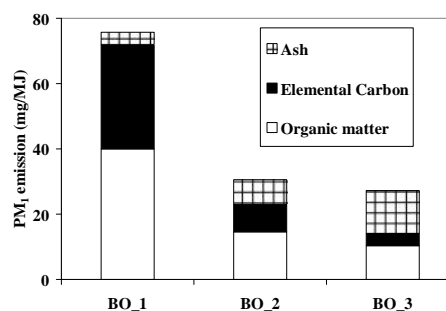


Figure 2. PM<sub>1</sub> composition from baking oven in the first (BO<sub>1</sub>) and the second (BO<sub>2</sub>) batches and during the burn out phase in the third batch (BO<sub>3</sub>).

This work was supported by the Finnish Funding Agency for Technology and Innovation (TEKES) and the Finnish Ministry of the Environment.

Lyyränen, J., Jokiniemi, J., Kauppinen, E. I. & Backman, U. (2004). *Aer. Sci. Technol.*, 38, 12–23.

Tissari, J. M., Hytönen, K. H., Sippula, O. M. J., Turrek, T. & Jokiniemi, J. (2007) The effects of operating conditions on emissions from masonry heaters and sauna stoves. *Submitted*.

## Fractional Efficiency in the Submicron range and control of heavy metals emission by means of a Hybrid Filter

S. Astarloa<sup>2</sup>, E. Peña<sup>2</sup>, Z. Elorriaga<sup>2</sup>, E. García<sup>2</sup>, J.A. Legarreta<sup>1</sup>, C. Gutiérrez-Cañas<sup>1</sup>, S.-C. Kim<sup>3</sup> and D.Y. Pui<sup>3</sup>

<sup>1</sup> Dpt. Chemical and Environmental Eng., U. of the Basque Country, A. de Urquijo s/n, 48013, Bilbao, Spain

<sup>2</sup> AIRg María Díaz de Haro, 48920, Portugalete, Spain

<sup>3</sup> Particle Technology Laboratory, Dpt Mechanical Engineering, UofM, 111 Church Str., Minneapolis, 55455MN, USA

**Keywords:** Fraccional Efficiency, Hybrid Filter, Heavy metals, Fine particle.

Trace metals (HM) emission from co-incineration plants is subjected to tighten regulations (Directive 94/67/EC). Ensuring the compliance of HM limits requires an effective control of the fine fraction, due to their high occurrence 2  $\mu\text{m}$ . Moreover, the emission of volatile metals –Cd, Tl and in less amount Pb- is linked with the presence of a secondary mode around 0.7  $\mu\text{m}$  of the aerodynamic diameter number distribution (Garcia *et al*, 2006). Electrostatic precipitators show a penetration window in the size range of target pollutants; therefore hybrid filters, as described in (Rinschler, 2002), taking advantage of both electrical deposition and bag filtration have been recently adopted. Systematic measurements of the fractional efficiency were performed in a coincinerating plant producing 2200 t/day and before/after revamping, and have been reported elsewhere (Garcia *et al*, 2006).

the filter (The fiber is the upper part, and the deposit between adjacent fibers the lower part of the picture).

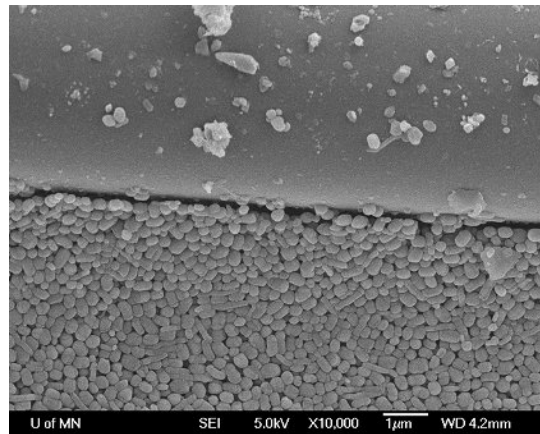


Figure 2 Downstream face of the bag after 1-year operation.

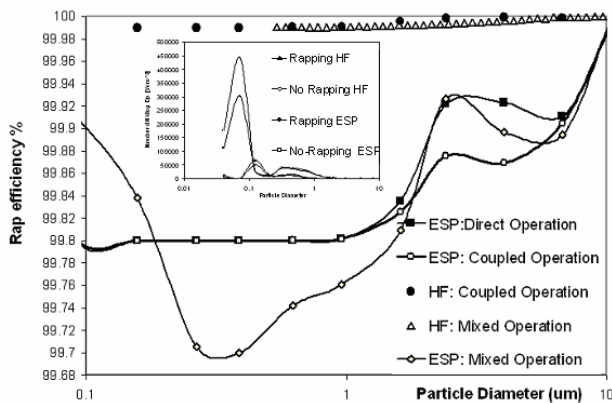


Figure 1: Fractional efficiency of the 2-field ESP and of the hybrid filter (HF) averaged over 2 hours. Short-term influence of electrode rapping (small graph).

Figure 1 shows the fractional efficiencies before (ESP) and after (HF) revamping. The U-shaped efficiency of the ESP –under both direct and coupled operation- is consistent with earlier results at coal- and biomass-fired boilers, (Lind *et al.*, 2003; Ferge *et al.*, 2004). In terms of heavy metal control, hybrid systems show a weaker dependence -that is a less pronounced mode in the size range of metals occurrence- on rapping cycles than electrostatic precipitator systems. Complementary evidence can be acquired observing the regular morphology of the stable deposits after 1 year of continuous operation of

However, as shown in Figure 3, the effect of SO<sub>2</sub> on the two intermediate modes is the opposite as in the case if ESP. This has been indirectly confirmed by the chemical analysis of collected dust; as the emission in the range 0.1-1  $\mu\text{m}$  decreases, its sulphate concentration increases. This suggests a layer reaction, to be confirmed/discarded by ongoing work.

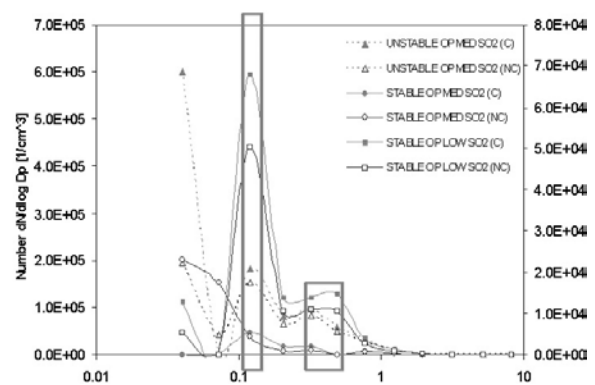


Figure 3 SO<sub>2</sub> concentration and size distribution.

### References

- Ferge T., Maguhn J., Felber H. and Zimmerman R., (2004), Environ. Sci. Technol, 38,1545-1553
- García E., Legarreta J., Astarloa S., Larrión M., Urcelay C., Peña E., Guede E. and Gutierrez-Cañas C., (2006) Int. Aerosol Conf., St Paul, MN
- Lind T., Hokkinen J. and Jokiniemi J. (2003) Environ. Sci. Technol., 37, 2482-2846
- Rinschler C. (2002) Advanced Hybrid™ Technology, World Cement, 80

## Direct Comparison of Four Different Measurement Methods Applied to Applied to Particle Emissions from Diesel Engines

H.-G. Horn

TSI GmbH, Neuköllner Straße 4, 52068, Aachen, Germany

Keywords: Aerosol instrumentation, Diesel soot particles, Measurement, Vehicle emissions.

Upcoming regulations for the type approval of internal combustion engine powered vehicles (Euro 5 and Euro 6) will exhibit a significant reduction of emission limits for particulate matter. A campaign of tail pipe measurements within the project “Emission Check 2010” by VDTÜV and DEKRA was run to investigate whether measurement techniques – both already available and under development – are applicable for regular vehicle inspections, especially with regard to the lower limits defined by the new regulations. All tests were run on the DEKRA chassis dynamometer in Klettwitz, Germany. Three different vehicles were tested during a one week campaign. New European drive cycle tests, steady state tests and a test sequence with 10 subsequent engine starts were run. In some of the 31 tests, DPF malfunction was simulated by means of a valve-controlled DPF bypass. In order to maintain confidentiality, only the results of the participating TSI instruments (a CPC 3010D, an Electrical Aerosol Detector EAD 3070A, a light scattering photometer DustTrak 8520 and an Engine Exhaust Particle Sizer EEPS 3090) are discussed in this paper. Several other measurement principles were investigated during the campaign as well. The measurements were backed up by gravimetric bag measurements and an AVL Micro Soot Sensor.

The parallel use of the four different measurement principles allowed an in depth analysis of the differences in response under transient conditions. All samples were taken from a sample splitter connected directly to the tail pipe of the vehicles. Figure 1 shows how the sample was conditioned and then split between the four TSI instruments.

In order to analyze the correlation of the four different measurement techniques, calibration factors were used to calculate both number concentrations and mass concentrations from the electrical current measured by the EAD. The particle number distribution measured by the EEPS was transferred to a mass distribution by means of a fractal density function (fractal dimension = 1.9,  $\rho_{max} = 2.2 \text{ g/cm}^3$ ). For the comparison, the arithmetic mean concentration of each test run was calculated. The mean values of all tests covered two orders of magnitude in both mass and number concentration. Table 1 summarizes the results of the correlation analysis. The results will be discussed in detail in the presentation.

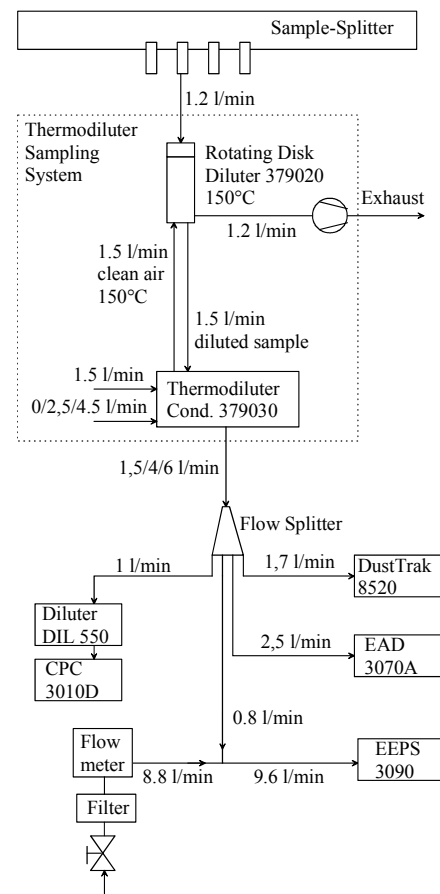


Figure 1: Setup of the subset of instruments discussed in this analysis.

Table 1. Results of the correlation analysis for number concentration and mass concentration measurements.

Number	CPC	Remarks
EEPS	$C_{EEPS} = 1.189 C_{CPC}$ $R^2 = 0.971$	EEPS size distribution truncated to match CPC efficiency
EAD	$C_{EAD} = 1.007 C_{CPC}$ $R^2 = 0.9687$	Calibration factor $1.78 \cdot 10^4 \text{ cm}^{-3} \text{ pA}^{-1}$
Mass	EEPS	Remarks
EAD	$C_{EAD} = 0.999 C_{EEPS}$ $R^2 = 0.9915$	Calibration factor $0.064 \text{ mg m}^{-3} \text{ pA}^{-1}$
DustTrak	$C_{DustTrak} = 0.998 C_{EEPS}$ $R^2 = 0.9245$	Calibration factor $2.11 \text{ mg}_{soot}/\text{mg}_{ISO}$

## Size distribution, morphology, fractal dimension , and elemental composition of soot particles emitted by commercial CFM-56 aircraft engines

D. Delhaye<sup>1</sup>, D. Ferry<sup>2</sup>, E. Ruiz<sup>1</sup>, J. Gouge<sup>3</sup>, G. Rollin<sup>3</sup>, B. Demirdjian<sup>2</sup>, and J. Suzanne<sup>2</sup>.

<sup>1</sup>ONERA, DMPH / EAG, BP72, F-92322, Châtillon, France

<sup>2</sup>CRMC-N / CNRS, Campus de Luminy, Case 913, F-13009, Marseille, France

<sup>3</sup>SNECMA, Villaroche Center, Rond-point René Ravaud, F-77550, Moissy-Cramayel, France

Keywords: Soot size distribution, Aggregates, Particle characterization, Electron microscopy.

Aircraft engines emissions of particulate matter is of growing concern since a few years because of their potential negative effects on the environment. Indeed, aircraft emissions can affect the health and welfare of people living in the neighborhood of airports through changes in the air quality but they can also affect the climate forcing by favoring the formation of condensation trails and cirrus clouds. An accurate knowledge of the physical and chemical properties of the emitted soot particles is therefore needed to assess the extent of these effects and to predict the impact of today's and the future's air traffic on the environment.

Within this context, our study is focused on the experimental characterization of soot physical and chemical properties. Our soot samples are collected by direct impaction on polycarbonate membranes and transmission electron microscope (TEM) grids that are located at 27 m behind an aircraft engine during Landing/Take-Off (LTO) cycles. Two different commercial aircraft engines, namely a CFM56-5C and a CFM56-5B, are used on a CFM56 aero-engine bench at SNECMA Villaroche center (France).

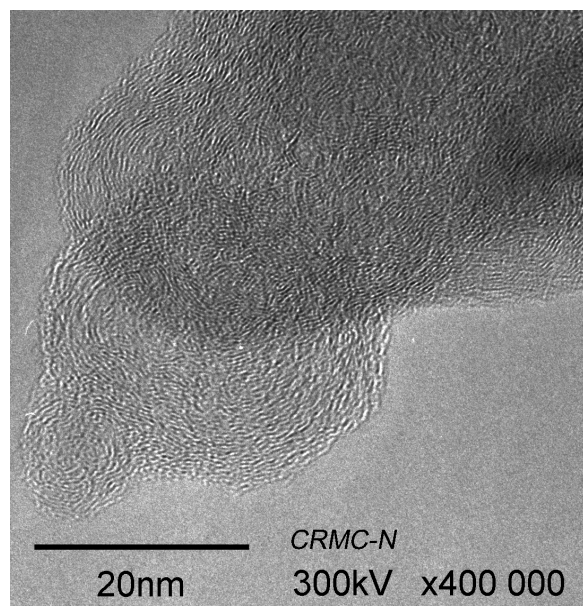


Figure 1. TEM micrograph of soot particles emitted by a CFM56-5B engine.

In addition to the aggregates fractal dimension, the soot primary particles and aggregates size distributions, morphology, structure and elemental composition are studied by using a scanning electron microscope (SEM) and a transmission electron microscope (TEM) that are both equipped with an energy dispersive X-ray detector (EDS).

Soot primary particles exhibit a spherical shape and have an “onion-like” structure, as shown in figure 1. Electron diffractograms show concentric diffuse rings, that are typical of such turbostratic structures, and allow us to determine interplane spacing values:  $d_{002} = 3.82 \pm 0.17 \text{ \AA}$ ,  $d_{10.} = 2.15 \pm 0.07 \text{ \AA}$  and  $d_{11.} = 1.25 \pm 0.02 \text{ \AA}$ .

Comparison of the primary particles size distributions, respectively determined from TEM and SEM micrographs, points out a significant difference due to the samples metallization required prior to the SEM analyses. It indicates that TEM is more suitable for determining the primary particles size distribution. This latter follows a lognormal law and the particles mean diameter value is  $d = 9.9 \pm 0.1 \text{ nm}$ . The size distribution of soot aggregates also follows a lognormal law and the aggregates fractal dimension is found to be  $D_f = 1.82 \pm 0.02$  following the method described by Neer *et al.* (2006). Aggregates are statistically made of  $66 \pm 3$  primary particles, which corresponds to a mean gyration diameter  $d_g = 73 \pm 3 \text{ nm}$ . Their elemental composition is about  $98.3 \pm 2.5 \%$  carbon atom,  $1.5 \pm 0.4 \%$  oxygen atom and  $0.12 \pm 0.05 \%$  sulphur atom.

Neer, A., Koylu U. O. (2006). *Combustion and Flame*, 146, 142-154.

### Influence of the sample preparation on the aircraft engine soot primary particles size distribution determined by Scanning Electron Microscopy.

D. Delhaye<sup>1</sup>, D. Ferry<sup>2</sup>, E. Ruiz<sup>1</sup>, B. Demirdjian<sup>2</sup>, J. Suzanne<sup>2</sup>, J. Gouge<sup>3</sup>, and G. Rollin<sup>3</sup>

<sup>1</sup>ONERA, DMPH / EAG, BP72, F-92322, Châtillon, France

<sup>2</sup>CRMC-N / CNRS, Campus de Luminy, Case 913, F-13009, Marseille, France

<sup>3</sup>SNECMA, Villaroche Center, Rond-point René Ravaud, F-77550, Moissy-Cramayel, France

Keywords: Electron microscopy, Particle size distribution, Soot particles.

The characterization of physical and chemical properties of particulate matter emitted by aircraft engines is of growing concern in the last few decades. This is due to the fact that these particles are suspected to favor the formation of condensation trails and cirrus clouds that influence the climate forcing. Moreover, particulates originating from aircraft engines have potential negative effects on the human health due to their submicrometer sizes. Despite great efforts of the scientific community, data on the relevant sizes of aircraft engine soot primary particles are very limited in the literature. Within this context, we present an experimental study devoted to determine the size distribution of soot primary particles emitted by CFM56-5B and CFM56-5C aircraft engines.

Soot particles are collected by direct impaction on polycarbonate membranes and transmission electron microscope (TEM) grids that are located at 27 m behind an aircraft engine during Landing/Take-Off (LTO) cycles on a CFM56 aero-engine bench at the SNECMA Villaroche center (France).

6320F. However, these membranes are not (electrically) conductive and have to be coated with an amorphous carbon film to enable SEM observations. We illustrate in figure 1 the influence of the amorphous carbon coating on the primary particles size distribution. The size distribution's behaviour is modified and the value of its maximum is shifted towards higher values with increasing carbon film thicknesses. Evolution of the primary particles size distributions versus the parameters that govern the carbon coating is presented in details.

Finally, comparison of the primary particles size distributions respectively determined from TEM and SEM micrographs points out a significant difference due to the samples carbon coating required prior to the SEM analyses. We conclude from our results that TEM, which allows a direct analysis, is a more suitable technique to determine the soot primary particles size distribution compared to SEM, which introduces artefacts through to the sample preparation phase.

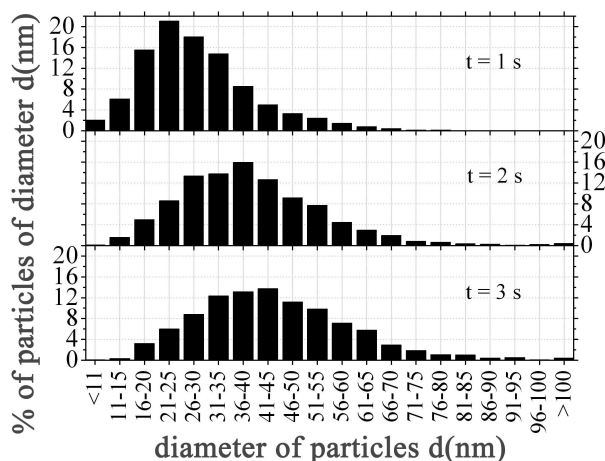


Figure 1. Soot primary particles size distributions of determined from SEM images and various carbon film thicknesses (the time duration t of carbon sublimation is indicated)

Polycarbonate membranes are used to determine the particles size distribution by using a scanning electron microscope (SEM) JEOL JSM-

## In-situ analysis of diesel nano PM, THC and SOF using multi DMAs-CPCs and FID in transient engine conditions

B. Han, H. J. Kim, Y. J. Kim \*

Environmental System Research Center, Korea Institute of Machinery and Materials  
171 Jang-dong, Yuseong-gu, Daejeon, 305-343, Korea

Keywords: In-situ measurement, nanoparticle, after treatment

Diesel particulate matter (PM) is one of the major sources of atmospheric contamination. Recently, much attention has been given to the influence of nanoparticles from diesel engines on human health. In order to reduce diesel particulate matters effectively, diesel particulate filter (DPF) is largely used for diesel exhaust after-treatment systems. Testing of DPF has shown that it is capable of sufficiently reducing diesel particulate matters by mass but not by number owing to the volatile nanoparticles. These nanoparticles are largely generated via gas to particle conversion during the cold start or abrupt speed-up. Therefore, it is necessary to monitor particle and gas emissions at the real time at the transient engine conditions. In this study, emissions of diesel nano PM were investigated with total hydrocarbon (THC), soluble organic fraction (SOF) and NO<sub>x</sub> by in-situ measurements using multi DMAs-CPCs and flame ionization detector (FID).

Test engine was a common rail diesel engine (1,991cc displacement, 25kg·m/2000rpm max. torque, and 112PS/2000rpm max. power). In-situ particle monitor was composed of four DMAs (Model 3081/3085, TSI) and CPCs (Model 3022/3025, TSI). THC and SOF were measured by a FID (MEXA 8120, Horiba) with two filters of 50°C, 190°C, respectively.

Table 1. Transient engine test mode

Mode	Load (%)	Speed (rpm)	Mode	Load (%)	Speed (rpm)
1	0	750	8	50	1500
2	25	1000	9	0	750
3	75	1000	10	25	2000
4	50	1000	11	75	2000
5	0	750	12	50	2000
6	25	1500	13	0	750
7	75	1500			

Table 1 shows the transient engine test mode used in this study. Each mode was operated during 40 seconds and change between modes was during 20 seconds.

Figure 1 shows the emission changes of THC, SOF, NO<sub>x</sub> and diesel PM in the transient engine mode without any after treatment. Hydrocarbon was usually generated as an engine speed increased from

mode 1 to 2, mode 5 to 6, and mode 9 to 10. SOF was generated as an engine load increased from mode 2 to 3, mode 6 to 7. However, SOF was little emitted for the engine load increase from mode 10 to 11 probably due to the high temperature of engine. NO<sub>x</sub> was a good indicator of engine load change. Therefore, the emission of SOF showed similar tendency as that of NO<sub>x</sub> at the low temperature engine conditions ( $T_{\text{emission gas}} < 300^{\circ}\text{C}$ ). The behaviour of volatile nano PM of 30 nm was similar as that of THC at the low temperature probably due to the condensation of HC during sampling, while it was adverse tendency as those of large diesel PM of 60, 90 and 120 nm due to the adsorption of HC on the large PM. However, for the conditions of high speed and high load, a lot of nano PM were generated unexpectedly.

At the rear of a diesel oxidation catalyst (DOC), THC was decreased by about 20-50% at the low temperature from mode 1 to 7, and by 70-80% at the high temperature from mode 8 to 13. However, a lot of nano PM of 30 nm were also emitted even at the high temperature due to the oxidation of sulfur components and their seed effect for condensation of HC after the DOC.

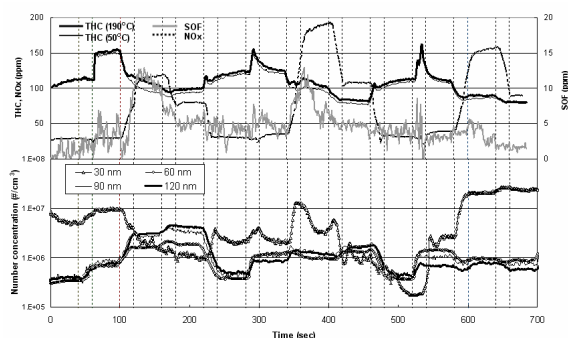


Figure 1. THC, SOF, NO<sub>x</sub> and PM emissions at the transient engine test mode

This work is part of the project "Development of Partial Zero Emission Technology for Future Vehicle" funded by Ministry of Commerce, Industry and Energy and we are grateful for its financial support.

Fukushima, H, Asano, I., Nakamura, S., Ishida, K. & Gregory, D. (2000). *SAE Technical Papers*, 922390

## Elemental content of traffic emitted PM<sub>2.5</sub>

S. Janhäll, J. Boman, M. Hallquist and E. Lakelayeh

Department of Chemistry, University of Göteborg, Department of Chemistry, Atmospheric Science, SE-412 96 Göteborg, Sweden

Keywords: traffic emissions, elemental content, PM<sub>2.5</sub>.

Traffic emitted particles comprises a large part of the particle content of urban air. As urban air quality is of great concern to the constantly growing urban population worldwide, further studies of traffic related particles are needed. PM<sub>2.5</sub> is one of the particle variables that is limited by guidelines, and is thus the focus in this study. Since a large part of it is being long distance transported it is also more difficult to use in emission factor calculations, as the calculations are sensitive to varying backgrounds. This study aims at quantifying the elemental content of particles emitted from traffic, and also includes a short literature study.

Table 1. The estimated emission factor (in  $\mu\text{g}/\text{m}^3$ ) for traffic related elements calculated from eight out of nine samples high in traffic.

Element	Fe	Ca	Cu	Mn	Ti	Cr
Emission	8400	400	500	130	120	20

During nine consecutive weeks sampling of PM<sub>2.5</sub> and nitrogen oxides was performed close to a main road in the city of Göteborg, Sweden. The ratio between nitric oxide and nitrogen dioxide decided if sampling was performed into one filter or the other (Svensson, 2003). During all times one cyclone particle collector was continuously operated. The content in the filters sampled during high NO to NO<sub>2</sub> ratios was then used as the traffic sample, and the continuous sampling as a background. In this way the elemental content of traffic emitted PM<sub>2.5</sub> was analysed. The difference between the concentrations of NO<sub>x</sub>, i.e. NO + NO<sub>2</sub>, during the sampling of traffic samples and the continuous sampling was used to describe the dilution of the traffic plume. By taking the median value of the calculated emission factors an approximation of the emissions of various elements was calculated. The method is a development of the size distributed particle number emission method described in Janhäll and Hallquist (2005).

Nitrogen oxides were measured on-line with chemiluminescence, Eco Physics CLD 700 AL, every minute, while particle collection was performed weekly by Casella cyclones onto Teflon filters, Pall 3.0  $\mu\text{m}$  pore size 25mm diameter, analysed by weighing for mass and by Energy Dispersive X-Ray Fluorescence (EDXRF) spectroscopy to find the elemental content. Filters were also collected for organic content analysis by GC-MS.

The elements associated with traffic emissions in this study was Fe, Ca, Cu, Mn, Ti and Cr. All of those elements were found in higher concentrations in the traffic samples than in the background. According to literature, e.g. Lough *et al* (2005), the elements are principally of two kinds, i.e. the ones normally related to soil, or, in this case, re-suspended dust (Fe, Ca, Mn, Ti), and the elements related to wear of the vehicle or road (Fe, Cu, Cr). The elements not related to traffic are mainly long distance transported (Pb, S), or from other known sources (Br, Sr), while some elements occasionally related to traffic according to these measurements, and also in literature related to both traffic and other sources (Rb, Zn, K, Cl, Ni), that was not possible to resolve by this simple method and short campaign. The quantification of the emissions of different elements from traffic was rather uncertain, but for the elements where literature data was available, the results obtained here was mainly in the same range as other studies.

Table 2. Number of samples showing traffic influence out of nine possible samples, for elements defined as non-traffic related.

Rb	Zn	K	Cl	Ni	Pb	Sr	S	Br
6	5	5	5	5	4	3	3	2

This method was proven useful for traffic emission studies, where the total sample volume needs to be high, implying the need of long time measurement scenarios. By selective sampling the integrated time in each collector is long enough to detect many elements, even if each single occasion with one situation is short.

This work was supported by MISTRA, the Swedish Foundation for Strategic Environmental Research.

Janhäll, S. & Hallquist, M. (2005) *Environmental Science & Technology*, 39, 7609-7615  
 Lough, G., Schauer, J. J., Park, J.S., Shafer, M.M., Deminter, J.T. & Weinstein, J.P. (2005). *Environ. Science & Technology*, 39, 826-836.  
 Svensson H. (2003). *Development of a selective sampling method for aerosol particles*. Thesis Göteborg University, Sweden

## Filter test with soot generation from 7.5 nm up to 200 nm

Martin Schmidt, Leander Mölter

Palas® GmbH, Greschbachstr. 3b, 76229 Karlsruhe, Germany

Keywords: aerosol generation, combustion particles, diesel soot particles, generation of combustion aerosols, generation of nanoparticles

The influence of soot particles on the human health and on our environment is a highly discussed topic in research, industry and politics. This fact opens a wide range of applications, as e.g. atmospheric research, test of diesel soot filters, inhalation studies, calibration of particle measuring devices and fire detectors, where soot particles of different sizes and concentrations are needed.

This can be accomplished with the new Variable Soot Generator series VSG which generates real soot particles from a flame with stable concentration and defined particle size. The VSG system is a licensed product of the Deutsches Zentrum für Luft- und Raumfahrt e. V. (German Centre for Aerospace), Stuttgart, Germany.

Already used in practice to the full satisfaction of the customer is the version **VSG-3000S**. It is a fully automated test generator which enables a large variety of different settings:

- particle sizes from 50 nm up to more than 200 nm
- mass concentration from 100 mg/h up to 2.5 g/h
- variable output temperature up to 300°C
- adjustable volume flow up to 60 m<sup>3</sup>/h



Figure 1. Variable Soot Generator VSG-3000S

Changing the set-up of the generator around the burner as well as the diameter of the burner gives the possibility to cover the specifications from many different applications concerning particle size and concentration. Mass flows from a few nanograms up to more than 2.5 g/h can be achieved easily in the different versions.

Flame-soot is formed in fuel rich zones of a flame. In a diffusion flame, the “two dimensional” flame-front is very thin and the local air-fuel mixtures vary from full-lean to full-rich! But soot formation is strongly influenced by the air-fuel mixture!

Therefore, the new developed soot generator works with a premixed flame. Compared to a

diffusion flame, the premixed flame has a well defined air-fuel mixture and a “three dimensional” flame-volume. The great advantage is that the premixed flame is less influenced by ambient conditions, as e.g. temperature and ambient pressure, and allows an extremely stable soot generation concerning particle size and concentration. This leads to the possibility to adjust the mean particle size distribution, generated in the flame, just by changing the fuel-air mixture.

A brand new version of the VSG-series, small and comparably very economical, has been already developed. The version **VSG-3010C** is especially made for calibration of measurement devices, as e.g. CPC-counters, SMPS-systems and Differential Mobility Analysers, and for testing the fractional efficiency of small filters and filter media.



Figure 2. Variable Soot Generator VSG-3010C

This version uses the advantages of the burner principle, the well defined aerosol generation and high reproducibility to generate soot particles with mean diameters of e.g. 7.5 nm up to 150 nm. The particle size distribution is a log-normal distribution.

In this paper we will explain the set-up of the different VSG-versions and show detailed measurement results concerning particle size, particle size distribution and mass flow output.

## Gas-particle distribution of PAH emission from masonry heater in wood combustion

K. Hytönen<sup>1</sup>, P. Yli-Pirilä<sup>1</sup>, J. Tissari<sup>1</sup> and J. Jokiniemi<sup>1,2</sup>

<sup>1</sup>Department of Environmental Science, University of Kuopio, Fine Particle and Aerosol Technology Laboratory, FI-70211 Kuopio, Finland

<sup>2</sup>VTT, Technical Research Centre of Finland, Fine Particles, FI-02044 VTT, Espoo, Finland

Keywords: PAHs, residential wood combustion, gas-particle distribution

The polycyclic aromatic hydrocarbons, PAHs, are of common interest because of their adverse health effects. In many countries, residential wood combustion is an important source of PAHs. Recently, the legislation concerning ambient air PAH concentration in PM10 has come into force in EU (European Parliament, Council, 2004). The phase distribution of PAH emission is of great interest due to the phase specific legislation.

PAHs were sampled from the emissions of a masonry heater, where birch wood was burned (Tissari *et al.*, 2006). The sampling was done with two methods (Table 1). The adsorbents and filters were extracted and 15 PAHs were analyzed with Agilent GC/MS operated in SIM mode (acenaphthylene (acy), acenaphthene (ace), fluorene (fle), phenanthrene (phe), anthracene (ant), fluoranthene (fla), pyrene (pyr), benz(a)anthracene (b(a)a), chrysene (chr), benzo(b)fluoranthene (b(b)f), benzo(k)fluoranthene (b(k)f), benzo(a)pyrene (b(a)p), indeno(1,2,3-cd)pyrene (i(1,2,3-cd)p), dibenz(a,h)-anthracene (d(ah)a), benzo(g,h,i)perylene (b(ghi)p)).

Table 1. PAH sampling methods.

Method	Sampling equipment	Dilution, temperature
Denuder method	Gas phase: 2 8-channeled annular denuders (XAD on the internal surface)	Porous tube diluter DR 80-120
	Particle phase: filter, PUF	T 21 °C
ISO 11338	Gas phase: XAD, condensate Particle phase: filter	non-diluted T 250 °C

The gas-particle distribution of PAHs in diluted exhaust gas was shifted to the particle phase (Fig. 1), whereas the distribution in non-diluted, hot exhaust gas showed that the emissions of all PAHs were mostly in the gas phase (Fig. 2). In the dilution, condensable PAHs condense on the surface of the particles. In addition, in ISO 11338 the adsorbent is placed after the filter, which may lead to incorrect determination of the phase distribution due to artifacts (Gundel *et al.*, 1995).

The total PAH emissions determined with the two methods were fairly close to each other. Instead, determined with the ISO method, the average emission of the particle phase PAHs was 90% lower than the emission determined with the denuder

method. The sampling method affects remarkably the emission of particle phase PAHs; this should be considered in the emission measurement in general.

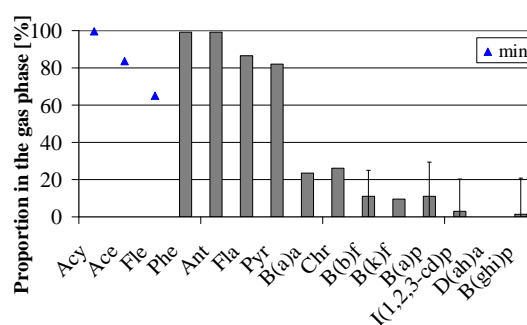


Figure 1. The proportion of the PAH emission in the gas phase sampled with denuder method from diluted exhaust gas.

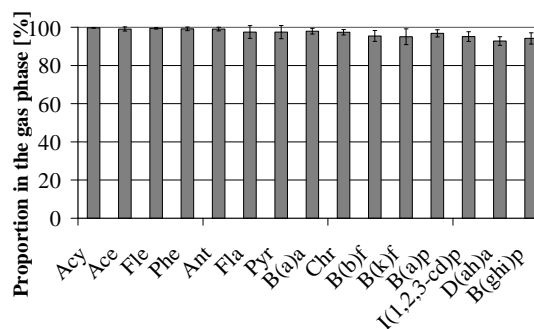


Figure 2. The proportion of the PAH emission in the gas phase sampled with ISO 11338 (raw gas).

This work was supported by Tekes- Finnish Funding Agency for Technology and Innovation, Graduate school in Physics, Chemistry, Biology and Meteorology of Atmospheric composition and climate change, and Maj and Tor Nessling Foundation.

European Parliament, Council. (2004). Directive 2004/107/EC.

Gundel, L. A., Lee, V. C., Mahanama K. R. R., Stevens, R. K., Daisey, J. M. (1995). *Atm. Env.*, 94, 1719-1733.

ISO 11338-1 (2003). Geneva, Switzerland.

Tissari, J., Hytönen, K., Yli-Pirilä, P., Suonmaa, V., Turrek, T., Willman, P., Jokiniemi, J. (2006). in: *Proc. 7th Int. Aerosol Conf.*, St. Paul, 252-253.

## Fine particulate emissions from combustion of woods common in Austria

C. Schmidl, A. Caseiro, H. Puxbaum and I.L. Marr

Institute of Chemical Technologies and Analytics, Vienna University of Technology, Getreidemarkt 9/164-UPA, 1060 Vienna, Austria

Keywords: Woodsmoke, Levoglucosan, PM10, Combustion particles

Wood smoke is increasingly being seen as an important component of airborne particulate matter (PM). As the new short time standard for PM10 – particles in ambient air, of  $50 \mu\text{g m}^{-3}$ , set by the European Union (EU-Directive 1999/30/EG) is frequently violated in most urban regions in Europe, we have to find effective measures to reduce these concentration levels. This requires detailed knowledge of the magnitudes of individual source contributions (Puxbaum *et al.*, 2004). Therefore the AQUELLA – project was started in Austria, using a chemical mass balance (CMB) – receptor model as source apportionment technique (Watson, 1984). This calls for chemical profiles of the source materials.

Additionally, a macro tracer model has been developed within the AQUELLA Project, which uses single numerical factors for each characteristic compound, in each of the source materials being considered. Ideally, these are compounds that are known to be emitted by only one source. Levoglucosan has been recommended as a single tracer for the PM10 source "wood combustion" (Simoneit *et al.*, 1999).

This study focuses on domestic wood combustion, which is thought to be a major source of particulate emissions in Europe to the north of the Alps. The aim was to characterise the wood smoke emitted in Austria, to obtain a chemical profile of the fine particles (PM10), and if possible, factors for individual macro-trace markers.

Large (30 cm) pieces of beech, oak, spruce, larch and softwood briquettes were burned in a closed domestic stove, and samples of the particulate emissions were analysed for trace metals, ions, carbon species, anhydrosugars and other trace organics, plus cellulose and HULIS.

Table 1. Anhydrosugars in woodsmoke, % m/m

	Beech	Oak	Spruce	Larch	Briquettes
Levo	4.1	13.3	10.7	15.1	10.1
Man	0.28	0.92	3.0	3.9	4.0
<i>R</i>	14.8	14.4	3.6	3.9	2.5
<i>n</i>	8	4	10	3	6

Table 1 summarises findings for the anhydrosugars levoglucosan and mannosan, also the ratio of the two, *R*, and the number of tests, *n*, for each wood. Beech emissions are significantly

different from those from spruce, and the SEM for the levoglucosan contents was < 3 % absolute.

Taking the mix of trees felled as 32 % beech, 9 % oak, 50 % spruce, 4 % of larch and 5 % briquettes, a suitable composite factor for Austrian woodsmoke, based on the levoglucosan to PM10 factor

$$F_w = 100 / \{ c_{\text{beech}} \times 4.1 + c_{\text{oak}} \times 13.3 + c_{\text{spruce}} \times 10.7 + c_{\text{larch}} \times 15.1 + c_{\text{briquettes}} \times 10.1 \}$$

works out at 11.2 which is close to a combination of 20/70/10 % (beech/spruce/briquettes) omitting oak and larch resulting in  $F_w = 10.7$ . From this, woodsmoke accounts, in winter, for typically 10 – 20 % m/m of PM10 collected in Vienna.

The levoglucosan to mannosan ratios were different and well defined and so permit the proportion of spruce to beech, approximating softwood to hardwood, to be estimated:

$$\% \text{ spruce} = (14.8 - R_{\text{levo/man}}) / (0.112)$$

Using this relationship we could show that smoke in ambient PM10 collected in Graz, Salzburg and Vienna, derived mainly from softwoods, was in the range 80 – 90 %. This demonstrates the utility of analysing for anhydrosugars in such samples, for source apportionment.

The comparison of chemical profiles from this study with literature data (Fine *et al.*, 2004) showed that while there were qualitative similarities, the actual concentrations of metals, for instance, could be quite different. Likewise, the values for OC and EC differed considerably from literature values, which has confirmed the need to establish in-house profiles for Austria and not to import profiles from elsewhere. The inorganic components measured here were not significantly different for the different woods, so that one profile could be derived for woodsmoke, appropriate for CMB modelling.

Puxbaum, H., Gomišček, B., Kalina, M., Bauer, H., Salam, A., Stopper, S., Preining, O., Hauck, H., (2004) *Atmos. Environ.* **38**, 3949-3958.

Watson, J.G. (1984). *J. Air Pollut. Control Assoc.*, **34**, 619-623.

Simoneit, B.R.T., Schauer, J.J., Nolte, C.G., Oros, D.R., Elias, V.O., Fraser, M.P., Rogge, W.F. & Cass, G.R. (1999). *Atmos. Environ.*, **33**, 173 – 182.

Fine, P.M., Cass, G.R. and Simoneit, B.R.T. (2004). *Environ. Eng. Sci.*, **21**, 387 – 409

## Particle Emissions from Heating Units Operating on Wood and Heavy Fuel Oil

O. Sippula<sup>1</sup>, J. Hokkinen<sup>2</sup>, P. Yli-Pirilä<sup>1</sup>, H. Puustinen<sup>2</sup>, J. Jokiniemi<sup>1,2</sup>

<sup>1</sup>University of Kuopio, Department of Environmental Sciences, Fine Particle and Aerosol Technology Laboratory, P.O. Box 1627, FI-70211 Kuopio, Finland.

<sup>2</sup>VTT Technical Research Centre of Finland, Fine Particles, P.O. Box 1602, 02044 VTT, Espoo, Finland

Keywords: Combustion particles, Emission factor, Chemical composition, Field Measurements

The use of biomass fuels is currently increasing rapidly in energy production in Finland. Also, the district heating units operating on heavy fuel oil (HFO) are replaced by ones using biomass fuels. This may have a significant impact on the atmospheric particle emissions because small heating units (<10 MW) are typically not equipped with effective particle filtration systems.

In this study, particle emissions from three wood fuel fired and two heavy fuel oil fired (HFO) district heating units were studied on the field. Two of the wood fired heating units were rotating grate boilers and one a gasification combustion boiler. The HFO boilers had no filtration devices in use. All of the wood-fired units had a cyclone to remove the coarse particles from the flue gas. In addition, one of the rotating grate boilers had a wet flue gas scrubber in use and the second one was equipped with an electrostatic precipitator (ESP).

The measurements included determinations of particle mass concentrations and particle number concentrations as a function of particle size, and analyses on particle chemical composition. The particle mass size distributions were measured using an 11 stage Berner Low Pressure Impactor (BLPI). The sample was diluted in a porous diluter which was inserted in the stack. A cyclone was used prior to the diluter to collect the coarse particles. ICP-MS analysis and ion chromatography were used to determine chemical compositions of the impactor samples. The particle number size distributions and number concentrations were measured using an Electric Low Pressure Impactor (ELPI). Particle organic carbon (OC), elemental carbon (EC) and carbonate was analyzed from separately collected PM1.0 filter samples, applying a thermal-optical carbon analyzer (Sunset Laboratory Inc.). The analyses were performed according to the NIOSH procedure (NIOSH, 1999).

Figure 1 presents the average fine particle (PM1.0) and total suspended particles (TSP) emissions measured from the heating units. Figure 2 shows the chemical compositions of the PM1.0 from different heating units. The particle emissions from wood fired heating units were higher than those from heavy fuel oil fired units, in case no effective particle filtration, as ESP for example, was used. The flue gas wet scrubber was found to capture 80-88 % of the TSP but only 37-51 % of PM1.0.

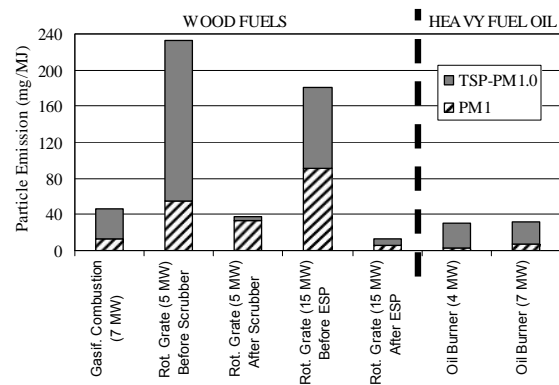


Figure 1. Average nominal emissions of PM1.0 and TSP from different heating units. Additionally, emission values before the filtration units are shown.

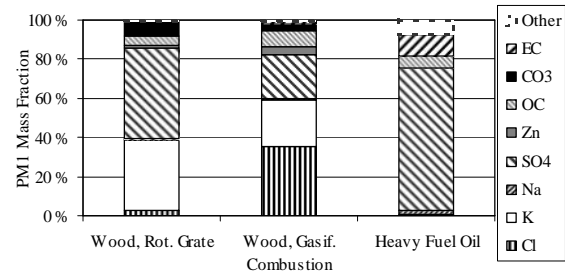


Figure 2. Chemical compositions of fine particles (PM1.0) from different sources.

The fine particle formation in wood combustion was mainly influenced by the vaporization of ash minerals from the fuel. Especially alkali metals, sulphur, chlorine and zinc were enriched in fine particles. In addition, OC compounds and carbonate contributed significantly to the PM1.0 emission. In heavy fuel oil combustion the main factor influencing the particle formation was the formation of sulphuric acid from the SO<sub>2</sub> gas. Around 4 % of the fuel sulphur was converted to sulphate and condensed to particle phase. In addition, soot (EC), OC compounds and a large variety of metals were analysed from the fine particles.

This work was supported by the Finnish Funding Agency for Technology and Innovation.

NIOSH (1999) Elemental Carbon (Diesel Particulate) Method 5040. In *NIOSH Manual of Analytical Methods (NMAM)*, The National Institute for Occupational Safety and Health, Atlanta.

## Detailed particle analysis in the hot flue gas of a municipal waste incineration plant

Christian Deuerling<sup>1</sup>, Jürgen Maguhn<sup>1</sup>, Hermann Nordsieck<sup>2</sup>, Ragnar Warnecke<sup>3</sup> and Ralf Zimmermann<sup>1,2,4</sup>

<sup>1</sup>Institut für Ökologische Chemie, GSF-Forschungszentrum für Umwelt und Gesundheit GmbH, Ingolstädter Landstrasse 1, D-85764 Neuherberg, Germany

<sup>2</sup>Abteilung Umweltchemie und Prozessanalytik, BfA-Bayerisches Institut für Angewandte Umweltforschung und -technik, Am Mittleren Moos 46, D-86167 Augsburg, Germany

<sup>3</sup>GKS Gemeinschaftskraftwerk Schweinfurt GmbH, Hafenstrasse 30, 97424 Schweinfurt

<sup>4</sup>Analytische Chemie, Institut für Physik, Universität Augsburg, Universitätsstrasse 1, D-86159 Augsburg

Keywords: Aerosol Measurement, Cascade Impactor, Combustion Particles, high temperature aerosols

High-temperature chlorine corrosion of super heaters is one of the main cost factors of running municipal solid waste incineration (MSWI) plants.

To setup a comprehensive model for corrosion in a MSWI plant, a measurement system was developed to analyse the complex processes the waste incineration raw gas is subjected to upon travel through the flue-gas duct of a MSWI boiler. Particles from 30 nm to 3 µm were sampled off-stack, size fractionated and analysed concerning mass concentration and chemical composition. Additionally, acidic components of the gas phase were analysed. Measurements were performed in the 1st (900 °C) and 2nd pass (700 °C), straight behind the first two super heater blocks in the 3rd pass (500 °C) and in the 4th pass (300 °C). Because of temporal variation of the fuel composition, each measurement was carried out in parallel at the reference point (2nd pass) and at the measuring point in question by two identical measurement systems.

In order to sample the particulate matter in its current state, rapid dilution of the raw gas was accomplished by a porous tube diluter positioned directly behind the inlet of the sampling probe. The probe is held at a constant temperature of 300 °C. The raw gas subsequently passes a cyclone, further diluters and enters the instruments for analysis of chemistry and morphology.

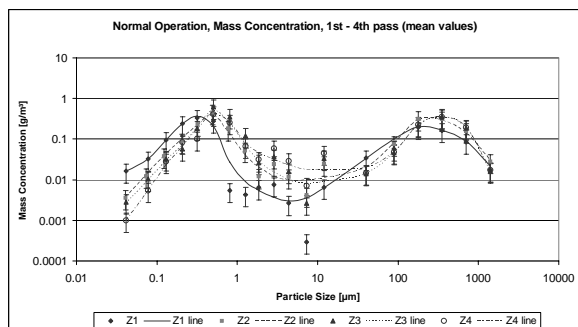


Figure 1. Size distribution of particle mass concentration in the four consecutive passes of the waste incineration boiler.

At normal operation conditions of the plant a bimodal size distribution of the particles can be observed (Fig. 1) showing growth of the particles

upon travel through the flue gas duct due to agglomeration and condensation effects.

The chemical composition of the particles also changes (Fig. 2) due to condensation of volatile compounds and chemical reactions. An increase of the sulphur content can be observed probably due to sulphatation of chlorides.

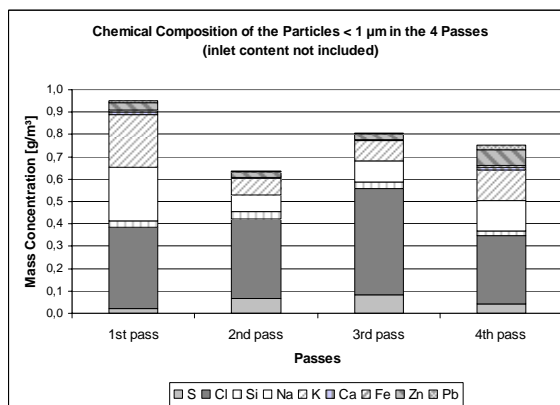


Figure 2. Changes in chemical composition of the fine particles upon travel through the flue-gas duct

Modifications of the operation conditions of the plant on corrosion parameters such as reduction of the length of the fire, changing of the rate of recirculated air, adding of sulphur to the waste and injection of SO<sub>2</sub> were performed resulting in changes of aerosol composition.

This project is funded by the Bayerisches Staatsministerium für Umwelt, Gesundheit und Verbraucherschutz within the scope of the European Regional Development Fund (ERDF).

The author wishes to thank Max-Buchner-Forschungsförderung for their kind support.

Deuerling, C., Maguhn, J., Nordsieck, H., Reznikov, G., Zimmermann, R. & Warnecke, R. (2005). *Proc. Europ. Aerosol Conf.*, Ghent, 373.

Schroer, C. & Konys, J. (2002). *Report*, Forschungszentrum Karlsruhe.

Maguhn, J., Karg, E., Kettrup, A. & Zimmermann, R. (2003). *Environ. Sci. Technol.*, 37, 4761-4770.

## Traffic Emissions and Micrometeorology near a Busy Road

G. Gramotnev, M. J. Burchill and D. K. Gramotnev

Applied Optics Program, School of Physical and Chemical Sciences,  
Queensland University of Technology, GPO Box 2434, Brisbane, QLD 4001, Australia

Keywords: Aerosol formation, Aerosol modelling, Evaporation, Meteorology, Traffic.

As has been shown by several recent papers, combustion aerosols resulting from transport emissions are strongly non-stable and experience rapid evolutionary processes (Zhu *et al*, 2002, Gramotnev & Ristovski, 2004, Zhang & Wexler, 2004, Gramotnev & Gramotnev, 2005). Such processes are likely to include condensation and evaporation, coagulation and fragmentation, nucleation, etc. Unfortunately a complete understanding of these processes has not been achieved so far with different models and mechanisms being considered in the literature. Therefore, further research in this direction and use of new approaches that may shed the light on the actual processes involved is an essential goal of aerosol science.

In this paper, we attempt to gain additional information about possible processes during evolution of combustion aerosols by undertaking a comprehensive study of the effect of transport emissions on micrometeorological factors near a busy road.

Monitoring of the local meteorological parameters (such as wind speed and direction, temperature and humidity) was conducted by means of a portable automatic weather station at the height of approximately 2 m above the ground level. Simultaneously, traffic conditions on the road were recorded by a video camera with the subsequent determination of the corresponding numbers of trucks and cars on the road. Monitoring was conducted at different wind conditions, ambient (background) humidity, temperature and solar radiation.

Detailed canonical and multi-variate statistical analyses of local humidity and temperature have been undertaken at different distances from the road, different traffic and atmospheric conditions. In particular, it is shown that typical traffic-related variations of temperature and humidity near a busy road may reach several degrees and several percent, respectively. Strong correlations of these parameters (especially humidity) with traffic conditions, such as numbers of heavy trucks and cars on the road, have been demonstrated and analyzed.

Significant attention has been focused on the analysis of the dependencies of humidity and temperature on distance from the road. The obtained results are linked to the expected

evolutionary processes in combustion aerosols. In particular, correlations between the determined micrometeorological parameters and particle size distributions are investigated, showing strong relationship between particle concentrations and local temperature. The obtained results are consistent with the model of particle fragmentation. On the other hand, correlations between particle concentrations in different channels and humidity were demonstrated to be largely non-stable. This may indicate that humidity does not play a significant role in evolution of combustion aerosol, at least at the considered evolutionary stage for the considered particle dimensions (largely below ~ 100 nm).

At the same time, local humidity levels have been linked to larger (~ 1  $\mu\text{m}$ ) composite liquid particles in combustion aerosols near a busy road. Theoretical modeling of evolution of such particles and their relationship to local humidity is carried out. In particular, the results are consistent with the direct observation of deposition of such larger composite liquid particles onto different surface with their subsequent microscopic analysis.

The results will be important for better understanding of evolutionary processes in different types of particles in combustion aerosols near busy roads.

Y. Zhu, et. al. (2002), *Atmospheric Environment*, vol.36, 4323-4335.

G. Gramotnev and Z. Ristovski (2004), *Atmospheric Environment*, vol.38, 1767-1776.

K. M. Zhang and A. S. Wexler, (2004) *Atmospheric Environment*, vol.38, 6643-6653.

D. K. Gramotnev and G. Gramotnev (2005), *J. Aerosol Sci.*, vol.36, 323-340.

## Cross-Correlations of Particle Modes at Different Distances from a Busy Road

G. Gramotnev and D.K. Gramotnev

Applied Optics Program, School of Physical and Chemical Sciences,  
Queensland University of Technology, GPO Box 2434,  
Brisbane, QLD 4001, Australia

Keywords: Statistical analysis, Combustion aerosols, Particle size distribution, Particle modes.

Understanding of mechanisms of evolution and interaction of combustion aerosols resulting from transport emissions in the real world environment is an important but complex task because of the instability of such aerosols and fast evolutionary processes undergone by different particle modes (Hu *et al.*, 2002, Gramotnev & Ristovski, 2004, Kiang & Wexler, 2004, Gramotnev & Gramotnev, 2005). Together with strong stochastic fluctuations and variability of source and external conditions (e.g., caused by atmospheric turbulence), this aspect presents a significant difficulty for the analysis of such aerosols and determination of the major physical/chemical processes guiding evolution of combustion aerosols. This is significant hurdle for the development of a reliable predictive model for the determination of population exposure to particulate transport emissions. New statistical methods of analysis may be the best answer to these serious problems.

Therefore, this paper presents a detailed analysis of the experimental monitoring data obtained near a busy road in the Brisbane metropolitan area, Australia, based on the newly developed statistical approach that combines determination of simple correlation coefficients between particle concentrations in different channels of the size distribution and moving average approach (Gramotnev & Gramotnev, 2007).

The monitoring data near a busy road were used for the monitoring campaign previously described in (Gramotnev and Ristovski, 2004).

In particular, it has been demonstrated that at some particular distances from the road, some of the modes/channels of the particle size distributions in combustion aerosols can be grouped in accordance with their cross-correlations with all other channels from the same size distribution. Cross-correlation coefficients between channels from one group with all other channels in the size distribution appear to have significantly similar features. At the same time cross-correlation coefficients for channels from the different groups tend to display significantly different (opposite) features. For example, Figure 1a shows the dependencies of the moving average cross-correlation coefficients for two channels from the two different groups, while Figure 1b shows the similar dependencies for the channels from the same group.

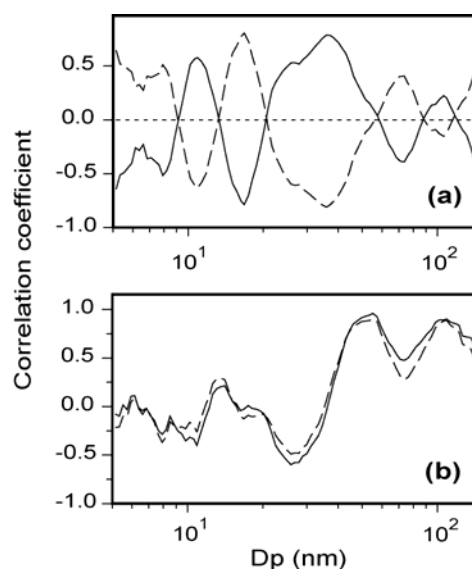


Figure 1. The dependencies of the moving average cross-correlation coefficients with all the channels in the size distribution: (a) for the 17 nm particles (dashed) and 37 nm particles (solid) (b) for the 55 nm particles (solid) and 109 nm particles (dashed). The distance from the centre of the road was 45 m.

The discussed distinctly different cross-correlations patterns for different channels in the size distribution have been analysed for distances from the road within the range from 45 to 300 m. The obtained results were explained on the basis of the fragmentation model of evolution of combustion aerosols.

The discussed approach will be useful not only for the consideration of particle fragmentation, but also for investigation of any other rapid evolutionary process in atmospheric aerosols.

- Y. Hu, *et al.* (2002), *Atm. Env.*, vol.36, 4323-4335.  
G. Gramotnev and D. Ristovski (2004), *Atm. Env.*, vol.38, 1767-1776.  
K. M. Kiang and A. S. Wexler, (2004) *Atm. Env.*, vol.38, 6643-6653.  
D. K. Gramotnev and G. Gramotnev (2005), *J. Aerosol Sci.*, vol.36, 323-340.  
G. Gramotnev, D. K. Gramotnev, *Atm. Env.* (online 07/02/2007  
doi:10.1016/j.atmosenv.2007.01.031).

## Exhausted particle concentration of charge injected two fluid combustion nozzle for non-conducting liquid

<sup>1</sup>Joong Hyuk Kim, <sup>1</sup>Youngjoo Choi, <sup>1</sup>Mingyu Park and <sup>1</sup>Sang Soo Kim

<sup>1</sup>Department of Mechanical Engineering, KAIST, 305-701, Daejeon, South Korea

In the liquid spray technology, droplet size and spatial dispersion are important characteristics to improve combustion efficiency. For well-atomized fine droplet spray, applying electrostatic force to droplets is a useful method. (Laryea & No, 2004) However non-conduction liquid such as diesel which is commonly used for combustion is not easy to charge. Charge injection method has been applied by introducing the needle electrode for high voltage in liquid. (Shrimpton & Yule, 2003) But sole charge injection method is still limited to atomize diesel widely, so it is difficult to apply combustion nozzle. To overcome this problem, the compressed air is used to break diesel in fine droplets in this study.

The two fluid, diesel and air, nozzle combined charge injection was designed, and its spray characteristics were described and the effect of charged liquid in combustion was investigated.

The experimental setup for combustion test which is cross sectional view is shown in Figure 1. The fuel, diesel, is supplied along the tungsten wire in the stainless steel orifice. The end of tungsten wire is sharpened like needle. The filtered air is supplied a ring shape and impinges on the liquid jet outside the liquid discharge orifice with high speed. Negative high voltage is applied to the tungsten wire and orifice is connected to ground. The nozzle is located in the closed chamber where cold water is supplied like boiler.

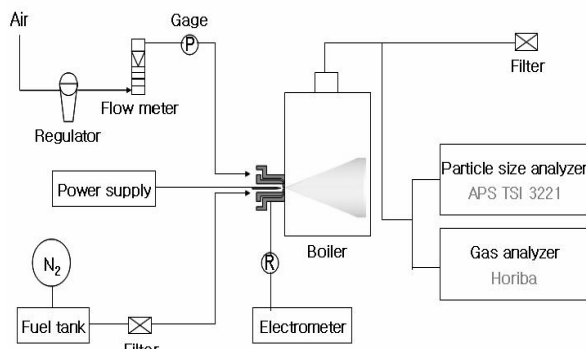


Figure 1. Schematic diagram of experimental setup.

The concentration of exhausted particles such as soot, unburned hydrocarbon, and etc. is measured by Aerosol Particle Sizer, TSI 3221.

When applied voltage to diesel, specific charge density increased and droplet size decreased slightly. This result means that the nozzle generates highly charged fine droplets effectively.

The number concentration of exhausted particle from the charged diesel combustion is shown in Figure 2. When applied voltage increased, the concentration decreased. Because unipolar charges generated by needle electrode resulted in well-dispersed spray and the suppression of particles by their electrical repulsive force.

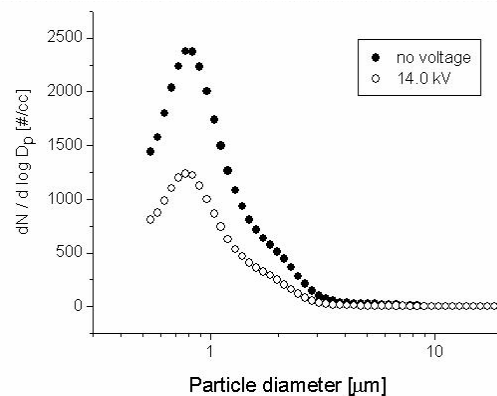


Figure 2. Exhausted particle number concentration for applied voltage.

This work was supported by the Brain Korea 21 Program of the Ministry of Education and the Eco-Technopia 21 Project of the Ministry of Environment

Laryea, G. N. and No. S. Y. (2004). *Journal of Electrostatics*, 60, 37-47.

Shrimpton, J. S. and Yule, A. J. (2003). *Atomization and Sprays*, 13, 173-190.

## Real-world particle number emission factors from residential wood burning

G. Olivares<sup>1,3</sup>, C., Johansson<sup>1</sup>, J., Ström<sup>1</sup> and L. Gidhagen<sup>2</sup>

<sup>1</sup>Department of applied environmental sciences, Stockholm University, S 10691, Stockholm, Sweden

<sup>2</sup>Swedish Meteorological and Hydrological Institute, 601 76 Norrköping, Sweden.

<sup>3</sup>National Institute of Water and Atmospheric Research Ltd. Newmarket, Auckland 1032, New Zealand.

Keywords: Ambient aerosols, combustion particles, DMA, emission factor, number size distribution.

Biomass burning has a severe impact on the air quality in several parts of the world, particularly in developing countries (Ludwig et al., 2003). Emissions from biofuels have been reported to be of similar magnitude as those from open vegetation fires (Ito and Penner, 2004). Emissions from residential wood combustion (RWC) are difficult to characterize due to the small scale and scattered nature of these sources and the range of fuels used.

Using air quality measurements from a campaign in Temuco (Chile) during the Chilean winter of 2005, we estimated the size resolved particle number emission factors from RWC. These estimates correspond to an average of the equipments used in the city and an average of the operating conditions in terms of quality of fuel and burning conditions.

The measurements were performed in Temuco (38°45'S; 72°40'W; 120 m.a.s.l.) between April 18<sup>th</sup> and June 15<sup>th</sup> of 2005. To separate the impact of traffic from RWC, two monitoring sites were used. The first site (Las Encinas) was located in a residential area relatively far from major roads while the second site (City) was located in a busy street in downtown Temuco. The measurements were performed with custom built Differential Mobility Analyzers (DMA) systems located one at each site. The systems were set up to scan particle sizes from 25nm to 600nm in 20 channels. These DMA were connected to condensation particle counters (TSI 3010 and TSI 3760).

To estimate the emission factors, a Gaussian model ([www.indic-airviro.smhi.se](http://www.indic-airviro.smhi.se)) was run and the emission factors were adjusted so the results fitted the hourly average measurements in the Las Encinas site. Meteorological information was available from the Las Encinas monitoring site. Information about average wood consumption in the residential areas of the city and traffic flows, with street locations, was incorporated to the model to reflect the spatial distribution of the emissions and give realistic relative impacts on the two measuring sites.

Figure 1 shows the obtained particle number emission factors as function of particle size. Results from emission measurement reported by Hedberg et al. (2002) for a residential woodstove are shown for comparison. The obtained size distribution

emission factor shows a main mode around 80nm, while direct emission measurements show a secondary mode below 30nm.

This result indicates that ambient measurements can be used to estimate emission factors using modelling tools, provided that the major sources are included in the model.

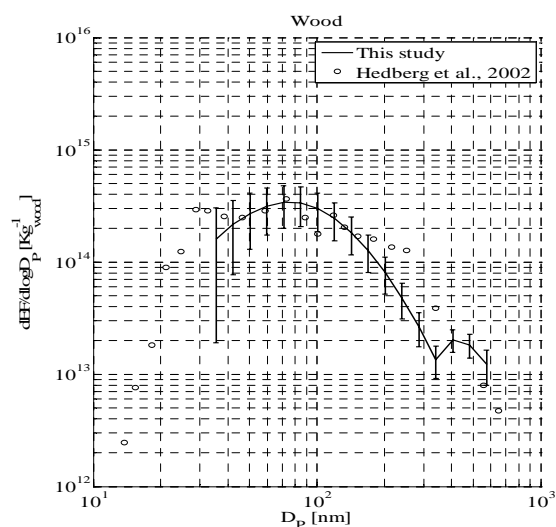


Figure 1. Particle number emission factor as function of particle size for residential wood combustion. The error bars indicate the 95% confidence interval for the emission factor estimates. Results from Hedberg et al (2002) are shown for comparison.

This work was supported by the Swedish International Development Agency (SIDA). Additional support was provided by NIWA Ltd (Auckland, New Zealand).

Hedberg, E., et al., 2002. Chemical and physical characterization of emissions from birch wood combustion in a wood stove. *Atmos. Env.*, 36, 4823 – 4837.

Ito A. and Penner J., 2004. Global estimates of biomass burning emissions based on satellite imagery for the year 2000. *J. Geophysical. Res.*, 109, D14S05, doi:10.1029/2003JD004423

Ludwig, et al., 2003. Domestic combustion of biomass fuels in developing countries: A major source of atmospheric pollutants. *J Atmos. Chem.* 44, 23 – 37.

## Fine Particle Emissions from Solid Biofuel Combustion Studied With Single Particle Mass Spectrometry

J. Pagels<sup>1,2</sup>, D.S. Gross<sup>3</sup>, D.D. Dutcher<sup>1</sup>, M.R. Stolzenburg<sup>1</sup> and P.H. McMurry<sup>1</sup>

<sup>1</sup>Particle Technology Laboratory, Department of Mechanical Engineering, 111 Church Street S.E. Minneapolis, MN 55455, USA.

<sup>2</sup>Div. of Aerosol Technology (EAT), Lund Institute Technology, Lund, Sweden.

<sup>3</sup>Department of Chemistry, Carleton College, Northfield, MN 55057 USA.

Keywords: Bio fuels, Single Particle Analysis

An increased use of biofuels in residential heating is desired to decrease net emissions of green house gases, such as CO<sub>2</sub> to the atmosphere. This includes conventional woody biofuels, as well as novel crop fuels such as corn. It is well established that the particle emissions during less optimised combustion in small scale wood combustion are most often dominated by products of incomplete combustion, i.e. organic and elemental carbon (OC/EC), McDonald et al. (2006). In contrast during optimised combustion in modern domestic pellet combustion systems, the aerosol can be dominated by ash compounds, especially KCl and K<sub>2</sub>SO<sub>4</sub> formed via heterogeneous reactions in the gas-phase.

However, little research has focused on the variations in physical and chemical particle properties over the combustion cycle. This is partly due to the lack of experimental methods with sufficient time resolution to follow the inherently transient nature of batch wise wood log combustion. Further, little information is available on emissions from novel fuels such as corn. For example, corn has higher ash content than conventional wood fuels.

In this work we used an Aerosol Time-of-Flight Mass Spectrometer (TSI Inc., Shoreview, MN, USA) to study chemical signatures of single particles from three wood log fuels (oak, pine and birch) and corn. The instrument was equipped with an aerodynamic focusing lens inlet. The wood fuels were combusted in a conventional wood stove, while the corn was combusted in a commercially available corn stove, which operates similarly to modern wood pellets stoves.

Each wood-combustion experiment involved start-up from a cold stove with a full load of fuel. Fuel was then added once and experiments were conducted until only glowing embers remained. Particles were sampled and diluted with particle free air using a three stage dilution system which allowed dilution ratios between 1:10 and 1:10000. In a few experiments a Differential Mobility Analyzer was used upstream of the ATOFMS to determine the particles effective density.

A Scanning Mobility Particle Sizer was used to determine the particle size distribution (20-800 nm). A gas analyzer (TSI CA-6215) was used to determine the flue gas composition (O<sub>2</sub>, NO<sub>x</sub>, CO).

Preliminary results show clear differences in the particle composition between:

1. The three different wood fuels
2. Wood and corn fuels
3. Different regions in the combustion cycle for the wood fuels

When the corn stove was operating optimally, markers for inorganic ash components were dominant. These included <sup>39</sup>K<sup>+</sup>, <sup>113</sup>K<sub>2</sub>Cl<sup>+</sup> and <sup>213</sup>K<sub>3</sub>SO<sub>4</sub><sup>+</sup>. Note that the corn combustion process is semi-continuous as opposed to batch-wise log combustion, where distinct combustion phases can be identified.

During the start-up phase and during throttling of the supply air in wood combustion, strong organic markers were present. Several of these, for example *m/z* = -45 (C<sub>3</sub>H<sub>3</sub>O<sub>2</sub><sup>-</sup>), -59 (C<sub>3</sub>H<sub>3</sub>O<sub>2</sub><sup>-</sup>) and -71 (C<sub>3</sub>H<sub>3</sub>O<sub>2</sub><sup>-</sup>) have previously been detected from pure levoglucosan (Silva et al. 1999), a dominant organic component from low temperature wood combustion. In the efficient combustion phase, many markers for organic compounds diminished, while e.g. <sup>113</sup>K<sub>2</sub>Cl<sup>+</sup> was strongly enhanced. A large number of high mass peaks in the positive spectrum (e.g. *m/z* +203, +209 and +235) were present during soft wood combustion (Pine). These are likely markers of polycyclic aromatic hydrocarbons (PAHs).

Overall the laser-desorption ionization approach used in the ATOFMS instrument enables us to detect signatures from both organic compounds and low volatility alkali salts, such as KCl and K<sub>2</sub>SO<sub>4</sub>. The combination of these two classes of signatures is promising for source receptor studies. The ATOFMS is also a promising tool to assess various fuels for their impact on emissions.

*Joakim Pagels' postdoc at UMN was supported by the Swedish Research Council FORMAS. Patience and help from Woodland Stoves, Minneapolis is warmly acknowledged.*

JD McDonald, RK White, EB Barr, B Zielinska, JC Chow and E Grosjean (2006) *Aerosol Sci. & Techn.* 40: 573-584.

P Silva, D Liu, CA Noble and KA Prather (1999) *Env. Sci. & Techn.* 33: 3068-3076.

## Comparison of fine particle emissions from a modern small-scale biomass boiler and from a large-scale coal-firing power plant

E. Lamminen, H. Isherwood

Dekati Ltd. Osuusmyllynkatu 13, 33700, Tampere, Finland

Keywords: Biomass burning, Combustion particles, ELPI, Particle size distribution

As the small- and large-scale use of fossil fuels is reduced throughout Europe and gradually replaced with alternative fuels, there is a need to assess the effect on emissions of particulate and gaseous pollution. Previous studies indicate that wood burning for example is an important source of particulate pollution into the atmosphere (1).

In this study we focused on comparing the particle number and mass size distributions and concentrations from a modern small-scale (7MW) biomass power plant and from a coal-firing large scale (360 MW) power plant fulfilling the current emission regulations.

The particle measurements were conducted with the same instrument setup at both locations during winter of 2006 and 2007. Fine Particle Sampler (FPS-4000, Dekati Ltd.) was used to dilute and condition the combustion aerosol and Electrical Low Pressure Impactor (ELPI, Dekati Ltd.) (2), was used to measure the particle size distributions and concentrations in real-time. The biomass boiler was equipped with gasification of wood, re-circulation of flue gas and flue gas cyclones to reduce the particle emissions. The coal-firing power plant flue gas was cleaned with an electrostatic precipitator, and additionally equipped with a sulphur reduction facility using wet scrubbers and a baghouse filter. All measurements in both locations were conducted after the flue gas pollution control devices.

Biomass burning via fuel gasification differs from typical biomass firing in that the heating power is not generated directly by burning the fuel but by firing the products of the gasification of the fuel. Gasification of the fuel occurs in a stable thick layer of embers on a grate where the fuel turns slowly into ash. Grate movement removes the ashes from the bottom of the embers layer, but also causes some stirring of the embers layer. In flue gas re-circulation part of the flue gas is blown back from the stack into the boiler in an attempt to improve gas mixing and stabilize the embers layer.

The measured particle size from the coal-firing power plant was found to be significantly larger than what was measured from the biomass power plant, which is shown in Figure 1 as normalized particle

number distributions. The emitted particle number concentration from the coal-firing power plant is lower than from the biomass plant. However, due to the larger particle size, the emitted particle mass is significantly higher from the coal-firing plant.

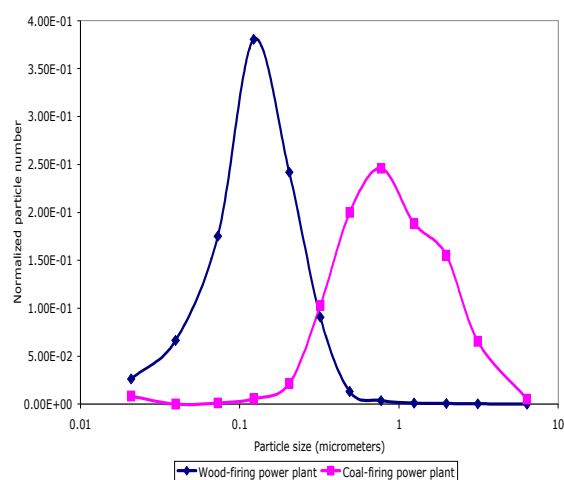


Figure 1. Measured normalized particle number distributions from a wood firing and from a coal firing power plant.

During emission peaks caused by grate movement in biomass plant and ESP rapping and baghouse cleaning in the coal-firing plant, particle size was found to increase due to re-entrainment of collected particles. In addition to these results, some considerations for performing particle measurements at sub-zero temperatures will be presented.

1. Tissari, J., Raunemaa, T., Jokiniemi, J., Sippula, O., Hytönen K., Linna, V., Oravainen, H., Pyykönen, J., Tuomi, S., Vesterinen, R., Taipale, R., Kolsi, A., Nuutinen, I., Kouki, J & Vuorio, K. 2005. Puun Pienpolton hiukkaspäästöt. Kuopion yliopiston ympäristötieteiden laitosten monistesarja 2/2005 (In Finnish, abstract available in English).
2. Keskinen, J., Pietarinen, K. & Lehtimäki, M. 1992. Electrical Low Pressure Impactor, Journal of Aerosol Science, vol 23, pp. 353-360.

## Particle emissions during pulsating combustion of biomass in a pilot reactor

C. Boman<sup>1,2</sup>, J. Hrdlicka<sup>3</sup>, A. Dahl<sup>4</sup>, S.-I. Möller<sup>3</sup> and E. Swietlicki<sup>1</sup>

<sup>1</sup>Division of Nuclear Physics, Lund University, P.O. Box 118, SE-221 00, Lund, Sweden

<sup>2</sup>Energy Technology and Thermal Process Chemistry, Umeå University, SE-901 87, Umeå, Sweden

<sup>3</sup>Division of Combustion Physics, Lund University, P.O. Box 118, SE-221 00, Lund, Sweden

<sup>4</sup>Division of Ergonomics and Aerosol Technology, Lund University, P.O. Box 118, SE-221 00, Lund, Sweden

Keywords: aerosol characterisation, aerosol size distribution, combustion particles, emission

An increased utilization of biomass as a renewable energy source is expected to play a vital role to mitigate global warming. However, concerns about atmospheric PM and adverse health effects, forces the development of efficient and low-polluting combustion systems. Pulsating combustion might be a potential option and due to interactions between acoustics and the combustion process this technology offers unique features related to improved mixing and increased heat transfer (Lindholm, 1999). The objective of the present study was to characterize the particle emissions during combustion of pelletized softwood at different operational conditions in a pilot scale Rijke type pulse reactor.

Combustion experiments were performed with systematic variations in load, air to fuel ratio and primary/secondary air distribution. Particle measurements included  $PM_{tot}$  ( $PM_{10}$  cyclone+filter), mass size distribution (LPI, 0.03-10  $\mu m$ ) and particle number concentrations/size distributions (SMPS, 15-700 nm). The  $PM_{tot}$  and impactor sampling were performed in the un-diluted exhaust while the aerosol for the SMPS measurements was diluted 150-300 times by a two-step ejector dilutor system (corrected for in the results).

The  $PM_{tot}$  emissions varied significantly between 12-390  $mg/Nm^3$  at 11% excess  $O_2$ , clearly influenced by the studied variables, with a varying fraction of coarse ( $>10 \mu m$ ) particles (5-78%). Large unburned fuel residues present in the flue gases under some experimental conditions contributed to the major part of  $PM_{tot}$ . However, a significant variation in "fine" PM ( $<PM_{10}$ ) were also determined (10-100  $mg/Nm^3$ ) presumably indicating the influence of combustion efficiency on the fine PM mass concentrations, as also seen by higher concentrations of CO in the cases with increased fine PM. The lowest level determined (12  $mg/Nm^3$ ) is rather low compared to reported emissions for normal residential wood pellet combustion (Johansson *et al.*, 2004) as well as lab-studies of fixed-bed combustion of wood pellets (Boman *et al.*, 2006).

The fine particle aerodynamic mass median diameters varied between 72 and 102 nm, with no obvious influence by the studied variations in combustion conditions. Number concentrations as well as count median mobility diameters were also relatively similar (CMD 101-110 nm) in all cases.

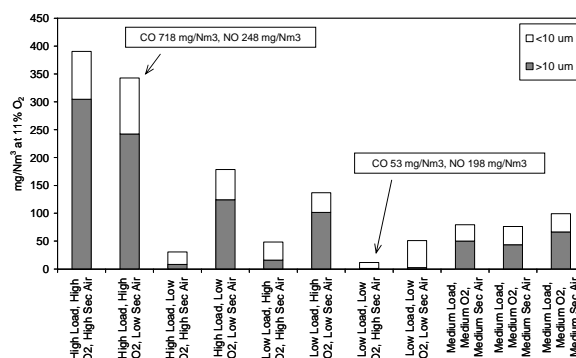


Figure 1. Total mass concentrations given as  $>10 \mu m$  and  $<10 \mu m$  fractions.

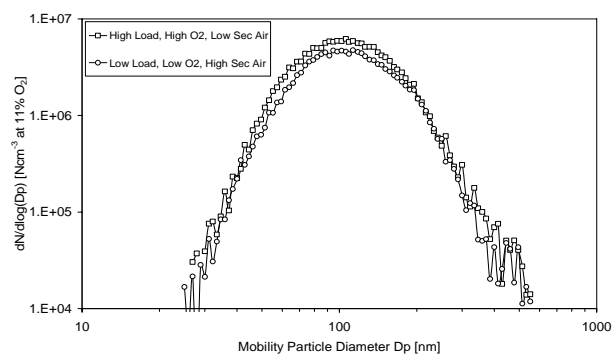


Figure 2. Typical particle number size distributions at two different combustion conditions.

Some influences of combustion conditions, mainly mass concentration, on particle emissions were determined, with different behaviour of the coarse and fine modes. The pulse reactor combustion may potentially enable reduced emissions of both CO, NO and fine particles during certain operational conditions, but further evaluation of data, including PM chemistry, are in progress and will be presented.

This work was partly supported by the Nordic Center of Excellence on Aerosols (BACCI).

Lindholm A. (1999). *Pulsating Combustion - Combustion Characteristics and Reduction of Emissions*. Dissertaion. Lund University.

Johansson, L.S., Leckner, B., Gustavsson, L. *et al.* (2004). *Atmos Environ*, 38, 4183-4195.

Boman, C., Pettersson, E., Lindmark, F. *et al.* (2006). In *Proc. 2nd World Conf on Pellets*, Jönköping, Sweden, 187-193. (Submitted to Biomass and Bioenergy)

## Water uptake by exhaust soot and its transformation through the interactions in the humid atmosphere

V.V.Tishkova<sup>1,3</sup>, A.M.Voloshuk<sup>1</sup>, O.B. Popovicheva<sup>2</sup>, and N.K.Shonija<sup>2</sup>  
B. Demirdjian<sup>3</sup>, D. Ferry<sup>3</sup> and J. Suzanne<sup>3</sup>

<sup>1</sup>Institute of Physical Chemistry, 119991, Moscow, Russia

<sup>2</sup>Moscow State University, 119992, Moscow, Russia

<sup>3</sup>CRMC-N / CNRS, Campus de Luminy, 13009 Marseille, France

Keywords: combustion particles, aerosol-surface interaction, hygroscopicity, microstructure

The phenomenon of aircraft contrail formation attracts much attention as a direct soot exhaust impact upon the atmosphere. It is now clear that aviation impact may be larger via cirrus cloud changes due to heterogeneous nucleation on emitted soot aerosols. But the fate of soot after emission has not been determined. It is important to know how the water uptake ability of aircraft soot changes when soot particles are first exposed to a saturated water vapor in the aircraft plume, then immersed into water droplets, after transformed into contrail ice and later left as residual particles when ice evaporates.

Previous work (Demirdjian et al., 2007) successfully helped to remove the lack of experimental data concerning the physico-chemical properties of original soot sampled at the outlet of aircraft engines operating at cruise conditions. The analysis showed that the composition and structure heterogeneities in aircraft engine combustor (AEC) soot separate its particles into two fractions: a relatively "pure" *main fraction* and a *fraction with impurities* containing soluble inorganics/organics sulfates and metal. TC1 aviation kerosene soot produced by an oil lamp was proposed as a laboratory surrogate for the hydrophobic main fraction of AEC aerosols in the atmosphere.

In this report we elucidate the modifications in the soot microstructure and water uptake at the conditions simulating the saturated plume and contrail processing. For these purposes AEC and TC1 *aged* soot samples are prepared in the laboratory under exposure to a water-saturated atmosphere, immersion into water and freezing. Surface area, micropore volume and size, and mesopore surface are determined by N<sub>2</sub> adsorption measurements.

Water uptake was measured by a gravimetric method at room temperature. The cycle of water adsorption-desorption and second adsorption are measured in a wide relative humidity (RH) range for original and aged samples. Irreversible adsorption and low pressure hysteresis indicate soot microstructure transformation and swelling. Figure 1 plots the isotherms of water adsorption in the first cycle for *original* TC1 soot; TC1 soot after exposure to saturated water vapor (*RH 100%*); TC1 soot after immersion into water and drying (*water*); TC1 soot after immersion into water, freezing and drying (*ice*).

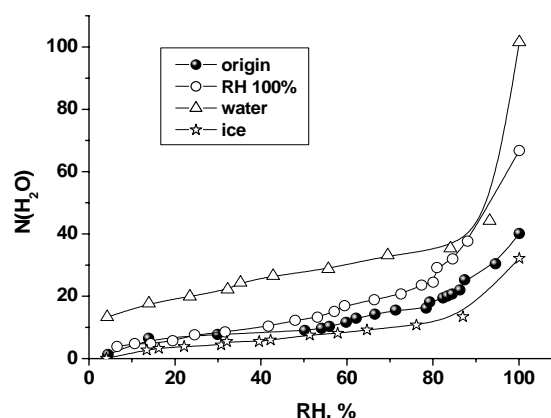


Fig.1. Water uptake by original and aged TC1 soot.

A significant increase in the water uptake is observed for TC1 soot exposed to saturated water vapor and especially (up to 2.6 times) after immersion into water, while ice processing decreases the water adsorbability.

It is shown that aircraft engine soot particles once emitted into the atmosphere exhibit irreversible changes in microstructure and water uptake ability as a result of saturated plume and contrail processing. These findings require an extended study using instruments to detect ice nucleation (FTIR NMR and neutron scattering) to examine whether the secondary ice nucleation in cirrus is more efficient than primary nucleation in contrails.

This work is partly supported by EC Quantify-TTC project under contract №003893. V.Tishkova gratefully acknowledge the French Ministry of Education and Research for providing her with a cotutorship thesis travelling grant.

I.Demirdjian.B., Ferry.D., Suzanne, Popovicheva. O.B., Persiantseva. N.M. & Shonija.N.K. (2007), *J.Atmos. Chem.*,56, 83-103

## Gaseous sulphuric acid and volatile nanoparticle formation by modern diesel vehicles

F. Arnold<sup>1</sup>, T. Schuck<sup>1</sup>, L. Pirjola<sup>2,3</sup>, J. Keskinen<sup>4</sup>, T. Rönkkö<sup>4</sup>, T. Lähde<sup>4</sup>,  
K. Hämeri<sup>2,5</sup>, H. Aufmhoff<sup>1</sup>, A. Sorokin<sup>1</sup>, and D. Rothe<sup>6</sup>

<sup>1</sup> Atmospheric Physics Division, Max Planck Institute for Nuclear Physics (MPIK), P.O. Box 103980, D-69029 Heidelberg, Germany

<sup>2</sup> Department of Physical Sciences, University of Helsinki, P.O. Box 64, FIN-00014 Helsinki, Finland

<sup>3</sup> Department of Technology, Helsinki Polytechnic, P.O. Box 4020, FIN-00099 Helsinki, Finland

<sup>4</sup> Aerosol Physics Laboratory, Institute of Physics, Tampere University of Technology, P. O. Box 692, FIN-33101 Tampere, Finland

<sup>5</sup> Department of Physics, Finnish Institute of Occupational Health, Topeliuksenkatu 41, FIN-00250 Helsinki, Finland

<sup>6</sup> MAN Nutzfahrzeuge AG, Abt. MTVN, Abgasnachbehandlung / Partikelmesstechnik, Vogelweiherstr. 33, D-90441 Nürnberg, Germany

Keywords: mass spectrometry, diesel exhaust, nucleation, sulphur particles, number concentration

Diesel vehicles are presently becoming increasingly fitted and refitted with modern oxidation catalyst Diesel filter (CDF) systems which remove from the exhaust most soot particles and organic molecules. However, during recent time it was found that CDF, as an undesired side effect, promote the emission of large numbers of volatile nanometer sized aerosol particles (VNP) whose nature is not well known. Due to their small diameters (around 10 nm) VNP have a maximum efficiency of intruding to the deepest and most vulnerable region (alveolar or air sacks) of the human lung. Therefore VNP are potentially harmful and their chemical nature and formation need to be investigated.

Here we report on pioneering measurements of gaseous sulphuric acid (GSA) in the exhaust of a diesel passenger vehicle and a heavy duty diesel vehicle engine on a test bench.

The measurements were made using a CIMS (Chemical Ionization Mass Spectrometer) instrument equipped with an ion trap mass spectrometer. The ion molecule reaction employed for GSA detection was originally introduced by our MPIK group.

The test bench measurements were made for two different fuel sulphur contents (FSC=7 and 36 ppmM) and for different engine load. These measurements included tests of three different after treatment scenarios: (a) no after treatment; (b) an oxidation catalyst OXICAT, (c) a coated catalytic diesel filter CDF.

It was found that the GSA concentration in the exhaust increases with increasing FSC and increasing engine load. When the OXICAT or CDF were used the GSA concentration was much higher compared to the case without after treatment.

The efficiency of fuel sulphur conversion to GSA increased with increasing engine load reaching up to 40% for the OXICAT case.

Besides GSA volatile aerosol particles and soot aerosol particles were also measured. The volatile particle had diameters mostly below 20 nm.

They were more abundant and larger in size when GSA was more abundant.

Our measurements indicate that VNP are formed by gaseous sulphuric acid (GSA) nucleation and grow by condensational uptake of GSA and organics (see also Arnold *et al.*, 2006). Obviously these condensable organics are not sufficiently removed by the OXICAT and CDF. Eventually they may even be formed by the exhaust after treatment system.

Since the condensable organics eventually also include carcinogenic compounds VNP may act as a “Trojan Horse” transporting harmful organics into the alveolar region of the human lung.

Our findings indicate that modern diesel vehicles equipped with an OXICAT or CDF and combusting low sulphur fuel (50 ppmM) emit more GSA than old diesel vehicles without OXICAT or CDF combusting high sulphur fuel (350 ppmM). The low sulphur fuel is obligatory in the European Union since 2005 while previously the mean fuel sulphur content was about 350 ppmM.

Our findings also indicate that present obligatory regulations of diesel vehicle exhaust are insufficient to avoid VNP emissions.

This work was supported by the Max Planck Society and the National Technology Agency of Finland (TEKES).

Arnold F., L. Pirjola, H. Aufmhoff, T. Schuck, T. Lähde, K. Hämeri, (2006). *Atmos. Environ.*, 40, 7097-7105.

## Experiences with ultra fine particle monitoring in air quality monitoring networks in Europe

C. Gerhart<sup>1</sup>, T. Petry<sup>1</sup>, T. Rettenmoser<sup>1</sup>, A. Kranapeter<sup>2</sup>, HP. ötscher<sup>3</sup>

<sup>1</sup>Grimm Aerosol Technik GmbH & Co. KG, Ainring, 83404, Germany

<sup>2</sup>Abteilung Immissionsschutz Stadt Salzburg, Salzburg, 5020, Austria

<sup>3</sup>Amt für Natur und Umwelt, Chur, 7001, Switzerland

Keywords: Combustion particles, Health effects of aerosols, Outdoor aerosols, PAH(s), SMPS

In air monitoring networks particles in the range of a few hundred nm are not measured. For mass related measurements the ultra fine particles are negligible. Nevertheless these small particles (below 500nm) contribute with 80% to the particle number concentration in ambient aerosols. Special in urban regions the total particle concentration is determined by very small particles like diesel soot, generated by combustion processes. In epidemiological discussions on air born particles the focus of interest has shifted from mass to number concentration in the recent years. Therefore it is a very interesting task to measure the ultra fine particles additionally to the coarse fraction and compare the data with the meteorological parameters and the values of important volatiles.

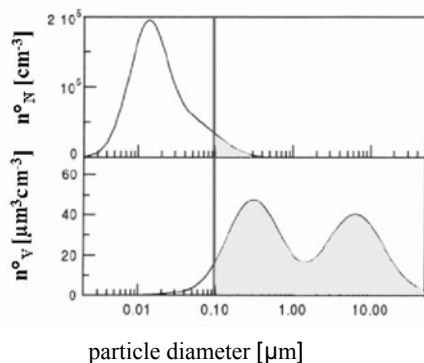


Figure 1. A typical volume and number distribution in an urban aerosol (Seinfeld and Pandis, 1997)

To compare the measurements of ultra fine particles with the data, obtained from the well proofed instrumentation of the air quality monitoring networks, it is essential to be sure that the devices for measuring nano particles are working stable and comparable. Such investigations were carried out in the last years for the GRIMM SMPS C instruments with good results (for example in December 2006 in Leipzig at the Leibniz Institute for Tropospheric Research).

There are also strong efforts at the moment in Germany to work out the details of measuring ultra fine particles for a VDI DIN directive. A first

draft defines already the use of a CPC (Condensation Particle Counter) and a DMA (Differential Mobility Analyser).

In the following, some examples of measuring campaigns are mentioned in which GRIMM instruments were used in air quality monitoring networks to obtain additional information about the aerosol particles. Where SMPS C means a combination of a CPC with a DMA for the size range between 5 and 1100 nm and WRAS (Wide Range Aerosol Spectrometer) the combination of a SMPS C with an OPC (Optical Particle Counter) for particle diameters up to 30 µm.

In April 2006 such measurements with a WRAS were done in Graz (Austria). The measured particle concentrations related strongly to the traffic and folkloric events (Easter fires).

In May 2006 during eight days a measurement in Salzburg (Austria) was carried out. Here additionally to the WRAS a PAH sensor was installed. The concentrations of the ultra fine particles and the values of the PAH sensor correlated strongly with the values for NO<sub>x</sub> and CO<sub>2</sub>, which were measured by the network.

In winter 2007 in Graubünden (Switzerland) a long-term measurement (over six weeks) was done. Here the particle concentration, measured with a SMPS C, in rural and urban regions were compared.

Special thanks to the involved networks.

Alexander, F. R., & Nathan J. O. (1986). *An Introduction to Ultrasonic Nebulisation*. Cambridge, U.K.: Cambridge University Press.

Chapman, D. H. (1975). *J. Aerosol Science*, 36, 3456-3467.

Finn, P., Diver, G. N., & Wake, K. T. (1998). In *Proc. 13th Int. Conf. on Marine Aerosols*, Reykjavik (Wiley, New York), 631-633.

## High-speed video observations of the alumina nanoparticle formation during combustion of Al microparticles

E.V. Karaseva<sup>1</sup>, A.A. Onischuk<sup>1</sup>, V.V. Karasev<sup>1</sup>, C.J. Tsai<sup>2</sup>

<sup>1</sup>Institute of Chemical Kinetics and Combustion SB RAS, 630090, Novosibirsk, Russia

<sup>2</sup>Institute of Environmental Engineering, National Chiao Tung University, 300 Hsinchu, Taiwan

Keywords: coagulation, combustion synthesis, heat and mass transfer, oxides nanoparticles.

Combustion of metal powder in the air can be an effective way of synthesis of semiconductor and ceramic oxide nanoparticles (Karasev V. V. et al., 2006). A single metal particle burning can be a starting point in understanding the metal oxide nanoparticles formation (Karasev V. V. et al., 2004). However the mechanism of nanoparticles formation is not understood completely yet, partially, due to the lack of experimental data. In this work using the high-speed video microscopy we studied the structure of the flame zone around a burning Al microparticle moving in the air. Fig. 1 shows a sequence of video images for the burning particle. The illuminating flame zone (where the reaction between O<sub>2</sub> and Al vapor occurs and alumina nanoparticles form) as well as Al<sub>2</sub>O<sub>3</sub> cap can be clear seen. One can also see the rotation of the particle with the frequency about 200 Hz. The probable reason for this rotation is in asymmetric vapor jets coming from under the cap. The particle velocity is decreasing with time due to the counter flow drag force.

The reaction zone radius  $R$  was measured from the video images as a function of the maternal particle radius  $r$  for different values of the particle velocity (Fig. 2). The solid line is the result of simulation in terms of the reduced layer approximation, based on the solution of the heat and mass transfer equations (see also Fig. 3). The size distributions for the primary alumina nanoparticles formed in the reaction zone were simulated by solving the Smoluchowsky equations. A typical size spectrum from these simulations is shown in Fig. 4. These simulation results are in a reasonable agreement with our experimental data (Karasev V. V. et al., 2006)

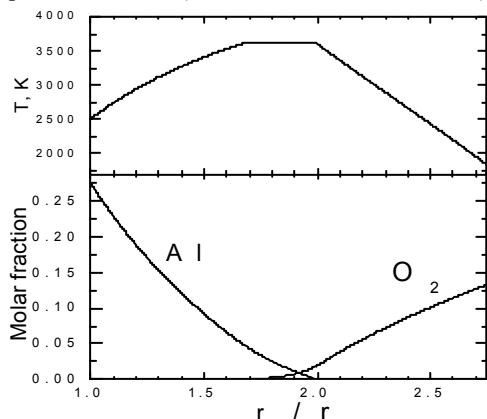


Fig. 3 Radial profiles of temperature and reagent concentrations around the burning Al droplet (radius  $r = 150 \mu\text{m}$ ), moving in air with a velocity of 2.5 m/s

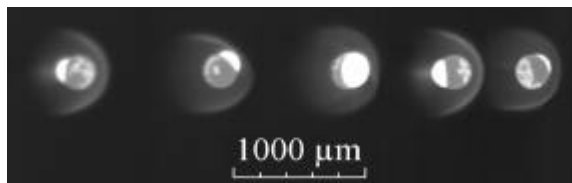


Fig.1. Series of consecutive images of a burning aluminum 250  $\mu\text{m}$  droplet, moving in air with a velocity of 2.5-1.5 m/s. Primary alumina nanoparticles are formed in the high-temperature reaction zone ( $\approx 3500\text{K}$ ) which has the form of halo around of a burning drop.

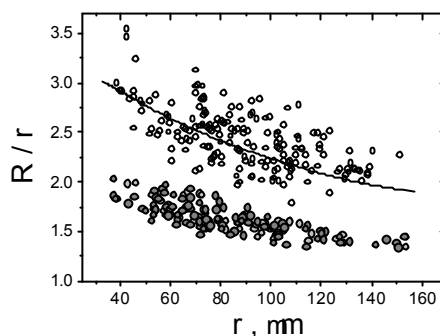


Fig.2. Relative ( $R/r$ ) radius of the reaction zone (halo) vs radius  $r$  of burning Al droplet.

Points - experimental data: hollow circles - for counter flow 2.5 m/s, gray circles - for counter flow 15 m/s.

Solid line - result of simulation for 2.5 m/s.

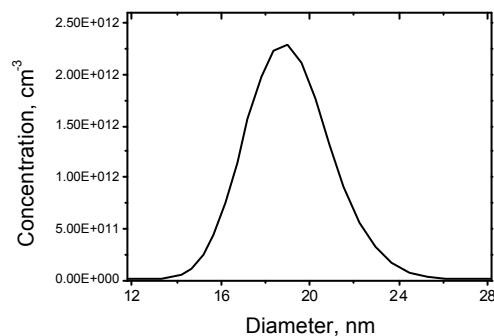


Fig. 4. Typical size spectrum of alumina nanoparticles formed in the reaction zone (simulation result).

Karasev V. V., Onischuk A. A., Khromova S. A. et al., (2006), *Combust., Expl., Shock Waves*, Vol. 42, No. 6, 649–662.

Karasev V. V., Onischuk A. A., Glotov O. G. et al., (2004), *Combust. Flame*, 138, 40–54.

Financial support for this work was provided by RFBR 05-03-90576-NSC a, grant of SB RAS No 78, NSC Taiwan-RFBR No. 94WFA0600016 Contract No. RP05E15.

## **T15 Abstracts**

## Copper a marker for non-tailpipe emissions from traffic?

P. Molnár<sup>1</sup>, T. Bellander<sup>2</sup>, J. Boman<sup>3</sup> and G. Sällsten<sup>1</sup>

<sup>1</sup>Department of Occupational and Environmental Medicine, Sahlgrenska Academy, Göteborg University, SE-405 30 Göteborg, Sweden

<sup>2</sup>Institute of Environmental Medicine, Karolinska Institutet, Stockholm, Sweden and Department of Occupational and Environmental Health, Stockholm County Council, Stockholm, Sweden

<sup>3</sup>Department of Chemistry, Atmospheric Science, Göteborg University, SE-412 96 Göteborg, Sweden

Keywords: PM<sub>2.5</sub>, trace elements, traffic, NO<sub>2</sub>, XRF.

Traffic is one of the major pollutants in cities today and NO<sub>2</sub> is known to be a marker for traffic emissions. Non-tailpipe particulate emissions from traffic have been proposed to be a potentially important factor to human health (Schlesinger et al., 2006).

Fine particles (PM<sub>2.5</sub>) and NO<sub>2</sub> were sampled outdoors at 40 sampling sites; outside ten classrooms in five schools, at ten preschools and 20 non-smoking homes, in three communities in Stockholm, Sweden, during nine 2-week periods. The sites were selected to represent local conditions, e.g. traffic intensity and population density. They were located in Stockholm city centre, in suburban municipalities located about 10 km NW of the city centre and in a detached municipality situated about 25 km NW of the city centre. Each sampling site was sampled twice, once during winter and once during spring. PM<sub>2.5</sub> was collected with Harvard impactors and analysed for elemental concentrations using X-ray fluorescence (XRF) spectroscopy while NO<sub>2</sub> was measured using diffusive samplers.

Table 1. Spearman correlations for Cu v. NO<sub>2</sub> for the total study, winter and spring season.

	Homes	Schools	Preschools
Total	0.64	0.91	0.80
Winter	0.61	0.86	0.86
Spring	0.69	0.96	0.82

A fourfold increase in Cu levels was found for the central areas compared to the detached area (medians: 4.1 v. 1.0 ng m<sup>-3</sup>). Significant correlations between the traffic marker NO<sub>2</sub> and Cu was found at all environments and during both winter and spring (Table 1). Vehicle brakes are known to contain Cu (Johansson & Burman, 2006; Lough et al., 2005), and therefore constitute a likely source of Cu. Zn (from tire wear) was also found to have significant correlations with NO<sub>2</sub> for all locations, but only for both winter and spring at preschools. Snow covered streets during winter and wet surfaces during periods of rain will likely trap some of the Zn particles and later release them through resuspension of road dust.

At homes and preschools, several more trace elements (K, Ca, Mn, and Fe) were found to be significantly correlated to NO<sub>2</sub>.

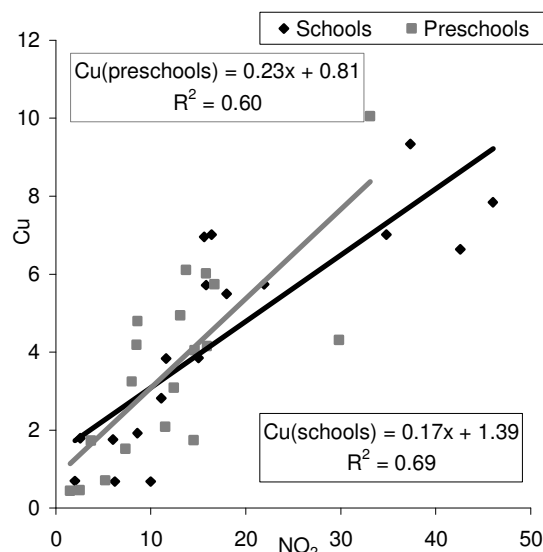


Figure 1. The relation at schools and preschools between NO<sub>2</sub> (in µg m<sup>-3</sup>) and Cu (in ng m<sup>-3</sup>).

In this study we found high and consistent correlations between NO<sub>2</sub> and Cu outdoors for all microenvironments and over both seasons studied. This suggests that outdoor Cu may be a suitable elemental marker for traffic-related aerosols in health studies in areas without other significant outdoor Cu sources (e.g. certain industries or Cu roofs). Lead has traditionally been used as a marker of vehicle exhaust, but it is of less value today when most petrol is unleaded.

This work was supported by the Swedish National Air Pollution and Health Effects Programme (SNAP), funded by the Swedish Environmental Protection Agency.

Johansson, C. & Burman, L., 2006. ITM-rapport 147, Department of Applied Environmental Science, Stockholm, Sweden.

Lough, G.C. et al., 2005. Environ Sci Technol., 39(3): 826-836.

Schlesinger, R.B., Kunzli, N., Hidy, G.M., Gotschi, T. & Jerrett, M., 2006. Inhal Toxicol., 18(2): 95-125.

## Characterization of aerosols produced by laser-matter interaction during paint stripping experiments by laser

P. Dewalle<sup>1,2,3,4</sup>, J. Vendel<sup>1</sup>, J.M. Weulersse<sup>2</sup>, P. Hervé<sup>3</sup> and G. Decobert<sup>4</sup>

<sup>1</sup>Institut de Radioprotection et de Sûreté Nucléaire, DSU/SERAC, B.P. 68, 91192 Gif-sur-Yvette Cedex, France.

<sup>2</sup>Commissariat à l'Énergie Atomique, DEN/DANS/DPC/SCP, 91191 Gif-sur-Yvette Cedex, France.

<sup>3</sup>Laboratoire d'Énergétique et d'Économie d'Énergie, Univ. Paris 10, 1 ch. Desvallières, 92140 Ville d'Avray, France.

<sup>4</sup>AREVA NC, Business Unit Traitement, 2 rue Paul Dautier, 78141 Valz Cedex, France.

Keywords: Nanoparticles : characterization, Particle size distribution, Particle Shape, Submicron particles, Laser Ablation.

A surface decontamination process is here considered: laser ablation. This technology is promising for paint stripping. During the process, particulate matter and gases resulting from interaction between the laser beam and the target are released. These aerosols can influence the process efficiency (Gillot *et al.*, 2004) and present a risk for the health of operators (Lee & Cheng, 2004). The aim of the study is to perform both a physical and a chemical characterization of laser produced aerosols during ablation of paints and as well as to understand their mechanisms of formation.

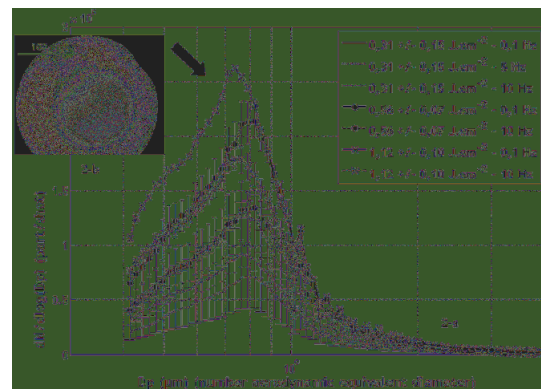
The experiments were carried out using a Nd:YAG laser working at 532 nm, the pulse duration was 5 ns. The repetition rate and the fluence have been varied respectively from 0,1 to 10 Hz and from 0,2 to 11 J.cm<sup>-2</sup>. The ablation took place in a cylindrical cell of 118 cm<sup>3</sup> in which is mounted the sample, a green acrylic paint. The particle number was measured with a Condensation Particle Counter (CPC) and their size distribution with an Engine Exhaust Particle Sizer (working range: 5,6-560 nm) and an Aerosizer (working range: 0,5-700 nm). In addition, we used a filtration system in order to collect the particles for Transmission Electronic Microscopy (TEM) and Energy Dispersive x-ray Spectroscopy (EDS) analyses.

Figures 1-a and 2-a show the mean number particle size distributions for a single laser shot on the paint at various fluences for two repetition rates: 0,1 Hz and 10 Hz obtained respectively with the EEPS and the Aerosizer. These results show that the aerosol produced during a laser shot is both composed of nanoparticles and submicronic particles. Indeed bimodal size distributions are observed. A mode around 70 nm was detected by the EEPS (figure 1-a) on which the fluence and the repetition rate have little influence (Dewalle *et al.*, 2006). A second mode around 717 nm was observed by the Aerosizer (figure 2-a) on which we have noticed an influence of the fluence and the repetition rate. Moreover, the TEM-EDS analyses allow us to suppose that the nanoparticles would be aggregates of primary particles composed mainly of carbon (figure 1-b). The submicronic particles would be large spherical particles (figure 2-b) composed mainly of titan (probably TiO<sub>2</sub>, coming from the

paint composition). These particles are likely produced by two different mechanisms.



Figures 1-a/b. Particle size distributions (EEPS results) (a) and TEM micrograph (b).



Figures 2-a/b. Particle size distributions (Aerosizer results) (a) and TEM micrograph (b).

The further work will be to perform complementary chemical analyses on particles and gases and to set up in-situ optical methods to follow the formation stages of the particles.

- Dewalle, P., Vendel, J., Weulersse, J.M., Hervé, P., Pina, V., & Decobert, G. (2006). *Acts of the 22th French Congress on Aerosols*. Paris, 113-118.
- Gillot, M., & Gensdarmes, F. (2004). *Acts of the 20th French Congress on Aerosols*, Paris, 141-146.
- Lee, D. W., & Cheng, M. D. (2004). *J. Aerosol Science*, 35, 1527-1540.

## Aerosol synthesis as a route to bulk nanocrystalline metals and composites with superior mechanical properties

R. N. Grass, W. J. Stark

<sup>1</sup>Department of Chemistry and Applied Biosciences, ETH Zurich, Wolfgang-Pauli-Strasse 10, 8093, Zurich, CH

Keywords: reducing flame spray, nanocomposites, bulk nanocrystalline, material synthesis, nanoparticles application

The increased hardness of nanocrystalline copper (Chokshi et al., 1989; Gleiter, 1989) has triggered a wealth of research in nanocrystalline bulk materials showing improved wear resistance, superplastic formability, material strength and shock resistance. Currently, such nanocrystalline metals are hard to synthesize at larger scale, so that their beneficial properties are only accessible to material science laboratories. Aerosol nanoparticle engineering has been the method of choice for the synthesis of nanoparticles at large-scale, and the very recent discovery of reducing flame synthesis expands the range of accessible materials to metal nanoparticles. (Grass and Stark, 2006a; Grass and Stark, 2006b)

We present the fabrication of bulk nanocrystalline cobalt (Grass et al., 2007b) as well as bismuth / ceria nanocomposites (Grass et al., 2007a) of highly increased hardness using aerosol derived nanoparticles as a precursor. The nanoparticles were synthesized at production rates of more than 70 g / hr using reducing flame synthesis and processed to bulk metals by compaction and sintering. The resulting nanocrystalline cobalt material (Fig. 1) exhibited a

hardness 4x exceeding the hardness of bulk cobalt and even exceeding the hardness of bulk stellite, a high wear cobalt/chromium/tungsten alloy.

Reducing flame synthesis further allowed the manufacture of metal matrix nanocomposites of an excellent homogeneity, offering increased mechanical properties in combination with a good electrical conductivity and a metallic appearance. We present the synthesis of bismuth/ceria nanocomposites with a ceramic loading of up to 15 vol% exhibiting a Vickers hardness of 120 HV, which is similar to the hardness of a coarse grained steel. The observed composite hardness strongly exceeded the hardness of bulk bismuth (15 HV), which can be deformed with a finger nail. The nanocomposites still maintained its metallic gloss and electrical conductivity, as can be seen in Figure 2 by the illumination of a LED.

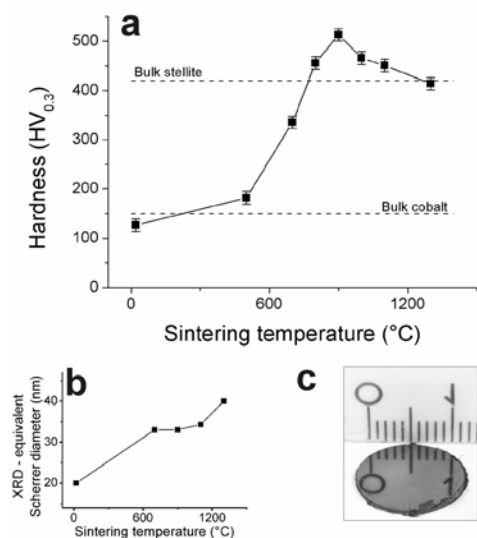


Figure 1. Hardness (a) and crystallite size (b) of compacted cobalt nanopowders after sintering at specified temperatures. Photograph of compacted cobalt nanopowder (c).

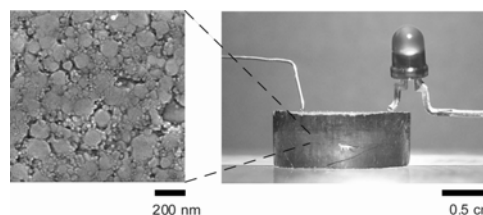


Figure 2. Scanning electron micrograph (left) and photograph (right) of a bismuth matrix nanocomposites with a ceria loading of 15 vol%.

The results suggest the use of aerosol synthesis for the fabrication of metal nanoparticles at large scale and show the application of these nanoparticles for the production of bulk nanocrystalline metals and nanocomposites.

### References

- Chokshi, A. H., Rosen, A., Karch, J., & Gleiter, H. (1989). *Scripta Metall.*, 23, 1679-1683.
- Gleiter, H., (1989). *Prog. Mater. Sci.*, 33, 223-315.
- Grass, R. N., Albrecht, T. F., Krumeich, F., & Stark, W. J. (2007a). *J. Mater. Chem.*, DOI:10.1039/B614317B.
- Grass, R. N., Dietiker, M., Spolenak, R., & Stark, W. J. (2007b). *Nanotechnology*, 18, 035703.
- Grass, R. N., & Stark, W. J. (2006a). *J. Nanopart. Res.*, 8, 729 - 736.
- Grass, R. N., & Stark, W. J. (2006b). *J. Mater. Chem.*, 16, 1825-1830.

## Capturing the effect of sulphur in diesel exhaust

M. Lemmetty<sup>1</sup>, L. Pirjola<sup>2,3</sup>, E. Vouitsis<sup>4</sup> and J. Keskinen<sup>1</sup>

<sup>1</sup>Institute of Physics, Tampere University of Technology, P.O. Box 629, FIN-33101 Tampere, Finland

<sup>2</sup>Department of Technology, Helsinki Polytechnic Stadia, P.O. Box 4020, FIN-00099 City of Helsinki, Finland

<sup>3</sup>Department of Physical Sciences, University of Helsinki, P.O. Box 64, FIN-00014 University of Helsinki, Finland

<sup>4</sup>Laboratory of Applied Thermodynamics, Aristotle University of Thessaloniki, P.O. Box 458, GR-54124 Thessaloniki, Greece

Keywords: Diesel exhaust, Nucleation mode, Aerosol modelling, Dilution

Diesel emissions are one of the most important sources of particulate matter in urban environment. The diesel aerosol consists of two modes: a solid, fractal-like soot mode formed during combustion, and a liquid, volatile nucleation mode which forms during the dilution of aerosol.

The formation of the nucleation mode takes place rapidly during the dilution. Although there is rather large amount of experimental data, the quantitative understanding of the nucleation mode formation is still lacking. The processes affecting the formation nucleation mode are condensation, nucleation and coagulation. In this work, two models are presented and used to reproduce a set of measurement data.

The Tampere University of Technology Exhaust Aerosol Model (TUTEAM) is a sectional model which considers two externally mixed modes, namely the soot mode and the nucleation mode, tracking their time development and size dependent chemical compositions separately. The AEROFOR model is a sectional model developed for atmospheric aerosols which considers a single particle number size distribution. The chemical models used in AEROFOR are updated for this study to reflect the situation in diesel exhaust.

The experimental data was selected from the measurements of Vaaraslahti et al (2005). The data was a set of SMPS measurements using a porous tube dilution system. The measurements were conducted on a EURO II heavy-duty diesel engine and Catalytic Regenerative Trap (CRT) aftertreatment. Five different lubricant sulphur – fuel sulphur concentration combinations were measured at 100 % load. In all cases, a nucleation mode attributed to sulphur was observed.

The models used the simple flow model of Lemmetty et al (2006), where the dilution process is described by two time constants: one for dilution and one for cooling. The chemical composition was calculated from the stoichiometry of the situation, assuming 100 % conversion of sulphur to sulphuric acid. The dilution time constant was held constant at all runs, while the cooling time constant was adjusted to fit the measurements, separately for TUTEAM and AEROFOR. The adjusting parameter was fitted for a

single measurement point and used for all measurement points.

Both TUTEAM and AEROFOR are capable of capturing the trends exhibited by the nucleation mode and reproducing the measured size distribution (Figure 1). The sulphuric acid–water nucleation mechanism and subsequent condensation and coagulation are sufficient to explain the development of the nucleation and soot mode observed in the experiment. The semivolatile organic component concentrations needed to affect the particle size distribution in the models exceed the organic gas concentration measured in the experiment.

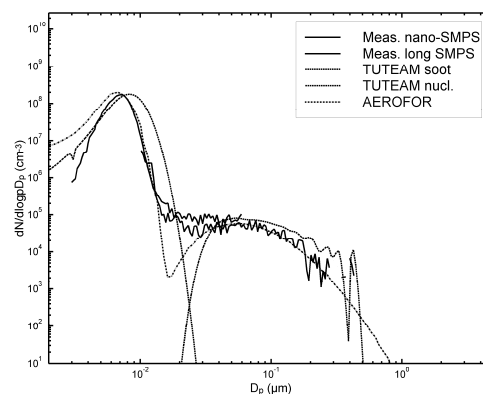


Figure 1. The measured and modelled size distributions using 1 ppm sulphur fuel and lubricant with 5100 ppm sulphur.

This work was supported by Finnish Academy of Science and Letters, Vilho, Yrjö and Kalle Väisälä Fund.

- Lemmetty, M., Pirjola, L., Vouitsis, E., Keskinen, J. (2007) The effect of sulphur in diesel exhaust aerosol: models compared with measurements. Submitted to *Aerosol Science and Technology*
- Lemmetty, M., Pirjola, L., Rönkkö, T., Mäkelä, J. M., Keskinen, J. (2006) *J. Aerosol Sci.* 37(11), 1596–1604.
- Vaaraslahti, K., Keskinen, J., Gieschaskiel, B., Solla, A., Murtonen, T., Vesala, H. *Environ Sci Technol.* 39, 8497–8504

## Mobile inhalation system for exposure to diluted diesel exhaust

J. Guénette<sup>1</sup>, D.J. MacIntyre<sup>2</sup>, K. Curtin<sup>1</sup> and R. Vincent<sup>1</sup>

<sup>1</sup>Inhalation Toxicology and AeroBiology Section, Health Canada, K1A 0K9, Ottawa, Canada

<sup>2</sup>Le Boisé Alternatives, Outaouais, J0X 1S0, Québec, Canada

Keywords: inhalation, diesel exhaust, environmental particles, outdoor aerosols, health effects of aerosols.

Transportation pollutants are responsible for 50% of ambient PM<sub>2.5</sub> experienced by Canadians in urban centres. The association between diesel engine exhaust and acute effects on cardio-respiratory morbidity and mortality is well established; additional work is needed to understand the pathophysiological mechanisms for these effects.

We have initiated a study under the Program of Energy Research and Development (PERD) of the Canadian federal government to examine the potential adverse health impacts of diesel particulate matter (DPM), generated under well defined conditions (fuels, engines, load etc), using an integrated *in vitro/in vivo* approach in animals and humans. The *in vitro* approach will assess the effects of a panel of DPM in animal and human cell lines. The results will provide an insight into the toxic potency of diesel emissions with respect to their source and conditions of generation. The *in vivo* bioassays will investigate the effects of respirable diesel emissions after intrapharyngeal nebulization of a subset of the DPM panel in mice and rats in order to validate potency ranking and support *in vitro/in vivo* extrapolations. Inhalation exposure of rodents to selected conditions of diesel emissions will provide insight into the magnitude and nature of physiological changes, and provide candidate endpoints for human studies. Finally, focussed, hypothesis-directed inhalation exposures of healthy human subjects will allow us to validate the key observations and critical endpoints of toxicity for human risk assessment. The study will provide invaluable information about the impacts of diesel emissions *in vivo* and will allow a comparison of the utility and efficacy of the three approaches in examining the effects of those emissions.

Key to the success of this project is the development of a mobile facility to perform inhalation exposures of rodents and human subjects in remote locations. The MITES Lab creates a unique opportunity to fill an information gap regarding the acute and long-term effects of exposure to airborne pollutants.

The trailer design includes distinct lab and office areas with controlled ambient temperature and on-board back-up power. A Labview™-based data acquisition system records environmental and exposure conditions and provides local and remote alarming and data viewing.

Although diluted diesel exhaust is provided under T/RH consistent with animal comfort, flow control and further dilution are required to provide appropriate exposure conditions and comfortable housing. Three 1000-litre whole-body inhalation chambers allow for simultaneous exposures to 2 doses of diluted diesel exhaust and one control. Each chamber has independent air handling as well as temperature, humidity and airflow monitoring. A custom manifold further dilutes the exhaust to achieve safe concentrations of NO<sub>x</sub>, CO and particulate matter within each chamber. The manifold also allows for removal of the particles using an optional HEPA filter for simultaneous comparative exposure to diluted exhaust with and without its constituent particulate matter.

Animals are monitored remotely on an ongoing basis, both through the data saved to an off-site server, and using a web-based security system that publishes camera images to a secure Internet host. The MITES trailer includes equipment to measure exposure concentrations of particulate, NO<sub>x</sub>, CO and O<sub>3</sub>.

This work is supported by the Program of Energy Research and Development, Natural Resources Canada, and by the Genomics R&D Initiative, Health Canada.

Vincent R, S Bjarnason, IY Adamson, C Hedgecock, P Kumarathasan, J Guénette, M Potvin, P Goegan, L Bouthillier. (1997). *Acute pulmonary toxicity of urban particulate matter and ozone*. *American Journal of Pathology*, 151, 1563-1570.

Chapman, D. H. (1975). *J. Aerosol Science*, 36, 3456-3467.

Brook RD, Brook JR, Urch B, Vincent R, Rajagopalan S, Silverman F. *Inhalation of fine particulate air pollution and ozone causes acute arterial vasoconstriction in healthy adults*. (2002) *Circulation*, 105, 1534-6.

Allan W, Brook JR, Graham L, Jiang W, Liu L, Smallwood G, Stieb D. *Transportation-related Particles Research and Development Cycle Report*. (2005). OERD, NRCan.

## Synthesis of yellow emitting silicate phosphor particles for white LED

H.S. Kang<sup>1</sup> and S.B. Park<sup>1</sup>

<sup>1</sup>Department of Chemical and Biomolecular Engineering & Center for Ultramicrochemical Process Systems, KAIST, 373-1, Guseong-dong, Yuseong-gu, Daejeon 305-701, Korea

Keywords: Optical properties, Particles, Spray pyrolysis, LED.

White lighting emitting diodes (LED) is one of candidates for new illuminator to replace conventional incandescent or fluorescent lamp, because white LED has advantages such as high brightness, long life time, small size and low power consumption. Most of commercial methods producing white LED is to combine blue LED and yellow YAG:Ce<sup>3+</sup> phosphor (Nakamura *et al.*, 1996). This method is presently the most efficient technique. However, this method is rather low color rendering index (CRI) because of its low red luminescence. In other words, the CRI of white LED can be improved further by addition of a red phosphor. Recently, oxinitride and silicate phosphors have been reported as new yellow phosphors to replace YAG:Ce<sup>3+</sup> because of high CRI. Li<sub>2</sub>SrSiO<sub>4</sub>:Eu<sup>2+</sup> was synthesized by sol-gel, solid-state reaction and combustion synthesis (Haferkorn *et al.*, 1998; Pardha Saradhi *et al.*, 2006; Toda *et al.*, 2006). In this paper, we introduced spray pyrolysis for synthesis of Li<sub>2</sub>SrSiO<sub>4</sub>:Eu<sup>2+</sup>. Spray pyrolysis is a promising way of synthesizing multi-component materials such as phosphor. In the present study, we synthesized orange-yellow emitting Li<sub>2</sub>SrSiO<sub>4</sub>:Eu<sup>2+</sup> phosphor particles by spray pyrolysis and investigated the photoluminescence (PL) properties.

Li<sub>2</sub>Sr<sub>1-x</sub>SiO<sub>4</sub>:Eu<sup>2+</sup><sub>x</sub> were synthesized by the spray pyrolysis using 1.7MHz ultrasonic vibrators which are used to generate droplets of the precursor solution. The temperature of the reactor was fixed at 900 °C. The flow rate of air was controlled at 45 l/min. The as-prepared particles were post-treated between 600 and 1100 °C for 3 hr under 10% H<sub>2</sub>/N<sub>2</sub> mixture gas. The starting materials used for the preparation of precursor solution were Sr(NO<sub>3</sub>)<sub>2</sub>, LiNO<sub>3</sub>, Eu(NO<sub>3</sub>)<sub>3</sub>·5H<sub>2</sub>O and tetraethyl orthosilicate (TEOS). The overall solution concentration was 0.5M, and Eu concentration was varied from 0.001 to 0.05mol% of strontium component. The crystal structure and morphology of Li<sub>2</sub>Sr<sub>1-x</sub>SiO<sub>4</sub>:Eu<sup>2+</sup><sub>x</sub> were investigated by X-ray diffractometry and scanning electron microscopy, respectively. The PL spectra of Li<sub>2</sub>Sr<sub>1-x</sub>SiO<sub>4</sub>:Eu<sup>2+</sup><sub>x</sub> were measured using a spectrofluorophotometer under the excitation of a 450 nm UV produced by a Xe flash lamp.

The effect of the amount of LiNO<sub>3</sub> on the crystal structure of Li<sub>2</sub>SrSiO<sub>4</sub>:Eu<sup>2+</sup> were investigated. In addition of 20 mol% excess LiNO<sub>3</sub>, Li<sub>2</sub>SrSiO<sub>4</sub>:Eu<sup>2+</sup> were confirmed to be a Li<sub>2</sub>EuSiO<sub>4</sub>

single phase (JCPDS #47-0120) with a hexagonal structure because of volatilization of Li content. PL spectra of Li<sub>2</sub>SrSiO<sub>4</sub>:Eu<sup>2+</sup> prepared by spray pyrolysis were shown in Figure 1. The excitation band is due to 4f<sup>7</sup> → 4f<sup>6</sup>5d<sup>1</sup> transitions, and the broad excitation band from 400 to 460nm matches well with emission band of GaN based LED. Li<sub>2</sub>SrSiO<sub>4</sub>:Eu<sup>2+</sup> showed an orange-yellow emission band with the maximum intensity at 570nm under 450nm excitation. PL intensity of Li<sub>2</sub>Sr<sub>1-x</sub>SiO<sub>4</sub>:Eu<sup>2+</sup><sub>x</sub> increased with x, reaching a maximum at x=0.005.

In summary, orange-yellow emitting Li<sub>2</sub>SrSiO<sub>4</sub>:Eu<sup>2+</sup> was successfully synthesized by spray pyrolysis. PL property, crystal structure and morphology of Li<sub>2</sub>SrSiO<sub>4</sub>:Eu<sup>2+</sup> were optimized in spray pyrolysis.

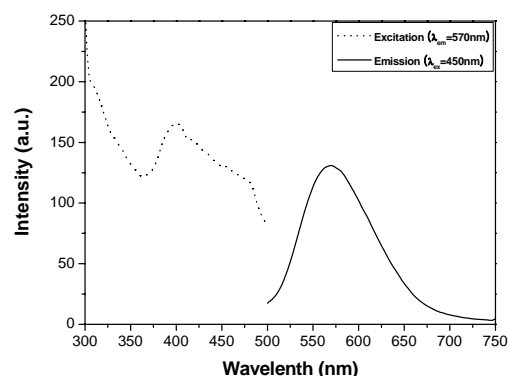


Figure 1. Excitation and Emission spectrum of Li<sub>2</sub>SrSiO<sub>4</sub>:Eu<sup>2+</sup> phosphor particles.

This work was partially supported by Center for Ultramicrochemical Process Systems (CUPS) sponsored by KOSEF. Travel express was supported by brain korea 21 program (Ministry of Education).

Nakamura, Y., & Fasol, G. (1996). *The blue laser diodes: GaN based light emitter and lasers* (Springer, Berlin).

Haferkorn, B., & Mayer, G. (1998). *Z. Anorg. Allg. Chem.*, 624, 1079-1081.

Pardha Saradhi, M., & Varadaraju, U. V. (2006). *Chem. Mater.*, 18, 5267-5272.

Toda, K., Kawakami, Y., Kousaka, S., Ito, Y., Komono, A., Uematsu, K., & Sato, M. (2006). *IEICE Trans. Electron.*, E89(10) 1406-1412.

## Synthesis of mesoporous SiO<sub>2</sub> using ultrasonic spray method

Lee-hwa Song, SeungBin Park\*

Department of Chemical and Biomolecular Engineering, Korea Advanced Institute of Science and Technology,  
373-1, Guseong-dong, Yuseong-gu, Daejeon 305-701, Republic of Korea  
\*SeungBinPark@kaist.ac.kr, +82-42-869-3928

Keywords: Mesoporous, SiO<sub>2</sub>, Surfactants, Ultrasonic spray

Mesoporous materials have high surface area and uniform pore size ranging from 2 to 50nm. Due to these properties, they are used for gas sensors, catalysis, separation processes, support of nano-materials and other various fields. In general, the most of mesoporous materials mainly have been synthesized by a sol-gel method that requires additional processes such as hydrothermal process, washing, drying and calcination with the long reaction time.

In this work, SiO<sub>2</sub> particles with well-defined mesopores were synthesized by an ultrasonic spray method, which does not require the additional process like a hydrothermal process in continuously producing mesoporous SiO<sub>2</sub> within 1 min.

The surfactant was dissolved in 1 M HNO<sub>3</sub> solvent of an ethanol/distilled water mixture. Thereafter, tetraethylortho silicate (TEOS, Aldrich) as precursor was dissolved in that surfactants solution. And then, this solution was stirred until it became transparent; it indicates that the hydrolysis reaction occurred. In this work, tri-block copolymer ((EO)<sub>20</sub>-(PO)<sub>70</sub>-(EO)<sub>20</sub>, Aldrich), Cetyltrimethylammonium bromide (CTABr, Aldrich) and Dodecylamine (Aldrich) were used as templating agents. The total concentration of precursor was 0.2 M.

The droplets of precursor were generated by the ultrasonic droplet generator and, by air such as carrier gas, were carried into the ultrasonic spray reactor which was composed of the dry reactor for the formation of composite between template and TEOS and the furnace reactor for the condensation reaction as well as the calcinations. The synthesized particles were collected into the back filter (Figure 1).

X-ray diffractometer (XRD, Model D/Max-IIC), scanning electron microscopy (SEM, Model Hitachi S4800), transmission electron microscopy (TEM, Model Tecnai F30 s-Twin) and surface area & pore size analyzer (Model NOVA 4200) were employed to study the pore structure and morphology, and to analyze pore size and surface area.

TEM images in Figure 2 show that SiO<sub>2</sub> without surfactants was non-porous, however SiO<sub>2</sub> with tri-block copolymer was porous. Figure 3 shows the pore size distribution for a mesoporous sample with CTABr. The surface area (BET) obtained the sample with CTABr is 1393m<sup>2</sup>/g, and BJH<sub>des</sub> average pore size is 3.38nm.

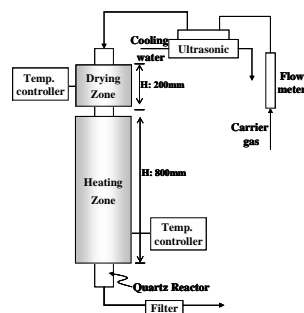


Figure 1. Schematic diagram of an ultrasonic spray reactor.

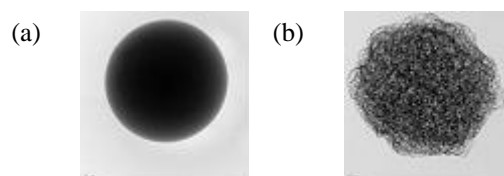


Figure 2. TEM images of the SiO<sub>2</sub> (a) without surfactants and (b) with tri-block copolymer as surfactant.

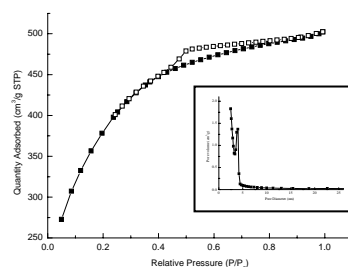


Figure 3. Nitrogen sorption isotherm and pore size distribution of SiO<sub>2</sub> with CTABr as a surfactant.

This work was partially supported by Center for Ultramicrochemical Process Systems (CUPS) sponsored by KOSEF. Travel expense was supported by Brain Korea 21 program (Ministry of education).

Lu, Y., Fan, H., Stump, A., Ward, T. L., Rieker, T., & Brinker, C. J. (1999). *Nature*, 398, 223-226.

Li, D., Zhang, J., & Ampo, M. (2006). *J. Lumin.* 116, 73-78.

Kao, H. M., Liao, Y. W., & Ting, C. C. (2007). *Micropor Mesopor Mat.* 98, 80-88.

## Characteristics of aerosol formation from pulverized coal pyrolysis

W.H. Chen and J.S. Wu

Department of Marine Engineering, National Taiwan Ocean University, Keelung 202, Taiwan, R.O.C.

Keywords: aerosol formation, pulverized coal, pyrolysis, drop tube furnace.

Pulverized coal (PC) pyrolysis is a fundamental and essential phenomenon in coal applications. In a coal-fired power plant, pulverized coal is generally blown into boilers through injectors. Because of intrinsic high-temperature environments in combustors where a high thermal-gradient in the vicinity of particle surface is exhibited, the pyrolysis of the coal particles is inevitably encountered initially, thereby liberating a large amount of volatiles (Smoot and Smith, 1985). While the volatiles are burned in furnaces, they are also likely to recombine, convert into carbonaceous agglomerates, and then produce a considerable number of aerosol particles such as tar and soot (Bockhorn, 1994.). When these fine particles are emitted into the atmosphere, air pollution problems are induced. Apart from the coal-fired power plant, PC is also extensively employed in ironmaking processes (Du and Chen, 2006). If the generated amount of aerosol particles in the blast furnace is large to a certain extent, especially for soot particles, gas permeability in the hearth will be retarded, whereby the furnace instability will be exhibited.

In order to recognize the above-mentioned phenomena, aerosol formations from pulverized coal pyrolysis in a drop tube furnace were studied in the present study. In the drop tube furnace, the reactor was heated by a SiC heater which can heat the furnace up to 1600°C. The heater was controlled by a PID temperature controller and a SCR power controller. An R-type thermocouple was mounted in the furnace to detect the temperature of the reaction zone which was used as the reference of the SCR. A cyclone and a filter were installed behind the reactor, sequentially. The former and the latter will capture larger (>0.5µm) and smaller particles (<0.5µm), respectively. Then, the smaller or aerosol particles were observed via a scanning electron microscope and analyzed by means of a thermogravimetry.

To recognize detailed characteristics of the generated particles, their thermogravimetric analysis (TGA) and derivative thermogravimetric (DTG) analysis from the reaction temperature of 1000°C are displayed in Figure 1. The heating temperature of TG is increased from 25°C to 1400°C and the heating rate is 20°C/min. The aerosol particles are in an environment of nitrogen with the volume flow rate of 500 mL/min. When the environmental temperature proceeds from 25°C to 500°C, it can be seen that the weight of the particles declines substantially. Specifically, the particles weight decreases from 100% to 68% and the maximum value of DTG

occurs at 360°C where the weight-loss intensity is 4.3%/°C. After reaching the heating temperature of 500°C, the decrease in TGA curve tends to slow down until 1000°C. During this heating period (i.e. 500-1000°C), only 6% of weight is lost. With further increasing the temperature from 1000 to 1400°C, the particles weight drops from 62% to 50% where it can be seen that DTG curve has been promoted to a certain extent compared with the previous heating period. According to the distribution of TGA or DTG curve, the entire reaction of the aerosol particles can be divided into three stages. In the first stage (i.e. 25°C-500°C), the pronounced drop in weight is due to the release of tar contained in the particles. Consequently, this stage is spoken of as the tar-reaction stage. In the second stage (i.e. 500°C-1000°C), because the weight-loss with respect to the heating temperature is weak, probably resulting from the reactions of heavier hydrocarbons, it is referred to as the weak-reaction stage. In the last stage (i.e. 1000°C-1400°C), it is inferred that the weight-loss is a consequence of soot reaction; it is thus named the soot-reaction stage

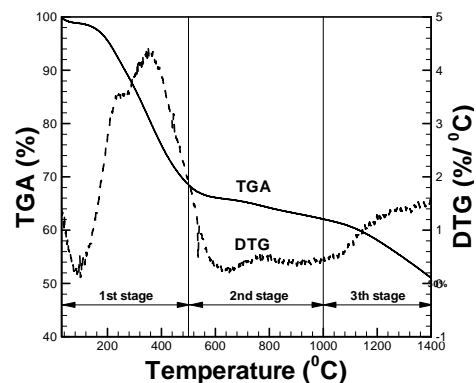


Figure 1. TG and DTG analyses of the generated aerosol particles at 1000°C.

The authors acknowledge the National Science Council, Taiwan, R.O.C., for supporting this work in part.

Smoot, L.D. and Smith, P.J. (1985) *Coal Combustion and Gasification*. Plenum, New York.

Bockhorn, H. (1994). *Soot Formation in Combustion*. Springer-Verlag, Berlin.

Du, S.W. and Chen, W.H. (2006). *Int. Comm. Heat Mass Transfer*, 33, 327-334.

## Interaction between meteorological quantities and particle concentrations in the suburban rural boundary layer during different weather episodes

S. Weber

Department of Applied Climatology and Landscape Ecology, University of Duisburg-Essen, Campus Essen, 45141 Essen, Germany

Keywords: turbulence, aerosol, surface layer, source area

### Introduction

Meteorological quantities can have contrasting influences on airborne particles concentrations depending on the aerosol physical characteristics, e.g. different effects of turbulent mixing on particles in different size classes (Weber et al., 2006). In order to study the interaction between aerosol and meteorology (i.e. turbulence parameters) within the suburban/rural surface layer, measurements at two heights above ground level were performed during winter/spring 2006.

### Study site and weather periods

The nine-week measurement period was conducted from 11 February to 18 April, 2006 at the regional airport Essen/Mülheim, Germany (51° 24' N, 6 56' E). The airport is situated in the SW of the city of Essen right on the city border of Essen/Mülheim. It comprises an area of about 141 ha and is situated at 124 m above sea level.

Three periods with different weather conditions were extracted from the data-set for further analysis. The first episode (SNOW) from March 1 to 6 was dominated by a trough over Central-Europe with cold arctic air masses entering the region. A permanent snow cover with a height of 6 - 7 cm was apparent at the site. The second episode (CLEAR) from Mar 12 - 19 was a clear and sunny period characterised by an anticyclonic high-pressure circulation pattern with north-easterly wind directions. The third episode (SWT) from Apr 06 - 09 was extracted due to its constant winds from SW with an average speed of 3.44 m s<sup>-1</sup>.

### Results

The periods were characterised by distinctly different particle concentration regimes and different influence of meteorology and turbulence on airborne particles. The highest particle mass concentrations for all size fractions were measured during CLEAR, e.g. PM<sub>10</sub> is larger by a factor of 1.5 and 1.62 at both measurement heights agl in comparison to SNOW and SWT, respectively. A clear relation of particle concentrations at the site and direction of the approaching flow was observed demonstrating a significant effect during time periods of advection of the urban plume towards the measurement site (urban area is situated to NE of the site).

A correlation analysis demonstrated significant differences of meteorological effects on particle concen-

tration during the episodes. In general, most distinct statistical relationships with particles can be observed for quantities indicating turbulent flow, namely  $\sigma_w$ ,  $u_*$ , and for the horizontal wind speed  $u$ . However, comparing the three episodes a contrasting behaviour of particle concentrations and turbulent flow was found. During SNOW and SWT a negative correlation of turbulence and particle concentrations was observed while CLEAR is characterised by a positive correlation.

Thermal turbulence shows a slight positive correlation to the particle mass fractions PM<sub>10</sub>, PM<sub>2.5</sub> and PM<sub>1</sub> during SNOW. Interestingly no such behaviour in CLEAR but a moderate negative correlation to the ratio PM<sub>1</sub>/PM<sub>10</sub> was found (Fig. 1). This can be satisfactorily described by a linear relationship ( $r = 0.76$ ) indicating smaller concentrations of submicrometer particles with increasing upward directed surface heat fluxes. This is believed to be governed by higher concentration increases of larger particles relative to smaller particles during daytime with drying soil surfaces.

Overall the experiment stated the important influence of site characteristics and meteorology on the resulting concentration regimes. This behaviour was shown not to be universal but a function of characteristics of the upwind (source) area, emission sources, measurement height and atmospheric boundary layer conditions.

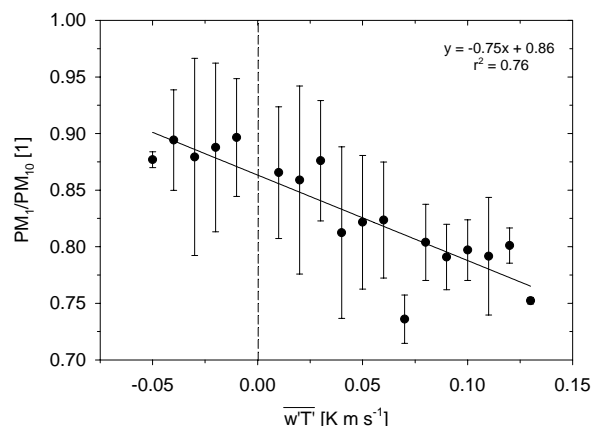


Fig. Relationship between kinematic surface heat flux and the particle mass ratio PM<sub>1</sub>/PM<sub>10</sub> during CLEAR grouped into 0.01 K m s<sup>-1</sup> classes.

Weber, S., Kuttler, W. and Weber, K. (2006). *Atmos Environ*, 40, 7565-7578.

## Temporal variation of apparent particle density in an urban aerosol

M. Pitz<sup>1,2</sup>, W. Birmili<sup>3</sup>, O. Schmid<sup>2</sup>, J. Heinrich<sup>2</sup>, R. Zimmermann<sup>2</sup>, H.-Erich Wichmann<sup>2</sup>, A. Peters<sup>2</sup> and J. Cyrys<sup>1,2</sup>

<sup>1</sup>WZU, Center for Science and Environment, University of Augsburg, 86159 Augsburg, Germany

<sup>2</sup>GSF National Research Center for Environment and Health, 85758 Neuherberg, Germany

<sup>3</sup>Institute for Tropospheric Research, 04318 Leipzig, Germany

Keywords: particle characterization, urban aerosol, apparent particle density, TDMPS, TEOM.

Epidemiological studies indicate that elevated mass concentrations of ambient particles below aerodynamic diameters of 10  $\mu\text{m}$  ( $\text{PM}_{10}$ ) or 2.5  $\mu\text{m}$  ( $\text{PM}_{2.5}$ ) are associated with health effects. However, additional aerosol parameters, such as particle surface area or chemical composition, have been recently discussed as being relevant for health effects studies.

Particle density is a parameter which might be influenced by physical properties, chemical composition and by the generation processes of particles. It might be considered when associations between health effects and ambient particles are investigated.

In this study, conducted in Augsburg, Germany, from January 1, 2005 to December 31, 2006, we calculated the apparent particle density using highly time-resolved measurements of particle number size distribution (converted to volume) and fine-particle mass concentration. Here, we show the day-to-day variation of the apparent particle density and we study the impact of the chemical composition and meteorological conditions on the apparent density by means of Spearman correlation coefficients ( $r$ ) and multiple linear regressions.

A Twin Differential Mobility Particle Spectrometer (TDMPS) and an Aerodynamic Particle Sizer (APS) were used for measuring the particle number size distribution.  $\text{PM}_{2.5}$  mass concentrations were measured in parallel with a Tapered Element Oscillating Microbalance (TEOM) equipped with a Filter Dynamic Measurement System (FDMS) to correct the measurement for the volatile particle mass fraction. For the estimation of the mean apparent density of particles, number size distributions were converted into volume size distributions, assuming that the particles were spherically shaped. Mean apparent particle density was calculated as the ratio of mass concentration and volume concentration up to an aerodynamic diameter smaller than 2.5  $\mu\text{m}$ . In addition, Black Carbon (BC) concentrations were measured by an Aethalometer, particle bound nitrate and sulfate concentrations were determined by Ambient Particulate Nitrate/Sulfate Monitors.

The mean apparent particle density on a daily base was  $1.6 \pm 0.4 \text{ g cm}^{-3}$  (Figure 1). We found a strong day-to-day variation of apparent density

ranging from 1.0 to 2.3  $\text{g cm}^{-3}$  (5<sup>th</sup> and 95<sup>th</sup> percentile). Moreover, a temporal pattern was visible. In the time period from June 2005 to February 2006 the apparent density was mostly below the average value, whereas in spring and summer 2006 the density was higher than the average value.

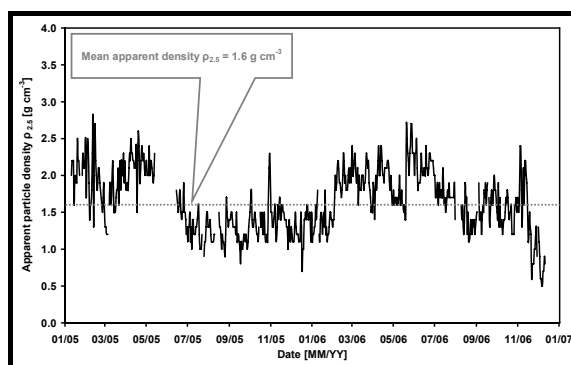


Figure 1. Day-to-day variations of apparent particle density of  $\text{PM}_{2.5}$  2005 - 2006 in Augsburg, Germany.

The correlations between the apparent density of  $\text{PM}_{2.5}$  and the physical properties, chemical composition as well as meteorological data were only moderate. The strongest correlation could be seen between the apparent density and the BC fraction associated with fine particles ( $r = -0.5$ ), followed by the relationship between density and the volatile particle mass fraction of  $\text{PM}_{2.5}$  ( $r = 0.4$ ).

A regression model using all relevant particle characteristics and meteorological data explained 61 % of the daily variability of the apparent particle density. A substantial portion of the variability was explained by the BC fraction of  $\text{PM}_{2.5}$  (27%), followed by particle number concentrations (16%) and the sulfate fraction of fine particles (12%).

In conclusion: Apparent density shows a pronounced day-to-day variation and a temporal pattern. It reflects the composition of particles and their interaction with the surrounding air. Hence, in addition to chemical composition, shape, and surface area of particles their density could play an important role when studying health risks of air pollutants and for clarifying the effects on human health and classifying the emission sources.

## PM Characterization by Carbon Isotope

C. Grassi<sup>1</sup>, V. Campigli<sup>3</sup>, L. Dallai<sup>2</sup>, S. Nottoli<sup>2</sup>, L. Tognotti<sup>3</sup>, M. Guidi<sup>2</sup>

<sup>1</sup> Department of Mechanical, Nuclear and Production Engineering, University of Pisa, 56126 Pisa (Italy)

<sup>2</sup> Geoscience and Georesources Institute, IGG-CNR of Pisa, Via G. Moruzzi 1, Pisa-I 56124.

<sup>3</sup> Department of Chemical Engineering, University of Pisa, 56126 Pisa (Italy)

Keywords: Carbonaceous Particles, Chemical Composition, Measurement, Urban Aerosol, Source Identification.

Isotopic characterization of PM can play an important role in the individuation of primary and secondary sources and also in the determination of the natural/biogenic or anthropogenic/combustion contribution to the measured concentration. As the matter of fact, a methodology to analyze the stable isotope of the carbonaceous fraction of PM10 has been developed.

The PM10 samples were collected during the PaTOS monitoring campaign Autumn 2005 – Spring 2006 in six sites located on the regional Tuscany territory: Arezzo Urban/Traffic (AR-UT), Lucca Urban/Background (LU-UB), Livorno Suburban/Background (LI-SB), Prato Urban/Traffic (PO-UT), Firenze Urban/Background (FI-UB) and Grosseto Urban/Background (GR-UB). A Low Volume Sampler (LVS), Tecora TCR, was used with sampling head USEPA-cfr part.50 to collect 24 hr daily aerosols samples on QUARTZ fibre filters.

The PM organic matter on the quartz fibre filters is converted into a combustion apparatus, Thermo Finnigan, Elemental Analyser-EA1108, into CO<sub>2</sub>. A mixed flow rate of helium and oxygen was used as carrier gas in the apparatus to send the CO<sub>2</sub> through the spectrometer, Thermo Finnigan-Delta Plus XP, for the determination of the isotope abundance. The hardware and software connected to the spectrometer allow to determine  $\delta^{13}C$  (‰) in relation to the PDB reference standard (“Pee Dee Belemite” CaCO<sub>3</sub>), applying the  $\delta^{13}C/\delta^{12}C$  ratio equation.

The PM10 concentrations, calculated as daily averaged values, show a significant variability from the urban to suburban sites varying from 50  $\mu\text{g}/\text{m}^3$  (AR-UT) to 20  $\mu\text{g}/\text{m}^3$  (LI-SB) as averaged concentration on the sampling period and from autumn 60  $\mu\text{g}/\text{m}^3$  (LU-UB) and spring 25  $\mu\text{g}/\text{m}^3$  (LU-UB) periods. Also the PM carbon content, on period average values, shows very different results from site to sites with a minimum in GR-UB of 20% up to the 60% of LU-UB.

In figure 1 the average values of the carbon content, expressed as weight percentage of the PM, versus the  $\delta^{13}C$  parameter were shown for each monitoring sites together with the two parameters variability. The analytical results in terms of  $\delta^{13}C$ 's values are comprised from -28 and -23 and show significant variation from the traffic and background sites; in fact, in the background and suburban sites (LI-SB, FI-UB and GR-UB) the  $\delta^{13}C$ 's show a bigger

variability than in the urban sites AR-UT, PO-UT, LU-UB, LI-UB were the results don't vary significantly, and this could be well correlated with the constant emissions from traffic. On the contrary the background sites both urban or rural, depending on the meteorology and atmospheric processes, show a wider variability in the  $\delta^{13}C$  values relating to the changing in the contribution from the natural, secondary and anthropogenic source emissions.

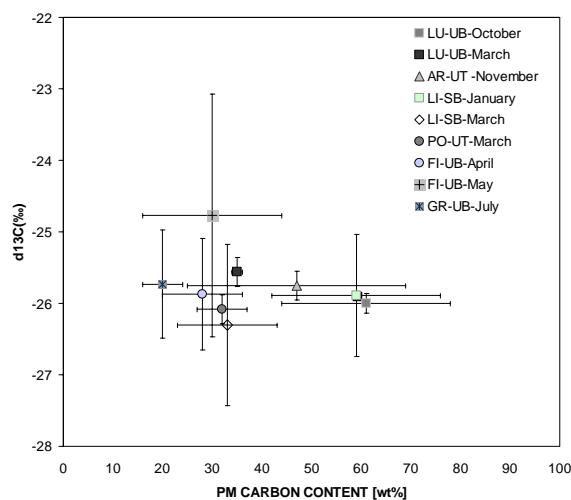


Figure 1.  $\delta^{13}C$  [‰] versus PM carbon content [wt%] for the monitoring sites, Tuscany.

The lower negativities of the  $\delta^{13}C$  values of the PO-UT compared to the AR-UT could be explained by the presence of industrial source that are negligible in the AR-UT and that concurred as lower negative  $\delta^{13}C$  values [Widory et al., 2004]. The  $\delta^{13}C$  values confirm the indication determined for the identification of the emissions from non stationary combustion sources as traffic vehicles and the differences shown between urban and rural sites [Huang et al., 2006].

Huang L., J.R. Brook, W. Zhang, S.M. Li, L. Graham, D. Ernst, A. Chivulescu, G. Lu. Atmospheric Environment 40 (2006) 2690–2705.  
Widory David, Stephane Roy, Yvon Le Moullec, Ghislaine Goupil, Alain Cocherie, Catherine Guerrot, Atmospheric Environment 38 (2004) 953–961.

## Chemical investigation of eight different types of carbonaceous particles using thermoanalytical techniques

G. Matuschek<sup>1</sup>, E. Karg<sup>2</sup>, A. Schröppel<sup>2</sup>, H. Schulz<sup>2</sup>, O. Schmid<sup>2</sup>

<sup>1</sup>GSF-National Research Center for Environment and Health, GmbH, Institute of Ecological Chemistry, Ingolstädter Landstraße 1, D-85764 Neuherberg, Germany

<sup>2</sup>GSF - National Research Center for Environment and Health, GmbH, Institute of Inhalation Biology, Ingolstädter Landstraße 1, D-85764 Neuherberg,

Keywords: Carbonaceous particles, Chemical analysis; Organic matter, Particle characterization.

The chemical composition of ambient aerosol particles affects numerous important physical aerosol parameters as well as their potentially adverse health effects. In recent years, numerous epidemiological studies have revealed an association between elevated levels of ambient particles and increases in all-cause morbidity or mortality. Recently, toxicological and epidemiological studies indicate that ultrafine particles (< 0.1 µm diameter) may be more harmful per unit mass than larger ones (Oberdörster 2000).

However, the studies suffer from a lack of detailed information on particle chemistry. Some newer studies (Stoeger et. al 2006, Schober et. al. 2006) try to overcome this limitation. These and other studies have characterized carbonaceous particles based on the thermooptically determined organic carbon (OC), elemental carbon (EC) content and the ratio of both. Unfortunately, the interpretation of the resulting OC/EC data is limited by the fact that, OC and EC are operationally defined parameters, i.e., the observed OC and EC content is method-dependent (Chow et. al. 2001). In addition, the methods can not provide detailed chemical speciation, a drawback that is particularly significant for toxicological or biological studies, and the organic matter content needs to be calculated from OC by conversion factors.

The objective of this study was to derive both detailed chemical speciation and useful proxies for the quantitative classification of the organic matter content of carbonaceous aerosol samples. Using three different techniques, a) thermal desorption - gas chromatography mass spectrometry (TD-GC/MS), b) evolved gas analysis with mass spectrometry (EGA-MS) and c) thermogravimetry with Fourier transform infrared spectroscopy (TG-FTIR), we investigated eight different carbonaceous particulate matter samples used for health effect studies. The samples include different types of surrogate soot particles, pigment black and spark-generated carbon particle as well as two ambient aerosol samples (diesel soot and particulates collected in a road tunnel). All samples showed an increasing mass desorption ( $M_d$ ) with rising temperature, but the desorption curves scattered heterogeneously allowing no reliable OC classification based  $M_d$  alone. However, as seen from

Fig. 1, the samples could be clearly distinguished based on their OC content (high/low OC samples = solid/open symbols) using a novel parameter, the "equivalent organic mass fraction"  $OMF_e$ , where  $OMF_e = OIR * M_d$  ("organic ion ratio" OIR is the ratio of the areas underneath the "organic" and total ion count signal of the EGA-MS).

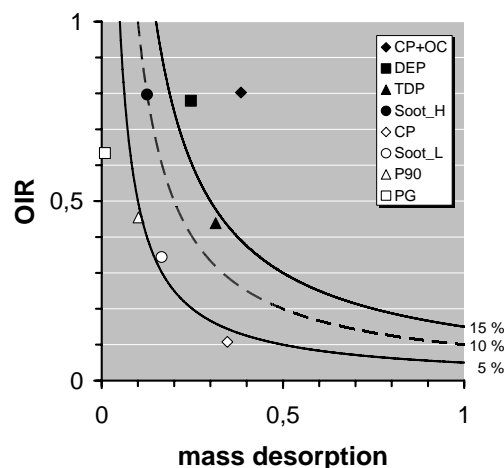


Figure 1. OIR versus  $M_d$ . The contour lines represent the 5%, 10% and 15% levels of the  $OMF_e$

The validity of this classification was confirmed with a second proxy parameter and information on the generation process of the particles. Both types of printex samples and the spark-generated carbon particles showed the lowest OC mass fraction (<8%), whereas for road tunnel and diesel emission particles <16 % and <19 % was estimated, respectively.

Chow, J.C., Watson, J.G., Crow, D., Lowenthal, D.H., Merrifield, T., *Aerosol Science and Technology* 34 (1) 2001, 23-34

Oberdörster, G. (2000) *Philosophical Transactions of the Royal Society of London A* 358, 2719-2740.

Schober, W., Belloni, B., Lubitz, S., Eberlein-König, B., Bohn, P., Saritas, Y., Lintelmann, J., Matuschek, G., Behrendt, H. and Buters, J. (2006) *Toxicological Sciences* 90 (2) 2006, 377-384

Stoeger, T., Reinhard, C., Takenaka, S., Schroepel, A., Karg, E., Ritter, B., Heyder, J., Schulz, H. (2006) *Environmental Health Perspectives* 114 (3) 328-333.

## Continuous measurements of particle number concentrations, in Athens, Greece

G. Grivas, A. Chaloulakou and N. Spyrellis

School of Chemical Engineering, National Technical University of Athens, Zografos, 15780, Athens, Greece

Keywords: Number concentration, Ultrafine particles, Submicron particles, PM measurements.

The association of increased particle number concentrations with detrimental health effects has been proposed since the mid-nineties and there has been a considerable number of studies even suggesting causal relationships between exposure to ultrafine particles and mortality, and respiratory health of sensitive population subgroups (Peters and Wichmann, 2002). The availability of number concentrations time-series is crucial for the investigation of these relationships through epidemiological studies. Moreover the importance of particle number monitoring is highlighted in the case of traffic impacted locations, where it is considered that such a metric, for which ambient concentrations is raised near emission sources would increase the effectiveness of mitigation measures. In this work, results from a bi-annual particle number concentration measurement campaign are presented, for a high PM recording location in Athens. It is one of the first to examine the variability of number concentrations in Athens (Grivas et al., 2004) for longer measurement periods and is intended to provide reference material for future research.

The monitoring site is located at the area of Lykovrissi, influenced from vehicular, industrial and natural particle sources. Total number concentrations (TNC) were measured for the period March-August 2006 by a TSI condensation particle counter, sensitive to ultrafine particle diameters down to 10nm. Submicron particle mass concentrations were also measured everyday, with a Partisol 2025 unit and ancillary measurements of PM<sub>2.5</sub> and PM<sub>10</sub> were conducted. The reflectance of PM<sub>1</sub> filters was determined and used for the calculation of the absorption coefficient, which represents the variation of black smoke (BS) concentrations.

The average total particle number concentration for the whole examination period was determined at 19800 particles cm<sup>-3</sup>, with daily mean values reaching up to 39200 particles cm<sup>-3</sup>, and recorded short term peaks up to 133900 particles/cm<sup>3</sup>. Particle numbers levels were comparable to those reported for sites impacted by traffic. (Noble et al., 2003). The examined diurnal variation of concentrations (Figure 1), by the occurrence of representative diurnal peak concentrations, characterizing morning go-to-work and afternoon return-from-work traffic. The importance of the particular source type is also reflected on the weekly variation, with concentrations being 17.8% lower during weekends as compared to weekdays.

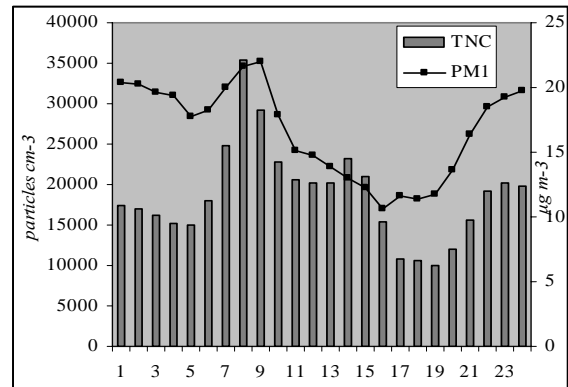


Figure 1. Diurnal variation of TNC and PM<sub>1</sub> levels.

Associations between particle number and particle mass concentrations were statistically significant but of moderate magnitude. Pearson correlation coefficients decreased by increased diameter of the particle metric, as processes other than ultrafine particle formation assume increased importance for fine and coarse particles. In the case of black smoke particles a stronger association is displayed, denoting the importance of vehicular emissions. The inverse association of particle numbers with atmospheric dilution and removal processes (scavenging) is reflected by TNC inverse correlations with wind speed and amount of rainfall while a different pattern is observed for correlations with temperature (T) and solar radiation (SR) intensity, during the warm months.

Table 1. Statistical significant (c.l.: 0.95) correlations of TNC with PM metrics and meteorological parameters.

	PM <sub>1</sub>	PM <sub>2.5</sub>	PM <sub>10</sub>	BS
<i>r</i>	0.50	0.39	0.31	0.60
	Wind speed	T	SR	Rainfall
<i>r</i>	-0.45	0.40*	0.37*	-0.19

\* Warm period (May-August)

This work presents results from the research project PYTHAGORAS II, co-funded by the European Social Fund (75%) and National Resources (25%).

Grivas G., Asteriou C., Chaloulakou A., Spyrellis N. (2004). *Journal of Aerosol Science*, 35, 553-554.

Noble C.A., et al. (2003). *Atmospheric Environment*, 37, 827-840.

Peters A., Wichmann H.E. (2002). *Epidemiology*, 13, 255.

## Submicron aerosol particles in a small settlement near highway

J. Hovorka, Z. Staňková

Institute for Environmental Studies, Faculty of Science, Charles University in Prague, Benátská 2,  
128 01, Prague 2, Czech Republic

Keywords: traffic, home heating, submicron particles, number size distribution, mass size distribution

Meeting the EU air quality standards for particulate matter (PM<sub>2.5</sub> and PM<sub>10</sub>) and tropospheric ozone is the most difficult task for the air quality administration of the Czech Republic. The limits for PM's concentrations are exceeded not only in highly urbanized/industrialized areas but also in rural areas (Braniš, 2003). The air quality of industrialized areas is generally well documented, while that of rural areas is monitored scarcely, despite the uniformity of the resident number distribution by the settlement size in the Czech Republic. It was well documented that air masses in cities are usually well-mixed (Hussein, 2005), contrary to the small settlements where local sources of air pollution often play a major role. The purpose of this study was to resolve contribution of local heating and highway to the mass and size of fine aerosol particles in the air of a small settlement situated near a highway.

Measurements were conducted in a small settlement Koberovice (49°35'N, 15°15'E, altitude 470 m). There are about 150 residents in the Koberovice, which uses for household heating solely brown coal and wood. The burning ratio of wood to coal is one to one approximately. The sampling station was located on the highway-facing edge of the settlement, on the field about 350 meters from the D1 highway. Sampling heads were positioned 3.5m above the field. Winter sampling campaign went from the 24<sup>th</sup> Nov to the 8<sup>th</sup> Dec. The 5 minute integrates of number-size distribution of particles in the size range of 14.6-736.5 nm (SMPS 3936, TSI) and 15 minute integrates of NO<sub>x</sub> concentrations (APNA-360, Horiba) were recorded. A yearly measurement of 5 minute integrates of meteorology data (wind speed/direction, temperature, humidity, global radiation) were also performed at the station.

Basic statistical data for total number and mass concentrations are summarized in Table 1.

Table 1. Basic statistical data of total number and mass ( $\rho=1.5 \text{ g cm}^{-3}$ ) concentrations recorded during winter campaign.

	Particle number # cm <sup>-3</sup>	Particle mass μg m <sup>-3</sup>
Min/max	7.0 10 <sup>2</sup> /2.5 10 <sup>5</sup>	2.4/132
Median	3.4 10 <sup>3</sup>	16.7
Geomean	3.5 10 <sup>3</sup>	14.9
Average	4.1 10 <sup>3</sup>	17.1

Both number and mass concentrations are not alarmingly high. The percentile of the highest mass concentrations was recorded in the late afternoons (17:30-20:00) what, also confirmed by wind directions, simply trace heating habits in the village. Contrary to mass concentration, the percentile of the highest number concentrations can be apportioned to both local heating and highway, when the traffic counts were higher (>1400 h<sup>-1</sup>).

Concerning number size distributions, we usually recorded bi-modal size distributions with two distinct modes in ultrafine (GMD 20-30nm) and accumulation (GMD 100 nm) size ranges. The first mode can be attributed to the traffic (Charron, 2003). However, during our measurements the situation was not such straightforward and, according to wind speed and direction, local heating emitted particles of this mode. In general, particles of the larger mode formed majority of aerosol mass and particles of the lower mode, when it was present, formed majority of the particle number.

During 15 days of our winter campaign emission from local heating sources formed majority of the mass concentrations of submicron particles with the exception of about 4 hours of traffic jam at the highway, when traffic emission prevailed over local heating emissions. Our measurement is in accord with studies discussing dispersion of the emission from traffic (Pirjola, 2006).

Traffic volumes were provided by Road and Motorway Directorate of the Czech Republic and are greatly acknowledged. The study was partially carried out under the project 90-901986 and institutional support of the Institute for Environmental Studies of FSCU in Prague.

Braniš, M., Domasová, M. (2003) *Atmos. Environ.*, 37, 83-92

Charron, A., Harrison, R.M. (2003) *Atmos. Environ.*, 37 4109-4119

Hussein, T., Hameri, K., Aalto, P.P., Paatero, P., Kulmala, M. (2005) *Atmos. Environ.*, 39, 1655-1668  
Pirjola, L., Paasonen P., Pfeiffer, D., Hussein, T., Hameri, K., Koskentalo, T., Virtanen, A., Ronkko, T., Keskinen, J., Pakkanen, T.A., Hillamo, R.E., (2006), *Atmos. Environ.*, 40 867-879

## Characteristics of particulate matter deposition from Port of Koper

Poljšak B.<sup>1</sup>, Jereb G.<sup>1</sup>, Marzi B.<sup>2</sup>, Cepak F.<sup>3</sup>, Dražič G.<sup>4</sup>

<sup>1</sup> University of Ljubljana, College of health studies, Poljanska 26 a, 1000 Ljubljana, Slovenia

<sup>2</sup> Port of Koper, Vojkovo Nabrežje 38, 6000 Koper, Slovenia

<sup>3</sup> Institute of public health Koper, Vojkovo Nabrežje 4a, 6000 Koper, Slovenia

<sup>4</sup> Jožef Stefan Institute, Jamova 39, 1000 Ljubljana, Slovenia

**Key words:** Particulate matter deposition, particle characterization, particle concentration, coal and iron ore

The basic activities performed in the Port of Koper are cargo handling and warehousing. At the European Energy Terminal in Port of Koper large amounts of coal and iron ore is handled and warehoused. The storage capacity of the landfill is 450.000 t for coal ore and 350.000 t for iron ore. Unloading daily capacity of coal (cape size vessel) is 17.000 t or 15.000 t (panamax vessel) and for iron ore (cape size vessel) is 25.000 t.

Due to coal and iron ore open stockpiles the area is directly exposed to environmental conditions and its location is close to urban areas, a study was conducted during October 2005- September 2006 with the aim to identify particulate matter concentration, characterization and distribution from Port of Koper to nearby residential sites of urban region of Ankaran city.

In the following study total particulate matter deposition, qualitative evaluation of the particulate matter shape, size and elemental chemical composition was analyzed.

Results of gravimetric analysis of particulate matter deposition showed increased values during particulate matter sampling periods (Figure 1).

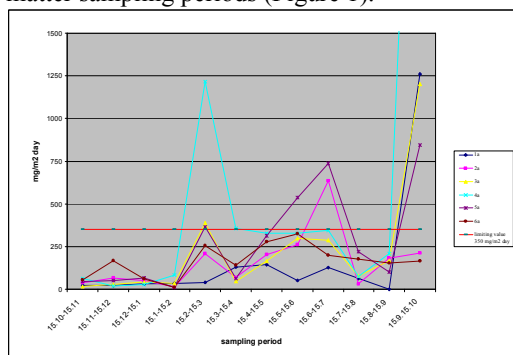


Figure 1: Particulate matter deposition ( $\text{mg}/\text{m}^2\text{day}$ ) at six different locations

By using electron microscope with energy dispersive X-ray spectroscopy shape, size and elemental chemical composition of collected particulate matter was measured. Results showed the presence of both iron and coal ore in the samples collected in urban area (Figure 2 and 3).

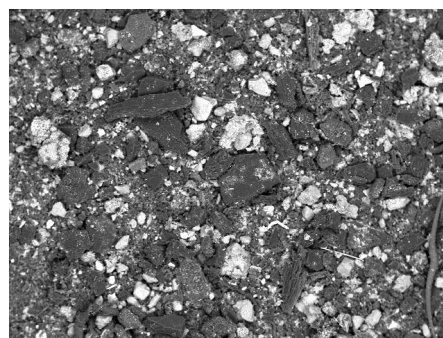


Figure 2: Picture of collected particulate matter under the electron microscope

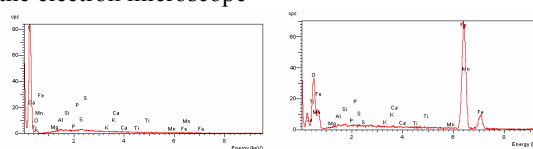


Figure 3: Typical spectrum of coal and iron ore using electron microscope with energy dispersive X-ray spectroscopy shape

In order to limit the negative influence of terminal operation, specially the amount of particulate matter, the following solutions have been introduced:

- a system of sprinkling towers and an Aluminium barrier (11 m high) was set up around the stockpiles
- ship loader is equipped with an anti-dust telescopic tube
- cleaning the transport path around the terminal twice a day

The efficiency of already taken steps will be controlled in the future study.

## Characteristics of the multiplexed grooved nozzles for high flow rate electrospray

Kyoungtae Kim<sup>1</sup>, Woojin Kim<sup>1</sup>, and Sangsoo Kim<sup>1</sup>

<sup>1</sup>Department of Mechanical Engineering, Korea Advanced Institute of Science and Technology, 373-1 Guseong-dong, Yuseong-gu, 305-701, Deajeon, Republic of Korea

Keywords: electrical effect, electrospray, extractor, fine particle, multiplexing.

The Electro spray has been adapted for many applications because it can generate the highly charged fine droplets. However, the low flow rate is available to get the monodisperse fine droplets. To increase the flow rate, a multiplexed nozzle system (Rulison & Flagan, 1993), and a grooved nozzle system (Duby *et al.*, 2006) were introduced. Electric field control was also reported (Park *et al.*, 2004). In this study, the multiplexed grooved-nozzle system was specially designed with the extractor to control the electric field. The droplet size and stable voltage regime of grooved mode were measured for several nozzle spacing.

The experiment device was composed of five stainless steel grooved nozzles (2.0mm I.D., 3.2mm O.D.) that have 12 grooves each, power supply, syringe pump (kdScientific 220) and extractor. The spacing of nozzles was from 10mm to 25mm and the location of extractor was changed at 2mm intervals to decide the optimum multi-jet condition using digital camera (OLYMPUS E300) and He-Ne laser (MELLES GRIOT 1135P). The distance between nozzle tip and mesh was fixed at 30mm. Ethanol was used for working liquid that was inserted into a syringe pump and sprayed through the nozzles. The grooves (0.5mm width, 0.5mm depth) were made by wire-EDM method and the flow rate of ethanol was 6ml/h. Droplet size distribution was measured by the phase doppler particle analyzer (PDPA, TSI) and the spray current was measure by a nano-ampere meter (keithley6415 Electrometer).

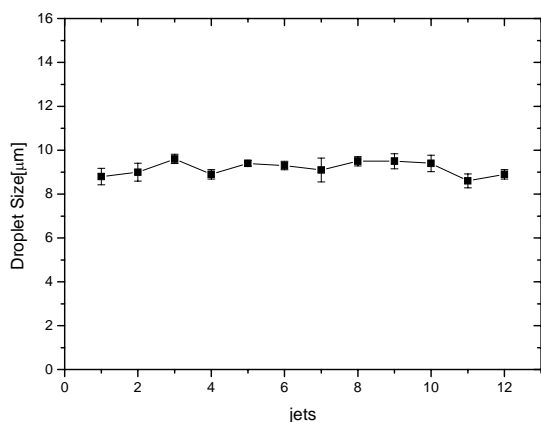


Figure 1. Average droplet size at flow rate of 6ml/h in individual jets of the grooved mode electro spray.

Figure 1 shows the droplet size of each jet and they are quite uniform. In addition, each jet has cone-jet mode characteristics.

Figure 2(a) shows that the inner nozzle didn't build up the same mode like outer nozzles caused by coulombic repulsion. Meanwhile, in the case of (b), all nozzles had a grooved mode perfectly and the voltage of the extractor was 10kV.

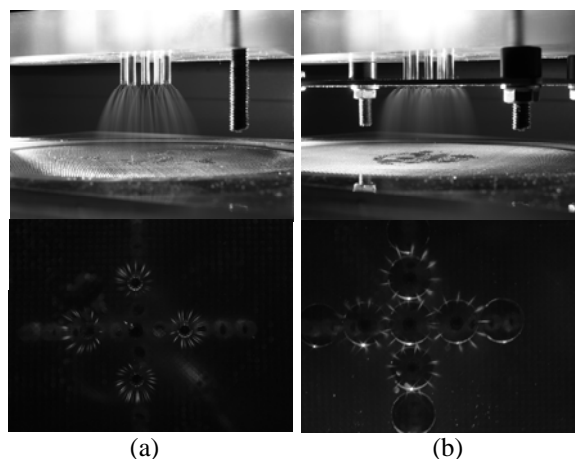


Figure 2. Electro spray visualization for 10mm nozzle spacing (a) with extractor and (b) without extractor.

The coulombic repulsion of highly charged liquids resulted nonuniform electric field. Therefore the multiplexing is impossible within 25mm nozzle spacing. Using the extractor, the multiplexed grooved mode at all nozzles was achieved on condition of wider than 10mm spacing. This high flow rate electro spray system can be realized simply and easily.

This work was supported by the Brain Korea 21 Program of the Ministry of Education and the Eco-Technopia 21 Project of the Ministry of Environment.

Rulison, A. J., & Flagan, R. C. (1993). *Review of Scientific*. 64, 683-686

Duby, M.-H., Deng, W., Kim, K., Gomez, T., & Gomez, A. (2006). *J. Aerosol Science*, 37, 306-322.

Park, H., Kim, K., & Kim, S. (2004). *J. Aerosol Science*, 35, 1295-1312.

## Highway exhaust aerosols and their effects on alpine lichen populations

E. Heinzlmann, P. Madl and W. Hofmann

Department of Materials Engineering & Physics, University of Salzburg, 5020 Salzburg, Austria

Keywords: aerosol sampling, combustion particles, lichens, size distribution, SMPS

Shortly after the oil crisis in the 1970's it was observed that incomplete combustion of fossil fuel resulted in thick grey-brown smog blankets covering the Salzach-valley in Salzburg, Austria (Hufnagel & Türk, 1998). The investigation of the net effect of airborne aerosol pollutants was studied with epiphytic lichen communities (Christ & Türk, 1981). Back then the most damaging component were  $\text{SO}_2$  and  $\text{H}_2\text{S}$  components resulting in loss of chlorophyll of the algal partner (Heber et al, 1994). With the gradual decrease of sulphur content in combustion fuel,  $\text{NO}_x$  and polycyclic aromatic HC components have taken over the chemical aspects of pollutant inventory. Being readily adsorbed by nano-particles, they provide the ideal agent to induce damage to lichen communities located near polluted areas, and in particular near high-traffic areas (Kasperowski & Frank, 1989). By investigating the particle inventory, it is possible to correlate epiphytic lichen populations with nearby aerosol line-sources like the Highway E55 (Tauernautobahn) and to estimate the potential damage to the adjacent Bluntau-valley.

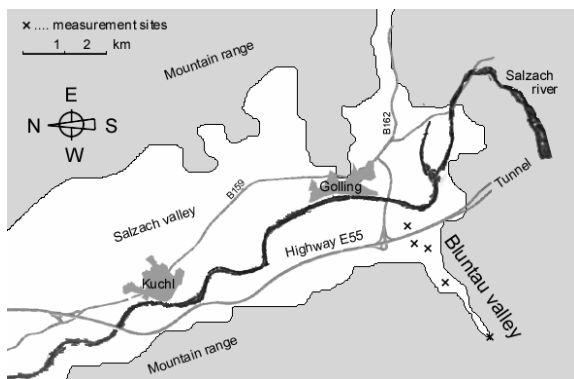


Figure 1. Topographical setting of the Bluntau-valley, highway and measurement sites.

SMPS-measurements were carried out repeatedly on several days during a six-month period. Measurement times were coordinated by taking into consideration the topography and the geographical orientation of the highway, i.e., the north-south orientation of the U-shaped Salzach-valley suggested to confine the monitoring window to the early morning or evening hours of bright, sunny days. Oscillatory motions of air masses occur perpendicularly to the valley's main orientation. The observed convective mass-flow of air driven by solar radiation and augmented by the western mountain

range fit nicely with the documented surface wind data recorded on these days.

Since the morning measurements of the transect stretched from the westbound area across the highway to the eastbound area and beyond into the Bluntau-valley, the documented particle inventory confirms the translocating effect thereby exerting an additional stress-factor on lichen populations (fig.2).

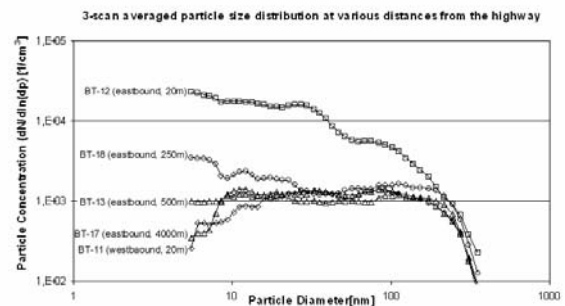


Figure 2. Size distributions of exhaust particles near Highway E55 (Tauernautobahn).

In conclusion, this investigation documents that particles from traffic emissions are translocated across the sound-protective barriers of the highway into the adjacent Bluntau-valley. This is obviously sufficient to negatively affect lichen populations as far as 500 m away from the high-traffic area and confirm biomonitoring investigations carried out almost 20 years ago (Kasperowski & Frank, 1989).

Heber, I., Heber, W., & Türk R. (1994). Die Luftqualität in der Stadt Linz (Oberösterreich, Österreich) von Oktober 1990 bis Oktober 1991 festgestellt anhand von Flechtenexponaten. *Naturk. Jahrb. Stadt Linz*, 37-39, 491-552 (in German).

Christ, R., & Türk, R. (1981). Die Indikation von Luftverunreinigungen durch  $\text{CO}_2$ -Gaswechsellmessungen an Flechtentransplantaten. *Mitt. Forstl. Bundesversuchsanstalt*, 137, 145-150 (in German).

Hufnagel, G., & Türk R. (1998). *Sauteria*, 9 (IAL3-Proceedings), 281-288.

Kasperowski, E., & Frank, E. (1989). *Boden- und Vegetationsuntersuchungen im Bereich der Scheitelstrecke der Tauernautobahn*. Umweltbundesamt Wien (Hrsg.), 1-126 (in German).

## Electrical and mechanical properties of alumina-MWNT nanocomposite synthesized by spray pyrolysis and spark plasma sintering

K.B. ee<sup>1</sup>, C.B. Mo<sup>2</sup>, S.H. Hong<sup>2</sup> and S.B. Park<sup>1</sup>

<sup>1</sup>Department of Chemical and Biomolecular Engineering, Korea Advanced Institute of Science and Technology, 373-1 Kusung-dong, Yujung-gu, 305-701, Dae on, Republic of Korea

<sup>2</sup>Department of Materials Science and Engineering, Korea Advanced Institute of Science and Technology, 373-1 Kusung-dong, Yujung-gu, 305-701, Dae on, Republic of Korea

Keywords: nanotubes, aerosol generation, sintering.

Alumina is one of the most widely used ceramic with its high hardness and good chemical and thermal stability. It has low fracture toughness which is an intrinsic characteristic of ceramic materials and low electrical conductivity. Wider range of applications of alumina is expected when these properties are improved. There have been many researches about alumina composite. Addition of second phase such as metal in ceramic matrix for the improvement of electrical properties deteriorates thermal and chemical stabilities or mechanical properties. Recently, carbon nanotubes (CNT) are thought to be fascinating materials as additive in composite owing to their outstanding properties (Harris, 2004). CNT have high Young's modulus with good flexibility and high aspect ratio, high electrical conductivity, and good thermal and chemical stability. Better mechanical and electrical properties of alumina were achieved by incorporation of CNT.

Alumina-CNT nanocomposites synthesized by different method have been reported. Alumina powder was physically blended with single-walled nanotube and sintered into dense nanocomposite (han et al., 2002). CNT were grew on Fe-Al<sub>2</sub>O<sub>3</sub> particle in situ, however, impurities such as Fe<sub>3</sub>C or Fe<sub>2</sub>C<sub>5</sub> were remained after sintering. Molecular level mixing was proposed for good adhesion between CNT and alumina matrix (Cha et al., 2005). They showed the increase of both hardness and fracture toughness. However, high loading of CNT is difficult in this method owing to time consuming reaction which leads to bundling of CNT. In this study, spray pyrolysis is applied to overcome this problem. Spray pyrolysis is effective for the prevention of CNT from bundling caused by van der Waals forces since it takes ust a few seconds for the reaction and ultrasonic used for aerosol generation maintains good dispersion of CNT in precursor solution.

Precursor solution is prepared by dispersing multi-walled nanotubes (MWNT) in aluminium nitrate melted water with surfactant using high energy tip sonicator. The amount of incorporated MWNT in alumina matrix is varied from 0 to 1.78wt . Amorphous alumina-MWNT composite powder synthesized by spray pyrolysis is heat-treated

to decompose surfactant. After ball milling, the nanocrystalline composite powder is sintered into pellet using spark plasma sintering (SPS) at 1375°C. The relative densities of final samples are measured by using Archimedes method. Electrical conductivity and mechanical properties are measured using two probe method and the Vicker's indentation method, respectively.

Figure 1. shows the morphologies of fractured surfaces of sintered alumina and alumina-MWNT composites. The grain sizes of the composites are gradually diminished as the amount of MWNT is increased. The network of MWNT is formed and the electrical conductivity is increased by the order of 13 in comparison with pure alumina when 0.178wt of MWNT is incorporated into alumina.

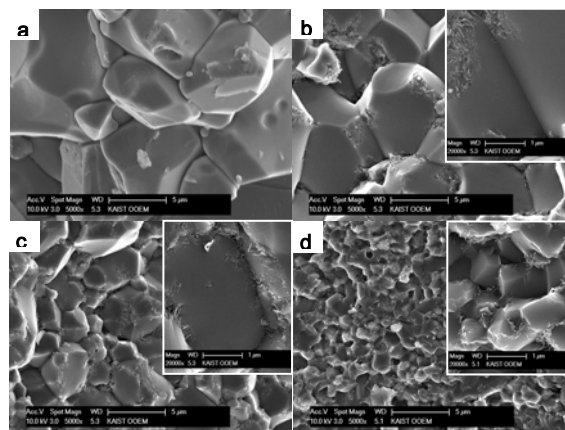


Figure 1. SEM images of fractured surface of the composites having (a) No MWNT (b) 0.38wt of MWNT (c) 0.71wt of MWNT (d) 0.178wt of MWNT.

Harris, P. J. F. (2004). *Int. Mater. Rev.*, 49, 31-43.

han, G. D., Kuntz, J. D., Wan, J., & Mukher ee, A. K. (2002). *Nat. Mater.*, 2, 38-42.

Cha, S. I., Kim, K. H, ee, K. H., Mo, C. B., & Hong, S. H, (2005). *Scripta Mater.*, 53, 793-797..

## **T16 Abstracts**

## Formation of TiO<sub>2</sub> nanoparticles by combustion of single titanium particles

V.V. Karasev<sup>1</sup>, A.A. Onischuk<sup>1</sup>, S. A. Khromova<sup>1</sup>, C.J. Tsai<sup>2</sup>

<sup>1</sup>Institute of Chemical Kinetics and Combustion SB RAS, 630090, Novosibirsk, Russia

<sup>2</sup>Institute of Environmental Engineering, National Chiao Tung University, 300 Hsinchu, Taiwan

Keywords: combustion synthesis, oxide nanoparticles, aggregates, fractals.

TiO<sub>2</sub> based photocatalytic nanomaterials are perspective for fog proof, and self cleaning glass production, anti-bacterial, anti-viral, fungicidal application, air purification and water treatment. In this work we have studied the TiO<sub>2</sub> nanoparticle formation during combustion of single Ti particles (of diameter 20 to 300 nm) when moving in the air with the velocity of about 1 m/s. The combustion was registered by the high speed video microscopy. Two consecutive frames illustrate the combustion in Fig. 1. TiO<sub>2</sub> nanoparticles can be seen as a tail which is formed due to the oxide evaporation from the droplet surface. To study the initial stages of the nanoparticle formation the combustion was frozen by the deposition of the maternal particle to the surface at small angle (see Fig. 2). The deposit from the reaction and aerogelation zone was analysed by a transmission Electron Microscope (TEM, Fig.3). The TiO<sub>2</sub> aerosol was formed as aggregates composed by small primary (10 – 40 nm) particles. The aggregate morphology was elaborated in terms of the fractal-like dimension  $D_f$  which can be evaluated from the power relationship between the aggregate mass  $M$  and radius  $R$ :  $M \propto R^{D_f}$ . One can see from Fig. 3 that  $D_f$  is high (2.8) for small aggregate due to the high temperature restructuring and small (1.6) for the large aggregates. The droplet temperature was measured in special experiments when the burning particle was fixed on a W-Re thermocouple. The temperature evolution is shown in Fig. 4. The X-ray diffraction analysis has shown that nanoparticle phase composition is 70% anatase, 30% rutile. The TEM data showed that nucleation of TiO<sub>2</sub> oxide vapor starts at the distance of 15 nm from the burning surface (for maternal particle of diameter 300 nm). The critical supersaturation was evaluated  $S = 3.5$ . The video observations have shown that the combustion follows via a series of bursts (Fig. 5). The maternal particle bursts to primary fragments later the primary fragments burst to secondary ones and so on. The element analysis of the maternal particle (being quenched in alcohol) with the SEM/ED-Integrated Analysis System showed that both oxygen and nitrogen dissolve in the burning liquid particle. The average composition before the primary particle burst was 60 at. % of oxygen and a few percent on nitrogen. A simple model was analysed assuming that the reason for bursts lies in the crystal TiO<sub>2</sub> shell formation followed by the nitrogen release inside and the droplet inner pressure increase as a consequence. Estimating the dispersion energy for the droplet as a sum of the debris kinetic energy and surface energy increase due to the newly formed surface we get the inner breaking pressure  $P_{inn} = 1.7 \cdot 10^5$  Pa which corresponds to the concentration

nitrogen dissolved in the liquid droplet to be about 8 at. %.

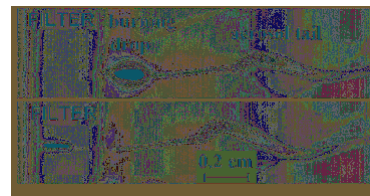


Fig. 1. Two consecutive frames (negatives) of the burning Ti droplet in the 90° scattered light. The droplet diameter is 200 μm. Frame frequency is 1 kHz, frame duration is 0.9 ms. The left side of the frame is filtered to avoid the droplet self-radiation (to measure the droplet diameter)



Fig. 2. Optical microscope image of a deposit formed at the surface due to the impact of burning Ti droplet at small angle. The diameter of maternal droplet is 330 μm.

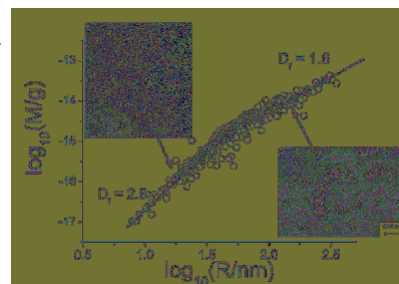


Fig. 3. Aggregate mass vs. radius. TEM images illustrating the morphology of small and large aggregates are inserted.

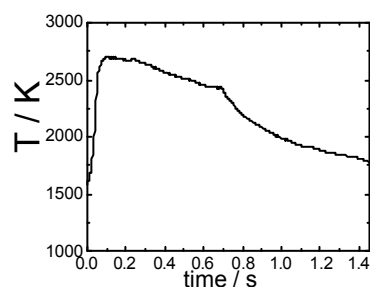


Fig. 4. Temperature evolution of maternal burning particle (with diameter of 600 μm)

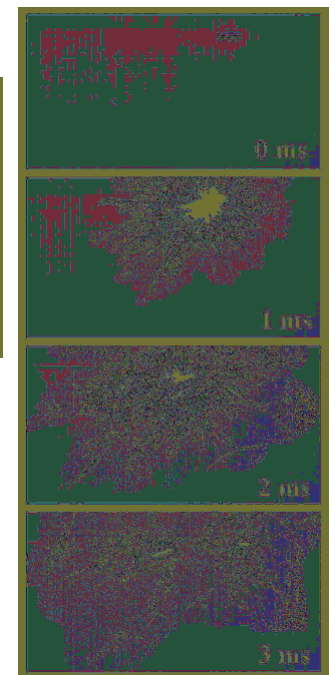


Fig. 5. Consequence of frames illustrating the burst at the last stage of combustion of Ti droplet. The droplet initial diameter is 200 μm, frame duration 0.9 ms. The initial time for each frame is shown in the figure.

Financial support for this work was provided by RFBR 05-03-90576-NSC a, grant of SD RAS No 78, NSC Taiwan-RFBR No. 94WFA0600016 Contract No. RP05E15.

## Characterisation of aerosols formed in high temperature experiments

A. Pintér Csordás<sup>1</sup>, P. Windberg<sup>1</sup>, I. Nagy<sup>1</sup>, Z. Hózer<sup>1</sup>, L. Matus<sup>1</sup>, M. Steinbrück<sup>2</sup> and J. Stuckert<sup>2</sup>

<sup>1</sup>Department of Fuel and Reactor Materials, HAS KFKI AEKI, 1121, Budapest, Hungary

<sup>2</sup>Forschungszentrum Karlsruhe, Institute für Materialforschung, Postfach 3640, 76021 Karlsruhe, Germany

Keywords: aerosol characterisation, aerosol chemistry, electron microscopy, particle characterisation, mass spectrometry.

Aerosols were formed in two QUENCH experiments (No. 10 and 11) performed in the Forschungszentrum Karlsruhe (Steinbrück et al., 2006) in frame of the LACOMERA project to simulate the main phases of a spent fuel pool accident. Twenty fuel rod simulators were heated by 6 mm diameter tungsten heaters installed in the rod centre and surrounded by annular ZrO<sub>2</sub> pellets to simulate fuel pellets. QUENCH-10 had the following steps: pre-oxidation in steam, air ingress period and final water quenching. In QUENCH-11 the water-filled bundle was boiled-off and subsequently flooded with a low water injection rate from the bottom.

Aerosols were collected by means of an integral collector (Ni plate with a pocket attached to its bottom) and by ten-stages impactor systems (Hózer, Z. et al., 2003), working in the most important steps of the experiments. The maximum temperature at aerosol sampling was 1632 °C in QUENCH-10 and 2024 °C in QUENCH-11. Mass change of the impactor plates and the Ni collector was measured. Morphological features (shape and size) were studied by SEM (Pintér-Csordás et al., 2000). EDX was applied for elemental analysis of aerosol particles and aggregates, while mass spectrometry (spark source and laser ionisation) was used for the chemical analysis of the aerosol settled on the quartz fibre filters (part of the impactor systems) and on the Ni plate.

Aerosol particles and aggregates were settled on each impactor plate, however the coverage of them was different and it was in correlation with the mass change of the collector plates. The amount of the collected aerosol was 5 % higher for QUENCH-10 than for QUENCH-11 and the weight of the powder settled in the pocket was ten times more in QUENCH-10. The highest amounts of aerosol and therefore the highest mass change were found for samples taken at the cooling stages of the experiments. The size of the individual aerosol particles was between a few tenth of µm and a few µm by SEM. Figure 1 shows two SEM images taken for the Ni plates.

In the aerosols of QUENCH-10 Zr, Sn and the elements of the steel components and some impurities were found. In the aerosols of the QUENCH-11 experiment, mostly W, Ta and Mo, further elements of the steel components and some

impurities were detected. These elements were originated from some structural materials such as heating rod, case of the thermometers, etc. Ten times more Zr was detected by SSMS in the pocket used in QUENCH-10 than in QUENCH-11. This can be due to the larger degree of cladding oxidation in QUENCH-10. In QUENCH-11 oxidation of the heating rods and some structural materials were more pronounced, therefore W, Mo, Sn and steel components were detected on the Ni plate by LIMS. All these results together with the data collected during the two experiments will be used for later model calculations.

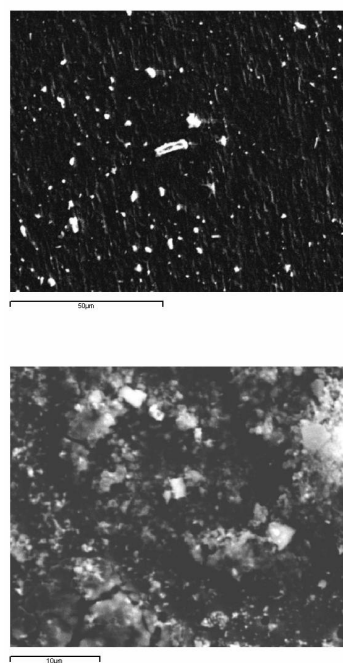


Figure 1. SEM images of the Ni plates applied in QUENCH-10 and -11, respectively.

Steinbrück, M. et al. (2006). *Nuclear Engineering and Design*, 236, 1709-1719.

Hózer, Z. et al. (2003). *Nuclear Technology*, 141, 244-256.

Pintér-Csordás, A. et al. (2000). *Journal of Nuclear Materials*, 282, 205-215.

## Behaviors of Polycyclic Aromatic Hydrocarbons during Vitrification in a Coke Bed Furnace

Y.M. Kuo<sup>1</sup>, C.H. Tsai<sup>2</sup> and C.T. Wang<sup>1</sup>

<sup>1</sup>Department of Safety Health and Environmental Engineering, Chung Hwa University of Medical Technology, Rende Shiang, 71703, Tainan County, Taiwan ROC.

<sup>2</sup>Department of Chemical and Material Engineering, National Kaohsiung University of Applied Sciences, Kaohsiung, Taiwan, ROC.

Keywords: PAHs; Coke bed furnace; Slag; Ash; Melting.

Incinerator ashes pose a particular environmental threat of dioxins and hazardous metals release. Direct landfilling has been identified as an inappropriate solution especially in long-term considerations. Recent research has shown that ash carries 80 to 90% of the total dioxins emission (Abe et al., 1997). Melting process can lead to a volume reduction (Kinto, 1996), a destruction of > 98% of dioxins (Ito, 1996), and metal can be separated for smelting by phase separation (Ecke et al., 2000). The mobility of hazardous metals in slag is also drastically reduced (Ecke et al., 2001). Therefore, the benefit is quite conspicuous if the ash melting process could be implemented extensively. Some polycyclic aromatic hydrocarbons (PAHs), well known for the carcinogenicity or DNA genotoxicity (Schoket, 1999), and indispensable contributors in de novo synthesis on fly ash (Wilhelm et al., 2001), deserve further investigation.

Fate of PAHs during the vitrification of ashes from the municipal waste incinerator in a coke bed furnace was investigated in this study. Twenty-one individual PAHs were divided into three categories: Low Molecular PAHs (LM-PAHs, 2~3-ring), Median Molecular PAHs (MM-PAHs, 4-ring) and High Molecular PAHs (HM-PAHs, 5~7-ring). In this system, both coke and lime were added to enhance the melting reaction. Figure 1a and 1b show the fractions of individual PAH input-mass and output-mass distributions. The major PAH sources were ash and coke, which respectively contributed 97 and 3% of PAHs in the input-mass. The percentage of total PAHs in ash, coke and lime averaged 97, 3 and < 0.1%. Among the total 21 PAHs, > 99% existed in flue gas, and < 1% of those were encapsulated in slag. The LM-, MM- and HM-PAHs had > 99, > 99 and 84% of their mass discharged by the flue gas, respectively, while < 1, < 1 and 16% of those were discharged from slag, respectively.

Figure 2 shows the O/I (output-mass/input-mass) ratio of LM-, MM- and HM-PAHs were 0.063, 0.002 and <0.001, respectively. The high distribution in flue gas and O/I ratio of LM-PAHs is reasonable since they are more easily evaporated, hence difficult to be removed by air pollution control devices. On the contrary, the HM-PAHs, having lower vapor pressure, primarily stays mainly in slag. Based on the 21 total PAH content in feeding ash and slag, the reduction efficiency of the coke bed furnace was

>99.9%. To minimize the secondary pollution, the efficiency of coke bed furnace should be improved to reduce the PAH emission into ambient air.

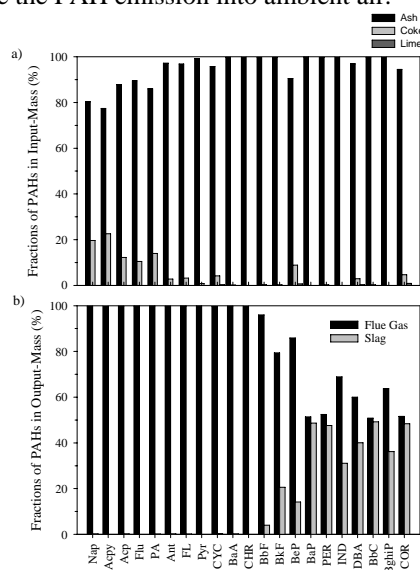


Figure 1. Fractions of PAHs in input-mass (a) and output-mass (b)

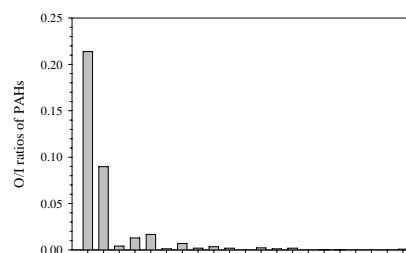


Fig. 2. O/I ratios of individual PAHs

- Abe, S., Kanbayashi, F., & Okada, M., (1996). *Waste Management*, 16, 431-443.
- Ecke, E., Sakanakura, H., Matsuto, T., Tanaka, N., & Lagerkvist, A. (2000). *Waste Management Research*, 18, 41-51.
- Ecke, H., Sakanakura, H., Matsuto, T., Tanaka, N., & Lagerkvist, A. (2001). *Environmental Science & Technology*, 35, 1531-1536.
- Ito, T. (1996). *Waste Management*, 16, 453-460.
- Kinto, K. (1996). *Waste Management*, 16, 423-430.
- Wilhelm, J., Stieglitz, L., Dinjus, E., & Will, R. (2001). *Chemosphere*, 42, 792-802.

## Aerosol synthesis as a route to metallic Ni-Mo alloys with enhanced mechanical properties

E. K. Athanassiou, R. N. Grass and W. J. Stark

<sup>1</sup>Department of Chemistry and Applied Biosciences, ETH Zurich, Wolfgang-Pauli-Strasse 10, 8093, Zurich, CH

Keywords: hastelloy, reducing flame synthesis, nanocrystalline material, enhanced Vickers hardness

Nanocrystalline metals and alloys have attracted considerable interest due to their exceptional electric, magnetic and mechanical properties (Gleiter, 1989). Among them nickel-molybdenum alloys, known as superalloys have triggered a wealth of research since they exhibit improved material strength, wear, shock and corrosion resistance. Therefore, they are widely used as coatings resulting in components with advanced service life and high temperature performances. Currently, such alloys are hard to synthesize at larger scales, so that their beneficial properties are only accessible to material science laboratories. Flame based processes have been established as an industrial scalable process for the manufacture of metal oxides. The recent extension of the process and the discovery of reducing flame synthesis expanded the range of accessible materials to nanocrystalline metal and metallic alloy nanoparticles (Grass and Stark, 2006; Grass et al., 2007).

Here we present the large-scale formation of nanocrystalline nickel-molybdenum alloy by reducing flame synthesis (Athanassiou et al., 2007). The nanoparticles were synthesized at production rates of about 40 g h<sup>-1</sup> exhibiting a highly air stability and a uniform particle size distribution compared to commercially applied materials (Figure 1). Thermogravimetric analysis showed that the metallic nanoparticles were covered by an amorphous oxide layer of about 5 nm protecting them from further oxidation and resulting in a total metal content of about 88 wt%.

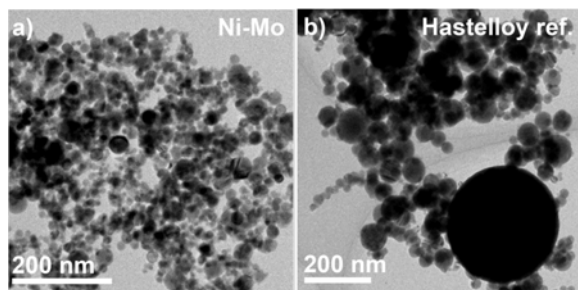


Figure 1. Electron microscopy images of Ni-Mo alloys produced by reducing flame synthesis (a) and commercially available, plasma-synthesized hastelloy.

However incorporation of the nickel, molybdenum liquids precursors with additional metals such as aluminium and chromium showed the limitations of the current flame process as the oxidized form of these metals was formed without having any further effect on the formation of the Ni-Mo alloy. Basic thermodynamic calculations verified the experimental results.

Further compression of the as prepared nanoalloy to pills and further sintered under reduced conditions resulted in a nanocrystalline material with a characteristic metallic gloss and Vickers hardness of 760-800 HV. The enhanced hardness properties could be attributed to the high density of twinning effects and twin boundaries (Figure 2).

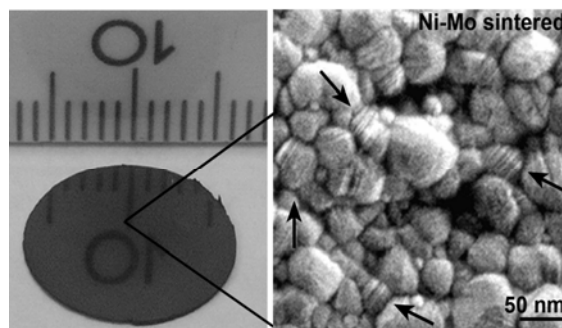


Figure 2. Compaction and sintering of the as prepared powder resulted to pills with characteristic metallic gloss and hardness properties. The advanced hardness properties may be associated to the high density of twins.

These results suggest the use of reducing flame synthesis for the fabrication of certain alloy materials at large scale production and show the application of these nanoparticles for the production of nanocrystalline materials with enhanced hardness properties.

### References

- Gleiter, A. H., Rosen, A., Karch, J., & Gleiter, H. (1989). *Scripta Metall.*, 23, 1679-1683.
- Grass, R. N., & Stark, W. J. (2006). *J. Mater. Chem.*, 16, 1825-1830.
- Grass, R.N., Dietiker, M., Spolenak, R., & Stark, W. J. (2007). *Nanotechnology*, 18, 035703.
- Athanassiou, E. K., Grass, R.N., & Stark, W. J. manuscript in preparation

## identification of byproduct species for destructing sulfur hexafluoride using a high-temperature plasma torch

Cheng-Hsien Tsai<sup>1</sup>, Hao-Hi Kuo<sup>1</sup>, Yuan-Chung Lin<sup>2</sup> and Kuan-Chuan Fang<sup>3</sup>

<sup>1</sup>Department of Chemical and Material Engineering, National Kaohsiung University of Applied Sciences, Kaohsiung 807, Taiwan.

<sup>2</sup>Department of Mechanical Science and Engineering, University of Illinois at Urbana-Champaign, IL 61801, USA.

<sup>3</sup>Department of Mechanical Engineering, National Cheng Kung University, Tainan 701, Taiwan.

Keywords: plasma, air pollution, generation of combustion aerosol, high temperature aerosols, sulphur particles.

Sulfur hexafluoride (SF<sub>6</sub>) is commonly used as an etching or etching-aid gas in fabricating the submicrometer features of modern integrated circuits. However, SF<sub>6</sub> has an extremely long atmospheric lifetime with a high global warming potential, abatement of SF<sub>6</sub> is needed to reduce the emissions. In this study, different additives were used to elevate the SF<sub>6</sub> conversion using a high-temperature microwave plasma torch. Moreover, the species of toxic byproducts were detected for further developing the treatment approach of the problem that caused by sequent secondary pollution.

The pulsed microwave plasma system is assembled by a commercially available magnetron (Toshiba 2M130, 2.45 GHz) with maximum stationary power of 2 kW. A quartz tube and an antenna are intersected the waveguide and the resonator perpendicularly. The composition of the byproducts were identified and quantified by an on-line Fourier transform infrared spectrometer and a residual gas analyzer equipped with a quadrupole Mass Spectrometer (Figure 1).

The experimental conditions are as follows: inlet molar fraction of SF<sub>6</sub> was 2000 ppm three inlet additive/reactant molar ratios were: H<sub>2</sub>/SF<sub>6</sub> 5/1, O<sub>2</sub>/SF<sub>6</sub> 5/1, and H<sub>2</sub>/O<sub>2</sub>/SF<sub>6</sub> 5/5/1 with N<sub>2</sub> as the balanced gas, system pressure was operated at 700 torr (93.1 kPa) applied MW power was set at 1.2 kW temperature of the feed was at room temperature and total flow rate was fixed at 20 slpm (standard liter/min).

The results showed that SF<sub>6</sub> conversion reached 43.4%, 36.4%, and 33.5% for adding H<sub>2</sub>/O<sub>2</sub>, H<sub>2</sub>, and O<sub>2</sub> as the additive, respectively, to be much higher than without additive condition (conversion 18.6%). The identification of byproducts revealed that the dominant byproduct was fluorine (F<sub>2</sub>) regardless of which additive was supplied. F<sub>2</sub> should be formed mainly at the afterglow discharge zone via the recombination reaction (F + F → F<sub>2</sub>) of F atoms that yielded via the electron impact dissociation or penning dissociation of SF<sub>6</sub>. Edelson & Flamm, 1984. In addition, SF<sub>x</sub> radicals reacted with S atoms, O atoms, H atoms, and OH radicals to form mainly SO<sub>2</sub>, sulfur aerosols St-Onge et al., 1995, and

SO<sub>2</sub>F<sub>2</sub> when added H<sub>2</sub>/O<sub>2</sub>, H<sub>2</sub>, and O<sub>2</sub> into the mixtures, respectively (Table 1).

In addition, minor and trace amount of byproducts were also measured for adding H<sub>2</sub> and O<sub>2</sub> (to yield sulfur depositions, HF, and NO<sub>x</sub>), H<sub>2</sub> (only formed HF), and O<sub>2</sub> (to produce sulfur oxyfluorides, such as SOF<sub>2</sub> and SOF<sub>4</sub>, sulfur deposition, SO<sub>2</sub>, and NO<sub>x</sub>) (Table 1).

The simultaneous addition of H<sub>2</sub> and O<sub>2</sub> seemed to inhibit the generation of Sulfur oxyfluorides (such as SO<sub>2</sub>F<sub>2</sub>, SOF<sub>2</sub>, and SOF<sub>4</sub>), and yield fewer HF than only adding H<sub>2</sub> by producing abundant SO<sub>2</sub> with trace amount of sulfur depositions. Hence, to simultaneously add H<sub>2</sub> and O<sub>2</sub> into SF<sub>6</sub>/N<sub>2</sub> mixtures not only enhanced the SF<sub>6</sub> conversion, but also produced fewer toxic byproducts.

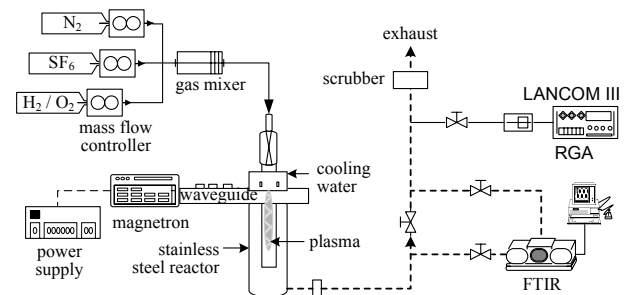


Figure 1. Experimental apparatus

Table 1. Byproducts of SF<sub>6</sub> abatement for adding various additives

byproducts	additive		
	H <sub>2</sub> and O <sub>2</sub>	H <sub>2</sub>	O <sub>2</sub>
Major	F <sub>2</sub> SO <sub>2</sub>	F <sub>2</sub> Sulfur	F <sub>2</sub> SO <sub>2</sub> F <sub>2</sub>
Minor or trace	Sulfur HF NO <sub>x</sub> H <sub>2</sub> O	HF	SOF <sub>2</sub> Sulfur SOF <sub>4</sub> SO <sub>2</sub> NO <sub>x</sub>

Edelson, D., Flamm, D. (1984). *J. Appl. Phys.*, 56, 1522-1531.

St-Onge, J., Sadeghi, N., Booth, J. P., Barbeau, C. (1995). *J. Appl. Phys.*, 78, 6957-6966.

## Zinc aerosols from steelmaking EAF: morphology and growth.

García E.<sup>1,2</sup>, Lopez Biain I<sup>3</sup>, Astarloa S<sup>2</sup>., Legarreta J.A.<sup>1</sup> and C. Gutiérrez-Cañas.<sup>1</sup>

<sup>1</sup> University of the Basque Country, Alameda de Urquijo s/n, 48013, Bilbao, Spain

<sup>2</sup> AIRg María Díaz de Haro, 48920, Portugalete, Spain

<sup>3</sup>ACB, Arcelor, Sestao, Spain

**Keywords:** high-T aerosols, air pollution, submicron particles

Controlling the emission of zinc from electric arc furnaces poses a challenge, either in terms of compliance or of filter performance. This aerosol occurs significantly within the penetration window of control devices (Flagan and Seinfeld, 1988). This could be compensated through the enhancement of other removal mechanisms, such as the use of adsorbents or the scavenging onto coarse particles coflowing with the Zn-rich fine fraction (Friedlander *et al.* 1991). The potential improvement -an engineered modification of inlet size distribution at the control device- should be carefully considered (Owens *et al.*, 1996; Linak *et al.*, 1993).

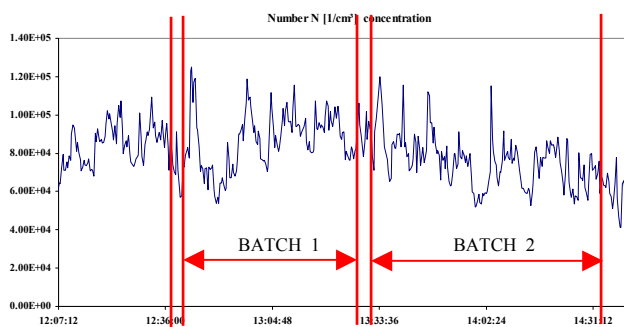


Figure 1 Dynamics of a full-scale furnace (70 t steel/batch) number concentration along 2 batches.

Zinc aerosol formation, speciation and growth is strongly linked to the furnace dynamics (Charging; Melting; O<sub>2</sub> refining and Liquid steel casting) and cooling rate upstream the filter. Precursors are related to volatilization and bursting of CO bubbles inside the furnace. Morphology derivation and evolution of ZnO along a duct under a non-constant cooling rate lead to a high variety of morphologies (porous, nanowires-nanorods, flower-like bundles), Figs 2 and 3 with different surface properties.

This work is the preliminary characterization of the variety and relative abundance of Zn-rich particles arising from a 70t steel/batch furnace, as the first step to control the size distribution of the aerosol along the line (upstream the filter). Theoretical basis to assess the intercoagulation on coarse particles is provided by (Lee and Wu, 2005; Whitby and McMurry, 1997). The experimental method is described elsewhere (García *et al.*, 2006) and uses near real-time aerosol size analyzers, and cascade impactors as size-resolved sample pre-separators for further analysis (chemical and morphological).

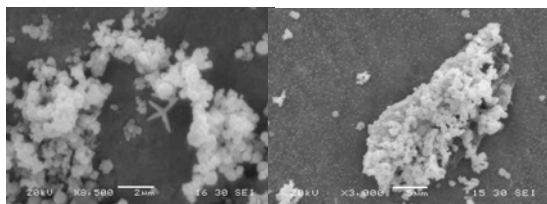


Figure 2 (left) ZnO tetrapod, formed during the very early stages. (See Zhang *et al.*, 2005 for similar structures). (Right) Scavenged Zn rich-particles over a coarse slag fragment after a medium residence time and a severe cooling (from 1800 to 60 °C).

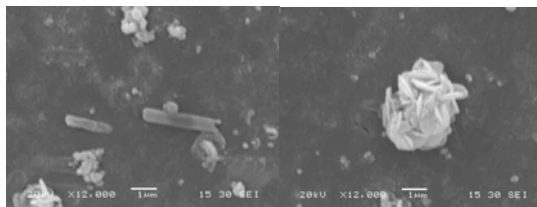


Figure 3. The influence of T-t history: (left) ZnO nanorods and (right) Zn-rich flower-like structure.

### Conclusions

Size-resolved emissions and zinc-rich fractions have been identified for different process conditions, as well as the most relevant operation parameters. The distribution of the Zn-aerosol entering to the filtration unit could significantly vary under slightly differences on process operation. The control of T-t history along the process line, as well as the injection of specific inorganic sorbents have been identified as the most promising measures to prevent this emissions.

### References

- Flagan R. and Seinfeld J., (1988), *Fundamentals of Air Pollution Engineering*, Prentice Hall, p 433-471
- Friedlander S.K., Koch W. and Main H.H. (1991), *J. Aerosol Sci.*, 22:1-8
- García E., Meléndez A., Peña E, Larrión M., Legarreta J.A., and Gutiérrez-Cañas C., Fine PM formation dynamics in three discontinuously operated ferrous foundry furnaces, *aaas (Adv. Atmos. Aerosol Symp.)*, Milan, November 2006
- Lee S.R. and Wu C.Y., (2005), *Aerosol Sci. Technol.* 39:358-370
- Linak, W. P.; Wendt, J. O. L., *Prog. Energy Combust. Sci.* **1993**, 19, 145.
- Owens T. and Biswas P., (1996), *Ind. Eng. Chem. Res.*, 35: 792-798
- Whitby E.R. and McMurry P.H., (1997), *Aerosol Sci. Technol.* 27(6), 673-688
- Zhang J. *et al.*, *J. Crystal Growth* (2005) 280, 509-515

## Measurements of high temperature particle charge

K. Reuter-Hack<sup>1</sup>, J. Meyer<sup>1</sup>, A. P. Weber<sup>2</sup> and G. Kasper<sup>1</sup>

<sup>1</sup> Institute for Mechanical Process Engineering and Applied Mechanics, University of Karlsruhe, Straße am Forum 8, 76131 Karlsruhe, Germany,

<sup>2</sup>Institute of Mechanical Process Engineering, Technical University of Clausthal, Leibnizstrasse 19, 33678 Clausthal, Germany

Keywords: High temperature aerosols, charged particles, charge measurement, electrical effects, ions.

### Introduction

Due to thermal emission of electrons, aerosol particles can acquire extreme high charge levels, if exposed to high temperatures (Schiel et al., 2002). However, due to fast recombination kinetics the real charge of the particles can hardly be deduced from low temperature measurements. Therefore, new techniques were employed to either measure in situ the particle charge at high temperature or to effectively quench charge recombination.

### Experimental

In a lab-scale experimental setup a size selected aerosol (for instance platinum particles in air) is fed to a  $\text{Al}_2\text{O}_3$ -tube in a vertical furnace with a working temperature up to  $1600^\circ\text{C}$ . After the furnace (at temperatures up to  $800^\circ\text{C}$ ) an electrode zone is located (Fig. 1), where an adjustable AC field perpendicular to the gas flow was applied, to selectively remove the gas ions (but not the particles) to avoid recombination during the cooling of the gas as far as possible. With this technique the resulting particle charge depends on the field strength that is applied to enable its measurement. After cooling, the mean particle charge is measured directly with a combination of CPC and FCE.

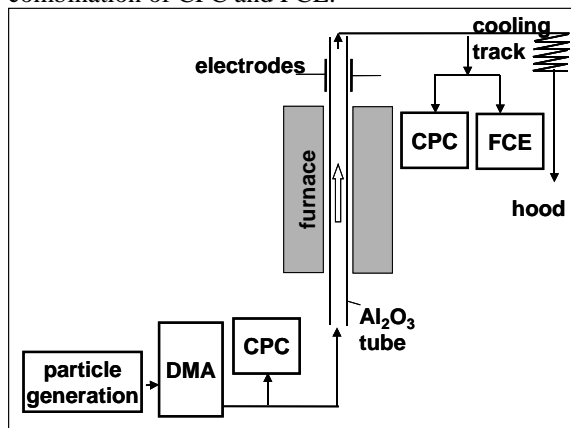


Figure 1. Experimental set-up to measure the particle charge after cooling by avoiding recombination processes.

Alternatively, the high temperature charge state was quenched by a sudden expansion of the gas through a critical orifice. After stripping the ions in a weak electric field, the particle charge was measured by an FCE. Additionally, in the particle free case, the ion concentration in the gas for different gases was determined, showing significant differences.

### Results and discussion

For air as carrier gas, at furnace temperatures higher than  $800^\circ\text{C}$  the mean particle charge was negative, as reported in case of gold particles by Magnusson et al., (1999). This is shown in Fig. 2 for platinum particles at a furnace temperature of  $1100^\circ\text{C}$ . This result can only be explained by an additional source of negative charges besides the particles.

This assumption is corroborated by the fact, that applying an external AC field in the electrode zone shifts the mean particle charge to even more negative values (not shown here). If the gasborne particles were the only origin of electrons, (and subsequently formed negative gas ions) the mean particle charge would be positive, and a removal of the gas ions would reduce the recombination yielding even higher positive mean particle charges.

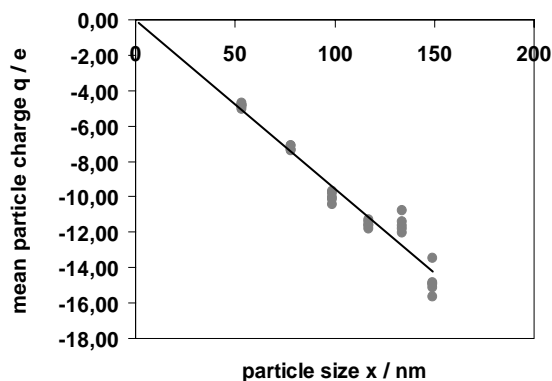


Figure 2. Dependence of the particle charge on the particle size (material: Platinum, furnace temperature  $1100^\circ\text{C}$ ).

Electron emission from the tube walls probably results in diffusion charging of the particles (Hinds, 1999), producing negative particle charges that increases linearly with the particle size as shown in Figure 2.

This work was supported by the DFG as research project We2331/3-3.

Magnusson, M. H., Deppert, K., Malm, J.-O., Bovin, J.-O., & L. Samuelson (1999) *J. Nanoparticle Res.*, 1, 243-251

Hinds, W. C. (1999) *Aerosol Technology*, Wiley Interscience Publication, New York (1999)

A. Schiel, A. P. Weber, G. Kasper, H.-J. Schmid (2002) *Part. Part. Syst. Charact.* 19, 410-418

## **T17 Abstracts**

## Characterization of aerosol emitted by impact of millimetric droplets onto a liquid film

C. Motzkus<sup>1,2</sup>, E. Gehin<sup>2</sup> and F. Gensdarmes<sup>1</sup>

<sup>1</sup>Institut de Radioprotection et de Sûreté Nucléaire/Service d'Etudes et de Recherches en Aérodispersion des polluants et en Confinement, B.P 68, 91192, Gif-sur-Yvette Cedex, France.

<sup>2</sup>Centre d'Etudes et de Recherches en Thermique, Environnement et Système, Université Paris XII, 61 av. du Général de Gaulle, 94010, Créteil Cedex, France.

Keywords : impact, droplet, airborne, resuspension

A liquid droplet impinging onto a liquid film is of both fundamental interest and practical importance to determine the potential sources of contamination in the case of scenarios of liquid falls such as dripping. During the impaction of droplets, three phenomena can occur: deposition, rebound or splash. The key parameters of these phenomena are the characteristics of the droplets (diameter  $d_i$ , velocity  $V_i$ , density  $\rho$ , viscosity  $\mu$  and surface tension  $\sigma$  of the liquid) and the thickness  $h_{\text{film}}$  of the liquid film. Cossali *et al.* (1997) and Vander Wal *et al.* (2006) have determined qualitatively the deposition/splash threshold for the impact of millimetric droplets as function of dimensionless numbers (Reynolds, Weber, Ohnesorge and the film parameter  $S_f = h_{\text{film}}/d_i$ ) by the visualization of droplets emitted larger than 50  $\mu\text{m}$ . The water droplets emitted with a diameter ( $d_e$ ) smaller than 50  $\mu\text{m}$  evaporate rapidly. If these droplets contain some solute, they give rise to dry airborne residues. The objectives of our work are to study experimentally the emission of airborne particles during the impaction of droplets onto a liquid film and to examine the relevance of existing relations to determine the presence or not of airborne particles.

The method used to measure the mass of airborne particles with a tracer (sodium fluorescein) and to observe the “deposition” and “splash” phenomena are detailed by Motzkus *et al.* (2006). We measure the mass and the size distribution of the dry residues produced during the impact of droplets onto a liquid film, whose thickness is maintained constant, with a drip frequency of 0.4 droplet/s during 60 min, in a ventilated closed vessel. The size distribution of dry residues is measured with an Aerodynamic Particle Sizer. When the splash is observed, we prove the presence of the dry residues stemming from the evaporation of droplets smaller than 50  $\mu\text{m}$ . Figure 1 represents the count distribution of dry residues produced by impact of a 4 mm-diameter droplet with  $V_i = 3.7 \text{ m}\cdot\text{s}^{-1}$  and  $S_f = 0.3$ .

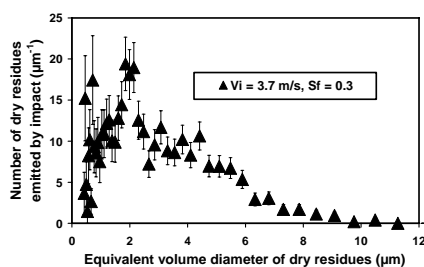


Figure 1. Count distribution of emitted dry residues

The diameters of emitted droplets are calculated from the residues diameters by using the concentration of the tracer (10 g/l). We study the influence of different parameters  $V_i$  (2.2, 3.1 and 3.7  $\text{m}\cdot\text{s}^{-1}$ ),  $d_i$  (2 and 4 mm),  $S_f$  (0.3, 0.6 and 1) and  $\sigma$  (66  $\text{mN}\cdot\text{m}^{-1}$ ) on the emission of droplets. We take into account the losses of particles by sedimentation to calculate the number of droplets produced by impact. Figure 2 represents the count distributions of droplets produced by impact of a 4 mm-diameter droplet with different parameter of  $V_i$  and  $S_f$ . These results show that the increase of  $V_i$  or the decrease of  $S_f$  involve an augmentation of the number of droplets emitted by impact in the range 2-50  $\mu\text{m}$ .

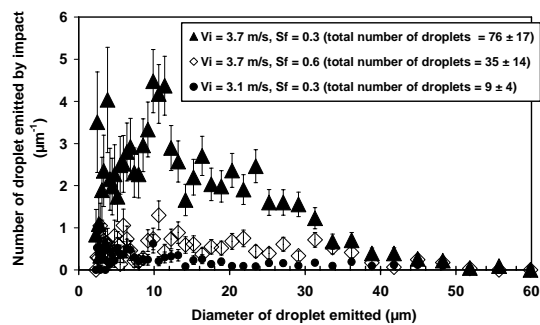


Figure 2. Count distributions of emitted droplets

Moreover, by comparing our visualizations with threshold relations, we note that the one of Vander Wal *et al.* (2006) describes correctly the threshold for small Ohnesorge numbers ( $< 3 \cdot 10^{-3}$ ) in contrary to the one of Cossali *et al.* (1997) that describes correctly the threshold for high Ohnesorge numbers ( $> 3 \cdot 10^{-3}$ ).

Cossali, G.E., Coghe, A. and Marengo, M. (1997).

The impact of a single drop on a wetted solid surface. *Exp. Fluids*, 22, 463-473.

Vander Wal, R.L., Berger, G.M. and Mozes, S.D. (2006) The splash/non-splash boundary upon a dry surface and thin fluid film. *Exp Fluids*, 40, 53-59.

Motzkus, C., Gehin, E. et Gensdarmes, F. (2006) Study of aerosol production by normal impaction of millimetric droplets onto a liquid film. *Proceeding of the Seventh International Aerosol Conference*, 834-835.

## FOG FORMATION DURING HYDROGEN BROMIDE ABSORPTION IN FLUE GAS CLEANING PROCESSES

A. Wix<sup>1</sup>, S. Sinanis<sup>1</sup> and K. Schaber<sup>1</sup>

<sup>1</sup> Institut für Technische Thermodynamik und Kältetechnik, Universität Karlsruhe (TH), Engler-Bunte-Ring 21, 76131 Karlsruhe, Deutschland

Keywords: aerosol formation, aerosol modelling, hydrogen bromide, absorption

Aerosol formation in flue gas cleaning processes is an undesired phenomenon due to the potential exceeding of emission limits or operational problems in downstream operation units.

In gas-liquid contact devices utilized for flue gas cleaning (e.g. absorbers, quench coolers) aerosols can be formed by spontaneous phase transitions in supersaturated gas-vapour mixtures. The supersaturation during the absorption of hydrogen bromide is induced by simultaneous heat and mass transfer processes and also it is additionally favoured by the phase equilibrium of the acid-water system which exhibits a strong azeotropic behaviour. Experimental and theoretical results of the aerosol characteristics (i.e. droplet diameter, number concentration) are presented.

The experimental investigations were carried out in a two-stage pilot plant (Fig. 1) where typical operating conditions of industrial gas cleaning equipment can be simulated (Gretschner et. al., 1999).

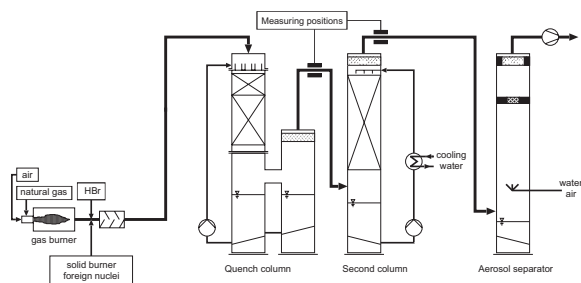


Figure 1. Process flow sheet of the pilot plant.

The flue gas (volume flux  $\sim 200 \text{ m}_N^3/\text{h}$ ) is generated from the burning of natural gas and enters the first column which is operated as co-current absorption stage with a temperature of  $200^\circ\text{C}$ . It is cooled down to the adiabatic saturation temperature, which is approximately  $45^\circ\text{C}$  at the given operating conditions. For the characterization of the aerosol (mean diameter and number concentration) only optical in situ methods can be used because the equilibrium between the droplets and the gas phase must not be disturbed. For this reason the Three-Wavelength-Extinction-Method (3WEM) is used. It can be applied to the characterization of aerosols with droplet diameters from  $500\text{nm}$  to  $3\mu\text{m}$  for non absorbing particles and droplet number

concentrations between  $10^4/\text{cm}^3$  and  $10^8/\text{cm}^3$ . The quench cooler is followed by a counter-current column with two possible operating modes. At first it can be used as a supplementary absorption column at adiabatic saturation temperature, secondly as a direct-contact cooler with recooled scrubbing water. In this mode it can be cooled externally thus acting as a direct condenser for the enlargement of the droplets in case they are too small for the characterization after the quench column. With the experimental setup hydrogen bromide concentrations in the raw gas from  $100 \text{ mg}/\text{m}_N^3$  to  $500 \text{ mg}/\text{m}_N^3$  can be realised.

The theoretical results were obtained with the simulation programme AerCoDe which was developed for the calculation of aerosol formation by spontaneous phase transitions in multi-component multi phase flows (Ehrig et. al., 2002). The modelling is based on three different control volumes (gas phase, liquid phase and aerosol), for which unsteady, differential total mass, component mass and energy balances were set up. With AerCoDe, heterogeneous nucleation as well as homogeneous nucleation can be calculated. By comparison of theory and experiment, it has been proven useful that when heterogeneous nucleation takes place a monodisperse description of the droplet size distribution is adequate.

The experimental results show that the fog is formed in the first stage of the pilot plant. The droplets are too small for characterization after the quench column and thus the direct contact cooler is used to enlarge the droplets. After the second column the droplet diameters are about  $1\mu\text{m}$  and the number concentration reaches up to  $10^6/\text{cm}^3$ .

The theoretical results show that the gas phase reaches noticeable supersaturations of up to 1.4 in the quench column, even for low hydrogen bromide concentrations in the raw gas.

The presentation will give a survey of the experimental and theoretical results on fog formation during absorption of hydrogen bromide and compare it to the absorption of other acid pollutants.

Gretschner, H., Schaber, K. (1999). Chemical Engineering and Processing, 38, 541-548  
 Ehrig, R., Ofenloch, O., Schaber, K., Deuffhard, P. (2002). Chemical Engineering Science, 57, 1151-1163

## Effect of Wastewater/Heavy Oil Emulsified fuel on the Emissions of Polycyclic Aromatic Hydrocarbons from the industrial boiler

Chung-Chi Chen<sup>1,2\*</sup>, Wen-Jhy Lee<sup>1,2</sup>, Oliver J. Hao,<sup>3</sup>

<sup>1</sup> Department of Environmental Engineering, National Cheng Kung University  
NO.1, University Rd, Tainan 70101, Taiwan, ROC

<sup>2</sup> Sustainable Environment Research Center, National Cheng Kung University  
NO.1, University Rd, Tainan 70101, Taiwan, ROC

<sup>3</sup> Department of Civil and Environmental Engineering, University of Maryland, College Park, MD 20742, USA

Keywords: emulsified fuel, boiler, PAHs.

The wastewater containing high-concentration organic compounds always caused treatment difficulty in the process. This study demonstrated that the wastewater from the wet scrubber of a waste oil vacuum/heating process can be used to produce the emulsified fuel for the industrial boiler. Heavy oil and wastewater (or water) are inherently immiscible and must be added surfactant to reduce the interfacial tension and increase the affinity among the three materials. In this study, the heavy oil, surfactant and water (or wastewater) were pumped into the mixing tank and mixed initially by mixer at 100 rpm and then was emulsified by a inline microemulsifier at 3600rpm. The fraction of surfactant was 0.1 wt% of total weight and main chemical compounds of the surfactant used in this study were described in our previous studies (Lin et al., 2006).

There are three test fuels used in this study: Pure heavy oil fuel (PHOF), water/oil emulsions Fuel (WOEF) (20% city tap-water +80% heavy oil) and wastewater/ heavy oil emulsions fuel (WWEF) (20% Wastewater + 80% heavy oil). Emissions of PAHs from industrial boiler by using the three different fuels, respectively, were measured. In the stack flue gases, PAHs samplings were adapted by the USEPA's sampling method 5 (MM5). The PAH contents were determined with a Hewlett-Packard (HP) gas chromatograph (GC) (HP 5890A; Hewlett-Packard, Wilmington, DE, USA), a mass selective detector (MSD) (HP 5972), and a computer workstation (Aspire C500; Acer, Taipei, Taiwan).

In the stack flue gases of boiler, when comparing with that of PHOF, the total PAH concentration was significantly reduced from  $451\mu\text{g Nm}^{-3}$  to 317 and  $283\mu\text{g Nm}^{-3}$  by using the WOEf and WwEf, respectively. Total BaP<sub>eq</sub> emission concentration in the boiler exhaust followed a similar tendency. The mean reduction fractions were 45.0% and 62.7% for WOEf and WwEf, respectively, compared with PHOF ( $5.04\mu\text{g Nm}^{-3}$ ). The addition of water in the form of emulsified fuel improved the combustion efficiency and resulted in the reduction of total PAH concentration in the stack flue gases.

Mean emission factors of PAHs from the stack flue gas of the boiler were 44.9, 39.7 and 38.1 mg/L by using PHOF, WOEf and WwEf, respectively. In the other word, being compared with that of PHOF, the mean PAHs emission factors were reduced to 88.4% and 84.9% by using WOEf and WwEf, respectively. The mean reduction fractions of total BaP<sub>eq</sub> (PHOF =  $501\mu\text{g/L}$ ) from the boiler exhaust were 31.9%, and 50.1% for WOEf and WwEf, respectively, compared with PHOF. A similar tendency in the mean reduction fraction of EF<sub>total-PAH</sub> and EF<sub>BaP<sub>eq</sub></sub> in ng/kJ can be presented. This was because the PAH content of water, wastewater, and the surfactant were close to zero and the combustion of emulsified fuel led to the micro-explosion, which improved the secondary atomization and resulted in a lower PAHs emission. Farfaletti et al found that the mean reduction fractions of total BaP<sub>eq</sub> emission from the exhaust of the heavy-duty engine were 14% and 39% for emulsions with up to 20% water and the Cerium-based additive, respectively. (Farfaletti et al., 2005) These results revealed that emulsified fuels with wastewater are a good way to decrease PAH emission from the stack flue gas of boiler.

The above results revealed that by using WwEf have the advantage of removing the organic compounds in the wastewater, improving combustion efficiency in the industrial boiler, and reducing the emissions of PAHs. It is a highly innovative and potential method for commercial application.

Lin, C. Y.; Wang, K. H. (2004), *Fuel*, 83, 507-515.

Lin Y. C., Lee W. J.; Chen C. C.; Chen C. B. (2006), *Environ. Sci. Technol.*, 40, 5553-5559.

Farfaletti A.; Astorga C.; Martini G.; Manfredi U.; Mueller A.; Rey M.; De Santi G.; Krasenbrink A.; Larsen B. R. (2005), *Environ. Sci. Technol.*, 39, 6792-6799.

## Wood dust particle size sampler: WODUSA

F.Belosi<sup>1</sup>, F.Prodi<sup>1,2</sup>, S. Agostini<sup>3</sup>, M. Casazza<sup>1</sup>, and L.Di Matteo<sup>1</sup>

<sup>1</sup>Institute for Atmospheric Science and Climate (ISAC-CNR), National Research Council, 40129, Bologna, Italy

<sup>2</sup>Physics Department, University of Ferrara, Italy,

<sup>3</sup>Bioikos Ambiente s.r.l., 40139, Bologna, Italy,

Keywords: aerosol instrumentation, particle size distribution, penetration, coarse particles, dust.

A knowledge of the size distribution of wood dust is of primary importance in order to estimate the behaviour of the personal samplers used to assess workers' exposure (Harper *et al.*, 2004; Sala *et al.*, 2002). WODUSA, WOOD DUST SAMPLER, allows the separation of particles into four fractions (< 30  $\mu\text{m}$ ; < 17  $\mu\text{m}$ ; < 10  $\mu\text{m}$  and < 3  $\mu\text{m}$  aerodynamic size). It consists of a vertical tunnel for sampling the particles from the environment. Inside the tunnel five nozzles, each connected to a specific inertial separator, sample the particles isokinetically. The inlet conditions of the tunnel (diameter and velocity) have been designed according to the Agarwal and Liu criteria (Agarwal *et al.*, 1980) for unit efficiency in calm air conditions. With a tunnel diameter of 35 cm and an inlet average velocity of 2 m/s, the criteria is respected up to 80  $\mu\text{m}$  aerodynamic size.

In the central nozzle (Fig. 1) particles are sampled directly onto a filter (quartz or glass fiber mats) to measure the total dust concentration inside the tunnel. The largest size fraction is obtained by means of a horizontal elutriator which is located outside the tunnel, and the particles are sent to the selector through a bend. The transmission efficiency of the elutriator-bend system has been theoretically designed (Mercer, 1973; Belosi *et al.*, 1984) and experimentally verified with glass spheres. The cut-size, defined as the aerodynamic diameter at 50% penetration, is 30  $\mu\text{m}$ . An inertial impactor provides the next size fraction. The impactor has been calibrated with PSL particles and the cut-off is 17  $\mu\text{m}$ . The last two fractions are obtained by means of two cyclones with penetration characteristics of 10  $\mu\text{m}$  and 3  $\mu\text{m}$ , respectively.

On the whole WODUSA requires five filters of the same size (47 mm diameter) to perform a complete scanning of wood dust particles. Since the sampling flow rate of each nozzle is set to 600 lph, the gravimetric assessment of the collected particle mass on the filters, also in relatively low environmental concentrations (less than 1  $\text{mg}/\text{m}^3$ ), can be determined after few sampling hours. WODUSA has been set up with the pneumatic components and the aspiration pump on a trolley (Fig.1). The results of preliminary samplings in wood factories show different cumulative size distributions, even though the environmental concentration is roughly the same (about 0.7  $\text{mg}/\text{m}^3$ ).

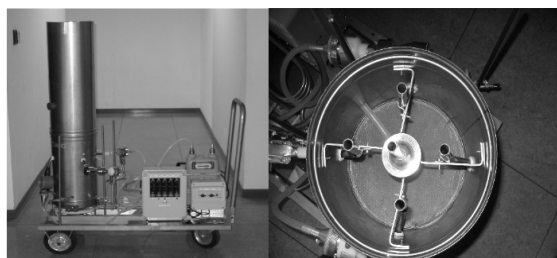


Figure 1. The WODUSA sampler (on the left). The internal nozzles for the five sampling lines (on the right).

In particular two different size distributions are discussed. In the first case, while the mass concentrations after the impactor and cyclones were lower than the Limit of Quantification (LOQ), above 30  $\mu\text{m}$  the cumulative mass distribution percentage was of 73%. In the second case, it was possible to measure the mass concentration downstream each size selector and the size distribution was fitted with a lognormal curve bearing a MMAD value of 24  $\mu\text{m}$  and a GSD of 2.2 (Fig. 2). Therefore, above 30  $\mu\text{m}$  the cumulative mass distribution percentage was only 59%.

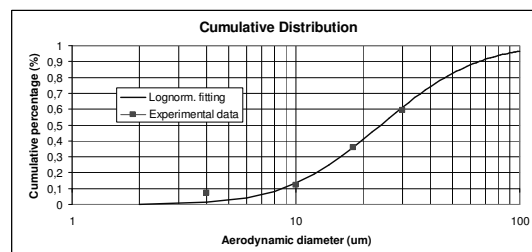


Figure 2. Cumulative size distribution of wood dust.

This work was supported by the ISPESL (National Health Service) under grant B72/DIL/03.

Agarwal J.K. & Liu B. Y.H. Liu. (1980). *American Industrial hygiene Association J.*, 41, 191-197.

Belosi F. & Prodi V. (1984). *J. Aerosol Science*, 15, 382-385.

Harper M., Akbar M.Z., & Andrew M.E. (2004). *J. Environ. Monit.*, 6, 18-22.

Mercer T.T. (1973). *Aerosol Technology in Hazard Evaluation*, Accademic Press..

Sala C. & Chiappino G. (2002). *Giornale degli Igienisti Industriali*, 27, 95-104.

## Real time wood dust sampling with particle size classification

F. Belosi<sup>1</sup>, F. Prodi<sup>1,2</sup>, G. Santachiara<sup>1</sup>

<sup>1</sup>Institute for Atmospheric Science and Climate (ISAC-CNR), National Research Council, 40129, Bologna, Italy

<sup>2</sup>Physics Department, University of Ferrara, Italy

Keywords: personal sampling, optical particle counter, particle size distribution, industrial aerosol, monitoring.

Personal inhalable collectors (among them IOM and GSP) have different aspiration efficiencies depending on the size distribution of the sampled particles (Aizenberg, 2000; Lidén 2000). In Italy alongside the IOM, a conical sampler (“conetto”) is widely used which resemble the GSP selector. In order to compare these selectors and gain real time information regarding the concentration and size distribution of wood dust, a calibrator manikin has been developed based on the results obtained during the European project SMT4-CT97-2254. Essentially, it consists of a modified manikin capable of housing the traditional IOM and “conetto” samplers, as well as two real time particle counters (Handheld 5016, LightHouse), each one connected to a modified version of the same samplers. Fig. 1 shows the front and back side of the manikin with the two counters mounted; Fig. 2 shows the manikin with all the samplers (IOM active, passive and modified, “conetto” active and modified).

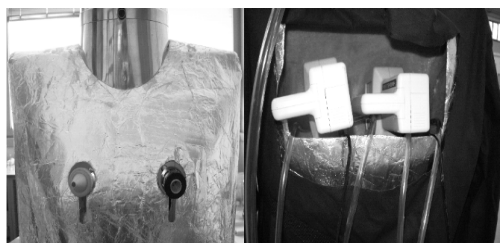


Fig. 1. Particle counters: front and back side.

The real time counters classify the particles into five size ranges from 0.5 µm to larger than 25 µm (optical size); in this way, both concentration and size distribution can be recorded as a function of time.

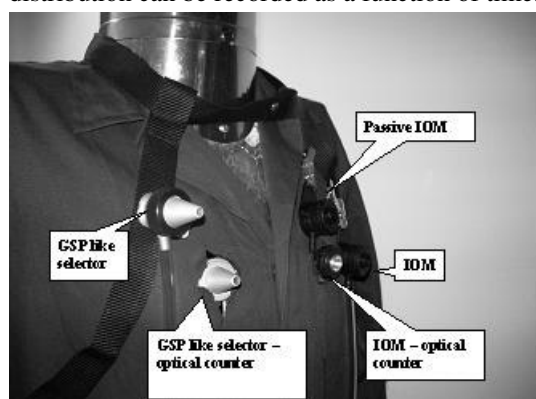


Fig. 2. Manikin with all the samplers mounted.

Table 1 shows the results of several samplings from different working machines (mainly sawing and sand-paper) in a wood factory. Test 5 shows the highest IOM/conetto ratio both for mass and number concentration (only the largest size fraction was considered).

Test	IOM (mg/m <sup>3</sup> )	“Conetto” (mg/m <sup>3</sup> )	IOM / “Conetto”	
			Mass	Number (> 10 µm)
1	0.56±0.07	0.53±0.08	1.06	1.07
2	0.68±0.04	0.61±0.04	1.11	1.29
3	0.57±0.05	0.57±0.04	1.00	1.14
4	0.53±0.05	0.55±0.05	0.96	1.29
5	0.66±0.05	0.55±0.07	1.20	1.47

Table 1. Results from samplings in a wood factory.

Fig. 3 shows, on a logarithmic scale, that the particles coming from sand paper machining have a smaller diameter than the ones coming from belt-saw processing.

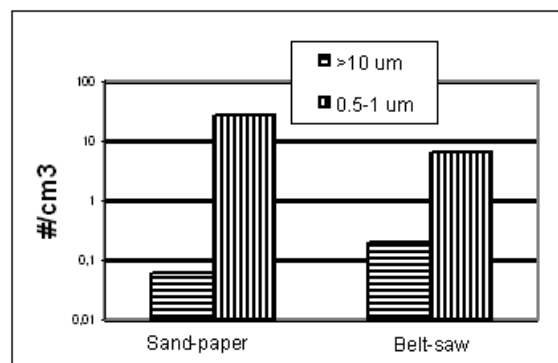


Figure 3. Differences in particle emission from sand-paper and belt-saw machining.

This work was supported by the ISPESL (National Health Service) under grant B72/DIL/03.

Aizenberg, V., Grinshpun S.A., Willeke K., Smith J. & Baron P.A.. (2000). *J. Aerosol Sci.*, 31, 169-179.  
Lidén, G., Jüringe L., Gudmundsson A., (2000). *J. Aerosol Sci.*, 31, 199-219, 2000.

## mission characteristics of polychlorinated diben *o-p*-dio ins and diben ofurans in the stac flue gases of electric arc furnaces

S.I. Shih<sup>1</sup>, W.J. ee<sup>2,3</sup>, C.C. Chen<sup>2,3</sup>, M.H. iu<sup>2,3</sup>, G.P. Chang-Chien<sup>4</sup> and .C. Wang<sup>4</sup>

<sup>1</sup>Department of Environmental Engineering, Kun Shan University, 949 Da-Wan Rd, 710, Yung-Kang, Tainan County, Taiwan

<sup>2</sup>Department of Environmental Engineering, National Cheng Kung University, 1 University Rd, 701, Tainan, Taiwan

<sup>3</sup>Sustainable Environment Research Centre, National Cheng Kung University, Tainan, 701, Tainan City, Taiwan

<sup>4</sup>Department of Chemical Engineering, Cheng Shiu University, 840 Chengching Rd, 833, Kaohsiung, Taiwan

Keywords: emission, PCDD/Fs, stack flue gas, electric arc furnace

Electric arc furnaces (EAFs) are extensively employed to produce carbon and steel alloys. In Taiwan, 24 EAFs are presently in operation. Some studies indicated that PCDD/F (polychlorinated dibenzo-*p*-dioxin and dibenzofuran) emission from EAFs was even higher than that from municipal waste incinerators (MWIs) (Chen, 2004 Sakai, 1999). The current study mainly reported the concentrations, congener profiles, and emission factors of PCDD/Fs in the stack flue gases of electric arc furnaces. The effects of PCDD/F emission from EAFs on the ambient air quality were also evaluated.

The PCDD/F samples from stack flue gas were collected according to US EPA modified Method 23. The sampling train adopted in this study was comparable with that specified by the US EPA modified Method 5. Prior to sampling, AD-2 resin was spiked with PCDD/F surrogate standards pre-labeled with isotopes. Each stack flue gas sampling lasted approximately 3 h. To ensure that the collected samples were free of contamination, one field blank was always taken when the field sampling was conducted.

Analyses of PCDD/Fs samples followed the US EPA modified Method 23, and were performed in the Super Micro Mass Research and Technology Center in Cheng Shiu University. This center is the first lab certified by the Taiwan EPA to analyze PCDD/Fs in Taiwan and passes the international inter-calibration on PCDD/Fs in fly ash, sediment, mother's milk, human blood and cod liver (Wang et al., 2003).

A high-resolution gas chromatography (HRGC), coupled with a high-resolution mass spectrometer (HRMS), were used for PCDD/Fs measurements. The HRGC is a Hewlett Packard 6970 Series gas chromatography, equipped with a DB-5 (J&W Scientific, CA, USA) fused silica capillary column (60 m, 0.25 mm ID, 0.25 μm film thickness), and splitless in action. An initial oven temperature was 150 °C and the electron energy was set at 35 eV.

Figure 1. shows the congener profiles of PCDD/Fs in the stack flue gas of electric arc furnaces. 2,3,4,7,8 PeCDF and 1,2,3,4,6,7,8-HpCDF were the

top two predominant species. Total PCDD/F concentrations ranged from 5.49 to 6.15 ng/Nm<sup>3</sup> (mean 5.81 ng/Nm<sup>3</sup>). With regard to toxicities, the ratios of PCDDs/PCDFs (I-TE) were less than unity, indicating that PCDFs were the primary toxicity distributors for PCDD/Fs. The mean total PCDD/F concentration in the stack flue gas of EAFs was 0.757 ng I-TE /Nm<sup>3</sup>, which was much lower than that regulated by the Taiwan EPA 5 ng I-TE /Nm<sup>3</sup>.

The emission factors of total PCDD/Fs in the stack flue gas from EAFs ranged from 21.6 to 24.4 μg/ton-feedstock (mean 23.0 μg/ton-feedstock). Based on the approximate evaluation, the annual emission of PCDD/Fs in the stack flue gas from EAFs was several times higher than those from other emission sources (e.g. large-scale MWIs), indicating the importance of the PCDD/F emission from EAFs on the ambient air quality.

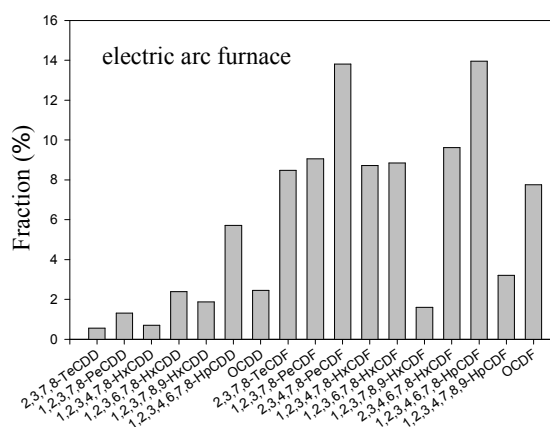


Figure 1. Congener profiles of PCDD/Fs in the stack flue gas of electric arc furnaces

Chen, C. M. (2004). *Chemosphere*, 54, 1413-1430.

Sakai, S. I. (1999). *Organohalogen Compd*, 40, 449-452.

Wang, . C., ee, W. J., ee, W. S., Chang-Chien G. P., & Tsai, P. J. (2003). *Environ. Sci. Technol.*, 37, 62-67.

## Characterization of ultrafine aerosol particles from aluminium smelter potrooms by electron microscopy

*N. Benker<sup>1</sup>, G. Miehe<sup>2</sup>, M. Ebert<sup>1</sup>, Y. Thomassen<sup>3</sup>, S. Weinbruch<sup>1</sup>*

<sup>1</sup> Institute of Applied Geosciences, Technical University of Darmstadt, Schnittspahnstr. 9, D-64287 Darmstadt

<sup>2</sup> Institute of Material Science, Technical University of Darmstadt, Petersenstr. 23, D-64687 Darmstadt

<sup>3</sup> National Institute of Occupational Health, P.O. Box 8149 DEP, N-0033 Oslo

Keywords: industrial aerosols, ultrafine particles, TEM, ESEM, single particle analysis.

Aluminium is produced by electrolysis of alumina ( $\text{Al}_2\text{O}_3$ ). To decrease the melting point cryolite ( $\text{Na}_3\text{AlF}_6$ ) is added. At present, the Norwegian aluminium industry uses two different technologies to produce aluminium: the so called Söderberg and Prebake processes (Nechev, 1997). In both cases, particles with variable composition, several gases and aromatic hydrocarbons (PAHs) are formed. Inhalation of these pollutants has adverse health effects for the workers. For better understanding of the toxicological relevance of the particulate matter present in the workrooms, individual particle analysis was performed. For this purpose, a combination of transmission electron microscopy (TEM) and environmental scanning electron microscopy (ESEM) was applied. Size, morphology, chemical and phase composition and the hygroscopic behaviour of different aerosol particles were analysed. In this contribution we focus on TEM investigation of ultrafine particles (diameters < 100 nm). Larger particles occurring in the potroom of the same refinery were studied recently by Höflich *et al.* (2005).

Aerosol samples of the two processes were collected on copper foils for ESEM investigations, and copper grids with conducting carbon foil for TEM investigations. A Jeol 3010 with a LaB<sub>6</sub> cathode equipped with a Gatan Imaging Filter (GIF) was used for TEM investigations. ESEM measurements were carried out with a FEI Quanta 200 FEG, equipped with an energy dispersive x-ray spectrometer (EDXS).

The phase composition of ultrafine particles was identified with high resolution (HRTEM) images. Fourier transformation (FT) of the HRTEM images gives "pseudo" diffraction pattern of the particles. These diffraction patterns were indexed with the ICSD databank and the software package PIEP (Miehe, 1997). Preliminary analysis shows the presence of cryolite and/or  $\text{AlF}_3$  in the ultrafine fraction.

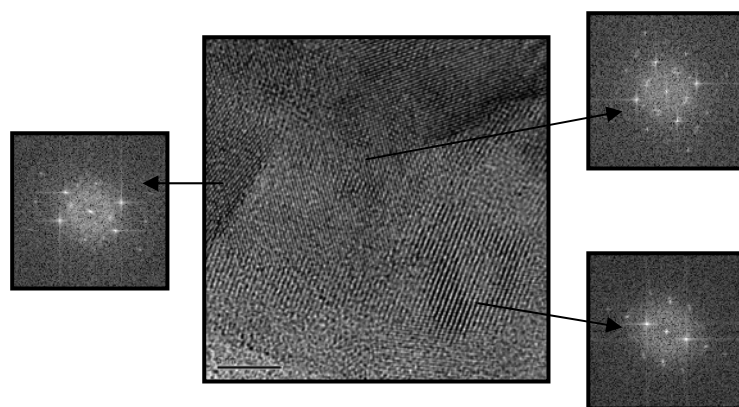


Figure 1. HRTEM and FFT images of an Al-rich particle.

ESEM was applied to particles in the size range 50 - 2000 nm. Due to beam damage no automation procedures could be applied for EDX analysis. Thus, all analyses (approximately 600) were carried out manually. Particles containing aluminium, fluorine, sodium and oxygen are dominant. In addition, carbonaceous particles with high oxygen content were also frequently observed.

Hygroscopic properties of the aerosol particles were investigated by changing the pressure (i.e., the relative humidity RH) in the sample chamber at a constant temperature of 5°C. All particles containing F, Na and Al developed a small water film at a RH > 95 %, showing the presence of surface coatings of soluble material.

G. Nechaev, S. Tsymbalov, L. E. Swartling and G. E. Volfson (1997). *Proceedings TMS Annual Meeting*, Orlando, FL, USA, pp. 201–205.

B. L. W. Höflich, S. Weinbruch, R. Theissmann, H. Gorzawski, M. Ebert, H. M. Ortner, A. Skogstad, D. G. Ellingsen, P. A. Drabløsd and Y. Thomassen (2005). *J. Environ. Monit.*, 7, 419–424.

G. Miehe (1997), *Ber. Dtsch Mineralogischen Ges. Beih. z. Eur. J. Mineral.*, 9, 250.

## Nanoparticulate construction materials via flame spray synthesis: Enhanced reactivity of nano-Portland cement and improved hardness of nano-gypsum

S. C. Halim<sup>1</sup>, N. Osterwalder<sup>1</sup>, S. Loher<sup>1</sup>, R. N. Grass<sup>1</sup>, T. J. Brunner<sup>1</sup>, L. K. Limbach<sup>1</sup>, M. Böhner<sup>2</sup> and W. J. Stark<sup>1</sup>

<sup>1</sup>Chemistry and Applied Biosciences, ETH Zurich, CH-8093, Zurich, Switzerland

<sup>2</sup>Dr Robert Mathys Foundation, CH-2544, Bettlach, Switzerland

Keywords: nanoparticle applications, combustion aerosols, physical properties, surface reaction.

Gypsum is one of the oldest known construction materials today accounting for a worldwide production of an estimated 100 million metric tons of calcium sulfate. Portland cement, on the other hand, represents one of the largest volume chemicals globally with an annual production of over 2.1 billion tons. Both materials are widespread due to their mechanical properties and the versatile fields of applications.

In this work, nano-sized anhydrous calcium sulfate (anhydrite) and nanoparticles with a typical Portland cement composition (68% CaO, 22% SiO<sub>2</sub>, 5.8% Al<sub>2</sub>O<sub>3</sub>, 2.6% Fe<sub>2</sub>O<sub>3</sub>, 1.5% MgO) were produced in a one-step preparation route based on flame spray synthesis. Latter has established itself as a reliable production process for mixed oxide nanoparticles of high phase homogeneity (Maedler, 2002; Stark, 2003; Stark, 2002). This continuous high temperature gas process uses suitable organic derivatives of the desired metals as homogeneous mixtures. The precursors are directly sprayed into a flame where they are rapidly converted into the corresponding mixed oxides.

The in-situ prepared gypsum and Portland cement nanoparticles were characterized with respect to particle size, crystal phases, morphology, and mechanical properties.

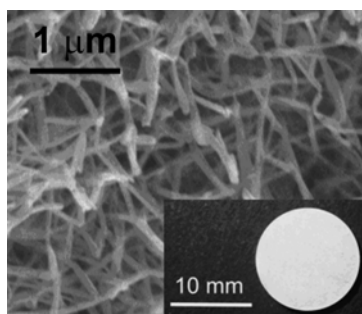


Figure 1. Scanning electron micrograph of nano-gypsum after setting; insert: pressed nano-gypsum pill.

After compaction and hardening by the addition of water, the anhydrite nanoparticles reacted to nano-gypsum which was confirmed by X-ray diffraction, diffuse reflectance IR spectroscopy and thermal analysis. Mechanical properties were

investigated in terms of Vickers hardness and revealed an up to three times higher hardness of nano-gypsum if compared to conventional micron-sized construction material (Osterwalder, 2006). The improved mechanical properties of nano-gypsum could in part be traced back to the presence of calcium sulfate nano-needles in the nano-gypsum as showed by electron microscopy (Figure 1).

The hardening process of the flame-derived Portland cement was followed in situ using isothermal calorimetry. The 20-50 nm sized Portland cement displayed an over 10 times faster hardening if compared to conventional cement (micrometer sized starting material, see Figure 2), yet showed poorer mechanical properties (Halim, 2007).

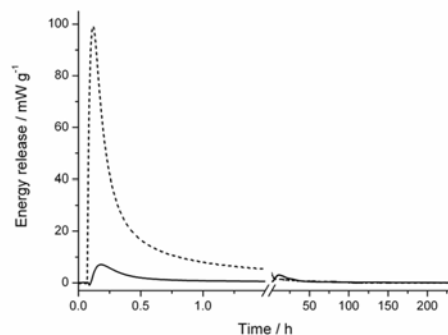


Figure 2. Heat release profile as measured by isothermal calorimetry for flame-made (dashed) and commercial Portland cement (solid).

This work was supported by the Gebert Rűf Foundation, grant no. GRS-048/04, and ETH Zurich.

### References

- Halim, S.C., Brunner, T. J., Grass, R. N., Böhner, M. & Stark, W. J. (2007). *Chem. Commun.*, submitted.
- Maedler, L., Stark, W. J. & Pratsinis, S. E. (2002). *J. Mat. Res.*, 17, 1356
- Osterwalder, N., Loher, S., Grass, R. N., Brunner, T. J., Halim, S. C., Limbach L. K. & Stark, W. J. (2006). *J. Nanopart. Res.*, DOI:10.1007/s11051-006-9149-7.
- Stark, W. J., Maciejewski, M., Mädler, L., Pratsinis, S. E. & Baiker, A. (2003). *J. Catal.I*, 220, 35-43.
- Stark, W. J., Maedler, L. & Pratsinis, S. E. (2002). *Flame Made Metal Oxides*, WO 2004/005184.

## CHARACTERISTICS OF OIL MIST CONTROL BY CORONA DISCHARGE

K.S.HWANG<sup>1</sup> and D.N.Shin<sup>2</sup>

<sup>1,2</sup>Environmental Research Team, Research Institute of Industrial Science & Technology  
Pohang P. O. Box 135, 790-330, Republic of Korea

Keywords: Oil Mist, Pre-ionizer, Electrostatic Precipitator, Collection Efficiency

### INTRODUCTION

There are a number of sources emitting fine oil mist and fume. One of them comes from metal working fluids which act as coolant, lubricator and flushing material of metal chips during the metal working process. The particle size of oil mist and fume produced by such process is so fine, such as 0.03-1.0  $\mu\text{m}$  in diameter, that oil mist and fume pose a serious hazard, for example, causing respiratory problems. Consequently, it is required to create safety and maintenance concerns as particles settle on expensive machinery, work surface and finished products. Among the control technologies of such oil mist and fume, electrostatic precipitator (ESP) is known to be the most effective way of the control of them. This paper presents the characteristics of collecting oil mist and fume by utilizing ESP system which consists of pre-ionizer and collection plates. The role of the pre-ionizer gives the charge into the oil mist before oil mist enters the collection plates, resulting in the enhancement of collection efficiency of oil mist.

### METHODS

The pilot scale experimental system was made for the control of oil mist and fume, where the available capacity of the system was about 15  $\text{m}^3/\text{min}$  of the flow rate. It is composed of an oil mist and fume generation section, pre-ionization section, collection section and measuring section. The pre-ionizer consists in metal wires having small diameters and operates with a positively direct current high voltage in the range of 0 - 15 kV. Such high voltage on the wire creates an electric field to charge the oil mists. The initially produced electrons in the pre-ionizer flow across the oil stream and in turn collide with or adhere to the particles, imparting a charge on them. The collection section is a series of parallel metal plates which are spaced apart with alternate plates charged and grounded. Charged oil mists are driven by a electric force from the charged plates toward the ground plate where they are collected. The metal working fluids oil investigated in this study was insoluble cutting oil in water.

### RESULTS

In this study, the performance of the system has been investigated as a function of voltage, inlet gas velocity, initial oil concentration, inlet gas

temperature. The effect of voltage applied to pre-ionizer on the removal efficiency has been represented in Figure 1, where the applied voltage was positive DC, inlet velocity was 1.3 m/sec, the inlet concentration was 500  $\text{mg}/\text{Nm}^3$  and the inlet temperature was 50°C, respectively. Under the condition of 13 kV, it has been observed that the removal efficiency of oil mist was achieved up to about 87%. The collection efficiency of oil mist was found to be largely enhanced as a result of applying voltage to the pre-ionizer. In this study, we have also examined the effect of inlet velocity on the removal efficiency represented in Figure 2.

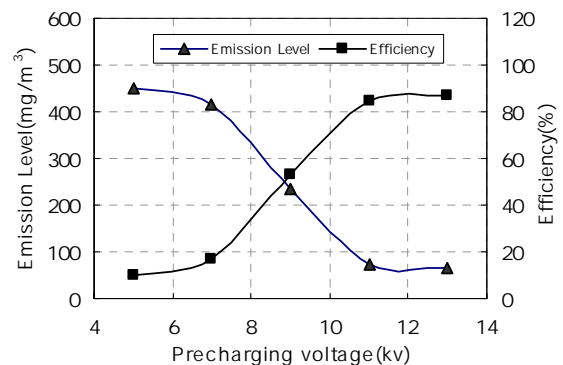


Figure 1. Effect of Applied Voltage on Removal Efficiency

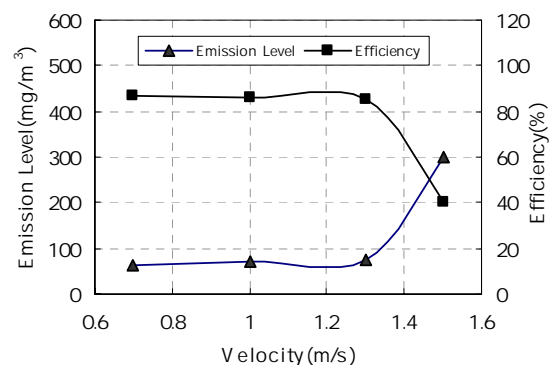


Figure 2. Effect of velocity on Removal Efficiency

Oglesby, Jr. S., and Nichols, G. B.(1978). *Electrostatic Precipitation*, marcel Dekker, Inc., New York and Basel(1978)

## Particle Collection Efficiency of a Vortex Scrubber with Opposing Nozzles

K. S. Lim, S. H. Lee and H. S. Park

<sup>1</sup>Department of Energy Conversion Research, Korea Institute of Energy Research, 71-2 Jang-dong, Yuseong-gu, 305-343, Daejeon, Korea

Keywords: Vortex scrubber, Opposing nozzle, Liquid spray, Collection efficiency

The vortex scrubber combines the advantages of a cyclone with those of wet scrubber for higher particle collection efficiency. In a vortex scrubber, exhaust gas enters the scrubber chamber where the shape of the entry, such as tangential, scroll or swirl vane entries, cause the gas to spin. After entering the chamber, the gas forms a vortex with a high tangential velocity that gives particles entrained in the gas a high centrifugal force, throwing them to the chamber wall for collection. At the same time, liquid is sprayed inside the chamber. Thus, there are two particle collection mechanisms in a vortex scrubber, by a centrifugal force formed from tangential inlet and by a particle impaction on liquid droplet sprayed from nozzle.

The particle collection of a vortex scrubber by two mechanisms was affected by several process variables, such as particle size, liquid droplet size, the relative velocity of particle and liquid droplets, liquid-to-gas ratio, and so on. Because the liquid droplet size and velocity depend on the nozzle shape and size, the nozzle spraying liquid droplets plays a very important role in all wet scrubbers as well as vortex scrubbers. The nozzles contain the impingement nozzle, solid cone nozzle, helical spray nozzle (Gerald et al., 1998). These spray nozzles are appropriate for different scrubbing systems because they have different spraying liquid size range and spraying angle.

In this study, the opposing nozzles were used as shown in Figure 1. Opposing nozzles can produce tiny and uniform-sized liquid droplets with high velocity by collisions of liquid from opposing nozzles. Moving from the center of scrubber chamber to the outer wall of scrubber, the liquid droplets with high velocity collect the particles which swirl around the chamber by impaction. This type of a scrubber with opposing nozzles has already been commercialized as V-tex<sup>TM</sup> by Accentus plc. In this study, The particle removing efficiencies of the vortex scrubber with these opposing nozzles were evaluated varying opposing nozzle diameter, distance between nozzles, liquid flow rate, and so on.

The particle removing efficiency in the vortex scrubber increased as the liquid flow rate ( $Q_l$ ) of scrubbing liquid increased and the distance between opposing nozzles ( $L$ ) decreased as shown in Figure 2. In addition, as the nozzle diameter ( $D$ ) decreased, the removing efficiency increased, but the liquid pressure drop of nozzles also increased. The large liquid flow

rate ( $Q_l$ ) and close distance of opposing nozzles ( $L$ ) lead to the strong collision between liquid from opposing nozzles, which produces the small and monodisperse liquid droplet.

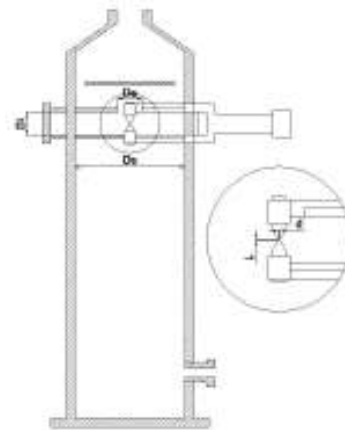


Figure 1. Vortex scrubber with opposing nozzles.

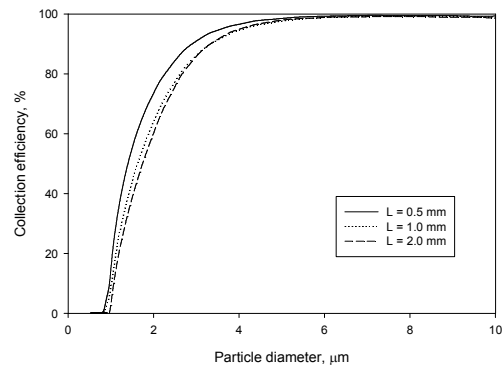


Figure 2. Particle removing efficiency of the vortex scrubber ( $D_i=65$  mm,  $D_s=250$  mm,  $D_e=60$  mm,  $d=1.8$  mm,  $Q_g=1.67$  m<sup>3</sup>/min,  $Q_l=3.4$  l/min).

Joseph, G. T., & Beachler, D. S. (1998). *Scrubber systems operation review; Self-Instructional Manual*. (APTI Course SI: 412C, 2nd ed.), Raleigh, US: North Carolina State University Press.

## Nanoparticles measurement in two workplaces

C.J. Tsai<sup>\*1</sup>, C.S. Chang<sup>1</sup>, C.H. Wu<sup>1</sup>, Y.H. Cheng<sup>2</sup>, S.C. Chen<sup>1</sup>, T.S. Shih<sup>3</sup>, S.N. Uang<sup>3</sup>

<sup>1</sup>Institute of Environmental Engineering, National Chiao Tung University, 300, Hsinchu, Taiwan

<sup>2</sup>Department of Safety, Health and Environmental Engineering, Mingchi University of Technology, 243, Taipei County, Taiwan

<sup>3</sup>Institute of Occupational Safety and Health, Council of labor Affairs, 221, Taipei County, Taiwan

Keywords: PM<sub>10</sub>, PM<sub>2.5</sub>, nanoparticles, aerosol sampling

This study measured PM<sub>10</sub>, PM<sub>2.5</sub>, and nanoparticle concentrations in a lead powder and a casting factory. The results showed that the relationship between PM<sub>10</sub> and PM<sub>2.5</sub> could be determined as  $PM_{2.5} = 0.6 \times PM_{10} + 14.63$  and the number concentrations of particles below 100nm was between  $7.76 \times 10^3 \text{ \#/cm}^3$  to  $4.65 \times 10^4 \text{ \#/cm}^3$  (average:  $1.78 \times 10^4 \text{ \#/cm}^3$ ). In the casting factory, the relationship between PM<sub>10</sub> and PM<sub>2.5</sub> was shown to be  $PM_{2.5} = 0.65 \times PM_{10} + 63.71$  while the number concentrations of particles below 100nm was between  $2.31 \times 10^4 \text{ \#/cm}^3$  to  $2.96 \times 10^5 \text{ \#/cm}^3$  (average:  $9.21 \times 10^4 \text{ \#/cm}^3$ ). The concentration of particles below 100 nm, or PM<sub>0.1</sub>, was found to be correlated well with PM<sub>10</sub> as  $PM_{0.1} = 0.03 \times PM_{10} + 4.88$ . We also evaluated the exposure of workers to nanoparticles in the casting factory by using the time-activity pattern measured by a RFID system and the number distribution measure by the SMPS. Figure 1 is shown that the average number and mass concentrations of worker's exposure to nanoparticles were found to range from  $5.17 \times 10^4 \text{ \#/cm}^3$  and  $11.39 \text{ \mu g/m}^3$ , respectively.

We also used MOUDI to measure mass distributions and SMPS to measure number distributions of nanoparticles in the casting factor. The MOUDI measures aerodynamic diameter while the SMPS measures the mobility diameter. Using the relationship between the mobility and aerodynamic diameters, the MOUDI's mass distributions as a function of aerodynamic size were converted to mass distributions as a function of mobility size using an effective particle density. Figure 2 shows that assuming the effective density of  $2 \text{ g/cm}^3$ , mass distributions measured by the MOUDI and SMPS are nearly the same.

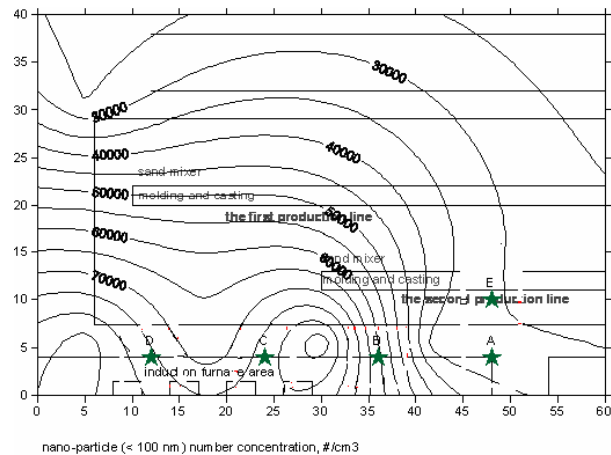


Figure 1. Nanoparticle number concentration in the workplace.

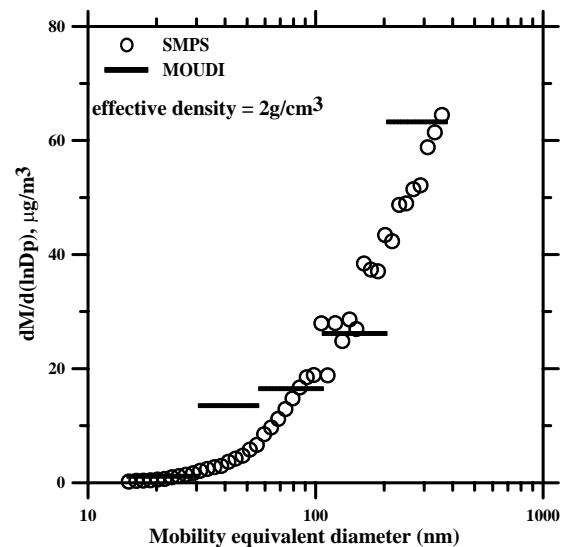


Figure 2. Mass size distributions measured with SMPS and MOUDI

The authors would like to thank for the support of the Taiwan Institute of Occupational Safety and Health

Biswas, P., & Flagan, R.C. (1984), *Environ. Sci. Technol.* 18, 611-616.

Park, K., Cao, F., Kittelson, D. B., & McMurry, P.H. (2003), *Environ. Sci. Technol.* 37, 577-583.

Sarder, S. B., Fine, P. M., Mayo, P. R. & Sioutas, C. (2005), *Environ. Sci. Technol.* 39, 932-944.

## The influence of process conditions on the efficiency of non-steady filtration of aerosols

T. Jankowski

Department of Chemical and Aerosol Hazards, Central Institute for Labour Protection – National Research Institute, 00-701 Warsaw, Poland

Keywords: aerosol filtration, fibrous filters, industrial aerosols, particle size distribution

Needled nonwovens are an important part of fibrous filters used in ventilation systems. When planning the use of fibrous filters to protect the human in the working environment, it is necessary to maintain optimal conditions for filtering industrial aerosol particles at different concentrations and velocities in ventilation systems.

This article presents some aspects of the influence of aerosol velocity and cumulative concentration on the efficiency of non-steady filtration process through needled nonwovens.

Tests were carried out using spunlace nonwovens used in ventilation systems. Below, the results concerning only one tested needled nonwoven are shown. A structural characteristic of this filter is given in Table 1.

Table 1. Structural characteristic of tested filter.

Filter thickness [mm]	Packing density [kg/m <sup>3</sup> ]	Fiber diameter [μm]	Porosity [%]
2.08 ± 0.01	273.98 ± 4.21	16.52 ± 0.54	80.76 ± 1.44

The investigations were conducted at two face velocities of a DEHS aerosol:  $U_1=5$  cm/s and  $U_2=20$  cm/s. The DEHS aerosol was generated in two cumulative concentrations:  $C_1=2.68 \cdot 10^5$  particles/cm<sup>3</sup> and  $C_2=2.44 \cdot 10^6$  particles/cm<sup>3</sup>. Particle size distributions were measured with SMPS 3936 (TSI DMA 3080L and CPC 3022A).

Figure 1 presents particle size distributions from tests carried out in different process conditions. When aerosol velocity increases, there is natural dilution of real concentration of aerosol particles which flow through the filter.

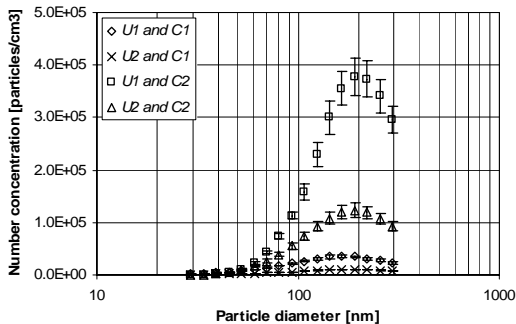


Figure 1. Particle size distributions of DEHS before filter at different aerosol concentrations and velocities.

The results of investigations of filtration efficiency during a continuous load of a filter with aerosol in different process conditions are illustrated in Figure 2.

It was found that filtration efficiency and fractional efficiency for the range of particles 40–300 nm in diameter decrease as the time of filter loading, aerosol velocity and cumulative particle concentration increase.

Moreover, fractional efficiency for most penetration particles (MPPS) was reduced by about 40% (for  $U_1$  and  $C_1$ , figure 3) and 45% (for  $U_2$  and  $C_2$ , figure 4).

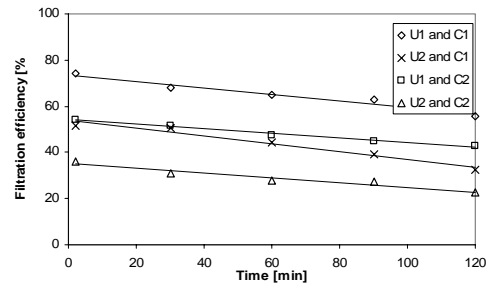


Figure 2. Effect of aerosol velocity and cumulative concentration on filtration efficiency of DEHS particles

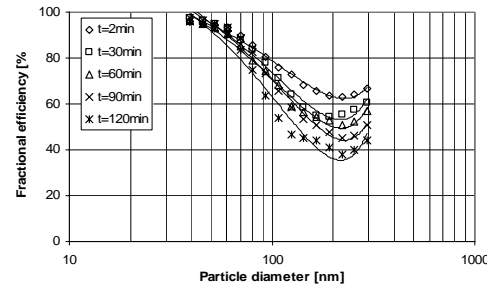


Figure 3. Fractional efficiency of the filter at  $U_1$  and  $C_1$ .

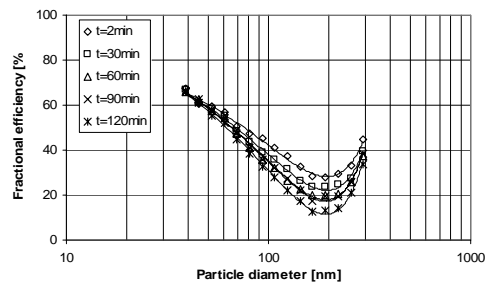


Figure 4. Fractional efficiency of the filter at  $U_2$  and  $C_2$ .

This study was part of the statutory activity of the Central Institute for Labour Protection – National Research Institute, Warsaw, Poland.

Albrecht, W., Fuchs, H. & Kittelmann, W. (2002). Nonwoven fabrics. Wiley-VCH.

## A multi-scale characterization of PM10 at an urban and industrialized coastal site

J. Rimetz-Planchon<sup>1,2</sup>, E. Perdrix<sup>1</sup>, S. Sobanska<sup>2</sup> and C. Brémard<sup>2</sup>

<sup>1</sup>Département Chimie et Environnement, Ecole des Mines de Douai, Douai, France

<sup>2</sup>Laboratoire de Spectrochimie Infrarouge et Raman (LASIR), Université des Sciences et Technologies de Lille, Villeneuve d'Ascq, France

Keywords: Aerosol characterization, anthropogenic aerosol, chemical composition, , Single particles analysis.

Atmospheric particulate matter has serious environmental and health-related consequences due to the development of anthropogenic activities in urban and industrialised areas. The knowledge of the physical and chemical composition of the aerosols is a key-issue to scrutinize the air pollution processes.

In this study, we propose a multi-techniques and multi-scales approach to characterise the composition of PM10, from the bulk sample to the individual particle scale. The evolution of the chemical composition under the influence of meteorological parameters and pollution sources is also investigated. Bulk analyses of PM10 consist in the determination of EC/OC, elemental and ionic composition of PM10 by thermo-optical method, ICP-AES/MS and chromatography, respectively. Special care was taken to check sampling artefacts for the inorganic ionic fraction (Keck & Wittmaack, 2005).

Through chemical imaging, the microscopic techniques bring information about the morphology, heterogeneity and chemical composition of individual particles. Particles were impacted on suitable substrates. Samples were analyzed without prior preparation by automated Raman microprobe and ESEM-EDS. Raman spectral mapping can be collected by computer-controlled scanning under *in situ* conditions. Applying multivariate curve resolution methods (MCR) to Raman mapping yields to specific molecular information with a spatial resolution imposed by the optical diffraction limit (~0.5  $\mu\text{m}$ ) (Batonneau et al, 2006). Analytical environmental scanning electron microscopy (ESEM-EDS) is used for elemental mapping in conditions limiting the particles damage linked to the chamber vacuum. Energy dispersive electron probe X-ray microanalysis (EPMA) has proven to be a powerful technique to provide the quantitative elemental composition of particles (Choël et al, 2006).

Located in the southern part of the North Sea, the coastal city of Dunkerque (200,000 inhabitants), Nord Pas-de-Calais, France (51°N 2°E) is a highly industrialised area (especially petrochemistry and steel production) combined with a heavy road traffic and the largest national harbour for trade. Dunkerque undergoes prevailing strong winds from the SW. However, in early spring and during summer, sea breezes appear characterised by anticyclonic

conditions and NNE air masses, influenced by the marine source and long range transport. During such events, inhabitants are exposed to the important industrial plume potentially inducing public health problems.

Samples were collected simultaneously upwind and downwind the industrial area during summer and winter periods. Under the observed meteorological conditions, no significant difference of composition is observed during summer and winter. Composition and size-resolved ionic concentrations are similar in both sites but sulphate, ammonium, chloride and potassium levels are high at the downwind site. The industrial influence is highlighted by the presence of minor elements e.g. Fe, Pb, Zn, Mn, and an increase of carbon concentrations.

EPMA is in good agreement with bulk analysis. Individual particles are composed of a deliquescent mixture of salts. Secondary nitrate and sulphate ( $\text{NaNO}_3$ ,  $\text{NH}_4\text{NO}_3$ ,  $(\text{NH}_4)_2\text{SO}_4$ ,  $\text{Na}_2\text{SO}_4$ ,  $\text{CaSO}_4$ ) in both sites are believed to be formed during heterogeneous reactions of anthropogenic gases (De Hoog et al, 2005). Numerous particles are observed at the downwind site and Raman mapping reveals a complex mixtures of iron oxides and hydroxides ( $\text{Fe}_2\text{O}_3$ ,  $\text{Fe}_3\text{O}_4$ ,  $\text{FeOOH}$ ) with these inorganic particles. These aggregates were probably generated by a rapid agglomeration of fine particles emitted by the steel industry with the atmospheric aerosols. This work shows that multi-scale techniques provide elemental and molecular imaging, essential to assess the chemical heterogeneity and ageing of aerosol particles.

Batonneau, Y., Sobanska, S., Laureys, J. & Brémard, C. (2006). *Environmental Science and Technology*, 40, 1300-1306.

Choël, M., Deboudt, K., Flament, P., Lecornet, G., Perdrix, E., Sobanska, S. (2006). *Atmospheric Environment*, 40, 4439-4449.

De Hoog, J., Osan, J., Szaloki, I., Eyckmans, K., Worobiec, A., Ro, C.-U. and Van Grieken, R. (2006). *Atmospheric Environment*, 40, 3231-3242

Keck, L. & Wittmaack, K. (2005). *Atmospheric Environment*, 39, 2157-2162.

## The effect of hygroscopicity on inhaled dose for aerosol species measured in an industrial workplace

C. Mitsakou<sup>1</sup>, A. Karanasiou<sup>1</sup>, S. Vratolis<sup>1</sup>, K. Eleftheriadis<sup>1</sup>, M. Lazaridis<sup>2</sup> and C. Housiadas<sup>1</sup>

<sup>1</sup>“Demokritos” National Centre for Scientific Research, 15310, Agia Paraskevi, Athens, Greece

<sup>2</sup>Department of Environmental Engineering, Technical University of Crete, 73100, Chania, Greece

Keywords: Industrial aerosols, lung deposition, soluble fraction.

Aerosol exposure by inhalation is of great interest in occupational health, as it represents a major potential source of hazard for workers in many industrial environments. Workers' inhaled dose assessment is far from being routinely performed in many workplaces. The aim of this study is to investigate the effect of hygroscopicity of specific aerosol species on the workers' inhaled dose. For this purpose the airborne particulate matter concentration and the distribution of health-relevant chemical species that are released in an industrial workplace were measured.

The measurements took place in February and July 2005 inside a detergent industry, located in Athens area. The purpose of the aerosol measurements was to obtain the chemically-resolved airborne particulate matter size distribution. The size distribution was then used in the calculation of the inhaled dose, in order to determine the extent of variation in the calculated dose due to the differences in hygroscopicity of common aerosol species.

The aerosol size distribution was obtained by means of a ten-stage Berner impactor. The inhaled dose is determined in terms of lung deposition, by using a mechanistic inhalation dosimetry model (Mitsakou *et al.*, 2005). The model accommodates full aerosol dynamics, thus enabling to address the effects due to hygroscopic growth of water-soluble particles. The particle deposited mass on lung regions (extrathoracic - ET, tracheobronchial - TB, alveolar - AI) per breath is depicted in Table 1.

TABLE 1. Fraction (%) of deposited mass to inhaled mass in the different regions (extrathoracic – ET, tracheobronchial – TB, alveolar – AI) of the respiratory tract for (NH<sub>4</sub>)<sub>2</sub>SO<sub>4</sub>, CaCO<sub>3</sub> and total aerosol mass.

	(NH <sub>4</sub> ) <sub>2</sub> SO <sub>4</sub>	CaCO <sub>3</sub>	Total aerosol mass
ET	0.2	3.5	8.6
TB	0.6	2.4	12.6
AI	1.4	3.3	26.2

The samples of the impactor were analyzed by ion chromatography and atomic absorption spectrometry (Karanasiou *et al.*, 2007), so as to determine the size distribution of water-soluble inorganic ions and metallic elements. The size

distributions of metallic elements were unimodal with their maximum found in coarse particles. Among the water-soluble aerosol components SO<sub>4</sub><sup>2-</sup>, NO<sub>3</sub><sup>-</sup>, Cl<sup>-</sup>, NH<sub>4</sub><sup>+</sup> and Ca<sup>2+</sup> were the major contributors to total particle mass. The chemical analyses showed that the water-soluble part of the produced aerosol consists mainly of (NH<sub>4</sub>)<sub>2</sub>SO<sub>4</sub> and CaCO<sub>3</sub>. The normalized distribution of the deposited mass on the thoracic part of the respiratory tract for the two soluble compounds is depicted in Figure 1. The calculations were performed by considering or neglecting their hygroscopic properties. In the later case the distributions representing the deposited mass appear significantly distorted in comparison to those calculated by considering the hygroscopic nature of these species. The determination of the lung deposition reveals the effect that chemically variable aerosol components have on the levels of the inhaled dose. The differences between the species appear mainly due to their different size distributions and water solubility.

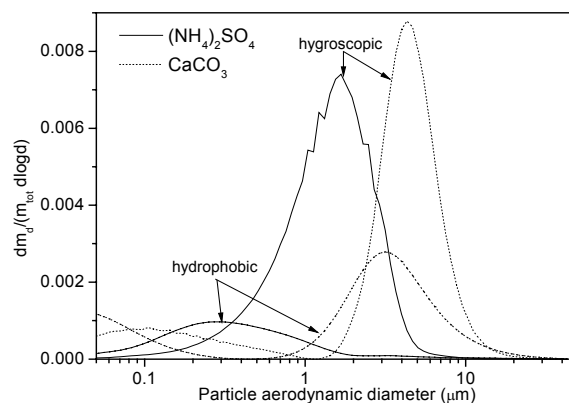


Figure 1. Normalized distribution of the deposited mass of (NH<sub>4</sub>)<sub>2</sub>SO<sub>4</sub> and CaCO<sub>3</sub>.

Work partially supported by GSRT through grant from the O.P. “Competitiveness”. This project is co-funded (75%) by the European Union - European Regional Development Fund (ERDF).

Karanasiou A., Eleftheriadis K., Vratolis S., Zarbas P., Mihalopoulos N., Mitsakou C., Housiadas C., Lazaridis M., Ondracek J., & Dzumbova L., (2007). *Water Air Soil Pollution Focus*, in press.  
Mitsakou, C., Helmis, C., & Housiadas, C. (2005). *J. Aerosol Sci.*, 36, 75-94.

## Modeling of *in-situ* Particle Coating at High Temperatures

B. A. Buesser, M. C. Heine and S. E. Pratsinis

Particle Technology Laboratory, Institute of Process Engineering,  
Department of Mechanical and Process Engineering, ETH Zurich, 8092 Zürich, Switzerland

Keywords: Aerosol coating, Coagulation, Condensation, Modeling, Surface reaction.

Aerosol coating is a promising one-step process to modify nanoparticle surfaces. Here gas-phase coating of SiO<sub>2</sub> particles with TiO<sub>2</sub> films is investigated which is important in making fillers with controlled refractive index for dental nanocomposites and photocatalytic particles.

This process is investigated theoretically accounting for TiO<sub>2</sub> monomer generation, coagulation, sintering and surface growth by TiCl<sub>4</sub> and TTIP (titanium tetraisopropoxide) precursors as there are available chemical kinetic expressions for gas phase and surface growth oxidation (Tsantilis & Pratsinis, 2004a). The evolution of the TiO<sub>2</sub> coating particle population is described by bimodal (Jeong & Choi, 2005) and sectional (Heine & Pratsinis, 2005) models to distinguish the fine and coarse modes of TiO<sub>2</sub> coating particles. The fine mode deposits fast on SiO<sub>2</sub> particles forming a smooth coating while the coarse deposits further downstream and may contribute to rough coatings depending on TiO<sub>2</sub> sintering kinetics.

Coating starts by injecting the TiO<sub>2</sub> precursor after the SiO<sub>2</sub> particles have reached their optimal primary particle size that no longer changes by sintering (Tsantilis & Pratsinis, 2004b). That way SiO<sub>2</sub> primary particles and aggregates have attained a self-preserving distribution that can be represented by a single size facilitating the simulations. Sintering may take place on the surface of the SiO<sub>2</sub> particles and transform rough into smooth coatings depending on process conditions.

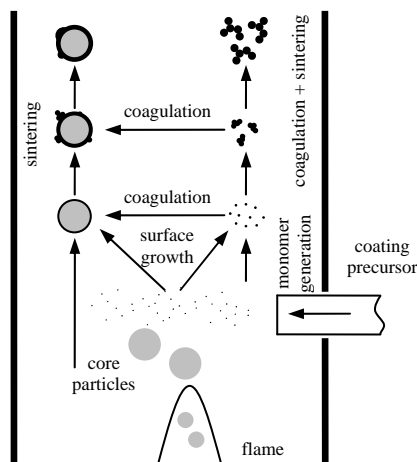


Figure 1. Pathways of gas-phase particle coating.

A second Damkohler number, Da<sub>2</sub>, is defined to compare the characteristic time of surface reaction with the characteristic time of diffusion to the SiO<sub>2</sub> surface. Figure 2 shows a diagram for diffusion (Da<sub>2</sub> > 1) or reaction (Da<sub>2</sub> < 1) limited TiO<sub>2</sub> particle growth by TTIP oxidation.

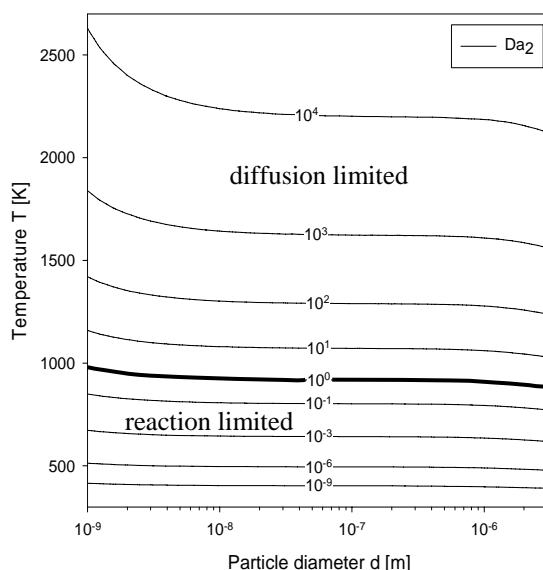


Figure 2. Regions of limiting growth of TiO<sub>2</sub> coatings made by TTIP oxidation on particles of various sizes and process temperatures.

The influence of SiO<sub>2</sub> particle size and concentration, process temperature, cooling rate, mixing delay and precursor concentration on TiO<sub>2</sub> coating thickness and texture are investigated. Especially the evolution of TiO<sub>2</sub> coating thickness and surface area of the rough TiO<sub>2</sub> coating on the SiO<sub>2</sub> core particles surface are discussed.

Financial support by ETH Zurich and the Swiss National Science Foundation (SNF) 200020-107947/1 is gratefully acknowledged.

Heine, M. C., & Pratsinis, S. E. (2005). *Ind. Eng. Chem. Res.*, 44, 6222-6232.

Jeong, J. I., & Choi, M. (2005). *J. Colloid Interface Sci.*, 281, 351-359.

Tsantilis, S., & Pratsinis, S. E. (2004a). *J. Aerosol Sci.*, 35, 405-420.

Tsantilis, S., & Pratsinis, S. E. (2004b), *Langmuir*, 20, 5933-5939.

## Physico-chemical characterization of atmospheric particulate emissions from an iron and steel works

H. Aversin<sup>1</sup>, D. Hleis<sup>1</sup>, D. Courcot<sup>1</sup>, F. Ledoux<sup>1</sup>, D. Courcot<sup>1</sup>, E.A. Bilinskaya<sup>1</sup>,  
F. Cazier<sup>2</sup>, S. Bouhsina<sup>1</sup>, A. Aboukassab<sup>1</sup>

<sup>1</sup> Laboratoire de Catalyse et Environnement (E.A. 2598), Université du Littoral Côte d'Opale,

<sup>2</sup> Centre Commun de Mesures de l'Université du Littoral Côte d'Opale

<sup>1,2</sup> 145, avenue Maurice Schumann, Dunkerque, 59140, France

Keywords: industrial aerosols, PM10, source identification, instrumentation/chemical characterization.

A physico-chemical characterization of different atmospheric particles samples collected at Dunkerque (France) under the influence of the city centre or a heavy industrialized area has been undertaken. Different techniques have been applied to evidence specific physico-chemical parameters that could be used to differentiate between the urban and the industrial particles, and particularly those emitted by different units of a steel works. In this study, the attention has been focused on particulate emissions with size  $< 10 \mu\text{m}$  from different manufacturing processes: a sintering plant, blast furnaces and a steel smelting plant. An iron ore storage area has also been considered.

The chemical analysis of metals was performed by inductively coupled plasma – mass spectrometry (ICP-MS). The morphology of particles and their individual composition have been studied by scanning electron microscopy coupled to X-ray microanalysis (SEM-EDX). Complementary investigation of the inorganic fraction has been undertaken with the use of X-ray diffraction (XRD), Infrared spectroscopy (FT-IR) and electron paramagnetic resonance (EPR), to specify the structure and the chemical environment of some metal elements.

Two kinds of Fe-rich particles were collected downwind of the steel manufacturing facilities. First, we detected iron ores particles with angular shape corresponding to hematite  $\alpha\text{-Fe}_2\text{O}_3$ . Because this phase possesses antiferromagnetic properties, such particles give a specific EPR signal intensity evolution versus the recording temperature (Ledoux *et al.*, 2004). On the other hand, Fe-rich spherules were observed under the influence of blast furnaces and the steel smelting plant. These particles are mainly composed of magnetite  $\text{Fe}_3\text{O}_4$  with their surface partly oxidized in hematite  $\alpha\text{-Fe}_2\text{O}_3$  and they are the result of the condensation of iron released into the atmosphere from processes at high temperature (Moreno *et al.*, 2004). Such particles contained also other metals as Zn and Mn incorporated in iron oxides. Particles from the sintering unit are mostly emitted from a point source.

The chemical analysis and SEM-EDX data indicate the association of K and Cl as a specific characteristic of this source and the presence of others elements with high concentration levels: Fe, Al, Si, Ca.

Under non industrial sectors, iron – rich particles that were detected correspond mostly to small particles ( $< 3 \mu\text{m}$ ) with angular shape or aged particles in which evidence of an interaction between iron oxide and sulphur dioxide could be revealed.

In this way, different tracers have been proposed for the different sources and could be validated after comparing these characteristics with physico-chemical data obtained for samples collected downwind of other influences as rural sector or urban agglomeration.

This work was supported by Arcelor Atlantique et Lorraine, Steel producer, Dunkerque (France). Nord Pas de Calais County Council is also acknowledged for financial support.

Ledoux, F., Bilinskaya, E.A., Courcot, D., Aboukassab, A., & Puskaric, E., (2004), *Atmospheric Environment*, 38, 1201-1210.  
Moreno, T., Jones, T.P., & Richards, R.J. (2004), *The Science of the Total Environment*, 334-335, 337-346.

## CHARACTERIZATION OF SALT AND ACID AEROSOLS USING RAMAN SPECTROSCOPY

S. Sinanis<sup>1</sup>, M. Aleksandrova<sup>1</sup> and K. Schaber<sup>1</sup>

<sup>1</sup>Institut für Technische Thermodynamik und Kältetechnik, Universität Karlsruhe (TH)  
Engler-Bunte-Ring 21, 76131 Karlsruhe, Deutschland

Keywords: Raman spectroscopy, aerosol measurement, aerosol characterization

In a multiplicity of technical processes absorption, cooling as well as condensation take place in the presence of inert gases. In this kind of processes simultaneous heat and mass transfer can lead to the supersaturation of the gas phase and aerosol formation initiated by homogeneous or heterogeneous nucleation. Typical examples are the absorption of acid components like HCl, HBr, HNO<sub>3</sub> and SO<sub>3</sub> in aqueous solutions and the condensation of vapors (Wix et. al., 2007). Furthermore chemical reactions in the gas phase between e.g. NH<sub>3</sub> and HCl, followed by desublimation of the generated components, can also cause undesired aerosol formation.

Despite the significance of aerosol formation for the design of gas scrubbing plants up to now knowledge on this topic is not yet sufficient. In order to understand the principles of the formation and behaviour of aerosols in wet scrubbing processes and to design suitable mist precipitators, the aerosol characteristic data like mean diameter and number concentration have to be known. Furthermore it is necessary to know the composition of the aerosols for the development of appropriate nucleation and growth models (Wix et. al., 2007).

It must be emphasized that for the characterization of aerosols containing liquid particles only optical in situ methods can be used because the equilibrium between the gas phase and the aerosol must not be disturbed due to e.g. dilution or cooling. Raman Spectroscopy can be used as an appropriate method to measure the composition of the droplets as well as the distribution of a species between the gas phase and the aerosol. This has been shown in several investigations mainly on single droplets (Schweiger et.al., 1990, Friedlander et. al., 2002).

For the generation of multicomponent salt and acid aerosols an apparatus has been developed in which salt particles like e.g. NH<sub>4</sub>Cl are formed due to the mixing followed by the reaction of NH<sub>3</sub> and HCl. A wet aerosol can be formed by adding a nitrogen stream with variable humidity to ammonia and hydrogen chloride. The Raman spectra of these aerosols give information about the distribution of NH<sub>3</sub> in the droplets and in the surrounding gas phase. Furthermore deliquescence points of mixed salt particles can be determined.

For the generation of salt aerosols from aqueous solutions containing nitrate and sulphate we used a two component jet. The aerosols produced in this way have a mean diameter of approximately 1 μm and number concentrations of up to 10<sup>7</sup> cm<sup>-3</sup> (Fig.1).

A solid state Nd:YVO<sub>4</sub> Laser with an output power up to 5 W operating at 532 nm was employed for excitation. The scattered Raman light was measured at 90° while the elastically scattered light is removed by two Notch Filters. Besides the measurement of the Raman intensities the mean diameter and the number concentration of the aerosols are measured with the Three Wavelength-Extinction Method (3-WEM). Due to this we can get information about the chemical as well as the mechanical state of the aerosol. In Fig. 1 the Raman spectrum in the aerosol phase of an aqueous solution mixture consisting of 20wt% SO<sub>4</sub><sup>2-</sup> and 10wt% NO<sub>3</sub><sup>-</sup> is shown. The two peaks at 1057 cm<sup>-1</sup> and 992 cm<sup>-1</sup> correspond to the vibrations of the nitrate and sulphate ions respectively.

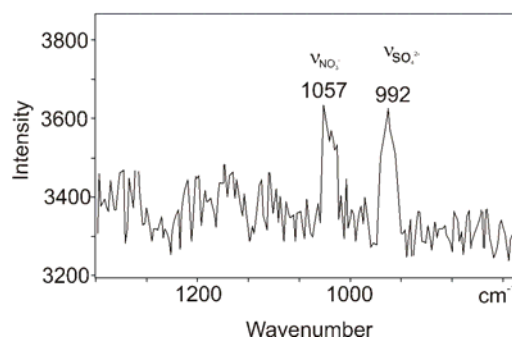


Figure 1. Raman spectrum of an aerosol consisting of 20wt% SO<sub>4</sub><sup>2-</sup> and 10wt% NO<sub>3</sub><sup>-</sup> in aqueous solution at T=298 K and a laser output power of 5W.

Schweiger, G. (1990). *J. Aerosol Sci.* 21 Nr. 4 S.483-509

Stowers, M.A., Friedlander S.K. (2002). *Aerosol Science and Technology* 36, 48-61

Wix, A., Schaber, K., Ofenloch, O., Ehrig, R., Deuffhard, P. (2007). *Chem. Eng. Comm.* 194, 565-577

## Effect of SO<sub>x</sub> gas on NO<sub>x</sub> removal process by Aerosol Driven NTPT Process

E. Nishino, K. Grzybowski, H. Takano and M. Itoh

Department of Chemical Engineering and Materials Science, Doshisha University,  
Kyo-Tanabe, Kyoto 610-0321, Japan.

Keywords: Aerosol-surface reactions, Corona discharge, NO<sub>x</sub>, Sulfur dioxide, Ammonia radical shower

To solve one of the environmental issues such as air pollutant caused by NO<sub>x</sub> and SO<sub>x</sub> gases, SO<sub>x</sub> disposal technology has been already developed, and non-thermal plasma technique (NTPT) is applied to the treatment of NO<sub>x</sub> gases. Itoh *et al.* (2003) proposed an injection method of foreign aerosols into the reaction zone so as to remove NO<sub>x</sub> without any activation of the main flue gases. The aerosol driven method combined with the NTPT might be effective to promote a removal process of both NO<sub>x</sub> and SO<sub>x</sub> gases under the heterogeneous nucleation and condensation of additional NH<sub>4</sub>NO<sub>3</sub> vapor. The aerosol driven NTPT improves removal efficiencies of NO<sub>x</sub> and SO<sub>x</sub> simultaneously, due to higher reactivity of SO<sub>x</sub> with water and NH<sub>3</sub> in aerosol formation. In this study, therefore the interference effect of SO<sub>x</sub> gas is investigated on the NO<sub>x</sub> removal process with aerosol driven NTPT.

Schematic diagram of experimental apparatus is shown in Figure 1. Carrier gas was supplied from a compressor via four cylinders of silica gel, activated charcoal, molecular sieve and Millipore filter. NO (NO: 1.01%, N<sub>2</sub> balance) and NH<sub>3</sub> (NH<sub>3</sub>: 1.98%, air balance) gases were fed from a standard gas cylinder. The temperature of electric furnace reaction chamber was maintained at 100°C.

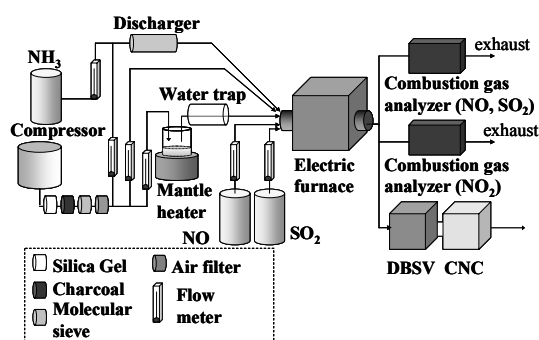


Figure 1. Schematic of experimental apparatus.

NH<sub>3</sub> and carrier gases were injected into a corona discharger. Water vapor was generated from heated ultra pure water with mantle heater, and was passing through a water trap with carrier gas. NO gas, SO<sub>2</sub> gas, discharged air, humid air and carrier gas were injected into the reaction chamber individually. Injected NO and NO<sub>2</sub> gases from the reaction chamber were measured by in-lined combustion analyzer (Series CA-6200 CA-C<sub>ALC</sub><sup>TM</sup>, TSI). The increased volumetric change of aerosol particles was estimated

from the particle size, which were distribution and particle number concentration measured with a Condensation Nuclei Counter (CNC, Model 3020, TSI) associated with an automatic diffusion battery (Model 3040+3042, TSI). All experiments have been performed under normal atmospheric pressure.

Figure 2. shows NO<sub>x</sub> and SO<sub>2</sub> removal rates with discharge in SO<sub>2</sub> concentration from 0-400ppm. Discharge worked on NO<sub>x</sub> removal comparing discharged or not. From this, discharge made NH<sub>3</sub> radical, acceleration of aerosol formation occurred. SO<sub>2</sub> gas was removed completely, both concentration 200 and 400ppm; SO<sub>2</sub> gas changed easily to be aerosols with water and NH<sub>3</sub>. According to the increase of SO<sub>2</sub> gas concentration, NO<sub>x</sub> removal rate was improved. Due to surface reaction promoted on aerosol from SO<sub>2</sub> gas, NO<sub>x</sub> reduction is increased. This means SO<sub>x</sub> aerosol affected as the condensation nuclei of NO<sub>x</sub> reduction. SO<sub>x</sub> gas affect on NTPT NO<sub>x</sub> removal process as aerosol. It can confirm that possibility of simultaneous effective removal NO<sub>x</sub> and SO<sub>x</sub> with the aerosol driven NTPT process.

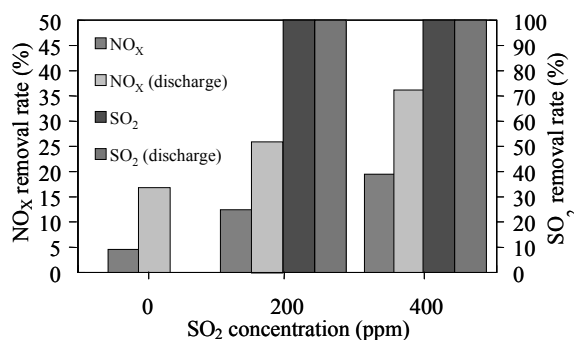


Figure 2. NO<sub>x</sub> and SO<sub>2</sub> removal rates with corona discharge in SO<sub>2</sub> concentration from 0 to 400ppm.

This study was supported by the Academic Frontier Research Project on "Next Generation Zero-emission Energy Conversion System" of Doshisha University & Ministry of Education, Culture, Sports, Science and Technology, Japan.

M. Itoh, et al (2003), Characterization of aerosol particles formed from corona discharge radical shower system during non-thermal plasma desulfurization process from flue gases, in *Proc. 3rd Asian-Pacific Intern. Symp on Basic and Appl. of Plasma Technology*, pp.66-71.

## Experimental analysis on the NO<sub>x</sub> reduction process assisted with ultraviolet irradiation

Yuji Emi, Hiroshi Takano and Masayuki Itoh

Department of Chemical Engineering and Materials Science, Doshisha University, Kyoto 610-0321, Japan

Keywords: nitrogen oxides (NO<sub>x</sub>), NO<sub>x</sub> reduction, photochemical reaction, aerosol

There are some conventional techniques for NO<sub>x</sub> reduction as catalyst method, adsorption method, condensation method, combustion thermal decomposition method and non-thermal plasma techniques (NTPT). NTPT is mostly efficient but usually high energy consumption process. One of the major processes utilizing NTPT is the reduction process of such gases by numerous aerosolizations based on heterogeneous nucleation. It precedes by gas phase chemical reactions accelerated with ions or radicals excited by electron beams and/or thermal electrons from corona discharge. The rate-determining step in such excitation processes is the collision process of electrons to gases molecule, and the efficiency is directly related to the number of electrons having sufficient kinetic energy. However, such excitation of gases can perform with photochemical process with ultraviolet irradiation.

In this study, the NO<sub>x</sub> removal efficiency associated with ultraviolet (UV) irradiation was investigated with a large tubular type Pyrex chemical reaction chamber (inner diameter: 145 mm, effective length: 1800 mm) to improve the energy efficiency in NTPT.

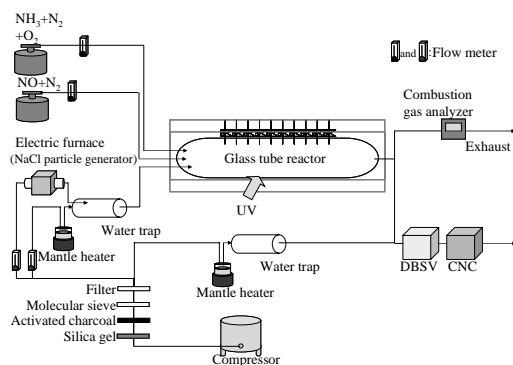


Figure 1. Schematic diagram of experimental system.

The schematic diagram of experimental system was shown in Figure 1. NaCl particles for aerosol driven process (Yamada, et al.), NO gas and NH<sub>3</sub> gas were mixed with aerosol free humid air in the glass tube reactor. The reactor was set at the center of UV tunnel (Peak wave length: 350nm). The UV intensity was ranged from 0 to 14.9Wm<sup>-2</sup>. Initial NO and NH<sub>3</sub> concentrations were set at 500ppmv. In the tubular reactor, temperature was equalized to room temperature (23°C). Residence time of the reactants in the reactor was about 520s. The NO gas and NO<sub>2</sub> gas concentrations were measured with combustion

gas analyzer (Series CA6200 and CA6000 TSI) from the chamber outlet. Particle number concentration was measured with CNC (MODEL 3020 TSI) attached with Diffusion Battery (MODEL3040 TSI).

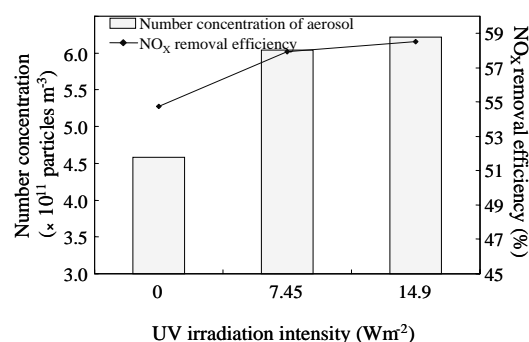


Figure 2. Number concentration of the generated aerosols and NO<sub>x</sub> removal efficiency.

The effects of UV on the particle generation and the NO<sub>x</sub> removal efficiency are shown in Figure 2 for three cases. Without any additional operation except mixing of NO<sub>x</sub> and NH<sub>3</sub>, some portion of NO<sub>x</sub> can be removed by the condensation on to the foreign NaCl particles following weak acid-base gas phase chemical reactions. Still, NO<sub>x</sub> removal efficiency increased so much via strong acid-base gas reaction enhanced under the UV irradiation. It is because resultant OH radical attacked on NO<sub>x</sub> to form HNO<sub>3</sub>; such NO<sub>x</sub>-water reaction path is very seldom without the radical.

In this experiment, the photon flux density was  $9.3 \times 10^{18}$  photons/s at  $7.45 \text{ Wm}^{-2}$  and the number of NO<sub>x</sub> molecule introduced into the reactor per unit time was  $6.7 \times 10^{17} \text{ s}^{-1}$ . So the photon density was saturated even at the middle point, and the removal efficiency seemed to be similar in the case of  $14.9 \text{ Wm}^{-2}$ . It is not so easy to compare the energy-based removal efficiency with usual NTPT. Still it will be possible to say that photon is absorbed for the molecule excitation but the electron parcels out its energy for the excitation and passing away.

This study was supported by the Academic Frontier Research Project on "Next Generation Zero-emission Energy Conversion System" of Doshisha University & Ministry of Education, Culture, Sports, Science and Technology, Japan.

K. Yamada, Y. Emi, H Takano and M. Itoh, (2006), in *Proc. ICLASS2006*, C1-10-216.

## Filter Cleaning Performance of a Cyclone-Baghouse Dust Collector

Hyun-Seol Park and Kyung Soo Lim

<sup>1</sup>Department of Energy Conversion Research, Korea Institute of Energy Research, 71-2 Jang-dong, Yuseong-gu, 305-343, Daejeon, Korea

Keywords: Bag Filter, Cyclone, Baghouse, Filter Cleaning, Dust Removal

Baghouse is one of the most efficient dust removal devices. The dust collection efficiency of baghouse is related to the properties of bag filter media, air to cloth ratio (filtration velocity), filter cleaning method, and others. Among them, the filter cleaning process is the key parameter having a great influence on filtration efficiency and filter life time. For a baghouse with a pulse-jet cleaning, most of dust particles are emitted at the instant of or in a few minutes after filter cleaning. Therefore, the elongation of filter cleaning interval decreases the emitted dust amount, consequently enhancing filtration efficiency. Smaller dust loading to bag filters is the best way to increasing filter cleaning interval and filter life time.

A hybrid dust collector combining a modified cyclone and a cylindrical baghouse has been developed. The cyclone-baghouse is aimed at reducing dust loading to bag filters, thus increasing filter cleaning interval and filtration efficiency, and elongating filter life time (Park et al., 2000). In this study, we have tried to examine the filter cleaning performance of the cyclone-baghouse, further to find out the effect of flow field introducing to bag filters (at the outlet of cyclone).

Fig. 1 shows the schematic diagram of the cyclone-baghouse. The outer diameter of the cylindrical collector was 520mm, the cyclone outlet diameter was 195/316 mm, and the bag filter was  $\phi$ 130 and 600 mm in length. The flow rates were 3.5 and 7.0 m<sup>3</sup>/min. A lattice flow distributor was installed inside the cyclone outlet for changing the flow pattern.

Filter cleaning interval with cleaning cycles, which is the elapsed time between pulse-jet cleanings, is plotted in Fig. 2. The residual pressure drop, which is the pressure drop across bag filters right after filter cleaning, is shown in Fig. 3. The flow rate is linearly proportional to the pressure drop, and higher flow rate means higher dust amount collected on filters, thus the residual pressure drop and cleaning interval were increased with flow rate. The lattice flow distributor breaks up the rotational flow, and changes it into somewhat straight upward flow. Our results show that the less rotational flow in the cyclone outlet gives higher cleaning efficiency (lower residual pressure drop) and longer cleaning frequency, which denotes the enhanced filtration performance of the cyclone-baghouse dust collector with a flow distributor.

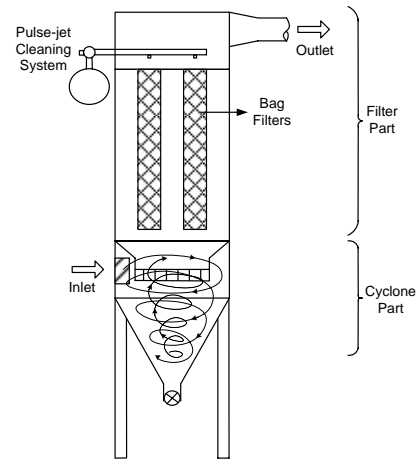


Figure 1. The cyclone-baghouse dust collector.

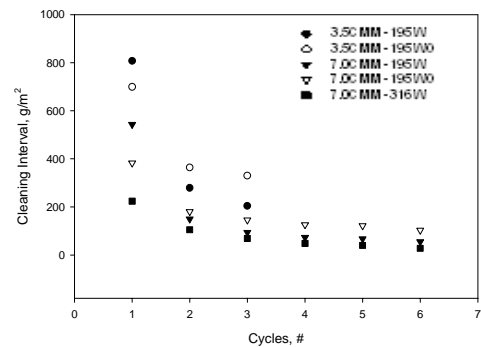


Figure 2. Filter cleaning intervals

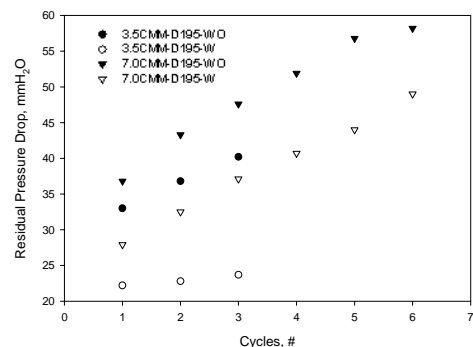


Figure 3. Residual pressure drop

Park, Y.O., Kim, S.D., Son, J.E., Rhee Y.W. & Choi, W.S. (2000). *Korean J. of Chem. Eng.*, 17(5): 579-584.

## **T18 Abstracts**

## Reentrainment and deaggregation of powder particles as a result of flow disarrangement

T.R. Sosnowski, J. Gac, and L. Gradoń

Faculty of Chemical and Process Engineering, Warsaw University of Technology, Waryńskiego 1, 00-645 Warsaw, Poland

Keywords: turbulence, dry powder inhaler, reentrainment, resuspension

Resuspension of powder particles by a stream of flowing air is a fundamental process for the operation of dry powder inhalers (DPI). Micronized particles of a drug and carrier (typically – lactose), which constitute the given pharmaceutical powder have strong tendency to aggregate due to van der Waals forces and electrostatic effects. A medical inhaler should release fine particles capable of penetrating to the lungs, so the effective deaggregation of powder grains during aerosolization process inside the DPI is essential.

In this work we report theoretical and experimental studies related to powder reentrainment and break-up of aerosol particles in turbulent flow, which is artificially induced due to the presence of turbulence promoters in the powder resuspension chamber. This study is an elaborated extension of our initial research reported recently (Sosnowski et al., 2006).

The eddy fluid particle model (EFPM) has been used to calculate the turbulent airflow field in the chamber of the given geometry, as described by Gac et al. (2007). Knowing the instantaneous airflow field, particle-particle interactions in the powder structure were considered utilising a modified Verlet algorithm.

In the experimental part of the study we compared three arrangements of the resuspension chamber: one without any flow disturbance, and two with different turbulence promoters. The powder of sodium cromoglicate was resuspended with air drawn with the flow rates in the range of 5-60 LPM. The PSD of emitted aerosol was determined with WELAS spectrometer.

Computational results, which illustrate the mechanism of particle reentrainment and consecutive break-up by turbulent eddies are depicted in Fig.1.

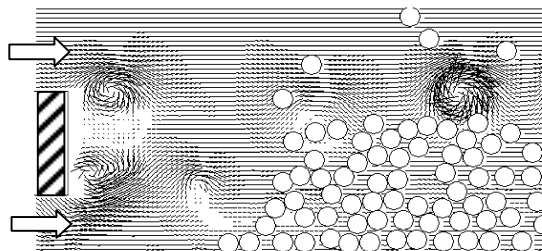


Figure 1. Computational prediction of particle reentrainment and break-up in turbulent flow field.

The measured effects of enhanced powder resuspension and deaggregation by disarrangement of aerosol flow are illustrated in Fig. 2 and 3.

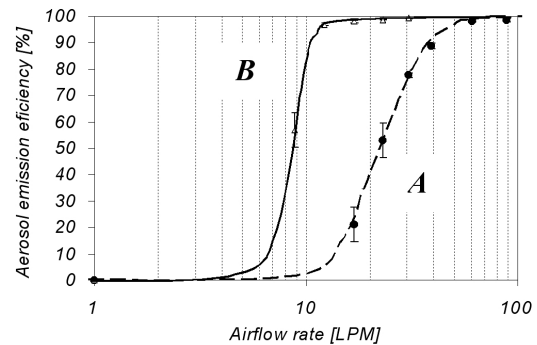


Figure 2. Aerosol resuspension efficiency for undisturbed (A) and disturbed (B) airflow.

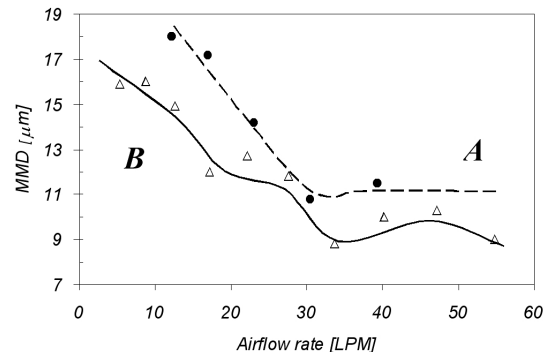


Figure 3. Mass median diameter for the system without (A) and with (B) flow disarrangement.

Both the theoretical predictions and experimental results indicate that powder resuspension is significantly improved in the systems where flow is disarranged by turbulence promoters. The reason is a more effective transfer of kinetic energy from air into the powder structure. The increase of pressure drop due to use of the promoters remains at a reasonable level from the viewpoint of DPI application.

This work was supported by the budget sources for science in the years 2005-2008 (MEiN grant 3 T09C 028 29).

Gac, J., Sosnowski, T.R., Gradoń, L. (2007). *J. Aerosol Science* - submitted

Sosnowski, T.R., Gradoń, L., & Bernatek, P. (2006). in *Proc. 5th Int. Aerosol Conf.*, St. Paul, 898-899.

## The effect of particle hygroscopicity on mouth and throat deposition

C. Mitsakou<sup>1</sup>, D. Mitrakos<sup>1,2</sup> and C. Housiadas<sup>1</sup>

<sup>1</sup>“Demokritos” National Centre for Scientific Research, 15310 Athens, Greece

<sup>2</sup>National Technical University of Athens, Faculty of Mechanical Engineering, 15780 Athens, Greece

Keywords: health aspects of aerosols, inhalation, aerosol dynamics.

The administration of pharmaceutical aerosols is commonly made through the oral route because of the lower filtering efficiency of the inspired aerosol along the oral pathway compared to the nasal pathway. In general, metered-dose inhalers include water-soluble compounds. Thus, the investigation of the effect of hygroscopicity on particle deposition in the mouth and throat region seems in order.

In this study a previously developed mathematical model (Mitsakou *et al.*, 2004) was further elaborated to address growth effects. The model is based on a one-dimensional representation of the aerosol flow along the mouth-throat extrathoracic flow-path. The geometrical model of Stapleton *et al.* (2000) was used as a basis for the mouth-throat geometry. The latter scheme was reduced to a sequence of three cylindrical tubes segments, describing the oral cavity, the pharynx and the larynx, joined together.

The aerosol flow is calculated by a Eulerian mechanistic description that takes into account aerosol deposition and dynamics, based on the modeling work of Mitsakou *et al.* (2005). The rate of particle diameter increase due to hygroscopic growth is described through a modified expression of Mason’s equation. The increase rate of particle diameter  $d$  is described as follows

$$\dot{d} = \frac{4}{d} \left( S - 1 - \frac{4\sigma}{d\rho_l R_v T_g} + \frac{6\chi n_s m_0 M_l}{\pi M_s \rho_l d^3} \right) \cdot \frac{f_{FS}}{f_{mass} + f_{heat}} \quad (1)$$

where  $S$  is the saturation ratio,  $\sigma$  the particle surface tension,  $\rho_l$  the water density,  $R_v$  the gas constant for water vapour,  $T_g$  the gas (air) temperature,  $\chi$  the aerosol soluble fraction,  $n_s$  the degree of ion dissociation,  $m_0$  the dry particle mass,  $M_l$  the water molecular weight and  $M_s$  the apparent molecular weight of the aerosol soluble components. The factors  $f_{FS}$ ,  $f_{mass}$ ,  $f_{heat}$  represent the Fuchs correction term, the contribution associated with mass transfer (vapor diffusion) and the contribution due to heat conduction respectively.

Figure 1 shows total deposition, as well as deposition in the oropharyngeal and laryngeal regions separately, as a function of the initial particle diameter. The extrathoracic deposition is calculated

for both inert and hygroscopic particles. For the hygroscopic aerosol we applied the physical properties of sodium chloride (molecular weight = 58.5 g mol<sup>-1</sup>, ion dissociation = 2) to maximize the effect. As shown, if hygroscopic growth is neglected, deposition of water-soluble particles may be significantly underestimated (e.g. by 50% for initially 6 μm particles). Thus, hygroscopic growth has to be taken into account to properly calculate deposition in the mouth-throat region.

In terms of regional deposition, the effect is more pronounced in the oropharyngeal region, in comparison to that in the laryngeal region. In general, higher deposition is calculated in the former region, due to the significant flow direction change (~ 115°) and constriction at the end of the oral cavity.

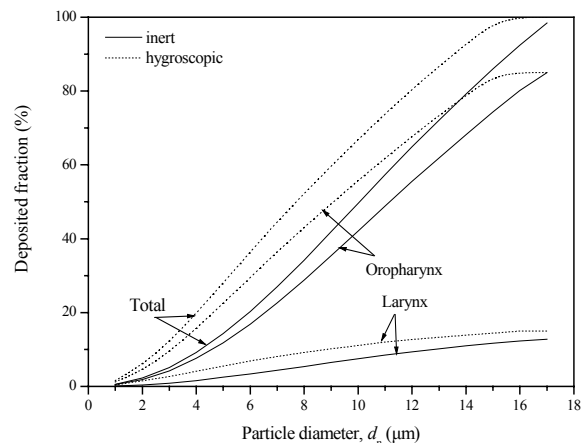


Figure 1. The impact of hygroscopic growth of water-soluble particles on deposition as a function of particle size, shown for the whole mouth and throat region, and separately in the oropharyngeal and laryngeal sub-regions.

Work partially supported by GSRT - O.P. “Competitiveness”, co-funded (75%) by the European Union - European Regional Development Fund (ERDF).

Mitsakou, C., Helmis, C., & Housiadas, C. (2004). *J. Aerosol Sci.*, 35, S1127-S1128 (Proc. EAC 2004).

Mitsakou, C., Helmis, C., & Housiadas, C. (2005). *J. Aerosol Sci.*, 36, 75-94.

Stapleton, K. W., Guentsch, E., Hoskinson, M. K., and Finlay, W. H. (2000). *J. Aerosol Sci.*, 31, 739-749.

## Numerical study of the transient behavior of cascade impactors

M. Chiruta, D. L. Roberts, F. J. Romay

MSP Corporation, Shoreview, MN 55126, USA

Keywords: Inertial impactor, Medicinal aerosols, Modeling

European Pharmacopoeia (EP) section 2.9.18 describes a method for testing dry-powder inhalers (DPIs) that is based on cascade impactors. The test method involves opening a solenoid valve to initiate the air flow, leaving the solenoid valve open for a few seconds, and then closing the solenoid valve. The goal of this flow transient is to simulate approximately the breathe-actuated discharge of particles that takes place when a DPI is used by a patient. However, the aerodynamic behavior of cascade impactors is understood only for steady-state flows, and therefore the flow transient prescribed in the EP method obscures the interpretation of the cascade impactor results.

This paper is aimed at elucidating the aerodynamic behavior of cascade impactors during transient flows of the type prescribed in the EP inhaler testing methods. We aim to provide a means for deducing the size distribution of particles emitted by a DPI when one knows the steady-state aerodynamics of the impactor, how long the solenoid valve is open, and how much mass of particles is captured in each stage. We make a number of approximations for other physical parameters characteristic of an EP DPI test method.

A typical cascade impactor consists of a series of impaction stages. Each stage collects the aerosol particles larger than a given size; the smaller particle can remain airborne and pass to the next stage. For a given set of steady flow conditions each collection stage has a well defined particle capture efficiency curve (Mitchell & Nagel, 1997). For example, Table 1 presents the seven NGI stage cut sizes ( $D_{50}$ ) for three different flow rates (Marple et. al., 2003).

Table 1 Stage cut sizes at 30, 60 and 100L/min

Stage	$D_{50}(\mu\text{m})$ at each flow rate		
	30 L/min	60 L/min	100 L/min
1	11.7	8.06	6.12
2	6.40	4.46	3.42
3	3.99	2.82	2.18
4	2.30	1.66	1.31
5	1.36	0.94	0.72
6	0.83	0.55	0.40
7	0.54	0.34	0.24

The EP DPI testing method consists of a cascade impactor with a vacuum pump, a two-port

solenoid valve, a timer, a flow control valve, and connecting vacuum tubing (European Pharmacopoeia, Section 2.9.18). The duration of the test is controlled by the timer.

If the duration of the test were much longer than the time to fully open and close the solenoid valve, the transient flow regime would not significantly influence the distribution of particles collected in each stage. However since a typical steady-state flow rate is 60 L/min, and since regulators want to see total volumes of 1 L, 2L, and 4L, it is typical for the solenoid valve to be open 1 sec, 2 sec, or 4 sec. The solenoid valves themselves tend to have 0.1 seconds opening time. Hence the duration of the test is comparable with the duration of the transient flow regime. The collection efficiency curves are different in the transient regime compared to the steady regime. This difference translates into an uncertainty in the size of the particles captured on each stage.

To describe the impactor performance in the transient regime, we developed a numerical model of a cascade impactor. The airflow is described by the unsteady Navier-Stokes equation. The individual aerosol particles behavior is described by equation of motion.

First we computed the airflow field through the impactor in the three functioning time stages: during the opening of the two-way solenoid valve, during the steady state functioning regime, and during the closing of the valve.

To quantify the effect of the transient regime on the cascade impactor, we ran a set of numerical experiments with the duration of the sampling time as a parameter. For short sampling times, the transient effect had a detrimental effect on the retrieved size distribution. The retrieved distribution was broadened and skewed towards larger particles sizes. As the sampling time increased the retrieved distribution resembled more and more the original distribution .

European Pharmacopoeia 5.1 Supplement (2004), 2.9.18, Preparations for inhalation, 2804.  
Mitchell, J. P., Nagel, M. W. (1997), Particle Sci. Technol., 15, 217-41.  
Marple, V. A., et. al (2003), J. Aerosol Med., 16, 283-99.

## Aerodynamic characterisation of new pharmaceutical inhalers

H. Wachtel<sup>1</sup>, Ö. Ertunç<sup>2</sup>, Ç. Köksoy<sup>2</sup>, and F. Durst<sup>2</sup>

<sup>1</sup>Boehringer Ingelheim Pharma GmbH & Co. KG, Binger Str. 173, D-55218 Ingelheim, Germany

<sup>2</sup>Lehrstuhl für Strömungsmechanik, Universität Erlangen-Nürnberg, D-91058 Erlangen, Germany

Keywords: Aerosol generation, inhalation, instrumentation, inhaler.

The rapidly increasing number of new inhalers on the market makes the selection of the optimum device difficult, both for doctors and patients. This choice is even more complicated at start of development of a new inhalative medication. It is imperative that the 'right' device be selected which will reproducibly generate aerosolised medication.

The aerodynamic design of inhalers decides on the patients' perception during inhalation and consequently influences the compliance. Apart from the subjective feeling, the performance of a device can be measured objectively by testing procedures described in the pharmacopoeia, e.g. EP or USP. During development, the pharmacopoeial tests must be supplemented by visualisation of the drug delivery process in the device and eventually the mouth-/throat region. Only the combination of both, the quantitative testing and aerodynamic analysis results in the complete understanding of the inhaler under consideration.

Methods of our analyses are computational fluid dynamics (CFD) and flow visualisation using scaled models based on the conservation of the Reynolds number. Figure 1 shows the cross-section through the HandiHaler®, a single dose dry powder inhaler which is used for the administration of powder in capsules. The advantage of visualisation of streamlines using a flow channel becomes clear when the rapid motion of the capsule inside the chamber is analysed. In this application, CFD would require dynamic meshing and would consume time and computing power in order to account for the motion of the capsule, while the scaled model can easily be filmed and even be modified on the fly, thus enabling faster development cycles.

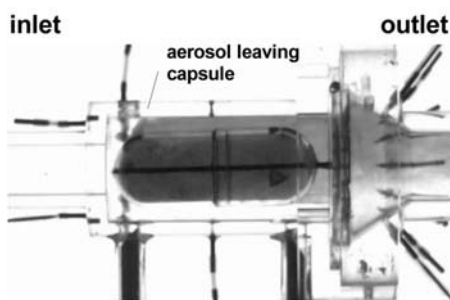


Figure 1. View into the transparent air duct of the HandiHaler® model in the flow channel.

The HandiHaler® is a passive device, i.e. the energy required for aerosolization of the powder is gained from the air flow sucked through the device. Motion and emptying of the capsule is governed by the hydrodynamic paradoxon. Based on typical breathing patterns of patients (flow profiles), the aerosolization process has been optimised. In contrast, the spray generation of the Respimat® soft mist inhaler (SMI) is independent of the patient. This inhaler is an example of an active device which uses mechanical energy of a spring to push a piston which presses a liquid through a nozzle. By its micro structured nozzle, drug solutions are atomized at high pressure (~200 bar) and presented to the air flow inhaled by the patient. Figure 2 shows the superposition of an image taken at the flow channel and the CFD simulation.

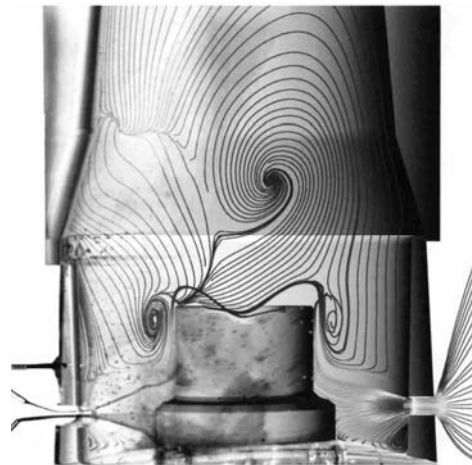


Figure 2. Superposition of flow visualisation in a transparent model (left) and CFD calculation (right) of the mouthpiece of Respimat® attached to the model of the USP inlet tube.

Concluding, computational fluid dynamics as well as flow visualisations using dedicated flow channels and scaled models are important tools during the development of new inhalers. The visualisations are extremely helpful with respect to the 'Quality by design' concept. Moreover, using throat models (Finlay et al.), mouth and throat deposition can be investigated, thus optimizing the inhaler / patient interface.

Finlay, W. H. et al. (2004). *Experiments in Fluids*, 37, 673-689.

## **T19 Abstracts**

## Seasonal variability in atmospheric aerosol levels and composition during 2006 at Uccle, Belgium

X. Chi<sup>1</sup>, W. Maenhaut<sup>1</sup>, W. Wang<sup>1</sup>, N. Raes<sup>1</sup>, H. De Backer<sup>2</sup> and A. Cheymol<sup>2</sup>

<sup>1</sup>Institute for Nuclear Sciences, Ghent University, Proeftuinstraat 86, B-9000 Gent, Belgium.

<sup>2</sup>Dept. of Observations, Royal Meteorological Institute of Belgium, 3 avenue Circulaire, B-1180 Uccle, Belgium.

Keywords: atmospheric aerosols, PM10/PM2.5, chemical composition, chemical mass closure, seasonality.

During 2006, a study was undertaken at Uccle, Belgium, to examine the relationship between the vertical column-integrated Aerosol Optical Depth (AOD) and the boundary layer aerosol characteristics. As part of this study, PM<sub>2.5</sub> and PM<sub>10</sub> aerosol samples were collected on 0.4 µm pore size Nuclepore polycarbonate filters and on pre-fired Whatman QM-A quartz fibre filters. The collections were done during the daytime only and on days with no or few clouds when 50% or more valid AOD data were to be expected. A total of 109 collections were performed with each sampler.

The particulate mass (PM) was obtained from weighing each filter before and after sampling with a microbalance. All quartz fibre filters were analysed for organic carbon (OC) and elemental carbon (EC) by a thermal-optical transmission (TOT) technique. The Nuclepore filters were analysed for 29 elements (from Na to Pb) by particle-induced X-ray emission spectrometry (PIXE) and for major anions and cations by ion chromatography (IC) (Maenhaut *et al.*, 2005).

Seasonal median atmospheric concentrations (ranges and other descriptive statistics) were calculated. From examining these data, it appeared that (for both PM<sub>2.5</sub> and PM<sub>10</sub>) the median atmospheric levels of the PM were about a factor of two higher in winter than in the other three seasons. Also the other major aerosol species (OC, ammonium, nitrate, and sulphate) exhibited higher medians in winter than in the other 3 seasons. The high levels in winter were due to the strong pollution episode at the end of January and beginning of February 2006, which persisted from western to central Europe. Nitrate and the Cl<sup>-</sup>/Na<sup>+</sup> ratio were clearly lowest in summer; for nitrate this is at least in part due to the fact that the volatile ammonium nitrate is rather in the gas phase than in the particulate phase within the atmosphere during this season, but volatilisation of nitrate from the aerosol collected on the filter may also play a role; the low Cl<sup>-</sup>/Na<sup>+</sup> ratios during summer (medians of 0.05 and 0.35 in PM<sub>2.5</sub> and PM<sub>10</sub>, resp., versus, for example, 0.82 and 1.25 in PM<sub>2.5</sub> and PM<sub>10</sub>, resp., in spring) indicate that the loss of Cl from the sea-salt aerosol (because of reactions with acidic species within the atmosphere or on the filter) is clearly most pronounced in this season. The medians for the crustal elements (Al, Si, Ca, Ti) were similar in all seasons, the primary biogenic element P had highest median in summer; and several (mostly an-

thropogenic) elements, including K, Mn, Fe, Cu, Zn, and Pb, had highest medians in winter, followed by fall; the medians for Zn and Pb in fall were about a factor of 2 higher than those in summer.

Aerosol chemical mass closure calculations were made for the PM<sub>2.5</sub> and PM<sub>10</sub> aerosol, and also for the coarse (PM<sub>10-2.5</sub>) size fraction, and this for each individual sampling. As gravimetric PM data we used the data from the Nuclepore polycarbonate filters. For reconstituting this PM, eight aerosol types (or components) were considered (Maenhaut *et al.*, 2005). The average concentrations of the various aerosol types (and of the unexplained gravimetric PM) in PM<sub>10</sub> for each season are shown in Figure 1. The percentage contributions of the various components to the seasonally averaged gravimetric PM were also calculated. Secondary inorganic aerosols (SIA), which is the sum of ammonium, nitrate and non-sea-salt (nss) sulphate, was the major component in each season for both PM<sub>2.5</sub> and PM<sub>10</sub>, in each case followed by organic matter (OM, calculated as 1.4 OC). For example, in PM<sub>2.5</sub>, SIA accounted for 59, 67, 46, and 42% of the mean PM in winter, spring, summer, and fall, respectively. The corresponding percentages for OM were 34, 20, 41, and 32%. Crustal matter was the major component in the coarse size fraction, with percentages in the range of 28 to 42%.

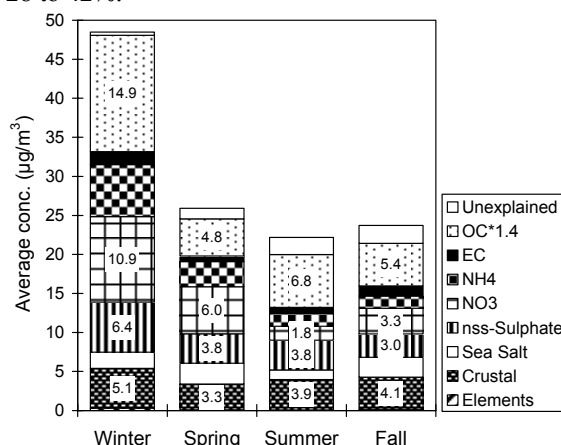


Fig. 1. Seasonally averaged concentrations of 8 aerosol types in PM<sub>10</sub> at Uccle during 2006.

Maenhaut, W., et al. (2005). *X-Ray Spectrom.*, 34, 290-296.

## Source Apportionments and Spatial Variability of Coarse Particle During the Regional Air Pollution Study (RAPS)

InJo Hwang<sup>1</sup>, Philip K. Hopke<sup>1</sup>, and Joseph P. Pinto<sup>2</sup>

<sup>1</sup>Department of Chemical and Biomolecular Engineering, Clarkson University, Potsdam, NY 13699-5708, USA

<sup>2</sup>U.S. Environmental Protection Agency, Research Triangle Park, North Carolina 27711, USA

Keyword: coarse particles, PMF, spatial variability, COD

Recently the U.S. Environmental Protection Agency (EPA) considered the promulgation of a National Ambient Air Quality Standard for inhalable coarse particulate matter (smaller than 10  $\mu\text{m}$  in diameter but larger than PM<sub>2.5</sub>). The new standard was to be limited to urban coarse particles (Edelman, 2006). Although they ultimately chose not to establish a new indicator at this time, there is a need to better understand the spatial variability of coarse particles across urban area and the variation in exposure to coarse particles arising from different sources.

The objective of this study is to characterize the spatial uniformity in coarse particle source contributions so that the potential for exposure characterization error in health outcome studies can be better understood. In the present study, Positive Matrix Factorization (PMF) was applied to an ambient coarse particles compositional data from ten RAPS/RAMS sites in St. Louis to identify the coarse particle sources and estimate their contributions to coarse particles mass concentrations in the St. Louis metropolitan area. Also, the spatial variability in contributions from source categories is discussed.

The ambient coarse particle samples were collected at ten sampling sites in St. Louis metropolitan area as part of the St. Louis Regional Air Pollution Study (RAPS) (Alpert & Hopke, 1981). The coarse particle samples were collected using the automatic dichotomous samplers between May 1975 and April 1977. Samples were analyzed for total mass concentration by  $\beta$ -gauge measurements and a total of 27 species were analyzed using Energy-Dispersive X-ray fluorescence (EDXRF) analysis (Chang et al., 1988). Positive Matrix Factorization (PMF) (Pattero, 1997) was applied to the data using the PMF2 program. PMF was described in detail in prior studies (Hwang & Hopke, 2007). Pearson correlation coefficients and the coefficients of divergence (COD) were used to evaluate the degree of spatial heterogeneity of source contributions among sampling sites (Kim et al., 2005).

Nine sources were identified for 8 of the 10 sites (exceptions were sites 122 and 124): soil, cement kiln/quarry, iron + steel, motor vehicle, incinerator, pigment plant, primary/secondary lead smelter, zinc smelter, and copper production source, respectively. Soil was the largest coarse particles source across the

study area (6.15  $\mu\text{g}/\text{m}^3$ , 29.3 %). Cement kiln/quarry, iron + steel, and motor vehicle source were the other large contributions to the coarse particles mass (5.27  $\mu\text{g}/\text{m}^3$ , 25.1 %; 3.53  $\mu\text{g}/\text{m}^3$ , 16.8 %; 2.72  $\mu\text{g}/\text{m}^3$ , 12.9 %). The analysis of spatial variability showed that point sources are the least well correlated among the source categories and, point sources are nonuniform in the St. Louis metropolitan area. The results of this study showed spatial distributions of coarse particles source contributions can be highly heterogeneous within a given region.

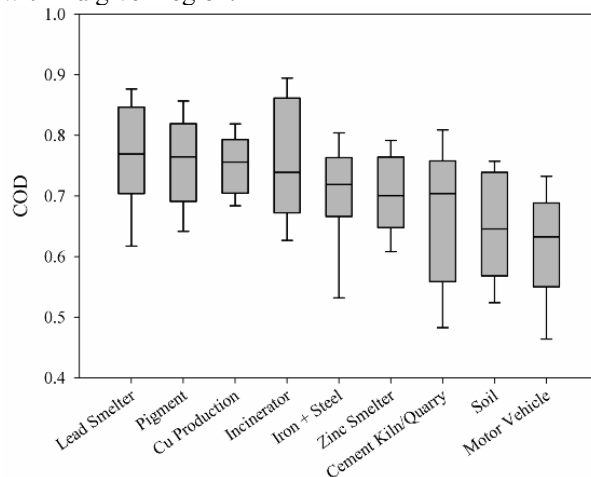


Figure 1. The average COD for source contributions between all of the site pairs.

This work was supported by the U.S. Environmental Protection Agency (EPA) under contract No. EP06C000004.

- Alpert, D.J., & Hopke, P.K. (1981). *Atmospheric Environment*, 15, 675-687.
- Chang, S.N., Hopke, P.K., Gordon, G.E., Rheingrover, S.W. (1988). *Aerosol Sci. Technol.*, 8, 63-80.
- Edelman, N. (2006). *Environmental Management*. June, 24-29.
- Hwang, I.J., & Hopke, P.K. (2007). *Atmospheric Environment*, 41, 506-518.
- Paatero, P. (1997). *Chemom. Intell. Lab. Syst.*, 37, 23-35.
- Kim, E., Hopke, P.K., Pinto, J.P., Wilson, W.E. (2005). *Environ. Sci. Technol.*, 39, 4172-4179.

## Analysis of temporal patterns of vertical turbulent fluxes of PM2.5 on the Venice lagoon

A. Donateo<sup>1</sup>, D. Contini<sup>1</sup>, D. Cesari<sup>1</sup>, F. Belosi<sup>2</sup>, F. Prodi<sup>2</sup>

<sup>1</sup>Institute of Atmospheric Science and Climate (ISAC-CNR), 73100, Lecce, Italy  
<sup>2</sup>Institute of Atmospheric Science and Climate (ISAC-CNR), 40100, Bologna, Italy

Keywords: PM2.5, aerosol measurement, dry deposition, fluxes, turbulence.

In this work an analysis of the aerosol local dynamics, for the PM2.5 fraction, is presented. Measurements have been carried out in the Mazzorbetto Island in the Venice Lagoon using a measuring station based on a 3D-ultrasonic anemometer and a real-time PM2.5 optical detector (pDR1200, Mie). Measurement system allows detecting fluctuations of the concentration and velocity fields that are also used to evaluate the vertical turbulent fluxes of PM2.5.

Data post-processing is based on 30 minutes averages in the streamlines reference system. The eddy-correlation method is used to estimate vertical turbulent of momentum, sensible heat and PM2.5 fluxes as described in (Donateo et al., 2006). Measured optical concentrations have been corrected with the procedure described in (Donateo et al., 2006) for the effect of relative humidity (RH). Corrected daily averaged concentrations have been compared with gravimetric detection of aerosol and a good correlation (Pearson 0.93) has been obtained. It has to be put in evidence that there is a great variability of PM2.5 concentrations caused by different meteorological events: rain, snow and changes in wind parameters and also by changes in the sources. It has been put in evidence a contribution from local industrial sources, a long-range transport from Pianura Padana and also some events of intrusion of African Dust. Correlation of concentration levels with wind direction shows that higher concentration are associated to wind blowing from the SW-W sectors and lower concentration are associated to wind coming from the Sea (SE). A seasonal pattern is present with higher winter concentrations, as it often happens in the north of Italy (Marcazzan et al., 2001). The vertical turbulent fluxes are mainly positive during the winter and mainly negative during the summer or spring (Figure 1). Results put in evidence also the presence of a daily pattern with diurnal (8-20) average PM2.5 concentration lower than nocturnal average (20-8). The pattern is also present in the turbulent fluxes with the maximum activity present in diurnal hours because of the more intense turbulence (Figure 1). The concentration daily pattern is analyzed in terms of typical day: averaging all data registered in a specified hour of the day. To put in evidence eventual trends, the analysis has also been carried out using the hourly fluctuations of concentrations  $C_f$  with respect to the daily average:

$$C_f = \frac{C - \langle C \rangle_{\text{daily}}}{\langle C \rangle_{\text{daily}}} \quad (1)$$

where  $C$  is the hourly concentration and  $\langle C \rangle_{\text{daily}}$  is the daily average. Results show a very similar pattern both in summer, winter and spring even if the original concentrations are quite different. The pattern has been found to be correlated with the pattern of prevalent wind direction, relative humidity and also boundary layer height. This confirms the relationships between concentration levels and local meteorology.

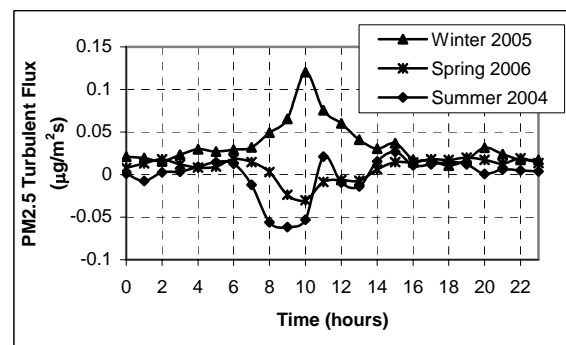


Figure 1. Daily pattern of vertical turbulent fluxes of PM2.5 on the Venice lagoon.

We used a one-dimensional model for the calculation of time dependent boundary layer height ( $H$ ), using one point surface data (Martano & Romanelli, 1997). Results indicate that there are several periods in which  $H$  and  $C$  are correlated (at hourly level), but also other in which this correlation is not present and this means that the growth of the boundary-layer is not the only driving force of concentration changes.

Financial contribution of CORILA is gratefully acknowledged. Authors wish to thank Dr. A. Gambaro and Dr. S. Ferrari for their precious contributions.

Donateo A., D. Contini, F. Belosi, 2006. *Atmospheric Environment*, 40, 2006, pp. 1346-1360  
 Marcazzan G.M., Vaccaro S., Valli G., Vecchi R. 2001. *Atmospheric Environment*, 35, 4639-4650.  
 Martano, P. & Romanelli, A. 1997. *Boundary Layer Meteorology*, 82, 105-117.

## Urban dust – chemical composition of PM<sub>10</sub> fraction in Prague tunnels

V. Tydlitát<sup>1</sup>, B.Kotlík<sup>2</sup>, J. Karban<sup>1</sup> and J. Janota<sup>3</sup>

<sup>1</sup>Institute of Chemical Process Fundamentals AS CR, v.v.i., Rozvojová 135, 165 02, Praha 6, Česká republika

<sup>2</sup>National Institute of Public Health, Šrobárova 48, 100 42, Praha 10, Česká republika

<sup>3</sup>Magistrát hl.m.Prahy, Jungmannova 35, 111 25, Praha 1, Česká republika

Keywords: PM, urban aerosols, chemical composition, diesel exhaust.

Airborne pollution in Prague is a serious issue. Exposure to excess PM<sub>10</sub> values is nationwide; in 2005, 97 % of the population in the monitored area were exposed to annual median values of 40 µg/m<sup>3</sup> whilst 99 % were exposed to a value in excess of 30 µg/m<sup>3</sup>.

Figure1. Estimated distribution of PM<sub>10</sub> airborne particle load in Prague (2005)

Median values of the particulate matter PM<sub>10</sub>, assessed period 2000-2004



Major aerosol sources include, apart from industrial sources, direct emissions (esp. combustion engines, abrasions and resuspended particles). The annual consumption of 424 000 tonnes of diesel fuel in Prague allows a minimal estimate of emission volume from diesel motors alone (assuming pollution at 0.1g of solid pollutants per km) of 716 tonnes of fine particles (< 2.5 µm)/annum. Consumption of diesel fuel in Europe is on the increase; in Prague, it is necessary to take into account the no. of diesel-powered vehicles in use (over 50% of those over 15 years old) as well as regular transit sources.

In two Prague urban road tunnels (2100 a 900 m long) with traffic load in excess of 30 000 vehicles/day, PM<sub>10</sub> airborne particles and sediments from the roads and ventilation systems were collected in the Spring and Summer seasons 2006. The advantage was the unambiguous identity of sources and high volume of samples.

Tab.1. PM<sub>10</sub> concentrations as µg/m<sup>3</sup> (2006)

Strahov tunnel		tunnel Mrázovka	
Spring	Summer	Spring	Summer
1170	850	430	310

Determinations were made for both macro elements largely originating from the earth's crust or from construction and building materials (C, N, H, S, Na,

Ca, Fe, Al), as well as micro elements (elements, anions and PAHs).

Table2. Distribution of microelements and PM<sub>10</sub> fractions in Prague road tunnels (Percentage by weight)

element	Strahov tunnel		tunnel Mrázovka	
	Spring	Summer	Spring	Summer
Cu	0,37	0,39	0,41	0,35
Zn	0,21	0,34	0,26	0,33
Cr	0,1	0,11	0,12	0,1
Mn	0,05	0,05	0,06	0,06
Mo	0,04	0,05	0,21	0,15
Ni	0,01	0,05	0,05	0,04
Pb	0,01	0,01	0,02	0,02
K	0,001	0,001	0,001	0,001
Cd	0,0002	0,0002	0,0004	0,0003
Mg	0,19	nd	nd	nd
SO <sub>4</sub> <sup>2-</sup>	1,5062	2,0387	2,08	2,3539
Cl <sup>-</sup>	0,6422	0,7409	1,4191	1,2443
NO <sub>3</sub> <sup>-</sup>	0,2982	0,6305	0,1447	1,0968
F <sup>-</sup>	0,0264	0,0384	0,0378	0,0366
PO <sub>4</sub> <sup>3-</sup>	0,0092	0,1772	0,1357	0,2072
Br <sup>-</sup>	0,0054	nd	nd	0,0263
NO <sub>2</sub> <sup>-</sup>	0,003	0,0089	nd	0,0085

Summary:

Aerosol composition in road tunnels (excepting carbon - Spring 43-57%, Summer 47-35%) correlates with the ratios of elements in heavily burdened urban traffic sites. Results thus gained can be used, by comparison with the composition of analysed urban aerosol, to identify the extent of traffic load.

This work was supported by the Committee for the Urban Environment of Prague.

Kazmarová H., a kol., (2006) Zdravotní důsledky a rizika znečištění ovzduší, ISBN 80-7071-268-6

Birch M.E., Cary R.A., (1996), *Aerosol Science and Technology* 25, 221-241

El-Fadel M., Hashisho Z, (2001), *Env.Sci. and Technol.* 31(2), 125-174

Laile E., Zahoransky R.A., Claussen M (2003), *J.of Aerosol Sci.*, 1055

Metz N., Resch G. et al. (2004), *in Proc EAC 2004* Budapest. 391

## Traffic contribution to PM in cities – size segregated characterization of EC/OC and organic species

K. Müller, T. Gnauk, E. Brüggemann, G. Spindler, D. van Pinxteren, H. Herrmann

Leibniz-Institut für Troposphärenforschung, Permoserstr. 15, 04318 Leipzig, Germany

Keywords: Aerosol sampling, carbonaceous particles, chemical composition, trajectory

Recent epidemiological studies in Europe and the US (Kappos et al., 2004) have determined strong correlations between long-term exposition of people to fine and ultra-fine dust and the risk of negative health effects. The traffic, especially emission of soot from diesel trucks and buses, is an important anthropogenic factor of PM in cities. Fine particles and the associated organic compounds are of current concern because of their putative health effects. Of particular concern are polycyclic aromatic hydrocarbons (PAH) which are mutagenic air pollutants formed as by-products of combustion. Studies of size-segregated analysis of PM from traffic sites already exist (Cass et al. 2000, Allen et al., 2001) but the focus of the present project was the investigation of the carbonaceous fraction of fine and ultrafine particles in a street canyon. Nano-particles ( $d_p < 100$  nm) and their effects on human health depend on their chemical constitution, water solubility or lipid solubility.

To investigate local and seasonal variation of the size-segregated PM impactor measurements were made on a traffic-site monitoring station in the street canyon of the Eisenbahnstraße (E) in the city of Leipzig during two summers and two winters. Simultaneous measurements were performed at IfT (I – urban background) and in Melpitz (M – rural background). During the experiment the street was reconstructed completely. The traffic volume changed within the measuring periods from about 20,000 cars per day via 2,000 during reconstruction works to 10,000 after the reconstruction.

PM sampling and chemical characterization was carried out using five-stage Berner impactors ( $0.05 < D_p < 10 \mu\text{m}$ ) and a 11-stage MOUDI (Micro Orifice Uniform Deposit Impactor;  $0.056 < D_p < 18 \mu\text{m}$ ). The MOUDI samples delivered additional information about sources because the greater number of impaction stages.

The investigation was directed mainly to the smallest particles of the Berner impactor (Figure 1 - stage 1:  $0.05 < D_p < 0.14 \mu\text{m}$ ) which are well known from previous experiments for primary traffic emissions. In nearly all periods of the experiment the determined mass of these ultra-fine particles decreased from Eisenbahnstraße via IfT to Melpitz. A similar observation was made for OC/EC, major ions, and alkanes, too. In Figure 1 the mean mass

concentration found in this size class is demonstrated for all periods and sites.

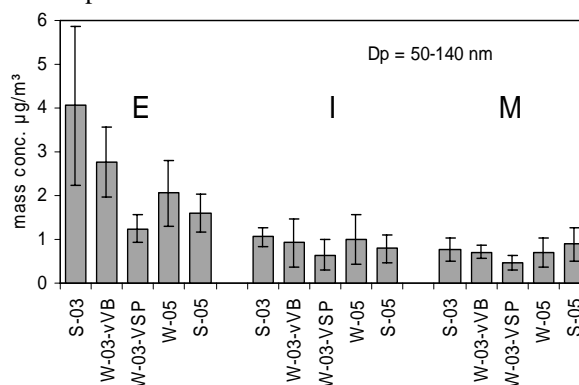


Figure 1. Mean mass concentration of BI stage 1 particles ( $d_p=0.05-0.14 \mu\text{m}$ ) at the sites E, I and M and the variability between and within periods (S-03 - summer 2003 before traffic reduction; W-03 vVB – winter 2003 before traffic reduction; W-03VSP – winter 2003 during the reconstruction work; W-05 – winter 2005 after reconstruction; S-05 – summer 2005 after reconstruction.)

The total effect of local traffic emission to the  $\text{PM}_{10}$  mass is between 33 % in summer 2003 and 17 % in summer 2005 at a traffic reduction to 50 % observed during our experiments. A traffic reduction to 50 % helps to diminish the exposition of people to ultra-fine PM to 30 % of the original value. The reduction of OC/EC is more important for health than the mass reduction because their putative effects on respiratory organs and the cardiovascular system.

This work was supported by the FAT – Forschungsvereinigung für Automobiltechnik e.V., Frankfurt/Main, Germany.

Allen, J. O., Mayo, P. R., Hughes, L. S., Salmon, L. G., and Cass, G. R. (2001). *Environ. Sci. Technol.* 35, 4189-4197.

Cass, G. R., Hughes, L. S., Bhave, P., Kleman, M. J., Allen, J. O., and Salmon, L. G. (2000). *Phil. Trans. R. Soc. Lond., A* 358: 2581-2592.

Kappos, A. D., Bruckmann, P., Eikmann, T., Englert, N., Heinrich, U., Höpfe, P., Koch, E., Krause, G. H., Kreyling, W., Rauchfuss, K., Rombout, P., Schulz-Klemp, V., Thiel, W. R., Wichmann, H.-E. (2004). *Intern. J. Hygiene and Env. Health* 207, 399-407.

## Chemical Mass Balance for PM10 at Sonnblick

C. Effenberger<sup>1</sup>, A. Kranabetter<sup>2</sup>, G. Schauer<sup>3</sup> and A. Kasper-Giebl<sup>1</sup>

<sup>1</sup>Institute for Chemical Technologies and Analytics, Getreidemarkt 9, 1060, Vienna, Austria

<sup>2</sup>Land Salzburg, Referat Immissionsschutz, Ulrich-Schreier-Str.18, 5020, Salzburg, Austria

<sup>3</sup>Central Institute for Meteorology and Geodynamics, Freisaalweg 16, 5020, Salzburg, Austria

Keywords: atmospheric aerosols, field measurements, organic carbon, PM10

The Sonnblick Observatory is located at 3106 m a.s.l. in the main ridge of the Austrian Alps. It has the ideal characteristics of a high alpine background site, situated 'above' the center of Europe surrounded by regions with large emission densities at distances of a few hundred kilometres.

Aerosol samples were taken weekly on quartz fibre filters using a Digital HiVol sampler. Sample change was performed manually. Sampling started in November 2005 and will be continued until spring 2008. The present sampling program is a continuation of earlier projects based on filterpack sampling. A comparison of the filterpack sampling with HiVol sampling yielded good results. HiVol data for this intercomparison are taken from the CARBOSOL project.

and major ions as well as the partitioning of total carbon to organic carbon and elemental carbon between will be quantified and compared to background sites at lower elevation. Further focus will be put on seasonal changes observed between the warm and the cold period.

This work was supported by the Federal Ministry for Education, Science and Culture.

Puxbaum, H., Rendl J., 1983. *Ein automatisches Analysatorensystem zur Bestimmung von Kohlenstoff und Schwefel in luftgetragenen Stäuben*. Microchemia Acta, 263-272

Cachier, H., Bremond, M.P., Buat-Manard, P., 1989. *Determination of atmospheric soot carbon with a simple thermal method*. Tellus 41B, 379-390

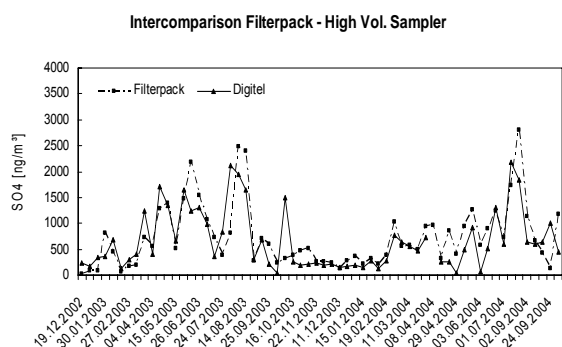


Figure 1. Intercomparison between Filterpack- and HiVol sampling method

Aerosol mass is determined by weighing of the filters prior and after sampling. Chemical analysis includes the determination of major anions and cations as well as organic acids by ion chromatography using standard procedures and the analysis of total carbon, organic carbon and elemental carbon using combustion methods (Puxbaum, H., Rendl J., 1983; Cachier, H. et al. 1989) as well as a thermo-optical method for selected samples. Furthermore a number of samples were analysed for cellulose and anhydrosugars such as levoglucosan to get information about 'living' biomass and 'biomass burning'.

We will present a simple mass balance for the weekly aerosol samples collected within more than one year. The relationship between organic matter

## The use of trajectory cluster analysis to interpret PM levels and composition at central Spain

P. Salvador<sup>1</sup>, B. Artíñano<sup>1</sup> and X. Querol<sup>2</sup>

<sup>1</sup>Department of Environment, CIEMAT, Avda. Complutense 22, 28040, Madrid, Spain

<sup>2</sup>Institute of Earth Sciences "Jaume Almera", CSIC, c) Lluis Solé y Sabaris s/n, 08028, Barcelona, Spain

Keywords: atmospheric aerosols, trajectory, PM10, PM2.5, long-range transport.

The present study uses an objective classification technique, cluster analysis, to identify the main synoptic patterns, that influence some properties of the air masses flowing over the center of the Iberian Peninsula. The relationship of the different meteorological scenarios on observed particulate matter (PM) levels and composition at a rural-background experimental site, have been examined.

Cluster analysis is a statistical method used to organize large data sets into smaller, similar groups. A non-hierarchical method known as k-means procedure has been utilized, using air masses trajectory coordinates as the clustering variables (Brankov *et al.*, 1998). A non-parametric technique, Kruskal-Wallis test, has been used for testing the significance of the inter-cluster variation in PM concentration. The Duncan's multiple sample comparison test, has also been performed.

During the 1999-2005 period, 5-day backward air trajectories arriving at 1400 m over Campisábalos monitoring site at 00:00, 06:00, 12:00 and 18:00 h UTC, were daily calculated using the FLEXTRA model (Stohl & Seibert, 1998). In all, 10,204 complete trajectories were available for analysis. Campisábalos is a regional background monitoring site included in the UNECE/LRTAP/EMEP air quality network. TSP, PM10 and PM2.5 samples were obtained at this station on a daily basis using high volume samplers. Concentrations of  $\text{SO}_4^{2-}$ ,  $\text{NO}_3^-$  and  $\text{NH}_4^+$  were chemically determined in TSP and PM10 samples.

8 clusters were obtained for the study period (Figure 1). Cluster 1 represented slow air circulation or regional transport. Cluster 2 grouped moderate moving westerly trajectories. Cluster 3 represented fast moving Northeasterly flow. Cluster 4 was characterised by trajectories from North-Africa. Cluster 5 indicates moderate flow to Madrid air basin from a Northwestern direction. Fast moving westerly trajectories were grouped in cluster 6. Cluster 7 represents the transport of air masses from the European Continent towards the Iberian Peninsula, through the Mediterranean sea. Finally a slow moving Northwesterly flow were represented by cluster 8.

Kruskal-Wallis non-parametric tests indicated significant differences ( $p \ll 0.05$ ) in TSP, PM10, PM2.5,  $\text{SO}_4^{2-}$ ,  $\text{NO}_3^-$  and  $\text{NH}_4^+$  concentrations among

clusters. The highest significant TSP and PM10 mean levels were associated with North-African air flows (cluster 4). This meteorological scenario can give rise to the transport of highly dust loaded air masses, from Northern Africa desertic regions. For PM2.5,  $\text{SO}_4^{2-}$ ,  $\text{NO}_3^-$  and  $\text{NH}_4^+$ , clusters 1 and 7 stand out as having significantly higher concentrations. Regional recirculating flows (cluster 1) have been typically produced in the summer, generating the transport and recirculation of PM from local and regional sources. The high sun insolation degree associated with these events also favours formation of secondary inorganic compounds by photochemical conversion. The fact that cluster 7 appears to influence PM2.5,  $\text{SO}_4^{2-}$ ,  $\text{NO}_3^-$  and  $\text{NH}_4^+$  concentrations in the monitoring site, suggests that a long-range transport of these compounds could be produced. Overall, the results show that PM mean concentrations associated with fast and moderate moving maritime air masses (clusters 2, 5 and 6) are significantly lower. These atmospheric transport scenarios favours scavenging processes, such as high precipitation rates and strong winds, producing a drop in surface PM concentration levels.

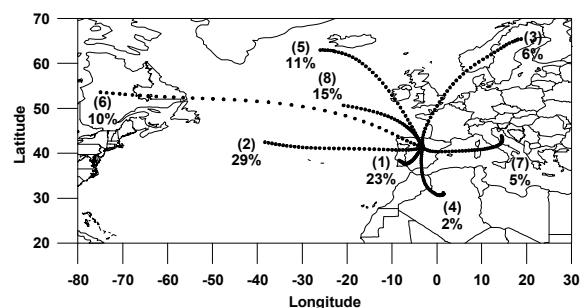


Figure 1. The 8 cluster centers resulting of the analysis. The percentage of trajectories occurring in each cluster is included.

Authors acknowledge to ECMWF, NILU and the FLEXTRA developers for the air mass trajectories.

Brankov, E., Rao S.T. & Porter P.S. (1998). *Atmospheric Environment*, 32, 1525-1534.  
Stohl A. & Seibert P. (1998). *Q.J.Roy.Met.Soc.*, 124,1465-1484.

## New sites for background air quality monitoring in Ireland

S. Leinert<sup>1,2</sup>, S. G. Jenninigs<sup>2</sup>

<sup>1</sup>EPA, Dublin 14, Ireland

<sup>2</sup>NUI Galway, Galway, Ireland

Keywords: atmospheric aerosols, PM10, chemical composition, monitoring

In this poster, new sites for background air quality monitoring in Ireland are presented, as well as first data for 2005 and 2006.

Between 2004 and 2006, new monitoring sites were set up in Ireland, for background air quality monitoring. These sites are located at Oak Park, Malin Head, and Carnsore Point. Additional precipitation samplers were deployed in Glenn Veagh National Park, and Johnstown Castle. The site locations are shown in Figure 1, which also includes existing sites at Mace Head and Valentia. The sites were set up to give information on background air pollution levels in Ireland, and they also contribute to the EMEP network.



Figure 1. Location of new sites (circles; precipitation sampler triangles) and existing sites (squares)

The main equipment are Digital PM10 samplers, collecting particles on filters, with a flow rate of 500 lpm. Filters are changed daily. They are then analysed for chemical compounds (SO<sub>4</sub>, NO<sub>3</sub>, NH<sub>4</sub>, Na, Mg, K, Ca) at Met Eireann laboratories.

Table 1. overview of new sites

Site	Type	since
Oak Park	Precip./aerosol	01/2005
Malin Head	aerosol	01/2005
Glenn Veagh	precipitation	08/2005
Johnstown Castle	precipitation	03/2006
Carnsore Point	aerosol	05/2005

At the precipitation sites, an Eigenbrodt wet only sampler is collecting precipitation, in a bottle for each day. Precipitation is then analysed for chemical

compounds (SO<sub>4</sub>, NO<sub>3</sub>, NH<sub>4</sub>, Na, Mg, K, Ca, Cl) as well as ph and conductivity.

Sites at Malin Head and Carnsore Point are also equipped with a CPC and an Aethalometer. In Carnsore Point, there is an additional TEOM for measuring PM10 mass concentration.

Mean PM10 mass concentrations for the chemical compounds analysed for are shown in Figure 2. Sea salt (calculated as 2.54\*Na) shows annual mean levels of up to 8 µg/m<sup>3</sup>, with daily means up to 38 µg/m<sup>3</sup> at coastal sites (Carnsore Point) and daily means up to 10 µg/m<sup>3</sup> inland (Oak Park).

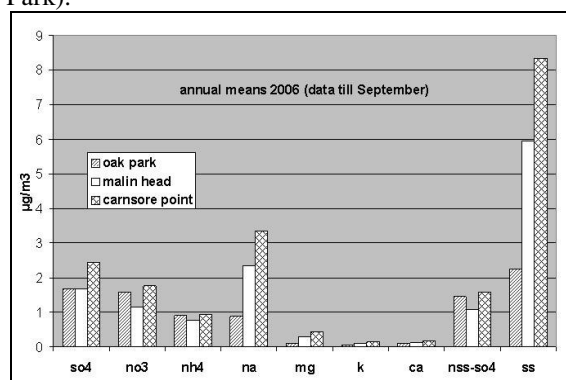


Figure 2. Mean concentration of chemical compounds in air, in PM10, for 2006

The data show episodes of elevated non sea salt SO<sub>4</sub> at all three sites simultaneously (see Figure 3). This indicates a regional rather than a local event, which could be caused by meteorological conditions or through long range transport.

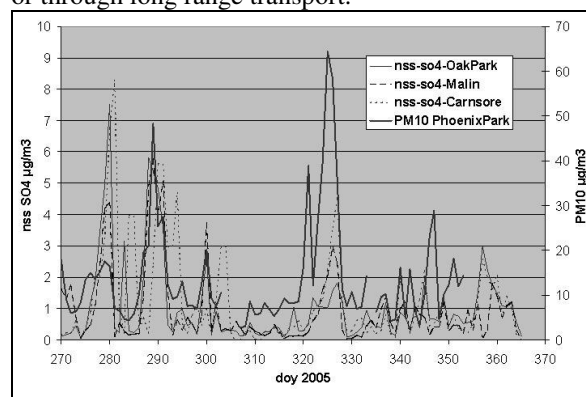


Figure 3. Episodes of elevated nss SO<sub>4</sub> at the three sites; PM10 at Phoenix Park, Dublin

## Mobile air quality monitoring trailer for developing countries

T. Petäjä<sup>1</sup>, A. Paakkio<sup>1</sup>, T. Pohja<sup>1</sup>, E. Siivola<sup>1</sup>, H. Paakkio<sup>1</sup>, P.P. Aalto<sup>1</sup>, P. Keronen<sup>1</sup>,  
N.A. Kgabi<sup>2</sup> and M. Kulmala<sup>1</sup>

<sup>1</sup>Department of Physical Sciences, University of Helsinki, PO Box 64, FI-00014 University of Helsinki, Finland

<sup>2</sup>North-West University, Republic of South Africa

Keywords: atmospheric aerosols, monitoring, field measurements.

Industrial countries have invested heavily on the air quality monitoring during the last decades. Significant emission and air quality regulations have been set and continuous monitoring in urban and industrial centers has been carried out. In the third world these issues are not yet at the same level (Paakkio et al. 2006) despite the fact that the poor air quality affects the lives of hundreds of millions of people, in particularly in the developing world.

In order to assess the role of different particulate sources in the air quality in the developing world, one has to know also the natural background conditions. Thus it is essential to conduct measurements in areas far enough from large industrial sites and cities, which is a challenging task due to very small infrastructure at these locations. In order to reach this goal, a mobile instrument trailer was constructed in Finland. Prior shipping a short comparison campaign was conducted at Hyytiälä, Finland, where the performance of the trailer instruments was evaluated against data obtained from a state-of-the-art atmospheric field station in Hyytiälä, Finland.

A mobile air quality trailer was designed and built in Finland. The trailer instrumentation include a Differential Mobility Particle Sizer (DMPS, Aalto et al. 2001), which measures aerosol number size distribution from 10 to 800 nm with 10 min time resolution. Mass concentration of particulate matter is monitored with a TEOM 1400a Ambient Particulate Monitor (Rupprecht & Patashnick). An automatic custom made inlet switch allows measurement of PM<sub>1</sub>, PM<sub>2.5</sub> and PM<sub>10</sub> with the same instrument in 20 min sampling interval for each mass fraction. Positive and negative air ions between 0.4 and 40 nm are detected with an Air Ion Spectrometer (AIS, Airel Ltd, Tartu, Estonia). Gaseous pollutants (SO<sub>2</sub>, O<sub>3</sub>, CO, NO<sub>x</sub>) and local meteorological parameters (temperature, relative humidity, wind speed, wind direction, precipitation rate and photosynthetically active radiation) are logged continuously. The trailer is equipped with a GPS-receiver to pin-point the measurement location. The measurement data is copied to a server via GPRS-modem wirelessly. This enables remote monitoring of data quality on everyday basis.

During spring 2006, test measurements with the trailer setup were conducted side by side with aerosol and gas phase equipment of SMEAR II (Vesala et al. 1998) station located at Hyytiälä,

Finland. An exemplary data of aerosol number size distribution and total number concentration measurements are presented in Figure 1. New particle formation and subsequent growth was detected by the trailer DMPS and at the station.

The instrument trailer is a mobile unit. In the future, measurements in background savannah environment are conducted and also in more polluted regions are planned in order to obtain data for a wide range of atmospheric conditions. This will enable assessment of human activities on the air quality of rapidly developing Republic of South Africa.

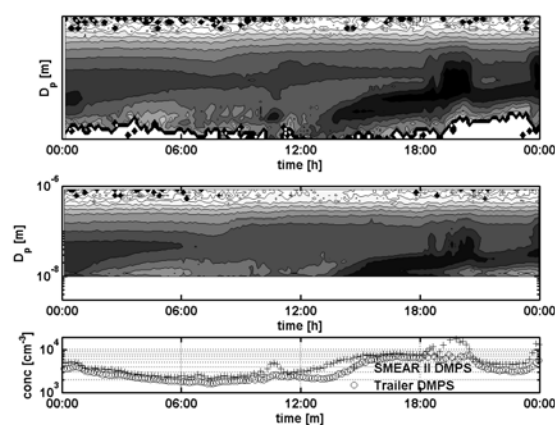


**Figure 1.** Number size distribution of sub-micron particles measured with SMEAR DMPS (top-most panel) and Trailer DMPS (middle panel) were in qualitative agreement on April 26, 2006. Total number concentration (lowest panel) showed that Trailer DMPS is unable to detect new particle formation event in full extent due to size range limitations.

### REFERENCES

- Aalto, P., et al. (2001). Physical characterization of aerosol particles during nucleation events. *Tellus*, 53B:344--358.
- Paakkio, A., et al. (2006) Aerosol particles in the developing world: a comparison between New Delhi in India and Beijing in China. *Water Air Soil Pollut.*, 173: 5–20.
- Vesala, T. et al. (1998). Long-term field measurements of atmosphere-surface interactions in boreal forest combining forest ecology, micrometeorology, aerosol physics and atmospheric chemistry. *Trends in Heat, Mass & Momentum Transfer*, 4:17--35.

## Effects of particle hygroscopicity on fine particle mass concentration at Seoul, Korea

E.K. Choi<sup>1</sup> and Y.P. Kim<sup>1</sup>

<sup>1</sup>Department of Environmental Science and Engineering, Ewha Womans University, Seoul, 120-750, Korea

Keywords: atmospheric aerosol, modelling, water soluble compounds.

Hygroscopicity of particles is an important factor that determines particle water content and, thus, particle mass concentration. Since particle mass concentration, especially, that of fine particles is closely related with various air pollution phenomena such as visibility reduction and lung disease, it is critical to understand hygroscopic properties of fine particles. It is known that inorganic ionic species in a particle and relative humidity affect particle water content. But direct measurement of particle water content is difficult because sampling and analytical techniques are inappropriate for the measurement of water. Thus, in this work, by using a gas/particle equilibrium model, (1) the relationship between relative humidity and particle water content is quantified to characterize particle hygroscopicity and (2) sensitivity of fine particle mass concentration to the change of the total ambient concentrations of sulfuric acid, nitric acid, and ammonia is studied. Then sensitivity of fine particle light scattering is also studied for the same cases by using a light extinction model.

The aerosol measurement data used in this study are from Kang (2003). He used an annular-denuder filterpack system with a PM<sub>2.5</sub> inlet to collect fine particles for 24 h. The sampling period was between April 2001 and February 2002. The number of the sampling data was 60. Meteorological data, T and RH, were obtained from the surface weather station near to the sampling site operated by the Korea Meteorological Administration. To ensure the quality of the data, we applied the quality assurance/quality control (QA/QC) procedure to the measurement data. Ion balance was used to check the validity of the data. The data with the ratio of the sum of the cation concentrations to the anion concentrations being within 30% were used for further data analysis. The criterion of 30% was chosen since the concentrations of organic and carbonates could be up to 30% of the total ion concentrations. After this process, 48 data were used in this study.

SCAPE2 (Simulating Composition of Atmospheric Particles at Equilibrium 2) model was used. This model estimates the state and composition of atmospheric inorganic ionic species between the gas and particle phases in chemical equilibrium. Input data for the SCAPE2 consist of total (the sum of the gaseous and particle phase) concentrations of sulfate, nitrate, ammonium, sodium, chloride, calcium, magnesium, potassium, and carbonate, and

temperature (T) and RH. Details of SCAPE2 are given by Kim *et al.* (1993ab) and Meng *et al.* (1998).

Figure 1 shows the relationship between particle size (assuming spherical particle with constant density) and ambient relative humidity for the Seoul data.

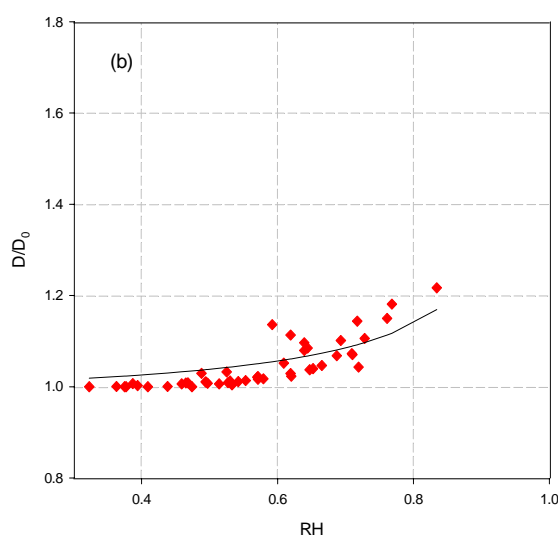


Figure 1. The relationship between aerosol size growth and relative humidity (diamond: SCAPE2 result, line: fitting line).

This work was supported by the Korea Science and Engineering Foundation (KOSEF) through the National Research Lab. Program funded by the Ministry of Science and Technology (No. M10600000221-06J0000-22110).

Kang, C. M. (2003). Characteristics of the fine particles and source apportionments using the CMB model in Seoul area, Ph.D. Thesis, Konkuk University, Seoul.

Kim, Y. P., Seinfeld, J. H., & Saxena, P. (1993a) *Aerosol Sci. Technol.*, 19, 157-181.

Kim, Y. P., Seinfeld, J. H. and Saxena, P. (1993b) *Aerosol Sci. Technol.*, 19, 182-198.

Meng, Z., Dabdub, D., & Seinfeld, J.H. (1998). *J. Geophys. Res.*, 103, 3419-3435.

## PM air pollution in urban agglomerations

M. Schwarzova<sup>1</sup>, M. Schmidt<sup>2</sup>, R. Licbinsky<sup>1</sup>, J. Huzlik<sup>1</sup>, V. Adamec<sup>1</sup> and W. Goessler<sup>2</sup>

<sup>1</sup>Transport Research Centre, Lisenska 33a, 636 00, Brno, Czech Republic

<sup>2</sup>Institut of chemistry – Analytical chemistry, University Graz, Universitaetsplatz 1, 8010 Graz, Austria

Keywords: aerosol sampling, agglomerates, particulate matter, size distribution, traffic.

Particulate matter (PM) is an important part of air quality monitoring. In the last ten years increasing concentrations of more than 12% and their negative health effects were observed (WHO, 2004). Especially in the large cities PM can be a problem due to the road transport that is an important source of these particles.

PM<sub>10</sub>, PM<sub>2.5</sub> and PM<sub>1.0</sub> concentrations, size distribution and the content of selected metals have been investigated during measuring campaigns in Brno and Graz in order to find seasonal variations. The first sampling campaign took place in September, the second one in November in both cities. It is planned to sample PM fractions in February (winter period) and at the end of April (spring period).

Urban localities in Brno with different burden by traffic and different morphology of surroundings were chosen. Locality 1 is considered to be a street canyon with high traffic intensity (36,000 vehicles per day). The second locality represents the area more opened with low burden by traffic (8,000 vehicles per day). Samplers (Leckel MVS6, EnvironCheck 107) were situated next to the street on both localities. The university building (locality 3) in Graz situated in the town centre next to street with 21,000 vehicles per day was chosen. The samplers (Leckel MVS6, EnvironCheck 107) were placed on the open terrace on the fourth floor. The open position should be representative for the overall situation in Graz concerning air quality with impact from traffic and all other influences such as house burning.

PM<sub>2.5</sub> concentrations were very similar in both localities from Brno in the first campaign whereas the content of PM<sub>1.0</sub> fraction was different. The share of this fraction on locality 1 was higher than on the second locality in Brno. Similar size distribution of separate PM fractions was observed also in the second campaign in November. Determined concentration values for PM<sub>10</sub> were two times higher in the autumn sampling campaign and daily concentrations exceeded the legislation limit (50 µg.m<sup>-3</sup>) in three days. Weekly average PM concentrations were in both campaigns higher on the locality with higher traffic intensity but absolute concentration values are also significantly influenced by meteorological conditions. Weekly average PM concentrations on locality 3 were slightly higher during the measurements in September but

legislation limit was not exceeded in any case. Very similar share of PM<sub>1.0</sub> on the overall PM<sub>10</sub> pollution was observed in both measuring campaigns. On the basis of obtained results it is possible to note that coarse particles have the main share on PM<sub>10</sub> pollution on locality 2 in Brno whereas the main share of PM<sub>1.0</sub> on PM<sub>10</sub> concentrations was observed on locality 3 probably due to location of samples on the terrace where the coarse particles are not easily transported from the street canyon. Metal concentrations will be also presented in the paper.

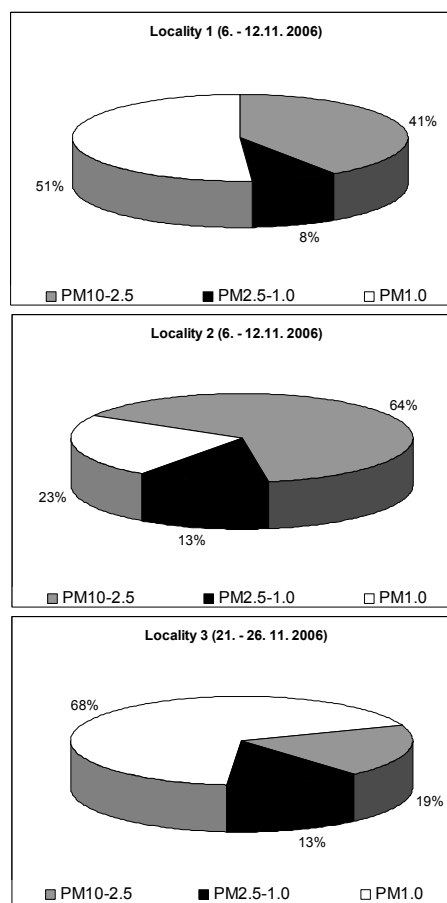


Figure 1. The share of separate PM fractions

Transport-related health effects with a particular focus on children, THE PEP, WHO, UNECE, 2004.

## Water soluble organic and inorganic compounds in PM10

G.A. Blanco-Heras<sup>1</sup>, M.C. Prieto-Blanco<sup>1</sup>, M.I. Turnes-Carou<sup>1</sup>, M. Piñeiro-Iglesias<sup>2</sup>, P.López-Mahía<sup>1,2(\*)</sup>, S. Muniategui-Lorenzo<sup>1</sup> and D. Prada-Rodríguez<sup>1,2</sup>

<sup>1</sup>Department of Analytical Chemistry, University of A Coruña, Campus A Zapateira, E-15071, A Coruña, Spain

<sup>2</sup>Institute of Environment, University of A Coruña, Pazo de Lóngora, Liáns, E-15179, Oleiros, A Coruña, Spain

Keywords: Water soluble compounds, organic compounds, PM10, urban aerosols, industrial aerosols

In this work we have compared water soluble compounds: inorganic (cations and anions) and organic species (carboxylic acids, PAH and carbonylic compounds) in PM10 from two distinctly different sites: urban and industrial areas. The major potential sources for the determined compounds under consideration are traffic emissions, industries activities (refinery, coal fired power station, alloy industry...) and secondary formation from anthropogenic gas phase precursors.

The carboxylic acids have been identified as major constituents of the water soluble organic aerosol. Dicarboxylic acids are likely to dominate in the two areas: oxalic acid was the dominant specie (ranged from 1.5 to 146.6ng/m<sup>3</sup> in urban site and 5.1 to 235.6 ng/m<sup>3</sup> in industrial area) followed by malonic, acetic, formic and succinic acids. Azelaic, glutaric, adipic and suberic acid have been detected in few samples and at lower cocentration.

Fluoranthene, pyrene, benzo(a)anthracene, chrysene and benzo(b)fluoranthene are the predominant PAH followed by benzo(a)pyrene, benzo(k)fluoranthene and dibenz(ah)anthracene. It is important to consider the PAH solubility from a bioavailability perspective because the predominant exposure pathway for airborne particles to humans is through the air/lung fluid interface. In this work the water soluble fraction of PAH ranged from 7 to 20% of the total PAH.

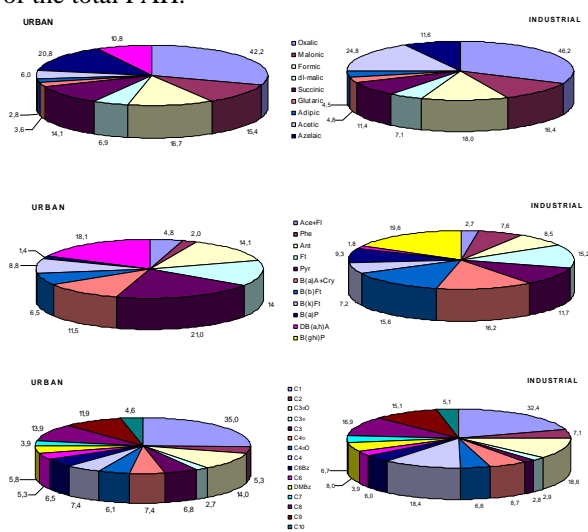


Figure 1. Mean of relative percentages of carboxylic acids, PAH and carbonylic compounds.

Lower carbonyl concentrations were measured. Formaldehyde, butanal, octanal, nonanal, acetaldehyde and acrolein were the most abundant carbonyls with concentrations ranged to 1.2 from 30.5ng/m<sup>3</sup>. The ratios C1/C2 were ranged from 5.2 to 6.3 and the ratio C2/C3 from 1.1 to 1.6 in the urban and industrial area, respectively.

Correlations were calculated between all the inorganic and organic acids. High correlations were observed between non-sea-sulphate, ammonium, nitrate, oxalate and malonate.

High correlation were also observed within PAH and between these and other organic compounds.

Also, the influence of atmospheric variables such us boundary layer height, predominant wind direction sector, precipitation, etc. was observed.

PCA analysis was performed in order to obtain an source contribution estimation. As shown in the figure below, compounds are grouped according to their origin.

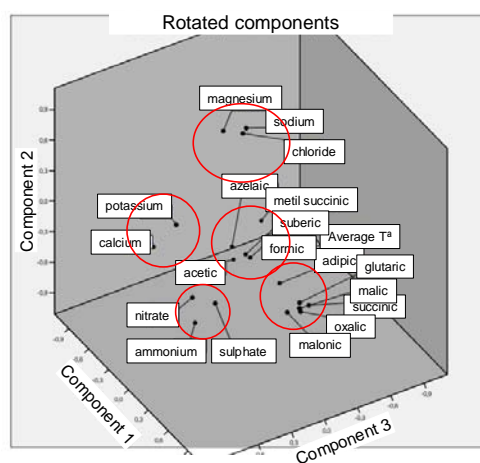


Figure 2. Components in the rotated space for inorganic and organic acids.

This work was supported by Spanish Ministry of Education and Science (REN2003-08603-C04-01) and for the FPI grant to G.A.B.-H. (BES-2004-320). They wish to thank the National Meteorological Institute (Centro Zonal de A Coruña).

G.A. Blanco Heras, M.I. Turnes Carou, P. López Mahía, S. Muniategui Lorenzo, D. Prada Rodríguez (2007). *J. Chromatogr. A*. In Press.

## What about water uptake by mixtures of four of the most important atmospheric aerosol ions: $\text{NH}_4^+$ , $\text{Na}^+$ , $\text{SO}_4^{2-}$ , and $\text{Cl}^-$ ?

Birgitta Svenningsson<sup>1,2</sup>, Merete Bilde<sup>1</sup>, Jenny Rissler<sup>3</sup>, and Erik Swietlicki<sup>3</sup>

<sup>1</sup> Dept. of Chemistry, Copenhagen Univ., Universitetsparken 5, DK-2100 Copenhagen, Denmark

<sup>2</sup> Dept. of Physical Geography and Ecosystems Analysis, Lund Univ., Sölvegatan 12, SE-223 62 Lund, Sweden

<sup>3</sup> Div. of Nuclear Physics, Lund Univ., Box 118, SE-221 00 Lund, Sweden

Keywords: hygroscopicity, ammonium sulphate, sodium chloride, marine aerosols

In this work, we have put some light on the lack of understanding of water uptake by mixtures of some of the most abundant salts in atmospheric aerosols. The hygroscopic growth of mixtures of  $\text{NH}_4^+$ ,  $\text{Na}^+$ ,  $\text{SO}_4^{2-}$ , and  $\text{Cl}^-$  ions depends strongly on the state of mixing of these ions: the hygroscopic growth is much smaller if they are all mixed compared to the case where sodium chloride and ammonium sulphate exist in separate particles.

This is of great atmospheric relevance since the interaction between water vapour and atmospheric aerosol particles has implications for several important processes: deposition (incl. lung deposition), cloud formation, and light scattering, thus influencing the radiation balance in the atmosphere and the climate

The ZSR mixing rule (Stokes and Robinson, 1966) relies on the assumption that the water uptake by a mixture can be described as the sum of the water that would have been attached to the individual compounds at the same water activity. This simple mixing rule can often adequately explain the water uptake by mixed aerosol particles. However, it does not work for  $(\text{NH}_4)_2\text{SO}_4$  and  $\text{NaCl}$  mixtures (Cohen et al. 1987; Svenningsson et al. 2006).

The hygroscopic growth of a mixture of all four ions (figure 1) resembles that of pure sodium sulphate. The main difference is that the mixed particles, starting as being dry, begin to take up water already at a water activity below 0.75. This fits well with the deliquescence point of ammonium chloride. However, if all ammonium and chloride was dissolved at this point, the hygroscopic growth factor is expected to be 1.3 instead of 1.05. ZSR based on ammonium chloride + sodium sulphate gives a good agreement for water activities below 0.8, but overestimates the hygroscopic growth for higher water activities.

Modelling of the crystals formed from ammonium, sodium, chloride, and sulphate ions (<http://mae.ucdavis.edu/~sclegg/aim.html>; Wexler and Clegg, 2002; Clegg et al., 1998) shows that these ions preferentially form ammonium chloride and sodium sulphate.

Sodium sulphate in itself has several different forms of crystals, with and without crystal water and with different solubilities and densities. In mixtures including ammonium ions, we will also have to consider the formation of sodium ammonium

sulphate ( $\text{NaNH}_4\text{SO}_4 \cdot 2 \text{H}_2\text{O}$ ), which has a relatively low density and high molar weight due to the crystal water.

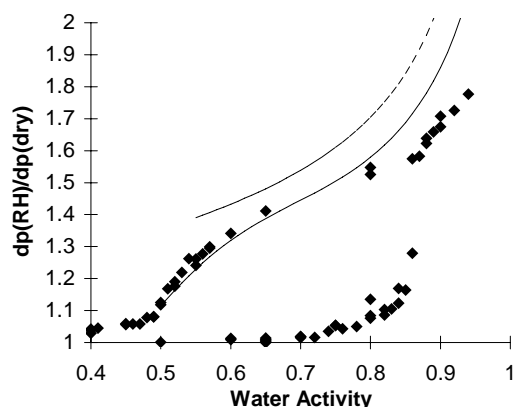


Figure 1: H-TDMA data on hygroscopic growth of a mixture containing 0.5 mole of ammonium sulphate per 1 mole of sodium chloride. The solid lines are calculated based on the ZSR method, under the assumption that the crystals formed are 1) sodium chloride and ammonium sulphate (upper curve) or 2) ammonium chloride and sodium sulphate (lower curve). H-TDMA data on hygroscopic growth of sodium sulphate, ammonium chloride, sodium chloride and ammonium sulphate are used as input to the ZSR model.

This work is supported by the Danish Natural Science Research Council, Åse og Ejnar Danielsens Fond, the Swedish Research Council, and the European Commission. We also want to thank the BACCI Nordic Center of Excellence for its support.

Clegg, S. L., Brimblecombe, P., and Wexler, A. S. (1998) *J. Phys. Chem. A*, 102, 2155-2171.

Cohen, M. D., Flagan, R. C., and Seinfeld, J. H. (1987) *J. Phys. Chem.*, 91, 4575-4582.

Stokes, R. H. and Robinson, R. A. (1966) *J. Phys. Chem.*, 70, 2126-2130.

Svenningsson, B., Rissler, J., Swietlicki, E., Mircea, M., Bilde, M., Facchini, C., Decesari, S., Fuzzi, S., Zhou, J., Mønster, J., and Rosenørn, T.: (2006) *Atm. Chem. Phys.* 6, 1937-1952.

Wexler, A. S. and Clegg, S. L. (2002) *J. Geophys. Res.*, 107, 4207.

## Profiles of road dust and its contribution to PM10 atmospheric aerosol

N. Jankowski, H. Puxbaum, I.L.Marr

Institute for Chemical Technologies and Analytics, Vienna University of Technology, Getreidemarkt 9/164-AC, 1060, Vienna, Austria

Keywords: mineral dust, PM10, source apportionment, modelling

As a result of the frequent exceedances of the 50  $\mu\text{g}/\text{m}^3$  limit adopted by the European Union for the PM10 inhaleable fraction of airborne particulates, questions are being asked about the sources and their contributions to PM collected in cities. One possibility for evaluating the contributions is the CMB model (Watson, 1984), for this, the compositions of all source emissions have to be known, and the selection of analytical parameters - the framework for a profile - must be the same for both sources and ambient air samples.

This study deals with the particulate emissions from paved roadways. Besides the direct emissions from vehicle tailpipes, there are particles from the abrasion of tyre material, the brakes, the binders and the mineral surface of the road as well. Further, in winter, salt and gritting minerals are also present. Particles which settle out on the street can be resuspended by passing vehicles and by wind, and thus get into the atmosphere, to be mixed with other material derived from remote sources. The street therefore presents a dynamic system of settling and resuspension of fine particulate matter.

Evaluation of the contribution of resuspended street dust to the PM10 particles in the atmosphere requires one or more chemical profiles. An important question is whether the profiles for different cities, or indeed for different sampling sites within one city, are the same or different. It would obviously be simpler to have one profile for all road dust, whatever the location. Therefore different road dust samples (for different seasons and locations) have been collected and resuspended in a specially constructed apparatus to get the fraction of interest: PM10. The resuspended particles have been sampled using PM10 sampling heads, with quartz fibre filters for the analysis of carbonaceous components such as TC, EC, OC, cellulose, humic like substances, anhydrosugars and trace semi-volatile organics, or cellulose ester membrane filters for the determination of trace metals by ICP-OES and macrocomponents such as silicon and aluminium by XRF.

Figure 1 shows ratios of a few selected components from the profiles for Vienna, Graz and Salzburg. EC and OC are similar for all, while Fe, Al and Si are higher for Graz. However, because of the high variability of the samples, even from any one site, most apparent differences are not significant and so one profile can be adopted for all sites.

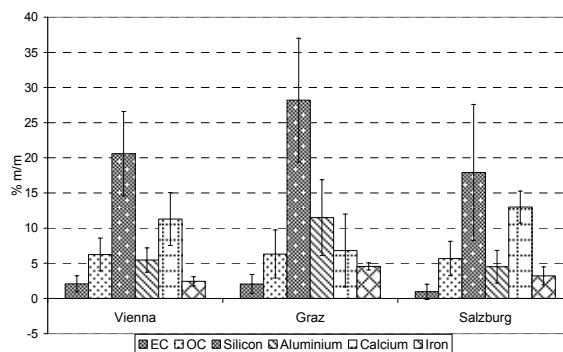


Figure 1. Comparison of selected components

It must be stressed that uncertainties in the profile levels are thus due to sample variability and not to analytical uncertainty. Differences between these figures for Austria and others in the literature (e.g. Hildemann *et al.*) are obvious, so own profiles for Austrian cities have to be established. Figure 2 shows the contribution of road dust, and for January also of salt, to the ambient PM10 level. For all cities the road dust burden is highest in April, at the time when the roads are being swept clean after winter. The fact that Vienna shows higher levels than the other two cities must be related to its size - the incoming air at each site has accumulated its burden over a greater distance of urban development.

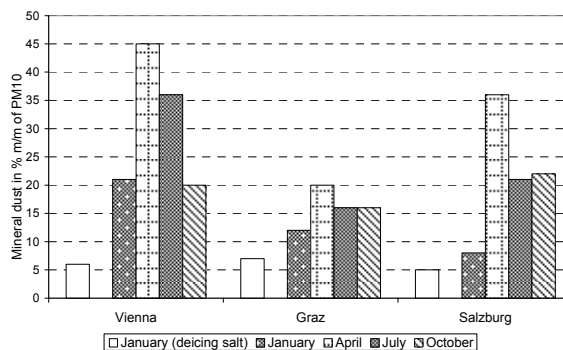


Figure 2. Contribution of road dust to ambient PM10

Watson, J.G. (1984). *J. Air Pollut. Control Assoc.*, 34, 619-623.

Hildemann, L.M., Markowski, G.R. and Cass, G.R. (1991). *Environ. Sci. Technol.* 25, 744-759.

## **Some aspects of fine inorganic aerosols (PM<sub>1</sub>, PM<sub>2.5</sub>) in the metropolitan area of Mexico City during the winters of 2003, 2005 and 2006 (MIRAGE-MILAGRO field campaign).**

**M. Moya<sup>1</sup> and Gregory Huey<sup>2</sup>**

<sup>1</sup>Centro de Ciencias de la Atmosfera, Universidad Nacional Autonoma de Mexico, Ciudad Universitaria, 04511, Mexico City, Mexico.

<sup>2</sup>School of Earth and Atmospheric Sciences Georgia Institute of Technology, 311 Ferst Drive, Atlanta, GA 30332-0100, USA

*Keywords:* fine particulate matter, inorganics, crustal elements, trace elements.

### INTRODUCTION

The air quality in the Valley of Mexico has become an issue in last decades due to high levels of particulated matter (PM) and ozone exceeding the Mexican 24-h standards several days of year (Edgerton et al., 1999, Molina and Molina, 2002). Aerosols play an important role in many areas including visibility reduction and radiative budget (IPCC Report, 2007). In addition, it is now recognized that aerosols, particularly the fine (PM with aerodynamic diameters less than 1 and 2.5  $\mu$ m) fraction, are associated with adverse health effects such as respiratory and cardiovascular issues. In this work, chemical characterization of fine collected particles in Mexico City during field studies conducted during the dry-winter seasons of 2003, 2005 and 2006, the latter in the context of the MIRAGE (MI AGRO) field campaign are presented.

### EXPERIMENTAL

PM<sub>1</sub>, PM<sub>2.5</sub> and size-resolved PM<sub>3</sub> (0.18-3.16 micrometers) were collected at a site near downtown Mexico City during 2003, 2005, 2006 and also during 2006, in the context of MIA GRO (<http://mirage-mex.acd.ucar.edu>) at the T1 site (19 N, 98 W). Details of the collection of particles and analytical methods for the determination of inorganic compounds (SO<sub>4</sub><sup>2-</sup>, NO<sub>3</sub><sup>-</sup>, Cl<sup>-</sup>, Na<sup>+</sup>, NH<sub>4</sub><sup>+</sup>, Ca<sup>2+</sup>, K<sup>+</sup> and Mg<sup>2+</sup>) are depicted in Moya et al., 2004. The duration of the sampling periods varied from 3h, 4 h, 6h and 24 h.

### RESULTS AND DISCUSSION

3 h, 4 h PM sulphate levels were up to 30  $\mu$ g m<sup>-3</sup> in downtown MC during 2003, 2005 and 2006 field studies. At the 2006 T1 MI AGRO site, located approximately 30 km from downtown

Mexico City, 6 h levels of this chemical species were up to 18  $\mu$ g m<sup>-3</sup>. The California Standard for PM sulphates (25  $\mu$ g m<sup>-3</sup>) were exceeded diurnally during the 2005 and 2006 field studies.

Crustal elements were of relative importance in the PM<sub>2.5-1</sub> size during all of the field campaigns.

Trace metals PM concentrations such as Pb, V and Mn were in limits very close to concentrations recommended by the World Health Organization (WHO, report 2005 Guidelines for Europe).

### ACKNOWLEDGEMENTS

This work has been supported by the PAPIIT-UNAM Projects: IN117906, I 106004 and IN107306, obtained during my first 3 years at UNAM (Mexico). MI AGRO sampling was funded by the National Science Foundation (Gregory Huey).

### REFERENCES

*Edgerton et al., 1999.* Journal of the Air & Waste Management Ass. 49, 1221-1229.

*IPCC 2007. Climate Change 2007: The Physics Science basis. Summary for Policymakers.* Contribution of Working Group I to the 4<sup>th</sup> Assessment Report of the Intergovernmental Panel on Climate Change.

*Molina, M. and Molina, L.T. 2002.* Air quality in the Mexico Megacity: An integrated assessment. Kluwer Academic Publishers, Dordrecht.

*Moya, M. et al. 2004.* Atmospheric Environment, 38, 5651-5661.

*Air Quality Guidelines for Europe.* 2<sup>nd</sup> Edition. World Health. Regional Office for Europe. Copenhagen, European Series, No. 91, 2005.

## Concentration and the chemical characterization of PM10 and PM2.5 in all the Italian territory

E. Bolzacchini<sup>1</sup>, . Ferrero<sup>1</sup>, C. o Porto<sup>1</sup>, M. G. Perrone<sup>1</sup>, G. de Gennaro<sup>2</sup>, P. Bruno<sup>2</sup>, M. Caselli<sup>2</sup>, P. R. Dambruoso<sup>2</sup>, B. E. Daresta<sup>2</sup>, C. M. Placentino<sup>2</sup>, M. Tutino<sup>2</sup>, M. Amodio<sup>2</sup>, D. Baldacci, M. Stracquadanio, . Tositti, S. appoli, D. Gullotto, V. ibrando, . Minniti, G. Perrini, G. Trincali, S. Becagli, A. Mannini, R. Udisti, C. Paradisi, A. Tapparo, P. Barbieri, . Capriglia, F. Cozzi, E. Maran, E. Reisenhofer, V. Sicardi. P. Fermo, A. Piazzalunga

<sup>1</sup>Department of Environmental Science and Technology, University of Bicocca, p.za della Scienza 1, 20126, Milan, Italy

<sup>2</sup>Department of Chemistry, University of Bari , p.za Umberto I, 70121 Bari

Keywords: Ions, PAH(s), Particle characterization, Particle concentration, PM10, PM2.5, Sulphate.

In order to studying the concentration and the chemical characterization of atmospheric particulate in the different season in all the Italian territory, inside the SITECOS project (PRIN 2004), a gravimetric sampling campaigns have been conducted. The PM10 and PM2.5 samplings were placed at the same time in different sites along the Italian peninsula. The sampling sites were: Bari, Taranto, Pollino (m.1800, remote site), Catania, Sesto Fiorentino, Florence, Arezzo, Grosseto, Capannori- U, Prato, Montale-PT (rural site), Bologna and Monte Cimone (m.2100, remote site on Italian Apennines), Padua, Milan, San Colombano (m.2300, remote site on Italian Alps), Trieste and San Rocco a Muggia (TS).

Daily PM2.5 and PM10 samples have been collected, to do a sampling bank , available for a further chemical / physical / toxicological characterization of atmospheric particulate. Samples have been chemically characterized according to their main species: PAHs, inorganic ions and EC/OC in the PM2.5 samples elements in the PM10 samples.

In the Padana plain (Milan, Bologna, Padua) the PM concentration is uniform and a strong seasonal trend is observed, with the highest values in winter time and the lowest values in summer while PM concentration in S. Colombano and Monte Cimone sites show an opposite seasonality, with the highest values in summer and the lowest ones in winter.

These data show a slight evolution during the winter s day because of the height of the dispersion layer, in connection with microclimatic parameters for example in Milan city during acute cases of pollution, the height is no more that 300m (Ferrero *et al.*, 2006). Remote sites of S. Colombano and Monte Cimone in the winter time are above the boundary layer while during summer period they are on it.

In the center of Italy PM seasonality concentration is less important while in the South Italy and in Sicily there is any seasonal trend. The reasons are, in part, linked to the different meteorological features present in the Italian peninsula.

Chemical composition data show a significant differences. In the North of Italy there is a strong seasonality of ionic component in particular, during the winter, the Nitrate concentration is higher than the Sulfate one while the situation is opposed in summer. Ammonium does not show a strong seasonality, but it remains pretty constant the same applies to Carbon. In the South of Italy cities,  $\text{SO}_4^-$ ,  $\text{NO}_3^-$  and  $\text{NH}_4^+$ , primary component of inorganic ions, they do not show a seasonality with a Sulfate concentration that is always higher than Nitrates. In the center of Italy the seasonality is less marked thanks to the inorganic ions. Sulfate and Nitrate are similar from a percentage point of view.

Also PAHs (expressed in weight/weight, quality of particulate), in the Padana plain, shows a strong seasonality, with a high percentage in the winter season and a lower one in summer (Ravindra *et al.*, 2006). Over the year concentrations are constant in South of Italy, while in the center area, the seasonality is less strong.

The vehicles traffic source is estimated to be one of the main PM source in the Padana plain, while in the South of Italy there are other sources like photochemistry reactivity, Saharan Dust events, etc.

These results show a different role of PM sources along the Italian peninsula and they carry fundamental information for a correct management of the complex problem on a national scale.

Ferrero, ., azzati, ., o Porto, C., Perrone, M.G., Petraccone, S., Sangiorgi, G., Bolzacchini, E., (2006) *Vertical distribution of particulate matter in the urban atmosphere of Milan*. Poster. International Aerosol Conference 2006.

Ravindra, K., Bencs, ., Wauters, E., Hoog, J., Deutsch, F., Roekens, E., Bleux, N., Berghmans, P., Van Grieken, R., (2006) *Seasonal and site-specific variation in vapour and aerosol phase PAHs over Flanders (Belgium) and their relation with anthropogenic activities*. Atmospheric Environment 40 (2006) 771-785.

## Summer 2006 events and their effect on PM<sub>10</sub> levels in Haifa Bay region, Israel

Yuval and David M. Broday  
Civil and Environmental Engineering, Technion, Haifa, Israel

Keywords: Air pollution, Urban aerosols, PM measurement

Summer 2006 events and the missiles launched against northern Israel caused dramatic changes in the economic and personal activity in Haifa and its surroundings. The larger industries, the refineries and the power plant continued to work more or less as usual, but smaller factories, the port and most of the commerce and the public institutions were closed down temporarily or shifted to reduced activity. These changes, the decrease in the population that resulted from people moving to stay with their relatives in the southern parts of Israel, and the dramatic change in the individual activity of those who stayed in the region brought about a dramatic decrease in traffic volumes for about a month. Monitoring data collected at stations of the Air Quality Monitoring Network from 1/6/06 to 31/8/06 reveal that the meteorological conditions were stable. In particular, the distributions of wind direction and velocity were very similar for the period before the war (1/6-15/6), during the war (16/6-14/7), and after the cease fire agreement (15/7-31/8). However, several air pollutants, including PM<sub>10</sub>, NO<sub>x</sub> and O<sub>3</sub> show a clear change during the war, with PM<sub>10</sub> and NO<sub>x</sub> levels significantly lower than in the control periods whereas ozone showing significant higher values. Average PM<sub>10</sub> concentrations during the war were lower by 3-9 µg/m<sup>3</sup> at all the 10 monitoring stations (10-30 µg/m<sup>3</sup>). PM<sub>2.5</sub> did not show a similar clear trend, with similar average readings in the three time periods. The 90<sup>th</sup> and 95<sup>th</sup> percentile concentrations at all the stations are lower during the war period for both PM<sub>10</sub> (in 2-12 µg/m<sup>3</sup>) and PM<sub>2.5</sub> (in 4-11 µg/m<sup>3</sup>). These changes are significant in spite of the relatively high background PM levels at the semi-arid climate experienced in the region. All these indexes suggest that transportation is a key contributor to PM emissions in the

study area, in agreement with our previous conclusions based on different methodology (Yuval and Broday, 2006) and in contrast to estimations of the municipal environmental unit and the local office of the environmental protection ministry. Detailed analysis of the data and further interpretations, relevant to possible abatement procedures, will be presented.

Yuval & Broday D. M. (2006). *Atmos. Environ.* 40, 3653–3664.

## Size-segregated physical-chemical Characterization of Particles Depending on Air Mass Origin at German lowlands (Melpitz site)

G. Spindler<sup>1</sup>, E. Brüggemann<sup>1</sup>, Th. Gnauk<sup>1</sup>, A. Grüner<sup>1</sup>, H. Herrmann<sup>1</sup>,  
K. Müller<sup>1</sup>, Th. M. Tuch<sup>2</sup>, B. Wehner<sup>1</sup>, M. Wallasch<sup>3</sup>, A. Wiedensohler<sup>1</sup>

<sup>1</sup>Leibniz-Institut für Troposphärenforschung e.V., Permoserstrasse 15, 04318 Leipzig, Germany

<sup>2</sup>Umweltforschungszentrum, Permoserstrasse 15, 04318 Leipzig, Germany

<sup>3</sup>Umweltbundesamt, Wörlitzer Platz 1, 06844 Dessau, Germany

Keywords: PM<sub>10</sub>/PM<sub>2.5</sub>, field measurements, Particle size distribution, Particle characterization, trajectory

The joint investigation (supported by the Umweltbundesamt, project 351 01 022) for a size-segregated physical-chemical characterization of tropospheric aerosol has started in spring 2004 at the research station of the Leibniz-Institut für Troposphärenforschung (IfT) in Melpitz situated in the vicinity of the city of Torgau in the river Elbe valley (12°56' E, 51°32' N, 86 m asl.). This spot is integrated in the EMEP activities and a supersite in the EUSAAR network (Flossmann *et al.*, 2006). 24 hour samples for PM<sub>10</sub>, PM<sub>2.5</sub> (every day) and PM<sub>1</sub> (at least every six days) were collected at quartz fibre filters (Munktell, S) using high volume samplers (DHA-80, DIGITEL Electronic AG, CH). Particle mass concentration was determined gravimetrically under constant conditions (24 hours: 50% relative humidity, temperature 20°C). Figure 1 shows exemplary the percentage of PM<sub>2.5</sub> in PM<sub>10</sub> with a typical seasonal variation.

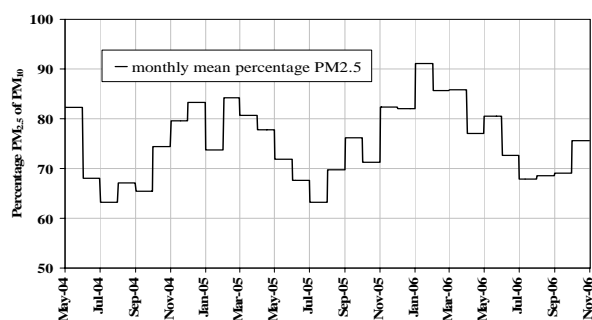


Figure 1. Time series of monthly percentage of PM<sub>2.5</sub> in PM<sub>10</sub>

The concentration of water-soluble ions was detected by ion chromatography (Metrohm, CH). Total carbon was quantified as sum of organic and elemental (TC=OC+EC) by a thermographic method applying a Ströhlein C-mat 5500 carbon analyzer (Spindler *et al.*, 2004). The particle number size distribution was measured in the range 3 to 800 nm and using a thermodenuder for evaporation of volatile particle mass (Wehner, *et al.*, 2003). During selected days in winter and summer with distinct air mass origin particles in the range of PM<sub>10</sub> up to PM<sub>0.05</sub> were sampled with a five stage BERNER-type low pressure impactor and analysed for mass, the content of water soluble ions, organic and black carbon and selected organic species.

Under the dominating wind direction southwest to northwest (W) air masses from the Atlantic Ocean with integrated showers are transported, often during low pressure situations, to Melpitz. They pass large parts of Germany. The second main wind direction is East (E). Then dry air masses are transported with moderate wind velocity during high pressure situations over long distances to Melpitz. The main sources regions for these air masses are in Russia, Poland, Belarus, Ukraine, and the North of Czech Republic. In these areas coal heated power plants sometimes with little exhaust treatment; old industry and older cars still exist as air pollution sources. The mean particle distribution for these main air mass directions are given in Table 1.

Table 1. Mean particle mass distribution in summer 2004 and 2005 and winter 2004/05 and 2005/06 for two air mass origins at Melpitz site

amo	PM	n	mass	SO <sub>4</sub> <sup>2-</sup>	NO <sub>3</sub> <sup>-</sup>	NH <sub>4</sub> <sup>+</sup>	TC
W <sub>summer</sub>	1	51	8.8	1.9	0.7	1.0	1.9
W <sub>summer</sub>	2.5	206	11.4	2.2	1.0	1.1	2.2
W <sub>summer</sub>	10	214	16.2	2.4	1.7	1.1	3.7
E <sub>summer</sub>	1	12	16.3	3.4	0.8	1.5	3.8
E <sub>summer</sub>	2.5	65	19.7	4.2	1.0	1.8	4.8
E <sub>summer</sub>	10	65	26.9	4.6	1.6	2.0	8.0
W <sub>winter</sub>	1	42	11.8	1.7	3.3	1.6	2.1
W <sub>winter</sub>	2.5	173	16.2	2.4	4.6	2.3	3.0
W <sub>winter</sub>	10	184	19.5	2.6	5.4	2.4	3.8
E <sub>winter</sub>	1	11	21.0	4.0	3.8	2.5	5.8
E <sub>winter</sub>	2.5	67	31.0	6.1	5.6	3.9	8.1
E <sub>winter</sub>	10	67	36.6	6.6	6.4	4.2	10.0

**summer:** May till September, **winter:** October till April; **amo**, air mass origin; **n**, number of measurements; for mass, ions and TC mass-concentrations in µg/m<sup>3</sup>

For identifying air mass source regions 96 hours backward trajectories (www.arl.noa.gov) were used.

Flossmann, A., Laj, P., the EUSAAR Partners (2006) *European Supersites for Atmospheric Aerosol Research (EUSAAR): a new FP6 Integrated Infrastructure Initiative*. Geophysical Research Abstracts, Vol. 8, 02357

Spindler, G., Müller, K., Brüggemann, E., Gnauk, T., Herrmann, H. (2004). *Atmos. Environ.*, 38, 5333-5347.

Wehner, B., Philippin, S., Wiedensohler, A. (2003). *Aerosol Science.*, 33, 1087-1093.

## PM10 in Ireland, 2002 to 2005

S. Leinert<sup>1,2</sup>, J. Finnan<sup>2</sup>, B. O’Leary<sup>2</sup>

<sup>1</sup>EPA, Dublin 14, Ireland

<sup>2</sup>NUI Galway, Galway, Ireland

Keywords: PM10, urban pollution, mass concentration, monitoring

PM10 data for Ireland for the years 2002 to 2005 is presented here. The data was collected as part of the PM10 network run by the Irish EPA and local authorities. Instruments used are mostly Partisol 2025 and Opsis SM-200. Some sites are continuous sites, whereas others were temporary only, with data available for part of a year. This study includes data from 19 sites.

Data were analysed for variation with site type, seasonal variation, and dependence on wind direction/air mass origin.

Data show a clear trend in PM10 mass concentration from background suburban on the lower end to traffic urban on the upper end, with large variations within one site category (Table 1). A Dublin kerbside and rural background value are included for comparison, from a study by Jennings et al (2006).

Table 1. PM10 in  $\mu\text{g}/\text{m}^3$  for different site types

Site type	Range of annual means (number)	Median of means
Dublin kerbside	35.4 (1)	35.4
Traffic urban	19.2 – 28.4 (12)	21.3
Traffic suburban	14.3 – 32.4 (15)	19.0
Industrial rural	16.7 – 16.8 (2)	16.7
Background suburban	12.1 – 21.4 (15)	15.5
Rural background	10.5 (1)	10.5

Phoenix Park site, located in a park in the centre of Dublin, shows the lowest values of the background suburban stations, with  $12.1 \mu\text{g}/\text{m}^3$  only slightly higher than the rural background value.

The data show an urban increment of about  $10 \mu\text{g}/\text{m}^3$ . Kerbside measurements by Jennings et al. (2006) yield an additional increment of about  $15 \mu\text{g}/\text{m}^3$ .

Seasonal variation is shown in Figure 1, for those sites with at least two years of data. Maximum values are observed in March. All sites are placed in Dublin or Cork (marked with -C), except for Kiltrough. Cork and Dublin sites show the same seasonal variation.

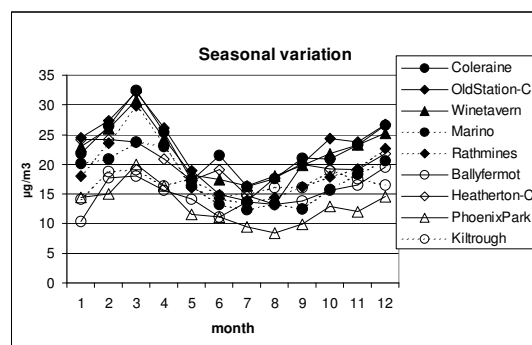


Figure 1. seasonal variation of PM10 concentration for sites with at least two years of data

Variation of PM10 concentration with wind direction is shown in Figure 2. Dublin airport wind direction data supplied by MetEireann were used for classification into eight sectors. The analysis shows a clear trend, with highest average PM10 levels associated with Easterly directions (90 degrees), and lowest levels associated with wind directions from SouthWest and West (225 and 270 degrees). This trend is similar for all locations, independent of site type and location.

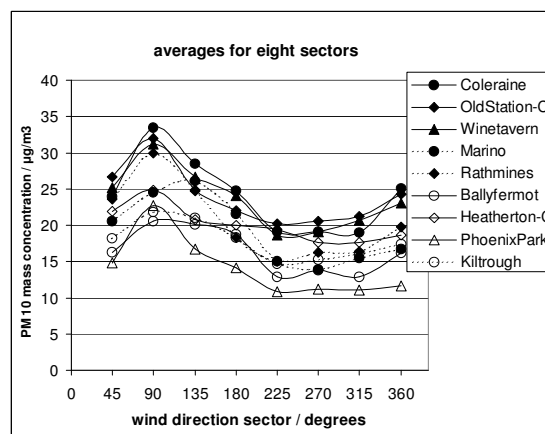


Figure 2. variation of PM10 concentration as function of wind direction

Jennings, S. G., et al. (2006), *Nature and Origin of PM10 and Smaller Particulate Matter in Urban Air*, published by the EPA, Ireland

## Interannual variation of particulate matter over Europe with emphasis on North Rhine-Westphalia: Impact of changing emissions and meteorological conditions

M. Memmesheimer<sup>2</sup>, S. Wurzler<sup>1</sup>, W. Kappert<sup>1</sup>, J. Friesel<sup>1</sup>, U. Hartmann<sup>1</sup>, A. Brandt<sup>1</sup>, U. Pfeffer<sup>1</sup>, M., E. Friese<sup>2</sup>, H. J. Jakobs<sup>2</sup>, H. Feldmann<sup>2</sup>, A. Ebel<sup>2</sup>, and C. Kessler<sup>2</sup>

<sup>1</sup>North Rhine-Westphalia State Agency for Nature, Environment and Consumer Protection (LANUV NRW), Leibnizstrasse 10, D-45659 Recklinghausen, Germany

<sup>2</sup>Rhenish Institute for Environmental Research (RIU), EURAD-Project, University of Cologne, Aachener Strasse 201-209, D-50931 Cologne, Germany

Keywords: Air Pollution, Atmospheric Aerosol, Aerosol Modelling, PM10, Regional Modelling

In short, the EC air quality framework directive and its daughters require that since 2002 the air quality has to be assessed and monitored area wide in each member state using the combined efforts of observational networks and modelling. Objectives of the EC air quality directives are SO<sub>2</sub>, NO<sub>x</sub>, NO<sub>2</sub>, CO, O<sub>3</sub>, benzene, Pb, and aerosol particles (PM10). Limit values have to be met for e.g., PM10 in 2005 and for e.g., NO<sub>2</sub> in 2010.

In this paper the results of long-term runs for the years 2002, 2003, 2004, 2005, and 2010 carried out with the European Air Pollution Dispersion Model (EURAD, Memmesheimer et al., 2004) are discussed with emphasis on atmospheric particulate matter over Europe and especially over North Rhine-Westphalia (NRW), the main centre of European integrated steel production. The model results allow the assessment of air quality in regions where observations are incomplete or missing.

The EURAD model predicts the transport, chemical transformation and deposition of air pollutants. Meteorological fields are provided by the meteorological model MM5, transport is modelled by solving the 3-D advection and diffusion equation. Gas-phase chemistry is handled with the RACM-MIM chemical mechanism, dry deposition is treated with a resistance model. The Modal Aerosol Dynamics Model (MADE) has been applied with extensions to account for the formation of secondary organic aerosols (Schell et al., 2002). MADE provides size resolved concentrations of secondary and primary aerosol species. The calculations are performed using a one-way nesting scheme. The horizontal grid resolution is 125 km on the European Scale, 25 km for an intermediate scale, and 5 km to simulate the region of NRW.

Model runs related to the years 2002, 2003, 2004, 2005, and 2010, have been successfully completed with different emission scenarios and meteorological fields. Model results have been analysed with respect to the requirements of the EC air quality directive on PM10 and compared to observations. Example results are given in Figs. 1 and 2. Fig. 1 shows the prognosis of the annual average PM10 concentration over Europe in 2002 and 2010. In most parts of Europe the PM10

background concentration assumes values higher than 50% of the limit value. The PM10 concentration decreases in 2010, but there persist areas with high particle load, e.g., NRW. Fig. 2 shows the impact of changing meteorological conditions. PM10 loads in 2003 are compared to those in 2005. Meteorological effects seem to be important for the exceedances of the daily average of 50 µg/m<sup>3</sup>.

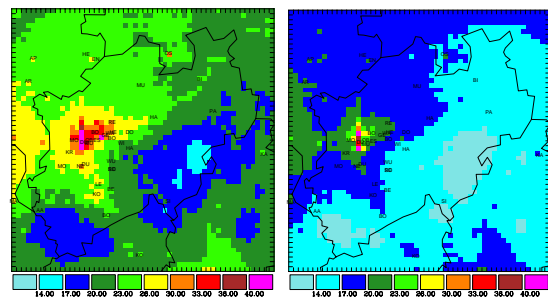


Figure 1. Annual average PM10 concentration over Europe in µg/m<sup>3</sup> in the years 2002 (left panel) and 2010 (right panel)

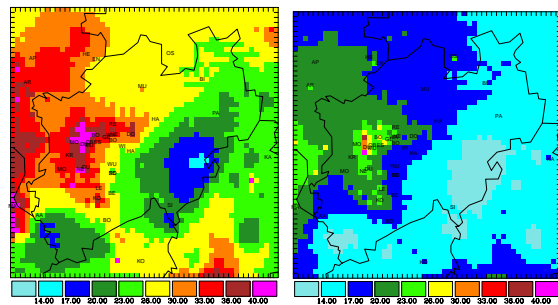


Figure 2. Annual average PM10 concentration over NRW in µg/m<sup>3</sup> in the years 2003 (left panel) and 2005 (right panel)

This work was supported by the LANUV NRW. Thanks also to UBA, EMEP, IIASA, ICG2, Research Center Jülich, ZAM/NIK, RRZK/ZAik Uni. Köln.

Memmesheimer, M., Friese, E., Ebel, A., Jakobs, H. J., Feldmann, H., Kessler, C., Piekorz, G. (2004), *IJEP*, **22**, 108 – 132.

Schell, B., Ackermann, I.J., Hass, H., Binkowski, F.S., and Ebel, A. (2002) *J. Geophys. Res.*, 106, 28275-28293.

### Positive Matrix Factorization on particulate matter daily data series

F. Mazzei<sup>1</sup>, A. D'Alessandro<sup>2</sup>, F. Lucarelli<sup>3</sup>, S. Nava<sup>3</sup>, P. Prati<sup>1</sup>, G. Valli<sup>2</sup>, R. Vecchi<sup>2</sup>

<sup>1</sup> Dipartimento di Fisica and INFN, via Dodecaneso 33, 16146 Genova – Italy

<sup>2</sup> Istituto di Fisica Generale Applicata and INFN, Via Celoria 16, 20133, Milano – Italy

<sup>3</sup> Dipartimento di Fisica and INFN, via Sansone 1, 50019, Sesto Fiorentino – Italy

Keywords: PMF, PM10, PM2.5, PM1, XRF

The use of Positive Matrix Factorization (PMF) to get profiles of emission sources, starting from concentration time series measured in urban and rural sites, is rapidly expanding. Nevertheless, as all the receptor models, PMF can produce artefacts, in particular when applied to daily data sets, and appropriate testing methodologies are desirable. Here, we present the results of a wide campaign conducted in the urban area of Genoa (Italy) where hundreds of PM10, PM2.5 and PM1 daily samples were collected in sites with different characteristics. Elemental concentrations were obtained by X-Ray Fluorescence (XRF) analysis and source profiles were calculated by PMF2. Source apportionment was then achieved directly including the PM mass in the PMF analysis. The sampling in different sites allowed us to perform several consistency tests on PMF profiles and to obtain average and stable values for tracers of specific sources in each PM fraction. In particular, we got typical ratios for tracers of traffic (Cu, Zn, Pb) and heavy oil combustion (V, Ni). We could also identify and quote the contamination of polluted PM in “natural” sources (sea salt, soil dust). The sampling in several sites in the same area, allowed us to resolve and to quote average characteristics and very local situations: this approach could suggest a general methodology to check receptor model and source apportionment results.

The PM concentration was determined using 47 mm Teflon membranes with 2 µm pore size. Sampling time was always 24 hours beginning at midnight. Filters, pre-conditioned for 2 days in a controlled room (temperature: 20 ± 1 °C, relative humidity: 50 ± 5 %), were weighed using an analytical balance (sensitivity: 1 µg); electrostatic effects were avoided using a de-ionizing gun. The weighing procedure included several reproducibility tests and controls with certified weights resulting in a typical accuracy of 3 - 5 µg, being the PM deposit on each filter in the range 300 - 2000 µg. The elemental composition of PM was detected by ED-XRF at the Physics Department of the Genoa University using an ED-2000 spectrometer by Oxford Instruments (Ariola et al., 2006).

PMF was applied to the data sets of elemental concentrations in the PM10, PM2.5 and PM1 size

fractions. The PMF methodology has been described in detail by its developers (Paatero and Tapper, 1997).

Samples have been collected in several sites in town and the major results is the profiles of some anthropogenic sources, as traffic and heavy oil combustion, which turned out to be fairly constant in all the sites. The town averages are given in Table 1

Size fraction	Tracers ratio	Town average
PM10	Cu:Pb	4.0 ± 0.5
PM2.5	Cu:Pb	2.7 ± 0.8
PM1	Cu:Pb	0.5 ± 0.3
PM10	Cu:Zn	1.0 ± 0.2
PM2.5	Cu:Zn	0.3 ± 0.1
PM1	Cu:Zn	0.09 ± 0.04
PM10	V:Ni	3.2 ± 0.9
PM2.5	V:Ni	3.7 ± 0.6
PM1	V:Ni	3.0 ± 0.9

Table 1. Tracer concentration ratios in the PMF profiles of the sources named as “traffic” and “oil combustion”

This work has been partly supported by Amministrazione Provinciale di Genova and by INFN.

Ariola, V., D'Alessandro, A., Lucarelli, F., Marazzan, G., Mazzei, F., Nava, S., Garcia Orellana, I., Prati, P., Valli, G., Vecchi, R., Zucchiatti, A., 2006.

*Elemental characterization of PM10, PM2.5 and PM1 in the town of Genoa (Italy).* Chemosphere 62, 226 – 232.

Paatero, P., Tapper, U., 1994.

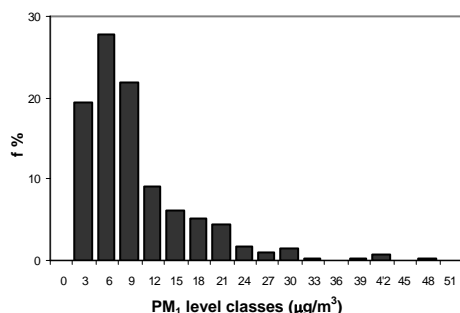
*Positive matrix factorization: a non-negative factor model with optimal utilization of error estimates of data values.*

Environmetrics 5, 111-126.

**PM<sub>1</sub> and trace element concentrations measured in Tito Scalo (Basilicata, Southern Italy)**S. Trippetta<sup>1</sup>, R. Caggiano<sup>1</sup>, M. Macchiato<sup>2</sup>, M. Ragosta<sup>3</sup>, S. Sabia<sup>1</sup> and G. Scardaccione<sup>1</sup><sup>1</sup>Istituto di Metodologie per l'Analisi Ambientale, CNR, C.da Santa Loja Zona Industriale, 85050, Tito Scalo (PZ), Italy<sup>2</sup>Dip. di Scienze Fisiche, Università Federico II, Via Cintia, 80126, Napoli, Italy<sup>3</sup>Dip. di Ingegneria e Fisica dell'Ambiente, Università della Basilicata, V.le dell'Ateneo Lucano, 85100, Potenza, Italy

Keywords: Fine particles, Seasonal patterns, trace elements, Source profiles

Nowadays level measurements, high event occurrence and chemical composition of atmospheric particulate matter represent main topics in pollution monitoring. Particularly evaluation and characterization of fine fractions (PM<sub>2.5</sub> and PM<sub>1</sub>) play a key role for upgrading and improving indoor and outdoor air quality monitoring systems. The adverse impact of fine particles on natural ecosystems and living organisms may be very significant. In urban, industrial and rural sites, it is very important to characterize the levels of these pollutants, substituting progressively TSP and PM<sub>10</sub> measurements. In this study we present the data collected from October 2005 to January 2007 in the industrial area of Tito Scalo (Basilicata, Southern Italy). The measurement campaign was aimed to evaluate daily concentrations of PM<sub>1</sub> and to characterize their trace element content. In this site, other measurement campaign were carried out, starting from 1997 in which TSP, PM<sub>10</sub> and PM<sub>2.5</sub> levels and corresponding heavy metal content were measured and analyzed. This area represents an optimal test site. It is a part of a rather unpolluted region. Moreover anthropogenic activities patterns and geomorphologic features of the area are well characterized. In table 1, a summary of explorative statistical parameters evaluated in the different field surveys is shown. We note that, for decreasing size of collected particles, the difference between standard limit values and observed values decreases significantly. Table 2 shows PM<sub>1</sub> levels measured in other Italian sites. These areas are characterized by different climatic, geomorphologic and anthropogenic features in comparison with our site. We observe low PM<sub>1</sub> levels in Tito Scalo and preliminary data analysis points out a different seasonal behavior.

Figure 1. PM<sub>1</sub> data frequency (%) distribution

In figure 1, data frequency distribution is shown; we may note the occurrence of concentration peaks (1% of data are higher than 40 µg/m<sup>3</sup>) which have to be investigated carefully.

Regarding the chemical composition, we determine the concentrations of Mn, Mg, Al, Ca, Si, Na, Cr e Zn with ICP-OES techniques and Cd, Cu, Fe, Pb e Ni concentration with GF-AAS techniques. Data analysis will be aimed to point out the relationships among metal concentrations and PM levels. Particularly correlation structure and source profile will be characterized and interpreted by means of a multivariate statistical procedure.

Table 1: Summary of explorative statistical parameters (data are expressed in µg/m<sup>3</sup>). Legend: *n* = sample number, *m* = mean value, *sd* = standard deviation, *min-max* = range, *sv* = standard value

	<i>n</i>	<i>m</i>	<i>sd</i>	<i>min</i>	<i>max</i>
PM <sub>1</sub>	290 (2005-07)	9	9	0.2	88.5
PM <sub>2.5</sub>	591 (2001-04)	13	12	0.1	117.0
PM <sub>10</sub>	101 (2001)	24	23	1.0	183.0
TSP	514 (1997-99)	60	46	1.0	218.0
<i>sv</i>					

Table 2: PM<sub>1</sub> levels (µg/m<sup>3</sup>) measured in Italian sites.

Milan <sup>a</sup>	Urban area	31
	Residential area	24
	Suburban area	18
Milan <sup>b</sup>	Urban area	29
Genoa <sup>c</sup>	Urban area	20
Florence <sup>d</sup>	Urban area	17

<sup>a</sup>Giugliano M., et al. (2005). *Atmos. Environ.*, 39, 2421-2431

<sup>b</sup>Vecchi R., et al.. (2004). *Atmos. Environ.*, 38, 4437-4446.

<sup>c</sup>Ariola V., et al. (2006). *Chemosphere*, 62, 226-232.

<sup>d</sup>ARPAT data, [www.arpat.toscana.it/news](http://www.arpat.toscana.it/news). n.182-2006.

## PM<sub>10</sub> and PM<sub>2.5</sub> in Ambient Soil Dust: Elemental Enrichment Factor

Krystyna Trzepla-Nabaglo, R.G. Flocchini and O.F. Carvacho  
Crocker Nuclear laboratory, University of California, One Shields Ave. Davis, CA. 95616 U.S.A.

Keyword: PM<sub>10</sub> PM<sub>2.5</sub> PESA RF heavy metals enrichment factor

In California's San Joaquin Valley, agricultural operations are highly complex and potentially significant sources of PM<sub>10</sub> and PM<sub>2.5</sub>. Furthermore, PM<sub>10</sub> and PM<sub>2.5</sub> are considered to be among the most harmful of all air pollutants. When inhaled these particles evade natural defenses of the respiratory system and lodge deep in the lungs causing serious health problems.

Our studies aim to characterize particulate concentrations and associated chemical species in rural atmosphere during agricultural processes and identify potential sources. Enrichment factors were calculated based on the elemental data.

A series of experiments with different soils characteristics were conducted to measure PM<sub>10</sub> and PM<sub>2.5</sub> emissions from agricultural operations in San Joaquin Valley. All samples were collected during summertime of 1999 under actual field conditions using a combination of upwind/downwind source isolation to quantify PM<sub>10</sub> and PM<sub>2.5</sub> concentrations. Ambient PM<sub>10</sub> and PM<sub>2.5</sub> were collected on Teflon filters using IMPROVE samplers for gravimetric and elemental analyses.

The aerosol mass concentrations were calculated using the gravimetric method. The elemental composition of the aerosol samples was determined using  $\gamma$ -ray fluorescence method for elements from sodium to lead and PESA (Proton Elastic Scattering Analysis) for hydrogen. The analyses were performed at Crocker Nuclear laboratory, University of California in Davis.

Figure 1 shows the mass concentration and fractional composition of the PM<sub>10</sub> dust collected from ambient samples downwind of agricultural operations. For all the soil types examined, mineral soil (i.e. the SOI parameter) accounts for 77 to 87 of the PM<sub>10</sub> mass in downwind ambient samples. Organic matter comprises 12 to 22 of the PM<sub>10</sub> mass for all soil types, with sulphate, metals, and other elements accounting for 1 or less.

The mass concentration and fractional composition of the PM<sub>2.5</sub> dust collected from ambient samples downwind of agricultural operations is shown in Figure 2. The PM<sub>2.5</sub> mass is 6 to 7 of the PM<sub>10</sub> mass for all soil types with the exception of loam, 12 of the PM<sub>10</sub> mass. Mineral soil accounts for 37 to 66 of the PM<sub>2.5</sub> mass for all soil types. Organic matter accounts for 32 to 41 of the PM<sub>2.5</sub> mass, and sulphate accounts for 2 to 21. Metals and other elements account for 3 or less of PM<sub>2.5</sub> mass. In general, the elemental composition of the ambient samples collected during agricultural operations suggests soil and organics as major

components of the aerosol. However, the presence of metals and sulphate in the collected aerosol samples is possibly due to the presence of those in the air or in very small amounts, in the underlying soil. The contribution from agricultural equipment may be a major source of these components.

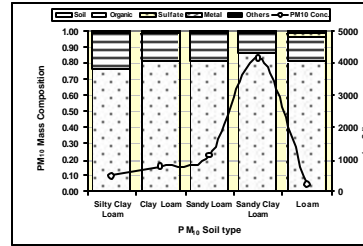


Figure 1. Concentration and composition of PM<sub>10</sub> in ambient samples

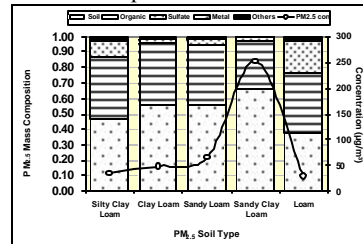


Figure 2. Concentration and composition of PM<sub>2.5</sub> in ambient samples

Enrichment factors for given element relative to silicon concentration were calculated using equation (1) for elements in PM<sub>2.5</sub> and PM<sub>10</sub> samples.

$$EF = \frac{E_{2.5} / Si_{2.5}}{E_{10} / Si_{10}} \quad (1)$$

In the equation above,  $EF$  is the enrichment factor,  $E_x$  is the elemental concentration in the PM<sub>2.5</sub> or PM<sub>10</sub> fraction, and  $Si_x$  is the silicon concentration in the PM<sub>2.5</sub> or PM<sub>10</sub> fraction.

Calculated enrichment factors for elements indicate that elements of anthropogenic pollution origins, like  $n$ , Pb, Se, Ni etc, are highly enriched with respect to crustal composition (Al, Fe, Ca, etc.) Calcium is enriched by approximately a factor of two, while some toxic and harmful elements, particularly V, Cr, Cu,  $n$ , Pb, Se, and Br are enriched by about an order of magnitude in the PM<sub>2.5</sub> fraction relative to the PM<sub>10</sub> fraction. Sulfur is enriched by a factor of 11 to 36 (18.4 on average).

It is noticed, that sulphate and metals are enriched in the PM<sub>2.5</sub> fraction compared to the PM<sub>10</sub> fraction by factors that vary depending on the soil type and test conditions.

Holmen et al., Atmospheric Environment, 35, 3265-3277, 2000.

## Statistical study of the secondary organic aerosol from countryside of Madrid (Spain)

O. Pindado, R.M. Perez, S. Garcia, A.I. Barrado

Chemistry Division, Department of Technology, CIEMAT, Avda. Complutense 22, 28040, Madrid, Spain

Keywords: Atmospheric aerosols, Biogenic particles, Organic compounds, PM10/PM2.5

During last years, there have been many works dedicated to study atmospheric aerosols, due to in urious effects that particulate matter produces on the human health and environment. These aspects were reflected in the IPCC of 1995.

At the moment, some studies have conducted the characterization of the organic fraction of atmospheric aerosols, one of them is the extensive work of Meinheng (Meng *et al.*, 2000), but less those able to study annual variability of secondary organic aerosol. Moreover, the number of studies about rural aerosol is less than those focused on urban or industrial areas, where organic emissions are large and have dramatic effects on air quality.

This study has taken a step more its objective was to investigate secondary aerosol components for a period of one year in a rural zone of Madrid (Spain).

For this purpose, an annual campaign of sampling of atmospheric aerosol from a rural area took place between April of 2004 to March of 2005, collecting two fractions of particulate matter PM2.5 and PM10. Briefly, sampling was performed using high-volume samplers and was collected over quartz filters. The inorganic and organic composition for both fractions was analysed.

For organic analysis, samples were Soxhlet extracted with a mixture of dichloromethane/acetone. After, extracts were concentrated and cleaned-up by silica gel column chromatography and four fractions were obtained, alkanes, PAHs, alcohols and acids respectively. Alkanes were analyzed by GC-MS, meanwhile polar compound were previously derivatised with BSTFA before chromatographic analysis. PAHs were submitted to HPLC with fluorescence detection.

Within organic fraction there have been studied some unsaturated fatty acids, as oleic and linoleic acids, a degradation product of stearic and palmitic acids, as azelaic acid, and finally several degradation products of  $\alpha$ -pinene, as pinic, pinonic and norpinonic acids. These compounds studied were chosen because of their significance as tracers for secondary organic fraction (Kavouras *et al.*, 1999).

In table I is shown the concentration range for each organic compound in PM2.5 fraction. It is important to note that pinonic acid is the most abundant secondary organic compound in both fractions. Normally, highest concentrations were found in summer, indicating the large biogenic contribution during these days.

Table 1. Concentrations range of secondary organic aerosol in PM2.5

Acid Compounds	Summer-Spring (ng/m <sup>3</sup> )	Winter-Autumn (ng/m <sup>3</sup> )
inoleic	0,2 – 63,9	10,5 – 65,5
Oleic	0,1 – 50,6	8,6 – 38,4
Azelaic	1,6 – 36,1	6,3 – 32,4
Pinonic	0,8 – 271,6	7,7 – 287,5
Pinic	1,0 – 45,2	6,8 – 35,2
Norpinonic	2,0 – 2,3	2,4 – 25,4

Correlations between the studied organic compounds detected in PM2.5 fraction are shown in table 2. There are excellent correlations between linoleic, oleic, azelaic and pinonic acids, and relatively good correlations between pinic and the rest of compounds. Therefore, these results confirm a similar source for all organic compounds considered in this work.

Table 2. Correlations between organic compounds in PM2.5 fraction

	inoleic	Oleic	Azelaic	Pinonic	Pinic
inoleic	1				
Oleic	0,97	1			
Azelaic	0,98	0,91	1		
Pinonic	0,96	0,91	0,96	1	
Pinic	0,69	0,52	0,64	0,8	1

Some multivariate statistical techniques, as Cluster analysis and Factor Analysis have been applied to the set of data in order to identify sources of atmospheric particles.

This work was funded by the Ministerio de Educaci n y Ciencia of Spain (REN2003-08603-C04-02). Authors would like too thank to the Conse eria de Medioambiente de la Comunidad de Madrid for their sampling and infrastructure support.

Intergovernmental Panel on Climate Change IPCC (1995). Climate Change, Cambridge University Press. New York

Kavouras I. G., Mihalopoulos N. & Stephanou E. G. (1999), Environ. Sci. Technol., 33, 1028-1037.

Meng M., Fang M., Wang F. & To K. . (2000), Atmos. Environ., 34, 2691-2702

## Fine Particles PM10 in the Mitrovica Urban Atmosphere and monitoring

Afrim M. Syl<sup>1</sup>, Kadri Berisha<sup>2</sup>, Agron Veliu<sup>2</sup>

<sup>1</sup>MESP – Ministry of Environment and Spatial Planning of Kosova, 10000 Prishtina, KOSOVA  
Universitet of Prishtina, Faculty of Technology and Environment, Mitrovica 40000 Mitrovica  
<sup>2</sup>University of Prishtina, Faculty of Mining and Metallurgy in Mitrovica, 40000 Mitrovica Kosova

Keywords: heavy metals, particulate matter

**Abstract:** The city of Mitrovica, approximately 40 km north of Prishtina, was the site of one of the largest lead smelters in Europe. The present environmental situation in Mitrovica, put as in front of the responsibility to act more rationally towards nature and to be more responsible towards the protection of the environment for future generations. The lack of protection of the environment during the last ten years, as well as the conflict in Kosova is the origin of huge problems regarding present environmental situation in Mitrovica (Kosova). Mitrovica has its air divided in two kinds, speaking in quality terms: air above rural and mountainous zones, which is clean, air above city urban of the center and nearby different plants, which is more polluted. Urban air contains dust particles and gases, added on it is as results of normal activity of the city and industries in them. Now Mitrovica can be cited as one of the capitals of Europe with worst air pollution. Exposure to airborne particulates PM10 and PM2.5 containing low concentrations of heavy metals, such as Pb, Cd and Zn, may have serious health effects. However, little is known about the specification and particle size of these airborne metals. Fine and PM10 particles size with heavy metals in aerosol samples from the Mitrovica urban area were examined in detail to investigate metal concentrations and speciation. The crystal structures of the particles containing Pb, Cd and Zn were determined from their electron diffraction patterns by XRF methods.

Atmospheric particles aerosols are some of the key components of the atmosphere. They influence the energy balance of the Earth's surface, visibility, climate, human health and environment as a whole. According to World Health Organization (WHO), ozone, particulate matter, heavy metals and some hydrocarbons present the priority pollutants in the troposphere. The results of the long-term studies confirm that the adverse health effects are mainly due to particulate matter, especially small particles—less than 10 microns in diameter (PM10). According to the 1999/30/EC Directive, the countries-members are obligated to reduce the emission of the particles in urban areas by some 50% over the existing levels in order to meet the health-based limit values by 2005 and 2010. The majority of particles of industrial origin

contain significant quantities of some potentially dangerous trace elements. As the result of condensation and adsorption processes, the elements as As, Cd, Mn, Ni, Pb and Zn can be found on the particle surface.

Sampling of suspended particulate matter, PM10 and PM2.5 started in July April 2003 and are still in progress at three sites in the very urban area of Mitrovica: roof of the FXM building MIP, roof of the elementary school "Bedri Gjina" at about 4m height; 40m far from heavy-traffic streets; on the platforms above entrance stairs to the faculty of Mining at the height above 3m from the ground. Suspended particles were collected on Pure Teflon filters, Whatman (37 mm diameter, 2µm pore size) and Pure Quartz, Whatman (37 mm diameter) filter paper, using the low volume air sampler Mini-Vol Airmetrics Co, Inc. (5 l min<sup>-1</sup> flow rate). The duration of each sampling period was 24 hours. The filter samples were sealed in plastic bags and kept in portable refrigerators, in horizontal position during transport back to the laboratory. Particle mass was gravimetrically determined by weighting loaded and unloaded filters, after 48 hours conditioning in a desiccator's, in clean room class at the temperature T=20 °C and constant relative humidity RH around 50%.

For a quality assurance procedure, the quality of sample collection was determined by collecting blank samples in the field and by three control filters. During the sampling, conventional meteorological parameters were regularly recorded at the Meteorological Station of the Hydrometeorological Institute of Kosova located inside central urban area.

## The episode of high particle loads in Europe in January and February 2006 with emphasis on Germany

S. Wurzler<sup>1</sup>, W. Kappert<sup>1</sup>, K. Mildenerger<sup>2</sup>, M. Memmesheimer<sup>3</sup>, H. Jakobs<sup>3</sup>, G. Spindler<sup>4</sup>, K. Drescher<sup>5</sup>, and P. Bruckmann<sup>1</sup>

<sup>1</sup>North Rhine Westphalia State Agency for Nature, Environment and Consumer Protection, Leibnizstrasse 10, D-45659 Recklinghausen, Germany

<sup>2</sup>Institute for Landscape Ecology, University of Muenster, Robert-Koch-Strasse 26, D-48149 Muenster, Germany

<sup>3</sup>Rhenish Institute for Environmental Research, EURAD-Project, University of Cologne, Aachener Strasse 201-209, D-50931 Cologne, Germany

<sup>4</sup>Leibniz Institute for Tropospheric Research, Permoserstrasse 15, D-04318 Leipzig, Germany

<sup>5</sup>Brandenburg State Office for Environment, Seeburger Chaussee 2, D- 14476 Potsdam, Germany

Keywords: Atmospheric Aerosol, Air Pollution, PM10.

Atmospheric aerosol particles with diameters smaller than 10  $\mu\text{m}$  belong to the pollutants of concern in the Clean Air For Europe strategie of the European Commission. The health effects of the particles are likely to vary depending on e.g., their composition and on the exposure time. It is now accepted widely that populations living in areas with higher particle concentrations show a difference in health to otherwise similar people. The effects include higher death rates, respiratory and circulatory effects and cancer. The aim of the European Air Quality Framework Directive and its daughters is to protect mens health and nature. This is done by setting mandatory limit values for air pollutants. The limit value for the annual average PM10 concentration is 40  $\mu\text{g}/\text{m}^3$  and the allowed number of days with average PM10 values higher than 50  $\mu\text{g}/\text{m}^3$  is limited to 35 per year.

Unusual high particle loads were observed in many parts of Europe during an episode lasting from midst of January to the beginning of February in 2006. In many places the daily averages of the PM10 values exceeded 50  $\mu\text{g}/\text{m}^3$  (see Fig. 1). Not only the particle loads were exceptionally high, but also the episode lasted for more than 2 weeks. This resulted in an exceedance of the allowed 35 days per year with daily averages of 50  $\mu\text{g}/\text{m}^3$  already at the beginning of April 2006 at numerous German measurement sites. Even remote areas such as Luneburg heath land, East Frisian Islands, and Munster land achieved scores of more than 10 exceedance days. The year 2006 started with a rather high PM10 burden. After more than two decades with mild winters in most parts of Germany, the winter of the year 2006 with several days of continuous frost, snow and low wind speeds raised memories of the last two big smog episodes in Germany in January 1985 and 1987. The PM10 episode days in 2006 are exceptional even compared to the particle loads of the last two decades. Scope of the paper is to analyse the PM10 episode in 2006, the origin of the high PM10 loads,

and the tradeoffs between transboundary transport processes and home made contributions.

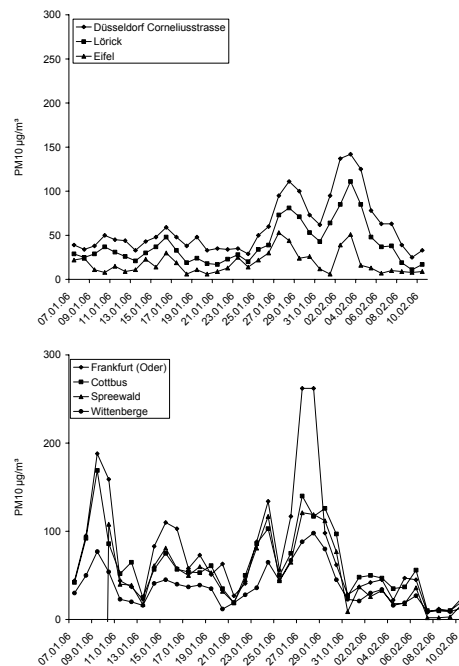


Figure 1. Particle concentrations during the episode in January and February 2006 in NRW (upper panel) and in Brandenburg (lower panel).

Observational data and model results were evaluated for Europe with emphasis on Germany and North Rhine Westphalia. During stationary temperature inversions daily average PM10 values of more than 100  $\mu\text{g}/\text{m}^3$  can be reached in major parts of Europe. These high particles loads result from a combination out of regional contributions and from a mix out of long range transport and local sources. While the high particle loads in eastern and southern parts of Germany were significantly influenced by long range transport, there is strong evidence that the pollution in western parts of Germany was mainly home made during the second part of the particle episode.

## High population density and heavy industry: The challenge for air quality management in North Rhine Westphalia: Are the measures effective?

S. Wurzler<sup>1</sup>, W. Kappert<sup>1</sup>, D. Glatke<sup>1</sup>, P. Bruckmann<sup>1</sup>, and M. Memmesheimer<sup>2</sup>

<sup>1</sup>North Rhine Westphalia State Agency for Nature, Environment and Consumer Protection (LANUV NRW), Leibnizstrasse 10, D-45659 Recklinghausen, Germany

<sup>2</sup>Rhenish Institute for Environmental Research (RIU), EURAD-Project, University of Cologne, Aachener Strasse 201-209, D-50931 Cologne, Germany

Keywords: Atmospheric Aerosol, Air Pollution, PM10.

Aim of the EC air quality framework directive and its daughters is to protect men's health and the environment. They require that the air quality has to be assessed in each member state using the combined efforts of monitoring networks and modelling. Limit values have to be met for e.g., PM10 in 2005. Plans and programmes to achieve this obligation have to be implemented if pollution levels are too high. In 2002 continuous measurements had shown that the PM10 burden was far too high in Duisburg. In 2004 a clean air plan was launched for this region. The present paper focuses on the changing situation in Duisburg due to the clean air plan.

The city of Duisburg (about 500,000 inhabitants) is located in the west of Germany at both sides of the river Rhine. The Rhine is the most important waterway in Europe and the inland port of Duisburg is the largest one in Europe. Duisburg is the place with the highest density of heavy industry and represents the main centre of European integrated steel production. In the year 2002 an exceedance of the annual average PM10 value was observed in Duisburg Bruckhausen. Directly west of the measurement site the industrial zone with steel mill, sinter plants, blast furnaces and a coking plant stretches out. Residential areas are located just to the east of the measurement site and connect to the industrial site. In order to identify the main source of PM10 at the measurement site model simulations were carried out. This source apportionment showed that the regional background contributed more than 50% to the total PM10 load (see Fig. 1). The industrial share was 39%. Traffic is to be found on the third place. Further source apportionment on the basis of measurement analysis shows that the main PM10 source was located in the west of the measurement station and is most likely related to the old coking plant (12% of the total load) of Thyssen. Additional contributions came from the blast furnaces in the west of Bruckhausen (12%).

In order to determine the development of the air quality, PM10 contributions of the years 2002 to 2006 and model simulations for the year 2010 were compared.

The industrial contribution to the PM10 load in Duisburg Bruckhausen has dropped significantly from 2002 ( $20\mu\text{g}/\text{m}^3$ ) to 2003 ( $13\mu\text{g}/\text{m}^3$ ) and 2004

( $12\mu\text{g}/\text{m}^3$ ), owing to the successful implementation of measures to reduce air pollution; especially the closing of the old coking plant west of the station had the main share of this effect ( $5\text{--}6\mu\text{g}/\text{m}^3$ ). After the coking plant was closed the amount of Benzo[a]pyrene in PM10 was reduced dramatically. In 2005 the PM10 concentration rose again, probably due to street construction work and demolition work nearby. But the increase of the mass of iron particles in PM10 in 2005 suggests also industrial processes.

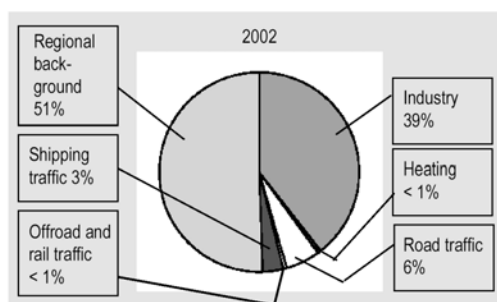


Figure 1. Cause analysis by model simulations for the PM10 load in the northern part of Duisburg.

At Duisburg Marxloh the industrial local contribution rose from  $14\mu\text{g}/\text{m}^3$  in 2003 to  $19\mu\text{g}/\text{m}^3$  in 2004, owing to high contributions out of the direction of the ore harbour in the northwest of the station on very few days. In 2005 the contribution dropped again. The data from 2005 and 2006 are at present subject to further analysis.

The clean air plan Duisburg North includes several measures to reduce the particle emission of the integrated steel industry in the region of Duisburg Bruckhausen. Up to now only the replacement of the coking plant has a large effect. In the years 2005 and 2006 the limit value for the annual average of PM10 was met for the first time. But the industry in this area emits still large amounts of PM10. An important problem remains: the allowed number of days with average PM10 values higher than  $50\mu\text{g}/\text{m}^3$  is exceeded every year in Bruckhausen and Marxloh. Especially on episode days it can be noted that there is not only a rather high contribution to the PM10 load during working hours but also a total background concentration which is already close to the limit value.

## The ratio of PM<sub>2,5</sub>/PM<sub>10</sub> concentrations of suspended particles at stations selected in the Czech Republic

I. Brožová

Air Pollution Laboratory, Czech Hydrometeorological Institute, Na Šabatce 17, 143 06, Prague 4, Czech Republic

Keywords: PM<sub>2,5</sub>/PM<sub>10</sub>, PM (general), PM measurements, Monitoring

The concentration of suspended particles ranks among air pollution components being monitored historically for a very long time. In the Czech Meteorological Institute, the network to monitor the concentrations of the components mentioned has been practising since the sixties of the last century. Numerous considerable changes have taken place over this time. A present-day form of the network corresponds to the relevant technical possibilities and contemporary requirements for information of the atmosphere quality. In 2004, the last extensive reconstruction of this network passed. At all stations, the concentration of the PM<sub>10</sub> fraction is routinely monitored—even PM<sub>2,5</sub> at stations selected. Two types of monitoring—automated and manual are in question. Both these programmes cover all the Czech Republic by dozens of the stations.

Four stations belonging to the manual network ( Košetice, Ústí nad Labem-Kočkov, Ostrava-Poruba, Ostrava-Přívoz) are further indicated. At every these stations are identically going the 24 hours intervals of sample collection, low-volume. A sample is collected by means of the continuous

filtration of the ambient air through a membrane filter consisting of the cellulose derivatives of the 47 mm radius (Millipore 1.2) by constant rate of 2.3 m<sup>3</sup> per hour. The respective concentration is gravimetrically determined in µg/m<sup>3</sup>, namely from the difference of the filter weight after and before exposure and the collected air volume converted to standard conditions. The weighting room equipment is in compliance with the standard EN 12341, the analytical microbalance used belongs in the category 10<sup>-6</sup>.

According to valid European Classification, the selected stations are ranged, as follows: Košetice – Background/Rural/Agricultural/Natural; Ústí nad Labem – Background/Suburban; Ostrava-Poruba – Background/Suburban; Ostrava-Přívoz – Industrial/Urban. For the station type given, the fraction ratio PM<sub>2,5</sub>/PM<sub>10</sub> concentration is characteristic. The more clean station, the closer is to the value of 1. In the following table, the annual averages of the aforesaid ratios are précised, being an example, inclusive of the applicable relative standard deviation, for the stations above-mentioned in years 2004 to 2006.

Table 1. The ratio of PM<sub>2,5</sub>/PM<sub>10</sub> concentration of suspended particles at selected stations

Station	Košetice		
Year	2004	2005	2006
Number of values	138	144	175
Annual average	0.90	0.90	0.90
RSD %	15	12	11

Station	Ostrava - Poruba		
Year	2004	2005	2006
Number of values	167	182	180
Annual average	0.70	0.74	0.80
RSD %	24	18	13

Station	Ústí nad Labem - Kočkov		
Year	2004	2005	2006
Number of values	0	129	173
Annual average	-	0.79	0.74
RSD %	-	16	16

Station	Ostrava - Přívoz		
Year	2004	2005	2006
Number of values	88	66	89
Annual average	0.73	0.70	0.71
RSD %	16	16	14

ISO 7708, 1998

EN ČSN 12341, 2000

EMEP Manual for Sampling and Chemical Analysis, 2002

Air Pollution Atmospheric Deposition in Data, Czech Republic 2004 – CHMI Yearbook

Air Pollution Atmospheric Deposition in Data, Czech Republic 2005 – CHMI Yearbook

## Source apportionment of PM10 in industrialized urban areas by automated electronmicroscopical particle analysis

M. Ebert, N. Benker, K. Kandler, D. Müller-Ebert, S. Weinbruch

Institute of Applied Geosciences, Technical University of Darmstadt, Schnittspahnstr. 9, D-64287 Darmstadt

Keywords: urban aerosols, soot particles, PM10/PM1, single particle analysis, source apportionment,

From April 2005 to February 2006, fortytwo aerosol particle samples were collected in Duisburg Marxloh. The sampling location is close to a heavy industrialized area (one of the largest steel plants in Europe).

From the daily PM10 measurements carried out by the Landesamt für Natur, Umwelt und Verbraucherschutz Nordrhein-Westfalen (LANUV) it is known that PM10 at this location is strongly increased in contrast to the urban background.

For the characterization of the particle composition, automated individual particle analysis (IPA) by scanning electron microscopy combined with energy dispersive X-ray analysis was used.

In total, the chemical composition, geometrical parameters and the size of almost 40000 particles (size range 500 nm – 10 µm) of 22 sampling days were automatically analyzed (at least 1000 particles per sampling day) by use of the EDAX Genesis particle automation software.

Based on the chemical composition, the particles were classified in 13 groups: aluminosilicates, iron oxides, other metal oxides, aged sea salt, soot, carbonates, Cl-rich, P-rich, calcium sulfate, three mixed groups (Ca/Si, Si/SO<sub>4</sub> and Fe-mixtures) and complex secondary material (complex mixtures of sulfates, nitrates, organics often with inclusions of primary particles, mainly iron oxides or soot).

As one main result, it was found that the day to day variation in the abundance of the individual particle groups is correlated with specific wind direction and not with PM10.

Depending on the wind direction, two different situations can be distinguished, urban background and industrial conditions. The urban background at this site is characterized by the dominance of complex secondary material and soot (often internally mixed, Fig.1a) for particles below 1 µm equivalent projected area diameter. Above 1 µm, additional silicates and silicate/sulfate mixtures are present in high amounts.

At days with winds coming from the industrialized area, large amounts of iron oxides (Fig.1b) and iron mixed particles are added to the urban background aerosol. In addition, other metal oxides and Cl-rich

particles are also enriched, and for particles below 1 µm diameter also silicate fly ashes and carbonates.

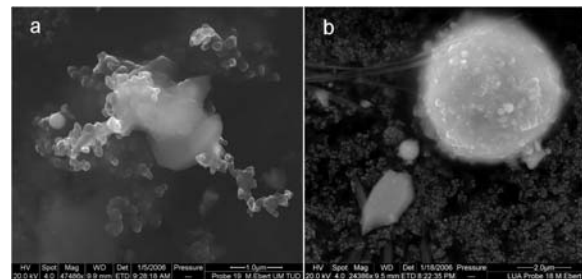


Figure 1: Secondary electron images of (a) a mixture of sulfate, organics and soot and (b) an iron oxide fly ash.

Based on the results of IPA, the average contribution of the different sources to PM10 for background and industrial conditions is quantified (Fig.2).

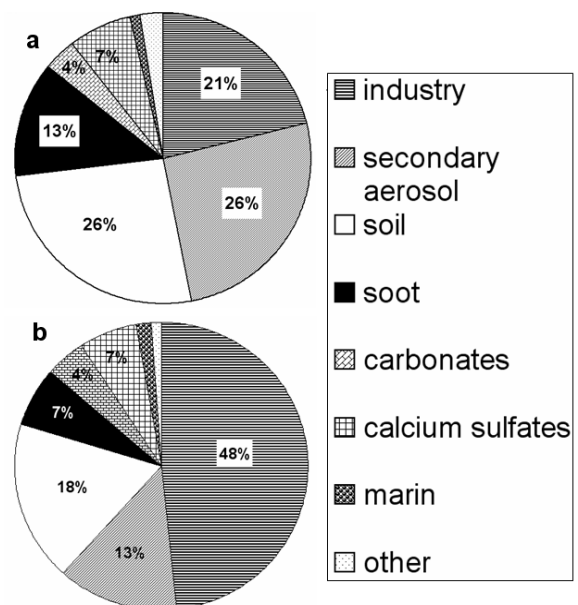


Figure 2: Average contribution of different sources to PM10 at Duisburg Marxloh under (a) background conditions and (b) industrial conditions.

## Characteristics of atmospheric aerosols in Cheonan area during

S. Oh and H. B. ee

Department of Civil and Environmental Engineering, Sangmyung University, San 98-20, Anseo-dong, 339-720, Cheonan, South Korea

Keywords: ambient aerosols, particle size distribution, PM10, PM2.5.

Currently, Korea has a regulation only on PM10 concentration for atmospheric particles, and the 250 National Air Quality Monitoring Stations measure only PM10 mass concentrations. Thus, relatively little data are available on characteristics of atmospheric aerosols in Korea. Furthermore, National air quality standard for the daily average PM10 concentration has been strengthened to 100  $\mu\text{g}/\text{m}^3$  from 150  $\mu\text{g}/\text{m}^3$  in 2007. Therefore, areas unsatisfied the new standards are required to set up the effective air quality control strategy, and characterizations of atmospheric aerosols are necessary. Cheonan is located at 83.6km south from Seoul with approximately 500 thousand people. It is a centre of transportation for the national roads and railroads, and has been changing into industrial areas. The daily average PM10 concentrations in Cheonan often exceeded the new PM10 standards (Oh, 2006). Thus, the purpose of this study is to characterize atmospheric aerosols, and provide the data concerning size fractions, trends, and concentrations of aerosols in Cheonan, Korea.

Size-differentiated mass concentrations of aerosols were determined using a high volume air sampler (Andersen, GV2360) equipped with a 5-stage cascade impactor (Andersen, Model 235) at a site about 1,000m away from heavy traffic highway in Cheonan. Samples were taken for 24 hours of the total 22 times during January and December of 2006. In addition to these manual operations, real time concentrations of PM10 and PM2.5 were monitored at an interval of 1 minute with a laser spectrometer (Grimm Model 1.107).

Sampled aerosols showed mostly bimodal distributions with a saddle point in 1.5–3.0  $\mu\text{m}$  range in diameter and a larger peak in the fine mode, indicating urban characteristics (Willeke & Whitby, 1975). A MMD of fine mode particles were  $0.56 \pm 0.17 \mu\text{m}$  with a GSD of  $2.65 \pm 0.82$ , and those of coarse mode particles were  $5.14 \pm 0.68 \mu\text{m}$  and  $2.15 \pm 0.28 \mu\text{m}$ , respectively. Errors represent 95 confidence intervals. As listed in Table 1, mean values of the daily average concentrations of TSP, PM10, and PM2.5 were 57.0, 50.7, and 39.5  $\mu\text{g}/\text{m}^3$ , respectively. The highest daily average PM10 concentration exceeded the new national standard. Fractions of PM10 and PM2.5 in TSP were  $88.9 \pm 1.8\%$  and  $69.3 \pm 3.9\%$ , and the fraction of PM2.5 in PM10 was  $77.9 \pm 2.2\%$ . The results indicate that

atmospheric aerosols in Cheonan were mainly fine mode particles.

Table 1. Daily average concentrations of TSP, PM10, and PM2.5 in  $\mu\text{g}/\text{m}^3$ .

	TSP	PM10	PM2.5
Mean	57.0	50.7	39.5
Highest	129.0	105.9	76.2
Lowest	10.1	9.4	7.7

Diurnal variations in 1-hr average concentrations of PM10, PM2.5 (fine particles), and PM2.5–10 (coarse particles) are shown in Figure 1. While PM2.5–10 variations were insignificant, PM10 and PM2.5 variations were remarkable and showed the similar pattern, highest in the commuting periods of between 6:00–9:00am and 7:00–9:00pm. The ratio of the highest to lowest concentrations of PM10, PM2.5, and PM2.5–10 were 2.05, 2.56, and 1.46, respectively. The results clearly indicate that secondary aerosols from mobile sources were major component in fine particles. Thus, control of fine particles focusing on mobile sources should be the primary concern for PM10 control strategy in Cheonan, Korea.

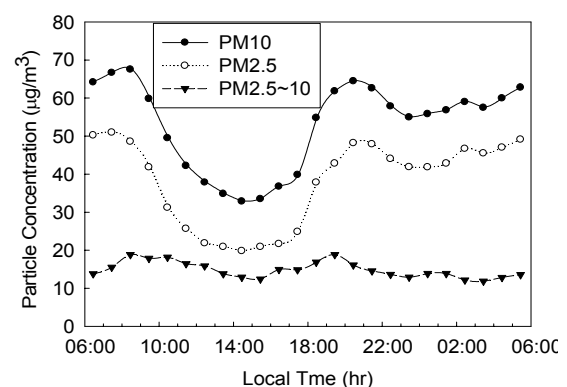


Figure 1. Diurnal variations in 1-hr average concentrations of PM10, PM2.5, and PM2.5–10.

This work was supported by Chungnam Environmental Technology Development Centre.

Willeke, K., & Whitby K. T. (1975). *Journal of the Air Pollution Control Association*, 25, 529-534.

Oh, S (2006). *Journal of Korean Society for Atmospheric Environment*, 22, E1, 45–48.

## Modification of commercially available whole body exposure chambers for rodents for exposure to fine and ultrafine aerosols.

Th. M. Tuch<sup>1</sup>, U. Franck<sup>1</sup>, M. Schilde<sup>1</sup>, M. Wilde<sup>2</sup>, V. Menzel<sup>2</sup>, P. Portius<sup>2</sup> and O. Herbarth<sup>1</sup>

<sup>1</sup>Department Human Exposure and Epidemiology, <sup>2</sup>Mechanical Workshop, Helmholtz Centre for Environmental Research – UFZ, Permoserstraße 15, 04318 Leipzig, Germany

Keywords: Health effects of aerosols, ultrafine particles, submicron particles, inhalation

**Introduction:** High concentrations of airborne particles have been associated with the development and the exacerbation of various diseases. Pathways from the exposure to ambient aerosols to the development of diseases are however not yet well understood. Animal models may help to understand underlying mechanisms and may help to identify susceptible groups. Most commercially available whole body exposure chambers have originally been designed for exposure to gaseous pollutants. Because of the typical high diffusivity of gases little attention has been paid to assure proper mixture of the pollutants with the carrier air. We have modified commercially available exposure chambers (TSE Systems, Germany) for long term exposure of rodents to a wide size range of aerosol particles.

**Design:** Originally TSE exposure chambers are designed for vertical top to bottom air flow. Pollutants are injected directly at the inlet of the chambers (Fig. 1).

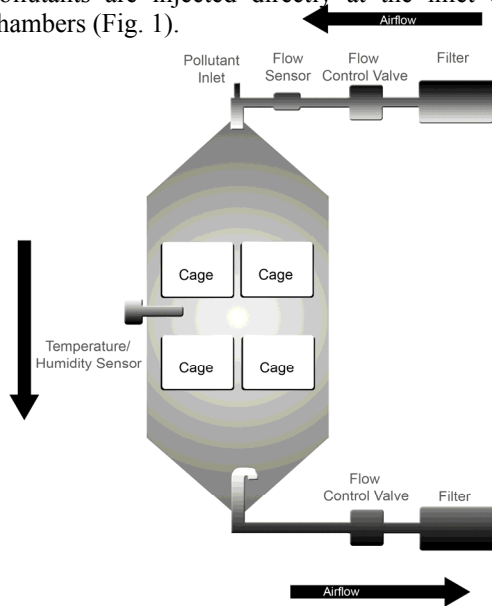


Fig. 1: Original design of TSE exposure chambers

We have changed the original air flow direction to horizontal flow to avoid aerosol losses at the bottoms of the cages. Stainless steel screens have been inserted at both inlet and outlet of the chambers for flow laminarization. A 1.3 m<sup>3</sup> mixing chamber has been added to allow for homogenous mixing of the aerosol and to provide a first (10 to 20 times) dilution of the aerosol to reduce coagulation of ultrafine particles. A schematic view of the modified system is shown in Fig. 2)

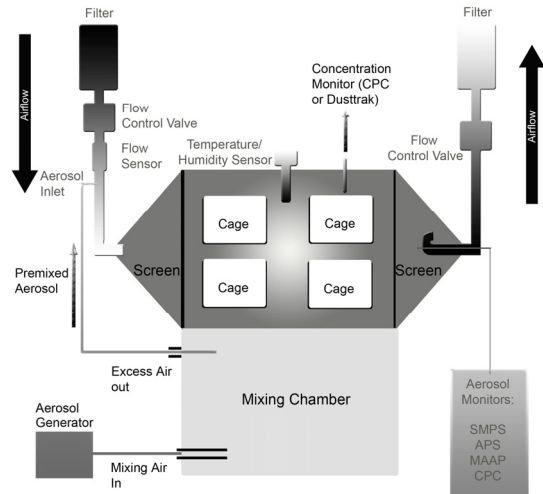


Fig. 2: Modified exposure chamber

**Performance:** Currently we have successfully tested the performance of the chambers with Printex 75 (ultrafine black carbon) and the ultrafine fraction of Arizona road dust for time periods of 24 hours. During these experiments aerosol concentrations varied by +/- 10% due to fluctuations of the generators. The concentration difference between different measurement points inside the chambers did not exceed 10%. Typical number and volume concentrations for the aerosols are shown in fig. 3.

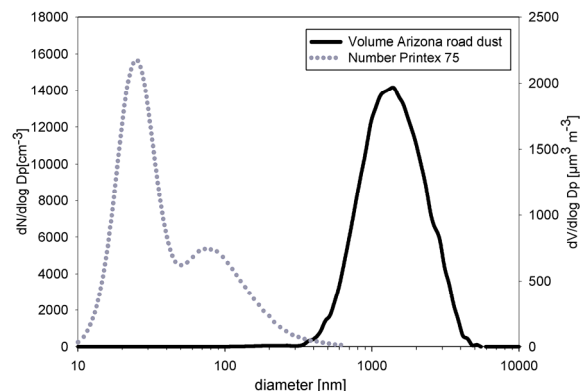


Fig. 3: Exemplary number and volume distributions.

First exposure experiments are scheduled to start in March 2007 in collaboration with the Institute of Laboratory Medicine, Clinical Chemistry and Molecular Diagnostics, University of Leipzig and the Institute of Environmental Toxicology, University of Halle-Wittenberg.

## PM<sub>10</sub> physical and chemical characterisation using high-time resolved samplings in an air pollution “hot-spot” area in Europe

*R. Vecchi<sup>1</sup>, G. Valli<sup>1</sup>, V. Bernardoni<sup>1</sup>, D. Cricchio<sup>1</sup>, A. D'Alessandro<sup>1</sup>, P. Fermo<sup>2</sup>,  
A. Piazzalunga<sup>2</sup>, C. Rigamonti<sup>2</sup>, S. Nava<sup>3</sup>, F. Lucarelli<sup>4</sup>, F. Mazzei<sup>5</sup>, P. Prati<sup>5</sup>*

<sup>1</sup>Inst. of Applied General Physics, University of Milan, and INFN-Milan, 20133, Milan, Italy

<sup>2</sup>Dep. of Inorganic, Metallorganic and Analytical Chem., University of Milan, 20133, Milan, Italy

<sup>3</sup>National Inst. of Nuclear Physics, Sesto Fiorentino, 50019, Florence, Italy

<sup>4</sup>Dep. of Physics, University of Florence, and INFN-Florence, 50019, Florence, Italy

<sup>5</sup>Dep. of Physics, University of Genoa, and INFN-Genoa, 16146, Genoa, Italy

Keywords: PM<sub>10</sub>, high-time resolution, aerosol characterisation, source apportionment

In this paper high-time resolved compositional analysis, aiming at PM<sub>10</sub> physical and chemical characterisation as well as at the identification of different aerosol sources and processes involving atmospheric particles, is shown. High-time resolved measurements of aerosols are necessary to have insights on phenomena like production, deposition, transport and chemical reactions in atmosphere, which can not be generally identified by standard 24-hours integrated filter-based methods.

Two intensive measurement campaigns have been performed in Milan (Italy), located in the Po valley, one of the largest air pollution “hot-spots” in Europe. PM<sub>10</sub> was sampled with 4-hours resolution and the aerosol mass concentration was determined by gravimetric analyses. The filters were analysed for elemental composition by ED-XRF technique, for soluble components by ion chromatography and for EC/OC fractions by TOT method. Fine and coarse PM fractions were also collected with hourly resolution obtaining the elemental composition by PIXE analysis. Particles number size distributions were measured by an Optical Particle Counter and the dataset was correlated with chemical components. Finally, the assessment of atmospheric dispersion conditions by means of Radon and meteorological parameters measurements was performed.

Beside the complete physical and chemical characterisation of PM<sub>10</sub>, these measurements allowed the identification of peculiar phenomena, like long-range transport events, and the evaluation of the impact of local and/or fugitive sources on atmospheric aerosol concentration and composition.

After particles removal due to a huge thunderstorm, the particles accumulation time was assessed; it varied from less than 3 hours for particles in the finest fractions to about 12 hours for bigger particles. Differences in the removal efficiency for different size ranges were also observed with experimental results in agreement with modelling previsions.

Chemical mass closure was carried out for each time interval during the day and in both season. Significant differences during daytime were observed for the crustal component and sulphates, while increases in nitrates percentages were registered during

the night especially during summertime. Considering adjacent time intervals only slight differences in composition were generally observed as particles residence times also play a relevant role.

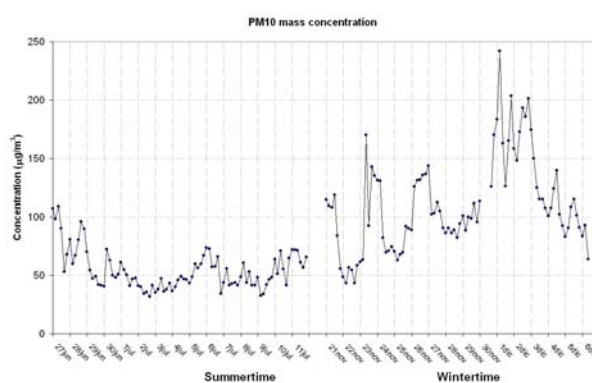


Figure 1: 4-hours resolution mass concentration

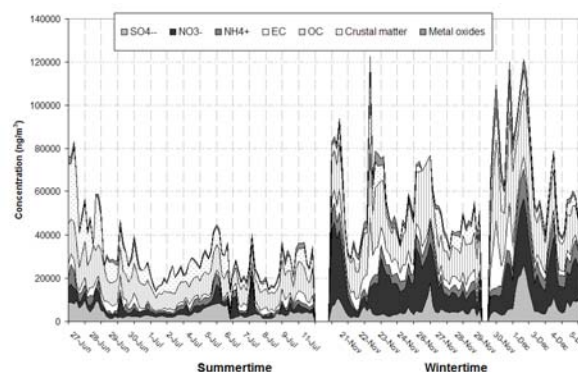


Figure 2: 4-hours resolution chemical composition

The whole data-set was analysed using Positive Matrix Factorization (PMF2) resolving 6 different sources: “nitrates”, “sulphates”, “resuspended soil dust”, “construction works”, “traffic (primary emissions)” and “industry”. The high-time resolved analyses give evidence to the variation in the contribution of the sources during the different parts of the day.

## Fireworks as a source of PM pollution: results of a case study

*R. Vecchi<sup>1</sup>, G. Valli<sup>1</sup>, V. Bernardoni<sup>1</sup>, A. D'Alessandro<sup>1</sup>, P. Fermo<sup>2</sup>,  
A. Piazzalunga<sup>2</sup>, S. Nava<sup>3</sup>, M. Chiari<sup>3</sup>, F. Lucarelli<sup>4</sup>*

<sup>1</sup>Inst. of Applied General Physics, University of Milan, and INFN-Milan, 20133, Milan, Italy

<sup>2</sup>Dep. of Inorganic, Metallorganic and Analytical Chem., University of Milan, 20133, Milan, Italy

<sup>3</sup>National Inst. of Nuclear Physics, Sesto Fiorentino, 50019, Florence, Italy

<sup>4</sup>Dep. of Physics, University of Florence, and INFN-Florence, 50019, Florence, Italy

Keywords: PM10, EDXRF, PIXE, number size distribution

In this paper high-time resolved compositional analysis of PM<sub>10</sub> aiming at the characterisation of aerosol generated by fireworks. Pyrotechnic displays are a source of air pollution: they create dense clouds of smoke and cause a huge increase both of the number of particles measured and of the concentration of different PM components, which then slowly disperse in the atmosphere.

The effect of pyrotechnic displays on air pollution was studied in Milan (Italy), during the night between 9 and 10 July 2006 when fireworks were burnt to celebrate the national football team, winner of the FIFA World Cup. A complete chemical characterisation (elements, ions, organic and elemental carbon) on PM<sub>10</sub> sampled with 4-hours resolution was carried out. Elemental concentrations with hourly resolution were also determined on the coarse and fine aerosol fractions collected by a streaker sampler and analysed by PIXE. Particles number size distributions were determined by an Optical Particle Counter in 32 size ranges (from 0.25 up to 32 µm). During the investigated night a sudden growth in concentration both of number concentration and chemical components of atmospheric aerosol was detected. A strong increase in concentration (more than 5.5 times in one hour, between 11.00pm and 12.00am, fig.1) was observed for particles in the 0.5µm-1µm size range. The same behaviour was registered for some elements (fig.2), measured by PIXE on the aerosol fine fraction: in particular, Sr concentration was 66 times (K: 12 times, Mg: 11 times, Cu: 6 times, Pb: 4 times) the average concentration measured during the previous day. Ba data were not available with hourly resolution; nevertheless, it showed a similar increase on 4-hours PM<sub>10</sub> samples (5 times in the 0.00-4.00 time interval). The sharp growth of these elements can be justified considering that pyrotechnical displays give origin to intense emission, but that they are not usually longer than half an hour.

Sr and Ba are used to colour fireworks (red and green, respectively), Pb gives white colored fireworks, while Mg makes sparkles brighter and more colourful and it is also a useful fuel. K salts provide the main oxidizer during burning. Also EC (measured by TOT method on quartz filters) had a 3-fold increase in its concentration in the same 0.00-4.00 time interval. It is noteworthy that Cu and EC can be produced both by fireworks burnt (Cu produces blue sparkles and EC is

in the black powder) and by vehicles emissions (the increase in traffic volume is typical during the celebrations of this event).

Using Sr as a tracer for pyrotechnical displays and comparing its growth with the number concentration one in the 0.65-0.7µm range, a very good correlation (fig.3) was observed, suggesting that emissions by fireworks are in this dimensional range. The evaluation of the time necessary for particles diffusion after the emission by fireworks, in a wind calm situation, was performed; it resulted 8-10 hours.

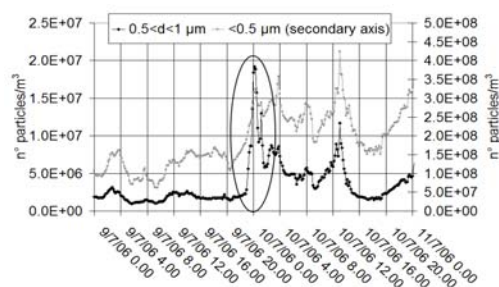


Figure 1: particle number concentration (size ranges:  $d < 0.5 \mu\text{m}$  and  $0.5 \mu\text{m} < d < 1 \mu\text{m}$ )

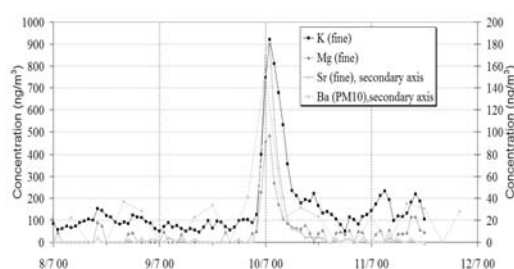


Figure 2: concentration of some tracers of fireworks

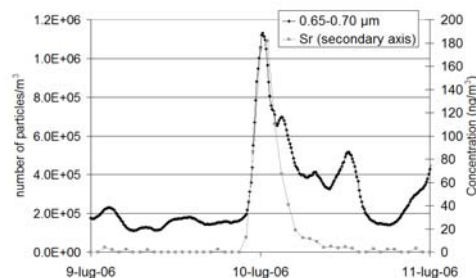


Figure 3: Sr concentration and particles in 0.65-0.7µm range

## Evaluation of the effectiveness of street sweeping on road dust removal

S. Han<sup>1</sup>, H. Jo<sup>1</sup>, J.S. Kim<sup>1</sup>, S.B. Lee<sup>2</sup> and Y.-W. Jung<sup>1</sup>

<sup>1</sup>Department of Environmental Engineering, Inha University, YonghyunDong, NamGu, 402-751, Incheon, Korea

<sup>2</sup>Air Pollution Cap System Division, National Institute of Environmental Research, Incheon, Korea

Keywords: fugitive dust, re-suspended road dust, silt loading, street sweeping, PM<sub>10</sub>

Re-suspended dust from paved roads in Seoul and Incheon metropolitan areas has been regarded an important contributor to ambient particulate matter (PM). Recently, these cities have practiced the enhanced street sweeping program as a means of controlling PM<sub>10</sub> emissions from paved roads. The effectiveness of street sweeping on ambient PM<sub>10</sub>, however, has not been clearly investigated thus far. Chang et al. (2005) found that street sweeping followed by washing can reduce ambient TSP up to 30%. But other studies (Chow et al., 1990; Etyemezian et al., 2003; Gertler et al., 2006) showed that street sweeping does not reduce PM<sub>10</sub> level or PM<sub>10</sub> re-entrainment rate.

The ultimately aim of our study is to quantitatively evaluate the effectiveness of street sweeping program for reducing PM<sub>10</sub> emissions. In this study, in order to evaluate the road dust removal effectiveness, silt loadings of test roads before and after street sweeping were measured by using EPA AP-42 vacuum swept method and real-time silt loading measurement system, which has been recently developed for estimation of fugitive dust emissions from paved road by our research group.

For the real-time measurement of silt loading on paved roads, the principle used in the TRAKER method (Kuhns et al., 2001) was employed and the entire sampling systems including data acquisition system combined with DGPS were designed for this purpose and mounted on a Hyundai SUV.

The evaluation of the road dust removal effectiveness is based on removal rate of silt loading, which is defined as silt (<75 μm) weight per unit road area swept by vacuum sweeper (TENNANT 3050) in this study. Silt loadings were measured on traffic lane and road shoulder of real roadways in Incheon, respectively. With these results, variations of spatial distribution of silt loading on traffic lanes were measured by real-time silt loading measurement system and were evaluated. Table 1 shows that the road dust removal rate by street sweeping depends on the size of road dust. And Figure 1 is the typical graphical representation showing silt loading values which were measured by using real-time measurement system in the test roads before and after street sweeping. With these data, repetitive measurements in a test road without traffic volumes will also be evaluated and presented.

Table 1. Removal rate (%) of road dust loading (g/m<sup>2</sup>) by street sweeping measured by using vacuum swept method on a test road in Incheon.

Size range	Removal rate (%)	
	Shoulder	Traffic lane
75 ~ 850 μm (dust loading)	85 %	75 %
< 75 μm (silt loading)	68 %	34 %

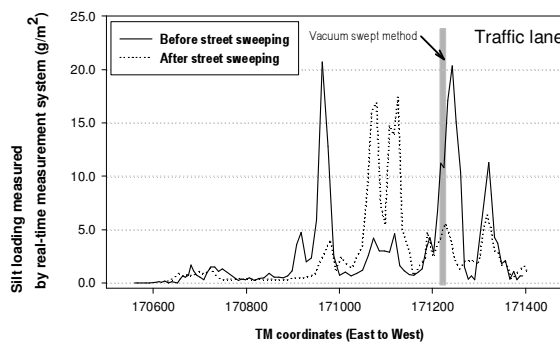


Figure 1. Variation of silt loading on a test road in Incheon before and after street sweeping.

This work was supported by the National Institute of Environmental Research and Incheon Regional Environmental Technology Developmental Center.

- Chang, Y.-M., Chou, C.-M., Su, K.-T., Tseng, C.-H. (2005). *Atmospheric Environment*, 39, 1891-1902
- Chow, J. C., Watson, J. G., Egami, R. T., Frazier, C. A. & Lu, Z. (1990). *J. Air Waste Manage. Assoc.*, 40, 1134-1142.
- Etyemezian, V., Kuhns, H., Green, M., Hendrickson, K., McCown, M., Barton, K., Pithford, M. (2003). *Atmospheric Environment*, 37, 4573-4582.
- Gertler, A., Kuhns, H., Abu-Allaban, M., Damm, C., Gillies, J., Etyemezian, V., Clayton, R., Proffitt, D. (2006). *Atmospheric Environment*, 40, 5976-5985.
- Kuhns, H., Etyemezian, V., Landwehr, D., MacDougall, C., Pitchford, M., Green, M. (2001). *Atmospheric Environment*, 35, 2815-2825.

## A European Quality Assurance program on PM measurements

L. Marelli, L. Emblico, F. Lagler, J. Theunis, D. Buzica and A. Borowiak,

European Commission - DG Joint Research Centre, Institute for Environment and Sustainability, Ispra, Italy

Keywords: PM10/PM2.5, PM1, Optical particle counter, Elemental carbon, Organic carbon

Although Standard methods to measure PM<sub>10</sub> and PM<sub>2.5</sub> have been validated, there are still difficulties at European scale in comparing data because of differences in methodology and reporting between countries, regions and cities: quality assurance and control (QA/QC) is thus an essential feature of any successful environmental assessment program. In support of the harmonization of PM measurements in Europe, the European Commission's Joint Research Centre (JRC) is carrying out an intercomparison and QA/QC exercise for PM in collaboration with the Network of Air Quality Reference Laboratories (AQUILA) and with local monitoring networks in the Member States. The main objectives of this program are: a) to provide further information on the comparability of PM<sub>10</sub> and PM<sub>2.5</sub> measurements in the networks, b) to verify the state of implementation of automatic PM monitors i.e. the practical use of correction factors reporting under the Council Directive 1999/30/EC and c) to assess the comparability of reference and equivalent methods and the respect of the Data Quality Objectives.

An urban background station is selected in each Member State, and parallel measurements are carried out for 14 days.

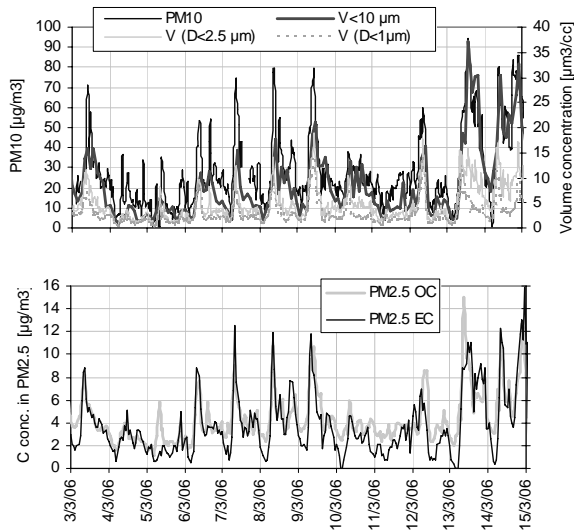


Fig. 1: mass and volume concentration and organic /elemental carbon in PM<sub>2.5</sub> during a measurement campaign in southern Europe

For the purpose of intercomparison, JRC uses two PM<sub>10</sub> sequential low-volume-samplers (LVS) equivalent to the reference method [2]. For a better PM characterization, the JRC mobile laboratory is also equipped with a PM<sub>2.5</sub> and a PM<sub>1</sub> sequential sampler, an Optical Particle Counter (0.3 – 20 µm), a TEOM-FDMS for PM<sub>10</sub> and an organic/elemental semi-continuous carbon analyzer (Fig.1). In some cases further chemical analysis on anions and cations are also performed on PM quartz filters by Ion chromatography.

Table 1 shows some results of orthogonal regressions calculated between JRC-PM<sub>10</sub> equivalent instruments and methods implemented by National Reference Laboratories (NRL) or local monitoring networks. Also shown in the table is the between-sampler uncertainty (u.b.s.) between JRC and local NRL or networks.

Sampler	Slope	Intercept	R <sup>2</sup>	u.b.s. (µg/m <sup>3</sup> )
NRL1 Ref.method	0.95	0.31	0.99	1.79
NRL1 Continuousr	0.96	-0.06	0.99	1.71
NRL2 Ref. method	0.86	0.67	0.99	3.40
NRL3 Continuous	1.04	-6.64	0.99	3.23
Local Network 1 Reference method.	1.04	0.19	0.96	1.61
Local Network 2 Continuous monitor	0.85	4.3	0.94	3.45

Table 1: Orthogonal regression and between-sampler uncertainty of local reference laboratories and monitoring networks with JRC equivalent method.

Results of the first ten campaigns evidenced that deviations between different methods may occur, depending on the composition of the particles and on the measurement capabilities of the laboratories and of the networks.

EN 12341 (1998) Determination of the PM<sub>10</sub> fraction of suspended particulate matter, Reference method and field test procedure to demonstrate reference equivalence of measurement methods

EN 14907 (2005) Standard gravimetric measurement method for the determination of PM<sub>2.5</sub> mass fraction of suspended particulate matter

Council Directive 1999/30/EC

## PM<sub>10</sub> Air Quality assessment at a Portuguese rural city using a TEOM instrument

S.N. Pereira<sup>1</sup>, F. Wagner<sup>1</sup> and A.M. Silva<sup>1,2</sup>

<sup>1</sup>Évora Geophysics Center, Rua Romão Ramalho, 59, 7000 Évora, Portugal

<sup>2</sup>University of Évora Physics Department, Rua Romão Ramalho, 59, 7000 Évora, Portugal

Keywords: Particulate matter, PM<sub>10</sub>, TEOM, aerosol sampling, air quality.

Health problems related with high levels of airborne particles (aerosols) have recently called the attention of scientists and policymakers. The EU first Daughter Directive (1999/30/CE) established thresholds for several atmospheric pollutants including atmospheric particles with aerodynamic diameter lower than 10 µm (PM<sub>10</sub>). The mass of particles per volume of air was the selected parameter for assessing the air quality in terms of aerosol loading. Daily PM<sub>10</sub> threshold of 50 µg m<sup>-3</sup> should not be exceeded more than 35 times per year (7 times by 2010) and an annual threshold of 40 µg m<sup>-3</sup> was also established (20 µg m<sup>-3</sup> by 2010).

Aerosol mass concentration (PM<sub>10</sub>) is being continuously measured in Évora Geophysics Center Observatory since January 2006 with a TEOM, Tapered Element Oscillating Microbalance, (Patashnick & Rupprecht, 1991). The instrument was calibrated by comparing its mass concentration measurements with the ones obtained with a HiVol gravimetric instrument. This work investigates the mass concentration measurements obtained with the TEOM during 2006 (305 days). Évora is a 60000 inhabitant Portuguese city and is located in a rural region SW of Iberian Peninsula (figure 1a). Anthropogenic aerosol production is mainly related to local road traffic as there are no major polluting industries in the region. Long term transport of anthropogenic aerosols from Northern Europe or Saharan desert dust can be observed regularly at Évora

The results show that the PM<sub>10</sub> levels were usually low. Almost 70% of PM<sub>10</sub> daily values stood below the 25 µg m<sup>-3</sup> (with 19 days with PM<sub>10</sub> less than 10 µg m<sup>-3</sup>). The minimum daily concentration was 5 µg m<sup>-3</sup> and the maximum daily concentration was almost 100 µg m<sup>-3</sup> during a dust episode. The average PM<sub>10</sub> obtained for the whole period was 24 µg m<sup>-3</sup> which is considerably lower than the annual threshold of 40 µg m<sup>-3</sup>. The 50 µg m<sup>-3</sup> limit was exceeded in 23 occasions, mainly during the dry season. These situations were related to aerosol advection from distant sources, i.e. desert dust particles from African Sahara and also forest fire/European pollution as suggested by back-trajectories analysis. Monthly PM<sub>10</sub> values were higher in the warmer period as a result of more frequent aerosol episodes (figure 1b). These values varied from 15/16 µg m<sup>-3</sup> in November/ December to 30/34 µg m<sup>-3</sup> in July/August. In spite of the low

average aerosol mass concentration values measured at Évora, the average diurnal variation (figure 1d) seems to reflect the traffic intensity with a well-defined morning (8:00-9:00) and evening peaks (19:00-20:00).

As a final remark it is interesting to verify that in 2010 the thresholds established by legislation would not be obeyed as they are nowadays in Évora.

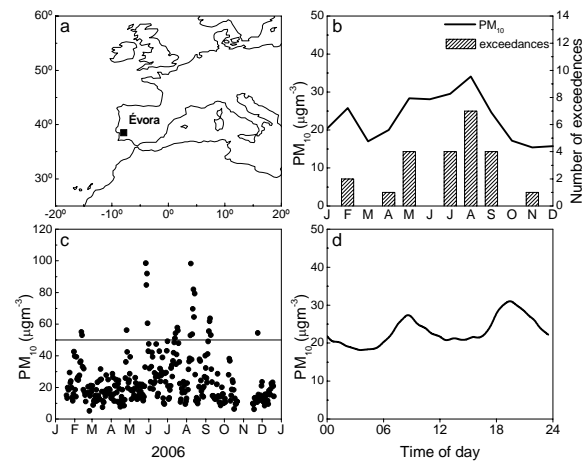


Figure 1. Geographical location of Évora (a), monthly PM<sub>10</sub> and number of **exceedances** per month (b), daily PM<sub>10</sub> and 50 µg m<sup>-3</sup> threshold (c) and averaged PM<sub>10</sub> diurnal variation (d).

This work was supported by FCT (Fundação para a Ciência e Tecnologia) under grant SFRH BPD 14508 2003 under POCTI and PDCTE/CTA/49828/2003.

Patashnick, H and Rupprecht, E. G., 1991. Continuous PM<sub>10</sub> Measurements Using the Tapered Element Oscillating Microbalance. *Journal of Air and Waster Management Association* 4 J (8), 1079-1084.

Pereira, S. Utilização de um monitor de partículas para a determinação da concentração mássica de aerossóis à superfície e validação das medições, 2006. Tese de mestrado, Univ. Évora.

## Characteristics of atmospheric particles collected near a wax apple waste open burning site

W.Y. Lin<sup>2</sup>, S.J. Chen<sup>1\*</sup>, K.L. Huang<sup>1</sup>, C.C. Lin<sup>1</sup> and J.H. Tsai<sup>1</sup>

<sup>1</sup> Department of Environmental Engineering and Science, National Pingtung University of Science and Technology, Nei Pu, 912, Pingtung, Taiwan

<sup>2</sup> Institute of Environmental Planning and Management, National Taipei University of Technology, Da An, 106, Taipei, Taiwan

Keywords: aerosol sampling, carbonaceous particle, PM<sub>2.5</sub>, PM<sub>10</sub>, water soluble compounds.

This study investigated the influence of wax apple branches waste open burning on the compositions and size distributions of particulates in surrounding atmosphere. Both MOUDI and Dichot samplers were used to collect the atmospheric particles during the wax apple waste burning in April, 2006. The compositions and size distributions of PM<sub>2.5</sub> and PM<sub>2.5-10</sub> were analyzed for the samples taken from different burning stages and compared with before-burning background values. The results show that burning wax apple branches significantly increased the concentrations of both fine and coarse particles, especially that of PM<sub>2.5</sub>. The concentrations of PM<sub>2.5</sub> and PM<sub>2.5-10</sub> decreased as the sampling distance from the burning source increased, but the ratio of PM<sub>2.5</sub>/PM<sub>10</sub> was higher than those before and after burning (Fig. 1).

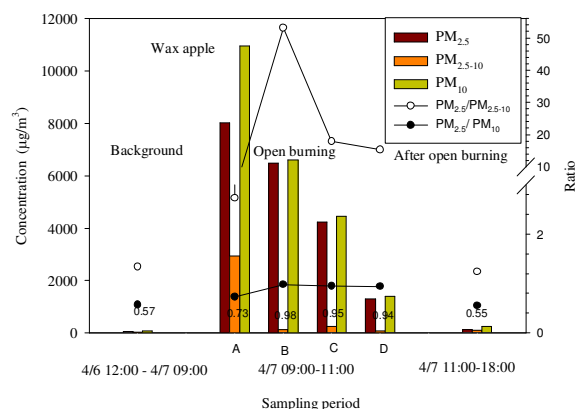


Figure 1. PM concentrations and ratios for the particles collected near the wax apple waste opening burning site.

The atmospheric particle size distributions before burning were bimodal with a background primary peak at the coarse size range of 3.2–5.6 µm and a secondary peak at the fine size range of 1–1.8 µm. However, during burning, atmospheric particle size distribution was uni-modal and peaked at a fine size range (1–1.8 µm). The fraction of 0.056–2.5 µm fine particles significantly increased when compared with that before burning, particularly for the submicron meter sized particles (increasing by about 38.9%).

Before burning the wax apple waste, the main water soluble ions in the atmospheric particles were secondary aerosols (NO<sub>3</sub><sup>-</sup>, SO<sub>4</sub><sup>2-</sup>, and NH<sub>4</sub><sup>+</sup>) and the contents of particulate Cl<sup>-</sup> and K<sup>+</sup> were small. During

burning, the contents of particulate Cl<sup>-</sup> and K<sup>+</sup> in PM<sub>2.5</sub> and PM<sub>2.5-10</sub> significantly increased. Cl<sup>-</sup> displayed the highest content among eight water soluble ions investigated, and sometimes the content of K<sup>+</sup> was higher than those of NO<sub>3</sub><sup>-</sup>, SO<sub>4</sub><sup>2-</sup>, and NH<sub>4</sub><sup>+</sup> (Table 1). After the burning, the dominant water soluble ions in the atmospheric particles changed back to NO<sub>3</sub><sup>-</sup>, SO<sub>4</sub><sup>2-</sup>, and NH<sub>4</sub><sup>+</sup>, indicating that Cl<sup>-</sup> and K<sup>+</sup> could be used as the indicator elements for the agricultural waste open burning. Pagels et al. (2003) also observed that the dominant elements were K, S, and Cl (with dominant ions of K<sup>+</sup>, SO<sub>4</sub><sup>2-</sup>, and CO<sub>3</sub><sup>2-</sup>) in the fine mode whereas Ca, K, and S dominated in the coarse mode during combusting moist forest residue.

Table 1. The water-soluble ion concentrations of PM<sub>2.5</sub> and PM<sub>2.5-10</sub> for the particles collected near the wax apple waste opening burning site

Sampling items	PM (µg/m <sup>3</sup> )	Water-soluble Ions (µg/m <sup>3</sup> )							
		Cl <sup>-</sup>	NO <sub>3</sub> <sup>-</sup>	SO <sub>4</sub> <sup>2-</sup>	Na <sup>+</sup>	NH <sub>4</sub> <sup>+</sup>	K <sup>+</sup>	Mg <sup>2+</sup>	Ca <sup>2+</sup>
<b>PM<sub>2.5</sub></b>									
Background	47.5	1.52	7.97	8.74	0.39	7.48	0.58	0.06	0.10
<b>Open burning</b>									
Sample A	8014	157	64.5	74.7	17.2	63.4	133	3.76	5.91
Sample B	6481	166	37.4	56.2	9.36	33.0	153	1.10	2.20
Sample C	4227	79.5	26.1	36.8	7.85	15.7	109	1.57	3.14
Sample D	1303	78.1	40.9	24.6	15.6	12.0	33.1	2.40	5.41
After open burning	133	5.85	14.2	17.1	0.92	11.4	0.95	0.13	0.26
<b>PM<sub>2.5-10</sub></b>									
Background	35.5	1.42	4.30	1.81	1.19	1.50	0.23	0.12	0.33
<b>Open burning</b>									
Sample A	2939	27.4	7.14	33.5	6.66	5.95	19.7	1.43	39.7
Sample B	122	9.85	7.46	4.46	4.46	1.76	6.12	0.73	0.62
Sample C	237	19.0	9.37	6.53	6.25	5.11	13.1	0.85	1.99
Sample D	85.1	5.46	4.39	1.66	3.32	2.25	2.13	0.47	0.71
After open burning	107	4.61	7.17	5.49	2.57	5.03	0.18	0.16	0.17

During the burning, the atmospheric fine and coarse particulate carbon contents were also significantly higher than those of background values, especially the organic carbon; additionally, the TC content in PM<sub>2.5</sub> (about 80%) was more than two times that of the background (23.7%).

Pagels, J., Strand, M., Lillieblad, L. (2003). *J. Aerosol Science*, 36, 1043–1059.

## Variations of particulate matter concentrations in dependence on climatic conditions

V. Adamec<sup>1</sup>, J. Huzlik<sup>1</sup>, R. Licbinsky<sup>1</sup> and M. Schwarzova<sup>1</sup>

<sup>1</sup>Transport Research Centre, 636 00 Brno, Czech Republic

Keywords: health effects, concentration, NO<sub>x</sub>, particulate matter, temperature.

Particulate matter (PM) become an actual part of research not only due to increasing concentrations in the ambient air but primarily because of their negative effects on human health (respiratory and cardiovascular diseases). 347,900 European died in accordance with the newest EU study (Watkiss et al., 2005) due to air pollution and life shortening of 8 months was statistically determined because of long exposure to PM.

PM sampling campaigns (LECKEL MVS6) took place in the years 2005-2006 on selected urban localities with different burden by traffic and with different morphology of surroundings. The sampling intervals and season periods were chosen to characterise average annual concentrations of PM<sub>2,5</sub> and PM<sub>10</sub>. Gravimetric analysis (Mettler-Toledo MX5/A) of each exposed filter was used for determination of the PM content. Meteorological conditions were also observed during the sampling campaigns.

Results shows the significant negative correlation between PM<sub>2,5</sub> concentrations and temperature (fig. 1). This was caused probably by the loss of volatile PM compounds (e.g. ammonia salts) in the summer. These compounds coagulate in colder periods and could be caught on the filter surface. The vertical stability of the atmosphere could be another reason. Particles were better dispersed due to better ventilation of localities in the warmer periods (convection) whereas in colder months the ventilation was limited and PM cumulated in the lower part of atmosphere near the source (inversion). Local furnace could be also the important contributors for PM air pollution in winter season.

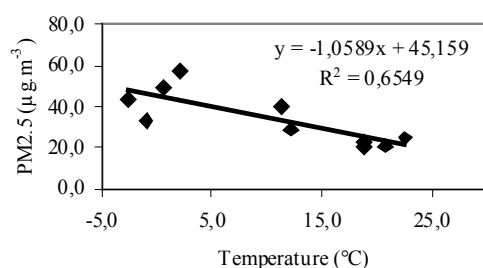


Figure 1. The dependency of PM<sub>2,5</sub> concentrations and temperature

Correlation between PM<sub>2,5</sub> and PM<sub>10</sub> fractions on both localities were very similar with statistically significant coefficients (0,967 for PM<sub>2,5</sub>, 0,879 for

PM<sub>10</sub>) that indicated similar behaviour of PM and so similar source - traffic. Statistically significant correlations were also determined between PM<sub>2,5</sub> - NO<sub>x</sub> and PM<sub>2,5</sub> - NO<sub>2</sub>. Relatively close correlation can be a prop for using NO<sub>x</sub> concentrations as indicator for PM air pollution. Correlation between PM<sub>2,5</sub> a NO<sub>2</sub> was not close as for NO<sub>x</sub> probably due to higher NO<sub>2</sub>/NO concentrations ratio dependency on actual physical conditions of atmosphere especially on temperature and the sunshine intensity.

Predominance of seasonal influences particularly temperature and atmospheric stability is well evident from the facts described in the text. Obtained results promote conclusions published in some studies (Charron & Harrison, 2006; Gertler et al., 2006; Duan et al., 2006) especially the dependency of PM concentrations on temperature that was observed during the measurements in London, Beijing and in Egypt though absolute concentration values are not comparable. We can also promote that pollution can come from other sources than traffic that are in the long distance. Upcoming limit for PM<sub>2,5</sub> concentrations (25 µg.m<sup>-3</sup>) in accordance with Directive of the European Parliament and council on ambient air quality and cleaner air for Europe would be exceeded on both localities.

- Duan F. K., He K. B., Ma Y. L., Yang F. M., Yu X. C., Cadle S. H., Chan T., & Mulawa P. A. (2006). Concentration and chemical characteristics of PM<sub>2,5</sub> in Beijing, China: 2001 – 2002, *Science of Total Environment*, 355, 264 – 267.
- Gertler A. W., Abu-Allaban M., & Lowenthal D. H. (2006). The mobile source contribution to observed PM<sub>10</sub>, PM<sub>2,5</sub> and VOCs in the greater Cairo area, In JOUMARD, R. (ed.) *Environnement & Transports / Environment & Transport: Vol. 1 Poster communications*. Actes INRETS n°107. Reims (France), June 12-14, 2006. Bron cedex (France), INRETS, 263-269.
- Charron A., & Harrison R. (2006). Interpretation of multi-metric particulate matter data monitored near busy London highway. In JOUMARD, R. (ed.) *Environnement & Transports / Environment & Transport: Vol. 1 Poster communications*. Actes INRETS n°107. Reims (France), June 12-14, 2006. Bron cedex (France), INRETS, 255-262.
- Watkiss, P., Pye, S., & Holland, M. (2005). *CAFE CBA: Baseline analysis 2000 to 2020*, CAFE Programme.

## EVALUATION OF PM10 SOURCES IN THREE COASTAL AREAS OF THE NORTHWEST OF SPAIN

M. Piñeiro-Iglesias<sup>1</sup>, P.López-Mahía<sup>1,2</sup>, S. Muniategui-Lorenzo<sup>2</sup>, D. Prada-Rodríguez<sup>1,2</sup> and E. Fernández-Fernández<sup>2</sup>

<sup>1</sup>Institute of Environment, University of A Coruña, Pazo de Lóngora, Liáns, 15179, Oleiros, A Coruña, Spain

<sup>2</sup>Department of Analytical Chemistry, University of A Coruña, Campus A Zapateira s/n, 15071, A Coruña, Spain

Keywords: aerosol chemistry, PM and source apportionment, PM10, principal component analysis, multiple linear regression analysis.

This study was conducted over a one-year period (May 2004-May 2005) at 3 sites located at the Northwest coast of Spain. A total of 267 PM10 samples were analysed for carbon, hydrogen, nitrogen, sulphur and 19 major, minor and trace elements. The arithmetic mean PM10 values were 57  $\mu\text{g m}^{-3}$  at the industrial site, 48  $\mu\text{g m}^{-3}$  at the urban site and 30  $\mu\text{g m}^{-3}$  at the rural site exhibiting significant spatial variations. The highest PM10 values at the industrial and urban sites would exceed the EC annual limit value of 40  $\mu\text{g m}^{-3}$ .

Principal component factor analysis (PCA) has been used for identification of the possible sources contributing to the PM10. Only the species quantified in more than 80% of the samples were retained for PCA analysis. For data below detection limit, half of the detection limit values were used for calculations. PCA was performed with and without samples with outliers. The conclusions obtained were identical, therefore all samples were considered except at the industrial site, where a sample of 334  $\mu\text{g m}^{-3}$  was discarded. Varimax rotated factor analysis complemented by additional tools (air mass back trajectories analysis, atmospheric temperature soundings and meteorological data) identified up to five possible sources depending upon the site comprising vehicular traffic with the influence of road dust, combustion sources, industrial activities like a petroleum refinery and power stations among others, soil erosion and marine aerosol.

The contribution of each source group was quantitatively assessed by applying multilinear regression analysis (MLRA) to the experimental data using as dependent variable PM10 concentrations and as independent variables the principal component scores (after being normalized by introducing an artificial sample with concentrations equal to zero for all variables).

MLRA shows that one of largest contribution to PM10 is marine aerosol which was to be hoped for because the proximity of these sampling sites to the coast, but also it was found a relative high contribution of industrial sources.

The modelled daily PM10 concentrations were correlated with the experimental values to test the accuracy of the model, with outstanding results ( $y = 0.92x + 0.56$ ,  $r^2 = 0.92$  at the urban site,

$y = 0.78x + 5.44$ ,  $r^2 = 0.78$  at the industrial site and  $y = 0.81x - 0.48$ ,  $r^2 = 0.81$  at the rural site).

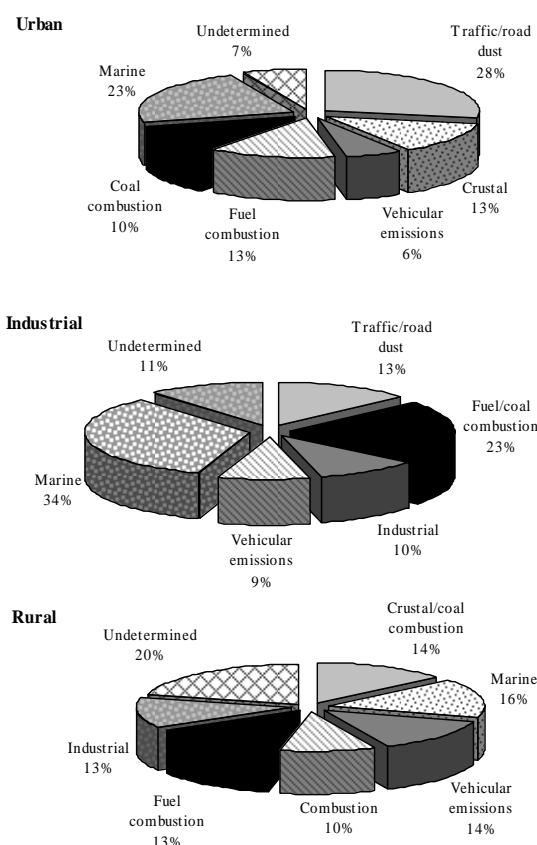


Figure 1. Source contribution analysis for PM10.

The authors thank financial support from Ministerio de Ciencia y Tecnología (REN2003-08603-C04-01) and Xunta de Galicia (PGIDT04PXIC16401PN). The authors thank to SAI (Universidade da Coruña) and Dept. Analytical Chemistry, Nutrition and Bromatology (University of Santiago de Compostela) for technical support and to P. Esperón and V. Juncal for their assistance and to the National Meteorological Institute (Centro Zonal de A Coruña).

Almeida S. M., Pio C. A., Freitas M. C., Reis M. A. & Trancoso M. A. (2005) *Atmospheric Environment*, 39, 3127-3138

Viana M., Querol X., Alastuey A., Gil J. I. & Menéndez M. (2006) *Chemosphere*, 65, 2411-2418.

## Impact of wood combustion on composition and concentrations of urban particulate matter

J.Schnelle-Kreis<sup>1,2</sup>, M.Sklorz<sup>2</sup>, J. Orasche<sup>1</sup>, J.J. Briedé<sup>4</sup>, T. M. de Kok<sup>4</sup> and R. Zimmermann<sup>1,2,3</sup>

<sup>1</sup> Department of Chemistry, Bavarian Institute of Applied Environmental Research and Technology, BifA GmbH, Am Mittleren Moos 46, 86167 Augsburg, Germany

<sup>2</sup> Institute of Ecological Chemistry, GSF – National Research Centre for Environment and Health, Ingolstädter Landstrasse 1, 86573 Neuherberg, Germany

<sup>3</sup> Department of Analytical Chemistry, University of Augsburg, Universitätsstraße 1, 86159 Augsburg, Germany

<sup>4</sup> Department of Health Risk Analysis and Toxicology, University Maastricht, P.O Box 616, 6200 MD Maastricht, The Netherlands

Keywords: Ambient Aerosol, biomass burning, chemical analysis, organic tracer, PM, source apportionment

Recently, the use of wood as renewable energy source is discussed contradictorily. On one hand the favourable CO<sub>2</sub>-balance does not enhance the global warming problem whereas on the other hand biomass combustion may contribute significantly to PM mass loading. Data presented here, will focus on concentrations of organic components and PM in urban particulate matter and tracers for domestic wood burning.

Since 2003 PM<sub>2.5</sub> samples are taken in Augsburg, Germany, day-to-day. Concentrations of low volatile organic compounds were analysed by direct thermal desorption – gas chromatography - time of flight mass spectrometry, DTD-GC-TOFMS. For the first two years, samples were analysed for PAH, oxidized PAH, n-alkanes, alkan-2-ones, n-alkanoic acid methylesters, hopanes, dehydroabietane and dehydroabietic acid methylester.

Using positive matrix factorization (PMF) for the statistical investigation of the data set five factors have been separated. These factors are dominated by the pattern of single sources or groups of similar sources, factor 1 – lubricating oil, factor 2 – emissions of diesel and heating oil consumption, factor 3 – wood combustion, factor 4 – brown coal combustion and factor 5 - biogenic emissions and transport components. Like the SVOC the factors showed strong seasonality with highest values in winter for factor 1 to 4 and in summer for factor 5 (Schnelle-Kreis et al. 2007).

Rapid variations up to one order of magnitude from day to day were measured. Highest concentrations were observed during episodes with low wind speeds and low mixing layer heights (most significant in November and December 2003). These episodes are accompanied with high PM mass loadings, measured by the Bavarian environmental state agency at a comparable urban site. In January 2004, similar

temperatures as in November predominated, but higher horizontal and vertical exchange led to low ambient concentrations, despite ongoing domestic heating period.

Since 2005 samples are taken at the GSF aerosol-research station in Augsburg, characterised as urban background, too. Additional data on particle mass and number concentrations as well as size distributions are available from this station and will be discussed together with data on organic composition of PM. As first preliminary result, a short, intensive summer campaign in 2005 indicated an association between concentration of biomass burning tracers, to PM, PAH, O-PAH as well as to free oxygen radical formation (Sklorz et al. 2007).

Actually, after extension of the analytical method by an (automated) derivatisation step the PM<sub>2.5</sub> samples are analysed for additional typical tracers of biomass and wood combustion like levoglucosan and phenolic compounds, too. PMF results concerning wood combustion will be crosschecked and correlated to PM mass.

This work was supported by the Bavarian State Ministry for Environment, Health and Customer Protection. The work was carried out in cooperation with the GSF-Focus-Network “Aerosols and Health” which coordinates aerosol-related research within the GSF Research Centre.

Schnelle-Kreis, J., Sklorz, M., Orasche, J., Stölzel, M., Peters, A., Zimmermann, R. (2007) *Environ. Sci. Technol.*, submitted.

Sklorz, M Briedé, J.J., Schnelle-Kreis, J., Liu, Y., Yongbo Liu<sup>1</sup>, Cyrus, J., de Kok, T.M., Zimmermann, R.. (2007) *J. Toxicol. Env. Health A*, in press.

## Concentrations of oxygenated PAH and other SVOC in relation to urban PM<sub>2.5</sub> derived formation of reactive oxygen species

M. Sklorz<sup>1</sup>, J.J. Briedé<sup>2</sup>, J. Schnelle-Kreis<sup>1,4</sup>, Y. Liu<sup>1</sup>, J. Orasche<sup>4</sup>, J. Cyrys<sup>1,4</sup>,  
T.M. de Kok<sup>2</sup> R. Zimmermann<sup>1,3,4</sup>

<sup>1</sup> Institute of Ecological Chemistry, GSF and Institute of Epidemiology– National Research Centre for Environment and Health, Ingolstädter Landstrasse 1, 86573 Neuherberg, Germany

<sup>2</sup> Department of Health Risk Analysis and Toxicology, University Maastricht, P.O. Box 616, 6200 MD Maastricht, The Netherlands

<sup>3</sup> Department of Analytical Chemistry and environmental science centre, University of Augsburg, Universitätsstraße 1, 86159 Augsburg, Germany

<sup>4</sup> Department of Chemistry, Bavarian Institute of Applied Environmental Research and Technology, BIfA GmbH, Am Mittleren Moos 46, 86167 Augsburg, Germany

Keywords: oxygenated PAH, SVOC, ROS, reactive oxygen species, PM

Exposure to increased levels of ambient particulate matter (PM) is associated with several adverse health effects. Especially PM mass loadings and combustion related organic compounds such as polycyclic aromatic hydrocarbons (PAH) and their oxygenated derivatives (O-PAH) are assumed to be involved in oxidative stress formation and inflammatory response. Here we present data of PM-derived formation of reactive oxygen species (ROS) from PM<sub>2.5</sub> and relate this to the individual PAH and O-PAH content as well as to the concentration of some source specific semi volatile organic compounds (SVOC)

PM<sub>2.5</sub> samples were taken in summer 2005 at the GSF measuring station in Augsburg, Germany. The sampling site is classified as urban background station. PM was collected on quartz fibre filters for 24 hr each, using a low volume sampler. The filters were cut into two parts: One aliquot of the filter was used for ROS formation measurements by electron spin resonance (ESR) (Briedé et al. 2005). The remaining part of the filters were analysed for PAH and O-PAH by using gas chromatography - high resolution mass spectrometry according to Liu et al (2006). Additional filter samples were screened by direct thermodesorption - gas chromatography - mass spectrometry for SVOC and source related tracers (Schnelle-Kreis et al. 2007)

Indeed highly significant correlations were observed between ROS formation and the concentration of the mainly particle associated O-PAH. They correlated even better than PAH,

particulate mass or particle number concentration. Correlations were most pronounced for some polycyclic aromatic monoketones as e.g. benz[de]anthracene-7-one.

The recently published association found between ESR measurements and the presence of specific SVOC (Sklorz et al. 2007) will be discussed. The amount of e.g. resin acid derivatives in the collected particulate matter suggested an important influence of wood burning in PM<sub>2.5</sub> related ROS formation.

This work was carried out in cooperation with the GSF-Focus-Network "Aerosols and Health" which coordinates aerosol-related research within the GSF Research Centre.

Briedé, J.J., De Kok, T.M.C.M., Hogervorst, J.G.F., Moonen, E.J.C., Op Den Camp, C.L.B., Kleinjans J.C.S. (2005) *Environ. Sci. Technol.* 39:8420-8426.

Liu, Y., Sklorz, M., Schnelle-Kreis, J., Orasche, J., Ferge, T., Kettrup A., Zimmermann, R. (2006) *Chemosphere* 62:1889-1898.

Schnelle-Kreis, J., Sklorz, M., Orasche, J., Stölzel, M., Peters, A., Zimmermann, R. (2007) *Environ. Sci. Technol.*, submitted.

Sklorz, M. Briedé, J.J., Schnelle-Kreis, J., Liu, Y., Cyrys, J., de Kok, T.M., Zimmermann, R. (2007) *J. Toxicol. Env. Health A*, in press.

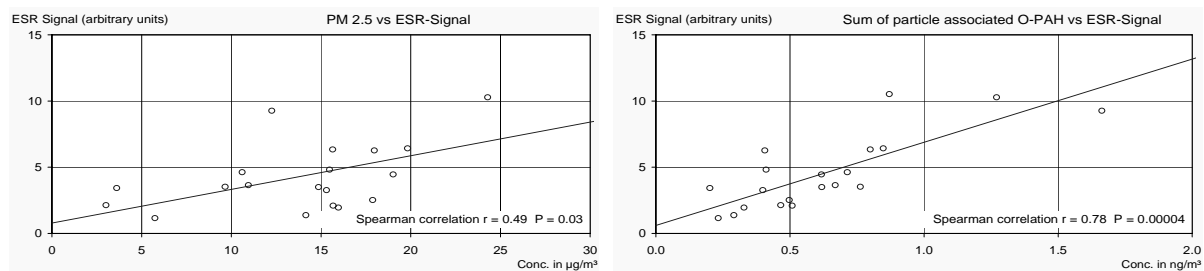


Figure 1: Spearman rank correlation plots between ESR signal and PM<sub>2.5</sub> and O-PAH concentration, resp.

## Air Pollution And Climate Change - Who Takes The Blame ? C(1s) NEXAFS spectroscopy on fine particulates "*Feinstaub*" could provide answers

A. Braun<sup>1,2</sup>

<sup>1</sup>University of Kentucky, Dept. of Chemical and Materials Engineering, and Consortium for Fossil Fuel Sciences, University of Kentucky, Lexington KY 40506, USA

<sup>2</sup>EMPA – Swiss Federal Laboratories for Materials Testing & Research, Laboratory for High Performance Ceramics, CH-8600 Dübendorf, Switzerland

Keywords: NEXAFS, urban PM, wood smoke, diesel soot, air pollution

Who contributes (most) to urban and rural air pollution with carbonaceous airborne particulate matter (PM) ?

Identification of source specific signatures is of utmost importance for subsequent source attribution and apportionment. Signatures are not easy to obtain for carbonaceous PM. Classification typically exists in terms of elemental and organic carbon only: EC and OC. This distinction appears too primitive for source apportionment. We propose use of soft X-ray techniques for characterization and molecular speciation of carbonaceous PM. Emphasized are recent results on diesel exhaust, wood smoke, urban PM and others with C(1s) NEXAFS spectroscopy, which appears superior to IR and TEM-EELS, and GC-MS.

Recent and current research activities on the chemical characterization of carbon in airborne carbonaceous particulate matter with near-edge X-ray absorption fine structure (NEXAFS) spectroscopy are reviewed. This relatively novel technique is often superior to TEM-EELS and FTIR spectroscopy. In the extreme case, one single PM particle is sufficient for characterization. Liquids, extracts, solid core and surface functional groups can be quantified. Preliminary data on combustion derived PM such as diesel soot, wood smoke and tobacco smoke are compared with ambient samples. Scanning transmission X-ray micro-spectroscopy and conventional C(1s) NEXAFS data of diesel particulate matter, and aqueous extracts thereof are presented. A significantly better spectral resolution of molecular species than with TEM-EELS is obtained and allows for source signature attribution.

Noteworthy observations are the absence of graphitic structures in woodsmoke. Graphitization of diesel soot can strongly depend on engine operation conditions and fuel doping; surprisingly, ferrocene prevents soot from graphitization. Preliminary results on combined toxicological bio-assay and NEXAFS studies on extracts are also shown. C(1s) NEXAFS for environmental applications is still in its infancy but has a good potential to become a useful analytical technique for atmospheric and environmental scientists and combustion engineers, who need to address carbon relevant issues like global climate change or human health impact of PM. This concerns

in particular soot, and similar combustion derived carbonaceous matter. The conjugated surface and bulk sensitivity of NEXAFS is superior to any of the aforementioned techniques and invaluable to researchers who have to tackle with a broad range of chemically and structurally complex carbonaceous PM. Extracts and solid residuals can be studied. Radiation damages are less significant than in TEM-EELS but harder than in IR spectroscopy. Intense probe techniques like STXM bear the risk of considerable radiation damages and hence alteration of the sample, as previously observed, but also the potential for atmospheric in situ studies. A disadvantage is that NEXAFS studies require access to synchrotron facilities, but more and more such facilities are built and equipped for soft X-ray experiments. A potentially interesting near-future application of STXM will be the study of the interaction between PM and biological cells. Biological cells are large enough for STXM to give high resolution, better than the IR microscope in terms of spatial resolution, and better than TEM-EELS in terms of chemical sensitivity with respect to carbon. Biofilms have already been studied with NEXAFS and STXM. Several research groups have mastered the problems that result from bringing samples in aqueous environment into the STXM. Mechanisms that govern adverse health effects when humans are exposed to PM are more likely to be elucidated with such experiments. This review was about carbon NEXAFS spectroscopy. The same technique applies to oxygen as well.

Financial support by National Science Foundation grant # CHE-0089133.

A Braun, *Carbon speciation in airborne particulate matter with C(1s) NEXAFS spectroscopy*, J. Env. Monitoring, *J. Environ. Monit.*, 2005, **7**(11), 1059-1065.

A Braun, BS Mun, FE Huggins, GP Huffman. *Carbon speciation of diesel exhaust and urban particulate matter NIST standard reference materials with C(1s) NEXAFS spectroscopy*, Environmental Science & Technology 2007, **41**, 173-178.

## Impact of ferrocene on the structure of diesel soot

A. Braun<sup>1,2</sup>

<sup>1</sup>University of Kentucky, Dept. of Chemical and Materials Engineering, and Consortium for Fossil Fuel Sciences, University of Kentucky, Lexington KY 40506, USA

<sup>2</sup>EMPA – Swiss Federal Laboratories for Materials Testing & Research, Laboratory for High Performance Ceramics, CH-8600 Dübendorf, Switzerland

Keywords: SAXS, NEXAFS, diesel soot, ferrocene, maghemite.

We report on the structure of a set of diesel exhaust samples that were obtained from reference diesel fuel and diesel fuel mixed with ferrocene. Characterization was carried out with X-ray absorption spectroscopy (C (1s) NEXAFS) and wide-angle X-ray scattering (WAXS). The reference diesel soot shows a pronounced graphite-like microstructure and molecular structure, with a strong (002) graphite Bragg reflex and a strong aromatic C=C resonance at 285 eV. The mineral matter in the reference soot could be identified as Fe<sub>2</sub>O<sub>3</sub> hematite. NEXAFS spectra of such soot barely show aromatics but pronounced contributions from aliphatic structures. The soot specimen from the diesel mixed with ferrocene has an entirely different structure and lacks significantly in graphite-like characteristics. NEXAFS spectra of such soot barely show aromatics but pronounced contributions from aliphatic structures. WAXS patterns show almost no intensity at the Bragg (002) reflection of graphite, but a strong aliphatic  $\gamma$ -side band. The iron from the ferrocene transforms to Fe<sub>2</sub>O<sub>3</sub> maghemite.

In summary, adding ferrocene to diesel fuel has a dramatic impact on soot formation processes and on the molecular structure and nano-structure of soot. The graphitic structure of soot is dramatically altered in favor of aliphatic structures. According to the WAXS data, aromatic graphene sheets still seem to be present, but at a very small stack height. The majority of the ordered carbon comes in aliphatic structures. The iron persists as maghemite, but in significantly greater quantity. The carbon NEXAFS data support findings about the carbonaceous material, in particular the formation of aliphatic structures during combustion in the presence of ferrocene. Higher engine speeds make a significant difference on the graphite-like carbon formation, this is, at higher engine speeds ferrocene suppresses formation of the nanocrystalline graphite-structures, and enhances the aliphatic structures. This holds at least for the speed range studied here: 1500 – 2200 rpm. The soot from non-doped fuel seems to be largely unaffected by the change in speed. A similar effect has been observed with oxygenated fuels [3]. Graphite, the thermodynamically and kinetically stable form of carbon, can persist for long times in the environment, the atmosphere and even in the universe. It resists more to oxidation than other forms of solid carbon. In contrast, aliphatic carbon can be

much more easily oxidized. Since mixing diesel fuel with ferrocene generates soot with less graphitic but more aliphatic structure, this may be a route to accelerating oxidation of soot in the atmosphere.

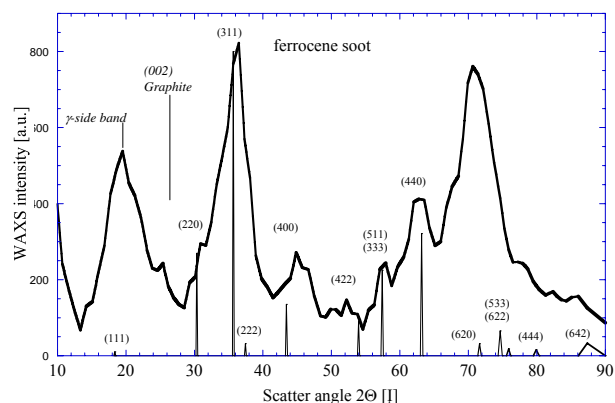


Figure 1. WAXS curves from diesel soot prepared from ferrocene doped diesel fuel.

Financial support by National Science Foundation grant # CHE-0089133.

A. Braun, N. Shah, F.E. Huggins, G.P. Huffman, K.E. Kelly, S.B. Mun, S.N. Ehrlich, *Impact of ferrocene on the structure of diesel exhaust soot as probed with wide-angle X-ray scattering and C(1s) NEXAFS spectroscopy*, Carbon (2006) **44/14** 2904-2911.

**PM<sub>10</sub>, PM<sub>2.5</sub>, PM<sub>1</sub> fractions of particulate matter in Prague during year 2006**

L. Štefancová, J. Schwarz, J. Smolík

Institute of Chemical Process Fundamentals, Academy of Sciences of the Czech Republic, v.v.i., Rozvojova 135, 165 02, Prague 6 – Suchbátka, Czech Republic

Keywords: urban aerosol, mass concentration, PM<sub>x</sub> fractions

PM<sub>10</sub>, PM<sub>2.5</sub>, PM<sub>1</sub> fractions of particulate matter were studied in Prague during year 2006, to get more information about content of secondary aerosol particles in PM<sub>10</sub> fraction of suspended particles. Current models used in the Czech Republic are counting with primary emissions emitted from urban and natural sources and do not comprise production of secondary aerosol and reemission of resuspended particles. Secondary aerosol particles are formed by chemical reaction of gaseous precursors followed by condensation of product. Those particles are mainly included in fine mode of PM<sub>10</sub> fraction, which is mostly retained inside respiratory system.

Samples of atmospheric particles were collected on the roof site located 285 m ASL at the northwest part of Prague in the campus of the Institute of Chemical Process and Fundamentals. PM<sub>10</sub>, PM<sub>2.5</sub> and PM<sub>1</sub> fractions were sampled for 24 hours every 6<sup>th</sup> day. Particles collection was provided by using PM<sub>10</sub> and PM<sub>2.5</sub> sampling heads (Leckel) and PM<sub>1</sub> cyclone sampling head (URG) with flow rate 1 m<sup>3</sup> per hour. Total flow rate through filters was measured by gas meter located downstream membrane pump for ambient air sampling. Zeflur teflon filters with 2 µm pore size and 47 mm in diameter (Pall, USA) were used to collect aerosol particles. In parallel, Leckel LVS3 sampler with PM<sub>2.5</sub> sampling head was used to collect PM<sub>2.5</sub> size fraction on quartz filter (QMA Whatmann). Meteorological data were monitored by CHMI monitoring station. Aerosol mass was determined by gravimetric analysis using a microbalance Sartorius with 1 µg sensitivity. The campaign started on February 23, 2006 and finished in January 2007.

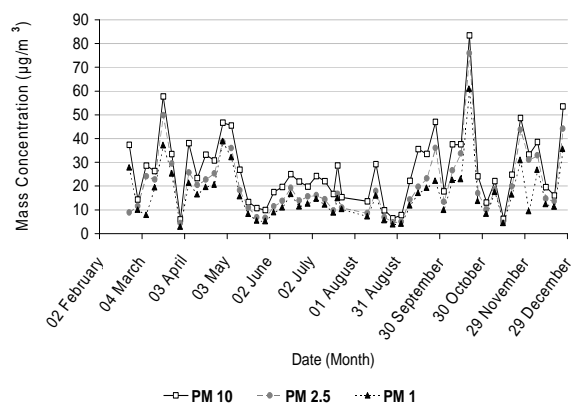


Figure 1. Mass concentrations of PM<sub>10</sub>, PM<sub>2.5</sub>, PM<sub>1</sub> fractions monthly collected during year 2006.

Table 1. Averages and standard deviations of ratios of PM fractions collected during year 2006.

Period Month '06	Heating Period	Unheating Period
	October, November December, March, April	May, June, July, August, September
PM <sub>1</sub> /PM <sub>2.5</sub>	0,78 ± 0,12	0,83 ± 0,05
PM <sub>1</sub> /PM <sub>10</sub>	0,63 ± 0,11	0,56 ± 0,05
PM <sub>2.5</sub> /PM <sub>10</sub>	0,81 ± 0,07	0,66 ± 0,06

Here we report results on mass concentration of PM<sub>x</sub>. Results for each PM fraction obtained during year 2006 are shown in the Figure 1. Average mass concentrations were 26,9±14,9 µg/m<sup>3</sup> for PM<sub>10</sub>, 20,3±13,5 µg/m<sup>3</sup> for PM<sub>2.5</sub>, 16,4±10,8 µg/m<sup>3</sup> for PM<sub>1</sub> fractions. These values are in the range commonly measured in Prague and elsewhere in Central and Western Europe (Civiš *et al.*, (2005), Schwarz *et al.*, (2006), Putaud *et al.*, (2004)). We can conclude that PM fractions collected in the heating period (October, November, December, March, April) are higher in their mass concentration comparing to results of samples obtained in unheating period (May, June, July, August, September). This could be caused by emissions coming from combustion sources used for heating and lower average mixing layer during winter comparing to summer. It is well known that those particles are in the fine size fraction. This is confirmed by results shown in the Table 1. The ratios PM<sub>2.5</sub> to PM<sub>10</sub> are higher in winter then in summer. In the opposite PM<sub>1</sub> to PM<sub>2.5</sub> ratio is slightly higher for summer probably due to lower average humidity, which shift accumulation mode to the smaller particles.

This work was supported by the Ministry of the Environment of the Czech Republic under project VaV- SM/9/86/05.

Civiš M., Hovorka J., & Schwarz J. (2005), in *European Aerosol Conference*, Ghent, 529.  
 Putaud J.P., Raes F., van Dingenen R., Baltenspelger U., Brüggemann E., Facchini M.C., Decesari S., Fuzzi S., Gehrig R., Hansson H.C., et al., (2004), *Atmospheric Environment*, 38, 2579-2595.  
 Schwarz J., Chi X., Maenhaut W., Hovorka J. & Smolík J. (2006), in *NOSA Aerosol symposium*, Helsinki, 335-339.

## Levels and chemical composition of PM10 and PM2.5 in “El Arenosillo” rural monitoring station (SW Spain)

Y. González Castanedo<sup>1,2</sup>, J.D. de la Rosa<sup>2</sup>, A.M. Sánchez de la Campa<sup>3,2</sup>, A. Alastuey<sup>4</sup>, X. Querol<sup>4</sup>, J.P. Bolivar<sup>5</sup>, V. Cachorro<sup>6</sup> and M. Sorribas<sup>1,6</sup>

<sup>1</sup>Instituto Nacional de Técnica Aeroespacial, Esat El Arenosillo, 21130 Huelva Spain

<sup>2</sup>Department of Geology, University of Huelva, Huelva, Spain.

<sup>3</sup>Department of Environment and Planning, University of Aveiro, 3810 Aveiro, Portugal

<sup>4</sup>Institute of Earth Sciences “Jaume Almera”, CSIC, C/ Lluís Sole i Sabaris s/n, 08028 Barcelona, Spain

<sup>5</sup>Department of Applied Physic, University of Huelva, Huelva, Spain

<sup>6</sup>Grupo de Óptica Atmosférica, Universidad de Valladolid, Valladolid, Spain

Keywords: PM10, PM2.5, chemistry, rural monitoring station, SW Spain

El Arenosillo rural monitoring station is located in the Gulf of Cádiz, near the Doñana National Park (Huelva, SW Spain). The frequency of African dust outbreak in this region is high (40-50 days per year as average) compare with other regions of the Iberian Peninsula, and due to the proximity of African continent.

Since the summer of 2004, PM10 was sampling using a Grasseby–Andersen high-volume sampler (68 m<sup>3</sup>/h). In 2006, simultaneous sampling of PM10 and PM2.5 was performed by using MCV high volume samplers (CAVF-PM1025, 30 m<sup>3</sup>/h), and equipped with MCV PM10 and PM2.5 inlets. QF20 Schleicher and Schuell quartz glass filters were used, at a rate of one sample daily per week during. A total of 102 filters of PM10 and 39 filters of PM2.5 samples were collected.

The analytical methodology comprise several instrumental techniques (ICP-OES, ICP-MS, Chromatography and elemental analysis of C by LECO) in order to know the concentrations of major and trace elements, and also, soluble anions, ammonium and total carbon. The procedure of digestion of the filter employ the method proposed by Querol *et al.* (2001)

Mean PM10 levels obtained for the sampling days were 26 µgPM10m<sup>-3</sup>, and 17 µgPM2.5m<sup>-3</sup>. The PM10 values are below the mean annual level described in the Directive 1999/30/EC. El Arenosillo is characterized by high concentration of PM10 compare with other rural sites of Spain (Querol *et al.*, 2006). Under the influence of the African dust outbreak, daily levels and crustal components analyzed were 3-5 times higher than the annual average. The mineral and marine components are high (6.0 and 2.8 µg/m<sup>3</sup> respectively) (Table 1).

High levels of As, Se, Cu, Pb, Bi and Ti were determined in El Arenosillo in PM10 and PM2.5 compare with other rural sites of Spain (op. sit). The average of As in PM10 and PM2.5 was 4.2 ng/m<sup>3</sup> and 3.9 ng/m<sup>3</sup> respectively implying as the emissions of the Industrial States near the city of Huelva can impact in the rural site of this region of the Iberian Peninsula.

Table 1. Levels and chemical composition of PM10 and PM2.5 in rural monitoring station in Spain (Querol *et al.*, 2006) and El Arenosillo.

µg/m <sup>3</sup>	Querol <i>et al.</i> 2006				
	MON	BEM	MONT	MOR (TSP)	ARENO
PM10	21	19	19	24	26,0
N	132	87	157	10	102
OM+EC	2,8	5,5	3,8	2,2	3,0
MINERAL	5,2	2,5	4,8	4,5	6,0
MARINO	0,7	2,6	0,5	1,7	2,8
nmSO <sub>4</sub> <sup>2-</sup>	3,7	3	2,8	3,4	4,2
NO <sub>3</sub> <sup>-</sup>	2,5	0,9	2	3,1	2,6
NH <sub>4</sub> <sup>+</sup>	1,3	1,3	1,2	0,4	1,1
INDET	4,8	3,2	3,9	7	7,6

µg/m <sup>3</sup>	Querol <i>et al.</i> 2006		
	BEM	MONT	ARENO
PM2.5	14	17	17,3
N	45	60	39
OM+EC	3,8	4,6	3,8
MINERAL	1,5	2,1	1,4
MARINO	1	0,3	0,8
nmSO <sub>4</sub> <sup>2-</sup>	2,9	2,9	3,5
NO <sub>3</sub> <sup>-</sup>	0,4	1,9	1,2
INDET	3,3	3,8	4,9

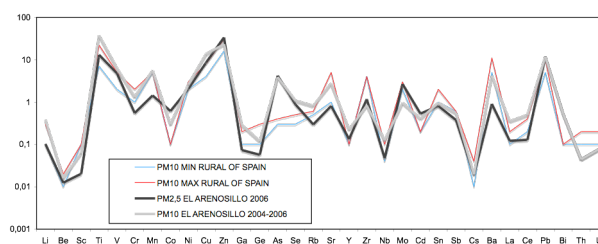


Figure 1. Spiderdiagram of PM10 and PM2.5 trace elements of El Arenosillo, and maximum and minimum PM10 of rural site in Spain (Querol *et al.*, 2006).

Querol X, et al. (2006). *Atmospheric particulate matter in Spain: levels, composition and source origin*. CSIC y Ministerio de Medio Ambiente. 41 pp.

## PM<sub>10</sub> and PM<sub>2,5</sub> ambient levels in the Czech Republic

I. Hůnová

Air Quality Section, Czech Hydrometeorological Institute, Na Šabatce 17, 143 06, Prague 4, Czech Republic

Keywords: monitoring, particle concentration, PM<sub>10</sub>, PM<sub>2,5</sub>, PM<sub>10</sub>/PM<sub>2,5</sub>.

Due to their health effects, particles currently constitute a serious threat for population of many regions of the world (e.g. Krzyzanowski et al., 2005). The health effect studies have not identified a clear no-effect threshold. The limit values in terms of 24h and annual mean concentrations are set up by European legislation.

Particles are monitored in the Czech Republic (CR) in the long run. After the evidence that health effects are related mostly to the fine fraction of PM, monitoring of TSP has been replaced by monitoring of PM<sub>10</sub>, and according to EU recommendations (1999/30/EC Directive) in 2005 fraction PM<sub>2,5</sub> monitoring started. Currently 104 sites monitor PM<sub>10</sub> and 25 PM<sub>2,5</sub> concentrations. Some of these also measure the aerosol chemical composition.

According to the latest nationwide ambient air quality assessment for 2005 (CHMI, 2006), the PM<sub>10</sub> limit values are significantly exceeded over the Czech territory. The limit value for 24-h concentration was exceeded over 35 %, the limit value for annual mean concentration over 1,5 % of the territory. This corresponds to about 66 % of population endangered. The most serious particle problem is encountered in the Moravian-Silesian region (area of Ostrava - Karviná) with maximal 24-h mean concentration of 430 µg.m<sup>-3</sup> (site Cesky Tesin, 2005) and maximal annual mean concentration of 62 µg.m<sup>-3</sup> (site Bohumin, 2005). In this region in addition to transport and local heating sources (which are the major emission sources of particles in other areas as well), local metallurgy and fuel processing are significant contributors. The load here is further enhanced by regional range air pollutant transport from the heavily industrialized Katowice area in Poland.

Apart from high PM concentrations in agglomerations and industrial areas, the increased levels are recorded also at rural background sites. This fact indicates the increasing total aerosol load over CR.

In 2005 we started to monitor fine PM<sub>2,5</sub> particle fraction at 25 sites over CR. The proposed limit value was exceeded at 12 sites, while 6 sites were closely below the limit value. The highest annual mean concentrations were recorded, similarly as for PM<sub>10</sub>, in the Ostrava-Karviná region.

Fig. 1 presents the seasonal variability of PM<sub>2,5</sub>/PM<sub>10</sub> ratio as a mean calculated from 23 sites where both fractions were measured in 2005. The results indicate that PM<sub>2,5</sub>/PM<sub>10</sub> ratio is not constant

through the year, but shows a distinct seasonal course. In 2005 the ratio ranged between 0,69–0,85, with higher values in winter. The seasonal course of PM<sub>2,5</sub>/PM<sub>10</sub> ratio reflects the seasonal character of emission sources. Emissions from combustion sources have higher share of PM<sub>2,5</sub> fraction than e.g. emissions from agriculture and reemissions during dry and windy weather. Consequently, heating in winter period can result in higher share of PM<sub>2,5</sub> fraction as compared to PM<sub>10</sub> fraction.

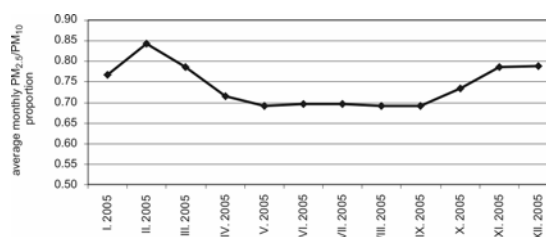


Figure 1. Seasonal course of PM<sub>2,5</sub>/PM<sub>10</sub> ratio calculated for 23 Czech sites in 2005.

In presented contribution PM<sub>2,5</sub>/PM<sub>10</sub> ratio is analysed for different types of sites (urban, traffic, industrial and rural) for 2005 and 2006 data sets. The preliminary results indicate differences as to the type of the site.

In compliance with the EU legislation, the major monitoring activities are focused on agglomerations in the CR. According to some recent studies (e.g. Branis & Domasova, 2003), however, it can be assumed that high PM concentrations exceeding limit values are to be expected in minor towns and villages, where the ambient air pollution is not monitored. Relatively high share of Czech population dwells right there. Due to burning coal and wood, increased emissions of particles, polycyclic aromatic hydrocarbons and toxic metals are released. Moreover, by burning refuse in local fireplaces, regrettably a common practice in small communities in the CR, dangerous dioxins are emitted and added to the toxic ambient air mixture.

Branis, M., & Domasova, M. (2003). *Atm. Env.* 37, 83–92.

CHMI (2006). *Air Pollution in the Czech Republic*. Prague, 216 p.

Krzyzanowski, M., Kuna-Dibbert, B., & Schneider, J. (2005). *Health effect of transport-related air pollution*. WHO, Copenhagen.

## Spatial and temporal variability in PM<sub>10</sub> data from Italian urban networks

A. Di Menno di Bucchianico, S. Bartoletti, A. Gaeta, G. Gandolfo and A.M. Caricchia, M.C. Cirillo

APAT – Italian National Environmental Protection Agency, Via Brancati 48, 00144, Rome, Italy

Keywords: PM<sub>10</sub>, traffic, urban pollution, air quality network.

The attention to airborne particulate matter pollution has constantly grown during the past years. This is due to its well-known health effects and to the high levels of mass concentration measured year-round, especially in urban sites.

PM<sub>10</sub> concentrations are monitored in all the main Italian urban areas through air quality networks, formed by a different number of stations, which are different in type. In fact, referring to the European Exchange of Information (EoI) classification, monitoring stations can be defined by type of area (urban, suburban and rural) and type of dominant emission sources (traffic, industrial and background).

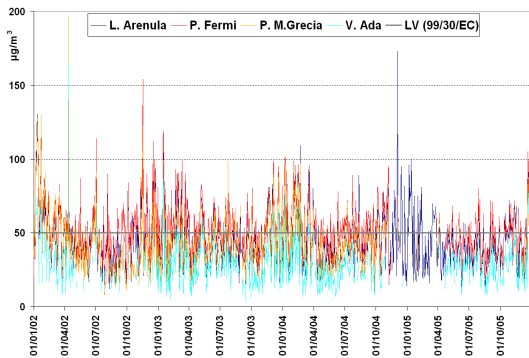


Figure 1. Temporal trend of PM<sub>10</sub> concentrations in Rome (2002-2005).

Consequently, frequently it is hard to compare data sets coming from dissimilar urban networks and obtained with different sampling devices. Above all, it is often demanding to define the spatial and temporal representativeness of data on whose basis anti-pollution measures, like traffic limitations, are taken.

In Italy, following the implementation of the European Directive 1999/30/EC, dated in 2002, the 24-hour and the annual limit values are defined in, respectively, 50 µg/m<sup>3</sup> (not to be exceeded more than 35 times a year) and 40 µg/m<sup>3</sup>.

With the aim to investigate this topic, four years sets of data (from 2002 to 2005), produced by urban air quality networks of the main Italian cities were examined. These cities have been chosen on the basis of geographic and data-coverage criteria.

Therefore, temporal trends and weekend/weekday differences in PM<sub>10</sub> mass concentrations (see figures 1 and 2 illustrating temporal and weekly trends in PM<sub>10</sub> levels in Rome) were analysed using statistical techniques so to delineate homogeneity of results among stations belonging to the same type (see table 1).

Table 1. Correlation between vectors of values from different stations (2002-2005).

Rome	Class.	A	F	G	Ad
A	<i>T</i> <i>U</i>	1.00			
F	<i>T</i> <i>U</i>	0.92	1.00		
G	<i>T</i> <i>U</i>	0.89	0.85	1.00	
Ad	<i>B</i> <i>U</i>	0.87	0.86	0.86	1.00

*T*: traffic; *B*: background; *U*: urban.

A: L. Arenula station; F: P. Fermi station; G: P. M. Grecia station; Ad: V. Ada station.

Although average PM<sub>10</sub> concentrations, from 2002 to 2005, have not clearly decreased or increased on a national scale, the four-year results showed a well-defined seasonal and spatial pattern.

Moreover, through the comparison between PM<sub>10</sub> and some primary pollutants levels (such as carbon monoxide, CO, and nitrogen monoxide, NO) was highlighted if and when PM<sub>10</sub> concentrations from traffic type stations were evidently connected to traffic sources.

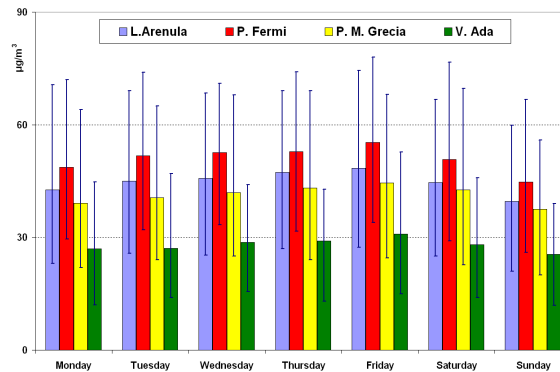


Figure 2. Weekly trend of PM<sub>10</sub> concentrations in Rome (2002-2005).

## Chemical composition and source apportionment of particulate matter in Elche, Spain

J. Crespo<sup>1</sup>, J. Nicolás<sup>1</sup>, S. Caballero<sup>1</sup>, E. Yubero<sup>1</sup>, M. Chiari<sup>2</sup>, F. Lucarelli<sup>2</sup>, S. Nava<sup>2</sup>, I. García Orellana<sup>3</sup>

<sup>1</sup>LCA - Miguel Hernández University, Elche, Spain

<sup>2</sup>Department of Physics, University of Florence and INFN, Florence, 50019, Italy

<sup>3</sup>University of Seville, Spain, and INFN, Florence, Italy

Keywords: PM<sub>10</sub>/PM<sub>2.5</sub>, source apportionment, PIXE, chemical analysis, mass concentration.

The chemical composition of particulate matter has been studied in Elche, a medium-size city (225,000 inhabitants), in the southeast of Spain, ~10 km inland from the Mediterranean coast. This area is characterised by very scarce annual precipitation, dryness of the soil (semi-arid surroundings) and frequent occurrence of episodes of African dust intrusions.

Samples of both PM<sub>10</sub> and PM<sub>2.5</sub> were collected daily, between December 2004 and December 2005, in an urban background location, 12 m above ground level, on a building roof. 47 mm diameter Quartz fibre filters were used in two low volume IND LVS.3.1 EN 12341 reference samplers. Total mass concentrations were obtained gravimetrically using an Ohaus AP250D microbalance (sensitivity 10 µg). A subset of 125 PM<sub>10</sub> and 125 PM<sub>2.5</sub> samples have been analysed by PIXE (Particle Induced X-ray Emission) at the 3 MV Tandem accelerator of the LABEC laboratory of the INFN in Florence to obtain the concentration of all the elements from Na to Pb, and by IC at the LCA laboratory of Miguel Hernández University of Elche, to obtain the ionic composition for SO<sub>4</sub><sup>2-</sup>, NO<sub>3</sub><sup>-</sup>, Cl<sup>-</sup>, Na<sup>+</sup>, Ca<sup>2+</sup>, NH<sub>4</sub><sup>+</sup> and Mg<sup>2+</sup>.

Although the mean PM levels are quite low (31.1 µg/m<sup>3</sup> for PM<sub>10</sub> and 14.7 µg/m<sup>3</sup> for PM<sub>2.5</sub>), several overcomings of the 50 µg/m<sup>3</sup> limit occurred. While in winter about 60% of PM<sub>10</sub> is in the fine fraction, in summer it is mainly in the coarse one, due to different composition and different predominant sources in the two periods.

S, V, Ni, Zn, Br and Pb are mainly in the fine fraction while crustal elements like Al, Ca, Ti, Fe, Sr and sea salt elements, like Na and Cl, are mainly in the coarse one.

Concerning the ionic composition of PM<sub>2.5</sub>, sulfate, nitrate and ammonium are the most abundant ions; the anions-cations balance is remarkable and ammonium well neutralizes sulfate and nitrate.

In PM<sub>10</sub> the contribution of crustal (Ca<sup>2+</sup>, K<sup>+</sup>, Mg<sup>2+</sup>) and sea salt (Cl<sup>-</sup>, Na<sup>+</sup>) ions becomes important. The ion balance shows an anion deficit of about 25% and this can be attributed to carbonates, which are not detected by IC. This high value of carbonates confirms the importance of the soil component in this area. NH<sub>4</sub><sup>+</sup> does not neutralize SO<sub>4</sub><sup>2-</sup> and NO<sub>3</sub><sup>-</sup>.

SO<sub>4</sub><sup>2-</sup> is mainly present in the fine fraction, while Na<sup>+</sup>, Mg<sup>2+</sup>, Cl<sup>-</sup> and Ca<sup>2+</sup> in the coarse one, whereas NO<sub>3</sub><sup>-</sup> is equally distributed in both fractions.

In order to identify the main PM sources we performed a PMF analysis (Paatero et al., 1997) on both PM<sub>10</sub> and PM<sub>2.5</sub> data sets. In PM<sub>10</sub> the soil dust source gives the main contribution (43% of the mass) and its weight becomes predominant in most of the 50 µg/m<sup>3</sup> limit overcomings (Fig.1). Looking at wind directions, dispersion models and satellite images, and calculating backward trajectories, we found that all these episodes were connected to Saharan dust intrusions. Secondary aerosols account for about 30% of the total mass, while the traffic contribution is only 16%. Sea spray aerosol gives a non-negligible contribution (12%).

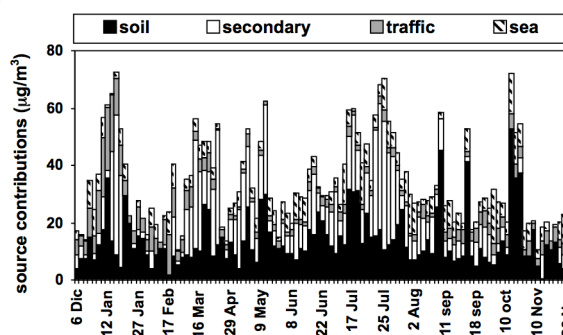


Figure 1. Daily contributions of the identified sources to PM<sub>10</sub>.

As far as PM<sub>2.5</sub> is concerned, secondary aerosols are the main source (52% of the total PM<sub>2.5</sub> mass), followed by traffic (22%).

Two fireworks events were detected with high concentrations of K<sup>+</sup> (~18 µg/m<sup>3</sup>), Cl<sup>-</sup> (~3 µg/m<sup>3</sup>), and SO<sub>4</sub><sup>2-</sup> (~19 µg/m<sup>3</sup>), mainly in the fine fraction.

Work supported by CICyT under the CGL2004-044019/CLI (RESUSPENSE) project.

Paatero, P. Least square Formulation of Robust Nonnegative Factor Analysis; *Chemomet. Intell. Lab. Systems* 1997, 37, 23-35.

## Urban contribution to trace metals in the PM10 in Salzburg and other Austrian cities

M. Handler, H. Zbiral, H. Puxbaum and A. Limbeck

Institute of Chemical Technologies and Analytics, Vienna University of Technology,  
Getreidemarkt 9/164, A-1060 Vienna, Austria

Keywords: Trace metals, Mineral dust, PM10, Urban aerosols.

Anthropogenically-induced mobilization of trace metals into the biosphere has become an important process in global geochemical cycling. This effect is most evident in urban areas where several as yet unidentified sources, both stationary and mobile, release quantities of trace metals into the atmosphere to produce urban PM levels much in excess of rural PM levels. (Bilos 2001)

The European Commission (EC) has included PM10 monitoring in the new air quality directive and established an annual average limit of  $40 \mu\text{g PM}_{10} \text{ m}^{-3}$ , and a 24 h limit value of  $50 \mu\text{g PM}_{10} \text{ m}^{-3}$ . Thirty days of exceedances are allowed per year, but this number is violated in several Austrian as well as in many other European and North American cities (Chow et al., 1992, Puxbaum et al., 2004). Trace elements will not usually contribute more than 1 % to total PM10 mass, but mineral elements like Si, Al and Fe can make up to 20 %

An important factor in environmental pollution is the extent to which local emissions, especially in a city, can increase the background levels brought in by large-scale air movement. In terms of total mass this is often small, but the contribution to the trace metals is not generally known.

During the AQUELLA-project (Jan to Dec 2004), airborne PM10-material was collected in Vienna, Graz and Salzburg on a daily basis. In each city three sampling sites have been operated: one urban site, heavily influenced by road traffic, one urban residential site and the third a local background site remote from the city. This experimental design gives the opportunity to study the impact of the urban area on a local scale.

PM10 samples (24 h mean values) were treated with *aqua regia* in a microwave oven to be analysed with ICP-AES for selected trace metals and mineral elements. Analysis of As, Sb and Pb was performed by GF-AAS. Prior to the digestion step, the concentrations of Si and Al were determined directly on the filters, by XRF.

PM10 levels in Salzburg city centre (Rudolfsplatz) are enhanced over background, with exceedances occurring in the early Spring. The observed increase on the PM10 concentration, called "Urban Impact", averages in Lehen, about 25% on top of the background level recorded at Anthering, and around 100% extra for Rudolfsplatz.

Figure 1 shows the annual average concentrations of selected trace metals at the three sampling sites in Salzburg. Urban Impacts for trace elements were much higher than for the PM10, with individual elements increased by up to 10-15 times the background levels, indicating, for these elements, a very significant local contribution from the urban environment.

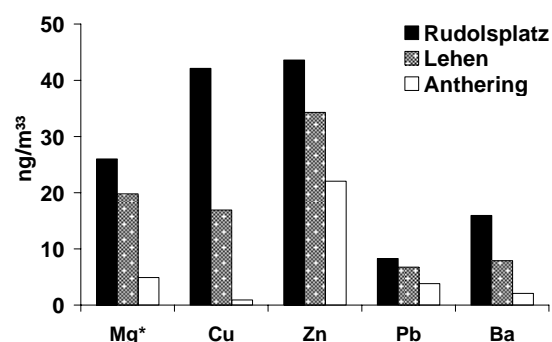


Figure 1: Concentrations of selected elements in Salzburg (annual average) (\*Mg scaled 1/10)

Ba, Sr, (and Fe) remain fairly constant though the year at Rudolfsplatz, but are significantly enhanced over the background levels. Copper shows a particularly large impact throughout the year, indicating that all the copper comes from urban sources while the zinc urban impact is about half that. Ca and Mg on the other hand show highs in the early spring associated with the use of dolomite for gritting the roads. At such times the urban impact factors can reach 20 compared with 4 in summer.

This work was financed by the provincial governments of Carinthia, Lower and Upper Austria, Salzburg, Styria and Vienna.

- Bilos, C., Colombo, J.C., Skorupka, C.N., Rodriguez Presa M.J. (2001) *Environ. Pollut.*, **111**, 149-158.  
Chow, J.C., Watson, J.G., Lowenthal, D.H., Solomon, P.A.; Magliano, K.L., Ziman, S.D., Richards, L.W. (1992) *Atmos. Environ.*, Part A: **26A**, 3335-3354.  
Puxbaum, H., Gomisček, B., Kalina, M., Bauer, H., Salam, A., Stopper, S., Preinig, O., Hauck, H. (2004). *Atmos. Environ.* **38**, 3949-3958.

## Source apportionment of fine and coarse aerosol in the Athens Metropolitan area

A.A Karanasiou<sup>1,2</sup>, P.A. Siskos<sup>2</sup> and K. Eleftheriadis<sup>1</sup>

<sup>1</sup>Institute of Nuclear Technology and Radiation Protection, Environmental Radioactivity Laboratory,  
N.C.S.R. Demokritos, Ag. Paraskevi, Attiki, 15310, Greece

<sup>2</sup>Department of Chemistry, Analytical Chemistry Laboratory, National and Kapodistrian University of Athens,  
Panepistimiopolis, 15771, Athens, Greece

Keywords: Source apportionment, Urban aerosols, Trace elements, PM<sub>10</sub>, PM<sub>2.5</sub>

The objective of this study was to identify the major pollution sources in the Athens urban area by means of factor analysis. Two different multivariable methods were used: Principal Component Analysis (PCA) and Positive Matrix Factorization (PMF).

Two aerosol-sampling campaigns were conducted during March 2002 - December 2002 at three sites in the Athens Metropolitan area, during the cold and warm period. PM<sub>10</sub> and PM<sub>2.5</sub> samples were collected simultaneously over a 24 h period. Black carbon concentrations (BC) were concurrently measured by means of an aethalometer (AE-9, Magee Sci). After gravimetric analysis the loaded PTFE membrane filters were subjected to microwave acid digestion and analysed for Cd, Pb, V, Ni, Mn, Cr, Cu, Fe, Al, Ca, Mg, K, and Na by atomic absorption spectrometry. In two out of three sites the water-soluble SO<sub>4</sub><sup>2-</sup> was also determined by ion chromatography.

Source apportionment by PCA is useful to a certain extent but suffers from the appearance of negative factor loadings and the assumption of nonrealistic standard deviations for the values of the data matrix (Paatero & Tapper 1993). However, it was used as a first approach in order to gain insight on the number of factors before the implementation of PMF.

PMF analysis was performed with a number of parameters adjusted, so that the optimum solution was obtained. The number of factors and the rotational state were selected after several runs of PMF. The main advantage of PMF over PCA is the computation of the individual error estimates  $S_{ij}$  for all variables. In this study  $S_{ij}$  were calculated by performing recovery and reproducibility tests.

For fine and coarse aerosol 5 and 3 factors were selected respectively. Table 1 shows the resolved factors for fine aerosol. For fine particles the first factor relating BC and SO<sub>4</sub><sup>2-</sup> with Cu, Fe, Al, Ca, Mg, and K was attributed to road dust in accordance to an earlier study (Karanasiou et al., 2007). The high percentage of Ca in this source implied the influence of construction activities in the area. Sulfates related to this factor are likely to originate from sulfate salts such as CaSO<sub>4</sub> and Al<sub>2</sub>(SO<sub>4</sub>)<sub>3</sub>, which are typical cement components. Given that BC was the predominant variable in the second factor, this was concluded to represent motor vehicles emissions. A

biomass-burning source was associated with factor 3 taking into account the high mass percentages of BC, K and SO<sub>4</sub><sup>2-</sup> in this factor. The fourth source (F4) was attributed to marine aerosol, since Na was the dominant element in this factor and the composition profile was comparable to that of sea-salt aerosol. The factor having high concentrations of Fe, BC, SO<sub>4</sub><sup>2-</sup> and a small contribution of Pb, V and Ni was assigned to oil combustion. V and Ni, which are characteristic fuel oil tracers, have the highest mass fraction relative to their total mass associated with this factor. For coarse aerosol three sources were identified: road dust, soil and an aged marine aerosol. Motor vehicles and road/construction dust were the major contributors to fine particle mass.

Table 1. Factor profiles for fine aerosol (in mass percentages) produced by PMF

Variable	Fine particles factors				
	F1	F2	F3	F4	F5
Cd	0.01	0.00	0.00	0.00	0.04
Pb	1.01	0.26	0.44	0.00	0.53
V	0.11	0.05	0.12	0.08	0.38
Ni	0.00	0.30	0.00	0.00	0.46
Mn	0.00	0.04	0.10	0.29	0.69
Cr	2.29	0.18	0.31	0.08	0.08
Cu	1.22	0.12	0.65	0.33	0.00
Fe	0.75	0.01	0.00	0.39	50.47
Al	4.91	0.34	0.00	0.35	6.94
Ca	16.91	0.04	0.00	0.00	2.52
Mg	1.45	0.00	0.00	1.52	3.13
K	0.00	0.00	17.80	3.82	10.03
Na	0.15	0.00	0.01	93.05	4.80
BC	44.87	98.66	27.45	0.08	9.93
SO <sub>4</sub> <sup>2-</sup>	26.31	0.00	53.11	0.00	10.01

Where: F1: Road dust F2: Vehicles F3: Biomass-Burning F4: Marine aerosol F5: Oil combustion

### References

- Paatero, P., & Tapper, U., (1993). *Chemom Intell Lab Syst*, 18, 183-194.  
Karanasiou A.A., Sitaras, I.E., Siskos P.A., & K. Eleftheriadis (2007). *Atmos Environ* (in press)

## INFLUENCE OF TYRE AND PAVEMENT ON PM<sub>10</sub> AND PARTICLE NUMBER EMISSIONS FROM ROAD WEAR

A. Gudmundsson<sup>1</sup>, A. Dahl<sup>1</sup>, E. Swietlicki<sup>2</sup>, G. Blomqvist<sup>3</sup>, P. Jonsson<sup>3</sup> and M. Gustafsson<sup>3</sup>

<sup>1</sup>Division of Aerosol and Technology, Lund University, Sweden

<sup>2</sup>Division of Nuclear Physics, Lund University, Sweden

<sup>3</sup>Swedish National Road and Transport Research Institute (VTI), Linköping, Sweden

Keywords: PM measurements, Ultrafine particles, Vehicles emissions, Wear particles

During the last years it has become evident that wear particles from road pavements and tyres strongly contribute to episodes with very high concentrations of inhalable particles in outdoor air. These episodes normally occur during dry periods in winter and spring when accelerated wear and particle production occurs due to the use of studded tyres and winter gritting. This problem has attracted attention in countries where studded are frequently used. The resulting wear and production of inhalable particles is dependent on a number of factors that are difficult to quantify in real world environments. Therefore, the objective of this study was to investigate the effects of pavement type, tyre type and speed on pavement wear in a controlled environment.

At the Swedish National Road and Transport Research Institute (VTI) a circular road simulator was used to generate wear particles. Particle sampling in the simulator hall makes it possible to sample pure wear particles, with very low contamination from ambient particles. The road simulator runs four wheels around a circular track. Each wheel axle is equipped with an electrical motor which drives the rotation of the simulator. The speed can be varied between 0–70 km/h. The simulator track can be equipped with any type of pavement and any type of light-duty vehicle tyre can be mounted on the axles. Three different sets of measurements were made in order to elucidate the effect of three factors on pavement wear and generation of PM<sub>10</sub>; these were 1) type of pavement, 2) type of tyres and 3) speed.

- 1) These included an asphalt concrete consisting of granite stone material with 16 mm maximum aggregate size (hereafter denominated “Granite <16”), a stone mastic asphalt of quartzite stone material with 16 mm maximum aggregate size (“Quartzite <16”) and another stone mastic asphalt (“Quartzite <11”) of another quartzite stone material with 11 mm maximum aggregate size.
- 2) Three types were chosen; studded winter tyres, friction (non-studded winter) tyres and summer tyres.

- 3) Speed was varied from 0–70 km/h in the road simulator. The increase between these speeds is made quickly in less than two minutes. Once the desired speed has been reached the road simulator is left to run for ~1.5 h.

Particle size distribution in the road simulator hall was sampled using a PM<sub>10</sub>-inlet and measured using different instrument as APS (model 3321, TSI), SMPS (CPC 3010 and DMA 3071, TSI), DustTrak (model 8520, TSI) and TEOM.

A granite pavement resulted in 70 % higher PM<sub>10</sub> concentration than a quartzite pavement of the same aggregate size. Out of two quartzite pavements with different aggregate sizes, the one with smaller stone material (Quartzite <11) led to lower PM<sub>10</sub> concentration than larger (Quartzite <16), indicating that other aggregate properties than size are more important for PM<sub>10</sub> production.

Studded tyres cause extreme concentrations of PM<sub>10</sub> that are tens of times higher than those associated with non-studded winter tyres. Summer tyres have a very little effect on PM<sub>10</sub> production in contrast.

Using a simple box model assumption mass emission and number emissions factors were estimated. Our estimated PM<sub>10</sub> emission for studded tyres at 70 km/h agrees with field measurements carried out in two cities in Sweden. The PM<sub>10</sub> emission was determined to ~1 g per vehicle kilometre.

Apart from the expected wear particle size ranges (>1 µm), an ultra-fine (<100 nm) fraction with a number maximum around 20–40 nm was found for studded tyres. No ultra-fine particle emission was detected from friction or summer tyres. The composition of the emitted particles is assumed to be winter tyre fillers and softening oils, which differ from summer tyres. For a given tyre the velocity and thereby the tyre temperature was the most significant parameter that affected the amount of generated particles.

The Swedish National Road Administration is acknowledged for financial support.

## Size-Selective Mass and Elemental Composition of Fine Particles in the Vicinity of a Major Freeway

Dainius Martuzevicius<sup>1,2</sup>, Sergey A. Grinshpun<sup>1</sup>, Anna L. Kelley<sup>3</sup>, Harry St. Clair<sup>3</sup>,  
Linus Kliucininkas<sup>2</sup>, Tomas A. Cahill<sup>4</sup>

<sup>1</sup>Center for Health-Related Aerosol Studies, Department of Environmental Health, University of Cincinnati, Cincinnati, Ohio, USA

<sup>2</sup>Department for Environmental Engineering, Kaunas University of Technology, Kaunas, Lithuania

<sup>3</sup>Hamilton County Department of Environmental Services, Cincinnati, Ohio, USA

<sup>4</sup>Department of Applied Sciences, University of California Davis, Davis, CA, USA

Keywords: Ambient aerosols, fine particles, mass size distribution, trace elements, traffic

### Introduction

The study was designed to address the transformation of fine particles in the vicinity of a major freeway with intense traffic. Previous research aimed at determining primarily the particle number concentrations, which was shown to be elevated at the distances of up to 100-400 m from the source, especially in the fine and ultrafine size ranges. Very little information is available about the size-fractionated concentrations of specific elements at different distances from the motorways. We have addressed this issue by utilizing a cascade impactor collecting with samples a high time resolution and suitable for subsequent elemental analyses.

### Methods

The measurement campaign was conducted near the 14th mile of Interstate freeway I-71 in the state of Ohio, USA. The average total traffic at the 6-lane freeway segment was 132330 vehicles per day (90.6% of these were light-duty and 9.4% were heavy-duty vehicles). Two sites were positioned at 45 m and 185 m from the highway shoulder.

The 8-Stage Rotating Drum Impactor, manufactured by DELTA Group at the University of California Davis, California, USA, was utilized to collect a size-resolved particulate matter with a time resolution of 3 hours. The deposit was later analyzed by soft  $\beta$  analysis (mass concentration) and S-XRF analysis (elemental concentrations)

### Results

The PM mass was mostly distributed bimodally, with the first mode peaking on stages 6-7 (0.26-0.56  $\mu\text{m}$ ) and the second mode occurring somewhere in the coarse size range (as seen from the increasing number of particles detected on stages 1 and 2). This type of mass distribution is common at sites of traffic influence (Pakkanen et al., 2003).

The summer campaign revealed that the PM size distribution may be tri-modal as shown in Fig. 1, which possibly reflects two major sources of particles – in size ranges of 0.26 - 0.34  $\mu\text{m}$  (stage 7) and 0.56-0.75  $\mu\text{m}$  (stage 5). The studies by Kleeman and Cass (1998) and Pakkanen et al. (2003) suggest that the traffic-influenced mode occurs at about 0.2–0.3  $\mu\text{m}$

and a long-range influenced mode at about 0.7–0.8  $\mu\text{m}$ . The size distributions of PM obtained at both distances are comparable, with a slight difference within one standard deviation.

The traffic-related trace elements, such as Cu, Mn, Zn, and Fe exhibited mostly single-modal size distributions. After averaging the data sets for these elements, a clear mode was observed representing larger particles while the fine particle mode appeared to be insignificant. In order to trace out a distinct spatial gradient of the particle concentration near the freeway, the data were analyzed with respect to the wind direction. When the wind was blowing from the highway, the above mentioned trace metals exhibited a significant mode on stage 4 (0.75-1.15  $\mu\text{m}$ ) at the 45 m site, while this mode was not present at the 185 m site. We attribute this to the traffic related aerosol emissions.

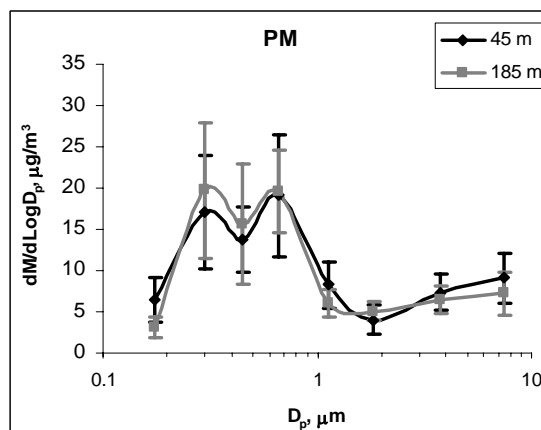


Figure 1. Average particle size distributions for PM, displaying tri-modal distribution.

The study was partially supported by the US EPA (Air Toxics Grant).

Pakkanen, T., Kerminen, V.-M., Korhonen, Loukkola, K., C., Hillamo, R., Aarnio, P., Koskentalo, T., Maenhaut, W. (2003). *Atmos. Environ.*, 37, 1673–1690.

Kleeman, M.J., Cass, G.R. (1998). *Atmos. Environ.*, 32, 2803–2816.

## Study of spatial variability of the particulate matter (PM) concentrations

<sup>1</sup>Sabina Stefan, <sup>2</sup>Cristina Mihaela Raicu

<sup>1</sup>University of Bucharest, Faculty of Physics, P.O. Box MG-11, Bucharest, Romania,  
Tel./Fax: +40 21 4574521, E-mail: sabina\_stefan@yahoo.com

<sup>2</sup>The National Research & Development Institute for Environmental Protection, Bucharest, Romania

keywords: atmospheric aerosol, meteorology, PM10, urban aerosols

The aim of this paper is to analyse temporal and spatial variability of aerosol (Particulate Matter, PM) data, which were obtained in Bucharest (Romania) region. Aerosol is considered at rural, near-city, urban, and kerbside sites, over one year. Data are available from 8 sites and include PM10 mass concentrations. The background wind speed and direction were analysed to determine the dominant direction for pollutant transport. The back-trajectories of air masses were also used to explain the transport of the aerosol. Such data sets are essential to elucidate the sources of the aerosols, their effect on human health, their role in the radiation balance of the atmosphere, and to validate atmospheric models.

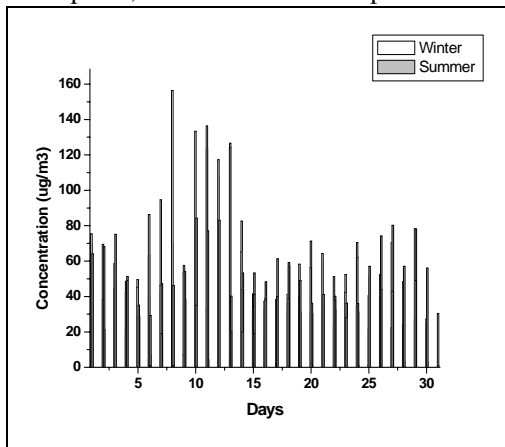


Fig.1. Evolution in time of PM10 concentrations for an urban site in the winter (DJF) and summer (JJA) seasons.

The results of the study show the following: (i) the background is not only due to natural sources, but also to long range transport of anthropogenic particles; (ii) in a few sites, PM10 in city is strongly affected by the regional aerosol background; (iii) the comparison between concentrations at different sites indicates that traffic is responsible for the high PM10 concentrations in urban sites; (iv) there is a correlation between PM mass concentration on the one hand, and the air mass trajectories on the other hand; (v) at polluted sites PM10 is significantly higher during winter (Fig. 1). This is at least partially due to meteorology, because the dispersion of pollutants is least in winter, when the mixed boundary layer height is reduced.

### Acknowledgments

This work is supported by the contract No. 734/2006 (TOP) of the research and development program CEEX-MENER. The authors thank to National Research & Development Institute for Environment Protection for the data used.

## PATOS: the first extensive field campaign for atmospheric aerosol characterisation in Tuscany (Italy)

F. Lucarelli<sup>1</sup>, F. Barzagli<sup>2</sup>, S. Becagli<sup>2</sup>, G. Calzolai<sup>1</sup>, A. Cincinelli<sup>2</sup>, M. Chiari<sup>1</sup>, M. Giannoni<sup>2</sup>, T. Martellini<sup>2</sup>, L. Lepri<sup>2</sup>, S. Nava<sup>1</sup>, L. Paperetti<sup>1</sup>, F. Rugi<sup>2</sup>, R. Traversi<sup>2</sup> and R. Udisti<sup>2</sup>

<sup>1</sup>Department of Physics and INFN, University of Florence, Sesto Fiorentino, 50019, Florence, Italy

<sup>2</sup>Department of Chemistry, University of Florence, Sesto Fiorentino, 50019, Florence, Italy

Keywords: chemical composition, PM<sub>10</sub>/PM<sub>2.5</sub>, urban aerosols, source apportionment.

The PATOS project (*Particolato Atmosferico in TOScana*), the first extensive field campaign for PM<sub>10</sub> characterisation in Tuscany, has been entrusted by the Regional Government mainly to investigate the aerosol composition and to identify its sources. The project is now ended and a complete overview of the more interesting results will be shown.

Aerosol samples have been collected, on a daily basis, from September 2005 and to September 2006, in seven sampling sites in Tuscany, representative of areas of different typology: Florence (urban background), Prato (urban traffic), Capannori-Lucca (urban background), Arezzo (urban traffic), Grosseto (urban background), Montale-Pistoia (rural background) and Livorno (suburban background). Four sequential samplers were used, each of them equipped with two inlets in order to collect aerosol on Teflon and Quartz fibre filters simultaneously, thus allowing the application of different analytical techniques. Three samplers were used to collect PM<sub>10</sub> (and were moved every 15 days), while the fourth sampler collected PM<sub>2.5</sub> in Florence.

PM<sub>10</sub> and PM<sub>2.5</sub> daily mass concentrations have been obtained gravimetrically.

Samples collected on Teflon filters have been analysed by PIXE to measure the concentrations of all the elements with atomic number  $Z > 10$  (Chiari *et al.*, 2005), by IC to quantify the soluble component of inorganic ions (Fattori *et al.*, 2005), and by ICP-MS to assess the soluble component of several metals. Samples collected on Quartz fibre filters were analysed by GC and GC-MS to determine n-alkanes and PAHs concentrations (Cincinelli *et al.*, 2003), and were also used for Total Carbon (TC) assessment.

During shorter periods both fine and coarse fractions of the aerosol were also collected by streaker sampler; PIXE analysis of these samples produced the elemental concentrations with hourly resolution.

Concerning PM<sub>10</sub> concentrations (Fig.1), the higher values were found in Capannori-Lucca, during wintertime, followed by Prato, whereas quite low levels were registered in Grosseto and Livorno.

Sulfate showed very similar temporal trends and concentration values in the different sites, indicating that the contribution of local sources is negligible in comparison to the regional background (mainly due to atmospheric oxidation of SO<sub>2</sub> mainly emitted by power plants).

Nitrate concentrations were higher in those sites (Prato, Capannori-Lucca, Firenze, Arezzo) which are more stressed by local anthropogenic sources like traffic.

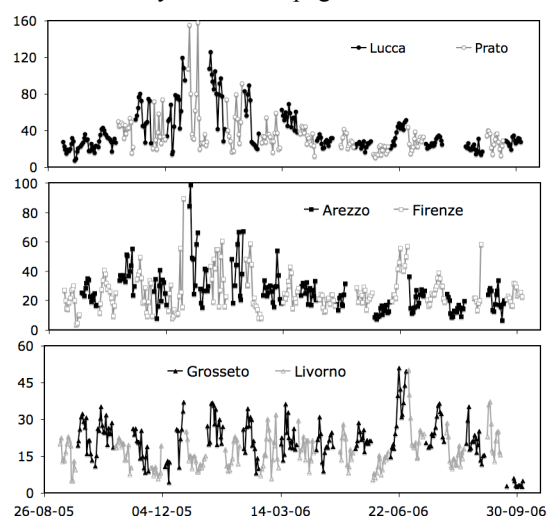


Figure 1. PM<sub>10</sub> daily contributions (µg/m<sup>3</sup>).

TC resulted the main PM<sub>10</sub> component in all the sites (~40% of the total mass), with higher concentrations in winter, especially in Capannori-Lucca.

PMF (Positive Matrix Factorisation) analysis, applied both on daily and hourly concentrations, allowed us to identify the main sources and to estimate their impact. As an example, the high C level in Capannori-Lucca during wintertime was ascribed to a biomass burning source (also traced by Glycolates and K, the latter with peculiar hourly time trend).

Concerning natural sources, Saharan dust intrusions and marine aerosol transport episodes have been well characterised by elemental composition and meteorological data.

Comparing data from PIXE and ICP-MS, we could assess the soluble fraction of several elements: Ni, Cu, Zn and V resulted mainly soluble, while an opposite behaviour was found for crustal metals (Al, Fe, Mn).

This work was supported by the Regional Government of Tuscany, Italy.

Chiari *et al.* (2005). *X-Ray Spectrometry* 34, 4, 323-329.

Cincinelli *et al.* (2003). *Atm. Env.*, 37, 3125-3133.

Fattori *et al.* (2005). *J. Environ. Monit.* 7, 12, 1265-1274.

## Atmospheric aerosol characterisation in Tuscany (PATOS project): identification of natural and anthropogenic episodes by PIXE analysis

F. Lucarelli<sup>1</sup>, G. Calzolai<sup>1</sup>, M. Chiari<sup>1</sup>, L. Lepri<sup>2</sup>, S. Nava<sup>1</sup>, L. Paperetti<sup>1</sup> and R. Udisti<sup>2</sup>

<sup>1</sup>Department of Physics and INFN, University of Florence, Sesto Fiorentino, 50019, Florence, Italy

<sup>2</sup>Department of Chemistry, University of Florence, Sesto Fiorentino, 50019, Florence, Italy

Keywords: PIXE, trace elements, urban aerosols, source identification.

Since aerosol particles retain elemental compositions characteristic of their origin, the simultaneous detection of groups of elements by multi-elemental techniques, like Proton Induced X-ray Emission (PIXE), can be of great help in the study of aerosol sources. Among PIXE detectable elements there are markers of specific components such as marine aerosol (Na, Cl), mineral dust (Al, Si, Ca, Ti, Sr), sulfates (S), biomass burning products or biogenic emissions (K, Zn, Rb), heavy oil combustion (V, Ni), incinerator emissions (K, Zn, Pb), traffic and industrial emissions (Mn, Ni, Cu, Zn, Pb). In particular, as regards natural sources, Saharan dust intrusion events can be well identified by an increase of the concentration of all crustal elements and by changes in their elemental ratios, and their impact can be estimated.

Furthermore, PIXE analysis (together with the use of specific continuous samplers, like the “streaker” sampler) can produce elemental concentrations with high temporal resolution (of the order of 1 hour). This feature is particularly useful for the study of fugitive or episodic sources. The high temporal resolution singles out sharp peaks lasting few hours and the knowledge of the hour of the day of the peak occurrence can suggest its origin.

In the framework of the PATOS project, the first extensive field campaign for the aerosol characterisation in Tuscany (Italy), PM<sub>10</sub> daily samples have been collected in six sampling sites for one year (September 2005 – September 2006), simultaneously on Teflon and Quartz filters, thus allowing the application of different analytical techniques (PIXE, IC, Total Carbon measurements, etc.). During shorter periods the fine and coarse fractions of particulate matter have been collected by a streaker sampler and analysed by PIXE.

In this poster will focus on those results obtained within the PATOS project by the application of PIXE.

While for most of the detected elements some differences among the various sampling sites are evident, S shows very similar trends and absolute values in all the sampling sites; this result indicates that the contribution of local S sources (diesel vehicles, domestic heating) are negligible in comparison to the regional background, mainly due to SO<sub>2</sub> oxidation in the atmosphere.

Very high K levels were found in PM<sub>10</sub> daily samples collected in the sampling site of Capannori—Lucca. Looking at the streaker data we found that K was mainly in the fine fraction, thus indicating a non-soil source, probably a combustion source. The hourly time trend of fine K (Fig.1) shows that the concentration of this element increases during late evening/night hours, thus evidencing a domestic heating source. A Positive Matrix Factorisation analysis of hourly and daily concentrations supported this hypothesis.

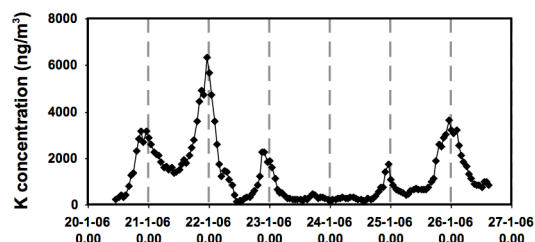


Figure 1. Fine fraction K hourly concentration in Capannori-Lucca sampling site. Vertical lines correspond to midnight.

Several Saharan dust intrusion and marine aerosol transport events were identified during the PATOS campaign. For example, three marine episodes occurring on February and March 2006 were detected in all sampling sites by an increase of Na and Cl concentrations (Fig.2), and were confirmed by backward trajectories calculations. Other examples will be shown.

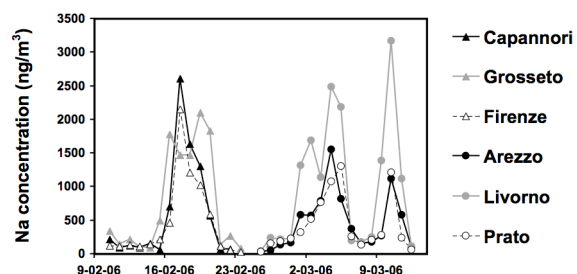


Figure 2. Na daily concentration.

This work was supported by the Regional Government of Tuscany, Italy.

## On the methodology to identify the origin of air masses arriving in a receptor site and determine their contribution to PM levels. A 7-year study in SE Spain.

M. Cabello, V. Galiano and J.A.G. Orza

SCOLab, Física Aplicada, Universidad Miguel Hernández, E-03202, Elche, Spain

Keywords: trajectory, atmospheric aerosols, long-range transport, meteorology, PM10/PM2.5

Cluster analysis has been used to classify air mass trajectories into non-predefined dominant groups by a number of authors. The procedures try to minimize within cluster variance and maximize between cluster variance.

A k-means cluster analysis of 96 hour trajectories arriving in Elche at 3000, 1500 and 500m for the 7-year period 2000-2006 has been performed to describe the main flows arriving in SE Spain and to relate them to PM10 and PM2.5 values and meteorological variables in this area.

Back-trajectories arriving at 12 UTC were computed using the HYSPLIT model v.4 with the FNL meteorological data. Hourly latitude and longitude were used as input variables in the clustering procedure.

There are some subjective decisions to make when performing a k-means clustering. The procedure described by Dorling et al. (1992) was used to reduce the *subjectivity in the selection of the appropriate number of clusters*. The percentage change in total RMSD (i.e. the sum of the Root Mean Square Deviation of every cluster) when the number of clusters is reduced from  $k$  to  $k-1$  by merging the two closest clusters was used to derive the optimum number. Unlike Dorling, we define this number as the smallest quantity that corresponds to the smallest total RMSD change.

Different sets of seed trajectories (i.e. initial centroids to begin the clustering process) have been used to study the *influence of the starting conditions in the final cluster classification*, both (**synthetic radial trajectories** (Mattis, 2001) starting in Elche and **real trajectories** (Dorling et al., 1992).

These approaches gave identical results for 3000 and 1500m, and quite similar solutions for 500m. Although this would show the robustness of the procedures, they do not necessarily lead to the smallest total RMSD, due to a lack of sampling of the trajectories' ensemble (especially when considering small number of clusters) to choose the initial seeds. The calculation of 100,000 clustering analyses for each  $k$ , taking the initial seeds from randomly chosen real trajectories, provides smaller total RMSDs and hence better solutions. Moreover, when the percentage change in total RMSD to extract the appropriate number of air mass types is applied, this last method obtains a different number of clusters for 3000 and 1500m than the Dorling and Mattis' procedures.

We have considered as best solution the one with the smallest RMSD; the 96h back-trajectories arriving at 3000, 1500 and 500m are found to be clustered into 6, 5, and 6 groups, respectively.

For the 3000m trajectories (fig. 1) there are several Northwesterly flows: fast (NWfast), moderate (NWmod) and slow (NWslow) polar maritime air masses, that account for 31% of the total number of trajectories. The southwesterly flows cluster (SW) is the major one (32%), followed by Mediterranean recirculations (MedR, 17%).

At 1500m there is an elevated occurrence of slow flows and recirculations due to situations with a low baric gradient that last several days: Mediterranean (23%) and Western (WR, 39%) recirculations. No SW flows are identified.

For the trajectories arriving at 500m, low baric gradient situations represent 70% of the cases: MedR, WR and slow flows from western Europe (N-Eu). Mediterranean flows are split into Med and MedR ones.

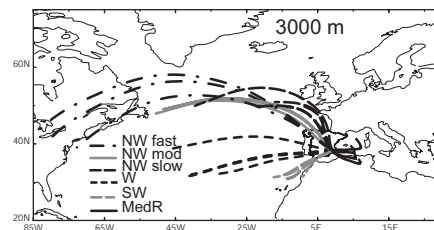


Figure 1. Cluster centroids from different initializations for 96h back-trajectories arriving at 3000m.

The Kruskal-Wallis and the Mann-Whitney tests were performed to detect significant differences on PM and meteorological variables according to the identified clusters. Correlation analysis and PCA were also applied to characterize the air masses in a more compact way. Air masses influence atmospheric parameters like precipitation, mixing height or surface wind speed, and these influence PM levels as well.

Work supported by the Ministerio de Educación y Ciencia under the CGL2004-04419/CLI (RESUSPENSE) project.

Dorling, S. R., Davies, T. D. & Pierce, C. E. (1992). *Atmos. Environ.*, 26a, 2575-2581.

Mattis, I. (2001). <http://lidarb.dkrz.de/earlinet/scirep1.pdf>

## Contribution of Soft and Hardwood combustion to the Austrian PM<sub>10</sub>

P. Kotianová, A. Caseiro and H. Puxbaum

Institute of Chemical Technologies and Analytics, Vienna University of Technology,  
Getreidemarkt 9/164-AC, A-1060 Vienna, Austria

Keywords: levoglucosane, retene, PM<sub>10</sub>

Many epidemiological studies consistently show a clear relationship between ambient atmospheric particulate matter (PM) concentrations and increased morbidity and mortality (e.g. Dockery *et al.*, 1993; Pope *et al.*, 2000). This has led European countries to establish 50 µg/m<sup>3</sup> as a limit for ambient PM<sub>10</sub>, which is commonly exceeded in major Austrian cities during the winter. Thus, there is a need to understand the aerosol sources and quantify them. Methods based on the analysis of ambient PM combined with the analysis of PM from different sources (e.g. Schauer *et al.*, 1996) have proved to be useful attempts to complete the knowledge about the magnitude of individual source contributions. This approach has identified wood burning as a ubiquitous source for atmospheric fine aerosol, and an important source of particulate matter in the atmosphere in certain communities during the cold season.

Among the organic tracers proposed so far, anhydrosaccharides (levoglucosan, mannosan and galactosan) seem to be particularly suitable for the quantification of wood burning due to their high emission rates, 100±50 mg/gOC reported by Fine *et al.* (2001), their atmospheric stability and their uniqueness as cellulose thermal degradation products. A careful examination of wood burning source analysis data points towards a difference in the ratio between levoglucosan and mannosan in hard and softwood. Another wood smoke tracer, retene, a resin acid derivative, has been proposed as typical for softwood (Fine *et al.*, 2001; Schauer *et al.*, 2001). There are then two potential approaches for the differentiation between hard and softwood. The goal of this work was to quantify the wood burning contribution to PM<sub>10</sub>, as well as to differentiate the inputs of soft and hardwood within that contribution using and comparing both approaches.

In the present study, ambient PM<sub>10</sub> from three Austrian cities was sampled for one year (2004) and chemically characterised for a selected set of tracers. The sampling networks accounted for urban, urban residential and background sites. Also, PM<sub>10</sub> from various sources was characterized in the same fashion, among them were wood burning samples of representative Austrian species.

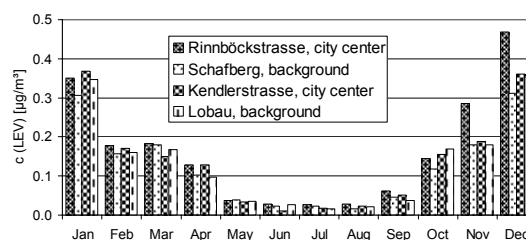


Figure 1. Monthly mean concentration of levoglucosan at Vienna sampling sites in 2004.

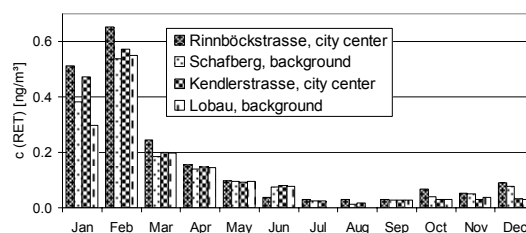


Figure 2. Monthly mean concentration of retene at Vienna sampling sites in 2004.

- Dockery, D. W., Pope III C. A., Xu, X., Spengler, J. D., Ware, J. H., Fay, M. E., Ferris, B. G. & Speizer, F. E. (1993). *The New England Journal of Medicine*, 329, 1573-1759.
- Pope, C. A. (2000). *Aerosol Sci. Technol.*, 36, 4-14.
- Schauer, J. J., Rogge, W. F., Hildemann, L. M., Mazurek, M. A., Cass, G. R. & Simoneit, B. R. T. (1996). *Atmos. Environ.*, 30, 3837-3855.
- Fine, P. M., Cass, G. R. & Simoneit B. R. T. (2001). *Environ. Sci. Technol.*, 35, 2665-2675.
- Schauer, J. J., Kleeman, M. J., Cass, G. R. & Simoneit B. R. T. (2001). *Environ. Sci. Technol.*, 35, 1716-1728.

## Vegetative input to the Austrian PM<sub>10</sub>

P. Kotianová, A. Caseiro, I.L. Maar, H. Bauer and H. Puxbaum

Institute of Chemical Technologies and Analytics, Vienna University of Technology,  
Getreidemarkt 9/164-AC, A-1060 Vienna, Austria

Keywords: PM<sub>10</sub>, bioaerosol, cellulose, n-alkanes, urban areas.

It has been proven that primary biological aerosol particles (PBAPs) are a principal component among the variety of aerosol sources. PBAPs comprise material that originally derives from biological processes, such as pollen, spores, bacteria, viruses, and plant debris.

Cellulose, the main constituent of vegetative material, has been proposed as a specific molecular marker for plant debris. Green leaves contain around 50% cellulose in the dry mass, while pollen contained only 3-7% and production of cellulose by some bacteria is assumed to be negligible. Thus, the portion of the plant debris in the aerosol is proposed to be estimated by the following relation: “plant debris” = 2 \* cellulose (Puxbaum *et al.*, 2003).

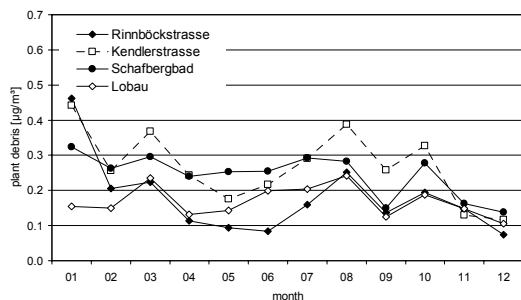


Figure 1. Monthly mean concentration of total cellulose at Vienna sampling sites in 2004.

Another class of compounds, n-alkanes, are in turn constituents of plant waxes, and have also been used to evaluate the contribution of vegetative detritus to PM<sub>10</sub>. However, other sources, such as automotive traffic, also account for the abundance of n-alkanes in the atmospheric aerosol. Through the use of the carbon preference index and plant wax number (% WNA), factors based on the concentrations of individual n-alkanes, it is possible to determine the biological fraction of n-alkanes (e.g. Lin *et al.*, 2004; Cheng *et al.*, 2006).

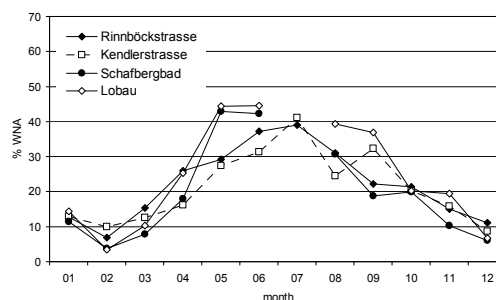


Figure 2. Monthly mean concentration of total cellulose at Vienna sampling sites in 2004.

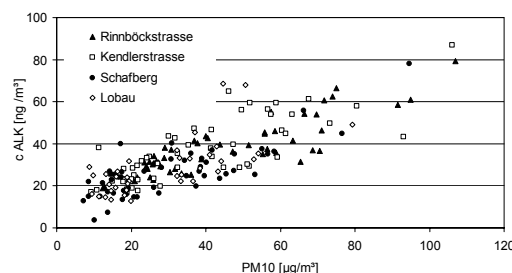


Figure 3. Total “plant wax” n-alkanes concentration versus PM<sub>10</sub> concentration in Vienna, 2004.

The aim of this study is to estimate input of vegetative detritus to PM<sub>10</sub> in three Austrian cities via known relationship between cellulose concentration and plant debris, characterize its contribution by CPI and %WNA numbers, as well as attempt to find a relation of n-alkanes to PM<sub>10</sub>.

The atmospheric aerosols were sampled at 10 sites, including urban, urban residential and background sites, within the AQUELLA projects framework for Vienna, Salzburg and Graz during the year 2004. Cellulose was determined using an enzymatic degradation method, followed by a photometrical measurement of the evolved glucose. n-Alkanes were determined by gas chromatography with a mass spectrometric detection.

Puxbaum, H. & Tenze-Kunit, M. (2003). *Atmos. Environ.*, 37, 3693-3699.

Lin, J. J. & Lee L.-Ch. (2004). *Atmos. Environ.*, 37, 3693-3699.

Cheng, Y., Lee S.-M., Leithead A. & Brook J. R. (2006). *Atmos. Environ.*, 40, 3693-3699.

## Speciation of semivolatile organics in the Veneto's bonfires aerosol

A. Latella<sup>1</sup>, L. Sperti<sup>2</sup>, E. Rampado<sup>3</sup> and A. Benassi<sup>1</sup>

<sup>1</sup>ARPAV (Veneto Region EPA) – Regional Air Observatory – Via Lissa, 6 – 30171 Mestre (Venice) – Italy

<sup>2</sup>Venice University – Chemistry Department – Dorsoduro 2137 – 30123 Venice

<sup>3</sup>Ente Zona Industriale di Porto Marghera – Via delle Industrie, 19 – 30175 Porto Marghera (Venice) - Italy

Keywords: biomass burning, PM10, DTD-GC-MS, SVOC

Direct Thermal Desorption (DTD) of PM samples hyphenated to gas chromatography – mass spectrometry (GC-MS) or comprehensive bidimensional gas chromatography Time Of Flight MS (GCxGC-TOF MS) have been proposed for the characterization studies of the particle-bound Semivolatile Organic Compounds (SVOC) (Waterman *et al.*, 2000; Falkovich *et al.*, 2001; Larsen *et al.* 2003; Hays *et al.*, 2003; Hays *et al.*, 2004) and the routine characterization of PM<sub>2,5</sub> on daily collected filters (Schnell-Kreis *et al.*, 2005).

An application is presented for this technique employing a filtering media (glass fiber) for PM that has not been conditioned thermally before sampling, adopting only the requirements of the current procedure for the gravimetric measurement of PM. Tentatively also samples of the glass fiber ribbon from PM10 analysers in the air quality monitoring network of the Ente Zona Industriale di Porto Marghera (Venice mainland industrial area) have been tested.

PM10 samples have been sequentially collected on a 4 hours basis (sample volume: 4 m<sup>3</sup>) starting from January 5 h00:00 for three days at an urban site in Mestre (Venice mainland). Automatic analysers collected 2 hours PM10 spots (sample volume: 4.6 m<sup>3</sup>) on their glass fiber ribbon starting from January 5 h12:00 for two days.

The major PM contributing source at the monitoring site is traffic. However its relevance decrease in the time series of collected filter as the chosen period of sampling include the Twelfth Night (eve of Epiphany, Jan 5-6 night) when thousands bonfires are lit in the Veneto Region at suburban and rural sites from evening to midnight. As reported for the U.K. bonfires (Harrison *et al.*, 1999; Farrar *et al.*, 2004) the air concentration of PM rised according to the widespread combustion sources, but the peculiar meteorological conditions (wind calm) induced a relevant pollution episode leading to a PM10 air concentration of 470 µg/m<sup>3</sup> between 00:00 and 04:00 January 6.

Aliquots of the collected PM10 filters (or ribbon) were thermally desorpted, without any preparation, directly to a gas chromatograph coupled with a quadrupole MS detector (DTD-GC-MS). The GC-MS chromatograms showed a rather complex pattern of SVOC according to the variety and different blend of raw materials used to build

and make up the bonfires, as well to the actual burning conditions of each of them. Selected ion traces (m/z) allowed an easy identification of several aliphatic homologues series (alkanes, esters, alkan-2-ones, alkenes), PAH(s), oxy-PAH(s), and thermal derivatives from terpenoids, lignin and vegetation waxes (Simoneit, 2002).

The results of the filters (4h sampling) are compared with those obtained from the PM spots on glass fiber ribbon sampled by the PM10 analysers of the survey network (2h sampling), allowing a better resolution of the different SVOC profile in the early traffic related samples and those collected during the bonfire flaming and smoldering phases. The the pros and cons of the technique as blank level of the DTD-GC introduction system and filtering media, lower and upper volatility range limits for the SVOC, and sensitivity will be discussed.

- Falkovich, A. H., & Rudich, Y. (2001). *Environ. Sci. Technol.* 2001,35, 2326–2333.
- Farrar, N. J., Smith, K. E. C., Lee, R. G. M., Thomas, G. O., Sweetman, A. J. & Jones, K. C. (2004). *Environ Sci. Technol.* 38, 1681-1685
- Harrison, R. M., Shi, J. P., & Jones, M.R. (1999). *Atmos. Environ.* 33, 1037–1047
- Hays, M. D., Smith, N. D.; Kinsey, J., Dong, Y. J. & Kariher, P. (2003). *J. Aerosol Science.* 34, 1061-1084.
- Hays, M. D., Smith, N. D. & Dong, Y. J. (2004). *J. Geophys. Res. Atmos.* 109, D14504.
- Larsen, R. K. & Baker, J. E. (2003). *Environ. Sci. Technol.* 2003, 37,1873–1881.
- Simoneit (2002), Simoneit, B. R. T., *Appl. Geochem.* 2002, 17, 129–162.
- Schnelle-Kreis J., Welthagen W. Sklorz M. & Zimmermann, R. (2005). *J. Separation Science*, 28, 1648–1657
- Waterman Waterman, D., Horsfield, B., Leistner, F., Hall & K., Smith, S. (2000). *Anal. Chem.* 2000, 72, 3563–3567.

## Exceptional urban air pollution episode from biomass burning

A. Latella, A. De Bortoli, G. Marson, E. Baraldo, P. Tieppo and A. Benassi

ARPAV (Veneto Region EPA) – Regional Air Observatory – Via Lissa, 6 – 30171 Mestre (Venice) - Italy

Keywords: biomass burning, SPAH(s), CPC, optical particle counter

On January 5, the eve of Epiphany, as usual in parts of Europe, a holiday is traditionally celebrated in the Veneto Region by lighting of bonfires in the countryside from evening to midnight.

A singular windless period settled just before the night of the last celebration (January 2007) and extreme bihourly PM10 concentration has been recorded at all the air quality monitoring stations within the Province of Venice (max 606  $\mu\text{g}/\text{m}^3$ ). The severe impact of the bonfires gave rise even to indoor pollution complaints in the Venice centre and mainland area, and as a consequence an average daily PM10 greater than 200  $\mu\text{g}/\text{m}^3$  lasted for days at many monitoring sites.

A description of the biomass burning aerosol properties monitored in Mestre (the densely populated Venice mainland), from the initial flaming phase to the overnight lasting smoldering of the bonfires, will be discussed with a fast time resolved (2 minutes) profiling of total Surface Polycyclic Aromatic Hydrocarbon concentration measured with a photoelectric aerosol sensor (SPAH(s) on particles with diameter in the 0.01-1  $\mu\text{m}$  range, Figure 1), particle number concentration (4nm – 3 $\mu\text{m}$ ) with a condensation particle counter (Figure 2.), and combustion gases CO, NOx, and O<sub>3</sub> with commercial standard analysers (Figure 1, 3)

Also the estimated PM mass concentration (five classes: PM1, PM2.5, PM7, PM10 and TSP) have been recorded, with the same time resolution, using an handheld optical particle counter (OPC, PM10 in Figure 2, PM1 in Figure 3). The commercial instrument has been custom upgraded with a sensor and heater to stabilise the relative humidity of the air sample before optical counting. The OPC PM10 values ranging in a wide interval from 13 to 770  $\mu\text{g}/\text{m}^3$ , averaged over a 4 hours period, have been adjusted to those obtained from gravimetric analysis of filter samples collected in parallel.

Gas chromatographic measurement of benzene and toluene were acquired every 30 minutes, however the time trend of the Volatile Organic Compounds (VOC) related to the biomass combustion event is evidenced by their positive interference in the nighttime O<sub>3</sub> values (Figure 3).

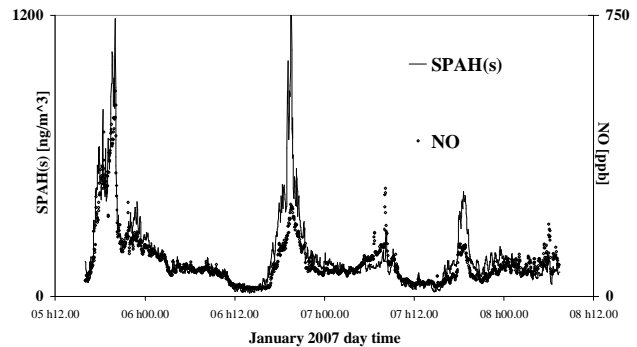


Figure 1. SPAH(s) and NO were always correlated.

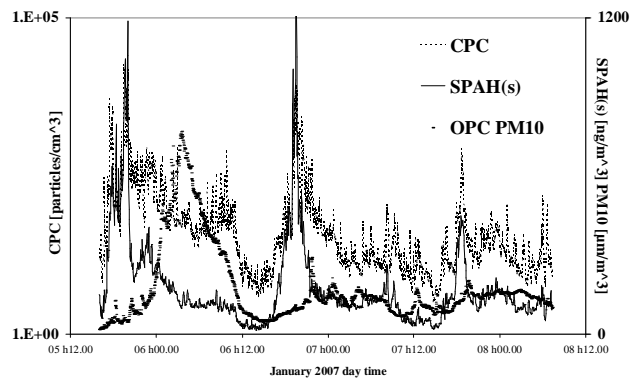


Figure 2. SPAH(s) concentration peaked at the flaming of the bonfire, the mass at the smoldering while particle number concentration decreased.

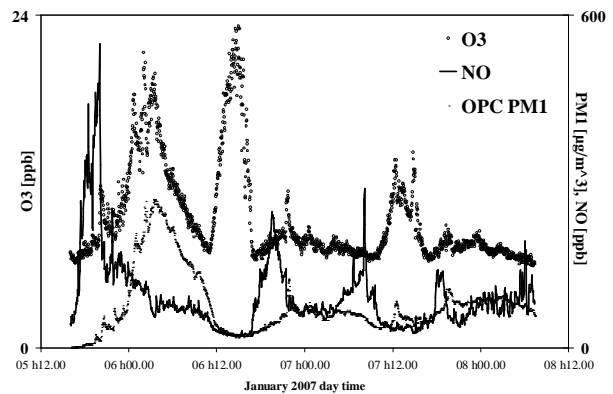


Figure 3. VOC related to the biomass burning event interfered with the O<sub>3</sub> measurement at 254 nm.

## Characterization of polycyclic aromatic hydrocarbons from different sources of urban areas in Germany

M.A. Bari<sup>1</sup>, G. Baumbach<sup>1</sup>, G. Scheffknecht<sup>1</sup>, B. Kuch<sup>2</sup>

<sup>1</sup> Institute of Process Engineering and Power Plant Technology, Department of Air Quality Control, Universitaet Stuttgart, Pfaffenwaldring 23, 70569 Stuttgart, Germany

<sup>2</sup> Institute of Sanitary Engineering, Water Quality and Solid Waste Management, Universitaet Stuttgart, Bandtaele 2, 70569 Stuttgart, Germany

Keywords: GC-MS, PM<sub>10</sub>, PAHs, vehicle emissions, wood burning.

The objectives of this study were to determine the particle phase polycyclic aromatic hydrocarbons (PAHs) concentrations as well as to characterize the major possible PAH emission sources in different urban areas of Germany. The PM<sub>10</sub> samplings were carried out from 1 November 2005 to 31 March 2006 in a residential site with low volume sampler. PAH samples collected on glass fibre filters were first extracted using toluene with ultrasonication and then analysed by GC-MS with Hewlett Packard 5890 Gas Chromatograph coupled with a HP 5971 Mass Selective Detector (MSD).

16 species specified by USEPA as priority pollutants which are naphthalene (Nap), acenaphthene (Ace), acenaphthylene (Acy), fluorene (Flu), phenanthrene (Phe), anthracene (Ant), fluoranthene (Fluo), pyrene (Py), chrysene (Chr), benzo[a]pyrene (BaP), benzo[a]anthracene (BaA), benzo[k]fluoranthene (BkF), benzo[b]fluoranthene (BbF), indeno[1,2,3-cd]pyrene (IP), dibenzo[a,h]-anthracene (DahA), benzo[ghi]perylene (BghiP) are considered for analysis. Additionally 5 species retene (Ret), benzo[j]fluoranthene (BjF), perylene (Pryl), triphenylene (Tpl) and benzo[e]pyrene (BeP) which were frequently used as reference PAH compounds are detected and quantified. The average value obtained for the sum of 21 PAHs in the 50 samples was 22.9 ng/m<sup>3</sup> where maximum value of 121.4 ng/m<sup>3</sup> and minimum value of 1.6 ng/m<sup>3</sup>. Daily levels of BaP, the most investigated PAH and often used as an indicator of total PAH, are in the range of 0.05 – 7.4 ng/m<sup>3</sup>. The average level of BaP over the winter period is 1.6 ng/m<sup>3</sup>.

In residential areas, where wood is frequently used for heating seasons, residential wood combustion is an important source for PAHs, mainly in winter. Figure 1 shows the comparison of relative average contribution of single PAH compounds to total PAHs for urban residential samples and for wood burning in the test facility. It can be seen that the compounds Fluo, Py, Ret, BaA, BjF, BeP, BaP and Pryl which were found in the ambient air show similar behaviour with the concentrations obtained from wood burning. The combustion derived PAHs (contributing 75% of total PAHs) and the carcinogenic compounds (contributing more than 45% of total PAHs) are highly pronounced in the

residential samples. The typical compounds for wood burning such as Ret, Fluo, Py, Ant, BaA, BaP, Chr (Ramdahl, 1983; Khalili et al., 1995; Marbach & Baumbach, 1998; Kulkarni & Venkataraman, 2000) show about 70% contribution whereas other compounds like BkF, BjF, BeP, IP and BghiP also show some proportions.

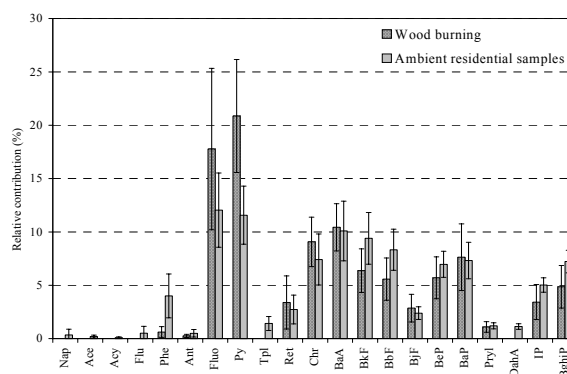


Figure 1. Relative average contribution of PAHs in urban residential and wood burning samples

To evaluate the chemical composition patterns as source fingerprints samplings were also carried out in oil burning source as well as urban traffic site. To investigate the sources of PAHs in ambient air, diagnostic analysis of ratios was developed. The results obtained from different ratios suggest that the major polluting sources in the residential area during winter were the burning of fuels like wood and oil, diesel and gasoline vehicles.

The authors would like to thank the institutes of Universitaet Stuttgart, for its material support for this work through a research project. Bari is receiving a doctoral grant from Baden-Wuerttemberg state. We would like to thank for this.

- Khalili, N. R., Scheff, P. A., Holsen, T. M. (1995). *Atmospheric Environment* 29, 533 – 542.  
Marbach, G., Baumbach, G. (1998). *Gefahrstoffe – Reinhaltung der Luft* 58, Nr.6, 257-261.  
Ramdahl, T. (1983). *Nature* 306, 580-582.  
Rogge, W. F., Hildemann, L., Mazurek, M. A., Cass, G. R., Simoneit, B. R. T. (1993a). *Environmental Science & Technology* 27, 636-651.

## Characterisation and size distribution of airborne particles in urban traffic and background sites at Stuttgart Neckartor

K.B. Ang<sup>1</sup>, G. Baumbach<sup>1</sup>, M.A. Bari<sup>1</sup>, G. Scheffknecht<sup>1</sup>, W. Dreher<sup>2</sup>, P. Pesch<sup>3</sup>

<sup>1</sup>Institute of Process Engineering and Power Plant Technology, Department of Air Quality Control, Universitaet Stuttgart, Pfaffenwaldring 23, 70569 Stuttgart, Germany

<sup>2</sup>Natural and Medical Science Institute at the University of Tuebingen, Markwiesenstraße 55, 72770 Reutlingen, Germany

<sup>3</sup>Landesanstalt für Umwelt, Messungen und Naturschutz Baden-Württemberg, 76231 Karlsruhe, Germany

Keywords: Cascade impactor, PM<sub>10</sub>, particle size distribution, SEM/EDX, vehicle emissions.

Traffic-induced particulate matter (PM) is an important contributor to ambient PM. At the traffic-impacted site of Stuttgart Neckartor, the 24h limit value of 50 µg/m<sup>3</sup> for PM<sub>10</sub> prescribed by the European legislation was exceeded 160 and 186 times in 2004 and 2005 respectively. In 2005, the PM<sub>10</sub> annual average value was 51 µg/m<sup>3</sup> which exceeded the limit value of 40 µg/m<sup>3</sup>. The problem with PM<sub>10</sub> exceedances at Neckartor arises predominantly in the months from January until April and September until December. A PM<sub>10</sub> seasonal pattern can also be observed, with highest concentrations in the winter months and lowest concentrations in the summer.

The contribution of traffic-related PM sources was previously determined by the computation of emissions' propagation from the surrounding PM<sub>10</sub> sources (UMEG 2005). The PM<sub>10</sub> contribution from traffic could also be determined from the differences of PM and its chemical components between the local influence of traffic on the adjacent street and the urban background station (Lenschow *et al.*, 2001). However, the emissions attributed from exhaust and abrasion could not be differentiated here. More detailed PM<sub>10</sub> source apportionment method could also be determined by chemical analyses of the PM<sub>10</sub> samples and followed by the factor analysis (Baumbach and Pfeiffer, 2004). However, this method is costly due to the required laboratory instrumentation and the final results are not always clear.

Thus, a novel method for investigating the characterisation and size distribution of airborne particles in high traffic and urban background areas in Stuttgart was developed. PM samplings were carried out from two sites by means of eight stage non-viable cascade impactors and PM<sub>10</sub> samplers in the city of Stuttgart from 12 January to 26 March 2006. The two sampling sites were characterised by different exposure to traffic emissions, enabling the assessment and comparison of PM concentration levels and particle size distributions between the traffic and urban background sites. After sampling, the morphology, composition and mineralogy of PM from the respective impactor stages were determined based on individual particle analysis with Scanning

Electron Microscopy (SEM) with an integrated Energy Dispersive X-ray analysis (EDX) system.

Three groups of potential PM sources could be identified from the results as shown in Figure 1. The PM coarse fraction from 2.1 to 10.0 µm was identified as resuspended road dust, the PM fraction from 0.7 to 2.1 µm as background and agglomerated particles with nitrogen and sulphur containing crystals, and the finer PM fraction smaller than 0.7 µm as agglomerated diesel soot particles with traces of sulphur. The presented results show that the method of the size-selective PM sampling coupled with the SEM/EDX analyses is suitable to determine the origin of the particles.

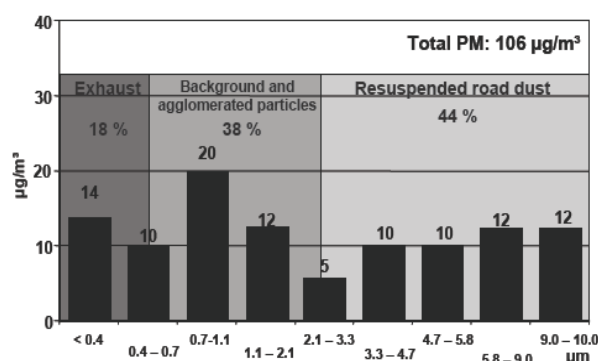


Figure 1. Average particle size distributions at Stuttgart Neckartor from 10 samplings during high PM<sub>10</sub> concentration (24 h PM<sub>10</sub> > 80 µg/m<sup>3</sup>)

The authors gratefully acknowledge the Ministry of Environment from the state of Baden-Wuerttemberg for funding this project.

Baumbach, G., Pfeiffer, H. (2004). *Final Report*, UNOPS project. Cyprus.

Lenschow, P., Abraham, H. J., Kutzner, K., Lutz, M., Preuss, J. D., Reichenbaecher, W. (2001). *Atmos. Environ.*, 35 (1), 23-33.

UMEG Zentrum für Umweltmessungen, Umwelterhebungen und Gerätesicherheit Baden-Württemberg. (2005). *Bericht Nr. 4-01/2005*. Karlsruhe.

## PM<sub>x</sub> mass and ionic composition of PM in the NW suburb of Prague in relation to meteorological conditions.

Jaroslav Schwarz<sup>1</sup>, Jiří Smolík<sup>1</sup>, Jan Hovorka<sup>2</sup>

<sup>1</sup>Institute of Chemical Process Fundamentals AS CR, Prague, Czech Republic  
<sup>2</sup>Charles University, Institute for Environmental Studies, Prague, Czech Republic

Keywords: urban aerosols, chemical composition, PM10.

To study atmospheric PM in Prague the measurement took place each third day from Feb 2004 till May 2005. The sampling site was located at northwest suburbs of 285 m ASL. Particles collection was provided by using PM<sub>10</sub>, PM<sub>2.5</sub> and PM<sub>1</sub> samplers and using Gent stack filter unit (SFU) described in Hopke et al. (1997). Meteorological data were provided by a meteo-station. We present our results from SFU as a sum of the results from both filters which gives PM<sub>10</sub> values. The SFU samples were analyzed for anion and cations using IC.

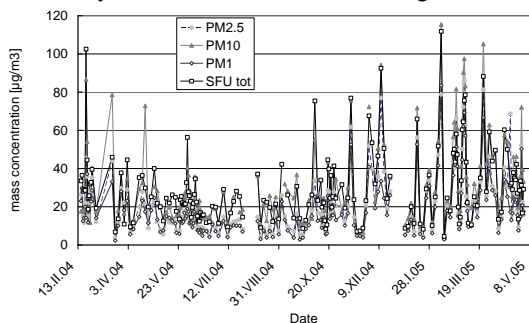


Fig.1: Time series of PM<sub>10</sub>, PM<sub>2.5</sub>, PM<sub>1</sub> and SFU<sub>TOT</sub>

The time series of PM<sub>10</sub>, PM<sub>2.5</sub>, PM<sub>1</sub> and SFU<sub>TOT</sub> are shown in the Fig.1. The data exhibits quite a bit of variability, and clear difference between colder and warmer period of the year. The average values for the whole period were 31.9±21.5 µg/m<sup>3</sup> (PM<sub>10</sub>), 29.0±18.6 µg/m<sup>3</sup> (SFU<sub>TOT</sub>), 21.1±16.4 µg/m<sup>3</sup> (PM<sub>2.5</sub>), and 17.6±13.6 µg/m<sup>3</sup> (PM<sub>1</sub>).

The average values of PM<sub>x</sub> and ions in PM<sub>10</sub> are shown in the Fig. 2 in dependence on average daily temperature (T<sub>av</sub>). This graph already shows many trends typical in Central Europe. All measured PM<sub>x</sub> fractions have highest concentration at the lowest temperatures. But then the trends are different for PM<sub>10</sub> comparing to PM<sub>2.5</sub> and PM<sub>1</sub>. While PM<sub>10</sub> was constant approximately for higher T<sub>av</sub>, the PM<sub>2.5</sub> and PM<sub>1</sub> were decreasing continuously with increasing T<sub>av</sub>. This also means an increasing importance of coarse (PM<sub>10</sub>-2.5) particles in PM<sub>10</sub> with increasing T<sub>av</sub>, probably due to lower average RH and possibly higher influence of primary biogenic particles during warmer season. In the opposite, snow cover in winter decreases resuspension of coarse particles. These effects correlate in temperature dependences of ions that are present mainly in coarse size fraction like Ca<sup>2+</sup> and Mg<sup>2+</sup>. Despite of partial decrease of PM<sub>10</sub>

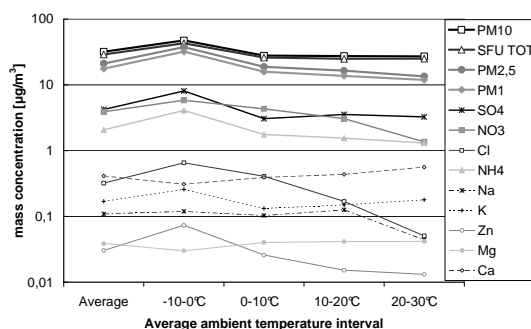


Fig. 2: Average concentration of PM<sub>x</sub> and ions in PM<sub>10</sub> for different temperature levels

mass with increasing T<sub>av</sub>, Ca<sup>2+</sup> and Mg<sup>2+</sup> ions have an opposite trend. Main ions - SO<sub>4</sub><sup>2-</sup>, NO<sub>3</sub><sup>-</sup> and NH<sub>4</sub><sup>+</sup> have their maximum at lowest T<sub>av</sub>, but their behavior differs for higher T<sub>av</sub>. While NH<sub>4</sub><sup>+</sup> copies behavior of fine fractions, SO<sub>4</sub><sup>2-</sup> is not decreasing further with increasing T<sub>av</sub>. The higher rate of photochemical production of SO<sub>4</sub><sup>2-</sup> at higher temperature is probable reason. We could even speculate about influence of natural production of dimethyl sulfide in the Atlantic Ocean, because of the local maximum of sulphates for T<sub>av</sub> between 10 and 20°C which coincides with local maximum of sodium, and those mild temperatures are often connected with westerly air mass trajectories.

The fate of NO<sub>3</sub><sup>-</sup> reflects its thermodynamic behavior. At the lowest T<sub>av</sub> when enough of sulfuric acid is available due to intensive local coal combustion, the NO<sub>3</sub><sup>-</sup> are partially depleted and dissociation of ammonium nitrate caused their depletion at the highest temperature above 25°C. K<sup>+</sup> behavior can be explained by biomass combustion. during cold days for heating, during warmest days barbecues and garden fires are the K<sup>+</sup> sources. Both Cl<sup>-</sup> and Zn<sup>2+</sup> are strongly inversely proportional on T<sub>av</sub>. Combustion sources are probable the most important for them, due to much lower than expected ratio Na<sup>+</sup>/Cl<sup>-</sup> during cold days.

The support by grant and Ministry of Environment CR No. VaV-SM/9/86/05 is gratefully acknowledged

Hopke, P.K., Xie, Y., Raunemaa, T., Biegalski, S., Landsberger, S., Maenhaut, W., Artaxo, P., Cohen, D., 1997, *Aerosol Sci. and Technol.*, 27, 726–735.

## Effectiveness of street cleaning for reducing ambient PM10 concentrations

A.C. John<sup>1</sup>, A. Hugo<sup>1</sup>, H. Kaminski<sup>1</sup>, A. Brandt<sup>2</sup>, W. Kappert<sup>2</sup>, E. Falkenberg<sup>2</sup>, T.A.J. Kuhlbusch<sup>1</sup>

<sup>1</sup>IUTA e. V., Bliersheimer Strasse 60, 45229 Duisburg, Germany

<sup>2</sup>LANUV NRW, 45023 Essen, Germany

Keywords: traffic emissions, PMx reduction, abatement strategies, street sweeping.

### Introduction

Exceedences of the PM10 limit values set by the EU are frequent at urban traffic hot spots, especially in street canyons\*. As street cleaning is discussed as a method to reduce ambient PMx concentrations in cities, a research project was initiated to evaluate its effectiveness.

### Methods

Street cleaning by high pressure watering was carried out from 03/08/04 until 19/09/05 in the Corneliusstrasse (4 lane main road, ca. 40.000 cars/day, street canyon) in Düsseldorf, Germany. Cleaning was carried out in the early morning hours, once a week until March 2005, then daily and from June 2005 twice per week.

PM10 concentrations were measured simultaneously at the site "Düsseldorf Corneliusstrasse" (DDCS/DENW082) of the North Rhine-Westphalian Air Quality Monitoring Network. Data of other traffic and urban monitoring sites in Düsseldorf were used for comparison and to correct for changes in meteorological conditions and DTV e.g. during holiday seasons.

### Results and Discussion

Different methods of data analyses showed reductions of ambient air PM10 concentrations on street cleaning days between 0,6 µg/m<sup>3</sup> and 5,8 µg/m<sup>3</sup> compared to non-cleaning days.

On average, the reduction of the daily mean PM10 concentration was 1,8 µg/m<sup>3</sup> per cleaning day, taking into account all days with and without precipitation. When only days without precipitation are considered, the average reduction was 2,9 µg/m<sup>3</sup>. This larger reduction potential for PM10 ambient air concentrations by street cleaning on "dry" days compared to "dry" and rainy days is important especially considering a cost/benefit analysis, as each cleaning of the Corneliusstrasse (length: 1,6 km) adds up to 460 € to 1.650 € depending on the amount of water used per m<sup>2</sup>.

Considering the effectiveness of street cleaning with respect to the PM10 yearly and daily limit values, a reduction of 1,8 µg/m<sup>3</sup> per cleaning day corresponds to a reduction of the yearly average of ca. 0,3 µg/m<sup>3</sup> for cleaning once per week and of ca. 0,5 µg/m<sup>3</sup> for cleaning twice per week.

With regard to the daily limit value of 50 µg/m<sup>3</sup>, figure 1 shows the distribution of PM10 in concentration classes of 1 µg/m<sup>3</sup>.

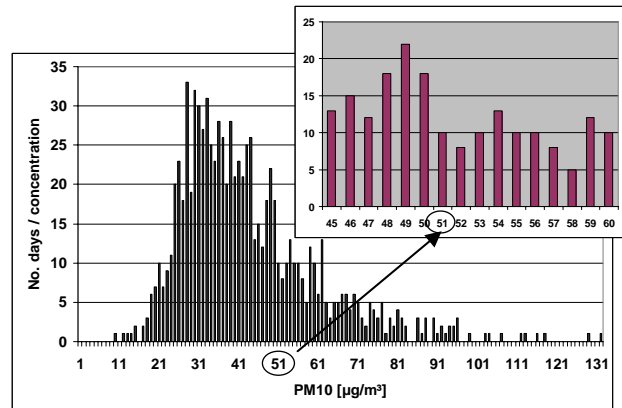


Figure 1: Number of days per PM10 concentrations for the Corneliusstrasse, Düsseldorf, 01/01/03-19/09/05.

About 6 % of the exceedences of the PM10 daily limit value could have been avoided assuming an average reduction of 1,8 µg/m<sup>3</sup> (ca. 9% for a reduction of 2,9 µg/m<sup>3</sup> on dry days). As these exceedence days are more or less evenly distributed over the days of the week, the effective reduction of daily limit value exceedences will be lower when routine cleaning (1-2x per week) is done. Additional street cleaning could be carried out when limit value exceedences are predicted.

A reduction of the daily PM10 average of about 2 µg/m<sup>3</sup> by street cleaning is quite effective being only a single action. However, this reduction is only achieved for a limited area, which has to be taken into account when evaluating different abatement strategies.

### Further Information

Together with detailed results from the street cleaning investigations, information on related aspects such as use of different water qualities, use of surfactants and different street cleaning technologies will be given in the presentation.

### Acknowledgement

This work was supported by the Environmental State Agency of North Rhine Westphalia (LUA NRW), now: North Rhine Westphalia State Agency for Nature, Environment and Consumer Protection (LANUV).

\* Corneliusstrasse: 83 days > 50 µg/m<sup>3</sup> and 41 µg/m<sup>3</sup> yearly average (2004); 69 days > 50 µg/m<sup>3</sup> and 38 µg/m<sup>3</sup> yearly average (2005)

## Non-exhaust PM emission from highway traffic

A.C. John<sup>1</sup>, U. Quass<sup>1</sup>, J. Lindermann<sup>1</sup>, M. Beyer<sup>1</sup>  
 M. & M. Sulkowski<sup>2</sup>, A.V. Hirner<sup>2</sup>, A. Baum<sup>3</sup>, T.A.J. Kuhlbusch<sup>1</sup>  
<sup>1</sup>IUTA e. V., Bliersheimer Straße 60, 45229 Duisburg, Germany

<sup>2</sup>University of Duisburg-Essen, Institute of Environmental Analytical Chemistry, Essen, Germany

<sup>3</sup>Federal Highway Research Institute (BASt), Brüderstraße 53, 51427 Bergisch-Gladbach

Keywords: emission factor, traffic, resuspension, PM10/PM1, chemical composition

### Introduction

A large uncertainty still exists with regard to non-exhaust PM emissions of traffic (tyre and brake wear, resuspension, street abrasion) and their contribution to PM concentrations close to roads. The uncertainty is even larger for roads outside urban areas and highways. Hence, a source apportionment study was initiated in order to gain further insights.

### Methods

Simultaneous upwind/downwind measurements of PM<sub>10</sub> and PM<sub>1</sub> (gravimetric and by TEOM), NO, NO<sub>2</sub>, NO<sub>x</sub>, traffic density and speed (separately for passenger cars and HDVs) as well as meteorological parameters were carried out at a four-lane highway (no speed limit) for several months (09/05-03/06, 06/06-12/06). NO<sub>x</sub> concentrations and wind directions were used to identify 72 days with upwind/downwind characteristics for further chemical analyses. This data subset is also used for the evaluations presented here.

### First results

The distribution of gravimetric mass concentrations (24h averages) of PM<sub>10</sub>, PM<sub>1</sub>, coarse particles (PM<sub>10</sub>-PM<sub>1</sub>) and their upwind/downwind differences are shown in the upper part of Figure 1. For the same set of sampling days the corresponding daily averages for NO and NO<sub>2</sub> are presented in the lower part. Both graphs show box-whisker plots with minimum/maximum values (whiskers), 10-, 90-percentiles (box) and median (bar). The traffic density (sum of both directions) ranged from ca. 30,000 to ca. 80,000 vehicles/day, with heavy duty vehicles representing 28% (median).

### Discussion

Downwind concentrations generally exceeded upwind values, thus indicating traffic induced PM<sub>x</sub> and NO<sub>x</sub> contributions.

The results compare reasonably well to values reported by Gehrig et. al. (2003) for similar investigations at two different sites<sup>1</sup> with however somewhat lower traffic densities. The concentration increments make up ca. 23%, 26% and 11% (median ratios) of the upwind levels for PM<sub>10</sub>, PM<sub>1</sub> and coarse particles, resp.. About 70% of the PM<sub>10</sub> increment is covered by PM<sub>1</sub>. Assuming that PM<sub>1</sub> contributions

are attributed to exhaust particles, non-exhaust emissions add about 1-2 µg/m<sup>3</sup> to the PM<sub>10</sub> concentrations downwind..

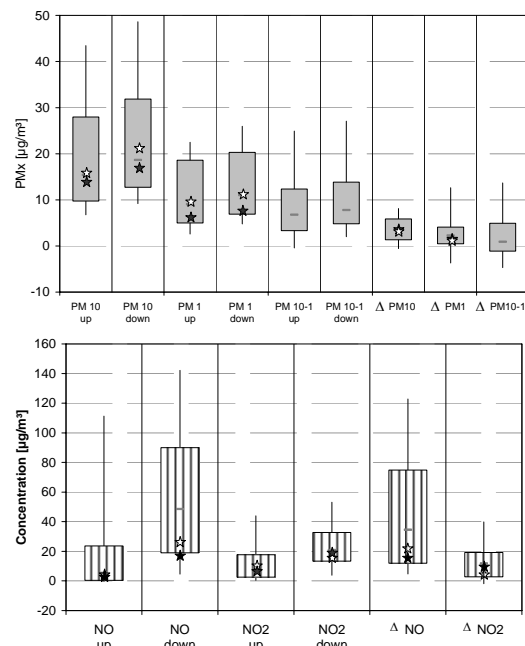


Figure 1. Box-whisker plots of measured PM<sub>x</sub> (upper graph) and NO/NO<sub>2</sub> concentrations (lower graph). Asterisks: values reported by Gehrig et al. (2003) for two different sites

### Further analyses

The filter samples were chemically analysed for 15 metals, 3 anions, ammonium and elemental/organic carbon. These parameters and the time resolved measurements are used for source apportionment studies with uni- and multivariate statistical methods. This statistical analysis is specifically focussed on separating non-exhaust PM contributions by traffic. Emission factors (EFs) for the PM fractions and identified source processes will be calculated by the NO<sub>x</sub> dilution factor approach.

### Acknowledgement

This work was financed by the Federal Highway Research Institute (BASt), Bergisch-Gladbach.

### References

Gehrig, R., Hill, M., Buchmann, B. Imhof, D. Weingartner, E. Baltensperger, U. (2003). *Report ASTRA 2000/415*

<sup>1</sup> Humlikon (highway/freeway with speed limits 100/80 km/h) and Birrhard (highway, speed limit 100 km/h)

## Gradients of PM10 mass concentrations analysed for major German conurbation areas

U. Quass<sup>1</sup>, U. Rating<sup>1</sup>, A. Hugo<sup>1</sup>, and T.A.J. Kuhlbusch<sup>1</sup>

<sup>1</sup>IUTA e.V., Bliersheimer Straße 60, 45229 Duisburg, Germany

Keywords: air pollution, monitoring, PM10, urban areas, hot-spots

An evaluation of the spatial variations observable for PM10 mass concentrations in the area of nine major German conurbations<sup>1</sup> was conducted for the years 2003-2005.

### Data base

As far as possible for two measurement sites per area type [regional (=least influenced by local sources), rural (= influenced by local, mainly agricultural activities), urban background, urban traffic, and industrially influenced sites] were selected per agglomeration area. Time resolved measurement data for the years 2003 to 2005 provided by the German Environmental Agency (UBA) from the selected sites were used. Overall, 17 (regional and rural background), 18 (urban background and traffic) and 3 (industry) sites were used in this study.

### Results

Average weekly variations were calculated for each site, then 24h-averages calculated per site type. (Figure 1, left graph). Separate averages for working (Mo-Fri) and weekend (Sa-Su) days were also computed (Figure 1, right graph).

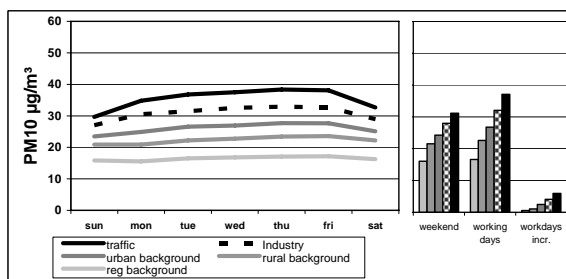


Figure 1. Average weekly variation of PM10 mass concentrations at different types of sites.

The variability of the PM10 concentrations in dependence of day and site type was also investigated. The results based on average weekly variations (per calendar year) are shown in Figure 2 as box-plots indicating minimum, 25-,50-,75-percentiles and maximum concentration values found.

### Discussion

Apparently, the differences between weekend and working days become more pronounced with increasing PM10 levels.

Average working day increments range from ca. 0.5 - 6 µg/m<sup>3</sup> for regional background and traffic sites,

resp. This increment increases to ~8 µg/m<sup>3</sup> if only Sundays are considered as weekend days.

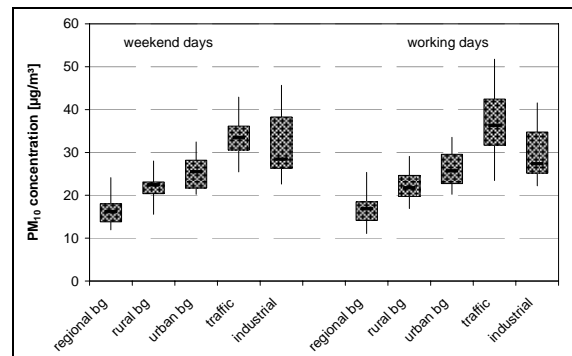


Figure 2.Box-plot showing the variability of PM10 mass concentrations for different site types, compared for weekend and working days

The expected gradients between remote sites and urban hot-spots could be verified for nearly all agglomeration regions investigated, except for one case with PM10 at the rural exceeding those measured at the urban background site. The PM10 increment from one site type to the next more polluted one is generally about 5 µg/m<sup>3</sup>, in case of traffic hot spots ca. twice that value. However, the increments for the three industrial sites included in the study are less pronounced.

The traffic-urban increment contributes by ca. 22% on weekends and ca. 28% on workdays to the PM10 concentrations found at traffic sites. This is complemented by the contributions from regional (48/42%), rural (18/16%) and urban (12/14%) background. These relations do not significantly vary between the considered years.

### Conclusion

Analysis of time resolved air quality measurement data from the German Länder networks proves that PM10 concentrations in the areas of various urban agglomerations exhibit common features regarding the weekly pattern and spatial profile. From these results the possibilities and the limitations for reducing exposure to particulate matter by local measures can be inferred.

### Outlook

PM10 chemical composition data available from Germany will be used to obtain information on the spatial gradients of main chemical compounds.

### Acknowledgement

This work was partly supported by the German Federal Environment Agency (FKZ 360 11 007)

<sup>1</sup> Berlin, Bremen, Frankfurt, Hannover/ Braunschweig, Hamburg, Leipzig/Dresden, Ludwigshafen/Mannheim, Munich, Ruhr-Area

### Magnetic measurements of PM10 and their potential for monitoring environmental stress

E. Petrovský<sup>1</sup>, B. Kotlík<sup>2</sup>, R. Zbořil<sup>3</sup>, J. Novák<sup>4</sup>, A. Kapička<sup>1</sup> and H. Fialová<sup>1</sup>

<sup>1</sup>Institute of Geophysics ASCR, Boční II/1401, 141 31 Praha 4, Czech Republic

<sup>2</sup>National Institute of Public Health, Šrobárova 48, 100 42 Praha 10, Czech Republic

<sup>3</sup>Center for Nanomaterial Research, Palacký University, Šlechtitelů 11, 783 71 Olomouc, Czech Republic

<sup>4</sup>Czech Hydrometeorological Institute, Na Šabatce 17, 143 06 Praha 4, Czech Republic

Keywords: PM10, monitoring, physical properties, magnetic properties, Fe-oxides.

Atmospheric particulate matter of anthropogenic origin contains significant portion of minerals with pronounced ferrimagnetic properties. These minerals, mostly iron oxides, can serve as tracers of industrial pollutants at the sites of PM10 collection and the neighbouring soils. Quite often, significant correlation can be found between magnetic parameters reflecting concentration of these particles (namely saturation magnetization and magnetic susceptibility) and concentration of heavy metals (e.g., Pb, Zn, Cd, etc.). This relationship has no general validity and is site-characteristic. Despite that, once determined, fast and cheap magnetic measurements can help in assessing the concentration of heavy metals and thus in monitoring the environmental stress at different sites. In our study, we have investigated PM10 collected in different periods of a year at sites characterized by various environmental circumstances (industrial, traffic, urban, urban background and regional background).

In this contribution, we will show and discuss regional variations in magnetic parameters, characterizing concentration of magnetic fraction of PM10, and those parameters related to grain-size distribution. For instance, our results clearly show that PM10 at the industrial site has constant mineralogy and grain-size distribution in different periods of a year (Figure 1), determined by constant composition of the pollutants emitted in the atmosphere from the close sources. Contrary to that, PM10 from urban and regional background sites can be clearly distinguished from the particles collected at the industrial site (Figure 1).

This work is supported by the Grant Agency of the Academy of Sciences of the Czech Republic under grant A300120606.

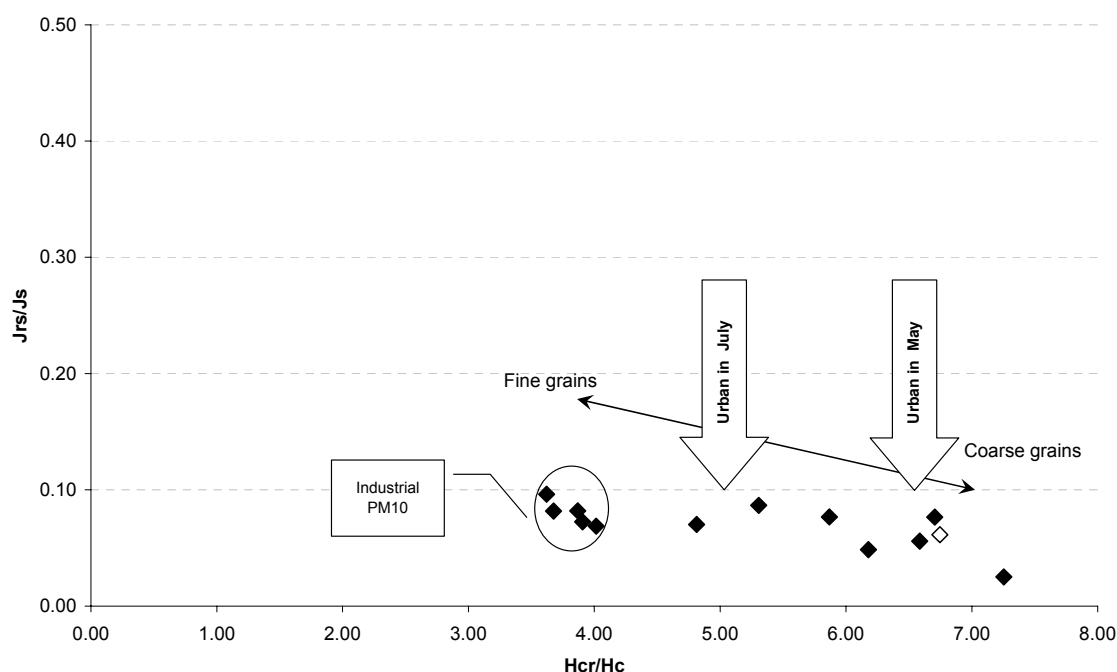


Figure 1. Combination of magnetic parameters, related to grain-size distribution, in a “Day plot”. PM10 from industrial site shows constant composition and grain-size distribution. Urban particles indicate trend towards finer grains in summer time compared to spring and autumn.

## HULIS over Vienna: investigations into water and alkaline extractable Humic Like Substances in airborne particulate matter

B.Klatzer, H.Bauer I.L.Marr and H.Puxbaum

Institute of Chemical Technologies and Analytics, Vienna University of Technology, Getreidemarkt 9/164, A 1060 Vienna, Austria

Keywords: Atmospheric aerosols, biomass burning, organic aerosols, PM10

As ambient aerosol plays an important role in atmospheric processes like cloud condensation, and is affecting the global radiation balance due to its light absorbing and scattering properties, great interest is focused on aerosol composition and formation mechanisms. Although organic material contributes up to 50 % to the total aerosol mass, only a small part is resolved on a molecular level. However, water-soluble materials of higher molecular weight, termed Humic Like Substances due to chemical similarities with soil extractables, are shown to account for often 10 % of the PM. (Havers et al. 1998). Two suggested precursors for HULIS are trimethylbenzene (Kalberer et al. 2004) and isoprene (Limbeck et al. 2003) which are of anthropogenic and biogenic origin, respectively. Polymerisation may take place in the gas phase, or, heterogeneously on particle surfaces. Biomass burning is known to be also a source for HULIS.

HULIS is determined by a two-step isolation procedure followed by measurement of HULIS carbon with a TOC analyser (Limbeck, 2005). An SPE step assures the removal of inorganic ions and organic hydrophilic compounds, while an ion-exchange step removes mono- and dicarboxylic acids. Aerosol samples on quartz fibre filters are extracted first with ultrapure water and then with dilute alkali. The latter should help to differentiate the HULIS fraction with more hydrophobic and more acidic character and higher molecular weight.

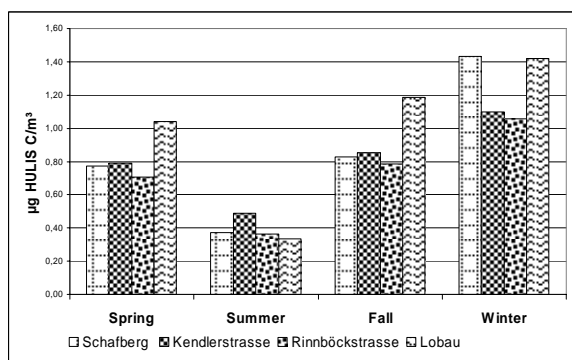


Fig. 1. Seasonal averaged (n=6-23) total HULIS concentrations for four Viennese sampling sites 2004

Figure 1 shows winter enrichment for HULIS by a factor of more than two for the urban sites and a factor of four for the urban fringe sites. This winter

enrichment would be in accordance with the observation that biomass burning is a major source for HULIS. The summer source could be secondary aerosol formation from biogenic and/or anthropogenic precursors. High concentrations at the fringe sites, even in winter, might be due to local biogenic sources.

Resolving the total HULIS into aqueous and alkaline soluble fractions, reveals a trend to higher contributions from the alkaline fractions at periods of higher PM10 loadings, seen in Fig. 2 for an urban site in January 2004.

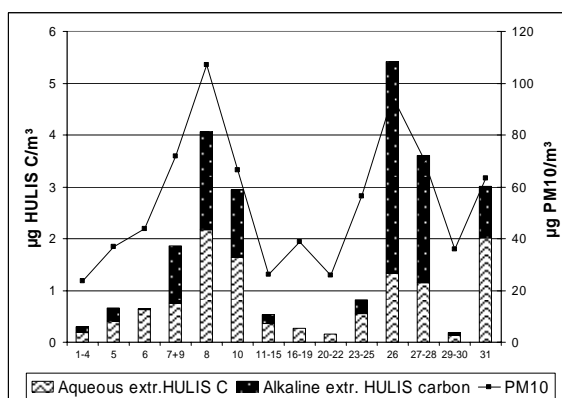


Fig.2. Urban aqueous and alkaline extracted HULIS carbon and PM10, January 2004

Elevated levels of the higher-molecular weight more acidic fraction appear to be associated with episodes of higher PM10 burdens. Thus, formation of HULIS on particle surfaces, rather than in the gas phase (which would predominate in clean air), might be responsible for this alkali extract fraction. These findings do confirm the idea that there are different sources for HULIS.

Havers N., Burba P., Lambert J., and Klockow D., (1998), *J.Atmos.Chem*, 29(1), 45-54.

Kalberer, M., Paulsen D., Sax M., Steinbacher M., Dommen J., Prevot A., Fisseha R., Weingartner E., Zenobi R. and Baltensperger U., (2004), *Science*, 303, 1659 – 1662.

Limbeck A., Kulmala M., and Puxbaum H., (2003) *Geophys.Res.Lett.* 30 (19)

Limbeck, A., Handler M., Neuberger B, Klatzer B. and H. Puxbaum, (2005) *Analytical Chemistry* 77(22), 7288-7293.

## A Novel Sampler for Large Particles

Sang-Rin Lee<sup>1</sup>, Suresh Dhaniyala<sup>2</sup> and Thomas M Holsen<sup>1</sup>

<sup>1</sup>Department of Civil & Environmental Engineering, Clarkson University, NY, 13699, Potsdam, USA

<sup>2</sup>Department of Mechanical and Aeronautical Engineering, Clarkson University, NY, 13699, Potsdam, USA

Keywords: Large particle inlet, inlet efficiency, PM

### INTRODUCTION

Large particles (greater than 10  $\mu\text{m}$ ) play an important role in pollutant cycling (deposition and resuspension) in the environment (Odabasi et al., 1999; Holsen et al., 1991; Eisenreich, 1999), because of their large deposition velocities. Also, in the study of cloud properties, particle sizes of interest are large compared to typical particles of interest in health-based studies. Instruments for aerosol analysis have, however, largely focused on analysis of PM10 particles and are not suitable for large particle studies. There is, therefore, an urgent need to develop an instrument to effectively sample and analyze large particles.

In this study, the design of a novel Inlet for accurate sampling of particles larger than 10  $\mu\text{m}$  (PM<sub>10</sub>) is presented. This inlet, called the Large Particle Inlet (LPI), is designed for sampling over a large range of wind velocities, and independent of wind direction. LPI is designed using Computational Fluid Dynamics (CFD) modeling, considering the importance of different geometry and operating parameters on the inlet performance. The inlet performance is tested in a aerosol wind-tunnel facility.

### DESIGN

A thin wall upward facing (vertical) inlet is used in many commercialized samplers in part because they do not require rotating parts and are easy to operate. However, this inlet cannot sample large particles efficiently. A novel LPI design has a upward facing, funnel type inlet with elliptically tapered inner wall and a top lid. The schematic drawing of the novel LPI is shown in Figure 1. The top lid in the LPI prevents rain drops and snow from entering the sample stream and also reduces sampling bias caused by the fast settling velocity of large particles. LPI entrance is same as the slot opening. Inlet efficiency as function of its geometry, operating parameters and the ambient wind conditions were investigated.

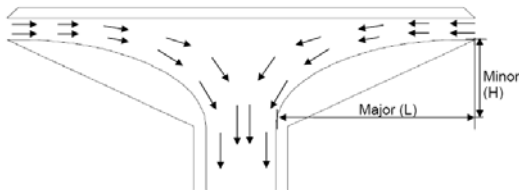


Figure 1 schematic drawing of LPI

### MODELING

The commercial CFD software FLUENT (Fluent Inc, NH) was used to model the flow and particle

trajectories in the LPI and wind tunnel. Three-dimensional, turbulent modeling was used to obtain the inlet performance considering typical sampling conditions.

### RESULTS AND DISCUSSION

LPI performance was investigated based on its geometry and operating conditions. Several types of elliptical tapering were applied and the results suggest that an inlet with 8cm major and 4 cm minor axis lengths had the best performance. One advantage of funnel type slot opening is counterflow effect. Since LPI samples air from all directions, particles entering the inlet along with the wind direction are turned into the inlet with the opposing force provided by the counterflowing sample stream. The extent of counterflow effect depends on the slot height, sampling flowrate and ambient wind velocity.

As shown in Figure 2, 1cm slot opening LPI can sample around 40% of 50 $\mu\text{m}$  at wind speed as fast as 7m/s. Noone et al (1992) used similar tapered inlet as ours but they showed inlet efficiency of 30  $\mu\text{m}$  was less than 10% at wind speed 4.9m/s. A novel LPI can sample particles as large as 100 $\mu\text{m}$  in low wind speeds, a significant improvement over existing designs.

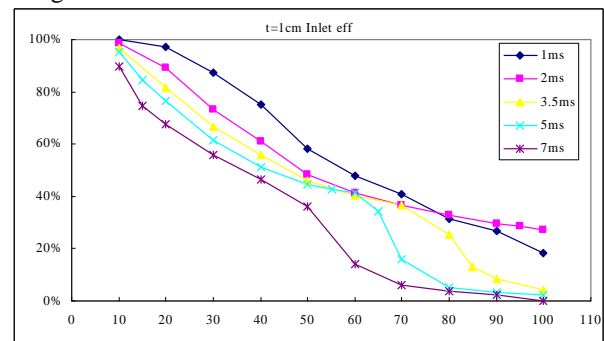


Figure 2 Inlet efficiency of LPI as function of particle size and wind speed

LPI performance was also evaluated in an aerosol wind tunnel at Clarkson University. Preliminary result with coarse Arizona road dust validated the prediction that LPI could sample large particles.

This project is supported by NSF (BES- 0521137).

### REFERENCES

- Eisenreich, S.J.,(1999), *Epidemiology* 10(4).
- Holsen et al.,(1991), *Env. Sci. Tech.*, 25, 1075-1081.
- Odabasi, et al., (1999), *Env. Sci. Tech.* 33, 426-434.
- Noone, K.J. et al., (1992), *J. Aer. Sci.*, 23, 153-164

## Mobile laboratory measurements of PM<sub>9</sub> and PM<sub>2.5</sub> in Helsinki, Finland

L. Pirjola<sup>1,2</sup>, K. Kupiainen<sup>3,4</sup> and H. Tervahattu<sup>3</sup>

<sup>1</sup> Department of Technology, Helsinki Polytechnic, P.O. Box 4020, FIN-00099 Helsinki, Finland

<sup>2</sup> Department of Physical Sciences, University of Helsinki, P.O. Box 64, FIN-00014 Helsinki, Finland

<sup>3</sup> Nordic Envicon Oy, Koetilantie 3, FIN-00790 Helsinki, Finland.

<sup>4</sup> Department of Biological and Environmental Sciences, University of Helsinki, P.O. Box 56, FIN-00014 University of Helsinki

Keywords: instrumentation, vehicles emissions, emission factor, mineral dust, resuspension.

Recent toxicological and epidemiological studies have associated high particulate concentrations (PM) in urban air with increased morbidity such as respiratory symptoms, lung cancer and cardiovascular diseases, and with increased mortality (e.g. Pope et al., 2002). Also recently reported is epidemiological evidence of effects of coarse non-exhaust airborne particles on health (Brunekreef and Forsberg, 2005). In Northern areas, e.g., in Scandinavia, street dust levels are especially high during spring due to the use of antiskid methods, like street sanding and studded tires.

The mobile laboratory SNIFFER was first developed to measure traffic emissions under real driving conditions as well as exhaust emissions of an individual vehicle with the chasing method (Pirjola et al., 2004; Rönkkö et al., 2006). The measurement set up was later extended to include also measurements of non-exhaust particles.

Dust sample is sucked from behind the left tire through a conical inlet into a vertical tube with a flow rate of 1600 lpm. The objective of the sampling was to catch most of the particles in the plume originated from the tire and road interaction.

A sampling air branch-off was constructed into particle mass monitors TEOM (Tapered Element Oscillating Microbalance) and ELPI (Electrical Low Pressure Impactor). TEOM collects isokinetically particles smaller than 9.2 µm, due to a cutoff of the used sampling cyclone, with a time resolution of 10 s. ELPI measures real time particle number concentration and size distribution (1 s time resolution). In this work we have eliminated the mass concentration of exhaust particles and calculated PM<sub>2.5</sub>-PM<sub>0.6</sub> by assuming particle density of 2000 kg m<sup>-3</sup>. Another ELPI sampling in front of the van is used to measure background PM<sub>2.5</sub>.

To evaluate the average road dust PM<sub>9</sub> emission factor (g km<sup>-1</sup>) for SNIFFER we performed flux tower measurements based on an upwind/downwind technique presented by e.g. Gertler et al. (2000). The measurements were performed on an asphalt field closed by other traffic in Helsinki. SNIFFER was passing the tower with the speed of 30 and 50 km h<sup>-1</sup>; the measurements were performed at different heights at the tower. On the other hand, the instrumented SNIFFER was driving the same lane

with a constant speed of 30 km h<sup>-1</sup> or 50 km h<sup>-1</sup>. From these measurements the SNIFFER signal was converted to emission factor (g km<sup>-1</sup>). As a result, the ratio of the PM<sub>9</sub> emission factor and SNIFFER signal was found to be around 0.39 (mg km<sup>-1</sup>/µg m<sup>-3</sup>).

The city route measurements were conducted in Helsinki during springtime in 2005-2006 before, during and after street cleaning activities on a route located in urban area. Figure 1 shows the average PM-concentrations over the whole route in 2006. PM<sub>2.5</sub> is 13-28% of PM<sub>9</sub> (Pirjola et al., 2007). The results show clear decreasing trend, however, high concentrations after street cleaning were observed.

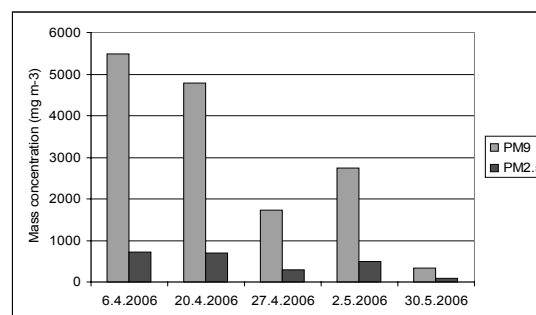


Figure 1. Average springtime PM concentrations over the Helsinki city route measured by SNIFFER.

This work was supported by the National Technology Agency of Finland (TEKES).

Brunekreef, B. and Forsberg, B. (2005). *European Respiratory Journal*, 26, 309-318.

Gertler, A.W., Gillies, J.A., Pierson, W.R. (2000). *Water Air and Soil Pollution* 123, 203-214.

Pirjola, L., Parviainen, H., Hussein, T., Valli, A., Hämeri, K., Aalto, P., Virtanen, A., Keskinen, J., Pakkanen, T., Mäkelä, T., Hillamo, R. (2004) *Atmos. Environ.*, 38, 3625-3635.

Pirjola, L., Perhoniemi, P., Kupiainen, K., Tervahattu, H., Vesala, H. (2007). Submitted to *Environ. Sci. and Technol.*

Pope III CA, Burnett RT, Thun MJ, Calle EE, Krewski D, Ito K, Thurnston GD. (2002). *American Medical Association* 287, 1132-40.

Rönkkö, T., Virtanen, A., Vaaraslahti, K., Keskinen, J., Pirjola, L., Lappi, M. (2006) *Atmos. Environ.* 40, 2893-2901.

## Characterization of traffic and by scanning electron microscopy

K. Slezakova<sup>1</sup>, M.C. Pereira<sup>1</sup>, J.C.M. Pires<sup>1</sup> and M.C. Alvim-Ferraz<sup>1</sup>

<sup>1</sup> EPAE, Faculdade de Engenharia, Universidade do Porto, Rua Dr. R. Frias, 4200-46, Porto, Portugal

Keywords: PM<sub>10</sub>, PM<sub>2.5</sub>, traffic, SEM.

Air pollution particulates currently present a serious risk to human health. Up to this date, most of the epidemiological studies researched particulate matter (PM) in relation to size of particles, as it seemed that size is the most health influencing factor. However, other parameters as chemical composition or morphology of particles have also an important role in possible health effects and one of the recent studies suggests that health effects may be related more to PM specific components rather than PM mass (Ghio & Devlin, 2001). Considering the relevance of that knowledge, for a further evaluation of the influence of traffic emissions on public health, this work included PM<sub>10</sub> and PM<sub>2.5</sub> characterization, with the specific objective to study the influence of traffic emissions on the morphology and elemental composition of PM<sub>10</sub> and PM<sub>2.5</sub> particles at one site directly influenced by traffic (one rural background site was used for comparison).

The traffic site (TR) was situated in the north of Portugal at a zone of Oporto city (Paranhos district) where traffic emissions are the main source of atmospheric pollutants (Pereira, 2005). The background site (BC) was situated approximately 13 km far from seacoast in a remote area, about 112 km north of Oporto.

PM<sub>10</sub> and PM<sub>2.5</sub> monitoring was performed for 21 consecutive days at each site during 2005 using TCR TECORA Bravo H2 constant flow samplers (with flow rate 2.3 m<sup>3</sup> h<sup>-1</sup>) and combined with PM<sub>10</sub> and PM<sub>2.5</sub> EN 12341. The particles were collected on polytetrafluoroethylene (PTFE) membrane filters with polymethylpentene support ring (2 m porosity, Pall Life Science Teflo<sup>TM</sup>). To determine the PM concentrations, PM masses were measured gravimetrically and then divided by the total volume of air that passed through filter (at 25 °C and 101.3 kPa). The analysis of individual particles was performed using a JEO JSM-6301F electron scanning microscope combined with energy dispersive spectrometer NORAN VOYAGER (EDS) analyzing elements from carbon to uranium. Elements with atomic number less than 11 were not determined, as well as carbon and fluorine due to their presence on the substrate. For each selected filter 1 cm<sup>2</sup> was cut and mounted with a double-side tape on an aluminum stub. For better conductivity and reduction of electron charge, the sample was coated with a carbon layer. The microscope magnification was set to 540 and 2000 which allowed the detection fields of

170 160 and 50 40 m, respectively. About 25 fields per each selected filter were observed with 10 randomly selected particles on each field, giving 250 manually characterised particles per filter. In total 500 particles for each site were analyzed. The X-ray spectrum was accumulated for 60 s with an acceleration voltage of 20 kV. The elemental composition of the analyzed particles, as well as the following morphological parameters were identified: particle area, shape aspect, physical diameter (maximum, minimum and mean), Ferret diameter (maximum, minimum, mean), perimeter, and particle roundness. Cluster analysis (CA) was applied to classify the set of particles using Euclidean distance to measure the similarity of particles.

PM<sub>10</sub> concentrations ranged from 20 to 85 g m<sup>-3</sup>, with a mean of 51 g m<sup>-3</sup> at site TR and from 1.8 to 23 g m<sup>-3</sup>, with a mean of 11 g m<sup>-3</sup> at site BC. The PM<sub>2.5</sub> ranged from 16 to 62 g m<sup>-3</sup>, with a mean of 37 g m<sup>-3</sup> at TR and from 1.3 to 17 g m<sup>-3</sup> with a mean of 8.2 g m<sup>-3</sup> at site BC. PM<sub>10</sub> and PM<sub>2.5</sub> concentrations were significantly lower at the background site than at the traffic one. The obtained results also showed that traffic related emissions increased about 5 times PM<sub>10</sub> and PM<sub>2.5</sub> concentrations.

Using SEM technique, the following 27 elements were identified at both sites in PM<sub>10</sub> and PM<sub>2.5</sub>: Na, Mg, Al, Si, P, S, Cl, K, Ca, Mn, Fe, Cu, Zn, Pb, Ti, V, Cr, Ni, Ba, Mo, Co, Sn, Sb, Sc, Sr, and Ce. At site BC the majority of particles were composed of Al and Si. These particles were mostly from granite soil of this region composed mainly of Al and Si. At the traffic site, the majority of particles were dominated by Fe, but also other metals such as Mn, Cu, Zn, Pb, Ni, Ti and Cr were present as minor elements in most of the particles.

This work was supported by Fundação Calouste Gulbenkian and by Fundação para a Ciência e Tecnologia under grant SFRH/BD/24228/2005.

Ghio, A. J. & Devlin, R. B. (2001). *Environ. Health Perspect.* *n*, 164, 704-708.

Pereira, M. C., Alvim-Ferraz, M. C. & Santos, R. C. (2005). *Environ. Health Perspect.* *n*, 101, 203-221.

## Chemical characterization of fine particulate matter in Bari and Taranto (South Italy).

M. Amodio, P. Bruno, M. Caselli, P. R. Dambruoso, B. E. Daresta, G. de Gennaro, P. Ielpo, V. Paolillo, C. M. Placentino, L. Trizio, M. Tutino

Department of Chemistry, University of Bari, Via E. Orabona, 4, 70126, Bari, Italy

Keywords: PM<sub>2.5</sub>/PM<sub>10</sub>, chemical composition, particulate nitrate, sulphate, source apportionment.

This contribution is part of the SITECOS (Integrated Study on national Territory for the characterization and Control of atmospheric pollutants) PRIN project 2004-2006. The principal goal of this project is the attainment of an organic vision of the air quality on national level, evaluating the effects of the meteorological and emissive differences of pollutants among North, Middle and South of Italy.

In order to reach this aim, summer and winter monitoring campaigns have been carried out in the principal Italian towns, extending the study to urban sites interested from industrial impacts and to remote sites, to verify the airborne transport effect. In particular our research group has carried out monitoring campaigns in Bari, Taranto and Mount Pollino (remote site) during the months of October 2005, February and July 2006. During these campaigns PM<sub>2.5</sub> and PM<sub>10</sub> daily samples have been collected and chemical characterization has been performed on them. The results obtained do not show a seasonal trend for PM<sub>10</sub> concentration, moreover in the several sampling sites is evident a common contribution to the PM<sub>10</sub> amount, apparently independent from local sources. In fact correlations of PM<sub>10</sub> among the several investigated sites are higher than the correlation of PM<sub>2.5</sub> in the same sites and than the correlation between PM<sub>2.5</sub> and PM<sub>10</sub> in each site. Such evidences are confirmed, in Bari, by applying multivariate statistical analysis (receptor models) to data collected by automatic monitoring networks of Bari Municipality, in fact automotive traffic doesn't follow PM<sub>10</sub> trend and contributes little to its amount.

The chemical investigation has dealt with analysis of inorganic component, polycyclic aromatic hydrocarbons (PAHs) and carbonaceous fraction (TC/OC/EC). The organic carbon is the principal constituent of PM<sub>2.5</sub> and PM<sub>10</sub>, and is characterized by OC/EC diagnostic ratio higher than 2.5 (Turpin *et al.*, 1995) in all sites, suggesting the secondary organic aerosol formation. The ionic fraction is a substantial part of PM, consisting of sulphate, ammonia, potassium in fine fraction, and of chloride, calcium, sodium and magnesium in coarse fraction, while nitrate is apportioned among the two fractions. Sulphate, nitrate in certain cases, and ammonia, prevalent components in ionic fraction, show a similar distribution in both Bari and Taranto sampling sites: this suggests an uniform distribution on wide area.

Experimental results, highlighted by characteristic diagnostic ratio magnesium/sodium (Seinfeld *et al.*, 1998 ; Wilson *et al.*, 1975), show the presence of marine aerosol in particulate matter. Marine salts don't contribute in significant way to PM<sub>10</sub>, while Saharan dust events cause considerable increments of particulate matter. During such events, confirmed by diagnostic ratio sulphate/calcium, the ionic coarse fraction percentage exceeds the 50%, compared to a mean contribution of 30%.

By observing the PAHs concentrations in the PM samples collected in Bari and Taranto, it has been possible to point out the prominent influence of Taranto industrial area: for these samples is evident a direct relation between wind direction coming from industrial area (North) and high PAHs concentrations. The study of PAHs concentrations ratio and in particular of benzo(b+j)fluoranthene/benzo(g,h,i)perylene has allowed to distinguish traffic source from the other possible ones. In particular it has been possible to understand that Taranto industrial area is the predominant PAHs source when the wind blows from North. The diagnostic ratio analysis shows that the predominant PAHs source in Bari is automotive traffic. The automotive and industrial emissions are not the only PM<sub>2.5</sub> source: such hypothesis is supported by the poor correlation between PAHs and PM<sub>2.5</sub>, for both cities.

Multivariate statistical analysis as receptor models (APCS, (Thurston *et al.*, 1985)) has been applied in order to identify the profile sources and their contributions. The results for Bari and Taranto showed the presence of recurrent sources in all sites, such as vehicular traffic, marine aerosol, secondary and resuspended particulate matter. The secondary particulate matter gives the most important contribution.

Turpin, B.J., Huntzicker, J.J. (1995). *Atmospheric Environment* 29, 3527-3544.

Seinfeld J.H., Pandis S.N. (1998). *Atmospheric Chemistry and Physics, from Air Pollution to Climate Change*, (Wiley, New York), 444.

Wilson, T.R.S. (1975). *Salinity and the major elements of sea water*. Riley, J.P., Skirrow, G. (Eds.), Chemical Oceanography Academic, Orlando, FL, 365-413.

Thurston G.D., Spengler J.D. (1985) *Atmospheric Environment*, 19, 9-25.

## Meteorological influence on relation between particulate matter and traffic flow.

M.Filice<sup>1</sup> and P. De Luca<sup>1</sup>

<sup>1</sup>Department of Pianificazione Territoriale, University of Calabria, Arcavacata di Rende, 87036, Cosenza, Italy

Keywords: Aerosol cloud interaction, anthropogenic aerosol, coarse particles, PM measurement, traffic

Complexity of Particulate Matter (PM) pollution is due to two principal factors: territorial sources and meteorological parameters (DeGaetano *et al.*, 2004). Many epidemiological studies show that PM inhalation is dangerous for human respiratory system (Kappos *et al.*, 2004), in particular particles inhalation with an aerodynamic diameter less than 10 micrometers.

This study is focused on determining the relation between PM concentration and traffic flow. Sampling was been in March 2006, in an urban area of Southern Italy with a vehicular pollution. We have placed the sampler in a canyon street at 4 meters from the ground, with an air flow of 20 lit/min. PM concentration has been determinate by gravimetric method. 5h morning sampling (08:30-13:30) has been divided in hourly bands. Simultaneously we have observed meteorological parameters (temperature, rainfall) and traffic flow.

Figure 1 shows meteorological screening in sampling time. We have determined temperature difference between maximum and minimum temperature values ( $\Delta T = T_{max} - T_{min}$ ). We have observed that exist a relation between  $\Delta T$  and rainfall.

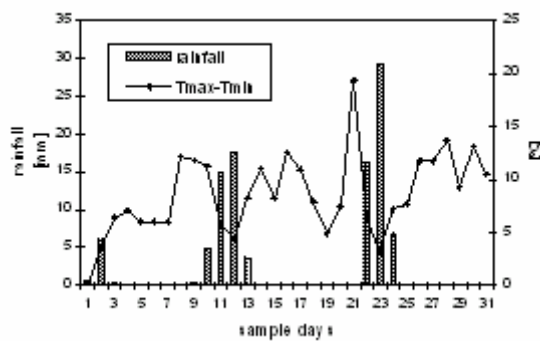


Figure 1. Comparison between rainfall and temperature trends.

Traffic analysis shows a flow time reduction due to citizen custom. To evaluate the relation between PM and traffic we have analysed rainy and sunny days. We observed two different trends.

Sunny days trend: there is not a direct relation between traffic flow and PM concentration: higher PM concentration corresponding lower traffic flow (Figure 2): this results is due to particles accumulating processes.

Rainy days trend: there is a direct relation between traffic flow and PM concentration: higher

PM concentration corresponding higher traffic flow (Figure 3). Rainfall has an air cleaning action with a double function: it hinders accumulating process and it emphasizes traffic flow contribution.

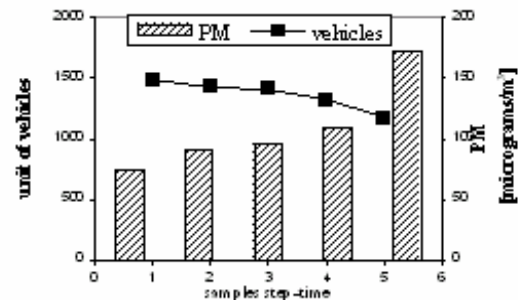


Figure 2. Relation between PM and traffic flow in a sunny day. Average Hourly trend.

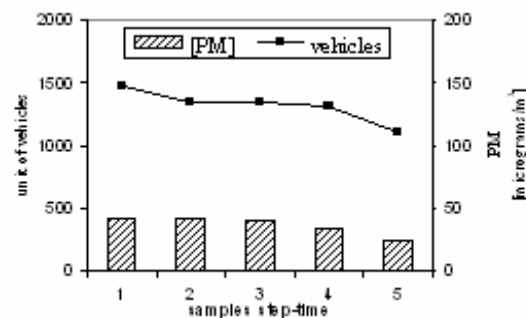


Figure 3. Relation between PM and traffic flow in a rainy day. Average Hourly trend.

We observed that PM concentration in a sampling time  $j$  is due to two different actions: accumulating process ( $A$ ) and local traffic emission ( $[PM]^*$ ).

$$[PM]_j = A + [PM]^* \quad A = \sum_{i=1}^{j-1} K_i [PM]_i$$

- $A$  represent accumulating particles process due to sources emission in a time previous sampling time. It is function of meteorological condition and PM concentration.

- $[PM]^*$  represent local traffic emission in sampling time.

- $K$  is function of meteorological parameters as wind direction, temperature, rain and pressure. It influences particles dispersion.

Kappos A.D., Brugkmann P., Eikmann T., Englert N., et al. (2004) *Int. J. Hyg. Environ. Health* 207, 399-407

DeGaetano A.T., Doherty O.M., (2004), *Atmospheric Environment* 38, 1547-1558

## **Chemical characterization of atmospheric PM sampled near an incinerator of urban solid waste located in Granarolo dell'Emilia, Bologna, Italy, and in the neighbours urban and rural areas of Bologna**

V. Poluzzi<sup>1</sup>, C. Maccone<sup>1</sup>, I. Ricciardelli<sup>1</sup>, L. Passoni<sup>1</sup>, M. Busetto<sup>1</sup>, D. Lucchini<sup>2</sup>, E. Errani<sup>2</sup>, M. Ridolfi<sup>2</sup>, S. Ruiba<sup>2</sup>, S. Tamburini<sup>2</sup>, P. Franceschi<sup>2</sup>, I. Scaroni<sup>3</sup>, G. Castellari<sup>3</sup>

<sup>1</sup> Excellence Urban and Industrial Ecosystem, <sup>2</sup> Environmental Analytical Area,

Environmental Protection Agency of Emilia-Romagna Region, (Arpa), I-40138 Bologna, Italy

<sup>3</sup> Excellence Organic Micro-pollutants, Environmental Protection Agency of Emilia-Romagna Region, (Arpa), I-48100 Ravenna, Italy

Keywords: Aerosol characterization, Air pollution, Chemical composition, PM<sub>10</sub>/PM<sub>2.5</sub>, PAH(s)

### INTRODUCTION

The incinerator of urban solid waste (IUSW) of Granarolo dell'Emilia is located in the Po Valley, immediately north-east to the Bologna urban area. The results reported in this paper are part of one big project, coordinated by the Provincial Administration of Bologna, aimed to study the impact on the environment of the IUSW.

We report here only the results of the chemical characterization of PM<sub>10</sub> and PM<sub>2.5</sub> sampled in 5 sites near the IUSW compared with the same parameters analysed in the monitoring stations of the neighbours urban and rural areas of Bologna.

The pollutants measured have been:

Mass concentration of TSP, PM<sub>10</sub>, PM<sub>2.5</sub>.

On the TSP filters the following elements have been searched: Pb, Ni, Mn, Cr, Cr (VI), Co, Zn, Cu, V, Cd, Sb, As, Hg.

On PM<sub>10</sub> and PM<sub>2.5</sub> filters the concentration of single molecular species of PAH(s) have been investigated.

For the only winter campaign PCDD and PCDF(s) on the TSP filters have been analysed.

NO<sub>2</sub> and HCl have been also measured with passive sampler.

### MEASUREMENTS

The measurements of the parameters of air quality have been conducted in five sites near the IUSW, in one (three for PAH(s)) in the urban area of Bologna and two in the rural areas.

The monitoring campaigns have been made in three different period of about 15 days each.

- Summer campaign: 12 - 26.7.2005

- Autumn campaign: 28.10 - 13.11.2005

- Winter campaign: 28.1 - 12.2.2006

During the air quality monitoring campaign the control of the flow emission at the IUSW has been made.

For each campaign a characterization of the meteorological parameters has been made using the pre-processor Calmet.

### RESULTS

The data obtained for PM<sub>10</sub> and PM<sub>2.5</sub> shows that the area near the incinerator is substantially similar to the one located in the urban area of Bologna. Differences are evident comparing the rural areas that show lower values for both aerosol fractions.

In general, excluding 2 sites during the summer campaign, over 80 % of total value of PAH(s) are found to be on the PM<sub>2.5</sub> confirming other studies. The comparison between the sites shows higher value in urban area monitoring stations, and the 5 sites near the IUSW result comparables with the data coming from the rural area.

The same behaviour are found for the metals investigated and for NO<sub>2</sub>.

The values of HCl result systematically lower to the limit of detection, except for the 2 sites in the summer campaign.

PCDD and PCDF(s) don't show critical values and are similar to that reported in literature for Italian urban areas.

High values of PAH(s), mass concentration of PM<sub>10</sub>, PM<sub>2.5</sub> and Zn in autumn and winter campaign in one of the station near the IUSW, don't exclude a possible local source of environmental pollution (civil heating or wood combustion).

Finally, even if fluoranthene ratio vs total PAH(s) at the emission of IUSW shows high levels, in the air quality of the five sites this ratio shows low data and a similarity with the rural area. On the contrary, higher values of fluoranthene ratio are found in the urban area meaning, for this sites, a different type of source for this molecular specie.

## **T20 Abstracts**

## Aerosol physical properties as an important factor in remote sensing of coastal areas

T. Zielinski, A. Ponczkowska

*Institute of Oceanology, PAS, Poland*

Keywords: Atmospheric aerosols, remote sensing, coastal area

Atmospheric aerosols originate from a wide variety of sources in both the marine and the continental environments. Aerosol content varies significantly depending upon whether the air mass is natural or modified anthropogenically, marine or continental, rural or urban. Therefore, characterizing aerosols not only requires describing their spatial and temporal distributions but their multi-component composition, particle size distribution and physical properties as well.

This is especially evident in coastal areas where aerosols are in the direct interaction zone between the atmosphere and the ocean surface and are characterized by rapid temporal and spatial changes in concentration. The spectrum of marine aerosol size distribution functions is complicated and depends heavily on weather conditions in the marine boundary layer, especially on wind speed, duration and direction as well as on relative humidity.

Since 1992 measurements have been taken at several stations on the Polish coast of the Baltic Sea. Additionally, the authors participated in a number of international experiments, such as EOPACE and SOAP. The objectives of the EOPACE (Electrooptical Propagation Assessment in Coastal Environments) effort, which was conducted in Duck, N.C. (USA) between 25 February and 11 March 1999, involved investigating, developing and evaluating ocean and coastal aerosol models and their effects on visibility; integrating and developing simple, realistic models for infrared propagation near the ocean surface and developing a consistent chemical/optical model for aerosol particles suitable for inclusion in navy meteorological models. The Studies Of Aerosol Properties - SOAP project was carried out in Crete between 28 July and 10 August 2006 and it aimed at a determination of the direct aerosol climatic effect including solar radiative closure between observed and calculated aerosol properties. During all experiments an ensemble of instruments were employed, including lidars, laser particle counters, sunphotometers etc.

It was discovered that the near-water layer in the coastal areas is significantly different from that over the open seas, both in terms of structure and physical properties. The aerosol composition and

concentrations are usually uniform over the open ocean.

In cases of coastal areas the composition can be changed over short periods of time, and the real aerosol concentrations depend on many factors, concerned with different particle origins. The coastal area aerosol can be divided into three groups: marine, a mixture of marine and continental and continental. The aerosol type depends on the history of air masses, wind speed and direction. Both horizontal and vertical aerosol concentrations and size distributions vary significantly seasonally and in short periods of time.

Depending on aerosol origin different light refraction indexes must be applied for calculations of particle optical properties. For marine aerosols the light refraction index is the same as for the water in the area, while the continental aerosols must be regarded as absorbing particles. The aerosol particles in the marine boundary layer over the coastal zones significantly influence the light extinction in the visible and infrared ranges. The difference between the extinction coefficients at the sea level and at the altitude of 30 m a.s.l. can reach a magnitude of up to two orders. Also the Angström coefficients show a significant variability, both short-term and seasonally.

### ACKNOWLEDGEMENTS

This work was supported by the ONR VSP and ACCENT programs.

Gulyaev, Y. N., Yershov, O. A., Smirnov, A. V., Shifrin, K. S. (1990). *The influence of air masses on spectral transmittance of air masses in typical maritime regions*, In: Atmospheric and marine optics, K. S. Shifrin (ed.) State Opt. Inst., Leningrad, 96-97

Smirnov, A., Villevalde, Y., O'Neill, T. N., Royer, A., Tarussov, A. (1995). *Aerosol optical depth over the oceans: analysis in terms of synoptic air mass types*. J. Geophys. Res. 100: 16,639-16,650.

Zielinski, T., Piskozub, J. (2005). *Studies of aerosols in the marine boundary layer in the coastal area during the EOPACE'99 campaign*. Boundary-Layer Meteorology, Vol. 116, No. 3, 533-541.

## A low-cost, telemetric LIDAR for the monitoring of PBL aerosols

<sup>1</sup>M.Del Guasta, <sup>1</sup>F.Castagnoli, M.Baldi, <sup>1</sup>V.Venturi

<sup>1</sup>Istituto Fisica Applicata “Nello Carrara”, National Research Council, Sesto Fiorentino, 50019, Florence, Italy

Keywords: LIDAR, backscatter, urban aerosol

An old-fashioned technology such as the “searchlight profiler”, which was used in the 1960s for the pioneering profiling of atmospheric backscatter (Rozenberg, 1960), has been revisited in our telemetric-LIDAR. The instrument is intended for the low-cost monitoring of aerosols, with a limited useful range of 100-200 meters. A modulated CW laser beam (532 nm) is used to probe the atmosphere. An 8-cm refractive telescope is used to collect the backscattered light, as in any ordinary LIDAR. A 10-nm bandwidth interference filter is used to block daylight, and a photodiode array placed in the focal plane of the lens is used as a detector. As in a telemetric system, the distance between the laser beam and the telescope determines the distance of the measurement volume for each photodiode pixel.

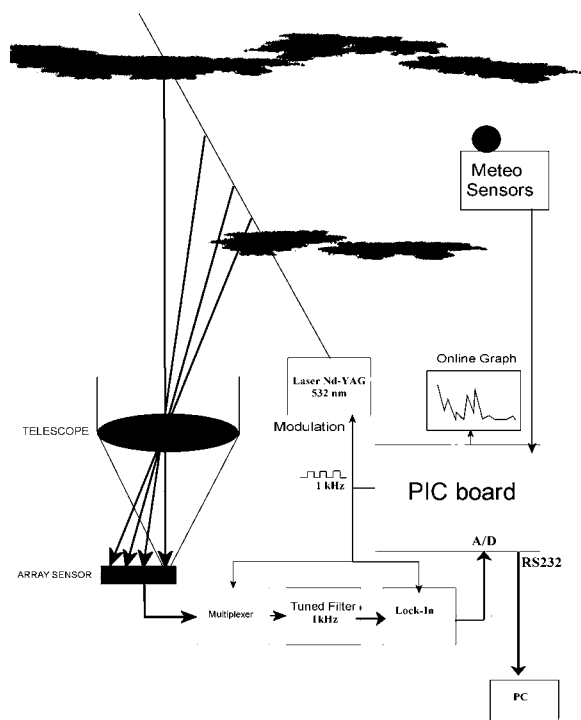


Figure 1. The basic schematics of the instrument

The modulated light received by each pixel is converted into a DC signal by means of a lock-in amplifier (gain 5E6). The DC signal is ultimately acquired by means of an inexpensive PIC18 board. The photodiode pixels are scanned in order to measure the aerosol backscatter at different distances. As in any telemetric system, the range resolution of

the instrument changes with the measurement distance. With a laser-telescope distance of 50 cm, and 1mm photodiode size, the resolution is approximately 3m at a measuring distance of 10m, but increases up to 30m at a distance of 100m. For this reason, the instrument is mainly suitable for the monitoring of urban aerosol pollution, because the range resolution is adequate and similar to that of an ordinary LIDAR in the surface layer, the region in which the monitoring of urban pollution is most important.

When compared with an ordinary LIDAR, the advantage of the instrument is seen to be the extremely low cost of both the instrument itself and its maintenance.

In the case of urban aerosols, light backscatter can be converted into aerosol mass concentration once the relative humidity is known (Del Guasta and Marini, 2000). As in the case of ordinary LIDARs, the measured mass is the mass of the “wet” aerosols: thus, the results are unreliable when  $RH \gg 90\%$ . For an interpretation of the results in terms of meteorological conditions, the instrument is equipped with ordinary meteorological sensors, the signals of which are automatically acquired together with the LIDAR data.

The instrument was run for a first field campaign in Prato (Italy), together with a Beta-attenuation PM10 instrument. The telemetric-LIDAR provided PM10 data every 5 minutes, while hourly data were supplied by the Beta-attenuation instrument. The instrument’s reliability as a monitoring tool, at least when  $RH < 90\%$ , was confirmed.

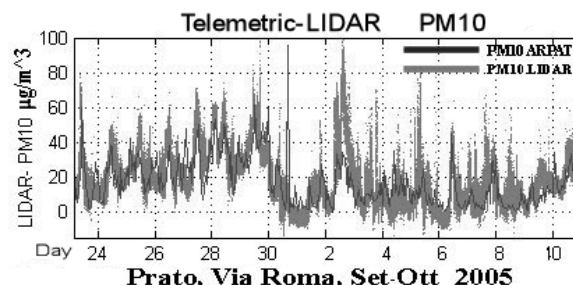


Figure.2 Comparison between Beta-attenuation PM10 and the telemetric-LIDAR data

Rozenberg, G.V., (1960). *Am. Inst. Physics*, 3, 346-371

Del Guasta, M., Marini, S.(2000). *J. Aerosol Sci.* 31, 1469-1488.

## CALIPSO and MISR Aerosol Data Available for Atmospheric Research

Nancy A. Ritchey<sup>1</sup>, Linda A. Hunt<sup>1</sup> and Michelle T. Ferebee<sup>2</sup>

<sup>1</sup>Science Systems and Applications, Inc., Atmospheric Science Data Center, 23681, Hampton, VA, USA

<sup>2</sup> Atmospheric Science Data Center, NASA Langley Research Center, 23681, Hampton, VA, USA

Keywords: Atmospheric Aerosol, Aerosol Characterization, Measurements, LIDAR, Spectroradiometer.

The Atmospheric Science Data Center (ASDC) at NASA Langley Research Center processes, archives and distributes data relating to aerosols, the Earth's radiation budget, clouds, and tropospheric chemistry. The ASDC was established in 1991 to support the Earth Observing System as part of NASA's Science Mission Directorate, and is one of several Distributed Active Archive Centers sponsored by NASA as part of the Earth Observing System Data and Information System.

Global aerosol measurements and aerosol characteristics are contained in many data products available from ASDC. This paper focuses on the satellite instruments Cloud-Aerosol Lidar and Infrared Pathfinder Satellite Observations (CALIPSO), part of the A-Train constellation, and Multi-angle Imaging SpectroRadiometer (MISR), currently orbiting on the Terra satellite.

CALIPSO was launched into a sun-synchronous orbit on April 28, 2006, where it joined the A-Train constellation of four other NASA Earth-orbiting satellites: Aqua, Aura, CloudSat and PARASOL. The primary objective of CALIPSO's three-year mission is to make a global survey of the vertical structure of clouds and aerosols and their physical properties needed to improve climate predictions.

CALIPSO comprises three instruments, the Cloud-Aerosol Lidar with Orthogonal Polarization (CALIOP), an Imaging Infrared Radiometer (IIR), and a Wide Field Camera (WFC). CALIOP is a two-wavelength, polarization-sensitive lidar that provides information about the composition of clouds, the abundance and sizes of aerosols, and the altitudes of cloud and aerosol layers. The IIR measures outgoing radiation at three wavelengths in the thermal infrared window (8.65  $\mu\text{m}$ , 10.6  $\mu\text{m}$ , and 12.0  $\mu\text{m}$ ) to determine cloud emissivity and particle size. The high resolution, nadir-viewing WFC images the region around the lidar footprint in a single spectral channel (645 nm).

CALIPSO Level 2 aerosol data products include an aerosol layer product at 5 km resolution (height, thickness, optical depth, and integrated attenuated backscatter) and an aerosol profile product with a horizontal resolution of 40 km and vertical resolution of 120 m (backscatter, extinction, and depolarization ratio).

MISR has been operating continuously since its launch on December 18, 1999 on the Terra satellite. MISR collects multi-angle as well as multi-spectral data never before obtained by satellite instruments. The additional information contained in these data make it possible to set limits on particle size and composition, as well as aerosol amount, measured over ocean. These data are also used to derive aerosol properties in the atmosphere over heterogeneous land and dense dark vegetation. Different methods to derive aerosol properties over different types of surface are used.

MISR also uses a systematic, global monitoring program to collect data about particle type and amount. This data product, known as "Clim-Likely", is used in studies of the planetary energy balance, and for modeling regional and global trends in Earth's climate.

MISR Level 2 aerosol data product contains tropospheric aerosol optical depth, aerosol physical model, Angstrom exponent and single scattering albedo on 17.6 km centers, aerosol mixture identifier and retrieval residuals ancillary meteorological data, and related parameters.

MISR Level 3 global aerosol optical depth is available on a 0.5° by 0.5° resolution grid averaged over daily, monthly, seasonal and annual time scales. This product is available in HDF-EOS and NetCDF file formats.

Additional information about all ASDC data products, images and software tools is available from the ASDC web site at <http://eosweb.larc.nasa.gov>. ASDC data are distributed free of charge. User assistance is available from the on-call help desk available via e-mail ([larc@eos.nasa.gov](mailto:larc@eos.nasa.gov)).

## Local Radiative forcing by Saharan Dust and Forest Fire Aerosols over Portugal

D. Santos<sup>1</sup>, M.J. Costa<sup>1,2</sup> and A.M. Silva<sup>1,2</sup>

<sup>1</sup>Évora Geophysics Centre, University of Évora, Rua Romão Ramalho 59, 7000-671 Évora, Portugal

<sup>2</sup>Department of Physics, University of Évora, Rua Romão Ramalho 59, 7000-671 Évora, Portugal

Keywords: Remote Sensing of Aerosols, Radiative properties, Remote sensing, Satellites.

It is well known that aerosols directly affect the climate by increasing back-scattered radiation and by absorbing solar and long wave radiation (IPCC, 2001).

Continental Portugal is often affected by the long-range transport of desert dust aerosols advected from Africa, and, frequently during summer, smoke from forest fires (Silva *et al.*, 2003). This fraction is very efficient at scattering and absorbing short-wave radiation, being then of primary importance the estimation of radiative forcing due to aerosols.

In order to understand climate change implications, in particular to identify major aerosol types, aerosol long-term monitoring is necessary. This is a good way to characterise their spatial and temporal distribution and their optical and physical properties, and to estimate their local and regional radiative forcing. Since 2002, long-term monitoring is being undertaken in Portugal with measurements from ground-based instruments at Évora, and, since December 2003, extended with measurements from Cabo da Roca.

The main objective of this work is to estimate the aerosol radiative forcing at the top of the atmosphere (TOA) over the south of Portugal, particularly in the region of Évora and of Cabo da Roca, due to significant aerosol events of desert dust and forest fires.

The methodology is based on radiative transfer calculations combined with surface and satellite measurements and its block diagram is presented in figure 1:

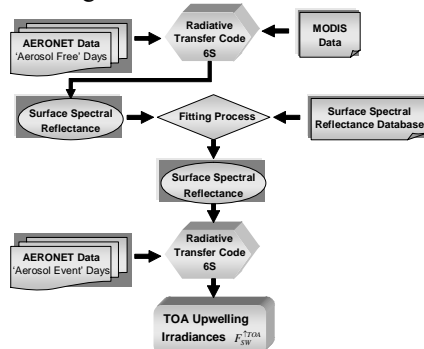


Figure 1. Methodology block diagram used in this work.

The surface measurements of the aerosol optical properties combined with the satellite-measured radiance provide the essential atmospheric

characterization, allowing for the retrieval of the surface spectral reflectance, which is also crucial for the calculation of the clear-sky irradiances. Once the surface characterization is retrieved, the irradiances are calculated (Costa *et al.*, 2004), and the TOA local aerosol radiative forcing calculated by the difference between the downwelling and up-welling irradiances (equation 1):

$$\Delta F^{TOA} = (F_{SW}^{\uparrow TOA})_{CLEAN} - (F_{SW}^{\uparrow TOA})_{AER} \quad (1)$$

$(F_{SW}^{\uparrow TOA})_{AER}$  is the up-welling irradiances at TOA that suffered an external perturbation due to aerosols and  $(F_{SW}^{\uparrow TOA})_{CLEAN}$  is the up-welling irradiances at TOA of a pristine atmosphere.

Another term that is very useful is the atmospheric forcing efficiency term,  $\Delta F_e$ , that depends only on the aerosol type and underlying surface. As expressed in equation (2),  $\Delta F_e$  is simply the radiative forcing per unit aerosol optical thickness,  $\tau$ :

$$\Delta F_e = \Delta F / \tau \quad (2)$$

For Desert Dust aerosols, in Évora land region the forcing efficiency is estimated  $-40.6 \text{ W/m}^2/\tau_{0.55}$  and for Cabo da Roca area the forcing efficiency is estimated  $-45.7 \text{ W/m}^2/\tau_{0.55}$ . In the presence of Forest Fire aerosols, in Cabo da Roca region the forcing efficiency is estimated  $-27.6 \text{ W/m}^2/\tau_{0.55}$  and in Évora region a forcing efficiency of  $-44.0 \text{ W/m}^2/\tau_{0.55}$  at TOA is found. The results obtained illustrate the importance of considering the actual aerosol properties, in this case measured by ground-based instrumentation, since different aerosol types may originate different forcings. The local aerosol radiative forcings obtained at TOA are negative, indicating a tendency for cooling the Earth.

Costa, M. J., Silva, A. M. & Levizzani, V. (2004), *Journal of Applied Meteorology*, 43, 1799-1817.

IPCC (2001). *International Panel for Climate Change Third Assessment Report. Climate Change 2001: The Scientific Basis. Contribution of Working Group I to the Third Assessment Report of IPCC.* Cambridge, U.K.: Cambridge University Press.

Silva, A.M., Costa, M.J., Elias T., Formenti P., Belo N., Pereira S. (2003). Ground based aerosol monitoring at Évora, Portugal. *Global Change Newsletter*, 56, 6-9.

## Aerosol optical properties in a rural site of South Italy from simultaneous measurements by CIMEL and Avantes radiometers

G. Pavese<sup>1</sup>, F. Esposito<sup>2</sup>, L. Leone<sup>3</sup>,  
 M. R. Perrone<sup>4</sup>, F. De Tomasi<sup>4</sup>, A. M. Tafuro<sup>4</sup>,  
 L. Alados-Arboledas<sup>5</sup>, H. Lyamani<sup>5</sup>

<sup>1</sup> I.M.A.A. – C.N.R., Tito Scalo, 85050, Italy

<sup>2</sup> DIFA, Università della Basilicata, Potenza, 85100, Italy

<sup>3</sup> C.R.A.B. – ARPAB, Potenza, 85100, Italy

<sup>4</sup> Dipartimento di Fisica, Università di Lecce

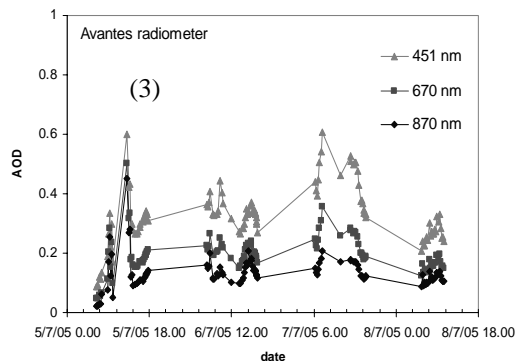
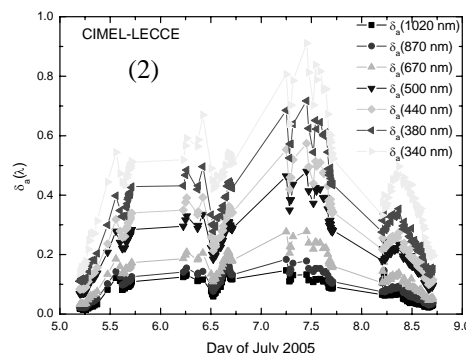
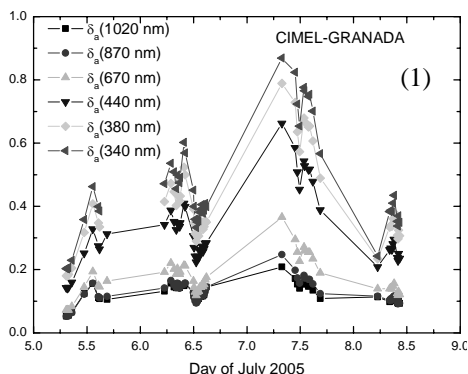
<sup>5</sup> Grupo de Física de la Atmósfera. C.E.A.MA. J.A.. Universidad de Granada, 18071, Granada, Spain.

Keywords: Atmospheric aerosols, aerosol size distributions, spectrometer.

In the framework of an Italian National Project (PRIN- 2004023854) and an “*Integrated Action Italy-Spain Project*”, ground-based, joint radiometric measurements have been performed from July, 4<sup>th</sup> to July, 8<sup>th</sup>, 2005 in the neighbourhood of Lecce (18.18° E, 40.38° N), a city located in South Italy and very close to both the Ionian and the Adriatic Sea. Especially, two CIMEL sunphotometers, one from Lecce- and one from Granada, and an Avantes high resolution radiometer (400 nm – 900 nm, 1.5 nm resolution) have been used. The CIMEL regularly operating in Lecce is part of the AERONET robotic network and calibrated according to the standard AERONET procedures, while the Granada’s CIMEL was calibrated few days before the measurement campaign. A first intercomparison study among the derived Aerosols Optical Depth has shown some differences in the estimated values, already discussed in Esposito et al., 2006 and due to degradation problems of the Lecce filter, mainly at 340 nm, and an offset problem for the Avantes radiometer.

A detailed analysis on the variation of the Ångström parameters and aerosol size distributions retrieved by three different inversion techniques will be provided.

This study has been supported by HYSPLIT back-trajectories tool and NAAPS models to investigate the variation of the aerosol properties under different advection patterns and hence aerosol types.



In figures 1-3 the AOD temporal evolution as obtained by the three radiometers at different wavelengths are shown.

**Acknowledgments.** Work partially supported by Ministero della Ricerca Universitaria of Italy, by the “Integrated Action Italy-Spain”, by HI-2004-0219 and Spanish Ministry of Education project CGL2004-05984-C07-03.

### References

F. Esposito, G. Pavese, L. Leone, M. R. Perrone, F. De Tomasi, A. M. Tafuro, L. Alados-Arboledas, H. Lyamani “ CIMEL and AVANTES high resolution spectrometers: a comparison study of aerosol parameters” , Conference on Visibility , Vienna, Sept. 2006

## Atmospheric aerosol characterization by lidar and sun-photometer measurements.

A. Boselli<sup>1</sup>, A. Amodeo<sup>1</sup>, C. Cornacchia<sup>1</sup>, G. D'Amico<sup>1</sup>, F. Madonna<sup>1</sup>, L. Mona<sup>1</sup>, G. Pappalardo<sup>1</sup>

<sup>1</sup>CNR - IMAA - Istituto di Metodologie per l'Analisi Ambientale C.da S. Loja, 85050, Tito Scalo (PZ), Italy

Keywords: LIDAR, aerosol measurement, Optical depth, AERONET

The current increasing interest in the study of atmospheric aerosols is related to the critical effects they play on air quality and climate change.

The large uncertainties in current estimates of aerosol properties are related to their inhomogeneity and to the complexity of the involved mechanisms, highly variable both in space and time. To overcome these difficulties, long-term measurements of vertical profiles of aerosol optical properties with high spatio-temporal resolution, and coordinated research strategy that integrates data from different techniques of measurement are needed to reduce these uncertainties.

In order to reach a more detailed knowledge of involved mechanisms and to study the variability of the optical and microphysical properties of atmospheric aerosols, we used a combined approach based on the integration of active and passive instruments. In the framework of the CNR-IMAA ground based facility for Earth Observation, a multi-wavelength lidar system and a Sun-photometer are operative.

At CNR-IMAA (40°36'N, 15°44' E, 760 m above sea level), a lidar system for aerosol study is operative since May 2000 in the framework of EARLINET (European Aerosol Research Lidar Network) (J. Bösenberg et al., 2003; Mona et al., 2006a). Until August 2005, it provided independent measurements of aerosol extinction and backscatter at 355 nm and aerosol backscatter profiles at 532 nm. After an upgrade of the system, PEARL (Potenza EARLINET Raman Lidar) provides independent measurements of aerosol extinction and backscatter profiles at 355 and 532 nm, and of aerosol backscatter profiles at 1064 nm and depolarization ratio at 532 nm. For these measurements, lidar ratio at 355 and 532 nm and Angstrom exponent profiles at 355/532 nm are also obtained. Lidar measurements are performed systematically 3 times per week and additional measurements are performed in order to investigate special cases such as Saharan dust intrusions, volcanic eruptions and forest fires (Mona et al., 2006b; Villani et al., 2006).

In addition, an AERONET sun photometer (Holben et al., 1998) is routinely operational at CNR-IMAA since December 2004. This instrument allows aerosol characterization in terms of columnar aerosol optical depth at several wavelengths (340, 380, 440, 500, 675, 870 e 1020 nm), of the Angstrom coefficient at 440-870 nm and of aerosol size distribution (Dubovik et al., 2000).

The integration of lidar and sun-photometer data allows to follow the temporal evolution of aerosol optical properties both in daytime and nighttime conditions. Ancillary information provided by the sunphotometer can be useful to improve the lidar retrieval for daytime measurements. On the other hand, information on the aerosol vertical distribution provided by the lidar can add important information at columnar observation provided by the sunphotometer.

J Bösenberg, et al., EARLINET: A European Aerosol Research Lidar Network to Establish an Aerosol Climatology, MPI-Report No. 348, Hamburg, Germany, 2003.

O. Dubovik, M.D. King, A flexible inversion algorithm for retrieval of aerosol optical properties from Sun and sky radiance measurements, *JGR Vol. 105, NO. D16*, 20,673-20,696, August 27, 2000.

B. Holben et al., AERONET- A federated instrument network and data archive for aerosol characterization - *Remote Sens. Environ.*, 66, 1-16, 1998.

Mona, L., et al. (2006a). Five years of lidar ratio measurements over Potenza, Italy – *Proc. SPIE, Lidar technologies, techniques, and measurements for atmospheric remote sensing II*, Stockholm, Sweden, 11-16 September, 2006.

Mona, L., et al. (2006b). Saharan dust intrusions in the Mediterranean area: three years of Raman lidar measurements, *J. Geophys. Res.*, Vol.111, doi:10.1029/2005JD006569.

Villani, M.G. et al., Transport of volcanic aerosol in the troposphere: The case study of the 2002 Etna plume, *J. Geophys. Res.*, 111, D21102, doi:10.1029/2006JD007126.

## Analysis of aerosol extinction coefficient using Lidar observation in urban area

Boyouk Neda<sup>3</sup>, Jean- Francois Leon<sup>1</sup>, and Herve Delbarre<sup>2</sup>

<sup>1</sup>Laboratoire d'Optique Atmospherique, Centre National de la Recherche Scientifique - universite des science et technologies de Lille1, Lille, France

<sup>2</sup>Laboratoire de Physico-Chimie de l'Atmosphère Université du Littoral Cote d'Opale, 59140, Dunkerque, France

Keywords: Atmospheric aerosol, Extinction coefficient, Lidar, urban pollution, Troposphere aerosol.

To understand the radiation budget of the atmosphere it is important to study aerosol optical properties. Aerosol Lidar measurement can deliver aerosol backscatter and extinction profiles and using inversion techniques. We are performing operational observation of the vertical profile of aerosol in Lille (50.61N, 3.14 E) in the North of France. The lidar system is a micropulse backscattering lidar by CIMEL and emitting at 532 nm. Figure 1 presents the diurnal evolution of the lidar signal recorded on December 12, 2006. We can observe a well developed boundary layer up to 1.2 km. Some cirrus clouds are also observed between 6.5 and 10.0 km.

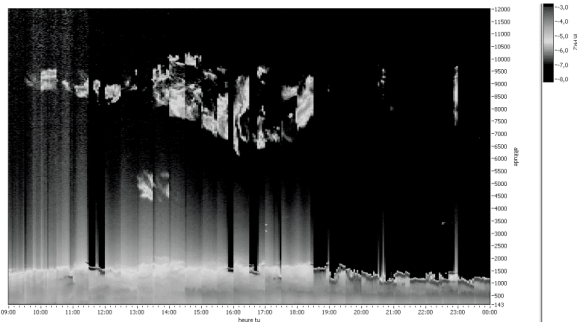


Figure 1. Profiles of the logarithm of the lidar signal as a function of time and altitude.

Simultaneous measurements of the aerosol optical thickness are performed by an automatic Sun photometer located close to the lidar. The aerosol optical thickness is then interpolated at 532 nm by using measurements performed at 440 and 670 nm and following the Angstrom law. We have selected the lidar data between 09:30 to 10:30 GMT. The aerosol optical thickness derived from the Sun photometer is 0.15 on average.

The lidar signal is then ranged corrected and calibrated versus the molecular backscattering at a given altitude of reference where we assume that there is no aerosol backscattering. The range of altitude for the normalization of the signal is between 6-6.5 km. This range will be adapted according to the vertical structure of aerosols. The Figure 2 presents the ranged corrected and calibrated lidar attenuated backscattering coefficient for the selected day.

Elastic back scatter Lidar detects the total atmospheric backscatter without separation of particle and molecular contributions. In order to retrieve the aerosol extinction coefficient from the attenuated backscattering coefficient, we have used the Klett's (1981) method. Mean value of the aerosol extinction coefficient between 210m- 6 km have been calculated. The observed lidar ratio for less absorbing aerosols is between 35 up to 70 sr (Ansmann and Muller, 2005). We have selected a value of 51 sr. This value is required to as close as possible to the aerosol optical thickness given by the Sun photometer.

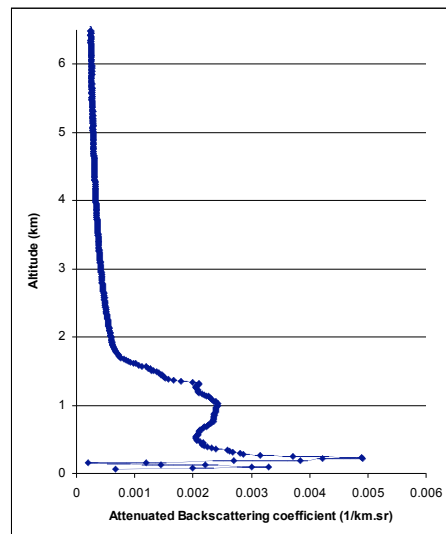


Figure 2. Vertical structure of Lidar data

Further investigated of the adequate lidar ratio will be performed and more days will be analysed and presented.

Ansmann, A, and D. Muller (2005). *Lidar and Atmospheric aerosol particles*, ed. C. Weitkamp, Springer.

Klett, J. D., (1981). *J. Appl. Opt.* 2, 211-220.

## Water vapour column content derived from a star photometer at Granada, Spain.

D. Pérez-Ramírez<sup>1,2</sup>, F.J. Olmo<sup>1,2</sup>, L. Alados-Arboledas<sup>1,2</sup>, J. Aceituno<sup>3</sup>

<sup>1</sup>Grupo de Física de la Atmósfera. CEAMA. Universidad de Granada. Junta de Andalucía. 18071 Granada. Spain

<sup>2</sup>Departamento de Física Aplicada. Universidad de Granada. 18071, Granada. Spain.

<sup>3</sup>Calar Alto Centro Astronómico Hispano Alemán, AIE, C\ Jesús Durbán Remón 2-2º. Almería (Spain).

Keywords: Columnar water vapour, Star photometer, measurements, optical instrumentation.

Solar transmittance methods allow us to obtain water vapour column content from direct sunlight measurements in spectral channels in and adjacent to water-vapour absorption bands. However, during night time this kind of procedure is not applicable unless one substitutes the Sun by a different star. In this sense, continuous measurements of water-vapour transmittance are possible using a star photometer measuring the direct star-light. First attempts have been carried out by Leiterer et al. (1998) who installed a star photometer at the Lindenberg Observatory (52.14°N; 14.14°E). Recently, we have developed a star photometer, using a CCD camera as detector. Our instrument has a filter wheel with six filters centred at 380, 436, 500, 670, 880 and 1020 nm to measure aerosol optical depth (AOD). An additional filter at 940 nm is used to retrieve water vapour column content,  $W$ .

For this purpose, we have adapted to the star photometer the methodology applied to derive the water vapour column content used in sun photometry. The theoretical approach is described in detail in Halthore et al. (1997), who proposed a modified expression of the Beer-Bougher-Lambert law, applicable to the water vapour that presents, around 940 nm, an absorption band having a large number of spectral lines that can be considered to be distributed randomly within the band:

$$V = V_0 \cdot \exp(-m \cdot \delta) \cdot \exp(a \cdot m^b \cdot W^b) \quad (1)$$

Where  $V$  and  $V_0$  are the signals measured by star-photometer at the station and out of atmosphere,  $\delta$  is the optical thickness from Rayleigh scattering and aerosol scattering and absorption in the 940-nm band,  $m$  is the air mass and  $W$  water vapour column content in cm (atm). This last method is known as modified Langley.

Constants 'a' and 'b' depend on the central filter wavelength, width and shape of 940-nm filter function and must be insensitive to changes in atmospheric conditions. To calculate these last constants, variation in water vapour column content is accomplished in MODTRAN-3, that is evaluated for a Mid-latitude atmosphere and varying the solar zenith angle of observation. Coefficients 'a' and 'b' are then obtained from water-vapour transmittance. We have obtained  $a = 0.6497 \pm 0.0017$  and  $b = 0.5470 \pm 0.0009$ . Next step is to get an accurate

value of  $V_0$ . For this purpose, a stable atmosphere is required and so we moved the instrument to Calar Alto Observatory (37.2236° N, 2.54625 ° W, 2168 m a.s.l.). The method consists into represent  $\log V - m \cdot \delta$  versus  $m^b$ . The ordinate intercept yields the the logarithm of  $V_0$  and the slope give us  $a \cdot W^b$  and so we can get  $W$  in cm.

The successful calibration factors have been applied to measurements performed at Granada (37.16°N, 3.60°W, 680 m a.s.), where a CIMEL CE-318 provides similar measurements during the daytime. Figure 1 shows the evolution of water vapour column content during the month of November 2006. A good agreement is encountered between day and night time measurements with water vapour content in the range between 1.5 and 0.5 cm.

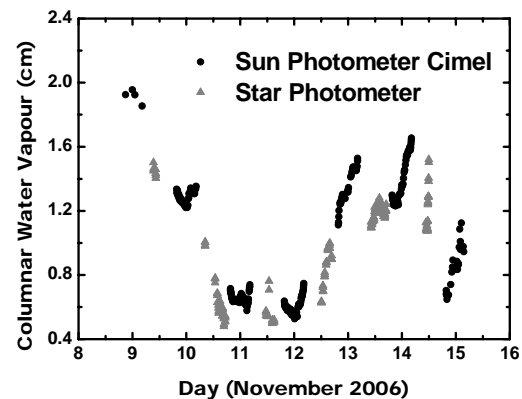


Figure 1: Day and night time measurements of water vapour column content at Granada, Spain.

*Acknowledgements:* This work was supported by the Spanish Ministry of Education project CGL2004-05984-C07-03 and by Andalusian Regional Government project P06-RNM-01503.

### References

- Halthore, R.N., Eck, T.F., Holben, B.N., Markham, B.L., 1997. Sun photometric measurements of atmospheric water vapor column abundance in the 940-nm band *J. Geophys. Res.* **102**, 4334-4352.
- Leiterer, U. et al., 1998. Water vapor column content and optical depths measurements by a Sun and star photometer. *Contributions to Atmospheric Physics* **71**, 401-420.

## MODIS satellite observations and meteorological surface characterization to evaluate PM<sub>2.5</sub> concentrations

W. Di Nicolantonio<sup>1</sup>, A. Cacciari<sup>1</sup>, E. Bolzacchini<sup>2</sup>, L. Ferrero<sup>2</sup>, B. Ferrini<sup>2</sup>, E. Pisoni<sup>3</sup>, M. Volta<sup>3</sup>

<sup>1</sup> Carlo Gavazzi Space S.p.A at ISAC-CNR, via Gobetti, 101, 40129 Bologna, Italy;

<sup>2</sup> Dipartimento di Scienze dell'Ambiente e del Territorio, University of Milano-Bicocca, P.za della Scienza 1, Milano, Italy;

<sup>3</sup> Dipartimento di Elettronica per l'Automazione, University of Brescia, via Branze 38, Brescia, Italy;

Keywords: remote sensing, optical depth, PM<sub>2.5</sub>.

Air Quality monitoring at urban and regional scale is typically performed using in-situ measurements. Also chemical transport models are employed to assess and predict air quality.

During the last years, attention has been devoted to evaluate the possibility to monitor surface particulate matter (PM) concentrations using satellite observations. In particular, the capability of NASA sensors MODIS - on board Terra and Aqua platforms - to retrieve tropospheric Aerosol Optical Depth (AOD) has been exploited to verify the degree of correlation between satellite AOD at 550 nm and surface PM<sub>2.5</sub> (Wang et al, 2003; Liu et al., 2005).

However, several factors affect the relationship between columnar AOD and surface PM concentrations. Among these, the two most important are the aerosol vertical distribution and the relative humidity of the suspended particles.

In our analysis, NASA official MODIS Aerosol Optical Properties at spatial resolution of 10x10 km<sup>2</sup> in terms of Aerosol Optical Depth at 550 nm due to fine fraction particles have been employed together with PM<sub>2.5</sub> concentrations measured at the ground in six sampling sites in Lombardia region.

Moreover, as ancillary meteorological parameters, relative humidity at surface and mixing layer height at spatial resolution of 5x5 km<sup>2</sup> derived from MM5 simulations has been considered in this study.

All the data refer to whole 2004 over an area of about 300x300 km<sup>2</sup> around Milan city involving a great part of the Po Valley in the Northern Italy.

In the above six sampling sites, best fit parameters were retrieved for the relationship between AOD and PM<sub>2.5</sub>, then, by means of a spatial interpolation they were extended to the whole analysed area.

In Figure 1, a preliminary evaluation of PM<sub>2.5</sub> based on satellite data is presented.

This work is carried out in the frame of ESA PROMOTE-2 (Protocol Monitoring for the GMES Service Element: Atmosphere) and ASI QUITSAT (Italian Space Agency Pilot Project for Air quality assessment through the fusion of Earth observations, ground-based and modeling data projects).

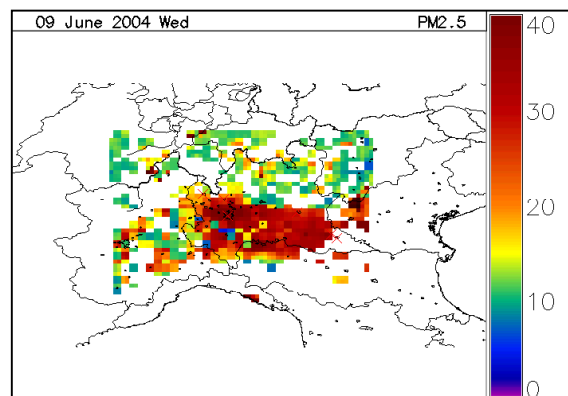


Figure 1. Satellite estimated PM<sub>2.5</sub> ( $\mu\text{g m}^{-3}$ ) at the resolution of 10x10 km<sup>2</sup>, derived from MODIS/Aqua data.

Wang, J., and Christopher, S.A., (2003), *Geophys. Res. Lett.*, 30, 21, 2095, doi: 10.129/2003GL018174.

Liu Y., Sarnat J.A., Kilaru V., Jacob D.J., and Kourakis P., (2005), *Environ. Sci. Technol.*, 39, 3269-3278.

## On the relation between AOD and PM<sub>2.5</sub> at the research station of Cabauw, The Netherlands

M. Schaap<sup>1</sup>, B. Henzing<sup>1</sup>, A. Apituley<sup>2</sup>, D. Swart<sup>2</sup>, R. Koelemeijer<sup>3</sup>, G. de Leeuw<sup>1</sup>

<sup>1</sup> TNO, Business unit Environment, Health and Safety, PO Box 342, 7300 AH Apeldoorn, The Netherlands

<sup>2</sup> National Institute for Public Health and the Environment, P.O. Box 1, 3720 AH Bilthoven, The Netherlands

<sup>3</sup> Netherlands Environmental Assessment Agency (MNP), P.O. Box 303, 3720 AH Bilthoven, The Netherlands

Keywords: Aerosol Optical Depth, PM<sub>2.5</sub>, Measurements, Remote sensing

Airborne particulate matter (PM) can lead to a wide range of detrimental health effects, including premature mortality. The Netherlands form a PM hot-spot in Europe. For the assessment of the exposure to PM<sub>2.5</sub>, the determination of the aerosol mass is mandatory. Traditionally, in situ observations are used to derive information on the large scale features of air pollutants. In case of PM<sub>x</sub> this approach is hampered by the difficulties in the sampling techniques and the highly variable concentrations. Satellite remote sensing may be a cost-effective method to monitor the highly variable aerosol fields on regional scales.

To construct maps of PM<sub>2.5</sub> based on AOD data it is crucial to understand the relation between AOD and PM. Koelemeijer et al. (2006) showed that the linear correlation between PM<sub>10</sub> and AOD is promising (on average 0.6) when accounting for meteorology (mixing layer depth and relative humidity). However, a substantial part of the variability in AOD was not explained by the variability of PM, which can be due to variations in meteorological parameters, aerosol vertical distribution, and aerosol properties.

To address the relation between AOD and PM<sub>2.5</sub> a study was set-up to monitor PM<sub>2.5</sub> using the artefact free FDMS technique at the site of Cabauw, which is located in a rural area in the central part of Netherlands (Cabauw, 51.97 N, 4.93 E). At this site long term time series of AOD and a range of optical and physical aerosol parameters such as size distribution, volatility and aerosol extinction coefficient are obtained. Furthermore, the vertical

aerosol distribution is monitored using a LIDAR. The combination of the instrumentation at Cabauw provides a unique opportunity to study the AOD-PM<sub>2.5</sub> relationship in the Netherlands.

During the summer of 2006 (July-August) the correlation between AOD and PM<sub>2.5</sub> is low (R=0.24). On the other hand, during the subsequent fall (Sep-Nov) the variability in the AOD and PM<sub>2.5</sub> track each other very well with a high correlation coefficient (R=0.77). The situation in fall (Fig. 1) illustrates the potential to define situations in which the AOD may be used to estimate PM<sub>2.5</sub> levels. LIDAR data showed that the period during fall is characterised by relatively well mixed conditions in which the presence of residual layers does not largely affect the AOD.

At the meeting we will present the results for a full year (Jul-2006 to Jul-2007). We will present the relation between AOD and PM<sub>2.5</sub> and how it is influenced by variations in meteorological parameters (like mixing layer height, relative humidity, wind speed/direction) and aerosol characteristics. Selected periods with high values for AOD or PM<sub>2.5</sub>, that show high and low correlations will be discussed. Finally, we hope to demonstrate the feasibility of constructing a map of PM<sub>2.5</sub> for the Netherlands using the established relationships between AOD and PM<sub>2.5</sub>.

R.B.A. Koelemeijer, C.D. Homan and J. Matthijsen, *Atmos Environ*, 40, 5304-5315.

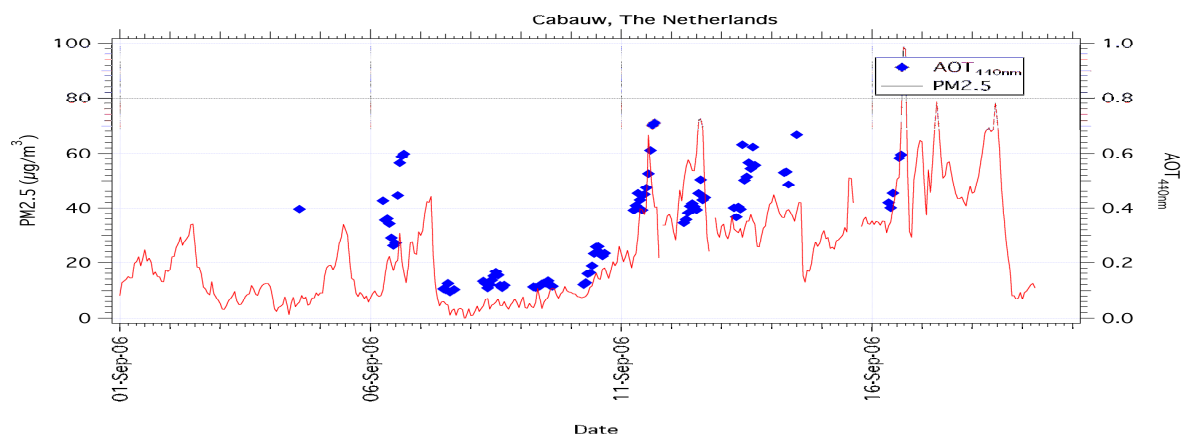


Figure 1. The temporal variability in AOD and PM<sub>2.5</sub> (µg/m<sup>3</sup>) during September, 2006, at Cabauw.

## **Influence of variability in aerosol vertical profile on retrievals of aerosol optical thickness from NOAA AVHRR measurements**

A. Rozwadowska

Institute of Oceanology, Polish Academy of Sciences, Powstancow Warszawy 55, 81-712, Sopot, Poland

Keywords: optical depth, remote sensing, atmospheric aerosols, vertical distribution

Upward radiances at the TOA are the main source of information on the atmosphere and the Earth's surface. Therefore the precise modelling of the atmospheric component of these radiances is an essential problem in remote sensing algorithms. Atmospheric aerosols control variability of TOA radiances over clear sky for given positions of the sun and a satellite. Vertical distribution of type and concentration of aerosol particles varies in time and space. Typically, variability of aerosol profiles is not included in remote sensing algorithms for AOT. Neither they are taken into account in sensitivity analysis of the algorithms. However, some works indicate that in some cases variability in aerosol profile may have significant impact on the TOA radiances (e.g. Meloni *et al.*, 2005, Mitchell *et al.*, 2006).

In the present study we analyse the possible influence of variability in atmospheric aerosol profiles on angular distributions of the TOA upward radiances, focusing on its possible impact on AOT retrievals. We do not intend to analyse any particular case but rather estimate the maximum uncertainty to be expected, and specify the conditions for which a maximum uncertainty may be expected.

The analysis is based on simulations by means of MODTRAN code (Berk *et al.*, 1999). The following tropospheric aerosol models were used in the study: urban/industrial, polluted maritime and clean maritime (d'Almeida *et al.*, 1991). TOA radiances were modelled for three kinds of vertical profiles of aerosol attenuation coefficient for  $\lambda=550$  nm. Profiles similar to those included in MODTRAN were used in the retrieval algorithm. „Real” TOA radiances in NOAA AVHRR channels 1 and 2 were calculated for the extreme cases when all aerosol is concentrated (profile 0) near the surface (0-1 km) and (profile 1) in a layer 5-7 km above the surface. Aerosol optical thickness retrieved from the simulated TOA radiances by means of the algorithm was compared to the actual AOT used in the modelling of the TOA radiances. The biases, i.e. the differences between the retrieved and the actual AOT, were simulated for various values of AOT, water vapour content (WV), solar zenith angle (SZA) satellite zenith angle and relative azimuth between the satellite and the sun. Atmospheric conditions and solar and satellite angles used in the bias simulation are similar to those in the Baltic region.

In the case of channel 1, concentration of the aerosol in the near-surface layer practically does not influence AOT retrievals under the assumption of

constant aerosol profile. The bias is negligible regardless of AOT, solar zenith angle, water vapour content and aerosol model. However, an appearance of a dominating aerosol layer at the altitude of several kilometres may result in a considerable bias in AOT retrievals from AVHRR radiances in channel 1. The maximum bias,  $\epsilon=-0.14$ , is found for AOT=1, SZA=65°, WV=0.5 g cm<sup>-1</sup> and absorbing aerosols, that is for urban and polluted maritime models. In the case of AOT=0.2 the maximum absolute value of the bias is about 0.02.

In channel 2, the bias is considerably higher than in channel 1. Generally, the bias is negative for the profile 0 and positive for the profile 1, regardless of the aerosol model, aerosol optical thickness, water vapour content, and sun-pixel-satellite geometry. Its absolute value increases with an increase in AOT, SZA and water vapour content, reaching its maximum value at AOT=1, SZA=65° and WV=3.0 g cm<sup>-1</sup> in these simulations. For profile 1 the maximum absolute value of the bias amounts to 0.4 for AOT=1 and about 0.04 for AOT=0.2, while for profile 0 it does not exceed 0.02 for AOT=0.2 and 0.06 for AOT=1.0 in our simulations.

Even though actual biases may vary from the values presented above, they should fall within the range of magnitude determined in his paper. Given that in the present bias estimation simplified “exaggerated” cases were considered and that AOT over the Baltic Sea typically is below 0.2 and only very rarely exceeds 0.5, the expected aerosol profile bias is negligible for channel 1 of NOAA AVHRR, while for channel 2 it may be significant.

Berk A. *et al.* (1999). *MODTRAN4 users manual*. Air Force Research Lab., Hanscom, AFB, Mass., USA.

d'Almeida, G. A., Koepke P. & Shettle E. P. (1991). *Atmospheric aerosols: global climatology and radiative characteristics*. Hampton, Virginia, USA: A. Deepak Publishing.

Meloni, D., di Sarra A., di Iorio T., & Fiocco G. (2005). *J. Q. Spect. Rad. Transfer*, 93, 397-413.

Mitchell R. M., O'Brien D. M., Campbell S. K. (2006). *J. Geophys. Res.*, 111, D02204, doi:10.1029/2005JD006304.

## Exact analytical solution of the vector radiative transfer equation for aerosols with an arbitrary scattering matrix

A. B. Gavrilovich

Institute of Physics, National Academy of Sciences,  
68, Nezavisimosti Prosp., 220072, Minsk, Belarus

KEYWORDS: aerosol, vector radiative transfer equation, polarization, scattering matrix.

Urgent problems of atmospheric optics call a necessity of fundamental investigations directed to the improvement of the analytical methods solution of the vector radiative transfer equation (VRTE) in dispersion medium with real scattering matrix. The problem of light scattering by an aggregation of randomly oriented nonspherical particles is one of the most complex problems of the aerosol optics. It is very difficult to mathematically describe the interaction of light with such a system when it is necessary to take into account the multiple scattering of light and radiation polarization. However, this is need for the most important problems of optical polarization diagnostics of dispersion media. Solution of these problems gives a reach information on a microstructure and optical constants of a substance, the component composition, and the form of particles and their orientation in space. Because of the multiparametricity and complexity of the light interaction with particles, the solution of such problems were based till now on the numerical methods and crude analytical approximations. The main difficulty of analytical solution of the VRTE, as is known, is taking into account the infinitely large number of generalized spherical functions. The known analytical approximations are very idealized and, as a rule, do not provide the obtaining of physically right results. For example, the method of spherical harmonics leads to significant losses of the information at small scattering angles. The method of small-angle approximation, by contrast, ignores the very informative region of large scattering angles. A new method developed by the author and presented in this work is free of the indicated drawbacks. We have realized a new method of solving the VRTE, which implies that the infinite system of generalized spherical functions is replaced by the finite orthogonal basis of G-functions satisfying the complexity conditions. The G-functions forms the class of functions belonging in the finite functional G-space. As the object of investigation, we used a volume of nonspherical chaotically oriented particles with an arbitrary scattering matrix. A monochromatic unidirectional polarized beam of rays incident on the three-dimensional volume of particles was considered. The problem of multiple scattering of polarized radiation on such an aggregation of

particles reduces to the solution of the vector integro-differential equation of transfer (VRTE), where  $\mathbf{I}(\mathbf{r}, \mathbf{\Omega})$  is the Stokes vector of diffuse radiation as a function of the space coordinates  $\mathbf{r} = \mathbf{r}(x, y, z)$ , and the direction of radiation propagation  $\mathbf{\Omega} = \mathbf{\Omega}(\mathcal{G}, \varphi)$ , where  $\mathcal{G}$  и  $\varphi$  are the polar and azimuth angles of the spherical coordinate system. The scattering matrix  $\mathbf{x}(\mu)$  is determined by the microstructural, optical, geometric, and orientational parameters of the particles.

The high sensitivity of the polarization effects to the properties of particles imposes very high requirements on the new method of solving the equation of transfer. Namely, the solution should involve the whole information contained in the real scattering matrix. The new method of solving the VRTE is based on the use of the system of special orthogonal basis G-functions. We have the found system of special basis function  $G_l^{mn}(\mathbf{R})$ , orthogonal on a unite sphere of directions. The system of orthogonal basis functions is sufficient for realization of G-function method for analytical solving the VRTE. The application of the system of the G-functions obtained to the vector radiative transfer equation made it possible to get the analytical solution for the components of the Stokes vector in the closed form:

$$I_i(\mathbf{r}, \mathbf{\Omega}) = \sum_{l=\sup(m,n)}^2 \sum_{m=-l}^l \sum_{n=-l}^l \mathbf{I}_l^{mn}(\mathbf{r}) \mathbf{G}_l^{mn}(\mathbf{\Omega}),$$

$i = 1, 2, 3, 4.$

### Conclusion

For the first time we found an exact analytical solution of the VRTE for the Stokes vector in the form of a finite series in class of the G-space functions.

## Mixing layer height determination by Lidar and radiosounding data

F. Navas-Guzmán<sup>1,2</sup>, J. L. Guerrero-Rascado<sup>1,2</sup>, A. B. Fernández-Medina<sup>1,2</sup>, J. A. Adame<sup>3</sup> and L. Alados-Arboledas<sup>1,2</sup>

<sup>1</sup>Grupo de Física de la Atmósfera. CEAMA. Universidad de Granada. Junta de Andalucía. 18006 Granada. Spain

<sup>2</sup>Departamento de Física Aplicada. Universidad de Granada. 18071, Granada. Spain.

<sup>3</sup>Instituto Nacional de Tecnología Aeroespacial (INTA), Huelva, Spain

Keywords: Mixed-layer Depth, Lidar, radiosounding

The atmospheric boundary layer (ABL) has a thickness quite variable in space and time, ranging from hundred of metres up to a few kilometres. For convective conditions, pollutants that are emitted into the mixed layer become gradually dispersed and mixed through the action of turbulence. In this sense the mixing height (MH) is a key parameter.

Different methods can be employed to determine the mixing height. For convective conditions the radiosoundings are the most common data source based on wind, temperature and pressure profiles. A description of the determination of mixing layer by means of radiosounding is presented by Hanna (1969).

Active remote sensing systems such as Lidars use aerosols as tracers where the received energy is proportional to the aerosol content of the atmosphere. The main advantage of the Lidar technique is the possibility of carrying out a continuous monitoring of the atmosphere that permits to obtain a mixing height temporal evolution.

The energy received by a Lidar system is proportional to the backscattered signal from particles and molecules present in the atmosphere. The range-squared-corrected signal can be expressed as:

$$RSCS = k[\beta^a(r) + \beta^m(r)]T(r)^2$$

where  $\beta^a$  and  $\beta^m$  are particular and molecular backscatter coefficients, respectively,  $k$  is the system constant,  $T$  is the atmospheric transmission and  $r$  is the distance between the laser source and the target.

Three derivative methods are used to estimate the mixing height (Sicard et al, 2005):

*Gradiente Method (GM):* For the marked transition between the Mixed Layer and the Free Troposphere, the derivative of RSCS exhibits a strong negative peak. This method assigns how mixing height where occurs the absolute negative minimum of the first derivative of the RSCS.

*The Inflection Point Method (IPM):* The mixing height corresponds to the minimum of the second derivative the RSCS just below altitude obtained by gradient method.

*The Logarithm Gradient Method (LGM):* this height,  $h_{LGM}$ , corresponds to the minimum of the first derivative of the RSCS is reached.

The mixing heights obtained on 29th June 2006 at 12:00 GMT in El Arenosillo station (Huelva, Spain, 37.1° N, 6.7° O, 0 m a.s.l.) for the different derivative methods are  $h_{GM} = 995 \pm 15$  m,  $h_{IPM} = 980 \pm 30$  m and  $h_{LGM} = 995 \pm 15$  m. These results show a good agreement with mixing height obtained through the Richardson method by radiosoundings in overlap spatial and temporal, which was  $1020 \pm 30$  m.

Figure 1 shows the RSCS temporal evolution on 29th June. Black points correspond to the mixing heights obtained by Lidar and white diamonds correspond to the mixing height by radiosoundings.

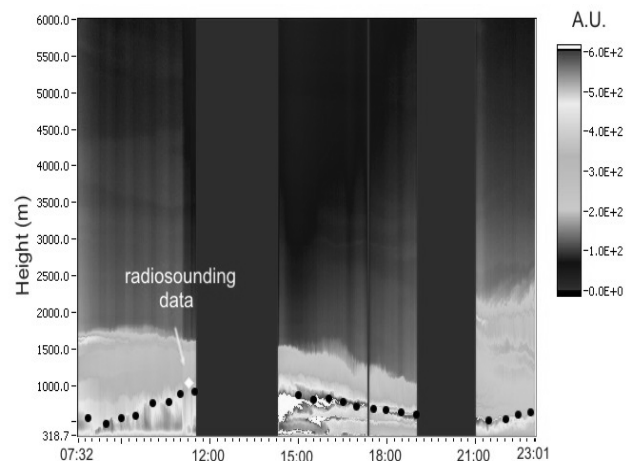


Figure 1: RSCS evolution on 29th June 2006, black points and white diamonds correspond to mixing heights by Lidar system and radiosounding, respectively.

*Acknowledgements:* This work was supported by the Spanish Ministry of Education project CGL2004-05984-C07-03 and by Andalusian Regional Government project P06-RNM-01503.

### References

- Hanna, S. R., 1969. The thickness of the planetary boundary layer, *Atmos. Environ.* **3**, 519-536.
- Sicard, M., Pérez, C., Rocadenbosch, F., Baldasano, J.M. y García-Vizcaino, D., 2005. Mixed-layer depth determination in the Barcelona coastal area from regular lidar measurements: methods, results and limitations, *Boundary-Layer Meteorol.*, **119**,135-157.

## **T21 Abstracts**

## Ice-nucleating ability of the most abundant mineral dust phases in the atmosphere

F. Zimmermann<sup>1</sup>, M. Ebert<sup>1</sup>, St. Weinbruch<sup>1</sup> and L. Schütz<sup>2</sup>

<sup>1</sup>Institute of Applied Geosciences, Technical University Darmstadt, Schnittspahnstr. 9, 64287 Darmstadt, Germany

<sup>2</sup>Institute for Atmospheric Physics, Johannes-Gutenberg University, Johann-Joachim-Becher-Weg 21, 55099 Mainz, Germany

Keywords: Mineral dust, ESEM, Ice nuclei, Heterogeneous ice nucleation

Ice nucleation occurs in the atmosphere in two primary ways: by homogeneous freezing of liquid solution droplets and by heterogeneous interaction with a particulate nucleus (e.g., Pruppacher and Klett, 1997). Heterogeneous freezing is initiated by the presence of solid particles with an appropriate structure, so called "ice nuclei" (IN) (e.g., Roddy and O'Connor, 1981). For both processes, nucleation efficiency varies with temperature and supersaturation with respect to ice.

Mineral dust has been identified as an abundant species in the troposphere and can act as efficient IN (DeMott, 2003) in the deposition mode. Mineral dust, however, can be composed of different minerals. Clay or silicate particles, contained in mineral aerosols, are particularly effective ice nuclei (Pruppacher and Klett, 1977).

Therefore we investigated the ice-nucleating ability of eight major minerals (quartz, feldspar, calcite, gypsum, illite, kaolinite, montmorillonite, and hematite; Claquin et al. 1999). We determine threshold temperature and threshold supersaturation values with respect to water or ice for the condensation freezing mode and for the deposition mode, respectively, using an environmental scanning electron microscope (ESEM).

Environmental scanning electron microscopy (ESEM) enables in-situ observation of interactions between water vapour and aerosol particles in the sub-micrometer range (e.g., Ebert et al, 2002). By varying the water partial pressure and using a Peltier element to realize temperatures below the freezing point it is possible to obtain supersaturated conditions relative to ice in the sample chamber of an environmental scanning electron microscope (Zimmermann et al., 2007).

All investigated mineral dust phases nucleated ice in the temperature range of -10°C to -25°C, relevant for mixed phase clouds in the lower troposphere. However, the ice forming ability of the various minerals differ largely from each other (table 1).

Kaolinite, hematite, and illite were the most efficient IN, whereas calcite and gypsum act as ice nuclei only at relative low temperatures. These findings are in good agreement with literature data.

Table 1. Activation temperatures of mineral dust particles as well as corresponding supersaturation with respect to ice

Dust species	temperature (°C)	RH <sub>i</sub> (%)
kaolinite	-10	113
montmori.	-13	116
illite	-12	115
quartz	-12	119
calcite	-15	110
orthoclase	-14	110
gypsum	-16	115
hematite	-11	114

We also investigated ambient aerosol samples from a rural background site (Kleiner Feldberg, Taunus, near Frankfurt a. M.) and Sahara aerosol samples. Both, the rural and the Sahara aerosol samples, were very efficient IN over the whole temperature range and over a broad RH<sub>i</sub> range due to the different minerals phases contained in ambient mineral dust. Further investigations will be focus on the influence of anthropogenic impurities on the IN efficiency of naturally occurring minerals.

Financial support by the German Science Foundation (Sonderforschungsbereich 641 "The tropospheric ice phase") is gratefully acknowledged.

- Claquin, T., Schulz, M. & Balkanski, Y.J. (1999). *J. Geophys. Res.* 104, 22243-22256
- DeMott, P.J., Sassen, K., Poellot, M.R., Baumgardner, D., Rogers, D.C., Brooks, S.D., Prenni, A.J., Kreidenweis, S.M. (2003). *Geophys. Res. Lett.* 30:doi:10.1029/2003GL017410.
- Ebert, M., Inerle-Hof, M., & Weinbruch S. (2002), *Atmos. Environ.* 36, 5909-5916.
- Pruppacher, H.R. & Klett, J.D. (1997). *Microphysics of Cloud and Precipitation*. Kluwer Academic Press.
- Roddy, A.F. & O'Connor, T.C. (Eds.) (1981). *Atmospheric Aerosols and Nuclei*, Galway Univ. Press, Galway, Ireland, 333-387
- Zimmermann, F., Ebert, M., Worrigen, A., Schütz, L., & Weinbruch, S. (2007). *Atmos. Environ.*, under review

## **The Meridional Gradient of Black Carbon in the Upper Troposphere and Lower Stratosphere over Northern Europe**

D.G. Baumgardner<sup>1</sup>, G.L. Kok<sup>2</sup> and M. Krämer<sup>3</sup>

<sup>1</sup>Centro de Ciencias de la Atmósfera, Universidad Nacional Autónoma de México, Mexico City, 04150 Mexico

<sup>2</sup>Droplet Measurement Technologies, Boulder, 80301, Colorado, USA

<sup>3</sup>Research Center Jülich, ICG-1, Germany

Keywords: atmospheric aerosols, aerosol chemistry, black carbon

As part of the Cirrus III campaign, conducted November 23-29, 2006, black carbon (BC) measurements were made with the single particle soot photometer (SP2) that was mounted on the Learjet operated by Envioscope for this field campaign. The SP2 measures the mass and mass equivalent diameter of BC contained in individual particles so that the properties of these climatically important particles can be characterized in great detail.

The BC mass shows a positive trend with latitude, increasing from 0.2 to 1.2 ng m<sup>-3</sup> from 55° to 70° N, and the number concentration of BC particles also increased from 0.2 to 0.4 cm<sup>-3</sup>. The extinction coefficient, estimated from the fraction of BC in the particles, increased from 0.2 to 1 Mm<sup>-1</sup> over this same latitude range.

The microstructure of the soot layers, properties of the BC particles and the implications for radiative forcing will be presented in this study.

## Dust Aerosol-Cloud Interaction Derived From A-Train Satellites and Ground Measurements

Jianping Huang<sup>1</sup>, Patrick Minnis<sup>2</sup>, Yuhong Yi<sup>3</sup>,  
Jing Su<sup>1</sup>, Jianrong Bi<sup>1</sup>, and Kirk Ayers<sup>3</sup>

<sup>1</sup>College of Atmospheric Sciences, anzhou University, anzhou, China 73000

<sup>2</sup>NASA Langley Research Center, Hampton, VA, 23681

<sup>3</sup>SSAI, One Enterprise Parkway, Hampton, VA, 23666

Key words: Dust aerosol, Indirect effect, Semi-direct effect, A-Train satellite

Recent studies have shown that aerosols can cause substantial alteration in the energy balance of the atmosphere and the Earth's surface, thus modulating the hydrologic cycle. Absorbing aerosols, such as dust and black carbon, can heat the atmosphere due to shortwave absorption and enhanced cloud evaporation (Huang et al., 2006 a, b). In this study, both the indirect and semi-direct effects of Asian dust aerosols on cloud and radiative properties are studied using A-train satellite data and ground-based measurements. The NASA A-train series of satellites includes CA IPSO, C OUDSAT, MODIS/Aqua, CERES/Aqua, OMI/Aura, which take nearly simultaneous measurements of aerosol radiative properties, vertical structure, cloud properties, temperature and water vapor profiles. Using CERES top-of-the-atmosphere fluxes, aerosol/cloud properties retrieved from MODIS, vertical distributions of aerosols and clouds from CA IPSO as well as measurements from surface sites as inputs, radiative transfer models are used to determine reliable estimates of dust radiative forcing.

The results show that the dust appears to reduce the ice cloud effective particle diameter and increase high cloud amount. The average ice cloud effective particle diameter of cirrus clouds under dust polluted conditions (dusty clouds) is 11 smaller than that derived from ice

clouds in dust-free conditions. Due to the effect of dust aerosol on cloud properties, the instantaneous net radiative forcing at the top of atmosphere (TOA) for dusty clouds is reduced compared to that for dust-free clouds. The reduced cooling effects of dust may lead to a net warming. The water paths of dusty clouds are also considerably smaller than those of dust-free clouds. Dust aerosols could warm clouds, thereby increasing the evaporation of cloud droplets resulting in reduced cloud water path (semi-direct effect). The semi-direct effect may be dominated by the interaction between dust aerosols and clouds over arid and semi-arid areas and partly contribute to reduced precipitation.

Huang, J., et al. (2006), Satellite-based assessment of possible dust aerosols semi-direct effect on cloud water path over East Asia, *Geophys. Res. Lett.*, **33**, doi:2006G 026561.

Huang, J., et al., (2006) Possible influences of Asian dust aerosols on cloud properties and radiative forcing observed from MODIS and CERES, *Geophys Res. Lett.* **33**, doi:10.1029/2005G 024724.

## Dynamics and ice nucleation behavior of water on kerosene soot, original and wetted by H<sub>2</sub>SO<sub>4</sub>: UT / LS implications.

B. Demirdjian<sup>1</sup>, D. Ferry<sup>1</sup>, J. Suzanne<sup>1</sup>, O.B. Popovicheva<sup>2</sup>, N.M. Persiantseva<sup>2</sup>, N.K. Shonija<sup>3</sup>

<sup>1</sup>CRMC-N / CNRS, Campus de Luminy, 13009 Marseille, France

<sup>2</sup>Institute of Nuclear Physics, Moscow State University, 119899 Moscow, Russia

<sup>3</sup>Chemistry Department, Moscow State University, 119992 Moscow, Russia

Keywords: Atmospheric aerosols, heterogeneous ice nucleation, particles characterisation, soot particles.

The heterogeneous nucleation mechanism is at the origin of most of ice formation in nature. In the polluted atmosphere combustion soot aerosols attract much attention as potential ice-forming nuclei. Because of their various structure and source-dependent surface organic coverage, soot particles may demonstrate a great variety of ice nuclei activities. Interaction with atmospheric particles (sulfate aerosols) enlarges the soot activity spectrum and therefore complicates estimations of possible climate impact of soot exhausts upon atmosphere.

Quasi-elastic neutron scattering (QENS) is a powerful tool to analyse the freezing phenomenon in the water-soot system (Ferry *et al.*, 2002). Complementary techniques (transmission electron microscopy, water adsorption isotherms, FTIR spectroscopy, gas chromatography, mass spectrometry) provide very useful information about the soot physico-chemical characteristics: microstructure, composition and surface chemistry. In this work original kerosene flame soot (figure 1) produced by burning an aviation kerosene is studied as a surrogate of the hydrophobic fraction of aircraft-generated soot aerosols (Popovicheva *et al.*, 2004).

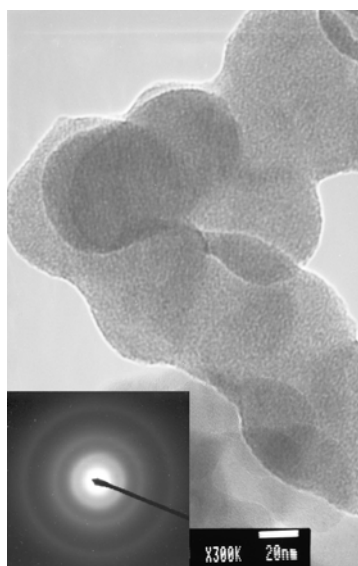


Figure 1. TEM (transmission electron microscopy) image and its SADP (selected area diffraction pattern) of kerosene soot particles.

Its water adsorbability is determined by the organic coverage which prevents the water access to the micropores.

Examination of QENS data of adsorbed water on original kerosene soot under UT/LS conditions allows a decomposition of spectra into a solid and a liquid components. The analysis shows a high fraction of unfrozen water, 70% and 60% at 240K and 220K respectively. Ice nucleation ability of original kerosene flame soot is changed by a soot treatment with 20 wt% of sulphuric acid. We find that the H<sub>2</sub>SO<sub>4</sub> interaction with the soot surface facilitates ice nucleation: the fraction of unfrozen water decreases down to 40% and 30% at 240K and 220K respectively. Therefore, the hydrophobic fraction of aircraft-generated soot particles may act as ice nuclei only at lower temperatures in the ice-saturated ranges of the upper troposphere but their ice-forming ability is sensitive to interaction with sulfate aerosols.

D. Ferry, J. Suzanne, S. Nitsche, O.B. Popovicheva, & N.K. Shonija, (2002). *Journal of Geophysical Research* 31 (11): Art. No. L11104

O.B. Popovicheva, N.M. Persiantseva, E.E. Lukhovitskaya, N.K. Shonija, N.A. Zubareva, B. Demirdjian, D. Ferry, & J. Suzanne (2004). *Geophysical Research Letters* 107 (D23): Art. No. 4734

## The Pacific Dust Experiment (PACDEX): Early Results

J.L. Stith<sup>1</sup>, V. Ramanathan<sup>2</sup>

<sup>1</sup>National Center for Atmospheric Research, Boulder, 80307, Colorado, USA

<sup>2</sup>Scripps Institute of Oceanography, La Jolla, 92037, California, USA

Keywords: aerosol chemistry, clouds, dust, radiative properties

The long range transport of dust and anthropogenic aerosols (e.g., black carbon, organics and sulfates, and air pollution from Eurasia) across the Pacific Ocean, into North America is one of the most widespread and major pollution events on the planet. This plume passes through the Pacific Ocean extra tropical cloud systems, which are important climate regulators through their large radiative cooling effect. The effect of this mixed dust-pollution plume on the Pacific cloud systems and the associated radiative forcing is an outstanding problem for understanding climate change and has not been explored. The primary reason is the lack of an airborne platform that can sample the evolution of this plume in situ all the way across the Pacific Ocean. The NSF/NCAR-HIAPER (High Performance Instrumented Airborne Platform for Environmental Research) platform fills this observational gap and opens new doors for observing this great natural/man made phenomenon.

The Pacific Dust Experiment (PACDEX) is a pilot study using quasi-Lagrangian sampling of this Eurasian-Pacific-North American dust plume. The following objectives will be the focus of the experiment:

- a) Identification of the principal cloud-active aerosol in the Asian plume. This will be done using Cloud Condensation Nuclei and Ice Nuclei measurements together with the basic aerosol package on HIAPER.
- b) Document the changes in the cloud hydrometeor size spectra in regions of enhanced cloud active aerosol.
- c) Document the solar changes in the plume vertical structure in clear air and cloudy regions.
- d) Document near source and far from source changes in the plume that might affect (a), (b) and (c). While the sampling cannot be truly Lagrangian, due to the effects of wind shear over the depth of the plume, we identify regions with various ages using trajectory analysis and model simulations.
- e) Compare the in-situ vertical structure observed from the aircraft upwind and near the ground stations.

The PACDEX science team consists of 27 scientists from four countries (US, China, Japan, Korea), and includes specialists in airborne in situ sampling (trace gases, aerosols, cloud active nuclei, cloud water and ice size distributions, upward and downward irradiance), ground based sampling (radiation characterization, aerosol characterization, lidar), satellite observations (e.g. A-train data), and modeling of plume chemical and physical properties.

A description of the PACDEX flight sampling strategy is shown in Figure 1.

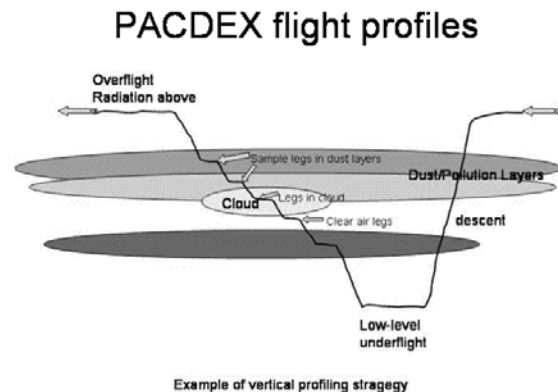


Figure 1. The PACDEX Flight Strategy. Racetrack Patterns will be done at various altitudes, depending on the locations of plume features.

PACDEX will follow the atmospheric transport of dust and pollution across the Pacific Ocean during April and May of 2007. This is the first time that a dust event will be sampled just before a dust event and across its entire transection across the Pacific Ocean. Hence, we hope to obtain unique insights into long range transport of dust and soot and their impacts on clouds and radiation in the Pacific Ocean and North America. In this presentation we describe (a) the science team for PACDEX and their roles in the project, (b) An overview of the major instruments and data products, (c) a summary of the missions that were accomplished, and (d) An overview of preliminary results and observations from the project.

Acknowledgements. The primary support for PACDEX is from the National Science Foundation (NSF). NCAR is supported by the National Science Foundation.

## Do aircraft black carbon emissions affect cirrus clouds on the global scale?

J. Hendricks<sup>1</sup>, B. Kärcher<sup>1</sup>, U. Lohmann<sup>2</sup> and M. Ponater<sup>1</sup>

<sup>1</sup>DLR-Institut für Physik der Atmosphäre, Oberpfaffenhofen, D-82234 Wessling, Germany

<sup>2</sup>ETH Zurich, Institute for Atmospheric and Climate Science, Universitätstr. 16, CHN O11, 8092 Zurich, Switzerland

Keywords: atmospheric aerosols, black carbon, ice nuclei, ice clouds, modelling

Potential modifications of cirrus clouds caused by aircraft-generated black carbon (BC) soot particles were investigated with the global atmospheric model ECHAM4 (Roeckner *et al.*, 1996) including aerosols, cloud microphysics, and aerosol-ice cloud interactions (Lohmann *et al.*, 2004).

The simulations reveal that BC from aviation can cause significant perturbations of the number concentration of potential ice nuclei (Fig.1; Hendricks *et al.*, 2004).

microphysics to aviation-induced BC was studied (Hendricks *et al.*, 2005). The model results suggest that aircraft BC particles could change the ice crystal number concentration at northern midlatitudes significantly (10–40% changes of annual mean zonal averages at main flight altitudes), provided that such BC particles serve as efficient ice nuclei. The sign of the effect depends on the specific assumptions on aerosol-induced ice nucleation.

These results demonstrate that significant cirrus cloud modifications by BC from aircraft and related climatic impacts cannot be excluded.

Table 1. Summary of scenarios analyzed.

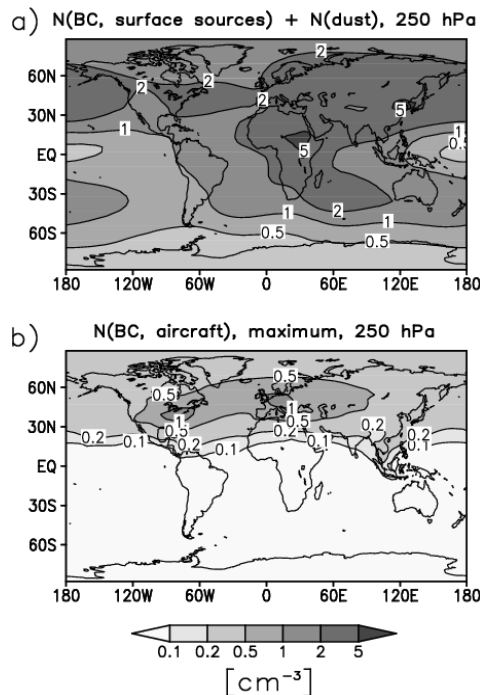


Figure 1. Annual mean number concentrations [particles/cm<sup>3</sup>] of potential ice nuclei at 250 hPa (within main aircraft flight level; approximately at 10 km altitude). (a) Mineral dust and hydrophilic BC particles originating from surface sources. (b) BC particles from aircraft (maximum estimate by Hendricks *et al.* (2004)). The Figure is adopted from a previous publication (Hendricks *et al.*, 2005).

Many details of the role of BC in cirrus cloud formation are currently not well known. Therefore, hypothetical scenarios based on various assumptions on the ice nucleation efficiency of background and aircraft-induced BC particles were considered (Table 1). Using these scenarios, the sensitivity of ice cloud

Assumptions on heterogeneous ice formation	Analysis strategy	Main result
<i>Scenario 1</i>		
Heterogeneous nucleation on mineral dust, BC from surface sources, and BC from aircraft	Comparison of simulations in/excluding ice formation of BC from aircraft	Aviation causes significant increase in ice crystal number concentrations
<i>Scenario 2</i>		
Heterogeneous nucleation on BC from aircraft only; background freezes homogeneously	As Scenario 1	Aviation causes significant decrease in ice crystal number concentrations

This research was performed within the DLR (German Aerospace Center) / HGF (Helmholtz Association of German Research Centers) project ‘‘Particles and Cirrus Clouds’’ (PAZI-2).

Hendricks, J., et al. (2004). *Atmos. Chem. Phys.*, 4, 2521–2541.

Hendricks, J., Kärcher, B., Lohmann, U., & Ponater, M. (2005). *Geophys. Res. Lett.*, 32, L12814, doi:10.1029/2005GL022740.

Lohmann, U., Kärcher, B., & Hendricks, J. (2004). *J. Geophys. Res.*, 109, D16204, doi:10.1029/2003JD004443.

Roeckner, E., et al. (1996). *Tech. Rep. 218*, Max-Planck-Inst. für Meteorol., Hamburg, Germany.

## Nitric acid uptake and supersaturations in different types of cirrus clouds: model case and sensitivity studies

I. Gensch<sup>1</sup>, H. Bunz<sup>2</sup>, D. Baumgardner<sup>3</sup>, L.E. Christensen<sup>4</sup>, J. Curtius<sup>5</sup>, R.L. Herman<sup>4</sup>, T. Peter<sup>6</sup>, P. Popp<sup>7</sup>, C. Schiller<sup>1</sup>, H. Schlager<sup>8</sup>, C. Voigt<sup>8</sup>, C.R. Webster<sup>4</sup>, J.C. Wilson<sup>9</sup>, M. Kraemer<sup>1</sup>

<sup>1</sup>Forschungszentrum Juelich, Institut fuer Chemie und Dynamik der Geosphaere, ICG-1,52425 Juelich, Germany

<sup>2</sup>Forschungszentrum Karlsruhe, Institut fuer Meteorologie und Klimaforschung, 76021 Karlsruhe, Germany

<sup>3</sup>Universidad Nacional Autonoma de Mexico, Ciudad Universitaria, Mexico City, DF 04150, Mexico

<sup>4</sup>Jet Propulsion Laboratory, California Institute of Technology, Pasadena, CA 91109, USA

<sup>5</sup>Institut fuer Physik der Atmosphaere, Universitaet Mainz, 55099 Mainz, Germany

<sup>6</sup>Institut fuer Atmosphaere und Klima, ETH Zuerich, 16 8092 Zuerich, Switzerland

<sup>7</sup>NOAA Earth System Research Laboratory, Chemical Sciences Division, Boulder, CO 80305, USA

<sup>8</sup>DLR-Institut fuer Physik der Atmosphaere Oberpfaffenhofen, 82234 Wessling, Germany

<sup>9</sup>University of Colorado at Denver, Denver, CO 80217, USA

Keywords: UT/LS Supersaturations, Nitric Acid, Homogeneous/Heterogeneous Freezing of Aerosols

### INTRODUCTION

The uptake of gas phase HNO<sub>3</sub> by super-cooled solution droplets plays an important role in the NO<sub>x</sub>/NO<sub>y</sub> budget in the upper troposphere and thus may affect the ozone chemistry. At temperatures below ~235K rapid cooling rates lead to high relative humidities with respect to ice RH<sub>ice</sub>. Depending on the aerosol particle composition **homogeneous** or **heterogeneous** ice nucleation occurs after reaching a specific freezing threshold. The partitioning of ambient water vapor and nitric acid among the gas phase, the liquid interstitial aerosols and the ice crystals is controlled by different parameters such as composition of the particles population, ambient temperature and pressure, as well as the concentration of the trace gases.

Case and sensitivity studies presented here accentuate the impact of freezing mechanism and temperature on the temporal evolution of RH<sub>ice</sub> and HNO<sub>3</sub> partitioning in ice clouds.

### MODEL STUDIES

A detailed micro-physical box model has been used here in order to follow the evolution (growth, uptake of trace gases, ice nucleation) of an aerosol population along an atmospheric trajectory.

The initialization of the simulations is based on data collected during the field campaigns **Polstar 1997**, **CIRRUS-III 2006** and **CR-AVE 2006**. The box model is advected along isentropic backward trajectories ending on the flight path, which have been calculated using ECMWF data.

The growth kinetics of the aerosol particles, in this case aqueous H<sub>2</sub>SO<sub>4</sub> droplets, is governed by the condensation/evaporation rates of the volatile compounds (water, nitric acid). At each time step parameters like particle composition, partial and saturation vapour pressures are calculated considering the mass balance among different condensing phases of the components (Bunz et al. 2003).

Homogeneous ice nucleation rate J<sub>hom</sub> depends only on the water activity and temperature (Koop et al. 2000). The simulation of heterogeneous ice

nucleation uses a “shifted” water activity scheme (Kärcher and Lohmann 2003). Experiments in the aerosol chamber AIDA provide information about supersaturations at freezing onset of soot particles coated with H<sub>2</sub>SO<sub>4</sub>/H<sub>2</sub>O films (Möhler et al. 2005).

### RESULTS

High RH<sub>ice</sub> and substantial amounts of nitric acid inside the particles are present at ice formation in all simulations.

High ice crystal number density inside ice clouds in case of homogeneous ice nucleation determines a rapid decrease of the RH<sub>ice</sub> after ice formation, followed by a fast partial release of HNO<sub>3</sub> from the interstitial particles.

Heterogeneous freezing generates lower ice crystal number densities. These together with higher cooling rates and lower temperatures can lead to supersaturations inside cirrus clouds that persist over longer time periods. Consequently, more HNO<sub>3</sub> is residing longer in the interstitial particles.

At very low temperatures the simulations show a steadily increasing amount of HNO<sub>3</sub> in the interstitial aerosol particles during cloud evolution.

### CONCLUSIONS

Comparison among model sensitivity studies and field observations help to give insight to the freezing mechanism of aerosols and to understand the role of different atmospheric parameters in the formation of ice clouds.

### REFERENCES

- Bunz, H. et al. (2003), in *EGS-AGU-EUG Joint Assembly*, Nice, France, 6-11th April 2003.  
Kärcher, B. and Lohmann U. (2003), *J. Geophys. Res.*, 108, D14, 4402-4416.  
Koop, Th., Luo, B., Tsias, A. and Peter Th. (2000), *Nature*, 406, 611-614.  
Krämer, M. et al. (2006), *Tellus B, Chem. Phys. Meteo.*, 58 (2), 141-147  
Möhler, O. et al. (2005), *J. Geophys. Res.*, 110, D11210.

## Impact of aerosols and dynamics on cirrus clouds - measurements and model studies

P. Spichtinger<sup>1</sup>, S. Schlicht<sup>2</sup>, C. Schiller<sup>2</sup>, N. Spelten<sup>2</sup>, M. de Reus<sup>3</sup>, J. Curtius<sup>3</sup>, H.-J. Vössing<sup>3</sup>, S. Borrmann<sup>3</sup> and M. Krämer<sup>2</sup>

<sup>1</sup>Institute for Atmospheric and Climate Science, ETH Zurich, 8092 Zurich, Switzerland

<sup>2</sup>ICG-I, FZ Jülich, Jülich, Germany

<sup>3</sup>Institute for Atmospheric Physics, University of Mainz, Mainz, Germany

Keywords: Ice clouds, Modelling, Measurements, Ice nuclei.

Cirrus clouds are important modulators of Earth's radiation budget; it is assumed that (thin) cirrus clouds can contribute to a net warming of the Earth-Atmosphere system. Usually, in large scale models cirrus clouds are treated as homogeneous layer clouds. However, even from surface observation the internal structure or "patchiness" of cirrus clouds is obvious, hence this could lead to additional radiative effects. It is not clear, if these structures are due to different amounts of ice nuclei or if slightly different dynamics could induce the internal structure of cirrus clouds. For further investigation of the "patchiness" we use data from recent measurement campaigns (CIRRUS II, November 2004 and CIRRUS III, November 2006) and a 2D/3D cloud resolving cirrus model.

During the aircraft campaigns CIRRUS II & III (base at Hohn, Northern Germany) cirrus clouds in frontal systems over Norway, North Sea and Germany were observed by means of the Lyman- $\alpha$ -hygrometer FISH (Fast In-situ Stratospheric Hygrometer), the water vapor tunable diode laser OJSTER (Open-path Jülich Stratospheric Tdl ExpeRiment) and an FSSP (Forward Scattering SPectrometer) mounted on board of a GFD-Learjet (FSSP300 during CIRRUS II and FSSP100 during CIRRUS III). Additional information about the aerosol background was available from the particle counters COPAS (COndensation PArticle Counter System during CIRRUS II) and MARIE (Mainz AeRosol Instrument, during CIRRUS III).

From theory (see e.g. Kärcher and Lohmann, 2002) one would expect quite low ice crystal number concentrations due to the moderate synoptic updrafts ( $w < 10$  cm/s) along fronts and weather systems. However, during a flight on 24th of November 2004 (CIRRUS II) the ice particle concentrations inside the observed cloud reached high values up to  $55 \text{ cm}^{-3}$  whereas, backward trajectory calculations based on CLaMS and ECMWF-data yield typical low synoptic vertical velocities of 1-3cm/s; homogeneous freezing of aqueous solution droplets (e.g. Koop et al., 2000) at these vertical velocities would produce ice crystal number concentrations about 2-3 orders of magnitude lower than the measured values. Additionally, inside the cirrus clouds horizontal gradients of ice crystal number density are often quite high, i.e. the cirrus

clouds are inhomogeneous or patchy.

For the investigation of the formation processes of this patchiness we use the non-hydrostatic an-elastic dynamical model EULAG (Smolarkiewicz and Margolin, 1997) with a recently developed and implemented two moment bulk ice microphysics (Spichtinger and Gierens, 2007), including the processes nucleation (homogeneous and heterogeneous, triggered explicitly by background aerosols), diffusion growth and evaporation and sedimentation of ice crystals. From simulations using different background aerosol number concentrations we could exclude heterogeneous nuclei as a source of high ice crystal number concentrations. From the vertical temperature profile obtained from the aircraft data we found a neutral or even slightly unstable layer. Using these environmental conditions in a superimposed synoptic updraft we found that latent heat release due to the growth of freshly nucleated ice crystals could induce small "convective" cells within the neutral layer. The vertical velocity within these cells can reach values of 1-2m/s. In this case also heterogeneous nucleation plays an important role, because of the lower threshold relative humidities for the initiation of nucleation. Additionally, further investigation of satellite images points to possible impact of orographic waves over Norway – this impact was tested in additional simulations. Hence, for this situation dominated by a large-scale flow additional mesoscale effects (turbulence due to stability, orographic waves) can change the patterns of cirrus clouds and induce patchiness.

We have also investigated frontal cirrus clouds during CIRRUS III in November 2006; here we found much lower values of ice crystal number densities to be more consistent with the synoptic updraft velocities. Here the observed patchiness was investigated as a possible result of dynamics and aerosol effects.

### References:

- Kärcher, B. and U. Lohmann (2002). *J. Geophys. Res.*, 107 (D23), 4698.  
Smolarkiewicz, P. and L. Margolin (1997). *Atmos.-Ocean special*, 35, 127-152.  
Spichtinger, P. and K. Gierens (2007). *Atmos. Chem. Phys.*, in preparation.

## Model calculations and experiments investigating freezing of UT/LS-aerosols

H. Bunz, S. Benz and O. Möhler

Department for Atmospheric Aerosol Research, Inst. for Meteorology and Climate Research, Research Centre Karlsruhe, P. O. Box 3640, 76021 Karlsruhe, Germany

Keywords: aerosol modelling, ice clouds, ice nuclei, mineral dust.

Freezing of aerosols changes their optical properties as well as their chemical and physical behaviour such as growth, surface reactions, uptake of trace gases etc.. Therefore, knowledge of the physical state and the conditions governing its formation is of great importance assessing the influence of the aerosol particles on the climate.

In recent years extensive experimental studies to investigate the freezing potential of different types of aerosol particles were performed (further work is still in progress) in the aerosol chamber AIDA (Möhler et al., 2003). The necessary water vapour supersaturation is achieved by adiabatic pumping of the chamber starting from conditions close to ice saturation. The experiments are accompanied by detailed model calculations. The model simulates on the one hand the important aerosol physical processes and on the other hand simultaneously the thermodynamics in the chamber during the experiments. Besides the temperature and pressure as function of the time the partial pressures of trace gases such as  $H_2O$  and  $HNO_3$  are of special importance and are balanced taking into account the fluxes to and from the walls as well as to and from the aerosol particles. A special version of the model is also used for air parcels moving along an atmospheric trajectory (Krämer et al., 2006)

Ice can be formed either homogeneously within pure water or solution droplets or heterogeneously initiated by surfaces of e.g. mineral dust, soot or other materials. Different formulations for these processes are implemented in our model and compared to the experimental results. Other formulations can be implemented easily.

Whereas quite a few experiments have already been performed for solution droplets, mainly  $H_2SO_4$  and  $(NH_4)_2SO_4$ , recent experiments concentrate on ice formation on mineral dust aerosols, which can be coated by  $H_2SO_4$ -solutions, and on the possible CCN and IN activity of soot particles with different degrees of organic coating.

In cases of coated mineral dust particles the results show that the ice formation at typical cirrus temperatures is governed by the sulphuric acid and the onset saturation level is very similar to the value for pure  $H_2SO_4$ -droplets for the experiments as well as for the model calculation. For most calculations the formulation in (Koop et al., 2000) was applied correlating the freezing probability to the water activity of the droplets. Whereas for temperatures

above about  $-50$  °C the agreement between the modelled and the experimental results is satisfactory, at lower temperatures the degree of water saturation necessary to initiate freezing tends to be higher by up to 20 % in the experiments compared to the model and accordingly the fraction of frozen particles is overestimated by the model. The water activity of the particles had to be reduced to get an agreement with the experimental results (Fig. 1). The reasons for this disagreement are not yet completely understood, some possible explanations are still being discussed.

In the cases of non-coated particles the freezing capacity depends strongly on the nature of the particle surfaces. For hydrophilic particles the onset of the freezing is quite similar to the homogeneous case whereas for hydrophobic particles quite high saturation levels are required.

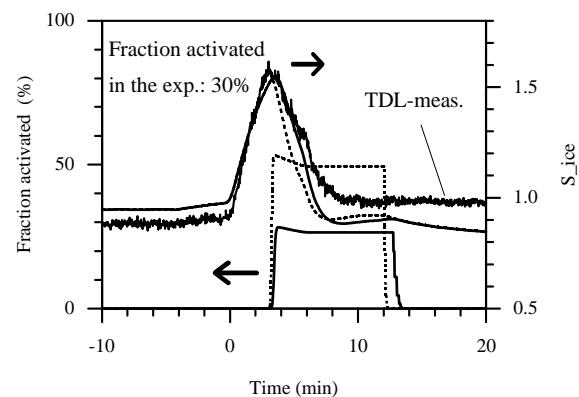


Figure 1. Calculated ice saturation and fraction of activated particles for an experiment with  $H_2SO_4$ -coated Illit particles. Solid lines:  $H_2O$  activity reduced,

Möhler O., Stetzer O., Schaefers S., Linke C., Schnaiter M., Tiede R., Saathoff H., Krämer M., Mangold A., Budz P., Zink P., Schreiner J., Mauersberger K., Haag W., Kärcher B., and Schurath U. (2003) *Atmospheric Chemistry and Physics* 3, 211-223

Krämer, M., Schiller, C., Ziereis, H., Ovarlez, J., & Bunz, H.. (2006). *Tellus* 58B, 141-147

Koop, Th., Luo., B., Tsias, A., & Peter, Th. (2000) *Nature* 406, 611-614

## Aerosol impact on supersaturations in cirrus: laboratory and field observations

M. Krämer<sup>1</sup>, S. Schlicht<sup>1</sup>, C. Schiller<sup>1</sup>, A. Mangold<sup>1,5</sup>, O. Möhler<sup>2</sup>, H. Saathoff<sup>2</sup>,  
V. Ebert<sup>3</sup> and N. Sitnikov<sup>4</sup>

<sup>1</sup>Research Center Jülich, Germany (m.kraemer@fz-juelich.de)

<sup>2</sup>Research Center Karlsruhe, Germany

<sup>3</sup>University Heidelberg, Germany

<sup>4</sup>Central Aerological Observatory, Moscow Region, Russia

<sup>5</sup>now at Royal Meteorological Institute, Brussel, Belgium

Keywords: aerosol cloud interaction, cirrus clouds, supersaturation.

Significant water vapor supersaturations over ice are frequently measured from aircraft and balloons in and around upper tropospheric cirrus. Such supersaturations may have significant impact on climate, e.g., decreasing the freezing threshold of ice clouds will lead to an increase in high cloud cover, which in turn feeds back to the radiation balance of the atmosphere (Gettelman and Kinnison, 2006). Subsequent supersaturations inside cirrus influence the clouds microphysics and also the vertical redistribution of water vapor through sedimentation of ice crystals.

Changes of the cirrus freezing threshold are caused by alterations in the aerosol population. To better understand potential aerosol indirect effects on climate, ice cloud nucleation and microphysics, including supersaturations, must be studied.

Here, we present temporal evolutions of supersaturations in cirrus clouds formed by different types of aerosol particles, namely liquid H<sub>2</sub>O-H<sub>2</sub>SO<sub>4</sub> particles, soot and mineral dust. The experiments were made at the large aerosol chamber AIDA in the temperature range 195-225K. In the case of homogeneously freezing liquid aerosol particles (as an example H<sub>2</sub>O-H<sub>2</sub>SO<sub>4</sub> particles are shown in Figure 1), the high initial threshold supersaturation is depleted very rapidly after ice formation at temperatures larger than 200K. For lower temperatures, the in-cloud supersaturation tends to stay high. For heterogeneously freezing aerosols like soot, the freezing threshold supersaturation is lower, but the in-cloud supersaturation is found to be higher than in the homogeneous case. These differences are attributed to the number of nucleated ice crystals, which is higher for homogeneously formed ice clouds.

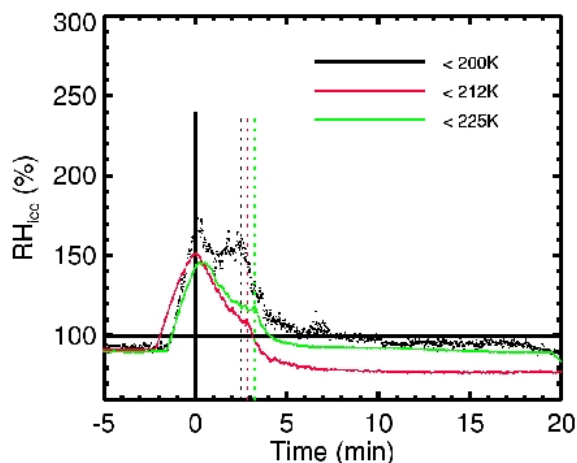


Figure 1. Temporal evolution of supersaturations in AIDA ice clouds nucleated on liquid H<sub>2</sub>SO<sub>4</sub>-H<sub>2</sub>O particles.

In addition, we present field observations of supersaturations in and outside of cirrus from several field campaigns. A comparison of the field measurements with the laboratory observations may give an impression of the aerosol type serving as ice nuclei in the atmosphere.

Gettelman, A. and D. E. Kinnison, (2006). The global impact of supersaturation in a coupled chemistry-climate model. *Atmos. Chem. Phys. Discuss.*, 6, 1243312468.

## Formation of Large (~100 $\mu\text{m}$ ) Ice Crystals Near the Tropical

E. J. Jensen<sup>1</sup>, L. Pfister<sup>1</sup>, T. V. Bui<sup>1</sup>, P. Lawson<sup>2</sup>, B. Baker<sup>2</sup>, Q. Mo<sup>2</sup>, D. Baumgardner<sup>3</sup>, E. M. Weinstock<sup>4</sup>, J. B. Smith<sup>4</sup>, E. J. Moyer<sup>4</sup>, T. F. Hanisco<sup>4</sup>, D. S. Sayres<sup>4</sup>, J. M. St. Clair<sup>4</sup>, R. L. Herman<sup>5</sup>, R. F. Troy<sup>5</sup>, M. J. Alexander<sup>6</sup>, O. B. Toon<sup>7</sup>, J. A. Smith<sup>7</sup>

<sup>1</sup>NASA Ames Research Center, Moffett Field, CA, USA

<sup>2</sup>Spec, Inc., Boulder, CO, USA

<sup>3</sup>Universidad Nacional Autonoma de Mexico, Circuito Exterior, Mexico

<sup>4</sup>Harvard University, Cambridge, MA, USA

<sup>5</sup>Jet Propulsion Laboratory, Pasadena, CA, USA

<sup>6</sup>Colorado Research Associates, Boulder, CO, USA

<sup>7</sup>University of Colorado, Boulder, CO, USA

Keywords: first, second, third, fourth, fifth.

Recent high-altitude aircraft measurements with in situ imaging instruments indicated the presence of relatively large (~100  $\mu\text{m}$  length), thin (aspect ratios of 6:1 or larger) hexagonal plate ice crystals near the tropical tropopause in very low concentrations ( $< \sim 0.01 \text{ L}^{-1}$ ). These crystals were not produced by deep convection or aggregation. Water vapor measurements were made with several instruments in the tropopause region where these large crystals must have grown. There are large discrepancies between the different instruments, with water concentrations ranging from  $< 2$  ppmv to  $\sim 3.5$  ppmv near the tropopause. The higher water vapor concentrations correspond to very large ice supersaturations (relative humidities with respect to ice of about 200%). We use simple growth-sedimentation calculations as well as detailed cloud simulations to evaluate the conditions required to grow the large crystals. Uncertainties in crystal aspect ratio leave a range of possibilities. If the aspect ratios of the hexagonal plate crystals are as small as the image analysis suggests (6:1) then growth of the large crystals before they sediment out of the supersaturated layer would only be possible if the water vapor concentration were on the high end of the range indicated by the different measurements ( $> 3$  ppmv). On the other hand, if the crystal aspect ratios are quite a bit larger ( $\sim 4$ ), then  $\text{H}_2\text{O}$  concentrations toward the low of the measurement range (2–2.3 ppmv) would suffice to grow the large crystals. Gravity-wave driven temperature and vertical wind perturbations only slightly modify the water concentrations needed to grow the crystals. We find that it would not be possible to grow the large crystals with water concentrations less than 2 ppmv, even with assumptions of a very high aspect ratio of 15 and steady upward motion of  $2 \text{ cm s}^{-1}$  to loft the crystals in the tropopause region. These calculations would seem to imply that the measurements indicating water vapor concentrations less than 2 ppmv are implausible, but we cannot rule out the possibility that higher humidity prevailed upstream

of the aircraft measurements and the air was dehydrated by the cloud formation. Simulations of the cloud formation with a detailed model indicate that the large crystals probably nucleated on very effective ice nuclei. Also, growth of the large crystals would not have been possible if homogeneous freezing of aqueous aerosols and subsequent ice crystal growth had rapidly depleted vapor in excess of saturation, implying either very slow cooling during cloud formation or that the aerosol physical state was different from those used in homogeneous freezing laboratory experiments such that the vast majority of aerosols present did not freeze even at very high ice supersaturations.

## Particle chemical composition measured at a high alpine field station in Switzerland: Impact on the phase of cold clouds

A.C. Targino<sup>1</sup>, K. Bower<sup>1</sup>, T.W. Choularton<sup>1</sup>, H. Coe<sup>1</sup>, J. Crosier<sup>1</sup>, I. Crawford<sup>1</sup>  
M.W. Gallagher<sup>1</sup>, M. Flynn<sup>1</sup>, J. Cozic<sup>2</sup>, B. Verheggen<sup>2</sup>, E. Weingartner<sup>2</sup> and U. Baltensperger<sup>2</sup>

<sup>1</sup>Centre for Atmospheric Science, School of earth Atmospheric and Environmental Sciences  
University of Manchester, Manchester, UK

<sup>2</sup>Laboratory of Atmospheric Chemistry, Paul Scherrer Institut, CH-5232, Villigen PSI, Switzerland.

Keywords: Aerosol-cloud interaction, ice nuclei, black carbon, sulphate, cloud phase

An experiment to determine the microphysical and chemical interactions between aerosols and cold cloud elements was carried out at the high alpine station Jungfraujoch, Switzerland. The 6<sup>th</sup> experiment in the project series called *Cloud-Aerosol Characterisation Experiment (CLACE)* was conducted during the period February to March 2004 and was designed to characterise the physical and chemical properties of particles that act as ice nuclei and to assess to what extent anthropogenic emissions modify cloud phase. Cloud particles were sampled using two complementary inlet systems: a heated total inlet, to sample both residual and interstitial particles, and an interstitial inlet, to sample particles smaller than 2  $\mu\text{m}$ . The results presented here are based on data from an Aerodyne Mass Spectrometer (AMS), deployed to measure the mass of volatile and semi-volatile components of submicron aerosol particles, the Cloud Particle Imager, used to take discrete images of cloud particles in the size range of 10 to 2000  $\mu\text{m}$  and to discriminate between liquid and ice elements, and the Multi-Angle Absorption Photometer (MAAP), installed to measure the particle absorption coefficient and from which black carbon (BC) mass concentration were derived.

During the experiment, some clouds events were captured and we focus here on events carefully chosen to illustrate the effects of BC particles on cloud phase. On March 6<sup>th</sup> and 8<sup>th</sup> the site was shrouded in clouds, which alternated between being predominantly in the ice or liquid phases throughout the day. During these events it was observed that BC mass was enhanced. This enhancement of BC mass was accompanied by an increase of sulphate and organic compounds concentration, as measured by the AMS (Fig. 1). The AMS data, segregated by cloud phase, showed that regions containing ice have higher loadings, especially of sulphate and organics. On March 23<sup>rd</sup> and 24<sup>th</sup>, the clouds were liquid and, despite a modest enhancement of BC mass, the AMS measured little mass of the volatile components.

It is hypothesized that the source of the ice is sulphate-coated black carbon particles, being carried to Jungfraujoch in plumes of polluted air.

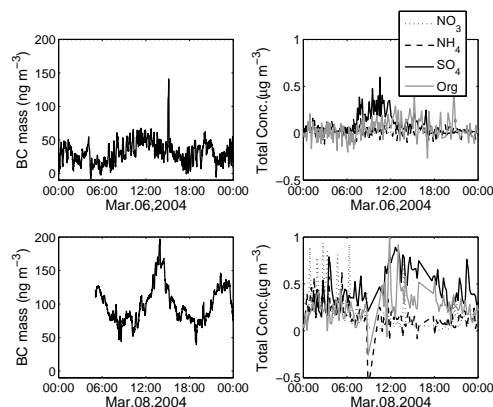


**Figure 1:** Time series of black carbon mass (measured with MAAP) and SO<sub>4</sub>, NO<sub>3</sub>, NH<sub>4</sub> and total organics mass concentrations (measured with the AMS) off the total inlet.

This might explain the different phases of the cloud as these plumes arrive at the observation site. A possible scenario is that first the coated soot may act as CCN and then the resultant drops freeze as a result of the presence of the soot encapsulated in the droplet. A few cloud chamber studies have investigated the ice nucleation efficiency of treated BC particles. DeMott et al. (1999) have shown that soot particles treated with sulphuric acid froze as solution droplets most readily compared with untreated soot particles. Möhler et al. (2005) found that BC could act as a deposition nucleus at low temperatures, and sulphate coatings considerably increased the effectiveness of the ice nuclei at water saturation when they first acted as CCN then causing the droplets to freeze. In these circumstances the carbon particles were effective as ice nuclei at  $-20\text{C}$ .

The results discussed here, *albeit* not conclusive, suggests that BC particles probably coated with sulphate have an increased tendency to form ice crystals.

### References

- DeMott, P.J. et al. (1999). *Geophys. Res. Lett.*, 26, 2429-2432.  
Möhler, O. et al. (2005). *J. Geophys. Res.*, 110, D11210, doi:10.1029/2004JD005169.

## **T22 Abstracts**

## Hot-air balloon measurements of vertical variation of boundary layer new particle formation

L. Laakso<sup>1</sup>, T. Grönholm<sup>1</sup>, S. Haapanala<sup>1</sup>, A. Hirsikko<sup>1</sup>, T. Kurtén<sup>1</sup>, M. Boy<sup>1</sup>, A. Sogachev<sup>1</sup>, I. Riipinen<sup>1</sup>, M. Kulmala<sup>1</sup>, L. Kulmala<sup>2</sup>, E. R. Lovejoy<sup>3</sup>, J. Kazil<sup>4</sup>, D. Nilsson<sup>5</sup> and F. Stratmann<sup>1,6</sup>

<sup>1</sup> Department of Physical Sciences, University of Helsinki, P.O. Box 64, FI-00014 Finland

<sup>2</sup> Department of Forest Ecology, University of Helsinki, P.O. Box 27, FI-00014 University of Helsinki, Finland

<sup>3</sup> NOAA Aeronomy Laboratory 325 Broadway, Boulder, CO 80303, USA

<sup>4</sup> NOAA Earth System Research Laboratory, 325 Broadway, Boulder, CO 80305, USA

<sup>5</sup> Department of Applied Environmental Research, Stockholm University, S-10691 Stockholm, Sweden

<sup>6</sup> Institute for Tropospheric Research, Permoserstrasse 15, D-04318 Leipzig, Germany

Keywords: New Particle formation and growth, Aerosol measurement, Atmospheric Aerosol

Boundary layer particle formation has been observed in diverse environments (Kulmala et al. 2004). Since exact location of particle formation is not known, we placed several devices in a hot-air balloon during spring 2006. The instrumentation included: air ion spectrometer (positive and negative ions 0.4-40 nm), CPC (particle number concentration >10nm), VOC- sampling with bottles, T, RH, p and CO<sub>2</sub>-concentration.

Together with the ground-based measurements from SMEAR II-station, the results provide new insights in a new particle formation in the boundary layer. The results show that:

- The concentration of 1.5-3 nm negative ions was several times higher than the concentration of positive ions of same size (Figure 1). This is an indication of ion-induced nucleation in favour of negative ions.
- Particles do not form at the top of boundary layer.
- During one of the days, particles were overcharged in the beginning and at the end of particle formation event whereas in the middle of event they are undercharged. This indicates that particle formation is, at least during the early winter, a combination of ion-induced and neutral nucleation. This observation is consistent with the theory of neutral and ion cluster activation.
- During some of the days, we observed negative ion-induced nucleation with growth stopping at around 3 nm, probably due to the lack of condensable (organic) vapours.

This work was supported by Maj and Tor Nessling foundation

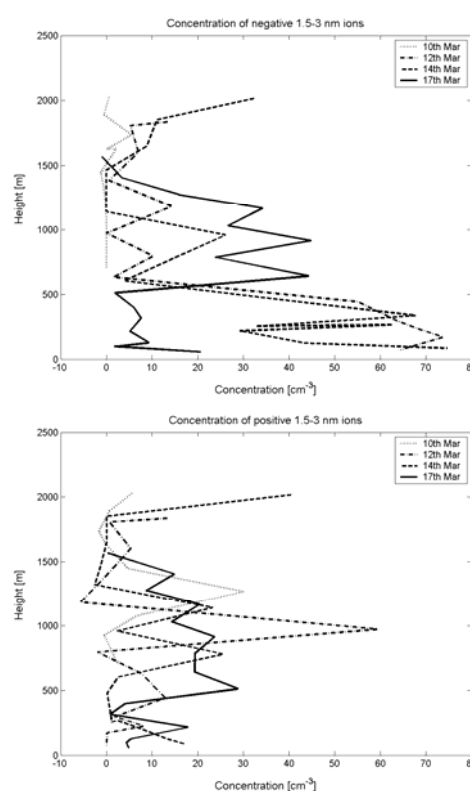


Figure 1. Vertical concentration profiles of 1.5--3 nm negative and positive ions

### References

- Kulmala M., Vehkamäki H., Petäjä T., Dal Maso M., Lauri A., Kerminen V.-M., Birmili W. & McMurry P.H. (2004) *Formation and growth rates of ultrafine atmospheric particles: A review of observations*. *J. Aerosol Sci.* **35**: 143--176
- Laakso, L., Grönholm, T., Kulmala, L., Haapanala, S., Hirsikko, A., Lovejoy, E.R., Kazil, J., Kurtén, T., Boy, M., Nilsson, E.D., Sogachev, A., Riipinen, I., Stratmann, F. and Kulmala, M. (2007) *Hot-air balloon measurements of vertical variation of boundary layer new particle formation*, Accepted to *Boreal Environment Research*

## New Statistical Methods of Analysis of Atmospheric Aerosols

G. Gramotnev and D. K. Gramotnev

Applied Optics Program, School of Physical and Chemical Sciences,  
Queensland University of Technology, GPO Box 2434, Brisbane, QLD 4001, Australia

Keywords: Atmospheric aerosols, Statistical analysis, Particle size distribution, Source identification.

A major problem with comprehensive analysis of atmospheric aerosols and particulate emissions is related to strong stochastic fluctuation and variability of the atmospheric, environmental and other external parameters. This results in major difficulties with the analysis of the obtained monitoring data and determination of sensible and reliable relationships between different polluting agents and their sources. If a monitoring dataset is large, then averaging over the whole set may give relatively consistent results. However, in this case, we lose all the dependencies of monitored parameters on different external factors (e.g., wind direction and speed, fluctuations of the source, etc.) varying stochastically on different time scales. If, on the contrary, a dataset is relatively small, then stochastically varying external parameters result in unpredictable and significant variations of the obtained results and tendencies. This is one of the main reasons for the current lack of detailed understanding of air pollution problems in the real-world environment. We believe that the only real way out of this difficulty is in the extensive use of statistical methods that should be specifically developed for the analysis of strongly dispersed monitoring data with multiple dependencies on various external and meteorological parameters.

In this paper, we demonstrate several new statistical approaches that have been recently developed for the multi-channel analysis of particle concentrations and their relationships in a size distribution for combustion and background aerosols in the real-world urban environment [1-4].

The developed statistical methods embrace a range of approaches focused on:

- optimal plotting of particle size distributions (using a moving average technique) [1,2,4],
- new statistical method for effective identification and investigation of particle modes in the presence of strong turbulent mixing and stochastic concentration fluctuations (when the conventional size distribution does not reveal any significant features) [1,2,4],
- canonical correlation analysis combined with the moving average approach for the comprehensive analysis of sources of particle

modes, their evolutionary tendencies and simultaneous dependence of numerous external and meteorological factors [2],

- cross-correlation between different particles modes combined with the moving average approach for identification and investigation of mutual interactions and transformations of particle modes during their evolution in the atmosphere [3,4],

- recently developed multi-channel statistical analysis of concentration fluctuations in different channels of the particle size distribution combined with the moving average technique.

In particular, all these different methods provide a unique opportunity for the detailed comprehensive analysis of various types of atmospheric aerosols from several different points of view, which will substantially improve reliability of the obtained results and conclusions. Therefore, these methods will provide a new tool and valuable physical insight into possible evolutionary processes in atmospheric aerosols.

So far these expectations have been successfully tested and validated on two significantly different time scales, involving detailed statistical analysis of combustion aerosols near the source (~ tens of meters from a busy road) and aged urban background aerosols (~ a few kilometres from the source). The obtained results and their consistency have clearly demonstrated high efficiency and accuracy of the developed methods in terms of determination of particle sources and their physical/chemical evolutionary processes [1-4].

D. K. Gramotnev and G. Gramotnev (2005), *J. Aerosol Sci.*, vol.36, pp.323-340.

G. Gramotnev, D. K. Gramotnev, *Atm. Env.* (online 07/02/2007; doi:10.1016/j.atmosenv.2007.01.031).

D. K. Gramotnev, G. Gramotnev, *Atm. Env.* (online 30/01/2007; doi:10.1016/j.atmosenv.2007.01.007).

G. Gramotnev, P. Madl, D. K. Gramotnev, M. J. Burchill, Urban background aerosols: Negative correlations of particle modes and fragmentation mechanism. *Geophysical Research Letters* (submitted).

## Caustics, Collisions and the Stokes Trap in Turbulent Aerosols

Michael Wilkinson<sup>1</sup> and Bernhard Mehlig<sup>2</sup>

<sup>1</sup>Department of Mathematics, Open University, Milton Keynes, MK7 6AA, England

<sup>2</sup>Department of Physics, Gothenburg University, 41296 Gothenburg, Sweden

Keywords: caustic, turbulence, collisions, fragmentation.

Collisions of suspended particles in an aerosol are fundamental to understanding the formation of raindrops from clouds (Shaw, 2003), or the growth of planets from dust in a protostellar environment (Armitage, 2007). Recently we have gained a comprehensive picture of the processes leading to collisions in turbulent aerosols.

When the Stokes number (the ratio of the stopping time due to drag to the correlation time of the turbulent flow) approaches unity, there is a dramatic increase in the relative velocity of suspended particles due to the formation of fold caustics in their velocity field, illustrated in figure 1. When faster particles overtake slower ones, the manifold representing the phase-space distribution of the particles develops folds, and the velocity field of the particles goes from being single valued to multi-valued (three-valued, in this illustration). Before the caustics form, the relative velocity of the particles is due to their Brownian diffusion or shearing motion of the fluid. After the folds have formed the relative velocity may be orders of magnitude higher, greatly increasing the collision rate.

We find that the collision rate may be described by the formula (Wilkinson *et al*, 2006)

$$R = R_d + R_a + \exp(-A/St) R_g \quad (1)$$

Here  $R_d$  is the rate of collision due to Brownian motion,  $R_a$  is the advective collision rate, estimated by Saffman & Turner (1956) and  $R_g$  is the collision rate predicted by a ‘gas-kinetic’ model, introduced by Abrahamson (1975), in which the suspended particles move with velocities which become uncorrelated with each other and with the gas flow. The exponential term describes the fraction of the coordinate space for which the velocity field is multi-valued:  $A$  is a ‘universal’ dimensionless constant. The rate  $R_g$  greatly exceeds  $R_d$  and  $R_a$ , but the gas-kinetic theory is only applicable when the velocity field of the suspended particles is multi-valued. The exponential term is analogous to the Arrhenius term  $\exp(-E/kT)$  in the expression for the rate of an activated chemical reaction. The abrupt increase of the collision rate as the Stokes number exceeds a threshold is illustrated in figure 2. A theory proposed by Falkovich *et al* (2002) is similar in structure, but does not allow accurate quantitative comparisons with numerically calculated collision rates.

We also describe a new theory, the Stokes trap, describing collisions of particles, which may fragment on impact, and which may be relevant to the formation of planets.

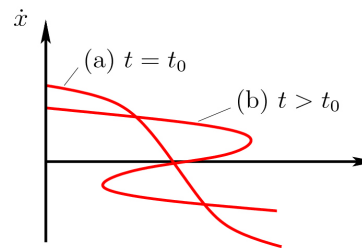


Figure 1. Velocity of suspended particles as a function of position may develop fold caustics.

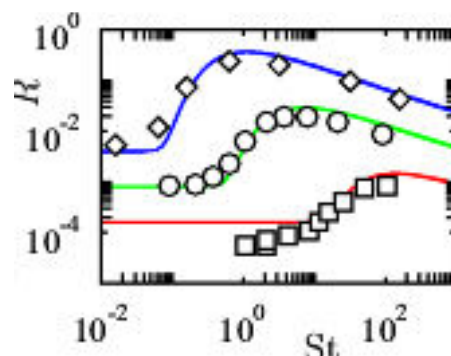


Figure 2. Numerical test of equation (1).

R. A. Shaw, (2003), *Annu. Rev. Fluid Mech.*, **35**, 183.

P. J. Armitage, (2007), arXiv: astro-ph/0701485.

P. G. Saffman and J. S. Turner, (1956), *J. Fluid Mech.*, **1**, 16-30.

J. Abrahamson, (1975), *Chem. Eng. Sci.*, **30**, 1371-9.

G. Falkovich, A. Fouxon and G. Stepanov, (2002), *Nature*, **419**, 151-154.

M. Wilkinson, B. Mehlig and V. Bezuglyy, (2006), *Phys. Rev. Lett.*, **97**, 048501.

## Aerosol fluctuations and condensation

C. F. Clement<sup>1</sup>

<sup>1</sup>15 Witan Way, Wantage, Oxon OX12 9EU, U.K.

Keywords: aerosol formation, atmospheric aerosols, condensation, fluctuations, heat and mass transfer.

Clouds are atmospheric aerosols which exhibit large fluctuations in space and time in which their concentrations in number and mass vary greatly. Fluctuations affect properties such as rainout and nucleation of new aerosol important to weather and climate. Processes which lead to these fluctuations include localized emissions and mixing of different air masses, but here we concentrate on their origins from condensation, particularly as it affects clouds.

In the simplest model of air mass rise leading to cloud formation with spatially uniform CCN (cloud condensation nuclei), one would expect a narrow droplet distribution to be formed. However, observations (e.g. Korolev et al 1994, 1995) show droplet spectra which vary widely over distances at least down to the scale of tens of meters and which are often multimodal. A large variety of explanations have been put forward to explain such phenomena, a recent one on wind velocity fluctuations being by Erlick et al (2005) who also discuss alternative ideas.

Possibly the simplest idea is to impose fluctuations in the local water vapour saturation,  $S(t)$ , around a mean value close to 1 on trajectories in time of realistic CCN and see what size distribution results. This approach was followed by Kulmala et al (1997) who found that droplet could grow into a wide distribution even with mean values of  $S$  less than 1.

However, this explanation, together with several of the others put forward, begs the question of the origin of the fluctuations. All the local variables which describe the system of nuclei in air containing water vapour are connected by deterministic equations. With the possible exception of local fluctuating velocities from turbulence which could be treated stochastically, it is unreasonable to impose a stochastic variation on an isolated variable.

We consider the two variables of vapour concentration,  $c$ , and temperature,  $T$ , which specify condensation in vapour-gas mixtures (Clement 1985). The supersaturation is specified by the difference between the actual vapour concentration and its equilibrium value at the local temperature,

$$u = c - c_e(T). \quad (1)$$

An equation for  $u$  is derived (Clement 1991) from the separate equations for  $c$  and  $T$  given by Clement (1985) is now augmented by additional terms for pressure change and interaction with radiation:

$$\frac{\partial u}{\partial t} + \mathbf{v} \cdot \nabla u + \nabla \cdot (-D \nabla u) = D c_e'' (\nabla T)^2 - (\frac{\partial p}{\partial t} - \nabla \cdot \mathbf{q}) / (L C_n) - c_e' (1 - Le^{-1}) (\frac{\partial T}{\partial t} + \mathbf{v} \cdot \nabla T) - (1 + C_n)^{-1} (dp_a/dt) / \rho, \quad (2)$$

where  $c_e'$  is  $dc_e/dT$ ,  $\mathbf{q}$  is the radiation current interacting with the aerosol, and  $C_n$  is the bulk condensation number:

$$C_n = k / (L D \rho c_e'(T)), \quad (3)$$

given in terms of the thermal conductivity,  $k$ , latent heat,  $L$ , vapour diffusivity,  $D$ , and gas density,  $\rho$ .

The source terms on the RHS of (2) lead to supersaturation and mass transfer to aerosols, the final term being the actual transfer rate proportional to increase in aerosol mass density,  $\rho_a$ , which is itself proportional to  $u = c - c_e$ . The first term on the RHS is proportional to the second derivative of  $c_e$ . It is essentially positive and its nonlinearity shows why supersaturations arise in temperature gradients. The proportionality to  $-\partial p/\partial t$  shows the effect of reduced pressure in rising air columns to produce supersaturation, but the radiative term can have either sign in adding or removing heat from the aerosol. Of great interest is the term depending on the Lewis number,  $Le$ ,

$$Le = k / (D \rho c_p). \quad (4)$$

For water vapour in air,  $Le \approx 0.85$  and the sign of the term depends on whether the temperature of the transported air at the point in question is rising or falling. In the atmosphere, air packets will exist which have opposite signs leading to highly local fluctuations in the water content. An example of this locality in aerosol formation produced is seen in the calculations for cooled laminar flow in a tube performed by Barrett and Fissan (1989). However, realistic calculations for both  $c$  and  $T$  for actual turbulent flows in the atmosphere are lacking.

## REFERENCES

- Barrett, J. C. and Fissan, H. (1989) *J. Colloid Inter. Sci.*, **130** 498-507.  
 Clement, C. F. (1985) *Proc. Roy. Soc., London A* **398**, 307-339.  
 Clement, C. F. (1991) Condensation and evaporation in clouds, in Workshop on Condensation, Helsinki 1991 (eds. M. Kulmala and K. Hämeri) *Report Series in Aerosol Science* No. **17**, Finnish Association for Aerosol Research, Helsinki.  
 Erlick, C., Khain, A., Pinsky, M. and Segal, Y. (2005) *Atmos. Res.* **75** 15-45.  
 Korolev, A. V. (1994) *Atmos. Res.* **32**, 143-170.  
 Korolev, A. V. (1995) *J. Atmos. Scis.* **52**, 3620-3634.  
 Kulmala, M., Rannik, Ü, Zapadinsky, E. L. and Clement, C. F. (1997). *J. Aerosol Sci.* **28**, 1395-1409.

## Homogeneous nucleation in wake flows

J. Pyykönen<sup>1</sup>, S. Garrick<sup>2</sup> and J. Jokiniemi<sup>1,3</sup>

<sup>1</sup>VTT, Fine Particles, P.O.Box 1000, 02044 VTT, Finland

<sup>2</sup>Department of Mechanical Engineering, University of Minnesota, 111 Church Street SE, MN 55455-0111, USA

<sup>3</sup>University of Kuopio, Department of Environmental Sciences, P.O.Box 1627, 70211 Kuopio, Finland

Keywords: aerosol modeling, nucleation, turbulence, CFD.

The effect of turbulent mixing on homogeneous nucleation is a major stumbling block in the application of theoretical particle formation models to real-world phenomena. As a continuation of our earlier direct numerical simulations of turbulent jets (Pyykönen and Garrick, 2004), we broaden the range of flows by modeling the details of particle formation in turbulent wakes. Homogeneous nucleation is typically extremely sensitive to local conditions, and the microstructure of turbulent eddies is an essential consideration. Various flow types generate different types of eddies, and a comparison of DNS simulations of nucleation in various flows provides indications of the sensitivity of the nucleation process to the flow type.

We have modeled a wake flow that is created by a lower velocity stream issuing from a planar nozzle into a faster flowing co-flow. The use of direct numerical simulation automatically takes care of all the scales of mixing, including the molecular processes that, in the end, generate the local conditions for nucleation. The simulations are in 2D, which makes the results somewhat qualitative, but still helpful in identifying the role of the flow microstructure. Two cases are considered: (a) Hot (400 K) lower velocity nozzle stream doped with a condensable species that nucleation during mixing with cold (300 K) co-flow, and (b) Cold nozzle stream issuing into hot vapor-laden co-flow. Following our previous studies, dibutylphthalate (DBP) was adopted as the nucleating agent and the nucleation model of Girshick and Chiu (1990) was used.

The simulations show that flow fields right at the nozzle outlet are essential since a great deal of mixing can take place there. In terms of turbulent eddy structure, in the case (a), the highest nucleation rates are predicted to occur in bridges of nozzle stream component that connect rolled eddy structures. Figure 1 presents time-averaged nucleation rate predictions with this setup. The nucleation rates are much lower than in the jet flow because of the absence of vortex pairing, a process that is responsible for generating the maximum nucleation rates in the jet flows we considered. In the case (b), nucleation mainly takes place inside the rolled eddies, and the nucleation rates are low.

These simulations together with our earlier studies of nucleation in turbulent jets demonstrate

that nucleation processes can be remarkably different in various kinds of turbulent flow and that care must be exercised when generalizing the results to other types of flows.

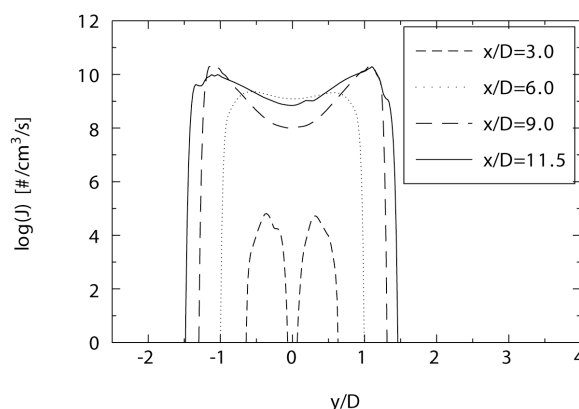


Figure 1. Simulated time-averaged nucleation rates in the case (a) with nozzle velocity 1/4 of the co-flow velocity and wake Reynolds number 500. Various positions  $x$  in the main flow direction relative to the nozzle diameter  $D$ .

We acknowledge the funding of Finnish Funding Agency for Technology and Innovation and a consortium of companies.

Girshick, S. and Chiu C.-P. (1990). Kinetic nucleation theory: A new expression for the rate of homogeneous nucleation from an ideal supersaturated vapor. *J. Chem. Phys.*, 93, 1273-1277.

Pyykönen, J. Garrick, S. (1994) Abstracts of the 1994 European Aerosol conference. *J. Aerosol Sci.* S419-S420.

## **T23 Abstracts**

## Overview of source apportionment methods in selected European COST633 Action member countries

M. Viana<sup>1\*</sup>, X. Querol<sup>1</sup>, T.A.J. Kuhlbusch<sup>2</sup>, A. Miranda<sup>3</sup>, M. Vallius<sup>4</sup>,  
A. Kasper-Giebl<sup>5</sup>, S. Szidat<sup>6</sup>, W. Winiwarter<sup>7</sup>, R.M. Harrison<sup>8</sup>

<sup>1</sup>Institute of Earth Sciences “Jaume Almera”, 08028 Barcelona, Spain (\*mviana@ija.csic.es)

<sup>2</sup>IUTA e.V. Bliersheimerstr. 60, 47229 Duisburg

<sup>3</sup>University of Aveiro, Campus Universitário de Santiago . 3810-193 Aveiro . Portugal

<sup>4</sup>National Public Health Institute, P.O.Box 95, FI-70701 Kuopio, Finland

<sup>5</sup>Institute for Chemical Technologies and Analytics, Getreidemarkt 9/164-AC, A-1060 Vienna

<sup>6</sup>University of Bern, Freiestrasse 3, CH-3012, Bern, Switzerland

<sup>7</sup>Austrian Research Centers - ARC, 1220 Vienna, Austria

<sup>8</sup>The University of Birmingham, Edgbaston, Birmingham B15 2TT, UK

Keywords: ambient PM, source contribution, receptor models, road dust, shipping emissions.

During the progress of COST Action 633 and within its Working Group 3 (Sources, Emissions, Modelling, Economic Aspects), a questionnaire was distributed amongst the Action's participant countries with the aim to compile data on the source apportionment methodologies used in the different countries. This questionnaire included data on the PM fraction targeted, sampling methodology and study area. Despite the fact that replies to the questionnaires were not obtained from all the member countries, the return may be seen as an overview on source apportionment activities in Europe before the year 2006. It should be noted, however, that this overview does not intend to provide the full set of all source apportionment studies performed in the European COST633 Action member countries.

The different member countries reported a total of 47 publications on source apportionment in 7 countries (Austria, Belgium, Finland, Germany, Portugal, Spain, Switzerland, UK), based on 10 different methodologies: Principal Component Analysis (PCA, Thurston & Spengler, 1985), CMB (Chemical Mass Balance, US-EPA, 1987), Positive Matrix Factorisation (PMF, Paatero & Tapper, 1994), UNMIX, ME (Multi-Linear Engine, Paatero, 1999), Lenschow approach (Lenschow et al., 2001), back-trajectory analysis, cluster analysis, COPREM (Constrained Physical Receptor Model, Wählin, 2003) and isotopic mass balance using C-14 (Szidat et al., 2004). The most frequently used method was PCA (30% of the studies), followed by back-trajectory analysis and the Lenschow approach (15%), and PMF (10%). The remaining methods were used in at most 2 studies each. Regarding the number of research groups applying the different techniques, PCA appeared to be most widely used (5 different countries), whereas PMF and the Lenschow approach were applied in 4 and 3 countries, respectively.

Aside from the techniques reported by COST633 member countries, it is also important to acknowledge the use of CMF (Constrained Matrix

Factorisation) and SOMs (Self-Organising Maps), as well as the relative increase in the use of PMF and CMB in Europe in the last year.

The evaluation of the data provided by the member countries showed a large number of PM10 and PM2.5 sources identified across Europe, as well as the different criteria adopted by researchers in order to interpret the nature of such sources. For example, some sources were interpreted as specific industrial processes such as “Metallurgy”, whereas in other regions more general sources such as “Trans-boundary pollution” were reported. Consequently, the inter-comparison of results is in such cases complicated. Achieving comparable results over Europe is certainly one major task to tackle. Another issue evidenced by this analysis is the relevance of regional background contributions to PM levels, which were identified at most of the monitoring sites although with different tracer elements. Traffic contributions, e.g. exhaust and road dust, were identified in urban areas only by certain models, evidencing a clear research need. This also applies to other combustion sources such as shipping emissions, unobserved in the reported source apportionment studies.

The authors would like to thank all the researchers who provided data for the questionnaires. This work was carried out under COST Action 633.

Lenschow P., Abraham H.J., Kutzner K. et al. (2001) *Atmos. Environ.* 35, 123-133.

Paatero, P. and Tapper, U. (1994). *Environmetrics*, 5, 111-126.

Paatero P. (1999) *J. Comput. Graph. Stat.* 8(4), 854-888.

Szidat S., Jenk T.M., Gäggeler H.W. et al. (2004) *Radiocarbon* 46, 475-484.

Thurston G.D. & Spengler J.D. (1985) *Atmos. Environ.* 19, 9-25.

US-EPA. (1987) *Protocol for applying and validating the CMB model* (ed. Office for AQPS).

Wählin, P. (2003) *Atmos. Environ.* 37, 4861-4867.

## **Cross-disciplinary approaches for critical issues in particulate air pollution**

R. Hittenberger<sup>1\*</sup>, J. Tursic<sup>2</sup>, J.-P. Putaud<sup>3</sup>, A. Berner<sup>4</sup>, R.O. Salonen<sup>5</sup>, W. Kreyling<sup>6</sup>, T.A.J. Kuhlbusch<sup>7</sup>,  
M. Amann<sup>8</sup>, F. Cassee<sup>9</sup>, W. Winiwarter<sup>10</sup> and COST633-Members

<sup>1</sup> Faculty of Physics, University of Vienna, Boltzmannngasse 5, A-1090 Vienna, Austria. <sup>2</sup> Environmental Agency of the Republic of Slovenia, Vojkova 1/b, SI-1000 Ljubljana, Slovenia.

<sup>3</sup> European Commission, DG JRC, Institute for Environment and Sustainability, I-21020 Ispra, Italy

<sup>4</sup> Austrian Academy of the Sciences, KRL, Dr. Ignaz-Seipel-Platz 1, A-1010 Vienna, Austria

<sup>5</sup> National Public Health Institute, Department of Environmental Health, Kuopio, Finland

<sup>6</sup> GSF - National Research Center for Environment and Health, P.O. Box 1129, D-85758 Neuherberg, Germany <sup>7</sup>.

IUTA e.V. Bliersheimerstr. 60, D-47229 Duisburg, Germany

<sup>8</sup> IIASA, Schlossplatz 1, A-2361 Laxenburg, Austria.

<sup>9</sup> National Institute for Public Health and the Environment, P.O. box 1, B-3720 BA Bilthoven, The Netherlands.

<sup>10</sup> Austrian Research Centers – ARC, Donau-City-Str. 1, A-1220 Vienna, Austria

Keywords: Particulate Matter, Measurements, Health aspects of Aerosols, Source apportionment, Modelling

The field of the COST Action 633 “Particulate matter (PM) – properties related to health effects”, is very broad and covers several disciplines. It includes, e.g. measurement techniques of PM, measurement artifacts, consideration of parameters to be measured, epidemiology, toxicology, modelling of exposure, emission inventories, source apportionment and dispersion modelling, and integrated assessment modelling.

All the various disciplines had and have accumulated a vast amount of knowledge was, and partially still is, hard to communicate to the public and decision-makers, and even between the researchers. The Action was especially initiated to enable communication and enhance the interactions between the various disciplines, since the progress needed for the improvement of air quality and quality of life can only be achieved by coordinated efforts. This was accomplished by the COST 633 Action bringing together a multidisciplinary team of scientists to tackle a faced with the complex problems posed by PM to society.

There are three working groups in the Action: WG1 - air quality and instrumentation, WG2 - Health related issues of particles, and WG3 - Sources, emission, modelling, economic aspects. In the Action, however, we a cross-disciplinary approach involving all the experts was taken.

The Action has already given some major recommendations:

- Extension of the current air quality monitoring network is needed in Europe. Additional particle parameters should be measured preferably in urbanized areas.
- A possible new focus could be the combination of emission inventories, chemical transport models and source apportionment methods into an integrated approach. While each tool separately is not capable of answering all questions, in combination they could provide a more detailed

insight to issues such as regional variability of contributions by traffic, wood burning, etc.

- There is a need to assess the uncertainty of existing models rather than to develop new models.
- Long-term exposure estimates need to be improved and developed, especially taking the indoor situation into account.
- Development of high resolution spatial exposure models for the estimation of chronic, long-term particle exposure and studies in selected regions in Europe on long-term effects of air pollution with standardized procedures in both health and exposure assessment are needed. To appropriately investigate chronic effects, such studies must focus on early pathophysiological or functional markers of chronic diseases rather than on terminal outcomes.
- Better integration of epidemiology and toxicology is needed, using for instance same health indicators (biomarkers of effect).
- Source-related toxicological studies should be conducted, preferably using real world mixed samples from different regions of Europe.
- There is an obvious need for collaboration and interdisciplinary approaches, and a call to conduct well organized concerted research studies in several regions in Europe comprising monitoring and research on air pollution, exposure, epidemiology with appropriate exposure-response functions, source-orientated toxicological studies as well as evaluation of the effectiveness of various abatement measures.

This work was supported by COST Action 633. Comprehensive information on the COST Action, including recent Conference Proceedings, can be downloaded from <http://cost633.dmu.dk>

## **Similarities and heterogeneities in exposure and health effects over Europe – Epidemiological results and research needs identified in COST Action 633**

M. Riediker<sup>1</sup>, N. Künzli<sup>2</sup>, G. Hoek<sup>3</sup>, J. Cyrys<sup>4,5</sup>, A. Peters<sup>4</sup>, R.O. Salonen<sup>6</sup>

<sup>1</sup> Institute for Occupational Health Sciences, University of Lausanne, 1005 Lausanne, Switzerland

<sup>2</sup> ICREA and Center for Research in Environmental Epidemiology (CREAL), 08003 Barcelona, Spain

<sup>3</sup> Institute for Risk Assessment Sciences IRAS, 3508 TD Utrecht, The Netherlands

<sup>4</sup> GSF- Ntl. Research Center for Environment and Health, Inst. of Epidemiology, 85758 Neuherberg, Germany

<sup>5</sup> WZU - Environmental Science Center of the University Augsburg, 86159 Augsburg, Germany

<sup>6</sup> National Public Health Institute, Department of Environmental Health, 70701 Kuopio, Finland

Keywords: airborne particles, aerosol characterization, epidemiology, health effects of aerosols, modelling.

Short-term and long-term exposure to ambient airborne particulate matter (PM) is associated with increased prevalence of respiratory and cardiovascular diseases and mortality.

Many acute health effect studies observed regional heterogeneities in the association of daily variations in mass concentrations of ambient airborne particulate matter (PM) such as black smoke, thoracic, or fine particles with cardiovascular or respiratory mortality and morbidity.

Heterogeneities can also be observed related to PM-sources. Particles from local combustion sources have more consistent and stronger relationships with both respiratory and cardiovascular outcomes than PM from other sources. However, there is currently not enough scientific evidence to declare any source or chemical composition as “non-toxic”, because even sea salt and soil-derived particles may interact in urban areas with local anthropogenic particles.

It is possible that physicochemical differences in PM mixtures contribute to these observed heterogeneities, but there may well be other reasons such as ambient temperature, differences in exposure patterns of the populations, and differences between the sites of monitoring stations in different countries. The role of population characteristics such as genetic and socio-economic differences is not known, while factors like dietary intake of antioxidants or use of such supplements could well have an impact.

Only few European studies investigated so far long-term health effects of exposure to ambient particles. The existing data allows the conclusion that chronic, long-term PM-exposure causes health effects that go beyond those expected for repeated short-term exposures. However, too few studies and data exist to draw conclusions about heterogeneities of long-term health effects in European populations and the relation of such heterogeneities to sources or particle characteristics. This gap of knowledge exists on a European as well as on a worldwide scale.

Understanding the heterogeneities over Europe will require a better spatial and physicochemical characterisation of particle exposure, a better description of the activity patterns, genetics and socioeconomics of exposed populations and the inclusion of markers of diseases.

Studies require sufficient exposure gradients to detect effects. Central monitoring sites were useful to examine acute health effects of PM in time-series studies because the temporal sequences of PM at different sites in a given region are usually well correlated. However, the understanding of source- and physicochemical- specific PM effects requires methods that capture contrasts in exposure to pollutants that are heterogeneously distributed. This is especially important for chronic effect studies. Given the inability to measure the personal exposure over long periods of time, combinations of measurements and modelling will play an important role in future research.

Genetic polymorphisms can modify the response to oxidative stress and/or systemic inflammation. However, we do not sufficiently understand how this translates into the risks, and other genes and pathways are expected to play a complementary role in the development of diseases.

Socioeconomic factors are proposed to affect the dose-response relationship between air pollutants and health in two ways: They can affect the exposure (e.g. low income housings near busy streets), and they can affect the susceptibility of the individuals to the pollutants (e.g. lifestyle factors such as smoking or dieting, and co-morbidities such as diabetes)

Finally, including preclinical markers of diseases and disease development will be important to distinguish between pathophysiological changes that contribute to chronic diseases and reversible changes that trigger acute events.

This work summarizes the findings of the epidemiology sessions of the COST633 Workshop in Vienna, 3 - 5 April 2006.

## Analysis of contribution of different sources to PM10 concentration levels at three different locations in Slovenia

T. Bolte<sup>1</sup>, J. Turšič<sup>1</sup>, A. Šegula<sup>1</sup> and B. Gomišček<sup>2</sup>

<sup>1</sup>Environmental Agency of the Republic of Slovenia, Vojkova 1b, SI-1000 Ljubljana, Slovenia

<sup>2</sup>University of Maribor, faculty of Organization Sciences, Kidričeva 55a, SI-4000 Kranj, Slovenia

Keywords: PM10, urban aerosols, chemical composition, source identification

Non-attainment of air quality standards regarding particulate matter is frequently observed in many cities in Europe. Urban areas contain a large concentration of people and also anthropogenic industrial and traffic activities. Several reports revealed elevated concentration levels of PM, its spatial and temporal distribution (Gomišček *et al.*, 2004) as well as significant correlation between particulate matter levels and adverse effects on human health (Pope, 2000). Therefore, it is great importance to understand chemical composition and source apportionment in order to control air pollution in these areas. For preparation of effective abatement strategies to reduce particulate matter levels, it is necessary to obtain contributions of different sources. Several techniques are available for this task. However, the most widely used are Principal Component Analysis, Chemical Mass Balance, Positive Matrix Factorisation, back-trajectory analysis, Lenschow approach (Lenschow *et al.*, 2001; Paatero and Trapper, 1994; Thurston and Spenger, 1985, US-EPA, 1987).

The present study is focused on detailed chemical characterization of PM10 sampled at three different locations in Slovenia followed by detailed interpretation of data using back trajectories and other relevant meteorological data. For source identification multivariate statistical technique will be applied.

Sampling of PM10 was performed at three different locations in the period between December 2006 and February 2007. The sampling site in Ljubljana, situated in a residential-commercial area, represents urban background location. The location in Maribor is a typical traffic location, while the location at Trbovlje is situated in rather closed valley and is predominantly influenced by traffic and a cement industry plant. Sampling was performed by low volume reference samplers (Leckel) on 24 hour basis. In addition continuous measurements of PM10 by TEOM and measurements of black carbon by Aehalometers were carried out. All measuring sites are equipped also with common meteorological sensors and monitors for SO<sub>2</sub>, NO<sub>x</sub> and O<sub>3</sub>. 5-days back trajectories were calculated for each day of the measuring period.

After sampling, filters were divided into three sub-samples. Following the extraction in Milli-Q water analysis of major ions was performed by ion

chromatography with one part of the filters. The second part was digested by HNO<sub>3</sub> and H<sub>2</sub>O<sub>2</sub> according to SIST EN 14902 in order to carry out the determination of selected trace elements by ICP-MS. The third part was used for the determination of total and elemental carbon.

In table 1 average yearly concentration of PM10 and number of days above the 24-hour limit value (50 µg m<sup>-3</sup>) in 2006 are presented for all three locations. For comparison data for background EMP-GAW station Iskrba are shown.

Table 1: Average yearly concentration of PM10 and number of exceedances of limit value (50 µg m<sup>-3</sup>) in 2006 for selected locations - Ljubljana, Maribor, Trbovlje and Iskrba.

	Average yearly concentration [µg m <sup>-3</sup> ]	Number of exceedances of limit value
Ljubljana	36	51
Maribor	45	117
Trbovlje	42	92
Iskrba	14	3

In this contribution the results of the intensive campaign regarding elevated PM10 concentration levels, chemical composition, principal contribution sources and paths as well as source apportionment will be presented and discussed.

This work was supported by the Ministry for Environment and Spatial Planning of the Republic of Slovenia and was done in the frame of COST-633 Action.

Gomišček B., Hauck H., Stopper S., Preining O. (2004). *Atmos. Environm.* 38, 3917-3934.

Lenschow P., Abraham H. J., Kutzner K., Lutz M., Preuß J. D., Reichenbacher W. (2001). *Atmos. Environm.* 35, 123-133

Paatero P., Trapper U. (1994). *Environmetrics* 5, 111-126.

Pope C.A. (2000). *Aerosol Sci. Technol.* 32, 4-14

Thurston G.D., Spengler J. D. (1985). *Atmos. Environm.* 19, 9-25

US-EPA. (1987) *Protocol for applying and validating the CMB model*

## Modelling exposure to atmospheric particulate matter– an overview

C. Borrego<sup>1</sup>, A.I. Miranda<sup>1</sup>, J. Ferreira<sup>1</sup>, O. Hänninen<sup>2</sup>, T. Kuhlbusch<sup>3</sup> and W. Winiwarter<sup>4</sup>

<sup>1</sup>CESAM - Department of Environment and Planning, University of Aveiro, 3810-193 Aveiro, Portugal

<sup>2</sup>KTL, Department of Environmental Health, PO Box 95, FI 70701, Kuopio, Finland

<sup>3</sup>IUTA e.V. Bliersheimerstr. 60, 47229 Duisburg, Germany

<sup>4</sup>ARC Austrian Research Centers

Keywords: modelling, air quality, exposure.

Exposure is one of the main factors determining risk assessment and risk management. According to the IPCS (2004) an exposure model is a conceptual or mathematical representation of the exposure process, designed to reflect real-world human exposure scenarios and processes, and thus, it combines information on personal activity patterns and media (indoor and outdoor) air concentrations. Ambient air concentration of particulate matter (PM) is then a key input variable for exposure models, and are generally obtained by direct measurements in air quality monitoring stations. However, depending on the location and dimension of the region to be studied, monitoring data could not be sufficient to characterize PM levels or to perform population exposure estimations. Numerical models are alternatives to measured concentration data. They simulate the changes of pollutant concentrations in the atmosphere using a set of mathematical equations characterizing the chemical and physical processes in the atmosphere.

Aiming to provide an overview of the application of PM models in European COST633 Action member states in a common usable framework, modellers were asked to answer to a questionnaire (Miranda *et al.*, 2006). A total of 30 case studies applications and 20 models were reported, covering different scopes and different modelling scales, from the local to the regional scale. Primary aerosols were simulated in all the case studies, whereas secondary aerosols were included in 50% of the cases, estimating not only PM<sub>10</sub>, but also PM<sub>2.5</sub> and SOA.

A number of exposure modelling studies based on air quality modelling results combined with population activity patterns have already been performed, namely in the scope of the European Project FUMAPEX. Fig 1 presents the results of the estimation of children exposure in Turin city area. A mesoscale model was used to obtain PM<sub>10</sub> ambient concentrations.

A methodology to estimate the population exposure to PM<sub>10</sub> in urban areas was developed and applied to a hot spot in Lisbon city centre. Results of PM<sub>10</sub> air concentration field predicted by VADIS local dispersion model and the population exposure expressed in terms of an accumulated index (APEI50) are presented in Fig 2.

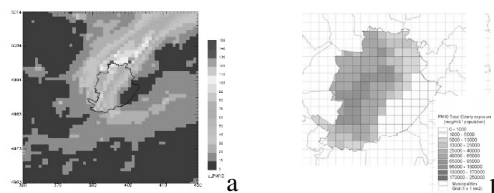


Figure 1. PM<sub>10</sub> simulated concentration field (a), and spatial distribution of 24-hours total PM<sub>10</sub> exposure (b) (Hänninen *et al.*, 2005).

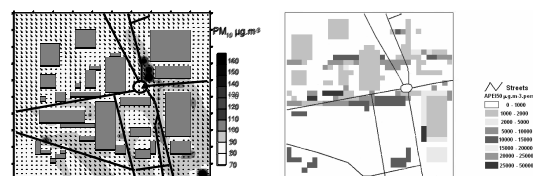


Figure 2. PM<sub>10</sub> simulated field and exposure results for an urban area in Lisbon (Borrego *et al.*, 2006).

From this overview we can conclude that air quality models are already used as input for exposure modelling and health related issues, but a wider effort is still needed to combine these PM air concentration models with personal activity patterns and indoor concentration values.

Borrego, C.; Tchepel, O.; Costa, A.M.; Martins, H.; Ferreira, J.; Miranda, A.I. (2006) *Traffic-related particulate air pollution exposure in urban areas*. Atmospheric Environment 40, 7205–7214.

IPCS (2004) *IPCS glossary of key exposure assessment terminology*. In: IPCS Risk Assessment Terminology. Geneva, World Health Organization, International Programme on Chemical Safety (Harmonization Project Document No. 1).

Hänninen, O.; Karppinen, A.; Valkama, I.; Kauhaniemi, M.; Kukkonen, J.; Kousa, A.; Aarnio, P.; Sokhi, R.; Skouloudis, A.; Jantunen, M. (2005) *Recommendations and best practices for population exposure assessment in the context of air quality modelling*. FUMAPEX Project Deliverable D7.4.

Miranda, A.I.; Ferreira, J.; Borrego, C.; Kuhlbusch, T.; Viana, M.; Winiwarter, W.; Ketzler, M. (2006) *Modelling Particulate Matter in European COST633 Action Member States*. COST Action 633. Ed: Thomas Kuhlbusch & Flemming Cassee.

## Generation and Quantification of Organic Peroxides in Aerosols to Study Cellular Responses on Oxidative Stress

A.A-M. Gaschen<sup>1</sup>, A. Praplan<sup>1</sup>, M. Savi<sup>2</sup>, D. Lang<sup>2</sup>, M. Geiser<sup>2</sup> and M. Kalberer<sup>1</sup>

<sup>1</sup>Department of Chemistry and Applied Biosciences, Swiss Federal Institute of Technology, ETH Zürich, Wolfgang-Pauli-Strasse 10, 8093 Zürich, Switzerland

<sup>2</sup>Institute of Anatomy, University of Bern, Bühlstr. 26, 3012 Bern, Switzerland

Keywords: Aerosol instrumentation, Deposition, Generation of aerosols, Lung/particle interaction, SOA

Ambient fine and ultrafine particles have, besides of impacts on atmospheric processes, a variety of adverse health effects, from which respiratory diseases have attracted a lot of attention in media. Up to about 50% of the ambient aerosol is composed of organic material. However, the highly complex organic mixture is chemically poorly characterized (Baltensperger *et al.* 2005; Kalberer 2006). The reaction of terpenes with ozone in the polluted troposphere mainly generates aldehydes, carboxylic acids and organic peroxides. The contribution of these peroxides to health risk is assumed to be especially important because of their high reactivity and oxidation potential.

The aim of this work is to characterize and quantify oxidizing agents in aerosols generated under controlled conditions in a flow tube setup (figure 1). In an accompanying project, lung cells are then examined for morphologic, biochemical and physiological changes after exposure to these aerosol particles.

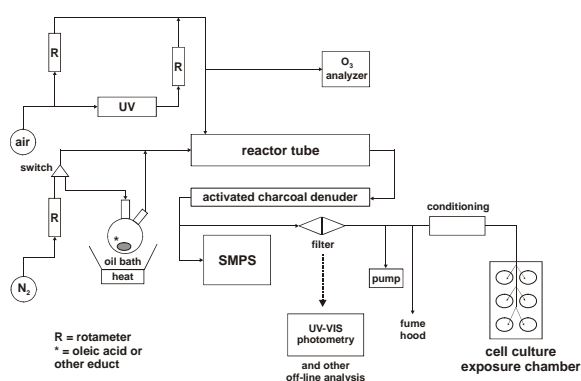


Figure 1. Scheme of the experimental setup.

First experiments were performed by reaction of ozone with oleic acid aerosol particles, which are often used as a model substance for terpenes due to its reactive double bond. Ozone was obtained by photolysis and radical reaction of oxygen from compressed air. Both components were led to the reaction chamber, a glass tube of about 1.5 l in volume. Then, ozone and other volatile products were removed by an activated charcoal diffusion denuder. The peroxide particles were collected on a

filter and their concentration was quantified off-line by UV-VIS spectrophotometry. The iodometric reaction used here allows to determine the total amount of -ROOR- groups in a sample (Docherty *et al.*, 2005). Oxidized oleic acid particles were produced with varying amounts of peroxides. Further analyses by chromatography and MS methods will elucidate the chemical composition of the generated aerosols. The particle size distribution was analysed by a scanning mobility particle sizer, SMPS.

Simultaneously to collecting the reaction products on a filter, the particles were also deposited directly onto the air-liquid interface of lung cell cultures. In this on-line particle deposition chamber, charged particles were deposited in an electrical field onto six parallel cell culture wells. The air flow was conditioned to a constant temperature, humidity and gas composition prior to contact with the cell cultures.

This setup can be easily adapted to study particle formation in various systems of organic aerosols. The functioning of the instrument has been tested thoroughly and first results indicate that test particles can be deposited evenly onto lung cell cultures. However, stable aerosol flow conditions are still difficult to achieve due to the sensitivity of the setup to temperature and pressure fluctuations. A comparison of the cellular responses to inert polystyrene test particles and to peroxide aerosol particles will be presented.

These analyses of oxidation properties of organic aerosols will greatly help to understand the cellular responses induced by fine and ultrafine particles. The main hypothesis of this project is, that the oxidation capacity of organic particles is mainly responsible for their biological effects.

This work was supported by SBF under grant Nr. C06.0075 as part of the COST Action 633.

Baltensperger, U. *et al.*, (2005). *Faraday Discuss.*, 130, 265-278

Docherty, K. S. *et al.*, (2005). *Environ. Sci. Technol.*, 39, 4049-4059.

Kalberer, M. (2006). *Anal Bioanal Chem.*, 385, 22-25.

## Differences and Similarities in PM Characteristics across Europe: Results of the COST633 Data Compilation Activity

J.P. Putaud<sup>1</sup>, A. Alastuey<sup>2</sup>, H. ten Brink<sup>3</sup>, R. Hitzenberger<sup>4</sup>, A. Jones<sup>5</sup>, A. Kasper-Giebl<sup>6</sup>, A. Kousa<sup>7</sup>, A. Molnar<sup>8</sup>, T. Moreno<sup>2</sup>, F. Palmgren<sup>9</sup>, C. Petaloti<sup>10</sup>, I. Salma<sup>11</sup>, J. Tursic<sup>12</sup>, and M. Viana Rodriguez<sup>2</sup>.

<sup>1</sup> European Commission, DG JRC, Institute for Environment and Sustainability, I-21020 Ispra, Italy

<sup>2</sup> Institute of Earth Sciences (Jaume Almera), CSIC, Solé i Sabarís, s/n. Barcelona 08028, Spain

<sup>3</sup> Energy Research Centre of the Netherlands (ECN), P.O. Box 1, Petten 1755 ZG, The Netherlands

<sup>4</sup> Faculty of Physics, University of Vienna, Boltzmannngasse 5, A-1090 Vienna, Austria.

<sup>5</sup> Univ. of Birmingham, Environmental Health and Risk Management, Edgbaston, Birmingham B15 2TT, UK

<sup>6</sup> Vienna University of Technology, Getreidemarkt 9/164-AC, A-1060 Vienna

<sup>7</sup> YTV Helsinki Metropolitan Area Council, Opastinsilta 6 A, FI-00520 Helsinki, Finland

<sup>8</sup> Hungarian Academy of Sciences, P.O.Box 158, H-8201 Veszprém, Hungary

<sup>9</sup> National Environmental Research Institute, Postboks 358, Frederiksborgvej 399, 4000 Roskilde, Denmark

<sup>10</sup> Aristotle University of Thessaloniki, Macedonia, Greece

<sup>11</sup> Eotvos University, Institute of Chemistry, P.O. Box 32, H-1518 Budapest, Hungary

<sup>12</sup> Environmental Agency of the Republic of Slovenia, Vojkova 1/b, SI-1000 Ljubljana, Slovenia.

Keywords: Particulate Matter, Measurements.

Epidemiologic studies have shown a close relationship between particulate matter (PM) mass concentrations and mortality and / or morbidity (e.g. Dockery et al., 1993). However, they have also pointed out spatial differences in the health impact of PM mass concentrations or mass concentration increments (e.g. Le Tertre et al., 2005). One of the reasons for this might be that PM characteristics (chemical composition, size distribution) do vary from place to place, both at a large scale (across a continent) and at a more regional / local scale (from rural background to kerbside sites). To test this hypothesis, the results of the epidemiological studies should be confronted to PM characterisation data, beyond the only PM mass concentrations reported by the air quality monitoring networks.

Such parameters (PM mass concentration, chemical composition and particle number concentration and / or size distribution) have been measured at various locations in Europe for many years. However, most of them rarely reach possible users such as epidemiologists, modellers, and policy makers.

We aimed at closing this gap by complementing the data compilations by Van Dingenen et al. (2004), and Putaud et al. (2004), based on a more systematic survey of the available aerosol data across Europe, made possible by the official collaboration of the 20 signatories of the COST633 Action. We identified 94 (+24) new data sets containing PM mass and chemistry for at least 1 year (or several weeks), and 21 (+7) data sets including PM mass and particle number data, which cover 13 countries. Up to now, 34 datasets from 8 countries have been delivered to the COST633 data bank (Fig. 1).

These data have been aggregated to the ones already available to highlight differences and

similarities in PM characteristics across various scales in Europe.

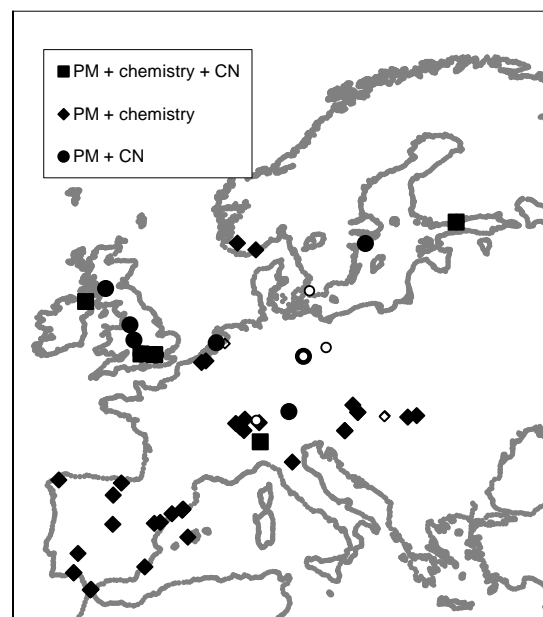


Figure 1. Location of the sites where PM mass and characterisation data were collected from.

This work was supported by COST Action 633 "Particulate matter (PM) – properties related to health effects"

Dockery D. W. et al. (1993), *N Engl J Med*; 329, 1753–1759

Le Tertre A., et al. (2005), *Risk Analysis*, 25, 711-718

Putaud J.P. et al. (2004), *Atmos Environ*, 38, 2579-2595

Van Dingenen R. et al. (2004), *Atmos Environ*, 38, 2561-2577

## Seasonal variability of air pollution and mortality in the Urban Area of Katowice, Poland

M. Kowalska<sup>1</sup>, J.E.Zejda<sup>1</sup>, L. Ośródk<sup>2</sup>, K. Kleinowski<sup>3</sup>, E. Krajny<sup>2</sup>

<sup>1</sup>Department of Epidemiology, Medical University of Silesia, Medyków Str.18 40-820 Katowice, Poland

<sup>2</sup>Institute of Meteorology and Water Management, Bratków Str. 10, 40-045 Katowice, Poland

<sup>3</sup>Institute of Environmental Engineering Bases of Polish Academy of Science, Department of Air Protection, M.Skłodowskiej-Curie Str. 34, 41-819 Zabrze, Poland

Keywords: mortality, ambient air pollution, time-series study.

Epidemiological evidence has proven a significant association between ambient air pollution (gaseous and particulate) and daily total and specific mortality. A number of papers have also indicated a strong impact of the season on the overall magnitude of the risk of additional death [1, 2]. The latter effect could be modified by the sources of air pollution and meteorological conditions [3,4].

The aim of the study was to analyze the current relationship between seasonal variability of the daily total and specific mortality (cardiovascular and respiratory mortality) and daily PM<sub>10</sub>, SO<sub>2</sub> and NO<sub>x</sub> average area concentrations in the ambient air in the Urban Area of Katowice.

Daily counts of deaths in 2001-2002, in the study region, were obtained from the Central Statistical Office in Warsaw. The records included total number of deaths, the number of deaths due to cardiovascular and respiratory diseases, for the entire population and in two age categories: <65 years and 65+ years of age. The classification of causes of death was based on the International Classification of Diseases ICD-10. Data concerning ambient air pollution and meteorological conditions (temperature, atmospheric pressure and relative humidity) were calculated as 24-hour area averages. The data set included also a four-level variable describing a climatic season ('winter', 'spring', 'summer' and 'fall').

Relationship between the daily number of deaths and daily concentrations of pollutants, and meteorological parameters in the defined seasons was estimated by means of Spearman correlation analysis. Analyses were performed with the use of procedures available in the Statistica 7.0 program.

Table 1 shows the average daily counts of deaths by season, in the Urban Area of Katowice in the period 2001-2002.

Figure 1 presents average daily concentrations of each other examined air pollution, by season, in the study area.

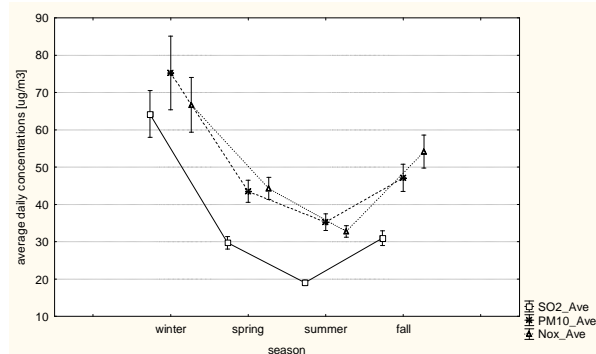
We noted statistically significant relationship between daily number of deaths due to cardiovascular/respiratory diseases and sulphur dioxide concentration in winter and in spring (Spearman correlation coefficient amounted: 0,24 and 0,21, respectively).

Similar effect was seen in the elderly (population aged 65+ years), but only in spring time. We observed also a high correlation between temperature and sulphur dioxide concentration in cold seasons (winter and fall).

Table 1. Average daily counts of deaths in the Urban Area of Katowice, by season (2001-02).

Season	Total number of deaths	Number of deaths from CVD and RD
Spring	53,8 ± 8,1	27,2 ± 5,7
Summer	50,5 ± 7,6	25,0 ± 5,3
Fall	52,7 ± 8,2	26,7 ± 5,5
Winter	57,8 ± 7,5	30,9 ± 6,1

Figure 1. Average daily concentration of air pollutants in Urban Area of Katowice, by season (2001-2)



This project was supported by the State Committee for Scientific Research, Poland (Grant: COS/87/2006)

1. Brunekreef B., Holgate S.T. (2002) *Lancet*, 360: 1233-42
2. Clancy L., Goodman P. at all (2002) *Lancet*, 360:1210-14
3. Peng R.D., Dominici F. Pastor-Barriuso R. at all (2005) *Am J Epidemiol*, 161: 585-594.
4. Schwartz J. (2004) *Occup Environ Med*, 61: 956-61

## **Heterogeneity in toxicity of particulate matter collected across Europe**

F.R. Cassee<sup>1</sup>, E. Dybing<sup>2</sup>, T. Sandström<sup>3</sup> and R.O. Salonen<sup>4</sup>

<sup>1</sup>Centre for Environmental Health Research, National Institute for Public Health and the Environment, Bilthoven, the Netherlands

<sup>2</sup>Division of Environmental Medicine, Norwegian Institute of Public Health, Oslo, Norway

<sup>3</sup>Department of Respiratory Medicine and Allergy, University Hospital, Umeå, Sweden

<sup>4</sup>Department of Environmental Health, National Public Health Institute, Kuopio, Finland

Keywords: Heterogeneity, Toxicity, Particulate Matter, Health, Air pollution.

The adverse health effects associated with ambient air pollution has triggered epidemiologists, toxicologists and aerosol scientists to combine their experience in investigation of the toxicity of ambient air particulate matter (PM) from European sites with differing traffic intensity and source mixture. The aim has been to increase the understanding of the role of fine and coarse PM, and their chemical characteristics, in relation to health effects. Under the European Union 5th Framework Programme (FP5), the HEPMEAP, RAIAP and PAMCHAR projects have utilised high volume cascade impactors to collect size-segregated PM in a variety of European locations during different seasons and performed a whole range of laboratory investigations. In general, the samples of both the coarse (2.5 - 10 µm) and fine (0.1 / 0.2 – 2.5 µm) thoracic PM were able to induce significant toxic effects. The sources and chemical composition of the PM samples have been suggested to play an important role in these responses.

### **Respiratory Allergy and Inflammation Due to Ambient Particles (RAIAP)<sup>a)</sup>**

The overall objective of the RAIAP research project (QLRT-2000-00792) has been to assess the role of ambient suspended particles in causing local inflammation in the respiratory tract and induction and elicitation of respiratory allergies, in order to understand the underlying mechanisms for involvement of particles in the development of these diseases. Coarse and fine PM were collected in four European cities during three seasons.

### **Health effects of particles from motor engine exhaust and ambient air pollution (HEPMEAP)<sup>b)</sup>**

The project (QLK-CT-1999-01582) focuses on the assessment of the inflammatory and toxic potential of ambient air suspended particles (collected at locations across Europe with contrasts in traffic intensity) in comparison with diesel engine exhaust PM. The investigators have assessed and compared the overall toxicity in vitro and in vivo in animals and humans. Moreover, these data and the physico-chemical characteristics of ambient air PM have been related to health effects noted in epidemiological studies.

### **Chemical and biological characterisation of ambient air coarse, fine, and ultrafine particles for human health risk assessment in Europe (PAMCHAR)<sup>c)</sup>**

The PAMCHAR project (QLK4-CT-2001-00423) investigates the physico-chemical and toxicological characteristics of ambient air coarse (PM<sub>10-2.5</sub>), fine (PM<sub>2.5-0.2</sub>) and ultrafine (PM<sub>0.2</sub>) particles in geographically and climatologically contrasting PM pollution situations in Europe. It focuses on comparison of the inflammatory, cytotoxic and genotoxic activities of PM samples in relation to their greatly varying chemical composition and sources.

### **Results and conclusions**

Oxidative and immunotoxic effects have been demonstrated in several in vitro and animal models. PM from traffic, and other local sources of incomplete combustion such as small-scale biomass and coal heating, have a high toxic potential. Coarse and fine PM have both been capable of inducing toxicity but via different modes of action. The chemical composition of PM seems to play an important role and although the view on causative components is not definite, metals and hydrocarbons appear to be consistently associated with toxic responses. Ambient PM has been shown to increase allergic responses in experimental animals. Asthmatics have been demonstrated to be particularly sensitive to diesel exhaust by showing clearly increased bronchial hyperresponsiveness. The acute inflammatory response in the airways of asthmatic subjects differed between the fine and coarse PM. This may indicate that the pre-existing asthmatic airway inflammation plays a role in the sensitivity of these subjects to air pollution, as suggested by epidemiological studies. The studies in cell lines and in animals have shown that the physico-chemical characteristics are generally more predictive for health effects than the PM mass. Decision-makers should integrate the PM composition and toxicity research findings into further refinement of the PM exposure and health risk assessment as well as into continuous improvement of management strategies for emission sources and urban air quality.

a) [www.raiap.org](http://www.raiap.org); b) [www.hepmeap.org](http://www.hepmeap.org); c) [www.pamchar.org](http://www.pamchar.org)

## PM<sub>2.5</sub> site/seasonal variability in Ireland: toxicological effects

D Healy<sup>1</sup>, V. Silvani<sup>2</sup>, E. Per-Trepat<sup>1</sup>, J. Lopez<sup>1</sup>, A. Whittaker<sup>1</sup>, I. O Connor<sup>1</sup>, J. Sodeau<sup>1</sup> and J. Heffron<sup>2</sup>

<sup>1</sup> Department of Chemistry and Environmental Research Institute, University College Cork, Ireland

<sup>2</sup> Department of Biochemistry, University College Cork, Ireland

Keywords: PM<sub>2.5</sub>, chemical composition, toxicity, health effects

Whilst internationally collected data demonstrating that adverse health effects correlate with Particulate Matter (PM), many questions, concerning the mechanisms by which they act, remain.

Chemical analysis shows PM to comprise of many inorganic, organic, and elemental materials, several of which promote adverse toxicological responses. For example, transition metals have long been recognised as toxic components of particles found in occupational settings and there are a number of well-characterised pathological diseases caused by the inhalation of particles of specific metallic compounds. (Samet *et al.*, 2007)

Therefore it is important to determine the contribution of metals and other chemical components, to the adverse health effects observed in PM epidemiology studies. Project ERITASK is the first of its kind in Ireland to encompass the four necessary stages to characterize ambient PM<sub>2.5</sub>: 1. Sampling 2. Physico-chemical compositional analysis. 3. Toxicological studies, and 4. Chemometrics/statistical analysis. The ultimate aims are to determine both the hypothesised link that exists between PM<sub>2.5</sub> composition and its potential toxicity and also to investigate any geographical and seasonal differences for PM<sub>2.5</sub> sampled in the urban area of Cork City.

PM<sub>2.5</sub> has been collected at three sites located throughout Cork, Ireland (Urban/City centre, urban background and a rural site). The collections were made on Polyurethane foam (PUF) filter substrates using a high volume cascade impactor sampler (900 min<sup>-1</sup>). Elemental concentrations of representative suites of 20 metals were determined using microwave extraction and ICP-OES spectrometry. In addition, aqueous extracts were analysed, after sequential agitation/sonication to quantify the solubility (bioavailability) of the different metal components (ICP-OES). This procedure was also utilised in the determination of the inorganic ion content of the PM<sub>2.5</sub> by ion chromatography. Both the total carbon was determined (CE440 Elemental Analyser) and the endotoxin content determined for the PM<sub>2.5</sub> sampled.

To investigate the biological effects of PM<sub>2.5</sub> at a sub-cellular level, the human epithelial pulmonary A549 cell line was exposed for 72hrs to different concentrations of PM<sub>2.5</sub> (0, 5.5, 11.0, 22.0

g/cm<sup>2</sup>). As an index of cytotoxicity after PM<sub>2.5</sub> exposure the activity of DH released from the cytosol of damaged cells into the supernatant was determined. *In vitro* cell proliferation and cytotoxicity after PM<sub>2.5</sub> exposure has also been determined using the resazurin assay. The reduced glutathione (GSH) assay (Hissin *et al.*, 1976) was employed to evaluate how GSH, one of the primary bio chemicals for cell defence, can be influenced by PM toxicity. In this study the ability of the 3 different concentrations of PM to induce release of the pro-inflammatory mediators, interleukin-6 (I-6), interleukin-8 (I-8) and tumor necrosis factor (TNF) from human epithelial lung cells (A549) was investigated. The most potent samples exhibited a relatively high content of transition metals (*e.g.* Fe and Mn) this was especially true for the summer samples of the three sites when looking at I-6. Significant cytotoxicity was noted only at higher concentrations of particle exposure which would indicate that chemical composition of PM<sub>2.5</sub> is a critical determinant for the marked differences in potency to induce cytokine responses in human epithelial lung cells. A concentration dependence was noted for the toxicological assays: ROS, I-6, DH. However the I-8 response did not always increase with increasing particle dose over the 5.5-22.0 g/cm<sup>2</sup> range. In these cases, the decrease in I-8 at higher particle concentrations could not be explained by loss of cell viability.

The application of Chemometric methods (*e.g.* Principle Component Analysis), investigated correlations between elemental content (*e.g.* metals) and toxicological endpoints (ROS, I-6, I-8).

This work was supported by the Irish Environmental Protection Agency and 6th Framework Program Marie Curie Transfer of Knowledge Programme.

Samet, J. M., & Ghio A. J. (2007). Chapter 8 *Particle Toxicology*. Taylor & Francis Group. CRC Press.

Hissin PJ, Hilf R: *Anal Biochem* (1976) 74:214-226.

## **T24 Abstracts**

## The processes prompting the contrasting behaviour between the aerosol number and mass concentrations at the Izaña Global Atmospheric Watch Observatory: new particles formation *versus* Saharan dust inputs

S. Rodríguez<sup>1,2</sup>, E. Cuevas<sup>1</sup>, R. Ramos<sup>1</sup>, P.M. Romero<sup>1</sup>

<sup>1</sup> Izaña Atmospheric Observatory, INM-CSIC, Santa Cruz de Tenerife, 38071, Canary Islands, Spain

<sup>2</sup> Department of Geology, University of Huelva, Huelva, 21071, Spain

Keywords: North Atlantic free troposphere, new particles formation, nucleation, Saharan dust

This study summarises some of the results obtained in the simultaneous monitoring of the aerosols number and mass concentrations at the Izaña Global Atmospheric Watch Observatory (28.47°N, 16.24°E), located in the free troposphere in Tenerife at 2367 m.a.s.l. (Canary Islands). At this site the mass concentrations of particles less than 10, 2.5 and 1  $\mu\text{m}$  (i.e. PM10, PM2.5 and PM1, respectively) and the number concentrations of particles coarser than 3 and 10 nanometres (i.e.  $N_{>3}$  and  $N_{>10}$ , respectively) are continuously monitoring in order to obtain information on the features, sources, transport patterns and origin-region of aerosols in the North Atlantic free troposphere.

At Izaña free troposphere site, the number concentrations  $N_{>3}$  &  $N_{>10}$  exhibit a strongly marked daily cycles with much higher levels during daylight than at night, exhibiting a high correlation with the solar radiation intensity. Daylight  $N_{>3}$  concentrations are one order of magnitude higher in summer than in winter:  $\sim 15 \cdot 10^3 \text{ cm}^{-3}$  in summer versus  $\sim 1.5 \cdot 10^3 \text{ cm}^{-3}$  in winter (Figure 1). Observe in Figure 1 how the whole daily evolution of  $N_{>3}$  is delayed in winter because the change in the solar radiation pattern. The  $N_{>3}$  and  $N_{>10}$  cross correlation analysis shows that the number concentrations  $N_{3-10}$  (3 to 10 nanometres) are very low at night ( $< 100 \text{ cm}^{-3}$ ), when the  $N_{>3}$  versus the  $N_{>10}$  data exhibits a slope equals to 0.995 ( $r^2=0.94$ ). In contrast,  $N_{3-10}$  concentrations exhibit extremely high values during daylight (up to  $35 \cdot 10^3 \text{ cm}^{-3}$ ), when  $N_{3-10}$  accounts for  $\sim 50\%$  of  $N_{>3}$ , and the  $N_{>3}$  versus the  $N_{>10}$  data exhibits a slope of  $\sim 2$  ( $r^2=0.89$ ). These results point that this behaviour is highly prompted by new particles formation during daylight by photo-chemically induced nucleation processes. These conclusions are also supported by  $dN/d\log D$  size distribution data collected during some intensive campaigns.

At Izaña, the PM10 concentrations exhibit a highly contrasting behaviour. PMx levels do not show a daily cycle as marked as that of the number concentration. The most important variations in PMx levels occurs under Saharan dust conditions, when PM10 levels experiences frequent increases from  $< 10$  to  $> 100 \mu\text{g}/\text{m}^3$  (Figure 2). Rodríguez et al. (2007) present more details on PMx features at Izaña in this proceeding.

These and other results obtained in this study evidence that the mass and number concentrations of aerosols at the Izaña North Atlantic free troposphere site are significantly influenced by different sources and processes. The number concentration is mainly affected by new particles formation by nucleation which originally occurs in the 3-10nm size range. A significant involvement of the biogenic emissions from the forest of pines in Tenerife is expected. In contrast, the mass concentrations of aerosols is mainly affected by mineral dust inputs from the Sahara desert mostly affecting the size range  $> 1 \mu\text{m}$ .

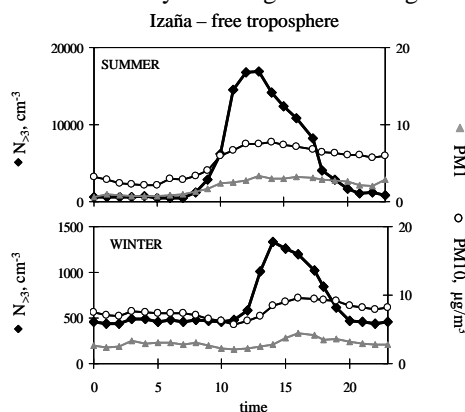


Figure 1. Daily mean evolution of  $N_{>3}$ , PM10 and PM1 at Izaña free troposphere site.

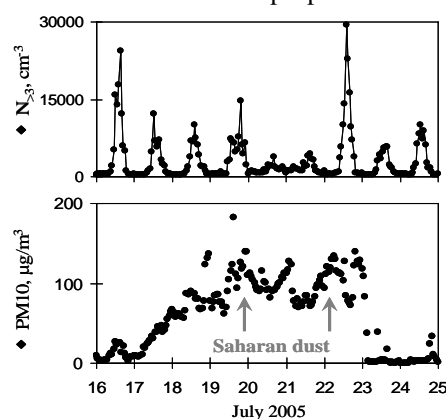


Figure 2. Hourly mean concentrations of  $N_{>3}$  and PM10 at Izaña in July 2005.

Rodríguez, S., Cuevas, E., Romero, P.M., Querol, X., Alastuey, A., Perez, N., Castillo, S. (2007). In *Proc. EAC 2007*. Included in this issue.

## Saharan dust observations in the Mediterranean-Adriatic confluence region

S. Rodríguez<sup>1,2</sup>, D. Đorđević<sup>3</sup>

<sup>1</sup> Department of Geology, University of Huelva, Huelva, 21071, Spain

<sup>2</sup> Izaña Atmospheric Observatory, INM-CSIC, Santa Cruz de Tenerife, 38071, Canary Islands, Spain

<sup>3</sup> Institute of Chemistry, Technology and Metallurgy – Centre for Chemistry, University of Belgrade, Studentski trg 12 - 16, 11000 Belgrade, Serbia

Keywords: mineral dust, Saharan dust, Mediterranean

Saharan dust transport over the Mediterranean is a topic of major interest because it is involved in the geological evolution of soils, in the nutrients supply to marine ecosystems and it influences on the radiation transfer and on the processes related clouds evolution. Years ago, these topics prompted field measurements campaigns for performing *in-situ* characterisation studies of mineral dust in central Mediterranean sites such as Sicily and Sardinia (Figure 1).

Moreover, during the last years Saharan dust transport has also been involved in the studies on air quality in Europe owing to it has been observed that the mineral dust transported from the Sahara desert result in high PM<sub>10</sub> and PM<sub>2.5</sub> concentrations interfering with the monitoring of urban and rural air quality. First observations pointing to this significant Saharan dust interference in the air quality monitoring were performed in Spain (Querol et al., 1998; Rodríguez et al., 2001), where the studies undertaken during the last years allowed to understand how this dust transport take place, and to quantify the typical mineral dust concentrations in TSP, PM<sub>10</sub> and PM<sub>2.5</sub> under Saharan dust events conditions. More recently, other studies describing similar ‘air quality impairment problems’ due to the Saharan dust transport to Portugal, Greece, Northern Italy and Turkey have been published. Most of our knowledge on the Saharan dust impact on the aerosol composition is based on observations mostly performed in the Western and Eastern Mediterranean’s sides (Figure 1).

In this study we present the results of 5 years (1995-2000) of Saharan dust observations in a coastal site (42.45°N, 18.55°E) located into the Herceg-Novi bay close to the Adriatic - Mediterranean confluence, a region where previous Saharan dust observations had not been performed. The content in major and minor aerosol components was determined by several analytical techniques. Saharan dust events in our data base were identified by using meteorological techniques, including back-trajectories and on-line available modelling (DREAM, NAAPS and SKIRON systems).

The result shows that the Saharan dust transport has a strong impact in the aerosol composition in this region. For example, the concentrations of Ti experiences frequent increases from 10 to >100 ng/m<sup>3</sup> owing to the Saharan input,

even reaching ~400 ng/m<sup>3</sup> during severe dust events. Similar increases are observed in other mineral dust components, such as Fe or Mn. These dust events may results in total aerosol mass concentrations of 100µg/m<sup>3</sup>.

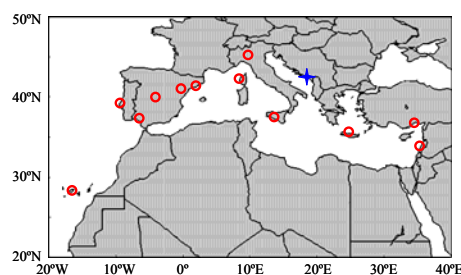


Figure 1. Map of the Mediterranean showing the location of our (★) and other sites (●) where Saharan dust observations have been performed.

The meteorological scenarios associated with the Saharan dust transport are into the framework of those identified in previous studies in the Eastern and Western Mediterranean. However, Saharan dust transport in this region appears to be more ‘irregular’ than in other regions of the Mediterranean (e.g. Spain). In general, Saharan dust events mostly occur in spring and summer, being most of the events associated with a southern dust transport owing to cyclonic activity over the Mediterranean - North Africa regions. However, it worth to be highlighted that anomalous Saharan dust events have been observed, such as a dust plume entering in the Adriatic sea from the Northeast owing to the dust recirculation over the Eastern Mediterranean.

These results, together with a literature review, have contributed to build a ‘general picture’ on the dust transport and its impact on the air quality in the Mediterranean.

Rodríguez, S., Querol, X., Alastuey, A., Kallos, & G., Kakaliagou, O. (2001). *Atmos. Environ.* 35, 2433–2447

Querol, X., Alastuey, A., Puicercus, J.A., Mantilla, E., Miro, J.V., López-Soler, A., Plana, F., Artíñano, B. (1998). *Atmos. Environ.* 32, 1963-1978.

## State of mixing of the Saharan dust sub- and supermicrometer aerosol

N. Kaaden<sup>1</sup>, A. Massling<sup>1</sup>, T. Müller<sup>1</sup>, A. Schladitz<sup>1</sup>, K. Kandler<sup>2</sup>, L. Schütz<sup>3</sup>, and A. Wiedensohler<sup>1</sup>

<sup>1</sup>Department of Physics, Leibniz-Institute for Tropospheric Research, Leipzig, Germany

<sup>2</sup>Institute of Applied Geosciences, Darmstadt University of Technology, Darmstadt, Germany

<sup>3</sup>Institute for Physics of the Atmosphere, Johannes-Gutenberg-University, Mainz, Germany

Keywords: Mineral dust, Hygroscopicity, Particle formation and growth, TDMA, APS.

### INTRODUCTION

Hygroscopic properties in terms of growth factors and state of mixing of sub- and supermicrometer particles were measured in May/June 2006 for characterization of the Saharan dust aerosol. Therefore, a measurement station was set up near Tinfou close to Zagora, Morocco, within the project SAMUM (SAharan Mineral dUst experiment).

### METHODS

In the submicrometer particle size range, hygroscopic properties were investigated using an H-TDMA system (Hygroscopicity - Tandem Differential Mobility Analyzer) consisting of two DMAs in series with a humidity conditioner in between (Massling et al., 2005).

For the supermicrometer particle size range, an H-DMA-APS system (Hygroscopicity - Differential Mobility Analyzer - Aerodynamic Particle Sizer) was used (Leinert & Wiedensohler, 2006). This system consists of a High Aerosol Flow DMA with two APS in series combined with a humidity conditioner downstream of the DMA and upstream of the second APS. Table 1 presents a list of the measurements performed during the experiment.

Table 1. List of systems and parameters obtained during SAMUM.

System	Size range	Measurement
H-TDMA	30, 50, 80, 150, 250, 350nm	Growth factor at RH = 85%
H-TDMA	30, 50, 80, 150, 250, 350nm	State of mixture, number fraction
H-DMA-APS	0.8, 1.0, 1.2 $\mu$ m	Growth factor at RH = 85%
H-DMA-APS	0.8, 1.0, 1.2 $\mu$ m	State of mixture, number fraction

### RESULTS

Lognormal fitting of the particle number size distributions resulted in three distinct particle modes (hydrophobic, less hygroscopic and more hygroscopic) for the submicrometer size range and just one particle mode (hydrophobic) for the

supermicrometer size range. Corresponding number fractions of these different particle types are illustrated in Figure 1, presenting a dust event observed during SAMUM. In general the number fractions of the hydrophobic particle group are increasing with increasing diameter. Most impressive is the hydrophobic number fraction of 250nm particles, reaching a value of more than 50%.

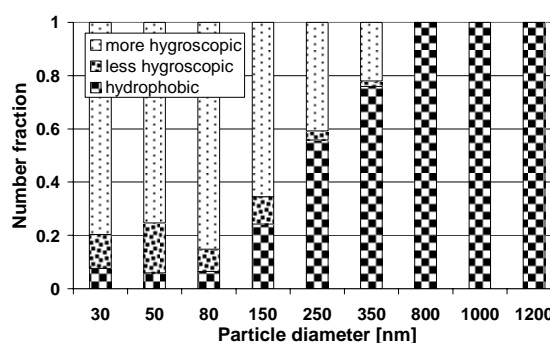


Figure 1. Number fractions of hygroscopically different sub- and supermicrometer particles reflecting a dust event in Zagora, Morocco.

First analyses suggest that the hydrophobic material consists of mineral dust (mostly feldspars, clay minerals, quartz, calcite, dolomite, gypsum and hematite) as well as carbonaceous material. Correlation between hygroscopic (hydrophobic number fraction) and optical data (single scattering albedo) was proved and affirmed ( $r_{nf-SSA} = -0.73$ ).

Growth factors for the more hygroscopic particle fraction in the submicrometer size range showed values close to that of ammonium sulphate, less hygroscopic particles had growth factors varying from 1.2 to 1.4.

Shape factors derived from H-DMA-APS measurements together with the hygroscopic behaviour of the particles are important inputs for optical closure experiments.

This work was supported by the Deutsche Forschungsgemeinschaft (DFG).

Leinert S., & Wiedensohler A. (2006). *J. Aerosol Science*, submitted.

Massling, A., Stock, M., & Wiedensohler, A. (2005). *Atm. Env.*, 39, 3911-3922.

## Chemical and mineralogical composition of Saharan dust over southeast Morocco

K. Kandler<sup>1</sup>, C. Deutscher<sup>2</sup>, M. Ebert<sup>1</sup>, H. Hofmann<sup>1</sup>, S. Jäckel<sup>1</sup>, A. Petzold<sup>3</sup>,  
L. Schütz<sup>2</sup>, S. Weinbruch<sup>1</sup>, B. Weinzierl<sup>3</sup>, S. Zorn<sup>2</sup>

<sup>1</sup>Institute of Applied Geosciences, Darmstadt University of Technology, Darmstadt, Germany

<sup>2</sup>Institute for Physics of the Atmosphere, Johannes-Gutenberg-University, Mainz, Germany

<sup>3</sup>Institute of Atmospheric Physics, German Aerospace Center, Wessling, Germany

Keywords: mineral dust, chemical composition, single particle analysis, electron microscopy.

The Saharan Mineral Dust Experiment (SAMUM) is dedicated to the understanding of the radiative effects of mineral dust. A joint field campaign focussed on the source-near investigation of Saharan dust was carried out in southern Morocco. Ground based measurements were performed near Tinfou and at the Ouarzazate airport; airborne measurements were carried out onboard a Falcon and a Partenvia aircraft. Together with Satellite observations, these measurements were performed from May 13<sup>th</sup> to June 7<sup>th</sup>, 2006.

Airborne as well as ground based samples were collected with a miniature impactor system on carbon coated substrates and carbon foils; additionally, filter samples for determination of the aerosol mass concentration were collected. The size-resolved particle aspect ratio and chemical composition is determined by means of electron-microscopical single particle analysis. The mineralogical composition of the filter samples is determined by x-ray diffraction. Additional information on single particles will be collected by transmission electron microscopy.

The bulk mineralogical composition is dominated by quartz, calcite, feldspars (plagioclase and K-spars), and clay minerals (illite/muscovite, kaoline, and chlorite). In addition, hematite is found as important minor component.

As an example, Fig. 1 shows the chemical composition of particles between 1 and 1.5  $\mu\text{m}$  in diameter as a function of measurement altitude over Tinfou for May 19, 2006, 11:24 to 11:42 h. On this day, the mineral dust layer extended up to approximately 4.5 km. The composition of the layer was quite homogeneous, except the sulfate-silicate mixtures on the ground and at the top of the layer being more abundant than within. The latter indicates anthropogeneous influence in the boundary layer as well as in the tropospheric background. On the other hand, the layer was not homogeneous in the horizontal as is shown in Fig. 2. 140 km to the northeast, a significantly higher content of calcium-bearing particles can be detected, appearing as a mode around 3  $\mu\text{m}$  diameter.

Further analysis of more samples will show more details on the variation of the mineral dust composition over Morocco.

Financial support by the Deutsche Forschungsgemeinschaft (research group SAMUM) is gratefully acknowledged.

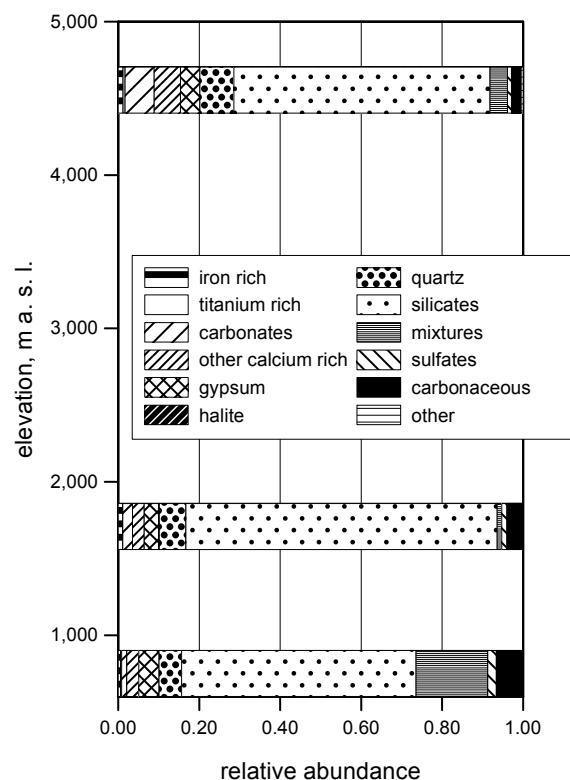


Fig. 1: Relative abundance of particle classes as function of altitude over Tinfou, Morocco

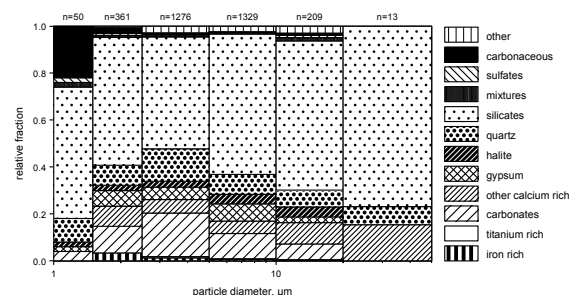


Fig. 2: Relative abundance of particles classes as function of particle diameter for a sample collected at 100 m altitude above the valley east of Ouarzazate, Morocco

## Reporting aerosol data about the most strong desert dust outbreak registered over the Iberian peninsula mixed with a forest fire episode. Columnar properties with remote sensing techniques.

V.E. Cachorro<sup>1</sup>, N. Prats<sup>1</sup>, M. Sorribas<sup>2</sup>, C. Toledano<sup>1,3</sup>, S. Mogo<sup>4</sup>, A. Berjón<sup>1</sup>, A.M. De Frutos<sup>1</sup>, and B.A. De la Morena<sup>2</sup>

<sup>1</sup> Atmospheric Optic Group GOA-UVA, University of Valladolid, 47071, Valladolid, Spain.

<sup>2</sup> Atmospheric Sounding Station 'El Arenosillo', Earth Observation, Remote Sensing and Atmosphere Department, INTA, 21130, Mazagón-Huelva, Spain.

<sup>3</sup> [Meteorological Institute](#), University of Munich, 80333, Munich, Germany.

<sup>4</sup> Department of Physics, University of Beira Interior, 6200, Covilha, Portugal.

Keywords: atmospheric aerosol, alpha Ångström coefficient, dust, particle size distribution, optical properties.

The Iberian Peninsula (IP) is frequently affected by air masses of desert origin, Sahara desert and Sahel areas in north Africa. These intrusions are the hardest episodes at atmospheric aerosol charge level. We present here the evaluation and analysis of the most strong North-African desert dust outbreak registered over the Iberian Peninsula (IP) during the last decades, with the modern techniques of remote sensing. This episode took place from 22 July to 3 August of 2004. The interest for the analysis of this event is increased by the apportioned or mixing with smoke particles due to the existing forest fires that occurred in IP at the same time, also very frequent in summer. We focus in this study on the columnar aerosol properties determined using the data provided by the Cimel-AERONET photometers at El Arenosillo (south-west) and Palencia (north-center) stations. Because of that we will have an interesting mixture of desert dust and biomass burning particles, with very different characteristics.

Although presented as a detailed case study, this is also part of the general characterization of aerosols or local climatology study carried out in the south-west of the IP, at the station of El Arenosillo, the ESA<sub>t</sub> (Atmospheric Sounding Station) belonging to INTA. This database runs since 2000 as a part of the photometric stations of the AERONET network and is managed together by the GOA-UVA and INTA. Also a general study or inventory of desert dust events is being carried out in this station since 2000 (Toledano, 2005). This study shows that 2004 was the year with the bigger number of desert dust outbreaks including the most important of them, not only because of the intensity as well as the duration.

The air masses of this event were originated in the area of Sahel and was transported via an Atlantic Arc through north-west Africa and Atlantic ocean entering the IP through the south-west during the early morning of 21 July and extend over the whole IP during the 22-23 July, following a SW-NE direction (depending on the IP areas). This results are supported by the analysis of daily backtrajectories at three different levels based on the HISPLIT model and Modis AOD maps. NAAPS (Navy Aerosol

Analysis and Prediction System) model was also used to better analysis the contribution of dust and smoke AOD values over the IP.

During the 22th July the aerosol optical depth (AOD) given by the Cimel at 440nm reached a maximum of 2.7 at El Arenosillo station and 1.3 at Palencia one day later, with the alpha Ångström coefficient values near zero during AOD peaks.

About the volume size distributions, product of the AERONET inversion of the almucantar data, it is worth noting that, like for the AOD, the 22 July was registered the highest volume concentration for the total of the particle size distribution (PSD) (1.42  $\mu\text{m}^3/\mu\text{m}^2$ ), increasing considerably the coarse mode (1.25) with regard to the fine (0.17). Under normal summer conditions the PSD shows certain bimodality in the coarse modes, with the biggest concentration in  $r=3.85 \mu\text{m}$  and other mode much less important in  $r=1.70 \mu\text{m}$ . This behavior almost disappears for the desert dust PSD, where the mode in  $r=3.85 \mu\text{m}$  is worthless, and the mode is centered in  $r=1.70 \mu\text{m}$ .

About the values of the optical parameters, as a desert dust aerosol, according to the bibliography (Dubovik, et. Al., 2002) we get high scattering, with values for the single scattering albedo of 0.96 and for the real part of the refraction index close to 1.5, and therefore low absorption, as show in the low values of the imaginary part of the refraction index, around 0.004 for 440 nm and 0.002 for bigger wavelengths. The asymmetry parameter is around 0.70 and has no spectral dependence.

This work was supported by MEC under project REN2002-00966 and Junta de Castilla y León VA001C05.

Dubovik, O., et al (2002). *Variability of absorption and optical properties of key aerosol types observed in worldwide locations*. J. Atmos. Sci. V.59, 590-608

Toledano, C. (2005) *Climatología de los aerosoles mediante la caracterización de propiedades ópticas y masas de aire en la estación "El Arenosillo" de la red AERONET*. PhD Tesis, University of Valladolid.

## Desert Aerosol Size Distributions and Mass Concentrations – Results from the Saharan Mineral Dust Experiment SAMUM 2006.

L. Schütz<sup>1</sup>, K. Kandler<sup>2</sup>, C. Deutscher<sup>1</sup>, R. Jaenicke<sup>1</sup>, P. Knippertz<sup>1</sup>, S. Zorn<sup>1</sup>, M. Ebert<sup>2</sup>, S. Weinbruch<sup>2</sup>, A. Maßling<sup>3</sup>, A. Schladitz<sup>3</sup>, and A. Wiedensohler<sup>3</sup>

<sup>1</sup>Institute for Physics of the Atmosphere, University of Mainz, 55099 Mainz, Germany

<sup>2</sup>Institute of Geosciences, Darmstadt University of Technology, 64287 Darmstadt, Germany

<sup>3</sup>Leibniz-Institute for Tropospheric Research, 04318 Leipzig, Germany

Keywords: mineral dust, size distributions, mass concentration, atmospheric aerosols, SAMUM.

Long-range transport of mineral dust is expected to influence the climatic system. Dust from the Saharan desert contributes significantly to the global dust burden. The Saharan Mineral Dust Experiment (SAMUM) is dedicated to the understanding of the radiative effects of mineral dust in a major source region. A first joint field campaign took place at Ouarzazate and at Tinfou near Zagora, southern Morocco, in 2006. Aircraft and ground based measurements were performed from May 13 to June 7. An experimental data set of surface and atmospheric columnar information was collected. This data set, combined with satellite data, will provide the base of the first thorough columnar radiative closure tests in Saharan dust. During the course of this campaign, a variety of aerosol physical and chemical properties were measured.

Surface-near aerosol size distributions from 20 nm to 500 µm were measured at the Tinfou ground station. The size range of 20 nm < d < 10 µm was investigated by a DMPS/APS combination, whereas particles with 4 µm < d < 500 µm were measured by impactor collection on coated glass substrates followed by automated microscopic image analysis of the individual particles. The DMPS/APS combination was measuring quasi-continuously; the large and giant particle range was investigated once a day. Various atmospheric conditions were encountered during the measurement period. Fig 1 shows a large range of variability due to local and regional mineral dust emissions for particles with d > 300 nm. Some anthropogenic influence can be detected in the submicron range. The largest concentration variations of approximately three orders of magnitude due to mineral dust were found in the range d > 100 µm. New approximations of desert aerosol size distributions can be deduced from these measurements. Together with aircraft data, they can be used in columnar radiative closure studies of Saharan mineral dust.

During the course of the measuring period, daily mass concentrations were determined from filter gravimetric analysis: For clear atmospheric conditions, mass concentrations of approximately 100 µg m<sup>-3</sup> for total, 80 µg m<sup>-3</sup> for “PM<sub>10</sub>” and 30 µg m<sup>-3</sup> for the “PM<sub>2.5</sub>” were found. During moderate dust storms, concentrations of up to 300000 µg m<sup>-3</sup>, 3000 µg m<sup>-3</sup> and 1000 µg m<sup>-3</sup>, respec-

tively, were encountered. Of the three measured mass concentrations, the total particulate matter correlates best with the local wind speed. This indicates mainly local production of the giant particles and significant contribution of advection to the concentration of the smaller ones. Under high dust concentrations giant particles with d > 10 µm account for more than 90 % of the total airborne aerosol mass.

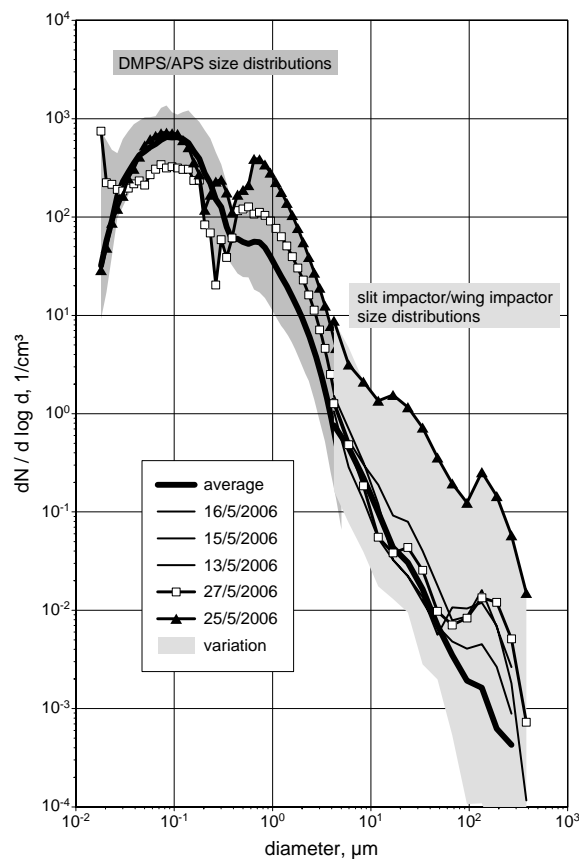


Fig. 1: Desert aerosol size distributions and range of variation at Tinfou, southern Morocco, during SAMUM 2006

This work was funded by the Deutsche Forschungsgemeinschaft (DFG) through its Forschergruppe SAMUM and by the Forschungsfond of the Johannes Gutenberg University, Mainz, Germany.

## Temporal variation of chemical compositions for aerosol samples collected during an Asian dust storm event in

H. Hwang, E. Choi, S. Kang, Y. Park, H. Kim, and C.-U. Ro

Department of Chemistry, Inha University, YonghyunDong, NamGu, 402-751, Incheon, Korea

Keywords: chemical analysis, single particle analysis, SEM/SE, Asian Dust.

In almost every spring, usually from March to May, Asian Dust originated from the arid areas in Central China is transported into the Korean Peninsular passing over industrialized regions in eastern China and the Yellow Sea. While Asian Dust travels a long-range distance, it can provide the reaction sites for the atmospheric reactions with diverse chemical species such as  $\text{SO}_x$  and  $\text{NO}_x$ . Hence, increasing attention has been devoted to study the physicochemical changes of Asian Dust particles during long-range transport.

A single particle analytical technique, named low-Z particle electron probe -ray microanalysis (low-Z particle EPMA) was applied to characterize Asian Dust aerosol samples collected in Incheon, Korea, on 7–9 April, 2006. To investigate the temporal variation of chemical compositions of Asian Dust, four samples were collected just before the Asian Dust storm event (sample A), in the middle of the storm event (sample B), at the peak time of the event (sample C), and at the end of the event (sample D). 3-stage Dekati PM10 sampler was used for the aerosol collection. The measurements were carried out on a Hitachi S-3500N V-SEM equipped with an Oxford Link SATW ultra-thin window ED detector.

In Figure 1, relative abundances of chemical species encountered (a) in coarse fraction ( $D_p$  2.5–10  $\mu\text{m}$ ) and (b) in fine fraction ( $D_p$  1.0–2.5  $\mu\text{m}$ ) are shown. The major chemical species encountered in Asian Dust samples are aluminosilicates (AlSi), silicon dioxides, calcium carbonates and their derivatives organic and carbon-rich species and reacted sea salt particles. In sample A, reacted sea-salts such as  $\text{NaNO}_3$ ,  $\text{Na}_2\text{SO}_4$  and their mixtures are most abundantly encountered with 51.3% and 56.6% in coarse and fine fractions, respectively. Reacted  $\text{CaCO}_3$  particles, such as  $\text{Ca}(\text{NO}_3, \text{SO}_4)$  and  $\text{Ca}(\text{CO}_3, \text{SO}_4)$ , are 15.9% and 8.8% in coarse and fine fractions, respectively. In sample B, the relative abundance of the reacted sea-salt particles decreases to 5% and that of AlSi-containing particles dramatically increases up to 70–80%. At the peak time of the event (sample C), the relative abundance of AlSi-containing particles is at its maximum (88% in coarse fraction). At the end of the storm event (sample D), it shows quite ordinary atmospheric composition such that the number fraction of soil-derived species decreases to 30–40%, while those of reacted sea-salt and organic species increased to 10–30% and 5–8%, respectively.

Based on this study for the temporal variation of the chemical compositions for the Asian Dust samples, the Asian Dust storm event seemed to be transported to Korea as follows i.e., in general, Asian Dust is transported to the Korean peninsular by strong wind. As Asian dust passed over industrialized eastern Chinese regions, the accompanying strong wind pushed away anthropogenic atmospheric pollutants such as  $\text{NO}_x$  and  $\text{SO}_x$  to the Yellow Sea. Then these gaseous pollutants can react with sea-salt particles over the Yellow Sea to produce  $\text{NaNO}_3$  and  $\text{Na}_2\text{SO}_4$  species. In addition,  $\text{CaCO}_3$  also reacted with gaseous  $\text{NO}_x$  and  $\text{SO}_x$  to produce  $\text{Ca}(\text{NO}_3)_2$  and  $\text{CaSO}_4$  species. And then these reacted sea-salts and reacted calcium carbonates arrived in the Korean Peninsular before Asian Dust mostly with pure minerals. As the Asian Dust storm event progressed, the air mass of Asian Dust arrived in the Korean Peninsular and the fraction of the soil particles such as aluminosilicate and silicon dioxide kept increasing and the maximum of their concentrations at the peak time of the storm event was observed.

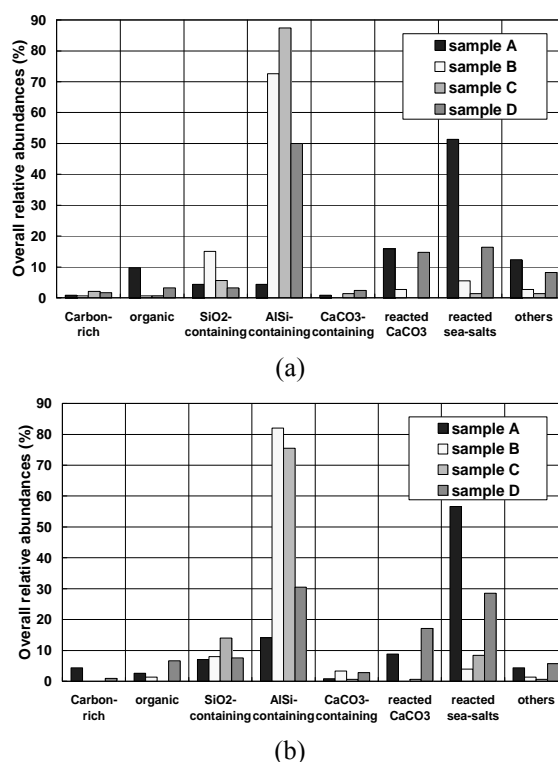


Figure 1. Overall relative abundances of particle types significantly encountered (a) in coarse fraction and (b) in fine fraction of Asian Dust samples

## MEASUREMENTS OF OPTICAL PROPERTIES OF DUST PARTICLES DURING THE SAHARAN MINERAL DUST EXPERIMENT SAMUM 2006

A. Schladitz, T. Müller, A. Maßling, N. Kaaden and A. Wiedensohler

Leibniz Institute for Tropospheric Research (IfT), 04318, Leipzig, Germany

Keywords: Mineral Dust, Optical Properties, Size Distribution, Refractive Index

During the SAMUM field campaign optical properties of mineral dust particles were investigated in southern Morocco. In-situ measurements of physical and optical parameters were performed near Zagora in southern Morocco from May 17 to June 7, 2006.

For measuring the scattering coefficient an Integrating Nephelometer ( $\lambda = 450, 550$  and  $700$  nm) was used. The absorption coefficient was determined with a Particle Soot Absorption Photometer (PSAP,  $\lambda = 530$  nm) and a Multi Angle Absorption Photometer (MAAP,  $\lambda = 637$  nm). Particle number size distributions were measured using a Differential Mobility Particle Sizer (DMPS) and an Aerodynamic Particle Sizer (APS) in the particle size range from  $20$  nm to  $10\mu\text{m}$ . The measured number size distribution was used to calculate the scattering and absorption coefficient using a Mie-code.

Periods with a low (case a) and a high (case b) particle number concentration in the dust-mode were selected. Assuming a log-normal size distribution the parameters for the dust-mode are  $\overline{D}_p \approx 600$  nm and  $\sigma \approx 1.74$ . Figure 1 shows the particle number concentration for the two cases.

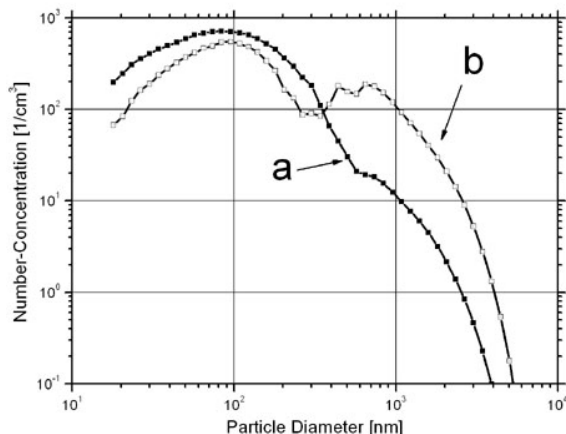


Figure 1: Particle number concentrations measured with a DMPS and an APS for case **a** (filled symbols) and **b** (open symbols).

High number concentrations in the dust-mode show increased values in the absorption and scattering coefficient (for the wavelengths see above). For calculating these optical parameters (assuming spherical particles) a refractive index for

dust (0% relative humidity) (GADS; Koepke et al., 1997) was used. Figure 2 shows measured and calculated absorption and scattering coefficients.

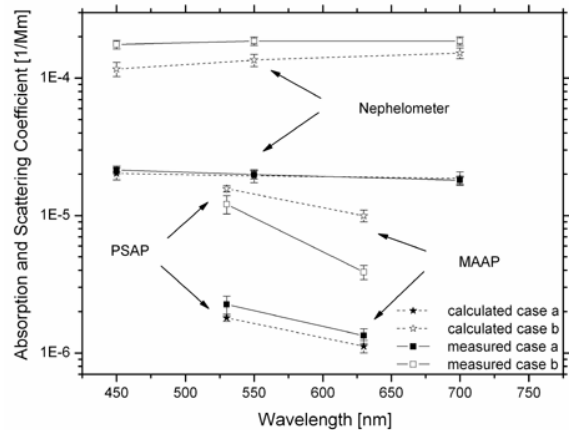


Figure 2: Calculated and measured scattering and absorption coefficients for case **a** (filled symbols) and for case **b** (open symbols).

Calculated absorption and scattering coefficients fitting well with measured absorption and scattering coefficients for case **a**. For case **b** the measured scattering coefficients are higher than the calculated ones. In contrast for case **b** the calculated absorption coefficients are higher than the measured ones for both wavelengths. We assume here a lower imaginary part of the refractive index of dust than the values given in Koepke et al. (1997).

The assumption of a lower imaginary part of the refractive index is in agreement with other authors. Haywood et al. (2003) point out an overestimation of absorption coefficients using a standard refractive index based on data of the SHADE field campaign in 2000.

### References:

- Koepke *et al.* (1997). Global Aerosol Data Set. MPI Meteorologie Hamburg Report No. 243, 44 Pages
- Haywood, J. *et al.* (2003). *J. Geophys. Res.*, 108 (D18), 8577.

## Size distribution vertical profiles of Saharan dust over the Eastern Atlantic during the 2005-2006 summer outbreaks from aircraft “in-situ” measurements

Andrey J.<sup>1</sup> Gil M.<sup>1</sup>, Serrano O.<sup>1</sup> and E. Cuevas<sup>2</sup>

<sup>1</sup>Instituto Nacional de Técnica Aeroespacial, Torrejón de Ardoz, 28850, Spain

<sup>2</sup>Instituto Nacional de Meteorología, Observatorio de Izaña, La Marina 20, 28071, Sta. Cruz de Tenerife, Spain

Keywords: Aerosol Size Distribution, dust, mass size distribution, extinction coefficient

Vertical profiles of aerosol size distribution have been obtained from measurements by a Passive Cavity Aerosol Spectrometer (PCASP-100X) from 6 flights carried out during the months of July 2005 and 2006 under Saharan dust outbreaks conditions. Observations were carried out in the Northern Subtropics near to the Canary Archipelago (28N, 16W) where high quality ancillary ground-based data are available.

The campaign was carried out during two large outbreaks (Aerosol Optical Thickness, AOT=0.7/1) in the frame of TROMPETA project and was triggered by the output of the DREAM/BSC aerosol diffusion model (Pérez *et al* 2006). PCASP provides particle concentration in 15 channels ranging from 0.1 to 3 μm with a high sampling rate of 1 cm<sup>3</sup> per second. The sonde was calibrated prior to the missions with polystyrene spheres (n=1.59).

Summer outbreaks on the Eastern Atlantic are characterised by transport at higher layers than in winter, resulting from strong convective activity over the Sahara under favourable meteorological conditions.

Results from the campaigns show a well defined and quite homogeneous vertical structure extending up to 5500-7000 m. In the 2005 event, the plume arrived the Canary Islands area within the free troposphere but extended to the sea surface in following days after the breaking of the inversion of the MBL. This feature can be observed in the flights of July-19, in which the lowest km present the signature of MBL distribution, and July-20 when all levels are dominated by the Saharan dust (see fig. 1).

In opposition with the first event, the 2006 campaign was largely variable in time and in vertical distribution as can be recognised by the large change in AOT during the days of the flights.

Vertical extinctions at 500 nm were estimated from mass loading through the empirical coefficient of 0.5215 obtained from AOT-mass correlation for previous episodes of Saharan aerosol (S. Chueca, private communication) and dust density of 2.6 gr/cm<sup>3</sup> from the literature. Integrated extinctions obtained in this way agrees to better than 10% with the CIMEL instrument of the Sta. Cruz nearby station (table 1).

Acknowledgements. This work has been funded by the Spanish I+D+I Plan (Project CGL2004-03669). Authors want to acknowledge

Carlos Pérez from BSC for the production of model forecasting.

Table 1. AOT from vertically integrated extinctions at 500 nm as computed from PCASP measurements and from CIMEL ground-based measurements

Flight day	PCASP	CIMEL
05 July 19	0.69	0.65
05 July 20	0.52	0.60
05 July 21	0.47	0.45-050
06 July 21	1.20	Not available
06 July 22	0.91	0.88
06 July 24	0.59	0.53

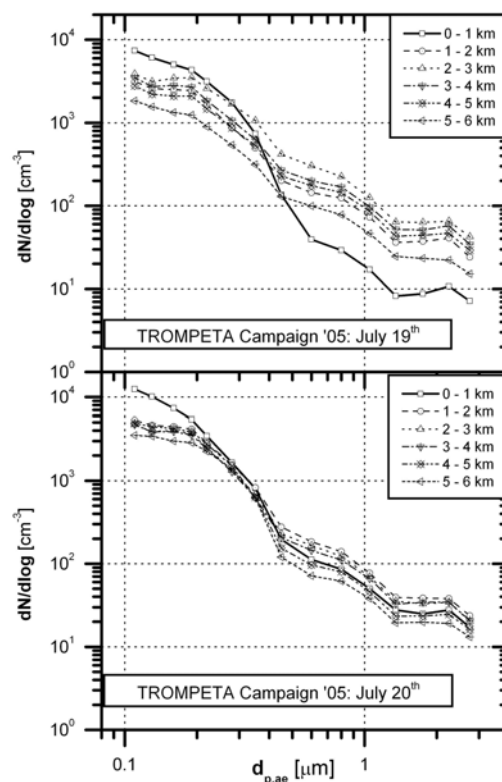


Fig.1 Aerosol size distribution in 1 km averaged layer

Pérez C., Nickovicv S, Pejanovic G., Baldasano J.M. and Özsoy E., *Interactive dust-radiation modeling: A step to improve weather forecasts*, J. Geophys. Res., 111, D16206, doi:10.1029/2005JD006717.

## Saharan Mineral Dust Experiment SAMUM 2006: Aerosol Optical Properties of Dust from Various Source Regions

A. Petzold<sup>1</sup>, K. Rasp<sup>1</sup>, T. Hamburger<sup>1</sup>, B. Weinzierl<sup>1</sup>, M. Fiebig<sup>1</sup>, A. Virkkula<sup>2</sup>

<sup>1</sup> Institute of Atmospheric Physics, German Aerospace Center (DLR), 82234 Wessling, Germany

<sup>2</sup> Finnish Meteorological Institute, 00560 Helsinki, Finland

Keywords: SAMUM, desert dust, optical properties, aerosol radiative forcing

In the framework of the Saharan Mineral Dust Experiment (SAMUM) optical, physical, chemical, and radiative properties of Saharan dust were studied close to a source region. The SAMUM intensive field phase was carried out in May/June 2006 in Southern Morocco. Dust plumes were probed with the DLR Falcon research aircraft which was equipped with an extensive set of aerosol physico-chemical instruments for size, volatility, and absorption measurements, impactor sampling for chemical analyses and with a nadir-looking high spectral resolution lidar (HSRL). Three large-scale dust events were probed which extended from southern Morocco to Portugal.

The optical properties of dust samples were studied by a  $3\lambda$  - PSAP and aerosol sizing instruments. Aerosol size information and absorption data were analysed with respect to the Ångström exponent of  $\sigma_{ap}$  and the effective diameter  $D_{eff}$ . Trajectory data were used for classifying air mass history and dust source regions.

Figure 1 shows several examples for the spectral dependence of the aerosol absorption coefficient for dust particles and particles from an urban atmosphere. The Ångström exponent of  $\sigma_{ap}$ ,  $\text{Å}_{ap}$ , was determined by a fitting procedure. Observed values varied between 2.0 for aged dust and 3 – 5 for pure dust. Laboratory data report a similar range of values. For urban pollution samples observed values were close to 1.0 as expected for combustion particles, see Figure 1.

Figure 2 shows the frequency of occurrence for  $\text{Å}_{ap}$  values of pure dust samples. The two distinguishable groupings correspond to different dust events. Effective diameters varied between 5 and 8  $\mu\text{m}$ . A statistical analysis will be presented demonstrating that clusters of  $\text{Å}_{ap}$  can be associated with different dust events.  $\text{Å}_{ap}$  may thus serve as another sensitive tool for the characterisation of aerosol particles of different types additional to size distributions. No similar patterns are observed in the effective diameters.

This work was supported by the Deutsche Forschungsgemeinschaft DFG, the European Space Agency ESA and the European Fleet for Airborne research EUFAR.

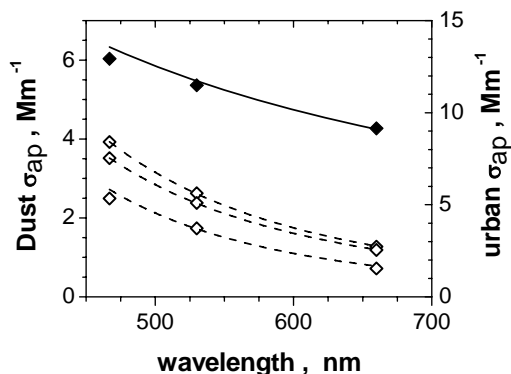


Figure 1. Ångström exponent of  $\sigma_{ap}$ ,  $\text{Å}_{ap}$ , for dust samples (open symbols, left Y-axis) and one urban pollution sample (filled symbols, right Y-axis)

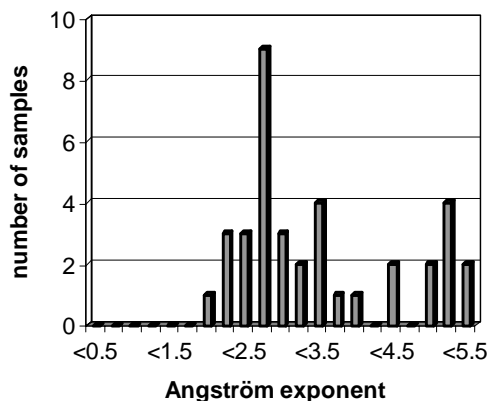


Figure 2. Frequency of occurrence for the Ångström exponent of  $\sigma_{ap}$ ,  $\text{Å}_{ap}$  of pure dust samples.

## Saharan Mineral Dust Experiment SAMUM 2006: Vertical profiles of dust particle properties from airborne in situ and LIDAR observations

B. Weinzierl<sup>1</sup>, K. Rasp<sup>1</sup>, M. Fiebig<sup>1</sup>, M. Esselborn<sup>1</sup>, F. Wagner<sup>2</sup>, A. Virkkula<sup>3</sup>, and A. Petzold<sup>1</sup>

<sup>1</sup> Institute of Atmospheric Physics, German Aerospace Centre (DLR), 82234 Wessling, Germany

<sup>2</sup> Centro de Geofísica, Universidade de Evora, 7000 Evora, Portugal

<sup>3</sup> Finnish Meteorological Institute, 00560 Helsinki, Finland

Keywords: SAMUM, desert dust, optical properties, aerosol radiative forcing

The Saharan Mineral Dust Experiment (SAMUM) is an initiative of several German universities and research establishments. Its goal is the characterisation of optical, physical, chemical, and radiative properties of Saharan dust close to a source region. The SAMUM intensive field phase was carried out in May/June 2006 in Southern Morocco. The DLR Falcon research aircraft was operating from Casablanca. The DLR Falcon was equipped with an extensive set of aerosol physico-chemical instruments for size, volatility, and absorption measurements, impactor sampling for chemical analyses and with a nadir-looking high spectral resolution lidar (HSRL).

In total eight mission flights were conducted from the Atlantic coast across the Atlas Mountains to the border of the Saharan desert where the ground sites Ouarzazate and Zagora were located, and from Morocco to Portugal. Three large-scale dust events were probed which extended from southern Morocco to Portugal. Vertical (0 - 10 km) and horizontal (Saharan border to southern Portugal) dust plume structures, aerosol optical depth as well as particle microphysical and optical properties were studied for all cases.

The upper boundary of the dust layers was found at altitudes between 4 and 6 km above sea level and coincided with the top of the well-mixed boundary layer. The internal structure of the dust layers varied from well mixed to stratified. Figure 1 shows averaged vertical profiles of aerosol number concentrations measured during SAMUM. Note the sharp upper boundary of the dust layers. Figure 2 shows an example for a dust size distribution measured at 3870 m above sea level close to the top of the dust layer. Extinction coefficients calculated from the size distribution and measured with the HSRL agree within 15%.

Presented results will cover profiles of dust size distributions and dust optical properties. Expected heating rates and their impact on atmospheric stability will be discussed.

This work was supported by the Deutsche Forschungsgemeinschaft DFG, the European Space Agency ESA and the European Fleet for Airborne research EUFAR.

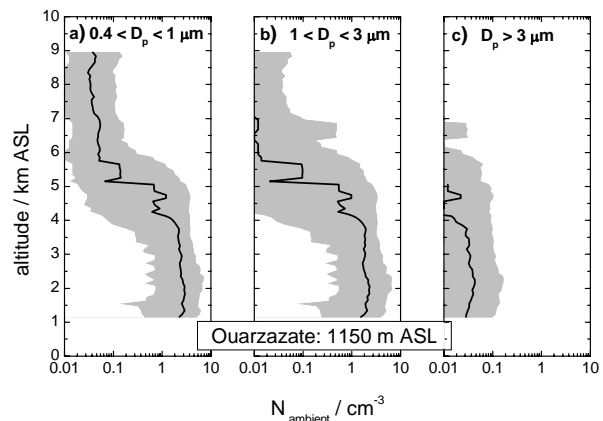


Figure 1. Mean vertical profiles of aerosol number concentrations measured during SAMUM: Median number concentrations (black line) of particles with diameters  $D_p$  (a)  $0.4 < D_p < 1 \mu\text{m}$ , (b)  $1 < D_p < 3 \mu\text{m}$  and (c)  $D_p > 3 \mu\text{m}$ . The shaded area represents the range within 10- and 90-percentile values.

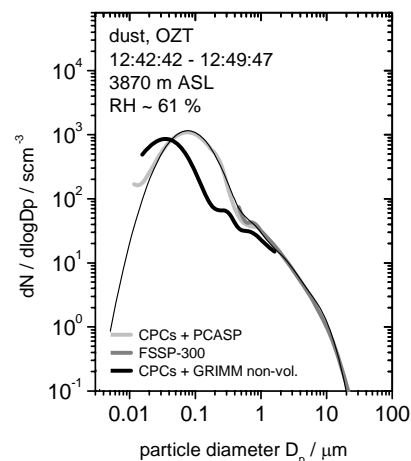


Figure 2. Composite size distribution of desert dust from condensation particle counters (CPC), DMA, and optical particle counters PCASP 100X and GRIMM 1.129. The GRIMM instrument measured the non-volatile fraction of the aerosol.

## **T25 Abstracts**

## Aerosol climatology of tropospheric aerosol profiles over Athens, Greece using an elastic-RAMAN lidar system (2000-2006)

R. E. Mamouri, G. Tsaknakis and A. Papayannis

National Technical University of Athens, Physics Department, Laser Remote Sensing Laboratory, Heroon Polytechniou 9, 15780 Zografou, Greece

Keywords: Tropospheric aerosols, lidar, lidar ratio, aerosol characterization, absorption coefficient

Tropospheric aerosols play an important role in earth's radiation budget through the scattering and absorption of the incoming and outgoing radiation. This can yield to local radiation balance and climate changes (local cooling or heating effects) depending on the aerosol chemical composition (Houghton *et al.*, 2001). Therefore, monitoring the optical properties of the aerosol particles is of crucial importance in studies of climate change, atmospheric modelling and satellite image correction.

Six-years of systematic measurements of aerosol backscatter, extinction, integrated backscatter, lidar ratio and optical depth using an elastic-Raman lidar system, at 355, 387 and 532 nm have been performed over Athens [37.9° N, 23.6° E, 200 m above sea level (asl.)], Greece. All lidar data were obtained in the frame of the EARLINET project (2000-2003) and also beyond (PENED-2003 Project), up to April 2007.

The lidar profiles were obtained in the lower troposphere typically from 500 m to 5000 m asl. The high quality of the lidar data has been previously assured by extensive inter-comparison at software (Böckmann *et al.*, 2004) and hardware level, within the frame of the EARLINET project (Bösenberg *et al.*, 2003). A large amount of the aerosol profiles has been recorded by the elastic lidar system during daytime and by the Raman lidar system during nighttime.

A statistical analysis has been performed to evaluate the optical properties of aerosol over Athens and observe their seasonal variations (Matthias *et al.*, 2004). Mean values and variances of the aerosol backscatter ( $\beta_{\text{aer}}$ ) and extinction ( $\alpha_{\text{aer}}$ ) profiles, integrated backscatter (IB), and optical depth (AOD) have been evaluated.

The corresponding seasonal cycle of these quantities shows highest values during the summer period and secondary maxima during the autumn/spring period. Small fluctuations have been found only during the winter months.

High aerosol integrated backscatter values were found during the summer period, due to larger

dust concentrations in the lower troposphere linked to long-rang transport activity of dust from the Saharan desert region.

Additionally, the seasonal variation of the lidar ratio (LR) at 355 nm was evaluated. Air mass back-trajectory analysis, along with a cluster analysis, related the lidar ratio and aerosol optical thickness values to air masses of different origin (i.e. Saharan dust, biomass burning, marine or continental aerosols). Thus, higher lidar ratio values in the free troposphere are generally correlated with air masses coming from southerly directions and this could be related to aerosols originating from the Saharan dust region and also from the NW directions (central Europe).

This lidar ratio climatology could also be useful for satellite data retrieval applications and for calibrating elastic backscatter lidar systems.

*Acknowledgements:* This work was co-funded by the European Union – European Social Fund (75%) and National Resources (25%) of the Greek Ministry of Development, GSRT/PENED (03-ED-169) Project and Raymetrics SA., in the frame of Measure 8.3 - Operational Program "COMPETITIVENESS" of the Community Support Framework (2000-2006).

Böckmann, C., Wandinger, U., Ansmann, A., et al. (2004). *Appl. Opt.*, 43, 977-989.

Houghton J. T., et al. (2001). *Climate Change 2001: The Scientific Basis*. Contribution of Working Group I to the Third Assessment Report of the Intergovernmental Panel on Climate Change (IPCC). Cambridge University Press.

Bösenberg, J. et al. (2003). A European aerosol research lidar network to establish an aerosol climatology, *MPI-Report 317*, Max-Planck Inst. für Meteorology, Hamburg, Germany.

Matthias V., et al. (2004). *J. Geophys. Res.*, 109, D18201, doi:10.1029/2004JD004638, 2004.

## Analysis of size-resolved atmospheric aerosol particle samples by Raman Microscopy

N.P. Ivleva<sup>1</sup>, U. McKeon<sup>1</sup>, U. Pöschl<sup>2</sup> and R. Niessner<sup>1</sup>,

<sup>1</sup>Technical University of Munich, Institute of Hydrochemistry, Marchioninstr. 17, D-81377 Munich, Germany

<sup>2</sup>Max Planck Institute for Chemistry, Biogeochemistry Department, Becherweg 27, D-55128 Mainz, Germany

Keywords: Atmospheric aerosols, ELPI, chemical composition, soot particles, Raman Microscopy (RM)

Aerosols are of great importance for atmospheric chemistry and physics, climate, and public health. Atmospheric particles scatter and absorb solar and terrestrial radiation, they are involved in the formation of clouds and precipitation. Moreover, airborne particles can cause or enhance respiratory, cardiovascular, infectious, and allergic diseases. The concentration, composition, and size distribution of atmospheric aerosol particles, are the primary parameters that determine the properties and effects of air particulate matter (Oberdörster, *et al.*, 2005).

Raman Microscopy (RM), which provides fingerprint spectra and allows the distinction of a wide range of chemical substances with the spatial resolution of an optical microscope, has been applied for the identification and semi-quantitative analysis of soot, humic-like substances (HULIS), nitrates, sulfates, and carbonate in size resolved samples of air particulate matter collected with an electrical low pressure impactor (ELPI).

Using several reference materials (graphite, Printex XE-2 soot, NIST 1650 diesel particulate matter, GfG spark discharge soot, humic acid), we found that spectral parameters determined by curve fitting with five bands (G, D1-D4) (Sadezky *et al.*, 2005) enable a discrimination of soot and HULIS and provide information about the relative abundance and structural order of graphite-like carbon. In particular, the D1 band width exhibited a near-linear negative correlation with the ratio of apparent elemental carbon to total carbon in different types of soot.

The spectral parameters of the ELPI samples of air particulate matter varied between those of standard diesel soot and humic acid (Ivleva *et al.*, 2006). The ELPI samples of sub-micrometer atmospheric particles exhibited essentially the same Raman spectra and parameters as standard diesel soot. In winter samples this was also the case for larger particles with aerodynamic diameters up to 4  $\mu\text{m}$ . Spring and autumn samples, however, exhibited increased D1 band widths and D3 band intensities, indicating a high prevalence of HULIS in the size range of 2-4  $\mu\text{m}$ . In addition, various nitrates and sulfates (mostly  $\text{NaNO}_3$  and  $(\text{NH}_4)_2\text{SO}_4$ ; some  $\text{NH}_4\text{NO}_3$ ,  $\text{Ca}(\text{NO}_3)_2$ ,  $\text{Na}_2\text{SO}_4$ , and  $\text{CaSO}_4$ ) and small amounts of  $\text{CaCO}_3$  were detected.

The relative abundance of different chemical components in different particle size ranges was quantified in mapping experiments. The proportion

of spectra with signals characteristic for soot or HULIS increased from ~10% for coarse particles to ~45% for fine particles (Figure 1), and a similar trend was observed for sulfates (mostly  $(\text{NH}_4)_2\text{SO}_4$ ; ~1 % of coarse and ~ 15 % of fine particle spectra). In contrast, the proportion of spectra with nitrate signals (mostly  $\text{NaNO}_3$ ) was as high as ~55% for coarse particles and dropped to zero for fine particles. Less than 1% of the spectra exhibited signals from calcite. The proportion of spectra with high fluorescence signals from organic components, increased from ~30% on ELPI stage 10 (2-4  $\mu\text{m}$ ) to ~60% on stage 7 (0.6-1  $\mu\text{m}$ ), indicating an increase of the organic fraction of air particulate matter with decreasing particle size. The results of this study demonstrate that RM and mapping can provide qualitative and quantitative (or at least semi-quantitative) information about the composition of ELPI aerosol samples.

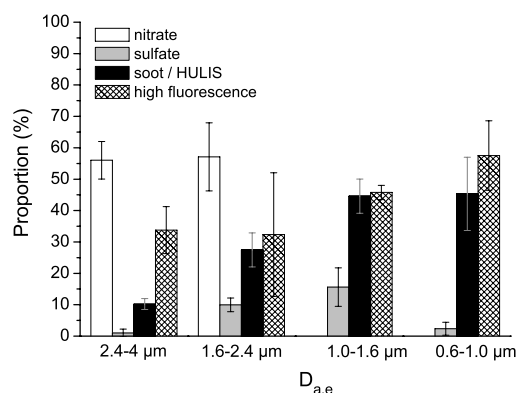


Figure 1. The proportion of the spectra ( $\lambda_0 = 514 \text{ nm}$ ) with signals characteristic for nitrates, sulfates, soot/HULIS, and high fluorescence in particles collected in May on ELPI stages 10-7 (0.6-4  $\mu\text{m}$ ).

This work was supported by the German Federal Ministry of Education and Research (BMBF, AFO2000 Project 07ATC05, CARBAERO).

Ivleva, N. P., McKeon, U., Niessner, R., & Pöschl, U. (2006) *Aerosol Science and Technology*, submitted.

Oberdörster, G., Oberdörster, E., & Oberdörster, J. (2005) *Environmental Health Perspectives*, 113, 823-839.

Sadezky, A., Muckenhuber, H., Grothe, H., Niessner, R., & Pöschl, U. (2005) *Carbon*, 43, 1731-1742.

## Single Particle Characterisation of Marine Aerosols at Mace Head, Ireland: Winter and Summer Data from the MAP Campaigns 2006

C. Grüning<sup>1</sup>, P. Cavalli<sup>1</sup>, N.R. Jensen<sup>1</sup>, D. Mira Salama<sup>1</sup>, F. Raes<sup>1</sup>

<sup>1</sup> European Commission, DG-JRC, Institute for Environment and Sustainability, Climate Change Unit, T.P. 290, I-21020 Ispra (VA), Italy

Keywords: single particle analysis, mass spectrometry, marine aerosols, field measurements, MAP-project

The Single Particle Analysis and Sizing System (SPASS) has been deployed at the Mace Head atmospheric research station of the National University of Ireland, Galway in the frame of the MAP project (Marine Aerosol Production: Primary & Secondary Marine Aerosol Production from Natural Sources). The SPASS characterized single aerosol particles with an aerodynamic diameter between 300 nm and  $\sim 3 \mu\text{m}$  during periods of low and high biological activity in the ocean, i.e. during winter and summer 2006. A technical description of the instrument and its characteristics can be found in Erdmann et al. (2005).

During the winter campaign from 9<sup>th</sup> till 29<sup>th</sup> of January 2006, the SPASS operated almost continuously and successfully acquired more than  $10^6$  single particle mass spectra during different meteorological conditions. To obtain a dataset with single particle mass spectra for marine aerosols during low biological activity in the Atlantic, the data analysis was focused on clean marine air masses that passed over the sampling site at Mace Head. Clean air periods were defined using wind directions, particle number concentrations and backward trajectories.

As expected, most particles characterized with the SPASS during clean air periods contain sea salt only. But more interestingly, 6 % of the particles consist of carbonaceous material that is internally mixed with sea salt (fig. 1). A summary of the marine particle population for clean air conditions is shown in table 1.

Remarkably, all carbonaceous particle classes have a size distribution that is approximately 30% smaller as compared to the pure sea salt particle class.

Table 1: Marine aerosol composition, averaged over all clean air periods in winter and summer 2006.

	winter	summer
sea salt	80 %	72 %
carbonaceous, total	14 %	15 %
mixed with sea salt	6 %	2 %
oxidized, mixed with potassium, sulfate	3 %	11 %
mixed with mainly sulfate, potassium	5 %	2 %
potassium, small sodium	6 %	11 %

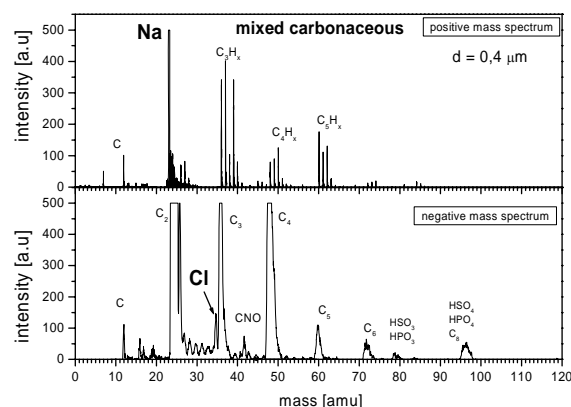


Figure 1: Mass spectrum of a single carbonaceous particle internally mixed with sea salt.

From June 5<sup>th</sup> till July 10<sup>th</sup> 2006 the SPASS sampled again several  $10^6$  single particles at Mace Head. The composition of the marine aerosol population is compared to the one in winter in table 1. Although the percentage of total carbonaceous material is rather similar in summer and in winter, more organic material is oxidized in summer and less is internally mixed with sea salt.

In addition to the analysis of clean air, looking at polluted air masses shows that particles predominantly contain  $\text{NO}_x$ ,  $\text{SO}_4$  and carbonaceous material. During one notable local nucleation event at Mace Head in winter, oxidized iodine has been observed on single particles.

The analysis of the huge data sets of single particle mass spectra is ongoing. It focuses on the internal and external mixing of sea salt with carbonaceous material and the amount of oxidized carbon present on particles during clean air conditions. Detailed results of the mass spectral data from marine aerosols that were obtained during the winter and summer measurement campaigns at Mace Head, Ireland will be presented.

This work was supported by the European Union under the FP6 STREP: MAP, project number GOCE-018332. The support of the NUIG personnel at Mace Head is thankfully acknowledged.

Erdmann, N., Dell'Acqua, A., Cavalli, P., Grüning, C., Omenetto, N., Putaud, J.-P., Raes, F., Van Dingenen, R. (2005). *Aerosol Science & Technology*, 39, 377–393.

## Size resolved mass and elemental composition of ground collected aerosols over south-east Italy

I. Carofalo and M. R. Perrone

Department of Physics, University of Lecce, Lecce, Italy

Keywords: aerosols characterization, air pollution, cascade impactor, elemental composition, PM measurements

Epidemiological studies have shown a significant association between exposure to particle pollution and health risks, including premature death. Besides the composition, the size of particles is directly linked to their potential for causing health problems, since it influences the site deposition in the respiratory system. Fine aerosols pose the greatest health risk: they can get deep into lungs and some of them may also get into the bloodstream.

Particle size is also closely linked to chemical properties of airborne particles, since it may reflect origin and formation: large particles are often originated from natural sources, while small particles are generally of anthropogenic origin or may derive from gas to particle conversion reactions in the atmosphere. The size-segregated sampling of aerosols represents the best way to get the size-resolved elemental composition of atmospheric particles.

In this work we present results on size-fractionated aerosol samples collected during 2005 at the Physics Department of Lecce's University (40° 20' N, 18° 06' E), which is located on a rural area of the flat Salentum peninsula in south-east Italy. The site that is away from large cities and/or industrial areas, is well suited to contribute to the aerosol characterization of the central-east Mediterranean basin. Bounded to the north by the European continent and to the south by North Africa, the Mediterranean basin offers unique conditions for aerosols studies, since atmospheric particles originating from natural, anthropogenic and marine sources are present at all times.

A 7-stage cascade impactor (OH-610-C, Kålmån System) has been used in this study to collect and characterize mass, morphology, and elemental composition of size-segregated aerosol particles. Especially, atmospheric particles have been collected on 7 quartz filters with 50% effective-cut-diameter at 5.7 µm, 2.7 µm, 1.4 µm, 0.65 µm, 0.35 µm, 0.14 µm and 0.08 µm. Morphological and elemental particle properties have been investigated by a scanning electron microscope (JSM-6480LV, JEOL) equipped with an energy-dispersive X-ray microanalysis system (EDS 2000, IXRF).

A main objective of this study is to investigate how particle size distributions and corresponding size-segregated elemental compositions are affected by the source regions of the air masses advected over the monitoring site. Air masses arriving over the monitoring site and hence in the central-east

Mediterranean, from N-NW are expected to contain particles from industrial and urban sources of the highly populated European countries, while those coming from Sahara desert to transport predominantly mineral and crustal aerosols. Long-range transported polluted air masses from the Atlantic Ocean and from the Mediterranean itself may instead cause marine aerosols pulses.

Figure 1 (solid line) shows as example the particle-mass plot as function of the 50% effective-cut-diameter of the impactor filters that has been retrieved during the Sahara dust outbreak occurred over the central Mediterranean on 30 June, 2005. The dashed line in Figure 1 represents the size-segregated mass distribution retrieved during a pollution event from north-east Europe occurred on 27 September, 2005. Mass peak-value is at 2.70 µm 50%-effective-cut-diameter during the dust event. On the contrary, mass peak-value is at 50%-effective-cut-diameters smaller than 0.65 µm during the pollution event from north-east Europe.

Morphological and elemental analyses performed by SEM on filters collected during the dust event, besides showing the dependence of particles' size, shape, and number on the 50%-effective-cut-diameter of the filters, have allowed inferring that nitrates, sulfates, and carbon were the main aerosol components of fine-mode particles, while sea-salts, carbonates, and minerals were the main aerosol components of coarse-mode particles. In particular, it has also been shown that dust particles mainly affect the coarse mode aerosol and that the anthropogenic fine mode particles can represent more than 50% of the aerosol load even during a dust outbreak.

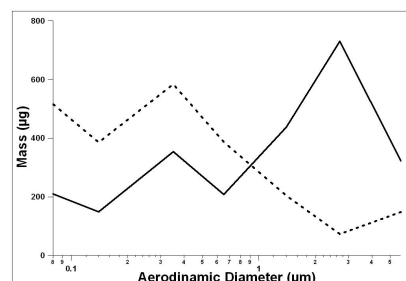


Figure 1. Particles mass plot as function of the 50%-effective-cut-diameter of the impactor filters. The solid line represents the mass size distribution retrieved on 30 June, 2005. The dashed line represents the mass size distribution retrieved on 27 September, 2005.

## Laminar Co-Flow Tube: A novel tool to study sulfuric acid – water nucleation

P. Krejčí<sup>1</sup>, T. Němec<sup>1</sup>, J. Hrubý<sup>1</sup> and V. Ždímal<sup>2</sup>

<sup>1</sup>Institute of Thermomechanics AS CR, v.v.i., Dolejškova 5, 182 00, Prague, Czech Republic

<sup>2</sup>Institute of Chemical Process Fundamentals AS CR, v.v.i., Rozvojová 135, 165 02, Prague, Czech Republic

Keywords: aerosol instrumentation, sulfuric acid, homogeneous nucleation, aerosol fundamentals.

Binary nucleation in the supersaturated vapor mixture of sulfuric acid and water is considered as one of the pathways of secondary aerosol particle formation in the atmosphere. The ongoing interest in this system is motivated by the need to better understand atmospheric processes (Clement *et al.*, 2006). Moreover, condensation of the flue gas, a process strongly related to the content of sulfuric acid and water in the system (VDI 4670, 2003) is in the interest of power industry, mainly due to the so-called low temperature corrosion (Dooley, 2006). Nucleation of sulfuric acid-water system has been studied experimentally for a long time, e.g. using a turbulent mixing (Wyslouzil *et al.*, 1991), and a flow chamber (Viisanen *et al.*, 1997). The quality and quantity of available experimental data is still unsatisfactory (Berndt *et al.*, 2005). A new device has been developed to provide more reliable data for applications in climatology, meteorology and power industry. Its experimental set-up and principle of operation are described in this study. The device is suitable for verification of theories on homogeneous nucleation and cavitation in binary and ternary systems.

The experimental set-up (see fig.1) consists of the Mixture Preparation Device (MPD) (Krejčí *et al.*, 2004), capable to prepare mixtures of up to three vapors, the Laminar Co-Flow Tube (LCFT) (Krejčí *et al.*, 2006), where nucleation and droplet growth take place, and an Ultrafine Condensation Particle Counter (TSI Inc., UCPC 3025A). Each of the vapors, prepared in the MPD by saturating a dry gas flowing above the liquid surface, proceed separately to the LCFT, where they are mixed by molecular diffusion. The operating conditions are chosen so that the flow is well within the stability limits as determined by flow visualization (Trávníček *et al.*, 2005). Due to high non-ideality of the sulfuric acid – water system, the vapor mixture becomes supersaturated. Binary homogeneous nucleation followed by droplet growth occurs in the co-flow region of the LCFT. Number concentration of the formed aerosol is determined by the UCPC. The resulting nucleation rate can be calculated using a computational fluid dynamics model of the flow and concentration fields in the LCFT, provided the known mixture composition, LCFT operating conditions and counted number concentration of droplets. Performed measurements confirmed expected dependency of droplet number concentrations on operating conditions.

Quantitative measurements of nucleation rates are in progress.

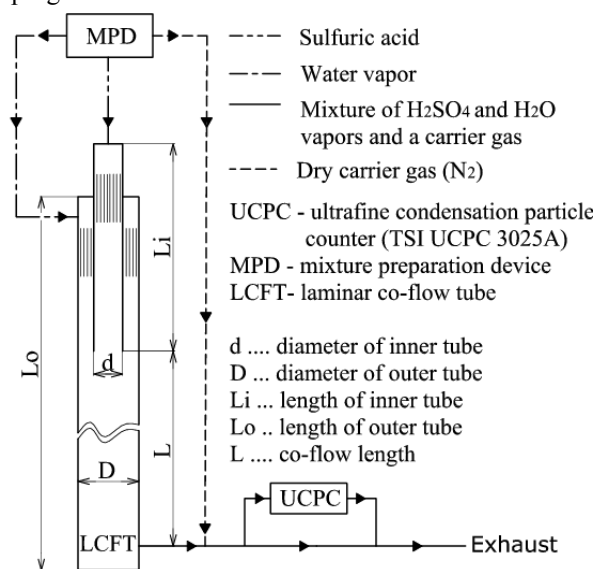


Figure 1. Schematics of the experimental setup, the binary case of sulfuric acid – water mixture depicted.

This work has been supported by the Grant Agency of the Academy of Sciences of the Czech Republic, grant no. IAA2076502, and the Czech Science Foundation grants no. 101/05/2524 and no. 101/07/1612.

- Berndt, T., Boge, O., Stratmann, F., Heintzenberg, J. and Kulmala, M. (2005). *Science*, **307**, 698-700.
- Clement, C. F., Pirjola, L., Twohy, C. H., Ford, I. J. and Kulmala, M. (2006). *Journal of Aerosol Science*, **37**, 1717.
- Dooley, B. (2006). *ICRN: Thermophys. Prop. of Humid Air and Comb.-Gas Mixt.*, <http://www.iapws.org/>.
- Krejčí, P., Hrubý, J. and Haartsen, J. (2004). in *Proc. Ann. Conf.*, Prague (Czech Aerosol Soc.), 47-49.
- Krejčí, P., Hrubý, J., Ždímal, V. and Trávníček, Z. (2006). in *Finnish-Czech Aerosol Symp.*, Helsinki (Finnish Assoc. for Aerosol Res.), 161-164.
- Trávníček, Z., Hrubý, J. and Vogel, J. (2005). *Developm. Machinery & Control*, **4**, 121-130.
- VDI 4670 (2003). VDI - Gesellschaft Energietechnik, Düsseldorf.
- Viisanen, Y., Kulmala, M. and Laaksonen, A. (1997). *J. Chem. Phys.*, **107**, 920-926.
- Wyslouzil, B. E., Seinfeld, J. H., Flagan, R. C. and Okuyama, K. (1991). *J. Chem. Phys.*, **94**, 6842-6850.

## Air quality in background savannah in Southern Africa

L. Laakso<sup>1</sup>, T. Petäjä<sup>1</sup>, H. Laakso<sup>1</sup>, P.P. Aalto<sup>1</sup>, E. Siivola<sup>1</sup>, P. Keronen<sup>1</sup>, S. Haapanala<sup>1</sup>, M. Kulmala<sup>1</sup>, H. Hakola<sup>2</sup>, N. Kgabi<sup>3</sup>, M. Molefe<sup>3</sup>, D. Mabaso<sup>3</sup>, K. Pienaar<sup>3</sup>, E. Sjöberg<sup>4</sup> and M. Jokinen<sup>4</sup>

<sup>1</sup>Department of Physics, University of Helsinki, PB 64, FI-00014, University of Helsinki, Finland

<sup>2</sup>Finnish Meteorological Institute, PB 503, FI-00101, Helsinki, Finland

<sup>3</sup>The North-West University, Republic of South Africa

<sup>4</sup>Department of Agriculture, Conservation and Environment, Mafikeng, Republic of South Africa

Keywords: Particle formation and growth, Aerosol measurement, Atmospheric Aerosol, Air Pollution

### Background

There are very few background air pollution measurements - and none of these are for longer periods - carried out in southern African savannah region (Laakso et al., 2006). For this reason, we started in July 2006 comprehensive air pollution monitoring measurements in background savannah environment approximately 300 km west of Johannesburg, South Africa. For this purpose, we built a wireless measurement trailer, which provides the following data:

- Basic meteorology: temperature, relative humidity, photosynthetically available radiation, wind direction, wind speed, precipitation
- Aerosol particle number size distribution 10-800 nm
- Air ion number size distribution 0.4-40 nm
- Aerosol mass: PM1, PM2.5, PM10
- Chemical analysis of PM10 and PM2.5 (inorganics, trace metals)
- Gases: NO<sub>x</sub>, SO<sub>2</sub>, CO, O<sub>3</sub>
- Volatile organic compounds (VOCs), (seasonally)

The measurements continue in the clean background savannah until the end of year 2007. Subsequently the trailer will be deployed to an area heavily impacted by mining (2008) and later to industrial background area (2009).



Figure 1. Our mobile measurement trailer in Botsalano game reserve, central Southern Africa

### Results

A preliminary data analysis from a period 23<sup>rd</sup> July-15<sup>th</sup> August 2006 indicated that

- New particle formation took place on every sunny day
- New particle formation produced  $1\text{-}3\cdot 10^4\text{ cm}^{-3}$  new particles in sizes above 10 nm.  $J_{10}$  was typically approximately  $1\text{ cm}^{-3}\text{ s}^{-1}$
- Typical night-time concentration of 10-840 nm particles was approximately  $1000\text{ cm}^{-3}$
- Particle growth rates were high, up to 15 nm/h

Table 1. Gases concentrations

Gas	Concentration [ppb]
O <sub>3</sub>	34.0
SO <sub>2</sub>	1.0
NO	0.1
NO <sub>x</sub>	0.9
CO	122.4

- Average mass concentrations were 12.8, 14.7 and 24.4  $\mu\text{g m}^{-3}$  for PM1, PM2.5 and PM10, respectively.
- The VOC concentrations were generally quite low. The sum of monoterpene concentrations varied from 0.3 to 1.6  $\mu\text{g m}^{-3}$ . Typical VOCs observed were  $\alpha$ -Pinene,  $\beta$ -pinene, benzene, nonane, isoprene and camphene

During the period discussed here, there were some plumes from distant field fires. Apart from these periods, air was very clean and there were no significant traces of anthropogenic influence.

This work was supported by the Finnish Academy of Sciences and Finnish Environment Institute.

Laakso, L., Koponen, I., Mönkkönen, P., Kulmala, M., Kerminen, V-M. Wehner, B., Wiedensohler, A., Wu, Z., Hu, M. (2006) *Aerosol particles in the developing world; a comparison between New Delhi in India and Beijing in China*, Water, Air and Soil Pollution, pages 1 - 16, DOI 10.1007/s11270-005-9018-5, 2006

## Characterization of ice residuals from the CLACE 5 experiment

A. Worringen<sup>1</sup>, N. Benker<sup>1</sup>, M. Ebert<sup>1</sup>, F. Zimmermann<sup>1</sup>, S. Mertes<sup>2</sup>, E. Weingartner<sup>3</sup>, and S. Weinbruch<sup>1</sup>

<sup>1</sup>Applied Geosciences, Technical University Darmstadt, D-64287, Darmstadt, Germany

<sup>2</sup>Leibniz-Institute for Tropospheric Research, D-04318, Leipzig, Germany

<sup>3</sup>Laboratory of Atmospheric Chemistry, Paul Scherrer Institut, CH-5232, Villigen PSI, Switzerland

Keywords: CLACE, ice nuclei, electron microscopy, single particle analysis.

In February/March 2006 an intensive Cloud and Aerosol Characterization Experiment (CLACE-5) was conducted at the high alpine research station Jungfraujoch (JFJ, 3580 m asl; 46.55°N, 7.98°E) in Switzerland.

The main focus of the single particle analysis approach is the chemical identification of the ice forming fraction and the remaining interstitial particle fraction of the total aerosol in mixed-phase clouds.

For particle sampling, we have used two self constructed 2-stage impactors (cut off diameters 0.7  $\mu\text{m}$  and 0.06  $\mu\text{m}$  for ice nuclei (IN) and 0.9  $\mu\text{m}$  and 0.06  $\mu\text{m}$  for interstitial particles) behind different inlet systems. The interstitial aerosol was sampled behind an interstitial inlet operated with a PM2 cyclone impactor. An ICE-CVI (Counterflow Virtual Impactor) inlet, which was designed and operated by the Institute for Tropospheric Research in Leipzig (Mertes et al., 2005), has been used to sample residual particles of small ice nuclei (IN).

The size, morphology, elemental composition, mixing state, and component of selected IN- and interstitial-samples were analysed by environmental scanning electron microscopy (ESEM) and transmission electron microscopy (TEM), each combined with energy dispersive X-ray microanalysis (EDX).

As dominant particle groups in the interstitial-samples carbon-dominated particles, sulphates, and/or mixtures of sulphates with nitrates, and carbon-dominated particles were observed. Silicates are a minor component in these samples. In the IN-samples (aged) sea salt, silicates and internal mixtures of carbon-dominated particles, sulphates, nitrates, and silicates are the main particle groups. Depending on the air mass history, soot and fly ash particles are present in the samples and can therefore be used as tracers for "polluted" air masses.

The most obvious difference between IN- and interstitial-samples is the occurrence of Pb-containing particles (Figure 1) in the IN-samples. These particles are predominantly internally mixed with (aged) sea salt, carbon-dominated particles or silicates. The relative number abundance of this particle group can reach up to 24 %.

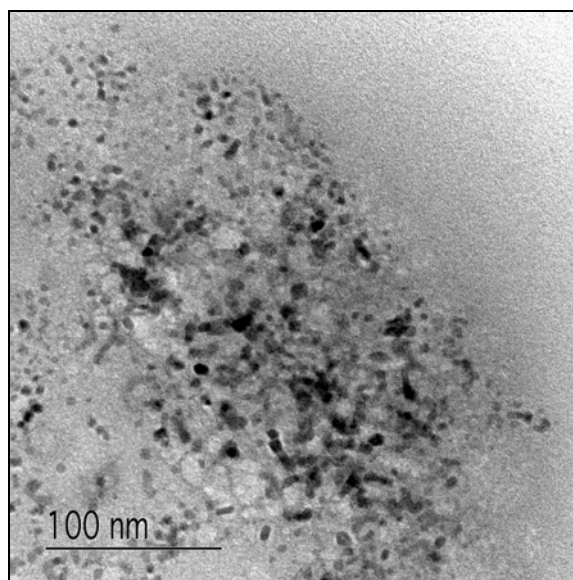


Figure 1: TEM-bright field image; section of an aged sea salt particle with Pb-containing particles (black dots).

The Pb inclusions are generally smaller than 10 nm and, therefore, difficult to characterize in more detail. According to high-resolution images and "pseudo" electron diffraction patterns (obtained by Fourier transformation of the bright field images), the Pb inclusions consist most likely of lead oxide. However, the presence of lead chloride and/or lead sulfide cannot be excluded up to now. The exact source of the lead inclusion is not yet known.

We thank the International Foundation High Altitude Research Stations Jungfraujoch and Gornergrat (HFSJG) for logistic and the German Science Foundation (Sonderforschungsbereich 641 "The tropospheric ice phase") for financial support.

Mertes S., B. Verheggen, J. Schneider, M. Ebert, S. Walter, A. Worringen, M. Inerle-Hof, J. Cozic, M. J. Flynn, P. Connolly, K. N. Bower, E. Weingartner, *Journal of Aerosol Science*, Abstract of EAC, Ghent, 2005, S130.

## Aerosol Elemental Mass Size Distributions at Baia Terra Nova (Antarctica): Individual Representations and Intersample Variability

P. Mittner, D. Ceccato, V. Trovò, F. Chiminello

Università di Padova, Dipartimento di Fisica «Galileo Galilei», Padova, Italy

Keywords: Antarctic aerosol, Coastal particles, Elemental composition, Mass size distribution, PIXE

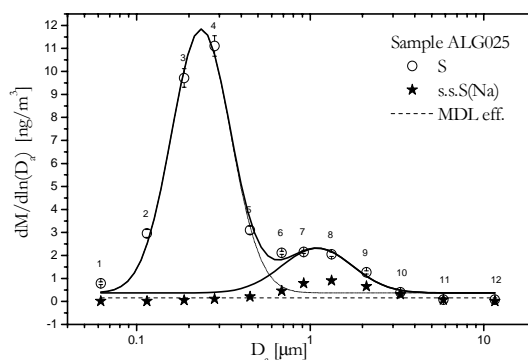
A multiannual experiment on Antarctic coastal aerosol is being performed during the summer season at the site Campo Icaro (Lat. 74°42'43"S, Long. 164°06'58"E). Size-segregated aerosol samples collected (48 hrs duration) with an SDI 12-stage impactor are submitted to PIXE analysis and the size distribution, EMSD, of the mass concentration ( $\text{ng m}^{-3}$ ) of up to 9 elements, (with  $Z \geq 11$ ) is obtained in the size range  $12. \pm 0.047 \mu\text{m}$ . More exactly, we consider the quantities:  $\Delta M_{ijk}$ , the mass concentration of element  $i$  in stage  $j$ , of sample  $k$ ;  $D_j$  and  $D_{j+1}$ , respectively the lower and upper cuts in aerodynamic diameter of stage  $j$ ,  $D_a^j$ , the geometric mean value of the above cut values;  $\Delta M_{ijk} / (\ln D_{j+1} - \ln D_j)$ . This last quantity – due to intrinsic SDI properties – nearly equals  $\Delta M_{ijk} / \Delta \ln D_a^j$ , a convenient expression for the EMSD, in view of analytical representations.

We present the partial results (11 samples) of the 2002/2003 campaign, which display a substantial reduction of the background levels (and thus of minimum detection limits and errors) with respect to the published [1] 1999/2000 results. In these conditions a successful representation of the EMSD's of 7 crucial elements (Na, Si, S, Cl, K, Ca, Fe) with one or two lognormal functions, in the full dimensional range, turns out to be possible for each individual sample (with few exceptions for K and Ca). Element Mg can also be represented in some cases. The EMSD's always include a dominant (with the exception of S) supermicrometric mode and, in some cases (for Na, Mg, K, Ca, Fe), a minor submicrometric mode, besides the dominant submicrometric S mode. The present results are thus much more detailed than the previous ones, which only concerned properties averaged over the full set of samples.

The scientific results concern properties and variability of a crustal component, cr, (identified by the strong correlation between Si and Fe and by the stable value of their ratio); the considerable stability of the parameters of the submicrometric S (accumulation) mode; the strong variability of the EMSD's of Na and Cl, the similarity of their shapes, displaying however a size-dependent Cl-depletion,  $\Delta \text{Cl}$ , of the sea-salt component, ss; a strongly variable size-dependence of the difference, nss (non-sea-salt S), between S (total) and ssS (sea-salt S) in

the supermicrometric region; the contributions of K and Ca to ss and cr.

Significant scientific problems include: (a) the strength of fluxes of S gaseous compounds to the ss aerosol as measured by the supermicrometric nssS; (b) the displacement of the supermicrometric nssS peak towards lower values of the particles aerodynamic diameter with respect to the ssS peak, as an indication of gas-particle interactions occurring preferentially at the particle surface rather than in their volume; (c) the relative strength of the supermicrometric and the submicrometric S peak, as a measure of the relative importance of the two corresponding S fluxes; (d) the absolute value of  $\Delta \text{Cl}$  as a measure of Cl flux from the (submicrometric) ss aerosol towards the atmosphere (biases due to Cl losses in the samples cannot however be completely excluded, at the moment, in this case); (e) use of size-distributions of  $\Delta \text{Cl}/\text{Cl}$  (relative Cl depletion) to investigate the preferential localization of the chemical interactions of the gas-particle interactions; (f) the time distributions (through the intersample variability) of the integrated quantities  $\text{Na}_{\text{tot}}$ ,  $\text{S}_{\text{tot}}$ ,  $\Delta \text{Cl}_{\text{tot}}$ , and their connections with the variability of meteorological and environmental parameters. Internal mixing of cr and ss components will be investigated by means of Principal Component Analysis, with the previously [1] described procedure.



[1] F. Chiminello, P. Mittner, A. Trevisiol and D. Ceccato. Proc. 16th Int. Conf. on Nucleation and Atmospheric Aerosols (ICNAA), Kyoto, 2004, pp.649-652

## Analysis of aerosol water-soluble organic compounds and humic-like substances by anion-exchange chromatography coupled to Total Organic Carbon determination

E. Finessi, S. Decesari, V. Mancinelli, M. Rinaldi, C. Carbone, M. Mircea, M.C. Facchini and S. Fuzzi

Istituto di Scienze dell' Atmosfera e del Clima, CNR, via Gobetti 101, 40129, Bologna, Italy

Keywords: Atmospheric aerosols, Organic carbon, Water soluble compounds, Chemical composition

Water-soluble organic carbon (WSOC) accounts for 20 to 70% of the organic carbon in atmospheric aerosol particles however its chemical composition is still largely unknown. Less than 20% (often less than 10%) of WSOC could be identified at the molecular level in spite of the great improvement of high resolution chromatographic techniques (Kourtchev, 2005). An alternative approach based on a combination between liquid chromatographic and spectroscopic techniques allows to simplify the initial complex WSOC mixture into a few main chemical classes.

Anion exchange liquid chromatography can be exploited for quantitatively resolving WSOC into neutral compounds (NC), mono- and di-acids (MDA) and polyacids (PA). On the basis of their retention coefficient, PA correspond to atmospheric humic-like substances (HULIS). Accurate and sensitive determination of this class of compounds would greatly benefit our understanding of HULIS effects on the optical and surface properties of aerosol particles.

So far, quantitative analysis of NC, MDA and PA was performed at both preparative scale (for samples containing > 100  $\mu\text{gC}$ ) and at the analytical scale employing UV detection. The use of a volatile buffer in low-pressure chromatography allowed subsequent analysis of total organic carbon (TOC) in the fractions. In the HPLC method instead, the concentrations were derived from peak areas in the UV chromatogram. Calibration of the UV detector was based on response factors determined empirically on reference samples fractionated by the low-pressure chromatographic method (Decesari, 2001).

Here, we report a new anion exchange HPLC method coupled to TOC analysis (Mancinelli, 2007). A completely inorganic mobile phase allows direct TOC analysis of the eluted fractions without any sample pre-treatment. The ability of the new method to elute organic compounds according to their neutral/acidic character has been tested on single standard solutions of water-soluble organic compounds commonly detected in atmospheric samples, as well as on the water extracts of real aerosol samples. With the new method, MDA could be resolved into MA (mono-acids) and DA (di-acids).

Samples collected in the QUEST-3 (Quantification of Aerosol Nucleation in the European Boundary Layer) field experiment held during spring 2004 at a polluted rural site in northern Italy and marine aerosol samples collected in pristine air masses over the North Atlantic ocean during spring 2006 during the MAP (Marine Aerosol Production) project have been analysed with the new HPLC method. In general marine samples contained lower amounts of PA (i.e., HULIS) with respect to continental polluted samples (Figure 1). The HPLC-TOC method can recover a substantial amount (> 86%) of WSOC from atmospheric aerosol extracts exceeding the recoveries provided by previously employed techniques, like solid phase extraction (Kiss, 2002).

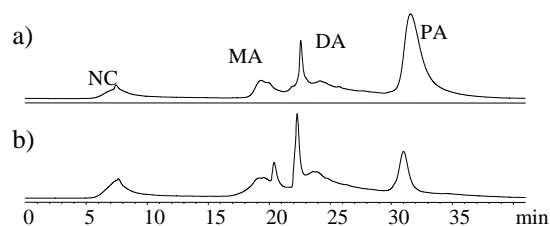


Figure 1. Resulting HPLC-chromatograms from the analysis of a continental aerosol sample (a) and a marine aerosol sample (b).

- Decesari, S., Facchini, M. C., Matta, E., Lettini, F., Mircea, M., Fuzzi, S., Tagliavini, E. & Putaud, J. - P. (2001). *Atmos. Environ.*, 35, 3691-3699.
- Kiss, G., Varga, B., Galambos, I. & Ganszky, I. (2002). *J. Geophys. Res.*, 107, 8339.
- Kourtchev, I., T. Ruuskanen, W. Maenhaut, M. Kulmala, M. Claeys. (2005) *Atmos. Chem. Phys. Discuss.*, 5, 2947-2971.
- Mancinelli, V., M. Rinaldi, E. Finessi, L. Emblico, M. Mircea, S. Fuzzi, M. C. Facchini, S. Decesari (2007), *J. Chrom. A*, accepted for publication.

**Long-term Observations of Aerosol Mass and Composition and Precursor Gas Concentrations in Pacific Background Air Masses at Coastal Atmospheric Monitoring Sites in Taiwan**

C. Junker and C.T. Lee

Graduate Institute of Environmental Engineering, National Central University, Jhongli, 32001, Taiwan, R.O.C.

Keywords: PM<sub>10</sub>/PM<sub>2.5</sub>, trace gases, measurements, long-range transport, trajectory.

Aerosol mass concentration and composition was measured since 2001 (Wang et al. 2004) to the present at the Shi-Men Atmospheric Research Station at the northern tip of Taiwan. 12-hour aerosol samples were collected during week-long campaigns in regular intervals. Atmospheric trace gas concentrations were measured continuously at two rural/remote coastal sites and one island site close to the Chinese mainland from 1993 to 2006 and at the GAW Yonaguni island site from 1997 to 2006.

Using back trajectory analysis (Draxler and Hess, 1998) and local wind speed and direction the effect of local air pollution was as far as possible removed from the data in order to obtain a time series of background pollution concentrations over the western Pacific. Comparing the gaseous measurements at the two coastal sites with those from the two island sites demonstrates that the measurements at the two rural/remote Taiwanese coastal sites are suitable for inferring Pacific background air pollution. Furthermore, each of the 12-hour aerosol sampling periods was classified according to the air mass origin in order to differentiate Asian continental long range air pollution transport from other Pacific pollution background.

The average concentrations found for Asian continental outflow conditions and other Pacific background conditions during the period 2001 to 2006 are listed in Table 1.

Table 1. Averages of aerosol mass, PM<sub>10</sub> components and precursor gas concentrations for continental outflow and other Pacific background conditions from 2001 to 2006. The trace gas concentrations from continuous measurements have been matched with the aerosol sampling dates.

		Other Pacific background	Continental outflow
PM <sub>10</sub>	g/m	39.9	67.1
PM <sub>2.5</sub>	g/m	17.5	31.1
EC	g/m	0.84	1.34
OC	g/m	3.58	5.00
nssSO <sub>4</sub> <sup>2-</sup>	g/m	5.57	9.39
NO <sub>x</sub>	g/m	2.24	3.03
CO	ppm	0.28	0.34
SO <sub>2</sub>	ppm	1.60	2.31
O <sub>3</sub>	ppb	37.8	46.7
NO <sub>x</sub>	ppm	7.93	6.67

With the exception of OC (40%) aerosol mass is on average enhanced by 70% for continental outflow conditions compared with other Pacific background. The highest enhancement of trace gas concentrations for continental outflow conditions is observed for sulphur dioxide (44%).

However, there is only moderate agreement between SO<sub>2</sub> and non-sea salt aerosol sulphate (nssSO<sub>4</sub><sup>2-</sup>) as shown in Figure 1. On the other hand the Figure shows near perfect agreement between elemental carbon (EC) and CO concentrations.

There is only moderate agreement between CO and OC mass concentrations (data not shown). It is possible that losses of primary OC occur during long-range transport.

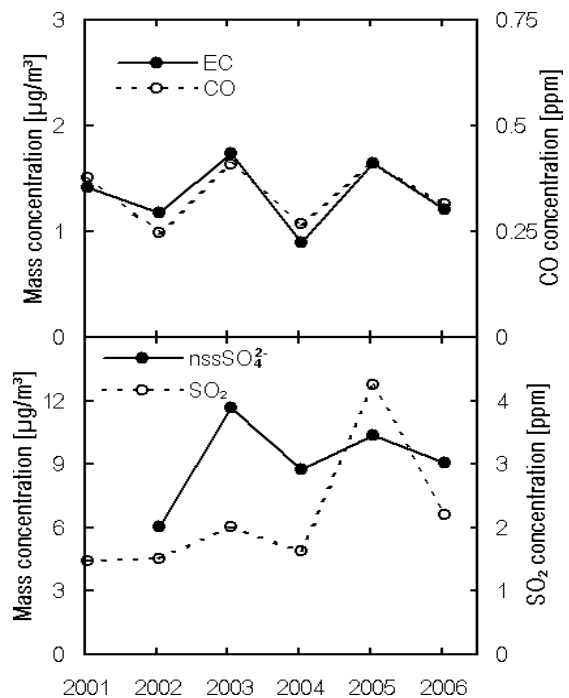


Figure 1. Year averages of EC, CO, sulphate and SO<sub>2</sub> of Pacific background air originating from mainland China

This work was supported by the Academia Sinica and the National Science Council of Taiwan.

Draxler, R.R. and G.D. Hess (1998). *Aust. Meteor. Mag.*, 47, 295-308.

Wang, C.-C., C.-T. Lee, S.C. Liu, and J.-P. Chen (2004). *TAO*, 15, 5, 839-855.

## Characteristic size distribution of sulphate aerosols influenced by Asian outflow

N. Kaneyasu<sup>1</sup>, A. Takami<sup>2</sup>, and S. Hatakeyama<sup>2</sup>

<sup>1</sup> National Institute of Advanced Industrial Science and Technology, Onogawa 16-1, 305-8569, Tsukuba, Japan

<sup>2</sup> National Institute for Environmental Studies, Onogawa 16-2, 305-8506, Tsukuba, Japan

Keywords: size distribution, sulphate, AMS, low-pressure-impactor, long-range transport

### Introduction

Reports on the size distributions of aerosol components are relatively sparse in the field campaigns conducted in Asia-Pacific rim region, where the emissions of air pollutants are expected to increase during this century. The focus of this study is the size distribution of sulfate aerosol, which is one of the most influential anthropogenic species in view of the climatic effects. The results of ground based and shipboard measurements are presented regarding the characteristics of size distribution in this region.

### Measurements

A low-pressure type cascade impactor (LPI, Tokyo Dylec LP-20) that consists of 12 impaction stages plus backup filter was operated at remote sites in Japan (Chichi-jima Island in 1998 winter, and Cape Hedo of Okinawa Island in 2006 spring), and during the 2001 cruise of the R/V *Hakuho-Maru* in the NW Pacific Ocean. The cutoffs sizes of each stage at 50% collection efficiency are 11, 7.8, 5.2, 3.5, 2.1, 1.2, 0.7, 0.49, 0.3, 0.2, 0.12, and 0.06  $\mu\text{m}$  in aerodynamic diameters at 24.6  $\text{L min}^{-1}$  flow rate. At Cape Hedo, an Aerodyne quadrupole aerosol mass spectrometer (AMS; Aerodyne Research) was operated to monitor both the mass spectra and size distribution of aerosols.

### Results and discussion

At the Cape Hedo station, seven samples of size-segregated aerosols were collected by LPI in 2006 spring, when Asian outflow is predominant. AMS was operated continuously during that period. Figure 1 compares the size distribution of LPI and AMS during March 14–21 period. Original AMS size distribution obtained at 10 min intervals were averaged according as the LPI sampling period. LPI size distribution yielded a mode in the submicron range at 0.5–0.7  $\mu\text{m}$  in aerodynamic diameter, which appears to be similar to the mode obtained by AMS. Impactor data divided for each stage were inverted into smooth mass size distribution by Twomey-algorithm, and then fitted to the sum of log-normal functions for fine and coarse modes. Geometric mean mass diameters  $d_{\text{gm}}$  of LPI in fine mode deduced as above are compared with those of AMS in Table 1. In this measure, the difference in  $d_{\text{gm}}$  between AMS and LPI-fine is within 0.11–1.13  $\mu\text{m}$ . The relative decrease in the mode diameter by AMS compared to

LPI can partly be attributed to that AMS measures “vacuum” aerodynamic diameter.

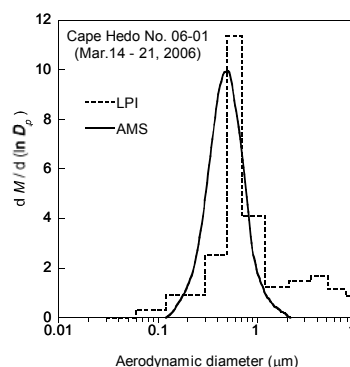


Figure 1. Mass size distribution of sulphate aerosol by LPI and AMS at Cape Hedo, Okinawa Island, Japan, during March 14–21, 2006.

It is noteworthy that the submicron mode of  $\text{SO}_4^{2-}$  resides in the stage of unexpectedly large sizes (0.5–0.7  $\mu\text{m}$  in aerodynamic or vacuum diameter) both by LPI and AMS measurements. The observed mode in 0.5–0.7  $\mu\text{m}$  range is similar to that found by Hering and Friedlander (1982) for sulfur aerosols in Los Angeles, which is referred to as the “droplet mode”. The same feature was also reported for the aerosols collected in the mid latitude zone of the North Pacific Ocean (on 175°E longitude line) in 1994 that was attributed to the long-range transport of Asian originated pollutants (Kaneyasu and Murayama, 2000). Similar results obtained by the shipboard measurement and at Chichi-jima Island are also discussed in the presentation.

Table 1. Comparison of geometric mass mean diameters measured by LPI and AMS at Cape Hedo.

Period	RH(%)	AMS $d_{\text{gm}}$ ( $\mu\text{m}$ )	LPI $d_{\text{gm}}$ ( $\mu\text{m}$ )
3/14 - 3/21	64.8	0.51	0.62
3/21 - 3/27	77.6	0.53	0.70
3/27 - 4/4	67.1	0.48	0.62
4/4 - 4/9	75.0	0.56	0.67
4/9 - 4/13	81.3	0.55	0.67
4/13 - 4/24	71.8	0.52	0.63

Hering, S. V., and Friedlander, S. K. (1982). *Atmos. Environ.*, 16, 2647–2656.

Kaneyasu, N., and Murayama, S. (2000). *J. Geophys. Res.*, 105(D15), 19,881–19,890.

## Chemical and morphological characterization of atmospheric particles in Mexico City and its classification in anthropogenic types

G.J. Labrada-Delgado, A. Aragón-Piña and A.A. Campos-Ramos

Instituto de Metalurgia, Universidad Autónoma de San Luis Potosí, Sierra Leona 550, Lomas 2ª Secc., 78210, San Luis Potosí, México.

Keywords: electron microscopy, PM10, particulate matter, anthropogenic aerosols.

Mexico City is one of the most populated cities in the world, and this region has a major problem of air pollution because of its great variety of socioeconomic activities. Although many studies about air quality have been done in this zone of Mexico, the most of them only describe the global chemical composition of the particulate matter by size classification (Raga et al., 2001), nevertheless; the individual characteristics of the atmospheric particles like morphology, shape, chemical composition and size distribution are unknown, these parameters have a very important role in the adverse effects caused to health and environment. The particle characterization of PM10 was done through techniques of scanning electron microscopy (SEM) and microanalyses, with the goal of knowing this individual information of the particles.

PM10 samples were analysed during 2004 in five stations of the Mexico City Metropolitan Area (MCMA). The analysis of the morphology and chemical composition of the particles allow its classification according to its origin in: natural and anthropogenic particles. Individual information of about 4,600 anthropogenic particles was obtained and an extensive classification of them in relation to its major element was conducted, identifying 20 groups. There are five predominant groups of anthropogenic aerosols which correspond to phases of iron, lead, barium, copper and elemental carbon. Anthropogenic aerosols were associated to particles emitted by diverse types of sources through reference of similar studies carried out in the city of San Luis Potosi, Mexico (Aragón et al., 2002 y 2006).

Particles with high content of iron presented metal associations with chromium, nickel and zinc as well as iron oxides with spherical morphology (Figure 1a). It was determined that these phases of iron come mainly from activities of the metal-mechanic industry. Around 55% of the lead phases presented size in the PM2.5 range and its typical morphology was agglomerates of nanometric spheres (Figure 1b), this generates a great interest because of the impact that these phases could cause to human health when they enter to the respiratory tract. The industries of melting, pigments and vehicle emission were the main source of particles rich in lead identified.

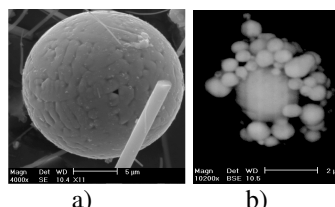


Figure 1. Anthropogenic aerosols a) Fe-rich particle, b) Pb-rich particles.

Barite was the predominant phase of barium, this mineral is widely used as source of barium in the industry. The particles containing copper presented association with zinc, and this indicates that its presence in the air is due to foundry processes in the obtaining of brass. The typical morphology of the elemental carbon particles was spherical and about 67% of them were in the PM2.5 range; this phase was associated to combustion processes emissions.

In general, the north region of the MCMA presented the biggest abundance of anthropogenic aerosols, and this is attributed to the great industrialization of this zone, nevertheless; the regional influence of the meteorological conditions generate the transport of this air contaminant to the south of Mexico City, where the residential zone is situated. This highlights the interest on identifying the main source of particles to contribute in mitigating the deterioration of the quality of the air that habitants of MCMA breathe.

This research has been sponsored by the Consejo Nacional de Ciencia y Tecnología of Mexico. CONACYT

Aragón, P.A., Torres, V.G., Santiago, J.P. & Monroy, F.M. (2002). *J. Atmos. Environ.*, 36, 5235-5243.

Aragón, P.A., Campos, R.A., Leyva, R.R., Hernández, O.M., Miranda, O.N. & Luszczewski, K.A. (2006). *Rev. Int. Contam. Ambient.*, 22, 5-19.

Raga, G.B., Baumgardner, D., Castro, T., Martínez, A.A. & Navarro, G.R. (2001). *J. Atmos. Environ.*, 35, 4041-4058.

## Surface tension properties of aerosol water extract and atmospheric humic-like substances

Imre Salma, Rita Ocskay, Nicolas Peron, Imre Varga

Eötvös University, Institute of Chemistry, H-1518 Budapest, P.O. Box 32, Hungary

Keywords: aerosol characterization, aerosol-surface interaction, SOA, water-soluble organic compounds.

Surface activity of droplets in the air alters droplet nucleation, growth, critical super-saturation, and multiphase water chemistry. One of the most important classes of compounds that influences the surface activity of the droplets are humic-like substances (HULIS). Surface tension properties of aerosol water extract and HULIS solutions were investigated.

Aerosol samples were collected by a high-volume sampler in the PM<sub>2.5</sub> size fraction at a kerbside site in downtown Budapest, Hungary in 2006. The samples were collected on Whatman QM-A quartz fibre filters. The filters were extracted by Milli-Q water for about 36 h, and the extracts were filtered through a membrane filter with a pore size of 0.22  $\mu\text{m}$ . Water-soluble organic carbon content was determined by a total organic carbon analyzer (Analytik Jena, Multi N/C 2100S, Germany) in two steps as the difference between the total carbon and total inorganic carbon. The aerosol water extract sample was obtained by freeze-drying one aliquot of the joint filtered water extract solutions. The HULIS sample was isolated from the second aliquot by a modified one-step version of a solid phase extraction (SPE) protocol on a pre-conditioned Oasis HLB column (hydrophilic-lipophilic-balanced water-wettable copolymer, Waters Inc., USA). The HULIS in pure organic form was eluted from the SPE column by methanol. The eluates from all samples were joined into a pool sample, and they were evaporated to dryness by a gentle nitrogen stream. The drying resulted in a dark yellow or brownish matter/pulp. The aerosol water extract and HULIS samples were dissolved in water yielding stock solutions. Two series of solutions with decreasing organic carbon concentrations were prepared from the stock solutions by sequential dilutions. Surface tension of the solutions was measured by a dynamic pendant drop shape method. A drop with clean and fresh surface and constant area was formed at the tip of a Teflon capillary within a closed temperature-controlled chamber with wetted walls and hydrophobic windows, and digital images of the drop were recorded and subjected to an edge detection and shape fitting computer program that calculated the temporal surface tension values. Surface tension relaxation curves were produced on line as well.

The solution of pure HULIS in concentration of 1 g/l decreased the surface tension of pure water by about 30%, and the major decrease occurred

within several tens of seconds. In diluted solutions (about 40 mg/l) of HULIS, the thermodynamic equilibrium in surface tension was only reached after several hours, but the equilibrium depression value was still remarkable, about 18%. Analysis of the surface tension relaxation curves implied that the kinetics of the surface tension depression can be described by a diffusion controlled process. The transport process in a real droplet can be more rapid than in the investigated system if the slightly soluble compounds occupy a distinct part of the particle surface, forming less and more hydrophilic areas. The particle hydration can start from the more hydrophilic area of the particle surface, and the slightly water-soluble components spread over the droplet by a surface diffusion which is thought to be much more rapid. Surface tension depression caused by the aerosol water extract is displayed in Fig. 1. The maximal decrease by the aerosol water extract is less than for the pure HULIS as the result of the interaction between the organic constituents and inorganic ions. The surface tension depended on the solution pH as well; the smallest depression for HULIS was observed at about pH = 5, and it was increased by an additional 13% for strong acidic or basic conditions; hence the role of surface tension in cloud droplet formation under acid rain conditions is further amplified.

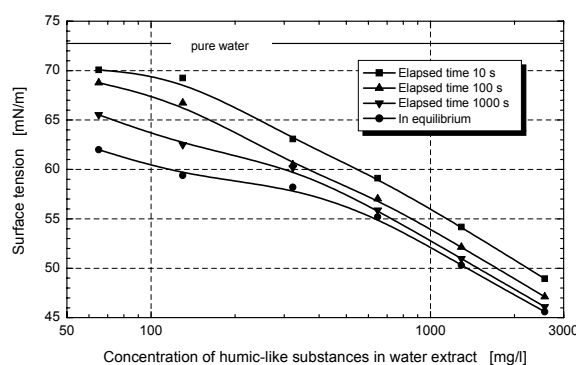


Figure 1. Dependence of the surface tension on the concentration of humic-like substances in the aerosol water extract after different elapsed times.

This work was supported by the Hungarian Scientific Research Fund under grant K061193.

Salma, I., Ocskay, R., Varga, I., & Maenhaut, W., (2006). *J. Geophys. Res.*, 111, D23205, doi: 10.1029/2005JD007015.

## Chemical characterization of all-year-round atmospheric aerosol at Dome C, East Antarctica

R. Udisti<sup>1</sup>, S. Becagli<sup>1</sup>, E. Castellano<sup>1</sup>, O. Cerri<sup>1</sup>, F. Lucarelli<sup>2</sup>, F. Marino<sup>3</sup>,  
A. Morganti<sup>1</sup>, S. Nava<sup>2</sup>, F. Rugi<sup>1</sup>, E. Salviotti<sup>1</sup>, M. Severi<sup>1</sup>, R. Traversi<sup>1</sup>.

<sup>1</sup>Department of Chemistry, University of Florence, Sesto F.no (FI), I-50019, Italy

<sup>2</sup>Department of Physics, University of Florence and INFN, Sesto F.no (FI), I-50019, Italy

<sup>3</sup>Department of Environmental Science, University of Milano Bicocca, Milano I-20126, - Italy.

Keywords: Antarctic aerosol, ions, long-range transport, cascade impactor, sources identification.

In the framework of Station Concordia network, an Italy-France joint program aiming to promote and support scientific activity at Dome C, size-segregated atmospheric aerosol was collected by cut-off samplers and multi-stage impactors during the 2004/05 Antarctic Campaign and following winter-over. Here we report the first results of the chemical composition of the Antarctic background aerosol reaching Dome C (Central East Antarctica, 3233 m a.s.l., about 1100 km far from the coast-line), pointing out the seasonal pattern and the temporal trend of some ionic components used as tracers of sea spray, marine biogenic and crustal emissions. The main goal of this study is understanding present-time sources, transport pathways, depositional processes and post-depositional effects of atmospheric particulate at Dome C, in order to better explain past changes in aerosol load and composition revealed by ice core stratigraphies. Indeed, a 3350 m depth ice core (EDC99 – EPICA project) was drilled in the 1999-2004 period at Dome C, allowing the reconstruction of paleo-atmosphere composition for the last 9 climatic cycles.

Aerosol particles were collected at Dome C, about 1 km south of the Station Concordia base (75° 06' S, 123° 23' E), upwind (with respect the dominant wind direction) to building and people activity, in order to minimise contamination by anthropic emissions. During the first all-year-round campaign (November 2004 - November 2005), aerosol samples were collected by using different low-volume sampling systems: 1. a stacked filter device (3.0 and 0.4 µm Teflon membranes separated by a nylon net); 2. a pre-selected cut-off collector with PM10 or PM2.5 head (used in alternate period); 3. a 8-stage (10-0.4 µm) sampler (Andersen 20-800 impactor). Sampling resolution and volume range from 2 to 7 days and from 1.7 to 2.3 m<sup>3</sup>/h, respectively.

A large number of samples, covering all the time period, was collected and used to describe seasonal pattern and temporal trend of load and chemical composition of aerosol at Dome C. Samples were analysed by Ion Chromatography for major inorganic cations and anions, methanesulphonic acid (MSA) and some short-chain carboxylic acids.

The atmospheric load in the summer is more than one order of magnitude lower than that

measured in coastal sites (Fattori *et al.*, 2005 - Terra Nova Bay – Northern Victoria Land) and chemical composition is dominated by secondary aerosol, mainly originated by biological marine activity (S-cycle), and distributed in the finest aerosol fractions. H<sub>2</sub>SO<sub>4</sub> from oxidation of biogenic DMS is the main component, while the contribution of HNO<sub>3</sub> to the ionic budget is difficult to reliably evaluate because of the re-emission into the atmosphere from the filter surface. Indeed, all the aerosol size-fractions collected in summer were very acidic. The ionic load was even lower in winter, when secondary biogenic aerosol decreases and larger particles from primary source (especially from sea spray) prevail, driving a different pattern between PM10 and PM2.5 fractions. Winter aerosol is almost neutralised and its composition shows a dominant contribution of sea spray species (Na<sup>+</sup>, Cl<sup>-</sup> and Mg<sup>2+</sup>). Nitrate is believed to be well preserved on the filter. Its relative contribution is higher in the finest fraction. Winter sulphate/Na ratio is similar to sea water, when biogenic activity is missing or negligible.

Fractionating effects leading to a reduction of SO<sub>4</sub><sup>2-</sup>/Na ratio (“frost flower” source) seem do not affect winter aerosol. The contribution of crustal components is always very low.

Multi-stage impactor samples revealed that sea-spray and crustal components peak in the 2-4 µm modes, while sulphate, MSA and ammonium show higher atmospheric concentration in the sub-micrometric fractions.

This work was supported by the Italian National Programme for Antarctic Research (PNRA) and was developed in the framework of the EPICA and Station Concordia projects.

Fattori, I., Becagli, S., Bellandi, S., Innocenti, M., Mannini, A., Severi, M., Vitale, V., & Udisti, R. (2005). *J. Environ. Monit.*, 7, 1265-1274.

Udisti, R., Becagli, S., Benassai, S., Castellano, E., Fattori, I., Innocenti, M., Migliori, A., & Traversi, R., (2004). *Ann. Glaciol.*, 39, 53-61.

## Characterization of aqueous solutions of atmospheric humic-like substances

R. Ocskay, I. Salma

Eötvös University, Institute of Chemistry., H-1518 Budapest, P.O. Box 32, Hungary

Keywords: water-soluble compounds, HULIS, molecular weight, aromaticity, solubility

Significant part of the water-soluble organic fraction of the atmospheric aerosol consists of humic-like substances (HULIS). It is increasingly recognized that they play an important role in the atmospheric system by influencing the physicochemical properties of the droplets in the air. Spectroscopic properties of pure HULIS samples and aquatic fulvic acids were investigated, compared and utilized further to estimate the average molecular weight and aromaticity, and water solubility of HULIS samples was studied.

Collection of the aerosol samples took place in downtown Budapest, Hungary at a kerbside site in 2–9 May (spring), and 17–24 July (summer) 2006. The samples were collected by a PM<sub>2.5</sub> high-volume sampler (Digitel DHA-80, Greenlab) on pre-baked Whatman QM-A quartz fibre filters for one-week. The HULIS samples were isolated by one-step solid phase extraction (SPE) method (Varga *et al.*, 2001). The filters were extracted with Milli-Q water. Separation of the HULIS was carried out with pre-conditioned Oasis HLB columns. The HULIS were eluted from the column with methanol, and were evaporated to dryness with a gentle nitrogen stream. The samples obtained (dark yellow-brown pulp) were dissolved in water for further investigations. Standard Suwannee River Fulvic Acid (SRFA, IHSS code: 2S101F), obtained from the International Humics Substances Society (IHSS), was dissolved in Milli-Q water, and was used for the spectroscopic measurements without any sample pre-treatment or fractionation.

The water-soluble organic carbon in the aqueous solutions was measured by total carbon analyzer (Analytik Jena Multi N/C 2100S, Germany) in two steps as the difference between the total carbon and inorganic carbon. UV/VIS spectra of the aqueous solutions were recorded in the range between 190 and 500 nm with an UV/VIS spectrophotometer (Lambda 12, Perkin-Elmer) in a 1-cm path length quartz cuvette.

The UV/VIS spectra of the HULIS and SRFA aqueous solutions were similar in general: the absorbance decreased monotonically from the maximum (around 220–240 nm) towards the longer wavelength, so the HULIS can be characterized by double-bounded aromatic structures. Specific molar absorptivities ( $\epsilon$ , L/mol/cm of organic carbon) were derived at 254 and 280 nm. We found linear relationship between the solute concentration and

absorbance for the diluted SRFA solutions only, and obtained molar absorptivities of 500 and 378 L/mol/cm at 254 and 280 nm, respectively. For the concentrated SRFA solutions (200–400 mg C/L), the absorptivity decreased with the concentration. For the HULIS aqueous solutions of about 10–130 mg C/L,  $\epsilon$  increased from 150 to 230 L/mol/cm at 254 nm, and from 100 to 170 L/mol/cm at 280 nm. Molar absorptivities were used to estimate the number-averaged molecular weight ( $M(N)$ ) and aromaticity ( $Ar$ ) (aromatic carbon content) of humic substances using the relationships that were established for humic substances originating from different terrestrial and aquatic sources (Chin *et al.*, 1994; Peuravuori & Pihlaja, 1997; Schäfer *et al.*, 2002). The correlations suggest that the relative amount of aromatic moieties (and so the absorptivity) increases with increasing molecular weight. As  $\epsilon$  changed with the concentration, we could not estimate constant values for  $M(N)$  and  $Ar$ . For SRFA, the average  $M(N)$  were 1036, 3848, and 636 AMU in the linear concentration range, while for the HULIS samples, the values of  $M(N)$  varied between 677–763, 596–933, and 373–432 AMU utilizing the correlations by Chin *et al.* (1994), Peuravuori & Pihlaja (1997), and Schäfer *et al.* (2002), respectively. The aromaticity of SRFA was estimated to be around 25%, while the aromaticity of atmospheric HULIS samples changed between 9 and 15%. The measured absorptivity of SRFA was greater compared to the HULIS, which corresponds to the lower molecular weight, and larger amount of aromatic moieties present.

The work was supported by the Hungarian Scientific Research Fund under grant K061193.

- Varga, B., Kiss, Gy., Ganszky, I., & Gelencsér, A., & Krivácsy, Z. (2001). *Talanta*, 55, 561–572.
- Chin, Y.P., Alken, G. & O'Loughlin, E., (1994). *Environ. Sci. Technol.* 28, 1853–1858.
- Peuravuori, J. & Pihlaja, K. (1997). *Anal. Chim. Acta*, 337, 133–149.
- Schäfer, A.I., Mauch, R., Waite, T.D. & Fane, A.G. (2002). *Environ. Sci. Technol.*, 36, 2572–2580.

## The atmospheric partitioning of PAHs and n-alkanes in urban (Milan) and remote (Alpe San Colombano, 2260 m agl) sites in Italy

G. Sangiorgi<sup>1</sup>, L. Ferrero<sup>1</sup>, Z. Lazzati<sup>1</sup>, C. Lo Porto<sup>1</sup>, M. G. Perrone<sup>1</sup>, S. Petraccone<sup>1</sup> and E. Bolzacchini<sup>1</sup>

<sup>1</sup>Department of Environmental Science and Technology, University of Bicocca, piazza della Scienza 1, 20126, Milan, Italy

Keywords: TSP, PAHs, n-alkanes, field measurements, long-range transport.

In the atmosphere a compound can partition between gaseous and particulate phase as a function of both its chemical-physical characteristics and atmospheric conditions. The partitioning of Semi-Volatile Organic Compounds (SVOCs) is a very important parameter in describing their atmospheric transport, reactivity, deposition and fate (Bidleman, 1988). Moreover, the gas-to-particle partitioning also is important for purpose of knowing and modelling their toxicity potential (e.g. PAHs), as well their contribution in secondary aerosol formation (Pankow, 1987).

During summer 2007, we collected TSP (Total Suspended Particulate) and gas samplers (ECHO PUF, TCR Tecora) at two different Italian sites: urban (Milan;  $n=8$ ) and remote (Alpe San Colombano, 2260 m a.g.l., SO;  $n=8$ ). The TSP was collected on quartz fiber filters and the gas on PUFs.

The solvent extraction was dichloromethane. The extraction was performed by 20 min of ultrasonic bath for quartz fiber filters and by Soxhlet extractor for the PUFs. We analysed all the samples by GC-MS to determine the Polycyclic Aromatic Hydrocarbons (PAHs) and the n-alkanes ( $C_{17}$  to  $C_{32}$ ).

The gas-to-particle partitioning is a function of both meteorological conditions ( $T$ ,  $p$ , RH,...) and molecular chemical-physical characteristics ( $K_{oa}$ ,  $p_L$ , MW,...) (Harner and Bidleman, 1998).

Considering the PAH results (Figure 1), the contribution of the particulate phase increased with the decrease of the compound's volatility.

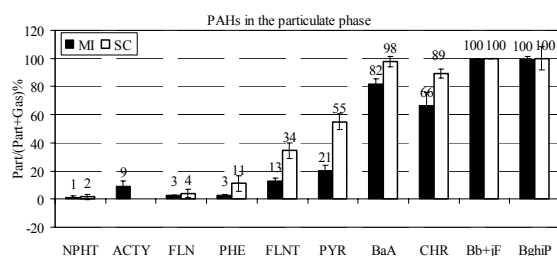


Figure 1. Concentrations (%) of PAHs in the particulate phase respect to their total (gas plus particulate) concentration.

The most volatile species (naphthalene) was almost totally in the gaseous phase, while the less volatile

species (benzo[a]anthracene to benzo[ghi]perylene) were in the particulate phase for more than 50% of their concentration. Phenanthrene, fluoranthene and pyrene were almost equally distributed between the two phases.

In general, at the remote site the PAHs were distributed more in the particulate phase than in the urban site. This may be due to the lower ambient temperature at Alpe San Colombano (average: 19°C) than in Milan (average: 31°C) during the sampling period, that forced the gas to condensate.

Concerning the n-alkanes, they showed an increasing preference for the particulate phase with the increasing number of C atoms. In Milan, the maximum carbon number was  $C_{20}$  and  $C_{29}$  in the vapour and the particulate phase, respectively. In Alpe San Colombano, the maximum carbon number was  $C_{21}$  and  $C_{31}$  in the vapour and the particulate phase, respectively.

A preference for the n-alkanes with an odd number of C atoms at both sites is also evident. This is an indication of the vegetal source apportion.

In conclusion, our field results showed that the gas-to-particle partitioning of SVOCs is first of all a function of the molecular chemical-physical properties, but also of the meteorological conditions ( $T$ ). This pattern is clear for the PAH compounds, that could be divided into three groups:

- volatile (naphthalene),
- semi-volatile (phenanthrene, fluoranthene pyrene),
- non-volatile (benzo[a]anthracene, chrisene, benzo[b]fluoranthene, benzo[j]fluoranthene, benzo[k]fluoranthene, benzo[e]pyrene, benzo[a]pyrene, indeno[1,2,3-cd]pyrene, dibenzo[ah]anthracene, benzo[ghi]perylene).

Bidleman, T. F. (1988). *Environ. Sci. Technol.*, 22 (4), 361-367.

Harner, T., & Bidleman T. (1998). *Environmental Science and Technology*, 32, 1494-1502.

Pankow, J.F., (1987). *Atmospheric Environment*, 21, 2275-2284.

## In-situ analysis of free tropospheric aerosol and small ice crystal residuals using a High Resolution Aerosol Mass Spectrometer (HR-ToF-AMS) at the Jungfraujoch during CLACE 5

J. Schneider<sup>1</sup>, S. Walter<sup>1</sup>, J. Curtius<sup>2</sup>, F. Drewnick<sup>1</sup>, S. Borrmann<sup>2,1</sup>, S. Mertes<sup>3</sup>,  
E. Weingartner<sup>4</sup>, M. Gysel<sup>4</sup>, J. Cozic<sup>4</sup>

<sup>1</sup>Particle Chemistry Dept., Max Planck Institute for Chemistry, Joh.-J.-Becherweg 27, 55128 Mainz, Germany

<sup>2</sup>Institute for Atmospheric Physics, University Mainz, Joh.-J.-Becherweg 21, 55128 Mainz, Germany

<sup>3</sup>Leibniz-Institute for Tropospheric Research, Permoser Str. 15, 04318 Leipzig, Germany

<sup>4</sup>Laboratory of Atmospheric Chemistry, Paul Scherrer Institute, CH-5232 Villigen, Switzerland

Keywords: Aerosol cloud interaction, Ice nuclei, Aerosol chemistry, Aerosol mass spectrometry

A High Resolution Time-of-Flight Aerosol Mass Spectrometer (HR-ToF-AMS) was operated during CLACE 5 (Cloud and Aerosol Characterization Experiment) at the High Alpine Research Station Jungfraujoch (Switzerland, 3500 m a.s.l.) to measure size resolved chemical composition of particles in the size range between 40 nm and 1.0  $\mu\text{m}$ .

This instrument sampled aerosol particles through three different inlet systems: an interstitial aerosol inlet (cut-off 2.5  $\mu\text{m}$ ), a heated total aerosol inlet, and an Ice-CVI, which is a counterflow virtual impactor designed to sample only small ice crystals (Fig. 1).

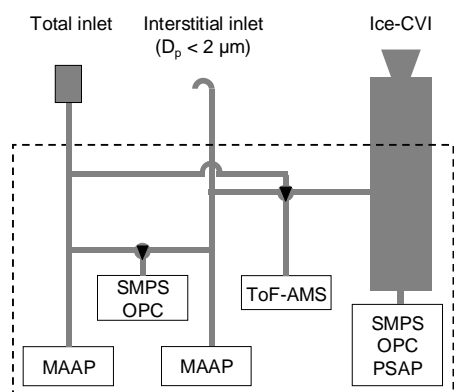


Figure 1. Simplified setup scheme of CVI, the interstitial and the total inlet and the instruments used in this work.

As an improvement to previous experiments (CLACE 3 and CLACE 4), where a similar setup was used, the HR-ToF-AMS allows to distinguish between hydrocarbon-like organic aerosol (HOA) and oxygenated organic aerosol (OOA) since the different elemental composition of ions with the same nominal  $m/z$  implies different exact molecular weights (DeCarlo et al., 2006). For example, the ion found at the integer  $m/z = 43$  can (amongst others) contain  $\text{C}_3\text{H}_7^+$  (exact  $m/z = 43.0548$ ) and  $\text{C}_2\text{H}_3\text{O}^+$  (exact  $m/z = 43.0184$ ).  $\text{C}_2\text{H}_3\text{O}^+$  is a fragment of an oxygen-containing organic molecule and can thereby be used as a marker for OOA, while  $\text{C}_3\text{H}_7^+$  can be a fragment as well of a larger hydrocarbon molecule as

of a larger oxygen-containing molecule (Fig. 2). A high contribution of oxygenated aerosol was found in the free tropospheric background aerosol, confirming the assumption that photochemical aging converts primary organic aerosol emissions into oxygenated aerosol.

The ice residual measurements confirmed the finding that was obtained in the previous CLACE campaigns: Ice nuclei (IN) are preferably composed of refractory material as mineral dust or black carbon that can not be detected by the HR-ToF-AMS. Additional black carbon measurements and a mass closure based on SMPS volume size distributions indicate that black carbon alone can not account for all the refractory material and that therefore most likely mineral dust is the major component of free tropospheric ice nuclei.

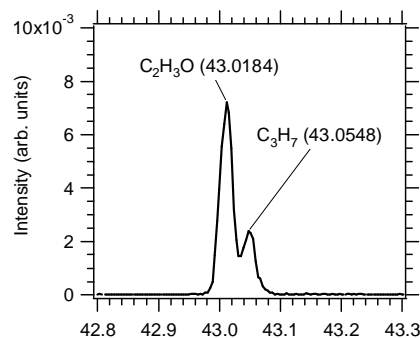


Figure 2. Example for a high-resolution mass peak at the nominal  $m/z = 43$ .

We thank the International Foundation High Altitude Research Stations Jungfraujoch and Gornergrat (HFSJG), the International Max Planck Research School for Atmospheric Chemistry and Physics and the German Research Foundation for funding this project through the Collaborative Research Center "TROPEIS" (SFB 641) and the grant HE 939/17.

DeCarlo, P., et al., Anal. Chem., 78, 8281-8289, 2006.

## **Season time modulation of Nitro-PAH in the air of Montelibretti RM, Italy**

A. Cecinato, C. Balducci, G. Nervegna, G. Tagliacozzo and A. Brachetti

Istituto Inquinamento Atmosferico CNR, Via Salaria km 29.3 – CP 10, 00016 Monterotondo Scalo RM, Italy;

Keywords: Airborne particles, Organic compounds, Source identification, PAH(s)

Nitro-PAH have been recognized strong mutagens as well as carcinogens. They occur in air at pg-ng per cubic meter concentrations, and are responsible for some percents of total long-term genotoxicity of airborne particulates. Looking to congener percent composition of the Nitro-PAH group, nitro-naphthalenes account for most of gas phase contents, whilst nitrated anthracene, fluoranthene and pyrene are the most abundant compounds associated to airborne particles. Atmospheric Nitro-PAH can have two kinds of sources, i.e. direct anthropogenic emission and in-situ generation involving parent PAH and nitrating species ( $\text{OH}+\text{NO}_2$ ,  $\text{NO}_3$ ,  $\text{HNO}_3$ ). These two way of release give raise to compounds isomerically different, allowing to discriminate primary from secondary sources. Similarly it occurs for in-air reactions developing in homogenous (gas) or heterogeneous (gas and particle) phase.

Several studies performed in Rome and other urban and rural areas worldwide found that the secondary 2-nitrofluoranthene usually prevails versus the directly emitted 1-nitropyrene. Despite that, a 2-year investigation conducted at Montelibretti seemed to demonstrate that Nitro-PAH present a pattern strictly dependent upon year time. Indeed, the sole 2-nitrofluoranthene was observed during the warm season, whilst 7-, 3- and 8-nitro isomers in winter. The diesel vehicle exhaust associated 1-nitropyrene existed at concentrations lesser than nitro-fluoranthenes, suggesting that these latter came out all from secondary reactions developing both in homogeneous and heterogeneous phase. In addition, within whatever time year substantial variations were observed among the Nitro-PAH burdens of aerosols in correspondence of different meteorological condition contours.

## **Detection and evaluation of Cocaine in ambient air particulates**

A. Cecinato, C. Balducci

Istituto Inquinamento Atmosferico CNR, Via Salaria km 29.3 – CP 10, 00016 Monterotondo Scalo RM, Italy

Keywords: Carbonaceous particles, Chemical analysis, Organic compounds, Urban aerosols

Cocaine was detected in the atmosphere at all sites investigated in downtown Rome (Italy) as well as in its outskirts, as associated to “pulmonary” fraction of particulates. Cocaine was also present in the air of Taranto, but it was not in the Algiers and its surrounding (Algeria R.P.). A dedicated analytical procedure, based upon solvent extraction, column chromatography and capillary gas chromatography coupled with mass spectrometric detection, was set-up in order to evaluate aerial cocaine with good

reliability ( $\pm 10\%$ ) for concentration ranges typically reached in Italian cities (0.02~1.0 ng m<sup>-3</sup>). Aerial contents of cocaine were usually 10 to 100 times lower than those of the regulated benzo(a)pyrene, on yearly average base; however, during shorter periods it could reach concentration ratios close to 1:1 with respect to it, suggesting that the drug abuse can play a unexpected role in terms “passive smoking” and negatively influence the air quality or toxicity.

## Size distributions of PAHs collected beside a heavily-trafficked road

C.C. Lin<sup>1</sup>, S.J. Chen<sup>1\*</sup>, K.L. Huang<sup>1</sup>, W.Y. Lin<sup>2</sup>

<sup>1</sup> Department of Environmental Engineering and Science, National Pingtung University of Science and Technology, Nei Pu, 912, Pingtung, Taiwan

<sup>2</sup> Institute of Environmental Planning and Management, National Taipei University of Technology, Da An, 106, Taipei, Taiwan

Keywords: aerosol sampling, particle characterization, PAHs, size distribution, traffic.

For health reasons and to accurately characterize atmospheric ultrafine particles, the chemical composition of actual atmospheric ultrafine particles and the effects of particle sizes must be determined. Accordingly, this study investigated the mass concentrations and determined the PAH components/concentrations in variously sized particles collected near a major road with busy traffic loadings in southern Taiwan. The particle size distributions and cumulative mass fractions of particles/PAHs were determined according to the roadside particles collected by a MOUDI and a Nano-MOUDI. The PAH species determined included five 3-ring (Acenaphthylene (AcPy), Acenaphthene (Acp), Fluorene (Flu), Phenanthrene (PA), Anthracene (Ant)), four 4-ring (Fluoranthene (FL), Pyrene (Pyr), Benzo(a)anthracene (BaA), Chrysene (CHR)), six 5-ring (Cyclopenta(c,d)pyrene (CYC), Benzo(b)fluoranthene (BbF), Benzo(k)fluoranthene (BkF), Benzo(e)pyrene (BeP), Benzo(a)pyrene (BaP), Perylene (PER)), four 6-ring (Indeno(1,2,3,-cd)pyrene (IND), Dibenzo(a,h)anthracene (DBA), Benzo(b)chrycene (BbC), Benzo(ghi)perylene (BghiP)), and a 7-ring (Coronene (COR)) PAH compounds.

The bi-modal or tri-modal size distributions of atmospheric particles and particulate PAHs collected from the traffic source were shown in Figure 1. The traffic-related particles exhibited a tri-modal distribution, with a major peak in coarse size (3.2–5.6  $\mu\text{m}$ ), a secondary peak in fine size (1–1.8  $\mu\text{m}$ ), and a minor peak in nano size (0.018–0.032  $\mu\text{m}$ ). The particulate total-PAHs (average of five times sampling) displayed a tri-modal distribution with a major peak in Aitken mode (0.032–0.056  $\mu\text{m}$ ), a secondary peak in accumulation mode (0.56–1  $\mu\text{m}$ ), and a minor peak in coarse mode (1.8–3.2  $\mu\text{m}$ ) (Figure 2). The major peak size of particulate total-PAHs (0.032–0.056  $\mu\text{m}$ ) was very different from that of atmospheric particles (3.2–5.6  $\mu\text{m}$ ). As suggested by John et al. (1990) and Rase et al. (2000), atmospheric fine particles usually have one or two peaks in the accumulation mode and ultrafine size range, which consists of nucleation and Aitken modes. The Aitken mode particles can be scavenged by clouds and rains or can grow by coagulation and become larger to shift their size distributions into accumulation mode. In general, particles with the Aitken mode in size distributions are referred to local origins.

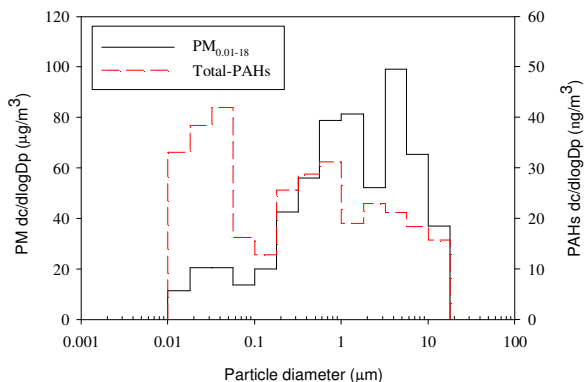


Figure 1. Size distributions of the  $\text{PM}_{0.01-18}$  and particle-bound total-PAHs.

Figure 2 showed the accumulation percentages of atmospheric particles and particulate total-PAHs collected near the traffic source. The accumulation percentages of the particles in nano (0.01 <  $D_p$  < 0.056  $\mu\text{m}$ ), ultrafine (0.01 <  $D_p$  < 0.1  $\mu\text{m}$ ), fine (0.01 <  $D_p$  < 2.5  $\mu\text{m}$ ), and  $\text{PM}_{0.01-10}$  size ranges were 8.74, 11.0, 62.2, and 93.7%, respectively, whereas those of particulate total-PAHs in the corresponding size ranges were 34.8, 39.9, 79.9, and 95.1%, respectively. The accumulation percentages of particulate total-PAHs in the nano and ultrafine size ranges were 4.34 and 4 times of those of PM, respectively. As can be seen from Figures 1 and 2, about 40% of particulate total-PAHs were distributed in the ultrafine size associated with the heavy traffic, which needs to be concerned for health impacts.

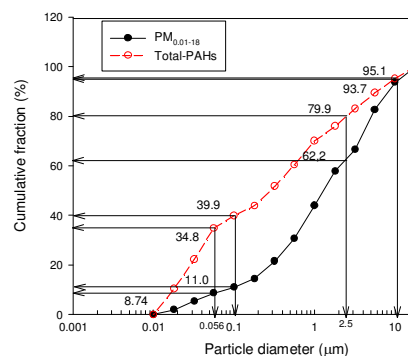


Figure 2. Cumulative mass fractions of the  $\text{PM}_{0.01-18}$  and particle-bound total-PAHs.

John, W. J., Wall, S. M., Ondo, J. L., Winklmayr, W. (1990). *Atmos. Environ.*, 24A, 2349–2359.

Raes, F., van Dingenen, R., Vignati, E., Wilson, J., Putaud, J. P., Seinfeld, J. H., Adams, P. (2000). *Atmos. Environ.*, 34, 4215–4240.

## Spring monitoring of the aerosol precursor isoprene and other biogenic volatile organic compounds (VOC) in a suburban area of A Coruña (NW Spain)

D. Pérez-Rial<sup>1</sup>, P. López-Mahía<sup>1,2</sup>, S. Muniategui-Lorenzo<sup>1</sup>, D. Prada-Rodríguez<sup>1,2</sup> and E. Fernández-Fernández<sup>1</sup>

<sup>1</sup>Department of Analytical Chemistry, University of A Coruña, Campus A Zapateira, E-15071, A Coruña, Spain

<sup>2</sup>Institute of Environment, University of A Coruña, Pazo de Lóngora, Liáns, E-15179, Oleiros, A Coruña, Spain

Keywords: isoprene, VOC, monitoring, organic compounds.

Volatile organic compounds (VOC) are emitted from vegetation into the atmosphere, where, in appropriated meteorological and chemical conditions, can take part in tropospheric ozone and particle formation chemistry (Owen *et al.*, 2001).

Among biogenic VOC, isoprene is one of the most abundant and it is well-known that its emissions are related to the plant photosynthetic activities. These emissions are both temperature and radiation dependent as a result of the isoprene synthase activity. Besides plants, anthropogenic sources of isoprene were sometimes found to be as equally important as biogenic sources in urban areas in winter (Borban *et al.*, 2001).

The aim of this work is to carry on a monitoring of the biogenic VOC concentrations in a suburban area of A Coruña (NW Spain) and study their relationships with the temperature and solar radiation. Especial attention has been paid to the isoprene concentrations because of its higher reactivity. The sampling area is surrounded by an eucalyptus plantation and during the most of the sampling days the weather was stable with humidity from 40 to 90%, diurnal solar radiation up to 2900 KJ m<sup>-2</sup> and average temperature of 19°C and without precipitation.

Air samples were taken using an automatic sequential sampler equipped with 24 Tenax TA<sup>®</sup> adsorbent cartridges. Samples were caught in 19 different days and in every sampling day twenty-four samples were collected pumping an air flow of 100 mL min<sup>-1</sup> through the adsorbent tubes. The sampling period was from the 1<sup>st</sup> of April to the 23<sup>th</sup> of June of 2006, sampling at least one day a week. Samples were analysed using thermal desorption in two steps coupled to gas chromatography with mass spectrometry detection (TD/GC/MSD). Isoprene was measured in a semi quantitative way because of its high volatility but other biogenic VOC as  $\alpha$ -pinene,  $\beta$ -pinene, limonene or eucalyptol were analysed quantitatively with instrumental detection limits lower than 2 ng.

In order to establish the relationships between these compounds and some meteorological variables such as temperature and radiation, meteorological data were analysed jointly with the concentration measurements.

Isoprene concentrations reached their maximums (up to 4.6  $\mu\text{g m}^{-3}$ ) at noon and decreased

near zero in the evening. But, in some cases, residual isoprene concentrations were also measured at night, probably due to anthropogenic sources. In order to establish the origin of these residual concentrations the ratios between isoprene and some anthropogenic VOC as benzene or toluene were also studied.

The highest concentrations of the quantitatively measured biogenic VOC were found for eucalyptol and  $\alpha$ -pinene with values sometimes close to 10  $\mu\text{g m}^{-3}$ .  $\beta$ -pinene and limonene were also found in several samples with lower values than those found for isoprene, eucalyptol or  $\alpha$ -pinene. In a few set of samples  $\alpha$ -phellandrene,  $\Delta^3$ -carene and  $\alpha$ -terpinene also appeared.

Figure 1 shows the patterns of measured isoprene concentrations, temperature and solar radiation.

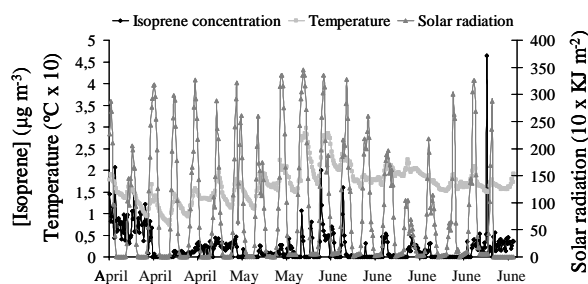


Figure 1. Monitoring of isoprene concentrations, temperature and solar radiation during the sampling time.

Summarising, the measured biogenic VOC concentrations are well correlated with temperature and radiation and it is easy to appreciate a daily emission cycle with maximums at the central hours of the day and minimums at night for the most of the analysed VOC.

D. Pérez Rial is very grateful to the Xunta de Galicia for the concession of a PhD Grant and the authors wish also to thank the National Meteorological Institute (Centro Zonal de A Coruña) the transferring of meteorological data.

Borban, A., Coddeville, P., Locoge, N. & Galloo, J. C. (2001). *Chemosphere*, 57, 931-942.

Owen, S.M., Boissard, C. & Hewitt, C. N. (2001). *Atm. Environm.*, 35, 5393-5409.

## Atmospheric aerosol characterization in Tuscany (PATOS Project): n-alkanes, PAHs and Total Carbon

T. Martellini<sup>1</sup>, A. Cincinelli<sup>1</sup>, M. Giannoni<sup>1</sup>, F. Barzagli<sup>1</sup>, D. Vannucchi<sup>1</sup>, L. Lepri<sup>1</sup>, R. Udisti<sup>1</sup> and F. Lucarelli<sup>2</sup>

<sup>1</sup>Department of Chemistry, University of Florence, Sesto Fiorentino, 50019, Florence, Italy

<sup>2</sup>Department of Physics and INFN, University of Florence, Sesto Fiorentino, 50019, Florence, Italy

Keywords: PM10, n-alkanes, PAHs, air pollution, urban areas

Polycyclic aromatic hydrocarbons (PAHs) comprise only a small fraction of atmospheric aerosols. However, they are a class of ubiquitous environmental pollutants, known to be mutagenic and/or carcinogenic (Dockery et al., 1993). Most PAHs emitted to the ambient air are formed during incomplete combustion, and the largest sources include motor vehicle exhaust, power generation via combustion of coal and oil, incineration of city waste, wood burning, domestic heating, cooking, smoking and industrial processes (Harrison et al., 1996). Atmospheric aliphatic hydrocarbons (i.e. n-alkanes) are not so toxic as PAHs, but they have negative impact on human health. N-alkanes may come from biogenic sources including particles shed from epicuticular waxes of vascular plants, direct suspension of pollen, microorganisms and incomplete combustion of fossil fuels and wood.

An intensive PM10 monitoring campaign was performed from September 2005 to January 2006 in six Tuscany urban areas (Firenze, Prato, Arezzo, Lucca, Grosseto, Livorno). Sampling sites were differently exposed to emission sources and classified as urban background, urban traffic and sub-urban area. This study is part of PATOS (Particolato Atmosferico in Toscana) project funded by Tuscany Region. Principal objectives of this study were to provide information on the airborne concentrations and emission sources for n-alkanes and PAHs. Total carbon (TC), consisting of elemental and organic carbon, was also measured. We believe that our results, together with the other studies which are part of PATOS, will be very useful for evaluating future air quality management in Tuscany.

A detailed description of the analytical procedure used for extraction, separation and analysis has been presented elsewhere (Cincinelli et al., 2003).

Results showed that PM10 and total carbon have a similar trend and the higher carbon concentration levels were observed in winter; in this period the larger proportion of carbonaceous species in PM10 is related to the higher degree of anthropogenic emissions (traffic, heating systems).

n-Alkanes concentrations were in accordance with those generally found in other urban areas in Europe. CPI, % WNA, UCM, Cmax were useful parameters for evaluating n-alkanes origin. CPI values approaching 1 and low %WNA, suggested the

importance of fossil fuels related emissions and the minor contribution of n-alkanes emitted directly from epicuticular waxes in urban area.

Gas chromatograms of the aliphatic hydrocarbon fraction showed characteristic profiles (see i.e. Figure 1) evidencing different petroleum origin. Diagnostic ratios of PAHs showed a high contribution of exhaust emissions from gasoline and diesel powered vehicles. Benzo(a)pyrene was also measured as requested by European Commission Directive and in some cases exceeded the guideline fixed by the Italian Ministry of Environment of  $\text{ng}/\text{m}^3$ .

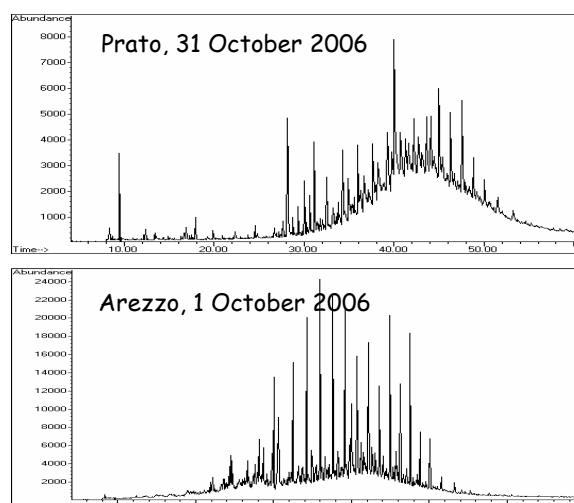


Figure 1. Gas-chromatogram of the aliphatic hydrocarbon fraction for two representative samples

Cincinelli, A., Mandorlo, S., Dickhut, R.M., Lepri, L., 2003. Particulate organic compounds in the atmosphere surrounding an industrialised area of Prato (Italy). *Atmos. Environ.*, 37, 3125-3133.

Dockery, D.W., Pope III, C.A., Xu, X., Spengler, J.D., Ware, J.H., Fay, M.F., Ferris, Jr, B.G., Speizer, F.E., 1993. An association between air pollution and mortality in six U.S. cities. *The New England Journal of Medicine* 329, 1753-1759.

Harrison, R.M., Smith, D.J.T., Luhana, L., 1996. Source apportionment of atmospheric polycyclic aromatic hydrocarbons collected from an urban location in Birmingham, U.K.. *Environ. Sci. Technol.*, 30, 825-832.

## Single particle characterization in the coarse mode from local, regional and long range transport episodes in Madrid by CCSEM and FE-SEM

E. Coz<sup>1</sup>, F.J. Gomez-Moreno<sup>1</sup>, M. Puadras<sup>1</sup>, T. Peters<sup>2</sup>, G. Casuccio<sup>2</sup> and B. Artano<sup>1</sup>

<sup>1</sup>Ciemat, Dept. Medio Ambiente, Av. Complutense 22, 28042, Madrid, Spain

<sup>2</sup>RJ Lee Group, Inc., 350 Hochberg Road, 15146, Monroeville, PA, USA

Keywords: SEM, CCSEM, PM<sub>10-2.5</sub>, mineral dust, particle shape.

High particle concentration events in the city of Madrid fall in three categories: events with high urban anthropogenic PM<sub>2.5</sub> concentrations, regional dust and African dust episodes (Artano et al., 2003). The dust episodes are characterized by high coarse PM concentrations. The African storms are associated with the highest PM<sub>10</sub> levels, causing additional exceedances of the daily EU standards. In addition, the transport of large amounts of mineral dust into the Iberian Peninsula could be contributing to soil aridity, the transport of other species such as organics, sulfates and trace metals, and the rising of asthma and allergic episodes. This work focuses on evaluating the extent of this foreign dust over Madrid and differentiating it from the native contribution.

Nine sampling periods have been studied covering seven different dust episodes. The meteorological scenarios, air mass trajectories, source location and the evolution of the PM concentration levels in local and regional scales have been investigated (table 1).

Table 1. Summary of episodes characterization (Air mass sector: A-Atlantic, AFR-Africa, MED-Mediterranean, REG-regional).

EVENT REF	SAMPLE	Date	Air mass sector	Major source contribution
ANT-1	ESEM-7	01/22/04	Stagnation	Urban local
AFR-1	ESEM-8	03/16/04	AFR-MED	Dust NW Algeria (Atlas)
	ESEM-9			
ATL-1	ESEM-10	03/23/04	A(NW)	Marine N Atlantic
REG-1	ESEM-13	07/22/04	REG	Dust Soil resusp.
AFR-2	ESEM-14	07/23/04	AFR-A(SW)-	Dust W Sahara & Mauritania
AFR-3	ESEM-15	07/28/04	A(W)	
AFR-4	ESEM-16	03/19/05	AFR-A(SW)	Dust S Algeria, Mali & Niger
	ESEM-17	03/21/05		

The sampling site was located at Ciemat, in a suburban area within the main city. More than 100,000 coarse particles (PM<sub>10-2.5</sub>) sampled with an 8-stage Anderson cascade impactor have been quantitatively analyzed by CCSEM (Computer-Controlled SEM, ASPE Personal SEM) and qualitatively characterized by a FE-SEM (Field Emission SEM, FEI Sirion400). Clustering methods based on the semi-quantitative chemical composition of 20 selected elements have allowed us to differentiate among events linked to the diverse sources. Size related morphology for each cluster has been studied too. Time distribution of the PM<sub>10</sub>,

PM<sub>2.5</sub> and PM<sub>1.0</sub> levels with a laser spectrometer (GRIMM-1107) and chemical analyses have been used to assist in the analysis of the measurements obtained by microscopy.

The concentration of aluminosilicates (clays), major components of the transported desert dust (Gatz and Prospero, 1996) with specific layered shape (Psfai and Molnar, 2002), is two times higher in the aerosol coming from Africa in comparison with the regional episode REG-1 (Figure 1).

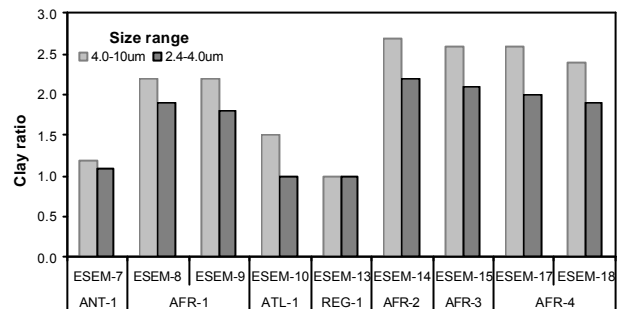


Figure 1. Relative abundance of clays for each size range, sample and event in relation to REG-1.

Cluster properties for all events have been analyzed and discussed. Significant differences within the clay group are found for each Sahara dust outbreak. These differences in clay type appear to be related to the clay composition at the source location in Africa.

Special thanks to Prof. Pandis and Prof. Robinson from Carnegie Mellon University for their help. This work was supported by the Spanish Ministry of Education and Science under Plan National program REN2003-02343.

Artano, B, P. Salvador, D. G. Alonso, ... Aerosol & A. Alastuey (2003), *Environ. Pollution*, 125, 453-465.

Gatz, D.F. & Prospero, J.M. (1996). *Atmos. Environ.*, V.30, No.22, 3789-3799.

Psfai, M. & Molnar, A. (2002) in EMU notes in Mineralogy (Vol.2): *Environmental Mineralogy*. D.J. Vaughan & R.A., Wogeliuspp., eds., 434 pages.

## The elemental analysis of size-fractionated particulate matter using TXRF - a tentative field study in Göteborg, Sweden -

Annemarie Wagner and Johan Boman

Department of Chemistry, Atmospheric Science, Göteborg University,  
SE-412 96 Göteborg, Sweden

Keywords: Cascade impactor, elemental composition, particle characterization, XRF

Size and chemical composition are considered as the most important properties of particulate matter with regard to human health and impact on climate. The aim of the present study was to investigate the elemental size distribution of aerosol particles collected in Göteborg, Sweden. A PIXE cascade impactor has been used to directly sample aerosol particles on Quartz plates at an air flow of 1 l/min. To avoid particle bounce-off, the Quartz plates were pre-treated with 2  $\mu$ l of a silicone solution. Prior to particle collection, 5  $\mu$ l of an Yttrium solution (1 ng/ $\mu$ l Y) were pipetted on the Quartz plates as an internal standard. The sampling periods chosen for this preliminary field study were 1 and 5 days, respectively. After sampling, the Quartz carriers were directly analysed by total-reflection X-ray fluorescence (TXRF). The rotating anode was operated at 45 kV and 100 mA and a livetime of 500 s was chosen for spectrum acquirement.

The spectra showed that diurnal sampling was sufficient to gain size distributions of the elements Cl, K, Ca, Fe, Ni, Cu, Zn, Br and Sr, whereas the 5-day sampling period resulted in additional information on particle size distribution for Cr and Mn. Our results classified the elements K, Ni and Zn as main contributors to the submicron peak in the total aerosol mass collected in Göteborg, suggesting a predominating influence of anthropogenic particle sources for these elements. The elements Ca, Cr and Fe contributed mainly to the supermicron range, indicating primarily natural sources, such as soil erosion, for these elements.

Bimodal distributions were found for Ni and Br with dominant peaks in the size range of 0.1 to 0.25  $\mu$ m, and for Cr with a main peak in the supermicron range, see fig. 1.

The bimodal size distributions of these elements are in agreement with the results of previous studies conducted at other sampling sites (Milford and Davidson, 1985). Further experiments are required to elucidate the range of variations in size distributions due to different particle sources in the study area.

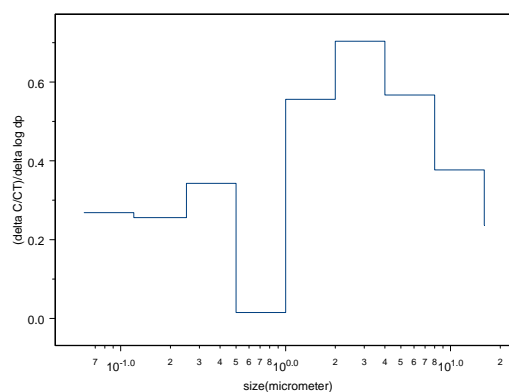


Figure 1. The size distribution for Cr in particulate matter collected in Göteborg, Sweden, under a 5 days period in January 2007.

We would like to thank Srinivas Srimantula and Satish Chandra Reddy Sareddy for their assistance in particle collection and TXRF analysis.

Milford, J.B., & Davidson, C.I. (1985).  
*Journal of the Air Pollution Control Association*, 35, No. 12, 1249-1260.

## Geochemical characterization of mineral aerosol reaching the East Antarctic Plateau

F. Marino<sup>1</sup>, S. Becagli<sup>2</sup>, E. Castellano<sup>2</sup>, O. Cerri<sup>2</sup>, F. Rugi<sup>2</sup>, R. Traversi<sup>2</sup>, S. Caporali<sup>2</sup>, S. Nava<sup>3</sup>, M. Chiari<sup>3</sup>,  
F. Lucarelli<sup>3</sup>, V. Maggi<sup>1</sup> and R. Udisti<sup>2</sup>

<sup>1</sup> Dept. of Environmental Science, University of Milano Bicocca. P.za della Scienza, 1. I-20126, Milano - Italy.

<sup>2</sup> Dept. of Chemistry, University of Florence. Via della Lastruccia, 3. I-50019, Sesto Fiorentino (FI) - Italy.

<sup>3</sup> Dept. of Physics and INFN, University of Florence. Via G Sansone, 1. I-50019, Sesto Fiorentino (FI) - Italy.

Keywords: Antarctic aerosols, chemical composition, mineral dust, source identification.

Dust recorded in ice cores stratigraphies is one of the main proxies of past climatic and environmental changes (e.g. EPICA community members, 2004). Together with dust mass and size distribution, the geochemical characterization of polar dust can reveal important aspects of the past climatic system dynamics, helping in identifying present and past dust source areas and atmospheric circulation patterns.

To date, results from ice cores mainly regarded dust deposited in glacial periods, when atmospheric concentrations were higher. For such periods, isotopic and geochemical data point to a dominant role of Southern South America as polar dust supplier, and rule out major contribution of other Southern Hemisphere possible source areas (SH-PSAs) (Delmonte *et al.*, 2004; Marino *et al.*, 2004; submitted).

Conversely, interglacial (and present day) dust characterization is far to be assessed. Due to the low amount of material deposited on the ice, available data do not depict a clear scenario, indicating a possible mix of sources for dust and a higher compositional variability.

In this context, an all-year-round collection of aerosol samples is going to be carried at Concordia Station (East Antarctic Plateau) in the framework of the Italian-French "Concordia" project.

The main difficulty to face is the extremely low aerosol atmospheric concentration that imposes to sample air at the highest rate. At this purpose, a high-volume sampler (12 m<sup>3</sup> h<sup>-1</sup>), specifically designed to work on extreme climatic conditions, was chosen. The sampler is equipped with PTFE-Fluoropore filters (diameter 142 mm; pores size 1 µm); filters features were selected in order to maximize the sampling volume, considering that the size of the Dome C mineral aerosol not exceed few µm.

Based on previous estimates of aerosol load at Dome C (Udisti *et al.*, 2004), we expect to collect on the filter about 100 µg of material, with a 30-days sampling, allowing us to collect 12 samples per year and to investigate possible changes in load and composition in different seasons. The first set of 12 filters, collected during the 2006 campaign, is currently (February 2007) en route to Europe.

Mineral particles collected on PTFE filters will be firstly extracted by sonification in water, then filtered on 0.45 µm polycarbonate filters (13 mm diameter) or digested in acids in order to have suitable samples for the chemical analyses. The quantitative particles recovery is not requested, since the main goal is the geochemical characterization of dust.

A filter quarter will be dedicated to PIXE measurements of major elements (Si, Al, Fe, Ca, Mg, Na, K and Ti,) to provide an overall geochemical imprint, helping in the identification of the different possible sources through comparison with SH-PSAs samples collected in different areas and analyzed after size selection (Marino *et al.*, 2004 and submitted).

A second filter quarter will be used for particles characterization by SEM-EDAX. Together with geochemical characterization of single particles, this technique will be used to produce images of significant areas of filters, for a particles size characterization.

The third part of the filter will be used for Rare Earth Elements (REEs) measurements by HR-ICP-MS. REEs dust composition also provides a powerful fingerprint of dust provenance and parent materials (e.g. Gaiero *et al.*, 2004).

Finally, the last fraction will be stored as archive or used for further possible characterizations.

Delmonte, B., Basile-Doelsch, I., Petit, J.-R., Maggi, V., Revel-Rolland, M., Michard, A., Jagoutz, E., & Grousset, F. (2004). *Earth-Sci. Rev.*, 66, 63-87.

EPICA community members (2004). *Nature*, 429, 623-628.

Gaiero, D.M., Depetris, P.J., Probst, J.-L., Bidart, S.M., & Leleyter, L. (2004). *Earth Planet. Sci. Lett.*, 219, 357-376.

Marino, F., Maggi, V., Delmonte, B., Ghermandi, G., & Petit, J.R. (2004). *Ann. Glac.*, 39, 110-118.

Marino, F., Castellano, E., Ceccato, D., Delmonte, B., De Deckker, P., Revel-Rolland, M., Ghermandi, G., Maggi, V., Udisti, R., & Petit, J.R.. submitted to *Earth Planet. Sci. Lett.*

Udisti, R., Becagli, S., Benassai, S., Castellano, E., Fattori, I., Innocenti, M., Migliori, A., & Traversi, R. (2004). *Ann. Glac.*, 39, 53.61.

## Single-particle characterization of aerosol samples collected over the Yellow Sea

Y. Park, H. Hwang, M.S.I. Khan, S. Kang, H. Kim and C.-U. Ro

Department of Chemistry, Inha University, YonghyunDong, NamGu, 402-751, Incheon, Korea

Keywords: Low-Z particle EPMA, single particle analysis, Yellow Sea, Asian Dust

The Yellow Sea surrounded by China and Korea has abundant anthropogenic pollution sources around it, in addition to marine source itself. Six sets of aerosol samples (samples S1-S6) were collected on the deck of a commercial ferryboat that plied between Incheon, Korea and Tianjin, China, in order to characterize marine aerosol particles over the Yellow Sea (see Figure 1). As shown in Figure 1, three samples were collected at Kyonggi-man (sample S1), Bo Hai Sea (sample S2), and in the sea near Tianjin (sample S3) when the ferryboat sailed from Incheon to Tianjin on 28-29 April, 2006. The other three samples (samples S4-S6) were collected when the ship returned from Tianjin back to Incheon on 30 April and 1 May, 2006. Samples S4-S6 happened to be collected when an Asian Dust storm event occurred in the sampling region. Particles were sampled on Ag foil using a three-stage cascade impactor (PM10 sampler, Dekati Ltd.). Three stages of the cascade impactor have aerodynamic cutoffs of 10, 2.5 and 1  $\mu\text{m}$ .

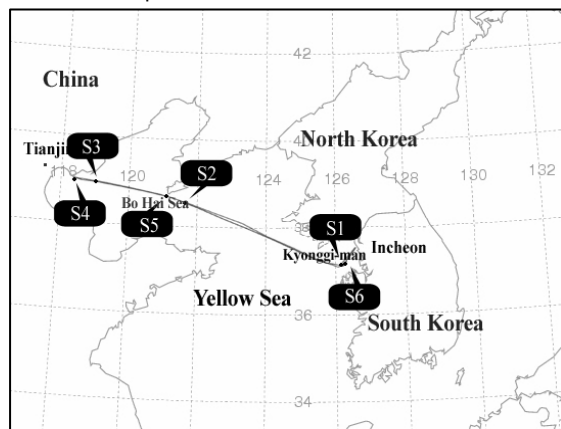


Figure 1. Ferryboat route and sampling places

For the characterization of the collected aerosol samples, a recently developed single particle analytical technique, named low-Z particle EPMA, was applied. The low-Z particle EPMA utilizes a SEM/EDX instrument equipped with an ultra-thin window and the technique can perform the quantitative determination of concentrations of even low-Z elements such as C, N, and O in individual particles of micrometer size.

As shown in Figure 2, sample S1 collected near the Korean peninsula contains ~25 % of reacted sea-salts such as  $\text{NaNO}_3$ ,  $\text{Na}_2\text{SO}_4$  and their mixture. For sample S2 which is collected at Bo Hai Sea, soil-derived particles such as aluminosilicates and  $\text{SiO}_2$

are major chemical species in coarse fraction ( $d_p = 2.5\text{-}10 \mu\text{m}$ ), and reacted sea-salts and reacted  $\text{CaCO}_3$  are abundant in fine fraction ( $d_p = 1.0\text{-}2.5 \mu\text{m}$ ). Soil-derived particles are mostly observed in coarse and fine fractions for sample S3. These results imply that sample S1 was somewhat marine influenced, sample S2 was influenced both by Yellow Sea and continental China, and sample S3 was mostly influenced by continental China.

Samples S4-S6 collected during an Asian Dust storm event have somewhat different characters from the samples S1-S3 that were collected when Asian Dust storm event did not happen. For samples S4-S6, it was observed soil-derived particles are major chemical species in coarse fraction whereas in fine fraction most abundantly encountered particles are reacted sea-salts. The characteristics of chemical compositions observed for samples S1-S6 can be related positively to results of backward trajectory analysis using the HYSPLIT model.

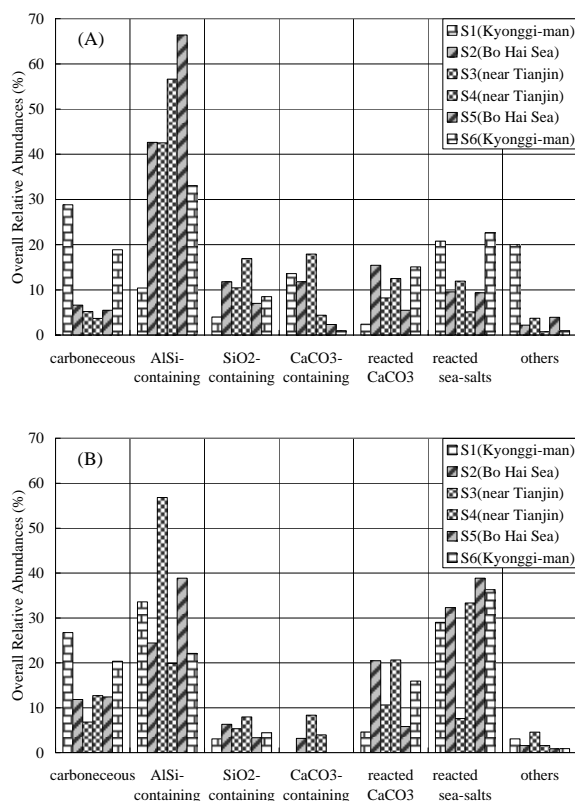


Figure 2. Overall relative abundances of particle types significantly encountered (A) in coarse fraction and (B) in fine fraction.

## **Atmospheric aerosol characterization in Tuscany (PATOS project): ionic composition and “soluble” fraction of selected metals**

S. Becagli<sup>1</sup>, E. Castellano<sup>1</sup>, O. Cerri<sup>1</sup>, L. Lepri<sup>1</sup>, F. Lucarelli<sup>2</sup>, F. Marino<sup>3</sup>,  
A. Morganti<sup>1</sup>, F. Rugi<sup>1</sup>, M. Severi<sup>1</sup>, R. Traversi<sup>1</sup>, and R. Udisti<sup>1</sup>

<sup>1</sup>Dept. of Chemistry, University of Florence. I-50019, Sesto F.no (FI) – Italy

<sup>2</sup>Dept. of Physics, University of Florence and INFN. I-50019, Sesto F.no (FI) – Italy

<sup>3</sup>Environmental Science, University of Milano Bicocca. I-20126, Milano - Italy.

Keywords: chemical composition, aerosol size distribution, anthropogenic aerosol, source identification, ions

In the framework of the PATOS project, one-year sampling campaign was carried out in seven sites in Tuscany (Central Italy), chosen as representative of different anthropic impact. The main goal was the characterization of atmospheric particulate (mainly PM<sub>10</sub>, with some spots of PM<sub>2.5</sub>) at regional scale in order to: 1. identify and, possibly, quantify primary and secondary sources, distinguishing between anthropic and natural contributions; 2. study temporal trends and possible seasonal patterns of source chemical markers; 3. understand emissive and meteorological conditions controlling high atmospheric concentration of natural and anthropic particulate (such as abrupt increase of human inputs, formation of temperature inversion layers, long-range transport – Saharan dust or sea spray events); 4. evaluate the natural and anthropic background level at regional scale in order to quantify local contributions. The achievement of these targets will allow to give to policymakers the knowledge and tools for a significant reduction of anthropic emissions.

Here, we focus on aerosol chemical characterization for ionic species and “soluble” fraction of metals, able to give information on primary (mainly from sea spray and continental dust) and secondary (mainly from human activity) sources. Analysis was carried out on Teflon filters collected with EN 12341 impactors (24 h, 2.3 m<sup>3</sup>/h) located in seven sites of Tuscany: Florence (urban background), Prato (urban traffic), Capannori-Lucca (urban background), Arezzo (urban traffic), Grosseto (urban background), Livorno (suburban background), Montale-Pistoia (rural background). Samplings were carried out from Sept. 2005 to Sept. 2006. Rotating three sampling devices, alternatively two sets of three stations were contemporaneously sampled for 15-day periods. Shorter PM<sub>10</sub> samplings were carried out in the Montale-Pistoia site. In Florence, PM<sub>2.5</sub> was also sampled, together with PM<sub>10</sub>, but for shorter time.

Teflon filters, after weighing, were cut in three parts under class-100 laminar flow hood. A quarter was devoted to Ion Chromatographic (IC) analysis, a quarter for HR-ICP-MS and the remaining half was devoted to PIXE measurements. The filter quarters were extracted in about 10 ml of ultra-pure water (IC) or of ultra-pure HNO<sub>3</sub> solution at pH = 1.5 (ICP-MS) by 20-min sonication. By IC, cations, inorganic

anions and some organic compounds (MSA and short-chain carboxylic acids) were determined. A set of 13 metals (Al, Fe, Mn, Cu, Zn, Cr, Ni, V, Mo, Pb, Cd, As, Hg) was analysed by HR-ICP-MS in the acidic solution.

We used as source markers: Na, chloride and Mg for sea spray; Ca and Al for continental dust; sulphate, ammonium and nitrate (together with minor components such as carboxylic acids) for secondary aerosol; MSA for marine biogenic activity; formate, glycolate and K for biomass burning processes. These associations were also confirmed by PCA analysis, unless different sources, atmospheric reactivity or transport lead to different distributions. For instance, nitrate is included in secondary aerosol but has different sources and atmospheric oxidation pathways with respect to sulphate. Indeed, spot-measurements of size-segregated aerosol showed that nitrate is distributed on size-classes larger than particles containing sulphate and ammonium. PCA analysis allowed to distinguish metals mainly coming from crustal source (Al, Mn and, partially, Fe) from those originated by human activity (especially Ni, Pb, Cd, As, Hg). The last ones show a soluble fraction, with respect the total metal content determined by PIXE, definitely higher than metals mainly originated by natural sources.

Results obtained for single stations were disaggregated by season, compared one to each other and with meteorological data in order to enlighten seasonal pattern at regional scale and focus particular emission features in the different station typologies. Sea spray components play a non-marginal role only in the marine stations (Grosseto and Livorno), especially in spring and fall, while their contribution is quite negligible in the internal sites. The contribution of secondary aerosol represented by sulphate and ammonium is homogeneously widespread with low seasonal pattern. On the contrary, nitrate shows maximum values in winter in all sites, revealing a relevant role of domestic heating systems in secondary aerosol production. Winter maxima were also observed for K, glycolate and formate, confirming heating by biomass burning is not a negligible input to atmospheric particulate.

This work was supported by the Regional Government of Tuscany, Italy.

## Sampling strategies and first results on chemical composition of size-segregated aerosol fractions at Dome C (Central East-Antarctica) during the 2006 winter-over campaign.

O. Cerri<sup>1</sup>, S. Becagli<sup>1</sup>, E. Castellano<sup>1</sup>, M. Chiari<sup>2</sup>, F. Lucarelli<sup>2</sup>, F. Marino<sup>3</sup>,  
A. Morganti<sup>1</sup>, S. Nava<sup>2</sup>, F. Rugi<sup>1</sup>, M. Severi<sup>1</sup>, R. Traversi<sup>1</sup>, and R. Udisti<sup>1</sup>

<sup>1</sup>Dept. of Chemistry, University of Florence. Via della Lastruccia, 3. I-50019, Sesto F.no (FI) – Italy

<sup>2</sup>Dept. of Physics, University of Florence and INFN. Via Sansone, 1. I-50019, Sesto F.no (FI) – Italy

<sup>3</sup>Environmental Science, University of Milano Bicocca. P.za della Scienza, 1. I-20126, Milano - Italy.

Keywords: Antarctic aerosol, ions, long-range transport, cascade impactor, sources identification.

During the second all-year-round campaign (November 2005 - November 2006) at Dome C (DC - Central East Antarctica, 3233 m a.s.l., about 1100 km far from the coast-line), size-segregated aerosol samples were collected at Concordia Station (75° 06' S, 123° 23' E) by using different low- or medium-volume devices: 1. pre-selected cutoff collectors with PM10, PM2.5 and PM1 heads (contemporaneous and alternate samplings); 2. a 4-stage (>10, 10-2.5, 2.5-1, <1 µm fractions), small-surface sequential impactor (Dekati PM-10 Impactor); 3. a 8-stage (10-0.4 µm) sampler (Andersen 20-800 Impactor); 4. a medium-volume (12 m<sup>3</sup>/h) PM10 collector (a modified version of Tecora Echo Puf) for long-time sampling. Sampling resolution ranged from one day to one month, and air-volume spanned from 2.3 to 12 m<sup>3</sup>/h. During the aerosol collection, continuous measurements of size distribution of the aerosol particles were carried out by using a laser-scattering Optical Particle Counter (OPC) device. OPC was able to classify aerosol particles in 32 size-classes in the range 16 - 0.3 µm with a 5-min resolution.

Aerosol measurements and samplings were carried out about 1 km upwind (with respect the dominant wind direction, mainly from southern sectors) to building and people activity, in order to minimise contamination by anthropic emissions (especially electrical power plants).

Although sampling activity was carried out all-year-round, severe weather conditions (especially air temperatures as low as -80 °C in winter) limited the continuous aerosol collecting, damaging pumps and electronic devices. Anyway, a large number of samples, covering all the time period, was collected and used to describe seasonal pattern and temporal trend of load and chemical composition of aerosol at DC.

Finally, fresh snow (when occurring), superficial snow and hoar (when occurring) samples were collected both in summer and winter to study atmosphere-snow interaction. In particular, superficial snow and hoar (when occurring) were collected two times per day (minimum and maximum solar irradiance), in order to understand the sublimation/condensation effects on snow chemical composition at DC. A reliable knowledge of the present sources, atmospheric transport and

depositional and post-depositional processes affecting snow and aerosol composition in high-altitude Antarctic plateau sites is propaedeutic for a correct interpretation of changes of paleo-atmosphere composition as a response to climate forcings.

The main goals of the scientific activity at DC were: 1. to describe all-year-round temporal profiles of chemical compounds usable as markers of source intensity or transport processes; 2. to identify seasonal pattern of chemical markers of biogenic productivity (sulphate, MSA), sea spray formation (Na, chloride, Mg), atmospheric processes (nitrate, carboxylic acids), continental dust inputs (Ca); 3. to enlighten particular events of aerosol production and/or long-range transport, such as phytoplanktonic bloom, abrupt advection of marine air masses in full winter, sea-ice formation, etc.; 4. to verify or discharge the hypothesis of a significant contribution of frost flower formation on pack ice in controlling atmospheric concentration sea-salt compounds in plateau sites (so correlating Na snow concentration to sea-ice extent); 5. to identify present Potential Source Areas (PSAs) of continental dust by geo-chemical and mineralogical analysis (PIXE, SEM-EDAX, ICP-MS) of insoluble dust monthly collected by the medium-volume sampler; 6. to study interchange processes between atmosphere and snow.

Here we report the first results obtained from the chemical analysis of filters collected with PM10, PM2.5 and PM1 samplers and multi-stage impactors.

This work was supported by the Italian National Programme for Antarctic Research (PNRA) and was developed in the framework of the EPICA and Station Concordia projects.

Fattori, I., Becagli, S., Bellandi, S., Innocenti, M., Mannini, A., Severi, M., Vitale, V., & Udisti, R. (2005). *J. Environ. Monit.*, 7, 1265-1274.

Udisti, R., Becagli, S., Benassai, S., Castellano, E., Fattori, I., Innocenti, M., Migliori, A., & Traversi, R., (2004). *Ann. Glaciol.*, 39, 53-61.

## Annual semicontinuous monitoring of surface PAH(s) in the Venice mainland

A. Latella and A. Benassi

ARPAV (Veneto Region EPA) – Regional Air Observatory – Via Lissa, 6 – 30171 Mestre (Venice)- Italy

Keywords: SPAH(s), PAS, submicron particles, urban area

Atmospheric monitoring of Surface Polycyclic Aromatic Hydrocarbons (SPAH(s)) can be achieved with a Photoelectric Aerosol Sensor (PAS). The PAS response is selective for aerosol particles with diameter in the 0.01-1  $\mu\text{m}$  range if organic compounds like PAH are present on the surface (properly SPAH according to Marr), the gas phase organic compounds being not detected. Despite of the hybrid physicochemical and structure-selective detection (Siegmann, Matter), if a PAS signal is recorded fine aerosol particles must be present and the provided information is given as total SPAH concentration in  $\text{ng}/\text{m}^3$  on  $\text{PM}_{<1}$ , (referred to the manufacturer's calibration). Correlation between the PAS signal and the concentration of individual PAH extracted from dust filters (low or high volume sampling) has been reported at urban sites where the traffic source is the main contributor (Agnesod, Chetwittayachan).

Results of urban air monitoring in Mestre (Venice mainland) for the SPAH(s) are presented on a 5 minutes time base (i.e. 288 data/day). Approximately 250000 measurements were recorded from winter 2003 to winter 2006 with a data availability of 62%, 66% and 94% for the years 2004, 2005 and 2006 respectively.

The monitoring site faces, in open path, the main ring road (500m distance) at the same height (10m) from ground level. This 6-lane elevated road (8 km long, toll-free) connects NW to NE Italy, W to SE Europe and Austria. Also used to bypass the urban road network it usually features a 60000 vehicles/day flux with peak values of 90000.

Parallel synchronous measurements with two extra PAS were also performed at the QCL (November 2003 – April 2004) and at different sites (traffic, industrial, suburban) for several months through the entire monitored period. A discussion is presented on a seasonal basis and daily trend of the SPAH concentration. For 12 days the correlation of the outdoor (Mestre) vs indoor (Venice historical centre, 9 Km distance) daily trend of SPAH has been recorded (Figure 1). The fast response rate of the PAS (down to 8s) allow to monitor transient pollution episodes missed by the time averaged PAH values obtained from particulate sampling. These events were typically recorded during the winter season (shallow inversion layer) leading exceptionally to an average daily concentration greater than 500  $\text{ng}/\text{m}^3$ .

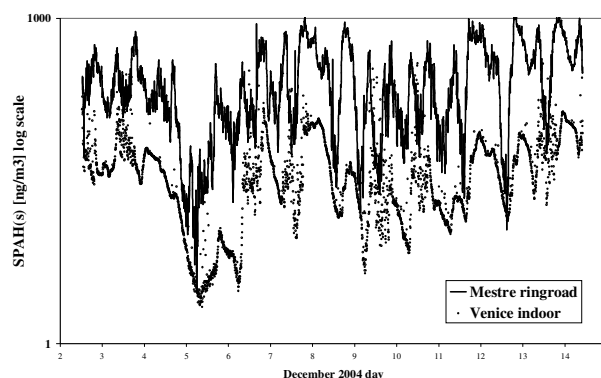


Figure 1. Outdoor (Mestre, upper trace) and indoor (Venice centre, lower dots) SPAH(s) concentration during the first half of December 2004. Log scale.

### References

- Agnesod 1996, G. Agnesod, R. De Maria, M. Fontana and M. Zublena, "Determination of PAH in airborne particulate: comparison between off-line sampling techniques and an automatic analyser based on a photoelectric aerosol sensor", *The Science of the Total Environment*, 189/190, 443-449, 1996
- Chetwittayachan 2002, T. Chetwittayachan, D. Shimazaki, K. Yamamoto: "A comparison of temporal variation of particle-bound polycyclic aromatic hydrocarbons (pPAHs) concentration in different urban environments: Tokyo, Japan, and Bangkok, Thailand, *Atmospheric Environment* 36 (2002) 2027-2037
- Marr 2005, Marr, L. C., Dzepina, K., Jimenez, J. L., Reisen, F., Bethel, H. L., Arey, J., Ganey, J. S., Marley, N. A., Molina, L. T., and Molina, M. J., 2005, *Atmos. Chem. Phys. Discuss.*, 5, 12741-12773
- Matter 1999, Matter, U. and Siegmann, H. C. "Dynamic Field Measurements of Submicron Particles from Diesel Engines", *Environ Sci. Technol.* 33 (1999), 1946-1952
- Siegmann K. 1999, K. Siegmann, L. Scherrer, H.C. Siegmann "Physical and chemical properties of airborne nanoscale particles and how to measure the impact on human health", *Journal of Molecular Structure (Theochem)* 458 (1999) 191-201

## Alkali metal content of individual particles in Mexico City during the MILAGRO campaign in 2006

Torbjörn L. Gustafsson, Jun Noda and Jan B. C. Pettersson  
Department of Chemistry, Atmospheric Science, Göteborg University, S-412 96 Göteborg, Sweden

Keywords: Real-time detection, AMS, alkali metal, MILAGRO, Mexico City

As the population of the world grows, urban areas expand rapidly and the number of very large metropolitan areas increases. The MILAGRO (Megacity Initiative: Local and Global Research Observations) field measurement campaign was conducted in Mexico City in March 2006. Aims of the campaign were to characterize the air quality in this densely populated area and the influence of the city on regional and global climate. The Mexico City Metropolitan Area (MCMA) is the second largest megacity in the world, with a population of more than 18 million people and it covers an area of 1,500 km<sup>2</sup>. MCMA has severe air pollution problems, which are influenced by several factors including the basin-like topography of the city, high altitude, meteorology, urban expansion, and demographic and industrial growth. The emissions of pollutants in MCMA routinely exceed the standards recommended by the World Health Organization. As a result air pollution has serious health consequences and large economic costs to society.

Traffic is known to be a major polluter in the MCMA, while the contributions from other sources including combustion of solid fuels are less well characterized. In the present study an aerosol mass spectrometer (AMS) was deployed to quantify the alkali metal content of the single particles. The AMS is based on orthogonal acceleration time-of-flight mass spectrometry combined with surface ionization (Svane et al. 2004; 2005) and it provides quantitative measurements of the alkali content of individual particles in the size range 20-1000 nm. Measured ratios of Na and K contents make it possible to distinguish particles emitted from biomass and waste burning from other sources.

The AMS was used together with a scanning mobility particle sizer (SMPS) to provide size information of the aerosol. The aerosol entered into the SMPS system, which was set to scan from 8 to 320 nm under 6 min periods. The monodisperse aerosol flow from the DMA unit of the SMPS was split and let into a CPC and the AMS. The aerodynamic lens system of the AMS produces a narrow particle beam that is directed towards a restively heated (1500 K) platinum surface in the vacuum system. Particles that impact on the hot surface decompose and the alkali content of the particles is efficiently ionised at the hot surface by

surface ionisation (Svane et al 2004). Alkali metals have unusually low ionisation potentials and the ionisation probability may approach 100%. The ions are accelerated into a time-of-flight unit and ions with different mass to charge ratio ( $m/z$ ) reaches the ion detector separated in time. Ions are detected with a multi channel plate (MCP) and the outgoing pulses from the MCP are amplified and counted by a computer-controlled Fastflight-2 Digital Signal Avarager. 1000 consecutive scans were added to a mass spectrum with a 13.5 ms long data collection period, and mass spectra were continuously stored to computer for further analysis.

The concentrations of alkali-containing particles were measured during the MILAGRO field campaign in Mexico City from March 7 to March 31, 2006. The measurements were performed on a roof-top site at the Instituto de Petroleo near the center of Mexico City. The concentrations of sodium- and potassium-rich particles were generally observed to be low compared to the total particle number concentrations of sub-micrometer particles. Measured Na:K ratios in individual particles indicated that biomass and waste burning, as well as sodium-rich mineral particles, make significant contributions to the aerosol in the MCMA. Typical AMS results will be presented and related to meteorological conditions in the Mexico City area and to other gas and particle measurements carried out during the field campaign.

### References

- Svane, M., Hagström, M., and Pettersson, J. B. C. (2004). Chemical Analysis of Individual Alkali-Containing Aerosol Particles: Design and Performance of a Surface Ionization Particle Beam Mass Spectrometer. *Aerosol Sci. Technol.* 38:655-663.
- Svane, M., Janhäll, S., Hagström, M., Hallquist, M., and Pettersson, J. B. C. (2005). On-line Alkali Analysis of Individual Aerosol Particles in Urban Air. *Atmospheric Environment.* 39:6919-6930.

## Characterization of compositions and size distributions of dicarboxylic acids in background and suburban aerosols

Y.I. Tsai<sup>1</sup>, T.-H. Weng<sup>1</sup>, S.-C. Kuo<sup>1</sup> and L.-Y. Hsieh<sup>2</sup>

<sup>1</sup>Department of Environmental Engineering and Science, Chia Nan University of Pharmacy and Science  
60, Sec. 1, Erh-Jen Rd., Jen-Te, Tainan 717, Taiwan, ROC

<sup>2</sup>Department of Chemistry, National Cheng Kung University, 1, Ta-Hsueh Rd., Tainan 701, Taiwan, ROC

Tel: +886-6-2660208; Fax: +886-6-2669090; Email: mtsaiyi@mail.chna.edu.tw

Keywords: particle size distribution, nanoparticles, organic compound, dicarboxylic acids

### 1. Introduction

Dicarboxylic acids in atmospheric aerosol have received much recent attention because of their potential role in affecting the global climate. Dicarboxylic acids in fact have even stronger cloud condensate capabilities than non-sea-salt sulfate (Cruz and Pandis, 1998; Abbatt *et al.*, 2005, Sun and Ariya, 2006). Due to their strong hydrophilic and hygroscopic properties, dicarboxylic acids are able to reduce surface tension and affect the formation of cloud condensates, and consequently affect the global radiation balance (Cruz and Pandis, 1998). Oxalic acid, succinic acid, and malonic acid are prominent in the research quoted above.

In this research, variations of characteristic composition as well as size distributions of the atmospheric inorganic salts and low-molecular-weight dicarboxylic acids (low- $M_w$  DCAs) in aerosol for the background Ali Mountain and Tainan suburban regions, Taiwan during June and December 2005.

### 2. Experimental

A Micro-Orifice Uniform Deposit Impactor (MOUDI, MOUDI-110, MSP) consisting of ten stages was used to collect particulate in the size fractions. Connecting the MOUDI, the NanoMOUDI (MSP) consisting of three stages was used to collect nanoparticles of 32nm, 18nm and 10nm. The dicarboxylic acid concentrations of aerosol were determined by ion chromatography (IC, Dionex).

### 3. Results and discussion

Oxalic acid is the most abundant low- $M_w$  DCAs in the Ali Mountain region followed by succinic acid and malonic acid. These low- $M_w$  DCAs are highly correlated with  $\text{NH}_4^+$  demonstrating that the aerosol low- $M_w$  DCAs in Ali Mountain are the photochemical products from natural emissions. In Tainan suburban region during high pollution period, concentrations of the daytime and nighttime low- $M_w$  DCAs are obviously higher. Similarly, oxalic acid during summer is the most abundant followed by succinic acid and maleic acid. Additionally, daytime concentrations of the six observed low- $M_w$  DCAs are 2 to 3 times higher than those during summer while during agricultural waste burning period, the diurnal variation tendency is quite similar to that during high pollution period. The concentration matrix reveals

that the correlation coefficients are 0.72 between oxalic acid and  $\text{NH}_4^+$  and 0.69 between oxalic acid and  $\text{K}^+$ . Since during the agricultural burning period, these three chemical species are more correlated than other seasons and periods indicating that the sol from agricultural waste burning contains a large quantity of oxalic acid.

As the atmospheric particle size distribution is concerned, the Ali Mountain background inorganic salts show droplet mode (concentration peaks between 0.46-2.4  $\mu\text{m}$ ), coarse mode (concentration peaks between 5.7-11.3  $\mu\text{m}$ ) and nuclei mode (concentration peaks between 4-90 nm). The low- $M_w$  DCAs are principally droplet mode with concentration peaks in 0.46-2.4  $\mu\text{m}$ ; the 4 nm peaks shows the beginning formation of low- $M_w$  DCA primary particles. For Tainan suburban region, the particle size distributions for both aerosol inorganic salts and low- $M_w$  DCAs change from single peak or double peaks in summer to triple or multiple peaks in autumn. During the high pollution period, the maximum concentration peaks for low- $M_w$  DCAs dominant in the condensation mode of 0.19-0.32  $\mu\text{m}$ . This reveals that particle coagulation and photochemical products contribute to the observed aerosols during the high pollution period. Additionally, the aerosol succinic ( $C_4$ ) and malonic acids ( $C_3$ ) have different maximum concentration peaks from oxalic acid ( $C_2$ ). During the autumn non-serious pollution period and high pollution period, the maximum concentration peak for oxalic acid shifts toward the nanometer range indicating that the autumn sol oxalic acid is an end photochemical product from  $C_4$  and  $C_3$  low- $M_w$  DCAs.

### Acknowledgements

This work was supported by the National Science Council of Taiwan ROC, through grant nos. NSC 94-2211-E-041-010 and NSC 95-2211-E-041-004.

### References

- Abbatt, J.P.D., Broekhuizen, K., & Pradeep Kumar, P. (2005). *Atmospheric Environment*, 39, 4767-4778.
- Cruz, C.N., & Pandis, S.N. (1998). *J. Geophysical Research*, 103, 13111-13123.
- Sun, J., & Ariya, P.A. (2006). *Atmospheric Environment*, 40, 795-820.

## Long term measurements of inorganic, organic and radionuclides at the puy de Dôme, 1465 m a.s.l.

L. Bourcier<sup>1</sup>, K. Sellegri<sup>1</sup>, O. Masson<sup>2</sup>, J.-M. Pichon<sup>1</sup>, P. Chausse<sup>1</sup>, P. Paulat<sup>2</sup> and P. Laj<sup>1</sup>

<sup>1</sup>Laboratoire de Météorologie Physique, Université Blaise Pascal / CNRS,  
24 avenue des Landais, 63 177 Aubière cedex, France

<sup>2</sup>Institut de Radioprotection et de Sûreté Nucléaire, BP 3, 13 115 Saint Paul lez Durance, France

Keywords: aerosol measurement, chemical composition, radioactive particles, long-range transport.

Meteorological parameters, chemical composition including inorganic and organic fractions and activity levels of  $\gamma$  emitters in aerosol are monitored throughout the year at the experimental site of the puy de Dôme (45° 46' 20'' N, 2° 57' 57'' E, 1465 m a.s.l.). The sampling period is about 3-4 days. The organic and inorganic compounds are sampled with total filters and a flow rate of 40 and 30 lpm (respectively). The radionuclides are collected with a high volume sampler (650 Nm<sup>3</sup>.h<sup>-1</sup>).

Levels of radionuclides are also determined at Opme, a rural site (660 m a.s.l.) next to the puy de Dôme. The comparison between these two sites (see figure 1) show similar variations with different range. For radionuclides, cesium-137 activity levels are larger at the high altitude site of the puy de Dôme than at the low altitude site of Opme. Consequently, we believe that the difference in concentrations between the two sites is due to long range transport reaching the puy de Dôme.

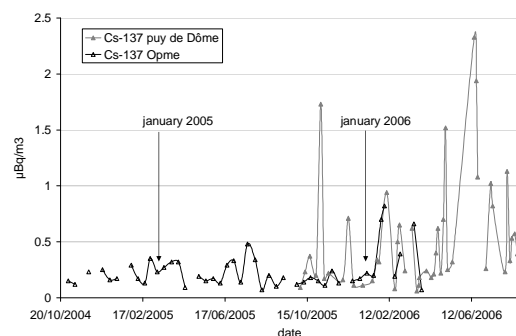


Figure 1. Level of <sup>137</sup>Cs at Opme and the puy de Dôme

The monitoring of <sup>137</sup>Cs at the puy de Dôme has shown a mean activity of 0.52 µBq.m<sup>-3</sup>, which is in the same order than in 1997 in the boundary layer. The activity of cesium should decrease on account of its emission due to resuspension from the soil and/or from biomass combustion. Hence such a high value at a high altitude site is rather unexpected.

On another hand, PTFE and quartz fibre filters have been analyzed since 2003 for the aerosol inorganic and organic content. We can observe seasonal variations for sulphate, oxalate, ammonium and organic carbon. The other

components do not present specific variations. Such variations have already been observed at the Sonnblick (Kasper, 1997). The mean concentrations are about 0.27 µg.m<sup>-3</sup> for the nitrate, 2.3 µg.m<sup>-3</sup> for the sulphate and 0.75 µg.m<sup>-3</sup> for the ammonium.

The comparison between the inorganic concentration and the level of activity of different radionuclide (shown in table 1) give us interesting information on the porter phase of <sup>137</sup>Cs, which is not well known.

Table 1. correlations between different components of the aerosol at the puy de Dôme

	Cs-137	Pb-210	Ca2+	NH4+ NO3- SO42-	Fe III	K biomasse
Cs-137	1					
Pb-210	0.8428	1				
Ca2+	0.4868	0.0027	1			
NH4+ NO3- SO42-	0.3427	0.6171	0.475	1		
Fe III	0.3985	0.3524	-0.1118	0.2626	1	
K biomasse	0.8311	0.7244	-0.008	0.3182	0.2387	1

The good correlation between the cesium and the potassium expresses a similar behaviour due to a similar origin that could originate from similar electronic configuration and subsequent similar absorption in plants. A co-emission of cesium-137 and potassium during biomass burning was already hypothesised by Wotawa et al. (2006).

The observation of chemical behaviour at puy de Dôme is in agreement with works on other sites concerning the inorganic and organic fractions. Concerning the <sup>137</sup>Cs, it is one of the first time that such low activity levels are usually measured in high altitude site. The comparison between these characteristics brings information concerning the actual source of <sup>137</sup>Cs and its transport from different origin air masses.

This work was supported by ADEME, IRSN.

Wotawa G. L.-E. De Geer, A. Becker, R. D'Amours, M. Jean, R. Servranckx and K. Ungar (2006). Inter- and intra-continental transport of radioactive cesium released by boreal forest fires, *Geophysical Research Letters*, 33, L12806, doi : 10.1029/2006GL026206.

Kasper A. and H. Puxbaum (1997). Seasonal variation of SO<sub>2</sub>, NHO<sub>3</sub>, NH<sub>3</sub> and selected aerosol components at Sonnblick (3106 m a.s.l.), *Atmos. Environ.*, 32, 3925-3939.

## **Chemical and Size Characteristics of Particles in the Lower Fraser Valley, British Columbia, Canada.**

Kurt Anlauf<sup>1</sup> and Shao-Meng Li<sup>1</sup>

<sup>1</sup> Environment Canada, 4905 Dufferin Street, Toronto, Canada M3H 5T4

Keywords: aerosol size distribution, chemical composition, aerosol characterization, field measurements.

During November/December 2004 and March/April 2005, extensive particle measurements were made by means of an impactor device (MOUDI) at Abbotsford in the Lower Fraser Valley of British Columbia, Canada (a rural site surrounded by relatively flat terrain and about 35 km inland from the Pacific Ocean the site was subject to coastal breezes frequently). This paper will present details on the particle size distributions and their chemical ionic characteristics.

Briefly, the size distributions exhibited a fine particle maximum in the size range 0.3-0.55  $\mu\text{m}$ , and another maximum of coarser particles at 3.1-6.2  $\mu\text{m}$ . This latter coarse mode was dominated by sodium, indicative of marine origin, but was depleted slightly of chloride (1-6.2  $\mu\text{m}$ ) and correspondingly augmented in nitrate, indicating nitric acid reaction on sea salt particles. The fine mode was characterized by  $\text{SO}_4$  and  $\text{NO}_3^-$ , ionically balanced by  $\text{NH}_4^+$ . There was some indication of nighttime formation of nitrate particles in the fine mode. These results contrast with an earlier 2001 mid-summer study (Anlauf et al., 2006) which showed more extensive coarse mode chloride depletion and a secondary fine mode particle maximum at 0.1-0.17  $\mu\text{m}$ .

Anlauf, K., Li, S-M., Leitch, R., Brook, J., Hayden, K., Toom-Sauntry, D., & Wiebe, A. (2006). Atmos. Environ. 40, 2662-2675.

## **T26 Abstracts**

## the role of road transport and industrial emission sources in daily distribution of concentrations in Wrocław air

J. Wozdzia<sup>1</sup>, A. Wozdzia<sup>1</sup>, I. Sowka<sup>1</sup>, A. Gzella<sup>1</sup> and A. Schady<sup>2</sup>

<sup>1</sup> Ecological and Atmosphere Protection Division, Institute of Environment Protection Engineering, Wrocław University of Technology, Wyb. Wyspińskiego 27, 50-370, Wrocław, Poland

<sup>2</sup> Institut für Physik der Atmosphäre, DLR-Oberpfaffenhofen, D-82234 Weßling, Germany

Keywords: urban areas, organic compounds, modelling.

The study of apportionment of BT to various sources and its implicated control strategies is usually conducted using the chemical mass balance (CMB) receptor model, provided that their major sources have been clearly characterized (McAreen et al., 1996; Watson et al., 2001). For species commonly found in Wrocław, such as BT, their relative abundances in some cases were significantly different from the vehicular emissions, confirming the existence of non-vehicular emissions. In principle, the contribution of non-vehicular and vehicular sources can be determined even for area without complete source profiles if there exists time series of BT concentrations which can exclusively serve as an indicator of vehicular emissions and a basis for identifying non-vehicular episodes.

Our approach to the data has been work with the basic hourly data of benzene, toluene and xylenes (m,p- and o-xylene) and other gaseous-phase pollutants (ozone, NO<sub>x</sub>, CO) measured over Wrocław area during September 2006 to distinguished from the general body of data events which characterize the impact of different emission sources (e.g. for two identified episodes in September, 18/19 and September, 8). BT concentrations showed diurnal variations with high concentrations in the morning and evening, and low concentrations during the daytime (Figure 1). The concentration rankings of the compounds closely associated with solvent usage such as toluene, m-/p-xylene, and o-xylene in the evening or night were higher than to those in the morning. The subset of BT data in the morning period is composed of primary pollutants, and their concentrations probably most closely reflect local traffic emissions.

To identify the contribution of the probable sources of VOC emission, mass balance analysis was performed for four cases: (1) gasoline exhaust emissions - solvent usage derived emissions and the monthly mean (September), (2) traffic related origin of pollutants from gas concentration measurements in ambient air - solvent usage emissions calculated from gas concentration measurements in ambient air and the monthly mean concentration, (3) traffic related origin of pollutants from measurements - solvent usage emissions calculated from

measurements on 18 September and the daily mean, (4) traffic related origin of pollutants from measurements - solvent usage emissions calculated from measurements on 8 September and the daily mean. The results from the CMB analysis showed that road traffic dominates the BT emissions in the city (Figure 2). The contribution was almost 100% for benzene and above 80% for toluene and xylenes when there were considered monthly means. Significant contributions from solvent emissions could only be observed during specific meteorological conditions, when the impact of solvent sources accounted on average for about 50% of measured toluene concentrations, and even above 90% of measured xylenes concentrations.

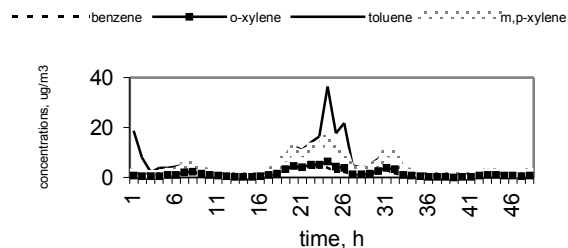


Figure 1. Diurnal variation of BT concentrations in September, 18-19, 2006.

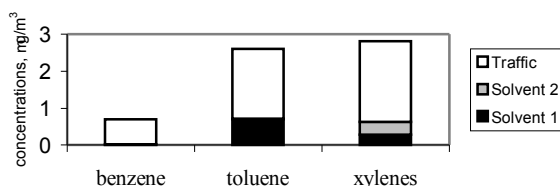


Figure 2. The monthly average mean of BT concentrations and the concentrations calculated by the CMB model for traffic and solvent use emissions.

This work was supported by the DBU under grant No. 21518

McAreen, R., Singleton, D., Bai, Y.K., Khou, B., Singer, E., Wu, J. & Niki, H (1996). *Environ. Sci. Technol.*, 30, 2219-2232.

Watson, J.G., Chow, J. C. & Fujita, E. (2001). *Environ. Sci. Technol.*, 35, 1567-1584.

## Source apportionment on time resolved particles number distributions

Federico Mazzei<sup>1</sup>, Franco Lucarelli<sup>2</sup>, Silvia Nava<sup>2</sup>, Paolo Prati<sup>1</sup>, Gianluigi Valli<sup>3</sup>, Roberta Vecchi<sup>3</sup>

<sup>1</sup> Dipartimento di Fisica and INFN, via Dodecaneso 33, 16146, Genova – Italy

<sup>2</sup> Dipartimento di Fisica and INFN, via Sansone 1, 50019, Sesto Fiorentino – Italy

<sup>3</sup> Istituto di Fisica Generale Applicata and INFN, Via Celoria 16, 20133, Milano – Italy

Keywords: streaker sampler, optical counter, PIXE, PMF

We describe a new experimental methodology based on the contemporary use of two-stage continuous streaker samplers and optical particle counters. This is a complementary approach to size-segregated particulate matter (PM) sampling, and it is able to give information on the elemental size distribution and to deduce the contribution to dimensional classes of major PM source. PM samples in the fine and coarse fraction of PM10 have been collected by a two-stage streaker sampler and analyzed by Particle Induced X-ray Emission (PIXE) to extract time series of elemental concentration values with hourly resolution. PM sources and profiles were obtained by Positive Matrix Factorization (PMF). A multi-linear regression of size-segregated number of particles versus the sources, resolved by PMF, made possible the apportionment of size-segregated particles number in a fast and direct way.

Particulate matter has been collected by two-stage streaker samplers, made by PIXE International Corporation. The streaker consists of a pre-impactor that removes particles with aerodynamic diameter  $D_{ae} > 10 \mu\text{m}$  from the incoming flux, a thin Kapton foil which collects particles with  $2.5 \mu\text{m} < D_{ae} < 10 \mu\text{m}$  and a Nuclepore film (pores size:  $0.4 \mu\text{m}$ ) that intercepts all smaller particles. The sampling produces a circular continuous deposit on the two stages. The deposits can be analyzed by Ion Beam Analysis to deduce elemental concentrations.

The particles number distribution was measured by a Grimm 1.108 optical particle counter (OPC), for diameters  $D_p$  between  $0.25 \mu\text{m}$  and  $32 \mu\text{m}$  in 32 size intervals with a 30-minutes time resolution. Particle Induced X-ray Emission analysis was performed on streaker deposits, using the external beam PIXE facility of the new I.N.F.N. Tandem accelerator at the Florence University. PIXE spectra were fitted for 25 elements using the GUPIX software package (Maxwell et al., 1995) and the elemental concentrations were obtained via a calibration curve from a set of thin standards of known areal density.

We applied the Positive Matrix Factorization (PMF) receptor model to the time series of hourly elemental concentrations. PMF is a least squares formulation of factor analysis developed by Paatero

(Paatero and Tapper, 1994). PMF analysis of the elemental concentration time series measured by streaker sampler resolved the number and profiles of major PM sources in three urban sites in the town of Genoa (Italy) site. For each dimensional class, a multi-linear regression between particles number and PMF sources temporal trends, gives the apportionment reported as synthetic columns plots in the example in Figure 1. In all sites, sea salt and re-suspended soil dust show larger contributions in the coarse fractions (soil: above  $D_p = 2 \mu\text{m}$ ; sea: around  $D_p = 2 \mu\text{m}$ ). Secondary compounds, which represent the major source of PM, and oil combustion are concentrated in the dimensional classes with  $D_p < 1 \mu\text{m}$ . Traffic emissions contribute in all dimensional classes.

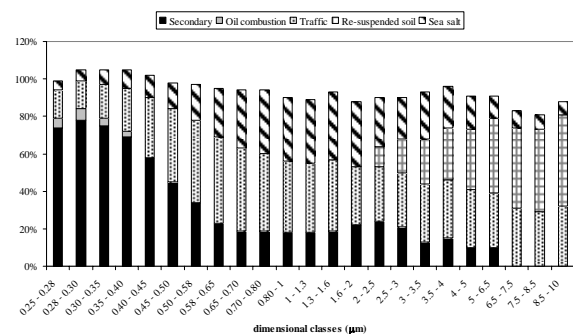


Figure 1. Apportionment of particles number in each dimensional class versus the PM sources identified by PMF in a “heavy traffic” site in Genoa .

This work has been partly supported by Amministrazione Provinciale di Genova and by I.N.F.N.

Maxwell, J. A., Teesdale, W. J., Campbell, J. L., 1995.

The Guelph PIXE package II.

Nuclear Instruments and Methods in Physics Research B95, 407-421.

Paatero, P., Tapper, U., 1994.

Positive matrix factorization: a non-negative factor model with optimal utilization of error estimates of data values.

*Environmetrics* 5, 111-126.

## Mass spectral signatures of aerosol particles from wood burning emissions

S. Weimer<sup>1,2</sup>, M.R. Alfarra<sup>2</sup>, D. Schreiber<sup>1</sup>, M. Mohr<sup>1</sup>, A.S.H. Prévôt<sup>2</sup>

<sup>1</sup>Laboratory for internal combustion engines, EMPA, Überlandstrasse 129, CH- 8600 Dübendorf, Switzerland

<sup>2</sup>Laboratory of Atmospheric Chemistry, Paul Scherrer Institute, CH- 5232 Villigen, Switzerland

Keywords: aerosol mass spectrometry, organics, measurements of combustion aerosol

During winter time wood burning for domestic heating is very common in many parts of the world.

As an example, Swedish homes are completely or partially heated using wood burning fire (Hedberg *et al.* 2002). In Switzerland it was found that wood burning emissions during periods of atmospheric temperature inversions contribute to elevated levels of particulate matter in Alpine Valleys (Alfarra *et al.* 2006). Those elevated levels do quite often exceed the daily Swiss air quality PM<sub>10</sub> standard of 50 µg m<sup>-3</sup>.

To characterise the chemical and physical composition of aerosol particles emitted from wood burning, a study was carried out at Empa (Swiss Federal Laboratories for Materials Testing and Research). The composition of aerosol particles emitted from the burning of beech, larch, fir, oak and chestnut wood in a small stove were investigated. Measurements of characteristic chemical components of the wood combustion aerosol were performed using an Aerodyne Aerosol Mass Spectrometer (Q-AMS). In addition, the aerosol total mass was measured by a TEOM (Tapered Element Oscillating Microbalance), the soot concentration was measured using a Micro Soot Sensor from AVL and the particle number concentration and size distribution were recorded using a condensation particle counter (CPC) and a scanning mobility particle sizer (SMPS), respectively.

The goal of this study was to identify and compare the mass spectral signatures of aerosol particles emitted from wood burning, and also to investigate the change in the mass spectral signature as a function of the burning cycle time and kind of wood. These signatures would then be used to distinguish wood burning emissions from traffic emissions in ambient air.

Markers related to levoglucosan which is the single most abundant compound (Jordan *et al.* 2005) associated with wood smoke emissions were produced by all of the studied wood types. These markers included m/z 29, 60 and 73.

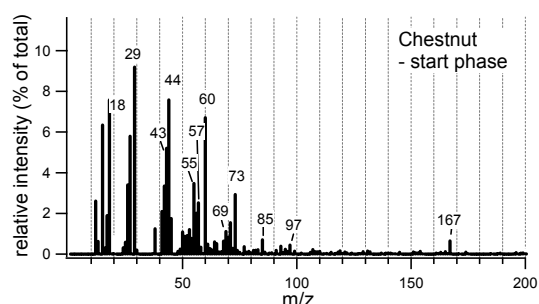


Figure 1. Normalised mass spectra of aerosol particles from burned chestnut wood.

However, these wood burning markers were more dominant during the first 10 minutes of the burning cycle (Fig. 1), which lasted for 45 minutes, and decreased towards the end of the cycle.

Comparison of mass spectra from these wood burning emissions will be compared and presented to mass spectra of traffic emissions and mass spectra of measurements performed with a mobile laboratory.

Alfarra, M.R. A.S.H. Prevot, S. Szidat, J. Sandradewi, S. Weimer, V. Lanz, D. Schreiber, M. Mohr, U. Baltensperger.: *Identification of the mass spectral signature of organic aerosols from wood burning emissions*. Submitted to ES&T September 2006.

Hedberg, E., A. Kristensson, M. Ohlsson, C. Johansson, P. Johansson, E. Swietlicki, V. Vesely, U. Wideqvist, R. Westerholm (2002): *Chemical and physical characterization of emissions from birch wood combustions in a wood stove*. Atmospheric Environment, 36, 4823-4837.

Jordan, T.B., A.J. Seen (2005): *Effect of Airflow Settings on the Organic composition of wood heater emissions*. Environmental Science and Technology 39, 3601-3610.

## An analysis of vehicular particle number emissions based on long-term roadside and urban background measurements

S. Klöse<sup>1</sup>, W. Birmili<sup>1</sup>, T. Tuch<sup>1,2</sup>, B. Wehner<sup>1</sup>, A. Wiedensohler<sup>1</sup>, U. Franck<sup>2</sup>, M. Ketzel<sup>3</sup>

<sup>1</sup> Leibniz-Institute for Tropospheric Research, Permoserstrasse 15, 04318 Leipzig, Germany

<sup>2</sup> UFZ – Centre for Environmental Research, Permoserstrasse 15, 04318 Leipzig, Germany

<sup>3</sup> National Environmental Research Institute, Frederiksborgvej 399, 4000 Roskilde, Denmark

Keywords: vehicle emissions, traffic, street canyon, DMPS

In complex urban landscapes, the probability to be exposed to anthropogenic particles increases along with traffic volume and decreasing ventilation. Exposure research and urban atmospheric modelling therefore need emission factors for vehicular traffic basing on particle number rather than particle mass concentration. Because a relevant fraction of ultrafine traffic aerosols are formed by gas-to-particle conversion in the atmosphere downstream the vehicle pipes, measurements near traffic sources are required to capture the full effects of traffic on urban particulate number. Here, we report on particle size distribution measurements in an urban street canyon, and the associated inverse modelling that leads to traffic emission factors.

Long-term particle number size distribution measurements (3-800 nm) were conducted over the entire years 2005 and 2006 inside a street canyon in Leipzig, Germany (“Eisenbahnstrasse”) using a twin differential mobility particle sizer. The street features a daily traffic volume of about 10.000 vehicles at driving speeds of about 30 km h<sup>-1</sup>, which were counted in live-time by a video detection system. The share of heavy duty vehicles was about 5 % during day-time. To obtain a measure for the urban background outside the canyon, measurements were also conducted at a second station not directly affected by traffic emissions (“lft”). By subtracting background from roadside concentrations, a measure for the true effect of traffic was obtained.

Figure 1 shows an exemplary diurnal cycle of particle number concentration on Mondays: Roadside concentrations exhibit two concentration maxima, which are associated with the morning and afternoon peak traffic times around 08:00 and 17:00.

The Operational Street Pollution Model (OSPM) was used to simulate atmospheric dispersion within the street canyon. The resulting dilution factor quantifies the degree of dilution of traffic aerosol before reaching the sampling point inside the street canyon. For each given large scale wind direction, OSPM also accounts for the turbulent transport induced by the topography as well as the moving traffic. Emission factors indicating the number of particles emitted by one vehicle per driven kilometre were calculated by dividing the concentration increment in the canyon by the dilution factor and the traffic volume (Ketzel et al., 2003).

The emission factor averaged over all vehicle types was found to vary between  $3 \cdot 10^{13}$  and  $7 \cdot 10^{14}$  veh<sup>-1</sup> km<sup>-1</sup>, depending on time of day, and also meteorological variables such as ambient temperature. We will provide a statistical summary of all observations and simulations, as well as their implications for the modelling of vehicular emissions.

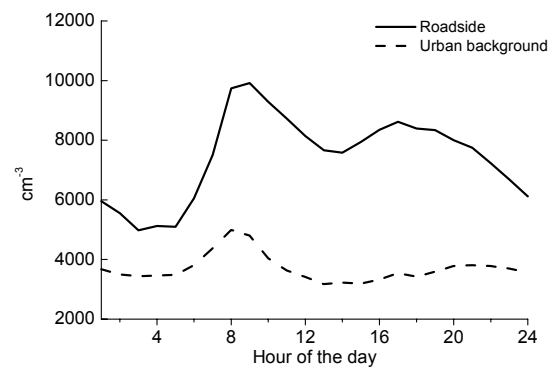


Figure 1: Mean diurnal cycle of particle number concentration (30-150 nm in diameter) on Mondays in 2005/06.

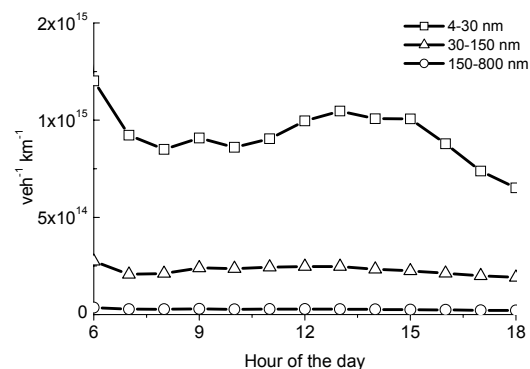


Figure 2: Mean emission factors averaged over all Mondays to Fridays in 2005/06.

Ketzel, M., Wählin, P., Berkowicz, R., Palmgren, F. (2003) Particle and trace gas emission factors under urban driving conditions in Copenhagen based on street and roof-level observations, *Atmos. Env.* **37**, 2735-2749.

## Wood burning aerosol during winter in an Alpine valley: Aethalometer and the Aerosol Mass Spectrometer measurements

J. Sandradewi<sup>1</sup>, M.R. Alfarra<sup>1</sup>, A.S.H. Prévôt<sup>1</sup>, E. Weingartner<sup>1</sup>, M. Gysel<sup>1</sup>, R. Schmidhauser<sup>1</sup>, S. Szidat<sup>2</sup> and U. Baltensperger<sup>1</sup>

<sup>1</sup>Laboratory of Atmospheric Chemistry, Paul Scherrer Institut, 5232 Villigen, PSI, Switzerland

<sup>2</sup>Department of Chemistry and Biochemistry, University of Bern, Freiestrasse 3, 3012 Bern, Switzerland

Keywords: AMS, biomass burning, field measurements, light absorption

In many regions of the world, wood burning is an important heating source especially during the cold winter period. Studies have shown that the gases and particles emitted from wood burning activities cause adverse health effects. Thus source apportionment studies to determine the fraction of wood burning aerosols in the atmospheric aerosol loading are needed.

In the AEROWOOD (Aerosol from wood burning) project, a multi-wavelength Aethalometer ( $\lambda=370, 470, 520, 590, 660, 880$  and  $950$  nm) was operated parallel to an Aerosol Mass Spectrometer (Aerodyne, Q-AMS) in various field campaigns within Switzerland. Table 1 gives an overview of these field campaigns.

Table 1. Field Campaigns

Locations	Characteristics	Dates (dd.mm.yy)
Roveredo	in an Alpine valley with high wood burning activities in winter	01–15.03.05 25.11–15.12.05
Zurich	urban	06–25.01.06
Reiden	near highway	27.01–13.02.06

The light absorption coefficients  $b_{abs}$  ( $\lambda$ ) from the Aethalometer were calculated and correction factors applied following the procedure of Weingartner *et al.* (2003). In Roveredo, we observed a very strong increase in  $b_{abs}$  (370 nm), indicating that there is a high fraction of UV absorbing organic material in wood smoke particles (Kirchstetter *et al.*, 2004). The wavelength dependence of  $b_{abs}$  was calculated using a power law fit. The power law exponent (also called the Ångström exponent)  $\alpha$  will be presented for all of these campaigns.

From the AMS data, we compared the organic mass concentration ( $\mu\text{g}/\text{m}^3$ ) with  $b_{abs}$  (370 nm) from the Aethalometer. Figure 1 describes this correlation for the Roveredo data. The higher slope in March compared to December might be interpreted by an increased contribution of secondary organic aerosols. Alfarra *et al.* (2006) reported that the mass fragment  $m/z$  60 measured by the AMS is a suitable marker for wood burning aerosols. Thus we compared  $m/z$  60 with  $b_{abs}$  (370 nm) as well. A rather high correlation

was observed in the Roveredo data (for clarity, the Zurich and Reiden data are not shown in Fig. 1 and 2). Further comparisons will include <sup>14</sup>C measurements of the EC and OC fractions.

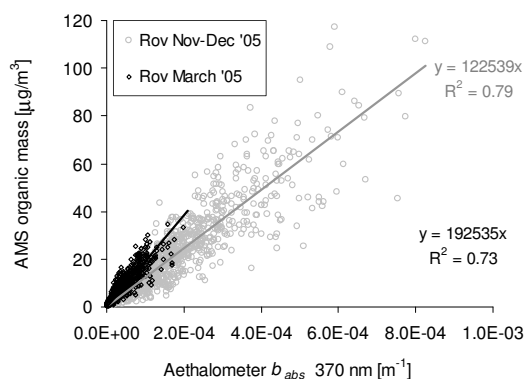


Figure 1. Correlation of the organic mass concentration and  $b_{abs}$  (370 nm). Only Roveredo data are shown.

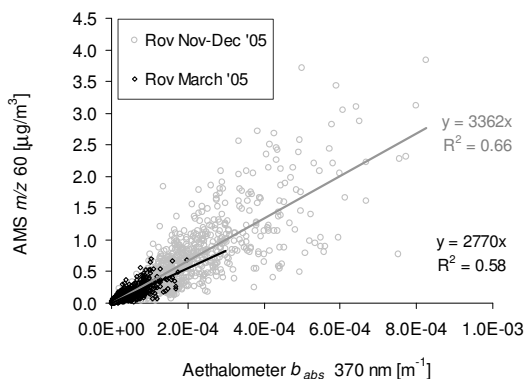


Figure 2. Correlation of  $m/z$  60 and  $b_{abs}$  (370 nm).

This work is supported by the Swiss Federal Office for the Environment (FOEN) and the Cantons Graubünden, Ticino, Lucerne and Zürich.

Alfarra, M. R., *et al.* (submitted, 2006) *Environ. Sci. Technol.*

Kirchstetter, T. W., *et al.* (2004) *J. Geophys. Res.*, 109, D21208.

Weingartner, E., *et al.* (2003) *J. Aerosol Science*, 34, 1445–1463.

## Chemical composition of primary marine aerosol: results from the Bubble Bursting laboratory experiment during MAP

C. Carbone<sup>1</sup>, E. Finessi<sup>1</sup>, M. Rinaldi<sup>1</sup>, S. Decesari<sup>1</sup>, M. Mircea<sup>1</sup>, M.C. Facchini<sup>1</sup>, S. Fuzzi<sup>1</sup>, D. Nilsson<sup>2</sup>, D. Ceburnis<sup>3</sup>, and C. O'Dowd<sup>3</sup>

<sup>1</sup>Institute of Atmospheric Sciences and Climate (ISAC-CNR), Bologna, Italy

<sup>2</sup>Department of Applied Environmental Science, Stockholm University, Stockholm, Sweden

<sup>3</sup>Department of Experimental Physics & Environmental change Institute, National University of Ireland, Galway, Ireland

Key words: aerosols size distributions, Berner impactor, marine aerosols, primary organic aerosols

The sources and properties of marine aerosols are of great interest as they have an important impact on both the Earth's albedo and climate.

Here we present the results of a bubble bursting experiment which was carried out within the Project MAP (Marine Aerosol Production Project) focused on primary marine aerosol sources, mechanisms and chemical composition. Recent measurements have revealed that both micro-physical and chemical properties of the North Atlantic marine aerosols possess a distinct seasonality pattern. Accumulation mode diameters increase from winter through summer, during periods of blooming phytoplankton, where they reach a maximum. Associated with the increasing mode diameters, an increase of the organic fraction in the sub-micron aerosol size interval was observed. Moreover, the increasing enrichment of the aerosol organic fraction with decreasing size is consistent with thermodynamic predictions of the bubble bursting process under conditions in which the ocean surface layer is rich of surfactant material of biogenic origin that can be incorporated into sea spray drops (C. Oppo et al. 1999).

The bubble bursting experiment took place during a 4-week ship-borne campaign over the North Atlantic, from the 11<sup>th</sup> of June to the 5<sup>th</sup> of July, 2006, and was carried out in the laboratory on board the Celtic Explore. Two Berner low pressure impactors were devoted to primary aerosol sampling from bubbles tanks purposely designed for the MAP experiment. The bubble bursting tanks were made of stainless steel and were filled with about 100 liters of sea water, directly supplied into the laboratory by a water system collecting with inlet below the sea surface. The flow rate of the water jet for generating the bubbles was 20 lpm in order to simulate sea-spray production. The water rate exchange in the tank was approximately 6-7 lpm. Samples run for approximately 12h with a continuous sea water flow through the tank. Nine samples were collected, covering a large variety of environmental conditions at the sea surface. Sampling substrates of both quartz and tedlar were adopted to allow the analysis of organic, inorganic and biological components. In order to characterize surfactants and primary aerosols precursors, sea water samples were also collected concurrently.

The size-segregated distributions of the aerosol inorganic fraction shows that concentration of nss-sulphate and nitrate are very low, thus evidencing that the bubble bursting experiment carried out during

MAP is effective at producing primary aerosol and is free of contaminations.

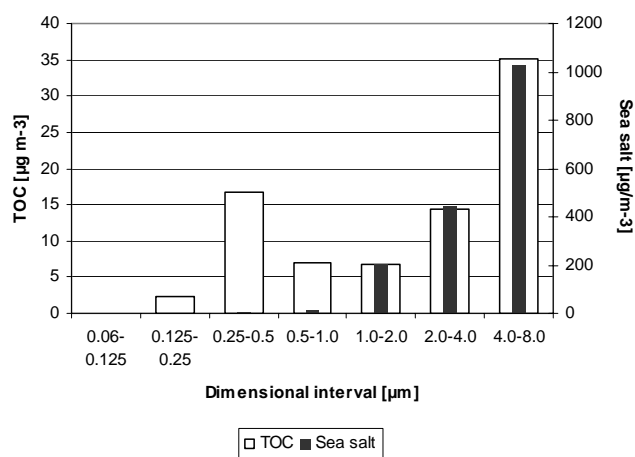


Figure 1. Size-segregated TOC and sea salt for a representative Bubble Bursting aerosol sample.

As expected, sea salt is enriched in the coarse fraction and, conversely, total organic carbon is significantly enriched in the sub-micrometer size range, representing from 60 to 80 % of the total aerosol mass in this size interval. Moreover, the organic carbon transferred into the aerosol particles by the bubble bursting experiment is mainly water insoluble and strongly surface active. This results are in agreement with the hypothesis that primary biogenic sources contribute significantly to the marine aerosol organic carbon concentration observed during periods of phytoplankton bloom.

O' Dowd, MC Facchini, F Cavalli, D Ceburnis, M Mircea, S Decesari, S Fuzzi, YJ Yoon, and JP Putaud (2004). Bionically-driven organic contribution to marine aerosol, *Nature* 676-680.

O'Dowd. Sea-Spray Fluxes and Chemical Compositions. In abstract of European Aerosol Conference, Ghent 2005.

C Oppo et al. (1999). Surfactants component of marine organic matter as agents for biogeochemical fractionation of pollutants transport via marine aerosol. *Marine Chemistry* 63, 235-253.

## Wood smoke contribution to aerosol concentrations in Northern Italy: levoglucosan determination by GC-MS and HPAEC-PAD

P. Fermo<sup>1</sup>, A. Piazzalunga<sup>1</sup>, R. Vecchi<sup>2</sup>, G. Valli<sup>2</sup>, M. A. De Gregorio<sup>3</sup>, S. Marengo<sup>4</sup>

<sup>1</sup>Dep. Inorganic, Metallorganic and Analytical Chem., University of Milan, Via Venezian 21, 20133, Milan, Italy

<sup>2</sup>Institute of General Applied Physics, University of Milan, Via Celoria 16 20133, Milan, Italy

<sup>3</sup>ARPA Lombardia-U.O.lab., Via Juvara 22, 20122, Milan, Italy

<sup>4</sup>Stazione Sperimentale per i Combustibili, Viale A. De Gasperi 3, 20097, S. Donato M., Milan, Italy

Keywords: levoglucosan, biomass burning, particulate matter, emission factor, HPAEC-PAD.

Very scarce data on the possible contribution of particles emitted by residential wood combustion in Italy are available. To achieve more information on this source of particulate matter, a study was carried out on wood smoke contribution by means of the chemical characterization of aerosol samples collected at different locations in Lombardy (Northern, Italy). It is noteworthy that in the literature potassium, oxalate and levoglucosan are regarded as good signatures of biomass/wood combustion in the atmosphere (Simoneit et al., 1999).

Measurement of collected samples included organic and elemental carbon analysis together with the wood smoke tracer levoglucosan. Levoglucosan arises from the pyrolysis of cellulose, the main building material of wood, at temperature higher than 300°C. It is emitted in large amounts, sufficiently stable and specific to cellulose-containing substances.

PM10 aerosol samples were collected in Milan and in other five cities in the Lombardy region in the frame of the ParFiL project (Particolato Fine in Lombardia). The sampling sites have been chosen according to the different contributions estimated for wood combustion to particulate matter emissions. The samples examined were collected during winter 2005, summer 2005 and winter 2006 using low volume EPA- samplers (flow rate: 1 m<sup>3</sup>/h) equipped with PM10 inlets. OC (organic carbon) and EC (elemental carbon) were measured by Thermal Optical Transmission method (TOT). Levoglucosan was quantified by two different techniques: Gas Chromatography coupled with Mass Spectroscopy (GC/MS) and High Performance Anion Exchange Chromatography (HPAEC) coupled with Pulsed Amperometric Detection (PAD). The two methods show fairly good agreement in mass concentration of levoglucosan ( $R^2 = 0.95$  for the linear regression between the two methods). Up to now GC/MS was the most commonly applied technique for levoglucosan quantification (Wang et al., 2005). Nevertheless, HPAEC-PAD is sensitive, precise and accurate (Gorin et al., 2006; Engling et al., 2006) and doesn't require any complex extraction procedure followed by derivatization such as those needed by GC-MS analyses.

Emission factors for levoglucosan were determined as percentage of tracer on OC. In the

examined sites it ranged from 3.6% (in a typical urban site) to 5.7% (at an Alpine town where per head consumption of wood for residential combustion is estimated to be the highest in Lombardy).

Using the correlation between levoglucosan and OC (i.e. extrapolating the least-square fit to zero levoglucosan) it is possible to quantify a "background" or "non-woodsmoke" contribution to OC, as reported in figure 1 for two of the examined sites during wintertime when levoglucosan concentrations are expected to be higher.

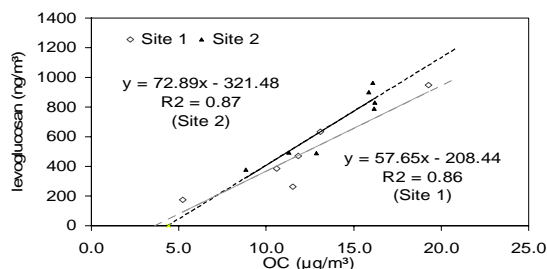


figure 1 – levoglucosan vs. OC concentrations for two of the examined sites during winter

More appropriate emission factors typical for the wood species present in Lombardy were also evaluated in order to make a correct assessment of wood burning contribution to OC. Through the analysis of the source test samples we estimated the contribution of levoglucosan to OC for different combustion systems (fireplaces and stoves) and different wood types.

### Acknowledgements

The authors are grateful to ParFiL Project for their financial support. We are thankful to all the people who have taken part to the collaboration.

Engling G., et al. (2006). *Atmos. Environ.*, 40, S299-S311

Gorin C. A., J. L. Collett (2006). *J. Air & Waste Manage. Assoc.*, 56, 1584-1590

Simoneit et al. (1999). *Atmos. Environ.*, 33, 173-182

Wang W. et al. (2005). *Mass. Spectrom.*, 19, 1343-1351

## Size distributions of aerosol particles in a food waste composting center

J.H. Byeon, C.W. Park, K.Y. Yoon, J.H. Park and J. Hwang

School of Mechanical Engineering, Yonsei University, 120-749, Seoul, Republic of Korea

Keywords: airborne particles, bioaerosols, particle size distribution, aerosol measurement, agglomerates.

In this study, we determined the size distributions of total airborne particles and bioaerosols in a food waste composting center using an optical particle counter and an agar-inserted six-stage impactor, respectively. The majority of the airborne particles were submicron-sized, while the bioaerosols were detected at all sizes ( $> 0.65\mu\text{m}$ ). The correlation,  $(\text{CFU}/\text{m}^3)/(\text{particles}/\text{m}^3)$ , was low at all particle sizes, but was shown to vary directly with the particle size. Even the highest correlation, 0.249 at a diameter of  $5.9\mu\text{m}$ , implies that the majority of the total airborne particles were comprised of non-biological matter. The bioaerosol concentration was found to depend significantly on the screening or airflow patterns at each of the sampling locations. The data obtained at 15 days and screening were higher than those obtained at any of the other sampling locations, and this was attributed to the tendency of the screening operation to cause microorganisms to become suspended in the air. Moreover, the data obtained on day 5 of composting were higher than those obtained on days 10 or 15, and this may be attributable to a higher flow rate of air, which harbored a significant quantity of microorganisms, toward stack 1.

From the bioaerosol samples collected at sampling location 1, 8 bacterial species, 5 fungi, and 1 actinomycete were isolated and identified. The concentrations of bacteria were significantly higher than the concentrations of fungi and actinomycetes at every sampling site. The aerodynamic diameters of the microorganisms detected by the impactor ( $0.73\text{--}5.12\mu\text{m}$ ,  $0.5\text{--}1.8\mu\text{m}$ , and  $0.5\text{--}2.4\mu\text{m}$ ) for Bacillus, Staphylococcus, and Streptomyces, respectively, were somewhat larger than those previously reported ( $0.5\text{--}2.5\mu\text{m}$ ,  $0.5\text{--}1.5\mu\text{m}$ , and  $0.5\text{--}2.0\mu\text{m}$ ). One of the reasons for this may be that the majority of bioaerosols in the composting facility were suspended, and existed as agglomerates (bioaerosols combined with certain kinds of dust and/or other bioaerosols).

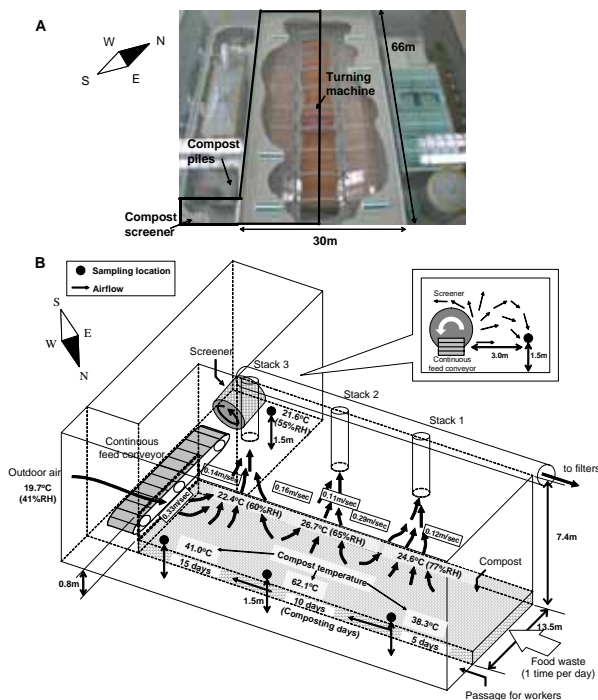


Figure 1. Layouts of the composting center (A) and air flow conditions (B).

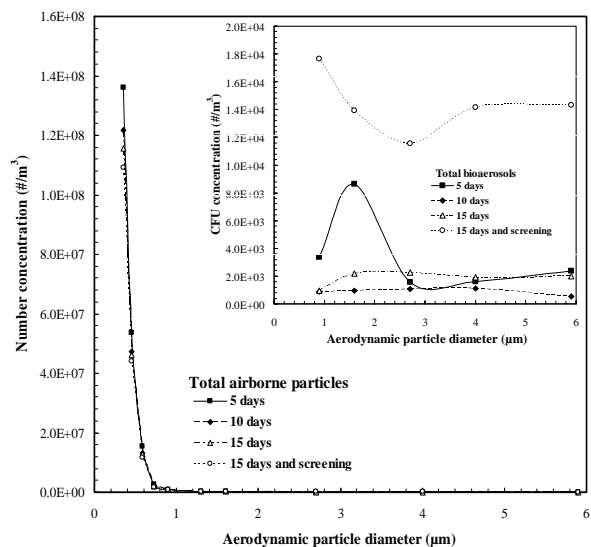


Figure 2. Size distributions.

This work was supported by grant No. 2006-8-0183 from the Agricultural Specified Research Project of the Rural Development Administration.

Folmsbee, M., & Strevett K. A. (1999). *Journal of the Air & Waste Management Association*, 49, 554-561.

Schlegelmilch, M., Streese, J., Biedermann, W., Herold, T., Stegmann, R. (2005). *Waste Management*, 25, 917-927.

Taha, M. P. M., Pollard, S. J. T., Sarkar, U., Longhurst, P. (2005). *Waste Management*, 25, 445-450.

## Road-side ultrafine particle and ion size distributions

Petri Tiitta<sup>1)</sup>, Pasi Miettinen<sup>1)</sup>, Petri Vaattovaara<sup>1)</sup> and Ari Laaksonen<sup>1)</sup>  
 Jorma Joutsensaari<sup>2)</sup>  
 Anne Hirsikko<sup>3)</sup>, Pasi Aalto<sup>3)</sup> and Markku Kulmala<sup>3)</sup>

<sup>1)</sup>Department of Physics, University of Kuopio, P.O.Box 1627, FI-70211 Kuopio, Finland

<sup>2)</sup>Department of Environmental Sciences, University of Kuopio, P.O.Box 1627, FI-70211 Kuopio, Finland

<sup>3)</sup>Department of Physical Sciences, University of Helsinki, P.O.Box 64, FI-00014 Helsinki, Finland

Keywords: traffic, vehicles emissions, aerosol size distribution, ions, clusters.

This work is focussing on investigation of ions and clusters in the vicinity of the road. The aim of this work is clarify how traffic related particles affect the air ions, their size distributions, and whether the vehicle exhausts are sources or sinks for air ions. Measurements were conducted both with high and low traffic densities, during upwind and downwind. We compare our results to the measurements in a boreal forest rural station-(SMEAR II).

Ion production rate can be estimated indirectly by the balance equation of cluster ions:

$$\frac{dN}{dT} = Q - \alpha n^2 - CS \cdot N(d_p, q) \quad (1)$$

where  $Q$  is the ion production rate,  $\alpha$  is the ion-ion recombination coefficient,  $n$  is concentration of positive and negative ions,  $CS$  is condensation sink and  $N(d_p, q)$  the concentration of aerosol particles of diameter  $d_p$  and charge  $q$  (Israel 1970). Thus cluster concentration is connected to condensation sink by the balance equation (Eq.1).

Savilahti measurement site was located between Savilahdentie road about 10 m from traffic lanes with traffic density around 15 000 vehicles per day and VT5 motorway about 100 m from traffic lanes with traffic density around 20 000 vehicles per day.

For detailed analysis, we grouped the air ions in three different size ranges; cluster ions (0.3-1.8 nm), intermediate ions (1.8-7.5 nm) and large ions (7.5-40 nm) (Figure 1). During the measurement period the average cluster ion concentrations were quite low, around 290 cm<sup>-3</sup> and 250 cm<sup>-3</sup> for negative and positive ions, respectively. The concentrations varied between 30 and 1 000 cm<sup>-3</sup> for negative cluster ions and between 30 and 720 cm<sup>-3</sup> for positive ones.

At the same time, the average cluster ion concentrations at SMEAR II station in Hyttiälä were almost three times higher than in Savilahti. The SMEAR II station is at rural site, where the cluster ion concentrations are affected more by the sink due to pre-existing aerosol particles than ion production by ionisation (Hirsikko *et al.*, 2006). Addition to aerosol sink and ion production, the composition of aerosols and gaseous compounds differ significantly between these two sites. Savilahti area is dominated

by local anthropogenic sources, especially by traffic exhaust, and Hyttiälä is a rural site, where forest emits organic secondary particle precursors.

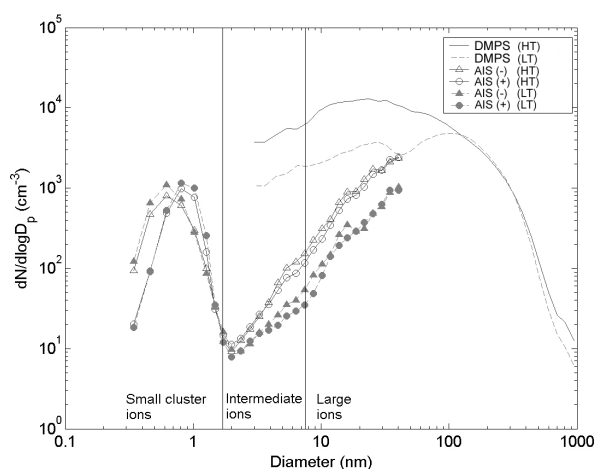


Figure 1. The size distribution of particles (TWIN-DMPS data) and ions (AIS data) during low traffic density (LT) (6500 vehicles 24 h<sup>-1</sup>) and higher traffic density (HT) conditions (14000 vehicles 24 h<sup>-1</sup>).

Negative intermediate ions (1.8-7.5 nm) had concentrations up to 620 cm<sup>-3</sup> in Savilahti with an average value of 70 cm<sup>-3</sup>. The corresponding values for positive ions were: maximum 190 cm<sup>-3</sup> and average 40 cm<sup>-3</sup>. Rain caused mainly the highest intermediate ion concentrations but we also observed intermediate ion bursts during fine weather, which indicates secondary particle formation.

Large ions (7.5-40 nm) followed the daily variation of ultrafine particle concentrations with an average concentrations of 680 and 630 cm<sup>-3</sup> for negative and positive ions, respectively. The average large ion concentrations were 2-3 times higher in Savilahti than at Hyttiälä SMEAR II.

Hirsikko A., Bergman T., Laakso L., Dal Maso M., Riipinen I., Hörrak U. & Kulmala M. 2006. Identification and classification of the formation of intermediate ions measured in boreal forest. *Atmos. Chem. Phys. Discuss.* 6: 9187-9212.  
 Israel H. 1970. Atmospheric electricity. *Israel Program for Scientific Translations*, 1, Jerusalem.

## Towards source apportionment of soot particles from wood and diesel combustion in ambient samples with X-ray microscopy

M.G.C.Vernooij<sup>1,2</sup>, M.Mohr<sup>1</sup>, R.Kaegi<sup>3</sup>, T.Huthwelker<sup>4</sup>, G.Tzvetkov<sup>5</sup>, R.Gehrig<sup>1</sup>

<sup>1</sup>Empa, Swiss Federal Laboratories for Materials Testing and Research, 8600 Dübendorf, Switzerland

<sup>2</sup>Institute for Mineralogy and Petrology, University of Fribourg, Ch. du Musée 6, 1700 Fribourg, Switzerland

<sup>3</sup>EAWAG, Swiss Federal Institute for Environmental Science and Technology, 8600 Dübendorf, Switzerland

<sup>4</sup>Laboratory for Environmental Chemistry, Paul Scherrer Institute, 5232 Villigen, Switzerland

<sup>5</sup>Swiss Light Source (SLS), Paul Scherrer Institute, 5232 Villigen, Switzerland

Keywords: source apportionment, atmospheric aerosols, soot particles, single particle analysis.

In urban areas, carbonaceous particulate matter typically accounts for 25-50% of the ambient PM 2.5. The major constituents of these carbonaceous aerosols are soot particles from diesel and wood combustion. Diesel and wood combustion emission samples can be distinguished based on C(1s) near edge x-ray absorption fine structure (NEXAFS) on bulk material (Braun, 2005). Characteristic resonances in the spectra allow for direct molecular speciation of the graphite-like solid core, surface functional groups, and aromatic and aliphatic components, depending on the origin of the soot. With scanning transmission X-ray microscopy (STXM) it is now for the first time possible to gain more detailed information on the variation in chemical structures of single soot particles depending on the combustion source.

The morphology of diesel and wood smoke soot particles is very similar. Both consist of chains of primary particles with a graphitic structure (Fig. 1a). First STXM results, however, indicate a clear difference between the chemical structures of the particles from the two different sources. Diesel soot particles contain a dominant spectral signature at 285 eV from unsaturated (multiple) carbon bonds in the solid cores of the primary particles and a very sharp exciton resonance at 290 eV (Fig. 1b). The spectra from graphite also show these features, confirming the partial graphitic nature of diesel soot. The spectra of wood soot have a less graphitic nature (Fig. 1b), but show a firm peak at 287 eV from C-OH bonds (Cody *et al.*, 1995). These source specific signatures may allow discrimination between wood and diesel soot particles in ambient air samples. We collected such samples (with particle sizes <1 μm) directly next to an arterial road in Zurich. First results show that the specific C(1s) NEXAFS peaks of the two combustion sources can be assigned to individual particles (Fig. 1c). The spectrum of particle 1 shows the characteristics of a diesel combustion source, the spectrum of particle 2 of wood combustion. Spectra, however, do not exactly match. Additional peaks are found, for example, between 295 and 300 eV in particle 1, which might be the result of particle aging. In the near future, measurements are planned to further investigate this aging effect and to quantify the relative abundance of diesel and wood

combustion particles in ambient samples from urban and rural locations.

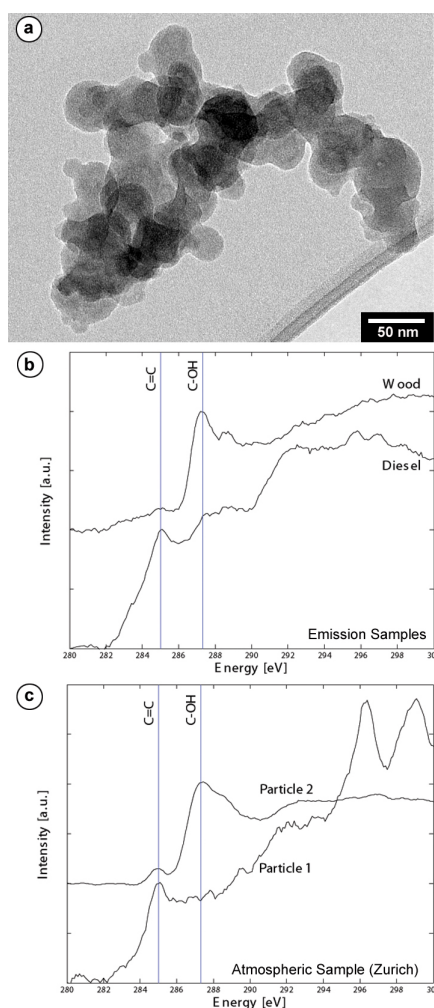


Figure 1. a) TEM bright field image of soot particle from wood combustion, b) C(1s) NEXAFS spectra of single soot particles from wood and diesel combustion, c) C(1s) NEXAFS spectra from two particles in an atmospheric sample that was collected along an arterial road in Zurich.

Braun, A. (2005). *J. Environ. Monit.*, 7, 1059-1065.

Cody, G.D., Botto, R.E., Ade, H., Behal, S., Disko M. and Wirick, S. (1995). *Energy & Fuels*, 525-533.

## Contribution of natural emissions to ambient aerosol concentration levels in the eastern Mediterranean

A. Spyridaki<sup>1</sup>, V. Aleksandropoulou<sup>1</sup>, M. Latos<sup>1</sup>, F. Flato<sup>2</sup>, T.M. Svendby<sup>3</sup>, and M. Lazaridis<sup>1</sup>

<sup>1</sup>Department of Environmental Engineering, Technical University of Crete, Crete, GR- 73100, Chania, Greece

<sup>2</sup>Bjerknes Centre for Climate Research, University of Bergen, N-5007, Bergen, Norway

<sup>3</sup>Norwegian Institute of Air-Research (NILU), N-2027, Kjeller, Norway

Keywords: Biogenic particles, Emission, Aerosol modelling, Marine aerosols, Mineral dust.

Natural emissions can have crucial importance for the overall atmospheric pollution burden for areas that lie close to such emission sources. A database for emissions of biogenic gases, sea-salt particles, DMS and resuspended mineral dust (e.g. Yay *et al.*, 2005) in Greece has been created for the year 2000. A database of forest fires in Greece during the period 1997-2003 has also been created and related gas/particle emissions have been estimated for the period of July 2000.

The contribution of natural vs anthropogenic (Vestreng *et al.*, 2005) particle emissions in the atmosphere of Greece has been examined (Figure 1). Natural PM emissions contribute up to 56% of total PM emissions in this area, during 13-16 July, 2000, with resuspended dust being the main constituent. PM emissions from forest fires at the same period, which consist mainly of fine EC, OM and sulfates are responsible for the 5.3 % of the total PM emissions.

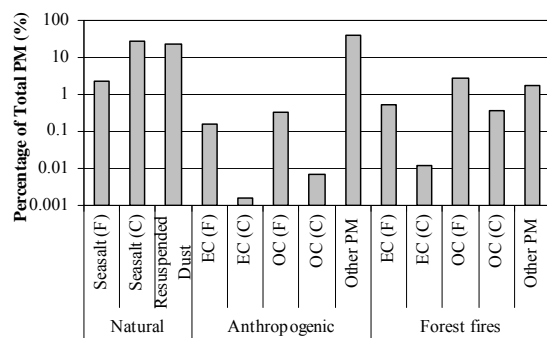


Figure 1. Contribution of marine aerosols, resuspended mineral dust, EC and OC emissions to Total PM emissions in Greece, 13-16 July 2000.

New temperature and initial organic mass dependent gas/aerosol partition coefficients have been implemented into the mesoscale air quality modelling system UAM-AERO (CBM-IV) for the oxidation reactions of BVOCs and aromatics (m-xylene, toluene). The above reactions lead to the production of significant amounts of COCs, precursors of OM. The potential of SOA formation by BVOCs (isoprene and monoterpenes ( $\alpha$ -pinene,  $\beta$ -pinene)) has been examined. An increase of ~103% to OM concentrations is found, due to elevated BVOCs emissions in the area for this period.

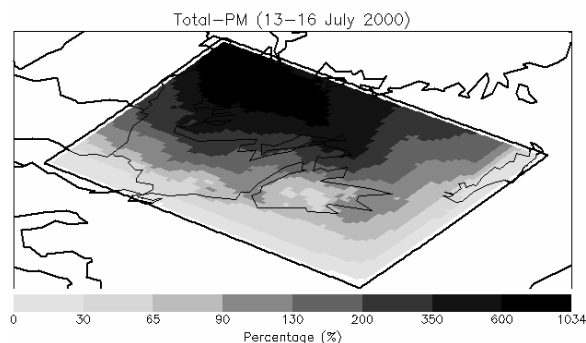


Figure 2. Percentage change of average PM concentrations due to BVOCs and marine aerosol emissions.

The modified mesoscale air quality modelling system UAM-AERO has been applied for 12-16 July, 2000 (10x10km<sup>2</sup>, 5 vertical layers), to study the dynamics of aerosols in the Eastern Mediterranean. The system is also used to validate the natural emissions database and to study their contribution to the local atmospheric air quality (e.g. Figure 2 - percentage change of average PM concentrations due to BVOCs and marine aerosol emissions).

The model results have been evaluated against measurements at the Finokalia station, Crete. Resuspended dust (32%), sea-salt (26%), SO<sub>4</sub><sup>2-</sup> (22%) and NO<sub>3</sub><sup>-</sup> (14%) are the main of total inorganic particulate matter concentrations in Greece, during 13-16 July, 2000. Sea-salt particles contribute to 44 % of total natural inorganic PM.

This work was supported by the Greek Ministry of Education and Religion and the European Union, under grant "Puthagoras – II".

Vestreng V., Breivik K., Adams M., Wagener A., Goodwin J., Rozovskaya O., Pacyna J.M. (2005). *Inventory Review 2005, Emission Data reported to LRTAP Convention and NEC Directive, Initial review of HMs and POPs*, Technical report MSC-W 1/2005, ISSN 0804-2446.

Yay O.D., Poupkou A., Symeonidis P., Gkantou A., Melas D., Döğeroğlu T.. (2005). in *Proc. 3d Int. Symp. on A.Q.M. at Urban, regional and Global Scales*, Regional studies, Istanbul, 16-24.

## Particulate organic compounds in the atmosphere surrounding a waste water treatment plant (Agliana-Pistoia, Italy)

T. Martellini<sup>1</sup>, A. Cincinelli<sup>1</sup>, M. Del Bubba<sup>1</sup>, L. Misuri<sup>1</sup>, A. Valentino<sup>1</sup> and L. Lepri<sup>1</sup>,

<sup>1</sup>Department of Chemistry, University of Florence, Sesto Fiorentino, 50019, Florence, Italy

Keywords: PM10, VOCs, n-alkanes, PAHs, Urban areas.

Organic compounds of anthropogenic or biogenic origin often represent a large fraction of particulate matter. Anthropogenic emissions generally include motor vehicles, industrial processes, waste incineration and tobacco smoke (Mandalakis et al., 2002); on the other hand, wind erosion of leaf epicuticular waxes, vegetation debris and microbial degradation are considered as the most important biogenic sources of organic compounds (Rogge et al., 1993). Organic compounds exist in ambient air as gases and adsorbed to airborne particulate matter; the distribution between gas-phase and particulate matter depends on the chemical-physical properties of the investigated organic compounds. Meteorological parameters (such as temperature, wind direction, wind speed, etc.) could also influence the distribution of the pollutants from the source in the ambient air so these parameters were also measured in this study.

A sampling field was performed in Agliana, near the city of Pistoia (Italy), during the period from May to July 2006. Aerosol samples were collected at 4 different sites located around a sewage treatment plant, because waste water treatment processes are considered responsible of the emissions of PM10 and associated pollutants (e.g. PAHs, alkyl phenols, etc.) (Cincinelli et al., 2003). The investigated area is also characterised by the presence of main arterial roads such as A11 and A1 highways, whose traffic is extremely high, and a residential area. The aims of this study were to evaluate the sources of organic pollutants and the impact of these on the surrounding area the waste water treatment plant.

To this aim the particulate matter amount and the aerosol-associated alkyl phenol mono and di-toxylates (waste water treatment plant markers), n-alkanes and PAHs were determined. Gas phase, total suspended particle (PTS), PM10 and VOCs (i.e. alkyl benzenes and tetrachloroethylene in particular). Sampling and analytical methods are described elsewhere (Cincinelli et al., 2003 – Cincinelli et al., 2007).

N-alkane concentrations varied from 13 to 165 ng/m<sup>3</sup> in the gas phase and from 16 to 101 ng/m<sup>3</sup> in the particulate matter. In figure 1 representative gas chromatographic profiles for the aliphatic hydrocarbons fraction are reported. N-alkanes origin were evaluated by specific parameters such as CPI, UCM, pristine and phytane, %WNA, Cmax.

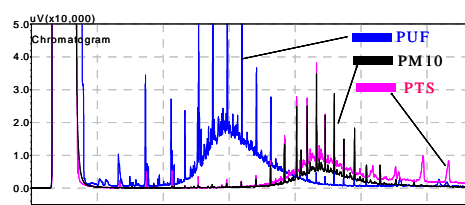


Figure 1- Gas Chromatograms of aliphatic hydrocarbons fraction for a representative sample

Alkyl phenols were also found in all samples, except for the PTS and PM10 of sample 1. These compounds are not produced naturally so their presence in the ambient might be due to anthropogenic activities such as the waste water treatment plant.

Total PAH concentrations ranged from 0.638 to 5 ng/m<sup>3</sup> for the gas phase and from 0.055 to 1.010 ng/m<sup>3</sup> for the particulate phase. Significant compositional differences were observed between gas and particulate phase. The gas phase percentage, generally, decreased with increasing molecular weight.

High concentrations of tetrachloroethylene were found in samples down wind to the plant. This result, together with the presence of alkylphenols in the same samples, evidences the impact of the plant in the surrounding area.

Cincinelli A., Mandorlo S., Dickhut R.M., Lepri L., 2003 – Particulate organic compounds in the atmosphere surrounding an industrialised area of Prato (Italy). *Atmospheric Environment* 37, 3125-3133

Cincinelli A., Del Bubba M., Martellini T., Lepri L., 2007 – Gas- particle concentration and distribution n-alkanes and polycyclic aromatic hydrocarbons in the atmosphere of Prato (Italy). *Chemosphere*, in press

Rogge W.F., Hildemann L., Mazurek M.A., Cass G.R., Simoneit B.R.T., 1993 - Sources of fine organic aerosol: 4. particulate abrasion products from leaf surfaces of urban plants. *Environmental Science and Technology* 27, 2700-2711

Mandalakis M., Tsapakis M., Tsoga A., Stephanou E.G., 2002 – Gas- particle concentrations and distribution of aliphatic hydrocarbons, PAHs, PCBs and PCDD/Fs in the atmosphere of Athens (Greece). *Atmospheric Environment* 36,4023-4035

## Monitoring station for ground based tropospheric aerosol properties in Southwest Spain

M. Sorribas<sup>1</sup>, S. Mogo<sup>2,3</sup>, V.E. Cachorro<sup>3</sup>, J. de la Rosa<sup>4</sup>, N. Prats<sup>3</sup>, J.F. López<sup>1</sup>, A.M. Sánchez de la Campa<sup>4</sup>, Y. González<sup>4</sup>, A.M. de Frutos<sup>3</sup> and B.A. De la Morena<sup>1</sup>.

<sup>1</sup> Atmospheric Sounding Station 'El Arenosillo', Earth Observation, Remote Sensing and Atmosphere Department, INTA, Mazagón, 21130, Huelva, Spain.

<sup>2</sup> Physics Department. University of Beira Interior, 6200, Covilhã, Portugal.

<sup>3</sup> Atmospheric Optics Group (GOA-UVA), University of Valladolid, 47071, Valladolid, Spain.

<sup>4</sup> Department of Geology, University of Huelva, 21071, Huelva, Spain.

Keywords: Tropospheric Aerosol, Aerosol Sampling, Monitoring, Coastal Particles, Mineral Dust.

The Atmospheric Sounding Station 'El Arenosillo' belongs to National Institute of Aerospace Technology (INTA). It is a platform to investigate about different atmospheric sciences: aerosols, gaseous pollutants, UV radiation, stratospheric ozone, etc., by in situ and remote sensing techniques. The aim of this work is the general presentation of the in situ aerosol activities in 'El Arenosillo' which are utilities to national and international institutes that take advantage of its good conditions as temporary or continuous observatory.

The station is located at Huelva, in the southwest Atlantic coast of Spain (37.1°N, 6.7°W, 40 m a.s.l.). The exceptional situation allows us to analyze the most frequent Atlantic maritime air masses and Saharan desert dust aerosol intrusions before its modification due to local sources. The Doñana National Park towards the northeast and the Atlantic Ocean towards the southwest, enable us to characterize the aerosol on meteorological local process like breezes, under non pollution conditions.

The surrounding is a homogeneous *Pinus Sylvestris* forest extending several kilometres, except to the south-west where the Atlantic Ocean is at a distance less than 1 km. Huelva City (160000 inhabitants) is located 35 km to the north-west of the station with an important industrial environment.

In situ measurements are carried out in the Atmospheric Aerosol Monitoring Station, a little home-laboratory about 75 m from the main building. The sampling inlet is located 8 meters above ground level and 3 meters over the top of the trees. The Aerosol Sampling System was designed for the extraction of the aerosol from its environment and the transportation to the instruments, with a well characterization of the efficiency, which is applied to the entire data set (Sorribas *et al.*, 2006).

Since July 2004, aerosol particle size distributions measurements are carried out in dry state, with a SMPS particle spectrometer (Scanning Mobility Particle Sizer) model 3936-TSI, in the sub-micrometric range (0.016–0.604)µm, (Sorribas *et al.*, 2007). Simultaneously measurements with an APS (Aerodynamic Particle Sizer) model 3321-TSI, are also performed in the super-micrometric range (0.542–10) µm.

Three wavelengths integrating nephelometer, model 3563-TSI, determines the scattering and backscattering coefficients of aerosols. A Dekati impactor with three stages, PM1, PM2.5 and PM10, permits to determine the mass concentration but also to use the impactor filters to determine the absorption coefficients and the black carbon concentration from an optical technique (Mogo *et al.*, 2005). Two MCV high volume samplers are used to determinate the concentration levels and chemical composition of PM10 y PM2.5. The analytical methodology is based in instrumental techniques in order to elucidate the contents of major and trace elements, soluble anions, ammonium, total carbon, etc, (Mogo *et al.*, 2007; De la Rosa *et al.*, 2006).

This kind of monitoring permits a detailed study of the aerosol particle size distribution, but also a statistical analysis, as monthly or seasonal characterization. This study is of great interest over an area like that of the southwest of the Mediterranean, linked with high level of solar radiation, high frequency of African desert dust intrusions and influenced by many different type of air masses. The statistical relations in terms of their relations to meteorology and synoptical-scale air masses help to understanding the effects of atmospheric particulates over regional climate.

This work was supported by the Spanish "Ministerio de Educación y Ciencia" by means of project CGL2005-05693-C03-02/CLI.

De la Rosa, *et al.* (2006). In Proc. 5<sup>a</sup> AHLGG. Sevilla, Spain, (In press).

Mogo, *et al.* (2005). Geophys. Res. Lett.,32,L13811.

Mogo, *et al.* (2007). *Aerosol Absorption and Chemical Properties during the 'El Arenosillo' 2004 summer campaign. Atmospheric Environment*, (submitted for publication).

Sorribas, *et al.* (2006). In Proc. 5<sup>a</sup> AHLGG. Sevilla, Spain, (In press).

Sorribas, *et al.* (2007). *Characterization of sub-micron number particle size distribution measurements at El Arenosillo Station (south-western, Spain) during periods with prevalence of the accumulation mode. Atmospheric Environment*, (submitted for publication).

## The effect of remote fire smokes on spectral behavior of the scale height of the aerosol atmosphere.

V.N. Uzhegov, Yu.A. Pkhalagov, D.M. Kabanov and S.M. Sakerin

Institute of Atmospheric Optics, Tomsk  
Siberian Branch of the Russian Academy of Sciences

Keywords: atmospheric aerosol, extinction coefficient, optical depth

The effect of the presence of smoke in different layers of air on the spectral behavior of the scale height of the aerosol atmosphere is studied. This term means the value  $Ho(\lambda) = \tau(\lambda) / \beta(\lambda)$ , where  $\tau(\lambda)$  is the optical depth of the aerosol atmosphere measured using Sun radiation at the wavelength  $\lambda$ ,  $\beta(\lambda)$  are the aerosol extinction coefficients obtained from measurements of the spectral transparency of the atmosphere on a near-ground path. Simultaneous measurements of  $\tau(\lambda)$  and  $\beta(\lambda)$  were carried out in summer and autumn 2003 at the outskirts of the city of Tomsk ( $56^{\circ}31'N$ ,  $85^{\circ}08'E$ ) in the wavelength range from 0.45 to 3.9  $\mu m$  (Uzhegov *et al.*, 2005). 480 individual spectra of  $\tau(\lambda)$  and  $\beta(\lambda)$  were obtained during four months, including the events of the presence of remote fire smokes in the atmosphere. Smoke plume of a remote fire can propagate at different heights, depending on meteorological conditions. Taking into account this fact, the total data array was divided into four sub-arrays with different contribution of smoke in the near-ground layer and in the atmospheric column, upon a specially created criterion. The parameters of the sub-arrays are shown in Table 1.

Table 1 *Characteristics of the presence of smoke in air in the near-ground layer and in the atmospheric column*

Curve in the fig. 1	Near-ground layer	Atmospheric column	Number of spectra
1	clean	clean	366
2	smoke	smoke	49
3	smoke	clean	49
4	clean	smoke	16

The greatest quantity of situations corresponded to the clean conditions (curves 1). Equal quantities of spectra were obtained under conditions when smoke was present either in the whole atmospheric column (curves 2) or only in the near-ground layer (curve 3). Finally, the cases were very rare, when smoke was present only on a slant path, but was not in near-ground air.

The spectral dependencies of the parameters  $\tau(\lambda)$ ,  $\beta(\lambda)$  and  $Ho(\lambda)$  averaged according to Table 1 are shown in the Fig. 1. It is seen that the effect of smoke is observed only in the short-wave parts of the dependencies  $\tau(\lambda)$  and  $\beta(\lambda)$ , and there are prac-

tically no differences in the range  $\lambda > 2 \mu m$ . However, slight increase of the scale height in IR wavelength range is seen in the spectral dependence of  $Ho(\lambda)$  in the cases of the presence of smoke in the lower and upper layers (curve 2).

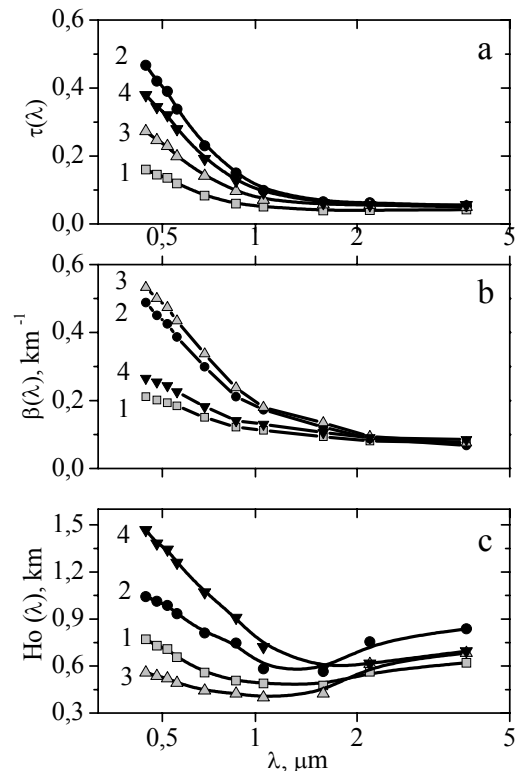


Figure 1. *Spectral behaviors of the parameters  $\tau(\lambda)$ ,  $\beta(\lambda)$  and  $Ho(\lambda)$  for different types of the presence of smoke in the atmosphere (see Table 1).*

On the whole, it follows from the figures that the scale height in visible and IR wavelength range strongly depends on the height location of the smoke layer. The minimum values of scale height are observed in the case when the smoke layer is situated just near the ground, and maximum is in the case then the smoke layer is situated at some height above the ground because of the temperature inversion.

Uzhegov V.N., Pkhalagov Yu.A., Kabanov D.M., Sakerin S.M. & Panchenko M.V. (2005) *Atmos. Ocean Opt.*, 18, N5-6, p. 367-372

## Determination of particle emission factors of individual vehicles under real-life conditions

C. Hak<sup>1</sup>, E. Ljungström<sup>1</sup>, M. Hallquist<sup>1</sup>, M. Svane<sup>1,2</sup> and J. B. C. Pettersson<sup>1</sup>

<sup>1</sup>Department of Chemistry, Atmospheric Science, Göteborg University, 412 96 Göteborg, Sweden

<sup>2</sup>now at Department of Applied Environmental Science, Stockholm University, 106 91 Stockholm, Sweden

Keywords: atmospheric aerosols, traffic, ultrafine particles, urban pollution, vehicles emissions.

Road traffic constitutes an important source of particulate matter and trace gases. Most particles in vehicle exhaust are in the ultrafine size range. In contrast to large particles which are a result of wear of road pavement, tyres and brakes, ultrafine particles are respirable and penetrate deep into the lungs, posing a threat to health. Especially in the densely populated urban areas, road traffic can lead to severe pollution of the ambient air. Since today half of the global population lives in urban areas, it is a matter of public and scientific concern to examine the emissions under real-life conditions.

Here we present an experimental setup for the measurement of particle emission factors (EF) from individual vehicles, which was designed for continuous on-road sampling. The measurement site was at a two-lane road at the periphery of Göteborg (Western Sweden). The measurements were performed monitoring the traffic on one of the two lanes, which is leading towards the city centre. The inlet of a sampling line was installed in the centre of the lane and attached to the street surface to extract air directly (*in-situ*) from the plumes of passing vehicles. To measure CO<sub>2</sub>, number density of particles > 10 nm and particle size distribution (30 nm – 10 µm) simultaneously, the collected air was distributed to a CO<sub>2</sub> monitor, a condensation particle counter (CPC) and an electrical low pressure impactor (ELPI), respectively.

Although the sampled air volume was diluted with a known amount of particle-free background air, the very high particle numbers within the vehicle exhaust plumes gave concentrations exceeding the upper limit of the particle counter. A solution to nevertheless quantify the excess particle numbers in the plume is presented and the particle EF's are derived from the enhancement ratios of particle number to CO<sub>2</sub> mixing ratio in the exhaust plumes of passing vehicles. When assuming a CO<sub>2</sub> emission of 164 g km<sup>-1</sup> veh<sup>-1</sup>, which is an average value for petrol-fuelled vehicles (cp. [www.starterre.fr/voiture-auto/emission\\_co2](http://www.starterre.fr/voiture-auto/emission_co2)), particle emission factors of the order  $2 \times 10^{13}$  part km<sup>-1</sup> veh<sup>-1</sup> were derived from the observed car passages. This value agrees well with those published in the literature for petrol-driven vehicles (e.g. Jones & Harrison, 2006), which constitute more than 90% of the Swedish fleet (Ahlvik, 2002). Given the obtained results, the used

setup proved appropriate to quantify particle emission factors from road traffic.

The characterisation of particle size distributions within vehicle emission plumes using ELPI data revealed three different classes of size distributions, as exemplified in Figure 1. Less than 10% of the particles detected in vehicle emission plumes had sizes > 0.3 µm.

From the measurements and observations from this study it is concluded that simultaneous measurements of CO<sub>2</sub> and particle number for the purpose of characterising individual vehicles' emissions is feasible. Furthermore, by using this method one can link the particle emission to other indicators for traffic exhaust such as NO<sub>x</sub>, VOC or CO in order to better understand real-world vehicle to vehicle variation in particle production.

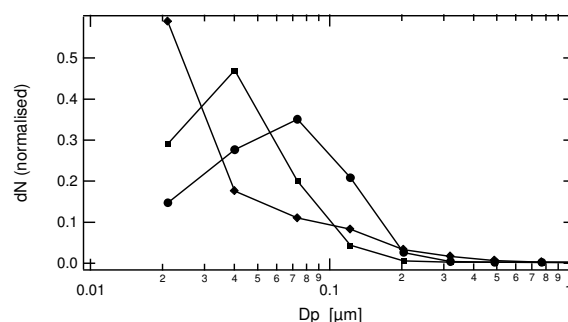


Figure 1. Different classes of particle size distributions for three selected vehicles.

This work was supported by the Swedish Foundation for Strategic Environmental Research MISTRA and the National Swedish Road Administration. We thank the Technical Research Institute of Sweden (SP) for lending the ELPI to us. Benny Lönn, Senior Research Engineer, is acknowledged for skilful technical support.

Jones, A. M., & Harrison, R. M. (2006). *Atmos. Environ.*, 40, 7125-7137.

Ahlvik, P. (2002). *Environmental and Health Impact from Modern Cars*, Report for the Swedish National Road Administration, Publication 2002:62.

## Chemical composition of fine particles in two major biomass burning episodes observed in Helsinki, 2006

S. Saarikoski, K. Saarnio, M. Sillanpää, H. Timonen, K. Teinilä, M. Sofiev, J. Kukkonen and R. Hillamo

Air Quality, Finnish Meteorological Institute, P.O.Box 503, FI-00101, Helsinki, Finland

Keywords: atmospheric aerosols, biomass burning, chemical composition, levoglucosan.

Biomass burning is the dominant source of particulate organic matter on a global basis. The quantity and the composition of particles emitted from biomass burning depend on various factors, such as the composition and structure of the fuel, terrain, weather, and the duration of flaming versus smoldering. Tracers, such as potassium, oxalate and levoglucosan, can be utilised in tracking the transport of particles from biomass burning.

Two episodes of biomass smokes were observed in Helsinki in 2006. The first episode started on April 25 and lasted 12 days. The second episode, in August 1–29, was a series of short-duration concentration peaks. The first episode is characterised more detailed in Saarikoski *et al.* (2007). The episodes observed in Helsinki in 2006 were exceptionally long compared to previously reported episodes (Niemi *et al.*, 2005).

In this study the measurements were performed at an urban background station in Helsinki. Common ions in aerosols and PM<sub>2.5</sub> were measured in real-time. In addition, elemental carbon (EC), organic carbon (OC), water-soluble organic carbon (WSOC), levoglucosan and inorganic ions were determined from the PM<sub>1</sub> filter samples.

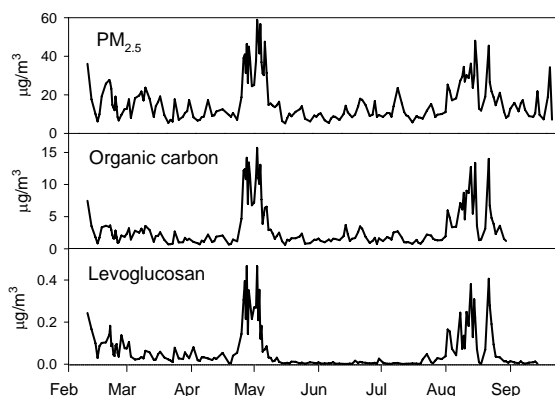


Figure 1. Daily mean concentrations of PM<sub>2.5</sub>, OC and levoglucosan in Helsinki from February to September, 2006.

The first episode is clearly seen in the PM<sub>2.5</sub> concentration (Fig. 1). The second episode had short-duration, high-concentration peaks and is not seen so clearly in the 24-h averaged data. The concentration of OC (Fig. 1) as well as that of WSOC increased remarkably during both episodes. EC was elevated

only during the first episode. The difference in the EC concentrations can be due to the different stages of the burning as well as the different material burnt during the episodes. In addition, the source area and the transport time differed between the episodes. Biomass burning origin for both episodes was evident on the basis of the tracer compound, levoglucosan (Fig. 1).

The chemical composition of fine particles was different during the two episodes. The contribution of WSOC, EC and inorganic ions to PM<sub>2.5</sub> was higher in the first episode than in the second one (Table 1). However, the contribution of OC to PM<sub>2.5</sub> was similar in both the episodes. Compared to the non-episodic period, the contributions of OC and WSOC to PM<sub>2.5</sub> were clearly higher during the episodes, whereas that of inorganic ions was lower. For EC, the contribution to PM<sub>2.5</sub> during the non-episodic period was close to that in the episode 1. The model computations showed that during the episodes the biomass smokes came from western part of Russia.

Table 1. The mean contribution of OC, WSOC, EC and inorganic ions to PM<sub>2.5</sub> during the episodes and the non-episodic period.

% of PM <sub>2.5</sub>	Non-episodic	Episode 1	Episode 2
OC	14	25	25
WSOC	7.0	16	14
EC	6.5	6.7	3.9
Ions	29	18	11

This work was supported by the Finnish Funding Agency for Technology and Innovation (grant no. 40531/04), the Academy of Finland (contract no. 201131), Maj and Tor Nessling Foundation (grant no. 2006167) and Graduate School in Environmental Health (SYTYKE).

Niemi J.V., Tervahattu H., Vehkamäki H., Martikainen J., Laakso L., Kulmala M., Aarnio P., Koskentalo T., Sillanpää M. and Makkonen U. (2005). *Atmos. Chem. Phys.* 5, 2299–2310.

Saarikoski S., Sillanpää M., Sofiev M., Timonen H., Saarnio K., Teinilä K., Karppinen A., Kukkonen J. and Hillamo R. (2007). *Atmos. Environ.* doi:10.1016/j.atmosenv.2006.12.053.

## Traffic and Meteorological Influence on Size Segregated Trace Elements at a Kerbside in Dresden, Germany

H. Gerwig<sup>1</sup>, E. Brüggemann<sup>2</sup>, Th. Gnauk<sup>2</sup>, K. Müller<sup>2</sup>, H. Herrmann<sup>2</sup>

<sup>1</sup>LfUG - Section Air Quality, Saxon State Agency for Environment and Geology, 01109 Dresden, Germany, Holger.Gerwig@smul.sachsen.de

<sup>2</sup>Leibniz-Institute for Tropospheric Research, 04318 Leipzig, Germany

Keywords: size segregated aerosols, trace elements, urban aerosols, ultrafine particles

High concentrations of PM<sub>10</sub> have been frequently measured at air quality monitoring stations in the agglomeration areas near road traffic. To understand the reasons for the adverse health effects it is very important to know more about the chemical composition of urban aerosols at kerbsides. Traffic is often the most important source for PM<sub>10</sub> and for toxic substances like antimony, copper and soot (Gerwig et al. 2006).

At roadside (55,000 vehicles per day, 8 % heavy duty vehicles, Dresden, Schlesischer Platz) 24h Berner Impactor samples were taken on Thursdays or Fridays (9), on Sundays (2) and on new years day between Aug-2003 and Aug -2004.

Additionally 2 samples were taken from a station of urban background (400 m to north east from traffic station at least 100 m away from streets with less than 5,000 vehicles per day).

Br, Cr, Cu, Fe, Mn, Ni, Pb, Si, Ti and Zn were analysed by PIXE. Ca, K, Mg and Na were analysed by special Ion Chromtography.

Crustal enrichment factors (CEFs) are calculated to assess anthropogenic contributions. For all elements CEFs are calculated by dividing the average concentration in the stages by their average abundance in the upper continental crust (UCC). We refer to UCC as described by Mason and Moore (1985). CEFs > 10 are commonly interpreted as PM sources different from natural origin. Si was chosen as reference element, because it is main component of silicate minerals. Often Al is used as reference element (Birmili et al. 2006).

Pb, Zn and Cu had crustal enrichment factors (CEFs) above 100 for all particle sizes.

The CEFs and concentrations of Fe and Cu are higher for workdays compared to Sundays. On working days Cu and Fe showed a concentration maximum on stage 4. When working day is compared to Sunday for Cu and Fe, the maximum of the normalised mass concentration shifted from coarse particles to fine particles.

3 Types of mass size distributions were found: unimodal in fine (stage 3): K, Pb, and Zn; unimodal in coarse: Na, Mg, Ca, Al, Si, Fe, Ti and Cu; Multimodal Mn, Cr and Ni.

Higher concentrations in winter were found for: mass, Pb, Zn, K and Cr, Ni, Ti. The higher concentrations for Pb, Zn and were mainly caused by fine particles. The Pb-concentration was more than two times higher in winter compared to summer. Ca,

Cu and Fe showed no relation to summer/winter as well as Si and Ti.

The anthropogenic elements Pb and K show highest concentration with air masses from the east. Greatest part of the sea salt elements Na and Mg came from northern or western air masses from the sea. The origin of air masses had almost no influence on concentrations of Cr, Cu, Zn, Ca, Ti, Si and Fe.

New Year's Day is characterised in Dresden by lowest number of vehicles during the whole year. Only 50% of the average numbers of vehicles were observed.

The daily average concentration of New Years Eve compared to the annual average was at least 3 times higher for K (24.1), Mg (6.0), Pb (5.3), Ti (4.2) and Cu (3.2). The size distribution maximum of Cu, Ti and Mg shifted from coarse particles to fine particles because of high concentration of firework burning products in the fine particulate range.

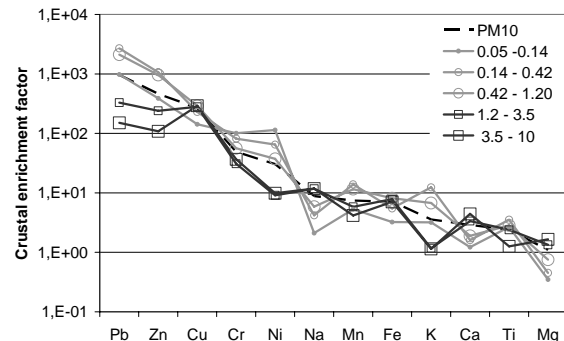


Figure 1: Crustal enrichment factors at traffic station

This work was supported by the Saxon State Agency for Environment and Geology. under reference number 13-8802-3520/10. The authors would like to thank the University of Lund (Per Kristiansson) for analysing the elements by PIXE.

Birmili, W., Allen, A. G., Bary, F., Harrison, R. M. (2006). *Environ. Sci. Technol.*, 40, 1144-1153.

Gerwig, H.; Bittner, H.; Brüggemann, E.; Gnauk, T.; Herrmann, H.; Löschau, G.; Müller, K. (2006). *Gef. Reinhalt. Luft*, 66, 175 – 180.

Mason, B., Moore, C.B. (1985). *Grundzüge der Geochemie*, Monographie; Ferdinand Enke Verlag Stuttgart.

## The natural aerosol field over Northern Europe - Implications of important climate feedbacks

P. Tunved<sup>1</sup>, H-C. Hansson<sup>1</sup>, B. Svenningsson<sup>2</sup>, V-M. Kerminen<sup>3</sup>, J. Ström<sup>1</sup>, M. Dal Maso<sup>4</sup>, H. Lihavainen<sup>3</sup>, Y. Viisanen<sup>3</sup>, P.P. Aalto<sup>4</sup>, M. Komppula<sup>4</sup> and M. Kulmala<sup>4</sup>

<sup>1</sup>Dep. of Applied Environmental Science (ITM), Stockholm University, SE-106 91, Stockholm, Sweden.

<sup>2</sup>Dept. of Physical Geography and Ecosystems Analysis, Lund Univ., P.O. Box 118, S-221 00 Lund, Sweden

<sup>3</sup>Finnish Meteorological Institute (FMI), Erik Palmenin Aukio 1, FI-00101, Helsinki, Finland.

<sup>4</sup>University of Helsinki, Department of Physical Sciences, Gustav Hällströmin katu, FI-00014, Helsinki, Finland

Keywords: Atmospheric aerosols, particle formation, second organic aerosol, natural aerosols, climate effect.

Aerosols in the atmosphere most likely have a large impact on climate due to both indirect and direct scattering of incoming solar radiation. The radiation forcing resulting from aerosol emissions (negative) and emission of greenhouse gases (positive) in the atmosphere is comparable in magnitude. Changes in particle emissions could therefore have substantial impact on earth's climate. Still, both particle sources and determining atmospheric processes are poorly quantified. It is therefore not yet possible to make precise estimates of the particles impact on the radiation balance of the atmosphere. The carbon containing fraction of the atmospheric aerosol has a central role in the atmosphere, making up 10-90% of the fine particle mass, and where 85% of the Volatile Organic Compounds (VOC's) comes from natural sources.

For the Scandinavian region, it has been shown that natural biogenic emissions of monoterpenes dominate VOC concentrations (Laurila and Lindfors., 1999). Monoterpenes emissions from pine and spruce are mainly controlled by temperature, and pool dependent emissions from spruce and pine are exponentially dependent on temperature (Guenther et al., 1995). There is increasing evidence that several of these compounds partake in gas-to-particle formation (Kavouras et al., 1998).

For the Scandinavian region, Tunved et al. (2006a, 2006b) have shown both qualitatively and quantitatively that the monoterpene emissions from the boreal forest at high latitudes in Europe potentially contribute to particle generation with an apparent yield in the range of approximately 5-10%. Oxidation products from monoterpenes have been identified in recently formed particles and several investigations of new particle formation events during the biologically active seasons indicate that biogenic aerosol precursor's gases are necessary to support the observed mass increase during particle formation events (Kulmala et al., 2000). Anthropogenic sources in this area are sparse. Together, the results indicate the biogenic emissions (most likely monoterpenes) completely dominate the evolution of the aerosol during transport of clean

marine air over Fenno-Scandinavia. Furthermore, increasing temperatures increase, at least initially, the monoterpene emission rates. Since the link between monoterpene emissions and aerosol formation is established it is also possible that increased forest emissions could provide cooling in times of a warming climate. The direct response of BVOC emissions to temperature is the result of enhanced production rate and increased vapour pressure of the compounds.

In this study we adopt a statistical approach to quantitatively investigate how the natural aerosol contributes to the regional aerosol fields over northern parts of Europe. We will make use of the simple but efficient parameterisation of particle formation potential resulting from monoterpene emissions described by Tunved et al (2006a). We will further investigate how the pool dependent monoterpene emissions changes with increased temperature, and thus move the knowledge forward towards projections on the future role of the boreal forest in a changing atmosphere.

This work was carried out within the frameworks of ASTA, Swedish Science Foundation and the Nordic Centre of Excellence BACCI.

European Commission: Biogenic VOC emissions and photochemistry in the boreal regions of Europe – Biphorep Edited by Tuomas Laurila and Virpi Lindfors, 1999 – 158 pp., ISBN 92-828-6990-3.

Kavouras, I.G., Mihalopoulos, N., Stephanou, E.G., Nature, 395, 683-686, 1998.

M. Kulmala *et al.*, *Tellus B* **53**, 324, (2001).

Guenther A, et al. , J Geophys Res., 104:8113–52, 1999

Tunved, P., Hansson, H.C., Kerminen, V.M., Ström, J., Dal Maso, M., Lihavainen, H., Viisanen, Y., Aalto, P.P., Komppula, M., Kulmala, M., Science, 312, 261-263, 2006a.

Tunved, P., Korhonen, H., Ström, J., Hansson, H-C., Lehtinen, K.E.J, Kulmala, M., Tellus, 58B, 129-140, 2006b.

## Coarse particles of probably volcanic origin collected with a passive sampler at NE-Greenland

E.Schultz<sup>1</sup>, B. Sittler<sup>2</sup> and V.Dietze<sup>1</sup>

<sup>1</sup>Deutscher Wetterdienst, Department of Human Biometeorology, 79104 Freiburg, Germany

<sup>2</sup>University of Freiburg, Institute for Landscape Management, 79085 Freiburg, Germany

Keywords: Arctic aerosol, volcanic particles, long-range transport, single particle analysis, sulphate

Particle deposition was measured with a passive sampler for nearly 15 years at NE Greenland. The sampling was conducted along with the long-term observation of lemming cycles within the Karupelv Valley Project running since 1988. The sampling site is located on Traill Island, in the NE Greenland National Park at about 72°30' north and 24° west. The sampling site is located more than 500 km apart from the next settlement possibly releasing particulate pollutants.

Weekly deposition samples were collected with the sampling device Sigma-2 according to VDI 2119-4 (1998) between end of June and end of August in the years 1991 to 2006, except 2000/2001. After transport back to Europe the samples were microscopically analysed with an automated image processing system at the facilities of the German Weather Service in Freiburg. Single particle analysis provided size and mean grey value of each particle between 3 µm to 100 µm geometric diameter. Additionally, sulphate deposition was analysed by ionchromatography.

Temporal analysis shows an obvious trend for the coarse particle fraction, in particular for a black component, and for sulphate. The latter components start on a high level in the years 1991 to 1993, afterwards continuously decrease till 1997 and remain on the achieved low level till the end of the period. The high level at the beginning coincides with two big volcano eruptions, one by the Hekla on Iceland in January 1991, and the other by the Pinatubo on the Philippines in June 1991.

Size distributions of the collected samples reflect the described trend in a more detailed manner. The temporal course is presented by the smallest particle fraction sampled between 3 and 10 µm particle diameter and is again most visual for the black component (Fig. 1).

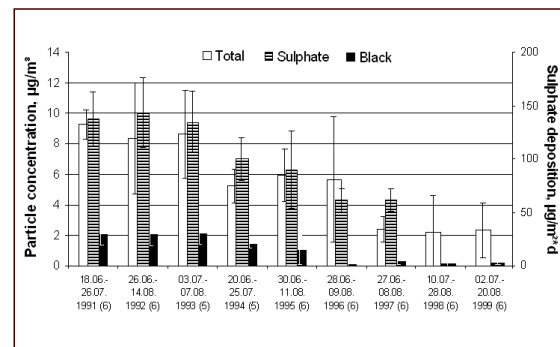


Figure 1. Concentration of total and black particles in the size range 3 – 10 µm and sulphate deposition in the summer seasons from 1991 – 1999.

The concentration of the bigger particles > 10µm keeps low over the whole period. The size distribution shows no systematic variation over the time for these particles.

The atmospheric residence time of particles between 3 and 10 µm is known to reach several weeks to months. Therefore, they may have been originated far away from the sampling site, e.g. by the mentioned eruptions. Also, the simultaneous increase of sulphate can be attributed to these sources. A microscopic inspection of selected black particles additionally revealed a porous, tephritic structure, another hint on the volcanic origin.

Volcanic particles of the Pinatubo eruption were recently reported to be found in snow samples of the Antarctic (Baroni et al., 2007). However, more detailed analysis has to confirm the volcanic origin of sampled particles in the present case. Morphological studies by confocal Laser Scan Microscopy and tracer element analysis by electron microprobe are in progress.

Baroni, M. et al., Science 315, 2007, 84

## Monitoring of atmospheric aerosols over Baikal Lake

V.A. Zagaynov<sup>1</sup>, T.V. Khodzher<sup>2</sup>, Yu.G. Biryukov<sup>1</sup>, V.A. Obolkin<sup>2</sup>, J.S. Lyubovtseva<sup>5</sup>, A.A. Lushnikov<sup>1</sup>

<sup>1</sup>Karpov Institute of Physical Chemistry, 10 Vorontsovo Pole str., 105064, Moscow, Russia

<sup>2</sup>Limnological Institute, Siberian Branch of RAS, 3 Ulanbatorskaya, 664033, Irkutsk, Russia

<sup>3</sup>Geophysical Center of RAS, Moscow, Russia

Keywords: atmospheric aerosols, size distribution, monitoring.

The problem of the particle birth in atmosphere is of great importance (Kulmala *et al.*, 2004). It is well known, that atmospheric aerosol impact on the local weather and global climate. The atmosphere is adjusted to natural aerosols, anthropogenic aerosol inserts new effects into exchange between sun radiation and Earth. To clear up the situation it is important to compare the nucleation in atmosphere of background, industrial and boundary regions. To this end the parameters of atmospheric aerosols were measured during one year.

Aerosol concentration, averaged particle radius and particle size distribution width were measured by diffusion aerosol spectrometers (Julanov *et al.*, 2002). This equipment was used because it covered wide range of particle sizes and time, required for one measuring, is in the interval between 2 – 4 minutes dependent on particle concentrations. To identify the sources of aerosol particles in atmosphere it air pressure, humidity, wind direction and velocity. Sometimes the SO<sub>2</sub> concentrations were measured in atmosphere too.

The measuring point was situated on the shore of Baikal Lake elevated over sea level at 700 m. Industrial centres of Irkutsk are 70 km away to north west and Baikal pulp and paper mill – 70 km away to south west. All the rest territory is covered by coniferous and deciduous forests.

The distance to opposite shore of the lake is approximately 40 – 50 km away. It means that wind direction defines aerosol mixture of the atmosphere. At the same time it has to be taken into account, that it was cases, when at different elevation wind direction was different.

The figure shows that particle concentration grows when SO<sub>2</sub> concentration grows too. It means, that SO<sub>2</sub> take part in particle nucleation. When particle concentration grows its size drops that is portion of most small particle at this time increased.

The analysis of these figures has shown, that (1) particle nucleation rate can reach up to 0.2 – 2 cm<sup>-3</sup> c<sup>-1</sup>. Some times nucleation rate may be much greater, but these periods are very short (less than 10 min.) and we regarded it as fluctuations. (2) Particle growth rate can reach up to 2 – 20 nm per hour, some times these values were exceeded, but during short periods. (3) The concentrations of vapours which provide this growth are in the range 10<sup>14</sup> – 10<sup>15</sup> m<sup>-3</sup>.

Comparison between particle concentrations, sizes, and SO<sub>2</sub> (07.07.05)

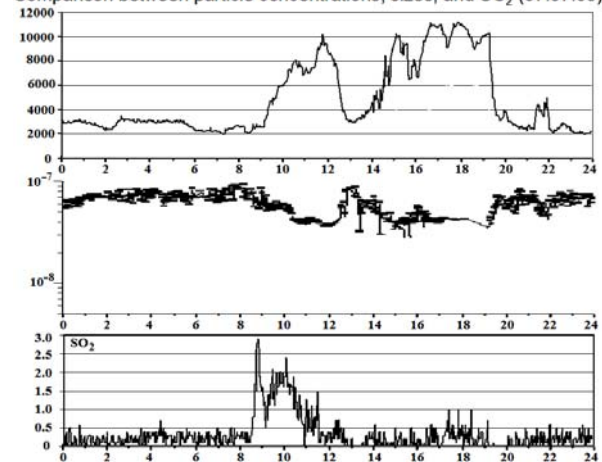


Figure 1. Evolution of particle total concentration on 07 of July 2005 with time (upper figure – particles per cm<sup>3</sup>) averaged particle size (middle figure – size in m) and SO<sub>2</sub> gas concentrations (lower figure – mass per m<sup>3</sup>). Horizontal line – time in hours.

These values are 2 orders of magnitude less, than concentrations of gas SO<sub>2</sub>. We did not find cases, when concentration NO<sub>x</sub> correlated with aerosol concentrations and particle size distributions.

It were found, that when wind went from industrial regions, concentration of nano aerosols correlated with concentrations of particles with size greater 0.1 micro m. When wind went from background regions, these correlations were absent.

This work was supported by International Science and Technology Center, project # 1908.

Kulmala, M., Vehkamäki, H., Petäjä, N., Dal Maso, M., Lauri, A., Kerminen, V.-M., Birmili, W., & McMurry, P.C. (2004), *J. Aerosol Science*, 35, 143-176.

Julanov, Yu.V., Lushnikov, A.A., & Zagaynov, V.A. (2002). *Atmospheric Research*, 62, 295-302.

## **Biomass Burning traces in Antarctic Ice.**

R. Zangrando<sup>a</sup>, A. Gambaro<sup>a,b</sup>, C. Barbante<sup>a,b</sup>, P. Gabrielli<sup>b</sup>, W. Cairns<sup>b</sup>, C. Turetta<sup>b</sup> and P. Cescon<sup>a,b</sup>.

<sup>a</sup>*Department of Environmental Sciences, University of Venice, Ca' Foscari, 30123 Venice, Italy*

<sup>b</sup>*Institute for the Dynamics of Environmental Processes-CNR, University of Venice, Ca' Foscari, 30123 Venice, Italy*

Keywords: antarctic aerosols, biomass burning, levoglucosan, long-range transport.

On a global basis biomass burning is a significant source of aerosol particles to the atmosphere that produce an impact on global climate by mostly absorbing radiation, but they also act as cloud condensation nuclei and often affect regional and local air quality. The chemical composition inventory of aerosol particulate matter is important for understanding the organic component contribution of biomass burning emissions to atmospheric chemistry, and complements existing data on the signatures of direct organic emissions from biomass sources.

Levoglucosan (1,6-anhydro- $\beta$ -D-glucopyranose) is a specific tracer, it is indeed source-specific to combustion of any fuel containing cellulose, it is stable in the atmosphere over a period of 10 days indicating the presence of emissions from biomass burning in atmospheric particulate matter. It is also a marker for long range transport of biomass combustion aerosols and can be used in sediment or ice for paleorecord and paleoclimatic studies.

The aim of this work was to develop a high performance liquid chromatography with triple

quadrupole tandem mass spectrometry (LC-MS/MS) method for the direct determination of Levoglucosan without the need of any kind of preconcentration.

The ice core sections analysed were retrieved from Antarctica at Dome C, within the framework of the European Project for Ice Coring in Antarctica (EPICA).

During the development of this method, contamination problems were carefully taken into account by adopting ultraclean procedures during the sample pre-treatment phases.

The ice core samples selected to test the developed method cover the last glacial age and the last interglacial period and the concentration of Levoglucosan in the inner ice core are within the picogram per gram range. An evident difference in the Levoglucosan concentration can be observed amongst these samples with inner ice core samples from the interglacial period showing lower concentrations than those from the glacial period.

The results obtained in this study are an important indication of the impact biomass burning aerosols have during different climatic periods, and highlights the need for more in depth studies.

## Aerosol sources apportionment at Lampedusa island (Central Mediterranean Sea)

S. Becagli<sup>1</sup>, E. Castellano<sup>1</sup>, M. Severi<sup>1</sup>, R. Traversi<sup>1</sup>, D.M. Sferlazzo<sup>2</sup>,  
C. Bommarito<sup>2</sup>, A. di Sarra<sup>3</sup>, F. Lucarelli<sup>4</sup>, F. Marino<sup>1</sup>, S. Nava<sup>4</sup>, F. Ruggi<sup>1</sup>, R. Udisti<sup>1</sup>

<sup>1</sup>Department of Chemistry, Scientific Pole, University of Florence, Sesto F.no, I-50019, Florence, Italy

<sup>2</sup>ENEA, Climate laboratory, I-90141, Palermo, Italy

<sup>3</sup>ENEA, C.R. Casaccia, I-00123, S. Maria di Galeria, Italy

<sup>4</sup>Department of Physics, University of Florence and INFN, Sesto F.no, I-50019, Florence, Italy

Keywords: Marine aerosol, ions, mineral dust, sources apportionments, principal component analysis.

Earth's climate is heavily affected by atmospheric aerosols. They attenuate the solar radiation, modify its vertical distribution, affect the infrared balance, and, indirectly, influence the cloud structure and properties. The uncertainties in the estimation of direct and indirect radiative forcing from aerosols are related to the insufficient knowledge of the high spatial and temporal variability of aerosol concentrations, of their microphysical, chemical and radiative properties (IPCC, 2001). Therefore, there is an urgent need for systematic studies of physical and chemical properties of the atmospheric aerosol. In particular, aerosol measurements in the Mediterranean basin are scarce. In order to fill this gap, a sampling campaign was carried out at the Station for Climate Observations located on a 45 m high plateau on the North-Eastern coast of Lampedusa (35° N, 12.6° E). At the station, continuous observations of greenhouse gases concentration, aerosol properties, total ozone, ultraviolet irradiance, and other climatic parameters are carried out (di Sarra *et al.*, 2002).

During the period June 2004- January 2006 aerosol sampling was performed with daily resolution by pre-selected cut-off sampler equipped alternatively with PM10, PM2.5 and PM1.0 heads. After mass determination, each filter was analyzed for main and trace ions (Na, NH<sub>4</sub><sup>+</sup>, K<sup>+</sup>, Mg<sup>2+</sup>, Ca<sup>2+</sup>, F<sup>-</sup>, Cl<sup>-</sup>, NO<sub>3</sub><sup>-</sup>, SO<sub>4</sub><sup>2-</sup> methanesulphonate – MSA, acetate, formate, glycolate, oxalate), and selected metals, (soluble fraction at pH = 1.5). Half filter was kept frozen for elemental analysis by PIXE.

The Absolute Principal Component Analysis (APCA) model (Swietlicki *et al.*, 1996) is applied to the chemical data in order to obtain the source apportionment of the soluble fraction of PM10 at Lampedusa. The dominant source from the measured species are primary marine, crustal, secondary and continental-anthropogenic. The sources temporal profiles are reported in figure 1.

Sea spray is the dominant source aerosol in this area and it is represented by the first factor containing large loadings of Na<sup>+</sup>, Mg<sup>2+</sup>, K<sup>+</sup>, Cl<sup>-</sup>.

Though here we consider only the soluble fraction of aerosol, the second factor is represented by crustal element such as Al, Mn, Fe and Ca, revealing how much continental dust contributes to the total aerosol load at Lampedusa Island. This

source shows several spikes that back-trajectory analysis allows to attribute to intrusion of air masses from the Sahara desert.

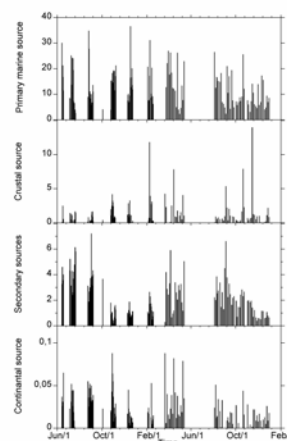


Figure 1. Time series of the daily sources contribution expressed as ng m<sup>-3</sup>.

The secondary inorganic aerosol is related to nssSO<sub>4</sub><sup>2-</sup>, MSA, oxalate and NH<sub>4</sub><sup>+</sup>. This source has a marked seasonal pattern with maximum values in summer. This pattern could be explained by an increase of natural (phytoplanktonic blooms) and anthropic (tourism) sources and by a higher efficiency in photochemical oxidation of its precursor SO<sub>2</sub>.

Linear regression analysis on PM2.5 and PM1 shows a close (R > 0.84) correlation between SO<sub>4</sub><sup>2-</sup> and NH<sub>4</sub><sup>+</sup> with a slope showing mol/mol ratios between 1 and 2, so revealing a contemporaneous contribution of (NH<sub>4</sub>)<sub>2</sub>SO<sub>4</sub> and NH<sub>4</sub>HSO<sub>4</sub>.

The last factor, containing glycolate, formate) and NO<sub>3</sub><sup>-</sup>, represents the continental anthropized aerosol. Back-trajectory analysis shows that spikes in this source are mainly related to air masses coming from polluted European areas.

This work was supported by "SNUMMAS" project.

IPCC, 2001. *Climate change 2001*. In: Watson, R., *et al.* (Eds.). U.K. Cambridge University Press, 98p.  
Swietlicki, S.P., Hansson H-C., & Edner, H. (1996). *Atmos. Environ.*, 30, 2795-2809.

di Sarra, A., and 9 others. (2002), *J. Geophys. Res.*, 107(D18), 8135, doi:10.1029/2000JD000139.

## Annual variability of aerosol load and chemical composition in two sites at different anthropic impact in Sesto F.no area (Florence-Italy) - PASF Project

R. Traversi<sup>1</sup>, S. Becagli<sup>1</sup>, E. Castellano<sup>1</sup>, O. Cerri<sup>1</sup>, M. Chiari<sup>3</sup>, F. Lucarelli<sup>3</sup>,  
F. Marino<sup>1,4</sup>, A. Morganti<sup>1</sup>, F. Rugi<sup>1</sup>, M. Severi<sup>1</sup> and R. Udisti<sup>1</sup>

<sup>1</sup>Chemistry Dept., University of Florence, Sesto F.no (Florence), I-50019, Italy

<sup>3</sup>INFN and Physics Dept., University of Florence, Sesto F.no (Florence), I-50019, Italy

<sup>4</sup>Environmental Science Dept., University of Milano-Bicocca, Milano, I-20126, Italy

Keywords: chemical composition, aerosol size distribution, anthropogenic aerosol, source identification, soluble fraction

In the framework of a collaboration agreement between the Chemistry Dept. of the University of Florence and municipality of Sesto Fiorentino, a 50,000-people city close to Florence (Italy), a project (PASF - Atmospheric Particulate in Sesto Fiorentino) on sampling and chemical analysis of atmospheric particulate has been started in 2004, aiming to the identification of emission sources and transport processes controlling particulate atmospheric concentration in Sesto F.no area.

PM10 aerosol has been collected daily in two sites at different anthropic impact. The first is located in an urbanised area, close to a trunk-road with a quite high traffic density; the sampler is on the roof of a building (Villa San Lorenzo – VSL, 50 m a.s.l.) about 10 m high. In the same site, PM2.5 has been also collected since 2005 and a study of chemical component distribution in different size classes through an 8-stage impactor was accomplished.

The second site is located in the hilly area north of Sesto F.no (Monte Morello - MM, about 750 m a.s.l.), about 8 km (as the crow flies) far from the first site. The geographical setting of this site, located above possible inversion layers occurring in winter over the Florence valley, makes it particularly useful for the evaluation of the atmospheric concentrations of the mid-scale background aerosol.

Sampling devices followed the EN 12341 European Directive collecting aerosol on Teflon filters for 24 h at the flow of 2.3 m<sup>3</sup>/h. Teflon filters, weighed in standard conditions, were analysed for ionic content by Ion Chromatography and for selected metals (Al, Fe, Mn, Zn, Cu, Cr, Ni, V, Pb, Cd, Mo, As and Hg) by HR-ICP-MS.

The urban site of VSL shows a relatively high PM10 load, sometimes (mainly in winter) exceeding the current law limit of 50 µg/m<sup>3</sup> (EU-Directive 1999/30/CE). PM2.5 annual mean values were about 70% of PM10 contemporaneously measured. Besides, PM10 and PM2.5 temporal trends were very similar.

The rural site of MM shows a lower PM10 load, never overtaking the 24-h limit of 50 µg/m<sup>3</sup>. PM10 mean concentrations are here higher in summer than in winter, probably due to higher crustal inputs, vegetative emissions and more frequent uplift

of air masses from Florence and Sesto F.no anthropized areas.

Sulphate, nitrate and ammonium dominate the ionic composition of both PM10 and PM2.5 at VSL. These ions, originated by secondary atmospheric processes, are mainly distributed in the finest fraction. On the contrary, Ca and Na, coming from primary sources (crustal and sea-spray, respectively), show higher concentrations in the PM10.

Mean annual PM10 at MM is about 2 times lower than at VSL showing, in percentage, similar values for nitrate and Na and higher contributions of ammonium and sulphate.

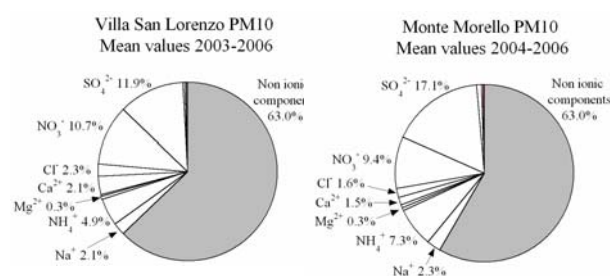


Figure 1. Mean ionic composition with respect to total particulate weight for PM10 collected in the urban (left) and rural (right) site in Sesto F.no.

Size-segregated aerosol collection at VSL by multi-stage impactor confirmed that Na and Ca are mainly distributed in the micrometric mode (centred around 2-4 and 4-6 µm, respectively) and sulphate and ammonium are contemporaneously present in finest fraction (0.3 µm). Interestingly, nitrate is mainly distributed in coarse particles (3-5 µm mode). In order to achieve information on the effect of the mixing layer height in concentrating local-sources anthropic emissions, Rn-family radioactive measurements were carried out with hourly resolution at VSL since 2006 by a FAI-PBL instrument. This measure is used as a proxy-marker of changes in mixing layer height, if Rn soil emission can be considered constant. Rn-family concentrations were compared with PM10 concentrations and local temperature, revealing that PM10 spikes in winter were mainly related to atmospheric conditions unfavourable for free atmospheric circulation (inversion layer formation).

## Primary Marine Aerosol emissions on the North Atlantic MAP-cruise 2006: combining eddy covariance flux measurements with in situ laboratory tank experiments

E. D. Nilsson<sup>1</sup>, K. Hultin<sup>1</sup>, E. M. Mårtensson<sup>1,2</sup>, R. Krejci<sup>2</sup>, D. Broman<sup>1</sup>, J. Hagström<sup>3</sup>, K. Rosman<sup>1</sup>, J. Bäcklin<sup>2</sup>, M. C. Facchini<sup>4</sup>, C. O'Dowd<sup>5</sup> and G. de Leeuw<sup>6</sup>

<sup>1</sup>Department of Applied Environmental Science, Stockholm University, Stockholm, Sweden

<sup>2</sup>Department of Meteorology, Stockholm University, Stockholm, Sweden

<sup>3</sup>Department of Biology and Environmental Science, Kalmar University, Kalmar, Sweden

<sup>4</sup>Institute of Atmospheric Sciences and Climate (ISAC-CNR), Bologna, Italy

<sup>5</sup>Department of Experimental Physics & Env. change Institute, National University of Ireland, Galway, Ireland

<sup>6</sup>Finnish Meteorological Institute/Department of Physical Sciences, University of Helsinki, Helsinki Finland

Key words: primary marine aerosols, sea spray, aerosol emissions, sea salt, primary organic aerosols, eddy covariance fluxes, bubble bursting, aerosol size spectra, aerosol laboratory experiments

Aerosol emissions from bubble bursting in breaking waves are the strongest aerosol source globally. It causes air-sea-transfer of sea salt, organics, pollutants and bacteria, and enriches surface-active compounds in the aerosol. These aerosol particles serve potentially as cloud condensation nuclei (CCN) influencing climate through their effect on cloud albedo. Sea salt is also the major remote marine light-scatterer. Most graduate students in atmospheric science are still taught that sea spray is all super micrometer sized and sea salt only, despite increasing experimental evidence that: 1. The number production is dominated by sub micrometer particles. 2. There is a large organic fraction (O'Dowd et al., 2004). Climate or transport models include so far only sea salt and until recently parameterisations valid only for the super micrometer, sometimes extrapolated into the sub micrometer. Mårtensson et al. (2003) and Clarke et al. (2006) offers new sub micrometer sea salt parameterisations, which global modellers have begun to use (Pierce and Adams, 2006), with results that emphasize the importance of sub micrometer sea salt particles as CCN. Nilsson et al. (2007) have validated the parameterisation of Mårtensson et al. (2003) by eddy covariance flux measurements in the OPC range (0.1-1.1  $\mu\text{m } D_p$ ). Despite this progress, two major problems remain: a) The emissions  $>100 \text{ nm}$  are not yet validated. b) The organic fraction is yet not quantified.

To overcome these problems, an integrated experiment with two main components was designed as part of the MAP-EU-project: I) in situ laboratory tank experiments with artificial bubble and aerosol production in water sampled on line simultaneously to II) eddy covariance flux measurements. This combination allows direct emission measurements of those aerosol parameters that can be used for eddy covariance (sensors response time not exceeding 1 second), while slow response instruments and aerosol sampling can be performed in the tank experiment. These included detailed aerosol distributions below the OPC range with a DMPS system, detailed (in)organic chemical aerosol analysis on Berner impactor samples, sampling of bacterial and intra cellular DNA, and of persistent organic pollutants (POPs), and bubble spectra. We used one smaller motion-stabilised, and four 200 l high-grade stainless steel tanks. Comparable aerosol instrumentation in the flux-system and laboratory and volatility measurements was used as a link between flux measurements, aerosol physics and detailed chemistry. Our hope is will allow us to scale slow measurements to the direct fluxes, and hence derive source

parameterisations for the organic and biological aerosol fractions, and for particles below the OPC range.

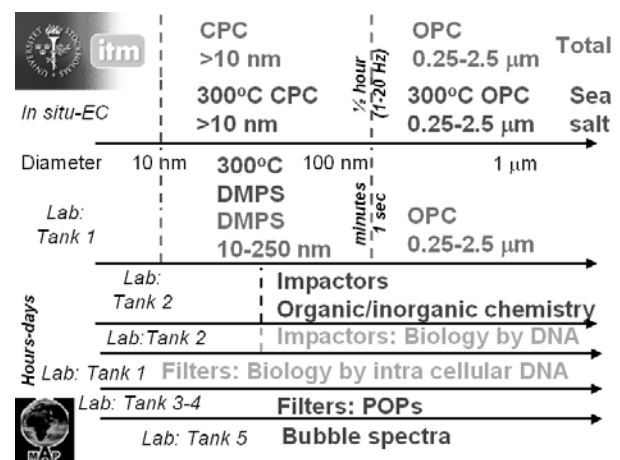


Figure 1 summarises schematically the various measurements involved and the different size ranges and time scales taken into account.

The approach was first tested on a smaller campaign in September 2005 by the Baltic Sea, before the main campaign during a 4-week ship-borne cruise over the North Atlantic, from the 11<sup>th</sup> of June to the 5<sup>th</sup> of July, 2006, on board the Celtic Explorer. The experiment required the collaboration of several research groups. We will focus on the first results with emphasis on weather the experiment appears to have fulfilled its objectives and those separate steps that are necessary to connect in situ fluxes, tank aerosol physics, chemistry and biology, dwelling on the possibility to derive a complete size resolved emission spectra from 10 nm to 2.5  $\mu\text{m } D_p$  and the quantification of the sea salt and organic fractions, and to compare these with existing sea salt parameterisations and outline the future construction of a primary marine organic aerosol source parameterisations. Detailed analysis of the aerosol fluxes, aerosol physics, chemistry, biology and bubble spectra will be presented elsewhere.

Acknowledgements. The European Commission, FORMAS, Swedish Research Council, and several national organisations.

Mårtensson, E.M., et al. (2003), *J. Geophys. Res.*, 108, 4297

Clarke, A.D. et al., (2006), *J. Geophys. Res.*, 111

Nilsson et al., (2007), manuscript in preparation for *Atm. Chem. Phys.*

O'Dowd, C. et al. (2004), *Nature*, 431, 676-680.

Pierce J.R., and P.J. Adams (2006), *J. Geophys. Res.*, 111

## Processing of Soot by Controlled Sulfuric Acid and Water Condensation – Mass and Mobility Relationship and Morphology

J. Pagels<sup>1,2</sup>, A. Khalizov<sup>3</sup>, M. Emery<sup>1</sup>, P.H. McMurry<sup>1</sup> and R.Y. Zhang<sup>3</sup>

<sup>1</sup>Particle Technology Laboratory, Dept. of Mechanical Eng., 111 Church St. S.E. Minneapolis, MN 55455, USA.

<sup>2</sup>Division of Aerosol Technology (EAT), Lund University, Lund, Sweden.

<sup>3</sup>Department of Atmospheric Sciences, Texas A&M University, College Station, TX 77843, USA.

Keywords: Soot Agglomerates, Condensation, Sulfur Particles, Fractals, Urban Particles

Soot particles are ubiquitous in the atmosphere and are of interest in studies related to adverse effects on human health and climate forcing. An important property of soot is its structure - or morphology. The morphology and mass-mobility relationship of fresh soot, such as diesel exhaust has been studied previously (e.g. Park et al. 2003). However, processing of soot undergoing condensation, simulating ageing in the atmosphere, has received much less attention.

We investigated the influence on morphology and the mass-mobility relationship of airborne soot particles upon coating with sulphuric acid and water. The main components of the experimental set-up were: 1. A Santoro burner, using propane as fuel to generate soot; 2. A Differential Mobility Analyzer (DMA) for selecting particles with given mobility size; 3. An "aerosol conditioner," which simulates processing similar to that which may occur in the atmosphere; 4. Either a second DMA or an APM (Aerosol Particle Mass Analyzer) to measure the altered mobility size or mass, respectively. This information also enabled us to determine the effective density and fractal dimension of fresh and processed soot. In the aerosol conditioner sulfuric acid was condensed onto the soot particles as described by Zhang and Zhang (2005). A heater was used to evaporate condensed material. A few experiments involved high RH cycling (a humidifier to increase the RH to 90% and a drier to reduce the RH to 5% before measurement).

$$\rho_{\text{eff}} = \frac{6m}{d_B^3 \pi} \quad (1), \quad m \propto d_B^{Df} \quad (2)$$

Typically the mass ( $m$ ) increased and the mobility diameter ( $d_B$ ) decreased as sulphuric acid was condensed onto the particles. The combined effects lead to an increased effective density ( $\rho_{\text{eff}}$ ; Eq. 1) and fractal dimension ( $Df$ ; Eq. 2). The influence on morphology depended strongly on the mass fraction of condensed material in the processed soot particles. Coating the particles with a low sulphuric acid mass fraction (~20%) resulted in a moderate influence on  $\rho_{\text{eff}}$  and  $Df$ . Results for a higher  $\text{H}_2\text{SO}_4$  mass fraction (~55%) are given in Figure 1. The fractal dimension increased from 2.11 upon coating with sulphuric acid. An additional high RH

cycling further increased  $Df$  to 2.80. For sizes below 100 nm, effective densities approached the estimated bulk density and dynamic shape factors approached 1, indicating a transformation from highly agglomerated to compact, nearly spherical particles.

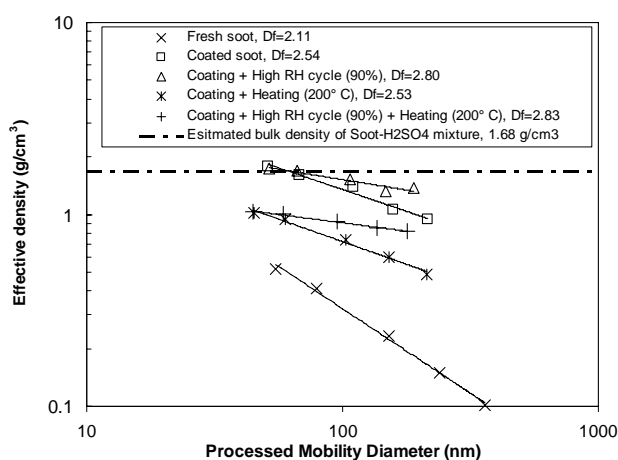


Figure 1. Effective density of fresh and processed soot.

Increased  $\rho_{\text{eff}}$  and  $Df$  were also observed when sulphuric acid was condensed on agglomerates and then removed by heating, indicating restructuring of the soot core. Soot with a hydrophilic coating, but not fresh hydrophobic soot, experienced restructuring upon RH cycling.

The atmospheric implication is that fresh (hydrophobic) soot will remain agglomerated when exposed to high RH cycles at subsaturation or upon low amounts of condensation. However as more mass condenses a gradual compaction takes place, which leads to full compaction at a mass ratio ( $m_{\text{processed}}/m_{\text{fresh}}$ ) of 2-3. If the condensate is hygroscopic then a high RH cycle even at RH below 100% can significantly progress the compaction.

*This research was supported by NSF Grant No. BES-0646507, the Swedish Research Council FORMAS, DOE - NIGEC, US EPA, and Robert A. Welch Foundation.*

Park K, Cao F, Kittelson DB and McMurry PH. *Env. Sci. & Techn.* 37: 577-583, 2003.

Zhang D and Zhang RY. (2005) *Env. Sci. & Techn.* 39: 5722-5728, 2005.

## The boreal forest canopy and aerosol eddy covariance fluxes

Ahlm<sup>1</sup>, S. Aunaiainen<sup>2</sup>, D. Nilsson<sup>1</sup>, T. Grönholm<sup>2</sup>, J. Rinne<sup>2</sup>, M. Mårtensson<sup>1</sup>, P. Aalto<sup>2</sup>, S. van Ekeren<sup>3</sup>, M. Kulmala<sup>2</sup> and T. Vesala<sup>2</sup>

<sup>1</sup>Department of Applied Environmental Research, Stockholm University, Sweden

<sup>2</sup>Department of Physical Sciences, University of Helsinki, Finland

<sup>3</sup>Laboratory for Atmospheric Chemistry, Paul Scherrer Institute, Switzerland

Keywords: eddy covariance, aerosol fluxes, aerosol deposition, boreal forest, forest canopy.

In this study data from Hyytiälä in southern Finland during late winter 2003 are used to compare the aerosol dry deposition above and below the forest canopy at this site. Additionally, data from Värriö in northern Finland during spring this same year are used to compare the aerosol deposition in Värriö, where the canopy is relatively thin, with the deposition in Hyytiälä where the canopy is more compact. Aerosol fluxes were determined by using the eddy covariance method, in Hyytiälä at altitudes of 23 m and 2 m (above and below canopy) and in Värriö at an altitude of 15 m (above the canopy), using similar ultrasonic anemometers and CPCs with a cut at 10 nm diameter.

In figure 1 below (Hyytiälä), canopy represents the difference between the fluxes at 23 m and 2 m and ground represents 2 m flux. In this figure fluxes have been separated to emissive (upper figure) and deposition fluxes (lower figure). For the deposition cases, fluxes to the canopy are larger than the fluxes to the ground, which means that a large part of the deposition takes place in the canopy. In fact around 80% of the deposition during this period was estimated to take place in the canopy and consequently only around 20% on the forest floor. Clearly this must be because the canopy offers a much larger surface for deposition than ground.

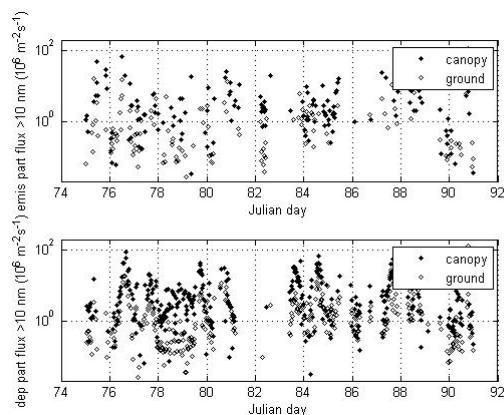


**Figure 1:** Emissive and deposition aerosol fluxes for canopy and ground in Hyytiälä from the middle of March to late March 2003.

For a period from late April to the middle of May 2003 aerosol fluxes were generally much larger in Hyytiälä than the fluxes in Värriö and at both sites the fluxes were mostly indicating net deposition. Since the friction velocities had similar mean values at the two sites during this period, the larger fluxes in Hyytiälä must be explained by the much higher number concentrations in Hyytiälä where the anthropogenic influence is more significant. Also the deposition velocities were higher in Hyytiälä. During this period the ground was snow covered most of the time in Värriö but not in Hyytiälä. Snow cover may be expected to reduce the deposition because of reduced leaf area. The higher presence of anthropogenic sources in Hyytiälä also affects the deposition since they generally result in smaller particles with a more efficient Brownian diffusion and thereby higher deposition velocities.

However our primary concern in this study is the influence of the canopy density on aerosol deposition. Therefore we now intend to compare the deposition during this period from late April to the middle of May 2003 in Värriö with other earlier periods this year in Hyytiälä with similar weather conditions at the two sites and also similar surface conditions regarding snow cover. In order to avoid the influence of particle size on deposition velocities we also will use data from differential mobility analysers (DMA) with size-dependent concentrations from both Hyytiälä and Värriö. A canopy model (Slinn, 1981) for aerosol dry deposition will be used and model results will be compared to measured data.

Slinn, W. G. N. (1982). Predictions for Particle Deposition to Vegetative Canopies. *Atmospheric Environment*, 16, 1785-1794

## Sea Spray Emission Function calculated from vertical aerosol concentration gradients over Arctic seas.

T. Petelski and A. Rozwadowska

Institute of Oceanology, PAS, Poland

Keywords: Arctic aerosols, sea spray , aerosol emission, marine aerosol

Sea spray emission fluxes were calculated on the basis of vertical of the aerosol concentration gradients from experimental data collected with a laser particle counter during four polar scientific cruises carried out in the summers of 2000, 2001, 2002 and 2003. The calculated flux values are the first obtained with a gradient method from data measured on the open ocean; such a method has a much better physical basis than any involving calculating fluxes from concentrations measured at one level only. The sea spray generation function we obtained was compared with other functions from the literature . We show that most literature sea spray generation functions are underestimated for the 1-8  $\mu\text{m}$  radius range, some of them by a factor of 6.

Breaking of the wind waves can be regarded as the main reason of the aerosol emission from the sea surface. This process is directly related to the wind speed in the case of the deep sea. Therefore aerosol emission from the sea surface should be well correlated to the wind speed.

On the other side, results of our measurements indicate that the correlation between an aerosol concentration in the atmospheric surface layer over sea and the wind speed is rather weak . Thus, we conclude that it is not possible to obtain a good estimation of aerosol emission only on the basis of the aerosol concentration and deposition velocity.

An aerosol flux from the sea surface can be determined from the vertical gradient of aerosol concentration. As it was shown, there is a range of aerosol sizes for which this vertical gradient is entirely defined by the aerosol emission from the sea surface.

Measurements which were conducted over several summer seasons in the North Polar Waters of the Atlantic showed that logarithmic vertical profiles of aerosol concentration are common for whitecap covered ocean areas. Aerosol flux values calculated from measured vertical concentration profiles may indicate an underestimation of emission values by literature SGFs for particles with radii between 1 and 8  $\mu\text{m}$ . The results of this study show also that the assumption, used often in the research of marine aerosol fluxes, that the SGF can be divided into two independent parts: the size spectrum and factor dependent on environmental parameters, may not be true. However, we need more

measurements for strong winds ( $U > 11$  m/s) in order to clarify this topic in a satisfactory manner.

The method of calculating aerosol fluxes from measured vertical concentration gradients, based on Monin-Obukhov scaling theory, gives a better approximation of turbulent aerosol fluxes than the dry deposition method. If used with data acquired from multiple particle counters, located at several altitudes with simultaneous measurement of additional parameters (especially wave parameters as well as momentum and heat turbulent fluxes), this method should make it possible to definitely solve the problem of coarse aerosol mode emission parametrization.

Andreas, E.L.(2002), *Volume 1, W.A. Perrie, Ed., WIT Press, Southampton, U.K., 1-46,*

Petelski, T.,(1996), *Water Resources 23, 2 145-148, 1996.*

Petelski, T.,(2003) , *Journal of Aerosol Science 34, 359-371, 2003.*

Petelski, T., (2005) *J. of Aerosol Sci. and Tech., 39:695–700, 2005*

Petelski, T., J. Piskozub(2006) , *J. Geophys. Res., doi:10.1029/2005JC003295, 2006*

Petelski, T., J. Piskozub & B. Paplinska-Swerpel, B. (2005), *J. Geophys. Res., 110, C10023, doi:10.1029/2004JC002800*

Stramska, M., and T. Petelski, *J. Geophys. Res., 108 (C3), 3086, doi:10.1029/2002JC001321, 2003.*

## Use of inventories of natural and artificial radionuclides in soils to estimate total aerosols deposition and origin in French mountains

Gaël Le Roux, Laurent Pourcelot, Olivier Masson,  
Céline Duffa, Françoise Vray, Philippe Renaud

Institut de Radioprotection et Sûreté Nucléaire, DEI/SESURE  
Laboratoire d'Etude Radioécologique du milieu Continental et Marin,  
CEN Cadarache Bât. 153 BP 3,13115 St Paul lez Durance

Keywords: aerosol characterization, air pollution, wet removal, particle deposition, radon decay products

Transport and deposition of aerosols are essential factors in climatic and environmental changes. Deposition of aerosols carrying contaminants mainly governs soil acidification and pollution. Most of the acid, heavy metals and anthropogenic radionuclides are delivered to the ground by wet deposition. However other mechanisms like dry and occult depositions can be essential, especially in forested and/or mountainous areas.

We use inventories of  $^{210}\text{Pb}$ , a natural radionuclide and artificial radionuclides ( $^{137}\text{Cs}$  and Pu) in undisturbed soils to quantify mechanisms influencing aerosol deposition in different French mountains. First, radionuclide and aerosol inventories are correlated with precipitations estimated by the Model AURELHY of Météo France: either annual rainfall ( $^{210}\text{Pb}$ ,  $^{137}\text{Cs}_{\text{nuclear tests}}$ ) or precipitation of may 1986 ( $^{137}\text{Cs}_{\text{Chernobyl}}$ ).

However, orographic clouds induce increased deposition on the mountain peaks. For example, high altitude sites show a >30% increase in  $^{210}\text{Pb}$  inventories compared to  $^{210}\text{Pb}$ -rainfall relationship established in the surrounding lowlands. Because artificial radionuclides and  $^{210}\text{Pb}$  have different past and present vertical distributions in the troposphere, we use  $^{137}\text{Cs}/^{210}\text{Pb}$  and  $\text{Pu}/^{210}\text{Pb}$  ratios to estimate occult deposition and aerosol origins. For example,  $^{210}\text{Pb}/^{239-240}\text{Pu}$  ratios of the soil inventories are increasing with altitude (Fig.1). We will show that is due to larger deposition of surface-air aerosols in mountainous areas.

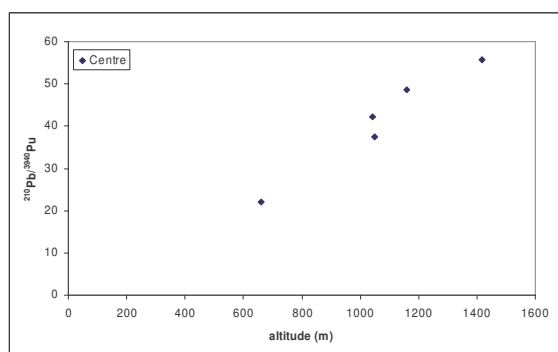


Fig.1:  $^{210}\text{Pb}/^{239-240}\text{Pu}$  in soil inventories vs. altitude in Massif Central

Occult deposition increases with altitude mainly due to cloud interception and the feeder-seeder effect scavenging aerosols from the surface air enriched in  $^{210}\text{Pb}$ .

Radionuclide inventories in undisturbed soils are therefore good estimators of total deposition of aerosols. Radionuclide ratios help to determine the origin of the aerosols. The combination of radionuclides inventories and ratios can therefore be used to assess the sensitivity of the different French mountains to local/global and discrete/continue atmospheric contaminations.

## Characterisation of Woodsmoke from Distant Forest Fires

T.H. Gan<sup>1</sup>, P.J. Hanhela<sup>1</sup>, W. Mazurek<sup>1</sup> and R. Gillett<sup>2</sup>

<sup>1</sup>Maritime Platforms Division, Defence Science and Technology Organisation, 506 Ormer St, Fishermans Bend, Victoria 3207, Australia

<sup>2</sup>Division of Marine and Atmospheric Research, Commonwealth Scientific and Industrial Research Organisation, Station St., Ascendale, Victoria 3195, Australia

Keywords: biomass burning, nanoparticles characterisation, PAH(s), particle size distribution, PM<sub>10</sub>

### Introduction

During the summer, on the 13<sup>th</sup> and 20<sup>th</sup> of December 2006, Melbourne was enveloped in clouds of biomass aerosol from bushfires in north-east (150 km) and eastern Victoria (200 km) which had been burning for two weeks. A characterisation of the outdoor and indoor woodsmoke was undertaken in real time.

### Experimental

Continuous measurements of outdoor and indoor PM<sub>10</sub> were made using the TSI DustTrak 8520 (0.1 µm to 10 µm) calibrated with the woodsmoke factor obtained by Kingham et al (2006). Fine particle size was determined using the Grimm 1109 optical aerosol spectrometer (OPC) in the size range 0.25 µm – 32 µm (31 size channels). Nanoparticle size distribution was obtained with the Grimm (Ainring, Germany) scanning mobility particle sizer (SMPS) (Reischl et al, 1997, Rettenmoser et al 2006, Winklmayr et al, 1990) and Grimm 5403 condensation particle counter (CPC). The SMPS size range was 11.1 nm – 1083.3 nm (0.011 µm – 1.083µm) in 44 channels and was only operated on 20 December without software-coupling to the OPC. In addition, polyaromatic hydrocarbon (PAH) concentrations were monitored continuously with the PAS 2000 (EcoChem Analytics, Tustin, USA).

### Results and Discussion

During the occurrence of the smoke haze on 13 December, outdoor PM<sub>10</sub> concentrations measured at Maribyrnong generally tracked the EPA Victoria 5-minute averaged values determined using a TEOM instrument located at the Footscray monitoring station 10 km away. Observed variations in outdoor levels were influenced by local wind conditions.

OPC and SMPS measurements on 20 December showed that the geometric mean particle size was 191.3 nm and the outdoor number concentration increased with woodsmoke concentrations (Figure 1).

PAH measurements in real time (Figure 2) indicate different sources, with nanoparticles from vehicles on two busy highways, 50 m south and two km north of the measuring site, and submicron particles from the smoke plume. Progress is underway to determine the chemical composition of

the smoke particles collected on Teflon and quartz filter samples.

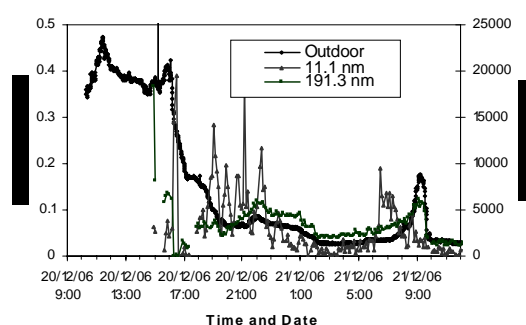


Figure 1. Comparison of woodsmoke concentration and particle size.

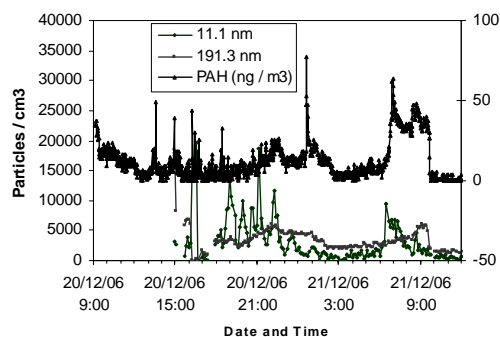


Figure 2. Correlation of PAH levels (ng m<sup>-3</sup>) and particle size.

We thank EPA Victoria for providing the TEOM and local weather data from Footscray monitoring station.

### References

- Kingham, S., Durand, M., Aberkane, T., Harrison, J., Wilson, J.G., and Epton, M. (2006). *Atmospheric Environment*, 40, 338-347.
- Reischl, G.P., Makela, J.M. and Nucid J. (1997), *Aerosol Sci. Tech.*, 27, 651-672.
- Rettenmoser, T., Gerhart, C., Richter, M., and Grimm H. (2006), in *7<sup>th</sup> International Aerosol Conference*, St. Paul, Minnesota (International Aerosol Research Assembly), 405.
- Winklmayr, W., Reischl, G.P., Lindner, A.O. and Berner, A. (1990), *J. Aerosol Sci.*, 22, 289-296.

## **T27 Abstracts**

## Influence of averaged vertical wind on transport of stratospheric aerosols

V.I. Gryazin, S.A. Beresnev

Aerosol Physics Laboratory, Ural State University, 620083, Ekaterinburg, Russia

Keywords: Aerosol dynamics, Fundamental aerosol physics, Modelling, Stratospheric aerosols, Vertical wind

One of permanent mechanisms of stratospheric aerosol transport is the vertical wind. The unique opportunity for the detailed spatio-temporal analysis of vertical wind is given with the database of NASA satellite UARS (Upper Atmosphere Research Satellite) included in assimilation atmospheric model UKMO (United Kingdom Meteorological Office) (Swinbank and O'Neill, 1992). The database UARS-UKMO contains the standard dataset for the certain time period (day or month) for fields of meteorological parameters: temperature, pressure, zonal, meridional, and vertical wind.

The latitudinal and seasonal dependences of vertical wind at different altitudes averaged for the various time intervals since 1992 to 2006 according to the model UKMO are analyzed. It is established, that monthly-averaged amplitudes of vertical wind make values  $\pm 5$  mm/s, and the annual-averaged are  $\pm 1$  mm/s. Ascending wind provides vertical lifting against gravity for the sufficiently large aerosol particles (up to  $3\div 5 \mu\text{m}$ ) with density up to  $1.0\div 1.5 \text{ g/cm}^3$  at stratospheric and mesospheric altitudes.

The vertical wind probably is the determining factor of particles motion up to altitudes  $30\div 40$  km and can change essentially the characteristics of sedimentation and residence times of atmospheric aerosols. The structure of the averaged vertical wind fields supposes the opportunity of formation of dynamically stable aerosol layers in the middle stratosphere.

Characteristics of motion for spherical particles and fractal-like aggregates are essentially different. The analysis of particle's gravitational sedimentation for model of stationary atmosphere without wind (Kasten, 1968) has been presented. For calculation of drag force of fractal-like aggregates the parameters of soot particles from data of Cai and Sorensen, 1994, Wang and Sorensen, 1999 have been used. In this case the essential distinctions in sedimentation velocities for particles of various structure are observed. Fractal-like structure of particles essentially increases residence times of aerosol particles in a stratosphere. Techniques of use of the average speed of a vertical wind in transport models for stratospheric aerosol are offered.

We are grateful to the BADC which provided us with access to the UKMO Stratospheric Assimilated Data. This work was supported by the Russian Foundation for Basic Research (RFBR) under grant 06-01-00669.

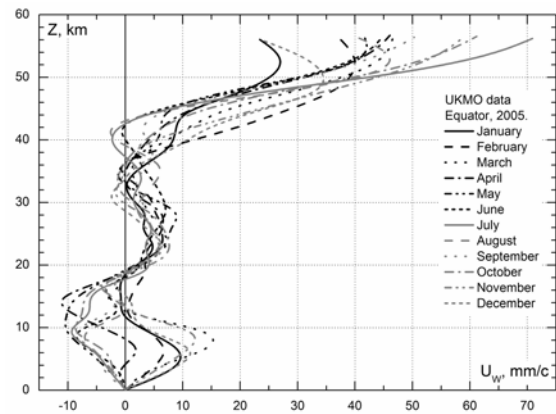


Fig.1. The months-averaged vertical wind for the equator from UARS-UKMO data.

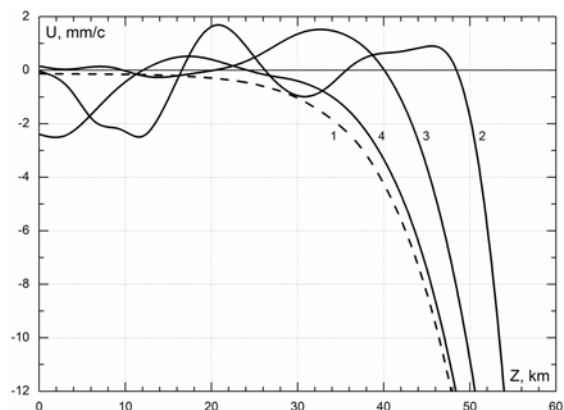


Fig.2. Velocity of particles with  $\rho = 1 \text{ g/sm}^3$  and  $R_p = 1 \mu\text{m}$ . 1 – gravitational sedimentation only; total velocity of particles under action of the annual-averaged vertical wind for: 2 – Equator, 3 – North Pole, 4 – South Pole.

Swinbank R., O'Neill A. A stratosphere-troposphere data assimilation system // *Mon. Weather Rev.* 1994. V.122. P.686-702.

Kasten F. Falling speed of aerosol particles // *J. Appl. Meteor.* 1968. V.7. N 10. P.944-947.

Cai J., Sorensen C.M. Diffusion of fractal aggregates in the free molecular regime // *J. Phys. Rev. E.* 1994. V.50. N.5. P.3397-3400.

Wang G.M., Sorensen C.M. Diffusive mobility of fractal aggregates over the entire Knudsen number range // *J. Phys. Rev. E.* 1999. V.60. N.30. P.3036-3044.

## Aerosols transport across the Central Mediterranean

D. Đorđević<sup>1</sup>, S. Rodríguez<sup>2-3</sup>, J.J. Rodríguez<sup>4</sup>, J.C. Guerra<sup>4</sup>, M. Todorović<sup>5</sup>,  
D. Relić<sup>5</sup>, A. Mihajilidi-Zelić<sup>5</sup>, D. Šegan<sup>5</sup>,

<sup>1</sup> Institute of Chemistry, Technology and Metallurgy – Centre for Chemistry, University of Belgrade, Studentski trg 12 - 16, 11000 Belgrade, Serbia

<sup>2</sup> Department of Geology, University of Huelva, Huelva, 21071, Spain

<sup>3</sup> Izaña Atmospheric Observatory, INM-CSIC, Santa Cruz de Tenerife, 38071, Canary Islands, Spain

<sup>4</sup> Department of Basic Physics, University of La Laguna, La Laguna, 38200, Tenerife, Canary Islands, Spain

<sup>5</sup> Department of Chemistry, University of Belgrade, Studentski trg 12-16, 11000 Belgrade, Serbia

Keywords: long range transport, Mediterranean aerosol, sulphate, Saharan dust

In this abstract some of the results obtained in a 5 years study on aerosol composition in a coastal site of the Central Mediterranean – Adriatic area are summarised. The study site (42.45°N, 18.55°E) was located in Montenegro (into the Herceg-Novi bay region). In this aerosol samples set, the content in  $\text{SO}_4^{2-}$ ,  $\text{NO}_3^-$ ,  $\text{NH}_4^+$ , Cd, Co, Cr, Cu, Ni, Pb, Hg, Se, Ti, Fe, Mn, Cl<sup>-</sup>, Na, K, Mg and Ca was determined by several analytical techniques. Data on local meteorology and air back-trajectories were also included in the data analysis.

The data treatment includes the following analysis:

- 1) identification of aerosol's sources profiles by statistical techniques,
- 2) study of the transport patterns and aerosol origin-region by meteorological analysis and back trajectories,

The analysis of the aerosol's sources profiles indicates a contribution of: 1) coal burning resulting in sulphate and elements associated with fly-ashes, 2) mineral dust derived from regional-resuspension and Saharan dust transport, 3) vehicles exhaust contributing with nitrate and lead, 4) sea salt, 5) industrial activities releasing Co and Hg, and 6) other anthropogenic sources contributing to Cd, Ni and Se concentrations.

The meteorological analysis evidences the existence of very well defined transport patterns of aerosols in this region, pointing to specific transport pathways for some of the aerosols components. Our analysis highlights these scenarios:

- 1) A north eastern transport pathway of sulphate from Eastern-Europe. Sulphate concentrations associated with this transport pattern are 1.5 to 3.0 higher than those associated with any other transport scenario.
- 2) Saharan dust transport. This mineral dust input results in sharp increases in the mineral dust

concentrations (e.g. Ti, Fe, and Mn among others).

- 3) A western sea-salt transport pattern. This pattern is associated with high wind speed events over the sea surface caused by easterly moving depressions from the Western Mediterranean.

The lowest levels of sulphate and total aerosol mass concentrations are associated with:

- 1) transport from the Eastern and Western Mediterranean owing to the fact that these are very frequently associated with rainy scenarios resulting in particle's scavenging.
- 2) a transport pattern from Northern Europe linked to abrupt entries, of northern and cold air from the Scandinavian countries, in the Adriatic sea region.

The study includes a detailed analysis of the meteorological scenarios associated with the different transport patterns and the seasonal distribution of these events.

This study contributes to understand the aerosols transport in the Mediterranean, including the "Southern export of anthropogenic aerosols from Europe to North-Africa" and the "Northern export of mineral dust from North Africa to Europe". These results evidence the important role of the aerosol exchange between Europe and North-Africa across the Mediterranean.

## Meteorological criteria for the accumulation, their transport and the range of a boundary layer of aerosols on the mesoscale

K. Weinhold<sup>1</sup>, W. Birmili<sup>1</sup>, C. Engler<sup>1</sup>, A. Sonntag<sup>1</sup>, A. Wiedensohler<sup>1</sup>, R. Wolke<sup>1</sup>,  
H. Hermann<sup>1</sup>, G. Löschau<sup>2</sup>

<sup>1</sup>Leibniz-Institute for Tropospheric Research, Permoserstr. 15, Leipzig, Germany

<sup>2</sup>Sächsisches Landesamt für Umwelt und Geologie

Keywords: tropospheric aerosol; boundary layer; number size distribution; DMPS

Although the levels of atmospheric pollution in Western industrialised regions, such as Central Europe, have declined over the past two decades, novel challenges have appeared, for instance in the context of PM regulation. Episodes of increased PM<sub>10</sub> concentrations are still occurring across Europe, and the complexity of the underlying processes, such as anthropogenic emissions and secondary formation are not straightforward to separate. Apart from PM<sub>10</sub>, only little information is available on the budget and life-time of atmospheric particle number concentration in the continental boundary layer. In addition, there has been a growing need for high quality aerosol data in order to validate atmospheric transport models.

To address the questions of spatial variability of boundary layer aerosols on the mesoscale, a comprehensive research project was designed using seven concurrent observation sites of particle size distributions within the state of Saxony, Germany. Continuous measurements at the seven sites were conducted between September 1, 2006 and February 28, 2007. Three observation sites are located in a rural environment (Schwartenberg, Niesky, Melpitz), whereas four additional stations measured urban aerosols within the two cities of Dresden and Leipzig. Due to the different geographic positions of the stations it is possible to examine the importance of aerosol emission, dispersion, and deposition during transit of an air mass through Saxony.

Ambient particle number size distributions between 3 nm and 10 µm in diameter were measured using Differential mobility particle sizers (DMPS/SMPS) and aerodynamic particle sizers (APS) at a time resolution of around 10 minutes. Several quality assurance measures, such as a Round Robin-Test using an additional SMPS system were made to ensure a maximum comparability of the measurement data at different stations.

An example of particle number size distributions (3 nm – 10 µm) is shown in Figure 1. An example for the wind directional dependence of particle number concentrations is shown in Figure 2; at the mountain station Schwartenberg, the by far highest number concentrations occurred from south-easterly wind direction. We will show a statistical analysis of the number size distributions for situations of connected flow between pairs of rural

background stations. A mesoscale atmospheric dispersion model (LM-MUSCAT) will also be used to examine the potential importance of aerosol emissions and deposition processes in more detail.

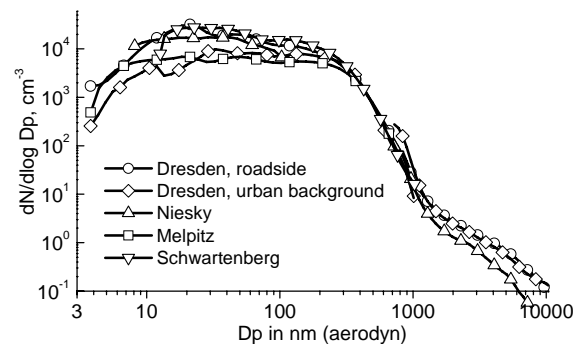


Figure 1: Particle number size distributions measured at 5 sites in Saxony on September 13, 2006.



Figure 2: Wind-directional dependence of the Aitken particle number concentration (40 nm < diameter < 120 nm; median values) at three rural observation sites within the state of Saxony, Germany.

### Acknowledgements

This work has been supported by the Environmental Office of Saxony (LfUG Dresden), grant “Einfluss des Ferneintrages auf die Feinstaubbelastung im Ballungsraum”.

## Back trajectories classification with columnar aerosol properties at southwest of Spain

C. Toledano<sup>1,3</sup>, V. Cachorro<sup>1</sup>, B. Torres<sup>1</sup>, N. Prats<sup>1</sup>, R. Rodrigo<sup>1</sup>, M. Sorribas<sup>2</sup>, A. Berjón<sup>1</sup> and A. De Frutos<sup>1</sup>

<sup>1</sup> Atmospheric Optic Group GOA-UVA, University of Valladolid, 47071, Valladolid, Spain.

<sup>2</sup> Atmospheric Sounding Station 'El Arenosillo', INTA, 21130, Mazagón-Huelva, Spain.

<sup>3</sup> Meteorological Institute, University of Munich, 80333, Munich, Germany.

Keywords: atmospheric aerosols, dust, marine aerosols, optical properties, remote sensing.

The AERONET site 'El Arenosillo', equipped with a Cimel sun photometer, is in operation since 2000. The aerosol database now available allows analyzing the atmospheric aerosols climatology over the region. Different aerosol types –marine, continental and desert dust– were detected at this site, thus suggesting to make an aerosol classification based on the sun photometer measurements. The aerosol types were distinguished by means of thresholds on the aerosol optical depth and the Ångström exponent (Toledano *et al.*, 2006).

The frequent intrusions of Saharan dust over the site, located in south-western Spain, suggested the use of back-trajectories to determine the air mass origin in these episodes of high turbidity. We wanted to analyze whether the air mass origin is a decisive issue for the aerosol properties in the study area. In this case, the back trajectory analysis could support the proposed aerosol classification.

Table 1. Frequency of the air masses according to the classification method based in the residence time, and mean AOD and AE for each type.

Type	freq.(%) 500m	freq.(%) 1500m	freq.(%) 3000m	AOD 440nm	Ång. exp
MP	41.4	41.6	38.4	0.13	1.00
MT	12.4	19.5	30.8	0.21	0.88
A	10.1	9.3	11.9	0.09	0.96
C	14.5	6.6	3.5	0.18	1.32
CT	5.2	12.7	10.4	0.30	0.72
L	4.6	5.5	3.9	0.25	1.13
Me	11.8	4.8	1.1	0.25	1.12

The aim of this work was to classify the air masses arriving at El Arenosillo by means of back-trajectories, and characterize the aerosols within each type by means of the optical depth (AOD) and its spectral dependence, given by the Ångström exponent (AE). For this purpose, two classification methods have been used, the first one based on sectors (residence time) and the second one based on cluster analysis. The analyzed period is 2000-2005, that is, the 6 years period in which AERONET level 2.0 data are available. The database of spectral AOD up to December 2005 includes more than 50000 cloud-free observations, and 1651 days with data, 77% of the days in the period. The results of both classification methods are shown and compared.

The back-trajectories have been calculated with the HYSPLIT model, locally run on a PC, with the following parameters: 1 trajectory per day at 12UTC, 5 days back in time, 3 altitude levels (500, 1500 and 3000m a.g.l.), the model vertical velocity and the FNL meteorological database.

The first classification method is based on the residence time of the trajectories over pre-defined regions. For that, 7 sectors are defined: Maritime Polar, Maritime Tropical, Arctic, Continental, Continental Tropical, Local and Mediterranean. The frequency of each air mass type is summarized in table 1. The aerosol properties within each air mass type show distinct features, allowing the discrimination of marine aerosols in the MP, MT and A air masses (low AOD and all range of AE), continental aerosols in the C air masses (medium AOD with high AE) and desert dust in the CT and MT air masses (high AOD and low AE), as reported in table 1. The L and Me air masses show a mixed aerosol type. These findings are in agreement with the classification proposed by Toledano *et al.* (2006) and confirm the relevance of the air mass type related to the aerosol properties.

The back-trajectories have been also classified with a second method, a non-hierarchical clustering algorithm. This analysis resulted in the identification of 7 clusters, in which we have also investigated the AOD and AE of the Cimel database. In 4 clusters different Atlantic back-trajectories are included, showing similar features to the MP and A sectors of the first classification, therefore giving a clear picture about the marine aerosols in the site. Another cluster includes local and North African air masses, with the aerosol features of desert dust, like the CT sector. A cluster of trajectories from central and north Europe shows the aerosol characteristics of the continental aerosol, and finally a cluster of short trajectories from the south-west is very similar to the MT sector, with a mixture of marine and desert dust aerosol.

This work was supported by MEC under project REN2002-00966 and Junta de Castilla y León VA001C05.

Toledano, C, V.E. Cachorro *et al.* *Aerosol optical depth and Ångström exponent climatology at 'El Arenosillo' AERONET site (Huelva, Spain)* (in press, 2006).

## VERTICAL MOVEMENT OF STRONG ABSORBING PARTICLES FOR STRATOSPHERIC PRESSURES DUE TO GRAVITOPHOTOPHORETIC FORCE AND THEIR MORPHOLOGY

O. Jovanovic and H. Horvath

*Institute for Experimental Physics, University Vienna, Boltzmanngasse 5, 1090 Vienna, Austria*

Keywords: gravito-photophoresis, stratosphere, black carbon, vertical transport, morphology.

Phenomenon of gravitophotophoresis for strong absorbing particles could explain the existence of black carbon particles in lower parts of stratosphere at heights of 20 km and perhaps in mesosphere at heights of 80 km.

Gravitophotophoresis is defined as phenomenon of vertical movement of particle when irradiated sideways by visible light.

Investigating this phenomenon multiple experiments were performed, whose goal was to establish the possibility of vertical transport of strong absorbing particles for pressures of 200 hPa and lower, which pressures correspond to heights from 12 km upward.

Experiments with particles which show gravitophotophoresis, particles that do not, and particles which show positive photophoresis (movement in direction of irradiation) were also performed. All particles were afterwards analyzed with scanning electronic microscope (SEM), in order to establish differences in shape.

Results show that the vertical transport of strongly absorbing particles for stratospheric range of pressures is possible for a flux density of one solar constant (1.357 kW/m<sup>2</sup>).

The vertical velocity **decreases** with pressure for range between 100 hPa and 200 hPa, fig. 1. For pressures between 15.9 hPa and 4.9 hPa the vertical velocity **increases** with pressure.

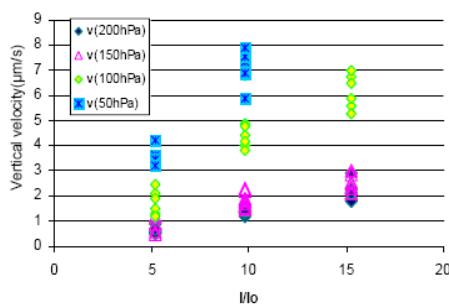


Figure 1: Vertical velocity of diesel black carbon particle for range of pressures from 50 hPa to 200 hPa compared to relative illumination intensity.

This results show very good agreement with calculations (Rohatschek, 1996) for mean gravitophotophoretic force  $F_g/G$  for model particle in standard atmosphere irradiated by one solar constant for all range of pressure. In all experiments the vertical velocity increases proportionally to the flux density.

Experiments analyzing the shape of particles showed a correlation between particle size and type of photophoresis: particles with greater diameter (e.g. 5 µm) are more likely to perform gravitophotophoresis.

There is no correlation between projected area of a particle and the type of photophoresis.

(gravitophotophoresis, positive photophoresis or none at all). On the other hand, experiments show that particles performing photophoresis have **significantly larger perimeter** than those performing positive photophoresis or those that do not perform photophoresis at all, fig. 2.

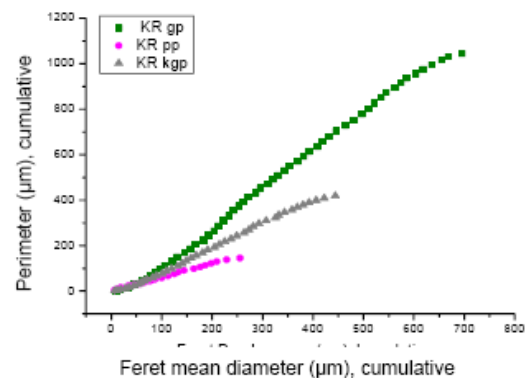


Figure 2.: Perimeter of particles is considerably greater for particles which exhibit gravito-photophoresis (squares) compared to particles which exhibit positive photophoresis (dots) or no-photophoresis (triangles).

It is possible to conclude that particles that perform positive photophoresis have very **irregular shape** compared to the other two groups of particles. In other words, particles that perform gravitophotophoresis for stratospheric range of pressures and reach higher layers of atmosphere must be strong absorbers and have very irregular, fractal-like shape.

Pueschel et al. (1992), Geophys. Res. Letter, 19, P. 1659-1662

Rohatschek, H. (1989), J. Aerosol. Sci., Vol. 20, No. 8, p. 903-906

Rohatschek, H. (1996), J. Aerosol. Sci., Vol. 27, No. 3, p. 467-475

Cheremisin A.A., Vassilyev Yu.V. and Horvath H., (2005), J. Aerosol Sci., Vol. 36, No. 11, p.1277-1299

## In-situ evidence for free-tropospheric long-range transport of a Siberian forest fire plume to the North Pole region

E. Swietlicki<sup>1</sup>, A. Wisthaler<sup>2</sup>, M. Tjernström<sup>3</sup>, A. Hansel<sup>2</sup> and C. Leck<sup>3</sup>

<sup>1</sup>Div. of Nuclear Physics, Lund University, P.O. Box 118, S-22100 Lund, Sweden

<sup>2</sup>Institute of Ion Physics and Applied Physics, Innsbruck University, A-6020 Innsbruck, Austria

<sup>3</sup>Department of Meteorology, Stockholm University S-10691 Stockholm, Sweden

Keywords: Arctic aerosols, vertical distribution, long-range transport, biomass burning.

We present the first in-situ evidence of free-tropospheric long-range transport of plumes originating from forest fires at lower latitudes (NE Siberia) to the summertime central Arctic (88.3°N). The elevated concentrations of acetonitrile (CH<sub>3</sub>CN) clearly point to a biomass burning source. Acetonitrile was also strongly correlated with aerosol particle number concentrations for sizes >300 nm in the same plume.

The summer 2001 Arctic Ocean Expedition (AOE-2001) led the Swedish icebreaker *Oden* to the central Arctic, mostly north of latitude 85°N in July-August 2001 (Leck *et al.*, 2004; Tjernström, 2005). The *Oden* was equipped with a helicopter to obtain vertical profiles of aerosol particle number concentrations in various size ranges (36 flights), as well as the gases acetone, acetonitrile and dimethyl sulfide (in 14 out of the 36 flights).

Here we focus on results obtained during a research flight (Flight #23) that reached the helicopter ceiling height of 3.6 km at 88.3°N, 2°W on August 8, 2001, 18:09-19:11 UTC. The aerosol particle size concentrations were measured at 1 Hz in several size ranges using two Condensation Particle Counters (TSI UCPC 3025, TSI CPC 3010) and an Optical Particle Counter (OPC, Climet CI-500, >300 nm). The particle concentrations of ultrafine particles (UF; diameters between 3-15 nm) were derived by taking the difference between the two CPCs operating with different lower cut-off sizes. During this flight, the helicopter also carried a PTR-MS instrument (Proton Transfer Reaction-Mass Spectrometry) measuring acetonitrile (CH<sub>3</sub>CN), a specific tracer for biomass burning. Considering the long atmospheric lifetime of acetonitrile (on the order of months) and the low levels observed in the Arctic boundary layer (ABL), the Arctic Ocean must act as a sink for acetonitrile. The positive acetonitrile gradient above the ABL can be explained by long-range transport from lower latitudes. The enhancement of acetonitrile in the layer at ~ 3 km may be explained by long-range transport of a Siberian forest fire plume.

On August 8, 2001, total aerosol particle number concentrations (>3 nm) typically decrease with altitude above the ABL, even when entering the plume. In the biomass smoke plume, the particles are shifted to larger sizes. The number concentrations of

particles detected in the OPC (>300 nm) increase drastically when entering the plume, at the expense of the number concentrations of smaller particles (<300 nm).

Aerosol number size distributions were calculated from the 1 Hz data obtained by the UCPC, CPC and OPC. The size resolution was sacrificed for improved time resolution, providing size bins of 3-15 nm, 15-300 nm, and several bins above 300 nm. The data were averaged over various altitude ranges. Except for the UF particles, number concentrations are much lower in the humid ABL than above. A shift towards larger particle sizes is clearly seen when moving from the slightly polluted layer immediately below the main plume, and the plume itself. The plume with increased aerosol and CH<sub>3</sub>CN concentrations sits in a layer which is neutrally stratified and even unstable to moist processes. This coincides with a sharp increase in RH from 2.6 to 3.7 km. These vertical profiles resemble those of a cloud layer, with the vertical mixing caused by in-cloud turbulence. The layer is capped by an inversion, possibly a very weak subsidence inversion, at 3.7 km altitude.

There is supporting evidence from fire maps and dispersion modelling that the plume intercepted during Flight #23 on 8 Aug 2001 above 2620 m altitude originated from NE Siberian forest fires. Various fire map products consistently show no or little large-scale biomass burning in Canada and Alaska, during August 2001, while there were large forest fires seen in NE Siberia. During the time period of interest (3-8 Aug 2001), TOMS and SeaWiFS images show large smoke plumes moving north-eastwards from Siberia, over the Bering Strait. The polar coverage of these remote sensing data is however poor.

Leck, C., M. Tjernström, P. Matrai, E. Swietlicki, and K. Bigg. (2004). Can Marine Microorganisms Influence Melting of the Arctic Pack Ice? *EOS*, Vol. 85, No. 3, pp. 25, 30, 32.

Tjernström, M., (2005). The summer Arctic boundary layer during the Arctic Ocean Expedition 2001 (AOE-2001). *Bound.-Layer Meteorol.*, 117, 5 - 36.

## Origin of the aerosol nanoparticles in the marine boundary layer over south-eastern Baltic Sea

V. Ulevičius<sup>1</sup>, K. Plauškaitė<sup>1</sup>, N. Prokopčiuk<sup>1</sup>, N. Špirkauskaitė<sup>1</sup>, T. Petelski<sup>2</sup> and T. Zielinski<sup>2</sup>

<sup>1</sup>Institute of Physics, Savanorių av. 231, LT-02300, Vilnius, Lithuania

<sup>2</sup>Institute of Oceanology, Polish Academy of Sciences (PAS), ul. Powstancow Warszawy 55, skr. poczt. 148, 81-712 Sopot, Poland

Keywords: aerosol formation, aerosol size distribution, marine aerosols, nucleation, particle formation and growth.

The aim of this study was to compare variation of marine aerosol size distribution and total aerosol concentration under the influence of different air masses over the south-eastern Baltic Sea and in the Lithuanian coastal zone. The measurements were performed at the Environmental pollution research station in Preila (Lithuania) and in the Baltic Sea about 10 km wide from the coast from 7 to 12 of May, 2006. The total aerosol particle concentration was measured by using condensation particle counter (CPC) UF-02, which can register 4.5 nm particles (Plauškaitė *et al.*, 2006). Over the same period the measurements of the aerosol particle number concentration and size distribution in the 10 – 200 nm size range were performed using differential mobility particle sizer (ELAS-5Mc; Ulevičius *et al.*, 2002) at the Preila station. The series of two-day air mass backward trajectories were calculated for the entire period using the Hybrid Single - Particle Lagrangian Integrated Trajectories model Version 4 (HY-SPLIT)(NOAA, [www.arl.noaa.gov/ready.html](http://www.arl.noaa.gov/ready.html)).

During the experiment the formation of aerosol particles and further their growth in the ambient air was observed on the 8, 9 and 11 of May, 2006. At the Preila station the aerosol particle concentration was lower and without such sharp short-term increases of particle concentration as in the Baltic Sea. These short-term increases of the particle concentration could be related to the air ionisation due to wave break and also to the pollution from ocean(sea)-going ships, which may influence the chemical composition of the marine boundary layer. However, due to enough strong mixing of air masses (median wind speed was over 5 m/s) and/or low condensation sink newly formed aerosol particles suddenly disappears. The aerosol size distributions were plotted as contour plots for each day (as a function of time). The nucleation event days were on 8, 9 and 11 of May, 2006.

For each event, the particle growth rate, new particle formation rate and the condensation sink were calculated graphically from the contour plots, and furthermore, from the growth rate the source rate of condensable vapour was estimated by using methodology given in Kulmala *et al.* (2001) (Table 1). Since the exact identity of the condensable

vapour is unknown, the source rate was estimated by using transport values of sulphuric acid.

Table 1. Calculated characteristics of the nucleation events.

Date	GR, nm/h	J, 1/(cm <sup>3</sup> s)	CS, 1/s	Q, 1/(cm <sup>3</sup> s)	Traj. dir.
2006.05.08	1.8	0.07	2.60·10 <sup>-2</sup>	6.41·10 <sup>5</sup>	NE
2006.05.09	2.9	1.53	3.26·10 <sup>-2</sup>	1.30·10 <sup>6</sup>	NE-N
2006.05.11	1.1	0.05	3.05·10 <sup>-2</sup>	4.60·10 <sup>5</sup>	N-NW

At the Preila station was observed new aerosol particle formation and growth events with enough low particle growth and formation rates (the means were 1.9 nm/h and 0.55 cm<sup>-3</sup>s<sup>-1</sup>, respectively). The mean condensation sink and the mean condensable vapour source rate values were 0.0297 s<sup>-1</sup> and 8,00·10<sup>5</sup> cm<sup>-3</sup>s<sup>-1</sup>, respectively. This type of nucleation seems to be typical for the marine and coastal environments. It was estimated, that the total aerosol particle concentration over the Baltic Sea was higher than at the Preila station. Before the start of nucleation process was observed the decrease of the total particle concentration. The short-term increases of the total particle concentrations in the marine environment could be related to the new particle formation, which could be accelerated by the air pollution from ships and ionization due to wave break. Usually the formation of new aerosol particles in the marine and coastal environments was observed when the clean air masses present at the site.

This work was supported by the FP6 project ACCENT and by the EUSAAR.

Kulmala, M., Dal Maso, M., Mäkelä, J.M., Pirjola, L., Väkevä, M., Aalto, P., Miikkulainen, P., Hämeri, K. and O'Dowd, C.D. (2001). *Tellus*, 53B, 479-490.

Plauškaitė, K., Mordas, G., Andriejauskienė, J. and Ulevičius, V. (2006). *Lithuanian J. Phys.*, 46, 489-496.

Ulevičius, V., Mordas, G. and Plauškaitė, K. (2002). *Environmental Chem. Phys.*, 24(2), 38-44.

## **Large-scale inhomogeneity of aerosol concentration at various humidity levels**

Jouravlev A.A., Teptin G.M.

Department of Physics, Kazan State University, Kremlevskaja 18, Kazan, Russia

Keywords: boundary layer, turbulence, impurity transport, electromagnetic waves propagation.

These work is devoted to empirical researches of large scales inhomogeneity structure of atmosphere ground layer. Macroturbulence of passive admixture in a ground layer has quasi two-dimensional structure, when height of inhomogeneity much less than its geometrical sizes along a surface of the ground more often. Such inhomogeneities as a whole to this day do not find the reliable theoretical description. At the same time it is rather long-living atmospheric formations capable to keep the structure long time and to transport impurity on distances up to 200 km.

Results of this work are based on unique prolonged data of every minute monitoring of ecological and meteorological parameters of an atmosphere. Measurements were obtained by 5 automatic stations be situated in a city and be apart on distances of 1-6 km. Stations measured specific mass concentration of an aerosol and the some aerosol generative atmospheric admixture gases. Use the measurements of atmospheric polluting substances concentration, has allowed to reveal empirical laws of aerosol concentration distribution such as spatial structural functions. Synchronous measurements of the basic meteoparameters are used for determination of significant distinctions in

behavior of spatial structural functions under various weather conditions. Influence of humidity on amplitude of spatial fluctuations of aerosol concentration is empirically established. Separations of data on seasons and time of day has essentially improved statistical reliability of structural function of aerosol concentrations and model of macroturbulence as a whole. Our work is researched a condition and dynamics of a ground layer and the macroturbulence characteristics. Besides the influence of aerosol particles and atmospheric inhomogeneities of aerosol concentration on propagation of electromagnetic waves is estimated in work.

This work was supported by the grant of the President of the Russian Federation for support of young Russian Scientists No MK-3183.2006.5.

O.G. Khutorova, G.M. Teptin Investigation of mesoscale variations in the troposphere by means of observing impurities concentration.//RAS. Meteorology and the ocean physics. 2001. V. 37. №6, p.853-856.

A.S. Monin., A.M. Yaglom. Statistical hydrodynamics. The turbulence theory. L.: Gidrometeoizdat, Vol. 1, 1992, 694 p.

## **T28 Abstracts**

## Influence of clouds on aerosol particle number concentrations in the upper troposphere – results from the CARIBIC project

A. Weigelt<sup>1</sup>, M. Hermann<sup>1</sup>, P. F. J. van Velthoven<sup>2</sup>,  
C. A. M. Brenninkmeijer<sup>3</sup>, J. Heintzenberg<sup>1</sup>, and A. Wiedensohler<sup>1</sup>

<sup>1</sup>Leibniz-Institute for Tropospheric Research, 04318, Leipzig, Germany

<sup>2</sup>Royal Netherlands Meteorological Institute (KNMI), 3730, AE De Bilt, Netherlands

<sup>3</sup>Atmospheric Chemistry Dep., Max Planck Institute for Chemistry, 55128, Mainz, Germany

Keywords: aerosol-cloud interaction, particle formation

From 1997 to 2001, 47 flights between Colombo (Sri Lanka) or Male (Maldives) and Germany were conducted as part of the CARIBIC project (Civil Aircraft for Regular Investigation of the Atmosphere Based on an Instrumentation Container, Brenninkmeijer et al., 1999, <http://www.caribic-atmospheric.com>). During these flights several trace gas and aerosol parameters were measured. Aerosol number concentrations for three different size ranges were obtained using three condensation particle counters (CPCs), i.e., ultrafine particles (4 to 12 nm,  $N_{4-12}$ ), particles larger than 12 nm ( $N_{12}$ ), and particle larger than 18 nm ( $N_{18}$ ). In this work, we investigate whether air parcels could have been in contact with clouds during a 48 hour period prior to interception by the aircraft and if this contact correlates with particle number concentrations.

For obtaining the air parcel history 3D kinematic 5-day backward trajectories (based on ECMWF input data) were calculated every three minutes along the flight route (<http://www.knmi.nl/samenw/campaign/support/CARIBIC/>) for all flights. To check for cloud contact along the trajectories we used satellite pictures from the ISCCP Project (International Satellite Cloud Climatology, Rossow and Schiffer, 1999, <http://isccp.giss.nasa.gov/>). These data sets (ISCCP\_DX) have a spatial resolution of about 30 km and are available every 3 hours. The great advantages of this product are that it is available for mayor parts of the globe and that it has the same standard, independent whether GOES- or METEOSAT-satellites were used. Furthermore, the DX product provides directly a cloud top high.

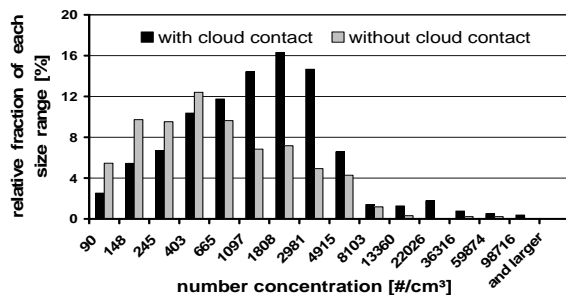


**Figure 1.** Histogram of ultrafine particle concentrations for tropical latitudes on the Indian route. Measurements where the air parcel encountered a cloud during the previous two days are displayed by black columns, measurements for air parcels that did not “see” a cloud are represented in grey.

A retrieval algorithm was written yielding the information whether there was a cloud contact, when this contact was, and for how long the contact existed. Using that information, we investigate how clouds influence the aerosol particle number concentration, i.e., do clouds act as particle source, particle sink, or vertical transporter. Figure 1 shows an example where in the tropics clouds act as particle source.

Using the time lag between the last cloud contact and measurement point, we can also describe the time behavior of the ultrafine particle concentration. When the average fraction of ultrafine particles is plotted against the time between cloud contact and measurement (Fig. 2), there is a clear trend. The longer the contact was ago, the smaller is the fraction of ultrafine particles. This is in agreement with the hypotheses that deep convective clouds lead to particle formation in the upper troposphere or rapidly transport UFPs to this level.

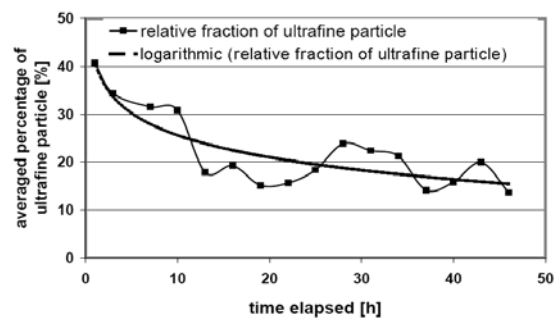


**Figure 2.** 3-hours average percentage of ultrafine particles plotted against time elapsed since cloud contact.

We thank the airlines LTU International Airways and German Lufthansa for their financial and logistical support. Also we thank Paul Carter from Langley Atmospheric Sciences Data Center for his help with the ISCCP data.

Brenninkmeijer C.A.M., et al., CARIBIC – Civil aircraft for global measurement of trace gases and aerosols in the tropopause region. *J. Atmos. Oceanic Technol.* 16, 1373-1383, 1999.

Rossow, W. B. and Schiffer, A. *Advances in Understanding Clouds From ISCCP. Bulletin of the American Meteorological Society* 80, 2261-2287, 1999.

## Thirty months of systematic measurements of tropospheric aerosol and ozone vertical profiles using a combined RAMAN-DIAL and a DOAS system over Athens, Greece (2005-2007)

G. Tsaknakis<sup>1</sup>, A. Papayannis<sup>1</sup>, P. D. Kalabokas<sup>2</sup>, I. Ziomas<sup>3</sup>, G. Chourdakis<sup>4</sup>, G. Georgousis<sup>4</sup> and P. Zanis<sup>2</sup>

<sup>1</sup>National Technical University of Athens, Laser Remote Sensing Laboratory, Heroon Polytechniou 9, 15780 Zografou, Greece

<sup>2</sup>Academy of Athens, Research Center for Atmospheric Physics and Climatology, 131, Tritis Septemvriou Str., 11251 Athens, Greece

<sup>3</sup>National Technical University of Athens, School of Chemical Engineering, 15780 Zografou, Greece

<sup>4</sup>Raymetrics S.A., Kanari 5, Glyka Nera, Athens, Greece

Keywords: Lidar, Tropospheric aerosols, Urban aerosols, Ozone, Raman-DIAL

Thirty months of regular measurements of tropospheric aerosol optical properties (backscatter, extinction and optical depth) and ozone vertical profiles using a combined ozone differential absorption (DIAL) and a Raman lidar system, in the ultraviolet spectral region, have been performed over Athens (37.9° N, 23.6° E, 220 m asl.), Greece, since January 2005, in the frame of the Pythagoras II project (2005-2007).

The lidar profiles were obtained in the lower troposphere typically from 500 m to 5000-6000 m above sea level (asl.) with a spatial raw resolution of 15 m and were complemented with ground-based DOAS measurements. The high quality of the lidar aerosol data has been previously assured by extensive inter-comparison at software (Böckmann *et al.*, 2004) and hardware levels within the frame of the EARLINET project (Bösenberg *et al.*, 2003) while the quality of the ozone DIAL data has been assured by extensive inter-comparison with local ozonesonde data, which showed a very good correlation between the two techniques.

In addition, the ozone mixing ratios obtained by lidar at the lowest available height (e.g. at 500 asl.) have been successfully inter-compared with ground ozone measurements obtained by a continuously operating DOAS system, showing a correlation coefficient  $R^2$  better than 0.92.

Mean values and variances of the ozone mixing ratios and aerosol optical properties have been evaluated during thirty months of systematic air quality measurements. The corresponding seasonal cycle of ozone and aerosols shows highest values during the spring and summer period and secondary maxima during the autumn period. Small fluctuations have been found only during the winter months.

More specifically, the mean ozone concentration varies from 40-50 ppbv during the winter period, and between 60-80 ppbv during the spring-summer period. The ozone concentration has been found to be approximately 1.5 times

higher at the top of the Planetary Boundary Layer (PBL), than at ground level.

The analysis of the vertical profiles of the aerosol optical properties shows that the aerosol backscatter coefficient, the integrated backscatter (IB) and the optical depth (AOD) show a seasonal cycle with highest values during the summer period and secondary maxima during the autumn/spring period (Figure 1). Small fluctuations have been found only during the winter months.

High aerosol IB values were equally found during the summer period, due to larger dust concentrations in the lower troposphere and in conjunction with wind trajectory patterns, mostly related to south-southwestern winds originating from the Saharan desert region.

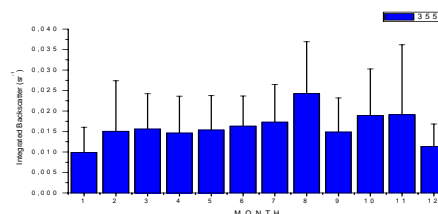


Figure 1. Mean monthly IB values ( $\text{sr}^{-1}$ ) at 355 nm in the period 2001-2005. The error bars correspond to the standard deviation of the individual values, representing the variability between them.

This project is co-funded by the European Social Fund (75%) and National Resources (25%)-Operational Program for Educational and Vocational Training II (EPEAEK II)-PYTHAGORAS Project.

Böckmann, C., Wandinger, U., Ansmann, A., et al. (2004). *Appl. Opt.*, 43, 977-989.

Bösenberg, J. et al. (2003). A European aerosol research lidar network to establish an aerosol climatology, *MPI-Report 317*, Max-Planck Inst. für Meteorology, Hamburg, Germany.

## The size segregated mass concentrations of aerosols in the North Atlantic free troposphere: 5 years observations at the Izaña Global Atmospheric Watch Observatory

S. Rodríguez<sup>1,2</sup>, E. Cuevas<sup>2</sup>, P.M. Romero<sup>2</sup>, X. Querol<sup>3</sup>, A. Alastuey<sup>3</sup>, N. Perez<sup>3</sup>, S. Castillo<sup>3</sup>

<sup>1</sup> Department of Geology, University of Huelva, Huelva, 21071, Spain

<sup>2</sup> Izaña Atmospheric Observatory, INM-CSIC, Santa Cruz de Tenerife, 38071, Canary Islands, Spain

<sup>3</sup> Institute of Earth Sciences “Jaume Almera”, CSIC, Lluís Sole i Sabaris S/N, Barcelona, 08028, Spain

Keywords: free troposphere, North Atlantic background aerosols, Saharan dust

In this study we summarise some of the results obtained in five years observations of the size segregated mass concentrations of aerosols at the Izaña Global Atmospheric Watch Observatory (28.47°N, 16.24°E), located at 2367 m.a.s.l. in Tenerife (Canary Islands). Because this site is about 1000 meters above the trade winds layer (~mixing layer in this region) during most of time, it has been recognised as a Global Atmospheric Watch station representative of the Subtropical North Atlantic free troposphere. At Izaña, the mass concentrations of aerosols less than 10, 2.5 and 1µm (i.e. PM10, PM2.5 and PM1, respectively) are being monitored since 2002. Moreover, two years of Total Suspended Particles (TSP) sampling has also been performed. The transport patterns and composition of TSP aerosols was previously studied in this region (Prospero et al., 1995). However, little is shown about the mass size distribution variations in the North Atlantic free troposphere.

At Izaña, PMx concentrations exhibit very low levels during most of time because the free troposphere conditions, resulting in PMx medians (50<sup>th</sup> percentile of daily means): 7.6µg/m<sup>3</sup> of PM10, 4.8µg/m<sup>3</sup> of PM2.5 and 2.3µg/m<sup>3</sup> of PM1. These “clean air free troposphere conditions” often disappear owing to the inflows of air masses from North Africa laden of mineral dust. The changes from “free troposphere” to “Saharan dust” conditions result in frequent increases from <10 to >200 µg/m<sup>3</sup> of PM10 hourly concentrations in a few hours period. As results of these Saharan dust events, the 99<sup>th</sup> percentile (of the daily mean values) reaches 208µg/m<sup>3</sup> of PM10, 61µg/m<sup>3</sup> of PM2.5 and 27µg/m<sup>3</sup> of PM1.

The analysis of these data evidences the coarse nature of the aerosols predominating in this region. PM10 accounts for a 90% of the TSP, however:

- PM2.5 only accounts for a ~20% of TSP.
- PM2.5 only accounts for a ~30% of PM10.
- PM1 accounts for an 8% of ~PM10.

Observe in Figure 1 how the contribution of PM1 to PM10 decreases when increases PM10 concentrations.

Annual mean PM10 concentrations exhibit significant year-to-year variations (Table 1). The strong Saharan dust events occurred in winter 2002 (>300µg/m<sup>3</sup> as daily mean) raised the annual mean PM10 concentrations to 41µg/m<sup>3</sup>. In contrast, the much lower number of Saharan dust events occurred in 2006 resulted in an annual mean of 15µg/m<sup>3</sup>. These year-to-year variations are less important in PM1 because the coarse nature of mineral dust. This data set allows understanding other features of the Saharan dust transport events over the North Atlantic Ocean.

Table 1. Annual mean concentrations of aerosols at Izaña North Atlantic free troposphere site (referred to ambient P & T conditions).

µg/m <sup>3</sup>	PM10	PM2.5	PM1
2002	41	14	4
2003	24	10	5
2004	20	9	5
2005	23	10	5
2006	15	6	4

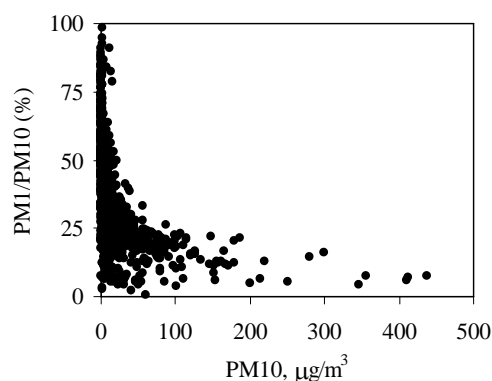


Figure 1. PM1 load in PM10 (in %) versus PM10 levels at Izaña free troposphere site. Analysis based in daily mean values.

Prospero, J. M., Schmitt, R., Cuevas, E., Savoie, D. L., Graustein, W. C., K. K. Turekian, Volz-Thomas, A. Díaz, A., Oltmans, S. J., & H. Levy II (1995), *Geophys. Res. Lett.*, 22-21, 2925– 2928.

## Differences between marine aerosol backscatter and size-distribution in Upwind and Downwind conditions with respect of the ship.

M.Del Guasta, F.Castagnoli, V.Venturi

Istituto Fisica Applicata “Nello Carrara”, National Research Council, Sesto Fiorentino, 50019, Florence, Italy

Keywords: LIDAR, MBL, marine aerosol

Within the framework of the Italian Antarctic Research Program (PNRA), an aerosol experiment was carried out on board the cargo ship ITALICA (Length 130 m, beam 17 m, Tonnage 6.000) in the Ross Sea (Antarctica) during the 2005-2006 winter. The experiment included three instruments developed at IFAC CNR (a PBL aerosol LIDAR, a telemetric-LIDAR with anti-rolly mounting, and an Optical Particle Sizer (OPS)). A commercial DMA sizer (Grimm) was also used. During the experiment, using remote-sensing, we continuously monitored the aerosol backscatter vertical distribution (LIDAR, 532 nm) and aerosol backscatter (5 m above sea level, 10 meters far from the ship left side, telemetric-LIDAR). By means of in-situ sampling (also performed on the left side of the ship, 5 meters a.s.l.), we derived the size distribution of aerosols in the 15 nm - 10  $\mu$ m range. The time resolution of all the measurements was approximately 5 minutes. The instruments operated in all weather conditions.

Taking advantage of the high time-resolution of the instruments and of the routine, bathymetric scan of the sea bottom performed by the ship, we ran an experiment in order to establish the differences in aerosol backscatter and size distribution when the aerosol lab was, respectively, downwind or upwind of the ship. Due to the zig-zag course of the ship, the aerosol lab was alternatively upwind and downwind of the ship. Results for one sample day (January 10, 2006) are shown. The speed of the ship was almost constant (~13 kt) during the scan, while the absolute wind speed was approximately 15 kt in the morning, and slowly decreased down to 5 kt in the evening. The DMA size distribution was almost unaffected by the direction of the relative wind, showing a maximum 20% increase in the concentration of particles in the 100-200 nm size range in downwind conditions. During the sample day, only a few events of direct contamination from the ship smokestack were observed: as the natural aerosol concentration of 50 nm particles in the Ross sea is very low, any aerosol contamination from the ship due to turbulent transport can be detected as a sharp increase in DMA concentrations in this size range, which is a fingerprint of the ship exhausts.

A much more marked downwind-upwind pattern was evidenced in the coarse particle concentration, as obtained from the OPS: 4 to 10 times larger concentrations were observed in downwind conditions throughout the size spectrum.

This difference cannot be explained by a difference in sampling efficiencies of the OPS in different wind directions. The telemetric-LIDAR data, which was measured approx. 10 meters far from the ship wall, confirmed this behaviour (Fig.1). The LIDAR is very sensitive to large particles, and the LIDAR signal showed the same pattern as the OPS, with a marked signal difference between upwind and downwind conditions.

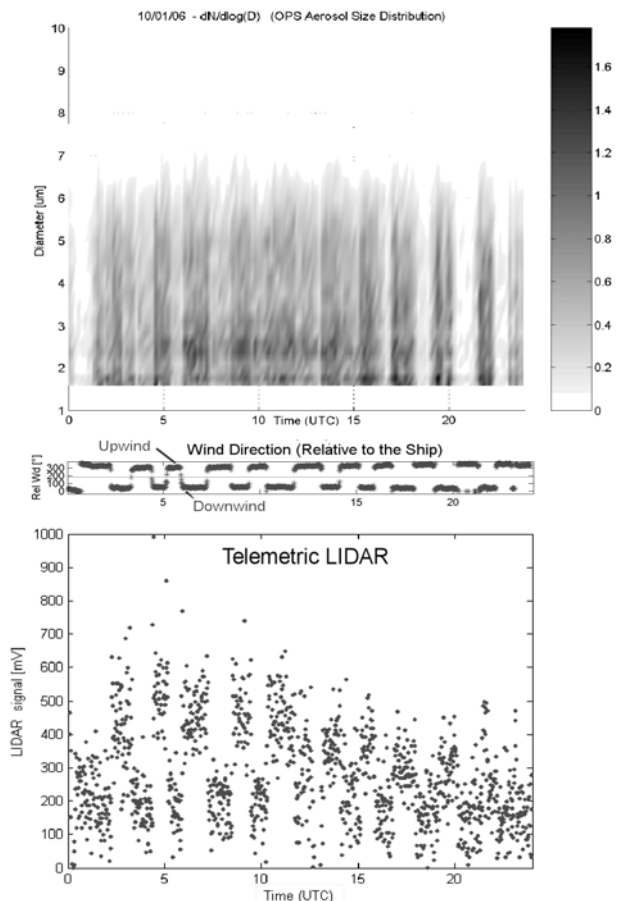


Figure.1 Daily time series of OPS size distribution, relative wind direction, and telemetric-LIDAR signal.

As a result, the ship acted as an efficient source of coarse-aerosols, thus spoiling the collection of natural marine aerosols when the laboratory was downwind of the ship. This effect extended for at least 10 meters away from the ship walls, as confirmed by the telemetric-LIDAR data.

## Meteorological processes affecting the atmospheric particle number size distribution at the high Alpine observatory "Schneefernerhaus"

K. König<sup>1</sup>, W. Birmili<sup>1</sup>, A. Sonntag<sup>1</sup>, L. Ries<sup>2</sup>, R. Sömer<sup>2</sup>, and A. Stöhl<sup>3</sup>

<sup>1</sup>Leibniz Institute for Tropospheric Research, Permoserstr. 15, 04318, Leipzig, Germany

<sup>2</sup>German Federal Environment Agency, Zugspitze 5, 83475, Zugspitze, Germany

<sup>3</sup>Norsk Institutt for Luftforskning, PO Box 100, 2027, Kjeller, Norway

Keywords: Atmospheric aerosols; Long-range transport; Number size distribution; SMPS; free troposphere

Transport of atmospheric aerosols over long distances has been of great interest as a pollution regulatory issue (Stöhl, 2004; WHO, 2004), since atmospheric aerosols may have a life-time of several weeks. Remote transport of aerosols also needs to be considered when quantifying aerosol radiative properties and their effects on regional climate (e.g., Haywood & Boucher, 2000).

In Europe, it is unclear to what extent source regions within, or even outside Europe may influence local aerosol concentrations and, therefore, air quality. In this work we examine the contributions of submicrometer particles that are imported over long distances into the Central European region.

Atmospheric particle number size distributions ( $10 \text{ nm} < \text{Diameter} < 600 \text{ nm}$ ) have been measured continuously since December 2004 at the Global Atmosphere Watch (GAW) observatory "Schneefernerhaus" (SFH), which is located on the Zugspitze mountain, Germany. Being situated at an altitude of 2650 m a.s.l. the SFH is ideally suited to observe free tropospheric air during much of the measurement time. Since the SFH is less influenced by tropospheric emissions than lowland observation sites the data can be screened for remote transport events as well as for footprints of the European main source regions. In addition, our data allow a close look on the influence of local mountain meteorology effects on the predominating particle spectrum.

Figure 1 shows the daily mean cycle of Aitken particle concentration (20-800 nm) for the four seasons, based on two years of observations (2005-2006). Generally, it can be seen that the mean concentrations are the lowest in winter and autumn, showing a diurnal cycle in all seasons. The observations are indicative of a diurnal evolution of the boundary layer, advecting tropospheric air more frequently after noon in a well mixed boundary layer. In winter, however, the boundary layer rarely reaches the altitude of the SFH, implying that these concentrations are more representative for free tropospheric air. Our observations are broadly consistent with former observations of aerosols at the Alpine mountain site Jungfraujoch (Weingartner et al., 1999).

In our data evaluation, air masses will be separated into free tropospheric, as opposed to

boundary layer air for the entire 2-year data set. Correlations between the particle data, trace gas ( $\text{CO}$ ,  $\text{NO}_x$ ,  $\text{NO}_y$ ) as well as radio isotope measurements will be examined to establish representative characteristics of different air masses. A Lagrangian dispersion model (FLEXPART) will be used to establish the source regions of ultrafine, Aitken, and accumulation mode particles on the basis of a two-year statistics.

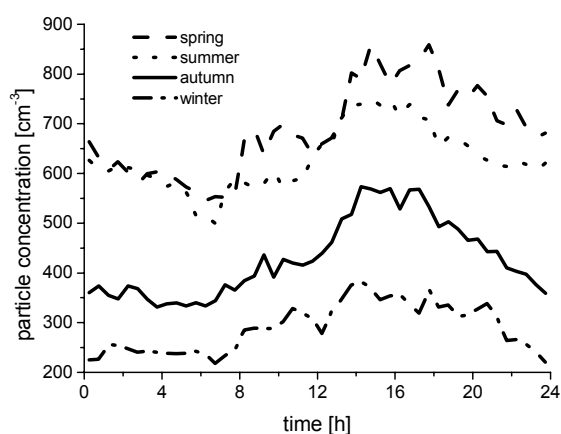


Figure 1. Daily cycles of Aitken particle concentration (20-80 nm) at Schneefernerhaus for all seasons, based on two years of observations (2005-2006).

Haywood J., Boucher O. (2000) Estimates of the direct and indirect radiative forcing due to tropospheric aerosols: A review, *Rev Geophys.*

Stöhl A. (2004) Intercontinental transport of air pollution, Springer.

Weingartner, E.; Nyeki, S.; Baltensperger, U. (1999) Seasonal and diurnal variation of aerosol size distributions ( $10 < D < 750 \text{ nm}$ ) at a high-alpine site (Jungfraujoch 3580 m asl), *J. Geophys. Res.*, 104, 26809-26820.

WHO (2004) Health Effects of Air Pollution Results from the WHO Project "Systematic Review of Health Aspects of Air Pollution in Europe", *WHO Report E83080*, June 2004, Geneva.

We acknowledge Reno Schaffranek from DWD Hohenpeissenberg for meteorological data, and Prof. Ingeborg Levin from the University of Heidelberg for radio isotope measurements. This work was supported by UBA contract UFOPLAN 20442202/01.

## Physico-chemical characterization of Venice lagoon aerosol

F.Prodi<sup>1,3</sup>, L.Di Matteo<sup>1</sup>, F.Belosi<sup>1</sup>, G.Santachiara<sup>1</sup>, S.Nava<sup>2</sup>, R.Udisti<sup>4</sup>, D.Contini<sup>5</sup>, A.Donateo<sup>5</sup>

<sup>1</sup>Institute ISAC-CNR, Bologna, Italy

<sup>2</sup>Physics Department, University of Florence and INFN, Scientific Pole, Florence, Italy

<sup>3</sup>Physics Department, University of Ferrara, Italy

<sup>4</sup>Chemistry Department, University of Florence, Italy

<sup>5</sup>Institute ISAC-CNR, Lecce, Italy

Keywords: Aerosol Chemistry, PIXE, Chemical composition.

The Venice lagoon, located along the northern Adriatic coast, represents a unique ecosystem in contact with an important historical city and a large industrial area. The centre of Venice has influenced the lagoon for more than 1000 years, while the industrial district, located on the inner edge of the lagoon and linked with the rest of the lagoon through its navigable canals, became active only at the beginning of the last century.

The main anthropogenic activities having an important influence on air quality in the Venice area can be summarized as follows: oil refining, metallurgy (e.g. production of Al), chemical plants producing a range of plastic materials (e.g. vinyl and polyvinyl chloride), energy generation (coal and oil), urban waste incineration, and traffic emission (e.g. ferry-boats). At present there is no waste water treatment facility.

In order to evaluate the contribution of aerosol in the transport of pollutants in the Venice lagoon system, an experimental campaign was carried out at Mazzorbetto (May 2006), in the north-east part of the lagoon.

Aerosol samplings were performed by means of an inertial spectrometer (INSPEC), which allows the collection on a filter of particles separated according to their aerodynamic diameter (V. Prodi et al., 1979). The filters were analysed with PIXE to obtain the concentration of chemical elements in different size range of aerosol. Crustal elements (Si, Fe) are present in higher percentages in the coarse fraction, while sulphur is present both in fine and coarse fraction.

By comparing the  $\text{SO}_4^{2-}$  concentration in the PM<sub>2.5</sub> fraction and the sulphur (S) concentration measured with PIXE in the same range, it can be deduced that in the fine fraction S is prevalently present as sulphate. In addition the PM<sub>2.5</sub> aerosol fraction was sampled, and filters were weighted in order to obtain the atmospheric aerosol concentration. Subsequently they were analysed with an Ion Chromatograph to assess the main inorganic water soluble ions, and organic compounds, i.e. formic acetic, oxalic and pyruvic acids, and methane-sulfonic acid (MSA).

A strong correlation was observed between  $\text{NH}_4^+$  and  $(\text{SO}_4^{2-} + \text{NO}_3^-)$ , indicating that the  $\text{NH}_4^+$  ion is mostly in the form of sulphate and nitrate. The ratio between the sum of the concentration of  $\text{NH}_4^+$ ,  $\text{SO}_4^{2-}$ ,  $\text{NO}_3^-$  (anthropogenic ions) and PM<sub>2.5</sub> ranges from 50 to 95% in the considered filters. Fig.1 shows the measured concentrations of  $\text{NH}_4^+$ ,  $\text{SO}_4^{2-}$ , and  $\text{NO}_3^-$ .

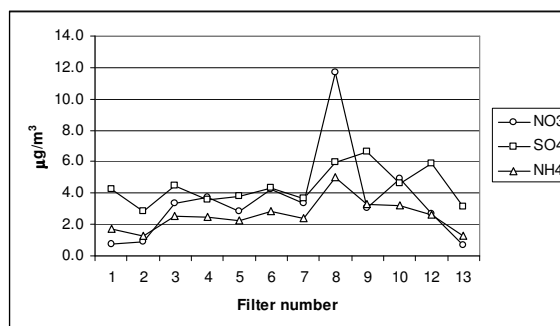


Fig.1- Concentration of  $\text{NH}_4^+$ ,  $\text{SO}_4^{2-}$ , and  $\text{NO}_3^-$

Diurnal and night sampling showed different ion concentrations, first of all for nitrate. By assuming Na as reference element for sea-salt aerosol, it can be inferred that the contribution of inorganic marine aerosol would be negligible. A contribution to non sea-salt sulphate ( $\text{nss-SO}_4^{2-}$ ) might come from the oxidation of dimethylsulfide (DMS), which flows from sea-water to the atmosphere (Sciare et al., 2000; Querol et al., 2001).

PM<sub>2.5</sub> was measured in real time also by optical counters (pDR 1200 and DustTrack 8520 TSI). The size distribution of the aerosol was obtained with an optical counter (Handheld 5016, Lighthouse), which classified particles in six channel: 0.5-1.0 µm, 1.0-3.0 µm, 3.0-5.0 µm, 5.0-10.0 µm, 10.0-25.0 µm, >25.0 µm.

Comparisons were made between elements and water-soluble ion concentrations measured in this campaign, and those deduced from samplings performed elsewhere. Meteorological parameters (temperature, relative humidity, wind speed and direction, back-trajectories of air masses, boundary layer height, etc) were considered in order to try to assess the sources of the pollutants.

V. Prodi et al. (1979) *J.Aerosol Science*, 101, 411-419.

Sciare, J. et al. (2000) *J.Geophys.Res.*, 105, 14433-14448.

Querol, X. et al. (2001) *Atmos.Environ.*, 35, 6407-6419.

## Atmospheric Aerosol Dynamics Obtained by Experiment Using Diffusion Battery

A. M. Baklanov<sup>1</sup>, G. I. Gorchakov<sup>2</sup>, T. E. Ovchinnikova<sup>3</sup>

<sup>1</sup> Institute of Chemical Kinetics and Combustion SB RAS, 630090 Novosibirsk, Russia

<sup>2</sup> Institute of Atmosphere Physics RAN, Moscow, Russia

<sup>3</sup> Institute for Water and Environmental Problems SB RAS, 630090 Novosibirsk, Russia

Keywords: atmospheric aerosol, diffusion battery, particle size distribution

Aerosol particle size distributions data obtained as a result of two-week experiment at a period October 4-18 are presented. The measurements using diffusion battery designed in the Institute of Chemical Kinetics and Combustion were fulfilled practically around the clock. The apparatus was placed in a locomotive that was bounded for the rout "Moscow—Vladivostok—Moscow". A spatio-temporal dynamics of aerosol particle size distributions was obtained. In the most part of measurement only low small-size particle count (diameter less than 10 nm) was observed. The size particle distribution dynamics at a part of the day October 11 is presented in the Figure 1.

An analysis of the data has shown that the distribution peaks correspond mainly to the diameters near 100 nm. In some cases the distributions with two peaks were observed (Figure 2).

The experiment has shown the possibility of diffusion battery using for a long time monitoring of atmosphere aerosol.

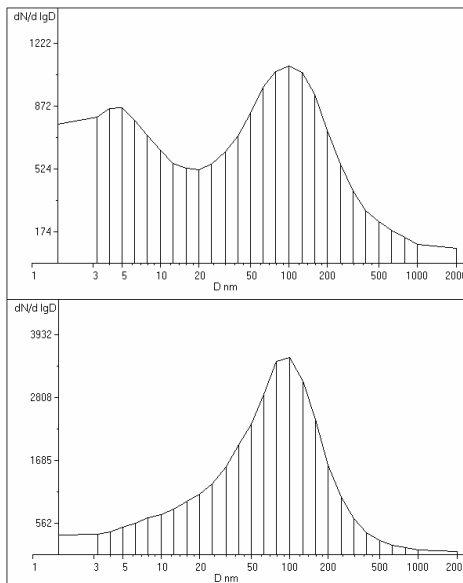


Figure 2. Typical particle size distributions with two and one peaks

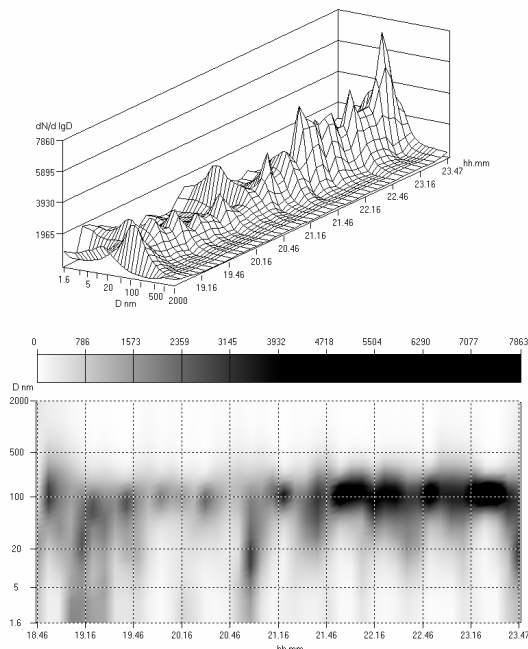


Figure 1. Particle size distribution dynamics obtained at October 11

Measuring data were processed by a program using multiple solutions averaging algorithm (Ovchinnikova *et al*, 2006). A peculiarity of the algorithm is that while obtaining particle size distributions the relative standard deviation of particle concentration is estimated. So the distribution can be calculated even in the cases of "wrong" data obtained under the conditions of abrupt fluctuations of aerosol concentrations leading to non-monotone data.

Ovchinnikova, T. E., Eremenko, S. I. & Baklanov, A.M (2006). in *Proc. 7th Int. Aerosol Conf.* St.Paul, Minnesota, 497-498.

## Similarity between aerosol physico-chemical properties at a coastal station and open ocean over the North Atlantic

M. Rinaldi<sup>1</sup>, C. Carbone<sup>1</sup>, E. Finessi<sup>1</sup>, S. Decesari<sup>1</sup>, M. Mircea<sup>1</sup>, M.C. Facchini<sup>1</sup>, S. Fuzzi<sup>1</sup>, D. Ceburnis<sup>2</sup> and C.D. O'Dowd<sup>2</sup>

<sup>1</sup>Istituto di Scienze dell'Atmosfera e del Clima – CNR, via P. Gobetti 101, 40129, Bologna, Italy

<sup>2</sup>Department of Experimental Physics & Environmental change Institute, National University of Ireland Galway, Ireland

Keywords: aerosol chemistry, biogenic particles, coastal particles, marine aerosols.

Organic marine aerosol (of both primary and secondary origin) represents a potentially important component of the marine biota and climate feedback system involving aerosols and clouds (O'Dowd et al., 2004; Cavalli et al., 2004).

In order to assess the potential influence of coastal environment on marine aerosol chemical composition, both organic and inorganic, two parallel aerosol data sets, collected in two campaigns in the framework of the EC project MAP, are compared in this work. The field experiments have been carried out from June 5<sup>th</sup> and July 5<sup>th</sup> 2006, during the period of high oceanic biological activity at Mace Head Atmospheric Research Station (coastal site) and on board of the oceanographic vessel "Celtic Explorer" (open ocean site). At both the sites the sampling has been fixed approximately at 10 m height above the sea level.

Aerosol samples were collected, under clean conditions (Cavalli et al., 2004) by means of 8-stages Berner impactors equipped with tedlar foils, collecting particles in eight size fractions between 0.060 and 16 µm diameter. In order to obtain a detailed chemical characterization of organic fraction, aerosol samples were also collected by high volume virtual impactors, segregating fine (a. d. less than 1 µm diameter) and coarse particles (a. d. between 1 and 10 µm diameter) on quartz filters.

Three parallel aerosol samples were collected during the campaigns as a result of sampling time of the order of 50 hours each. WSOC (Water Soluble Organic Carbon) and main inorganic ions analyses were performed on tedlar foils, while high volume samples were used for Total Carbon (TC) analyses and for organics chemical characterization (HPLC fractionation, HNMR functional group analyses and tensioactive properties analysis).

Non-sea-salt (nss) sulphate is the dominant species in submicron fraction in both samples sets, showing a similar trend both in coastal and in open ocean samples. For each stage of the fine fraction coastal site samples show an average nssSO<sub>4</sub><sup>-2</sup> concentration higher than the open ocean samples.

On the contrary, average WSOC concentration in the fine fraction is very similar for samples collected at Mace Head Station and at the open ocean site. The ratio between WSOC and

WIOC (Water Insoluble Organic Carbon) is slightly lower in samples collected at the coastal site, being WSOC the dominant fraction of organics in both samples sets.

Coarse fraction is dominated by sea salt in all the size intervals; however, in terms of absolute mass the coastal samples result enriched in sea salt as compared to open ocean samples.

Concerning WSOC chemical characterization, HNMR analyses show that functional groups distribution in samples collected during the cruise is consistent with the one of samples collected at Mace Head Station, suggesting the same chemical composition and the same origin. Moreover, the investigation of tensioactive properties of fine fraction isolated WSOC highlights the same behaviour for both samples collected in middle ocean and at the coastal site.

In conclusion, our results show strong similarity between aerosol physico-chemical properties at coastal station and open ocean site, especially for the main organic components thus excluding potential effects of the shore line environment on marine organic aerosol.

Cavalli, F., Facchini, M.C., Decesari, S., Mircea, M., Emblico, L., Fuzzi, S., Ceburnis, D., Yoon, Y.J., O'Dowd, C.D., Putaud, J.P. & Dell'Acqua, A. (2004). *Advances in characterization of size-resolved organic matter in marine aerosol over the North Atlantic*. J. of Geophysical Research, 109, doi: 10.1029/2004JD005137.

O'Dowd, C.D., Facchini, M.C., Cavalli, F., Ceburnis, D., Mircea, M., Decesari, S., Fuzzi, S., Yoon, Y.J. & Putaud, J.P. (2004). *Biogenically driven organic contribution to marine aerosol*. Nature, 431, 676-680.

## Characterization by electronic microscopy of particulate matter in different places of Mexico influenced by different pollutants emissions.

A. Aragón, A. A. Campos and G. J. Labrada

Instituto de Metalurgia, Universidad Autónoma de San Luis Potosí. Av. Sierra Leona 550, Col. Lomas 2<sup>a</sup>  
Sec. San Luis Potosí, S.L.P. 78210. Tel/Fax: (52) 4448254326, e-mail: [aragon@uaslp.mx](mailto:aragon@uaslp.mx).

Keywords: airborne particles, electron microscopy, morphology, particle characterization

During last years, Mexico has had a great development in industrial activity and population environment in the metallurgic-mining area, which has generated concern about the quality of air in many regions of the country. The knowledge of the individual characteristics of the particles, about their size distribution, chemical composition and morphology provides the identification of emission sources and information about the possible alterations and differences the particulate matter presents according to the climatic and geographic conditions of the different regions.

In this work the results obtained from the period 2000 to 2006 were compiled. It describes the morphologic characteristics and chemical composition of the particle associated to different sources of pollutants (Aragón et al, 2000, 2002, 2006). The samples were subjected to X-ray microanalysis (EDS) coupled with a scanning (SEM) and transmission (TEM) electron microscope to classify individual particles according to their chemical or mineralogical composition. As sample sites, three regions with different geo-environmental conditions in Mexico were considered.

One of the most important sampling sites is the Metropolitan Zone of the Valle of Mexico (ZMVM), which is considered one of the most populated areas of the world, in which a great contribution of particles rich in iron associated to elements like chromium, nickel and zinc with an aerodynamic diameter below 10 $\mu$ m, and particles rich in lead and elemental carbon clusters with an aerodynamic diameter below 2.5 $\mu$ m were observed, the majority associated to the industrial activity and of the vehicles traffic respectively.

To the north of the country, in the city of San Luis Potosí (S.L.P.) these particles of anthropogenic origin like sulphates and lead oxides with average diameter (1 $\mu$ m), arsenic trioxide (5 $\mu$ m), metallic copper (2 $\mu$ m), calcium sulphates (10 $\mu$ m), iron oxides or ferrites (5 $\mu$ m) and particles corresponding to fluorite mineral (15 $\mu$ m) were also found. Most of these come from copper refinery, melting of iron and lead, wastes of chemical industries and transport and storage in the industrial zone of fluorite.

It has to be pointed that for the identification of the sources a direct sampling was done in the different types of enterprises, getting as a result the type of particles that originates every industrial area.

On the other hand, in the western of the county at 30km of the Pacific Ocean coast the city of Colima (CLM) was also taken into account, here, a great abundance of carbonaceous and silicate agglomerates particles generally of coarse size were found and had a high relative humidity, originated by the intense volcanic activity that takes place in the region, besides some other particles of marine aerosol were observed (Cl-Na/K) which were transported by action of the wind, coming from the Pacific Ocean. Other particles rich in elemental carbon with vanadium and nickel associations were also present with a diameter below 15 $\mu$ m, originated mainly from the oil-fuel burning that a thermoelectric and sugar cane harvest season use as a source of energy located at 35 and 20km far from the city respectively. A collecting of samples of anthropogenic emissions for origins identification was also done.

It is important to mention that the presence of the particulate matter in the different regions is going to depend mainly in the weather conditions such as the speed, direction, relative humidity and temperature. As a result of their taking into account and the results obtained by SEM, during a great part of the year the population living far from the main sources of pollutants is also exposed to the particulate matter. That, because of their aerodynamic diameter and chemical composition could produce some effects in health of people and changes in the ecosystems.

These researches have been sponsored by the Consejo Nacional de Ciencia y Tecnología of Mexico. CONACYT

Aragón, P. A., Campos, R. A., Leyva, R. R., Hernández, O. M., Miranda, O. N. & Luszczewski, K. A. (2006). *Rev. Int. Contam. Ambientat*, 22, 5-19.

Aragón, P. A., Torres, V. G., Santiago, J. P. & Monroy, F. M. (2002). *J. Atmos. Environ.*, 36, 5235-52

Aragón P. A., Villaseñor T. G., Monroy F. M., Luszczewski T. A. & Leyva R. R., 2000, . *Atmospheric Environment*, 34, 4103-4112.

## Mass size distribution by gravimetric measurements in a rural site in South-Italy

M. Calvello<sup>1,2</sup>, F. Esposito<sup>1</sup>, L. Leone<sup>3</sup>, G. Pavese<sup>2</sup>, R. Restieri<sup>3</sup>

<sup>1</sup>Department of Environmental Engineering, University of Basilicata, , 85100, Potenza, Italy

<sup>2</sup>CNR-IMAA, C.da S.Loya, 85050, Tito Scalco (PZ), Italy

<sup>3</sup>ARPAB, Via della Fisica 18 C/D, 85100, Potenza, Italy

Keywords: cascade impactor, filters, mass size distribution.

Mass size distributions of atmospheric aerosol have been sampled in a rural site in South of Italy ( Tito Scalco, 40° 35' N, 15° 41' E) with few anthropogenic aerosol source impacting the sampling location. The measurement site is characterised mainly by continental air-masses but marine aerosol from the Mediterranean Sea and, sometimes, mineral dust from North Africa (Pavese *et al.*, 2006) may impact on this area too. The aerosol have been collected by a 13 stages DLPI cascade impactor from May 2006 to January 2007. The DLPI cascade impactor has a flow rate of 30 l/min, and a size range from 0.030 to 10.0 µm with stages cut-off diameters  $D_{50}$  listed in table 1 below. All size are aerodynamic equivalent diameters.

Table 1. Cut-off diameters of DLPI Impactor.

Stage number	$D_{50}$ ( µm)
End filter	0.010
1	0.029
2	0.056
3	0.095
4	0.158
5	0.264
6	0.383
7	0.610
8	0.939
9	1.577
10	2.354
11	3.928
12	6.471
13	9.769

A first wide data set of mass size distribution, quite weekly collected, has been analysed. Sampling period was about 25 h, corresponding to sample volumes of about 56.250 m<sup>3</sup>. Aerosol have been collected on 25 mm diameter polycarbonate filters.

As a first step, many proofs have been performed both to characterize the instrument and to optimize the gravimetric protocol and a special care has been spent to control the effects of relative humidity on mass determination. In fact, as atmospheric aerosols are known to absorb water under conditions of elevated relative humidity, the mass obtained from weighing depends, to some

extent, on the relative humidity in the laboratory. Moreover, as volatile and semivolatile compounds are present in the aerosol, the temperature also is important. These considerations led to the development of a weighing protocol which is the following.

Filters were stored into a conditioned room for 24 hours before and after exposure at  $50 \pm 5\%$  relative humidity (RH) and  $20 \pm 5$  °C (Baron & Willeke, 2001). After equilibration, before and after exposure, filters were weighted on a microbalance (Mettler Toledo MX5 Type , weighing accuracy of  $\pm 1$  µg) for the gravimetric analysis. Weighing was performed in the same conditioned room. Repeated weighing were performed for each filter with a third weighing when the first two were not within 5 µg. The mean of the two closest weighings was used for the analysis. Field blanks were used to calculate the limit of detection (LOD) for the whole procedure (Demokritou *et al.*, 2004).

Finally, an example of mass size distribution measured is showed in Fig.1.

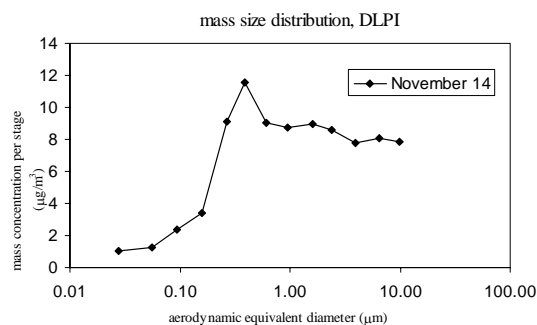


Figure 1. Typical mass distribution obtained by means of the DLPI. The stages are on logarithmic scale.

Pavese G., Leone L., Esposito F., Restieri R., Calvello M. (2006). In *Abstracts of Conference on Visibility, Aerosols, and Atmospheric Optics*, 71, Vienna.

Baron, P. A. & Willeke K. (2001). *Aerosol Measurements. Principles, Techniques, and Application*. Wiley & Sons, Inc., Publication.

Demokritou P., Seung J., Ferguson S., Koutrakis P., *J. Aerosol Science*, 35 , 281-299.

## Variability and long-term trends of aerosol parameters at the Jungfraujoch

M. Collaud Coen<sup>1</sup>, E. Weingartner<sup>2</sup>, S. Nyeki<sup>2</sup>, J. Cozic<sup>2</sup>, B. Verheggen<sup>2</sup> and U. Baltensperger<sup>2</sup>

<sup>1</sup>MeteoSwiss, CH-1530 Payerne, Switzerland

<sup>2</sup> Laboratory of Atmospheric Chemistry, Paul Scherrer Institut, CH-5232 Villigen, Switzerland

Keywords: long-term trend, tropospheric aerosol, optical properties, atmospheric aerosol, monitoring.

Continuous measurements of aerosol parameters have been performed since 1995 at the high alpine research station Jungfraujoch (JFJ, 3580 m asl), enabling a 11-year long-term trend analysis to be performed. The JFJ is prevalently situated in the free troposphere, but is often influenced by thermal convection of planetary boundary layer (PBL) air during warmer months (Ugauer *et al.*, 1998). The JFJ is therefore well suited to estimate the variability of the background aerosol load above a continental area.

Since the aerosol parameters are approximately lognormally distributed, a non-parametric test, the seasonal Kendall test, and a non-parametric slope estimator, the Sen's slope estimator, were applied to detect the long-term trends and their magnitudes for each month (Gilbert, 1987). With this method, an annual trend can be estimated only if the monthly trends are homogeneous in direction and magnitude, which is seldom the case in our study. The global trend was estimated by a least-mean square (LMS) fit of the data (or on the data logarithms if they are lognormally distributed).

Figure 1 shows that an increase of the scattering coefficient is clearly visible in the LMS fit of the data logarithms (at 95% confidence level). The same procedure applied to the scattering coefficient itself (rather than the logarithm) allows for estimating a positive trend magnitude of 3 to 4 % yr<sup>-1</sup>. Careful examination of Figure 1 shows that no visible increase of the scattering coefficient is found for the warmest months (June to August monthly medians, shown as dark grey squares) while a strong increase can be observed for November and December (light grey circles). A more detailed analysis of the long-term trend was therefore performed with the seasonal Kendall test.

The most significant trend detected with the seasonal Kendall test is the increase (2-4 % per year) of the aerosol light scattering coefficients at 450, 550 and 700 nm during the September to December period. The backscattering and absorption coefficients, and to a lesser extent the condensation nuclei concentration, also have significant positive trends in autumn. This increase of most of the aerosol parameters in the September-December period does not directly depend on the aerosol loading in nearby valleys, but probably relates to a European-wide increase in injection of PBL air masses into the lower FT coupled with large-scale transport. In this sense

the positive trend of the extensive aerosol properties in autumn can be described as an increase of the background aerosol concentration in the lower free troposphere.

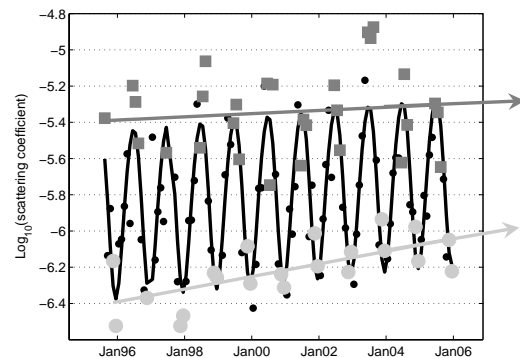


Figure 1. Scattering coefficient logarithm as a function of time, with June, July and August represented by dark grey squares and November and December by light grey circles. The black line is the LMS fit of the data.

In general, the summer months, which are strongly influenced by the PBL, do not show any significant long-term trend. It seems therefore that the measured decrease of anthropogenic aerosol emissions in Europe is not reflected in the summer mixed air masses found at the JFJ in summer.

The hemispheric backscattering fractions (backscattering coefficient/scattering coefficient) and the scattering exponent show an increase in size of small particles during the whole year, except during summer, with the size of large particle remaining constant.

Most of the described trends are significant at the 95% confidence level for both statistical methods. We can therefore conclude that, due to the large magnitude of the detected long-term trends, our dataset is long enough to estimate the aerosol variability in the lower free troposphere.

Collaud Coen, M., Weingartner, E., Nyeki, S., Cozic, J., Henning, S., Verheggen, B., Gehrig, R., and Baltensperger, U. (2006) *J. Geophys. Res.*, submitted.

Gilbert, R. O. (1987), Van Nostrand Reinhold Company, New York.

Ugauer, M., Baltensperger, U., Furger, M., Gägeler, H.W., Jost D.T., Schwikowski, M., and Wanner, H. (1998), *Tellus Series B*, 50B, 76-92.

## Size distributions of atmospheric ions in the Baltic Sea region

M. Komppula<sup>1</sup>, M. Vana<sup>2,3</sup>, V.-M. Kerminen<sup>1</sup>, H. Lihavainen<sup>1</sup>, Y. Viisanen<sup>1</sup>, U. Hörrak<sup>2,3</sup>, K. Komsaare<sup>2</sup>, E. Tamm<sup>2</sup>, A. Hirsikko<sup>3</sup>, L. Laakso<sup>3</sup> and M. Kulmala<sup>3</sup>

<sup>1</sup>Finnish Meteorological Institute, Research and Development, P.O. Box 503, 00101, Helsinki, Finland

<sup>2</sup>Institute of Environmental Physics, University of Tartu, 18 Ülikooli St., 50090, Tartu, Estonia

<sup>3</sup>Department of Physical Sciences, University of Helsinki, P.O. Box 64, 00014, Helsinki, Finland

Keywords: atmospheric aerosols, DMPS, ions, nucleation, particle formation and growth.

The formation and growth of ultrafine aerosol particles in the atmosphere have been studied during the last decade at many different locations around the world (Kulmala *et al.*, 2004). Despite the frequent observations of particle formation events, the microphysical mechanisms responsible for this phenomenon have remained unclear because mainly of instrumental limitations. The conventional instruments can only detect neutral particles larger than about 3 nm in diameter. Recently, the interest in air ions has increased because ions provide the only means for measuring the very initial steps of atmospheric aerosol formation (down to about 0.4 nm), and because ions themselves may be involved in the aerosol formation process (Laakso *et al.*, 2004). The knowledge about the behaviour of ion clusters, particles and their charged fraction (air ions) during nucleation events could help us to find out the role of different nucleation mechanisms.

The ion production comes from cosmic ray ionization occurring throughout the troposphere, from ionization by gamma radiation from the ground, and from the radioactive decay of compounds such as radon. The two latter processes typically dominate near the ground level over land surfaces and cosmic ray ionization dominates over the oceans.

This work presents ion measurements from three measurement sites in the Baltic Sea region: Utö in an island at Baltic Sea, Hyytiälä in continental Finland about 150 km from the Baltic Sea, and Tahkuse about 30 km from the coast in Estonia (Komppula *et al.*, 2007). Particle number size distribution was also measured simultaneously in all the three sites. The measurements were conducted in April-May 2004.

Different behaviour of cluster ion (diameter <1.6 nm) concentrations at the sites revealed clearly the competition between ion sources and sinks. Utö island with a minimum land area around it had the lowest cluster ion concentrations (Table 1). Hyytiälä had the highest cluster ion concentrations probably due to the granite soil as a source of radon, whereas the Tahkuse had a cluster ion concentration mostly in between the two other sites. Cluster ion concentrations were observed to be about three times smaller in Utö compared to Hyytiälä. The lower cluster ion concentrations over the Baltic Sea may be due to lower ionization rate in the cleaner marine

environment and also due to higher wind speeds than over the continent. It was estimated that during the measurement period the cosmic rays contributed about 30 % on average to the total ion production rate in Hyytiälä and about 60-70 % in Utö and in Tahkuse.

Mean concentrations of intermediate ions in the diameter interval of 1.6-7 nm were generally low (Table 1), but reached several hundreds during nucleation episodes in all the three locations. Mean values of total particle number concentration during the measuring period were 9900 cm<sup>-3</sup> in Tahkuse, 4800 cm<sup>-3</sup> in Utö and 3700 cm<sup>-3</sup> in Hyytiälä.

Table 1. Mean values ( $\pm$  standard deviation) of cluster and intermediate ion concentrations in Utö, Hyytiälä and Tahkuse. All values are given in cm<sup>-3</sup>.

	Utö	Hyytiälä	Tahkuse
Cluster ions (+) (<1.6 nm)	250 $\pm$ 110	840 $\pm$ 250	390 $\pm$ 120
Cluster ions (-) (<1.6 nm)	280 $\pm$ 120	770 $\pm$ 260	280 $\pm$ 120
Interm. Ions (+) (1.6-7 nm)	6 $\pm$ 14	13 $\pm$ 32	110 $\pm$ 130
Interm. Ions (-) (1.6-7 nm)	10 $\pm$ 24	21 $\pm$ 63	93 $\pm$ 150

The charged fractions of aerosol particles as a function of their size were calculated. The charging probabilities in diameter range below 8 nm were observed to be close to the steady state in all three sites. This suggests that, at least in this time period, ion-induced nucleation was not playing a major role.

Komppula, M., Vana, M., Kerminen, V.-M., Lihavainen, H., Viisanen, Y., Hörrak, U., Komsaare, K., Tamm, E., Hirsikko, A., Laakso, L., & Kulmala M. (2007). *Boreal Env. Res.* (in press).

Kulmala, M., Vehkamäki, H., Petäjä, T., Dal Maso, M., Lauri, A., Kerminen, V.-M., Birmili, W., & McMurry, P. H. (2004). *J. Aerosol Sci.*, 35, 143-176.

Laakso, L., Anttila, T., Lehtinen, K. E. J., Aalto, P. P., Kulmala, M., Hörrak, U., Paatero, J., Hanke, M., & Arnold F. (2004). *Atmos. Chem. Phys.*, 4, 2353-2366.

## Comparison of columnar aerosol properties in Moscow and Moscow region

M.A. Sviridenkov<sup>1</sup>, N.Ye. Chubarova<sup>2</sup> and P.P. Anikin<sup>1</sup>

<sup>1</sup>A.M. Obukhov Institute of Atmospheric Physics Russian Academy of Sciences,  
Pyzhevsky 3, 119017, Moscow, Russia

<sup>2</sup>Faculty of Geography, Moscow State University, Vorobyevy Gory, 119992, Moscow, Russia

Keywords: light extinction, optical depth, aerosol size distribution

One of the ways to investigate the effects of megalopolis on the content and optical and microphysical characteristics of the aerosol in atmospheric column is to perform simultaneous measurements of the aerosol extinction and sky radiance over city and in near-by rural region free of significant sources of aerosol pollution. In the present work we compare the results of measurements by two CIMEL sunphotometers – at the Meteorological Observatory of the Moscow State University (MO MSU) and at the Zvenigorod Scientific Station (ZSS) of the Institute of Atmospheric Physics located at 50 km to the west from MO MSU. Meteorological Observatory is situated to the south-west from the city center, far from the local industrial zones. So, the data records, obtained at MO MSU, characterize the general effect of the city on the aerosol properties. Both photometers are the parts of the AEROSOL ROBOTIC NETWORK (AERONET). Measurements at MO MSU started in 2001 and in 2006 at ZSS. Time shift between measurements at two sites is about 3 min due to the difference in their coordinates. Thus, the observations can be considered as quasi-simultaneous ones. Comparison of the measured aerosol optical depths (AOD) showed a good correlation between two sites, increasing with decrease of the wavelength. One of the reasons of such behaviour of correlation may be the cirrus clouds influence on the aerosol retrievals relatively more pronounced in IR and not eliminated by the standard AERONET algorithm (Smirnov et al., 2000). The differences between AOD at two wavelengths correlate better than AOD themselves. Correlation plots for AOD(500 nm), AOD(1020 nm) and their difference are shown in Figure 1. Additional screening of high level clouds from 1-hour visual cloud observations in MO MSU enabled to separate clear-sky cases. Some excess of the AODs at MO MSU is observed especially in the shortwave region. The possible explanations of these differences (additional NO<sub>2</sub> absorption in Moscow, or (and) enlarged content of the submicrometer aerosol fraction) are discussed.

Water vapour contents retrieved from measurements at the wavelength of 935 nm are also matched in clear-sky conditions. Aerosol size distributions and radiative characteristics, retrieved from the sunphotometer measurements at two sites, were compared. A rather good correlation between

volume concentrations was revealed. Calculated values of the asymmetry factors of the aerosol phase function are also connected at two measurement points. In addition to AERONET retrieval algorithm (Dubovik & King, 2000), some simplified techniques developed by authors were applied. Distinctions in standard AERONET and our approaches to the aerosol properties retrievals are considered.

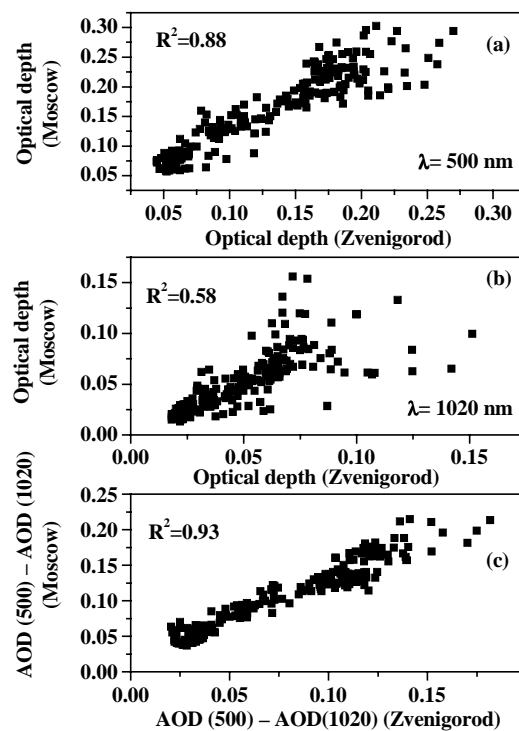


Figure 1. Correlation between aerosol optical depths at wavelength of 500 nm (a), 1020 nm (b), and their differences (c).

This work was supported in part by ISTC under Project No. 3254.

Smirnov, A., Holben, B.N., Eck, T.F., Dubovik, O., & Slutsker, I. (2000). *Remote Sensing of Environment*, 73, 337 – 349.

Dubovik, O., & King, M.D. (2000) *JGR*, 105, D 16, 20,673 – 20,696.

## Real-time Observation of Deliquescence and Efflorescence Behaviour of Individual Aerosol Particles

S.M. Kim<sup>1</sup>, J.H. Kuk<sup>1</sup>, K.H. Ahn<sup>1</sup>, S. Kang<sup>2</sup>, H. Hwang<sup>2</sup>, and C.U. Ro<sup>2</sup>

<sup>1</sup>Department of Mechanical Engineering, Hanyang University, Sa 1-dong, Ansan, 425-791, Korea

<sup>2</sup>Department of Chemistry, Inha University, Incheon, 402-751, Korea

Keywords: Hygroscopicity, Optical microscope, Impactor, Single Particle Analysis, Relative Humidity.

The study on heterogeneous chemistry of aerosol particles in the air is important. Since mineral and sea-salt particles, which are major components of airborne aerosols, can react in the air with gaseous pollutants such as SO<sub>x</sub> and/or NO<sub>x</sub> and their physicochemical properties can be modified through the heterogeneous chemical reactions, the modified chemical properties of mineral dust and sea-salt particles can change climate through their modified direct radiative forcing property and their modified effectiveness to serve as cloud condensation nuclei. In addition, the chemistry of the Earth's atmosphere is influenced by reducing photolysis rates of important atmospheric gas-phase species, through heterogeneous chemical reaction of mineral dust and sea-salt particles. Hence, increasing attention has been devoted to the study of physicochemical characteristic changes of aerosol particles (Rossi, 2003).

In this work, an analytical technique which can be useful for the study of hygroscopic characteristics of individual particle is introduced. A conventional inertial impactor is modified for real time observation of particles collected on an impaction plate as it is shown in Fig. 1. This device can observe particles collected on an impaction plate through a window (Yook, et. al., 2002). Using this device, NaCl, and KCl particles are collected on the impaction plate and observed in-situ to investigate the size changes of hygroscopic particles by varying the relative humidity inside the impactor.

NaCl or KCl salt is dissolved in Deionized (DI) water and aerosolized with ultrasonic nebulizer. The aerosolized salt droplet is then dried with diffusion dryer. This salt particle is introduced into the impactor to deposit on the impaction plate. All of this process is performed near room temperature and pressure. To observe the hygroscopic characteristics of individual particle, the particle generation and collection line is switched by three-way valve to humidity control line. By introducing the humidity control air, the particle hygroscopic change behavior is observed and recorded directly by CCD device.

Figure 2 shows the particle size changes with relative humidity on a glass plate used as an impaction plate. The growth rate is the ratio between the observed projected area over the observed projected area for solid particle. For NaCl particle, it is observed that DRH of ~75.4 % and ERH of 46.4-

47.9 %. In case of KCl, DRH of 82.4-85.2 % and ERH of 56.9-61.9 % are observed. These values for NaCl and KCl are very similar to those reported by Lee and Hsu (2000).

During these experiments, the surface roughness of the impaction plate and the contact angle of water on the impaction plate show the different DRH and ERH values for NaCl and KCl single particles. Higher hydrophobicity of the impaction plate shows the higher ERH and DRH values for NaCl and KCl single particles. Further discussion will be presented at the seminar.

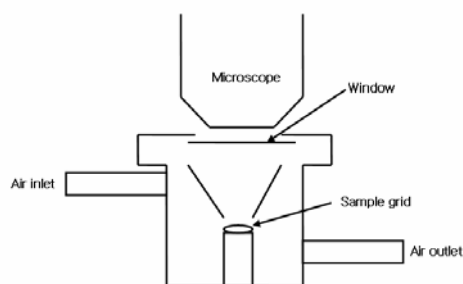


Figure 1. Schematic diagram of an impactor with observation window.

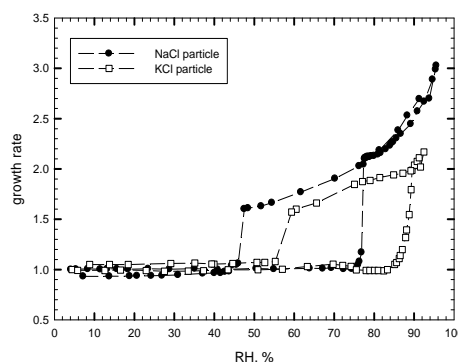


Figure 2. Growth rate changes of NaCl and KCl particles on a glass impaction plate with humidity.

This work was supported by the Second Brain Korea 21 Project in 2006.

Lee, C.T., Hsu, W.C., *J. Aerosol Sci.* (2000), 31, 189.

Rossi, M. J. *Chem. Rev.* (2003), 103, 4823-4882.

S.J. Yook, G.Y. Choi, K.H. Ahn, *6<sup>th</sup> International Aerosol Conference* (2002), 453-454.

## Database driven web-application for atmospheric data visualization

H. Junninen<sup>1</sup>, M. Kulmala<sup>1</sup>

<sup>1</sup>Department of Physical Sciences, University of Helsinki, P.O. Box 64, FIN-00014, Helsinki, Finland

Keywords: Atmospheric aerosols, Modeling, Monitoring, Data mining

Data measured from an atmospheric measurement station can be simple time series and straight forward to understand. However, degree of complexity increases drastically when more instruments are added, different sampling heights are used and lots of researchers are involved. If also air mass back-trajectories and potential emission sources are added the whole system can be extremely complex.

In order to get a good overview of the data researcher must consider all measured parameters at current moment of time. To do that, one must be able to handle data with different formats and in different time and spatial resolutions. Unfortunately, this task is often difficult, time consuming and resulting neglected.

This motivated us to build a tool that makes a comparison of different parameters as easy and simple as possible, and to make a better use of precious working hours of researches. As a first step the web application was built to make easy use of SMEAR database.

Continuous atmospheric measurements have been conducted in SMEAR II station in Hyytiälä, Finland over 10 years now. Measurements of 50 meteorological and 30 air quality parameters, aerosol size range from 3 to 1000 nm are collected with 1 to 30 minute time resolution. Additionally for each hour 4 day back-trajectories are calculated for multiple arriving heights using HYSPLIT 4 model. All this data is collected to a SMEAR database. The database is also coupled with European Pollutant Emission Registry (EPER) that covers approx. 12,000 facilities in the 25 Member States of the EU and Norway for the year 2004.

For convenient use of the complex database the web-based user interface was built and called smart SMEAR (Figure 1).

The user interface of smart SMEAR is minimized to a selection panel and graphs. User can select a date and the web-application makes number of database queries and presents the result in 20+ graphs, all visible at the same time on screen. The tool is designed for extreme easy of use and speed. With one click user can see air mass origin, meteorological conditions during the air mass travel and at site, gas concentrations, aerosol size distributions and concentrations for selected day.

To evaluate effect of industrial emissions on air quality in SMEAR II station air mass back-trajectories are plotted together with industrial facilities on an interactive map provided by Google (Figure 2). The map is fully functional (zoomable and movable) Google map with capability to switch on also a satellite image view. The last mentioned is very usable for spotting e.g. airports.

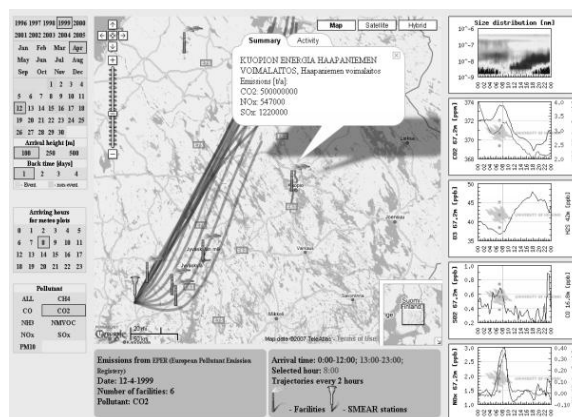


Figure 2. Screen capture of a part of the smart SMEAR's main view

All work was done using MySQL-database, php and JavaScript scripting languages.

The smart SMEAR is available from: <http://www.atm.helsinki.fi/~junninen>

EPER: <http://www.eper.cec.eu.int/eper/>  
 Google: <http://maps.google.com/>  
 HYSPLIT4: <http://www.arl.noaa.gov/ready/hysplit4.html>

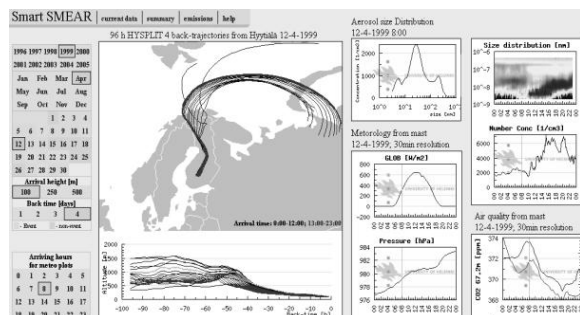


Figure 1. Screen capture of a part of the smart SMEAR's main view

## Seasonal variation of particle size distributions of PAHs at Seoul, Korea

J.Y. Lee<sup>1</sup>, C.-H. Kang<sup>2</sup> and Y.P. Kim<sup>1</sup>

<sup>1</sup>Department of Environmental Science and Engineering, Ewha Womans University, Seoul, 120-750, Korea

<sup>2</sup>Department of Chemistry, Cheju National University, Jeju, 690-756, Korea

Keywords: aerosol size distribution, atmospheric aerosol, PAHs, urban aerosols.

Particle size distributions of individual PAH compound can provide information on major emission sources of the PAHs, residence time in atmosphere, and the health effect of PAHs. In Korea, only two studies have been reported on the size distributions of PAH in Korea (Lee *et al.*, 2006a; Bae *et al.*, 2002). They found that most of PAHs were in small particles ( $D_p < 9\mu\text{m}$ ). Also they observed the ambient PAHs concentrations in the rural areas were comparable to those in the urban areas in Korea. They suggested that there might be local emission sources of PAHs in rural areas in Korea in addition to the transport from urban areas. However, they could not observe and explain seasonal difference of particle size distribution of PAHs.

In this study, the particles size distributions of PAHs were measured at Seoul, a representative urban areas in Korea in summer and winter 2003 (1) to characterize the seasonal variation of particle size distribution of particulate matter smaller than  $10\mu\text{m}$  in diameter (PM10) and PAHs in Seoul and (2) to determine the major factor affecting the seasonal variation of the observed particle size distributions of PAHs.

Measurement was carried out in June and December, 2003 at Seoul, Korea. The sampling site in Seoul is located in Asan hall, Ewha Womans University. The size distributions of PM10 were measured for 48 or 72 hr on pre-fired quartz fiber filters (QFFs, QM-A, Whatman) by an eight-stage Andersen 1 ACFM Nonviable Ambient Cascade Impactor equipped with a size-selective inlet. Detailed sampling procedure was given in Lee *et al.* (2006a) and the analytical procedures used in this study were described in detail in Lee *et al.* (2006b).

The average PM10 concentration in summer was  $85.8\mu\text{g m}^{-3}$  ranged from  $65.1$  to  $117\mu\text{g m}^{-3}$  and in winter  $97.0\mu\text{g m}^{-3}$  from  $45.5$  to  $223\mu\text{g m}^{-3}$ , respectively. A highest concentration of PM10 ( $223\mu\text{g m}^{-3}$ ) was observed in 23-26 December, 2003 (sample number W-5 in Figure 1). Seasonal variation of PM10 concentrations was not observed. The size distributions of PM10 in summer and winter were similar as shown in Figure 1. The PM10 size distribution was bimodal with the peaks in the  $0.65$ - $1.1\mu\text{m}$  diameter range in accumulation mode ( $0.1 < D_p < 1\mu\text{m}$ ) and  $4.7$ - $5.8\mu\text{m}$  in coarse mode ( $D_p > 2.5\mu\text{m}$ ), respectively, a typical size distribution for an urban atmosphere. The concentrations of total PAHs were ranged from  $4.32$  to  $5.48\text{ng m}^{-3}$  in summer and from  $25.6$  to  $35.9\text{ng m}^{-3}$  in winter, respectively. The

PAHs concentrations in winter were about one order higher than those in summer. About a half (41 ~ 65 wt %) of the PAHs concentrations were found on sub-micrometer particles ( $D_p < 1.1\mu\text{m}$ ) and average 75 wt % on fine particles ( $D_p < 2.1\mu\text{m}$ ).

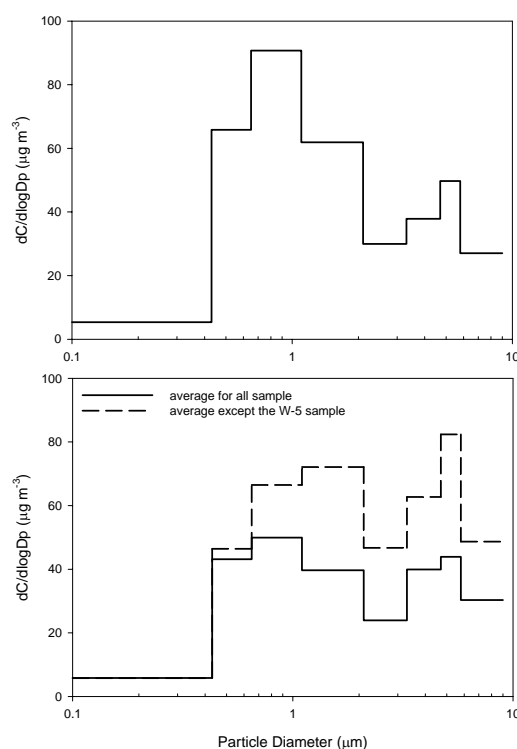


Figure 1. Average size distributions of PM10 in summer (upper) and winter (lower).

This work was supported by the Korea Science and Engineering Foundation (KOSEF) through the National Research Lab. Program funded by the Ministry of Science and Technology (No. M10600000221-06J0000-22110).

Bae, S. Y., Yi, S. M., & Kim, Y. P. (2002). *Atmos. Environ.*, 36, 5491-5500.

Lee, J. Y., Kim, Y. P., & Yi, S. M. (2006a). *Environ. Eng. Sci.*, 23, 393-404.

Lee, J. Y., Kim, Y. P., Kang, C. H., Ghim, Y. S., & Kaneyasu, N. (2006b). *J. Geophys. Res.*, 111, doi:10.1029/2005JD006537

## Observations of different events with high particle number size distributions at the coastal Atlantic area of southwest Spain

M. Sorribas<sup>1</sup>, V.E. Cachorro<sup>2</sup>, B. Wehner<sup>3</sup>, W. Birmili<sup>3</sup>, N. Prats<sup>2</sup>, J.F. López<sup>1</sup>, A. Wiedensohler<sup>3</sup>, A.M. De Frutos<sup>2</sup> and B.A. De la Morena<sup>1</sup>

<sup>1</sup> Atmospheric Sounding Station 'El Arenosillo', Earth Observation, Remote Sensing and Atmosphere Department, INTA, Mazagón, 21130, Huelva, Spain.

<sup>2</sup> Atmospheric Optics Group (GOA-UVA), University of Valladolid, 47071, Valladolid, Spain.

<sup>3</sup> Leibniz-Institute for Tropospheric Research, 04318, Leibniz, Germany.

Keywords: Particle Size Distributions, Atmospheric Aerosol, SMPS, Anthropogenic Aerosol, Particle Formation and Growth.

The Atmospheric Sounding Station 'El Arenosillo' is located at the southwest of Spain (coastal Atlantic area named Gulf of Cadiz). The sampling site is situated in a forest and coastal area, under the influence of the Huelva City with a population of one hundred and sixty, 35 km north westwards. Extensive measurements of the sub-micrometric number particle size distributions are being made since July 2004, using a particle spectrometer (SMPS-TSI, size range 16.5 – 604 nm). A long-term data set is used, from 15<sup>th</sup> July 2004 to 25<sup>th</sup> July 2005, to analyse the characteristic of the 10 min scan evolution.

This task is very difficult because different aerosol types are present in this area and it causes an enormous variation of the shape of the distributions, in short and long temporal scale. The excellent site of 'El Arenosillo' allows us to characterize the marine, continental and desert air masses. The variability in the shape of the size distributions monitored is attributed to appearance and disappearance of nucleation and Aitken modes. In previous studies, periods with prevalence of the accumulation mode are studied together with the atmospheric conditions (synoptic and local meteorological conditions: air masses, wind direction and speed, solar radiation, etc, (Sorribas *et al.*, 2007)

The carefully manual inspection of the size distributions has permitted to distinguish various types of short time events, in an effort to characterize their behaviour. In this case, the presence of local sources and re-circulations and high level of solar radiation encourages an increase of the Aitken mode concentration. The diurnal evolution of these processes allows classifying three kinds of events which take place around midday.

- Pollution events – Secondary particle formation is produced in the industrial areas around Huelva City. Because of the effect of wind, these anthropogenic pollution with a continuous high level of sub-micrometric particles cause an increase of the concentration in nucleation and Aitken modes in our sampling site in an elapsed time between two and eight hours. No growth of the particles towards higher diameters is produced.

- Events by breeze – The regional re-circulations is a factor, which can increase particle concentration. Our station is situated in a coastal place where meso-scale processes like breeze are very frequent during spring and summer (Adame, 2005). This type of events gives rise to a fast increase of particle concentration in all size ranges: nucleation, Aitken and accumulation modes. As the coarse mode hardly has impact on the number concentration, it is negligible in this study. The event lasts two or four hours and then the particle concentration return to initial level. There is no growth of the particles toward higher diameters.

- New particle formation events – The formation of new particles by gas-to-particle conversion enhances the concentration of particles at diameters below the detection limit of our particle spectrometer. The growth toward greater diameters causes an increase of concentration, at first in the nucleation mode. Later, the new particles growth towards Aitken mode and finally to the accumulation mode. The duration of this kind of events can be from two to eight hours. In future, nucleation process may be examined in a coastal environment.

The aim of this work is to study the diurnal evolution of these three different and particular events, using the modal parameters of the size distribution and their relations to meteorology and synoptical-scale air masses.

This work has been supported by the Spanish "Ministerio de Educación y Ciencia" by means of project CGL2005-05693-C03-02/CLI, and European Union as part of the project AEROTOOLS.

Adame (2005). *Caracterización y comportamiento del ozono superficial en la provincial de Huelva*. Ph. Dissertation. University of Huelva. Spain.

Sorribas *et al.* (2007). *Characterization of sub-micron number particle size distribution measurements at El Arenosillo Station (south-western, Spain) during periods with prevalence of the accumulation mode*. Atmospheric Environment, (submitted for publication).

## Density of boreal forest aerosol particles as a function of mode diameter

J. Kannosto<sup>1</sup>, A. Virtanen<sup>1</sup>, T. Rönkkö<sup>1</sup>, P.P. Aalto<sup>2</sup>, M. Kulmala<sup>2</sup>, J. Keskinen<sup>1</sup>

<sup>1</sup> Aerosol Physics Laboratory of institute of Physics, Tampere University of Technology, P. O. Box 692, FIN-33101 Tampere, Finland

<sup>2</sup> Department of Physical Sciences, P.O.Box 64, FIN-00014, University of Helsinki, Finland

Keywords: ambient aerosol, atmospheric aerosol, ELPI, nucleation mode, outdoor aerosol.

Detailed characterization of atmospheric aerosol particles is needed to understand their effects. Chemical composition of the smallest particles is not easy because of small particle size and low particle concentration. In spite of the recent development of analytical single particle measurement methods, they still do not effectively reach much below 50 nm in particle diameter. Measuring the density of the particles offers an indirect way of obtaining information of the composition of ultrafine particles, but there are not many studies on that either (Saarikoski et al, 2005). We report density values down to less than 20 nm, obtained from aerosol instrument data with a computational method (Virtanen et al, 2006, Kannosto et. al, 2006).

The method is based on simultaneous measurement by ELPI (Electrical Low Pressure Impactor) and SMPS (Scanning mobility particle sizer) and further on the relationship between particle aerodynamic size, mobility size and effective density. First, multimode distribution is fitted to the measured SMPS data. This is done to get separate modes that are then each allocated an average density value. Using the density values, the size distribution modes, and a mathematical model of the instrument, the current values on each ELPI channel are then simulated. The simulated values are compared to the measured ones. The modal density values providing the best agreement between simulated and measured signals are then sought computationally. The method has been reported by Virtanen et al. (2006).

To our knowledge, we have presented the first measured values for particle density of boreal forest aerosols in the range of 10-150nm. The average density value of boreal forest nucleation mode is 1.1g/cm<sup>3</sup>. The density value of nucleation mode decreases with increasing GMD. The density value of Aitken mode is approximately 0.8 g/cm<sup>3</sup>. The Aitken and nucleation modes seem to have the same origin and the nucleation mode particles seem to grow into Aitken mode by condensation of some lighter compound. The density obtained for accumulation mode is ab. 1.5 g/cm<sup>3</sup> and it seems to increase slightly with increasing particle size (Kannosto et al., 2006). These values are preliminary and further analysis of the data is underway. These density results are average values of two weeks measurement campaign in Hyttiälä, Finland. Currently, we are looking at the possibility to follow the evolution of particle density of nucleation mode particles during an event.

Table 1. Average density results of boreal forest aerosols.

	Nucleation	Aitken	Accumulation
$\rho$ (g/cm <sup>3</sup> )	1.1	0.8	1.5

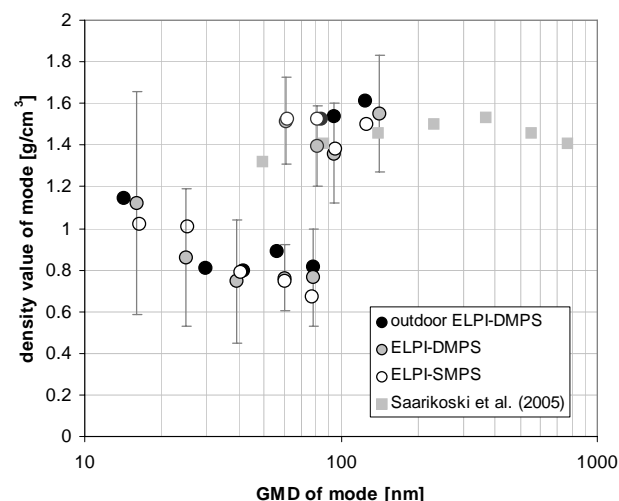


Figure 1. Density values of boreal forest aerosol particles as a function of mode diameter. Three different instrument pairs and result of Saarikoski et. al (2005).

- J. Kannosto, J. Ristimäki, A. Virtanen, J. Keskinen, P.P. Aalto, M. Kulmala (2006) Density analysis of boreal forest aerosols. *Chemical Engineering Transactions*, Vol 10, 2006, 95-99
- S. Saarikoski, T. Mäkelä, R. Hillamo, P.P. Aalto, V-M. Kerminen, M. Kulmala, (2005), Physico-chemical characterization and mass closure of size-segregated atmospheric aerosol in Hyttiälä, Finland, *Boreal Environment research*, 10, 385-400
- A. Virtanen, T. Rönkkö, J. Kannosto, J. Ristimäki, J. M. Mäkelä, J. Keskinen, T. Pakkanen, R. Hillamo, L. Pirjola, K. Hämeri, (2006), Winter and summer time size distributions and densities of traffic-related aerosol particles at a busy highway in Helsinki, *Atmos. Chem. Phys.*, 6, 2411-2421

## The coating of soot with levoglucosan

T. F. Mentel<sup>1</sup>, A. Kiendler-Scharr<sup>1</sup>, R. Tillmann<sup>1</sup>, A. Kiselev<sup>2</sup>, H. Wex<sup>2</sup>, F. Stratmann<sup>2</sup>, T. Hennig<sup>2</sup>, J. Schneider<sup>3</sup>, S. Walter<sup>3</sup>

<sup>1</sup>Research Centre Jülich, ICG-2: Troposphere, 52425 Jülich, Germany

<sup>2</sup>Institute for Tropospheric Research, Department of Physics, Permoser Str. 15, 04318 Leipzig, Germany

<sup>3</sup>Max Planck Inst. for Chemistry, Particle Chemistry Department, Joh.-J.-Becher-Weg 27, 55128 Mainz, Germany

Keywords: Atmospheric Aerosols, Carbonaceous Particles, Coatings, Hygroscopicity, Mass Spectrometry

Combustion of biomass generates carbonaceous aerosols which contain black carbon and organic components. Levoglucosan has been detected in such aerosols and is utilized as a tracer for biomass burning. Levoglucosan is a glucose derivative, thus contributes to the water soluble mass of biomass burning aerosols.

In November 2005, the measurement campaign LExNo (LACIS Experiment in November) was conducted at the ACCENT infrastructure site LACIS (Leipzig Aerosol Cloud Interaction Simulator, Wex et al. 2006). The goal of this campaign was to study the hygroscopic growth and activation of laboratory-generated model aerosol particles that imitate aged biomass burning aerosols. Here we focus on mass spectroscopic measurements (Aerodyne Research Inc., Q-AMS) of soot coated by levoglucosan and the impact of the coatings on size and shape of the particles as observed during the LExNO (2005) campaign.

Soot particles were generated by a sparc generator (PALAS GfG100), size selected by a first DMA, and coated with levoglucosan vapor. The levoglucosan vapor pressure was varied by adjusting the temperature of the coating device. After the coating process particles were again size selected by a second DMA and distributed to the analytical instruments. The amount of condensed levoglucosan, thus the water soluble mass, was determined from the MS-mode of the Q-AMS (Figure 1).

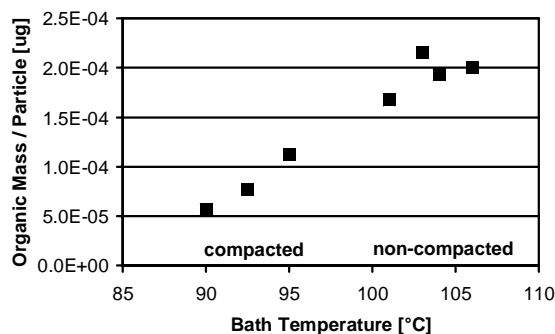


Figure 1. The organic mass per soot particle increases with increasing temperature of the coating device.

In some cases the soot was compacted before the coating process by pre-treating with propanol.

The propanol was removed by a diffusion tube filled with active charcoal.

The vacuum aerodynamic diameter  $D_{vae}$ , for the compacted soot particles increased with increasing levoglucosan mass, whereas  $D_{vae}$  in the case of non-compacted soot remained approximately constant,

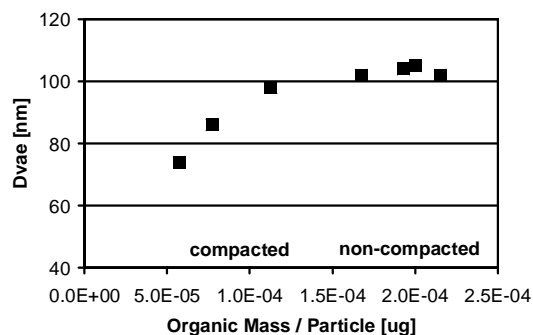


Figure 2. The vacuum aerodynamic diameter  $D_{vae}$  increases with the levoglucosan load for compacted soot particles and remains unaffected for non-compacted soot particles.

independent of the condensed amount of levoglucosan. This effect of compaction and coating on the aerodynamic diameter of soot was confirmed by two independent measurements of the  $D_{vae}$  by a Low Pressure Impactor and the particle ToF-mode of the Q-AMS.

As could be confirmed by TEM, levoglucosan filled mainly the voids of the non-compacted soot. In both cases the growth factors of the particles and critical supersaturations (inversely) scale with the amount Levoglucosan.

This work was supported by ACCENT EU-Network of Excellence.

Wex, H., Kiselev, A., Stratmann, F., & Ziese, M. (2006). *Atmos. Chem. Phys.*, 6, 4519–4527.

## The variability of the atmospheric aerosol in the planetary boundary layer for a subtropical, polluted environment in Southern China

A. Nowak<sup>1</sup>, A. Wiedensohler<sup>1</sup>, W. Birmili<sup>1</sup>, P. Achtert<sup>1</sup>, M. Hu<sup>2</sup>, Y. Zhang<sup>2</sup>

<sup>1</sup>Leibniz Institute for Tropospheric Research, 04318 Leipzig, Germany

<sup>2</sup>College of Environmental Science, Peking University, 100871 Beijing, P.R. China

Keywords: aerosol size distribution, aerosol characterization, atmospheric aerosol, anthropogenic aerosol, nucleation

The influence of atmospheric aerosols on climate is one of the central questions of current atmospheric and climate research. Especially the entrance of anthropogenic aerosols from urban environments plays an important role for understanding of transformation process, the identification of sources and also for the life cycle of atmospheric aerosols in the planetary boundary layer (PBL). To understand this life cycle better, a detailed characterization of the atmospheric aerosol is essential.

An intensive study to obtain highly time-resolved aerosol properties and per-cursor gases has been carried out in the Pearl River Delta north of Guangzhou in July 2006. This region is one of the densely populated and economically fastest growing areas in China. During this study, we measured aerosol size distributions with the mobility and aerodynamic size spectrometer covering the size range from 0.003 to 10  $\mu\text{m}$ . This study was part of the "Program of Regional Integrated Experiments of Air Quality over the Pear River Delta (PRIDE-PRD).

The data set of the campaign was separated into two parts, which represented the typical meteorological condition during the monsoon season in southern China. The first part was analyzed as high convective period with daily variations of minima and maxima in mass concentration (see Fig. 1). In this period, we frequently observed nucleation events (see Fig. 2) and relatively low particle mass concentration during noon time forced by the developing mechanism in the PBL. The second part was identified as polluted period during a longer dry cycle (see Fig 3). In this time period, we measured the highest mass concentration. We also observed typical noon minima in aerosol number concentration and relatively low concentration of ultrafine particles (see Fig 4).

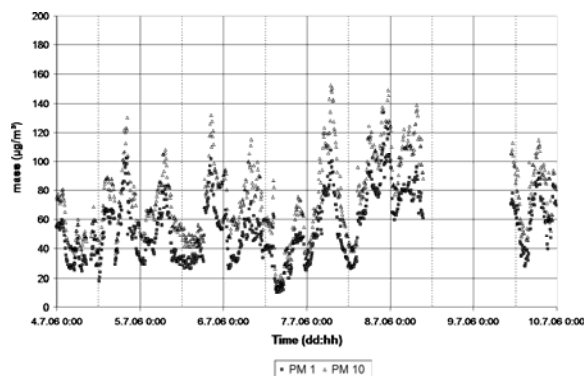


Figure 1. Calculated mass concentration (PM 1 and PM 10) of TDMPS and APS measurements for active convective period (clean period)

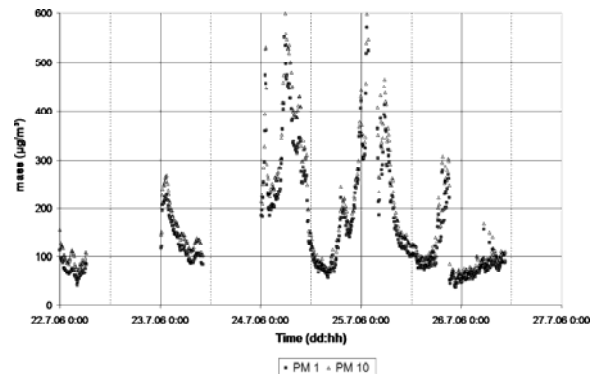


Figure 3. Calculated mass concentration (PM 1 and PM 10) of TDMPS and APS measurements for dry period (polluted days)

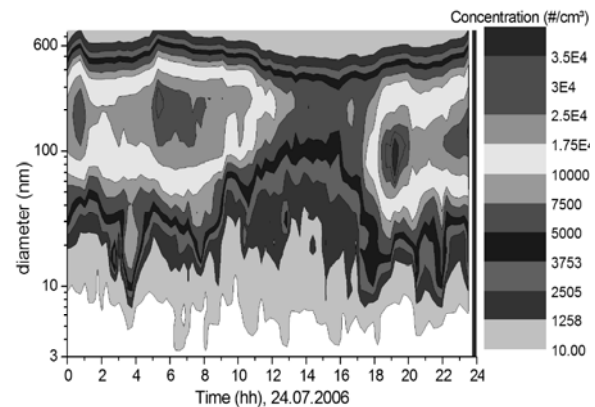


Figure 4. Example of polluted period measured with TDMPS, biomass burning day

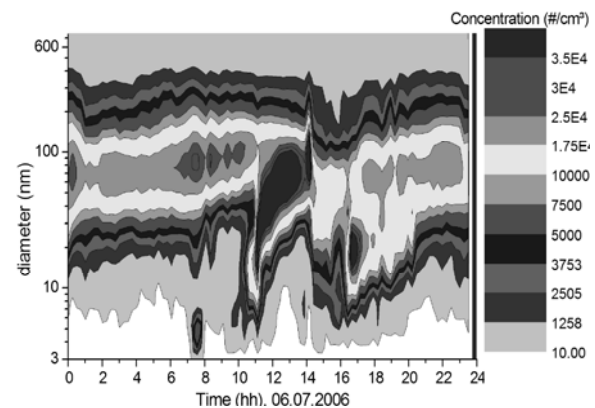


Figure 2. Example of day in the clean period measured with TDMPS, nucleation event interrupted by rain fall

## Comparison of the seasonal variation of the aerosol size distribution at high altitude research stations in France and Nepal

Hervé Venzac<sup>1</sup>, K. Sellegri<sup>1</sup>, P. Villani<sup>1</sup>, D. Picard<sup>1</sup>, P. Bonasoni<sup>2</sup> and P. Laj<sup>1</sup>

<sup>1</sup>Laboratoire de Météorologie Physique, Université Blaise Pascal, 63170 Aubière, France  
<sup>2</sup>CNR - Institute for Atmospheric Sciences and Climate, Bologna, Italy

Keywords: long range transport, vertical transport, free troposphere.

Regional and long range transport can be evaluated by studying the long term evolution of the atmospheric composition at high altitude research stations. Hence, the monitoring of the atmospheric aerosol content is very valuable for this purpose and can play a relevant role in evaluating the background conditions of the free troposphere and the vertical transport from the boundary layer.

Aerosol size distributions were continuously monitored during a full year at two high altitude research stations in Europe, France (1465 m a.s.l.), and Nepal (5079 m a.s.l.). Measurements were performed using Scanning Mobility Particle Sizers specially designed to be controlled by remote login and to operate for long-term periods in adverse weather conditions. The results show that the diurnal profiles of the aerosol size distribution have a seasonal variability on both sites (Figures 1 and 2). At the puy de Dôme station, we observe an increase of particle concentrations of the 50 nm size in the late morning during summer, which would be representative of a significant vertical transport from polluted air masses to the free tropospheric background concentrations. Additionally to the transport of these relatively large particles, we observe the formation of new ultrafine particles from the size of below 10 nm which are growing during the day to the 50 nm range, this all through the year. The annual variation of particle size distribution will be examined in a comparative study of the two high altitude stations.

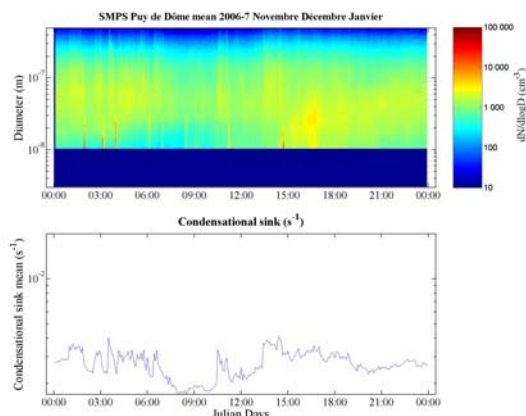


Figure 1. Mean winter (Nov-Dec-Jan) daily variation of the aerosol size distribution.

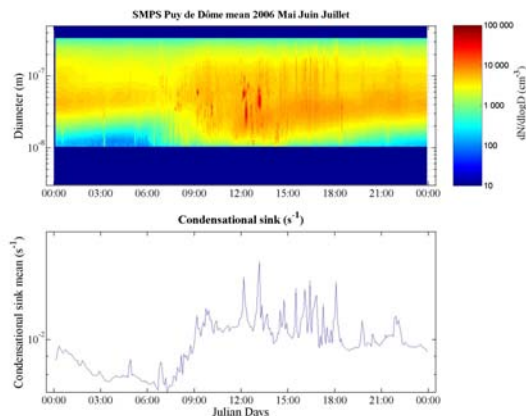


Figure 2. Mean summer (May-Jun-Jul) daily variation of the aerosol size distribution.

## Latitudinal variation in aerosol size distribution in the Eastern Atlantic

P. I. Williams, M. W. Gallagher and G. McFiggans

Centre for Atmospheric Science, SEAES, University of Manchester, Manchester, M60 1QD, UK

Keywords: marine aerosol, aerosol size distribution, condensational loss rate

Aerosol number size distributions were made on board the German research vessel FS-Polarstern, sailing from Bremerhaven, Germany to Cape Town, South Africa covering sizes from  $\sim 3\text{nm}$  to  $20\mu\text{m}$  in October – November 2003. The measurements were made using a combination of optical and mobility methods, with sizes greater than  $30\text{nm}$  recorded at close to ambient RH. It was found that for most of the Northern latitudes, the aerosols could be categorised into “clean” or “polluted”; clean cases were observed when the air mass back trajectory showed little anthropogenic influence, polluted with some continental influences. In the cases where the aerosol had not passed over land for several days, the data generally agreed with other studies of marine aerosol, with a persistent bimodality in the sub-micron range. Evidence of the larger jet and spume modes were also evident.

The data was separated according to wind speed and size, as shown in fig 1.

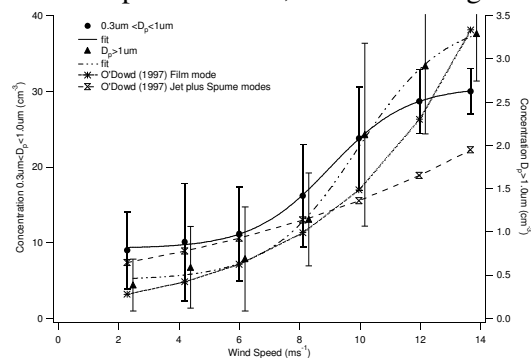


Fig 1. Aerosol number concentration as a

function of wind speed. Also shown, modelled results from O’Dowd (1997)

The results shown in figure 1 indicate that as wind speed increases the number concentration increases, but reaches a plateau at the highest wind speeds. Analysis of the size distribution (not shown) suggests that a separate mode is seen to develop with increasing wind speed.

The aerosol size distribution data were also used to investigate the loss rate of condensing gases with potentially important consequences for heterogeneous marine photochemical cycles, based on the equation given by Schwartz (1986).

This poster aims to present a summary of the characteristics of the clean marine aerosol in the Eastern Atlantic in October-November 2003, and the modelling of the loss rates, and hence lifetimes, of potential important photochemical species.

O’Dowd, C. D. Smith, M. H., Consterdine, I. E., Lowe (1997). *Marine aerosol sea-salt, and the marine sulphur cycle: a short review*, Atmos. Env. Vol 31, No 1, pp 73-80.

Schwartz, S.E. (1986). *Mass - transport considerations pertinent to aqueous phase reactions of gases in liquid-water clouds, in Chemistry of Multiphase Atmospheric Systems*. Nato ASI Series, G6, Berlin, 415 – 471.

## Air quality, particle size distribution and trace metal composition of aerosols from an urban area near an iron smelting facility

M.A. Barrero and L. Cantón

Chemical Engineering Group, Department of Applied Chemistry, University of the Basque Country, P. Manuel de Lardizabal, 20018, San Sebastián, Spain

Keywords: industrial aerosols, particle size distribution, PM<sub>10</sub>/PM<sub>2.5</sub>, trace elements, urban pollution.

Suspended particulate matter in the atmosphere is widely considered as one of the most important factors contributing to the increasing incidence of certain diseases in humans. This is particularly enhanced in urban areas, where the population is exposed to high levels of particulates (Schwartz, 2004). However, the mechanisms of particulate matter toxicity are unclear, partly because of its complex composition. In this context, recent studies have linked transition metal content of airborne particulate matter to increased toxicity (Schwarze et al., 2006). Metallurgical operations such as smelting, founding, refining and industrial combustion are important potential sources of particulates and metals. This work deals with the air particulate matter and metals levels in an urban industrial site in the Basque Country, in the north of Spain, with an active industry mainly related with metallurgical processes.

The aerosol samples were collected using a High Volume sampler equipped with quartz fibre filters over 24 h, once per week for a period of one year. In order to obtain the particle size distribution a cascade impactor (MCV-ICR) with six stages (>10 µm; 4.9 - 10 µm; 2.7 - 4.9 µm; 1.3 - 2.7 µm; 0.61 - 1.3 µm; and <0.61 µm) and equipped with quartz fibre filters was used once a month at the same site. Trace metals (cadmium, copper, iron, lead, manganese, nickel and zinc) were determined by atomic absorption spectrophotometry.

In addition, a measurement campaign was performed with a mobile unit equipped with automatic analysers that continuously measured the concentrations of the major pollutants (CO, NO<sub>x</sub>, O<sub>3</sub>, PM<sub>10</sub> and SO<sub>2</sub>) and the meteorological conditions.

In average, PM<sub>10</sub> (gravimetric method) included 78% of the total particles, while PM<sub>2.7</sub> was 46%, giving a PM<sub>2.7</sub>/PM<sub>10</sub> ratio of 0.59, suggesting additional sources of coarse particles to the typical urban ones. Fe and Zn were major metals with mean concentrations of 3000 ng/m<sup>3</sup> and 776 ng/m<sup>3</sup>, respectively. The metal content of particulates was high compared with those reported for typical urban areas (Figure 1.a).

When hourly measurements of PM<sub>10</sub> were examined for each day of the week, a different pattern was evident for weekdays compared to weekends. Furthermore, background levels were seen to increase as the week passed with a maximum

obtained on Friday followed by an abrupt decrease on the weekend.

The continuous measurement campaign in the proximity of the smelting facility allowed the detection of acute peaks of PM<sub>10</sub> on several days. A classification of days into categories led to the relationship of those PM<sub>10</sub> peaks with days when smelting operations were carried out. Other pollutants that abruptly increased their concentrations on smelting days were carbon monoxide and sulphur dioxide (Figure 1.b). Those peaks were detected associated with high atmospheric pressure conditions and winds from the North direction (upwind from the factory).

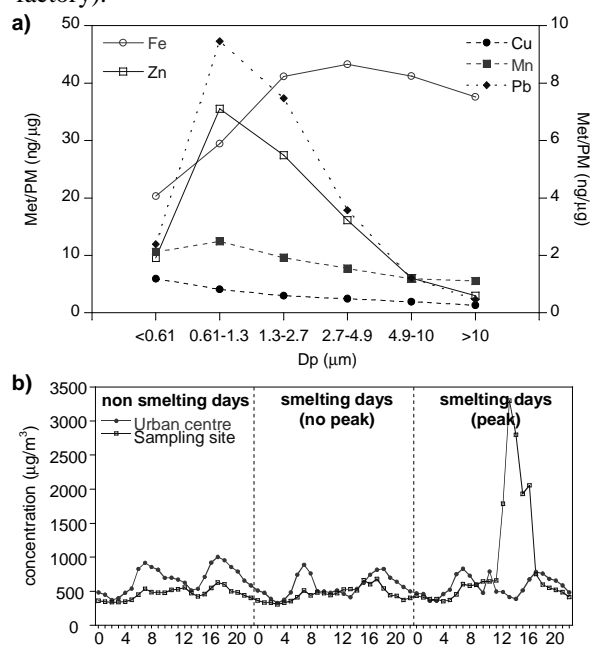


Figure 1. a) Average metal content of each particulate size fraction. b) Diurnal profiles of carbon monoxide concentrations on smelting and non smelting days.

This work was supported by the Department of Environment of the Basque Government.

Schwartz J. (2004). *Environ. Health Perspect*, 112, 557-561.

Schwarze P.E., Øvrevik J., Låg M., Refsnes M., Nafstad P., Hetland R.B. & Dybing E. (2006). *Hum Exp Toxicol*, 25, 559-579.

## Integrating LIDAR profiles and surface Particulate Matter mass concentration for atmospheric aerosol characterisation

R. Caggiano<sup>1</sup>, A. Boselli<sup>1</sup>, M. Macchiato<sup>2</sup>, L. Mona<sup>1</sup>, G. Pappalardo<sup>1</sup>, S. Sabia<sup>1</sup> and S. Trippetta<sup>1</sup>

<sup>1</sup>CNR - IMAA - Istituto di Metodologie per l'Analisi Ambientale C.da S. Loja, 85050, Tito Scalo (PZ), Italy

<sup>2</sup>DSF - Dipartimento di Scienze Fisiche, Università Federico II, Via Cintia, 80126, Napoli, Italy

Keywords: PM, LIDAR, aerosol, long-range transport.

Aerosol particles have been found to play a key role in human health, in pollution problems and in global climate change. Continuous monitoring of atmospheric aerosol properties is very much essential in view of their wide variability in space and time. Particularly, the integrated use of Lidar techniques and direct (in situ) measurements allows to obtain a better characterization of aerosols as function of altitude and to study the exchanges between planetary boundary layer (PBL) and earth surface.

In this study we present the first results of the integration of systematic backscattering and extinction coefficient profiles obtained by a Raman/elastic lidar operating in the framework of EARLINET (European Aerosol Research Lidar NETwork) with the daily concentrations and the chemical composition of particulate matter measured at the ground level. In particular, starting from the climatology of Saharan dust intrusions over Potenza, based on 3 years of Raman lidar measurements (Mona et al., 2006), the impact of Saharan dust on PM concentrations has been investigated. A strong relationship between the increase of the PM level and Saharan dust transport has been found (figure 1).

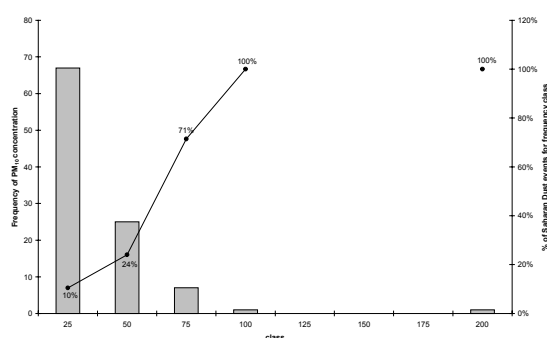


Figure 1. Percentage of Saharan dust events distributed for frequency classes of PM.

With the elastic/Raman lidar, vertical profiles of the backscatter coefficient at two wavelengths ( $\lambda=355\text{nm}$  and  $\lambda=532\text{nm}$ ) and the independent measurement in the UV of aerosol extinction are obtained. This allows us to obtain profiles of the lidar ratio (i.e. extinction/backscatter ratio), that does not depend on the aerosol quantity and is related only to aerosol microphysical

properties (Matis et al., 2003). A qualitative comparison can be carried out between the PM values and the backscatter Angström exponent, obtained from the backscatter profiles at 2 wavelengths, that is generally used as qualitative indicator of aerosol particle size, that can be

The high correlation between the aerosol optical properties measured by LIDAR and the PM levels suggested a detailed study of the chemical composition of the PM (Cd, Cr, Cu, Fe, Mn, Ni, Pb and Zn) (Ragosta et al., 2006). This study allowed us to discriminate natural and/or anthropical contribution and to verify as Saharan Dust transport phenomena can influence the measured PM concentrations.

The European Commission under grant RICA-025991 supported this work. The authors also thank the German Weather Service for the air mass back-trajectory analysis.

Matis I., et al. (2003). Unexpectedly high aerosol load in the free troposphere over central Europe in spring/summer 2003, *Geophys. Res. Lett.*, 30(22), 2178, doi:10.1029/2003GL018442.

Mona, L., et al. (2006). "Saharan dust intrusions in the Mediterranean area: three years of Raman lidar measurements", *J. Geophys. Res.*, Vol.111, doi:10.1029/2005JD006569.

Ragosta, M., et al. (2006). "PM<sub>10</sub> and heavy metal measurements in an industrial area of Southern Italy", *Atmospheric Research*, 81, 304-319.

## Weekly cycles of atmospheric variables and a possible link to the aerosol load

D. Bäumer, and B. Vogel

Institut für Meteorologie und Klimaforschung, Forschungszentrum Karlsruhe/Universität Karlsruhe, Postfach 3640, 76021 Karlsruhe, Germany

Keywords: atmospheric aerosols, climate change, optical depth, weekly cycles

Today, great effort is undertaken to understand and ideally quantify the anthropogenic impact on the climate in past, present and future (IPCC, 2007). However, the error bars with respect to the effect of aerosol particles on global climate are still large. One reason for that is that operational aerosol observations started only a few decades before. In opposite to investigations of the most likely current long-term climate change, the study of weekly cycles of meteorological and chemical variables offers an unequally higher degree of statistical reliability and present-day state-of-the-art measurement quality.

We carried out statistical analyses of data from 12 German meteorological stations meeting WMO standards focusing on the occurrence of a weekly cycle. These stations represent different local climate conditions in terms of both meteorology and pollution situation. For the average over data of all stations, we identified significant weekly periodicities in many variables such as temperature, daily temperature range, sunshine duration, cloud amount, precipitation, and precipitation frequency.

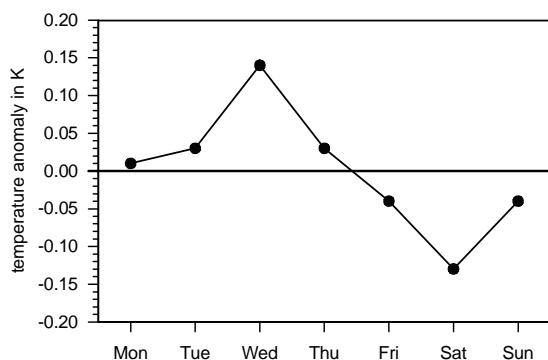


Figure 1. Temperature anomaly for the DWD Station Karlsruhe for the years 1991-2005.

Figure 1 shows as an example the temperature anomaly during the week for the station Karlsruhe, Germany. It shows that the average temperature reaches its maximum on Wednesday and its minimum on Saturday. Not only data of stations situated in congested urban areas, but also data of remote stations as e.g. on Mount Zugspitze 2960 m above sea level in the Alps show significant in-phase

weekly cycles (Bäumer & Vogel, 2007). These weekly periodicities cannot be explained completely by local pollution effects or local heat emissions. We tend towards the hypothesis that the anthropogenic weekly emission cycle and the subsequent aerosol cycle interacts with the atmospheric dynamics on a larger scale which leads to a forcing of a naturally existing 7-day period among the spectrum of atmospheric periods. Since there is no known natural process that creates a periodicity of seven days that prevails for a long time, the existence of such a periodicity is a strong indication of human influence on climate.

In order to elucidate the role of the amount of aerosol on the observed weekly cycle of the atmospheric variables, we evaluated the data of several AERONET (Holben et al., 1998) stations which are spread over Europe. The measurements at the AERONET station give the aerosol optical depth as an integral measure of the aerosol load. We found that most of them show a distinct weekly cycle.

Although no final conclusion can be drawn with respect to the influence of the aerosol on the observed weekly cycle of the atmospheric variables we will give some evidence that there is at least a link between those two quantities.

Bäumer, D., & B. Vogel (2007), *Geophys. Res. Lett.*, 34, L03819, doi:10.1029/2006GL028559.

Holben, B.N., T.F. Eck, I. Slutsker, D. Tanre, J.P. Buis, A. Setzer, E. Vermote, J.A. Reagan, Y. Kaufman, T. Nakajima, F. Lavenu, I. Jankowiak, A. Smirnov, (1998), *Remote Sensing Environment* 66, 1-16.

## Ultrafine Particle Exposure Control Measurement Techniques

Heinz Fissan, Christof Asbach, Heinz Kaminski, Burkhard Stahlmecke, and Thomas A.J. Kuhlbusch

Institut für Energie- und Umwelttechnik (IUTA), Bliersheimer Str. 60, 47229 Duisburg, Germany

Keywords: Ambient Aerosols, Ultrafine Particles, Exposure, Particle Surface Area Measurement

The increasing interest in engineered and unintended nanoparticles from combustion and other man-made sources released into the environment raised the question about the exposure control of ultrafine particles in the environment. The existing standards are based on mass concentration measurements from which the dose taken into human lungs is described. In case of ultrafine particles the mass contribution is very small. Toxicological studies also showed that number or surface area concentrations may be more relevant for health effects, especially for ultrafine particles.

In case of number concentrations we deal with a very sensitive measure, but it especially puts emphasis on the very small particles of a few nanometer in size, which are difficult to measure because of diffusional losses in pipes and sampling devices. In case of surface area concentrations the upper size limit, and therefore the definition of upper size limits of ultrafine particles becomes important. A well defined pre-separation with respect to the collection efficiency curve is needed.

For effective exposure control measurements, a single value is recommended in order to assess a potential exceedance of particle concentration limits affecting health. The instruments hence need to integrate over the number or surface area size distributions within defined size limits to obtain the respective concentrations. These abovementioned limit values can be applied to either emission or exposure situations. While for emissions these limit values usually are for the total airborne

concentration, exposure limits may be weighted according to e.g. particle size dependent deposition probability in different compartments of human lungs.

The monitors have to have a sensitivity per particle, which corresponds to the needed response function different for the different concentration measures. Needed response functions for a device measuring particle surface area (either total or deposited in a lung compartment) are illustrated in Figure 1 for spheres and agglomerates. For the response function for agglomerates, a theory developed by Lall & Friedlander (2006) was used. Primary particles were assumed to be spherical with a radius of 5 nm.

In this presentation the needed response functions (sensitivity as a function of particle size) are presented for different measures for spherical particles as well as for agglomerates based on different models and reference quantities (Rogak *et al.*, 1993; Lall and Friedlander, 2006). The response functions of available instruments (Condensation Particle Counter, Diffusion charger, Lung Deposited Nanoparticle Surface Area Monitor) are compared with the needed ones and the importance of deviations on the accuracy of the measurements of ultrafine particles is discussed.

Rogak, S.N.; Flagan, R.C.; Nguyen, H.V. (1993) *Aerosol Sci. Technol.* **18**:25

Lall, A.A.; Friedlander, S.K. (2006) *J. Aerosol Sci.* **37**:260

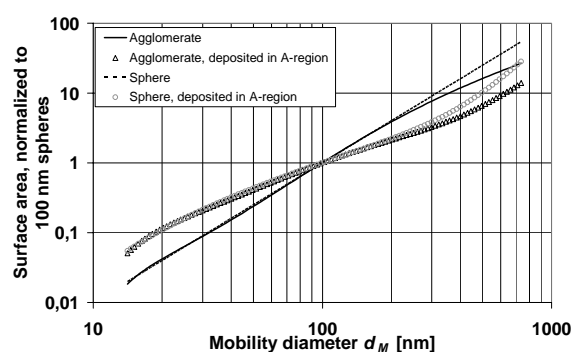


Figure 1: Needed response functions for particle surface area (total and deposited in alveolar region of human lung) for spheres and agglomerates, based on Lall & Friedlander (2006) with primary particle radius 5 nm

## First results of a simple method for directional coarse particulate matter monitoring

J.A.G. Orza, M. Cabello and J. Mateo

<sup>1</sup>SCOLab, Física Aplicada, Universidad Miguel Hernández, E-03202, Elche, Spain

Keywords: Coarse particles, mineral dust.

Directional assessment is a complement to concentration measures. The knowledge of the direction from which dust is coming provides useful information to identify local sources. It combines the existence of specific dust sources and wind directions at the study site.

First results are presented on the use of an inexpensive and simple passive system for directional dust measurement. Dust is collected on a transparent adhesive film fixed completely around a vertically mounted cylinder. Following exposure, the samples are scanned and images are saved as BMP files on a computer for later image analysis. Dust levels are calculated from the scanned images using two complementary methods: recording the presence (also its colour) or absence of dust for each pixel, and recording the position and size (area) of individual coarse particles (greater than 20 microns).

Previous use of sticky pads includes dust quantification by reflectance measurements (percentage reduction in reflectance; Beaman & Kingsbury, 1981) and by the proportion of pixels that have been dusted (Farnfield & Birch, 1997). These methods have higher directional resolution than the BS1747 directional dust gauge, the latter allowing gravimetric measurement.

Vertical array of samplers have been used to estimate the vertical distribution of horizontal particle flux, that corresponds to a combination of saltation and suspension. Samplers are stacked at six heights: 0.05, 0.16, 0.27, 0.38, 0.55 and 1.05 m above the ground.

Just to show one example, Fig. 1 depicts the sandrose and the vertical particle number profile for a 5-day measurement on windy conditions in a plane terrain partially covered with brush. The interaction with the vegetal cover leads to differences with the vertical profiles usually found in sandy areas.

Measurements on sites influenced by aeolian erosion and by dust sources like unpaved roads and stock piles have been performed. We relate them to PM10 values.

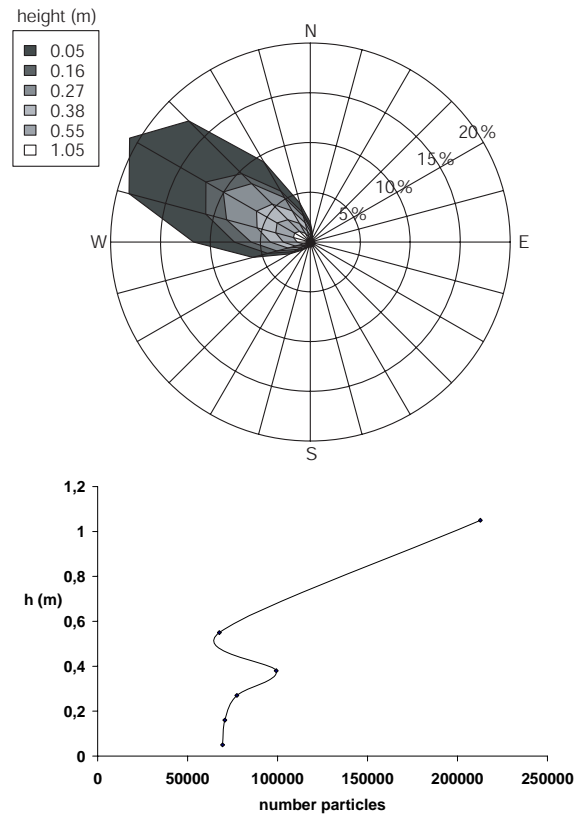


Figure 1. Sandrose at different heights (top) and vertical particle number profile (bottom)

This work was supported by the Ministerio de Educación y Ciencia under the CGL2004-04419/CLI (RESUSPENSE) project.

Beaman, A.L. & Kingsbury, R.W.S.M. (1981). *Clean Air*, 11, 77-81.

Farnfield, R.A. & Birch, W.J. (1997). *Clean Air*, 27, 73-76.

## Comparison of particle number concentrations and size distributions at Dome Concordia in the high Antarctic plateau and at Aboa in Queen Maud Land, Antarctica

A. Virkkula<sup>1</sup>, R.Hillamo<sup>1</sup>, M.Busetto<sup>2</sup>, V. Vitale<sup>2</sup>, P. Aalto, and M.Kulmala<sup>3</sup>

<sup>1</sup>Air Quality Research, Finnish Meteorological Institute, FIN-00880 Helsinki, Finland

<sup>2</sup>Institute of Atmospheric Sciences and Climate (CNR-ISAC), I-40129 Bologna, Italy.

<sup>3</sup>Department of Atmospheric Sciences, University of Helsinki, 00014 University of Helsinki, Finland

Keywords: Field measurements, Atmospheric aerosols, Antarctic aerosols, Aerosol size distribution, CPC

### INTRODUCTION

Dome Concordia (75°S, 123°E) is located on the Antarctic Plateau at an altitude of 3200 m above sea level, approximately 1100 km inland from the coast. Antarctic research stations. The International Polar Year project "POLAR-AOD: a network to characterize the climate-forcing properties of aerosols in polar regions" aims at establishing a bipolar network to obtain data needed to quantify properties of aerosols at high latitudes.

In this work first results of number concentrations and size distributions are presented. The results are compared with similar ones obtained at and around the Finnish Antarctic research station Aboa (73°S, 13°W) in western Queen Maud Land, approximately 150 km inland from the open Weddell Sea. To study the representativeness of the particle measurements at Aboa particle number concentrations and number size distributions were measured during the austral summer 2004/2005 at several locations at distances starting from less than 10 km from the coast up to about 200 km from Aboa and more than 300 km from the coast.

### MEASUREMENTS

As a preparative step for the aerosol measurements at Dome C new aerosol instrumentation were installed at the station in December 2006. Aerosol number concentrations are measured with a TSI 3010 CPC, aerosol number size distribution in the size range 0.3 – 20  $\mu\text{m}$  with a Grimm 1.108 optical particle counter and light absorption coefficient with a Radiance Research 3-wavelength Particle Soot Absorption Photometer. At the time of writing the abstract only one week of data was available from Dome C.

The same OPC and a CPC were used also at Aboa in 2004/2005. Measurements were also made during a special 4-day inland expedition towards the plateau and a 2-day expedition to the coast.

### PRELIMINARY RESULTS

The number concentrations measured with the CPC were remarkably similar at Dome C and Aboa. Median and the 95% range at Dome C was 217 (141 – 352)  $\text{cm}^{-3}$ , which is comparable with the number concentrations measured at Aboa (Figure 1). The big differences can be observed in the larger particle

(Figure 2). The site closest to the coast was clearly dominated by sea-salt particles that get deposited on the way inland. At Dome C no particles larger than 5  $\mu\text{m}$  were observed and also the volume concentrations of 1  $\mu\text{m}$  particles were about 2 orders of magnitude lower than at the coastal site.

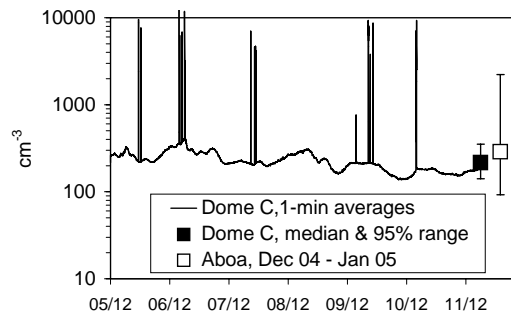


Figure 1. Particle number concentrations measured with a 3010 at Dome C in December 2006 and the median concentration at Aboa during December 2004 - January 2005.

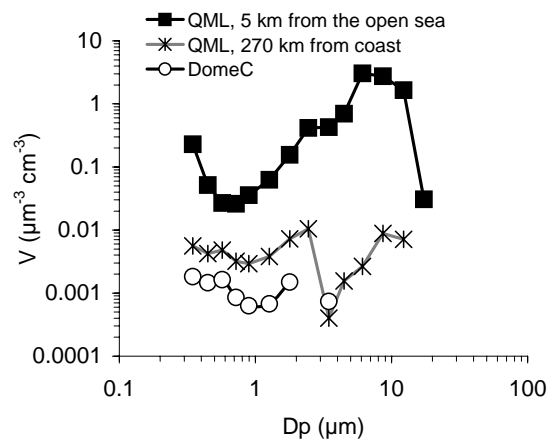


Figure 2. Average volume size distributions measured with a Grimm optical particle counter at two locations (6 – 12 hours) in Queen Maud Land in January 2005 and at Dome C in December 2006.

### Acknowledgement

The project was funded by the Academy of Finland (Finnish Antarctic Research Program, contracts no. 53669 and 2110998)

**Influence of the Mixing Layer on the concentration and size distribution of Particulate Matter over Milan**

Ferrero<sup>1</sup>, E. Bolzacchini<sup>1</sup>, M. G. Perrone<sup>1</sup>, S. Petraccone<sup>1</sup>, G. Sangiorgi<sup>1</sup>, C. Porto<sup>1</sup>, B.S. Ferrini<sup>1</sup>, Mazzati<sup>1</sup>, A. Riccio<sup>2</sup>, E. Previtali<sup>3</sup>, M. Clemenza<sup>3</sup>, F. Bruno<sup>4</sup>, D. Cocchi<sup>4</sup>, F. Greco<sup>4</sup>

<sup>1</sup>Department of Environmental Sciences, University of Milano-Bicocca, Piazza della Scienza 1, 20126, Milano, Italy

<sup>2</sup>Department of Applied Science, University Parthenope, Via De Gasperi 5, 80133, Napoli, Italy

<sup>3</sup>Department of Physics, University of Milano-Bicocca, INFN Milano Bicocca, P.zza della Scienza 3, 20126, Milano, Italy

<sup>4</sup>Department of Statistics P. Fortunati, University of Bologna, Via delle Belle Arti 41, 40126, Bologna, Italy.

Keywords: Atmospheric aerosols, vertical distribution, mixing layer, optical particle counter, size analysis

Urban activities affect air quality directly the highest values of PM<sub>10</sub> and PM<sub>2.5</sub> in Europe are reached in urban areas (Van Dingenen, 2004). The Po Valley, and in particular the city of Milan, are a good example of this scenario. In addition, the meteorology of this area plays an important role on PM pollution levels (Ferrero, 2007). In 2006, in Milan, PM<sub>2.5</sub> concentrations reached a mean value of 43 µg/m<sup>3</sup> in particular from December 2005 to February 2006, during winter times, a mean value of PM<sub>2.5</sub> of 83 µg/m<sup>3</sup> (range: 17–250 µg/m<sup>3</sup>) has been measured. For investigating the influence of atmospheric dispersion conditions on PM pollution levels, vertical profiles of particle number concentrations and particle size distributions (14 classes between 0.3 to 20 µm) were monitored at Torre Sarca site (45° 31' 19" N, 9° 12' 46" E) in Milan, starting from December 2005, using an optical particle counter (OPC GRIMM 1.108 "Dustcheck") and a portable meteorological station deployed on a 4 m tethered balloon (Ferrero, 2006–2007). This method provides the direct measure of the PM profile along height, with a direct evaluation of the Mixing layer (M) height (Seibert, 2000). Estimation of M has been performed using both MM5 model and <sup>222</sup>Rn measurements. The behaviour of the M was investigated in 12 days of acute episodes of PM<sub>2.5</sub> concentration (102±28 µg/m<sup>3</sup>), collecting 94 PM vertical profiles. In Figure 1 a couple among those 12 days are shown those M heights lead to high concentrations of particulate matter (100 and 133 µg/m<sup>3</sup> of PM<sub>2.5</sub>, 117 and 166 µg/m<sup>3</sup> of PM<sub>10</sub> respectively for the two days) due to low air volume available for dilution in addition accumulation processes are possible.

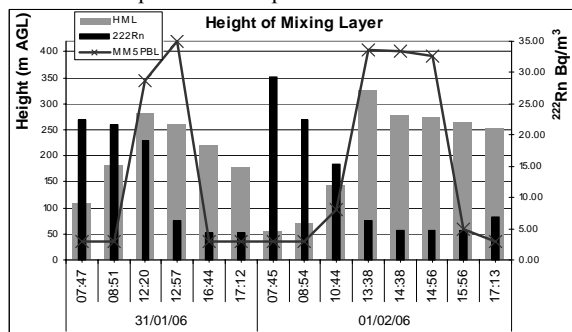


Fig. 1 Heights of ML measured by vertical profiles; MM5 PBL height predictions and <sup>222</sup>Rn measurements.

In order to explore also the physical behaviour of particles along height, a cluster analysis of the OPC original size classes was performed on data taken at three different levels: near the ground, in the M and over the M the first cluster corresponds to particles with a diameter of 0.3–0.5 µm at ground level and 0.3–1.6 µm over the M the mean particle diameter of the cluster 0.3–1.6 µm was calculated and inspected for each profile. A good correspondance between a rapid increase in the mean particle diameter of this cluster (0.3–1.6 µm) and the height of the M (fig. 2) in all the winter profiles, has been observed, with an R<sup>2</sup> of 0.883.

This agreement suggests that the M, under stable conditions, separates two zones in the lower troposphere:

the lower one in which an influence of directly emitted PM is evident, and the upper one where aged PM is present.

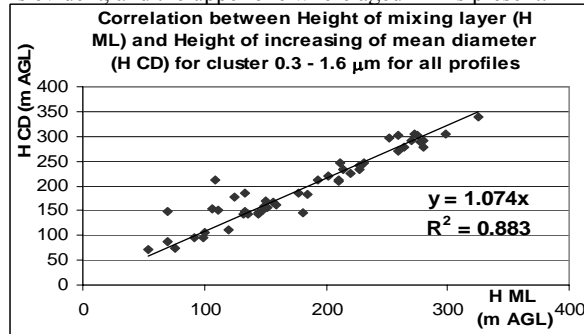


Fig. 2 Correlation between height of ML and height of mean particle diameter increase for cluster 0.3–1.6 µm

In order to check this feature we analyse jointly the proportions of PM classified according to particle size, following the theory of compositional data (Aitchison, 1986) according to two complementary perspectives. First, the relative proportions of particle sizes (compositions) are modelled as linear functions of meteorological variables. Their influence is stronger above M, likely because only the oldest particles arrive at such heights and dilution occurs. It is lower below M since particulate emission and persistence of older particulate intertwine and accumulation processes occur. Then, the evolution of the PM compositions are studied along the vertical profile. A hierarchical model which includes random effects related to launch, composition and height, is constructed. By means of this model, data belonging to launches considered as homogeneous are jointly used for evaluating the evolution of compositions with respect to height by means of probabilistic tools (Figure 3). The finest compositions are more relevant below M, whereas the largest particles become more influent above M. As a conclusion, the levels of M are crucial in both approaches, in the three vertical regions: below, within and above M.

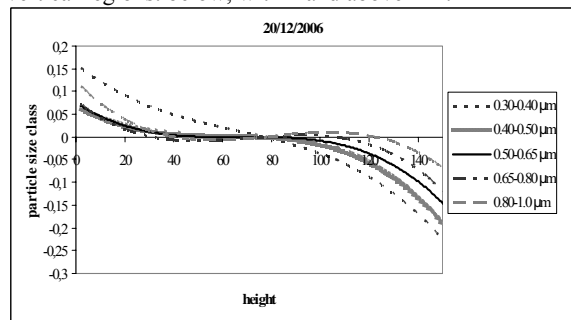


Fig. 3 Outcome of modelling the evolution of PM compositions along height for one launch.

Thanks to AERA fundation for financial support

Aitchison J. (1986), *The statistical analysis of compositional data*, Chapman and Hall.

Ferrero & al. (2007), *FEB*, Vol. 16 N 6 (in press).

Ferrero (2006), *IAC2006 abstract*, pp 1796-1797

Van Dingenen R. & al. (2004), *Atm. Env.*, 38, 2561-2577.

Seibert P. & al. (2000), *Atm. Env.*, 34, 1001-1027.

## Mass balance of total suspended particles over the coal burning power production area of western Macedonia, Greece

E. Terzi<sup>1</sup>, Ch. Anatolaki<sup>2</sup>, R. Tsitouridou<sup>2</sup> and C. Samara<sup>1</sup>

<sup>1</sup>Department of Chemistry, Aristotle University, Environmental Pollution Control Laboratory, G-541 24 Thessaloniki, Greece

<sup>2</sup>Department of Chemical Engineering, Polytechnic School, Aristotle University, Laboratory of Analytical Chemistry, G-541 24 Thessaloniki, Greece

Keywords: TSP, Ions, Trace elements, PAH(s), Trajectory.

Lignite-fired power plants are the main source of electricity in Greece. Four thermal power stations with more than 4000 MW total installed capacity are located in the Eordea basin, in western Macedonia, Greece (Triantafyllou & Kasomenos, 2002; Samara, 2005). Ambient suspended particles (TSP) were collected from January to June 2001 at seven sampling sites in this area. Sampling was performed by high volume air samplers at a flow rate of  $1.1\text{m}^3\text{m}^{-1}$ .

TSP samples were chemically characterized for trace elements (P, Cd, Cr, Cu, Mn, Pb, V, Zn, Te, Co, Ni, Se, Sr, As, and Sb), minerals (Fe, Al, Mg, Ca, K, Ti and Si), water-soluble ions ( $\text{Cl}^-$ ,  $\text{NO}_3^-$ ,  $\text{SO}_4^{2-}$ ,  $\text{Na}^+$ ,  $\text{K}^+$ ,  $\text{NH}_4^+$ ,  $\text{Ca}^{2+}$ ,  $\text{Mg}^{2+}$ ), carbon (OC/EC) and polycyclic aromatic hydrocarbons (PAHs).

Spatial variations of atmospheric concentrations were investigated in relation to the relative distance of sites from the power plants and related activities (mining, lignite and fly ash transport) (Tzimou-Tsitouridou, 2004). Correlations among TSP constituents were examined at each site. The study of chemical composition of TSP in relation to air mass trajectories showed that 44% of air masses had a North-West origin, 28% North-East and 28% Southeast-Southwest. The higher concentrations of the majority of the species were observed at the two latest sectors, indicating possibly additional enrichment from transported pollutants. Finally, the mass balance of TSP at each site was calculated.

Correlations among TSP constituents varied among sites. In general, PAHs were found to be significantly correlated with Cd, Sn, S, As, Br and V. Electrolytes did not show significant correlations with minerals and trace elements except at the site located closest to the power stations.

The total contribution of the identified chemical classes accounted for 47-58% to TSP mass in the individual sampling sites, while 42-53% remained unidentified. At all sites trace elements were the least abundant chemical class, contributing for 0.3-0.5% to TSP. Electrolytes, minerals and carbonaceous materials exhibited small differences in their contributions among the various sites.

This work was financially supported by the Public Power Corporation (PPC) of Greece.

Samara, C. (2005). *Atmos. Environ.*, 39, 6430-6443.

Triantafyllou, G.A., & Kassomenos, P. (2002). *Sci Total Environ.*, 297, 85-103.

Tzimou-Tsitouridou, R. (2004). *Talanta*, 62, 115-122.

## **T29 Abstracts**

## Particle formation events observed at the King Sejong Station, Antarctica

Y. J. Yoon<sup>1</sup>, B. Y. Lee<sup>1</sup>, T. J. Choi<sup>1</sup>, T. G. Seo<sup>2</sup>, and S. S. Yum<sup>3</sup>

<sup>1</sup> Korea Polar Research Institute, KORDI, Songdo Techno Park, 7-50, Songdo-dong, Incheon 406-540, Korea

<sup>2</sup> Korea Meteorological Administration, 460-18, Sindaebang-dong Seoul 156-720, Korea

<sup>3</sup> Dep. Of Atmospheric Sciences, Yonsei Uni., 134 Sinchon-dong, Seoul 120-749, Korea

Keywords: Antarctic aerosols, particle formation, nanoparticles, growth.

Aerosols affect the global radiation budget, directly through scattering incoming solar radiation (Charlson, et al., 1992), and indirectly through modulation of cloud albedo (Twomey, 1974). Secondary particle formations have been observed ubiquitously, over coastal environments (Yoon et al., 2006, O'Dowd, et al., 2002), the marine boundary layer (Clarke, et al., 1998), boreal forests (Makela, et al., 1997), Antarctica (Koponen, et al., 2003).

In this abstract, we report secondary particle formation events observed at the King Sejong Station (KSJ, 62.22 °S, 58.78 °W), Antarctica. Climatic effects of these newly formed particles are also proposed from detected increases in the accumulation mode particle number size concentrations.

Condensation Particle Counters (CPC) with different cut-off diameters (TSI CPC model 3025:  $D > 3\text{ nm}$  and 3010:  $D > 10\text{ nm}$ ) and an Optical Particle Counter (OPC, Grimm model 1.108) were deployed at the King Sejong station during an austral summer (6 Dec. 2005 - 7 Jan. 2006). The KSJ OPC measured particle number size distribution for 32 channels ranging from 0.3  $\mu\text{m}$  to 20  $\mu\text{m}$  with a time resolution of 5 minutes. Particle formation events were observed 18 days out of 33 days (55%) during the measurement period. During the events the total particle number concentration increased from 200 – 300  $\text{cm}^{-3}$  up to 50,000  $\text{cm}^{-3}$ , and the nucleation lasted for more than 4-5 hours depending on the availability of the direct solar radiation (Figure 1).

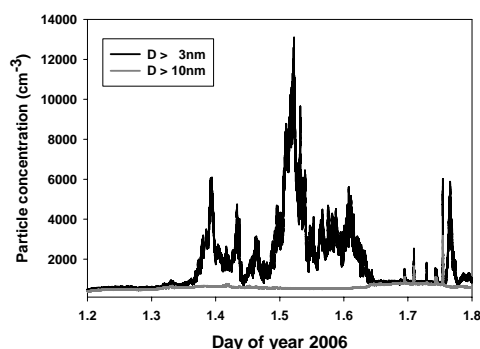


Figure 1. Particle formation event (1 January 2006).

Under clean marine air mass condition, nucleation events were observed only when the direct solar radiation is available, implying that photochemical reactions of the precursor gases are required to induce the observed events. Accumulation mode aerosol number concentration

increased dramatically after nucleation events (refer to Figure 2). These results suggest effects of particle formation in the Antarctic regions on climate through direct aerosol effect.

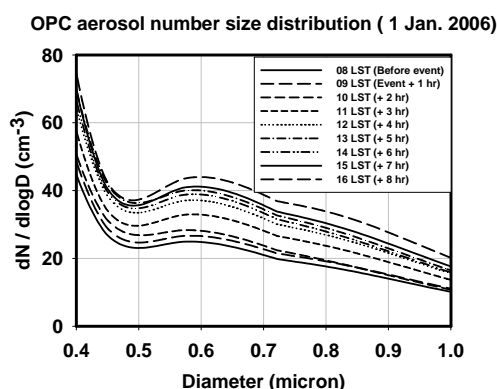


Figure 2. Aerosol number size distribution from KSJ OPC for a nucleation event day (1 January 2006).

This study was supported by ‘Integrated research on the Composition of Polar Atmosphere and Climate Change (COMPAC)’ (PE07030 of Korea Polar Research Institute). S. S. Yum is supported by Grant No. R01-2005-000-11228-0 from the Basic Research Program of the Korea Science and Engineering Foundation.

- Charlson, R. J., Lovelock, J. E., Andreae, M. O., & Warren, S. G. (1987). *Nature*, 326, 655-661.
- Clarke, A. D., Davis, D., Kapustin, V. N., Eisele, F., Chen, G., Paluch, I., Lenschow, D., Bandy, A. R., Thornton, D., Moore, K., Mauldin, L., Tanner, D., Litchy, M., Carroll, M. A., Collins, J., & Albercook, C. (1998). *Science*, 282, 89-92.
- Koponen, I. K., Virkkula, A., Hillamo, R., Kerminen, V. M., & Kulmala, M. (2003). *J. Geophys. Res.*, 108(D18), 4587, doi:10.1029/2003JD003614.
- Makela, J. M., Aalto, P., Jokinen, V., Pohja, T., Nissinen, A., Palmroth, S., Markkanen, T., Seitsonen, K., Lihavainen, H., & Kulmala, M. (1997). *Geophys. Res. Lett.*, 24, 1219-1222.
- O'Dowd, C. D. et al. (2002). *J. Geophys. Res.*, 107(D19), 8108, doi:10.1029/2001JD000555.
- Twomey, S. (1974). *Atmos. Environ.*, 8, 1251-1256.
- Yoon, Y.J., O'dowd, C.D., Jennings, S.G., & Lee, S.H. (2006). *J. Geophys. Res.*, 111, D13, D13204.

## Formation of particles in aircraft plumes using a multi trajectory box model and LES

X. Vancassel, E. Maglaras and E. Ruiz

ONERA-DMPH, 29 avenue de la division Leclerc, BP 72, 92322 Châtillon Cedex, France

Keywords: Aerosol modelling, Particle formation and growth, aircraft plumes

Aircraft emissions at flight levels (250-350hPa) may be responsible for atmospheric chemical changes as well as cloud coverage increase due to the formation of contrails. In spite of numerous studies conducted mainly during the last 10 years, uncertainties remain concerning particle formation and growth in aircraft plumes. Most of the models fail to reproduce field campaigns measurements for various reasons: lack of precise data concerning emissions of organic compounds, uncertainties on the fuel sulphur conversion rate to sulphuric acid, influence of the plume early mixing phase. Generally, trajectory box models are used: an aerosol model is run along a single trajectory representing the overall plume dilution ratio evolution due to the entrainment of ambient air. However, this approach tends to inhibit aerosol properties changes due to temperature and water vapour turbulent evolution. To improve the description of aerosol formation in a turbulent aircraft plume, aerosol dynamics or simplified ice particles growth schemes can be fully coupled with aerodynamics codes. Unfortunately some of important plume aerosol processes are not taken into account in these models because of their implementation complexity and computation efficiency problems. Therefore in order to give a better description of particle formation in aircraft plumes, we have used an intermediate method between the trajectory box model and the fully coupled aerodynamics-microphysics model.

A LES code has been used to describe an Airbus A340 wake in the near field of the aircraft (from engine exit up to 10 seconds downstream). The plume has been discretised into 25000 fluid particles randomly chosen, so that at each time step a fluid parcel is defined by its position, temperature, water vapour pressure and dilution ratio.

A detailed microphysical model based on previous studies (Kärcher, 1995; Yu and Turco, 1997; Sorokin *et al.*, 2001) has been run along each of the 25000 trajectories, considered independent. The code has been optimised and parallelised in order to process the large number of cases. The different processes considered are: nucleation (collision mechanisms), coagulation, condensation, ion-ion recombination, ion-neutral particles attachment, heterogeneous freezing. The different types of particles considered here are volatile

particles (water-sulphuric acid), dry soot particles, activated soot particles, and ice particles.

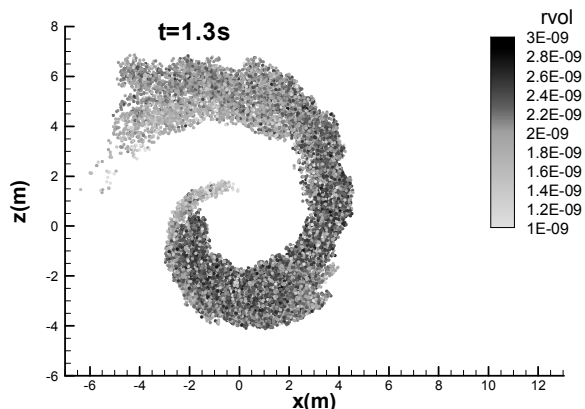


Figure 1. Volatile particles mean radius (nm) at 1.3s in the plume.

Our results mainly show the inhomogeneous spatial distribution of particle properties in the plume, as a function of the mixing efficiency (determined by the LES simulations). Figure 1 depicts the volatile particles mean radius within the plume at 1.3s. Particles grow slowly or even evaporate (high dilution) at the head and the tail of the vortex or grow faster in the centre. The influence of using an average trajectory or using an ensemble of trajectories on the volatile particles size distribution has also been studied. For the A340 case study, significant differences have been found at 1s, affecting the sulphate aerosol specific area density.

The impact of mixing on particle properties in aircraft plumes is known but the effect remains hardly defined quantitatively. We have proposed improvements and the results will be used to contribute to address the question of plume processes influence on aviation impact.

This work was supported by the French DPAC-CAAT project contract 05/01.

Kärcher, B., (1995). *J. Geophys. Res.*, 100, 18835-18844.  
 Yu F., Turco R.P., (1997). *Geophys. Res. Let.*, 24, 1927-1930.  
 Sorokin, A., Vancassel, X., & Mirabel, P., (2001). *Phys. Chem. Earth(C)*, 26, 557-561.

## Binary Homogenous Nucleation of Sulfuric Acid and Water Mixture: Experimental Device and Setup

David Brus<sup>1</sup>, Antti-Pekka Hyvärinen<sup>1</sup>, Heikki Lihavainen<sup>1</sup>, Yrjö Viisanen<sup>1</sup>, and Markku Kulmala<sup>2</sup>

<sup>1</sup>*Finnish Meteorological Institute, Erik Palménin aukio 1, P.O. Box 503, FIN-00100 Helsinki, Finland*

<sup>2</sup>*Department of Physical Sciences, University of Helsinki, P.O. Box 64, FIN-00014 Helsinki, Finland*

Keywords: Homogeneous nucleation; particle formation, sulfuric acid – water.

New particle formation in the atmosphere has received considerable attention lately both from atmospheric scientists and aerosol researchers. Atmospheric new particles have been observed to form by self-condensing or nucleating homogeneously in events lasting a couple of hours nearly all around the world (Kulmala *et al.*, 2004).

The first step of new particle formation or any first order phase transition is nucleation. It has been calculated that in the atmosphere the equilibrium vapor pressure of sulfuric acid is low enough for it to be a likely candidate to nucleate homogeneously, (e.g. Seinfeld and Pandis, 1998).

All recent experiments on homogeneous sulfuric acid and water nucleation have relied on a flow-based measurement technique (e.g. Wyslouzil *et al.* 1991, Viisanen *et al.*, 1997, Ball *et al.*, 1999, Zhang *et al.*, 2004 and Berndt *et al.*, 2006). In general the results are in fair agreement with each other, although somehow dependent on the method of generating the sulfuric acid vapor.

A New laminar flow chamber built recently in Finnish Meteorological Institute is presented here. It is designed for homogeneous nucleation experiments of binary and ternary compounds such as sulfuric acid and water.

The laminar flow chamber is positioned vertically and experimental setup consists of an atomizer, a furnace, a mixing unit, a nucleation chamber and measurement unit.

A known amount of studied solution is introduced to furnace with HPLC Pump through a ruby micro-orifice (20  $\mu\text{m}$ ). The dispersion is then vaporized in a Pyrex glass tube wrapped with resistant heating wires. The furnace temperature is kept at 380 °C, and the temperature of vapor inside furnace is 235 °C. After furnace, the vapor is filtered with Teflon filter, introduced to mixing unite and cooled by turbulent mixing with particle free air to 60 °C. The vapor gas mixture is then cooled to wanted nucleation temperature in nucleating chamber which is kept at constant temperature with two liquid circulating baths. The nucleation chamber is made of stainless steel and its whole length is 200 cm. Temperature of the stream is registered along the nucleation chamber using six PT100 probes. For nucleation at room temperature, 25 °C is achieved at

a distance approximately 115 cm from the mixing unit. The measured temperature profile is shown in Fig 1.

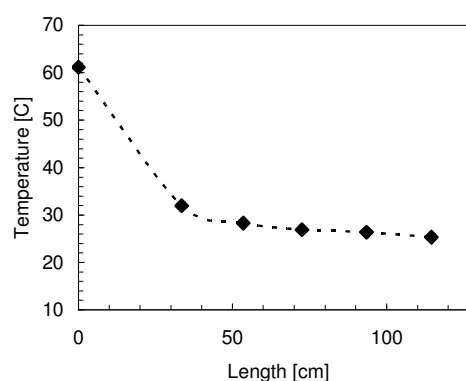


Figure 1. Temperature profile in the axis of laminar tube as a function of distance from mixing unit.

Concentration of water vapor is measured at the end of nucleation chamber with a dew point monitor. The applicable range of relative humidity is from 10 to 65 %. Sulfuric acid concentration is determined from samples taken inside the tube. The aerosol number concentration is measured with an ultrafine condensation nucleus counter (TSI 3025).

- Kulmala M., Vehkamäki H., Petäjä T., Dal Maso M., Lauri A., Kerminen V.-M., Birmili W., and McMurry P. H. (2004), *J. Aerosol Sci.*, 35, 143.
- Seinfeld J. H., and Pandis S. N. (1998), *Atmospheric Chemistry and Physics: From Air Pollution to Climate Change*, John Wiley & Sons Inc, NY.
- Wyslouzil B. E., Seinfeld J. H., Flagan R. C., and Okuyama K. (1991), *J. Chem. Phys.*, 94, 6842-68.
- Viisanen Y., Kulmala M., and Laaksonen A. (1997), *J. Chem. Phys.* 107, 920.
- Ball S. M., Hanson D. R., and Eisele F. L., and McMurry P. H. (1999), *J. Geophys. Res.* 104, D19, 23.709-23.718.
- Zhang R., Suh I., Zhao J., Zhang D., Fortner E. C., Tie X., Molina L. T., and Molina M. J. (2004), *Science* 304, 1487.
- Berndt T., Böge O., and Stratmann F. (2006), *Geophys. Res. Lett.*, 33, L15817.

## Mechanistic investigations on the formation of atmospheric H<sub>2</sub>SO<sub>4</sub>/H<sub>2</sub>O particles

T. Berndt, O. Böge and F. Stratmann

Leibniz-Institut für Troposphärenforschung e.V., Permoserstr. 15, 04318 Leipzig, Germany

Keywords: H<sub>2</sub>SO<sub>4</sub>, nucleation, particle formation.

Atmospheric particles have a strong impact on the Earth's radiation budget due to their radiative properties and the fact that they can act as condensation nuclei for clouds. Field measurements at ground level show atmospheric nucleation events for H<sub>2</sub>SO<sub>4</sub> concentrations of  $\sim 10^7$  molecule cm<sup>-3</sup> (Weber *et al.*, 1999). Despite intensive research activities in the last decade, the mechanism leading to new particles has not been unambiguously revealed yet.

In a previous investigation from this laboratory, experimental evidence for the formation of new particles under near-atmospheric conditions was found with H<sub>2</sub>SO<sub>4</sub> concentrations of  $\sim 10^7$  molecule cm<sup>-3</sup> (Berndt *et al.*, 2005). Here, H<sub>2</sub>SO<sub>4</sub> was produced in situ via the reaction of OH radicals with SO<sub>2</sub> in the presence of water vapour. In contrast, taking H<sub>2</sub>SO<sub>4</sub> from a liquid sample  $\sim 10^{10}$  molecule cm<sup>-3</sup> of H<sub>2</sub>SO<sub>4</sub> are needed for producing new particles (Ball *et al.*, 1999).

In the atmosphere, the gas-phase oxidation of SO<sub>2</sub> is initiated by the attack of OH radicals. The following reaction sequence is currently accepted leading finally to H<sub>2</sub>SO<sub>4</sub> vapour.



Subject of this study is to investigate the formation of new particles in the system H<sub>2</sub>SO<sub>4</sub>/H<sub>2</sub>O starting either from OH + SO<sub>2</sub> or from SO<sub>3</sub> or taking H<sub>2</sub>SO<sub>4</sub> vapour from a liquid H<sub>2</sub>SO<sub>4</sub> sample.

The experiments have been performed in the *Ift*-LFT (*Institute for Tropospheric Research – Laminar Flow Tube*; i.d. 8 cm; length 505 cm) at atmospheric pressure and  $293 \pm 0.5$  K using synthetic air as the carrier gas. Particle size distributions ( $dp > 2$  nm) were determined using a differential mobility particle sizer (DMPS) consisting of a short Vienna-type differential mobility analyzer (DMA) and an ultrafine particle counter (UCPC, TSI 3025). Total particle numbers were measured by means of different types of UCPC's to be directly attached at the outlet of the *Ift*-LFT. In the case of in situ H<sub>2</sub>SO<sub>4</sub> formation via OH + SO<sub>2</sub> the needed OH radicals were formed either by O<sub>3</sub> photolysis in the presence of water vapour or by ozonolysis of *t*-butene (dark reaction), c.f. (Berndt *et al.*, 2005). In experiments starting with SO<sub>3</sub>, this species was produced outside the *Ift*-LFT in a pre-reactor oxidizing SO<sub>2</sub> in a

catalytic reaction on a Pt surface at 525°C. The conversion of SO<sub>2</sub> to SO<sub>3</sub> was followed by on-line UV spectroscopy. For experiments using H<sub>2</sub>SO<sub>4</sub> vapour from a liquid sample, H<sub>2</sub>SO<sub>4</sub> concentrations were measured at the outlet of the saturator by means of a denuder system with subsequent analysis of SO<sub>4</sub><sup>2-</sup> ions by ion chromatography.

Figure 1 shows the experimental results using the different approaches for H<sub>2</sub>SO<sub>4</sub> formation. Roughly the same behaviour is observed using SO<sub>3</sub> or starting with H<sub>2</sub>SO<sub>4</sub> from a liquid sample. From these findings it can be speculated that in the course of SO<sub>2</sub> conversion to SO<sub>3</sub> via pathways (1) and (2) other, additional steps probably take place being important for the particle formation observed.

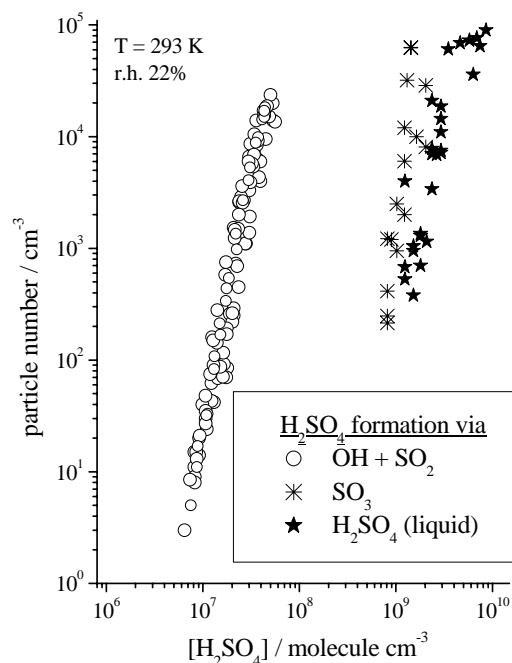


Figure 1. Measured particle numbers vs. H<sub>2</sub>SO<sub>4</sub> concentration for different formation ways.

- Ball, S. M., Hanson, D. R., Eisele, F. L. & McMurry, P. H. (1999), *J. Geophys. Res.*, 104(D19), 1999JD900411, 23709-23718,  
 Berndt, T., Böge, O., Stratmann, F., Heintzenberg, J. & Kulmala, M. (2005), *Science*, 307, 698-700.  
 Weber, R. J., McMurry, P. H., Mauldin III, R. L., Tanner, D. J., Eisele, F. L., Clarke, A. D. & Kapustin, V. N. (1999), *Geophys. Res. Lett.*, 26, 307-310.

## Investigating the composition of newly formed atmospheric aerosols with CPC battery

H.E. Manninen<sup>1</sup>, M. Kulmala<sup>1</sup>, I. Riipinen<sup>1</sup>, T. Petäjä<sup>1</sup>, T. Grönholm<sup>1</sup>, P.P. Aalto<sup>1</sup>, M. Sipilä<sup>1</sup> and K. Hämeri<sup>1</sup>

<sup>1</sup>Department of Physical Sciences, University of Helsinki, P.O. Box 64, FI-00014 Helsinki, Finland

Keywords: Atmospheric aerosols, aerosol formation, nanoparticles, chemical composition, activation.

A better understanding of various effects of atmospheric aerosols on air quality and climate change requires more comprehensive knowledge on their sources, processes and sinks. New particle formation by nucleation of supersaturated vapours and subsequent particle growth to detectable sizes is one of the key processes controlling the number concentration of aerosols in the atmosphere (Kulmala, 2003). A direct determination of the composition of these nucleation mode particles is difficult due to minuscule amounts of matter available for chemical analysis.

The Condensation Particle Counter Battery (CPCB) examines the activation properties of atmospheric nanoparticles in different vapours (Kulmala et al., 2006). It provides a method to estimate chemical composition of growing nucleation mode particles through different activation diameters. Our CPCB consists of four CPCs: two butanol CPCs (TSI-3025; TSI-3010) and two water CPCs (TSI-3785; TSI-3786) with cut-off sizes adjusted in calibrations to 3 nm and 11 nm using insoluble silver particles (Petäjä et al., 2006). TSI-3025 and TSI-3786 measured at cut-off size 3 nm and correspondingly TSI-3010 and TSI-3785 at 11 nm. Indirect information on the chemical composition of the particles is obtained as the solubility of the particles to the condensing vapour lead to changes in the cut-off sizes of the CPCs.

CPCB field measurements were performed in a rural background station in Finland (SMEAR II station located in Hyytiälä) between March 7 and May 31, 2006. The measurements showed that atmospheric particles that were newly formed during nucleation burst were more efficiently activated by the water CPCs compared to butanol CPCs. The results indicated that growing nucleation mode particles were water-soluble both at 3 and 11 nm.

Figure 1 shows the variation of the particle number concentrations measured by the CPCB on May 16, 2006 in Hyytiälä. New particle formation event (nucleation) occurred on that day starting around 9:30 a.m. local time. During the event the ratio between water and butanol CPCs increased in both pairs. The increase in concentrations measured by the TSI 3786 and TSI 3785 had 35 min time difference. After 1 p.m. the concentration difference between water and butanol CPCs started to decrease again. At the night time the ratio was normalised to one.

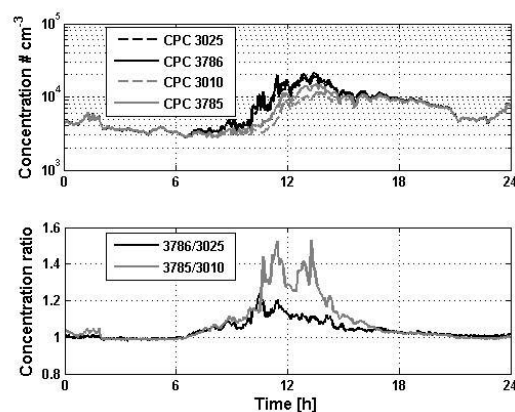


Figure 1. The aerosol particle number concentration with the CPCB on May 16, 2006 (top) and the ratio of the particle number within the pairs of water and butanol CPCs (bottom).

As this setup was used to measure number concentration of atmospheric aerosol particles, only the composition of the particles and resulting change in heterogeneous activation diameter, can explain the difference in their concentration readings. Thus water-soluble (hygroscopic) particles will be detected down to lower particle size in the water CPCs due to increased activation probability in water vapour. There for increased count rate will be measured in comparison to the butanol CPCs. The detection efficiency of the CPC depends both on the saturation ratio inside the CPC and on chemical composition of sampled aerosol particles.

An increase in the ratio between water and butanol CPCs is detected during every nucleation event (in 32 cases out of 32) in the investigated period. During non-event days the ratio is also usually close to unity except during pollution episodes when water-soluble material is present (e.g. SO<sub>2</sub>). Water-insoluble pollutants (e.g. NO<sub>x</sub>) do not cause any signal in the CPCB.

- Kulmala, M. (2003). *Science*, 302, 1000-1001.  
Kulmala, M. et al. (2006). *J. Aerosol Science*, doi:10.1016/j.jaerosci.2006.11.008.  
Petäjä, T. et al. (2006). *Aerosol Sci. Technol.*, 40, 1090-1097.

## Comparison of $\text{H}_2\text{SO}_4$ concentrations and new particle formation during 26 months in Hyytiälä, Finland

T. Nieminen, M. Kulmala, I. Riipinen, M. Boy and L. Laakso

Department of Physical Sciences, University of Helsinki, P.O. Box 64, 00014 Helsinki, Finland

Keywords: particle formation, sulfuric acid, ions, nucleation

Formation of new aerosol particles in the atmosphere has been observed in many locations. This process is currently not completely understood. Especially the nucleation of the initially 1–2 nm diameter particles cannot be directly observed because commonly used instruments (such as the Differential Mobility Particle Sizer DMPS) are able to detect only particles larger than 3 nm. It is possible however to measure naturally charged particles (ions) as small as 0.5 nm using ion spectrometers.

Since March 2003 air ion size distributions have been measured in Hyytiälä SMEAR II station in southern Finland using the Balanced Scanning Mobility Analyzer BSMA (Tammet 2006). The BSMA detects ions in the size range 0.4–7.5 nm. Between April 2003 and May 2005 we have seen new particle formation on 125 days in negative ions and 92 days in positive ions. To get information about the role of sulphuric acid in new particle formation we have calculated  $\text{H}_2\text{SO}_4$  concentrations for this period using a so-called pseudo steady state model (Boy *et al.* 2005). Since sulphuric acid is not measured regularly this is the only way to get a long time series of the behaviour of its ambient concentrations. When compared to the available measured values during the spring in 2003 and 2005 the measured and calculated concentrations agree quite well.

In Figure 1 is shown the saturation ratio of sulphuric acid (calculated according to Kulmala & Laaksonen 1990) and temperature during new particle formation events of negative ions and also at times when there is no new particle formation. The event points are mean values between start and end times of new particle appearance in the smallest sizes 1.4–2.4 nm. Non-event points are mean values from non-event days during the average time of events, which is 09:30–14:30 for negative ions. There is a clear difference in saturation ratio between events and non-events in the case of negative ions. In all temperatures the saturation ratio, which is related to the free energy change in nucleation, is on average higher during events of negative ions. With positive ions this difference is not so clear. Another difference between negative and positive ions is that on some days there is new particle formation seen in negative ions but not in positive ions. This indicates that in

ion-induced nucleation the negative ions are important and sulphuric acid is participating in the first stages of new particle formation.

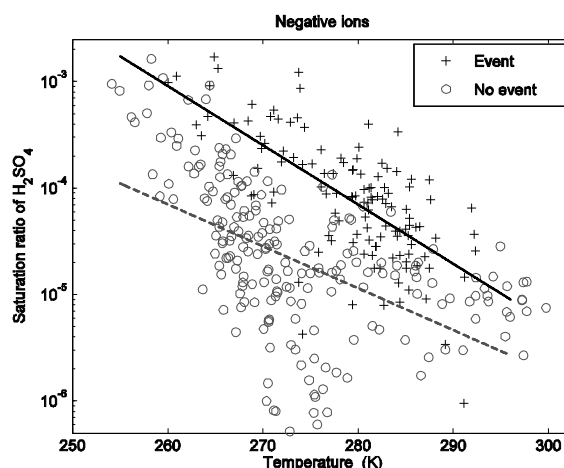


Figure 1. Comparison of  $\text{H}_2\text{SO}_4$  saturation ratio and temperature during new particle formation of negative ions and at times when there is no new particle formation. The solid and dashed lines are fitted to the event and no-event points, respectively.

Boy M., Kulmala M., Ruuskanen T. M., Pihlatie M., Reissel A., Aalto P. P., Keronen P., Dal Maso M., Hellen H., Hakola H., Jansson R., Hanke M., and Arnold F. 2005. Sulphuric acid closure and contribution to nucleation mode particle growth. *Atmos. Chem. Phys.* 5: 863–878.

Kulmala, M., and Laaksonen, A. 1990. Binary nucleation of water-sulfuric acid system: Comparison of classical theories with different  $\text{H}_2\text{SO}_4$  saturation vapour pressures. *J. Chem. Phys.* 93: 696–701.

Tammet, H. 2006. Continuous scanning of the mobility and size distribution of charged clusters and nanometer particles in atmospheric air and the Balanced Scanning Mobility Analyzer BSMA. *Atmos. Res.* 82: 523–535.

## Air Ion Spectrometer measurements of marine/coastal secondary particle formation

M. Ehn<sup>1</sup>, T. Petäjä<sup>1</sup>, H. Vuollekoski<sup>1</sup>, P. Aalto<sup>1</sup>, M. Vana<sup>1</sup>, G. de Leeuw<sup>1,2</sup>, D. Ceburnis<sup>3</sup>, C. D. O'Dowd<sup>3</sup> and M. Kulmala<sup>1</sup>

<sup>1</sup>Division of Atmospheric Sciences, Dept. of Physical Sciences, University of Helsinki, P.O. Box 64, FI-00014 University of Helsinki, Finland

<sup>2</sup>Finnish Meteorological Institute, Research and Development, Climate and Global Change Unit, P.O. Box 503, 00101 Helsinki, Finland

<sup>3</sup>Dept. of Experimental Physics and Environmental Change Institute, National University of Ireland, Galway, Ireland

Keywords: Nucleation, ions, coastal particles

Secondary particle formation occurs frequently on the west coast of Ireland (O'Dowd, et al. 2002a). These nucleation events usually coincide with low-tide and the presence of solar radiation. Sulfuric acid concentrations may be high enough to explain the nucleation, but not the subsequent growth, and therefore it has been suggested that biogenic iodine oxides can participate in the growth and perhaps also in the nucleation (O'Dowd, et al. 2002b).

Currently the lower detection limit for aerosol particles is around 3 nm, but if we only measure the charged particles (i.e. ions), the observed size spectrum can be extended to 1 nm and below. As part of the EU-project MAP (Marine Aerosol Production), we deployed an Air Ion Spectrometer (AIS, Airel Ltd., Estonia) at the Mace Head Atmospheric Research Station in Western Ireland in January 2006. The AIS measures the size distribution of positive and negative ions from 0.4 to 40 nm.

The measurements have continued over 1 year, and the aim is to get more information on what happens in the sub 3-nm range during nucleation events, and to detect a possible seasonal variation in the particle formation.

The one-year dataset was analyzed based on daily figures of both positive and negative ion spectra. Days were divided into six groups depending on whether new particle formation events were detected or not. If an event was observed, the type of event was characterized. If a specific day could not be characterized due to high noise or other uncertainties, it was placed in an "undefined" category.

Comparing days with and without events separately for each month, we concluded that all months, except December, showed particle formation during more than half of the days (Figure 1). During the summer months (June-September), the relative occurrence of event days was around 75%, and during the spring months (April-May) it was around 85%. This result excludes "undefined" or missing days, and for months 1, 10, 11 and 12 this means that up to half of the days were discarded, adding to the uncertainty.

As the station at Mace Head is located on the coast, the occurrence of new particle formation above the ocean or at the coast line will only be detected when the wind is on-shore. Wind direction data and tide calendars will be used to get a more precise picture of the new particle formation in further analysis.

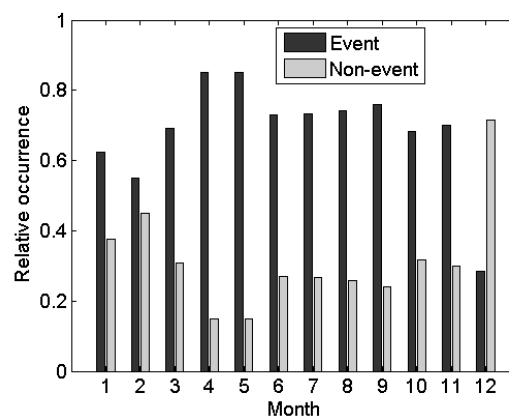


Figure 1. The relative occurrence of new particle formation events in Mace Head during 2006.

This work was funded by the EU (FP6, project number 018332).

O'Dowd, C., Hämeri, K., Mäkelä, J., Väkevä, M., Aalto, P., de Leeuw, G., Kunz, G., Becker, E., Hansson, H.-C., Allen, A., Harrison, R., Berresheim, H., Kleefeld, C., Geever, M., Jennings, S., and Kulmala, M. (2002a). Coastal new particle formation: Environmental conditions and aerosol physicochemical characteristics during nucleation bursts. *J. Geophys. Res.*, 107:10.1029/2001JD000206.

O'Dowd, C., Jimenez, J., Bahreini, R., Flagan, R., Seinfeld, J., Hämeri, K., Pirjola, L., Kulmala, M., Jennings, S., and Hoffmann, T. (2002). Marine aerosol formation from biogenic iodine emissions. *Nature*, 417, 632-636.

## Observations of secondary particle formation above the North Atlantic

M. Ehn<sup>1</sup>, T. Petäjä<sup>1</sup>, P. Aalto<sup>1</sup>, G. de Leeuw<sup>1,2</sup>, C. O'Dowd<sup>3</sup> and M. Kulmala<sup>1</sup>

<sup>1</sup>Division of Atmospheric Sciences, Dept. of Physical Sciences, University of Helsinki, P.O. Box 64, FI-00014 University of Helsinki, Finland

<sup>2</sup>Finnish Meteorological Institute, Research and Development, Climate and Global Change Unit, P.O. Box 503, FI-00101 Helsinki, Finland

<sup>3</sup>Dept. of Experimental Physics and Environmental Change Institute, National University of Ireland, Galway, Ireland

Keywords: Marine aerosols, nucleation, field measurements

The oceans produce large numbers of aerosol particles into the atmosphere (see for example O'Dowd, et al. 1997). The primary formation mechanism for these particles is bursting bubbles on the ocean surface. This primary particle production is fairly easily detectable although not as easily quantifiable. O'Dowd et al., (2002) have demonstrated a secondary formation mechanism under coastal conditions, resulting from marine algae emissions. These biogenic iodocarbons can photolyze into iodine oxides that, in turn, produce new particles.

The Marine Aerosol Production (MAP) project set out to quantify the primary sea-spray aerosol flux and elucidate the dominant condensable vapors driving the secondary aerosol formation. A more detailed knowledge of these parameters are essential for determining the impact of the oceans on the global climate. During June and July 2006, the most intense algae bloom period, the Research Vessel Celtic Explorer mapped the aerosol and gaseous phase concentrations in the marine boundary layer and the ocean-atmosphere interactions off the west coast of Ireland. This study focuses on the number size distribution measurements conducted on board the Celtic Explorer, and the detection of secondary particle formation.

A twin Differential Mobility Particle Sizer (DMPS) measured the size distribution from 3 to 1000 nm. During the 20-day measurement period, we observed particle bursts in the sub-20 nm size range during 4 days (13.6 and 29.6-1.7). Trajectory analysis showed that the particles detected during the last three days had probably been formed on the coast and transported to the ship. However, during the first day the air mass came from the northwest and had not passed over land for at least 36 hours prior to the detection of the new particles, which infers that the particles indeed were of marine origin. The size distribution observed that day is plotted in figure 1. A mode appears in the afternoon and grows during the evening.

Preliminary discussions with other groups have revealed that the sulfuric acid concentrations were high during 13.6, which often is the case during

new particle formation. Further analysis and comparison with supporting data will hopefully give a better insight into the vapors involved. Furthermore, the trajectories passing over the ship, continued south-east and reached an atmospheric research station at Mace Head, Western Ireland, around 10 hours later. A concurrent measurement campaign was conducted there during this time, and a comparison with the data measured there will be of large benefit.

Secondary particle formation in clean marine air masses has, to our knowledge, not previously been measured in the marine boundary layer above the North Atlantic.

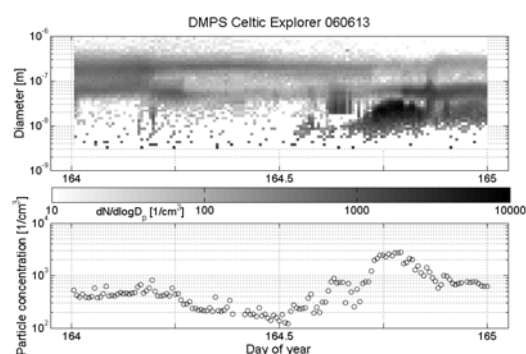


Figure 1. Number size distribution for 13 June.

We wish to acknowledge the crew of the Celtic Explorer for their assistance during the cruise. This work was funded by the EU (FP6, project number 018332).

O'Dowd, C., Smith, M., Consterdine, I. and Lowe, J. (1997). Marine Aerosol, sea-salt, and the marine sulphur cycle: A short review. *Atm. Env.*, 31, 73-80.

O'Dowd, C., Jimenez, J., Bahreini, R., Flagan, R., Seinfeld, J., Hämeri, K., Pirjola, L., Kulmala, M., Jennings, S., and Hoffmann, T. (2002). Marine aerosol formation from biogenic iodine emissions. *Nature*, 417, 632-636.

## New particle formation above a sub-arctic wetland-forest mosaic: analysis of high growth rates

Birgitta Svenningsson<sup>1,2)</sup>, Almut Arneth<sup>1)</sup>, Sean Hayward<sup>1)</sup>, Thomas Holst<sup>1)</sup>, Andreas Massling<sup>3)</sup>, Erik Swietlicki<sup>3)</sup>, Anne Hirsikko<sup>4)</sup>, Marko Vana<sup>4)</sup>, Tommi Bergman<sup>4)</sup>, Ilona Riipinen<sup>4)</sup>, Miikka Dal Maso<sup>4)</sup>, Tareq Hussein<sup>4)</sup>, Markku Kulmala<sup>4)</sup>

<sup>1)</sup>Dept. of Physical Geography and Ecosystems Analysis, Geobiosphere Science Centre, Lund Univ., Sölvegatan 12, SE-223 62 Lund, Sweden

<sup>2)</sup> Dept. of Chemistry, Copenhagen Univ., Universitetsparken 5, DK-2100 Copenhagen, Denmark

<sup>3)</sup>Div. of Nuclear Physics, Lund Univ., Box 118, SE-221 00 Lund, Sweden

<sup>4)</sup>Div. of Atmospheric Sciences, Univ. of Helsinki, P.O. Box 64, FIN-00014 University of Helsinki, Finland

<sup>5)</sup> Institute of Environmental Physics, Univ. of Tartu, Ülikooli 18, 50090, Tartu, Estonia

Keywords: particle formation and growth, atmospheric aerosols, biogenic particles, ions, aerosol size distributions

Atmospheric particle formation has been observed in sites all over the world (Kulmala et al 2004). Nevertheless, the first stage of growth (1-3 nm in particle diameter) has only been studied in a limited number of sites. Also, many of the observations do only cover short time periods (1-3 months).

We present classification statistics for nucleation events from measurements taken at a sub-arctic mire in northern Sweden, covering the period May 2005 to September 2006, with a break over the winter period.

The data were obtained in a remote area, far away from obvious pollution sources. The measurement site is the Stordalen mire, located about 15 km east of Abisko Scientific Research Station (68°21'N, 18°49'E, <http://www.ans.kiruna.se/>) in northern Sweden, next to the lake Torne Träsk (341 masl). Mountains surround the area, the highest one being 1991 masl. Total particle number concentrations (10-500 nm in diameter) were between fifty and a few thousand cm<sup>-3</sup>.

Aerosol particle number size distributions (10 nm < dry particle diameter < 500 nm) are measured using a Scanning Mobility Particle Spectrometer (SMPS). An Air Ion Spectrometer (AIS #5, Airel Ltd., Estonia, Mirme et al., 2006) is used to determine spectra of charged aerosol particles and clusters ions in the size range of 0.4-40 nm.

New particle formation in the atmosphere was found to be a frequent phenomenon also in this sub-arctic wetland-forest environment. The observed seasonal pattern was somewhat different compared to what is typically observed in boreal forests, the main difference being a much later onset of particle formation events in the spring. Some very high growth rates were observed in both the SMPS (see figure 1 for an example) and AIS (figure 2) data.

This work is supported by the European Commission via a Marie Curie Excellence Team Grant and by the Swedish Research Council. We would also like to acknowledge the support from BACCI Nordic Centre of Excellence and Abisko Scientific Research Station.

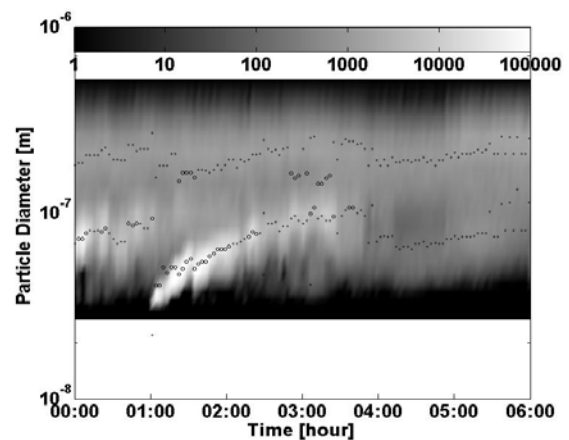


Figure 1. Example of a particle formation event (July 19, 2005) with high growth rate as seen by the SMPS. The maximum total particle concentration during the event was 3000 cm<sup>-3</sup>.

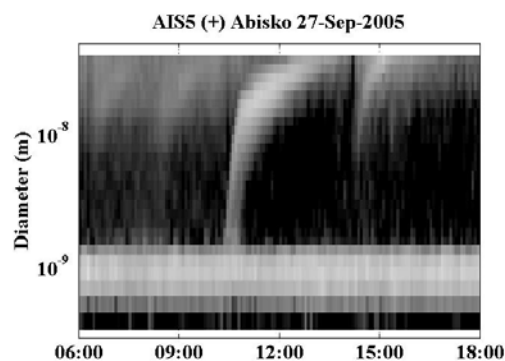


Figure 2. Also the data from the AIS showed high growth rates during several events as for example during a week in late September 2005. Black and white represent low and high concentrations, respectively.

Kulmala, M., Vehkamäki, H., et al. (2004), *J. Aerosol Sc.* 35 143-176,

A. Mirme, E. Tamm, et al. (2007) Submitted to *Boreal Environmental Research*.

## Aerosol particle and air ion number size distributions along the Trans-Siberian railroad

E. Vartiainen<sup>1</sup>, M. Kulmala<sup>1</sup>, M. Ehn<sup>1</sup>, T. Petäjä<sup>1</sup>, S. Kuokka<sup>2</sup>, R. Hillamo<sup>2</sup>, A. I. Skorokhod<sup>3</sup>,  
I. B. Belikov<sup>3</sup>, N. F. Elansky<sup>3</sup> and V.-M. Kerminen<sup>2</sup>

<sup>1</sup>Department of Physical Sciences, University of Helsinki, P.O. BOX 64, FIN-00014 Helsinki, Finland

<sup>2</sup>Finnish Meteorological Institute, Erik Palmenin aukio, FI-00560, Helsinki, Finland

<sup>3</sup>Obukhov Institute of Atmospheric Physics, Pyzhevsky 3, 119017, Moscow, Russia

Keywords: Ambient aerosols, DMPS, Ions, Number size distribution, Ultrafine particles.

Russia covers a large area of the earth's surface. Aerosol particle concentrations over Russia, and properties of these particles, have a major effect on global climate. Yet, there currently exist only few studies with information on aerosols measured in Russia. Thus, with our measurements we aimed to increase knowledge of aerosol particles in a broad area of Russia.

In October, 2005, we travelled two weeks along the Trans-Siberian railway from Moscow to Vladivostok and back. Measurements were made during TROICA-9 (TRAns-Siberian Observations Into the Chemistry of the Atmosphere) expedition. The idea of TROICA expeditions and information on previous TROICA trips can be found e.g. from publications by Crutzen *et al.*, 1998 and Oberlander *et al.*, 2002.

Earlier TROICA measurements in Russia have mostly concentrated on meteorological observations and aerosol chemistry. This time we also made extensive measurements on physical properties of aerosol particles. The differential mobility particle sizer (DMPS) measured the particle number size distribution from 3 nm to 950 nm every ten minutes. The air ion spectrometer (AIS) measured the size distribution of positive and negative ions from 0.4 nm to 40 nm. The measuring interval was 5 minutes. In addition, our Russian associates established our location with the GPS and marked all extraordinary events, such as oncoming trains or forest fires, to the electronic diaries.

Concentration of aerosol particles varied hugely in different parts of Russia while the total concentration was mainly between 500 and 50 000 cm<sup>-3</sup> (Fig 1). In industrial areas, and in vicinity of towns, concentrations were the highest. In rural areas, concentrations were lower but were, however, often influenced by local sources such as biomass burning or forest fires. Most of the particles were in the Aitken mode.

Distribution of ions showed many similarities with earlier ion distribution measurements in Boreal forest (e.g. Hirsikko *et al.*, 2005). However, concentrations of cluster ions were sometimes unusually high. The sum of positive and negative cluster ions was in maximum around 10 000 cm<sup>-3</sup>. Cluster ion concentrations also correlated well with ion pair production by <sup>222</sup>Rn.

The distribution of larger ions often followed the pattern of particle distribution of sub-40 nm particles. The ratio of positive to negative ions, however, changed according to particle origin. In addition, we detected increasing intermediate ion concentrations during rain and snowfall.

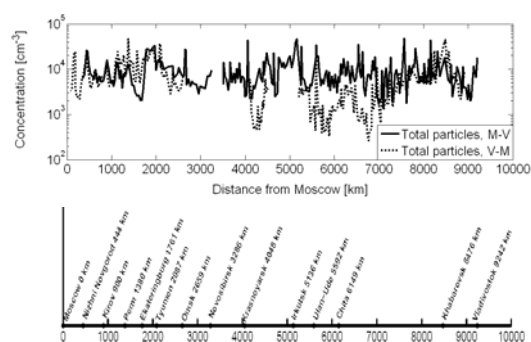


Figure 1. Half an hour average total aerosol particle concentration as a function of distance from Moscow. The solid line represents the concentration on the way to Vladivostok and the dotted line on the way back to Moscow. In a lower panel, the biggest cities along the railway are marked.

All together, we achieved much new information on the aerosol concentrations, sources, and processes in Russia.

This study was funded by the Academy of Finland grant no. 208208. The TROICA expedition was partly funded by the ISTC Project #2773.

Crutzen, P.J., Elansky, N.F., Hahn, M., Golitsyn, G.S., Brenninkmeijer, C.A.M., Scharffe, D.H., Belikov, I.B., Maiss, M., Bergamaschi, P., Röckmann, T., Grisenko, A.M. & Sevostyanov, V.M. (1998). *Journal of Atmospheric Chemistry*, 29(2), 179-194.

Hirsikko, A., Laakso, L., Hörrak, U., Aalto, P.P., Kerminen, V.-M. & Kulmala, M. (2005). *Boreal Environment Research*, 10, 357-369.

Oberlander, E.A., Brenninkmeijer, C.A.M., Crutzen, P.J., Elansky, N.F., Golitsyn, G.S., Granberg, I.G., Scharffe, D.H., Hofmann, R., Belikov, I.B., Parezke, H.G. & van Velthoven, P.E.J. (2002). *Journal of Geophysical Research*, 107(D14), 4 206-4 221.

## Aerosol particle and ion measurements in Queen Maud Land, Antarctica

E. Vartiainen<sup>1</sup>, M. Ehn<sup>1</sup>, P.P. Aalto<sup>1</sup>, A. Frey<sup>2</sup>, A. Virkkula<sup>2</sup>, R. Hillamo<sup>2</sup>, A. Arneth<sup>3</sup> and M. Kulmala<sup>1</sup>

<sup>1</sup>Department of Physical Sciences, University of Helsinki, P.O. BOX 64, FI-00014 Helsinki, Finland

<sup>2</sup>Finnish Meteorological Institute, Erik Palmenin aukio, FI-00560, Helsinki, Finland

<sup>3</sup>Dep. of Physical Geography and Ecosystems Analysis, Lund University, Sölvegatan 12, 223 62, Lund, Sweden

Keywords: Antarctic aerosols, Hygroscopicity, Ions, Particle formation and growth, Particle size distribution.

We studied a number of aerosol particle properties during Antarctic summer 2006/2007 at a Finnish research station Aboa. The station is located in Queen Maud Land, Antarctica (73°03'S, 13°25'W) approximately 130 km from the coast on a nunatak Basen.

We made the measurements in a separate laboratory container, 250 m uphill from the station and about 500 m above the sea level. The station was located southwest of the laboratory which was then the polluted sector. We ran the measurements continuously starting on 28 December 2006 and ending on 29 January 2007.

The measured quantities included e.g. distributions of particles and ions, hygroscopic growth factors of aerosol particles, light absorption and scattering by aerosol particles, and chemical analysis of collected filter samples. Here we will briefly present a part of the measurements and also very preliminary results.

We measured aerosol particle number size distributions from 3 to 1000 nm with a differential mobility particle sizer (DMPS). Time resolution of the measurement was 10 min. Hygroscopic growth of particles of diameters 10, 25, 50, and 90 nm was measured with a humidity-tandem differential mobility analyzer (H-TMDA) at a relative humidity of 90 %. The H-TDMA scanned one diameter spectra in about 10 min. Mobility size distributions of positively and negatively charged particles from 0.4 to 40 nm were also measured each five minutes using an air ion spectrometer (AIS). In addition, we could utilize the data from the year-round weather station next to our laboratory.

Even though the results are only preliminary some observations could already be made. The total number of particles on most measurement days was around 300 cm<sup>-3</sup> with the minimum being below 100 cm<sup>-3</sup>. When new particle formation was observed, the particle concentration could exceed 1000 cm<sup>-3</sup>. The detected particle concentration levels coincide well with the earlier measurements made in Aboa (e.g. Koponen *et al.*, 2003). In addition, particle concentration increased clearly when the wind blew from the direction of the station, which was presumed.

The measured particles were hygroscopic (GF ~ 1.7-1.8) and often showed very stable one-modal hygroscopic growth. Thus we could assume that particles were internally mixed. Detailed analysis of

the H-TDMA data, together with air-mass origin and weather data, will be done and is expected to reveal more detailed information on the composition of the particles.

Measurements of air ion mobility distributions aimed to examine concentrations of different sized ions, their charging state and relative abundance of positive and negative ions, and evolution of ion distribution with time. Especially the behaviour of ions during incidents like storms, nucleation, and different air masses was interesting. Figure below presents positive and negative ion distributions during one day (Figure 1.). This specific day showed very high ion concentrations due to a nucleation event. The different behaviour of positive and negative ions during nucleation is also detectable.

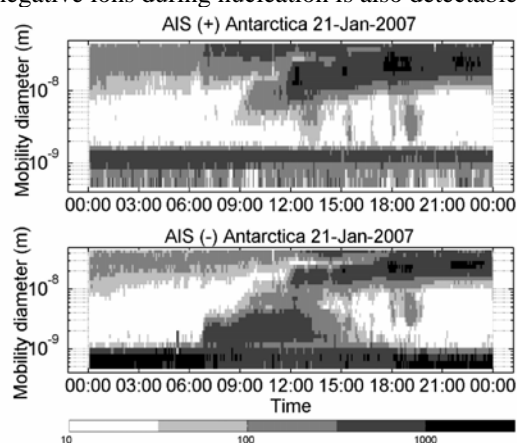


Figure 1. Positive and negative air ion number size distributions measured at Aboa on 21 January 2007. The color indicates the number of ions divided by the width of the mobility diameter range.

At this state of the analysis it is too early to draw too many conclusions. However, we achieved plenty of new information of Antarctic aerosols. Among them are ion distributions that have been measured in Antarctica only once before and hygroscopicity of aerosols that, in my knowledge, has earlier never measured in Antarctica. These new results, combined with our extensive aerosol data set will certainly lead to interesting results.

This work was supported by the Academy of Finland.

Koponen, I.K., Virkkula, A., Hillamo, R., Kerminen, V.-M. & Kulmala, M. (2003). *Journal of Geophysical Research*, 108, AAC8.1-AAC8.10.

## Presence of cluster ions in low ambient temperatures

A.-K. Viitanen<sup>1</sup>, T. Mattila<sup>2</sup>, J.M. Mäkelä<sup>1</sup>

<sup>1</sup>Aerosol physics laboratory, Tampere University of Technology, P.O.Box 692, FI-33101 Tampere, Finland

<sup>2</sup>Envionics Oy, P.O.Box 1199, FI-70211 Kuopio, Finland

Keywords: ion mobility, ion clusters, time-of-flight

Ion mobility distributions of certain trace compounds have been measured at temperatures reaching below 0°C. Our primary interest is in using calibration compounds for instrument testing in cold Northern European field conditions. Therefore, the attention of this study is especially towards low ambient temperatures. Understanding the temperature effects provides information also for better understanding of ion molecule reactions and processes in atmosphere. Atmospheric ions are also known to be linked with formation of new ambient aerosol particles (Kulmala et al., 2004).

Ion mobility spectrometry (IMS) is an *in-situ* technique for detecting and identifying gas phase compounds in low detection limits (Eiceman & Karpas, 2005). The IMS-device used, is a commercial RAID I (Bruker Daltonics GmbH) based on time-of-flight (TOF) technique. The device has been tuned for scientific use by removing the membrane. The sample gas is ionized using radioactive source. The pulse of ions enters the drift chamber due to electric field, arriving at the collector plate at different times. Knowing the electric field ( $E$ ), the length of the drift chamber ( $l$ ), the time of flight of an ion ( $t_d$ ) and the measurement conditions ( $P$  and  $T$ ) the reduced mobility ( $Z_0$ ) can be determined according to equation 1.

$$Z_0 = \frac{l}{Et_d} \frac{273 K}{T} \frac{P}{101.3 kPa} \quad (1)$$

The measurement set-up is shown in Figure 1. The TOF-device was placed in a chamber with controlled thermal conditions. The sample was introduced into the system using injection or diffusion tube method. The temperature of the gas was measured from the surface of the drift chamber.

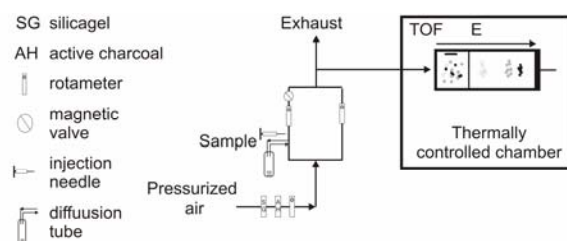


Figure 1. Measurement set-up.

Two gaseous compounds were studied, 2-propanol, a common solvent, and 2,6-di-tertbutyl pyridine (2,6-DtBP), used as a mobility reference with a unimodal mobility distribution (Eiceman et al.,

2003). The gas concentration was kept constant, being at ppm-level in case of 2-propanol and ppb-level in case of 2,6-DtBP, while temperature was varied between  $-7^{\circ}\text{C}$  –  $+80^{\circ}\text{C}$ . The results (Figure 2) show a strong temperature dependence for 2-propanol, forming trimers at low ambient temperatures. The mobility of a trimer is  $1.45 \text{ cm}^2/\text{Vs}$  corresponding to particle size  $\sim 0.7 \text{ nm}$  (Tammet, 1995). The results with 2,6-DtBP do not show such strong temperature dependence, but dimer-ion was detected in low ambient temperatures with the mobility of  $1.2 \text{ cm}^2/\text{Vs}$  ( $\sim 0.9 \text{ nm}$ ).

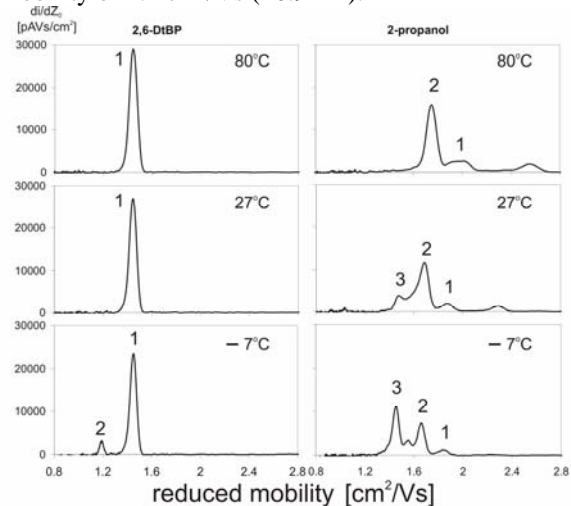


Figure 2. Mobility distribution for 2,6-DtBP and 2-propanol in different temperatures. The numbers 1-3 refers to the number of multimer.

The results show that the ion cluster mobility distribution is affected by temperature. Lower temperatures favor ion clustering. Understanding of temperature effects is important especially when adapting IMS-technique for environmental analysis.

Eiceman et al. (2003). Chemical standards for ion mobility spectrometry. *Anal. Chim. Acta*, 493, 185.

Eiceman, G.A., Karpas, Z. (2005). *Ion mobility spectrometry*. 2. edition. CRC Press, Taylor & Francis Group. Boca Raton, FL.

Kulmala et al. (2004). Formation and growth rates of ultrafine atmospheric particles: a review of observations. *Aerosol Science* 35 (2004) 143-176.

Tammet H. (1995). Size and mobility of nanometer particles, clusters and ions *J. Aerosol Sci.* 26, 459-475

## A comparison of new particle formation events in Eastern Germany and in Northern east Italy based on a three-year-analysis

A.Hamed<sup>1</sup>, B.Weher<sup>2</sup>, W.Birmili<sup>2</sup>, A.Wiedensohler<sup>2</sup>, F. Cavalli<sup>3</sup>, M.C. Facchini<sup>3</sup>,  
J. Joutsensaari<sup>1,+</sup> and A. Laaksonen<sup>1,4</sup>

<sup>1</sup>Department of Physics (+department of Environmental Sciences), University of Kuopio, P. O. Box 70211

<sup>2</sup>Institute for Tropospheric Research, Leipzig, Germany

<sup>3</sup>Instituto di Scienze dell'Atmosfera e del Clima Consiglio Nazionale delle Ricerche, Bologna, Italy

<sup>4</sup>Finnish Meteorological Institute, P.O. Box 503, 00101 Helsinki, Finland

Keywords: Nucleation, Aerosol formation, DMPS, Particle formation and growth.

New particle formation from supersaturated vapors (nucleation) can occur almost everywhere in the atmosphere, in clean areas, rural, coastal and polluted areas Kulmala et al. (2004). A direct chemical analysis of particles < 5 nm is technically not feasible at the moment; therefore, knowledge on the atmospheric nucleation and particle growth mechanism and its governing circumstances has only been gathered indirectly, for instance by time series analysis of the number concentration of freshly formed particles, gas phase precursor, and meteorological variables. A comparison of sufficiently long atmospheric data sets in different environments is expected to reveal useful information on the atmospheric conditions governing new particle formation events.

This study has been designed to compare the occurrence of new particle formation events (particles > 3 nm) in two anthropogenically influenced boundary layer regimes in Central Europe (Melpitz, Eastern Germany) and Southern Europe (San Pietro Capofiume "SPC" in the Po Valley). The analysis encompasses three years of data at each observation site, between July 2003 and June 2006; Particle size distribution measurements were carried out using twin DMPS systems (Differential Mobility Particle Sizers) at each site, with particle size ranges of 3-800 nm, and 3-600 nm at Melpitz and SPC, respectively.

In a first step, the particle formation events were identified and classified into different categories i.e., event and non-event days according to the particle number concentrations and the particle formation and growth rate. For nucleation event days, increase of the particle number concentrations in the nucleation mode showing clear growth of the new formed particle for a several hours were so remarkable. The classification method of nucleation events we followed here is based on the method described by (Hamed et al., 2007).

Out of a total of three years data from (2003-2006) the nucleation event days in SPC was (32%) that was higher than in Melpitz (30%) data while for non event days, (54% was found in Melpitz to 42% in SPC). 26% of the data in SPC respect to 16% in

Melpitz which a clear decision was not possible whether nucleation has taken place or not.

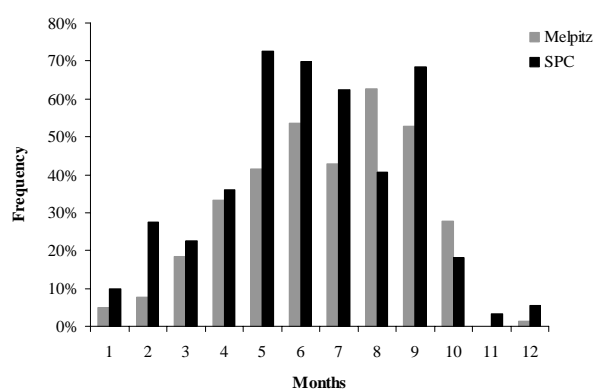


Figure1: Monthly frequency of nucleation events in Melpitz and in SPC stations for three years data set.

Figure 1 illustrates that nucleation events can take place throughout the whole years in different seasons for SPC with maximum frequencies during late spring and summertime, i.e. from May till August (on average, the frequency ratios during those formation months were ~65%). While in Melpitz, no nucleation events observed during November months at all, while the highest frequencies were between May and September (maximum frequencies values were on August and September months with ~55%). Where minimum values were during wintertime (~3%) in Melpitz and as well in SPC (~20%).

We will show a comprehensive statistical comparison of the two data sets with respect to meteorological and trace gases of nucleation events to elucidate the different process govern nucleation for the both station.

This work was supported by ACCENT (*Atmospheric Composition Change: an European Network*). Data in Melpitz were collected under the grant "Feinstaubmessung" by Umweltbundesamt, Dessau.

Hamed, A., et al. (2007). *Atmos. Chem. Phys.*, 7, 355-376.

Kulmala, M., et al. (2004). *J Aerosol Sci*, 35,143-176

## Nucleation events in Melpitz, Germany, as a source of cloud condensation nuclei

A.Hamed<sup>1</sup>, B.Wehner<sup>2</sup>, W.Birmili<sup>2</sup>, T.Tuch<sup>2</sup>, G.Spindler<sup>2</sup>, A.Wiedensohler<sup>2</sup>, J. Joutsensaari<sup>1</sup> and A. Laaksonen<sup>1</sup>

<sup>1</sup>Department of Physics, University of Kuopio, P. O. Box 70211 Kuopio, Finland

<sup>2</sup>Institute for Tropospheric Research, Leipzig, Germany

Keywords: CCN, Nucleation, Particle formation and growth

Atmospheric nucleation events due to gas-to-particle conversion have received increasing attention as a potentially important global source of new aerosol particles, thereby affecting both, climate and human health. After nucleating at diameters of about 1 nm, the new particles may grow by condensation and coagulation, and eventually reach particle sizes where they may act as cloud condensation nuclei (CCN). This growth of particles may take several days, and since many aerosol dynamical as well as meteorological effects interact during such a time span, it has been difficult to determine CCN production rates on the basis of experimental observations.

Here, we study the CCN production due to secondary particle formation based on the characteristics of nucleation events observed in a polluted continental boundary layer. The analysis makes use of continuous particle size distribution measurements at the rural observation site Melpitz (Eastern Germany), a region characterized by the presence of diffuse anthropogenic sources, such as vehicular traffic, agricultural and regulated industrial emissions. While particle formation at Melpitz had been studied during an earlier experiment between 1996 and 1997 (Birmili and Wiedensohler, 2000), this study concentrates on the new data, collected continuously between July 2003 and June 2006.

In a first step, the particle formation events were identified and classified into different categories i.e. event days and non event days. For the three-year Melpitz data, this procedure yielded 278 nucleation event days, 498 non event days, and 146 days for which a clear decision was not possible. From 57% of nucleation events, those particles grow up to 50 nm, we applied the same procedure as described before in (Laaksonen et.al.2005) to investigate the significance of the nucleation events as a source of CCN in Melpitz area. Firstly, we calculated the increases in concentrations of particles in the 50-600 nm, 100-600 nm, and 200-600 nm size ranges on nucleation event days. The average increase of number concentrations in those size ranges together with the average concentrations are presented in table 1. Secondly, we consider the CCN production of particles larger than 50 nm and by assuming that particle nucleation and growth occur in a well mixed boundary layer of 600 m height, the yield of 50-600 nm particles shown in Table 1 corresponds to annual particle production of  $1 \times 10^{14}$  particles per square meter of the Earth's surface. Radke and Hobbs (1976) estimated that

globally, the total annual CCN production from primary sources is on the order of  $10^{14} \text{ m}^{-2}$ , which has same order to the values we calculate for 50-600 nm particles for Melpitz. For further analysis of the importance of the nucleation events, we calculated hypothetical particle source rates (for more details see Laaksonen et al., 2005) that needed to support the average concentrations. As a result we obtain simple estimates of particle source strengths in the different size ranges the results are shown on the last row of Table 1. The steady state assumption (SS-assumption) is highly simplified, however, it can be seen that the actual annual particle production in the nucleation events is on the same order as the hypothetical steady-state production. By comparing the ratios of (nucleation production to particle source rate in the steady state we will refer to it as (SS-production), that calculate for 100-600 nm particles in Melpitz (see table 1) to the values obtained before for (San Pietro Capofiume "SPC" in the Po Valley, Northern east Italy) by Laaksonen et al, (2005). It is clear that in SPC the ratio was 0.38 while for Melpitz the ratio is  $0.7/1.2 = 0.58$ . The obtained results clearly show that in SPC the values are two times higher than in Melpitz. We believe that this comparison indicates that nucleation events can be an important source of CCN in the Saxony region, in Germany as in SPC, however it is more significantly pronounced in SPC than in Melpitz due to high amount of anthropogenic contributions in Po Valley area than in Saxony area.

Table1. The annual yield of particles, the average yield per one nucleation event, the average particle concentrations and hypothetical steady-state particle production rate needed to support the average concentrations for different size ranges.

Size Range (nm)	50-600	100-600	200-600
Annual yield/cc	1.6E+05	7.0E+04	2.2E+04
Average yield/Event	3.1E+03	1.3E+03	4.2E+02
Average			
Concentration/cc	2.4E+03	1.3E+03	4.4E+02
SS-production/cc/Year	2.2E+05	1.2E+05	3.9E+04

This work was supported by ACCENT and IfT.

Birmili, W. & Wiedensohler, A. (2000). *Geophys. Res. Lett.*, 27, 3325–3328.

Laaksonen A.et.al., (2005).*Geophys Res Lett.* 32, 1-4.

Radke, L.F. & Hobbs, P.V. (1976). *Science*, 193, 999-1002.

## Characterisation of air ions during a cruise over the Eastern Atlantic and Southern Ocean

M. Vana<sup>1,3</sup>, A. Virkkula<sup>2</sup>, A. Hirsikko<sup>1</sup>, P. Aalto<sup>1</sup>, M. Kulmala<sup>1</sup> and R. Hillamo<sup>2</sup>

<sup>1</sup>Department of Atmospheric Sciences, University of Helsinki, FIN-00014 Helsinki, Finland

<sup>2</sup>Air Quality Research, Finnish Meteorological Institute, FIN-00101 Helsinki, Finland

<sup>3</sup>Institute of Environmental Physics, University of Tartu, 50090 Tartu, Estonia

Keywords: Field measurements, Marine aerosols, Ions, Particle formation.

### INTRODUCTION

Formation of new particles and their further growth are important processes in the atmosphere (Kulmala, 2003). To understand particle nucleation mechanisms, measurements of the below 3 nm size particles are important. Air ion spectrometers are able to measure charged clusters and aerosol particles in this measurement range providing valuable information about particle formation and growth in the atmosphere. Air ion measurements in the marine boundary layer are rare so far (Siingh et al., 2005).

### DATA ACQUISITION

In this study we present a unique dataset about measurements of air ion mobility distribution onboard the Russian research vessel Akademik Fedorov during a cruise from Europe to Antarctica. The measurements were part of the FINNARP-2004 expedition and lasted from Nov 3 to Dec 9, 2004.

We measured air ion mobility distribution using an Air Ion Spectrometer (AIS) manufactured by AIREL Ltd, Estonia (Mirmé et al., 2007). The AIS has mobility range  $3.2-0.00134 \text{ cm}^2\text{V}^{-1}\text{s}^{-1}$  which corresponds to particle diameter range 0.4–40 nm. The time resolution of the measurements was 5 minutes. The air ion data were partly accompanied by the measurements of aerosol size distribution in the diameter range large than about 10 nm using a differential mobility particle sizer (DMPS), and by the measurements of black carbon using a two-wavelength Magee Scientific Aethalometer (AE-20).

### RESULTS

Several interesting results have been obtained from these measurements. We classified the measured ion mobility distributions according to air mass back-trajectories and meteorological conditions. We also identified and separated the data, which were contaminated, either by direct emissions from the chimney of ship or by other activities on board the ship.

In earlier studies, Koponen et al. (2002) observed the weak particle formation episodes above the pack-ice region of the Southern Ocean. During our cruise, we also observed few particle formation and growth episodes: mainly in higher northern and in higher southern latitudes. Small ions (0.4–1.5 nm) were found to present all the time and their

concentration were measured typically between  $100-600 \text{ cm}^{-3}$ . Concentrations of intermediate ions (1.5–7.4 nm) were most of the time below  $20 \text{ cm}^{-3}$ . Concentrations of large ions (7.4–22 nm) were mostly below  $100 \text{ cm}^{-3}$ .

One special effect, which we observed, is the formation of intermediate ions during rain. Figure 1 shows the formation of negative intermediate ions accompanied by sudden decrease in temperature during short-time showers in the tropical marine boundary layer. A potential way to obtain charged particles from a waterfall is described by Laakso et al. (2006).

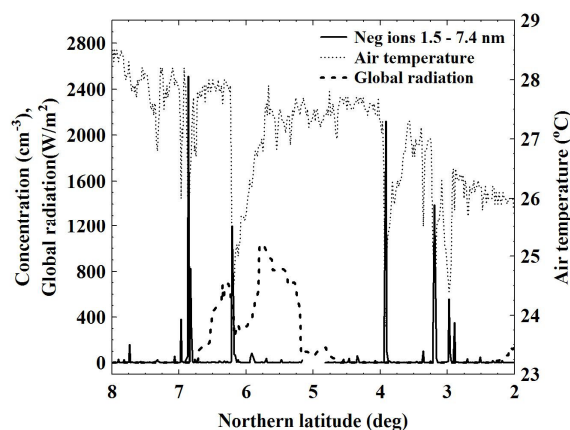


Figure 1. Formation of negative intermediate air ions during rain in the tropical marine boundary layer.

This work was supported by the Academy of Finland (Finnish Antarctic Research Program, contract no. 53669)

Koponen, I. K., Virkkula, A., Hillamo, R., Kerminen, V.-M., & Kulmala, M. (2002). *J. Geophys. Res.*, 107, 4753, doi:10.1029/2002JD002533.

Kulmala, M. (2003). *Science*, 302, 1000-1001.

Laakso, L., Hirsikko, A., Grönholm, T., Kulmala, M., Luts, A., & Parts, T.-E. (2006). *Atm. Chem. Phys. Discuss.*, 6, 9297-9314.

Mirmé, A., Tamm, E., Mordas, G., Vana, M., Uin, J., Mirmé, S., Bernotas, T., Laakso, L., Hirsikko, A., & Kulmala, M. (2007). *Boreal Env. Res.*, 12.

Siingh, D., Pawar, S. D., Gopalakrishnan, V., & Kamra, A. K. (2005). *J. Geophys. Res.*, 110, doi:10.1029/2005JD005765.

## Investigating ion-induced nucleation with the ion-

S. Gagn<sup>1</sup>, T. Petäjä<sup>1</sup>, Erkki Siivola<sup>1</sup>, Pekka Pihlakka<sup>1</sup>, V.-M. Kerminen<sup>2</sup>, Aalto, P.P.<sup>1</sup> and M. Kulmala<sup>1</sup>

<sup>1</sup>University of Helsinki, Dept. of Physical Sciences, PO Box 64, FI-00014 Helsinki, Finland

<sup>2</sup>Finnish Meteorological Institute, Climate and Global Change, Erik Palmenin Aukio 1, P.O. Box 503, FI-00101 Helsinki, Finland

Keywords: Particle formation and growth, Field measurements, Ion-induced nucleation, Ion-DMPS

Aerosol particle formation takes place frequently in the atmosphere (Kulmala et al., 2004). Despite great efforts, the exact nucleation mechanisms are not well known. Ion-induced nucleation is among the proposed mechanisms.

Information on the importance of neutral/ion-induced nucleation can be obtained with a special instrumental set-up called ion-DMPS (Pihlakka et al., 2007), which measures the charging state of atmospheric aerosol particles.

Charging state is the number of charged particles in a given sample divided by the measured number of particles corresponding to the steady-state charge distribution (equilibrium). In ion-DMPS this ratio is obtained with a neutralizer which can be switched either on or off. The size-range of our instrument is from 3 nm to 15 nm. The data presented here is from over one year measurement in Hyytiälä, Finland (Boreal forest).

Recently, Kerminen et al., (2007) developed a new method to calculate the contribution of ion-induced nucleation from the ion-DMPS-measurements. The resulting, simplified equation which can be used in the analysis has a following form:

$$S(d_p) = 1 - \frac{1}{kd_p} + \frac{(S_0 - 1)kd_0 + 1}{kd_p} \exp(-k(d_p - d_0))$$

where  $S(d_p)$  and  $S_0$  are the charging states at sizes  $d_p$  and  $d_0$ , where  $d_0$  is the diameter at which the new particle form. The parameter  $k$  is defined as:

$$k = \frac{\alpha N_{\pm}^c}{GR}$$

where  $\alpha$  is the recombination coefficient,  $N_{\pm}^c$  is the number of cluster ions and GR is the growth rate of particles. By fitting the equation to the ion-DMPS-data, we can estimate the contribution of ion-induced nucleation on total new particle formation rate.

Median initial charging state  $S_0$  at 1.5 nm during new particle formation events observed during one year with the ion-DMPS yielded values of 5.8 and 6.1 for negative and positive particles, respectively. Thus, in median, slightly less than 10% of the particle flux at this size resulted from ion-induced nucleation. However, the annual

variation was large and in some cases the fraction reached slightly less than 40%.

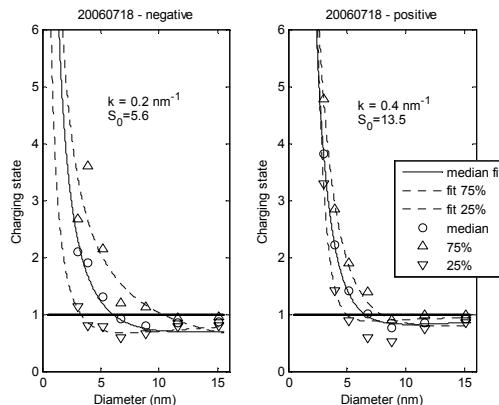


Figure 1. Charging state as a function of diameter together with fitted values on the earlier equation.

Erkki Siivola and Pekka Pihlakka are acknowledged for his work on the Ion-DMPS. Vei o Hiltunen and Heikki Pihlakka are acknowledged for their efforts maintaining the instrument during the field measurements. This work was supported by Biosphere-Aerosol-Cloud-Climate Interactions (BACCI).

Kulmala M., Vehkamäki H., Petäjä T., Dal Maso M., Siivola E., Kerminen V.-M., Birmili W. & McMurry P.H. (2004) *Formation and growth rates of ultrafine atmospheric particles: A review of observations*. J. Aerosol Sci. 35: 143–176

Pihlakka, P., Gagn, S., Petäjä, T., Hirsikko, A., Aalto, P., Kulmala, M. and Kerminen, V.-M. (2006) *Detecting charging state of ultra-fine particles: instrumental development and ambient measurements*, Atmospheric Chemistry and Physics - Discussions, p. 6401-6429. SRef-ID: 1680-7375/acpd/2006-6-6401

Kerminen, V. M. et al. (2007). Manuscript in preparation.

## Overview of nucleation events based on air ion measurements at Tahkuse observatory

Kaupo Komsaare<sup>1</sup>, Devendraa Siingh<sup>1,2</sup>, Aadu Mirme<sup>1</sup> and Urmas Hõrrak<sup>1</sup>

<sup>1</sup>Institute of Environmental Physics, University of Tartu, Ülikooli 18, 50090 Tartu, Estonia

<sup>2</sup>Indian Institute of Tropical Meteorology, Pune-411 008, India

Keywords: air ions, nucleation, electric effects, atmospheric aerosols

The importance of new particle formation on the Earth climate has been discussed in many of the recent papers (e.g. Kulmala et al., 2004), but the mechanism and species responsible for the nucleation are not well known so far. Air ions (cluster ions and electrically charged aerosol particles) mainly determine the electrical state of the atmosphere, but they can be involved also in the nucleation process.

In this paper we present the results of a statistical analysis of the nucleation events based on long-term measurements of air ion mobility distributions from July 2003 to December 2006 at the Tahkuse Observatory (58°31.4'N, 24°55.5'E), Estonia. The total number of analyzed days was 1154. The air ion spectrometers covered the mobility range of 0.00041–3.2 cm<sup>2</sup> V<sup>-1</sup> s<sup>-1</sup> (corresponding size range is 0.36–79 nm).

We have classified the intermediate air ion (or 1.6–7.4 nm charged particle) formation events at Tahkuse using similar classification principles as given by Hirsikko et al. (2007).

Class I. The formation and subsequent growth of particles had a clear shape. The concentration of new generated particles was sufficiently high and their growth starting from the cluster ion mode up to the size range of 40–50 nm was clearly seen during several hours. The gap between the cluster ion mode and larger ions was filled with ions indicating that cluster ions were involved in the nucleation process.

Class II. Similarly to class I, the formation of particles started from the cluster ion mode, but due to some reason, the growth of particles was suppressed in the size range below 5–10 nm. The reason might be consumption of nucleating vapors.

Class III. The particle formation did not start from the cluster ion mode and we saw a gap between cluster ions and larger charged particles at about 1.6 nm. The growth of particles could be followed starting from about 2–4 nm during 2–4 hours. The event might be due to the particle formation by homogeneous nucleation with a subsequent charging of neutral particles by cluster ions.

Class IV. During the nucleation event the concentrations of intermediate ions was quite low. The event lasted for 1–6 hours. These events can be considered also as uncertain cases.

Class V. Events of this type were observed during rain and sometimes also during snowfall with sleet. Commonly, the concentration of negative intermediate ions was higher than that of positive ones. In the

case of “rain events”, the concentration of intermediate ions depended on rainfall duration and intensity (Hõrrak et al., 2006).

Results of the statistical analysis of all categories of events are given in Figure 1. As follows, the most pronounced events (class I) with clear formation and growth of nanometer particles occurred most frequently during spring, the second maximum was recorded in autumn.

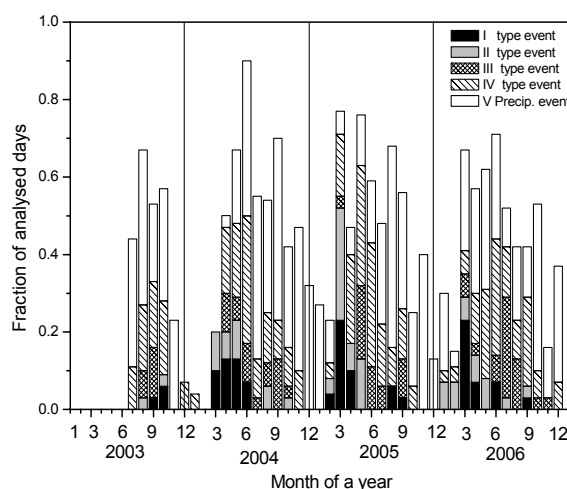


Figure.1 Monthly distributions of the fraction of days when the nucleation events or precipitation induced intermediate ion formation were observed.

This work was supported by the Estonian Science Foundation under grant 6223.

Hirsikko, A., Bergman, T., Laakso, L., Dal Maso, M., Riipinen, I., Hõrrak, U., & Kulmala, M. (2007). Identification and classification of the formation of intermediate ions measured in boreal forest. *Atmos. Chem. Phys.*, 7, 201–210, 2007.

Hõrrak, U., Tammet, H., Aalto, P.P., Vana, M., Hirsikko, A., Laakso, L., Kulmala, M. (2006). Formation of charged nanometer aerosol particles associated with rainfall: atmospheric measurements and lab experiment. *Report Series in Aerosol Science*, 80, 180–185.

Kulmala, M., Vehkamäki, H., Petäjä, T., Dal Maso, M., Lauri, A., Kerminen, V.-M., Birmili, W., & McMurry, P. H. (2004) Formation and growth rates of ultrafine atmospheric particles: A review of observations, *J. Aerosol Sci.*, 35, 143–176.

## Atmospheric particle formation rates below 3 nm

I. Riipinen, H.E. Manninen, T. Nieminen, M. Sipilä, T. Petäjä and M. Kulmala

Department of Physical Sciences, University of Helsinki, P.O. Box 64, FI-00014, University of Helsinki, Finland

Keywords: atmospheric aerosols, particle formation and growth, nucleation rate

To understand the atmospheric particle formation and growth processes, information on the very first steps of these processes is crucially needed. The current commercial instruments are typically able to measure down to 3 nm particles, whereas the atmospheric nucleation and cluster activation processes take place close to 1 – 2 nm (see e.g. Kulmala *et al.*, 2006a).

Air ions even smaller than 1 nm, on the other hand, can be detected with e.g. Air Ion Spectrometer (AIS) and Balanced Scanning Mobility Analyzer (BSMA). The concentrations of the small ions, however, are typically so low that they cannot alone explain the observed new particle formation events.

Significant effort has recently been made to develop instruments that measure neutral particles smaller than 3 nm. In this study we use such instruments, CPCB (Condensation Particle Counter Battery, see Kulmala *et al.*, 2006b and Manninen *et al.*, 2007), UF-02proto CPC pair (see Mordas *et al.*, 2005) and NAIS (Neutral Cluster Air Ion Spectrometer), to calculate new atmospheric particle formation rates close to 2 nm. The formation rates of 2 – 3 nm ions are also calculated for comparison, based on BSMA and AIS data. We aim to study the magnitude of the particle formation rates closer to the sizes where the real atmospheric nucleation and activation occurs, as well as investigate the relative contribution of neutral and charged particles to the particle formation.

The composition and therefore the activation properties of the freshly formed nucleation mode can be investigated using CPCB. The instrument consists of four CPCs, two with butanol (TSI3010 and TSI3025) and two with water (TSI3785 and TSI3786) used as the working fluid. In the case of highly water-soluble particles, the water CPCs detect them at smaller sizes than the instruments based on butanol. During new particle formation in Hyytiälä, Finland, the cut-off diameter of the CPCB is typically close to 2 nm (see Kulmala *et al.*, 2006b). UF-02proto is a novel condensation particle counter, which, according to recent calibrations, has the potential to detect particles as small as 1.8 nm. NAIS is similar to AIS, but the aerosol sample is charged with a corona charger before the electrical detection.

All the data studied in this work has been measured in Hyytiälä, southern Finland, during 10

weeks in spring 2006. We have calculated the formation rates of the 2 nm ( $J_2$ ) particles from the particle concentrations measured in the size range of 2 – 3 nm, taking into account the coagulation losses to the pre-existing particles, as well as the growth out of the size range. In the case of ions, also the ion-ion recombination and the charging of neutral particles were corrected for.

An exemplary plot on the behaviour of the  $J_2$  during new particle formation is presented in Figure 1. The charged particle formation rates in 2 nm are typically 1 – 2 orders of magnitude lower than the total formation rates. Also, the different activation properties of charged and neutral particles are visible in the data: the ion formation rates typically rise somewhat before a clear increase in the total  $J_2$  is seen, indicating that lower supersaturations are needed to activate charged clusters compared to neutral ones.

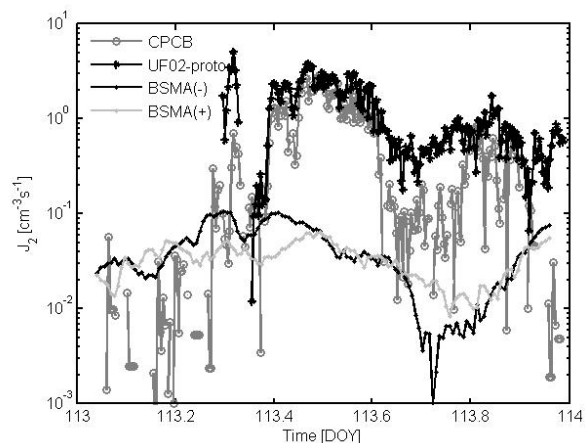


Figure 1. Comparison of 2 nm formation rates during new particle formation on 23.4.2006 in Hyytiälä, Finland. Dark grey: CPC-Battery; Black with circles: UF-02proto CPC pair; Black with dots: BSMA (negative ions); Light grey with dots: BSMA (positive ions)

Kulmala, M., Lehtinen, K.E.J. & Laaksonen, A. (2006a). *Atmos. Chem. Phys.*, 6, 787–793.

Kulmala, M. *et al.* (2006b). *J. Aerosol Sci.*, in press.

Manninen, H.E. *et al.* (2007). *These proceedings*.

Mordas, G. *et al.* (2005). Design and performance characteristics of a condensation particle counter UF-02proto, *Bor. Env. Res.*, 10, 543-552.

## The effect of clouds on ion cluster concentrations and new particle formation at 1465 m. a.s.l.

H.Venzac, K. Sellegri and P.Laj

Laboratoire de Météorologie Physique, Université Blaise Pascal, 63170 Aubière, France

Keywords: aerosol nucleation, precursors, free troposphere.

Our ability to predict the aerosol size and concentration in time and space is dependant on our knowledge of the aerosol sources. The secondary aerosol formation processes are complex and extremely variable according to the environment. Ultrafine aerosols formations, i.e. nucleation events, were observed in many environments (marine, boreal forest, antarctica) (Kulmala et al, 2004) but very few data have been reported at high elevation sites.

We propose to present here a unique set of measurements of charged aerosol particles performed by an Air Ion Spectrometer (AIS) (0.4–44 nm ion size distribution) at the summit of the puy de Dôme Research Station during spring 2006. This device provides us with the measurements of air ions at sizes which witness the very initial steps of aerosol formation. The goals were to investigate (1) the vertical extent of nucleation in the atmosphere, and (2) the effect of clouds on nucleation. The puy de Dôme station is located at 1 465 m a.s.l. and lies in a region where both the upper part of the boundary layer (BL) and the free troposphere (FT) can be sampled. All together, nucleation events were observed at the site more than one third of the days during the spring period. Because the puy de Dôme station is in-cloud for more than 50 % of the time, it offers a valuable opportunity to study the interaction between new particle formation processes and clouds.

Cluster ions (<1.4 nm) concentrations vary typically between 100 and 1 000 ions  $\text{cm}^{-3}$ , intermediate ions (1.4–6 nm) concentrations are usually lower than 500 ions  $\text{cm}^{-3}$  but can exceed 3 000 ions  $\text{cm}^{-3}$  during nucleation events. Large concentrations of intermediate ions seem to be appropriate to detect the occurrence of most of nucleation events. A statistical analysis of the concurrent presence of ion clusters and cloud droplets on one hand, and intermediate ions and cloud droplets on another hand, brings new information regarding our current understanding of atmospheric aerosol dynamics. In cloud, the cluster ions concentrations are significantly lower than during clear sky periods, presumably because they are efficiently scavenged by cloud droplets, but the intermediate ions concentrations remain unchanged (Figure 1). This result would lead to the conclusion that the limiting factor for new particle formation is

not the amount of precursors (clusters) but other parameters such as non-soluble condensing gases.

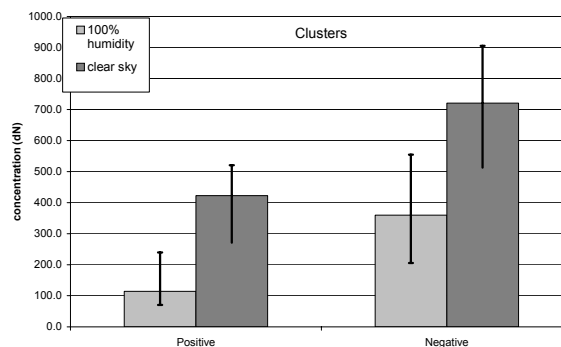


Figure 1. Median cluster concentrations in-cloud compared to clear sky periods for both positive and negative ions.

This work was supported by the mi-lourd INSU.

Kulmala M., Vehkamäki H., Petäjä T., Dal Maso M., Lauri A., Kerminen V.-M., Birmili W., & McMurry P.H. (2004) *Journal of Aerosol Science*, 35, 143–176.

## One-Year Observations of New Particle Formation at Two Stations in Central Siberia

M. Dal Maso<sup>1</sup>, L. Sogacheva<sup>1</sup>, A. Vlasov<sup>2</sup>, A. Staroverova<sup>2</sup>, A. Lushnikov<sup>1</sup>, M. Anisimov<sup>3</sup>, V.A. Zagainov<sup>4</sup>, T.V. Khodzer<sup>5</sup>, V.A. Obolkin<sup>5</sup>, Yu. S. Lyubovtseva<sup>1,6</sup>, I. Riipinen<sup>1</sup> and M. Kulmala<sup>1</sup>

<sup>1</sup>Division of Atmospheric Sciences, Dept. of Physical Sciences, 00014 University of Helsinki, Finland

<sup>2</sup>Russian State Hydrometeorological University, 195196 St Petersburg, Russia

<sup>3</sup>Institute of Catalysis, SB RAS, 630090, Novosibirsk, Russia,

<sup>4</sup>Karpov institute of physical Chemistry, Vurontsovo Pole, 105064 Moscow, Russia

<sup>5</sup>Limnological institute, Siberian branch of RAS, 3. Ulanbatroskaja, 664043 Irkutsk, Russia

<sup>6</sup>Geophysical Center RAS, 3. Molodezhnaya, 119296 Moscow, Russia

Keywords: Aerosol Formation, Atmospheric Aerosols, Nucleation mode

Formation of new atmospheric aerosol particles by nucleation events is a significant source of new atmospheric particles. The formed particles have, after growing by condensation, the potential to act as cloud condensation nuclei and thus affect the Earth's radiative balance as well as the hydrological cycle. Particle formation events have been observed in widely variable environments and conditions all around the world (Kulmala *et al.*, 2004).

The western part boreal forest has been an area where particle formation has been studied intensively, in part because it has been an area where long time series of atmospheric submicron size distributions have been measured (Tunved *et al.*, 2003; Dal Maso *et al.*, 2007). Studies on these measurements have revealed that the boreal forest is source of new particle number and mass (Tunved *et al.*, 2006). However, these studies are concentrated on the western part of the European boreal forest area, while data of the vast forested areas of the Siberian forests is still scarce.

In this work we present two one-year datasets from the Siberian boreal forest, where submicron aerosol size distributions have been measured. We also present an analysis of the frequency of new particle formation at these stations as well as characteristics for the formation events.

The first of the stations, the Listvyanka measurement station (51.9°N 104.7°E), is located on the south-western shore of Lake Baikal, a great freshwater basin surrounded by mountains. The station is situated ca. 70 km southeast from the city of Irkutsk on the top of a hill, ca 300 m over the surface of Lake Baikal. The sampling site is surrounded by coniferous forest consisting mainly of pine, cedar and spruce, with an admixture of deciduous trees.

The Tomsk measurement station (56.5°N 85.1°E) is situated near the city of Tomsk. The station itself is surrounded by mixed forest consisting mainly of birch, pine, spruce and larch. There are no roads or industrial activity in the immediate vicinity of the station.

The aerosol size distributions data was measured using Diffusion Aerosol Spectroscopes (DAS). The DAS consists of a set of grid diffusion

batteries and a condensation particle counter. By measuring the penetration with varying numbers of grids, the aerosol size distribution can be inverted from the measured grid penetrations. The data cover the time period March 2005-February 2006.

To determine the extent of the observed new particle formation, the size distributions resulting from the data inversion were analyzed visually on a day-to-day basis. Each day was classified into one of three classes: event, non-event or undefined, based on similar criteria as presented in Dal Maso *et al.*, (2005).

We found particle formation events occurring at both stations; 55 event days in Listvyanka and 33 in Tomsk. Particle formation was most frequent in springtime, in Listvyanka also summertime was an active period. The formation rates of new particles were on the average 0.4 and 0.8 cm<sup>-3</sup>s<sup>-1</sup> in Listvyanka and Tomsk, respectively. The growth rates of the formed particles were from 0.4 to 17 nm/h, on average 2 nm/h and 7 nm/h for the two stations, respectively. These observations are very similar to the particle formation frequencies and characteristics reported in the more western parts of the boreal forest area.

This work has been supported by the Maj and Tor Nessling Foundation

Dal Maso, M., *et al.*, (2005) Formation and growth of fresh atmospheric aerosols: eight years of aerosol size distribution data from SMEAR II, Hyytiälä, Finland, *Bor. Env. Res.* 10, 323-336.

Dal Maso, M., *et al.*, (2007) Aerosol size distribution measurements at four Nordic field stations: identification, analysis and trajectory analysis of new particle formation bursts. *Tellus B*, in press.

Kulmala, M., *et al.*, (2004) Formation and growth rates of ultrafine atmospheric particles: A review of observations *Aerosol Science* 35, 143-176.

Tunved, P. *et al.*, (2003) One year boundary layer aerosol size distribution data from five nordic background stations *Atmos. Chem. Phys.*, 3, 2183-2205

Tunved, P. *et al.*, (2006) High Natural Aerosol Loading over Boreal Forests *Science* 14, 261-263

## Formation of secondary organic aerosols by ozonolysis of plant-released volatiles

J. Joutsensaari<sup>1</sup>, P. Yli-Pirilä<sup>1</sup>, D.M. Pinto<sup>1</sup>, P. Tiiva<sup>1</sup>, J. Heijari<sup>1</sup>, A.-M. Nerg<sup>1</sup>, J.K. Holopainen<sup>1</sup>, P. Miettinen<sup>2</sup>, P. Tiitta<sup>2</sup>, J. Rautiainen<sup>2</sup>, H. Kokkola<sup>3</sup>, D.R. Worsnop<sup>4</sup> and A. Laaksonen<sup>2</sup>

<sup>1</sup>Department of Environmental Science, <sup>2</sup>Department of Physics, University of Kuopio, P.O. Box 1627, FIN-70211 Kuopio, Finland.

<sup>3</sup>Finnish Meteorological Institute, Unit Kuopio, P.O.Box 1627, FI-70210 Kuopio, Finland

<sup>4</sup>Aerodyne Research Inc., 45 Manning Road, Billerica, Ma 01821-3976, USA

Keywords: organic aerosols, SOA, particle formation, VOCs, biogenic particles.

Formation of secondary organic aerosols (SOA) is one of the main processes that affect the composition and properties of atmospheric particles. Volatile monoterpenes and isoprene are known to contribute to SOA formation (Kanakidou *et al.*, 2004) and the current evidence from reaction chamber studies (Bonn and Moortgat, 2003) suggests that inducible VOCs with low volatility such as sesqui- and homoterpenes might be even more effective in reactions with O<sub>3</sub> and subsequent formation of aerosol particles.

In a previous study, we have demonstrated in growth chamber conditions that particle nucleation by ozonolysis of plant volatiles takes place more efficiently over plants that are emitting inducible VOCs after elicitor triggering than over non-treated plants (Joutsensaari *et al.*, 2005). However, in the previous study, the plants were also exposed to O<sub>3</sub> therefore possible reactions between O<sub>3</sub> and terpenes or other compounds present in plant surfaces were not excluded. Thus, we have conducted new experiments to measure the reactions between O<sub>3</sub> and plant-emitted VOCs in separate reaction chambers (Pinto *et al.*, 2007).

In the experiments, two different type of continuous flow reactor systems were used: i) a Teflon chamber (1.2x1.4x1.2 m<sup>3</sup>, ~2 m<sup>-3</sup>, residence time ~2 h) and ii) a Teflon tube (278 cm, Ø 11 cm, ~26 l, ~20 min). Scots pine and Norway spruce seedlings (intact and methyl jasmonate treated) were used as VOC emitters in the first case and white cabbage plants (intact and herbivore-damaged) in the second case. In the both cases, plant-emitted VOCs were conducted into the separate reaction chamber and they were mixed with an air-flow enriched with ozone (100-400 ppb) at the inlet of the reactor. Particle size distributions were measured with scanning and fast mobility particle sizers (SMPS, FMPS). Ozone and VOC concentrations were measured at the reactor inlet and outlet. VOC samples were collected on Tenax-TA adsorbent and subsequently analyzed by gas chromatography-mass spectrometry (GC-MS). Furthermore, composition of formed particles were analysed with an Aerosol mass spectrometer (AMS, Aerodyne) (case i) and the monoterpene reactions with O<sub>3</sub> and OH were modelled using reaction kinetics equations (case ii).

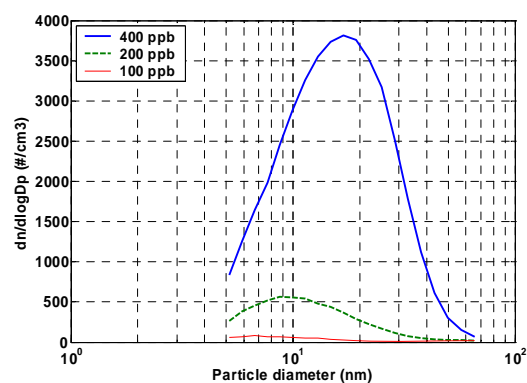


Figure 1. Average particle number size distributions at O<sub>3</sub> of 100, 200, 400 ppb (case ii, cabbage plants)

In the experiments with cabbage plants (case ii, Fig 1.), the average total number concentration (40 to 2400 #/cm<sup>3</sup>) as well as the mode diameter of the size distributions (8 to 17 nm) increased with increasing O<sub>3</sub> concentration. At 100 ppb, the particle concentrations were very low and, practically, no new particles were formed in some of the trials. At higher O<sub>3</sub> concentrations, the concentrations of formed particles were higher and they were larger in size. Formation of SOA was also observed in experiments with Scots pine and Norway spruce seedlings (case i) at O<sub>3</sub> level of 200 ppb. The results confirm that particle formation takes place in the air of chamber by reactions of VOCs and ozone, not as a result of reactions between O<sub>3</sub> and plant surface compounds, which could be possible in the previous experiments.

The work was supported by the Academy of Finland and by Emil Aaltonen Foundation.

- Bonn B. and Moortgat G.K. (2003) *Geophys. Res. Lett.* 30 (11), 1585, doi:10.1029/2003GL017000  
 Joutsensaari, J. *et al.* (2005). *Atmos. Chem. Phys.* 5, 1489-1495.  
 Kanakidou, M. *et al.* (2004). *Atmos. Chem. Phys.* 5, 1053-1123.  
 Pinto, D.M. *et al.* (2007) The effects of increasing atmospheric ozone on biogenic monoterpene profiles and the formation of secondary aerosols. *Atmos. Environ.*, accepted.

## Aerosol composition after a clean air nucleation event in Hyttiälä, Finland

T. Raatikainen<sup>1</sup>, P. Vaattovaara<sup>2</sup>, J. Rautiainen<sup>2</sup>, P. Tiitta<sup>2</sup>, A. Laaksonen<sup>1,2</sup> and D. Worsnop<sup>3</sup>

<sup>1</sup>Finnish Meteorological Institute, 00101, Helsinki, Finland

<sup>2</sup>Department of Physics, University of Kuopio, 70211, Kuopio, Finland

<sup>3</sup>Aerodyne Research Inc., Billerica, MA, USA

Keywords: AMS, Growth, Organic aerosols

Aerodyne aerosol mass spectrometer (AMS) is a nearly online instrument able to detect non-refractory species (e.g. ammonia, nitrate, sulphate and organics) from submicron aerosol particles (e.g. Jimenez *et al.*, 2003). A quadrupole AMS was one of the instruments used in a spring 2005 measurement campaign in Hyttiälä, Finland.

We selected for a closer look a 24 hour clean air period starting at March 31, 15:00. A nucleation event was observed to start a few hours before the beginning of this period. The nucleated particles continued growing, and accumulated mass enough to be detected by the AMS at 19:00. Particle mass increased the whole night, until it rapidly decreased in the following morning.

Most of the measured particle mass was organic and organics were also the main reason for the increasing mass (Fig. 1). It is possible that 10 °C temperature decrease after the sunset enhanced condensation of semi-volatile organics. The most likely reason for the decreasing concentration in the morning is increased vertical mixing.

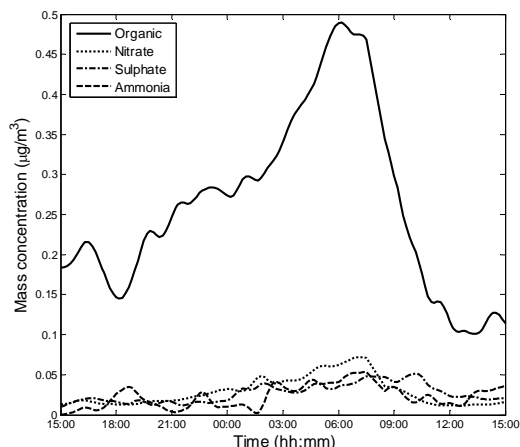


Figure 1. Mass concentrations of the four main species measured by AMS.

Because only a small fraction of the mass was inorganic, we concentrate on the organic fraction. Organic mass spectrum, which is similar to spectrum measured in 2003 campaign (Allan *et al.*, 2006), was divided to two different mass spectra by the method of Zhang *et al.* (2005). One spectrum is common for oxidized (aged) and the other is common for less oxidized (fresh) organic aerosols. Mass

concentrations and mass spectra of the two organic groups are presented in Figure 2.

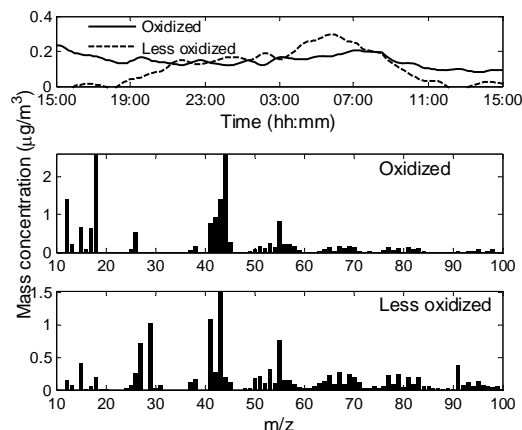


Figure 2. Mass concentrations and spectra of oxidized and less oxidized organics as a function of time and mass to charge ratio, respectively.

The lower spectrum is typical for less oxidized organics. The peak at  $m/z$  57 (mainly  $C_4H_9^+$ ) is quite small, which means that longer alkyl chains are rare. These organics are responsible for the increased organic mass concentration. Because the time period was selected based on clean conditions and less oxidized organics are mainly from local sources, these organics are likely to originate from the local forest.

The upper spectrum contains less hydrocarbon peaks, but there is a strong peak at  $m/z$  44, which is indicative of strongly oxidized organics. Oxidized organics (aged background aerosol) had relatively steady concentrations during the growth.

This work was supported by the Maj and Tor Nessling foundation under grant number 2007083.

- Allan, J., Alfarra, M., Bower, K., Coe, H., Jayne, J., Worsnop, D., Aalto, P., Kulmala, M., Hyötyläinen, T., Cavalli, F. & Laaksonen, A. (2006). *Atmos. Chem. Phys.*, 6, 317-327.
- Jimenez, J., Jayne, J., Shi, Q., Kolb, C., Worsnop, D., Yourshaw, I., Seinfeld, J., Flagan, R., Zhang, X., Smith, K., Morris, J. & Davidovits, P. (2003). *J. Geophys. Res.*, 108, 8425.
- Zhang, Q., Alfarra, M., Worsnop, D., Allan, J., Coe, H., Canagaratna, M. & Jimenez, J. (2005). *Environ. Sci. Technol.*, 39, 4938-4952

## CCN properties of ambient aerosol particles during nucleation events

U. Dusek<sup>1</sup>, J. Curtius<sup>2</sup>, G.P. Frank<sup>1</sup>, F. Drewnick<sup>3</sup>, A. Kürten<sup>2</sup>, J. Schneider<sup>3</sup>, M.O. Andreae<sup>1</sup>, and U. Pöschl<sup>1</sup>

<sup>1</sup>Biogeochemistry Department, Max Planck Institute for Chemistry, Box 3060, 55020 Mainz, Germany

<sup>2</sup>Institut für Physik der Atmosphäre, Universität Mainz, J.-J.-Becher-Weg 22, 55099 Mainz, Germany

<sup>3</sup>Particle Chemistry Department, Max Planck Institute for Chemistry, Box 3060, 55020 Mainz, Germany

Keywords: nucleation, CCN, SOA, number size distribution, ambient aerosol.

Nucleation events are ubiquitous in the atmospheric boundary layer. In remote areas the nucleated particles can grow into the size range of cloud condensation nuclei (CCN) (Kerminen *et al.*, 2005). Recently it has been proposed that biogenic secondary organic aerosol (SOA) plays an important role in the growth of freshly nucleated particles to larger sizes (Tunved *et al.*, 2006), which might impact their CCN properties. It is therefore important to directly determine the CCN activity of particles formed in nucleation events.

During the FACE-2005 experiment, carried out on the Kleiner Feldberg near Frankfurt in the summer of 2005, nucleation events occurred nearly every day. Between June 24 and July 6 2005, we measured size-resolved CCN efficiencies, by using a differential mobility analyzer upstream of a CCN counter as described in Frank *et al.* (2006). Size-resolved CCN spectra can be used to derive critical supersaturations of the particles formed during nucleation events, after they have grown to the CCN size range. The resulting CCN data are complemented by particle number size distributions and particle chemical composition measured by aerosol mass spectrometers.

Preliminary case studies indicate that particles are less CCN active during nucleation events than outside nucleation events. Figure 1 gives an example of a nucleation event observed on June 25th, 2005 between 5:30 and 19:00. The particle size distribution before, during and after the nucleation event is shown in Figure 1a. The nucleation mode did not show a continuous growth to larger sizes during the course of the day, but shows a tail that extends to sizes of around 60nm. Figure 1b compares size-resolved CCN spectra at  $S = 0.54\%$  before, during and after the nucleation event. The CCN efficiencies are clearly lower during the nucleation event than before or after that.

The preliminary results are in agreement with the hypothesis that organic compounds contribute to the growth of nucleation particles. This hypothesis will be further explored by making use of AMS data to investigate the change in particle chemical composition during nucleation events.

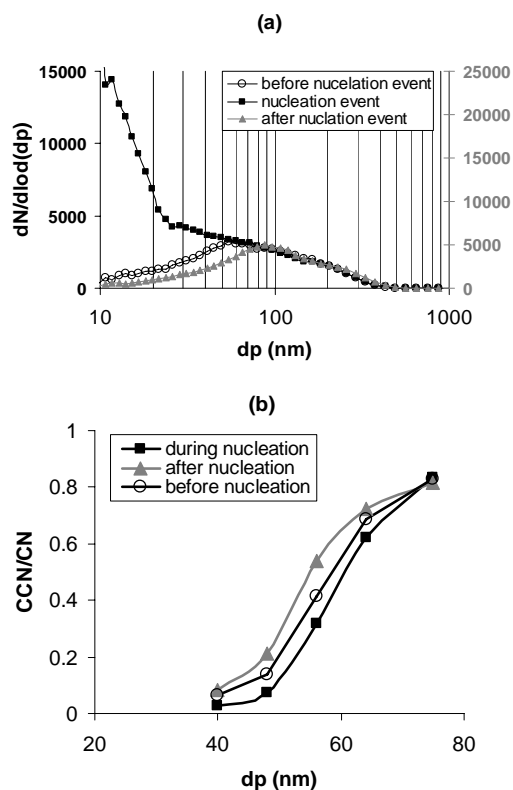


Figure 1. Particle number size distributions and CCN efficiencies at  $S = 0.54\%$  before during and after the nucleation event.

### References:

- Kerminen, V.-M., Lihavainen, H., Komppula, M Viisanen, Y., & Kulmala, M. (2005). Direct observational evidence linking atmospheric aerosol formation and cloud droplet activation. *Geophys. Res. Lett.*, 32, L14803, doi:10.1029/2005GL023130.
- Tunved, P., Hansson, H.-C., Kerminen, V.-M., Strom, J., Dal Maso, M., Lihavainen, H., Viisanen, Y., Aalto, P., Komppula, M., Kulmala, M. (2006). High Natural Aerosol Loading over Boreal Forests. *Science*, 312, 261-263.
- Frank, G. P., Dusek, U., & Andreae, M. O. (2006). Technical note: A method for measuring size-resolved CCN in the atmosphere. *Atmos. Chem. Phys. Discuss.*, 6, 4879-4895.

## Newly-formed nucleation mode particles composition change at boreal forest atmosphere

P. Vaattovaara<sup>1</sup>, T. Petäjä<sup>2</sup>, D.R. Worsnop<sup>3</sup> and A. Laaksonen<sup>1,4</sup>

<sup>1</sup>Department of Physics, University of Kuopio, POB 1627, 70211 Kuopio, Finland

<sup>2</sup>Department of Physical Sciences, University of Helsinki, Helsinki, Finland

<sup>3</sup>Aerodyne Research Inc., 45 Manning Road, Billerica, Ma 01821-3976, USA

<sup>4</sup>Finnish Meteorological Institute

Keywords: boreal forest, nucleation mode, particle formation, field measurements, chemical properties

The boreal forests forming a circum polar band throughout the Northern hemisphere continents and covering up approximately 15% of the Earth's land surface are large natural environment with a huge potential to affect climate processes. Boreal forests are known to emit numerous different volatile and semivolatile organic gases which are able to react with air oxidants and thus, forming secondary compounds and taking part into ultrafine particles formation and growing processes. Thus they are expected to affect both directly and indirectly Earth's radiative budget and thus, contribute to the climate change. However, in order to be able to better understand and predict the climatic effects of boreal forests, the newly-formed nucleation mode sized particles (i.e.  $d < 20$  nm) composition behavior should be better understood during new particle formation bursts (i.e. nucleation event).

In this work the changes in the nucleation mode particles (i.e. 10 nm in diameter) composition during new particles formation bursts and the composition differences of newly-formed nucleation mode particles between various boreal forest nucleation events were studied at research station SMEAR II in Southern Finland during spring 2003. These measurements were carried out using parallel the UFO-TDMA (ultrafine organic tandem differential mobility analyzer; Vaattovaara *et al.*, 2005) and UFH-TDMA (ultrafine hygroscopicity tandem differential mobility analyzer; Hämeri *et al.*, 2000) methods.

The comparison of the UFO-TDMA derived growth factors (EGFs, ethanol growth factors) and the UFH-TDMA derived hygroscopic growth factors (HGFs) to each other is presented in Figure 1. In clean air masses i.e. when gaseous pollutant levels of  $\text{SO}_2$  and  $\text{NO}_x$  were very low (Boy *et al.* 2005), the observed EGFs and HGFs were typically high and low, respectively. So, the EGFs show their highest and the HGFs their lowest values during the cleanest events. In contrast to that, the EGFs shows the lowest and HGFs the highest values during more polluted cases (i.e. a higher  $\text{SO}_2$  and  $\text{NO}_x$  concentrations; typically  $\text{SO}_2$  explain very well HGF values and thus hygroscopicity). Previously Petäjä *et al.* (2006) showed at suburban environment (Athens, Greece) that freshly formed particles were more water soluble

under polluted air masses than under relatively clean condition.

The composition change during separate new particle formation events were related to a decreasing trend of gas phase sulfuric acid ( $\text{H}_2\text{SO}_4$  data from Boy *et al.*, 2005) concentrations and consequently on an increased fraction of organics. Furthermore, quick air mass change from clean to less clean or dirty direction had an effect on the composition of nucleation mode particles. It is also expectable that the organic fraction composition change all the time during events, because also surrounding conditions and thus air chemistry is changing during the events.

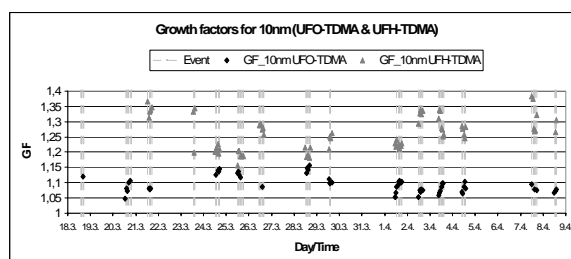


Figure 1. EGF and HGF values measured for 10 nm particles during 15 new particle formation event at a boreal forest site, Hyytiälä, Finland, spring 2003.

This work was supported by EU 5<sup>th</sup> Framework Programme through the QUEST project.

Boy, M., Kulmala, M., Ruuskanen, T.M, Pihlatie M., Reissel A., Aalto, P.P., Keronen, P., Dal Maso, M., Hellen, H., Hakola, H., Jansson, R., Hanke, M. & Arnold, F. (2005). *Atmos. Chem. Phys.*, 5, 863-878.

Hämeri, K., Väkevä, M., Hansson, H.-C., and Laaksonen, A. (2000). *J. Geophys. Res.*, 105(D17), 22231-22242.

Petäjä, T., Kerminen, V.-M., Dal Maso, M., Junninen, H., Koponen, I.K., Hussein, T., Aalto, P.P., Andronopoulos, S., Robin, D., Hämeri, K., Bartzis, J.G. & Kulmala, M. (2006). *Atmos. Chem. Phys. Discuss.*, 6, 8605-8647.

Vaattovaara, P., Räsänen, M., Kühn, T., Joutsensaari, J., and Laaksonen, A. (2005). *Atmos. Chem. Phys.*, 5, 3277-3287.

## Cosmic Ray Induced Formation of Atmospheric Aerosol Particles and Cloud Condensation Nuclei: New Insights from Atmospheric Trace Gas and Ion Measurements and Laboratory Investigations of Ion Induced Nucleation

F. Arnold<sup>1</sup>, V. Fiedler<sup>1,2</sup>, H. Aufmhoff<sup>1</sup>, T. Schuck<sup>1</sup>, R. Nau<sup>1</sup>, L. Pirjola<sup>3,4</sup>,  
T. Jurkat<sup>1</sup>, U. Reichel<sup>1</sup>, A. Roiger<sup>2</sup>, A. Sorokin<sup>1</sup>, and H. Schlager<sup>2</sup>

<sup>1</sup> Atmospheric Physics Division, Max Planck Institute for Nuclear Physics, P.O. Box 103980, D-69029 Heidelberg, Germany

<sup>2</sup> Institute for Physics of the Atmosphere, German Center for Air and Space DLR, Oberpfaffenhofen, Germany

<sup>3</sup> Department of Physical Sciences, University of Helsinki, P.O. Box 64, FIN-00014 Helsinki, Finland

<sup>4</sup> Department of Technology, Helsinki Polytechnic, P.O. Box 4020, FIN-00099 Helsinki, Finland

Keywords: nucleation, ions, mass spectrometry, sulphuric acid, aerosol dynamics.

Cosmic ray induced aerosol formation represents a potentially important physical mechanism which may connect clouds and climate with cosmic rays and solar activity. It involves three major steps: (a) cosmic ray induced formation of atmospheric molecular and atomic ions (Eichkorn *et al.*, 2002); (b) clustering of certain atmospheric trace gas molecules  $X$  to ions eventually leading to large cluster ions; (c) ion-ion recombination of large cluster ions eventually leading to stable molecular clusters which represent already small aerosol particles which grow further by condensation and coagulation and may eventually grow sufficiently to become cloud condensation nuclei (CCN). The only trace gas  $X$  so far detected in the atmosphere is gaseous sulphuric acid ( $H_2SO_4$ ) which is formed from the sulphur-bearing precursor gas  $SO_2$ .

We have made new measurements of  $SO_2$ , gaseous  $H_2SO_4$  (hereafter termed GSA), and cluster ions. The aircraft-based and ship-based state of the art  $SO_2$  measurements took place in polluted and also in remote regions including Europe, South America, South East Asia, and Equatorial Africa.

We have also made laboratory investigations of sulphuric acid cluster ions and model simulations of ion-induced  $H_2SO_4$  nucleation.

Our work indicates that cosmic ray induced aerosol formation is particularly efficient in the upper troposphere and that a substantial fraction of newly formed particles may indeed become CCN.

Figure 1 shows as an example some results of our laboratory flow reactor experiments. Here mass distributions of positive and negative cluster ions were measured in a flow reactor through which was passed synthetic air (1024 hPa and 293 K) with controlled traces of water vapour and gaseous sulphuric acid. In the flow were introduced reagent cluster ions of the form  $H^+W_w$  and  $NO_3^-(HNO_3)_n$  (curve  $SO_2 = 0$  ppm in Fig. 1). After introduction of gaseous sulphuric acid the reagent ions experienced conversion to  $H^+A_aW_w$  and  $HSO_4^-A_aW_w$  cluster ions (here  $A=H_2SO_4$  and  $W=H_2O$ ). The mass distributions of these sulphuric acid containing cluster ions are

broader and bi-modal. The second mode represents nucleated ions whose growth is hardly affected by thermal detachment of  $A$  molecules. As the GSA concentration increases the second mode increases. The ultimate decrease of the second mode reflects the limited growth due to the limited residence time (0.9 seconds) of the ions in the flow reactor.

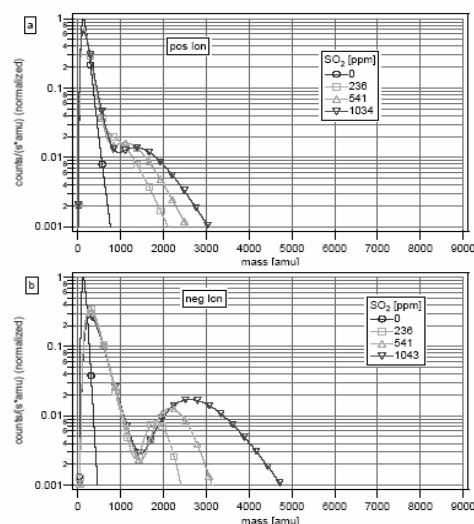


Figure 1: Mass distributions of positive and negative cluster ions of the form  $H^+A_aW_w$  and  $HSO_4^-A_aW_w$  measured in our flow reactor experiment. Different curves correspond to different gaseous sulphuric acid abundances. From Sorokin & Arnold (2007).

Eichkorn, S., Wilhelm, S., Aufmhoff, H., Wohlfrom, K.H., Arnold, F. (2002). *Geophysical Research Letters* 29, 10.1029/2002GL015044, 43-1 – 43-4.

Sorokin, A. and Arnold, F. (2007). *Atmos. Environ.*, (in print).

## **FINE AND ULTRAFINE AEROSOLS IN SOUTHWESTERN AUSTRALIA, INFLUENCE OF LAND SURFACE, LAND USE AND VEGETATION ON SIZE AND NUMBER DISTRIBUTIONS**

W. Junkermann<sup>1</sup>, J. Hacker<sup>2</sup>, T. Lyons<sup>3</sup> and Udaysankar Nair<sup>4</sup>

<sup>1</sup>F. K. IMK-IFU, Garmisch-Partenkirchen, 82467, Garmisch-Partenkirchen, Germany

<sup>2</sup>Airborne Research Australia, Flinders University, Adelaide, zip Code, City, Australia

<sup>3</sup>Murdoch University, South Street, Murdoch, 6150, Murdoch, WA, Australia

<sup>4</sup>National Space Science Technology Center, Huntsville, Alabama, 35805, USA

Keywords: Nucleation, Aerosol Size Distribution, Aerosol Characterisation

Fine particles act as an important link in the planetary boundary layer between surface water budget and cloud microphysics and subsequently precipitation. The number of cloud condensation nuclei within the planetary boundary layer originating either from advection or from local production of particles controls the droplet size distribution in the clouds and may also effectively modify precipitation probability. It affects cloud albedo and the radiation balance in a cloudy atmosphere (Flossmann, 1998) and use, surface structure and vegetation will significantly modify the local population of aerosols as well from wind blown dust which consists mainly from coarse particles as well as from local particle production from gas phase precursors which produces fine and ultrafine particles. It has been shown that ultrafine particles from nucleation can be a significant source for cloud condensation nuclei even in otherwise already heavily polluted environments (Jaakkola et al, 2005). In clean environments nucleation is considered to be the main source for particles in the accumulation mode. As modifications of the water budget have to be expected with climate change and are critical for future land use and agriculture, climate models need detailed information on the distribution of particle sources and source strength. This holds especially for semiarid areas where slight changes in the water budget can hamper agriculture. Investigations on production mechanisms and fine particle budget have been performed in the last decade in several areas in the northern hemisphere (Kulmala et al, 2004). Particle production and growth has been attributed to reactions of sulphur components and volatile organic compounds. In the southern hemisphere measurements are sparse and due to the lower sulphur concentrations new particle production may be different. Within this project (BUFE) measurements were performed from December 6 to December 14 in south-western Australia in the area of Lake King close to the Rabbit Fence which divides the area into agricultural and natural vegetation. The area was shown previously to develop clouds above either the agriculture or above the natural vegetation on several occasions. The location allows to perform regional scale

measurements comparing the different land use and surface structure and their impact on the local aerosol population within the planetary boundary layer using instrumented aircraft as mobile research platforms. It can be used as a natural laboratory as on both sides of the fence for several hundred kilometers well defined homogeneous surface structures and ground albedo are observed. Two aircraft were involved in the study equipped with instrumentation for aerosol size distribution, surface albedo, radiation balance and turbulent fluxes of water and CO<sub>2</sub> as well as with remote sensing equipment for land surface characterisation. Measurements were performed under low wind conditions on both sides of the fence comparing the aerosol budget and related processes on a regional scale. While no nucleation could be observed above the natural vegetation, a considerable local production of new particles has been found above the harvested agricultural land and the scattered salt lakes in the area.

Flossmann, A. I. (1998). *J. Atmospheric sciences*, 55, 879-887.

Jaakkola, A., Hamed, A., Joutsensaari, J., Hiltunen, J., Cavalli, F., Junkermann, W., Asmi, A., Fuzzi S., and Facchini, M.C. (2005) *Geophys. Res. Lett.*, 32, 6, 06812, 10.1029/2004G022092,

Kulmala, M., V.-M. Kerminen, T. Anttila, A. Jaakkola, and C. O Dowd (2004), *J. Geophys. Res.*, 109, D04205, doi:10.1029/2003JD003961.

## Atmospheric fronts, cloudiness and aerosol particle formation in Hyttiälä, Southern Finland.

L.Sogacheva<sup>1</sup>, L. Saukkonen<sup>2</sup>, G. de Leeuw<sup>1,2</sup> and M.Kulmala<sup>1</sup>

<sup>1</sup>Department of Physical Sciences, University of Helsinki, PO Box 64 FIN-00014, Helsinki, Finland

<sup>2</sup>Finnish Meteorological Institute, Erik Palménin aukio, FI-00560 Helsinki, Finland

Keywords: particle formation, atmospheric fronts, cloudiness

The mechanism of new particle formation and growth in the atmosphere has been a topic of research for several years (Kulmala *et al.*, 2004). Atmospheric chemical composition, water content, and the amount of solar radiation are among the key variables that are known to influence the formation of aerosol particles.

In the present study we have analyzed different types of synoptic situation in Hyttiälä for the period of 2003-2005, focusing mainly on atmospheric fronts passages and cloudiness for days that were classified according to the intensity of new particle formation.

The particle number concentration and size distribution has been measured at the SMEAR II station in Hyttiälä, southern Finland. Days were classified either as event days, nonevent days or undefined days. Event days were further classified into separate classes (class Ia, class Ib, and class II) regarding the possibility to drive the characteristics from size distribution (Dal Maso *et al.*, 2005). For class I days the growth rate could be determined with good confidence level; while for class II the derivation of these parameters was not possible or the accuracy of the results was questionable.

To investigate the passage of atmospheric fronts the synoptic maps of the surface and 850 hPa layers (“Berliner Wetterkarte”) have been analyzed together with the satellite images from the AVHRR five channel scanning radiometer. The cloudiness over Southern Finland has been estimated in octas.

The results (figure 1) show that the most typical situation for event days (78% to 65% of all cases for classes Ia to II respectively) is the absence of frontal passages during days when new particle formation occurred. The second typical situation for event days is particle formation in the rear of a cyclone, after the cold front passage. Particle formation classified as class Ib and class II often (in 15% and 10% respectively) starts prior to frontal passages; cloudiness, associated with atmospheric fronts, decrease the amount of solar radiation and particle growth slows down.

In about 40% of cases the atmospheric fronts and several frontal passages have been observed in Hyttiälä during the days classified as nonevent or undefined days.

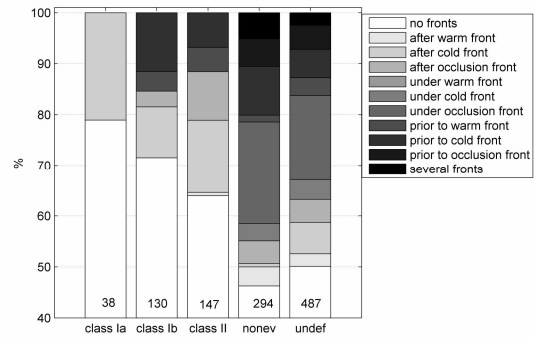


Figure 1. Fraction of the different types of the synoptic situations classified according to atmospheric fronts passages for event days (class Ia, class Ib, class II), nonevent (nonev) and undefined (undef) days. Number on the bar is the number of days in each group of days.

About 90% of the event classes Ia and 45% of the event classes II are clear sky days and days with very low (1-2 octas) cloudiness (figure 2). Clear sky conditions average 10% for nonevent and undefined days. This fact confirms the importance of solar radiation in new particle formation.

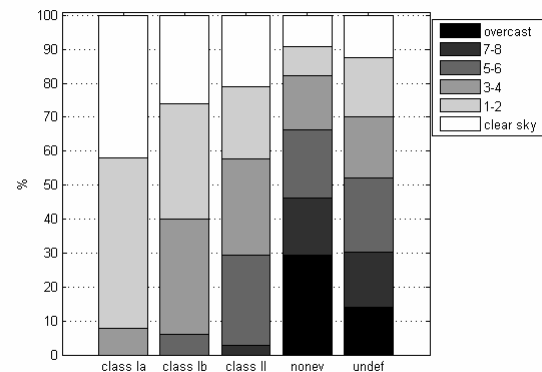


Figure 2. Cloudiness (color, in octas) for event days (class Ia, class Ib, class II), nonevent (nonev) and undefined (undef) days.

Kulmala, M., Vehkamäki, H., Petäjä, T., Dal Maso, M., Lauri, A., Kerminen, V.-M., Birmili, W., McMurry, P.H. (2004). *J. Aerosol Science*, 35, 143-176.

Dal Maso, M., Kulmala, M., Riipinen, I., Wagner, R., Hussein, T., Aalto, P. P., and Lehtinen, K. E. J. (2005). *Boreal Env. Res.*, 10, 323-336.

## **T30 Abstracts**

## Retrieval of water vapor and of the optical-microphysical-chemical properties of tropospheric aerosols using a compact 6-wavelength Raman-lidar system

A. Papayannis<sup>1</sup>, R. E. Mamouri<sup>1</sup>, A. Nenes<sup>2</sup>, G. Avdikos<sup>1</sup>, G. Chourdakis<sup>3</sup>, G. Georgoussis<sup>3</sup>, C. Böckmann<sup>4</sup>, A. Kirsche<sup>4</sup>, K. Eleftheriadis<sup>5</sup>, G. Tsaknakis<sup>1</sup> and C. Schneidenbach<sup>6</sup>

<sup>1</sup>National Technical University of Athens, Physics Department, Laser Remote Sensing Laboratory, Greece

<sup>2</sup>Georgia Institute of Technology, School of Earth and Atmospheric Sciences and Chemical & Biomolecular Engineering, Atlanta GA, USA

<sup>3</sup>Raymetrics S.A., Glyka Nera, Athens, Greece

<sup>4</sup>University of Potsdam, Institute of Mathematics (IMP), 14469 Potsdam, Germany

<sup>5</sup>N.C.S.R. Demokritos, GR-15310 Ag. Paraskevi, Attiki, Greece

<sup>6</sup>University of Potsdam, Institute of Computer Sciences, 14469 Potsdam, Germany

Keywords: lidar, Aerosol thermodynamics, aerosol size distribution, index of refraction, relative humidity

Atmospheric aerosols have large influence on earth's radiation budget. Recent estimations on the possible impact of aerosols (both direct and indirect effects) on the radiative forcing (cooling effect) in a global average are of the same order of magnitude as the CO<sub>2</sub> effect (warming effect). However, high uncertainties still exist concerning the indirect and direct effects, which are connected with the aerosol influence on climate. Water vapor is the most influential greenhouse gas, since it absorbs infrared radiation emitted from Earth's surface and lower atmosphere more than any other constituent, thereby causing about two third of the natural greenhouse effect of the Earth's atmosphere.

The compact 6-wavelength Raman lidar system of the National Technical University of Athens was used for the retrieval of water vapor and of the optical and microphysical properties of aerosol in the troposphere over Athens, Greece. The elastically backscattered lidar signals (at 355, 532 and 1064 nm), as well as those generated by Raman scattering by atmospheric N<sub>2</sub> and H<sub>2</sub>O (at 387, 607 and 407 nm, respectively) were used to derive the aerosol backscatter (at 355, 532 and 1064 nm) and the extinction (at 355 and 532 nm) coefficient profiles. The Raman lidar system has been validated both at hardware and software level during the EAR-INET project. A specially developed software code was also used to retrieve the water vapor, as well as the optical (extinction, backscatter, optical depth) and the microphysical properties of aerosols in the troposphere.

For the latter case, the hybrid regularization technique developed at IMP was used (Böckmann C. and Kirsche, 2006). This model was used with vertical profiles of elastic and Raman backscattered lidar signals (obtained at 5 different wavelengths), to derive the aerosol microphysical properties, such as the effective radius, the surface-area concentration and the volume concentration, as well as the single-scattering albedo and the mean complex refractive index.

The first regularization step is performed with discretization, in which the investigated distribution function is approximated by variable B-spline functions via a collocation method. The projection dimension (number of base function) and the order of the used B-splines serve, roughly speaking, as regularization parameters. In the second step, regularization is controlled by the level of truncated singular-value decomposition. The highly nonlinear problem of the determination of the complex refractive index as a second unknown is handled by introducing a grid of wavelength- and size-independent mean complex refractive indices and by enclosing the area of possible real/imaginary-part combinations through inversion and back-calculation of optical data.

The final data set of the aerosol optical and microphysical properties along with the water vapor profiles, were incorporated into the thermodynamic model ISORROPIA (Nenes *et al.*, 1998; Nenes *et al.*, 1999). This model, combined with a minimization algorithm, was used to infer the chemical parameters of the aerosols (water content, dry chemical composition) that are consistent with the retrieved single-scattering albedo, refractive index and volume concentration parameters.

Acknowledgements: This work was funded by the GSRT/05-NON-EU-95 Project and Raymetrics S.A., and also by the PEP Project from the HGF Impuls und Vernetzungsfond under grant VH-VI-100.

Böckmann C. and Kirsche A. (2006). *Comp. Phys. Comm.* 174, 607–615.

Nenes A. *et al.* (1998). *Aquat. Geochem.*, 4, 123–152, 1998.

Nenes A. *et al.* (1999). *Atmos. Environ.*, 33, 1553–1560, 1999.

## Studies of the impact of Arctic aerosols on climate modifications

T. Zielinski<sup>1</sup>, J. Piskozub<sup>1</sup>, T. Petelski<sup>1</sup>, A. Rozwadowska<sup>1</sup>, S. Malinowski<sup>2</sup>, T. Stacewicz<sup>2</sup>, K. Markowicz<sup>2</sup>,  
A. K. Jagodnicka<sup>2</sup>, M. Posyniak<sup>2</sup>, M. Gausa<sup>3</sup>, S. Blindheim<sup>3</sup>, R. Neuber<sup>4</sup>

<sup>1</sup>*Institute of Oceanology, PAS, Poland*

<sup>2</sup>*Warsaw University, Poland*

<sup>3</sup>*ALOMAR Laboratory, Norway*

<sup>4</sup>*AWI, Potsdam, Germany*

Keywords: Arctic aerosols, optical properties, remote sensing, lidar

Absorption and scattering of radiation by aerosols directly affect the radiation balance of the Arctic, which is thought to be very sensitive to changes in radiative fluxes. This is due to small amount of solar energy normally absorbed in the polar regions. These regions represent sensitive ecosystems, which are susceptible to even small changes in the local climate. Thus, for a given aerosol distribution, the specific optical properties are enhanced in these regions. In order to improve the knowledge about the origin, transport pathways, vertical structure of aerosol physical and chemical properties as well as the impact on climate in the polar regions, a combined effort of surface-based and remote sensing measurements is needed.

The Arctic studies of aerosol properties the authors originated in 1996 during the ARctic EXperiment (AREX) campaigns using the r/v *Oceania* vessel. Every year the vessel cruised for seven weeks (June-August) in the area of the Arctic between 0 and 14°E and 69 and 79°N. In 2002 the measurements were also carried out from the station in Ny-Alesund in Spitsbergen. The aerosol studies were conducted using an ensemble of instruments, including lidars, laser particle counters, sunphotometers and ozonometers. During the ship studies laser particle counter was placed on a mast of the vessel and moved vertically, which facilitated the determination of the vertical structure of aerosol concentrations and their size distribution at altitudes of up to 20 m a. s. l. Simultaneously, lidars provided the vertical profiles of aerosol concentrations. Those were further used for the calculation of aerosol optical thickness. Then the campaigns were launched in 2004 and 2006, within a framework of ASTAR (2004), POLAR-AOD and DAMOCLES (2006) international experiments, during which an ensemble of lidars and sunphotometers were applied.

Such measurement set ups facilitated the obtaining of data with good accuracy and well calibrated. The full meteorological coverage was always provided by the ship meteo station or from different meteo services, such as the British Atmospheric Data Center.

The Arctic aerosols in the Spitsbergen area show significant temporal and vertical variability. The results collected during the campaigns can be divided into two groups, the spring data and the summer data. Each winter, cold dense air settles over the Arctic. In the darkness, the Arctic seems to become more and more polluted by a buildup of mid-latitude emissions from fossil fuel combustion, smelting and other industrial processes. Then, in spring, when the light appears, there is a smog-like haze in the Arctic region. The values of aerosol optical thickness, e.g. at 500 nm, exceed 0.1 and they can be as high as 0.35.

In summer the situation differs from that in spring. The main problem in aerosol optical studies is related to cloud coverage over the region. Also the air mass trajectories can vary significantly which also influences the aerosol optical thickness. The summer values at 500 nm can also be high, up to even 0.3 (land origin of air masses) but majority of data are below 0.1, which indicates very clean air conditions, with very few aerosol particles suspended in it.

In order to fully describe the impact of aerosols on radiative budget it is necessary to continue the investigations of the vertical structure of physical and optical properties of aerosol particles, including solar radiative closure between observed and calculated aerosol properties also in different seasons, mainly in summer. Thus a new campaign is being prepared (summer 2007) during which r/v *Oceania* and an ensemble of lidars (ALOMAR, IOPAS, Warsaw University) and sunphotometers as well as other supporting instruments will be applied for measurements in the Arctic and the area of Andoya.

Herber, A., L. W. Thomason, H. Gernandt, U. Leiterer, D. Nagel, K.-H. Schulz, J. Kaptur, T. Albrecht, J. Notholt (2002), *Continuous day and night aerosol optical depth observations in the Arctic between 1991 and 1999*, Jour. Geophys. Res., 107, D10, 14 S, AAC 6-1-6-14, 10.1029/2001JD000536.

## Impact of different aerosol sources on particle optical properties – Experiment SOAP

T. Zielinski<sup>1</sup>, J. Remiszewska<sup>2</sup>, G. Chourdakis<sup>3</sup>, N. Mihalopoulos<sup>4</sup>

<sup>1</sup>*Institute of Oceanology, PAS, Poland*

<sup>2</sup>*Warsaw University, Poland*

<sup>3</sup>*Raymetrics S. A., Greece*

<sup>4</sup>*University of Crete, Greece*

Keywords: Atmospheric aerosols, sources, remote sensing, coastal area

In the marine boundary layer aerosols comprise of a mixture of components, each varying in number, size distribution and composition. The two major components to aerosols in the marine environment are: continental and locally generated sea-spray droplets and therefore, they include both natural and anthropogenic material which may be transported vast distances. Over the global oceans the concentrations and fluxes of atmospheric particulates produced at the sea surface predominantly by the action of the wind or carried out from the continents with the wind are of interest due to their significant impact upon various important atmospheric processes. The contribution of these particles to moisture and energy exchange processes at the sea surface, to the global salt flux, their role in cloud droplet formation processes and their influence upon the maritime atmospheric radiation balance are of increasing concern. The thorough understanding of such phenomena is essential to an accurate assessment of many processes for the development of coupled ocean-atmosphere global circulation models, including pollution problem.

The Studies Of Aerosol Properties - SOAP project aimed at a determination of the direct aerosol climatic effect including solar radiative closure between observed and calculated aerosol properties. The scientific objectives of the project included:

- Determination of the vertical structure of the chemical, physical and optical properties of aerosol particles, including solar radiative closure between observed and calculated aerosol properties (direct climate effect),
- Using the above information to define the role of absorbing and non-absorbing aerosol particles in coastal regions,
- Improve the knowledge on aerosol particle life cycle and transport pathways across Europe, including the Saharan dust events.

The measurement campaign started on July 28 2006 using the lidar LB series provided by Raymetrics S.A. from Greece which was located at Finokalia station (35° 20'N and 25° 40'E). Those were later supported by the measurements using the Microtops and a CIMEL CE-318 sunphotometers.

During the entire SOAP measurement period a series of measurements on aerosol chemical composition, light scattering coefficient, black carbon and PM10 were performed by the University of Crete. The full meteorological coverage (wind speed, direction, relative humidity, air temperature, etc.) was provided by the local meteo stations. Additionally, air mass backtrajectories were obtained for each selected day from the British Atmospheric Data Center. The campaign was completed on 9 August 2006.

The values of aerosol optical thickness measured at 500 nm varied from around 0.15 to around 0.5 during the entire measurement period. The preliminary results show that local emissions are not always most important factors, which influence the composition of marine aerosol in the near water atmospheric layer, even for the coarse mode aerosols, also known as the sea salt mode.

The high values of aerosol optical thickness indicate the impact of aerosol particles of continental origin or, in some cases, perhaps presence of thin cirrus clouds, invisible to the measurement performer. However, in majority of cases, the air mass backtrajectories for such days show that the particles were carried from over Europe.

The comparison of the results obtained during this campaign with the results of the MINOS campaign which was carried out at Finokalia station in summer 2001 will be made in the near future.

### ACKNOWLEDGEMENTS

This work was supported by the ACCENT program.

Li, X.H., Moring, Savoie, D., Voss, K., Prospero, M. (1996). *Dominance of mineral dust in aerosol light-scattering in the North Atlantic trade winds*. Nature 380, 416-419

Smirnov, A., Villevalde, Y., O'Neill, T. N., Royer, A., Tarussov, A. (1995). *Aerosol optical depth over the oceans: analysis in terms of synoptic air mass types*. J. Geophys. Res. 100: 16,639-16,650.

Zielinski T. (2004). *Studies of aerosol physical properties in coastal areas*. Aerosol Sci.&Tech., 38: 513-524.

## Model-predicted and satellite-derived aerosol optical properties in East Asia

Chul H. Song<sup>1</sup>, Yoojin Lee<sup>1</sup>, Jin Y. Kim<sup>2</sup>, Young J. Kim<sup>1</sup>, Kwon H. Lee<sup>1</sup>

<sup>1</sup>Department of Environmental Science and Engineering, Gwangju Institute of Science and Technology (GIST), 500-712, Gwangju, Korea

<sup>2</sup>Hazardous Substance Research Center, Korea Institute of Science and Technology (KIST), 136-791, Seoul, Korea

Keywords: aerosol optical depth, 3D chemistry-transport model, MODIS, CMAQ model

Spatial and seasonal distributions of Aerosol Index (AI) from the Total Ozone Mapping Spectrometer (TOMS) and Aerosol Optical Depth (AOD,  $\tau$ ) from the Moderate Resolution Imaging Spectroradiometer (MODIS) were compared with those of model-derived  $\tau$  and aerosol column loading for four different episodes in East Asia. In order to simulate  $\tau$  for major types of aerosols in the atmosphere, US EPA Models-3/CMAQ v4.3 model was employed together with the PSU/NCAR MM5 meteorological model and ACE-Asia/TRACE-P official emission inventory for East Asia. Firstly, a comparison study of CMAQ-derived aerosol column loading with TOMS AI was performed, since TOMS AI is a good indicator of UV absorbing particles typically transported through the free troposphere such as black carbon and mineral dust. The model-predicted high aerosol column loading mostly composed of mineral dust during the spring episode concurrently occurred with high TOMS AI over Manchuria and northern part of Korean peninsula where the dust storm had erupted and then transported. Secondly, MODIS-derived  $\tau$  ( $\tau_{\text{MODIS}}$ ) was retrieved, using the Bremen Aerosol Retrieval (BAER) algorithm, and CMAQ-derived  $\tau$  ( $\tau_{\text{CMAQ}}$ ) was also estimated, using a reconstructed extinction-coefficient based method from the mass concentrations of particulate species. In general, both  $\tau_{\text{MODIS}}$  and  $\tau_{\text{CMAQ}}$  showed high values around Chinese urban/industrial centers, such as Sichuan Basins (Chengdu / Chongqing), Bohai Bay (Beijing/Tianjin), and Yangzi Delta (Shanghai/Nanjing/ Hangzhou) regions and also around agricultural and livestock farming areas. For the four season episodes selected in this study, the CMAQ model generated similar levels of  $\tau_{\text{CMAQ}}$  to those of  $\tau_{\text{MODIS}}$  throughout the domain with relative differences ranging between -15% (spring episode) and 10% (summer episode). In particular, during the spring episode  $\tau_{\text{CMAQ}}$  was under-predicted compared to  $\tau_{\text{MODIS}}$  over the areas where a dust storm passed through. This could be due to the fact that the extinction-coefficient calculations employed in this

study has a tendency to be more or less insensitive to the coarse-mode dust concentrations. Except for the spring episode the levels of  $\tau_{\text{CMAQ}}$  is in general comparable to or slightly higher than those of  $\tau_{\text{MODIS}}$ . During the summer episode both high  $\tau_{\text{MODIS}}$  and  $\tau_{\text{CMAQ}}$  are related to high concentrations of  $(\text{NH}_4)_2\text{SO}_4$  produced over the Chinese urban/industrial centers. In contrast, during the winter episode high  $\tau_{\text{MODIS}}$  and  $\tau_{\text{CMAQ}}$  appear to be related to possibly over-predicted  $\text{NH}_4\text{NO}_3$  concentrations over Chinese agricultural and livestock farming areas. In future analysis, the accuracy of both  $\tau_{\text{CMAQ}}$  and  $\tau_{\text{MODIS}}$  will be further evaluated by the comparisons with different types of  $\tau$ , such as  $\tau$  estimated from Mie-theory based parametric approximation and  $\tau_{\text{AERONET}}$  obtained from Sun photometer network in East Asia like AERONET (or Sky Radiometer networks).

The authors gratefully acknowledge the financial support provided by a project from ADEMRC (Advanced Environmental Monitoring Research Center, NN02412).

Chin, M., P. Ginoux, S. Kinne, O. Torres, B. N. Holben, B. N. Buncan, R. V. Martin, J. A. Logan, A. Higurashi, and T. Nakajima (2002), *J. Atmos. Sci.*, 59, 461-483.

Chin, M., A. Chu, R. Levy, L. Remer, Y. Kaufman, B. Holben, T. Eck, P. Ginoux, and Q. Gao (2004), *J. Geophys. Res.*, 109 (D23S90), doi:10.1029/2004JD004829.

von Hoyningen-Huene W., M.F., and J. B. Burrows (2003), *J. Geophys. Res.*, 108(D9), doi: 10.1029/2001JD002018.

## Seasonal variability of vertical profiles of the single scattering albedo of submicron aerosol

V.S. Kozlov and M.V. Panchenko

Institute of Atmospheric Optics SB RAS, 1, Academicheskii ave., 634055, Tomsk, Russia

Keywords: tropospheric aerosols, submicron particles, Black carbon, mass concentration, single scattering albedo.

Improvement of radiative-climatic models for cloudless atmosphere significantly depends on correct modeling of the single scattering albedo of submicron aerosol. Solution of this problem requires carrying out detailed investigations of the aerosol absorption characteristics in the troposphere.

Measurements of the directed aerosol scattering coefficient of the dry matter of submicron particles at the angle of  $45^\circ$  at the wavelength of  $0.51 \mu\text{m}$  and the mass concentration of Black carbon (BC) were carried out in 1999-2006 from onboard the AN-30 "Optic-E" aircraft-laboratory. Measurements were carried out at the south of Novosibirsk region. The 3-hour long flights were performed once a month in the daylight time. Main attention in analysis were paid for measurements at horizontal flights at the heights of 0.5, 1.0, 1.5, 2.0, 3.0, 4.0, 5.5 and 7.0 km.

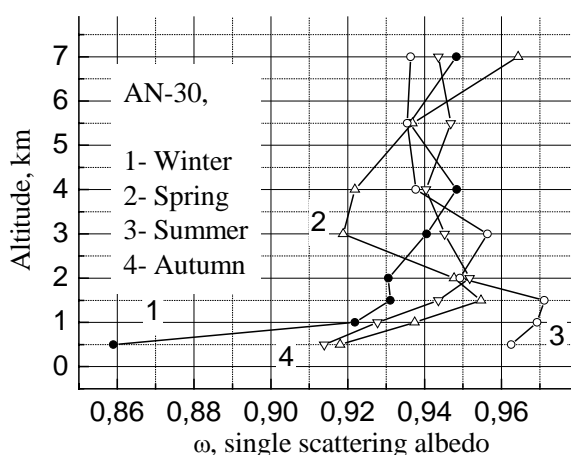


Figure 1. Seasonal mean vertical profiles of the single scattering albedo  $\omega$  of the dry matter of submicron aerosol (West Siberia, 1999-2006).

Vertical profiles of the black carbon fraction  $P$ , single scattering albedo  $\omega$  and the absorption index of the particulate matter  $\chi$  were estimated from the data on the directed aerosol scattering coefficient and the mass concentration of black carbon.

It is revealed that in autumn and winter the concentration of black carbon at the heights lower than 1-1.5 km decreases with height much faster than the aerosol mass concentration. Above 1.5 km the differences in the gradients are small. Variations of

the gradients at all heights in spring and summer are comparable.

Analysis of the data enabled to reveal that the near-ground layer up to the height of 1-1.5 km and the layer above 1.5 km have qualitatively different peculiarities of the vertical and seasonal variability of the absorption properties of submicron aerosol.

The black carbon fraction in autumn and winter in the lower layer varies strongly, decreasing with height from 13 to 4%. The range of variations of  $P$  in the upper layer is small in all seasons: 2-5%. Seasonal and vertical dynamics of  $P$  leads to the changes of the single scattering albedo (Fig. 1) and the absorption index of the particulate matter (Fig. 2). The values of the single scattering albedo of the dry matter of submicron particles in the layer up to 1.5 km in winter vary in the limits 0.86 - 0.93.

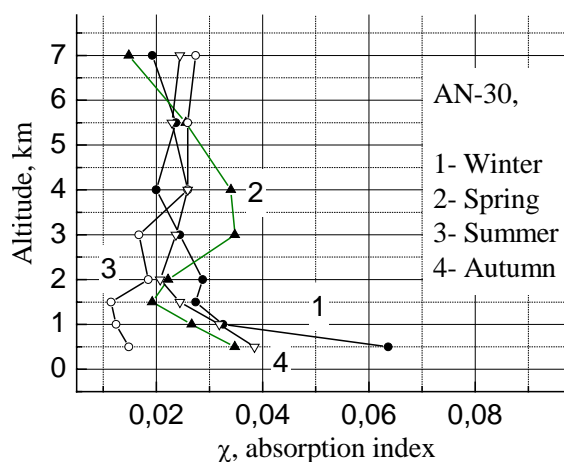


Figure 2. Seasonal mean vertical profiles of the absorption index  $\chi$  of the dry matter of submicron aerosol (West Siberia, 1999-2006).

The range of variations of the albedo in warm seasons becomes narrower: 0.92 - 0.97. It is seen in Fig. 2 that aerosol is the most absorbing in winter at the heights up to 1.5 km: the values of the effective absorption index are 0.03 - 0.065. However, particles at the heights above 1.5 km in all seasons have comparably weak absorption  $\chi \leq 0.03$ .

The work was supported by Russian Foundation for Basic Researches (grant No. 06-05-64393).

## Refractive index measurements of size separated aerosol particles with a polar nephelometer

F.Prodi<sup>1,2</sup>, G.Santachiara<sup>1</sup>, L.Di Matteo<sup>1</sup>, F.Belosi<sup>1</sup> and M.R.Perrone<sup>3</sup>

<sup>1</sup>Institute ISAC-CNR, Bologna, Italy

<sup>2</sup>Physics Department, University of Ferrara, Italy

<sup>3</sup>Physics Department, University of Lecce, Italy

Keywords: Refractive Index, Light Scattering, Light Absorption, Optical Properties.

Aerosol particles affect the radiative balance of the Earth-atmosphere system directly because they scatter and absorb radiation, and indirectly because they act as condensation and ice nuclei, thus modifying the radiative properties and lifetime of clouds.

The absorption of radiation by particles causes local heating of the atmosphere, while the backscattering of solar radiation to space may cause a cooling of the Earth-atmosphere system.

Therefore, the knowledge of the radiative properties of aerosol, in particular the complex refractive index of aerosol particles, is of great importance for environmental purposes. This parameter, defined as  $n = n_r - in_i$  ( $n_r$  is the real part responsible for scattering,  $n_i$  the imaginary part responsible for absorption), depends on the chemical composition and the wavelength of the incident radiation.

There are many methods that allow the measurements of the refractive index: combined use of satellite and surface observations, and an inversion algorithm based on measurements of direct Sun radiation and diffuse sky radiance. Such techniques evaluate the average values of the complex refractive index of aerosol in the columnar atmosphere, while laboratory measurements allow the calculations of values of  $n$  for specific compounds.

We followed a procedure which allows the examination of atmospheric aerosol sampled on a filter (Mennella and Prodi, 1993).

During a field campaign performed in southern Italy (Lecce, 2005) atmospheric aerosol was sampled with INSPEC, an inertial spectrometer which allows the collection on a filter of particles separated according to their aerodynamic diameter (V. Prodi et al., 1979). The refractive index measurements were performed using the following light scattering technique:

a) Each membrane filter was cut, and one half was examined under SEM in order to measure the geometric particle diameter. The chemical analysis of single particles, permitted by this technique, was not made.

b) The remaining half was treated with acetone vapours. This treatment makes the filter transparent and permits measurements of scattering by particles on the filter.

c) The He-Ne laser ( $\lambda = 632 \text{ nm}$ ;  $P = 20 \text{ mW}$ ) has a spot of about  $1.5 \text{ mm}$ , which illuminates zones of the filter

containing particles which were shown by the SEM analysis to be monodisperse.

d) The polarized plane of the incident light was set perpendicular to the scattering plane and the measurements of the forward light scattered were performed in a range between  $30^\circ$  and  $60^\circ$ .

e) The analysis of scattering data requires a single and independent scattering by particles, considered as spheres and the computation of the Mie scattering coefficient. In order to obtain the complex refractive index, a function (called  $\chi^2$ ) had to be minimized in the  $(n_r, n_i)$  space.

The experimental set-up of the nephelometer is shown in Fig. 1.

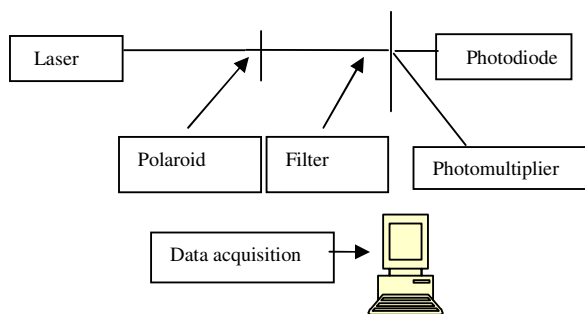


Fig.1 –A schematic of the apparatus used for the measurements of angular light scattering properties of the aerosol

Calibration of the nephelometer was done using sodium chloride and polystyrene latex particles captured on filters and treated with acetone.

Values of refractive index obtained show variation of both the real and imaginary part of aerosol sampled in different zones of the same filter, thus indicating a variation in the chemical composition for particles with different diameter. An event of dust particle originating from Sahara has been examined.

Mennella, A. & Prodi F. (1993) *Pure Appl.Optics*, 2, 471-488.

Prodi V. et al.(1979) *J.Aerosol Science*, 101, 411-419.

## **Aerosol optical properties measurements from two Chinese megacities, Beijing and Guangzhou**

RM Garland<sup>1</sup>, H Yang<sup>1</sup>, O Schmid<sup>2</sup>, D Rose<sup>1</sup>, SS Gunthe<sup>1</sup>, M Hu<sup>3</sup>, M Shao<sup>3</sup>, L Zeng<sup>3</sup>, Y Zhang<sup>3</sup>, T Zhu<sup>3</sup>, MO Andreae<sup>1</sup> and U Pöschl<sup>1</sup>

<sup>1</sup> Max Planck Institute for Chemistry, Department of Biogeochemistry, Mainz, Germany

<sup>2</sup> GSF-National Research Center for Environment and Health, Institute for Inhalation Biology, Neuherberg/Munich, Germany

<sup>3</sup> College of Environmental Sciences, Peking University, Beijing, China

Keywords: optical properties, field measurements, megacity

The extinction of solar radiation by aerosol particles is of great importance for the Earth's radiative balance and climate. The optical properties of atmospheric aerosols are, however, highly variable and not well characterized. In this study, aerosol optical properties were measured in two locations in China. The first site was in a rural area approximately 60 km northwest of the megacity Guangzhou in south China and was part of the "Program of Regional Integrated Experiments of Air Quality over the Pearl River Delta" intensive campaign in July 2006 (PRIDE-PRD2006). The second site was a suburban site approximately 40 km south of Beijing and was part of "Campaigns of Air Quality Research in Beijing" (CAREBeijing-2006) in August 2006.

Prior to the aerosol optical measurements, the sampled air was dried to below 40% RH (generally 20-40 % RH). Three instruments were used to measure light absorption and scattering by aerosol particles. Aerosol scattering coefficients at 450 nm, 550 nm, and 700 nm were determined with a TSI three-wavelength nephelometer. Aerosol absorption coefficients were measured with a DRI Photoacoustic Spectrometer in situ at 532 nm and with a Carusso/MAAP instrument on a glass fiber filter tape at 670 nm.

In both 30-day measurement campaigns, a variety of different types of air masses and meteorological conditions were encountered. In PRIDE-PRD2006 this included high pollution events from local biomass burning. Compared to the Guangzhou optical data, the trends in Beijing were less episodic, with lower maximum values, but higher average values.

In PRIDE-PRD2006 the average scattering coefficient (550 nm) was  $199 \text{ Mm}^{-1}$  and the maximum was  $1900 \text{ Mm}^{-1}$ . Comparatively, the average scattering coefficient (550 nm) for CAREBeijing was  $333 \text{ Mm}^{-1}$  and the maximum was  $1440 \text{ Mm}^{-1}$ . Similar trends were noted for black

carbon concentration and aerosol absorption coefficient.

The average single scattering albedo for both campaigns was  $\sim 0.83$  (at 532 nm); however, there were many instances where significantly lower single scattering albedo values were measured (as low as  $\sim 0.6$ ). In PRIDE-PRD2006, diurnal cycles of single scattering albedo and Angstrom exponents were observed. Both parameters showed a minimum value, 0.79 for single scattering albedo and 1.39 for the Angstrom exponent, in the early morning ( $\sim 6:00$ ).

These measurement results suggest that the local aerosol emissions may have a large impact on the radiative balance of both the Pearl River Delta and Beijing region.

## **“Preliminary estimations of Aerosol Optical Depth (AOD) over Spain obtained from the INM CIMEL sun-photometers measurements”**

M. D. Gil<sup>1</sup>, B. Navascúes<sup>1</sup>, M. López<sup>1</sup>, A. Cansado<sup>1</sup>, M. Antón<sup>2</sup>, M. L. Cancillo<sup>2</sup>

<sup>1</sup>Área de Proyectos. Subdirección de Climatología y Aplicaciones  
Instituto Nacional de Meteorología. Madrid. Spain

<sup>2</sup>Departamento de Física. Universidad de Extremadura. Badajoz. Spain

Keywords: aerosol, AOD, CIMEL

The Spanish National Meteorological Service, Instituto Nacional de Meteorología (INM), has recently deployed a CIMEL sun-photometer national network over Spain with instruments located at La Coruña, Madrid, Murcia, Palma de Mallorca and Zaragoza.

Aerosol measurements are performed with three types of CIMEL sun photometers measuring at least at the four nominal aerosols wavelengths 440 nm, 670 nm, 870 nm and 1020 nm.

A software package has been developed at INM to automatically collect the raw counts from each station, retrieve the Aerosol Optical Depth (AOD), perform quality control and archive both the raw and processed data on the computing facilities at the INM headquarters in Madrid.

As part of the data processing the Angström exponent is calculated using the cloud free AOD at 440, 500, 670 and 870 nm.

The developed processing system is now being updated to include daily estimations of the extraterrestrial constant (ETC) for each instrument by using Langley plot method.

A cloud-screening procedure is routinely applied to raw AOD values following the AERONET algorithm (Smirnov et al., 2000).

The retrieval and quality control software developed has been validated against 1.5 level AOD data from AERONET at the Caceres station, owned by the Extremadura University and belonging to the AERONET network.

The poster presented describes the data processing, including the algorithm developed to derive the AOD and Angstrom parameter, and the quality control procedure.

In order to complement AOD estimations over the Iberian Peninsula, FLEXTRA model has been installed on INM computers and backward trajectories are calculated at the network stations on a daily basis, making use of the 6-hour analysis fields from the INM NWP operational system, HIRLAM.

In this work we also present the preliminary results obtained since the beginning of August 2006.

## The angle-dependent light scattering by soot-water drop agglomerates

S.S. Vlasenko<sup>1</sup>, E.F. Mikhailov<sup>1</sup> and M.Yu. Igonin<sup>1</sup>

<sup>1</sup>Atmospheric Physics Department, Research Institute of Physics, St.Petersburg State University, Peterhof, 198904, St.Petersburg, Russia

Keywords: Soot particles, optical properties, hygroscopicity.

It has become evident over the last decade that absorbing aerosols play a crucial role in impacting global and regional climate. Soot-containing aerosol is known to be one of the largest contributors to aerosol absorption in the atmosphere, but its radiative properties reveal a great deal of variability resulting from diversity of morphology, mixture state and affinity to water vapour. The last property determines the hygroscopic growth of aerosol particles and their interaction with water droplets. These processes account for aerosol scattering dependence on relative humidity in the atmosphere. The dependence shows up both in variation of aerosol volumetric scattering coefficient and in redistribution of scattering energy within scattering angles. The first item has been already dealt with in (Mikhailov *et al.*, 2006), the last one, i.e. change of the soot aerosol scattering phase function due to soot - water interaction, is the subject of present work.

Soot particles are generated with a diffusion acetylene burner. The fresh soot particles are hydrophobic. When required the affinity of particles to vapour is further modified by condensing glutaric acid at the the surface of the particles in a ring gap-mixing nozzle. An adsorption of glutaric acid by the soot surface transforms the particles from hydrophobic to hydrophilic. The water droplets are produced by nebulizer. The aerosol scattering is measured by polar nephelometer with 535 nm diode laser as light source and photomultiplier as detector.

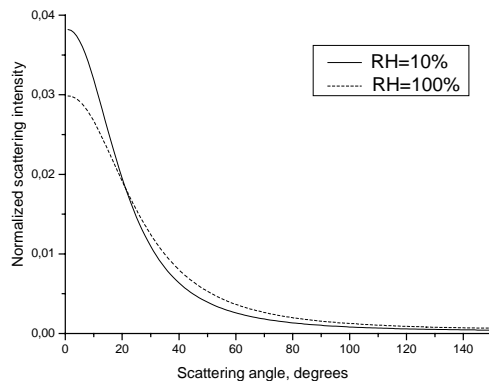


Figure 1. Phase function for hydrophilic soot.

The scattering phase function was measured for both hydrophilic and hydrophobic soot particles in dry (RH 10%) and humid (RH 100%) conditions. It has been found that covering of hydrophilic soot particles with water shell in the humid atmosphere resulted in redistribution of scattering radiation from small angles to larger (fig.1). In case of hydrophobic soot there was no difference in phase functions for dry and humid conditions.

The light scattering by soot particles + water droplets systems is revealed to be not additive. There is a difference between measured scattering signal for soot-droplets mixture and sum of scattering signals for soot and droplets individually (fig.2). The concentration of soot particles and water droplets remains constant during the measurements.

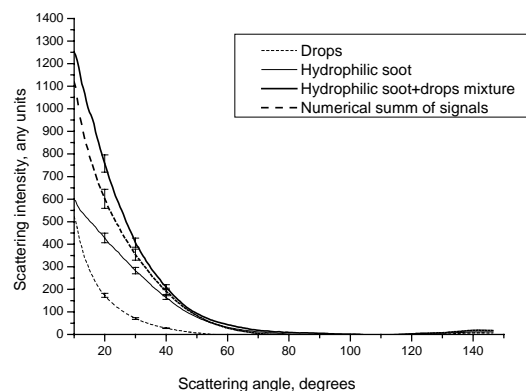


Figure 2. Phase function for soot-drops mixture.

The measured non-additivity is most likely to be attributable to coagulation of soot particles with water droplets

This work was supported by Russian Fund for Basic Research grants 05-05-64756, 06-05-65155.

Mikhailov, E.F., S.S.Vlasenko, I.A.Podgorny, V.Ramanathan, and C.E.Corrigan (2006) Optical properties of soot-water drop agglomerates: An experimental study, *J.Geophys.Res.*, *111*, D07209, doi:10.1029/2005JD006389.

## Measurement of the Optical and Physical Properties of Light-duty and Heavy-Duty Vehicle Particulate Emissions

AW. Strawa<sup>a</sup>, AG. Hallar<sup>b</sup>, TW. Kirchstetter<sup>c</sup>, GA. Ban-Weiss<sup>d</sup>, JP. McLaughlin<sup>e</sup>, RA. Harley<sup>d</sup>, MM. Munden<sup>c</sup>, AJ. Kean<sup>f</sup>, ED. Stevenson<sup>g</sup> and GR. Kendall<sup>g</sup>

<sup>a</sup>NASA-Ames Research Center, Moffett Field, CA 94035

<sup>b</sup>Desert Research Institute, Storm Peak Laboratory, Steamboat Spring, CO 80488

<sup>c</sup>Lawrence Berkeley National Laboratory, Atmospheric Science Dept., Berkeley, CA 94720

<sup>d</sup>University of California, Dept. of Mechanical Engineering, Berkeley, CA 94720

<sup>e</sup>University of California, Dept. of Civil & Environmental Engineering, Berkeley, CA 94720

<sup>f</sup>California Polytechnic State University, Dept. of Mechanical Engineering, San Luis Obispo, CA 93407

<sup>g</sup>Bay Area Air Quality Management District, Technical Services Division, 939 Ellis St., San Francisco, CA 94109

Keywords: Absorption Coefficient, Atmospheric Aerosol, Black Carbon, Vehicle Emissions, Diesel soot particles, Size Distribution

This paper discusses the measurement of climate relevant physical and optical properties of aerosols emitted from motor vehicles during the summer of 2004 and 2006 at the Caldecott Tunnel in the San Francisco Bay Area. Measurements were made in two separate traffic bores: one carrying only light-duty (LD) vehicles and the other carrying a mix of LD vehicles and heavy-duty (HD) diesel trucks. A unique instrument that uses cavity ring-down (CRD) techniques and a reciprocal nephelometer to simultaneously measure the aerosol extinction and scattering coefficients, respectively, facilitated calculation of the aerosol absorption coefficient and single scattering albedo. These quantities are important in determining the radiative forcing of aerosols on climate. Aerosol size distributions were measured with a TSI scanning differential mobility spectrometer. In addition, real-time measurements of ultrafine particle number, black carbon (BC), CO, CO<sub>2</sub>, and NO<sub>x</sub> concentrations and time-integrated measurements of PM<sub>2.5</sub>, EC, and OC mass concentrations were made.

As expected, the aerosol in the tunnel was dominated by fresh black carbon emissions in the accumulation mode. This paper will compare climate relevant properties (aerosol single scattering albedo, BC mass absorption efficiency, and the effect of relative humidity on the aerosol optical coefficients (*fRH*)) of LD and HD vehicle aerosol emission, including the aerosol absorption emission factor, which is derived by normalizing absorption to fuel consumption using measured CO and CO<sub>2</sub> levels inside the tunnel. Measured values will be compared to those reported in emission inventories, used in climate models, and measured in other field campaigns.

The measured particle size distributions show three modes: a nucleation mode due to the condensation of volatile exhaust gas, an accumulation mode composed of soot aggregates, and a larger mode of

modal diameter of about 600 nm, whose origin is unknown at present. The nucleation mode measured in these experiments is not as high as previous measurements in the Caldecott Tunnel (Geller et al., 2005) or in other tunnels, e.g. Plabutsch and Kingsway Tunnel (Imhof et al., ACP, 2006).

Average Mass Absorption Efficiencies (MAE) are determined to be at the low end of typically reported values. This is fresh emission, however. The Mass Absorption Efficiency will likely increase as the aerosols age and scattering material condenses on the BC as discussed in Bond et al. (2006).

Table 1. Comparison of Mass absorption Efficiencies.

Bore	Abs. Coef. Mm <sup>-1</sup>	BC μg-m <sup>-3</sup>	MAE m <sup>2</sup> -g <sup>-1</sup>
Mixed	241	44.5	5.4
D	103	14	7.3

Table 2. Diesel Emission Factors by Integration Method.

Abs. Coef Mm-1	NO <sub>x</sub> EF g-kg fuel-1	Abs EF Mm-1-kg fuel-1
1312	54.3	58.9

This work was supported by the NASA Radiation Sciences Program.

Geller, M.D., et al., (2005) Environ. Sci. Technol., 39, 8653-8663.

Imhof, D., et al., (2006) Atmos. Chem. Phys. 6, 2215-2230.

Bond, T.C., et al., (2006) J. Geophys. Res., 111, D20211.

## The Estimation of Light Scattering Coefficient of Atmospheric Aerosols Using Source Area Analysis for Particle Size Distributions

P. Kolmonen<sup>1</sup>, V. Aaltonen<sup>1</sup>, J. Hatakka<sup>1</sup>, A. Hyvärinen<sup>1</sup>, T. Kaurila<sup>2</sup>, K. E. J. Lehtinen<sup>3</sup>, H. Lihavainen<sup>1</sup>

<sup>1</sup>Finnish Meteorological Institute, P.O. Box 503, 00101, Helsinki, Finland

<sup>2</sup>Defence Forces Technical Research Centre, P.O. Box 5, 34111 Lakiala, Finland

<sup>3</sup>Finnish Meteorological Institute, P.O. Box 1627, 70211 Kuopio, Finland

Keywords: light scattering, optical properties, aerosol size distribution, source identification, trajectory.

Quantitative knowledge of optical properties of atmospheric aerosols is vital for air and sea traffic. The most important property for these needs is the horizontal visibility. In addition, some measurement devices, such as laser based techniques, require the knowledge of the optical properties for reliable results. The forecasting of the optical properties enables e.g. low visibility warnings.

Here, we present a method to estimate the light scattering coefficient of atmospheric aerosols. The coefficient serves as an example of the optical properties of the aerosols. The development of the estimation method is based on an assumption that the path that air mass follows has a sizable effect on the observed aerosol size distribution. The size distribution can then be used for the determination of the light scattering coefficient. To track the air mass, backward trajectories were used. They were computed using the FLEXTRA model (Stohl *et al.*, 1995).

The used source analysis method is described in Kolmonen *et al.* (2006). Briefly: trajectories and their corresponding measured size distributions are used to form a linear model of source areas where a measured size distribution is a linear combination of size distributions of the areas where the corresponding trajectory has passed. The inversion of this model is first used to determine size distributions of the areas. Then, the model can be applied to any trajectory which is based on analyzed or forecasted meteorological data. The source area analysis has been previously used for tracking of certain aerosol particles (Asbaugh, 1983; Stohl, 1996); the novelty here is that the size distributions of aerosols are used.

Previously, using aerosol size distributions that were determined by the above described method, the estimations of the light scattering coefficient were not satisfactory. The time series comparison of the estimated and correct coefficients showed quite good temporal agreement but the amplitude of the estimated coefficient was too small.

Here, to enhance the results, we have not modified the source area method, but brought more data to the model. Previously, the source areas were determined using measured size distributions and computed trajectories for Pallas measurement site in Northern Finland. The data in the model can, however, include arbitrary number of measurement

sites. We have utilized this by using data from two Finnish measurement sites: the previously used Pallas and the Southern Finland situated Utö.

Figure 1 shows the estimated and correct light scattering coefficients during autumn 2003 at Pallas. As can be seen, the agreement is quite good.

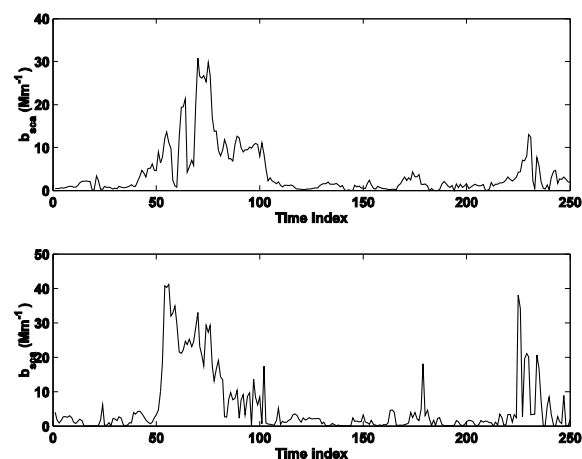


Figure 1. Time series of the light scattering coefficient at 550 nm during autumn 2003 at Pallas. Higher panel: The coefficient determined from the measured aerosol size distributions. Lower panel: The coefficient determined from the estimated aerosol size distributions.

This work was supported by the MATINE project: The effect of aerosol optical properties on the light propagation in the atmosphere.

Ashbaugh, L. L. (1983). *J. Air Pollut. Control Assoc.*, 33, 1096-1098.

Kolmonen, P., and Lihavainen, H. (2006). *Proc. of the NOSA 2006 Aerosol symposium, Helsinki* (Finnish association for aerosol research, Helsinki), 153-154.

Stohl, A., Wotawa, G., Seibert, P., and Kromp-Kolb, H. (1995). *J. Appl. Meteor.*, 34, 2149-2165.

Stohl, A. (1996). *Atmos. Environ.*, 30, 579-587.

## Aerosol refractive index and extinction coefficient calculated from chemical data

D. Benkő<sup>1</sup>, A. Molnár<sup>2</sup> and K. Imre<sup>1</sup>

<sup>1</sup>Department of Earth and Environmental Sciences, University of Pannonia, H-8201 Veszprém, Hungary

<sup>2</sup>Air Chemistry Group of the Hungarian Academy of Sciences, H-8201 Veszprém, Hungary

Keywords: refractive index, volume mixing rule, size distribution, hygroscopic growth, extinction coefficient

Aerosol particles take important part in the control of the short wave radiation balance of the atmosphere. This interaction results in scattering and absorption of the light by the aerosol. The effect of aerosol particles on the radiation transfer depends on their size and chemical composition, i.e. the refractive index. Hygroscopicity of the particles can modify both aerosol parameters. Owing to water uptake, particle size can increase significantly, and the absorbed water can also change the refractive index of the aerosol. In climate forcing estimations, the enlargement of the particles are generally considered, while the variation of the refractive index as the function of the size and the hygroscopicity is not usually involved. The aim of this work is to present our results on the size distribution of refractive index, and to show the effect of hygroscopic growth on the refractive index. We also show comparison between the scattering and absorption coefficients calculated from refractive index data and those of measured directly.

Ambient aerosol samples were taken at K-puszta, in rural Hungary by means of electric low pressure (ELPI) and Berner impactors in 8 size ranges from 31 nm up to 1.7 µm and from 62nm up to 16 µm, respectively. The particles were collected on aluminium foils. First the dry mass -and in case of the Berner samples- the mass growth of the samples was determined by applying gravimetric method. The samples were measured in an isolated box where the relative humidity was adjusted by saturated solutions of different inorganic salts, silica gel and water. Then the samples were chemically analyzed. The amount of the total organic carbon was measured by a TOC solid analyzer, the ion concentrations ( $\text{NH}_4^+$ ,  $\text{K}^+$ ,  $\text{Ca}^{2+}$ ,  $\text{Na}^+$ ,  $\text{Mg}^{2+}$ ,  $\text{Cl}^-$ ,  $\text{SO}_4^{2-}$ ,  $\text{NO}_3^-$ ) by capillary electrophoresis.

In the estimation of the complex refractive index first the mass closure of the size selected aerosol was established. The concentrations of the main inorganic compounds were estimated by applying stoichiometry. The total carbon concentrations were differentiated to EC (10% of TC mass), HULIS (35%) and the rest of TC was considered as non-absorbing organic carbon (Kiss et al., 2002). We also assumed that the missing mass in the balance is  $\text{SiO}_2$ . Then, the refractive indices of different compounds were regarded. On

the basis of these two data sets the complex refractive indices of the dry aerosol were estimated applying volume mixing rule (Horvath, 1998). In case of Berner samples considering the amount of absorbed water, the refractive index was recalculated. Scattering and absorption efficiency values were calculated with the application of the Mie-theory (Reist, P.C., 2000). Scattering and absorption coefficients were determined applying number concentrations measured by ELPI. For comparison we also measured directly scattering and absorption coefficient values by means of a nephelometer and PSAP respectively.

Our results show that:

- In the optically active size range (0.1-1 µm) the real part of the refractive index increases with the particle size from 1.499 to 1.527 according to ELPI samples. For Berner samples the increasing tendency is the same.
- In the optically active range there is a significant decrease in the imaginary refractive index, its value falls from 0.025 to 0.008, and has a local minimum around particle diameter of 1 µm.
- Water uptake decreases the refractive index of the particles, by 4% at 85% RH compared to the dry aerosol. Moreover, changes in the size distribution can also be observed.
- It makes a considerable difference regarding extinction coefficient if we don't take into account the size distribution of the refractive index.
- As our preliminary results show the difference between calculated and measured absorption coefficients is 26% on average. This relation is worse in case of scattering coefficient.

This work was supported by the Hungarian Research Fund (OTKA, project numbers TS 40903 T 047222).

Kiss, G., Varga, B., Galambos, I., Ganszky, I.: Characterization of water soluble organic matter isolated from atmospheric fine aerosol, *Journal of Geophysical Research*, 107(D21),8339, doi:10.1029/2001JD000603, 2002.

Horvath, H.: Influence of atmospheric aerosols upon the global radiation balance. Atmospheric Particles IUPAC Series on Analytical and Physical Chemistry of Environmental Systems, *John Wiley, New York*, vol. 5, 543-596, 1998.

Reist, P.C., 2000. PC Mie Program (version 3.13)

## Ambient single scattering albedo at the high alpine site Jungfraujoch

M. Collaud Coen<sup>1</sup>, E. Weingartner<sup>2</sup>, R. Nessler<sup>2</sup> and U. Baltensperger<sup>2</sup>

<sup>1</sup>MeteoSwiss, CH-1530 Payerne, Switzerland

<sup>2</sup>laboratory of Atmospheric Chemistry, Paul Scherrer Institut, CH-5232 Villigen, Switzerland

Keywords: Single scattering albedo, tropospheric aerosol, absorption coefficient, atmospheric aerosol, long-term trend.

Continuous measurements of aerosol optical properties have been performed since 1995 at the high alpine research station Jungfraujoch (JFJ) situated at 3580 m asl. The JFJ is prevalently situated in the free troposphere (FT), but is often influenced by thermal convection of planetary boundary layer (PB) air during the warmer months. Consequently all measured aerosol parameters show a clear annual cycle with maximum values in summer and minimum values in winter. The JFJ is therefore well suited to measure the background aerosol above a continental area.

Due to the hard weather conditions, the inlet is heated and the measured optical properties relate therefore to dry aerosol. Nessler *et al.* (2005a and b) gave an RH correction for the scattering and backscattering coefficients and showed that the correction of the absorption coefficient for ambient humidity can be neglected for the calculation of the single scattering albedo (SSA). Taking into account the ambient relative humidity at the JFJ, these corrections were applied to obtain ambient scattering and backscattering coefficients. The absorption coefficient measured by the multiwavelength aethalometer was corrected for the shadowing effect and for the scattering offset according to Arnott *et al.* (2005) and Schmid *et al.* (2006):

$$B_{abs,n} = \frac{SG BC_n - \alpha B_{scat,n}}{C R} \quad (1)$$

where  $SG(\lambda)$  is the multiplying factor used by the manufacturer,  $BC$  is the measured black carbon concentration,  $\alpha(\lambda)$  depends on the scattering exponent and the filter properties,  $C(\lambda)$  depends on the SSA and on a  $C_{ref}$  value, and  $R(\lambda)$  depends on the filter loading, the flow rate, the spot area and filter properties. Since April 2003, a MAAP (Multiangle Absorption Photometer) has also been used to measure the absorption coefficient at the JFJ.  $C_{ref}$  value was therefore determined from Weingartner *et al.* (2003), taking the MAAP as reference.

The RH correction has a greater impact on the SSA than the aethalometer correction. With both corrections the 5-year means of the SSA vary between 0.943 and 0.916 depending on the wavelength.

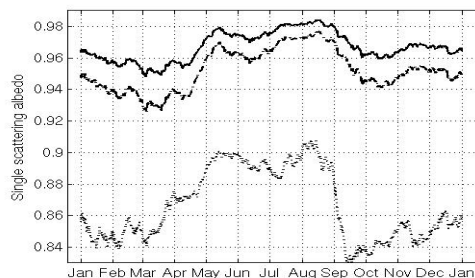


Figure 1. SSA seasonal cycle for dry condition (.-.), with RH correction(--), and with both RH and aethalometer corrections (full line).

Even if the cycle amplitude is smaller, the corrected seasonal cycle becomes clearer, the SSA being highest with the maximum PB influence from May to August, and lowest at the end of February, the coldest month. A diurnal cycle of the SSA is clearly visible only in spring, when the FT or PB influence is well defined. A trend analysis with the seasonal Kendall method and with a least-mean square fit will be performed on the SSA and all other corrected parameters.

Table 1. Five years mean, 10 and 90 percentiles of SSA (nephelometer  $B_{scat}$  values were extrapolated to the aethalometer wavelengths).

$\lambda$ nm	370	520	660	950
10 percentile	0.888	0.876	0.855	0.809
Mean SSA	0.943	0.939	0.932	0.916
90 percentile	0.992	0.992	0.992	0.993

Arnott, W.P., Hamasha, K., Mossm ller, H., Sheridan, P.J., and Ogren, J.A. (2005), *Aerosol Sci. Technol.*, 39, 17-29.

Nessler, R., Weingartner, E., and Baltensperger, U. (2005), *Environ. Sci. Technol.*, 39, 2219-2228.

Nessler, R., Weingartner, E., and Baltensperger, U. (2005), *J. Aerosol Sci.*, 36,958-972.

Schmid, O., et al., (2006), *Atmos. Chem. Phys.*, 6, 3443-3462.

Weingartner, E., Saathoff, H., Schnaiter, M., Streit, N., Bitnar, B., and Baltensperger, U. (2003), *Aerosol Sci.*, 34, 1445-1463.

## Comparison of surface and satellite derived aerosol optical depth measurements in Finland

T. Mielonen<sup>1</sup>, A. Arola<sup>1</sup>, P. Kolmonen<sup>2</sup>, H. Lihavainen<sup>2</sup>, T. Kaurila<sup>3</sup>, E. Parmes<sup>4</sup> and K. E. J. Lehtinen<sup>1,5</sup>

<sup>1</sup>Finnish Meteorological Institute, Kuopio Unit, P.O. Box 1627, FIN-70211, Kuopio, Finland

<sup>2</sup>Finnish Meteorological Institute, P. O. Box 503, FIN-00101, Helsinki, Finland

<sup>3</sup>Finnish Defence Forces Technical Research Centre, P.O. Box 5, FIN-34111, Lakiala, Finland

<sup>4</sup>VTT Technical Research Centre of Finland, P.O. Box 1000, FIN-02044, Espoo, Finland

<sup>5</sup>Department of Physics, University of Kuopio, P.O. Box 1627, FIN-70211, Kuopio, Finland

Keywords: Atmospheric aerosols, Remote sensing, Optical depth, Light extinction, Measurements.

When the reflectance of the ground is evaluated from satellite measurements, it is extremely important to know the contribution of the atmosphere, since satellites measure the backscattered radiance from the surface-atmosphere system. Attenuation of radiation in the atmosphere deteriorates the quality of satellite images of land surfaces, thus the effect of atmosphere has to be removed from the data. The effect of aerosols is especially challenging to estimate due to their large spatial and temporal variability. Aerosol optical depth (AOD) is a quantity which describes the amount of total aerosol attenuation (scattering and absorption).

In this study AOD values calculated from the Moderate Resolution Imaging Spectroradiometer (MODIS) measurements are compared with AOD values measured with ground-based Precision Filter Radiometers (PFR) located in Sodankylä and Jokioinen. Comparisons are done over a long time-period and in a wide range of weather conditions.

MODIS instruments are aboard the Terra and Aqua satellites. Terra MODIS and Aqua MODIS cover Earth's surface every 1 to 2 days. These instruments have 36 spectral bands and they measure near-nadir radiance over a 2300-km wide swath. The resolution of the measurements varies between 0.25 to 1 km. (Anderson *et al.*, 2005)

The PFR measures direct solar irradiance in four narrow spectral bands (862, 500, 412 and 368 nm). The resolution of the instrument is 5 nm.

The Cloud-Aerosol Lidar with Orthogonal Polarization (CALIOP) on board CALIPSO satellite, launched April 28th 2006, is a three-channel backscatter lidar. It is optimized for aerosol and cloud profiling. CALIOP transmits linearly polarized laser pulses at 532 nm and 1064 nm. The receiver at 1064 nm is insensitive for the polarization of the backscatter signal, whereas the receiver at 532 nm measures separately the components polarized perpendicular and parallel to the outgoing beam. The lidar measurement provides the vertical distribution of aerosols and clouds, cloud ice/water phase (via the ratio of signals in two orthogonal polarization channels), and a qualitative classification of aerosol size (via the wavelength dependence of the backscatter). CALIOP measures only at nadir providing a curtain of data along the orbit track. Maximum resolution is 30 m vertical and 300 m

along-track. (Winker and Hunt, 2004; Anderson *et al.*, 2005) CALIOP has the advantage of not being sensitive to surface reflectance. Therefore AOD values, integrated from CALIOP-measured vertical profiles, are also included in the comparison.

Anderson, T. L., Charlson, R. J., Bellouin, N., Boucher, O., Chin, M., Christopher, S. A., Haywood, J., Kaufman, Y. J., Kinne, S., Ogren, J. A., Remer, R. A., Takemura, T., Tanre, D., Torres, O., Trepte, C. R., Wielicki, B. A., Winker, D. A., and Yu, H. (2005). An "A-Train" Strategy for Quantifying Direct Climate Forcing by Anthropogenic Aerosols. *Bulletin of the American Meteorological Society*, 18, 1795-1809.

Winker, D., and Hunt, B. (2007). First Results from CALIOP. Available at: [ams.confex.com/ams/pdfpapers/121113.pdf](http://ams.confex.com/ams/pdfpapers/121113.pdf).

## Comparison of aerosol characteristics retrieved from measurements of scattering in local volume and extinction on horizontal path

S.A. Terpugova, M.V. Panchenko, V.N. Uzhegov, T.A. Dokukina and Yu.A. Pkhalagov

V.E. Zuev Institute of Atmospheric Optics, 1, Academicheskii ave., 634055, Tomsk, Russia

Keywords: atmospheric aerosol, light scattering, light extinction, aerosol size distribution

Nephelometers with limited scattering volume are widely used in practice of aerosol optical research. However, due to some reasons, the optical parameters measured with the nephelometers represent, first of all, the submicron aerosol fraction. The data on spectral transparency of the atmosphere in visible and infrared wavelength range enable to extend the size range of aerosol under study.

The results of parallel measurements of light extinction on a horizontal near-ground path and the light scattering parameters in a local air volume in 2005 – 2006 are considered in this paper, as well as the retrieved aerosol refractive indices and size distributions.

The spectral extinction coefficient  $\varepsilon(\lambda)$  was measured by means of the multi-wavelength transparency meter on 830 m long near-ground path in the wavelength range 0.45 to 3.91  $\mu\text{m}$ . Then the aerosol extinction coefficients  $\beta(\lambda)$  were isolated using the original statistical technique developed by authors (Pkhalagov & Uzhegov, 1988).

The coefficients of directed scattering, at the angle of 45° at three wavelengths (0.41, 0.5, and 0.63  $\mu\text{m}$ ) and polarized and cross polarized components of the scattered light at 90° scattering angle at two wavelengths (0.44 and 0.51  $\mu\text{m}$ ), were measured by means of the nephelometer equipped with the device for artificial humidification in the range of relative humidity from  $RH = 20 - 30$  to 90% (Panchenko et al, 2004).

Comparison of the two datasets has shown that the correlation coefficient between aerosol scattering and extinction in visible wavelength range is  $\sim 0.7$ .

The measured optical parameters (spectral extinction coefficients measured on the near-ground path and seven parameters of light scattering obtained with the nephelometer) were inverted to the size spectrum and the refractive index of the aerosol particles. Measurements of spectral transparency do not provide for obtaining the refractive index  $n$  of particulate matter. Solution of the inverse problem in this case needs its a priori setting. In our study,  $n$  was evaluated by the inversion of nephelometric data. It was done both for the dried particles (at relative humidity  $RH \sim 20 - 30\%$ ) and for humidified aerosol at  $RH \sim 90\%$ . Then the refractive index *in situ* was estimated, i.e. at outdoor relative humid-

ity. To do it, the light scattering parameters *in situ* were retrieved from the data of measurements at two values of humidity using the Kasten's parameterization (Kasten, 1969):

$$\mu_i = \mu_{0,i}(1 - RH)^{-\gamma_i},$$

where  $\mu$  is the directed scattering coefficient,  $\mu_0$  is the directed scattering coefficient of the dry aerosol fraction,  $RH$  is relative humidity of air,  $\gamma$  is the parameter of condensation activity, the index “ $i$ ” means the respective measured scattering characteristics. Parameters  $\gamma_i$  were determined from this formula using the initial and final values of the respective directed scattering coefficient or its polarized component, as well as the initial and final values of relative humidity. Then the parameters  $\mu_i$  at outdoor relative humidity were calculated. Solution of the inverse problem for these data provided for the *in situ* refractive index and size distribution of accumulative aerosol fraction. The obtained values  $n$  were used for inverting the data on the spectral extinction coefficient on horizontal path.

Analysis of the results of inversion has shown that, in significant part of cases, in the radius range  $r = 0.1 - 0.5 \mu\text{m}$ , the particle size distributions retrieved from the aerosol extinction coefficients are close to those obtained from the light scattering brought to outdoor humidity. At the same time, the data on extinction, which cover the wider wavelength range including near IR, make it possible to obtain also the size spectrum of intermediately dispersed aerosol fraction. However, the correctness of estimation of the size distribution function in the range  $r > 1 \mu\text{m}$  significantly depends on how close the refractive index of these particles to the value  $n$  of submicron particles retrieved from nephelometric measurements.

The work was supported by Russian Foundation for Basic Research under grant No. 06-05-64393.

Kasten, F. (1969). *Tellus* 21, 631–635.

Pkhalagov, Yu.A. & Uzhegov, V.N. (1988). *Atmos. Ocean Optics*, 1, 3–11.

Panchenko, M.V., Sviridenkov, M.A., Terpugova, S.A., & Kozlov, V.S. (2004). *Atmos. Ocean Optics*, 17, 378–386.

## Aerosol optical properties in Granada from simultaneous measurements by LIDAR, Nephelometer, CIMEL, Avantes and FieldSpec radiometers

F. Esposito<sup>2</sup>, M.R. Calvello<sup>1,2</sup>, L. Leone<sup>3</sup>, G. Pavese<sup>1</sup>, R. Restieri<sup>3</sup>,  
H. Lyamani<sup>4,5</sup>, J.L. Guerrero-Rascado<sup>4,5</sup>, F.J. Olmo<sup>4,5</sup>, L. Alados-Arboledas<sup>4,5</sup>

<sup>1</sup> I.M.A.A. – C.N.R., Tito Scalo, 85050, Italy

<sup>2</sup> DIFA, Università della Basilicata, Potenza, 85100, Italy

<sup>3</sup> C.R.A.B. – ARPAB, Potenza, 85100, Italy

<sup>4</sup> Grupo de Física de la Atmósfera. CEAMA. Universidad de Granada. Junta de Andalucía. 18071 Granada. Spain

<sup>5</sup> Dep. Física Aplicada. Universidad de Granada. Fuentenueva s/n. 18071, Granada. Spain.

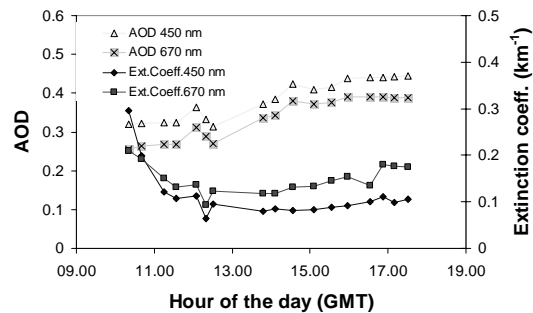
Keywords: Aerosol Optical Depth, aerosol size distributions, aerosol scale height.

In the framework of the “Integrated Action Italy-Spain” a joint radiometric measurements campaign was held in Granada from July, 10<sup>th</sup> 2006 to July, 19<sup>th</sup> 2006. The instruments used were two CIMELs CE318C, one located in Granada (37.18°N, 3.58°W, 680 m a.s.l), as a part of the AERONET robotic network, the other in Sierra Nevada (37.06°N, 3.38°W, 2896 m a.s.l), an Avantes high resolution radiometer (400 nm – 900 nm, 1.5 nm resolution) to measure direct solar irradiance; a FieldSpec to measure Horizontal Aerosol Extinction Coefficient in the range 400-700 nm, a LIDAR system to measure vertical aerosol profile, a TSI-3563 Integrating Nephelometer and a Multi Angle Absorption Photometer (MAAP). Avantes spectrometer was calibrated few days before the campaign following the Langley procedure. The horizontal extinction coefficient has been obtained by using a contrast measurement, avoiding the necessity of absolute calibration.

The joint measurement of vertical Aerosol Optical Depth by Avantes and HAEC has been exploited to obtain aerosol scale height, compared to the values obtained by LIDAR observations.

From the vertical AODs estimation, the Angstrom parameters and the Aerosol Size Distribution have been derived for columnar aerosol content both for CIMEL and Avantes spectrometers.

The following figure reports the AOD and the horizontal Extinction coefficient for two wavelengths as a function of the hour of the day for 17<sup>th</sup>, July.

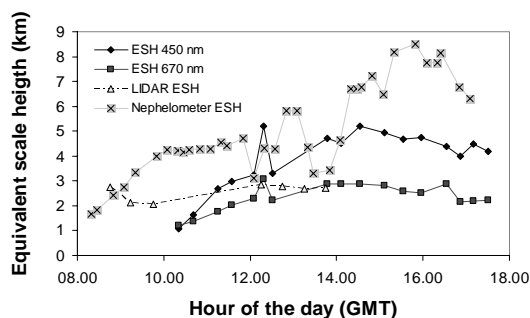


In the figures above the equivalent scale height obtained by vertical and horizontal measurements is reported, together with scale height obtained by LIDAR and combination of CIMEL CE-318C, Integrating Nephelometer and MAAP data.

*Acknowledgments.* Work partially supported by P.R.I.N. “Characterization of the optical and microphysical aerosol properties by several experimental and numerical techniques: a key tool to assess aerosol climatology”, “Integrated Action Italy-Spain” HI-2004-0219 and by CICYT from the Spanish Ministry of Science and Technology through project CGL2004-05984-C07-03 and by Andalusian Regional Government project P06-RNM-01503.

### References

- F. Esposito, G. Pavese, L. Leone, M. R. Perrone, F. De Tomasi, A. M. Tafuro, L. Alados-Arboledas, H. Lyamani “ CIMEL and AVANTES high resolution spectrometers: a comparison study of aerosol parameters” , Conference on Visibility , Vienna, Sept. 2006
- F. Esposito, H. Horvath, F. Romano, C. Serio: Vertical and horizontal aerosol spectral extinction coefficient at a rural location in southern Italy. *Jour. Of Geop. Res.* Vol. 101, No. D14, 19285-19292 (1996)



## Aerosol scattering and mass concentration for different aerosol types

S.N. Pereira<sup>1</sup>, F. Wagner<sup>1</sup>, A.M. Silva<sup>1,2</sup> and N. Belo<sup>1</sup>

<sup>1</sup>Évora Geophysics Center, Rua Romão Ramalho, 59, 7000 Évora, Portugal

<sup>2</sup>University of Évora Physics Department, Rua Romão Ramalho, 59, 7000 Évora, Portugal

Keywords: particulate matter, light scattering, mass scattering efficiency, PM<sub>10</sub>.

The mass scattering efficiency,  $E_s(r,\lambda,m)$ , is one of the aerosol properties relevant to radiative forcing (IPCC, 2001). It is defined as the ratio between aerosol scattering coefficient and mass concentration and represents the increase of scattered radiation per unit mass increase of suspended particles.  $E_s(r,\lambda,m)$  depends on the particle size, wavelength of incident radiation and particle composition (index of refraction).

The experimental setup is based on an integrating nephelometer (TSI 3563) measuring continuously the aerosol spectral scattering coefficients,  $\sigma_\lambda$ , at three wavelengths (450, 550 and 700 nm) and a TEOM (Tapered Element Oscillating Microbalance) Series1400 monitor which measures the aerosol mass concentration,  $C_m$ , continuously. Both instruments were provided with PM<sub>10</sub> sampling heads for removing particles with aerodynamic diameter larger than 10  $\mu\text{m}$ . The TEOM was calibrated by comparing its mass concentration measurements with the ones obtained by a High Volume (HiVol) gravimetric instrument.

Nearly one year of measurements in 2006 were investigated. The mass scattering efficiencies for various aerosol types were derived for so-called aerosol episodes when the aerosol load at the measuring site was significantly higher than the background level. The episodes studied included one desert dust outbreak (27<sup>th</sup> – 30<sup>th</sup> May 2006) followed by continental pollution (30<sup>th</sup> May – 2<sup>nd</sup> June 2006), forest fire plume (7<sup>th</sup> – 8<sup>th</sup> August 2006) and another desert dust episode (23<sup>rd</sup> -24<sup>th</sup> November 2006).

Figure 1 shows the scattering coefficient at 550 nm as a function of mass concentration. It shows a clear distinction between desert dust and forest fire aerosols with the former values between 0.6 and 1  $\text{m}^2\text{g}^{-1}$  and the later values between 2.5 - 3  $\text{m}^2\text{g}^{-1}$ . The difference is more visible as the aerosol load increases and so do PM<sub>10</sub> and  $\sigma_{550}$ . During the continental polluted period (likely a mixture with desert dust aerosols) the mass scattering efficiency values exhibited higher variability and range from 1 up to 3  $\text{m}^2\text{g}^{-1}$ . The mass scattering efficiencies for the other two wavelengths were also derived.

Additionally the experimentally derived mean mass scattering efficiencies were then compared with theoretical calculated ones. Hereby particle optical and microphysical properties were taken from the database OPAC (Optical Properties of Aerosols and Clouds, Hess et al., 1998). The mass scattering

efficiencies were calculated not only for PM<sub>10</sub> but also for PM<sub>2.5</sub> and PM<sub>1</sub>. The results show that  $E_s$  is nearly independent on the cut off size for all aerosol types consisting mainly of small particles. On the other side the cut-off-size influences strongly the mass scattering efficiency, when large particles significantly contribute to the total mass and the scattering coefficient (e.g. desert dust). These findings will be helpful when mass scattering efficiencies from different places with various cut-off-sizes should be compared.

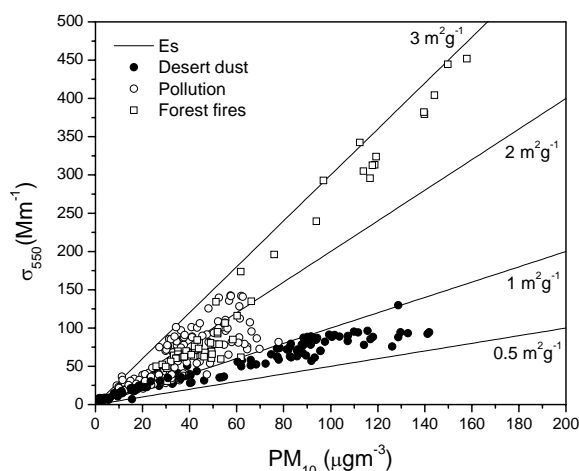


Figure 1. Aerosol scattering coefficient at 550 nm as a function of aerosol mass concentration. The lines corresponds to different mass scattering efficiencies.

This work was supported by FCT (Fundação para a Ciência e Tecnologia) under grant SFRH BPD 14508 2003 under POCTI and PDCTE/CTA/49828/2003.

- Hess, M., Koepke, P. and Schult, I., 1998. Optical Properties of Aerosols and clouds: The software package OPAC, *Bull. Am. Met. Soc.*, 79, 831-844.
- Intergovernmental Panel on Climate Change (IPCC): Climate Change 2001: Radiative Forcing of Climate Change, edited by Houghton, J. T., Ding, Y., Griggs, D. J., Noguera, M., van der Linden, P. J., and Xiaosu, D., Cambridge Univ. Press, Cambridge, 2001.
- Patashnick, H and Rupprecht, E. G., 1991. Continuous PM<sub>10</sub> Measurements Using the Tapered Element Oscillating Microbalance. *Journal of Air and Water Management Association* 4 J (8), 1079-1084.

## Seasonal variability in the physical and optical properties of atmospheric aerosols over a coastal zone

Auomeet Saha, J. Piazzola and S. Despiou\*

LSEET-LEPI, UMR 6017, Université du Sud Toulon-Var, BP 20132, 83957 La Garde, France

Keywords: atmospheric aerosols, black carbon, particle concentration, PM10

Between October 2005 and 2006 we measured various physical and optical properties of atmospheric aerosols in the French Mediterranean coastal zone. BC mass concentration, wavelength dependency of absorption, scattering coefficient, concentration and number-size distributions of fine and coarse particles and PM10 concentrations were continuously measured at ground level along with meteorological parameters and SO<sub>2</sub>, NO<sub>x</sub> and O<sub>3</sub> concentrations. We present here the main results obtained.

All the parameters examined in the present study depicted significant seasonal variations. Typical variations for BC mass concentrations and scattering coefficients are shown in Fig.1. Large aerosol concentrations and higher values of scattering and absorption coefficients occurred during the winter months, followed by lower concentrations during spring and summer. Monthly mean BC concentrations varied between ~ 300 and 1000 ng.m<sup>-3</sup> and PM10 between ~10 and 60 µg.m<sup>-3</sup> during the study period. The aerosol absorption coefficient showed relatively weak wavelength dependency and didn't show any significant seasonal changes, thereby indicating that BC was the dominant absorbing aerosol component in that region during the study period.

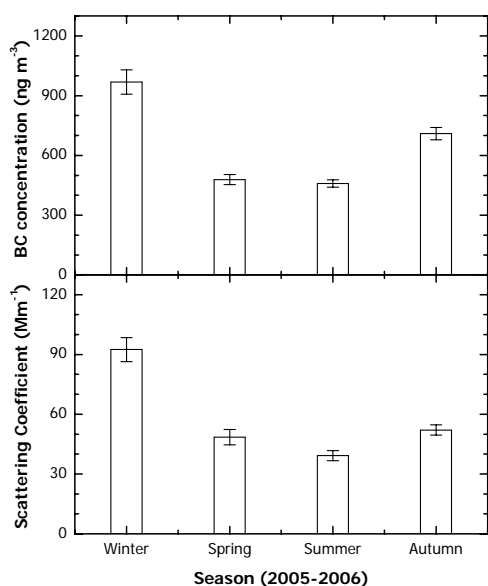


Figure 1. Seasonal variation of BC (top panel) and scattering coefficient (bottom panel).

In addition to the seasonal variations, BC and fine particle (0.01 – 0.41 µm) concentration showed strong diurnal variations, with two peaks, one in the morning and the other in the evening, and mid afternoon minimum. The diurnal variations are also found to be seasonal dependent, with the maximum diurnal amplitude occurring during the winter months. Typical diurnal variations are shown in Fig.2 for BC and fine particle concentrations for the month of February (representing winter) and July (representing summer).

Both diurnal and seasonal variations of aerosol physical and optical properties are found to be significantly influenced by the anthropogenic activities, local meteorology and boundary-layer dynamics.

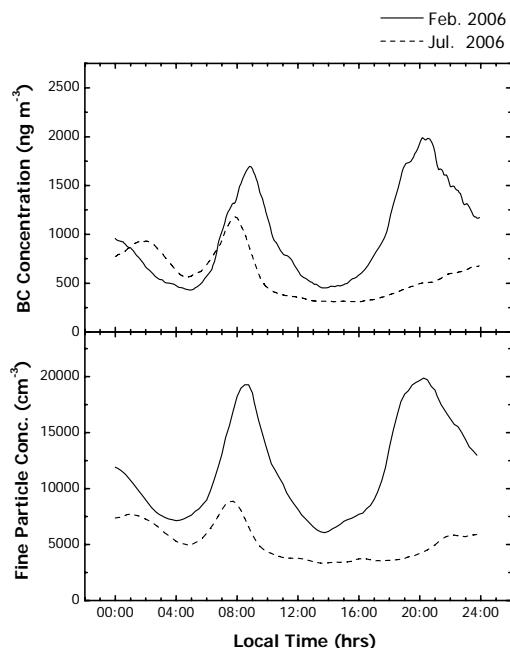


Figure 2. Diurnal variation of BC (top panel) and fine particle concentration (bottom panel) for February and July 2006.

This work is supported by French CNRS, INSU, and PNTS Projects. One of the authors (AS) would like to acknowledge the French Ministry for Education & Research and the Université du Sud Toulon-Var for providing the financial assistance.

Study of inter-annual variability of atmospheric aerosol as assessed from the data of spectral measurements of aerosol extinction on near-ground path.

E. V. Makienko, Y.A. Pkhalagov, R.F. Rakhimov, V.N. Uzhegov  
*Institute of Atmospheric Optics, Tomsk*

Keywords: atmospheric aerosol, extinction coefficient, particle size distributions

Inter-annual variability of the aerosol extinction coefficients  $\beta(\lambda)$  is studied based on the data of measurements of the transparency of the near-ground atmosphere in the wavelength range  $\lambda = 0.44-3.9 \mu\text{m}$  carried out in 2000-2005 in the region of Tomsk ( $56^{\circ}31'N - 85^{\circ}08'E$ ). The main quantity of measurements (3891 realizations) were carried out in seasons with positive monthly mean temperature of air.

Histograms of the distribution density  $\xi(\beta)$  within the range of annual variability were used for analysis of the inter-annual variations of  $\beta(\lambda)$ . An example of histograms of the distribution density of the coefficient  $\beta(\lambda)$  at the wavelength of  $\lambda = 0.56 \mu\text{m}$  is shown in Fig. 1.

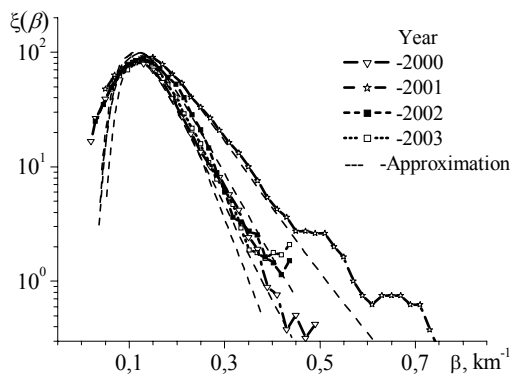


Fig. 1. histograms of the distribution density of the values of the coefficient  $\beta(0.56)$  in different years.

It is seen that the amplitudes and half-widths of the histograms  $\xi(0.56)$  in different years are significantly different, but their maxima lie approximately in the same range of the values of the coefficient  $\beta(0.56)$ . By definition, the range of the values lying in the close vicinity of the maximum of the distribution, corresponds to the most probable value (MPV) of the aerosol extinction coefficient  $\beta^*(\lambda)$  for the considered region. Let us note that inter-annual differences in the distribution of the parameter  $\xi(\beta)$  become apparent mainly in the range of the enhanced values  $\beta(0.56)$ . It occurred that the histograms shown in Fig. 1 are well approximated in the range of the most probable values by the lognormal distribution. Correlation coefficient between  $\xi(\beta)$  and the approximating curve in the range of the values close to MPV is 88-97%. It enables to quite accurately estimate MPV at all wavelengths. In particular, such approach gives the estimate of the most probable value at  $\lambda = 0.56 \mu\text{m}$

$\beta^*(0.56)=0.116 \text{ km}^{-1}$ . According to the long-term data, the coefficients  $\beta(0.56)$  in 84% of events indeed do not exceed the level of  $0.2 \text{ km}^{-1}$ .

The most probable values of the aerosol extinction coefficients  $\beta^*(\lambda)$  in  $\text{km}^{-1}$  in the entire wavelength range were determined using analogous approach for each year (see Table).

$\lambda, \mu\text{m}$	Year			
	2000г	2001г	2002г	2003г
0.44	0.139	0.153	0.166	0.146
0.48	0.127	0.144	0.160	0.136
0.52	0.118	0.130	0.140	0.124
0.56	0.106	0.117	0.125	0.116
0.69	0.089	0.093	0.094	0.089
0.87	0.075	0.078	0.087	0.080
1.06	0.064	0.076	0.082	0.069
1.60	0.060	0.067	0.072	0.069
2.17	0.059	0.056	0.062	0.060
3.91	0.053	0.038	0.053	0.056

The results of inverting the mean spectra  $\beta^*(\lambda)$  obtained in 2000-2003 (Fig. 2) show stability of the shape of the size spectra of accumulative and intermediately dispersed ( $0.45 < r < 1.8 \mu\text{m}$ ) fractions.

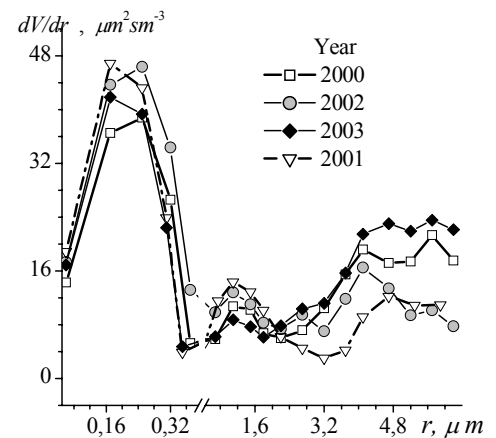


Fig. 2. Retrieved volume size distributions  $dV/dr$ .

Realizations of the most probable values of the atmospheric transparency in 2000-2003 in the same range is evidently related with the absence of essential inter-annual trend of the conditions of formation of the accumulative fraction of particles in this period of observations.

## MieCalc program for calculation of light scattering and absorption characteristics on particles continental and coastal aerosol

G.A. Kaloshin,<sup>1</sup> L.B. Kochneva,<sup>2</sup> S.A. Beresnev<sup>2</sup>

<sup>1</sup>V.E. Zuev Institute of Atmospheric Optics SB RAS,  
1, Academicheskii ave., 634055, Tomsk, Russia

<sup>2</sup>Ural State University, Ekaterinburg, 620083, Russia

Keywords: Mie scattering, Size parameter, Refractive index.

In 1908, Gustav Mie developed a rigorous method to calculate the intensity of light scattered by uniform spheres. Although Mie's solution was precise, it involved a huge number of calculations for spheres and was rarely used until the 1980s when powerful computers became available for scientific research.

Now there are number PC programs for calculation of light scattered characteristics on water drops, glass, and air spheres, and surrounding medium in air, vacuum and in water accordingly.

In the report the MieCalc program for calculation of light scattered characteristics on particles continental and coastal aerosol is submitted (Kaloshin & Serov, 2006). The MieCalc program can produce graphs of the intensity of scattered light as a function of scattering angle, where 0° implies forward-scattering (i.e. in the original direction) and 180° implies back-scattering (i.e. back towards the source of the light); radius, wavelength, and refractive index. In addition, it can produce graphs of scattering cross-sections ( $C_{ext}$ ,  $C_{sca}$  &  $C_{abs}$ ) and scattering efficiencies ( $Q_{ext}$ ,  $Q_{sca}$  &  $Q_{abs}$ ) as functions of radius of the scattering sphere, size parameter or wavelength.

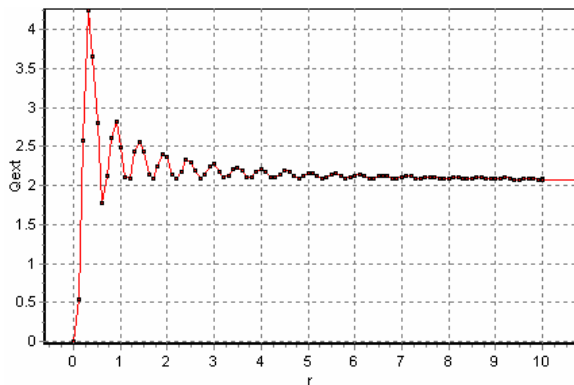


Fig. 1. Scattering efficiency  $Q_{ext}$  vs aerosol particle radius  $r$ ,  $\mu\text{m}$  for marine aerosol.

On Figs.1-3 as an example result of calculation by MieCalc program scattering efficiency  $Q_{ext}$ , inner field intensity  $I_{avg}$ , and absorption efficiency  $Q_{abs}$  for marine aerosol are shown.

The MieCalc program has been designed with an "intuitive" interface – which should be simple to use. On it is present three functional areas:

- area for input of the initial data: input parameters are the radius of the scattering sphere, size parameter or

- wavelength, a step of scattering angle and relative humidity;

- area for display of scattering matrix elements: the choice of scattering matrix for various particles is carried out by means of corresponding bookmarks;

- area for display of calculation results: the intensity of light scattered, values of size parameter, refractive index, scattering efficiencies ( $Q_{ext}$ ,  $Q_{sca}$  &  $Q_{abs}$ ) and back-scattering.

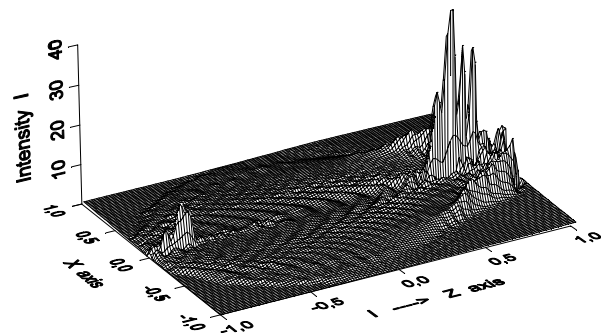


Fig. 2. Inner field intensity  $I_{avg}$  for marine aerosol droplet at  $\lambda=0,5 \mu\text{m}$  and  $\rho=100$ .

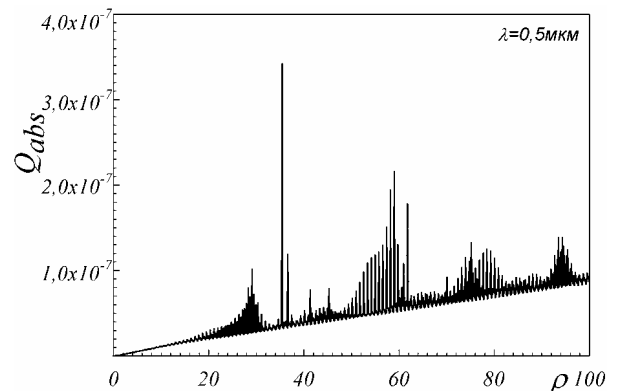


Fig. 3. Absorption efficiency  $Q_{abs}$  for marine aerosol droplet at  $\lambda=0,5 \mu\text{m}$ .

G.A. Kaloshin, S.A. Serov. MieCalc program for calculation of light scattering characteristics on particles sea and coastal aerosol Proc. XIII International Symp. «Atmospheric and Ocean Optics. Atmospheric Physics». Tomsk, July 2-6, 2006. P. 137.

## ESTIMATION OF AEROSOL IMPACT ON EXTREME WEATHER AND CLIMATE EVENTS

A.V.Andronova<sup>1</sup>, D.P.Gubanova<sup>1</sup>, V.M. Minashkin<sup>1</sup>,

<sup>1</sup>Karpov Institute of Physical Chemistry, Moscow, Russian Federation

Keywords: . catastrophes, climate, aerosol-impacts

The offered report is devoted to existing methods and consequences of aerosol influence analysis on various hydrometeorological processes, and also to basic principles of construction of hierarchy of opportunities of influence to extremal hydrometeorological processes and situations by various physical properties and chemical structures aerosols.

Besides, the estimation of possible consequences of mass emission (600 000 ò.) sulphate aerosol in stratosphere cite as an example in the report, that would allow to prevent global change [Israel et al., 2006].

In view of that the similar experiment on delivery to stratosphere and burning in it a plenties of sulphur with subsequent SO<sub>3</sub> hydrolysis can be carried out by our available means, the estimation of consequences of such experiment was carried out.

The account of aerosols extinction coefficient was made under the Mi theory and the integrated factors extinction and reflection of radiation from aerosol layer paid off under the program, which described in [Ivanov et.al., 1985]. The estimation of albedo change and radiation balance and also the change of ground surface temperature was carried out on basis of radiative-convective model for the moment of time, when all quantity of aerosol will be stirred in regular intervals in atmosphere of Northern hemisphere [Ginzburg et al., 1985]. The results of estimation are given in table.1,2.

But SO<sub>3</sub> hydrolysis and sulphuric acid particles condensation, accompanying by allocation 4-8 x 1E9 calories of heat, will result to aerosols carry-over in top layers of stratosphere, to water reduction, to convection in stratosphere and to possible increase of stratospheric clouds, as shown in work [Gostinzev,1884]. This will result to additional ozone destruction since ozone adsorbtion coefficient of such particles makes about E-2- E-6. The ozone quantity will have large change (6000 tones for ice particles and 0.6 tones for liquid particles) that will result to increase a flow of short-wave solar radiation and to appreciable change of radiation balance.

Spectral range, [mkm]	Extinction coefficient, [m <sup>2</sup> /g]
0.55	5.5
7-12	0.5

Table 1. Parameters of aerosols elementary scattering volume.

Table 2. The result of calculation of temperature decrement estimation.

Albedo	Temperature change of	C
0.1	Surface	0
	Atmosphere above ground	12
	Atmosphere above ocean	6
0.3	Surface	2
	Atmosphere above ground	18
	Atmosphere above ocean	8

1. Israel, Ya.A. et al. (2006) *Meteorology and Hydrology*, v.6, , pp.21-27 (in Russian)
2. Ivanov, A.P., Zege, E.P., Cazev, I.L. (1985) *Optics of scattering enviroments*. Minsk. (in Russian)
3. Ginzburg, A.S., Golyzin, G.S., Demchenko, P. Ph., (1985) *Evolution of turbid convective border layer*. – In 9-th International conference of clouds physic. Vol. 4. –S.-Pb.: Hydrometheoizat. (in Russian)
4. Gostinzev, Yu.A., et al. (1984) *Turbulently thermic in stratifying atmosphere*. -Moscow., Preprint of Institute of Chemical Physics, 46p. (in Russian)

## CAPEX – AEROPOR Overview : objectives and first results

A.M. Silva<sup>1,2</sup>, M.J.Costa<sup>1,2</sup>, F.Wagner<sup>2</sup>, D. Bortoli<sup>2</sup>, S. Pereira<sup>2</sup>, N. Belo<sup>2</sup>, L. Bugalho<sup>2</sup>, L. Alados-Arboledas<sup>3</sup>, H. Lyamani<sup>3</sup>, J.L. Guerrero-Rascado<sup>3</sup>, D. Kindred<sup>4</sup> and M. Smith<sup>5</sup>

<sup>1</sup>Department of Physics, University of Évora, 7000, Évora, Portugal

<sup>2</sup> Évora Geophysics Centre, University of Évora, 7000, Évora, Portugal

<sup>3</sup> Grupo de Física de la Atmósfera, Universidad de Granada, Granada, Spain

<sup>4</sup> EU Aircraft Liaison Officer, Observations Based Research, Met Office, Ex1 3PB, Exeter, United Kingdom

<sup>5</sup> CAPEX Detachment Manager, from FAAM, Cranfield, MK43 0AL, United Kingdom

Keywords: aerosol characterization, optical properties, measurements

CAPEX (Clouds and Aerosols over Portugal Experiment) is an European project, coordinated by Évora Geophysics Centre, to investigate aerosol particles, radiation, cloud properties, precipitation and radioactivity over Portugal using both airborne and ground based instrumentation. The airborne measurements were obtained with the BAe-146 aircraft, provided by the Met Office (UK) and operated by FAAM, based at Beja Air Force Base, in the south of Portugal; the ground based remote sensing and “in situ” measurements were obtained at Geophysics Centre Observatory at Évora and at the Cabo da Roca site, respectively, located 70 km northern of Beja and at the sea coast 20 km northwest of Lisbon. This project, funded by EC under the 6<sup>th</sup> Framework Program within the EUFAR Initiative, took place from 30<sup>th</sup> May up to 18<sup>th</sup> June 2006 over central and south Portugal, and consisted of three individual projects: AEROPOR (AERosols Over Portugal: Optical and Radiation Measurements), CLAPREC (Clouds, Aerosols, Precipitation) and VPRACOP (Vertical Profiles of Radioactive Aerosol Constituents Over Portugal). Within AEROPOR project two teams were involved, the one from Évora Geophysics Centre, and the other one from Granada University

Within the framework of AEROPOR, about 10 flight hours were used to obtain stack profiles and some radiation runs over different sites in order to **derive aerosol properties and their vertical distribution**, for different aerosol situations (European pollution from Central Europe and Iberian Peninsula, Saharan desert dust, remote continental aerosols), **perform aerosol radiative calculations** for different aerosol situations, and **to validate surface reflectance algorithms and contribute** to regional surface reflectance data base. Within AEROPOR project, the following airborne measurements were made: broadband solar radiation and spectral irradiances (up and downwelling) the latest with a SWS and SHIM radiometers, spectral radiances (up and down welling) with an ARIES interferometer, volume scattering and absorption coefficients respectively with a nephelometer and a PSAP instrument, size distribution measurements with a PCASP instrument and temperature, humidity and wind measurements. At the Évora site, the following

measurements were made continuously: volume scattering and absorption coefficients, respectively with a three wavelength nephelometer and a MAAP instrument, aerosol mass concentration with a TEOM instrument, aerodynamic particle size distribution with an APS instrument, spectral aerosol optical thicknesses and spectral almucantar measurements, with a sunphotometer within the AERONET network, spectral global and diffuse solar irradiances with a MFR shadowband radiometer, broad-band solar and thermal down-welling irradiances and the cloud base heights with a ceilometer; during the flight profiles, LIDAR measurements were also determined and for the entire time period of the campaign during night time period, water vapour mixing ratio profiles were also measured. At the Cabo da Roca site (another AERONET site), spectral aerosol optical thicknesses and spectral almucantar measurements were continuously taken, and at the Beja site, spectral aerosol optical thicknesses were made at certain periods with a handheld sunphotometer instrument. At all sites, meteorological information was provided at the surface, and the 5-days back-trajectories analysis at different pressure levels, ending at Évora site were also computed, using the HYSPLIT model (Draxler & Rolph, 2003).

From the ground based measurements at Évora site it was possible to identify, a mixture of different aerosol types at different altitudes even when the remote continental aerosol situation prevailed. The aerosol events, which occurred during CAPEX campaign were clearly identified both with the airborne and ground based instruments. Different aerosol distributions were clearly identified within a 50 km horizontal distance, during the desert dust episode event over different underlying surfaces.

This research has been partially funded by EUFAR, by the Spanish Projects HP-2003-0013, CGL2004-05984-C07-03 and P06-RNM-01503 and by FCT under grant SFRH BPD 14508 2003 under POCTI.

Draxler, R.R. and G.D. Rolph (2003): HYSPLIT (HYbrid Single-Particle Lagrangian Integrated Trajectory). Model access via the website <http://www.arl.noaa.gov/ready/hysplit4.html>

## CAPEX-AEROPOR: Aerosol Measurements derived from airborne and ground-based measurements

F. Wagner<sup>1</sup>, S. Pereira<sup>1</sup>, D. Bortoli<sup>1</sup>, M.J. Costa<sup>1,2</sup>, N. Belo<sup>1</sup>, A.M. Silva<sup>1,2</sup>, J.L. Guerrero-Rascado<sup>3,4</sup>,  
H. Lyamani<sup>3,4</sup>, and L. Alados-Arboledas<sup>3,4</sup>

<sup>1</sup>Évora Geophysics Centre, University of Évora, 7000, Évora, Portugal

<sup>2</sup>Department of Physics, University of Évora, 7000, Évora, Portugal

<sup>3</sup>Grupo de Física de la Atmósfera, CEAMA, Universidad de Granada, Junta de Andalucía, 18071 Granada, Spain

<sup>4</sup>Departamento de Física Aplicada, Universidad de Granada, 18071 Granada, Spain

Keywords: Aerosol measurement, mineral dust, European pollution

The experiment AEROPOR (Aerosols over Portugal) is part of the measuring campaign CAPEX (Clouds and Aerosols over Portugal Experiment) and was conducted in June 2006 in the South of Portugal. Airborne measurements of aerosol optical and microphysical parameters were obtained for a variety of different aerosol types.

On the 4<sup>th</sup> of June 2006 an aerosol plume from the European Continent, originating in Spain and France, brought higher particle concentrations to Portugal. On the 7<sup>th</sup> of June 2006 an outbreak of African air transporting mineral particles to Portugal could be observed. Various aerosol particle properties were measured, with a variety of ground-based and airborne instruments, for both different situations. Whereas on the 4<sup>th</sup> June the aircraft was flying directly over the ground station (Évora Geophysics Observatory) and on the 7<sup>th</sup> June there was a horizontal difference of about 100 km between the aircraft and the Évora site.

Figure 1 shows the total scattering coefficient at 550 nm observed with a Nephelometer onboard the aircraft Bae146 and the extinction coefficient at 532 nm derived from the Lidar operated by the Spanish team at the Évora Geophysics Observatory, Portugal. The height of the particle plume is about 3 km with slightly higher values for the desert dust case compared to the European pollution case. The general vertical particle profile differs very much between the two cases; having a quasi continuously decay with height on the 04<sup>th</sup> June day and demonstrating a nearly constant vertical profile in the aerosol layer on the 7<sup>th</sup> June with a sharp upper boundary.

The differences in the vertical extend of the desert dust plume derived from airborne Nephelometer and ground-based Lidar can likely be attributed to the horizontal distance between the two instruments. Note that from Lidar data the extinction coefficient and from Nephelometer measurements the scattering coefficient is derived. However there is a remarkable agreement between the vertical trends above 1500 m for the 4<sup>th</sup> of June.

A Nephelometer at the ground observed values of about 30 Mm<sup>-1</sup> on the 4<sup>th</sup> of June and 50 Mm<sup>-1</sup> on the 7<sup>th</sup> June, respectively. These values agree quite well with the airborne Nephelometer

measurements at the lowest altitude. The scattering Angstrom exponent, derived from the blue and the red channel of the two Nephelometers, show values between 1.3 and 1.5 for the European pollution case and between 0.5 and 1.0 for the desert dust case. These values are similar to the Angstrom exponent derived from sun photometer which ranging between 1.3 and 1.4 on 4<sup>th</sup> June and between 0.7 and 0.9 on 7<sup>th</sup> June 2006.

At the conference further aerosol optical and microphysical particle parameters, obtained for the two aerosol situations will be presented. This will also include Ceilometer, APS and MAAP.

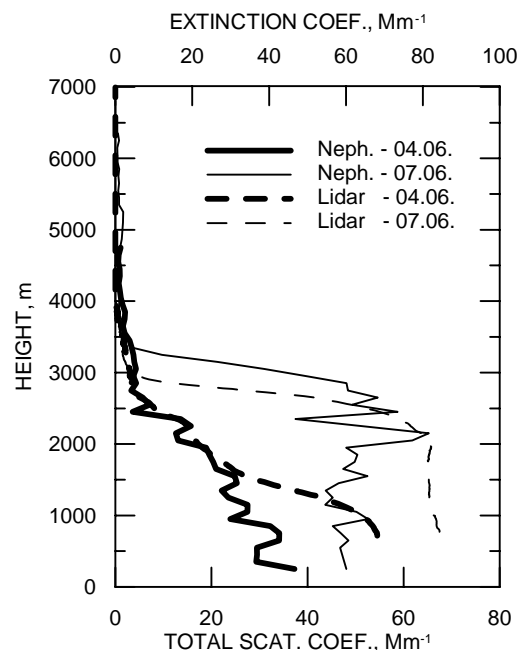


Figure 1: Extinction Coefficient at 532 nm derived at Évora on 4<sup>th</sup> and 7<sup>th</sup> June 2006 with a ground-based Lidar and total scattering coefficient measured with airborne Nephelometer.

This work was supported by FCT, Portugal under grant SFRH BPD 14508 2003 under POCTI. Partial support has been obtained by EUFAR and from Spanish grants: CGL2004-05984-C07-03 and P06-RNM-01503, and by the Acciones Integradas Program Spain-Portugal HP-2003-0013.

## Seasonal and diurnal variations of scattering and absorption properties of aerosols in an urban area, Granada, Spain.

H. Lyamani<sup>1,2</sup> and L. Alados-Arboledas<sup>1,2</sup>

<sup>1</sup>Grupo de Física de la Atmósfera. Centro Andaluz de Medio Ambiente. Universidad de Granada. Junta de Andalucía. Avda. del Mediterráneo s/n. 18071 Granada. Spain

<sup>2</sup>Departamento de Física Aplicada. Facultad de Ciencias. Universidad de Granada. Fuentenueva s/n. 18071, Granada. Spain.

Keywords: scattering coefficient, absorption coefficient, urban aerosols.

Atmospheric aerosols have a significant impact on regional air pollution as well as on the radiation budget. Furthermore, atmospheric aerosols have been shown to have adverse effects on human health and environmental quality including visibility. Understanding the climatic and environmental effects of atmospheric aerosols requires knowledge of the optical properties of the aerosols, such as scattering and absorption coefficients. In this paper, surface measurements of aerosol optical properties at Granada (37.18°N, 3.58°W, 680 m a.s.l), Spain, obtained during winter (December-February) and summer (Jun-August) 2006 are presented. Measurements include scattering and absorption coefficients as well as aerosol concentration. Seasonal, diurnal and weekday variations of these parameters are analyzed and explained and the effects of local meteorological parameters and anthropogenic activities are also examined.

The scattering,  $\sigma_{\text{sca}}$ , and backscattering,  $\sigma_{\text{bsca}}$ , coefficients were measured with an integrating nephelometer (TSI, model 3563) in three wavelengths 450, 550 and 700 nm. No idealities due to non-lambertian and truncation errors were corrected using the method described by Anderson and Ogren (1998). Light absorption coefficient at 670 nm,  $\sigma_{\text{abs}}(670 \text{ nm})$ , was recorded with Multi-Angle Absorption Photometer (Thermo ESM Andersen Instruments, Erlangen, Germany). Particle size distribution in the diameter range 0.50-20  $\mu\text{m}$  was obtained by an aerodynamic aerosol sizer (APS-3222, TSI).

All aerosol parameters show large variability in their values in the winter and summer seasons (Table 1). The values of aerosol properties obtained in this study are similar to those obtained in other moderately polluted urban areas. High values of  $\sigma_{\text{abs}}$ ,  $\sigma_{\text{sca}}$  and aerosol concentration were obtained during winter and low values were measured during summer season. The Angström exponent,  $\alpha$ , presented an average value of  $1.8 \pm 0.2$  during winter and  $1.5 \pm 0.3$  during summer, suggesting a large fraction of submicron particles at the site during winter season, an observation confirmed by aerosol size distribution

measurements made by APS. Urban aerosols in Granada contain a large fraction of absorbing material as indicated by an average single-scattering albedo,  $\omega_{0A}(670 \text{ nm})$ , of  $0.66 \pm 0.06$  and  $0.71 \pm 0.05$  obtained during winter and summer respectively, indicating that about 30-35% of the aerosol light extinction was accounted for by absorption. A clear diurnal pattern was observed, in both season, in  $\sigma_{\text{abs}}$ ,  $\sigma_{\text{sca}}$  and aerosol concentration with two local maxima occurring in early morning and late evening. This diurnal cycle was mainly attributed to local anthropogenic activities and meteorological conditions. In both season, significant reduction in  $\sigma_{\text{abs}}$  values has been found on weekends compared to weekdays indicating a strong impact of traffic emissions on absorbing aerosol concentrations. The highest  $\sigma_{\text{sca}}$  and  $\sigma_{\text{abs}}$  values were associated with air mass originated from Africa and Central Europe and also to local stagnation conditions.

Parameter	Summer	Winter
$\sigma_{\text{sca}}(450 \text{ nm}) \text{ Mm}^{-1}$	$69 \pm 23$	$117 \pm 57$
$\sigma_{\text{sca}}(550 \text{ nm}) \text{ Mm}^{-1}$	$52 \pm 18$	$83 \pm 42$
$\sigma_{\text{sca}}(700 \text{ nm}) \text{ Mm}^{-1}$	$37 \pm 14$	$53 \pm 27$
$\alpha [450-700]$	$1.5 \pm 0.3$	$1.8 \pm 0.2$
$\sigma_{\text{abs}}(670 \text{ nm}) \text{ Mm}^{-1}$	$15.5 \pm 4.8$	$27.8 \pm 10.6$
$\omega_{0A}(670 \text{ nm})$	$0.71 \pm 0.05$	$0.66 \pm 0.06$

Table1: Summary of aerosol properties (average  $\pm$  standard deviation).

*Acknowledgements:* This work was supported by CICYT from the Spanish Ministry of Science and Technology through project CGL2004-05984-C07-03 and by Andalusian Regional Government project P06-RNM-01503..

### References

Anderson, T.L., Ogren, J.A., 1998. *Determining aerosol radiative properties using the TSI 3563 integrating nephelometer. Aerosol. Sci. Tech*, 29, 57-69.

## Characterization of the atmospheric aerosol properties during ESTIO2005 field campaign: an interdisciplinary approach.

Alados-Arboledas, L.<sup>1,2</sup>, H. Horvath<sup>3</sup>, Querol X.<sup>4</sup>, Olmo, F.J.<sup>1,2</sup>, Guerrero-Rascado, J.L.<sup>1,2</sup>, Lyamani, H.<sup>1,2</sup>, Gangl, M.<sup>3</sup>, S. Castillo<sup>4</sup>, A. Alastuey<sup>4</sup>

<sup>1</sup>Grupo de Física de la Atmósfera. CEAMA. Universidad de Granada. Junta de Andalucía. 18071 Granada. Spain

<sup>2</sup>Departamento de Física Aplicada. Universidad de Granada. 18071, Granada. Spain.

<sup>3</sup>Experimental Physics Institute, University of Vienna, Vienna, Austria.

<sup>4</sup>Institute of Earth Sciences "Jaume Almera"-CSIC (Spain)

**Keywords:** Atmospheric aerosols, Optical properties, columnar properties, Chemical composition, Special field campaigns Radiative properties, Remote sensing, Retrieval of aerosol properties

This paper presents the results concerned with the characterization of the atmospheric aerosol from a multidisciplinary point of view during the field campaign ESTIO2005 (Experimental Study of the atmospheric aerosol in urban environment), developed at Granada, Spain, during the month of September 2005.

A relevant fraction of the experimental set up used in this study is routinely operated at the Andalusian Center for Environmental Studies (CEAMA), located in South-eastern Spain in the urban area of Granada, a non-industrialised medium size city (37.18°N, 3.58°W and 680 m a.m.s.l.).

Thus a Raman Lidar system based on a Nd:YAG laser source operating at 1064, 532 y 355 nm and including elastic, polarized and Raman shifted detection has been used to derive profiles of several atmospheric aerosol properties.

Column integrated properties of the atmospheric aerosol has been derived by a CIMEL CE-318 radiometer operating at several wavelengths: 340, 380, 440, 670, 870, 940 and 1020.

In situ characterization of the atmospheric aerosol has been accomplished by an integrating nephelometer, TSI-3563, that operates at 450, 550 and 700 nm with possibility to determine the backscattering coefficient. Aerosol absorption coefficient at 670 nm has been determined by means of a Multi Angle Absorption Photometer. An Aerosol Particle Sizer APS-322 (TSI) has been used to determine the aerosol size distribution in the diameter range 0.50-20  $\mu\text{m}$ .

Sampling of PM10 and PM2.5 was simultaneously performed using high volume samplers (MCV 30m<sup>3</sup>/h) with PM10 and PM1 cut off inlets with 15cm quartz microfibre filters (QF20 Schleicher and Schuell), to determine major and trace aerosol components.

During the campaign the University of Vienna operates a custom made Polar Nephelometer with a design similar to that proposed by Waldram (1945). Finally, the University of Vienna Telephotometer [Horvath, 1981] has measured the average of the horizontal aerosol extinction coefficient between the instrument and the target at wavelengths in the range 366-700 nm.

Temporal evolution of the different aerosol properties are presented and interpreted using additional information on synoptic situations and evidences of long range transport. The connections between chemical and physical properties sampled in the bottom of the urban planetary layer have been analyzed. On the other hand, information on column integrated aerosol properties is combined with surface in situ and vertically resolved features retrieved by Lidar analyses to describe the urban atmosphere analyzed.

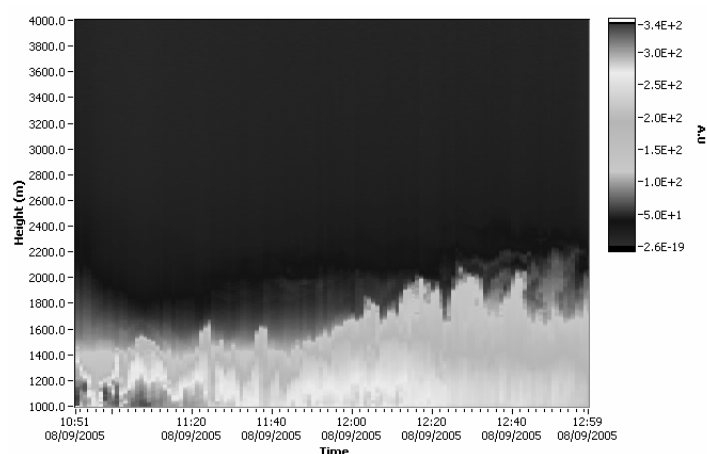


Figure 1. Range corrected signal at 532 nm obtained by LIDAR during the morning of 8 September, showing the evolution of the PBL.

**Acknowledgements:** This work was supported by CICYT from the Spanish Ministry of Science and Technology through project CGL2004-05984-C07-03 and by Andalusian Regional Government project P06-RNM-01503, and by the Acciones Integradas Program Spain-Austria, HU2001-0022.

### References

Lyamani, H., Olmo, F. J., Alcántara, A. and Alados-Arboledas, L., 2006. Atmospheric aerosols during the 2003 heat wave in southeastern Spain. *Atmos. Environ.*, 40-33, 6465-6476.

Waldram, J.M., 1945. *Trns.Illum.Eng.Soc.*, 10, 147-188.

## **Arctic smoke – aerosol characteristics during a record air pollution event in the European Arctic and its radiative impact**

R. Treffeisen<sup>1</sup>, P. Turnved<sup>2</sup>, J. Ström<sup>2</sup>, A. Herber<sup>3</sup>, J. Bareiss<sup>4</sup>, A. Helbig<sup>4</sup>, R. S. Stone<sup>5</sup>, W. Hoyningen-Huene<sup>6</sup>, R. Krejci<sup>7</sup>, A. Stohl<sup>8</sup>, and R. Neuber<sup>1</sup>

<sup>1</sup>Alfred Wegner Institute for Polar and Marine Research, Telegrafenberg A45, 14473 Potsdam, Germany

<sup>2</sup>ITM - Department of Applied Environmental Science, Stockholm University, S 106 91 Stockholm, Sweden

<sup>3</sup>Alfred Wegner Institute for Polar and Marine Research, Am Handelshafen 12, 27570 Bremerhaven, Germany

<sup>4</sup>University of Trier, Department of Climatology, 54286 Trier, Germany

<sup>5</sup>Cooperative Institute for Research in Environmental Sciences, University of Colorado, Boulder 80309

<sup>6</sup>University of Bremen, Institute of Environmental Physics, Otto-Hahn-Allee 1, 28334 Bremen, Germany

<sup>7</sup>Department of Meteorology (MISU), Stockholm University, S 106 91 Stockholm, Sweden

<sup>8</sup>Norwegian Institute for Air Research, Instituttveien 18, 2027 Kjeller, Norway

**Keywords:** Arctic aerosols, biomass burning, long-range transport, radiative properties, tropospheric aerosols.

In early May 2006 a record high air pollution event was observed at Ny-Ålesund, Spitsbergen. An atypical weather pattern established a pathway for the rapid transport of biomass burning aerosols from agricultural fires in Eastern Europe to the Arctic. Atmospheric stability was such that the smoke was constrained to low levels, within 2 km of the surface during the transport. This study puts emphasis on the radiative effect of the smoke. The aerosol size distribution was characterized as having an accumulation mode centered at 165-185 nm and almost 1.6 for geometric standard deviation of the mode. Nucleation and small Aitken mode particles were almost completely suppressed within the smoke plume measured at Ny-Ålesund. Chemical and microphysical aerosol information obtained at Mt. Zeppelin (474 m.a.s.l) was used to derive input parameters for a one-dimensional radiation transfer model to explore the radiative effects of the smoke. The daily mean heating rate calculated on 2 May 2006 for the average size distribution and measured chemical composition reached 0.55 K day<sup>-1</sup> at 0.5 km altitude for the assumed external mixture of the aerosols but showing much higher heating rates for an internal mixture (1.7 K day<sup>-1</sup>). In comparison a case study for March 2000 showed that the local climatic effects due to Arctic haze, using a regional climate model, HIRHAM, amounts to a maximum of 0.3 K day<sup>-1</sup> of heating at 2 km altitude.

## Comparisons between the AERONET products and those derived from aerosols optic and chemistry in Beijing

Roger J.C.<sup>1</sup>, Dubovik O.<sup>2</sup>, Guinot B.<sup>3</sup>, Mallet M.<sup>4</sup>, Lin L.<sup>1</sup>, Vermote E.<sup>5</sup>, Cachier H.<sup>3</sup>,  
Chen H.<sup>6</sup>, Tong Y.<sup>7</sup>, Holben B.<sup>8</sup>

<sup>1</sup>LAMP/OPGC, Université Blaise Pascal, Aubière, France

<sup>2</sup>LOA, Université de Lille 1, Villeneuve d'Ascq, France

<sup>3</sup>LSCE/CEA, IPSL, Gif-sur-Yvette, France

<sup>4</sup>LA, Université Paul sabatier, Toulouse, France

<sup>5</sup>University of Maryland, Dept Geography, College Park, Md, USA

<sup>6</sup>Institute of Atmospheric Physics, Beijing, China

<sup>7</sup>Municipal Environmental Monitoring Center, Beijing, China

<sup>8</sup>NASA GSFC, Biospheric Sciences Branch, Greenbelt, USA

Keywords: Aerosol Characterisation, Aerosol measurement, Optical properties, Radiative properties, Instrumentation/physical Char.

The AERONET network provides new aerosol products from the version 2. The work presented here takes place in the frame of a validation exercise. We chose urban environment in a mega-city because it allows a homogeneous atmosphere with high concentration and then allows us a direct comparison between ground-based measurements and vertically integrated data.

During 3 campaigns held in Beijing between January 2003 and August 2004, we performed aerosols optical, microphysical and chemical measurements. Optical measurements have been realized from nephelometer and aethalometer, while size distributions were acquired from DPS and GRIMMS. In synergy with optical measurements, aerosols have been collected on filters using 13 levels DKTI impactors. After chromatographic and carbon analysis, we get the massic size-distribution for ions, black carbon and organic carbon. Using a methodology developed by authors, we were able to determine the aerosol optical and radiative properties (Mallet et al., 2003; Roger et al., 2006).

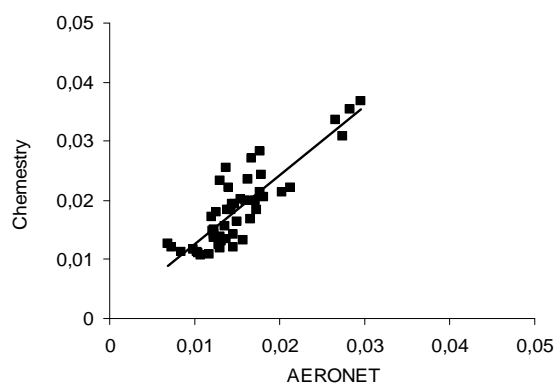


Figure 1. Aerosols imaginary refractive indexes derived from AERONET and chemistry

Globally, results are very satisfying and encouraging. Regarding microphysical properties, le

size-distribution is well inverted particularly for the accumulation mode (the coarse mode is not totally observed by optical and chemical ground based measurements). Comparisons for the complex refractive index are good, especially for the imaginary part (Figure 1). We will also show comparisons for the single scattering albedos (Figure 2) and for the aerosol direct radiative forcing obtained from AERONET, from direct optical measurements and from chemical properties.

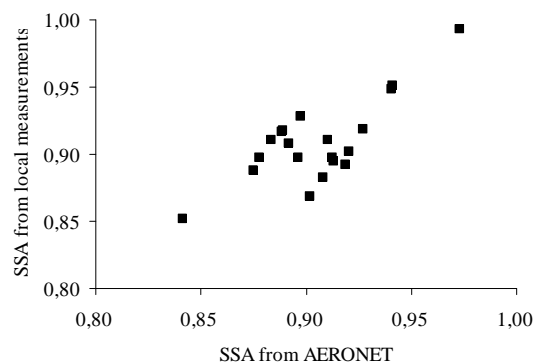


Figure 2. Aerosols single scattering albedos derived from AERONET and from local measurement

Mallet M., Roger J.C., Despiiau S., Dubovik O., Putaud J.P., 2003, Microphysical and optical properties of aerosol particles in urban zone during ESCOMPTE, *Atmospheric research*, 69, 73-97.

Roger J.C., Mallet M., Dubuisson P., Cachier H., Vermote E., Dubovik O., Despiiau S., 2006, "A synergetic approach for estimating the local direct aerosol forcing. Application to an urban zone during the ESCOMPTE Experiment", *J. Geophys. Res.*, 111, D13208, doi:10.1029/2005JD006361

## Results of spring aerosol campaigns in Hornsund, Spitsbergen, 2004 and 2007

A. Rozwadowska<sup>1</sup>, T. Petelski<sup>1</sup>, K. Migala<sup>2</sup> and T. Zielinski<sup>1</sup>

<sup>1</sup>Institute of Oceanology, Polish Academy of Sciences, Powstancow Warszawy 55, 81-712, Sopot, Poland

<sup>2</sup>Institute of Geography and Regional Development, University of Wroclaw, Kosiby 6/8, 51-670, Wroclaw, Poland

Keywords: Arctic aerosols, aerosol size distribution, optical depth, vertical distribution, trajectory

Aerosols and clouds reflect, absorb and emit solar and terrestrial radiation in the atmosphere and thus affect radiative balance and climate of the earth. They influence radiances at the TOA, which are the source of information in the remote sensing methods. Moreover, aerosol and cloud particles interact with each other, which influences their microphysical and optical properties. In the Arctic, usually high spectral surface albedo and low solar elevation cause enhanced aerosol effects due to multiple scattering.

Aerosol measurement at the Polish polar station in Hornsund has been performed since 2004. Since 2005 Hornsund is a site of Aerosol Robotic Network (AERONET, Holben *et al.*, 1998). The main objectives of the aerosol research in Hornsund performed by the Institute of Oceanology are as follows:

1. to determine the impact of air mass history on physical and optical properties of tropospheric aerosols in the Arctic,
2. to investigate contribution of the boundary layer aerosols to the total aerosol optical thickness in the Arctic,
3. to investigate vertical profiles of aerosol concentration in the boundary layer and determine factors that control them.

During May and June 2004, aerosol measurements at Hornsund were carried out within the campaign ASTAR 2004 (Herber, 2004). Exemplary results from 2004 campaign shown in Fig. 1 illustrate strong impact of air mass history on aerosol size distribution. Aerosol measurements will be continued this spring. The following properties are measured at the Hornsund station during the campaign:

1. spectral aerosol optical thickness (Microtops II sunphotometer)
2. aerosol concentration and size distributions (coarse mode, Classical Scattering Aerosol Spectrometer Probe CSASP-100-HV-SP, Handilaz Aerosol Particle Counter, Airnet 310 Particle Counter)
3. vertical profiles of aerosol concentration (FLS-12 lidar) in the boundary layer
4. boundary layer structure (SODAR)
5. solar radiation fluxes (UV, VIS, IR; Precision Spectral Pyranometer with Schott filters 295, 395 and 695 nm, Eppley)

6. upward and downward shortwave and longwave radiative fluxes (CNR-1 NET-radiometer, Kipp & Zonen)

7. total ozone content (Microtops II Ozonometer)

The aerosol and flux measurements are accompanied by the standard meteorological observations.

In the present paper, selected results of the measurements performed in Hornsund in spring seasons of 2004 and 2007 are presented.

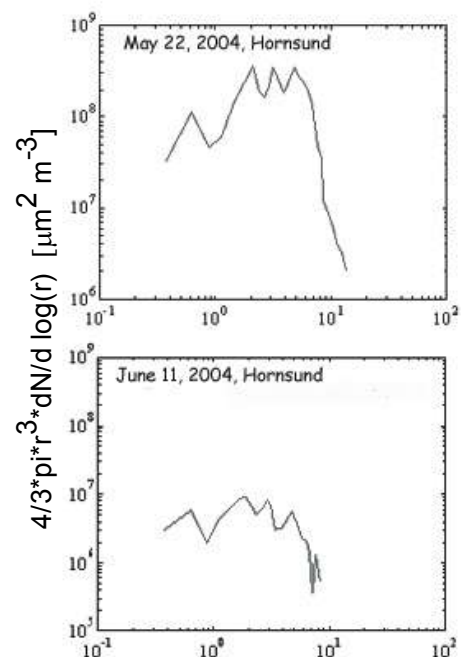


Figure 1. Daily mean aerosol size distributions for the case of advection of air mass from Europe (top) and from the polar seas (bottom) in Hornsund, Spitsbergen.

Herber, A. *et al.* (2004) in *Abstracts of the European Aerosol Conference 2004, Budapest, J. Aerosol Science*, 595-596

Holben, B. *et al.* (1998). *Rem. Sens. Environ.*, 66, 1-16.

## **T31 Abstracts**

## A gas/aerosol pollutant study in urban and rural atmosphere of Rome during the ITALIA campaigns. Monitoring and characterization.

P. Di Filippo<sup>1</sup>, C. Riccardi<sup>1</sup>, D. Pomata<sup>1</sup>, F. Incoronato<sup>1</sup>, S. Spicaglia<sup>1</sup>, A. Cecinato<sup>2</sup> and C. Balducci<sup>2</sup>

<sup>1</sup>DIPIA/ISPESL, Monteporzio Catone, 00040, Rome, Italy

<sup>2</sup>IIA/CNR, Montelibretti, 00016, Rome, Italy

Keywords: PM10, PAHs, VOCs, SOA, organic compounds.

Rome is a typical Mediterranean metropolitan region experiencing meteo-climatic conditions that frequently promote pollution characterized by high concentrations of ozone and particulate matter. These episodes are typically associated with hot sunny days in late spring and summer, and slow-moving or stagnant high-pressure air system. From the emission rate point of view, Rome is characterized by duty and all-the-day-persistent flows of vehicle traffic, with reduced average speed both in downtown and across the principal ways entering the city.

This paper describes an intensive monitoring study carried out in the framework of the ITALIA project, funded by the Italian Health Ministry. The ITALIA project was aimed to select a list of indexes based on concentration of pollutants, suitable for describing environmental quality and toxicity exposition of population. The corresponding maps would be also developed. For this purpose, the monitoring of a set of pollutants [both gas (Fig. 1) and particle-associated (Fig. 2), criteria and non-criteria] was performed in four urban sites located in downtown Rome and in one non-urban location in the Latium region. The present work presents the preliminary results of the sampling campaign carried out in June 2005.

The list of target compounds selected for our study includes C5~C9 volatile hydrocarbons (VOC), and ten gaseous aldehydes and ketones, as well as organic (polynuclear aromatic hydrocarbons PAHs, nitro-PAHs, methyl-PAHs, and n-alkanes) components associated to airborne particulates.

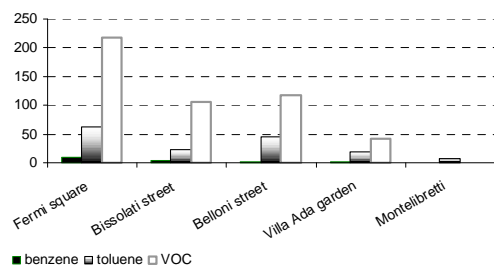


Fig 1. VOC concentrations in  $\mu\text{g}/\text{m}^3$  at the five sites.

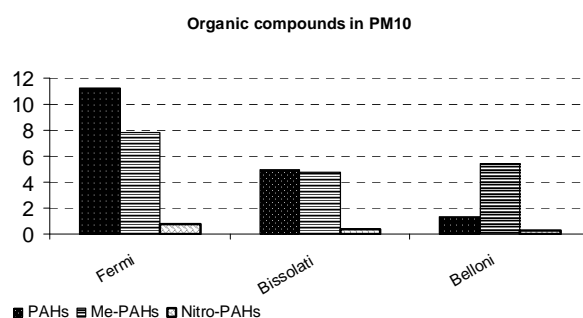


Fig 2. Particulate Organic PAHs, Methyl-PAHs, Nitro-PAHs downtown Rome in June 2005

The main purpose of the present study was to more accurately describe the environment as important tool to investigate the relationship of ambient toxic concentrations and health impacts.

This work was supported by the Italian Health Ministry, in the frame of the ITALIA project (PMS/025/2003) It is still in progress..

Heiden, A. C., Kobel, K., Komenda, M. Koppmann, R. & Shao, M. (1999). *Geophysical Research Letters*, 26, 9, 1283-1286.

Di Filippo, P.; Riccardi, C.; Incoronato, F.; Cecinato, A.; Sallusti, F. (2005). *Polycyclic Aromatic Compounds*. 25, 5, 393 – 406

Gariazzo, C.; Pelliccioni, A.; Di Filippo, P.; Sallusti, F.; Cecinato, A. (2005). *Water, Air and Soil Pollution*. 167, 17-3.

## Descriptive time series analysis of fine carbonaceous aerosol at Potsdam, New York

Ramya Sunder Raman and Philip K. Hopke

Department of Chemical and Biomolecular Engineering, and Centre for Air resources Engineering and Science, Clarkson University, Potsdam, NY, 13699-5708, USA

Keywords: Potsdam, NY, carbonaceous aerosol, auto-correlation function, cross-correlation function, SOC.

Samples of fine particulate matter (PM<sub>2.5</sub>) were collected on multiple filters in a speciation network sampler near Potsdam, NY from November 2002 to August 2005.

The Teflon filters were analyzed for PM<sub>2.5</sub> mass by gravimetry, black carbon (BC) by light transmittance, and elemental composition by XRF. Nylasorb and Teflon filters were leached and analyzed for anions and cations, respectively, by IC. The quartz fiber filters were analyzed for organic and elemental carbon (OC and EC) by a thermal-optical method and the remaining filter was leached and analyzed for short-chain, water-soluble acids by IC. Ozone concentrations measured at Perch River, NY (approximately 130 km southwest of Potsdam) were also used in the time series analysis.

Ambient air data usually display serial correlations. The auto-correlation function (ACF) of mass and carbonaceous species and cross-correlation function (CCF) between temperature, ozone and carbonaceous species concentrations were used to assess the importance of secondary organic carbon (SOC) formation during different seasons.

The analyses were performed using statistical software STATGRAPHICS Plus (Version 5.0, November 2000). The ACF measures the degree to which a time series variable  $y_t$  is correlated to its own past  $y_{t-k}$ , where  $y_{t-k}$  denotes the series measured 'k' time units in the past.

As an illustrative example, the seasonal differences in ACF during the period between November 2002 and October 2003 are discussed in detail. For this study, November 2002- April 2003 was considered as the warm months, while May 2003- October 2003 was considered as the cooler months. Figure 1 shows the lag-k ACF for mass and all of the carbonaceous species between November 2002 and April 2003 while Figure 2 shows same information between May 2003 and October 2003. In these figures the dotted lines indicate the 95% confidence level. Any ACF value outside the dotted lines indicates a significant value.

The observed differences in ACF values for carbonaceous species during the cooler months (Figure 1) and warm months (Figure 2) indicate that secondary sources are important contributors to the observed concentrations of mass, OC, formic, and oxalic acid during the photochemically active time of the year. This hypothesis was reinforced by the

observed autocorrelation of the oxidant, ozone during the warm months (Figure not shown). Mass, OC, formic, and oxalic acids (major species likely to have secondary sources) showed ACF trends similar to that exhibited by ozone.

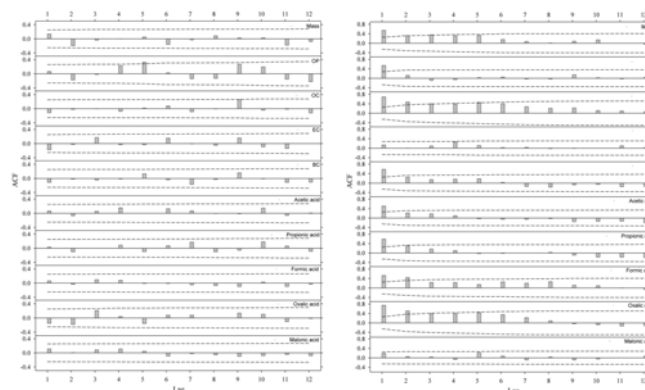


Figure 1 Lag-k ACF for mass and carbonaceous species at Potsdam from November 2002 - April 2003

Figure 2 Lag-k ACF for mass and carbonaceous species at Potsdam from May 2003 - October 2003

In order to assess the possible impact of temperature and ozone concentrations on the measured concentrations of mass, OC, and ions, the cross-correlation between these species during the warm and cooler months were examined.

During the cooler months OC and sulfate showed a statistically significant CCF with temperature. These values however were much lower than those observed during the warm months. During the warm months, all of the species except nitrate showed significant CCF's with temperature, extending over several lags. Further, an examination of CCF between OC, sulfate, mass and ozone concentrations also indicated significant CCF's at several lags during the warm months. These observations suggest the importance of temperature and oxidant driven secondary aerosol formation during the warm months compared to the cooler months.

This work was supported by NYSERDA, through grants 6083 and 7919. However, this work does not necessarily reflect the views of the agency and no official endorsement should be inferred.

## A inter-year climatology of urban aerosol and minor gas impurities in the east European region of Russia

O.G. Khutorova, G.M. Teptin

<sup>1</sup>Kazan State University, 18 Kremlevskaya St., Kazan, 420008, Russia

Keywords: atmospheric aerosols, synoptic variations

In this work we used a databank of measurements of aerosol and gaseous impurities concentrations by the net of automatic stations in urban region of Eastern Europe (54° N, 49° E), (53° N, 51° E). Distance between stations is 260 km. It allows investigating both temporal and spatial structure of variations of an aerosol. The measurement of the mass concentration of the aerosol by filter has the measurement accuracy - 1 µg/m<sup>3</sup>. Measurements are made at height of 2.4 m. The same point simultaneously concentrations of CO, NO, NO<sub>2</sub>, H<sub>2</sub>S, SO<sub>2</sub> and meteoroparameters - wind velocity and direction, temperature, relative humidity, pressure are measured. At present data for 1996-2006 are collected.

It is known that variations of atmospheric aerosols connected with weather systems. This work shows the inter-year climatology of synoptic processes on the variability of impurities concentration and on other atmospheric parameters.

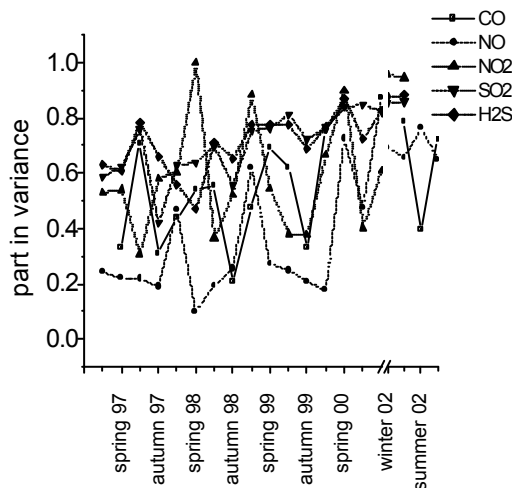
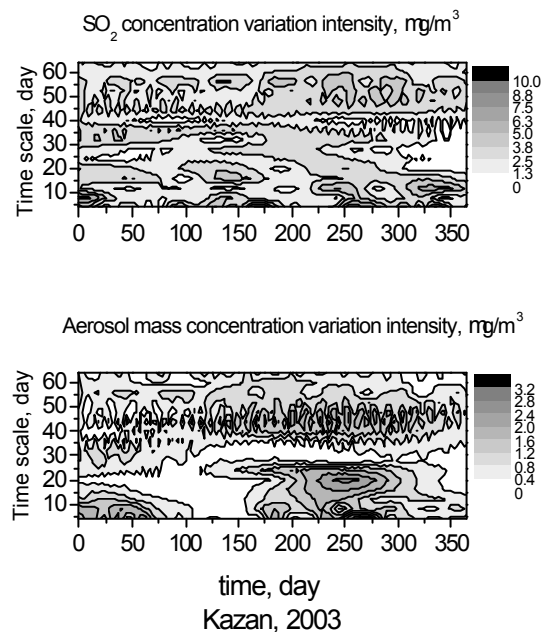


Figure1 Part of synoptic processes in the common variance for gaseous impurities

For each season of 1996-2005 we calculated the contributions of synoptic variability components into total variance of air pollutions. It is 10-45% of total variance. Cluster analysis allows us to find different magnitudes as similar. This work shows that a synoptic variation gives the significant part in the common variance of measured concen-

tration of minor gas impurities and aerosol concentration.

By the wavelet transform we analyze the series of concentrations simultaneously in temporal - frequency space (Figure 2). The wavelet transformations module (Mallat S.G., 1989) in case of a complex wavelet characterizes a time variation of the relative contribution a component of different time synoptic scales. For each impurity and meteoroparameter wavelet representation of synoptic variations intensity was built. Both in aerosol and gaseous impurities concentration variations with temporal scales 3-5, 7-10, 15, 30-35, 40-45 day were found.



The authors wish to thank the Russian Foundation of Basic Research (07-05-00862) and Academy of Science RT (09-9.5-32, 06-6.3-13) for supporting this work.

Mallat S.G., 1989, A theory for multisresolution signal decomposition: the wavelet representation. IEEE Trans. Pattn. Anal. Mach. Intell. 11, 5.

## Monitoring the road traffic aerosol pollution in urban air: a comparative study between several aerosol concentration metrics

S. Rodríguez<sup>1,2</sup>, E. Cuevas<sup>1</sup>, P.M. Romero<sup>1</sup>, R. Ramos<sup>1</sup>, X. Querol<sup>3</sup>, A. Alastuey<sup>3</sup>

<sup>1</sup> Izaña Atmospheric Observatory, INM-CSIC, Santa Cruz de Tenerife, 38071, Canary Islands, Spain

<sup>2</sup> Department of Geology, University of Huelva, Huelva, 21071, Spain

<sup>3</sup> Institute of Earth Sciences “Jaume Almera”, CSIC, Lluís Sole i Sabaris S/N, Barcelona, 08028, Spain

Keywords: road traffic, urban aerosols, black carbon, ultra-fine particles

This abstract summarises some of the results obtained in an intensive field campaign focused on assessing the ‘sensitivity’ of several metrics representative of the aerosol concentration to road traffic emissions in urban air. The campaign took place in a central urban background site in “Santa Cruz de Tenerife” city (Canary Islands, 28.47°N, 16.24°E): SCO - Santa Cruz Observatory. In this campaign the road traffic intensity was monitored in the main roads of the city. At SCO site, the following aerosol concentration metrics were monitored:

1. PM<sub>x</sub> = PM<sub>10</sub>, PM<sub>2.5</sub> and PM<sub>1</sub>, by ‘24-h sampling on filter’ and by ‘1-min Optical Particle Counter measurements (subsequently converting the aerosol volume to aerosol mass concentrations by experimentally conversion factors)’,
2. Black-Carbon = 1-min concentrations of BC less than 10µm (aerodynamic diameter) by placing a PM<sub>10</sub> impactor in the inlet of a Multi-Angle Absorption Photometer - MAAP,
3. Total number concentration of particles coarser than 3nanometer = N<sub>>3</sub> by an ultrafine condensation particle counter.

The results evidence that the N<sub>>3</sub> and (secondarily) BC concentration are much more sensitive to road traffic emissions than any PM<sub>x</sub> aerosol metrics. The mean “morning rush hours to nocturnal-background” ratio is about 5 for N<sub>>3</sub> and BC and ≈1.5 for all PM<sub>x</sub> concentrations metrics, and around 25 for road traffic intensity. Moreover, the correlation coefficient between the daily mean evolution of the “road traffic intensity” and the “aerosol concentration metrics” is 0.8-0.9 for N<sub>>3</sub> and BC and about 0.0 for PM<sub>x</sub>. The much more sensitivity of the number concentration N<sub>>3</sub> to road traffic is highlighted when correlating all data collected during the campaign, road traffic intensity exhibits a much higher correlation with N<sub>>3</sub> than with any other aerosol metrics (Figure 1).

The availability of simultaneous BC and N<sub>>3</sub> data allowed to identify the microphysical processes involved in the high N<sub>>3</sub> events. High concentrations of N<sub>>3</sub> during daylight were associated with high N<sub>>3</sub>/BC ratio under high solar radiation conditions,

which points to a significant involvement of new particles formation by photo-chemically induced nucleation processes.

The different behaviour we observe in the number N<sub>>3</sub>, BC and PM<sub>x</sub> aerosol metrics is due to the different influence of the ultrafine (<0.1µm), accumulation-mode (0.1-1µm) and coarse (>1µm) particles on these aerosol metrics. These results evidenced that road traffic emissions mostly affect to ultrafine particles which are the most important contributors to N<sub>>3</sub>. Our results together with a review of recent studies have been used to produce a conceptual model for understating how road traffic emission affects the different part of the aerosol’s size spectrum. This has implications on how road traffic aerosol pollution should be monitored in urban air.

Table 1. Mean concentration aerosols metrics at Santa Cruz de Tenerife during the 1 month intensive measurements campaign in 2006.

		mean
N <sub>&gt;3</sub>	cm <sup>-3</sup>	26305
BC	µg/m <sup>3</sup>	1.9
PM <sub>10</sub>	µg/m <sup>3</sup>	20
PM <sub>2.5</sub>	µg/m <sup>3</sup>	14
PM <sub>1</sub>	µg/m <sup>3</sup>	9

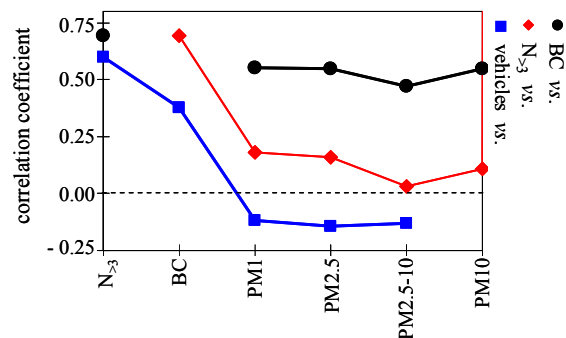


Figure 1. Correlation coefficient between road traffic intensity and several metrics of the aerosol concentration (based on 515 hourly and 3092 10-minutes data).

## Dispersion of Fine and Ultrafine Particles near the Berlin Urban Motorway: Derivation of Vehicular Emission Factors

W. Birmili<sup>1</sup>, B. Alaviippola<sup>1,2</sup>, D. Hinneburg<sup>1</sup>, O. Knöth<sup>1</sup>, K. König<sup>1</sup>,  
A. Sonntag<sup>1</sup>, D. Bake<sup>3</sup>, Th. Tuch<sup>4</sup>, S. Warwel<sup>5</sup>, J. Borcken<sup>5</sup>

<sup>1</sup>Leibniz Institute for Tropospheric Research, Permoserstrasse 15, 04318 Leipzig, Germany

<sup>2</sup>Finnish Meteorological Institute, P.O. Box 503, 00101 Helsinki, Finland

<sup>3</sup>UBA – Federal Environment Agency, Corrensplatz 1, 14195 Berlin, Germany

<sup>4</sup>UfZ – Centre for Environmental Research, Permoserstrasse 15, 04318 Leipzig, Germany

<sup>5</sup>DLR – German Aerospace Center, Rutherfordstrasse 2, 12489 Berlin, Germany

Keywords: urban aerosol, vehicle emission, traffic, microscale modelling

Atmospheric particles from traffic exhaust have been recognised as an environmental health hazard due to their small particle size as well as their fractions of soot and toxins. Besides direct emissions of soot, additional particles, mostly < 100 nm in diameter, may be formed as a result of gas-to-particle conversion in the free atmosphere downstream the vehicle pipes. To capture the real effects of traffic emissions on atmospheric particle number, measurements near traffic sources are required. Here, we report on particle size distribution measurements near an urban motorway and the associated small-scale dispersion modelling.

The field experiment PURAT 2 (*Particles in the Urban Atmosphere*) was conducted between July and September 2005 near the A115 motorway in Berlin, Germany. The six-lane motorway passes through densely populated residential areas about 7 km west of the city centre, carrying about 190000 vehicles a day. Airborne particle number size distributions of 10-500 nm in diameter were collected simultaneously at three observation sites using scanning mobility particle sizers (SMPS). Particle number size distributions at roadside showed a number maximum around a diameter of 30 nm, clearly related to the motorway emissions. The average particle number concentration at roadside was 28000 particles cm<sup>-3</sup>, decreasing to 10000 particles cm<sup>-3</sup> at two background measurement stations 40 and 800 m apart, respectively.

To characterise the atmospheric air flow in the vicinity of the motorway, the three-dimensional fluid model ASAM (All-Scale Atmospheric Model; Hinneburg and Knöth, 2005) was applied over a model domain of 500×500×100 meters in size (see Figure 1). Generally, the simulations were able to reproduce the spatial distribution pattern of traffic-related particles under different wind directions as suggested by the experiments.

Using the dispersion simulations and the measured particle number concentrations and traffic volumes, the method of inverse modelling was applied to derive emission factors for the motorway traffic. An average vehicle was determined to emit  $1.7 (\pm 0.5) \times 10^{14}$  particles per km driven, which is similar to values reported in former studies (Jamriska

and Morawska, 2001; Ketzel et al., 2003). Further analysis will include the derivation of particle number emission factors separately for passenger cars and light and heavy duty vehicles. Preliminary results indicate that heavy duty vehicles on the motorway emit 30–40 times more particles than passenger cars.

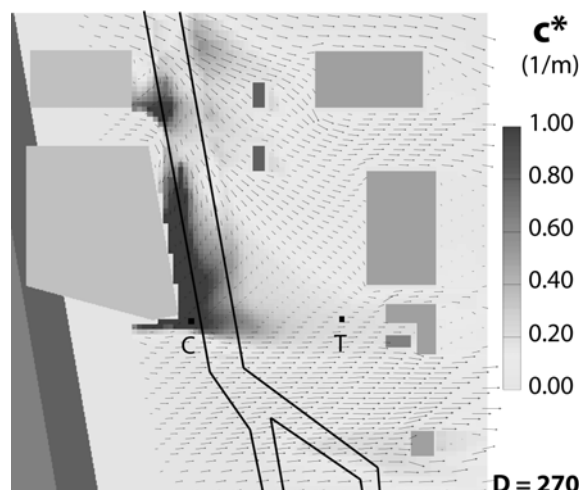


Figure 1: Three-dimensional simulation of the dispersion of traffic emissions near the A115 Berlin motorway, as indicated by normalized concentrations  $c^*$ . “C” and “T” denote the locations of roadside and background measurements, respectively.

Hinneburg, D. and Knöth, O. 2005. Non-dissipative cloud transport in Eulerian grid models by the volume-of-fluid (VOF) method. *Atmos. Env.* **39**, 4321-4330.

Jamriska, M. and Morawska, L. 2001. A model for determination of motor vehicle emission factors from on-road measurements with a focus on submicrometer particles. *Sci. Total Environ.* **264**, 241-255.

Ketzel, M., Wählin, P., Berkowicz, R. and Palmgren, F. 2003. Particle and trace gas emission factors under urban driving conditions in Copenhagen based on street and roof-level observations. *Atmos. Env.* **37**, 2735-2749.

This work was supported by the German Environmental Agency, UBA, project UFOPLAN 204-422-04/03 and the EU Marie Curie host fellowship contract number EVK2-CT-2002-57005.

## Urban particle number size distributions of ambient-state and non-volatile aerosols in Augsburg, Germany

K. Heinke<sup>1</sup>, W. Birmili<sup>1</sup>, A. Wiedensohler<sup>1</sup>, M. Pitz<sup>2,3</sup>, J. Cyrys<sup>2,3</sup>, and A. Peters<sup>2</sup>

<sup>1</sup>Leibniz Institute for Tropospheric Research, 04318 Leipzig, Germany

<sup>2</sup>GSF National Research Center for Environment and Health,  
Institute of Epidemiology, 85758 Neuherberg/Munich, Germany

<sup>3</sup>WZU - Environmental Science Center of the University Augsburg, 86159 Augsburg, Germany

Keywords: aerosol size distribution, urban aerosols, soot particles

Fine and ultrafine (< 100 nm) aerosol particles in the environment have moved into the interest of public health research due to their presumed adverse effects upon human health, such as cardiovascular and respiratory disease. While the adverse effects of ambient particles are in general widely acknowledged, there has been only little epidemiological evidence on the role of particular sub-fractions of the aerosol.

The city of Augsburg in Southern Germany hosts a centre of environmental medical research for the quantification of air pollutants and their effects on sensitive parts of the population (KORA; Holle et al. 2005). Specialized aerosol particle measurements were started in November 2004 in order to support future epidemiological studies within KORA.

As ambient particles are a complex mixture of a myriad of chemical compounds, there is a growing need to characterise and isolate those particular sub-fractions that are relevant to human health. Volatility analysis is a method that makes use of different volatilisation temperatures of chemical compounds, thereby separating volatile compounds, such as organic matter, sulfates and nitrates, from non-volatile compounds, such as soot and mineral dust. A volatilisation temperature of 300°C allows to identify soot particles in the ultrafine size range emitted from vehicular traffic (Wehner et al., 2004; Rose et al. 2006).

At the GSF research station Augsburg ambient state and non-volatile particle size distributions (3- 800 nm) have been measured continuously since 11/2004 using a twin differential mobility particle sizer (TDMPS).

Figure 1 presents median particle number size distribution for ambient and non-volatile compounds during the rush hour traffic; while the ambient particle number distribution peaks in the Aitken mode (~40 nm), the curve of non-volatile residues peaks in the nucleation mode (~10 nm) and in less-volatile particle mode (~80 nm) which presents the externally mixed population of soot particles. These measurements imply that within the measurement accuracy, every ambient particle contains a non-volatile core. The chemical composition of the non-volatile residues < 20 nm is, however, not known yet.

We will present a statistical summary of the 2-year data set, including an analysis of the relationship between total and non-volatile particle size distributions, and the meteorological factors that cause high concentrations of total and non-volatile particle fractions, such as wind direction, mixed layer height, and remote transport.

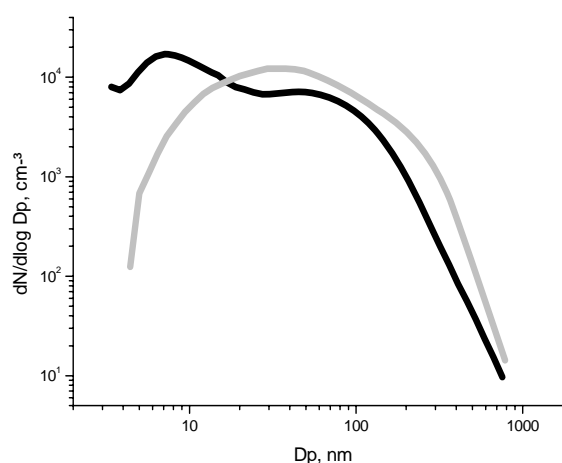


Figure 1: Median particle number size distribution of total (grey) and non-volatile (black) aerosol between 7:00 – 9:00 am.

- Holle, R., Happich, M., Löwel, H., Wichmann, H. E. (2005): KORA – A Research platform for population based health research, *Gesundheitswesen* 2005, 67 Sonderheft 1, S19-S25.
- Wehner, B., Philippin, S., Wiedensohler, A., Scheer, V., Vogt, R. (2004): Variability of non-volatile fractions of atmospheric aerosol particles with traffic influence, *Atmos. Env.*, 38, 6081-6090.
- Rose, D., Wehner, B., Ketzel, M., Engler, C., Voigtländer, J., Tuch, T., Wiedensohler, A. (2006): Atmospheric number size distributions of soot particles and estimation of emission factors, *Atmos. Chem. Phys.*, 6, 1021-1031.

## Microscale variations of atmospheric particle number size distributions in a densely built-up city area: Implications for exposure to traffic particles

M. Merkel<sup>1</sup>, S. Klöse<sup>1</sup>, W. Birmili<sup>1</sup>, A. Wiedensohler<sup>1</sup>, D. Hinneburg<sup>1</sup>, O. Knöth<sup>1</sup>, T. Tuch<sup>1,2</sup>, and U. Franck<sup>2</sup>

<sup>1</sup>Leibniz Institute for Tropospheric Research, Permoserstr. 15, 04318 Leipzig, Germany

<sup>2</sup>UFZ – Helmholtz Centre for Environmental Research, Permoserstr. 15, 04318 Leipzig, Germany

Keywords: DMPS, number size distribution, traffic, urban aerosols, exposure

The dominant source of aerosol particle number concentration in urban areas is combustion of fossil fuel in motor vehicles. Particle number size distributions near roads with high traffic are dominated by particles smaller than 100 nm in diameter. These anthropogenic submicron ( $< 1 \mu\text{m}$ ) and ultrafine ( $< 0.1 \mu\text{m}$ ) particles have moved into the focus of public health interest because they are suspected to contribute to acute and chronic disease in susceptible parts of the population.

To investigate the spatial and temporal variability of fine and ultrafine aerosol particles in the microscale environment around a street canyon, a specialised field experiment (PURAT: *Particles in the urban atmosphere*) was conducted. The measurements took place in the residential area around Eisenbahnstrasse in Leipzig, Germany. Particle number size distributions were measured continuously using differential mobility particle sizers over a time period of five months in winter 2005/2006 at the points (1)-(3) as indicated in Figure 1. Additional measurements at street level (4) between 06:00 and 10:00 were carried out to characterize microscale variations within the street canyon during a second period in July and August 2006. Regular direct intercomparisons between the instruments were made to ensure a maximum comparability of the size distributions at different points.

Our main findings are that the particle number concentrations at all four sites generally followed the general trend with concentrations backyard (3)  $<$  roof-top level (2)  $<$  street canyon (height 6 m) (1)  $<$  street canyon (ground level) (4) (see Figure 2). Particle concentrations in the backyard (3) were the lowest ( $\sim 5000 \text{ cm}^{-3}$ ), but particles on street level reached mean levels of  $25000 \text{ cm}^{-3}$ . The ratio of concentrations measured at different points did reach values of 10:1. Inside the street canyon, the measured concentrations were strongly influenced by the wind direction. The flow vortex in the street canyon (especially for northerly winds) influences the measurement points (1) and (4) directly. In this case they are downwind of the vehicular traffic as also shown by Voigtländer et al., 2006.

These first results suggest that the exposure to traffic-related particles in the outdoor environment of a densely built-up residential area exhibits substantial spatial variations. These variations need

to be considered in practical exposure assessments. The experimental results will be placed into context with simulations by a three-dimensional fluid model ASAM (All-Scale Atmospheric Model), which describes the dispersal of traffic aerosols within the domain at a spatial resolution down to 1.5 metres.

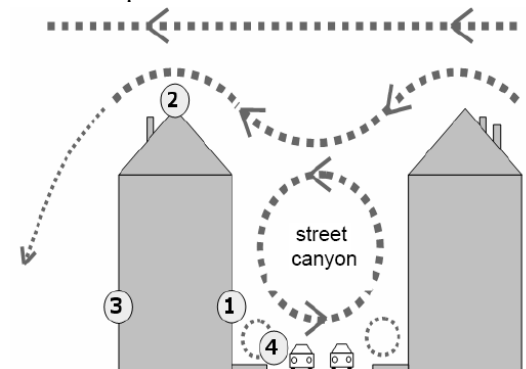


Figure 1. Sketch of the atmospheric air flow in the vicinity of the street canyon “Eisenbahnstrasse” in Leipzig, Germany. The numbers 1-4 indicate the measurement points for particle size distributions.

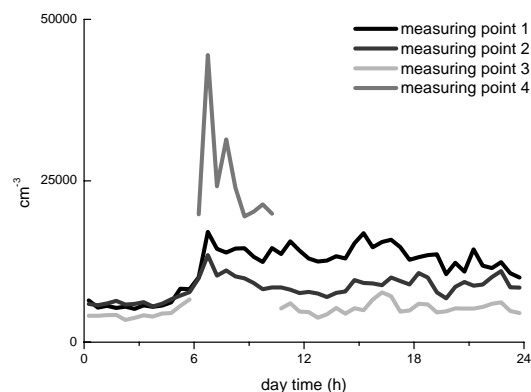


Figure 2. Mean diurnal cycle of particle number concentration (10-500 nm) at the four measurement points in the Eisenbahnstrasse, Leipzig.

Voigtländer J., T. Tuch, W. Birmili, and A. Wiedensohler. Correlation between traffic density and particle size distribution in a street canyon and the dependence on wind direction. *Atmos. Chem. Phys.*, 6:4275-4286, 2006.

This work was supported by UBA contract UFOPLAN No. 20442204/03 and the EU Marie Curie Reintegration Grant FP6-2002-Mobility-11 contract No. 510583.

## Nano/ultrafine particle behavior near intersection of busy roadway observed using a rapid type PM sizer

Hiroaki Minoura<sup>1,2</sup>, Shigeo Terada<sup>1,2</sup>, and Tomonori Takada<sup>1,3</sup>

<sup>1</sup>Petroleum Energy Center, 3-9, Toranomon 4-Chome, Minato-ku, Tokyo 105-0001, Japan

<sup>2</sup>Toyota Central R&D Labs., Inc., Nagakute, Aichi, 480-1192, Japan

<sup>3</sup>Japan Energy Corporation, Niizo-Minami, Toda, Saitama, 335-8502, Japan

Keywords: Ultrafine particles, Nanoparticles, Particle size distribution, Roadside

**1. Introduction** The behavior of nano/ultrafine PM in the roadside atmosphere has not been clarified in spite of its health influence attracting attention. Vehicle emissions are regarded as the dominant origin of nanoparticles (NPs) at roadside areas while photochemical nucleation has the potential to be another source in the summer (Minoura & Takekawa, 2005). The size distribution of NPs observed near intersections is variable due to the traffic conditions. The spatial distribution of NPs was observed by SMPSs multipoint observations (Minoura & Takada, 2005). However, the size distribution changes rapidly more than the SMPS scanning time when a vehicle pass by. In this study, we used the rapid type PM sizer and focused on the time variation of the NPs including volatile components (VCs) change.

**2. Observation** The observations were carried out at the curbside of the Ring 8 in Tokyo (average traffic volume is 2,400 vehicles/hr and the HDV type ratio is 11%). The PM was measured by an EEPS (TSI, Inc.) A thermo denuder (TD; Dekati, Ltd.) heated at 350 degrees Celsius was installed upstream of one EEPS, so that the VCs of the PM were removed. The sampling point was just curbside of Ring 8 and 50m behind (site A) and 5m beyond (site C) the intersection. Two sets of two EEPSs (with/wo TD) placed on the sidewalk were used. The number concentration (NC) was continuously monitored every 0.1sec. The 3D supersonic anemometer was used at the two sites. The traffic condition was monitored by four sets of video cameras and each vehicle movement was analyzed. Also, a micro traffic simulation model (Paramics; Edinburgh Univ.) was used to analyze the traffic flow.

### 3. Results

(1) The signal cycle of the intersection was 140sec. When the observed time series data was averaged every 140sec, a very smooth distribution of all the data could be obtained (Fig.1). Upstream of the measuring site, there is an offramp of expressway, and the traffic volume showed two peaks. The 1<sup>st</sup> peak of traffic volume (TV) in Fig.1v is due to vehicles from the express offramp, and 2<sup>nd</sup> peak is from the Ring 8. The NC showed two peaks also corresponding to TV change. However, the NC height showed a different tendency ( $NC_A < NC_C$  at 1<sup>st</sup>

peak;  $NC_A > NC_C$  at 2<sup>nd</sup> peak). The difference in driving condition at each site is one reason.

(2) The geometric mean diameter (GMD) of PM at site C located in downstream of the intersection, was big in comparison with site A, but, the tendency of GMD of non-volatile was opposite (Fig.1ii).

(3) The volume of VC at site C was larger than that at site A (Fig.1iii). It is thought that a lot of VC is emitted from a vehicle at a spot with much acceleration or jerk driving. (Fig.1iv).

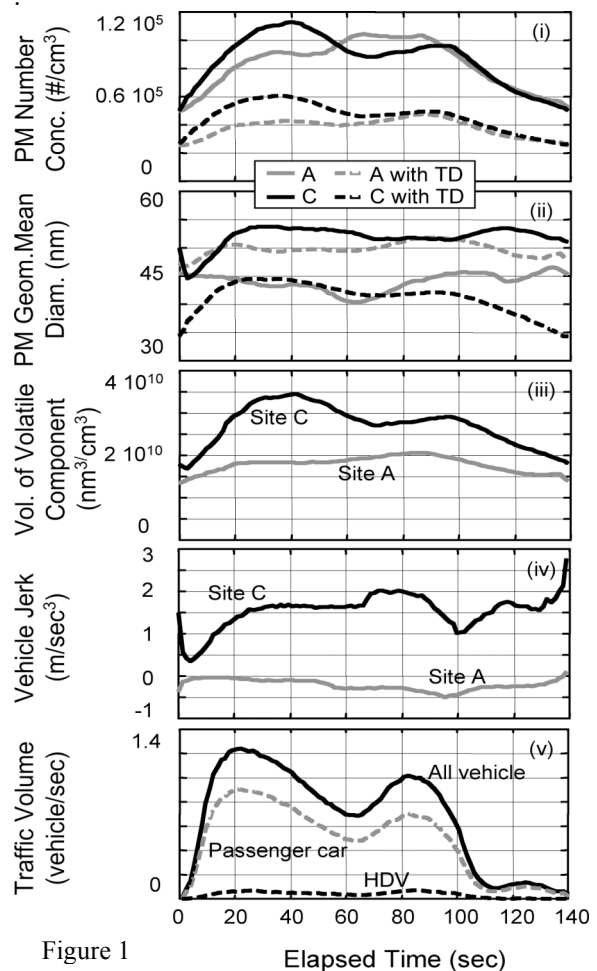


Figure 1

This work was supported by the Japan Clean Air Program of Ministry of Economy, Trade and Industry.

Minoura H. and Takekawa, H. (2005), Atmospheric Environment, 39, 5806-5816.  
 Minoura H. and Takada, T. (2005), EAC2005.

## Chemical characterization and source attribution of size-segregated aerosol collected at an urban site in Mediterranean basin

M. Rinaldi<sup>1</sup>, L. Emblico<sup>1</sup>, V. Mancinelli<sup>1</sup>, S. Decesari<sup>1</sup>, M. C. Facchini<sup>1</sup>, S. Fuzzi<sup>1</sup> and V. Librando<sup>2</sup>.

<sup>1</sup>Istituto di Scienze dell'Atmosfera e del Clima – CNR, via P. Gobetti 101, 40129, Bologna, Italy

<sup>2</sup>Dipartimento di Scienze Chimiche, Università di Catania, Viale A. Doria 6, 95125, Catania, Italy

Keywords: aerosol characterization, source apportionment, urban aerosols.

In this work, we carried out a detailed characterization of size segregated chemical composition of aerosol samples collected in typical urban street canyon conditions at Catania (Italy), representative of the Mediterranean environment and in proximity of large active volcano (Mount Etna). In this work we show that, with this detailed chemical study, it is possible to identify different aerosol sources, contributing to the total particles load, beside vehicular traffic.

Twelve aerosol samples were collected from 16<sup>th</sup> March to 13<sup>th</sup> June 2005. The sampling was performed using an 80 L/min five-stages Berner cascade impactor, operating with the following size intervals: 0.05 – 0.14  $\mu\text{m}$ , 0.14 – 0.42  $\mu\text{m}$ , 0.42 – 1.2  $\mu\text{m}$ , 1.2 – 3.5  $\mu\text{m}$ , 3.5 – 10  $\mu\text{m}$ . The samples were analysed for total aerosol mass, Water Soluble Organic Carbon (WSOC), Total Carbon (TC) and the main inorganic ionic species. The Water-Insoluble Carbon (WINC) was derived by difference: TC – WSOC.

The samples exhibit some common features: ammonium sulphate and carbon-containing species (both soluble and insoluble) are the largest contributors of fine particle mass, while coarse particles are essentially composed of sea-salt, sodium nitrate and unaccounted PM (probably crustal material). The WINC/WSOC ratio decreases from the smallest size range to the large accumulation mode range (0.42 – 1.2  $\mu\text{m}$ ), while  $\text{nssSO}_4^{2-}$  and  $\text{NH}_4^+$  concentration increases as the size decreases. The water-insoluble carbonaceous matter is the dominant component (70 % of PM) in smallest particles (0.05-0.14  $\mu\text{m}$ ), but its contribution to particle mass strongly decreases at larger diameters: 13% in large accumulation mode particles and 7% in coarse particles. By contrast, WSOC concentration and total aerosol mass exhibit a peak in the large accumulation mode size range (0.42 – 1.2  $\mu\text{m}$ ), therefore showing a size distribution typical of the secondary inorganic aerosol species (as ammonium sulphate).

In conclusion, we identified four different aerosol types, corresponding to different sources, contributing to the total particles load of the investigated urban environment. The first source identified is vehicular traffic, producing primary carbonaceous insoluble particles with maximum air concentration in Aitken particles and in the smallest

accumulation mode particles. Secondary aerosols dominate, instead, the composition of accumulation mode particles (aerodynamic diameters between 0.14 and 1.2  $\mu\text{m}$ ) with main components being WSOC and ammonium sulphate. Organic matter in this mode is mainly soluble indicating the presence of more oxidized functional groups, likely due to gas-to-particle conversion of semi-volatile photo-oxidized gaseous organic compounds. Finally, modified (e.g., nitrate-containing) sea salt particles and mineral dust are the dominant component of coarse particles. While the insoluble carbon particles emitted by local traffic constantly occur in the low size intervals, the concentrations of the secondary organic and inorganic components, as well as of sea-salt particles vary between samples according to different wind regimes and occurrence of regional pollution episodes in the central Mediterranean Basin.

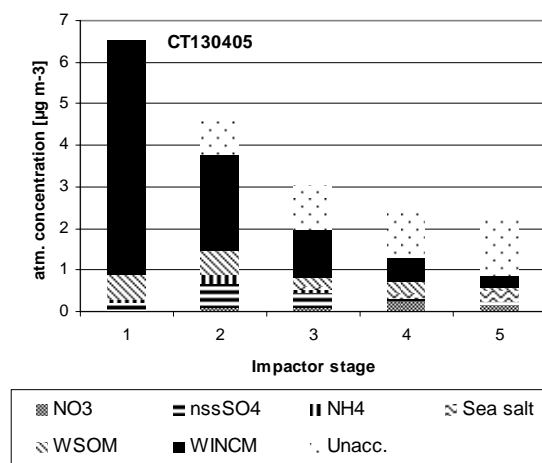


Figure 1. Size segregated chemical composition of a sample (13 April 2005) dominated by traffic emissions.

## Determination of particulate carbonaceous species in an urban background aerosol in Nairobi, Kenya.

M. J. Gatari<sup>1</sup>, M. D. Hays<sup>2</sup>, R. J. Lavrich<sup>2</sup> and S. M. Gaita<sup>1</sup>

<sup>1</sup>Institute of Nuclear Science & Technology, College of Architecture and Engineering, University of Nairobi, P. O. Box 30197-00100, Nairobi, Kenya

<sup>2</sup>U. S. Environmental Protection Agency, National Risk Management Research Laboratory, 109 TW Alexander Drive, Research Triangle Park, NC 27711

Keywords: Alkanes, PAHs, thermal desorption, polycyclic aromatic compounds, urban aerosols

Tropospheric carbonaceous pollutants play an important role in the physical and chemical processes in the atmosphere. Some of the polycyclic aromatic compounds (PACs) are mutagenic and genotoxic carcinogens and any level of exposure may increase risks of cancer. These pollutants are poorly understood and their characterization in the African aerosol is very low. The following work is a preliminary solution to jump start their investigation in Nairobi aerosol (Figure 1).

A Hi-Vol sampler was used to collect airborne particles on quartz fibre filters at a site that was 25 m above ground level. The sampler cut off aerodynamic diameter was about 30-50  $\mu\text{m}$ . The filters were preconditioned at 550 °C before use and after sampling they were well parked and sent to U. S. Environmental Protection Agency (USEPA) laboratories in California for analysis. A direct thermal desorption-gas chromatography-mass spectrometry was used to quantify alkanes and PAHs while a thermal method was used for organic (OC) and elemental carbon (EC).

The measured mean concentrations in  $\mu\text{g m}^{-3}$  were  $153 \pm 13$ ,  $25 \pm 2$ ,  $15 \pm 1$  and  $40 \pm 4$  for particulate mass (PM), OC, EC and total carbon (TC) respectively. Twenty one alkane species with 12 to 35 carbons (n-dodecane to n-pentatriacontane) were detected in the samples. Their mean concentrations ranged from  $0.02 \pm 0.02 \text{ ng m}^{-3}$  of 17A(H)-22,29,30-Trisnorhopane to  $7.2 \pm 0.7 \text{ ng m}^{-3}$  of n-nonacosane. The concentrations of polycyclic aromatic hydrocarbons (PAHs) are shown in Figure 2. These concentrations are artefacts affected due to adsorption and absorption on the filters besides environmental changes during transport. The mean total carbon content in the PM was 26 % while EC was 10 %. These values were lower than those previously measured at the same site in  $\text{PM}_{2.5}$ . However the cut off size of the previously sampled particles were < 3 decades in size than in this study. High resolution quantification of atmospheric hydrocarbons (HCs) could play a major role in aerosol source identification and apportionment especially those originating from energy provisioning activities. The carbon contents of HCs that are emitted from these products are well understood in geochemistry. Cholestane is a biomarker of refined

petroleum products. Particulate alkanes of 27 to 33 carbons are predominantly in biogenic emissions. The obtained background concentrations are precursors of possible higher levels in the urban aerosol of Nairobi and it needs priority investigation.

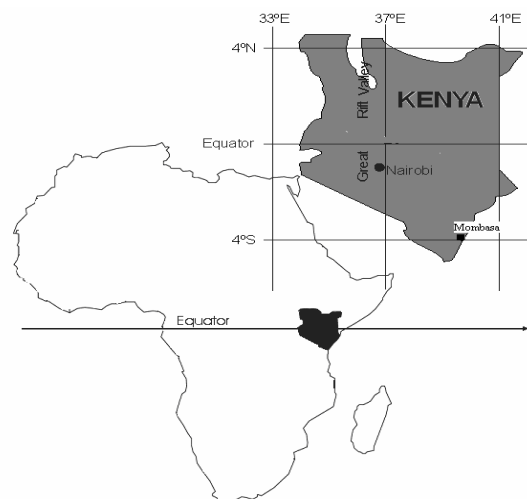


Figure 1. Geographical location of Kenya

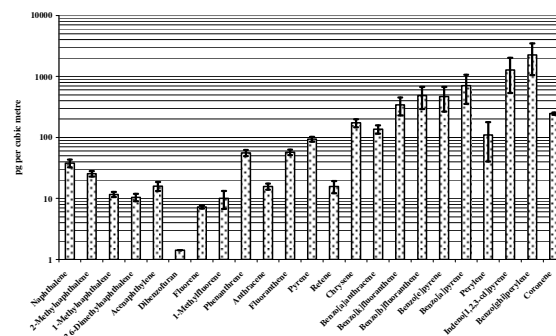


Figure 2. Mean concentrations of PAHs in  $\text{pg m}^{-3}$ .

This work was supported by USEPA and International Science Programs, Sweden.

Finlayson-Pitts, B. J., & Pitts Jr J. N. (2000). *Chemistry of the Upper and Lower Atmosphere*. San Diego, U.S.A.: Academic Press

Hays, M. D., & Lavrich, R. J. (2006). in *Trends in analytical Chemistry*, doi:10.1016/j.tac.2006.08.007

## A wintertime study of atmospheric aerosols collected in São Paulo, Brazil.

P.C. Vasconcellos<sup>1</sup>, L. Ogura<sup>1</sup>, W. Lopes<sup>2</sup>, P. A. Pereira<sup>2</sup>, J. Andrade<sup>2</sup>, O. Sanchez-Ccoyllo<sup>3</sup>.

<sup>1</sup>Department of Chemistry, University of São Paulo, Av. Lineu Prestes 748, 05508-000, São Paulo, Brazil

<sup>2</sup>Department of Chemistry, Federal University of Bahia, Rua Barão de Geremeoabo 147, 40170-290, Salvador, Brazil

<sup>3</sup>Department of Atmospheric Sciences, University of São Paulo, Rua do Matão, 05508-000, São Paulo, Brazil

Keywords: gravimetric analysis, PAH, organic compounds, megacity, atmospheric pollution.

Atmospheric pollution has become a significant problem for urban areas worldwide. In megacities aerosols are released by different emissions sources. These sources can emit particles in a large variety of sizes. Size distributions provide information on the sources and the sources processes of particles or species (Maenhaut et al. 2002).

In the wintertime (2005) twenty PM<sub>10</sub> samples were collected in São Paulo city using hi-vol sampler and fine particles (from 6 to 18,000 nm) were collected using NanoMoudi impactor.

Polycyclic aromatic hydrocarbons (PAH) recognised as mutagen and carcinogen compounds were identified in PM<sub>10</sub> samples and gravimetric concentrations were calculated for fine particles.

The results showed PAH total concentrations ranged from 0.27 to 43.8 ng m<sup>-3</sup> (Figure 1). Phenanthrene (7.3 ng m<sup>-3</sup>) and anthracene (2.2 ng m<sup>-3</sup>), lighter compounds were the most abundant PAH; benz(a)pyrene (1.4 ng m<sup>-3</sup>) mutagenic compound was found in higher concentration than previous work (Vasconcellos et al., 2001).

For PM<sub>10</sub> concentrations, 60% of the samples (n=12) are higher than WHO standards (50 µg m<sup>-3</sup>).

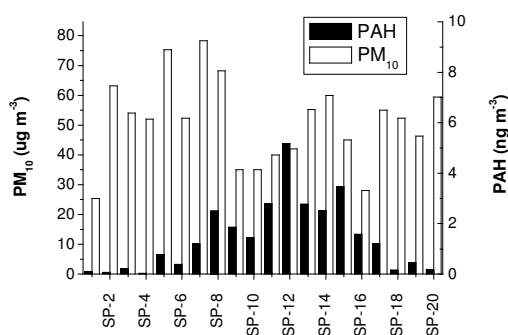


Figure 1. PAH and PM<sub>10</sub> concentrations

Figure 2 presents the particle size distribution of the samples collected in the cascade impactor. Three modes can be found in the particles with mean diameter: 44 nm, 440 nm and 14000 nm. It is in agreement with the fact this site is located inside a large green area (campus of the University of São

Paulo), which can be source of particles between 25 and 440 nm (Finlayson-Pitts and Pitts, 2000).

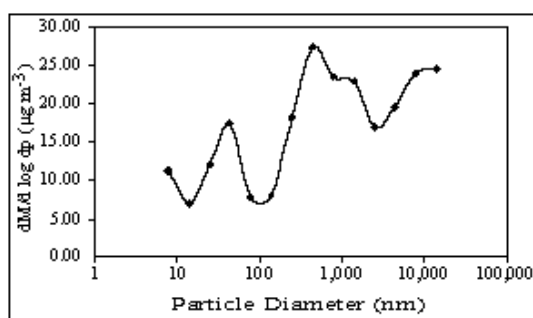


Figure 2. Mass size distribution for the sampling during winter 2005 campaign.

We conclude that at this urban site vehicular emissions are indicated as being the most important PAH emitters. For fine particles, soil resuspension and biogenic emissions seem to be the most important sources.

This work is supported by Fundação de Amparo à Pesquisa do Estado de São Paulo.

Finlayson-Pitts, B.J & Pitts Jr, J.N. (2000). Chemistry of Upper and Lower Atmosphere, Academic Press, USA.

Maenhaut, W., Cafmeyer, J., Dubtsov, S. & Chi, X. (2002). Nuclear Instruments and Methods in Physics Research B189, 238-242.

Vasconcellos, P.C., Zacarias, D., Pool, C. & Carvalho, L. (2001). Atmospheric Environment, 37,3009-3018.

## UFIPOLNET: Concentration of Particle Number Distributions at 4 Stations in Europe

H. Gerwig<sup>1</sup>, G. Löschau<sup>1</sup>, L. Hillemann<sup>2</sup>, B. Wehner<sup>3</sup>, A. Wiedensohler<sup>3</sup>, A. Zschoppe<sup>4</sup>, C. Peters<sup>4</sup>, A. Rudolph<sup>4</sup>, C. Johansson<sup>5</sup>, J. Cyrys<sup>6</sup>, M. Pitz<sup>6</sup>, R. Rückerl<sup>6</sup>, J. Novak<sup>7</sup>, H.G. Horn<sup>8</sup>, R. Caldow<sup>9</sup>, G.J. Sem<sup>9</sup>

<sup>1</sup>LfUG - Section Air Quality, Saxon State Agency for Environment and Geology, 01109 Dresden, Germany

<sup>2</sup>UBG – Staatliche Umweltbetriebsgesellschaft, 01445 Radebeul, Germany

<sup>3</sup>Leibniz-Institute for Tropospheric Research, 04318 Leipzig, Germany

<sup>4</sup>Topas GmbH, 01279 Dresden, Germany

<sup>5</sup>ITM – Department of Applied Environmental Science, Stockholm University, 106 91 Stockholm, Sweden

<sup>6</sup>GSF National Research Centre for Environment and Health, 85764 Neuherberg, Germany

<sup>7</sup>CHMI – Czech Hydrometeorological Institute, 14306 Prague, Czech Republic

<sup>8</sup>TSI GmbH, 52068 Aachen, Germany

<sup>9</sup>TSI Inc., Shoreview, Minnesota, 55126, USA

Keywords: number concentration, number size distribution, particle concentration, urban aerosols

Several studies show a decline of particle mass concentrations in Central Europe of TSP and PM10 since 1990. In contrast, particle number concentrations of ultrafine particles (< 100 nm = UFP) were not changed during winter periods 1991 – 1999 in Erfurt/Germany (Cyrys et al. 2002). There are however only a limited number of long-term UFP measurements in Europe. Epidemiological studies showed a relationship between high number concentrations of UFP and adverse health effects.

The European Commission needs therefore more information about UFP concentrations for evaluation processes within the CAFE process and the Thematic Strategy on Air Pollution.

The project UFIPOLNET (Ultrafine Particle Size Distributions in Air Pollution Monitoring Networks) intends to demonstrate that the newly developed Ultrafine Particle Monitor UFP 330 is able to perform adequately in routine network operation.

The instrument produces a number size distribution from 20 to 500 nm. Only 6 size classes >20, > 30, > 50, > 70, > 100, >200 (N1 – N6) are transferred to the central measurement network stations to reduce the amount of data collected in the databases.

First comparisons with a DMPS for ambient aerosols (Wehner et al. this issue) show a good correlation with a DMPS measuring in parallel at a street canyon site.

Since December 2006 in Dresden and February 2007 in Augsburg, Stockholm and Prague, the UFP 330 will run continuously until October. It is planned to run the instruments on a permanent basis for a longer period. All sites are near busy roads; Augsburg is an urban background site.

The number concentrations will be correlated with nitrogen oxides, benzene and other continuously measured parameters in a routine measuring network. In some places, traffic numbers will be correlated with the measurements.

At three stations, SMPS/DMPS size spectrometers have been monitoring for several years. Figure 1 compares the annual mean

concentrations of total number concentrations per station (2003 – 2005). Augsburg shows about half, Stockholm twice as many particles as Dresden. Prague and Dresden show almost the same concentration of NOx in 2005, while the street canyon of Stockholm shows almost twice the concentration. The correlation with NOx indicates the traffic influence (Birmili, 2006).

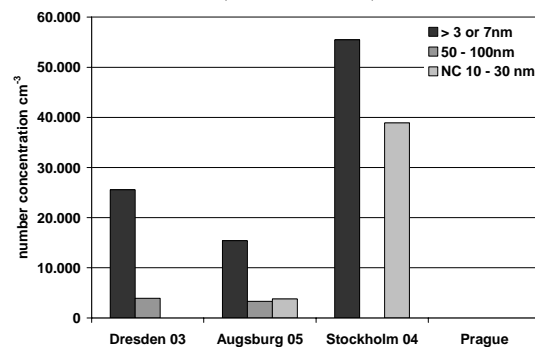


Figure 1: Number concentrations at the 3 stations with reference instruments

One aim of UFIPOLNET is to harmonise the sampling conditions (particle pre-impaction and humidity) as well as the evaluation of identical size classes. In this way, interpretations of particle number concentrations and size distributions will be facilitated. Comparable results will permit analysis of absolute differences between ultrafine aerosol size distributions at many polluted sites over long periods.

UFIPOLNET ([www.ufipolnet.eu](http://www.ufipolnet.eu)) is financed by the LIFE financial instrument of the European Community under No. LIFE04 ENV/D/000054.

J. Cyrys, J. Heinrich, A. Peters, W. Kreyling, and H.E. Wichmann (2002). *Umweltmed Forsch Prax.*, 7, 67-77.

Birmili, W. (2006). Editor: D. Bake; *Forschungsbericht* 203 43 257/05 UBA-FB 000942 ; *UBA Texte* 26 – 06, Umweltbundesamt, Berlin.

## Time evolution of fine and ultrafine ambient particles in a Madrid suburban site.

M. Puadas<sup>1</sup>, F.J.G. Mez-Moreno<sup>1</sup>, J. Plaza<sup>1</sup>, J. Rodríguez-Maroto<sup>1</sup>, M. Sánchez<sup>2</sup>, E. Coz<sup>1</sup> and B. Artano<sup>1</sup>

<sup>1</sup>Department of Environment, CIEMAT, Avda. Complutense 22, E-28040, Madrid, Spain

<sup>2</sup>Department of Technology, CIEMAT, Avda. Complutense 22, E-28040, Madrid, Spain

Keywords: aerosol size distribution, chemical composition, particle growth, ultrafine particles, urban aerosols

This work summarizes one year (Feb 2006-Feb 2007) of continuous and semi-continuous measurements of physico-chemical properties of fine and ultrafine ambient aerosol at CIEMAT, a place located in a suburban area of Madrid.

The main goal of this campaign was to document the time evolution of the aerosol size distribution and its linked phenomena. The particle size distribution has been measured by a TSI-SMPS (DMA 3071 and CNC 3025) (Stainer et al., 2004) and the particle chemical composition by the R&P carbonaceous aerosol and particulate nitrate monitors, MOUDI and denuder/filter sampling techniques coupled to ion chromatography analysis. Different gaseous pollutants, which could participate in the aerosol chemical transformation, have been measured by a DOAS spectrometer (OPSIS AR-500).

The observed changes in the distributions have been related to the growth and chemical changes of fine particles during air pollution episodes. This growth of the particle mean diameter has been studied by automatic fitting the size measurements (20-600 nm) to bimodal distributions (Van Dingenen et al., 2005). The results have shown the typical presence of two modes: one centred around 35-45 nm and other located around 80-100 nm. During daytime, the first mode, associated to coagulated primary particles, did not vary essentially its position, although its presence was much more intense during emission hours. On the other hand the second mode, corresponding to secondary aerosol, experienced an increase of its relative weight along the time and showed a clear change of its position from 80 to 110 nm. This behaviour was observed especially during pollution episodes and in a time scale of 4-5 hours (fig. 1). This evolution in poor atmospheric dispersion situations used to be associated to increases of PM<sub>2.5</sub> nitrate, sulphate and organic carbon and a remarkable photochemical activity.

Some MOUDI measurements have shown that the increase in the particulate nitrate concentration can be mainly found in the size range 300-800 nm. At the same time, the evolution of the corresponding volume distributions clearly reflects the continuous concentration increase of the secondary particle size in the accumulation range (i.e. at 500 nm) (fig. 2).

These simultaneous increases suggest that this aerosol growth could be related to this chemical change. Some condensation processes, for both water soluble inorganic compounds and low volatile organic photooxidation products, would play a main role, pointing out the relevance of the condensation-aggregation processes.

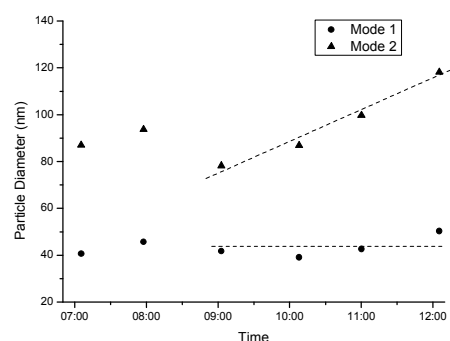


Figure 1. Evolution of two mode diameters during a pollution episode (9 Feb 2006)

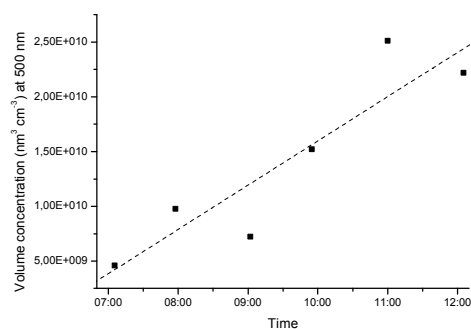


Figure 2. Evolution of the volume concentration for 500-nm particles (9 Feb 2006)

This work has been developed in the framework of the EFFESO project funded by the Spanish Ministry of Education and Science (Plan Nacional I D I, CG 2004-05984-C07-07).

Stanier, C.O., A.Y. Khlystov and S.N. Pandis, 2004. Atmos. Environ. 38, 3275.

Van Dingenen, R., J.P. Putaud, S. Martins-Dos Santos and F. Raes, 2005. Atmos. Chem. Phys. 5, 2203.

## Contribution of anthropogenic and biogenic aerosol sources in three Austrian cities

P. Kotianová, I. L. Maar and H. Puxbaum

Institute of Chemical Technologies and Analytics, Vienna University of Technology,  
Getreidemarkt 9/164-AC, A-1060 Vienna, Austria

Keywords: PAHs, n-alkanes, PM10, source identification.

The EU short term limit for the PM10 concentration is  $50 \mu\text{g}/\text{m}^3$  daily mean and for years 2005-2009 it may not be exceeded more than 30 times a year. In fact, at many urban sites the EU PM10 daily mean is exceeded many more times in the year, which raises the questions, what is this PM and where does it come from? Knowing what the sources are could help to reduce air pollution by more effective regulation of emission sources.

The primary sources are either connected with human activity or they have natural origin and the estimation of individual source contribution to the PM10 fraction is based on utilization of a specific species, markers. The aim of this study was to evaluate some sources contribution via determination of non-polar and semi-polar organic compounds.

The atmospheric aerosols were collected at urban, urban-fringe and rural sites in Vienna, Graz, and Salzburg during the year 2004. Selected polycyclic aromatic hydrocarbons (PAHs) and their derivatives were determined, which serve as tracers of vehicle exhaust, wood combustion, natural gas combustion. Furthermore, normal alkanes  $\text{C}_{24}\text{-C}_{33}$  were quantified to differentiate vegetative detritus.

The differentiation of sources is possible via known PAHs ratios in source emissions. Thus, it was found out, that non-traffic sources have higher input to polycyclic aromatic hydrocarbons in winter season and that the traffic emissions come predominantly from diesel engines.

The specific marker for natural gas burning, benzo(de)anthracene-7-one, showed high concentrations in January-February and in November-December 2004 (up to  $5 \text{ ng}/\text{m}^3$  in Vienna and Salzburg, up to  $16 \text{ ng}/\text{m}^3$  in Graz), while in summer it was often below the detection limit of  $0.1 \text{ ng}/\text{m}^3$ . This is in keeping with the suggestion that it can be used as a marker for natural gas combustion. The wood combustion is reported to be identified via retene. However, the concentrations did not always show the expected yearly trend. So, the usage of retene as wood smoke marker is questionable.

The relatively high value of urban impact for total n-alkanes  $\text{C}_{24}\text{-C}_{33}$  (e.g. 30% for Vienna) suggests that a high proportion of them come from local sources. Among normal alkanes sources, traffic emissions and vegetative detritus are proposed to be the strongest. Basically on their composition differences, the origin of n-alkanes can be assigned. The strong contribution of vegetative detritus was identified summer according carbon preference index (CPI) values higher than 2.0, typical for urban areas, and via higher plant wax number (% WAX). The plant wax contribution to total n-alkanes is in winter usually less than 15%, but in summer it can be over 40%. Although CPI and % WAX numbers were higher at not inner city sampling sites, it was found out that relative composition of total n-alkanes varied more with time than with a location.

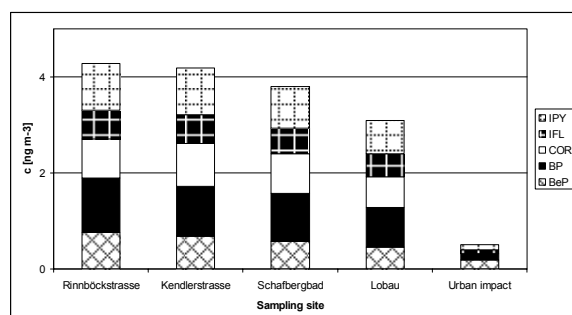


Figure 1. Yearly mean concentrations of selected 5-7 rings PAHs at Vienna sampling sites in year 2004.

The yearly mean concentrations of selected PAHs were only slightly higher at urban sites than at the rural sites, suggesting that long range transport plays the main role in distribution of PAHs in the atmosphere. A little bit higher urban impact was found for retene and benzo(de)anthracene-7-one, what indicates contribution of local sources as well as role of transport, probably at regional level.

As the main source of selected 5-7 rings PAHs is considered vehicle exhaust. Other sources are also anthropogenic and are connected with

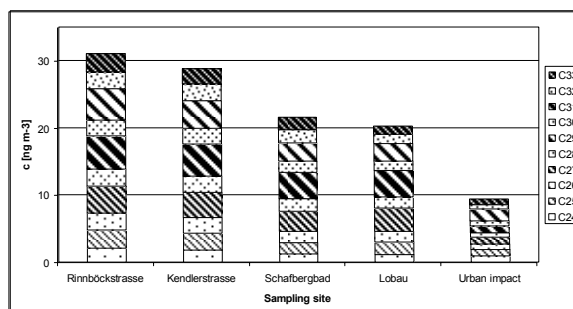


Figure 2. Yearly mean concentrations of n-alkanes  $\text{C}_{24}\text{-C}_{33}$  at Vienna sampling sites in year 2004.

## Characterization of different pollution levels in Beijing, China with relation to air mass classification

B. Wehner<sup>1</sup>, F. Ditas<sup>1</sup>, W. Birmili<sup>1</sup>, A. Wiedensohler<sup>1</sup>,  
 J. Wu<sup>2</sup>, M. Hu<sup>2</sup>

<sup>1</sup> Leibniz-Institute for Tropospheric Research, 04318 Leipzig, Germany

<sup>2</sup> College of Environmental Sciences, Peking University, Beijing 100871, P. R. China

Keywords: number size distribution, back trajectories, mega city

Beijing with approximately 15 million inhabitants is one of the megacities in the world. Along with rapid economic growth and vehicle increase (11% per year in China), the features of air pollution in Beijing are changing from typical coal-combustion pollution to a compound pollution case.

Since March 2003, number size distributions from 3 nm to 10 μm have been measured using a Twin DMPS in conjunction with an APS (TSI 3321). The measurement site is located on the Campus of Peking University in the urban area of Beijing (Wehner et al., 2004). Within this study 2 years of data have been analyzed. Number size distributions as resulting integral number and volume concentrations have been classified according to air mass history, i.e. direction of the backtrajectories calculated by the HYSPIT model.

All measurement days were classified according to the direction of the backtrajectory during the last 3 days before arriving at the site. Three main directions were defined: Northwest (NW), northeast (NE), and south (S), covering all of the observed cases. More polluted regions are located south and east of Beijing while the northern surroundings are densely polluted and characterized by mountain. In addition a fourth type has been defined containing the backtrajectories which spent the last two days within the urban area of Beijing (local, loc). The dominating types were NW (331 days), S (205 days), and loc (37 days) and will be analysed in more detail here.

Figure 1 shows the calculated mass concentration ( $< 10 \mu\text{m}$ ) divided into the three main air mass types. The length of the 3-day backtrajectory was also used to calculate the mean air mass transportation speed ( $v$ ). This  $v$  shows significant differences between the individual classes, which reflects the wind climatology in Northern China: for air masses coming from the south or local areas  $v$  is  $1.5 \text{ m s}^{-1}$  while for air masses from the north it is on average  $2.5 \text{ m s}^{-1}$ . Also, air masses from the north are connected with lower aerosol mass concentration. This has probably two reasons: 1. there are less pollution sources north of Beijing, 2. the air masses travel faster and thus they have less time to accumulate aerosol mass.

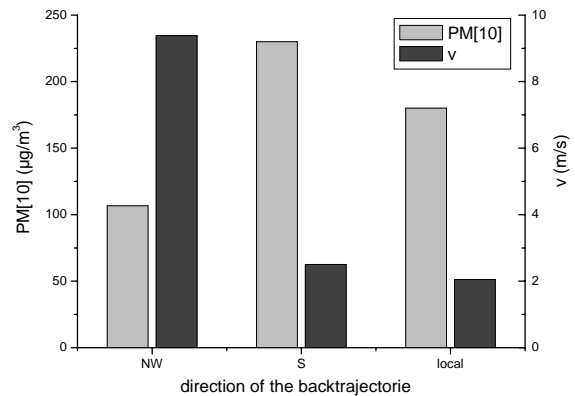


Figure 1: Calculated PM10 mass concentration and air mass transportation speed in relation to direction of the backtrajectory.

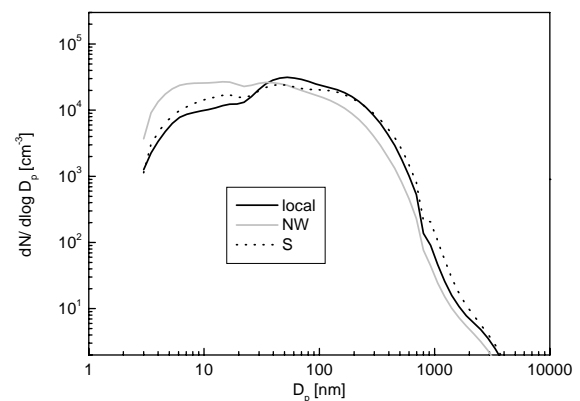


Figure 2: Mean number size distributions at 14:00 local time for the three classes.

Figure 2 shows the mean number size distributions at 14:00 local time for the three air mass classifications. Accumulation and coarse mode is highest for local and southern air masses while nucleation mode particle concentration is higher for northern air masses. Due to the lower condensation sink new particle formation is more frequent for these cases.

### Reference

Wehner, B., A. Wiedensohler, T.M. Tuch, J. Wu, M. Hu, J. Slanina, C.S. Kiang (2004). Variability of the aerosol number size distribution in Beijing, China: New particle formation, dust storms, and high continental background. *Geophys. Res. Lett.* **31**(22): 22108, doi:10.1029/2004G021596.

## Mixing state of non volatile particle fractions in two Chinese mega city areas

B. Wehner<sup>1</sup>, M. Berghof<sup>1</sup>, P. Achtert<sup>1</sup>, A. Nowak<sup>1</sup>, A. Wiedensohler<sup>1</sup>,  
Y.F. Cheng<sup>2</sup>, M. Hu<sup>2</sup>, Y.H. Zhang<sup>2</sup>, T. Zhu<sup>2</sup>

<sup>1</sup>Leibniz-Institute for Tropospheric Research, 04318 Leipzig, Germany

<sup>2</sup>College of Environmental Sciences, Peking University, Beijing 100871, P. R. China

Keywords: volatility, mixing state, mega city

Along with the increasing population density in China, the urbanization increases leading to a growing number of so-called mega cities. In China, these large cities are mainly located within three distinct areas, so called city clusters. Here the problems of urban air pollution are extended to a whole region. Very frequent the pollution is obvious as hazy layer covering a large area and decreasing the visibility. To estimate the effect on regional and global climate the knowledge of absorbing and scattering compounds as well as their mixing state is important to know.

A Volatility Tandem DMA (VTDMA) has been used to measure the non volatile fraction (at 300°C) of submicrometer aerosol particles. A first DMA selects one particle diameter between 30 and 320 nm. This quasi monodisperse size fraction passes a heating column followed by a DMPS system measuring the size distribution of the remaining fraction. This size distribution can be typically divided into two fractions: a less volatile one including those particles changing their diameter by less than 5% due to heating and a more volatile one including those particles with significant size change due to heating. The less volatile fraction is equivalent with externally mixed non volatile material, in the size range from 30 to 350 nm most likely elemental carbon. The second group consists of internally mixed non volatile material. In combination with number size distribution the number concentration of e.g. the externally mixed non volatile particles was calculated.

To experiments have been performed: PRIDE PRD between July 4 and 25, 2006 in Backgarden located 70 km northwest of Guangzhou in the Pearl River Delta and Carebeijing between August 12 and September 9, 2006 in Yufa located 60 km south of Beijing.

Figure 1 shows the evolution of externally mixed non volatile particles, i.e. elemental carbon for three selected diameters during PRIDE PRD. The fraction varies between ~ 10% at 50 nm and ~40 % at 180 nm. During certain periods the fraction of non volatiles shows a clear diurnal cycle with a maximum during night time and the minimum after noon.

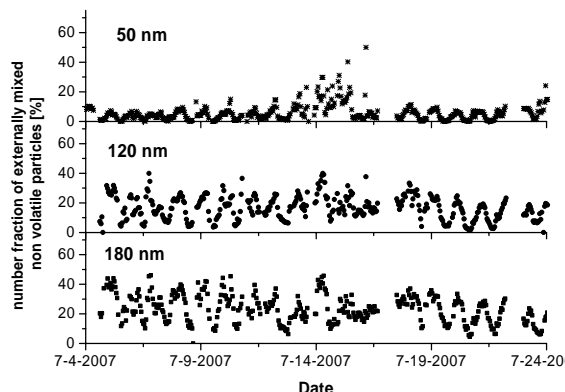


Figure 1: Evolution of number fractions of externally mixed non volatile particles of three selected diameters during PRIDE PRD.

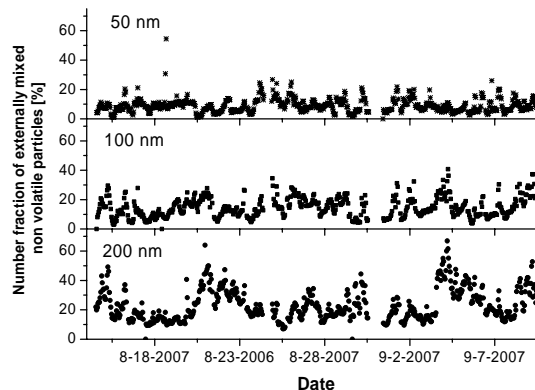


Figure 2: Evolution of number fractions of externally mixed non volatile particles of three selected diameters during Carebeijing.

Figure 2 shows the evolution of externally mixed non volatile particles during Carebeijing. The fractions show also significant variations but no clear diurnal cycles. Here, differences in the mixing state are usually caused by variations in air mass history and meteorological conditions: those air masses containing a high fraction of aged aerosol have low number fractions of externally mixed particles, those with a high fraction of fresh emissions have more externally mixed elemental carbon.

## Chloride ion in urban atmospheric aerosols

Ana Filipa Ferreira, Paulo Portela, Cristina Oliveira, Liliana Quintão, M. Filomena Camões

CCMM-Department of Chemistry and Biochemistry, Faculty of Sciences, University of Lisbon, Edifício C8 – Campo Grande, 1749-016, Lisboa, PORTUGAL

Keywords: urban aerosols, chloride, size distribution, soluble fraction, ion chromatography

Apart from major gas species, atmospheric air contains minor constituents, present as gas and as liquid or solid aerosol particles. Urban atmospheres contain a high number of chemical species from both natural and anthropogenic origins, which originate from local sources and/or from more remote continental or oceanic origins

In this work, a study is presented of the composition of an urban atmosphere at Lisbon city; air was actively sampled from above the roof of building C1 of the Faculty of Sciences-University of Lisbon, at Campo Grande, between October 2004 and August 2006. The sampling site, close to one main avenue, a ring road with heavy traffic, two hospitals with incineration of residues, on the route of the airport and next to a horse riding field and a city garden is located at about 30 km from the open Atlantic Ocean. For this reason, the impact of marine air masses on this area of the city has been investigated.

The composition of marine aerosols is correlated to that of seawater, with particle size classified as coarse fraction (1-10  $\mu\text{m}$ ). Conventionally sodium ions are adopted as the tracer element, with origin being solely attributed to the seawater. Comparison of the ratios of other ionic species present in the aerosols water soluble fraction and sodium ion to those characteristic of seawater indicate the extent of sea salt in the sampled air masses.

Sodium chloride being the major component of seawater is the expected prevailing source of chloride ions, well correlated with sodium ion. Nevertheless, a chloride deficiency due to aerosol processing is often referred in the literature [von Glasow *et al.*, 2002; Sander *et al.* 2003].

Owing to the fact that we are dealing with an urban atmosphere, where both marine (coarse fraction) and anthropogenic (fine fraction  $\leq 1 \mu\text{m}$ ) sources are likely to be found, particulate matter was collected on a 4-stage filter pack system with filters placed in decreasing order of porosity, Nuclepore (8  $\mu\text{m}$ ), Teflon 1 (1  $\mu\text{m}$ ),

Teflon 0.5 (0.5  $\mu\text{m}$ ) and Whatman 41, aiming at assessing aerosol size distribution. Analysis of the water soluble fraction was performed by Ion Chromatography.

Analysis of results showed good correlation with seawater composition for aerosol fraction collected in the filters of higher porosity, allowing conclusions about the marine influence in the area.

On the other side, results for chloride ion from lower porosity filters, showed high concentration of these ions, not correlated with seawater.

These observations support the indication of the presence of other sources of halogenated water soluble compounds in the aerosol form. The small size of such particles is characteristic of secondary aerosols, resulting from gas phase chemical reactions or from gas-particle interaction.

Results time series are shown and critically discussed in terms of the identification of pollution episodes.

- von Glasow, R., Sander, R., Bott, A., Crutzen, P.J., *Journal of Geophysical Research* (2002) 107 (D17), 4341-4356.

- Sander, R., Keene, W.C., Pszenny, A.A.P., Arimoto, R., Ayers, G.P., Baboukas, E., Cainey, J.M., Crutzen, P.J., Duce, R.A., Hönninger, G., Huebert, B.J., Maehaut, W., Mihalopoulos, N., Turekian, V.C., van Dingenen, R., *Atmospheric Chemistry and Physics* (2003) 3, 1301-1336.

- Sienfeld, J. H., Pandis, S. N. (1998), *Atmospheric chemistry and physics: from air pollution to climate change*, New York, USA, Wiley-Interscience, John Wiley & Sons, Inc.

This work was supported by the FCT under the Project POCI/CTE-ATM/60036/2004.

## On aerosol characterization at the research station of Cabauw, The Netherlands

B. Henzing, M. Moerman, M. Schaap, and G. de Leeuw

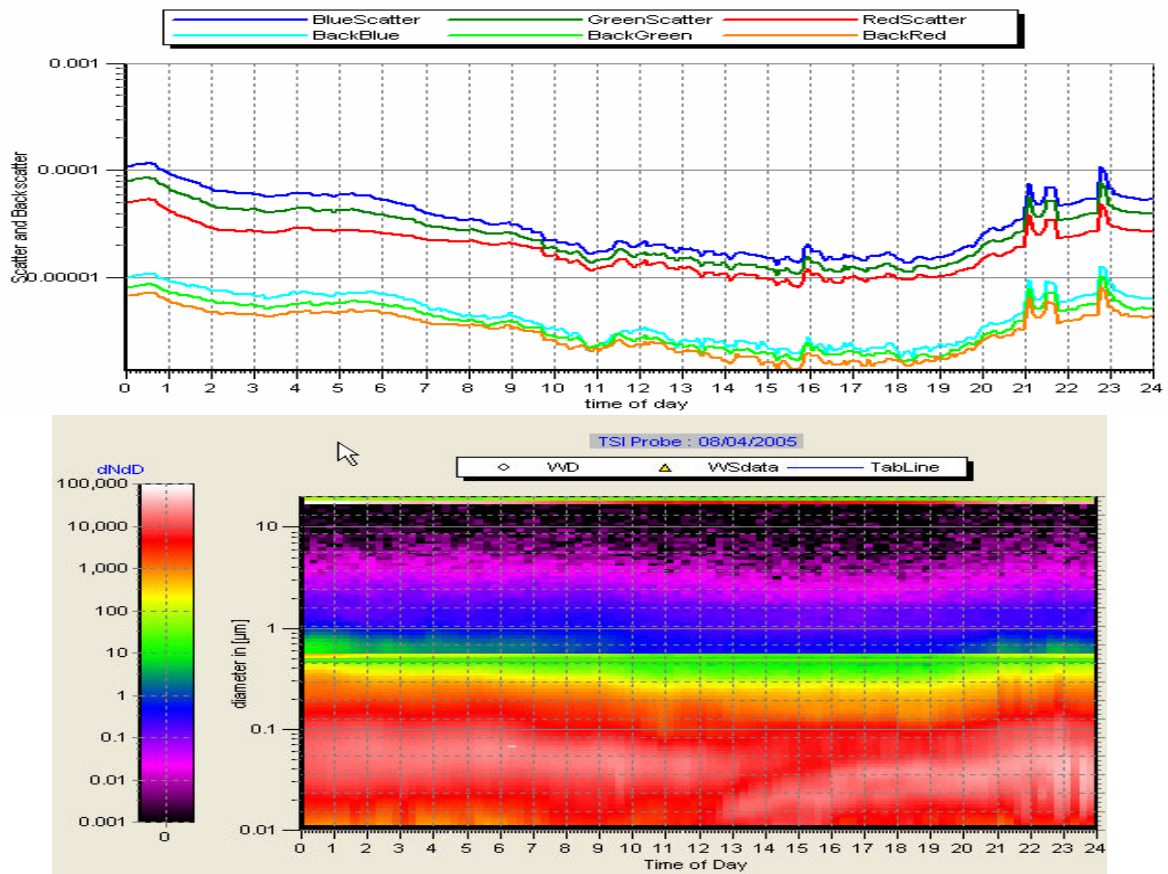
TNO, Business unit Environment, Health and Safety, PO Box 342, 7300 AH Apeldoorn, The Netherlands

Keywords: aerosol characterization, aerosol formation, number size distribution, optical properties

The single most important source of uncertainty in understanding and predicting climate change is the existing of airborne particles. Aerosols and greenhouse gases have competing effects on climate change. Through, their radiative effects greenhouse gases tend to warm the atmosphere, whereas the net aerosol effect is to cool the atmosphere. With respect to precipitation, the competition is such that greenhouse gases are believed to speed up the hydrological cycle, whereas aerosols tend to suppress precipitation. To study the role of aerosols in our climate a permanent measurement site is set-up in the central part of the Netherlands (Cabauw, 51.97 N, 4.93 E). The Cabauw Experimental Site for Atmospheric Research (CESAR) is the focal point of experimental atmospheric research in The Netherlands. The CESAR goal is to set-up and operate at the Cabauw site an observational facility with a comprehensive set of remote sensing and in-situ equipment. CESAR as atmospheric reference site is of international importance in the European and global research networks.

At the site long term time series of a range of optical and physical aerosol parameters such as particle number size distribution, volatility and aerosol extinction coefficient are obtained. The combination of the instrumentation at Cabauw provides a unique opportunity to characterise the atmospheric aerosol composition. Various instruments complement each other (e.g. SMPS for particle size distribution [10nm-500nm] and APS [0.5 micron – 20 micron]) other instruments give different estimates of the same quantity (integrated particle size distribution and PM monitors).

At the meeting we will present uncertainty estimates of aerosol optical and physical properties that are based on various estimates of these quantities that are based on different instruments. The results are based on two full years (May-2005 to May-2007). Despite the fact that the Netherlands form a hot-spot in aerosol load, we frequently observe new particle formation in the year 2005. In the presentation, we will therefore focus on the special aerosol characteristics in cases with new particle formation and we will relate these results to aerosol characteristics in clean-air regions.



New particle formation at Cabauw, The Netherlands. [top] temporal variability in scatter and backscattering coefficient [m<sup>-1</sup>] and [bottom] particle number size distribution as measured by SMPS and APS at August 4, 2005 at Cabauw.

## Seasonal variation of submicron aerosol number size distributions at urban and suburban sites of Prague in 2004/2005

J. Hovorka<sup>1</sup>, V. Ždímal<sup>2</sup>, J. Schwarz<sup>2</sup>, Z. Wagner<sup>2</sup>, P. Dohányosová<sup>2</sup>, M. Braniš<sup>1</sup>, J. Smolík<sup>2</sup>

<sup>1</sup> Institute for Environmental Studies, Faculty of Science, Charles University in Prague, Benátská 2, 128 01 Prague 2, Czech Republic

<sup>2</sup>Institute of Chemical Process Fundamentals, Academy of Sciences of the Czech Republic, Rozvojova 2, 165 02 Prague 6 – Suchbát, Czech Republic

Keywords: air pollution, urban aerosols, number size distribution, nucleation

There are many records in scientific literature on ubiquity of transient particulate matter (PM) events mainly in urban atmosphere in which PM mass concentrations rapidly rise and fall over a period of few hours (Weber, 2003). Their causes are sudden temporal variation of meteorology parameters, emission source strengths and formation of new particles. Highly time resolved measurements of sub-micron aerosol number size distribution should provide sufficient datasets for the evaluation of such transient events (Zhou, 2005).

Roof-top sampling stations, equipped with similar instrumentation (SPMS, TSI), were used to measure 5 minute averages of aerosol number size distributions within the size range approximately 14-700 nm at two localities for three seasons. The urban locality was situated in a large botanic garden of the University in Prague center. The suburban locality, on the premises of Academy of Science of the Czech Republic, was situated in NW direction within 8 km of air distance from the urban locality. Total concentrations measured at the IES site were divided by a factor of 1.4 due to the fact, that the Kr-85 source was damaged. The correction factor was determined experimentally by a long-term comparison of concentrations obtained with and without the source at the same location under similar meteorological conditions.

Table 1. Campaign dates and basic statistic data (#cm<sup>-3</sup>) of number size distributions recorded at suburban - ICPF and urban - IES sites

	Fall 2004		Winter 2005		Spring 2005	
Dates	11.-26.10		22.2.-9.3.		19.4.-3.5.	
Station	ICPF	IES	ICPF	IES	ICPF	IES
25%	3.7e3	4.9e3	4.2e3	7.9e3	4.6e3	5.9e3
Median	6.0e3	7.9e3	7.1e3	1.2e4	6.4e3	7.9e3
75%	8.9e3	1.2e4	10.4e3	1.7e4	8.9e3	1.1e4
Mean	6.8e3	9.3e3	8.1e3	1.3e4	7.8e3	9.3e3
Stdev	4.2e3	6.2e3	5.5e3	6.4e3	5.9e3	5.9e3

The total number concentrations were usually higher, as was expected, at the urban than at the suburban locality (Table 1). Additionally, the difference had a seasonal pattern. While during the

fall and spring the values recorded were higher by approximately 30% and 20% respectively at urban than at suburban locality, in winter the difference was more than 70%. The causes are presumably less favorable conditions for pollution dispersion at the urban locality than at the suburban one. The Prague city centre was situated on the bottom of the Vltava river valley, with frequent appearance of the temperature–inverse stratification of the air. The suburb site was situated at the edge of the valley, which favors air pollution dispersion.

Seasonally, winter campaign values were significantly higher at the urban locality than those in fall or spring. This does not apply to the seasonally averaged size distribution recorded in the suburban locality. Regarding the modality of the size distributions, mainly monomodal then less bimodal distributions and rarely threemodal distributions were set down at urban and suburban localities.

Four nucleation events were recorded within the sampling campaign. They were on the 11<sup>th</sup> and 12<sup>th</sup> of October 2004 and on the 10<sup>th</sup> and 11<sup>th</sup> April 2005 at both the localities. Typical condition for nucleation were relative humidity below 60%, cloudlessness, high UV values and very low particle number count for more than one hour right before the nucleation is registered. Nucleation events were nearly coincident at both the localities. Moreover, these nucleation events, as drawn in time series colored maps, had almost identical shapes and, before the nucleation events when the total particle concentration drops, the number concentrations were nearly equal at both the localities. This indicated well-mixed air masses in the urban airshed, which is in contrast to the results of total number concentrations discussed previously. Our results stress the eminent importance of the meteorology conditions for the urban air quality.

This work was supported by the Grant Agency of Czech Republic under project number 205/03/1560

Weber, R. (2003) *J. Air & Waste Manage. Assoc.* 53, 84

Zhou, L.M., Hopke, P.K., Stanier, C.O., Pandis, S.N., Ondov, J.M., Pancras, J.P., (2005) *J. Geophys. Res.-Atmos.* 110, D07S18

## Human basophils are target cells for urban aerosol-associated polycyclic aromatic hydrocarbons (PAHs)

W. Schober<sup>1</sup>, S. Lubitz<sup>1</sup>, B. Belloni<sup>1</sup>, G. Gebauer<sup>1</sup>, B. Eberlein<sup>1,2</sup>, J. Lintelmann<sup>3</sup>, H. Behrendt<sup>1</sup> and J. Buters<sup>1</sup>

<sup>1</sup>Division of Environmental Dermatology and Allergy GSF/TUM, ZAUM – Center for Allergy and Environment, Technical University Munich, 80802, Munich, Germany

<sup>2</sup>Department of Dermatology and Allergy, Technical University Munich, 80802, Munich, Germany

<sup>3</sup>Institute of Ecological Chemistry, GSF-National Research Center for Environment and Health, 85764, Neuherberg, Germany

Keywords: urban aerosols, traffic, PM2.5, PAHs, health effects of aerosols.

**Background:** Airborne particulates and gases related to human activities, or ambient air pollution, are important environmental issues that affect human health. Diesel exhaust particles (DEPs) have been implicated in the worldwide increased incidence of asthma and allergic rhinoconjunctivitis over the past century (Heinrich and Wichmann, 2004). There is growing evidence that PAHs from traffic emissions participate in the development and maintenance of IgE-mediated allergic diseases. To address this issue we investigated the impact of PAH containing airborne extracts and single U.S. EPA priority PAHs on human basophils, which markedly contribute to allergic inflammation through the release of preformed and granule-derived mediators.

**Methods:** Atmospheric fine dust was collected using an Andersen High-Volume Sampler equipped with a 2.5 µm head. Particles were collected on quartz-fibre filters at an average flow rate of 52 m<sup>3</sup>/h. The sampler was located near a highly frequented six-lane road (approx. 44.000 motor vehicles/day) in the north of Munich, Germany. Filters were heated for 2 hours at 100 °C and the aqueous condensate was online extracted by dropping through 2 ml n-hexane. After steam distillation n-hexane was replaced by DMSO yielding two organic extracts of urban aerosol (AERex) with similar concentrations of air equivalents per ml. Variance of PAH composition was analyzed as described in detail elsewhere (Schober *et al.*, 2006). Whole blood samples from birch pollen allergic and control subjects were incubated in the presence of AERex or EPA-PAH standard with or without rBet v 1. Basophils were analyzed for CD63 expression as a measure of basophil activation by using multiparameter flow cytometry. In addition, purified basophils from birch pollen allergic subjects and non-atopic donors were incubated with phenanthrene (Phe), benzo[a]pyrene (B[a]P) or their redox-active derivatives (Phe-9,10-hydroquinone, B[a]P-1,6-quinone) for 2 hours prior to rBet v 1 stimulation. Supernatants were assayed for IL-4, IL-8 and histamine by means of ELISA.

**Results:** Basophils exposed *in vitro* simultaneously to AERex or EPA-PAH standard and rBet v 1 expressed CD63 significantly more than with antigen alone. Both AERex and EPA-PAH standard synergized with rBet v 1 dose-dependently, but did not activate basophils from non-allergic donors. Moreover, B[a]P and Phe at concentrations of 0.1 – 5 µM drove IL-8 secretion from purified basophils in a dose-dependent manner. The effect was more significant for B[a]P ( $p = 0.0004$ ) than for Phe and could be observed with and without antigen added. Both PAHs significantly enhanced IL-4 secretion ( $p = 0.02$ ) from purified basophils in the absence of antigen suggesting an adjuvant role of DEP-PAHs in allergic sensitization. No relevant further increase in IL-4 secretion was seen in the presence of specific antigen. Phe but not B[a]P significantly enhanced histamine release ( $p = 0.04$ ) from basophils of birch pollen allergic individuals in absence of rBet v 1. In contrast, stimulation with PAH derivatives had virtually no influence on mediator release. None of basophil samples from healthy controls showed any PAH effect on cytokine or histamine secretion.

**Conclusion:** Since basophils are mediator cells of allergy being involved in the initiation and propagation of allergic inflammation, including asthma, it is important to understand how traffic-related air pollutants affect their functional responses and signalling pathways. Our data suggest that urban aerosol-associated PAHs can not only drive proallergic processes through enhanced FcεRI-coupled mediator release from human basophils, but also initiate a proinflammatory Th2 dominated immune response via direct action of single PAHs on sensitized basophils.

Heinrich, J., and Wichmann, H. E. (2004). *Curr Opin Allergy Clin Immunol*, 4, 341-348.

Schober, W., Belloni, B., Lubitz, S., Eberlein-König, B., Bohn, P., Saritas, Y., Lintelmann, J., Matuschek, G., Behrendt, H., and Buters, J. (2006). *Toxicol Sci*, 90, 377-384.

## **T32 Abstracts**

## Cubic and hexagonal ice and high humidity in low-temperature cirrus

A. Bogdan

Division of Atmospheric Sciences, Department of Physical Sciences, University of Helsinki,  
P.O. Box 64, FIN-00014, Helsinki, Finland

Keywords: cubic ice, hexagonal ice, cirrus clouds, H<sub>2</sub>SO<sub>4</sub>/H<sub>2</sub>O aerosol.

Recently there have been debates about the nature of unusual high relative humidity with respect to ice (RH<sub>i</sub>) observed in low-temperature cirrus clouds (Gao et al., 2004; McGraw, 2004; Murray et al., 2005; Shilling et al., 2006). Shilling et al. (2006) reported that the measured water vapor pressure of cubic ice P<sub>I<sub>c</sub></sub> was ~10.5±2.5 % higher than that of hexagonal ice P<sub>I<sub>h</sub></sub>. Basing on this the authors proposed that “the formation of cubic ice at T < 202 K may significantly contribute to the persistent in-cloud water supersaturations ...” It has been the second attempt to explain the high RH<sub>i</sub> (up to 180 % in cold cirrus. The first attempt, which was based on a new class of HNO<sub>3</sub>-containing ice particles (Δ-ice), was unsuccessful because it was in violation of the second law of thermodynamics (McGraw, 2004). Cubic ice cannot either explain the high RH<sub>i</sub> for the reasons described below. Here we also present our explanation of the high RH<sub>i</sub> in low-temperature cirrus.

For calculation of enthalpy of transition I<sub>c</sub> → I<sub>h</sub>, ΔH<sub>I<sub>c</sub>→I<sub>h</sub></sub>, Shilling et al., used their measured data for the P<sub>I<sub>c</sub></sub> in the formula

$$\ln \frac{P_{I_c}}{P_{I_h}} = \frac{\Delta H_{I_c \rightarrow I_h}}{RT}$$

where P<sub>I<sub>c</sub></sub> and P<sub>I<sub>h</sub></sub> are the vapour pressures of cubic and hexagonal ice at the same temperature T, and R the gas constant. Although there is a doubt about the formula, because it is the integrated form of the Clausius-Clapeyron equation which is only applied when one of the phases in the phase transition is a gas, we will use it for calculation of the P<sub>I<sub>c</sub></sub> using the generally accepted value of ΔH<sub>I<sub>c</sub>→I<sub>h</sub></sub> ≈ 50 J/mol (Handa et al., 1986; Kohl et al., 2000). The calculation gives that the P<sub>I<sub>c</sub></sub> is only ~3 % larger than the P<sub>I<sub>h</sub></sub>. The small difference between the P<sub>I<sub>c</sub></sub> and P<sub>I<sub>h</sub></sub> is physically more reasonable than the measured value of 10.5±2.5%, because the lattice energy of the I<sub>c</sub> and I<sub>h</sub> differs only by ~0.5% (Steytler et al. 1983).

The small difference in the lattice energy of ~0.5%, quite a wide temperature range over which the transition I<sub>c</sub> → I<sub>h</sub> occurs, and the dependence of the rate of the transition on the thermal history and temperature can be the reasons that the transition itself had not always been observed and enthalpy change accompanying the transition had not been

detected at all (Bogdan, 2006; Bogdan, 2007). The small difference in the lattice energy of ~0.5% cannot satisfactorily explain why the hexagonal form of ice should be more stable than the cubic. The said above can be considered as arguments against the great difference in the water vapor pressures of I<sub>c</sub> and I<sub>h</sub>.

Shilling et al. re-analyzed the field measured data of RH<sub>i</sub> from Gao et al. (2004). The re-analysis reduced the RH<sub>i</sub> by ~10 %. Assuming that the P<sub>I<sub>c</sub></sub> is really ~10 % larger than the P<sub>I<sub>h</sub></sub>, the cubic ice particles cannot account for the ‘reduced’ average of RH<sub>i</sub> ≈ 120 % below 202 K (see Fig.3 in Shilling et al.). Nor can they account for the excursion of the RH<sub>i</sub> up to 160 % observed between 195 and 210 K.

Our recent publications reported that cirrus ice particles formed from H<sub>2</sub>SO<sub>4</sub>/H<sub>2</sub>O aerosol drops can be coated with unfrozen residual solution (Bogdan et al. 2006). The coating is formed independently whether the I<sub>c</sub> or I<sub>h</sub> lattice are formed within the solution drops. The coating can serve as a shield which reduces a number of H<sub>2</sub>O molecules condensing on the coating and subsequently diffusing to the ice core in comparison with that which would deposit directly on the ice surface (Bogdan, 2007). For example, at 188 K it is smaller by ~1000 times (Bogdan, 2007). The reduction is due to the fact that water pressure of the coating is larger than that of pure ice, either cubic or hexagonal. Therefore the rate of ice growth of the coated particles is smaller than that of the uncoated ones. The slow rate of ice growth slowly depletes the ambient water vapor and explains the high RH<sub>i</sub> observed in low-temperature cirrus.

Bogdan, A., M. J. Molina, K. Sassen, M. Kulmala (2006). *J. Phys. Chem. A*, 110, 12541-12542.

Bogdan, A. (2006). *J. Phys. Chem. B*, 110, 12205-12206.

Bogdan, A., (2007), (Submitted).

Gao, R. S., et al. (2004). *Science*, 303, 516-520.

Handa, P. Y., D. D. Klug, and E. Whalley (1986). *J. Chem. Phys.* 84, 7009-7010.

Kohl, I., E. Mayer, & A. Hallbrucker (2000). *Phys. Chem. Chem. Phys.* 2, 1579-1586.

McGraw, R. (2004). *Science*, 961.

Murray, B. J., D. A. Knopf & A. K. Bertram, (2005). *Nature*, 202-205.

Shilling, J. E. et al. (2006). *Geophys. Res. Lett.* 33, L17801, doi:1029/2006GL026671.

Steytler, B. C., J. C. Dore, & C. J. Wright (1983). *J. Phys. Chem.* 87, 2458-2459.

## ature of high relative humidity with respect to ice in cold cirrus clouds

A. Bogdan

Division of Atmospheric Sciences, Department of Physical Sciences, University of Helsinki,  
P.O. Box 64, FIN-00014, Helsinki, Finland

Keywords: cirrus clouds, relative humidity,  $\text{H}_2\text{SO}_4/\text{H}_2\text{O}$  aerosol, greenhouse effect.

Low-temperature high-altitude cirrus clouds, being globally widespread, affect Earth's climate through modulation of incoming solar and outgoing terrestrial radiation, due to their potential for chlorine activation with concomitant ozone loss in the tropopause, and regulation of water content in the upper troposphere. According to climate models, the amount of atmospheric water vapor, which is the dominant greenhouse gas, will be doubled by the end of the century due to increasing emissions of anthropogenic greenhouse gases (Sodden et al., 2005).

In situ observations often reveal a high relative humidity with respect to ice ( $\text{RH}_i$ ) (up to 170 %) in upper-tropospheric low-temperature cirrus (Gao et al., 2004). An attempt to explain the high  $\text{RH}_i$  by the formation of new type of ice, so called 'Δ-ice' (Gao et al. 2004), was unsuccessful because it was in violation of the second law of thermodynamics (McGraw, 2004). The second attempt to explain the high  $\text{RH}_i$  by the formation of metastable cubic ice ( $\text{I}_c$ ) instead of stable hexagonal ice ( $\text{I}_h$ ) (Murray et al., 2005; Shilling et al., 2006) does not work either, because water vapor pressure of the  $\text{I}_c$  is only ~10 % larger than that of the  $\text{I}_h$  (Shilling et al., 2006) and therefore cannot explain the observed high  $\text{RH}_i$  (Bogdan, 2007). We think that culprits of the elevated  $\text{RH}_i$  can be  $\text{H}_2\text{SO}_4$  and  $\text{HNO}_3$  which increase the thickness of the solution coating around ice particles (Bogdan et al. 2006). The solution coating slows down the rate of ice growth and maintains the high  $\text{RH}_i$ , thus adding to the greenhouse effect (Bogdan, 2007).

The increasing content of  $\text{H}_2\text{SO}_4$  and  $\text{HNO}_3$  in the upper troposphere, due to volcanic or anthropogenic emissions, will increase concentration of the aerosol droplets. The larger concentration of the droplets will enhance the cloud humidity because more concentrated droplets freeze at lower temperature, Figure 1. After the freezing, the formed solution coating will maintain the cloud humidity because the number of  $\text{H}_2\text{O}$  molecules condensing on the coating and then diffusing to the ice core is much smaller than that which would deposit directly on the ice surface. The smaller number of the  $\text{H}_2\text{O}$  molecules condensing on the solution coating is due to the fact that water vapor pressure of the coating is much smaller than that of ice at equilibrium.

Mechanism of growth of the coated ice particles differs from that of pure ice particles. The coated ice

particles grow much slower than the uncoated ones, which experience rapid growth due to  $\text{H}_2\text{O}$  condensation on the ice surface. In the case of the coated particles,  $\text{H}_2\text{O}$  molecules first condense on the coating, dilute it, diffuse to the ice core, and only then become incorporated into the ice lattice. But despite that viscosity of  $\text{H}_2\text{SO}_4/\text{H}_2\text{O}$  solution increases very steeply with decreasing temperature, the diffusion process is not a dominant factor slowing down the rate of ice growth because the coating is very thin. The dominant factor reducing the rate of ice growth is the smaller flux of water molecules condensing on the coating in comparison with condensing on ice (Bogdan, 2007).

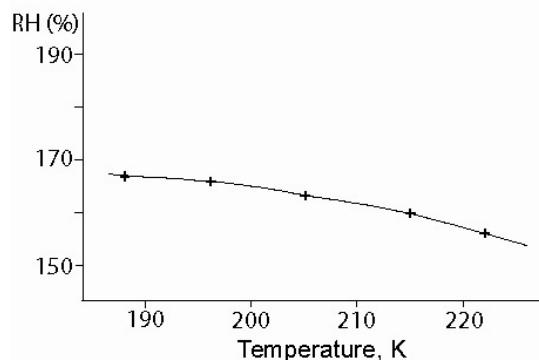


Figure 1. Relative humidity with respect to ice ( $\text{RH}_i$ ) calculated at the freezing temperatures of  $\text{H}_2\text{SO}_4/\text{H}_2\text{O}$  aerosol droplets taken from Bogdan (2006). Concentration of the droplets was 10;15;20;23, and 25 wt %  $\text{H}_2\text{SO}_4$ . More concentrated droplet freeze at colder temperature.

Bogdan, A., M. J. Molina, K. Sassen, M. Kulmala (2006). *J. Phys. Chem. A*, 110, 12541-12542.

Bogdan, A. (2006). *J. Phys. Chem. B*, 110, 12205-12206.

Bogdan, A., (2007), (Submitted).

Gao, R. S., et al. (2004). *Science*, 303, 516-520.

McGraw, R. (2004). *Science*, 961.

Murray, B. J., D. A. Knopf & A. K. Bertram, (2005). *Nature*, 435, 202-205.

Shilling, J. E. et al. (2006). *Geophys. Res. Lett.* 33, L17801, doi:10.29/2006GL026671.

Sodden, B. J. et al. *Science*, 310, 841-844.

## The composition of ice residue in clean mixed phase clouds

L. Keller, H. Herich, D.J. Cziczo, U. Lohmann

Institute for Atmospheric and Climate Science, ETH Zurich, 8092 Zurich, Switzerland  
livia.keller@env.ethz.ch

Key words: Ice nuclei, Aerosol mass spectrometry, Mixed phase clouds, CLACE, Atmospheric aerosol

Aerosols play an important role in the radiation budget of the atmosphere (IPCC Report 2001). Particles interact directly with radiation (direct aerosol effect) or they can influence the formation and lifetime of clouds, which in turn influence the radiation budget of the Earth (indirect effect). Many of the aspects of aerosol – cloud interaction are presently uncertain and the indirect effect of aerosols on climate is poorly known. The indirect effect of aerosols could possibly compensate for a part of global warming by greenhouse gases as the aerosol radiative forcing through clouds cools climate globally (IPCC Report 2001; Lohmann and Feichter, 2005)

Our knowledge and understanding of the role of aerosols in mixed phase clouds is still rather poor. Ice nuclei in these clouds are especially insufficiently investigated. An ideal site to study mixed phase clouds is the high alpine research station on the Jungfrauoch, which lies 3580 m asl. The air measured there can be regarded as representative of the continental lower free troposphere during winter, with only a very small influence of boundary layer air and pollution (Baltensperger et al., 1997). The Jungfrauoch is frequently covered in clouds during winter. In the beginning of 2007, a large field campaign took place on the Jungfrauoch research station, the Cloud and Aerosol Characterization Experiment (CLACE 6).

In order to investigate only those aerosols that are activated in mixed phase clouds, a special inlet can be applied. Such a special inlet is a Counterflow virtual impactor (CVI) (Boulter et al., 2006). A CVI uses a counterflow of inert gas for inertial separation and allows only particles above a certain inertia to pass. Thus, it can be set that only aerosols that formed ice or droplets and thus grew in size can pass. Such a CVI can be modified to an ICE CVI (Mertes et al., submitted). Ice inlets stop droplets from entering by the use of a cold plate before the actual CVI. Ice particles and interstitial aerosols can bounce off of this cold plate, while water droplets freeze onto it. The interstitial aerosols are then removed in a normal CVI. As a result, only ice particles of a certain size range can pass the inertial separation.

To investigate the chemical composition of the ice residue after inertial separation, single parti-

cle mass spectrometry was applied. This allowed us to qualitatively investigate the composition of single particles in situ and in real time. The instrument used was an Aerosol Time-of-Flight Mass Spectrometer (ATOFMS, TSI Model 3800), a bipolar time of flight mass spectrometer, which gives the spectra for both polarities simultaneously.

We acknowledge that the International Foundation High Altitude Research Stations Jungfrauoch and Gornergrat (HFSJG), 3012 Bern, Switzerland, made it possible for us to carry out our experiments at the High Altitude Research Station at Jungfrauoch.

Baltensperger, U., Gäggeler, H.W., Jost, D.T., Lugauer, M., Schwikowski, M., Weingartner, E. and Seibert, P. (1997). Aerosol Climatology at the High-Alpine Site Jungfrauoch, Switzerland. *J. Geophys. Res.* 102(D16): 19707 – 19715.

Boulter, J.E., Cziczo, D.J., Middlebrook, A.M., Thomson, D.S. and Murphy, D.M. (2006). Design and Performance of a Pumped Counterflow Virtual Impactor. *Aerosol Sci. Technol.* 40 (11):969 – 976.

Intergovernmental Panel on Climate Change (IPCC) (2001): Climate Change 2001: The Scientific Basis. IPCC Third Assessment Report Cambridge, Cambridge University Press.

Lohmann, U. and Feichter, J. (2005). Global Indirect Aerosol Effects: A Review. *Atmos. Chem. Phys.* 5: 715 – 737.

Mertes, S., Verheggen, B., Walter, S., Connolly, P., Ebert, M., Schneider, J., Bower, K.N., Inerle-Hof, M., Cozic, J., Baltensperger, U. and Weingartner, E. (submitted 2006). Counterflow virtual impactor based collection of small ice particles in mixed-phase clouds for the physico-chemical characterization of tropospheric ice nuclei: sampler description and first case study. *Aerosol Sci. Technol.*

## Surface tensions of multi-component mixed inorganic/organic aqueous systems of atmospheric significance: Measurements, model predictions and importance for cloud activation predictions.

D.O. Topping<sup>1</sup>, G.B. McFiggans<sup>1</sup>, G. Kiss<sup>2</sup>, Z. Varga<sup>3</sup>, M.C. Facchini<sup>4</sup>, S. Decesari<sup>4</sup> and M. Mircea<sup>4</sup>

<sup>1</sup>School of Earth, Atmospheric and Environmental Sciences, The University of Manchester, The Sackville street building, Sackville street, Manchester, M60 1QD,UK

<sup>2</sup>Air Chemistry Group of the Hungarian Academy of Sciences, University of Pannonia, 8201 Veszprém, P.O. Box 158, Hungary

<sup>3</sup>Department of Earth and Environmental Sciences, University of Pannonia, 8201 Veszprém, P.O. Box 158, Hungary

<sup>4</sup>Instituto di Scienze dell Atmosfera e del Clima, Consiglio Nazionale delle Ricerche, Via Gobetti, Bologna, Italy

Keywords: Aerosol chemistry, Hygroscopicity, Clouds, Modelling, Surface activity.

In order to predict the physical properties of aerosol particles, it is necessary to adequately capture the behaviour of the ubiquitous complex organic components. One of the key properties which may affect this behaviour is the contribution of the organic components to the surface tension of aqueous particles. Unfortunately, our quantitative understanding on mixed organic and mixed inorganic / organic systems is limited. Furthermore, it is unclear whether models that exist in the literature can reproduce surface tension variability.

The current study aims to resolve both issues to some extent. Surface tensions of single and multiple solute aqueous solutions were measured and compared with predictions from a number of model treatments. On comparison with binary organic systems, two predictive models found in the literature provided a range of predicted values resulting from sensitivity to calculations of pure component surface tensions. Results indicate that a fitted model can capture the variability of the measured data very well, producing the lowest average percentage deviation for all compounds studied. The performance of the other models varies with compound and choice of model parameters. The behaviour of ternary mixed inorganic/organic systems was unreliably captured by using a predictive scheme and this was composition dependent.

For higher order systems, entirely predictive schemes performed poorly. It was found that use of the binary data in a relatively simple mixing rule, or modification of an existing thermodynamic model with parameters derived from binary data, was able to accurately capture the surface tension variation with concentration of this system. Thus, it would appear that in order to model multi-component surface tensions involving compounds in this study one requires the use of appropriate binary data. The effect of deviations between predicted and measured surface tensions on predicted cloud activation properties was quantified, by firstly incorporating the surface tension models used in this study into an existing thermodynamic framework based on the

'fundamental' kohler equation. Critical saturation ratios as a function of dry size for all of the multi-component systems were computed and it was found that deviations between predictions increased with decreasing particle dry size. As expected, use of the surface tension of pure water, rather than calculate the influence of the solutes explicitly, led to a consistently higher value of the critical saturation ratio indicating that neglect of the compositional effects will lead to significant differences in activation behaviour even at large particle dry sizes. However, the effect of bulk to surface partitioning was then explored for some case studies (figure1). Results suggest that the critical saturation ratio can be significantly increased by removal of material from the bulk phase. Indeed, results were closer to predictions assuming the surface tension of pure water whilst there were still some deviations. Such findings suggest the need for further studies in the laboratory to highlight the important processes taking place within droplets.

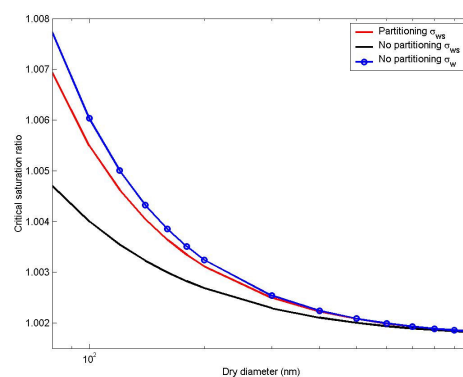


Figure1: Critical saturation ratio versus dry diameter for Suwannee River Fulvic acid treating non-ideality (red, black, blue), accurate surface tension variability (black,red) and with(red)/without(black,blue) bulk to surface partitioning calculations

David Topping is currently funded by DIAC/NCAS and this work was sponsored by the ACCENT Joint Research Programme on Aerosols: Air quality & Climate.

## The first aerosol-cloud experiment at the Puijo semi-urban measurement station

A. Leskinen<sup>1</sup>, T. Raatikainen<sup>3</sup>, A.-P. Hyvärinen<sup>3</sup>, A. Kortelainen<sup>2</sup>, P. Miettinen<sup>2</sup>, N. Pietikäinen<sup>1</sup>, H. Portin<sup>1</sup>, J. Rautiainen<sup>2</sup>, R. Sorjamaa<sup>2</sup>, P. Tiitta<sup>2</sup>, P. Vaattovaara<sup>2</sup>, A. Laaksonen<sup>2,3</sup>, K.E.J. Lehtinen<sup>1,2</sup>, H. Lihavainen<sup>3</sup>, and Y. Viisanen<sup>3</sup>

<sup>1</sup>Finnish Meteorological Institute, Kuopio Unit, P.O. Box 1627, FI-70211 Kuopio, Finland

<sup>2</sup>Department of Physics, University of Kuopio, P.O. Box 1627, FI-70211 Kuopio, Finland

<sup>3</sup>Finnish Meteorological Institute, Research and Development, P.O. Box 503, FI-00101 Helsinki, Finland

Keywords: Aerosol cloud interaction, Aerosol mass spectrometry, Clouds, Measurements, Urban aerosols.

Atmospheric fine particles affect the climate directly by scattering and absorbing energy, and indirectly through cloud formation and cloud optical properties. The latter are reported to have an uncertain though cooling effect on the climate (IPCC, 2001). In order to make climatic model estimations more accurate, more experimental data are needed, e.g. from measurement stations, which are at times in cloud. These kinds of stations are, for example, the GAW (Global Atmospheric Watch) stations at Jungfraujoch in Switzerland and at Pallas in Finland.

Similar particle and cloud research was recently started in Kuopio, Finland at the Puijo measurement station, which is located on the top of a 75 m high observation tower (62°54'32" N, 27°39'31" E, 306 m asl, 224 m above surrounding lake level). Measurements at Puijo produce data from a semi-urban environment for climatic models and particle formation studies. The data from Puijo are compared with those measured at the Pallas background station (Hatakka *et al.*, 2003).

During the first aerosol-cloud experiment (PUCE1), Oct 16, 2006 to Nov 17, 2006, a dozen of cloud events, lasting 1-8 hours, were observed. The cloud events were characterized by a sudden drop in visibility (Vaisala FD12P) below 200 m and changes in scattering coefficient (TSI 3563 Nephelometer) and cloud interstitial particle size distribution (DMPS, 10-500 nm), and onset of cloud droplets (DMT, 2-50 μm). Events with precipitation intensity (Vaisala FD12P) more than 0.2 mm/h were omitted. The activated fraction was also measured with a cloud condensation nuclei counter (DMT) in 0.1-2 % supersaturations. Aerosol mass spectrometer (Aerodyne Quadrupole AMS, 50-600 nm) was used to get the aerosol chemical composition.

As an example, cloud interstitial and total particle size distributions and concentrations of organics, sulphate, ammonium and nitrate on one day with a cloud event are shown in Figure 1. When the cloud event started at around 8 a.m., a part of the accumulation mode particles were seen to disappear as they were activated into cloud droplets. The onset of the cloud event can be seen as increase of cloud droplet concentration. In this event the cloud droplet size ranged to 30 μm. During the cloud event the concentrations of organics and sulphate were seen to decrease.

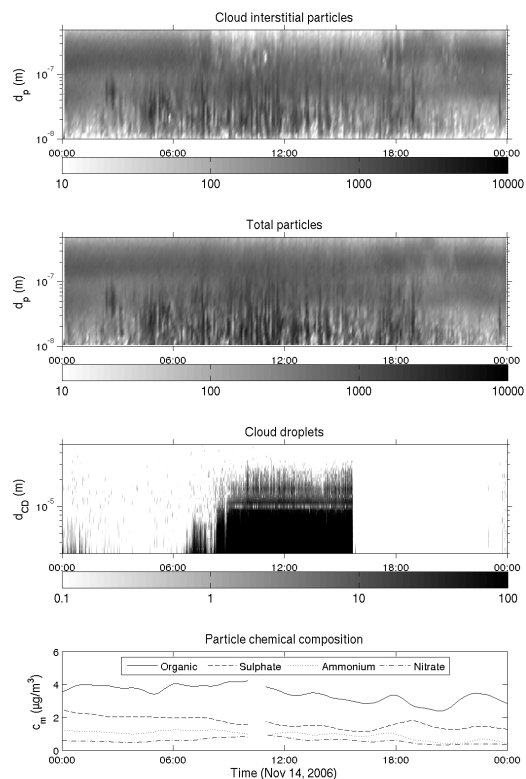


Figure 1. Cloud interstitial particle size distribution (top), total particle size distribution (middle), and particle chemical composition (bottom) on Nov 14, 2006. The horizontal bars denote particle and cloud droplet concentration ( $1/\text{cm}^3$ ).

Hatakka, J., Aalto, T., Aaltonen, V., Aurela, M., Hakola, H., Komppula, M., Laurila, T., Lihavainen, H., Paatero, J., Salminen, K. & Viisanen, Y. (2003). Overview of the atmospheric research activities and results at Pallas GAW station. *Boreal Env. Res.*, 8, 365-383.

IPCC (2001) Climate Change 2001: Synthesis Report. A Contribution of Working Groups I, II, and III to the Third Assessment Report of the Intergovernmental Panel on Climate Change [Watson, R.T. and the Core Writing Team (Eds.)], Cambridge, U. K.: Cambridge University Press.

### **Observations of the role of organic aerosol in the initiation of ice and liquid clouds**

K.Bower<sup>1</sup>, E. Weingartner<sup>2</sup>, T.W.Choularton<sup>1</sup>, M. R. Alfarra<sup>2</sup>, M.W.Gallagher<sup>1</sup>, H.Coe<sup>1</sup>, J.Crosier<sup>1</sup>, J. Allan<sup>1</sup>, A.Targino<sup>1</sup>, I.Crawford<sup>1</sup>, P.Connolly<sup>1</sup>, B. Verheggen<sup>2</sup>, M.Gysel<sup>2</sup>, S. Sjogren<sup>2</sup>, U. Baltensperger<sup>2</sup>, J. Cozic<sup>2</sup>

<sup>1</sup>School of Earth, Atmospheric and Environmental Sciences, University of Manchester, Manchester, M60 1QD, UK

<sup>2</sup>Laboratory of Atmospheric Chemistry, Paul Scherrer Institut, CH-5232, Villigen PSI, Switzerland

Keywords: organic, CLACE, clouds, ice nuclei, ice clouds.

In this paper we will present results from 2 major field campaigns where we examined the impact of internally mixed organic and inorganic aerosol on the initiation of cloud droplets in warm and supercooled cloud. In the supercooled cloud cases we will also present results concerning the role of these aerosol in the nucleation of the ice phase. Results will be presented from experiments that continue the Cloud-Aerosol Characterisation Experiment (CLACE) series held at the high alpine research station Jungfraujoch (JFJ, 3580 m asl; 46.55°N, 7.98°E), Switzerland. The experiments are designed to investigate the chemical composition of aerosol particles, their hygroscopic properties and their interaction with clouds. The experiments will be referred to as CLACE2 (warm clouds) and CLACE3 (supercooled clouds). In this experiment detailed measurements were made of the cloud properties including the cloud droplet size distribution and liquid water content, the size distribution and habit of ice crystals and the ice water content. Measurements were made of the aerosol interstitial to the cloud and the size resolved composition of the total aerosol including cloud particle residues. A wide variety of instrumentation was used but key to the results presented here were measurements made by an Aerodyne Aerosol Mass spectrometer, of the size resolved aerosol composition.

The second experiment was the CLOud Processing of regional Air Pollution, (CLOPAP), advecting over land and sea. In this experiment the instrumented FAAM research aircraft, a BAE 146, made measurements of the cloud microphysics and aerosol composition within the stratocumulus capped boundary layer being impacted by the urban plume from London, UK. Horizontal transects were made perpendicular to the plume at 50 km distance intervals moving away from London. At each distance a pass was made below within and above cloud. Within cloud the droplet residuals were sampled using a CVI. A key measurement for the results presented here was again the Aerodyne AMS providing size resolved aerosol composition. Only warm clouds were sampled in this project.

It was found that in all these experiments the aerosol in the size range 0.1  $\mu\text{m}$  to 3  $\mu\text{m}$  were mostly an internally mixed mixture of nitrate, organics, sulphate and ammonium. The proportions of the species did vary, however, during CLACE 2 organics

were dominant with sulphate dominant in CLACE-3. During CLOPAP the plume was rather inhomogeneous with sulphate, organics and nitrate dominating at different times.

In all the experiments, including CLOPAP 50km from London (the closest we flew), the organics were dominated by highly oxygenated secondary material, in contrast to the properties of newly formed organic aerosol found within the urban environment. It was found that the species were nucleation scavenged by the cloud droplets in the same ratio as they were present in the out of cloud aerosol, confirming that they were internally mixed particles and that all the particles were effective CCN. For example, during the CLOPAP experiment it was found within a transect 100 km from London that one plume contained predominantly sulphate aerosol internally mixed with a small amount of organic material whilst a neighbouring plume consisted of predominantly organic material internally mixed with sulphate. Both plumes resulted in increased droplet number in the cloud to roughly the same degree.

During CLACE-3 temperatures were typically between  $-10\text{C}$  &  $-20\text{C}$ . The clouds consisted of regions made almost entirely of supercooled water together with neighbouring regions consisting of mixed phase ice and water clouds or in some cases ice crystals only. The transitions between these regions were often very sharp with clouds switching from being composed of entirely supercooled water to entirely ice in a few seconds or less.

To attempt to explain this behaviour the AMS aerosol data was conditionally sampled for ice cloud and water cloud. It was found that the ice cloud contained significantly higher loadings of sulphate, nitrate and organics. CO concentrations were also higher on average in the ice clouds. As discussed above the aerosol components were largely internally mixed. These observations suggest that polluted clouds contain more ice. Recent measurements at the AIDA chamber have shown that soot aerosol coated with sulphate is an effective ice nucleus when it operates in the condensation-freezing mode. (Möhler et al 2005). Very recent measurements suggest a further enhancement in nucleation efficiency when a coating of highly oxidised organic material is present. These findings would appear to offer an explanation for the intermittent presence of the ice phase in these clouds.

Möhler et al 2005 *J. Geophys. Res.* **110** (D11), 11210

## European Integrated Project on Aerosol Cloud Climate and Air Quality Interactions - C

M. Kulmala<sup>1</sup>, A. Asmi<sup>1</sup>, H. appalainen<sup>1</sup>

<sup>1</sup>Department of Physical Sciences, University of Helsinki, 00014, Helsinki, Finland

Keywords: research integration, atmospheric aerosols, modelling, measurements

The European Integrated project on Aerosol Cloud Climate and Air Quality Interactions, EUCAARI, is an integrated project in the Sixth Framework Programme of the European Union. The project lasts from 2007 to the end of 2010. It brings together European research groups, state-of-the-art infrastructure and key players from third countries to investigate the role of aerosol on climate and air quality.

The objectives of EUCAARI are

- (I) Reduction of the current uncertainty of the impact of aerosol particles on climate by 50 and quantification of the relationship between anthropogenic aerosol particles and regional air quality, and
- (II) quantification of the side effects of European air quality directives on global and regional climate, and provide tools for future quantifications for different stakeholders.

EUCAARI will also contribute to technological developments in the aerosol measurements, enhancing future experiments and air-quality monitoring networks.

The project is organized into four scientific elements designed to maximize the integration of methodologies, scales and ultimately our understanding of air quality and climate (see Figure 1). New ground-based, aircraft and satellite measurements will be integrated with existing data to produce a global consistent dataset with the highest possible accuracy.

A European measurement campaign will be designed around simultaneous multi-station observations, stratospheric aircraft measurements and carefully selected super-sites. A hierarchy of models will be developed based on the results of the laboratory and theoretical investigations. The models will be used to interpret the measurements and will be integrated in regional air quality and global climate models.

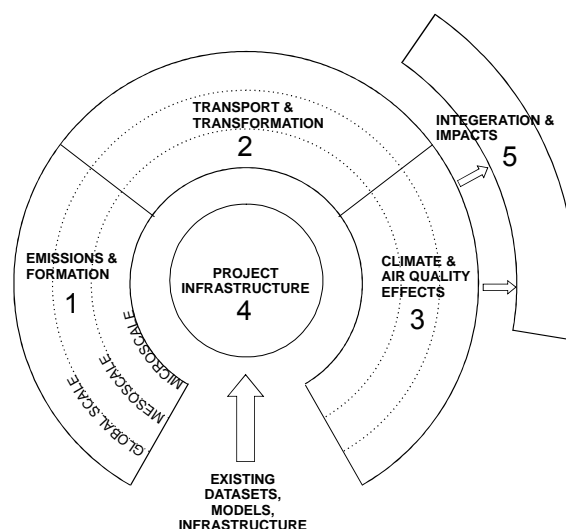


Figure 1. Schematic of the five major elements of EUCAARI. In first three elements all scales from micro (and nano) to global scale are involved (Kulmala *et al.*, 2007).

The project team is strengthened by the inclusion of institutes from developing countries: China, India, Brazil, and South Africa. The consortium consists of 48 partners from 25 countries (18 EU countries, 3 associated states, 4 developing countries with 3rd country status, one SME, and the Joint Research Centre of the EU Commission).

The result will be measurable improvements in the project's climate and air quality models. The outcomes (scenarios, recommendations, models, harmonized datasets and new knowledge) will be disseminated to authorities, policy makers, the research community, industry, instrument designers, and the EU-ESA Global Monitoring for Environment and Security (GMES) Program.

Kulmala, M., Asmi A. & appalainen H. (2007). *EUCAARI - Description of Work*. Helsinki Finland. ISBN: 978-952-10-3679-8

## Partitioning of aerosol particles in mixed-phase clouds at a high alpine site

E. Weingartner<sup>1</sup>, J. Cozic<sup>1</sup>, B. Verheggen<sup>1</sup>, M. Gysel<sup>1</sup>, U. Baltensperger<sup>1</sup>, S. Mertes<sup>2</sup>, K.N. Bower<sup>3</sup>, I. Crawford<sup>3</sup>, M. Flynn<sup>3</sup>, P. Connolly<sup>3</sup>, M. Gallagher<sup>3</sup>, T. Choulaton<sup>3</sup>, U. Lohmann<sup>4</sup>, D. Cziczo<sup>4</sup>, J. Schneider<sup>5</sup>, S. Walter<sup>5</sup>, J. Curtius<sup>6</sup>, S. Borrmann<sup>5,6</sup>, A. Petzold<sup>7</sup>

<sup>1</sup> Laboratory of Atmospheric Chemistry, Paul Scherrer Institut, CH-5232, Villigen PSI, Switzerland

<sup>2</sup> Leibniz-Institute for Tropospheric Research, D-04318, Leipzig, Germany

<sup>3</sup> University of Manchester, M60 1QD, Manchester, United Kingdom

<sup>4</sup> Institute of Atmospheric and Climate Sciences, ETH Zürich, CH-8093, Switzerland

<sup>5</sup> Max Planck Institute for Chemistry, D-55128, Mainz, Germany

<sup>6</sup> Johannes Gutenberg University, D-55099, Mainz, Germany

<sup>7</sup> German Aerospace Centre, D-82234, Wessling, Germany

Keywords: Aerosol cloud interaction, scavenging, CCN, ice nuclei, black carbon.

In international collaborations, a series of intensive field experiments were carried out at the Jungfraujoch station (3580 m asl) in Switzerland under the name CLACE (Cloud and Aerosol Characterization Experiment). A main focus of CLACE is the investigation of the aerosol-cloud interaction processes in mixed-phase clouds.

State-of-the-art instrumentation was employed to characterize the aerosol size distribution (SMPS, OPC), size segregated chemical composition (AMS, ATOFMS), black carbon (BC) mass concentration (Aethalometer, PSAP, MAAP), and cloud microphysics (PVM, FSSP, CPI, ADA).

Different inlets were used for these instruments: A total inlet (tot) designed to evaporate cloud constituents at an early stage of sampling (i.e. sampling both cloud residuals and interstitial particles), an interstitial inlet (int) collecting only unactivated aerosol particles and an Ice-Counterflow Virtual Impactor (Ice-CVI) (Mertes *et al.*, 2007) designed to sample residual particles of small ice crystals (i.e. particles that served as ice nuclei). Differencing the response downstream of the different inlets provides insight into the partitioning of the aerosol particles into cloud droplets and ice crystals.

A result from the latest CLACE campaigns is that the partitioning of aerosol particles to the cloud phase is strongly dependent on the relative fraction of ice in the mixed-phase clouds. Figure 1a shows that the scavenged volume fraction (derived from the size distribution measurements and defined as  $(V_{\text{tot}} - V_{\text{int}})/V_{\text{tot}}$ ) is about 60% in liquid clouds. The fraction of scavenged particles decreases with increasing cloud ice mass fraction (IMF) (Verheggen *et al.* 2007). This can be explained by the Wegener-Bergeron-Findeisen process, which describes the effect of a water vapor flux from liquid droplets to ice crystals. The higher the IMF in mixed-phase clouds is, the more liquid droplets evaporate and a higher fraction of cloud condensation nuclei are released back to the interstitial aerosol phase. Figure 1b shows that black carbon (BC) mass is scavenged into the cloud phase to the same extent as the bulk

aerosol. Such a behavior is not expected for freshly emitted soot particles because they have a hydrophobic nature. Most soot particles on the Jungfraujoch experienced aging processes which transformed them into an internally mixed hygroscopic aerosol (Cozic *et al.*, 2006).

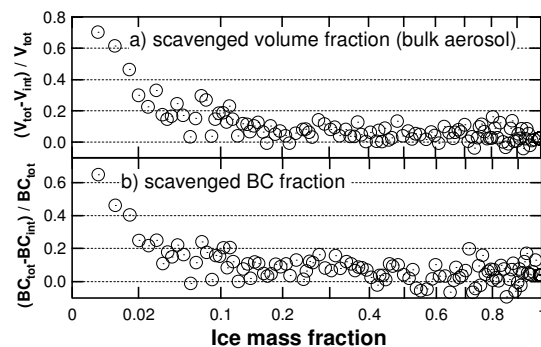


Figure 1: Scavenged fraction of aerosol volume (a) and black carbon mass (b) vs. the ice mass fraction of mixed-phase clouds. Each point is based on an average over 100 min of measurements.

Measurements downstream of the Ice-CVI confirmed that only a very small subset of atmospheric particles serve as ice nuclei. We found that BC is significantly enriched in the ice phase compared to the bulk aerosol indicating that some BC particles act as ice nuclei. This result is highly important for climate modeling since BC has a predominately anthropogenic origin.

This work was supported by MeteoSwiss in the framework of the Global Atmosphere Watch program, the German Research Foundation DFG, and the Natural Environment Research Council NERC.

Mertes, S., et al. (2007). *Environ. Sci. Technol.* (submitted).

Verheggen, B., et al. (2007). *J. Geophys. Res.* (submitted).

Cozic, J., et al. (2006). *Atmos. Chem. Phys. Discuss.*, 6, 11877–11912.

## Are the cloud condensation nuclei (CCN) properties in polluted air different from those in a remote region?

D. Rose<sup>1</sup>, G. P. Frank<sup>1</sup>, U. Dusek<sup>1</sup>, M. O. Andreae<sup>1</sup>, and U. Pöschl<sup>1</sup>

<sup>1</sup>Max Planck Institute for Chemistry, Biogeochemistry Department, 55128 Mainz, Germany

Keywords: CCN, size segregated aerosol, clean air, air pollution.

The influence of aerosol particles on clouds and precipitation is one of the central questions of current atmospheric and climate research. The cloud condensation nuclei (CCN) activity and its relation to other properties of aerosol particles from different sources and regions are, however, not yet well characterized.

In our study, CCN concentrations and efficiencies were measured as a function of water vapor supersaturation and particle diameter (Frank *et al.*, 2006, Rose *et al.*, 2007) in a polluted and in a remote continental region.

The polluted aerosol was measured approximately 60 km northwest of the megacity Guangzhou in south China. These measurements were part of the “Program of Regional Integrated Experiments of Air Quality over the Pear River Delta” intensive campaign in July 2006 (PRIDE-PRD2006).

The remote location was on Mt. Jungfrauoch (3570 m asl) in the Swiss Alps. These measurements were part of the Cloud and Aerosol Characterization Experiment (CLACE-5) and took place in February and March 2006.

The two measurement sites were characterized by aerosols of different sources and state of ageing. Nevertheless, the average CCN efficiency spectra (CCN/CN vs. particle size) were very similar for supersaturations of 0.5% and higher, which are required to efficiently activate particles with diameters  $\leq 80$  nm. This similarity has been found also for other aerosol types as published by Dusek *et al.*, 2006.

At small supersaturations (0.1-0.3%), however, we discovered that the CCN efficiencies in polluted air were on average significantly lower than under remote conditions.

Since low supersaturations are most typical for the atmosphere, the observed differences should be considered in the modeling of CCN activation and cloud formation. They may have a strong influence on aerosol-cloud interactions and on the effects of air pollution on climate.

### References

Dusek, U., Frank, G. P., Hildebrandt, L., Curtius, J., Schneider, J., Walter, S., Chand, D., Drewnick, F., Hings, S., Jung, D., Borrmann, S., & Andreae, M. O. (2006). *Science*, 312, 1375-1378.

Frank, G. P., Dusek, U., & Andreae, M. O. (2006). *Atm. Chem. Phys. Dis.*, 6, 4879-4895.

Rose, D., Frank, G. P., Dusek, U., Andreae, M. O., and Pöschl, U. (2007). to be submitted to *Atm. Chem. Phys. Dis.*

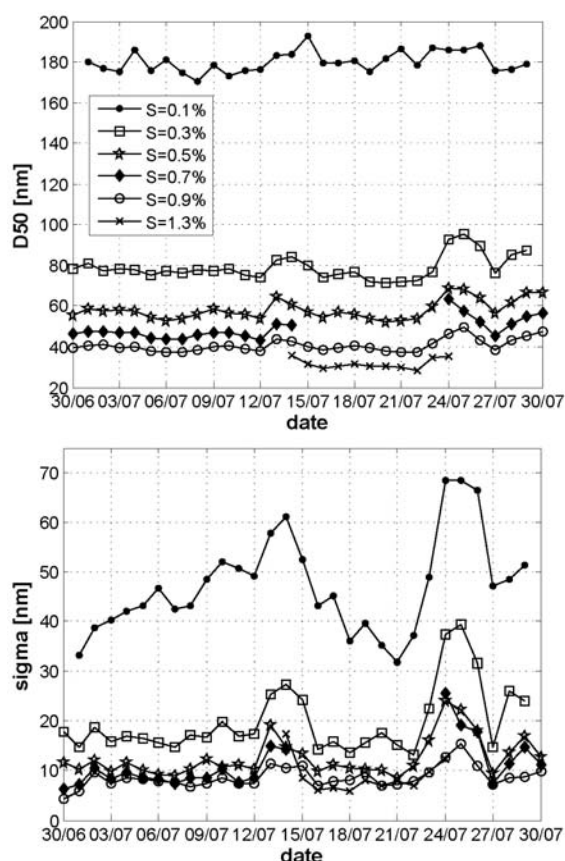


Figure 1: Time series of parameters from the CCN efficiency spectra recorded during the PRIDE-PRD2006 campaign: a) D50, the diameter at which half of the monodisperse particles are activated (decreases with particle solubility), b) sigma, the half width of a fitted error function to the spectra (decreases with particle homogeneity).

## Cloud condensation nucleus activity of secondary organic aerosol particles mixed with sulfate

S.M. King, T. Rosenoern, J.E. Shilling, Q. Chen and S.T. Martin

School of Engineering and Applied Sciences, Harvard University, Cambridge, MA 02138 USA

Keywords: CCN, SOA, smog chamber, ammonium sulphate, alpha-pinene oxidation

The cloud condensation nucleus (CCN) activity of organic-sulfate particles was investigated using a steady-state environmental chamber. The organic component consisted of secondary organic aerosol (SOA) generated in the dark from  $24 \pm 2$  ppb  $\alpha$ -pinene for conditions of  $300 \pm 5$  ppb ozone,  $40 \pm 2\%$  relative humidity, and  $25 \pm 1^\circ\text{C}$ , with the organic mass loading in the chamber ranging from 23 to 37  $\mu\text{g m}^{-3}$ . CCN analysis was performed for 80- to 150-nm particles having variable organic-sulfate volume fractions, estimated from the diameter of the organic-sulfate particle relative to that of the seed as well as independently from mass spectra. Critical supersaturation, which increased for greater SOA volume fraction and smaller particle diameter, was well predicted by a Köhler model having two components, one for ammonium sulfate and another for SOA. The entire data set could be successfully modeled by a single suite of effective chemical parameters for SOA. The results show that the effects of limited organic solubility may be reliably omitted in the treatment of cloud droplet formation, at least for the range of conditions studied.

$S_c$  values for each organic volume fraction ( $\epsilon_{SOA}^d$ ) are shown in Figure 1. The lines in Figure 1 show the least-squares fit of the model. The effective SOA molecular weight ( $M_{SOA}$ ) was obtained as an optimized model fit to the entire data set for fixed values of surface tension ( $\sigma$ ), effective SOA density ( $\rho_{SOA}$ ), and effective van't Hoff factor of SOA ( $v_{SOA}$ ) (Table 1). The optimization had no sensitivity to the effective saturation concentration of the organic component ( $C_{sat,SOA}$ ) provided that a lower limit of  $0.085 \text{ g g}^{-1} \cdot \text{H}_2\text{O}$  was exceeded. The value of  $\rho_{SOA}$  ( $1.4 \pm 0.1 \text{ g cm}^{-3}$ ) was determined by comparing the mode diameter of the vacuum-aerodynamic size distribution to the mode diameter of the mobility size distribution and assuming a spherical particle shape, including a correction for the density of ammonium sulfate. The values of  $v_{SOA}$  and  $\sigma$  were assumed equal to 1 and  $0.0725 \text{ N m}^{-1}$ , respectively.  $M_{SOA}$ , the target of the global optimization, was constrained as  $230 \pm 3 \text{ g mol}^{-1}$  based on the least-squares fit of the entire data set using a Monte Carlo method to vary  $S_c$  values within their uncertainty.

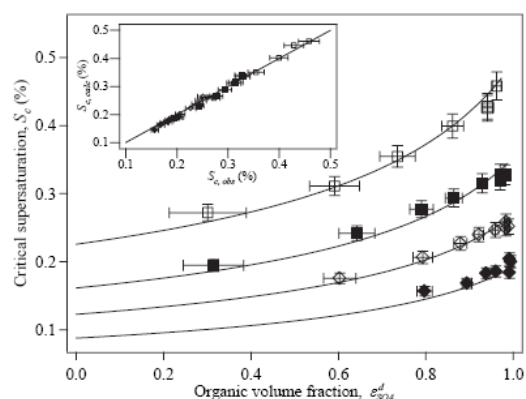


Figure 1. Critical supersaturation ( $S_c$ ) for 50% CCN activation of SOA particles internally mixed with sulfate. Data are shown for four particle mobility diameters ( $\square$ , 80 nm;  $\blacksquare$ , 100 nm;  $\diamond$ , 120 nm;  $\blacklozenge$ , 150 nm) for increasing organic volume fraction ( $\epsilon_{SOA}^d$ ). Lines represent modeled values using a single set of parameters (cf. Table 1). Lines for each diameter are drawn from  $\epsilon_{SOA}^d = 0$  to the largest measured  $\epsilon_{SOA}^d$ . Inset: Comparison of modeled  $S_c$  to observed  $S_c$  for all particle diameters. Comparison to the shown 1:1 line yields an r-squared value of 0.99.

Table 1. Parameters used in Köhler model to calculate  $S_c$ .

Parameter	Value
Surface tension, $\sigma$	$0.0725 \text{ N m}^{-1}$
van't Hoff factor of $(\text{NH}_4)_2\text{SO}_4$ , $v_{AS}$	2.2
Effective SOA density, $\rho_{SOA}$	$1.4 \text{ g cm}^{-3}$
Effective SOA van't Hoff factor, $v_{SOA}$	1
Effective SOA molecular weight, $M_{SOA}$	$230 \text{ g mol}^{-1}$
Saturation concentration (lower limit) of SOA, $C_{sat,SOA}$	$0.085 \text{ g g}^{-1} \text{ H}_2\text{O}$

## **T33 Abstracts**

## LACIS-Measurements of hygroscopic growth and activation of sea-salt particles

D. Niedermeier, H. Wex and F. Stratmann

Leibniz-Institute for Tropospheric Research, Department of Physics,  
Permoser Str. 15, 04318, Leipzig, Germany

Keywords: aerosol cloud interaction, marine aerosols, hygroscopicity, activation.

Sea-salt particles produced through the evaporation process of sea spray are important for the marine boundary layer. Depending on the present relative humidity, these particles scatter the incoming solar radiation. Under moderate wind conditions the production rate of sea-salt particles is high enough, so that they contribute to the number of cloud condensation nuclei (CCN) (O'Dowd *et al.*, 1997). Therefore it is important to study the hygroscopic behaviour and activation of these particles at different locations.

LACIS (Leipzig Aerosol Cloud Interaction Simulator) (Stratmann *et al.*, 2004) was used to measure the hygroscopic growth and activation of sea-salt particles which were generated from three different seawater samples. Sample I and II were taken from the Baltic Sea, the first one in the bay of Mecklenburg and the second one in the east of Gotland. The third sample was gathered from the Atlantic Ocean at 45°N latitude.

The Köhler equation was used to model the hygroscopic growth of the particles. Some parameters used in this equation are unknown for sea-salt. They are combined in an "ionic density"  $\rho_{ion}$  (Wex *et al.*, 2007):  $\rho_{ion} = (\Phi v \rho_s) / M_s$  with the osmotic coefficient  $\Phi$ , the number of ions  $v$  in which the salt dissociates, the solute density  $\rho_s$  and the molecular mass  $M_s$ . For each sea-salt sample a mean  $\rho_{ion}$  was determined by using the Köhler equation and the measured grown particle sizes.

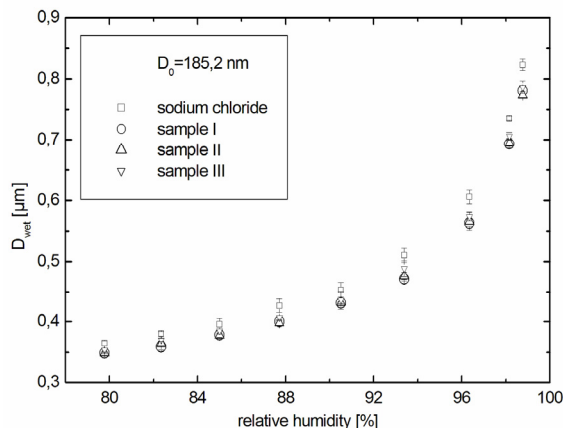


Figure 1. Hygroscopic growth of sea-salt particles generated from three different seawater samples at different values of RH in comparison to pure NaCl.

In Figure 1 the measured equilibrium diameters of the generated sea-salt particles (dry

diameter: 185,2 nm) is shown for different relative humidities. For comparison the growth of sodium chloride particles with the same dry size is presented, too. The values of the grown diameters for the three sea-salt samples agree within the measurement tolerances. But the hygroscopic growth of the sea-salt particles is less than that of the NaCl particles. At the highest RH studied, the difference amounts 4%.

LACIS was also used to measure the activation of the sea-salt particles at two different supersaturations  $S$ : 0,1% and 0,3%. At these two supersaturations, the critical diameters for the sea salt particles also were calculated, using the Köhler equation and the corresponding ionic density as derived from the hygroscopic growth.

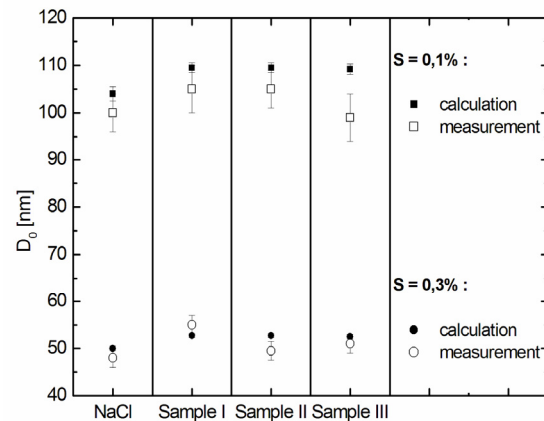


Figure 2. Comparison between calculated and measured critical dry diameters for the activation at super-saturations of 0,1% and 0,3%.

In Figure 2 the measured and calculated critical dry diameters for the activation of the different sea-salt and NaCl particles are shown. Besides two exemptions (sea-salt particles of sample III at  $S = 0,1\%$  and particles of sample II at  $S = 0,3\%$ ) the measurements are in agreement with the calculations within the error ranges.

O'Dowd, C. D. *et al.* (1997). *Atmos. Environ.*, 31 (1), 73-80.

Stratmann, F. *et al.* (2004). *J. Atmos. Oceanic Technol.*, 21, 876-887.

Wex, H. *et al.* (2007). *Geophys. Res. Lett.*, 34, L02818, doi: 10.1029/2006GL028260.

## Comparison of the hygroscopic growth and activation of urban aerosol and HULIS

M. Ziese<sup>1</sup>, E. Nilsson<sup>2</sup>, H. Wex<sup>1</sup>, T. Hennig<sup>1</sup>, I. Salma<sup>3</sup>, R. Ocskay<sup>3</sup>, F. Stratmann<sup>1</sup> and A. Massling<sup>1</sup>

<sup>1</sup>Leibniz-Institute for Tropospheric Research, Permoser Straße 15, 04318, Leipzig, Germany

<sup>2</sup>Lund University, Division of Nuclear Physics, P.O. Box 118, SE-221 00 Lund, Sweden

<sup>3</sup>Eotvos University, Institute of Chemistry, P.O. Box 32, 1518 Budapest, Hungary

Keywords: atmospheric aerosols, hygroscopicity, Aerosol cloud interaction, activation, supersaturation

Atmospheric aerosol particles influence the radiation transfer in the atmosphere directly via scattering the radiation and indirectly when they act as cloud condensation nuclei. For these effects, the hygroscopic properties of the particles are important. Among the substances that influence the hygroscopic properties are humic like substances (HULIS). Only a few investigations were performed on the hygroscopic growth and activation of HULIS particles, e.g. Wex et al. (2007).

Aerosol particles were sampled in downtown Budapest, Hungary. From the filters, two samples were prepared, one containing all soluble material, the other one containing only HULIS. Both samples were redissolved in Milli-Q water and atomized to generate particles. The hygroscopic growth and activation of particles from both samples were compared to each other.

Investigations regarding the hygroscopic growth up to 98% relative humidity were performed using a HHTDMA (Hennig et al., 2005). For relative humidities between 98% and 99.36% LACIS was applied (Stratmann et al., 2004; Wex et al., 2005). Also LACIS was utilised to investigate the activation of the particles between 0.2% and 1% supersaturation (Wex et al., 2006).

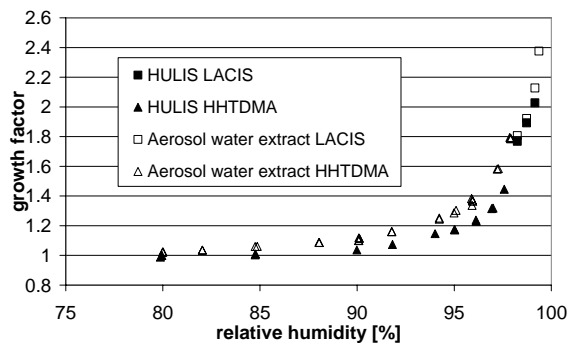


**Figure 1: Hygroscopic growth of HULIS and aerosol water extract particles measured with a HHTDMA (relative humidities up to 98%) and LACIS (relative humidities above 98%). The growth factor is defined as the ratio of wet diameter to dry diameter.**

HULIS particles grow continuously with increasing relative humidity above 85%. They show no deliquescence behaviour. The growth factor at 99.16% relative humidity is 2.03 (see Figure 1). At the same relative humidity the particles produced

from the aerosol water extract sample have a growth factor of 2.13. These particles grow continuously at relative humidities above 85%. The aerosol water extract particles also show no deliquescence behaviour (see Figure 1).

The activation of the HULIS and aerosol water extract particles was also measured. For this investigation the supersaturation was held constant and the dry diameter of the particles was varied. At the same supersaturation the HULIS particles activate at larger dry diameters than the aerosol water extract particles. The results are shown in Figure 2.

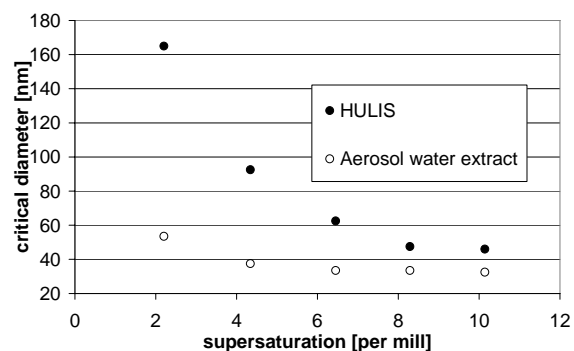


**Figure 2: Critical diameter for the activation of HULIS and aerosol water extract particles at several supersaturations.**

The hygroscopic growth of the HULIS sample is similar to the aerosol water extract sample. However, the activation behavior is different. This can be an effect of the surface tension, which is influenced by organic substances like HULIS (Salma et al., 2006). We will investigate this effect in the future.

Hennig, T. et al. (2005). *Journal of Aerosol Science*, 36(10), 1210-1223

Salma, I. et al. (2006). *Journal of Geophysical Research*, 111, D23205, DOI:10.1029/2005DJ007015

Stratmann, F. et al. (2004). *Journal of Atmospheric and Oceanic Technology*, 21, 876-887.

Wex, H. et al. (2005). *Journal of Geophysical Research*, 110, D21212, DOI:10.1029/2004JD005507

Wex, H. et al. (2006). *Atmospheric Chemistry and Physics*, 6, 4519-4527

Wex, H. et al. (2007). *Geophysical Research Letters*, 34, L02818, DOI:10.1029/2006GL028260

## The effects of aerosol composition on the hygroscopicity of atmospheric aerosols collected at three sites in Taiwan

C.T. Lee<sup>1</sup> and M.J. Chen<sup>1</sup>

<sup>1</sup>Graduate Institute of Environmental Engineering, National Central University, Zhongli, 32001, Taiwan

Keywords: Atmospheric aerosol, aerosol hygroscopicity, aerosol composition, relative humidity.

Aerosol hygroscopicity is one of the most fundamental properties of atmospheric aerosols. The variations of aerosol mass change (AMC) due to water uptake will affect aerosol deposition characteristics, size distribution, optical property, and heterogeneous chemical reactions. In this study, PM<sub>2.5</sub> at a rural (Shi-Men at northern tip of Taiwan), an urban (Northern Aerosol Supersite in northern Taiwan), and a mountain (Mt. Yu in middle Taiwan) sites are collected for measuring aerosol water uptake by using a water-mass measuring system (Lee and Chang, 2002) at high humid (90 RH) environment. The rural and the urban samples were collected during Asian dust transport, while mountain sample collections were made during biomass burning transport from Southeast Asia in March 2006.

Figure 1 shows the measured aerosol water mass, W<sub>mea</sub>, at 90 RH, correlated well with PM<sub>2.5</sub> concentration. It indicates that hygroscopic components of aerosol are correlated linearly with aerosol water uptake. Among these aerosol hygroscopic components, sulfate is the one dominates aerosol water mass as can be seen from Figure 2.

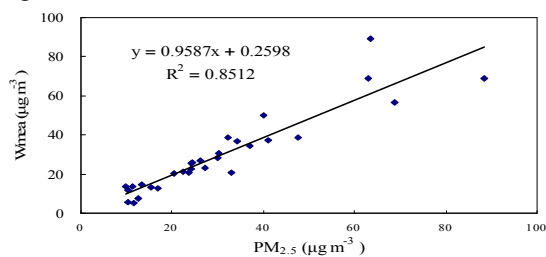


Figure 1. The measured aerosol water mass, W<sub>mea</sub>, and PM<sub>2.5</sub> concentration at the three sampling sites.

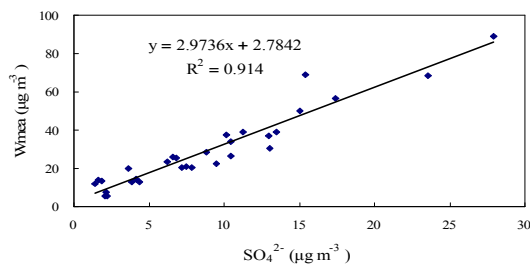


Figure 2. The measured aerosol water mass, W<sub>mea</sub>, and PM<sub>2.5</sub> sulfate concentration at the three sampling sites.

To investigate aerosol composition in affecting AMC, this study analyzes water-soluble inorganic ions, organic and elemental carbons, and water-soluble organic carbon (WSOC) in the collected aerosols. Meanwhile, the aerosol water mass of water-soluble inorganic ions simulated from the ISORROPIA model (Nenes et al., 1998), W<sub>model</sub>, is compared with W<sub>mea</sub> at 90 RH. This will enable the study on water uptake from the influence of aerosol organics.

For the investigation of the influence of aerosol organic components on aerosol water mass, Figure 3 shows the difference between W<sub>mea</sub> and W<sub>model</sub> for various WSOC mass ratios. It shows that the unaccounted aerosol water mass is weakly correlated with aerosol organic fraction. However, for aerosol organic fraction below a certain limit, e.g., 0.11 in Figure 3, the effect of organic fraction is uncertain or even shows an inhibition of aerosol water uptake.

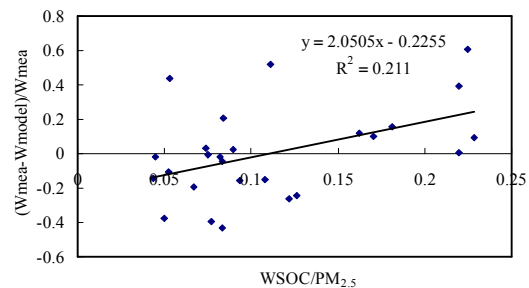


Figure 3. The difference of aerosol water mass between measured and modelled for various WSOC mass ratios at the three sampling sites.

For an environment controlled at 25°C and 30 RH, AMC is found ranging from 1.00-1.41 in this study. It suggests that filter-based aerosol mass determined from weighing may frequently be overestimated unless the weighing room is completely dry. High fraction of WSOC in aerosol tends to help increase aerosol water uptake under low RH environment in the deliquescence mode. This high fraction of WSOC in aerosol also inhibits complete water release even in the 20 RH environment in the efflorescence mode.

Lee, C. T., & Chang, S. Y., (2002). *Atmospheric Environment*, 36, 1883-1894.

Nenes A., Pandis S. N., & Pilinis C., (1998). *Aquatic Geochemistry*, 4, 123-152.

## Closure between chemical composition and hygroscopic growth of aerosol particles

M. Gysel<sup>1,2</sup>, J. Crosier<sup>1</sup>, D.O. Topping<sup>1</sup>, J.D. Whitehead<sup>1</sup>, K.N. Bower<sup>1</sup>, M.J. Cubison<sup>1</sup>, P.I. Williams<sup>1</sup>, M.J. Flynn<sup>1</sup>, G.B. McFiggans<sup>1</sup>, H. Coe<sup>1</sup>

<sup>1</sup>Atmospheric Sciences Group, SEAES, University of Manchester, P.O. Box 88, Manchester, M60 1QD, UK

<sup>2</sup>Now at Laboratory of Atmospheric Chemistry, Paul Scherrer Institut, 5232 Villigen PSI, Switzerland

Keywords: hygroscopicity, atmospheric aerosols, HTDMA, AMS, on-line measurements.

Aerosol physical and chemical properties have been investigated during the TORCH2 field campaign in Weybourne, UK, on the North Norfolk coast (Gysel *et al.*, 2006). An Aerodyne aerosol mass spectrometer (Q-AMS) was employed to measure highly time and size resolved chemical composition of the non-refractory compounds in PM<sub>1</sub>. Hygroscopic growth factors (HGF) of particles with different dry sizes have been measured using a Hygroscopicity Tandem Differential Mobility Analyser (HTDMA).

Clean air masses not exposed to contact with land over the course of several days were encountered from 11-13 and 21-23 May, during which the aerosol composition showed little variation and the particles were sulphate dominated with an organic mass fraction of 20% or less. Accordingly the HGFs were quite constant and as high as 1.6-1.8 for 60 to 217 nm particles (thick black lines in Fig. 1). Aged polluted air masses originating from the Northeastern Atlantic and transported across Ireland and mid or north England were encountered from 14-20 May, where the organic fraction was still roughly constant at ~30, 50, and 70% for dry diameters 217, 137, and 60 nm, respectively. Accordingly, the overall inorganic fraction was also roughly constant, but the respective contributions from ammonium sulphate (AS) and ammonium nitrate (AN) showed a distinct diurnal pattern with maxima of AS and AN during the day and night. The HGFs also showed a distinct diurnal pattern, which is surprising regarding the roughly constant ratio of inorganic to organic compounds.

Predictions of expected HGFs, based on the size-resolved chemical composition obtained by the AMS, were made using the Zdanovskii-Stokes-Robinson

(ZSR) rule for calculating the water activity of mixtures from pure compound properties. HGFs of pure AS and AN were taken from thermodynamic models, whereas a bulk HGF of 1.20 was assumed for the organics with small reductions accounting for the Kelvin effect. The black lines with markers in Fig. 1 show that predicted growth factors agree well with measurements in the clean air mass, but there is a clear disagreement at larger sizes during the aged polluted event. However, very good agreement between measurement and AMS/ZSR prediction at any size and any time is achieved when assuming that ~60% of the particulate AN evaporated in the HTDMA (grey lines in Fig. 1). A long residence time of ~60 s in the HTDMA was chosen to ensure full equilibration with water vapour, which, in retrospect, is likely to have caused the AN artefact in the HGF measurements.

This study has shown that high time and size resolution is a crucial prerequisite for a valid hygroscopicity closure. The ZSR rule along with a constant organic HGF is an adequate simplification of the thermodynamic modelling in case of aged air masses, because more detailed chemical characterisation for comprehensive thermodynamic modelling typically undermines time and size resolution.

This work was supported by the British Natural Environment Research Council through grant number NER/T/S/2002/00494 and by the Swiss National Science Foundation.

Gysel, M., Crosier, J., Topping, D. O. *et al.* (2006). *Atmos. Chem. Phys. Discuss.*, 6, 12503–12548.

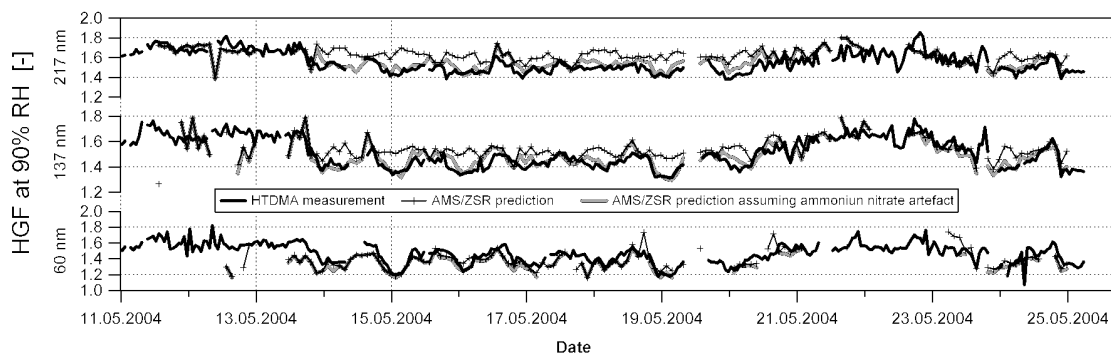


Figure 1. Closure between measured HGFs and prediction based on AMS chemical composition.

## Hygroscopic properties of secondary organic aerosol formed from plant emissions

T. F. Mentel<sup>1</sup>, E. Dinar<sup>3</sup>, P. Griffiths<sup>2</sup>, R. Tillmann<sup>1</sup>, R. Fisseha<sup>1</sup>, T. Hohaus<sup>1</sup>, A. Kiendler-Scharr<sup>1</sup>, E. Kleist<sup>1</sup>, A. Mensah<sup>1</sup>, M. Miebach<sup>1</sup>, Y. Rudich<sup>3</sup>, R. Uerlings<sup>1</sup>, and J. Wildt<sup>1</sup>

<sup>1</sup>Institut für Chemie und Dynamic der Geosphäre, Forschungszentrum Jülich, D-52425 Jülich, Germany

<sup>2</sup>Cambridge University, Center of Atmospheric Science, Cambridge, UK

<sup>3</sup>Weizmann Institute of Science, Department of Environmental Science, 76100 Rehovot, Israel

Keywords: Biogenic Particles, CCN, SOA, Hygroscopicity

The largest portion of atmospheric volatile organic compounds (VOC) is of biogenic origin. Atmospheric oxidation of VOCs emitted by plants, in particular that of mono- and sesquiterpenes, leads to a substantial fraction of low volatile products that form secondary organic aerosols (SOA). Since aerosols scatter sunlight and are essential for cloud formation, they are important players in the climate system. A shift in climate zones could affect plant emissions and the resulting particle production. Kulmala et al. (2004) discussed if and how biogenic particle production from forests can contribute to a feed back between air chemistry, climate and vegetation.

Previous laboratory studies of hygroscopic properties and CCN activation of biogenic SOA focus on single compounds or simple mixtures (Varutbangkul et al. 2006, Huff-Hartz et al. 2005). In our experiments we used plants as complex VOC sources and investigated the formation of secondary organic particles directly from the plant emissions. The idea is to account for the multi-component and highly mixed character of natural systems. Hygroscopic growth and CCN activity of the particles were directly measured.

to a reaction chamber and SOA formation was initiated there by UV-photolysis of ozone in the presence of water (60% RH). The chamber was operated as a stirred flow reactor with about 1 h residence time. The vapor phase in the reactor was monitored by PTR-MS (Ionicon), the composition of the particles by aerosol mass spectrometry (AMS, Aerodyne Research)

As soon as the freshly formed particles reached diameters of 50 nm, growth factors  $G_f$  as a function of the relative humidity RH were measured by a Hygroscopicity Tandem Differential Mobility Analyzer (Figure 1). Moreover, the CCN activity of the particles was monitored by a combination of a CCN spectrometer (DMT), SMPS and a CPC.  $G_f(\text{RH}90)$  for all tree species were around 1.1 as observed in laboratory studies for monoterpenes. In the case where emissions were dominated by sesquiterpenes the smallest  $G_f(\text{RH}90)$  of 1.08 was observed. The critical diameters of CCN activation varied during the formation and condensation process. E.g. for particles from pine emissions the critical diameter varied from 90 nm to 110 nm at 0.4% supersaturation.

This work was supported by the ACCENT EU Network of Excellence and the ESF INTROP program.

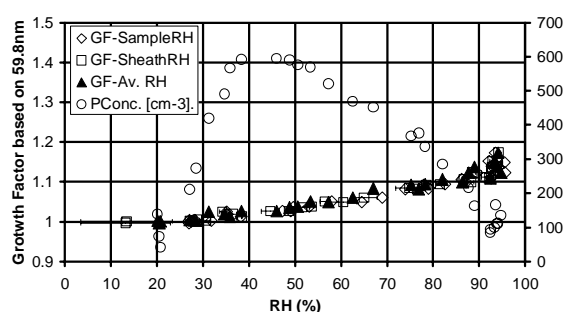


Figure 1. Growth factors of particles generated from emissions of a Mediterranean Oak. The number density of the selected particles is given on the right hand scale.

The experiments were performed using plants kept under well defined conditions in the plant chamber in Juelich (Research Center Juelich, ICG-3). Mediterranean oak, and species from the boreal forest, spruce, pine, and birch, were used as model plants. The plant emissions were characterized by GC-MS. Air from the plant chamber was transferred

Kulmala, M., et al. (2004), *Atmos. Chem. Phys.*, 4, 557-562.

Varutbangkul, V. et al., (2006), *Atmos. Chem. Phys.* 6, 2367-2388.

Huff-Hartz, K. E., et al. (2005), *J. Geophys. Res.*, 110, D14208, doi:10.1029/2004JD005754.

## Aerosol hygroscopicity as the function of the size and the chemical composition

K. Imre<sup>1</sup>, A. Molnár<sup>2</sup> and D. Benkő<sup>1</sup>

<sup>1</sup>Department of Earth and Environmental Sciences, University of Pannonia, Egyetem 10, 8200, Veszprém, Hungary

<sup>2</sup>Air Chemistry Group, Hungarian Academy of Sciences, Egyetem 10, 8200, Veszprém, Hungary

Keywords: atmospheric aerosols, chemical composition, hygroscopicity, size distribution.

The hygroscopic behavior of the particles is determined by the inorganic as well as by the organic species. Although the organic fraction of the aerosol particles is rather high, our knowledge on their role in aerosol hygroscopicity is limited. The aim of this work is to study the hygroscopic growth of the particles as the function of their size and chemical composition, and to estimate the effect of organic compounds on the aerosol hygroscopicity.

In summer of 2001 and 2002, 13 size-selected ambient aerosol samples were taken at K-pusztá station, Hungary. The sampling site is located on a forest clearing on the Great Hungarian Plain. The air was sampled by a 9-stage Berner impactor. Gravimetric method was applied for the determination of the aerosol particle mass under different relative humidities. The relative humidity was controlled by saturated solutions of different inorganic salts. Finally, the samples were chemically analyzed; the concentrations of inorganic ions and total carbon were measured.

Beside measured mass growth, on the basis of the inorganic composition of the aerosol, the mass growth of the particles in different size ranges were calculated by means of Aerosol Inorganic Model (AIM) (Clegg *et al.*, 1998): Then, the measured and calculated mass growth factors were transformed to diameter growth factors considering volume mixing rule for dry particle mass and absorbed water mass.

Particle growth  $G(RH)$  is generally estimated as the function of relative humidity ( $RH$ ) (Zhou *et al.*, 2001):

$$G(RH) = 10^c \cdot \left( \frac{1 - RH}{100} \right)^{-\gamma}$$

Table 1:  $\gamma$  exponents in different particle sizes for both measured and calculated data sets.

Geometric particle diameter ( $\mu\text{m}$ )	$\gamma$ exponent	
	measured	calculated
0.088	0.185	0.273
0.18	0.096	0.164
0.35	0.078	0.206
0.71	0.182	0.268
1.4	0.178	0.205
2.8	0.201	0.192
5.7	0.196	0.092
11.3	0.147	0.140

The growth rate is mostly governed by  $\gamma$ , since  $10^c$  varies around 1. In Table 1 the summary of fitted  $\gamma$  exponents are given for both the measured and for the calculated data sets. The results show that the particle growth ( $\gamma$  exponent) strongly depends on the particle size. One can suppose that  $\gamma$  is mainly controlled by the chemical composition of the particles. We assumed that the measured  $\gamma$  exponent ( $\gamma_m$ ) – the growth factor (G) – can be estimated by the inorganic ion and the total carbon concentrations of the aerosol particles. We considered that the hygroscopic behavior of the inorganic compounds is well estimated by the AIM model, i.e. the hygroscopic effect of inorganic ions is correctly described by the “calculated”  $\gamma$  exponent ( $\gamma_c$ ). On the other hand we also supposed that the hygroscopic effect of carbonaceous compounds can be estimated by the TC concentration. As a first approximation, linear function of two variables is considered:

$$\gamma_m = m_1 \cdot \gamma_c + m_2 \cdot TC + b$$

The calculation is based on multilinear approach, where parameter “b” could be interpreted as the hygroscopic effect of other constituents which are not determined. The results for fine and coarse mode aerosol show statistically significant relationship among the parameters considered:

$$\text{Fine mode: } \gamma_m = 0.78 \cdot \gamma_c + 0.07 \cdot TC - 0.01$$

$$\text{Coarse mode: } \gamma_m = 0.58 \cdot \gamma_c + 0.12 \cdot TC - 0.13$$

The results indicate that in the fine mode  $\gamma_m$  can be estimated by the inorganic and the total carbon concentrations, since the unknown constituents (“b”) do not play important role (<10%) in the control of  $\gamma_m$ . On the other hand, for coarse mode aerosol same conclusion cannot be drawn because of the high contribution of non-defined compounds (the share of “b” is > 70%).

This work was supported by the Hungarian Science Foundation (OTKA, project numbers: T 047222 and TS 049845). This work was done in the frame of ESF COST 633 program.

Clegg S. L., Brimblecombe P. & Wexler A. S. (1998). *J. Phys. Chem.* 102A, 2155-2171.

Zhou, J., Swietlicki, E., Berg, O., Aalto, P.P. Hämeri, K., Nilsson, E.D. & Leck, C. (2001). *J. Geophys. Rech.*, 106, D23, 32,111-32,123.

This document was created with Win2PDF available at <http://www.win2pdf.com>.  
The unregistered version of Win2PDF is for evaluation or non-commercial use only.  
This page will not be added after purchasing Win2PDF.

## Measurement of Size Resolved Hygroscopic and Cloud Activation Aerosol Properties

N. Good<sup>1</sup>, J. Crosier<sup>1</sup>, P. Williams<sup>1</sup>, H. Coe<sup>1</sup>, G. McFiggans<sup>1</sup>

<sup>1</sup>Centre for Atmospheric Science, SEAES, University of Manchester, P.O. Box 88, Manchester, M60 1QD, UK

Keywords: Aerosol Cloud Interaction, Hygroscopicity, CCN.

Aerosol hygroscopic and cloud activation properties were measured during the MAP (Marine Aerosol Production) Celtic Explorer campaign in the North East Atlantic in Summer 2006.

A HTDMA (Hygroscopic Tandem Differential Mobility Analyser) (Cubison et al 2005) was employed to measure the size resolved hygroscopic growth distribution of aerosol at 90% relative humidity. Aerosols with dry diameters from 30nm to 300nm were selected in the HTDMA covering the dry size range most likely to include the critical dry size for droplet activation at reasonable marine stratocumulus supersaturations (McFiggans et al 2006).

The number of particles forming cloud droplets at a given supersaturation was measured using a Droplet Measurement Technologies (DMT) CCN (Cloud Condensation Nucleus) Counter (Nenes et al 2005). The design of the instrument allows high time resolution measurements at atmospherically realistic supersaturations. An inlet switching system enabled the size resolved activated fraction as well as the activation behaviour of the entire aerosol population below  $4\mu\text{m}$  diameter to be measured. On alternate hours the counter i) sampled polydisperse aerosol and then ii) switched so that a scanning DMA supplied it with monodisperse aerosol. Using this arrangement aerosol activation distributions from 10nm to 300nm at 5 different supersaturations were measured over a 1 hour period during alternate hours. Comparing the activation distribution to the aerosol

number size distribution enabled calculation of the activated fraction as a function of size.

An Aerodyne time-of-flight aerosol mass spectrometer (ToF-AMS) was used to provide size resolved measurements of chemical composition of the non-refractory aerosol. Along with offline measurements, this allowed differences in aerosol composition with size to be directly related to the measured subsaturated and supersaturated behaviour. From the measured hygroscopic growth distributions and the activated fraction distributions it is then possible to reconcile subsaturated and supersaturated measurements.

This work was supported by the European Commission under GOCE 018332. NG receives a UK NERC studentship.

Cubison, M.J. et al. (2005). *A modified hygroscopic tandem DMA and a data retrieval method based on optimal estimation*. Journal of Aerosol Science 36 (7): 846-865.

McFiggans, G. et al. (2006). *The effect of physical and chemical aerosol properties on warm cloud droplet activation*. Atmospheric Chemistry and Physics 6: 2593-2649.

Roberts, G.C. & Nenes, A. (2005). *A continuous-flow streamwise thermal-gradient CCN chamber for atmospheric measurements*. Aerosol Science and Technology, 39(3): 206-221.

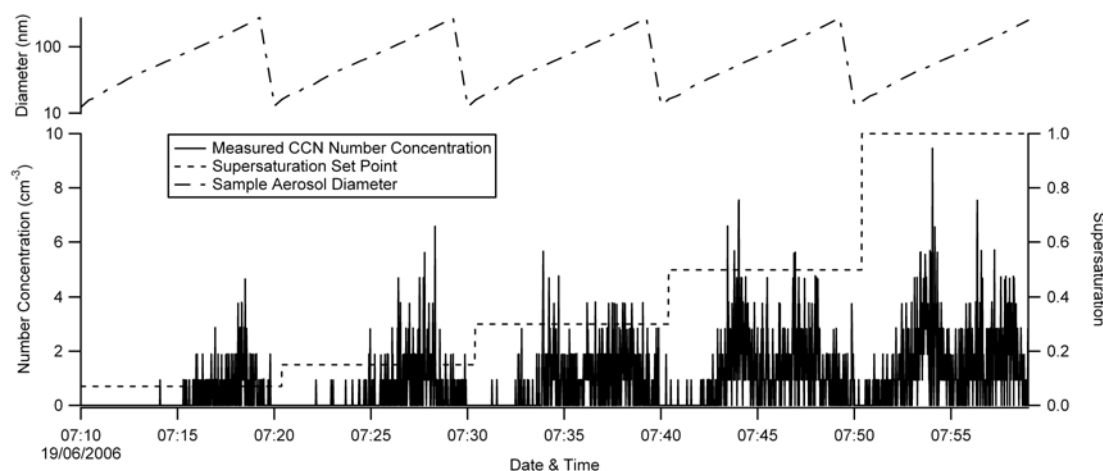


Figure 1. Top Panel - Sample particle dry diameter. Bottom Panel - Number of particles activating as a function of supersaturation and size during a 1 hour cycle.

## Hygroscopic properties of sub-micrometer atmospheric aerosol particles measured with H-TDMA instruments in various environments - A review

E. Swietlicki<sup>1</sup>, H.-C. Hansson<sup>2</sup>, A. Massling<sup>3</sup>, T. Petäjä<sup>4</sup>, P. Tunved<sup>2</sup>, K. Hämeri<sup>4</sup>, E. Weingartner<sup>5</sup>, U. Baltensperger<sup>5</sup>, P.H. McMurry<sup>6</sup>, G. McFiggans<sup>7</sup>, B. Svenningsson<sup>8</sup>, A. Wiedensohler<sup>3</sup> and M. Kulmala<sup>4</sup>

<sup>1</sup>Div. of Nuclear Physics, Lund University, P.O. Box 118, S-22100 Lund, Sweden

<sup>2</sup>Department of Applied Environmental Science, Stockholm University, S-10691 Stockholm, Sweden

<sup>3</sup>Department of Physics, Leibniz-Institute for Tropospheric Research, D-04318 Leipzig, Germany

<sup>4</sup>Div. of Atmospheric Sciences, P.O. Box 64, FI-00014 University of Helsinki, Finland

<sup>5</sup>Laboratory of Atmospheric Chemistry, Paul Scherrer Institut, 5232, Villigen PSI, Switzerland

<sup>6</sup>Univ Minnesota, Dept. of Mechanical Engineering, 111 Church St SE, Minneapolis, MN 55455, USA

<sup>7</sup>Atmospheric Sciences Group, SEAES, Univ. of Manchester, P.O. Box 88, Manchester, M60 1QD, UK

<sup>8</sup>Dept. of Physical Geography and Ecosystems Analysis, Lund Univ., P.O. Box 118, S-221 00 Lund, Sweden

Keywords: Atmospheric aerosols, hygroscopicity, relative humidity, H-TDMA.

The hygroscopic properties of atmospheric sub-micrometer aerosol particles are vital for a proper description of how the particles interact with water vapour at sub- and super-saturated conditions, and are thus of major importance in describing the life cycle of the aerosol and the direct and indirect effects of aerosols on climate. These hygroscopic properties can be measured in great detail using H-TDMA instruments (Hygroscopic Tandem Differential Mobility Analyzers).

The H-TDMA is one of the few instruments capable of providing on-line and in-situ information regarding the extent of external versus internal mixing of the atmospheric aerosol, since the H-TDMA determines the hygroscopic growth of individual aerosol particles. Although this state of mixing strictly refers only to the hygroscopic properties, it nevertheless implies the extent of chemical mixing of the aerosol.

The primary parameters measured with an H-TDMA as a function of dry particle diameter are i) the ratio between humidified and dry particle diameter at a well-defined relative humidity  $RH$  - often denoted hygroscopic growth factor; ii) the number fraction of particles belonging to each of the observed and separable groups of hygroscopic growth; and often also iii) the spread of diameter growth factors around the arithmetic mean value. Alternatively, the H-TDMA measurements can also be presented as distributions of hygroscopic growth factors for each given dry particle diameter.

While the bulk of H-TDMA data is available for a nominal and high  $RH$  (often between 80-90%), some field studies have performed scans in  $RH$  to explore the aerosol deliquescence and efflorescence behaviour and water uptake at low  $RH$ .

Over the last 25 years, H-TDMA instruments have been used in several field measurements in various air masses around the globe. These include remote marine environments (Atlantic Ocean, Pacific Ocean, Indian Ocean, Arctic Ocean), background continental sites (Amazon rain forest, Nordic boreal

forest, the Alps, North America), polluted continental sites (Italy, United Kingdom, Germany), and polluted urban sites (Germany, North America, Mexico, Asia). Air masses influenced by fresh as well as aged biomass burning have been studied in North and South America. Emission studies include fresh diesel vehicle and jet engine exhaust and flue gases from biomass combustion. Secondary organic aerosol has been investigated in a variety of smog chamber experiments.

While H-TDMA instruments are normally operated in a size interval that covers the Aitken and accumulation modes of the atmospheric aerosols (from ~30 nm to a few hundred nm), there are a limited number of field studies on nucleation mode particles (<~30 nm) in some environments (boreal forest, coastal, urban) where new particle formation has been frequently observed.

A combination of volatility and hygroscopic TDMA techniques has recently provided new insights regarding the processes that shape the atmospheric aerosol. In several so called hygroscopic and CCN closure studies, efforts have been made to reconcile H-TDMA data with size-resolved chemical composition data and the ability of the aerosol particles to act as cloud condensation nuclei.

This work reviews and summarizes the existing H-TDMA data sets, with an emphasis on those published so far in peer-reviewed journals. The aim is to present the data in a way that will make it useful in evaluating models on various spatial and temporal scales incorporating a more detailed aerosol description than simply aerosol mass. To facilitate comparison between sites, growth factors are recalculated to an  $RH$  of 90% whenever possible, and classified according to the air mass properties and geographical location.

This work was carried out within the frameworks of the EU FP6 Integrated Project EUCAARI, the EU FP6 Infrastructure Project EUSAAR as well as the NOS-N Nordic Centre of Excellence BACCI.

## Hygroscopic properties of summertime central Arctic sub-micrometer aerosol particles and prediction of their CCN activity

E. Swietlicki<sup>1</sup>, J. Rissler<sup>1</sup>, J. Zhou<sup>1</sup>, E.K. Bigg<sup>2</sup> and C. Leck<sup>3</sup>

<sup>1</sup>Div. of Nuclear Physics, Lund University, P.O. Box 118, S-22100 Lund, Sweden

<sup>2</sup>12 Wills Ave., Castle Hill 2154, Australia

<sup>3</sup>Department of Meteorology, Stockholm University S-10691 Stockholm, Sweden

Keywords: Arctic aerosols, hygroscopicity, clouds, H-TDMA.

The central Arctic Ocean is a region that is particularly sensitive to changes in climate due to various feedback mechanisms that exist there. During the Arctic summer, aerosol particles influence the radiative balance primarily by acting as cloud condensation nuclei (CCN). Therefore, knowledge of the sources and physical/chemical properties of these particles are essential for an adequate assessment of future climate changes in the Arctic region.

In the summer 2001 Arctic Ocean Expedition (AOE-2001), the Swedish icebreaker *Oden* was used as a measurement platform in the central Arctic, mostly north of latitude 85°N in July-August 2001 (Leck *et al.*, 2004; Tjernström, 2005). Measurements of the hygroscopic and cloud-nucleating properties of the aerosol and the size distribution were conducted on *Oden* using an H-TDMA (Hygroscopic Tandem Differential Mobility Analyzer), a CCN counter and a DMPS (Differential Mobility Particle Sizer). A summary of the aerosol particle size distributions are given in Heintzenberg *et al.* (2006). Continuous and uninterrupted measurements in the pristine Arctic environment were greatly facilitated by mooring the icebreaker to an ice floe and drifting with the trans-polar current. The ice drift started on 1 August 2001 near 89.0° N, 1.8° E and ended on 22 August at 88.2° N, 9.4° W.

The H-TDMA often showed an external mixture during the ice drift period for particles with dry diameters between 20-165 nm. More-hygroscopic particles were nearly always present (83-92% frequency) with hygroscopic growth factors (dry to  $RH=90\%$ ) between 1.49-1.61 and increasing with dry size. Less-hygroscopic particles were less frequent (23-42%) with growth factors between 1.11-1.01 and decreasing with dry size. Since periods of pollution from the icebreaker were carefully excluded, the appearance of near-hydrophobic particles in the Aitken and accumulation mode size ranges indicate a surface source of aerosol particles within the pack ice region.

Concentrations of CCN were predicted based on the DMPS and H-TDMA data (Rissler *et al.*, 2004), and compared with parallel measurements at supersaturations of 0.3 and 0.8% (Bigg & Leck, 2001).

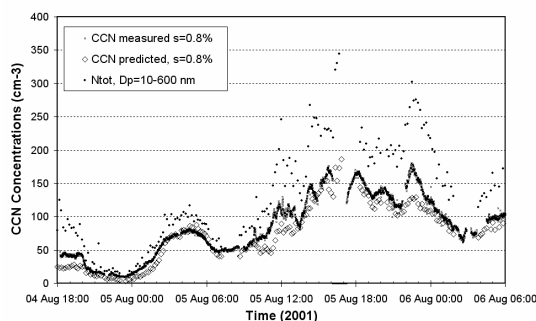


Figure 1. Comparison between predicted and measured CCN concentrations at  $s=0.8\%$  for a time period during the ice drift.

Figure 1 shows a 36-hour time series of predicted and measured CCN concentrations at 0.8% supersaturation. Agreement was in general good despite very low particle number concentrations, with ratios of predicted/measured CCN concentrations in general between 0.7-1.3 at both supersaturations. Time periods during which the CCN prediction failed may be indicative of the existence of poorly water-soluble compounds or surface tension depression at the point of activation. Particles with these properties might be linked to biogenic activity in the Arctic Ocean or the surface microlayer of the open leads during summer (Leck & Bigg, 2005).

- Bigg E.K. and Leck C. (2001). *J. Geophys. Res.* 106, 32155-32166.
- Heintzenberg J., Leck C., Birmili W., *et al.* (2006). *Tellus* B58, 41-50.
- Leck, C., M. Tjernström, P. Matrai, E. Swietlicki, and K. Bigg. (2004). *EOS*, Vol. 85, No. 3, pp. 25, 30, 32.
- Leck C, Bigg EK. (2005). *Tellus* B57, 305-316.
- Rissler J, Swietlicki E, Zhou J, *et al.* (2004) *Atm. Chem. Phys.*, 4, 2119-2143.
- Tjernström, M. (2005). *Bound.-Layer Meteorol.* 117, 5-36.
- Zhou J.C., Swietlicki E., Berg O.H., *et al.* (2001) *J. Geophys. Res.* 106, 32111-32123.

## Mixing states and hygroscopicity of aerosol particles in West Africa: Based on AMMA aircraft campaign in summer 2006

A. Matsuki<sup>1</sup>, A. Schwarzenboeck<sup>1</sup>, H. Venzac<sup>1</sup>, P. Laj<sup>1</sup>, O. Laurent<sup>1</sup>, G. Momboisse<sup>1</sup>,  
S. Crumeyrolle<sup>2</sup>, L. Gomes<sup>2</sup> and T. Bourrienne<sup>2</sup>

<sup>1</sup> Laboratoire de Météorologie Physique, Université Blaise Pascal, 63177, Clermont-Ferrand, France

<sup>2</sup> Centre National de Recherches Météorologiques, Météo-France, 31057, Toulouse, France

Keywords: aerosol-cloud interactions, CCN, hygroscopicity, inertial impactor, single particle analysis.

While West Africa is recognized as being the region with highest aerosol optical thickness in the entire globe, the heterogeneity arising from the mixing and cloud processing of various aerosol species (mineral dust, biomass burning, sulphates etc.) further complicates the accurate prediction of the aerosol direct effect, cloud life cycle and consequently the indirect effect.

In order to address the issue as to how the mixing and cloud processes modify the physico-chemical characteristics, especially the hygroscopic property of the aerosols, the French ATR-42 research aircraft equipped both with a counterflow virtual impactor (CVI) and community aerosol inlets was deployed in Niamey, Niger (13°30' N, 02°05' E) in August 2006 during one of the special observation periods (SOP) of the African Monsoon Multidisciplinary Analysis (AMMA) project.

Continuous exploration of both the aerosol particles and the cloud residual particles (can be considered as those activated as CCN) was performed by choosing between the two inlets depending on whether the aircraft was outside, or inside the cloud.

Table 1. list of instruments downstream the two inlets

- 
- Aerosol spectrometer (GRIMM model 1.108)
  - Scanning Mobility Particle Spectrometer SMPS (10nm < Dp < 300nm)
  - An oven upstream the other pair of GRIMM and SMPS for particle volatility measurement
  - CN counter (TSI 3010)
  - Lyman-alpha hygrometer
  - Particle soot / absorption photometer PSAP (Radiance Research)
  - Impactors for individual particle analysis (Dp > 0.2µm)
  - Filter packs for bulk chemistry analysis
- 

The CVI was operated partly in 9 of the 15 flights (each flight lasting 3-4 hours) during cloud encounter, accounting for the total period of about 4 hours. Due to the patchy nature of the clouds, it was difficult to direct the aircraft to always stay well inside the dense and homogeneous cloud for the entire CVI operation. Nevertheless, droplet concentration inside stratiform cloud layers estimated

from the average counts of cloud residual particles ranged between 50-250 particles/cm<sup>3</sup>. This is roughly the range of droplet concentration expected inside non-polluted, continental clouds and hence suggesting no major breakup of droplets inside the CVI inlet.

The impactor samples are analyzed using transmission electron microscope (TEM) and scanning electron microscope coupled with energy dispersive X-ray spectroscopy (SEM-EDS). It is probable that some interstitial particles with larger inertia (e.g. fraction of dust particles with particularly larger sizes) may penetrate into CVI inlet and mimic the cloud residual particles. However, the number of coarse particles (Dp > 1µm) found on the CVI samples seemed to vary independently from the duration of the filter exposure, but rather in accordance with the average concentration of residual particles during cloud sampling. Thus, heavier interstitial particles may not be solely responsible for the coarse particles collected via CVI, and current samples should be able to show, if any, the characteristics of the cloud residual particles.

The preliminary results of the analysis will be presented at the conference. The comprehensive set of physical parameters and the mixing states of individual particles collected in- and out-cloud is expected to provide deeper insights into the characteristics of the CN fraction which eventually became CCN, and their possible cloud processing.

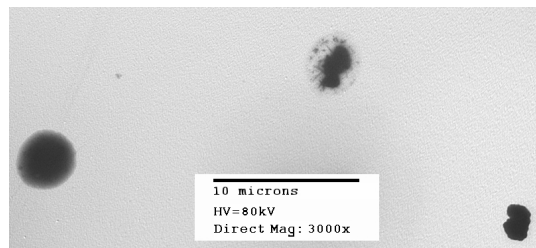


Figure 1. Representative TEM micrograph of the coarse particles (Dp > 1µm) collected via CVI

This work was supported by INSU, JSPS as well as the following funding agencies:  
<http://amma-international.org/fundorg/index>

## **WGLPI Abstracts**

## Size partitioning of airborne particles to compare their proinflammatory effect in airway epithelial cells.

K. Ramgolam<sup>1</sup>, O. Favez<sup>2</sup>, L. Martinon<sup>3</sup>, H. Cachier<sup>2</sup>, A. Person<sup>4</sup>, A. Gaudichet<sup>5</sup>, F. Marano<sup>1</sup> and A. Baeza-Squiban<sup>1</sup>

1 : Laboratoire de Cytophysiologie et Toxicologie Cellulaire (LCTC), Université Paris 7, 75005 Paris, France

2 : Laboratoires des Sciences du Climat et de l'Environnement (LSCE), 91191- Gif sur Yvette, France

3 : Laboratoire d'Etude des Particules Inhalées (LEPI), 11 rue Georges Eastman, 750013-Paris, France

4 : Laboratoire d'Hygiène de la Ville de Paris (LHVP) 11 rue Georges Eastman, 750013-Paris, France

5 : Laboratoire Interuniversitaire des Systèmes Atmosphériques (LISA), Université Paris 12, Créteil, France

Keywords: urban aerosols, fine and ultrafine fractions, lung-particle interactions, health effects of aerosols.

Paris background aerosol is almost exclusively composed of fine (PM 2.5; PM 1) and ultra fine (PM 0.1) particles, originating mainly from combustion processes including traffic exhausts. Epidemiological and experimental investigations underlined the role of the aerosol size, in particular the ultra fine one.

The aim of the present study was to investigate which size-fraction of the urban particulate matter is the most relevant regarding to the biological effect considering the proinflammatory response of airway epithelial cells *in vitro*. This response is characterized by the release of mediators that would explain the inflammation observed in exposed subjects.

Human bronchial epithelial cells (16HBE) and primary cultures of nasal epithelial cells (HNE) that are the main target cells of airborne particles were exposed to the different size-fractions. The release of GM-CSF, a cytokine involved in allergic process was used as a proinflammatory biomarker of PM exposure and the cytochrome P450 1A1 (CYP1A1) that metabolizes xenobiotics, which activity was used as a biomarker of polyaromatic hydrocarbon (PAH) bioavailability.

Downtown Paris, four co-located 13-stage Dekati cascade impactors running in parallel were used to selectively collect particles from 30nm to 10µm on polycarbonate filters and were allocated to biological and physico-chemical (black carbon, particulate organic matter and water soluble organic compounds, major ions, PAH) investigations. 11 samplings were conducted in order to investigate whether the seasonal variability (summer and winter) and diurnal evolution related to photochemistry of the urban aerosol composition modulate the biological effects of some or all size-fractions.

*In vitro* biological assays were conducted with particles from pooled stages (1 to 3 representing ultra fine fraction [0.1-0.03µm], 4 to 7 the [1-0.1µm], 8 to 9 the [2.5-1µm] fine fraction and 10 to 13 the [10-2.5µm] coarse fraction). Particles were recovered from collection filters by brief sonications directly in the same volume of cell culture medium for each

size-fractions. Two experimental strategies were used: cells were exposed for 24 hours either at isovolume of particles suspension in order to respect the proportion of the different size-fraction in the sampled-air volume or at isomass.

When cells are exposed to an isovolume of particles suspension, the highest GM-CSF secretion was induced by PM1-0.1 that is the most important fraction in Paris background aerosol (up to 71% of the total PM10 mass). With a cell exposure at an isomass of particles, GM-CSF secretion was significantly induced by fine and ultra-fine particles with a dose-dependent increase from 1µg/cm<sup>2</sup> (5µg/mL) to 10µg/cm<sup>2</sup>, without inducing any cytotoxicity. Whatever the season or diurnal sampling, the finer the aerosol fraction, the higher the GM-CSF secretion was, whereas coarse particles displayed no or fewer effect. Moreover, endotoxins were not involved in the ultrafine particle-induced GM-CSF secretion whereas they partially contributed to the fine particle ones as assessed by the use of endotoxin neutralizing recombinant protein. Considering PAH bioavailability, PM1-0.1 from winter samples induced the higher CYP1A1 activity whereas the CYP 1A1 activity increases as the size decreases with summer samples.

Chemical analyses enlightened the major presence of carbonaceous species in Paris aerosols especially in the ultra-fine and fine fractions where PAH are also predominant (90% in these fractions).

To conclude, we observed that the proinflammatory response of bronchial epithelial cells *in vitro* was closely related to particle size with ultrafine particles exhibiting the highest effect.

This work was supported by ADEME, the french environmental agency, under the PRIMEQUAL grant n° 0462C0056.

## Prolonged retention of ultrafine carbon particles from human airways and the lung periphery

W. Möller<sup>1</sup>, K. Felten<sup>1</sup>, K. Sommerer<sup>3</sup>, G. Scheuch<sup>3</sup>, G. Meyer<sup>2</sup>, K. Häussinger<sup>2</sup>, and W.G. Kreyling<sup>1</sup>

<sup>1</sup>GSF National Research Center for Environment and Health – Clinical Research Group ‘Inflammatory Lung Diseases’ and Institute for Inhalation Biology, Gauting and Neuherberg, Germany

<sup>2</sup>Asklepios Hospital for Respiratory Diseases, Gauting, Germany

<sup>3</sup>Inamed Research GmbH, Gauting, Germany

Keywords: Air pollution, ultrafine particles, bolus technique, clearance, translocation

**Introduction:** A growing body of epidemiological studies have shown consistent associations between the exposure to particulate air pollution and increases in morbidity and mortality rates, especially for persons with obstructive pulmonary and cardiovascular diseases (Samet, J.M. *et al.*, 2000). The causality of the exposure by inhalation and the noxious effects on the cardiovascular system is still under debate. Ultrafine particles may play a specific role in this causality, because they contribute little to the mass concentration (PM10 or PM2.5), but are dominant in the number of airborne particles.

In this study we report on deposition, clearance and translocation of 100 nm radiolabeled carbon particles in healthy human volunteers and in patients with chronic obstructive pulmonary disease (COPD). Because the conducting airways and the alveoli are anatomically different structures with different clearance mechanisms, we targeted the ultrafine test particles to either of these regions by using the aerosol bolus technique.

**Methods:** 99m-Tc radiolabeled 100 nm diameter carbon particles (Technegas (Möller, W. *et al.*, 2006)) were inhaled by healthy non-smokers, asymptomatic smokers and by patients with chronic obstructive pulmonary disease (COPD). Using a bolus inhalation technique particle deposition was targeted either to the airways or to the lung periphery, and retention, clearance and translocation were measured using retained radiotracer imaging (shielded lung counter and gamma camera).

**Results and discussion:** In vitro leaching of the 99mTc-radiotracer after 24 hours was 4.10±2.6%, and 24-hour cumulative urine 99mTc-activity excretion was 1.09±1.25% of deposited activity. Activity in the blood after 1 h and after 5 hours was 0.22±0.17 % and 0.23±0.25 % of the deposited activity, respectively. In the lung periphery particle retention was not affected by smoking or disease; retention was 96.0±2.8 % after 24h (see Figure 1). The inverse correlation of retention with in vitro leaching, blood activity and 24-h urine activity excretion suggests negligible clearance of particles deposited in the lung periphery. In the airways

particle retention and clearance show two phases. Fast mucociliary clearance removes particles within the first 24 hours. In non-smokers retention of particles targeted to the airways was 89.3±5.7 % and 74.8±10.2 % after 1.5 h and 24 h, respectively. There was no further clearance between 24 hours and 48 hours, indicating that the remaining fraction (75 %) is persistent. Retention was significantly increased in smokers (after 1.5 h) and in COPD patients (at all measurement points).

Particle translocation to the liver could not be identified above the detection limit of the gamma camera (0.5 % of deposited activity).

**Conclusions:** Ultrafine carbon particles are prolonged retained in the lung periphery and in the conducting airways (only about 25 % were cleared within 24 hours), and may accumulate after chronic exposure. This may imply increased risks for susceptible individuals, such as patients with chronic diseases

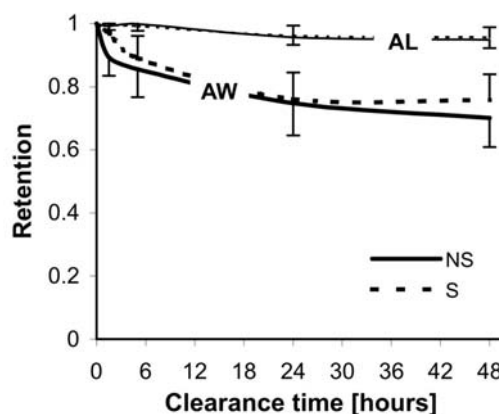


Figure 1. Clearance of 100 nm carbon particles after shallow (AW) and after deep (AL) bolus inhalation in non-smokers (NS) and in asymptomatic smokers (S) during a 48-h post inhalation period..

This study was supported in part by the CEC (FIGD-CT-2000-00053).

Möller, W., *et al.* 2006. *J. Aerosol Sci.* 35, 631-644.  
Samet, J. M., *et al.* 2000. *Research report / HEI* 94, 5-70; discussion 71-9.

